ORGANOMETALLICS

Volume 14, Number 5, May 1995

Communications

Synthesis and Crystal Structure of $Ph_3Ln(THF)_3$ (Ln = Er, Tm)

Leonid N. Bochkarev* and Tatyana A. Stepantseva

Department of Chemistry, Nizhny Novgorod State Pedagogical University, Ulyanova 1, Nizhny Novgorod 603600, Russia

Lev N. Zakharov and Georgy K. Fukin

Institute of Organometallic Chemistry, Russian Academy of Sciences, Tropinina 49, Nizhny Novgorod 603600, Russia

Alexander I. Yanovsky and Yuri T. Struchkov

A. N. Nesmeyanov Institute of Organoelement Compounds, Russian Academy of Sciences, Vavilova 28, Moscow 117813, Russia

Received October 11, 1994[⊗]

*Summary: Triphenyllanthanoids $Ph_3Ln(THF)_3$ (Ln = Er (**1**), Tm (**2**)) were synthesized in THF by reaction of metallic lanthanoids with Ph_2Hg or Ph_3Bi in the presence of catalytic amounts of LnI_3. The X-ray diffraction studies of **1** and **2** have shown that these species represent monomeric complexes with a distorted fac-octahedral arrangement of ligands around the Ln atom.*

Known synthetic pathways to homoleptic lanthanoid aryls of R_2Ln and R_3Ln type are not of general utility for the entire lanthanoid series. Thus, the reaction of PhLi and $LnCl_3$ yields Ph_3Sc and Ph_3Y, whereas the anionic $[Ph_4Ln]Li$ complexes were isolated in the case of La and Pr.[1] Chelating (aminotolyl)lithium reagents allowed the synthesis of σ-aryls $[o\text{-}Me_2NCH_2C_6H_4]_3Ln$ of Sc, Y, Pr, Yb and Lu);[2-4] however, no characterizable products have been isolated in the case of Pr, Nd, Sm, and Tb.[3]

Transmetalation reactions of R_2Hg and metallic lanthanoids have been successfully used for preparation of polyfluorophenyl complexes R_2Ln ($R = C_6F_5$, $o\text{-}HC_6F_4$, $p\text{-}HC_6F_4$; Ln = Sm, Eu, Yb)[5-7] and (benzene)tricarbonylchromium derivatives $[(OC)_3CrPh]_2Ln(THF)_n$ (Ln = Sm, Eu, Yb; n = 1, 2).[8] Diphenylmercury was found to be unreactive toward free Yb,[6] while slow interaction was observed with the amalgamated metal,[8] and violent reaction has been reported[9] for ytterbium activated with CH_2I_2. Phenylytterbium species are formed in these processes in 35–75% yields and identified *in situ* by reactions with H_2O, Ph_3SnCl, and 9-fluorenone. They have been formulated as Ph_2Yb.[8,9]

[⊗] Abstract published in *Advance ACS Abstracts,* March 15, 1995.

(1) Hart, F. A.; Massey, A. G.; Saran, M. S. *J. Organomet. Chem.* **1970**, *21*, 147.
(2) Manzer, L. E. *J. Am. Chem. Soc.* **1978**, *100*, 8068.
(3) Wayda, A. L.; Atwood, J. L.; Hunter, W. E. *Organometallics* **1984**, *3*, 939.
(4) Booij, M.; Kiers, N. H.; Heeres, H. J.; Teuben, J. H. *J. Organomet. Chem.* **1989**, *364*, 79.
(5) Deacon, G. B.; Vince, D. G. *J. Organomet. Chem.* **1976**, *112*, C1.
(6) Deacon, G. B.; Raverty, W. D.; Vince, D. G. *J. Organomet. Chem.* **1977**, *135*, 103.
(7) Deacon, G. B.; Koplick, A. J.; Raverty, W. D.; Vince, D. G. *J. Organomet. Chem.* **1979**, *182*, 121.
(8) Suleimanov, G. Z.; Khandozhko, R. N.; Mekhdiev, R. Yu.; Petrovsky, P. V.; Agdamsky, T. A.; Kolobova, N. E.; Beletskaya, I. P. *Dokl. Akad. Nauk SSSR* **1985**, *284*, 1376.
(9) Starostina, T. A.; Shifrina, R. R.; Rybakova, L. F.; Petrov, E. S. *Zh. Obshch. Khim.* **1987**, *57*, 2402.

0276-7333/95/2314-2127$09.00/0

It has been recently reported that the (naphthalene)-ytterbium compound $C_{10}H_8Yb(THF)_2$ reacts readily with Ph_2Hg to form the binuclear complex $(THF)Ph_2Yb(\mu\text{-}Ph)_3Yb(THF)_3$ as a major product, with only a small amount of $Ph_3Yb(THF)_3$.[10] Among $(aryl)_3Ln$ compounds, X-ray structural data are available only for $(o\text{-}Me_2NCH_2C_6H_4)_3Lu$[3] and the binuclear derivative $(THF)Ph_2Yb(\mu\text{-}Ph)_3Yb(THF)_3$[10]. The latter compound is thought to consist of associated $Ph_2Yb^{II}(THF)$ and $Ph_3Yb^{III}(THF)_3$ units.

We have recently observed the enhanced activity of lanthanoid metals in some reactions with organic and organometallic substrates in the presence of catalytic amounts of lanthanoid halides.[11-13] This catalytic activity of lanthanoid salt appears to be operative also in transmetalation of Ph_2Hg or Ph_3Bi and metallic lanthanoids. The reactions proceed in THF at room temperature in the presence of lanthanoid triiodides and lead to $Ph_2Ln(THF)_2$ (Ln = Eu, Yb) and $Ph_3Ln(THF)_3$ complexes (Ln = Ho, Er, Tm, Lu) in 75–95% yields. Herein we report the synthesis and the crystal structure of $Ph_3Ln(THF)_3$ (Ln = Er, Tm). The reactions of Eu, Yb, Ho, and other lanthanoids with Ph_2Hg and Ph_3Bi are currently under detailed investigation.

Er and Tm were found to react with Ph_2Hg in the presence of appropriate lanthanoid triiodides (3.0–5.0 mol %) over a period of 120–150 h. The yields of crude complexes **1** and **2** are usually 90–95%.[14]

$$3Ph_2Hg + 2Ln \xrightarrow[20\ ^\circ C]{THF,LnI_3} 2Ph_3Ln(THF)_3 + 3Hg$$

$$Ln = Er, Tm$$

The reaction of Er with Ph_3Bi in the presence of ErI_3 (4.0 mol %) is completed in ca. 200 h with the formation of complex **1** in 70% yield. The course of the reactions was monitored by the yield of metallic mercury or bismuth. After recrystallization from THF, complexes **1** and **2** were isolated in 40–45% yields as air-sensitive pale pink (**1**) and colorless (**2**) crystals. They are sparingly soluble in THF, poorly soluble in toluene, and insoluble in hexane. They decompose at 95–100 °C (**1**) and 120–125 °C (**2**). IR spectra of **1** and **2** are essentially identical and show the absorption bands of phenyl rings (3010 w, 1405 m, 1225 w, 1065 w, 1045 m, 1015 s, 985 w, 910 w, 715 m, 700 s, 670 s, 665 m, 625 m, 425 m cm^{-1}) and coordinated THF (1035 w, 865 br, s cm^{-1}).

The structures of **1** and **2** were determined by X-ray diffraction method.[15] Crystals of **1** and **2** are isostructural and consist of monomeric molecules. The Ln atoms in complexes **1** (Ln = Er) and **2** (Ln = Tm) have a distorted *fac*-octahedral environment (Figure 1). The C(1)–Ln–C(7), C(1)–Ln–C(13), and C(7)–Ln–C(13) angles (99.2(2), 99.8(2), and 103.5(2)° for Ln = Er; 99.8-(2), 101.4(2), and 102.9(2)° for Ln = Tm) are significantly more than 90°, whereas the O(1)–Ln–O(2), O(1)–Ln–O(3), and O(2)–Ln–O(3) angles (80.6(1), 79.3(1), 77.7-(1)° for Ln = Er; 81.0(2), 79.5(1), 78.0(2)° for Ln = Tm) are significantly less than 90°. Similar patterns in the O(R)–Ln–O(R) and O(THF)–Ln–O(THF) angles were found in the *fac*-octahedral complexes $Y(OSiPh_3)_3(THF)_3$ (100.8–102.3 and 79.6–82.2°)[16] and $Ce(OSiPh_3)_3(THF)_3$ (100.4–103.3° and 76.5–83.1°).[17]

The Ln–C(1), Ln–C(7), and Ln–C(13) distances are 2.412(5), 2.442(5), and 2.440(6) Å for Ln = Er in **1** and 2.421(6), 2.425(6), and 2.416(7) Å for Ln = Tm in **2**. The difference between the average Er–C (2.431(14) Å) and Tm–C (2.421(4) Å) distances in **1** and **2** is equal to the difference in the radii for six-coordinate Er^{3+} and Tm^{3+}, 0.01 Å, given by Shannon.[18] The Er–C and Tm–C distances in **1** and **2** may be compared with the Ln–C(aryl) distances found in other organolanthanoid complexes: the average Lu–C distance, 2.435 Å, in $(o\text{-}Me_2NCH_2C_6H_4)_3Lu$;[3] the average Yb–C distance, 2.42 Å, for terminal Ph groups in $(THF)Ph_2Yb(\mu\text{-}Ph)_3Yb(THF)_3$;[10] the Gd–C distance, 2.412 Å, in $PhGdCl_2(THF)_4$;[19] the Sm–C distance, 2.511 Å, in $(Me_5C_5)_2SmPh(THF)$;[20] the Lu–C distance, 2.345 Å, in $Cp_2LuC_6H_4Me\text{-}p(THF)$;[21] the average Y–C distance,

(10) Bochkarev, M. N.; Khramenkov, V. V.; Rad'kov, Yu. F.; Zakharov, L. N.; Struchkov, Yu.T. *J. Organomet. Chem.* **1992**, *429*, 27.
(11) Bochkarev, L. N.; Grachev, O. V.; Zhiltsov, S. F.; Zakharov, L. N.; Struchkov, Yu. T. *J. Organomet. Chem.* **1992**, *436*, 299.
(12) Bochkarev, L. N.; Grachev, O. V.; Zhiltsov, S. F. *Metalloorg. Khim.* **1993**, *6*, 249.
(13) Bochkarev, L. N.; Molosnova, N. E.; Zakharov, L. N.; Fukin, G. K.; Yanovsky, A. I.; Struchkov, Yu. T. *J. Organomet. Chem.* **1995**, *485*, 101.

(14) All operations in the synthesis and isolation of **1** and **2** were performed in vacuo in sealed ampules using thoroughly dried solvents. Preparation of **1**: A mixture of Ph_2Hg (0.5 g, 1.41 mmol), ErI_3 (0.03 g, 0.06 mmol), and erbium in the form of filings (1.35 g, 8.07 mmol) in 15 mL of THF was stirred using a magnetic stirrer for ca. 120 h at room temperature. The excess Er and the metallic mercury formed were separated from the brown solution by centrifugation and washed with warm THF (2 × 15 mL); 0.27 g (95.5%) of mercury was found in the excess erbium. The reaction solution and washings were combined and evaporated to dryness in vacuo at room temperature to yield 0.55 g (94.8%) of crude complex **1** as a brown solid. Anal. Calcd for $C_{30}H_{39}ErO_3$: C, 58.60; H, 6.39; Er, 27.20. Found: Er, 28.5. Crude complex **1** was dissolved in 5 mL of THF at 50 °C and slowly cooled to 0 °C to yield 0.26 g (45.0%) of **1** in the form of pale-pink hexagonal prisms. Dec pt: 95–100 °C. Anal. Found: C, 58.33; H, 6.34; Er, 26.95. Complex **2** was synthesized in a similar way from 0.5 g (1.41 mmol) of Ph_2Hg and 1.40 g (8.29 mmol) of Tm in the presence of 0.03 g (0.06 mmol) of TmI_3. The reaction time was 150 h. Yield of crude complex **2**: 0.53 g (91.4%). Anal. Calcd for $C_{30}H_{39}TmO_3$: C, 58.44; H, 6.38; Tm, 27.40. Found: Tm, 29.00. After recrystallization from THF complex **2** was obtained as colorless crystals (0.22 g, 40.0%). Dec pt 120–125 °C. Anal. Found: C, 58.31; H, 6.10; Tm, 27.17.
(15) X-ray data for **1** and **2** were collected at 153 K on a Siemens P3/PC diffractometer (Mo Kα radiation, graphite monochromator, Θ–2Θ scan mode, $2 \le \Theta \le 25$ and $2 \le \Theta \le 24°$, 5001 and 4911 independent reflections measured, 3958 ($F > 4\sigma(F)$) and 3626 ($F > 6\sigma(F)$) reflections observed for **1** and **2**, respectively). Crystal data at 153 K for **1**: $C_{30}H_{39}O_3Er$, fw 614.9, space group $C2/c$, $a = 36.047(7)$ Å, $b = 11.244(2)$ Å, $c = 14.029(3)$ Å, $\beta = 102.12(3)°$, $V = 5559(3)$ Å^3, $Z = 8$, $D_{calc} = 1.469$ g/cm^3, $\mu = 3.085$ mm^{-1}. Crystal data at 153 K for **2**: $C_{30}H_{39}O_3Tm$, fw 616.5, space group $C2/c$, $a = 36.128(12)$ Å, $b = 11.257(5)$ Å, $c = 14.026(5)$ Å, $\beta = 102.07(3)°$, $V = 5578(4)$ Å^3, $Z = 8$, $D_{calc} = 1.468$ g/cm^3, $\mu = 3.239$ mm^{-1}. The structures of **1** and **2** were solved by direct methods. In both structures all non-H atoms were refined anisotropically. The phenyl H atoms were located in the difference Fourier maps (refined isotropically), and the tetrahydrofuran H atoms were calculated (refined in riding model with fixed isotropic parameters $U = 0.08$ Å^2). Absorption was taken into account by the DIFABS program (Walker, N.; Stuart, D. *Acta Crystallogr., Sect. A* **1983**, *39*, 158). The final refinements converged at $R = 0.044$, $R_w = 0.049$, and $S = 1.18$ for **1** and $R = 0.036$, $R_w = 0.046$, and $S = 1.33$ for **2**, for observed reflections. The $(\Delta/\sigma)_{av}$ values in the final cycles are 0.006 (**1**) and 0.002 (**2**). All calculations were performed using the SHELXTL-Plus package (Sheldrick, G. M. Structure Determination Software Program Package (PC version); Siemens Analytical X-ray Instruments, Inc., Madison, WI, 1989).
(16) McGeary, M. J.; Coan, P. S.; Folting, K.; Streib, W. E.; Caulton, K. G. *Inorg. Chem.* **1989**, *28*, 3283.
(17) Gradeff, P. S.; Yunlu, K.; Deming, T. J.; Olofson, J. M.; Doedens, R. J.; Evans, W. J. *Inorg. Chem.* **1990**, *29*, 420.
(18) Shannon, R. D. *Acta Crystallogr., Sect. A* **1976**, *A32*, 751.
(19) Lin, G.; Jin, Z.; Zhang, Y.; Chen, W. *J. Organomet. Chem.* **1990**, *396*, 307.
(20) Evans, W. J.; Bloom, I.; Hunter, W. E.; Atwood, J. L. *Organometallics* **1985**, *4*, 112.
(21) Schumann, H.; Genthe, W.; Bruncks, N.; Pickardt, J. *Organometallics* **1982**, *1*, 1194.

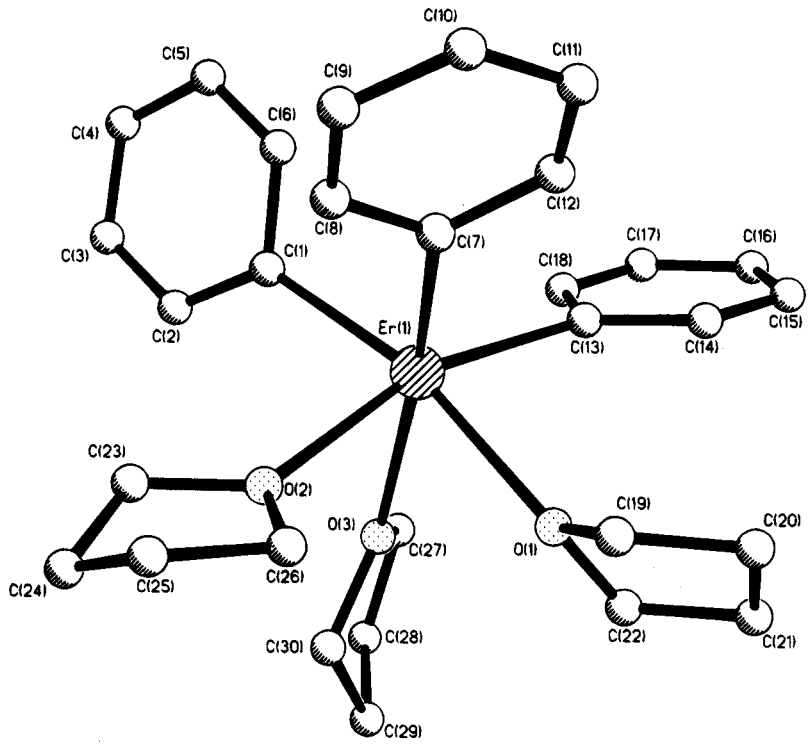

Figure 1. General view of **1** and atom labeling (**2** has a similar structure). Pertinent parameters (distances in Å and angles in deg): Ln–C(1), Ln–C(7), Ln–C(13) 2.412(5), 2.442(5), 2.440(6) (Ln = Er) and 2.421(6), 2.425(6), 2.416(7) (Ln = Tm); Ln–O(1), Ln–O(2), Ln–O(3) 2.423(3), 2.408(4), 2.419(3) (Ln = Er) and 2.429(4), 2.391(5), 2.401(4) (Ln = Tm); C(1) Ln–C(7), C(1)–Ln–C(13), C(7)–Ln–C(13) 99.2(2), 99.8(2), 103.5(2) (Ln = Er) and 99.8(2), 101.4(2), 102.9(2) (Ln = Tm); O(1)–Ln–O(2), O(1)–Ln–O(2), O(2)–Ln–O(3) 80.6(1), 79.3(1), 77.7(1) (Ln = Er) and 81.0(2), 79.5(1), 78.0(2) (Ln = Tm).

2.41 Å, in $Cp_2YC_6H_4CH_2NMe_2$-*o*.[22] The Yb–C distances for μ-bridging Ph groups in $(THF)Ph_2Yb(\mu\text{-}Ph)_3Yb(THF)_3$[10] (2.48–2.75 Å) and in $(THF)_2Ph_3SnYb(\mu\text{-}Ph)_3Yb(THF)_3$[23] (2.60–2.66 Å) are longer than the lengths of the above-mentioned terminal Ln–C bonds.

The Ln–O(1), Ln–O(2), and Ln–O(3) distances (2.423(3), 2.408(4), 2.419(3) Å for Ln = Er and 2.429(4), 2.391(5), 2.401(4) Å for Ln = Tm) in **1** and **2** are somewhat shorter than the average Ln–O(THF) distances for the $Ln(THF)_3$ *cis* fragment in the complexes $(THF)Ph_2Yb(\mu\text{-}Ph)_3Yb(THF)_3$[11] (2.44 Å) and $(THF)_2Ph_3SnYb(\mu\text{-}Ph)_3Yb(THF)_3$[24] (2.468 Å) with an octahedral environment around the Yb atom. The Er(Tm)-O(THF) distances in **1** and **2** are longer than those in cyclopentadienyllanthanoid complexes[24] if the differences in metal size and coordination number are considered. The steric crowding seems to be the predominant factor in such Ln–O(THF) bond lengthening. However, the trans influence of the *fac* phenyl groups can also be a reason. Unfortunately, the available X-ray data are not sufficient to evaluate such an influence in **1** and **2**.

Acknowledgment. We thank the Russian Foundation of Fundamental Research (Grant 93-03-5722) for financial support of this work.

Supplementary Material Available: Tables of crystallographic data, data collection, and solution and refinement details, positional and thermal parameters, and bond distances and bond angles for **1** and **2** (16 pages). Ordering information is given on any current masthead page.

OM940784N

(22) Rausch, M. D.; Foust, D. F.; Rogers, R. D.; Atwood, J. P. *J. Organomet. Chem.* **1984**, *265*, 241.
(23) Bochkarev, M. N.; Khramenkov, V. V.; Rad'kov, Yu.F.; Zakharov, L. N.; Struchkov, Yu. T. *J. Organomet. Chem.* **1991**, *421*, 29.
(24) Deacon, G. B.; Mackinnon, P. I.; Hambley, T. W.; Taylor, J. C. *J. Organomet. Chem.* **1983**, *259*, 91.

Synthesis of Very Large Organoruthenium Dendrimers

Yi-Hsien Liao and John R. Moss*

Department of Chemistry, University of Cape Town, Rondebosch 7700, South Africa

Received January 11, 1995[⊗]

Summary: A dendrimer containing 48 ruthenium atoms has been prepared by the convergent approach. The organoruthenium functional groups are attached exclusively at the periphery of a poly(benzyl phenyl ether) dendritic structure.

Synthesis of dendritic macromolecules has attracted much attention in recent years.[1] Also, there is a growing interest in the preparation of organometallic macromolecules, which may have novel properties and applications.[2]

Organometallic dendrimers containing Ge,[3] Si,[4] Fe,[5] and Pt[6] have recently been reported. Previously, we have prepared a dendrimer containing 12 organoruthenium functional groups.[7] We have now extended this methodology and prepared some very large metal complexes (VLMC's). In this way, a new dendritic macromolecule containing 48 organoruthenium functional groups ($CpRu(CO)_2CH_2CH_2CH_2-$), located exclusively at the periphery of the dendritic structure, has been prepared by a stepwise approach. As far as we know, this dendrimer is the largest organotransition-metal complex ever reported. It has a nominal molecular mass of 18 438 amu and an estimated diameter of about 5 nm. The size has been measured using a computer-generated molecular model.[8] The synthesis of these dendritic macromolecules and some of their properties are described below.

We have prepared the organoruthenium dendritic macromolecules using the convergent approach, as developed by Hawker and Fréchet.[9] Previously we have reported the synthetic methodology for this type of dendrimer, but only up to the second generation.[7] Thus, the available[7] second-generation dendritic wedge **Rp3G2Br** (Figure 1) is reacted with the dendritic building block 3,5-dihydroxybenzyl alcohol to give the third-generation dendritic wedge **Rp3G3OH**. In the next step, **Rp3G3OH** was converted to the analogous benzyl bromide complex **Rp3G3Br** by reaction with a large excess of PPh_3 and CBr_4 (Scheme 1). We have been able to construct dendritic wedges up to the fourth

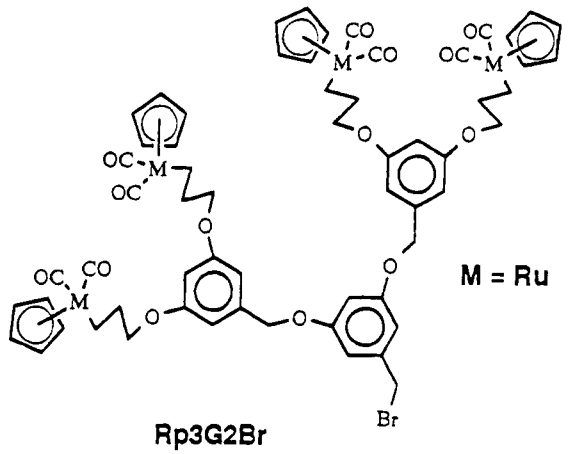

Figure 1. Molecular representation of the second-generation organoruthenium dendritic wedge. The notation we have used for these dendrimers is of the form Rpn1Gn2x, where Rp = $(\eta^5\text{-}C_5H_5)Ru(CO)_2$, n1 is the number of methylene groups in the polymethylene chain (which is 3 in all complexes described in this paper), G is a character that stands for "generation", n2 is the generation number of the dendrimer, and x is the functional group at the focal point of the dendrimer.

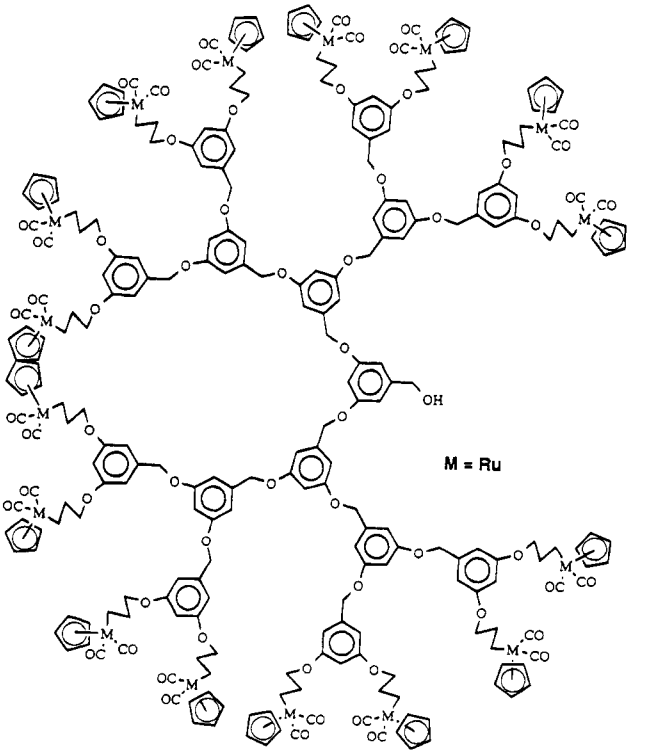

Figure 2. Molecular representation of the fourth-generation organoruthenium dendritic wedge, **Rp3G4OH**.

[⊗] Abstract published in *Advance ACS Abstracts,* April 1, 1995.

(1) (a) Kim, Y. H. *Adv. Mater.* **1992,** *4,* 764. (b) Dagani, R. *Chem. Eng. News* **1993,** *71* (Feb. 1), 28. (c) Hodge, P. *Nature* **1993,** *362,* 18. (d) Mekelburger, H. B.; Jaworek, W.; Vogtle, F. *Angew. Chem., Int. Ed. Engl.* **1992,** *31,* 1571.

(2) Sheats, J. E.; Carraher, C. E., Jr.; Pittman, C. U., Jr.; Zeldin, M.; Currell, B. *Inorganic and Metal-Containing Polymeric Materials*; Plenum Press: New York, 1990.

(3) Bochkarev, M. N. *Metalloorg. Khim. (USSR)* **1988,** *1,* 115.

(4) (a) Zhou, L.-L.; Roovers, J. *Macromolecules* **1993,** *26,* 963. (b) Seyferth, D.; Son, D. Y.; Rheingold, A. L.; Ostrander, R. L. *Organometallics* **1994,** *13,* 2682.

(5) Moulines, F.; Djakovitch, L.; Boese, R.; Gloaguen, B.; Thiel, W.; Fillaut, J.-L.; Delville, M.-H.; Astruc, D. *Angew. Chem., Int. Ed. Engl.* **1993,** *32,* 1075.

(6) (a) Achar, S.; Puddephatt, R. J. *Angew. Chem., Int. Ed. Engl.* **1994,** *33,* 847. (b) Achar, S.; Puddephatt, R. J. *J. Chem. Soc., Chem. Commun.* **1994,** 1895.

(7) Liao, Y.-H.; Moss, J. R. *J. Chem. Soc., Chem. Commun.* **1993,** 1774.

(8) The computer-assisted molecular models have been generated using Hyperchem.

(9) Hawker, C.; Fréchet, J. M. J. *J. Chem. Soc., Chem. Commun.* **1990,** 1010. (b) Hawker, C.; Fréchet, J. M. J. *J. Am. Chem. Soc.* **1990,** *112,* 7638.

0276-7333/95/2314-2130$09.00/0

Scheme 1[a]

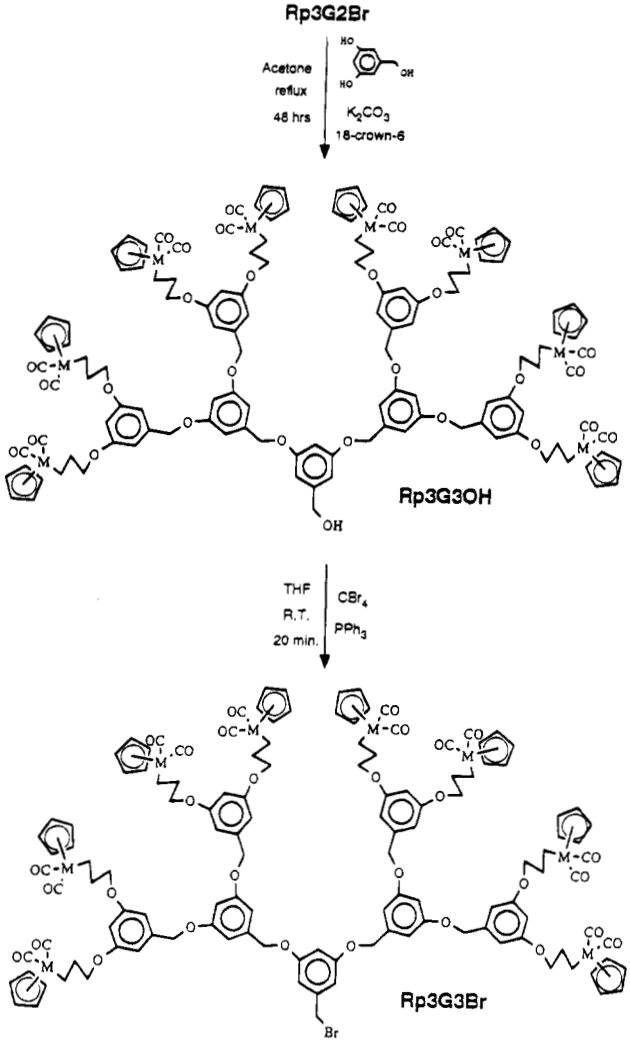

[a] M = Ru.

generation, *viz.* **Rp3G4OH** and **Rp3G4Br** (Figure 2), using a similar reaction sequence. Although the reaction steps are similar to those reported for earlier generations, it is found that the yields of the reactions decrease somewhat as the size of the dendritic wedges increases. This may be due to the increasing steric congestion, which reduces the reactivity of functional groups at the focal point.

In the convergent approach, the dendritic wedges **Rp3Gx Br** ($x = 3, 4$) can be reacted with a polyfunctional core molecule. Here, the chosen trifunctional core molecule is 1,1,1-tris(4-hydroxyphenyl)ethane. Thus, in a typical reaction[10] 3 molar equiv of the dendritic wedge **Rp3Gx Br** ($x = 3, 4$) is reacted with 1 molar equiv of the core molecule in the presence of potassium carbonate and 18-crown-6 in refluxing acetone for 48 h. The resulting products **Rp3G3C** and **Rp3G4C** have 24 and 48 organoruthenium functional groups, respectively, attached to the surface of the dendritic structure. (In the notation we have used in this paper, **Rp3G3C** and **Rp3G4C** refer to three third-generation dendritic wedges and three fourth-generation dendritic wedges, respectively, attached to the core.)

All of the new complexes were purified by column chromatography, followed by several recrystallizations from CH_2Cl_2/hexane mixtures. The complexes are air-stable in the pure state but slowly decompose in solution on exposure to air. The organoruthenium dendrimers described in this paper are soluble in most common organic solvents, except hexane, and they are sparingly soluble in methanol.

The novel organoruthenium dendrimers have been characterized by IR and ^1H and ^{13}C NMR spectroscopy, as well as elemental analysis and mass spectrometry.[11] ^1H NMR spectroscopy has proved to be particularly crucial for the characterization of these new dendritic complexes. For example, Figure 3 shows the 400 MHz

(10) **Experimental procedure for the synthesis of Rp3G4C:** A mixture of **Rp3G4Br** (110 mg, 0.018 mmol), 1,1,1-tris(4-hydroxyphenyl)ethane (1.8 mg, 0.0058 mmol), potassium carbonate (320 mg, excess), and 18-crown-6 (49 mg, excess) in acetone (30 mL) was stirred vigorously and heated at reflux for 48 h. After this time, another portion of 1,1,1-tris(4-hydroxyphenyl)ethane (22 mg, excess) was added, and the reaction mixture was stirred and heated at reflux for another 24 h. The solvent was then removed under reduced pressure. The residue was extracted with CH_2Cl_2 (*ca.* 20 mL) and filtered. The pale yellow filtrate was concentrated and transferred to an alumina column, with a 60% CH_2Cl_2/40%/hexane solution as eluent. The major colorless fraction was collected and concentrated. A pale yellow oil separated out from the solution at −15 °C and the final white glassy solid was obtained after drying this oil under high vacuum. Yield: 70 mg, 66%.

(11) **Rp3G3OH:** yield 74%; IR (CH_2Cl_2) ν 2012, 1948 cm^{-1} (CO); ^1H NMR (400 MHz, $CDCl_3$, 25 °C) δ 6.66 (d, ^4J(H,H) = 2 Hz, 4H, Ar), 6.59 (d, ^4J(H,H) = 2 Hz, 2H, Ar), 6.54 (d, ^4J(H,H) = 2 Hz, 11H, Ar), 6.40 (t, ^4J(H,H) = 2 Hz, 4H, Ar), 5.23 (s, 40H, Cp), 4.96 (s, 4H, $ArCH_2O$), 4.95 (s, 8H, $ArCH_2O$), 4.62 (d, ^3J(H,H) = 6 Hz, 2H, CH_2-OH), 3.85 (t, ^3J(H,H) = 7 Hz, 16H, CH_2O), 2.00 (m, 16H, CH_2), 1.69 (m, 16H, $RuCH_2$); ^{13}C NMR (100 MHz, $CDCl_3$, 25 °C) δ 202.10 (CO), 160.54, 160.16, 160.10, 138.94, 106.37, 105.69, 100.80 (Ar), 88.55 (Cp), 71.06, 70.18 (CH_2O), 38.47 (CH_2), −9.31 ($RuCH_2$); MS (FAB) *m/z* 2922 (M^+ − 2CO). Anal. Found: C, 51.4; H, 4.2. Calcd for $C_{129}H_{124}O_{31}Ru_8$ (M_r 2979.09): C, 52.0; H, 4.2. **Rp3G4OH:** yield 66%; IR (CH_2Cl_2) ν 2012, 1948 cm^{-1} (CO); ^1H NMR (400 MHz, $CDCl_3$, 25 °C) δ 6.66 (d, ^4J(H,H) = 2 Hz, 4H, Ar), 6.59 (d, ^4J(H,H) = 2 Hz, 2H, Ar), 6.53 (d, ^4J(H,H) = 2 Hz, 23H, Ar), 6.38 (t, ^4J(H,H) = 2 Hz, 4H, Ar), 5.21 (s, 80H, Cp), 4.96 (s, 4H, $ArCH_2O$), 4.94 (s, 8H, $ArCH_2O$), 4.93 (s, 16 H, $ArCH_2O$), 4.57 (d, ^3J(H,H) = 6 Hz, 2H, $ArCH_2OH$), 3.83 (t, ^3J(H,H) = 6 Hz, 32H, CH_2O), 1.98 (m, 32H, CH_2), 1.67 (m, 32H, $RuCH_2$); ^{13}C NMR (100 MHz, $CDCl_3$, 25 °C) δ 202.13 (CO), 177.24, 160.54, 160.15, 160.10, 139.13, 138.92, 106.48, 106.46, 106.43, 105.71, 100.79 (Ar), 88.56 (Cp), 71.04, 70.17, 70.07 ($ArCH_2O$), 38.47 (CH_2), −9.37 ($RuCH_2$). Anal. Found: C, 52.7; H, 4.5. Calcd for $C_{265}H_{252}O_{63}Ru_{16}$ (M_r 6062.00): C, 52.5; H, 4.2. **Rp3G3Br:** yield 73%; IR (CH_2Cl_2) ν 2012, 1948 cm^{-1} (CO); ^1H NMR (400 MHz, $CDCl_3$, 25 °C) δ 6.66 (d, ^4J(H,H) = 2 Hz, 4H, Ar), 6.62 (d, ^4J(H,H) = 2 Hz, 2H, Ar), 6.57 (t, ^4J(H,H) = 2 Hz, 3H, Ar), 6.55 (d, ^4J(H,H) = 2 Hz, 8H, Ar), 6.40 (t, ^4J(H,H) = 2 Hz, 4H, Ar), 5.23 (s, 40H, Cp), 4.96 (s, 12H, $ArCH_2O$), 4.41 (s, 2H, CH_2Br), 3.86 (t, ^3J(H,H) = 7 Hz, 16H, CH_2O), 2.01 (m, 16H, CH_2), 1.69 (m, 16H, $RuCH_2$); ^{13}C NMR (100 MHz, $CDCl_3$, 25 °C) δ 202.10 (CO), 160.56, 160.18, 138.92, 106.46, 105.70, 100.80 (Ar), 88.55 (Cp), 71.05 (CH_2O), 70.21, 70.11 ($ArCH_2O$), 38.48 (CH_2), −9.30 ($RuCH_2$); MS (FAB) *m/z* 2988 (M^+ − 2CO). Anal. Found: C, 50.5; H, 4.4. Calcd for $C_{129}H_{123}O_{30}BrRu_8$ (M_r 3041.84): C, 50.8; H, 4.1. **Rp3G4Br:** yield 66%; IR (CH_2Cl_2) ν 2012, 1948 cm^{-1} (CO); ^1H NMR (400 MHz, $CDCl_3$, 25 °C) δ 6.67(d, ^4J(H,H) = 2 Hz, 8H, Ar), 6.63 (d, J = 2 Hz, 4H, Ar), 6.54 (d, ^4J(H,H) = 2 Hz, 25H, Ar), 6.40 (t, ^4J(H,H) = 2 Hz, 8H, Ar), 5.22 (s, 80H, Cp), 4.96, 4.94 (s, 30H, $ArCH_2O$), 4.38 (s, 2H, CH_2Br), 3.85 (t, ^3J(H,H) = 7 Hz, 32H, CH_2O), 2.00 (m, 32H, CH_2), 1.68 (m, 32H, $RuCH_2$); ^{13}C NMR (100 MHz, $CDCl_3$, 25 °C) δ 202.11 (CO), 160.54, 160.16, 139.08, 138.92, 106.49, 105.70, 100.79 (Ar), 88.55 (Cp), 71.02 (CH_2O), 70.16, 70.07 ($ArCH_2O$), 38.46 (CH_2), −9.30 ($RuCH_2$). Anal. Found: C, 52.1; H, 4.2. Calcd for $C_{265}H_{251}O_{62}BrRu_{16}$ (M_r 6124.89): C, 52.0; H, 4.1. **Rp3G3C:** yield 54%; IR (CH_2Cl_2) ν 2012, 1948 cm^{-1} (CO); ^1H NMR (400 MHz, $CDCl_3$, 25 °C) δ 7.01 (d, ^3J(H,H) = 9 Hz, 6H, Ar^{CORE}), 6.87 (d, ^3J(H,H) = 9 Hz, 6H, Ar^{CORE}), 6.69 (d, ^4J(H,H) = 2 Hz, 6H, Ar), 6.67 (d, ^4J(H,H) = 2 Hz, 12H, Ar), 6.54 (d, ^4J(H,H) = 2 Hz, 33H, Ar), 6.39 (t, ^4J(H,H) = 2 Hz, 12H, Ar), 5.21 (s, 120H, Cp), 4.94 (s, 42H, $ArCH_2O$), 3.84 (t, ^3J(H,H) = 7 Hz, 48H, CH_2O), 2.04 (s, 3H, CCH_3), 1.99 (m, 48H, CH_2), 1.67 (m, 48H, $RuCH_2$); ^{13}C NMR (100 MHz, $CDCl_3$, 25 °C) δ 202.13 (CO), 160.54, 160.16, 139.09, 138.92, 106.53, 105.70, 100.79 (Ar + Ar^{CORE}), 88.56 (Cp), 71.03, 70.17, ($ArCH_2O$), 38.47 (CH_2), −9.30 ($RuCH_2$). Anal. Found: C, 53.3; H, 4.4. Calcd for $C_{407}H_{384}O_{93}Ru_{24}$ (M_r 9189.15): C, 53.2; H, 4.2. **Rp3G4C:** yield 66%; IR (CH_2Cl_2) ν 2012, 1948 cm^{-1} (CO); ^1H NMR (400 MHz, $CDCl_3$, 25 °C) δ 7.01 (br d, 6H, Ar^{CORE}), 6.84 (br d, 6H, Ar^{CORE}), 6.65 (br, 42H, Ar), 6.52 (br, 69H, Ar), 6.37 (br, 24H, Ar), 5.17 (s, 240H, Ar), 4.91 (br, 90H, $ArCH_2O$), 3.82 (br, 96H, CH_2O), 1.96 (m, 99H, CH_2 and CH_3), 1.66 (m, 96H, $RuCH_2$); ^{13}C NMR (100 MHz, $CDCl_3$, 25 °C) δ 202.13 (CO), 160.53, 160.13, 138.93, 106.51, 105.70, 101.63, 100.80 (Ar + Ar^{CORE}), 88.56 (Cp), 71.03, 70.17 ($ArCH_2O$), 38.47 (CH_2), −9.29 ($RuCH_2$). Anal. Found: C, 52.9; H, 4.3. Calcd for $C_{815}H_{768}O_{189}Ru_{48}$ (M_r 18438.31): C, 53.1; H, 4.2.

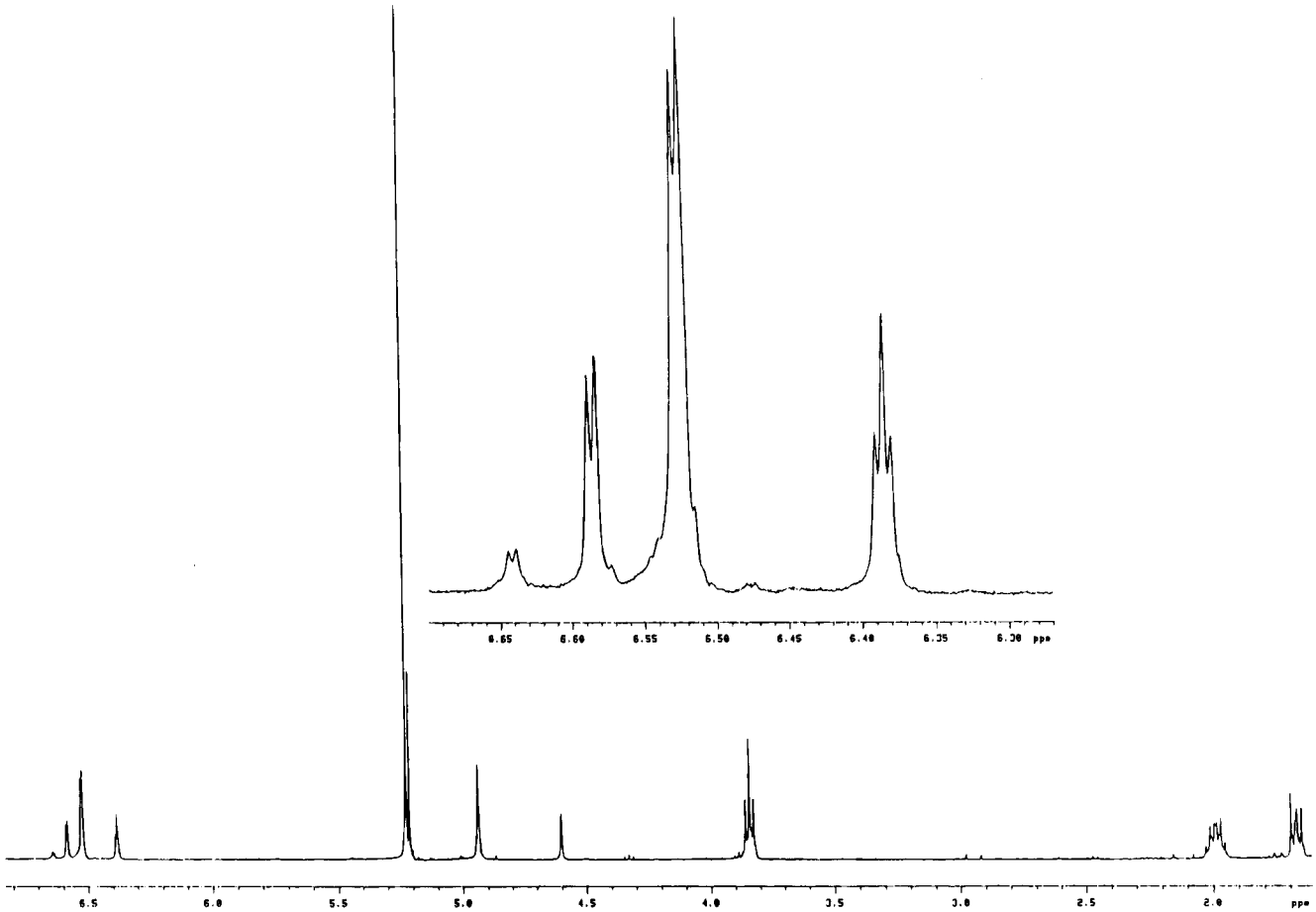

Figure 3. ^{1}H NMR spectrum (400 MHz, $CDCl_3$) of Rp3G3OH.

^{1}H NMR spectrum of **Rp3G3OH**. The organoruthenium functional groups give four sets of resonances at δ 5.23 (Cp), 3.85 (CH_2O), 2.01 (CH_2), and 1.70 ppm ($RuCH_2$). The triplet observed at δ 3.85 ppm is important, since it confirms the formation of the anticipated product (**Rp3G1OH**) from the (bromopropyl)ruthenium complex [$CpRu(CO)_2(CH_2CH_2CH_2Br)$], as we reported previously.[7] Also, the exponential growth in intensity of the resonances during the course of the synthesis indicates that the number of organoruthenium groups is correspondingly increasing in the growing dendritic structure. The ^{1}H NMR resonances occurring in the region of δ 6.3–6.7 ppm were assigned to the aromatic protons of the dendritic building blocks. Separate resonances, corresponding to each "layer" of dendritic monomer, were observed. This is demonstrated in Figure 3, from which the generation number can be easily identified by the number of doublet peaks (thus, three doublets were observed for the third-generation benzyl alcohol **Rp3G3OH**). In all cases, the integration of resonances was employed to further confirm the generation number and to ascertain whether the reaction of **Rp3G*x*Br** with the core molecule (or with 3,5-dihydroxybenzyl alcohol) had gone to completion.

The molecular masses of the dendrimers (up to 4500 amu) have been confirmed using fast atom bombardment (FAB) mass spectrometry, as reported in ref 11. We have made repeated attempts to try and observe molecular ions for the dendrimers with higher masses, including the use of matrix-assisted laser desorption ionization (MALDI) mass spectrometry. However, these attempts have so far been unsuccessful and we believe that this is due to two factors: (1) the low intensity of the molecular ions (this is already seen with smaller dendrimers of this type) and (2) the large number of naturally occurring isotopes of ruthenium, resulting in increasingly broad peaks as the number of ruthenium atoms increases. It is thus anticipated that the molecular ion peaks of large ruthenium dendrimers will be both very weak and very broad and thus very difficult to observe.

We are currently exploring the synthesis and properties of organometallic dendrimers with other metals as well as block copolymers and heterobimetallic dendrimers. We will report on these and other results in forthcoming papers.

Acknowledgment. We thank the University of Cape Town and the Foundation for Research Development of South Africa for support.

OM950020N

Crystal Structure of a Carbanion–Amide Combination with Lithium and Sodium Cations†

Sjoerd Harder,*,‡ Martin Lutz,‡ and Thomas Kremer§

Universität Konstanz, Postfach 5560, M738, 78434 Konstanz, Germany, and Institüt für Organische Chemie, Henkestrasse 42, 91054 Erlangen, Germany

Received February 21, 1995⊗

Summary: In analogy with RLi / MOR′ (M = Na, K, Rb, Cs) superbases, metal exchange in mixtures of $(RLi)_2$ and $(MNR'_2)_2$ to give $(RM)_2$ and $(LiNR'_2)_2$ is calculated to be exothermic. A small energy difference between complete metal exchange and the formation of mixed aggregates, RM / LiNR′$_2$, suggests a significant role of the latter. We prepared a mixed Li / Na carbanion–amide and studied the structure by single-crystal X-ray diffraction. The structure of this Li / Na carbanion–amide complex can be described as a tetrameric cluster from units in which Li and Na cations bridge the carbanion and amide functionalities. The carbanion–amide bonding interactions with the Li cations are of major importance, whereas the Na cations are involved in weaker bonding. The different influence of amide anions and alkoxide anions on the structure of mixed aggregates provoked a comparative study on the superbasic properties of such systems.

Enhanced reactivity of organo alkali-metal species with mixed metals initiated the structural study of such systems.[1] While several X-ray structures of mixed-metal species have been determined,[2] only a few complexes are known in which both different metals *and* different anions occur.[3] We reported the first structure of an organosodium/lithium alkoxide compound, an intramolecular superbase model with both functionalities attached to the same molecule.[3b] Superbasicity (*i.e.* enhanced deprotonating power)[1e,f] of RLi/R′OM (M = Na, K, Rb, Cs) mixtures is generally ascribed to metal exchange,[4] which gives the more reactive RM/R′OLi combination. The driving force for this exothermic exchange reaction (note the *ab initio* results of eq 1)[4] is the greater electrostatic attraction between cations and anions: the larger cation (M^+) prefers to be associated with the larger anion (C^-) and the smaller cation (Li^+) with the smaller anion (O^-).[3b,5] Indeed, the structure of the only known mixed organosodium/lithium alkoxide compound shows a strong preference for Li–O bonding.[3b]

$$(MeLi)_2 + (NaOH)_2 \rightarrow (MeNa)_2 + (LiOH)_2 \quad (1)$$

$$\Delta E = -8.3 \text{ kcal/mol}$$

$$(MeLi)_2 + (NaNH_2)_2 \rightarrow (MeNa)_2 + (LiNH_2)_2 \quad (2)$$

$$\Delta E = -7.0 \text{ kcal/mol}$$

$$(MeLi)_2 + (NaOH_2)_2 \rightarrow 2(MeNa/LiNH_2) \quad (3)$$

$$(\Delta E) = -5.3 \text{ kcal/mol}$$

In analogy with RLi/MOR′ superbases, mixtures of RLi and MNR′$_2$ (M = Na, K, Rb, Cs) also should exchange metals to form RM/LiNR′$_2$, in which the smaller lithium cation interacts with the smaller amide anion. *Ab initio* calculations on dimeric species (eq 2) show this metal exchange to be exothermic by 7.0 kcal/mol.[4] The smaller exothermicity, compared to the Li/Na exchange in eq 1, is due to the larger radius of the amide anion compared to that of the alkoxide anion. Since formation of a mixed aggregate ($MeNa/LiNH_2$) is only 1.7 kcal/mol less favorable than complete transmetalation (eq 3), mixed aggregates may well be significant components under experimental conditions.

Equilibria between many different species (and crystallization only of the least soluble species) has hindered a structural study of a mixed alkali-metal carbanion–amide system. Therefore, we chose to study an intramolecular system in which carbanion and amide functionalities are incorporated in the same molecule. We determined the X-ray structure of the crystalline product (**2**·tmeda) obtained in the reaction of sodium methyl(4-methylbenzyl)amide (**1**) with *n*-butyllithium/*N,N,N′,N′*-tetramethylethylenediamine (tmeda).[6] A structure in which Li and Na are doubly bridging the carbanion and amide units (as in **2**) resembles a mixed aggregate, whereas a compound in which distinct N–Li and C–Na bonds can be recognized (*e.g.* **3**) resembles a situation of complete metal exchange.

† Dedicated, with all best wishes, to Professor Paul von Ragué Schleyer on the occasion of his 65th birthday.

‡ Universität Konstanz.

§ Institüt für Organische Chemie.

⊗ Abstract published in *Advance ACS Abstracts,* May 1, 1995.

(1) (a) Morton, A. A.; Claff, C. E., Jr.;*J. Am. Chem. Soc.* **1954**, *76*, 4935. (b) Wittig, G.; Ludwig, R.; Polster, R. *Chem. Ber.* **1955**, *88*, 294. (c) Wittig, G.; Bickelhaupt, F. *Chem. Ber.* **1958**, *91*, 865. (d) Wittig, G.; Benz, E. *Chem. Ber.* **1958**, *91*, 873. (e) Lochmann, L.; Pospísil, J.; Lím, D. *Tetrahedron Lett.* **1966**, 257. (f) Schlosser, M. *J. Organomet. Chem.* **1967**, *8*, 9.

(2) (a) Cambillau, C.; Bram, G.; Corst, J.; Riche, C. *Nouv. J. Chim.* **1979**, *3*, 9. (b) Weiss, E.; Sauermann, G.; Thirase, G. *Chem. Ber.* **1983**, *116*, 74. (c) Clegg, W.; Mulvey, R. E.; Snaith, R.; Toogood, G. E.; Wade, K. *J. Chem. Soc., Chem. Commun.* **1986**, 1740. (d) Momany, C.; Hackert, M. L.; Sharma, J.; Poonia, N. S. *J. Inclusion Phenom.* **1987**, *5*, 3443. (e) Schuhmann, U.; Weiss, E. *Angew. Chem.* **1988,** *100*, 573; *Angew. Chem., Int. Ed. Engl.* **1988**, *27*, 584. (f) Barr, D.; Clegg, W.; Mulvey, R. E.; Smith, R. *J. Chem. Soc., Chem. Commun.* **1989**, 57. (g) Lorenzen, N. P.; Kopf, J.; Olbrich, F.; Schümann, U.; Weiss, E. *Angew. Chem.* **1990,** *102*, 1481; *Angew. Chem., Int. Ed. Engl.* **1990**, *29*, 1441. (h) Williard, P. G.; Hintze, M. J. *J. Am. Chem. Soc.* **1990**, *112*, 8602. (i) Williard, P. G.; Nichols, M. A. *J. Am. Chem. Soc.* **1991**, *113*, 9671. (j) Baker, D. R.; Mulvey, R. E.; Clegg, W.; O'Neil, P. A. *J. Am. Chem. Soc.* **1993**, *115*, 6472. (k) Baker, D. R.; Clegg, W.; Horsburgh, L.; Mulvey, R. E. *Organometallics* **1994**, *13*, 4170 and references cited therein.

(3) (a) Williard, P. G.; MacEwan, G. J. *J. Am. Chem. Soc.* **1989**, *111*, 7671. (b) Harder, S.; Streitwieser, A. *Angew. Chem.* **1993**, *105*, 1108; *Angew. Chem., Int. Ed. Engl.* **1993**, *32*, 1067.

(4) MP4SDTQ/6-31+G*//6-31+G* calculations.

(5) Grovenstein, E., Jr. In *Recent Advances in Anionic Polymerization*; Hogen-Esch, T. E., Smid, J., Eds., Elsevier:Amsterdam, **1987**, p 3.

0276-7333/95/2314-2133$09.00/0

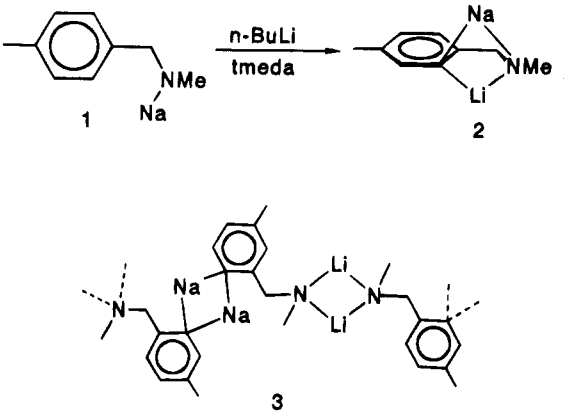

A single-crystal X-ray structure analysis[7] of **2**·tmeda reveals a centrosymmetric tetrameric aggregate which consists of four distinct monomeric units of **2** in which both Li and Na bridge the same carbanion and amide functionalities (this Li/Na double bridging within these units is indicated by darkened bonds in Figure 1).

The core of the aggregate is formed by the four Li cations, which are arranged on the corners of a planar (centrosymmetric) rhomboid. The negatively charged carbon atoms C11 and C11′ bridge the two available triangular Li_3 faces on opposite sides of the rhomboid. The other two negatively charged carbon atoms bridge opposing Li_2 sides of the rhomboid. All C-Li distances are in the narrow range of 2.26(1)–2.37(1) Å. The remaining coordination sites on the Li cations are occupied by the negatively charged amide functionalities, so that all the Li cations have a distorted-tetrahedral coordination environment.

The Na cations are more weakly bound and are positioned in the outer regions of the tetrameric cluster. Each Na cation bridges one amide and two aryl functionalities and is additionally solvated by tmeda to complete the coordination sphere. The C(ipso)–Na bond distances range widely from 2.660(6)–3.049(6) Å. For comparison, the C(ipso)–Na distances in phenylsodium compounds range from 2.566 to 2.756 Å.[2e,8] This suggests a weak electrostatic C–Na bonding in the structure of **2**·tmeda, which is due to the enormous crowding of Li and Na cations around the negatively charged C(ipso) centers (C11 and C12), as can be seen in Figure 2. Repulsive interactions between Li2–Na2 and Li1′–Na1 bends the Na cations away from σ-electron density on C(ipso) and weakens the electrostatic C^-/Na^+ interaction. Less bending of the Na cations is observed in the metal coordination geometry for C12, which only binds two Li cations. Even though the electrostatic C–Na bonding is weakened due to crowding, the *seven-coordinate* carbons C11 and C11′ are remarkable.

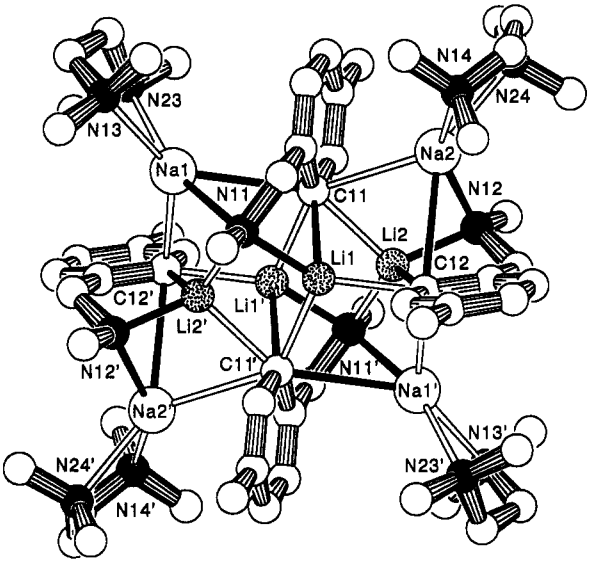

Figure 1. Crystal structure of (**2**·tmeda)$_4$. Nitrogens are black, and lithiums are speckled. Hydrogens have been omitted; atoms marked with a prime are symmetry-related by a center of inversion. Selected distances (Å): Li1–C11, 2.36(1); Li1–C12, 2.26(1); Li1–C11′, 2.27(1); Li1–N11, 2.09(1); Li2–C11, 2.34(1); Li2–C12, 2.37(1); Li2–N12, 1.95(1); Li2–N11′, 2.04(1); Na1–C11, 3.025(6); Na1–C12′, 2.660(6); Na1–N11, 2.594(5); Na1–N13, 2.583(6); Na1–N23, 2.550(6); Na2–C11, 2.904(6); Na2–C12, 3.049(6); Na2–N12, 2.380(5); Na2–N14, 2.669(6); Na2–N24, 2.512(6); Li1–Li2, 2.49(1); Li1–Li1′, 2.45(2); Li1′–Li2, 2.59(1).

The short distances of the Na cations to other carbon atoms in the aryl rings implies an interaction of Na with the aryl π-system which is especially important for Na2. Such bonding plays a dominant role in anionic benzylic systems (particularly those of the higher alkali metals)[9] in which the benzylic negative charge is strongly delocalized into the π-system. The negative charge in **2** will be mainly localized on C(ipso), which therefore is of major significance in bonding of the Na cations.

The amide functionalities either bridge two metal cations or bridge triangular arrangements of three alkali-metal cations. The Li–NR_2 and Na–NR_2 bond distances are in the normal range for lithium and sodium amides.[10]

(6) All experiments were carried out under an inert argon atmosphere using Schlenk techniques and syringes. Solvents were freshly destilled from sodium/benzophenone prior to use. *n*-Butyllithium (1.6 M in hexane, 2.8 mL, 4.58 mmol) is added to a solution of **1**·tmeda (1.0 g, 3.66 mmol) in 80 mL of hexane and 3.0 mL of tmeda. Air-sensitive orange crystals of **2**·tmeda suitable for X-ray diffraction are formed overnight at room temperature (0.53 g; yield 52%). Crystals dissolved in toluene-d_8 show ^{1}H NMR spectra with many overlapping, extremely broadened signals (temperature range −50 to +80 °C) which are due to slow exchange processes. Extreme line broadening prohibited the recording of ^{13}C NMR spectra. Dissolving and quenching the crystals in methanol-d_4 give clean spectra of the deuterated product, 4-Me-2-D(C_6H_3)CH_2N(D)Me, and tmeda in a 1/1 ratio. ^{1}H NMR (250 MHz, methanol-d_4, 25 °C, TMS): δ 2.24 (s, 12 H, tmeda Me), 2.30 (s, 3 H, NMe), 2.33 (s, 3H, Me), 2.45 (s, 4H, tmeda CH_2), 3.62 (s, 2H, NCH_2), 7.05 (d, ^3J(H,H) = 7.2 Hz, 1H, arom), 7.06 (s, 1H, arom), 7.14 (d, ^3J(H,H) = 7.2 Hz, 2H, arom). ^{13}C NMR: δ 21.2 (Me), 35.5 (NMe), 45.9 (tmeda Me), 56.1 (NCH_2), 57.9 (tmeda CH_2), 129.3 (t, ^1J(C,D) = 23.6 Hz), 129.6, 130.0, 130.1, 137.3, 137.9 (arom).

(7) Crystal structure determination of **2**·tmeda: the crystal was covered with high-grade paraffin oil and mounted on a glass fiber in a cold N_2 stream; a = 13.752(3) Å, b = 21.940(4) Å, c = 12.188(3) Å, β = 107.12(1)°, V = 3514(1) Å^3, space group $P2_1/c$, formula C_9H_{11}-NLiNa·$C_6H_{16}N_2$, M_r = 279.33, Z = 8, ϱ_{calcd} = 1.056, μ(Mo Kα) = 0.79 cm^{-1}; 7974 unique reflections were measured on a Enraf-Nonius CAD4 diffractometer (Mo Kα radiation, graphite monochromator, T = −75 °C); solution by direct methods with SHELXS-86,[11] refinement with 361 parameters and 2767 observed reflections ($F^2 > 2.0\sigma(F^2)$) to $R_w(F^2)$ = 0.179 and R1(F) = 0.078; non-hydrogen atoms anisotropic, hydrogen atoms located in difference Fourier maps and included with fixed parameters during refinement; refinement with SHELXL-93[12] and plots with the EUCLID package.[13]

(8) Schümann, U.; Behrens, U.; Weiss, E. *Angew. Chem.* **1989**, *101*, 481; *Angew. Chem., Int. Ed. Engl.* **1989**, *28*, 476.

(9) Hoffmann, D.; Bauer, W.; Hampel, F.; van Eikema Hommes, N. J. R.; Schleyer, P. v. R.; Otto, P.; Pieper, U.; Stalke, D.; Wright, D. S.; Snaith, R. *J. Am. Chem. Soc.* **1994**, *116*, 528.

(10) (a) Lappert, M. F.; Slade, M. J.; Singh, A.; Atwood, J. L.; Rogers, R. O.; Shakir, R. *J. Am. Chem. Soc.* **1983**, *105*, 302. (b) Haase, M.; Sheldrick, G. M. *Acta Crystallogr., Sect. C* **1986**, *42*, 1009. (c) Williard, P. G.; Salvino, J. M. *J. Org. Chem.* **1993**, *58*, 1. (d) Barr, D.; Clegg, W.; Mulvey, R. E.; Snaith, R.; Wright, D. S. *J. Chem. Soc., Chem. Commun.* **1987**, 716.

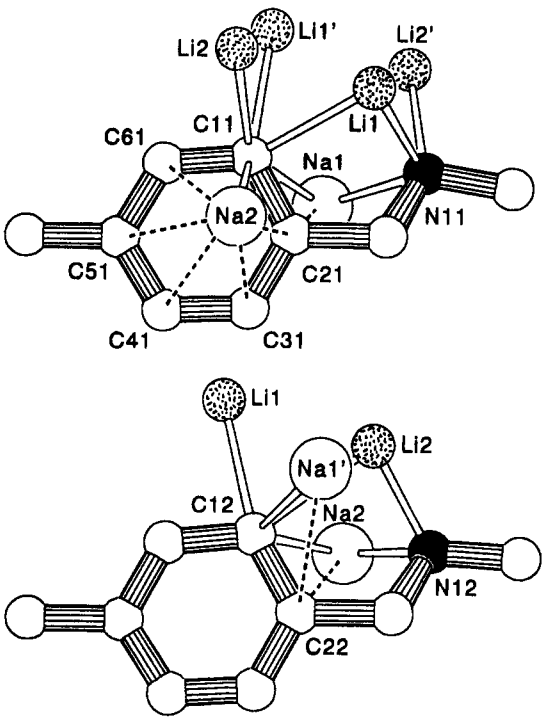

Figure 2. 2. Partial structures showing the complete metal surroundings for the two different $Ar^{(-)}CH_2N^{(-)}Me$ dianions (views are perpendicular to the aryl ring plane). Short Na–C distances to the aryl system (upper part; Å): Na1–C11, 3.025(6); Na1–C21, 2.768(6); Na2–C11, 2.904(6); Na2–C21, 2.889(6); Na2–C31, 3.119(6); Na2–C41, 3.315(6); Na2–C51, 3.338(6); Na2–C61, 3.089(6). Short Na–C distances to the aryl system (lower part; Å): Na1′–C12, 2.660(6); Na1′–C22, 3.142(6); Na2–C12, 3.049(6); Na2–C22, 3.015(6).

In summary, the Li/Na carbanion–amide compound can be described as a cluster of intramolecular mixed aggregates (**2**) in which carbanion–amide bonding to the Li cations is of major importance and weaker bonding interactions are observed with the Na cations. In contrast with the structure of the organosodium/lithium alkoxide combination,[3b] there seems to be no particular preference for interaction of Li with the smaller anion (*i.e.* the R_2N^- functionality) in the structure of **2**·tmeda.

To our knowledge, no research results on the use of $BuLi/MNR_2$ mixtures as superbases have been described in the literature. The structurally different behavior between amide anions and alkoxide anions has provoked a study of the possible superbase potential of $BuLi/MNR_2$ (M = Na, K) and is currently under investigation.

Acknowledgment. S.H. thanks the Alexander von Humboldt Foundation for the award of a fellowship. Professors H.-H. Brintzinger, G. Müller, and P. v. R. Schleyer are kindly acknowledged for discussions and for providing laboratory facilities.

Supplementary Material Available: For **2**·tmeda, tables of crystal and structure refinement data, coordinates, bond lengths and angles, anisotropic displacement parameters, and hydrogen atom coordinates and *U*(eq) values and an ORTEP plot (12 pages). Ordering information is given on any current masthead page.

OM950137B

(11) Sheldrick, G. M. SHELXS-86. In *Crystallographic Computing*; Sheldrick, G. M., Krüger, C., Goddard, R., Eds.; Oxford University Press: Oxford, U.K., 1985; Vol. 3, p 175.
(12) Sheldrick, G. M. SHELXL-93: Program for the Refinement of Crystal Structures; Institute für Anorganische Chemie, Göttingen, Germany, 1993.
(13) Spek, A. L. EUCLID Package. In *Computational Crystallography*; Sayre, D., Ed.; Clarendon Press: Oxford, U.K., 1982.

Organometallic Chemistry of Ambident Dianions. Reactions of Organosilicon Dihalides with Acetone Dianions. Remarkable Difference in Reactivity between Diorganodichlorosilanes and Diorganodifluorosilanes

Dietmar Seyferth,*,† Tao Wang,† Robert L. Ostrander,‡ and Arnold L. Rheingold‡

Departments of Chemistry, Massachusetts Institute of Technology, Cambridge, Massachusetts 02139, and University of Delaware, Newark, Delaware 19716

Received January 26, 1995®

Summary: The $[CH_2C(O)CPh_2]^{2-}$ dianion reacted with R_2SiCl_2 (R = Ph, CH_3, Et) to give cyclic products of type ***5****, but with R_2SiF_2* ***4*** *(R = Ph, Et) was formed. The structures of* ***5*** *and* ***4*** *(R = Ph) were determined by single-crystal X-ray diffraction. A reason for the difference in the regioselectivity of the reactions of the dianion with R_2SiCl_2 and R_2SiF_2 is suggested.*

In a previous communication[1] we reported that the ambident $[CH_2C(O)CR_2]^{2-}$ (R = Ph, H) dianions (**1**) react with the oxophilic bis(cyclopentadienyl) dichlorides of zirconium and hafnium as C,O-dinucleophiles, giving 1,5-dimetalla-2,6-dioxacyclooctanes (**2**), which appear to dissociate in solution to form 2-metallaoxacyclobutanes.

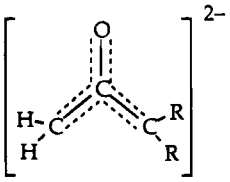

1 a, R = C_6H_5
b, R = H

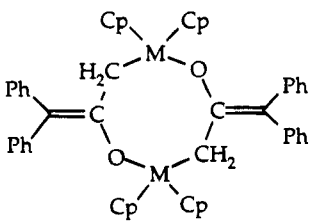

2, M = Zr, Hf

In contrast, the dianion derived from dibenzyl ketone reacted with *cis*-$[L_2PtCl_2]$ and *trans*-$[L_2PdCl_2]$ complexes as a C,C-dinucleophile, giving 3-metallacyclobutanones.[2] In view of the oxophilicity of silicon, it was expected that such acetone dianions also would react with dichlorosilanes (R_2SiCl_2) as C,O-dinuleophiles. We report here our studies of such reactions in which we have encountered a remarkable difference in reactivity between R_2SiCl_2 and R_2SiF_2 compounds.

In one such experiment, a THF solution of the dianion derived from 1,1-diphenylacetone[3] was added to 1 molar equiv of diphenyldichlorosilane.[4] In time, the red dianion color was discharged. Workup of the resulting

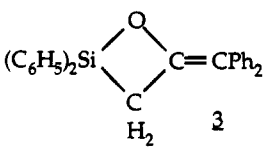

3

yellow suspension gave a white, air-stable solid, mp 189–191 °C, in 40% yield. Although a monomer, i.e., the 2-silaoxacyclobutane (a silaoxetane) **3**,could in principle have been formed, the EI mass spectrum of the solid product indicated that it was a "dimer". The $(C_6H_5)_2Si$ analog of **2** ($(C_6H_5)_2Si$ in place of Cp_2M), **4a**, would be an obvious possibility for the structure of this dimer. However, its ^{29}Si NMR spectrum could not be reconciled with this structure, since it indicated that two different kinds of $(C_6H_5)_2Si$ units were present, while the $(C_6H_5)_2Si$ groups in **4a** are equivalent. An alternate structure for the "dimer" is **5a**, in which the $(C_6H_5)_2Si$ groups are in different environments.

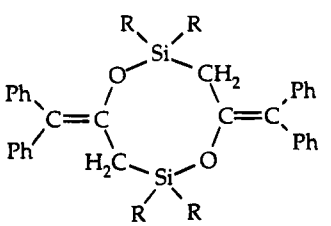

4 a, R = C_6H_5
b, R = C_2H_5

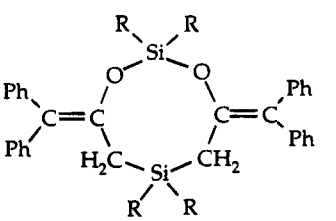

5 a, R = C_6H_5 c, R = CH_3
b, R = C_2H_5

Similar products that were "dimers" by mass spectrometry and that contained (by ^{29}Si NMR) two silicon atoms which were in different environments were

† Massachusetts Institute of Technology.
‡ University of Delaware.
® Abstract published in *Advance ACS Abstracts,* March 15, 1995.

(1) Seyferth, D.; Wang, T.; Davis, W. M. *Organometallics* **1994**, *13*, 4134.

(2) Chiu, K. W.; Henderson, W.; Kemmitt, R. D. W.; Prouse, L. J. S.; Russell, D. R. *J. Chem. Soc., Dalton Trans.* **1988**, 427.

(3) Trimitsis, G. B.; Hinkley, J. M.; TenBrink, R.; Poli, M.; Gustafson, G.; Erdman, J.; Rop, D. *J. Am. Chem. Soc.* **1977**, *99*, 4838.

(4) Dianion **1** was prepared by the method of ref 3 using 12.5 mmol of 1,1-diphenylacetone and 12.5 mmol each of KH and *n*-BuLi. The red THF solution of **1** was added dropwise to 3.16 g (12.5 mmol) of Ph_2SiCl_2 in 100 mL of THF at 0 °C. The resulting mixture was stirred at room temperature for 10 h to give a yellow suspension. Removal of volatiles at reduced pressure was followed by extraction of the residue with hexane. Filtration and evaporation was followed by crystallization of the residue from CH_2Cl_2/hexane at −23 °C during 1 week to give 2.0 g (40%) of a colorless solid. Single crystals of X-ray quality were obtained by dissolving in methylene chloride and allowing the solution slowly to evaporate: mp 189–191 °C; ^1H NMR (300 MHz, $CDCl_3$) δ 2.62 (s, 4 H, CH_2), 6.61–7.42 (m, 40 H, Ph); ^{13}C NMR (75.4 MHz, $CDCl_3$) δ 22.8 (t, ^1J = 122 Hz, CH_2SiPh_2), 122.5 (s, $CH_2C{=}CPh_2$), 125.7–141.2 (m, Ph), 145.4 (t, ^2J = 5.8 Hz, $CH_2C{=}CPh_2$); ^{29}Si NMR (59.59 MHz, $CDCl_3$) δ −36.1, −9.1; MS (70 eV) *m/z* 780 (M^+). Anal. Calcd for $C_{54}H_{44}O_2Si_2$: C, 83.03; H, 5.69. Found: C, 82.72; H, 5.76. Mol wt (VPO, $CHCl_3$): 830 (calcd 781).

0276-7333/95/2314-2136$09.00/0

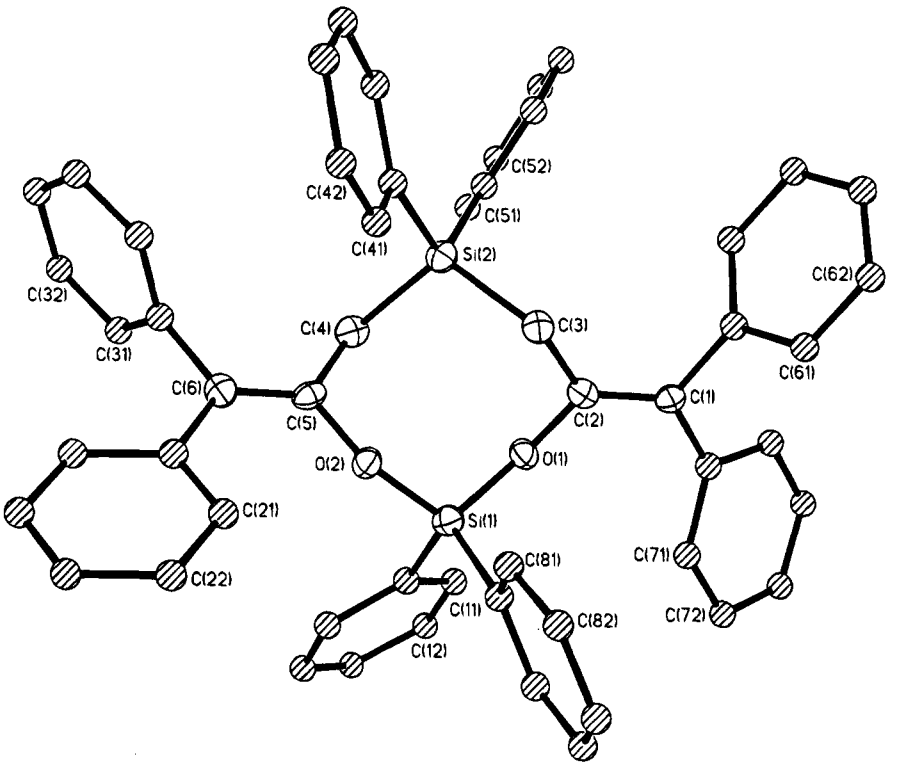

Figure 1. ORTEP plot of the structure of **5a** showing 35% probability ellipsoids. Important bond distances (Å) and angles (deg): Si(1)–O(1) = 1.648(6); Si(1)–O(2) = 1.633(6); Si(2)–C(3) = 1.910(8); Si(2)–C(4) = 1.895(8); O(1)–C(2) = 1.390(10); O(2)–C(5) = 1.382(10); C(2)–C(3) = 1.492(11); C(4)–C(5) = 1.490(12); C(1)–C(2) = 1.340(11); C(5)–C(6) = 1.358(12); O(1)–Si(1)–O(2) = 112.6(2); Si(1)–O(1)–C(2) = 129.3(5); Si(1)–O(2)–C(5) = 132.9(5); O(2)–Si(1)–C(16) = 112.4(3); C(3)–Si(2)–C(4) = 111.4(4); Si(2)–C(3)–C(2) = 117.5(5); Si(2)–C(4)–C(5) = 113.8(5); O(1)–C(2)–C(3) = 113.1(7); O(2)–C(5)–C(4) = 114.6(7); O(1)–C(2)–C(1) = 119.7(7); O(2)–C(5)–C(6) = 118.7(7); C(1)–C(2)–C(3) = 127.2(7); C(4)–C(5)–C(6) = 126.3(8); C(26)–C(6)–C(36) = 115.4(7); C(66)–C(1)–C(76) = 115.8(7).

obtained in reactions of the $[CH_2C(O)CPh_2]^{2-}$ dianion with $(C_2H_5)_2SiCl_2$[5] and $(CH_3)_2SiCl_2$.[5] An X-ray diffraction study of **5a**[6] confirmed the structure as written (Figure 1). The Si–O and Si–C bond distances (1.648(6), 1.633(6) Å and 1.910(8), 1.895(8) Å) are normal and are in the ranges (1.630–1.677 and 1.872–1.894 Å, respectively) observed in diverse cyclic silicon compounds containing Si–O and Si–C(sp^3) bonds in the ring.[7]

The reaction of the $[CH_2C(O)CPh_2]^{2-}$ anion with diphenyl*difluoro*silane appeared to be slower than that with Ph_2SiCl_2.[8] It was immediately apparent that the white crystals isolated in 21% yield from this reaction were not the expected **5a**, since their melting point was 239–240 °C. Combustion analysis, however, established the same composition and the EI mass spectrum indicated a "dimeric" formulation. The ^{29}Si NMR spectrum showed that the two silicon atoms were chemically equivalent. This evidence suggested that the product was **4a**, i.e., a positional isomer of **5a**, and this was confirmed by an X-ray diffraction study.[9] Figure 2 shows an ORTEP plot of **4a**. The Si–O (1.643(6) and 1.641(6) Å) and Si–C (1.873(8) and 1.862(7) Å) bonds are normal, within the ranges for tetrahedral silicon. In chloroform solution all compounds of types **4** and **5** were found by vapor pressure osmometry to be "dimer-

(5) Characterization details are given in the supplementary material.

(6) Crystal data for **5a**: colorless block, orthorhombic, a = 11.676(4) Å, b = 23.057(11) Å, c = 31.850(15) Å, V = 8575(7) Å^3, space group $Pbca$, Z = 8, fw = 781.1, calcd density 1.210 Mg/m^3. Data in the range 4–42° were collected at 238 K using Mo Kα radiation on a Siemens P4 diffractometer. The structure was solved by direct methods and refined by full-matrix least-squares techniques. The non-hydrogen atoms were refined anisotropically. An absorption correction was not applied. Final R = 0.0739 and R_w = 0.0807 for 2501 observed reflections ($F > 4.0\sigma(F)$) and 283 variables. The largest peak on the final difference Fourier map was 0.51 e Å^{-3}.

(7) Lukevics, E.; Pudova, O.; Strukovich, R. *Molecular Structure of Organosilicon Compounds*; Ellis Horwood: Chichester, U.K., 1989; Chapter 1.4.

(8) The same procedure was used in the reaction of 2.75 g (12.5 mmol) of Ph_2SiF_2 with dianion **1** in THF at 0 °C. The red color of the dianion was discharged very slowly. A red suspension remained after the reaction mixture had been stirred at room temperature overnight. All volatiles were evaporated at reduced pressure. The residue was extracted with hexane (2 × 100 mL) and then with toluene (3 × 50 mL). The orange hexane solution was evaporated at reduced pressure, leaving 2.5 g of a yellow oligomeric mixture (mol wt 500–2400 by GPC vs polystyrene standards) which has not been identified. The toluene extract was filtered through Celite. Evaporation of the yellow filtrate and recrystallization of the residue from CH_2Cl_2 gave 1.0 g (21%) of **4b**, mp 239–240 °C. Single crystals of X-ray quality were obtained by dissolving in a minimum amount of methylene chloride, adding 2 equiv of hexane, and storing the solution at −23 °C. ^1H NMR (300 MHz, $CDCl_3$): δ 2.56 (s, 4 H, CH_2), 6.71–7.38 (m, 40 H, Ph). ^{13}C NMR (75.4 MHz, $CDCl_3$): δ 24.4 (t, ^1J = 120.4 Hz, CH_2SiPh_2), 122.3 (s, $CH_2C{=}CPh_2$, 124.4–141.7 (m, Ph), 144.8 (t, ^2J = 5.8 Hz, $CH_2C{=}CPh_2$). ^{29}Si NMR (59.59 MHz, $CDCl_3$): δ −10.8. MS (70 eV): m/z 780 (M^+). IR (KBr, cm^{-1}): Si–O 1005. Anal. Calcd for $C_{54}H_{44}O_2Si_2$: C, 83.03; H, 5.69. Found: C, 82.72; H, 5.76. Mol wt (VPO, $CHCl_3$): 813 (calcd 781).

(9) Crystal data for **4a**: colorless block, monoclinic, a = 10.384(2) Å, b = 19.762(4) Å, c = 21.513(5) Å, β = 96.65(2)°, V = 4384.9(16) Å^3, space group $P2_1/n$, Z = 4, fw = 781.1, calcd density 1.1839 Mg/m^3. Data in the range 4–42° were collected at 296 K using Mo Kα radiation on a Siemens P4 diffractometer. The structure was solved by direct methods and refined by full-matrix least-squares techniques. The non-hydrogen atoms were refined anisotropically. An absorption correction was not applied. Final R = 0.0549 and R_w = 0.0642 for 2022 observed reflections ($F > 5.0\sigma(F)$) and 427 variables. The largest peak on the final difference Fourier map was 0.22 e Å^{-3}.

(10) A reaction in which only 1 molar equiv of Me_3SiCl added to a solution of dianion **1**, followed by aqueous workup, gave $Ph_2CHC(O)CH_2SiMe_3$ (~30%), $Ph_2CHC(O)CH_3$ (~30%), and $Ph_2C{=}C(OSiMe_3)CH_2SiMe_3$ (15%) seems to provide support for this assumption. A separate experiment showed $Ph_2C{=}C(OSiMe_3)CH_2SiMe_3$ to be stable to hydrolysis under acidic conditions: Langer, P. Diplomarbeit, University of Hannover, 1994.

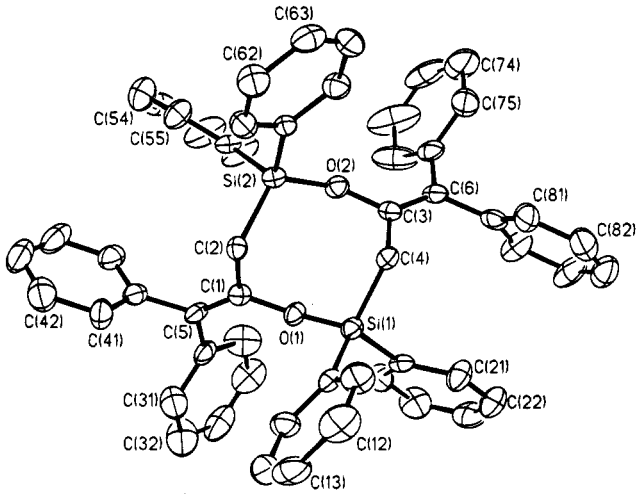

Figure 2. ORTEP plot of the structure of **4a** showing 35% probability ellipsoids. Important bond distances (Å) and angles (deg): Si(1)–O(1) = 1.643(6); Si(1)–C(4) = 1.873(8); Si(2)–O(2) = 1.641(6); Si(2)–C(2) = 1.862(7); O(1)–C(1) = 1.388(10); O(2)–C(3) = 1.384(11); C(1)–C(2) = 1.510(12); C(3)–C(4) = 1.507(11); C(1)–C(5) = 1.321(13); C(3)–C(6) = 1.321(13); O(1)–Si(1)–C(4) = 112.2(3); Si(1)–O(1)–C(1) = 129.0(5); Si(1)–C(4)–C(3) = 113.5(6); O(1)–Si(1)–C(16) = 109.1(4); C(4)–Si(1)–C(16) = 109.5(4); O(2)–Si(2)–C(2) = 113.4(3); Si(2)–C(2)–C(1) = 115.1(5); Si(2)–O(2)–C(3) = 133.5(5); O(2)–Si(2)–C(56) = 104.7(3); O(1)–C(1)–C(2) = 114.7(7); O(1)–C(1)–C(5) = 118.0(8); O(2)–C(3)–C(4) = 114.4(7); O(2)–C(3)–C(6) = 118.1(8); C(2)–C(1)–C(5) = 127.1(8); C(36)–C(5)–C(46) = 116.1(7).

Scheme 1

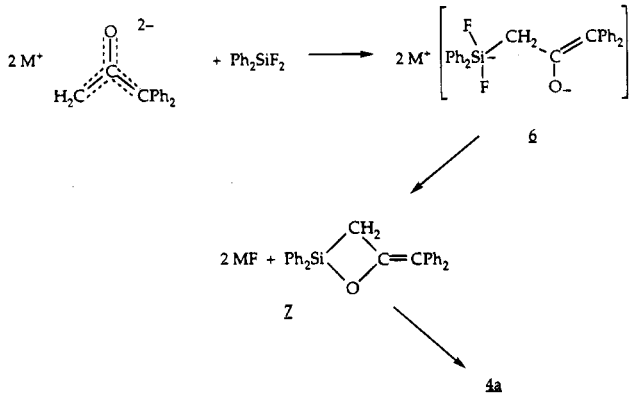

ic". Thus, in contrast to what was found in the case of the $(\eta^5\text{-}C_5H_5)_2Zr$ analog of **4**,[1] **5a–d** and **4b** do not dissociate to give 2-silaoxetanes in solution.

The differing regioselectivities of the reactions of $[CH_2C(O)CPh_2]^{2-}$ with dichlorosilanes and with diphenyl- and diethylfluorosilane require an explanation. Of the two reaction sites of the $[CH_2C(O)CPh_2]^{2-}$ dianion, $-CH_2^-$ and $-O^-$, the former may be expected to be the more reactive in nucleophilic substitution at silicon.[10] In the case of diphenyldifluorosilane we suggest that initial formation of a hypervalent, anionic intermediate, **6**, occurs first (Scheme 1). Such intermediates have enhanced reactivity,[11] and in the case of **6**, rapid intramolecular ring closure *via* displacement of F^- by $-O^-$ to give the 2-silaoxetane **7** is facilitated. The latter

Scheme 2

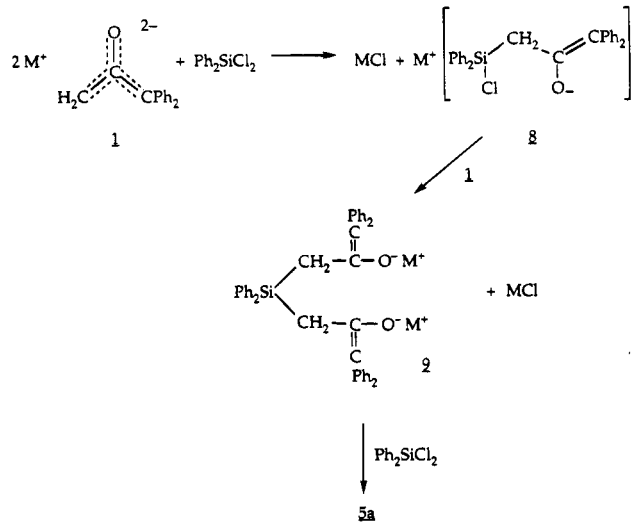

then undergoes ring-opening cyclodimerization to the observed product **4a**. On the other hand, in the case of Ph_2SiCl_2, a hypervalent intermediate is not formed and such enhancement of reactivity does not obtain. The result is that intermediate **8** (Scheme 2) is sufficiently long-lived to undergo attack by another dianion **1a**. The resulting intermediate **9** then reacts with another molecule of Ph_2SiCl_2 to give **5a**. The 2-silaoxetane is not an intermediate.

These suggestions concerning possible mechanisms are speculation, but they seem reasonable in terms of known chemistry. 2-Silaoxetanes generally are not stable, decomposing to olefin and silanone, but sterically hindered 2-silaoxetanes are stable (e.g., 2,2-bis(trimethylsilyl)-4,4-diphenyl-3-adamantyl-3-(trimethylsiloxy)-2-silaoxetane is a crystalline solid[12]). While ring-opening cyclodimerization appears not to have been observed for a 2-silaoxetane, such a process is known for 2-silaoxacyclopentanes.[13]

In any case, this marked difference in the regiochemistry of Ph_2SiCl_2 and Ph_2SiF_2 in reactions with the same reagent is remarkable. Further studies of the reactions of the $[CH_2C(O)CPh_2]^{2-}$ anion of organohalosilanes are in progress.

Acknowledgment. The MIT authors are grateful to the National Science Foundation for support of this work.

Supplementary Material Available: Text giving synthetic details and characterization data for **5b**, **5c**, and **4b** and tables giving structure determination summaries, atomic coordinates and equivalent isotropic displacement coefficients, anisotropic displacement coefficients, H-atom coordinates, bond distances, and bond angles for **4a** and **5a** (32 pages). Ordering information is given on any current masthead page.

OM9500679

(11) Bréfort, J.-L.; Corriu, R. J. P.; Guérin, C.; Henner, B. J. L.; Wong Chi Man, W. W. C. *Organometallics* **1990**, *9*, 2080.
(12) Brook, A. G.; Chatterton, W. J.; Sawyer, J. F.; Hughes, D. W.; Vorspohl, K. *Organometallics* **1987**, *6*, 1246.
(13) Rossmy, G.; Koerner, G. *Makromol. Chem.* **1964**, *73*, 85.

Reaction of a Germylene with Ethylene: A Stable Digermacyclobutane via a Germirane Intermediate

Harunobu Ohgaki, Yoshio Kabe, and Wataru Ando*

Department of Chemistry, University of Tsukuba, Tsukuba, Ibaraki 305, Japan

Received December 1, 1994[⊗]

*Summary: 1,2-Digermacyclobutane (**2**) is formed by reaction of a stable germylene (**1**) with ethylene. The crystal structure of **2** has been determined by single-crystal X-ray diffraction. The ^1H NMR spectrum of the reaction mixture revealed the presence of a germirane having no substituents on the ring carbon.*

Numerous studies have been concerned with the synthesis of small-ring compounds containing the heavier group 14 elements.[1] Recently we have reported the first substituent-stabilized germiranes with alkylidene and acyl groups on the ring carbons.[2] However, the reaction of simple olefins such as ethylene, propylene, 2-butene, etc. with a germylene remained to be studied. We attempted reactions of a stable germylene[3] with propylene and 2-butene, but the expected products were not detected. On the other hand, the reaction of a stable germylene with ethylene afforded a 1,2-digermacyclobutane.

When ethylene gas was bubbled into a toluene solution of the stable germylene (**1**; 1.70 mmol), the yellow color of **1** was immediately discharged. The mixture was stirred in excess ethylene at room temperature for 24 h. After removal of the solvent, purification of the residue by silica gel column chromatography (hexane) followed by recrystallization in hexane gave colorless crystals of 1,2-digermacyclobutane (**2**), an air- and moisture-stable compound in 55% yield. The ^1H NMR spectrum of **2** exhibits signals due to one CH and two $SiMe_3$ groups of the $(Me_3Si)_2CH$ substituents and to one $GeCH_2$ group at 2.19 ppm, and the ^{13}C NMR spectrum exhibits a signal due to the $GeCH_2$ groups at 27.2 ppm.[4] These observations support the presence of diastereotopic $(Me_3Si)_2CH$ groups and equivalent CH_2 groups.

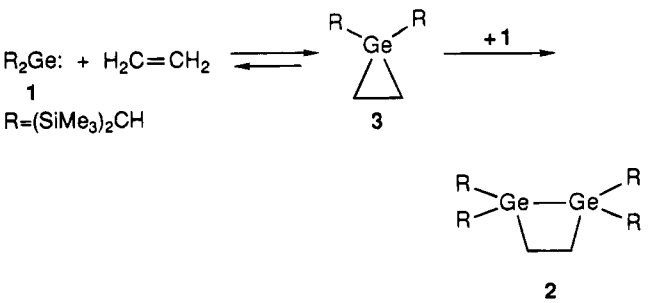

The results of the X-ray structure analysis of **2** are shown in Figure 1. The molecule possesses an approximate C_2 axis which bisects both C–C and Ge–Ge bonds. The C_2Ge_2 trapezoidal core deviates from planarity with a C–Ge–Ge–C torsion angle of 12.7°. This deviation is due to the sterically demanding $(Me_3Si)_2CH$ groups on the two germanium atoms.

In order to detect spectral changes associated with the first stage of the reaction, UV–vis spectra were measured immediately after the reaction of germylene **1** with ethylene. No significant absorptions for **1** at 418 nm nor for **2** at 278 nm were observed. However, removal of excess ethylene from the mixture by bubbling argon caused appearance of a peak at 418 nm. These findings indicate that an intermediate species is in thermal equilibrium in solution with **1** and the ethylene fragment. This species could be either the germylene–ethylene π complex or the germirane.

An NMR study of the reaction mixture at the first stage of the reaction of **1** with excess ethylene revealed the presence of only one species, to which we assign the germirane (**3**) structure shown in Figure 2. The peaks

⊗ Abstract published in *Advance ACS Abstracts,* April 1, 1995.

(1) (a) Review: Ando, W.; Kabe. Y. Small-Ring Organo-Silicon, Germanium and Tin Compounds. *Adv. Strain Org. Chem.* **1993**, *3*, 59. (b) Siliranes: Delker, G. L.; Wang, Y.; Stucky, G. D., Jr.; Lambert, R. L.; Hass, C. K.; Seyferth, D. *J. Am. Chem. Soc.* **1976**, *98*, 1779. (c) Seyferth, D.; Annarelli, D. C.; Vick, S. C.; Ducan, P. *J. Organomet. Chem.* **1980**, *201*, 179. (d) Ando, W.; Fujita, M.; Yoshida, H.; Sekiguchi, A. *J. Am. Chem. Soc.* **1988**, *110*, 3310. (e) Boudjouk, P.; Black, E.; Kumarathasan, R. *Organometallics* **1991**, *10*, 2095. (f) Pae, D. H.; Xiao, M.; Chiang, M. Y.; Gasper, P. P. *J. Am. Chem. Soc.* **1991**, *113*, 1281. (g) Alkylidene–siliranes: Saso, H.; Ando, W.; Ueno, K. *Tetrahedron* **1989**, *45*, 1929. (h) Bis(alkylidene)silirane: Yamamoto, T.; Kabe, Y.; Ando, W. *Organometallics* **1993**, *12*, 1996. (i) Silirenes: Conlin, R. T.; Gaspar, P. P. *J. Am. Chem. Soc.* **1976**, *98*, 3715. (j) Seyferth, D.; Annarelli, D. C.; Vick, S. C. *J. Am. Chem. Soc.* **1976**, *98*, 6382. (k) Sakurai, H.; Kamiyama, Y.; Nakadaira, Y. *J. Am. Chem. Soc.* **1977**, *99*, 3879. (l) Hirotsu, K.; Higuchi, T.; Ishikawa, M.; Sugisawa, M.; Kumada, M. *J. Chem. Soc., Chem. Commun.* **1982**, 726. (m) Seyferth, D.; Annarelli, D. C.; Vick, S. C. *J. Organomet. Chem.* **1984**, *272*, 123. (n) Germirenes: Krebs, A.; Berndt, J. *Tetrahedron Lett.* **1983**, *24*, 4083. (o) Egorov, M. P.; Kolesnikov, S. P.; Struchkov, Y. T.; Antipin, M. Y.; Sereda, S. V.; Nefedov, O. M. *J. Organomet. Chem.* **1985**, *290*, C27. (p) Stannirenes: Sita, L. R.; Bickerstaff, R. D. *J. Am. Chem. Soc.* **1988**, *110*, 5208.

(2) Ando, W.; Ohgaki, H.; Kabe, Y. *Angew. Chem., Int. Ed. Engl.* **1994**, *33*, 659 and references cited therein.

(3) Goldbeg, D. E.; Hitchcock, P. B.; Lappert, M. F.; Thomas, K. M.; Thorne, A. J.; Fjeldberg, T.; Haaland, A.; Schilling, B. E. R. *J. Chem. Soc. Dalton Trans.* **1986**, 2387.

(4) **2**: colorless crystals; decpt 170 °C; ^1H NMR (C_6D_6, 400 MHz) δ 0.36 (s, 36H), 0.42 (s, 36H), 0.61 (s, 4H), 2.19 (s, 4H); ^{13}C NMR (C_6D_6, 100 MHz) δ 4.2 (d), 5.2 (q), 5.6 (q), 27.2 (t); LRMS (*m/z*) 810 (M^+), 795 (M^+ – Me); UV (hexane) λ_{max} (ϵ) 278 nm (6900). Anal. Calcd for $C_{30}H_{80}Si_8Ge_2$: C, 44.44; H, 9.94. Found: C, 44.43; H, 9.99. **3**: ^1H NMR (C_6D_6, 500 MHz) δ −0.41 (s, 2H), 0.18 (s, 36H), 0.78 (s, 4H); ^{13}C NMR (C_6D_6, 125 MHz) δ 2.5 (t), 2.7 (d), 3.0 (q). **4**: colorless oil; ^1H NMR (C_6D_6, 90 MHz) δ 0.35 (s, 18H), 0.36 (s, 18H), 0.40 (s, 18H), 0.41 (s, 18H), 0.55 (s, 4H), 2.02 (s, 4H); ^{13}C NMR (C_6D_6, 22.5 MHz) δ 4.0 (q), 4.1 (q), 14.3 (d), 21.8 (t); LRMS (*m/z*) 867 (M^+ – Me), 427 (ClGe[CH(SiMe$_3$)$_2$]$_2^+$). **5**: colorless crystals; mp 298–301 °C, ^1H NMR (C_6D_6, 90 MHz) δ −0.18 (s, 2H), 0.25 (s, 36H), 1.80 (s, 6H), 1.95 (s, 4H); ^{13}C NMR (C_6D_6, 22.5 MHz) δ 3.5 (q), 5.5 (d), 19.6 (q), 30.7 (t), 131.6 (s); LRMS (*m/z*) 474 (M^+), 459 (M^+ – Me).

(5) Crystal data of **2**: fw 810.84, monoclinic, a = 8.901(1) Å, b = 13.948(2) Å, c = 37.645(4) Å, β = 90.43(1)°, V = 4673.5 Å^3, space group $P2_1/c$, Z = 4, μ(Mo Kα) = 14.9 cm^{-1}, ϱ(calcd) = 1.15 g/cm^3. The 3674 independent reflections ($2\theta \le 50°$; $|F_o^2| \ge 3\sigma|F_o^2|$) were measured on an Enraf-Nonius CAD4 diffractometer using Mo Kα irradiation and an ω–2θ scan. An empirical absorption correction based on a series of ψ scans were applied to the data 0.83/1.00. The structure was solved by direct methods, and hydrogen atoms were added to the structure factor calculations but their positions were not refined anisotropically to R = 0.067 (R_w = 0.086).

(6) In stannirene and a thiastannirane thermal equilibria between stannylene and acetylene or thioketene were reported: (a) Boatz, J. A.; Gordon, M. S.; Sita, L. R. *J. Phys. Chem.* **1990**, *94*, 5488. (b) Ohtaki, T.; Kabe, Y.; Ando, W. *Organometallics* **1993**, *12*, 4.

0276-7333/95/2314-2139$09.00/0

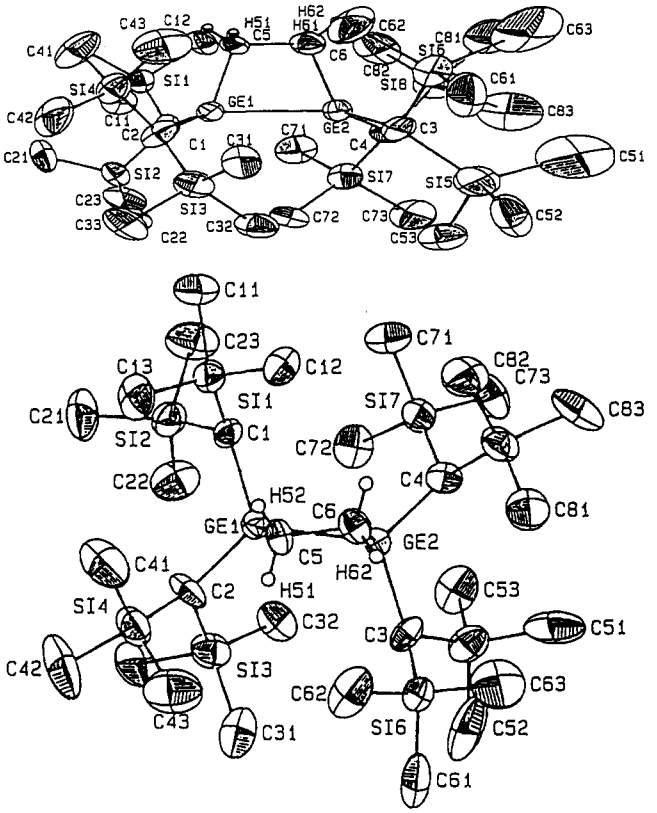

Figure 1. Crystal structure of **2** (ORTEP). Selected bond lengths (Å) and angles (deg): Ge(1)–Ge(2) = 2.554(2), Ge(1)–C(5) = 2.01(1), Ge(2)–C(6) = 2.01(1), C(5)–C(6) = 1.57(2), Ge(1)–C(1) = 2.04(1), Ge(1)–C(2) = 2.03(1), Ge(2)–C(3) = 2.04(1), Ge(2)–C(4) = 2.00(1); Ge(1)–Ge(2)–C(6) = 74.7(4), Ge(2)–Ge(1)–C(5) = 75.3(4), Ge(1)–C(5)–C(6) = 102.2(8), Ge(2)–C(6)–C(5) = 103.1(8); torsion angle C(5)–Ge(1)–Ge(2)–C(6) = 12.74.

were assigned by DEPT and C-H COSY spectra (ppm): $CHSiMe_3$ (^1H, −0.41; ^{13}C, 2.7), $GeCH_2$ (^1H, 0.78; ^{13}C, 2.5), $SiCH_3$ (^1H, 0.18; ^{13}C, 3.0).[4] A single $SiMe_3$ resonance is consistent with a highly symmetrical structure (C_{2v}) such as that of the germirane, not with a π complex. In the latter the two substituents on the Ge atom bend inward to the ring skeleton in order to maximize the overlap between the vacant p orbital of **1** and the π orbital of ethylene. Furthermore, ^{13}C NMR signals due to the ring carbons of the intermediate exhibited an upfield shift similar to that of cyclopropane (δ −2.6) and 1,1-di-*tert*-butylsilirane (δ −5.0).[1e] The $^1J(^{13}C-^1H)$ coupling constant was estimated to be 153 Hz by ^1H-coupled ^{13}C spectra, which was large and comparable to that in cyclopropane (J = 160 Hz) and 1,1-di-*tert*-butylsilirane (J = 154 Hz).[1e] When the reaction mixture was allowed to stand for a few days, the intermediate germirane (**3**) gradually was converted to **2**, as shown in Figure 2. However, attempts to isolate **3** was unsuccessful. Removal of ethylene and solvent resulted in the disappearance of **3**.

The photochemical sensitivity of the Ge–Ge bond[7] results in changes in the UV–vis spectrum upon irradiation (>300 nm) using a high-pressure mercury lamp. Loss of the absorbance due to **2** at 278 nm was

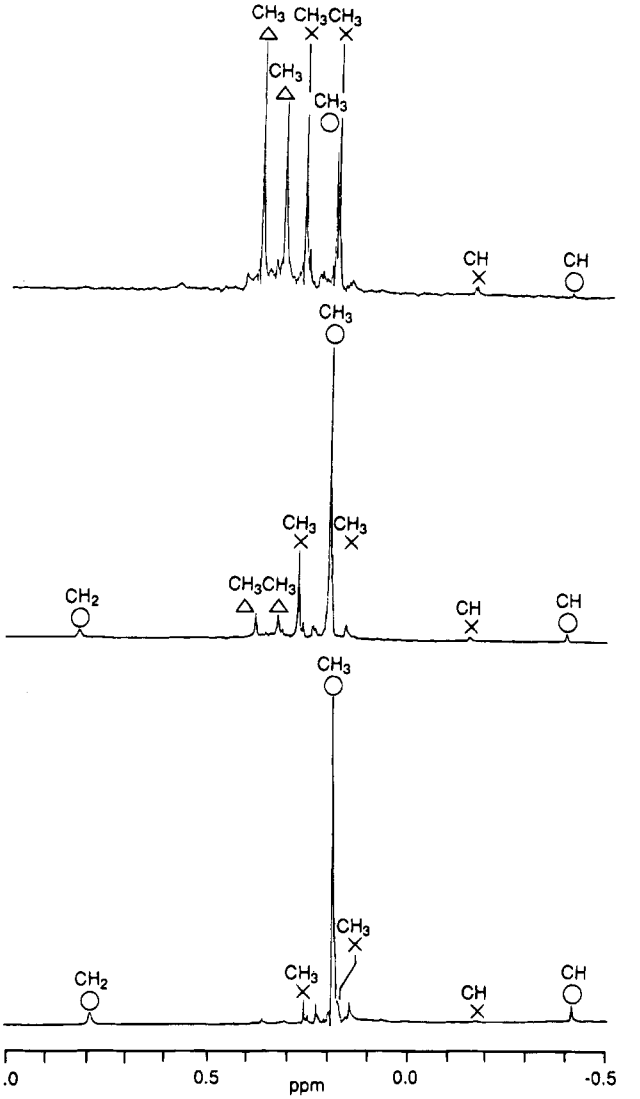

Figure 2. ^1H NMR spectra of **1** and C_2H_4 in benzene-d_6: (○) **3**; (△) **2**; (×) $[(Me_3Si)_2CH]_2GeH(OH)$ as a minor product derived from **1** and adventious water. Measuring times of the spectra are as follows: (bottom) after 30 min; (middle) after 6 h; (top) after 24 h.

observed with concomitant growth of peaks due to free germylene **1** at 418 nm. Similarly, photolysis of **2** in carbon tetrachloride afforded 1,4-digerma-1,4-dichlorobutane (**4**) quantitatively,[4] and photolysis in 2,3-dimethyl-1,3-butadiene yielded 1-germacyclopent-3-ene (**5**) quantitatively.[4] These results indicated that Ge–

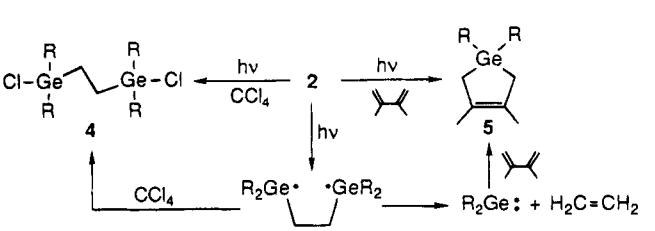

Ge bond dissociation is the dominant primary photoprocess.[8] The diradical which is formed reacts with

(7) (a) Mochida, K.; Kikkawa, H.; Nakadaira, Y. *Chem. Lett.* **1988**, 1089. (b) Bobbitt, K. L.; Maloney, V. M.; Gasper, P. P. *Organometallics* **1991**, *10*, 2772.

(8) (a) Kira, M.; Sakamoto, K.; Sakurai, H. *J. Am. Chem. Soc.* **1983**, *105*, 1469. (b) Sakurai, H.; Sakamoto, K.; Kira, M. *Chem. Lett.* **1984**, 1213. (c) Sakurai, H.; Sakamoto, K.; Kira, M. *Chem. Lett.* **1984**, 1379. (d) Sakurai, H.; Sakamoto, K.; Kira, M. *Chem. Lett.* **1987**, 983.

carbon tetrachloride more rapidly than does 2,3-dimethyl-1,3-butadiene. On the other hand, in the presence of the butadiene, with which the diradical reacts only slowly, it undergoes germylene extrusion. The latter reacts with the butadiene to give the 1-germacyclopent-3-ene.

Acknowledgment. We are grateful to Asai Germanium Institute and Shin-Etsu Co. Ltd. for their gifts of trichlorogermane and chlorosilanes. This work was supported by a Grant-in-Aid for Scientific Research from the Ministry of Education, Science and Culture of Japan.

Supplementary Material Available: Text describing crystallographic procedures, tables of crystallographic data, atomic coordinates and thermal parameters, and bond length and angles for **2**, a figure showing the ORTEP structure, and figures showing UV–vis spectra and ^{1}H, ^{13}C, DEPT, ^{1}H-decoupled ^{13}C, and C-H COSY NMR spectra of **3** (42 pages). Ordering information is given on any current masthead page.

OM940918X

Photochemical Additions of *cyclo*-$(Ar_2Si)_4$ and $(Ar_2Ge)_4$ to C_{60}

Takahiro Kusukawa, Yoshio Kabe, and Wataru Ando*

Department of Chemistry, University of Tsukuba, Tsukuba, Ibaraki 305, Japan

Received December 29, 1994[⊗]

Summary: The photochemical reaction of cyclotetrasilane ***1a*** *with* C_{60} *afforded stable 1:1 adducts* ***2a*** *and* ***3a****; the latter was obtained from a rearrangement of the cyclotetrasilane unit. Similarly, cyclotetragermane* ***1c*** *gave* ***2c*** *and the rearranged product* ***3c****. In the case of cyclotetrasilane* ***1b****, only the rearranged product* ***3b*** *was obtained in high yield. The structures of all compounds were determined by spectroscopic methods, including* $^{29}Si-^{1}H$ *HMBC hetero nuclear shift correlation experiments.*

The unique structure of C_{60} and its derivatives has sparked much research activity bridging the disciplines of chemistry, physics, and material science.[1-5] Recently, Wang and West reported that fullerene-doped polysilane displays enhanced photoconductivity.[6] Fullerene-bonded polysilane derivatives might be expected to show higher conductivity. However, only a few examples of the formation of fullerene–silicon derivatives have been reported to date.[7] Among the attractive targets are the fullerene-bonded polysilanes (Scheme 1). We now report the synthesis of fullerene–silicon derivatives bearing Si–Si and Ge–Ge rings, whose thermal or catalyzed ring opening may be expected to provide fullerene-substituted polysilanes and polygermanes.

Irradiation of a solution of 70.1 mg (83.3 μmol) of cyclotetrasilane[8] **1a** and 60.0 mg (83.3 μmol) of C_{60} in 60 mL of toluene with a high-pressure mercury lamp (λ > 300 nm) for 6 h under an argon atmosphere, followed by purification by means of gel-permeation chromatography (Jaigel 1H and 2H columns, Japan Analytical Industry Co. Ltd.; eluent toluene), afforded the brown

Scheme 1

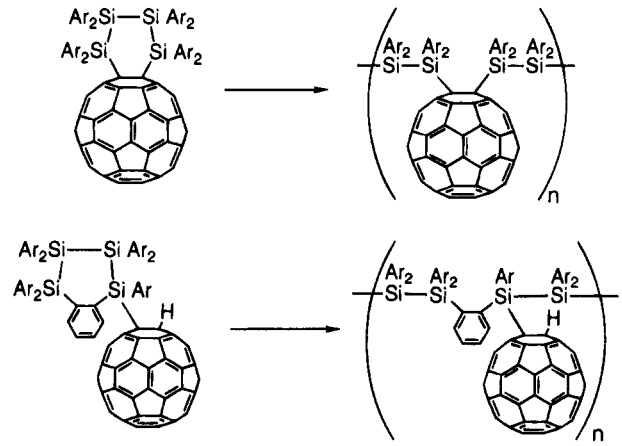

adducts **2a**[9] and **3a**[10] in 13% and 46% yields, respectively (based on unreacted C_{60}; Scheme 2). Under identical conditions, only **3b** was obtained from **1b** in 87% yield.

The FAB mass spectrum of **2a** exhibits one peak at m/z 1560–1563 ($C_{116}H_{56}Si_4$, M^+, molecular cluster ion), as well as one for C_{60} at m/z 720–723.

⊗ Abstract published in *Advance ACS Abstracts,* April 1, 1995.

(1) (a) Kroto, H. W.; Allaf, A. W.; Balm, S. P. *Chem. Rev.* **1991**, *91*, 1213. (b) Kroto, H. W.; Heath, J. R.; O'Brien, S. C.; Curl, R. F.; Smalley, R. E. *Nature* **1985**, *318*, 162. (c) Krätschmer, W.; Lamb, L.; Fostiropoulos, K.; Huffman, D.R. *Nature* **1990**, *347*, 354. (d) Krätschmer, W.; Fostiropoulos, K.; Huffman, D. R. *Chem. Phys. Lett.* **1990**, *170*, 167.

(2) See the entire third issue: *Acc. Chem. Res.* **1992**, *25*, 98–175.

(3) (a) Haufler, R. E.; Conceicao, J.; Chibante, L. P. F.: Chai, Y.; Byren, N. E.; Flanagan, S.; Haley, M. M.; O'Brien, S. C.; Pan, C.; Xiao, Z.; Billups, W. E.; Ciufolini, M. A.; Hauge, R. H.; Margrave, J. L.; Wilson, L. J.; Curl, R. F.; Smalley, R. E. *J. Phys. Chem.* **1990**, *94*, 8634. (b) Allemand, P. M.; Koch, A.; Wudl, F.; Rubin, Y.; Diederich, F.; Alvarez, M. M.; Anz, S. J.; Whetten, R. L. *J. Am. Chem. Soc.* **1991**, *113*, 1050. (c) Dubois, D.; Kadish, K. M.; Flanagan, S.; Wilson, L. J. *J. Am. Chem. Soc.* **1991**, *113*, 7773.

(4) Hirsch, A. *Angew. Chem., Int. Ed. Engl.* **1993**, *32*, 1138.

(5) *Fullerenes: Synthesis, Properties, and Chemistry of Large Carbon Clusters*; Hammond, G., Kuck, V. J., Eds.; ACS Symposium Series 481; American Chemical Society: Washington, DC, 1992.

(6) Wang, Y.; West, R.; Yuan, C.-H. *J. Am. Chem. Soc.* **1993**, *115*, 3844.

(7) (a) Akasaka, T.; Ando, W.; Kobayashi, K.; Nagase, S. *J. Am. Chem. Soc.* **1993**, *115*, 10366. (b) Akasaka, T.; Ando, W.; Kobayashi, K.; Nagase, S. *J. Am. Chem. Soc.* **1993**, *115*, 1605. (c) Akasaka, T.; Mitsuhida, E.; Ando, W.; Kobayashi, K.; Nagase, S. *J. Am. Chem. Soc.* **1994**, *116*, 2627. (d) Kusukawa, T.; Kabe, Y.; Erata, T.; Nestler, B.; Ando, W. *Organometallics* **1994**, *13*, 4186.

(8) (a) Pink, H. S.; Kipping, F. S. *J. Chem. Soc.* **1923**, *123*, 2830. (b) Jarvie, A. W. P.; Winkler, H. J. S.; Peterson, D. J.; Gilman, H. *J. Am. Chem. Soc.* **1961**, *83*, 1921.

(9) $(C_{56}H_{56}Si_4)C_{60}$ (FAB MS, m/z 1560–1563): ^{1}H NMR (500 MHz, 1:1 $CDCl_3$–CS_2) δ 2.21 (s, 6H, Si–C_6H_4*Me*), 2.25 (s, 6H, Si–C_6H_4*Me*), 2.30 (s, 6H, Si–C_6H_4*Me*), 2.32 (s, 6H, Si–C_6H_4*Me*), 6.76 (d, 4H, J = 7.7 Hz), 6.87 (d, 4H, J = 7.7 Hz), 6.92 (d, 4H, J = 7.7 Hz), 6.98 (d, 4H, J = 7.7 Hz), 7.33 (d, 4H, J = 7.7 Hz), 7.37 (d, 4H, J = 7.7 Hz), 7.45 (d, 4H, J = 7.7 Hz), 7.62 (d, 4H, J = 7.7 Hz); ^{13}C NMR (126 MHz, $CDCl_3$) δ (number of quaternary carbons) 62.18 (2), 127.35 (2), 128.65 (2), 132.94 (4), 136.67 (2), 139.21 (2), 139.49 (2), 139.62 (4), 140.14 (1), 140.41 (2), 141.43 (2), 141.62 (2), 141.91 (1), 142.00 (2), 142.03 (1), 142.85 (2), 142.98 (2), 143.31 (2), 143.36 (2), 143.51 (2), 144.48 (2), 144.52 (2), 144.56 (2), 144.70 (2), 144.92 (2), 145.02 (2), 145.23 (2), 145.26 (2), 145.71 (2), 146.11 (1), 147.14 (2), 147.50 (2), 148.11 (2), 148.55 (2), 148.64 (2), 151.02 (2), 151.20 (2), 165.03 (2), side chain δ 21.54 (q), 21.60 (q), 21.63 (q, two carbons), 128.31 (d), 128.35 (d), 128.53 (d), 128.58 (d), 135.74 (d), 135.83 (d), 137.77 (d), 138.07 (d); ^{29}Si NMR (400 MHz 1:1 $CDCl_3$–CS_2) δ −22.25, −11.34.

(10) $(C_{56}H_{56}Si_4)C_{60}$ (FAB MS, m/z 1560–1563): ^{1}H NMR (500 MHz, 1:1 $CDCl_3$–CS_2) δ 2.02 (s, 3H, Si–C_6H_4*Me*), 2.16 (s, 3H, Si–C_6H_4*Me*), 2.19 (s, 3H, Si–C_6H_4*Me*), 2.22 (s, 3H, Si–C_6H_4*Me*), 2.230 (s, 3H, Si–C_6H_4*Me*), 2.233 (s, 3H, Si–C_6H_4*Me*), 2.26 (s, 3H, Si–C_6H_4*Me*), 2.40 (s, 3H, Si–C_6H_4*Me*), 6.53 (d, 2H, J = 7.6 Hz), 6.57 (d, 2H, J = 7.6 Hz), 6.68 (d, 2H, J = 7.6 Hz), 6.81 (d, 2H, J = 7.6 Hz), 6.83 (d, 2H, J = 7.6 Hz), 6.85 (d, 4H, J = 7.6 Hz), 6.90 (d, 2H, J = 7.6 Hz), 6.91 (s, 1H), 6.99 (d, 2H, J = 7.6 Hz), 7.00 (d, 2H, J = 7.6 Hz), 7.03 (d, 2H, J = 7.6), 7.08 (d, 2H, J = 7.6 Hz), 7.38 (d, 2H, J = 7.6 Hz), 7.49 (d, 2H, J = 7.6 Hz), 7.56 (d, 1H, J = 7.8 Hz, H^b), 7.66 (s, 1H, H^d), 9.13 (d, 1H, J = 7.8 Hz, H^a); ^{13}C NMR (126 MHz, 1:1 $CDCl_3$–CS_2) δ (number of quaternary carbons) 127.24 (1), 128.04 (2), 129.52 (1), 130.08 (1), 136.32 (1), 137.52 (1), 138.15 (1), 138.18 (1), 138.36 (1), 138.43 (2), 138.52 (1), 138.99 (1), 139.14 (1), 139.26 (1), 139.43 (1), 139.45 (1), 139.54 (1), 140.51 (1), 141.16 (1), 141.17 (1), 141.27 (1), 141.39 (1), 141.60 (1), 141.63 (1), 141.68 (1), 141.72 (1), 141.75 (1), 141.78 (1), 142.26 (1), 142.29 (1), 142.32 (1), 142.35 (1), 142.96 (2), 143.23 (1), 143.28 (1), 144.25 (1), 144.39 (1), 144.45 (1), 144.52 (3), 144.58 (1), 144.85 (1), 145.13 (1), 145.18 (2), 145.26 (3), 145.86 (1), 145.87 (1), 145.95 (1), 145.97 (1), 146.01 (1), 146.04 (1), 146.07 (1), 146.12 (3), 146.20 (1), 146.23 (1), 146.52 (1), 147.05 (1), 147.37 (3), 147.48 (1), 148.27 (1), 153.26 (1), 155.08 (1), 156.61 (1), 157.67 (1), side chain δ 60.35 (d, C^e), 63.02 (s, C^f), 128.04 (d), 128.17 (d), 128.26 (d), 128.35 (d), 128.58 (d), 128.61 (d), 128.68 (d), 129.24 (d, C^b), 136.44 (d), 136.71 (d), 136.78 (d), 137.42 (d), 137.68 (d), 137.70 (d), 138.32 (d), 139.92 (d, C^a), 141.36 (d, C^d); ^{29}Si NMR (400 MHz, 1:1 $CDCl_3$–CS_2) δ −44.83, −41.26, −24.30, −12.66.

0276-7333/95/2314-2142$09.00/0

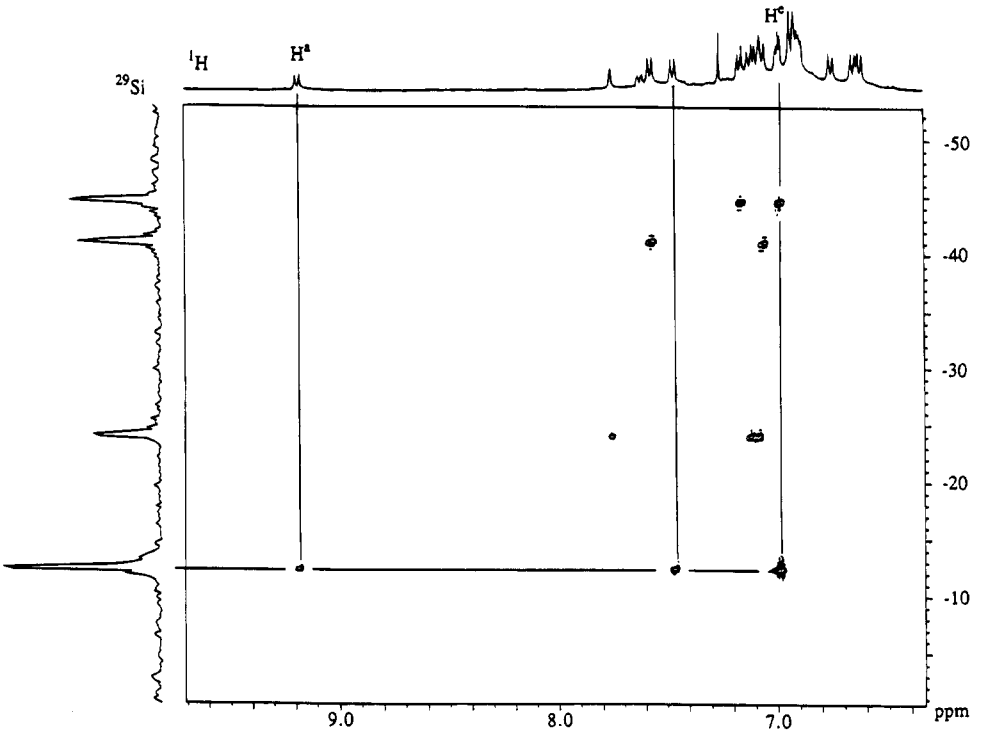

Figure 1. ^{1}H−^{29}Si HMBC spectrum of **3a**.

Scheme 2

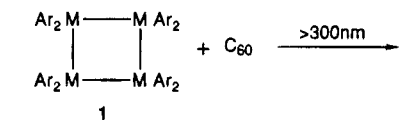

1

a: Ar = 4-Me-C$_6$H$_4$-, M = Si
b: Ar = Ph, M = Si
c: Ar = Ph, M = Ge

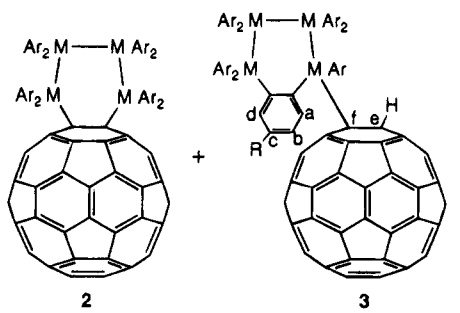

2 3

a: Ar = 4-Me-C$_6$H$_4$-, M = Si, R = Me
b: Ar = Ph, M = Si, R = H
c: Ar = Ph, M = Ge, R = H

The ^{13}C NMR spectrum of **2a** displays 38 signals for all quaternary carbons. Of the 38, one fullerene carbon atom resonates at 62.18 ppm. The signals of all other carbons appear in the region between δ 125 and 165 ppm. The ^{1}H NMR spectrum of **2a** displays 4 methyl signals and 4 pairs of AB quartets, supporting C_s symmetry for the molecule. The ^{29}Si NMR spectrum of **2a** shows two peaks at −22.25 and −11.34 ppm, which are assigned to the silicon atoms of **2a**.

Symmetry arguments support the following possibilities: (i) a 5,6-ring junction or 1,4-addition to the C_{60} with ring inversion (in the case of a 5,6-ring junction or 1,4-addition on the C_{60} with frozen conformer; formation of two diastereomeric adducts would have to be expected) and (ii) a 6,6-ring junction on the C_{60} with a frozen conformer (no ring inversion).[7b] To obtain further information concerning the structure of **2a**, a variable-temperature ^{1}H NMR measurement was carried out. A chemical shift change of the *p*-tolyl groups, reflecting a conformational change of the molecule, was observed.[11] From these findings, a 6,6-ring junction on the C_{60} with a frozen conformer is most probable for **2a**.

The FAB mass spectrum of **3a** exhibits one peak at *m*/*z* 1560−1563 ($C_{116}H_{56}Si_4$, M^+, molecular cluster ion), as well as one for C_{60} at *m*/*z* 720−723.

The ^{13}C NMR spectrum of **3a** displays 64 signals for all quaternary carbons, which indicates the absence of any symmetry element in this molecule. Of the 64, one fullerene carbon atom resonates at 60.35 ppm. The signals of all other carbons appear in the region between δ 125 and 160 ppm.

The partial structure of the fragment annulated to the C_{60} moiety can be derived from the NMR spectroscopic properties for **3a**: For *one 4-methyl-o-phenylene group*, three doublets at δ 129.24 (C^{b}), 139.92 (C^{a}), and 141.36 (C^{d}) appear in the ^{13}C NMR spectrum. As evidenced by homo- (^{1}H−^{1}H) and heteronuclear (^{1}H−^{13}C) shift correlation (COSY) experiments, the corresponding methine protons resonate at 7.56 (H^{b}), 9.13 (H^{a}), and 7.66 (H^{d}) ppm, and one methyl signal appears in the ^{1}H NMR spectrum.

The other *seven 4-Me-C$_6$H$_4$ groups* give rise to 14 doublets in the ^{13}C NMR spectrum and 13 doublets (overlapping might obscure one signal) and 7 methyl signals in the ^{1}H NMR spectrum.

The presence of *one hydrogen connected to C_{60}* is deduced from one doublet at 60.35 (C^{e}) ppm and one singlet at δ 6.91 (H^{e}) in the ^{13}C NMR and ^{1}H NMR spectra, respectively. The ^{29}Si NMR spectrum of **3a** shows four peaks at −44.83, −41.26, −24.30, and

(11) Variable-temperature ^{1}H NMR measurement was carried out in toluene-d_8 in the range 25−80 °C. However, these conditions are not enough to effect complete ring inversion of adduct **2a**.

−12.66 ppm, which are assigned to the silicon atoms of **3a**. The connectivities between these structural elements were determined by a $^{29}Si-^{1}H$ HMBC experiment.[7d] It was shown that the silicon resonance at −12.66 ppm correlated with both H^a and H^e methylene proton signals (Figure 1).

Regarding the addition pattern of the fullerene moiety, a 6,6-ring junction of the tetrasilacyclohexane fragment is most probable.[7a,12] In the case of a 5,6-junction, formation of two diastereomeric adducts would have to be expected.[13,14] The possibility of 1,4-addition can be eliminated by $^{13}C-^{1}H$ COLOC (correlation spectroscopy via long-range coupling). It was shown that the proton resonance at 6.91 ppm (H^e) correlates with the C^f quaternary carbon on the C_{60} group.

In order to obtain information concerning the mechanistic pathway for the formation of **2** and **3**, we carried out the photochemical reaction (λ > 300 nm) of **1b** in the presence of CCl_4, to give 1,4-dichloro-1,1,2,2,3,3,4,4-octaphenyltetrasilane (**4b**) and 1,3-dichloro-1,1,2,2,3,3-hexaphenyltrisilane (**5b**) in 37% and 31% yields, respectively. Under identical photolytic conditions adduct **2a** did not convert to **3a** in a control experiment. These findings indicate that a biradical (**6**) might be involved in the course of the reaction (Scheme 3).

Scheme 3

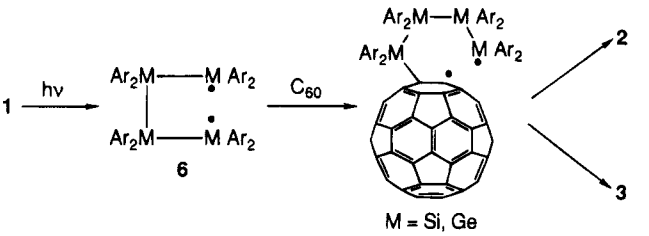

In the case of cyclotetragermane[15] **1c**, products **2c** (43%) and **3c** (37%, based on unreacted C_{60}) were obtained. The structures of the adducts **2b**, **2c**, and **3c** were determined in a similar manner by use of one- and two-dimensional NMR techniques; for details, see the supplementary material.

Further investigations of the synthesis of fullerene-bonded polysilane derivatives are in progress.

Acknowledgment. We are grateful to Dr. K. Ishikawa (National Chemical Laboratory for Industry, Tsukuba, Japan) for FAB mass measurements. This work was supported by a Grant-in-Aid for Scientific Research from the Ministry of Education, Science, and Culture of Japan.

Supplementary Material Available: Text giving NMR data for **2** and **3** and figures giving additional NMR spectra for **3a−c** (15 pages). Ordering information is given on any current masthead page.

OM940997C

(12) Dixon, D. A.; Matsuzawa, N.; Fukunaga, T.; Tebbe, F. N. *J. Phys. Chem.* **1992**, *96*, 6107.

(13) (a) Suzuki, T.; Li, Q.; Khemani, K. C.; Wudl, F.; Almarsson, Ö. *Science* **1991**, *254*, 1186. (b) Prato, M.; Lucchini, V.; Maggini, M.; Stimpfl, E.; Scorrano, G.; Eiermann, M.; Suzuki, T.; Wudl, F. *J. Am. Chem. Soc.* **1993**, *115*, 8479. (c) Smith, A. B., III; Strongin, R. M.; Brard, L.; Furst, G. T.; Romanow, W. J. *J. Am. Chem. Soc.* **1993**, *115*, 5829.

(14) Komatsu, K.; Kagayama, A.; Murata, Y.; Sugita, N.; Kobayashi, K.; Nagase, S.; Wan, T. S. M. *Chem. Lett.* **1993**, 2163.

(15) Ando, W.; Tsumuraya, T. *J. Chem. Soc., Chem. Commun.* **1987**, 1514.

Insertion Reactions of Isocyanides with Dioxodimesitylmolybdenum(VI): Crystal and Molecular Structure of the μ-Oxo η^2-Iminoacyl Dinuclear Complex $[(C_6H_2Me_3\text{-}2,4,6)Mo[C(C_6H_2Me_3\text{-}2,4,6)=NBu^t](O)]_2(\mu\text{-}O)$

Richard Laï,*,† Olivier Desbois,† Florence Zamkotsian,† Robert Faure,† Janine Feneau-Dupont,‡ and Jean-Paul Declercq‡

ENSSPICAM URA CNRS 1410, Faculté des Sciences / Saint-Jérôme, 13013 Marseille, France, and Laboratoire de Chimie Physique et de Cristallographie, Université Catholique de Louvain la Neuve, 1348 Louvain, Belgium

Received February 21, 1995®

Summary: Isocyanides react with dioxodimesitylmolybdenum(VI), $Mo(O)_2mes_2$ (mes = mesityl = $C_6H_2Me_3$-2,4,6), affording three different compounds identified as dimesityl imine $mes_2C{=}NR$, mesityl amide mesCONHR, and dinuclear μ-oxo η^2-iminoacyl complexes $[(C_6H_2Me_3\text{-}2,4,6)Mo[C(C_6H_2Me_3\text{-}2,4,6){=}NR](O)]_2(\mu\text{-}O)$ ($R = Bu^t$, C_6H_{11}, $CH_2C_6H_5$). These new complexes which have been characterized by spectroscopic methods and by X-ray crystallography in the case of $R = Bu^t$ represent the first examples of compounds in which bound to a high-valent metal is an η^2-iminoacyl group together with terminal and oxo-bridged ligands. Furthermore, they constitute a new structural type for the $Mo_2O_3^{4+}$ systems in which an oxo-bridged complex possesses a metal–metal bond and one terminal oxo group on each metal atom.

Insertion of isonitriles into metal–alkyl bonds leads to η^1- or η^2-iminoacyls, and this is comparable with CO reactivity.[1,2] However, in contrast to the extensive studies reported on the spectroscopic and structural properties of the η^2-acyl function, the study of the isoelectronic η^2-iminoacyl ligand formed by the migration insertion of isocyanides into metal–carbon bonds is much less thorough,[3] and sometimes more complicated reactions can occur by way of multiple insertion and coupling reactions.[4,5] Although the chemistry of complexes of the d-transition elements containing multiple-bonded ligands constitutes a rapidly expanding area of research,[6] apart from a few exceptions,[7,8] these complexes do not give stable compounds with π-acid ligands. Indeed, in such species, $d \rightarrow \pi^*$ back-bonding is very weak or totally absent because of the high oxidation state of the metal. Consequently, in spite of the growing number of examples of d^0 CO complexes only very few have been isolated.[9,10] Furthermore, only two examples of high-valent η^2-iminoacyl complexes containing multiple-bonded ligands have been reported until now.[7,11]

We have recently shown that $Mo(O)_2mes_2$ (mes = mesityl = $C_6H_2Me_3$-2,4,6) reacts with CO in the presence of pyridines affording dihydropyridine dimers[12] and tentatively explained this reactivity via electrophilic η^2-acyl species. In this context we thought it could be of interest to compare the reactivity of carbon monoxide with isoelectronic isonitriles.

The reaction of $Mo(O)_2mes_2$ with 1 equiv of *tert*-butyl isocyanide in pyridine at 0 °C results in an immediate color change from yellow to brown. After stirring of the mixture overnight at room temperature, the brown residue left after pyridine removal under reduced pressure is chromatographed under nitrogen on a silica gel column affording three principal fractions. The first and the third ones have been identified by IR, NMR, and mass spectroscopic means as a dimesityl imine $mes_2C{=}NBu^t$ (**3a**) (55%) and a mesityl amide mesCONHBu^t (**6a**) (15%), respectively. The second fraction is a red-brick solid (**4a**) (25%) which exhibits a strong absorption band around 1678 cm^{-1} (ν_{CN}) and one at 954 cm^{-1} ($\nu_{MO=O}$) in the IR spectrum. The absorption at 1678 cm^{-1} and a peak at δ 207.4 ppm in the $^{13}C\{^1H\}$ NMR spectrum (C_6D_6) are consistent with an η^2-iminoacyl functionality.[3,13,14] This complex **4a** appears through the FAB$^+$ mass spectrum to be dimeric (*m/z* 884 corresponding to MH$^+$ for isotope ^{96}Mo), and its structure, solved by an X-ray diffraction study,[15] confirmed this observation. A view of the molecule is depicted in

† ENSSPICAM, Marseille, France.
‡ Université de Louvain, Louvain, Belgium.
® Abstract published in *Advance ACS Abstracts,* April 15, 1995.

(1) Durfee, L. D.; Rothwell, I. P. *Chem. Rev.* **1988**, *88*, 1059.
(2) Braterman, P. S. *Reactions of Coordinated Ligands*; Plenum Press: New York, 1986.
(3) Chamberlain, L. R.; Durfee, L. D.; Fanwick, P. E.; Kobriger, L.; Latesky, S. L.; McMullen, A. K.; Rothwell, I. P.; Folting, K.; Huffman, J. C.; Streib, W. E.; Wang, R. *J. Am. Chem. Soc.* **1987**, *109*, 390.
(4) Chiu, K. W.; Jones, R. A.; Wilkinson, G.; Galas, A. M. R.; Hursthouse, M. B. *J. Chem. Soc., Dalton Trans.* **1981**, 2088.
(5) Chiu, K. W.; Jones, R. A.; Wilkinson, G.; Galas, A. M. R.; Hursthouse, M. B. *J. Am. Chem. Soc.* **1980**, *102*, 7978.
(6) Nugent, W. A.; Mayer, J. M. *Metal-Ligand Multiple Bonds*; Wiley: New York, 1988.
(7) Sullivan, A. C.; Wilkinson, G.; Motevalli, M.; Hursthouse, M. B. *J. Chem. Soc., Dalton Trans.* **1988**, 53.
(8) Su, F.-M.; Cooper, C.; Geib, S. J.; Rheingold, A. L.; Mayer, J. M. *J. Am. Chem. Soc.* **1986**, *108*, 3545.
(9) Guram, A. S.; Swenson, D. C.; Jordan, R. F. *J. Am. Chem. Soc.* **1992**, *114*, 8991.
(10) Antonelli, D. M.; Tjaden, E. B.; Stryker, J. M. *Organometallics* **1994**, *13*, 763.
(11) Vivanco, M.; Ruiz, J.; Floriani, C.; Chiesi-Villa, A.; Rizzoli, C. *Organometallics* **1993**, *12*, 1802.
(12) Laï, R.; Le Bot, S.; Djafri, F. *J. Organomet. Chem.* **1991**, *410*, 335.
(13) Carmona, E.; Palma, P.; Paneque, M.; Poveda, M. L. *Organometallics* **1990**, *9*, 583.
(14) Adams, R. D.; Chodosh, D. F. *Inorg. Chem.* **1978**, *17*, 41.
(15) Crystal data for $Mo_2N_2O_3C_{46}H_{62}$: prallelepiped red crystals, 0.15 × 0.17 × 0.35 mm, monoclinic, space group $P2_1/c$, a = 10.927(5) Å, b = 18.560(6) Å, c = 23.863(11) Å, β = 99.69(5)°, V = 4770(3) Å^3, Z = 4, D_x = 1.23 g cm^{-3}, μ = 5.56 cm^{-1}. X-ray diffraction data were collected on a Huber four-circle diffractometer using graphite-monochromatized Mo Kα radiation (λ = 0.710 69 Å). A total of 8383 independent reflections were collected ($(\sin\theta)/\lambda \leq 0.60$ Å^{-1}). A total of 4035 reflections with $I \geq 2.5\sigma(I)$ were used in the structure solution. The structure was solved by direct methods using SHELXS86.[16] H atoms were placed in computed positions. Anisotropic least squares refinement (SHELX76[17]) using F led to R = 0.063 and R_w = 0.062. Atomic scattering factors were taken from *International Tables for X-ray Crystallography.*

0276-7333/95/2314-2145$09.00/0

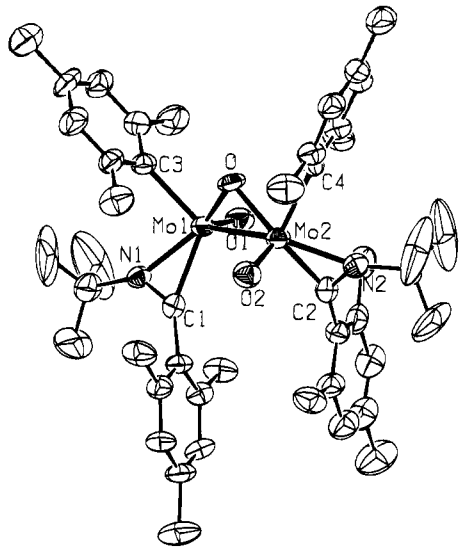

Figure 1. ORTEP drawing of **4a**. Selected bond distances (Å) and angles (deg) are as follows: Mo1O1 = 1.671(7), Mo1O 1.928(6), Mo1Mo2 = 2.772(1), Mo1C1 = 2.131(10), Mo1N1 = 2.093(8), Mo1C3 = 2.176(9), C1N1 = 1.254(12), Mo2O2 = 1.682(7), Mo2O = 1.926(6), Mo2C2 = 2.105(9), Mo2N2 = 2.104(8), Mo2C4 = 2.199(10), C2N2 = 1.260(14); Mo1OMo2 = 92.0(2), OMo1Mo2 44.0(2), OMo2Mo1 = 44.0(2), Mo2Mo1O1 = 102.5(2), Mo1Mo2O2 = 104.0(2), C2Mo2N2 = 34.8(4), C2N2Mo2 = 72.6(6), N2C2Mo2 = 72.5(6), O2Mo2C2 = 107.4(4), O2Mo2O = 109.6(3), O2Mo2N2 = 110.1(3), C1Mo1N1 = 34.5(3), C1N1Mo1 = 74.4(6), N1C1Mo1 = 71.1(6), O1Mo1C1 = 108.8(3), O1Mo1O = 108.9(3), O1Mo1N1 = 108.8(3).

Figure 1 with the most relevant bond distances and angles.

This complex is formed by two equivalent molybdenum moieties bound by a bent oxo bridge and a metal–metal bond, the Mo–Mo distance of 2.772(1) Å being consistent with a single bond. Each moiety contains one molybdenum atom, one terminal oxo ligand, and one mesityl group as well as an η^2-iminoacyl ligand. The terminal oxo ligands at each molybdenum atom are in the anti position with respect to each other, and they are sitting symmetrically on each side of the Mo–O–Mo plane. The usual conventions indicate a Mo(V) d^1 formulation to each molybdenum atom, the diamagnetism of the complex being explained by spin-pairing between the two molybdenum atoms. The distances in two Mo–η^2-iminoacyl linkages are identical within experimental error and lie in the range generally found for η^2-iminoacyl ligands.[3] They are also very similar to those reported for the only η^2-iminoacyl imido d^0 chromium complex.[7]

Complex **4** is remarkable for two reasons: first, it constitutes the unique example of an η^2-iminoacyl functionality linked to a metal bearing terminal and bridging oxo groups, and, second, to our knowledge, the bent oxo-bridged complex possessing a molybdenum–molybdenum bond and one terminal oxo group on each metal atom represents a completely new structural type for the $Mo_2O_3^{4+}$ systems.[18–20] The only example of a complex containing such a framework reported to date concerns a rhenium(IV) species.[21] When $Mo(O)_2mes_2$ was reacted with $C_6H_{11}NC$ or $C_6H_5CH_2NC$, the same reactivity was observed and the corresponding compounds were isolated and characterized.

The NMR spectroscopic properties of **4** are consistent with the solid-state structure[22] (see Figure 2 for the numbering scheme), and the presence of only one absorption around 954 cm^{-1} in the IR spectrum is well in accord with terminal oxo groups with a trans structure.[19]

Restricted rotation about the mesityl–molybdenum bond and about the mesityl–carbon bond of the iminoacyl functionality was shown by variable-temperature NMR experiments. The fact that neither coalescence nor line broadening was observed up to 110 °C indicated barriers to rotation about the mesityl–Mo and mesityl–CN bonds higher than 75 kJ·mol^{-1}.

(16) Sheldrick, G. M. SHELX86. Program for the Solution of Crystal Structures, 1985.
(17) Sheldrick, G. M. SHELX76, Program for crystal structure determination, 1976.
(18) West, B. O. *Polyhedron* **1989**, *8*, 219.
(19) Stiefel, E. I. *Progress in Inorganic Chemistry*; Lippard, S. G., Ed.; Wiley: New York, 1977.
(20) Holm, R. H. *Chem. Rev.* **1987**, *87*, 1401.
(21) Herrmann, W. A.; Felixberger, J. K.; Kuchler, J. G.; Herdtweck, E. *Z. Naturforsch.* **1990**, *45b*, 876.
(22) Selected NMR data for **4a**: As far as mesityl I and II are concerned, ^1H and ^{13}C assignments have been determined using a combination of inverse detection techniques. These techniques are the ^1H detected one-bond (C,H) heteronuclear multiple quantum coherence (HMQC) and the long-range (two and three bonds) (C,H) heteronuclear quantum bond connectivity (HMBC) experiments.[23] ^1H ($CDCl_3$): δ 1.06 (s, 18 H, *tBu*), 1.07 (s, Me(6) mes II), 1.43 (s, 6 H, Me(6) mes I), 1.93 (s, 6 H, Me(2) mes II), 2.23 (s, 6 H, Me(4) mes II), 2.42 (s, 6 H, Me(4) mes I), 2.64 (s, 6 H, Me(2) mes I), 6.48 (s, 2 H, CH(5) mes II), 6.49 (s, 2 H, CH(5) mes I), 6.81 (s, 2 H, CH(3) mes II), 6.97 (s, 2 H, CH(3), mes I). $^{13}C\{^1H\}$: δ 19.5 (Me(6) mes II), 20.8 (Me(2) mes II), 21.0 (Me(4) mes II), 21.3 (Me(4) mes I), 22.4 (Me(6) mes I), 28.5 ($(CH_3)_3C$), 29.5 (Me(2) mes I), 65.4 ($(CH_3)_3C$), 126.9 (CH(3) mes I), 128.0 (CH(3) mes II), 128.2 (CH(5) mes I), 129.0 (CH(5) mes II), 132.1 (Cqu(4) mes II), 133.1 (Cqu(6) mes II), 133.7 (Cqu(4) mes I), 134.0 (Cqu(1) mes II), 137.8 (Cqu(2) mes II), 137.9 (Cqu(2) mes I), 143.3 (Cqu(6) mes I), 172.7 (Cqu(1) mes I), 206.5 (C=N). One can assume that for mesityl I the most shielded ortho methyl group (Me(6)) is in the proximity of the shielding cone of the MoOMo ring, whereas the other one (Me(2)) is deshielded because of the anisotropic effect of the Mo=O bond. In the case of mesityl II one ortho methyl (Me(2)) has a normal δ value, whereas the other one (Me(6)) being located in the shielding cone of mesityl II bound to the other molybdenum atom is shielded at higher field in the ^1H NMR spectrum. We have also noticed that when C_6D_6 is used as a solvent, important differences are shown in the ^1H NMR spectra which are due to the AIS effect.[24] ^1H (C_6D_6): δ 0.99 (s, 18 H, *tBu*), 1.51 (s, 6 H, Me(6) mes II), 1.53 (s, 6 H, Me(6) mes I), 2.06 (s, 6 H, Me(2) mes II), 2.26 (s, 6 H, Me(4) mes II), 2.33 (s, 6 H, Me(4) mes I), 3.18 (s, 6 H, Me(2) mes I), 6.51 (s, 2 H, CH(5) mes II), 6.66 (s, 2 H, CH(5) mes I), 6.70 (s, 2 H, CH(3) mes II), 7.30 (s, 2 H, CH(3), mes I). $^{13}C\{^1H\}$: δ 19.5 (Me(6) mes II), 20.9 (Me(2) mes II), 21.1 (Me(4) mes II), 21.2 (Me(4) mes I), 23.4 (Me(6) mes I), 28.4 ($(CH_3)_3C$), 30.1 (Me(2) mes I), 65.3 ($(CH_3)_3C$), 127.7 (CH(3) mes I), 128.5 (CH(3) mes II), 128.8 (CH(5) mes I), 129.1 (CH(5) mes II), 132.7 (Cqu(4) mes II), 133.3 (Cqu(6) mes II), 134.1 (Cqu(4) mes I), 134.6 (Cqu(1) mes II), 137.9 (Cqu(2) mes II), 138.3 (Cqu(2) mes I), 143.9 (Cqu(6) mes I), 173.0 (Cqu(1) mes I), 207.4 (C=N). Data for **4b** are as follows. ^1H ($CDCl_3$): δ 1.10 (s, 6H, Me, mes), 1.14 (s, 6H, Me, mes), 1.80 (s, 6H, Me, mes), 2.20 (s, 6H, Me, mes), 2.30 (s, 12 H, Me, mes), [4.47 (d, 2 H, J_{HH} = 11 Hz), 4.70 (d, 2 H, J_{HH} = 11 Hz), $CH_2C_6H_5$ AB type spectrum], 6.45–7.27 (m, 10 H, C_6H_5). $^{13}C\{^1H\}$: δ 18.9 (Me(6) mes II), 20.0 (Me(2) mes II), 21.0 (Me(4) mes II), 21.3 (Me(4) mes I), 21.6 (Me(6) mes I), 29.3 (Me(2) mes I), 54.6 ($CH_2C_6H_5$), 127.0–141.1 (CH and Cqu C_6H_5 and mes), 172.9 (C ipso mes I, 209.8 (C=N). Data for **4c** are as follows. ^1H (C_6D_6): δ 0.59 (m, 4 H, CH_2 in C_6H_{11}), 0.87 (m, 4 H, CH_2 in C_6H_{11}), 1.09 (m, 4 H, CH_2 in C_6H_{11}), 1.24 (m, 4 H, CH_2 in C_6H_{11}), 1.55 (s, 6 H, Me(2) mes II), 1.61 (s, 6 H, Me(6) mes I), 1.63 (m, 4 H, CH_2 in C_6H_{11}), 2.11 (s, 6 H, Me(2) mes II), 2.18 (s, 6 H, Me(4) mes II), 2.33 (s, 6 H, Me(4) mes I), 3.13 (s, 6 H, Me(2) mes I), 3.82 (m, 2 H, CHN), 6.46 (s, 2 H, CH(5) mes II), 6.65 (s, 2 H, CH(5) mes I), 6.69 (s, 2 H, CH(3) mes II, 7.27 (s, 2 H, CH(3), mes I). $^{13}C\{^1H\}$: δ 19.5 (Me(6) mes II), 20.8 (Me(2) mes II), 21.0 (Me(4) mes II), 21.3 (Me(4) mes I), 21.8 (Me(6) mes I), 24.7 (CH_2, cyclohexyl), 25.0 (CH_2, cyclohexyl), 29.6 (Me(2) mes I), 30.5 (CH_2, cyclohexyl), 30.8 (CH_2, cyclohexyl), 62.7 (CHN), 127.0 (CH(3) mes I), 128.0 (CH(3) mes II), 128.4 (CH(5) mes I), 128.8 (CH(5) mes II), 131.5–142.0 (Cqu mes), 171.5 (C ipso mes I), 207.9 (C=N).
(23) Martin, G. E.; Zekter, A. S. *Two-Dimensional NMR methods for establishing molecular Connectivity*; VCH Publishers, Inc.: New York, 1988.
(24) Gunther, H. *La Spectroscopie de RMN*; Masson: Paris, 1994.

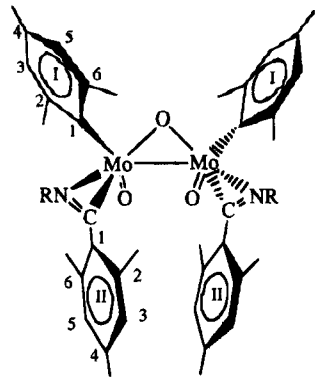

Figure 2. Adopted numbering scheme for the mesityl groups of **4**.

When the above reaction was effected in the presence of an excess of isocyanide, only monoinserted products were isolated. A terminal isocyanide complex $Mo(O)_2(mes)_2(CNBu^t)$ (**1a**), which is likely intermediate in the reaction leading to **4a**, can, however, be isolated as a dark-violet solid (ν_{CN} 2190 cm^{-1} and $\nu_{Mo=O}$ 910 and 924 cm^{-1}) by treating $Mo(O)_2mes_2$ with 1 equiv of Bu^tNC in Et_2O at −50 °C and precipitation with hexane. This species is stable in the solid state, but in contrast with its osmium analogue,[25] it evolves rapidly in solution to form compounds **3a**, **4a**, and **6a**, respectively.

When $Mo(O)_2mes_2$ is reacted with Bu^tNC in a sealed NMR tube in C_5D_5N, spectral changes occur as the temperature is raised from −33 to 25 °C. At −33 °C, in the $^{13}C\{^1H\}$ NMR spectrum, a singlet is shown at 204.8 ppm. At 25 °C, this peak disappears and new peaks characteristic of **3a** and **4a** appear at 162.9 and 207 ppm. The signal at 204.8 ppm can possibly be assigned to an unstable intermediate mononuclear η^2-iminoacyl **2** complex which could be at the origin of the different products found in this reaction (Scheme 1). Although this study has unambiguously established the structure of compound **4**, both in the solid state and in solution, the precise mechanism of the reaction leading to **4** and **6** remains to be clarified and Scheme 1 can be seen as a rationalization rather than a true mechanism. Formation of the imine **3** can be easily explained via a double migration of mesityl groups[1,26] followed by a reductive elimination pathway. Complex **4** is the result of the dimerization of the mononuclear η^2-iminoacyl moiety with loss of an oxygen. Insertion of oxygen into the molybdenum carbon bond of the iminoacyl function of **2** could afford an oxazametallacycle **5** which upon hydrolysis would then generate the amide.

Insertion of oxygen in a metal−carbon bond followed by amide formation has been reported once.[27] Furthermore, such metallacycles as **5** could be common intermediates in reactions between CO and imido complexes[7,12] or between isocyanates and imido- and oxomolybdenum complexes. In this last case they have been characterized by NMR.[28]

Scheme 1

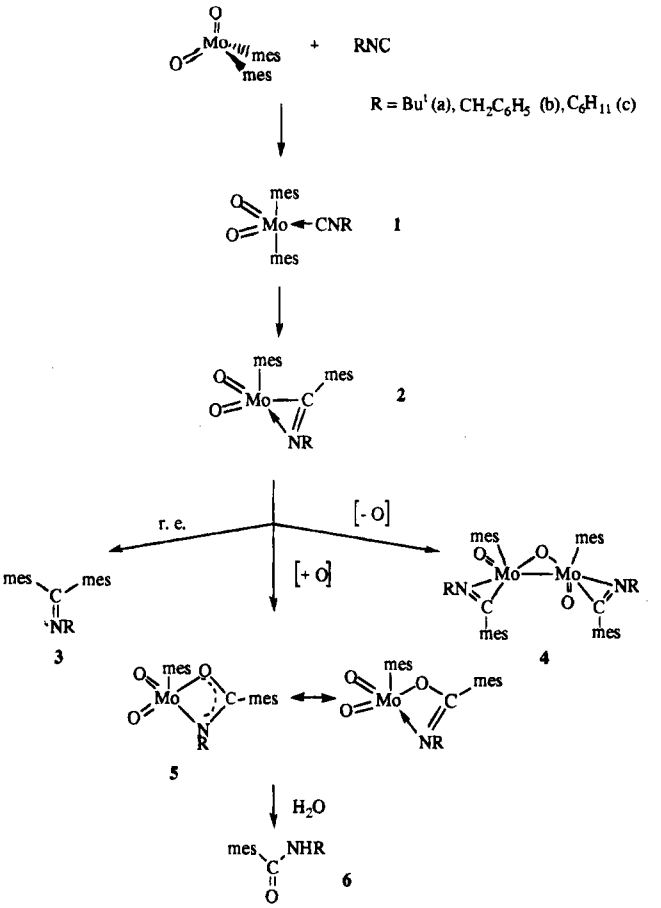

Acknowledgment. We are grateful to Dr. G. Salmona and Dr. D. Nuel for helpful discussions and valuable cooperation.

Supplementary Material Available: A fully labeled ORTEP diagram and tables of positional parameters, thermal parameters, bond lengths, bond angles, torsion angles, and crystal data for **4a** (7 pages). This material is contained in many libraries on microfiche, immediately follows this article in the microfilm version of the journal, and can be ordered from the ACS; see any current masthead page for ordering information.

OM950134Z

(25) McGilligan, B. S.; Arnold, J.; Wilkinson, G.; Hussain-Bates, B.; Hursthouse, M. B. *J. Chem. Soc., Dalton Trans.* **1990**, 2465.
(26) Koschmieder, S. U.; Hussain-Bates, B.; Hursthouse, M. B.; Wilkinson, G. *J. Chem. Soc., Dalton Trans.* **1991**, 2785.
(27) Vivanco, M.; Ruiz, J.; Floriani, C.; Chiesi-Villa, A.; Guastini, C. *Organometallics* **1990**, *9*, 2185.
(28) Laï, R.; Mabille, S.; Croux, A.; Le Bot, S. *Polyhedron* **1991**, *10*, 463.

New Copper and Rhodium Cyclopropanation Catalysts Supported by Chiral Bis(pyrazolyl)pyridines. A Metal-Dependent Enantioselectivity Switch

David L. Christenson, Christopher J. Tokar, and William B. Tolman*

Department of Chemistry, University of Minnesota, 207 Pleasant Street S.E., Minneapolis, Minnesota 55455

Received February 9, 1995

Summary: Copper and rhodium complexes of new optically pure bis(pyrazolyl)pyridines catalyze the cyclopropanation of styrene with moderate to high enantioselectivities, but the sense of asymmetric induction observed depends on the nature of the metal ion, implicating interesting mechanistic differences between the copper- and rhodium-based systems.

Optically active N-donor ligands have been demonstrated to be useful auxiliaries for metal-promoted asymmetric reactions,[1] particularly notable examples being the highly enantioselective cyclopropanations of alkenes by alkyl and aryl diazo carboxylates catalyzed by copper complexes of chiral semicorrins, 5-aza-semicorrins,[2] and bis(oxazolines).[3,4] Although the detailed mechanisms of these reactions are unclear, similarities among the pathways followed are suggested by the analogous topologies of the bidentate ligands used and a common relation between ligand absolute configuration and product stereochemistry. Thus, in every instance, ligands with stereogenic centers adjacent to the metal-bound N atom with an *S* configuration (e.g., **1**) favor production of 1*R*,2*R* and 1*R*,2*S* forms of *trans*- and *cis*-cyclopropanes (e.g., **2** and **3**), respectively. The

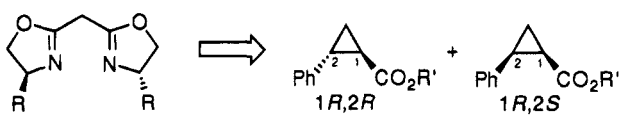

1 **2** **3**

same sense of asymmetric induction was reported recently for a bis(oxazolinyl)pyridine–ruthenium catalyst.[5] Here we report that, in efforts directed toward comparing the efficacy of C_2- and C_3-symmetric polypyrazole ligands in promoting stereoselective transformations,[6] we have prepared a set of Cu(I) and Rh(III) complexes of optically active bis(pyrazolyl)pyridines and have found that they catalyze the enantioselective cyclopropanation of styrene. We have also discovered that, for a given ligand diastereomer, the absolute configuration of the favored cyclopropane product changes with the nature of the metal ion, implicating an interesting difference between the copper and rhodium systems in the relative orientation of carbenoid species and olefin during the reaction step that defines product stereochemistry.

Ligands **4**–**6** were prepared by heating solutions of the appropriate potassium pyrazolates[6] with 2,6-dibromopyridine in diglyme via a precedented procedure (Scheme 1).[7,8] All three ligands formed stable $LRhCl_3$ complexes (**7**–**9**) whose structural formulations are based on combined analytical, NMR spectroscopic, and, in one instance, preliminary X-ray crystallographic data.[9–11] Solutions of active cyclopropanation catalysts were prepared by addition of 2 equiv of silver triflate to $LRhCl_3$ in THF, a method analogous to that used by Nishiyama and co-workers to generate bis(oxazolinyl)pyridine–rhodium catalysts used for the asymmetric hydrosilylation of ketones.[12,13] Copper catalysts were generated *in situ* by stirring Cu(I) triflate and the chosen ligand L in $CHCl_3$. Selected results from the reaction of ethyl diazoacetate (EDA) with excess styrene in the presence of the copper or rhodium catalysts (2 mol %) are listed in Table 1.

The cyclopropanes recovered from the reactions catalyzed by the copper complexes were obtained in moderate yield as a mixture of *trans* and *cis* isomers in a ratio (~2:1) that did not vary appreciably with the nature of L or with temperature. Enantioselectivities were also

* To whom correspondence should be addressed. E-mail: tolman@chemsun.chem.umn.edu. FAX: (612) 624-7029.

⊗ Abstract published in *Advance ACS Abstracts,* April 1, 1995.

(1) Togni, A.; Venanzi, L. M. *Angew. Chem., Int. Ed. Engl.* **1994**, *66*, 497–526.

(2) (a) Pfaltz, A. *Acc. Chem. Res.* **1993**, *26*, 339–345. (b) Pflatz, A. In *Modern Synthetic Methods*; Scheffold, R., Ed.; Springer-Verlag: Berlin, 1989; Vol. 5, pp 198–248.

(3) (a) Evans, D. A.; Woerpel, K. A.; Hinman, M. M.; Faul, M. M. *J. Am. Chem. Soc.* **1991**, *113*, 726–728. (b) Lowenthal, R. E.; Masamune, S. *Tetrahedron Lett.* **1991**, *32*, 7373–7376.

(4) For recent reviews on catalytic asymmetric cyclopropanations, see: Doyle, M. P. In *Catalytic Asymmetric Synthesis*; Ojima, I., Ed.; VCH: New York, 1993; pp 63–99.

(5) Itoh, K.; Itoh, Y.; Matsumoto, H.; Nishiyama, H.; Park, S.-B. *J. Am. Chem. Soc.* **1994**, *116*, 2223–2224.

(6) (a) LeCloux, D. D.; Tokar, C. J.; Osawa, M.; Houser, R. P.; Keyes, M. C.; Tolman, W. B. *Organometallics* **1994**, *13*, 2855–2866. (b) LeCloux, D. D.; Keyes, M. C.; Osawa, M.; Reynolds, V.; Tolman, W. B. *Inorg. Chem.* **1994**, *33*, 6361–6368.

(7) Jameson, D. L.; Goldsby, K. A. *J. Org. Chem.* **1990**, *50*, 4992–4994.

(8) LeCloux, D. D.; Tolman, W. B. *J. Am. Chem. Soc.* **1993**, *115*, 1153–1154.

(9) Synthetic procedures and analytical and spectroscopic data for all new compounds are reported in the supplementary material.

(10) Preliminary X-ray data for **7**: $C_{27}H_{37}N_5Cl_3Rh$, fw 640.89, cubic, space group $I23$ (No. 197), at −96 °C, $a = b = c = 23.802(9)$ Å, $V = 13485$ Å^3, $Z = 12$, $R = 0.089$, and $R_w = 0.121$ for 1053 reflections with $I > 2\sigma(I)$ and 85 parameters. The high residuals apparently resulted from the fact that the crystal diffracted X-rays only weakly and contained highly disordered solvent molecules (crudely modeled as five carbon atoms per complex). Nonetheless, confirmation of the overall topology of the molecule was obtained. See the supplementary material for a drawing of the structure.

(11) Structurally analogous ruthenium complexes of achiral bis(pyrazolyl)pyridines have been reported: Bessel, C.; See, R. F.; Jameson, D. L.; Churchill, M. R.; Takeuchi, K. J. *J. Chem. Soc., Dalton Trans.* **1993**, 1563–1576.

(12) (a) Nishiyama, H.; Kondo, M.; Nakamura, T.; Itoh, K. *Organometallics* **1991**, *10*, 500–508. (b) Nishiyama, H.; Sakaguchi, H.; Nakamura, T.; Horihata, M.; Kondo, M.; Itoh, K. *Organometallics* **1989**, *8*, 846–848.

(13) Hydrosilylations of acetophenone with Ph_2SiH_2 using **7**–**9** as catalyst precursors under the exact conditions cited in ref 12 were successful (89% yield of 1-phenylethanol after hydrolysis), but no enantioselectivity was observed. There was no reaction when the reaction was performed in the presence of excess L (4 equiv). These results suggest that catalysis of hydrosilylation is promoted by a rhodium species present in solution that does not contain **4**–**6**.

0276-7333/95/2314-2148$09.00/0

Scheme 1

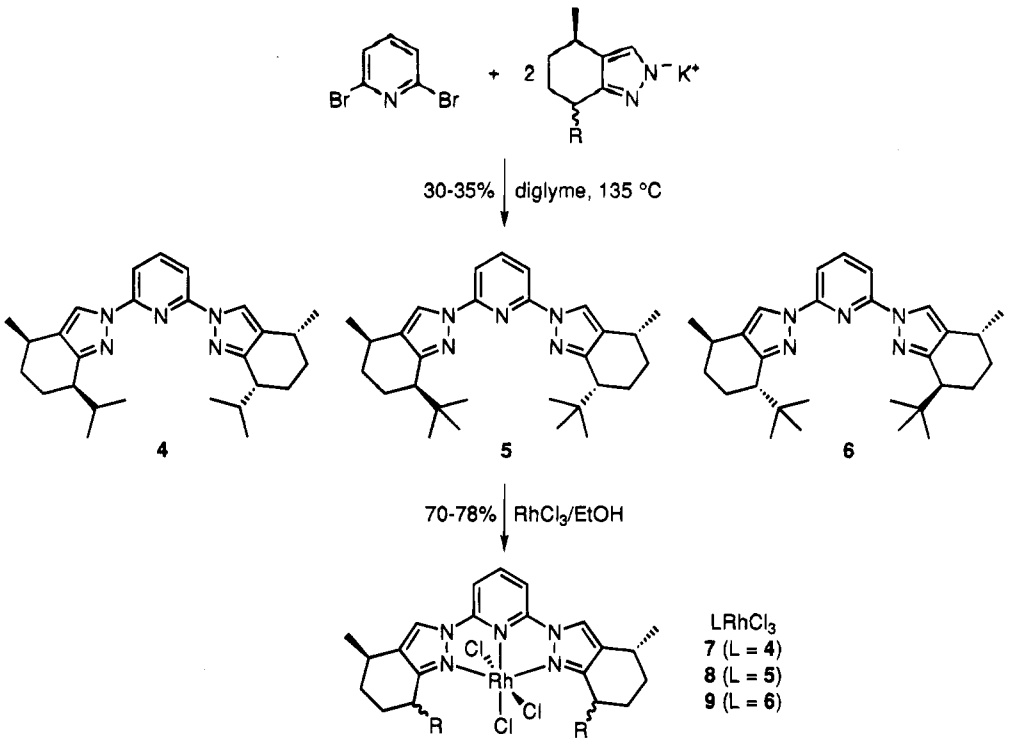

Table 1. Catalytic Cyclopropanation of Styrene with Ethyl Diazoacetate (EDA)[a]

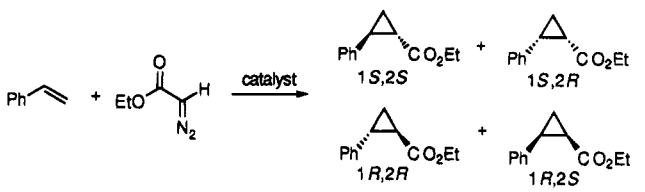

catalyst precursor	temp (°C)	yield (%)[b]	trans/cis ratio[c]	ee trans[d,e] (%)	ee cis[d,f] (%)
4/CuOTf (2.5:1)	25	73	63:37	40 (1*R*,2*R*)	41 (1*R*,2*S*)
4/CuOTf (1:1)	25	58	61:39	20 (1*R*,2*R*)	16 (1*R*,2*S*)
5/CuOTf (2.5:1)	25	82	66:34	15 (1*R*,2*R*)	12 (1*R*,2*S*)
5/CuOTf (2.5:1)	0	63	65:35	24 (1*R*,2*R*)	22 (1*R*,2*S*)
6/CuOTf (2.5:1)	25	49	64:36	48 (1*S*,2*S*)	50 (1*S*,2*R*)
6/CuOTf (2.5:1)	0	77	64:36	67 (1*S*,2*S*)	66 (1*S*,2*R*)
7[g]	25	43	42:58		33 (1*S*,2*R*)
8[g]	25	44	48:52	85 (1*S*,2*S*)	82 (1*S*,2*R*)
9[g]	25	37	49:51	83 (1*R*,2*R*)	80 (1*R*,2*S*)

[a] All reactions were performed by slowly (6 h) adding a solution of EDA to a solution of styrene (~8 equiv) and the catalyst (2 mol % based on EDA). The solvent was $CHCl_3$ or THF for the Cu- or Rh-catalyzed reactions, respectively. [b] Isolated yield after Kugelrohr distillation. [c] Determined by ^1H NMR and GC/MS analysis. [d] Absolute configurations of the major enantiomers are written in parentheses. [e] Determined by ^1H NMR and GC/MS analysis of the amides derived from (*S*)-1-phenylethylamine according to the procedure of Evans et al.[3a] [f] Determined by GC analysis (Chiraldex G-TA column). [g] AgOTf (2 equiv based on catalyst) was added prior to EDA addition.

moderate, with the best results obtained when L was used in excess for the system derived from **6** at 0 °C. The preferred absolute configurations of the products were as expected, on the basis of the extensive data available for cyclopropanations catalyzed by copper complexes of other C_2-symmetric chiral N-donor ligands.[2,3]

Lower *trans*/*cis* ratios (~1:1) and slightly better enantioselectivities (as high as 85%) were observed for the products of the rhodium-catalyzed reactions, which did not proceed unless **7**–**9** were pretreated with Ag^+. Surprisingly, the favored enantiomers in the reactions promoted by rhodium were opposite to the ones preferred in the reactions catalyzed by the copper complexes of the identical ligands. Thus, for example, 1*S*,2*S* and 1*S*,2*R* cyclopropanes were favored when **6** was complexed to Cu(I), but the 1*R*,2*R* and 1*R*,2*S* products were preferred when **9** was used as the catalyst precursor.

In the absence of definitive mechanistic evidence at this early point in our studies, we can only speculate as to the origin of the unusual[14] metal-dependent enantioselectivity "switch" we have observed. According to the model cited by Pfaltz,[15] an electrophilic metal carbene is the key cyclopropanating agent and the preferred approach of the incoming alkene to the metal carbene is governed by developing steric interactions between the substituents on the carbene and those on the chiral ligand as carbenoid pyramidalization occurs (and *not* by preferential blocking of a M=C face) (**A** in Figure 1). We can rationalize our observation of the same sense of asymmetric induction as seen for the bis(oxazoline) and semicorrin catalysts by applying this model to the reactions catalyzed by the **4**–**6**/Cu(I) systems, although likely bidentate coordination of **4**–**6** (via one pyrazolyl N and the pyridine N) to Cu(I) reduces the symmetry of our system and complicates the analysis.[16] If the assumption is made that the Pfaltz model can be applied to the rhodium-based system, in which

(14) Other examples of reversal of enantioselectivity in reactions performed with identical chiral auxiliaries: (a) Kawano, H.; Ikariya, T.; Ishii, Y.; Saburi, M.; Yoshikawa, S.; Uchida, Y.; Kumobayashi, H. *J. Chem. Soc., Perkin Trans. 1* **1989**, 1571–1575. (b) Kobayashi, S.; Ishitani, H. *J. Am. Chem. Soc.* **1994**, *116*, 4083–4084.

(15) Fritschi, H.; Leutenegger, U.; Pfaltz, A. *Helv. Chim. Acta* **1988**, *71*, 1553–1565.

(16) Similar arguments may explain recent results obtained with catalysts complexed to chiral bi- and terpyridine ligands: Chelucci, G.; Cabras, M. A.; Saba, A. *J. Mol. Catal.* **1995**, *95*, L7–L10.

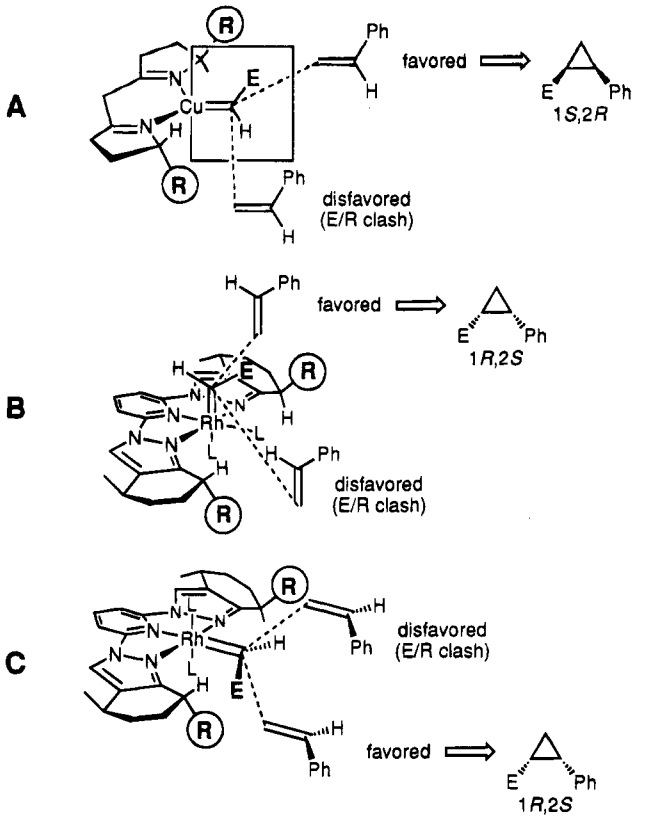

Figure 1. (**A**) Model based on arguments proposed by Pfaltz et al.[15] to explain preferential formation of *cis*-1*S*,2*R* enantiomer in cyclopropanation of styrene with a Cu(I) catalyst of a generic C_2-symmetric ligand analogous to a semicorrin or a bis(oxazoline). (**B**) Model involving an axial carbene to explain preferential formation of the *cis*-1*R*,2*S* enantiomer in the cyclopropanation of styrene using **9** (R = *t*-Bu). (**C**) Model involving an equatorial carbene (rotated 90° relative to that in **A**) to explain preferential formation of the *cis*-1*R*,2*S* enantiomer in the cyclopropanation of styrene using **9** (R = *t*-Bu).

meridional tridentate coordination can be assigned with more confidence, then in order to explain the asymmetric induction observed one is forced to postulate that either (i) the carbene occupies the axial instead of the equatorial position in the octahedral Rh complex (**B**, Figure 1) or (ii) the metal carbene is in the equatorial position but is rotated by 90° relative to the orientation in **A** (**C**, Figure 1). Alternative carbene orientations either predict product stereochemistry opposite to that observed or involve negligible E/R interactions during the course of the reaction, thus offering no apparent rationale for the observed enantioselectivities via the Pfaltz model.

These postulates comprise the framework for future studies of the mechanism and scope of the cyclopropanation reactions mediated by our new chiral rhodium catalysts. In addition, it will be particularly interesting to extend the chemistry of **7**–**9** to other substrates, with a view toward drawing reactivity comparisons to known dirhodium(II) catalysts for synthetically useful α-diazo carbonyl compound decompositions.[4,17]

Acknowledgment. We thank Professor Doyle Britton for his work on the X-ray crystal structure of **7** and Colleen Havlin for technical assistance. Financial support was provided by the National Science Foundation (Grant No. CHE-9207152 and a National Young Investigator Award), the donors of the Petroleum Research Fund, administered by the American Chemical Society, and the Alfred P. Sloan Foundation (fellowship to W.B.T.).

Supplementary Material Available: Text giving synthetic procedures and characterization data for compounds **4**–**9** and representative procedures for performing and analyzing the products of catalytic cyclopropanation and hydrosilylation reactions[13] and an ORTEP drawing of the preliminary X-ray crystal structure of **7** (6 pages). Ordering information is given on any masthead page.

OM9501081

(17) Padwa, A.; Austin, D. J. *Angew. Chem., Int. Ed. Engl.* **1994**, *33*, 1797–1815 and references cited therein.

Observation of a Non-H-Bond-Stabilized Tautomeric Imine–Enamine Equilibrium in Iminoacyl–Palladium Complexes

Juan Cámpora, Sarah A. Hudson, and Ernesto Carmona*

Departamento de Química Inorgánica, Instituto de Ciencia de Materiales, Universidad de Sevilla, Consejo Superior de Investigaciones Científicas, Apdo. 553, 41071 Sevilla, Spain

Received January 18, 1995[⊗]

Summary: Iminoacyl complexes of the type trans-Pd(C(=NBu^t)(CH$_2$C$_6$H$_4$-p-X))Cl(PR$_3$)$_2$ exist in solution as equilibrium mixtures of their imine and enamine forms. The position of the equilibria can be tuned by varying the X substituent of the aryl ring and the phosphine ligands, allowing in some cases the isolation of compounds that exist as the less common enamine form, both in solution and in the solid state.

Prototropic tautomerism is an important process that is involved in many organic transformations.[1] Of the different kinds, keto–enol and imine–enamine tautomerism have been the subject of numerous investigations due to their importance not only in organic but also in biological processes.[2] Although organometallic acyl and iminoacyl complexes are widespread and their chemical behavior has been thoroughly studied,[3] they are almost invariably encountered in their keto and imine forms, respectively.[4] In transition-metal–iminoacyl chemistry, imine-to-enamine tautomerism has been invoked to account for the nature of the product of the reaction of the iminoacyl *trans*-Pd(C(=NC$_6$H$_4$-*p*-Me)Me)Cl(PEt$_3$)$_2$ with MeO$_2$CC≡CCO$_2$Me,[5] but tautomerization to a stable enamine structure is uncommon and requires stabilization by hydrogen bonding,[6] extensive electron delocalization,[7a] or formation of more complex structures.[7b,c] A similar situation is found for organic imines and enamines, where the imine form usually predominates.[1a,2,8] In this communication we wish to report the first observation of a quantifiable imine–enamine equilibrium in the system arising from the insertion of CNBu^t into the Pd–C bond of complexes of the type Pd(CH$_2$C$_6$H$_4$-*p*-X)Cl(PR$_3$)$_2$. The position of this equilibrium can be varied by modifying the nature of the X group and the phosphine ligands, thereby allowing the study of the factors that affect the equilibrium constant and of the complexes that exist as the more uncommon enamine tautomer.

Reaction of the benzylpalladium derivative **1al** with *tert*-butyl isocyanide yields a yellow product, **1im**,[9] whose NMR and IR spectra[5] display features typical for a η^1-iminoacyl complex.[10] However, NMR spectra also show a second set of signals associated with a minor product, **1en**,[9] which amounts to ca. 8% of the overall mixture and could not be separated by recrystallization. Careful examination of the ^{1}H NMR spectrum of **1en** (acetone-d_6, 20 °C) revealed the presence of resonances at δ 5.65 (t, J_{HP} = 2.8 Hz) and 4.82 (br s) attributable to an olefinic and an NH proton, respectively. These signals strongly suggest that **1en** has the enamine structure shown in Scheme 1. Since the low concentration of **1en** in solution prevented the observation, under ordinary conditions, of the ^{13}C resonance corresponding

[⊗] Abstract published in *Advance ACS Abstracts,* April 1, 1995.

(1) (a) March, J. *Advanced Organic Chemistry: Reactions, Mechanisms and Structure*; Wiley: New York, 1992. (b) Lowry, M. T.; Richardson, K. S. *Mechanism and Theory in Organic Chemistry*; Harper and Row: New York, 1987.

(2) Lammersma, K.; Pasad, B. V. *J. Am. Chem. Soc.* **1994**, *116*, 642 and references therein.

(3) (a) Durfee, L. D.; Rothwell, I. P. *Chem. Rev.* **1988**, *88*, 1059. (b) Crociani, B. In *Reactions of Coordinated Ligands*; Braterman, P., Ed.; Plenum Press: New York, 1986; Chapter 9. (c) Alexander, J. J. In *The Chemistry of the Metal-Carbon Bond*; Hartley, F. R., Patai, S., Eds.; Wiley: New York, 1985; Vol. 2, Chapter 5.

(4) We are not aware of any well-documented example of M–C(O)-CHR ⇌ M–C(OH)=CR$_2$ tautomerism. However, transition-metal enolates are an important and synthetically useful class of organometallic compounds. For some examples see: (a) Rusik, C. A.; Collins, M. A.; Gamble, A. S.; Tonker, T. L.; Templeton, J. L. *J. Am. Chem. Soc.* **1989**, *111*, 2550. (b) Heah, P. C.; Patton, A. T.; Gladysz, J. A. *J. Am. Chem. Soc.* **1986**, *108*, 1185. (c) Liebeskind, L. S.; Welker, M. E.; Fengl, R. W. *J. Am. Chem. Soc.* **1986**, *108*, 6328. (d) Davies, S. G.; Walker, J. C. *J. Chem. Soc., Chem. Commun.* **1985**, 209. (e) Theopold, K. H.; Becker, P. N.; Bergman, R. G. *J. Am. Chem. Soc.* **1982**, *104*, 5250. (f) Ho, S. C. H.; Straus, D. A.; Armantrout, J.; Schaefer, W. P.; Grubbs, R. H. *J. Am. Chem. Soc.* **1984**, *106*, 2210.

(5) Clark, H. C.; Milne, C. R. C.; Payne, N. C. *J. Am. Chem. Soc.* **1978**, *100*, 1164.

(6) (a) Veya, P.; Floriani, C. *Organometallics* **1993**, *12*, 4899. (b) Bertani, R.; Castellani, C. B.; Crociani, B. *J. Organomet. Chem.* **1984**, *269*, C15.

(7) (a) Belderraín, T. R.; Paneque, M.; Carmona, E., to be submitted for publication. (b) Bellachioma, G.; Cardaci, G.; Zanazzi, P. *Inorg. Chem.* **1987**, *26*, 84. (c) Werner, H.; Heiser, B.; Kühn, A. *Angew. Chem., Int. Ed. Engl.* **1981**, *20*, 300.

(8) de Jeso, B.; Pommier, J. C. *J. Chem. Soc., Chem. Commun.* **1977**, 565.

(9) Procedure, analytical and selected spectroscopic data for compounds **1im/1en**, **2im/2en**, and **3im/3en** are as follows. **1im/1en**: To a stirred solution of Pd(CH$_2$C$_6$H$_5$)Cl(PMe$_3$)$_2$ (0.2 g, 0.57 mmol) in THF (40 mL) at room temperature was added CNBu^t (0.6 mL, 1 M solution in THF). There was an immediate color change from dark yellow to light yellow. The mixture was stirred at room temperature for 4 h and then evaporated *in vacuo*. The solid residue was crystallized from diethyl ether (20 mL) at −20 °C, giving a yellow crystalline material in 71% yield. **2im/2en** and **3im/3en** were prepared in the same manner, also giving yellow crystalline products in 71% and 73% yields, respectively. **1im**: IR (cm^{-1}, Nujol) $\nu_{C=N}$ 1637; ^{1}H NMR (20 °C, acetone-d_6) δ 3.84 (s, 2 H, CH$_2$); ^{13}C{^{1}H} NMR (20 °C, acetone-d_6) δ 56.0 (t, $^3J_{CP}$ = 12.5 Hz, CH$_2$), 176.9 (s, C=N); ^{31}P{^{1}H} NMR (20 °C, acetone-d_6) δ −18.3. **1en**: ^{1}H NMR (20 °C, acetone-d_6) δ 4.67 (br s, 1 H, NH), 5.65 (t, 1 H, $^4J_{HP}$ = 2.8 Hz, =CH); ^{13}C{^{1}H} NMR (20 °C, acetone-d_6) δ 101.8 (s, =CH); ^{31}P{^{1}H} NMR (20 °C, acetone-d_6) δ −18.2. Anal. Calcd for C$_{18}$H$_{34}$NClPdP$_2$: C, 46.2; H, 7.3; N, 3.0. Found: C, 46.5; H, 7.5; N, 2.8. **2im**: IR (cm^{-1}, Nujol) $\nu_{C=N}$ 1640; ^{1}H NMR (20 °C, acetone-d_6) δ 3.93 (s, 2 H, CH$_2$); ^{13}C{^{1}H} NMR (20 °C, acetone-d_6) δ 55.4 (t, $^3J_{CP}$ = 13.0 Hz, CH$_2$), 175.9 (s, C=N); ^{31}P{^{1}H} NMR (20 °C, acetone-d_6) δ −19.5. **2en**: ^{1}H NMR (20 °C, acetone-d_6) δ 5.20 (s, 1 H, NH), 5.70 (t, $^4J_{HP}$ = 2.9 Hz, 1 H, =CH); ^{13}C{^{1}H} NMR (20 °C, acetone-d_6) δ 101.1 (s, =CH), 166.3 (s, Pd–C–N); ^{31}P{^{1}H} NMR (20 °C, acetone-d_6) δ −20.0. Anal. Calcd for C$_{19}$H$_{33}$NClF$_3$PdP$_2$: C, 42.5; H, 6.2; N, 2.6. Found: C, 42.3; H, 6.1; N, 2.6. **3im**: undetected by NMR. **3en**: IR (Nujol, cm^{-1}) ν_{N-H} 3400, $\nu_{C=C}$ 1540; ^{1}H NMR (20 °C, acetone-d_6) δ 4.45 (s, 1 H, NH), 5.68 (t, $^4J_{HP}$ = 2.8 Hz, 1 H, =CH); ^{13}C{^{1}H} NMR (20 °C, acetone-d_6) δ 102.2 (s, =CH), 164.4 (s, Pd–C–N); ^{31}P{^{1}H} NMR (20 °C, acetone-d_6) δ 10.0. Anal. Calcd for C$_{25}$H$_{45}$NClF$_3$PdP$_2$: C, 48.4; H, 7.3; N, 2.3. Found: C, 48.3; H, 7.3; N, 2.4.

(10) (a) Carmona, E.; Palma, P.; Paneque, M.; Poveda, M. L. *Organometallics* **1990**, *9*, 583. (b) Reference 5. (c) Otusaka, S.; Ataka, K. *J. Chem. Soc., Dalton Trans.* **1976**, 327.

(11) The cationic carbene complex formed upon protonation of compound **3im/3en** by triflic acid has been isolated and characterized.

0276-7333/95/2314-2151$09.00/0

Scheme 1

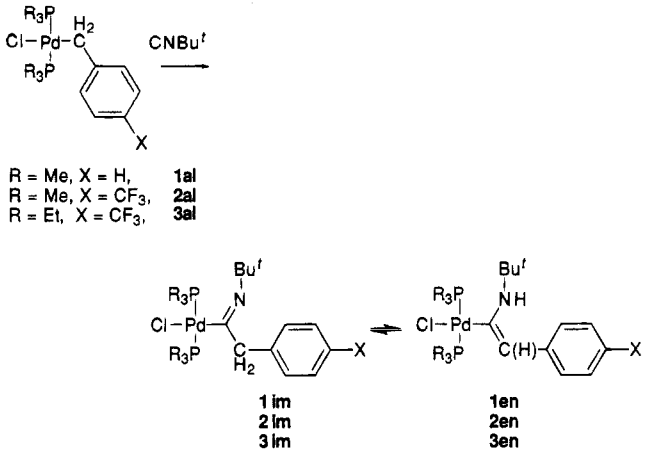

to the enaminic Pd—*C*(NHBu^t) carbon atom as well as the IR NH absorption, we sought a means of increasing the equilibrium concentration of the enamine form. The use of various solvents was of little help, since only a small difference in the tautomer ratio was observed when compound **1im/1en** was dissolved in benzene or chloroform as compared to more polar solvents such as acetone, the enamine form being slightly more favored in the latter.

The ground state of organic enamines has been described as a resonance hybrid of the neutral enamine form **A** and the 1,3-dipolar iminium salt form **B**.[1] For

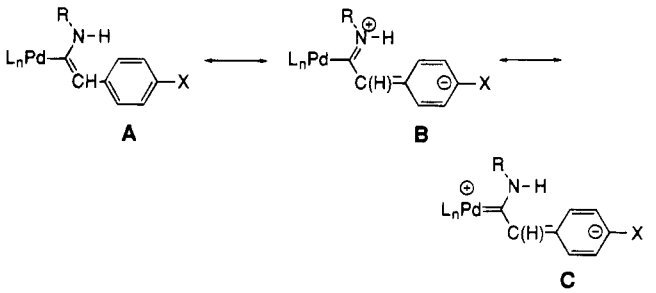

compounds **1en**–**3en**, a dipolar carbene form, **C**, could also be taken into account. From this picture, it can be readily understood that the presence of electron-releasing substituents on the nitrogen or palladium atoms, or of electron-withdrawing substituents on the aryl ring, should increase the relative stability of the enamine form. In agreement with these expectations, the concentration of the enamine tautomer is markedly increased for complexes **2**, which bear a *p*-trifluoromethyl fragment. NMR spectra for these tautomers, recorded in acetone-d_6 at 20 °C, showed a 3:4 equilibrium mixture of **2im** and **2en**.[9]

Although the structural and spectroscopic properties of late-transition-metal iminoacyl complexes do not suggest an important contribution of the amidocarbene resonance form to the electronic ground-state structure of these compounds,[12] the participation of such a dipolar carbene form **C**, particularly in the case of the enamines **2en** and **3en**, cannot be disregarded. Accordingly, compound **3im/3en**, in which the more basic ligand triethylphosphine replaces the trimethylphosphine of compound **2im/2en**, shows an even stronger preference for the enaminic form, **3en**, lowering the concentration

Scheme 2

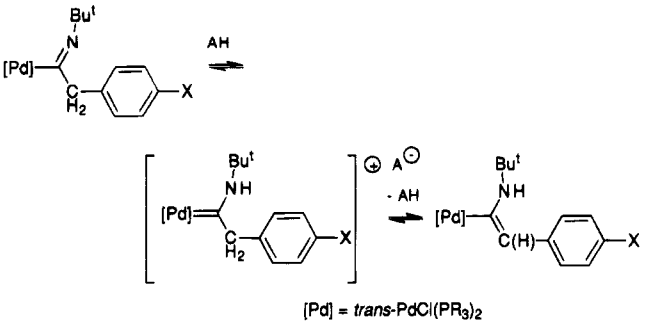

of the imine form **3im** to undetectable levels. This observation is in accord with the stabilizing effect exerted by electron-releasing ligands on resonance form **C**.

The $^{13}C\{^1H\}$ NMR spectrum of the enamine isomer **2en** displays resonances at 166.3 and 100.7 ppm, attributable respectively to the Pd—*C* and Pd—C=*C*H atoms; corresponding resonances can be found for compound **3en** at δ 164.4 and 102.2 ppm. This assignation has been confirmed by gated-decoupling and HETCOR spectroscopy (^1H—^{13}C) and is consistent with the chemical shifts expected for such derivatives. Whereas the crystallized mixtures of **1im** ⇌ **1en** and **2im** ⇌ **2en** display a prominent IR band at 1640 cm^{-1} which is characteristic of η^1-iminoacyl ligands, this absorption is absent in the spectrum of **3** and is replaced by new bands at 3450 and 1540 cm^{-1}, associated with the N—H and C=C bonds, respectively. The imine form **3im** has not been detected for this system; thus, pure enamine **3en** exists in the solid state.

Although we still do not have enough data to confirm a mechanism for the proton exchange, we have observed that these iminoacyl complexes are readily protonated to the corresponding cationic products (Scheme 2).[11] This behavior has previously been observed in related iminoacyl complexes,[6a,12] and is in accord with the expected basicity of the nitrogen atom. Even though tautomer exchange may occur by an intramolecular hydrogen shift, as has been proposed for other prototropies involving the iminoacyl functionality,[13] it seems more likely that it is promoted by trace quantities of an acid catalyst such as water present in the solvent, as shown in Scheme 2. Supporting this hypothesis, exchange of the NH, =CH, and CH_2 protons with deuterium occurs when D_2O is added to solutions of **2im** ⇌ **2en** in acetone-d_6.

In summary, we have demonstrated that the enamine structure of simple Pd—iminoacyl complexes can be stabilized by appropriately modifying the electronic characteristics of the metal center and the alkyl ligand.

Acknowledgment. We thank the Dirección General de Investigación Científica y Técnica (Grant No. PB-91-0612-C03-01) and Junta de Andalucía for the award of research fellowships. S.A.H. thanks the Commission of the European Communities for a grant from the HCM program (Project No. ERCHBICT920061). Thanks are also due to the University of Sevilla for free access to its analytical and NMR facilities.

OM950041H

(12) Carmona, E.; Palma, P.; Poveda, M. L. *Polyhedron* **1989**, *12*, 1447.

(13) Beshouri, S. M.; Chebi, D. E.; Fanwick, P. E.; Rothwell, I. P.; Huffman, J. C. *Organometallics* **1990**, *9*, 2375.

Synthesis and Structure of a Dinuclear η^1:η^2-μ_2-Butenynyl Complex Which Catalyzes Di- and Trimerization of Ferrocenylacetylene at the Thiolate-Bridged Diruthenium Center

Hiroyuki Matsuzaka,† Yukihiro Takagi, Youichi Ishii, Masayuki Nishio, and Masanobu Hidai*

Department of Chemistry and Biotechnology, The University of Tokyo, Hongo, Tokyo 113, Japan

Received January 12, 1995⊗

*Summary: Treatment of [Cp*RuCl(μ_2-SPr^i)$_2$RuCp*][OTf] (**1**; Cp* = η^5-C_5Me_5, OTf = OSO_2CF_3) with HC≡CFc (Fc = ferrocenyl) at room temperature afforded the dinuclear butenynyl complex [Cp*Ru{η^1:η^2-μ_2-C(=CHFc)C≡CFc}(μ_2-SPr^i)$_2$RuCp*][OTf] (**4a**), the molecular structure of which has been determined by X-ray diffraction analysis of the corresponding BPh_4^- salt **4b**. Complex **4a** is an effective catalyst for di- and trimerization of the alkyne to yield the head-to-head Z dimer CHFc=CHC≡CFc (**5**) and the linear Z,Z trimer CHFc=CHCFc=CHC≡CFc (**6**).*

Multisite interactions between a substrate molecule and more than one adjacent metal center can facilitate activation and transformation of the substrate, which offers a promising approach to new types of catalytic processes.[1] In a recent study on transition-metal–sulfur cluster compounds, we have shown that a series of dinuclear Cp*Ru–thiolate complexes (Cp* = η^5-C_5Me_5)[2–4] provide well-defined bimetallic reaction sites for unique transformations of alkynes,[5] organic halides,[2c] and hydrazines.[6] In a previous paper, we described facile coupling of HC≡CR (R = $\overline{CCH(CH_2)_3CH_2}$, Tol) on [Cp*RuCl($\mu_2$-SPr^i)$_2$RuCp*][OTf] (**1**; OTf = OSO_2CF_3), affording the five-membered metallacycles **2** and **3**.[7] These reactions have been believed to proceed via

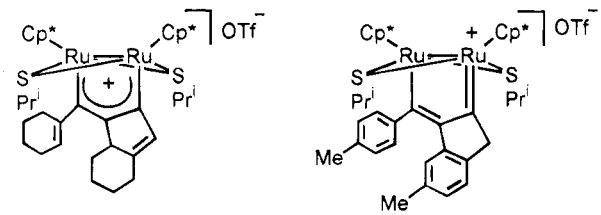

2 **3**

a vinylidene-alkynyl combination pathway at the diruthenium center.[5d,7,8] However, no intermediates could be detected in these conversions even at low temperature with a limited amount of alkynes. We report herein the isolation and characterization of the dinuclear butenynyl complex [Cp*Ru{η^1:η^2-μ_2-C(=CHFc)C≡CFc}(μ_2-SPr^i)$_2$RuCp*][OTf] (**4a**; Fc = ferrocenyl), which corresponds to a key intermediate of the above coupling reactions, and its unique catalytic activity for linear di- and trimerization of HC≡CFc.

Treatment of **1** with 6 equiv of HC≡CFc in CH_2Cl_2 at room temperature gave the dinuclear butenynyl complex **4a** in 83% yield (eq 1), which was obtained as a dark brown crystalline solid;[9] its corresponding BPh_4^- salt **4b** has been fully characterized by X-ray crystallography (Figure 1).[10] The most characteristic feature of its structure is the bridging butenynyl moiety formed by head-to-head coupling of two HC≡CFc molecules on the diruthenium-thiolate template. The two Ru atoms

† Present address: Department of Chemistry, Tokyo Metropolitan University, Minami-osawa, Tokyo 192–03, Japan.

⊗ Abstract published in *Advance ACS Abstracts,* April 15, 1995.

(1) (a) Süss-Fink, G.; Meister, G. *Adv. Organomet. Chem.* **1993**, *35*, 41 and references cited therein. (b) Gates, B. C., Guzci, L., Knözinger, V. H., Eds. *Metal Clusters in Catalysis*: Elsevier: Amsterdam, 1986.

(2) (a) Dev, S.; Imagawa, K.; Mizobe, Y.; Cheng, G.; Wakatsuki, Y.; Yamazaki, H.; Hidai, M. *Organometallics* **1989**, *8*, 1232. (b) Dev, S.; Mizobe, Y.; Hidai, M. *Inorg. Chem.* **1990**, *29*, 4797. (c) Takahashi, A.; Mizobe, Y.; Matsuzaka, H.; Dev, S.; Hidai, M. *J. Organomet. Chem.* **1993**, *456*, 243. (d) Matsuzaka, H.; Ogino, T.; Nishio, M.; Hidai, M.; Nishibayashi, Y.; Uemura, S. *J. Chem. Soc., Chem. Commun.* **1994**, 223. (e) Hidai, M.; Mizobe, Y.; Matsuzaka, H. *J. Organomet. Chem.* **1994**, *473*, 1.

(3) Some dinuclear CpRu and Cp*Ru complexes have been recently reported. See: (a) Kuhlman, R.; Streib, K.; Caulton, K. G. *J. Am. Chem. Soc.* **1993**, *115*, 5813. (b) Rauchfuss, T. B.; Rodgers, D. P. S.; Wilson, S. R. *J. Am. Chem. Soc.* **1986**, *108*, 3114. (c) Loren, S. D.; Campion, B. K.; Heyn, R. H.; Tilley, T. D.; Bursten, B. E.; Luth, K. W. *J. Am. Chem. Soc.* **1989**, *111*, 4712. (d) Suzuki, H.; Omori, H.; Lee, D.-H.; Yoshida, Y.; Fukushima, M.; Tanaka, M.; Moro-oka, Y. *Organometallics* **1994**, *13*, 1129. (e) Knox, S. A. R. *J. Organomet. Chem.* **1990**, *400*, 255 and references cited therein. (f) Kölle, U.; Kang, B.-S.; Thewalt, U. *Organometallics* **1992**, *11*, 2893. (g) Chang, J. C.; Bergman, R. G. *J. Am. Chem. Soc.* **1987**, *109*, 4298. (h) Hubbard, J. L.; Morneau, A.; Burns, R. M.; Zolch, C. R. *J. Am. Chem. Soc.* **1991**, *113*, 9176.

(4) For pertinent examples of Ru–sulfur complexes, see: (a) Houser, E. J.; Amarasekera, J.; Rauchfuss, T. B.; Wilson, S. R. *J. Am. Chem. Soc.* **1991**, *113*, 7440. (b) Amarasekera, J.; Rauchfuss, T. B.; Wilson, S. R. *J. Chem. Soc., Chem. Commun.* **1989**, 14. (c) Koch, S. A.; Millar, M. *J. Am. Chem. Soc.* **1983**, *105*, 3362. (d) Millar, M. M.; O'Sullivan, T.; Vries, N.; Koch, S. A. *J. Am. Chem. Soc.* **1985**, *107*, 3714. (e) Shaver, A.; Plouffe, P.-Y.; Lilles, D. C.; Singleton, E. *Inorg. Chem.* **1992**, *31*, 997. (f) Hörnig, A.; Englert, U.; Kölle, U. *J. Organomet. Chem.* **1994**, *464*, C25.

(5) (a) Matsuzaka, H.; Mizobe, Y.; Nishio, M.; Hidai, M. *J. Chem. Soc., Chem. Commun.* **1991**, 1011. (b) Nishio, M.; Matsuzaka, H.; Mizobe, Y.; Hidai, M. *J. Chem. Soc., Chem. Commun.* **1993**, 375. (c) Nishio, M.; Matsuzaka, H.; Mizobe, Y.; Tanase, T.; Hidai, M. *Organometallics* **1994**, *13*, 4214. (d) Matsuzaka, H.; Hirayama, Y.; Nishio, M.; Mizobe, Y.; Hidai, M. *Organometallics* **1993**, *12*, 36. (e) Matsuzaka, H.; Koizumi, H.; Takagi, Y.; Nishio, M.; Hidai, M. *J. Am. Chem. Soc.* **1993**, *115*, 10396.

(6) Kuwata, S.; Mizobe, Y.; Hidai, M. *Inorg. Chem.* **1994**, *33*, 3619.

(7) Matsuzaka, H.; Takagi, Y.; Hidai, M. *Organometallics* **1994**, *13*, 13. The structure **1** is more appropriate than the structure Ru(μ_2-Cl)-Ru proposed in the previous paper,[7] because the ^{1}H NMR spectrum taken at −50 °C exhibited resonances at δ 1.59 and 1.63 assigned to two nonequivalent Cp* methyl groups.

(8) Formation of mononuclear butenynyl complexes by vinylidene–alkynyl combination has been observed. See: (a) Hughes, D. L.; Jimenez-Tenorio, M.; Leigh, G. J.; Rowley, A. T. *J. Chem. Soc., Dalton Trans.* **1993**, 3151. (b) Field, L. D.; George, A. V.; Purches, G. R.; Slip, I. H. M. *Organometallics* **1992**, *11*, 3019. (c) Bianchini, C.; Peruzzini, M.; Zanobini, F.; Frediani, P.; Albinati, A. *J. Am. Chem. Soc.* **1991**, *113*, 5453. (d) Wakatsuki, Y.; Yamazaki, H.; Kumegawa, N.; Satoh, T.; Satoh, J. Y. *J. Am. Chem. Soc.* **1991**, *113*, 9604. (e) Jia, G.; Rheingold, A. L.; Meek, D. W. *Organometallics* **1989**, *8*, 1378. (f) Gotzig, J.; Otto, H.; Werner, H. *J. Organomet. Chem.* **1985**, *287*, 247. (g) Dobson, A.; Moore, D. S.; Robinson, S. D. *J. Organomet. Chem.* **1979**, *177*, C8.

0276-7333/95/2314-2153$09.00/0

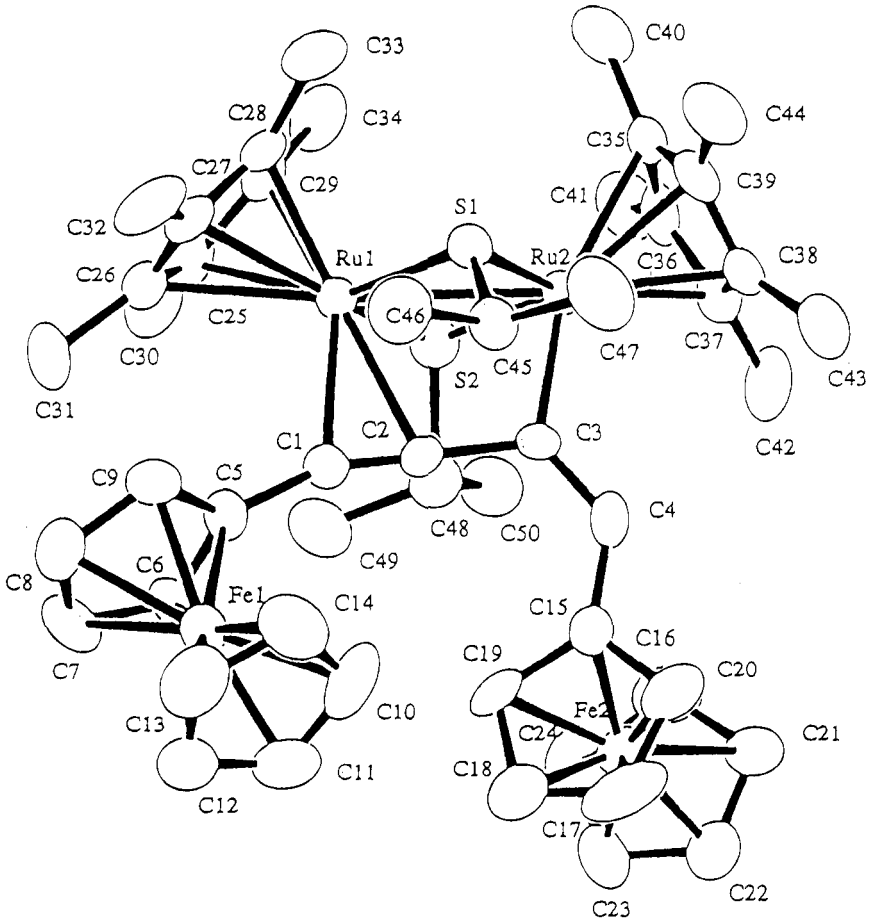

Figure 1. ORTEP drawing of the cationic part of complex **4b**.

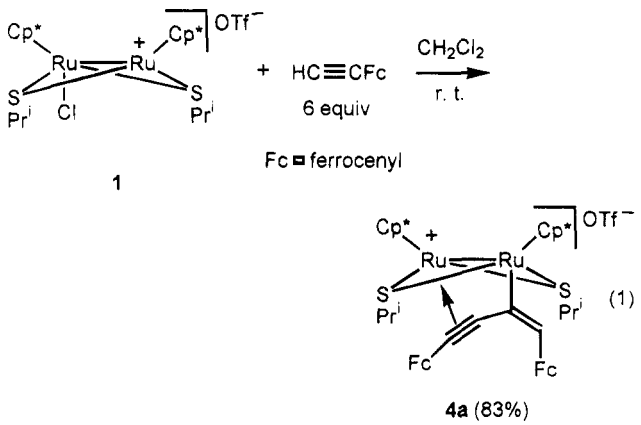

form an almost planar ring system with C(1), C(2), and C(3). The distances between Ru(1) and C(1) (2.40(1) Å) and C(2) (2.384(10) Å) are longer in comparison with the metal–carbon lengths in common π-alkyne complexes.[11] This is reflected in the relatively short C(1)–C(2) distance of 1.22(1) Å. Although several mononuclear butenynyl complexes have appeared in the literature,[8] **4** is, to the best of our knowledge, the first example of a well-characterized dinuclear butenynyl complex and sheds light on the mechanism of alkyne coupling reactions involving vinylidene–alkynyl combination at the thiolate-bridged diruthenium site.[12]

Complex **4a** has proved to be an efficient catalyst for linear di- and trimerization of HC≡CFc under mild conditions (eq 2: in $ClCH_2CH_2Cl$, 60 °C, 30 h, HC≡CFc: **4a** = 20:1).[13] A mixture of the head-to-head dimer **5** and the linear trimer **6** was produced with high regioselectivity and stereoselectivity, which were isolated in 62% and 32% yields, respectively, and spectroscopically

(9) To a CH_2Cl_2 (20 mL) solution of **1** (502 mg, 0.622 mmol) was added HC≡CFc (0.63 mL, 3.7 mmol), and the reaction mixture was stirred overnight at room temperature. After removal of the solvent, the resultant solid was washed with hexane (5 mL × 3) and recrystallized from CH_2Cl_2/ether (5 mL/15 mL) to give **4a** as dark brown crystals (618 mg, 0.519 mmol); yield 83%. ^1H NMR ($CDCl_3$): δ 5.51 (s, 1H, vinyl), 4.32, 4.27, 4.26, 4.19 (t, 2H each, J = 1.9 Hz, C_5H_4), 4.09, 3.73 (s, 5H each, Cp), 3.99 (sep, 2H, J = 6.7 Hz, SC*H*Me_2), 1.87, 1.46 (s, 15H each, Cp*), 1.68, 1.67 (d, 6H each, J = 6.7 Hz, SCHMe_2). A small amount of dimer **5** and trimer **6** (eq 2) were also observed in the reaction mixture. Single crystals of **4b** suitable for X-ray structural analysis were prepared by recrystallization from CH_2Cl_2/hexane after the anion metathesis of **4a** by BPh_4^-.

(10) Crystal data: $P\bar{1}$ (triclinic), a = 15.005(2) Å, b = 17.693(3) Å, c = 15.020(2) Å, α = 95.95(1)°, β = 107.53(1)°, γ = 98.49(1)°, V = 3714-(1) Å, Z = 2, $R(R_w)$ = 5.4% (4.4%) for 5606 reflections ($|I| > 3\sigma(I)$). Bond distances (Å) and angles (deg): Ru(1)-Ru(2), 2.767(1); Ru(1)-C(1), 2.40(1); Ru(1)-C(2), 2.384(10); Ru(2)-C(3), 2.091(10); C(1)–C(2), 1.22-(1); C(2)–C(3), 1.46(1); C(3)–C(4), 1.33(1); Ru(2)–Ru(1)–C(1), 97.1-(3); Ru(2)–Ru(1)–C(2), 67.9(2); Ru(1)–Ru(2)–C(3), 78.4(3); Ru(1)–C(1)–C(2), 74.6(7); Ru(1)–C(1)–C(5), 124.6(8); C(2)–C(1)–C(5), 160(1); Ru(1)–C(2)–C(1), 75.8(7); Ru(1)–C(2)–C(3), 105.8(7); C(1)–C(2)–C(3), 172(1); Ru(2)–C(3)–C(2), 107.8(7); Ru(2)–C(3)–C(4), 129.8(8); C(2)–C(3)–C(4), 122.3(10); C(3)–C(4)–C(15), 130(1).

(11) Ittel, S. D.; Ibers, J. A. *Adv. Organomet. Chem.* **1976**, *14*, 33.

(12) Several coupling reactions between the vinylidene ligand and the organic moiety at mononuclear sites have also been reported. See: (a) Wiedemann, R.; Steinert, P.; Schäfer, M.; Werner, H. *J. Am. Chem. Soc.* **1993**, *115*, 9864. (b) Selnau, H. E.; Merola, J. S. *J. Am. Chem. Soc.* **1991**, *113*, 4008.

(13) A solution of HC≡CFc (303 mg, 1.44 mmol) and **4a** (82 mg, 0.069 mmol; 5 mol % of the alkyne) in $ClCH_2CH_2Cl$ (5 mL) was stirred at 60 °C for 30 h. After removal of the solvent, the resultant solid was chromatographed on silica gel with benzene/hexane (2/1). The first band (yellow) contained unreacted HC≡CFc (19 mg, conversion 94%). Solvents were evaporated from the second (orange) and the third (orange) bands, from which dimer **5** (188 mg) and trimer **6** (96 mg) were obtained, respectively.

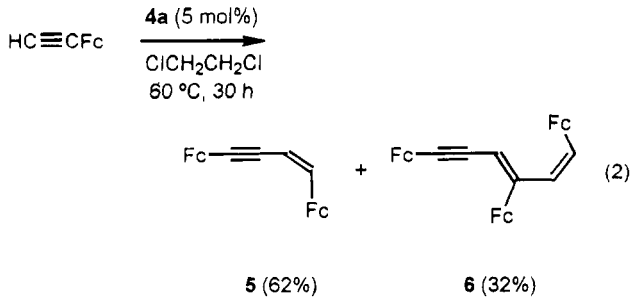

characterized.[14] Further, the structure of **6** has been unequivocally determined by X-ray analysis.[15]

Particularly interesting is the formation of the linear trimer **6**, which has never been observed in oligomerization with mononuclear complex catalysts.[16] No byproducts such as cyclic oligomers were detected, and **4a** was recovered from the reaction solution in high yield. These results strongly suggest that the reaction proceeds at the diruthenium core, which remains intact during the catalysis. Klein et al. recently reported the highly selective linear trimerization of HC≡CPh in the presence of *triangulo*-$Co_3(\mu_3\text{-}H)(\mu_2\text{-}CO)_3(PMe_3)_6$ (**7**) to give the *E,E* linear trimer Ph(PhC≡C)C=CH-CH=CHPh.[17] However, it was not certain whether a tricobalt derivative of **7** or a mononuclear species is the active catalyst. Furthermore, it should be noted that the configuration of the latter trimer is essentially different from that of **6**.

A plausible mechanism for the formation of dimer **5** is shown in Scheme 1. The butenynyl complex **4a** would first react with incoming HC≡CFc molecules to liberate **5** and form the monoalkynyl–alkyne intermediate **8**.

Scheme 1

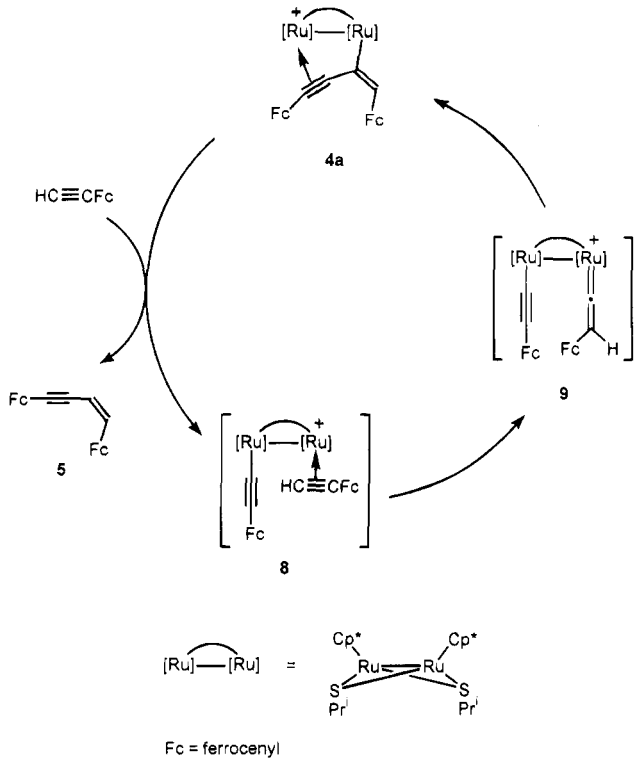

Complex **8** is then converted into the vinylidene–alkynyl intermediate **9**, which is further transformed back to the starting compound **4a**. If the *trans* migratory insertion of two HC≡CFc molecules into the Ru–alkynyl bond in **8** proceeds at the diruthenium site, the linear trimer **6** may be formed. However, we must await further investigations to elucidate a detailed reaction mechanism.

Acknowledgment. The Ministry of Education, Science and Culture of Japan is gratefully acknowledged for support of this research.

Supplementary Material Available: Text giving experimental details, including results of elemental analyses, and tables of crystal data and data collection parameters, atomic coordinates, anisotropic thermal parameters, and bond distances and angles for **4b** and **6** (27 pages). Ordering information is given on any current masthead page.

OM950024S

(14) **5**: yield 62%; ^{1}H NMR ($CDCl_3$) δ 6.44, 5.58 (d, 1H each, J = 11.5 Hz, alkenyl), 4.87, 4.52, 4.33, 4.27 (t, 2H each, J = 1.9 Hz, C_5H_4), 4.28, 4.18 (s, 5H each, Cp); ^{13}C NMR ($CDCl_3$) δ 137.2, 104.6, 93.9, 85.7, 81.1, 71.0, 69.8, 69.4, 69.2, 69.1, 68.8, 66.0; MS (EI) m/z 420 (M^+). **6**: yield 32%; ^{1}H NMR ($CDCl_3$) δ 6.26 (d, 1H, J = 12.0 Hz, vinyl), 6.21 (dd, 1H, J = 12.0, 1.0 Hz, vinyl), 5.94 (d, 1H, J = 1.0 Hz, vinyl), 4.97, 4.51, 4.44, 4.36, 4.26, 4.21 (t, 2H each, J = 1.7 Hz, C_5H_4), 4.28, 4.23, 4.13 (s, 5H each, Cp); ^{13}C NMR ($CDCl_3$) δ 145.0, 128.6, 127.2, 105.2, 95.3, 86.5, 82.8, 80.6, 70.9, 70.0, 69.9, 69.6, 69.4, 69.2, 69.0, 68.8, 68.6, 66.4; MS (EI) m/z 630(M^+).

(15) Crystal data: $P2_1/c$ (monoclinic), a = 11.623(1) Å, b = 18.341(2) Å, c = 12.814(1) Å, β = 91.855(7)°, V = 2730.1(4) Å^3, Z = 4, R (Rw) = 4.9% (2.3%) for 2330 reflections ($|I|>3\sigma(I)$).

(16) Oligomerization of HC≡CFc by using $(PPh_3)_2Ni(CO)_2$ gave a mixture of the head-to-head dimer **5**, the acyclic branched trimer CHFc=CHC(C≡CFc)=CHFc, and 1,2,4-triferrocenylbenzene: Pittman, C. U., Jr.; Smith, L. R. *J. Organomet. Chem.* **1975**, *90*, 203.

(17) Klein, H.-F.; Mager, M.; Isringhausen-Bley, S.; Flörke, U.; Haupt, H.-J. *Organometallics* **1992**, *11*, 3174.

Bifunctional Carriers of Polar Organometallics Using Transition-Metal–Schiff Base Complexes: A Very Easy Access to Manganese(II)–Carbon Functionalities

Emma Gallo,[†] Euro Solari,[†] Carlo Floriani,*[,†] Angiola Chiesi-Villa,[‡] and Corrado Rizzoli[‡]

Institut de Chimie Minérale et Analytique, BCH, Université de Lausanne, CH-1015 Lausanne, Switzerland, and Dipartimento di Chimica, Università di Parma, I-43100 Parma, Italy

Received February 7, 1995[⊗]

*Summary: This report details a conceptual approach to the use of bifunctional complexes for carrying ion pair reagents, such as lithium alkyls or others. This study led to the first crystallographic characterization of organometallic [Mn(Schiff base)RLi(DME)] compounds (R = CH_3, **2**; R = Ph, **3**; R = Mes (≡2,4,6-$Me_3C_6H_2$), **3**). The importance of these complexes lies in the electronic and steric modification of lithium alkyl chemistry. Preliminary studies with PhCHO and PhCN show how complexes **2**–**4** react in a bifunctional fashion with organic substrates.*

The unique behavior of organocuprates[1] as key synthons in organic synthesis is built on, among others, two major characteristics: (i) they act as carriers of lithium organometallics; (ii) they exhibit a bifunctional nature, expressed by the intervention of both lithium and copper during the reactions. Such characteristics are rarely found in other organometallic reagents.[2] We tried to mimic this conceptual approach and in the meantime apply it to a transition metal undergoing a real renaissance in coordination chemistry,[3] catalysis,[4] and organometallic applications,[5] namely manganese. We exploited the binding properties of metal–Schiff base complexes which allow them to act as ligands for alkali-metal cations[6] and of Mn(II) as a metal which cannot be easily reduced in this kind of ligand environment.[7] Very recently, manganese–Schiff base complexes have been tuned by Jacobsen in an elegant stereochemical approach to obtain extraordinarily selective oxidation catalysts.[8]

The model complex we have considered as a carrier for polar organometallic functionalities is [Mn_2(acacen)$_2$] (**1**; acacen = *N*,*N*′-ethylenebis(acetylacetiminato) dianion).[9] This compound is easily accessible in high yield and is very soluble in aromatic hydrocarbons. The dimeric structure has been determined in the solid state by an X-ray analysis and has been confirmed in solution by a molecular weight determination in benzene.

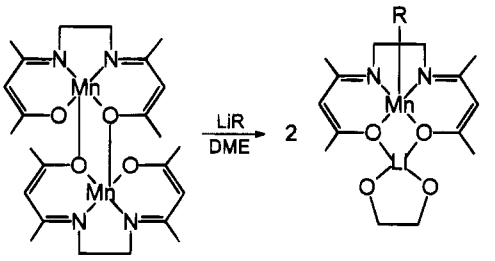

[Mn_2(acacen)$_2$], **1** [Mn(acacen)(R){Li(DME)}]

R = Me, **2**

R = Ph, **3**

R = Mes = 2,4,6-$Me_3C_6H_2$, **4**

Complex **1** can be the source of the monomeric bifunctional unit [Mn(acacen)] in the presence of appropriate ion pairs.

* To whom correspondence should be addressed.

† Université de Lausanne.

‡ Università di Parma.

⊗ Abstract published in *Advance ACS Abstracts,* April 1, 1995.

(1) (a) Lipshutz, B. H.; Sengupta, S. In *Organic Reactions*; Paquette, L. A., Ed.; Wiley: New York, 1992; Vol. 41, Chapter 2. (b) Lipshutz, B. H. In *Organometallics in Synthesis: A Manual;* Schlosser, M., Ed.; Wiley: New York, 1994; Chapter 4.

(2) (a) Reetz, M. T. In *Organotitanium Reagents in Organic Synthesis*; Springer: Berlin, Germany, 1986. (b) Reetz, M. T.; Steinbach, R.; Westermann, J.; Peter, R.; Wenderoth, B. *Chem. Ber.* **1985**, *118*, 1441. (c) Reetz, M. T.; Wenderoth, B. *Tetrahedron Lett.* **1982**, *23*, 5259. (d) Morris, R. J.; Girolami, G. S. *Organometallics* **1991**, *10*, 792. (e) Quan, R. W.; Bazan, G. C.; Kiely, A. F.; Schaefer, W. P.; Bercaw, J. E. *J. Am. Chem. Soc.* **1994**, *116*, 4489.

(3) (a) Wieghardt, K. *Angew. Chem., Int. Ed. Engl.* **1989**, *28*, 1153. (b) Pecoraro, V. L.; Baldwin, M. J.; Gelasco, A. *Chem. Rev.* **1994**, *94*, 807.

(4) (a) Srinivasan, K.; Michaud, P.; Kochi, J. K. *J. Am. Chem. Soc.* **1986**, *108*, 2309. (b) Menage, S.; Collomb-Dunand Sauthier, M. N.; Lambeaux, C.; Fontecave, M. *J. Chem. Soc., Chem. Commun.* **1994**, 1885. (c) Eilmes, J. *Polyhedron* **1992**, *11*, 581. (d) O'Connor, K. J.; Wey, S. J.; Burrows, C. J. *Tetrahedron Lett.* **1992**, *33*, 1001. (e) Evans, D. A.; Faul, M. M.; Bilodeau, M. T.; Anderson, B. A.; Barnes, D. M. *J. Am. Chem. Soc.* **1993**, *115*, 5328. (f) Reddy, D. R.; Thornton, E. R. *J. Chem. Soc., Chem. Commun.* **1992**, 172.

(5) (a) Normant, J. F.; Cahiez, G. In *Modern Synthetic Methods*; Scheffold, R., Ed.; Wiley: Chichester, U.K., 1983, Vol. 3, p 173. (b) Cahiez, G.; Alami, M. *Tetrahedron* **1989**, *45*, 4163. (c) Cahiez, G.; Marquais, S. *Synlett* **1993**, 45. (d) Cahiez, G.; Figadere, B.; Clery, P. *Tetrahedron Lett.* **1994**, *35*, 3065. (e) Cahiez, G.; Chau, K.; Clery, P. *Tetrahedron Lett.* **1994**, *35*, 3069. (f) Corey, E. J.; Posner, G. H. *Tetrahedron Lett.* **1970**, 315. (g) Reetz, M. T.; Haning, H. *Tetrahedron Lett.* **1993**, *34*, 7395. (h) Reetz, M. T.; Haning, H.; Stanchev, S. *Tetrahedron Lett.* **1992**, *33*, 6963. (i) Reetz, M. T.; Rölfing, K.; Griebenow, N. *Tetrahedron Lett.* **1994**, *35*, 1969.

(6) (a) Floriani, C.; Calderazzo, F.; Randaccio, L. *J. Chem. Soc., Chem. Commun.* **1973**, 384. (b) Bresciani-Pahor, N.; Calligaris, M.; Delise, P.; Nardin, G.; Randaccio, L.; Zotti, E.; Fachinetti, G.; Floriani, C. *J. Chem. Soc., Dalton Trans.* **1976**, 2310. (c) Arena, F.; Floriani, C.; Zanazzi, P. *J. Chem. Soc., Chem. Commun.* **1987**, 183 and references therein.

(7) Gallo, E.; Solari, E.; De Angelis, S.; Floriani, C.; Re, N.; Chiesi-Villa, A.; Rizzoli, C. *J. Am. Chem. Soc.* **1993**, *115*, 9850.

(8) (a) Zhang, W.; Jacobsen, E. N. *J. Org. Chem.* **1991**, *56*, 2296. (b) Jacobsen, E. N.; Zhang, W.; Muci, A. R.; Ecker, J. R.; Deng, L. *J. Am. Chem. Soc.* **1991**, *113*, 7063. (c) Larrow, J. F.; Jacobsen, E. N. *J. Org. Chem.* **1994**, *59*, 1939. (d) Brandes, B. D.; Jacobsen, E. N. *J. Org. Chem.* **1994**, *59*, 4378.

(9) Procedure for **1**: $MnCl_2$·1.5THF (39.3 g, 168 mmol) was added to a THF (1000 mL) suspension of acacenNa_2 (45 g, 168 mmol) at room temperature. The orange suspension was refluxed for 12 h, the solvent was evaporated to dryness, and the orange residue was recrystallized from toluene to remove NaCl and to obtain a crystalline solid (65%). Anal. Calcd for $C_{24}H_{36}Mn_2N_4O_4$: C, 51.99; H, 6.54; N, 10.10. Found: C, 51.81; H, 6.62; N, 9.85. μ = 5.78 μ_B at 295 K.

0276-7333/95/2314-2156$09.00/0

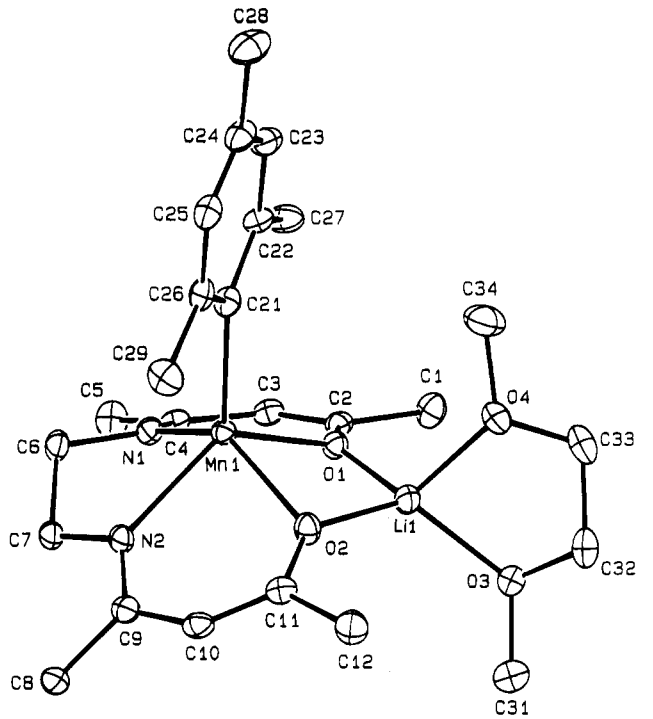

Figure 1. ORTEP view of complex **4** (30% probability ellipsoids). Selected bond distances (Å) and angles (deg): Mn1–O1, 2.151(2); Mn1–O2, 2.173(2); Mn1–N1, 2.188(3); Mn1–N2, 2.223(3); Mn1–C21, 2.181(4); Li1–O1, 1.887(6); Li1–O2, 1.894(6); Li1–O3, 2.003(8); Li1–O4, 1.957(7); N1–Mn1–N2, 75.8(1); O2–Mn1–N2, 83.5(1); O1–Mn1–N1, 82.5(1); O1–Mn1–O2, 77.9(1); O1–Li1–O2, 91.9(3); O3–Li1–O4, 83.5(3); Mn1–O1–Li1, 93.1(2); Mn1–O2–Li1, 92.2(2).

The reaction of **1** with LiR in DME (dimethoxyethane) at −60 °C and then at room temperature gave a red solution from which the alkylated product (**2**–**4**)[10] crystallized upon addition of Et_2O. The proposed structures have been confirmed by X-ray analysis. Details are given only for **4**.[11] The structure is shown in Figure 1 with a selection of structural parameters. The [Mn(acacen)] fragment has an umbrella conformation with the dihedral angles between the O–Mn–N planes being 69.0(1)°. The distance of Mn from the N_2O_2 plane (0.919(1) Å) is remarkably longer than those in other five-coordinate d^1–d^2 [M^{III}(acacen)R] organometallic derivatives.[12] The Mn–C bond distance is not affected by lithium coordination and is close to those of other Mn–Mes fragments.[13] The binding of the lithium cation does, however, strongly reduce the O···O bite angle from 109.7(2)° (complex **1**) to 77.9(1)°. The tetrahedral coordination around lithium is completed by DME. The short Li–O1 and Li–O2 distances support the premise of highly basic ligand oxygens.[14] The structure of **2** is similar and also shows how the LiR reagents may be carried by a bifunctional complex. Mn(II) does not undergo any reduction in the reaction with LiR, as it does in the corresponding Mn(III) complex.[15] Reaction 1 represents an easily accessible route to rare organometallic derivatives of Mn(II) which can be useful in organic synthesis. The bifunctional reactivity of **2** can be exemplified in its reaction with benzaldehyde, leading to **5**.[16]

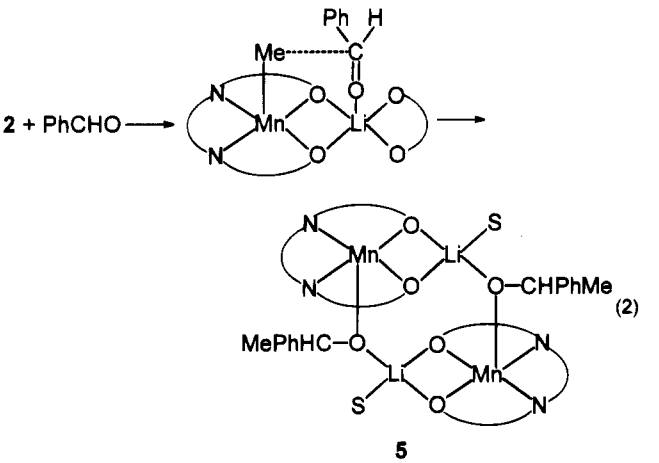

S = solvent or an oxygen from an intermolecular interaction;

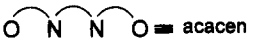

An analogous pathway can be proposed for the reaction of **2** with PhCN to give [Mn(acacen)Li{N=C(Ph)(Me)}]$_2$ (**6**). Complexes **5** and **6** have been hydrolyzed to the corresponding alcohol (Ph(Me)CHOH)[17] and ketone (Ph(Me)CO). The pathway of reaction 2 and the structure of **5** are supported by the following: (i) the reaction is slowed in the presence of 12-crown-4, which competes with the Schiff base in binding the lithium

(10) Procedure for **2**: To an orange DME (250 mL) suspension of **1** (10.01 g, 36.1 mmol) was added MeLi (20.7 mL, 36.1 mmol) in a dropwise manner at −40 °C. A red solution was obtained, which was stirred at room temperature for 12 h. The solvent was evaporated to dryness and the orange residue treated with Et_2O (150 mL). The Et_2O suspension was chilled to −25 °C, yielding an orange product (76%). Crystals suitable for X-ray analysis were grown in DME/Et_2O. Anal. Calcd for $C_{17}H_{31}LiMnN_2O_4$: C, 52.45; H, 8.03; N, 7.20. Found: C, 52.52; H, 8.15; N, 7.27. μ = 5.80 μ_B at 295 K. Procedure for **3** and **4**: Complexes **3** (60% yield) and **4** (70% yield) were prepared in a manner similar to complex **2**. The analytical data for **3** and **4** were satisfactory.

(11) Crystal data for **4**: $C_{25}H_{39}LiMnN_2O_4$, triclinic, space group $P\bar{1}$, a = 11.004(5) Å, b = 13.286(4) Å, c = 9.883(2) Å, α = 103.50(2)°, β = 95.08(3)°, γ = 70.36(2)°, V = 1323.2(8) Å^3, Z = 2, ϱ_{calcd} = 1.239 g cm^{-3}, Cu Kα radiation (λ = 1.54178 Å), μ(Cu Kα) = 43.08 cm^{-1}, crystal dimensions 0.18 × 0.31 × 0.40 mm. The structure was solved by the heavy-atom method and anisotropically refined for all non-hydrogen atoms. The hydrogen atoms were located from a difference map and introduced as fixed contributors in the last stage of refinement (U_{iso} = 0.06 Å^2). For 3278 unique observed reflections ($I > 2\sigma(I)$) collected at T = 143 K ($6 < 2\theta < 140°$) and corrected for absorption the final R value was 0.045 (R_w = 0.053). All calculations were carried out with use of SHELX-76 on an Encore E91 computer. See the supplementary material for more details.

(12) Rosset, J. M.; Floriani, C.; Mazzanti, M.; Chiesi-Villa, A.; Guastini, C. *Inorg. Chem.* **1990**, *29*, 3991.

(13) (a) Gambarotta, S.; Floriani, C.; Chiesi-Villa, A.; Guastini, C. *J. Chem. Soc., Chem. Commun.* **1983**, 1128. (b) Bartlett, R. A.; Olmstead, M. M.; Power, P. P.; Shoner, S. C. *Organometallics* **1988**, *7*, 1801. (c) Morris, R. J.; Girolami, G. S. *Organometallics* **1991**, *10*, 799.

(14) Fachinetti, G.; Floriani, C.; Zanazzi, P. F.; Zanzari, A. R. *Inorg. Chem.* **1979**, *18*, 3469.

(15) The reaction of the [Mn^{III}(acacen)Cl] complex with a lithium alkyl afforded a crystallographically characterized reduced product.

(16) A toluene solution (100 mL) of **1** (1.58 g, 4.06 mmol) was cooled to −70 °C, and a toluene solution (50 mL) of PhCHO (0.41 mL, 4.06 mmol) was added in a dropwise manner. The yellow solution was warmed to room temperature and stirred for 12 h. The solvent was removed and the remaining residue was treated with hexane. The yellow solid which precipitated was collected and dried in vacuo (79%). Anal. Calcd. for $C_{40}H_{54}Li_2Mn_2N_4O_6$: C, 59.27; H, 6.71; N, 6.91. Found: C, 58.65; H, 6.91; N, 7.18. μ = 5.78 μ_B at 295 K and μ = 1.75 μ_B at 2 K. Complex **6** (65% yield) was prepared in a manner similar to that for complex **5**. The analytical data were satisfactory.

(17) The organic products from the hydrolysis of compounds **5** and **6** were obtained by quenching with HCl/H_2O, purified by flash chromatography, and identified by NMR and GC–MS.

cation; (ii) the dimeric compounds **5** and **6** have a reduced magnetic moment for Mn(II), as expected for an antiferromagnetically coupled dimer;[18] (iii) dimers such as **5** or **6** have been structurally characterized in the reaction of $[Fe_2(acacen)_2]$, isostructural with **1**, with alkali-metal alkoxides.[19]

The bifunctional approach reported here for carrying polar organometallics implies the potential application of coordination compounds as catalysts in reactions involving ion pairs, such as lithium alkyls or alkali-metal enolates. Our approach is now being extended to properly sterically designed Schiff base complexes of Mn(II)[8] and to other fundamental ion pair moieties, such as the alkali-metal enolates.

Acknowledgment. We thank the Fonds National Suisse de la Recherche Scientifique (Grant No. 20-33420-92) for financial support.

Supplementary Material Available: Tables giving crystal data and details of the structure determination, fractional atomic coordinates, thermal parameters, bond lengths, and bond angles for complex **4** (Tables 1–5) (7 pages). Ordering information is given on any current masthead page.

OM950096J

(18) Mabad, B.; Cassoux, P.; Tuchagues, J. P.; Hendrickson, D. N. *Inorg. Chem.* **1986**, *25*, 1420.

(19) Floriani, C.; Solari, E.; Corazza, F.; Chiesi-Villa, A.; Guastini, C. *Angew. Chem., Int. Ed. Engl.* **1989**, *28*, 64.

Formation of a Metalaaziridine Ring and Dinitrogen Fixation Promoted by a Niobium Amide Complex

Pietro Berno, and Sandro Gambarotta

Organometallics, **1995**, 14 (5), 2159-2161• DOI: 10.1021/om00005a012 • Publication Date (Web): 01 May 2002

Formation of a Metallaaziridine Ring and Dinitrogen Fixation Promoted by a Niobium Amide Complex

Pietro Berno and Sandro Gambarotta*

Department of Chemistry, University of Ottawa, Ottawa, Ontario K1N 6N5, Canada

Received February 27, 1995[⊗]

*Summary: Reaction of $NbCl_4(THF)_2$ with 3 equiv of Cy_2NLi in toluene formed $(Cy_2N)_2Nb(CyNC_6H_{10})Cl$ (**1**), where one cyclohexyl ring was metalated to form a niobaaziridine ring. Further reaction of **1** with $NaHBEt_3$ in toluene led to the formation of the end-on dinitrogen complex $[(Cy_2N)_3Nb]_2(N_2)$, which was isolated as pale yellow crystals in good yield.*

The interest in the chemistry of medium-valent niobium and tantalum has been stimulated by the variety of transformations performed by these species which range from alkyl chain dehydrogenation,[1] to oxidative addition reactions,[2] formation of stable CO_2[3] and N_2[4] adducts, metal-promoted organic synthesis,[5] reductive couplings,[6] and formation of polyhydrides.[7] In contrast, medium-valent niobium and tantalum complexes are very rare[8] and, besides the polynuclear halides[9a] and the cyclopentadienyl systems,[9b] have been poorly characterized or prepared *in situ*. We thus became interested in the preparation and characterization of low- and medium-valent niobium complexes supported by anionic organic amides. The employment of these anions as supporting ligands was suggested by their well-known characteristics, which include the ability to stabilize low oxidation states[10] of the metal, their electronic flexibility, the possibility of fine-tuning the steric hindrance, and their ability to engage in C–H σ-bond metathesis reactions to form highly reactive cyclometallaazabutane rings.[11] In addition, organic amide ligands have recently been proven to be involved in H-transfer reactions[12] and to sufficiently enhance the reactivity of the metal center to support coordination of dinitrogen.[13]

In this paper we describe the reaction of $NbCl_4(THF)_2$ with Cy_2NLi to form a niobaaziridine ring and its further reaction with hydride to form a dinitrogen complex.

The reaction of $NbCl_4(THF)_2$ with 3 equiv of Cy_2NLi in toluene gave a brown oil which, upon crystallization from hexane, yielded orange crystals of $(Cy_2N)_2Nb(CyNC_6H_{10})Cl$ (**1**; 43%).[14] The formulation was indicated by consistent combustion analysis data and the correct Nb/Cl ratio as determined by X-ray fluorescence. The complex is diamagnetic, which implies that the metal center has undergone oxidation to the pentavalent state. The ^1H NMR spectrum of **1** showed the presence of two different cyclohexyl groups, as indicated by two triplets of triplets at 3.60 and 3.41 ppm which are integrated in the ratio 1:4. In addition, the ^{13}C NMR spectrum showed the presence of a quaternary carbon atom at 82.4 ppm, thus indicating that partial dehydrogenation of one cyclohexyl ring had occurred. Ac-

⊗ Abstract published in *Advance ACS Abstracts,* April 1, 1995.

(1) (a) Yu, J. S.; Fanwick, P. E.; Rothwell, I. P. *J. Am. Chem. Soc.* **1990**, *112*, 8171. (b) Bishop, P. T.; Dilworth, J. R.; Nicholson, T.; Zubieta, J. A. *J. Chem. Soc., Chem. Commun.* **1986**, 1123. (c) Steffey, B. D.; Chamberlain, L. R.; Chesnut, R. W.; Chebi, D. E.; Fanwick, P. E.; Rothwell, I. P. *Organometallics* **1989**, *8*, 1419. (d) Chamberlain, L. R.; Kerschner, J. L.; Rothwell, A. P.; Rothwell, I. P.; Huffman, J. C. *J. Am. Chem. Soc.* **1987**, *109*, 6471.

(2) (a) Curtis, M. D.; Real, J.; Kwon, D. *Organometallics* **1989**, *8*, 1644. (b) Arnold, J.; Tilley, T. D.; Rheingold, A. L.; Geib, S. J. *Organometallics* **1987**, *6*, 473. (c) Neithamer, D. R.; LaPointe, R. E.; Wheeler, R. A.; Richeson, D. R.; Van Duyne, G. D.; Wolczanski, P. T. *J. Am. Chem. Soc.* **1989**, *111*, 9056. (d) Neithamer, D. R.; Parkanyi, L.; Mitchell, J. F.; Wolczanski, P. T. *J. Am. Chem. Soc.* **1988**, *110*, 4421.

(3) Fu, P. F.; Khan, M. A.; Nicholas, K. M. *J. Am. Chem. Soc.* **1992**, *114*, 6579.

(4) (a) Dilworth, J. R.; Henderson, R. A.; Hills, A.; Hughes, D. L.; McDonald, C.; Stephen, A. N.; Walton, D. R. M. *J. Chem. Soc., Dalton Trans.* **1990**, 1077. (b) Rocklage, S. M.; Schrock, R. R. *J. Am. Chem. Soc.* **1982**, *104*, 3077. (c) Green, D. W.; Hodges, R. V.; Gruen, D. M. *Inorg. Chem.* **1976**, *15*, 970. (d) Turner, H. W.; Fellmann, J. D.; Rocklage, S. M.; Schrock, R. R.; Churchill, M. R.; Wassermann, H. J. *J. Am. Chem. Soc.* **1980**, *102*, 7809. (e) Rocklage, S. M.; Turner, H. W.; Fellman, J. D.; Schrock, R. R. *Organometallics* **1982**, *1*, 703. (f) Schrock, R. R.; Wesolek, M.; Liu, A. H.; Wallace, K. C.; Dewan, J. C. *Inorg. Chem.* **1988**, *27*, 2050.

(5) (a) Roskamp, E. J.; Pedersen, S. F. *J. Am. Chem. Soc.* **1987**, *109*, 6551. (b) Roskamp, E. J.; Dragovich, P. S.; Hartung, J. B.; Redersen, S. F. *J. Org. Chem.* **1989**, *54*, 4736.

(6) (a) Etienne, M.; White, P. S.; Templeton, J. L. *Organometallics* **1993**, *12*, 4010. (b) Bianconi, P.A.; Williams, I. D.; Engeler, M. P.; Lippard, S. J. *J. Am. Chem. Soc.* **1986**, *108*, 311. (c) Cotton, F. A.; Hall, W. T. *Inorg. Chem.* **1978**, *17*, 3525. (d) Bruck, M. A.; Copenhaver, A. S.; Wigley, D. E. *J. Am. Chem. Soc.* **1987**, *109*, 6525.

(7) (a) Profilet, R. D.; Rothwell, A. P.; Rothwell, I. P. *J. Chem. Soc., Chem. Commun.* **1993**, 42. (b) Steffey, B. D.; Rothwell, I. P. *J. Chem. Soc., Chem. Commun.* **1990**, 213. (c) Yu, S. J.; Rothwell, I. P. *J. Chem. Soc., Chem. Commun.* **1992**, 632. (d) Steffey, B. D.; Chesnut, R. W.; Kerschner, J. L.; Pellechia, P. J.; Fanwick, P. E.; Rothwell, I. P. *J. Am. Chem. Soc.* **1989**, *111*, 378. (e) Tebbe, F. N.; Parshall, G. W. *J. Am. Chem. Soc.* **1971**, *93*, 3793. (f) Foust, D. F.; Rogers, R. D.; Rausch, M. D.; Atwood, J. L. *J. Am. Chem. Soc.* **1982**, *104*, 5646.

(8) Coffindaffer, T. W.; Steffy, B. D.; Rothwell, I. P.; Folting, K.; Huffman, J. C.; Streib, W. J. *J. Am. Chem. Soc.* **1989**, *111*, 4742.

(9) (a) Cotton, F. A.; Walton, R. R. *Multiple Bonds Between Metal Atoms*; Clarendon Press: Oxford, U.K., 1993. (b) Wilkinson, G. *Comprehensive Organometallic Chemistry Update*; Pergamon Press: Oxford, U.K., in press.

(10) Duchateau, R.; Beydoun, N.; Gambarotta, S.; Bensimon, C. *J. Am. Chem. Soc.* **1991**, *113*, 8986.

(11) (a) Berno, P.; Hao, S.; Minhas, R.; Gambarotta, S. *Organometallics* **1994**, *13*, 1052. (b) Berno, P.; Gambarotta, S. *J. Chem. Soc., Chem. Commun.*, in press.

(12) (a) Khulman, R.; Folting, K.; Caulton, K. G. *J. Am. Chem. Soc.* **1993**, *115*, 5813. (b) Planalp, P. R.; Andersen, R. A.; Zalkin, A. *Organometallics* **1983**, *2*, 16. (c) Simpson, S. J.; Andersen, R. A. *J. Am. Chem. Soc.* **1981**, *103*, 4063. (d) Sonnenberger, D. C.; Mintz, E. A.; Marks, T. J. *J. Am. Chem. Soc.* **1984**, *106*, 3484. (e) Cummins, C. C.; Schrock, R. R.; Davis, W. M. *Organometallics* **1992**, *11*, 1452. (f) Berno, P.; Gambarotta, S. *Organometallics* **1994**, *13*, 2569.

(13) Song, J.; Berno, P.; Gambarotta, S. *J. Am. Chem. Soc.* **1994**, *116*, 6927.

(14) The addition of $LiNCy_2$ (10.1 g, 53.8 mmol) to a suspension of $NbCl_4(THF)_2$ (6.8 g, 17.9 mmol) in toluene (100 mL) at room temperature turned the color orange-brown. The suspension was stirred at 60 °C for 3 h and then filtered. The clear solution was evaporated to dryness, and the brown oily residue was heated overnight at 44 °C in vacuo. The resulting brown solid was crystallized from hexane (120 mL), affording orange crystalline **1** (5.1 g, 43%). IR (Nujol mull, cm^{-1}): ν 2802 (sp), 1660 (w), 1353 (m), 1265 (br), 1209 (w), 1182 (w), 1159 (w), 1145 (sp), 1113 (br), 1054 (w), 1025 (sp), 981 (sp), 947 (s), 894 (sp), 842 (sp), 807 (m), 781 (sp), 687 (s), 620 (w), 588 (w), 513 (w), 498 (w), 451 (w). ^1H NMR (C_6D_6, 500 MHz, 25.4 °C): δ 3.60 (tt, 1H), 3.41 (tt, 4H), 2.7–0.95 (m, 60H). ^{13}C NMR (C_6D_6, 75 MHz, 25.4 °C): δ 82.40, 64.49, 59.00, 39.68, 36.32, 36.13, 35.11, 27.46, 27.15, 27.12, 26.63, 26.06, 25.99, 25.93. Anal. Calcd (found) for $C_{36}H_{65}N_3NbCl$: C, 64.70 (64.66); H, 9.80 (9.61); N, 6.29 (6.21).

0276-7333/95/2314-2159$09.00/0

Scheme 1[a]

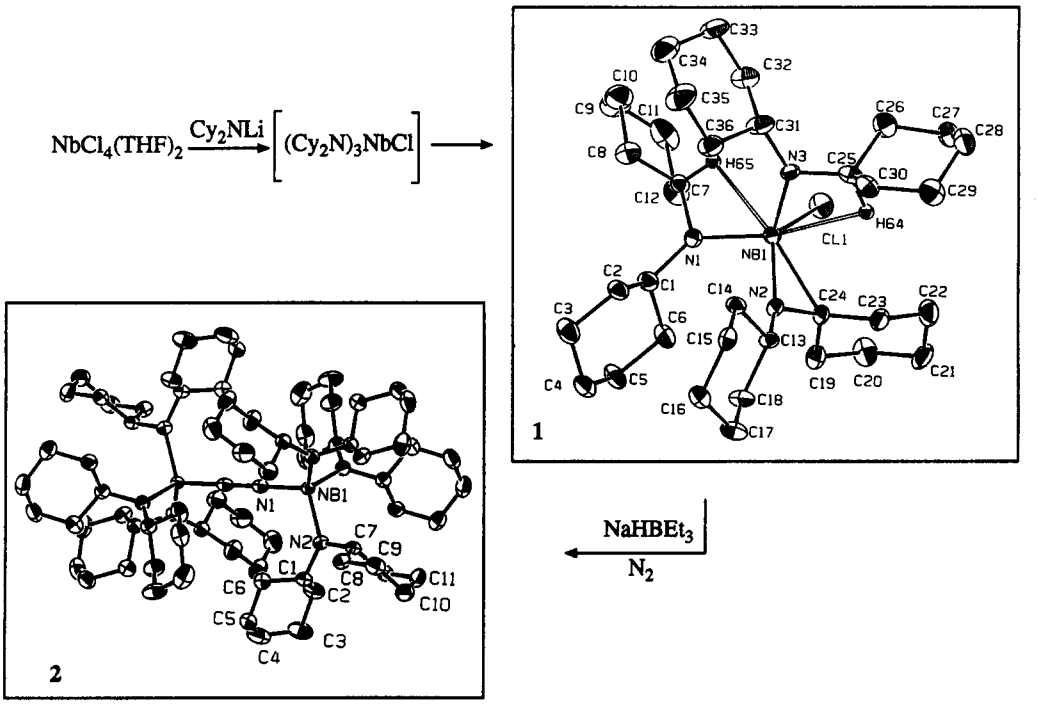

[a] Selected values of bond distances (Å) and angles (deg) are as follows. Complex **1**: Nb1–N1 = 1.977(5), Nb1–N2 = 1.956(5), Nb1–N3 = 1.984(5), Nb1–Cl1 = 2.415(2), Nb1–C24 = 2.196(6), N2–C24 = 1.432(7), N2–C13 = 1.466(7), N1–C1 = 1.483(7); N2–Nb1–C24 = 39.8(2), N1–Nb1–Cl1 = 102.1(1), Cl1–Nb1–N3 = 101.2(1), Nb1–N1–C7 = 108.9(3), Nb1–N1–C1 = 137.6(4), Nb1–N2–C13 = 150.8(4); Nb1···H64 = 2.46, Nb1···H65 = 2.54. Complex **2**: Nb1–N1 = 1.812(6), N1–N1a = 1.34(1), Nb1–N2 = 2.020(3), N2–C1 = 1.477(5); N1–Nb1–N2 = 108.96(9), Nb1–N1–N1a = 180.00, C1–N2–Nb1 = 132.7(3), C7–N2–Nb1 = 115.0(2), C1–N2–C7 = 112.3(3), N2–Nb1–N2a = 109.98(9).

cordingly, hydrogen gas was found in the atmosphere of the reaction mixture (0.47 equiv/Nb). Conversely, chemical degradation of **1** carried out with gaseous HCl did not produce H_2, thus ruling out the possibility that **1** might be a hydride species.

The salient feature of the molecular structure of **1**, as elucidated by an X-ray crystallographic study,[15] is the metalation of one cyclohexyl ring to form a niobaaziridine ring. The structure of **1** may be regarded to be composed of a $(Cy_2N)_2NbCl$ moiety coordinated side-on to a $CyN{=}C_6H_{10}$ imine (Scheme 1), although the Nb–C and Nb–N bond distances are significantly different. The steric interaction between cyclohexyl rings is responsible for the significant distortion of the trigonal-planar geometry around each nitrogen atom, with one of the two rings significantly bent toward the less crowded chlorine. This bending causes the methyne hydrogen atom of one cyclohexyl ring of each of the two amide groups to form short Nb–H contacts.

A reasonable pathway for the formation of **1** from $NbCl_4(THF)_2$ involves the intermediate formation of $(Cy_2N)_3NbCl$ followed by elimination of hydrogen, and formation of the Nb–C bond. There are only a very few examples of this type of transformation described in the literature of niobium and tantalum[1a,7a,b,16] which, being promoted by *in situ* generated trivalent Nb and Ta complexes, involve two-electron-transfer processes. The formation of **1** provides the first case where such a transformation is performed by a Nb(IV) metal center.

Attempts to reduce **1** by reaction with $NaHBEt_3$ in toluene yielded a yellowish red solution from which pale yellow crystals of the diamagnetic dinitrogen complex $[(Cy_2N)_3Nb]_2(\mu\text{-}\eta^1{:}\eta^1\text{-}N_2)$ (**2**) were isolated in reasonable yield (57%).[17] Both the ^1H- and ^{13}C NMR spectra showed the presence of only one type of cyclohexyl ring, while the presence of the dinitrogen moiety was demonstrated by the formation of N_2 (25%) during degradation experiments carried out with anhydrous HCl in a closed vessel connected to a Toepler pump.

The molecular structure of **2**, as clarified by X-ray diffraction methods, consists of two pyramidal $[Cy_2N]_3$-Nb moieties connected by a bridging end-on dinitrogen molecule.[18] The very short Nb–N distance formed by the N_2 moiety suggests a significant contribution of Nb–N multiple-bond character, while the elongated

(15) Crystal data are as follows: **1**, $C_{36}H_{65}N_3NbCl$, fw 668.29, triclinic, $P\bar{1}$, a = 10.067(1) Å, b = 18.7588(6) Å, c = 9.7431(8) Å, α = 93.89(1)°, β = 105.26(1)°, γ = 88.579(9)°, V = 1707.9(6) Å^3, Z = 2, d_{calc} = 1.253 g cm^{-3}, μ = 4.27 cm^{-1}, $F(000)$ = 720, R = 0.057 (R_w = 0.062) for 519 parameters and 4624 unique reflections. Non-hydrogen atom positions were refined anisotropically. All the hydrogen atom positions were located in different Fourier maps. However, isotropic refinement was possible for only some of the H atoms due to the unfavorable parameter/observation ratio.

(16) (a) Ballard, K. R.; Gardiner, I. M.; Wigley, D. E. *J. Am. Chem. Soc.* **1989**, *111*, 2159. (b) Shickler, J. R.; Wexler, P. A.; Wigley, D. E. *Organometallics* **1988**, *7*, 2067.

(17) An orange suspension of **1** (2.6 g, 3.9 mmol) in toluene (50 mL) was treated with a solution of $NaHBEt_3$ (4 mL, 1 M) in toluene. The mixture was stirred overnight at room temperature under N_2. The resulting reddish orange suspension was filtered and evaporated to dryness. The yellow residue was crystallized from hot hexane, yielding pale yellow crystals of **2** (1.45 g, 57%). IR (Nujol mull, cm^{-1}): ν 1344 (sp), 1242 (br), 1155 (sp), 1144 (sp), 1093 (s), 1030 (br, s), 949 (vs), 888 (sp), 849 (s), 835 (sh), 801 (w), 782 (w), 681 (s), 584 (br), 506 (sp), 484 (sp), 447 (sp). ^1H NMR (C_6D_6, 500 MHz, 25.4 °C): δ 2.58 (tt, 1H), 1.83–0.86 (m, 10H). ^{13}C NMR (C_6D_6, 75 MHz, 25.4 °C): δ 53.13, 34.86, 26.72, 25.45. Anal. Calcd (found) for $C_{36}H_{66}N_4Nb$: C, 66.74 (66.69); H, 10.27 (10.19); N, 8.65 (8.58).

(18) Crystal data: $C_{36}H_{66}N_4Nb$, fw 647.85, hexagonal, $R\bar{3}$(h), a = 18.998(1) Å, c = 16.652(1) Å, Z = 6, d_{calc} = 1.240 g cm^{-3}, μ = 3.59 cm^{-1}, R = 0.043 (R_w = 0.045) for 128 parameters and 1410 unique reflections. Non-hydrogen atom positions were refined anisotropically. All the hydrogen atom positions were located but not refined.

N−N distance (N1−N1* = 1.34(1) Å; the longest ever found for an end-on complex) suggests a significant extent of dinitrogen reduction.

Complex **2** is exceedingly robust, as may be expected on the basis of previous observations carried out on other niobium dinitrogen complexes formed by the reaction of niobium halides with hydrazines or Schiff bases.[4] Similar to the case of the isostructural vanadium amide dinitrogen complex,[13] dinitrogen could not be displaced by coordinating ligands such as pyridine or phosphine. In addition, the cyclic voltammogram of **2** in THF−(TBA)BF_4 solution ((TBA)BF_4 = *n*-tetrabutylammonium tetrafluoborate; $E_{pa} - E_{pc}$ = 71 mV vs Fc/Fc^+, room temperature, scan rate 200 mV s^{-1}) did not show any oxidation wave up to 1.2 V, possibly indicating that, in agreement with the structural data, a significant extent of dinitrogen reduction occurred in this complex.

Although we do not know the mechanism of formation of complex **2**, it is reasonable to expect that the reaction proceeds via a two-electron reduction operated by one hydride, forming an intermediate $(Cy_2N)_3Nb^{III}$ complex. Although there are a few examples of dinitrogen complexes of niobium in the literature,[4] complex **2** provides the first example where the N_2 moiety is actually derived from elemental nitrogen.

Acknowledgment. This work was supported by the Natural Sciences and Engineering Research Council of Canada (operating and strategic grants).

Supplementary Material Available: Tables giving details on the structure determination, atomic positional parameters, anisotropic thermal parameters, and bond distances and angles (24 pages). Ordering information is given on any current masthead page.

OM9501541

Synthesis and X-ray Structure of $[(\eta^5\text{-}C_5Me_5)Ti(\mu_3\text{-}O)_3\{Rh(COD)\}_3]$ (COD = Cycloocta-1,5-diene). Organometallic Approach to Strong Metal–Support Interaction in Heterogeneous Catalysis

Rosa Fandos,*,† José Luis G. Fierro,‡ Marek M. Kubicki,§ Antonio Otero,|| Pilar Terreros,‡ and María Asunción Vivar-Cerrato‡

Departamento de Química Inorgánica y Bioquímica, Universidad de Castilla-La Mancha, Facultad de Químicas, Campus de Toledo, San Lucas, 6, 45001 Toledo, Spain, Departamento de Química Inorganica, Organica y Bioquímica, Universidad de Castilla-La Mancha, Facultad de Químicas, Campus de Ciudad Real, 13071 Ciudad Real, Spain, Instituto de Catálisis y Petroleoquímica, CSIC, Campus Universidad Autónoma, Cantoblanco, 28049 Madrid, Spain, and Laboratoire de Synthèse et d'Electrosynthèse Organométalliques associé au CNRS (URA 1685), Faculté des Sciences, 6 bd. Gabriel, 21000 Dijon, France

Received January 13, 1995[⊗]

*Summary: $[(\eta^5\text{-}C_5Me_5)TiMe_3]$ (**1**) reacts with $[Rh(\mu_2\text{-}OH)(COD)]_2$ (**2**) to yield $[(\eta^5\text{-}C_5Me_5)Ti(\mu_3\text{-}O)_3\{Rh(COD)\}_3]$ (**3**). The molecular structure of **3** shows that it can be compared to the cubane type structures M_4X_4 in which the fourth X ligand position is absent.*

Metal polarization by interaction with supports such as oxides is an idea proposed 60 years ago by Adadurov,[1] but a very special effect was proposed by Tauster et al.[2] in 1978. They found that H_2 and CO chemisorptions were dramatically inhibited for metals supported on TiO_2 when the reduction temperature was ca. 770 K. This effect applicable to group 8–10 metals supported on reducible oxides (V_2O_5, TiO_2, CeO_2, Nb_2O_5) was called thereafter strong metal–support interaction (SMSI),[3] and many studies are based on TiO_2-supported catalysts. One of the explanations of the SMSI effect is based in the fact that Ti^{4+} is partially reduced and the reduced species TiO_x migrate over metal particles, blocking active sites. Activity and selectivity in Fischer–Tropsch synthesis and related catalytic reactions are severely affected.

Homometallic complexes have been widely studied[4] to elucidate the cooperative effect between both metal centers. More recently, heterometallic compounds containing an early metal and a late one have been in the focus[5] to elucidate the mechanism for activation of small molecules such as CO. These complexes contain an oxophilic center and an electron-rich metal which may act as a H_2 activation site, a situation which mimics SMSI. Many heterometallic complexes have been prepared up to now, but relatively few of them contain bridging oxo ligands between the different metals.[6] Such compounds are particularly important when the oxo ligands bridge a group 4–6 transition metal and those from groups 8–10, in part because such compounds can provide insight into the chemistry that occurs at the interface between a metal and its oxide support during catalytic reactions.

Herein, we report the synthesis and characterization of a d^0–d^8 heterometallic complex in which both metal centers are exclusively bridged by oxo ligands. Therefore, it could be envisaged as a close model unit for rhodium catalyst supported on titania.

Reaction of $(\eta^5\text{-}C_5Me_5)TiMe_3$ (**1**) with 3 equiv of $[Rh(\mu_2\text{-}OH)(COD)]_2$ (**2**) in toluene at room temperature affords $[(\eta^5\text{-}C_5Me_5)Ti(\mu_3\text{-}O)_3\{Rh(COD)\}_3]$ (**3**)[7] in 70% yield (eq 1). Complex **3** is moderately air stable in the solid state, partially soluble in alkanes, and very soluble in toluene or THF.

$$(\eta^5\text{-}C_5Me_5)TiMe_3 + {}^3/_2[Rh(\mu_2\text{-}OH)(COD)]_2 \rightarrow [(\eta^5\text{-}C_5Me_5)Ti(\mu_3\text{-}O)_3\{Rh(COD)\}_3] + 3MeH \quad (1)$$

Yellow crystals suitable for X-ray diffraction of compound **3** were obtained by slow diffusion of pentane in a saturated toluene solution of **3**. Figure 1 shows an ORTEP diagram of the molecule along with some selected bond lengths and bond angles.

The structure[10] is built up of discrete tetrametallic ($TiRh_3$) organometallic molecules. The tetrametallic core forms a tetrahedron in which the three μ_3-O oxygen

† Campus de Toledo, Universidad de Castilla-La Mancha.
‡ CSIC, Instituto de Catálisis.
§ CNRS (URA 1685), Faculté des Sciences.
|| Campus de Ciudad Real, Universidad de Castilla-La Mancha.
⊗ Abstract published in *Advance ACS Abstracts,* April 1, 1995.

(1) Adadurov, I. J. *J. Phys. Chem. USSR* **1935**, *6*, 206.
(2) Tauster, S. J.; Fung, S. C.; Garten, R. L. *J. Am. Chem. Soc.* **1978**, *100*, 170.
(3) (a) Haller, G. L.; Resaco, D. E. *Adv. Catal.* **1989**, 173. (b) *Metal-Support Interactions in Catalysis, Sintering and Redispersion*; Van Nostrand Reinhold Catalysis Series; Van Nostrand-Reinhold: New York, 1987. (c) *Strong Metal Support Interactions*; American Chemical Society: Washington DC, 1986.
(4) See for example: Kalck, Ph. *Polyhedron* **1988**, *7*, 2441.
(5) See for example: (a) Stephan, D. W. *Coord. Chem. Rev.* **1989**, *95*, 41 and references therein. (b) Choukroun, R.; Dahan, F.; Gervais, D.; Rifai, C. *Organometallics* **1990**, *9*, 1982. (c) Baker, R. T.; Fultz, W. C.; Mader, T. B.; Williams, I. D. *Organometallics* **1990**, *9*, 2357. (d) Stephan, D. W. *J. Chem. Soc., Chem. Commun.* **1991**, 129. (e) Vites, J. C.; Steffey, B. D.; Giuseppetti-Dery, M. E.; Cutler, A. R. *Organometallics* **1991**, *10*, 2827. (f) Baranger, A. M.; Hollander, F. J.; Bergman, R. G. *J. Am. Chem. Soc.* **1993**, *115*, 7890.
(6) (a) Rau, M. S.; Kretz, C. M.; Geoffroy, G. L.; Rheingold, A. L.; Haggerty, B. S. *Organometallics* **1994**, *13*, 1624 and references therein. (b) Xi, R.; Wang, B.; Abe, M.; Ozawa, Y.; Isobe, K. *Chem. Lett.* **1994**, 1177. (c) Xi, R.; Wang, B.; Abe, M.; Ozawa, Y.; Isobe, K. *Chem. Lett.* **1994**, 323. (d) Isobe, K.; Yagasaki, A. *Acc. Chem. Res.* **1993**, *26*, 524.
(7) A solution of complex **1**[8] (95 mg, 0.42 mmol) in 4 mL of toluene was added to 280 mg (0.61 mmol) of **2**.[9] The reaction mixture was stirred for 3 h. After this time the solvent was removed under vacuum and the solid washed with pentane (3 × 2 mL), yielding 254 mg (0.29 mmol) of a yellow microcrystalline solid which was characterized as complex **3**.
(8) Mena, M.; Pellinghelli, M. A.; Royo, P.; Serrano, R.; Tiripicchio, A. *J. Chem. Soc., Chem. Commun.* **1986**, 1118.
(9) Usón, R.; Oro, L. A.; Cabeza, J. A. *Inorg. Synth.* **1985**, *23*, 126.

0276-7333/95/2314-2162$09.00/0

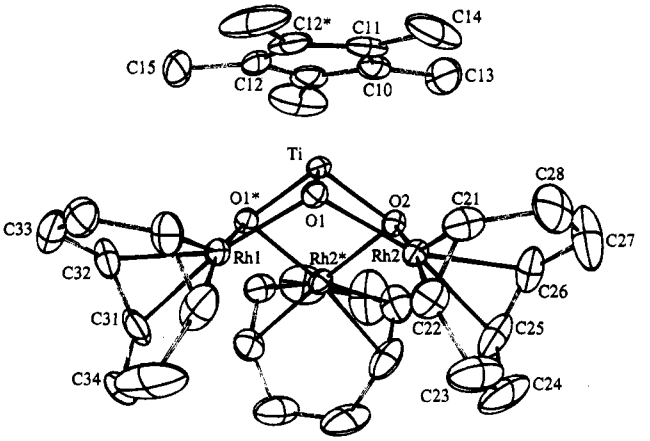

Figure 1. Labeled ORTEP drawing (30% probability level) of **3**. The Rh1, Ti, C10, and C13 atoms are located on the symmetry plane. Selected bond distances (Å) and angles (deg): Rh1–Ti, 2.731(2); Rh2–Ti, 2.760(1); Ti–O1, 1.842(5); Ti–O2, 1.849(7); Rh1–O1, 2.092(4); Rh2–O1, 2.094(5); Rh2–O2, 2.101(3); Rh2–O1–Ti, 88.8(2); Rh2–O2–Ti, 88.4(2).

atoms are bridging. The structure of **3** may be compared to the cubane-type structures M_4X_4, in which the fourth X ligand position is absent. The titanium atom has the usual tetrahedral geometry, while the rhodium atoms are approximately planar. The midpoints of the two C=C (COD) bonds, the two oxygen atoms bound to the rhodium, and the rhodium are coplanar within 0.1 Å. However, the dihedral angle between the O/Rh/O plane and that formed by the midpoints of the C=C double bonds of the COD ligand and the Rh atom is close to 11°. Ti, Rh1, O2, C10, and C13 atoms are on the mirror plane in the *Pnma* space group.

The intermetallic Rh1–Ti and Rh2–Ti distances are 2.731(2) and 2.760(1) Å, respectively. They are shorter than the Ti–Rh distance in μ-methylene μ-phenyl complexes[11] and close to that found in μ-thiolate complexes.[12] The Ti–Rh distance in **3** is sufficiently short so that a direct metal–metal interaction is possible. For comparison, the Ti–Rh distance in an alloy of the metals[13] is 2.68 Å and the Ti–Rh distance in a highly reduced Rh on titania[14] is 2.55 Å.

The distance from titanium to the plane containing the cyclopentadienyl ring (2.061 Å) is normal for titanium complexes.[15] Ti–O1 and Ti–O2 distances are 1.842(5) and 1.849(7) Å, which are comparable to that in titanium complexes with oxo bridging groups.[16] On the other hand, the Ti–O–Rh angles are around 88°.

Complex **3** has been characterized by elemental analysis,[17] ^{1}H and ^{13}C NMR,[18] FT IR and FT Raman, and XPS spectroscopic techniques. ^{1}H and ^{13}C NMR spectra are consistent with the structure. Both spectra show that the three COD groups are equivalent. Each COD group shows two different olefinic signals, as expected for an asymmetrical group. Olefinic carbon atoms are coupled to rhodium, and the coupling constants ($^1J_{C-Rh}$ = 14.64 Hz and $^1J_{C-Rh}$ = 13.73 Hz) as well as the shifts observed (73.26 and 78.58 ppm) are normal for Rh(I) complexes.[19]

The FT IR spectrum shows absorptions at 668 (s), 651 (m), and 622 (m) cm^{-1} which can be tentatively assigned to Ti–O–Rh vibrations. The FT Raman spectrum shows a strong absorption at 668 cm^{-1}, but those at 651 and 622 cm^{-1} are very weak. Binding energies of Rh $3d_{5/2}$ and Ti $2p_{3/2}$ core levels at 308.6 and 456.9 eV are consistent with the expected values for Rh(I) complexes and Ti[(μ_3-O)Rh]$_3$ bridging structures, respectively. The Rh/Ti atomic ratio of 2.8 agrees well with the stoichiometric ratio (Rh/Ti = 3) expected for a type **3** structure.

In line with these results, the structure of complex **3** can serve as a model not only for the interpretation of the SMSI effect in titania-supported metals but also as a basis for delineating the active sites which are involved in hydrogenation and Fischer–Tropsch synthesis.

The catalytic performance of compound **3** in syngas conversion under high-pressure conditions was investigated.[20] CO conversion was rather high (30.0%), and the products identified were methane (52.0%), C_2–C_7 hydrocarbons (7.6%), methanol (1.4%), ethanol (34.0%), propanol (1.5%), butanol (1.3%), other oxygenated products (1.0%), and carbon dioxide (1.2%). These results, although preliminary nicely illustrate the ability of compound **3** to convert in a rather selective way syngas into ethanol, a desired product from this reaction.[21] A detailed study of the catalytic behavior of this compound will be reported in our next contribution.

Acknowledgment. We acknowledge financial support from the Dirección General de Investigación Científica y Técnica (Grant No. PB92-0715) and from the CE Project JOU2-CT92-0040. Thanks are due to Dr. M. López Granados for his help in catalytic experiments.

Supplementary Material Available: Tables giving details of the X-ray structure analysis, anisotropic thermal parameters, atom coordinates, and complete bond distances and angles for **3** (6 pages). Ordering information is given on any current masthead page.

OM950026C

(10) Crystallographic data for **3**: orthorhombic, space group *Pnma* (No. 62), a = 18.010(4) Å, b = 18.38(4) Å, c = 10.32(4) Å, V = 3441.7 Å^3, d_{calc} = 1.668 g cm^{-3}, Z = 4, and μ = 16.44 cm^{-1}. A yellow crystal having the approximate dimensions 0.3 × 0.3 × 0.1 mm was used for data collection, carried out at 296 K on an Enraf-Nonius CAD4 diffractometer with Mo Kα radiation (λ = 0.710 73 Å). Intensity data were collected for 3349 reflections. The Enraf-Nonius Molen library was used for data reductions, solution (Patterson and Multan), and refinement of the structure. All non-hydrogen atoms were refined with anisotropic temperature factors, and the hydrogen atoms were placed in calculated positions. These last atoms were riding on the carbon atoms bearing them and included in the final calculations with B_{iso} fixed at values equal to 1.3B_{eq} for the corresponding carbon atoms. Full-matrix least-squares refinement based on 2282 unique reflections with $I > 3\sigma(I)$ converged at R = 0.036.

(11) Park, J. W.; Henling, L. M.; Schaefer, W. P.; Grubbs, R. H. *Organometallics* **1991**, *10*, 171.

(12) Nadasdi, T. T.; Stephan, D. W. *Inorg. Chem.* **1994**, *33*, 1532.

(13) Tauster, S. J. *Acc. Chem. Res.* **1987**, *20*, 389.

(14) Sakellson, S.; McMillan, M.; Haller, G. L. *J. Phys. Chem.* **1986**, *90*, 1733.

(15) Mena, M.; Pellinghelli, M. A.; Royo, P.; Serrano, R.; Tiripicchio, A. *J. Chem. Soc., Chem. Commun.* **1986**, 1118.

(16) Garcia Blanco, S.; Gomez Sal, M. P.; Martinez Carreras, S.; Mena, M.; Royo, P.; Serrano, R. *J. Chem. Soc., Chem. Commun.* **1986**, 1572.

(17) Anal. Calcd for $C_{34}H_{51}O_3Rh_3Ti$: C, 47.24; H, 5.95. Found: C, 47.11; H, 5.88.

(18) ^{1}H NMR (benzene-d_6, 20 °C, 200 MHz): δ 1.63 (m, 12 H, CH_2 COD), 2.15 (m, 12H, CH_2 COD), 2.32 (s, 15H, Cp*), 3.95 (m, 6H, =CH COD), 4.11 (m, 6H, =CH COD). ^{13}C{^{1}H} NMR (benzene-d_6, 20 °C, 50.3 MHz): δ 11.48 (s, Cp*), 30.71 (s, CH_2), 73.26 (d, $^1J_{C-Rh}$ = 14.64 Hz, =CH), 78.58 (d, $^1J_{C-Rh}$ = 13.73 Hz, =CH), 117.35 s, (Cp*).

(19) Mackenzie, P. B.; Coots, R. J.; Grubbs, R. H. *Organometallics* **1989**, *8*, 8.

(20) Catalytic activity experiments have been performed in a stainless steel reactor (10 mm i.d.) working at 20 bar (2 × 10^6 Pa) total pressure and 523 K. The reactor is dessigned so that very low dead volume is present downstream of the catalyst bed (45 mg of compound **3** diluted with SiC up to 0.7 mL). The reaction mixture consisted of 67% of H_2 and 33% of CO with a total flow of 50 mL min^{-1}. The composition of the effluent products after 12 h on stream was analyzed online by GC. An HP 5890 chromatograph equipped with FID, TCD, and two molecular sieves on Poraplot Q columns was used.

(21) Xiaoding, Xu; Doesburg, E. B. M.; Scholten, J. J. F. *Catal. Today* **1987**, *2*, 125.

Synthesis and Characterization of a (Ketenyl)metal Cluster Complex, an Intermediate in the Oxidative Decarbonation of an Acetylide Ligand

Te-Kun Huang,[†] Yun Chi,*[,†] Shie-Ming Peng,*[,‡] Gene-Hsiang Lee,[‡] Sue-Lein Wang,[†] and Fen-Ling Liao[†]

Departments of Chemistry, National Tsing Hua University, Hsinchu 300, Taiwan, and National Taiwan University, Taipei 107, Taiwan

Received January 17, 1995[⊗]

*Summary: Oxidation of the acetylide cluster Cp*WOs$_3$(CO)$_9$(C$_2$)(C$_2$Ph) (**2**) in toluene produced the ketenyl complex Cp*WOs$_3$(CO)$_9$(C$_2$)(OC$_2$Ph) (**3**). Compound **3** releases a CO group to afford the alkylidyne cluster Cp*WOs$_3$(CO)$_9$(C$_2$)(CPh) (**4**) upon heating, which provides an example of sequential conversion of acetylide to ketenyl and alkylidyne.*

Many examples of transition-metal complexes containing ketenyl ligands have been prepared, and their chemistry is under active investigation.[1] However, one important reaction that has not been well-documented is C–C bond cleavage to afford a coordinated alkylidyne (eq 1). Such ketenyl complexes have been proposed as speculative intermediates for the oxidative decarbonation of acetylide complexes by Vahrenkamp[2] and may be of relevance to oxygen-induced ligand fragmentation[3] and oxo–hydrocarbyl ligand coupling reactions.[4] Herein we report the studies of the ketenyl cluster Cp*WOs$_3$(CO)$_9$(C$_2$)(OC$_2$Ph), which was prepared from direct reaction of the acetylide cluster with oxygen and shows a reversibe equilibrium with the alkylidyne cluster. The overall reaction provides a model for the involvement of a ketenyl ligand in the acetylide to alkylidyne transformation (eq 2) via consecutive oxygen atom transfer and elimination of a CO ligand on metal clusters.

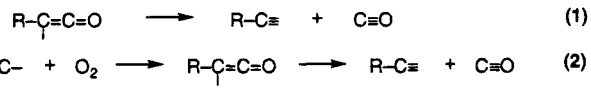

During our investigation on the interaction of highly unsaturated substrates on polynuclear cluster compounds,[5] we were able to synthesize the novel diynyl cluster Os$_3$(CO)$_{10}$[PhC$_4$WCp*(CO)$_3$] (**1**), in which the remote acetylenic C–C triple bond is tightly coordinated to the Os$_3$ triangular core via a $2\sigma + \pi$ mode (Scheme 1). Compound **1** was prepared by a 1:1 combination of Os$_3$(CO)$_{10}$(NCMe)$_2$ and the mononuclear diyne complex Cp*W(CO)$_3$(C$_4$Ph) in refluxing toluene.[6] Further thermolysis of **1** in toluene (110 °C, 1 h) leads to the formation of the acetylide–dicarbide cluster Cp*WOs$_3$(CO)$_9$(C$_2$)(C$_2$Ph) (**2**) in 57% yield as a result of the cleavage of the diynyl C(sp)–C(sp) single bond.[7] Red, needle-shaped single crystals of **2** were obtained from a methanol–dichloromethane solution, and definitive proof of the structure was elucidated by X-ray crystallography.[8]

Scheme 1

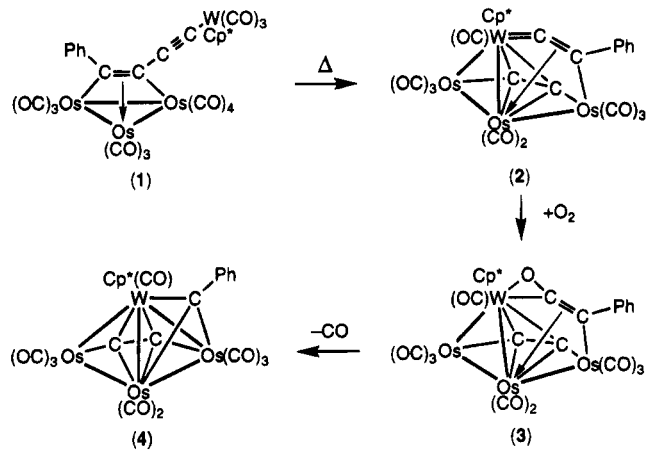

† National Tsing Hua University.

‡ National Taiwan University.

⊗ Abstract published in *Advance ACS Abstracts,* April 1, 1995.

(1) (a) Geoffroy, G. L.; Bassner, S. L. *Adv. Organomet. Chem.* **1988,** *28,* 1. (b) Casey, C. P.; Fagan, P. J.; Day, V. W. *J. Am. Chem. Soc.* **1982,** *104,* 7360. (c) Chisholm, M. H.; Huffman, J. C.; Marchant, N. S. *J. Chem. Soc., Chem. Commun.* **1986,** 717. (d) Kreissl, F. R.; Sieber, W.; Wolfgruber, M. *Angew. Chem., Int. Ed. Engl.* **1983,** *22,* 493.

(2) (a) Bernhardt, W.; Vahrenkamp, H. *Organometallics* **1986,** *5,* 2388. (b) Bernhardt, W.; Vahrenkamp, H. *J. Organomet. Chem.* **1990,** *383,* 357. (c) Shaposhnikova, A. D.; Stadnichenko, R. A.; Kamalov, G. L.; Pasynskii, A. A.; Eremenko, I. L.; Nefedov, S. E.; Struchkov, Y. T.; Yanovsky, A. I. *J. Organomet. Chem.* **1993,** *453,* 279.

(3) (a) Boyar, E.; Deeming, A. J.; Kabir, S. E. *J. Chem. Soc., Chem. Commun.* **1986,** 577. (b) Doherty, E. D.; Filders, M. J.; Forrow, N. J.; Knox, S. A. R.; Macpherson, K. A.; Orpen, A. G. *J. Chem. Soc., Chem. Commun.* **1986,** 1335.

(4) (a) Herrmann, W. A. *Angew. Chem., Int. Ed. Engl.* **1988,** *27,* 1297. (b) Carney, M. J.; Walsh, P. J.; Hollander, F. J.; Bergman, R. G. *Organometallics* **1992,** *11,* 761. (c) Herrmann, W. A.; Roesky, P. W.; Scherer, W.; Kleine, M. *Organometallics* **1994,** *13,* 4536.

(5) (a) Chiang, S.-J.; Chi, Y.; Su, P.-C.; Peng, S.-H.; Lee, G.-H. *J. Am. Chem. Soc.* **1994,** *116,* 11181. (b) Peng, J.-J.; Horng, K.-M.; Cheng, P.-S.; Chi, Y.; Peng, S.-H.; Lee, G.-H. *Organometallics* **1994,** *13,* 2365.

(6) Selected data for **1** are as follows. IR (C_6H_{12}): ν(CO) 2097 (w), 2064 (vs), 2053 (s), 2025 (vs), 2004 (m), 1945 (s), 1935 (s), 1838 (br, vw) cm^{-1}. ^{13}C NMR ($CDCl_3$, 294 K): CO, δ 232.8 (J_{W-C} = 124 Hz), 215.7 (J_{W-C} = 144 Hz, 2CO), 177.4 (br, 10C, Os–*C*O); δ 151.2 (*i*-C_6H_5), 146.3 (C_δ), 141.8 (J_{W-C} = 20 Hz, C_β), 129.0 (*o,m*-C_6H_5, 2C), 127.7 (*m,o*-C_6H_5, 2C), 127.4 (*p*-C_6H_5), 119.2 (C_γ), 104.8 (C_5Me_5), 101.0 (J_{W-C} = 90 Hz, C_α), 10.8 (Me). Anal. Calcd for $C_{33}H_{20}O_{13}Os_3W$: C, 28.74; H, 1.46. Found: C, 28.61; H, 1.48.

(7) Spectral data for **2** are as follows. MS (FAB, ^{192}Os, ^{184}W): *m/z* 1272 (M^+). IR (C_6H_{12}): ν(CO) 2082 (s), 2067 (w), 2059 (vs), 2012 (s), 1999 (vs), 1981 (m), 1964 (m), 1949 (w) cm^{-1}; ^{1}H NMR ($CDCl_3$, 294 K): δ 7.34 (d, 2H, J_{H-H} = 8.0 Hz), 7.26 (t, 2H, J_{H-H} = 8.0 Hz), 7.15 (t, 1H, J_{H-H} = 8.0 Hz), 2.29 (s, 15H, Cp*). ^{13}C NMR ($CDCl_3$, 294 K): CO, δ 217.2 (J_{W-C} = 171 Hz), 184.4, 181.7, 179.2, 177.6 (3C), 175.3, 173.5; δ 306.4 (J_{W-C} = 158 Hz, *C*CPh), 172.2 (μ_4-C_2), 145.9 (μ_4-C_2), 138.8 (*i*-C_6H_5), 129.2 (*o,m*-C_6H_5, 2C), 128.2 (*m,o*-C_6H_5, 2C), 127.1 (*p*-C_6H_5), 105.7 (C_5Me_5), 67.1 (C*C*Ph), 12.4 (Me). Anal. Calcd for $C_{29}H_{20}O_9Os_3W$: C, 27.49; H, 1.59. Found: C, 27.45; H, 1.64.

(8) Crystal data for **2**: $C_{29}H_{20}O_9Os_3W$, monoclinic, $P2_1/n$, a = 14.053(5) Å, b = 10.255(2) Å, c = 22.495(7) Å, β = 106.35(3)°, V = 3110(2) Å^3, Z = 4, $F(000)$ = 2272, μ(Mo Kα) = 15.95 mm^{-1}, 2812 reflections with $I > 3\sigma(I)$ and 380 parameters, R = 0.041, R_w = 0.035, GOF = 0.99.

0276-7333/95/2314-2164$09.00/0

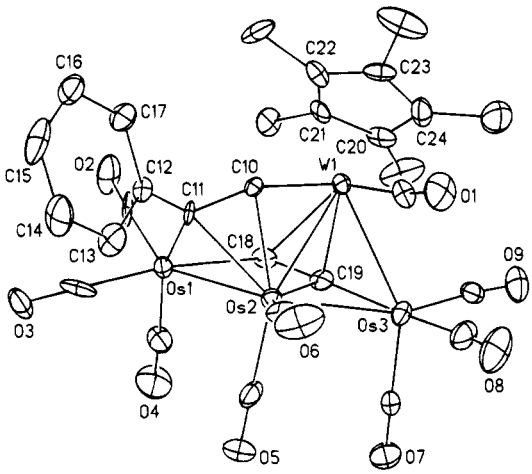

Figure 1. Molecular structure of **2**. Selected bond lengths (Å) are as follows: Os(1)–Os(2) = 2.760(2), Os(2)–Os(3) = 2.809(2), Os(2)–W(1) = 2.801(2), Os(3)–W(1) = 2.846(2), Os(2)–C(10) = 2.19(2), W(1)–C(10) = 1.92(2), Os(1)–C(11) = 2.09(2), Os(2)–C(11) = 2.29(2), C(10)–C(11) = 1.36(2), C(11)–C(12) = 1.52(3), Os(1)–C(18) = 2.13(2), Os(2)–C(18) = 2.20(2), W(1)–C(18) = 2.43(2), Os(2)–C(19) = 2.26(2), Os(3)–C(19) = 1.99(3), W(1)–C(19) = 2.25(3), C(18)–C(19) = 1.25(3).

The structure of **2** consists of a spiked-triangular core arrangement with the Os(3) atom located at the pivotal position (Figure 1). The dicarbide ligand adopts a novel μ_4 mode, in which the carbon atoms are linked to the Os(1) and Os(2) atoms via two σ-bonds and coordinated to the metal atoms Os(3) and W(1) via π-interactions. The atoms Os(1), Os(2), and Os(3) and the dicarbide fragment C(18)–C(19) are close to coplanar. The C(18)–C(19) length (1.25(3) Å), which is intermediate between the C–C distances of the complexes $CpW(CO)_3(C_2)W(CO)_3Cp$ (1.18(3) Å)[9] and $CpWOs_3(CO)_{11}(\mu_4\text{-}C_2Ph)$ (1.38(2) Å)[10] and resembles that of the complexes $Co_2Re_2(C_2)(CO)_{14}$ (1.28(2) Å)[11] and $CpWOs_2(CO)_8(C_2Ph)$ (1.23(5) Å),[12] confirms the presence of C–C multiple-bond character, which is also similar to that observed in $Ru_4(\mu\text{-}PPh_2)_2(C_2)(CO)_{12}$.[13] The dicarbide ligand showed signals at δ 172.2 and 145.9 in the ^{13}C NMR spectrum. These chemical shifts are similar to those observed for $[Fe_3(CO)_9\{C_2Fe(CO)_2Cp\}]^-$ (δ 172.9, 132.2) and $[CpFeCo_2(CO)_6\{C_2Fe(CO)_2Cp\}]$ (δ 207.7, 154.4).[14] In addition, the acetylide ligand adopts a novel $\mu_3\text{-}\eta^1\text{:}\eta^2\text{:}\eta^2$ mode,[15] in which the β-carbon is linked to the Os(1) and Os(2) atoms via two single bonds (Os(1)–C(11) = 2.09(2) Å and Os(2)–C(11) = 2.29(2) Å) and the α-carbon is linked to the W(1)–Os(1) edge with substantial carbynic character (Os(2)–C(10) = 2.19(2) Å and W(1)–C(10) = 1.92(2) Å). In accordance with the above description, the signals for the μ-C_2Ph ligand in the ^{13}C NMR spectrum are found at δ 306.4 (C_α, J_{W-C} = 158 Hz) and 67.1 (C_β). The downfield shift and the large J_{W-C} coupling constant of its α-carbon suggests that there is considerable multiple-bond character in this tungsten–carbon bond.

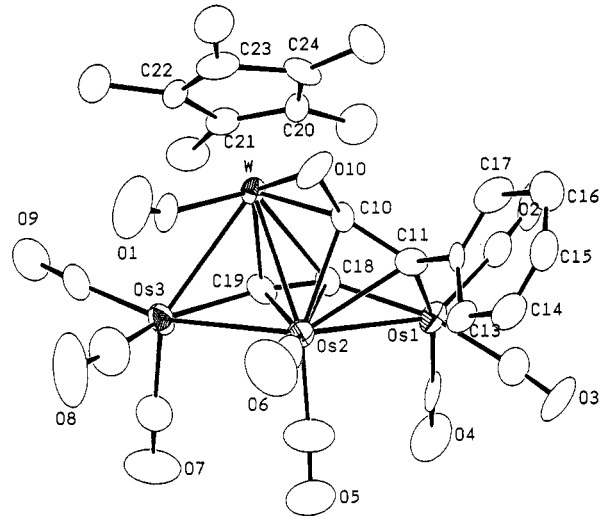

Figure 2. Molecular structure of **3**. Selected bond lengths (Å) are as follows: Os(1)–Os(2) = 2.769(2), Os(2)–Os(3) = 2.789(2), W–Os(2) = 2.795(2), W–Os(3) = 2.871(2), W–O(10) = 2.18(2), C(10)–O(10) = 1.25(3), Os(2)–C(10) = 2.27(3), W–C(10) = 2.01(3), Os(1)–C(11) = 2.06(3), Os(2)–C(11) = 2.40(3), C(10)–C(11) = 1.48(4), C(11)–C(12) = 1.47(3), Os(1)–C(18) = 2.08(3), Os(2)–C(18) = 2.19(2), W–C(18) = 2.47(3), Os(2)–C(19) = 2.23(3), Os(3)–C(19) = 2.04(3), W–C(19) = 2.21(3), C(18)–C(19) = 1.20(4).

Treatment of **2** with oxygen in toluene solution (1 atm, 110 °C, 1 h) afforded the ketenyl cluster $Cp^*WOs_3(CO)_9(C_2)(OC_2Ph)$ (**3**), which was isolated in 70% yield after recrystallization.[16] The X-ray diffraction study[17] confirms that it possesses a $WOs_3(\mu_4\text{-}C_2)$ core identical with that of **2**, on which the acetylide of **2** has converted into a ketenyl ligand with the oxygen atom bridging the W–C(10) bond (Figure 2). The insertion of an oxygen atom weakens the bonding capability of the C(10)C(11)-Ph unit, increasing the W–C(10) distance from 1.92(2) to 2.01(3) Å, the Os(2)–C(11) distance from 2.29(2) to 2.40(3) Å, and the C(10)–C(11) distance from 1.36(2) to 1.48(4) Å with respect to the structural data of **2**. The ^{13}C NMR spectrum exhibits dicarbide resonance signals at δ 141.4 and 119.9 and ketenyl signals at δ 210.9 (C_α, J_{W-C} = 51 Hz) and 137.4 (C_β). Of note are the chemical shift and the J_{W-C} coupling constant of the ketenyl α-carbon, which are consistent with the lengthening of the W–C(10) distance with respect to that in **2**.

The reactivity of **3** was examined. As expected, complex **3** was found to react slowly in refluxing toluene

(9) Chen, M.-C.; Tsai, Y.-J.; Chen, C.-T.; Lin, Y.-C.; Tseng, T.-W.; Lee, G.-H.; Wang, Y. *Organometallics* **1991**, *10*, 378.

(10) Chi, Y.; Wu, C.-H.; Peng, S.-M.; Lee, G.-H. *Organometallics* **1990**, *9*, 2305.

(11) Weidmann, T.; Weinrich, V.; Wanger, B.; Robl, C.; Beck, W. *Chem. Ber.* **1991**, *124*, 1363.

(12) Hwang, D.-K.; Chi, Y.; Peng, S.-M.; Lee, G.-H. *Organometallics* **1990**, *9*, 2709.

(13) Bruce, M. I.; Snow, M. R.; Tiekink, E. R. T.; Williams, M. L. *J. Chem. Soc., Chem. Commun.* **1986**, 701.

(14) (a) Jensen, M. P.; Sabat, M.; Shriver, D. F. *J. Cluster Sci.* **1990**, *1*, 75. (b) Akita, M. Terada, M.; Moro-oka, Y. *Organometallics* **1992**, *11*, 1825.

(15) The common bonding of the μ_3-acetylide ligand involves the $\sigma + 2\pi$ mode; see: Sappa, E.; Tiripicchio, A.; Braunstein, P. *Chem. Rev.* **1983**, *83*, 203.

(16) Spectral data for **3** are as follows. MS (FAB, ^{192}Os, ^{184}W): *m/z* 1288 (M^+). IR (C_6H_{12}): ν(CO) 2086 (m), 2067 (vs), 2017 (s), 2009 (m), 2001 (s), 1982 (m), 1973 (m), 1950 (w), 1882 (br, w) cm^{-1}; ^1H NMR ($CDCl_3$, 294 K): δ 7.09–7.27 (m, 5H, Ph), 2.02 (s, 15H, Cp*). ^{13}C NMR ($CDCl_3$, 294 K): CO, δ 221.7 (J_{W-C} = 169 Hz), 185.6, 179.9 (2C), 177.3, 175.9 (br, 3C), 173.4; δ 210.9 (J_{W-C} = 51 Hz, *C*CPh), 148.1 (*i*-C_6H_5), 141.4 (μ_4-C_2), 137.4 (C*C*Ph), 128.2 (*o,m*-C_6H_5, 2C), 127.9 (*m,o*-C_6H_5, 2C), 126.8 (*p*-C6H5), 119.9 (μ_4-C_2), 109.1 (C_5Me_5), 11.2 (Me). Anal. Calcd for $C_{29}H_{20}O_{10}Os_3W$: C, 27.15; H, 1.57. Found: C, 27.10; H, 1.63.

(17) Crystal data for **3**: $C_{29}H_{20}O_{10}Os_3W$, monoclinic, $P2_1/c$, a = 20.906(3) Å, b = 14.274(4) Å, c = 10.634(3) Å, β = 97.20(2)°, V = 3148-(1) Å^3, Z = 4, $F(000)$ = 2283, μ(Mo Kα) = 15.85 mm^{-1}, 3449 reflections with $I > 2\sigma(I)$ and 389 parameters, R = 0.066, R_w = 0.073, GOF = 2.83.

under N_2 to form the alkylidyne cluster $Cp^*WOs_3(CO)_9(C_2)(\mu_3\text{-CPh})$ (**4**; 5 h, 56%) (Scheme 1). However, thermolysis of **3** under CO at 1 atm produced **4** in much higher yield (92%). Complex **4** was fully characterized by an X-ray analysis and spectroscopic methods.[18] The key spectral feature involves the observation of five CO signals at 207.0 (J_{W-C} = 141 Hz), 189.9, 183.1, 177.0 (br, 3C), and 175.5 (3C), two dicarbide signals at δ 162.5 and 155.3, and an alkylidyne C_α signal at δ 315.3 (J_{W-C} = 93 Hz) in its ^{13}C NMR spectrum.

In conclusion, this work provides the crucial mechanistic evidence for the oxidative decarbonation of acetylide ligands. Although the acetylide → ketenyl → alkylidyne sequence is the dominant pathway in our experiment and other systems comprising metal cluster compounds,[2] generation of a stable ketenyl derivative from acetylide and its subsequent conversion to alkylidyne ligands has never been achieved in mononuclear and dinuclear metal complexes; only the reversals were documented.[19] The oxophilic W atom appears to be the site for initial O_2 attack, as the oxygen atom of the ketenyl ligand is directly bonded to the W atom. Further evidence comes from the study of the selective ^{13}CO exchange of **2** under ^{13}C-labeled carbon monoxide (95 °C, 3 h). This experiment indicated that the W−CO ligand exhibits an exchange rate 2−6 times faster than that observed for other Os−CO ligands and implied that the W atom is more susceptible to direct chemical attack. Finally, we speculate that the production of a ketenyl fragment is a consequence of the W=C double-bond character of the acetylide ligand in **2**. In the absence of this unusual W=C bonding, the oxidation would give rise to an energetically more favorable bridging W=O → Os functional group or terminal W≡O unit. This type of bonding was clearly noted in the oxo−acetylide compound $Cp^*WRe_2(CO)_8(O)(CCPh)$, generated by the treatment of its precursor $Cp^*WRe_2(CO)_9(CCPh)$ with the oxidants O_2 or N_2O.[20]

Acknowledgment. We thank the National Science Council of the Republic of China for support (Grant No. NSC 84-2113-M007-020).

Supplementary Material Available: Tables of crystal data, bond distances, atomic coordinates, and anisotropic thermal parameters for **2** and **3** and an ORTEP diagram including selective bond distances for **4** (9 pages). Ordering information is given on any current masthead page.

OM950034T

(18) Selected data for **4** are as follows. MS (FAB, ^{192}Os, ^{184}W): *m/z* 1260 (M^+). IR (C_6H_{12}): ν(CO) 2074 (vw), 2054 (vs), 2043 (vw), 2004 (s), 1997 (m), 1984 (vw), 1978 (vw), 1962 (w), 1937 (vw) cm^{-1}. ^1H NMR ($CDCl_3$, 294 K): δ 7.62 (d, J_{H-H} = 7.5 Hz, 2H), 7.39 (t, J_{H-H} = 7.5 Hz, 2H), 7.29 (t, J_{H-H} = 7.5 Hz, 1H), 2.21 (s, 15H, Cp*). Crystal data: $C_{28}H_{20}O_{19}Os_3W{\cdot}CH_2Cl_2$, triclinic, $P\bar{1}$, a = 11.022(2) Å, b = 11.304(2) Å, c = 13.488(3) Å, α = 78.84(2)°, β = 77.28(2)°, γ = 88.46(2)°; R = 0.027. Details of the structure determination will be given in a full publication.

(19) (a) Kreissl, F. R.; Frank, A.; Schubert, U.; Lindner, T. L.; Huttner, G. W. *Angew. Chem., Int. Ed. Engl.* **1976**, *15*, 632. (b) Kreissl, F. R.; Eberl, K.; Uedelhoven, W. *Angew. Chem., Int. Ed. Engl.* **1978**, *17*, 860. (c) Uedelhoven, W.; Eberl, K.; Kreissl, F. R. *Chem. Ber.* **1979**, *112*, 3376. (d) Jeffery, J. C.; Ruiz, M. A.; Stone, F. G. A. *J. Organomet. Chem.* **1988**, *355*, 231.

(20) Chi, Y.; Cheng, P.-S.; Wu, H.-L.; Hwang, D.-K.; Peng, S.-H.; Lee, G.-H. *J. Chem. Soc., Chem. Commun.* **1994**, 1839.

A Triosmium Cluster with a Novel Mode of Metallacyclopentadiene Fragment Bonding. X-ray Structure and Reactivity of $Os_3\{\mu_3\text{-}\eta^1\text{:}\eta^1\text{:}\eta^2\text{:}\eta^2\text{-}C(SiMe_3)C(Me)C(H)C(Ph)\}(CO)_9$

Avth'andil A. Koridze,* Nadezhda M. Astakhova, Fedor M. Dolgushin, Aleksandr I. Yanovsky, Yuri T. Struchkov, and Pavel V. Petrovskii

Institute of Organoelement Compounds, Russian Academy of Sciences, 28 Vavilov Street, Moscow 117813, Russian Federation

Received November 1, 1994[⊗]

Summary: The molecular structure of $Os_3\{\mu_3\text{-}\eta^1\text{:}\eta^1\text{:}\eta^2\text{:}\eta^2\text{-}C(SiMe_3)C(Me)C(H)C(Ph)\}(CO)_9$ *(**3**), obtained from* $Os_3(\mu_3\text{-}Me_3SiC_2Me)(\mu\text{-}CO)(CO)_9$ *(**2**) and PhC≡CH in hot hexane, involves an osmacyclopentadiene ring π-coordinated to the remaining two osmium atoms of the cluster. Heating of **3** in refluxing benzene yields two new compounds,* $Os_3(\mu\text{-}H)\{\mu_3\text{-}C(SiMe_3)C(Me)C(H)C(C_6H_4)\}(CO)_8$ *(**4**) with a rearranged, coordinated on one cluster edge osmacyclopentadiene fragment, and* $Os_2\{\mu\text{-}\eta^1\text{:}\eta^1\text{:}\eta^4\text{-}C(SiMe_3)C(Me)C(H)C(Ph)\}(CO)_6$ *(**5**). Compound **4** reacts with* PPh_3 *at room temperature to form* $Os_3\{\mu\text{-}\eta^1\text{:}\eta^1\text{:}\eta^4\text{-}C(SiMe_3)C(Me)C(H)C(Ph)\}(CO)_8(PPh_3)$ *(**8**).*

It is well-known[1] that all triosmium clusters with osmacyclopentadiene fragments characterized thus far have the structure of the B type (Figure 1), and although the alternative structure A had been suggested earlier[1a] for $Os_3(C_4Ph_4)(CO)_9$ (**1**), it has never been proved. Later, it was shown by an X-ray diffraction study[2] that this complex has the structure B, $Os_3(\mu\text{-}\eta^1\text{:}\eta^1\text{:}\eta^4\text{-}C_4Ph_4)(CO)_9$. It may be noted, however, that $\mu_3\text{-}\eta^1\text{:}\eta^1\text{:}\eta^2\text{:}\eta^2$ coordination of an organic fragment to a triangular array of osmium atoms has been found for the cluster $Os_3\{C(Me)C(Me)C(O)C(Me)C(Me)\}(CO)_8\{P(OMe)_3\}$ with an osmacyclohexadienone ring.[3]

In the course of our study of silylalkyne transformations on triruthenium and triosmium clusters[4] we obtained and fully characterized a triosmium cluster of the structure A, $Os_3\{\mu_3\text{-}\eta^1\text{:}\eta^1\text{:}\eta^2\text{:}\eta^2\text{-}C(SiMe_3)C(Me)C(H)C(Ph)\}(CO)_9$ (**3**).

Reaction of the alkyne complex $Os_3(\mu_3\text{-}Me_3SiC_2Me)(\mu\text{-}CO)(CO)_9$ (**2**) with phenylacetylene in hot hexane yields the red compound **3** in 65% yield (Scheme 1).

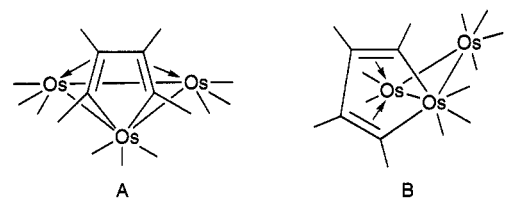

Figure 1. Two possible structures for $Os_3(C_4R_4)(CO)_9$ complexes.

Scheme 1

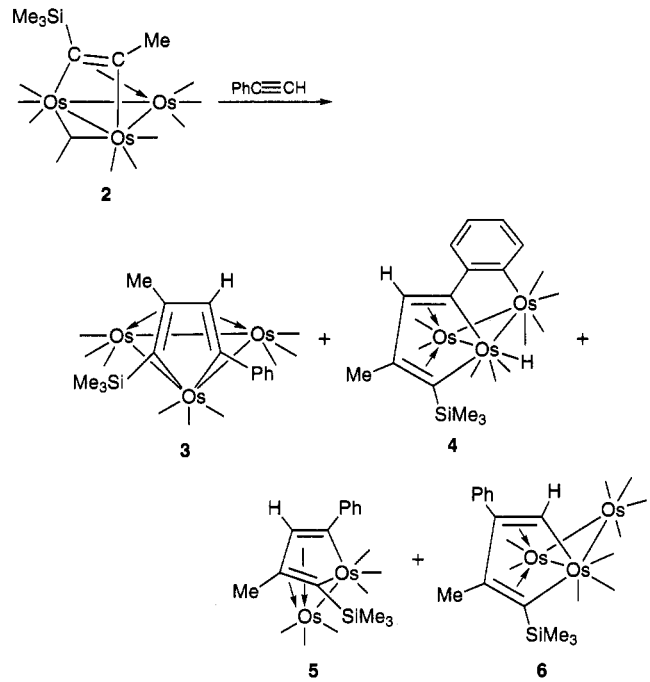

Compound **3** was characterized by IR and ^1H NMR spectra and elemental analysis.[5] The IR spectrum of **3** is distinctly different from that of **1** and related osmium complexes $Os_3(\mu_3\text{-}\eta^1\text{:}\eta^1\text{:}\eta^4\text{-}C_4R_4)(CO)_9$ with side-on-coordinated osmacyclopentadiene.[1a–e]

The X-ray diffraction study[6] of compound **3** has shown that this complex represents a triosmium cluster involving the osmacyclopentadiene moiety (Figure 2). In contrast to all previously structurally characterized trimetal clusters with metallacyclopentadiene frag-

[⊗] Abstract published in *Advance ACS Abstracts,* February 15, 1995.

(1) (a) Gambino, O.; Vaglio, G. A.; Ferrari, R. P.; Cetini, G. *J. Organomet. Chem.* **1971**, *30*, 381. (b) Gambino, O.; Ferrari, R. P.; Chinone, M.; Vaglio, G. A. *Inorg. Chim. Acta* **1975**, *12*, 155. (c) Ferrari, R. P.; Vaglio, G. A.; Gambino, O.; Valle, M.; Cetini, G. *J. Chem. Soc., Dalton Trans.* **1972**, 1998. (d) Deeming, A. J.; Hasso, S.; Underhill, M. *J. Chem. Soc., Dalton Trans.* **1975**, 1614. (e) Tachikawa, M.; Shapley, J. R.; Pierpont, C. G. *J. Am. Chem. Soc.* **1975**, *97*, 7172. (f) Johnson, B. F. G.; Khattar, R.; Lahoz, F. J.; Lewis, J.; Raithby, P. R. *J. Organomet. Chem.* **1987**, *319*, C51.

(2) Ferraris, G.; Gervasio, G. *J. Chem. Soc., Dalton Trans.* **1974**, 1813.

(3) Johnson, B. F. G.; Khattar, R.; Lewis, J.; Raithby, P. R.; Smit, D. N. *J. Chem. Soc., Dalton Trans.* **1988**, 1421.

(4) (a) Koridze, A. A.; Astakhova, N. M.; Yanovsky, A. I.; Struchkov, Yu. T. *Metalloorg. Khim.* **1992**, *5*, 886. (b) Yanovsky, A. I.; Struchkov, Yu. T.; Astakhova, N. M.; Koridze, A. A. *Metalloorg. Khim.* **1990**, *3*, 704. (c) Koridze, A. A.; Astakhova, N. M.; Dolgushin, F. M.; Yanovsky, A. I.; Struchkov, Yu. T. *Izv. Akad. Nauk, Ser. Khim.* **1993**, 2011. (d) Koridze, A. A.; Astakhova, N. M.; Petrovskii, P. V.; Dolgushin, F. M.; Yanovsky, A. I.; Struchkov, Yu. T. *J. Organomet. Chem.* **1994**, *481*, 247.

(5) Compound **3** is air-stable and was isolated by TLC on silica gel using a 1:9 benzene/petroleum ether (40–70 °C) solvent mixture. IR (ν(CO), cm^{-1}; in hexane): 2085 (m), 2049 (vs), 2026 (vw), 2011 (s), 1996 (w), 1984 (m). ^1H NMR (δ; in C_6D_6): 7.06–7.40 (m, 5H), 5.69 (s, 1H), 2.14 (s, 3H), 0.34 (s, 9H). Anal. Calcd (found): C, 26.63 (26.39); H, 1.75 (1.66); Os, 55.02 (55.36); Si, 2.71 (2.71).

0276-7333/95/2314-2167$09.00/0

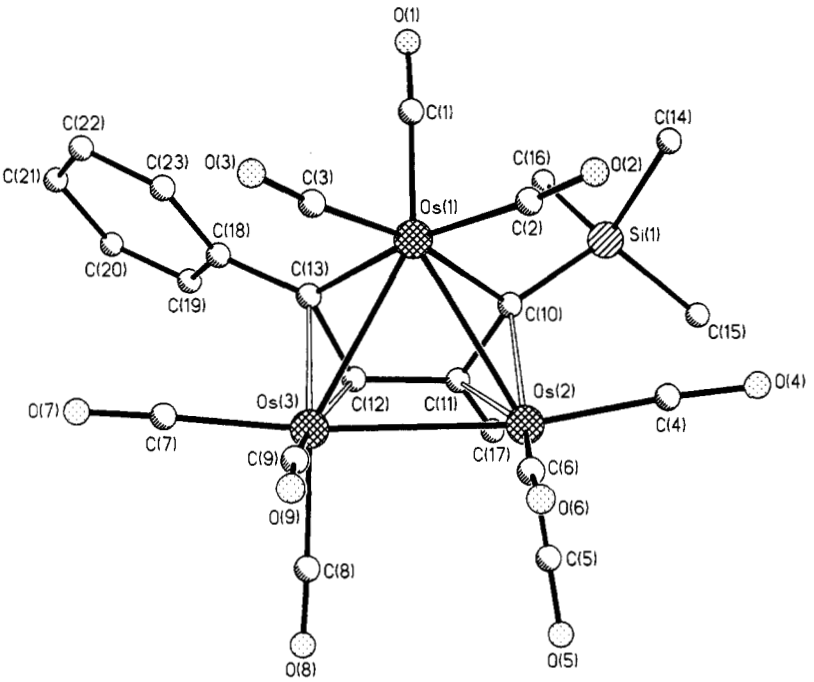

Figure 2. Molecular structure of $Os_3\{\mu_3\text{-}\eta^1\text{:}\eta^1\text{:}\eta^2\text{:}\eta^2\text{-}C(SiMe_3)C(Me)C(H)C(Ph)\}(CO)_9$ (**3**). Open bonds correspond to π coordination. Selected interatomic distances (Å) are as follows: Os(1)–Os(2) = 2.811(1), Os(1)–Os(3) = 2.811(1), Os(2)–Os(3) = 2.825(1), Os(1)–C(10) = 2.19(1), Os(1)–C(13) = 2.12(1), Os(2)–C(10) = 2.18(1), Os(2)–C(11) = 2.42(2), Os(3)–C(12) = 2.25(1), Os(3)–C(13) = 2.22(1), C(10)–C(11) = 1.44(2), C(11)–C(12) = 1.46(2), C(12)–C(13) = 1.48(2).

ments, the hydrocarbon ligand in **3** is directly bonded to all three metal atoms, its two double bonds being coordinated by two different Os atoms, each of them bearing three terminal carbonyl groups—*i.e.*, **3** has a structure of type A.

The osmacyclopentadiene ring has an envelope conformation, its folding angle along the C(10)–C(13) line being equal to 28.8°. The Os(1) atom is displaced from the C(10)C(11)C(12)C(13) group, which is planar within 0.02 Å, by 0.794 Å; the other osmium atoms Os(2) and Os(3) are displaced from this plane in the same direction as Os(1) by 2.133 and 2.093 Å, respectively.

In spite of the apparent symmetry of the central nucleus of the cluster involving the Os_3 triangle and osmacyclopentadiene ring, some geometrical parameters show considerable differences between both wings of the complex evidently caused by the different substituents at the carbon atoms of the osmacyclopentadiene moiety. Thus, one of the π bonds is characterized by distinctly nonequivalent Os–C bonding distances (Os(2)–C(10) = 2.18(1) Å and Os(2)–C(11) = 2.42(2) Å), whereas another π bond exhibits a quite normal symmetrical mode of coordination (Os(3)–C(12) = 2.25(1) Å and Os(3)–C(13) = 2.22(1) Å). A noticeable difference is also observed between the metal–carbon σ bonds within the osmacyclopentadiene ring (Os(1)–C(10) = 2.19(1) Å and Os(1)–C(13) = 2.12(2) Å).

Other products obtained in the reaction of **1** with phenylacetylene are yellow $Os_3(\mu\text{-}H)\{\mu_3\text{-}C(SiMe_3)C(Me)C(H)C(C_6H_4)\}(CO)_8$ (**4**; 8% yield), colorless $Os_2\{\mu\text{-}\eta^1\text{:}\eta^1\text{:}\eta^4\text{-}C(SiMe_3)C(Me)C(H)C(Ph)\}(CO)_6$ (**5**; 12% yield), and amethyst-violet $Os_3\{\mu\text{-}\eta^1\text{:}\eta^1\text{:}\eta^4\text{-}C(SiMe)_3C(Me)C(Ph)C(H)\}(CO)_9$ (**6**; 5% yield). All three compounds were characterized by ^1H NMR and IR spectra.[8]

The ^1H NMR spectrum of compound **6** shows a single proton resonance in the substantially low-field region at δ 7.93 ppm, which is characteristic for hydrogen atoms at the σ,π-coordinated carbons. This feature allows to assign to complex **6** the structure shown in Scheme 1.

The similarities in the shielding of Me_3Si, Me, and H substituents of the osmacyclopentadiene ring in the ^1H NMR spectra of compounds **3**–**5** suggest that the last two complexes are derived from **3**. Indeed, when **3** was heated in refluxing benzene, **4** and **5** were formed in the ratio 1:1.6. Although the yellow hydride **4** does not react with CO with formation of $Os_3\{\mu\text{-}\eta^1\text{:}\eta^1\text{:}\eta^4\text{-}C(SiMe_3)C(Me)C(H)C(Ph)\}(CO)_9$ (**7**) (in contrast to the

(6) Red crystals of **3** were grown from hexane at −5 °C. Crystal data for **3**: $C_{23}H_{18}O_9Os_3Si$, M_r = 1037.1, monoclinic, space group $P2_1/c$, at 296 K, a = 8.996(3) Å, b = 13.450(5) Å, c = 22.082(9) Å, β = 93.88(3)°, V = 2669(2) Å^3, D_{calcd} = 2.580 g/cm^3 for Z = 4. Intensities of 5614 independent reflections and cell parameters were measured at 296 K with a Siemens P3/PC automated diffractometer using Mo Kα radiation (λ = 0.710 73 Å, graphite monochromator, $\theta/2\theta$ scan, $\theta \leq 27°$, semiempirical absorption correction on the basis of ψ scans, minimum transmission factor 0.4142). The structure was solved by direct methods and refined by the least-squares technique in the anisotropic approximation. H atoms were placed geometrically and included in the structure factor calculation in the riding motion approximation with the common refined U_{iso} = 0.07(2) Å^2. The refinement of 326 parameters against 4539 reflections with $I > 3\sigma(I)$ converged at R = 0.0593 and R_w = 0.0705. All calculations were carried out with an IBM PC AT computer using the SHELXTL PC program package.[7]

(7) Robinson, W.; Sheldrick, G. M. SHELX. In *Crystallographic Computing-Techniques and New Technologies*; Isaacs, N. W., Taylor, M. R., Eds.; Oxford University Press: Oxford, England, 1988; p 366.

(8) Compounds **4**–**6** are isolated by TLC on silica gel using a 1:10 benzene/petroleum ether (40–70 °C) solvent mixture. IR (ν(CO), cm^{-1}; in hexane): for **4**, 2095 (s), 2055 (s), 2029 (vs), 2017 (s), 2012 (m), 1995 (m), 1985 (m), 1972 (m); for **5**, 2080 (s), 2049 (vs), 2010 (s), 2000 (vs), 1979 (s), 1968 (s); for **6**, 2108 (m), 2053 (vs), 2035 (m), 2030 (s), 2011 (vs), 1994 (m), 1982 (m), 1936 (m). ^1H NMR (δ; in C_6D_6): for **4**, 6.9–8.0 (m, 4H), 6.11 (s, 1H), 2.29 (s, 3H), 0.34 (s, 9H), −14.76 (s, 1H); for **5**, 6.98–7.21 (m, 5H), 6.28 (s, 1H), 2.15 (s, 3H), 0.33 (s, 9H); for **6**, 7.93 (s, 1H), 7.06–7.20 (m, 5H), 2.30 (s, 3H), 0.50 (s, 9H). Satisfactory elemental analyses (C, H) have been obtained for **4**–**6**.

(9) Compound **8** was isolated by TLC on silica gel using a 1:4 benzene/petroleum ether (40–70 °C) solvent mixture. IR in hexane solvent (ν(CO), cm^{-1}): 2069 (m), 2038 (s), 1995 (vs), 1980 (vs), 1965 (s), 1915 (m). ^1H NMR (C_6D_6; δ): 6.99–7.77 (m, 20H), 6.80 (s, 1H), 2.47 (s, 3H), 0.66 (s, 9H). Anal. Calcd (found): C, 37.79 (37.85); H, 2.62 (2.76).

Scheme 2

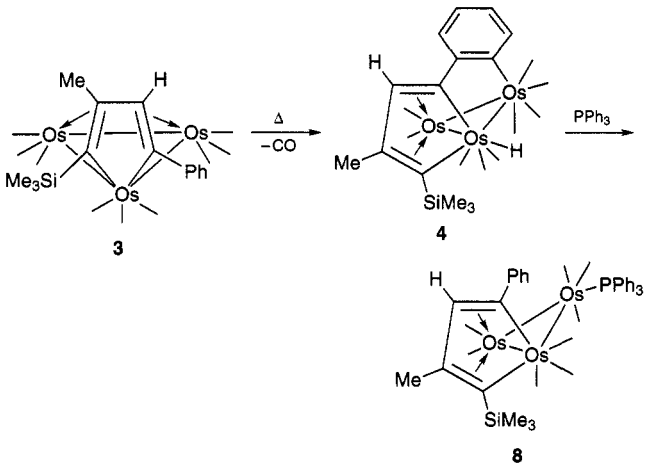

related compound $Os_3(\mu\text{-}H)(\mu_3\text{-}C_4Ph_3C_6H_4)(CO)_8$, which adds CO instantaneously[1a] to yield **1**), it slowly reacts with PPh_3 at room temperature to give the phosphine derivative of **7**, *viz.*, the violet-black compound $Os_3\{\mu\text{-}\eta^1\text{:}\eta^1\text{:}\eta^4\text{-}C(SiMe_3)C(Me)C(H)C(Ph)\}(CO)_8(PPh_3)$ (**8**; 85% yield)[9] (Scheme 2).

It still remains unclear whether the observed **3** → **4** transformation involves the decarbonylation of complex **3** with subsequent face-on → side-on rearrangement accompanied by the *ortho* metalation of the phenyl group or, alternatively, this reaction proceeds through the formation of complex **7**, the unstable intermediate with side-on osmacyclopentadiene coordination.

Acknowledgment. We are indebted to Dr. M. G. Ezernitskaya for recording of the IR spectra and helpful discussion. This work was supported by the Russian Foundation of Fundamental Research (Grant Nos. 94-03-08167 and 94-03-08338) and the International Science Foundation (Grant No. MO 4000). A.I.Y. is pleased to thank the American Crystallographic Association for financial support within the framework of the ACA/USNCCr grants program.

Supplementary Material Available: Tables giving the structure determination summary, positional and thermal parameters, and bond distances and angles for **3** (8 pages). Ordering information is given on any current masthead page.

OM9408324

A Novel Synthetic Approach to Cycloocta-1,5-diynes and Cyclooct-3-ene-1,5-diynes via Cobalt-Complexed Propargyl Radicals

Gagik G. Melikyan,* Masood A. Khan, and Kenneth M. Nicholas*

Department of Chemistry and Biochemistry, University of Oklahoma, Norman, Oklahoma 73019

Received January 20, 1995[⊗]

Summary: A novel synthetic strategy has been elaborated to produce $Co_2(CO)_6$-complexed 1,5-cyclooctadiynes and the first cyclooct-3-ene-1,5-diyne derivative. Eight-membered rings are formed with high dl-diastereoselectivity (de ≥98%) by reduction of the corresponding propargyl dication complexes under hetero- (Zn) and homogeneous (Na/Ph_2CO) conditions. A novel "red-ox" decomplexation method has been developed for 1,5-cyclooctadiynes.

Eight-membered carbocycles constitute the characteristic molecular fragment of natural *cyclooctanoids*, including those containing one or two double bonds, e.g. precapnelladiene, basemenone, fusicoccin, dactylol, and ophiobolin F,[1-5] as well as the saturated taxol.[6] Retrosynthetically, 1,5-cyclooctadiynes are attractive precursors to such compounds since the 1,5-disposition of the triple bonds could be used to develop the remaining ring functionality. At present, however, *there is no synthetically useful approach to 1,5-cyclooctadiyne derivatives which includes construction of the eight-membered ring.*[7] Decades ago 1,5-cyclooctadiyne itself was isolated in 2.6% yield from the spontaneous [4 + 4] cyclocondensation of butatriene.[8] Recently, its synthesis from 1,5-cyclooctadiene was achieved using a classical bromination/dehydrobromination sequence,[9] but this methodology is limited by the requirement of a preformed ring and the low selectivity of the elimination step. Additional incentives for the synthesis of cyclic diynes come from discovery of the remarkable ene–diyne antibiotics[10] which effect double-stranded DNA cleavage via cyclization to arene 1,4-diradicals.[11] Among them, calicheamicin, esperamicin, and dynemicin contain a *ten-membered ene–diyne* unit, while the neocarzinostatin chromophore possesses a *nine-membered ring*. No eight-membered homologs are known, and their highly strained nature raises interesting questions regarding their ease of Bergman cyclization.[12] We report here a novel method for the construction of eight-membered carbocycles applied to the preparation of metal-complexed 1,5-cyclooctadiynes and cyclooct-3-ene-1,5-diyne, *the first eight-membered ene–diyne derivative.*

Our strategy is based on intramolecular coupling of $Co_2(CO)_6$-complexed bis(propargyl) radicals **1** and **2**, part of a continuing investigation of the chemistry of little studied π-bonded organometallic radicals.[13-15] Complexation of the triple bonds of **1** and **2** was considered advantageous for overcoming the poor regioselectivity associated with classical propargyl/propargyl coupling[16] and for facilitating the formation and stabilization of the eight-membered ring by taking advantage of the bent geometry of the coordinated alkyne unit.[17-19]

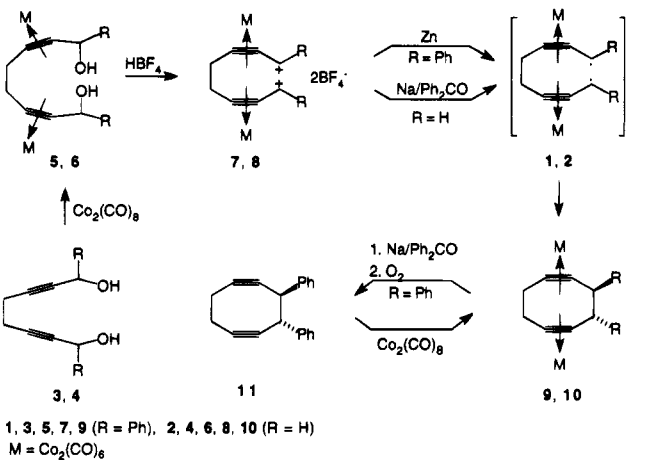

Diacetylenic diols **3** and **4** were synthesized by condensation of 1,5-hexadiyne with benzaldehyde and paraformaldehyde, respectively.[20] Complexation of **3** and **4** with $Co_2(CO)_8$ (ether, 20 °C) produced bis com-

[⊗] Abstract published in *Advance ACS Abstracts,* April 1, 1995.

(1) Ayanoglu, E.; Gebreyesus, T.; Beechan, C. M.; Djerassi, C. *Tetrahedron* **1979**, *35*, 1035. Mehta, G.; Murty, A. N. *J. Chem. Soc. Chem. Commun.* **1984**, 1058.

(2) Wahlberg, I.; Eklund, A. M.; Nishid, T.; Enzell, C. R.; Berg, J. E. *Tetrahedron Lett.* **1983**, 843.

(3) Cordell, G. A. *Phytochemistry* **1974**, *13*, 2343.

(4) Schmitz, F. J.; Hollenbeak, K. H.; Vanderah, D. J. *Tetrahedron* **1978**, *34*, 2719. Paquette, L. A.; Ham, W. H.; Dime, D. S. *Tetrahedron Lett.* **1985**, 4983.

(5) Hough, E.; Hursthouse, M. B.; Neidle, S.; Rodgers, D. *J. Chem. Soc. D* **1968**, 1197. Barrow, K. D.; Barton, D. H. R.; Chain, E. B.; Ohnsorge, U. F. W.; Thomas, R. *J. Chem. Soc. D* **1968**, 1198.

(6) Review: Nicolaou, K. C.; Dai, W.-M.; Guy, R. K. *Angew. Chem., Int. Ed. Engl.* **1994**, *33*, 15.

(7) 1,5-Cycloocta*diene* derivatives have been synthesized via Ni-mediated [4 + 4] diene cycloaddition. Review: Rigby, J. H. In *Comprehensive Organic Synthesis*; Trost, B. M., Ed.; Pergamon Press: Oxford, U.K., 1991; Vol. 5, Chapter 5.2, pp 639–641.

(8) Kloster-Jensen, E.; Wirz, J. *Angew. Chem.* **1973**, *85*, 723.

(9) Detert, H.; Rose, B.; Mayer, W.; Meier, H. *Chem. Ber.* **1994**, *127*, 1529.

(10) Review: Nicolaou, K. C.; Dai, W. M. *Angew. Chem., Int. Ed. Engl.* **1991**, *30*, 1387.

(11) Review: Bergman, R. G. *Acc. Chem. Res.* **1973**, *6*, 25. Koga, N.; Morokuma, K. *J. Am. Chem. Soc.* **1991**, *113*, 1907.

(12) Ring strain and the distance between the connecting 1,6-carbons primarily determine the ease of cyclization; see ref 10 and references cited therein.

(13) Melikyan, G. G.; Vostrowsky, O.; Bauer, W.; Bestmann, H. J. *J. Organomet. Chem.* **1992**, *423*, C24.

(14) Melikyan, G. G.; Vostrowsky, O.; Bauer, W.; Bestmann, H. J.; Khan, M.; Nicholas, K. M. *J. Org. Chem.* **1994**, *59*, 222.

(15) Melikyan, G. G.; Combs, R. C.; Lamirand, J.; Khan, M.; Nicholas, K. M. *Tetrahedron Lett.* **1994**, 363.

(16) Review: Badanyan, S. O.; Voskanyan, M. G.; Chobanyan, Z. A. *Russ. Chem. Rev. (Engl. Transl.)* **1981**, *50*, 1080.

(17) Typical bond angles for the coordinated alkyne of (alkyne)$Co_2(CO)_6$ are about 145°: Saha, M.; Muchmore, S.; van der Helm, D.; Nicholas, K. M. *J. Org. Chem.* **1986**, *51*, 1960 and references therein.

(18) Complexes of cycloalkynes generally have been produced from cycloalkene precursors: Bennett, M. A.; Schwemlein, H. P. *Angew. Chem., Int. Ed. Engl.* **1989**, *28*, 1296.

0276-7333/95/2314-2170$09.00/0

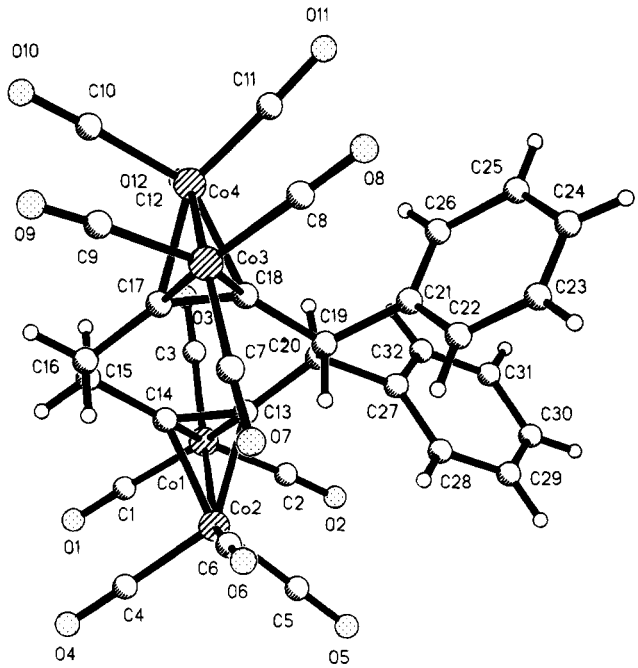

Figure 1. X-ray molecular structure of **9**. Selected bond distances (Å) and angles (deg): Co(1)–Co(2) = 2.464(3), Co(3)–Co(4) = 2.467(3), C(13)–C(14) = 1.382(17), C(17)–C(18) = 1.333(18); C(13)–C(14)–C(15) = 142.1(10), C(14)–C(13)–C(20) = 143.9(10), C(14)–C(15)–C(16) = 112.7(9), C(16)–C(17)–C(18) = 143.8(11), C(17)–C(18)–C(19) = 140.9(9), C(18)–C(19)–C(20) = 110.4(8); C(21)–C(19)–C(20)–C(27) = 41.6(1.2).

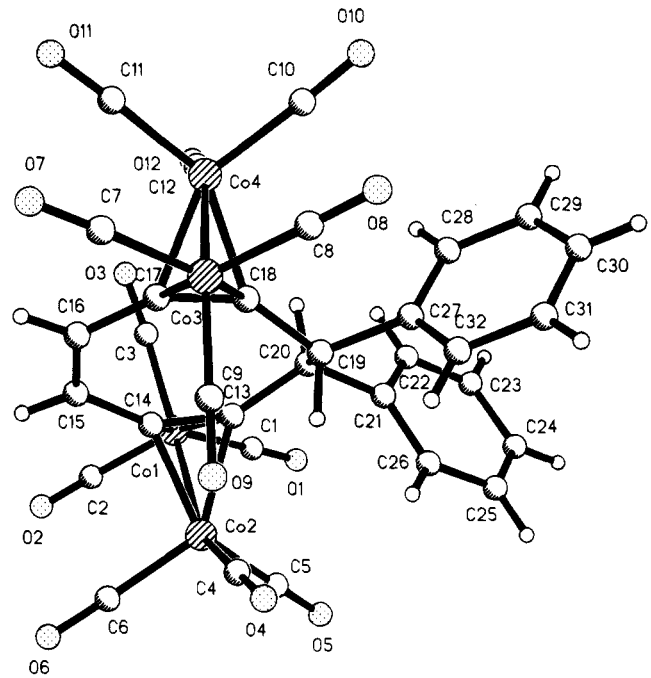

Figure 2. X-ray molecular structure of **15**. Selected bond distances (Å) and angles (deg): Co(1)–Co(2) = 2.471(2), Co(3)–Co(4) = 2.483(2), C(13)–C(14) = 1.335(10), C(17)–C(18) = 1.351(12); C(13)–C(14)–C(15) = 146.4(8), C(14)–C(13)–C(20) = 142.9(6), C(14)–C(15)–C(16) = 124.3(8), C(16)–C(17)–C(18) = 146.6(6), C(17)–C(18)–C(19) = 141.1-(7), C(18)–C(19)–C(20) = 111.3(8); C(27)–C(19)–C(20)–C(21) = 39.8(0.8), H(19)–C(19)–C(20)–H(20) = 167.4(5.7).

plexes **5** and **6**, the former as an inseparable mixture of diastereomers (2:1). Preparation of the dark red, sparingly soluble bis cation salts **7** and **8** was accomplished by treatment of **5** and **6** with HBF_4 and subsequent precipitation with Et_2O.[21] Reduction of **7** with Zn dust (325 mesh, 1:70) in CH_2Cl_2 (room temperature, 2 h) smoothly produced *dl*-1,5-cyclooctadiyne complex **9** in 48% isolated yield (from **5**), together with 0.6% of the *meso* isomer. The configuration of the major isomer **9** was established as *dl* by X-ray diffraction (Figure 1);[22] the structure features diequatorial phenyl rings and an *anti* disposition of H(19) and H(20). Other noteworthy structural features include (a) a typically bent geometry of the coordinated triple bond (140–146°),[17] (b) a lengthened coordinated triple bond (1.33 and 1.35 Å vs 1.21 Å for C≡C), (c) essentially undistorted bond angles for the sp^3-hybridized ring carbons (109–115°), and (d) a C2 symmetric orientation of the two $-Co_2(CO)_6$ units.

In short, the coordinated diyne appears to be nearly strain-free.

Formation of the eight-membered ring of **9** occurs with remarkably high stereoselectivity (de 97.6%), exceeding by far that obtained typically in radical dimerizations,[23,24] including most pinacol couplings,[25] as well as the corresponding Co-mediated *inter*molecular reactions (de 50%)[15] and *intra*molecular variants producing ten-membered 1,5-diynes (de 80%).[15] This selectivity can be explained on the basis of conformational analysis of the putative intermediates, diradicals **A** and **B**. The former, which gives rise to the *dl* isomer,

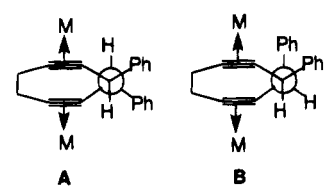

features *two gauche* interactions between the bulkier substituents, while in conformation **B** *three gauche* interactions are involved, rendering the *meso* isomer kinetically disfavored. Molecular mechanics calculations (PCMODEL) of the *dl*-/*meso*-3,4-diphenyl-1,5-cyclooctadiynes and their Co complexes indicate the *dl* isomer to be more stable in both the uncomplexed (ΔE = 2.3 kcal) and complexed (ΔE ca. 3.5 kcal) forms.

Corresponding reduction of primary dication salt **8** (from **6**) with Zn in CH_2Cl_2 gave 1,5-cyclooctadiyne complex **10** as a minor product along with a preponderance of (2,6-octadiyne)$[Co_2(CO)_6]_2$ (1:4, total yield 20%), derived from H-atom abstraction by the intermediate diradical. To minimize the latter and thus furnish a

(19) Cyclization of (alkyne)$Co_2(CO)_6$ to cycloalkyne complexes via (propargylium)$Co_2(CO)_6^+$ has been illustrated: Schreiber, S. L.; Sammakia, T.; Crowe, W. E. *J. Am. Chem. Soc.* **1986**, *108*, 3128. Magnus, P.; Pitterna, T. *J. Chem. Soc., Chem. Commun.* **1991**, 541. Magnus, P.; Fortt, S. M. *J. Chem. Soc., Chem. Commun.* **1991**, 544. Magnus, P.; Carter, P.; Elliott, J.; Lewis, R.; Harling, J.; Pitterna, T.; Bauta, W. E.; Fortt, S. *J. Am. Chem. Soc.* **1992**, *114*, 2544.

(20) Brandsma, L. *Preparative Acetylenic Chemistry*; Elsevier: Amsterdam, 1988.

(21) Varghese, V.; Saha, M.; Nicholas, K. M. *Org. Synth.* **1988**, 141.

(22) *Crystal data for* **9** *and* **15** (details of data collection and refinement are provided in the supplementary material): For **9** reflection data were collected at 295 K and the structure was refined to R = 0.08. There are two independent molecules and a half of a benzene solvent molecule present in the asymmetric unit. H atoms for the disordered benzene molecule were not included in the refinement; all other hydrogens were included in the idealized positions. Data for **15** were collected at 163 K, and the solution and refinement proceeded routinely to an R factor of 0.05. Hydrogen atoms attached to C(19) and C(20) were located and refined anisotropically, and all other hydrogens were fixed.

general method for efficient coupling of *complexed primary propargyl radicals*, we sought a reducing system which would not supply an effective H-atom source. A series of experiments led to the dramatically improved cyclization of **8** to **10** using Na/Ph_2CO in benzene (**6**/Ph_2CO = 1/4; 5 °C, 1.5 h; 52% from **6**) with complete exclusion of the H-atom-abstraction product.

Decomplexation of Co–alkyne complexes is usually accomplished oxidatively, using Ce(IV), Fe(III), and Me_3NO.[26] To date all attempts to utilize such methods on **9** and **10** to produce the corresponding uncomplexed diynes have failed, possibly due to their instability under the reaction conditions. We turned therefore to an unproven approach, i.e. *reductive decomplexation*, suggested by the detection of free alkynes during electrochemical reduction of (alkyne)$Co_2(CO)_6$.[27] Treatment of **9** with up to 10 equiv of Na/Ph_2CO in THF (−78 → 0 °C), while causing its complete consumption (TLC monitoring), apparently results in formation of a metastable reduced complex[28] without the production of organic products. Only upon *oxidation* of this reduced species, e.g. with molecular oxygen (3 h, 20 °C), was diyne **11** detected. The latter could be isolated following preparative TLC on silica gel (4 °C) as an unstable white solid which was characterized spectroscopically (^1H NMR, MS). Recomplexation of **11** with $Co_2(CO)_8$ regenerated the bis cluster **9** in 44% overall yield (**9** → **11** → **9**), establishing the integrity of the diyne during the decomplexation procedure.

To test the scope and versatility of the intramolecular coupling reaction, we chose an even more challenging target, eight-membered ene–diyne complex **15**. Starting diyne–diol **12** was synthesized by established methods from 1,2-dichloroethylene and 1-phenyl-2-propynol[29] and then treated with $Co_2(CO)_8$ to produce easily separable (SiO_2) diastereomeric diols **13** and **14**. Independent generation of dication salts from **13** and **14** and subsequent Zn-induced reductive cyclizations were carried out as above. Cyclic ene–diyne complex **15** was produced (38–42% overall from **13** or **14**) *as a single isomer (de ≥99%) by starting from either isomeric diol*. The configuration of **15**, like that of **9**, was found to be *dl* by X-ray diffraction (Figure 2).[22] The structure of **15**, *vis à vis* the bond lengths and angles within the cluster units and the disposition of the phenyl and $-Co_2(CO)_6$ groups, is similar to that of the "saturated" derivative **9**. Although atoms C(14)–C(18) lie in a plane, the carbocycle of **15** is distinctly puckered with the other atoms deviating significantly: C(13) (+0.17 Å), C(18) (−0.10 Å), C(19) (−0.43 Å), and C(20) (+0.50 Å). Only modest deviations from ideality are seen for the bond angles and lengths of the nominally sp^2 and sp^3 carbons of the ring, revealing little strain. The formation of **15** is thus *completely diastereoselective but not stereospecific*. Epimerization could take place during intervention of the Co-complexed propargyl cation, given their known fluxional behavior,[30] or with the corresponding radical.

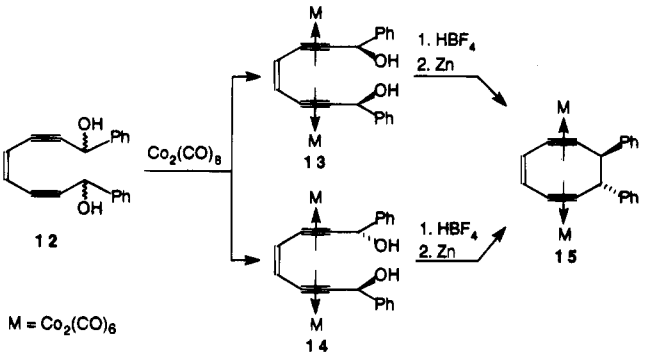

Initial decomplexation attempts with **15** have also provided unexpected results. Although transient organic compounds have been detected by TLC during the reactions of **15** with *N*-methylmorpholine *N*-oxide and with Na/Ph_2CO followed by oxygenation, no stable organics have been isolated. Remarkably, treatment of **15** with *excess* $(NH_4)_2Ce(NO_3)_6$ fails to induce decomplexation at all but instead produces a series of as yet unidentified complexes in which the ene–diyne unit appears to be intact.[31] Efforts are continuing to effect the release and isolation of these and other novel cycloalkynes produced by cobalt-mediated cyclizations.

Acknowledgment. Financial support from the Petroleum Research Fund (Grant No. 27375-AC1) and the Oklahoma Center for the Advancement of Science and Technology (Grant No. HR4-074) is greatly appreciated. We thank Mr. John Lamirand for technical assistance.

Supplementary Material Available: Text giving experimental procedures and spectral data for all synthesized compounds and tables of crystal data, atomic positional parameters and isotropic thermal parameters, bond lengths, and bond angles for complexes **9** and **15** (36 pages). Ordering information is given on any current masthead page.

OM950046E

(23) Review: Porter, N. A.; Krebs, P. J. *Top. Stereochem.* **1988**, *18*, 97.

(24) Reductive cyclization of a 1,5-bis[tricarbonyl(pentadienylium)-iron] complex produces a single isomer upon crystallization, but the composition of the crude product(s) was not reported. Sapienza, R. S.; Riley, P. E.; Davis, R. E.; Pettit, R. *J. Organomet. Chem.* **1976**, *121*, C35.

(25) Review: McMurry, J. E. *Chem. Rev.* **1989**, *89*, 1513. McMurry, J. E.; Rico, J. G. *Tetrahedron Lett.* **1989**, *30*, 1169. Mundy, B. P.; Buss, D. R.; Kim, Y.; Larsen, R.; Warnet, R. J. *Tetrahedron Lett.* **1985**, *26*, 3927. Swindel, C. S.; Fan, W.; Klimko, P. G. *Tetrahedron Lett.* **1994**, *35*, 4959. Nicolaou, K. C.; Yang, Z.; Liu, J. J.; Ueno, H.; Nantermet, P. G.; Guy, R. K.; Claiborne, C. F.; Renaud, J.; Couladouros, E. A.; Paulvannan, K.; Sorensen, E. J. *Nature* **1994**, *367*, 630.

(26) Review: Nicholas, K. M. *Acc. Chem. Res.* **1987**, *20*, 207.

(27) Arevgoda, M.; Rieger, P. H.; Robinson, B. H.; Simpson, J.; Visco, S. J. *J. Am. Chem. Soc.* **1982**, *104*, 5636.

(28) This species may be the 38-electron complex $\{(cycloalkadiyne)[Co_2(CO)_6]_2\}^{2-}$ by analogy with the 19-electron species $(alkyne)Co_2(CO)_6^-$, implicated in the electrochemical reduction of $(alkyne)Co_2(CO)_6$.[27]

(29) Alami, M.; Crousse, B.; Linstrumelle, G. *Tetrahedron Lett.* **1994**, 3543. Ratovelomanana, V.; Linstrumelle, G. *Tetrahedron Lett.* **1981**, 315.

(30) Padmanabhan, S.; Nicholas, K. M. *J. Organomet. Chem.* **1984**, *268*, C23. Schreiber, S. L.; Klimas, M. T.; Sammakia, T. *J. Am. Chem. Soc.* **1987**, *109*, 5749.

(31) Treatment of **15** with $(NH_4)_2Ce(NO_3)_6$ in acetone/1,4-cyclohexadiene at room temperature produces an isolable red complex which slowly converts to a yellow compound which, in turn, reverts to **15** upon exposure to air. Full characterization of these compounds is under investigation.

Articles

Interference of Phosphino Enolato Ligands in the 1-Alkyne-to-Vinylidene Rearrangement: Syntheses of the Isomeric {(mesitylene)Ru[η^3-CH=CHC(PPh$_2$)(Me)C(Bu^t)=O]}[PF$_6$] and {(mesitylene)Ru[η^3-C(=CH$_2$)C(PPh$_2$)(Me)C(Bu^t)=O]}[PF$_6$] Ruthenium(II) Complexes

Pascale Crochet and Bernard Demerseman*

Laboratoire de Chimie de Coordination Organique, URA-CNRS 415, Campus de Beaulieu, Université de Rennes, 35042 Rennes Cédex, France

Received January 25, 1995[⊗]

The (phosphino enolato)ruthenium(II) complex (η^6-mesitylene)[Ph$_2$PC(Me)=C(Bu^t)O]RuCl, **1**, reacts in methanol with ethyne or (trimethylsilyl)acetylene, and NH$_4$PF$_6$, to afford the isomeric complexes {(mesitylene)Ru[η^3-CH=CHC(PPh$_2$)(Me)C(Bu^t)=O]}[PF$_6$], **2**, and {(mesitylene)Ru[η^3-C(=CH$_2$)C(PPh$_2$)(Me)C(Bu^t)=O]}[PF$_6$], **3**, respectively. The formation of **2** and **3** consists formally of the coupling of the carbon enolate from the functional ligand with coordinated ethyne but at a distinct stage of the ethyne-to-vinylidene rearrangement. In ethanol at reflux, **3** undergoes transformation to {(mesitylene)(Ph$_2$PF)Ru[η^2-C(CH$_3$)=C(Me)C(Bu^t)=O]}[PF$_6$], **4**.

Introduction

The 1-alkyne-to-vinylidene rearrangement is a key process in the coordination chemistry of terminal alkynes on a metallic center, especially in the iron triad.[1] The process has been demonstrated to provide a thermal equilibrium between the two isomeric rhenium complexes [Cp(NO)(L)Re(η^2-HC≡CR)]$^+$ and [Cp(NO)(L)Re=C=CHR]$^+$.[2] Both the η^2-coordinated ethyne and corresponding vinylidene complexes were isolated[3] and structurally characterized[4] when starting from cyclopentadienylruthenium precursors, but the formation of (vinylidene)ruthenium complexes from 1-alkynes is often so fast that no intermediate could be detected.[1] Of peculiar interest, (trimethylsilyl)acetylene provides a more convenient access than ethyne to the [Cp(PMe$_3$)$_2$Ru=C=CH$_2$]$^+$ vinylidene derivative.[3] Reactive ligands may react with coordinated alkynes and thus interpose in the 1-alkyne-to-vinylidene rearrangement. We have recently reported the reaction of (η^6-arene)(phosphino enolato)ruthenium(II) precursors, **I** (Chart 1), with phenylacetylene leading to complexes **II**, according to a coupling reaction between the phosphino enolato ligand and the alkyne.[5]

The irreversible formation of complexes **II** precluded the observation of interaction between nucleophilic phosphino enolato and electrophilic vinylidene ligands. In order to better understand the formation of complexes **II**, of interest is to specify how phosphino enolato ligands prevent the vinylidene rearrangement of phenylacetylene. We report herein (a) the first example of a derivative of type **II** incorporating ethyne and (b) starting from (trimethylsilyl)acetylene, the formation of the isomeric complex of type **III** where a four-membered phosphametallacycle is likely the result of an intramolecular coupling reaction involving a vinylidene intermediate. Since a derivative **IV** including a three-membered phosphametallacycle was readily obtained[5] by heating the parent complex **II**, of interest was the examination of the thermal stability of the novel complex **III**.

Results and Discussion

The (phosphino enolato)ruthenium(II) derivative (η^6-mesitylene)[Ph$_2$PC(Me)=C(Bu^t)O]RuCl, **1**, obtained starting from [(mesitylene)RuCl$_2$]$_2$ and the β-keto phosphine Ph$_2$PCH(Me)C(=O)Bu^t,[5] reacted with a solution of ethyne and NH$_4$PF$_6$ in methanol to afford selectively **2**, isolated as orange crystals (eq 1).

[⊗] Abstract published in *Advance ACS Abstracts,* April 1, 1995.

(1) (a) Bruce, M. I. *Chem. Rev.* **1991**, *91*, 197. (b) Bruce, M. I.; Swincer, A. G. *Adv. Organomet. Chem.* **1983**, *22*, 59.

(2) Kowalczyk, J. J.; Arif, A. M.; Gladysz, J. A. *Organometallics* **1991**, *10*, 1079.

(3) Bullock, R. M. *J. Chem. Soc., Chem. Commun.* **1989**, 165.

(4) Lomprey, J. R.; Selegue, J. P. *J. Am. Chem. Soc.* **1992**, *114*, 5518.

(5) Demerseman, B.; Guilbert, B.; Renouard, C.; Gonzalez, M.; Dixneuf, P. H.; Masi, D.; Mealli, C. *Organometallics* **1993**, *12*, 3906.

0276-7333/95/2314-2173$09.00/0

Chart 1

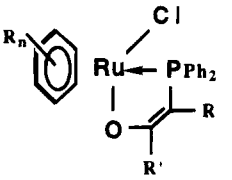

I

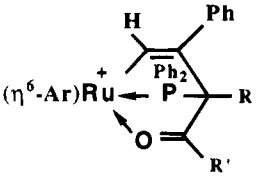

II

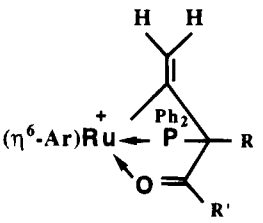

III

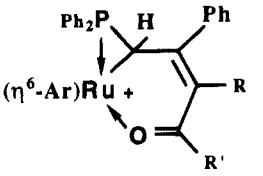

IV

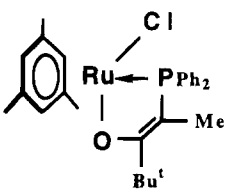

1

$HC{\equiv}CH$, MeOH, NH_4PF_6

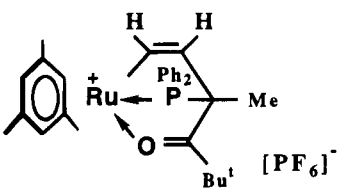

2

The reaction of **1** with (trimethylsilyl)acetylene and NH_4PF_6 in methanol was then experimented and was found fast as monitored by the observation of a light yellow precipitate. Subsequent work resulted in the isolation of bright yellow crystals of **3** in 62% yield (eq 2).

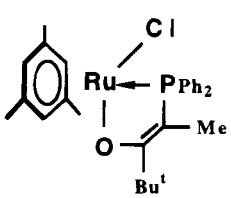

1

$HC{\equiv}C\text{-}SiMe_3$, MeOH, NH_4PF_6

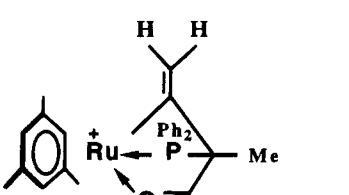

3

Complexes **2** and **3** are air stable in the solid state, and their structures were elucidated by NMR spectroscopy. Besides the trivial characterization of the $(PF_6)^-$ anion, the spectroscopic data collected for **2** gave evidence of a structure of type **II**. The ^1H NMR spectrum of **2** exhibited the expected low-field resonance of the vinylic RuCH= proton at $\delta = 9.02$ ppm. As reported for complexes **II** incorporating phenylacetylene, the $^{31}P\{^1H\}$ resonance ($\delta = 145.1$ ppm) is highly deshielded. In agreement with the formation of a smaller ring,[6] the $^{31}P\{^1H\}$ resonance observed for **3** ($\delta = 72.7$ ppm) is less deshielded and is found close to the resonance observed for the starting phosphino enolato derivative **1** ($\delta = 74.8$ ppm). The $^{13}C\{^1H\}$ NMR spectra of complexes **2** and **3** gave evidence of the incorporation of two additional carbon nuclei into **2** and **3** relative to the number of carbons in precursor **1** and were found significantly similar to indicate that the formation of **3** also involved the transformation of the phosphino enolato metallacycle in **1** into a phosphino keto metallacycle (Ru–P–C=C–O → Ru–P–C–C=O). Thus, the resonances attributable to the keto-carbon nuclei are found at $\delta =$ 228.5 for **2** and 231.8 ppm for **3**. The ^1H NMR spectroscopy gave straightforwardly evidence of the loss of the $SiMe_3$ group while the formation of **3** occurred, and the ^1H NMR spectra of **2** and **3** indicated for both two additional protons relative to the number in the starting compound **1**. The complexes **2** and **3** thus arose formally from the removal of the chloride anion to allow the coordination of the alkyne and a subsequent formation of a *Ru*–(C_2H_2)–*(P)*C bridge. The $^{13}C\{^1H\}$ NMR resonances attributable to the bridging carbon atoms compared closely ($\delta = 174.3$ and 132.2 for **2**, 165.3 and 113.8 ppm for **3**), but ^{13}C NMR spectroscopy allowed us to specify the expected *Ru*–CH=CH–*(P)C* bridge in **2** and a novel *Ru*–C(=CH_2)–*(P)C* bridge in **3**.

Previous work had emphasized the easiness of hydrolysis of the C–$SiMe_3$ bond in vinylidene complexes,[3,7] and the formation of **3** is likely the result of the intramolecular coupling of the carbon enolate of the functional ligand with the electrophilic C_α carbon of a vinylidene intermediate (see Scheme 1). Such a coupling between an O-bound enolate and a vinylidene

(6) Garrou, P. E. *Chem. Rev.* **1981**, *81*, 229.
(7) Werner, H.; Baum, M.; Schneider, D.; Windmüller, B. *Organometallics* **1994**, *13*, 1089.

Scheme 1. Proposal of Mechanism To Account for the Formation of Complexes 2 and 3

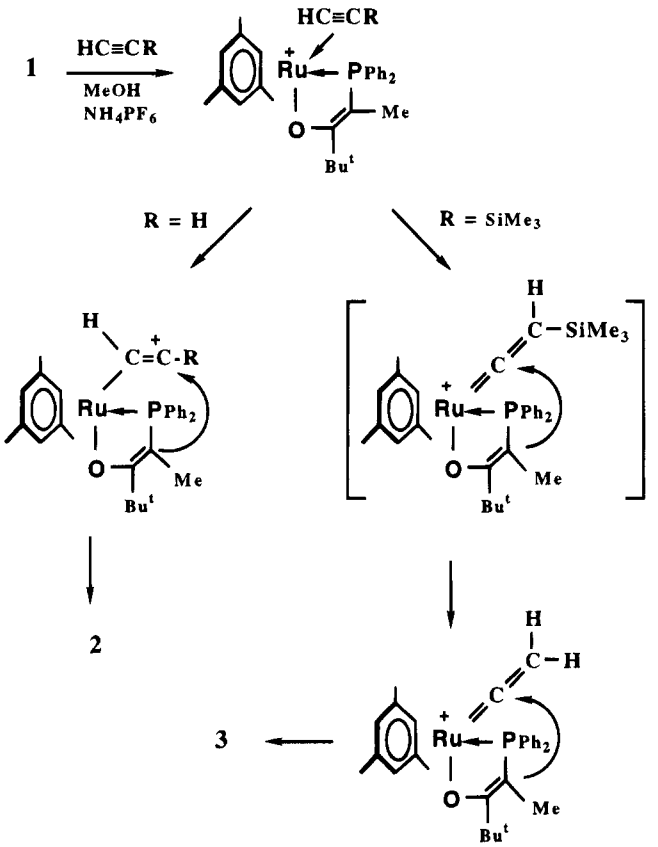

ligand has been proposed to account for the formation of rhenium 2-metallafuran complexes.[8]

The formation of **3** gave evidence that the vinylidene rearrangement of (trimethylsilyl)acetylene occurred despite the closeness of the phosphino enolato ligand, suggesting that the formation of **2** may result from the interference of the functional ligand while the vinylidene rearrangement of ethyne initiated. According to the theoretical mechanism,[9] the 1-alkyne-to-vinylidene rearrangement transiently involves a $RuCH{=}CR^+$ intermediate where the alkyne is η^1-coordinated as depicted in Scheme 1. Further coupling of the β electrophilic carbon atom with the carbon enolate of the functional ligand accounts attractively for the formation of **2**. However, the vinylidene rearrangement of ethyne at a ruthenium center is slow and even requires a thermal activation in the Cp series[3,4] and there is no evidence that the process occurred easily when starting from an η^6-arene precursor such as **1**. At the opposite, the vinylidene rearrangement of phenylacetylene would be fast,[1] but ethyne and phenylacetylene produce both derivatives of type **II** in high yields and not surprising is the observed regioselectivity (Ru−**CH**=**CPh**− pattern) of the reaction when the alkyne was phenylacetylene.[5] The formation of **2** was not detected when starting from (trimethylsilyl)acetylene which yields **3** selectively, and the bulky $SiMe_3$ group may be assumed to hinder the coupling process. The achievement of the 1,2-hydrogen shift and subsequent removal of the $SiMe_3$ group allow the coupling reaction resulting in the formation of **3**. To summarize, the formation of **2** and **3** would formally consist of the coupling reaction of the carbon enolate of the functional ligand with coordinated ethyne but at a distinct stage of the ethyne-to-vinylidene rearrangement.

Since we have reported[5] one example of a thermally induced **II** to **IV** isomerization, the behavior of **3** in similar conditions was investigated. After the heating of complex **3** in ethanol at reflux, complex **4** was isolated as yellow crystals in 45% yield (eq 3).

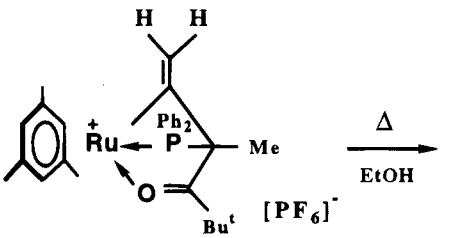

3

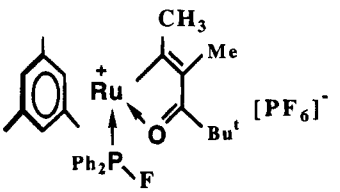

4

The comparison of the $^{31}P\{^1H\}$ and $^{19}F\{^1H\}$ NMR spectra of **4** gave evidence of the formation of a fluorinated Ph_2PF ligand. The ^1H NMR spectrum is consistent with the preservation of a five-membered metallacycle but involving the protonation of the $=CH_2$ group in **3**. The $^{13}C\{^1H\}$ NMR spectrum of **4** exhibited a deshielding vinylic RuC= resonance (δ = 245.3 ppm) relevant to the contribution of the resonance forms **A** and **B** as reported previously for numerous 2-metallafuran complexes.[10]

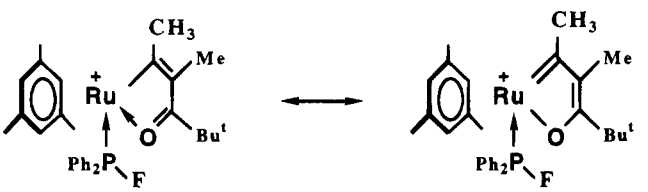

A B

The formation of **4** consisted of the formal addition of HF (from PF_6^- and the solvent) resulting in the cleavage of the bridging phosphorus−carbon bond in **3**. Complex **3** was found unaffected by aqueous HCl, suggesting the cleavage of the phosphorus−carbon bond (*vs* protonation of the $=CH_2$ carbon) to be the first step of the reaction. The partial consumption of the counterion in **3** to generate the Ph_2PF ligand might reduce the formation of **4**, but the additional presence of NH_4PF_6 (in excess; molar ratio 1.5) shows the yield of the reaction unaffected.

(8) Stack, J. G.; Simpson, R. D.; Hollander, F. J.; Bergman, R. G.; Heathcock, C. H. *J. Am. Chem. Soc.* **1990**, *112*, 2716.

(9) Silvestre, J.; Hoffmann, R. *Helv. Chim. Acta* **1985**, *68*, 1461. A first experimental evidence was inferred from the study of bimetallic alkynyl complexes: Akita, M.; Ishii, N.; Takabuchi, A.; Tanaka, M.; Moro-oka, Y. *Organometallics* **1994**, *13*, 258 and related references.

(10) For leading to relevant references: Shih, K.-Y.; Fanwick, P. E.; Walton, R. A. *Organometallics* **1994**, *13*, 1235.

Experimental Section

All chemicals were reagent grade and were used as received or synthesized as described below. The reactions were performed according to Schlenk type techniques. Solvents were dried according to conventional methods and distilled under inert atmosphere before use. Infrared spectra were recorded as Nujol mulls. NMR spectra (^{1}H, 300.13 MHz; ^{13}C, 75.47; ^{19}F, 282.41 MHz; ^{31}P, 121.50 MHz; δ in ppm; coupling constant values in Hz) were referenced internally to the solvent peak.

(η^6-mesitylene)[$Ph_2PC(Me)$=$C(Bu^t)O$]RuCl, 1. The experimental details concerning the synthesis of **1** were already reported.[5] Supplementary NMR spectroscopic data are given as following. $^{31}P\{^1H\}$ NMR, CD_2Cl_2, δ: 74.8 (s). $^{13}C\{^1H\}$ NMR, CD_2Cl_2, δ: 190.9 (d, $^2J_{PC}$ = 17.8, =CO), 138.9 (d, $^1J_{PC}$ = 42.0, ipso), 135.0 (d, $^2J_{PC}$ = 9.4, ortho), 132.9 (d, $^3J_{PC}$ = 10.0, meta), 131.2 (d, $^1J_{PC}$ = 56.6, ipso), 130.0 (d, $^4J_{PC}$ = 2.7 para), 129.9 (d, $^4J_{PC}$ = 2.6, para), 128.6 (d, $^3J_{PC}$ = 9.7, meta), 128.0 (d, $^2J_{PC}$ = 10.4, ortho), 104.3 (d, $^2J_{PC}$ = 2.3, *C*Me, mesitylene), 82.9 (d, $^2J_{PC}$ = 3.7, CH, mesitylene), 78.9 (d, $^1J_{PC}$ = 58.0, P*C*Me), 39.5 (d, $^3J_{PC}$ = 11.8, *C*Me$_3$), 29.2 (s, C*Me*), 18.5 (s, C$_6$*Me*$_3$), 15.2 (s, PC*Me*).

{(mesitylene)Ru[η^3-CH=CHC(PPh_2)(Me)C(Bu^t)=O]}-[PF_6], 2. A 120 mL Schlenk flask containing a 0.39 g (0.70 mmol) sample of **1** and 0.14 g (0.86 mmol) of NH_4PF_6 was filled with ethyne (1 atm), and 30 mL of methanol was added *via* a syringe. The mixture was stirred overnight and then evaporated to dryness. The residue was extracted with dichloromethane (20 mL) to obtain an orange solution that was filtered and then covered with diethyl ether (100 mL) to afford orange crystals of **2**. Yield: 0.43 g, 89%. $^{31}P\{^1H\}$ NMR, CD_2Cl_2, δ: 145.1 (s). ^{1}H NMR, CD_2Cl_2, δ: 9.02 (dd, 1 H, $^3J_{HH}$ = 6.3, $^3J_{PH}$ = 2.8, RuCH), 7.61–7.42 (m, 10 H, Ph), 5.97 (dd, 1 H, $^3J_{PH}$ = 18.1, PCCH), 5.22 (s, 3 H, C$_6$H$_3$), 2.10 (s, 9 H, C$_6$Me$_3$), 1.86 (d, 3 H, $^3J_{PH}$ = 11.9, PCMe), 1.01 (s, 9 H, Bu^t). $^{13}C\{^1H\}$ NMR, CD_2Cl_2, δ: 228.5 (d, $^2J_{PC}$ = 9.1, C=O), 174.3 (d, $^2J_{PC}$ = 11.6, RuC=), 135.1 (d, $^3J_{PC}$ = 9.1, meta), 133.2 (d, $^4J_{PC}$ = 2.0, para), 132.9 (d, overlapped, $^4J_{PC}$ < 2.6, para), 132.9 (d, $^3J_{PC}$ = 10.1, meta), 132.2 (d, $^2J_{PC}$ = 13.8, RuC=*C*), 130.0 (d, $^2J_{PC}$ = 9.0, ortho), 129.3 (d, $^2J_{PC}$ = 9.9, ortho), 129.1 (d, $^1J_{PC}$ = 22.2, ipso), 125.9 (d, $^1J_{PC}$ = 47.8, ipso), 110.1 (d, $^2J_{PC}$ = 1.6, *C*Me, mesitylene), 85.9 (d, $^2J_{PC}$ = 3.8, CH, mesitylene), 75.2 (d, $^1J_{PC}$ = 28.1, P*C*Me), 47.0 (d, $^3J_{PC}$ = 2.6, *C*Me$_3$), 26.3 (s, C*Me*$_3$), 19.4 (s, C$_6$*Me*$_3$), 16.4 (d, $^2J_{PC}$ = 5.4, PC*Me*). ^{13}C NMR, CD_2Cl_2, δ: 174.3 (dd, $^1J_{HC}$ = 156, $^2J_{PC}$ = 11.6, RuCH), RuC=*C*H overlapped with phenyl groups. Anal. Calcd for $C_{30}H_{36}F_6OP_2Ru$: C, 52.25; H, 5.26; P, 8.98. Found: C, 52.32; H, 5.24; P, 9.08.

{(mesitylene)Ru[η^3-C(=CH_2)C(PPh_2)(Me)C(Bu^t)=O]}-[PF_6], 3. A mixture consisting of 1.71 g (3.09 mmol) of **1**, 0.54 g (3.31 mmol) of NH_4PF_6, and 0.50 mL (3.54 mmol) of Me$_3$SiC≡CH in 30 mL of methanol was stirred for 4 h. Diethyl ether (30 mL) was added to the resulting slurry and the yellow precipitate separated by filtration. This solid was extracted with dichloromethane (30 mL) to obtain a yellow solution that was filtered and then covered with diethyl ether (120 mL) to afford yellow crystals of **3**. Yield: 1.32 g, 62%. IR, ν(C=C): 1529 cm^{-1}. $^{31}P\{^1H\}$ NMR, CD_2Cl_2, δ: 72.7 (s). ^{1}H NMR, CD_2Cl_2, δ: 7.80–7.44 (m, 10 H, Ph), 5.77 (dd, 1 H, $^2J_{HH}$ = 2.0, $^4J_{PH}$ = 5.7, =CH$_2$, H$_a$), 5.69 (dd, 1 H, $^4J_{PH}$ = 8.6, =CH$_2$, H$_b$), 5.31 (s, 3 H, C$_6$H$_3$), 2.19 (d, 9 H, $^4J_{PH}$ = 0.7, C$_6$Me$_3$), 1.70 (d, 3 H, $^3J_{PH}$ = 12.5, PCMe), 0.77 (s, 9 H, Bu^t). $^{13}C\{^1H\}$ NMR, CD_2Cl_2, δ: 231.8 (d, $^2J_{PC}$ = 4.5, C=O), 165.3 (d, $^2J_{PC}$ = 65.4, RuC=), 134.8 (d, $^3J_{PC}$ = 12.2, meta), 134.1 (d, $^3J_{PC}$ = 9.8, meta), 133.8 (d, $^4J_{PC}$ = 2.4, para), 133.3 (d, $^4J_{PC}$ = 3.0, para), 129.9 (d, $^2J_{PC}$ = 9.8, ortho), 129.7 (d, $^2J_{PC}$ = 10.4, ortho), 126.1 (d, $^1J_{PC}$ = 43.3, ipso), 123.1 (d, $^1J_{PC}$ = 20.1, ipso), 113.8 (d, $^3J_{PC}$ = 11.1, =CH$_2$), 107.8 (d, $^2J_{PC}$ = 1.7, *C*Me, mesitylene), 87.7 (d, $^1J_{PC}$ = 26.8, P*C*Me), 84.6 (d, $^2J_{PC}$ = 3.8, CH, mesitylene), 46.5 (s, *C*Me$_3$), 25.7 (s, C*Me*$_3$), 19.9 (s, C$_6$*Me*$_3$), 15.2 (d, $^2J_{PC}$ = 4.2, PC*Me*). ^{13}C NMR, CD_2Cl_2, δ: 165.4 (d, $^2J_{PC}$ = 65.3, RuC), 113.8 (ddd, $^1J_{HC}$ = 161 and 154, $^3J_{PC}$ = 11.0, =CH$_2$). Anal. Calcd for $C_{30}H_{36}F_6OP_2Ru$: C, 52.25; H, 5.26; P, 8.98. Found: C, 52.08; H, 5.18; P, 8.72.

Behavior of 3 toward Aqueous HCl. To a saturated solution of 0.50 g (0.70 mmol) of **3** in 30 mL of methanol was added 1.0 mL of a 2 M aqueous HCl solution, and the mixture was stirred for 1 day. A yellow solid was separated by filtration, recrystallization of which from dichloromethane (15 mL)/diethyl ether (100 mL) afforded yellow crystals (yield: 0.37 g, 74%) identified as **3** by NMR spectroscopy.

{(mesitylene)(Ph_2PF)Ru[η^2-C(CH_3)=C(Me)C(Bu^t)=O]}-[PF_6], 4. A slurry of 0.38 g (0.55 mmol) of **3** in a mixture of ethanol (30 mL) and dichloromethane (5 mL) was heated at reflux for 12 h to lead to a red brown solution that deposited a yellow crystalline precipitate upon cooling to −20 °C. The solid was collected by filtration, and subsequent work as above afforded yellow crystals of **4**. Yield: 0.18 g, 45%. $^{31}P\{^1H\}$ NMR, CD_2Cl_2, δ: 185.2 (d, $^1J_{FP}$ = 926). $^{19}F\{^1H\}$ NMR, CD_2Cl_2, δ: −73.4 (d, $^1J_{PF}$ = 713, PF_6), −142.8 (d, $^1J_{PF}$ = 925, Ph_2PF). ^{1}H NMR, CD_2Cl_2, δ: 7.63–7.03 (m, 10 H, Ph), 5.39 (s, 3 H, C$_6$H$_3$), 2.85 (s, 3 H, RuCMe), 2.11 (s, 9 H, C$_6$Me$_3$), 1.68 (s, 3 H, RuCCMe), 0.94 (s, 9 H, Bu^t). $^{13}C\{^1H\}$ NMR, CD_2Cl_2, δ: 245.3 (dd, $^2J_{PC}$ = 18.8, $^3J_{FC}$ = 2.7, RuC), 221.4 (s, C=O), 139.5 (s, RuC=*C*), 136.4 (dd, $^1J_{PC}$ = 48.5, $^2J_{FC}$ = 13.5, ipso), 133.3 (d, $^4J_{PC}$ = 1.8, para), 133.1 (dd, $^1J_{PC}$ = 53.0, $^2J_{FC}$ = 16.2, ipso), 132.2 (s, para), 130.7 (dd, $^2J_{PC}$ = 14.4, $^3J_{FC}$ = 3.6, ortho), 129.6 (dd, $^2J_{PC}$ = 12.6, $^3J_{FC}$ = 3.6, ortho), 129.4 (d, $^3J_{PC}$ = 11.7, meta), 128.9 (d, $^3J_{PC}$ = 10.8, meta), 114.3 (d, $^2J_{PC}$ = 1.2, *C*Me, mesitylene), 91.9 (d, $^2J_{PC}$ = 2.6, CH, mesitylene), 43.4 (s, *C*Me$_3$), 34.4 (s, RuC*Me*), 27.0 (s, C*Me*$_3$), 19.6 (s, C$_6$*Me*$_3$), 15.0 (s, RuCC*Me*). Anal. Calcd for $C_{30}H_{37}F_7OP_2Ru$: C, 50.78; H, 5.26; P, 8.73. Found: C, 51.05; H, 5.30; P, 8.65.

Acknowledgment. This work was supported by the "Centre National de la Recherche Scientifique". The "Conseil Régional de Bretagne" is gratefully acknowledged for a grant to P.C.

OM950062B

Reactions of Low-Valent Group V Dicarbonyl Phosphine Complexes with Carbon-Based Electrophiles To Produce Metal Alkyl, Acyl, Carbyne, and Acetylene Complexes

Brian S. Bronk, John D. Protasiewicz, Laura E. Pence, and Stephen J. Lippard*

Department of Chemistry, Massachusetts Institute of Technology, Cambridge, Massachusetts 02139

Received December 22, 1994[⊗]

The $[V(CO)_2(dmpe)_2]^-$ anion reacts with Et_3OBF_4 and EtOTf to afford the unexpected product of formal C-alkylation, $[V(\eta^2\text{-}C(O)Et)(CO)(dmpe)_2]$, which has been structurally characterized by X-ray crystallography (space group $Pna2_1$, a = 12.917(2) Å, b = 12.335(2) Å, c = 14.331(2) Å, V = 2283.4(5) Å^3). The formation of species derived by O-acylation of the CO ligands in the $[Ta(CO)_2(dmpe)_2]^-$ and $[Ta(CO)_2(depe)_2]^-$ anions was indirectly established by isolation and characterization of products in which two CO ligands had coupled to form acetylene complexes. Addition of 2 equiv of acetyl chloride to $Na[Ta(CO)_2(dmpe)_2]$ or $Na[Ta(CO)_2(depe)_2]$ yielded the acetylene complexes [Ta(AcOC≡COAc)(dmpe or depe)$_2$Cl]. The structure of the dmpe derivative was confirmed in a single-crystal X-ray determination (space group $C2$, a = 14.964(2) Å, b = 11.960(2) Å, c = 31.710(5) Å, β = 102.77(1)°, V = 5535(1) Å^3). Additional proof of direct alkylation at terminal CO ligands was provided by isolation of mixed siloxy/alkoxyacetylene coupled products $[M(R'_3SiOC{\equiv}COR)(dmpe)_2X]$ (R = Et, Ac, CO_2Me; R'_3Si = ^{t}BuPh$_2$Si, ^{i}Pr$_3$Si) and $[M(R'_3SiOC{\equiv}COR)(depe)_2X]$ (R = Et, Ac; R'_3Si = ^{t}BuPh$_2$Si, ^{i}Pr$_3$Si, Me$_3$Si) from reactions of the siloxycarbyne precursors $[M(COSiR'_3)(CO)(dmpe)_2]$ and $[M(COSiR'_3)(CO)(depe)_2]$ (M = Nb, Ta) with carbon-based electrophiles. The proper choice of carbon-based electrophile and reaction conditions is crucial in order to avoid oxidation of these low-valent metal complexes to $[M(CO)_2(dmpe)_2X]$, which can occur competitively or exclusively.

Introduction

The reductive coupling of two carbon monoxide ligands in $[M(CO)_2(Me_2PCH_2CH_2PMe_2)_2X]$ complexes occurs according to the mechanism outlined in Scheme 1.[1] This transformation was originally discovered[2] following studies of reductive coupling in related isocyanide complexes[3,4] and has since been applied by us and others in the synthesis of a wide variety of related metal acetylene complexes.[2,5–21] As indicated in the scheme, the reaction proceeds by electrophilic attack of a silyl reagent on the carbonyl oxygen atoms of the highly reduced dicarbonyl anion in two sequential steps. The first step leads to a siloxycarbyne and the second to the coupled product. This mechanism differs from that commonly encountered in the coupling of carbyne and CO ligands in many other systems, which often involves

Scheme 1

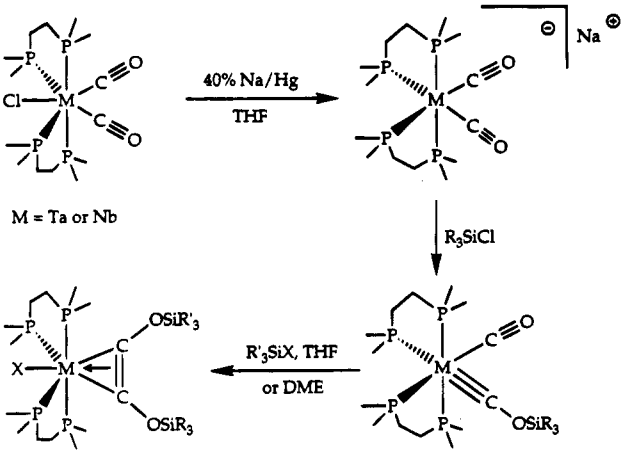

[⊗] Abstract published in *Advance ACS Abstracts,* April 1, 1995.

(1) Carnahan, E. M.; Protasiewicz, J. D.; Lippard, S. J. *Acc. Chem. Res.* **1993**, *26*, 90.
(2) Bianconi, P. A.; Williams, I. D.; Engeler, M. P.; Lippard, S. J. *J. Am. Chem. Soc.* **1986**, *108*, 311.
(3) Lam, C. T.; Corfield, P. W. R.; Lippard, S. J. *J. Am. Chem. Soc.* **1977**, *99*, 617.
(4) Lam, C. T.; Novotny, M.; Lewis, D. L.; Lippard, S. J. *Inorg. Chem.* **1978**, *17*, 2127.
(5) Vrtis, R. N.; Liu, S.; Rao, C. P.; Bott, S. G.; Lippard, S. J. *Organometallics* **1991**, *10*, 275.
(6) Acho, J. A.; Lippard, S. J. *Organometallics* **1994**, *13*, 1294.
(7) Bianconi, P. A.; Vrtis, R. N.; Rao, C. P.; Williams, I. D.; Engeler, M. P.; Lippard, S. J. *Organometallics* **1987**, *6*, 1968.
(8) Bronk, B. S.; Protasiewicz, J. D.; Lippard, S. J. *Organometallics* **1995**, *14*, 1385.
(9) Carnahan, E. M.; Lippard, S. J. *J. Am. Chem. Soc.* **1990**, *112*, 3230.
(10) Carnahan, E. M.; Lippard, S. J. *J. Chem. Soc., Dalton Trans.* **1991**, 699.
(11) Carnahan, E. M.; Lippard, S. J. *J. Am. Chem. Soc.* **1992**, *114*, 4166.
(12) Protasiewicz, J. D.; Lippard, S. J. *J. Am. Chem. Soc.* **1991**, *113*, 6564.
(13) Protasiewicz, J. D.; Bronk, B. S.; Masschelein, A.; Lippard, S. J. *Organometallics* **1994**, *13*, 1300.
(14) Vrtis, R. N.; Lippard, S. J. *Isr. J. Chem.* **1990**, *30*, 331.
(15) Warner, S.; Lippard, S. J. *Organometallics* **1986**, *5*, 1716.
(16) Filippou, A. C.; Grünleitner, W. *J. Organomet. Chem.* **1990**, *393*, C10.
(17) Filippou, A. C.; Grünleitner, W. *Z. Naturforsch.* **1991**, *46B*, 216.
(18) Filippou, A. C.; Grünleitner, W.; Völkl, C.; Kiprof, P. *Angew. Chem., Int. Ed. Engl.* **1991**, *30*, 1167.
(19) Filippou, A. C.; Völkl, C.; Grünleitner, W.; Kiprof, P. *J. Organomet. Chem.* **1992**, *434*, 201.
(20) Pombeiro, A. J. L.; Richards, R. L. *Coord. Chem. Rev.* **1990**, *104*, 13.
(21) Fraústo da Silva, J. J. R.; Pellinghelli, M. A.; Pombeiro, A. J. L.; Richards, R. L.; Tiripicchio, A.; Wang, Y. *J. Organomet. Chem.* **1993**, *454*, C8.

0276-7333/95/2314-2177$09.00/0

Scheme 2

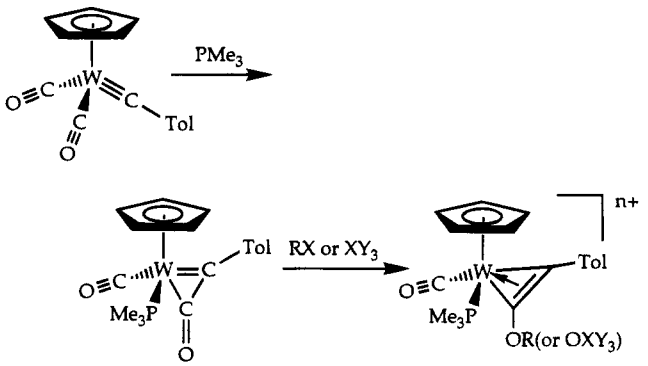

RX = Me_3OBF_4, MeOTf, Et_3OBF_4 (n = 1)
XY_3 = $AlEt_3$, $AlCl_3$, $InCl_3$, BCl_3, BH_3 (n = 0)

an η^2-ketenyl intermediate, as illustrated for one case in Scheme 2.[22,23] A metal-bound ketenyl oxygen atom is significantly more activated toward electrophilic attack compared even to the electron-rich carbonyl complexes used in the reductive coupling reaction of Scheme 1. A detailed kinetic analysis clearly indicated, however, that the first step in converting the siloxycarbyne to the coupled product was silylation of the adjacent CO ligand, and no evidence was found to indicate the participation of an η^2-ketenyl species.[13,24]

One conspicuous facet of the CO-coupling chemistry in Scheme 1 is the fact that, up to the present, silyl-based electrophiles have been required. Reactions of carbon-based electrophiles with complexes containing terminal CO ligands usually occur at the metal center.[25] Previous work established that treatment of Na[Ta(CO)$_2$(dmpe)$_2$] with alkylating reagents affords a tantalum alkyl species (eq 1) rather than the carbyne or

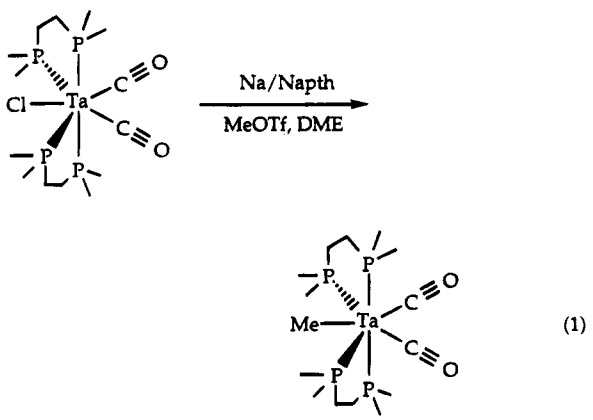

(1)

coupled product.[26] The success of silyl-based electrophiles was attributed to the extra driving force obtained by formation of Si–O bonds, which are considerably stronger than M–Si bonds. This difference might direct electrophilic attack at the oxygen atom of the terminal CO ligand, rather than the metal center. Alternatively, it might be argued that silyl-based reagents are more sterically encumbered than alkylating reagents, hindering formation of a metal–silicon bond. The importance of such steric factors is underscored by reactions of the vanadium compound Na[V(CO)$_2$(dmpe)$_2$] with Me_3SiOTf and EtOTf to produce respectively the novel species [V($Me_3SiOC{\equiv}COSiMe_3$)(dmpe)$_2$]OTf, communicated previously,[12] and [V(η^2-C(O)Et)(CO)(dmpe)$_2$], described in the present article.

Electrophilic attack at the oxygen atom of metal carbonyl species is most facile for complexes having bridging CO ligands. A variety of electrophiles has been employed,[27] including mineral acids,[28,29] Lewis acids, and alkylating[28,30–33] or acylating reagents.[28] In complexes with terminal CO ligands, the metal center appears to be the preferred site of attack by protic acids, although Lewis acids can exhibit some affinity for the oxygen atom. Reactions of this kind have most frequently been probed with anionic carbonyl complexes and alkylating reagents.[34–37] Attempts to acylate these complexes gave exclusive addition to the metal center.[35,36] Acylation reactions have not received as much attention, however, since acyl complexes can be readily prepared by alkylation at the metal center, followed by alkyl migration to a carbonyl ligand.

In the present work we have achieved the reductive coupling of two CO ligands by using acyl groups as carbon-based electrophiles. This reaction significantly extends the scope of reductively coupled products accessible by the chemistry outlined in Scheme 1. In addition, we have delineated some of the conditions which dictate the site of carbon-based electrophilic attack on low-valent metal carbonyl complexes.

Experimental Section

General Considerations. All reactions and manipulations were carried out either in a Vacuum Atmospheres drybox under a dinitrogen atmosphere or by standard Schlenk techniques under an argon atmosphere. Solutions were stirred magnetically with a Teflon-covered stirbar unless noted otherwise. Solvents (THF, DME, Et_2O, and pentane) were distilled under dinitrogen from sodium benzophenone ketyl. Benzene-d_6 was dried by passage through a column of alumina and stored under dinitrogen. Tetramethylsilane was distilled from calcium hydride and stored under dinitrogen. Acetyl chloride and methyl chloroformate were distilled and stored under dinitrogen. All other reagents were used as received after degassing. Proton chemical shifts were referenced to residual solvent peaks. ^{31}P NMR spectra were referenced to external phosphoric acid. ^{1}H, ^{31}P, and ^{13}C NMR spectra were recorded on a Varian XL 300 instrument at 300, 121, and 75.5 MHz, respectively. Infrared (IR) spectra were recorded on a Biorad FTS-7 spectrophotometer. Elemental analyses were performed by Oneida Research Laboratories, Whitesboro, NY.

(22) Kreissl, F. R.; Frank, A.; Schubert, U.; Lindner, T. L.; Huttner, G. *Angew. Chem., Int. Ed. Engl.* **1976**, *15*, 632.
(23) Kreissl, F. R.; Eberl, K.; Uedelhoven, W. *Chem. Ber.* **1977**, *110*, 3782.
(24) Protasiewicz, J. D.; Masschelein, A.; Lippard, S. J. *J. Am. Chem. Soc.* **1993**, *115*, 808.
(25) King, R. B. *Acc. Chem. Res.* **1970**, *3*, 417.
(26) Datta, S.; Wreford, S. S. *Inorg. Chem.* **1977**, *16*, 1134.
(27) Adams, R. D.; Horvath, I. T. *Prog. Inorg. Chem.* **1985**, *33*, 133.
(28) Hodali, H. A.; Shriver, D. F. *Inorg. Chem.* **1979**, *18*, 1236.
(29) Whitmore, K.; Shriver, D. F. *J. Am. Chem. Soc.* **1980**, *102*, 1456.
(30) Shriver, D. F.; Lehman, D.; Strope, D. *J. Am. Chem. Soc.* **1975**, *97*, 1594.
(31) Green, M.; Mead, K. A.; Mills, R. M.; Salter, I. D.; Stone, F. G. A.; Woodward, P. *J. Chem. Soc., Chem. Commun.* **1982**, 51.
(32) Johnson, B. F. G.; Lewis, J.; Orpen, A. G.; Raithby, P. R.; Süss, G. *J. Organomet. Chem.* **1979**, *173*, 187.
(33) Gavens, P. D.; Mays, M. J. *J. Organomet. Chem.* **1978**, *162*, 389.
(34) Gladysz, J. A.; Williams, G. M.; Tam, W.; Johnson, D. L.; Parker, D. W.; Selover, J. C. *Inorg. Chem.* **1979**, *18*, 553.
(35) Heck, R. F.; Breslow, D. S. *J. Am. Chem. Soc.* **1962**, *84*, 2499.
(36) Hieber, W.; Duchatsch, H. *Chem. Ber.* **1965**, *98*, 1744.
(37) Lai, C.-K.; Feighery, W. G.; Zhen, Y.; Atwood, J. D. *Inorg. Chem.* **1989**, *28*, 3929.

$[Ta(CO)_2(dmpe)_2Cl]$,[38] $[Ta(CO)_2(depe)_2Cl]$,[38] $[Nb(CO)_2(dmpe)_2Cl]$,[38] $Na[V(CO)_2(dmpe)_2]$,[12] $[Ta(COSi^tBuPh_2)(CO)(dmpe)_2]$,[13] and $[Ta(COSi^iPr_3)(CO)(dmpe)_2]$[5] were prepared by following literature procedures. $[Ta(^{13}CO)_2(dmpe)_2Cl]$ was prepared with ^{13}CO (99%, Cambridge Isotopes Lab).

$[Ta(EtOC{\equiv}COSi^tBuPh_2)(dmpe)_2OTf]$ (1a). A 25-mL, one-necked, pear-shaped flask fitted with a rubber septum was charged with $[Ta(COSi^tBuPh_2)(CO)(dmpe)_2]$ (0.117 g, 0.15 mmol) and 10 mL of DME. Upon dissolution, EtOTf (0.020 mL, 0.027 g, 0.15 mmol) was added in one portion via syringe. The reaction mixture was stirred for 1.5 h, during which time the color changed from deep red to green-brown. The solvents were removed under vacuum, and the residue was triturated with two 10-mL portions of pentane. The product was extracted with 15 mL of pentane, the extract was filtered, and the solvents were removed under vacuum to provide a green-brown solid. Recrystallization from pentane at −30 °C afforded 0.043 g (30%) of **1a** as a dark green solid. IR (Nujol): 1609, 1318, 1236, 1204, 1166, 1101, 1024, 970, 937, 732, 703 cm^{-1}. ^1H NMR (300 MHz, C_6D_6): δ 7.59−7.63 (m, 4 H), 7.13−7.16 (m, 6 H), 2.76 (q, J = 7.0 Hz, 2 H), 1.83 (bs, 8 H), 1.61 (bs, 12 H), 1.48 (s, 12 H), 1.07 (s, 9 H), 0.29 (t, J = 7.0 Hz, 3 H). ^{31}P NMR (121 MHz, C_6D_6): δ 34.2. Anal. Calcd for $C_{33}H_{56}F_3O_5P_4SSiTa$: C, 41.51; H, 5.91; N, 0.00. Found: C, 41.86; H, 5.84; N, 0.00.

$[Ta(EtOC{\equiv}COSi^iPr_3)(dmpe)_2OTf]$ (1b). A 25-mL, one-necked, pear-shaped flask fitted with a rubber septum was charged with $[Ta(CO)_2(dmpe)_2Cl]$ (0.143 g, 0.25 mmol) and 10 mL of THF. Upon dissolution, excess 40% sodium amalgam was added and the reaction mixture was stirred vigorously for 4 h. The resulting orange solution was decanted into a second 25-mL, one-necked, pear-shaped flask fitted with a rubber septum, and $^iPr_3SiCl$ (0.054 mL, 0.048 g, 0.25 mmol) was added in one portion via syringe, resulting in a dark red solution. After the mixture was stirred for an additional 15 min, the solvents were removed under vacuum, the product was triturated with two 10-mL portions of pentane and extracted with 10 mL of pentane, the extract was filtered, and the solvents were removed under vacuum to provide 0.166 g (0.24 mmol) of a red solid, unpurified $[Ta(COSi^iPr_3)(CO)(dmpe)_2]$. This material was dissolved in 5 mL of DME in a 25-mL, one-necked, pear-shaped flask fitted with a rubber septum, and EtOTf (0.031 mL, 0.043 g, 0.24 mmol) was added in one portion via syringe. The reaction mixture was stirred for 40 min, during which time the color changed from deep red to green-brown. The solvents were removed under vacuum, the product was extracted with 15 mL of pentane, the extract was filtered, and the pentane was removed under vacuum. Crystallization from pentane at −30 °C provided 0.092 g (42% for two steps) of **1b** as green-brown crystals. IR (Nujol): 1606, 1322, 1233, 1202, 1171, 1116, 1018, 971, 942, 928, 884, 722 cm^{-1}. ^1H NMR (300 MHz, C_6D_6): δ 3.75 (bq, 2 H), 1.51−1.86 (m, 20 H), 1.36 (s, 12 H), 1.11−1.25 (m, 3 H), 1.05 (d, J = 7.0 Hz, 18 H), 1.04−1.05 (m, 3H). ^{13}C NMR (75.5 MHz, C_6D_6): δ 205 (bs) (prepared from $[Ta(^{13}CO)_2(dmpe)_2Cl]$). ^{31}P NMR (121 MHz, C_6D_6): δ 32.2. Anal. Calcd for $C_{26}H_{58}F_3O_5P_4SSiTa$: C, 35.78; H, 6.70; N, 0.00. Found: C, 35.82; H, 6.48; N, 0.00.

$[Ta(COSi^tBuPh_2)(CO)(depe)_2]$ (2). A 25-mL, one-necked, pear-shaped flask fitted with a rubber septum was charged with $[Ta(CO)_2(depe)_2Cl]$ (0.212 g, 0.31 mmol) and 10 mL of THF. Upon dissolution, excess 40% sodium amalgam was added and the reaction mixture was stirred vigorously for 3.5 h. The solution was decanted into a second 25-mL, one-necked, pear-shaped flask, and $^tBuPh_2SiCl$ (0.081 mL, 0.085 g, 0.31 mmol) was added in one portion via syringe, resulting in a deep red solution. The reaction mixture was stirred for an additional 0.75 h, after which the solvents were removed under vacuum, the product was extracted with pentane, and the pentane solution was filtered and concentrated, providing the crude product as a red oil. Crystallization from pentane at −30 °C afforded 0.220 g (80%) of **2** as a red solid. An analytically pure sample was obtained by recrystallization from TMS at −30 °C. IR (Nujol): 1786, 1418, 1291, 1263, 1245, 1114, 1027, 863, 822, 811, 758, 700 cm^{-1}. ^1H NMR (300 MHz, C_6D_6): δ 8.21 (m, 2 H), 7.98 (m, 2 H), 7.47 (t, J = 6.8 Hz, 2 H), 7.34 (m, 4 H), 2.15 (m, 2 H), 0.8−1.9 (m, 43 H), 1.26 (s, 9 H), 0.64 (dt, J = 7.4, 12.7 Hz, 3 H). ^{31}P NMR (121 MHz, C_6D_6): δ 48.5, 48.1, 36.1, 21.4. Anal. Calcd for $C_{38}H_{67}O_2P_4SiTa$: C, 51.35; H, 7.60; N, 0.00. Found: C, 51.02; H, 7.60; N, 0.00.

$[Ta(EtOC{\equiv}COSi^tBuPh_2)(depe)_2OTf]$ (3a). A 25-mL, one-necked, pear-shaped flask fitted with a rubber septum was charged with $[Ta(CO)_2(depe)_2Cl]$ (0.205 g, 0.30 mmol) and 10 mL of THF. Upon dissolution, excess 40% sodium amalgam was added and the reaction mixture was stirred vigorously for 4.6 h. The solution was decanted into a second 25-mL, one-necked, pear-shaped flask, and $^tBuPh_2SiCl$ (0.078 mL, 0.082 g, 0.30 mmol) was added in one portion via syringe, resulting in a deep red solution. The reaction mixture was stirred for an additional 1 h, after which the solvents were removed under vacuum, the product was extracted with pentane, and the pentane solution was filtered and concentrated, providing a red oil (0.253 g), unpurified $[Ta(COSi^tBuPh_2)(CO)(depe)_2]$. A 25-mL, one-necked, pear-shaped flask was charged with the crude carbyne and 7 mL of DME. Upon dissolution, ethyl triflate (0.035 mL, 0.048 g, 0.27 mmol) was added in one portion and the reaction mixture was stirred for 2.5 h. Upon removal of the solvents under vacuum, the product was extracted with pentane and the pentane solution was filtered and concentrated under vacuum to provide a gummy green solid. After trituration with pentane, recrystallization from pentane at −30 °C afforded 0.176 g (55% for two steps) of green crystalline **3a**. IR (Nujol): 1623, 1427, 1322, 1233, 1205, 1168, 1107, 1020, 973, 869, 730, 701 cm^{-1}. ^1H NMR (300 MHz, C_6D_6): δ 7.58−7.61 (m, 4 H), 7.12−7.14 (m, 6 H), 2.79 (q, J = 7.0 Hz, 2 H), 2.11−2.22 (m, 4 H), 1.71−2.04 (m, 18 H), 1.02−1.17 (m, 26 H), 1.05 (s, 9 H), 0.31 (t, J = 7.0 Hz, 3 H). ^{31}P NMR (121 MHz, C_6D_6): δ 52.8. Anal. Calcd for $C_{41}H_{72}F_3O_5P_4SSiTa$: C, 46.15; H, 6.80; N, 0.00. Found: C, 46.54; H, 6.77; N, 0.00.

$[Ta(EtOC{\equiv}COSiPh_3)(depe)_2OTf]$ (3b). A 25-mL, one-necked, pear-shaped flask fitted with a rubber septum was charged with $[Ta(CO)_2(depe)_2Cl]$ (0.068 g, 0.12 mmol) and 5 mL of THF. Upon dissolution, excess 40% sodium amalgam was added and the reaction mixture was stirred vigorously for 3.5 h. The solution was decanted into a second 25-mL, one-necked, pear-shaped flask, and Ph_3SiCl (0.029 g, 0.10 mmol) was added in one portion via syringe, resulting in a deep red solution. The reaction mixture was stirred for an additional 1 h, after which the solvents were removed under vacuum, the product was extracted with pentane, and the pentane solution was filtered and concentrated, providing a red oil (0.084 g), unpurified $[Ta(COSiPh_3)(CO)(depe)_2]$. A 25-mL, one-necked, pear-shaped flask was charged with the unpurified carbyne and 5 mL of DME and cooled to −30 °C. Upon dissolution, ethyl triflate (0.012 mL, 0.016 g, 0.09 mmol) was added in one portion and the reaction mixture was stirred for 0.5 h. Upon removal of the solvents under vacuum, the product was extracted with pentane and the pentane solution was filtered and concentrated under vacuum to provide a gummy green solid. After trituration with pentane, recrystallization from pentane at −30 °C afforded 0.018 g (14% for two steps) of green crystalline **3b**. IR (Nujol): 1622, 1428, 1317, 1230, 1208, 1167, 1114, 1102, 1084, 1019, 982, 870, 806, 732 cm^{-1}. ^1H NMR (300 MHz, C_6D_6): δ 7.57−7.60 (m, 6 H), 7.10−7.19 (m, 9 H), 3.27 (q, J = 7.0 Hz, 2 H), 1.58−2.10 (m, 22 H), 1.00−1.24 (m, 26 H), 0.54 (t, J = 7.0 Hz, 3 H). ^{31}P NMR (121 MHz, C_6D_6): δ 51.1. Anal. Calcd for $C_{43}H_{68}F_3O_5P_4SSiTa$: C, 47.51; H, 6.31; N, 0.00. Found: C, 47.98; H, 5.93; N, 0.00.

(38) Protasiewicz, J. D.; Bianconi, P. A.; Williams, I. D.; Liu, S.; Rao, C. P.; Lippard, S. J. *Inorg. Chem.* **1992**, *31*, 4134.

[Ta(EtOC≡COSiMe$_3$)(depe)$_2$OTf] (3c). A 25-mL, one-necked, pear-shaped flask fitted with a rubber septum was charged with [Ta(CO)$_2$(depe)$_2$Cl] (0.103 g, 0.15 mmol) and 8 mL of THF. Upon dissolution, excess 40% sodium amalgam was added and the reaction mixture was stirred vigorously for 4 h. The solution was decanted into a second 25-mL, one-necked, pear-shaped flask, and Me$_3$SiCl (0.019 mL, 0.016 g, 0.15 mmol) was added in one portion via syringe, resulting in a deep red solution. The reaction mixture was stirred for an additional 30 min, after which the solvents were removed under vacuum. The product was extracted with pentane, and the pentane solution was filtered and concentrated, providing a red oil (0.108 g), unpurified [Ta(COSiMe$_3$)(CO)(depe)$_2$]. A 25-mL, one-necked, pear-shaped flask was charged with the unpurified carbyne and 5 mL of DME. With rapid stirring, EtOTf (0.019 mL, 0.027 g, 0.15 mmol) was added in one portion and the reaction mixture was stirred for 1.5 h. After removal of the solvents under vacuum, the product was extracted with pentane and the pentane solution was filtered and concentrated under vacuum to provide a green-brown solid. Recrystallization from pentane at −30 °C afforded **3c** (0.031 g, 23%) as green crystals. IR (Nujol): 1591, 1324, 1202, 1167, 1036, 1016, 988, 841, 723 cm^{-1}. ^{1}H NMR (300 MHz, C$_6$D$_6$): δ 3.68 (q, J = 7.0 Hz, 2 H), 1.97−2.14 (m, 8 H), 1.71−1.86 (m, 12 H), 1.53−1.61 (m, 4 H), 0.97−1.12 (m, 24 H), 0.99 (t, J = 7.0 Hz, 3 H), 0.05 (s, 9 H). ^{31}P NMR (121 MHz, C$_6$D$_6$): δ 50.2.

[Ta(AcOC≡COSi^{t}BuPh$_2$)(depe)$_2$Cl] (4). A 25-mL, one-necked, pear-shaped flask fitted with a rubber septum was charged with [Ta(COSi^{t}BuPh$_2$)(CO)(depe)$_2$] (0.088 g, 0.1 mmol) and 5 mL of DME. Upon dissolution, the reaction vessel was cooled to −30 °C, acetyl chloride (0.007 mL, 0.008 g, 0.08 mmol) was added in one portion via syringe, and the reaction mixture was stirred for 10 min, providing a green solution. The solvents were removed under vacuum, the product was extracted with pentane, and the pentane solution was filtered and concentrated under vacuum to afford 0.084 g of the crude product as a green solid. Recrystallization from pentane at −30 °C provided 0.062 g (64%) of **4** as green crystals. IR (Nujol): 1723, 1538, 1365, 1234, 1227, 1114, 1083, 1031, 1019, 964, 927, 868, 804, 757, 722 cm^{-1}. ^{1}H NMR (300 MHz, C$_6$D$_6$): δ 7.68−7.71 (m, 4 H), 7.18−7.20 (m, 6 H), 1.81−2.10 (m, 16 H), 1.62−1.67 (m, 8 H), 1.07−1.22 (m, 24 H), 1.17 (s, 9 H), 1.12 (s, 3 H). ^{31}P NMR (121 MHz, C$_6$D$_6$): δ 43.0. Anal. Calcd for C$_{40}$H$_{70}$ClO$_3$P$_4$SiTa: C, 49.66; H, 7.29; N, 0.00. Found: C, 49.35; H, 7.20; N, 0.00.

[Ta(AcOC≡COSi^{t}BuPh$_2$)(dmpe)$_2$Cl] (5). A 25-mL, one-necked, pear-shaped flask fitted with a rubber septum was charged with [Ta(COSi^{t}BuPh$_2$)(CO)(dmpe)$_2$] (0.078 g, 0.1 mmol) and 5 mL of DME. Upon dissolution, the reaction vessel was cooled to −30 °C, acetyl chloride (0.007 mL, 0.008 g, 0.08 mmol) was added in one portion via syringe, and the reaction mixture was stirred for 15 min, providing a green solution. The solvent was removed under vacuum, the product was extracted with pentane, and the pentane solution was filtered and concentrated under vacuum to afford 0.072 g of the crude product as a green solid. Recrystallization from pentane at −30 °C provided 0.044 g (51%) of **5** as a green solid. IR (Nujol): 1724, 1540, 1430, 1365, 1291, 1276, 1234, 1113, 1098, 1033, 979, 938, 929, 889, 821, 794, 744, 731, 699 cm^{-1}. ^{1}H NMR (300 MHz, C$_6$D$_6$): δ 7.64−7.67 (m, 4 H), 7.13−7.16 (m, 6 H), 1.52−1.72 (m, 8 H), 1.52 (m, 12 H), 1.41 (m, 12 H), 1.12 (s, 9 H), 1.01 (s, 3 H). ^{31}P NMR (121 MHz, C$_6$D$_6$): δ 26.4. Anal. Calcd for C$_{32}$H$_{54}$ClO$_3$P$_4$SiTa: C, 44.95; H, 6.36; N, 0.00. Found: C, 44.39; H, 6.08; N, 0.00.

[Nb(AcOC≡COSi^{t}BuPh$_2$)(dmpe)$_2$Cl] (6). A 25-mL, one-necked, pear-shaped flask fitted with a rubber septum was charged with [Nb(CO)$_2$(dmpe)$_2$Cl] (0.048 g, 0.10 mmol) and 10 mL of THF. Upon dissolution, excess 40% sodium amalgam was added and the reaction mixture was stirred vigorously for 3.5 h. The solution was decanted into a second 25-mL, one-necked, pear-shaped flask, and ^{t}BuPh$_2$SiCl (0.026 mL, 0.027 g, 0.10 mmol) was added in one portion via syringe, resulting in a deep red solution. The reaction mixture was stirred for an additional 1 h, after which the solvents were removed under vacuum, the product was extracted with pentane, and the pentane solution was filtered and concentrated, providing unpurified [Nb(COSi^{t}BuPh$_2$)(CO)(dmpe)$_2$] as a red oil (0.068 g). A 25-mL, one-necked, pear-shaped flask fitted with a rubber septum was charged with the unpurified [Nb(COSi^{t}BuPh$_2$)(CO)(dmpe)$_2$] and 5 mL of DME. Upon dissolution, the reaction vessel was cooled to −30 °C, acetyl chloride (0.007 mL, 0.008 g, 0.08 mmol) was added in one portion via syringe, and the reaction mixture was stirred for 10 min, providing a green solution. The solvent was removed under vacuum, the product was extracted with pentane, and the pentane solution was filtered and concentrated under vacuum to afford the product as a green solid. Recrystallization from pentane at −30 °C provided 0.031 g (40%) of **6** as a green solid. IR (Nujol): 1725, 1544, 1430, 1365, 1292, 1280, 1232, 1113, 1095, 1032, 979, 938, 929, 890, 821, 791, 744, 730, 700 cm^{-1}. ^{1}H NMR (300 MHz, C$_6$D$_6$): δ 7.62−7.65 (m, 4 H), 7.11−7.15 (m, 6 H), 1.55−1.80 (m, 8 H), 1.40 (t, J = 2.7 Hz, 12 H), 1.35 (t, J = 2.7 Hz, 12 H), 1.13 (s, 9 H), 1.02 (s, 3 H). Anal. Calcd for C$_{32}$H$_{54}$ClO$_3$P$_4$SiNb: C, 50.10; H, 7.10; N, 0.00. Found: C, 50.29; H, 6.90; N, 0.00.

[Ta(MeO$_2$COC≡COSi^{t}BuPh$_2$)(dmpe)$_2$Cl] (7). A 25-mL, one-necked, pear-shaped flask fitted with a rubber septum was charged with [Ta(COSi^{t}BuPh$_2$)(CO)(dmpe)$_2$] (0.038 g, 0.05 mmol) and 5 mL of THF. Upon dissolution, methyl chloroformate (0.004 mL, 0.005 g, 0.05 mmol) was added in one portion via syringe and the reaction mixture was stirred for 1 h, providing a green solution. The solvents were removed under vacuum, the product was extracted with pentane, and the pentane solution was filtered and concentrated under vacuum to afford the product as a green solid. Recrystallization from pentane at −30 °C provided 0.031 g (71%) of **7** as a green solid. IR (Nujol): 1738, 1560, 1425, 1366, 1292, 1277, 1254, 1114, 1074, 1020, 973, 941, 927, 889, 829, 802, 748, 733, 699 cm^{-1}. ^{1}H NMR (300 MHz, C$_6$D$_6$): δ 7.71−7.74 (m, 4 H), 7.10−7.17 (m, 6 H), 2.93 (s, 3 H), 1.51−1.68 (m, 8 H), 1.48 (s, 12 H), 1.39 (s, 12 H), 1.16 (s, 9 H). ^{31}P NMR (121 MHz, C$_6$D$_6$): δ 26.1. Anal. Calcd for C$_{32}$H$_{54}$ClO$_4$P$_4$SiTa: C, 44.12; H, 6.25; N, 0.00. Found: C, 44.23; H, 6.19; N, 0.00.

[V(η^2-C(O)Et)(CO)(dmpe)$_2$] (8). To a stirred solution of Na[V(CO)$_2$(dmpe)$_2$] (0.155 g, 0.360 mmol) in 10 mL of DME was added Et$_3$OBF$_4$ (0.072 g, 0.380 mmol). The solution turned immediately dark brown-black. After the solution was stirred for several minutes, the solvent was removed under vacuum, leaving a red-brown material which was extracted into a few milliliters of pentane. Cooling the solution to −30 °C yielded a mixture of red crystals ([V(CO)$_2$(dmpe)$_2$], identified by FTIR) and very dark brown crystals of **8**, which were collected by filtration and dried (0.079 g). ^{1}H NMR (300 MHz, C$_6$D$_6$): δ 3.39 (m), 3.24 (m), 1.80 (bs), 1.58 (bs), 1.41 (bs), 1.27 (bs), 0.71 (bs), 0.62 (bs). ^{31}P NMR (121 MHz, C$_6$D$_6$): δ 71 (m), 40−58 (m, two overlapping signals), 29 (m).

[Ta(AcOC≡COAc)(dmpe)$_2$Cl] (9). A 25-mL, one-necked, pear-shaped flask fitted with a rubber septum was charged with [Ta(CO)$_2$(dmpe)$_2$Cl] (0.115 g, 0.2 mmol) and 10 mL of DME. Upon dissolution, excess 40% sodium amalgam was added in one portion and the reaction mixture was stirred vigorously for 4 h. The orange solution was decanted into a second 25-mL, one-necked, pear-shaped flask fitted with a rubber septum, the reaction vessel was cooled to −30 °C, and acetyl chloride (0.028 mL, 0.031 g, 0.4 mmol) was added in one portion via syringe. The reaction mixture was stirred for 2 min, providing a green solution. Upon removal of the solvents under vacuum, the green product was extracted with pentane and the pentane solution was filtered and concentrated under vacuum to provide a green solid. Recrystallization from pentane at −30 °C yielded 0.063 g (48%) of **9** as green crystals. IR (Nujol): 1742, 1566, 1420, 1361, 1293, 1282, 1216, 1088, 1008, 943, 925, 891, 733, 699 cm^{-1}. ^{1}H NMR (300 MHz, C$_6$D$_6$): δ 1.82 (s, 6 H), 1.50−1.61 (m, 16 H), 1.23−1.44 (m, 16

H). ^{13}C NMR (75.5 MHz, C_6D_6): δ 200.4 (p, J = 14.7 Hz) (**9b**, prepared from [Ta(^{13}CO)$_2$(dmpe)$_2$Cl]). ^{31}P NMR (121 MHz, C_6D_6): δ 24.5. Anal. Calcd for $C_{18}H_{38}ClO_4P_4Ta$: C, 32.82; H, 5.81; N, 0.00. Found: C, 32.67; H, 5.90; N, 0.00. Spectral data for material prepared from 99% $CH_3{}^{13}C(O)Cl$, [Ta($CH_3C^*(O)OC{\equiv}COC^*(O)CH_3$)(dmpe)$_2$Cl] (**9a**): IR (Nujol) 1702, 1564, 1421, 1360, 1293, 1282, 1186, 1085, 1007, 942, 924, 890, 836, 733, 699 cm^{-1}; ^1H NMR (300 MHz, C_6D_6) δ 1.82 (d, J = 6.3 Hz, 6 H), 1.50−1.61 (m, 16 H), 1.23−1.44 (m, 16 H); ^{13}C NMR (75.5 MHz, C_6D_6) δ 166.6.

[Ta(AcOC≡COAc)(depe)$_2$Cl] (10). A 25-mL, one-necked, pear-shaped flask fitted with a rubber septum was charged with [Ta(CO)$_2$(depe)$_2$Cl] (0.068 g, 0.1 mmol) and 10 mL of DME. Upon dissolution, excess 40% sodium amalgam was added in one portion and the reaction mixture was stirred vigorously for 3 h. The orange solution was decanted into a second 25-mL, one-necked, pear-shaped flask fitted with a rubber septum, the reaction vessel was cooled to −30 °C, and acetyl chloride (0.014 mL, 0.016 g, 0.2 mmol) was added in one portion via syringe. The reaction mixture was stirred for 15 min, providing a green solution. Upon removal of the solvents under vacuum, the green product was extracted with pentane and the pentane solution was filtered and concentrated under vacuum to provide a green solid. Recrystallization from pentane at −30 °C yielded 0.033 g (43%) of **10** as green crystals. IR (Nujol): 1749, 1569, 1419, 1365, 1211, 1080, 1030, 1008, 965, 869, 807, 761, 728 cm^{-1}. ^1H NMR (300 MHz, C_6D_6): δ 1.83−2.01 (m, 16 H), 1.83 (s, 6 H), 1.63−1.67 (m, 4 H), 1.39−1.43 (m, 4 H), 1.01−1.18 (m, 24 H). ^{31}P NMR (121 MHz, C_6D_6): δ 41.5. Anal. Calcd for $C_{26}H_{54}ClO_4P_4Ta$: C, 40.50; H, 7.06; N, 0.00. Found: C, 40.50; H, 7.00; N, 0.00. Spectral data for material prepared from 99% $CH_3{}^{13}C(O)Cl$, [Ta($CH_3C^*(O)OC{\equiv}COC^*(O)CH_3$)(depe)$_2$Cl] (**10a**): IR (Nujol) 1709, 1567, 1415, 1365, 1183, 1080, 1037, 1006, 963, 866, 807, 727 cm^{-1}; ^1H NMR (300 MHz, C_6D_6): δ 1.83−2.03 (m, 16 H), 1.83 (d, J = 7.1 Hz, 6 H), 1.62−1.69 (m, 4 H), 1.36−1.42 (m, 4 H) 1.01−1.18 (m, 24 H); ^{13}C NMR (75.5 MHz, C_6D_6) δ 166.8.

X-ray Crystallography. [Ta(AcOC≡COSi^{t}BuPh$_2$)(depe)$_2$Cl] (4). Green crystals were grown by cooling a saturated solution of **4** in pentane at −30 °C. The crystals were removed from the glovebox in a pool of Exxon Paratone-N oil to minimize decomposition. An irregularly shaped crystal (dimensions 0.35 × 0.38 × 0.43 mm) was cut from a larger specimen and mounted with silicon grease on the end of a quartz fiber. Unit cell parameters and intensity data were obtained by standard methods in our laboratory, details of which are provided in Table 1. The crystal was judged to be acceptable on the basis of open counter ω-scans of several low-angle reflections ($\Delta\bar{\omega}_{1/2}$ = 0.24°) and by axial photographs. The tantalum atom was located by the SIR-92[39] direct methods option in the teXsan software package.[40] The remaining non-hydrogen atoms were revealed by initial cycles of DIRDIF[41] followed by alternating least-squares refinements and difference Fourier maps. All non-hydrogen atoms were refined anisotropically, except for the carbon atoms C300−C305 of the phenyl ring, which were treated as a rigid group. This ring and an ethyl group (C34 and C35) were disordered over two positions. The site occupancies of the latter were refined, resulting in a 70/30 population distribution. The populations of the two ethyl sites were fixed, and then this same distribution was applied to the phenyl ring positions. Hydrogen atoms were placed at calculated positions in the final refinement cycles. The largest residual peak in the final difference Fourier map was 1.49 e/Å^3 near the tantalum atom.

[V(η^2-C(O)Et)(CO)(dmpe)$_2$] (8). Very dark brown crystals of **8** and light red crystals of *trans*-[V(CO)$_2$(dmpe)$_2$] were grown from a mixture of the two complexes in pentane at −30 °C. A crystal of dimensions 0.20 × 0.20 × 0.20 mm was mounted from a cold stage onto the end of a quartz fiber with silicon grease. Unit cell parameters and intensity data were obtained by standard methods, details of which are provided in Table 1. The crystal was judged to be acceptable on the basis of open counter ω-scans of several low-angle reflections ($\Delta\bar{\omega}_{1/2}$ = 0.24°). The vanadium atom positional parameters were determined by the SHELXS-86[42] option in the TEXSAN[43] structure solution package. The remaining non-hydrogen atoms were located by iterations of the DIRDIF[41] program followed by subsequent least-squares refinements and difference Fourier maps. All non-hydrogen atoms were refined anisotropically. Hydrogen atoms were placed at calculated positions in the final refinement cycles. The largest residual peak in the final difference Fourier map was 0.38 e/Å^3 located near the vanadium atom.

Table 1. Experimental Details of the X-ray Diffraction Studies of [Ta(AcOC≡COSi^{t}BuPh$_2$)(depe)$_2$Cl] (4), [V(η^2-C(O)Et)(CO)(dmpe)$_2$] (8), and [Ta(AcOC≡COAc)(dmpe)$_2$Cl] (9)[a]

	4	8	9
empirical formula	$C_{40}H_{70}O_3P_4SiTaCl$	$C_{16}H_{37}O_2P_4V$	$C_{18}H_{38}O_4P_4TaCl$
fw	967.37	436.3	658.79
a, Å	21.553(5)	12.917(2)	14.964(2)
b, Å	10.893(1)	14.331(2)	11.960(2)
c, Å	20.213(2)	12.335(2)	31.710(5)
β, deg	117.86(2)	90	102.77(1)
V, Å^3	4569(2)	2283.4(6)	5535(1)
T, °C	−110	−78	−60
Z	4	4	8
ϱ_{calc}, g cm^{-3}	1.41	1.27	1.58
space group	$P2_1/n$	$Pna2_1$	$C2$
2θ limits, deg	3−50	3−48	3−46
data limits	$-h,-k,\pm l$	$+h,+k,+l$	$+h,+k,\pm l$
scan type	$\omega/2\theta$	$\omega/2\theta$	$\omega/2\theta$[b]
μ, cm^{-1}	26.6	7.0	43.1
no. of total data	8838	2658	6084
no. of unique data[c]	6034	2067	4069
no. of params	427	207	407
p factor	0.05	0.03	0.03
abs corr	empirical (ψ)		empirical (ψ)
transmissn range	0.818−1.00	0.956−1.00	0.826−1.00
R_{merge}	0.025	0.032	0.096
GOF	1.810	1.21	1.898
R[d]	0.041	0.040	0.063
R_w	0.044	0.044	0.071

[a] Data were collected on an Enraf-Nonius CAD-4F κ geometry diffractometer using Mo Kα radiation. [b] This choice of scan type may have led to some reflection overlap, diminishing the accuracy of the data. [c] Observation criterion $I > 3\sigma(I)$. [d] $R = \sum||F_o| - |F_c||/\sum|F_o|$ and $R_w = [\sum w(|F_o| - |F_c|)^2/\sum w|F_o|^2]^{1/2}$, where $w = 1/\sigma^2(F)$, as defined in: Carnahan, E. M.; Rardin, R. L.; Bott, S. G.; Lippard, S. J. *Inorg. Chem.* **1992**, *31*, 5193.

[Ta(AcOC≡COAc)(dmpe)$_2$Cl] (9). Green crystals were grown by cooling a saturated solution of **9** in pentane at −30 °C. An irregularly shaped crystal (dimensions 0.35 × 0.38 × 0.43 mm) was cut from a larger specimen, coated with Exxon Paratone-N oil, and mounted on the end of a quartz fiber with silicon grease. Unit cell and data collection parameters are summarized in Table 1. The crystal was judged to be acceptable on the basis of open counter ω-scans of several low-angle reflections ($\Delta\bar{\omega}_{1/2}$ = 0.29°) and by axial photographs. The tantalum atom was located by direct methods. The remaining non-hydrogen atoms were revealed by subsequent least-squares refinements and difference Fourier maps. Anisotropic refinement of non-hydrogen atoms produced several non-positive-definite temperature factors, and some bond distances

(39) Altomare, A.; Burla, M. C.; Camalli, M.; Cascarano, G.; Giacovazzo, C.; Guagliardi, A.; Polidori, G. *J. Appl. Crystallogr.* **1994**, *27*, 435.

(40) *TeXsan: Single Crystal Structure Analysis Software, Version 1.6c*; Molecular Structure Corp.: The Woodlands, TX, 1994.

(41) Parthasarathi, V.; Beurskens, P. T.; Slot, H. J. B. *Acta Crystallogr.* **1983**, *A39*, 860.

(42) Sheldrick, G. M. In *Crystallographic Computing*; Sheldrick, G. M., Krüger, C., Goddard, R. Eds.; Oxford University Press: Oxford, U.K., 1985; p 175.

(43) *TEXSAN: Single Crystal Structure Analysis Software, Version 5.0*; Molecular Structure Corp.: The Woodlands, TX, 1989.

and angles for the two independent molecules in the asymmetric unit were inconsistent with one another. This inconsistency persisted irrespective of whether or not the absorption and decay corrections were applied, and whether refinement was carried out using F or F^2. Attempts to solve the structure in the alternative space groups *Cm* or *C2/m* were not successful, and packing diagrams were consistent only with *C*2 as the space group. Although the unit cell contains both enantiomers, they are not related by a crystallographic symmetry element. The choice of polarity was made following refinement with both orientations. The largest residual peak in the final difference Fourier mp was 1.94 e/Å^3, situated near Ta1.

Results and Discussion

Siloxycarbyne–CO Coupling. Previous work demonstrated that siloxycarbynes of the type [M(≡COSiR$_3$)(CO)(dmpe)$_2$] react with a variety of silylating reagents (R'$_3$SiX) to afford the corresponding coupled products [M(R$_3$SiOC≡COSiR'$_3$)(dmpe)$_2$X]. More recently, we have shown that addition of AlEt$_3$ to [Ta(≡COSi^{t}BuPh$_2$)(CO)(dmpe)$_2$] produces the unusual carbene–carbyne species [Ta(≡COSi^{t}BuPh$_2$)(=C=O-AlEt$_3$)(dmpe)$_2$].[13,24] Attempts to add nucleophiles (Nu) to this species to promote C–C bond formation and yield products of the kind [M(R$_3$SiOC≡COAlEt$_3$)(CO)(dmpe)$_2$-Nu] have thus far not resulted in carbene–carbyne coupling, but rather in removal of AlEt$_3$ to regenerate [Ta(≡COSi^{t}BuPh$_2$)(CO)(dmpe)$_2$]. These results suggested that the carbyne–CO coupling process depends on the nature of the electrophile and led us to expand the range of electrophiles that might result in O-alkylation of the CO ligand in [M(≡COSiR$_3$)(CO)-(dmpe)$_2$]. Since the bond angle between the coordinated carbon atoms of the carbene and carbyne ligands in [Ta-(≡COSi^{t}BuPh$_2$)(=C=OAlEt$_3$)(dmpe)$_2$] decreased to 73.4-(4)° from its value of 88.5(6)° in [Ta(≡COSi^{t}BuPh$_2$)-(CO)(dmpe)$_2$], we were interested to know whether O-alkylation by a carbon-based electrophile would generate the [Ta(≡COSiR$_3$)(=C=OR')(dmpe)$_2$]$^+$ analogue or possibly lead to coupled products [M(R$_3$SiOC≡COR')-(CO)(dmpe)$_2$]$^+$ or [M(R$_3$SiOC≡COR')(CO)(dmpe)$_2$X].

Reactions of [Ta(≡COSi^{t}BuPh$_2$)(CO)(dmpe)$_2$] with a series of alkylating reagents were therefore investigated. Addition of Et$_3$OBF$_4$, BnBr, or allyl iodide to [Ta(≡COSi^{t}BuPh$_2$)(CO)(dmpe)$_2$] produced yellow solutions, signaling oxidation to [Ta(CO)$_2$(dmpe)$_2$X] species. Analysis of the IR spectra of the yellow solids isolated from the reaction mixtures confirmed the presence of two *cis*-CO ligands, whereas ^{1}H NMR spectroscopy indicated the absence of resonances attributable to metal alkyls. In this manner, we identified the capping ligands (X) in these [Ta(CO)$_2$(dmpe)$_2$X] complexes as halide ion. Similar results were obtained irrespective of the solvents or reaction temperatures employed. Reaction of MeOTf with [Ta(≡COSi^{t}BuPh$_2$)(CO)(dmpe)$_2$], however, provided [Ta(CO)$_2$(dmpe)$_2$Me], as revealed by the characteristic Ta–Me signal in the ^{1}H NMR spectrum at −1.59 ppm.[26]

Very different results were obtained when DME solutions of [Ta(≡COSi^{t}BuPh$_2$)(CO)(dmpe)$_2$] were treated with ethyl triflate. The deep red color of the carbyne complex changed to green-brown, mimicking the well-established behavior of silyl-induced coupling processes. Removal of solvent and extraction of the product mixture with pentane led to isolation of a green-brown compound that was recrystallized as brown crystals from pentane. Analysis of the IR spectrum of this new complex showed no terminal CO stretches and a new band at 1609 cm^{-1}, which was assigned to the acetylene ligand in [Ta(EtOC≡COSi^{t}BuPh$_2$)(dmpe)$_2$OTf] (**1a**). The ^{31}P NMR spectrum consisted of a single resonance at 34.2 ppm, as observed in other four-electron-donor acetylene complexes.[44] A similar product, [Ta-(EtOC≡COSi^{i}Pr$_3$)(dmpe)$_2$OTf] (**1b**), was isolated from the reaction of [Ta(≡COSi^{i}Pr$_3$)(CO)(dmpe)$_2$] with ethyl triflate, although the yields of both **1a** and **1b** were somewhat lower than for analogous reactions with silyl reagents (eq 2).

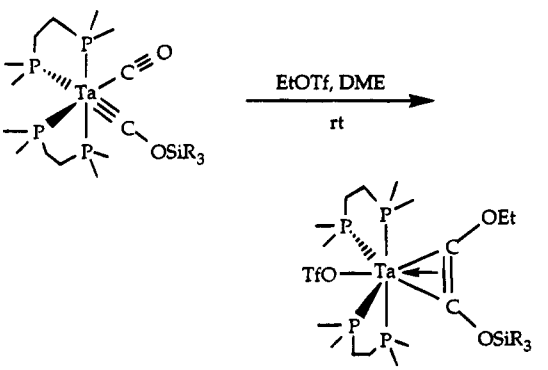

(2)

Analogous siloxy–ethoxy acetylene complexes could be prepared from complexes containing the chelating phosphine ligand depe. Addition of EtOTf to a DME solution of [Ta(≡COSi^{t}BuPh$_2$)(CO)(depe)$_2$] afforded [Ta(EtOC≡COSi^{t}BuPh$_2$)(depe)$_2$OTf] (**3a**) in slightly higher yields. Longer reaction times were required, presumably owing to the increased steric bulk about the metal center. Similarly, the (triphenylsiloxy)- and (trimethylsiloxy)carbynes [Ta(≡COSiPh$_3$)(CO)(depe)$_2$] and [Ta(≡COSiMe$_3$)(CO)(depe)$_2$] reacted with EtOTf, yielding [Ta(EtOC≡COSiPh$_3$)(depe)$_2$OTf] (**3b**) and [Ta-(Me$_3$SiOC≡COEt)(depe)$_2$OTf] (**3c**), respectively (eq 3).

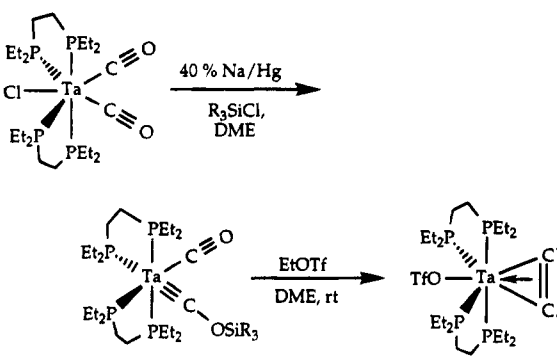

(3)

The ethylations proceeded in modest yields, ranging from 17 to 58%, indicating the lower propensity of the carbynes to couple with ethylating versus silylating reagents. Attempts to extend the reaction to larger alkylating reagents, such as ^{i}PrBr, led only to oxidized products, [M(CO)$_2$(dmpe)$_2$X]. Although the systems described above allowed for the first examples of carbyne–CO coupling, the reaction could not be achieved with a wider variety of electrophiles. To some extent, the reductive coupling reaction mimics the reactivity of

(44) Templeton, J. L. *Adv. Organomet. Chem.* **1989**, *29*, 1.

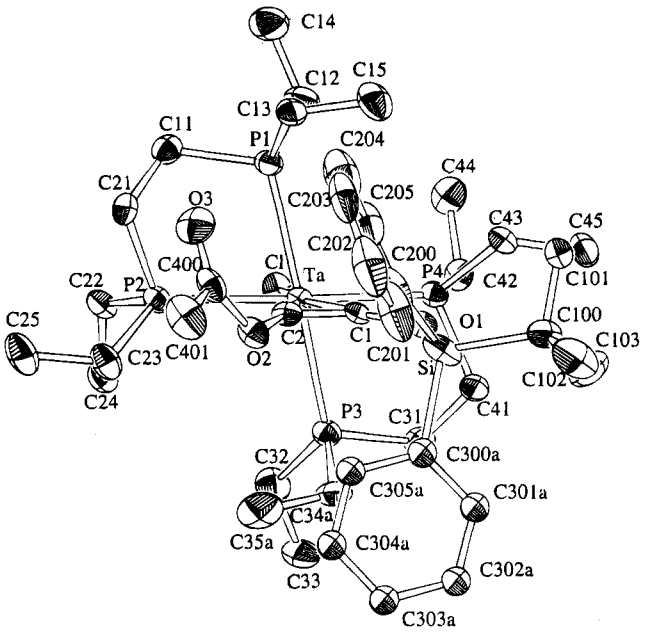

Figure 1. ORTEP diagram of [Ta(AcOC≡COSi^{t}BuPh$_2$)(depe)$_2$Cl] (**4**) showing 40% thermal ellipsoids for all non-hydrogen atoms. The disordered atoms are shown at the sites of highest occupancy.

Scheme 3

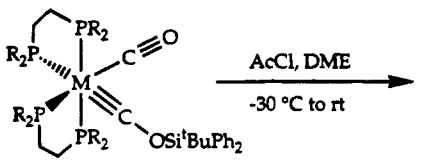

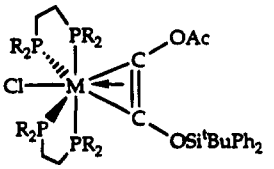

M	R	Compound
Ta	Me	**4**
Ta	Et	**5**
Nb	Me	**6**

enolates.[45] Trapping enolates as the corresponding silyl enol ethers is well-precedented, and these same silylating reagents afforded the best yields of reductively coupled products. In contrast, O-alkylation of enolates can be difficult,[46] a characteristic that applies to the carbyne–CO coupling reaction. These considerations prompted us to examine acyl chlorides, another reagent commonly employed to trap enolates as the corresponding enol ester.[47]

When acetyl chloride was added to a cooled solution of [Ta(≡COSi^{t}BuPh$_2$)(CO)(depe)$_2$] or [M(≡COSi^{t}BuPh$_2$)(CO)(dmpe)$_2$] (M = Nb, Ta), the color changed to green, consistent with carbyne–CO coupling. Recrystallization from pentane afforded green crystals, the spectroscopic properties of which were consistent with the formation of [M(AcOC≡COSi^{t}BuPh$_2$)(depe or dmpe)$_2$Cl] (**4–6**) (Scheme 3). Most striking in the IR spectra are two bands at ca. 1724 and 1539 cm^{-1}. The more intense, higher energy mode can be assigned to the C=O stretch of the acetyl unit, whereas the lower energy band is ascribed to the bound acetylene ligand. The ^{31}P NMR spectra for **4** and **5** displayed characteristic singlets at 43.0 and 25.4 ppm, respectively.

X-ray analysis of **4** revealed the geometry of the reductively coupled product in the solid state (Figure 1). This compound is the first structurally characterized product resulting from carbyne–CO coupling on a group V metal center with carbon-based electrophiles. The geometry of the seven-coordinate complex is very similar to that of niobium and tantalum complexes prepared by reductive coupling of carbon monoxide ligands with the use of silyl reagents. Tables 2 and 3 list fractional

Table 2. Positional Parameters and Equivalent Isotropic Thermal Parameters for the Non-Hydrogen Atoms in [Ta(AcOC≡COSi^{t}BuPh$_2$)(depe)$_2$Cl] (4)[a]

atom	*x*	*y*	*z*	*B*(eq), Å$^{2\,b}$
Ta	0.28380(2)	0.18380(3)	0.60311(1)	2.07(1)
Cl	0.2938(1)	0.2373(2)	0.7190(1)	3.05(7)
P1	0.2028(1)	0.3733(2)	0.5627(1)	2.70(8)
P2	0.3716(1)	0.3629(2)	0.6331(1)	2.57(7)
P3	0.3654(1)	0.0062(2)	0.6693(1)	2.63(7)
P4	0.1981(1)	0.0240(2)	0.6073(1)	2.41(7)
Si	0.2271(1)	−0.0733(2)	0.4012(1)	3.6(1)
O1	0.2232(2)	−0.0113(5)	0.4682(2)	2.6(2)
O2	0.3324(2)	0.1873(5)	0.4730(2)	3.1(2)
O3	0.2890(3)	0.3762(6)	0.4352(3)	4.6(3)
C1	0.2557(3)	0.0859(6)	0.5124(3)	2.0(3)
C2	0.2995(4)	0.1728(7)	0.5165(3)	2.4(3)
C11	0.2560(4)	0.5164(7)	0.5873(4)	3.1(3)
C12	0.1393(4)	0.4074(8)	0.5950(4)	3.9(4)
C13	0.1502(4)	0.3917(7)	0.4701(4)	3.4(3)
C14	0.1043(5)	0.533(1)	0.5773(5)	5.0(4)
C15	0.0906(4)	0.298(1)	0.4365(4)	4.9(4)
C21	0.3242(4)	0.4996(7)	0.5830(4)	3.5(3)
C22	0.4112(4)	0.4352(7)	0.7186(4)	3.1(3)
C23	0.4469(4)	0.352(1)	0.6152(4)	3.7(4)
C24	0.4642(4)	0.3582(8)	0.7772(4)	3.5(3)
C25	0.4925(4)	0.465(1)	0.6289(5)	4.9(4)
C31	0.3153(4)	−0.1166(7)	0.6851(4)	3.2(3)
C32	0.4383(4)	0.023(1)	0.7556(4)	4.5(4)
C33	0.4032(4)	−0.0780(8)	0.6231(4)	3.7(3)
C34a	0.4711(6)	−0.083(1)	0.7968(6)	4.6(6)
C34b	0.514(1)	0.062(3)	0.746(1)	5(1)
C35a	0.4601(7)	−0.006(1)	0.6177(7)	5.5(7)
C35b	0.444(1)	−0.200(3)	0.640(1)	3(1)
C41	0.2415(4)	−0.1295(7)	0.6246(4)	3.0(3)
C42	0.1707(4)	0.0246(7)	0.6749(4)	3.0(3)
C43	0.1147(3)	−0.0063(7)	0.5303(3)	2.7(3)
C44	0.1193(5)	0.1269(8)	0.6672(4)	4.2(4)
C45	0.0725(4)	−0.117(1)	0.5314(5)	4.5(4)
C100	0.1523(4)	−0.1849(8)	0.3654(4)	3.4(3)
C101	0.0845(4)	−0.1127(7)	0.3394(4)	3.6(3)
C102	0.1525(5)	−0.273(1)	0.4206(5)	5.7(4)
C103	0.1497(5)	−0.257(1)	0.3056(5)	6.1(5)
C200	0.2102(4)	0.042(1)	0.3347(4)	4.7(4)
C201	0.2245(5)	0.013(1)	0.2792(5)	6.6(5)
C202	0.2058(6)	0.090(1)	0.2261(6)	8.2(7)
C203	0.1722(5)	0.201(1)	0.2232(5)	5.9(5)
C204	0.1591(6)	0.234(1)	0.2780(6)	7.8(6)
C205	0.1787(5)	0.152(1)	0.3326(4)	5.2(4)
C400	0.3226(4)	0.289(1)	0.4358(4)	3.4(3)
C401	0.3599(5)	0.277(1)	0.3922(4)	5.1(4)
C300a	0.3142(3)	−0.1628(6)	0.4304(3)	2.9
C305a	0.3714(3)	−0.0954(4)	0.4351(3)	2.9
C304a	0.4361(3)	−0.1527(6)	0.4561(4)	2.9
C303a	0.4437(3)	−0.2774(6)	0.4723(4)	2.9
C302a	0.3865(3)	−0.3449(4)	0.4676(3)	2.9
C301a	0.3218(3)	−0.2876(6)	0.4466(3)	2.9
C300b	0.320(1)	−0.094(2)	0.418(1)	5.6
C305b	0.359(1)	−0.022(2)	0.395(1)	5.6
C304b	0.428(1)	−0.055(2)	0.412(1)	5.6
C303b	0.458(1)	−0.159(2)	0.452(1)	5.6
C302b	0.420(1)	−0.231(2)	0.474(1)	5.6
C301b	0.351(1)	−0.198(2)	0.457(1)	5.6

[a] Atoms are labeled as indicated in Figure 1. Estimated standard deviations in the least significant figure are given in parentheses. [b] $B(\text{eq}) = {}^4/_3[a^2\beta_{11} + b^2\beta_{22} + c^2\beta_{33} + 2ab(\cos\gamma)\beta_{12} + 2ac(\cos\beta)\beta_{13} + 2bc(\cos\alpha)\beta_{23}]$.

(45) Semmelhack, M. F.; Tamura, R. *J. Am. Chem. Soc.* **1983**, *105*, 4099.
(46) Tardella, P. A. *Tetrahedron Lett.* **1969**, 1117.
(47) Ladjama, D.; Riehl, J. J. *Synthesis* **1979**, 504.

Table 3. Selected Intramolecular Bond Distances (Å) and Angles (deg) Involving the Non-Hydrogen Atoms for [Ta(AcOC≡COSi^{t}BuPh$_2$)(depe)$_2$Cl] (4)[a]

Bond Distances			
Ta–P1	2.579(2)	Ta–P2	2.580(2)
Ta–P3	2.562(2)	Ta–P4	2.570(2)
Ta–C1	2.088(7)	Ta–C2	2.090(8)
Ta–Cl	2.526(2)	C1–C2	1.31(1)
C1–O1	1.386(8)	C2–O2	1.44(1)
Si–O1	1.660(6)	C400–O2	1.33(1)
Bond Angles			
Ta–C1–O1	152.5(6)	Ta–C2–O2	159.9(4)
C1–Ta–C2	36.6(3)	Si–O1–C1	135.7(5)
C400–O2–C2	120.9(7)	Cl–Ta–P2	82.00(7)
Cl–Ta–P1	83.56(7)	Cl–Ta–P4	81.01(7)
Cl–Ta–P3	83.56(7)	Cl–Ta–C2	163.9(2)
Cl–Ta–C1	160.1(1)	P1–Ta–P3	167.10(7)
P1–Ta–P2	77.31(7)	P1–Ta–C1	103.4(2)
P1–Ta–P4	99.94(7)	P2–Ta–P3	101.50(6)
P1–Ta–C2	95.9(2)	P2–Ta–C1	118.8(2)
P2–Ta–P4	162.99(7)	P3–Ta–P4	77.38(7)
P2–Ta–C2	82.2(2)	P3–Ta–C2	96.6(2)
P3–Ta–C1	88.5(2)	P4–Ta–C2	114.8(2)
P4–Ta–C1	78.2(2)	O2–C400–O3	126(1)
O2–C400–C401	110.0(8)	O3–C400–C401	123.8(9)

[a] Atoms are labeled as indicated in Figure 1. Estimated standard deviations in the least significant figure are given in parentheses.

coordinates and important distances and angles, respectively. The mean Ta–P bond length of 2.573(8) Å is elongated when compared to the mean value of 2.553(2) Å in [Ta(Me$_3$SiOC≡COSiMe$_3$)(dmpe)$_2$Cl],[7] although this difference in part reflects the choice of chelating phosphine ligand, since a similar difference occurs in the structures of [Ta(CO)$_2$(dmpe)$_2$Cl] (2.58(2) Å)[7] and [Ta(CO)$_2$(depe)$_2$Cl] (2.60(2) Å).[38] The C1–C2 bond distance of 1.31(1) Å is similar to the reported values for disiloxyacetylene ligands (1.31–1.33 Å).[5,13]

Methyl chloroformate was also used to induce the coupling of siloxycarbyne and CO ligands (eq 4). This

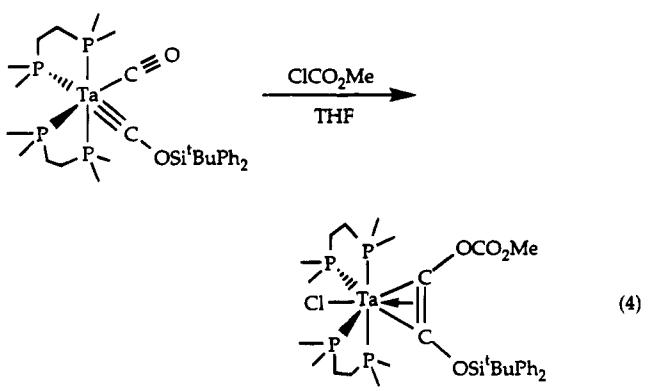

(4)

conversion proceeded at a much slower rate compared to reactions involving acetyl chloride and was best performed at room temperature. The spectroscopic properties of [Ta(MeO$_2$COC≡COSi^{t}BuPh$_2$)(dmpe)$_2$Cl] (**7**), notably the strong IR bands at 1738 and 1560 cm^{-1}, are similar to those in the acetyl chloride species described above.

Attempts to couple any of the siloxycarbyne complexes by addition of benzoyl chloride were unsuccessful, resulting instead in formation of the corresponding [M(CO)$_2$(R$_2$PCH$_2$CH$_2$PR$_2$)$_2$X] dicarbonyl species. Preliminary analysis of the products by IR spectroscopy indicated the presence of two CO stretches at 1829 and 1763 cm^{-1}.

Reactions of Dicarbonyl Anions with Alkylating Reagents. Having demonstrated that carbyne–CO coupling can be effected with carbon-based electrophiles, we were interested to determine whether coupling with such electrophiles could accomplished by starting with Na[M(CO)$_2$(dmpe)$_2$] (M = Nb, Ta). Irrespective of the reaction conditions employed, however, the predominant products resulting from the reaction of Na[M(CO)$_2$(dmpe)$_2$] or Na[M(CO)$_2$(depe)$_2$] (M = Nb, Ta) with alkylating agents, such as MeOTf and EtOTf, were metal–alkyl species, as determined by ^{1}H NMR spectroscopy. Similarly, the reaction of Na[V(CO)$_2$(dmpe)$_2$] with MeOTf afforded mixtures of [V(CO)$_2$(dmpe)$_2$Me] and [V(CO)$_2$(dmpe)$_2$].[48] Presumably, direct electrophilic attack of the alkylating reagent on the highly reduced metal center occurs for the Nb and Ta complexes, but electron-transfer reactions may be important for the vanadium complexes (see below).

Different results were obtained, however, when Na[V(CO)$_2$(dmpe)$_2$] was allowed to react either with EtOTf or Et$_3$OBF$_4$ (eq 5). A mixture of two products in com-

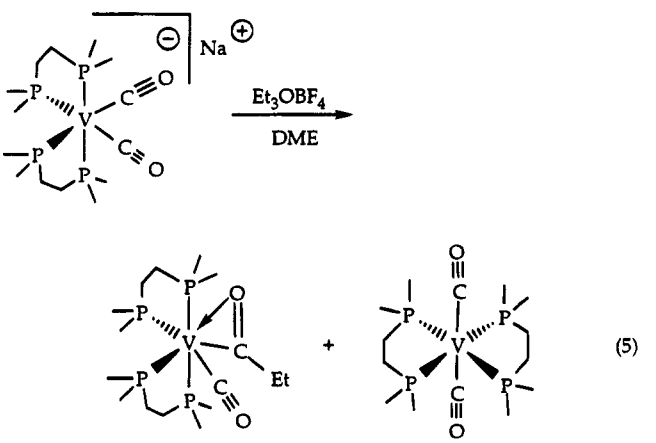

(5)

parable amounts invariably formed, one of which was readily identified as [V(CO)$_2$(dmpe)$_2$] by infrared spectroscopy and X-ray crystallography.[49] Recrystallization of the mixture from pentane at −30 °C yielded two distinct types of crystals, from which a specimen of the unidentified complex was selectively chosen. An X-ray crystal structure determination revealed incorporation of an ethyl group to provide the η^2-acyl complex [V(η^2-C(O)Et)(CO)(dmpe)$_2$] (**8**), the structure of which is depicted in Figure 2. Tables 4 and 5 provide the fractional atomic coordinates and some important distances and angles, respectively.

Although the solid-state structure resembles that of other η^2-acyl complexes,[50–52] the mechanism by which compound **8** forms is unclear. A review of the literature revealed no previous reports of direct electrophilic attack on the carbon atom of a coordinated CO ligand. Instead, a transient intermediate is typically formed, which rearranges to afford the isolated product. In the case of **8**, a vanadium alkyl species might form initially and then undergo ethyl migration to reduce steric congestion. Refluxing or photolyzing solutions of either

(48) Wells, F. J.; Wilkinson, G.; Motevalli, M.; Hursthouse, M. B. *Polyhedron* **1987**, *6*, 1351.
(49) Girolami, G. S.; Wilkinson, G.; Galas, A. M. R.; Thornton-Pett, M.; Hursthouse, M. B. *J. Chem. Soc., Dalton Trans.* **1985**, 1339.
(50) Franke, U.; Weiss, E. *J. Organomet. Chem.* **1979**, *165*, 329.
(51) Schiemann, J.; Weiss, E. *J. Organomet. Chem.* **1983**, *255*, 179.
(52) Durfee, L. D.; Rothwell, I. P. *Chem. Rev.* **1988**, *88*, 1059.

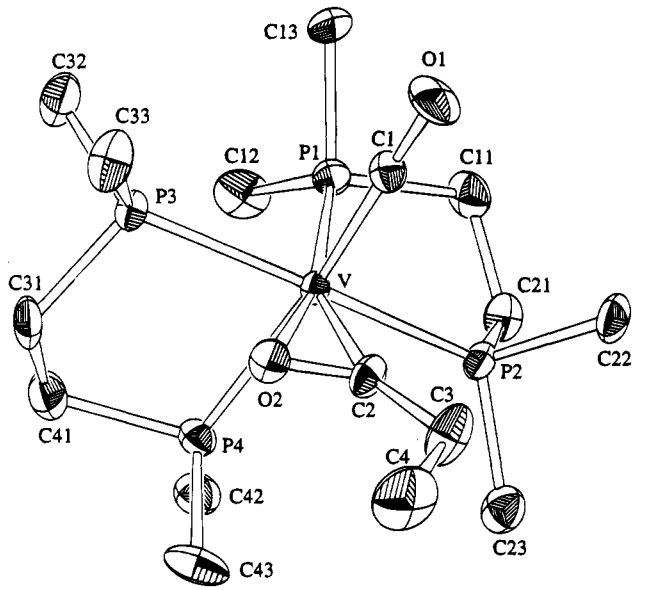

Figure 2. ORTEP diagram of $[V(\eta^2\text{-}C(O)Et)(CO)(dmpe)_2]$ (**8**) showing 40% thermal ellipsoids for all non-hydrogen atoms.

Table 4. Positional Parameters and Equivalent Isotropic Thermal Parameters for $[V(\eta^2\text{-}C(O)Et)(CO)(dmpe)_2]$ (8)[a]

atom	*x*	*y*	*z*	*B*(eq), Å^2 [b]
V	0.29850(9)	0.9581(1)	0.75	1.46(5)
P1	0.3028(1)	1.1428(2)	0.6883(2)	2.18(9)
P2	0.1939(1)	0.9425(2)	0.6143(2)	2.04(9)
P3	0.3865(1)	1.0155(2)	0.8933(2)	2.02(8)
P4	0.1489(1)	0.9746(2)	0.8559(2)	2.15(9)
O1	0.5023(4)	0.9206(5)	0.6481(5)	4.1(3)
O2	0.3214(4)	0.8062(4)	0.8295(4)	2.6(3)
C1	0.4239(6)	0.9369(6)	0.6876(6)	2.3(4)
C2	0.2877(6)	0.8000(6)	0.7465(7)	2.5(3)
C3	0.2742(8)	0.6906(7)	0.7034(7)	4.1(5)
C4	0.2724(9)	0.5967(7)	0.7668(9)	5.9(6)
C11	0.2504(7)	1.1488(7)	0.5681(6)	3.1(4)
C12	0.2323(7)	1.2572(6)	0.7408(7)	3.8(4)
C13	0.4286(7)	1.2077(6)	0.6687(6)	3.3(4)
C21	0.1564(7)	1.0724(7)	0.5617(6)	3.0(4)
C22	0.2532(7)	0.8761(7)	0.5126(6)	3.2(4)
C23	0.0687(7)	0.8735(7)	0.6167(6)	3.3(4)
C31	0.2989(7)	0.9934(8)	0.9928(6)	3.8(5)
C32	0.4399(7)	1.1503(7)	0.9187(6)	3.7(4)
C33	0.4957(7)	0.9337(7)	0.9284(6)	3.9(5)
C41	0.1929(7)	1.0292(9)	0.9703(6)	4.0(5)
C42	0.0349(6)	1.0593(6)	0.8383(6)	3.2(4)
C43	0.0880(7)	0.8466(7)	0.8920(7)	4.1(5)

[a] Atoms are labeled as indicated in Figure 2. Estimated standard deviations in the least significant figure are given in parentheses. [b] $B(eq) = {}^4/_3[a^2\beta_{11} + b^2\beta_{22} + c^2\beta_{33} + 2ab(\cos\gamma)\beta_{12} + 2ac(\cos\beta)\beta_{13} + 2bc(\cos\alpha)\beta_{23}]$.

$[V(CO)_2(dmpe)_2Me]$ or $[Ta(CO)_2(dmpe)_2Et]$, however, did not result in the formation of an acyl complex, making this possible reaction pathway unlikely. A second possibility is that an intermediate ethoxycarbyne complex forms which then undergoes a 1,2-alkyl shift to produce the acyl complex. It also is possible that the reaction proceeds through initial one-electron transfer to afford $[V(CO)_2(dmpe)_2]$ and an ethyl radical, followed by inefficient recombination to afford the metal alkyl, the ethoxycarbyne, or the acyl complex, with the isolated species being the acyl complex. Attempts to alkylate $Na[V(CO)_2(dmpe)_2]$ with ^{i}PrBr under a variety of conditions produced only *trans*-$[V(CO)_2(dmpe)_2]$.

Table 5. Selected Intramolecular Bond Distances (Å) and Angles (deg) Involving the Non-Hydrogen Atoms for $[V(\eta^2\text{-}C(O)Et)(CO)(dmpe)_2]$ (8)[a]

	Bond Distances		
V–P1	2.444(2)	V–P2	2.377(2)
V–P3	2.452(2)	V–P4	2.466(2)
V–C1	1.869(8)	V–C2	1.956(7)
V–O2	2.213(5)	C2–O2	1.27(1)
C1–O1	1.177(9)	C3–C4	1.47(1)
C2–C3	1.49(1)		
	Bond Angles		
V–C1–O1	178.1(7)	V–C2–O2	83.8(5)
C1–V–C2	84.8(3)	V–C2–C3	156.9(7)
C2–C3–C4	117.3(8)	O2–C2–C3	118.8(7)
C1–V–O2	90.7(3)	C2–V–O2	34.8(3)
P1–V–P2	77.99(8)	P1–V–P3	91.37(8)
P1–V–P4	99.41(8)	P1–V–C1	86.4(2)
P1–V–C2	157.1(3)	P1–V–O2	166.5(2)
P2–V–P4	93.70(8)	P2–V–P3	166.58(9)
P2–V–C1	95.2(3)	P2–V–C2	81.8(3)
P2–V–O2	115.4(2)	P3–V–P4	79.87(8)
P3–V–C1	92.2(2)	P3–V–C2	110.0(3)
P3–V–O2	75.6(1)	P4–V–C1	170.2(2)
P4–V–C2	92.4(3)	P4–V–O2	81.8(1)

[a] Atoms are labeled as indicated in Figure 2. Estimated standard deviations in the least significant figure are given in parentheses.

Very recently it was reported that vanadium alkyls of the form $[V(CO)_2(dmpe)_2R]$ (R = 2,4,4-trimethyl-1-pentyl, 3-methyl-2-butyl, 3,3-dimethyl-1-butyl) can be prepared by photolyzing $[V(CO)_2(dmpe)_2H]$ in the presence of alkenes.[53] It is not clear why the hydrovanadation of alkenes would yield vanadium alkyls whereas ethylation of $[V(CO)_2(dmpe)_2]^-$ provides an acyl complex. Obviously steric constraints cannot be the only factor that determines which species is favored, since the insertion products contain alkyls sterically more demanding than an ethyl group. From this comparison, we suggest that ethylation proceeds via initial O-alkylation of the terminal CO ligand followed by subsequent migration of the ethyl group to form the η^2-acyl species. It is also interesting to note that, as in our alkylation reactions, $[V(CO)_2(dmpe)_2]$ forms as a byproduct in the hydrovanadation of alkenes by $[V(CO)_2(dmpe)_2H]$.[53]

Carboxycarbyne–CO Coupling. Attempts to isolate carboxycarbyne complexes by alkylation of $Na[M(CO)_2(dmpe)_2]$ or $Na[M(CO)_2(depe)_2]$ (M = V, Nb, Ta) were unsuccessful. We nonetheless attempted to couple two CO ligands in these anions with carbon-based electrophiles, with the expectation that the desired intermediate M≡COR species might have sufficient lifetime to be trapped with a second equivalent of alkylating reagent to generate a stable acetylene complex. Since acetyl chloride gave excellent results in promoting siloxycarbyne–CO coupling, we focused on use of this reagent.

Treatment of a THF solution of $Na[Ta(CO)_2(dmpe)_2]$ with acetyl chloride at room temperature gave a yellow solution, indicating formation of $[Ta(CO)_2(dmpe)_2X]$. Analysis of the product by IR and ^{1}H NMR spectroscopy revealed only $[Ta(CO)_2(dmpe)_2Cl]$, and not $[Ta(CO)_2(dmpe)_2Ac]$. Markedly different results were obtained, however, when the reaction was run at −30 °C in DME. Rather than the yellow solution obtained at room

(53) Süssmilch, F.; Olbrich, F.; Rehder, D. *J. Organomet. Chem.* **1994**, *481*, 125.

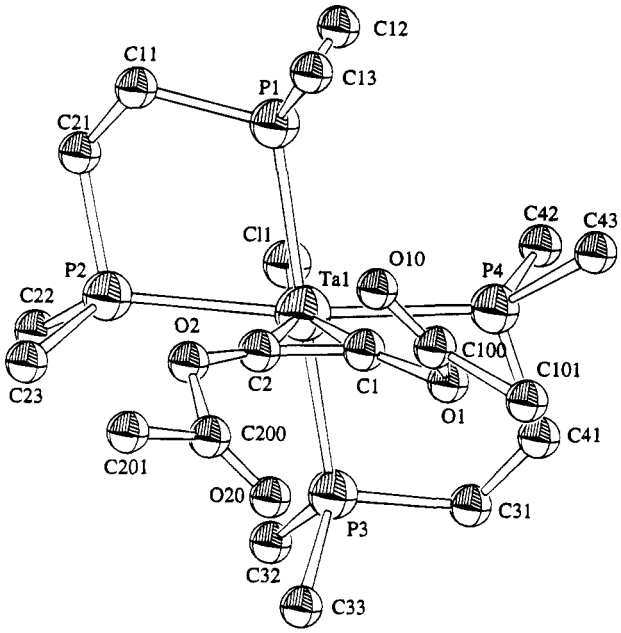

Figure 3. ORTEP diagram of [Ta(AcOC≡COAc)(dmpe)$_2$Cl] (**9**) showing 40% isotropic thermal ellipsoids for all non-hydrogen atoms.

temperature, a deep red color formed initially, which then rapidly turned green. After workup, green crystals of **9** were obtained from pentane at −30 °C. Similarly, addition of 2 equiv of acetyl chloride to a DME solution of Na[Ta(CO)$_2$(depe)$_2$] at −30 °C allowed isolation of a green crystalline product (**10**). Complexes **9** and **10** both exhibited two significant stretches in the infrared spectrum, intense bands at 1742 and 1749 cm^{-1}, respectively, attributed to the CO stretch of an acetyl group and weaker bands at 1566 and 1569 cm^{-1} for **9** and **10**, respectively, similar to values reported for the $\nu_{C\equiv C}$ stretch in previously reported disiloxyacetylene ligands. By using 2 equiv of $CH_3{}^{13}C(O)Cl$ in the syntheses of **9** and **10**, compounds **9a** and **10a** were obtained having CO stretches at 1702 and 1709 cm^{-1}, respectively, confirming the assignment of these bands. The ^{13}C NMR spectra of **9a** and **10a** have single resonances at 166.6 and 166.8 ppm, respectively. Correspondingly, their ^{1}H NMR spectra display doublets at 1.82 (J_{CH} = 6.3 Hz) and 1.83 (J_{CH} = 7.1 Hz) ppm, rather than the singlets observed for the unlabeled materials. Employing [Ta(^{13}CO)$_2$(dmpe)$_2$Cl] as the starting material afforded **9b**, which had a five-line pattern in its ^{13}C NMR spectrum centered at 200.4 ppm (J_{CP} = 14.7 Hz), in agreement with values reported for other disiloxyacetylene ligands (212.5 ppm (J_{CP} = 15 Hz) for [Ta(Me$_3$SiOC≡COSiMe$_3$)(dmpe)$_2$Cl]).[7]

Definitive structural assignment of **9** as the bis(acetoxyacetylene) complex was provided through a single-crystal X-ray analysis, an ORTEP diagram from which is presented in Figure 3. The highlight of the structure is the newly formed acetylene with two acetoxy substituents, confirming **9** as the first product of reductive coupling of two CO ligands on a group V metal promoted solely by carbon-based electrophiles. Presumably, formation of the acetylene proceeds through the acetoxy−carbyne complex [Ta(≡COAc)(CO)(dmpe)$_2$] (Scheme 4), as evidenced by the deep red solution obtained upon initial addition of acetyl chloride. This pathway is analogous to that elucidated for reductive

Scheme 4

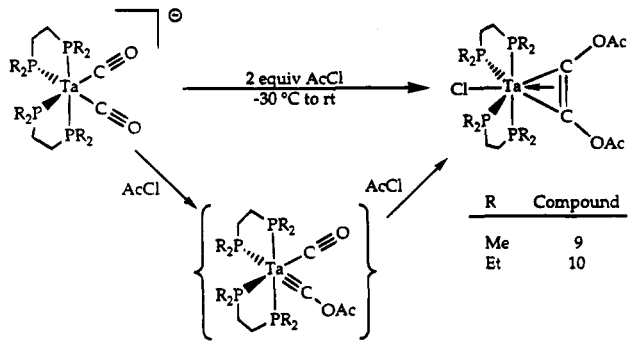

coupling with silyl reagents. Initial attempts to isolate this complex provided to be difficult, owing to its instability.

Attempts to effect coupling by treatment of Na[Ta(CO)$_2$(dmpe or depe)$_2$] with benzoyl chloride or methyl chloroformate, or by reaction of Na[Nb(CO)$_2$(dmpe)$_2$] with acetyl chloride, led instead to the corresponding dicarbonyl complexes as the major products. Efforts were also made to use carbon-based electrophiles in coupling chemistry that would result in acetylenes having a cyclic structure, analogous to cyclic coupled products of the type [M(Me$_2$SiOC≡COSiMe$_2$)(L-L)$_2$Cl] (M = V, Ta; L-L = dmpe, depe).[8] This approach was attempted to determine whether intramolecular trapping of an unstable carboxycarbyne intermediate might be faster than the corresponding intermolecular process. This strategy was unsuccessful, however, regardless of whether triphosgene, oxalyl chloride, dimethylmalonyl chloride, or succinyl chloride was employed.

Despite our inability to generalize reactions of carbon-based electrophiles for O-alkylation of the CO ligands in these complexes, the present work has established that direct O-alkylation can occur and can be used to induce new C−C bond-forming processes. Thus, earlier speculations that the formation of strong Si−O bonds is *required* to drive the silyl-based coupling process are not borne out. In this regard, it should be mentioned that proton sources react with the metal carbonyl anions [M(CO)$_2$(dmpe)$_2$]$^-$ (M = V, Nb, Ta) to afford hydrides [M(CO)$_2$(dmpe)$_2$H].[26] Hydride ligands have limited steric requirements; therefore, the formation of metal hydrides is accompanied by little or no steric barrier. Only O-silylation occurs for reactions of trialkylsilyl reagents with these complexes, consistent with the difficulty of reacting a quaternary silicon with these metal centers. On the other hand, the carbon-based electrophiles bind either at the metal center or at the carbon or oxygen atom of the CO ligand. As the size of such an electrophile increases, the likelihood of metal alkylation decreases and the formation of O-alkylated species, or complexes derived therefrom, increases. At the same time, however, the probability of electron-transfer processes increases and oxidized products of the form [M(CO)$_2$(L-L)$_2$X] or [M(CO)$_2$(L-L)$_2$] are isolated.

Summary. The reductive coupling reaction of a siloxycarbyne with an adjacent CO ligand on a group V metal has been extended to include a variety of carbon-based electrophiles. The reaction proceeded with ethyl triflate, and improved yields occurred with the bulky depe phosphine ligand. With more oxophilic reagents,

such as methyl chloroformate and acetyl chloride, high yields of coupled products were obtained, irrespective of the phosphine ligand. An X-ray crystal structure of [Ta(AcOC≡COSi^{t}BuPh$_2$)(depe)$_2$Cl] revealed the geometry about the metal center, as well as the new acetylene ligand, to be quite similar to that in the bis(siloxyacetylene) derivatives. Attempts to effect reductive coupling directly from the dicarbonyl anion with alkylating reagents normally resulted in the formation of metal alkyls or halides. One notable exception is the reaction of Na[V(CO)$_2$(dmpe)$_2$] with Et_3OBF_4, which afforded an η^2-acyl complex. In addition, under the appropriate reaction conditions, reductive coupling was achieved directly from the tantalum dicarbonyl anions Na[Ta(CO)$_2$(dmpe)$_2$] and Na[Ta(CO)$_2$(depe)$_2$] with acetyl chloride as the trapping reagent, providing the first examples of this chemistry with purely carbon-based electrophiles. In addition to extending the reductive coupling chemistry, these reactions add to the relatively scarce number of examples of direct attack of carbon-based electrophiles on carbon monoxide ligands.

Acknowledgment. This work was supported by a grant from the National Science Foundation. L.E.P. is grateful for a National Institutes of Health National Research Service Award (CA-59223).

Supplementary Material Available: Tables of bond distances and angles and anisotropic thermal parameters for **4**, **8**, and **9**, as well as structural diagrams and a table of positional parameters for **9** (21 pages). Ordering information is given on any current masthead page.

OM940981M

Stable Organoplatinum(IV) Complexes with Pendant Free Radicals

Louis M. Rendina, Jagadese J. Vittal, and Richard J. Puddephatt*

Department of Chemistry, The University of Western Ontario, London, Ontario, Canada N6A 5B7

Received November 29, 1994[⊗]

Oxidative addition of 2-bromoacetamido derivatives of the stable, free-radical nitroxides tempo and proxyl (2,2,6,6-tetramethylpiperidinyl-*N*-oxyl and 2,2,5,5-tetramethylpyrrolidinyl-*N*-oxyl, respectively) to [$PtMe_2$(bpy)] (bpy = 2,2′-bipyridine) affords the novel organoplatinum(IV) complexes [Pt{$CH_2C(O)NH$-tempo}$BrMe_2$(bpy)] (**1**), [Pt{$CH_2C(O)NH$-proxyl}$BrMe_2$(bpy)] (**2**), [Pt{$CH_2C(O)NHCH_2$-proxyl}$BrMe_2$(bpy)] (**3**), [Pt{$CH_2C(O)NHCH_2C(O)NH$-proxyl}-$BrMe_2$(bpy)] (**4**), and [Pt{$CH_2C(O)NH(CH_2)_3$ $NHC(O)$-proxyl}$BrMe_2$(bpy)] (**5**) in good yields. The complexes exist as a mixture of *trans* (**a**) and *cis* (**b**) isomers and are the result of *trans* and *cis* oxidative addition, respectively. The broad ^1H NMR spectra and distinctive three-line pattern in the ESR spectra conclusively demonstrate the paramagnetic nature of the complexes. The X-ray structure of **1a** was determined. Crystals of **1a** are monoclinic, space group $P2_1/c$, with a = 13.401(2) Å, b = 16.979(1) Å, c = 11.199(1) Å, β = 93.01(1)°, Z = 4, and R = 0.0499. The bromo and Pt–C σ-bonded 4-(2-acetamido)-tempo ligands occupy a mutually *trans* arrangement about the octahedral platinum(IV) center. Complexes **1**–**5** are rare examples of stable organometallic species with pendant free radicals.

Introduction

Stable nitroxide free radicals are essential tools in the study of organized systems by ESR spectroscopy.[1] If the organic free radical is covalently attached to specific sites on a macromolecule, then it is commonly known as a "spin label". Alternatively, the macromolecule is studied with a "spin probe", i.e. a small molecule containing the free radical. The nitroxide group can provide valuable information on its environment, including local ordering, structure, and motional dynamics. Furthermore, the extremely high sensitivity of ESR spectroscopy allows one to use extremely low concentrations (micromolar) of free-radical compound.

Recently, octahedral $[Ru(phen)_3]^{2+}$ (phen = 1,10-phenanthroline) complexes that are functionalized at one of the phen ligands by a pendant nitroxide moiety have been used as ESR probes to study micellar solutions[2] and the B-form of DNA.[3] Several examples of nitroxide radicals acting as O-donor ligands to high-oxidation-state metal centers are reported,[4] but very few cases are known of stable free radicals that are tethered to diamagnetic organometallic complexes,[5] e.g., ferrocene derivatives.[6]

In this paper we report the preparation and characterization of novel organoplatinum(IV) complexes with pendant tempo and proxyl (2,2,6,6-tetramethylpiperidinyl-*N*-oxyl and 2,2,5,5-tetramethylpyrrolidinyl-*N*-oxyl, respectively) spin labels by the oxidative addition of their 2-bromoacetamido derivatives to the electron-rich organoplatinum(II) precursor [$PtMe_2$(bpy)] (bpy = 2,2′-bipyridine). This is perhaps the simplest synthetic route to stable radicals containing transition metal fragments.

Experimental Section

All reactions were performed under a N_2 atmosphere using standard Schlenk techniques. All solvents were freshly distilled, dried, and degassed prior to use. NMR spectra were recorded by means of a Varian Gemini (^1H at 300.10 MHz) or Varian XL300 (^{195}Pt at 64.38 MHz) spectrometer. Chemical shifts are reported to ppm with respect to TMS reference (^1H) or external aqueous $K_2[PtCl_4]$ (^{195}Pt). All ^1H NMR spectra are referenced to the residual protons of the deuterated solvents. The calculated values for ^{195}Pt NMR line widths ($\Delta\nu_{1/2}$) equal the width of the signals at half-height (in hertz) minus 20.0 Hz used for line-broadening (in the data processing). ESR spectra were recorded at room temperature on a Bruker ESP300 spectrometer, typically with a modulation amplitude of 0.2 mT and, for selected complexes, 0.005 mT. The field controller was calibrated by taping dpph (2,2-diphenyl-1-picrylhydrazyl radical)[7] powder to the outside of the ESR tube. Elemental analyses were determined by Guelph Chemical Laboratories, Canada.

The complex [$PtMe_2$(bpy)] was prepared according to the literature method.[8] The 2-bromoacetamido spin labels were obtained commercially (Aldrich).

Preparation of complexes. [4-(Acetamido-C^2)-2,2,6,6-tetramethylpiperidinyl-*N*-oxyl](2,2′-bipyridine)bromo-

[⊗] Abstract published in *Advance ACS Abstracts,* April 15, 1995.

(1) (a) Aurich, H. G. In *Nitrones, Nitronates and Nitroxides*; Patai, S., Rappoport, Z.; Eds.; Wiley: New York, 1989; p 313. (b) *Bioactive Spin Labels*; Zhdanov, R. I. Ed.; Springer-Verlag: Berlin, 1992. (c) Keana, J. F. W. *Chem. Rev.* **1978**, *78*, 37.

(2) Ottaviani, M. F.; Ghatlia, N. D.; Turro, N. J. *J. Phys. Chem.* **1992**, *96*, 6075.

(3) Ottaviani, M. F.; Ghatlia, N. D.; Bossmann, S. H.; Barton, J. K.; Dürr, H.; Turro, N. J. *J. Am. Chem. Soc.* **1992**, *114*, 8946.

(4) (a) Eaton, S. S.; Eaton, G. R. *Coord. Chem. Rev.* **1988**, *83*, 29. (b) Eaton, S. S.; Eaton, G. R. *Coord. Chem. Rev.* **1978**, *26*, 207. (c) Caneschi, A.; Getteschi, D.; Rey, P. *Prog. Inorg. Chem.* **1991**, *39*, 331.

(5) For example, see: Symons, M. C. R. *Specialist Periodical Reports (Royal Society of Chemistry);* Alden Press: London, U.K.; 1993; Vol. 13B, p 200.

(6) (a) Forrester, A. R.; Hepburn, S. P. *J. Chem. Soc., Chem. Commun.* **1969**, 698. (b) Owtscharenko, W. I.; Huber, W.; Schwarzhans, K. E. *Monatsch. Chem.* **1987**, *118*, 955.

(7) Weil, J. A.; Bolton, J. R.; Wertz, J. E. *Electron Paramagnetic Resonance: Elementary Theory and Practical Applications*; Wiley: New York, 1994; p 511.

(8) Puddephatt, R. J.; Monaghan, P. K. *Organometallics* **1984**, *3*, 444.

0276-7333/95/2314-2188$09.00/0

Table 1. Selected ^{1}H NMR Spectroscopic Data for Complexes 1–5[a]

complex	*trans* isomer (**a**) δ(Pt–Me)	*cis* isomer (**b**) δ(Pt–Me)	*trans* isomer (**a**) δ(CH$_2$)[b]	ratio a:b[c]
1	1.45 (s, $^2J_{PtH}$ = 70, $\Delta\nu_{1/2}$ = 11.4)	0.77 (s, $^2J_{PtH}$ = 74, $\Delta\nu_{1/2}$ = 16.4)[d]	2.99 (s, $^2J_{PtH}$ = 94, $\Delta\nu_{1/2}$ = 17.9)	1.8:1
2	1.46 (s, $^2J_{PtH}$ = 68, $\Delta\nu_{1/2}$ = 25.6)	0.77 (s, $^2J_{PtH}$ = 68.5, $\Delta\nu_{1/2}$ = 26.6)[d]	3.07 (s, $\Delta\nu_{1/2}$ = 32.9)[f]	1:2
3	1.44 (s, $^2J_{PtH}$ = 69, $\Delta\nu_{1/2}$ = 14.9)	0.76 (s, $^2J_{PtH}$ = 73, $\Delta\nu_{1/2}$ = 21.4)[d]	2.99 (s, $^2J_{PtH}$ = 96, $\Delta\nu_{1/2}$ = 23.1)	1:1.2
4	1.46 (s, $^2J_{PtH}$ = 68, $\Delta\nu_{1/2}$ = 11.6)	0.67 (s, $^2J_{PtH}$ = 72, $\Delta\nu_{1/2}$ = 12.8); 1.53 (s, $^2J_{PtH}$ = 68)[e]	2.97 (s)[e,f,g]	1:1
5	1.43 (s, $^2J_{PtH}$ = 69, $\Delta\nu_{1/2}$ = 9.0)	0.73 (s, $^2J_{PtH}$ = 73, $\Delta\nu_{1/2}$ = 11.9); 1.47 (s, $^2J_{PtH}$ = 69)[e]	2.99 (s, $^2J_{PtH}$ = 100, $\Delta\nu_{1/2}$ = 16.1)	1:1.4

[a] Measured in acetone-d_6 (*ca.* 0.1 M). Quoted multiplicities do not include ^{195}Pt satellites. ^{195}Pt–^{1}H coupling constants and $\Delta\nu_{1/2}$ in parentheses (Hz). [b] The Pt–CH$_2$ signal of the *cis* isomer could not be resolved. [c] Ratio calculated by integration of signals. [d] Remaining Pt–Me resonance is masked by the Pt–Me signal of the *trans* isomer. [e] $\nu_{1/2}$ not determined. [f] $^2J_{PtH}$ not determined. [g] Very broad peak.

dimethylplatinum(IV), [Pt{CH$_2$C(O)NH-tempo}BrMe$_2$(bpy)] (1). To a stirred solution of [PtMe$_2$(bpy)] (0.026 g, 0.069 mmol) in acetone (5 mL) was added BrCH$_2$C(O)NH-tempo (0.020 g, 0.068 mmol). The deep-red solution immediately changed to pale yellow. Evaporation of the solvent *in vacuo* gave a pale-yellow powder (0.044 g, 95.4%). Recrystallization of the solid is usually unnecessary, although it may be recrystallized from acetone/diethyl ether to afford pale-yellow microcrystals with an orange tinge. Anal. Calcd for $C_{23}H_{34}BrN_4O_2Pt$: C, 41.02; H, 5.09; N, 8.32. Found: C, 41.14; H, 5.15; N, 8.10. ESR (acetone): g = 2.0062; a_N = 1.565 mT. NMR in CD_2Cl_2: $\delta(^{195}Pt)$ = −961 and −900 (**1a** and **1b**, respectively; $\Delta\nu_{1/2}$ = *ca.* 50 Hz).

The remaining complexes were prepared similarly to give the following: [3-(acetamido-C^2)-2,2,5,5-tetramethylpyrrolidinyl-*N*-oxyl](2,2′-bipyridine)bromodimethylplatinum(IV), [Pt{CH$_2$C(O)NH-proxyl}BrMe$_2$(bpy)] (**2**) (yield 89%) [Anal. Calcd for $C_{22}H_{32}BrN_4O_2Pt$: C, 40.07; H, 4.89; N, 8.50. Found: C, 39.62; H, 4.91; N, 8.25. ESR (acetone): g = 2.0059; a_N = 1.445 mT]; [3-(acetamidomethyl-C^2)-2,2,5,5-tetramethylpyrrolidinyl-*N*-oxyl](2,2′-bipyridine)bromodimethylplatinum(IV), [Pt{CH$_2$C(O)NHCH$_2$-proxyl}BrMe$_2$(bpy)] (**3**) (yield 90%) [Anal. Calcd for $C_{23}H_{34}BrN_4O_2Pt$: C, 41.02; H, 5.09; N, 8.32. Found: C, 41.10; H, 5.12; N, 8.07. ESR (acetone): g = 2.0059; a_N = 1.445 mT]; [3-{2-(acetamido-C^2)acetamido}-2,2,5,5-tetramethylpyrrolidinyl-*N*-oxyl](2,2′-bipyridine)bromodimethylplatinum(IV), [Pt{CH$_2$C(O)NHCH$_2$C(O)NH-proxyl}BrMe$_2$(bpy)] (**4**) (yield 87%) [Anal. Calcd for $C_{24}H_{35}BrN_5O_3Pt$: C, 40.23; H, 4.92; N, 9.77. Found: C, 40.08; H, 4.95; N, 9.51. ESR (acetone): g = 2.0059; a_N = 1.445 mT]; [3-{[2-(acetamido-C^2)propyl]carbamoyl}-2,2,5,5-tetramethylpyrrolidinyl-*N*-oxyl](2,2′-bipyridine)bromodimethylplatinum(IV), [Pt{CH$_2$C(O)NH(CH$_2$)$_3$NHC(O)-proxyl}BrMe$_2$(bpy)] (**5**) (yield 91%) [Anal. Calcd for $C_{26}H_{39}BrN_5O_3Pt$: C, 41.94; H, 5.28; N, 9.41. Found: C, 41.28; H, 5.23; N, 9.11. ESR (acetone): g = 2.0059; a_N = 1.445 mT]. Selected ^{1}H NMR data for **1**–**5** are presented in Table 1.

X-ray Structure Determination of 1a. Light-yellow blocklike crystals were grown by diffusion of diethyl ether into an acetone solution of **1** at room temperature. A suitable crystal (0.12 × 0.17 × 0.23 mm) was selected, wedged inside a Lindemann capillary tube, flame sealed, and used in the diffraction experiments. The density of the crystal was measured by the neutral buoyancy method. The diffraction experiments were carried out on a Siemens P4 diffractometer with the XSCANS software package[9] using graphite-monochromated Mo Kα radiation at 23 °C. The cell constants were obtained by centering 25 high-angle reflections (24.7 ≤ 2θ ≤ 25.0°). The Laue symmetry 2/*m* was determined by merging symmetry-equivalent reflections. A total of 4220 reflections were collected in the θ range 2.0–22.5° (−14 ≤ h ≤ 14, −18 ≤ k ≤ 1, −1 ≤ l ≤ 12) in the θ–2θ scan mode at variable scan speeds (2–10 °/min). Background measurements were made at the ends of the scan range. Three standard reflections were monitored at the end of every 297 reflections collected. A numerical absorption correction was applied to the data after the faces of the data crystal were indexed, and the distances between them were measured (μ = 7.11 mm^{-1}). The maximum and minimum transmission factors were 0.625 and 0.0345, respectively. The space group $P2_1/c$ was determined from the systematic absences ($h0l$, l = 2n + 1 and 0k0, k = 2n + 1). The data processing, solution, and the initial refinements were done using SHELXTL-PC programs.[10] The final refinements were performed using SHELXL-93 software programs.[11] Only 25 out of the 34 hydrogen atoms in the neutral molecule were located in the difference Fourier routine; atoms H(1a), H(1b), H(3), H(5), H(9), H(10), H(12), H(13), and H(20) were not located. All the hydrogen atoms were placed in the calculated positions and they were included for the purpose of structure factor calculations only. A common isotropic thermal parameter was refined for all the hydrogen atoms. All the non-hydrogen atoms except the carbon atoms in the bipyridyl ligand were refined anisotropically. In the final least-squares refinement cycles on F^2, the model converged at $R1$ = 0.0499, $wR2$ = 0.1041 and GoF = 1.037 for 2368 observations with $F_o \geq 4\sigma(F_o)$ and 250 parameters, and $R1$ = 0.0823, $wR2$ = 0.1191 for all 3314 data. In the final difference Fourier synthesis, the electron density fluctuated in the range +1.31 to −0.97 e Å^{-3}; the top six peaks were associated with the Pt atoms at distances of 1.17–1.30 Å. The mean and the maximum shift/esd in the final cycles were 0.000 and −0.003.

Results and Discussion

Oxidative addition of 2-bromoacetamido nitroxide free radicals to the organoplatinum(II) complex [PtMe$_2$(bpy)] affords the novel platinum(IV) complexes **1**–**5** in high yields (Scheme 1). All the complexes are air- and moisture-stable at room temperature and are stable with respect to loss of the free radical, e.g. by redox processes.

Selected ^{1}H NMR spectroscopic data for complexes **1**–**5** (*ca.* 0.1 M in acetone-d_6) are presented in Table 1. The ^{1}H NMR spectrum of **1** is shown in Figure 1. The spectra show considerable line broadening due to the interaction of the unpaired electron with the ^{1}H nuclear spins (Table 1). This results in the very rapid intra- and intermolecular relaxation of protons. The line broadening is dependent on the concentration of the solution; higher concentrations lead to narrower line widths.[12] The proton resonances of the piperidine (**1**) and pyrrolidine (**2**–**5**) moieties could not be detected between δ = +50 and −50 due to their close proximity to the unpaired electron.[11] Reduction of the N–O$^\bullet$ group with phenylhydrazine to afford the diamagnetic N–OH complex[14] occurred cleanly but did not assist in the characterization of complexes by NMR spectroscopy

(9) *XSCANS*; Siemens Analytical X-ray Instruments Inc.: Madison, WI, 1990.

(10) Sheldrick, G. M. *SHELXTL-PC Software*; Siemens Analytical X-ray Instruments Inc.: Madison, WI, 1990.

(11) Sheldrick, G. M. SHELXL-93. *J. Appl. Crystallogr.*, in press.

(12) (a) Kreilick, R. W. *J. Chem. Phys.* **1966**, *45*, 1922. (b) Kreilick, R. W. *J. Chem. Phys.* **1967**, *46*, 4260.

(13) (a) Briere, R.; Lemaire, H.; Rassat, A.; Dunand, J.-J. *Bull. Soc. Chim. Fr.* **1970**, 4220. (b) Briere, R.; Lemaire, H.; Rassat, A.; Rey, P.; Rousseau, A. *Bull. Soc. Chim. Fr.* **1967**, 4479.

(14) Lee, T. D.; Keana, J. F. W. *J. Org. Chem.* **1975**, *40*, 3145.

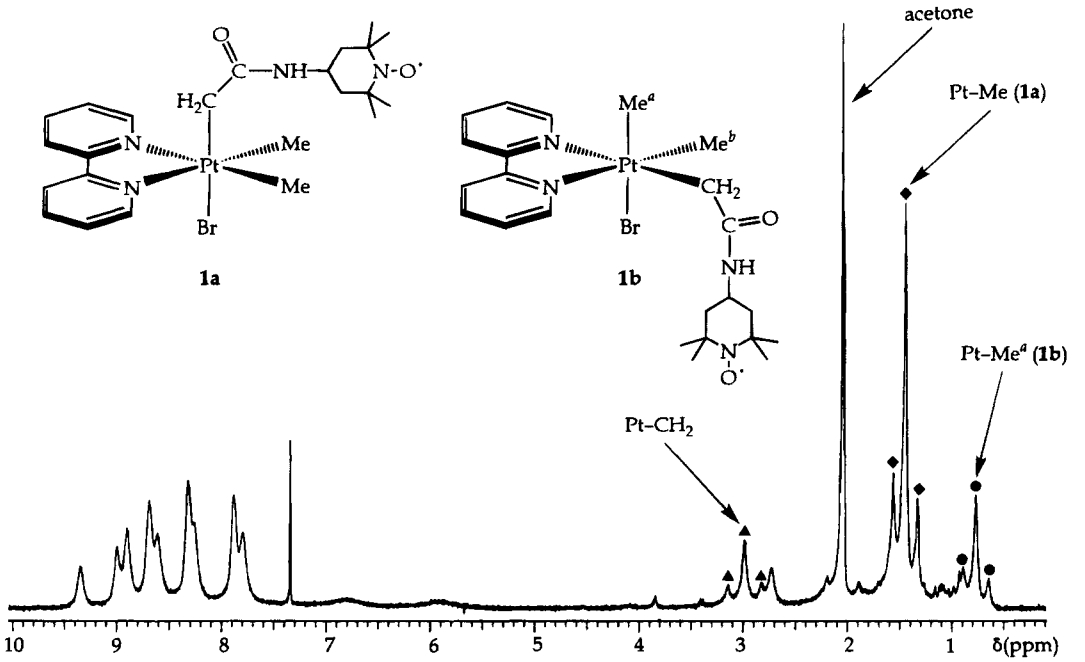

Figure 1. ^{1}H NMR spectrum of **1** in acetone-d_6. The Pt−Me^b (**1b**) signal is masked by the Pt−Me (**1a**) signal.

Scheme 1

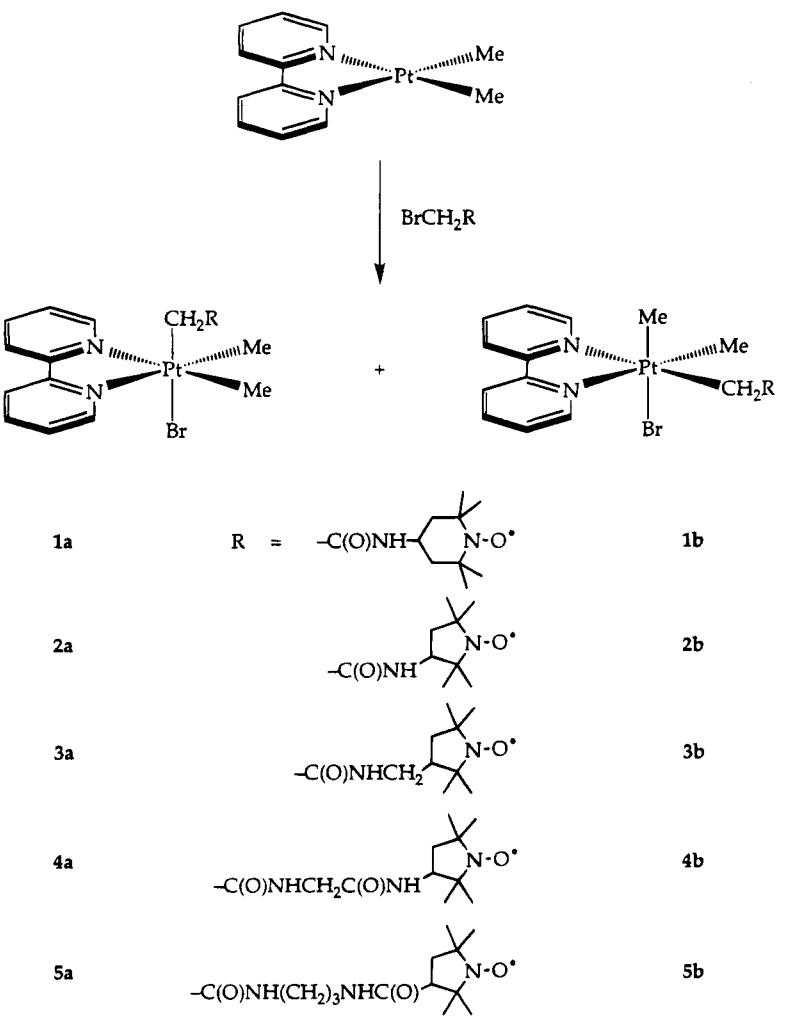

owing to the complicated nature of the resonances of the piperidine or pyrrolidine fragments. Thus, only the NMR spectroscopic data of the paramagnetic species are presented here.

Resonances of protons that are far removed from the N−O• group, i.e. those closest to the platinum(IV) center, provide valuable structural information. Thus the bpy, Pt−Me and Pt−CH_2 signals were observed in the ^{1}H

NMR spectra, although the Pt−CH_2 resonance was not observed in all cases due to its broadness. As expected, the line broadening that is associated with the Pt−alkyl resonances diminishes considerably as the intramolecular distance between the N−O• moiety and platinum(IV) center increases (Table 1). The distinct Pt−Me signal(s) at high field are flanked by ^{195}Pt satellite signals. The decrease in magnitude of $^2J_{PtH}$ (*ca.* 69 Hz) for the Pt−Me signal(s) of **1**−**5** compared to the platinum(II) precursor ($^2J_{PtH}$ = 86 Hz) is consistent with the decreased s character of the platinum hybrid orbital used in bonding to the methyl ligand on oxidation from platinum(II) to platinum(IV).[15] As noted elsewhere, the magnitude of $^2J_{PtH}$ is dependent on the nature of the ligands *trans* to the methyl group, and the stereochemistry about the platinum center can thus be established readily.[15c]

The complexes are shown by ^{1}H NMR spectroscopy to exist as a mixture of two isomers, the major product in **2**, **3**, and **5** corresponding to that of *cis* oxidative addition. For the *cis* isomer, there are two Pt−Me resonances. The Pt−Me signal with the higher value of $^2J_{PtH}$ (*ca.* 73 Hz) and lower chemical shift (δ = *ca.* 0.8) is assigned to the methyl group *trans* to Br, while the other (δ = *ca.* 1.45, $^2J_{PtH}$ = *ca.* 68 Hz) is assigned to the Pt−Me group *trans* to N. For **1b**−**3b**, the second Pt−Me signal (at δ = *ca.* 1.45) is masked by the Pt−Me signal of the *trans* isomer, but it is observed for **4b** and **5b**. For example, in **4a** δ(Pt−Me) = 1.46, $^2J_{PtH}$ = 68 Hz, while **4b** has δ(Pt−Me, *trans* to Br) = 0.67 and δ(Pt−Me, *trans* to N) = 1.53 with $^2J_{PtH}$ values of 72 and 68 Hz, respectively. The Pt−CH_2 resonance appears at δ = *ca.* 3.0 with a $^2J_{PtH}$ value of *ca.* 98 Hz. This signal is shifted approximately 1 ppm downfield compared to that of the analogous but diamagnetic complexes of the type [$PtBrMe_2(CH_2X)(bpy)$] (X = CO_2Me; CO_2Et; CO_2H; CN; $CONH_2$).[16] Again, the changes in line-broadening as a function of tether length, as noted earlier for the Pt−Me signals, are also evident for the Pt−CH_2 signals.

The room temperature ESR spectra of complexes **1**−**5** in acetone solution show the expected three lines of equal intensity that are due to the interaction of the free electron with the ^{14}N (I = 1) nucleus and are characteristic of nitroxide radicals.[1] The ESR parameters of **2**−**5** are identical with those of the parent free-radical compounds (g = 2.0059; a_N = 1.445 mT). This is convincing evidence that little electronic interaction exists between the metal center and the distant proxyl moiety. In particular, no ^{195}Pt coupling is resolved even at very low modulation amplitudes (0.005 mT). Similarly, the ESR spectrum of **1** is identical to that of the 4-(2-bromoacetamido)-tempo precursor (g = 2.0062; a_N = 1.565 mT). To check that the ESR spectra were not due to partial dissociation of the parent radical, the spectra of complexes and parent radicals were recorded at equal concentrations and shown to have equal intensities.

The ^{195}Pt NMR spectra of **1a** and **1b** are essentially identical to those of the diamagnetic analogues that are generated by addition of phenylhydrazine to a solution of the complexes in CD_2Cl_2 solution.[12] Thus two signals are observed at δ = −961 and −900 which correspond to **1a** and **1b**, respectively, for both the free radical (N−O•) and diamagnetic (N−OH) complexes. Furthermore, both the chemical shifts and line widths of the signals do not show any significant concentration dependence.

Table 2. Summary of Crystallographic Data for *trans*-[Pt{$CH_2C(O)NH$-tempo}$BrMe_2$(bpy)] (1a)

chem formula	$C_{23}H_{34}Cl_3N_4O_2BrPt$
fw	673.54
space group	$P2_1/c$
a, Å	13.401(2)
b, Å	16.979(1)
c, Å	11.199(1)
V, Å^3	2544.7(7)
β, deg	93.01(1)
Z	4
T, K	296
ϱ_{calc}, g cm^{-1}	1.758
ϱ_{obs}, g cm^{-1}	1.77(5)
μ, mm^{-1}	7.11
F(000)	1316
R^a	0.0499
S^b	1.037

^{a} $R = \Sigma||F_o| - |F_c||/\Sigma|F_o|$×fa. ^{b} S = goodness of fit = $[(\Sigma w(F_o^2 - F_c^2)^2/(n-p)]^{1/2}$ where n = number of unique reflections and p = number of parameters.

Table 3. Bond Lengths (Å) and Angles (deg) for 1a

Pt(1)−C(2)	2.044(14)	Pt(1)−C(3)	2.056(13)
Pt(1)−C(1)	2.079(12)	Pr(1)−N(1)	2.140(11)
Pt(1)−N(2)	2.171(9)	Pt(1)−Br(1)	2.581(2)
C(3)−C(4)	1.51(2)	C(4)−O(1)	1.20(2)
C(4)−N(3)	1.37(2)	N(3)−C(5)	1.48(2)
C(5)−C(6)	1.50(2)	C(5)−C(9)	1.51(2)
C(6)−C(7)	1.56(2)	C(7)−N(4)	1.48(2)
C(7)−C(10)	1.50(2)	C(7)−C(11)	1.51(2)
C(8)−N(4)	1.47(2)	C(8)−C(13)	1.52(2)
C(8)−C(12)	1.53(2)	C(8)−C(9)	1.53(2)
N(4)−O(2)	1.310(13)	N(1)−C(18)	1.35(2)
N(1)−C(14)	1.36(2)	C(14)−C(15)	1.35(2)
C(15)−C(16)	1.34(2)	C(16)−C(17)	1.37(2)
C(17)−C(18)	1.39(2)	C(18)−C(19)	1.49(2)
N(2)−C(19)	1.34(2)	N(2)−C(23)	1.35(2)
C(19)−C(20)	1.39(2)	C(20)−C(21)	1.37(2)
C(21)−C(22)	1.34(2)	C(22)−C(23)	1.39(2)
C(2)−Pt(1)−C(3)	85.9(6)	C(2)−Pt(1)−C(1)	86.0(6)
C(3)−Pt(1)−C(1)	90.3(5)	C(2)−Pt(1)−N(1)	174.2(5)
C(3)−Pt(1)−N(1)	94.8(5)	C(1)−Pt(1)−N(1)	99.8(5)
C(2)−Pt(1)−N(2)	98.4(5)	C(3)−Pt(1)−N(2)	91.8(5)
C(1)−Pt(1)−N(2)	175.2(5)	N(1)−Pt(1)−N(2)	75.8(4)
C(2)−Pt(1)−Br(1)	92.3(4)	C(3)−Pt(1)−Br(1)	178.1(4)
C(1)−Pt(1)−Br(1)	90.1(4)	N(1)−Pt(1)−Br(1)	87.0(3)
N(2)−Pt(1)−Br(1)	87.9(2)	C(4)−C(3)−Pt(1)	114.9(9)
O(1)−C(4)−N(3)	121.7(12)	O(1)−C(4)−C(3)	124.0(12)
N(3)−C(4)−C(3)	114.3(12)	C(4)−N(3)−C(5)	123.8(11)
N(3)−C(5)−C(6)	109.4(11)	N(3)−C(5)−C(9)	11.4(11)
C(6)−C(5)−C(9)	109.9(11)	C(5)−C(6)−C(7)	114.2(11)
N(4)−C(7)−C(10)	108.8(11)	N(4)−C(7)−C(11)	109.0(11)
C(10)−C(7)−C(11)	111.6(11)	N(4)−C(7)−C(6)	107.3(10)
C(10)−C(7)−C(6)	108.5(12)	C(11)−C(7)−C(6)	111.4(12)
N(4)−C(8)−C(13)	110.4(11)	N(4)−C(8)−C(12)	111.7(12)
C(13)−C(8)−C(12)	107.8(12)	N(4)−C(8)−C(9)	107.9(11)
C(13)−C(8)−C(9)	109.3(12)	C(12)−C(8)−C(9)	109.7(11)
C(5)−C(9)−C(8)	114.4(11)	O(2)−N(4)−C(8)	114.1(10)
O(2)−N(4)−C(7)	114.6(10)	C(8)−N(4)−C(7)	127.6(11)
C(18)−N(1)−C(14)	116.3(12)	C(18)−N(1)−Pt(1)	116.6(8)
C(14)−N(1)−Pt(1)	127.1(9)	C(15)−C(14)−N(1)	122.9(14)
C(16)−C(15)−C(14)	120(2)	C(15)−C(16)−C(17)	120.0(14)
C(16)−C(17)−C(18)	118.3(13)	N(1)−C(18)−C(17)	122.7(12)
N(1)−C(18)−C(19)	116.0(11)	C(17)−C(18)−C(19)	121.3(12)
C(19)−N(2)−C(23)	118.7(11)	C(19)−N(2)−Pt(1)	116.0(8)
C(23)−N(2)−Pt(1)	124.0(9)	N(2)−C(19)−C(20)	120.7(12)
N(2)−C(19)−C(18)	115.1(10)	C(20)−C(19)−C(18)	124.0(12)
C(21)−C(20)−C(19)	119.0(14)	C(22)−C(21)−C(20)	121(2)
C(21)−C(22)−C(23)	118(2)	N(2)−C(23)−C(22)	122.2(14)

(15) (a) Pregosin, P. S.; Omura, H.; Venanzi, L. M. *J. Am. Chem. Soc.* **1973**, *95*, 2047. (b) Appleton, T. G.; Hall, J. R. *Inorg. Chem.* **1971**, *10*, 1717. (c) Anderson, C. M.; Crespo, M.; Jennings, M. C.; Lough, A. J.; Ferguson, G.; Puddephatt, R. J. *Organometallics* **1991**, *10*, 2672.

(16) Achar, S.; Scott, J. D.; Vittal, J. J.; Puddephatt, R. J. *Organometallics* **1993**, *12*, 4592.

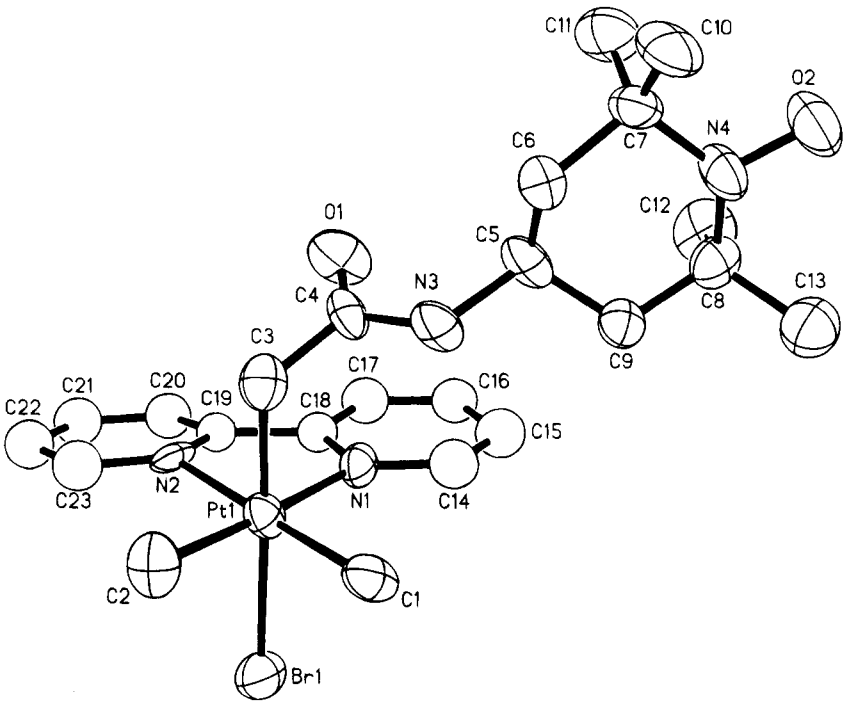

Figure 2. Molecular structure of *trans*-[Pt{$CH_2C(O)NH$-tempo}$BrMe_2$(bpy)] (**1a**). Hydrogen atoms are omitted for clarity. Thermal ellipsoids are represented at the 50% level.

The line widths are higher for the paramagnetic complexes, the difference being *ca.* 20 Hz for both **1a** and **1b**. These results show that the free radical marginally interacts with the platinum(IV) center, although this interaction must be extremely small in both **1a** and **1b** as their ESR spectra show no remarkable features (*vide supra*). The assignment of the ^{195}Pt signals to the *cis* and *trans* isomers was made by analogy to the assignment for the diamagnetic complex [$PtBrMe_2(CH_2CO_2$-$CH{=}CH_2)(^tbu_2bpy)$] ($^tbu_2bpy$ = 4,4′-*tert*-di-butyl-2,2′-bipyridine) which exists as a 7:1 mixture of *trans* (δ = −972) and *cis* (δ = −896) isomers,[16] thus making the assignment straightforward based on peak intensity.

The X-ray structure of **1a** consists of discrete molecules of complex separated by normal Van der Waals contacts. The molecular structure of **1a** is presented in Figure 2 with the atom labeling scheme. A summary of crystallographic data, important bond geometries, and atomic coordinates of the non-hydrogen atoms for **1a** is presented in Tables 2−4, respectively.

The platinum atom is coordinated to two methyl groups, a bromine atom, a chelating bpy ligand, and the methylene group of the 4-(acetamido-C^2)-tempo moiety in an octahedral geometry. The bromo and Pt−C σ-bonded 4-(acetamido-C^2)-tempo ligands occupy a mutually *trans* arrangement. The N−O• bond length (1.31-(1) Å) is similar to that reported for other nitroxides.[15] Furthermore, the N(4)−C(8) and N(4)−C(7) bond lengths (1.47(2) and 1.48(2) Å, respectively) and C(7)−N(4)−C(8), O(2)−N(4)−C(7), and O(2)−N(4)−C(8) bond angles (127.6(11), 114.6(10), and 114.1(10)°, respectively) are close to those determined for other tempo compounds.[17ab] The molecular dimensions of the platinum coordination sphere show no unusual features and are comparable to those of the related complexes [$PtBrMe_2(CH_2CO_2Me)$-(bpy)] and [{$PtBrMe_2$(bpy)}$_2$(μ-$CH_2CO_2CH_2CH_2O_2$ C-CH_2)].[14] There are no short intramolecular contacts in **1a**, and so rotation about the Pt−CH_2 bond is not expected to be hindered in any way.

In conclusion, oxidative addition of 2-bromoacetamido

Table 4. Atomic Coordinates ($\times 10^4$) and Equivalent Isotropic Displacement Parameters (Å^2 $\times$ 10^3) for 1a

atom	*x*	*y*	*z*	*U*(eq),[a] Å^2
Pt(1)	7427.1(4)	532.1(30	1007.8(5)	37.1(2)
Br(1)	5893.3(11	1024.7(9)	2091.7(15)	63.0(2)
C(1)	6915(11)	−620(7)	1123(12)	50(4)
C(2)	8213(10)	311(8)	2586(13)	57(4)
C(3)	8678(10)	145(9)	197(12)	50(4)
C(4)	8536(9)	11(8)	−1136(12)	42(3)
O(1)	8701(8)	497(6)	−1873(9)	61(3)
N(3)	8181(8)	−720(6)	−1147(9)	47(3)
C(5)	8058(10)	−1005(8)	−2698(11)	45(3)
C(6)	8894(10)	−1558(8)	−2944(12)	51(4)
C(7)	8854(9)	−1893(8)	−4242(12)	47(4)
C(8)	6886(10)	−1727(7)	−4210(13)	49(4)
C(9)	7065(9)	−1414(7)	−2913(12)	43(3)
C(10)	9508(10)	−2613(9)	-4262(14)	65(4)
C(11)	9165(12)	−1282(9)	−5127(13)	69(5)
C(12)	6913(11)	−1047(10)	−5055(14)	70(5)
C(13)	6010(11)	−2301(9)	−4250(15)	69(5)
N(4)	7805(8)	−2129(7)	−4546(10)	51(3)
O(2)	7686(7)	−2576(7)	−5497(9)	71(3)
N(1)	6651(7)	885(6)	−624(10)	40(3)
C(14)	6083(10)	421(8)	−1388(12)	51(4)
C(15)	5624(10)	697(8)	−2408(14)	56(4)
C(16)	5753(9)	1452(8)	−2730(13)	49(4)
C(17)	6310(10)	1947(8)	−2000(13)	53(4)
C(18)	6750(8)	1644(7)	−948(11)	36(3)
N(2)	7853(7)	1755(5)	790(9)	36(3)
C(19)	7385(8)	2142(7)	−123(11)	34(3)
C(20)	7447(10)	2959(8)	−206(13)	50(4)
C(21)	8019(10)	3361(9)	636(13)	55(4)
C(22)	8506(10)	2982(8)	1541(13)	53(4)
C(23)	8389(10)	2173(8)	1623(13)	52(4)

[a] *U*(eq) is defined as one-third of the trace of the orthogonalized U_{ij} tensor.

(17) (a) Shibaeva, R. N. *Zh. Strukt. Khim.* **1975**, *16*, 330. (b) Bordeaux, D.; Lajzerowicz, J. *Acta Crystallogr., Sect. B* **1977**, *33*, 1837. (c) Boeyens, J. C. A.; Kruger, G. J. *Acta Crystallogr., Sect. B* **1970**, *26*, 668.

derivatives of proxyl and tempo to [$PtMe_2$(bpy)] occurs cleanly and rapidly to afford the novel organoplatinum(IV) complexes **1**–**5**. To our knowledge, these are the first organoplatinum complexes with appended free-radical substituents. The oxidative addition route provides a particularly simple synthesis of a range of such stable radical complexes. Their use as ESR probes in the study of organized systems is anticipated. For example, substitution of bpy by other diimine ligands such as phen or phi (phenanthroquinonediimine) may lead to organometallic agents that are capable of binding to DNA.[18] Furthermore, because the complexes are neutral, rather than ionic as in $[Ru(phen)_3]^{2+}$ derivatives, they are well suited to studies of macromolecular structures in organic rather than aqueous media.

(18) (a) Pyle, A. M.; Barton, J. K. *Prog. Inorg. Chem.* **1990**, *38*, 413. (b) Long, E. C. *J. Inorg. Organomet. Polym.* **1993**, *3*, 3.

Acknowledgment. We thank Drs. Aitken Hoy and P. A. W. Dean for their generous assistance with the ESR and ^{195}Pt NMR experiments, respectively. We also thank the NSERC (Canada) for financial support to R.J.P. and a Canada International Fellowship to L.M.R.

Supplementary Material Available: Tables of non-bonded contacts, atomic anisotropic displacement parameters, positional parameters for the hydrogen atoms, torsion angles for non-hydrogen atoms, and selected weighted least-squares planes (5 pages). Ordering information is given on any current masthead page.

OM940911F

Models for Bimetallic Catalysts: Anion Additions to Pt_3Re Cluster Cations

Jianliang Xiao, Leijun Hao, and Richard J. Puddephatt*

Department of Chemistry, University of Western Ontario, London, Ontario, Canada N6A 5B7

Ljubica Manojlović-Muir, Kenneth W. Muir,* and Ali Ashgar Torabi

Department of Chemistry, University of Glasgow, Glasgow, Scotland G12 8QQ

Received January 10, 1995[⊗]

The complexes $[Pt_3(\mu_3\text{-}ReL_3)(\mu\text{-}dppm)_3]^+$ (L = CO (**1**), O (**2**)) add halide ions at the Pt_3 face opposite to the ReL_3 fragments to give $[Pt_3(\mu_3\text{-}X)(\mu_3\text{-}ReL_3)(\mu\text{-}dppm)_3]$ (L = CO, X = Cl (**3a**), Br (**3b**), I (**3c**); L = O, X = Cl (**4a**), X = Br (**4b**), X = I (**4c**)). The reactions are easily reversible, with complex stability following the series $X^- = I^- > Br^- > Cl^-$ and L = O > CO. Complex **2** also reacts with SnX_3^- to give $[Pt_3(\mu_3\text{-}SnX_3)(\mu_3\text{-}ReO_3)(\mu\text{-}dppm)_3]$ (X = F, Cl), in which the SnX_3 group caps the Pt_3 triangle. The iodide adduct of **1**, $[Pt_3(\mu_3\text{-}I)\{\mu_3\text{-}Re(CO)_3\}(\mu\text{-}dppm)_3]$ (**3c**), has been characterized by an X-ray crystal structure analysis of **3c**·CH_2Cl_2·H_2O (monoclinic, space group $C2/c$, $a = 34.911(4)$ Å, $b = 19.965(6)$ Å, $c = 24.101(3)$ Å, $\beta = 117.98(1)°$, $Z = 8$, $R = 0.0393$, $R_w = 0.0420$ for 10 848 unique reflections with $I \geq 3\sigma(I)$). The molecular structure of **3c** contains a distorted-tetrahedral Pt_3Re center with the Pt_3 face capped by a weakly bound iodide ligand to form a trigonal-bipyramidal Pt_3ReI core of approximate C_3 symmetry (Pt–Pt = 2.586(1)–2.613(1) Å, Pt–Re = 2.728(1)–2.771(1) Å, and Pt–I = 3.113(1)–3.343(1) Å); the iodide is bound to Pt and not Re as previously proposed.

Introduction

In the $Pt–Re–Al_2O_3$ catalysts used in petroleum reforming, the platinum is present in the metallic state but rhenium may exist in one or more of the oxidation states Re(0), Re(II), and Re(IV).[1-3] In attempts to model these catalysts, the synthesis and chemistry of several coordinatively unsaturated Pt_3Re clusters have been described.[4] In particular, the oxidation of $[Pt_3\{\mu_3\text{-}Re(CO)_3\}(\mu\text{-}dppm)_3]^+$ (**1**) with O_2 led to the remarkable cluster complex $[Pt_3(\mu_3\text{-}ReO_3)(\mu\text{-}dppm)_3]^+$ (**2**).[4] Since both CO and terminal oxo ligands are 2-electron donors, both complexes **1** and **2** are coordinatively unsaturated 54-electron clusters and they have similar structures, each having a tetrahedral Pt_3Re core.[4] However, while the formal oxidation states of the metals in **1** may be described as $Pt^0{}_3Re^I$, those in **2** can be considered as $Pt^0{}_3Re^{VII}$.[4] The unprecedented existence of two cluster complexes with the same geometry but such widely divergent metal oxidation states gives us an opportunity to study cluster chemistry as a function of the rhenium oxidation state. There is a possibility that such studies may provide clues to how the oxidation state of rhenium in the bimetallic catalysts may influence reactivity. In a preliminary communication, it was shown that neutral ligands such as CO and $P(OR)_3$ add to the rhenium center in **1** but to the Pt_3 center in **2**.[5] The same selectivity was suggested for addition of halide ions on the basis of some spectroscopic properties and by analogy with the neutral ligand additions.[5] However, it has now proved possible to grow crystals of the iodide adduct of **1**, and an X-ray structure determination shows that addition of halide to the Pt_3 center occurs. This paper describes the details of the halide addition reactions to **1** and **2** and also describes some related chemistry of the anions SnX_3^- (X = F, Cl).

With respect to the Pt–Re bimetallic catalysts, it is noted that the alumina-supported re-forming catalysts are chlorinated before use. While one major function of this treatment is to adjust the acidity of the support,[6] it is also thought that chloride also interacts with the metals, influencing the degree of PtRe alloying for example.[7] It is not known how chloride interacts with the metals; perhaps the halide adducts of **1** and **2** may mimic halide coordination of the catalysts.

Results

Synthesis and Spectra of Halide Adducts. Complexes **1** and **2** reacted with halide ions to give the neutral clusters **3** and **4** as shown in eqs 1 and 2.

These reactions are easily reversible, and solutions in CH_2Cl_2 were shown to contain mixtures of starting

[⊗] Abstract published in *Advance ACS Abstracts,* April 15, 1995.

(1) (a) Mingos, D. M. P.; Wales, D. J. *Introduction to Cluster Chemistry*; Prentice-Hall: Englewood Cliffs, NY, 1990. (b) *The Chemistry of Metal Cluster Complexes*; Shriver, D. F., Kaesz, H. D., Adams, R. D., Eds.; VCH: New York, 1990.

(2) Sinfelt, J. H. *Bimetallic Catalysts: Discoveries, Concepts and Applications*, Wiley: New York, 1983.

(3) (a) Fung, A. S.; McDevitt, M. R.; Tooley, P. A.; Kelley, M. J.; Koningsberger, D. C.; Gates, B. C. *J. Catal.* **1993**, *140*, 190. (b) Hilbrig, F.; Michel, C.; Haller, G. L. *J. Phys. Chem.* **1992**, *96*, 9893. (c) Godbey, D. J.; Somorjai, G. A. *Surf. Sci.* **1988**, *202*, 204. (d) Augustine, S. M.; Sachtler, W. M. H. *J. Catal.* **1989**, *116*, 184. (e) Tysoe, W. T.; Zaera, F.; Somorjai, G. A. *Surf. Sci.* **1988**, *200*, 1.

(4) (a) Xiao, J.; Vittal, J. J.; Puddephatt, R. J.; Manojlović-Muir, L.; Muir, K. W. *J. Am. Chem. Soc.* **1993**, *115*, 7882. (b) Xiao, J.; Puddephatt, R. J.; Manojlović-Muir, L.; Muir, K. W.; Torabi, A. A. *J. Am. Chem. Soc.* **1994**, *116*, 1129.

(5) Xiao, J.; Hao, L.; Puddephatt, R. J.; Manojlović-Muir, L.; Muir, K. W. *J. Chem. Soc., Chem. Commun.* **1994**, *2221*.

(6) Gates, B. C. *Catalytic Chemistry*; Wiley: New York, 1992.

(7) (a) Malet, P.; Munuera, G.; Caballero, A. *J. Catal.* **1989**, *115*, 567. (b) Augustine, S. M.; Alameddin, G. N.; Sachtler, W. M. H. *J. Catal.* **1989**, *115*, 217.

0276-7333/95/2314-2194$09.00/0

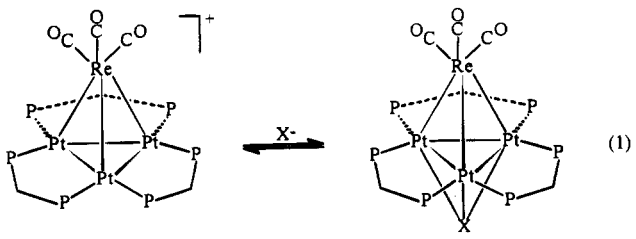

(1)

X = Cl, **3a**; Br, **3b**; I, **3c**

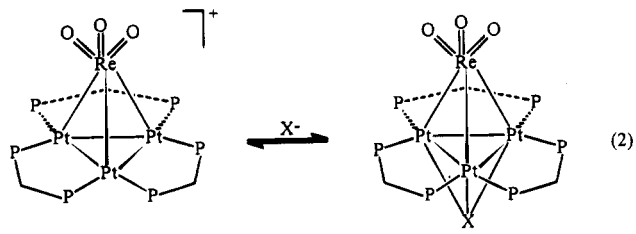

(2)

X = Cl, **4a**; Br, **4b**; I, **4c**

materials and products. However, when the reactions were conducted in acetone solution and in the presence of excess halide, the equilibrium strongly favored product formation and, since the clusters **3** and **4** were sparingly soluble in acetone, they precipitated in high yield. This property makes the isolation of the products easy. The exchange between starting materials and products (eqs 1 and 2) was fast on the NMR time scale, and so only an average signal was observed in either the ^1H or ^{31}P spectra. The NMR parameters of the products **3** and **4** were therefore obtained in CD_2Cl_2 by using excess halide such that the spectroscopic parameters no longer changed with the addition of more halide salt. For each complex **3** or **4**, each ^{31}P NMR spectrum contained only a singlet for the phosphorus atoms of the dppm ligands (an average value for starting materials and products of eq 1 or 2) and the chemical shift moved progressively toward the limiting values quoted for **3** or **4** as more halide was added. Thus, for example, the limiting ^{31}P chemical shifts of **1** and **3b** are δ 7.9 and 4.3, respectively, and in the reaction of **1** with Br^-, the singlet was observed at δ 5.6, 5.2, 4.5, and 4.3 when **1** in CD_2Cl_2 was treated with 1, 1.5, 4, and 10 equiv of bromide, respectively. Qualitatively, when pure **3** or **4** was dissolved in CD_2Cl_2, the equilibrium of eq 1 or 2 lay well to the left when X = Cl, both species were present when X = Br, and the equilibrium lay well to the right when X = I. The halide exchange (eqs 1 and 2) could not be frozen out at temperatures as low as −90 °C. For example, the ^{31}P NMR spectrum of **3b** in CD_2Cl_2 at −90 °C contained a very broad resonance at δ 7.3 with $^1J(PtP)$ = 2472 Hz, tentatively interpreted as being due to an intermediate rate of exchange between **1** and **3b** (Figure 1). The broadening of the spectra at low temperature was initially interpreted in terms of intramolecular fluxionality of an unsymmetrical structure formed by halide addition to the rhenium center,[5] but this is now shown to be incorrect by the X-ray structure determination described below. The broadening at low temperature was much less for **3c**, for which the equilibrium constant is much larger and so which is mostly present as **3** in solution.

The IR spectra of complexes **3** (Nujol mull) contained three bands due to ν(CO) in the terminal carbonyl region. The ν(CO) frequencies were 15−20 cm^{-1} lower in energy than for the parent cluster **1**,[4a] consistent with

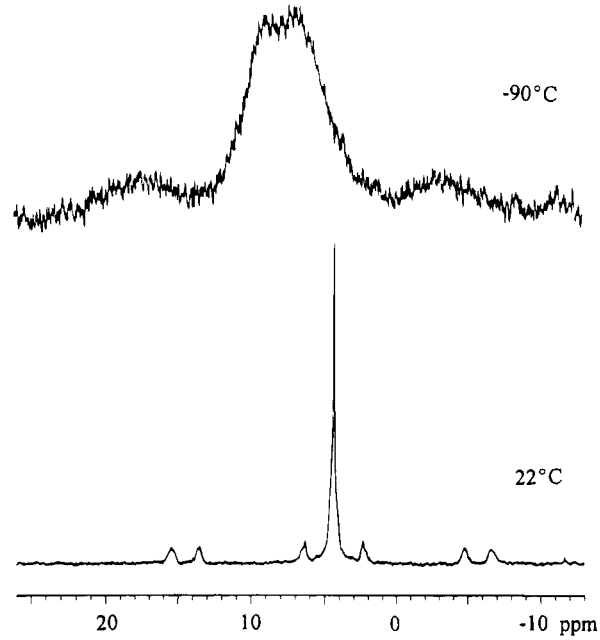

Figure 1. ^{31}P NMR spectra of cluster **3b** in CD_2Cl_2 at 22 °C in the presence of excess bromide to prevent dissociation to **1** and at −90 °C in the absence of excess Br^-. The broadness is interpreted in terms of an intermediate rate of exchange between **1** and **3**. In the room-temperature spectrum, the doublet appearance of the ^{195}Pt satellite spectrum arises from $^3J(PP)$.

slightly stronger Re−CO back-bonding in the neutral clusters **3** compared to the cationic **1**.

The room-temperature ^1H NMR spectra of **3** displayed two resonances of equal intensity for the $CH^aH^bP_2$ protons of the dppm ligands, and the ^{31}P NMR spectra gave singlet resonances at δ 7.0, 4.3, and −5.7 for **3a**−**c**, respectively, with satellites due to coupling to ^{195}Pt, indicative of C_{3v} symmetry on the NMR time scale. The coupling constants $^1J(PtP)$ for **3**, ranging from 2462 to 2520 Hz, are similar to that observed for cluster **1** ($^1J(PtP)$ = 2445 Hz). The ^{195}Pt satellite spectra show a doublet splitting due to the *trans*-like coupling $^3J(PPtPtP)$ through each metal−metal bond (P(1)P(4), P(2)P(5), P(3)P(6) in Figure 2). The long-range couplings $^2J(PtP)$ and $^3J(PP)$, which reflect the strength of Pt−Pt bonding, are similar in magnitude to those found for **1**,[4a] indicating that halide addition does not affect the strength of the Pt−Pt bonds.[8]

The IR spectra of clusters **4** were very similar to that of **2**. For example, the spectrum of **4a** contained bands due to ν(Re=O) at 926 and 890 cm^{-1}, similar to those for cluster **2** (925 and 893 cm^{-1}).[4b] The ReO_3 fragment is also found in [(η^5-C_5Me_5)ReO_3] where the ν(Re=O) bands appear at 909 and 878 cm^{-1}.[9]

The room-temperature ^1H NMR spectra of **4** contained two broad resonances for the $CH^aH^bP_2$ protons and the ^{31}P NMR spectra contained singlets at δ −7.8, −13.9, and −15.2 for **4a**−**c**, respectively, consistent with 3-fold symmetry. The magnitude of the coupling $^1J(PtP)$, ranging between 3210 and 3292 Hz, is slightly larger than that observed for cluster **2** ($^1J(PtP)$ = 3134 Hz).

(8) (a) Rashidi, M.; Puddephatt, R. J. *J. Am. Chem. Soc.* **1986**, *108*, 7111. (b) Ling, S. S. M.; Hadj-Bagheri, N.; Manojlović-Muir, Lj.; Muir, K. W.; Puddephatt, R. J. *Inorg. Chem.* **1987**, *26*, 231.

(9) Herrmann, W. A.; Serrano, R.; Bock, H. *Angew. Chem., Int. Ed. Engl.* **1984**, *23*, 383.

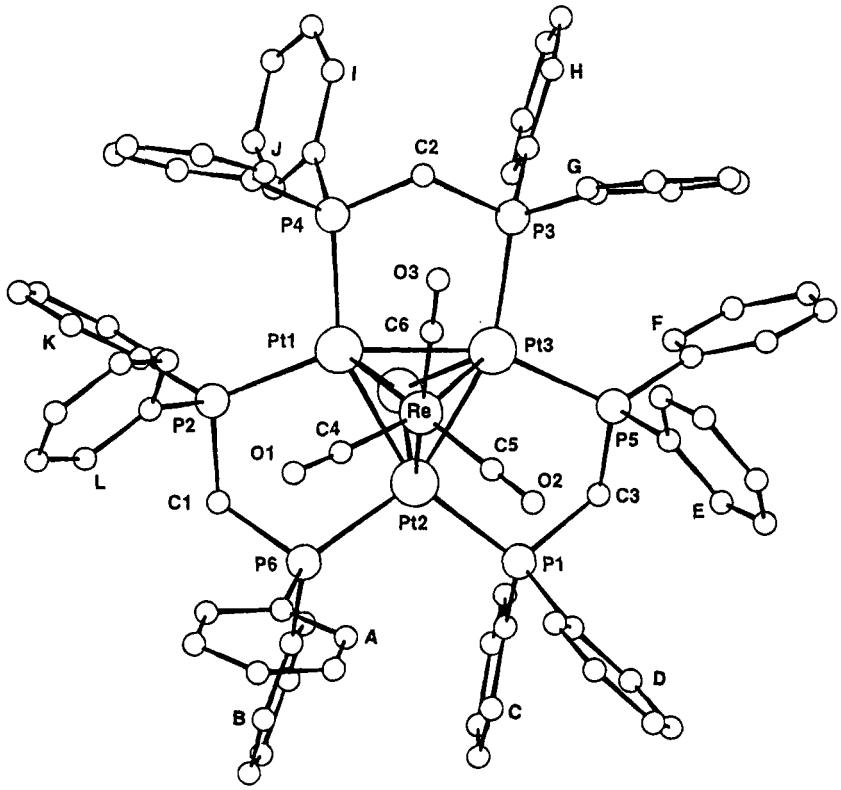

Figure 2. View of the molecular structure of **3c**, with atoms represented by spheres of arbitrary size. In the phenyl rings carbon atoms are numbered in sequences C(n1) to C(n6) (n = A–L) starting with the P-substituted atoms, and the ring labels indicate the positions of the C(n2) atoms. The hydrogen atoms are omitted for clarity.

The values of ^1J(PtP) were significantly higher than in the corresponding complexes **3**.

Structure of Complex 3c. The molecular structure of **3c**, illustrated in Figure 2 and characterized by the atomic parameters listed in Table 1, was determined by an X-ray diffraction study of **3c**·CH_2Cl_2·H_2O. It showed that the addition of halide to the parent complex **1** occurs at the Pt_3 site and not at the Re center as previously thought.[5]

The structure of **3c** contains a triangular Pt_3 unit capped by a $Re(CO)_3$ fragment to form a distorted-tetrahedral Pt_3Re cluster and complete a highly distorted octahedral coordination geometry around the Re center (C–Re–C = 84.1(5)–85.3(5)°, Pt–Re–Pt = 56.0(1)–57.1(1)°). The other face of the Pt_3 cluster is capped by a weakly bound iodide ligand, resulting in a trigonal-bipyramidal $Pt_3(\mu_3\text{-I})(\mu_3\text{-Re})$ core with approximate C_3 symmetry. The Pt_3 triangle is edge-bridged by three dppm ligands to form a $Pt_3(\mu\text{-dppm})_3$ fragment with an essentially planar Pt_3P_6 skeleton. All three Pt_2P_2C rings adopt envelope conformations with the methylenic carbon atom at the flap and two flaps lying above the $Re(CO)_3$-capped face and the third above the I-capped face of the Pt_3 plane (Figure 3). Such a conformation of the $Pt_3(\mu\text{-dppm})_3$ fragment is characterized by different numbers of axial and equatorial phenyl groups surrounding the opposite faces of the Pt_3 cluster,[10] and the iodide ligand is present on the triangular face associated with lower steric hindrance. It results in approximate C_s symmetry of the $Pt_3(\mu_3\text{-I})\{\mu_3\text{-Re}(CO)_3\}(\mu\text{-P-C-P})_3$ unit, the mirror plane passing through the Pt(2), Re, I, and C(2) atoms and bisecting the Pt(1)–Pt(3) bond. The Pt–P and Re–C bond lengths are unexceptional (Table 2).

In the Pt_3Re core both Pt–Pt (2.586(1), 2.598(1), 2.613(1) Å) and Pt–Re (2.728(1), 2.739(1), 2.771(1) Å) distances display small variations. The mean Pt–Pt (2.60 Å in both **1** and **3c**) and Pt–Re (2.75 Å in **3c** and 2.67 Å in **1**[4a]) distances show that the addition of the iodide donor to the Pt_3 cluster in **3c** has no effect on Pt–Pt bonding but causes lengthening of the Pt–Re bonds. In contrast, addition of the $P(OPh)_3$ donor to the Re site to give the cluster $[Pt_3\{\mu_3\text{-Re}(CO)_3\}\{P(OPh)_3\}(\mu\text{-dppm})_3]^+$ lengthens both Pt–Pt and Pt–Re bonds (mean values 2.64 and 2.84 Å, respectively),[5] and the effect on the Pt–Re bonds is substantially higher than in **3c**.

The Pt–I distances in **3c** (Table 2), which also display small variations, are much longer than the Pt–I bonds (2.806(2)–2.825(2) Å) in $[Pt(\mu_3\text{-I})Me_3]_4$ (where no direct Pt–Pt bonding is observed).[11] It is, however, interesting to compare them with analogous distances in the molecular structures of the closely related complexes $[Pd_3(\mu_3\text{-I})(\mu_3\text{-CO})(\mu\text{-dppm})_3]^+$ and $[Au_3(\mu_3\text{-I})(\mu_3\text{-AuI})(\mu\text{-dppm})_3]$, in which the $Re(CO)_3$ fragment is replaced respectively by CO[12] and AuI[13] units. In all these complexes the $M-(\mu_3\text{-I})$ distances are too long to be ascribed to normal covalent bonds. Nevertheless, the Pd–I (2.591(1)–3.083(1) Å), Pt–I (3.113(1)–3.343(1) Å), and $Au-(\mu_3\text{-I})$ [3.132(2)–3.668(2) Å] distances follow the order of the metal atom radii Pd < Pt < Au, and both Pd–I and $Au-(\mu_3\text{-I})$ distances are considered indicative

(10) Puddephatt, R. J.; Manojlović-Muir, L.; Muir, K. W. *Polyhedron* **1990**, *9*, 2767.

(11) Allman, R.; Kuchazczyk, D. *Z. Kristallogr.* **1983**, *165*, 227.

(12) Lloyd, B. R.; Manojlović-Muir, L.; Muir, K. W.; Puddephatt, R. J. *Organometallics* **1993**, *12*, 1231.

(13) Van der Velden, J. W. A.; Bour, J. J.; Pet, R.; Bosman, W. P.; Noordick, J. H. *Inorg. Chem.* **1983**, *22*, 3112.

of some degree of covalency.[12,13] It would thus appear that there is some covalent character in the Pt–I bonds in **3c**.

Adducts with SnF_3^- and $SnCl_3^-$. The cluster **1** failed to react with SnX_3^- (X = F, Cl), but reaction of **2** with SnX_3^- occurred readily to give **5** as shown in eq 3. The SnX_3^- reagents were generated *in situ* by reaction of SnX_2 with X^-, and with X = F a similar result could also be obtained by making use of $Na[SnF_3]$. No further reaction occurred when excess SnX_3^- was used, in contrast to the similar reaction of $[Pt_3(\mu_3\text{-CO})(\mu\text{-dppm})_3]^{2+}$ shown in eq 4.[14–16]

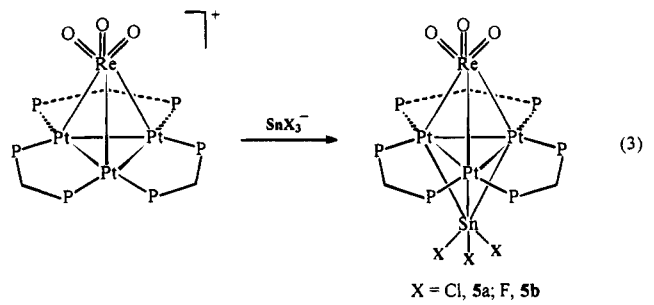

(3)

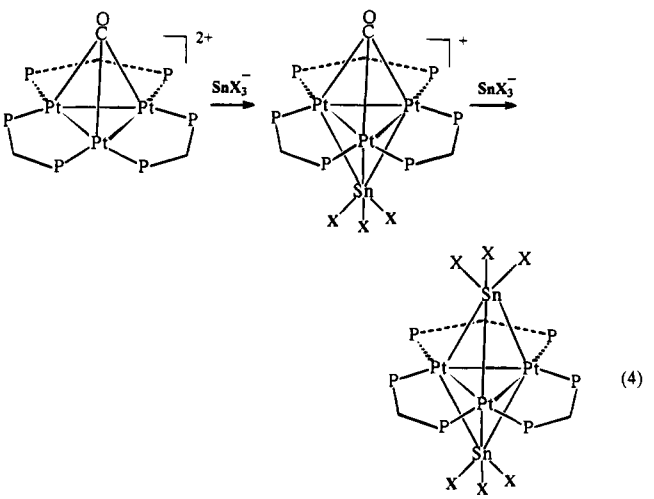

(4)

The IR spectra of **5a** (946 and 937 cm^{-1}) and **5b** (946 and 937 cm^{-1}) each contained two bands assigned to ν(Re=O), the bands occurring at slightly higher energy than in **2** or **4**. The ^{31}P NMR spectra of **5** contained singlet resonances due to the dppm phosphorus atoms, with satellites due to coupling to ^{195}Pt. The couplings $^1J(PtP)$ = 3144 (for **5a**) and 3099 Hz (for **5b**) are close to that for cluster **2** ($^1J(PtP)$ = 3134 Hz).[4] These data support the structure shown in eq 3. In addition, since the NMR spectra in CD_2Cl_2 are independent of added SnX_3^-, it is clear that the equilibrium in eq 3 lies well to the right. It is not clear why **1** fails to form an adduct with SnX_3^-.

Further Studies of the Halide Addition and Exchange Reactions. Consistent with the easy reversibility of the reactions of eqs 1 and 2, anion exchange takes place readily. Thus, in CH_2Cl_2 solution, the chloride ion in **3a** or **4a** was readily replaced by bromide ion to give **3b** or **4b** and the bromide ion in **3b** or **4b** was readily replaced by iodide ion to give **3c** or **4c**, as shown by ^{31}P NMR studies. For example, addition of iodide to a solution of **3b** in CH_2Cl_2, in the presence of excess bromide to prevent dissociation to **1**, led to complete conversion to **3c**. These experiments confirm the ease of the reversibility of the reactions of eqs 1 and 2 and also demonstrate that the equilibrium constants for formation of **3** and **4** follow the sequence $I^- \gg Br^- \gg Cl^-$. This is the sequence expected if the $Pt_3(\mu_3\text{-X})$ group formed has covalent character in the Pt–X bonding.

It was of interest to determine if **1** or **2** possessed the greater ability to bind halide. This could be studied by using a competition between **1** and **2** for a limited amount of halide. A convenient way to carry out this experiment was to dissolve equimolar amounts of complexes **3b** and **2** in CD_2Cl_2 and to monitor by using ^{31}P NMR. The resulting solution will contain the rapidly equilibrating pairs of compounds **1** (δ 7.9) and **3b** (δ 4.3), and of **2** (δ −2.5) and **4b** (δ −13.9). The ^{31}P NMR spectrum contained two singlets at δ 6.8 for **1** and **3b** and δ −13.8 for **2** and **4b**. Because of the small scale of these reactions, it was difficult to control the stoichiometry accurately and so no attempt was made to obtain the equilibrium constants; nevertheless, it should be clear that bromide is selectively complexed by **2** in competition with **1**. From several experiments, the ratio $K(\mathbf{2})/K(\mathbf{1})$ was estimated to be >10 in competition for the bromide ion.

Discussion

The rhenium centers in complexes **1** and **2** have markedly different oxidation states, but the structures are similar and the cluster electron counts are the same. The neutral ligands CO and $P(OR)_3$ add selectively to the rhenium atom of **1** but to the Pt_3 triangle of **2**.[5] This paper shows that the halide ions add to the Pt_3 triangle of both **1** and **2** while SnX_3^- adds to the Pt_3 triangle of **2** but fails to react with **1**. The cluster **2** therefore shows a consistent pattern of selective reaction at platinum, whereas the cluster **1** may react at either platinum or rhenium, or neither in the case of SnX_3^-. The cluster **2** thus reacts in a way similar to that for the dication $[Pt_3(\mu_3\text{-CO})(\mu\text{-dppm})_3]^{2+}$, which adds both neutral and anionic ligands at the Pt_3 triangle opposite to the μ_3-CO group.[10,14] In a comparison of **1** and **2**, the platinum centers in **2** should be more electrophilic, since the ReO_3 group will be more electron withdrawing than the $Re(CO)_3$ group in **1**. This is supported by the observation that the Pt $4f_{7/2}$ binding energy increases from 72.6 to 73.0 eV on going from **1** to **2** and is fully consistent with the observation that **2** binds halide ions more strongly than does **1** and that **2** binds SnX_3^- whereas **1** does not. The coordinative unsaturation in both 54-electron cluster cations **1** and **2** can be considered to be located at a vacant $6p_z$ orbital at each platinum center. If a μ_3-X^- ligand is considered to donate 6 electrons, the clusters **3** and **4** may be considered as coordinatively saturated 60-electron clusters, formed by donation of 2 electrons into each $6p_z$ orbital. The metal–metal bonding in the cluster cation need not be, and indeed appears not to be, perturbed significantly in this process. However, if

(14) Jennings, M. C.; Schoettel, G.; Roy, S.; Puddephatt, R. J.; Douglas, G.; Manojlović-Muir, Lj.; Muir, K. W. *Organometallics* **1991**, *10*, 580.

(15) (a) Lindsey, R. V., Jr.; Parshall, G. W.; Stolberg, U. G. *Inorg. Chem.* **1966**, *5*, 109. (b) Guggenberger, L. J. *J. Chem. Soc., Chem. Commun.* **1968**, 512.

(16) Douglas, G.; Jennings, M. C.; Manojlović-Muir, Lj.; Muir, K. W.; Puddephatt, R. J. *J. Chem. Soc., Chem. Commun.* **1989**, 159.

Table 1. Atomic Fractional Coordinates and Equivalent Isotropic Displacement Parameters (Å²)

	x	*y*	*z*	*U*[a]		*x*	*y*	*z*	*U*[a]
Pt(1)	0.13055(1)	0.17229(2)	0.09200(2)	0.027	C(E5)	0.2003(4)	0.4045(3)	0.3928(6)	0.074
Pt(2)	0.09864(1)	0.27702(2)	0.12092(2)	0.027	C(E6)	0.1680(3)	0.3600(6)	0.3564(5)	0.052
Pt(3)	0.14642(1)	0.19153(2)	0.20692(2)	0.027	C(F1)	0.1318(3)	0.1959(3)	0.3462(4)	0.053
Re	0.18542(1)	0.27467(2)	0.15567(2)	0.037	C(F2)	0.1595(4)	0.2056(7)	0.4093(4)	0.071
I	0.04361(2)	0.15004(4)	0.10935(4)	0.054	C(F3)	0.1520(5)	0.1733(7)	0.4539(3)	0.096
P(1)	0.07402(8)	0.33616(12)	0.17986(11)	0.033	C(F4)	0.1167(3)	0.1313(3)	0.4354(3)	0.142
P(2)	0.09668(8)	0.18906(12)	−0.01508(11)	0.031	C(F5)	0.0890(5)	0.1216(7)	0.3724(4)	0.151
P(3)	0.18981(8)	0.10092(12)	0.24955(11)	0.031	C(F6)	0.0965(5)	0.1539(7)	0.3278(3)	0.083
P(4)	0.16879(8)	0.07501(12)	0.11432(11)	0.033	C(G1)	0.2386(4)	0.1177(7)	0.3256(3)	0.039
P(5)	0.13727(8)	0.24237(12)	0.28437(11)	0.035	C(G2)	0.2769(3)	0.1414(3)	0.3292(4)	0.052
P(6)	0.06567(8)	0.32040(12)	0.02274(11)	0.032	C(G3)	0.3100(2)	0.1622(5)	0.3861(4)	0.066
Q(1)	0.2075(3)	0.3406(4)	0.0605(4)	0.074	C(G4)	0.3049(3)	0.1593(6)	0.4394(3)	0.067
Q(2)	0.2309(3)	0.3969(5)	0.2352(5)	0.093	C(G5)	0.2666(3)	0.1356(2)	0.4359(4)	0.076
Q(3)	0.2765(3)	0.2175(5)	0.2077(4)	0.084	C(G6)	0.2335(3)	0.1148(6)	0.3789(4)	0.053
C(1)	0.0551(3)	0.2540(5)	−0.0341(4)	0.037	C(H1)	0.1694(3)	0.0226(3)	0.2656(3)	0.036
C(2)	0.2110(3)	0.0735(5)	0.1960(4)	0.037	C(H2)	0.1978(3)	−0.0273(6)	0.3008(4)	0.049
C(3)	0.0847(3)	0.2863(5)	0.2492(5)	0.042	C(H3)	0.1820(3)	−0.0868(5)	0.3111(5)	0.062
C(4)	0.1977(3)	0.3170(5)	0.0949(5)	0.044	C(H4)	0.1379(3)	−0.0963(3)	0.2862(3)	0.076
C(5)	0.2132(4)	0.3512(6)	0.2056(5)	0.056	C(H5)	0.1095(3)	−0.0463(6)	0.2511(5)	0.074
C(6)	0.2411(4)	0.2400(6)	0.1879(5)	0.056	C(H6)	0.1253(3)	0.0131(5)	0.2407(6)	0.053
C(A1)	0.0970(3)	0.3857(5)	0.0077(3)	0.039	C(I1)	0.1395(4)	−0.0049(5)	0.1028(4)	0.038
C(A2)	0.1193(3)	0.4309(3)	0.0554(4)	0.058	C(I2)	0.1602(3)	−0.0633(7)	0.1322(4)	0.057
C(A3)	0.1455(4)	0.4785(5)	0.0487(4)	0.072	C(I3)	0.1376(3)	−0.1229(5)	0.1180(5)	0.081
C(A4)	0.1494(2)	0.4809(4)	−0.0056(3)	0.081	C(I4)	0.0942(3)	−0.1241(4)	0.0744(3)	0.082
C(A5)	0.1271(3)	0.4356(4)	−0.0533(4)	0.073	C(I5)	0.0735(3)	−0.0657(6)	0.0450(5)	0.069
C(A6)	0.1009(4)	0.3880(6)	−0.0466(4)	0.053	C(I6)	0.0961(3)	−0.0060(4)	0.0592(6)	0.054
C(B1)	0.0102(3)	0.3541(7)	−0.0106(6)	0.038	C(J1)	0.1983(3)	0.0600(3)	0.0688(5)	0.035
C(B2)	−0.0021(3)	0.4136(5)	−0.0435(3)	0.069	C(J2)	0.2398(4)	0.0838(5)	0.0887(3)	0.049
C(B3)	−0.0451(3)	0.4331(4)	−0.0720(5)	0.103	C(J3)	0.2588(3)	0.0787(5)	0.0499(3)	0.059
C(B4)	−0.0757(3)	0.3930(6)	−0.0677(5)	0.083	C(J4)	0.2363(3)	0.0499(3)	−0.0087(4)	0.065
C(B5)	−0.0635(2)	0.3335(4)	−0.0348(3)	0.058	C(J5)	0.1948(3)	0.0261(5)	−0.0286(3)	0.056
C(B6)	−0.0205(3)	0.3140(5)	−0.0062(6)	0.052	C(J6)	0.1758(3)	0.0312(6)	0.0102(4)	0.046
C(C1)	0.0150(3)	0.3528(7)	0.1470(6)	0.043	C(K1)	0.0635(4)	0.1217(5)	−0.0688(3)	0.035
C(C2)	−0.0010(3)	0.4153(5)	0.1228(2)	0.056	C(K2)	0.0741(3)	0.0948(5)	−0.1126(4)	0.054
C(C3)	−0.0449(3)	0.4277(4)	0.0962(5)	0.074	C(K3)	0.0492(3)	0.0439(2)	−0.1516(5)	0.073
C(C4)	−0.0729(2)	0.3775(6)	0.0939(5)	0.070	C(K4)	0.0139(3)	0.0198(4)	−0.1467(3)	0.066
C(C5)	−0.0568(3)	0.3151(4)	0.1181(3)	0.059	C(K5)	0.0033(2)	0.0467(4)	−0.1029(4)	0.061
C(C6)	−0.0129(3)	0.3026(5)	0.1447(6)	0.052	C(K6)	0.0281(4)	0.0976(3)	−0.0640(5)	0.046
C(D1)	0.0980(5)	0.4172(5)	0.2154(5)	0.042	C(L1)	0.1280(3)	0.2167(4)	−0.0538(4)	0.039
C(D2)	0.0814(3)	0.4557(6)	0.2465(4)	0.072	C(L2)	0.1085(3)	0.2458(7)	−0.1126(6)	0.058
C(D3)	0.1012(4)	0.5152(4)	0.2743(6)	0.100	C(L3)	0.1331(3)	0.2631(5)	−0.1415(4)	0.080
C(D4)	0.1377(4)	0.5362(5)	0.2707(4)	0.106	C(L4)	0.1772(3)	0.2512(3)	−0.1116(4)	0.095
C(D5)	0.1543(3)	0.4977(5)	0.2395(5)	0.091	C(L5)	0.1967(3)	0.2221(6)	−0.0528(5)	0.081
C(D6)	0.1345(5)	0.4382(3)	0.2119(7)	0.055	C(L6)	0.1721(3)	0.2049(5)	−0.0239(4)	0.056
C(E1)	0.17775(4)	0.3058(6)	0.3295(3)	0.037	C(7)	0.0575(10)	0.2447(14)	0.6676(13)	0.20(1)
C(E2)	0.2193(4)	0.2961(3)	0.3390(6)	0.050	Cl(1)	0.1130(3)	0.2690(5)	0.6968(5)	0.263(4)
C(E3)	0.2516(3)	0.3406(5)	0.3753(5)	0.065	Cl(2)	0.0359(3)	0.2159(5)	0.7070(5)	0.267(4)
C(E4)	0.2421(3)	0.3948(5)	0.4023(2)	0.068	O(4)	0.5050(7)	0.1112(11)	0.2983(9)	0.25(1)

[a] $U = {}^1/_3\Sigma_{i=1}^3\Sigma_{j=1}^3 U_{ij}a^*_i a^*_j(\bar{a}_i\bar{a}_j)$. For the atoms in solvent molecules, C(7), Cl(1), Cl(2), and O(4), *U* is the isotropic displacement parameter.

a ligand adds to the 18-electron rhenium center of **1** or **2**, it must lead to cleavage or weakening of at least one Pt−Re bond. We suppose that this is only possible if the Re−L bond formed is significantly stronger than the Pt−Re bond broken. This appears to be the case for reaction of **1** with L = CO, $P(OPh)_3$ but not with L = X^-, SnX_3^-. One remaining puzzle is that the binding to **2** follows the sequence $SnX_3^- > I^- > Br^- > Cl^-$ but to **1** the series is $I^- > Br^- > Cl^- > SnX_3^-$.

To gain further insight into the above reactions, an analysis of the interaction of I^- with the model clusters $[Pt_3(\mu_3\text{-}ReL_3)(\mu\text{-}H_2PCH_2PH_2)_3]^+$ (L = CO, O) to give simplified analogues of **3c** and **4c**, $[Pt_3(\mu_3\text{-}I)(\mu_3\text{-}ReL_3)(\mu\text{-}H_2PCH_2PH_2)_3]^+$, has been made using the EHMO method.[17-19] There are bonding interactions between the filled *p* orbitals of I^- and the unoccupied platinum p_z orbitals as shown in **A**. The p_z orbital of I^- interacts

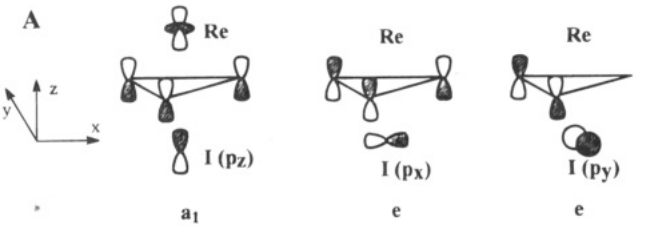

with the a_1 combination of p_z orbitals as shown in **A**, while the p_x and p_y orbitals overlap more weakly with the e combination of p_z orbitals which lie at higher energy. Because of the mismatch in energies of the donor and acceptor orbitals, these bonding interactions are limited and there are also strong interactions involving the filled p orbitals of I^- and filled d orbitals of the Pt_3 unit which cannot lead to a net bonding in either **3c** or **4c**. The a_1 combination of p_z orbitals for cluster **2** is calculated to be more than 1 eV lower in energy than for cluster **1**, and hence a greater bonding interaction is observed for **2**. The calculation for **4c**

(17) For previous theoretical work on Pt_3L_6 clusters, see: (a) Evans, D. G. *J. Organomet. Chem.* **1988**, *352*, 397. (b) Mealli, C. *J. Am. Chem. Soc.* **1985**, *107*, 2245.

(18) Albright, T. A.; Burdett, J. K.; Whangbo, M.-H. *Orbital Interactions in Chemistry*; Wiley: New York, 1985; Chapter 20.

(19) Schoettel, G.; Vittal, J. J.; Puddephatt, R. J. *J. Am. Chem. Soc.* **1990**, *112*, 6400.

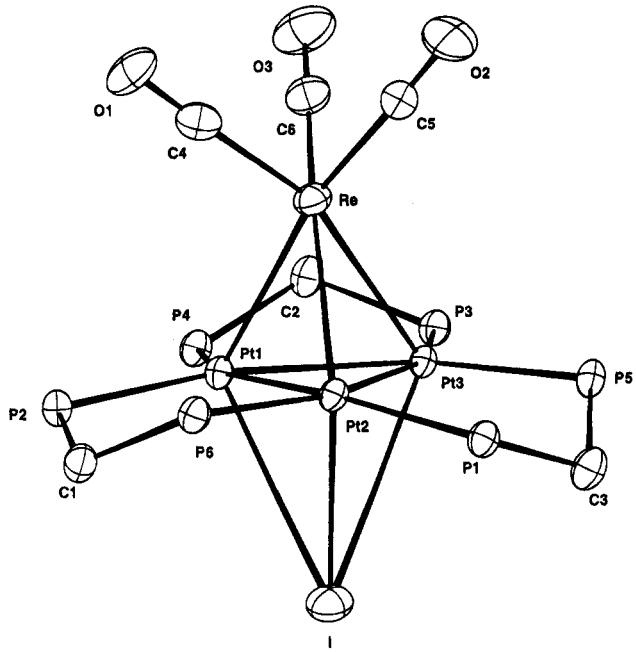

Figure 3. View of the inner core of **3c**, with displacement ellipsoids showing 50% probability.

suggests a charge of only −0.15 e on the coordinated iodide, while the occupation of each $6p_z$ orbital of platinum increased from 0.03 to 0.16 e on addition of iodide. These calculations therefore suggest that, although the net bonding is weak, the $Pt_3(\mu_3\text{-}I)$ interaction is covalent in nature and that iodide can act as a weak six-electron donor by using all of its filled p orbitals in bonding. These results are then in accord with the structural study on **3c** and with the competition experiments between **1** and **2** for halide coordination.

A similar interaction is seen in adding SnF_3^- to the model clusters, but this ligand can act only as a two-electron donor. The donor orbital is the lone pair on tin(II) having mostly tin 5s character.

It may be speculated that halide interacts with the PtRe clusters present in supported bimetallic PtRe catalysts in a way similar to that established here, that is by preferential coordination to platinum.[6,7,20]

Experimental Section

The compounds $[Pt_3\{Re(CO)_3\}(\mu\text{-dppm})_3][PF_6]$ (**1**$[PF_6]$) and $[Pt_3\{ReO_3\}(\mu\text{-dppm})_3][PF_6]$ (**2**$[PF_6]$) were prepared by previously reported procedures.[4] IR spectra were recorded by using a Perkin-Elmer 2000 spectrometer, and the NMR spectra were recorded, unless otherwise indicated, in CD_2Cl_2 solution at ambient temperature by using a Varian Gemini-300 spectrometer; chemical shifts are referenced to TMS (^1H) and 85% H_3PO_4($^{31}P\{^1H\}$). Elemental analysis were performed by Guelph Chemical Laboratories and Galbraith Laboratories.

$[Pt_3(\mu_3\text{-}Cl)\{Re(CO)_3\}(\mu\text{-dppm})_3]$ (3a). To a solution of **1**$[PF_6]$ (41 mg, 0.019 mmol) in acetone (5 mL) was added tetraethylammonium chloride (3.2 mg, 0.019 mmol). A red-brown precipitate formed almost immediately. The mixture was stirred for 10 min. The solution was then concentrated, followed by adding hexane to completely precipitate the product, which was then washed with acetone (0.5 mL) to give the product as a red-brown powder. Yield: 60%. Anal. Calcd for $C_{78}H_{66}ClO_3P_6Pt_3Re$: C, 45.83; H, 3.25. Found: C, 44.52; H, 4.75. IR (Nujol): ν(CO) 1973 (s), 1862 (s), 1831 (s) cm^{-1}. The NMR spectra of **3a** were obtained by the addition of excess (~10-fold) tetraethylammonium chloride in CD_2Cl_2 solution. Since no detectable change was observed in the NMR spectrum on further addition of the halide, it was assumed that the data given below are the limiting values for **3a**. NMR in CD_2Cl_2: ^1H, δ 6.44 [br, 3H, H^aCP_2], 4.50 [br, 3H, H^bCP_2]; $^{31}P\{^1H\}$, δ 7.0 [s, ^1J(PtP) = 2478 Hz, ^2J(PtP) = 262 Hz, ^3J(PP) = 228 Hz, dppm].

Table 2. Selected Bond Lengths (Å) and Angles (deg)

Pt(1)–Pt(2)	2.613(1)	Pt(1)–Pt(3)	2.586(1)
Pt(1)–Re	2.728(1)	Pt(1)–I	3.283(1)
Pt(1)–P(2)	2.304(3)	Pt(1)–P(4)	2.274(3)
Pt(2)–Pt(3)	2.598(1)	Pt(2)–Re	2.739(1)
Pt(2)–I	3.113(1)	Pt(2)–P(1)	2.301(3)
Pt(2)–P(6)	2.262(3)	Pt(3)–Re	2.777(1)
Pt(3)–I	3.343(1)	Pt(3)–P(3)	2.272(3)
Pt(3)–P(5)	2.275(3)	Re–C(4)	1.905(11)
Re–C(5)	1.905(13)	Re–C(6)	1.857(12)
O(1)–C(4)	1.137(14)	O(2)–C(5)	1.144(16)
O(3)–C(6)	1.185(15)		

Pt(2)–Pt(1)–Pt(3)	60.1(1)	Pt(2)–Pt(1)–Re	61.7(1)
Pt(2)–Pt(1)–I	62.5(1)	Pt(2)–Pt(1)–P(2)	97.1(1)
Pt(2)–Pt(1)–P(4)	153.8(1)	Pt(3)–Pt(1)–Re	62.9(1)
Pt(3)–Pt(1)–I	68.3(1)	Pt(3)–Pt(1)–P(2)	156.6(1)
Pt(3)–Pt(1)–P(4)	93.8(1)	Re–Pt(1)–I	118.5(1)
Re–Pt(1)–P(2)	112.2(1)	Re–Pt(1)–P(4)	109.1(1)
I–Pt(1)–P(2)	98.2(1)	I–Pt(1)–P(4)	109.2(1)
P(2)–Pt(1)–P(4)	109.0(1)	Pt(1)–Pt(2)–Pt(3)	59.5(1)
Pt(1)–Pt(2)–Re	61.2(1)	Pt(1)–Pt(2)–I	69.3(1)
Pt(1)–Pt(2)–P(1)	154.8(1)	Pt(1)–Pt(2)–P(6)	95.7(1)
Pt(3)–Pt(2)–Re	62.7(1)	Pt(3)–Pt(2)–I	71.0(1)
Pt(3)–Pt(2)–P(1)	97.5(1)	Pt(3)–Pt(2)–P(6)	155.1(1)
Re–Pt(2)–I	124.1(1)	Re–Pt(2)–P(1)	120.0(1)
Re–Pt(2)–P(6)	105.9(1)	I–Pt(2)–P(1)	94.6(1)
I–Pt(2)–P(6)	103.2(1)	P(1)–Pt(2)–P(6)	107.2(1)
Pt(1)–Pt(3)–Pt(2)	60.5(1)	Pt(1)–Pt(3)–Re	61.0(1)
Pt(1)–Pt(3)–I	65.8(1)	Pt(1)–Pt(3)–P(3)	97.4(1)
Pt(1)–Pt(3)–P(5)	154.6(1)	Pt(2)–Pt(3)–Re	61.2(1)
Pt(2)–Pt(3)–I	61.791)	Pt(2)–Pt(3)–P(3)	157.9(1)
Pt(2)–Pt(3)–P(5)	94.4(1)	Re–Pt(3)–I	115.1(1)
Re–Pt(3)–P(3)	108.4(1)	Re–Pt(3)–P(5)	112.6(1)
I–Pt(3)–P(3)	112.9(1)	I–Pt(3)–P(5)	99.8(1)
P(3)–Pt(3)–P(5)	107.7(1)	Pt(1)–Re–Pt(2)	57.1(1)
Pt(1)–Re–Pt(3)	56.0(1)	Pt(1)–Re–C(4)	104.6(4)
Pt(1)–Re–C(5)	166.3(4)	Pt(1)–Re–C(6)	106.1(4)
Pt(2)–Re–Pt(3)	56.2(1)	Pt(2)–Re–C(4)	111.9(3)
Pt(2)–Re–C(5)	110.0(4)	Pt(2)–Re–C(6)	157.7(4)
Pt(3)–Re–C(4)	160.2(4)	Pt(3)–Re–C(5)	114.2(4)
Pt(3)–Re–C(6)	103.1(4)	C(4)–Re–C(5)	84.1(5)
C(4)–Re–C(6)	85.3(5)	C(5)–Re–C(6)	84.9(5)
Pt(1)–I–Pt(2)	48.1(1)	Pt(1)–I–Pt(3)	45.9(1)
Pt(2)–I–Pt(3)	47.3(1)	Pt(2)–P(1)–C(3)	108.1(4)
Pt(2)–P(1)–C(C1)	119.3(4)	Pt(2)–P(1)–C(D1)	121.2(5)
C(3)–P(1)–C(C1)	101.3(5)	C(3)–P(1)–C(D1)	101.6(5)
C(C1)–P(1)–C(D1)	102.3(7)	Pt(1)–P(2)–C(1)	108.2(3)
Pt(1)–P(2)–C(K1)	120.1(3)	Pt(1)–P(2)–C(Li)	120.1(4)
C(1)–P(2)–C(K1)	100.2(5)	C(1)–P(2)–C(L1)	104.6(4)
C(Ki)–P(2)–C(Li)	101.0(5)	Pt(3)–P(3)–C(2)	108.7(3)
Pt(3)–P(3)–C(G1)	114.3(5)	Pt(3)–P(3)–C(H1)	122.2(4)
C(2)–P(3)–C(G1)	105.1(5)	C92)–P(3)–C(H1)	122.2(4)
C(G1)–P(3)–C(H1)	102.3(5)	Pt(1)–P(4)–C(2)	110.9(4)
Pt(1)–P(4)–C(I1)	118.7(4)	Pt(1)–P(4)–C(J1)	115.3(3)
C(2)–P(4)–C(I1)	104.9(4)	C(2)–P(4)–C(J1)	104.2(5)
C(I1)–P(4)–C(J1)	101.2(5)	Pt(3)–P(5)–C(3)	109.2(4)
Pt(3)–P(5)–C(E1)	115.7(4)	Pt(3)–P(5)–C(F1)	123.2(3)
C(3)–P(5)–C(E1)	105.5(6)	C(3)–P(5)–C(F1)	98.7(5)
C(E1)–P(5)–C(F1)	102.2(4)	Pt(2)–P(6)–C(1)	109.5(4)
Pt(2)–P(6)–C(A1)	114.8(3)	Pt(2)–P(6)–C(B1)	120.7(5)
C(1)–P(6)–C(A1)	107.3(4)	C(1)–P(6)–C(B1)	97.9(6)
C(A1)–P(6)–C(B1)	104.8(5)	P(2)–C(1)–P(6)	118.1(5)
P(3)–C(2)–P(4)	111.4(6)	P(1)–C(3)–P(5)	114.2(6)
Re(1)–C(4)–O(1)	175.9(9)	Re(1)–C(5)–O(2)	178.0(11)
Re(1)–C(6)–O(3)	179.1(11)		

(20) (a) Godbey, D. J.; Garin, F.; Somorjai, G. A. *J. Catal.* **1989**, *117*, 144. (b) Augustine, S. M.; Sachtler, W. M. H. *J. Catal.* **1987**, *106*, 417. (c) Meitzner, G.; Via, G. H.; Lytle, F. W.; Sinfelt, J. H. *J. Chem. Phys.* **1987**, *87*, 6354.

$[Pt_3(\mu_3\text{-Br})\{Re(CO)_3\}(\mu\text{-dppm})_3]$ (3b). A procedure similar to that for **3a** was followed with the use of tetraethylammonium bromide instead of tetraethylammonium chloride. The red-brown solid **3b** was obtained in 76% yield. Anal. Calcd for $C_{78}H_{66}BrO_3P_6Pt_3Re$: C, 44.86; H, 3.19. Found: C, 44.47; H, 3.38. IR (Nujol): ν(CO) 1972 (s), 1861 (s), 1828 (s) cm^{-1}. NMR in CD_2Cl_2: ^1H, δ 6.10 [br, 3H, H^aCP_2], 4.41 [br, 3H, H^bCP_2]; $^{31}P\{^1H\}$, δ 4.3 [s, ^1J(PtP) = 2462 Hz, ^2J(PtP) = 259 Hz, ^3J(PP) = 231 Hz, dppm].

$[Pt_3(\mu_3\text{-I})\{Re(CO)_3\}(\mu\text{-dppm})_3]$ (3c). Complex **3c** was prepared by the same procedure as for **3a**, except that tetrabutylammonium iodide was used instead of tetraethylammonium chloride. The product was obtained as a dark red-brown powder in 82% yield. Anal. Calcd for $C_{78}H_{66}IO_3P_6Pt_3Re$: C, 43.87; H, 3.12. Found: C, 44.21; H, 3.12. IR (Nujol): ν(CO) 1977 (s), 1866 (s), 1832 (s) cm^{-1}. NMR in CD_2Cl_2: ^1H, δ 5.84 [d, 3H, ^2J(HH) = 13.1 Hz, ^2J(PH) = 66 Hz, H^aCP_2], 5.26 [d, 3H, ^2J(HH) = 13.1 Hz, H^bCP_2]; $^{31}P\{^1H\}$, δ = −5.7 [s, ^1J(PtP) = 2520 Hz, ^2J(PtP) = 209 Hz, ^3J(PP) = 240 Hz, dppm]; ^1H at −90 °C, δ 5.87 [br, 3H, H^aCP_2], 5.24 [br, 3H, H^bCP_2]; $^{31}P\{^1H\}$ at −90 °C, δ −6.9 [s, br, ^1J(PtP) = 2543 Hz, ^2J(PtP) = 197 Hz, ^3J(PP) = 217 Hz, dppm].

$[Pt_3(\mu_3\text{-Cl})\{ReO_3\}(\mu\text{-dppm})_3]$ (4a). To a solution of **2**$[PF_6]$ (31 mg, 0.015 mmol) in acetone (15 mL) was added tetraethylammonium chloride (9.7 mg, 0.059 mmol). A red-brown precipitate formed almost immediately. The solution was stirred for 15 min and was then concentrated to *ca.* 2 mL. Hexane was added to precipitate the product, which was washed with methanol (0.5 mL) and diethyl ether (2 mL) and then dried under high vacuum to give a red-brown solid. Yield: 70%. Anal. Calcd for $C_{75}H_{66}ClO_3P_6Pt_3Re$: C, 44.86; H, 3.31. Found: C, 44.81; H, 3.37. IR (Nujol): ν(Re=O) of ReO_3 925 (m), 890 (s, br) cm^{-1}. The NMR spectra of **4a** were obtained by the addition of excess tetraethylammonium chloride (15-fold). In the absence of added tetraethylammonium chloride, the NMR spectrum of **4a** in CD_2Cl_2 was very similar to that of **2**, indicating extensive dissociation of chloride under these conditions. NMR for **4a** in CD_2Cl_2: ^1H, δ 5.81 [br, 3H, H^aCP_2], 5.30 [br, 3H, H^bCP_2]; $^{31}P\{^1H\}$, δ −7.8 [s, ^1J(PtP) = 3210 Hz, ^3J(PP) = 166 Hz, dppm].

$[Pt_3(\mu_3\text{-Br})\{ReO_3\}(\mu\text{-dppm})_3]$ (4b). The procedure was the same as for **4a**, except that tetraethylammonium bromide was used instead of tetraethylammonium chloride. The red-brown solid **4b** was obtained in 80% yield. In order to characterize **4b** in CD_2Cl_2 solution, a 4-fold excess of tetraethylammonium bromidw was used. Anal. Calcd for $C_{75}H_{66}BrO_3P_6Pt_3Re$: C, 43.89; H, 3.24. Found: C, 43.80; H, 3.42. IR (Nujol): ν(Re=O) of ReO_3 924 (m), 890 (s, br) cm^{-1}. NMR in CD_2Cl_2: ^1H, δ 5.80 [br, 3H, H^aCP_2], 5.32 [br, 3H, H^bCP_2]; $^{31}P\{^1H\}$, δ −13.9 [s, ^1J(PtP) = 3292 Hz, ^3J(PP) = 158 Hz, dppm].

$[Pt_3(\mu_3\text{-I})\{ReO_3\}(\mu\text{-dppm})_3]$ (4c). A procedure similar to that for **4b** was followed with the use of **2**$[PF_6]$ and tetrabutylammonium iodide. A red-brown product was obtained. Yield: 90%. **4c** is slightly soluble in dichloromethane. Anal. Calcd for $C_{75}H_{66}IO_3P_6Pt_3Re\cdot{}^1/_2CH_2Cl_2$: C, 42.33; H, 3.15. Found: C, 42.27; H, 2.94. IR (Nujol): ν(Re=O) of ReO_3 926 (m), 892 (s, br) cm^{-1}. NMR in CD_2Cl_2: ^1H, δ 5.80 [br, 3H, H^aCP_2], 5.30 [br, 3H, H^bCP_2]; $^{31}P\{^1H\}$, δ −15.2 [s, ^1J(PtP) = 3264 Hz, ^3J(PP) = 174 Hz, dppm]. NMR confirmed the presence of CH_2Cl_2.

$[Pt_3(\mu_3\text{-SnCl}_3)\{ReO_3\}(\mu\text{-dppm})_3]$ (5a). To a solution of **2**$[PF_6]$ (36 mg, 0.017 mmol) in THF (15 mL) was added an equimolar mixture of NaCl (1.0 mg) and $SnCl_2$ (3.2 mg). After 16 h of stirring, the solvent was removed under vacuum. The brown residue was extracted with dichloromethane to give a brown solution, which was then concentrated to *ca.* 2 mL; the product was precipitated with hexane and then dried under vacuum to give the product in 80% yield. Black platelike crystals of complex **5a** could be obtained from CH_2Cl_2/diethyl ether. Anal. Calcd for $C_{75}H_{66}Cl_3O_3P_6Pt_3ReSn$: C, 40.99; H, 3.03. Found: C, 41.78; H, 3.09. IR (Nujol): ν(Re=O) of ReO_3 946 (m), 937 (s) cm^{-1}. NMR in CD_2Cl_2: ^1H, δ 6.05 [br, 3H, H^aCP_2], 5.70 [br, 3H, H^bCP_2]; $^{31}P\{^1H\}$, δ −7.1 [s, ^1J(PtP) = 3144 Hz, ^3J(PP) = 193 Hz, dppm].

Table 3. Crystallographic Data for $[Pt_3(\mu_3\text{-Re(CO)}_3)(\mu_3\text{-I})(\mu\text{-dppm})_3]\cdot CH_2Cl_2\cdot H_2O$

empirical formula	$C_{79}H_{70}Cl_2IO_4P_6Pt_3Re$
fw	2238.5
space group	C_2/c
a, Å	34.911(4)
b, Å	19.965(6)
c, Å	24.101(3)
β, deg	117.98(1)
V, Å^3	14835(5)
Z	8
D_{calc}, g cm^{-3}	2.004
cryst dimens, mm	0.42 × 0.10 × 0.03
temp, °C	25
radiation	Mo Kα
wavelength, Å	0.71073
μ(Mo Kα), cm^{-1}	80.1
data collection range, θ, deg	2.1−30.0
no. of unique reflns ($I \geq 3\sigma(I)$)	10 848
no. of params refined	701
R	0.0393
R_w	0.0420
largest shift/esd ratio	0.06
observn of unit wt	1.37
final diff synthesis, e Å^{-3}	−1.6 to +1.9

$[Pt_3(\mu_3\text{-SnF}_3)\{ReO_3\}(\mu\text{-dppm})_3]$ (5b). The same procedure was followed as for **5a** with the use of NaF and SnF_2 instead of NaCl and $SnCl_2$. A yellow-black product was obtained. Yield: 76%. Anal. Calcd for $C_{75}H_{66}F_3O_3P_6Pt_3ReSn$: C, 41.93; H, 3.10. Found: C, 41.67; H, 3.21. IR (Nujol): ν(Re=O) of ReO_3 965 (m), 926 (s) cm^{-1}. NMR in CD_2Cl_2: ^1H, δ 5.96 [br, 3H, H^aCP_2], 5.68 [br, 3H, H^bCP_2]; $^{31}P\{^1H\}$, δ −6.6 [s, ^1J(PtP) = 3099 Hz, ^3J(PP) = 122 Hz, dppm].

X-ray Crystal Structure Analysis of $[Pt_3(\mu_3\text{-I})\{Re(CO)_3\}(\mu\text{-dppm})_3]\cdot CH_2Cl_2\cdot H_2O$ (3c·CH_2Cl_2·H_2O). A black, needlelike crystal of dimensions ~0.42 × 0.10 × 0.03 mm was used in this analysis. All X-ray crystallographic measurements were made with graphite-monochromated Mo Kα radiation and an Enraf-Nonius CAD4 diffractometer.

The unit cell constants, listed in Table 3, were determined by a least-squares treatment of 25 reflections with Bragg angles 11 < θ < 21°. The intensity data were measured by continuous $\theta/2\theta$ scans of $(0.73 + 0.58 \tan\theta)°$ in θ, and the scan speeds were adjusted to give $\sigma(I)/I \leq 0.03$ subject to a time limit of 30 s. The stability of the crystal and diffractometer was monitored throughout the experiment by measuring three reflections every 2 h. Their mean intensity showed only random variations not exceeding 3.5%. The integrated intensities of all reflections, derived in the usual manner (q = 0.03),[21] were corrected for Lorentz, polarization, and absorption effects. The last correction was made by the empirical method of Walker and Stuart at the end of the isotropic refinement.[22] The internal agreement factor, R_{int}, for measuring 634 duplicate intensities was 0.034. Of 21 563 unique reflections measured, only 10 848 for which $I \geq 3\sigma(I)$ were used in the structure analysis.

The positions of the Pt and Re atoms were determined from a Patterson function and those of the remaining non-hydrogen atoms from the subsequent Fourier difference syntheses. Hydrogen atoms of the dppm ligands were included in the structural model in calculated positions, with C−H = 0.96 Å and U(H) = 1.2U(C), where U(C) is the isotropic displacement parameter of the carbon atom to which the hydrogen is bonded. No allowance was made for scattering of the hydrogen atoms

(21) Manojlović-Muir, Lj.; Muir, K. W. *J. Chem. Soc., Dalton Trans.* **1974**, 2427.
(22) Walker, N.; Stuart, D. *Acta Crystallogr.* **1983**, *A39*, 158.
(23) *International Tables for X-ray Crystallography*; Kynoch Press: Birmingham, England, 1974; Vol. IV.
(24) Mallinson, P. R.; Muir, K. W. *J. Appl. Crystallogr.* **1985**, *18*, 51.

of CH_2Cl_2 and H_2O molecules. The structure was refined by full-matrix least-squares, minimizing the function $\sum w(|F_o| - |F_c|)^2$, where $w = \sigma(|F_o|)^{-2}$. The 11 C and H atoms of each phenyl group were refined as a rigid group constrained to D_{6h} symmetry and C–C = 1.38 Å. In the CH_2 groups the hydrogen atoms were allowed to ride on the carbon atoms. All non-hydrogen atoms in the metal complex **3c** were refined with anisotropic, and those in the solvent molecules with isotropic, displacement parameters. The atomic scattering factors and anomalous dispersion corrections were taken from ref 23. The refinement, involving 701 parameters and 10 848 unique reflections with $I \geq 3\sigma(I)$, converged at $R = 0.0393$ and $R_w = 0.0420$.

All calculations were performed using the GX program package.[24]

Acknowledgment. We thank the NSERC (Canada) for financial support and the SERC (U.K.) for an equipment grant and the Iranian government for a studentship (to A.A.T.).

Supplementary Material Available: Tables of hydrogen atom coordinates, anisotropic displacement parameters, and bond lengths and angles for **3c** (7 pages). Ordering information is given on any current masthead page.

OM950016B

Mechanism of Formation of Platinum(0) Complexes Containing Silicon–Vinyl Ligands

Larry N. Lewis,*,† Robert E. Colborn,*,† Hans Grade,† Garold L. Bryant, Jr.,†,‡ Chris A. Sumpter,† and Robert A. Scott§

GE Corporate Research and Development Center, Schenectady, New York 12301, and Center for Metalloenzyme Studies, Chemistry Building, The University of Georgia, Athens, Georgia 30602-2556

Received October 14, 1994⊗

Reactions are described in detail between H_2PtCl_6 and vinyl–silicon-containing compounds such as 1,3-divinyltetramethyldisiloxane ($M^{vi}M^{vi}$) and divinyldimethylsilane ($(CH_3)_2Si(CH{=}CH_2)_2$). The structures of the platinum and silicon products were examined from these reactions with $M^{vi}M^{vi}$ and 1,3,5,7-tetravinyltetramethylcyclotetrasiloxane (D_4^{vi}). The platinum products were all Pt(0)–olefin complexes. The reaction of chloroplatinic acid with $M^{vi}M^{vi}$ gave a mixture of platinum complexes containing $M^{vi}D_xM^{vi}$ ligands (**1**; $x = 0-11$). Some complexes are polynuclear with bridging ligands and no metal–metal bonds, such as $Pt_2(M^{vi}M^{vi})_3$ (**2**). The conversion of Pt(IV) complexes to Pt(0) species resulted in the net conversion of a silicon–vinyl group to a silicon–oxygen group. The reaction of H_2PtCl_6 with $(CH_3)_2Si(CH{=}CH_2)_2$ gave both a Pt(0) (**4**) and a Pt(II) (**5**) product. A three-dimensional, X-ray crystal structure of **5** was solved, which showed a doubly chloro bridged platinum dimer with no metal–metal bond of stoichiometry $C_{18}H_{38}Cl_2Pt_2Si_3$. The dimer contained a bridging $(CH_3)_2Si(CH{=}CH_2)_2$ ligand. Additionally each Pt atom had a chelating $(CH_3)_2Si(\eta^2\text{-}CH{=}CH_2)(\eta^1\text{-}CH_2CH_2)$ ligand, resulting from formal protonation of one of the vinyl groups. Crystallographic data: $a = 6.799(3)$ Å, $b = 19.830(8)$ Å, $c = 18.847(10)$ Å, $\beta = 95.43(4)°$; space group $P2_1/c$; $Z = 4$. The structure of **4** was determined by spectroscopic analysis to be a Pt(0)–olefin complex. The structures of **4** and **5** were further confirmed by preparation of chemical derivatives with $P(C_6H_5)_3$, which formed known platinum phosphine compounds. Compound **4** converted to compound **5** by reaction with HCl. A mechanism for the reaction of Pt(IV) with silicon–vinyl is presented based on the analysis of platinum, silicon, and gaseous products. Mechanistic experiments included reactions with D_2PtCl_6 and reactions in the presence of added C_2H_4 or C_2D_4.

Introduction

The hydrosilylation reaction (eq 1) has been the subject of several extensive reviews.[1-8] The reaction is employed for the synthesis of monomers with Si–C bonds and for forming cross-linked networks by using multifunctional polymers.[9]

$$R_3SiH + H_2C{=}CHR' \xrightarrow{\text{catalyst}} R_3SiCH_2CH_2R' \quad (1)$$

The most active catalysts for hydrosilylation are complexes of the platinum-group metals; among these, platinum complexes are the most active.[10,11] An example of a highly active catalyst is Karstedt's catalyst;[12] this catalyst is typically prepared via the procedure shown in eq 2. Details of such a synthesis were recently described.[13,14] Lappert and co-workers have recently described some of the chemistry from eq 2, including a

$$H_2PtCl_6 + \text{excess } M^{vi}M^{vi} \xrightarrow[2.\ NaHCO_3]{1.\ EtOH,\ heat} Pt(M^{vi}D_xM^{vi})_y + M^{vi}D_xM^{vi} \quad (2)$$

1

$x = 0-11$, $y = 2-4$

1a: $x = 0$, $y = 2$

$M^{vi}M^{vi} = CH_2{=}CH{-}Si(CH_3)_2{-}O{-}Si(CH_3)_2{-}CH{=}CH_2$ $\quad D = {-}Si(CH_3)_2{-}O$

† GE Corporate Research and Development Center.

‡ Present address: Physical & Analytical Chemistry Research, The Upjohn Co., Kalamazoo, MI 49001-0199.

§ The University of Georgia.

⊗ Abstract published in *Advance ACS Abstracts,* April 1, 1995.

(1) Marciniec, B.; Gulinski, J.; Urbaniak, W.; Kornetka, Z. W. In *Comprehensive Handbook on Hydrosilylation*; Marciniec, B., Ed.; Pergamon: Oxford, U.K., 1992.

(2) Pukhnarevich, V. B.; Lukevics, E.; Kopylova, L. I.; Voronkov, M. G. *Perspectives of Hydrosilylation*; Institute of Organic Synthesis: Latvia: Riga, Latvia, 1992.

(3) Ojima, I. In *The Chemistry of Organic Silicon Compounds*; Patai, S., Rappoport, Z., Eds.; Wiley-Interscience: New York, 1989; Vol. 2, Chapter 25, pp 1479–1526.

(4) Armitage, D. A. In *Comprehensive Organometallic Chemistry*; Wilkinson, G., Stone, F. G. A., Abel, E. W., Eds.; Pergamon: Oxford, U.K., 1982; Vol. 2, pp 117–120.

(5) Speier, J. L. In *Advances in Organometallic Chemistry*; Stone, F. G. A., West, R., Eds.; Academic Press: New York, 1979; Vol. 17, pp 407–447.

(6) Lukevics, E.; Belyakova, Z. V.; Pomeransteva, M. G.; Voronkov, M. G. *J. Organomet. Chem. Libr.* **1977,** *5,* 1.

(7) Eaborn, C.; Bott, R. W. In *The Bond to Carbon*; MacDiarmid, A. G., Ed.; Marcel Dekker: New York, 1968.

(8) Harrod, J. F.; Chalk, A. J. In *Organic Synthesis via Metal Carbonyls*; Wender, I., Pino, P., Eds.; Wiley: New York, 1977; Vol. 2, pp 673–703.

(9) Stein, J.; Lewis, L. N.; Smith, K. A.; Lettko, K. X. *J. Inorg. Organomet. Polym.* **1991,** *1,* 325. The use of M, D, T, and Q shorthand has been described in this paper.

(10) Lewis, L. N.; Lewis, N. *Chem. Mater.* **1989,** *1,* 106–114.

(11) Lewis, L. N.; Uriarte, R. J. *Organometallics* **1990,** *9,* 621–625.

(12) Karstedt, B. D. U.S. Patent 3,775,452, 1973.

0276-7333/95/2314-2202$09.00/0

description of the gaseous products[14] and the oligosiloxanes.[14,15] The structure of the platinum product(s) (**1**) from eq 2 has been discussed.[10,16] Willing had previously reported the reaction of H_2PtCl_6 with $M^{vi}M^{vi}$.[17] However, Willing's reaction conditions did not use ethanol or the sodium bicarbonate workup procedure. It is well-known in the synthetic literature for platinum that complexes of the type L_2PtX_2, where L is an olefin, alkyne, or diene and X is a halogen, may be prepared from alcoholic solutions of H_2PtCl_6 and ligand.[18,19] The alcohol serves as a reducing agent to give Pt(II) complexes and the corresponding aldehyde. An unusual feature of the procedure of eq 2 is the formation of a Pt(0) compound. Indeed, the dihalides are often replaced by carbonate, e.g., $[PtL_2(CO_3)]$, to make the Pt(0) olefin complex from a Pt(II) precursor.[20]

This article describes our efforts to further identify the products from the reaction in eq 2 and understand their mechanism of formation. The critical question is to resolve the formation of the Pt(0) complexes from the vinyl–siloxane ligands; this is important both from a synthetic perspective and for their role as industrial catalysts. We have used ligands other than $M^{vi}M^{vi}$ in the direct synthesis of Pt(0) olefin complexes from Pt(IV) precursors. A subsequent report will describe the catalytic performance of some of these new platinum complexes.

Results and Discussion

Synthesis and Structure of Pt Complexes with $(CH_3)_2(CH_2{=}CH)SiOSi(CH{=}CH_2)(CH_3)_2$. The reaction in eq 2 was originally reported by Karstedt.[12] Earlier, Willing[17] had described the reaction between H_2PtCl_6 and $M^{vi}M^{vi}$ at reflux temperature. Willing's workup procedure involved aqueous extraction of the product until the extractant was neutral, presumably removing residual acid and chloride. Ashby and Modic[16] reported a field desorption mass spectroscopic (FDMS) analysis of two chromatographically separated fractions obtained from eq 2. Their FDMS analysis suggested the empirical formulas $Pt(M^{vi}M^{vi})_2$ (**1a**) and $Pt(M^{vi}M^{vi})(M^{vi}M^{OH})$. Lappert defined "solution A" as the combined product mixture from eq 2.[15]

The Lappert group[15] reported the dimeric structure of the platinum product $Pt_2(M^{vi}M^{vi})_3$ (**2**), obtained from the reaction of $Pt(COD)_2$ (COD = 1,5-cyclooctadiene) with $M^{vi}M^{vi}$ (eq 3). Dimer **2** has no Pt–Pt bond and one bridging $M^{vi}M^{vi}$, and each Pt atom has a chelating $M^{vi}M^{vi}$ ligand. It is not clear if **2** is a true representative of the platinum species in solution from eq 2. We shall address this question in our experiments described below.

$$2Pt(COD)_2 + 3M^{vi}M^{vi} \rightarrow \underset{\mathbf{2}}{Pt_2(M^{vi}M^{vi})_3} \qquad (3)$$

Many Pt(0) olefin complexes have been prepared and studied as hydrosilylation catalysts.[21] One recent report described an unusual Pt(0) complex with DBA ligands (DBA = dibenzylideneacetone) and summarized most of the structural data for Pt(0)–olefin complexes.[22] These platinum complexes generally are planar and three-coordinate. The four-coordinate, tetrahedral complex $Pt(COD)_2$ appears to be an exception.[23] Only a few examples exploiting the synthetic methodology of eq 2 to make Pt(0) complexes have appeared.[14,15,24] One problem is that the reaction of H_2PtCl_6 with most olefins gives Pt(II) compounds.[25,26] Some limited work using other silicon–vinyl sources has been reported: 1,3,5,7-tetravinyltetramethylcyclotetrasiloxane (D_4^{vi}),[12,14,27] $(CH_3)_2Si(CH{=}CH_2)_2$,[12,27] $(C_6H_5)_2Si(CH{=}CH_2)_2$,[12,27] and 1,3-divinyl-1,3-diphenyldimethyldisiloxane.[28]

Due to the possible role of ethanol in the reduction of Pt(IV), the great majority of the reactions described in this paper were carried out with no ethanol in the presence of excess vinylsilane. In the standard reaction with $M^{vi}M^{vi}$ (eq 2), such a process leads to the same Pt species in the same yield with a similar family of oligosiloxanes.

Since it is difficult to obtain rigorously dry chloroplatinic acid, one also needs to consider the possible role of water in the reduction of the platinum species. By analogy to Wacker chemistry, one might propose a scheme to convert the silyl olefin to an aldehyde with concomitant production of HCl. However, in an analysis of the volatile fraction by both NMR spectroscopy and GC/MS, no organic products based on oxygen addition at the olefin are observed. Moreover, smooth reduction of anhydrous $PtCl_4$ takes place to produce the same distribution of platinum compounds (vide infra). In such a reaction, silyl chlorides are observed as the primary reaction products.

In the present work, NMR analysis of solution A was carried out after first concentrating it in vacuo. The ^1H NMR spectrum of the solution A concentrate showed a 1:1 ratio of free vinyl to Pt-bound vinyl. The bound vinyl protons exhibit a complex multiplet from δ 2.8 to 4.2 significantly upfield from the free vinyl protons. FDMS analysis of the recovered distillate showed mostly oligomers of the formula $M^{vi}D_xM^{vi}$ (x = 0–11). The FDMS analysis of solution A concentrate showed that **1**, specifically including **1a**, was present, but no dimer **2** was observed.

In contrast, the FDMS analysis of the product from eq 3, when 6 equiv of $M^{vi}M^{vi}$ was used (relative to Pt), showed that both **2** and **1a** were formed. The ^1H NMR spectrum of the reaction product between $Pt(COD)_2$ and 6 equiv of $M^{vi}M^{vi}$ is quite different from that of solution A concentrate; the region for the Pt–vinyl protons for

(13) Lewis, L. N.; Lewis, N.; Uriarte, R. J. In *Homogeneous Transition Metal Catalyzed Reactions*; Adv. Chem. Ser. 230; Moser, W. R., Slocum, D. W., Eds; American Chemical Society: Washington, DC, 1992; p 541.
(14) Chandra, G.; Lo, P. Y.; Hitchcock, P. B.; Lappert, M. F. *Organometallics* **1987**, *6*, 191–192.
(15) Hitchcock, P. B.; Lappert, M. F.; Warhurst, N. J. W. *Angew. Chem., Int. Ed. Engl.* **1991**, *30*, 438–440.
(16) Ashby, B. A.; Modic, F. J. U.S. Patent 4,288,345, 1981.
(17) Willing, D. N. U.S. Patent 3,419,593, 1968.
(18) Zeise, W. C. *Mag. Pharm.* **1830**, 35, 105.
(19) Hartley, F. R. *Inorg. Chim. Acta* **1971**, *5*, 197.
(20) Hayward, P. J.; Blake, D. M.; Wilkinson, G.; Nyman, C. J. *J. Am. Chem. Soc.* **1970**, *92*, 5873.
(21) Marciniec, B.; Gulinski, J.; Urbaniak, W.; Nowicka, T.; Mirecki, J. *Appl. Organomet. Chem.* **1990**, *4*, 27–34.
(22) Lewis, L. N.; Krafft, T. A.; Huffman, J. C. *Inorg. Chem.* **1992**, *31*, 3555–3557.
(23) Howard, J. A. K. *Acta Crystallogr., Sect. B* **1982**, *38*, 2896–2898.
(24) Chandra, G.; Lo, P. Y. K. U.S. Patent 4,593,084, 1986.
(25) McAfee, R. C.; Adkins, J.; Miskowski, R. L. U.S. Patent 4,394,317, 1983.
(26) Cavezzan, J. U.S. Patent 4,699,813, 1987.
(27) Karstedt, B. D. U.S. Patent 3,814,730, 1974.
(28) Saruyama, T.; Takeda, H.; Togashi, T. U.S. Patent 5,098,980, 1992.

solution A has many more peaks than the product from $Pt(COD)_2$. The complex nature of the ^1H NMR spectrum for solution A concentrate suggested that a mixture of platinum species was present. These might include a variety of bridging divinyloligosiloxane ligands.

Further spectroscopic analyses were employed to determine the species in the solution A mixture. Typical ^{195}Pt NMR spectra for solution A showed a pair of resonances, as reported by Lappert,[14] at −6148 and −6149 ppm in a 2:1 ratio, respectively. Lappert suggested that these resonances were due to isomers of **2**, i.e., *rac* and *meso* forms. In our experiments, when additional $M^{vi}D_xM^{vi}$ oligomers were added to a solution A concentrate, only a single ^{195}Pt NMR signal was observed at −6148 ppm. Thus, another interpretation for the 2:1 set of resonances observed in the solution A concentrate is an equilibrium between complexes of different nuclearity, such as **2** and **1a** (shown in eq 4).

change in nuclearity

$$\underset{\mathbf{1a}}{2Pt(M^{vi}M^{vi})_2} \rightleftharpoons \underset{\mathbf{2}}{Pt_2(M^{vi}M^{vi})_3} + M^{vi}M^{vi} \qquad (4)$$

FDMS analysis of solution A showed the silicon products were $M^{vi}D_xM^{vi}$ (x = 0−11). The platinum-containing products in the spectrum were identified on the basis of the characteristic isotope pattern for platinum. Clusters of peaks were separated by 74 amu corresponding to D units ($(CH_3)_2SiO_{2/2}$). FDMS also demonstrated the presence of **1a** and other monomeric platinum complexes where the ligands $M^{vi}D_xM^{vi}$ varied in composition from x = 0 to x = 5. However, because we failed to detect **2** by FDMS, yet another equilibrium based on ligand exchange as in eq 5 may be operative.

ligand exchange

$$Pt(M^{vi}M^{vi})_2 + 3M^{vi}D_xM^{vi} \rightleftharpoons Pt(M^{vi}D_xM^{vi})_3 + 2M^{vi}M^{vi} \qquad (5)$$

In a related experiment, solution A was combined with $MD^{vi}M$. No ^{195}Pt NMR signal was observed when 10 mol equiv was added (based on Pt), presumably due to a broadening based on exchange between different sites; however, when 100 equiv of $MD^{vi}M$ was added, a new resonance was observed at −6155 ppm. New ^{13}C NMR signals were also observed for the mixture containing 100 equiv of $MD^{vi}M$ and 1 equiv of solution A, replacing those observed for solution A. These results confirm replacement of $M^{vi}M^{vi}$ with $MD^{vi}M$ when 100 equiv of the latter was added.

Extended X-ray absorption fine structure (EXAFS) analysis was carried out on a Karstedt's catalyst solution (Figure 1a). The first platinum shell contained carbon, d_{Pt-C} = 2.17 Å, with a Pt−C coordination number of 6. The EXAFS data also showed the absence of a significant amount of chlorine in the coordination sphere around platinum. The second coordination shell contained silicon (d_{Pt-Si} = 3.41 Å) with a Pt−Si coordination number of 3. The near-edge region was consistent in shape and area with Pt(0) species.[29]

In summary, the platinum compounds in solution A are best viewed as zerovalent and as a mixture of vinyl-

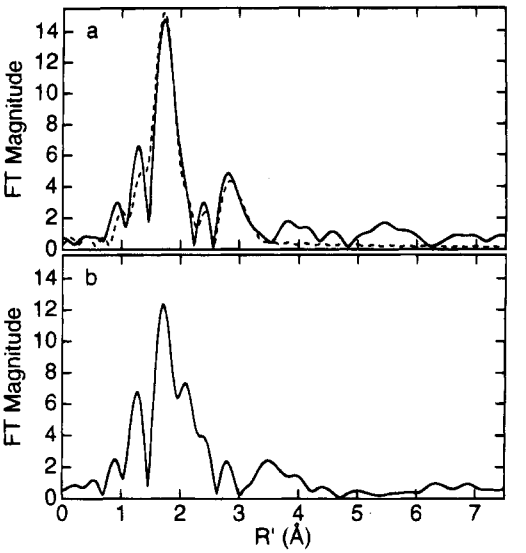

Figure 1. Fourier transforms (k = 2−13 Å^{-1}, k^3 weighting) of the Pt EXAFS of **1** (a) and **4** (b). The dashed line in (a) is the Fourier transform of a simulated EXAFS spectrum composed of six Pt−C at 2.17 Å (σ^2 = 0.0021 Å^2) and two Pt−Si at 3.40 Å (σ^2 = 0.0031 Å^2).

coordinated siloxane species similar to **1** and **2**. The exact composition is undoubtedly a function of the ratio of platinum to ligand and the extent of hydrolysis in the siloxanes.

Analysis of Gaseous Products from Eq 2. The synthesis of **1** (eq 2) was repeated except that D_2PtCl_6 was employed in the reaction with $M^{vi}M^{vi}$. The gaseous products were then analyzed and compared to those observed for the reaction with H_2PtCl_6. These experiments showed that the main volatile products were ethylene and butadiene, while lesser amounts of products included ethane, butane, hydrogen chloride, and vinyl chloride. The ethylene had substantial C_2H_3D, while the ethane had significantly more deuterium, $C_2H_xD_{6-x}$ (x = 3,4 predominated). Butadiene had significant deuterium incorporation as well, but it was not possible to obtain quantitative data about these products. The hydrogen chloride had no detectable deuterium, while the vinyl chloride had small amounts of the monodeuterated species but mostly contained all protio material. Absence of observable DCl by GC/MS could be due to exchange with hydrogen on the walls of the ion source. Finally, butenes were not observed but may have been present though masked by butadiene.

The reaction of eq 2 was rerun except that K_2PtCl_4 was used in place of H_2PtCl_6. Analysis of the gases from this reaction showed essentially only butadiene was produced with only a trace of ethylene. This result strongly suggests that H_2PtCl_6 provided the hydrogen atom required to form ethylene in the reaction as derived from the Si−vinyl species.

Analysis of Polysiloxane Products from the Reaction of Platinum Halides with Silicon−Vinyl Compounds. Analysis of the polysiloxane products from eq 2 (as discussed above) showed mainly $M^{vi}D_xM^{vi}$ oligomers. A lesser series of oligomeric products were observed as high-retention-time shoulders in the GC and GC/MS analyses for each oligomer x of $M^{vi}D_xM^{vi}$; these products were identified as $M^{Et}D_xM^{vi}$. When D_2PtCl_6 was used in place of H_2PtCl_6 in eq 2 as described

(29) Chang, Y. H.; Choi, K. H.; Ford, W. T.; Cho, S. J.; Ryoo, R. *J. Chem. Soc., Chem. Commun.* **1994**, 785−787.

above in the gas analysis section, some deuterium incorporation was noted in the $M^{Et}D_xM^{vi}$ set of oligomers but not in the $M^{vi}D_xM^{vi}$ set. $M^{Et}DM^{vi}$ contained molecules where 79% were all protio, 14% contained one deuterium, and 4% contained two deuterium atoms. For $M^{Et}D_2M^{vi}$, 76% of the molecules were all protio, 16% were monodeuterated, 5% were doubly deuterated, and 3% were triply deuterated.

The reaction of eq 2 was repeated except that in one case MM ($(CH_3)_3Si-O-Si(CH_3)_3$) was added to $M^{vi}M^{vi}$ and in another case MM^{vi} was used in place of $M^{vi}M^{vi}$. In both cases the oligomeric mixture of products was the same and was more complicated than in the case of eq 2. The results in eq 6 show the typical

$$H_2PtCl_6 + MM^{vi} \xrightarrow[2.\ NaHCO_3]{1.\ reflux} Pt(MD_xM^{vi})_a(M^{vi}D_xM^{vi})_b + MD_xM + MD_xM^{vi} + M^{vi}D_xM^{vi} \quad (6)$$

product distribution for the reaction of H_2PtCl_6 with either $M^{vi}M^{vi}$ or MM or of H_2PtCl_6 with MM^{vi}. The results in eq 6 show that each of the siloxane units can exchange with each other, reminiscent of the well-known[43] Lewis-acid-catalyzed exchange of siloxy units; in this case the platinum species served as the Lewis acid.

Reactions were carried out with added C_2H_4 or C_2D_4 to probe the effects on the reduction process and oligosiloxane formation. The latter experiment was complementary to the experiments above using D_2PtCl_6. The effect of ethylene pressure on the oligomer product distribution is shown graphically in Figure 2. Here it is shown that when eq 6 was run under a pressure of C_2H_4 (60 equiv based on Pt), the population of higher oligomers increased vs the case when no ethylene was present. A similar pattern was observed for the reaction of eq 2 run with and without ethylene (Figure 3). When eq 2 was run under pressure of C_2H_4, analysis of the gases showed C_2H_4, as well as C_2H_6, C_4H_6, and C_4H_8. The presence of added C_2H_4 led to more saturated products; C_2H_4 was apparently a proton source for the formation of ethane and butene (from butadiene). In the reaction of eq 2 run under ethylene, if the platinum concentration was increased 5-fold, a higher yield of gases (ethane, butadiene, and butene) was noted. Clearly platinum was involved in the formation of these additional gas products. When eq 2 was run under C_2D_4, no deuterium incorporation was noted in any of the silicon-containing products. Analysis of the gases from the reaction of H_2PtCl_6 with $M^{vi}M^{vi}$ under C_2D_4 showed both C_2D_4 and C_2H_4 with no evidence of H–D exchange; e.g., no $C_2H_{4-x}D_x$ was observed. Some deuterium incorporation was noted in the hydrogenated gaseous products as $C_2D_{6-x}H_x$ and $C_4D_{8-x}H_x$. Hence, hydrogenated products, e.g., ethyl oligosiloxane, ethane, or butene, may derive hydrogen atoms from the H_2PtCl_6 or ethylene. No deuterium incorporation was noted in any vinyl polysiloxane product. Thus, there is no significant pathway to exchange free ethylene with a vinyl hydride coordinated material.

Synthesis and Structure of Pt Complexes with $[(CH_3)(CH_2{=}CH)SiO]_4$. Another common ligand for platinum used in polysiloxane applications is $[(CH_3)(CH_2{=}CH)SiO]_4$, known as D_4^{vi}. H_2PtCl_6 was reacted with D_4^{vi} (eq 7) in a fashion analogous to the reaction in eq 2. The platinum products were assigned as Pt(0) olefin complexes **3** on the basis of the following analysis. ^{195}Pt NMR spectroscopy showed an envelope 10 ppm wide centered at −6166 ppm consistent with a mixture of Pt(0)–olefin complexes. EXAFS analysis was practically identical with that from the reaction with disiloxane; it showed that the first coordination shell around platinum contained carbon (d_{Pt-C} = 2.18 Å) with a Pt–C coordination number of 6. The second coordination shell around platinum contained silicon (d_{Pt-Si} = 3.40 Å) with a coordination number of 3. By analogy to the work of Lappert using $M^{vi}M^{vi}$ to give solution A, we call the product solution from eq 7 solution B. Solution B was subjected to vacuum stripping to remove volatile compounds. The ^1H NMR spectrum of the solution B concentrate showed broad resonances from 2 to 4 ppm in the region of Pt–vinyl. The ^{13}C NMR spectrum of solution B concentrate also showed resonances characteristic of Pt–vinyl at 54–59 ppm. The NMR spectra for solution B concentrate showed broad envelopes rather than individually resolved peaks, suggestive of a mixture of compounds of related structure.

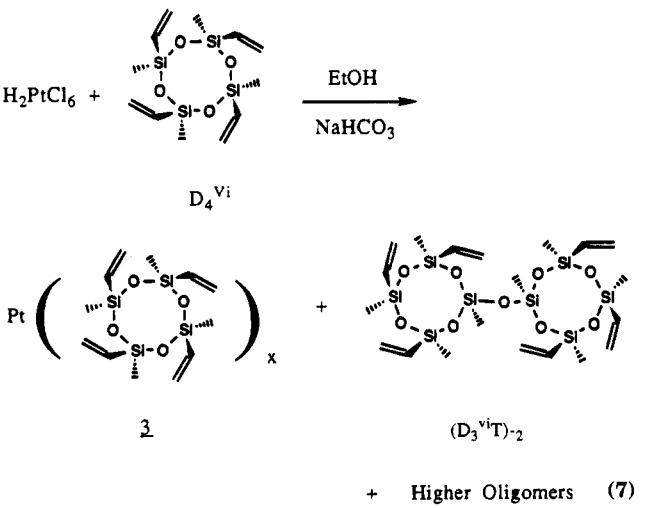

As shown in eq 2, some of the M^{vi} ($(H_2C{=}CH)Si(CH_3)_2O_{1/2}$) functionality was converted to a D ($(CH_3)_2SiO_{2/2}$–) group, thus giving rise to the oligomeric product $M^{vi}D_xM^{vi}$. Likewise, in the reaction of eq 7 some of the D^{vi} groups of D_4^{vi} were changed to T ($(CH_3)SiO_{3/2}$–) groups. Analysis of the silicon-containing products in solution B concentrate by gas chromatography/mass spectroscopy (GC/MS) and by FDMS showed the presence of two types of products: higher cyclics, D_x^{vi} (x = 4–6), and T-containing oligomers, such as $(D_3^{vi}T-)_2$ (as shown in eq 7), $D_4^{vi}T-TD_3^{vi}$, and $(D_4^{vi}T-)_2$. Thus, with D_4^{vi} if one D^{vi} group transformed into a SiOH and then reacted with an identical molecule eliminating water, $(D_3^{vi}T-)_2$ would form.

Reactions with $(CH_3)_2Si(CH{=}CH_2)_2$. In eq 2, a Pt(IV) starting material is reduced to Pt(0). No Pt(II) intermediate is isolated or observed by ^{195}Pt NMR; the Pt(0) region is roughly upfield of −4000 ppm, while Pt(II) compounds have resonances in the region of −2500 to −4500 ppm (some overlap exists in the literature).[30,31] When a mixture of H_2PtCl_6 and $M^{vi}M^{vi}$ was stirred and heated to 80 °C for 2 h (with no ethanol or $NaHCO_3$ added), ^{195}Pt NMR analysis showed the Pt(0) resonances and a new broad resonance at −3470 ppm.

(30) Pregosin, P. S. *Coord. Chem. Rev.* **1982**, *44*, 247.
(31) Pregosin, P. S. *Annu. Rep. NMR Spectrosc.* **1986**, *17*, 285.

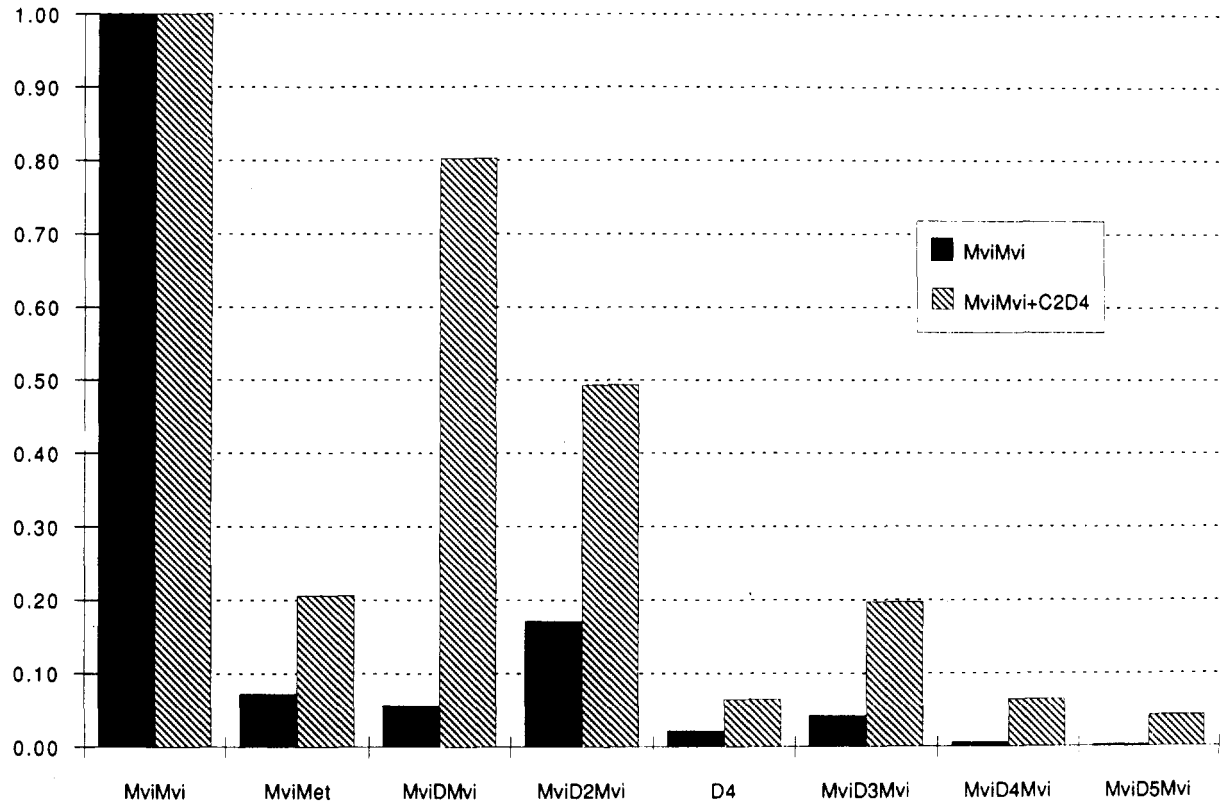

Figure 2. Histogram giving the distribution of polysiloxane products from eq 6 run with and without added C_2H_4 pressure.

Different silicon–vinyl compounds were employed as reducing agents in place of $M^{vi}M^{vi}$ to possibly isolate a Pt(II) intermediate. When $(CH_3)_2Si(CH{=}CH_2)_2$ was reacted with H_2PtCl_6 (eq 8), two platinum products were observed. The silicon-containing products were similar to those observed in the reaction of eq 2. In particular, no D^{vi}-containing species were observed.

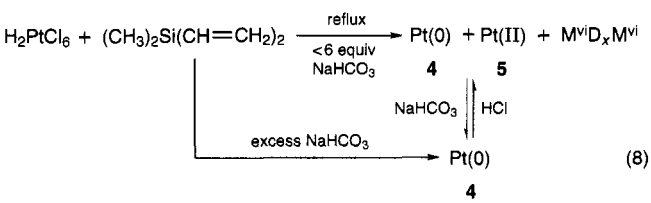

(8)

When excess $NaHCO_3$ was employed in the reaction sequence of eq 8, **4** was produced (>90% recovered yield) to the exclusion of **5**. Even under favorable conditions for the production of **5**, approximately 90% of the platinum material was **4**, as determined by integrating the ^{195}Pt NMR signals. The ^{195}Pt NMR resonance for **5** occurred at −3603 ppm, while the resonance for **4** was observed at −6152 ppm.

Structure of 5. The presence of **5** was noted when it crystallized from reaction solutions (of eq 8) containing less than 6 equiv of sodium bicarbonate at −15 °C. The structure of **5** was determined by single-crystal X-ray crystallography. Table 1 summarizes the crystal data. Table 2 provides the solution and refinement information. Table 3 lists the atomic coordinates and isotropic displacement coefficients. Tables 4 and 5 show bond lengths and angles, while the anisotropic displacement coefficients and H-atom coordinates are given in the supplementary material.

Compound **5** (Figure 4) is a platinum dimer with two bridging chlorine atoms and a bridging $(CH_3)_2Si(CH{=}CH_2)_2$ ligand. The most surprising aspect of **5** is the $\eta^1{:}\eta^2$-$(CH_3)_2Si(CH{=}CH_2)(CH_2CH_2)$ ligand. Apparently one of the vinyl groups in $(CH_3)_2Si(CH{=}CH_2)_2$ was protonated to a σ-bound $Si{-}CH_2CH_2$ group, thereby forming a platinum–alkyl linkage as part of a chelating σ,π ligand. In the typical oxidation-state formalism, one counts chloride as −1 and the substituted ethyl linkage as −1; thus, each Pt is in the +2 oxidation state.

Compound **5** displays a distorted-trigonal-bipyramidal (TBP) arrangement around each platinum. Figure 5 shows the structure of **5** with the emphasis around the Pt coordination environment. In the TBP arrangement, the silyl ethyl and one of the chlorine atoms occupied the axial positions while the other chlorine atom and the centroids of the two vinylic linkages occupied the equatorial positions. As shown in Figure 5, the axial angle formed for C(13)–Pt(1)–Cl(2) was nearly 180°. Three points defined the equatorial portion of the TBP, where X(1A) and X(1B) were the centroids of the C=C bonds. The two Cl(1)–Pt–X angles were 109.9 and 112.8°, while the angle X–Pt–X was larger, 137.2°. The origin of the larger equatorial angle was probably due to steric repulsion by the olefin ligands.

The C=C bond lengths in the vinyl groups averaged 1.398 Å. This C=C distance was similar to that found in a number of other platinum–olefin structures.[14,15,17,22,23,32–35] One unusual feature was the

(32) Howard, J. A. K.; Spencer, J. L.; Mason, S. A. *Acta Crystallogr., Sect. A* **1978**, *34* (Suppl.), S 129.
(33) Green, M.; Howard, J. A. K.; Spenser, J. L.; Stone, F. G. A. *J. Chem. Soc., Chem. Commun.* **1975**, 449–451.
(34) Boag, N. M.; Howard, J. A. K.; Spencer, J. L.; Stone, F. G. A. *J. Chem. Soc., Dalton Trans.* **1981**, 1051–1056.

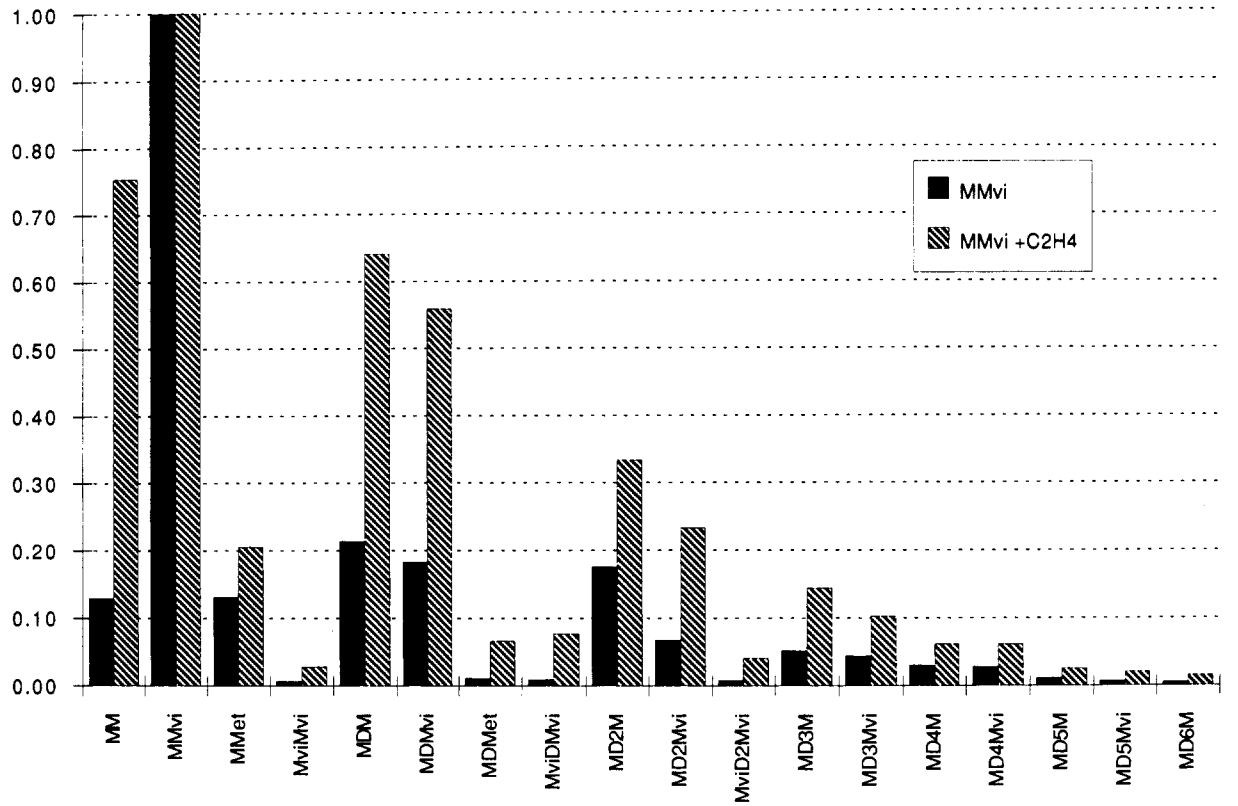

Figure 3. Histogram giving distribution of polysiloxane products from eq 2 run with and without added C_2H_4 pressure.

Table 1. Experimental Data for the Crystallographic Analysis of 5

empirical formula	$C_{18}H_{38}Cl_2Pt_2Si_3$
color, habit	clear flat needle
a, Å	6.799(3)
b, Å	19.830(8)
c, Å	18.847(10)
β, deg	95.43(4)
V, Å^3	2530(2)
Z	4
$F(000)$	1516
space group	$P2_1/c$
T, K	158
λ(Mo Kα), Å	0.710 73
ϱ(calc), g cm^{-3}	2.103
abs coeff, mm^{-1}	11.521
diffractometer used	Siemens R3m/V
monochromator	highly oriented graphite cryst
2θ range, deg	3.5–55.0
scan type	Wyckoff
scan speed in ω, deg min^{-1}	variable; 1.50–14.65
scan range (ω), deg	0.60
std rflns	3 meas every 47 rflns
index ranges	$0 \le h \le 8$, $0 \le k \le 25$, $-24 \le l \le 24$
no. of rflns collected	6475
no. of indep rflns	5806 (R_{int} = 3.02%)
no. of obs rflns	4365 ($F > 6.0\sigma(F)$)
no. of abs cor	face-indexed numerical

Table 2. Solution and Refinement Data for 5

syst used	Siemens SHELXTL PLUS (VMS)
soln	direct methods
refinement method	full-matrix least squares
quantity minimized	$\sum w(F_o - F_c)^2$
extinction coeff	$\chi = -0.000011(10)$, where $F^* = F[1 + 0.002\chi F^2/(\sin 2\theta)]^{-1/4}$
H atoms	riding model, fixed isotropic U
weighting scheme	$w^{-1} = \sigma^2(F) + 0.0012F^2$
no. of param refined	227
final R indices (obs data), %	R = 3.28, R_w = 4.34
R indices (all data), %	R = 4.87, R_w = 4.92
goodness of fit	1.00
largest and mean Δ/σ	1.127, 0.070
data-to-param ratio	19.2:1
largest diff peak, e Å^{-3}	3.45
largest diff hole, e Å^{-3}	−1.45

Pt–C bond lengths found in **5** between Pt and the C=C groups. While the average distance of 2.16 Å agreed with the similar distance of 2.17 Å in (COD)$PtCl_2$,[35] the spread in the distances (see Table 5) was quite large. This apparent asymmetry in the Pt–vinyl distances may represent some strain in the molecule.

The Pt–Cl distances in **5** average 2.52 Å, slightly longer than in square-planar bridging Pt(II) halides such as bis(μ-chloro)dichlorobis(olefin)diplatinum(II) (2.32–2.36 Å)[36] or the tetrameric allylchloroplatinum (2.37–2.46 Å).[37] The Pt–Cl bonds trans to the σ-carbon averaged 2.505 Å, consistent with a strong trans influence previously observed.[38,39] The other Pt–Cl bond was 2.54 Å, which was quite long but again consistent with reduced electron density due to the presence of two olefins in the pseudo-equatorial plane, i.e., five versus four-coordination.

The silyl–ethyl linkage was truly saturated, as noted by the C–C bond lengths of 1.519 Å. The Pt–C distances for the silyl–ethyl ligand were 2.06 Å (0.1 Å shorter than the Pt–C distance to the vinyl groups) but were consistent with the former having a true metal–

(35) Syed, A.; Stevens, E. D.; Cruz, S. G. *Inorg. Chem.* **1984**, *23*, 3674–3674.

(36) Bordner, J.; Wertz, D. W. *Inorg. Chem.* **1974**, *13*, 1639–1643.

(37) Raper, G.; McDonald, W. S. *J. Chem. Soc., Chem. Commun.* **1979**, 655.

(38) Whitla, W. A.; Powell, H. M.; Venanzi, L. M. *J. Chem. Soc., Chem. Commun.* **1966**, 310–311.

(39) Anderson, G. K.; Cross, R. J.; Manojlovic-Muir, L.; Muir, K. W.; Solomun, T. *J. Organomet. Chem.* **1979**, *170*, 385–397.

Table 3. Atomic Coordinates ($\times 10^4$) and Equivalent Isotropic Displacement Coefficients ($Å^2 \times 10^3$) for 5

	x	y	z	U(eq)[a]
Pt(1)	8510(1)	−1594(1)	2683(1)	19(1)
Cl(1)	5911(3)	−893(1)	1963(1)	24(1)
Cl(2)	9858(3)	−492(1)	3166(1)	21(1)
Pt(2)	6849(1)	150(1)	2688(1)	18(1)
C(1)	6155(12)	462(4)	3720(4)	27(2)
C(2)	5307(12)	−169(3)	3596(4)	23(2)
Si(1)	6089(3)	−946(1)	4110(1)	22(1)
C(3)	8041(12)	−741(4)	4844(5)	30(2)
C(4)	3859(13)	−1231(4)	4521(5)	31(3)
C(5)	6755(12)	−1705(4)	3586(4)	24(2)
C(6)	8566(12)	−2052(4)	3713(5)	27(2)
C(7)	4392(12)	665(4)	2251(5)	29(2)
C(8)	4230(12)	658(4)	1435(4)	29(2)
Si(2)	6685(3)	877(1)	1117(1)	25(1)
C(9)	6863(14)	1805(4)	959(6)	37(3)
C(10)	7253(15)	408(5)	309(6)	42(3)
C(11)	8527(11)	628(4)	1894(4)	25(2)
C(12)	8697(12)	1001(4)	2519(5)	27(2)
C(13)	7442(16)	−2503(4)	2280(5)	37(3)
C(14)	7195(15)	−2521(5)	1477(6)	40(3)
Si(3)	9320(3)	−2104(1)	1083(1)	24(1)
C(15)	11214(14)	−2704(5)	813(6)	42(3)
C(16)	8329(18)	−1591(5)	302(6)	49(4)
C(17)	10435(11)	−1566(4)	1820(5)	24(2)
C(18)	11457(11)	−1850(4)	2431(5)	28(2)

[a] Equivalent isotropic U, defined as one-third of the trace of the orthogonalized U_{ij} tensor.

Table 4. Bond Lengths (Å) for 5

Pt(1)−Cl(1)	2.539(2)	Pt(1)−Cl(2)	2.507(2)
Pt(1)−C(5)	2.180(8)	Pt(1)−C(6)	2.139(9)
Pt(1)−C(13)	2.061(8)	Pt(1)−C(17)	2.183(9)
Pt(1)−C(18)	2.163(8)	Cl(1)−Pt(2)	2.527(2)
Cl(2)−Pt(2)	2.504(2)	Pt(2)−C(1)	2.135(9)
Pt(2)−C(2)	2.183(8)	Pt(2)−C(7)	2.062(8)
Pt(2)−C(11)	2.182(8)	Pt(2)−C(12)	2.146(8)
C(1)−C(2)	1.388(11)	C(2)−Si(1)	1.870(8)
Si(1)−C(3)	1.868(8)	Si(1)−C(4)	1.854(9)
Si(1)−C(5)	1.879(8)	C(5)−C(6)	1.411(11)
C(7)−C(8)	1.531(12)	C(8)−Si(2)	1.877(9)
Si(2)−C(9)	1.870(8)	Si(2)−C(10)	1.856(11)
Si(2)−C(11)	1.899(8)	C(11)−C(12)	1.388(12)
C(13)−C(14)	1.507(14)	C(14)−Si(3)	1.878(11)
Si(3)−C(15)	1.860(10)	Si(3)−C(16)	1.862(11)
Si(3)−C(17)	1.856(8)	C(17)−C(18)	1.406(11)

alkyl linkage. Related Pt(II) olefin−alkyl chelating ligands have Pt−C σ bonds of 2.04 and 2.05 Å.[40,41]

Solutions of crystals of **5** or mixtures which contained **4** and **5** were analyzed spectroscopically to confirm that the crystal structure of **5** is maintained in solution. In the ^{1}H NMR of **5**, which also contained the oligomeric products from the reaction in eq 8, namely $M^{vi}D_xM^{vi}$, the free vinyl resonance from the oligomeric product appeared from 6.3 to 5.4 ppm. The coordinated vinyl proton peaks occurred from 4.0 to 2.8 ppm. The protons on the methylene group coordinated to Pt were observed at 1.9 ppm ($J_{Pt-H} = 50$ Hz), while the methylene protons of the ethyl group adjacent to Si were observed at 0.94 ppm. The Si−methyl proton resonances were present from 0.2 to −0.35 ppm.

The ^{13}C spectrum of **5** showed the *C*H of the coordinated vinyl (determined from a separate APT experiment) at 81.39 ppm ($J_{Pt-C} = 150$ Hz) and the *C*H$_2$ resonance at 70.30 ppm ($J_{Pt-C} = 120$ Hz). In the upfield region of the ^{13}C NMR spectrum of **5**, the silyl−ethyl resonances were observed at 11.17 and 9 ppm. The broadness of the latter peak suggested that it was the resonance associated with the CH$_2$ bound to Pt. The silyl−methyl resonances appeared from 1.3 to −3.1 ppm.

Crystals of **5** had a sharp decomposition point at 37 °C. The C,H analysis for **5** was low by over 50% vs the calculated expected value. The error in the elemental analysis suggested incomplete combustion in the analysis. Platinum analysis was performed at the GE research center, where much time and effort was devoted to ensuring complete dissolution of the analyte. Platinum bis(acetylacetonate) was employed as an organic-soluble Pt standard. For **5** the calculated percentage of Pt was 48.8% and the measured value was 49.8%.

Attempts were made to analyze **5** via FDMS. The FDMS spectrum for crystals of **5** (Figure 6) showed an isotope pattern whose relative intensities matched a computer-generated model for $C_{12}H_{28}Cl_2Pt_2Si_2$. The mass spectrum is consistent with loss of $(CH_3)_2Si$-

Table 5. Bond Angles (deg) for 5

Cl(1)−Pt(1)−Cl(2)	85.9(1)	Cl(1)−Pt(1)−C(5)	93.9(2)
Cl(2)−Pt(1)−C(5)	90.7(2)	Cl(1)−Pt(1)−C(6)	132.0(2)
Cl(2)−Pt(1)−C(6)	93.8(2)	C(5)−Pt(1)−C(6)	38.1(3)
Cl(1)−Pt(1)−C(13)	94.5(3)	Cl(2)−Pt(1)−C(13)	179.1(3)
C(5)−Pt(1)−C(13)	90.0(3)	C(6)−Pt(1)−C(13)	86.5(3)
Cl(1)−Pt(1)−C(17)	91.3(2)	Cl(2)−Pt(1)−C(17)	91.3(2)
C(5)−Pt(1)−C(17)	174.5(3)	C(6)−Pt(1)−C(17)	136.6(3)
C(13)−Pt(1)−C(17)	87.9(3)	Cl(1)−Pt(1)−C(18)	128.6(2)
Cl(2)−Pt(1)−C(18)	88.3(2)	C(5)−Pt(1)−C(18)	137.3(3)
C(6)−Pt(1)−C(18)	99.4(3)	C(13)−Pt(1)−C(18)	90.9(4)
C(17)−Pt(1)−C(18)	37.7(3)	Pt(1)−Cl(1)−Pt(2)	91.8(1)
Pt(1)−Cl(2)−Pt(2)	93.1(1)	Cl(1)−Pt(2)−Cl(2)	86.2(1)
Cl(1)−Pt(2)−C(1)	131.5(2)	Cl(2)−Pt(2)−C(1)	93.6(2)
Cl(1)−Pt(2)−C(2)	94.1(2)	Cl(2)−Pt(2)−C(2)	90.4(2)
C(1)−Pt(2)−C(2)	37.5(3)	Cl(1)−Pt(2)−C(7)	92.0(2)
Cl(2)−Pt(2)−C(7)	177.5(3)	C(1)−Pt(2)−C(7)	88.9(3)
C(2)−Pt(2)−C(7)	91.5(3)	Cl(1)−Pt(2)−C(11)	96.1(2)
Cl(2)−Pt(2)−C(11)	90.3(2)	C(1)−Pt(2)−C(11)	132.4(3)
C(2)−Pt(2)−C(11)	169.9(3)	C(7)−Pt(2)−C(11)	88.1(3)
Cl(1)−Pt(2)−C(12)	133.2(2)	Cl(2)−Pt(2)−C(12)	89.1(2)
C(1)−Pt(2)−C(12)	95.2(3)	C(2)−Pt(2)−C(12)	132.5(3)
C(7)−Pt(2)−C(12)	90.9(3)	C(11)−Pt(2)−C(12)	37.4(3)
Pt(2)−C(1)−C(2)	73.2(5)	Pt(2)−C(2)−C(1)	69.4(5)
Pt(2)−C(2)−Si(1)	120.7(4)	C(1)−C(2)−Si(1)	124.2(6)
C(2)−Si(1)−C(3)	110.6(4)	C(2)−Si(1)−C(4)	105.3(4)
C(3)−Si(1)−C(4)	108.0(4)	C(2)−Si(1)−C(5)	117.3(4)
C(3)−Si(1)−C(5)	111.9(4)	C(4)−Si(1)−C(5)	102.9(4)
Pt(1)−C(5)−Si(1)	120.5(4)	Pt(1)−C(5)−C(6)	69.4(5)
Si(1)−C(5)−C(6)	123.5(6)	Pt(1)−C(6)−C(5)	72.5(5)
Pt(2)−C(7)−C(8)	112.0(6)	C(7)−C(8)−Si(2)	109.7(5)
C(8)−Si(2)−C(9)	110.6(4)	C(8)−Si(2)−C(10)	114.0(4)
C(9)−Si(2)−C(10)	109.9(5)	C(8)−Si(2)−C(11)	103.6(4)
C(9)−Si(2)−C(11)	109.3(4)	C(10)−Si(2)−C(11)	109.2(4)
Pt(2)−C(11)−Si(2)	107.0(4)	Pt(2)−C(11)−C(12)	69.9(5)
Si(2)−C(11)−C(12)	120.8(6)	Pt(2)−C(12)−C(11)	72.7(5)
Pt(1)−C(13)−C(14)	113.1(6)	C(13)−C(14)−Si(3)	111.7(7)
C(14)−Si(3)−C(15)	113.9(4)	C(14)−Si(3)−C(16)	108.6(5)
C(15)−Si(3)−C(16)	110.0(5)	C(14)−Si(3)−C(17)	103.4(4)
C(15)−Si(3)−C(17)	109.2(4)	C(16)−Si(3)−C(17)	111.7(4)
Pt(1)−C(17)−Si(3)	108.2(4)	Pt(1)−C(17)−C(18)	70.3(5)
Si(3)−C(17)−C(18)	121.2(6)	Pt(1)−C(18)−C(17)	71.9(5)

Table 6. ^{195}Pt NMR Shifts

reacn	eq	^{195}Pt NMR shift, ppm
H_2PtCl_6 + $M^{vi}M^{vi}$ (soln A)	2	−6148, −6149
soln A + excess $M^{vi}DM^{vi}$	4	−6148
soln A + excess $MD^{vi}M$		−6155
H_2PtCl_6 + $M^{vi}M^{vi}$, no $NaHCO_3$	2	−6148, −6149, −3470
H_2PtCl_6 + $[(CH_3)(CH_2{=}CH)SiO]_4$	7	−6166
H_2PtCl_6 + $(CH_3)_2Si(CH_2{=}CH)_2$	8	−6152, −3603

(40) Panattoni, C.; Bombieri, G.; Forsellini, E.; Crociani, B. *J. Chem. Soc., Chem. Commun.* **1969**, 187.
(41) Pedone, C.; Benedetti, E. *J. Organomet. Chem.* **1971**, *31*, 403−414.

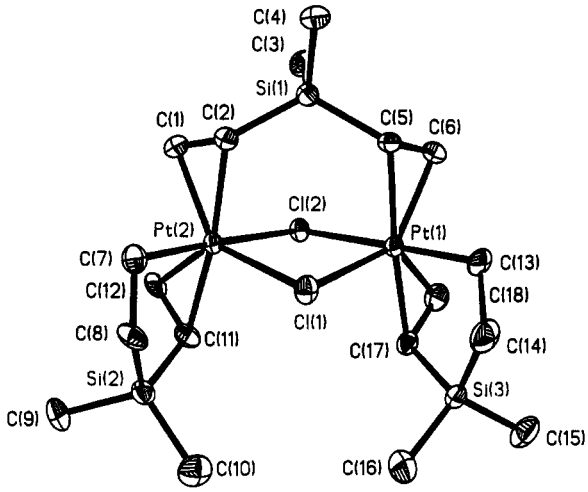

Figure 4. Thermal ellipsoid plot for **5**.

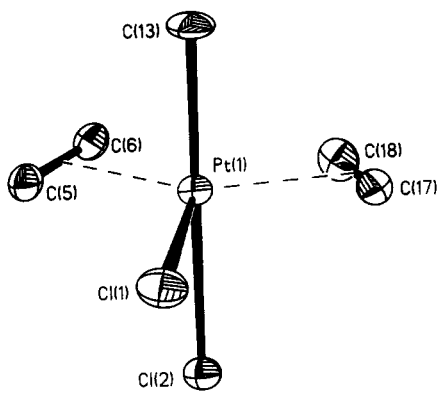

Figure 5. Coordination environment for Pt(1) in **5** emphasizing the TBP geometry at platinum. X(1A) = centroid between C(17) and C(18) and X(1B) = centroid between C(5) and C(6). Pt–Cl(1) = 2.540 Å, Pt–Cl(2) = 2.508 Å, Pt–C(13) = 2.061 Å, Pt–X(1A) = 2.056 Å, Pt–X(1B) = 2.041 Å. C(13)–Pt–Cl(2) = 179°, X(1A)–Pt–X(1B) = 137.2°, X(1A)–Pt–Cl(1) = 109.9°, X(1B)–Pt–Cl(1) = 112.8°.

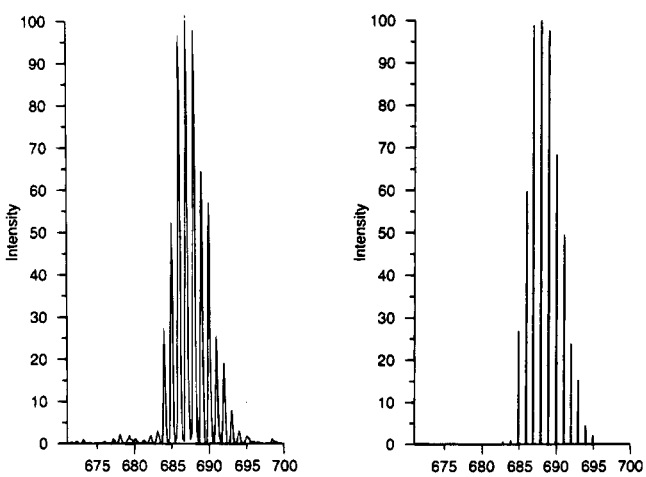

Figure 6. Field desorption mass spectrum of **5** (left) and modeled spectrum for $C_{12}H_{27}Cl_2Pt_2Si_2$ (right; this fragment corresponds to **5** with loss of the bridging ligand $(CH_3)_2Si(CH{=}CH_2)_2$).

$(CH{=}CH_2)_2$ from the parent molecule **5**, followed by protonation. Note the proposed assignment for the observed pattern is composed of contributions due to two platinum atoms and two chlorine atoms and therefore is likely to be a correct match. GC/MS analysis of the

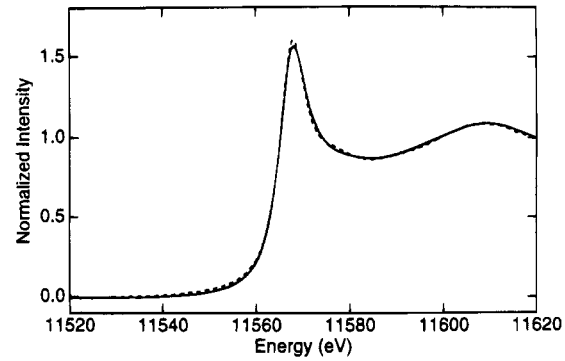

Figure 7. Pt K X-ray absorption edge spectra for **1** (—) and **4** (- - -).

products from eq 8 showed that $M^{vi}M^{vi}$ and higher oligomers of $M^{vi}D_xM^{vi}$ ($x > 0$) were formed as well.

Structure of 4. In the proton NMR spectrum of **4**, the silyl–ethyl resonances of **5** are absent. Moreover, no resonances are observed for free vinyl protons when the sample was subjected to vacuum stripping for 3 days. It was never possible in the synthesis of Karstedt's catalyst to completely remove all of the free vinyl due to the higher molecular weight of the $M^{vi}D_xM^{vi}$ formed in the preparation of **1**. However, the volatility of the vinyl-stopped oligosiloxane formed in eq 8 was sufficiently high for it to be completely removed under vacuum (0.01 mmHg). Samples of **4** did not crystallize from solution at −15 °C for over 6 months.

The ^{13}C NMR spectrum of **4** shows coordinated vinyl at nearly the same resonance as the bound vinyl of **1**, consistent with a Pt(0) complex. As in the ^1H spectrum, the resonances due to the vinyl and silyl–ethyl groups of **5** were absent. These spectra demonstrated that no **5** was present when excess $NaHCO_3$ was employed in the reaction of eq 8.

A solution of **4** was added to CH_2Cl_2 and stirred vigorously with 0.1 M HCl(aq) for 1 h. The CH_2Cl_2 layer was separated from the aqueous layer, and then the CH_2Cl_2 was removed in vacuo to leave an oil. The oil was placed in a freezer compartment of a refrigerator (ca. −15 °C), and crystals of **5** formed within 4 days. These results can be summarized by the lower portion of eq 8. The spectroscopically observed yield described above for **5** was 10%, while the recovered yield of the crystals was 1–2%.

EXAFS and X-ray absorption near edge spectroscopy (XANES) analyses were carried out on solutions of **4**. The XANES analysis clearly showed that the platinum oxidation state of **4** was identical with that of **1** (Figure 7). As shown in Figure 1b, the EXAFS of **4** was far more complicated than that of **1** but appeared to contain Pt–C in the first coordination sphere and Pt–Si in the second coordination sphere.

The mixture obtained from eq 8 was reacted with 1.2 equiv of $P(C_6H_5)_3$ to derivatize the platinum products and learn more about the structure of **4** (eq 9). Lappert's

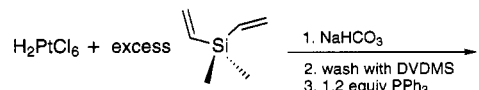

$$(M^{vi}M^{vi})Pt(PPh_3) + (PPh_3)_2PtCl_2 \quad (9)$$

6, 81% **7**, 19%

group carried out similar experiments with phosphines and solution A, which generated analogs of complex **6**.[14] The product ratios from eq 9 were determined by ^{31}P NMR integration and confirmed by isolated yields. The presence of compounds **6**[42] and **7** was determined by ^{31}P NMR spectroscopy. Both **6** and **7** were isolated as crystalline products; **7** crystallized first, and large crystals of **6** were then obtained by slow evaporation of the filtrate. The identity of **6** was confirmed by ^{1}H and ^{13}C NMR and FDMS.[42] ^{1}H and ^{13}C NMR analysis of **7** showed phenyl resonances, shifted from those of free triphenylphosphine. The NMR data for **6** showed resonances for the bound vinyl of $M^{vi}M^{vi}$; these resonances were absent in the NMR of **7**. Compound **7** was further identified by FDMS analysis, which showed a molecular ion centered at 790 amu.

All known Pt(0) olefin compounds are three- or four-coordinate. It seems likely that **4** is a Pt(0) complex with three or four olefin ligands in the coordination sphere of platinum derived from some combination of $(CH_3)_2Si(CH{=}CH_2)_2$ and $M^{vi}M^{vi}$, e.g. $Pt_2(M^{vi}M^{vi})_x((CH_3)_2Si(CH{=}CH_2)_2)_y$ (x and/or $y = 2$).

We suggest that **5** (the Pt(II) complex) is NOT an intermediate in the formation of **4** (the Pt(0) complex) from H_2PtCl_6 and $(CH_3)_2Si(CH{=}CH_2)_2$, although one might argue that hydrolysis of **5** occurs to give a bound silanol, eliminating ethylene and HCl, which were both observed during decomposition of **5**. Rapid condensation of the silanols would lead to formation of the Si–O–Si bond. However, when anhydrous $PtCl_4$ was reacted with $(CH_3)_2Si(CH{=}CH_2)_2$ under anhydrous conditions,^{195}Pt NMR analysis showed only Pt(0) was present (no Pt(II) signal was observed). Analysis of the silicon-containing products by ^{29}Si NMR showed that, besides unreacted $(CH_3)_2Si(CH{=}CH_2)_2$, the major product was $(CH_3)_2Si(CH{=}CH_2)Cl$. After exposure to air, analysis by GC/MS confirmed the presence of $(CH_3)_2Si(CH{=}CH_2)Cl$ and the formation of $M^{vi}M^{vi}$ ($M^{vi}M^{vi}$ was present in only trace amounts before exposure to air). Thus, silicon–vinyl reacted with Pt–Cl to give Si–Cl and Pt–vinyl (vide infra). Therefore, we conclude that the more likely scenario is that **5** results from the reaction of **4** with HCl generated by the hydrolysis of silyl chloride species.

Mechanism of Formation of Pt(0) Complexes with Si–Vinyl Reducing Agents. The most important step in the chemistry described here is the reduction of platinum by silicon–vinyl. Under anhydrous conditions, silicon–chloride products were formed directly from reaction of silicon–vinyl with platinum chloride. Formation of the silicon–chloride bond constitutes a thermodynamic driving force. This piece of the chemistry is shown in Scheme 1, where X can be Cl, H, or D. Scheme 1 explains the formation of the silicon products. There is ample precedent for such a transformation, particularly in palladium and platinum systems.[44–47] Fitch and co-workers have noted the relative instability of dichloro–Pt(II) vinylsilane com-

Scheme 1

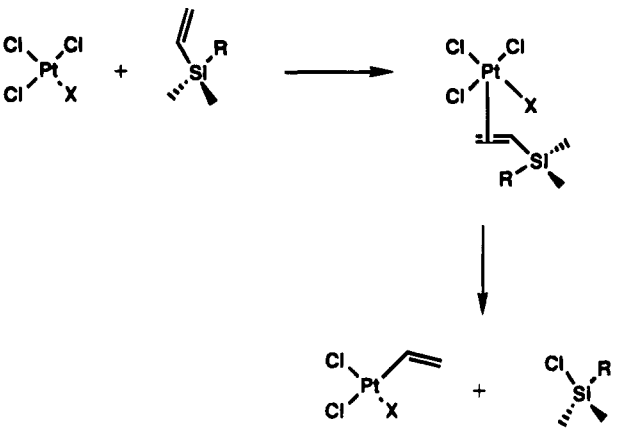

12

plexes relative to the Pt(0) species.[48,49] Hydrolysis of the chlorosilane produced in Scheme 1 gives the observed siloxane products. The reactions in Scheme 2 show the hydrolysis, condensation, and equilibration reactions that account for the methyl- and vinyl-containing siloxane products.

A method for formation of ethylene and butadiene and for further reduction of platinum is shown in Scheme 3. Note that when the platinum source was D_2PtCl_6, then **8** reacted with DCl to form $PtCl_4$ and C_2H_3D. Compound **8** can also react with more vinylsiloxane to make the divinyl compound **9**. Note that if X = H or D, formation of Si–Cl was always observed and that formation of Si–H (or Si–D) was never observed nor were any products based on addition of Si–H to vinyl observed. Again, the chlorosilane product reacts as shown in Scheme 2. Compound **13** may react via a reductive-elimination path to give butadiene and the Pt(II) product. Recall that when K_2PtCl_4 was used in place of H_2PtCl_6, butadiene was the main gaseous product and ethylene was only formed when H_2PtCl_6 was the platinum source.

The molecular weight of the $M^{vi}D_xM^{vi}$ oligomers was higher when H_2PtCl_6 was reacted with $M^{vi}M^{vi}$ in the presence of added ethylene than when no ethylene was added. $M^{vi}M^{vi}$ can take part in one of two reactions. If $M^{vi}M^{vi}$ reacts with platinum as shown in Scheme 1, then

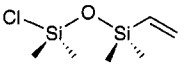

$M^{Cl}M^{vi}$

forms, which then reacts as in scheme 2 to form

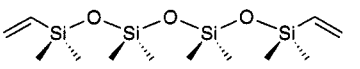

$M^{vi}D_2M^{vi}$

Alternatively, $M^{vi}M^{vi}$ can react with $M^{vi}D_2M^{vi}$ (or any other oligomer) in the Lewis-acid-catalyzed equilibration reaction of Scheme 2 to form 2 equiv of $M^{vi}DM^{vi}$. When

(42) Beuter, G.; Heyke, O.; Lorenz, I.-P. *Z. Naturforsch., B: Chem. Sci.* **1991**, *46*, 1694–1698.
(43) Odian, G. *Principles of Polymerization*, 2nd ed.; Wiley: New York, 1981; p 549.
(44) Kliegman, J. M. *J. Organomet. Chem.* **1971**, *29*, 73–77.
(45) Mansuy, D.; Pusset, J.; Chottard, J. C. *J. Organomet. Chem.* **1976**, *105*, 169–178.
(46) Akhrem, I. S.; Chistovalova, N. M.; Mysov, E. I.; Vol'pin, M. E. *J. Organomet. Chem.* **1974**, *72*, 163–170.
(47) Akhrem, I. S.; Chistovalova, N. M.; Malysheva, A. V.; Vol'pin, M. E. *Izv. Akad. Nauk SSSR, Ser. Khim.* **1983**, *12*, 2696–2702.
(48) Fitch, J. W.; Chan, K. C.; Froelich, J. A. *J. Organomet. Chem.* **1978**, *160*, 477–497.
(49) Haschke, E. M.; Fitch, J. W. *J. Organomet. Chem.* **1973**, *57*, C93–C94.

Scheme 2

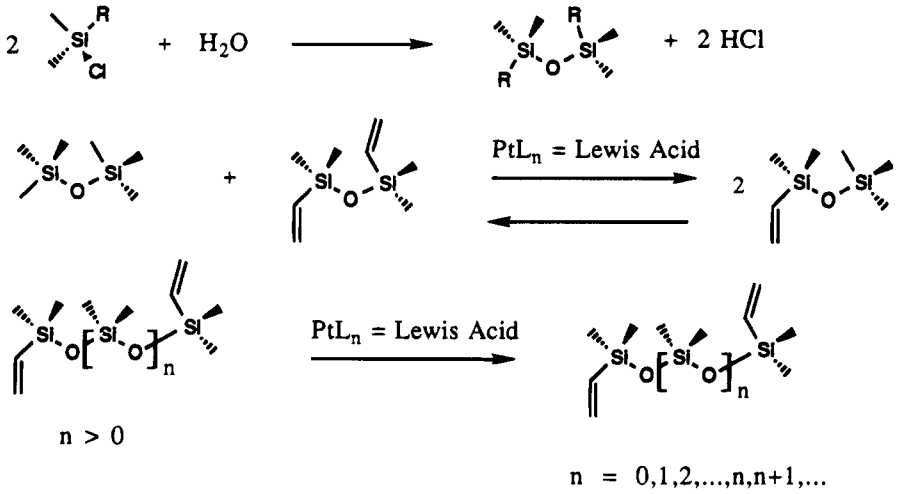

Scheme 3

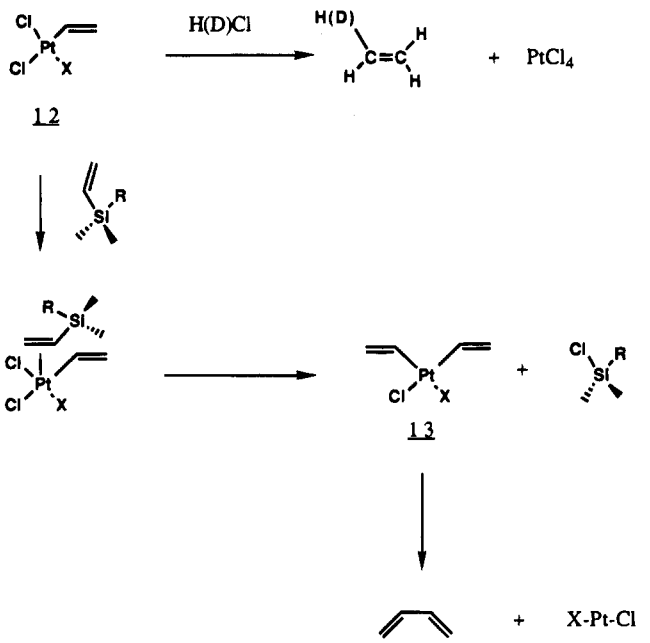

$M^{vi}M^{vi}$ was reacted with H_2PtCl_6 in the presence of ethylene, the reaction of silicon–vinyl with platinum was inhibited because silicon–vinyl must compete with ethylene for coordination sites on platinum. Thus, the $M^{vi}M^{vi}$ equilibration reaction with higher oligomers was more likely when ethylene was present. The equilibration reaction must consume $M^{vi}M^{vi}$ at a faster rate than did the reaction in Scheme 1. The histograms in Figures 2 and 3 may simply show that $M^{vi}M^{vi}$ was more rapidly consumed when ethylene was present than when ethylene was absent.

The other observed products are explained by the following observations. Equation 2 gave mostly ethylene and butadiene gaseous products with lesser amounts of ethane, butenes, and butane. The main polysiloxane products were $M^{vi}D_xM^{vi}$ oligomers with lesser amounts of $M^{vi}D_xM^{Et}$. The hydrogen source which converted the unsaturated olefins to the observed saturated species was from the hydrogen atoms of chloroplatinic acid and from ethylene. When D_2PtCl_6 was reacted with $M^{vi}M^{vi}$, the observed ethylene contained C_2H_3D. This result suggested that the deuterium of D_2PtCl_6 would react with the vinyl ligand. Indeed, the HCl observed at the end of the reaction contains only protio material, because the gas is generated ultimately by the reaction between water and silyl chloride (also, DCl is difficult to detect because of exchange as discussed above). When D_2PtCl_6 was reacted with $M^{vi}M^{vi}$, deuterium was observed in the $M^{vi}D_xM^{Et}$ oligomers as well as in the gaseous products ethane and butenes. The products derived from hydrogenation of unsaturated groups were formed in very low yield relative to ethylene, butadiene, and the vinyl–polysiloxane products. The reactions in Scheme 4, which attempt to explain these results, must have occurred with low efficiency. In summary, there is a pathway to exchange hydrogen atoms from vinyl to ethyl on ligands, but there does not seem to be a reversible shuttle from olefin to vinyl.

When C_2D_4 was present during the reaction of H_2PtCl_6 with $M^{vi}M^{vi}$, GC/MS analysis of the ethylene product showed only C_2H_4 and C_2D_4. This result confirms that the steps that occurred in Scheme 4 happen to a very small extent. The presumed mixed ethylene, e.g. C_2D_3H, was present in small quantities compared to C_2H_4 and C_2D_4. Deuterated ethyl–silicon, ethane, etc. were observed because these products were only formed from the exchange processes shown in the schemes.

Experimental Section

General Considerations. All operations were carried out in air with standard reagents unless otherwise noted. ^1H and ^{13}C NMR spectra were recorded on a GE QE-300 instrument at 300.15 and 75.48 MHz, respectively. Additional ^{13}C, ^{29}Si, and ^{195}Pt NMR spectra were recorded on a GE GN-Omega 500 NMR instrument at 125.8, 76.77, and 107.512 MHz, respectively. ^{29}Si NMR spectra were all recorded with 1% $Cr(acac)_3$ relaxation reagent and employed gated decoupling. In order to record ^{195}Pt NMR spectra where peaks were separated by more than 2000 ppm, the transmitter offset had to be moved and the probe retuned. GC measurements were made with a Hewlett-Packard Model 5890 instrument coupled to a Model 3393 integrator and Model 7673A auto sampler and using a 6-ft, 3% OV-101 column with a thermal conductivity detector. GC/MS analysis was carried out using a JEOL SX 102 high-resolution, double-focusing magnetic sector instrument; for liquid samples a 30 m DB 5 capillary column was employed, and for gas samples a 10 ft Supelco Fluorocol $^1/_8$ in. packed column was used. FDMS measurements were made using a JEOL Model HX 110 instrument. Platinum analyses were

Scheme 4

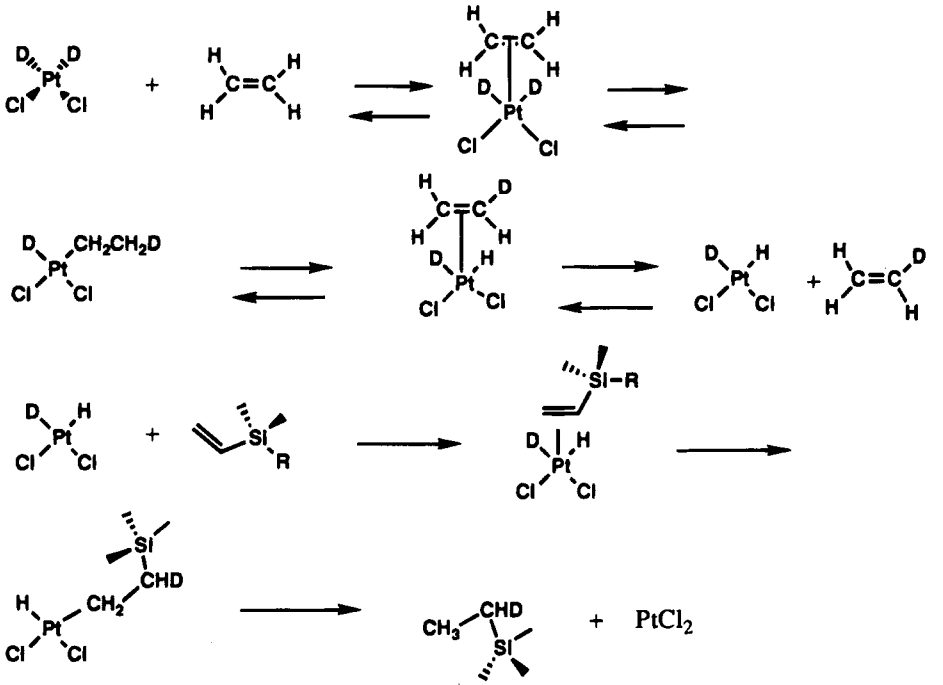

Table 7. PtL_{III} EXAFS Data Collection and Reduction for Platinum Samples

SR facility	SSRL
beam line	7–3
monochromator cryst	Si[220]
energy resolution, eV	~1
detection method	fluorescence
detector type	13-element solid state array[a]
scan length, min	21
scans in average	12
temp, K	10
energy std	Pt foil (inflection)
energy calibration, eV	11563
E_0, eV	11580
pre edge bkgd energy range eV (polynomial order)	11240–11725 (2)
spline bkgd energy range eV (polynomial order)	11580–11725 (2), 11725–11948 (3), 11948–12250 (3)

[a] Maintained by NIH Biotechnology Research Resource at SSRL.[54]

performed by ICP (inductively coupled plasma) by digesting the samples in refluxing aqua regia, after which aqueous NaOH was added to dissolve the polysiloxane portion. $Pt(acac)_2$ was used as a spike standard. $Pt(COD)_2$[50,51] and $Cl_2Pt(PPh_3)_2$[52] were made by literature methods.

EXAFS Analysis. X-ray absorption spectroscopic data collection was performed at Stanford Synchrotron Radiation Laboratory (SSRL). Data reduction was performed using XFPAK software developed as described.[53] Details of the data collection and reduction are summarized in Table 7. On beam line X10C at NSLS, the beam was also focused horizontally and vertically downstream of the monochromator and the vertical beam position was stabilized by feedback control of the mirror tilt angle using an in-hutch beam position monitor.

Curve-fitting analyses of the EXAFS data used scattering functions calculated by the FEFF program (v3.25).[54] In all FEFF calculations, the amplitude reduction factor was set to 0.9, the Debye–Waller factor (σ^2) was set to zero, the coordination numbers for central and scattering atoms were left as 1, and the muffin-tin potential overlap was set to 1.0 (no overlap). All other parameters were defaulted to values recommended by the FEFF authors.[54] The resulting FEFF scattering parameters were ported to XFPAK and used in curve-fitting optimizations that varied only absorber–scatterer distance (R_{as}) and Debye–Waller factor (σ_{as}^2). Tests of such FEFF parameters on a series of model compounds determined that a ΔE_0 of +10 eV was required (i.e., 10 eV must be *added* to the calculated phase functions) to match these parameters to our arbitrary selection of E_0 = 11 580 eV used in extracting the experimental EXAFS. These tests also confirmed that the FEFF parameters yield bond distance to an accuracy better than ±0.02 Å.

Chloroplatinic Acid + Vinyl–Polysiloxanes. The reaction of H_2PtCl_6 with $M^{vi}M^{vi}$ has been described.[14] A representative reaction of H_2PtCl_6 with a vinyl–polysiloxane is given here. H_2PtCl_6 (1 g, 2.0 mmol) was combined with pentamethylvinyldisiloxane, MM^{vi} (20 g, 115 mmol), and heated to 80 °C with stirring for 2 h. At this point $NaHCO_3$ (1.3 g, 15.4 mmol) was added and gas evolution was noted. The solution was then stirred an additional 1 h at ambient temperature and then filtered and washed with 0.7 g of MM^{vi} to give 18.2 g of a maroon solution, 1.68% Pt by weight. If a lower amount of MM^{vi} was used (9.4 g), then the resultant solution was 0.07% Pt by weight; i.e., most of the platinum is filtered off as insoluble material.

$Pt(COD)_2$ + $M^{vi}M^{vi}$. $Pt(COD)_2$ (0.0074 g, 0.018 mmol) was dissolved in C_6D_6 (0.5 mL) in an NMR tube, and then $M^{vi}M^{vi}$ (0.0197 g, 0.106 mmol) was added. The NMR data are discussed in the text.

Reaction of H_2PtCl_6 with $(CH_3)_2Si(CH{=}CH_2)_2$. (a) H_2PtCl_6 (1 g, 2 mmol) was combined with $(CH_3)_2Si(CH{=}CH_2)_2$ (15 g, 134 mmol) and heated at 85 °C with stirring for 2.5 h. $NaHCO_3$ (0.35 g, 4.1 mmol) was then added, and this mixture was stirred an additional 1 h at ambient temperature. This solution was filtered and the filtrate washed with $(CH_3)_2Si(CH{=}CH_2)_2$ (2 g) to give 11.1 g of a yellow solution, 3.37% Pt by weight. This solution was stored in a freezer (−15 °C) in

(50) Wright, L. L. Furman University, personal communication, 1984.
(51) Herberich, G. E.; Hessner, B. *Z. Naturforsch., B: Anorg. Chem., Org. Chem.* **1979**, *34B*, 638–639.
(52) Bailar, J. C., Jr.; Itatani, H. *Inorg. Chem.* **1965**, *4*, 1618–1620.
(53) Scott, R. A. *Methods Enzymol.* **1985**, *117*, 414.
(54) Rehr, J. J.; Leon, J. M. d.; Zabinsky, S. I.; Albers, R. C. *J. Am. Chem. Soc.* **1991**, *113*, 5135–5140.

the dark, and white crystals of **5** formed after about 2 weeks. A 0.025 g amount of white crystals was obtained: 3% isolated yield based on H_2PtCl_6; mp. 37 °C dec. The crystals were stored in the freezer in the dark and were used for the single-crystal X-ray and FDMS analyses.

(b) The reaction was carried out as in (a) except that 8 equiv of $NaHCO_3$ (1.4 g) was used. A yellow solution, 9.8 g, 3.78% Pt by weight, was obtained.

(c) The reaction was carried out as in (a) except that ethanol (2 mL) was added initially. A yellow solution, 9.6 g, 3.93% Pt by weight, was obtained. No crystals formed using methods b or c.

Reaction of H_2PtCl_6 with $(CH_3)_2Si(CH{=}CH_2)_2$ in the Presence of PPh_3. H_2PtCl_6 (1 g) and $(CH_3)_2Si(CH{=}CH_2)_2$ (15 g, 134 mmol) were combined and heated as described in method a above to give a yellow solution. Then 11.32 g (1.96 mmol of Pt) of this yellow solution was combined with PPh_3 (0.64 g, 2.4 mmol) dissolved in CH_2Cl_2 (10 mL). White crystals were initially obtained, which precipitated. These were collected by filtration and washed with hexane and then dried in vacuo. The yield was 0.3 g (0.38 mmol) of **7** (19%). The ^1H NMR spectrum and FDMS agreed with those obtained for $(PPh_3)_2PtCl_2$ made according to a literature procedure.[52] The residual mother liquor was allowed to sit several days, from which crystals of **6** deposited, 1 g, 1.5 mmol, 81% yield.

Reaction of D_2PtCl_6 with $M^{vi}M^{vi}$. H_2PtCl_6 (2 g) was dissolved in D_2O (10 mL) and then heated in an oven at 100 °C until a dry free-flowing solid was obtained, which was assumed to be mostly D_2PtCl_6. D_2PtCl_6 (1 g, 2 mmol) and $M^{vi}M^{vi}$ (25 g, 0.13 mol) were heated at ca. 120 °C for 7 h. The polysiloxane product from this reaction was then analyzed by GC/MS.

Reaction of H_2PtCl_6 with $M^{vi}M^{vi}$ and MM. H_2PtCl_6 (1 g, 2 mmol) was combined with $M^{vi}M^{vi}$ (10 g, 53.8 mmol) and MM (4.3 g, 26.5 mmol) and then heated at 70 °C for 90 min. Some insoluble black solid formed. $NaHCO_3$ (1 g) was added, and the mixture was stirred an additional 30 min. The mixture was then filtered, and a yellow liquid was obtained (1.64% Pt).

Reaction of H_2PtCl_6 with $M^{vi}M$. H_2PtCl_6 (1 g, 2 mmol) was combined with $M^{vi}M$ (9.4 g, 54 mmol) and then heated for 90 min at 70 °C to give a maroon solution. $NaHCO_3$ (1 g) was added, and the solution was stirred an additional 30 min. The solution was filtered to give a pale yellow solution (690 ppm of Pt).

Reaction of H_2PtCl_6 with $M^{vi}M^{vi}$ under an Ethylene Atmosphere. Reactions were carried out with either C_2H_4 or C_2D_4; a representative experiment is described. A 90 mL Fischer–Porter thick-walled glass bottle, equipped with a magnetic stirbar, was charged with H_2PtCl_6 (0.5 g, 1.2 mmol) and $M^{vi}M^{vi}$ (5 g, 26.9 mmol). The bottle was then subjected to three cycles of degassing and readdition of N_2; the last step left the bottle under reduced pressure. C_2H_4 (54 psig, 13.5 mmol) was added to the evacuated, degassed bottle, and the contents were stirred while the pressure was monitored to ensure no leak was present in the system. The tube was then heated behind a protective shield to 70 °C for 17 h. After the system was cooled to ambient temperature, the pressure in the bottle exceeded 100 psig, indicating that gas was produced in the reaction. The gases were collected by condensing with dry ice and then analyzed by GC/MS. The solution remaining had a dark precipitate.

Acknowledgment. Paul Donahue and Joanne Smith carried out some of the NMR measurements. Steve Dorn and Woody Ligon recorded the FDMS spectra. Eileen Skelly-Frame, Denise Anderson, and Winnie Balz developed and carried out the ICP Pt analysis method. The XAS data were collected at the Stanford Synchrotron Radiation Laboratory, which is operated by the Department of Energy, Division of Chemical Sciences. The SSRL Biotechnology Program is supported by the National Institutes of Health, Biomedical Resource Technology Program, Division of Research Resources. Support for the X-ray fluorescence detector is from NIH BRS Shared Instrument Grant RR05648.

Supplementary Material Available: Figures giving additional NMR spectra for the compounds discussed in this paper (8 pages). Ordering information is given on any current masthead page.

OM940794O

Regioselectivity of the Insertion of 4,4-Dimethyl-2-Pentyne into the Pd–C Bond of Cyclopalladated Complexes†

John Spencer and Michel Pfeffer*

Laboratoire de Synthèses Métallo-Induites, URA 416 du CNRS, Université Louis Pasteur, 4 rue Blaise Pascal, F-67070 Strasbourg, Cédex, France

Nathalie Kyritsakas and Jean Fischer‡

Laboratoire de Cristallochimie, URA 424 du CNRS, Université Louis Pasteur, 4 rue Blaise Pascal, F-67070 Strasbourg, Cédex, France

Received November 14, 1994®

The mono-insertion of 4,4-dimethyl-2-pentyne into the Pd–C bond of a series of cyclopalladated complexes has been studied. In most cases these reactions were found to be highly regioselective, and stable organometallic complexes could often be isolated. Two basic trends were found for these reactions. When chelation of the donor atom to palladium was relatively important, the regioisomer obtained had the t-Bu fragment on the same carbon as the palladium atom. In the absence of such coordination, the opposite regiochemistry was observed. These results were interpreted by taking into account the pre-insertion scenario involving η^2-coordination of the alkyne to the metal. The X-ray crystal structures of [PdC(t-Bu)=C(Me)C_6H_4-2-CH_2SMe(C_5H_5N)Cl], **7a**, [PdC(Me)=C(t-Bu)C_6H_4-2-CH_2S-t-Bu(C_5H_5N)I], **7c**, and [PdC(t-Bu)=C(Me)-2-$C_6H_4C_6H_4$-2′-SMe(C_5H_5N)Cl], **10b**, were determined.

Introduction

The insertion of an alkyne in the metal–carbon bond of metal alkyl or aryl complexes, known as the carbometalation reaction, is of both synthetic and mechanistic interest, enabling the formation of substituted olefins with a high degree of regio- and stereocontrol.[1] Cyclopalladated complexes can react with disubstituted alkynes *via syn* addition of the Pd–C fragment to the alkyne, and this procedure, which can also be considered as a special type of carbometalation, has proved to be attractive for the selective syntheses of both carbo- and heterocycles.[2] One major asset of these reactions is that organometallic complexes, resulting from the insertion of the alkyne in the Pd–C bond, can be isolated, and these have often been shown to be genuine intermediates in the formation of the organic products. With disymmetric alkynes, these insertions are usually regioselective and on the basis of the following observations it was concluded that steric factors would appear to have a more dominant influence than electronic effects on the regiochemistry of these reactions.

(i) An electronically biased insertion of phenylpropynoate derivatives would be expected to afford a cyclopalladated complex in which the palladium is linked to the same carbon as the ester function, a reaction akin to a 1,4-Michael addition. In the majority of cases the regiochemistry of the insertion of these alkynes is such that the ester function ends up away from the palladium (see (a) in Scheme 1).[2b,c,3] Nevertheless, in what must be considered as an atypical example, a cyclopalladated azobenzene complex was found to react with methyl 3-phenylpropynoate to afford a product that was assumed to result from a 1,4-Michael type addition of the metalated aryl group on the alkyne (see (b) in Scheme 1).[4]

(ii) An electronic biased insertion of nonsymmetric arylalkynes, such as (4-methoxyphenyl)-2-phenylacetylene or (4-nitrophenyl)-2-phenylacetylene, whereby one of the aryl groups is substituted by a strong electron-donating or -withdrawing group, in the Pd–C bond would be expected to occur with a high regioselectivity. However, these reactions have been shown on many occasions to be nonregioselective.[5,6]

Having established that electronic factors are of little influence, we decided to test to what extent steric factors might affect the regiochemical outcome of these insertions. The archetypal metalation of 4,4-dimethyl-2-

* Author to whom correspondance should be addressed.

† Part of the Ph.D. thesis of J.S. (Université Louis Pasteur, Strasbourg, 1994).

‡ Address correspondence pertaining to crystallographic studies to this author.

® Abstract published in *Advance ACS Abstracts,* April 1, 1995.

(1) (a) Negishi, E. *Acc. Chem. Res.* **1987**, *20*, 65. (b) Normant, J. F.; Alexakis, A. *Synthesis* **1981**, 841. (c) Knochel, P. In *Comprehensive Organic Synthesis. Selectivity, Strategy and Efficiency in Modern Organic Chemistry*; Trost, B. M., Fleming, I., Eds.; Pergamon Press: Oxford, U.K., 1991; Chapter 4.4. (d) Heck, R. F. *Org. React.* **1982**, *27*, 325. (e) Nakamura, E.; Miyachi, Y.; Koga, N.; Morokuma, K. *J. Am. Chem. Soc.* **1992**, *114*, 6686.

(2) (a) Pfeffer, M. *Pure Appl. Chem.* **1992**, *64*, 335. (b) Pfeffer, M. *Recl. Trav. Chim. Pays-Bas* **1990**, *109*, 567. (c) Pfeffer, M.; Rotteveel, M. A.; Le Borgne, G.; Fischer, J. *J. Org. Chem.* **1992**, *57*, 2147. (d) Pfeffer, M.; Sutter, J. P.; Rotteveel, M. A.; De Cian, A.; Fischer, J. *Tetrahedron* **1992**, *48*, 2427. (e) Tao, W.; Rheingold, A. L.; Heck, R. F. *Organometallics* **1989**, *8*, 2550. (f) Pfeffer, M.; Sutter, J. P.; De Cian, A.; Fischer, J. *Organometallics* **1993**, *12*, 1167. (g) Dupont, J.; Pfeffer, M.; Rotteveel, M. A.; De Cian, A.; Fischer, J. *Organometallics* **1989**, *8*, 1116.

(3) Maassarani, F.; Pfeffer, M.; Le Borgne, G. *Organometallics* **1987**, *6*, 2029.

(4) Wu, G.; Rheingold, A. L.; Heck, R. F. *Organometallics* **1987**, *6*, 2386.

(5) Beydoun, N.; Pfeffer, M. *Synthesis* **1990**, 729.

(6) Huggins, J. M.; Bergman, R. G. *J. Am. Chem. Soc.* **1981**, *103*, 3002.

0276-7333/95/2314-2214$09.00/0

Scheme 1

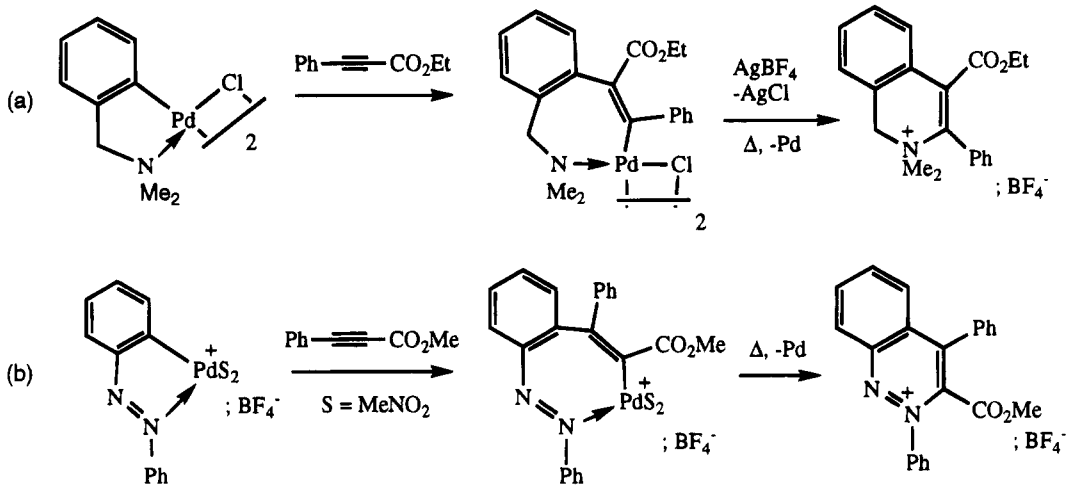

Scheme 2

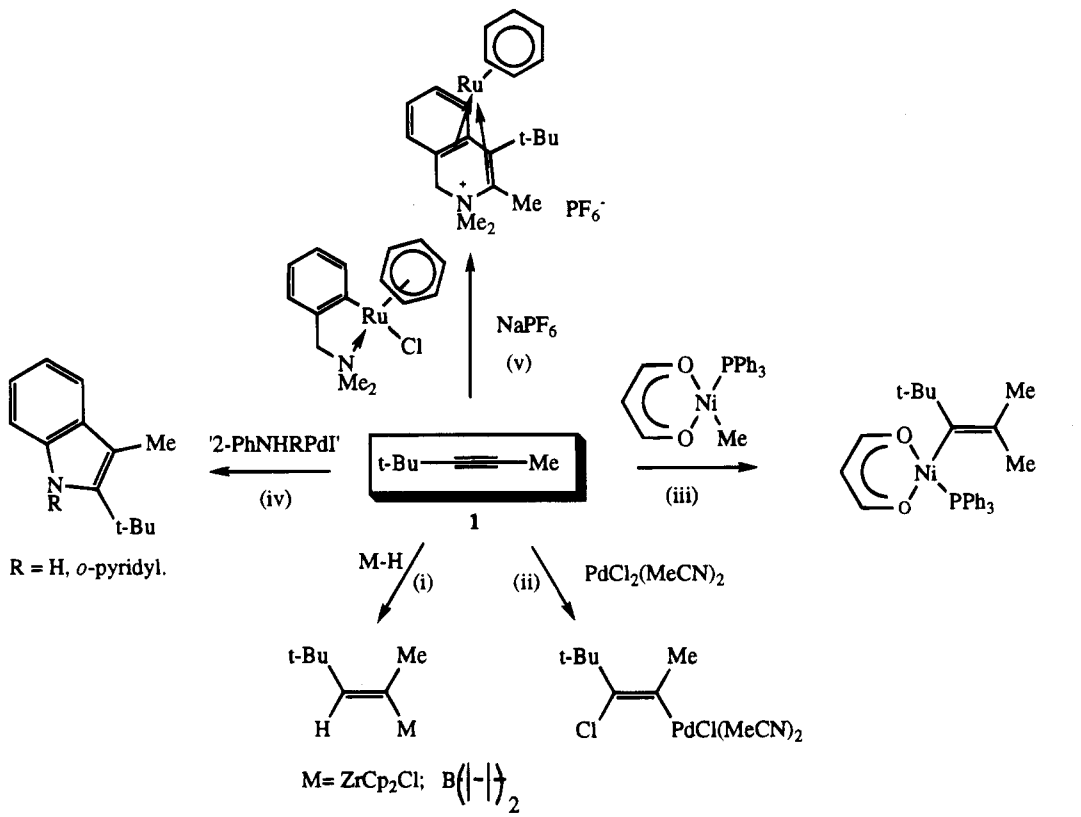

pentyne, **1**, an alkyne containing two very different sterically demanding groups, has been studied by many groups for different reaction types. It has already been shown, for example, that **1** can insert in *syn* fashion in M−Cl[7] or M−H[8] bonds in such a way that the "large" metal fragment ends up adjacent to the "small" methyl group (see (i) and (ii) in Scheme 2).

With nickel(II) complexes a different regioselectivity for the insertion of this alkyne in the Ni−C bond was observed, with the *t*-Bu group ending up on the carbon next to the metal in the final product (see (iii) in Scheme 2). In this case, however, the overall stereochemical outcome of the reaction was established as a *trans* addition.[6]

The reaction of **1** or similar alkynes with true[9] primary amines or masked secondary amines[10] was shown to afford indoles regioselectively, with the larger substituent ending up next to nitrogen in the final product (see (iv) in Scheme 2). Here, the addition of the amine function onto the metal-coordinated alkyne was proposed to explain the formation of the heterocycles.[10]

1 reacted with a cycloruthenated complex to afford a cationic heterocyclic derivative which was η^4-bonded to

(7) Maitlis, P. M. *J. Organomet. Chem.* **1980**, *200*, 161.
(8) (a) Hart, D. W.; Blackburn, T. F.; Schwartz, J. *J. Am. Chem. Soc.* **1975**, *97*, 679. (b) Zweifel, G.; Clark, G. M.; Polston, N. L. *J. Am. Chem. Soc.* **1971**, *93*, 3395.
(9) Larock, R. C.; Yum, E. K. *J. Am. Chem. Soc.* **1991**, *113*, 6689.
(10) Maassarani, F.; Pfeffer, M.; Spencer, J.; Wehman, E. *J. Organomet. Chem.* **1994**, *466*, 265.
(11) Abbenhuis, H. C. L.; Pfeffer, M.; Sutter, J. P.; De Cian, A.; Fischer, J.; Li Ji, H.; Nelson, J. H. *Organometallics* **1993**, *12*, 4464.

Chart 1

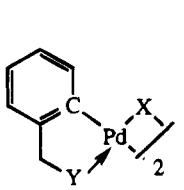

2a:Y= SMe, X=Cl.
2b:Y= SMe, X=I.
2c: Y=St-Bu, X=Cl.
2d: Y=St-Bu, X=I.
3 : Y= NMe_2, X=Cl.

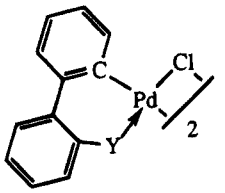

4: Y= SMe
5: Y= NMe_2

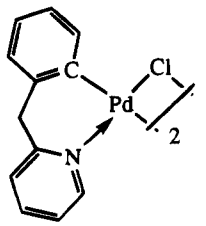

6

the ruthenium(0) center, as in (v) of Scheme 2, and in this particular example, the t-Bu group is oriented away from the newly formed C–N bond.[11] We can assume that this reaction proceeds by initial alkyne insertion in the Ru–C bond whereby the "small" Me group of the alkyne is adjacent to ruthenium.

Faced with the complexity of the insertions of **1** into metal–carbon bonds, each reaction being very regioselective yet changing as a function of the organometallic reagent employed, we decided to study the behavior of this alkyne toward a series of cyclopalladated compounds. The palladium-containing starting materials employed in our study, **2-6**, were selected in order to satisfy various requirements (see Chart 1). Both five- and six-membered sulfur- and nitrogen-containing metallacycles were chosen to be reacted with **1**. The sulfur-containing derivatives were selected as they are prone to undergoing mono-insertion reactions with alkynes.[12] We were especially interested in avoiding the possibility of the frequently observed multiple insertions of alkynes in the Pd–C bond.[2b,7]

It is generally accepted that the migratory insertions of alkynes in the metal–carbon bond are preceded by an η^2-interaction of the alkyne to the metal, the alkyne being *cis* relative to the metal–carbon bond.[13] More recently, and much more relevant to our work, the reactions of disubstituted alkynes with cyclopalladated complexes were shown by kinetic studies to involve a halide bridge-splitting reaction, followed by a migratory insertion of the alkyne into the Pd–C bond of the resulting dimeric complex.[14] With this model in hand we predicted that the regioselectivity of the reaction of **1** with cyclopalladated complexes ought to be influenced by the diverse structural permutations present in **2-6**. Our goal was to study the possible influence of ring size, geometry, and the nature of the donor group, in these palladium-containing starting materials, on the regioselectivity observed.

Results and Discussion

Reactions of Five-Membered Sulfur-Containing Cyclopalladated Complexes with 1. The five-membered sulfur-containing chelated complex **2a** reacted with **1** in refluxing chlorobenzene (PhCl) over a 1 h period. The addition of pyridine and crystallization in hexane at −20 °C gave a yellow solid/oil that analyzed as being a pyridine-containing palladium complex incorporating both the original ligand and a single unit of **1**. We undertook a ^{1}H NMR nOe study to confirm the regiochemical outcome of this reaction. The most significant effects observed upon irradiation of the t-Bu group were enhancements of the neighboring Me group (5.7%) and of two equivalent protons of the coordinated pyridine atom (8% on H° at δ = 8.84 ppm). Similar irradiation of the methyl group (δ = 2.14 ppm) gave a small enhancement of the t-Bu group (2.6%), an effect on both aromatic protons (7.8% of multiplet at δ = 7.47 ppm), and a small effect on the pyridine protons (1.3% effect on H° at δ = 8.84 ppm) (eq 1).

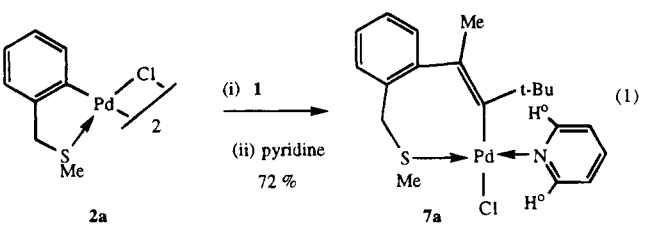

(1)

The unequivocal regiochemical assignment of the structure of **7a** was achieved by a single crystal X-ray structural determination study of crystals obtained by slow hexane diffusion into a dilute CH_2Cl_2 solution of **7a**. It is immediately apparent from the ORTEP diagram of **7a**, shown in Figure 1, that alkyne insertion into the Pd–C bond of **2a** has occurred and that the t-Bu group, as predicted by the nOe experiment, is on the carbon adjacent to the metal in **7a**. The palladium atom is in a near square planar environment and is part of a boat-shaped seven-membered ring in which the sulfur atom is coordinated to the metal center. The sulfur–palladium bond distance is in the normal range (2.273 Å),[15] and the pyridine atom is *trans* to the SMe group with a Pd–N distance of 2.099 Å.

The iodo-bridged dimers **2b,d** were obtained by the oxidative addition of an *ortho*-iodo thioether on $Pd(dba)_2$, both in ca. 60% yield.[16] With these starting materials it was tempting to study the possible influence of a change in the halogen bridges on the regiochemistry of these reactions. When we reacted **2b** with **1**, followed by pyridine addition, the product obtained displayed a very complicated ^{1}H NMR spectrum which included a multitude of peaks between δ = 1 and 3 ppm. Reaction of the iodo derivative **2d** with **1**, and then with pyridine,

(12) Dupont, J.; Pfeffer, M.; Theurel, L.; Rotteveel, M. A. De Cian, A.; Fischer, J. *New J. Chem.* **1991**, *15*, 551.
(13) (a) Samsel, E. G.; Norton, J. R. *J. Am. Chem. Soc.* **1984**, *106*, 5505. (b) de Vaal, P.; Dedieu, A. *J. Organomet. Chem.* **1994**, *478*, 121.
(14) Ryabov, A. V.; van Eldik, R.; Le Borgne, G.; Pfeffer, M. *Organometallics* **1993**, *12*, 1386.
(15) Dupont, J.; Pfeffer, M.; Daran, J. C.; Jeannin, Y. *Organometallics* **1987**, *6*, 5505.
(16) Spencer, J.; Pfeffer, M.; DeCian, A.; Fischer, J. *J. Org. Chem.* **1995**, *60*, 1005.

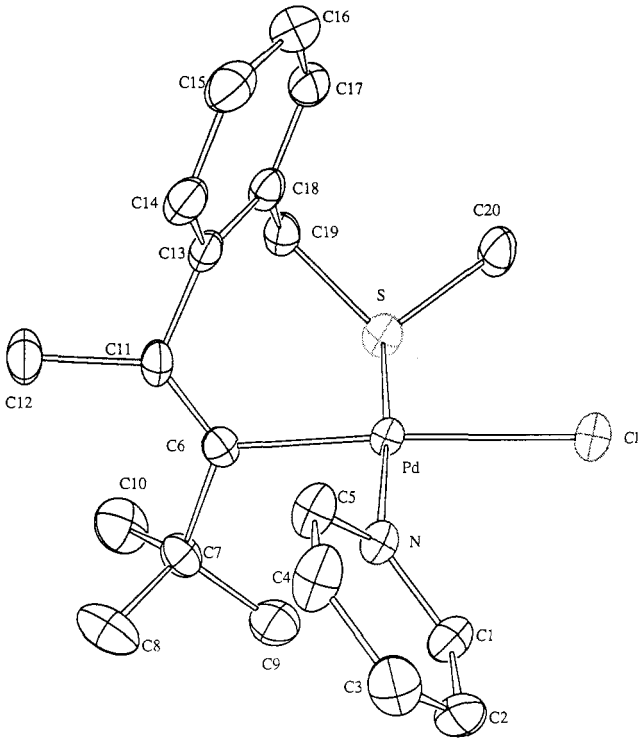

Figure 1. ORTEP diagram of **7a** using the adopted numbering scheme. Hydrogen atoms have been omitted for clarity.

Table 1. Selected Bond Distances (Å) and Angles (deg) for Compound 7a[a]

	Distances		
Pd–S	2.273(1)	Pd–N	2.099(4)
Pd–Cl	2.439(1)	C(6)–C(11)	1.326(7)
Pd–C(6)	2.011(4)	C(11)–C(13)	1.485(7)
	Angles		
Cl–Pd–N	89.0(1)	N–Pd–C(6)	89.6(2)
Cl–Pd–C(6)	176.4(1)	N–Pd–S	176.1(1)
Cl–Pd–S	94.83(5)	C(6)–Pd–S	86.6(1)

[a] Numbers in parentheses are estimated standard deviations in the least significant digits.

yielded a monomeric pyridine-containing palladium complex. Its ^{1}H NMR spectrum was much more complicated than that of **7a** and was quite similar to that of the product of **2b** and **1**. The presence of a large number of signals for the t-Bu and Me groups, in the bulk product, all pointed to a nonregioselective insertion of the alkyne in the Pd–C bond. We anticipated that in solution the pyridine atom was likely to be in both *cis* and *trans* positions with respect to the S-t-Bu group. Another possibility, which is moreover reflected by the repeatedly poor combustion analyses obtained for **7c**, is the presence of both monomeric (i.e. **7c**) and iodo-bridged dimeric species in the bulk compound. An nOe study was unconceivable for such a complex spectrum at rt (room temperature), and variable-temperature ^{1}H NMR (in $CDCl_3$ or benzene-d_6) was unhelpful. It was concluded rather tentatively that **2d** reacted with **1** to give **7c** as a mixture of regioisomers, the pyridine molecule being either *cis* or *trans* to the S-t-Bu unit in each case (see eq 2).

Crystallization of the bulk product in CH_2Cl_2/hexane afforded two types of crystals. Large orange blocks were formed along with a small amount of small red needles, and the two sets were rather difficult to separate. Once

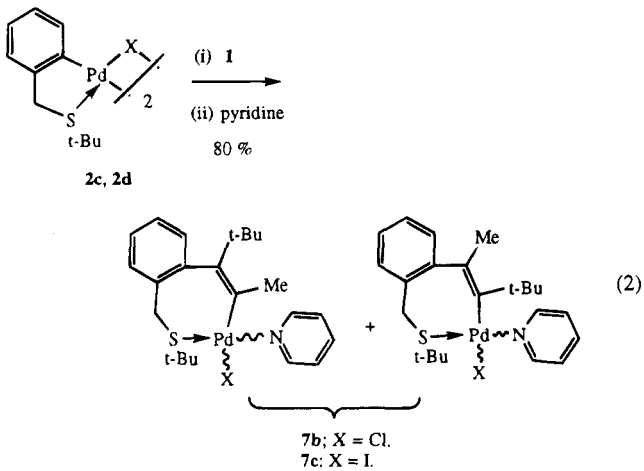

a sample of the orange blocks was dissolved in $CDCl_3$ solution, the ^{1}H NMR spectrum of the resulting solution was still very complicated. A single crystal X-ray diffraction study could be carried out on one of these orange crystals. The ORTEP diagram shown in Figure 2 shows that, for the particular crystal chosen, the pyridine is located in a *cis* position relative to the S-t-Bu group in **7c**, even though this position would appear to be sterically rather crowded in the square planar complex. The Pd–N distance of 2.24 Å is significantly longer than that of the *trans* (SMe–pyridine) ligated complex **7a** (Pd–N = 2.099 Å), reflecting the high *trans* influence of the vinylic carbon, C1, in **7c**.[17] The methyl group of the inserted alkyne is now found on the carbon atom adjacent to palladium in the seven-membered metallacyclic product. This result has, however, to be treated with some circumspection as we will see later that this regioisomer is the minor product of the insertion reaction.

The chloride-containing monomeric pyridine complex **7b** was formed by the reaction of **1** with **2c**, followed by pyridine addition, and its ^{1}H NMR spectrum revealed the presence of two regioisomers in a ca. 6:1 ratio.

Formation of S-Heterocycles from the Reaction of 2 with 1. We predicted that the reactions of **2** with **1** might be clarified by simply removing the metal. Using our recently developed demetalation procedure for the formation of sulfur-containing heterocycles,[16] we were able to form organic products from these reactions. This procedure relies on the destabilization of the compounds obtained *in situ* from the reaction of **1** with **2** by halide abstraction using a silver salt in a weakly coordinating solvent (THF). The resulting solvated monomeric complexes are then more labile toward thermolysis. **2a–d** were thus reacted with **1** in refluxing PhCl. Following $AgBF_4$ treatment in THF and thermolysis, palladium black was deposited and organic products were obtained after the usual workup procedure. **2a** and **2b** yielded seemingly the same heterocyclic product **8** as one regioisomer in 78% and 86% isolated yields, respectively. Moreover, when the two

(17) Pyridine usually bonds *cis* to palladated carbon atoms: (a) Ryabov, A. D.; Kazankov, G. M.; Yatsimirsky, A. K., Kuz'mina, L. G.; Burtseva, O. Y.; Dvortsova, N. V.; Polyakov, V. A. *Inorg. Chem.* **1992**, *31*, 3083. (b) Maassarani, F.; Pfeffer, M.; Le Borgne, G.; Grandjean, D. *Organometallics* **1986**, *5*, 1511. (c) Deeming, A. J.; Rothwell, I. P.; Hursthouse, M. B.; New, L. *J. Chem. Soc., Dalton Trans.* **1978**, 1490. For a pyridine *trans* to a carbon atom; see: Pfeffer, M.; Sutter-Beydoun, N.; De Cian, A.; Fischer, J. *J. Organomet. Chem.* **1993**, *453*, 139.

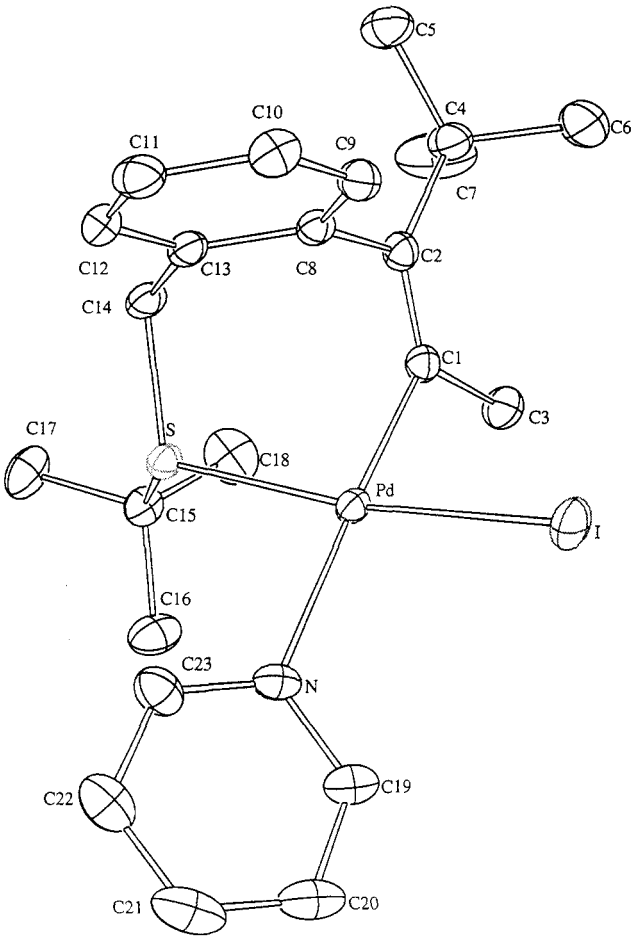

Figure 2. ORTEP plot of **7c** using the adopted numbering scheme. Hydrogen atoms have been omitted for clarity.

Table 2. Selected Bond Distances (Å) and Angles (deg) for Compound 7c[a]

	Distances		
I–Pd	2.6319(5)	Pd–N	2.240(4)
Pd–C(1)	1.994(5)	C(1)–C(2)	1.322(7)
Pd–S	2.326(1)	C(13)–C(14)	1.510(7)
	Angles		
I–Pd–C(1)	86.2(1)	C(1)–Pd–N	176.6(2)
I–Pd–S	168.96(4)	S–Pd–N	90.2(1)
I–Pd–N	92.8(1)	Pd–C(1)–C(2)	121.5(4)
C(1)–Pd–S	91.4(1)	Pd–C(1)–C(3)	109.5(4)

[a] Numbers in parentheses are estimated standard deviations in the least significant digits.

separate products were mixed together, the ^{1}H NMR spectrum of the mixture was that of one single product. This unstable, and difficult to purify, organic product was characterized by ^{1}H NMR which revealed the presence of a single t-Bu group (δ = 1.52 ppm) and two methyl groups that resonate at virtually the same chemical shift (δ = 2.56 and 2.57 ppm). An AB spin system for the diastereotopic methylene protons around δ = 4.6 ppm was diagnostic of a S-methylated 1*H*-2*S*-benzothiopyrilium salt, and the orientation of the t-Bu and Me groups was inferred from the structural determination of **7a**.

When **2d** was reacted with **1** and subjected to the same depalladation conditions, a mixture of two regioisomeric heterocyclic products was obtained in a ca. 4:1 ratio. The ^{1}H NMR spectrum of the major product displayed singlets for the t-Bu and Me groups of the original alkyne at δ = 1.40 ppm and δ = 2.37 ppm, respectively, and the methylene protons were found as a singlet at δ = 3.54 ppm. We can note the absence of a t-Bu group on the sulfur atom, which is lost during the reaction as isobutene.[16] We assigned the 1*H*-2*S*-benzothiopyran structure **9a/9b** to the products obtained. **2c** under identical conditions gave **9** although it was difficult to calculate the regiomeric composition of the products due to purification problems. The major regioisomer, however, corresponded to the predominant one obtained from the reaction of **2d** and **1**.

Demethylation of **8** (PhCl reflux, 48 h) afforded the corresponding 1*H*-2*S*-benzothiopyran derivative **9b**, as shown in eq 3. The ^{1}H NMR spectrum of the latter included singlets at δ = 1.39, 2.37, and 3.54 ppm for the t-Bu, Me, and CH_2 groups, respectively. Here, we were, therefore, able to establish that the reactions of **2a,d** with **1** both yield the same heterocycle, **9b**, as major product, the reaction involving **2d** being somewhat less regioselective. Given that the reactivities of **2a,b** are very similar toward **1**, another pertinent point is that a change in the halogen bridges from chloride to an iodide has little effect on the regiochemistry of these reactions.

Reactions of a Six-Membered Sulfur-Containing Cyclopalladated Complex with 1. When the thioether-chelated six-membered complex **4** was reacted with **1** in refluxing PhCl over a short period of time, a yellow solid **10a** was obtained which analyzed as containing the original cyclopalladated fragment along with the alkyne in a 1:1 ratio. Its ^{1}H NMR spectrum was very complicated, although in the presence of deuterated pyridine (i.e. the monomeric complex **10b** is formed) it displayed singlets for the t-Bu, Me, and SMe groups in the high-field region. Traces of a possible

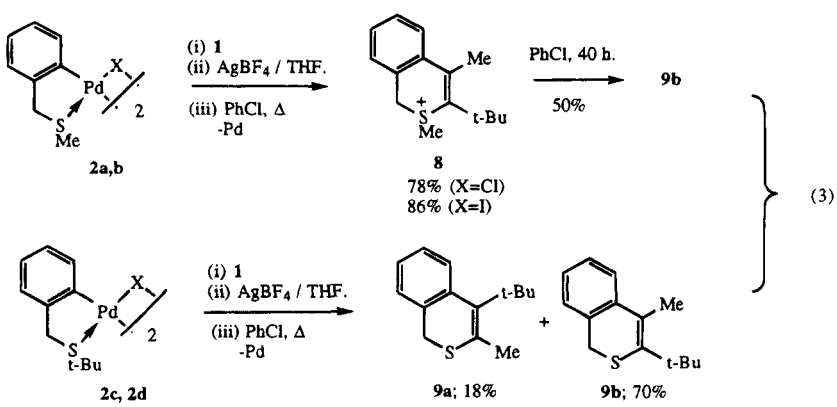

Table 3. Selected Bond Distances (Å) and Angles (deg) for Compound 10b[a]

	Distances		
S(1)–Pd(1)	2.2761(9)	S(1)–C(24)	1.788(3)
Pd(1)–Cl(1)	2.4271(9)	S(1)–C(25)	1.815(4)
Pd(1)–C(6)	2.013(3)	C(6)–C(7)	1.544(4)
Pd(1)–N(1)	2.085(3)	C(6)–C(11)	1.329(4)
	Angles		
Cl(1)–Pd(1)–S(1)	89.54(3)	S(1)–Pd(1)–C(6)	92.58(9)
Cl(1)–Pd(1)–N(1)	90.19(7)	N(1)–Pd(1)–C(6)	87.6(1)
Cl(1)–Pd(1)–C(6)	177.75(9)	C(24)–S(1)–C(25)	100.1(2)
N(1)–Pd(1)–C(6)	87.6(1)	C(6)–C(11)–C(12)	127.5(3)
S(1)–Pd(1)–N(1)	173.04(7)		

[a] Numbers in parentheses are estimated standard deviations in the least significant digits.

second regioisomer were apparent in its ^{1}H spectra. Moreover, addition of triphenylphosphine to **10a** yielded the expected monomeric phosphine complex **10c** which gave two singlets in its ^{31}P NMR spectrum of ca. 10:1 ratio (see eq 4).

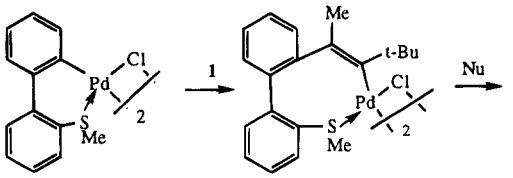

4 **10a** (major regioisomer)

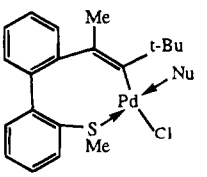

(4)

10b: Nu = pyridine-d_5
10c: Nu = PPh_3

The orientation of the t-Bu and Me groups in **10b** was investigated by nOe spectroscopy in $CDCl_3$ solution. Irradiation of the t-Bu group caused an enhancement of the adjacent methyl group (6.3%) and a small effect on an aromatic proton (1.6% on H at δ = 7.5 ppm). Irradiation of the Me group (at δ = 1.73 ppm) caused a significant effect on two distinct aromatic protons (6.2% on δ = 7.18 ppm and 4.1% on δ = 7.47 ppm), and irradiation of the SMe group (δ = 2.68 ppm) led to an enhancement of two aromatic protons (5.3% on δ = 7.3 ppm and 5.7% on δ = 7.54 ppm). Once more, we concluded that the t-Bu group was on the carbon atom next to the palladium atom in the major product, and this was confirmed by an X-ray diffraction study of the monomeric adduct **10b**, the crystals of which were obtained in an analogous fashion to **7a**. The pyridine unit is located in a *trans* position with respect to the thioether group, and the palladium atom is in a near square planar environment in the eight-membered ring (see Figure 3).

At this stage, we can draw an early conclusion in that **1** inserts into the Pd–C bond of both five- and six-membered SMe-bound palladocycles in a regioselective manner whereby the t-Bu group of the alkyne is on the carbon adjacent to the metal in the inserted product. We next focused our attention on palladacycles containing nitrogen donor groups.

Reactions of Nitrogen-Containing Cyclopalladated Complexes with 1. The reaction of **3** with **1** in

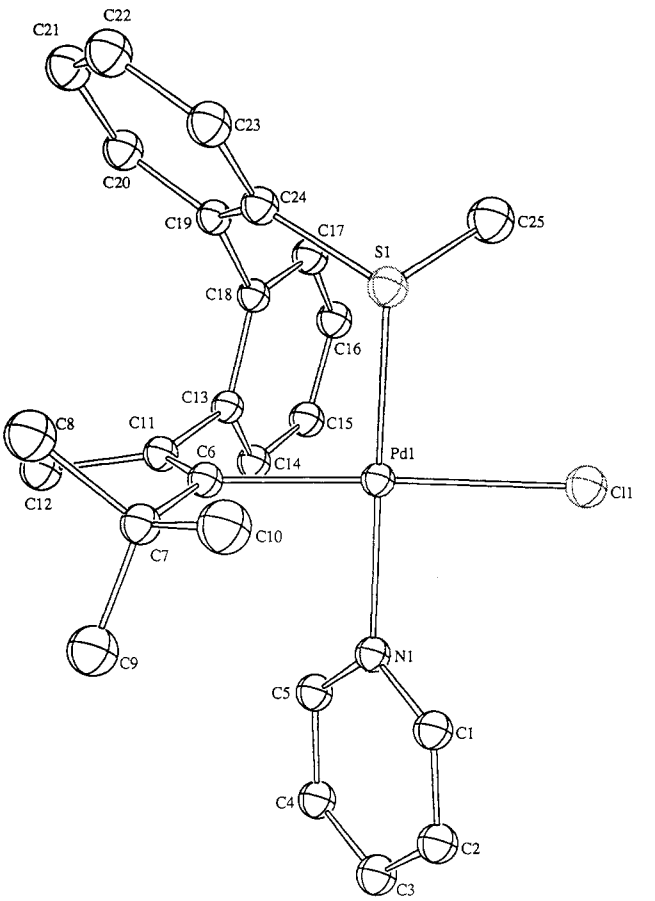

Figure 3. ORTEP plot of one of the independent molecules of **10b** using the adopted numbering scheme. Hydrogen atoms have been omitted for clarity.

CH_2Cl_2 overnight at rt afforded an n-hexane-soluble solid which analyzed as a 2:1 inserted alkyne cyclopalladated complex adduct. It is pertinent to note that the ^{1}H NMR spectrum of this compound was characteric of a complicated mixture of regioisomers. All our efforts aimed at separating or crystallizing these regioisomers did not meet with success.

We anticipated that **5***, formed by chloride abstraction of **5** with a silver salt, would react with **1** to give an organic product according to the known procedure.[12] Indeed, during the reaction, palladium metal was formed and the organic product obtained displayed the typical ^{1}H NMR and analytical data of the expected spirocyclic cationic compound **11** (see eq 5). A ^{1}H NMR

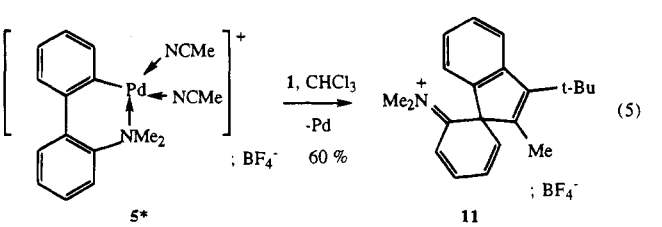

5* **11** (5)

nOe experiment confirmed the orientation of the t-Bu and Me groups. Irradiation of the t-Bu group led to a large enhancement of an aromatic proton (16% at δ = 7.7 ppm), and irradiation of the Me group led to a small enhancement of one of the cyclohexadienyl protons (3% on an H at δ = 5.45 ppm). Here, the t-Bu group is found to be orientated away from the newly formed spirocyclic C–C junction.

Scheme 3

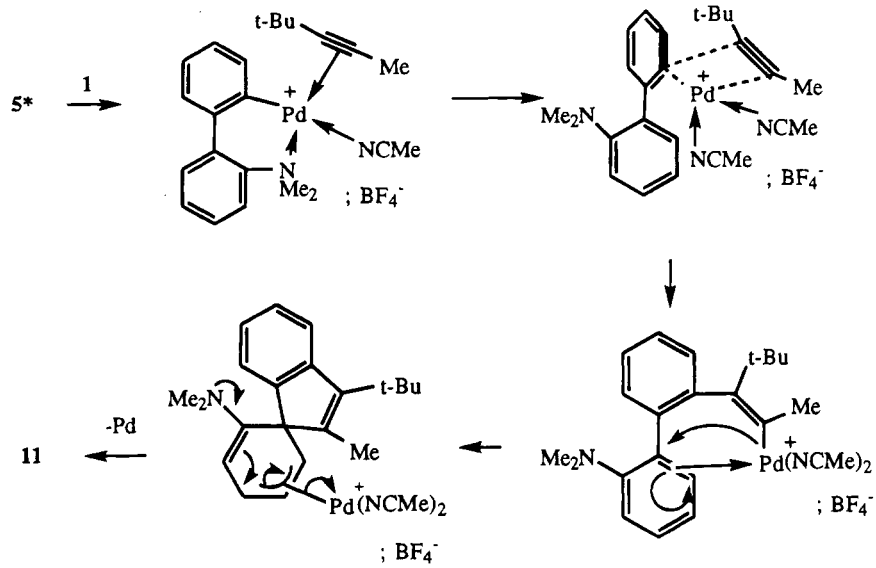

A final candidate for our study was the six-membered palladacycle **6**. In this complex, the pyridine entity is known to be a relatively good chelating ligand, and it has already been shown that **6** can react with alkynes to afford chelated eight-membered metallacycles and in some special instances heterocyclic products.[18] When we reacted **6** with **1** in refluxing CH_2Cl_2 overnight, followed by pyridine addition, a yellow solid could be obtained along with traces of unreacted **6** (see eq 6).

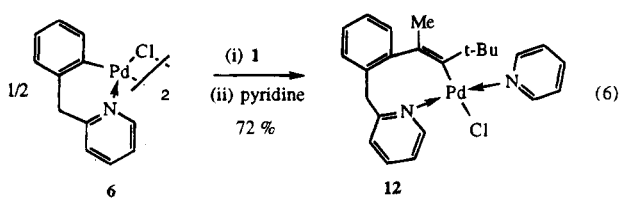

6 12

Attempts to shorten the reaction time led to incomplete reaction. The product analyzed as being a mono-inserted, pyridine-containing, organometallic complex, and its ^1H NMR spectrum compared with those of similar reported compounds. Irradiation of the t-Bu group, using nOe spectroscopy, led to an enhancement of the adjacent Me group (2.6%), a large effect on the two *ortho* pyridine protons (4.4% effect on H° at $\delta = 8.8$ ppm), and a significant effect on the H° of the pyridine atom of the benzylpyridine fragment (6.6% on H° at $\delta = 9.52$ ppm). Similar irradiation of the Me group led to a large effect on the aromatic proton (6.2% on H at $\delta = 6.97$ ppm). Given the successful combination of nOe spectroscopy and X-ray diffraction studies above, we declined in this case from undertaking a crystal structure determination and attributed the product as having the structure **12**.

Discussion

We have shown herein that the reaction of **1** with a series of five- and six-membered palladacycles, with the exception of **2c,d**, can indeed be very regioselective and that both organometallic and organic products can be isolated, often in very good yields. Although one slight disadvantage of our study is that the conditions employed often change from one substrate to another, we can still infer certain conclusions on the relationship between the structure of the starting material and that of the product obtained.

(i) The "Palladium Effect": Lack of Coordination to the Metal. **1** reacts with **5*** to give the organic product **11**. According to the proposed mechanism, adapted for the insertion of **1** (see Scheme 3), this reaction involves alkyne insertion in the Pd–C bond, followed by η^2-coordination of the aryl group to palladium.[12] The activated olefinic fragment of the aryl group can then undergo a nucleophilic attack by the vinyl-palladated group, leading to the formation of a C–C bond by an intramolecular spirocyclization process. Following palladium loss, the organic carbocyclic product is obtained.

We can reasonably assume that chelation of the amine function to palladium is relatively weak in **5***. This had already been shown[12] with the inserted complex $[PdC(CO_2Me)=C(CO_2Me)\text{-}2\text{-}C_6H_4C_6H_4\text{-}2'\text{-}NMe_2\text{-}(\mu\text{-}Cl)]_2$ in which the dative bond between the amine group and palladium was readily displaced by an external nucleophile, pyridine, to give $[PdC(CO_2Me)=C\text{-}(CO_2Me)\text{-}2\text{-}C_6H_4C_6H_4\text{-}2'\text{-}NMe_2(pyr)_2Cl]$.

The regiochemistry of this reaction parallels that observed earlier for the insertion of **1** in the Pd–Cl bond.[7] The steric control is likely to be due to a "palladium effect"; i.e. the regiochemical outcome is such that the steric interactions between the two large entities, the t-Bu group and palladium, are minimized. For this to be possible the orientation of the alkyne prior to insertion in the Pd–C bond is of crucial importance, and we can consider this as being the rate-determining step of this reaction as the ensuing C–C bond formation should be irreversible. Scheme 3 provides a useful model for explaining the regiochemistry observed. We can corroborate this argument by invoking the decoordination of the amine group from the metal. The insertion of **1** can then occur perpendicular to the plane of the aryl group linked to palladium, with the flat aryl face presenting little steric hindrance toward the t-Bu group.

(ii) Chelate Control. The reactions of **1** with **2a**, **4**, and **6** are regioselective, affording chelated organome-

(18) Maassarani, F.; Pfeffer, M.; Le Borgne, G. *Organometallics* **1987**, *6*, 2043.

Scheme 4

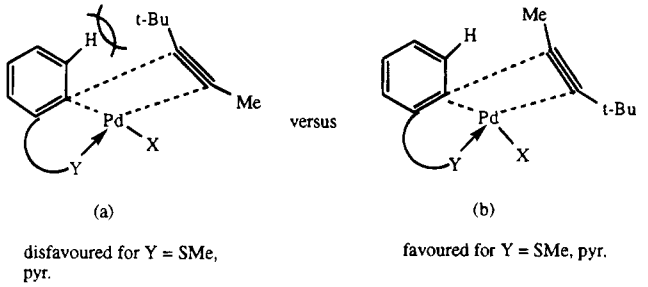

tallic complexes whereby the t-Bu group is located on the carbon atom next to palladium. This "chelate control", therefore, directs the alkyne insertion in the Pd–C bond such that the "large" alkyne substituent ends up on the carbon next to the metal, the most blatant example being illustrated by the fact that **4** reacts with **1** to give a chelated organometallic complex with the t-Bu group near to palladium whereas the same alkyne adopts the opposite orientation with the nonchelating **5***.

The two hypothetical pre-insertion possibilities that dictate the orientation of the regioselective insertions of **1** in the Pd–C bond of **2**, **4**, and **6** are illustrated in Scheme 4. The cyclopalladated complexes are shown as monomeric species for simplification. According to (a), the resulting inserted product will contain the Me group adjacent to the metal, the main steric interactions occurring between the t-Bu group and the metalated aryl group in the pre-inserted intermediate. (b) is the situation prior to the insertion of **1** which leads to the t-Bu group next to the metal in the final product. Here, the principal encumbrance can be found between the t-Bu group and the metal.

In this particular example, the subtle difference between these reactions and the one shown in Scheme 3 is that, due to the coordination of Y (Y = pyr, SMe) to palladium, the insertion of **1** now has to occur in the same plane as the aryl group bonded to palladium. Of the two orientations possible prior to the insertion of **1** in the Pd–C bond, (b) would now appear to be favored since in (a) there is steric hindrance between the t-Bu group of **1** and the coplanar aromatic proton situated in an *ortho* position with respect to palladium. This interaction would appear to counterbalance the "palladium effect" discussed above, and hence, the t-Bu group ends up on the carbon next to the metal in the final product.

The reactions of **2c,d** with **1** are rather unselective in comparison with those of **2a,b** with the same alkyne. We can, therefore, reasonably conclude that the S-t-Bu group of the thioether is at least partially responsible for this loss of regioselectivity. Using the model given above, we suggest that the greater *trans* influence of the S-t-Bu group, as compared to a SMe group for example, leads to an elongation of the Pd–alkyne bond in the pre-inserted intermediate (a) or (b). According to the situation (a) in Scheme 4, the t-Bu substituent of the alkyne should now be less sensitive toward steric interactions with the protons of the metalated aryl group. The greater steric bulk around the metal due to the presence of the S-t-Bu group may also enhance the contribution of such a "palladium effect". It is likely that the nonselectivity of these reactions is due to a contribution of both (a) and (b) prior to the insertion of **1** in the Pd–C bond of **2c** or **2d**. Indeed, this reaction represents a "halfway house" situation, with both the chelate and palladium effects seemingly having an influence on the orientation of the alkyne insertion.

Our "chelate model" may also provide an alternative explanation for the regioselective insertion of **1** in metal–carbon bonds observed for similar reactions. For example, **1** was found to react with *o*-iodobenzaldehyde in the presence of $Pd(OAc)_2$ as catalyst to give a 2-t-Bu-substituted carbocyclic, indenone product **13** (see Scheme 5).[19a] The essential part of the mechanism is likely to involve the intramolecular nucleophilic attack of a palladated vinyl group onto an activated carbonyl function, as proposed elsewhere.[10,19b,20,21] Here, and also with a similar manganese-promoted carbocyclization (which led to **14** for example, using n-hexyne as alkyne),[20] an alternative explanation for the orientation of the disymmetric alkyne prior to insertion in the metal–carbon bond is very well accommodated by our "chelate model" shown in Scheme 5 (although chelation of the carbonyl function to the metal would appear to be less obvious in the case of Pd[19b]). Once again, the favored alkyne orientation is such that the large substituent R_L is adjacent to the metal in the inserted product, and the pre-inserted scenario resembles situation (b) in Scheme 4. Although genuine metallacyclic complexes, resulting from alkyne insertion in the Mn–C bond, have been isolated in the case of the manganese-mediated reactions,[21] these results were somewhat tarnished by the total lack of regioselectivity observed when using disymmetric alkynes.

Scheme 5

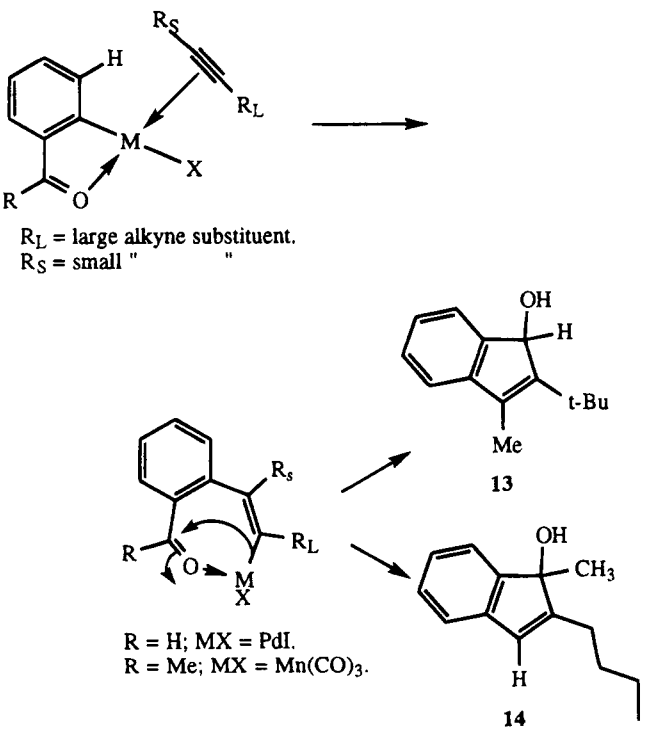

(19) (a) Larock, R. C.; Doty, M. J.; Cacchi, S. *J. Org. Chem.* **1993**, *58*, 4579. (b) Vicente, J.; Abad, J. A.; Gil-Rubio, J. *J. Organomet. Chem.* **1992**, *436*, C9.

(20) Liebeskind, L. S.; Gasdaska, J. R.; McCallum, J. S.; Tremont, S. J. *J. Org. Chem.* **1989**, *54*, 669.

(21) Grigsby, W. J.; Main, L.; Nicholson, B. K. *Organometallics* **1993**, *12*, 397.

Table 4. X-ray Experimental Data[a]

	7a	7c	10b
formula	$C_{20}H_{26}NSClPd$	$C_{23}H_{33}NSPdI$	$C_{25}H_{28}NSClPd$
M_r	454.4	588.9	516.4
cryst system	monoclinic	monoclinic	triclinic
a (Å)	13.698(4)	10.041(3)	9.658(2)
b (Å)	9.809(2)	16.149(4)	15.195(4)
c (Å)	15.674(4)	15.332(4)	17.096(5)
α (deg)			74.52(2)
β (deg)	101.76(2)	94.18(2)	85.71(2)
γ (deg)			89.23(2)
V (Å^3)	2061.8	2479.6	2411.1
Z	4	4	4
D_{calc} (g cm^{-3})	1.464	1.577	1.423
μ (cm^{-1})	11.174	20.592	9.646
space group	$P2_1/n$	$P2_1/n$	$P\bar{1}$
cryst dimens (mm)	0.38 × 0.20 × 0.12	0.30 × 0.22 × 0.20	0.38 × 0.30 × 0.10
scan width (deg)	1.05 + 0.34 tan θ	1.39 + 0.34 tan θ	1.20 + 0.34 tan θ
octants	$\pm h,+k,+l$	$+h,+k,\pm l$	$\pm h,\pm k,+l$
no. of data collcd	3983	4704	8483
no. of data with $I > 3\sigma(I)$	2275	2970	6339
no. of variables	217	244	523
abs min/max	0.88/1.00	0.94/1.00	0.88/1.00
$R(F)$	0.031	0.029	0.025
$R_w(F)$	0.042	0.044	0.037
p	0.06	0.06	0.06
largest peak in final diff (e Å^{-3})	0.16	0.26	0.15
GOF	1.045	1.133	1.006

[a] In common: color, yellow; wavelength (Å), 0.7107; diffractometer, Enraf-Nonius CAD4-F; radiation, Mo Kα graphite monochromated; scan mode, $\theta/2\theta$; scan speed, variable; $\theta_{min/max}$ (deg), 2/24.

Conclusion

Chelation of the donor atom to palladium, irrespective of whether it is an amine or thioether group, directs the insertion of **1** in the Pd−C bond to give an enlarged metallacycle in which the t-Bu group is found on the carbon atom next to the metal. In the absence of this chelation, as with **5***, this regiochemistry is reversed. Apart from the reactions of **2c,d** with **1**, which exhibit a relatively poor regioselectivity, attributed to the high *trans* effect and no doubt greater steric bulk of the *tert*-butylated thioether group, these reactions are highly regioselective.

Experimental Section

General Comments. Unless stated otherwise, all reactions were performed in air using either distilled (CH_2Cl_2 over P_2O_5, *n*-hexane and *n*-pentane over sodium) or commercial grade solvents (PhCl, $ClCH_2CH_2Cl$). ^1H NMR spectra were recorded at 200.13 and 300.13 MHz on SY200 and AC300 Bruker instruments respectively, and externally referenced to TMS. Elemental analyses were performed by the Service Central de Microanalyses du CNRS. Column chromatography was carried out on either Al_2O_3 90 (activity II-III mesh, Merk) or on silica gel (Kieselgel 60). **2a**,[22] **2b**,[16] **2d**[16], **2c**,[23] **3**[24], **4**,[22] **5**,[12] and **6**[25] were made according to given procedures. 4,4-Dimethyl-2-pentyne was purchased from Lancaster and used without purification. NOe spectra were recorded on freeze−pump−thaw degassed samples in sealed tubes.[26]

(22) Dupont, J.; Beydoun, N.; Pfeffer, M. *J. Chem. Soc., Dalton Trans.* **1989**, 1715.
(23) Fuchita, Y.; Hiraki, K.; Yamaguchi, T.; Maruta, T. *J. Chem. Soc., Dalton Trans.* **1981**, 2405.
(24) Pfeffer, M. *Inorg. Synth.* **1989**, *26*, 211.
(25) Hiraki, K.; Fuchita, Y.; Takechi, K. *Inorg. Chem.* **1981**, *20*, 4316.
(26) *Modern NMR Techniques for Chemistry Research*; Derome, A. E., Ed.; Pergamon Press: Oxford, U.K., 1987; Chapter 5, p 97.

Table 5. Positional Parameters and *B* Values and Their Esd's for 7a

atom	x	y	z	B^a (Å^2)
Pd	0.44228(2)	0.24553(3)	0.25995(2)	2.941(6)
Cl	0.36925(9)	0.2307(1)	0.38914(7)	4.34(3)
N	0.4937(3)	0.0446(4)	0.2828(2)	3.34(8)
C(1)	0.5395(4)	0.0043(5)	0.3623(3)	4.3(1)
C(2)	0.5646(4)	−0.1284(5)	0.3820(3)	4.9(1)
C(3)	0.5382(4)	−0.2259(5)	0.3200(4)	5.0(1)
C(4)	0.4909(4)	−0.1866(5)	0.2393(3)	5.0(1)
C(5)	0.4701(4)	−0.0517(5)	0.2225(3)	4.4(1)
C(6)	0.5110(3)	0.2570(4)	0.1584(3)	3.43(8)
C(7)	0.6254(3)	0.2883(5)	0.1828(3)	4.2(1)
C(8)	0.6849(4)	0.1629(6)	0.1621(5)	7.1(2)
C(9)	0.6582(4)	0.3162(7)	0.2786(4)	6.3(2)
C(10)	0.6501(4)	0.4136(6)	0.1349(4)	7.0(2)
C(11)	0.4574(3)	0.2320(4)	0.0795(3)	3.66(9)
C(12)	0.4959(4)	0.2220(6)	−0.0064(3)	5.6(1)
C(13)	0.3470(3)	0.2221(4)	0.0623(3)	3.5(1)
C(14)	0.2982(4)	0.1037(5)	0.0283(3)	4.5(1)
C(15)	0.1958(4)	0.0953(6)	0.0098(3)	5.3(1)
C(16)	0.1394(4)	0.2060(4)	0.0248(4)	5.6(1)
C(17)	0.1862(4)	0.3217(6)	0.0579(3)	4.9(1)
C(18)	0.2884(3)	0.3341(5)	0.0764(3)	3.8(1)
C(19)	0.3367(4)	0.4657(5)	0.1096(3)	4.3(1)
S	0.3893(1)	0.4622(1)	0.22608(8)	4.14(3)
C(20)	0.27560(4)	0.4868(4)	0.2652(3)	6.8(1)

[a] Anisotropically refined atoms are given in the form of the isotropic equivalent displacement parameter defined as + $ac(\cos\beta)\beta(1,3)$ + $bc(\cos\alpha)\beta(2,3)$].

[PdC(t-Bu)=C(Me)C$_6$H$_4$-2-CH$_2$SMe(C$_5$H$_5$N)Cl], 7a. 2a (140 mg, 0.5 mmol) and **1** (73 mg, 0.76 mmol) were heated to reflux temperature for 1 h in chlorobenzene (20 mL). After Celite filtration and solvent concentration (to *ca.* 5 mL), excess pyridine was added (0.1 mL) and the solvent was evaporated to dryness. Overnight crystallization in hexane/pyridine (20 mL/2 mL) at −20 °C gave a yellow solution and near white precipitate. After decantation of the solution, the remaining solid was dried and dissolved in CH_2Cl_2 (10 mL). Slow evaporation *in vacuo* gave an analytically pure yellow solid/oil **7a** (164 mg, 72%). Anal. Calcd for $C_{20}H_{26}NClPdS$: C, 52.87; H, 5.77; N, 3.08. Found: C, 52.37; H, 5.79; N, 2.84. ^1H NMR (200.13 MHz, $CDCl_3$, 25 °C): δ 1.25 (s, 9H, t-Bu), 2.14 (s, 3H, Me), 2.58 (s, 3H, SMe), 3.10, 3.94 (AB, 2H, CH_2, $^2J(HH)$ = 12.8), 7.17−7.69 (m, 6H, Ar), 7.73 (dt, 1H, H*p* pyr, $^3J(HH)$ = 7.6), 8.84 (dd, 2H, H° pyr, $^3J(HH)$ = 4.9, $^4J(HH)$ = 1.5).

[PdC(*t*-Bu/Me)=C(Me/*t*-Bu)C$_6$H$_4$-2-CH$_2$S-t-Bu(C$_5$H$_5$N)Cl], 7b. This was obtained as a yellow solid in 89% yield by the method described below for **7c**. ^1H NMR (300.13 MHz, $CDCl_3$, 25 °C) (major isomer): δ 1.27 (s, 9H, t-Bu), 1.67 (s, 9H, t-Bu), 2.13 (s, 3H, Me), 3.47, 3.81 (AB, 2H, CH_2, $^2J(HH)$ = 12.8), 7.15−7.71 (m, 6H, Ar), 8.85 (dd, 2H, H*o* pyr, $^3J(HH)$ = 4.9, $^4J(HH)$ = 1.5). A second isomer was present with attributable signals at δ = 1.25, 1.56, (2 t-Bu), 2.01 (Me) (AB and aromatics hidden under major regioisomer), and δ = 8.57 (bs).

[PdC(t-Bu/Me)=C(Me/t-Bu)C$_6$H$_4$-2-CH$_2$S-t-Bu(C$_5$H$_5$N)I], 7c. 2d (102 mg, 0.25 mmol) and **1** (43 mg, 0.45 mmol) were heated to reflux temperature in 1,2-dichloroethane (20 mL) for 1.75 h. After concentration of the resulting red solution to ca. 5 mL *in vacuo*, pyridine addition (0.1 mL) gave rise to an immediate yellow coloration. Hexane was added (20 mL), the combined solvents were evaporated to dryness, and the pale yellow solid obtained, **7c** (118 mg, 80%), was dried in vacuo. Slow hexane diffusion into a dilute CH_2Cl_2 solution of the latter solid over 48 h gave a virtually inseparable mixture of red (ca. 5 mg) and orange crystals (73 mg) which were removed from the residual solution by decantation. Anal. Calcd for $C_{23}H_{32}NIPdS$: C, 46.99; H, 5.49; N, 2.38. Found: C, 46.01; H, 5.54; N, 2.18. ^1H NMR (300.13 MHz, $CDCl_3$, 25 °C) (orange crystals): δ 1.25, 1.27, 1.38, 1.44, 1.49, 1.51, 1.57, 1.60, 1.75 (9 s, t-Bu), 2.02, 2.04, 2.04, 2.06, 2.13 (4s, Me), 3.30,

Table 6. Positional Parameters and *B* Values and Their Esd's for 7c

atom	*x*	*y*	*z*	B^a (Å^2)
Pd	0.37455(4)	0.23739(2)	0.04458(2)	3.071(7)
I	0.59832(4)	0.27292(3)	−0.02661(2)	5.209(9)
C(1)	0.3896(5)	0.3496(3)	0.0988(3)	3.5(1)
C(2)	0.4393(5)	0.3601(3)	0.1802(3)	3.5(1)
C(3)	0.3457(6)	0.4146(4)	0.0310(3)	4.9(1)
C(4)	0.4580(6)	0.4439(3)	0.2281(3)	4.7(1)
C(5)	0.4880(7)	0.4333(4)	0.3258(4)	5.8(2)
C(6)	0.5759(9)	0.4909(4)	0.1928(5)	8.6(2)
C(7)	0.3325(9)	0.4975(4)	0.2168(5)	9.9(2)
C(8)	0.4826(5)	0.2841(3)	0.2317(3)	3.3(1)
C(9)	0.6166(5)	0.2663(3)	0.2508(3)	4.0(1)
C(10)	0.6571(5)	0.1971(4)	0.2980(4)	4.7(1)
C(11)	0.5633(6)	0.1435(4)	0.3276(4)	5.1(1)
C(12)	0.4299(6)	0.1605(3)	0.3095(3)	4.5(1)
C(13)	0.3885(5)	0.2294(3)	0.2627(3)	3.5(1)
C(14)	0.2420(5)	0.2455(4)	0.2398(3)	4.0(1)
S	0.2034(1)	0.20145(8)	0.13172(7)	3.29(2)
C(15)	0.0337(5)	0.2394(3)	0.0966(3)	4.0(1)
C(16)	0.0037(6)	0.1992(5)	0.0084(4)	5.8(1)
C(17)	−0.0608(6)	0.2080(5)	0.1613(4)	6.0(2)
C(18)	0.0297(7)	0.3319(4)	0.0885(5)	7.3(2)
N	0.3541(4)	0.1150(3)	−0.0239(3)	4.06(9)
C(19)	0.3829(6)	0.1084(4)	−0.1073(4)	5.1(1)
C(20)	0.3833(7)	0.0335(4)	−0.1501(4)	6.8(2)
C(21)	0.3552(7)	−0.0364(4)	−0.1068(5)	7.1(2)
C(22)	0.3222(6)	−0.0309(4)	−0.0216(5)	6.0(2)
C(23)	0.3238(6)	0.0468(4)	0.0169(4)	5.0(1)

[a] See footnote *a* of Table 5.

3.32, 3.35, 3.42, 3.74, 3.80, 3.86, 3.97 (4 AB, CH_2), 7.09−7.61 (m, Ar), 8.40 (bs, H*pyr*), 8.95 (d, H° pyr, $^3J(HH)$ = 5.2).

1*H*-2*S*-Methyl-3-*tert*-butyl-4-methylbenzothiopyrilium Tetrafluoroborate, 8. (Under N_2) **2b** (190 mg, 0.51 mmol) and **1** (90 mg, 0.94 mmol) were heated to reflux in 1,2-dichloroethane (20 mL) for 1.75 h. After solvent evaporation *in vacuo* and dissolution in THF (20 mL), $AgBF_4$ (130 mg, 0.67 mmol) was added. After 1 h of stirring and filtration of the AgI precipitate over a Celite pad, the resulting orange filtrate was evaporated to dryness. Reflux in PhCl (30 mL) for 1 h afforded a dark solution due to the formation of metallic palladium, which was removed by filtration over Celite. Evaporation of the solvent afforded a brown oil **8** (160 mg, 86%) which was not further purified. ^{1}H NMR (300.13 MHz, $CDCl_3$, 25 °C): δ 1.52 (s, 9H, t-Bu), 2.56, 2.57 (2s, 6H, Me), 4.40, 4.83 (AB, CH_2, $^2J(HH)$ = 16.1), 7.49−7.60 (m, 4H, Ar).

1*H*-2*S*-4-*tert*-Butyl-3-methylbenzothiopyran, 9a/1*H*-2*S*-3-*tert*-Butyl-4-methylbenzothiopyran, 9b. (Under N_2) **2d** (195 mg, 0.47 mmol) and **1** (60 mg, 0.62 mmol) were heated to reflux in 1,2-dichloroethane for 1.5 h. After $AgBF_4$ treatment (130 mg, 0.66 mmol) in THF, followed by PhCl reflux, according to the procedure employed for **8**, a brown oil **9** was obtained (90 mg, 88%) as a 4:1 mixture of regioisomers. ^{1}H NMR (300.13 MHz, $CDCl_3$, 25 °C): major isomer **9b**, δ 1.44 (s, 9H, t-Bu), 2.37 (s, 3H, Me), 3.53 (s, 2H, CH_2), 7.09−7.62 (m, 4H, Ar), minor isomer **9a**, δ 1.46 (s, 9H, t-Bu), 2.23 (s, 3H, Me), 3.44 (s, 2H, CH_2), 7.09−7.62 (m, 4H, Ar). MS: *m/z* (M^+, 100%) 218.

Demethylation of 8. **8** (250 mg, 0.78 mmol), obtained from **2a** and **1** in 78% yield according to the method employing **2b** outlined above, was heated to reflux temperature in PhCl (40 mL) for 40 h. After solvent evaporation the residue was extracted with diethyl ether (60 mL) and the extracts were evaporated. A brown oil corresponding to **9b** (110 mg, 50%) was obtained.

[PdC(*t*-Bu)=C(Me)-2-$C_6H_4C_6H_4$-2′-SMe(μ-Cl)]$_2$, 10a. A suspension of **4** (340 mg, 1.0 mmol) and **1** (100 mg, 1.04 mmol) was refluxed for 0.5 h in chlorobenzene (30 mL). After cooling, the resulting orange solution was evaporated to dryness. Stirring in pentane (20 mL) afforded a yellow solid **10a** which was collected by filtration and dried (320 mg, 73%). Anal. Calcd for $C_{20}H_{23}ClPdS$: C, 54.93; H, 5.30. Found: C, 55.05; H, 5.47. ^{1}H NMR (200.13 MHz, $CDCl_3$ and pyr-d_5, 25 °C) for **10b**: δ 0.89 (s, 9H, t-Bu), 1.73 (s, 3H, Me), 2.69 (s, 3H, SMe), 7.18−7.58 (m, 8H, Ar). Traces of a second regioisomer could be observed at δ = 1.29, 1.88, 2.19. **10c** (made in an analogous fashion to **10b** but with PPh_3 instead of pyridine-d_5) ^{1}H NMR (very broad): δ 1.35 (s, 9H, t-Bu), 1.73, 1.89 (2s, 6H, Me), 7.18−7.81 (m, 23H, Ar). ^{31}P: 12.53 (s), 13.11 (s) in a 10:1 ratio.

2-(*N*,*N*-Dimethyliminium)-2-*tert*-butyl-1-methylspiro-[3,5-cyclohexadiene-1,1-indene], 11. 5* (150 mg, 0.31 mmol) and **1** (30 mg, 0.31 mmol) were heated to reflux

Table 7. Positional Parameters and *B* Values and Their Esd's for 10b

atom	*x*	*y*	*z*	B^a (Å^2)	atom	*x*	*y*	*z*	B^a (Å^2)
Pd(1)	0.23486(2)	0.12877(1)	0.30281(1)	3.098(4)	Pd(2)	−0.25328(2)	0.47290(1)	0.30640(1)	3.147(5)
Cl(1)	0.2843(1)	0.20176(6)	0.40787(5)	4.83(2)	Cl(2)	−0.2063(1)	0.34634(6)	0.42136(5)	5.22(2)
S(1)	0.43093(8)	0.19310(5)	0.22856(5)	4.08(2)	S(2)	−0.05027(8)	0.44425(5)	0.24074(5)	4.04(2)
N(1)	0.0430(3)	0.0843(2)	0.3639(1)	3.41(5)	N(2)	−0.4482(3)	0.4860(2)	0.3631(2)	3.64(5)
C(1)	−0.0432(3)	0.1433(2)	0.3874(2)	3.91(7)	C(26)	−0.4924(3)	0.5643(2)	0.3776(2)	4.13(7)
C(2)	−0.1675(3)	0.1172(2)	0.4315(2)	4.46(8)	C(27)	−0.6124(3)	0.5705(2)	0.4239(2)	4.34(7)
C(3)	−0.2037(3)	0.0268(3)	0.4543(2)	4.53(8)	C(28)	−0.6941(4)	0.4943(3)	0.4551(2)	4.76(8)
C(4)	−0.1173(3)	−0.0344(2)	0.4311(2)	4.18(7)	C(29)	−0.6524(4)	0.4147(3)	0.4383(2)	4.90(8)
C(5)	0.0045(3)	−0.0034(2)	0.3852(2)	3.77(7)	C(30)	−0.5296(4)	0.4120(2)	0.3932(2)	4.16(7)
C(6)	0.1860(3)	0.0676(2)	0.2175(2)	3.27(6)	C(31)	−0.3004(3)	0.5783(2)	0.2126(2)	3.44(6)
C(7)	0.0851(3)	0.1190(2)	0.1552(2)	4.19(7)	C(32)	−0.3960(4)	0.5581(3)	0.1516(2)	4.73(8)
C(8)	0.1396(4)	0.1196(3)	0.0682(2)	6.4(1)	C(33)	−0.3335(5)	0.5990(3)	0.0640(2)	6.7(1)
C(9)	−0.0603(4)	0.0778(3)	0.1746(3)	6.7(1)	C(34)	−0.4108(5)	0.4553(3)	0.1623(2)	6.5(1)
C(10)	0.0731(5)	0.2192(3)	0.1563(3)	7.1(1)	C(35)	−0.5421(4)	0.5947(4)	0.1631(3)	7.3(1)
C(11)	0.2364(3)	−0.0158(2)	0.2249(2)	3.31(6)	C(36)	−0.2539(3)	0.6603(2)	0.2138(2)	3.79(7)
C(12)	0.1950(4)	−0.0854(2)	0.1807(2)	4.99(8)	C(37)	−0.2922(5)	0.7530(3)	0.1610(3)	6.2(1)
C(13)	0.3470(3)	−0.0527(2)	0.2816(2)	3.24(6)	C(38)	−0.1482(3)	0.6681(2)	0.2719(2)	3.58(6)
C(14)	0.3209(3)	−0.1213(2)	0.3532(2)	3.86(7)	C(39)	−0.1810(4)	0.7005(2)	0.3397(2)	4.48(8)
C(15)	0.4245(4)	−0.1566(2)	0.4045(2)	4.29(7)	C(40)	−0.0818(4)	0.7084(2)	0.3919(2)	4.84(8)
C(16)	0.5590(4)	−0.1252(2)	0.3833(2)	4.36(7)	C(41)	0.0522(4)	0.6862(2)	0.3763(2)	4.71(8)
C(17)	0.5888(3)	−0.0597(2)	0.3110(2)	4.18(7)	C(42)	0.0895(3)	0.6587(2)	0.3070(2)	4.27(7)
C(18)	0.4849(3)	−0.0233(2)	0.2589(2)	3.38(6)	C(43)	−0.0098(3)	0.6494(2)	0.2544(2)	3.54(6)
C(19)	0.5234(3)	0.0406(2)	0.1776(2)	3.49(6)	C(44)	0.0363(3)	0.6264(2)	0.1768(2)	3.61(6)
C(20)	0.5837(4)	0.0038(2)	0.1171(2)	4.40(8)	C(45)	0.0957(3)	0.6946(2)	0.1124(2)	4.30(7)
C(21)	0.6178(4)	0.0577(3)	0.0389(2)	5.11(9)	C(46)	0.1412(4)	0.6778(3)	0.0393(2)	5.15(9)
C(22)	0.5924(4)	0.1485(3)	0.0194(2)	5.17(9)	C(47)	0.1303(4)	0.5922(3)	0.0293(2)	5.34(9)
C(23)	0.5345(4)	0.1878(2)	0.0784(2)	4.73(8)	C(48)	0.0726(4)	0.5228(2)	0.0912(2)	4.84(8)
C(24)	0.5013(3)	0.1344(2)	0.1570(2)	3.74(7)	C(49)	0.0238(3)	0.5396(2)	0.1651(2)	3.82(7)
C(25)	0.5734(4)	0.1814(3)	0.2940(3)	6.2(1)	C(50)	0.0870(4)	0.4221(3)	0.3102(3)	6.3(1)

[a] See footnote *a* of Table 5.

temperature in $CHCl_3$ (20 mL) for 0.5 h. After Celite filtration and solvent evaporation, **11** was obtained as an orange oil (70 mg, 60%) that could be partially crystallized from CH_2Cl_2/ether. Anal. Calcd for $C_{21}H_{26}NBF_4$: C, 66.51; H, 6.91; N, 3.69. Found: C, 66.07; H, 6.55; N, 3.62. ^{1}H NMR (200.13 MHz, $CDCl_3$, 25 °C): δ 1.49 (s, 9H, t-Bu), 2.03 (s, 3H, Me), 3.00, 3.72 (2s, 6H, NMe), 5.45 (d, 1H, H_{diene}, $^3J(HH)$ = 8.9 Hz), 6.55 (dd, 1H, H_{diene}, $^3J(HH)$ = 6.1), 6.90–7.28 (m, 3H, Ar), 7.40 (dt, 1H, $^3J(HH)$ = 6.1, $^4J(HH)$ = 2.6), 7.63 (dd, H_{diene}, $^3J(HH)$ = 6.4), 7.73 (dd, Ar, $^3J(HH)$ = 8.0). IR (KBr pellet): 1080 cm^{-1} (BF_4^-).

[PdC(*t*-Bu)=C(Me)C_6H_4-2-CH_2-2′-$C_5H_5N(C_5H_5N)Cl$], 12. **6** (200 mg, 0.66 mmol) and **1** (65 mg, 0.68 mmol) were refluxed overnight in CH_2Cl_2 (20 mL). After Celite filtration and solvent concentration (to ca. 5 mL), excess pyridine was added. The resulting yellow solution was layered with pentane (50 mL) and refrigerated at −20 °C. A yellow solid **12** (230 mg, 72%) was collected by filtration and dried. Anal. Calcd for $C_{24}H_{27}N_2ClPd$: C, 59.49; H, 5.62; N, 5.79. Found: C, 59.33; H, 5.53; N, 5.42. ^{1}H NMR (200.13 MHz, $CDCl_3$, 25 °C) δ 1.16 (s, 9H, t-Bu), 2.16 (s, 3H, Me), 3.98, 4.35 (AB, 2H, CH_2, $^2J(HH)$ = 15.0), 6.9–7.77 (m, 10 H, Ar), 8.80 (d, 2H, H° pyr, $^3J(HH)$ = 6.4), 9.52 (d, 1H, H° pyr, $^3J(HH)$ = 7.0).

Structural Determination and Refinement of 7a, 7c, and 10b. Suitable single crystals of **7a**, **7c**, and **10b** were obtained by slow diffusion of hexane into CH_2Cl_2 solutions at room temperature. For each complex, one single crystal was cut out from a cluster of crystals and mounted on a rotation-free goniometer head. Systematic searches in reciprocal spaces using a Enraf-Nonius CAD4-F automatic diffractometer showed that crystals of **7a** and **7c** belong to the monoclinic system, whereas **10b** belongs to the triclinic system.

Quantitative data were obtained at room temperature. All experimental parameters used are given in Table 4. The resulting data sets were transfered to a VAX computer, and for all subsequent calculations the Enraf-Nonius VAX/Molen package[27] was used.

Three standard reflections measured every 1 h during the entire data collection periods showed no significant trend. The raw data were converted to intensities and corrected for Lorentz and polarization factors.[28] Absorption corrections derived from ψ scans of 4 reflections were applied.

The structures were solved using the heavy atom method. After refinement of the heavy atoms, difference-Fourier maps revealed maximas of residual electronic density close to the positions expected for hydrogen atoms. They were introduced in structure factor calculations by their computed coordinates (C−H = 0.95 Å) and isotropic temperature factors such that B(H) = 1.3 B_{eqv}(C) Å^2 but not refined. Full least-squares refinements followed; $\omega = 1/\sigma^2(F^2)$ and $\sigma^2(F^2) = \sigma^2_{counts} + (pI)$.[2] Final difference maps revealed no significant maxima. The scattering factor coefficients and anomalous dispersion coefficients come respectively from ref 29a,b.

Acknowledgment. The Commission of the European Communities is thanked for financial support of this project (Grant No. ERBSCC*CT000011).

Supplementary Material Available: Tables of bond distances and angles, H atom coordinates, and thermal parameters for **7a**, **7c**, and **10b** (26 pages). Ordering information is given on any current masthead page.

OM9408573

(27) Molen, An Interactive Structure Solution Procedure, Enraf-Nonius, Delft, The Netherlands, 1990.
(28) Walker, N.; Stuart, D. *Acta Crystallogr., Sect. A* **1983**, *A39*, 158.
(29) Cromer, D. T.; Waber, J. T. *International Tables for X-ray Crystallography*; Kynoch Press: Birmingham, U.K., 1974; Vol. IV: (a) Table 2.2b; (b) Table 2.3.1.

The ^{60}Co γ-Radiation-Induced Polymerization of Vinylalkoxysilanes

Dietmar Seyferth,* David Y. Son, and Miklos Tasi

Department of Chemistry, Massachusetts Institute of Technology, Cambridge, Massachusetts 02139

Received December 8, 1994[⊗]

The ^{60}Co γ-radiation-induced polymerization of CH_2=$CHSi(OEt)_3$ gave, according to analytical and spectroscopic (IR, ^1H and ^{29}Si NMR) data, as well as similar data for its $LiAlH_4$ reduction product, a polymer of composition R–[–CH_2–$CH(Si(OEt)_3)$–]$_a$–[–$C(CH_3)(OSi\equiv)$–]$_y$–[–CH_2–$CH(Si(OEt)_3)$–]$_b$–R, where $b \gg a$ and the end groups R = $-CH_2CH_2Si(OEt)_3$, $(EtO)_3Si(C-)HCH_3$, and $-CH(OSi\equiv)CH_3$. A similar polymer was obtained by γ-ray-induced polymerization of CH_2=$CHSi(OMe)_3$, but less chain transfer involving the alkoxy groups occurred in this case. Similar polymerization of CH_2=$CHSiCH_3(OEt)_2$ and CH_2=$CHSi(CH_3)_2OEt$ was less facile, giving polymers of similar composition and of lower molecular weight in much lower yield for a given radiation dose.

Introduction

In previous papers we have reported the ^{60}Co γ-radiation-initiated polymerization of vinyltrichlorosilane,[1] vinylmethyldichlorosilane,[2] and vinyldimethylchlorosilane[2] and the conversion of the resulting vinyl polymers, $PVSiCl_3$, $PVSiMeCl_2$, and $PVSiMe_2Cl$, to the corresponding silicon hydride polymers, $PVSiH_3$, $PVSiMeH_2$, and $PVSiMe_2H$. To complement this work, we have investigated the ^{60}Co γ-radiation-initiated polymerization of analogous vinylethoxy- and vinylmethoxysilanes. The polymerization of vinylalkoxysilanes has received extensive study by previous workers, the first report being published by Wagner, Bailey, Pines, Dunham, and McIntire in 1953[3] on the di-*tert*-butyl peroxide-initiated polymerization of vinyltriethoxysilane. It was found that soluble, viscous, liquid polymers of low molecular weight (M_n *ca.* 5000–8000) were produced in high yield when the polymerization was carried out at 130 °C. A later study by Mixer and Bailey[4] provided chemical evidence for a polymer composition of $R[(EtO)_2SiOCH(CH_3)]_m[CH_2CH(Si(OEt)_3)]_nH$ (R = vinyl or polymer chain) resulting from chain transfer by α-hydrogen atom abstraction from an ethoxy group (Scheme 1). Such chain transfer to monomer or polymer would be expected to result in high yields of polymers of low molecular weight, as had been observed.

Japanese workers[5] polymerized vinyltrimethoxy- and vinyltriethoxysilane using ^{60}Co γ-radiation initiation. A 60 Mrad dose resulted in degrees of polymerization ($\overline{DP}$) of 4.3–7.4, respectively, for CH_2=$CHSi(OMe)_3$ and CH_2=$CHSi(OEt)_3$. The information provided by IR and ^1H NMR studies was not sufficient to allow any conclusions concerning the composition of the polymers.

Andrianov and his co-workers carried out di-*tert*-butyl peroxide-initiated polymerizations of a number of CH_2=$CHSi(R)(OR')_2$ compounds, including CH_2=$CHSi(R)(OCH_3)_2$ (R = *n*-C_3H_7, *n*-C_4H_9, *n*-C_5H_{11}, and *p*-ClC_6H_4)[6] and CH_2=$CHSi(CH_3)(OR')_2$ (R' = CH_3, C_2H_5, *n*-C_3H_7, *n*-C_4H_9, and C_6H_5).[7] The molecular weights of the polymers obtained (M_n) were low, ranging from 720 to 2670, depending on the monomer. IR studies indicated that chain transfer of the type shown in Scheme 1 is slight at the early stages of the polymerization but becomes important at higher conversions. Later, detailed ^{13}C NMR studies of poly(vinylmethyldiethoxysilane)[8] and other poly(vinylmethyldialkoxysilanes) (RO = CH_3O, *n*-C_3H_7O, and *i*-C_3H_7O)[9] prepared by this procedure were reported by Zhdanov and his co-workers. It was concluded that in the case of CH_2=$CHSi(CH_3)(OC_2H_5)_2$ polymerization only about 30% of the initial vinyl groups were present as [–$CH_2CH(Si(CH_3)(OC_2H_5)_2$–] units; 3% were present as unchanged CH_2=CH groups, 2% as CH_2=$C(Si(CH_3)(OC_2H_5)_2)CH_2$– groups, and 60% as fragments in which the α-carbon atom had become a CH group by hydrogen atom abstraction from an ethoxy group. It was estimated that some 20% of the OC_2H_5 groups had in this way been converted into $CH_3(C-)HO$ and $CH_3(C<)O$ units. Thus, as in the case of CH_2=$CHSi(OEt)_3$, degradative chain transfer was a major process that competed with the desired vinyl polymerization. Structural units of types $\equiv SiOCH(CH_3)-$, $-CH_2CH_2Si\equiv$, $\equiv SiOCH(CH_3)CH_2CH-$

Scheme 1

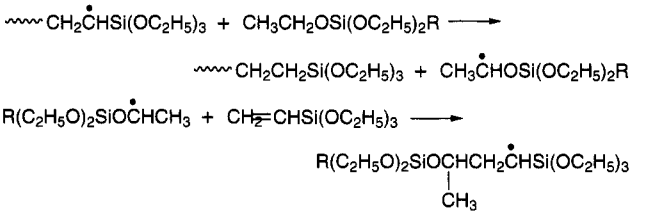

[⊗] Abstract published in *Advance ACS Abstracts,* April 15, 1995.

(1) Seyferth, D.; Tasi, M.; Woo, H.-G. *Chem. Mater.* **1995**, *7*, 236.
(2) Seyferth, D.; Son, D. Y. Submitted for publication.
(3) Wagner, G. H.; Bailey, D. L.; Pines, A. N.; Dunham, M. L.; McIntire, D. B. *Ind. Eng. Chem.* **1954**, *45*, 367.
(4) Mixer, R. Y.; Bailey, D. L. *J. Polym. Sci.* **1955**, *18*, 573.
(5) (a) Hayakawa, K.; Kawase, K.; Yamakita, H.; Inagaki, S. *Polym. Lett.* **1967**, *5*,1077. (b) Hayakawa, K.; Kawase, K.; Yamakita, H.; Yumoto, T. *J. Polym. Sci., Polym. Chem. Ed.* **1981**, *19*, 3145.
(6) Andrianov, K. A.; Delazari, N. V.; Yemel'kina, N. A.; Kramarenko, T. P. *Vysokomol. Soyedin.* **1975**, *A17*, 2325; *Polym. Sci. USSR* **1975**, *17*, 2679.
(7) Andrianov, K. A.; Delazari, N. V.; Yemel'kina, N. A.; Pecherkina, Z. V.; Leites, L. A. *Vysokomol. Soyedin.* **1977**, *A19*, 749; *Polym. Sci. USSR* **1977**, *19*, 868.
(8) Lavrukhin, B. D.; Chernyavskaya, N. A.; Strelkova, T. V.; Zhdanov, A. A. *Vysokomol. Soyedin.* **1986**, *A28*, 272; *Polym. Sci. USSR* **1986**, *28*, 296.
(9) Lavrukhin, B. D.; Strelkova, T. V.; Chernyavskaya, N. A.; Zhdanov, A. A. *Vysokomol. Soyedin.* **1987**, *A29*, 272; *Polym. Sci. USSR* **1987**, *29*, 299.

0276-7333/95/2314-2225$09.00/0

Table 1. ^{60}Co γ-Radiation-Initiated Polymerization of Vinyltriethoxysilane

Mrad		mol wt (GPC)	
total dosage	yield of polymer, %	no. avg	wt avg
6	44(44)[a]	4416	10 788
9	60	8326	16 246
12	74	3661	10 291
15	85	3937	12 136
18	85	4544	13 855

[a] With added 1 wt % di-*tert*-butyl peroxide.

(Si≡)$-CH_2CH_2Si$≡, ≡$SiOC(CH_3)CH_2CH_2Si$≡, and ≡$SiOC(CH_3)CH_2CH$(Si≡)CH_2CH_2Si≡ were claimed to be the main components resulting from the chain transfer reactions, with lesser contributions from ≡$SiCH_2CH_2CH_2Si$≡ and ≡$SiCH_2CH$(Si≡)CH_2CH_2Si≡.

The composition of the polymers formed by initiation of CH_2=$CHSi(R)(OR')_2$ (R = alkyl or OR') polymerization by ^{60}Co γ-radiation rather than by radicals derived from di-*tert*-butyl peroxide thermolysis probably is somewhat different since γ-radiation can result in the formation of diradicals, $^{\bullet}CH_2\dot{C}HSi$≡, whose reactions will complicate the structure of the polymer further, in addition to the complications introduced by chain transfer processes.

Since the composition of the polymer obtained by the ^{60}Co γ-radiation-initiated polymerization of vinyltriethoxysilane (in terms of the structural components of the polymer) had not been established, it was of interest to study the polymers resulting from such a CH_2=$CHSi(OEt)_3$ polymerization in greater detail. We report here the results of such studies as well as the results of similar studies carried out with vinyltrimethoxysilane and vinylmethyldiethoxysilane and vinyldimethylethoxysilane.

Results and Discussion

Polymerization of Vinyltriethoxysilane. The polymerization of vinyltriethoxysilane was carried out using a 1.03 Mrad/day ^{60}Co γ-ray source. The yield of polymer (which we will call γ-$PVSi(OEt)_3$ to distinguish it from the polymer obtained by *t*-BuOOBu-*t* initiated polymerization, which we will call $PVSi(OEt)_3$) was dependent on the radiation dose, as shown in Table 1. Noteworthy is the fact that the yields were much higher than those obtained in the ^{60}Co γ-radiation-initiated polymerization of vinyltrichlorosilane[1] and that much lower radiation doses served to achieve these higher yields. As expected, the greater the total radiation dose, the higher the yield of polymer. Di-*tert*-butyl peroxide did not accelerate the γ-radiation-induced polymerization of CH_2=$CHSi(OEt)_3$. That the polymer yield did not increase on going from the 15 to the 18 Mrad polymerization may be attributed to the low concentration of residual monomer in the very viscous polymer.

The polymers in all of these experiments were very thick, clear, colorless materials. In the case of the 15 and 18 Mrad polymerizations, the contents of the ampules had to be heated to make them sufficiently fluid for transfer to a Schlenk flask. The molecular weights of the γ-$PVSi(OEt)_3$ samples prepared were not very high (Table 1), the M_n corresponding to degrees of polymerization of around 18–44. These polymers are soluble in common organic solvents. Gel formation occurred rapidly when the polymers were treated with aqueous acid or base. The elemental analysis of the polymers was in good agreement with that calculated for the simplest composition, $[CH_2CH\ Si(OEt)_3]_n$. However, NMR spectroscopic study of the polymer and of the γ-$PVSiH_3$ derived from it showed that this was not the structure.

Table 2. Characterization Data for γ-$PVSiH_3$

elemental analysis	Calcd for C_2H_6Si: C, 41.34; H, 10.33; Si, 48.33. Found: C, 43.41; H, 9.88; Si, 34.80
IR (cm^{-1}, thin film)	3446 (br), 2971 (m), 2922 (s), 2147 (s), 1376 (w), 1078 (m), 920 (s), 740 (m)
^{1}H NMR (ppm)	0.72 (s), 0.79 (s), 1.2 (s), 1.3 (s), 1.6 (br s), 3.2 (s), 3.5 (s), 3.8 (br s), 3.9–4.2 (br), 4.5–4.9 (br)
^{13}C NMR (ppm)	0.93, 5.0, 5.3, 7.0, 17.8, 19.0, 23.5, 26.5, 27.0, 31.9, 37.6, 38.4, 40.4, 43.7, 58.4, 68.5, 71.0
^{29}Si NMR (ppm)	−58.2, −56.6, −49.9; J_{Si-H} = 196 Hz
ceramic residue yield (TGA), %	27
mol wt (GPC)	no. avg, 682; wt avg, 1800; polydispersity, 2.6

The ^{1}H NMR spectrum of γ-$PVSi(OEt)_3$ is unexceptional. It shows strong signals due to the ethoxy group protons and broad resonances in the δ 0.2–2.0 region due to the alkyl protons of the backbone carbon atoms. The ^{29}Si NMR spectrum of the polymer shows a number of resonances in the δ_{Si} −42 to −48 region, with principal signals at −44.4 and −44.1 ppm. (For comparison, the ^{29}Si NMR resonance of $CH_3Si(OEt)_3$ occurs at −44.5 ppm.[10])

Neither the ^{29}Si nor the ^{1}H or ^{13}C NMR spectra provided much useful information concerning the composition of γ-$PVSi(OEt)_3$. This also had been the case with $PVSiCl_3$, the polymer derived from the ^{60}Co γ-radiation-initiated polymerization of CH_2=$CHSiCl_3$.[1] However, reduction of $PVSiCl_3$ to $PVSiH_3$ provided a product whose NMR spectra were more informative and, in fact, allowed us to conclude that $PVSiH_3$ had the composition CH_2=$C(SiH_3)(-CH_2-CH(SiH_3)-)_x(-CH_2-CH(SiH_3)-CH(SiH_3)-CH_2-)_y(-(C-)H-CH_2-SiH_2-)_z-$ ($x > y \gg z$).[1] Accordingly, γ-$PVSi(OEt)_3$ was reduced with $LiAlH_4$ in THF to γ-$PVSiH_3$, which was isolated as a clear, colorless, very thick material, soluble in organic solvents and stable to atmospheric oxygen and moisture.

The analytical, IR and NMR spectroscopic, and molecular weight data collected for γ-$PVSiH_3$ are given in Table 2. They suggest that some other mode of propagation occurred during the polymerization besides normal vinyl polymerization. The indication of this is the large discrepancy in the elemental analysis. If only simple vinyl polymerization had occurred and if the reduction went to completion, the γ-$PVSiH_3$ would contain only carbon, hydrogen, and silicon. However, the analyses for C, H, and Si added up to only 88.09%, and these analyses were reproducible. The reduction was repeated under more strenuous conditions (refluxing THF) to ensure that complete reduction occurred, but the same analytical results were obtained for the polymer that was isolated. In another experiment γ-$PVSi(OEt)_3$ was converted to γ-$PVSiCl_3$ by treatment with acetyl chloride and the resulting polymer then was reduced with $LiAlH_4$. However, the analytical results were essentially the same. The infrared spectrum of γ-$PVSiH_3$ showed the expected Si–H stretching frequency at 2147 cm^{-1}. However, a broad peak at 3446 cm^{-1} also was present, which suggests the presence of OH groups in the polymer. The ^{1}H NMR spectrum of γ-$PVSiH_3$ showed the expected signals for the SiH_3 protons as well as the C–H signals for the polymer

(10) Schraml, J.; Chuy, N. D.; Chvalovsky, V.; Mägi, M.; Lippmaa, E. *J. Organomet. Chem.* **1973**, *51*, C5.

Scheme 2[a]

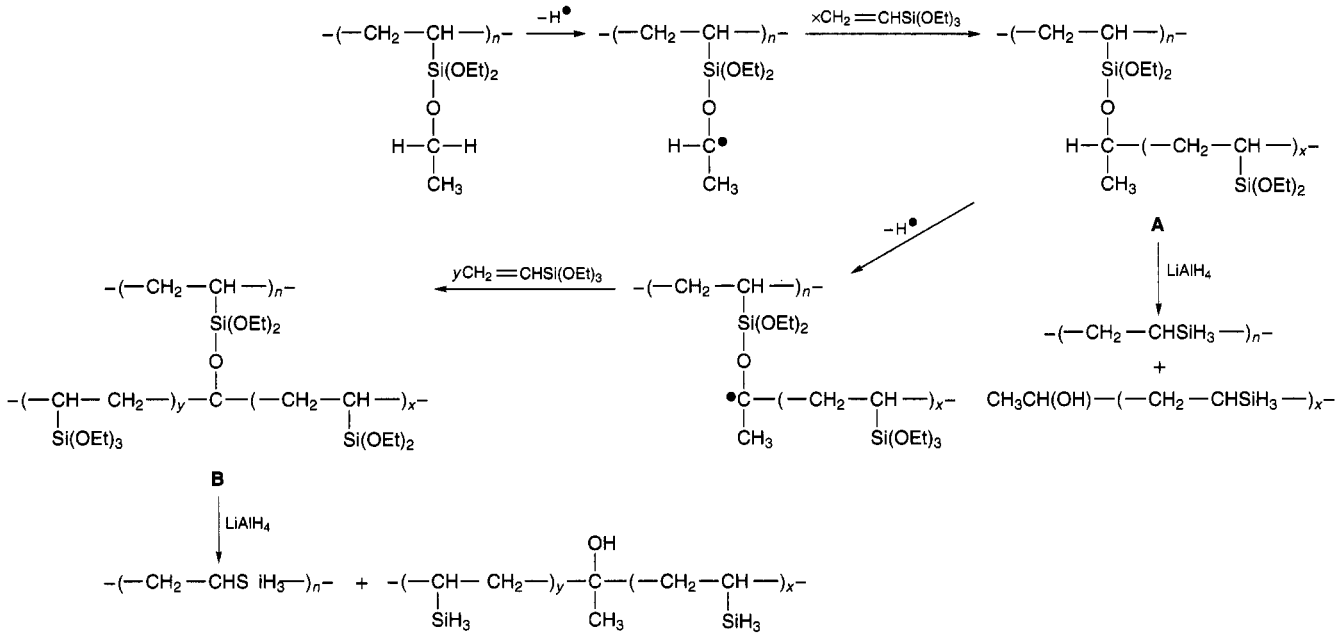

[a] Minor amounts of coupling between $R-(CH_2CHSi(OEt)_3)_n-CH_2-\dot{C}H-Si(OEt)_3$ radical species and $CH_3\dot{C}HOSi\equiv$ and $CH_3\dot{C}(OSi\equiv)(-CH_2CHSi(OEt)_3)_x-$ type radicals may result in connectivity of the opposite type:

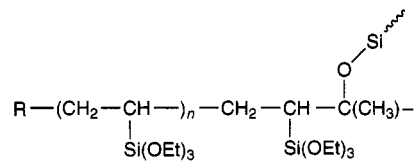

Thus, we will write the composition of γ-PVSi(OEt)$_3$ as

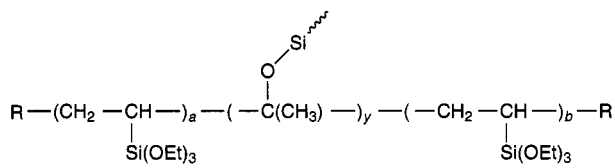

where $b \gg a$ and the end groups R = $-CH_2CH_2Si(OEt)_3$, $(EtO)_3Si(C-)HCH_3$, and $-CH(OSi\equiv)CH_3$.

backbone. However, the CH to SiH integration ratio was not the expected 1, as it was in $PVSiH_3$ derived from $PVSiCl_3$;[1] rather it was 2.0, which indicates that additional C−H protons were present in the polymer. The ^{29}Si NMR spectrum of γ-$PVSiH_3$ was relatively clean, showing two large resonances at δ_{Si} −58.2 and −56.6 and a smaller resonance at −49.9. These resonances are in the region where signals due to $RSiH_3$ compounds usually are observed.[11] Further studies using DEPT sequences showed that none of these resonances were due to SiH_2 groups, in contrast to the $PVSiH_3$ derived from $PVSiCl_3$ whose ^{29}Si NMR spectrum contained resonances of low intensity due to SiH_2 groups.[1]

These results may be rationalized as shown in Scheme 2. Single and double H atom abstraction from α-carbon atoms of ethoxy groups on silicon would result in extensive chain branching to give species of types A and B in γ-PVSi(OEt)$_3$ in addition to the expected $[CH_2CHSi(OEt)_3]_n$. $LiAlH_4$ reduction of such a branched polymer would reduce branching Si−O−C units, giving, after hydrolysis, a less branched polymer with pendant SiH_3 groups. The components of γ-$PVSiH_3$ resulting from reduction of fragments A and B will have a higher CH/SiH ratio and, due to the presence of $CH_3(C-)HOH$ and $CH_3(C<)OH$ units, will not give an elemental analysis in agreement with $[CH_2CHSiH_3]_n$. Its IR spectrum will show an absorption due to ν(OH), and its ^{29}Si NMR spectrum will show more than one resonance due to the presence of the $CH_3(C<)OH$ units in the polymer chain. Also, since the reaction with $LiAlH_4$ will cleave all the branches present in γ-PVSi(OEt)$_3$ as shown in Scheme 2, the resulting γ-$PVSiH_3$ should have a lower molecular weight than the γ-PVSi(OEt)$_3$ from which it was derived, and this is what was observed.

The presence of $CH_3(C-)HOH$ end groups and of $CH_3(C<)OH$ groups in the polymer chain would explain the ν(OH) band observed in the the IR spectrum of γ-$PVSiH_3$. In its ^{1}H NMR spectrum one of the two singlets in the δ 1.0−1.5 region now can be assigned to the $CH_3(C<)OH$ methyl protons (compare δ 1.26 for the CH_3 protons of $(CH_3)_3COH$[12]).

An approximate calculation can be made to determine the relative amounts of each unit in the polymer. If x is the fraction of CH_2CHSiH_3 units, then $1 - x$ equals the fraction of $CH_3(C<)OH$ units. The resonance cor-

(11) Harris, R. K.; Kennedy, J. D.; McFarlane, W. In *NMR and the Periodic Table*; Harris, R. K., Mann, B. E., Eds.; Academic: London, 1978; Chapter 10a.3. See also the papers of Schmidbaur and coworkers, e.g.,: Schmidbaur, H.; Dörzbach, C. *Z. Naturforsch.* **1987**, *42B*, 1088. Schmidbaur, H.; Ebenhöch, J. *Z. Naturforsch.* **1987**, *42B*, 1543. Schmidbaur, H.; Zech, J. *Eur. J. Solid State Inorg. Chem.* **1992**, *29*, 5.

responding to the OH protons is in the δ 0.5–2.0 region (as determined by shaking a solution of the polymer with D_2O). Thus, the following equation may be derived:

$$\frac{3x + 4(1 - x)}{3x} = 2$$

where 2 is the CH/SiH ratio as determined by integration of the ^1H NMR spectrum of γ-$PVSiH_3$. Solving this equation gives $x = 0.57$ and $1 - x = 0.43$.

The end groups are not included in the calculations, as it is impossible to determine their exact nature. The weight percent of each element now can be calculated for formula **1**: C, 46.15; H, 9.88; Si, 30.76; O, 13.22%. These values are in fairly close agreement with the experimental values: C, 43.41; H, 9.88; Si, 34.80; O (by difference), 11.91%, considering that end groups are not included. Finally, the structure of γ-$PVSiH_3$ can be depicted as **1**, where $b \gg a$ and $(a + b) = 0.57$; $y = 0.43$;

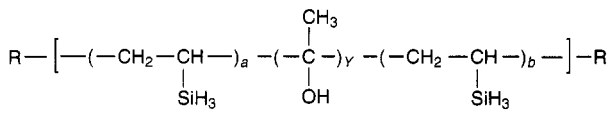

1

$n = 13$ (from the molecular weight data, and R = the end groups, which could be $CH_2CH_2SiH_3$, $CH(SiH_3)CH_3$, or $CH(OH)CH_3$. The $CH_3(C<)OH$ groups may or may not be adjacent to each other; most likely, most of them will be separated rather than adjacent. Vinylic end groups do not appear to be present. In view of the fact that initiation by γ irradiation generates diradicals from olefin monomers,[13] the presence of some head-to-head units, $CH_2CH(SiH_3)CH(SiH_3)CH_2$, in the polymer is a real possibility.

If formula **1** depicts the composition of γ-$PVSiH_3$, then γ-$PVSi(OEt)_3$, from which it is derived, must have the composition shown in formula **2**.

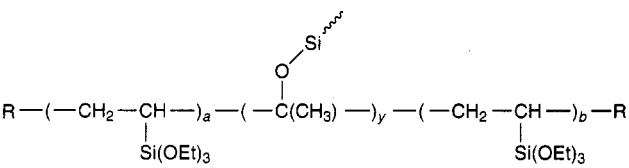

2

$b \gg a$ and end groups R = $-CH_2CH_2Si(OEt)_3$, $(EtO)_3SiCHCH_3$, and $-CH(OSi\equiv)CH_3$

For comparison's sake, CH_2=$CHSi(OEt)_3$ also was polymerized by the procedure of Wagner, Bailey, and their co-workers,[3,4] using di-*tert*-butyl peroxide as the initiator at 125 °C. A very viscous polymer, which we shall call UC-$PVSi(OEt)_3$, was obtained in 96% yield. Its molecular weight was 5970 by VPO. Lithium aluminum hydride reduction of UC-$PVSi(OEt)_3$ gave a polymer, UC-$PVSiH_3$, whose spectroscopic properties (IR, ^1H and ^{29}-Si NMR) were very similar to those of γ-$PVSiH_3$. Accordingly, it is likely that UC-$PVSi(OEt)_3$ is formed by much the same mechanism as is γ-$PVSi(OEt)_3$ and that its composition is very similar. The fact that for the UC-$PVSiH_3$ polymer the CH/SiH ratio is 3, while this ratio is 2 for γ-$PVSiH_3$, suggests that chain transfer occurred to a greater extent in the case of the di-*tert*-butyl peroxide-initiated polymerization.

In addition to γ-$PVSi(OEt)_3$ and the Union Carbide $PVSi(OEt)_3$ discussed in the Introduction, we have prepared still another compositionally different poly(vinyltriethoxysilane). The $PVSiCl_3$ obtained by ^{60}Co γ-radiation-initiated polymerization of CH_2=$CHSiCl_3$ was treated with LiOEt in ethanol to give, after appropriate workup, a light yellow, viscous oil whose C,H analysis agreed well with that calculated for $[CH_2$=$CHSi(OEt)_3]_n$. Its molecular weight (M_n, by VPO) was 1139. The composition of $PVSiCl_3$ was deduced to be that shown in formula **3**.[1] Nucleophilic ethoxy-for-chlorine substitution should not cause changes in the polymer skeleton, so the poly(vinyltriethoxysilane) prepared in this manner should be **4**, i.e., there should be no $CH_3(C<)OH$ units in the polymer chain and no $CH_3(C-)HOH$ end groups.

Like the $PVSiH_3$ derived from $PVSiCl_3$,[1] γ-$PVSiH_3$, although somewhat different in composition, should be an effective pyrolytic precursor for silicon carbide. As indicated in Table 2, the ceramic residue yield obtained when it was pyrolyzed to 950 °C in a stream of argon in a thermogravimetric analysis (TGA) experiment was only 27%. Thus some cross-linking prior or during pyrolysis of the polymer was required. The latter was effected by refluxing a sample of γ-$PVSiH_3$ in hexane solution with a catalytic amount of $(\eta^5$-$C_5H_5)_2TiCl_2$. The resulting green, soluble semisolid gave a ceramic residue yield of 79% in a TGA experiment. (The green color resulted from reduction of the Ti(IV) complex to Ti(III) by the silicon hydride polymer.)

The UC-$PVSiH_3$ polymer also was cross-linked, but with $[(\eta^5$-$C_5H_5)_2ZrH_2]_n$, which had been found very effective in the case of $PVSiH_3$ prepared from $PVSiCl_3$.[1] A 1 h reflux in hexane solution with 0.5 mol % of the zirconium catalyst gave a yellow, semisolid product whose pyrolysis to 950 °C in argon (TGA experiment) left a ceramic residue in 69% yield. Extending the reflux time to 3 h resulted in an insoluble solid.

Polymerization of Vinyltrimethoxysilane. Hayakawa et al. reported that the ^{60}Co γ-radiation-initiated polymerization of vinyltrimethoxysilane was slower than that of vinyltriethoxysilane,[5] a finding which our experiments confirmed. Using the procedure described above for vinyltriethoxysilane, a dose of 9.36 Mrad gave

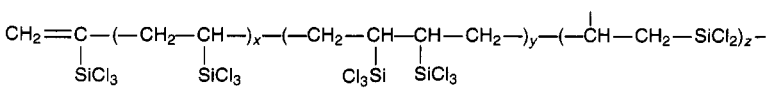

3 ($x \rangle y \rangle\rangle z$)

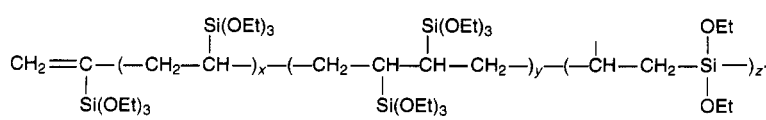

4

Table 3. Characterizing Data for PVSi (OMe)$_3$

appearance	immobile, clear, colorless, material
elemental analysis	Calcd for $C_5H_{12}O_3Si$: C, 40.54; H, 8.10. Found: C, 40.53; H, 8.21
IR (cm^{-1}, thin film)	2943 (s), 2839 (s), 1456 (m), 1191 (s), 1085 (s), 796 (s)
^{1}H NMR (ppm)	0.0−2.0 (broad), 3.34 (s)
^{13}C NMR (ppm)	49.8
^{29}Si NMR (ppm)	−44.1, −43.6, −41.1, −40.7
mol wt (GPC)	no. avg, 607; wt avg, 1436; polydispersity, 2.4

Table 4. Characterizing Data for MeOPVSiH$_3$

appearance	clear, colorless, slightly viscous oil
elemental analysis	Calcd for C_2H_6Si: c, 41.34; H, 10.33, Si, 48.33. Found: C, 36.02; H, 10.13; Si, 44.68
IR (cm^{-1}, thin film)	3445 (broad), 2898 (m) 2843 (m), 2142 (s), 1449 (w), 1069 (m), 914 (s)
^{1}H NMR (ppm)	0.40−2.2 (broad, unresolved), 3.5 (s, with satellites at 3.2 and 3.8)
^{13}C NMR (ppm)	5.1, 21.7, 29.2, 36.8
^{29}Si NMR (ppm)	−58.2, −57.2, −56.6, −53.4, −52.3
ceramic residue yield (TGA), %	24
mol wt (GPC)	no. avg, 963; wt avg, 2862; polydispersity, 2.9

poly(vinyltrimethoxysilane), an immobile, clear, colorless material, in only 16% yield (compared with a 60% yield of poly(vinyltriethoxysilane) after a 9 Mrad dose). Increasing the total dosage to 19 Mrad resulted in a yield increase to 29%. Characterizing data for poly(vinyltrimethoxysilane) are given in Table 3. The ^{1}H NMR spectrum shows signals due to the backbone protons at δ 0.0−2.0 as a broad, unresolved feature and the methoxy proton resonance as a singlet at δ 3.34. Vinylic proton signals were absent. The ^{29}Si NMR spectrum shows several closely spaced peaks in the δ_{Si} −45 to −40 region. These values are close to the ^{29}Si NMR resonance of $CH_3Si(OCH_3)_3$, δ −39.8 ppm.[14]

If chain transfer as occurred in the case of vinyltriethoxysilane is an important process in the polymerization of vinyltrimethoxysilane, then the slower rate of polymerization of the latter is understandable. Hydrogen atom abstraction from an Si−OCH_3 function should be much less favorable than H atom abstraction from an Si−OCH_2CH_3 function since in the former case a primary, in the latter case a more highly stabilized secondary, radical would be formed.

To obtain more information about PVSi(OMe)$_3$, the polymer was reduced with $LiAlH_4$ to the SiH_3 derivative (which we designate MeO−PVSiH$_3$ to make clear its antecedent). Characterizing data for MeO−PVSiH$_3$ are given in Table 4. As in the case of γ-PVSiH$_3$, it is clear from the analysis (ΣC,H,Si = 90.83%) that this polymer is not the simple $[CH_2$−$CHSiH_3]_n$. The IR spectrum shows ν(OH) at 3445 cm^{-1}. In the ^{1}H NMR spectrum the CH/SiH ratio is 1.33 rather than 1, so here also an excess of C−H bonds is present. The ^{29}Si NMR spectrum only shows signals in the $RSiH_3$ region. These

Table 5. Characterizing Data for PVSiCH$_3$(OEt)$_2$

appearance	clear, colorless, very viscous material
elemental analysis	Calcd for $C_7H_{16}O_2Si$: C, 52.49; H, 9.99. Found: c, 52.40; H, 10.02
IR (cm^{-1}, thin film)	2970 (s), 2924 (s), 1442 (m), 1390 (m), 1256 (m), 1095 (vs), 951 (s), 794 (s)
^{1}H NMR (ppm)	−0.026 (s), 1.08 (s), 0.2−1.9 (broad unresolved peaks), 3.62 (d)
^{13}C NMR (ppm)	−5.2, 18.2, 57.7
^{29}Si NMR (ppm)	−4.87, −4.52, −4.12, −3.84
mol wt (GPC)	no. avg, 1610; wt avg, 4559; polydispersity, 2.8

observations suggest that the composition of MeO−PVSiH$_3$ is very similar to that of γ-PVSiH$_3$, i.e., that shown in formula **1**, with the difference that chain transfer involving all three C−H bonds of the methoxy group should, in principle, be possible. In that case, PVSi(OMe)$_3$ would have the composition shown in **5**. It is difficult to make an estimate of the percentage of each unit in PVSi(OMe)$_3$ since there are more variables compared to γ-PVSi(OEt)$_3$. The mechanism of the polymerization of CH_2=$CHSi(OMe)_3$ must be the same as that of CH_2=$CHSi(OEt)_3$, the main difference between them being that hydrogen atom abstraction from OCH_3 is less facile than that from OCH_2CH_3. For synthetic purposes, because of the higher polymer yield for a given γ radiation dose and the higher molecular weight, CH_2=$CHSi(OEt)_3$ is the preferred vinyltrialkoxysilane monomer.

One experiment was carried out using CH_2=$CHSi(OCMe_3)_3$ as the monomer. However, a 12 Mrad γ-radiation dose produced essentially no polymerization. This is not surprising. The vinyltri-*tert*-butoxysilane monomer has no C−H bonds α to oxygen, so chain transfer is less favorable and, more important, the $RCH_2\dot{C}HSi(OCMe)_3$ radical is so sterically hindered that the normal vinyl polymerization propagation steps are impossible.

Polymerization of Vinylmethyldiethoxysilane and Vinyldimethylethoxysilane. The polymerization of vinyltriethoxysilane provides a polyethylene chain with trifunctional Si(OEt)$_3$ substituents. For some purposes it is desirable to have only mono- or difunctional silicon substituents, and for this reason, we have investigated the ^{60}Co γ-radiation-induced polymerization of CH_2=$CHSi(CH_3)(OEt)_2$ and CH_2=$CHSi(CH_3)_2OEt$.

Exposure of CH_2=$CHSi(CH_3)(OEt)_2$ to a 9.36 Mrad γ-radiation dose gave a polymer in only 26% yield as a clear, colorless, very viscous material. The slower polymerization rate, compared with that of CH_2=$CHSi(OEt)_3$, was expected since the likelihood of chain transfer involving OCH_2CH_3 groups is one-third less. Characterizing data for PVSiCH$_3$(OEt)$_2$ are given in Table 5. The composition of the polymer is assumed to

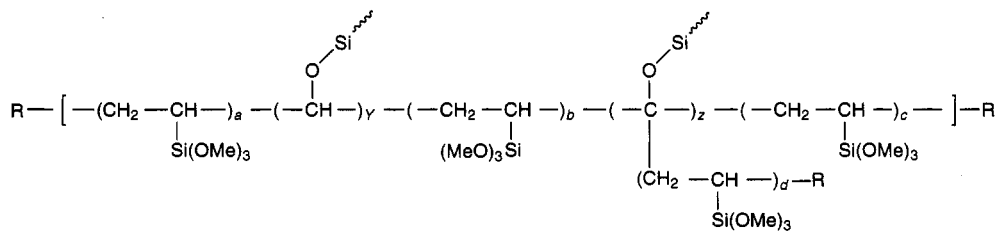

5

c, *d* ⟩⟩ *a*, *b*, and end groups R = $-CH_2CH_2Si(OMe)_3$, $(MeO)_3SiCHCH_3$, and $CH_2OSi\equiv$

Table 6. Characterizing Data for $PVSi(CH_3)_2OEt$

appearance	clear, pale yellow, viscous liquid
elemental analysis	Calcd for $C_6H_{14}OSi$: C, 55.37; H, 10.76. Found: C, 54.92; H, 10.76
IR (cm^{-1}, thin film)	2970 (s), 2924 (s), 1390 (m), 1250 (s), 1109 (s), 1082 (s), 947 (m), 826 (s), 777 (s)
^1H NMR (ppm)	0.021 (s), 0.3–1.0 (broad), 1.11 (s), 1.1–1.7 (broad), 3.57 (s), 3.59 (s)
^{13}C NMR (ppm)	−2.3, 18.4, 58.0
^{29}Si NMR (ppm)	16.8, 17.6[15]
mol wt (GPC)	no. avg, 490; wt avg, 873; polydispersity, 1.8

follow from a mechanism of formation similar to that for CH_2=$CHSi(OEt)_3$ (Scheme 2), so formula **6** should

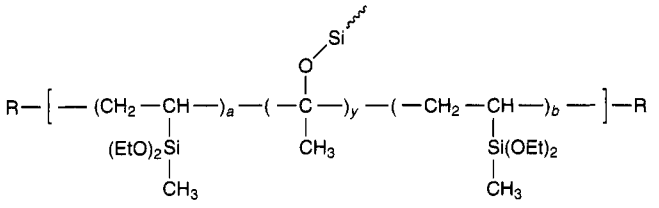

6

end groups R = $-CH_2CH_2SiCH_3(OEt)_2$, $-CHCH_3$, $CH_3Si(OEt)_2$ or $-CH(OSi{\equiv})CH_3$, *b* ⟩⟩ *a*

be an appropriate description of the polymer. $PVSiCH_3(OEt)_2$ is of relatively low molecular weight with a broad distribution. Its ^1H NMR spectrum shows intense resonances for the $SiCH_3$ and $SiOCH_2CH_3$ protons and broad signals due to the protons of the CH_2CH backbone. The ^{29}Si NMR spectrum shows four signals of about equal intensity between δ_{Si} −3.84 and −4.87. For comparison, the reported ^{29}Si NMR chemical shift of $(CH_3)_2Si(OEt)_2$ is −6.1 ppm.[10]

Vinyldimethylethoxysilane was polymerized in the same manner. A 9.36 Mrad γ-radiation dose gave an even lower polymer yield of 8.4%. The characterizing data for $PVSi(CH_3)_2OEt$, which was isolated as a clear, pale yellow, viscous oil, are given in Table 6. The lower polymerization rate may be attributed to the fact that there is only one OCH_2CH_3 group per monomer available for chain transfer and, of course, also to the steric hindrance to normal vinyl-type chain propagation due to the bulky $Si(CH_3)_2OEt$ group. Assuming that the polymerization/chain transfer mechanism shown in Scheme 2 is applicable to the polymerization of CH_2=$CHSi(CH_3)_2OEt$, the composition of this polymer then would be **7**.

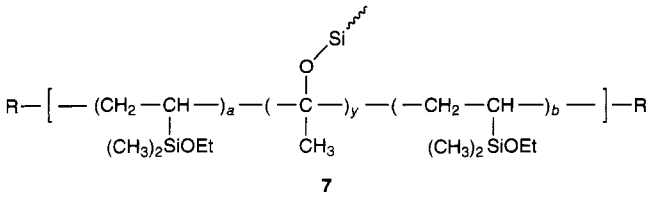

7

end groups R = $-CH_2CH_2Si(CH_3)_2OEt$, $-CHCH_3$, $(CH_3)_2SiOEt$ $-CH(OSi{\equiv})CH_3$, *b* ⟩⟩ *a*

The yields (for approximately the same γ-radiation doses) and the molecular weights of γ-$PVSi(OEt)_3$, $PVSiCH_3(OEt)_2$, and $PVSi(CH_3)_2OEt$ follow regular trends, as the data in Table 7 show. In view of the approximately same steric factor of the silyl groups in all three monomers, the decisive factor responsible for these differences appears to be the availability of OCH_2CH_3 groups in the monomer for chain transfer. It appears that all these polymers are composed of polymer chains that contain branching $CH_3(C<)OSi{\equiv}$ units in addition to the expected $CH_2CHSi(CH_3)_n(OEt)_{3-n}$ (n = 0–2) units. γ-$PVSi(OEt)_3$ contains such branching units in a substantial amount. If these are undesirable, then the $PVSiCl_3$ obtained by γ-radiation-induced polymerization of CH_2=$CHSiCl_3$[1] is preferred. This polymer does contain some branching (via a different mechanism), but there is much less of it.

Table 7. Polymer Yield and Molecular Weight Data for γ-$PVSi(OEt)_3$, $PVSiCH_3(OEt)_2$, and $PVSi(CH_3)_2OEt$

polymer	dose, Mrad	yield, %	mol wt (GPC)
γ-$PVSi(OEt)_3$	9	60	M_n 4416, M_w 10 788
$PVSiCH_3(OEt)_2$	9.36	26	M_n 1610, M_w 4559
$PVSi(CH_3)_2OEt$	9.36	8.4	M_n 490, M_w 873

The polymerization experiments with CH_2=$CHSiCH_3(OEt)_2$ and CH_2=$CHSi(CH_3)_2OEt$ were limited to a radiation dose of 9.36 Mrad for the sake of comparison. Higher doses should give higher polymer yields, as was demonstrated in the case of CH_2=$CHSi(OEt)_3$.

Experimental Section

General Comments. All reactions were performed under an argon atmosphere unless otherwise indicated. All reaction solvents were distilled from the appropriate drying agents. Infrared spectra were recorded on a Perkin-Elmer 1600 Fourier transform infrared spectrophotometer. All NMR spectra were recorded on either a Bruker-250 or Varian-300 instrument and are referenced to tetramethylsilane. Thermogravimetric analysis (TGA) of samples was performed using a Perkin-Elmer TGS-2 system under a 100 mL/min argon flow. Samples were heated from 50 to 950 °C at 10 °C/min.

GPC molecular weight determinations were made using a Waters Millipore 150-C ALC/GPC chromatograph equipped with a Waters Millipore Ultrastyragel 10^3 Å column with toluene solvent. Elemental analyses were performed by Scandinavian Microanalytical Laboratories, Herlev, Denmark, and Galbraith Laboratories, Knoxville, TN.

Vinyltrichlorosilane, vinylmethyldichlorosilane, vinyldimethylchlorosilane, vinyltriethoxysilane, vinylmethyldiethoxysilane, vinyldimethylethoxysilane, and vinyltrimethoxysilane were obtained from Hüls America and distilled and degassed before use.

γ-Ray polymerizations were carried out at 25 °C with exposure to a ^{60}Co source. The dosage rate was approximately 1.03 Mrad/day.

Polymerization of Vinyltriethoxysilane. A thick-walled glass ampule was charged with 31.6 g of CH_2=$CHSi(OEt)_3$ and subsequently was cooled in a liquid nitrogen bath and sealed under vacuum. The ampule was placed in the ^{60}Co γ reaction chamber and irradiated for the desired dosage at a rate of approximately 1.03 Mrad/day. After the desired dosage had been attained, the ampule was cooled again and broken open. The contents were poured into a Schlenk flask, and all volatiles were removed under full vacuum with heating to 120 °C. The residue, γ-$PVSi(OEt)_3$, was a thick, clear, colorless material.

(12) *Aldrich Library of ^{13}C and ^1H FT NMR Spectra*, ed. 1, Pouchert, C. J., Behnke, J., Eds.; Aldrich: Milwaukee, WI, 1993; p 188.

(13) Allcock, H. R.; Lampe, F. H. *Contemporary Polymer Chemistry*; Prentice-Hall: Englewood Cliffs, NJ, 1981; p 103.

(14) Van den Berghe, E. V.; Van der Kelen, G. P. *J. Organomet. Chem.* **1976**, *122*, 329.

(15) For comparison, δ_{Si} for $(CH_3)_3SiOEt$ = 14.53 ppm: Englehardt, G.; Schraml, J. *Org. Magn. Reson.* **1977**, *9*, 239.

Table 1 gives polymer yields and molecular weight data for various dosages.

γ-PVSi(OEt)$_3$. IR (thin film, cm^{-1}), 2974 (s), 2764 (m), 1884 (m), 1483 (s), 1456 (s), 1393 (s), 1078 (s), 764 (s). ^{1}H NMR (300 MHz, $CDCl_3$): δ 0.3−1.0 (broad, unresolved peaks), 1.11 (s), 1.2−2.0 (broad, unresolved peaks), 3.70 (s), 3.72 (s), 3.74 (sh). ^{13}C NMR (75.5 MHz, $CDCl_3$): δ_C 22.5, 58.0. ^{29}Si NMR (59.59 MHz, $CDCl_3$): δ_{Si} −47.0, −44.4, −44.1, −42.8. Anal. (6 Mrad sample) Calcd for $C_8H_{18}O_3Si$: C, 50.53; H, 9.47. Found: C, 50.48; H, 9.61.

Polymerizations of CH_2=$CHSi(OMe)_3$, CH_2=$CHSiCH_3(OEt)_2$, and CH_2=$CHSi(CH_3)_2OEt$ were carried out using the same procedure on about the same (30−35 g) scale. Characterizing data for $PVSi(OMe)_3$, $PVSiCH_3(OEt)_2$, and $PVSi(CH_3)_2OEt$ are given in Tables 3, 5, and 6, respectively.

Preparation of Poly(vinyltriethoxysilane) from Poly(vinyltrichlorosilane). $PVSiCl_3$[1] (6.76 g, equivalent to 0.126 mol of monomer) was dissolved in a mixture of 250 mL of diethyl ether and 14 mL of ethanol (0.38 mol). To the stirred solution was added in small portions 6.55 g (0.128 mol) of lithium ethoxide. A vigorous reaction ensued. After completion of the addition, the reaction mixture was stirred for 4 h at room temperature. Filtration was followed by removal of solvents from the filtrate at reduced pressure. The residue was extracted with 150 mL of diethyl ether. Evaporation of the ether extracts in vacuum left 6.92 g (87% yield) of a pale yellow, viscous oil. IR (thin film, cm^{-1}): 2975 (vs), 2921 (s), 2888 (s), 1877 (vw), 1480 (w), 1447 (w), 1387 (m), 1360 (vw), 1292 (w), 1167 (s), 1095 (vs) 1007 (s), 960 (s), 770 (s). ^{1}H NMR ($CDCl_3$): δ 0.80 (broad), 1.17 (broad s), 1.55 (broad s), 3.78 (broad s). ^{13}C NMR ($CDCl_3$): δ_C 18.00, (q, J_{C-H} = 126 Hz), 57.94 (t, J_{C-H} = 142 Hz). ^{29}Si NMR ($CDCl_3$): δ_{Si} −44.39 (broad, $Si(OEt)_3$), −47.32 (broad, $Si(OEt)_2$). Mol wt (M_n via VPO): 1139. Anal. Calcd for $C_8H_{18}O_3Si$: C, 50.53; H, 9.47. Found: C, 50.34; H, 9.49.

Lithium Aluminum Hydride Reduction of γ-PVSi(OEt)$_3$. A solution of 19.35 g (0.10 mol as monomer) of γ-PVSi(OEt)$_3$ in 70 mL of THF was added dropwise to an ice-cooled suspension of 5.8 g (0.15 mol) of $LiAlH_4$ in 350 mL of THF. The reaction mixture was stirred and allowed to warm to room temperature. After it had been stirred for 18 h, the mixture was filtered through a pad of Celite and the filtrate was added cautiously (!) to 400 mL of ice-coled 2 N aqueous HCl. The layers were separated, and the aqueous layer was washed twice with diethyl ether. The combined organic layers were washed twice with distilled water and once with saturated aqueous NaCl. The solution was dried over anhydrous $MgSO_4$ and subsequently the volatiles were removed at reduced pressure. The residue was taken up in 400 mL of hexane. The resulting cloudy solution was filtered through a pad of silica gel. Removal of hexane at reduced pressure left γ-$PVSiH_3$ as a clear, colorless, thick material in 85% yield. Characterization data are in given in Table 2.

A similar procedure served in the reduction of $PVSi(OMe)_3$ to MeO−$PVSiH_3$ in 66% yield. The reaction mixture from the $LiAlH_4$ reduction of the Union Carbide $PVSi(OEt)_3$[3,4] was hydrolyzed with cold 20% aqueous H_2SO_4 instead of 2 N HCl. The UC-$PVSiH_3$ was isolated in 67% yield as a thick oil.

UC-PVSiH$_3$. Mol wt (M_n via VPO): 1755. IR (thin film, cm^{-1}): 3470 (broad), 3070 (vw), 2968 (m), 2895 (m), 2840 (m), 2147 (vs), 1445 (w), 1374 (w), 1287 (w), 1069 (m), 920 (vs, broad), 739 (m), 620 (m). ^{1}H NMR ($CDCl_3$): δ 0.69, 1.24, 1.61, 3.49 (Si−H) (all broad s), CH/SiH = 3. ^{29}Si NMR ($CDCl_3$): δ_{Si} −50.0, −56.71, −58.35 (all broad). Ceramic residue yield (TGA): 19%.

Cross-Linking Reactions. (a) γ-PVSiH$_3$ with (η^5-C_5H_5)$_2$TiCl$_2$.[16] A 100 mL round-bottomed flask was charged with 0.5 g of γ-$PVSiH_3$, 11 mg of the titanium compound, and 30 mL of hexane. The solution was stirred and heated at reflux for 14 h. Volatiles were removed from the resulting pale green solution at reduced pressure, leaving a quantitative yield of a green semisolid. Ceramic residue yield (TGA): 79%.

(b) UC-PVSiH$_3$ with [(η^5-C_5H_5)$_2$ZrH$_2$]$_n$. In a similar experiment, a solution of UC-$PVSiH_3$ in hexane containing 0.5 mol % (based on Si) of the zirconium hydride was stirred and heated at reflux under argon for 1 h. Subsquently, the yellow reaction mixture was filtered and the filtrate was evaporated at reduced pressure. A soluble yellow solid was obtained in quantitative yield. CH/SiH = 4.5 (by integration of the ^{1}H NMR spectrum). Ceramic residue yield (TGA) = 69%. A 3 h reflux period resulted in an insoluble yellow solid. Ceramic residue yield: 74%.

Acknowledgment. This work was supported by the U.S. Air Force Office of Scientific Research (AFSC) and the Office of Naval Research.

Supplementary Material Available: Figures giving ^{1}H, ^{13}C, and ^{29}Si NMR spectra of compounds prepared in this paper (8 pages). Ordering information is given on any current masthead page.

OM940935M

(16) Based on the catalytic dehydrogenative coupling of $RSiH_3$: Aitken, C. A.; Harrod, J. F.; Samuel, E. *J. Organomet. Chem.* **1985**, *279*, C11. See also: Mu, Y.; Aitken, C. A.; Cote, B.; Harrod, J. F.; Samuel, E. *Can. J. Chem.* **1991**, *69*, 264. Aitken, C. A.; Barry, J.-P.; Gauvin, F.; Harrod, J. F.; Malck, A.; Rousseau, D. *Organometallics* **1989**, *8*, 1732.

Cluster Synthesis. 45. Syntheses and Structural Characterizations of Gold Phosphine Derivatives of the Layer-Segregated Cluster $Pt_3Ru_6(CO)_{21}(\mu_3\text{-}H)(\mu\text{-}H)_3$

Richard D. Adams,* Thomas S. Barnard, and Jeffrey E. Cortopassi

Department of Chemistry and Biochemistry, University of South Carolina, Columbia, South Carolina 29208

Received December 29, 1994[⊗]

Treatment of the compound $Pt_3Ru_6(CO)_{21}(\mu_3\text{-}H)(\mu\text{-}H)_3$ (**1**) with $[Bu_4N]OH$ followed by $[Au(PEt_3)][PF_6]$ yielded two new layer-segregated platinum–ruthenium cluster complexes, $Pt_3Ru_6[Au(PEt_3)](CO)_{21}(\mu\text{-}H)_3$ (**2**; 22% yield) and $Pt_3Ru_6[Au(PEt_3)]_2(CO)_{21}(\mu_3\text{-}H)_2$ (**3**; 5% yield), by the replacement of one and two of the hydride ligands in **1** with $Au(PEt_3)$ groupings, respectively. The yield of **3** can be increased to 18% by using larger amounts of $[Bu_4N]OH$ and $[Au(PEt_3)][PF_6]$. Both compounds were characterized by IR, ^1H NMR, and single-crystal X-ray diffraction analyses. Compound **2** was formed from **1** by the substitution of the triply bridging hydride ligand with an $Au(PEt_3)$ grouping as a triple bridge on one of the Ru_3 triangles. The structure of the cluster of **3** is similar to that of **2**, but the $Au(PEt_3)$ groups have assumed triply bridging positions across Ru_2Pt triangles on opposite sides of the cluster and the two hydride ligands have adopted triply bridging sites on the two Ru_3 triangles. Crystal data: for **2**, space group $P2_1/a$, $a = 17.520(2)$ Å, $b = 11.867(2)$ Å, $c = 20.987(4)$ Å, $\beta = 92.46(1)°$, $Z = 4$, 3348 reflections, $R = 0.041$; for **3**, space group $P2_1/c$, $a = 11.740(2)$ Å, $b = 17.351(4)$ Å, $c = 25.543(6)$ Å, $\beta = 90.89(2)°$, $Z = 4$, 3527 reflections, $R = 0.051$.

Introduction

We have recently prepared series of mixed-metal cluster complexes that contain the first examples of layer-segregated triangular stacks of platinum combined with ruthenium[1,2] or osmium.[3] An acetylene derivative of the platinum–ruthenium complex $Pt_3Ru_6(CO)_{21}(\mu\text{-}H)_3(\mu_3\text{-}H)$ (**1**) has been found to exhibit an unusual ability to hydrogenate diphenylacetylene to (*Z*)-stilbene catalytically.[4]

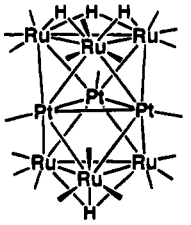

1

In an effort to explore the unusual properties of these layer-segregated mixed-metal cluster complexes further, we have prepared the derivatives $Pt_3Ru_6[Au(PEt_3)](CO)_{21}(\mu\text{-}H)_3$ (**2**) and $Pt_3Ru_6[Au(PEt_3)]_2(CO)_{21}(\mu_3\text{-}H)_2$ (**3**) by the replacement of one and two of the hydride ligands in **1** with $Au(PEt_3)$ groupings. The syntheses and characterizations of these new compounds are reported here.

Experimental Section

General Procedures. Reagent grade solvents were stored over 4 Å molecular sieves. $Pt_3Ru_6(CO)_{21}(\mu\text{-}H)_3(\mu_3\text{-}H)$ (**1**) was prepared by our previously reported procedure.[1] All other reagents were purchased from Aldrich and were used as received. All reactions were performed under a nitrogen atmosphere unless specified otherwise. Infrared spectra were recorded on a Nicolet 5DXB FTIR spectrophotometer. ^1H NMR spectra were recorded on a Bruker AM-500 FT-NMR spectrometer. Elemental microanalyses were performed by Oneida Research Services Inc., Whitesboro, NY. TLC separations were performed in air on Analtech 0.25 mm silica gel 60 Å F_{254} plates.

Synthesis of $Pt_3Ru_6[Au(PEt_3)](CO)_{21}(\mu\text{-}H)_3$ (2) and $Pt_3Ru_6[Au(PEt_3)]_2(CO)_{21}(\mu_3\text{-}H)_2$ (3). A 20.4-mg amount of **1** (0.0114 mmol) was dissolved in 20 mL of CH_2Cl_2 in a 100-mL three-necked round-bottom flask. A 7.5-μL amount of $[Bu_4N]OH$ (40 wt % aqueous solution, 1.0 equiv) was added via syringe. The solution was stirred at room temperature for 30 min. A solution of $[Au(PEt_3)][PF_6]$ was prepared by stirring 4.0 mg of $Au(Cl)PEt_3$ (0.0114 mmol) and 4.2 mg of $TlPF_6$ (0.0120 mmol) in 5 mL of CH_2Cl_2 for 5 min and then filtering to remove TlCl. This solution was then added to the previously prepared solution of **1** plus OH^-; see above. The mixture was stirred at room temperature for 30 min, and the solvent was then removed. The residue was transferred to TLC plates using a minimum of CH_2Cl_2 and then separated by using a hexane/CH_2Cl_2 (1/1) solvent mixture. This yielded the following, in order of elution: a dark brown band of $Pt_3Ru_6[Au(PEt_3)](CO)_{21}(\mu\text{-}H)_3$ (**2**; 5.2 mg, 22%) and a brown band of $Pt_3Ru_6[Au(PEt_3)]_2(CO)_{21}(\mu_3\text{-}H)_2$ (**3**; 1.5 mg, 5%). IR for **2**: (ν(CO), cm^{-1}; in hexane): 2094 (w), 2054 (s, sh), 2049 (vs), 2035 (m), 2021 (w), 1986 (w). ^1H NMR for **2** (δ; in $CDCl_3$): 2.02 (dq, 6H, CH_2, $^3J_{H-H} = 7.7$ Hz, $^2J_{P-H} = 16.6$ Hz), 1.23 (dt, 9H, CH_3, $^3J_{H-H} = 7.6$ Hz, $^3J_{P-H} = 18.2$ Hz), −17.32 (s, 3H, RuH, $^2J_{Pt-H} = 39.1$ Hz). Anal. Calcd (found) for **2**: C, 15.45 (15.13); H, 0.86 (1.02). IR for **3** (ν(CO), cm^{-1}; in hexane): 2081 (w), 2049 (s), 2044 (s, sh), 2037 (vs), 2027 (s), 1982 (w, br). ^1H NMR for **3** (δ; in CD_2Cl_2): 2.01 (dq, 18H, CH_2, $^3J_{H-H} = 7.6$ Hz, $^2J_{P-H} = 9.2$ Hz), 1.21 (dt, 12H, CH_3, $^3J_{H-H} = 7.6$ Hz, $^3J_{P-H} = 18.2$ Hz), −18.63 (s, 2H, RuH). Anal. Calcd (found) for **3**: C, 16.43 (16.00); H, 1.34 (1.33).

⊗ Abstract published in *Advance ACS Abstracts,* April 1, 1995.

(1) Adams, R. D.; Li, Z.; Wu, W.; Yamamoto, J. *Organometallics* **1994**, *13*, 2357.
(2) Adams, R. D.; Li, Z.; Wu, W. *Organometallics* **1992**, *11*, 4001.
(3) (a) Adams, R. D.; Lii, J.-C.; Wu, W. *Inorg. Chem.* **1991**, *30*, 3613. (b) Adams, R. D.; Lii, J.-C.; Wu, W. *Inorg. Chem.* **1992**, *31*, 2556. (c) Adams, R. D.; Lii, J.-C.; Wu, W. *Inorg. Chem.* **1991**, *30*, 2257.
(4) Adams, R. D.; Barnard, T. S.; Li, Z.; Wu, W.; Yamamoto, J. *J. Am. Chem. Soc.* **1994**, *116*, 9103.

0276-7333/95/2314-2232$09.00/0

Table 1. Crystal Data for Compounds 2 and 3

	2	3
formula	$AuPt_3Ru_6PO_{21}C_{27}H_{18}$	$Au_2Pt_3Ru_6P_2O_{21}C_{33}H_{32}$
fw	2098.06	2412.17
cryst syst	monoclinic	monoclinic
lattice params		
a (Å)	17.520(2)	11.740(2)
b (Å)	11.867(2)	17.351(4)
c (Å)	20.987(4)	25.542(6)
α (deg)	90	90
β (deg)	92.46(1)	90.89(2)
γ (deg)	90	90
V (Å^3)	4359(1)	5202(2)
space group	$P2_1/a$ (No. 14)	$P2_1/c$ (No. 14)
Z	4	4
ϱ_{calc} (g/cm^3)	3.20	3.08
μ(Mo Kα) (cm^{-1})	150.4	155.0
temp (°C)	20	20
$2\theta_{max}$ (deg)	43.0	43.0
no. of obs rflns ($I > 3\sigma(I)$)	3348	3527
goodness of fit (GOF)	2.16	2.02
residuals:[a] R; R_w	0.041; 0.034	0.051; 0.046
max shift/error on final cycle	0.25	0.37
largest peak in final diff map	1.80	2.66
abs cor, max/min	DIFABS, 1.56/0.77	empirical, 1.0/0.19

[a] $R = \sum_{hkl}(||F_o| - |F_c||/\sum_{hkl}|F_o|$; $R_w = [\sum_{hkl}w(|F_o| - |F_c|^2)/\sum_{hkl}F_o^2]^{1/2}$, $w = 1/\sigma^2(F_o)$; GOF $= [\sum_{hkl}(|F_o| - |F_c|/\sigma(F_o)]/(n_{data} - n_{vari})$.

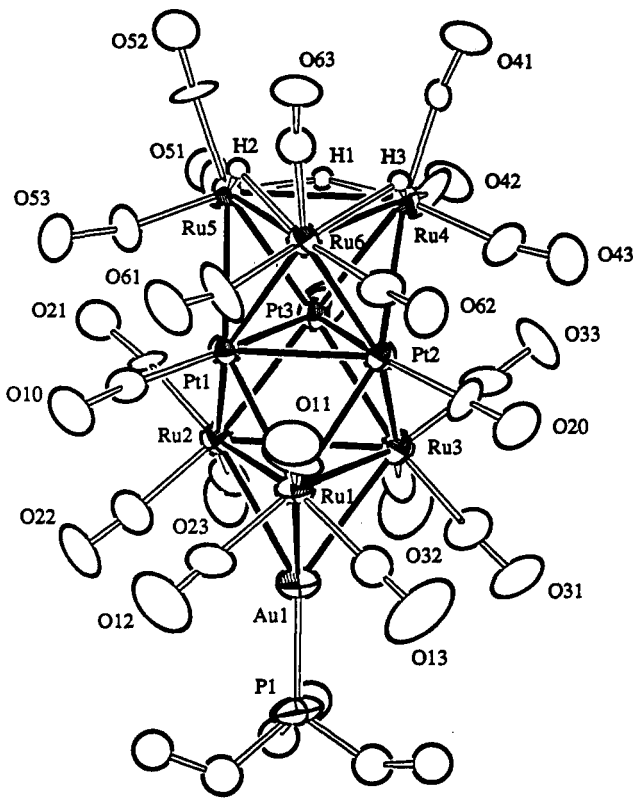

Figure 1. ORTEP diagram of $Pt_3Ru_6[Au(PEt_3)](CO)_{21}(\mu\text{-}H)_3$ (**2**) showing 40% probability thermal ellipsoids.

Improved Synthesis of $Pt_3Ru_6[Au(PEt_3)]_2(CO)_{21}(\mu_3\text{-}H)_2$ (3). An 18.9-mg amount of **1** (0.0106 mmol) was dissolved in 20 mL of CH_2Cl_2 in a 50-mL three-necked flask. A 14.6-μL amount of $[Bu_4N]OH$ (40 wt % aqueous solution, 2.1 equiv) was added via syringe. The solution was stirred at room temperature for 30 min. An IR spectrum of the solution taken at this time showed a single broad absorption at 2006 cm^{-1}. A solution of $[Au(PEt_3)][PF_6]$ was prepared by stirring 11.0 mg of $Au(Cl)PEt_3$ (0.031 mmol) and 22.0 mg of $TlPF_6$ (0.063 mmol) in 7 mL of CH_2Cl_2 for 5 min and then filtering to remove TlCl.

Table 2. Positional Parameters and B(eq) Values (Å^2) for $Ru_6Pt_3[Au(PEt_3)](CO)_{21}(\mu\text{-}H)_3$ (2)

atom	x	y	z	B(eq)
Au(1)	0.64579(6)	−0.14294(9)	0.14703(5)	3.74(5)
Pt(1)	0.79581(5)	−0.08624(8)	0.32937(5)	2.42(4)
Pt(2)	0.82759(5)	0.07940(8)	0.25136(5)	2.49(4)
Pt(3)	0.70509(5)	0.09092(8)	0.31817(5)	2.41(4)
Ru(1)	0.7956(1)	−0.1276(2)	0.2027(1)	3.1(1)
Ru(2)	0.6507(1)	−0.1143(1)	0.2809(1)	2.8(1)
Ru(3)	0.6876(1)	0.0767(2)	0.1894(1)	3.0(1)
Ru(4)	0.8255(1)	0.2519(2)	0.3486(1)	2.7(1)
Ru(5)	0.7888(1)	0.0629(1)	0.4377(1)	2.5(1)
Ru(6)	0.9306(1)	0.0502(1)	0.3608(1)	2.7(1)
P(1)	0.5856(4)	−0.2343(7)	0.0632(4)	5.1(4)
O(10)	0.813(1)	−0.332(1)	0.358(1)	6(1)
O(11)	0.966(1)	−0.162(2)	0.225(1)	6(1)
O(12)	0.781(1)	−0.382(2)	0.188(1)	8(1)
O(13)	0.827(1)	−0.101(2)	0.061(1)	9(1)
O(20)	0.914(1)	0.143(2)	0.137(1)	6(1)
O(21)	0.604(1)	−0.129(2)	0.419(1)	5(1)
O(22)	0.635(1)	−0.370(1)	0.269(1)	6(1)
O(23)	0.479(1)	−0.084(2)	0.246(1)	5(1)
O(30)	0.544(1)	0.179(2)	0.330(1)	5(1)
O(31)	0.708(2)	0.097(2)	0.046(1)	9(1)
O(32)	0.518(1)	0.109(2)	0.157(1)	8(1)
O(33)	0.701(1)	0.334(1)	0.195(1)	7(1)
O(41)	0.906(1)	0.437(2)	0.426(1)	6(1)
O(42)	0.676(1)	0.384(1)	0.349(1)	5(1)
O(43)	0.872(1)	0.371(1)	0.229(1)	5(1)
O(51)	0.627(1)	0.126(1)	0.4717(8)	4.0(9)
O(52)	0.848(1)	0.123(1)	0.568(1)	6(1)
O(53)	0.769(1)	−0.174(1)	0.4862(9)	5(1)
O(61)	0.979(1)	−0.194(1)	0.374(1)	6(1)
O(62)	1.0334(9)	0.087(2)	0.248(1)	5(1)
O(63)	1.054(1)	0.123(1)	0.4588(9)	5(1)
C(10)	0.807(1)	−0.240(2)	0.350(1)	3(1)
C(11)	0.900(1)	−0.148(2)	0.218(2)	5(2)
C(12)	0.781(1)	−0.286(2)	0.194(1)	4(1)
C(13)	0.810(1)	−0.111(2)	0.114(1)	4.1(6)
C(20)	0.881(1)	0.119(2)	0.180(1)	3(1)
C(21)	0.625(1)	−0.116(2)	0.368(1)	3(1)
C(22)	0.640(1)	−0.277(2)	0.271(1)	4(1)
C(23)	0.546(1)	−0.089(2)	0.256(1)	4(1)
C(30)	0.605(1)	0.144(2)	0.328(1)	3(1)
C(31)	0.702(1)	0.084(3)	0.101(1)	5(2)
C(32)	0.576(2)	0.098(2)	0.174(1)	5(1)
C(33)	0.696(1)	0.239(2)	0.194(1)	4(1)
C(41)	0.874(1)	0.366(2)	0.401(1)	3(1)
C(42)	0.731(1)	0.326(2)	0.347(1)	5(1)
C(43)	0.853(2)	0.318(2)	0.270(1)	4(2)
C(51)	0.685(1)	0.099(2)	0.454(1)	3(1)
C(52)	0.820(2)	0.100(2)	0.519(1)	4(1)
C(53)	0.778(1)	−0.088(2)	0.460(1)	3(1)
C(61)	0.957(2)	−0.107(2)	0.361(2)	7(2)
C(62)	0.990(1)	0.073(2)	0.288(1)	4(1)
C(63)	1.008(1)	0.093(2)	0.424(1)	3.5(5)
C(71)	0.588(6)	−0.38(1)	0.053(6)	34(5)
C(72)	0.597(2)	−0.447(4)	0.102(2)	11(1)
C(73)	0.484(2)	−0.236(3)	0.059(2)	10(1)
C(74)	0.443(2)	−0.147(3)	0.072(2)	10(1)
C(75)	0.594(5)	−0.195(7)	−0.010(5)	27(3)
C(76)	0.661(2)	−0.152(3)	−0.039(2)	11(1)

This solution was then added to the above reaction solution. The resulting solution was stirred at room temperature for 30 min, and the solvent was removed. The residue was transferred to TLC plates using a minimum amount of CH_2Cl_2. The product was isolated using a hexane/CH_2Cl_2 (1/1) solvent mixture to yield a dark brown band of **3** (4.7 mg, 18%), and no **2** was obtained.

Crystallographic Analyses. Crystals of **2** suitable for X-ray diffraction analysis were grown from a solution in a dichloromethane/hexane (1/1) solvent mixture by slow evaporation of the solvent at 25 °C. Crystals of **3** suitable for X-ray diffraction analysis were grown from a solution in a dichloromethane/heptane (1/1) solvent mixture by slow evaporation of the solvent at 25 °C. The crystals used for intensity measurements were mounted in thin-walled glass capillaries. Diffraction measurements were made on a Rigaku AFC6S

Table 3. Intramolecular Distances for 2[a]

Au(1)–Ru(1)	2.833(2)	Ru(1)–C(13)	1.91(3)
Au(1)–Ru(2)	2.828(3)	Ru(2)–Ru(3)	3.059(3)
Au(1)–Ru(3)	2.840(2)	Ru(2)–C(21)	1.89(3)
Au(1)–P(1)	2.285(8)	Ru(2)–C(22)	1.95(3)
Pt(1)–Pt(2)	2.633(1)	Ru(2)–C(23)	1.92(2)
Pt(1)–Pt(3)	2.640(1)	Ru(3)–C(31)	1.88(3)
Pt(1)–Ru(1)	2.703(3)	Ru(3)–C(32)	1.98(3)
Pt(1)–Ru(2)	2.717(2)	Ru(3)–C(33)	1.94(3)
Pt(1)–Ru(5)	2.888(2)	Ru(4)–Ru(5)	3.008(3)
Pt(1)–Ru(6)	2.915(2)	Ru(4)–Ru(6)	3.025(3)
Pt(1)–C(10)	1.88(2)	Ru(4)–C(41)	1.91(3)
Pt(2)–Pt(3)	2.617(1)	Ru(4)–C(42)	1.87(2)
Pt(2)–Ru(1)	2.710(2)	Ru(4)–C(43)	1.91(3)
Pt(2)–Ru(3)	2.726(2)	Ru(4)–H(1)	1.62
Pt(2)–Ru(4)	2.891(2)	Ru(4)–H(3)	1.78
Pt(2)–Ru(6)	2.880(2)	Ru(5)–Ru(6)	3.024(3)
Pt(2)–C(20)	1.85(3)	Ru(5)–C(51)	1.91(2)
Pt(3)–Ru(2)	2.718(2)	Ru(5)–C(52)	1.83(3)
Pt(3)–Ru(3)	2.713(2)	Ru(5)–C(53)	1.86(2)
Pt(3)–Ru(4)	2.896(2)	Ru(5)–H(1)	1.71
Pt(3)–Ru(5)	2.870(2)	Ru(5)–H(2)	1.91
Pt(3)–C(30)	1.88(2)	Ru(6)–C(61)	1.92(3)
Ru(1)–Ru(2)	3.085(3)	Ru(6)–C(62)	1.91(3)
Ru(1)–Ru(3)	3.080(3)	Ru(6)–C(63)	1.93(3)
Ru(1)–C(11)	1.85(2)	Ru(6)–H(2)	1.82
Ru(1)–C(12)	1.90(3)	Ru(6)–H(3)	2.01

[a] Distances are in angstroms. Estimated standard deviations in the least significant figure are given in parentheses.

automatic diffractometer by using graphite-monochromated Mo Kα radiation. Unit cells were determined from 25 randomly selected reflections obtained by using the AFC6 automatic search, center, index, and least-squares routines. Crystal data, data collection parameters, and results of the analyses are listed in Table 1. All data processing was performed on a Digital Equipment Corp. VAXstation 3520 computer by using the TEXSAN structure-solving program library obtained from the Molecular Structure Corp., The Woodlands, TX. Lorentz–polarization (*Lp*) and absorption corrections were applied to the data in each analysis. Neutral atom scattering factors were calculated by the standard procedures.[5a] Anomalous dispersion corrections were applied to all non-hydrogen atoms.[5b] Both structures were solved by a combination of direct methods (MITHRIL) and difference Fourier syntheses. Full-matrix least-squares refinements minimized the function $\sum_{hkl} w(|F_o| - |F_c|)^2$, where $w = 1/\sigma(F)^2$, $\sigma(F) = \sigma(F_o^2)/2F_o$, and $\sigma(F_o^2) = [\sigma(I_{raw})^2 + (0.02I_{net})^2]^{1/2}/Lp$. For all four analyses, the positions of the hydrogen atoms on the ligands were calculated by assuming idealized geometry, C - H = 0.95 Å.

Compound **2** crystallized in the monoclinic crystal system. The space group $P2_1/a$ was established on the basis of the patterns of systematic absences observed in the data. All non-hydrogen atoms were refined with anisotropic thermal parameters. The positions of the three hydride ligands were obtained in difference Fourier syntheses. They were partially refined but would not converge and were therefore fixed on the final cycles of refinement. The positions of the hydrogen atoms on the ethyl groups were calculated by assuming idealized geometries and C–H = 0.95 Å. Their scattering contributions were added to the structure factor calculations, but their positions were not refined.

Compound **3** crystallized in the monoclinic crystal system. The space group $P2_1/c$ was established on the basis of the patterns of systematic absences observed in the data. Except for the carbon atoms of the ethyl groups, all non-hydrogen atoms were refined with anisotropic thermal parameters. The carbon atoms of the ethyl groups exhibited considerable disorder. They were refined partially with isotropic thermal parameters and were subsequently added as fixed contributions in the final cycles using the partially refined values. Reasonable positions of the two hydride ligands were obtained from difference Fourier maps. They were refined to a suitable convergence on their positional parameters using a fixed isotropic thermal parameter. The hydrogen atoms on the ethyl groups were ignored in this analysis.

(5) (a) *International Tables for X-ray Crystallography*; Kynoch Press: Birmingham, England, 1975; Vol. IV, Table 2.2B, pp 99–101. (b) *Ibid.*, Table 2.3.1, pp 149–150.

Table 4. Intramolecular Bond Angles for 2[a]

Ru(1)–Au(1)–Ru(2)	66.05(6)	Ru(4)–Pt(3)–Ru(5)	62.88(6)
Ru(1)–Au(1)–Ru(3)	65.78(6)	Au(1)–Ru(1)–Pt(1)	112.31(8)
Ru(1)–Au(1)–P(1)	137.5(2)	Au(1)–Ru(1)–Pt(2)	112.75(7)
Ru(2)–Au(1)–Ru(3)	65.33(6)	Au(1)–Ru(1)–Ru(2)	56.91(6)
Ru(2)–Au(1)–P(1)	144.6(2)	Au(1)–Ru(1)–Ru(3)	57.23(5)
Ru(3)–Au(1)–P(1)	141.3(2)	Pt(1)–Ru(1)–Pt(2)	58.22(5)
Pt(2)–Pt(1)–Pt(3)	59.52(3)	Pt(1)–Ru(1)–Ru(2)	55.52(6)
Pt(2)–Pt(1)–Ru(1)	61.02(5)	Pt(1)–Ru(1)–Ru(3)	85.50(7)
Pt(2)–Pt(1)–Ru(2)	94.49(6)	Pt(2)–Ru(1)–Ru(2)	85.12(7)
Pt(2)–Pt(1)–Ru(5)	92.83(5)	Pt(2)–Ru(1)–Ru(3)	55.73(6)
Pt(2)–Pt(1)–Ru(6)	62.31(5)	Ru(2)–Ru(1)–Ru(3)	59.50(6)
Pt(3)–Pt(1)–Ru(1)	94.68(5)	Au(1)–Ru(2)–Pt(1)	112.02(8)
Pt(3)–Pt(1)–Ru(2)	60.95(5)	Au(1)–Ru(2)–Pt(3)	112.88(7)
Pt(3)–Pt(1)–Ru(5)	62.37(5)	Au(1)–Ru(2)–Ru(1)	57.05(6)
Pt(3)–Pt(1)–Ru(6)	93.25(5)	Au(1)–Ru(2)–Ru(3)	57.53(6)
Ru(1)–Pt(1)–Ru(2)	69.39(7)	Pt(1)–Ru(2)–Pt(3)	58.13(5)
Ru(1)–Pt(1)–Ru(5)	152.52(7)	Pt(1)–Ru(2)–Ru(1)	55.09(6)
Ru(1)–Pt(1)–Ru(6)	106.87(7)	Pt(1)–Ru(2)–Ru(3)	85.68(6)
Ru(2)–Pt(1)–Ru(5)	107.40(6)	Pt(3)–Ru(2)–Ru(1)	85.00(6)
Ru(2)–Pt(1)–Ru(6)	152.68(6)	Pt(3)–Ru(2)–Ru(3)	55.63(6)
Ru(5)–Pt(1)–Ru(6)	62.81(6)	Ru(1)–Ru(2)–Ru(3)	60.18(6)
Pt(1)–Pt(2)–Pt(3)	60.38(4)	Au(1)–Ru(3)–Pt(2)	112.01(7)
Pt(1)–Pt(2)–Ru(1)	60.77(6)	Au(1)–Ru(3)–Pt(3)	112.65(8)
Pt(1)–Pt(2)–Ru(3)	94.49(6)	Au(1)–Ru(3)–Ru(1)	56.99(6)
Pt(1)–Pt(2)–Ru(4)	94.61(6)	Au(1)–Ru(3)–Ru(2)	57.14(6)
Pt(1)–Pt(2)–Ru(6)	63.66(5)	Pt(2)–Ru(3)–Pt(3)	57.53(5)
Pt(3)–Pt(2)–Ru(1)	95.05(6)	Pt(2)–Ru(3)–Ru(1)	55.23(5)
Pt(3)–Pt(2)–Ru(3)	60.98(5)	Pt(2)–Ru(3)–Ru(2)	85.34(7)
Pt(3)–Pt(2)–Ru(4)	63.21(5)	Pt(3)–Ru(3)–Ru(1)	85.17(7)
Pt(3)–Pt(2)–Ru(6)	94.55(6)	Pt(3)–Ru(3)–Ru(2)	55.79(6)
Ru(1)–Pt(2)–Ru(3)	69.04(6)	Ru(1)–Ru(3)–Ru(2)	60.32(6)
Ru(1)–Pt(2)–Ru(4)	154.02(7)	Pt(2)–Ru(4)–Pt(3)	53.77(4)
Ru(1)–Pt(2)–Ru(6)	107.68(6)	Pt(2)–Ru(4)–Ru(5)	85.43(6)
Ru(3)–Pt(2)–Ru(4)	107.84(6)	Pt(2)–Ru(4)–Ru(6)	58.22(6)
Ru(3)–Pt(2)–Ru(6)	154.04(7)	Pt(3)–Ru(4)–Ru(5)	58.14(5)
Ru(4)–Pt(2)–Ru(6)	63.21(6)	Pt(3)–Ru(4)–Ru(6)	86.09(6)
Pt(1)–Pt(3)–Pt(2)	60.11(4)	Ru(5)–Ru(4)–Ru(6)	60.17(6)
Pt(1)–Pt(3)–Ru(2)	60.92(5)	Pt(1)–Ru(5)–Pt(3)	54.58(5)
Pt(1)–Pt(3)–Ru(3)	94.64(6)	Pt(1)–Ru(5)–Ru(4)	87.13(7)
Pt(1)–Pt(3)–Ru(4)	94.34(5)	Pt(1)–Ru(5)–Ru(6)	59.04(6)
Pt(1)–Pt(3)–Ru(5)	63.05(5)	Pt(3)–Ru(5)–Ru(4)	58.98(6)
Pt(2)–Pt(3)–Ru(2)	94.84(6)	Pt(3)–Ru(5)–Ru(6)	86.57(7)
Pt(2)–Pt(3)–Ru(3)	61.49(5)	Ru(4)–Ru(5)–Ru(6)	60.20(6)
Pt(2)–Pt(3)–Ru(4)	63.02(5)	Pt(1)–Ru(6)–Pt(2)	54.03(4)
Pt(2)–Pt(3)–Ru(5)	93.56(5)	Pt(1)–Ru(6)–Ru(4)	86.31(6)
Ru(2)–Pt(3)–Ru(3)	68.57(7)	Pt(1)–Ru(6)–Ru(6)	58.14(5)
Ru(2)–Pt(3)–Ru(4)	153.80(6)	Pt(2)–Ru(6)–Ru(4)	58.57(6)
Ru(2)–Pt(3)–Ru(5)	107.87(6)	Pt(2)–Ru(6)–Ru(6)	85.32(6)
Ru(3)–Pt(3)–Ru(4)	108.07(7)	Ru(4)–Ru(6)–Ru(5)	59.63(6)
Ru(3)–Pt(3)–Ru(5)	153.53(6)	M–C–O (av)	173(3)

[a] Angles are in degrees. Estimated standard deviations in the least significant figure are given in parentheses.

Results and Discussion

Although the hydride ligands in many metal compounds are often regarded as hydride (H^-) donors, it is also well-known that the hydride ligands in many metal carbonyl complexes can often be abstracted as the positively charged ion H^+ by suitable bases.[6] The conjugate bases are metal carbonyl anions, and such anions are widely used for the synthesis of new organometallic complexes.[7] In this study we have used the tetrahydride complex **1** to synthesize some $Au(PEt_3)$-substituted derivatives of **1** by treatment of **1** with a series of $[Bu^n_4N]OH$ and $[(PEt_3)Au][PF_6]$. Infrared

(6) (a) Pearson, R. G.; Ford, P. C. *Comments Inorg. Chem.* **1982**, *1*, 279. (b) Walker, H. W.; Kresge, C. T.; Ford, P. C.; Pearson, R. G. *J. Am. Chem. Soc.* **1979**, *101*, 7428.

(7) King, R. B. *Acc. Chem Res.* **1970**, *3*, 182.

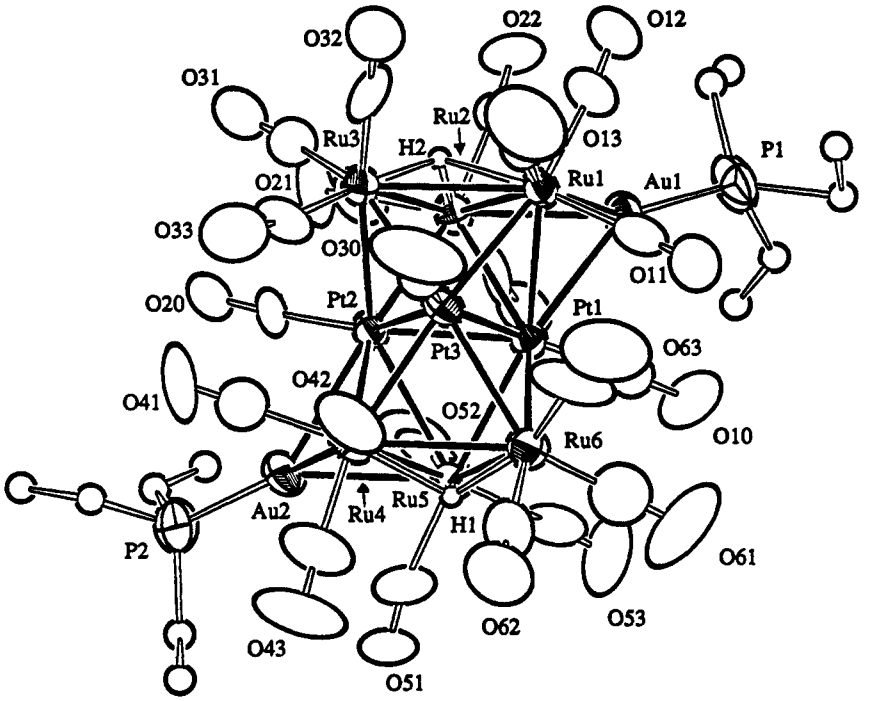

Figure 2. ORTEP diagram of $Pt_3Ru_6[Au(PEt_3)]_2(CO)_{21}(\mu_3\text{-}H)_2$ (**3**) showing 40% probability thermal ellipsoids.

spectra of solutions of **1** treated with 1 and 2 equiv of $[Bu^n{}_4N]OH$ show a progressive shift of the dominant absorption in **1** at 2067 cm^{-1} to 2020 and 2006 cm^{-1}, respectively. This shift to lower frequency is indicative of a greater back-bonding to the CO ligands and is consistent with the formation of negatively charged cluster species.

The addition of $[(PEt_3)Au][PF_6]$ to solutions of **1** treated with 1.0 equiv $[Bu^n{}_4N]OH$ provided two new gold-containing complexes after chromatographic work-up: $Pt_3Ru_6[Au(PEt_3)](CO)_{21}(\mu\text{-}H)_3$ (**2**; 22% yield) and $Pt_3Ru_6[Au(PEt_3)]_2(CO)_{21}(\mu_3\text{-}H)_2$ (**3**; 5% yield). The yield of **3** could be increased to 18% at the expense of **2** when larger amounts of $[Bu^n{}_4N]OH$ were used in the initial treatment of **1**. Both products were characterized by a combination of IR, ^1H NMR, and single-crystal X-ray diffraction analyses.

An ORTEP diagram of the molecular structure of **2** is shown in Figure 1. Final atomic positional parameters are listed in Table 2, and selected intramolecular distances and angles are listed in Tables 3 and 4. The molecule is structurally very similar to that of **1**. The

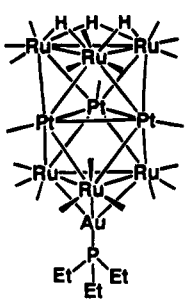

2

cluster consists of a stacked layer-segregated arrangement of six ruthenium and three platinum atoms with the platinum triangle in the center. Each metal triangle is rotated 60° from that of its nearest neighbor, which produces a staggered arrangement of the three triangles. This differs from that of the stacked Pt_3 triangular clusters $[Pt_3(CO)_6]_n{}^{2-}$ (n = 2–5) that were studied by Chini and Dahl.[8] The three hydride ligands are chemically equivalent and exhibit a single resonance in the ^1H NMR spectrum at δ −17.32 ppm with the appropriate long-range coupling to platinum, $^2J_{Pt-H}$ = 39.1 Hz. They were located and partially refined in the X-ray analysis. They occupy bridging positions across each of the three Ru–Ru bonds on one of the Ru_3 triangles. The associated Ru–Ru bond distances are elongated (Ru(4)–Ru(5) = 3.008(3) Å, Ru(4)–Ru(6) = 3.025(3) Å, and Ru(5)–Ru(6) = 3.024(3) Å) as expected. Similar elongation of the hydride-bridged Ru–Ru bonds was observed in **1** (Ru(4)–Ru(5) = 3.002(2) Å, Ru(4)–Ru(6) = 3.024(2) Å, and Ru(5)–Ru(6) = 3.033(2) Å).[1] The gold atom is bonded equally to all three ruthenium atoms of the other Ru_3 triangle (Ru(1)–Au = 2.833(2) Å, Ru(2)–Au = 2.828(3) Å, and Ru(3)–Au = 2.840(2) Å). These distances are similar to those that have been reported for a variety of other gold–ruthenium cluster complexes.[9–11] In **1** the site of the gold atom is occupied by a triply bridging hydride ligand. The platinum–platinum and platinum–ruthenium distances in **2** are similar to those found in **1**. The Pt_3 triangle does not lie midway between the two Ru_3 triangles but is positioned about 0.23 Å closer to the Au-bridged triangle (2.15 Å) than to the hydride-containing triangle (2.38 Å). In **1** the Pt_3 triangle was found to lie 0.23 Å closer to the Ru_3 triangle that contained the single hydride ligand (2.15 Å vs 2.38 Å).[1] As found in **1**, each ruthenium atom contains three linear terminal carbonyl ligands and each platinum atom has only one linear terminal carbonyl ligand. Overall, the molecule contains a total of 124 valence electrons about the 9 Pt_3Ru_6 atoms (gold excluded), which is precisely the

(8) (a) Longoni, G.; Chini, P. *J. Am. Chem. Soc.* **1976**, *98*, 7225. (b) Calabrese, J. C.; Dahl, L. F.; Chini, P.; Longoni, G.; Martinengo, S. *J. Am. Chem. Soc.* **1974**, *96*, 2614.

(9) Salter, I. D. *Adv. Organomet. Chem.* **1989**, *29*, 249.

(10) Orpen, A. G.; Salter, I. D. *Organometallics* **1991**, *10*, 111 and references therein.

(11) Bruce, M. I.; Nicholson, B. K. *Organometallics* **1984**, *3*, 101.

Table 5. Positional Parameters and *B*(eq) Values (Å²) for $Ru_6Pt_3[Au(PEt_3)]_2(CO)_{21}H_2$ (3)

atom	*x*	*y*	*z*	*B*(eq)
Au(1)	0.5489(1)	0.22774(7)	0.40865(6)	5.03(8)
Au(2)	0.9113(1)	0.12628(7)	0.19464(6)	5.46(8)
Pt(1)	0.7469(1)	0.15752(6)	0.36119(5)	3.73(7)
Pt(2)	0.7244(1)	0.10216(6)	0.26502(5)	3.71(7)
Pt(3)	0.7470(1)	0.00624(6)	0.34596(6)	4.09(7)
Ru(1)	0.5623(2)	0.0663(1)	0.3983(1)	4.0(1)
Ru(2)	0.5328(2)	0.1739(1)	0.3035(1)	4.2(1)
Ru(3)	0.5475(2)	0.0042(1)	0.2885(1)	4.5(1)
Ru(4)	0.9285(2)	0.0152(1)	0.2763(1)	4.8(2)
Ru(5)	0.9273(2)	0.1891(1)	0.2964(1)	4.6(2)
Ru(6)	0.9465(2)	0.0758(1)	0.3841(1)	4.8(2)
P(1)	0.480(1)	0.3254(5)	0.4582(5)	7.8(7)
P(2)	0.956(1)	0.1484(6)	0.1106(4)	7.9(7)
O(10)	0.817(2)	0.280(1)	0.439(1)	13(2)
O(11)	0.692(3)	0.102(2)	0.497(1)	9(2)
O(12)	0.330(2)	0.101(1)	0.442(1)	7(2)
O(13)	0.534(3)	−0.096(1)	0.437(1)	13(2)
O(20)	0.645(2)	0.092(2)	0.153(1)	8(2)
O(21)	0.454(3)	0.204(2)	0.196(1)	10(2)
O(22)	0.290(2)	0.212(2)	0.335(1)	10(2)
O(23)	0.619(2)	0.340(1)	0.303(1)	7(1)
O(30)	0.738(2)	−0.159(1)	0.378(1)	14(2)
O(31)	0.403(3)	0.026(2)	0.197(1)	9(2)
O(32)	0.373(3)	−0.104(1)	0.333(1)	11(2)
O(33)	0.654(2)	−0.134(1)	0.240(1)	12(2)
O(41)	0.838(3)	−0.064(1)	0.179(1)	11(2)
O(42)	0.968(2)	−0.141(1)	0.323(1)	9(2)
O(43)	1.174(3)	0.011(2)	0.240(2)	14(3)
O(51)	1.150(2)	0.218(2)	0.240(1)	8(2)
O(52)	0.803(2)	0.309(1)	0.232(1)	9(2)
O(53)	1.016(3)	0.312(2)	0.369(1)	14(3)
O(61)	1.044(3)	0.187(2)	0.460(2)	15(3)
O(62)	1.167(3)	−0.013(2)	0.390(1)	11(2)
O(63)	0.862(3)	−0.026(2)	0.471(2)	14(3)
C(10)	0.788(3)	0.233(2)	0.411(1)	5.3(8)
C(11)	0.641(4)	0.094(2)	0.460(2)	6(3)
C(12)	0.418(3)	0.089(2)	0.428(2)	6(2)
C(13)	0.542(3)	−0.036(2)	0.416(1)	5(2)
C(20)	0.678(3)	0.099(2)	0.195(1)	6(2)
C(21)	0.482(4)	0.186(3)	0.233(2)	8(3)
C(22)	0.381(3)	0.199(2)	0.326(1)	5(2)
C(23)	0.593(3)	0.273(2)	0.304(1)	5(2)
C(30)	0.742(3)	−0.093(2)	0.361(1)	5.4(7)
C(31)	0.459(4)	0.022(3)	0.235(2)	8(3)
C(32)	0.441(3)	−0.064(2)	0.316(2)	7(2)
C(33)	0.621(3)	−0.080(2)	0.259(2)	7(2)
C(41)	0.868(3)	−0.029(2)	0.212(2)	7(1)
C(42)	0.949(3)	−0.080(2)	0.306(2)	7(2)
C(43)	1.081(4)	0.014(2)	0.252(2)	9(3)
C(51)	1.068(3)	0.202(2)	0.257(2)	7(2)
C(52)	0.850(3)	0.261(2)	0.257(2)	7(2)
C(53)	0.983(3)	0.263(2)	0.346(2)	9(3)
C(61)	1.003(4)	0.146(2)	0.429(2)	10(1)
C(62)	1.089(4)	0.019(2)	0.387(2)	8(3)
C(63)	0.885(3)	0.015(2)	0.435(2)	10(3)
C(71)	0.5628	0.4089	0.4607	22.5
C(72)	0.6100	0.4448	0.4220	11.4
C(73)	0.3191	0.3385	0.4383	19.1
C(74)	0.2886	0.3727	0.4400	35.2
C(75)	0.5156	0.3388	0.5305	27.3
C(76)	0.4696	0.2716	0.5469	11.9
C(81)	0.9407	0.0550	0.0784	24.2
C(82)	0.8963	0.0837	0.0205	14.1
C(83)	1.0968	0.1965	0.0981	12.2
C(84)	1.1929	0.1303	0.1182	14.2
C(85)	0.8638	0.2231	0.0733	26.3
C(86)	0.8162	0.2788	0.0923	19.3
H(1)	0.99(2)	0.10(1)	0.32(1)	4.0
H(2)	0.49(2)	0.08(1)	0.321(9)	4.0

number predicted by the polyhedral skeletal electron pair theory for an arrangement of 9 metal atoms in a face-shared bioctahedral structure.[12]

(12) Mingos, D. M. P.; May, A. S. In *The Chemistry of Metal Cluster Complexes*; Shriver, D. F., Kaesz, H. D., Adams, R. D., Eds.; VCH: New York, 1990; Chapter 2.

Table 6. Intramolecular Distances for 3[a]

Au(1)−Pt(1)	2.907(2)	Ru(1)−C(12)	1.91(4)
Au(1)−Ru(1)	2.818(3)	Ru(1)−C(13)	1.85(3)
Au(1)−Ru(2)	2.847(3)	Ru(1)−H(2)	2.2(2)
Au(1)−P(1)	2.274(9)	Ru(2)−Ru(3)	2.973(3)
Au(2)−Pt(2)	2.889(2)	Ru(2)−C(21)	1.89(5)
Au(2)−Ru(4)	2.844(3)	Ru(2)−C(22)	1.93(3)
Au(2)−Ru(5)	2.821(3)	Ru(2)−C(23)	1.86(3)
Au(2)−P(2)	2.25(1)	Ru(2)−H(2)	1.7(2)
Pt(1)−Pt(2)	2.647(2)	Ru(3)−C(31)	1.74(4)
Pt(1)−Pt(3)	2.654(2)	Ru(3)−C(32)	1.87(4)
Pt(1)−Ru(1)	2.857(3)	Ru(3)−C(33)	1.87(3)
Pt(1)−Ru(2)	2.908(3)	Ru(3)−H(2)	1.8(2)
Pt(1)−Ru(5)	2.763(3)	Ru(4)−Ru(5)	3.061(3)
Pt(1)−Ru(6)	2.793(3)	Ru(4)−Ru(6)	2.953(4)
Pt(1)−C(10)	1.89(3)	Ru(4)−C(41)	1.93(4)
Pt(2)−Pt(3)	2.664(2)	Ru(4)−C(42)	1.83(3)
Pt(2)−Ru(2)	2.764(3)	Ru(4)−C(43)	1.90(4)
Pt(2)−Ru(3)	2.756(3)	Ru(4)−H(1)	2.0(2)
Pt(2)−Ru(4)	2.843(3)	Ru(5)−Ru(6)	2.986(4)
Pt(2)−Ru(5)	2.921(3)	Ru(5)−C(51)	1.97(4)
Pt(2)−C(20)	1.85(4)	Ru(5)−C(52)	1.82(4)
Pt(3)−Ru(1)	2.768(3)	Ru(5)−C(53)	1.91(4)
Pt(3)−Ru(3)	2.744(3)	Ru(5)−H(1)	1.9(2)
Pt(3)−Ru(4)	2.802(3)	Ru(6)−C(61)	1.79(5)
Pt(3)−Ru(6)	2.797(3)	Ru(6)−C(62)	1.94(4)
Pt(3)−C(30)	1.76(3)	Ru(6)−C(63)	1.84(4)
Ru(1)−Ru(2)	3.071(4)	Ru(6)−H(1)	1.7(2)
Ru(1)−Ru(3)	3.006(4)	O−C (av)	1.15(4)
Ru(1)−C(11)	1.88(5)		

[a] Distances are in angstroms. Estimated standard deviations in the least significant figure are given in parentheses.

An ORTEP diagram of the molecular structure of **3** is shown in Figure 2. Final atomic positional parameters are listed in Table 5, and selected intramolecular distances and angles are listed in Tables 6 and 7. This molecule also possesses the stacked arrangement of the six ruthenium and three platinum atoms with the three platinum atoms as a triangle sandwiched between two triruthenium triangles. There are two $AuPEt_3$ groups that occupy triply bridging sites on $PtRu_2$ triangles on opposite sides of the Pt_3 triangle. The gold−ruthenium distances are similar to those found in **2** and other gold−ruthenium cluster complexes[9−11] (Ru(1)−Au(1) = 2.818(3) Å, Ru(2)−Au(1) = 2.847(3) Å, Ru(4)−Au(2) = 2.844(3) Å, and Ru(5)−Au(2) = 2.821(3) Å). The gold−platinum distances are slightly longer than the gold−ruthenium distances (Au(1)−Pt(1) = 2.907(2) Å and Au(2)−Pt(2) = 2.889(2) Å). These distances are significantly longer than those found for gold-capped Pt_3 clusters, such as $[AuPt_3(\mu\text{-}CO)_3(PPh_3)_5][NO_3]$[13a] ($Au-Pt_{av}$ = 2.84 Å), $[AuPt_3(\mu\text{-}CO)_3\{P(C_6H_{11})_3\}_4][PF_6]$[13b] ($Au-Pt_{av}$ = 2.758(5) Å), $[AuPt_3(\mu\text{-}CO)_2(\mu\text{-}SO_2)\{P(C_6H_{11})_3\}_4][PF_6]$[13c] ($Au-Pt_{av}$ = 2.757(1) Å), and $[AuPt_3(\mu\text{-}Cl)(\mu\text{-}SO_2)_2\{P(C_6H_{11})_3\}_3\{P(C_6H_4\text{-}p\text{-}F)_3\}][PF_6]$ ($Au-Pt_{av}$ = 2.769(1) Å).[13c] The longer distances in **3** may be produced by steric effects, since each of the gold-bound platinum atoms have seven neighboring metal atoms. Compound **3** contains two triply bridging hydride ligands that were located and refined in the structural analysis. They bridge the Ru_3 triangles on opposite sides of the cluster and exhibit the characteristic strongly shielded shift (δ −18.63 ppm) but show no discernible coupling to the platinum atoms. Due to the presence of the hydride ligands, all of the Ru−Ru bond distances are unusually long (Ru(1)−Ru(2) = 3.071(4) Å, Ru(1)−Ru(3) = 3.006(4) Å, Ru(2)−Ru(3) =

(13) (a) Bour, J. J.; Kanters, R. P. J.; Schlebos, P. P. J.; Bos, W.; Bosman, W. P.; Behm, H.; Beurkers, P. T.; Steggerda, J. J. *J. Organomet. Chem.* **1987**, *329*, 405. (b) Briant, C. E.; Wardle, R. W. M.; Mingos, D. M. P. *J. Organomet. Chem.* **1984**, *267*, C49. (c) Mingos, D. M. P.; Wardle, R. W. M. *J. Chem. Soc., Dalton Trans.* **1986**, 73.

Table 7. Intramolecular Bond Angles for 3[a]

Pt(1)–Au(1)–Ru(1)	59.86(6)	Pt(2)–Pt(3)–Ru(4)	62.61(7)
Pt(1)–Au(1)–Ru(2)	60.70(7)	Pt(2)–Pt(3)–Ru(6)	94.21(7)
Pt(1)–Au(1)–P(1)	147.2(3)	Ru(1)–Pt(3)–Ru(3)	66.08(9)
Ru(1)–Au(1)–Ru(2)	65.65(8)	Ru(1)–Pt(3)–Ru(4)	153.48(8)
Ru(1)–Au(1)–P(1)	144.5(3)	Ru(1)–Pt(3)–Ru(6)	109.1(1)
Ru(2)–Au(1)–P(1)	138.7(3)	Ru(3)–Pt(3)–Ru(4)	108.2(1)
Pt(2)–Au(2)–Ru(4)	59.44(6)	Ru(3)–Pt(3)–Ru(6)	153.47(9)
Pt(2)–Au(2)–Ru(5)	61.52(7)	Ru(4)–Pt(3)–Ru(6)	63.7(1)
Pt(2)–Au(2)–P(2)	144.1(3)	Au(1)–Ru(1)–Pt(1)	61.62(6)
Ru(4)–Au(2)–Ru(5)	65.41(8)	Au(1)–Ru(1)–Pt(3)	117.72(9)
Ru(4)–Au(2)–P(2)	143.0(3)	Au(1)–Ru(1)–Ru(2)	57.63(7)
Ru(5)–Au(2)–P(2)	143.0(3)	Au(1)–Ru(1)–Ru(3)	116.2(1)
Au(1)–Pt(1)–Pt(2)	118.03(6)	Pt(1)–Ru(1)–Pt(3)	56.26(6)
Au(1)–Pt(1)–Pt(3)	118.55(5)	Pt(1)–Ru(1)–Ru(2)	58.61(7)
Au(1)–Pt(1)–Ru(1)	58.53(6)	Pt(1)–Ru(1)–Ru(3)	85.55(9)
Au(1)–Pt(1)–Ru(2)	58.63(7)	Pt(3)–Ru(1)–Ru(2)	85.9(1)
Au(1)–Pt(1)–Ru(5)	142.39(7)	Pt(3)–Ru(1)–Ru(3)	56.57(8)
Au(1)–Pt(1)–Ru(6)	143.08(9)	Ru(2)–Ru(1)–Ru(3)	58.58(9)
Pt(2)–Pt(1)–Pt(3)	60.35(5)	Au(1)–Ru(2)–Pt(1)	60.67(7)
Pt(2)–Pt(1)–Ru(1)	92.36(7)	Au(1)–Ru(2)–Pt(2)	116.2(1)
Pt(2)–Pt(1)–Ru(2)	59.47(7)	Au(1)–Ru(2)–Ru(1)	56.72(8)
Pt(2)–Pt(1)–Ru(5)	65.32(7)	Au(1)–Ru(2)–Ru(3)	116.3(1)
Pt(2)–Pt(1)–Ru(6)	94.68(8)	Pt(1)–Ru(2)–Pt(2)	55.57(6)
Pt(3)–Pt(1)–Ru(1)	60.18(6)	Pt(1)–Ru(2)–Ru(1)	57.02(7)
Pt(3)–Pt(1)–Ru(2)	91.40(6)	Pt(1)–Ru(2)–Ru(3)	85.25(9)
Pt(3)–Pt(1)–Ru(5)	96.11(7)	Pt(2)–Ru(2)–Ru(1)	85.68(8)
Pt(3)–Pt(1)–Ru(6)	61.74(7)	Pt(2)–Ru(2)–Ru(3)	57.27(7)
Ru(1)–Pt(1)–Ru(2)	64.37(8)	Ru(1)–Ru(2)–Ru(3)	59.61(9)
Ru(1)–Pt(1)–Ru(5)	154.28(8)	Pt(2)–Ru(3)–Pt(3)	57.95(6)
Ru(1)–Pt(1)–Ru(6)	106.74(8)	Pt(2)–Ru(3)–Ru(1)	87.11(9)
Ru(2)–Pt(1)–Ru(5)	110.0(1)	Pt(2)–Ru(3)–Ru(2)	57.55(7)
Ru(2)–Pt(1)–Ru(6)	150.64(9)	Pt(3)–Ru(3)–Ru(1)	57.35(8)
Ru(5)–Pt(1)–Ru(6)	65.03(9)	Pt(3)–Ru(3)–Ru(2)	88.3(1)
Au(2)–Pt(2)–Pt(1)	117.32(6)	Ru(1)–Ru(3)–Ru(2)	61.81(9)
Au(2)–Pt(2)–Pt(3)	120.39(6)	Au(2)–Ru(4)–Pt(2)	61.06(7)
Au(2)–Pt(2)–Ru(2)	141.84(7)	Au(2)–Ru(4)–Pt(3)	117.2(1)
Au(2)–Pt(2)–Ru(3)	143.80(8)	Au(2)–Ru(4)–Ru(5)	56.94(8)
Au(2)–Pt(2)–Ru(4)	59.50(7)	Au(2)–Ru(4)–Ru(6)	116.5(1)
Au(2)–Pt(2)–Ru(5)	58.10(7)	Pt(2)–Ru(4)–Pt(3)	56.32(6)
Pt(1)–Pt(2)–Pt(3)	59.95(5)	Pt(2)–Ru(4)–Ru(5)	59.17(7)
Pt(1)–Pt(2)–Ru(2)	64.96(7)	Pt(2)–Ru(4)–Ru(6)	87.3(1)
Pt(1)–Pt(2)–Ru(3)	94.96(8)	Pt(3)–Ru(4)–Ru(5)	86.71(9)
Pt(1)–Pt(2)–Ru(4)	91.54(8)	Pt(3)–Ru(4)–Ru(6)	58.09(8)
Pt(1)–Pt(2)–Ru(5)	59.26(7)	Ru(5)–Ru(4)–Ru(6)	59.5(1)
Pt(3)–Pt(2)–Ru(2)	94.41(8)	Au(2)–Ru(5)–Pt(1)	115.8(1)
Pt(3)–Pt(2)–Ru(3)	60.80(7)	Au(2)–Ru(5)–Pt(2)	60.37(7)
Pt(3)–Pt(2)–Ru(4)	61.07(7)	Au(2)–Ru(5)–Ru(4)	57.65(8)
Pt(3)–Pt(2)–Ru(5)	92.23(7)	Au(2)–Ru(5)–Ru(6)	116.1(1)
Ru(2)–Pt(2)–Ru(3)	65.18(7)	Pt(1)–Ru(5)–Pt(2)	55.43(6)
Ru(2)–Pt(2)–Ru(4)	153.1(1)	Pt(1)–Ru(5)–Ru(4)	84.87(8)
Ru(2)–Pt(2)–Ru(5)	109.55(9)	Pt(1)–Ru(5)–Ru(6)	57.96(8)
Ru(3)–Pt(2)–Ru(4)	106.70(8)	Pt(2)–Ru(5)–Ru(4)	56.68(7)
Ru(3)–Pt(2)–Ru(5)	150.8(1)	Pt(2)–Ru(5)–Ru(6)	85.27(9)
Ru(4)–Pt(2)–Ru(5)	64.14(8)	Ru(4)–Ru(5)–Ru(6)	58.4(1)
Pt(1)–Pt(3)–Pt(2)	59.71(5)	Pt(1)–Ru(6)–Pt(3)	56.68(6)
Pt(1)–Pt(3)–Ru(1)	63.56(6)	Pt(1)–Ru(6)–Ru(4)	86.4(1)
Pt(1)–Pt(3)–Ru(3)	95.09(7)	Pt(1)–Ru(6)–Ru(5)	57.01(8)
Pt(1)–Pt(3)–Ru(4)	92.31(6)	Pt(3)–Ru(6)–Ru(4)	58.25(8)
Pt(1)–Pt(3)–Ru(6)	61.58(6)	Pt(3)–Ru(6)–Ru(5)	88.3(1)
Pt(2)–Pt(3)–Ru(1)	94.01(7)	Ru(4)–Ru(6)–Ru(5)	62.0(1)
Pt(2)–Pt(3)–Ru(3)	61.25(7)	M–C–O (av)	173(4)

[a] Angles are in degrees. Estimated standard deviations in the least significant figure are given in parentheses.

2.973(3) Å, Ru(4)–Ru(5) = 3.061(3) Å, Ru(4)–Ru(6) = 2.953(4) Å, and Ru(5)–Ru(6) = 2.986(4) Å), but those Ru–Ru bonds that are bridged by the gold atoms (Ru(1)–Ru(2) and Ru(4)–Ru(5)) are the longest, which indicates that the gold atom also seems to produce a lengthening of the associated metal–metal bonds, as found in **2** above. It is notable that the gold-bridged Pt–Ru bonds are also longer than the others: Pt(1)–Ru(1) = 2.857(3) Å, Pt(1)–Ru(2) = 2.908(3) Å, Pt(2)–Ru(4) = 2.843(3) Å, and Pt(2)–Ru(5) = 2.921(3) Å versus Pt(1)–Ru(5) = 2.763(3) Å, Pt(1)–Ru(6) = 2.793(3) Å, Pt(2)–Ru(2) = 2.764(3) Å, Pt(2)–Ru(3) = 2.756(3) Å, Pt(3)–Ru(1) = 2.768(3) Å, Pt(3)–Ru(3) = 2.774(3) Å, Pt(3)–Ru(4) = 2.802(3) Å, and Pt(3)–Ru(6) = 2.797(3) Å. The bonding similarities between H and Au(PR$_3$) groupings have been investigated theoretically.[14] Both are well-known to bond to one, two, or three transition-metal atoms. However, Au(PR$_3$) grouping appears to exhibit a preference for the μ_3-bridging coordination when three or more additional transition-metal atoms are present in the molecule.[9] It seems thus that this preference may have had a directing influence on the formation of the structure observed in **3**. For example, compounds **1** and **2** each have one triple bridge (H or Au(PR$_3$)) and three edge-bridging hydride ligands. Compound **3**, on the other hand, has four μ_3 groups. It is suspected that this result is directed, in a large part, by the tendency of the Au(PR$_3$) groups to adopt the μ_3-bonding modes.

As expected, the Pt$_3$ triangle in **3** lies midway between the two Ru$_3$ triangles. Each ruthenium atom contains three linear terminal carbonyl ligands, each platinum atom has only one terminal carbonyl ligand, and the cluster contains the expected 124 valence electrons.[12]

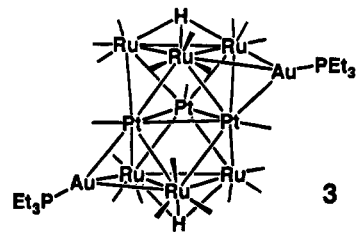

3

Overall, the molecule has an approximate C_2 symmetry with the C_2 axis passing through the atom Pt(3) and the midpoint of the Pt(1)–Pt(2) bond. The molecule is thus chiral, and as a result the methylene groups on the PEt$_3$ ligands are diastereotopic. Curiously, their inequivalence was not revealed in the ^{1}H NMR spectra, even when recorded at −80 °C. Either the molecule is engaging in a rapid dynamic process that averages their environments or the chiral environment is simply too weak to reveal their inequivalence spectroscopically.

We presume that compound **3** was formed by the addition of 2 equiv of [(PEt$_3$)Au]$^+$ to the corresponding dianion of **1** formed by removal of two protons. The reactions of metal carbonyl anions with [(PR$_3$)Au]-containing reagents is a well-established method for the preparation of gold-containing metal carbonyl cluster complexes.[15] We have not yet been able to isolate either the mono- or the dianion of **1** in a pure form as a salt, but these efforts are still in progress.

Acknowledgment. This research was supported by the National Science Foundation.

Supplementary Material Available: Tables of positional parameters for the hydrogen atoms for **2** and anisotropic thermal parameters for **2** and **3** (5 pages). Ordering information is given on any current masthead page.

OM9409940

(14) Evans, D. G.; Mingos, D. M. P. *J. Organomet. Chem.* **1982**, *232*, 171.

(15) (a) Hay, C. M.; Johnson, B. F. G.; Lewis, J.; McQueen, R. C. S.; Raithby, P. R.; Sorrell, R. M.; Taylor, M. J. *Organometallics* **1985**, *4*, 202. (b) Johnson, B. F. G.; Kaner, D. A.; Lewis, J.; Raithby, P. R.; Sorrell, R. M.; Taylor, M. J. *J. Chem. Soc., Chem. Commun.* **1982**, 314. (c) Johnson, B. F. G.; Kaner, D. A.; Lewis, J.; Raithby, P. R.; Sorrell, R. M.; Taylor, M. J. *Polyhedron* **1982**, *1*, 105.

Coordination and Transformations of Benzothienyl Ligands by Triosmium Cluster Complexes

Richard D. Adams* and Xiaosu Qu

Department of Chemistry and Biochemistry, University of South Carolina, Columbia, South Carolina 29208

Received January 9, 1995[⊗]

The reactions benzothiophene and 1-bromobenzothiophene with $Os_3(CO)_{10}(NCMe)_2$ have been investigated. The reaction of benzothiophene with $Os_3(CO)_{10}(NCMe)_2$ at 25 °C yielded two products $Os_3(CO)_{10}(\mu\text{-}SCCHC_6H_5)(\mu\text{-H})$, **1** (10%), and $Os_3(CO)_9(\mu_3\text{-}SCCC_6H_5)(\mu\text{-H})_2$, **2** (8%). Both products were characterized by single crystal X-ray diffraction analyses. Both products contain benzothiophene ligands transformed by the activation of one and two of the C–H bonds, respectively, of the benzothiophene molecule. Compound **1** consists of a closed triosmium cluster with a μ-η^2-benzothienyl ligand coordinated to an edge of the cluster through the C–C double bond in the five-membered ring of the ligand. Compound **2** contains a μ_3-η^2-benzothiophyne ligand coordinated to the face of a closed triosmium cluster. Compound **1** was transformed to **2** in 80% yield by heating to 125 °C in octane solvent. The reaction of 1-bromobenzothiophene with $Os_3(CO)_{10}(NCMe)_2$ at 25 °C yielded two products: $Os_3(CO)_{10}(\mu\text{-}SCCHC_6H_5)(\mu\text{-Br})$, **3** (32%), and $Os_3(CO)_9(\mu_3\text{-}SCCHC_6H_5)(\mu\text{-Br})$, **4** (10%). Both products were characterized by single crystal X-ray diffraction analyses. Both products contain benzothienyl ligands formed by the oxidative addition of the C–Br bond of the bromobenzothiophene to the cluster. In **3** the benzothienyl ligand is coordinated across the open edge of an open triosmium cluster through the sulfur and adjacent carbon atom. In **4** the benzothienyl ligand is a triply bridging ligand using the sulfur atom and the C–C double bond of the five-membered ring. Compound **3** was transformed to **4** in 74% yield by heating to 97 °C in heptane solvent for 30 min. Crystal data for **1**: space group = $P2_1/n$, a = 7.668(2) Å, b = 31.464(5) Å, c = 9.452(2) Å, β = 105.48(2)°, Z = 4, 2563 reflections, R = 0.035. Crystal data for **2**: space group = $P\bar{1}$, a = 9.791(1) Å, b = 14.576(2) Å, c = 8.094(1) Å, α = 95.44(1)°, β = 107.47(1)°, γ = 95.23(1)°, Z = 2, 2218 reflections, R = 0.024. Crystal data for **3**: space group = $P2_1/c$, a = 9.116(2) Å, b = 15.577(3) Å, c = 16.270(3) Å, β = 100.16(1)°, Z = 4, 2193 reflections, R = 0.038. Crystal data for **4**: space group = $P2_1/n$, a = 7.796(1) Å, b = 15.543(3) Å, c = 17.640(2) Å, β = 90.48(1)°, Z = 4, 2288 reflections, R = 0.028.

Introduction

Interest in the coordination and transformations of thiophene and its derivatives by metal complexes[1,2] is derived from the desire to understand the nature of the important reactions involved in the metal-catalyzed hydrodesulfurization of these molecules in petroleum purification processes.[3] The reactions of thiophene and derivatives with cluster complexes of the iron subgroup have not received a great deal of study even though it has been shown that the reactions of thiophenes with $Fe_3(CO)_{12}$ and $Ru_3(CO)_{12}$ lead to ring opening and ultimately to desulfurization of the thiophenes.[4]

Following our studies of the ring opening of tetrahydrothiophene by a triosmium cluster,[5] we undertook investigations of the reactions of benzothiophene and 1-bromobenzothiophene with $Os_3(CO)_{10}(NCMe)_2$. Both compounds undergo oxidative addition of the C–X bond at the carbon atom adjacent to the sulfur atom to yield products $Os_3(CO)_{10}(\mu\text{-}SCCHC_6H_5)(\mu\text{-X})$, **1**, X = H, and **3**, X = Br, which contain benzothienyl ligands. Interestingly, the benzothienyl ligands are coordinated to the clusters in two different ways. Both products undergo decarbonylation when heated. Compound **1** was transformed into the complex $Os_3(CO)_9(\mu_3\text{-}SCCC_6H_5)(\mu\text{-H})_2$,

[⊗] Abstract published in *Advance ACS Abstracts,* April 15, 1995.

(1) (a) Angelici, R. J. *Coord. Chem. Rev.* **1990**, *105*, 61. (b) Rauchfuss, T. B. *Prog. Inorg. Chem.* **1991**, *39*, 259. (c) Angelici, R. J. *Acc. Chem. Res.* **1988**, *21*, 387.

(2) (a) Riaz, U.; Curnow, O. J.; Curtis, M. D. *J. Am. Chem. Soc.* **1994**, *116*, 4357. (b) Jones, W. D.; Chin, R. M. *J. Am. Chem. Soc.* **1994**, *116*, 198. (c) Bianchini, C. Meli, A.; Peruzzini, M.; Vizza, F.; Moneti, S.; Herrera, V.; Sáchez-Delgado, R. A. *J. Am. Chem. Soc.* **1994**, *116*, 4370. (d) Chen, J.; Angelici, R. J. *Appl. Organomet. Chem.* **1992**, *6*, 479. (e) Luo, S.; Ogilvy, A. E.; Rauchfuss, T. B. *Organometallic* **1990**,*10*, 1002.

(3) (a) Schuman, S. C.; Shalit, H. *Catal. Rev.* **1970**, *4*, 245. (b) Gates, B. C.; Katzer, J. R.; Schuit, G. C. A. *Chemistry of Catalytic Processes*, McGraw-Hill: New York, 1978; Chapter 5. (c) Topsøe, H.; Clausen, B.; Topsøe, N.-Y.; Pedersen, E.; Niemann, W.; Müller, A.; Bögge, H.; Lengeler, B. *J. Chem. Soc., Faraday Trans.* **1987**, *83*, 2157. (d) Friend, C. M.; Roberts, J. T. *Acc. Chem. Res.* **1988**, *21*, 394. (e) Markel, E. J.; Schrader, G. L.; Sauer, N. N.; Angelici, R. J. *J. Catal.* **1989**, *116*, 11. (f) Prins, R.; De Beer, V. H. H.; Somorjai, G. A. *Catal. Rev. Sci. Eng.* **1989**, *31*, 1. (g) Sauer, N. N.; Markel, E. J.; Schrader, G. L.; Angelici, R. J. *J. Catal.* **1989**, *117*, 295. (h) Kwart, H.; Schuit, G. C. A.; Gates, B. C. *J. Catal.* **1980**, *61*, 128. (i) Curtis, M. D.; Penner-Hahn, J. E.; Schwank, J.; Beralt. O.; McCabe, D. J.; Thompson, L.; Waldo, G. *Polyhedron* **1988**, *7*, 2411. (j) Curtis, M. D. *Appl. Organomet. Chem.* **1992**, *6*, 429. (k) Roberts, J. T.; Friend, C. M. *J. Am. Chem. Soc.* **1987**, *109*, 7899.

(4) (a) Kaesz, H. D.; King, R. B.; Manuel, T. A.; Nichols, L. D.; Stone, F. G. A. *J. Am. Chem. Soc.* **1960**, *82*, 4749. (b) King, R. B.; Treichel, P. M.; Stone, F. G. A. *J. Am. Chem. Soc.* **1961**, *83*, 3600. (c) Ogilvy, A. E.; Draganjac, M.; Rauchfuss, T. B.; Wilson, S. R. *Organometallics* **1988**, *7*, 1171. (d) Arce, A. J.; Arrojo, P.; Deeming, A. J.; DeSanctis, Y. *J. Chem. Soc., Dalton Trans.* **1992**, 2423. (e) Arce, A. J.; DeSanctis, Y.; Karam, A.; Deeming, A. J. *Angew. Chem., Int. Ed. Engl.* **1994**, *33*, 1381.

(5) Adams, R. D.; Pompeo, M. P.; Wu W.; Yamamoto, J. H. *J. Am. Chem Soc.* **1993**, *115*, 8207.

0276-7333/95/2314-2238$09.00/0

Table 1. Crystal Data for Compounds 1–4

	compound			
	1	**2**	**3**	**4**
formula	$OS_3SO_{10}C_{18}H_6$	$Os_3SO_9C_{17}H_6$	$Os_3BrSO_{10}C_{18}H_5$	$Os_3BrO_9C_{17}H_5$
fw	984.90	956.89	1063.80	1035.79
cryst system	monoclinic	triclinic	monoclinic	monoclinic
lattice params				
a (Å)	7.668(2)	9.791(1)	9.116(2)	7.796(1)
b (Å)	31.464(5)	14.576(2)	15.577(3)	15.543(2)
c (Å)	9.452(2)	8.094(1)	16.270(3)	17.640(3)
α (deg)	90	95.44	90	90
β (deg)	105.48(2)	107.47(1)	100.16(1)	90.48(1)
γ (deg)	90	95.23(1)	90	90
V (Å^3)	2197.8(8)	1088.2(3)	2274.1(7)	2137.3(5)
space group	$P2_1/n$ (No. 14)	$P\bar{1}$ (No. 2)	$P2_1/c$ (No. 14)	$P2_1/n$ (No. 14)
Z value	4	2	4	4
ϱ_{calc} (g/cm^3)	2.98	2.92	3.11	3.22
μ(Mo Kα) (cm^{-1})	174.4	176.0	186.2	198.0
temp (°C)	20	20	20	20
$2\theta_{max}$ (deg)	47.0	43.0	43.0	45.0
no. obs ($I > 3\sigma$)	2563	2218	2193	2288
GOF[a]	1.91	1.73	2.45	1.50
residuals:[a] R; R_w	0.035; 0.038	0.024; 0.027	0.038; 0.043	0.028; 0.030
abs corr	DIFAB	empirical	empirical	empirical
largest peak in final diff map	1.08	1.06	1.83	1.03

[a] $R = \sum_{hkl}(||F_o| - |F_c||)/\sum_{hkl}|F_o|$; $R_w = [\sum_{hkl}w(|F_o| - |F_c|^2)/\sum_{hkl}F_o^2]^{1/2}$, $w = 1/\sigma^2(F_o)$; GOF = $[\sum_{hkl}(|F_o| - |F_c|/\sigma(F_o)]/(n_{data} - n_{vari})$.

2, containing a triply bridging benzothiophyne ligand by a second C–H activation step. Compound **3** was transformed to the complex $Os_3(CO)_9(\mu_3\text{-}\overline{SCCHC_6H_5})(\mu\text{-Br})$, **4**, simply by engaging the uncoordinated C–C double bond of the benzothienyl to form a triply bridging benzothienyl ligand. Details of these studies are reported herein.

Experimental Section

General Procedures. All reactions were performed under a dry nitrogen atmosphere. Reagent grade solvents were purified by distillation under nitrogen from the appropriate drying agents (CaH_2 for CH_2Cl_2 and heptane) and stored over molecular sieves and deoxygenated by purging with nitrogen prior to use. $Os_3(CO)_{10}(NCMe)_2$ was prepared from $Os_3(CO)_{12}$ by the standard procedure.[6] 1-Bromobenzothiophene was prepared according to the published procedure.[7] IR spectra were recorded on a Nicolet 5DXB FT-IR spectrophotometer. ^{1}H NMR spectra were recorded on Bruker AM-300 FT-NMR spectrometer. Elemental microanalyses were performed by Desert Analytics Organic Microanalysis, Tucson, AZ. TLC separations were performed in air by using silica gel (60 Å, F_{254}) on glass plates (Analtech, 0.25 mm).

Reaction of $Os_3(CO)_{10}(NCMe)_2$ with Benzothiophene. A 100.0-mg amount of $Os_3(CO)_{10}(NCMe)_2$ (0.107 mmol) and a 28.7-mg amount of benzothiophene (0.214 mmol) were dissolved in 25 mL of CH_2Cl_2, and the resulting solution was stirred at room temperature for 4 days. The solvent was then removed in vacuo, and the residue was separated by TLC using hexane as solvent to yield in the order of elution 10.4 mg of a yellow band of $Os_3(CO)_{10}(\mu\text{-}\overline{SCCHC_6H_5})(\mu\text{-H})$, **1** (10%), and 8.2 mg of a yellow band of $Os_3(CO)_9(\mu_3\text{-}\overline{SCCC_6H_5})(\mu\text{-H})_2$, **2** (8%). Spectroscopic data for the products are as follows. IR (ν_{CO} in hexane, cm^{-1}) for **1**: 2106 (m), 2069 (vs), 2055 (s), 2023 (vs), 2013 (s), 2001 (m), 1995 (s), 1984 (m). ^{1}H NMR (δ in $CDCl_3$) for **1**: 7.96 (d, 1H, $^3J_{HH}$ = 7.7 Hz), 7.67 (d, 1H, $^3J_{HH}$ = 7.7 Hz), 7.42 (dt, 1H, $^3J_{HH}$ = 7.5 Hz, $^4J_{HH}$ = 1.4 Hz), 7.34 (dt, 1H, $^3J_{HH}$ = 7.5 Hz, $^4J_{HH}$ = 1.4 Hz), 7.33 (s, 1H), −15.39 (s,1H). Anal. Calc (found) for **1**: C, 21.95 (21.23); H, 0.61 (0.53). IR (ν_{CO} in hexane, cm^{-1}) for **2**: 2112 (m), 2085 (s), 2062 (s), 2039 (s), 2034 (sh, w), 2025 (s), 2014 (s), 2005 (s), 1996 (w), 1991 (m). ^{1}H NMR (δ in $CDCl_3$) for **2**: 7.74–7.63 (m, 2H), 7.33–7.30 (m, 2H), −18.95 (s, 2H). Anal. Calc (found) for **2**: C, 21.34 (21.12); H, 0.63 (0.55).

Transformation of 1 to 2. A 15.0-mg amount of **1** (0.015 mmol) was dissolved in 10 mL of octane. The solution was heated to reflux for 30 min. The solvent was then removed in vacuo, and the residue was separated by TLC using hexane solvent. This yielded 11.5 mg of yellow compound **2** (80%).

Reaction of $Os_3(CO)_{10}(NCMe)_2$ with 1-Bromobenzothiophene. A 100.0-mg amount of $Os_3(CO)_{10}(NCMe)_2$ (0.107 mmol) and a 35.0-mg amount of 1-bromobenzothiophene (0.164 mmol) were dissolved in 25 mL of CH_2Cl_2. The solution was stirred at room temperature for 3 days. The solvent was then removed in vacuo, and the residue was separated by TLC on silica gel using hexane as solvent to yield in the order of elution 36.5 mg of an orange band of $Os_3(CO)_{10}(\mu\text{-}\overline{SCCHC_6H_5})(\mu\text{-Br})$, **3** (32%), and 11.1 mg of a yellow band of $Os_3(CO)_9(\mu_3\text{-}\overline{SCCHC_6H_5})(\mu\text{-Br})$, **4** (10%). Spectroscopic data for the products are as follows. IR (ν_{CO} in hexane, cm^{-1}) for **3**: 2107 (m), 2075 (vs), 2058 (m), 2025 (s), 2017 (m), 2014 (sh, m), 2003 (m), 1998 (m), 1989 (w), 1983 (w). ^{1}H NMR (δ in CD_2Cl_2) for **3**: 7.75 (d, 1H, $^3J_{HH}$ = 7.9 Hz), 7.70 (d, 1H, $^3J_{HH}$ = 7.9 Hz), 7.51 (s, 1H, br), 7.46 (dt, 1H, $^3J_{HH}$ = 7.7 Hz, $^4J_{HH}$ = 1.1 Hz), 7.32 (t, 1H, $^3J_{HH}$ = 7.9 Hz). Anal. Calc (found) for **3**: C, 20.32 (20.13); H, 0.47 (0.64). IR (ν_{CO} in hexane, cm^{-1}) for **4**: 2093 (w), 2072 (vs), 2034 (vs), 2017 (s), 2006 (m), 1991 (m), 1969 (w). ^{1}H NMR (δ in $CDCl_3$) for **4**: 7.77(d, 1H, $^3J_{HH}$ = 7.60 Hz), 7.67 (dd, 1H, $^3J_{HH}$ = 7.80 Hz, $^5J_{HH}$ = 1.0 Hz), 7.40 (td, 1H, $^3J_{HH}$ = 7.60 Hz, $^5J_{HH}$ = 1.0 Hz), 7.28 (dd, 1H, $^3J_{HH}$ = 7.60 Hz, $^5J_{HH}$ = 1.0 Hz), 5.20 (s, 1H). Anal. Calc (found) for **4**: C, 19.70 (19.72); H, 0.48 (0.50).

Pyrolysis of 3. A 60.0-mg amount of **3** (0.056 mmol) was dissolved in 15 mL of heptane. The solution was heated to reflux for 30 min. The solvent was then removed in vacuo, and the residue was separated by TLC using hexane solvent to yield 42.9 mg of yellow **4** (74%).

Crystallographic Analyses. Crystals of **3** suitable for X-ray diffraction analysis were grown from a solution of a solvent mixture of dichloromethane and hexane by slow evaporation of the solvent at −14 °C. Crystals of **4** suitable for X-ray diffraction analysis were grown from a solution of benzene by slow evaporation of the solvent at 25 °C. Crystals of **1** suitable for X-ray diffraction analysis were grown from a

(6) Nicholls, J. N.; Vargas, M. D. *Inorg. Synth.* **1989**, *28*, 232.
(7) Shirley, D. A.; Cameron, M. D. *J. Am. Chem. Soc.* **1952**, *74*, 664.

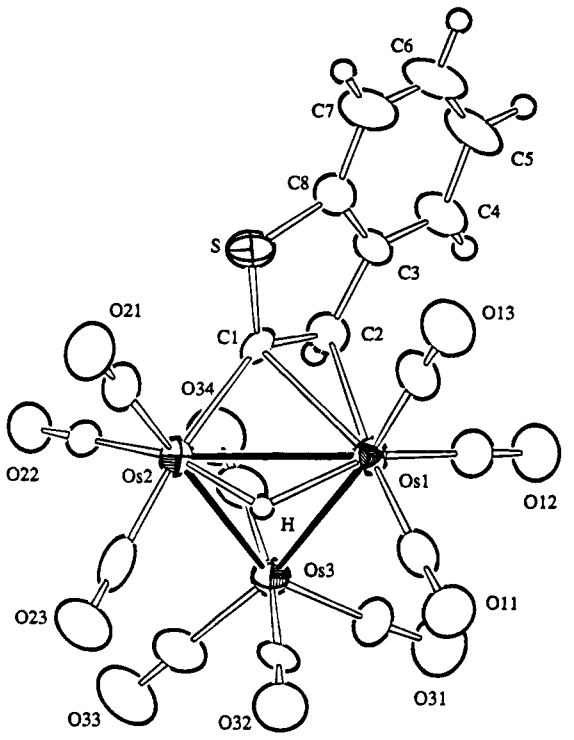

Figure 1. ORTEP diagram of $Os_3(CO)_{10}(\mu\text{-}\overline{SCCHC_6H_5})(\mu\text{-}H)$, **1**, showing 50% probability thermal ellipsoids.

solution of a solvent mixture of dichloromethane and hexane by slow evaporation of the solvent at −14 °C. Crystals of **2** suitable for X-ray diffraction analysis were grown from a solution in hexane by slow evaporation of the solvent at −5 °C. All crystals were mounted in thin-walled glass capillaries. Diffraction measurements were made on a Rigaku AFC6S automatic diffractometer by using graphite-monochromated Mo Kα radiation. Unit cells were determined from 15 randomly selected reflections obtained by using the AFC6 automatic search, center, index, and least-squares routines. Crystal data, data collection parameters, and results of the analyses are listed in Table 1. All data processing was performed on a Digital Equipment Corp. VAXstation 3520 computer by using the TEXSAN structure solving program library obtained from the Molecular Structure Corp., The Woodlands, TX. Lorentz–polarization (*Lp*) and absorption corrections were applied to the data in each analysis. Neutral atom scattering factors were calculated by the standard procedures.[8a] Anomalous dispersion corrections were applied to all non-hydrogen atoms.[8b] All structures were solved by a combination of direct methods (MITHRIL) and difference Fourier syntheses. Full matrix least-squares refinements minimized the following function: $\Sigma_{hkl} w(|F_o| - |F_c|)^2$, *where* $w = 1/\sigma(F)^2$, $\sigma(F) = \sigma(F_o^2)/2F_o$, *and* $\sigma(F_o^2) = [\sigma(I_{raw})^2 + (0.02I_{net})^2]^{1/2}/Lp$.

Compounds **1** and **4** crystallized in the monoclinic crystal system. The space group $P2_1/n$ was established for both compounds on the basis of the patterns of systematic absences observed in the data. All nonhydrogen atoms of the complex were refined with anisotropic thermal parameters. The hydrogen atoms on the benzothienyl ligand were calculated by assuming idealized geometries with C−H = 0.95 Å. The probable position of the hydride ligand in **1** was obtained from a difference Fourier map, but it could not be refined to a convergence. Thus, the hydride ligand and the hydrogen atoms on the benzothienyl ligand in both analyses were added to the structure factor calculations without refinement.

(8) (a) *International Tables for X-ray Crystallography*; Kynoch Press: Birmingham, England, 1975; Vol. IV, Table 2.2B, pp 99–101. (b) *Ibid.*, Table 2.3.1, pp 149–150.

Table 2. Positional Parameters and *B*(eq) Values (Å²) for 1

atom	*x*	*y*	*z*	*B*(eq)
Os(1)	0.09550(8)	0.10727(2)	0.11754(7)	2.58(2)
Os(2)	0.22124(8)	0.15647(2)	0.37710(7)	2.59(3)
Os(3)	0.34386(9)	0.17639(2)	0.12529(7)	3.02(3)
S	0.1914(6)	0.0553(1)	0.4668(5)	3.8(2)
O(11)	−0.194(2)	0.1519(4)	−0.110(2)	6.5(7)
O(12)	0.219(2)	0.0606(4)	−0.120(1)	6.2(7)
O(13)	−0.179(2)	0.0408(5)	0.149(2)	6.7(8)
O(21)	0.023(2)	0.1408(4)	0.610(1)	5.2(6)
O(22)	0.588(2)	0.1775(4)	0.578(1)	4.7(6)
O(23)	0.091(2)	0.2486(4)	0.364(2)	6.6(7)
O(31)	0.392(2)	0.1582(5)	−0.176(2)	6.6(8)
O(32)	0.006(2)	0.2302(5)	0.021(1)	6.5(7)
O(33)	0.566(2)	0.2571(5)	0.200(2)	8(1)
O(34)	0.688(2)	0.1302(5)	0.302(2)	5.6(7)
C(1)	0.279(2)	0.0903(5)	0.360(1)	2.3(5)
C(2)	0.354(2)	0.0657(5)	0.268(2)	2.8(6)
C(3)	0.344(2)	0.0197(5)	0.285(2)	2.9(6)
C(4)	0.413(2)	−0.0122(5)	0.215(2)	3.8(7)
C(5)	0.388(2)	−0.0532(5)	0.249(5)	5(1)
C(6)	0.299(3)	−0.0624(6)	0.358(3)	6(1)
C(7)	0.235(2)	−0.0315(6)	0.429(2)	4.9(9)
C(8)	0.259(2)	0.0103(5)	0.394(2)	3.5(7)
C(11)	−0.081(2)	0.1354(5)	−0.024(2)	3.9(7)
C(12)	0.175(2)	0.0781(6)	−0.029(2)	4.1(8)
C(13)	−0.071(3)	0.0656(6)	0.138(2)	4.5(8)
C(21)	0.099(2)	0.1453(6)	0.527(2)	3.9(8)
C(22)	0.448(2)	0.1699(5)	0.504(2)	3.2(7)
C(23)	0.143(2)	0.2149(7)	0.369(2)	4.2(8)
C(31)	0.374(2)	0.1668(6)	−0.061(2)	3.6(8)
C(32)	0.128(2)	0.2093(5)	0.059(2)	3.4(7)
C(33)	0.480(3)	0.2271(6)	0.174(2)	5(1)
C(34)	0.556(2)	0.1456(5)	0.231(2)	3.9(8)

Compound **2** crystallized in the triclinic crystal system. The space group $P\bar{1}$ was assumed and confirmed by the successful solution and refinement of the structure. All non-hydrogen atoms of the complex were refined with anisotropic thermal parameters. The hydrogen atoms on the benzothiophyne ligand were calculated by assuming idealized geometries. The probable position of the two hydride ligands were obtained from a difference Fourier map, but they could not be refined to a convergence. Thus, the hydride ligands and the hydrogen atoms on the benzothiophyne ligand were added to the structure factor calculations without refinement.

Compound **3** crystallized in the monoclinic crystal system. The space group $P2_1/c$ was established on the basis of the patterns of systematic absences observed in the data. All non-hydrogen atoms were refined with anisotropic thermal parameters. The hydrogen atoms on the benzothienyl ligand were calculated by assuming idealized geometries and were added to the structure factor calculations without refinement.

Results

The reaction of $Os_3(CO)_{10}(NCMe)_2$ with benzothiophene in CH_2Cl_2 at 25 °C for 4 days yielded two new compounds $Os_3(CO)_{10}(\mu\text{-}\overline{SCCHC_6H_5})(\mu\text{-}H)$, **1**, and $Os_3(CO)_9(\mu_3\text{-}\overline{SCCC_6H_5})(\mu\text{-}H)_2$, **2**, in rather low yields 10% and 8%, respectively. Both compounds were characterized by a combination of IR, ^1H NMR, and single-crystal X-ray

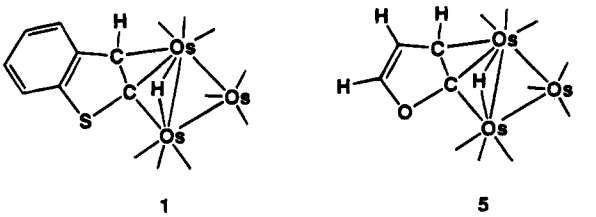

1 **5**

Table 3. Intramolecular Distances for 1[a]

Os(1)–Os(2)	2.843(1)	C(3)–C(4)	1.38(2)
Os(1)–Os(3)	2.8788(9)	C(3)–C(8)	1.39(2)
Os(1)–C(1)	2.41(1)	C(4)–C(5)	1.36(2)
Os(1)–C(2)	2.48(1)	C(5)–C(6)	1.41(3)
Os(2)–Os(3)	2.853(1)	C(6)–C(7)	1.34(3)
Os(2)–C(1)	2.14(1)	C(7)–C(8)	1.38(2)
S–C(1)	1.75(1)	Os–C(av)	1.90(2)
S–C(8)	1.71(2)	C–O(av)	1.14(2)
C(1)–C(2)	1.40(2)	Os(1)–H	2.01
C(2)–C(3)	1.46(2)	Os(2)–H	1.76

[a] Distances are in angstroms. Estimated standard deviations in the least significant figure are given in parentheses.

Table 4. Intramolecular Bond Angles for 1[a]

Os(2)–Os(1)–Os(3)	59.80(2)	C(3)–C(4)–C(5)	119(2)
Os(1)–Os(2)–Os(3)	60.72(2)	C(4)–C(5)–C(6)	120(2)
Os(1)–Os(3)–Os(2)	59.48(2)	C(5)–C(6)–C(7)	122(2)
C(1)–S–C(8)	95.0(8)	C(6)–C(7)–C(8)	119(2)
S–C(1)–C(2)	107(1)	S–C(8)–C(3)	112(1)
C(1)–C(2)–C(3)	116(1)	C(3)–C(8)–C(7)	120(2)
C(2)–C(3)–C(8)	110(1)	Os–C(av)–O	177(2)
C(4)–C(3)–C(8)	121(1)		

[a] Angles are in degrees. Estimated standard deviations in the least significant figure are given in parentheses.

diffraction analyses. An ORTEP diagram of the molecular structure of compound **1** is shown in Figure 1. Final atomic positional parameters are listed in Table 2, and selected interatomic distances and angles are listed in Tables 3 and 4. The molecule consists of a closed triangular cluster of three osmium atoms with 10 linear terminal carbonyl ligands. The most interesting ligand is a μ-η^2-benzothienyl ligand coordinated to an edge of the cluster through the C–C double bond in the five-membered ring in a $\sigma + \pi$ coordination mode. The reaction of $Os_3(CO)_{10}(NCMe)_2$ with furan and thiophene has been reported to yield similar complexes $Os_3(CO)_{10}(\mu\text{-}\overline{OCCHCHCH})(\mu\text{-H})$, **5**,[9] and $Os_3(CO)_{10}(\mu\text{-}\overline{SCCHCHCH})(\mu\text{-H})$, **6**,[10] containing μ-η^2-furyl and thienyl ligands, respectively, and the furyl complex **5** has been characterized crystallographically,[9] but this appears to be the first example of this coordination for a benzothienyl ligand.

The metal–carbon σ-bonding distance, Os(2)–C(1) = 2.14(1) Å, is similar to that found in **5**, Os–C = 2.11(1) Å. The metal–carbon π-bonding distances, Os(1)–C(1) = 2.41(1) Å and Os(1)–C(2) = 2.48(1) Å, are not greatly different from those found in **5**, 2.34(1) and 2.63(1) Å, respectively, although the distances are considerably more asymmetric in **5**. The μ-η^2-benzothienyl ligand has adopted a conformation similar to that of the furyl ligand in **5** in which the sulfur atom points away *(anti)* from the $Os(CO)_4$ grouping in the cluster. This is different from most σ–π coordinated alkenyl ligands where the substitutent on the bridging carbon atom is oriented *syn* to the $Os(CO)_4$ grouping.[11] Compound **1** contains one hydride ligand, $\delta = -15.39$ ppm. It was located crystallographically in a bridging position across the same metal–metal bond as the benzothienyl ligand, but it could not be refined. Interestingly, the metal–metal bond distance, Os(1)–Os(2) = 2.843(1) Å, is no longer than that of a normal Os–Os single bond, 2.877(3) Å.[12] It is possible the usual bond lengthening effect produced by hydride ligands may be counteracted by the bridging benzothienyl ligand. The hydride ligand in **5** occupied a similar position.[9]

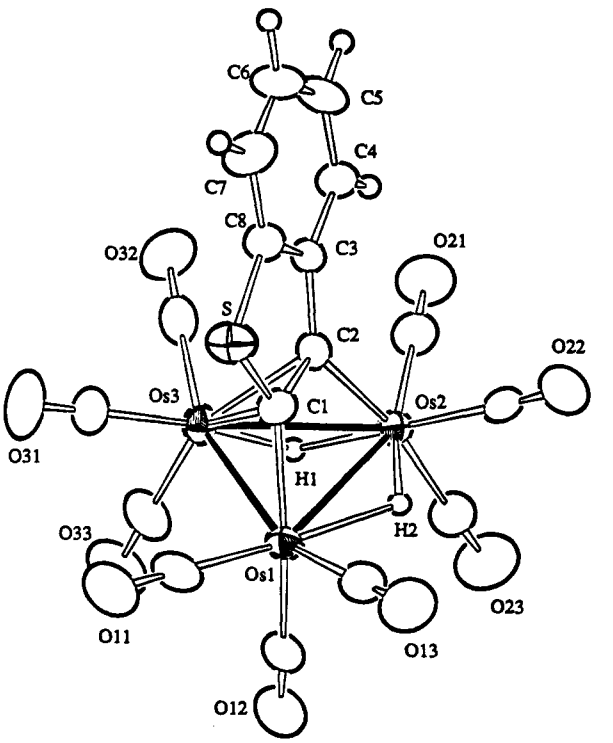

Figure 2. ORTEP diagram of $Os_3(CO)_9(\mu_3\text{-}\overline{SCCC_6H_5})(\mu\text{-H})_2$, **2**, showing 50% probability thermal ellipsoids.

Compound **1** is a precursor to **2**, and **2** was obtained in 80% yield when octane solutions of **1** were heated to reflux (125 °C) for 30 min. An ORTEP diagram of the molecular structure of compound **2** is shown in Figure 2. Final atomic positional parameters are listed in Table 5, and selected interatomic distances and angles are listed in Tables 6 and 7. This molecule also contains a closed triangular cluster of three osmium atoms but has only nine linear terminal carbonyl ligands, three on each metal atom. Compound **2** contains a benzothiophyne ligand formed by the cleavage of the carbon–hydrogen bond of the carbon of the coordinated C–C double bond and a transfer of the hydrogen atom to the cluster. The C(1)–C(2) bond in **2** is formally triple, but the C–C distance of 1.43(1) Å is longer than that of an uncoordinated triple bond as a result of the coordination. The ligand is coordinated to the face of the cluster through the C–C triple bond in the usual μ-|| or di-σ +

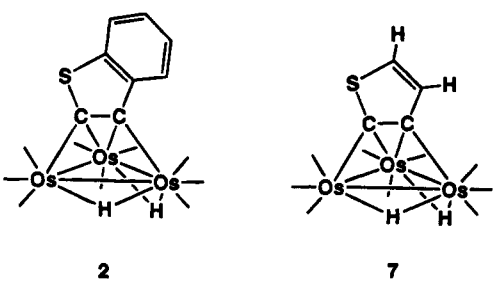

2 **7**

(9) Himmelreich, D.; Müller, G. *J. Organomet. Chem.* **1985**, *297*, 341.
(10) Arce, A. J.; Deeming, A. J.; De Sanctis, Y.; Machado, R.; Manzur, J.; Rivas, C. *J. Chem. Soc., Chem. Commun.* **1990**, 1568.
(11) (a) Deeming, A. J. *Adv. Organomet. Chem.* **1986**, *26*, 1. (b) Orpen, A. G.; Pippard, D.; Sheldrick, G. M. *Acta Crystallogr.* **1978**, *B34*, 2466. (c) Guy, J. J.; Reichert, B. E.; Sheldrick, G. M. *Acta Crystallogr.* **1976**, *B32*, 3319. (d) Sappa, E.; Tiripicchio, A.; Manotti, A. M. *J. Organomet. Chem.* **1983**, *249*, 391.
(12) Churchill, M. R.; DeBoer, B. G. *Inorg. Chem.* **1977**, *16*, 878.

Table 5. Positional Parameters and *B*(eq) Values (Å²) for 2

atom	*x*	*y*	*z*	*B*(eq)
Os(1)	0.80331(4)	0.12036(3)	0.21405(6)	3.13(2)
Os(1)	0.60719(4)	0.23345(3)	0.35926(6)	3.03(2)
Os(3)	0.91279(4)	0.27759(3)	0.45336(5)	3.03(2)
S	0.8622(3)	0.3105(2)	−0.0057(4)	4.2(1)
O(11)	1.087(1)	0.0947(6)	0.149(1)	6.8(5)
O(12)	0.829(1)	−0.0269(7)	0.464(1)	7.3(5)
O(13)	0.626(1)	0.0034(7)	−0.127(1)	7.3(4)
O(21)	0.530(1)	0.3971(6)	0.560(1)	6.8(5)
O(22)	0.342(1)	0.2135(7)	0.041(2)	7.9(5)
O(23)	0.477(1)	0.1029(8)	0.563(2)	9.1(6)
O(31)	1.190(1)	0.3173(7)	0.361(1)	7.3(5)
O(32)	0.933(1)	0.4733(6)	0.638(1)	5.6(4)
O(33)	1.059(1)	0.1748(7)	0.757(1)	7.9(5)
C(1)	0.797(1)	0.2521(7)	0.140(1)	3.5(4)
C(2)	0.727(1)	0.3118(7)	0.231(1)	2.9(4)
C(3)	0.723(1)	0.4031(6)	0.169(1)	2.7(4)
C(4)	0.664(1)	0.4801(7)	0.221(1)	3.9(5)
C(5)	0.676(1)	0.5614(8)	0.152(2)	4.7(5)
C(6)	0.747(1)	0.5705(8)	0.033(2)	5.1(5)
C(7)	0.805(1)	0.4967(9)	−0.026(2)	4.9(5)
C(8)	0.794(1)	0.4120(7)	0.043(1)	3.3(4)
C(11)	0.979(1)	0.1041(8)	0.172(2)	4.8(5)
C(12)	0.818(1)	0.0237(9)	0.369(2)	4.7(5)
C(13)	0.591(1)	0.0468(8)	0.003(2)	5.0(5)
C(21)	0.558(1)	0.3373(8)	0.483(2)	4.3(5)
C(22)	0.438(1)	0.2201(7)	0.162(2)	4.6(5)
C(23)	0.525(1)	0.1491(9)	0.488(2)	5.0(5)
C(31)	1.086(1)	0.3039(8)	0.396(2)	4.3(5)
C(32)	0.928(1)	0.3990(9)	0.572(1)	3.7(5)
C(33)	1.006(1)	0.213(1)	0.642(2)	5.1(5)

Table 6. Intramolecular Distances for 2[a]

Os(1)−Os(2)	3.0581(7)	C(1)−C(2)	1.43(1)
Os(1)−Os(3)	2.7600(7)	C(2)−C(3)	1.46(1)
Os(1)−C(1)	2.07(1)	Os−C(av)	1.92(1)
Os(2)−Os(3)	2.8522(7)	C−O(av)	1.14(1)
Os(2)−C(2)	2.12(1)	Os(1)−H(2)	1.96
Os(3)−C(1)	2.42(1)	Os(2)−H(1)	1.77
Os(3)−C(2)	2.27(1)	Os(2)−H(2)	1.60
S−C(1)	1.75(1)	Os(1)−H(1)	1.82
S−C(8)	1.74(1)		

[a] Distances are in angstroms. Estimated standard deviations in the least significant figure are given in parentheses.

Table 7. Intramolecular Bond Angles for 2[a]

Os(2)−Os(1)−Os(3)	58.44(2)	C(1)−C(2)−C(3)	111.5(9)
Os(1)−Os(2)−Os(3)	55.54(2)	C(2)−C(3)−C(8)	112.6(8)
Os(1)−Os(3)−Os(2)	66.01(2)	S−C(8)−C(3)	112.0(7)
C(1)−S−C(8)	92.7(5)	Os−C(av)−O	177(1)
S−C(1)−C(2)	111.1(7)		

[a] Angles are in degrees. Estimated standard deviations in the least significant figure are given in parentheses.

π mode. The thiophyne ligand in the complex $Os_3(CO)_9(\mu_3\text{-}\overline{SCCCHCH})(\mu\text{-}H)_2$, **7**,[13,14] that was formed by the decarbonylations of **6**[10] and the μ-acyl complex $Os_3(CO)_{10}(\mu\text{-}O{=}CC\overline{SCHCHCH})(\mu\text{-}H)$, **8**, is similarly coordinated. Compound **7** has been characterized crystallographically also. The Os−C σ-bond distances, Os(1)−C(1) = 2.07(1) Å and Os(2)−C(2) = 2.12(1) Å, are similar to those found in **7**, 2.14(2) Å [2.16(2) Å] and 2.13(2) Å [2.17(2) Å], respectively. The Os−C π-bonding is quite unsymmetrical, Os(3)−C(1) = 2.42(1) Å and Os(3)−C(2) = 2.27(1) Å, but similar asymmetry was found in **7**, 2.43(2) Å [2.46(2) Å] and 2.31(2) Å [2.23(2) Å] with the longest Os−C bond being to the sulfur-substituted carbon atom, as found in **2**. Compound **2** contains two hydride ligands. They were located in reasonable positions as bridges across the Os(1)−Os(2) and Os(2)−Os(3) bonds, but they could not be refined to convergence and were fixed in the final analysis. Although they are inequivalent, only one hydride resonance of intensity two was observed in the ^{1}H NMR spectrum, δ = −18.95 (2H). It is believed that the hydride ligands are dynamically averaged in the NMR spectrum at room temperature. A similar dynamical averaging of the inequivalent hydride ligands was also observed in **7**.[14]

(13) Arce, A. J.; De Sanctis, Y.; Deeming, A. J. *J. Organomet. Chem.* **1986**, *311*, 371.
(14) Deeming, A. J.; Arce, A. J.; De Sanctis, Y.; Day, M. W.; Hardcastle, K. I. *Organometallics* **1989**, *8*, 1408.

Table 8. Positional Parameters and *B*(eq) Values (Å²) for 3

atom	*x*	*y*	*z*	*B*(eq)
Os(1)	0.19110(8)	0.14994(5)	0.27477(5)	2.42(3)
Os(2)	0.43679(8)	−0.04318(5)	0.28044(5)	2.57(4)
Os(3)	0.25137(8)	0.03996(5)	0.13874(5)	2.55(4)
Br	0.2340(2)	0.0097(1)	0.3627(1)	3.04(9)
S	0.5522(5)	0.0965(3)	0.2961(3)	2.5(2)
O(11)	0.131(2)	0.257(1)	0.423(1)	6(1)
O(12)	0.191(2)	0.307(1)	0.169(1)	5.2(8)
O(13)	−0.137(2)	0.108(1)	0.201(1)	5.7(9)
O(21)	0.624(2)	−0.110(1)	0.444(1)	5.2(8)
O(22)	0.652(2)	−0.088(1)	0.166(1)	4.8(8)
O(23)	0.273(2)	−0.212(1)	0.244(1)	5.8(9)
O(31)	0.359(2)	−0.078(1)	0.013(1)	6(1)
O(32)	0.013(2)	−0.083(1)	0.188(1)	5.0(8)
O(33)	−0.002(2)	0.121(1)	0.017(1)	5.0(8)
O(34)	0.468(2)	0.185(1)	0.1128(9)	4.7(8)
C(1)	0.422(2)	0.168(1)	0.330(1)	2.7(8)
C(2)	0.488(2)	0.208(1)	0.396(1)	2.6(9)
C(3)	0.636(2)	0.182(1)	0.432(1)	2.4(8)
C(4)	0.730(2)	0.211(1)	0.503(1)	4(1)
C(5)	0.870(2)	0.173(1)	0.526(1)	4(1)
C(6)	0.917(2)	0.108(1)	0.480(1)	4(1)
C(7)	0.828(2)	0.078(1)	0.408(1)	3(1)
C(8)	0.686(2)	0.116(1)	0.386(1)	2.3(8)
C(11)	0.154(2)	0.215(1)	0.368(1)	4(1)
C(12)	0.189(2)	0.246(1)	0.209(1)	3(1)
C(13)	−0.014(3)	0.123(1)	0.231(1)	4(1)
C(21)	0.555(2)	−0.086(1)	0.381(1)	3(1)
C(22)	0.572(2)	−0.074(1)	0.206(1)	3(1)
C(23)	0.337(2)	−0.150(2)	0.255(1)	4(1)
C(31)	0.321(2)	−0.038(2)	0.062(1)	4(1)
C(32)	0.103(2)	−0.040(1)	0.171(1)	4(1)
C(33)	0.098(2)	0.094(1)	0.063(1)	3(1)
C(34)	0.393(2)	0.130(1)	0.125(1)	3(1)

The reaction 1-bromobenzothiophene with $Os_3(CO)_{10}(NCMe)_2$ at 25 °C yielded two products: $Os_3(CO)_{10}(\mu\text{-}\overline{SCCHC_6H_5})(\mu\text{-Br})$, **3** (32%), and $Os_3(CO)_9(\mu_3\text{-}\overline{SCCHC_6H_5})(\mu\text{-Br})$, **4** (10%). Both products were characterized by IR, ^{1}H NMR, and single crystal X-ray diffraction analyses. An ORTEP diagram of the molecular structure of compound **3** is shown in Figure 3. Final atomic positional parameters are listed in Table 8, and selected interatomic distances and angles are listed in Tables 9 and 10. This molecule contains an open triangular cluster of three osmium atoms with ten linear terminal carbonyl ligands. There are only two metal−metal bonds, Os(1)−Os(3) = 2.926(1) Å and Os(2)−Os(3) = 2.911(1) Å. There is a S-coordinated μ-η^2-benzothienyl ligand and bromo ligand that bridge the open edge of the cluster, Os(1)···Os(2) = 3.742(1) Å. Both of these ligands serve as three electron donors; thus, the cluster has a total of 50 valence electrons and in order for each of the metal atoms to have 18 electron configurations there can be no more than two metal−metal bonds between the three metal atoms. The osmium−sulfur bond distance of 2.411(5) Å is typical of the the os-

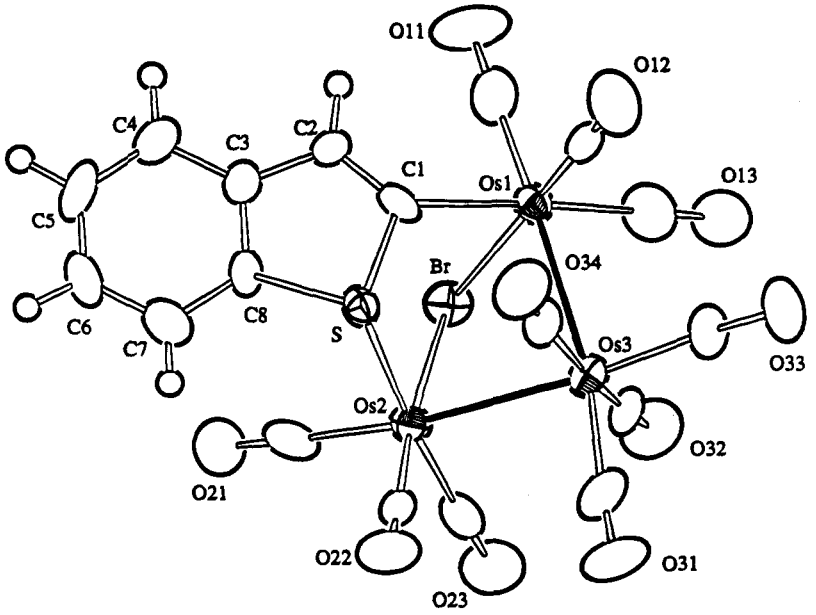

Figure 3. ORTEP diagram of $Os_3(CO)_{10}(\mu\text{-}\overline{SCCHC_6H_5})(\mu\text{-Br})$, **3**, showing 50% probability thermal ellipsoids.

Table 9. Intramolecular Distances for 3[a]

Os(1)–Os(3)	2.926(1)	C(3)–C(4)	1.40(3)
Os(1)–Br	2.602(2)	C(3)–C(8)	1.40(2)
Os(1)–C(1)	2.16(2)	C(4)–C(5)	1.39(3)
Os(2)–Os(3)	2.911(1)	C(5)–C(6)	1.38(3)
Os(2)–Br	2.600(2)	C(6)–C(7)	1.38(3)
Os(2)–S	2.411(5)	C(7)–C(8)	1.40(2)
S–C(1)	1.78(2)	Os–C(av)	1.91(2)
S–C(8)	1.76(2)	C–O(av)	1.14(2)
C(1)–C(2)	1.30(2)	Os(1)–Os(2)	3.742(1)
C(2)–C(3)	1.43(2)		

[a] Distances are in angstroms. Estimated standard deviations in the least significant figure are given in parentheses.

Table 10. Intramolecular Bond Angles for 3[a]

Os(3)–Os(1)–Br	83.94(5)	C(1)–C(2)–C(3)	118(2)
Os(3)–Os(1)–C(1)	95.3(5)	C(2)–C(3)–C(8)	112(2)
Br–Os(1)–C(1)	80.7(5)	C(4)–C(3)–C(8)	118(2)
Os(3)–Os(2)–Br	84.28(5)	C(3)–C(4)–C(5)	119(2)
Os(3)–Os(2)–S	82.2(1)	C(4)–C(5)–C(6)	122(2)
Br–Os(2)–S	89.8(1)	C(5)–C(6)–C(7)	121(2)
Os(1)–Os(3)–Os(2)	79.73(3)	C(6)–C(7)–C(8)	117(2)
Os(1)–Br–Os(2)	91.98(6)	S–C(8)–C(3)	109(1)
S–C(1)–C(2)	109(1)	Os–C(av)–O	176(2)

[a] Angles are in degrees. Estimated standard deviations in the least significant figure are given in parentheses.

mium–sulfur bond distances found in other S–C-bridged triosmium clusters (e.g. $Os_3(CO)_{10}(\mu\text{-}\overline{SCHCH_2CH_2CH_2})(\mu\text{-H})$, Os–S = 2.37(1) Å,[5] and $Os_3(CO)_9(PPh_3)(\mu\text{-}\overline{SCHCH_2CH_2CH_2})(\mu\text{-H})$, Os–S = 2.407(1) Å.[15] The S–C(1) distance, 1.78(2) Å, is typical of a carbon–sulfur single bond. The C(1)–C(2) bond is double, and the distance 1.30(2) Å is in accord with this assignment. There appear to be no previous reports of μ-S–C–η^2-thienyl or benzothienyl ligands. The bromide ligand symmetrically bridges the Os(1) and Os(2) atoms, Os(1)–Br = 2.602(2) Å and Os(2)–Br = 2.600(2) Å.

When heated to reflux in a heptane solution (97 °C), compound **3** was decarbonylated and transformed to **4** in 74% yield in 30 min. An ORTEP diagram of the molecular structure of compound **4** is shown in Figure 4. Final atomic positional parameters are listed in Table 11 and selected interatomic distances and angles are listed in Tables 12 and 13. This molecule also contains of a open triangular cluster of three osmium atoms but has only nine linear terminal carbonyl ligands, three on each metal atom. The metal–metal bonds, Os(1)–Os(3) = 2.8125(8) Å and Os(2)–Os(3) = 2.8873(8) Å, are shorter than those in **3** presumably because the benzothienyl ligand now bridges these bonds. However, the nonbonding Os(1)···Os(2) distance of 3.8798(8) Å is slightly longer than that in **3**. The benzothienyl ligand in **4** bridges all three metal atoms

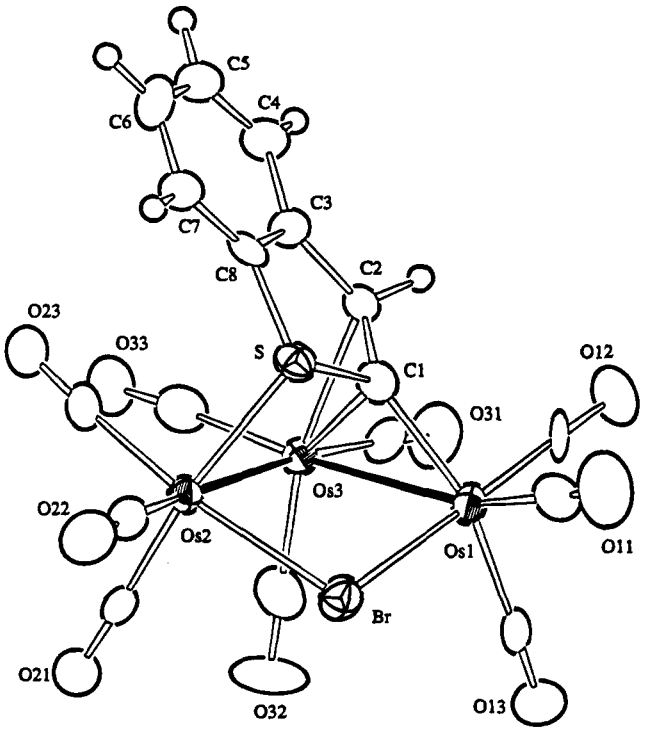

Figure 4. ORTEP diagram of $Os_3(CO)_9(\mu_3\text{-}\overline{SCCHC_6H_5})(\mu\text{-Br})$, **4**, showing 50% probability thermal ellipsoids.

(15) Glavee, G. N.; Daniels, L. M.; Angelici, R. J. *Organometallics* **1989**, *8*, 1856.

Table 11. Positional Parameters and *B*(eq) Values (Å²) for 4

atom	*x*	*y*	*z*	*B*(eq)
Os(1)	0.24807(7)	0.17113(3)	0.03962(3)	2.71(3)
Os(2)	0.26757(6)	0.32214(3)	0.21461(3)	2.29(2)
Os(3)	0.01307(6)	0.20397(3)	0.15622(3)	2.24(2)
Br	0.4735(2)	0.22711(9)	0.13700(8)	3.34(7)
S	0.2102(4)	0.3808(2)	0.0894(2)	2.7(2)
O(11)	0.494(2)	0.222(1)	−0.0849(7)	7.3(8)
O(12)	−0.017(1)	0.1051(7)	−0.0698(6)	5.6(6)
O(13)	0.372(2)	−0.0127(7)	−0.0721(6)	5.2(6)
O(21)	0.335(1)	0.2203(6)	0.3585(6)	4.7(6)
O(22)	0.567(1)	0.4443(6)	0.2586(6)	4.6(6)
O(23)	−0.013(1)	0.4280(7)	0.2848(6)	4.2(5)
O(31)	−0.225(1)	0.0655(7)	0.0902(6)	5.2(6)
O(32)	0.205(1)	0.0742(7)	0.2535(7)	6.0(7)
O(33)	−0.242(1)	0.2614(7)	0.2765(6)	4.3(5)
C(1)	0.109(2)	0.2816(8)	0.0590(7)	2.7(6)
C(2)	−0.069(2)	0.2965(8)	0.0553(7)	2.4(6)
C(3)	−0.120(2)	0.3862(8)	0.0723(7)	2.4(6)
C(4)	−0.284(2)	0.4223(9)	0.0673(8)	3.1(7)
C(5)	−0.300(2)	0.506(1)	0.0843(8)	3.7(8)
C(6)	−0.167(2)	0.559(1)	0.1052(8)	4.3(8)
C(7)	0.000(2)	0.5245(8)	0.1085(8)	3.7(8)
C(8)	0.014(2)	0.4382(8)	0.0922(7)	2.8(6)
C(11)	0.402(2)	0.199(1)	−0.039(1)	4.3(8)
C(12)	0.081(2)	0.1312(9)	−0.0282(7)	3.3(7)
C(13)	0.330(2)	0.054(1)	0.0590(7)	3.2(7)
C(21)	0.307(2)	0.2564(9)	0.3036(8)	3.0(7)
C(22)	0.456(2)	0.401(1)	0.2385(8)	3.3(7)
C(23)	0.098(2)	0.3897(9)	0.2601(7)	2.9(7)
C(31)	−0.140(2)	0.119(1)	0.1128(8)	3.3(7)
C(32)	0.135(2)	0.124(1)	0.2170(8)	3.5(7)
C(33)	−0.145(2)	0.244(1)	0.2298(9)	3.5(7)

Table 12. Intramolecular Distances for 4[a]

Os(1)−Os(3)	2.8125(8)	C(2)−C(3)	1.48(2)
Os(1)−Br	2.598(1)	C(3)−C(4)	1.39(2)
Os(1)−C(1)	2.06(1)	C(3)−C(8)	1.36(2)
Os(2)−Os(3)	2.8873(8)	C(4)−C(5)	1.34(2)
Os(2)−Br	2.583(2)	C(5)−C(6)	1.37(2)
Os(2)−S	2.427(3)	C(6)−C(7)	1.41(2)
Os(3)−C(1)	2.23(1)	C(7)−C(8)	1.38(2)
Os(3)−C(2)	2.37(1)	Os−C(av)	1.91(2)
S−C(8)	1.77(1)	C−O(av)	1.14(2)
C(1)−C(2)	1.41(2)	Os(1)···Os(2)	3.8798(8)

[a] Distances are in angstroms. Estimated standard deviations in the least significant figure are given in parentheses.

Table 13. Intramolecular Bond Angles for 4[a]

Os(3)−Os(1)−Br	84.08(4)	C(4)−C(3)−C(8)	118(1)
Os(3)−Os(2)−Br	82.85(3)	C(3)−C(4)−C(5)	118(1)
Os(3)−Os(2)−S	78.07(8)	C(4)−C(5)−C(6)	125(1)
Os(1)−Os(3)−Os(2)	85.79(2)	C(5)−C(6)−C(7)	119(1)
Os(1)−Br−Os(2)	97.00(5)	C(6)−C(7)−C(8)	116(1)
S−C(1)−C(2)	107(1)	C(3)−C(8)−C(7)	125(1)
C(1)−C(2)−C(3)	114(1)	Os−C(av)−O	176(1)
C(2)−C(3)−C(8)	114(1)		

[a] Angles are in degrees. Estimated standard deviations in the least significant figure are given in parentheses.

by using sulfur atom and the C−C double bond C(1)−C(2) in the five-membered ring. The sulfur atom is bonded to Os(2) as in **3**, Os(2)−S = 2.427(3) Å, and the C(1)−C(2) double bond has a μ-η^2 σ + π coordination across the Os(1)−Os(2) bond with C(1) σ-bonded to Os(1), Os(1)−C(1) = 2.06(1) Å, and C(1) and C(2) π-bonded to Os(3), Os(3)−C(1) = 2.23(1) Å and Os(3)−C(2) = 2.37(1) Å. The C(1)−C(2) distance of 1.41(2) Å in **4** is significantly longer than that in **3** as a result of the effect of coordination. There appear to be no previous reports of μ-S-C-η^2-thienyl or benzothienyl ligands. The Os−Br distances, Os(1)−Br = 2.598(1) Å and Os(2)−Br = 2.583(2) Å, are similar to those in **3**. The benzothienyl ligand in **4** serves formally as a 5 electron donor, but the cluster with one less CO ligand still has a total of 50 valence electrons just as in **3**.

Scheme 1

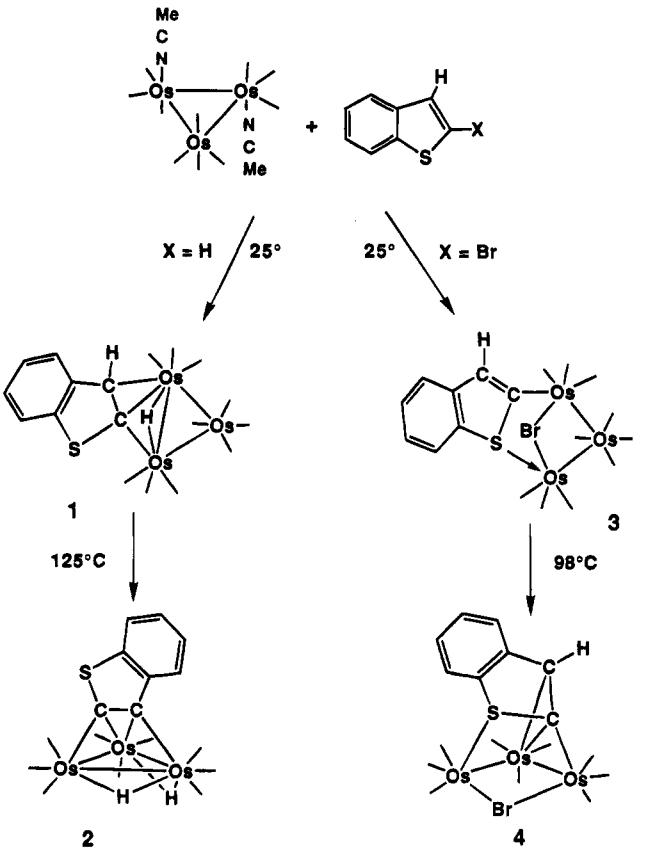

A summary of the results of this study is shown in Scheme 1. Both benzothiophene and 1-bromobenzothiophene react with $Os_3(CO)_{10}(NCMe)_2$ at 25 °C by displacement of the two NCMe ligands and oxidative addition of the benzothiophene at the C−X bond to form the benzothienyl triosmium complexes **1** and **3**, X = H and Br, respectively. The higher yield of **3** relative to **1** can probably be attributed to a higher reactivity of the C−Br bond in the 1-bromobenzothiophene compared to the C−H bond in benzothiophene, itself. In both reactions the X atom is transferred to the cluster and becomes a bridging ligand. Likewise, the benzothienyl ligand becomes a bridging ligand in each cluster. Interestingly, however the benzothienyl ligands bridge the clusters in two different ways in **1** and **3**. This is probably related to the distance between the two metal atoms that are bridged. In **1** the metal atoms are separated at a normal bonding distance, whereas in **3** the metal−metal bond was cleaved and the bridged metal atoms are 0.90 Å farther apart than those in **1**. As a result, the benzothienyl ligand cannot adequately bridge these two metal atoms in **3** using the C−C double bond in the usual σ + π coordination mode since one of the carbon atoms C(1) must be bonded to both metal atoms, and the metal atoms are simply too far apart to form a stable strucutre. Instead the benzothienyl in **3** adopted a configuration that uses two atoms to span the metal atoms, the sulfur atom, and neighboring carbon atom.

Both **1** and **3** undergo loss of on CO ligand when heated. The transformation of **3** leads to the formation

of a triply bridging benzothienyl ligand serving as a five electron donor by engaging the uncoordinated C–C double bond. In contrast the decarbonylation of **1** does not result in coordination of the sulfur atom but instead results in the oxidative addition of the remaining C–H bond on the carbon of the coordinated C–C double bond.

Unlike the reaction of benzothiophene with $Fe_3(CO)_{12}$[4b,c] and $Ru_3(CO)_{12}$,[4e] we have found no evidence for ring opening in the formation of compounds **1** and **2** or in their transformations into compounds **3** and **4** under the conditions that we have used. Likewise, it was reported that there was no evidence for ring opening of the thiophene ring in studies of the reactions of thiophene with $Os_3(CO)_{10}(NCMe)_2$.[10]

Acknowledgment. This research was supported by the Office of Basic Energy Sciences of the U.S. Department of Energy.

Supplementary Material Available: Tables of hydrogen atom positional and thermal parameters and anisotropic thermal parameters for all three structural analyses (10 pages). Ordering information is given on any current masthead page.

OM950011E

Synthesis, Structure, and Properties of the η^2 P⌒O-Chelated Mono(ether–phosphine)ruthenium Complex [Cp*Ru(CO)(P⌒O)][BPh$_4$]

Ekkehard Lindner,* Michael Haustein, Hermann A. Mayer, Karlheinz Gierling, Riad Fawzi, and Manfred Steimann

Institut für Anorganische Chemie der Universität, Auf der Morgenstelle 18, D-72076 Tübingen, Germany

Received September 12, 1994[⊗]

The 16-electron complex Cp*RuCl(P∼O) (**2**; Cp* = η^5-C_5Me_5; P∼O = η^1(P)-coordinated ligand) was synthesized by reaction of oligomeric [Cp*RuCl$_2$]$_n$ (**1**) with the basic ether–phosphine $(C_6H_{11})_2PCH_2CH_2OCH_3$ (O,P) in the presence of zinc. Carbonylation of **2** afforded the chloro carbonyl species Cp*RuCl(CO)(P∼O) (**3**), which was converted into the cationic, monochelated compound [Cp*Ru(CO)(P⌒O)][BPh$_4$] (**4**[BPh$_4$]; P⌒O = η^2(O,P)-chelated ligand) by chloride abstraction with NaBPh$_4$. The structure of **4** was elucidated by a single-crystal X-ray structural analysis. **4** crystallizes in the monoclinic space group $P2_1/c$ with $Z = 4$. The cell dimensions are $a = 11.739(3)$ Å, $b = 17.620(5)$ Å, $c = 22.919(6)$ Å, and $\beta = 98.80(2)°$. The cleavage of the Ru–O bond was achieved by 2 bar pressure of carbon monoxide, resulting in the formation of the dicarbonyl complex [Cp*Ru(CO)$_2$(P∼O)][BPh$_4$] (**5**[BPh$_4$]). By treatment of **4** with triphenylphosphine the mixed-phosphine derivative [Cp*Ru(CO)(P∼O)(PPh$_3$)][BPh$_4$] (**6**[BPh$_4$]) was formed. A single-crystal X-ray structural determination of **6** shows that it crystallizes in the monoclinic space group *Cc* with $Z = 4$. The cell dimensions are $a = 25.683(6)$ Å, $b = 15.496(4)$ Å, $c = 15.653(7)$ Å, and $\beta = 110.96(3)°$.

Introduction

The interest in coordinatively unsaturated transition-metal complexes stems from the fact that they represent very reactive intermediates in catalytically operating processes. The introduction of bifunctional ether–phosphines (O,P) instead of "classical" tertiary phosphines has significantly affected the isolation and thus the examination of such undercoordinated species.[1] These ligands are provided with oxygen atoms incorporated in open-chain or cyclic ether moieties which form a weak metal–oxygen contact while the phosphorus atom is strongly coordinated to the central atom. From this "hemilabile" character, it has been reported that the ether oxygen donor may be regarded as an intramolecular solvent molecule stabilizing the empty coordination site and hence make these complexes much more stable than simple solvent adducts.[1] In a recent study we investigated half-sandwich cyclopentadienyl- and (pentamethylcyclopentadienyl)ruthenium(II) complexes containing monodentate (P∼O) and bidentate (P⌒O) ether–phosphines (P∼O = η^1(P)-coordinated ligand; P⌒O = η^2 (O,P)-chelated ligand) in order to obtain experimental information about the ruthenium–oxygen bond strength in these systems.[2] The strength of the metal–oxygen bond is responsible for the ease of the dissociation of the O,P chelating ligand and hence for the reactivity of the complex toward an incoming substrate. As one result of these studies we observed a significant decrease of the Ru–O interaction by replacement of the Cp with the more basic, electron-donating Cp* ligand.[2] In addition we determined the different chelating abilities of a variety of diphenyl(ether–phosphine) ligands in dependence on the kind of ether moiety, the ring size of the cyclic ethers, and the number and position of the ether atoms in the ring via ^{31}P DNMR spectroscopy and line-shape analyses.[2] The last target was now to clear up the influence of the phosphorus basicity on the Ru–O bond strength in complexes of this type. The use of the basic O,P ligand $Cy_2PCH_2CH_2OCH_3$ has already been reported to be responsible for a weaker metal–oxygen bond in Rh(III) complexes, compared to the case for the diphenyl analogues.[3] Therefore, the present paper reports the synthesis and structure of the η^2(O,P)-chelated complex [Cp*Ru(CO)(P⌒O)][BPh$_4$] (**4**[BPh$_4$]; O,P = $Cy_2PCH_2CH_2OCH_3$). In order to examine the reactivity of the Ru–O bond, complex **4** was allowed to react with carbon monoxide and triphenylphosphine.

Experimental Section

General Procedures. All manipulations were carried out under an atmosphere of argon by use of standard Schlenk techniques. Solvents were dried over appropriate reagents and stored under argon. IR data were obtained with a Bruker IFS 48 instrument. FD mass spectra were taken on a Finnigan MAT 711 A instrument (8 kV, 60 °C), modified by AMD; FAB mass spectra were recorded on a Finnigan MAT TSQ 70 (10 kV, 50 °C). Elemental analyses were performed with a Carlo Erba 1106 analyzer; Cl analyses were carried out according to Schöniger[4] and analyzed as described by Dirscherl and Erne.[5] Ru was determined according to the literature.[6] ^{31}P-

[⊗] Abstract published in *Advance ACS Abstracts,* April 15, 1995.

(1) Bader, A.; Lindner, E. *Coord. Chem. Rev.* **1991**, *108*, 27.
(2) Lindner, E.; Haustein, M.; Mayer, H. A.; Kühbauch, H.; Vrieze, K.; de Klerk-Engels, B. *Inorg. Chim. Acta* **1994**, *215*, 165.
(3) Lindner, E.; Wang, Q.; Mayer, H. A.; Fawzi, R.; Steimann, M. *Organometallics* **1993**, *12*, 1865.
(4) (a) Schöniger, W. *Microchim. Acta* **1955**, 123. (b) Schöniger, W. *Microchim. Acta* **1956**, 869.
(5) Dirscherl, A.; Erne, F. *Microchim. Acta* **1961**, 866.

0276-7333/95/2314-2246$09.00/0

{^{1}H} NMR spectra were measured on a Bruker AC 80 spectrometer operating at 32.44 MHz; the external standard (coaxial insert) at low temperatures (0 to −80 °C) was 1% H_3PO_4 in acetone-d_6 and above 0 °C was 1% H_3PO_4 in D_2O. ^{13}C{^{1}H} NMR spectra were measured on Bruker DRX 250 and Bruker AMX 400 spectrometers at 62.90 and 100.62 MHz, respectively. ^{13}C chemical shifts were measured relative to partially deuterated solvent peaks which are reported relative to TMS. The ^{1}H/^{31}P HETCOR spectrum of compound **6** was recorded on a Bruker AMX 400 spectrometer (400.14 MHz for ^{1}H, 161.98 MHz for ^{31}P) using a standard pulse sequence.[7] The starting compounds $[Cp^*RuCl_2]_n$ (**1**)[8] and $(C_6H_{11})_2PCH_2CH_2OCH_3$ (O,P)[9] were prepared as described in the literature.

Chloro[dicyclohexyl(2-methoxyethyl)phosphine-*P*](pentamethylcyclopentadienyl) ruthenium(II) (2). To a solution of $[Cp^*RuCl_2]_n$ (**1**; 1.0 g, 3.26 mmol) in toluene (30 mL) were added 836 mg (3.26 mmol) of the ligand $(C_6H_{11})_2PCH_2CH_2OCH_3$ (O,P) and zinc (1.0 g). After it was stirred for 4 h at 60 °C, the dark reaction mixture had turned color to dark purple. $ZnCl_2$ and excess Zn were separated by filtration (G3). After concentration of the solution under reduced pressure to ~10 mL, the reaction mixture was purified by column chromatography on activated silica gel (length of the column 25 cm). With *n*-hexane/diethyl ether (1/1) a dark purple fraction was eluted which contained pure **2**. The solvent was removed completely and the residue was dried under vacuum to give 551 mg (32%) of a dark purple precipitate, which was very air-sensitive: mp 62 °C dec; MS (FAB, 50 °C) *m/e* 528 [M$^+$]. Anal. Calcd (found) for $C_{25}H_{44}ClOPRu$: C, 56.86 (56.52); H, 8.40 (8.22); Cl, 6.71 (6.67); Ru, 19.14 (18.92). ^{31}P{^{1}H} NMR (32.44 MHz, toluene, −30 °C): δ 36.6 (s). ^{13}C{^{1}H} NMR (62.90 MHz, C_6D_6, 22 °C): δ 75.6 (s, C_5Me_5), 70.1 (s, CH_2O), 59.7 (s, OCH_3), 34.2 (d, $^1J_{PC}$ = 18.2 Hz, PCH), 29.6−26.5 (m, CH_2 of C_6H_{11}), 23.2 (d, $^1J_{PC}$ = 16.4 Hz, PCH_2), 11.0 (s, C_5Me_5).

Carbonylchloro[dicyclohexyl(2-methoxyethyl)phosphine-*P*](pentamethylcyclopentadienyl)ruthenium(II) (3). Carbon monoxide was bubbled into a solution of **2** (550 mg, 1.04 mmol) in 20 mL of toluene at ambient temperature. The solution was stirred for 10 min resulting in a dark yellow color. After concentration of the solution to ~10 mL under reduced pressure, the reaction mixture was purified by column chromatography on activated silica gel (length of the column 20 cm). With *n*-hexane/diethyl ether (1/1) a yellow fraction was eluted which contained pure **3**. The solvent was removed under vacuum. Compound **3** was obtained as a yellow air-stable powder after recrystallization from methanol: yield 486 mg (84%); mp 154 °C; MS (FD, 60 °C) *m/e* 557 [M$^+$]. Anal. Calcd (found) for $C_{26}H_{44}ClO_2PRu$: C, 56.16 (55.81); H, 7.98 (8.21); Cl, 6.38 (6.65); Ru, 18.17 (17.84). IR (KBr, cm^{-1}): ν(CO) 1920 (vs). ^{31}P{^{1}H} NMR (32.44 MHz, CH_2Cl_2, −30 °C): δ 38.1 (s). ^{13}C{^{1}H} NMR (100.62 MHz, $CDCl_3$, 22 °C): δ 207.9 (d, $^2J_{PC}$ = 20.0 Hz, CO), 95.6 (s, C_5Me_5), 69.1 (s, CH_2O), 58.3 (s, OCH_3), 37.3 (d, $^1J_{PC}$ = 22.3 Hz, PCH), 29.7−26.2 (m, CH_2 of C_6H_{11}), 23.6 (d, $^1J_{PC}$ = 21.1 Hz, PCH_2), 10.1 (s, C_5Me_5).

Carbonyl[dicyclohexyl(2-methoxyethyl)phosphine-*O,P*](pentamethylcyclopentadienyl)ruthenium(II) Tetraphenylborate (4[BPh$_4$]). To a solution of **3** (500 mg, 0.90 mmol) in 20 mL of dichloromethane was added $NaBPh_4$ (308 mg, 0.90 mmol) in one portion. The reaction mixture was stirred for 3 days at ambient temperature. After removal of the solvent under vacuum the residue was redissolved in 20 mL of dichloromethane. NaCl was separated by filtration (G4). The solvent was again completely removed under vacuum. The residue was stirred in 20 mL of *n*-pentane to give a yellow air-stable powder, which was collected by filtration (G3) and dried in vacuo: yield 711 mg (94%); mp 148−150 °C; MS (FD, 60 °C) *m/e* 521 [M$^+$ − BPh_4]. Anal. Calcd (found) for $C_{50}H_{64}BO_2PRu$: C, 71.50 (71.26); H, 7.68 (7.84); Ru, 12.03 (11.74). IR (KBr, cm^{-1}): ν(CO) 1940 (vs). ^{31}P{^{1}H} NMR (32.44 MHz, CH_2Cl_2, −30 °C): δ 56.8 (s). ^{13}C{^{1}H} NMR (100.62 MHz, CD_2Cl_2, 22 °C): δ 205.4 (d, $^2J_{PC}$ = 16.5 Hz, CO), 164.6 (q, $^1J_{CB}$ = 48.3 Hz, *ipso*-C of BPh_4), 136.5−122.2 (m, CPh), 96.2 (s, C_5Me_5), 78.5 (s, CH_2O), 71.0 (s, OCH_3), 38.1, 35.0 (d, $^1J_{PC}$ = 26.7 and 19.1 Hz, PCH), 29.7−26.4 (m, CH_2 of C_6H_{11}), 22.6 (d, $^1J_{PC}$ = 21.6 Hz, PCH_2), 10.9 (s, C_5Me_5).

Dicarbonyl[dicyclohexyl(2-methoxyethyl)phosphine-*P*](pentamethylcyclopentadienyl)ruthenium(II) Tetraphenylborate (5[BPh$_4$]). A solution of **4** (300 mg, 0.36 mmol) in 10 mL of dichloromethane was treated with carbon monoxide (2 bar) at ambient temperature. The solution turned from yellow to colorless within 30 min. Subsequently the solvent was removed under vacuum. The residue was stirred in 20 mL of *n*-pentane to give a white air-stable powder, which was collected by filtration (G3) and dried in vacuo: yield 312 mg (100%); mp 206 °C; MS (FD, 60 °C) *m/e* 549 [M$^+$ − BPh_4]. Anal. Calcd (found) for $C_{51}H_{64}BO_3PRu$: C, 70.58 (70.92); H, 7.43 (7.62); Ru, 11.65 (11.38). IR (CH_2Cl_2, cm^{-1}): ν(CO) 2043 (vs), 1994 (vs). ^{31}P{^{1}H} NMR (32.44 MHz, CH_2Cl_2, −30 °C): δ 46.6 (s). ^{13}C{^{1}H} NMR (100.62 MHz, CD_2Cl_2, 22 °C): δ 199.7 (d, $^2J_{PC}$ = 15.3 Hz, CO), 164.4 (q, $^1J_{CB}$ = 49.6 Hz, *ipso*-C of BPh_4), 136.3−122.0 (m, CPh), 103.1 (s, C_5Me_5), 67.9 (s, CH_2O), 58.7 (s, OCH_3), 38.3 (d, $^1J_{PC}$ = 24.2 Hz, PCH), 29.9−26.1 (m, CH_2 of C_6H_{11}), 25.1 (d, $^1J_{PC}$ = 26.7 Hz, PCH_2), 10.6 (s, C_5Me_5).

Carbonyl[dicyclohexyl(2-methoxyethyl)phosphine-*P*](pentamethylcyclopentadienyl)(triphenylphosphine)ruthenium(II) Tetraphenylborate (6[BPh$_4$]). To a solution of **4** (500 mg, 0.60 mmol) in 20 mL of dichloromethane was added PPh_3 (315 mg, 1.20 mmol). The reaction mixture was stirred for 1 h at ambient temperature. Excess PPh_3 was separated by column chromatography on activated silica gel (length of the column 20 cm) with diethyl ether as eluent. The pale yellow fraction which contained pure **6** was eluted with dichloromethane/diethyl ether (1/1) and evaporated to dryness. The residue was stirred in 20 mL of *n*-pentane to give a pale yellow air-stable powder, which was collected by filtration (G3) and dried in vacuo: yield 602 mg (91%); mp 168−169 °C; MS (FD, 60 °C) *m/e* 783 [M$^+$ − BPh_4]. Anal. Calcd (found) for $C_{68}H_{79}BO_2P_2Ru$: C, 74.02 (73.78); H, 7.22 (7.36); Ru, 9.17 (9.39). IR (KBr, cm^{-1}): ν(CO) 1939 (vs). ^{31}P{^{1}H} NMR (32.44 MHz, $CHCl_3$, 33 °C): δ 47.1 (d, $^2J_{PP}$ = 26.9 Hz, PPh_3), 30.9 (d, $^2J_{PP}$ = 26.9 Hz, P∼O). ^{13}C{^{1}H} NMR (100.62 MHz, CD_2Cl_2, 22 °C): δ 209.1 (dd, $^2J_{PC}$ = 17.2 Hz, CO), 164.5 (q, $^1J_{CB}$ = 49.6 Hz, *ipso*-C of BPh_4), 136.6−122.0 (m, CPh), 101.3 (s, C_5Me_5), 68.3 (s, CH_2O), 58.5 (s, OCH_3), 38.4, 37.7 (d, $^1J_{PC}$ = 22.9 and 19.1 Hz, PCH), 29.3−26.0 (m, CH_2 of C_6H_{11}), 24.9 (d, $^1J_{PC}$ = 20.3 Hz, PCH_2), 10.9 (s, C_5Me_5).

Crystallographic Analyses. Single crystals of **4** were grown from a 2/1 diethyl ether/dichloromethane solvent mixture at −30 °C. Single crystals of **6** were obtained by slow diffusion of diethyl ether into a concentrated dichloromethane solution at ambient temperature. Both crystals were mounted on a glass fiber and transferred to a P4 Siemens diffractometer, using graphite-monochromated Mo Kα radiation. The lattice constants were determined with 25 precisely centered high-angle reflections and refined by least-squares methods. The final cell parameters and specific data collection parameters for **4** and **6** are summarized in Table 1. Intensities were collected with the ω-scan technique with scan speed varying from 8 to 30° min^{-1} in ω. Scan ranges for **4** and **6** were 1.5 and 1.0°, respectively. All structures were solved by Patterson methods[10] and refined by least squares with anisotropic thermal parameters for all non-hydrogen atoms. Hydrogen atoms were included in calculated positions (riding model). Maximum and minimum peaks in the final difference synthe-

(6) Lindner, E.; Bader, A.; Mayer, H. A. Z. *Anorg. Allg. Chem.* **1991**, *598/599*, 235.
(7) Bax, A.; Subramanian, S. *J. Magn. Reson.* **1986**, *67*, 565.
(8) Oshima, N.; Suzuki, H.; Moro-Oka, Y. *Chem. Lett.* **1984**, 1161.
(9) Lindner, E.; Meyer, S.; Wegner, P.; Karle, B.; Sickinger, A.; Steger, B. *J. Organomet. Chem.* **1987**, *335*, 59.
(10) Sheldrick, G. M. SHELXL 93 program; University of Göttingen, Göttingen, Germany, 1993.

Table 1. Crystal Data and Refinement Details for Compounds 4 and 6

compd	4[BPh_4]·H_2O	6[BPh_4]
formula	$C_{50}H_{64}BO_2PRu$	$C_{68}H_{79}BO_2P_2Ru$
fw	857.9	1102.1
color	red plates	yellow plates
cryst dimens	0.15 × 0.3 × 0.3	0.15 × 0.2 × 0.2
cryst syst	monoclinic	monoclinic
space group	$P2_1/c$	Cc
a, Å	11.739(3)	25.683(6)
b, Å	17.620(5)	15.496(4)
c, Å	22.919(6)	15.653(7)
β, deg	98.80(2)	110.96(3)
V, Å^3	4685(2)	5817(3)
Z	4	4
d_{calcd}, g cm^{-3}	1.216	1.259
T, °C	−100	−100
F(000), e	1816	2328
μ(Mo K$_\alpha$), mm^{-1}	0.405	0.373
2θ limits, deg	4−50	4−50
no. of rflns measd	16 452	11 761
no. of unique data with $I \geq 2\sigma(I)$	5511	4231
no. of variables	498	667
S	1.28	1.36
R1[a]	0.054	0.038
wR2[b]	0.135	0.080

[a] $R1 = \sum||F_o| - |F_c||/\sum|F_o|$. [b] $wR2 = [\sum[w(F_o^2 - F_c^2)^2]/[\sum[w(F_o^2)^2]]^{0.5}$.

sis were 2.24 and −1.31 e Å^{-3} (**4**), and 0.53 and −0.41 e Å^{-3} (**6**), respectively. The asymmetric unit of compound **4** contains one molecule of H_2O. The high maximum peak in the final difference Fourier map of **4** was located around the H_2O molecule. Final atomic coordinates are collected in Tables 2 and 3.

Results and Discussion

The generation of bis(ether−phosphine) derivatives Cp*RuCl(P∼O)$_2$ (P∼O = η^1(P)-coordinated diphenyl(ether−phosphine) was achieved by treatment of oligomeric [Cp*RuCl$_2$]$_n$ (**1**) with an excess of the O,P ligand in the presence of Zn.[2] No evidence for the formation of an analogous 18-electron complex with the basic and large ether-phosphine $Cy_2PCH_2CH_2OCH_3$ was obtained by following the same reaction pathway. Thus, the treatment of **1** with a stoichiometric amount and even with a 2-fold excess of this ligand resulted in the development of a dark purple color of the reaction mixture from which a dark purple precipitate analyzed as the very air-sensitive, 16-electron complex Cp*RuCl(P∼O) (**2**) (Scheme 1) can be isolated. This behavior is obviously due to the steric demand of the O,P ligand employed, which is in agreement with reports on the syntheses of mono(phosphine) complexes of the type Cp*RuCl(PR$_3$) (R = Cy, iPr, tBu).[11,12] Compound **2** reveals a single peak in the $^{31}P\{^1H\}$ NMR spectrum at 36.6 ppm. The ^{13}C NMR resonances of the methylene (δ_C 70.1) and the methyl group (δ_C 59.7) of the ether chain in **2** are quite comparable to those observed for Cp*RuCl(CO)(P∼O) (**3**) and are in the typical range of an η^1(P)-coordinated O,P ligand (*vide infra*). This is surprising, because the coordinatively unsaturated metal center in **2** would be expected to allow the bidentate O,P ligand to chelate, leading to a significant stabilization of the complex. However, the electron-rich ruthenium seems to prevent the contact of a further donor. Attempts to force the η^2(O,P) chelation at this system via chloride abstraction with NaBPh$_4$ failed, resulting in the decomposition of the compound.

The corresponding 16-electron complexes provided with "classical" tertiary phosphines have been reported to react with carbon monoxide, leading to stable, 18-electron species under mild reaction conditions.[11,12] Thus, the treatment of **2** with CO in toluene afforded the yellow air-stable compound Cp*RuCl(CO)(P∼O) (**3**) (Scheme 1), which was anticipated to be a suitable precursor for the generation of an η^2(O,P)-coordinated species. The η^1(P)-coordinated O,P ligand in complex

Table 2. Atomic Coordinates (×10^4, Esd's in Parentheses) of 4 with Equivalent Isotropic Displacement Coefficients (Å^2 × 10^3)[a]

atom	x	y	z	U_{eq}
Ru(1)	4033(1)	1722(1)	790(1)	22(1)
P(1)	2537(1)	2207(1)	1254(1)	26(1)
O(2)	2860(3)	227(2)	478(2)	41(1)
O(1)	2901(3)	2349(2)	80(1)	33(1)
B(1)	1416(4)	7669(3)	1573(2)	28(1)
C(1)	176(5)	6459(3)	1136(3)	42(1)
C(2)	−244(5)	5969(4)	677(3)	56(2)
C(3)	146(5)	6009(3)	141(3)	52(2)
C(4)	963(5)	6538(3)	72(2)	45(1)
C(5)	1371(4)	7029(3)	524(2)	39(1)
C(6)	995(4)	7012(3)	1082(2)	32(1)
C(7)	1183(4)	7995(3)	2685(2)	39(1)
C(8)	1235(4)	7820(4)	3283(2)	50(2)
C(9)	1416(4)	7086(5)	3482(2)	58(2)
C(10)	1553(5)	6524(4)	3079(3)	54(2)
C(11)	1512(4)	6692(4)	2487(2)	42(1)
C(12)	1321(4)	7435(3)	2260(2)	31(1)
C(13)	878(4)	8927(3)	941(2)	35(1)
C(14)	153(5)	9519(3)	728(2)	39(1)
C(15)	−907(4)	9610(3)	914(2)	42(1)
C(16)	−1225(4)	9100(3)	1322(2)	41(1)
C(17)	−492(4)	8506(3)	1530(2)	33(1)
C(18)	586(4)	8395(3)	1355(2)	29(1)
C(19)	3601(4)	7297(3)	1501(2)	33(1)
C(20)	4769(4)	7429(3)	1551(2)	40(1)
C(21)	5208(4)	8147(4)	1702(2)	43(1)
C(22)	4462(4)	8713(3)	1807(2)	42(1)
C(23)	3279(4)	8568(3)	1751(2)	35(1)
C(24)	2801(4)	7858(3)	1592(2)	30(1)
C(25)	1316(4)	2274(3)	648(2)	39(1)
C(26)	1675(4)	2187(3)	46(2)	37(1)
C(27)	3237(5)	2324(4)	−497(2)	49(1)
C(28)	3232(4)	824(3)	594(2)	29(1)
C(29)	1672(5)	3522(4)	1786(3)	54(2)
C(30)	1961(6)	4318(4)	2052(4)	69(2)
C(31)	2359(7)	4848(4)	1608(4)	70(2)
C(32)	3399(6)	4517(3)	1346(3)	59(2)
C(33)	3094(5)	3724(3)	1080(3)	43(1)
C(34)	2728(4)	3193(3)	1544(2)	36(1)
C(35)	2706(5)	1778(4)	2434(2)	44(1)
C(36)	2168(7)	1359(4)	2912(3)	62(2)
C(37)	1969(6)	530(4)	2759(3)	60(2)
C(38)	1218(5)	433(3)	2166(3)	45(1)
C(39)	1750(5)	841(3)	1683(2)	38(1)
C(40)	1948(4)	1686(3)	1834(2)	31(1)
C(41)	5731(3)	2354(3)	781(2)	28(1)
C(42)	5588(3)	2230(3)	1379(2)	29(1)
C(43)	5487(3)	1427(3)	1469(2)	28(1)
C(44)	5649(3)	1061(3)	929(2)	28(1)
C(45)	5768(3)	1632(3)	498(2)	28(1)
C(46)	5937(5)	3099(3)	507(3)	41(1)
C(47)	5683(4)	2815(3)	1858(2)	40(1)
C(48)	5511(4)	1023(3)	2047(2)	41(1)
C(49)	5800(4)	229(3)	854(2)	38(1)
C(50)	6095(4)	1503(3)	−105(2)	38(1)
O(3)	5000	5000	0	144(5)

[a] Equivalent isotropic U, defined as one-third of the trace of the orthogonalized $\mathbf{U}_{ij}$ tensor.

(11) Arliguie, T.; Border, C.; Chaudret, B.; Devillers, J.; Poilblanc, R. *Organometallics* **1989**, *8*, 1308.
(12) Campion, B. K.; Heyn, R. H.; Tilley, T. D. *J. Chem. Soc., Chem. Commun.* **1988**, 278.

Table 3. Atomic Coordinates (×10⁴, Esd's in Parentheses) of 6 with Equivalent Isotropic Displacement Coefficients (Å² × 10³)[a]

atom	x	y	z	U_{eq}
Ru(1)	10000(1)	8407(1)	0	18(1)
P(1)	10937(1)	8370(1)	51(1)	18(1)
P(2)	9961(1)	6882(1)	109(2)	22(1)
O(1)	10331(2)	8688(3)	2018(3)	36(1)
O(2)	12016(2)	7568(3)	2567(3)	31(1)
C(25)	10242(3)	8532(4)	1264(4)	23(1)
C(26)	10567(4)	6271(6)	1878(6)	51(2)
C(27)	10998(5)	5834(8)	2527(8)	83(4)
C(28)	11402(5)	5416(8)	2292(10)	92(5)
C(29)	11375(4)	5446(7)	1405(10)	78(4)
C(30)	10948(3)	5887(5)	738(7)	46(2)
C(31)	10537(3)	6302(5)	978(5)	35(2)
C(32)	9922(3)	5349(4)	−920(5)	30(2)
C(33)	9829(3)	4912(5)	−1741(6)	40(2)
C(34)	9661(3)	5342(5)	−2571(6)	40(2)
C(35)	9603(3)	6224(5)	−2581(5)	34(2)
C(36)	9706(3)	6682(5)	−1763(4)	26(1)
C(37)	9861(3)	6255(4)	−938(5)	25(2)
C(38)	9250(3)	6977(5)	1115(5)	30(2)
C(39)	8801(3)	6734(5)	1355(4)	35(2)
C(40)	8447(3)	6066(5)	887(5)	34(2)
C(41)	8555(3)	5641(5)	190(5)	31(2)
C(42)	9010(3)	5868(5)	−39(5)	30(2)
C(43)	9355(2)	6540(5)	415(4)	22(1)
C(44)	11568(3)	7316(4)	−812(5)	26(2)
C(45)	11505(3)	6766(5)	−1647(5)	36(2)
C(46)	11308(3)	7293(5)	−2523(5)	35(2)
C(47)	10765(3)	7749(5)	−2640(4)	31(2)
C(48)	10821(3)	8303(5)	−1805(4)	27(2)
C(49)	11012(3)	7761(4)	−933(4)	21(1)
C(50)	11805(3)	9513(4)	−14(5)	28(2)
C(51)	11933(3)	10447(5)	−202(5)	32(2)
C(52)	11899(3)	11048(5)	546(5)	31(2)
C(53)	11327(3)	10980(4)	627(6)	35(2)
C(54)	11176(3)	10053(4)	772(5)	28(2)
C(55)	11213(3)	9461(4)	7(4)	22(1)
C(56)	11492(3)	7872(5)	1032(5)	23(2)
C(57)	11536(3)	8025(5)	2018(4)	26(2)
C(58)	12091(4)	7604(6)	3522(5)	49(2)
C(59)	9187(3)	9059(5)	−113(5)	30(2)
C(60)	9069(3)	8523(4)	−900(5)	27(2)
C(61)	9378(3)	8853(4)	−1444(5)	26(2)
C(62)	9680(3)	9590(4)	−981(4)	24(1)
C(63)	9562(3)	9709(4)	−167(5)	28(2)
C(64)	8868(3)	9064(5)	535(6)	42(2)
C(65)	8616(3)	7846(6)	−1219(6)	35(2)
C(66)	9252(3)	8665(4)	−2449(4)	27(2)
C(67)	9939(3)	10230(4)	−1418(5)	32(2)
C(68)	9707(3)	10497(5)	450(5)	39(2)
B(1)	3442(3)	12264(5)	3820(5)	24(2)
C(1)	3468(3)	10705(4)	3124(4)	22(1)
C(2)	3247(3)	9902(5)	2777(5)	30(2)
C(3)	2724(3)	9678(4)	2746(4)	29(2)
C(4)	2421(3)	10259(4)	3056(4)	27(2)
C(5)	2644(3)	11063(4)	3394(4)	24(1)
C(6)	3186(3)	11306(4)	3449(4)	20(1)
C(7)	2738(3)	12795(5)	2198(5)	34(2)
C(8)	2505(3)	13405(6)	1498(6)	52(2)
C(9)	2714(4)	14223(6)	1575(8)	67(3)
C(10)	3161(4)	14431(6)	2351(8)	61(3)
C(11)	3403(3)	13826(5)	3046(6)	40(2)
C(12)	3192(3)	12984(5)	2994(5)	29(2)
C(13)	4461(3)	12558(4)	3698(5)	30(2)
C(14)	5037(3)	12453(5)	3991(5)	36(2)
C(15)	5307(3)	12007(5)	4777(6)	36(2)
C(16)	5003(3)	11656(5)	5267(4)	36(2)
C(17)	4442(3)	11752(5)	4966(5)	33(2)
C(18)	4134(3)	12222(4)	4177(5)	27(2)
C(19)	3224(3)	11955(5)	5349(5)	32(2)
C(20)	3046(3)	12156(6)	6066(5)	41(2)
C(21)	2879(3)	12985(6)	6158(6)	47(2)
C(22)	2901(3)	13606(5)	5521(6)	44(2)
C(23)	3081(3)	13388(5)	4807(5)	35(2)
C(24)	3252(3)	12547(4)	4696(5)	28(2)

[a] Equivalent isotropic U, defined as one-third of the trace of the orthogonalized U_{ij} tensor.

Scheme 1

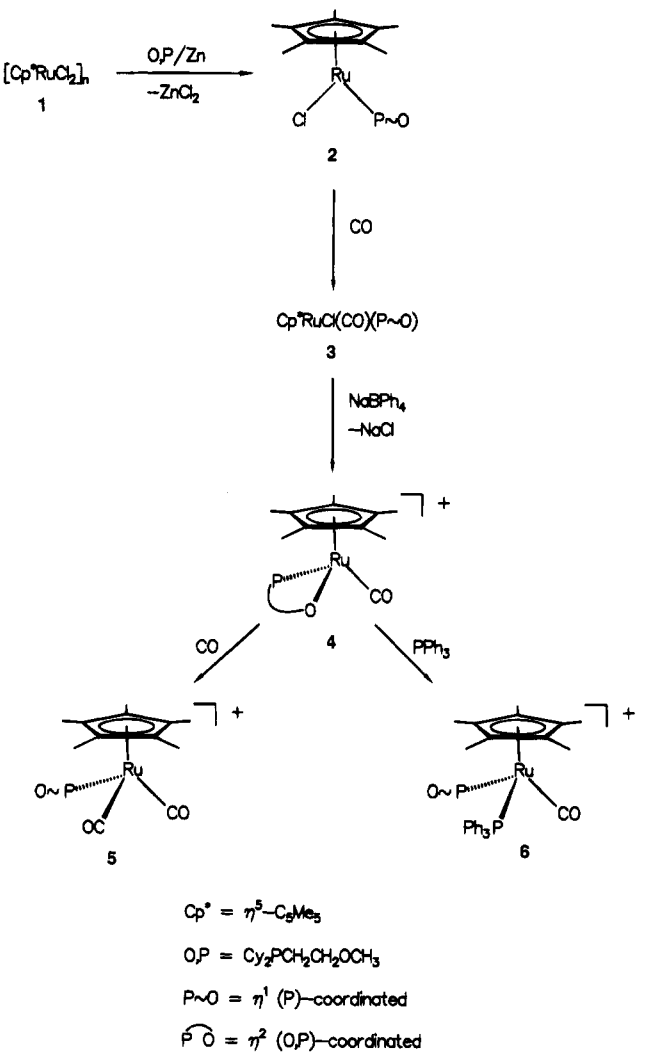

3 exhibits a single resonance at 38.1 ppm in the $^{31}P\{^1H\}$ NMR spectrum. One strong IR absorption at 1920 cm^{-1} is observed for the CO ligand. In the $^{13}C\{^1H\}$ NMR spectrum[13] of **3** the low-intensity doublet at 207.9 ppm is assigned to the carbonyl group. Moreover, the two singlets at 69.1 and 58.3 ppm, respectively, are attributed to the two carbon nuclei adjacent to the ether oxygen atom. The two diastereotopic methine carbon atoms of the cyclohexyl fragments appear as only one doublet due to the coupling to the phosphorus atom in the high-field range of the spectrum.

Synthesis and Spectroscopic Data of [Cp*Ru(CO)(P⌒O)][BPh₄] (4[BPh₄]). The intramolecular coordination of the ether function involving the cleavage of the Ru−Cl bond from complex **3** was attempted according to a previously published study.[14] However, the quantitative formation of the η^2(O,P)-chelated complex [Cp*Ru(CO)(P⌒O)][BPh_4] (**4[BPh₄]**) (Scheme 1) was found to require a prolonged reaction time (3 days) compared to the synthesis of the corresponding bis(phosphine) derivative [Cp*Ru(P~O)(P⌒O)][BPh_4] (O,P = (1.3-dioxan-2-ylmethyl)diphenylphosphine).[14] This

(13) The assignment of the ^{13}C NMR resonances was supported by ^{13}C DEPT 135 NMR spectroscopy: Günther, H. *NMR-Spektroskopie*; Thieme Verlag: Stuttgart, Germany, 1992.

(14) Lindner, E.; Haustein, M.; Mayer, H. A.; Schneller, T.; Fawzi, R.; Steimann, M. *Inorg. Chim. Acta* **1995**, *231*, 201.

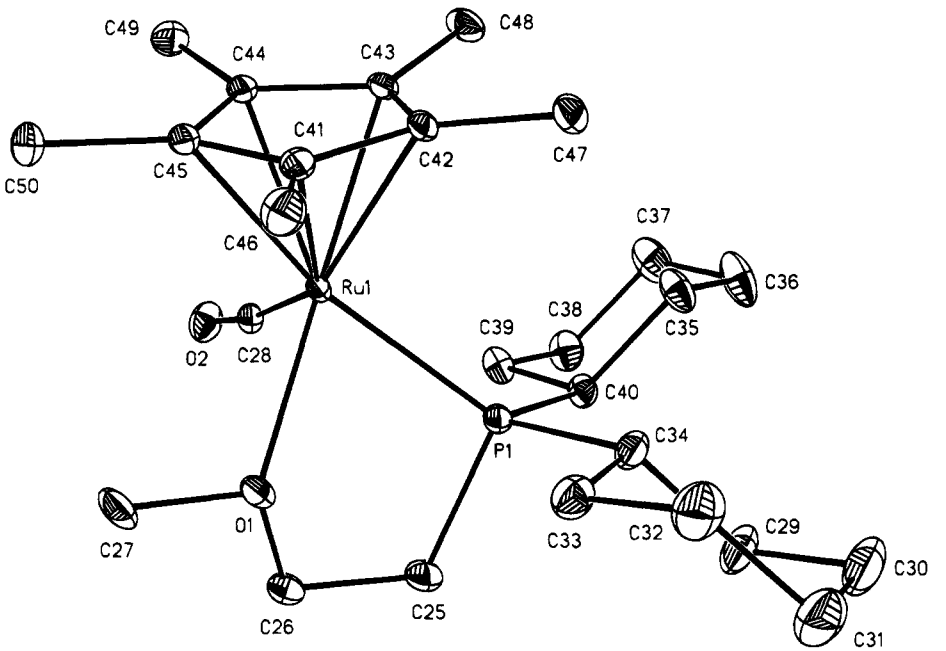

Figure 1. ORTEP plot of **4**.

indicates a strong Ru−Cl bond in complex **3**. Complex **4**, which represents an η^2(O,P)-coordinated mono(ether−phosphine) ruthenium complex, was obtained as a yellow air-stable powder in 94% isolated yield. Its ^{31}P-{^{1}H} NMR spectrum displays a single peak at 56.8 ppm which is shifted ($\Delta\delta$ ~19 ppm) to lower field due to the ring contribution Δ_R.[15] Due to the η^2(O,P)-coordination of the ligand the ^{13}C NMR resonances[13] of the two carbon atoms of the ether moiety in positions α to the oxygen are also significantly shifted to lower field (~9 ppm (CH_2O), ~13 ppm (OCH_3)) compared to the corresponding signals of the η^1(P)-coordinated ether moiety in **3**. Moreover, the two inequivalent methine carbon atoms of the two cyclohexyl groups reveal two doublets (δ_C 38.1 and 35.0, $^1J_{PC}$ = 26.7 and 19.1 Hz) which are caused by their different positions above and below the five-membered chelate ring. The CO ligand in **4** appears as a low-intensity doublet at 205.4 ppm ($^2J_{PC}$ = 16.5 Hz). In the IR spectrum the CO stretching frequency at 1940 cm^{-1} is shifted 20 cm^{-1} to higher wavelengths relative to the neutral species **3**, demonstrating the decreased electron density at the ruthenium center.

Crystal Structure of 4. A single-crystal X-ray determination of **4** was undertaken to determine the coordination geometry about ruthenium. The ORTEP drawing of the cation of **4** is shown in Figure 1. A listing of selected bond distances and angles is given in Table 4. The environment about the Ru atom corresponds to that of a three-legged piano stool with near 90° angles between P(1)−Ru(1)−C(28) and C(28)−Ru(1)−O(1). However, the O(1)−Ru(1)−P(1) angle (75.35(9)°) of the η^2-(O,P)-coordinated ligand is significantly smaller but is comparable with the corresponding angle reported for [Cp*Ru(P~O)(P^O)][BPh$_4$], 77.2 (2)°.[14] The five-membered chelate ring consists of two planes, which are determined by the atoms P(1), C(25), C(26), O(1) and P(1), Ru(1), O(1). These planes form an angle of 143.5° at their common edge, which is defined by P(1) and O(1),

(15) Garrou, P. E. *Chem. Rev.* **1981**, *81*, 229.

Table 4. Selected Interatomic Distances (Å) and Angles (deg) for 4

	Bond Lengths		
Ru(1)−P(1)	2.349(1)	P(1)−C(25)	1.840(5)
Ru(1)−O(1)	2.231(3)	C(25)−C(26)	1.512(7)
Ru(1)−C(28)	1.861(5)	C(26)−O(1)	1.457(6)
C(28)−O(2)	1.155(6)	O(1)−C(27)	1.436(6)
	Bond Angles		
P(1)−Ru(1)−C(28)	91.9(1)	Ru(1)−P(1)−C(25)	103.4(2)
C(28)−Ru(1)−O(1)	91.2(2)	P(1)−C(25)−C(26)	112.9(3)
O(1)−Ru(1)−P(1)	75.35(9)	C(25)−C(26)−O(1)	110.0(4)
Ru(1)−C(28)−O(2)	172.0(4)	C(26)−O(1)−Ru(1)	114.5(3)

giving an envelope conformation with Ru(1) at the top. The Ru−C−O unit deviates from the expected linear geometry, forming an angle of 172.0(4)°. The ruthenium−oxygen distance (Ru(1)−O(1) = 2.231(3) Å) is slightly shorter relative to that of [Cp*Ru(P~O)(P^O)]-[BPh$_4$] (2.262 (6) Å), which is indicative of an increased Ru−O bond strength.

Reactivity of 4 toward Carbon Monoxide and Triphenylphosphine. The strength of the Ru−O bond and hence the chelating ability of an η^2(O,P)-coordinating ether−phosphine ligand is of interest with regard to the easy dissociation and protective effect of the functional oxygen. In complexes with at least two "hemilabile" ether−phosphine ligands the oxygen donors compete for one coordination site. This reveals a fluxional behavior in solution which can be studied by variable-temperature ^{31}P NMR spectroscopy. Therefore, the determination of the Ru−O bond strength in complexes of the type [Cp*Ru(P~O)(P^O)]$^+$ (O,P = diphenyl(ether−phosphine)) was achieved by evaluation of the thermodynamic data based on line-shape analyses.[2] An alternative route to give a qualitative estimation of the chelating properties of bifunctional O,P ligands is to study the reactivity of such complexes toward incoming substrates. Hence, we reported the use of [Cp*Ru-(P~O)(P^O)][BPh$_4$] (O,P = (1,3-dioxan-2-ylmethyl)-diphenylphosphine) as a reactive precursor for the

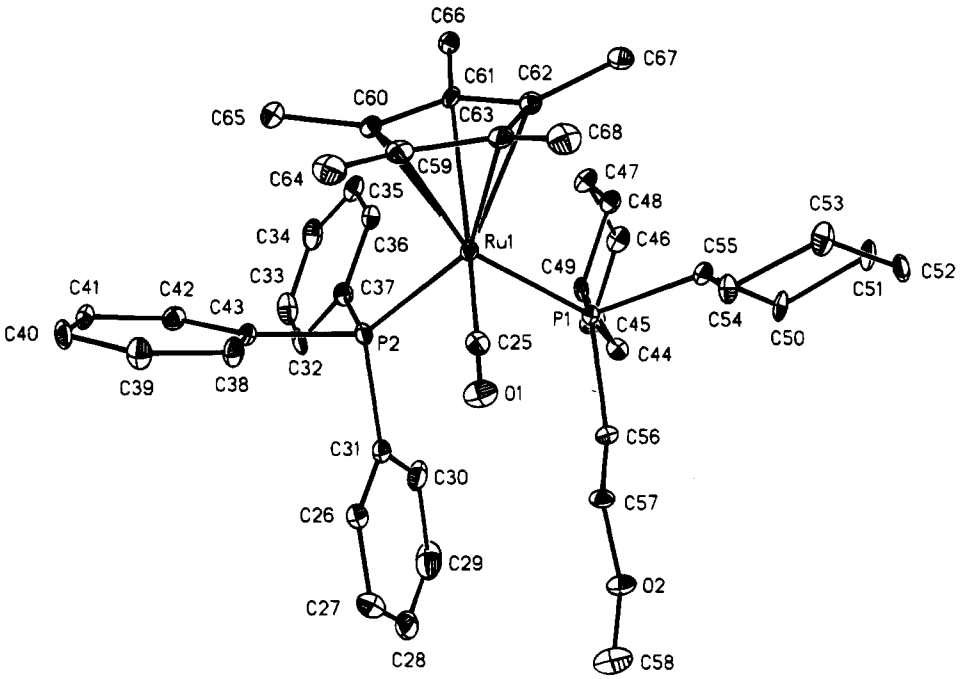

Figure 2. ORTEP plot of **6**.

coordination of a variety of small molecules.[16] In the case of the η^2(O,P)-chelated mono(ether–phosphine) complex **4** information concerning the strength of the Ru–O bond can be obtained by investigations of the reactivity of **4** toward simple molecules such as carbon monoxide and triphenylphosphine.

If carbon monoxide is bubbled into a solution of **4** in dichloromethane at ambient temperature, only slight conversion is observed after 10 min. This is in marked contrast to the fast coordination of CO to the corresponding bis(phosphine) derivative.[2] However, treatment of **4** with CO under forced reaction conditions (2 bar) resulted in the quantitative formation of the dicarbonyl species **5** (Scheme 1) within 30 min. The reaction was monitored by the appearance of a single peak at 46.6 ppm in the $^{31}P\{^1H\}$ NMR spectrum. Complex **5** is an air-stable white powder; the two CO stretching frequencies are observed at 2043 and 1994 cm^{-1}, respectively, in the IR spectrum. The two equivalent carbon monoxide ligands reveal a low-intensity doublet at 199.7 ppm ($^2J_{PC}$ = 15.3 Hz) in the $^{13}C\{^1H\}$ NMR spectrum. Moreover, the single resonances of the methylene (δ_C 67.9) and the methyl (δ_C 58.7) carbon atoms of the ether moiety are in the range of the corresponding signals of compounds **2** and **3**, respectively, indicating the η^1(P) coordination of the O,P ligand in complex **5**.

The addition of a 2-fold excess of triphenylphosphine to a solution of **4** in dichloromethane at ambient temperature is accompanied by a continuous color change from bright yellow to pale yellow. The complete conversion into the new complex [Cp*Ru(CO)(P~O)(PPh_3)][BPh_4] (**6[BPh_4]**) (Scheme 1) required approximately 60 min. Compound **6** was obtained as a pale yellow air-stable powder after separation of excess PPh_3 via column chromatography in 91% yield and represents an example for a mixed-phosphine complex. Its $^{31}P\{^1H\}$ NMR spectrum at 33 °C displays an AB pattern caused by PPh_3 (δ_P 47.1, $^2J_{PP}$ = 26.9 Hz) and the O,P ligand (δ_P 30.9, $^2J_{PP}$ = 26.9 Hz). The assignment of the two phosphorus nuclei was supported by a $^1H/^{31}P$ HETCOR spectrum[7] at room temperature. At −30 °C the doublet due to the phosphorus atom of the O,P ligand is broadened. Further cooling to −80 °C gives rise to two doublets of different intensities. The signal which is assigned to the PPh_3 ligand remains sharp in the whole temperature range. This dynamic phenomenon is consistent with a restricted Ru–P rotation which was also observed in Cp*Ru(P~O)$_2$ systems provided with sterically encumbering ancillary ligands such as chlorine[2] or ethene.[16] Therefore, no further investigations were carried out concerning the observed decoalescence in the present case. The fact that only the rotation around the metal–(ether–phosphine) bond axis can be frozen at −80 °C is reasonable with regard to the increased steric constraint of the $Cy_2PCH_2CH_2OCH_3$ ligand relative to PPh_3. The coordinated carbon monoxide in **6** reveals a strong absorption at 1939 cm^{-1} in the IR spectrum and a low-intensity doublet of doublets (δ_C 209.1, $^2J_{PC}$ = 17.2 Hz) due to the coupling with two inequivalent phosphines in the $^{13}C\{^1H\}$ NMR spectrum. The two single peaks at 68.3 and 58.5 ppm are respectively assigned to the methylene and methyl carbon atoms of the ether chain and are in the typical range observed for η^1(P) coordination (*vide supra*). The two diastereotopic methine carbon atoms of the cyclohexyl fragments of **6** display two resonances (δ_C 38.4 and 37.7, $^1J_{PC}$ = 22.9 and 19.1 Hz).

To determine the coordination geometry about ruthenium and to get an impression of the sterically encumbered ruthenium center, a single-crystal X-ray determination of **6** was carried out. The ORTEP drawing of the cation of **6** is shown in Figure 2. A listing of selected bond distances and angles is presented in Table 5. The geometry of **6** is octahedral about the metal center, with the Cp* occupying three coordination sites. This is evidenced by the near-90° angles between P(1)–Ru(1)–P(2), P(1)–Ru(1)–C(25), and P(2)–Ru(1)–C(25), respec-

(16) Lindner, E.; Haustein, M.; Fawzi, R.; Steimann, M.; Wegner, P. *Organometallics* **1994**, *13*, 5021.

Table 5. Selected Interatomic Distances (Å) and Angles (deg) for 6

	Bond Lengths		
Ru(1)–P(1)	2.379(2)	P(1)–C(56)	1.849(7)
Ru(1)–P(2)	2.373(2)	C(56)–C(57)	1.525(9)
Ru(1)–C(25)	1.860(6)	C(57)–O(2)	1.415(7)
C(25)–O(1)	1.144(7)	O(2)–C(58)	1.438(8)
	Bond Angles		
P(1)–Ru(1)–P(2)	92.44(7)	Ru(1)–P(1)–C(56)	120.5(2)
P(1)–Ru(1)–C(25)	91.0(2)	P(1)–C(56)–C(57)	122.1(5)
P(2)–Ru(1)–C(25)	92.0(2)	C(56)–C(57)–O(2)	105.7(5)
Ru(1)–C(25)–O(1)	170.5(6)	C(57)–O(2)–C(58)	112.2(5)

tively. The distances between ruthenium and each of the two different phosphorus atoms are nearly equivalent (Ru(1)–P(1) = 2.379(2) Å, Ru(1)–P(2) = 2.373(2) Å) and only slightly longer compared with the Ru–P bond length in **4** (2.349(1) Å). The coordination geometry of the Ru–C–O unit is in good agreement with that of compound **4**. The CO bond lengths as well as the IR data for both complexes are comparable, indicating almost the same back-donation from the metal to the carbonyl ligand and hence a similar electron density at both ruthenium centers.

Conclusion

The employment of the basic O,P ligand $Cy_2PCH_2CH_2OCH_3$ in the synthesis of (ether–phosphine)(pentamethylcyclopentadienyl)ruthenium complexes was taken into consideration with the intention of creating an electron-rich ruthenium center relative to the corresponding diphenyl(ether–phosphine) derivatives. Therefore, a very weak Ru–O contact was anticipated if the O,P ligand is allowed to function as a bidentate chelate. The steric constraint of this ligand reveals the formation of the 16-electron mono(ether–phosphine) complex **2**. A potential η^2(O,P) chelation in this compound is prevented, which is attributed to the increased electron density at the ruthenium. However, the stabilization of the coordinatively unsaturated metal center with carbon monoxide has led to a valuable precursor for the generation of the η^2(O,P)-chelated mono(ether–phosphine) complex **4**. The cleavage of the Ru–O bond in **4** was achieved by treatment of **4** with carbon monoxide and triphenylphosphine. In the case of the latter the sterically encumbering mixed-phosphine complex **6** was obtained. In general, however, the reactivity of **4** toward an incoming substrate is slowed down compared to the analogous bis(ether–phosphine) systems. This is further evidence for the increased metal–oxygen contact in **4** beside the shortened Ru–O bond length and is equivalent to a reduced electron density at the metal. These results may be best interpreted with a compensation of the electronically enriched ruthenium (caused by the basic O,P ligand employed) by the electron-withdrawing effect of the carbonyl group.

Acknowledgment. The support of this research by the Fonds der Chemischen Industrie is gratefully acknowledged. We thank the BASF Aktiengesellschaft for starting materials.

Supplementary Material Available: Tables of crystal data and refinement details, hydrogen atom positional parameters, anisotropic thermal parameters, and interatomic distances and angles for **4** and **6** (14 pages). Ordering information is given on any current masthead page.

OM940712W

Addition and Substitution Reactions and Structures of Heterobimetallic Phosphido-Bridged Fe–W Complexes—Adjacent Metal Assisted Substitution and Reaction Site Switching via Metal–Metal Bond Formation

Shin-Guang Shyu,* Pei-Jung Lin, Kuan-Jiuh Lin, Ming-Chi Chang, and Yuh-Shang Wen

Institute of Chemistry, Academia Sinica, Taipei 11529, Taiwan, Republic of China

Received October 6, 1994[⊗]

The metal–metal bond in $CpFe(CO)(\mu\text{-}PPh_2)(\mu\text{-}CO)W(CO)_4$ (**1**) was cleaved by Lewis bases L (L = PMe_3, PPh_2H, CH_3CN) to produce $CpFe(CO)_2(\mu\text{-}PPh_2)W(CO)_4L$ (**3**), in which L regioselectively and stereospecifically coordinates to W cis to the phosphido bridge. When L was PPh_3 or $P(OMe)_3$, both cis and trans isomers were obtained. When $CpFe(CO)_2(\mu\text{-}PPh_2)W(CO)_5$ (**2**) reacted with PMe_3, one CO ligand on Fe was replaced by PMe_3 to produce $CpFe(CO)(PMe_3)(\mu\text{-}PPh_2)W(CO)_5$ (**4**). Structures of $CpFe(CO)_2(\mu\text{-}PPh_2)W(CO)_4(PMe_3)$ (**3b-*cis***), $CpFe(CO)_2(\mu\text{-}PPh_2)W(CO)_4(P(OMe)_3)$ (**3c-*trans***), and **4** were determined by single-crystal X-ray diffraction studies. Crystal data for **3b-*cis***: $C_{26}H_{15}FeO_6P_2W$, space group $P2_1/c$, a = 9.832(4) Å, b = 16.027(3) Å, c = 18.264(4) Å, β = 103.87(2)°, V = 2794(1) Å^3, and Z = 4. The structure was refined to R = 0.026 and R_w = 0.031. Crystal data for **3c-*trans***: $C_{26}H_{24}FeO_9P_2W$, space group $Pna2_1$, a = 22.779(4) Å, b = 11.669(2) Å, c = 10.580(1) Å, V = 2812.7(7) Å^3, and Z = 4. The structure was refined to R = 0.023 and R_w = 0.026. Crystal data for **4**: $C_{26}H_{24}FeO_6P_2W$, space group $P2_1/n$, a = 15.768(2) Å, b = 10.7111(2) Å, c = 17.784(2) Å, β = 114.10(1)°, V = 2741.8(7) Å^3, and Z = 4. The structure was refined to R = 0.021 and R_w = 0.024. UV irradiation of **3** removed one CO to form $CpFe(CO)(\mu\text{-}PPh_2)W(CO)_4L$ (**5**). The structure of $CpFe(CO)(\mu\text{-}PPh_2)W(CO)_4(PPh_3)$ (**5e-*trans***) was determined by a single-crystal X-ray diffraction study. Crystal data for **5e-*trans***: $C_{40}H_{30}FeO_5P_2W$, space group $P2_1/c$, a = 18.6696(8) Å, b = 12.6178(6) Å, c = 18.195(1) Å, β = 118.220(5)°, V = 3777.5(3) Å^3, and Z = 4. The structure was refined to R = 0.028 and R_w = 0.030.

Introduction

In bimetallic phosphido-bridged complexes, one metal may exert an activating influence on the adjacent metal.[1] We recently reported that the metal–metal bond in the heterobimetallic phosphido-bridged complex $CpW(CO)_2(\mu\text{-}PPh_2)Mo(CO)_5$ activated the Mo carbonyl ligand toward substitution by Lewis bases L (L = PMe_3, PPh_2H, $P(OMe)_3$) at ambient temperatures via the opening of the metal–metal bond to produce $CpW(CO)_3(\mu\text{-}PPh_2)Mo(CO)_4L$ with the intramolecular transfer of one Mo carbonyl to the adjacent W.[1a] For the complex $CpW(CO)_2(\mu\text{-}PPh_2)W(CO)_5$, similar activation of the W carbonyl toward substitution by Lewis bases L by the adjacent metal through the metal–metal bond was also observed at a higher reaction temperature to produce $CpW(CO)_2(\mu\text{-}PPh_2)W(CO)_4L$.[1b]

Investigation on the influence of one metal on the chemistry of its adjacent metal in bimetallic complexes would be of importance for the understanding of the cooperativity effect in binuclear complexes and clusters. It would be of interest to evaluate the cooperativity effect by using different kinds of metal fragments and study their influence on a similar metal moiety. Since the intramolecular CO transfer from Mo to W during the addition reaction of $CpW(CO)_2(\mu\text{-}PPh_2)Mo(CO)_5$ is assisted by the adjacent W moiety,[1a] selecting a metal fragment which has a stronger interaction with the adjacent metal carbonyl may facilitate the addition reaction such that the addition product can be obtained under relatively mild conditions.

We recently synthesized the heterobimetallic phosphido-bridged complex $CpFe(CO)(\mu\text{-}CO)(\mu\text{-}PPh_2)W(CO)_4$ (**1**), which has a strong iron–tungsten carbonyl interaction, as revealed by its structure.[2] Reactions between **1** and Lewis bases L (L = CH_3CN, PPh_3, PMe_3, PPh_2H, $P(OMe)_3$) produced addition products with L regiospecifically coordinated to W under very mild conditions. Interestingly, reaction between $CpFe(CO)_2(\mu\text{-}PPh_2)W(CO)_5$ (**2**) and PMe_3 produced $CpFe(CO)(PMe_3)(\mu\text{-}PPh_2)W$-

[⊗] Abstract published in *Advance ACS Abstracts,* April 15, 1995.

(1) (a) Shyu, S.-G.; Hsu, J.-Y.; Lin, P.-J.; Wu, W.-J.; Peng, S. M.; Lee, G. H.; Wen, Y.-S. *Organometallics* **1994**, *13*, 1699. (b) Shyu, S. G.; Wu, W.-J.; Peng, S. M.; Lee, G. H.; Wen, Y.-S. *J. Organomet. Chem.* **1995**, *489*, 113. (c) Regragui, R.; Dixneuf, P. H.; Taylor, N. J.; Carty, A. J. *Organometallics* **1986**, *5*, 1. (d) Mercer, W. C.; Whittle, R. R.; Burkhardt, E. W.; Geoffroy, G. L. *Organometallics* **1985**, *4*, 68. (e) Powell, J.; Sawyer, J. F.; Stainer, M. V. R. *Inorg. Chem.* **1989**, *28*, 4461. (f) Powell, J.; Coutoure, C.; Gregg, M. R. *J. Chem. Soc., Chem. Commun.* **1988**, 1208.

(2) Shyu, S. G.; Lin, P.-J.; Dong, T.-Y.; Wen, Y.-S. *J. Organomet. Chem.* **1993**, *460*, 229.

0276-7333/95/2314-2253$09.00/0

Scheme 1

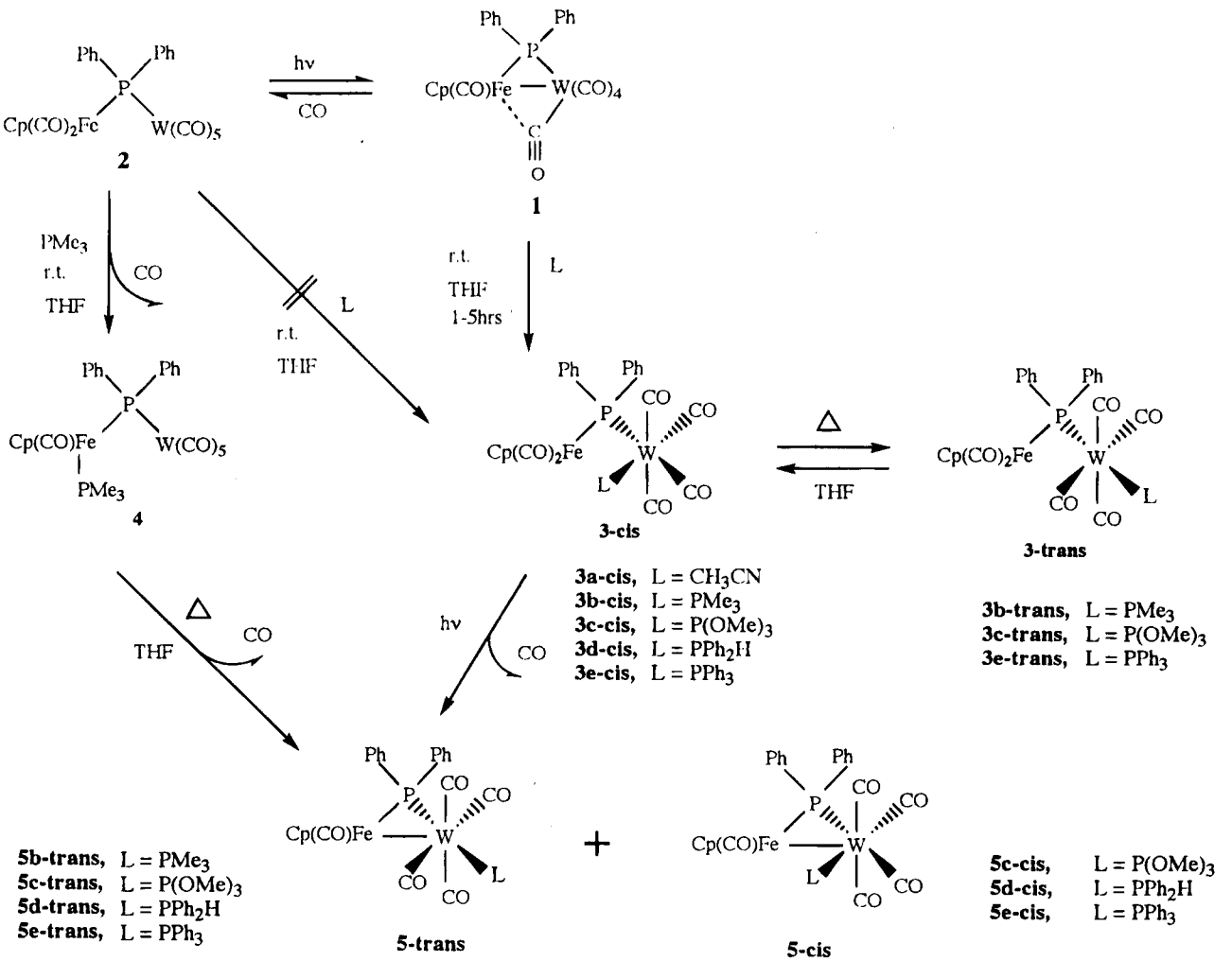

$(CO)_5$ (**4**) with PMe_3 regioselectively coordinated to Fe. For other Lewis bases, no reaction was observed when **2** was allowed to react with them under similar conditions. These observations indicated three interesting features: First, the Fe moiety in **1** could enhance substitution of the adjacent tungsten carbonyl through the formation of the metal–metal bond. Second, the cooperativity effect in binuclear complexes could be tailored by carefully selecting the adjacent metal such that a stronger interaction between the metal carbonyl ligand and the adjacent metal facilitated the reaction. Third, reaction site switching was observed through the formation of the metal–metal bond in the system. Reported herein are the reactivity studies of complexes **1** and **2**. Scheme 1 shows reactions that comprise the main focus of our work. The products of the addition reaction have been characterized spectroscopically, and the structures of complexes $CpFe(CO)_2(\mu\text{-}PPh_2)W(CO)_4(PMe_3)$ (**3b-*cis***), $CpFe(CO)_2(\mu\text{-}PPh_2)W(CO)_4(P(OMe)_3)$ (**3c-*trans***), **4**, and $CpFe(CO)(\mu\text{-}PPh_2)W(CO)_4(PPh_3)$ (**5e-*trans***) were also determined by complete single-crystal X-ray diffraction studies.

Experimental Section

Unless otherwise stated, all reactions and manipulations of air-sensitive compounds were carried out at ambient temperatures under an atmosphere of purified N_2 with standard procedures. A 450-W Hanovia medium-pressure quartz mercury-vapor lamp (Ace Glass) and a Pyrex Schlenk tube as a reaction vessel were used in the photoreactions. Infrared (IR) spectra were recorded on a Perkin-Elmer 882 infrared spectrophotometer. ^1H, ^{13}C, and ^{31}P NMR spectra were measured by using Bruker AMX-500, MSL-200, AC-200, and AC-300 spectrometers. ^{31}P NMR shifts are referenced to 85% H_3PO_4. Except as noted, NMR spectra were collected at room temperature. Electron impact (EI) and fast-atom bombardment (FAB) mass spectra were recorded on a VG 70-250S or a JEOL JMS-HX 110 mass spectrometer. Microanalyses were performed by the Microanalytic Laboratory at National Cheng Kung University, Tainan, Taiwan. $^{31}P\{^1H\}$ and ^1H NMR and IR spectroscopic data for complexes **3**–**5** are summarized in Table 1.

Materials. THF was distilled from potassium and benzophenone under an atmosphere of N_2 immediately before use. Other solvents were purified according to established procedures.[3] The metal carbonyls $M(CO)_6$ (M = Mo, W) and PMe_3, PPh_2H, and PPh_3 were obtained from Strem, $P(OMe)_3$ was purchased from Merck, and ^{13}CO (99 atom % ^{13}C) was obtained from Isotec. Other reagents and solvents were obtained from various commercial sources and used as received. Complexes $CpFe(CO)(\mu\text{-}CO)(\mu\text{-}PPh_2)W(CO)_4$ and $CpFe(CO)_2(\mu\text{-}PPh_2)W(CO)_5$ were prepared by literature procedures.[4]

Synthesis of $CpFe(CO)_2(\mu\text{-}PPh_2)W(CO)_4(NCCH_3)$ (3a). To a solution of 0.10 g (0.15 mmol) of **1** in 30 mL of THF was added 10 mL of $NCCH_3$ under N_2 at ambient temperature.

(3) Perrin, D. D.; Armarego, W. L. F.; Perrin, D. R. *Purification of Laboratory Chemicals*; Pergamon: Oxford, U.K., 1966.
(4) Shuy, S.-G.; Lin, P.-J.; Wen, Y.-S. *J. Organomet. Chem.* **1993**, *443*, 115.

Table 1. Spectroscopic Data for 1–5[a]

complex	$^{31}P\{^1H\}$ NMR,[b,c] δ	^1H NMR,[b,d] δ	IR, ν(CO),[e] cm^{-1}
3a-*cis*	14.0 (s)[f]	4.7 (s, 5H), 1.6 (s, 3H)[g]	2020 m, 2000 m, 1974 m, 1888 s, 1834 m[f]
3b-*cis*	−41.4 (d, $^2J_{P-P}$ 24.5, J_{P-W} 206, PMe_3), 4.69 (d, $^2J_{P-P}$ 24.5, J_{P-W} 219, μ-PPh_2)	4.67 (d, $^3J_{P-H}$ 1.5, 5H), 1.04 (d, $^3J_{P-H}$ 7.4, 9H)	2020 m, 2001 s, 1969 m, 1898 sh, 1882 s, 1852 m
3b-*trans*[h]	9.63 (d, $^2J_{P-P}$ 49.2, μ-PPh_2), −34.69 (d, $^2J_{P-P}$ 48.8, PMe_3)		
3c-*cis*	4.00 (d, $^2J_{P-P}$ 31.3, J_{P-W} 205.3, μ-PPh_2), 139.4 (d, $^2J_{P-P}$ 31.2, J_{P-W} 375.4, $P(OMe)_3$	4.63 (d, $^3J_{P-H}$ 1.5, 5H), 3.37 (d, $^3J_{P-H}$ 11.2, 9H)	2025 m, 2009 s, 1972 m, 1893 s, 1870 s
3c-*trans*	6.8 (d, $^2J_{P-P}$ 93.5, J_{P-W} 237.2, μ-PPh_2), 147.5 (d, $^2J_{P-P}$ 89.3, J_{P-W} 444.9, $P(OMe)_3$)	4.63 (d, $^3J_{P-H}$ 1.3, 5H), 3.57 (d, $^3J_{P-H}$ 11.3, 9H)	2026 m, 2010 m, 1969 m, 1945 vw, 1886 s
3d-*cis*	5.6 (d, $^2J_{P-P}$ 19.0, J_{P-W} 226.0, J_{P-H} 326, PPh_2H), 9.1 (d, $^2J_{P-P}$ 19.0; J_{P-W} 199.3, μ-PPh_2)	4.66 (d, $^3J_{P-H}$ 1.4, 5H), 5.2 (dd, $^1J_{P-H}$ 336, $^3J_{P-H}$ 8.3, 1H)	2023 m, 2007 s, 1971 m, 1902 s, 1860 s
3e-*cis*[h]	20.01 (d, $^2J_{P-P}$ 28.1, J_{P-W} 227), −3.03 (d, $^2J_{P-P}$ = 27.5 Hz)	4.49 (d, $^3J_{P-H}$ 1.2)	
3e-*trans*	8.2 (d, $^2J_{P-P}$ 56.0, J_{P-W} 244), 27.1 (d, $^2J_{P-P}$ 56.0 Hz, J_{P-W} 284)	4.60 (d, $^3J_{P-H}$ 1.6, 5H)	2019 s, 1997 w, 1968 m, 1936 m, 1876 vs
4	−4.42 (d, $^2J_{P-P}$ 33.0, J_{P-W} 195, μ-PPh_2), 21.5 (d, $^2J_{P-P}$ 33.0, PMe_3)	4.38 (d, $^3J_{P-H}$ 1.6, 5H), 1.25 (d, $^3J_{P-H}$ 9.2, 9H)	2057 m, 1939 m, 1915 s, 1896 s
5b-*trans*	−34.2 (d, $^2J_{P-P}$ 30.5, J_{P-W} 248, PMe_3), 165.7 (d, $^2J_{P-P}$ 33.6, J_{P-W} 221, μ-PPh_2)[j]	4.31 (d, $^3J_{P-H}$ 1.3, 5H), 1.81 (d, $^3J_{P-H}$ 8.1, 9H)	2010 m, 1932 s, 1884 s
5c-*cis*[h,i]	140.18 (d, $^2J_{P-P}$ 35.8, J_{P-W} 225.0), 130.92 (d, $^2J_{P-P}$ 35.8, J_{P-W} 410.0)	4.41 (s, 5H), 3.63 (d, $^3J_{P-H}$ 11.2 Hz, 9H)	
5c-*trans*[h]	163.95 (d, $^2J_{P-P}$ 61.0, J_{P-W} 205.0), 137.76 (d, $^2J_{P-P}$ 61.0, J_{P-W} 432.5)	4.35 (d, $^3J_{P-H}$ 1.1 Hz, 5H), 3.71 (d, $^3J_{P-H}$ 11.6 Hz, 9H)	
5d-*cis*[h,j]	161.23 (d, $^2J_{P-P}$ 40.2, J_{P-W} 234.9, μ-PPh_2), −1.93 (d, $^2J_{P-P}$ 35.2, J_{P-W} 243.0, J_{P-H} 350.3, PPh_2H)[k]	4.44 (s)	
5d-*trans*[h]	135.02 (d, $^2J_{P-P}$ 29.3, J_{P-W} 218.0, μ-PPh_2), −22.56 (d, $^2J_{P-P}$ 27.1, J_{P-W} 235.0, J_{P-H} 365.2, PPh_2H)[k]	4.40 (s)	
5e-*cis*[h,l]	128.04 (d, $^2J_{P-P}$ 24.3, μ-PPh_2), 16.96 (d, $^2J_{P-P}$ 24.3, PPh_3)[m]	4.47 (s)	
5e-*trans*	162.52 (d, $^2J_{P-P}$ 34.8, μ-PPh_2), 21.25 (d, $^2J_{P-P}$ 35.7, PPh_3)[m]	4.33 (s, 5H)	2015 m, 1932 s, 1891 s

[a] At room temperature. [b] J values in Hz. [c] In THF solution unless otherwise indicated. [d] In $CDCl_3$ solution unless otherwise indicated. Cp and Me groups only. Abbreviations: s, singlet; d, doublet. [e] In THF solution unless otherwise indicated. Abbreviations: vs, very strong; s, strong; m, medium; w, weak; br, broad; sh, shoulder. [f] In $NCCH_3$. [g] In $CDCl_3/NCCH_3$ (10:1). In solution, **3a-*cis*** is only stable in the presence of $NCCH_3$. [h] Not separated pure. [i] Cis:trans = 1:5. [j] Cis:trans = 1:2. [k] 233 K in CD_2Cl_2. [l] Cis:trans = 1:7. [m] In $CDCl_3$.

After it was stirred for 10 min, the solution changed from dark brown to red. The ^{31}P NMR of the solution indicated that **3a** was the only product. After the solvent was removed, a red solid of **3a** was obtained. Anal. Calcd for $C_{25}H_{18}O_6NPFeW$: C, 42.95; H, 2.58; N, 2.00. Found: C, 42.49; H, 2.67; N, 1.56. $^{13}C\{^1H\}$ NMR ($CDCl_3/CH_3CN$): δ 214.4 (d, $^2J_{P-C}$ = 15 Hz, 2CO), 210.3 (s, J_{W-C} = 115.0 Hz, 1CO), 208.5 (d, $^2J_{P-C}$ = 30.2 Hz, J_{W-C} = 129.8 Hz, 1CO), 203.4 (d, $^2J_{P-C}$ = 5.9 Hz; J_{W-C} = 130.4 Hz, 2CO), 144.53 (d, J_{P-C} = 9.9 Hz, *ipso*-C PPh_2), 133.37 (d, $^2J_{P-C}$ = 9.6 Hz, *o*-C, PPh_2), 127.4 (m, *m*-C, *p*-C, PPh_2), 88.1 (s, C_5H_5), 2.79 (s, $NCCH_3$).

Synthesis of $CpFe(CO)_2(\mu$-$PPh_2)W(CO)_4(PMe_3)$ (3b). To a solution of **1** (0.26 g, 0.40 mmol) in 30 mL of THF was added 122 μL (1.2 mmol) of PMe_3 under N_2 at ambient temperature in the dark. After 1 h, the solution changed from dark brown to red. Solvent was then removed and the residue was chromatographed on silica gel. Elution with CH_2Cl_2/hexane (1:4) afforded two fractions. The first band, which was yellow, was trace in amount and was not identified. The second band was red. The tail of the second band contains mostly **3b-*cis*** and a small amount of impurities as indicated by the ^{31}P NMR and was not collected. After the solvent was removed from the second band, pure **3b-*cis*** was obtained as a red solid. Yield: 0.16 g (54%). Anal. Calcd for $C_{26}H_{24}O_6P_2FeW$: C, 42.54; H, 3.30. Found: C, 42.40; H, 3.12. MS (FAB): M − CO^+ *m/z* 707.

Synthesis of $CpFe(CO)_2(\mu$-$PPh_2)W(CO)_4(P(OMe)_3)$ (3c). To a solution of **1** (0.32 g, 0.50 mmol) in 30 mL of THF was added 150 μL (1.2 mmol) of $P(OMe)_3$ under N_2 at ambient temperature in the dark. After 2 h, the solution changed from dark brown to red. Solvent was then removed, and the residue was chromatographed on silica gel. Elution with CH_2Cl_2/hexane (1:4) afforded two fractions. The first band, which was yellowish orange, was a mixture of **1** and **2**. The second band was red. After the solvent was removed, pure **3c-*cis*** was obtained as a red solid. Yield: 0.25 g (65%). Anal. Calcd for $C_{26}H_{24}O_9P_2FeW$: C, 39.93; H, 3.09. Found: C, 39.88; H, 3.02. $^{13}C\{^1H\}$ NMR ($CDCl_3$): δ 214.6 (d, $^2J_{P-C}$ = 14.7 Hz, 2CO), 207.6 (dd, $^2J_{P-C}$ = 3.7 Hz, $^2J_{P-C}$ = 45.3 Hz, 1CO), 206.3 (dd, $^2J_{P-C}$ = 20.9 Hz, $^2J_{P-C}$ = 9.4 Hz, 1CO), 203.2 (dd, $^2J_{P-C}$ = 6.1 Hz, $^2J_{P-C}$ = 11.0 Hz, J_{P-W} = 137.4 Hz, 2CO), 146.51 (d, J_{P-C} = 12.0 Hz, *ipso*-C, PPh_2), 133.47 (d, $^2J_{P-C}$ = 9.86 Hz, *o*-C, PPh_2), 127.5 (s, *p*-C, PPh_2), 127.0 (d, $^2J_{P-C}$ = 8.0 Hz, *m*-C, PPh_2), 88.2 (s, C_5H_5), 51.4 (d, $^2J_{P-C}$ = 4.0 Hz, $P(OMe)_3$). MS (FAB): M^+ *m/z* 782.

After the solvent was removed from the tail of the second band, 0.07 g of red solid which was identified as a mixture of **3c-*cis*** and **3c-*trans*** by ^{31}P NMR and ^{13}C NMR was obtained.

In order to obtain pure **3c-*trans***, 3.5 g of **1** was allowed to react with 1 equiv of $P(OMe)_3$ by following the above procedure. In the purification procedure by chromatography, the tail of the second band was collected. After the solvent was removed, pure **3c-*trans*** was obtained as a red solid. Yield: 0.34 g (8%). Anal. Calcd for $C_{26}H_{24}O_9P_2FeW$: C, 39.93; H, 3.09. Found: C, 40.10; H, 3.08. $^{13}C\{^1H\}$ NMR ($CDCl_3$): δ 214.8 (d, $^2J_{P-C}$ = 15.5 Hz, 2CO), 202.9 (dd, $^2J_{P-C}$ = 8.3 Hz, $^2J_{P-C}$ = 6.1 Hz, J_{W-C} = 129.3 Hz, 4CO), 147.6 (d, J_{P-C} = 14.4 Hz, *ipso*-C, PPh_2), 132.7 (d, $^2J_{P-C}$ = 9.8 Hz, *o*-C, PPh_2), 127.53 (s, *p*-C, PPh_2), 127.44 (d, $^2J_{P-C}$ = 8.8 Hz, *m*-C, PPh_2), 88.3 (s), 51.6 (s). MS (FAB): M − CO^+ *m/z* 754.

Synthesis of $CpFe(CO)_2(\mu$-$PPh_2)W(CO)_4(PPh_2H)$ (3d). To a solution of **1** (0.37 g, 0.58 mmol) in 30 mL of THF was added 122 μL (0.70 mmol) of PPh_2H under N_2 at ambient temperature in the dark. After 1 h, the solution changed from dark brown to red. Solvent was then removed, and the residue was chromatographed on silica gel. Elution with CH_2Cl_2/hexane (1:4) afforded two fractions. The first band, which was yellow, was a mixture of **1** and **2**. The third band was red. The ^{31}P NMR indicated that it was a mixture of **3d-*cis*** and **5d**. The second band was red. After the solvent was removed, pure **3d-*cis*** was obtained as a solid. Yield: 0.31 g (64%). Anal. Calcd for $C_{35}H_{26}O_6P_2FeW$: C, 49.80; H, 3.10. Found: C, 49.40; H, 3.05. $^{13}C\{^1H\}$ NMR ($CDCl_3$): δ 214.7 (d, $^2J_{P-C}$ = 14.7 Hz,

Table 2. Crystal and Intensity Collection Data for 3b-*cis*, 3c-*trans*, 4, and 5c-*trans*

	3b-*cis*	3c-*trans*	4	5e-*trans*
mol formula	$C_{26}H_{24}FeO_6P_2W$	$C_{26}H_{24}FeO_9P_2W$	$C_{26}H_{24}FeO_6P_2W$	$C_{40}H_{30}FeO_5P_2W{\cdot}CH_2Cl_2$
mol wt	734.12	782.11	734.11	977.25
space group	$P2_1/c$ (No. 14)	$Pna2_1$ (No. 33)	$P2_1/n$ (alt $P2_1/c$, No. 14)	$P2_1/a$ (No. 14)
a (Å)	9.832(4)	22.779(4)	15.768(2)	18.6696(8)
b (Å)	16.027(3)	11.669(2)	10.7111(2)	12.6178(6)
c (Å)	18.264(4)	10.580(1)	17.784(2)	18.195(1)
α (deg)	90	90	90	90
β (deg)	103.87(2)	90	114.10(1)	118.220(5)
γ (deg)	90	90	90	90
V (Å^3)	2793(1)	2812.2(7)	2741.8(7)	3777.5(3)
ϱ(calcd) (Mg m^{-3})	1.745	1.847	1.778	1.718
Z	4	4	4	4
cryst dimens (mm)	0.51 × 0.44 × 0.38	0.25 × 0.25 × 0.25	0.45 × 0.44 × 0.38	0.31 × 0.18 × 0.06
abs coeff μ (Mo Kα) (mm^{-1})	4.87	4.85	4.98	3.76
temp	room temp	room temp	room temp	room temp
radiation λ(Mo Kα) (Å)	0.710 73	0.710 73	0.710 73	0.710 73
2θ range (deg)	45	50	45	45
scan type	$\omega-2\theta$	$\omega-2\theta$	$\omega-2\theta$	$\omega-2\theta$
ω scan speed (deg)	1.04–8.24	0.90–8.24	1.50–8.24	1.50–8.24
no. of unique rflns	3645	2599	3574	4926
no. of obsd rflns	2982 ($>2.0\sigma(I)$)	2153 ($>2.5\sigma(I)$)	3005 ($>2.0\sigma(I)$)	3706 ($>2.5\sigma(I)$)
R_{int}[a]	0.013	0.014	0.011	0.014
no. of variables	325	351	325	454
R	0.026	0.023[b]	0.021	0.028
R_w	0.031	0.026	0.024	0.030
S	1.61	1.29	1.34	1.23
ΔF (e/Å^3)	<1.210	<0.470	<0.910	<0.720

[a] Merging after absorption correction. [b] Space group $Pna2_1$ is chiral, and refinement with $\eta = -1$ converged with higher values of R and R_w (0.029 and 0.034, respectively) than were found for $\eta = +1$; thus, the absolute configuration is as shown.

2CO), 210.2 (dd, $^2J_{P-C}$ = 3.7 Hz, $^2J_{P-C}$ = 25.6 Hz, 1CO), 208.3 (dd, $^2J_{P-C}$ = 7.3 Hz, $^2J_{P-C}$ = 22.0 Hz, 1CO), 203.5 (dd, $^2J_{P-C}$ = 6.1 Hz, $^2J_{P-C}$ = 6.1 Hz, 2CO), 88.3 (s, C_5H_5). MS (FAB): M^+ *m/z* 844.

Synthesis of CpFe(CO)$_2$(μ-PPh$_2$)W(CO)$_4$(PPh$_3$) (3e). To a solution of **1** (0.47 g, 0.73 mmol) in 30 mL of THF was added 0.25 g (0.90 mmol) of PPh_3 under N_2 at ambient temperature in the dark. After 4 h, the solution changed from dark brown to red. The solvent was then removed, and the residue was chromatographed on silica gel. Elution with CH_2Cl_2/hexane (1:4) afforded three fractions. The first band, which was yellow, was unreacted **1**. The third band was red. The ^{31}P NMR of the mixture indicated that it was a mixture of **3e** and CpFe(CO)(μ-PPh$_2$)W(CO)$_4$(PPh$_3$) (**5e**). The second band was red. After the solvent was removed, pure **3e** was obtained as a red solid. Yield: 0.19 g (29%). Anal. Calcd for $C_{41}H_{30}O_6P_2FeW$: C, 53.51; H, 3.29. Found: C, 53.52; H, 3.49. $^{13}C\{^1H\}$ NMR ($CDCl_3$): δ 215.1 (d, $^2J_{P-C}$ = 15.4 Hz, 2CO), 205.6 (t, $^2J_{P-C}$ = 5.1 Hz, J_{P-W} = 128.3 Hz, 4CO), 88.3 (s, C_5H_5). MS (FAB): M^+ *m/z* 920.

Synthesis of CpFe(CO)(PMe$_3$)(μ-PPh$_2$)W(CO)$_5$ (4). To a solution of **1** (0.26 g, 0.40 mmol) in 30 mL of THF was added 92 μL (0.91 mmol) of PMe_3 under N_2 at ambient temperature in the dark. After it was stirred for 3 h, the solution changed from dark brown to red. The solvent was then removed, and the residue was chromatographed on silica gel. Elution with CH_2Cl_2/hexane (1:4) afforded two fractions. The first band, which was yellow, was unreacted **2** as identified by ^{31}P NMR. The second band was red. After the solvent was removed, pure **4** was obtained as a red solid. Yield: 0.12 g (52%). Anal. Calcd for $C_{26}H_{24}O_6P_2FeW$: C, 42.54; H, 3.30. Found: C, 42.44; H, 3.29. $^{13}C\{^1H\}$ NMR ($CDCl_3$): δ 219.2 (dd, $^2J_{P-C}$ = 21.8 Hz, 30.5 Hz), 201.6 (d, $^2J_{P-C}$ = 17.2 Hz), 200.6 (d, $^2J_{P-C}$ = 4.4 Hz), 148.6 (d, J_{P-C} = 6.2 Hz, *ipso*-C PPh_2), 142.1 (d, J_{P-C} = 4.6 Hz, *ipso*-C′, PPh_2), 133.8 (d, $^2J_{P-C}$ = 9.0 Hz, *o*-C, PPh_2), 133.2 (d, $^2J_{P-C}$ = 9.4 Hz, *o*-C′, PPh_2), 127.4 (m, *p*-C, *p*-C′, *m*-C, *m*-C′, PPh_2), 85.4 (s, C_5H_5), 20.75 (d, J_{P-C} = 29.2 Hz, PMe_3).

Reaction of 2 with PR$_3$ (R = Ph, OMe) and PPh$_2$H. To a yellow solution containing 0.50 g of **2** in 20 mL of THF was added 90 μL of $P(OMe)_3$. The solution was stirred in the dark at ambient temperature overnight. No color change was observed. The result of a ^{31}P NMR study of the reaction mixture indicated the existence of unreacted **2** and $P(OMe)_3$.

Similar reaction conditions were applied to the reaction between **2** and PPh_3 or PPh_2H. No complex **3** was observed in the reaction product according to ^{31}P NMR spectra of the reaction mixtures.

Synthesis of CpFe(CO)(μ-PPh$_2$)W(CO)$_4$(PMe$_3$) (5b). A red solution of **3b** (0.40 g) in 30 mL of THF was irradiated with UV for 15 min. The solution changed to dark brown. The ^{31}P NMR of the solution indicated that **5b-*trans*** was the only product. After the solvent was removed, a quantitative amount of **5b** was obtained. Anal. Calcd for $C_{25}H_{24}O_5P_2FeW$: C, 42.49; H, 3.40. Found: C, 42.70; H, 3.63. $^{13}C\{^1H\}$ NMR ($CDCl_3$): δ 215.0 (d, $^2J_{P-C}$ = 17.2 Hz, Fe–CO), 200 (vb, W–CO), 145.6 (d, J_{P-C} = 31.4 Hz, *ipso*-C, PPh_2), 143.0 (d, J_{P-C} = 42.0 Hz, *ipso*-C′, PPh_2), 134.4 (d, $^2J_{P-C}$ = 9.0 Hz, *o*-C, PPh_2), 132.9 (d, $^2J_{P-C}$ = 10.5 Hz, *o*-C′, PPh_2), 128.7 (s, *p*-C, PPh_2), 128.2 (s, *p*-C′, PPh_2), 128.1 (d, $^2J_{P-C}$ = 10.4 Hz, *m*-C, *m*-C, PPh_2), 127.5 (d, $^2J_{P-C}$ = 9.6 Hz, *m*-C′, PPh_2), 83.9 (s, C_5H_5), 20.1 (d, J_{P-C} = 30.6 Hz, PMe_3). MS (FAB): $M^+ - CO$ *m/z* 679.

Synthesis of CpFe(CO)(μ-PPh$_2$)W(CO)$_4$(P(OMe)$_3$) (5c). A red solution of **3c** (0.205 g) in 30 mL of THF was irradiated with UV light for 100 min. The solution changed to dark brown. The ^{31}P NMR of the solution indicated that there were two isomers (**5c-*cis*** and **5c-*trans***) in the solution. The solvent was then removed, and the residue was chromatographed on grade III Al_2O_3 and eluted with CH_2Cl_2/hexane (1:4) to afford two fractions. Only a trace amount of yellow oil was obtained from the first fraction, and it was not identified. After the solvent was removed from the second band, a mixture of cis and trans isomers of **5c** was obtained as a brown solid. Yield: 0.103 g (52%). Anal. Calcd for $C_{25}H_{24}O_8P_2FeW$: C, 39.82; H, 3.21. Found: C, 40.21; H, 3.38. MS (FAB): M^+ *m/z* 754.

Synthesis of CpFe(CO)(μ-PPh$_2$)W(CO)$_4$(PPh$_2$H) (5d). A red solution of **3d** (0.80 g) in 50 mL of THF was irradiated with UV light for 100 min. The solution changed to dark brown. The ^{31}P NMR of the solution indicated that there were two isomers in the solution. The solvent was then removed, and the residue was chromatographed on Al_2O_3. Elution with CH_2Cl_2/hexane (1:4) afforded two fractions. A trace amount

Table 3. Atomic Coordinates and Isotropic Thermal Parameters (Å²) for 3b-*cis*

atom	*x*	*y*	*z*	B_{iso}[a]
W	0.19540(3)	0.10079(2)	0.11788(1)	3.20(1)
Fe	0.07628(10)	0.29442(7)	0.24274(6)	4.54(5)
P1	0.13995(17)	0.25800(10)	0.13238(9)	3.30(7)
P2	0.45866(19)	0.11327(12)	0.13865(11)	4.47(9)
O1	0.2433(6)	0.0566(4)	0.2917(3)	7.4(3)
O2	−0.1185(5)	0.0497(4)	0.0978(3)	6.7(3)
O3	0.2374(7)	−0.0870(3)	0.0860(3)	7.1(3)
O4	0.1803(7)	0.1349(4)	−0.0543(3)	7.8(4)
O5	0.1436(7)	0.4700(4)	0.2327(4)	8.4(4)
O6	0.3427(6)	0.2467(5)	0.3421(3)	8.0(4)
C1	0.2283(7)	0.0748(4)	0.2289(4)	4.3(3)
C2	−0.0037(8)	0.0708(4)	0.1032(4)	4.8(4)
C3	0.2240(8)	−0.0182(4)	0.0981(4)	4.7(4)
C4	0.1794(8)	0.1228(4)	0.0062(4)	4.5(4)
C5	0.1216(8)	0.3999(6)	0.2365(5)	6.1(4)
C6	0.2403(9)	0.2649(5)	0.3020(4)	5.5(4)
C7	−0.1119(8)	0.2297(7)	0.1990(5)	6.2(5)
C8	−0.0468(8)	0.1938(6)	0.2642(5)	5.8(5)
C9	−0.0320(10)	0.2525(8)	0.3223(5)	7.4(6)
C10	−0.0902(11)	0.3255(8)	0.2906(8)	8.9(7)
C11	−0.1394(8)	0.3136(8)	0.2122(6)	7.4(6)
C12	0.5319(8)	0.1742(5)	0.0746(5)	6.2(4)
C13	0.5576(8)	0.1493(6)	0.2299(5)	7.5(5)
C14	0.5409(9)	0.0128(5)	0.1316(6)	8.3(6)
C21	−0.0061(6)	0.3018(4)	0.0582(4)	3.6(3)
C22	−0.0270(8)	0.3872(4)	0.0530(5)	5.3(4)
C23	−0.1416(10)	0.4215(5)	0.0019(5)	6.3(5)
C24	−0.2379(8)	0.3693(5)	−0.0437(4)	5.6(4)
C25	−0.2172(8)	0.2861(5)	−0.0395(4)	5.1(4)
C26	−0.1020(7)	0.2521(4)	0.0109(4)	4.0(3)
C31	0.2826(6)	0.3256(4)	0.1166(4)	3.8(3)
C32	0.3867(8)	0.3580(5)	0.1744(5)	5.4(4)
C33	0.4979(8)	0.4039(5)	0.1582(6)	7.0(5)
C34	0.5032(9)	0.4191(5)	0.0859(7)	7.3(6)
C35	0.4022(10)	0.3873(5)	0.0283(6)	6.5(5)
C36	0.2918(7)	0.3414(4)	0.0430(4)	4.7(4)

[a] $B_{iso} = {}^8/_3\pi^2\sum_{i,j}U_{ij}a_ia_ja_i^*a_j^*$.

Table 4. Atomic Coordinates and Isotropic Thermal Parameters (Å²) for 3c-*trans*

atom	*x*	*y*	*z*	B_{iso}[a]
W	0.13568(1)	0.52344(3)	0.81599	2.37(2)
Fe	0.10412(6)	0.89906(12)	0.72502(18)	2.91(6)
P1	0.07612(9)	0.72694(19)	0.83525(32)	2.48(9)
P2	0.18519(10)	0.32548(20)	0.79843(31)	2.73(11)
O1	0.2482(4)	0.6475(8)	0.7069(10)	7.0(5)
O2	0.1987(4)	0.5574(8)	1.0555(8)	5.7(4)
O3	0.0321(3)	0.3812(7)	0.9431(8)	5.1(4)
O4	0.0871(4)	0.4790(9)	0.5653(8)	6.0(4)
O5	0.0466(3)	1.0746(7)	0.8804(7)	4.6(3)
O6	0.2206(2)	0.9100(6)	0.8292(11)	4.7(4)
O12	0.2537(2)	0.3296(5)	0.8293(10)	3.9(3)
O13	0.1836(3)	0.2538(6)	0.6772(7)	3.6(3)
O14	0.1618(3)	0.2048(6)	0.8678(6)	3.9(3)
C1	0.2064(5)	0.6043(10)	0.7450(11)	4.5(5)
C2	0.1745(4)	0.5493(9)	0.9685(10)	3.2(4)
C3	0.0691(4)	0.4338(9)	0.8965(9)	3.2(4)
C4	0.1023(4)	0.4955(9)	0.6557(10)	3.4(4)
C5	0.0708(4)	1.0036(7)	0.8160(16)	3.1(5)
C6	0.1738(4)	0.9028(8)	0.7896(8)	2.8(4)
C7	0.0900(6)	1.0175(11)	0.5859(11)	5.3(6)
C8	0.1424(5)	0.9516(13)	0.5679(12)	5.4(6)
C9	0.1270(7)	0.8215(16)	0.5652(11)	5.2(7)
C10	0.0671(7)	0.8111(12)	0.5804(10)	5.1(7)
C11	0.0452(5)	0.9311(13)	0.5930(10)	4.6(6)
C12	0.2869(4)	0.2133(9)	0.8272(16)	4.7(6)
C13	0.2104(5)	0.3116(12)	0.5781(10)	5.2(6)
C14	0.1596(7)	0.2108(12)	0.9891(11)	5.3(7)
C21	0.0729(4)	0.7721(9)	0.9905(9)	2.9(4)
C22	0.1135(5)	0.8503(13)	1.0369(9)	3.8(6)
C23	0.1120(6)	0.8810(12)	1.1525(11)	5.2(6)
C24	0.0689(6)	0.8291(11)	1.2205(9)	4.8(6)
C25	0.0287(5)	0.7476(11)	1.1746(10)	4.3(5)
C26	0.0312(5)	0.7201(9)	1.0605(9)	3.9(5)
C31	−0.0043(3)	0.7088(8)	0.8069(11)	2.5(4)
C32	−0.0430(4)	0.8032(8)	0.8392(11)	3.5(5)
C33	−0.1023(4)	0.7899(8)	0.8199(14)	4.2(5)
C34	−0.1241(4)	0.6800(12)	0.7693(10)	4.4(5)
C35	−0.0858(4)	0.5861(10)	0.7384(10)	4.1(5)
C36	−0.0264(4)	0.6022(10)	0.7576(9)	3.4(4)

[a] $B_{iso} = {}^8/_3\pi^2\sum_{i,j}U_{ij}a_ia_ja_i^*a_j^*$.

of yellow oil was obtained from the first fraction, and it was not identified. After the solvent was removed from the second band, a brown solid was obtained. It was identified by ^{31}P NMR as a mixture of cis and trans isomers of **5d**. Yield: 0.56 g (73%). Anal. Calcd for $C_{34}H_{26}O_5P_2FeW$: C, 50.03; H, 3.21. Found: C, 50.40; H, 3.14. MS (FAB): M^+ *m/z* 817.

Synthesis of CpFe(CO)(μ-PPh₂)W(CO)₄(PPh₃) (5e). A red solution of **3e** (0.116 g) in 10 mL of THF was irradiated with UV light for 30 min. The solution changed to yellowish brown. The ^{31}P NMR of the solution indicated that there were two isomers (**5e-*cis*** and **5e-*trans***) in the solution. Separation of the isomers by chromatography on grade III Al_2O_3 failed. After the solvent was removed, the mixture was obtained as a yellowish brown solid. Yield: 0.097 g (86%). The trans isomer was crystallized as single crystals by slow diffusion of hexane into the saturated solution of the mixture in CH_2Cl_2. Anal. Calcd for $C_{40}H_{30}O_5P_2FeW$: C, 53.84; H, 3.39. Found: C, 53.71; H, 3.37. $^{13}C\{^1H\}$ NMR ($CDCl_3$): δ 215.4 (d, $^2J_{P-C}$ = 15.4 Hz), 199 (vb) 83.9 (s, C_5H_5). MS (FAB): M^+ *m/z* 893.

Structure Determination of CpFe(CO)₂(μ-PPh₂)W(CO)₄(PMe₃) (3b-*cis*), CpFe(CO)(PMe₃)(μ-PPh₂)W(CO)₅ (4), CpFe(CO)₂(μ-PPh₂)W(CO)₄(P(OMe)₃) (3c-*trans*), and CpFe(CO)(μ-PPh₂)W(CO)₄(PPh₃) (5e-*trans*). Crystals of complexes **3b-*cis***, **4**, and **3c-*trans*** were grown by slow diffusion of hexanes into the saturated CH_2Cl_2 solution of the relevant complex at −15 °C in the air. Crystals of **5e-*trans*** were obtained by slow diffusion of hexanes into the saturated CH_2Cl_2 solution of the mixture **5e-*trans*** and **5e-*cis***. Diffraction measurements were made using an Enraf-Nonius CAD4 diffractometer and Mo Kα radiation. All data reduction and refinements were carried out on a MicroVax 3600 computer using NRCVAX programs. Intensities were collected and corrected for decay, absorption (empirical, ψ-scan), and Lp effects. Structures were solved by direct methods and refined on *F* by using full-matrix least-squares techniques. An *E* map from the starting set with the highest combined figure of merit revealed coordinates for W and Fe atoms. The remaining non-H atoms were located from successive difference Fourier maps and were refined anisotropically. The atomic parameters for all H atoms were excluded in the least-squares refinements, the hydrogen positions were displaced along the C–H vector to make the C–H distance of 1.08 Å.

Crystal data and details of data collection and structure analysis are summarized in Table 2. The final positional parameters for all atoms are listed in Tables 3 (**3b-*cis***), 4 (**3c-*trans***), 5 (**4**), and 6 (**5c-*trans***). Selected interatomic distances and bond angles are given in Tables 7 (**3b-*cis*** and **4**) and 8 (**3c-*trans*** and **5e-*trans***). The thermal parameters for these complexes are provided in the supplementary material.

Results and Discussion

Reactions of 2 with Phosphines and Molecular Structure of 4. The complex **2** remained intact after stirring with L (L = PPh_3, PPh_2H, $P(OMe)_3$) in THF at ambient temperature in the dark overnight. However, it reacted with PMe_3 to form **4** in THF at ambient temperatures within several hours. The upfield position of the phosphido bridge signal and the absence of the J_{P-W} satellites of the PMe_3 signal in the ^{31}P NMR indicates the absence of a metal–metal bond and the coordination of PMe_3 to the Fe atom in the complex.[5]

Table 5. Atomic Coordinates and Isotropic Thermal Parameters (Å²) for 4

atom	x	y	z	B_{iso}[a]
W	0.59218(1)	0.51543(2)	0.84810(1)	2.93(1)
Fe	0.66027(5)	0.89366(6)	0.92594(4)	3.52(4)
P1	0.70733(8)	0.68543(11)	0.94218(7)	2.65(6)
P2	0.76722(11)	0.97647(13)	1.03786(9)	4.49(8)
O1	0.7675(3)	0.3479(4)	0.8741(3)	7.1(3)
O2	0.5729(3)	0.3841(4)	1.0003(3)	6.4(3)
O3	0.4233(3)	0.6921(4)	0.8307(2)	5.1(2)
O4	0.5840(3)	0.6010(5)	0.6753(2)	7.2(3)
O5	0.4567(3)	0.3032(4)	0.7488(2)	5.7(2)
O6	0.5322(3)	0.8682(4)	1.0024(3)	7.0(3)
C1	0.7047(4)	0.4097(5)	0.8652(3)	4.4(3)
C2	0.5829(4)	0.4360(5)	0.9491(3)	3.9(3)
C3	0.4840(4)	0.6292(5)	0.8374(3)	3.6(3)
C4	0.5894(4)	0.5742(5)	0.7397(3)	4.4(3)
C5	0.5068(4)	0.3820(5)	0.7848(3)	4.0(3)
C6	0.5859(4)	0.8748(5)	0.9741(4)	4.4(3)
C8	0.5592(6)	0.9155(9)	0.8037(5)	8.0(5)
C9	0.6409(8)	0.8788(7)	0.8025(4)	7.9(6)
C10	0.7078(6)	0.9630(9)	0.8399(5)	7.2(5)
C11	0.6691(7)	1.0589(6)	0.8664(4)	7.1(5)
C12	0.5777(7)	1.0325(8)	0.8469(5)	8.0(5)
C13	0.8732(5)	1.0292(6)	1.0318(4)	7.4(4)
C14	0.8131(4)	0.8965(5)	1.1356(3)	5.1(3)
C15	0.7258(6)	1.1171(6)	1.0689(4)	9.2(5)
C21	0.7402(3)	0.6159(4)	1.0456(3)	2.7(2)
C22	0.8090(4)	0.5250(5)	1.0752(3)	3.7(3)
C23	0.8288(4)	0.4657(5)	1.1485(3)	4.8(3)
C24	0.7804(4)	0.4921(6)	1.1946(3)	5.3(3)
C25	0.7104(4)	0.5786(6)	1.1667(3)	5.0(3)
C26	0.6908(3)	0.6387(5)	1.0928(3)	3.9(3)
C31	0.8204(3)	0.6823(4)	0.9335(3)	3.0(2)
C32	0.9028(4)	0.7074(5)	0.9998(3)	4.2(3)
C33	0.9869(4)	0.7080(6)	0.9916(4)	5.0(3)
C34	0.9892(4)	0.6883(6)	0.9171(4)	5.4(4)
C35	0.9087(5)	0.6651(6)	0.8504(4)	5.8(4)
C36	0.8249(4)	0.6604(5)	0.8584(3)	4.5(3)

[a] $B_{iso} = {}^8/_3\pi^2\sum_{ij}U_{ij}a_ia_ja_i^*a_j^*$.

The structure of **4** was further characterized by a single-crystal X-ray diffraction study (Figure 1).

The long distance between Fe and W (4.2741(10) Å) in **4** indicates the absence of a metal–metal bond (Table 7). The replacement of the Fe carbonyl in **2** with PMe_3 does not increase the repulsion between the Fe and the W moieties in **4**, as shown by the observation that the distance between W and Fe and the Fe–P–W angle (118.75(5)°) in **4** are almost the same as the distance between Fe and W (4.2110(9) Å) and the Fe–P–W angle (118.42(6)°) in **2**.[2]

That only PMe_3 can substitute the Fe carbonyl ligand is explained by the small cone angle and the high basicity of the phosphine ligand.[6] For the other phosphines, greater steric factors or poor basicity may inhibit the substitution.

Addition Reactions of 1 with Phosphines and CO. Reactions of **1** with Lewis bases L (L = PMe_3, PPh_2H, $P(OMe)_3$) at room temperature yielded $CpFe(CO)_2(\mu\text{-}PPh_2)W(CO)_4L$ (**3**) with L regiospecifically coordinating to W. When L was CH_3CN, PMe_3, or PPh_2H, only the cis isomer (**3-*cis***) was obtained. For PPh_3 and $P(OMe)_3$, both cis and trans (**3-*trans***) isomers were produced (Scheme 1).

Table 6. Atomic Coordinates and Isotropic Thermal Parameters (Å²) for 5e-*trans*

atom	x	y	z	B_{iso}[a]
W	0.236431(17)	−0.183485(23)	0.061107(18)	2.433(15)
Fe	0.16202(6)	−0.33176(9)	0.12257(6)	3.19(5)
P2	0.21491(11)	0.00249(15)	0.00705(12)	2.79(9)
P1	0.25782(11)	−0.37227(15)	0.09110(12)	2.93(10)
O1	0.3329(4)	−0.1088(5)	0.2489(4)	6.5(4)
O2	0.4024(3)	−0.2048(5)	0.0548(5)	6.8(5)
O3	0.1251(4)	−0.2578(5)	−0.1251(4)	5.7(4)
O4	0.0789(3)	−0.1131(4)	0.0745(4)	4.9(4)
O5	0.0282(3)	−0.3899(5)	−0.0375(4)	5.6(4)
C1	0.2988(5)	−0.1361(6)	0.1802(5)	4.0(5)
C2	0.3418(5)	−0.1937(6)	0.0550(5)	4.1(5)
C3	0.1660(5)	−0.2311(6)	−0.0583(5)	3.3(4)
C4	0.1340(5)	−0.1554(6)	0.0739(5)	3.4(4)
C5	0.0824(5)	−0.3648(6)	0.0255(5)	3.7(4)
C6	0.0967(6)	−0.3137(10)	0.1897(6)	5.7(6)
C7	0.1698(6)	−0.2612(8)	0.2326(5)	5.0(6)
C8	0.2328(5)	−0.3336(8)	0.2533(5)	4.7(5)
C9	0.1991(6)	−0.4347(7)	0.2242(6)	5.3(6)
C10	0.1139(7)	−0.4226(9)	0.1838(6)	6.4(7)
C11	0.2336(4)	−0.4661(6)	0.0051(4)	3.2(4)
C12	0.2689(5)	−0.4550(7)	−0.0464(5)	4.8(5)
C13	0.2497(7)	−0.5250(8)	−0.1123(6)	6.1(7)
C14	0.1981(7)	−0.6075(8)	−0.1234(6)	5.9(7)
C15	0.1633(6)	−0.6209(7)	−0.0736(6)	5.5(6)
C16	0.1813(5)	−0.5506(6)	−0.0077(5)	4.0(5)
C21	0.3542(4)	−0.4261(6)	0.1720(5)	3.7(4)
C22	0.4137(5)	−0.3598(7)	0.2271(6)	5.2(5)
C23	0.4854(5)	−0.4007(9)	0.2904(6)	6.6(6)
C24	0.4997(6)	−0.5053(10)	0.2984(7)	6.6(7)
C25	0.4419(6)	−0.5743(8)	0.2441(7)	6.7(7)
C26	0.3683(5)	−0.5347(7)	0.1803(6)	5.4(5)
C31	0.1226(4)	0.0271(6)	−0.0924(4)	2.9(4)
C32	0.0519(4)	−0.0300(6)	−0.1128(5)	4.0(4)
C33	−0.0173(4)	−0.0125(7)	−0.1887(5)	4.5(5)
C34	−0.0177(5)	0.0615(7)	−0.2435(5)	4.1(5)
C35	0.0513(5)	0.1196(7)	−0.2239(5)	4.4(5)
C36	0.1207(5)	0.1013(6)	−0.1486(5)	3.7(4)
C41	0.2078(4)	0.0985(5)	0.0786(4)	2.9(4)
C42	0.1365(5)	0.1513(6)	0.0609(5)	4.1(4)
C43	0.1342(6)	0.2241(8)	0.1169(6)	5.8(6)
C44	0.2017(7)	0.2438(7)	0.1903(7)	5.7(7)
C45	0.2736(6)	0.1907(7)	0.2101(5)	5.4(6)
C46	0.2759(5)	0.1196(6)	0.1547(5)	4.0(5)
C51	0.2927(4)	0.0591(6)	−0.0158(4)	3.2(4)
C52	0.3222(5)	0.1617(7)	0.0061(5)	4.5(5)
C53	0.3795(6)	0.2011(8)	−0.0158(7)	6.7(7)
C54	0.4056(6)	0.1414(11)	−0.0600(7)	7.0(8)
C55	0.3763(6)	0.0389(9)	−0.0834(6)	6.3(7)
C56	0.3203(5)	−0.0012(7)	−0.0605(5)	4.8(5)
C60	0.4669(12)	−0.4112(17)	0.9603(15)	18.8(8)
CL1	0.4835(6)	−0.5627(9)	0.9228(7)	24.9(4)
CL2	0.4989(17)	−0.471(3)	0.9359(18)	16.0(8)

[a] $B_{iso} = {}^8/_3\pi^2\sum_{ij}U_{ij}a_ia_ja_i^*a_j^*$.

The regiospecific assignment is revealed by the observation of the J_{P-W} satellites for the signal of L in the ^{31}P NMR of **3**. An upfield shift of the phosphido bridge phosphorus signal in the ^{31}P NMR indicates the cleavage of the metal–metal bond.[5]

For the assignment of the stereoisomers, a large J_{P-P} value in the W complex usually indicates the phosphine ligands are trans to each other.[7] However, this method of assignment can be used only when L is a phosphine and both isomers are obtained. When L is not a phosphine or only one isomer is produced, the ^{13}C NMR spectrum can be used to support the cis and the trans assignment. For **3a-*cis***, the ^{13}C NMR spectrum showed four terminal carbonyl signals (a–d) with an intensity ratio of 2:1:1:2 (Figure 2A). Signal a (214.4 ppm, J_{P-C}

(5) (a) Carty, A. J.; Maclaughlin, S. A.; Nucciarone, D. In *Phosphorus-31 NMR Spectroscopy in Stereochemical Analysis: Organic Compounds and Metal Complexes*; Verkade, J. G., Quin, L. P., Eds.; VCH: New York, 1987; Chapter 16, and references cited therein. (b) Carty, A. J. *Adv. Chem. Ser.* **1982**, *No. 196*, 163. (c) Garrou, P. E. *Chem. Rev.* **1981**, *81*, 229.

(6) Tolman, C. A. *Chem. Rev.* **1977**, *77*, 313.

(7) Ogilvie, F. B.; Jenkins, J. M.; Verkade, J. G. *J. Am. Chem. Soc.* **1970**, *92*, 1916.

Table 7. Selected Bond Lengths (Å) and Bond Angles (deg) in 3b-*cis* and 4

3b-*cis*		4	
	Bond Lengths		
Fe···W	4.1812(11)	Fe···W	4.2741(10)
W–P1	2.6047(17)	W–P1	2.6327(12)
W–P2	2.5322(20)	W–C1	2.021(6)
W–C1	2.019(8)	W–C2	2.045(6)
W–C2	1.970(8)	W–C3	2.041(6)
W–C3	1.974(7)	W–C4	2.011(6)
W–C4	2.038(8)	W–C5	1.970(5)
Fe–P1	2.3238(19)	Fe–P1	2.3309(14)
Fe–C5	1.758(9)	Fe–P2	2.2026(16)
Fe–C6	1.778(9)	Fe–C6	1.724(6)
C1–O1	1.157(9)	C1–O1	1.146(7)
C2–O2	1.159(9)	C2–O2	1.132(7)
C3–O3	1.139(9)	C3–O3	1.136(7)
C4–O4	1.125(9)	C4–O4	1.151(7)
C5–O5	1.151(11)	C5–O5	1.156(6)
C6–O6	1.131(11)	C6–O6	1.151(8)
	Bond Angles		
Fe–P1–W	115.96(7)	Fe–P1–W	118.75(5)
P1–W–P2	98.03(6)	P1–W–C1	87.50(15)
P1–W–C1	94.86(19)	P1–W–C2	90.44(14)
P1–W–C2	91.39(21)	P1–W–C3	88.83(13)
P1–W–C3	174.75(21)	P1–W–C4	97.58(15)
P1–W–C4	88.06(18)	P1–W–C5	175.96(16)
P1–Fe–C5	93.4(3)	P1–Fe–C6	94.20(17)
P1–Fe–C6	93.89(24)	P1–Fe–P2	100.71(5)
W–C1–O1	176.8(6)	W–C1–O1	178.7(5)
W–C2–O2	176.0(6)	W–C2–O2	173.8(4)
W–C3–O3	178.5(7)	W–C3–O3	179.3(4)
W–C4–O4	175.2(7)	W–C4–O4	175.3(5)
Fe–C5–O5	176.0(7)	W–C5–O5	179.0(5)
Fe–C6–O6	177.4(7)	Fe–C6–O6	175.2(5)

Table 8. Selected Bond Lengths (Å) and Bond Angles (deg) in 3c-*trans* and 5e-*trans*

3c-*trans*		5e-*trans*	
	Bond Lengths		
Fe–W	4.1757(15)	Fe–W	2.8548(11)
W–P1	2.5547(22)	W–P1	2.4343(20)
W–P2	2.3877(23)	W–P2	2.5023(19)
W–C1	2.003(14)	W–C1	2.007(8)
W–C2	2.006(11)	W–C2	2.027(8)
W–C3	2.021(10)	W–C3	2.027(8)
W–C4	2.040(12)	W–C4	2.063(8)
Fe–P1	2.319(3)	Fe–P1	2.1809(21)
Fe–C5	1.715(16)	Fe–C5	1.738(8)
Fe–C6	1.758(10)		
C1–O1	1.146(16)	C1–O1	1.154(10)
C2–O2	1.158(14)	C2–O2	1.142(10)
C3–O3	1.146(12)	C3–O3	1.139(10)
C4–O4	1.125(15)	C4–O4	1.164(10)
C5–O5	1.193(18)	C5–O5	1.158(10)
C6–O6	1.164(13)		
	Bond Angles		
Fe–P1–W	117.83(12)	Fe–P1–W	76.20(7)
P1–W–P2	176.09(8)	P1–W–P2	169.94(6)
P1–W–C1	95.9(3)	P1–W–C1	95.70(23)
P1–W–C2	92.4(3)	P1–W–C2	83.64(23)
P1–W–C3	87.5(3)	P1–W–C3	85.53(22)
P1–W–C4	90.3(3)	P1–W–C4	101.84(21)
P1–Fe–C5	92.3(4)	P1–Fe–C5	95.2(3)
P1–Fe–C6	91.6(3)		
W–C1–O1	177.4(11)	W–C1–O1	178.3(7)
W–C2–O2	175.9(9)	W–C2–O2	175.7(7)
W–C3–O3	178.6(9)	W–C3–O3	178.6(6)
W–C4–O4	176.0(9)	W–C4–O4	161.9(6)
Fe–C5–O5	178.5(8)	Fe–C5–O5	177.1(7)
Fe–C6–O6	176.8(8)		

= 15.0 Hz) is assigned to the two CO ligands on Fe on the basis of its position compared with that of the CO ligands on Fe in **2** (214.0 ppm).[4] Signal c (208.5 ppm) is assigned to the CO ligands trans to the phosphido bridge on the basis of its larger J_{P-C} value (30.19 Hz).[8] Signal d (203.4 ppm, J_{P-C} = 5.9 Hz) is assigned to the two CO ligands trans to each other and cis to the CH_3CN. Finally, signal b is assigned to the CO ligand trans to the CH_3CN. For **3c-*trans***, only two carbonyl signals were observed in its spectrum. The signal at 214.8 ppm is assigned to the Fe CO's on the basis of the favorable comparison with the reported resonances at 214.0 ppm for the Fe CO's in the ^{13}C NMR of **2**.[4] The signal at 202.9 ppm is assigned to the four fluxional cis W CO's on the basis of the observed J_{P-W} satellites (J_{P-W} = 129.3 Hz) (Figure 2B). The absence of the trans W CO signal indicates the phosphine ligand occupies the trans position. The structures of **3b-*cis*** and **3c-*trans*** were further characterized by single-crystal X-ray diffraction studies. Their structures are shown in Figures 3 and 4.

The long distances between Fe and W in **3b-*cis*** (4.1812(11) Å) and in **3c-*trans*** (4.1756(15) Å) indicate that there is no metal–metal bond in either complex. In **3c-*trans***, the $P(OMe)_3$ ligand is coordinated to the W trans to the phosphido bridge. In **3b-*cis***, the PMe_3 ligand is cis to the phosphido bridge. One can consider the metallophosphine $CpFe(CO)_2PPh_2$ to be a ligand similar to PR_3. Thus, four CO's, $CpFe(CO)_2PPh_2$, and the PR_3 group (R = Me, OMe) coordinate to the W atom to form a distorted octahedron. The replacement of a CO in **2** with PMe_3 does not increase the repulsion between the Fe and the W moieties in **3b-*cis***, as shown by the observations that the distance between W and Fe (4.1812(11) Å) and the Fe–P–W angle (115.96(7)°) in **3b-*cis*** are almost the same as the distance between Fe and W (4.2110(9) Å) and the Fe–P–W angle (118.42(6)°) in **2**.[2]

The addition reaction was stereospecific, with L cis to the phosphido bridge. The observed **3-*trans*** was formed from the kinetic product **3-*cis***. This was demonstrated by the variable-temperature ^{31}P NMR experiments on **3c-*cis*** in THF. At 280 K, no **3c-*trans*** was observed. At 300 K, a trace amount of **3c-*trans*** was observed in the spectrum. As the temperature went up, the amount of **3c-*trans*** increased. Also, after the complex was heated to reflux temperature in THF overnight, the signal intensity ratio of cis to trans isomers was increased to 1:1. A similar phenomenon was also observed when **3b-*cis*** was heated to reflux temperature in THF overnight. Interestingly, no **3d-*trans*** was observed after heating **3d-*cis*** in THF at reflux temperature overnight. Heating the complex at higher temperature (refluxing in toluene) only resulted in the formation of the metal–metal-bonded complex **5d**.

The regiospecific addition on W may be due to a steric effect because of the bulky Cp, the μ-PPh_2 ligand, and the incoming phosphine. Compared with the $^{13}C\{^1H\}$ NMR spectrum of **2** which had been stirred under ^{13}CO overnight, the $^{13}C\{^1H\}$ NMR spectrum of ^{13}CO-enriched **2** which was prepared by stirring **1** under ^{13}CO showed addition of CO to **1** was predominantly on W and was stereospecifically cis to the phosphido bridge (Figure 5).[9]

(8) (a) Braterman, P. S.; Milne, D. W.; Randall, E. W.; Rosenberg, E. *J. Chem. Soc., Dalton Trans.* **1973**, 1027. (b) Bonder, G. M. *Inorg. Chem.* **1975**, *14*, 2694. (c) Todd, L. J.; Wilkinson, J. R. *J. Organomet. Chem.* **1974**, *77*, 1.

(9) The NOE effect was avoided by using the inverse gate decouple technique.

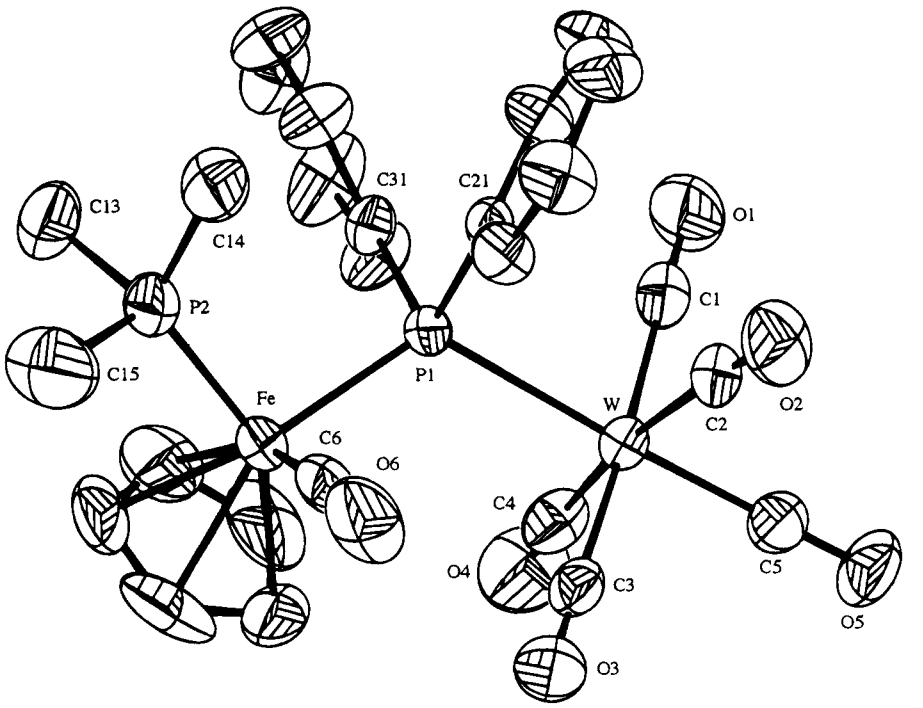

Figure 1. ORTEP drawing of **4**. Hydrogen atoms are omitted.

A small amount of ^{13}CO was coordinated to the Fe site, as shown by the spectrum which indicates that the addition reaction was not totally dominated by the electronic factor.

The phosphine may initially coordinate to Fe to form the kinetic product and further migration of the phosphine to the adjacent W to form **3**, as in the case of $(CO)_4Fe(\mu\text{-}AsMe_2)Co(CO)_2L_2$ (L = PMe_3, $P(OMe)_3$).[10] This possibility is eliminated because of the following observations. First, complex **3b** was not observed in the reaction between **2** and PMe_3 and only complex **4** was isolated at room temperature. Second, after the THF solution of **4** was heated at reflux temperature overnight, only **5b** and unreacted **4** were observed according to the ^{31}P NMR spectrum of the product solution. One may suspect that **3b** was formed as an intermediate which converted immediately to **5b** under the reaction conditions so that **3b** was not detected. However, heating ***3b-cis*** in THF at reflux temperature only resulted in a mixture of ***3b-cis*** and ***3b-trans*** according to the ^{31}P NMR spectrum of the product solution. This excludes the possibility that **3b** was an intermediate in the formation of **5b** from **4** (Scheme 2).

The formation of **3** from **1** requires the loss of one CO from W and the addition of one CO to Fe. There are two possible sources for this added Fe CO ligand. One possibility is that a carbon monoxide on W may first be substituted by the phosphine ligand to form the metal–metal-bonded complex **5d**. Free CO from the environment may react with **5d** to form **3** (Scheme 3). The other possibility is the intramolecular migration of the semibridging CO on W to the adjacent Fe during the reaction. A reaction between **1** and PPh_2H under ^{13}CO was carried out to produce **3c**. Both the mass spectrum and ^{13}C NMR of the product indicated that no ^{13}CO was introduced into the product. These observations exclude the intermolecular CO addition to the W atom in the reaction.

Substitution Enhancement and Switching of the Reaction Site—Role of the Metal–Metal Bond. One can consider the Fe–W bonding as a dative bond (donor–acceptor bond from W^0 to Fe^{II}) which acts as a ligand to replace the Fe carbonyl ligand in **2** to form **1** after photolysis, since the semibridging carbonyl ligand in **1** is primarily bonded to the W atom.[1c,11] The addition reaction usually occurs with the incoming ligand occupying the coordination side where the dative metal–metal bond was originally coordinated, as demonstrated by the addition of a Lewis base to heterobimetallic phosphido-bridged[1c,12] and arsino-bridged complexes.[13] Nevertheless, the addition of L to **1** did not occur at Fe as expected but proceeded regiospecifically at the W atom. Therefore, we suggest that the metal–metal dative bond in the addition reaction of L to **1** behaves as more than just a built-in intramolecular leaving group. In addition, it also has two important impacts on the reactivity of the complex.

First, the metal–metal bond enhances the substitution reaction of the carbonyl ligands on W. If we consider $Cp(CO)_2FePPh_2$ in complexes **2** and **3** as a ligand, complex **3** can be considered as a disubstituted $W(CO)_4LL'$ complex with L′ = $Cp(CO)_2FePPh_2$ and L = PPh_3, PPh_2H, PMe_3, $P(OMe)_3$. The substitution of the W carbonyl ligand usually requires high temperature.[14] The metallophosphine ligand $Cp(CO)_2FePPh_2$ did not activate the $W(CO)_5$ moiety for further substitution,

(10) Langenbach, H.-J.; Vahrenkamp, H. *Chem. Ber.* **1979**, *112*, 3390.

(11) Roberts, D. A.; Steinmetz, G. R.; Breen, M. J.; Shulman, P. M.; Morrison, E. D.; Duttera, M. R.; DeBrosse, C. W.; Whittle, R. R.; Geoffroy, G. L. *Organometallics* **1983**, *2*, 846.

(12) (a) Jenkins, H. A.; Loeb, S. J.; Stephan, D. W. *Inorg. Chem.* **1989**, *28*, 1998. (b) Baker, R. T.; Calabrese, J. C.; Krusic, P. J.; Therien, M. J.; Trogler, W. C. *J. Am. Chem. Soc.* **1988**, *110*, 8392.

(13) Langenbach, H.-J.; Vahrenkamp, H. *Chem. Ber.* **1979**, *112*, 3773.

(14) Keiter, R. L.; Keiter, E. A.; Mittelberg, K. N.; Martin, J. S.; Meyers, V. M.; Wang, J. G. *Organometallics* **1989**, *8*, 1399.

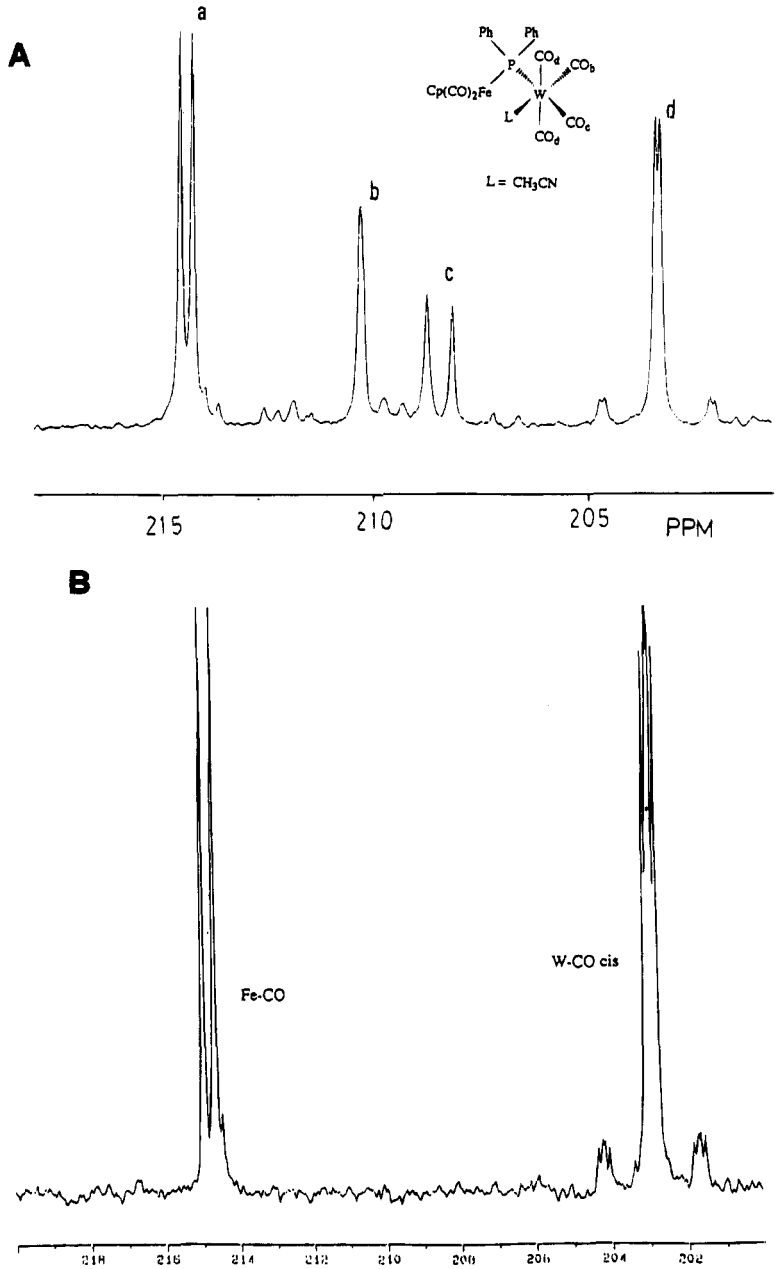

Figure 2. $^{13}C\{^1H\}$ NMR spectra of (A) **3a-*cis*** in $CH_3CN/CDCl_3$ and (B) **3c-*trans*** in $CDCl_3$. Only carbonyl regions are shown in both spectra.

since no **3** was observed when **2** was allowed to react with L in THF overnight. However, addition reactions between **1** and phosphine ligands to form **3** proceeded at ambient temperatures within several hours. Second, the reaction site for substitution is switched by the metal–metal bond. In **2**, an Fe CO ligand was substituted by PMe_3 to form **4** at room temperature. However, L substituted the W CO in complex **1** to form **3** under similar conditions.

The metal–metal bond can influence the reactivity of the bimetallic complex in two ways. One way is electron donation from the filled t_{2g} orbital of the W atom to the iron atom through the metal–metal bond. Powell suggested that the net result of this interaction will be a decrease in $d_{xy}(W) \rightarrow \pi^*(CO)$ bonding to the equatorial CO's.[1f] This may result in the weakening of the W–CO bond in **1**. The second way is that the metal–metal bond can bring the two metals together such that the adjacent iron is able to activate one of the W carbonyl ligands through the donation of the electron from the electron-rich iron atom to the π^* orbital of the adjacent tungsten CO to form a semibridging carbonyl ligand.[15]

Formation of the metal–metal dative bond in **1** thus can be considered as a switch, which not only triggers the substitution of the W carbonyl by the activation of one of the W carbonyls through the adjacent Fe atom but also switches the reaction site from the Fe metal to the adjacent tungsten. These two effects which originated from the influence of one metal to the adjacent metal through the metal–metal bond can be considered as cooperativity effects of the adjacent metal in heterobimetallic complexes.

Synthesis, Spectroscopic Characterization, and Molecular Structure of $CpFe(CO)(\mu\text{-}PPh_2)W(CO)_4L$ (5; L = PPh_3, PPh_2H, PMe_3, $P(OMe)_3$). One of the carbonyl ligands in **3** can be removed by UV irradiation

(15) Cotton, F. A. *Prog. Inorg. Chem.* **1976**, *21*, 1.

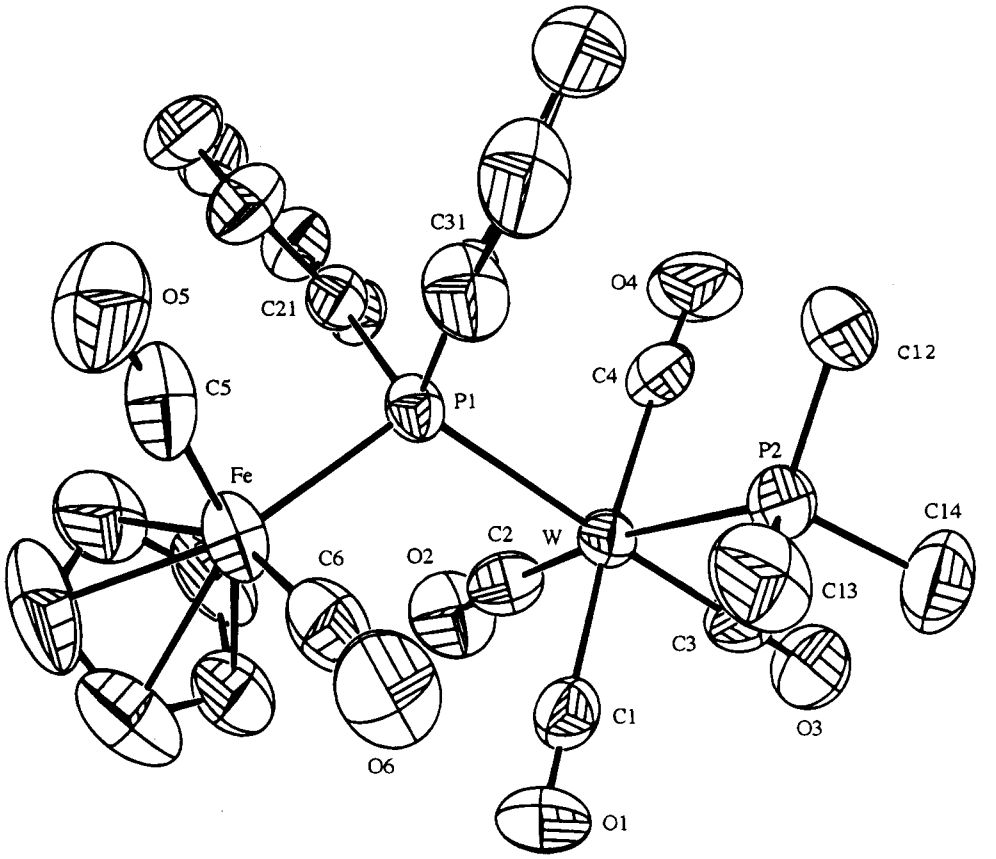

Figure 3. ORTEP drawing of **3b-*cis***. Hydrogen atoms are omitted.

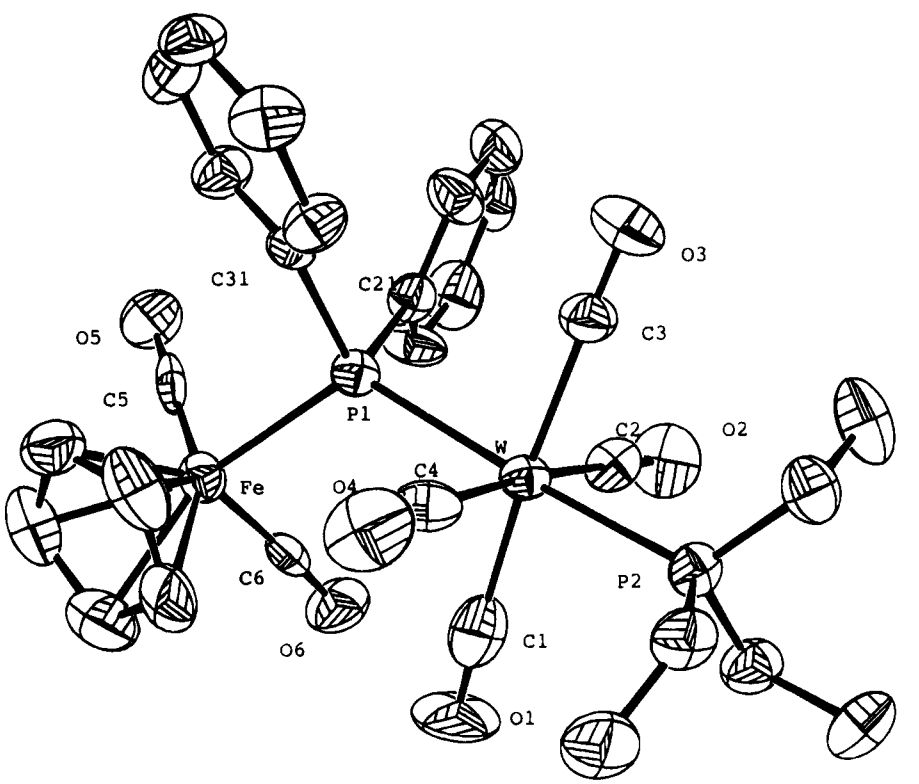

Figure 4. ORTEP drawing of **3c-*trans***. Hydrogen atoms are omitted.

to re-form the metal–metal bond to produce **5**. Actually, during the preparation of **3**, a small amount of **5** was always observed in **3** if laboratory fluorescent light was not avoided during chromatography. The downfield resonance in the ^{31}P NMR of the phosphido phosphorus indicates the presence of a metal–metal bond in **5**. The phosphine ligand remains coordinated to the W because J_{P-W} satellites were observed.

Both cis and trans isomers of **5** were observed, and only **5b-*trans*** and **5e-*trans*** were separated pure through recrystallization. The assignments of the cis and trans isomers were based on the magnitude of the

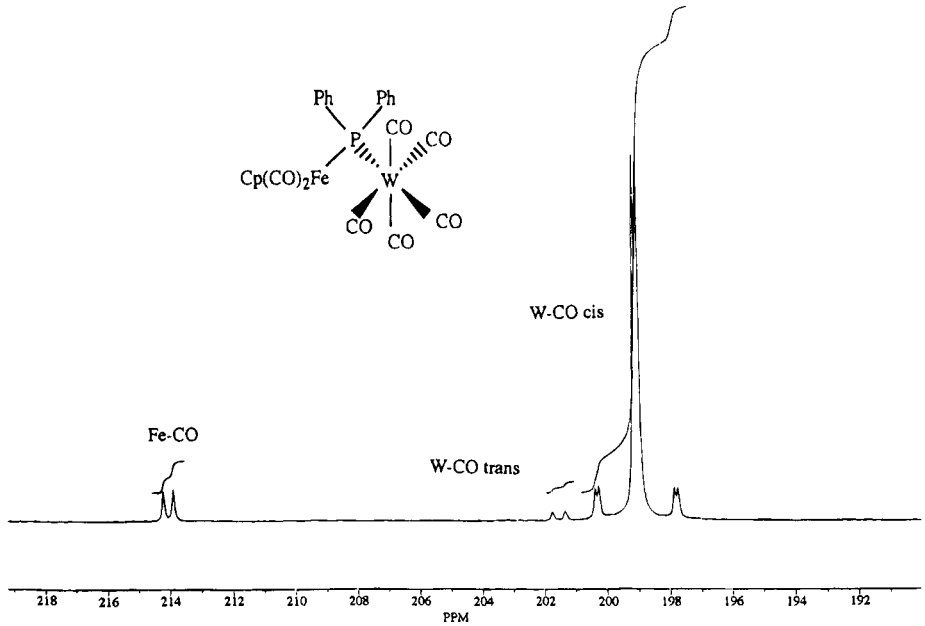

Figure 5. $^{13}C\{^1H\}$ NMR spectrum of ^{13}CO-enriched **2**. Only the carbonyl region is shown.

Scheme 2

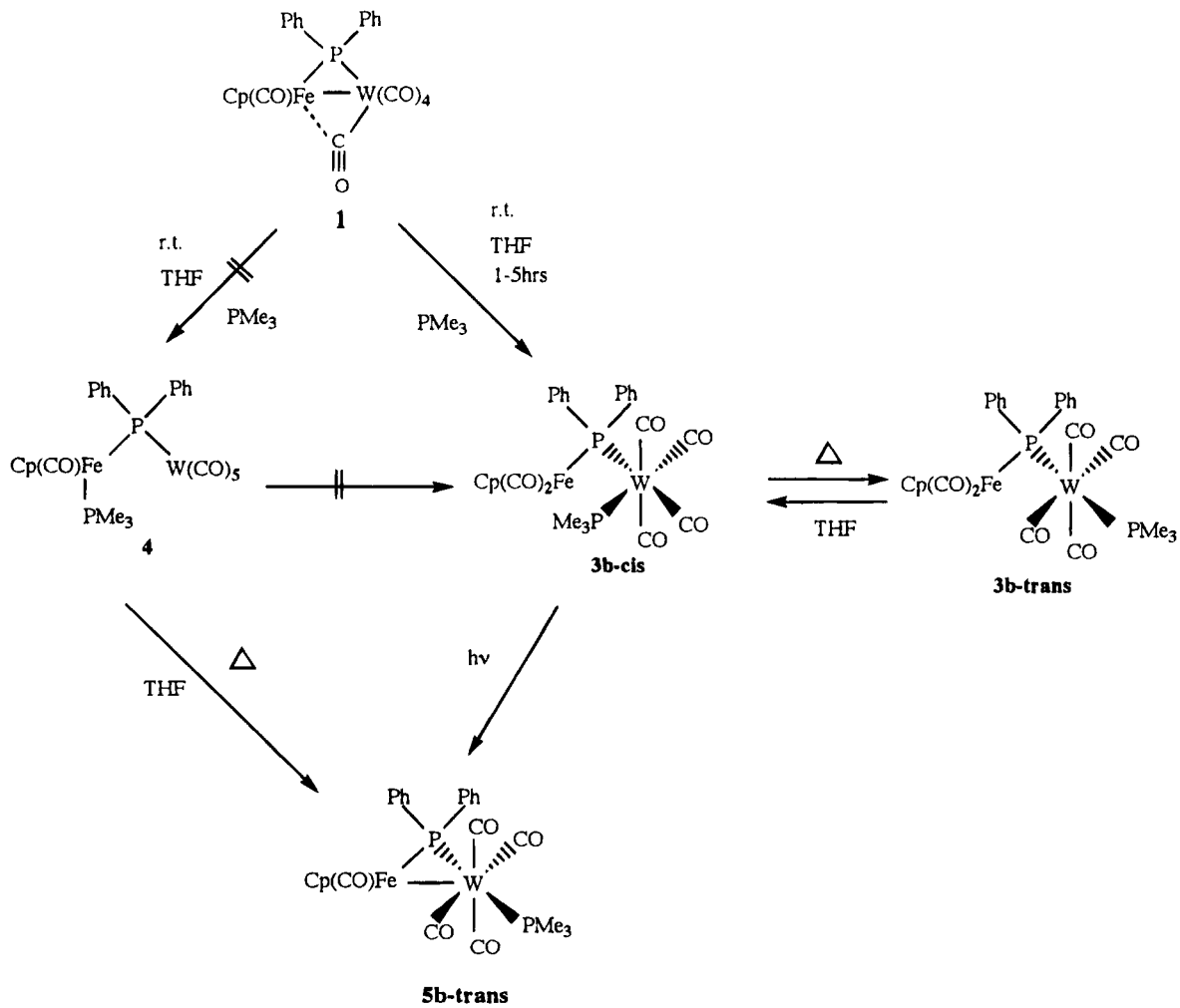

J_{P-P} value, since the trans isomer usually has a large J_{P-P} value in W complexes.[7] The structure of **5e-*trans*** was further characterized by a single-crystal X-ray diffraction study (Figure 6).

The distance between W and Fe (2.8507(20) Å) indicates a metal–metal bond. The W(4)–C(4)–O(4) angle (161.0(13)°) indicates a semibridging carbonyl with CO(4) primarily coordinated to the W atom. The trans PPh_3 does not increase the repulsion between the W and the Fe moieties in the complex, as shown by the W–P–Fe angle (76.12(12)°) and the W–Fe distance (2.8548(10) Å) in **5e-*trans***. They are almost the same

Scheme 3

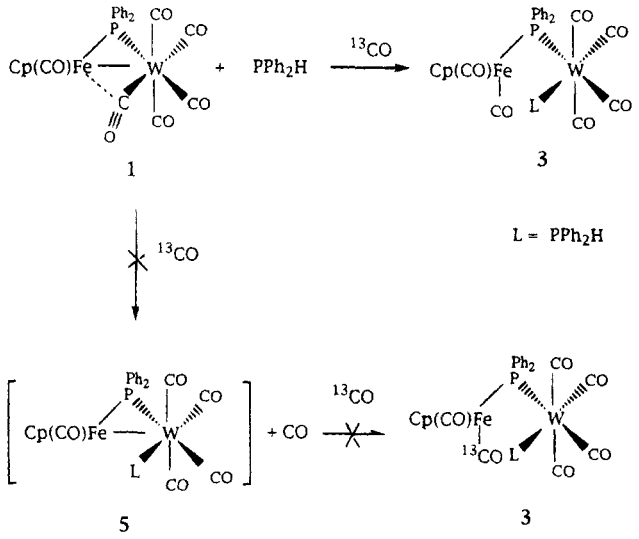

as the W–P–Fe angle (75.06(22)°) and the distance between W and Fe (2.851(3) Å) in **1**.[2]

The four W CO ligands cis to the phosphido bridge in ***5e-trans*** are fluxional. Only one doublet of the Fe carbonyl signal at 215.4 ppm ($^2J_{P-C}$ = 15.4 Hz) and a very broad hump for the W carbonyl signal at 199.0 ppm were observed in the ^{13}CO NMR spectrum. The assignment was based on their favorable comparison with the Fe CO signal at 212.6 ppm ($^2J_{P-C}$ = 12.6 Hz) and the W carbonyl signal at 192.0 ppm (broad hump) of **1**.[4] No trans W CO signal was observed. This kind of fluxional behavior has been observed for several monophosphido-bridged complexes with a metal–metal bond, and the trans CO ligand was usually not involved in the fluxional behavior. Thus, the absence of the trans CO signal is consistent with the molecular structure where the phosphine ligand occupies the trans position. The structure of ***5b-trans***, the only product obtained from the reaction between **1** and PMe_3, was determined by the only observation of the Fe CO resonance in its ^{13}C NMR spectrum.

Conclusions

Reactions of $CpFe(CO)(\mu\text{-}PPh_2)(\mu\text{-}CO)W(CO)_4$ (**1**) and Lewis bases L (L = CH_3CN, PMe_3, PPh_2H, $P(OMe)_3$, PPh_3) at ambient temperatures resulted in the addition products $CpFe(CO)_2(\mu\text{-}PPh_2)W(CO)_4L$ (**3**) with L regiospecifically on W. UV irradiation of **3** resulted in the formation of **5**. Structures of ***3b-cis***, ***3c-trans***, and ***5e-trans*** were determined by single-crystal X-ray studies.

No reaction was observed when $CpFe(CO)_2(\mu\text{-}PPh_2)W(CO)_5$ (**2**) was stirred with L under similar conditions. However, reaction of **2** with PMe_3 produced **4** with PMe_3 coordinating to Fe. The adjacent metal was believed to assist the addition reaction and switched the reaction site from Fe to W through the metal–metal bond.

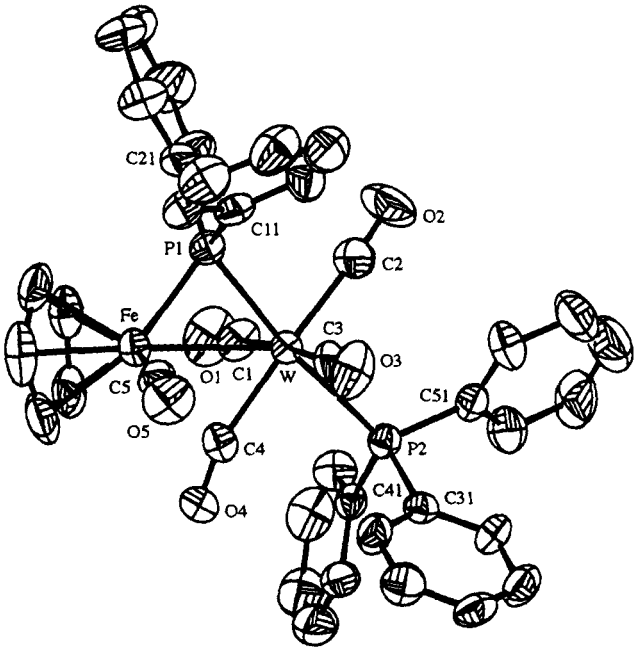

Figure 6. ORTEP drawing of ***5e-trans***. Hydrogen atoms are omitted.

Acknowledgment. We thank the National Science Council, Republic of China, and Academia Sinica for financial support of this work.

Supplementary Material Available: Listings of crystal data and refinement details, atomic coordinates, anisotropic thermal parameters, and bond distances and angles and figures giving additional views of ***3b-cis***, ***3c-trans***, **4**, and ***5e-trans*** (43 pages). Ordering information is given on any current masthead page.

OM940775E

Cationic Arylmanganese(II) Derivatives Occurring in Ion-Pair Forms with Tetraphenylborate Anions: Synthetic, Structural, and Magnetic Studies

Euro Solari, Fabrizio Musso, Emma Gallo, and Carlo Floriani*,[1]

Institut de Chimie Minérale et Analytique, BCH, Université de Lausanne, CH-1015 Lausanne, Switzerland

Nazzareno Re

Dipartimento di Chimica, Università di Perugia, I-06100 Perugia, Italy

Angiola Chiesi-Villa and Corrado Rizzoli

Dipartimento di Chimica, Università di Parma, I-43100 Parma, Italy

Received December 21, 1994[⊗]

We report a class of cationic manganese(II) aryl compounds stabilized by weak donor solvents or by interactions with the counteranion BPh_4^- to form ion-pair species. The parent compound used was Mn_3Mes_6 (**1**; Mes = 2,4,6-$Me_3C_6H_2$), which can be synthesized on a large scale by a conventional method and conveniently used as starting material. Reaction of **1** with BPh_3 in Et_2O gave the cationic derivative $[MesMn(OEt_2)_3]^+BPh_4^-$ (**2**), containing a single Mn–C bond and three weakly bonded Et_2O molecules. In order to avoid coordinating solvent, the reaction between **1** and BPh_3 was then carried out in toluene. This reaction gave, depending on the reaction time and the BPh_3/Mn ratio, the monomeric $[MesMn(\eta^3\text{-}Ph)_2\text{-}BPh_2]$ (**3**) and the dimeric $[Ph_2B(\eta^2\text{-}Ph)_2(\mu\text{-}MnPh)_2(\eta^2\text{-}Ph)_2BPh_2]$ (**4**) ion pairs. Temperature-dependent magnetic measurements showed that for **1** and **4** a strong antiferromagnetic coupling exists between the d^5 ions brought about by the bridging aryl groups and/or the short Mn···Mn distance (2.851(2) Å, **1**; 2.796(1) Å, **4**). Such a coupling, much greater than that observed in several Mn(II)–Mn(II) dimers, has J values of 55.4 cm^{-1} (complex **4**) and 40.4 cm^{-1} (complex **1**). Crystallographic details: **1** is triclinic, space group $P\bar{1}$, with a = 12.850(3) Å, b = 20.327(4) Å, c = 11.407(3) Å, α = 95.11(2)°, β = 114.00(2)°, γ = 98.77(2)°, Z = 2, and R = 0.052; **2** is triclinic, space group $P\bar{1}$, with a = 11.237(2) Å, b = 19.035(2) Å, c = 10.991(1) Å, α = 99.30(1)°, β = 106.66(1)°, γ = 104.58(1)°, Z = 2, and R = 0.070; **3** is monoclinic, space group $P2_1/n$, with a = 10.070(1) Å, b = 15.901(1) Å, c = 20.876(2) Å, β = 101.94(1)°, Z = 4, and R = 0.054; **4** is monoclinic, space group $P2_1/c$, with a = 15.074(4) Å, b = 13.289(4) Å, c = 20.139(5) Å, β = 98.39(2)°, Z = 4, and R = 0.055.

Introduction

The organometallic and coordination chemistry of manganese has undergone a renaissance due to the role of this metal in a number of naturally occurring systems,[2] in very efficient catalytic oxidation systems,[3] and, to a lesser extent, in organometallic chemistry.[4] The major objectives of the last class have essentially been focused on (i) the *in situ* synthesis of the Mn–C functionality with the aim of exploiting it in organic synthesis[4] and (ii) the stabilization of complexes with Mn–C functionalities. The organometallic complexes of manganese which have attracted the most attention in recent years are the homoleptic alkyl and aryl derivatives.[5] A quite successful strategy, which has been applied mainly to zirconium organometallics, has been the generation of coordinatively unsaturated species in the form of cationic alkyls, having Lewis acid properties.[6–8] Although the homoleptic alkyl or aryl complexes of manganese are very reactive, one synthetic challenge would be the generation of cationic analogues for their utilization in catalysis.[6] In addition, with particular regard to the preparation of manganese organometallics, *in situ*,[4] we feel that under some of the

⊗ Abstract published in *Advance ACS Abstracts,* April 15, 1995.

(1) To whom correspondence should be addressed.

(2) (a) *Manganese Redox Enzymes*; Pecoraro, V. L., Ed.; VCH: New York, 1992. (b) Wieghardt, K. *Angew. Chem., Int. Ed. Engl.* **1989**, *28*, 1153. (c) Pecoraro, V. L.; Baldwin, M. J.; Gelasco, A. *Chem. Rev.* **1994**, *94*, 807.

(3) (a) Srinivasan, K.; Michaud, P.; Kochi, J. K. *J. Am. Chem. Soc.* **1986**, *108*, 2309. (b) Menage, S.; Collomb-Dunand Sauthier, M. N.; Lambeaux, C.; Fontecave, M. *J. Chem. Soc., Chem. Commun.* **1994**, 1885. (c) Eilmes, J. *Polyhedron* **1992**, *11*, 581. (d) O'Connor, K. J.; Wey, S. J.; Burrows, C. J. *Tetrahedron Lett.* **1992**, *33*, 1001. (e) Evans, D. A.; Faul, M. M.; Bilodeau, M. T.; Anderson, B. A.; Barnes, D. M. *J. Am. Chem. Soc.* **1993**, *115*, 5328. (f) Reddy, D. R.; Thornton, E. R. *J. Chem. Soc., Chem. Commun.* **1992**, 172. (g) Zhang, W.; Jacobsen, E. N. *J. Org. Chem.* **1991**, *56*, 2296. (h) Jacobsen, E. N.; Zhang, W.; Muci, A. R.; Ecker, J. R.; Deng, L. *J. Am. Chem. Soc.* **1991**, *113*, 7063. (i) Larrow, J. F.; Jacobsen, E. N. *J. Org. Chem.* **1994**, *59*, 1939. (j) Brandes, B. D.; Jacobsen, E. N. *J. Org. Chem* **1994**, *59*, 4378.

(4) (a) Normant, J. F.; Cahiez, G. In *Modern Synthetic Methods*; Scheffold, R., Ed.; Wiley: Chichester, U.K., 1983; Vol. 3, p 173. (b) Cahiez, G.; Alami, M. *Tetrahedron* **1989**, *45*, 4163. (c) Cahiez, G.; Marquais, S. *Synlett* **1993**, 45. (d) Cahiez, G.; Figadere, B.; Clery, P. *Tetrahedron Lett.* **1994**, *35*, 3065. (e) Cahiez, G.; Chau, K.; Clery, P. *Tetrahedron Lett.* **1994**, *35*, 3069. (f) Corey, E. J.; Posner, G. H. *Tetrahedron Lett.* **1970**, 315. (g) Reetz, M. T.; Haning, H. *Tetrahedron Lett.* **1993**, *34*, 7395. (h) Reetz, M. T.; Haning, H.; Stanchev, S. *Tetrahedron Lett.* **1992**, *33*, 6963. (i) Reetz, M. T.; Rölfing, K.; Griebenow, N. *Tetrahedron Lett.* **1994**, *35*, 1969.

0276-7333/95/2314-2265$09.00/0

reaction conditions employed, the protolysis or ionization of the Mn−C bond can occur, with the consequent formation of cationic species. Among the various strategies used for that purpose,[6-8] i.e. controlled protolysis or reaction with a Lewis acid, the latter one is preferred since the resulting cation can be generated under noncoordinating conditions.

This report concerns the synthesis and structural characterization of the parent compound $[Mn_3Mes_6]$, which has been previously communicated,[5h] and its conversion into masked cationic forms of the $[Mn-Ar]^+$ fragment by the use of BPh_3. Such compounds have been isolated as monomers or dimers in the ion-pair form, with BPh_4^- as the counteranion. A magnetic study on the monomer, dimer, and trimer of this series completes our investigation.

Results and Discussion

Synthesis of Cationic Arylmanganese Derivatives. The synthesis of **1** has been performed by following the conventional method outlined in eq 1.

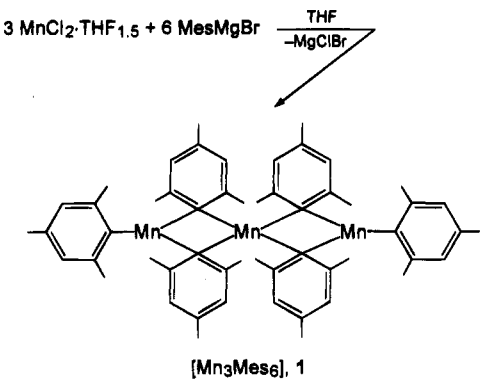

[Mn3Mes6], 1 (1)

Complex **1** is usually recrystallized from toluene and contains solvent of crystallization. The successful isolation of **1** in a pure form (without traces of chloride ions) requires a number of precautions, especially when the synthesis is carried out on a large scale. The use of very pure, crystalline $MnCl_2$·1.5THF is compulsory, as is the recrystallization of the crude product, at least twice, from toluene. Polynuclear structures such as **1** containing bridging hydrocarbyl ligands are not unusual in the organometallic chemistry of manganese.[4] In contrast to these examples, however, **1** can be produced in a large quantity and represents a very useful starting material for the metalation of active proton-containing substrates.[9]

The trimeric structure proposed for **1** is based on the solid-state X-ray analysis. In the presence of even weakly coordinating solvents, such as aromatic hydrocarbons, we expect a breakdown of the structure with a significant interaction of the arenes with the manganese ion. At present, much more attention has been devoted to the weakly stabilized, rather than to the ligand overstabilized, forms of organometallics. A general method which has been successfully used for this type of stabilization is the induced ionization of a metal−aryl bond by an appropriate Lewis acid such as $B(C_6F_5)_3$.[10] This procedure has been employed mainly in the case of cyclopentadienylmetal alkyl derivatives but not for homoleptic metal alkyl compounds. The organometallic cations thus formed showed a very high reactivity.[6-8]

The reaction of **1** has been studied with a relatively weak Lewis acid, BPh_3, under various conditions. Initial attempts were carried out in weakly binding solvents such as Et_2O.

Reaction 2 produces a weakly solvated form of the $[Mn-Mes]^+$ functionality with the BPh_4^- counteranion, instead of the expected $MesBPh_3^-$ anion. Analyzing the

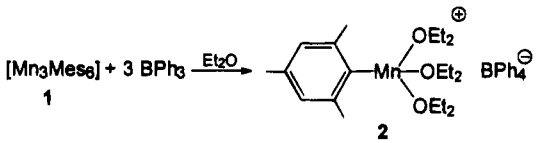

1 2 (2)

mother liquor of reaction 2 helped us identify $MesBPh_2$ as a major component. We assume that aryl scrambling occurs between BPh_3 and $MesBPh_3^-$, leading preferentially to BPh_4^- and the identified $MesBPh_2$. Complex **2** is a very rare example of a weakly solvated monomeric cationic form of the $[Mn-aryl]^+$ functionality, and its chemistry has not yet been explored. We then turned our attention to the ionization of **1** in toluene, to avoid any binding solvent containing donor atoms. Depending on the Mn/BPh_3 ratio and the reaction time, the products reported in reactions 3 (compound **3**) and 4 (compound **4**) were obtained.

(5) (a) Andersen, R. A.; Carmona-Guzman, E.; Gibson, J. F.; Wilkinson, G. *J. Chem. Soc., Dalton Trans.* **1976**, 2204. (b) Howard, C. G.; Wilkinson, G.; Thornton-Pett, M.; Hursthouse, M. B. *J. Chem. Soc., Dalton Trans.* **1983**, 2025. (c) Howard, C. G.; Girolami, G. S.; Wilkinson, G.; Thornton-Pett, M.; Hursthouse, M. B. *J. Chem. Soc., Dalton Trans.* **1983**, 2631. (d) Girolami, G. S.; Wilkinson, G.; Thornton-Pett, M.; Hursthouse, M. B. *J. Am. Chem. Soc.* **1983**, *105*, 6752. (e) Belforte, A.; Calderazzo, F.; Englert, U.; Strähle, J.; Wurst, K. *J. Chem. Soc., Dalton Trans.* **1991**, 2419. (f) Bartlett, R. A.; Olmstead, M. M.; Power, P. P.; Shoner, S. C. *Organometallics* **1988**, *7*, 1801. (g) Morris, R. J.; Girolami, G. S. *Organometallics* **1991**, *10*, 792, 799. (h) Gambarotta, S.; Floriani, C.; Chiesi-Villa, A.; Guastini, C. *J. Chem. Soc., Chem. Commun.* **1983**, 1128.

(6) Collins, S.; Kuntz, B. A.; Collins, S. *J. Org. Chem.* **1989**, *54*, 4154. Jordan, R. F. *Adv. Organomet. Chem.* **1991**, *32*, 325. Grossman, R. B.; Davis, W. M.; Buchwald, S. L. *J. Am. Chem. Soc.* **1991**, *113*, 2321. Guram, A. S.; Swenson, D. C.; Jordan, R. F. *J. Am. Chem. Soc.* **1992**, *114*, 8991. Guram, A. S.; Guo, Z.; Jordan, R. F. *J. Am. Chem. Soc.* **1993**, *115*, 4902. Guram, A. S.; Jordan, R. F. *J. Org. Chem.* **1993**, *58*, 5595. Hong, Y.; Kuntz, B. A.; Collins, S. *Organometallics* **1993**, *12*, 964.

(7) Pino, P.; Cioni, P.; Wei, J. *J. Am. Chem. Soc.* **1987**, *109*, 6189. Waymouth, R. M.; Pino, P. *J. Am. Chem. Soc.* **1990**, *112*, 4911. Morken, J. P.; Didiuk, M. T.; Hoveyda, A. H. *J. Am. Chem. Soc.* **1993**, *115*, 6997. Rodewald, S.; Jordan, R. F. *J. Am. Chem. Soc.* **1994**, *116*, 4491 and references therein.

(8) Kaminsky, W.; Külper, K.; Brintzinger, H. H.; Wild, F. R. W. P. *Angew. Chem., Int. Ed. Engl.* **1985**, *24*, 507. Ewen, J. A. Haspeslagh, L.; Atwood, J. L.; Zhang, H. *J. Am. Chem. Soc.* **1987**, *109*, 6544. Ewen, J. A.; Jones, R. L.; Razavi, A.; Ferrara, J. D. *J. Am. Chem. Soc.* **1988**, *110*, 6255. Hlatky, G. G.; Turner, H. W.; Eckman, R. R. *J. Am. Chem. Soc.* **1989**, *111*, 2728. Yang, X.; Stern, C. L.; Marks, T. *J. Am. Chem. Soc.* **1991**, *113*, 3623. Collins, S.; Gauthier, W. J.; Holden, D. A.; Kuntz, B. A.; Taylor, N. J.; Ward, D. G. *Organometallics* **1991**, *10*, 2061. Resconi, L.; Piemontesi, F.; Franciscano, L.; Abis, L.; Fiorani, T. *J. Am. Chem. Soc.* **1992**, *114*, 1025. Burger, P.; Diebold, J.; Gutmann, S.; Hund, H. U.; Brintzinger, H. H. *Organometallics* **1992**, *11*, 1319. Marks, T. *Acc. Chem. Res.* **1992**, *25*, 57. Coates, G. W.; Waymouth, R. M. *J. Am. Chem. Soc.* **1993**, *115*, 91. Erker, G.; Aulbach, M.; Knickmeier, M.; Wingbermühle, D.; Krüger, C.; Nolte, M.; Werner, S. *J. Am. Chem. Soc.* **1993**, *115*, 4590. Guerra, G.; Cavallo, L.; Moscardi, G.; Vacatello, M.; Corradini, P. *J. Am. Chem. Soc.* **1994**, *116*, 2988.

(9) Gallo, E.; Solari, E.; De Angelis, S.; Floriani, C.; Re, N.; Chiesi-Villa, A.; Rizzoli, C. *J. Am. Chem. Soc.* **1993**, *115*, 9850.

(10) (a) Brookhart, M.; Grant, B.; Volpe, A. F., Jr. *Organometallics* **1992**, *11*, 3920. (b) Yang, X.; Stern, C. L.; Marks, T. J. *J. Am. Chem. Soc.* **1994**, *116*, 10015. (c) Pellecchia, C.; Grassi, A.; Zambelli, A. *J. Chem. Soc., Chem. Commun.* **1993**, 947. (d) Pellecchia, C.; Immirzi, A.; Pappalardo, D.; Peluso, A. *Organometallics* **1994**, *13*, 3773. (e) Jia, L.; Yang, X.; Stern, C.; Marks, T. J. *Organometallics* **1994**, *13*, 3755. (f) Quyoum, R.; Wang, Q.; Tudoret, M.-J.; Baird, M. C. *J. Am. Chem. Soc.* **1994**, *116*, 6435. (g) Yang, X.; Stern, C. L.; Marks, T. J. *Angew. Chem., Int. Ed. Engl.* **1992**, *31*, 1375.

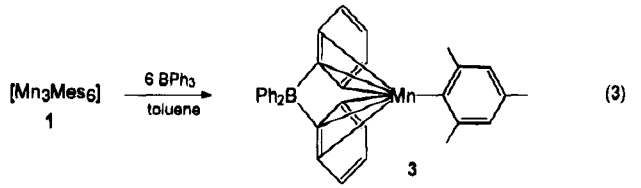

(3)

3

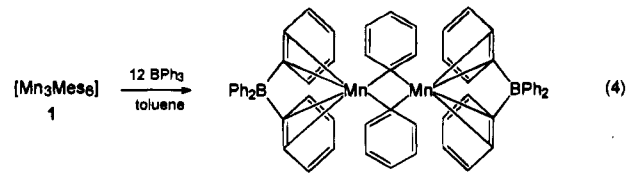

(4)

4

Longer reaction times and higher BPh_3/Mn ratios produce exclusively **4**, instead of **3** (see Experimental Section). Both compounds represent masked forms of cationic arylmanganese(II), but with some major differences. In complex **3**, the coordinatively unsaturated metal ion is, to some extent, satisfied by its interaction with BPh_4^-. The formation of BPh_4^- indicates that a facile mechanism exists for the scrambling (see above) of the aryl groups around boron. In the case of **4**, such scrambling occurs not only between boron–aryl units but also with manganese–aryl units, giving only phenyl groups in its structure. This complex contains a dimeric cationic manganese–phenyl $[Mn_2Ph_2]^{2+}$ fragment weakly complexed by two BPh_4^- anions. The occurrence of the $[Mn_2Ph_2]^{2+}$ cation in the dimeric complex **4** rather than $[Mn–Mes]^+$ in the monomeric form **3** may be due to a difference in steric hindrance of the aryl groups, the mesityl preferring to bond in a terminal rather than in a bridging fashion like the phenyl group.

In recent years, a number of cases have been reported in which BPh_4^- does not behave as an innocent anion but rather as a protecting group for coordinatively unsaturated transition-metal ions. BPh_4^- is capable of displaying different binding modes, going from η^2 to η^6 binding of a phenyl group to two bent η^6-phenyls surrounding a single metal ion.[11]

A general method for the generation of masked cationic organometallics is by reaction of BPh_3 with the organometallic to produce, *via* ionization reaction, a weakly binding anion. Nevertheless, the occurrence of ion-pair forms **3** and **4** is rather unique in organometallic chemistry in the absence of an ancillary ligand such as a cyclopentadienyl group. In addition, we should mention that for this purpose we only need a rather weak Lewis acid, instead of the much more powerful $B(C_6F_5)_3$.[10]

Structural Studies in the Solid State. The high lability of the Mn(II) coordination sphere makes a solid-state/solution-state structural correlation quite difficult, especially in the absence of any spectroscopic solution information. This is particularly true with some polynuclear or ion-pair species such as those dealt with in the present report.

The structure of **1** is given in Figure 1. Selected bond distances and angles are listed in Table 6. The molecule consists of a linear trimer (Mn2–Mn1–Mn3 = 178.8(1)°) with four bridging and two terminal mesityl groups. The central Mn1 atom has a distorted-tetrahedral coordination, while the two end Mn2 and Mn3 atoms achieve a trigonal coordination through a terminal mesityl ligand. The deviations from the plane defined by the three carbon atoms are 0.150(1) and 0.177(2) Å for Mn2 and Mn3, respectively. The two four-membered dinuclear rings are planar within experimental errors, the outer metal atoms lying nearly on the plane (*i.e.* Mn3 is 0.047(2) Å from the plane through Mn1, C1, Mn2, and C11; Mn2 is 0.026(2) Å from the plane through Mn1, C21, Mn3, and C31). They form a dihedral angle of 75.9(3)°. The internal C–Mn1–C and Mn–C–Mn angles (mean values 98.1(3) and 77.9(3)°, respectively) result in Mn···Mn distances (Mn1–Mn2 = 2.851(2) Å and Mn1–Mn3 = 2.852(2) Å) which are longer than those observed in $[Mn_2Ph_6]^{2-}$ [5f] anions (2.733(1) and 2.763(1) Å). The bridging aromatic rings are nearly perpendicular to the respective Mn_2C_2 dimetallacyclobutanes, forming dihedral angles of 85.2(2)° for both C1···C6 and C11···C16 with respect to the Mn1,Mn2,C1,C11 plane and of 89.7(2)° (C21···C26) and 88.2(2)° (C31···C36) with respect to the Mn1,Mn3, C21,C31 plane. The remarkable distortion from tetrahedral coordination around the Mn1 atom (Table 6) is most likely due to the steric hindrance from the bridging mesityl group. The terminal (average 2.122(7) Å) and bridging (average 2.331(5) Å) Mn–C bond distances are close to those in some monomeric, *e.g.* $[MnMes_3]^-$ [5f] ($Mn–C_{av}$ = 2.141(6) Å), and dimeric, *e.g.* $[Mn_2Ph_6]^{2-}$ [5f] ($Mn–C_{av}$ = 2.255(4) and 2.285(4) Å), arylmanganese complexes. The coordinative unsaturation of Mn2 and Mn3 is partially completed by some significant Mn···H interactions (Å): Mn2···H91, 2.71; Mn2···H171, 2.90; Mn···H491, 2.95; Mn3···H271, 2.75; Mn3···H391, 2.81; Mn3···H591, 2.94 Å. The Mn2 and Mn3 atoms are displaced remarkably from the terminal mesityl ring plane, the displacements from C41···C46 and C51···C56 rings being 0.360(1) and 0.646(2) Å for Mn2 and Mn3, respectively. These rings are tilted by 21.6(3) and 22.5(3)° with respect to their coordination planes. All the aromatic rings deviate slightly but significantly from planarity and show the longest C–C bonds at the carbon bonded to Mn. All the methyl groups lie significantly out of their respective aromatic ring planes in a range of 0.05(1)–0.25(1) Å for the bridging mesityls and of 0.03(1)–0.14(1) Å for the terminal ones.

Complex **2** crystallizes as separated monomeric cations $[Mn(Mes)(Et_2O)_3]^+$ and BPh_4^- anions. The structure of the cation is given in Figure 2. Selected bond distances and angles are listed in Table 7. The manganese atom displays a distorted-tetrahedral coordination involving a terminal mesityl ligand and three oxygen atoms from diethyl ether molecules. The direction of the Mn–C1 bond is nearly perpendicular to the plane of the oxygen atoms (dihedral angle 80.1(2)°), from which the Mn protrudes by 1.051(2) Å. The aromatic ring is perpendicular to the oxygen plane, the dihedral angle they form being 84.6(2)°. Distortions from an idealized coordination geometry appear to be related to intraligand steric effects involving the *o*-methyl substituents and the diethyl ethers. Thus, the angles O1–Mn1–C1 (121.1(2)°) and O2–Mn1–C1 (127.8(3)°) are opened beyond 109°, leading to closure of the O–Mn1–O

(11) (a) Bochmann, M. *Angew. Chem., Int. Ed. Engl.* **1992**, *31*, 1181. (b) Bochmann, M.; Karger, G.; Jaggar, A. J. *J. Chem. Soc., Chem. Commun.* **1990**, 1038. (c) Horton, A. D.; Frijns, J. H. G. *Angew. Chem., Int. Ed. Engl.* **1991**, *30*, 1152. (d) Calderazzo, F.; Englert, U.; Pampaloni, G.; Rocchi, L. *Angew. Chem., Int. Ed. Engl.* **1992**, *31*, 1235. (e) Strauss, S. H. *Chem. Rev.* **1993**, *93*, 927. (f) Pasquali, M.; Floriani, C.; Gaetani-Manfredotti, A. *Inorg. Chem.* **1980**, *19*, 1191.

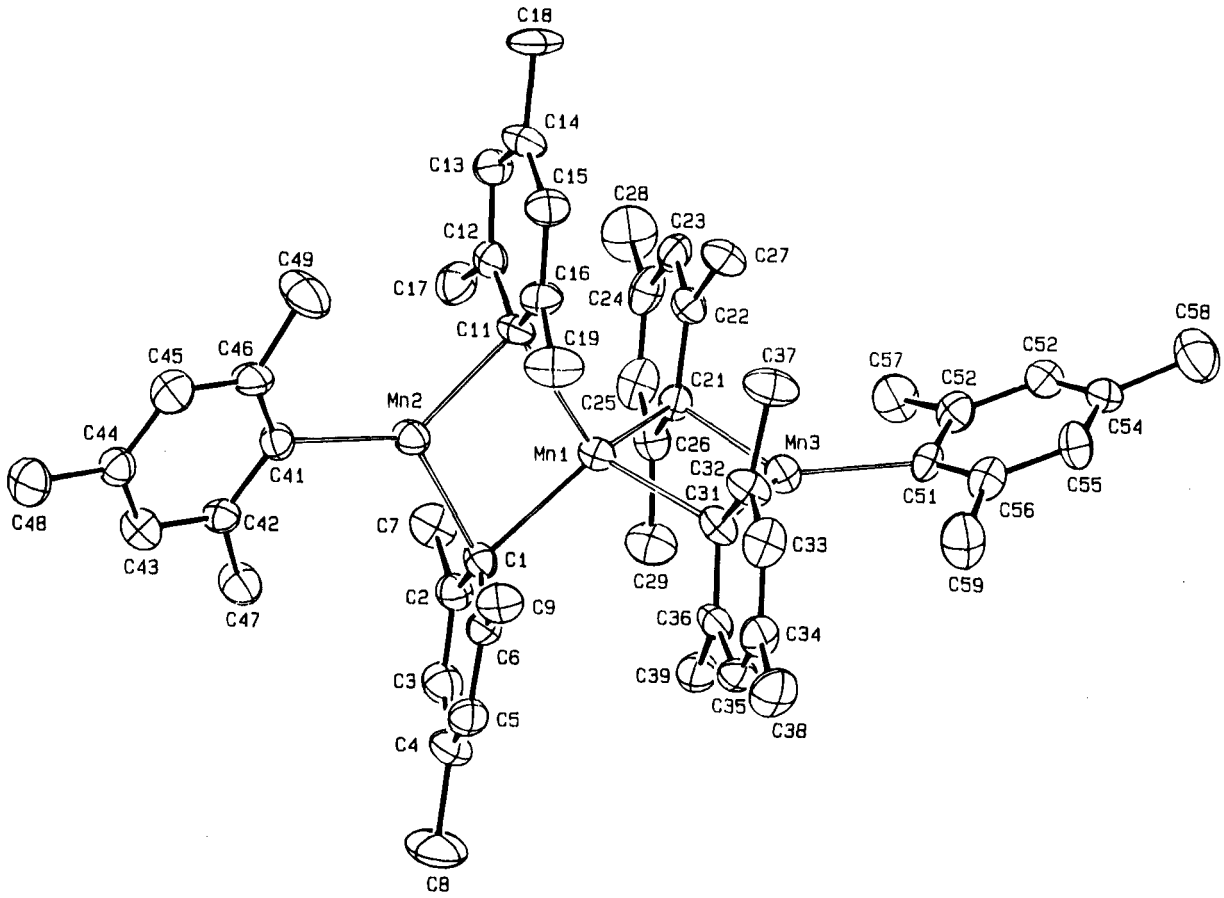

Figure 1. ORTEP drawing for complex **1** (30% probability ellipsoids).

Table 1. Experimental Data for the X-ray Diffraction Studies on Crystalline Compounds 1–4

	1	**2**	**3**	**4**
formula	$C_{54}H_{66}Mn_3{\cdot}C_7H_8$	$C_{21}H_{41}MnO_3{\cdot}C_{24}H_{20}B$	$C_{33}H_{31}BMn{\cdot}C_7H_8$	$C_{60}H_{50}B_2Mn_2{\cdot}1.5C_7H_8$
a, Å	12.850(3)	11.237(2)	10.070(1)	15.074(4)
b, Å	20.327(4)	19.035(2)	15.901(1)	13.289(4)
c, Å	11.407(3)	10.991(1)	20.876(2)	28.139(5)
α, deg	95.11(2)	99.30(1)	90	90
β, deg	114.00(2)	106.66(1)	101.94(1)	98.39(2)
γ, deg	98.77(2)	104.58(1)	90	90
V, Å^3	2652.2(12)	2109.3(5)	3270.4(5)	5576.4(25)
Z	2	2	4	4
fw	972.1	715.7	585.5	1040.8
space group	$P\bar{1}$ (No. 2)	$P\bar{1}$ (No. 2)	$P2_1/n$ (No. 14)	$P2_1/c$ (No. 14)
t, °C	22	22	22	22
λ, Å	0.710 69	1.541 78	1.541 78	1.541 78
ϱ_{calc}, g cm^{-3}	1.217	1.127	1.189	1.240
μ, cm^{-1}	7.1	28.1	34.6	40.0
transmissn coeff	0.938–1.000	0.603–1.000	0.547–1.000	0.662–1.000
R^a	0.052	0.058	0.054[e]	0.055[e]
$R_w{}^b$	0.060	0.070	–	–
wR2[c]	–	–	0.171[f]	0.175[f]
GOF[d]	0.961	1.250	0.820	0.805

[a] $R = \Sigma|\Delta F|/\Sigma|F_o|$. [b] $R_w = [\Sigma w^{1/2}|\Delta F|/\Sigma w^{1/2}|F_o|]$. [c] wR2 $= [\Sigma(w\Delta F^2)^2/\Sigma(wF_o^2)^2]^{1/2}$. [d] GOF $= [\Sigma w|\Delta F|(NO - NV)]^{1/2}$. [e] For unique observed data. [f] For unique total data.

angles, in particular for the O1–Mn1–O2 angle (89.4(2)°). The Mn–C distance is in agreement with that observed in complex **1** for the terminal Mn–Mes bond. The Mn atom is significantly displaced from the plane of the aromatic ring by 0.088(1) Å.

Structures of **3** and **4** are displayed in Figures 3 and 4, respectively, and the corresponding structural parameters are listed in Tables 8 and 9, respectively. Both compounds contain, in masked form, the cationic functionality [Mn–aryl]$^+$ as a monomer in **3** and as a dimer in **4**, the steric hindrance of the aryl moiety determining either the monomeric or the dimeric arrangement. The Mn–C(mesityl) distance in **3** is particularly short (2.066(5) Å) compared to those reported for all the other terminal Mn–Mes derivatives, including **1** and **2**. An equally short Mn–C distance is observed for the bridging phenyl (Mn–C_{av} = 2.197(6) Å) in **4** compared to the other bridging manganese–aryl complexes, including **1** (Mn–C_{av} = 2.331(5) Å). The two bridging phenyl rings give rise to a dinuclear four-membered ring which is signicantly puckered, the displacements of atoms from the least-squares mean plane being as follows (Å): Mn1,

Table 2. Fractional Atomic Coordinates ($\times 10^4$) for Complex 1

atom	*x/a*	*y/b*	*z/c*	atom	*x/a*	*y/b*	*z/c*
Mn1	−14.5(11)	2491.7(6)	2639.3(12)	C33	792(9)	1291(5)	5826(9)
Mn2	−1742.4(11)	1691.6(6)	266.5(13)	C34	1643(9)	983(5)	5732(8)
Mn3	1736.6(11)	3268.1(6)	5026.6(12)	C35	2260(8)	1269(4)	5116(9)
C1	166(7)	1814(4)	1013(7)	C36	2010(8)	1844(4)	4534(8)
C2	728(8)	2167(4)	319(8)	C37	−248(9)	2237(5)	5676(10)
C3	1584(8)	1923(5)	79(9)	C38	1837(10)	320(5)	6236(10)
C4	1903(8)	1315(5)	447(9)	C39	2793(8)	2142(5)	3952(9)
C5	1290(8)	947(4)	1013(9)	C41	−2923(7)	937(4)	−1323(8)
C6	466(8)	1190(4)	1306(8)	C42	−2568(7)	639(4)	−2238(8)
C7	350(9)	2773(5)	−253(9)	C43	−3260(8)	75(4)	−3132(9)
C8	2846(10)	1054(6)	157(13)	C44	−4351(8)	−215(4)	−3216(8)
C9	−158(8)	727(4)	1904(9)	C45	−4715(7)	93(5)	−2389(10)
C11	−2033(7)	2319(4)	1756(8)	C46	−4045(7)	658(5)	−1487(9)
C12	−2547(7)	2852(4)	1165(8)	C47	−1412(8)	926(5)	−2247(9)
C13	−3505(8)	3027(4)	1309(9)	C48	−5091(8)	−839(5)	−4229(10)
C14	−3959(8)	2709(5)	2053(10)	C49	−4572(9)	966(6)	−645(12)
C15	−3501(8)	2172(5)	2596(9)	C51	2732(7)	3857(4)	6905(8)
C16	−2594(8)	1971(4)	2429(9)	C52	2909(7)	4567(5)	7068(8)
C17	−2090(8)	3226(5)	343(9)	C53	3227(8)	4957(5)	8279(9)
C18	−4962(9)	2930(6)	2292(11)	C54	3424(8)	4652(5)	9384(9)
C19	−2259(9)	1324(5)	2884(11)	C55	3296(8)	3970(5)	9213(8)
C21	722(7)	3658(4)	3254(7)	C56	3003(7)	3576(5)	8049(8)
C22	−87(8)	4019(4)	3450(8)	C57	2763(9)	4934(5)	5921(9)
C23	−290(8)	4610(5)	2968(8)	C58	3733(9)	5074(6)	10644(10)
C24	275(9)	4883(5)	2283(9)	C59	2976(10)	2821(5)	7988(9)
C25	1109(9)	4583(5)	2134(9)	C61	5978(9)	3620(4)	6246(8)
C26	1340(8)	3978(4)	2608(8)	C62	5415(9)	3182(4)	6780(8)
C27	−722(9)	3773(4)	4248(9)	C63	5723(9)	2560(4)	7001(8)
C28	46(11)	5524(5)	1734(11)	C64	6593(9)	2376(4)	6689(8)
C29	2364(9)	3718(5)	2538(10)	C65	7156(9)	2814(4)	6155(8)
C31	1131(8)	2170(4)	4594(8)	C66	6849(9)	3436(4)	5934(8)
C32	558(8)	1879(4)	5328(8)	C67	5650(15)	4218(9)	6002(15)

Table 3. Fractional Atomic Coordinates ($\times 10^4$) for Complex 2[a]

atom	*x/a*	*y/b*	*z/c*	atom	*x/a*	*y/b*	*z/c*
Mn1	1936.3(11)	2057.3(6)	1145.8(11)	C19B	5448(33)	2237(20)	2041(30)
B1	3767(8)	6826(4)	2325(8)	C20B	3567(27)	3278(13)	3198(28)
O1	2207(4)	1248(2)	−264(5)	C21B	4384(28)	4107(15)	3499(29)
O2	1528(5)	2681(3)	−289(5)	C31	4816(7)	3337(4)	−2755(7)
O3	3885(6)	2704(4)	2316(5)	C32	4750(8)	4049(4)	−2351(9)
C1	835(7)	1718(4)	2335(6)	C33	3604(10)	4242(5)	−2758(10)
C2	−153(7)	2025(4)	2469(7)	C34	2457(9)	3699(6)	−3589(10)
C3	−923(7)	1780(4)	3214(7)	C35	2460(8)	2992(5)	−3984(8)
C4	−743(8)	1228(5)	3858(7)	C36	3628(8)	2813(4)	−3570(7)
C5	254(8)	948(4)	3785(7)	C41	2943(7)	6556(4)	3280(6)
C6	1030(7)	1175(4)	3041(7)	C42	2159(8)	6945(5)	3678(7)
C7	−391(10)	2667(5)	1869(9)	C43	1379(9)	6691(7)	4403(8)
C8	−1595(10)	961(6)	4634(10)	C44	1410(10)	6039(7)	4792(9)
C9	2133(8)	846(5)	3063(8)	C45	2138(10)	5643(5)	4425(10)
C10	2973(9)	1419(5)	−1128(10)	C46	2926(8)	5895(4)	3696(8)
C11	2154(12)	1149(6)	−2562(10)	C51	4011(6)	7732(4)	2420(7)
C12	1507(8)	458(4)	−500(8)	C52	3793(6)	8031(4)	1314(7)
C13	2372(11)	−24(5)	−297(10)	C53	4063(8)	8811(5)	1437(10)
C14	2503(9)	3335(5)	−337(8)	C54	4539(9)	9305(4)	2659(11)
C15	2176(11)	4034(5)	−77(11)	C55	4751(10)	9032(5)	3755(10)
C16	245(9)	2494(5)	−1324(8)	C56	4491(8)	8266(4)	3636(8)
C17	−564(8)	1719(5)	−1448(8)	C61	2873(7)	6343(3)	792(6)
C18A	5098(14)	2615(9)	2088(15)	C62	3441(8)	6302(4)	−186(7)
C19A	5388(16)	1922(8)	2509(16)	C63	2694(11)	5910(5)	−1488(8)
C20A	4189(16)	3052(8)	3713(11)	C64	1375(10)	5566(5)	−1836(8)
C21A	3772(18)	3748(9)	3610(18)	C65	788(8)	5601(4)	−906(8)
C18B	5027(38)	2534(30)	3170(24)	C66	1523(7)	5990(4)	382(7)

[a] The site occupation factors for C18, C19, C20, and C21 are 0.65 and 0.35 for A and B, respectively.

−0.002(1) Å; Mn2, −0.002(1) Å; C81, 0.079(7) Å; C91, 0.085(7) Å. The internal C−Mn−C and Mn−C−Mn angles (mean values 100.9(3) and 79.0(3)°, respectively) result in a Mn···Mn distance of 2.796(1) Å. The C81···C86 and C91···C96 bridging rings form dihedral angles of 91.6(2) and 107.2(2)° with the Mn_2C_2 core indicating some structural distortions.

The very important, novel feature of the structures of **3** and **4** is the interaction between Mn and the BPh_4^- anions, acting in both cases as a bent-sandwich ligand. In both cases, we observe rather long Mn−C(BPh_4^-) distances, implying rather weak interactions, as expected for the kind of ion pairing held by electrostatic interactions. The interaction modes are, however, significantly different in **3** and **4**. Although varying over a large range (see Table 8), the Mn−C(BPh_4^-) distances in complex **3** suggest a η^3 bonding to the C11···C16 and C21···C26 phenyl rings. The manganese experiences a kind of bent bis(allyl) binding. The C11,C12,C16 centroid and the C21,C22,C26 centroid to Mn distances

Table 4. Fractional Atomic Coordinates ($\times 10^4$) for Complex 3

atom	x/a	y/b	z/c	atom	x/a	y/b	z/c
Mn1	428.2(8)	1646.6(5)	2844.1(4)	C32	1415(6)	4684(3)	3457(2)
B1	51(5)	3567(3)	2636(3)	C33	1567(7)	5284(4)	3943(3)
C1	540(4)	427(3)	3193(3)	C34	440(9)	5475(4)	4217(3)
C2	246(4)	−270(3)	2768(3)	C35	−761(8)	5073(4)	3995(3)
C3	243(5)	−1078(4)	3023(4)	C36	−879(6)	4482(3)	3508(2)
C4	496(5)	−1228(4)	3686(4)	C41	−314(4)	4096(3)	1952(2)
C5	822(5)	−544(4)	4101(3)	C42	678(5)	4421(3)	1645(2)
C6	819(5)	268(3)	3867(2)	C43	366(6)	4900(3)	1084(2)
C7	−82(6)	−160(4)	2027(2)	C44	−963(6)	5083(3)	800(2)
C8	403(7)	−2100(4)	3951(4)	C45	−1973(5)	4783(3)	1096(2)
C9	1142(6)	981(4)	4350(3)	C46	−1640(5)	4292(3)	1658(2)
C11	1422(4)	2978(3)	2687(2)	C51A	5502(9)	3160(5)	4848(6)
C12	1633(5)	2525(3)	2130(3)	C52A	5369(14)	2405(7)	5169(7)
C13	2622(6)	1923(4)	2178(3)	C53A	4135(13)	2272(8)	5357(7)
C14	3477(6)	1734(4)	2767(4)	C54A	3084(15)	2856(7)	5301(8)
C15	3311(6)	2165(4)	3318(3)	C55A	3288(10)	3661(8)	5073(7)
C16	2302(5)	2772(3)	3274(2)	C56	4455(7)	3743(4)	4817(4)
C21	−1105(4)	2840(3)	2684(2)	C57A	6679(14)	3389(10)	4513(8)
C22	−1384(5)	2544(3)	3282(3)	C51B	3913(9)	3048(5)	5081(5)
C23	−2227(7)	1866(4)	3318(4)	C52B	4682(12)	2326(7)	5267(7)
C24	−2824(6)	1452(4)	2748(4)	C53B	6003(13)	2237(8)	5169(7)
C25	−2570(5)	1706(3)	2156(4)	C54B	6524(13)	2878(7)	4837(7)
C26	−1728(5)	2378(3)	2134(3)	C55B	5748(9)	3607(7)	4694(7)
C31	215(5)	4250(3)	3229(2)	C57B	2446(11)	3133(11)	5181(9)

[a] The site occupation factor is 0.5 for the A and B positions of C51, C52, C53, C54, C55, and C57.

Table 5. Fractional Atomic Coordinates ($\times 10^4$) for Complex 4[a]

atom	x/a	y/b	z/c	atom	x/a	y/b	z/c
Mn1	1605.9(6)	−859.8(7)	1888.8(3)	C61	−1119(3)	−919(4)	1776(2)
Mn2	3169.3(6)	−772.0(7)	2558.1(4)	C62	−902(4)	−711(4)	2263(2)
B1	4499(4)	−588(5)	3442(2)	C63	−1518(4)	−802(4)	2582(2)
B2	−361(4)	−861(5)	1406(2)	C64	−2376(5)	−1104(5)	2428(3)
C1	4514(3)	−8(4)	2921(2)	C65	−2627(4)	−1306(5)	1950(3)
C2	5014(4)	−414(5)	2577(2)	C66	−1999(4)	−1211(4)	1628(2)
C3	5066(4)	42(6)	2134(2)	C71	−860(4)	−903(5)	853(2)
C4	4613(5)	939(6)	2024(3)	C72	−1182(4)	−1802(5)	638(3)
C5	4110(5)	1349(5)	2342(3)	C73	−1682(5)	−1820(7)	193(3)
C6	4063(4)	895(5)	2777(2)	C74	−1866(7)	−976(10)	−57(3)
C11	3770(3)	−1550(4)	3376(2)	C75	−1568(7)	−64(8)	133(4)
C12	3764(4)	−2259(4)	3017(2)	C76	−1073(5)	−42(6)	579(3)
C13	3240(4)	−3115(5)	2984(3)	C81	1793(3)	−300(5)	2625(2)
C14	2689(4)	−3297(5)	3322(3)	C82	1429(4)	−874(5)	2971(2)
C15	2681(4)	−2625(6)	3692(3)	C83	1003(4)	−445(6)	3315(3)
C16	3195(4)	−1772(5)	3721(2)	C84	923(4)	587(7)	3327(3)
C21	4218(4)	204(4)	3848(2)	C85	1272(4)	1183(5)	3009(3)
C22	4790(4)	474(5)	4255(2)	C86	1705(4)	746(5)	2670(2)
C23	4549(5)	1137(5)	4597(3)	C91	2999(4)	−1220(5)	1796(3)
C24	3708(6)	1554(5)	4527(3)	C92	3229(5)	−581(6)	1407(4)
C25	3123(5)	1311(5)	4132(3)	C93	3753(6)	−855(8)	1062(3)
C26	3363(4)	632(5)	3802(2)	C94	4129(7)	−1771(9)	1073(4)
C31	5495(4)	−1056(4)	3632(2)	C95	3973(6)	−2446(7)	1434(4)
C32	5615(4)	−1942(4)	3903(2)	C96	3427(5)	−2154(6)	1755(3)
C33	6448(4)	−2267(5)	4115(2)	C1SA	8115(10)	1163(11)	5144(5)
C34	7199(4)	−1713(5)	4070(2)	C1SB	9066(17)	1167(16)	5318(9)
C35	7110(4)	−849(5)	3807(2)	C2S	8523(8)	299(8)	5262(4)
C36	6282(4)	−525(4)	3592(2)	C3SA	9435(13)	205(15)	5452(7)
C41	358(4)	−1814(4)	1506(2)	C3SB	7570(17)	556(18)	5021(8)
C42	555(3)	−2298(4)	1944(2)	C4S	9952(10)	1183(12)	5506(5)
C43	1146(4)	−3111(4)	2023(2)	C5SA	9575(13)	2000(13)	5371(6)
C44	1545(4)	−3470(5)	1652(3)	C5SB	7947(16)	2231(16)	5007(8)
C45	1380(5)	−3023(5)	1210(3)	C6S	8734(9)	2100(9)	5199(4)
C46	804(4)	−2208(5)	1135(2)	C7S	7210(9)	1373(11)	4936(5)
C51	204(4)	210(4)	1487(2)	C8S	4782(7)	889(7)	0(4)
C52	991(4)	366(4)	1282(2)	C9S	5498(15)	1055(16)	349(8)
C53	1453(4)	1282(5)	1320(2)	C10S	6034(9)	320(12)	565(5)
C54	1142(4)	2062(5)	1554(2)	C11S	5869(12)	−669(15)	339(7)
C55	364(4)	1951(4)	1758(2)	C12S	4601(14)	−107(19)	−203(8)
C56	−83(4)	1049(4)	1723(2)				

[a] The site occupation factor is 0.5 for C1SA, C1SB, C3SA, C3SB, C5SA, C5SB, C9S, C11S, and C12S.

are 2.294(5) and 2.347(5) Å, respectively, while the centroid−Mn−centroid angle is 88.1(2)° and the dihedral angle between the corresponding phenyl rings is 84.7(1)°.

In the case of complex **4**, for both Mn1 and Mn2 the bonding mode of the two adjacent phenyl rings to the metal is η^2 (see Table 9) and occurs at rather long distances (from 2.362(5) to 2.659 Å) by rather weak interactions. There are a number of recent and significant examples in which BPh_4^- acts as a ligand.[11]

Table 6. Selected Interatomic Distances (Å) and Angles (deg) for Complex 1

Mn1–Mn2	2.851(2)	Mn3–C31	2.189(8)
Mn1–Mn3	2.852(2)	Mn3–C51	2.123(7)
Mn1–C1	2.321(9)	C1–C2	1.439(14)
Mn1–C11	2.324(8)	C1–C6	1.410(12)
Mn1–C21	2.343(8)	C11–C12	1.432(12)
Mn1–C31	2.334(8)	C11–C16	1.414(15)
Mn2–C1	2.209(9)	C21–C22	1.436(15)
Mn2–C11	2.220(10)	C21–C26	1.414(14)
Mn2–C41	2.121(7)	C31–C32	1.432(15)
Mn3–C21	2.207(8)	C31–C36	1.415(15)
C21–Mn1–C31	97.8(3)	Mn2–C11–C16	116.6(6)
C11–Mn1–C31	124.2(3)	Mn2–C11–C12	107.2(6)
C11–Mn1–C21	107.6(3)	Mn1–C11–C16	117.2(6)
C1–Mn1–C31	106.0(3)	Mn1–C11–C12	116.8(6)
C1–Mn1–C21	124.8(3)	C12–C11–C16	115.4(8)
C1–Mn1–C11	98.8(3)	Mn1–C21–Mn3	77.6(3)
Mn2–Mn1–Mn3	178.8(1)	Mn3–C21–C26	117.4(6)
C11–Mn2–C41	130.4(4)	Mn3–C21–C22	111.0(5)
C1–Mn2–C41	122.6(3)	Mn1–C21–C26	118.2(6)
C1–Mn2–C11	105.5(3)	Mn1–C21–C22	112.7(6)
C31–Mn3–C51	126.0(3)	C22–C21–C26	114.7(8)
C21–Mn3–C51	125.4(3)	Mn3–C31–C36	110.8(6)
C21–Mn3–C31	106.5(3)	Mn3–C31–C32	116.9(6)
Mn1–C1–Mn2	78.0(3)	Mn1–C31–C36	114.1(6)
Mn2–C1–C6	108.6(6)	Mn1–C31–C32	117.9(7)
Mn2–C1–C2	117.8(6)	C32–C31–C36	114.1(8)
Mn1–C1–C6	116.0(5)	Mn2–C41–C46	123.5(6)
Mn1–C1–C2	115.1(5)	Mn2–C41–C42	120.9(7)
C2–C1–C6	115.8(8)	Mn3–C51–C56	122.3(6)
Mn1–C11–Mn2	77.7(3)	Mn3–C51–C52	120.2(6)

Table 7. Selected Bond Distances (Å) and Angles (deg) for Complex 2

Mn1–O1	2.145(5)	O2–C16	1.473(9)
Mn1–O2	2.138(6)	O3–C18A	1.499(19)
Mn1–O3	2.117(5)	O3–C20A	1.473(13)
Mn1–C1	2.111(8)	O3–C18B	1.500(45)
O1–C10	1.475(13)	O3–C20B	1.521(32)
O1–C12	1.452(8)	C1–C2	1.410(12)
O2–C14	1.456(11)	C1–C6	1.412(11)
O3–Mn1–C1	110.6(2)	C14–O2–C16	113.4(6)
O2–Mn1–C1	127.8(3)	Mn1–O3–C20B	97.5(13)
O2–Mn1–O3	100.9(3)	Mn1–O3–C18B	134.3(22)
O1–Mn1–C1	121.1(2)	Mn1–O3–C20A	119.5(8)
O1–Mn1–O3	102.4(2)	Mn1–O3–C18A	126.0(7)
O1–Mn1–O2	89.4(2)	C18B–O3–C20B	106.8(16)
Mn1–O1–C12	119.2(4)	C18A–O3–C20A	109.9(9)
Mn1–O1–C10	125.8(4)	Mn1–C1–C6	122.8(6)
C10–O1–C12	114.8(6)	Mn1–C1–C2	121.4(5)
Mn1–O2–C16	123.7(5)	C2–C1–C6	115.7(7)
Mn1–O2–C14	122.9(5)		

Included among these are the stabilization of the $[Zr(CH_2Ph)_3]^+$ cation[11b] by a η^6 interaction of one of the phenyl rings from BPh_4^-, the complex $[\{Ph_2B(\eta^6\text{-}Ph)_2\}Nb(\eta^2\text{-}C_2Me_2)]$[11d] containing a BPh_4^- ligand acting as a 12-electron donor and behaving as a bent bis(η^6-arene) ligand, and the η^2-bonding mode in some cationic indenyl zirconium complexes[11c] and in copper(I) complexes.[11f]

In spite of the fact that the structural parameters seem to indicate a rather weak interaction in such ion-pair forms, the BPh_4^- cannot be displaced by electron-rich neutral arenes, an indication of the importance of electrostatic interactions within complexes of this kind.[11a]

Magnetic Properties. The magnetic properties of organometallics is a poorly studied field, because a relationship has not been found between the magnetic properties and the chemical behavior, *i.e.* how much the chemistry of the [M–R] fragment depends on the magnetic properties of the metal. On the other hand, the magnetic properties could give vital information on

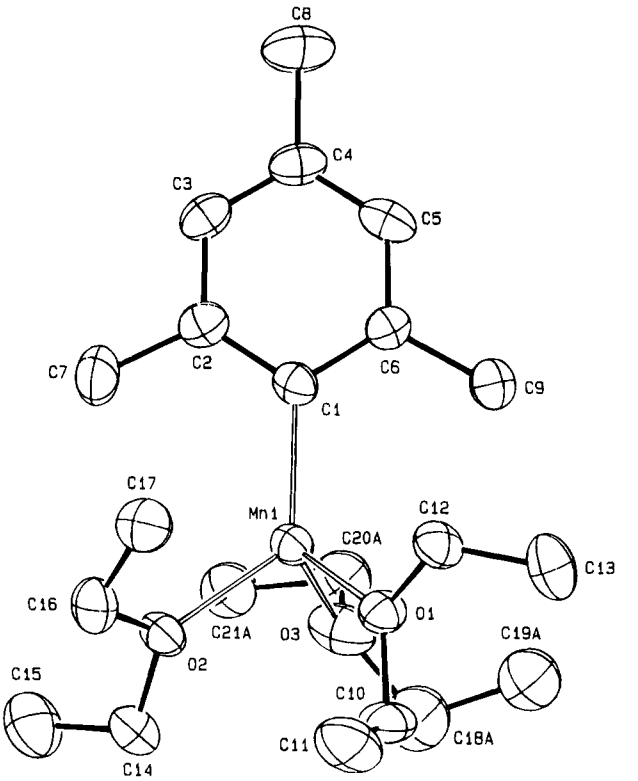

Figure 2. ORTEP drawing for complex **2** (30% probability ellipsoids). For clarity only the A position is given for the disordered C18–C21 carbon atoms.

the nature of alkyl–metal or aryl–metal aggregates, an area of increasing interest both for chemical reactivity and for precursors of solid-state materials.[12] Magnetic studies can also be diagnostic in some cases for the existence of metal–metal bonds.[13] In the present report we deal with a homogeneous class of manganese(II) aryls possessing monomeric, dimeric, and trimeric examples, with the last having a rather short Mn···Mn distance.

Magnetic susceptibility data for complexes **1**, **3**, and **4** were collected in the temperature range 1.9–300 K, and those for **4** and **1** are displayed in Figures 5 and 6, respectively.

For complex **3** the magnetic moment per manganese ion is essentially constant down to about 60 K with a value of 5.79 μ_B, which falls in the typical range for Mn(II) complexes,[14,15] and then shows a slight reduction due to a small zero-field splitting.

The susceptibility data for the dimer complex **4** were fitted with the simple theoretical equation[16]

$$\chi_{dim} = \frac{Ng^2\mu_B{}^2}{kT}\,\frac{2e^{2x} + 10e^{6x} + 28e^{12x} + 60e^{20x} + 110e^{30x}}{1 + 3e^{2x} + 5e^{6x} + 7e^{12x} + 9e^{20x} + 11e^{30x}}$$

where $x = J/kT$, obtained assuming that the interaction

(12) Trogler, W. C. *Organometallic Radical Processes*; Elsevier: Amsterdam, The Netherlands, 1990.
(13) Klose, A.; Solari, E.; Floriani, C.; Chiesi-Villa, A.; Rizzoli, C.; Re, N. *J. Am. Chem. Soc.* **1994**, *116*, 9123.
(14) Carlin, R. L. *Magnetochemistry*; Springer-Verlag: Berlin, 1986.
(15) Casey, A. T.; Mitra, S. In *Theory and Applications of Molecular Paramagnetism*, Bodreaux, E. A., Mulay, L. N., Eds.; Wiley: New York, 1976, p 135.
(16) O'Connor, C. J. *Prog. Inorg. Chem.* **1982**, *29*, 203.

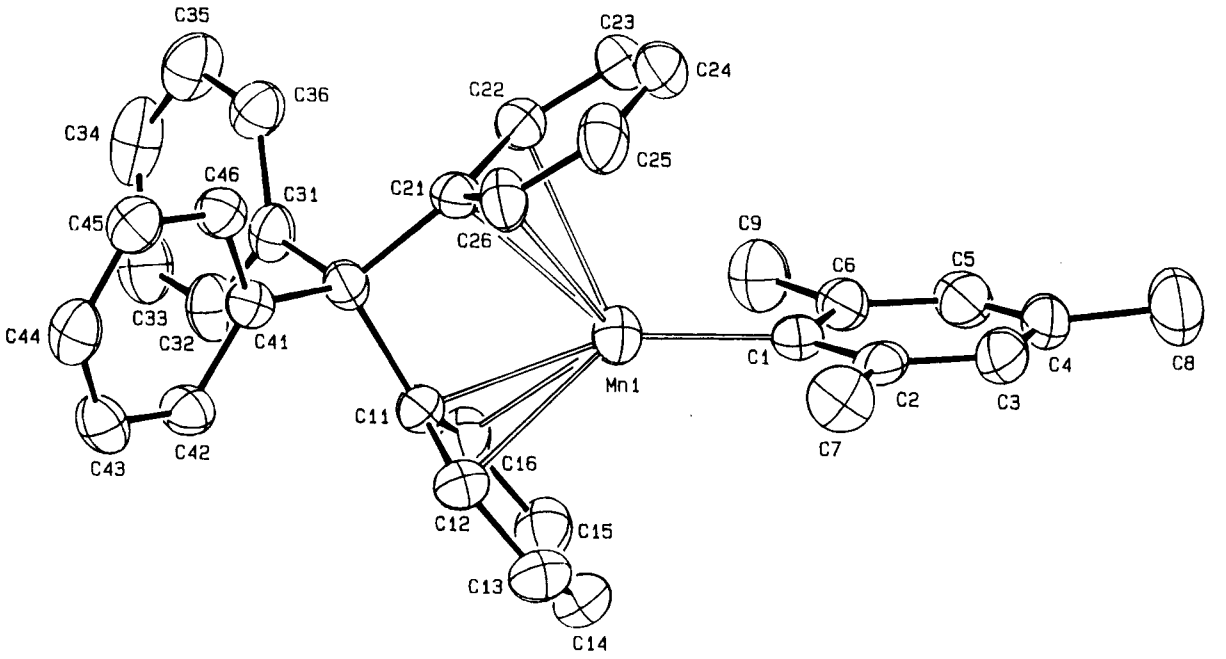

Figure 3. ORTEP drawing for complex **3** (30% probability ellipsoids).

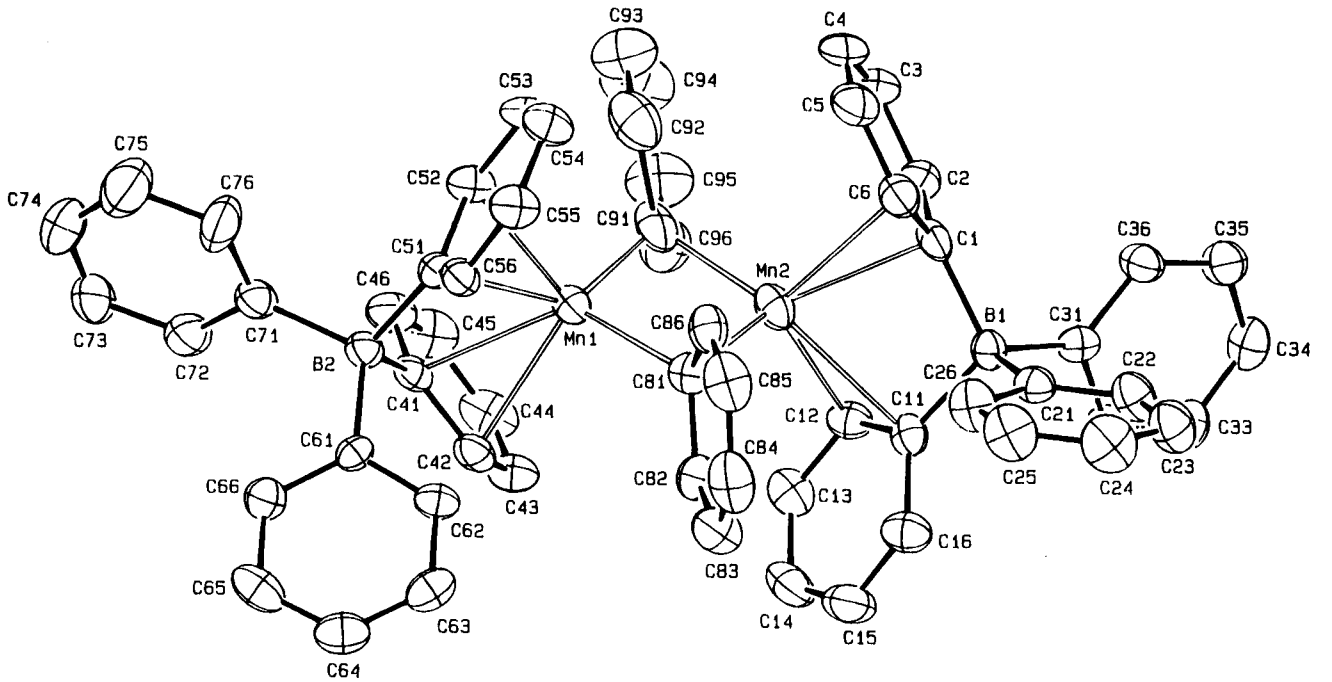

Figure 4. ORTEP drawing for complex **4** (30% probability ellipsoids).

between the the two spin centers were described by the Heisenberg spin Hamiltonian $H_{ex} = -2J\hat{S}_1\cdot\hat{S}_2$, with $\hat{S}_1 = \hat{S}_2 = {}^5/_2$.

The presence of a small Curie tail in the magnetic susceptibility data at low temperature for two of our complexes requires a correction for a small quantity of monomeric Mn(II) impurities which were assumed to obey Curie law. The following equation is therefore obtained for the total susceptibility:

$$\chi = \frac{1}{2}(1-p)\chi_{dim} + p\frac{Ng'^2\mu_B{}^2S(S+1)}{3kT} \qquad (1)$$

where S and g' are the spin and the g factors of the impurity (assumed to be the same as for the Mn(II) ion in the dimer) and p is the monomeric impurity fraction. A good fit ($R = 9 \times 10^{-4}$) to the collected data was obtained for $g = 1.98$, $J = -55.4$ cm^{-1}, and $p = 1.8\%$ (see Figure 5).

The situation is more complicated for the trimeric complex **1**, for which the temperature dependence of μ_{eff} shows a plateau at about 3.4 μ_B below 100 K and a very limited increase above that temperature (3.65 μ_B at 310 K). These values are much smaller than that expected for three uncoupled Mn(II) ions (5.92 μ_B). This behavior clearly indicates a strong antiferromagnetic coupling between the three Mn(II) centers, with spin frustration, leading to an overall $S = {}^5/_2$ ground state. Only at very low temperatures, less than 4 K, does μ_{eff} show a very

Table 8. Selected Interatomic Distances (Å) and Angles (deg) for Complex 3

Mn1–C1	2.066(5)	Mn1–C23	3.057(8)
Mn1–C11	2.393(5)	Mn1–C24	3.254(6)
Mn1–C12	2.528(6)	Mn1–C25	3.065(5)
Mn1–C13	2.877(7)	Mn1–C26	2.633(5)
Mn1–C14	3.110(7)	C1–C2	1.412(7)
Mn1–C15	2.983(6)	C1–C6	1.400(7)
Mn1–C16	2.621(5)	C11–C12	1.421(8)
Mn1–C21	2.425(5)	C11–C16	1.395(6)
Mn1–C22	2.625(6)	C21–C22	1.416(8)
C21–C26	1.398(7)		
C21–Mn1–C26	31.7(1)	Mn1–C1–C2	121.7(4)
C21–Mn1–C22	32.2(1)	C2–C1–C6	117.5(4)
C11–Mn1–C21	64.0(1)	Mn1–C11–B1	98.2(3)
C11–Mn1–C16	31.9(1)	Mn1–C11–C16	83.1(3)
C11–Mn1–C12	33.4(1)	Mn1–C11–C12	78.5(3)
C1–Mn1–C21	140.3(2)	Mn1–C21–B1	96.8(3)
C1–Mn1–C11	152.2(2)	Mn1–C21–C26	82.3(3)
Mn1–C1–C6	120.6(3)	Mn1–C21–C22	81.7(3)

Table 9. Selected Interatomic Distances (Å) and Angles (deg) for Complex 4

Mn1–Mn2	2.796(1)	Mn2–C13	3.332(7)
Mn1–C41	2.391(6)	Mn2–C14	4.106(7)
Mn1–C42	2.502(5)	Mn2–C15	4.180(8)
Mn1–C43	3.106(6)	Mn2–C16	3.527(6)
Mn1–C44	3.531(7)	Mn2–C81	2.202(5)
Mn1–C45	3.441(7)	Mn2–C91	2.204(8)
Mn1–C46	2.902(6)	C1–C2	1.417(8)
Mn1–C51	2.659(6)	C1–C6	1.409(8)
Mn1–C52	2.443(5)	C11–C12	1.380(8)
Mn1–C53	3.257(7)	C11–C16	1.423(8)
Mn1–C54	4.032(7)	C21–C22	1.377(8)
Mn1–C55	4.170(6)	C21–C26	1.397(9)
Mn1–C56	3.576(6)	C31–C32	1.400(8)
Mn1–C81	2.180(6)	C31–C36	1.399(8)
Mn1–C91	2.206(7)	C41–C42	1.383(8)
Mn2–C1	2.362(5)	C41–C46	1.421(9)
Mn2–C2	2.814(6)	C51–C52	1.408(9)
Mn2–C3	3.430(7)	C51–C56	1.398(8)
Mn2–C4	3.622(8)	C81–C82	1.409(9)
Mn2–C5	3.252(7)	C81–C86	1.404(9)
Mn2–C6	2.619(7)	C91–C92	1.466(13)
Mn2–C11	2.565(5)	C91–C96	1.411(10)
Mn2–C12	2.457(5)		
C81–Mn1–C91	101.1(2)	Mn1–C41–B2	97.0(3)
C52–Mn1–C91	109.4(2)	Mn1–C41–C46	95.8(4)
C52–Mn1–C81	114.8(2)	Mn1–C41–C42	78.0(3)
C41–Mn1–C91	122.1(2)	C42–C41–C46	114.8(5)
C41–Mn1–C81	126.4(2)	Mn2–C42–C41	69.2(3)
C41–Mn1–C42	32.7(2)	Mn2–C42–C43	101.9(4)
C51–Mn1–C52	31.7(2)	C41–C42–C43	123.4(5)
C81–Mn2–C91	100.5(3)	Mn1–C51–B2	87.7(3)
C12–Mn2–C91	106.0(2)	Mn1–C51–C56	129.4(4)
C12–Mn2–C81	117.4(2)	Mn1–C51–C52	65.7(3)
C1–Mn2–C91	120.5(2)	C52–C51–C56	114.5(5)
C1–Mn2–C81	126.9(2)	Mn1–C52–C51	82.6(3)
C1–Mn2–C6	32.3(2)	C51–C52–C53	122.5(5)
C11–Mn2–C12	31.8(2)	Mn1–C52–C53	113.1(4)
Mn2–C1–B1	93.5(3)	C62–C61–C66	115.4(5)
Mn2–C1–C6	83.9(3)	C72–C71–C76	115.3(6)
Mn2–C1–C2	92.8(3)	Mn1–C81–Mn2	79.3(2)
C2–C1–C6	114.2(5)	Mn2–C81–C86	113.1(4)
Mn2–C11–B1	86.1(3)	Mn2–C81–C82	111.8(4)
Mn2–C11–C16	121.7(4)	Mn1–C81–C86	115.0(4)
Mn2–C11–C12	69.8(3)	Mn1–C81–C82	117.5(4)
C12–C11–C16	114.7(5)	C82–C81–C86	115.0(5)
Mn2–C12–C11	78.4(3)	Mn1–C91–Mn2	78.7(2)
C11–C12–C13	123.7(6)	Mn2–C91–C96	109.1(6)
Mn2–C12–C13	117.8(4)	Mn2–C91–C92	124.3(5)
C22–C21–C26	115.3(5)	Mn1–C91–C96	130.9(5)
C32–C31–C36	115.1(5)	Mn1–C91–C92	107.2(5)

small decrease, indicating an almost negligible zero-field splitting effect. These data were fitted using the theoretical equation corresponding to the spin Hamiltonian

$$\hat{H} = -2J(\hat{S}_1 \cdot \hat{S}_2 + \hat{S}_1 \cdot \hat{S}_3) + g\mu_B H \cdot \hat{S} \qquad (2)$$

where $\hat{S}_1$ is the spin of the central ion, $\hat{S}_2$ and $\hat{S}_3$ are the spins of the terminal ions, all being $^5/_2$, and $\hat{S}$ is the total spin. In this Hamiltonian we assumed equivalent g factors for the three ions and neglected the coupling between the two terminal ions, both approximations being quite reasonable on the basis of the structure. The spin energy levels may be calculated by Kambe methods,[17] which gives

$$E(S',S) = -J[S(S+1) - S'(S'+1) - s(s+1)] \qquad (3)$$

in which $s = {}^5/_2$ and S' is the quantum number

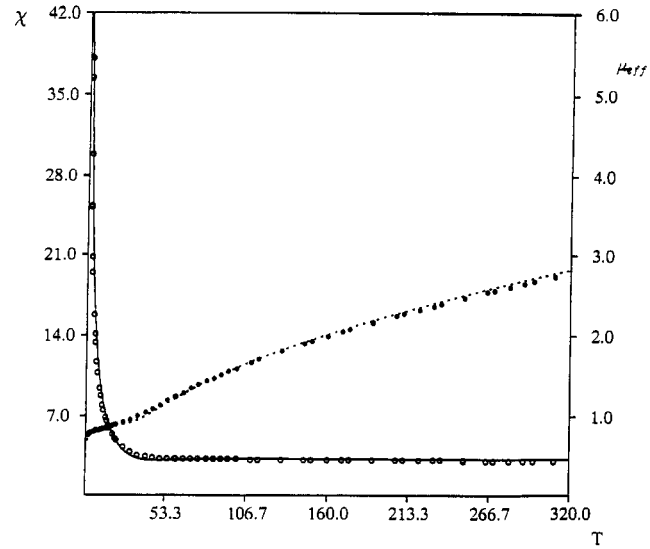

Figure 5. Magnetic susceptibility (○; 10^{-3} cm^3 mol^{-1}) and effective magnetic moment (●; μ_B) per Mn for **4** as a function of the temperature. The solid and dashed lines are the best theoretical fits (see text) to the experimental data.

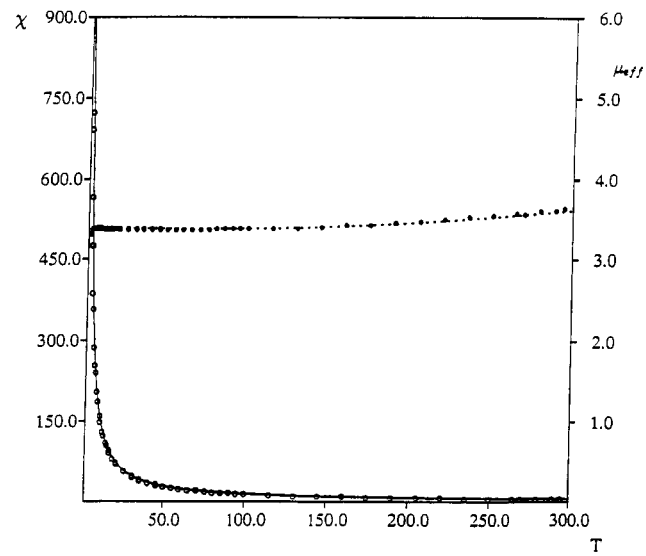

Figure 6. Magnetic susceptibility (○; 10^{-3} cm^3 mol^{-1}) and effective magnetic moment (●; μ_B) per Mn for **1** as a function of the temperature. The solid and dashed lines are the best theoretical fits (see text) to the experimental data.

(17) Kambe, C. *J. Phys. Soc. Jpn.* **1950**, *5*, 48.

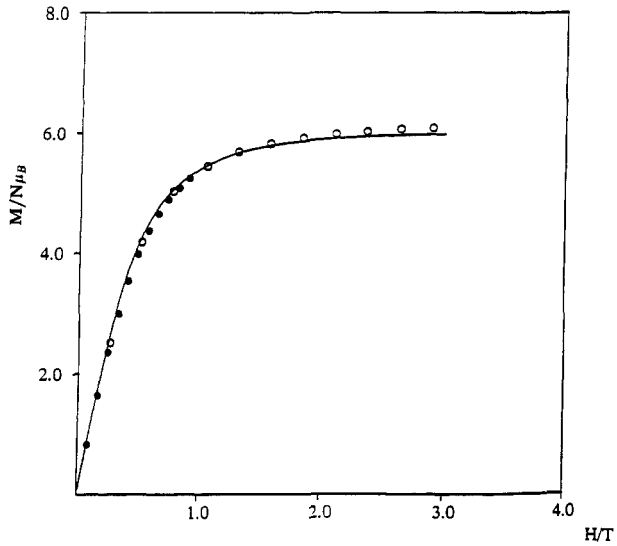

Figure 7. Reduced magnetization, $M/N\mu_B$, for **4** as a function of H/T (10^{-4} G K^{-1}) collected at two temperatures: (○) 1.9 K; (●) 6 K. The solid line is the best theoretical fit (see text) to the experimental data.

corresponding to $\hat{S}' = \hat{S}_2 + \hat{S}_3$. S' and S must satisfy the conditions $0 \le S' \le 5$, $|S' - {}^5/_2| \le S \le S' + {}^5/_2$. We use the expression obtained by inserting these energy levels into the van Vleck equation[18]

$$\chi = \frac{Ng^2\mu_B{}^2}{3kT} \frac{\sum_S \sum_{S'} S(S+1)(2S+1) \exp[-E(S,S')/kT]}{\sum_S \sum_{S'} (2S+1) \exp[-E(S,S')/kT]}$$

to fit the temperature dependence of χ and μ_{eff}. A good fit, $R = 5 \times 10^{-4}$, was obtained for $g = 1.99$ and $J = -40.4$ cm^{-1} and is shown in Figure 6.

In terms of an energy level scheme, the results above indicate that the $S = {}^5/_2$ ground state is fairly isolated, with the next excited levels ($S = {}^3/_2$ at 101 cm^{-1} and $S = {}^7/_2$ at 141.4 cm^{-1}) being high enough in energy to be negligibly populated below 60 K. On the other hand, these energy levels become slightly populated above 100 K, giving rise to a small increase in μ_{eff}. This energy level pattern has been confirmed by isothermal variable-field magnetization measurements taken at 1.9 and 6.0 K. The data are shown in Figure 7 and can both be fitted well with the expression

$$M = Ngm_B S B_{5/2}(z)$$

where $z = gm_B H/kT$ and $B_{5/2}(z)$ is the Brillouin function for a $S = {}^5/_2$ state.[14] In particular, the good fit for the 6 K data clearly indicates that excited energy levels are not populated at that temperature and confirms that they are high in energy.

Complexes **1** and **4** have unique trinuclear and binuclear cores in which dimanganese(II) units held by bridging aryl groups exhibit unusually large negative J values. Indeed, the coupling constant values found for complexes **1** and **4** show a strong antiferromagnetic coupling for these $(\mu_2\text{-Ar})_2Mn^{II}$ species. It is worth noting that these values are higher than those usually found for μ-alkoxo and μ-carboxylato Mn^{II}–Mn^{II} dimers[19–22] intensively studied within the investigation of inorganic model complexes of manganese-containing metalloproteins.[22] This strong interaction could be due either to a shorter Mn–Mn distance (2.8–2.9 Å) observed in compounds **1** and **4** versus the longer distances (3.3–4.3) usually observed in the μ-alkoxo and μ-carboxylato complex or to the higher efficiency for electron exchange of the aromatic carbon bridge. The only previously magnetically characterized manganese trimer containing unsaturated carbon bridges is tetrakis (3-methylpentadienyl)trimanganese.[23] However, it cannot be directly related to complex **1**, as its magnetic behavior has been interpreted in terms of a high-spin (ionic) central Mn^{2+} and two low-spin diamagnetic Mn(I) units.1 A vew aryl-bridged manganese(II) complexes are known,[5f] but these have not been magnetically well characterized. The only available value is the magnetic moment at room temperature of $[Ph_2Mn(\mu\text{-}Ph)_2MnPh_2]$, which at 2.3 BM indicates a considerable antiferromagnetic metal–metal coupling. To date only two other examples of magnetically characterized, mesityl-bridged, dimetal units are known to us: $[(Mes)Fe(\mu\text{-}Mes)_2Fe(Mes)]$,[13] with $J = -31.5$ cm^{-1}, and $[(Mes)Co(\mu\text{-}Mes)_2Co(Mes)]$,[24] where J is on the order of -500 cm^{-1}. In the latter case the first triplet excited state is thermally inaccessible but is low enough to give rise to a relevant temperature-independent paramagnetism.

The difference between the J values obtained for the dimer **4** (55.4 cm^{-1}) and the trimer **1** (40.4 cm^{-1}) reveals that the coupling constant due to these μ-aryl bridges is very sensitive to the metal–metal bond distance (2.851(2) and 2.796(1) Å, respectively, for **1** and **4**). The weaker interaction in complex **1** could be related equally to the larger Mn–Mn distance or to the larger Mn–C–Mn bond angle.

Experimental Section

General Procedure. All operations were carried out under an atmosphere of purified nitrogen using modified Schlenk techniques or in a Braun drybox. Solvents were dried and distilled before use by standard methods. The synthesis of BPh_3 was carried out as reported in the literature.[25]

Synthesis of 1. The Grignard reagent MesMgBr (380 mL, 0.334 mmol) was added to a THF (50 mL) solution of $MnCl_2$·1.5THF (37.2 g, 0.159 mmol) cooled to −30 °C. The brown suspension was then warmed to room temperature, stirred for 10 h, and refluxed for 5 h more. When dioxane (250 mL) was added to the suspension, a white solid suddenly formed. The resulting supension was stirred for 10 h and then left to stand for 2 h. The white solid was filtered out, and the

(18) van Vleck, J. H. *The Theory of Electric and Magnetic Susceptibilities*; Oxford University Press: Oxford, U.K., 1932.

(19) Menage, S.; Vitols, S. E.; Bergerat, P.; Codjovi, E.; Kahn, O.; Girerd, J.-J.; Guillot, M.; Solans, X.; Calvet, T. *Inorg. Chem.* **1991**, *30*, 2666.

(20) Wieghardt, K.; Bossek, K.; Nuber, B.; Weiss, J.; Bonvoisin, J.; Corbella, M.; Vitols, S. E.; Girerd, J.-J. *J. Am. Chem. Soc.* **1988**, *110*, 7398.

(21) Wieghardt, K.; Bossek, K.; Bonvoisin, J.; Beauvillain, P.; Girerd, J.-J.; Nuber, B.; Weiss, J.; Heinze, J. *Angew. Chem., Int. Ed. Engl.* **1986**, *25*, 1030.

(22) Wieghardt, K. *Angew. Chem., Int. Ed. Engl.* **1989**, *28*, 1153.

(23) Böhm, M. C.; Ernst, R. D.; Gleiter, R.; Wilson, D. R. *Inorg. Chem.* **1983**, *22*, 3815.

(24) Theopold, K. N.; Silvester, J.; Byrne, E. K.; Richeson, D. S. *Organometallics* **1989**, *8*, 2001.

(25) Pelter, A.; Smith, K.; Brown, H. C. *Borane Reagents;* Academic: London, 1988; p 227.

solution was evaporated to dryness to give a green solid. This solid was dissolved in warm toluene (150 mL) and the small amount of undissolved solid was filtered out while the solution was kept warm. When it was cooled, the solution gave crystals of **1**, which were further recrystallized from hot toluene (58.3%). Anal. Calcd for $C_{54}H_{66}Mn_3{\cdot}C_7H_8$: C, 75.36; H, 7.68. Found: C, 75.67; H, 7.34. The consistency of the composition of the obtained trimer has been proved (i) by the unit cell determination (the same result) on crystals of five different preparations and (ii) by measuring the magnetic susceptibilities for each crystalline sample used for reactivity studies.

Synthesis of 2. BPh_3 (2.59 g, 10.70 mmol) was added to a Et_2O (400 mL) suspension of **1** (3.50 g, 3.57 mmol). The suspension suddenly became a deep-red solution. Within 30 min, a white solid formed and the red solution turned yellow. The stirring was continued for 12 h at room temperature. The white solid was filtered out and collected (4.7 g, 62.0%). Anal. Calcd for $C_{45}H_{61}BMnO_3$: C, 75.52; H, 8.53. Found: C, 75.72; H, 8.63. The mother liquor, analyzed by GC–MS, showed the presence of large amounts of BPh_2Mes.

Synthesis of 3. Complex **1** (13.81 g, 14.0 mmol) was added as a solid to a toluene (400 mL) solution of BPh_3 (21.98 g, 90.0 mmol). The suspension was stirred overnight to give a yellow solution and a white insoluble solid. The suspension was then cooled to −15 °C, and the white solid was collected (10.6 g, 51.2%). Anal. Calcd for $C_{33}H_{31}BMn$: C, 80.34; H, 6.33. Found: C, 81.19; H, 6.76. The crystallization solvent (toluene) was lost while drying in vacuo. Crystals suitable for X-ray analysis were obtained from the mother liquor kept at 3–4 °C for 3 days. They contain one molecule of toluene of crystallization. The mother liquor was evaporated to dryness and the solid collected with pentane (100 mL). The very small amount of unidentified undissolved solid was filtered out and the yellow solution, analyzed by GC–MS, showed the presence of large amounts of BPh_2Mes.

Synthesis of 4. Complex **1** (3.38 g, 3.47 mmol) was added as a solid to a toluene (100 mL) solution of BPh_3 (10.1 g, 41.7 mmol). The suspension was stirred at room temperature for 2 weeks to give **4** as a light green solid (50%). The mother liquor gave crystals suitable for X-ray analysis. Anal. Calcd for $C_{60}H_{50}B_2Mn_2{\cdot}1.5C_7H_8$: C, 81.36; H, 6.00. Found: C, 81.50; H, 6.07.

X-ray Crystallography for Complexes 1–4. Suitable crystals of compounds **1**–**4** were mounted in glass capillaries and sealed under nitrogen. The reduced cells were obtained with the use of TRACER.[26] Crystal data and details associated with data collection are given in Tables 1 and SI (supplementary material). Data were collected at room temperature (295 K) on a single-crystal diffractometer (Philips PW1100 for **1** and Rigaku AFC6S for **2**–**4**). For intensities and background the "three-point technique" was used for **1**, while individual reflection profiles[27] were analyzed for **2**–**4**. The structure amplitudes were obtained after the usual Lorentz and polarization corrections,[28] and the absolute scale was established by the Wilson method.[29] The crystal quality was tested by ψ scans, showing that crystal absorption effects could be neglected for complex **1**. The data for complexes **2**–**4** were corrected for absorption using a semiempirical method.[30] The function minimized during the least-squares refinement was $\sum w|\Delta F|^2$ for **1** and **2** and $\sum w(\Delta F^2)^2$ for **3** and **4**. Weights were applied according to the scheme $w = k/\sigma^2(F_o) + g|F_o|^2$ with g = 0.005 and 0.010 for complexes **1** and **2**, respectively.[31a] The weighting scheme $w = 1/[\sigma^2(F_o^2) + (aP)^2]$ $(P = (F_o^2 + 2F_c^2)/3)$ was used for **3** and **4**, with a = 0.0911 and 0.0956, respectively.[31b] Anomalous scattering corrections were included in all structure factor calculations.[32b] Scattering factors for neutral atoms were taken from ref 32a for non-hydrogen atoms and from ref 33 for hydrogens. Among the low-angle reflections, no correction for secondary extinction was deemed necessary.

Solutions were based on the observed reflections. Refinement was based on the observed reflections for **1** and **2** using SHELX76[31a] and on the unique total data for **3** and **4** using SHELXL92.[31b] All the structures were solved by the heavy-atom method, starting from three-dimensional Patterson maps. Refinements were first done isotropically and then anisotropically for all non-H atoms, except for the disordered atoms. In complex **2** the C18–C21 carbon atoms of a diethyl ether molecule were found to be disordered over two positions (A and B), which were isotropically refined with site occupation factors of 0.65 and 0.35 for A and B, respectively. During the refinement, the C–O and C–C bond distances of the diethyl ether molecules were constrained to be 1.48(1) and 1.54(1) Å, respectively. In **3**, the toluene solvent molecule of crystallization was affected by disorder, which was solved by considering the molecule to be distributed over two positions (A and B) sharing the C56 carbon atom. The disordered carbon atoms were isotropically refined with a site occupation factor of 0.5 and with constraints imposed on the C_{sp^2}–C_{sp^2} bond distances (1.395 Å). In complex **4**, one toluene solvent molecule of crystallization was found to be statistically distributed over two positions (A and B); the second toluene molecule was distributed around an inversion center. The disordered carbons were isotropically refined with a site occupation factor of 0.5. During the refinement the aromatic ring of the toluene molecule in complex **1** was constrained to be a regular hexagon (C–C = 1.395 Å).

All the hydrogen atoms, partially found from difference Fourier maps and partially put in geometrically calculated positions, were introduced in the final refinement as fixed-atom contributions with isotropic U's fixed at 0.12 Å^2 for **1** and **2** and equal to 1.2 times the U_{eq} value of the corresponding carbon atom for **3** and **4**. The hydrogens related to the disordered ethyl groups in **2** and to the toluene molecules in **3** and **4** were ignored. The final difference maps showed no unusual features, with no significant peak having chemical meaning above the general background. Final atomic coordinates are listed in Tables 2–5 for non-H atoms and in Tables SII–SV (supplementary material) for hydrogens. Thermal parameters are given in Tables SVI–IX and bond distances and angles in Tables SX–XIII (supplementary material).[34]

Magnetic Measurements for Complexes 1, 3, and 4. Magnetic susceptibility measurements were made on a MPMS5 SQUID susceptometer (Quantum Design Inc.) operating at a magnetic field strength of 3 kG. Corrections were applied for diamagnetism calculated from Pascal constants. Effective magnetic moments were calculated by the equation $\mu_{eff} = 2.828(\chi_{Mn}T)^{1/2}$, where χ_{Mn} is the magnetic susceptibility per manganese. Variable-field magnetization data were measured on the same susceptometer at 1.9 and 6.0 K, in the range 3–55 kG. Fitting of the magnetic data to the theoretical expression

(26) Lawton, S. L.; Jacobson, R. A. TRACER (a Cell Reduction Program); Ames Laboratory, Iowa State University of Science and Technology: Ames, IA, 1965.
(27) Lehmann, M .S.; Larsen, F. K. *Acta Crystallogr., Sect. A: Cryst. Phys., Diffr., Theor. Gen. Crystallogr.* **1974**, *A30*, 580–584.
(28) Data reduction, structure solution, and refinement were carried out on an IBM AT personal computer equipped with an Inmos T800 transputer and on an Encore 91 computer.
(29) Wilson, A. J. C. *Nature* **1942**, *150*, 151.
(30) North, A. C. T.; Phillips, D. C.; Mathews, F. S. *Acta Crystallogr., Sect. A: Cryst. Phys., Diffr., Theor. Gen. Crystallogr.* **1968**, *A24*, 351.
(31) (a) Sheldrick, G. M. SHELX-76: Program for Crystal Structure Determination; University of Cambridge, Cambridge, U.K., 1976. (b) Sheldrick, G. M. SHELXL-92. Program for crystal structure refinement. University of Göttingen, Göttingen, Germany, 1992.
(32) (a) *International Tables for X-ray Crystallography*; Kynoch Press: Birmingham, U.K., 1974; Vol. IV, p 99. (b) *Ibid.*, p 149.
(33) Stewart, R. F.; Davidson, E. R.; Simpson, W. T. *J. Chem. Phys.* **1965**, *42*, 3175.
(34) See paragraph at the end of the paper regarding supplementary material.

were performed by minimizing the agreement factor, defined as

$$R = \sum \frac{[\chi_i^{\text{obsd}}T - \chi_i^{\text{calcd}}T]^2}{(\chi_i^{\text{obsd}}T)^2}$$

through a Levenberg–Marquardt routine.[35]

Acknowledgment. We thank the "Fonds National Suisse de la Recherche Scientifique" (Grant No. 20-40268.94), Ciba-Geigy Co. (Basel, Switzerland), and Action COST D3 (European Program for Scientific Research) for financial support.

(35) Press, W. H.; Flannery, B. P.; Teukolsky, S. A.; Vetterling, W. T. *Numerical Recipes*; Cambridge University Press: Cambridge, U.K., 1989.

Supplementary Material Available: Tables of experimental details associated with data collection and structure refinement (Table SI), hydrogen atom coordinates (Tables SII–SV), thermal parameters (Tables SVI–SIX), and bond distances and angles (Tables SX–SXIII) for **1–4** (21 pages). Ordering information is given on any current masthead page.

OM940977A

Reactions of Di- and Polynuclear Complexes. 14.[1] Synthesis of Permethylated-Cyclopentadienyl Chalcogeno-Bridged Compounds: A Route to the Stable Thiolatosulfidocarbonyldimolybdenum(III) Complex $[Cp^*_2Mo_2(CO)_2(\mu\text{-}SMe)_2(\mu\text{-}S)]$. Crystal Structure Determination of $[Cp^*_2Mo_2(CO)_2(\mu\text{-}SMe)_2(\mu\text{-}SH)][BF_4]$

Philippe Schollhammer, François Y. Pétillon,* Roger Pichon, Sylvie Poder-Guillou, and Jean Talarmin

URA CNRS 322 "Chimie, Electrochimie Moléculaires et Chimie Analytique", Faculté des Sciences, Université de Bretagne Occidentale, B.P. 809, 29285 Brest-Cedex, France

Kenneth W. Muir* and Ljubica Manojlović-Muir

Department of Chemistry, University of Glasgow, Glasgow G12 8QQ, Great Britain

Received October 21, 1994[⊗]

The new diamagnetic carbonyl-containing sulfido complex $[Cp^*_2Mo_2(CO)_2(\mu\text{-}SMe)_2(\mu\text{-}S)]$ (**8**) has been obtained by the thermal reaction of the pentamethylcyclopentadienyl compound $[Cp^*_2Mo_2(CO)_4]$ (**1**) with MeSSMe; the other predominant product of the reaction, $[Cp^*_2Mo_2(CO)_4(\mu\text{-}SMe)_2]$ (**3**), results from the oxidative addition of dimethyl disulfide across the Mo_2 center. Monitoring this thermal reaction by IR spectroscopy indicated that **8** arises from decarbonylative dimerization of $[Cp^*Mo(CO)_3(SMe)]$ (**2**). Reactions with other dialkyl and diaryl chalcogenides, REER (ER = SPh, SeMe), and with thiol (HSBz) and selenol (HSePh) led only to the formation of tetracarbonyl chalcogenato-bridged derivatives $[Cp^*_2Mo_2(CO)_4(\mu\text{-}ER)_2]$ (ER = SPh (**4**), SBz (**5**), SeMe (**6**), SePh (**7**)). A thermolysis study showed the degradation of **3** to $[Cp^*_2Mo_2(\mu\text{-}SMe)_4]$ (**12**) *via* $[Cp^*_2Mo_2(CO)_2(\mu\text{-}SMe)_2]$ (**9**); **8** was decarbonylated directly to **12**. Investigation of the reaction between **8** and electrophilic reagents showed that dinuclear molybdenum(III) complexes $[Cp_2{}^*Mo_2(CO)_2(\mu\text{-}SMe)_2(\mu\text{-}SH)]X$ [X = BF_4 (**16**), Cl (**17**), F(**18**)] were formed stereospecifically as the *cis* isomers. **16** has been structurally characterized by X-ray diffraction. Crystals of **16** are orthorhombic, space group *Pcab*, a = 15.655(5) Å, b = 16.173(3) Å, c = 23.662(5) Å, and Z = 8. The complex cation has approximate C_{2v} symmetry and the Mo–Mo bond length is 2.772(2) Å. Complex **3** was readily oxidized by $Ag[BF_4]$ to yield the dicationic product $[Cp^*_2Mo_2(CO)_4(\mu\text{-}SMe)_2][BF_4]_2$ (**21**). All new thiolato-bridged complexes have been characterized by spectroscopic analyses.

Introduction

The continuing interest in sulfur-containing transition metal complexes reflects their importance in biology and catalysis.[2] Dinuclear thiolato-bridged complexes, in particular those of molybdenum, have been widely studied,[3-6] since they have found applications both as synthons for the production of heteronuclear clusters[4] and as models of sulfur–metal sites in biological or catalytic systems. We have focused on μ-thiolato cyclopentadienyl (Cp) complexes,[5] particularly on their electrochemistry and on their ability to electrogenerate reactive sites[6].

Group 6 metal carbonyl compounds, such as $[CpM(CO)_3]_2$, $[CpM(CO)_2]_2$, or $[CpM(CO)_3X]$ (M = Cr, Mo, W; X = H, Cl), are known to react with REER or REH (E = S, Se, Te), and under vigorous conditions the non-

[⊗] Abstract published in *Advance ACS Abstracts,* April 15, 1995.

(1) Schollhammer, P.; Pétillon, F. Y.; Pichon, R.; Poder-Guillou, S.; Talarmin, J.; Muir, K. W.; Girdwood, S. E. *J. Organomet. Chem.* **1995**, *486*, 183.

(2) (a) Wachter, J. *J. Coord. Chem.* 1987, *15*, 219. (b) Stiefel, E. I. *Prog. Inorg. Chem.* 1977, *22*, 1. (c) Holm, R. H. *Chem. Soc. Rev.* 1981, *10*, 455. (d) Coucouvanis, D. *Acc. Chem. Res.* 1991, *24*, 1. (e) Rakowski Dubois, M. *Chem. Rev.* 1989, *89*, 1. (f) Curtis, M. D. *Appl. Organomet. Chem.* 1992, *6*, 429. (g) Wiegand, B. C.; Friend, C. M. *Chem. Rev.* 1992, *92*, 491.

(3) (a) Poli, R. *J. Coord. Chem.* 1993, *29*, 121. (b) Deavenport, J. L.; Stubbs, R. T.; Powell, G. L.; Sappenfield, E. L.; Mullica, D. F. *Inorg. Chim. Acta* 1994, *215*, 191. (c) Hughes, D. L.; Lane, J. D.; Richards, R. L.; Shortman, C. *J. Chem. Soc., Dalton Trans.* 1994, 621. (d) Shin, J. H.; Parkin, G. *Polyhedron* 1994, *13*, 1489. (e) Adams, H.; Bailey, N. A.; Brisson, A. P.; Morris, M. J. *J. Organomet. Chem.* 1993, *444*, C34. (f) Matsuzaka, H.; Hirayama, Y.; Nishio, M.; Mizobe, Y.; Hidai, M. *Organometallics* 1993, *12*, 36. (g) Chojnacki, S. S.; Hsiao, Y. M.; Darensbourg, M. Y.; Reibenspies, J. H. *Inorg. Chem.* 1993, *32*, 3573. (h) Green, M. L. H.; Ng, D. K. P. *J. Chem. Soc., Dalton Trans.* 1993, 11. (i) Kuhn, N.; Zauder, E.; Boese, R.; Bläser, D. *J. Chem. Soc., Dalton Trans.* 1988, 2171.

(4) (a) Curtis, M. D.; Williams, P. D.; Butler, W. M. *Inorg. Chem.* 1988, *27*, 2853. (b) Li, P.; Curtis, M. D. *Inorg. Chem.*1990, *29*, 1242. (c) Robin, F.; Rumin, R.; Pétillon, F. Y.; Folley, K.; Muir, K. W. *J. Organomet. Chem.* 1991, *418*, C33. (d) Eremenko, I. L.; Berke, H.; Kolobkov, B. I.; Novotortsev, V. M. *Organometallics* 1994, *13*, 244.

(5) (a) Guerchais, J. E.; Le Quéré, J. L.; Pétillon, F. Y.; Manojlović-Muir, Lj.; Muir, K. W.; Sharp, D. W. A. *J. Chem. Soc., Dalton Trans.* 1982, 283. (b) Gomes de Lima, M. B.; Guerchais, J. E.; Mercier, R.; Pétillon, F. Y. *Organometallics* 1986, *5*, 1952. (c) Pétillon, F. Y.; Schollhammer, P.; Talarmin, J. *J. Organomet. Chem.* 1991, *411*, 159.

(6) (a) Courtot-Coupez, J.; Guéguen, M.; Guerchais, J. E.; Pétillon, F. Y.; Talarmin, J.; Mercier, R. *J. Organomet. Chem.* 1986, *312*, 81. (b) Guéguen, M.; Pétillon, F. Y; Talarmin, J. *Organometallics* 1989, *8*, 148. (c) El Khalifa, M.; Guéguen, M.; Mercier, R.; Pétillon, F. Y.; Saillard, J. Y.; Talarmin, J. *Organometallics* 1989, *8*, 140. (d) Gloaguen, F.; Le Floc'h, C.; Pétillon, F. Y.; Talarmin, J.; El Khalifa, M.; Saillard, J. Y. *Organometallics* 1991, *10*, 2004.

0276-7333/95/2314-2277$09.00/0

carbonyl complexes $[CpM(ER)_x]_2$ [x = 1.5 (Cr) or 2 (Mo, W)] are isolated.[7] It has been shown that dimeric intermediates, $[CpM(CO)_x(ER)]_2$, are involved in these reactions though only those with x = 1 and 2 have so far been characterized.[7b,8] It is also established that the ease of carbonyl loss from the mononuclear species $[CpM(CO)_3ER]$ depends on E, R, and M as well as on the severity of the conditions;[8i-m] Abrahamson et al.[8k] consider that the σ-inductive effect of ER is critical: carbonyl is lost more easily if ER is electron-rich. If this view is correct, replacement of Cp by the more electron-rich pentamethylcyclopentadienyl (Cp*) should influence the ease and possibly the course of decarbonylation reactions.

Accordingly, we describe here the decarbonylation reaction of the pentamethylcyclopentadienyl complex $[Cp^*Mo(CO)_2]_2$ (**1**) in the presence of dialkyl and diaryl sulfides and selenides, thiols, or selenols. The results permit the effect of replacing Cp by Cp* to be assessed: reactions of CpMo–carbonyl complexes with RSSR, RSH, RSeSeR, and RSeH have been thoroughly studied[7,8] whereas the reactions of analogous Cp*–carbonyl complexes with chalcogenide compounds have not previously been reported.

Results and Discussion

1. Synthetic Studies and Spectroscopic Characterization. A red solution of $[Cp^*_2Mo_2(CO)_4]$ (**1**) in toluene reacted with Me_2S_2 at 80 °C within 2 h to give a yellow-brown solution from which were isolated two main products: $[Cp^*_2Mo_2(CO)_2(\mu\text{-SMe})_2(\mu\text{-S})]$ (**8**) in 35% yield and $[Cp^*_2Mo_2(CO)_4(\mu\text{-SMe})_2]$ (**3**) in 40% yield. The reaction gave also significant amounts of four side products[9,12-14] (Scheme 1). No reaction between **1** and dimethyl disulfide was observed at ambient temperature.

Thermal or photochemical treatment of complex **1** with REER (ER = SPh, SeMe) or REH (ER = SBz, SePh) gave the corresponding chalcogenato-bridged molybdenum complexes $[Cp^*_2Mo_2(CO)_4(\mu\text{-ER})_2]$ (**4–7**), and when ER = SPh $[Cp^*_2Mo_2(CO)_2(\mu\text{-ER})_2]$ (**10**) was obtained in moderate yield (Scheme 2). In the reaction with benzyl mercaptan a significant amount (10%) of the monomeric complex $[Cp^*Mo(CO)_3SBz]$ (**15**) was also formed.

The new compounds **3–15** have been characterized by various spectroscopic methods (^1H and ^{13}C NMR, and IR), elemental analysis, and mass measurements. The spectroscopic data and assigments (Table 1) will not be further discussed, except where interpretation is not straightforward. The structures proposed for the new compounds are shown in Schemes 1–3.

The ^1H NMR spectrum of **8** exhibits only two peaks, which indicates that this compound has a *cis–syn* geometry. Elemental analyses and mass data accord with the proposed stoichiometry. We have not been able to obtain crystals of **8** suitable for X-ray analysis; however, a structural analysis of the cationic complex $[Cp^*_2Mo_2(CO)_2(\mu\text{-SMe})_2(\mu\text{-SH})][BF_4]$ (**16**) (see below), which was obtained by reaction of **8** with $H[BF_4]$, is consistent with the proposed geometry for **8** (Scheme 1). ^1H and ^{13}C NMR spectroscopy of **3–7** shows equivalence of the C_5Me_5 rings and ER groups, which implies that these complexes are *cis–syn* isomers. Unlike the cyclopentadienyl analogues,[6a] the *trans* permethylated isomers were not obtained here. The NMR spectra of **9–11** show inequivalent C_5Me_5 groups and equivalent alkyl groups on the bridging S atoms, which is consistent with a *trans–syn* form. Compounds **13** and **14** have been identified by comparison of their spectroscopic data with those of the analogous cyclopentadienyl complexes $[Cp(CO)Mo(\mu\text{-SMe})_3Mo(CO)_3]$[8f] and $[Cp(CO)Mo(\mu\text{-SMe})_3Mo(CO)_2(\mu\text{-SMe})Mo(CO)_2Cp]$,[9] respectively. The ^1H NMR spectrum of **14** (Table 1) suggests the presence of a mixture of two inseparable isomers in solution; *syn–anti* isomerism related to the orientation of the methyl groups on the bridging S atoms could account for the spectral pattern. The IR of **15** [ν(CO) (cm^{-1}) 2015 (s) and 1930 (s)] is indicative of a mononuclear geometry.[8j,k,10] The presence in the ^1H NMR spectrum of **15** of two sets of singlets of different intensities attributable to the C_5Me_5 rings and to the $CH_2C_6H_5$ protons (Table 1) suggests the existence of two isomers due to a different orientation of the benzyl group relative to the CO plane.[15]

2. Possible Mechanisms of Formation of Products. As described above, the thermal or photochemical reactions of $[Cp^*_2Mo_2(CO)_4]$ (**1**) with dialkyl or diaryldichalcogenides REER or with thiol or selenol HER have yielded several complexes depending on the nature of E and R. Scheme 3 presents a possible sequence of reactions ensuing from addition of 2 equiv of REER or HER to **1**.

First, it should be noted that the μ-sulfido complex **8** is only obtained when ER = SMe and that the main products of the oxidation of **1** with dimethyl disulfide are **8** [Mo(III)] and **3** [Mo(II)]. Decarbonylation of **3** by heating it in either tetrahydrofuran (66 °C) or toluene solution (110 °C) gave the dinuclear product **9** in low (<3%) and good yields (60%), respectively, together with untransformed reactant, but no **8** was formed in these

(7) (a) King, R. B. *J. Am. Chem. Soc.* 1963, *85*, 1587. (b) Tillay, E. W.; Schermer, E. D.; Baddley, H. *Inorg. Chem.* 1968, *7*, 1925. (c) Connelly, N. G.; Dahl, L. F. *J. Am. Chem. Soc.* 1970, *92*, 7470. (d) Rakoczy, H.; Schollenberger, M.; Nuber, B.; Ziegler, M. L. *J. Organomet. Chem.* 1994, *467*, 217.

(8) (a) Treichel, P. M.; Morris, J. H.; Stone, F. G. A. *J. Chem. Soc.* 1963, 720. (b) Havlin, R.; Knox, G. R. *Z. Naturforsch. B* 1966, *21*, 1108. (c) Ehrl, W.; Vahrenkamp, H. *Chem. Ber.* 1972, *105*, 1471. (d) Davidson, J. L.; Sharp, D. W. A. *J. Chem. Soc., Dalton Trans.* 1972, 107. (e) Watkins, D. D., Jr.; George, T. A. *J. Organomet. Chem.* 1975, *102*, 71. (f) Pétillon, F. Y.; Le Quéré, J. L.; Roué, J.; Guerchais, J. E.; Sharp, D. W. A. *J. Organomet. Chem.* 1980, *204*, 207. (g) Benson, I. B.; Killops, S. D.; Knox, S. A. R.; Welch, A. J. *J. Chem. Soc., Chem. Commun.* 1980, 1137. (h) Jaitner, P. *J. Organomet. Chem.* 1982, *233*, 333. (i) Jaitner, P.; Wohlgenannt, W. *Inorg. Chim. Acta* 1985, *101*, L43. (j) Grobe, J.; Haubold, R. *Z. Anorg. Allg. Chem.* 1985, *522*, 159. (k) Weinmann, D. J.; Abrahamson, H. *Inorg. Chem.*1987, *26*, 2133. (l) Shaver, A.; Lum, B. S.; Bird, P.; Livingstone, E.; Schweitzer, M. *Inorg. Chem.* 1990, *29*, 1832. (m) Goh, L. Y.; Tay, M. S.; Mak, T. C. W.; Wang, R. J. *Organometallics* 1992, *11*, 1711. (n) Nefedov, S. E.; Pasynskii, A. A.; Eremenko, I. L.; Papoyan, G. A.; Rubinstein, L. I.; Yanovskii, A. I.; Struchkov, Yu. T. *Zh. Neorg. Khim.* 1993, *38*, 76.

(9) Poder-Guillou, S.; Schollhammer, P.; Pétillon, F. Y.; Muir, K. W. Unpublished results.

(10) Goh, L. Y.; Tay, M. S.; Wei, C. *Organometallics* 1994, *13*, 1813.

(11) Rakowski Dubois, M.; Van Derveer, M. C.; Dubois, D. L.; Haltiwanger, R. C.; Miller, W. K. *J. Am. Chem. Soc.* 1980, *102*, 7456.

(12) Orpen, A. G.; Brammer, L.; Allen, F. H.; Kennerd, O.; Watson, D. G.; Tailor, R. *J. Chem. Soc., Dalton Trans.* 1982, S1.

(13) Abrahamson, H. B.; Marxen, H. *Organometallics* 1993, *12*, 2835.

(14) (a) Boorman, P. M.; Fait, J. F.; Freeman, G. K. W. *Polyhedron* 1989, *8*, 1762. (b) Burrow, T. E.; Hills, A.; Hughes, D. L.; Lane, J. D.; Lazarowych, N. J.; Maguire, M. J.; Morris, R. H.; Richards, R. L. *J. Chem. Soc., Chem. Commun.* 1990, 1757. (c) Green, M. L. H.; Mountford, P. *Chem. Soc. Rev.* 1992, 29.

(15) Ashby, M. T.; Enemark, J. H. *J. Am. Chem. Soc.* 1986, *108*, 730.

Scheme 1[a]

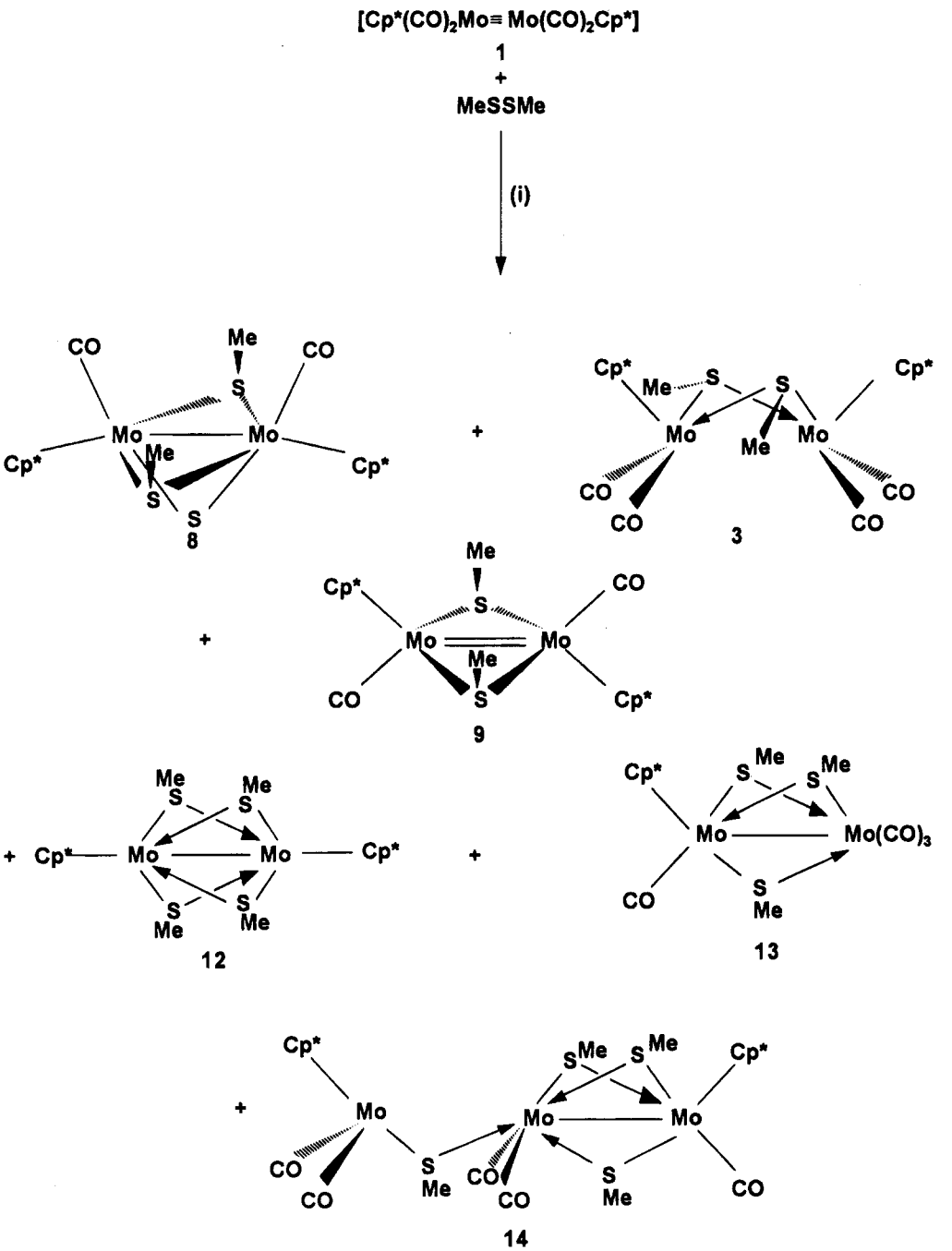

[a]Conditions: (i) in toluene at 80 °C for 2 h.

reactions. This observation clearly indicates that formation of **8** does not proceed *via* initial formation of **3**. In addition, prolonged heating of **9** in refluxing toluene gave only the completely decarbonylated compound $[Cp^*_2Mo_2(\mu\text{-SMe})_4]$ (**12**).[16] IR monitoring of thermolytic degradation of **9** showed that **8** was not formed in the reaction; this observation indicates that **9** is not the precursor complex to **8**.

The dialkyl or diaryl chalcogenide REER has directly coupled to the dimolybdenum site in **1** to produce **3**–**7** by oxidative addition. Concomitantly, $[Cp^*Mo(CO)_3ER]$ (**2** with, e.g., ER = SMe, SBz) was formed, as has been ascertained by monitoring the progress of the reaction by occasional withdrawal of samples for IR examination, although only the compound with ER = SBz has been isolated. Thus, the formation of **8** from **1** and MeSSMe can be understood in terms of their redox behavior. Initially, MeSSMe oxidized **1** to give $[Cp^*Mo(CO)_3SMe]$ (**2**). The cationic tris(thiolato)-bridged complex $[Cp^*(CO)Mo(\mu\text{-SMe})_3Mo(CO)Cp^*]^+$, resulting from dimerization and subsequent decarboxylation of **2**, can be reasonably envisaged as an intermediate of the formation of **8**: heating of an authentic sample of this complex, obtained according to a different route (see below), gave **8** quantitatively. Dealkylation of one thiolato group of the cationic intermediate provided a μ-S ligand. The dealkylation of thiolato ligands at mono- and dinuclear molybdenum centers has been previously reported for a few compounds,[3e,11] but in each case the presence of a hydride ligand has been consid-

(16) Complex **12** was also obtained from **8** under prolonged heating.

Scheme 2[a]

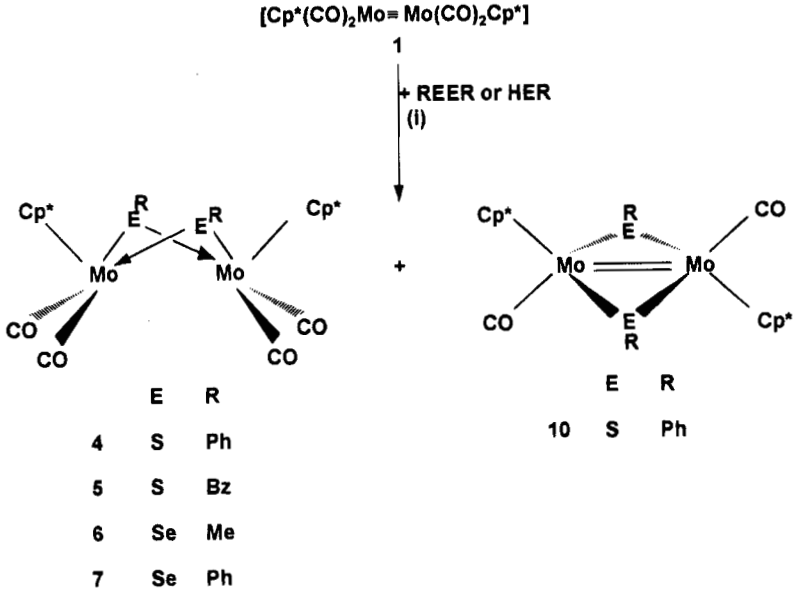

[a]Reagents and conditions: (i) in toluene, for **4** and **10**, and for **6** with diphenyl disulfide and dimethyl diselenide, respectively, at 80 °C for 2 h; for **7** with benzeneselenol at 40-50 °C for 1 h; for **5**, with benzyl mercaptan on irradiation for 2 days.

Table 1. Spectroscopic Data for Complexes $[Cp^*_2Mo_2(CO)_4(\mu\text{-}ER)_2]$ (3–7), $[\{Cp^*_2Mo_2(CO)_2(\mu\text{-}SMe)_2\}(\mu\text{-}S)]$ (8), $[Cp^*_2Mo_2(CO)_2(\mu\text{-}ER)_2]$ (9–11), $[Cp^*_2Mo_2(\mu\text{-}SMe)_4]$ (12), $[Cp^*Mo_2(CO)_4(\mu\text{-}SMe)_3]$ (13), $[Cp^*_2Mo_3(CO)_5(\mu\text{-}SMe)_4]$ (14), and $[Cp^*Mo(CO)_3SBz]$ (15)

complex	IR[a]	^{1}H NMR[b]	^{13}C NMR[c]
3 (ER = SMe)	1940 (s), 1845 (s)	1.81 (s, 6H, S–CH_3), 1.76 (s, 30H, $C_5(CH_3)_5$)[d]	260.97 (*C*O), 107.28 ($C_5(CH_3)_5$), 17.58 (S–CH_3), 10.74 ($C_5(CH_3)_5$)[d]
4 (ER = SPh)	1940 (s), 1845 (s)	7.60–7.15 (m, 10H, C_6H_5), 1.67 (s, 30H, $C_5(CH_3)_5$)	262.00 (*C*O), 138.91, 135.28, 127.54, 126.60 (S–C_6H_5); 107.87 ($C_5(CH_3)_5$), 10.61 ($C_5(CH_3)_5$)[d]
5 (ER = SBz)	1940 (s), 1840 (s)	7.38–7.18 (m, 10H, C_6H_5), 3.48 (s, 2H, CH_2–C_6H_5), 1.55 (s, 30H, $C_5(CH_3)_5$)	
6 (ER = SeMe)	1935 (s), 1835 (s)	1.90 (s, 6H, Se–CH_3), 1.82 (s, 30H, $C_5(CH_3)_5$)	257.43 (*C*O), 106.26 ($C_5(CH_3)_5$), 10.79 ($C_5(CH_3)_5$), 0.07 (SeCH_3)[d]
7 (ER = SePh)	1930 (s), 1840 (s)	7.60–7.20 (m, 10H, C_6H_5), 1.74 (s, 30H, $C_5(CH_3)_5$)	256.82 (*C*O), 136.11 (Se–C_6H_5),[e,f] 106.11 ($C_5(CH_3)_5$), 10.59 ($C_5(CH_3)_5$)
8 (ER = SMe)	1925 (s)	2.17 (s, 6H, S–CH_3), 1.92 (s, 30H, $C_5(CH_3)_5$)	247.39 (*C*O), 101.31 ($C_5(CH_3)_5$), 24.80 (S–CH_3), 12.11 ($C_5(CH_3)_5$)
9 (ER = SMe)	1815 (s)	2.22 (s, 6H, S–CH_3), 2.00 (s, 15H, $C_5(CH_3)_5$), 1.88 (s, 15H, $C_5(CH_3)_5$)	251.32, 246.18 (*C*O), 102.91, 102.27 ($C_5(CH_3)_5$), 25.26 (q,[g] S–CH_3, J_{CH} = 137.7 Hz), 11.30 (q,[g] $C_5(CH_3)_5$, J_{CH} = 127.2 Hz), 10.62 (q,[g] $C_5(CH_3)_5$, J_{CH} = 127.2 Hz)
10 (ER = SPh)	1870 (m), 1825 (s)	7.20 (m, 10H, C_6H_5), 1.85 (s, 15H, $C_5(CH_3)_5$), 1.72 (s, 15H, $C_5(CH_3)_5$)	254.73, 246.32 (*C*O); 144.74, 131.50, 127.27, 125.96 (S–C_6H_5); 103.02, 102.11 ($C_5(CH_3)_5$), 16.43, 10.43 ($C_5(CH_3)_5$)
11 (ER = SePh)	1870 (m), 1810 (s)	7.33–7.20 (m, 10H, C_6H_5), 2.03 (s, 15H, $C_5(CH_3)_5$), 1.76 (s, 15H, $C_5(CH_3)_5$)	
12 (ER = SMe)		2.28 (s, 30H, $C_5(CH_3)_5$), 2.25 (s, 12H, S–CH_3)	
13 (ER = SMe)	2000 (s), 1955 (m), 1945 (m)	2.59 (s, 3H, S–CH_3), 2.52 (s, 3H, S–CH_3), 2.00 (s, 15H, $C_5(CH_3)_5$), 1.29 (s, 3H, S–CH_3)	235.86, 226.59, 226.29, 220.6 (*C*O), 104.02 ($C_5(CH_3)_5$), 24.26, 24.10, 5.88 (SCH_3), 11.95 ($C_5(CH_3)_5$)
14a (40%)[h] (R = SMe)	1970 (sh), 1950 (s), 1910 (s), 1830 (s)	2.73, 2.37, 2.26, 1.42 (s, 3H, S–CH_3), 1.97, 1.96 (s, 15H, $C_5(CH_3)_5$)	250.75, 250.50, 250.21, 246.48, 241.09, 238.35, 237.68, 236.60, 227.98, 221.66 (*C*O)
14b (60%) (R = SMe)		2.68, 2.32, 2.74, 1.56 (s, 3H, S–CH_3), 2.03, 1.92 (s, 15H, $C_5(CH_3)_5$)	105.65, 104.84, 103.67, 103.39 ($C_5(CH_3)_5$), 27.31, 26.93, 23.13, 21.11, 19.11, 7.27, 5.90, 5.82 (SCH_3), 11.96, 10.73 ($C_5(CH_3)_5$), 11.65, 10.55 ($C_5(CH_3)_5$)
15a (56%)[h] (R = SBz)	2015 (s), 1930 (s)	7.11 (m, 5H, (s, 2H, CH_2–C_6H_5), 2.57 (s, 2H, CH_2–C_6H_5), 2.26 (s, 15H, $C_5(CH_3)_5$)	
15b (44%) (R = SBz)		7.00 (m, 5H, CH_2–C_6H_5), 2.63 (s, 2H, CH_2-C_6H_5), 2.21 (s, 15H, $C_5(CH_3)_5$)	

[a] (cm^{-1}) in CH_2Cl_2 solution. [b] Chemical shifts (δ) in ppm measured in $CDCl_3$ at 293 K. [c] Hydrogen-1 decoupled. [d] In CD_2Cl_2. [e] In C_6D_6. [f] Partially obscured by solvent peaks. [g] Without hydrogen-1 decoupling. [h] Relative percentages of isomers **a** and **b** given in parentheses.

ered significant. In the present case the alkyl could be eliminated as MeSMe. Other intermediates were considered, for example complex $[Cp^*_2Mo_2(CO)_6(\mu\text{-}S)]$,[17] but it has been shown by Herberhold et al. that the corresponding cyclopentadienyl compound[18] is observable only at a low temperature (−40 °C).

Scheme 3[a]

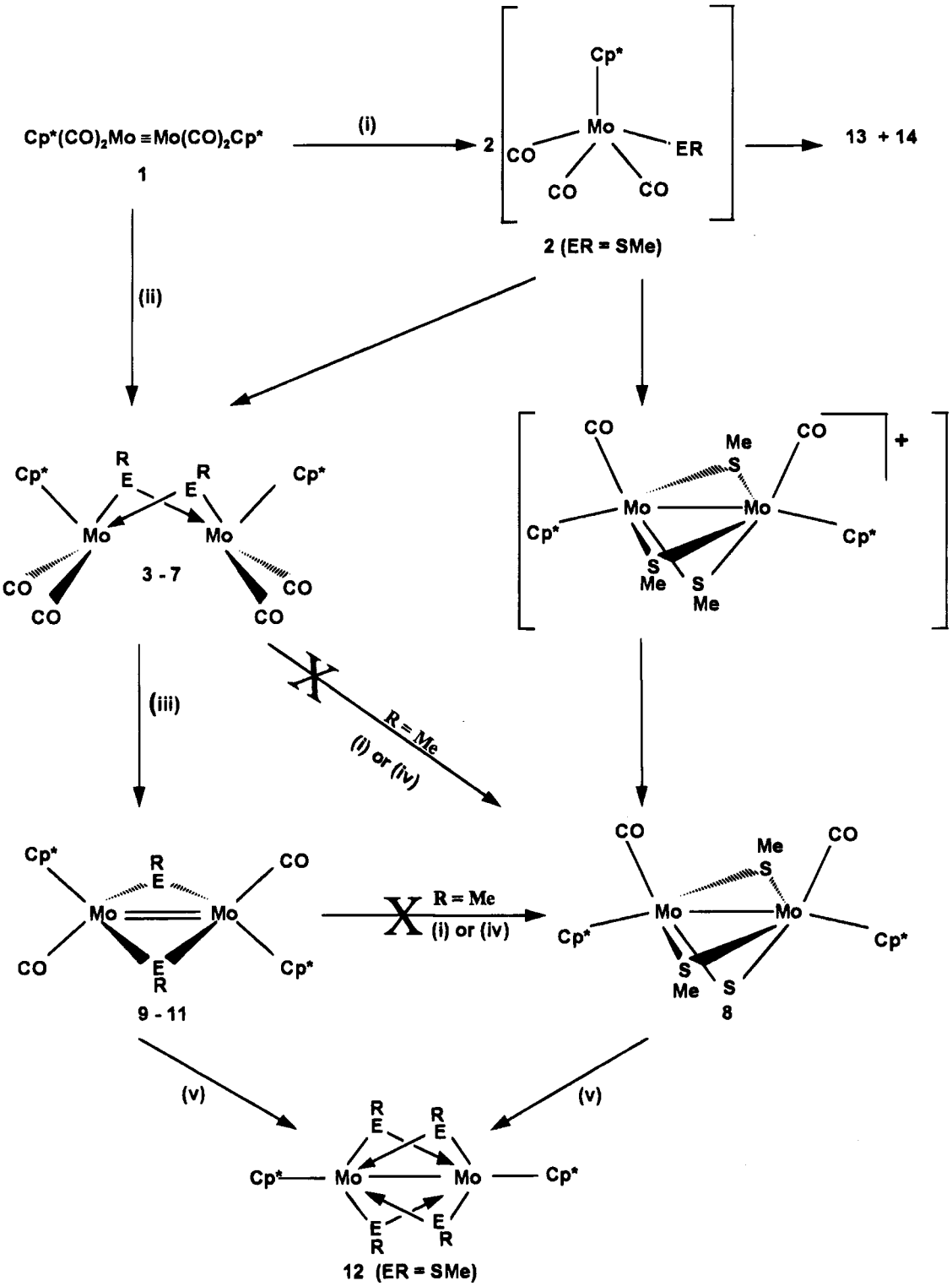

[a]Conditions: (i) MeSSMe/toluene, 80 °C, 2 h; (ii) REER or HER/toluene, 80 °C, 2 h; (iii) refluxing toluene, 4 h; (iv) toluene, 80 °C, 2 h and 3 days; (v) refluxing toluene, 3 days.

Kinetic (a) and electronic (b) arguments provide an explanation for the absence of μ-sulfido complexes in the reaction mixture when ER = SPh, SBz, SeMe, or SePh.

(a) We postulate above that $[Cp^*_2Mo_2(CO)_2(\mu\text{-}ER)_2(\mu\text{-}E)]$ (ER = SMe) derives from the mononuclear species $[Cp^*Mo(CO)_3ER]$. This implies that a significant amount of the mononuclear complex is present in the reaction mixture. Now, we have shown that oxidation of **1** with REER or HER (ER = SBz, SeMe, SePh) to $[Cp^*_2Mo_2(CO)_4(\mu\text{-}ER)_2]$ occurred under conditions (in toluene, at 30–50 °C for 1 h) milder than those required when MeSSMe is the oxidant (in toluene, at 80 °C for 2 h). Thus less $[Cp^*Mo(CO)_3ER]$ is available for transformation into $[Cp^*_2Mo_2(CO)_2(\mu\text{-}ER)_2(\mu\text{-}E)]$ when ER = SBz, SeMe, or SePh than when ER = SMe.

(b) Although it is possible that some mononuclear complex $[Cp^*Mo(CO)_3ER]$ would be obtained in the reaction of **1** with REER or HER (ER = SBz, SeMe,

Table 2. Spectroscopic Data for Complexes $[Cp^*_2Mo_2(CO)_2(\mu\text{-}SMe)_2(\mu\text{-}SR)]X$ (R = H, X = BF_4 (16), Cl (17), F (18); R = Me, X = I (19)), $[Cp^*_2Mo_2(CO)_4(\mu\text{-}SMe)_2][BF_4]$ (21), and $[Cp^*_2Mo_2(\mu\text{-}SH)_2(\mu\text{-}S)_2]$ (22)

complexes	IR (cm^{-1})	^1H NMR (ppm)	^{13}C NMR (ppm)[a]
16[b,c]	2470 (w) ν(SH), 1985 (b) ν(CO), 1150–1000 (s) ν(BF)	2.333 (s, 3H, S–CH_3), 2.331 (s, 3H, S–CH_3), 1.95 (s, 30H, $C_5(CH_3)_5$), −2.13 (s, 1H, S*H*)	239.39 (*C*O), 106.39 ($C_5(CH_3)_5$), 24.47 (S*C*H_3), 25.11 (S*C*H_3), 12.28 ($C_5(CH_3)_5$)
17[d]	1980 ν(CO)	2.33 (s, 6H, S–CH_3), 1.98 (s, 30H, $C_5(CH_3)_5$), −2.12 (s, 1H, S*H*)	
18[d]	1980 ν(CO)	2.35 (s, 6H, S–CH_3), 1.97 (s, 30H, $C_5(CH_3)_5$), −2.13 (s, 1H, S*H*)	
19[d,e]	1980 ν(CO)	2.46 (s, 3H, S–CH_3), 2.44 (s, 3H, S–CH_3), 2.07 (s, 30H, $C_5(CH_3)_5$), 1.63 (s, 3H, S–CH_3)	238.82 (*C*O), 106.00 ($C_5(CH_3)_5$), 25.98 (q, S*C*H_3, J_{CH} = 140.3 Hz),[g] 23.72 (q, S*C*H_3, J_{CH} = 139.8 Hz),[g] 11.98 (q, $C_5(CH_3)_5$, J_{CH} = 129.0 Hz),[g] 4.87 (q, S*C*H_3, J_{CH} = 141.5 Hz)[g]
21[e,f]	2080 (s), 2040 (s) ν(CO)	2.75 (s, 6H, S–CH_3), 2.30 (s, 30H, $C_5(CH_3)_5$)	221.67 (*C*O), 110.99 ($C_5(CH_3)_5$), 25.95 (S*C*H_3), 11.45 ($C_5(CH_3)_5$)
22[b,e]	2410 ν(SH)	2.23 (s, 30H, $C_5(CH_3)_5$), −1.95 (s, 1H, S*H*), −2.03 (s, 1H, S*H*)	111.09 ($C_5(CH_3)_5$), 14.03 ($C_5(CH_3)_5$)

[a] Hydrogen-1 decoupled. [b] IR in KBr pellets. [c] NMR in CD_3CN solution. [d] IR in CH_2Cl_2 solution. [e] NMR in CD_3COCD_3 solution. [f] IR in CH_3CN solution. [g] Without hydrogen-1 decoupling.

SePh), we believe that electronic effects could hinder the subsequent formation of a sulfidodimolybdenum(III) complex. Indeed, it has been shown that ease of carbonyl loss from $[CpM(CO)_3ER]$ (M = Mo, W) increases along the series ER = SeMe < SePh ≅ SBz < SMe < SPh, and thus correlates with the frequency of the highest energy ν(C≡O) absorption in the complexes.[7b, 8f,j,k] These data suggest that the stability of the mononuclear derivatives may be correlated with the softness of the ER groups so that decarbonylative dimerization of $[Cp^*Mo(CO)_3ER]$ into $[Cp^*_2Mo_2(CO)_2(\mu\text{-}ER)_2(\mu\text{-}E)]$, *via* $[Cp^*(CO)Mo(\mu\text{-}SMe)_3Mo(CO)Cp^*]^+$, is less likely when ER = SBz, SeMe, or SePh than that it is when ER = SMe. Now, assuming that the mechanism for the formation of $[Cp^*_2Mo_2(CO)_2(\mu\text{-}ER)_2(\mu\text{-}E)]$ from $[Cp^*M(CO)_3ER]$ involves initial dealkylation or dearylation of a μ-ER group, we believe that conjugation across the C–S bond when R = Ph makes its rupture less likely than when R = Me, thereby rationalizing the absence of the SPh analogue of **8**.

No Cp analogue of **8** is known and it is possible that the greater electron release from the Cp* ring stabilizes this (μ-sulfido)dicarbonyldimolybdenum(III) compound. It has been shown that CpCr analogues of **3** and **5**, e.g. $[Cp_2Cr_2(CO)_4(\mu\text{-}SPh)_2]$ and $[Cp_2Cr_2(CO)_2(\mu\text{-}SPh)_2]$, were the precursor complexes to the carbonyl-free unsaturated sulfido compound $[Cp_2Cr_2(\mu\text{-}SPh)_2(\mu\text{-}S)]$,[8m] but no carbonyl-containing sulfido compound was detected in the thermolytic reaction of the (thiolato)chromium complexes. Similarly, complete thermal decarbonylation of $[CpCr(CO)_3TePh]$ to give $[Cp_2Cr_2(\mu\text{-}TePh)_2(\mu\text{-}Te)]$ was very recently observed by Goh et al.[12]. These data and those described here clearly demonstrate that the ease of dimerization of $[LM(CO)_3ER]$ (L = Cp, Cp*; M = Cr, Mo; ER = SMe, SPh, TePh) with loss of CO follows the order M = Cr > Mo and L = Cp > Cp*. Above all, they show that the influence of the π-donating effect of the Cp* ring is more important than that of ER groups in these reactions. Thus, replacement of L = Cp by Cp* in $[LM(CO)_3ER]$ is a major factor governing the decarbonylative dimerization reactions of group 6 metal carbonyls.

3. Reactivity of Sulfido Ligands in $[Cp^*_2Mo_2(CO)_2(\mu\text{-}SMe)_2(\mu\text{-}S)]$ (8). The unusual nature of **8**, particularly the nucleophilic character of the sulfido ligand suggested that it might be highly reactive, and we have therefore investigated its behavior with electrophilic and alkylating agents. Addition of either HX (X = BF_4, Cl, F) or $[Me_3O][BF_4]$ or MeI to a dichloromethane solution of **8** rapidly formed a red color. Following addition of ether, red powders of **16** or **17**–**20** form from the solution at ambient temperature in good yields. Elemental analysis of **16** and **19** indicated the presence of a monocation with three sulfur atoms per two molybdenum atoms and **16** has been shown by X-ray crystallography (see below) to be $[Cp^*_2Mo_2(CO)_2(\mu\text{-}SMe)_2(\mu\text{-}SH)][BF_4]$. The *syn* disposition of the methyl substituents of the equatorial sulfur atoms, which is observed in the solid state (and in **8**), is maintained for **16** in solution, as shown by the very small difference of their chemical shifts ($\Delta\delta$ = 0.002 ppm; see Table 2). The other compounds (**17**–**20**) were formulated as shown (Scheme 4) by comparison of their spectroscopic data (Table 2) with those of **16**.

$[Cp^*_2Mo_2(CO)_2(\mu\text{-}SMe)_2(\mu\text{-}SH)]X$ (**16**–**18**) can be deprotonated with bases such as triethylamine to regenerate the sulfido complex **8**. Prolonged heating of a suspension of the cationic tris(thiolato)-bridged complex $[Cp^*_2Mo_2(CO)_2(\mu\text{-}SMe)_3]I$ (**19**) in refluxing toluene gave quantitatively compound **8**. In the same conditions, the reaction with cyclopentadienyl analogues $[Cp_2Mo_2(CO)_2(\mu\text{-}SMe)_3]X$ (X = Cl, Br) led to the insertion of the

(17) The mechanism shown in eqs 1–4, suggested by one referee has been considered:

$$[Cp^*_2Mo_2(CO)_6(\mu\text{-}SMe)]^+ + Nu^- \rightarrow [Cp^*_2Mo_2(CO)_6(\mu\text{-}S)] + MeNu \quad (1)$$

$$[Cp^*_2Mo_2(CO)_6(\mu\text{-}S)] \rightarrow [Cp^*_2Mo_2(CO)_4(\mu\text{-}S)] + 2CO \quad (2)$$

$$[Cp^*_2Mo_2(CO)_4(\mu\text{-}S)] + S_2Me_2 \rightarrow [Cp^*_2Mo_2(CO)_4(\mu\text{-}SMe)_2(\mu\text{-}S)] \quad (3)$$

$$[Cp^*_2Mo_2(CO)_4(\mu\text{-}SMe)_2(\mu\text{-}S)] \rightarrow [Cp^*_2Mo_2(CO)_2(\mu\text{-}SMe)_2(\mu\text{-}S)] + 2CO \quad (4)$$

Although it cannot be completely ruled out, it appears unlikely for the following reason: the Cp analogue of the $[Cp^*_2Mo_2(CO)_6(\mu\text{-}S)]$ intermediate, observed only at low temperatures,[18] decomposes to $[Cp_2Mo_2(CO)_6]$ at room temperature. The decarbonylation reaction shown in eq 2 should be even less favored for the Cp* derivative than for its Cp counterpart for which this reaction has not been observed.

(18) Herberhold, M.; Jellen, W.; Murray, H. H. *J. Organomet. Chem.* 1984, *270*, 65.

Scheme 4[a]

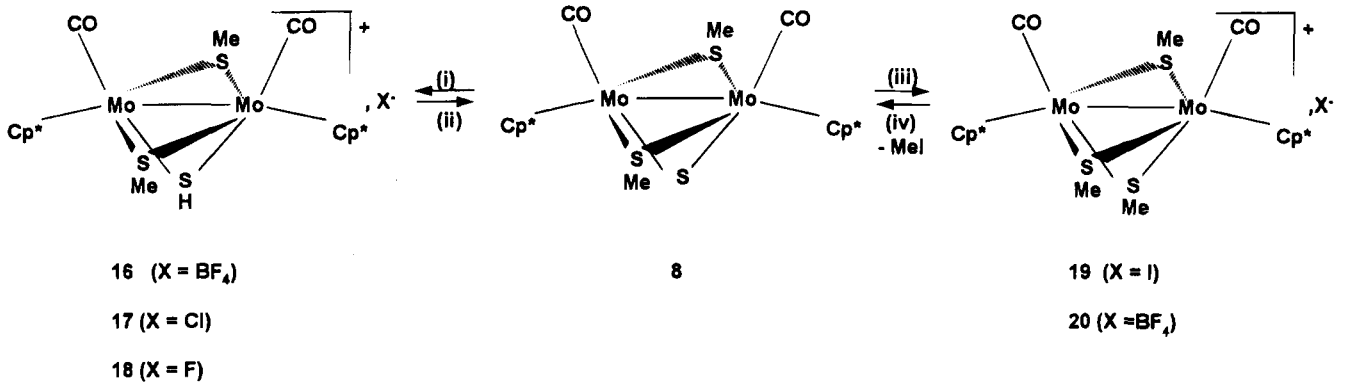

[a]Reagents and conditions: (i) HX (X = BF_4, Cl, F), in CH_2Cl_2; (ii) Et_3N, in CH_2Cl_2 at room temperature; (iii) $[Me_3O][BF_4]$, or MeI, in CH_2Cl_2 at room temperature; (iv) X = I, in refluxing toluene, 3 days.

Scheme 5[a]

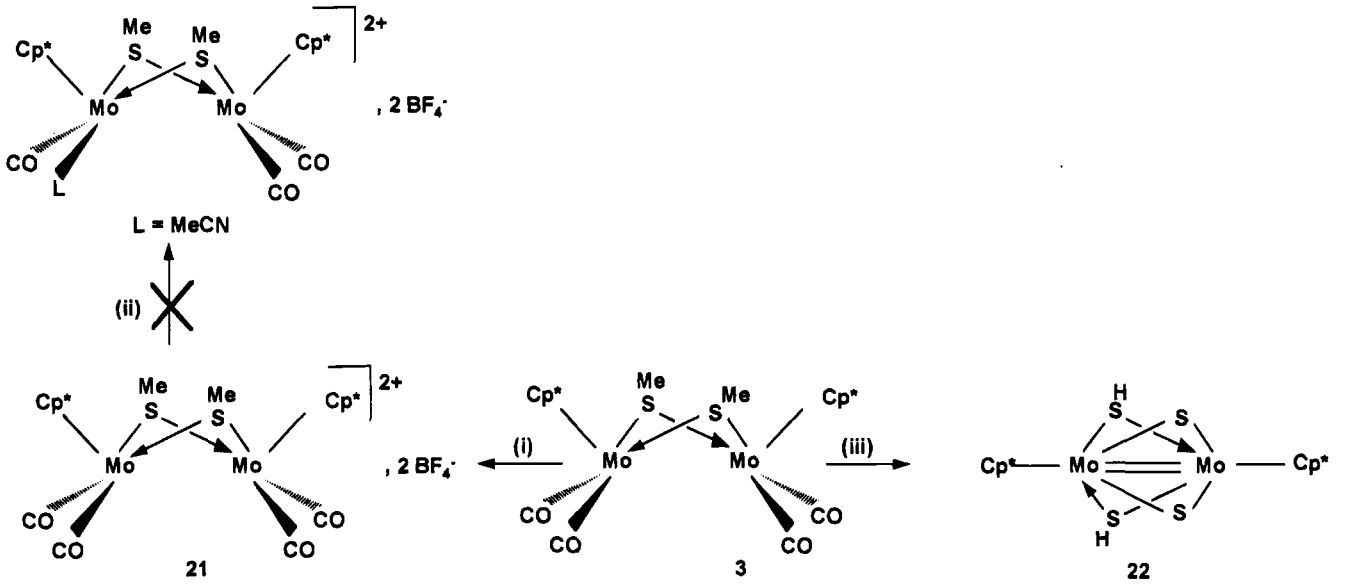

[a]Reagents and conditions: (i) 2 equiv of $Ag[BF_4]$, in CH_2Cl_2 at room temperature; (ii) in refluxing MeCN; (iii) H_2S, in toluene at 353 K, 5 days.

counterion into the Mo–Mo bond to give the decarbonylated product $[Cp^*_2Mo_2(\mu\text{-SMe})_3(\mu\text{-X})]$;[5b] this is consistent with the higher lability of the carbonyls in cyclopentadienyl carbonyl-containing compounds in comparison with pentamethylcyclopentadienyl analogues.

4. Reactions of $[Cp^*_2Mo_2(CO)_4(\mu\text{-SMe})_2]$ (3). Like the cyclopentadienyl analogue,[6a] complex **3** was readily oxidized by $Ag[BF_4]$ to yield the dicationic product $[Cp^*_2Mo_2(CO)_4(\mu\text{-SMe})_2][BF_4]_2$ (**21**). The spectroscopic data (Table 2) of **21** are consistent with a *cis–syn* geometry. Unlike its cyclopentadienyl analogue,[6c] no substitution of carbonyl by acetonitrile was observed when **21** was stirred in refluxing MeCN; this again accords with Cp* compounds showing greater resistance to decarbonylation than their Cp analogues.

Complex **3** reacted with dihydrogen sulfide in refluxing toluene (see Scheme 5) to yield the decarbonylated complex $[Cp^*_2Mo_2(\mu\text{-SH})_2(\mu\text{-S})_2]$ which has been previously characterized.[13]

5. Solid State Structure of $[Cp^*_2Mo_2(CO)_2(\mu\text{-SMe})_2(\mu\text{-SH})](BF_4)$ (16). X-ray analysis of **16** (Figure 1, Table 3) reveals that the $[Cp^*_2Mo_2(CO)_2(\mu\text{-SMe})_2(\mu\text{-SH})]^+$ cation is structurally closely analogous to the cation in the cyclopentadienyl complex $[Cp_2Mo_2(CO)_2(\mu\text{-SMe})_3]Br$.[5b] Thus the cation of **16** contains two nearly identical Cp*Mo(CO) units which eclipse each other when viewed along the Mo–Mo vector. The Mo1–Mo2 bond is supported by two bridging μ-SMe groups and a bridging μ-SH unit. The cation approximates quite closely C_{2v} symmetry: the diad axis is defined by S1 and the midpoint of the Mo1–Mo2 vector; atoms Mo1, Mo2, S1, C1, C2, O1, and O2 together with C(Cp1) and C(Cp2) (the centroids of rings C5–C9 and C10–C14) are nearly coplanar (rms displacement 0.05 Å), the slight deviation of the C(Cp1)–Mo1–Mo2–C(Cp2) torsion angle from zero (Table 3) being the most significant distortion from planarity; this plane is normal (dihedral angle 90.1°) to the plane defined by the three bridging sulfur atoms (from which methyl carbons C3 and C4 are only slightly displaced). The metal atoms are nearly coplanar with S2 and S3, the methane thiolate sulfur atoms [S3–Mo1–S2–Mo2 = −1.6(1)°]; both CO ligands and both thiolate methyl C atoms lie on the same side of this plane with the Mo–CO and S–Me bonds nearly parallel to one another. S1 makes short nonbonded contacts of 2.96 and 2.85 Å with S2 and S3, a feature also present in $[Cp_2Mo_2(CO)_2(\mu\text{-SMe})_3]Br$.[5b]

The metal coordination can be described as a Cp*-

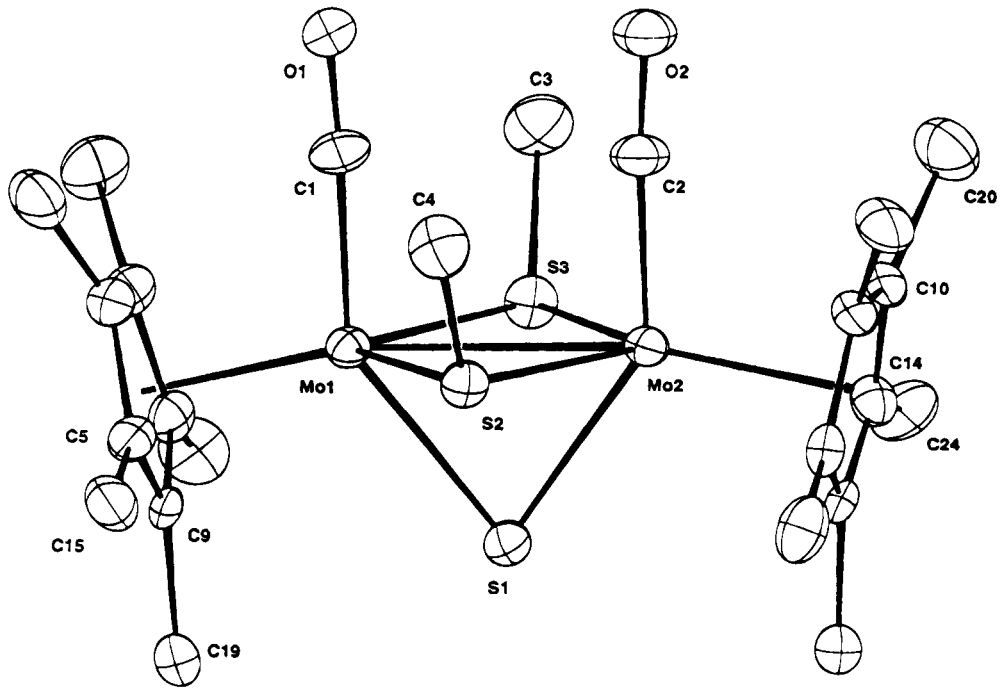

Figure 1. View of the $[Cp^*_2Mo_2(CO)_2(\mu\text{-SMe})_2(\mu\text{-SH})]^+$ cation of **16**. 50% probability ellipsoids are displayed, and hydrogens are omitted. Ring carbon atoms C5–C9 and C10–C14, and their associated methyl carbon atoms C15–C19 and C20–C24, are numbered in sequence around each ring.

$Mo(CO)S_3$ piano stool with S2–Mo–S3 [both 111.3(1)°] somewhat narrowed by the bridge constraint and S1–Mo–CO rather obtuse [145.8(3) and 146.2(4)°]. The single Mo–Mo bond required by the 18-electron rule points nearly toward the centroids of the Cp* rings (Cp–Mo–Mo 159 and 167°). Bond lengths in Table 3 agree quite well with established values: e.g. Mo–Cp* 2.034, μ-Mo–SR (R = alkyl) 2.460, Mo–CO 1.979 Å.[14] In particular, all three sulfur bridges are nearly symmetrical and the Mo–S1 distances are not notably different from those involving S2 and S3. This is strong indirect proof that S1 has been protonated (the H atom on S1 was not located experimentally) since μ-S(sulfido)–Mo distances are typically 0.13 Å shorter than μ-SR–Mo (R = alkyl) distances, even when both types of bridging unit are present in the same molecule.[14,19]

A survey of the structural literature for dimeric Mo complexes containing μ-SMe groups[3i,5b,9,13,19,20] suggests that the Mo–Mo distance is mainly determined by the number of bridging ligands: complexes containing a $Mo_2(\mu\text{-S})_4$ core have Mo–Mo bond lengths in the range 2.573–2.626 Å with acute Mo–S–Mo angles of 62–65°; species with three bridging groups, such as **16**, show slightly less acute S–Mo–S angles of 68–70° and rather longer Mo–Mo distances of 2.755–2.800 Å, the distance in $[Cp_2Mo_2(CO)_2(\mu\text{-SMe})_3]Br$[5b] being virtually identical to that in **16**. Finally, in the trimolybdenum chain

Table 3. Selected Bond Lengths (Å) and Angles (deg) in 16

(a) Bond Lengths

Mo1–Mo2	2.772(2)	Mo1–S1	2.458(3)
Mo1–S2	2.443(3)	Mo1–S3	2.473(3)
Mo1–C1	1.969(10)	Mo1–C(Cp1)[a]	1.980
Mo2–S1	2.466(3)	Mo2–S2	2.449(3)
Mo2–S3	2.466(3)	Mo2–C2	1.946(10)
Mo2–C(Cp2)	2.019	S2–C4	1.836(11)
S3–C3	1.824(12)	O1–C1	1.147(12)
O2–C2	1.182(13)		

(b) Bond Angles

Mo2–Mo1–S1	55.9(1)	Mo2–Mo1–S2	55.6(1)
Mo2–Mo1–S3	55.7(1)	Mo2–Mo1–C1	90.1(3)
Mo2–Mo1–C(Cp1)1	167.0	S1–Mo1–S2	73.8(1)
S1–Mo1–S3	70.5(1)	S1–Mo1–C11	145.8(3)
S1–Mo1–C(Cp1)1	111.4	S2–Mo1–S31	111.3(1)
S2–Mo1–C1	89.8(3)	S2–Mo1–C(Cp1)1	121.9
S3–Mo1–C1	88.7(3)	S3–Mo1–C(Cp1)1	125.2
C1–Mo1–C(Cp1)1	102.8	Mo1–Mo2–S1	55.6(1)
Mo1–Mo2–S2	55.4(1)	Mo1–Mo2–S3	56.0(1)
Mo1–Mo2–C2	90.6(4)	Mo1–Mo2–C(Cp2)1	158.9
S1–Mo2–S2	73.6(1)	S1–Mo2–S3	70.5(1)
S1–Mo2–C21	146.2(4)	S1–Mo2–C(Cp2)1	104.3
S2–Mo2–S31	111.3(1)	S2–Mo2–C2	88.9(4)
S2–Mo2–C(Cp2)1	116.5	S3–Mo2–C2	90.2(4)
S3–Mo2–C(Cp2)1	128.0	C2–Mo2–C(Cp2)1	109.4
Mo1–S1–Mo2	68.5(1)	Mo1–S2–Mo2	69.0(1)
Mo1–S2–C41	114.3(4)	Mo2–S2–C41	115.4(4)
Mo1–S3–Mo2	68.3(1)	Mo1–S3–C31	114.0(4)
Mo2–S3–C31	114.0(4)	Mo1–C1–O11	175.5(9)
Mo2–C2–O21	176.2(9)		

(c) Torsion Angles

C1–Mo1–Mo2–S1	−177.0(3)
C1–Mo1–Mo2–S2	89.8(3)
C1–Mo1–Mo2–S3	−88.4(3)
C1–Mo1–Mo2–C2	1.4(5)
C1–Mo1–Mo2–C(Cp2)	163.2(4)
C(Cp1)–Mo1–Mo2–C(Cp2)	−9.6
S3–Mo1–S2–Mo2	−1.6(1)

[a] C(Cp1) and C(Cp2) are the centroids of the five-membered rings C5–C9 and C10–C14, respectively.

(19) Casewit, C. J.; Haltiwanger, R. C.; Hoordik, J.; Rakowski Dubois, M. *Organometallics* 1985, *4*, 119.

(20) A search of the Cambridge Structural Database using the Chemical Database Service, EPSRC Daresbury Laboratory, Warrington WA4 4AD, Great Britain for species containing $Mo_2(\mu\text{-SMe})$ residues yielded, in addition to refs 3i, 5b, 13, and 15: (a) McKenna, M.; Wright, L. L.; Miller, D. J.; Tanner, L.; Haltiwanger, R. C.; Rakowski Dubois, M. *J. Am. Chem. Soc.* 1983, *105*, 5329. (b) Brunner, H.; Meier, W.; Wachter, J.; Weber, P.; Ziegler, M. L.; Enemark, J. H.; Young, C. G. *J. Organomet. Chem.* 1986, *309*, 313. (c) Hadjikyriacou, A. I.; Coucouvanis, D. *Inorg. Chem.* 1989, *28*, 2169. (d) Bernatis, P.; Haltiwanger, R. C.; Rakowski Dubois, M. *Organometallics* 1992, *11*, 2435.

Scheme 6. Thermal Decomposition of [LMo(CO)$_3$ER] (L = Cp, Cp*)

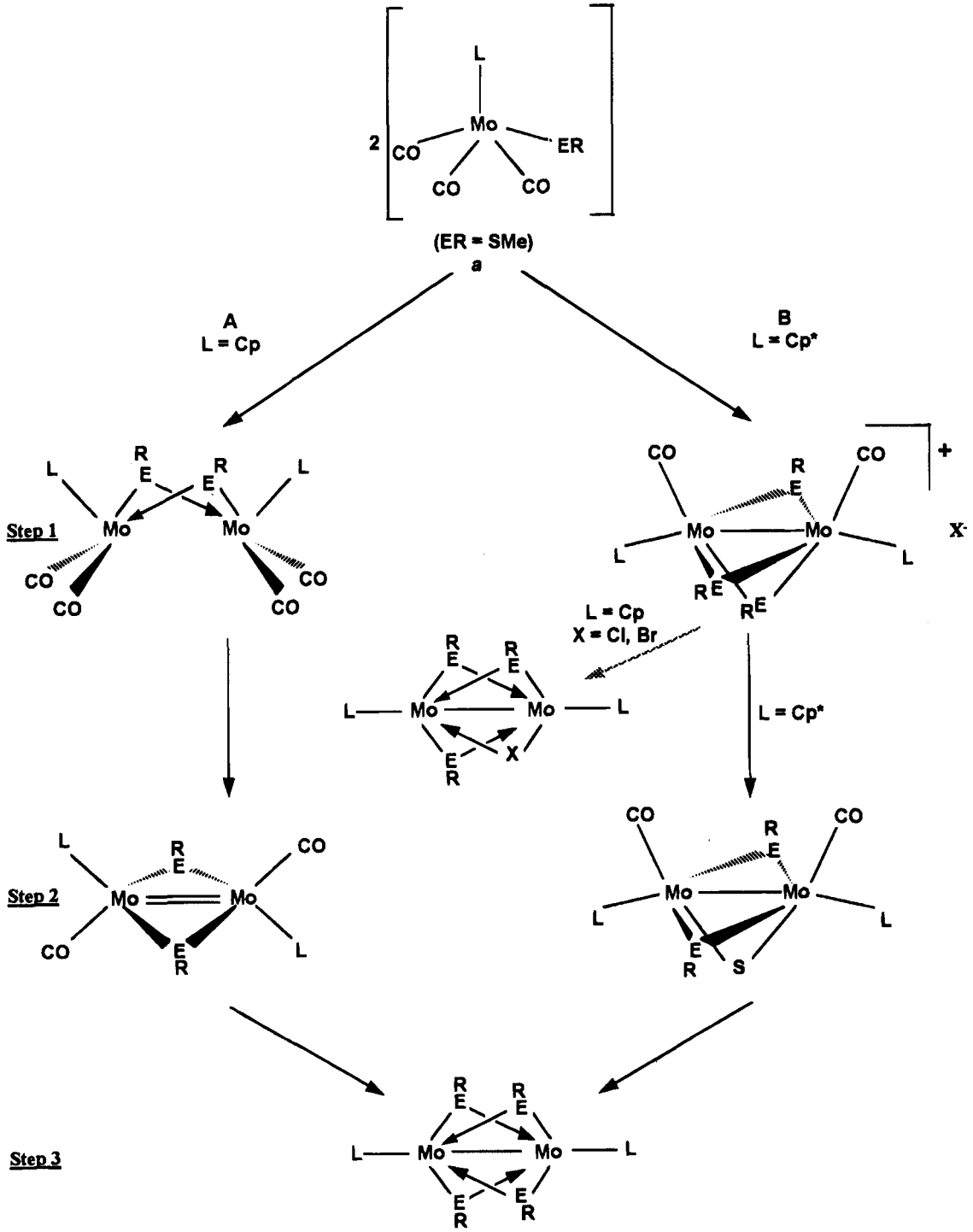

complex [Cp(CO)Mo(μ-SMe)$_3$Mo(CO)$_2$(μ-SMe)Mo(CO)-Cp] the Mo–Mo distance supported by a single μ-SMe bridge is 3.116(1) Å with an angle of 80° at the bridging sulfur atom.[9]

Conclusion

Our study on the thermal decomposition of [LMo(CO)$_3$-ER] (***a***) (L = Cp, Cp*) has shown that L takes a prominent part in the ease of dimerization and decarbonylation of these complexes. When L is the cyclopentadienyl ligand, authors[4b,5a,b,7b,d,8e,g,n] have shown that the thermal decomposition of ***a*** gives rise to the decarbonylated molybdenum(III) products [Cp$_2$Mo$_2$(μ-ER)$_4$] *via* successively the carbonylmolybdenum(II) complexes [Cp$_2$Mo$_2$(CO)$_4$(μ-ER)$_2$] and [Cp$_2$Mo$_2$(CO)$_2$(μ-ER)$_2$]. The more electron-releasing Cp* ring promotes the oxidation of the molybdenum atoms which occurs during the course of the first decarbonylation step of ***a***. Such an oxidation phenomenon is only observed during the last decarbonylation step when L is the cyclopentadienyl ring. The control exerted by the L (Cp or Cp*) rings on the course of the thermal reactions is summarized in Scheme 6.

The nucleophilic character of the sulfido atom in **8** is shown by the formation of tris(thiolato) compounds [Cp*$_2$Mo$_2$(CO)$_2$(μ-SMe)$_2$(μ-SR)]X on reacting the sulfido complex **8** with electrophilic reagents.

Experimental Section

1. General Procedures. The reactions were performed under either nitrogen or an argon atmosphere using standard Schlenck techniques; solvents were deoxygenated and dried by standard methods. Literature methods were used for the preparation of $C_5(CH_3)_5H$[21] and $[Cp^*_2Mo_2(CO)_4]$(**1**)($Cp^* = C_5(CH_3)_5$).[22]

Infrared spectra were obtained with a Perkin-Elmer 1430 spectrophotometer, and NMR spectra were recorded on a Bruker AC300 spectrophotometer. Peak positions are relative to tetramethylsilane as an internal reference. The mass spectra were measured on a GC/MS Helwett-Packard 5595C. Chemical analyses were performed by the "Centre de Microanalyses du CNRS, Vernaison". UV irradiations were performed by using a Hanau TQ 150 mercury vapor lamp placed approximately 10 cm from a Pyrex vessel.

2. Synthesis of Permethylated Cyclopentadienyl Complexes. Reaction of $[Cp^*_2Mo_2(CO)_4]$ with Me_2S_2. A red nitrogen-purged toluene solution containing 1 g (1.74 mmol) of $[Cp^*_2Mo_2(CO)_4]$ (**1**) and 0.28 g (3 mmol) of dimethyl disulfide, was heated at 80 °C to give, after 2 h, a brown suspension. Filtration removed a brown solid $[Cp^*_2Mo_2(CO)_4(\mu\text{-SMe})_2]$ (**3**) (465 mg, 40% yield) which was washed with pentane.

The filtrate was concentrated to ca. 2 mL and chromatographed on a silica gel column prepared in *n*-hexane. Elution gave five fractions: (i) a yellowish brown solution in 3:2 hexane–CH_2Cl_2, which yielded crystals of $[Cp^*_2Mo_2(CO)_2(\mu\text{-SMe})_2]$ (**9**) (107 mg, 10% yield), (ii) a dark brown solution in 3:2 hexane–CH_2Cl_2, which afforded $[Cp^*_2Mo_2(\mu\text{-SMe})_4]$ (**12**) (33 mg, 3% yield), (iii) a green solution in 1:1 hexane–CH_2Cl_2, which yielded green crystals of $[Cp^*_2Mo_2(CO)_5(\mu\text{-SMe})_3]$ (**13**) (53 mg, 5% yield), (iv) a red solution in 1:1 hexane–CH_2Cl_2, which gave a red powder of $[Cp^*_2Mo_3(CO)_4(\mu\text{-SMe})_4]$ (**14**) (77 mg, 5% yield), and (v) a green solution in 10:1 CH_2Cl_2–Et_2O, which afforded a green powder of $[Cp^*_2Mo_2(CO)_2(\mu\text{-SMe})_2(\mu\text{-S})]$ (**8**) (392 mg, 35% yield).

3. Anal. Found: C, 47.1; H, 5.4; S, 10.8. $C_{26}H_{36}Mo_2O_4S_2$ Calc: C, 46.7; H, 5.4; S, 9.6. Mass Spectrum: m/z 668 (M^+).

8. Anal. Found: C, 44.7; H, 5.6; S, 14.2. $C_{24}H_{36}Mo_2O_2S_3$ Calc: C, 44.7; H, 5.6; S, 14.9. Mass Spectrum: m/z 644 (M^+).

9. Anal. Found: C, 46.8; H, 6.0; S, 10.4; Mo, 30.9. $C_{24}H_{36}Mo_2O_2S_2$ Calc: C, 47.0; H, 5.9; S, 10.9; Mo, 31.4. Mass Spectrum: m/z 612 (M^+).

13. Anal. Found: C, 35.3. $C_{17}H_{24}Mo_2O_4S_3$ Calc: C, 35.2. Mass Spectrum: m/z 580 (M^+).

Reaction of $[Cp^*_2Mo_2(CO)_4]$ with Ph_2S_2 or Me_2Se_2. These reactions were conducted at 80 °C, in the manner described above using $[Cp^*_2Mo_2(CO)_4]$ and diphenyl disulfide or dimethyl diselenide, respectively. Brown solids, $[Cp^*_2Mo_2(CO)_4(\mu\text{-SPh})_2]$ (**4**) (410 mg, 30% yield) or $[Cp^*_2Mo_2(CO)_4(\mu\text{-SeMe})_2]$ (**6**) (597 mg, 45% yield), precipitated and were collected by filtration and then washed with pentane.

When Ph_2S_2 was used as reagent, a brown product $[Cp^*_2Mo_2(CO)_2(\mu\text{-SPh})_2]$ (**10**) (0.385 mg, 30% yield) was obtained from the filtrate and purified by chromatography on a silica gel column.

We should note that product **6** was also obtained at lower temperatures (30–50 °C) but the yield was higher at 80 °C.

4. Anal. Found: C, 53.5; H, 5.0; S, 7.9. $C_{36}H_{40}Mo_2O_4S_2$ Calc: C, 54.5; H, 5.0; S, 8.1.

6. Anal. Found: C, 41.1; H, 4.8; Se, 20.9. $C_{26}H_{36}Mo_2O_4Se_2$ Calc: C, 41.0; H, 4.7; Se, 20.7.

10. Anal. Found: C, 53.3; H, 5.3; S, 8.0. $C_{34}H_{40}Mo_2O_2S_2$ Calc: C, 55.4; H, 5.4; S, 8.7. Mass Spectrum: m/z 736 (M^+).

Reaction of $[Cp^*_2Mo_2(CO)_4]$ with HSBz. A toluene solution containing 0.5 g (0.87 mmol) of $[Cp^*_2Mo_2(CO)_4]$ and 0.32 g (2.6 mmol) of benzyl mercaptan was irradiated for 2 days. There was precipitation of a brown solid, which was allowed to settle, and the supernatant liquor was filtered off. The solid, $[Cp^*_2Mo_2(CO)_4(\mu\text{-SBz})_2]$ (**5**) (215 mg, 30% yield), was washed with pentane and dried *in vacuo*.

The filtrate was concentrated to ca. 2 mL and chromatographed on a silica gel column. Elution with a mixture of CH_2Cl_2–hexane (2:3) gave an orange band, which afforded $[Cp^*Mo(CO)_3SBz]$ (**15**) (76 mg, 10% yield).

5. Anal. Found: C, 53.8; H, 5.4. $C_{38}H_{44}Mo_2O_4S_2$ Calc: C, 55.6; H, 5.4.

Reaction of $[Cp^*_2Mo_2(CO)_4]$ with HSePh. A toluene solution containing 0.5 g (0.87 mmol) of $[Cp^*_2Mo_2(CO)_4]$ and 0.4 g (2.6 mmol) of benzeneselenol was heated at 50 °C for 1 h. After the solvent was removed *in vacuo*, the residue was extracted with 3 mL of dichloromethane and then was chromatographed on a silica gel column. Elution with a mixture of hexane–CH_2Cl_2 (1:1) removed a brown band, which gave brown crystals of $[Cp^*_2Mo_2(CO)_4(\mu\text{-SePh})_2]$ (**7**) (230 mg, 30% yield).

7. Anal. Found: C, 46.8; H, 4.3; Se, 17.8. $C_{36}H_{40}Mo_2O_4Se_2$ Calc: C, 48.7; H, 4.3; Se, 17.8.

3. Reactivity of $[Cp^*_2Mo_2(CO)_2(\mu\text{-SMe})_2(\mu\text{-S})]$ (8) and $[Cp^*_2Mo_2(CO)_4(\mu\text{-SMe})_2]$ (3). 3.1. Synthesis of $[Cp^*_2Mo_2(CO)_2(\mu\text{-SMe})_2(\mu\text{-SR})]X$ (16–20). (a) A dichloromethane solution (5 mL) of $[Cp^*_2Mo_2(CO)_2(\mu\text{-SMe})_2(\mu\text{-S})]$ (**8**) (0.1 g, 0.25 mmol) was added to a solution of $H[BF_4]$ (0.25 mmol in 5 mL of Et_2O) and $[Me_3O][BF_4]$ (0.25 mmol in 5 mL of MeCN) or to an excess of MeI. After stirring for a few minutes at ambient temperature, the color of the mixture readily changed from green to red. Then the solution was concentrated to ca. 3 mL, and 3 mL of Et_2O was added. Red solids $[Cp^*_2Mo_2(CO)_2(\mu\text{-SMe})_2(\mu\text{-SH})][BF_4]$ (**16**) (108 mg, 95% yield), $[Cp^*_2Mo_2(CO)_2(\mu\text{-SMe})_3][BF_4]$ (**20**) (116 mg, 100% yield), or $[Cp^*_2Mo_2(CO)_2(\mu\text{-SMe})_3]I$ (**19**) (116 mg, 95% yield) precipitated and were collected by filtration and then washed with pentane.

(b) Gaseous hydrogen chloride was bubbled through a dichloromethane solution containing 0.1 g (0.25 mmol) of $[Cp_2{}^*Mo_2(CO)_2(\mu\text{-SMe})_2(\mu\text{-S})]$ (**8**). There was rapid precipitation of a light red material. Then, the solution was concentrated and 3 mL of Et_2O was added to give some red microcrystals of $[Cp^*_2Mo_2(CO)_2(\mu\text{-SMe})_2(\mu\text{-SH})]Cl$ (**17**) (105 mg, 100% yield), which were collected by filtration and then washed by pentane.

(c) A 3 mL aliquot of a solution of hydrogen fluoride (40%) was added to a dichloromethane solution containing 0.1 g (0.25 mmol) of $[Cp_2{}^*Mo_2(CO)_2(\mu\text{-SMe})_2(\mu\text{-S})]$ (**8**). The mixture readily turned reddish. Addition of 3 mL of Et_2O to the reduced solution gave red crystals of $[Cp^*_2Mo_2(CO)_2(\mu\text{-SMe})_2(\mu\text{-SH})]F$ (**18**) (103 mg, 100% yield), which were collected by filtration and then washed by pentane.

16. Anal. Found: C, 39.1; H, 5.1; S, 12.8; Mo, 25.2. $C_{24}H_{37}BF_4Mo_2O_2S_3$.Calc: C, 39.3; H, 5.0; S, 13.1; Mo, 26.2.

19. Anal. Found: C, 38.3; H, 5.1; S, 12.1; I, 15.5. $C_{25}H_{39}IMo_2O_2S_3$ Calc: C, 38.2; H, 5.0; S, 12.2; I, 16.2.

3.2. Synthesis of $[Cp^*_2Mo_2(CO)_4(\mu\text{-SMe})_2][BF_4]_2$ (21). The literature method was used.[6c] **3** was dissolved in CH_2Cl_2 (0.5 g, 0.75 mmol), and a solution of $Ag[BF_4]$ (1.5 mmol) in THF was added. The mixture was stirred for 15 min. Then the solvents were removed under vacuum and $[Cp^*_2Mo_2(CO)_4(\mu\text{-SMe})_2][BF_4]_2$ (**21**) (567 mg, 90% yield) was extracted with acetonitrile (20 mL) and then recrystallized in MeCN–ether (1:1).

21. Anal. Found: C, 37.2; H, 4.3; S, 7.5. $C_{26}H_{36}B_2F_8Mo_2O_4S_2$ Calc: C, 37.0; H, 4.3; S, 7.6.

3.3. Reaction of $[Cp^*_2Mo_2(CO)_4(\mu\text{-SMe})_2]$ (3) with H_2S. Complex **3** (0.5 g, 0.75 mmol) was dissolved in toluene (50 mL) and the solution was heated (at 80 °C) in the presence of H_2S for 2 days. The solution was then evaporated to dryness, and the residue was chromatographed on a silica gel column. Elution with a mixture CH_2Cl_2 hexane (1:1) gave $[Mo_2Cp^*_2(\mu\text{-S})_2(\mu\text{-SH})_2]$ (**22**) (133 mg, 30% yield) which was washed with pentane.

(21) Koll, F. X.; Jutzi, P. *J. Organomet. Chem.* 1983, *243*, 119.
(22) King, R. B.; Iqbal, M. Z.; King, A. D., Jr. *J. Organomet. Chem.* 1979, *171*, 53.

22. Anal. Found: C, 40.6; H, 5.1; S, 20.7. $C_{20}H_{32}Mo_2S_4$ Calc: C, 40.6; H, 5.4; S, 21.6.

4. Thermolysis Reactions. [Cp*$_2$Mo$_2$(CO)$_4$(μ-ER)$_2$] (ER = SMe, SePh). A brown solution of [Cp*$_2$Mo$_2$(CO)$_4$(μ-ER)$_2$] [ER = SMe (**3**), SePh (**7**)] (0.5 g) in toluene (40 mL) was heated at 80 °C for 4 h. The resultant solution was concentrated to ca. 2 mL. Chromatography on a silica gel column afforded mainly one fraction: (i) for E = SMe, a yellowish brown solution in 3:2 hexane–CH_2Cl_2, which gave [Cp*$_2$Mo$_2$(CO)$_2$(μ-SMe)$_2$] (**9**) (275 mg, 60% yield); (ii) for ER = SePh, a red solution in 2:1 hexane–CH_2Cl_2, which afforded [Cp*$_2$Mo$_2$(CO)$_2$(μ-SePh)$_2$] (**11**) (70 mg, 15% yield).

11. Anal. Found: C, 49.0; H, 4.7; Se, 18.0. $C_{34}H_{40}Mo_2O_2Se_2$ Calc: C, 49.2; H, 4.8; Se, 19.0.

[Cp*$_2$Mo$_2$(CO)$_2$(μ-SMe)$_2$] (9) and [Cp*$_2$Mo$_2$(CO)$_2$(μ-SMe)$_2$(μ-S)] (8). A solution of **8** (0.1 g) or **9** (0.1 g) in toluene was maintained at 110 °C under nitrogen. This caused total decomposition of the reactants after 3 days. Chromatography on a silica gel column of the reduced solution gave only one fraction: a pink-red solution in 3:2 hexane–CH_2Cl_2, which yielded [Cp*$_2$Mo$_2$(μ-SMe)$_4$] (**12**) (15 mg, 15% yield). A brown band could not be removed even by washing the column with methanol.

[Cp*$_2$Mo$_2$(CO)$_2$(μ-SMe)$_3$]I (19). A suspension of **19** was heated in refluxing toluene for 3 days. The solution became green and then was evaporated under high vacuum. Elution with CH_2Cl_2 on a silica gel column gave [Cp*$_2$Mo$_2$(CO)$_2$(μ-SMe)$_2$(μ-S)] (**8**) in quantitative yields.

5. X-ray Analysis of [Cp*$_2$Mo$_2$(CO)$_2$(μ-SMe)$_2$ (μ-SH)][BF$_4$] (16). Measurements were made at 20 °C on an Enraf-Nonius CAD4 diffractometer with graphite-monochromatized Mo Kα radiation, λ = 0.710 73 Å, using an orange-red crystal of dimensions 0.15 × 0.08 × 0.02 mm. Our inability to obtain a larger crystal has had a slightly adverse effect on the quality of the results.

Crystal Data. $C_{24}H_{37}BF_4Mo_2O_2S_3$, M = 732.41, orthorhombic, space group *Pcab* (No. 61) a = 15.655(5) Å, b = 16.173(3) Å, c = 23.662(5) Å^3, V = 5991(3) Å^3, Z = 8, D_c = 1.624 g cm^{-3}, μ(Mo Kα) = 1.091 mm^{-1}.

Measurements. Cell dimensions are based on the setting angles of 25 reflections with 7 < θ(Mo Kα) < 11°. The intensities of 3668 unique relections with 2 < θ(Mo Kα) < 22°, 0 ≤ h ≤ 16, 0 ≤ k ≤ 16, and 0 ≤ l ≤ 24 were estimated from $\omega/2\theta$ scans and corrected for *Lp* and absorption (empirical correction factors on F 0.88–1.13).[23]

Structure Analysis. The structure was solved by Patterson and Fourier methods. Refinement on F with $w = 1/\sigma^2(F)$ of 325 parameters (Table 4) using all reflections converged (Δ/σ < 0.14) at R = 0.044, R_w = 0.083 for 1623 reflections with $I > 2\sigma(I)$ and to R = 0.168, R_w = 0.094 for all 3668 reflections, S = 0.82. Anisotropic U_{ij} values were used for all non-H atoms. The H atom bonded to S1 was not located. Other H-atom positions were calculated using stereochemical criteria (with C–H = 0.96 Å) after the methyl group orientations had been assessed from $\Delta\rho$ syntheses. All H atoms were then constrained to ride on their parent C atoms with U(H) = 1.5U_{eq}(C). Final $\Delta\rho$ values were −0.37 to +0.42 e Å^{-3}. The GX package was used for the final calculations.[24] Scattering factors and anomalous dispersion corrections were taken from ref 25.

Table 4. Fractional Coordinates for 16

atom	x	y	z
Mo1	0.17487(5)	0.01227(5)	0.17165(3)
Mo2	0.22738(5)	−0.09381(5)	0.08645(3)
S1	0.32510(17)	−0.01855(16)	0.14996(10)
S2	0.19686(15)	0.05348(15)	0.07341(10)
S3	0.20154(17)	−0.13718(16)	0.18490(11)
F1	0.4598(4)	−0.3996(4)	0.4357(3)
F2	0.5205(5)	−0.2744(4)	0.4402(3)
F3	0.4130(5)	−0.2987(5)	0.3839(3)
F4	0.5360(6)	−0.3521(5)	0.3646(4)
O1	−0.0163(5)	−0.0283(5)	0.1482(3)
O2	0.0386(4)	−0.1372(4)	0.0551(3)
C1	0.0547(6)	−0.0138(6)	0.1545(4)
C2	0.1090(6)	−0.1181(6)	0.0675(4)
C3	0.1048(7)	−0.1986(7)	0.1944(5)
C4	0.0980(6)	0.0771(6)	0.0348(4)
C5	0.1803(7)	0.1502(6)	0.2010(4)
C6	0.0984(7)	0.1145(7)	0.2127(5)
C7	0.1090(7)	0.0541(7)	0.2530(5)
C8	0.1979(7)	0.0461(6)	0.2652(4)
C9	0.2398(5)	0.1080(6)	0.2343(4)
C10	0.2385(7)	−0.2132(6)	0.0340(4)
C11	0.2353(7)	−0.1426(6)	−0.0036(4)
C12	0.3118(6)	−0.0966(6)	0.0062(4)
C13	0.3593(6)	−0.1398(7)	0.0476(5)
C14	0.3139(7)	−0.2082(6)	0.0650(4)
C15	0.1996(6)	0.2229(6)	0.1628(4)
C16	0.0143(7)	0.1567(6)	0.1949(5)
C17	0.0395(7)	0.0109(8)	0.2843(5)
C18	0.2378(8)	−0.0091(7)	0.3093(5)
C19	0.3314(6)	0.1324(6)	0.2408(4)
C20	0.1759(8)	−0.2850(7)	0.0304(5)
C21	0.1763(7)	−0.1288(6)	−0.0545(5)
C22	0.3412(7)	−0.0233(7)	−0.0269(4)
C23	0.4487(6)	−0.1197(6)	0.0660(4)
C24	0.3412(7)	−0.2729(7)	0.1074(5)
B	0.4854(10)	−0.3310(10)	0.4082(8)

Acknowledgment. We thank the CNRS, EPSRC, and the Universities of Brest and Glasgow for financial support.

Supplementary Material Available: Tables of crystal data, anisotropic displacement parameters, atomic parameters, and complete bond lengths and angles (10 pages). Ordering information can be found on any current masthead page.

OM940809I

(23) Walker, N.; Stuart, D. *Acta Crystallogr.* 1983, *A39*, 158.

(24) Mallinson, P. R.; Muir, K. W. *J. Appl. Crystallogr.* 1985, *18*, 51.

(25) *International Tables for X-ray Crystallography*; Kynoch Press: Birmingham, U.K., 1974; Vol. IV, pp 99–119.

Oxidative Insertion as Frontside S_N2 Substitution: A Theoretical Study of the Model Reaction System Pd + CH_3Cl

F. Matthias Bickelhaupt,*,† Tom Ziegler,* and Paul von Ragué Schleyer†

Department of Chemistry, University of Calgary, Calgary, Alberta, Canada T2N 1N4

Received December 7, 1994®

The potential energy surface of the model reaction system Pd + CH_3Cl has been explored using density functional theory based on the local density approximation (LDA) and its nonlocal extension NL-SCF. Oxidative insertion (OxIn) of Pd into the C–Cl bond has the lowest activation barrier ($\Delta E^{\ddagger} = -1.5$ kcal/mol relative to the separated reactants; NL-SCF) and leads to exothermic production of CH_3PdCl ($\Delta E_r = -7.7$ kcal/mol). The "straight" S_N2 substitution is not competitive as it leads to the highly endothermic formation of $PdCH_3^+ + Cl^-$ ($\Delta E_r = 145.2$ kcal/mol). However, in combination with a concerted rearrangement of the Cl^- leaving group from C to Pd, the substitution process (S_N2/Cl-ra) leads to the exothermic formation of CH_3PdCl via a still high but much lower energy barrier ($\Delta E^{\ddagger} =$ 29.6 kcal/mol). Furthermore, radical mechanisms proceeding via single electron transfer (SET) have been considered. Solvent effects, estimated using a simple electrostatic continuum model, tend to favor the straight S_N2 substitution because of the charge separation in the products, but oxidative insertion remains dominant. In order to explain the intrinsic preference of the Pd atom to react via oxidative insertion, a detailed analysis of the bonding mechanism between Pd and CH_3Cl has been carried out. It is argued that oxidative insertion in organometallic chemistry corresponds to frontside S_N2 substitution in organic chemistry, in spite of obvious differences. Finally, possible effects of ligands are discussed.

1. Introduction

Oxidative addition and reductive elimination (the reverse process) represent a fundamental class of organometallic reactions which occur in nearly all homogeneous, catalytic processes (eq 1).[1] Therefore, these

$$ML_n + R\text{–}X \underset{\text{Reductive Elimination}}{\overset{\text{Oxidative Addition}}{\rightleftharpoons}} R\text{–}ML_n\text{–}X \qquad (1)$$

processes are of major significance for synthesis and industrial processes and have been the subject of many experimental[1–5] and theoretical[6–8] studies. There are basically two different approaches to the investigation of oxidative addition. In the first approach, particular transition metal complexes are studied experimentally[1–3c] as well as theoretically,[6] using more or less realistic model systems in the latter case. In the second and more recent approach, the intrinsic reactivity of the metal ions or atoms is studied in the absence of ligands or solvent molecules, the effects of which may be added stepwise at later stages. Experimentally, this has been achieved using mass spectrometric[3,4] (metal ions) or spectroscopic[5] (metal atoms) techniques. Theoretical methods[7,8] play a key role in this approach. They enable the study of model reaction systems, which are indispensable for the achievement of a real understanding

† Present address: Computer Chemie Centrum, Universität Erlangen-Nürnberg, Nägelsbachstr. 25, D-91052 Erlangen, Germany.

® Abstract published in *Advance ACS Abstracts,* April 1, 1995.

(1) (a) Collman, J. P.; Hegedus, L. S.; Norton, J. R.; Finke, R. G. *Principles and Applications of Organotransition Metal Chemistry*; University Science Books: Mill Valley, CA, 1987. (b) Elschenbroich, Ch.; Salzer, A. *Organometallics. A Concise Introduction*, 2nd ed.; VCH: Weinheim, Germany 1992.

(2) (a) Janowicz, A. H.; Bergman, R. G. *J. Am. Chem. Soc.* **1982**, *104*, 352. (b) Janowicz, A. H.; Bergman, R. G. *J. Am. Chem. Soc.* **1983**, *105*, 3929. (c) Jones, W. D.; Feher, F. J. *J. Am. Chem. Soc.* **1982**, *104*, 4240. (d) Sakakura, T.; Sodeyama, T.; Sasaki, K.; Wada, K.; Tanaka, M. *J. Am. Chem. Soc.* **1990**, *112*, 7221. (e) Casalnuovo, A. L.; Calabrese, J. C.; Milstein, D. *J. Am. Chem. Soc.* **1988**, *110*, 6738. (f) Wright, M. W.; Smalley, T. L.; Welker, M. E.; Rheingold, A. L. *J. Am. Chem. Soc.* **1994**, *116*, 6777. (g) Grushin, V. V.; Alper, H. *Chem. Rev.* **1994**, *94*, 1047. (h) Ellis, P. R.; Pearson, J. M.; Haynes, A.; Adams, H.; Bailey, N. A.; Maitlis, P. M. *Organometallics* **1994**, *13*, 3215.

(3) (a) Armentrout, P. B.; Beauchamp, J. L. *Acc. Chem. Res.* **1989**, *22*, 315. (b) Eller, K.; Schwarz, H. *Chem. Rev.* **1991**, *91*, 1121. (c) van den Berg, K. J.; Ingemann, S.; Nibbering, N. M. M.; Gregor, I. K. *Rapid Commun. Mass Spectrom.* **1993**, *7*, 769. (d) Wesendrup, R.; Schröder, D.; Schwarz, H. *Angew. Chem.* **1994**, *105*, 1232. (e) Chen, Y.-M.; Clemmer, D. E.; Armentrout, P. B. *J. Am. Chem. Soc.* **1994**, *116*, 7815.

(4) (a) Jones, R. W.; Staley, R. H. *J. Am. Chem. Soc.* **1980**, *102*, 3794. (b) Jones, R. W.; Staley, R. H. *J. Phys. Chem.* **1982**, *86*, 1669. (c) Weil, D. A.; Wilkins, C. L. *J. Am. Chem. Soc.* **1985**, *107*, 7316. (d) Chowdhury, A. K.; Wilkins, C. L. *J. Am. Chem. Soc.* **1987**, *109*, 5336.

(5) (a) Mitchell, S. A.; Hackett, P. A. *J. Chem. Phys.* **1990**, *93*, 7822. (b) Ritter, D.; Weisshaar, J. C. *J. Am. Chem. Soc.* **1990**, *112*, 6425. (c) Chertihin, G. V.; Andrews, L. *J. Am. Chem. Soc.* **1994**, *116*, 8322.

(6) (a) Ziegler, T.; Tschinke, V.; Fan, L.; Becke, A. D. *J. Am. Chem. Soc.* **1989**, *111*, 9177. (b) Bickelhaupt, F. M.; Baerends, E. J.; Ravenek, W. *Inorg. Chem.* **1990**, *29*, 350. (c) Ziegler, T. *Chem. Rev.* **1991**, *91*, 651. (d) Koga, N.; Morokuma, K. *Chem. Rev.* **1991**, *91*, 823. (e) Low, J. J.; Goddard, W. A., III. *J. Am. Chem. Soc.* **1984**, *106*, 6928. (f) *Ibid.* **1984**, *106*, 8321. (g) *Ibid.* **1986**, *108*, 6115. (h) Irikura, K. K.; Goddard, W. A., III. *J. Am. Chem. Soc.* **1994**, *116*, 8733. (i) Perry, J. K.; Goddard, W. A., III. *J. Am. Chem. Soc.* **1994**, *116*, 5013.

(7) (a) Siegbahn, P. E. M.; Blomberg, M. R. A. *J. Am. Chem. Soc.* **1992**, *114*, 10548. (b) Siegbahn, P. E. M.; Blomberg, M. R. A.; Svensson, M. *J. Am. Chem. Soc.* **1993**, *115*, 1952. (c) Siegbahn, P. E. M. *Organometallics* **1994**, *13*, 2833. (d) Carter, E. A.; Goddard, W. A., III. *J. Phys. Chem.* **1988**, *92*, 5679. (e) Perry, J. K.; Ohanessian, G.; Goddard, W. A., III. *Organometallics* **1994**, *13*, 1870.

(8) (a) Blomberg, M. R. A.; Siegbahn, P. E. M.; Svensson, M. *J. Am. Chem. Soc.* **1992**, *114*, 6095. (b) Siegbahn, P. E. M.; Blomberg, M. R. A.; Svensson, M. *J. Am. Chem. Soc.* **1993**, *115*, 4191. (c) Svensson, M.; Blomberg, M. R. A.; Siegbahn, P. E. M. *J. Am. Chem. Soc.* **1991**, *113*, 7076. (d) Blomberg, M. R. A.; Siegbahn, P. E. M.; Svensson, M. *Inorg. Chem.* **1993**, *32*, 4218. (e) Siegbahn, P. E. M.; Blomberg, M. R. A.; Svensson, M. *J. Phys. Chem.* **1993**, *97*, 2564. (f) Siegbahn, P. E. M. *J. Am. Chem. Soc.* **1994**, *116*, 7722.

0276-7333/95/2314-2288$09.00/0

of the reaction mechanism, but which often cannot be realized experimentally. In the past, theoretical investigations were mainly focused on the oxidative addition reactions of organotransition metal systems to H–H,[6b–f] C–H,[6a,c,d,f,g,7b,c,e,8a–c] and C–C[6d,f,g,7a] bonds but also to F–F,[6c] N–H,[8d] and O–H[8e] bonds.

In the present study, we have carried out a high-level density-functional theoretical (DFT)[9] investigation on the intrinsic reactivity of palladium-d^{10} toward chloromethane. Thus, we follow the second approach (*vide supra*) using the model system Pd + CH_3Cl. The calculations were carried out with the ADF program.[10,11] First, the oxidative insertion (*cis* oxidative addition) of Pd to the C–Cl bond (OxIn, eq 2) is considered.

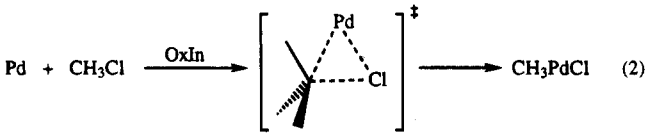

(2)

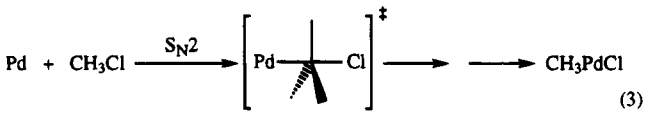

(3)

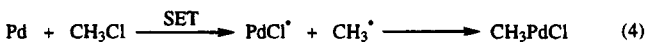

(4)

Furthermore, the competing backside nucleophilic substitution on carbon (S_N2, eq 3) and a radical mechanism proceeding via a single electron transfer (SET) and Cl abstraction (eq 4) are investigated. Solvent effects have been estimated using a simple electrostatic continuum model.[12]

One objective is to arrive at a better understanding of the important class of oxidative addition reactions in which a metal center inserts into the polar, electrophilic carbon–halogen bond.[13] It is noted, that our model reactions are closely related to the famous Monsanto acetic acid process in which the rate-determining step is oxidative addition of a Rh(I) complex to CH_3I.[14] The question is addressed if nucleophilic substitution or a radical mechanism can be competitive in the formation of the apparent oxidative insertion product, CH_3PdCl, as indicated in eqs 3 and 4.

Another main objective is to get insight into mechanistic and electronic differences and analogies between our organometallic (Pd + CH_3Cl) and related organic reaction systems involving main group bases (B + CH_3Cl). For this purpose, we have performed an advanced analysis[11] of the electronic structure of Pd + CH_3Cl in selected stationary points on the potential energy surface. This analysis enables us to interpret our quantitative results in familiar terms from MO theory.[15]

2. Methods

A. General Procedure. All calculations were performed using the Amsterdam-Density-Functional (ADF) program,[10] developed by Baerends *et al.*[10a–c] and vectorized by Ravenek.[10d] The numerical integration was performed using the procedure developed by te Velde *et al.*[10e,f] The MOs were expanded in an uncontracted set of Slater type orbitals (STOs).[10g] For H and C the basis is of double-ζ quality, augmented with a 2p and a 3d polarization function, respectively. For Cl the basis is of triple-ζ quality, augmented with two 3d polarization functions. For Pd the basis is of double-ζ quality for the 4s shell and of triple-ζ quality for the 4p, 4d, 5s, and 5p shells. The core shells of carbon (1s), chlorine (1s2s2p), and palladium (1s2s2p3s3p3d) were treated by the frozen-core approximation.[10a] An auxiliary set of s, p, d, f, and g STOs was used to fit the molecular density and to represent the Coulomb and exchange potentials accurately in each SCF cycle.[10h]

Geometries and frequencies were calculated at the LDA level. Equilibrium structures were optimized using analytical gradient techniques.[10i] Frequencies[10j] were calculated by numerical differentiation of the analytical energy gradients. Transition state structures[10k] were optimized using the algorithm developed by Simons[10l] in the implementation due to Baker.[10m]

Energies were evaluated using the local density approximation (LDA) as well as density functionals including nonlocal corrections (NL). At the LDA level exchange is described by Slaters Xα potential[9c] and correlation is treated in the Vosko–Wilk–Nusair (VWN) parameterization.[10n] At the NL level nonlocal corrections for the exchange due to Becke[10o,p] and for correlation due to Perdew[10q] are added self-consistently.[10r]

B. Solvent Effects. Solvent effects have been estimated using a simple electrostatic continuum model[12] based on the expressions derived by Onsager[12a] and Born.[12b] The solute is considered as a point dipole, μ, and/or point charge, Q, which is located in the center of a spherical cavity with radius a_0. This cavity is surrounded by the solvent which is represented as a dielectric continuum with relative dielectric constant ϵ_r. The solvation energy, ΔE_{solv}, is the sum of a dipole ($\Delta E_{solv,\mu}$) and a charge ($\Delta E_{solv,Q}$) term (eq 5). These terms are given in

$$\Delta E_{solv} = \Delta E_{solv,\mu} + \Delta E_{solv,Q} \quad (5)$$

(9) (a) Dreizler, R. M.; Gross, E. K. U. *Density Functional Theory, An Approach to the Quantum Many-Body Problem*; Springer-Verlag: Berlin, 1990. (b) Parr, R. G.; Yang, W. *Density-Functional Theory of Atoms and Molecules*; Oxford University Press: New York, 1989. (c) Slater, J. C. *Quantum Theory of Molecules and Solids*; McGraw-Hill: New York, 1974; Vol. 4.

(10) (a) Baerends, E. J.; Ellis, D. E.; Ros, P. *Chem. Phys.* **1973**, *2*, 41. (b) Baerends, E. J.; Ros, P. *Chem. Phys.* **1975**, *8*, 412. (c) Baerends, E. J.; Ros, P. *Int. J. Quantum Chem., Quantum Chem. Symp.* **1978**, *S12*, 169. (d) Ravenek, W. In *Algorithms and Applications on Vector and Parallel Computers*; Riele, H. H. J., Dekker, Th. J., van de Vorst, H. A., Eds.; Elsevier: Amsterdam, 1987. (e) Boerrigter, P. M.; te Velde, G.; Baerends, E. J. *Int. J. Quantum Chem.* **1988**, *33*, 87. (f) te Velde, G.; Baerends, E. J. *J. Comp. Phys.* **1992**, *99*, 84. (g) Snijders, J. G.; Baerends, E. J.; Vernooijs, P. *At. Nucl. Data Tables* **1982**, *26*, 483. (h) Krijn, J.; Baerends, E. J. Fit-Functions in the HFS-Method, Internal Report (in Dutch), Vrije Universiteit Amsterdam, The Netherlands, 1984. (i) Versluis, L.; Ziegler, T. *J. Chem. Phys.* **1988**, *88*, 322. (j) Fan, L.; Versluis, L.; Ziegler, T.; Baerends, E. J.; Ravenek, W. *Int. J. Quantum Chem., Quantum Chem. Symp.* **1988**, *S22*, 173. (k) Fan, L.; Ziegler, T. *J. Chem. Phys.* **1990**, *92*, 3645. (l) Banerjee, A.; Adams, N.; Simons, J.; Shepard, R. *J. Phys. Chem.* **1985**, *89*, 52. (m) Baker, J. *J. Comput. Chem.* **1986**, *7*, 385. (n) Vosko, S. H.; Wilk, L.; Nusair, M. *Can. J. Phys.* **1980**, *58*, 1200. (o) Becke, A. D. *J. Chem. Phys.* **1986**, *84*, 4524. (p) Becke, A. D. *Phys. Rev. A* **1988**, *38*, 3098. (q) Perdew, J. P. *Phys. Rev. B* **1986**, *33*, 8822. Erratum: *Ibid.* **1986**, *34*, 7406. (r) Fan, L.; Ziegler, T. *J. Chem. Phys.* **1991**, *94*, 6057.

(11) (a) Bickelhaupt, F. M.; Nibbering, N. M. M.; van Wezenbeek, E. M.; Baerends, E. J. *J. Phys. Chem.* **1992**, *96*, 4864. (b) Ziegler, T.; Rauk, A. *Inorg. Chem.* **1979**, *18*, 1558. (c) Ziegler, T.; Rauk, A. *Inorg. Chem.* **1979**, *18*, 1755. (d) Ziegler, T.; Rauk, A. *Theoret. Chim. Acta* **1977**, *46*, 1.

(12) (a) Born, M. *Z. Phys.* **1920**, *1*, 45. (b) Onsager, L. *J. Am. Chem. Soc.* **1936**, *58*, 1486. (c) Wong, M. W.; Frisch, M. J.; Wiberg, K. B. *J. Am. Chem. Soc.* **1991**, *113*, 4776.

(13) Reference 1a, Chapter 5.

(14) (a) Forster, D. *J. Am. Chem. Soc.* **1976**, *98*, 846. (b) Forster, D. *Adv. Organomet. Chem.* **1979**, *17*, 255. (c) Reference 1a, Chapter 12. (d) Forster, D. *J. Am. Chem. Soc.* **1975**, *97*, 951. (e) Hickey, C. E.; Maitlis, P. M. *J. Chem. Soc., Chem. Commun.* **1984**, 1609.

(15) (a) Albright, T. A.; Burdett, J. K.; Whangbo, M.-H. *Orbital Interactions in Chemistry*; Wiley-Interscience: New York, 1985. (b) Rauk, A. *Orbital Interaction Theory of Organic Chemistry*; Wiley-Interscience: New York, 1994. (c) Fleming, I. *Grenzorbitale und Reaktionen organischer Verbindungen*; VCH Verlagsgesellschaft: Weinheim, Germany 1990.

$$\Delta E_{\mathrm{solv},\mu} = -\frac{(\epsilon_r - 1)}{(2\epsilon_r + 1)}\frac{1}{4\pi\epsilon_0}\frac{\mu^2}{a_0^3} \quad (6)$$

$$\Delta E_{\mathrm{solv},Q} = -{}^1/_2\left(1 - \frac{1}{\epsilon_r}\right)\frac{1}{4\pi\epsilon_0}\frac{Q^2}{a_0} \quad (7)$$

SI units in eqs 6 and 7. Overall charges, Q, and dipole moments, μ, calculated at the NL-SCF level with respect to the center of electronic charge were used.[12c] The effective cavity radius a_0 for a molecule or ion was calculated[12c] as the sum of the greatest internuclear distance and the van der Waals radii[16,17] of the two atoms involved. The expressions were evaluated for two values of the relative dielectric constant corresponding to diethyl ether (ϵ_r = 4.34 at 20 °C) and water (ϵ_r = 78.54 at 25 °C).[18]

C. Bonding Energy Analysis. The bonding mechanism between Pd and CH_3Cl was analyzed in selected stationary points using an extended transition state (ETS) method.[11] The overall bond energy ΔE is made up of two major components (eq 8). The preparation energy ΔE_{prep} is the amount of energy

$$\Delta E = \Delta E_{\mathrm{prep}} + \Delta E_{\mathrm{int}} \quad (8)$$

required to deform the separated fragments from their equilibrium structure to the geometry which they acquire in the overall molecule. The interaction energy ΔE_{int} corresponds to the actual energy change when the prepared fragments are combined to form the overall molecule. The interaction energy is further split up in two physically meaningful terms (eq 9).[11]

$$\Delta E_{\mathrm{int}} = \Delta E_{\mathrm{elst}} + \Delta E_{\mathrm{Pauli}} + \Delta E_{\mathrm{oi}} = \Delta E^0 + \Delta E_{\mathrm{oi}} \quad (9)$$

The term ΔE_{elst} corresponds to the classical electrostatic interaction between the unperturbed charge distributions of the prepared fragments and is usually attractive. The Pauli repulsion $\Delta E_{\mathrm{Pauli}}$ comprises the 4-electron destabilizing interactions between occupied orbitals and is responsible for the steric repulsion. For neutral fragments, it is useful to combine ΔE_{elst} and $\Delta E_{\mathrm{Pauli}}$ in the steric interaction ΔE^0 (eq 9). The orbital interaction ΔE_{oi} accounts for charge transfer (interaction between occupied orbitals on one moiety with unoccupied orbitals of the other, including the HOMO–LUMO interactions) and polarization (empty/occupied orbital mixing on one fragment).

3. Results and Discussion

The results are summarized in Figure 1 (geometries), Table 1 (energies), and Table 2 (analysis). In the following, we will discuss the competition between the various reaction mechanisms (subsection A) and the possible influences of solvation (subsection B). Furthermore, a detailed analysis of the electronic structure of the reaction system Pd + CH_3Cl is presented (subsection C) and analogies with related organic systems involving main group bases (subsection D) as well as expectations for ligand effects (subsection E) are discussed. Energies were evaluated at the LDA and NL-SCF level using LDA geometries. At the LDA level, molecular complexes are stronger bound and transition state energies are lower than at the NL-SCF level (Table 1), in agreement with the general tendency of LDA methods to lead to overbinding.[6c] This overbinding is (partly) compensated by the introduction of gradient corrections in the NL-SCF scheme. The discussion is therefore based on the nonlocal results!

Table 1. Energies (in kcal/mol) of Stationary Points Relative to the Reactants Pd + CH_3Cl (LDA, NL-SCF and NL-SCF+solv)

System[a]	LDA	NL-SCF	NL-SCF+solv[b]	
			diethyl ether	water
Reactants				
Pd + CH_3Cl	0.0	0.0	0.0	0.0
Reactant Complexes				
[CH_3Cl, Pd]	-23.0	-9.9	-9.9	-9.8
[Pd, CH_3Cl]	-16.2	-3.7	-3.7	-3.7
Transition States				
TS(Pd-ra)	-16.1	-1.5	-1.4	-1.4
TS(S_N2/Cl-ra)	22.9	29.6	28.9	28.5
TS(OxIn)	-16.1	1.7	1.7	1.7
Radical Intermediates				
$PdCl^{\bullet}$ + $CH_3^{\bullet}$	35.2	29.3	28.9	28.7
$PdCH_3^{\bullet}$ + $Cl^{\bullet}$	50.6	46.9	46.9	46.9
Products				
$PdCH_3^+$ + Cl^-	149.0	145.2	50.6	23.8
CH_3PdCl	-25.3	-7.7	-7.8	-7.9

[a] See Figure 1 for structures. [b] Solvent effects were calculated using the Onsager–Born model (section 2.B). Diethyl ether: ϵ_r = 4.34. Water: ϵ_r = 78.54.

A. Reaction Mechanisms. Oxidative Addition. First, the oxidative insertion of Pd to CH_3Cl is considered (eq 2, OxIn). The corresponding reaction energy profile is depicted in Figure 2. The reactants Pd + CH_3Cl can combine in two different ways to give the reactant complexes [CH_3Cl, Pd], in which Pd coordinates to Cl, and [Pd, CH_3Cl], in which Pd coordinates to the CH_3 backside (Figure 1). The most stable reactant complex is [CH_3Cl, Pd] with a complexation energy ΔE = −9.9 kcal/mol (Table 1, NL-SCF). In this C_s symmetric complex, the Pd–Cl bond is oriented staggered with respect to CH_3 (Figure 1). The Pd–Cl bond length is 2.258 Å while the Pd–Cl–C angle amounts to 112.05°. The C–Cl bond is only slightly extended from 1.750 Å (in CH_3Cl) to 1.781 Å.

The oxidative addition reaction proceeds from [CH_3Cl, Pd] via a strong bending of Cl toward a C–H bond, leading to the C_s symmetric transition state TS(OxIn) which is 8.4 kcal/mol higher in energy (Figure 2) and is characterized by one imaginary frequency of i 161.7 cm^{-1} (Figure 1). The overall activation energy, $\Delta E^{\ddagger}$ = 1.7 kcal/mol (Table 1), is rather low. In TS(OxIn) the C–Cl and Pd–Cl bonds are elongated to 1.896 and 2.361 Å, respectively (Figure 1). The Pd–C bond is being formed and comes to 2.227 Å while the Pd–C–Cl angle amounts to 69.33°. Palladium is involved in an agostic interaction with a C–H bond, as indicated by a relatively short Pd–H bond of 1.857 Å and an elongated C–H bond of 1.154 Å. The oxidative addition is completed by further insertion of Pd into the C–Cl bond and results in the product CH_3PdCl which is at −7.7 kcal/mol with respect to the reactants (Table 1). During this final stage of the reaction the C–Cl bond further elongates to 2.374 Å, whereas the Pd–C and Pd–Cl bonds are shortened to 2.008 and 2.192 Å, respectively.

S_N2 Substitution. The reaction energy profile for nucleophilic substitution is shown in Figure 3. The reactant complex [Pd, CH_3Cl] is relatively weakly bound by ΔE = −3.7 kcal/mol and can be formed either directly from the separated reactants or by rearrangement of the more stable complex [CH_3Cl, Pd]. During this

(16) *CRC Handbook of Chemistry and Physics*, 63rd ed.; Weast, R. C., Ed.; CRC Press: Boca Raton, FL, 1982; p D-195.
(17) Greenwood, N. N.; Earnshaw, A. *Chemistry of the Elements*; Pergamon Press: Oxford, U.K., 1990.
(18) Reference 16, pp E-51, E-52.

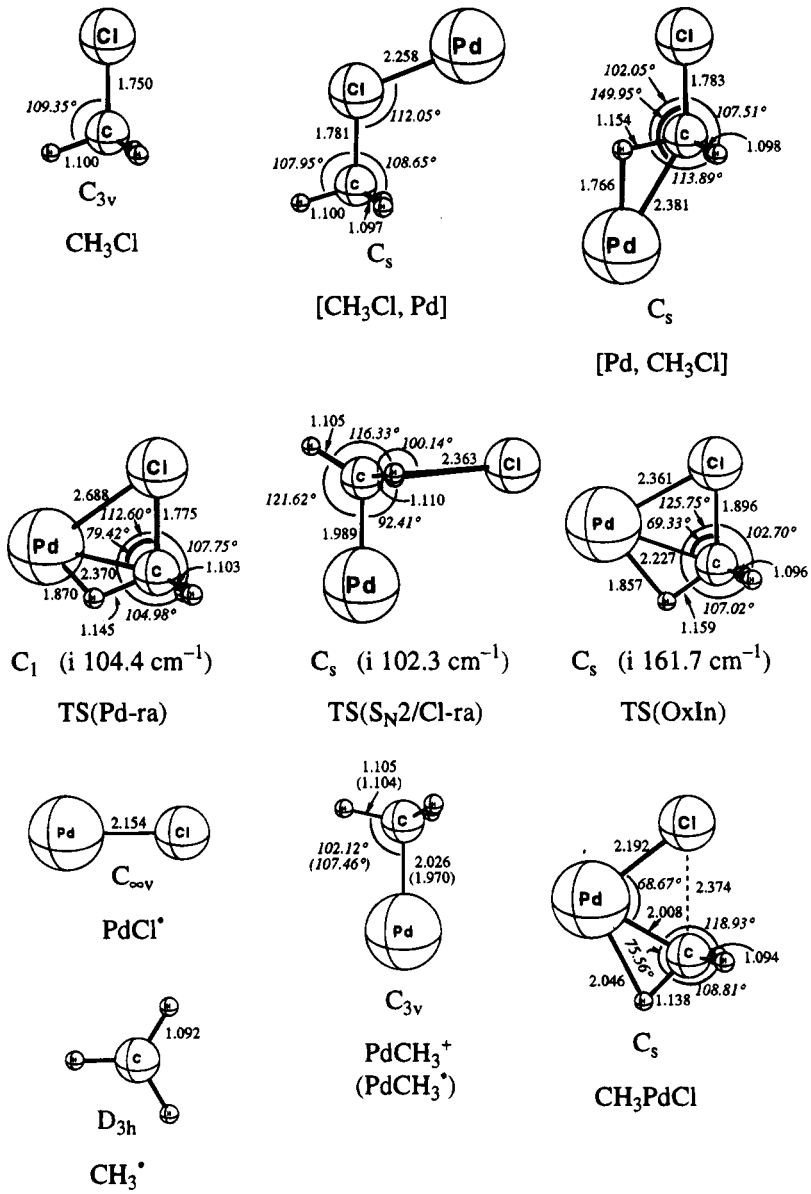

Figure 1. Optimized geometries (LDA; in Å and degrees) for stationary points of the Pd + CH_3Cl reaction system.

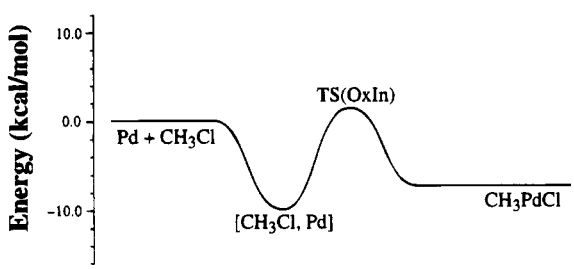

Figure 2. Reaction energy profile (NL-SCF; in kcal/mol) for the oxidative insertion (OxIn) of Pd + CH_3Cl.

rearrangement, Pd moves from Cl to the CH_3 backside via the C_1 symmetric transition state TS(Pd-ra) (*i* 104.4 cm^{-1}) in which Pd interacts weakly with Cl and a C−H bond (Figure 1: d_{Pd-Cl} = 2.688 Å, d_{Pd-C} = 2.370 Å, d_{Pd-H} = 1.870 Å). In the C_s symmetric reactant complex [Pd, CH_3Cl], palladium is involved in an agostic interaction with a C−H bond at the backside of the methyl group (d_{Pd-C} = 2.381 Å, d_{Pd-H} = 1.766 Å, d_{C-H} = 1.154 Å). The C−Cl bond is slightly extended to 1.783 Å.

The "straight" S_N2 substitution proceeds via attack of Pd on carbon and expulsion of the Cl^- leaving group

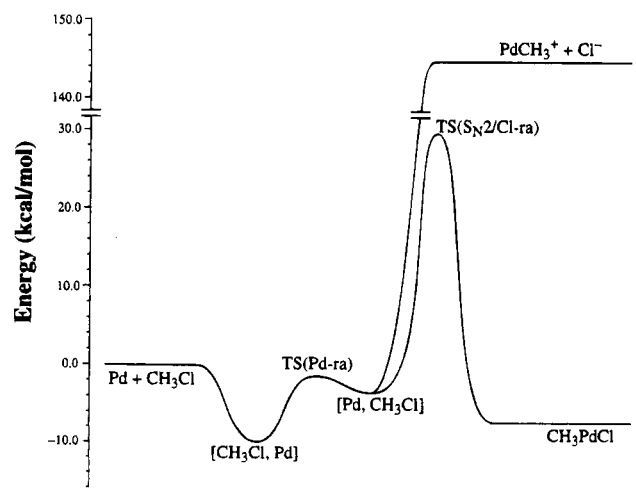

Figure 3. Reaction energy profile (NL-SCF; in kcal/mol) for the nucleophilic substitution (S_N2) of Pd + CH_3Cl.

(eq 10). The Pd−C bond length in $PdCH_3^+$ is 2.026 Å.

$$Pd + CH_3Cl \xrightarrow{S_N2} PdCH_3^+ + Cl^- \qquad (10)$$

This reaction is highly endothermic, i.e. $\Delta E = +145.2$ kcal/mol, due to the charge separation in the products $PdCH_3^+ + Cl^-$. The reverse process, backside S_N2 attack by Cl^- on $PdCH_3^+$, proceeds barrierless (Figure 3). The high endothermicity of the S_N2 process of eq 10 prevents this route to be a competitive alternative for the formation of CH_3PdCl, e.g. by recombination of $PdCH_3^+$ and Cl^- via palladium (eq 11).

$$Cl^- + PdCH_3^+ \longrightarrow CH_3PdCl \qquad (11)$$

There appears to be an alternative S_N2 pathway in which the Cl^- leaving group undergoes concerted rearrangement to palladium during the Pd–C bond formation (eq 12). This one-step substitution/rearrangement

$$Pd + CH_3Cl \xrightarrow{S_N2/Cl\text{-}ra} [Pd\cdots CH_3\cdots Cl]^{\ddagger} \longrightarrow CH_3PdCl \qquad (12)$$

process advances via transition state TS(S_N2/Cl-ra) (i 102.3 cm^{-1}), which is 33.3 kcal/mol above [Pd, CH_3Cl] (Figure 3). The overall barrier is $\Delta E^{\ddagger} = 29.6$ kcal/mol. In the C_s symmetric TS(S_N2/Cl-ra), the Cl^- ion binds electrostatically to $PdCH_3^+$ in an η^2 fashion, i.e. via two bridging H-atoms (Figure 1: $d_{Cl-H} = 2.363$ Å, $d_{C-H} = 1.110$ Å). The Pd–C bond length equals 1.989 Å and is thus somewhat shorter than in the final product (CH_3PdCl: $d_{Pd-C} = 2.192$ Å). The activation barrier (29.6 kcal/mol) is still too high for the S_N2/Cl-ra process (eq 12) to be competitive with oxidative insertion (1.7 kcal/mol, eq 2). This result shows however than an ion-pair mechanism dramatically reduces the extremely high energy found for the straight dissociation process (145.2 kcal/mol).

Radical Mechanisms. Next, we discuss briefly two conceivable radical mechanisms which proceed via single electron transfer (SET), focusing on the reactive intermediates. The reaction energy profiles are displayed in Figure 4. Starting from the most stable reactant complex, [CH_3Cl, Pd], this leads apparently to Cl atom abstraction (actually Cl^- abstraction by $Pd^{+\bullet}$) and the formation of $PdCl^{\bullet} + CH_3^{\bullet}$ (eq 4, Figure 1: $d_{Pd-Cl} = 2.154$ Å), which is 29.3 kcal/mol endothermic (Table 1). Recombination of the radical intermediates via palladium results in the exothermic formations of CH_3PdCl (eq 4). Alternatively, SET can occur in the less stable complex [Pd, CH_3Cl], inducing methyl radical transfer to palladium and formation of $PdCH_3^{\bullet} + Cl^{\bullet}$ (eq 13, Figure 1: $d_{Pd-C} = 1.970$ Å). This process is

$$Pd + CH_3Cl \xrightarrow{SET} PdCH_3^{\bullet} + Cl^{\bullet} \longrightarrow CH_3PdCl \qquad (13)$$

endothermic by 46.9 kcal/mol (Table 1) and is thus 17.6 kcal/mol less favorable, and not competitive, with respect to $Cl^{\bullet}$ abstraction (eq 4), reflecting the difference in Pd–C and Pd–Cl bond strengths. Again, recombination of the intermediates, $PdCH_3^{\bullet} + Cl^{\bullet}$, results in the formation of CH_3PdCl (eq 13).

Comparison of OxIn/S_N2/SET. The *intrinsic* reactivity of Pd toward CH_3Cl is clearly in favor of *oxidative insertion* (eq 2, OxIn). Nucleophilic substitution may only become a viable pathway for oxidative addition (e.g. through its S_N2/Cl–ra ion-pair mechanism, eq 12) after adjustment of additional reaction parameters (ligands, solvent). The SET mechanism proceeding via Cl atom abstraction by palladium and recombination of the intermediates (eq 4) has a comparable barrier as the S_N2/Cl-ra process and is thus neither competitive with respect to oxidative insertion, for our model system.

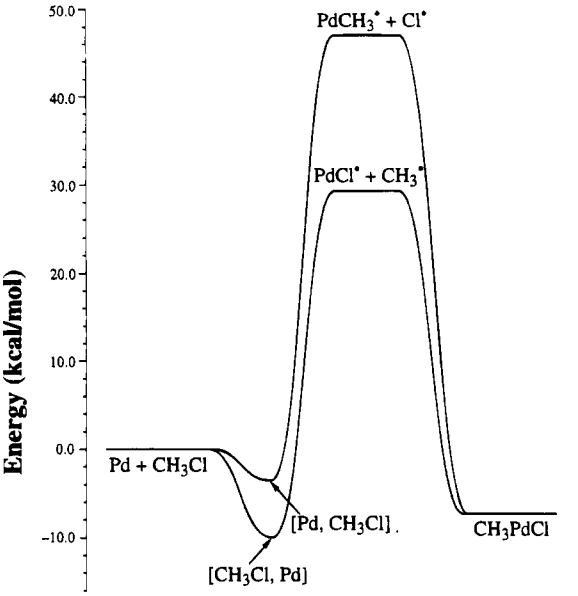

Figure 4. Reaction energy profile (NL-SCF; in kcal/mol) for radical pathways of Pd + CH_3Cl.

B. Solvent Effects. Solvent effects were estimated for diethyl ether ($\epsilon_r = 4.34$) and water ($\epsilon_r = 78.54$), i.e. for a weakly and a strongly polar solvent, using a simple electrostatic continuum model (Table 1, NL-SCF + solv; see also section 2.B). These simple calculations can give a good impression of the effects that can be expected, although a full understanding of the phenomenon of solvation requires the rather expensive incorporation of discrete solvent molecules in the quantum chemical calculation.[19] In general, complexation, activation and reaction energies change only very slightly (0–0.6 kcal/mol) upon introduction of solvent effects, as long as only neutral species are involved. Oxidative insertion (eq 2), for example, remains the dominating process in both diethyl ether and water, with an unchanged activation energy ($\Delta E^{\ddagger} = 1.7$ kcal/mol). An exception is seen for the activation energy of the S_N2/Cl-ra mechanism (eq 12) which is reduced by ca 1 kcal/mol to 28.9 and 28.7 kcal/mol for ether and water, respectively. This has to be ascribed to the rather large dipole moment ($\mu_{NL-SCF} = 7.108$ D) in the strongly polarized TS (S_N2/Cl–ra).

In contrast, the reaction endothermicity for the straight S_N2 substitution (eq 10) is dramatically reduced from 145.2 kcal/mol in the gas phase to 50.6 kcal/mol in diethyl ether and 23.8 kcal/mol in water (Table 1). This enormous change is mainly (>99.9%) caused by the Born term (eq 7), thus by the strong solvation of the separated charges in $PdCH_3^+ + Cl^-$. In diethyl ether, the (solvent caged) ion-pair S_N2/Cl-ra mechanism (eq 12) is still the faster substitution process with a lower activation energy than the straight S_N2 substitution

(19) Bickelhaupt, F. M.; Baerends, E. J.; Nibbering, N. M. M. To be published.

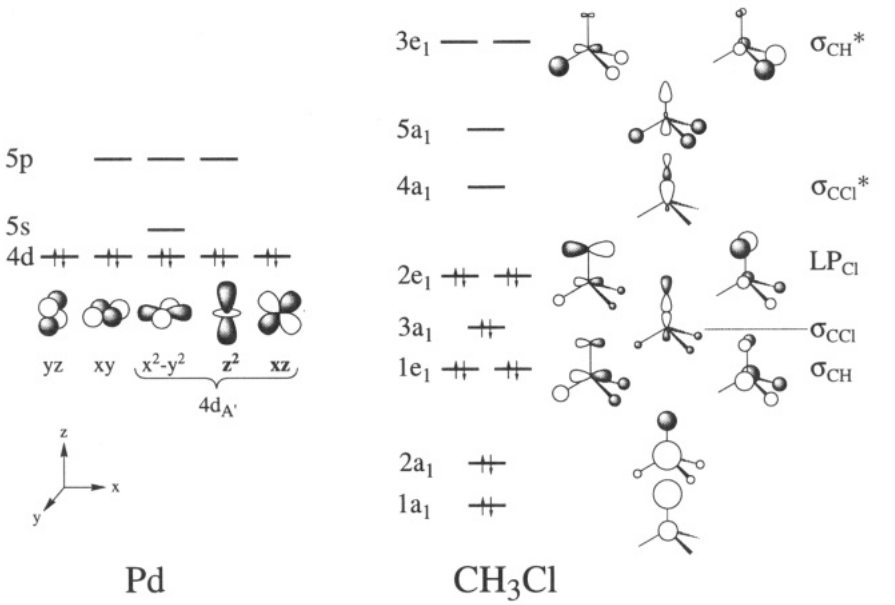

Figure 5. Valence MO scheme of Pd and CH_3Cl (for CH_3Cl the orbital counting begins with the lowest *valence* orbital).

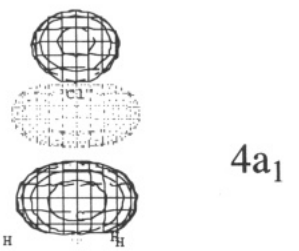

Figure 6. Realistic 3D representation of the $4a_1$-LUMO of CH_3Cl. Note that there is no "normal" backside lobe!

(Table 1). In water, however, the reaction energy of the straight S_N2 substitution (ΔE_r = 23.8 kcal/mol) falls below the activation energy of the S_N2/Cl-ra process ($\Delta E^{\ddagger}$ = 28.5 kcal/mol). This shows that solvation favors the straight S_N2 substitution (eq 10) and that the two substitution processes may become competitive with respect to each other in strongly polar solvents. However, an accurate assessment of the solvent dependence of this competition requires more quantitative methods for the evaluation of solvent effects,[19] e.g. a search for and optimization of a possible transition state of the straight S_N2 substitution in the presence of a (small) number of solvent molecules.

Summarizing, the preference of palladium to insert into the C−Cl bond is preserved under (electrostatic) solvation, although S_N2 substitution becomes less unfavorable. We conclude that still other reaction parameters, e.g. ligands, must be invoked to shift the reactivity toward substitution.

C. Electronic Structure and Bonding. We have analyzed the electronic structure of and bonding between Pd and CH_3Cl for the reactant complexes [CH_3-Cl, Pd] and [Pd, CH_3Cl], the transition state TS(OxIn), and the product CH_3PdCl (Figures 5 and 6, Table 2). As mentioned before, there is no TS structure corresponding to the straight S_N2 substitution, as shown in eq 3. For the sake of clarity, we use C_{3v} symmetry labels for the CH_3Cl orbitals, even though this fragment has the lower C_s point group symmetry in the four analyzed systems.

Separated Reactants. First, we inspect the valence electronic structures of the separated reactants, which

Table 2. Analysis of the Bonding Mechanism between Pd and CH_3Cl in Selected Stationary Points

	[CH_3Cl, Pd]	[Pd, CH_3Cl]	TS(OxIn)	CH_3PdCl
Energy (in kcal/mol) [a]				
ΔE^0	26.6	25.8	51.4	84.8
ΔE_{oi}	−36.5	−31.0	−57.2	−132.2
ΔE_{int}	−9.9	−5.2	−5.8	−47.4
ΔE_{prep}	0.0	1.5	7.5	39.7
ΔE	−9.9	−3.7	1.7	−7.7
Fragment Orbital Overlaps ⟨Pd|CH_3Cl⟩ [b]				
⟨$4d_{A'}$|$2e_{1-y}$⟩	0.21	0.09	0.21	0.17
⟨$4d_{A'}$|$4a_1$⟩	0.08	0.06	0.10	0.18
⟨$4d_{A'}$|$5a_1$⟩	0.05	0.17	0.09	0.14
⟨5s|$2e_{1-y}$⟩	0.19	0.06	0.11	0.15
Fragment Orbital Populations (in eL) [c]				
$P(4d_{A'})$	5.73	5.74	5.57	5.23
P(5s)	0.23	0.12	0.09	0.14
$P(2e_{1-y})$	1.89	1.99	1.93	1.85
$P(4a_1)$	0.08	0.01	0.18	0.61
$P(5a_1)$	0.00	0.08	0.02	0.01
Fragment Charges (in eL) [d]				
Q(Pd)	0.03	0.15	0.38	0.64
$Q(CH_3)$	−0.09	−0.21	−0.23	−0.22
Q(Cl)	0.06	0.06	−0.15	−0.42

[a] ΔE^0 = steric interaction, ΔE_{oi} = orbital interaction, ΔE_{prep} = preparation energy, required to deform the separated fragments to their geometry in the overall molecule (section 2.C). [b] Overlaps between Pd and CH_3Cl orbitals; $\langle 4d_{A'}|\varphi\rangle = \langle 4d_{xz}|\varphi\rangle + \langle 4d_{z^2}|\varphi\rangle + \langle 4d_{x^2-y^2}|\varphi\rangle$. [c] Gross Mulliken populations of Pd and CH_3Cl orbitals; $P(4d_{A'}) = P(4d_{xz}) + P(4d_{z^2}) + P(4d_{x^2-y^2})$. [d] Sums of gross Mulliken charges of the constituting atoms.

are schematically displayed in Figure 5. Palladium has a closed $4d^{10}$ shell containing the five degenerate HOMOs of the metal. The 5s LUMO is only 1.3 eV higher in energy, followed by the 5p orbitals at 4.1 eV above the HOMOs. The 4d orbitals can act as electron donors in all reactions, whereas the 5p orbitals play essentially no role. Next, the substrate (CH_3Cl) is considered for which the orbital counting begins with the lowest *valence* orbital. Thus, the two lowest valence MO levels, $1a_1$ and $2a_1$, are essentially the bonding and antibonding combinations of carbon 2s and chlorine 3s orbitals: $2s_C \pm 3s_{Cl}$. The $1e_1$ and $3a_1$ levels are σ_{CH} and σ_{CCl} bonding, respectively, while the $2e_1$ HOMOs are the

chlorine lone pairs, LP_{Cl}. The $4a_1$ LUMO has strong σ_{CCl}* antibonding character, while the unoccupied $5a_1$ and $3e_1$ orbitals are mainly σ_{CH}* antibonding. The $4a_1$ LUMO represents the well-known σ_{CCl}* orbital which is also involved in the donor/acceptor interaction between nucleophile and substrate in organic S_N2 reactions.[15b,c]

Interestingly, we find that the CH_3Cl $4a_1$ LUMO has essentially no backside lobe as shown by its 3D representation in Figure 6. This is in line with the relatively poor $\langle 4d_{A'}|4a_1\rangle$ overlap of 0.06 in [Pd, CH_3Cl] (Table 2). This result differs from the general view in which the HOMO of an approaching nucleophile can overlap with the pronounced backside lobe of the σ_{CX}* of a substrate CH_3X, which is the onset to S_N2 substitution.[15b,c]

Frontier Orbitals in the Pd/CH_3Cl Interaction. Next, we consider which are the most important frontier orbitals in the bonding between Pd and CH_3Cl (Table 2). The orbital interactions (ΔE_{oi}) in the C_s symmetric [Pd + CH_3Cl] species occur mainly (ca. 90%) in A′ symmetry. The frontier orbitals appear to be $4d_{xz}$, $4d_{z^2}$, and 5s for Pd and $2e_{1-y}$, $4a_1$, and $5a_1$ for CH_3Cl (Figure 5). Other orbitals play no important role due to poor overlap or energy mismatching with orbitals of the other fragment. Note, that in all calculations Pd keeps its orientation as in Figure 5, whereas CH_3Cl may be rotated around the z-axis by an arbitrary amount. This means, that the palladium $4d_{xz}$, $4d_{z^2}$, and $4d_{x^2-y^2}$ (all in A′ symmetry) interchange their function in the Pd/CH_3-Cl interaction from case to case in the actual calculation and must be treated as one set, i.e. $4d_{A'}$, as far as overlaps and populations are involved. Therefore, we use the sum of their overlaps with a specific CH_3Cl orbital φ, $\langle 4d_{A'}|\varphi\rangle$, and the sum of their populations, $P(4d_{A'})$, in the discussion (see footnotes to Table 2).

Reactant Complexes. The bonding orbital interaction (ΔE_{oi} = −36.5 kcal/mol) in [CH_3Cl, Pd] is caused by a synergic combination of "back-donation" **1** from

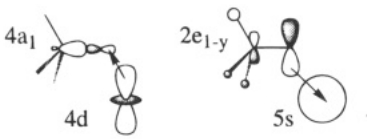

1 **2**

metal $4d_{A'}$ to substrate $4a_1$ LUMO (σ_{CCl}*) and "donation" **2** from a substrate lone pair (LP_{Cl}) to metal 5s (Figure 5, Table 2). This is also reflected by the populations of the orbitals involved (Table 2: $P(4d_{A'})$ = 5.73, $P(4a_1)$ = 0.08 el.; $P(2e_{1-y})$ = 1.89, $P(5s)$ = 0.23 el.). The bonding donation/back-donation interaction is counteracted by the steric interaction (ΔE^0 = 26.6 kcal/mol) of $4d_{A'}$ with LP_{Cl}, leading to an overall interaction $\Delta E = \Delta E_{int}$ = −9.9 kcal/mol (the preparation energy is zero, because CH_3-Cl is hardly deformed).

If we examine the backside complex [Pd, CH_3Cl], the overall interaction is reduced to ΔE = −3.7 kcal/mol, mainly because of a weaker orbital interaction (ΔE_{oi} = −31.0 kcal/mol) which is now provided by donation **3** into the higher energy $5a_1$ ($P(5a_1)$ = 0.08 el.). This is the agostic interaction leading to C−H bond lengthening (Figure 1). Note, that overlap and interaction **4** of $4d_{A'}$

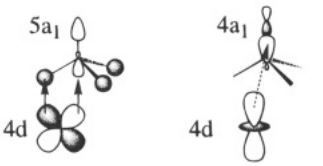

3 **4**

with the $4a_1$ LUMO are very poor ($P(4a_1)$ = 0.01 el.). The back-donation into 5s is also strongly reduced, because of the poor overlap of 0.06 with the chlorine lone pair, $2e_{1-y}$, which is only slightly depopulated: $P(2e_{1-y})$ = 1.99 el. (Table 2, Figure 5).

We conclude that the electronic structure of the metal is more suitable for frontside than for backside complexation to the C−Cl bond of the substrate.

Oxidative Insertion. The orbital interaction (−57.2 kcal/mol) and more so the steric interaction (51.4 kcal/mol) increase strongly when going from the reactant complex [CH_3Cl, Pd] to the transition state TS(OxIn), resulting in an reduced interaction of ΔE_{int} = −5.8 kcal/mol between palladium and chloromethane (Table 2). The deformations of the substrate increase the preparation energy to ΔE_{prep} = 7.5 kcal/mol, leading to an overall energy difference ΔE = 1.7 kcal/mol relative to the reactants. The increase in orbital interaction is due to the favorable overlap of interaction **5** between $4d_{A'}$

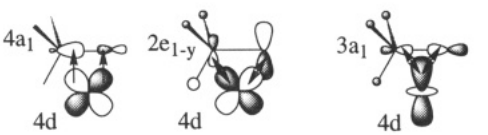

5 **6** **7**

and $4a_1$ ($\langle 4d_{A'}|4a_1\rangle$ = 0.10), which leads to effective population of the C−Cl antibonding $4a_1$ ($P(4a_1)$ = 0.18 el., Table 2). The resulting C−Cl bond elongation further amplifies interaction **5** because of the lowering of the $4a_1$ orbital energy. Similarly, the favorable overlap and interaction **6** between $4d_{A'}$ and the chlorine lone pair ($\langle 4d_{A'}|2e_{1-y}\rangle$ = 0.21) causes the relatively strong steric repulsion. Note, that the $\langle 4d_{A'}|4a_1\rangle$ overlap in TS(OxIn), 0.10, is nearly two times larger than in the backside complex [Pd, CH_3Cl], 0.06, whereas the C−Cl bond length is approximately equal, i.e. 2.3 ± 0.1 Å. This illustrates again the suitability of the metal electronic structure for frontside and not for backside reaction with the C−Cl bond.

Mainly due to **5**, the orbital interaction (−132.2 kcal/mol) increases very strongly, when the oxidative insertion completes and CH_3PdCl is formed. This is reflected by the strong depopulation and population of $4d_{A'}$ and 4a1, respectively (Table 2: $P(4d_{A'})$ = 5.23 el., $P(4a_1)$ = 0.61 el.). The reason is a further increase of the overlap to $\langle 4d_{A'}|4a_1\rangle$ = 0.18 as well as the extra lowering of the $4a_1$ energy, caused by further C−Cl elongation. The $4a_1$ undergoes a slight but significant change, as 1s lobe develops on H, out-of-phase with the frontside lobe on C (not illustrated). This modifies the nature of **5** in the sense that it also provides the agostic interaction which elongates the C−H bond (Figure 1). The steric interaction (84.8 kcal/mol) also increases considerably, but less so then ΔE_{oi}. It is provided by a somewhat weaker interaction **6** ($\langle 4d_{A'}|2e_{1-y}\rangle$ = 0.17) and by Pauli repulsion

Scheme 1

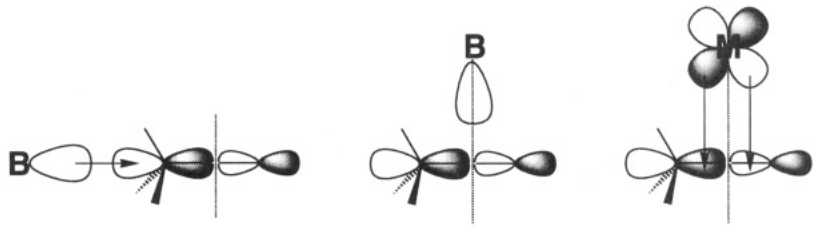

Backside Attack | Frontside Attack (Main Group Base) | Frontside Attack (Metal Base)

7 between palladium 4d and the substrate $3a_1$, i.e. the σ_{CCl} orbital whose energy is increased during C−Cl bond breaking. Due to the larger increase of bonding interaction **5** than of repulsive **6** and **7**, the net interaction ($\Delta E_{int} = -47.4$ kcal/mol) is strong enough to make the overall energy change exothermic ($\Delta E = -7.7$ kcal/mol), in spite of the unfavorable preparation energy ($\Delta E_{prep} = 39.7$ kcal/mol) connected with the heavy deformation of the substrate. During the insertion process the charge Q(Pd) on palladium increases continuously from 0.03 in [CH_3Cl, Pd] via 0.38 in TS(OxIn) to 0.64 el. in CH_3PdCl (Table 2). The fragment charges of CH_3 and Cl in CH_3PdCl are −0.22 and −0.42 el, respectively. This is in line with the oxidation of the metal. The formal charges are, of course, more pronounced and the final product CH_3PdCl can be conceived as Pd(II), coordinated by CH_3^- and Cl^-.

Summarizing, the electronic structure analysis ascribes the intrinsic preference of Pd for frontside attack on the C−Cl bond to the better 4d/σ_{CCl}* overlap in **5** than in **4**.

D. Analogies with Related Organic Reactions. It is interesting to compare our results for Pd + CH_3Cl with the related organic system B + CH_3Cl, where B represents a main group base. In general, the backside S_N2 substitution dominates in the organic reaction system,[20] which is explained on the basis of overlap arguments.[20a] Principally, a main group base B has a p- or sp^x-type HOMO, which favorably overlaps and interacts with the backside of the σ^*_{CCl} orbital of the substrate (Scheme 1). In the case of frontside attack, however, the interaction is very poor due to the well-known cancellation of overlap, as the HOMO lobe approaches on a nodal surface of σ^*_{CCl} (Scheme 1). Yet, our results show that this frontside attack becomes favorable for a metal base M, because the d-type HOMO is ideally suitable for frontside interaction with the σ^*_{CCl} of the substrate (Scheme 1). In this sense, oxidative insertion can be conceived as frontside S_N2 substitution which is favored by metal bases. We believe that the recognition of this analogy can be a helpful concept for the understanding and also the designing of organometallic and organic reactions. We stress that this concept should not be overestimated. Of course, there are obvious differences between the reactions of M + CH_3Cl and B + CH_3Cl, the most important one being the strong binding of the leaving group to the base in the final stage of the metal reaction. This difference is due to the special bonding capabilities of M, in particular the large flexibility to change the oxidation state. Nevertheless, one should also be aware not to overrate the differences. The reaction of B + CH_3Cl too can proceed via a product complex [CH_3B^+, Cl^-], in which the expelled leaving group is bound either to B or CH_3. The interaction here is only weaker and more electrostatic in nature than in the metal case.

E. Expectations for Ligand Effects. In this investigation, we have tried to understand the *intrinsic* reactivity of palladium toward CH_3Cl. This is the necessary basis for the next step, namely the development of insight into the working of ligands.[7,8] First, we take a look at the changes in the electronic structure of the Pd−d^{10} center upon introduction of one Cl^- ligand in $PdCl^-$. The Pd−Cl bond is provided by a donor/acceptor interaction between chlorine $3p_z$ and palladium 5s. The introduction of an overall negative charge causes all 4d orbital energies to rise by ca. 5 eV. This charge effect generally increases the reactivity, as it improves backside interaction **4** as well as frontside interaction **5**. However, the $4d_{z^2}$ rises the most and ends up as the HOMO, due to the Pauli repulsion with Cl $3p_z$. This effect strengthens backside interaction **4** and shifts the reactivity of the metal system from frontside to backside S_N2 substitution (eq 14). Furthermore, CH_3PdCl is directly formed; *no* Cl^- rearrangement (eq 12) is necessary and *no* charge separation (eq 10) occurs in the products.

$$ClPd^- + CH_3Cl \xrightarrow{\text{anion assisted } S_N2} ClPdCH_3 + Cl^- \qquad (14)$$

Finally, it is pointed out that ligands can also influence the reactivity of a metal center by changing the character or appearance of the frontier d orbitals. This is clearly demonstrated by the preference of the square planar d^8 system $PtCl_4^{2-}$ to coordinate end-on, but *not* side-on, to F_2 or I_2, in spite of the fact that the $5d_\pi$ orbitals ($5d_{xz}$, $5d_{yz}$) are higher in energy than the $5d_\sigma$ orbital ($5d_{z^2}$).[6b] We have shown previously that the reason is the special nodal structure of the metal/ligand hybrid $5d_\pi$ orbitals, which results in poor overlap with σ_{F-F}* or σ_{I-I}* in the side-on coordination mode.[6b]

4. Conclusions

The *intrinsic* reactivity of palladium strongly favors oxidative insertion (eq 2) over backside S_N2 substitution (eq 3) in the model system Pd + CH_3Cl, as has been shown by our NL-SCF density-functional investigation. The reason is that the metal 4d orbitals are more suitable for frontside ($4d_{xz}$) than backside ($4d_{z^2}$) overlap with the σ_{CCl}* LUMO of the substrate. We have argued that it can be a useful concept to conceive oxidative insertion as frontside S_N2 substitution, in spite of

(20) (a) March, J. *Advanced Organic Chemistry*; Wiley-Interscience: New York, 1992. (b) Deng, L.; Branchadell, V.; Ziegler, T. *J. Am. Chem. Soc.* **1994**, *116*, 10645.

obvious differences. Thus, frontside S_N2 attack is favored by (bare) metal bases due to the presence of valence d orbitals, whereas for main group bases only backside S_N2 substitution is feasible (Scheme 1).

The backside S_N2 substitution of Pd + CH_3Cl can proceed in two ways: (i) The "straight" S_N2 process (eq 10) is highly endothermic due to charge separation in the products $PdCH_3^+ + Cl^-$. (ii) In the S_N2/Cl-ra process (eq 12), substitution occurs with concerted rearrangement of the Cl^- leaving group and leads to the exothermic formation of CH_3PdCl via a still high but much lower energy barrier. A similar activation barrier has been found for a radical mechanism (eq 4) proceeding via single electron transfer (SET) and Cl^- abstraction by $Pd^{+\bullet}$, followed by recombination of the intermediates $CH_3^\bullet$ + $PdCl^\bullet$ to form CH_3PdCl.

Solvent effects, estimated using a simple electrostatic continuum model, tend to favor the straight S_N2 substitution due to the charge separation in the products. However, oxidative insertion remains dominant and other reaction parameters, namely ligands, must be invoked to shift the reactivity toward substitution.

Ligands can effect the reactivity of a metal center in two different ways: (i) by changing the (relative) energy of the d orbitals; (ii) by changing their character. The combined action of both mechanisms explains, for example, the working of the square planar d^8 system $[Rh(CO)_2I_2]^-$, i.e. the catalytic species of the well-known Monsanto acetic acid process. In the rate-determining step, $[Rh(CO)_2I_2]^-$ reacts specifically via backside S_N2 substitution with CH_3I. This reactivity is further enhanced by prior coordination with I^-, under formation of the pentacoordinate d^8 complex $[Rh(CO)_2I_3]^{2-}$.[13,14d,e] It will be the subject of our future efforts to quantitatively analyze the nature of ligand effects on the reactivity of different metal centers.

Acknowledgment. This investigation was supported by the Deutsche Forschungsgemeinschaft (DFG), the Netherlands Organization for Scientific Research (NCF/NWO), and the Natural Sciences and Engineering Research Council of Canada (NSERC). F.M.B. gratefully acknowledges a postdoctoral DFG fellowship.

OM940931H

Competitive Reductive Elimination of C–H and Si–H Bonds from $IrH(SiHPh_2)(mes)(CO)(dppe)$. Comparison of the Kinetic Activation Parameters for Reductive Eliminations in Ir^{III}(dppe) Complexes

Brian P. Cleary, Rajeev Mehta, and Richard Eisenberg*

Department of Chemistry, University of Rochester, Rochester, New York 14627

Received January 13, 1995[⊗]

The complex $IrH(SiHPh_2)(mes)(CO)(dppe)$ (**1**; mes = 2,4,6-trimethylphenyl; dppe = bis(diphenylphosphino)ethane) undergoes competing irreversible mesitylene and reversible diphenylsilane reductive eliminations in benzene, leading to the known Ir complexes Ir(mes)(CO)(dppe) and $IrH(SiHPh_2)_2(CO)(dppe)$ (**2**). The kinetics for the C–H vs Si–H competitive reductive eliminations have been studied and indicate that both reactions follow simple first-order kinetics. For mesitylene reductive elimination, $\Delta H^{\ddagger} = 21.8 \pm 0.3$ kcal mol^{-1}, $\Delta S^{\ddagger} = -5.0 \pm 1.1$ eu, and $\Delta G^{\ddagger}_{298} = 23.3 \pm 0.4$ kcal mol^{-1}, while for diphenylsilane reductive elimination, $\Delta H^{\ddagger} = 15.6 \pm 0.5$ kcal mol^{-1}, $\Delta S^{\ddagger} = -25.2 \pm 1.1$ eu, and $\Delta G^{\ddagger}_{298} = 23.1 \pm 0.6$ kcal mol^{-1}. A striking similarity exists among the kinetic parameters for diphenylsilane reductive elimination from **1** and for H_2 reductive eliminations from $IrH_2(C_2H_5)(CO)(dppe)$ (**5**) and $IrH_2(C(O)C_2H_5)(CO)(dppe)$ (**6**). To determine if a kinetic similarity for silane and H_2 reductive eliminations exists among Ir^{III} (dppe) complexes, the kinetic parameters for triethylsilane reductive elimination from $IrH_2(Si(C_2H_5)_3)(CO)(dppe)$ (**7**) and H_2 reductive elimination from $IrH_2(SiHPh_2)(CO)(dppe)$ (**8**) were determined. For triethylsilane reductive elimination from **7**, $\Delta H^{\ddagger} = 29.2 \pm 0.3$ kcal mol^{-1}, $\Delta S^{\ddagger} = 12.8 \pm 0.9$ eu, and $\Delta G^{\ddagger}_{298} = 25.4 \pm 0.4$ kcal mol^{-1}. For H_2 reductive elimination from **8**, $\Delta H^{\ddagger} = 25.2 \pm 0.7$ kcal mol^{-1}, $\Delta S^{\ddagger} = -4.2 \pm 2.1$ eu, and $\Delta G^{\ddagger}_{298} = 26.4 \pm 0.9$ kcal mol^{-1}. The negative entropies of activation for Si–H and H–H reductive eliminations are rationalized in terms of σ-complex formation prior to dissociation.

Platinum-group transition-metal complexes are known to catalyze the hydrosilation of olefins, acetylenes, aldehydes and ketones efficiently.[1–3] Several mechanisms have been postulated to describe catalytic hydrosilation. In the Chalk–Harrod mechanism,[4] hydrosilation occurs by oxidative addition of a silane Si–H bond to a metal–alkene complex followed by olefin insertion into the metal hydride bond (eq 1); reductive elimination then generates the organic product by Si–C bond formation as in eq 2. In an alternative mechanism,

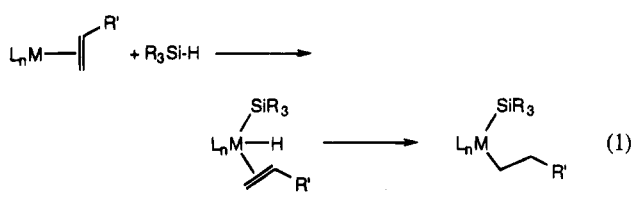

Si–H oxidative addition to the metal–olefin complex is followed by olefin insertion into the metal–silyl bond, yielding a β-silylalkyl hydride intermediate (eq 3) which gives the product after C–H reductive elimination.[5–7]

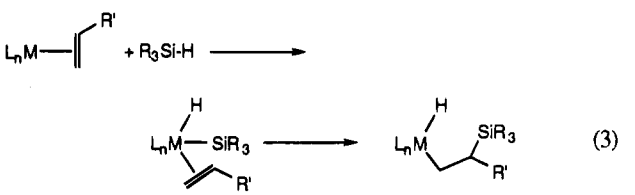

Formation of vinylsilane and alkane, common byproducts of hydrosilation catalysis, are also accounted for by this mechanism: the former via β-hydride elimination from the β-silylalkyl hydride intermediate (eq 4) and the latter from the dihydride intermediate generated in β-elimination, which serves as a catalyst for olefin hydrogenation. Finally, a third mechanism involving two silanes has been proposed for hydrosilations catalyzed by $Co(CO)_4SiR_3$ and $CpRh(C_2H_4)(SiR_3)H$ (Cp = cyclopentadienide).[8,9]

[⊗] Abstract published in *Advance ACS Abstracts,* April 15, 1995.

(1) Collman, J. P.; Hegedus, L. S.; Norton, J. R.; Finke, R. G. *Principles and Applications of Organotransition Metal Chemistry*; University Science Books: Mill Valley, CA, 1987.

(2) Speier, J. L. In *Advances in Organometallic Chemistry: Catalysis and Organic Syntheses* Stone, F. G. A., West, R., Eds.; Academic Press: New York, 1979; Vol. 17, p 407.

(3) Lukevics, E.; Belyakova, Z. V.; Pomerantseva, M. G.; Voronkov, M. G. In *Organometallic Chemistry Reviews*; Seyferth, D., Davies, A. G., Fischer, E. O., Normant, J. F., Reutov, O. A., Eds.; Elsevier: Amsterdam, Oxford, New York, 1977; pp 1–179.

(4) Chalk, A. J. *J. Organomet. Chem.* **1970,** *21,* 207–213.

(5) Schroeder, M. A.; Wrighton, M. S. *J. Organomet. Chem.* **1977,** *128,* 345–358.

(6) Brookhart, M.; Grant, B. E. *J. Am. Chem. Soc.* **1993,** *115,* 2151–2156.

(7) Wakatsuki, Y.; Yamazaki, H.; Nakano, M.; Yamamoto, Y. *J. Chem. Soc., Chem. Commun.* **1991,** 703–704.

(8) Seitz, F.; Wrighton, M. S. *Angew. Chem., Int. Ed. Engl.* **1988,** *27,* 289–291.

0276-7333/95/2314-2297$09.00/0

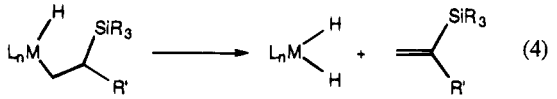

(4)

Regardless of the mechanism operating during hydrosilation, reductive eliminations involving formation of C–H, Si–H, and H–H bonds may be occurring at the metal center, leading to product formation in the catalysis or exchange reactions.[1,10,11] Since the distribution of the organic products is influenced in part by *relative* rates of reductive elimination, it is important to acquire kinetic information about these processes. Toward this end, mechanistic and kinetic data for C–H,[12–50] H–H,[51–57] and Si–H[58–69] reductive eliminations have been reported for a number of transition-metal compounds. Relative rates of C–H and Si–H bond formation can be obtained by investigating either (1) reductive eliminations of R-H and R'_3Si–H from related alkyl hydride and silyl hydride complexes to yield the *same* L_nM fragment, or (2) competitive reductive eliminations of R-H and R'_3Si–H from the *same* alkyl silyl hydride complex, $L_nMH(SiR_3')(R)$. The latter approach was employed by us to examine and establish the rate constants and activation parameters for the formation of H_2 and ethane from $IrH_2(C_2H_5)(CO)(dppe)$ (**5**; dppe = 1,2-bis(diphenylphosphino)ethane) and the formation of H_2 and propionaldehyde from $IrH_2(C(O)C_2H_5)(CO)(dppe)$ (**6**) via competitive H–H and C–H reductive elimination reactions according to eq 5.[70,71]

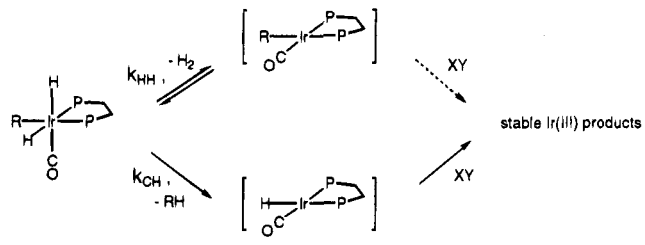

R = Et (**5**), EtC(O) (**6**) (5)

In the course of continuing investigations on iridium complexes containing the chelating ligand dppe, and in particular the Ir(I) dppe complex containing a mesityl (mes) ligand, Ir(mes)(CO)(dppe), we observed oxidative addition of SiH_2Ph_2 to generate the six-coordinate Ir(III) complex $IrH(SiHPh_2)(mes)(CO)(dppe)$ (**1**), as shown

(9) Duckett, S. B.; Perutz, R. N. *Organometallics* **1992**, *11*, 90–98.
(10) Cotton, F. A.; Wilkinson, G. *Advanced Inorganic Chemistry*, 5th ed.; Wiley: New York, 1988; p 1455.
(11) Stille, J. K. In *The Chemistry of the Metal-Carbon Bond: The Nature and Cleavage of Metal-Carbon Bonds*; Hartley, F. R., Patai, S., Eds.; Wiley: New York, 1985; Vol. 2, p 625.
(12) Jones, W. D.; Hessell, E. T. *J. Am. Chem. Soc.* **1992**, *114*, 6087–6095.
(13) Jones, W. D.; Kuykendall, V. L. *Inorg. Chem.* **1991**, *30*, 2615–2622.
(14) Jones, W. D.; Feher, F. J. *J. Am. Chem. Soc.* **1985**, *107*, 620–631.
(15) Jones, W. D.; Feher, F. J. *J. Am. Chem. Soc.* **1984**, *106*, 1650–1663.
(16) Jones, W. D.; Feher, F. J. *Acc. Chem. Res.* **1989**, *22*, 91–100.
(17) Hostetler, M. J.; Bergman, R. G. *J. Am. Chem. Soc.* **1992**, *114*, 7629–7636.
(18) Periana, R. A.; Bergman, R. G. *J. Am. Chem. Soc.* **1986**, *108*, 7332–7346.
(19) Buchanan, J. M.; Stryker, J. M.; Bergman, R. G. *J. Am. Chem. Soc.* **1986**, *108*, 1537–1550.
(20) Wax, M. J.; Styker, J. M.; Buchanan, J. M.; Kovac, C. A.; Bergman, R. G. *J. Am. Chem. Soc.* **1984**, *106*, 1121–1122.
(21) Nappa, M. J.; Santi, R.; Diefenbach, S. P.; Halpern, J. *J. Am. Chem. Soc.* **1982**, *104*, 619–621.
(22) Chan, A. S. C.; Halpern, J. *J. Am. Chem. Soc.* **1980**, *102*, 838.
(23) Abis, L.; Sen, A.; Halpern, J. *J. Am. Chem. Soc.* **1978**, *100*, 2915–2916.
(24) Halpern, J. *Acc. Chem. Res.* **1982**, *15*, 332–338.
(25) Bullock, R. J.; Headford, C. E. L.; Hennessy, K. M.; Kegley, S. E.; Norton, J. R. *J. Am. Chem. Soc.* **1989**, *111*, 3897–3908.
(26) Bullock, R. M.; Headford, C. E. L.; Kegley, S. E.; Norton, J. R. *J. Am. Chem. Soc.* **1985**, *107*, 727–729.
(27) Okrasinski, S. J.; Norton, J. R. *J. Am. Chem. Soc.* **1977**, *99*, 295–297.
(28) Schwartz, J.; Cannon, J. B. *J. Am. Chem. Soc.* **1974**, *96*, 2276–2278.
(29) Norton, J. R. *Acc. Chem. Res.* **1979**, *12*, 139.
(30) Milstein, D. *J. Am. Chem. Soc.* **1982**, *104*, 5227–5228.
(31) Milstein, D. *Acc. Chem. Res.* **1984**, *17*, 221–226.
(32) Gould, G. L.; Heinekey, D. M. *J. Am. Chem. Soc.* **1989**, *111*, 5502–5504.
(33) Michelin, R. A.; Faglia, S.; Uguagliati, P. *Inorg. Chem.* **1983**, *22*, 1831–1834.
(34) McAlister, D. R.; Erwin, D. K.; Bercaw, J. E. *J. Am. Chem. Soc.* **1978**, *100*, 5966–5968.
(35) Pedersen, A.; Tilset, M. *Organometallics* **1993**, *12*, 3064–3068.
(36) Basato, M.; Longato, B.; Morandini, F.; Bresadola, S. *Inorg. Chem.* **1984**, *23*, 3972–3976.
(37) Basato, M.; Morandini, F.; Longato, B.; Bresadola, S. *Inorg. Chem.* **1984**, *23*, 649–653.
(38) Bianchini, C.; Masi, D.; Meli, A.; Peruzzini, M.; Zanobini, F. *J. Am. Chem. Soc.* **1988**, *110*, 6411–6423.
(39) Bianchini, C.; Barbaro, P.; Meli, A.; Peruzzini, M.; Vacca, A.; Vizza, F. *Organometallics* **1993**, *12*, 2505–2514.
(40) Smith, G. M.; Carpenter, J. D.; Marks, T. J. *J. Am. Chem. Soc.* **1986**, *108*, 6805–6807.
(41) Werner, H.; Gotzig, J. *J. Organomet. Chem.* **1985**, *284*, 73–93.
(42) Gibson, V. C.; Kee, T. P.; Carter, S. T.; Sanner, R. D.; Clegg, W. *J. Organomet. Chem.* **1991**, *418*, 197–217.
(43) Price, R. T.; Andersen, R. A.; Muetterties, E. L. *J. Organomet. Chem.* **1989**, *376*, 407–417.
(44) Roper, W. R.; Wright, L. J. *J. Organomet. Chem.* **1982**, *234*, C5-C8.
(45) Thompson, J. S.; Bernard, K. A.; Rappoli, B. J.; Atwood, J. D. *Organometallics* **1990**, *9*, 2727–2731.
(46) Atwood, J. D. *Coord. Chem. Rev.* **1988**, *83*, 93–114.
(47) Bianchini, C.; Meli, A.; Peruzzini, M.; Zanobini, F. *J. Chem. Soc., Chem. Commun.* **1987**, 971–973.
(48) Cooper, N. J.; Green, M. L.; Mahtab, R. *J. Chem. Soc., Dalton Trans.* **1979**, 1557–1562.
(49) Hartwig, J. F.; Andersen, R. A.; Bergman, R. G. *Organometallics* **1991**, *10*, 1710–1719.
(50) McFarland, J. M.; Churchill, M. R.; See, R. F.; Lake, C. H.; Atwood, J. D. *Organometallics* **1991**, *10*, 3530–3537.
(51) Evans, J.; Norton, J. R. *J. Am. Chem. Soc.* **1974**, *96*, 7577–7578.
(52) Packett, D. L.; Trogler, W. C. *Inorg. Chem.* **1988**, *27*, 1768–1775.
(53) Duggan, T. P.; Golden, M. J.; Keister, J. B. *Organometallics* **1990**, *9*, 1656–1665.
(54) Nevinger, L. R.; Keister, J. B.; Maher, J. *Organometallics* **1990**, *9*, 1900–1905.
(55) Strohmeier, W.; Muller, F. J. *Z. Naturforsch.* **1969**, *24B*, 931–932.
(56) Bitterwolf, T. E.; Raghuveer, K. S. *Inorg. Chim. Acta* **1990**, *172*, 59–64.
(57) Collman, J. P.; Hutchison, J. E.; Wagenknecht, P. S.; Lewis, N. S.; Lopez, M. A.; Guilard, R. *J. Am. Chem. Soc.* **1990**, *112*, 8206–8208.
(58) Harrod, J. F.; Smith, C. A.; Than, K. A. *J. Am. Chem. Soc.* **1972**, *94*, 8321–8325.
(59) Harrod, J. F.; Smith, C. A. *J. Am. Chem. Soc.* **1970**, *92*, 2699–2701.
(60) Zhang, S.; Dobson, G. R.; Brown, T. L. *J. Am. Chem. Soc.* **1991**, *113*, 6908–6916.
(61) Aizenberg, M.; Milstein, D. *Angew. Chem. Int. Ed. Engl.* **1994**, *33*, 317–319.
(62) Hill, R. H.; Wrighton, M. S. *Organometallics* **1987**, *6*, 632–638.
(63) Hester, D. M.; Sun, J.; Harper, A. W.; Yang, G. K. *J. Am. Chem. Soc.* **1992**, *114*, 5234–5240.
(64) Hostetler, M. J.; Butts, M. D.; Bergman, R. G. *Organometallics* **1993**, *12*, 65–75.
(65) Rappoli, B. J.; McFarland, J. M.; Thompson, J. S.; Atwood, J. D. *J. Coord. Chem.* **1990**, *21*, 147–154.
(66) Schubert, U. *Angew. Chem., Int. Ed. Engl.* **1994**, *33*, 419–421.
(67) Schubert, U.; Scholz, G.; Müller, J.; Ackermann, K.; Wörle, B. *J. Organomet. Chem.* **1986**, *306*, 303–326.
(68) Schubert, U. In *Advances in Organometallic Chemistry*; Academic Press: New York, 1990; Vol. 30, pp 151–187.
(69) Kraft, G.; Kalbas, C.; Schubert, U. *J. Organomet. Chem.* **1985**, *289*, 247–256.
(70) Deutsch, P. P.; Eisenberg, R. *J. Am. Chem. Soc.* **1990**, *112*, 714–721.
(71) Deutsch, P. P.; Eisenberg, R. *Organometallics* **1990**, *9*, 709–718.

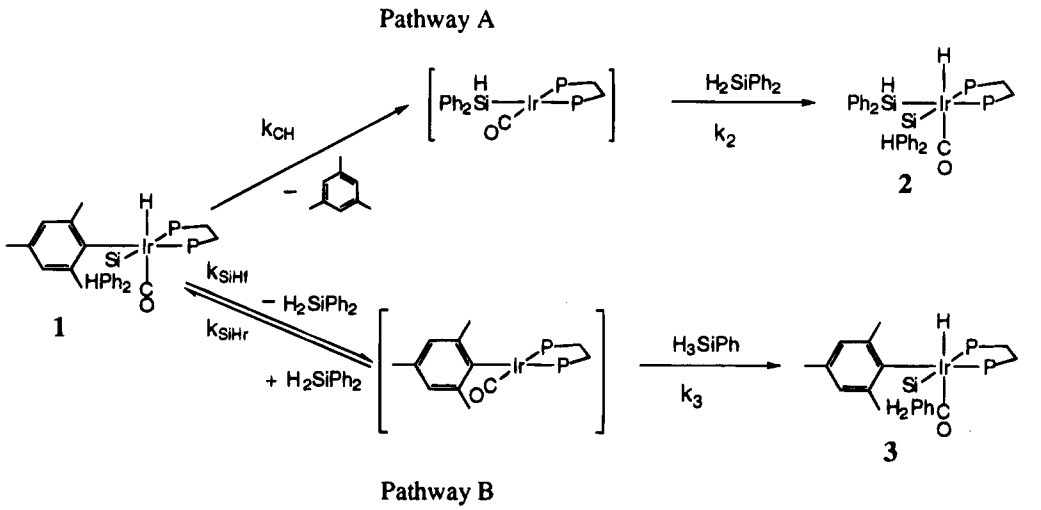

Figure 1. Kinetic pathways possible for the reductive elimination of diphenylsilane and mesitylene from $IrH(SiHPh_2)(mes)(CO)(dppe)$, **1**.

in eq 6. Complex **1** was found to be unstable in toluene

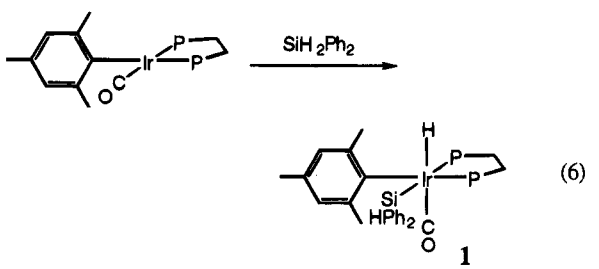

(6)

and benzene solutions at room temperature, leading to regeneration of the original Ir(I) complex as well as formation of $IrH(SiHPh_2)_2(CO)(dppe)$ (**2**) and mesitylene after several days, (eq 7). The observation of eq 7

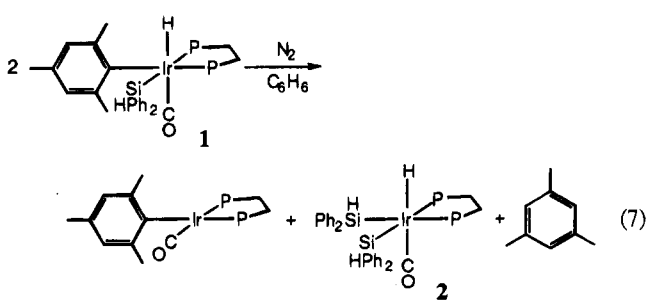

(7)

indicated that **1** was undergoing facile reaction chemistry that proceeded via reductive elimination. Moreover, the fact that the two complexes Ir(mes)(CO)(dppe) and $IrH(SiHPh_2)_2(CO)(dppe)$ were formed as the metal-containing products established that two different reductive eliminations were occurring competitively. Complex **1** thus provided a rare opportunity to investigate by kinetic methods competitive reductive elimination of aryl C–H and Si–H bonds.

Herein we describe the results of that study and compare the kinetic and activation parameters of this competitive reductive elimination with those reported previously by us for H–H and C–H bonds. Additionally, we describe kinetic studies that compare Si–H reductive elimination with that of H_2 in related Ir^{III}(dppe) systems.

Results

Kinetics of Competitive Reductive Elimination of Mesitylene and Diphenylsilane from 1. In competitive reductive elimination, two unimolecular reaction pathways exist and the kinetic parameters for each can be determined. The two specific routes of elimination observed during this study are illustrated in Figure 1, while the overall rate equation describing the disappearance of **1** is shown in eq 8. Four-coordinate Ir(I)

$$-d[\mathbf{1}]/dt = (k_{CH} + k_{SiH_f})[\mathbf{1}] - k_{SiH_r}[SiH_2Ph_2][Ir(mes)(CO)(dppe)] \quad (8)$$

intermediates in the reaction sequence such as Ir(CO)(mes)(dppe) and $[Ir(SiHPh_2)(CO)(dppe)]$ were not detected, since an excess of silane trapping agent (relative to **1**) was used during the kinetic runs. The silane trapping agent was either SiH_2Ph_2, when experiments were run to determine k_{CH}, or SiH_3Ph, when the sum of $k_{CH} \pm k_{SiH_f}$ was the kinetics objective (*vide infra*).

Since Ir(mes)(CO)(dppe) is not detected when SiH_2Ph_2 is present in large excess, it is possible under these conditions to apply the steady-state approximation to [Ir(CO)(mes)(dppe)], leading to $[Ir(CO)(mes)(dppe)] = k_{SiH_f}[\mathbf{1}]/k_{SiH_r}[SiH_2Ph_2]$. After substitution of the steady-state approximation into eq 8, the simple first-order integrated rate law for the determination of C–H reductive elimination shown in eq 9 is obtained. The

$$-\ln([\mathbf{1}]/[\mathbf{1}]_0) = k_{CH}t \quad (9)$$

rate constant for the elimination of mesitylene (k_{CH}) is thus determined by monitoring the disappearance of **1** in the presence of *excess* diphenylsilane (SiH_2Ph_2). Under these conditions diphenylsilane reductive elimination from **1** is "transparent" because any Ir(CO)(mes)(dppe) generated reacts rapidly with SiH_2Ph_2 to re-form **1**. Therefore, only mesitylene elimination contributes to the decay of signal intensity due to **1**.

The reductive elimination of mesitylene was followed by ^1H NMR spectroscopy between the temperatures of 295 and 323 K. For each experimental run, the decrease in signal intensity for the hydride resonance of **1** followed first-order kinetics through at least 3 half-lives. Changes in the concentration of either **1** or diphenylsilane (10–80 equiv relative to **1**) did not affect the rate of mesitylene elimination. Plots of $-\ln([\mathbf{1}]/[\mathbf{1}]_0)$ vs time were linear and are shown in Figure 2, while rate constants for mesitylene reductive elimination are listed in Table 1.

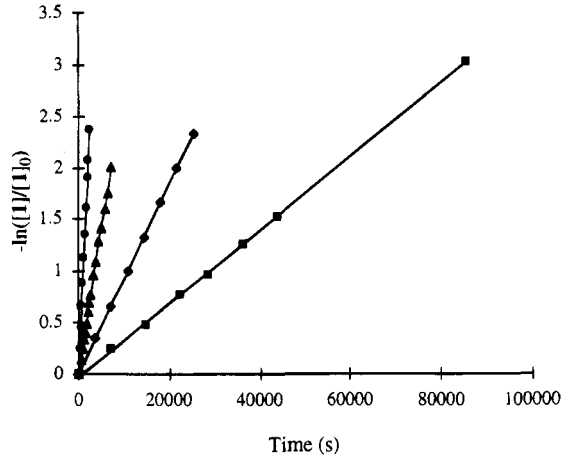

Figure 2. Plot of $-\ln([\mathbf{1}]/[\mathbf{1}]_0)$ vs time for the reductive elimination of mesitylene from **1**: (■) 295 K; (◆) 303 K; (▲) 313 K; (●) 323 K.

Table 1. Rate Constants for Mesitylene and Diphenylsilane Reductive Eliminations from IrH(SiHPh$_2$)(mes)(CO)(dppe), (1)

temperature (K)	k_{CH} ($\times 10^5$ s^{-1})[a,c]	k_{SiH_f} ($\times 10^5$ s^{-1})[d]	k_{obs} ($\times 10^5$ s^{-1})[b,c]
295	3.43 ± 0.03	5.26 ± 0.09	8.69 ± 0.08
303	9.41 ± 0.03	10.9 ± 0.4	20.3 ± 0.4
313	31.0 ± 0.3	25.8 ± 0.7	56.8 ± 0.6
323	94.6 ± 0.1	57.9 ± 0.4	152.5 ± 0.4

[a] Reaction conditions: [**1**] = 0.027 M in C_6D_6; 0.270 M diphenylsilane. [b] Reaction conditions: [**1**] = 0.027 M in C_6D_6; 0.540 M phenylsilane. [c] Values obtained from a least-squares fit of lines from plots of $-\ln[\mathbf{1}]/[\mathbf{1}]_0$ vs time. [d] Values calculated from $k_{SiH_f} = k_{obs} - k_{CH}$.

The overall rate constant (k_{obs}) for the disappearance of **1** is equal to the sum of the rate constants for both reductive-elimination processes ($k_{obs} = k_{CH} \pm k_{SiH_f}$). Monitoring the reaction in the presence of *excess* phenylsilane (SiH_3Ph), which reacts more rapidly with IrY(CO)(dppe) (Y = mes and $SiHPh_2$) than does SiH_2Ph_2 allows for the determination of k_{obs}. Under these conditions, regeneration of **1** via the back-reaction of Ir(CO)(mes)(dppe) with diphenylsilane is eliminated because any Ir(CO)(mes)(dppe) generated quickly undergoes oxidative addition with phenylsilane ($k_{SiH_f}[SiH_2Ph_2] \ll k_3[SiH_3Ph]$). Under these conditions, the integrated rate equation describing the disappearance of **1** simplifies to that shown in eq 10, yielding $k_{obs} = k_{CH} + k_{SiH_f}$, and the rate constant for diphenylsilane reductive elimination (k_{SiH_f}) can be calculated using k_{CH} determined from the previous experiment.

$$-\ln([\mathbf{1}]/[\mathbf{1}]_0) = (k_{CH} + k_{SiH_f})t \qquad (10)$$

The combined reductive elimination of mesitylene + diphenylsilane was monitored by ^{1}H NMR spectroscopy between the temperatures of 295 and 323 K. All reactions followed first-order kinetics and were unaffected by changes in concentration of **1** or phenylsilane (20–80 equiv relative to **1**). The plots of $-\ln([\mathbf{1}]/[\mathbf{1}]_0)$ vs time, shown in Figure 3, were linear through at least 3 half-lives. Included in Table 1 are the overall rate constants (k_{obs}) for the disappearance of **1** as well as calculated values for k_{SiH_f}.

The temperature dependence of the rate constants for mesitylene and diphenylsilane reductive eliminations (k_{CH} and k_{SiH_f}) allowed for calculation of the kinetic activation parameters for both processes.[72,73] Plots of $\ln(k/T)$ vs $1/T$ for the two processes are linear and are

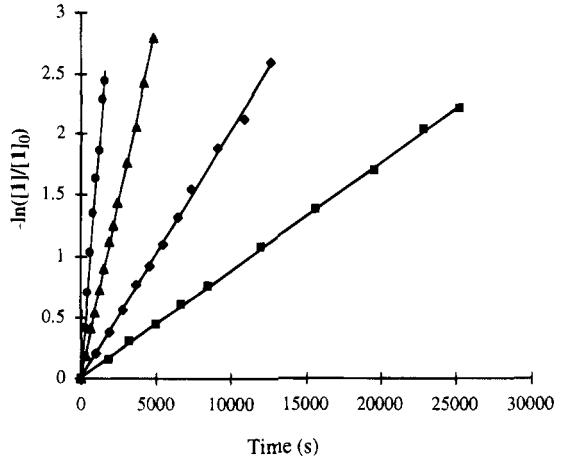

Figure 3. Plot of $-\ln([\mathbf{1}]/[\mathbf{1}]_0)$ vs time for the reductive elimination of mesitylene + diphenylsilane from **1**: (■) 295 K; (◆) 303 K; (▲) 313 K; (●) 323 K.

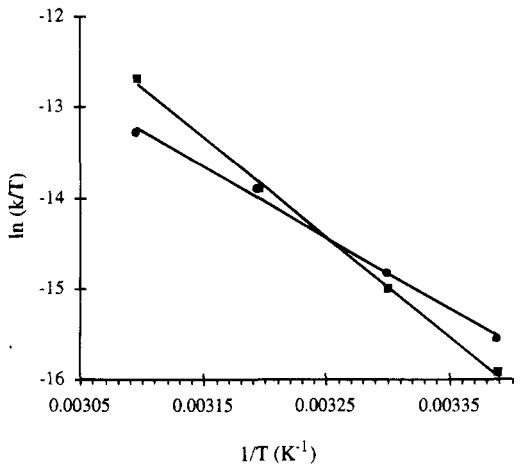

Figure 4. Eyring plot for the reductive eliminations of mesitylene (■) and diphenylsilane (●) from **1**.

pictured in Figure 4, while Table 2 lists the corresponding Eyring parameters.

Kinetics of Reductive Elimination of Triethylsilane from IrH$_2$(Si(C$_2$H$_5$)$_3$)(CO)(dppe) (7) and of Dihydrogen from IrH$_2$(SiHPh$_2$)(CO)(dppe) (8). With competitive reductive elimination for H–H and C–H bonds established in the previous study by Deutsch *et al.* and that for Si–H and aryl C–H bonds here, our attention focused on the possibility of comparing H–H and Si–H reductive elimination within the same system. However, not all Ir^{III} (dppe) complexes that have facial arrangements of ligands compatible with competitive reductive elimination exhibit both pathways under normal laboratory conditions and time scales. For example, complex **7**, Ir(H)$_2$(SiEt$_3$)(CO)(dppe), in toluene-d_8 showed little or no change in its ^{1}H NMR spectrum after being heated for several days in the presence of excess triethylsilane. However, when the silane was changed to phenylsilane, the known complex Ir(H)$_2$(SiH$_2$Ph)(CO)(dppe) was observed to form, indicating that **7** undergoes facile triethylsilane reductive elimination (eq 11) but is inert to hydrogen reductive elimination. Conversely, Ir(H)$_2$(SiHPh$_2$)(CO)(dppe) (**8**) under-

(72) Benson, S. W. *Thermochemical Kinetics: Methods for the Estimation of Thermochemical Data and Rate Parameters*; Wiley: New York, 1968.
(73) Avery, H. E. *Basic Reaction Kinetics and Mechanisms*; Macmillan: London, 1974.

Table 2. Activation Parameters for Reductive-Elimination Reactions in Ir^{III} (dppe) Complexes

eliminating fragment	$\Delta H^{\ddagger}$ (kcal mol^{-1})	$\Delta S^{\ddagger}$ (cal K^{-1} mol^{-1})	$\Delta G_{298}^{\ddagger}$ (kcal/mol)
Mes−H from **1**[a]	21.8 ± 0.3	−5.0 ± 1.1	23.3 ± 0.4
Ph_2HSi−H from **1**[a]	15.6 ± 0.5	−25.2 ± 1.1	23.1 ± 0.6
C_2H_5−H from **5**[b]	20.2 ± 0.4	−10.9 ± 1.3	23.4 ± 0.8
H−H from **5**[b]	15.5 ± 1.1	−23.7 ± 3.5	22.5 ± 2.1
$C_2H_5C(O)$−H from **6**[c]	22.3 ± 0.9	−11.0 ± 2.8	25.6 ± 1.7
H−H from **6**[c]	16.5 ± 1.6	−23.3 ± 4.8	23.4 ± 3.0
Et_3Si−H from **7**[d]	29.2 ± 0.3	12.8 ± 0.9	25.4 ± 0.4
H−H from **8**[e]	25.2 ± 0.7	−4.2 ± 2.1	26.4 ± 0.9

[a] Activation parameters for mesitylene reductive elimination determined from reactions with [**1**] = 0.027 M in C_6D_6 and 0.270 M diphenylsilane. Activation parameters for diphenylsilane reductive elimination determined from reactions with [**1**] = 0.027 M in C_6D_6 and 0.540 M phenylsilane. Eyring values obtained from a least-squares fit of lines from plots of $\ln(k/T)$ vs $1/T$. [b] Values determined in ref 70. [c] Values determined in ref 71. [d] Activation parameters determined from reactions with [**7**] = 0.027 M in toluene-d_8 and 0.540 M phenylsilane. [e] Activation parameters determined from reactions with [**8**] = 0.024 M in toluene-d_8 and 0.500 M phenylsilane.

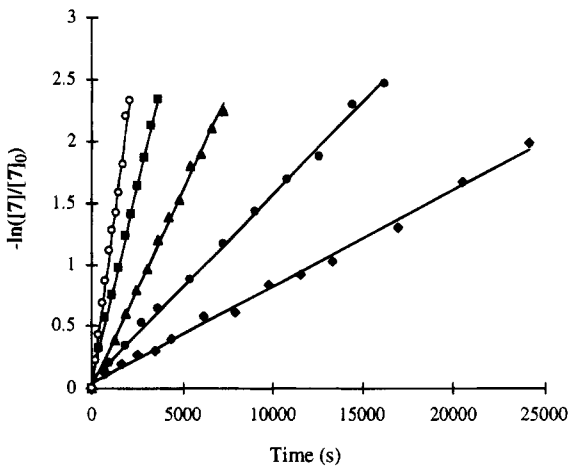

Figure 5. Plot of $-\ln([\mathbf{7}]/[\mathbf{7}]_0)$ vs time for the reductive elimination of triethylsilane from **7**: (◆) 323 K; (●) 328 K; (▲) 333 K; (■) 338 K; (○) 343 K.

goes reversible hydrogen reductive elimination but is inert to elimination of diphenylsilane (eq 12).

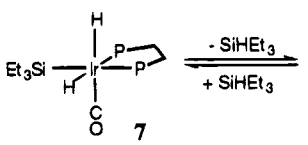

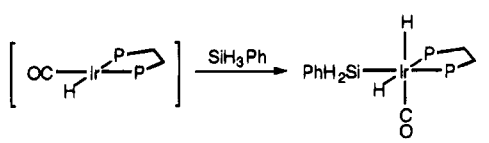

(11)

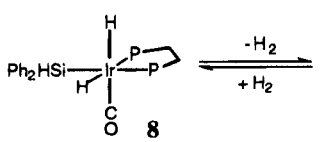

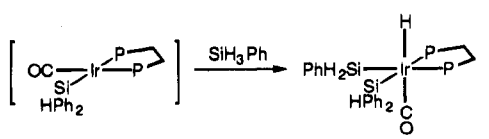

(12)

The kinetics of reductive elimination of triethylsilane from **7** and of hydrogen from **8** were monitored separately by ^{1}H NMR spectroscopy in toluene-d_8 between 323 and 363 K. Plots of $-\ln[\mathbf{7}]/[\mathbf{7}]_0$ and $-\ln[\mathbf{8}]/[\mathbf{8}]_0$ vs time are shown in Figures 5 and 6, respectively. The reactions were monitored for at least 3 half-lives, displayed linear first-order kinetics, and were unaffected by either initial changes in concentration of **7** or **8** or changes in concentration of phenylsilane as the trapping agent. The rate constants for triethylsilane reductive elimination (k_{SiH}) and hydrogen reductive elimination (k_{HH}) are listed in Tables 3 and 4, respectively. Plots of $\ln(k/T)$ vs $1/T$ were linear for both processes and are shown in Figure 7, while activation parameters are listed in Table 2.

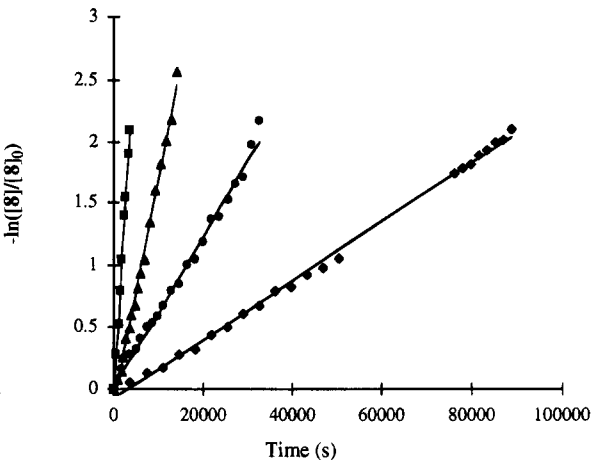

Figure 6. Plot of $-\ln([\mathbf{8}]/[\mathbf{8}]_0)$ vs time for the reductive elimination of dihydrogen from **8**: (◆) 333 K; (●) 343 K; (▲) 353 K; (■) 363 K.

Table 3. Rate Constants for Triethylsilane Reductive Elimination from $IrH_2(SiEt_3)(CO)(dppe)$, (7)[a]

temp (K)	k_{SiH} (x10^5 s^{-1})	temp (K)	k_{SiH} (x10^5 s^{-1})
323	7.8 ± 0.1	338	63.6 ± 0.9
328	15.0 ± 0.3	343	113 ± 3
333	31.7 ± 0.5		

[a] Reaction conditions: [**7**] = 0.027 M in toluene-d_8; 0.540 M phenylsilane. Values obtained from a least-squares fit of lines from plots of $-\ln[\mathbf{7}]/[\mathbf{7}]_0$ vs time.

Discussion

Due to the facial disposition of the mesityl, diphenylsilyl, and hydride ligands of **1**, two unimolecular reductive eliminations are possible thermally, leading to diphenylsilane (**A**) and mesitylene (**B**), respectively. The

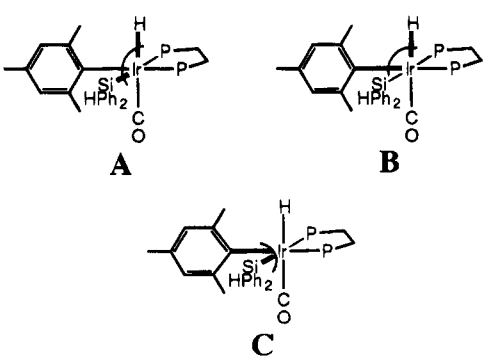

bonds which are cleaved in each process are shown in boldface. Thermal reductive elimination of mesityldiphenylsilane (**C**) does not occur because of the cis

Table 4. Rate Constants for Dihydrogen Reductive Elimination from $IrH_2(SiHPh_2)(CO)(dppe)$, (8)[a]

temp (K)	k_{HH} (x10^5 s^{-1})	temp (K)	k_{HH} (x10^5 s^{-1})
333	2.40 ± 0.03	353	18.5 ± 0.3
343	6.1 ± 0.1	363	61 ± 1

[a] Reaction conditions: [8] = 0.025 M in toluene-d_8; 0.500 M phenylsilane. Values obtained from a least-squares fit of lines from plots of $-\ln[8]/[8]_0$ vs time.

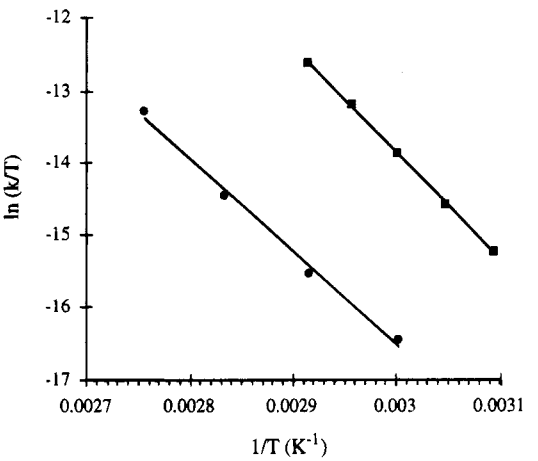

Figure 7. Eyring plot for the reductive eliminations of triethylsilane from **7** (■) and of hydrogen from **8** (●).

constraint imposed by the dppe ligand and the fact that in a concerted reductive elimination the ligands trans to the leaving ligands move into mutually trans positions in the resultant four-coordinate complex.[70,71] Complex **1** is representative of intermediates postulated to exist during hydrosilation catalysis, and the observation of eq 7 indicated that competitive reductive elimination of Si–H and aryl C–H bonds was occurring. A kinetics study of this reductive-elimination chemistry was therefore carried out. At lower temperatures, the rate of diphenylsilane reductive elimination is faster than that of mesitylene reductive elimination. However, as the temperature of the solution is raised, the rate of mesitylene reductive elimination increases and surpasses that of diphenylsilane elimination at temperatures greater than 307 K. This rate crossover indicates a significant difference between the activation parameters for the two elimination processes. For mesitylene reductive elimination, $\Delta H^{\ddagger} = 21.8 \pm 0.3$ kcal mol^{-1} and $\Delta S^{\ddagger} = -5.0 \pm 1.1$ cal K^{-1} mol^{-1}, while for diphenylsilane elimination, $\Delta H^{\ddagger} = 15.6 \pm 0.5$ kcal mol^{-1} and $\Delta S^{\ddagger} = -25.2 \pm 1.1$ cal K^{-1} mol^{-1}. At 298 K the free energy of activation, $\Delta G^{\ddagger}_{298}$, for mesitylene and diphenylsilane eliminations are 23.3 ± 0.4 and 23.1 ± 0.6 kcal mol^{-1}, respectively, which are identical within experimental error.

The most noteworthy result from this study is that negative entropies of activation are obtained for both Si–H and aryl C–H reductive eliminations from **1**. This indicates that the transition states for both processes are highly ordered and probably contain nonlinear, three-centered interactions. In this context, loss of rotational degrees of freedom in the transition state leads to a more constrained structure and hence a negative activation entropy.[74] Since $\Delta S^{\ddagger}$ for mesitylene reductive elimination is less negative than $\Delta S^{\ddagger}$ for diphenylsilane elimination, the transition state leading to C–H bond formation can be considered *looser* or less constrained relative to the transition state leading to diphenylsilane formation. The larger value of $\Delta H^{\ddagger}$ observed for mesitylene reductive elimination may reflect that (a) more bond breaking has preceded the transition state leading to mesitylene formation than for Si–H reductive elimination and (b) the Ir-C(mes) bond is stronger than the Ir–Si bond in these Ir(III) systems.[64,75] These conclusions regarding a larger $\Delta H^{\ddagger}$ and a less negative $\Delta S^{\ddagger}$ for C–H bond formation than for Si–H formation suggest that the eliminating mesitylene moiety is further removed from the metal center in the activated complex.[72] On the basis of this interpretation, feasible representations of the transition states leading to Si–H and C–H bond formation are shown as **D** and **E**, respectively.

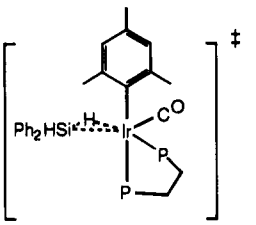

D

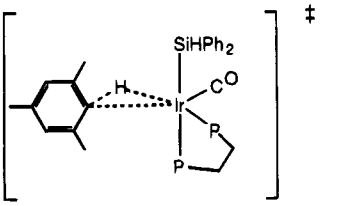

E

As shown in Table 2, the activation parameters for mesitylene reductive elimination from **1** are comparable to those found for ethane and propionaldehyde reductive eliminations from $IrH_2(C_2H_5)(CO)(dppe)$ (**5**) and $IrH_2(C(O)C_2H_5)(CO)(dppe)$ (**6**), respectively, and indicate with high probability that these three complexes have similar transition states leading to C–H bond formation. Furthermore, a striking similarity exists among the activation parameters for diphenylsilane reductive elimination from **1** and H_2 reductive eliminations from **5** and **6**.[70,71] Stimulated by earlier results that showed a similarity between the oxidative-addition reactions of silanes and H_2 with IrX(CO)(dppe) complexes (both additions proceed under kinetic control over the P–Ir–CO axis, leading stereoselectively to the product shown as **F**),[76–78] the reductive elimination study was expanded to determine if kinetic parameters for Si–H and H–H reductive eliminations from Ir^{III}(dppe) complexes were similar. However, it was not possible to find a silyl dihydride complex that would allow competitive reductive elimination on an accessible time frame. Therefore, we carried out a kinetics study of Si–H and H–H reductive eliminations from different complexes, specifically of triethylsilane from $IrH_2(SiEt_3)(CO)(dppe)$ (**7**) and of dihydrogen from $IrH_2(SiHPh_2)(CO)(dppe)$ (**8**).

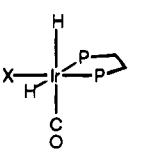

F

For triethylsilane reductive elimination from **7**, $\Delta H^{\ddagger} = 29.2 \pm 0.3$ kcal mol^{-1} and $\Delta S^{\ddagger} = 12.8 \pm 0.9$ eu, while for H_2 elimination from **8**, $\Delta H^{\ddagger} = 25.2 \pm 0.7$ kcal mol^{-1} and $\Delta S^{\ddagger} = -4.2 \pm 2.1$ eu. It is apparent by comparison

(74) Carpenter, B. K. *Determination of Organic Reaction Mechanisms*; Wiley: New York, 1984.

(75) Martinho Simoes, J. A.; Beauchamp, J. L. *Chem. Rev.* **1990**, *90*, 629.

of the activation parameters in Table 2 that the activation enthalpy and entropies for the reductive elimination of triethylsilane from **7** differ significantly from those found for diphenylsilane reductive elimination from **1**. The larger value of $\Delta H^{\ddagger}$ and the *positive* value for $\Delta S^{\ddagger}$ are consistent with a transition state that exhibits a great degree of bond breaking and is more dissociative in nature. A similar difference in activation parameters is observed for H_2 reductive elimination from **8** relative to those reported earlier, and the observed activation entropy seems to be in better agreement with those found by Deutsch *et al.* for C−H reductive eliminations rather than with H−H elimination.

There are only a few reports which describe the kinetics of silane reductive elimination from transition-metal complexes. In two seminal studies by Harrod which elucidated the reversibility of silane oxidative addition, kinetic parameters for the reductive elimination of various silanes from different iridium complexes were determined.[58,59] In the first, THF and acetonitrile solutions of $IrH(Si(OC_2H_5)_{3-n}(CH_3)_n)(dppe)_2$ (n = 0−2) were found to have similar activation parameters for silane reductive elimination with ranges of activation enthalpies varying between 19.2 ± 0.9 and 25.3 ± 0.8 kcal mol^{-1} and activation entropies between −0.3 ± 1.5 and 8.2 ± 2.5 eu. In the second, activation parameters for silane reductive elimination from toluene solutions of $IrH_2(Si(OC_2H_5)_{3-n}(CH_3)_n)(CO)(PPh_3)_2$ (n = 1, 3) were found to be similar to parameters obtained for phosphine dissociation from $IrH(CO)(PPh_3)_3$. For silane reductive elimination with n = 1, $\Delta H^{\ddagger}$ = 28.1 ± 0.9 kcal mol^{-1} and $\Delta S^{\ddagger}$ = 15.4 ± 2.5 eu, while for n = 3, $\Delta H^{\ddagger}$ = 23.9 ± 0.6 kcal mol^{-1} and $\Delta S^{\ddagger}$ = 3.4 ± 7.5 eu. The corresponding parameters for PPh_3 dissociation from $IrH(CO)(PPh_3)_3$ yield average values for $\Delta H^{\ddagger}$ and $\Delta S^{\ddagger}$ of 25.5 kcal mol^{-1} and 14.9 eu, respectively.

Hart-Davis and Graham investigated the reductive elimination of $SiHPh_3$ from $CpMnH(SiPh_3)(CO)_2$ (Cp = cyclopentadienyl) in *n*-heptane and found it to be unimolecular with $\Delta H^{\ddagger}$ = 29.2 ± 0.6 kcal mol^{-1}, $\Delta S^{\ddagger}$ = 3.8 ± 7.5 eu, and essentially no kinetic isotope effect (KIE = 0.97).[79] The authors speculated that the kinetic data support a late transition state which contains a significant amount of Si−H bond character. A similar transition state has been proposed independently by Wrighton and Yang for the reductive elimination of triethylsilane from $CpMnH(SiEt_3)(CO)_2$.[62,63] A neutron diffraction study of the closely related complex Cp′MnH(CO)$_2$(SiPh$_2$F) (Cp′ = methylcyclopentadienide) reveals a close Si−H contact of 1.802 ± 0.005 Å and a Mn−H bond distance of 1.569 ± 0.004 Å, suggestive of a Mn−H−Si *agostic* interaction.[68,80] This three-centered, two-electron interaction may be representative of transients formed along the reaction coordinate during silane reductive eliminations from the Cp analogs. For the complexes Cp′MnH(CO)(PR$_3$)(HPh$_2$Si) (R = *p*-ClC$_6$H$_4$, Ph, *p*-MeC$_6$H$_4$, Me, Bu), the activation parameters for diphenylsilane reductive elimination have been determined: $\Delta H^{\ddagger}$ ranges from 33.2 ± 1.0 to 25.4 ± 0.1 kcal mol^{-1} while $\Delta S^{\ddagger}$ varies between 17.2 ± 3.1 and 3.3 ± 3.8 eu.[69] For these reductive eliminations, $\Delta H^{\ddagger}$ and $\Delta S^{\ddagger}$ exhibit a compensating relationship—*i.e.*, as $\Delta H^{\ddagger}$ increases, $\Delta S^{\ddagger}$ becomes more positive—similar to that observed in the present study, except for the more positive values of $\Delta S^{\ddagger}$. In a recent study by Bergman, the kinetic parameters for the reductive elimination of triethylsilane from $Cp_2Ta(\mu\text{-}CH_2)_2IrH(SiEt_3)(CO)_2$ were determined: $\Delta H^{\ddagger}$ = 20.6 ± 0.2 kcal mol^{-1}, $\Delta S^{\ddagger}$ = 3.9 eu, and the reaction displayed a primary KIE of 1.45.[64] The authors proposed that the kinetic parameters are consistent with either a nonlinear three-centered transition state or the formation of a σ-complex intermediate preceding dissociation of silane product.

While studies involving the formation of silanes by reductive elimination are few, there are several reports which describe the kinetics of C−H bond formation by cis reductive elimination from $L_nMH(R)$ complexes. With regard to the formation of alkyl C−H bonds, the reductive eliminations of methane from $PtH(CH_3)(PPh_3)_2$ and trifluoroethane from *cis*-$PtH(CH_2CF_3)(PPh_3)_2$ both display normal KIE's while the temperature dependence of the rate of reductive elimination for the latter reaction yielded $\Delta H^{\ddagger}$ = 24.6 ± 0.6 kcal mol^{-1} and $\Delta S^{\ddagger}$ = 4.9 ± 2 eu.[23,33] Heinekey has reported that $[Cp_2ReH(CH_3)]^+$ undergoes intramolecular reductive elimination of methane with $\Delta H^{\ddagger}$ = 28.1 ± 1.2 kcal mol^{-1} and $\Delta S^{\ddagger}$ = 27 ± 6 eu[32] and concluded that methane elimination is preceded by the formation of a Re−CH_4 σ-complex on the basis of an inverse KIE of 0.8 ± 0.1 for the reductive elimination and the observation of a facile equilibrium between $[Cp_2ReH(CD_3)]^+$ and $[Cp_2ReD(CHD_2)]^+$.

The kinetics of cyclohexane elimination from Cp*IrH(Cy)(PMe_3) (Cp* = pentamethylcyclopentadienide) were studied and found to be first-order in Cp*IrH(Cy)(PMe_3) and inhibited by the addition of cyclohexane.[19] The reductive elimination of Cy−H displays an inverse KIE of 0.7 ± 0.5, while the kinetic parameters were determined to be $\Delta H^{\ddagger}$ = 35.6 ± 0.5 kcal mol^{-1} and $\Delta S^{\ddagger}$ = 10 ± 2 eu. On the basis of these results, the authors concluded that cyclohexane elimination proceeds either via a mechanism that is dissociative, producing [Cp*Ir(PMe_3)] and free cyclohexane from a three-centered transition state, or through the intermediacy of a cyclohexane−[Cp*Ir(PMe_3)] σ-complex.

More germane to the question of aryl C−H reductive eliminations are the studies by Jones and co-workers for the reductive eliminations of arene from Cp*RhH(PMe_3)(aryl) complexes and benzene from Tp′RhH(C_6H_5)(CN-neopentyl) (Tp′ = hydrotris(3,5-dimethylpyrazoyl)borate).[12,14,15] For the Cp*RhH(PMe_3)(aryl) complexes, arene eliminations were found to proceed through an η^2-arene intermediate via C−H reductive elimination and subsequent arene dissociation, yielding [Cp*Rh(PMe_3)]. Kinetic parameters for benzene elimination from Cp*RhH(PMe_3)(C_6H_5) were determined to be $\Delta H^{\ddagger}$ = 30.5 ± 0.8 kcal mol^{-1} and $\Delta S^{\ddagger}$ = 14.9 ± 2.5 eu. Since these kinetic parameters reflect both C−H reductive elimination *and* benzene dissociation, the kinetic parameters for the actual C−H reductive elimination process were determined by monitoring the temperature dependence of the rate of [1,2]-xylyl shifts in Cp*RhH(PMe_3)(2,5-$C_6H_3(CH_3)_2$). The reaction was monitored between 285 and 306 K and yielded $\Delta H^{\ddagger}$ =

(76) Johnson, C. E.; Fisher, B. J.; Eisenberg, R. *J. Am. Chem. Soc.* **1983**, *105*, 7772−7774.
(77) Johnson, C. E.; Eisenberg, R. *J. Am. Chem. Soc.* **1985**, *107*, 3148−3160.
(78) Johnson, C. E.; Eisenberg, R. *J. Am. Chem. Soc.* **1985**, *107*, 6531−6540.
(79) Hart-Davis, A. J.; Graham, W. A. G. *J. Am. Chem. Soc.* **1971**, *94*, 4388−4393.
(80) Schubert, U.; Ackermann, K.; Wörle, B. *J. Am. Chem. Soc.* **1982**, *104*, 7378−7380.

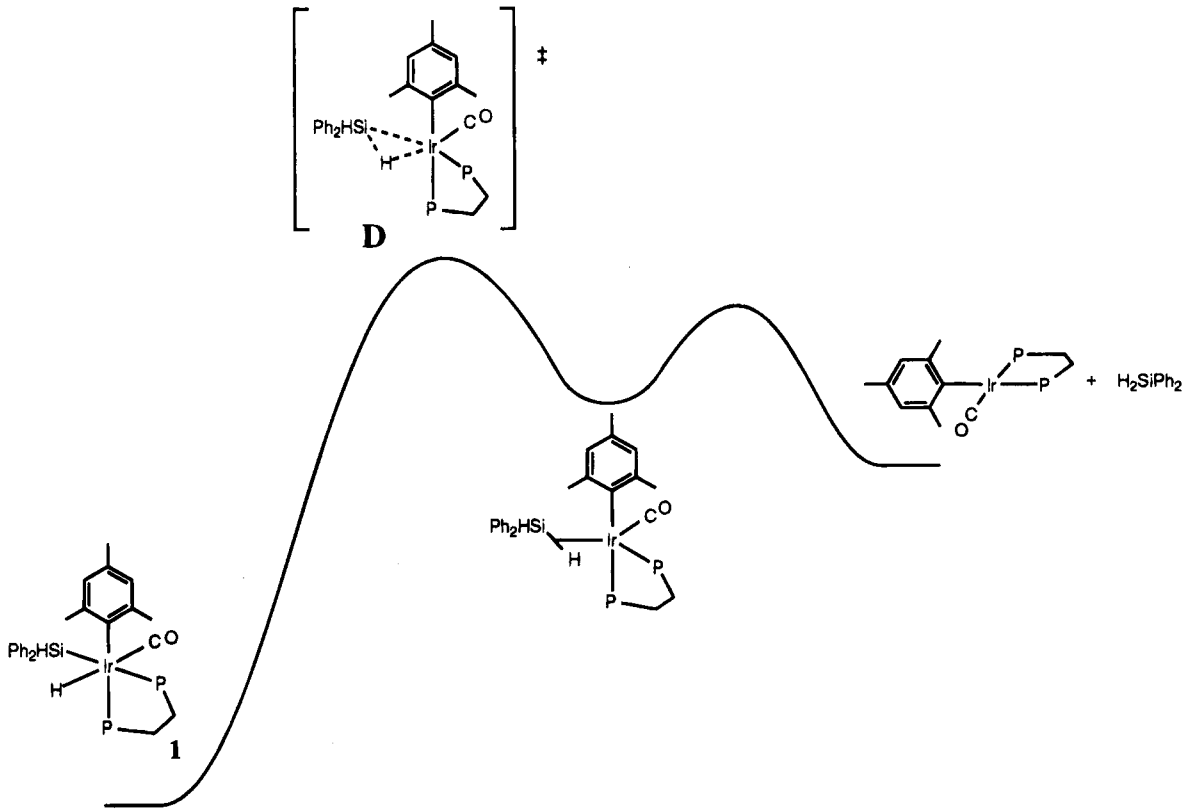

Figure 8. Proposed reaction coordinate for the reductive elimination of diphenylsilane from **1**.

16.3 ± 0.2 kcal mol^{-1} and $\Delta S^{\ddagger} = -6.3 \pm 0.8$ eu. In a similar analysis of benzene elimination from Tp'RhH(C_6H_5)(CN-neopentyl) the authors determined the reaction to proceed sequentially via C–H reductive elimination and η^2-benzene dissociation. The activation parameters for the *overall* elimination were determined to be $\Delta H^{\ddagger} = 37.8 \pm 1.1$ kcal mol^{-1} and $\Delta S^{\ddagger} = 23 \pm 3$ eu.

The previously studied reductive eliminations of Si–H and aryl C–H bonds provide a basis on which to analyze and interpret the activation parameters of Table 2. Clearly, the most striking difference between present and previous results involves the entropies of activation and specifically the moderate-to-large negative $\Delta S^{\ddagger}$ values seen here for an elimination reaction. A clue to understanding and rationalizing this difference comes from the work by Jones and Feher, who were able to probe separately the conversion of an aryl hydride complex to an η^2-species and subsequent arene dissociation.[14] The essential point is that formation of an η^2 intermediate via C–H reductive elimination proceeds with a negative $\Delta S^{\ddagger}$.

If similar logic is applied to the present results, we conclude that the negative $\Delta S^{\ddagger}$ values are suggestive of the formation of an intermediate on the pathway to reductive elimination. The intermediates we propose for these eliminations contain three-center interactions as are found in dihydrogen and σ-silane complexes. The reaction coordinate diagram for reductive elimination would thus possess a local minimum corresponding to the H_2 or Si–H σ-complex followed by a barrier for dissociation, as shown in Figure 8 for silane reductive elimination. On the basis of qualitative observations that show the reaction of either H_2 or silane with IrX(CO)(dppe) to be essentially complete,[76–78] and Vaska's quantitative assessment of the equilibrium constant for H_2 oxidative addition to $IrCl(CO)(PPh_3)_2$,[81] the corresponding reductive elimination is shown as an endothermic reaction. The relative heights of the two barriers in Figure 8, the first for formation of the silane σ-complex and the second for silane dissociation, control the kinetics and activation parameters of the process. If the initial barrier is larger, then the σ-complex is kinetically irrelevant but the activation parameters will reflect its formation rather than the overall dissociation process. We believe this is the case in the present study, where negative $\Delta S^{\ddagger}$ values suggest the formation of σ-complex intermediates on the path to reductive elimination. For previously reported systems in which $\Delta S^{\ddagger}$ values are positive, σ-complex intermediates may still exist, but it is the second barrier that controls the overall kinetics of the reductive-elimination reaction.

Summary

Discerning the rates of competitive reductive eliminations of facially disposed ligands in a transition-metal complex is essential when designing or rationalizing the product distributions from a catalytic cycle. Here, we have determined the rate and activation parameters for the competitive reductive elimination of diphenylsilane and mesitylene from the model hydrosilation intermediate IrH($SiHPh_2$)(mes)(CO)(dppe) (**1**). At lower temperatures, diphenylsilane reductive elimination is more facile than mesitylene elimination, but due to differences in activation parameters for the two reactions, the rate of mesitylene elimination surpasses that of diphenylsilane above 307 K. The activation parameters for mesitylene reductive elimination compare favorably to those found for ethane and propionaldehyde elimina-

(81) Vaska, L. *Acc. Chem. Res.* **1968**, *1*, 335–344.

tions from $IrH_2(C_2H_5)(CO)(dppe)$ (**5**) and $IrH_2(C(O)C_2H_5)(CO)(dppe)$ (**6**), respectively, suggesting that the transition states leading to C–H reductive eliminations for these Ir^{III}(dppe) complexes are similar. Although the activation parameters for diphenylsilane elimination from **1** are similar to those found for H_2 reductive eliminations from **5** and **6**, the results from triethylsilane reductive elimination from $IrH_2(Si(C_2H_5)_3)(CO)(dppe)$ (**7**) and H_2 elimination from $IrH_2(SiHPh_2)(CO)(dppe)$ (**8**) suggest that the kinetic factors describing the transition states for Si–H and H_2 reductive eliminations are variable for Ir^{III} (dppe) complexes. The more negative $\Delta S^{\ddagger}$ determined for Si–H reductive elimination from **1** and H–H reductive eliminations from **5** and **6** are rationalized in terms of σ-complex formation prior to dissociation.

Experimental Section

Reactions and sample preparations were completed in a nitrogen-filled glove box or under the appropriate gas using a high-vacuum line or Schlenk line. All solvents were reagent grade or better and were dried and degassed prior to use by accepted methods. Hydrogen (99.99%, Air Products) was used as received. Diphenylsilane (Hüls of America), triethylsilane (Hüls of America), and phenylsilane (Hüls of America) were dried over calcium hydride (Aldrich), vacuum-transferred and stored under nitrogen in amber bottles. Ir(CO)(mes)(dppe),[82] $IrH_2(SiEt_3)(CO)(dppe)$ (**7**),[83] and $IrH_2(SiHPh_2)(CO)(dppe)$ (**8**)[83] were prepared according to literature procedures.

NMR samples were prepared using resealable NMR tubes fitted with J. Young Teflon valves (Brunfeldt) and high-vacuum-line adapters. ^1H, ^{13}C, and ^{31}P NMR spectra were recorded at 400.13, 100.62, and 161.98 MHz, respectively, on a Bruker AMX 400 NMR spectrometer. Temperature control was achieved using a B-VT 1000 variable-temperature unit with a Cu–Constantan temperature sensor and was calibrated for high temperatures using an ethylene glycol standard. ^1H NMR chemical shifts are reported in ppm downfield of tetramethylsilane but measured from the residual ^1H signal in the deuterated solvents. ^{13}C NMR spectra are reported in ppm downfield of tetramethylsilane and referenced to a known carbon signal in the solvent. ^{31}P NMR spectra are reported in ppm downfield of an external 85% solution of phosphoric acid. Benzene-d_6 (MSD) was dried and distilled from a purple solution of sodium benzophenone ketyl. The KBr (Aldrich) mull infrared spectrum was recorded on a Matteson 6020 Galaxy FT-infrared spectrometer. Elemental analysis was performed by Desert Analytics Laboratory, Tucson, AZ.

$IrH(SiHPh_2)(CO)$(mesityl)(dppe) (1). The complex Ir(mes)(CO)(dppe) (50 mg, 0.0683 mmol) was dissolved in 1 mL of toluene along with a magnetic stirbar and cooled to 0 °C. To the orange solution was added 1.1 equiv (14.0 μL, 0.0751 mmol) of diphenylsilane, which after 2 min of stirring became colorless. The product precipitated after the addition of 6 mL of ethanol and the reduction of the volume to 3 mL under a stream of nitrogen. After an additional 3 mL of ethanol was added, the product was isolated as an air-stable cream-colored powder in 65% yield.

Spectroscopic data for **1**: IR (KBr, cm^{-1}) 2173 (w) (Si–H), 2048 (m) (Ir–H), 1968 (s) (CO); ^1H NMR (400 MHz, C_6D_6) δ 7.86 (m, 2H, Ph), 7.58 (d, 2H, Ph), 7.53 (m, 2H, Ph), 7.45 (m, 2H, Ph), 7.23 (m, 2H, Ph), 7.13-7.00 (m, 12 H, Ph), 6.91 (m, 4H, Ph), 6.81 (m, 3H, Ph), 6.75 (m, 3H, Ph), 5.76 (m, 1H, Si–H), 2.46 (s, 3H, $-CH_3$), 2.25 (s, 3H, $-CH_3$), 2.12 (s, 3H, $-CH_3$), 1.92 (m, 4H, $-PCH_2CH_2P-$), −8.42 (t, $^2J_{P-P}$ = 18.8 Hz, 1H, Ir–*H*); $^{31}P\{^1H\}$ NMR (162 MHz, C_6D_6) δ 22.7 (d, $^2J_{P-P}$ = 3 Hz), δ 15.4 (d, $^2J_{P-P}$ = 3 Hz); $^{13}C\{^1H\}$ NMR (100.6 MHz, C_6D_6) δ 180.7 (t, $^2J_{C-P}$ = 4 Hz, CO).

Kinetic Studies of Mesitylene Reductive Elimination from 1. In a nitrogen-filled glovebox a resealable NMR tube was charged with 10.0 mg of **1** and 0.50 mL of C_6D_6 (0.0136 mmol of **1**, 0.027 M) delivered by a 0.5 mL syringe. The sample was sealed and shaken to ensure complete dissolution, after which 25.0 μL (0.136 mmol, 0.270 M) of diphenylsilane was added. The tube was sealed, immediately removed from the glovebox, and inserted into a preheated NMR probe. The elimination of mesitylene was monitored by the disappearance of the hydride signal of **1** at δ −8.42. The reactions were monitored for at least 3 half-lives in the temperature range 295–323 K.

Kinetic Studies of Mesitylene + Diphenylsilane Reductive Eliminations from 1. In a nitrogen-filled glovebox a resealable NMR tube was charged with 10.0 mg of **1** and 0.50 mL of C_6D_6 (0.0136 mmol of **1**, 0.027 M) delivered by a 0.5 mL syringe. The sample was sealed and shaken to ensure complete dissolution, after which 33.7 μL (0.272 mmol, 0.540 M) of phenylsilane was added to the solution of **1**. The tube was sealed and immediately placed in a preheated NMR probe. The elimination of mesitylene and diphenylsilane was determined by monitoring the disappearance of the hydride signal of **1** at −8.42 ppm. The reactions were monitored for at least 3 half-lives in the temperature range of 295–323 K.

Kinetic Studies of Triethylsilane Reductive Elimination from 7. In a nitrogen-filled glovebox a resealable NMR tube was charged with 10.0 mg of **7** and 0.50 mL of toluene-d_8 (0.0136 mmol of **7**, 0.027 M) delivered by a 0.5 mL syringe. The sample was sealed and shaken to ensure complete dissolution, after which 33.8 μL (0.272 mmol, 0.540 M), phenylsilane was added. The tube was sealed and immediately placed in a preheated NMR probe. The elimination of triethylsilane was determined by monitoring the disappearance of the hydride signal of **7** centered at -10.20 ppm. The reactions were monitored for at least 3 half-lives in the temperature range 323–343 K.

Kinetic Studies of Dihydrogen Reductive Elimination from 8. In a nitrogen-filled glovebox a resealable NMR tube was charged with 10.0 mg of **8** and 0.50 mL of toluene-d_8 (0.0124 mmol of **8**, 0.025 M) delivered by a 0.5 mL syringe. The sample was sealed and shaken to ensure complete dissolution, after which 30.8 μL (0.248 mmol, 0.500 M), phenylsilane was added. The tube was sealed and immediately placed in a preheated NMR probe. The elimination of dihydrogen was determined by monitoring the disappearance of the hydride signal of **8** centered at −9.62 ppm. The reactions were monitored for at least 3 half-lives in the temperature range 333–363 K.

Acknowledgment. We wish to thank the National Science Foundation (Grants CHE 89-09060 and CHE 94-04991) for support of this work, the Johnson Matthey Co. Inc. for a generous loan of iridium trichloride, and Drs. William Jones, Paul Deutsch, and Simon Duckett for helpful discussions. B.P.C. gratefully acknowledges Sherman Clarke, Bristol Myers-Squibb, and Arnold Weissberger Fellowships.

OM9500275

(82) Cleary, B. P.; Eisenberg, R. *Organometallics* **1992**, *11*, 2335–2337.

(83) Hays, M. K.; Eisenberg, R. *Inorg. Chem.* **1991**, *30*, 2623–2630.

Activation of Ethers and Sulfides by Organolanthanide Hydrides. Molecular Structures of $(Cp^*_2Y)_2(\mu\text{-}OCH_2CH_2O)(THF)_2$ and $(Cp^*_2Ce)_2(\mu\text{-}O)(THF)_2$

Berth-Jan Deelman,[†] Martin Booij,[†] Auke Meetsma,[†] Jan H. Teuben,*[,†] Huub Kooijman,[‡] and Anthony L. Spek[‡,§]

Groningen Center for Catalysis and Synthesis, Department of Chemistry, University of Groningen, Nijenborgh 4, 9747 AG Groningen, The Netherlands, and Bijvoet Center for Biomolecular Research, Crystal and Structural Chemistry, University of Utrecht, Padualaan 8, 3584 CH Utrecht, The Netherlands

Received December 27, 1994[⊗]

Dialkyl ethers, ROR′, are cleaved by hydrides $(Cp^*_2LnH)_2$ (Ln = Y **1a**, La **1b**, Ce **1c**) to form alkoxides Cp^*_2LnOR (**2**), Cp^*_2LnOR', R′H, and RH. The extent to which either of the C–O bonds of asymmetric substituted dialkyl ethers ROR′ is attacked strongly depends on the alkyl substituents but is relatively insensitive to the nature of the metal. Ring opening is observed with THF or 1,4-dioxane leading to $Cp^*_2YO^nBu$ (**6a**) and $(Cp^*_2Y)_2(\mu\text{-}OCH_2CH_2O)(THF)_2$ (**8**), respectively. The molecular structure of **8** was determined by X-ray diffraction. Space group *Pbcn* had unit cell parameters $a = 21.7483(12)$ Å, $b = 14.2806(12)$ Å, $c = 16.726(2)$ Å and $Z = 4$. Least-squares refinement based on 4163 reflections converged to $R = 0.063$. Unsaturated ethers, vinyl ethyl ether and allyl ethyl ether, are cleaved instantaneously by **1a** to form Cp^*_2YOEt. Also, the C–O bonds of Cp^*_2LnOEt are attacked by $(Cp^*_2LnH)_2$ to give the oxo bridged compound $(Cp^*_2Ln)_2(\mu\text{-}O)$ and ethane. The molecular structure of the THF adduct of the cerium analogue $(Cp^*_2Ce)_2(\mu\text{-}O)(THF)_2$ (**12**) was determined by X-ray diffraction: spacegroup $P\bar{1}$ had unit cell parameters $a = 13.399(2)$ Å, $b = 14.864(4)$ Å, $c = 15.812(6)$ Å, $\alpha = 70.75(2)°$, $\beta = 85.15(2)°$, $\gamma = 63.78(2)°$, and $Z = 2$. Least-squares refinement based on 6294 reflections converged to $R = 0.038$. In contrast to ethers, organic sulfides RSR′ are metallated by **1a** to produce products $Cp^*_2YCH_2SMe$ (**13**, R = R′ = Me), $Cp^*_2YCH(SMe)Ph$ (**15**, R = Me, R′ = Ph), $Cp^*_2Y(SC_4H_3)$ (**18**, RR′ = CH=CHCH=CH), and dihydrogen. Only Et_2S underwent C–S cleavage to form Cp^*_2YSEt (**16**) and ethane. Reaction of **1a** with allyl methyl sulfide is not clean, but **1a** is a modest catalyst for the hydrogenation of allyl methyl sulfide.

Introduction

Organometallic compounds of group 3 and lanthanide metals are very active catalysts for polymerization[1] and hydrogenation[2] of olefins. Also, cyclization of 1,4-, 1,5-, and 1,6-dienes is very efficiently catalyzed by scandium and yttrium complexes.[3] However, in general, these catalytic processes have severe limitations, since they can only be performed with nonfunctionalized olefins. Only very recently have some examples appeared of catalytic conversions of olefins bearing functional groups. For instance, the hydrogenation of olefins with ether and thioether functions can be achieved.[4] Also, the cyclization of some functionalized dienes starting from $Cp^*_2YMe(THF)$ can be performed without severe deactivation of the catalyst.[3b] The living polymerization of methyl methacrylate (MMA) by organolanthanides shows that in some cases even carbonyl groups are tolerated.[5]

Some examples of C–X activation have been reported. For instance, the activation of alkyl halides leading to selective dehalogenation has been studied.[6] Several authors have reported on C–O cleavage, which resulted in the formation of Ln–O bonds.[7] The question remains

[†] University of Groningen.
[‡] University of Utrecht.
[§] Address correspondence pertaining to crystallographic studies of compound **8** to this author.
[⊗] Abstract published in *Advance ACS Abstracts,* April 15, 1995.

(1) (a) Thompson, M. E.; Baxter, S. M.; Bulls, A. R.; Burger, B. J.; Nolan, M. C.; Santarsiero, B. D.; Schaefer, W. P.; Bercaw, J. E. *J. Am. Chem. Soc.* **1987**, *109*, 203. (b) Watson, P. L.; Parshall, G. W. *Acc. Chem. Res.* **1985**, *18*, 51. (c) Watson, P. L. *J. Am. Chem. Soc.* **1982**, *104*, 337. (d) Watson, P. L. *J. Am. Chem. Soc.* **1982**, *104*, 6471. (e) Jeske, G.; Lauke, H.; Mauermann, H.; Swepston, P. N.; Schumann, H.; Marks, T. J. *J. Am. Chem. Soc.* **1985**, *107*, 8091. (f) Bunel, E.; Burger, B. J.; Bercaw, J. E. *J. Am. Chem. Soc.* **1988**, *110*, 976. (g) Burger, B. J.; Thompson, M. E.; Cotter, W. D.; Bercaw, J. E. *J. Am. Chem. Soc.* **1990**, *112*, 1566.

(2) (a) Jeske, G.; Lauke, H.; Mauermann, H.; Schumann, H.; Marks. T. J. *J. Am. Chem. Soc.* **1985**, *107*, 8111. (b) Conticello, V. P.; Brard, L.; Giardello, M. A.; Tsuji, Y.; Sabat, M.; Stern, C. L.; Marks, T. J. *J. Am. Chem. Soc.* **1992**, *114*, 2761.

(3) (a) Bunel, E.; Burger, B. J.; Bercaw, J. E. *J. Am. Chem. Soc.* **1988**, *110*, 976. (b) Molander, G. A.; Hoberg, J. O. *J. Am. Chem. Soc.* **1992**, *114*, 3123.

(4) Molander, G. A.; Hoberg, J. O. *J. Org. Chem.* **1992**, *57*, 3266.

(5) Yasuda, H.; Yamamoto, H.; Yokota, K.; Miyake, S.; Nakamura, A. *J. Am. Chem. Soc.* **1992**, *114*, 4908.

(6) (a) Schumann, H. *Angew. Chem.* **1984**, *96*, 475, and references cited therein. (b) Finke, R. G.; Keenan, S. R. *Organometallics* **1989**, *8*, 263. (c) Watson, P. L.; Tulip, T. H.; Williams, I. *Organometallics* **1990**, *9*, 1999. (d) Burns, C. J.; Andersen, R. A. *J. Chem. Soc., Chem. Commun.* **1989**, 136. (e) Deacon, G. B.; MacKinnon, P. I. *Tetrahedron Lett.* **1984**, *25*, 783. (f) Yasuda, H.; Yamamoto, H.; Yokota, K.; Nakamura, A. *Chem. Lett.* **1989**, 1309.

(7) (a) Evans, J. E.; Ullibarri, T. A.; Ziller, Z. W. *Organometallics* **1991**, *10*, 134. (b) Watson, P. L. *J. Chem. Soc., Chem. Commun.* **1983**, 276. (c) Evans, W. J.; Chamberlain, L. R.; Ulibarri, T. A.; Ziller, J. W. *J. Am. Chem. Soc.* **1988**, *110*, 6423. (d) Evans, J. W.; Dominguez, R.; Hanusa, T. P. *Organometallics* **1986**, *5*, 1291.

0276-7333/95/2314-2306$09.00/0

Table 1. Results of the Ether Cleavage Reactions with (Cp^*_2LnH)

$(Cp^*_2LnH)_2$	ROR′	Cp^*_2LnOR, Cp^*_2LnOR'
1a	Et_2O	**2a** Cp^*_2YOEt
1b	Et_2O	**3b** $Cp^*_2LaOEt(Et_2O)$
1c	Et_2O	**3c** $Cp^*_2CeOEt(Et_2O)$
1a	^{t}BuOMe	**4a** $Cp^*_2YOMe(^t$BuOMe)
1a	^{t}BuOEt	**2a** Cp^*_2YOEt
		5a $Cp^*_2YO^t$Bu (1:1)
1a	^{n}BuOEt	**6a** $Cp^*_2YO^n$Bu
1b	^{t}BuOMe	**4b** $Cp^*_2LaOMe(^t$BuOMe)
1b	^{t}BuOEt	**2b** Cp^*_2LaOEt
		5b $Cp^*_2LaO^t$Bu (2:3)
1b	^{n}BuOEt	**6b** $Cp^*_2LaO^n$Bu(^{n}BuOEt)

why some functional groups are tolerated in catalytic cycles and others are not. To understand the processes involved, we started a program directed to the interaction of some well-known catalytically active lanthanide hydride complexes $(Cp^*_2LnH)_2$ (Ln = Y, La, and Ce) with molecules R–X (X = OR, SR, NR_2, PR_2, COOR, $CONR_2$, etc.).

In this study we focus on C–O and C–S-containing molecules. Selective C–O cleavage by transition metal complexes can have considerable impact on organic synthesis.[8] For instance, the zirconium-mediated deprotection of allyl-protected hydroxyl functions was recently reported.[9] Also, C–S bond activation is especially interesting because of its relevance to hydrodesulfurization (HDS).[10] Recently we showed that C–H activation can compete effectively with C–X activation in substituted arenes.[11] We now direct our attention to nonaromatic and heteroaromatic substrates. In particular, the possible competition between C=C, C–H, and C–X activation is an interesting subject.

Results

Activation of Ethers. In an exploratory study the interactions of group 3 and lanthanide hydrides $(Cp^*_2LnH)_2$ (Ln = Y (**1a**), La (**1b**), Ce (**1c**)) with ethers (ROR′) were monitored by ^{1}H NMR (0.03–0.08 M, benzene-d_6, room temperature). Later, some of the experiments were carried out on a preparative scale. In general, clean reactions were observed with formation of alkoxides Cp^*_2LnOR, Cp^*_2LnOR', and alkanes (eq 1, Table 1).

$$(Cp^*_2LnH)_2 + 2\ ROR' \longrightarrow Cp^*_2LnOR + Cp^*_2LnOR' + R'H + RH \quad (1)$$

1a: Ln = Y
1b: Ln = La
1c: Ln = Ce

For yttrium, splitting of Et_2O was quantitative when 1 equiv of Et_2O per Y was applied. Addition of an excess of Et_2O resulted in the formation of adduct $Cp^*_2YOEt(Et_2O)$ (**3a**). For lanthanum and cerium the products Cp^*_2LnOEt show an increased tendency to complex Et_2O, resulting in the formation of the adducts $Cp^*_2LnOEt(Et_2O)$. Dissociation of Et_2O in these adducts appears to be difficult because the complexed ether is unavailable for reaction with **1b** and **1c**. As a consequence, complete conversion of **1b** and **1c** to the alkoxides requires at least 2 equiv of Et_2O per Ln. Within a few minutes after addition of a stoichiometric amount of Et_2O to **1a** in benzene-d_6, resonances were observed which were assigned to an intermediate ether adduct $Cp^*_2YD(Et_2O)$.[12] This intermediate was completely converted to Cp^*_2YOEt (**2a**) and ethane as the reaction progressed.

In principle, ether splitting is a good synthetic method for the preparation of the ether free alkoxide **2a** and ether adducts $Cp^*_2LnOEt(Et_2O)$ (Ln = La (**3b**) and Ce (**3c**)). However, with increased steric bulk of the ether substituents the rate of cleavage decreased dramatically. The half-lives of **1a** with different ethers were determined as follows: diethyl ether and *n*-butyl ethyl ether, <5 min; *tert*-butyl methyl ether, 45 min; and *tert*-butyl ethyl ether, >24 h at 50 °C. With asymmetric ethers such as *tert*-butyl methyl ether, *tert*-butyl ethyl ether, and *n*-butyl ethyl ether the selectivity of C–O activation by **1a** showed remarkable differences. *tert*-Butyl methyl ether gave selectively $Cp^*_2YOMe(^t$BuOMe) (**4a**), and with *tert*-butyl ethyl ether a 1:1 mixture of **2a** and $Cp^*_2YO^t$Bu (**5a**) was obtained. Complete conversion took 4 days at 50 °C. When *tert*-butyl ethyl ether was added in a ratio Y:^{t}BuOEt = 1:5, reaction was complete within 14 h at room temperature, yielding the same product ratio. There was no sign of complexation of *tert*-butyl ethyl ether to product Cp^*_2LnOR or to the starting compound **1a**, which is probably a consequence of the high steric requirements of the ether. With *n*-butyl ethyl ether the C–O activation process became selective again, leading to quantitative formation of **6a** and ethane. Analogous to the reaction with diethyl ether, there were resonances present in the ^{1}H-NMR spectrum which were assigned to an intermediate ether adduct $Cp^*_2YD(^n$BuOEt).

To understand better the mechanism of C–O activation, the kinetics of the cleavage of Et_2O by **1a** were determined in methylcyclohexane-d_{14} by ^{1}H NMR under pseudo-first-order conditions in Et_2O. It was found that at 0 °C $Cp^*_2YH(Et_2O)$ (**7**) was the only species present immediately after addition of Et_2O. The compound is a monomer since the signal observed in the ^{1}H-NMR spectrum for the hydride ligand (δ 5.62) appears as a doublet due to coupling with one yttrium nucleus ($^1J_{HY}$ = 83.1 Hz). This hydride species reacted quantitatively to **3a** and ethane with a first-order dependence in $[Cp^*_2YH(Et_2O)]$ at 0 °C for more than 5 half-lives ($[\mathbf{1a}]_0$ = 0.026 M, $[Et_2O]_0$ = 0.25 M, $k_{obs} = 7.4 \pm 0.1 \times 10^{-4}$ s^{-1}; $[\mathbf{1a}]_0$ = 0.12 M, $[Et_2O]_0$ = 1.21 M, $k_{obs} = 6.7 \pm 0.1 \times 10^{-4}$ s^{-1}). This shows that the actual C–O activation involves dissociation of dimeric **1a** to form **7**, which then intramolecularly converts to products.

To study the influence of increased ionic radius of the Ln center on C–O activation, reactions of aliphatic ethers with **1b** were performed. The reactivity order diethyl ether ≈ *n*-butyl ethyl ether > *tert*-butyl methyl ether ≈ *tert*-butyl ethyl ether is in good agreement with that found for **1a**, although rates are in all cases higher for **1b**. The selectivity pattern found for cleavage of *tert*-butyl ethyl ether and *n*-butyl ethyl ether is very similar to the one found for **1a** (Table 1). For *tert*-butyl ethyl

(8) Yamamoto, A. *Adv. Organomet. Chem.* **1992**, *34*, 111.
(9) Ito, H.; Taguchi, T.; Hanzawa, Y. *J. Org. Chem.* **1993**, *58*, 774.
(10) (a) Wiegand, B. C.; Friend, C. M. *Chem. Rev.* **1992**, *92*, 491. (b) Angelici, R. J.; Chol, M.-G. *Organometallics* **1993**, *11*, 3328. (c) Rosoni, G. P.; Jones, W. D. *J. Am. Chem. Soc.* **1992**, *114*, 10767.
(11) Booij, M.; Deelman, B.-J., Duchateau, R.; Postma, D. S. Meetsma, A.; Teuben, J. H. *Organometallics* **1993**, *12*, 3531.

(12) Formation of this adduct can be explained by fast H/D scrambling between the solvent benzene-d_6 and **1a**, see ref 11.

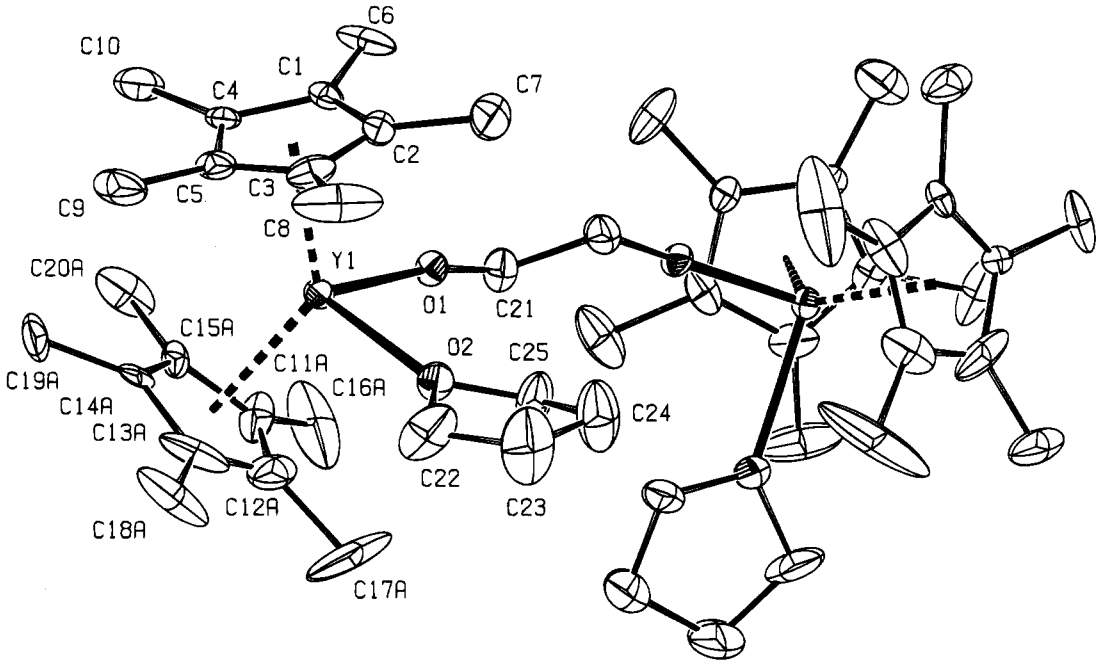

Figure 1. ORTEP drawing (30% probability level) and atom-labeling scheme for $(Cp^*_2Y)_2(\mu\text{-}OCH_2CH_2O)(THF)_2$ (**8**). Only the major-disorder component is shown. Hydrogen atoms and the noncoordinating THF molecule are omitted for clarity.

ether a 2:3 ratio of Cp^*_2LaOEt (**2b**) and $Cp^*_2LaO^tBu$ (**5b**) was found, which differs slightly from the corresponding reaction for **1a**. Since no dramatic difference between Ln = Y and La was found, from this point onward we only studied hydride **1a** for convenience.

Cyclic ethers gave, as expected, ring opening with **1a**. With THF initially the THF adduct $Cp^*_2YH(THF)$ was formed, which subsequently converted to a mixture of products (24 h at room temperature) of which **6a** could be identified as the major component (60% by ^1H NMR, eq 2).[13] In benzene-d_6 the reaction appeared to be more

$$(Cp^*_2YH)_2 \xrightarrow{THF} Cp^*_2YH(THF) \longrightarrow Cp^*_2YO^nBu \quad (2)$$
1a **6a**

complicated due to H/D scrambling between the hydride, the α-methylene hydrogen atoms of THF, and the solvent,[11] but apart from this, no indications were obtained for a different reactivity.

1,4-Dioxane and **1a** reacted to give a white precipitate which was recrystallized from THF and identified as the bimetallic glycolate complex $(Cp^*_2Y)_2(\mu\text{-}OCH_2CH_2O)(THF)_2$ (**8**) (eq 3). The gas evolved was collected by

$$(Cp^*_2YH)_2 + \text{O}\square\text{O} \xrightarrow[THF]{\text{- ethane}} \overset{THF}{Cp^*_2Y}\text{—O—}\square\text{—O—}\overset{THF}{YCp^*_2} \quad (3)$$
1a **8**

Töpler pump and analyzed as ethane (0.50 mol/mol Y, GC).[14] When the reaction was monitored by ^1H NMR, it became clear that the product was formed practically instantaneously.

(13) There are three other resonances in the Cp* area (δ = 2.1–1.9 ppm). Assignment is not well possible but products originating from secondary ether splitting or from metalation on the α-position of the complexed THF followed by enolate formation have to be reckoned with. See also ref 7d.

(14) Also a minor amount of dihydrogen (<0.05 mol/mol of Y) was detected. This can be attributed to conversion of **1a** to the bridged fulvene hydride $Cp^*_2Y(\mu\text{-}H)(\mu\text{-}Fv)YCp^*$[11], but metalation of 1,4-dioxane cannot be excluded.

Table 2. Selected Bond Distances (Angstroms), Bond Angles (Degrees), and Torsion Angles (Degrees) for $(Cp^*_2Y)_2(\mu\text{-}OCH_2CH_2O)(THF)_2$ (8)

Y1–O1	2.042(4)	O1–C21	1.359(9)
Y1–O2	2.398(5)	C21–C21[a]	1.484(9)
Y1–Ct1[b]	2.413(3)	Y1–Ct2	2.421(7)
O1–Y1–O2	89.54(16)	Y1–O1–C21	168.2(4)
Ct1–Y1–Ct2	133.18(19)	O1–C21–C21[a]	116.0(7)
O1–C21–C21[a]–O1[a]	163.1(6)		

[a] Denotes symmetry operation $-x, y, 1/2 - z$. [b] Ct1 = C1–C5 centroid, Ct2 = C11A–C15A centroid (=major disorder component).

The ^1H- and ^{13}C-NMR spectra of **8** show one resonance for all Cp* ligands. For the methylene groups in the OCH_2CH_2O bridge also one resonance is observed in both ^1H and ^{13}C NMR. This methylene resonance appears as a doublet in the ^1H-decoupled ^{13}C-NMR spectrum due to a $^2J_{CY}$ coupling of 5 Hz. These data suggest a structure with either a twofold rotation axis or an inversion center. A dynamic process, which is fast on the NMR time scale, might also account for the observed equivalence of the Cp* and OCH_2 groups. A structure that places the oxygen atoms of the OCH_2-CH_2O bridge in bridging positions between two yttrium centers can be excluded because each OCH_2 group is coupled to only one yttrium nucleus.

To elucidate the bonding of the glycolate ligand in **8**, a single-crystal X-ray structure determination was undertaken. An ORTEP diagram of the resulting molecular structure is shown in Figure 1. Besides compound **8**, the crystal also contains a noncoordinating THF molecule in a 1:1 ratio with the yttrium complex. Selected bond distances and angles are listed in Table 2. Both **8** and the THF molecule are situated on a crystallographic twofold rotation axis, which is in agreement with the NMR data. The molecule consists of two $Cp^*_2Y(THF)$ units, which have a distorted tetrahedral arrangement and which are bridged by the glycolate ligand. The bonding of THF and Cp* ligands to yttrium is not unusual. The Y1–Ct1 (2.413(3) Å) and Y1–Ct2

(2.421(7) Å) distances are close to that of $Cp^*_2YCH(SiMe_3)_2$ (2.381(3) and 2.382(3) Å), for instance.[15] The Y1–O1 distance compares well with Y–O distances in alkoxides $Cp^*Y(OC_6H_3{}^tBu_2)_2$ (2.096(4) and 2.059(3) Å)[16] and $[Cp^*Y(\mu\text{-}O^tBu)(O^tBu)]_2$ (1.995(10) and 2.018(9) Å).[17] Also, the almost linear Y1–O1–C21 angle due to π-overlap of the oxygen lone pairs with d orbitals of yttrium has been observed in $Cp^*Y(OC_6H_3{}^tBu_2)_2$.[16]

As opposed to THF and 1,4-dioxane, furan was not ring opened by **1a**. Instead, C–H activation of furan in the α-position to form $Cp^*_2Y(2\text{-}OC_4H_3)$ (**9**) was observed (^{1}H NMR, eq 4). This compound was characterized as the bis THF adduct $Cp^*_2Y(2\text{-}OC_4H_3)(THF)_2$ (**10**) which could be prepared independently from $Cp^*_2YCl_2Li(Et_2O)_2$ and 2-lithiofuran.

$$(Cp^*_2YH)_2 \xrightarrow[-H_2]{} Cp^*_2Y\text{-}(2\text{-}OC_4H_3) \quad (4)$$
1a **9**

C–O activation in the unsaturated ethers vinyl ethyl ether and allyl ethyl ether was found to be very rapid ($t_{1/2}$ < 2 min). With vinyl ethyl ether **2a** was formed in essentially quantitative yield (eq 5). Only a minor amount of gas was collected by Töpler pump (0.05 mol of ethylene/mol of Y, GC). The fate of the missing CH_2-CH_2 fragments was determined by GC/MS after the reaction mixture had been quenched with methanol. The mixture contained higher alkanes in the range C_{16}–C_{22} with exclusively even numbers of carbon atoms. This indicates that the ethylene evolved is oligomerized under the reaction conditions applied. This is most likely caused by reaction with **1a**, which is an extremely active ethylene polymerization catalyst.[18] Attempts to observe an intermediate at −80 °C were unsuccessful (^{1}H NMR). The yttrium hydride **1a** had already been converted to **2a** when a solution of **1a** in toluene-d_8, to which vinyl ethyl ether had been added at −196 °C, was warmed to −80 °C. With allyl ethyl ether the main product formed was **1a** (57% by ^{1}H NMR, eq 6). The gas evolved (0.56 mol/mol of Y) was analyzed as a mixture of propene (79%) and propane (21%) by GC.

$$(Cp^*_2YH)_2 \xrightarrow[-\text{ethylene}]{} Cp^*_2YOEt \quad (5)$$
1a **2a**

$$(Cp^*_2YH)_2 \xrightarrow[-\text{propene}]{} Cp^*_2YOEt \quad (6)$$
1a **2a**

Attempted hydrogenation of vinyl ethyl ether under mild conditions (dihydrogen atmosphere, 1 bar, room temperature) was carried out with a 10-fold excess of vinyl ethyl ether. This led to quantitative formation of the vinyl ether adduct of **2a**. Hydrogenation to diethyl ether was not observed, however. Also, attempted hydrogenation of allyl ethyl ether led to fast formation of the allyl ethyl ether adduct of **2a**, and again no hydrogenation was observed.

Scheme 1

$$(Cp^*_2LnH)_2 + 2\,Et_2O \longrightarrow 2\,Cp^*_2LnOEt + 2\,\text{ethane}$$
1a-c **2a-c**

$$(Cp^*_2LnH)_2 + 2\,Cp^*_2LnOEt \longrightarrow 2\,Cp^*_2Ln\text{-}O\text{-}LnCp^*_2 + 2\,\text{ethane}$$
2a-c **11a-c**

C–O Cleavage in Alkoxides Cp^*_2LnOR. Not only ethers are activated by hydrides **1a–c** but even the C–O bonds of alkoxides Cp^*_2LnOEt (Ln = Y, La, Ce (**2a–c**)) are attacked, leading to bimetallic complexes $(Cp^*_2Ln)_2(\mu\text{-}O)$ (Ln = Y, La, Ce (**11a–c**), Scheme 1). When diethyl ether was added to a solution of **1a** in a 1:1 ratio, the diethyl ether was completely converted to **2a** and ethane within a few minutes (^{1}H NMR). The excess **1a** was still present then. At 80 °C, **1a** reacted in about 4 days with **2a** to form **11a** and ethane. In a preparative experiment, 0.49 mol of ethane/mol of Y was collected after 0.5 h at room temperature. After 4 days at 80 °C, another 0.47 mol of ethane/mol of Y was collected. This is in agreement with the two-step reaction sequence depicted in Scheme 1 and the NMR experiment. Crystallization from THF afforded unsolvated **11a** as white crystals. Reactions of **1b** and **1c** with diethyl ether to form **11b** and **11c** proceeded analogously (^{1}H NMR). For cerium we were able to obtain single crystals of the THF adduct $(Cp^*_2Ce)_2(\mu\text{-}O)(THF)_2$ (**12**) and the X-ray crystal structure was determined.

Compound **12** crystallized from THF/pentane (1:1) in the triclinic space group $P\bar{1}$ with $Z = 2$. The asymmetric unit cell contains two additional THF solvate molecules. The molecule (Figure 2) is built from two Cp^*_2Ce fragments linked by a nearly linear oxygen bridge (Ce1–O3–Ce2 = 175.9(2)°, Table 3). The coordination sphere of each metal atom is completed by a THF molecule. The two Cp^*_2Ce moieties have the usual bent metallocene configuration[19] with the two oxygen atoms in the equatorial plane. The Cp* ligands have a dish-shaped conformation and the metal-to-ring distances are comparable to those in $Cp^*_2CeCH(SiMe_3)_2$.[20] The distances of the two cerium atoms to the μ-oxygen are equal (Ce1–O3 = 2.185(4) Å, Ce2–O3 = 2.183(5) Å), as are the cerium THF–oxygen distances (Ce1–O1 = 2.605(5) Å, Ce2–O2 = 2.603(5) Å). In the alkoxide $Cp^*_2Ce(2,6\text{-di-}tert\text{-butylphenoxide})_2$[21] the Ce–O distances are slightly longer (2.245(3) Å and 2.257(3) Å). For $(Cp^*_2Sm)_2(\mu\text{-}O)$ the Sm–O–Sm angle is 180° and the Sm–O distance is 2.094(1) Å.[22] When corrected for the difference in ionic radii of cerium and samarium (0.05 Å),[23] the Ce–O3 distance for **12** is somewhat longer (0.04 Å) than the corresponding distances in the unsolvated samarium complex. The small deviation from 180° for the Ce–

(15) Den Haan, K. H.; De Boer, J. L.; Teuben, J. H. *Organometallics* **1986**, *5*, 1726.
(16) Schaverien, C. J.; Frijns, J. H. G.; Heeres, H. J.; Van den Hende, J. R.; Teuben, J. H.; Spek, A. L. *J. Chem. Soc., Chem. Commun.* **1991**, 642.
(17) Evans, W. J.; Boyle, T. J.; Ziller, J. W. *Organometallics* **1993**, *12*, 3998.
(18) Eshuis, J. J. W. Thesis, University of Groningen, Groningen, 1991.
(19) Lauher, J. W.; Hoffmann, R. *J. Am. Chem. Soc.* **1976**, *98*, 1729.
(20) Heeres, H. J.; Renkema, J.; Booij, M.; Meetsma, A.; Teuben, J. H. *Organometallics* **1988**, *7*, 2495.
(21) Heeres, H. J.; Meetsma, A.; Teuben, J. H. *J. Chem. Soc., Chem. Commun.* **1988**, 962.
(22) Evans, W. J.; Grate, J. W.; Bloom, I.; Hunter, W. E.; Atwood, J. L. *J. Am. Chem. Soc.* **1985**, *107*, 405.
(23) Shannon, R. D. *Acta Crystallogr.* **1976**, *A32*, 751.

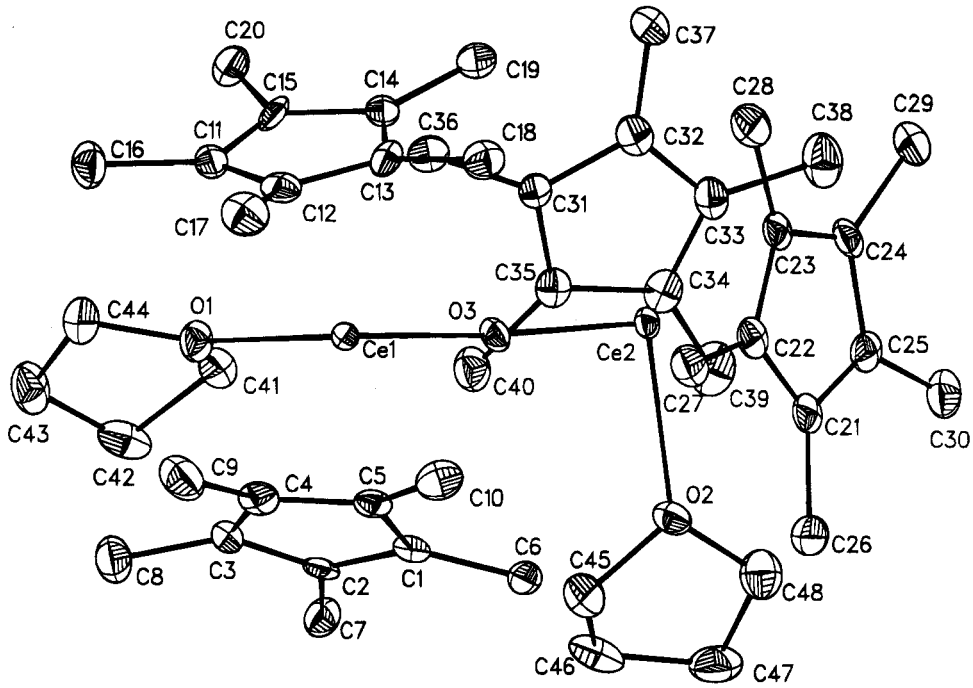

Figure 2. ORTEP drawing (50% probability level) and atom-labeling scheme for $(Cp^*_2Ce)_2(\mu\text{-}O)(THF)_2$ (**12**). Hydrogen atoms are omitted for clarity.

Table 3. Selected Bond Distances (Angstroms), Bond Angles (Degrees), and Torsion Angles (Degrees) for $(Cp^*_2Ce)_2(\mu\text{-}O)(THF)_2$ (12)

Ce1–Ct1	2.598(3)	Ce1–Ct2	2.601(3)
Ce2–Ct3	2.588(3)	Ce2–Ct4	2.604(3)
Ce1–O1	2.605(5)	Ce1–O3	2.185(4)
Ce2–O2	2.603(5)	Ce2–O3	2.183(5)
O1–Ce1–O3	103.9(2)	O2–Ce2–O3	103.0(2)
Ce1–O3–Ce2	175.9(2)		

[a] Ct1 = C1–C5 centroid, Ct2 = C11–C15 centroid, Ct3 = C21–C25 centroid, Ct4 = C31–C35 centroid.

O–Ce angle and the longer Ce–O3 distances indicate a weaker interaction with the μ-oxo ligand lone pairs. This is caused by the coordination of THF to the cerium centers in **12**, which makes the metal less electron deficient. Consequently, the interactions with the oxygen lone pairs of the μ-O ligand are weaker than in $(Cp^*_2Sm)_2(\mu\text{-}O)$.

Activation of Sulfides. In contrast to ethers, organic sulfides are activated predominantly by C–H activation to form the corresponding metalation products. Reaction of **1a** with Me_2S led to formation of $Cp^*_2YCH_2SMe$ (**13**) (eq 7). The product could be isolated as

$$(Cp^*_2YH)_2 \xrightarrow[-H_2]{Me_2S} Cp^*_2YCH_2SMe \quad (7)$$
1a **13**

the THF adduct $Cp^*_2YCH_2SMe(THF)$ (**14**) in reasonable yield. NMR tube experiments revealed that the reaction is very rapid at room temperature and essentially quantitative with excess Me_2S. When smaller amounts of Me_2S are used (Me_2S:Y $\leq$ 1), formation of an unidentified product, resulting from consecutive reaction of **13** with **1a**, was observed.[24]

(24) Crystalline material was obtained from THF. On the basis of ^{13}C-NMR data and elemental analysis this compound was provisionally identified as the double metalation product $(Cp^*_2Y)_2(\mu\text{-}CH_2SCH_2)(THF)_2$, but the purity of the material was low.

Metalation was also observed with benzyl methyl sulfide and $Cp^*_2YC(H)(SMe)Ph$ (**15**) was obtained (eq 8). However, Et_2S, in contrast to dimethyl sulfide and

$$(Cp^*_2YH)_2 \xrightarrow[-H_2]{PhCH_2SMe} Cp^*_2Y(SMe)(Ph) \quad (8)$$
1a **15**

benzyl methyl sulfide, was not metalated but underwent C–S cleavage instead. No signs for C–H activation of Et_2S were present (^1H NMR), and clean formation of Cp^*_2YSEt (**16**) was observed (eq 9). The product was isolated and identified as the THF adduct $Cp^*_2YSEt(THF)$ (**17**).

$$(Cp^*_2YH)_2 \xrightarrow[-\text{ethane}]{Et_2S} Cp^*_2YSEt \quad (9)$$
1a **16**

Thiophene behaves analogously to furan, dimethyl sulfide, and benzyl methyl sulfide and was metalated selectively in the α-position to form $Cp^*_2Y(2\text{-}SC_4H_3)$ (**18**) (eq 10). The product could be isolated in high yield as the THF adduct $Cp^*_2Y(2\text{-}SC_4H_3)(THF)$ (**19**).

$$(Cp^*_2YH)_2 \xrightarrow[-H_2]{\text{thiophene}} Cp^*_2Y(2\text{-}SC_4H_3) \quad (10)$$
1a **18**

Allyl methyl sulfide was studied to examine whether activation took place at the C–S, C=C, or C–H bonds. ^1H-NMR studies showed the complete conversion of **1a** to a mixture of compounds within several minutes at room temperature. A doublet of triplets ($^3J_{HH}$ = 7.1 Hz, $^2J_{HY}$ = 3.7 Hz) at δ −0.30 and a triplet at δ 2.66 ($^3J_{HH}$ = 6.8 Hz) in the ^1H-NMR spectrum were assigned to YCH_2CH_2 and CH_2S moieties, respectively. From this and a Cp* resonance (δ 1.91) we concluded that the

Scheme 2

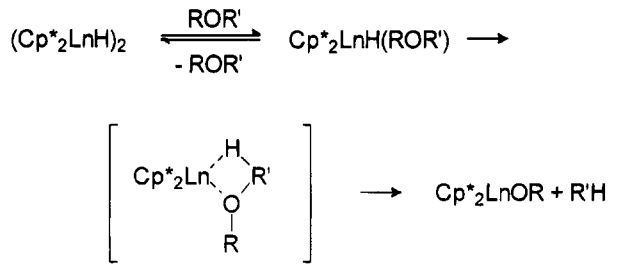

insertion product $Cp^*_2YCH_2CH_2CH_2SMe$ (**20**) was formed in 53% yield.[25]

No polymerization was observed with excess allyl methyl sulfide (NMR, GC), which is probably due to blocking of the metal center by the internal coordination of the SMe group. However, under H_2 atmosphere (1 bar) it was possible to hydrogenate catalytically allyl methyl sulfide to *n*-propyl methyl sulfide in moderate yield (30%).

Discussion

In analogy with C–H activation reactions, C–O activation by Lewis acidic lanthanide complexes, $(Cp^*_2LnH)_2$ (Ln = Sm,[26] Lu[27]), has been explained in terms of σ-bond metathesis[1a,28] (Scheme 2). First the ether molecule is coordinated, forming monomeric $Cp^*_2LnH(R_2O)$, which renders the α-C atom of the ether molecule susceptible to nucleophilic attack by the hydride ligand in the second step. Our observations for Y, La, and Ce are in good agreement with the results for Sm and Lu, emphasizing the strong similarities between group 3 metals and lanthanides. For yttrium, the intermediate ether hydride adducts $Cp^*_2LnH(ROR')$ and $Cp^*_2YD(ROR')$ were observed by ^1H NMR, which supports the proposed dissociation of dimeric $(Cp^*_2LnH)_2$ in the first step of Scheme 2. This is confirmed by the observed first-order dependence in **7**.

The reactivity order diethyl ether ≈ *n*-butyl ethyl ether > *tert*-butyl methyl ether > *tert*-butyl ethyl ether reflects the increasing steric requirements of the ethers involved. Approach and complexation of ether to $(Cp^*_2LnH)_2$ become more difficult with increasing steric bulk on the ether molecule. This is in line with the fact that monomeric ether adducts $Cp^*_2YH(R_2O)$ and $Cp^*_2YD(R_2O)$ could only be observed for the less bulky ethers (Et_2O, ^{n}BuOEt, and THF). The observation that the bulkiest ether, *tert*-butyl ethyl ether, reacts slightly faster with **1b** than with **1a** can be rationalized by the fact that La has a larger ionic radius than Y,[29] which makes complexation of the ether molecule more favorable.

For aliphatic nucleophilic substitution reactions it is well-known that alkyl substituents on the α-C atom of the substrate RX can have an enormous effect on reactivity.[30] In S_N2 type substitution, the reactivity order for different R is Me > Et > Pr > Np > Bu, whereas for S_N1 substitution the order Bz ≈ allyl > tertiary C > secondary C > primary C > Me is observed. In S_N2 substitution the reactivity is governed by steric characteristics of R, whereas in S_N1 substitution the stabilization of a positive charge on the α-C atom is of dominating importance. Ether cleavage of the S_N2 type has been observed with hydrohalic acids (HX) proceeding by S_N2 attack of X^- on the less hindered C–O bond.[31] Ether cleavage by strong Lewis acids such as boron trihalogenides is an example of a S_N1 type mechanism.[31]

Our systems show similarities with both of these nucleophilic aliphatic substitution reactions. The observation that *tert*-butyl methyl ether is attacked at the more substituted α-C atom indicates that electronic rather than steric factors are important and suggests an S_N1 mechanism. However, from reaction of *tert*-butyl ethyl ether, in which both C–O bonds are cleaved at comparable rates, and from the reaction of *n*-butyl ethyl ether, which is cleaved at the Et–O bond, it is clear that steric requirements of the ether molecules are important as well.

Only a small effect on the selectivity of ether splitting is found when the results for **1a** are compared with those for **1b**, although the ionic radii of Y and La are very different.[29] From this it is concluded that steric and electronic characteristics of the ether itself and not those of the $(Cp^*_2LnH)_2$ system determine the selectivity of the ether splitting.

The ring opening observed with 1,4-dioxane and THF fits well within the σ-bond metathesis scheme described above. Ring opening of THF has also been reported for $(Cp^*_2SmH)_2$.[26] With 1,4-dioxane the first step is most likely formation of $Cp^*_2YOCH_2CH_2OEt$. Formation of **8** requires the selective cleavage of the O–Et bond in the second step.

The complete deoxygenation of ethers by nucleophilic metal hydride complexes is to our knowledge without precedent. There have been some reports, however, concerning formation of μ-oxo species which might be attributed to the deoxygenation of THF. For instance, $Cp^*_2Sm(\mu\text{-}O)SmCp^*_2$ was obtained as a side product in the ring opening of THF by $(Cp^*_2SmH)_2$.[26] Another example is the isolation of $Cp_2Lu(THF)(\mu\text{-}O)(THF)LuCp_2$ from attempted crystallization of $Cp_2LuAsPh_2(THF)$ from THF, which was explained by hydrolysis due to traces of water.[32] A more plausible explanation in our opinion is that the μ-oxo ligand originates from double C–O cleavage of THF. This explanation is even more likely when the ring opening of THF by $Cp_2LuPPh_2(THF)$, leading to $Cp_2LuO(CH_2)_4PPh_2$, is considered.[32] The slower formation of the μ-oxo species for Y compared to La and Ce can be understood on the basis of the smaller ionic radius of Y.[29] Attack on the C–O

(25) S*Me* and $CH_2CH_2CH_2$ were not observed, probably due to overlap with other signals in the region δ = 2.2–1.8 ppm.

(26) Evans, J. E.; Ullibarri, T. A.; Ziller, Z. W. *Organometallics* **1991**, *10*, 134.

(27) Watson, P. L. *J. Chem. Soc., Chem. Commun.* **1983**, 276.

(28) (a) Thompson, M. E.; Bercaw, J. E. *Pure Appl. Chem.* **1984**, *56*, 1. (b) Steigerwald, M. L.; Goddard, W. A. *J. Am. Chem. Soc.* **1984**, *106*, 308. (c) Rabaâ, H.; Saillard, J.-Y.; Hoffmann, R. *J. Am. Chem. Soc.* **1986**, *108*, 4327.

(29) Ionic radii for eight coordinate complexes: Y^{3+} = 1.16 Å, La^{3+} = 1.30 Å, Ce^{3+} = 1.28 Å. See Shannon, R. D. *Acta Crystallogr.* **1976**, *A32*, 751.

(30) (a) McMurry, J. *Organic Chemistry*; Brook/Cole Publishing: Monterey, 1985. (b) Lowry, T. H.; Richardson, K. S. *Mechanism and Theory in Organic Chemistry*, 2nd ed.; Harper and Row: New York, 1985. (c) March, J. *Advanced Organic Chemistry*, 3rd ed.; Wiley: New York, 1985.

(31) (a) Bhatt, M. V.; Kulkarni, S. U. *Synthesis* **1983**, 249. (b) Meerwein, H. In *Methoden der Organischen Chemie*, 4th ed.; Müller, E., Ed.; Thieme Verlag: Stuttgart, 1965; Vol. VI, Part 3, Chapter 1. (c) Burwell, R. L., Jr. *Chem. Rev.* **1954**, *54*, 615.

(32) Schumann, H.; Palamidis, E.; Loebel, J. *J. Organomet. Chem.* **1990**, *384*, C49.

Scheme 3

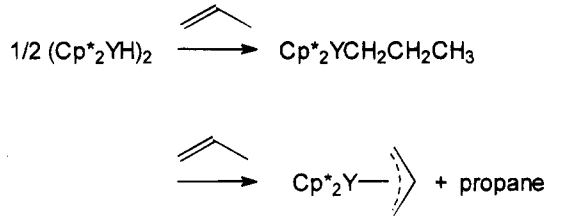

bond of the alkoxide to reach a four-centered transition state will be easier for La and Ce as a result of the larger coordination sphere of these metal ions.

The C−O activation of vinyl ethyl ether does not necessarily have to follow the same route as proposed in Scheme 2. An alternative mechanism involving insertion of the double bond into the Y−H bond followed by β-alkoxide elimination and evolution of ethylene cannot be ruled out *a priori*. Insertion might also play an important role in the reaction of allyl ethyl ether. However, attempts to observe an insertion product were unsuccessful. The fast formation of ethoxide **2a** also kills the polymerization and hydrogenation activity of **1a** since no hydrogenation or polymerization products of vinyl ethyl ether and allyl ethyl ether were observed. This is in remarkable contrast to the very high activity of $(Cp^*_2LnH)_2$ systems in hydrogenation[2] and polymerization[1] of nonfunctionalized olefins.

The formation of propene in the cleavage of allyl ethyl ether by **1a** is most likely the result of direct attack on the allyl−O bond, although a six-membered transition state has also been suggested for C−O activation in allyl ethers.[8] A plausible explanation for the formation of propane is allylic C−H activation of propene and $Cp^*_2Ln(\eta^3\text{-allyl})$, which is well-known for Cp^*_2LnR complexes (Ln = Y,[18] Lu,[1b] La, Nd[1]). The propene formed by C−O activation of allyl ethyl ether reacts with **1a** to form $Cp^*_2YCH_2CH_2CH_3$ (Scheme 3). Next, propane and $Cp^*_2Y(\eta^3\text{-allyl})$ are formed by reaction of $Cp^*_2YCH_2CH_2CH_3$ with propene. Attempts to observe $Cp^*_2Y(\eta^3\text{-allyl})$ in the ^{1}H-NMR spectrum were frustrated by overlap with resonances of unidentified material.

As shown by Marks and co-workers,[33] the driving force for the cleavage of C−X bonds is undoubtedly the formation of very stable Ln−X bonds. The overall reaction enthalpies ($\Delta H°$) of C−X cleavage in ethers and sulfides with $(Cp^*_2SmH)_2$ were calculated to be −48 kcal/mol (Me_2O) and −53 kcal/mol (Me_2S), respectively. These values are significantly more exothermic than those for C−H activation of hydrocarbons. For instance, the reaction enthalpy for metalation of benzene by Cp^*_2ScH was determined to be slightly endothermic by 6.7(3) kcal/mol.[1a]

From this it follows that C−X activation would be the thermodynamically favored process. However, the observed metalation of RX suggests that kinetic parameters are important as well. Both from experimental and from theoretical work it has become clear that σ-bond metathesis strongly depends on steric requirements in the transition states. It was found that metalations of hydrocarbons by $(Cp^*_2LnH)_2$ have low activation energies.[28bc,34] Especially, increasing substitution on the atoms participating in the four-centered transition state leads to a dramatic increase in activation energy. Since for C−H activation there are two hydrogens participating in the four-centered transition state, whereas for C−X activation only one hydrogen is involved (Figure 3), the steric requirements for C−H activation are expected to be less than for C−X activation. This could explain why, although the thermochemistry for both processes is very different, competition between C−H and C−X activation is possible. In addition, this effect can be enhanced by the increased acidity of the α-H's compared to hydrogens of hydrocarbons.

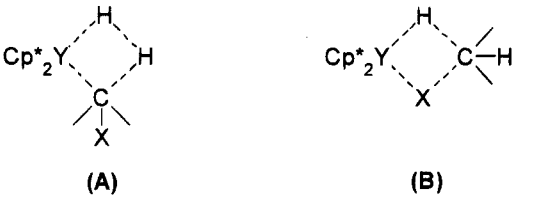

Figure 3. Transition states for C−H (A) and C−X activation (B).

From a comparison of the activation of ethers and sulfides it is clear that C−X cleavage is more facile for ethers than for sulfides, which could be the result of the lower BDE's of Ln−SR bonds vs Ln−OR bonds and the lower electronegativity of S vs O.[33] The result is that C−H activation and formation of metalated species can compete better. The observation of the insertion product and the hydrogenation of allyl methyl sulfide also indicate that deactivation is less important compared to unsaturated ethers.

Conclusions

It was shown that C−O cleavage of ethers (open and cyclic, saturated, and olefin functionalized) with $(Cp^*_2LnH)_2$ complexes is a general reaction. Only furan was found to react differently because of the facile ortho C−H activation pathway available. The cleavage pattern observed with asymmetric substituted ethers can be explained by a σ-bond metathesis mechanism, and in some cases very selective cleavages can be achieved. The unique activation of alkoxide C−O bonds by $(Cp^*_2LnH)_2$ complexes is a good synthetic route to bimetallic $(Cp^*_2Ln)_2(\mu\text{-O})$ complexes. As a consequence of the facile formation of alkoxides and oxides, molecules containing ether functions give very fast deactivation of the catalyst in hydrogenation and polymerization. For sulfides, C−S cleavage is less favorable and C−H activation can compete more effectively, allowing the formation of interesting metalation products. The successful hydrogenation of allyl methyl sulfide shows that deactivation of organolanthanide catalysts by C−X activation is less important for sulfur functions in the substrate molecule.

Experimental Section

General Considerations. All experiments were performed under nitrogen using standard Schlenk, glovebox (Braun MB200), and vacuum line techniques. Et_2O, pentane, THF, cyclohexane, benzene, benzene-d_6, toluene-d_8, and THF-d_8 were distilled from Na/K alloy and degassed prior to use. Compounds **1a**−**c**,[35,1e,20] $Cp^*_2YCl(LiCl)(Et_2O)_2$,[36] 2-lithiofuran,[37] and ^{t}BuOEt[31] were prepared according to published proce-

(33) Nolan, S. P.; Stern, D.; Marks, T. J. *J. Am. Chem. Soc.* **1989**, *111*, 7844.

(34) (a) Rappé, A. K. *Organometallics* **1990**, *9*, 466. (b) Ziegler, T.; Folga, E.; Berces, A. *J. Am. Chem. Soc.* **1993**, *115*, 636.

dures. H_2 (99.9995%, Hoek-Loos) was used without further purification. ^{t}BuOEt, ^{n}BuOEt, vinyl ethyl ether, and allyl ethyl ether were distilled twice from Na sand. Other reagents and cyclohexane-d_{12} were stored over molecular sieves (4 Å). NMR spectra were recorded on Bruker WH90 (^{1}H, 90 MHz), Gemini 200 (^{1}H, 200 MHz), and Varian VXR-300 (^{1}H, 300 MHz; ^{13}C, 75.4 MHz) spectrometers at ambient temperatures. GC analyses were carried out on a Hewlett-Packard HP5890-A instrument equipped with a Hewlett-Packard HP 3390 integrator using Porapack Q and Porasil B columns. GC/MS analyses were carried out on a Ribermag R 10-10 C instrument using a CP Sil 5 CB column, and MS spectra were recorded on an AEI MS 902 mass spectrometer. IR spectra were recorded as Nujol mulls between KBr disks on a Mattson Instruments Galaxy 4020 FT-IR spectrophotometer. Elemental analyses were carried out at the Micro-Analytical Department of the University of Groningen. The determinations are the average of at least two independent determinations.

NMR Tube Reaction of $(Cp^*_2YH)_2$ (1a) with Et_2O. In an NMR tube 0.020 g (0.028 mmol) of **1a** was dissolved in a mixture of 5.8 μL (0.056 mmol) of Et_2O and 0.5 mL of benzene-d_6. ^{1}H NMR after 10 min at room temperature showed the formation of $Cp^*_2YD(Et_2O)$ and **2a** (1:3). After 20 min at room temperature, ^{1}H NMR showed the formation of **2a** (100%) and ethane (δ 0.79). **2a**: ^{1}H NMR (300 MHz, benzene-d_6) δ 4.28 (q, $^3J_{HH}$ = 6.9 Hz, 2H, OCH_2CH_3), 1.93 (s, 30H, C_5Me_5), 1.31 (t, $^3J_{HH}$ = 6.9 Hz, 3H, OCH_2CH_3); ^{13}C NMR (75.4 MHz, benzene-d_6) δ 118.01 (s, C_5Me_5), 62.10 (td, $^1J_{CH}$ = 136 Hz, $^2J_{CY}$ = 6 Hz, OCH_2CH_3), 22.40 (q, $^1J_{CH}$ = 123 Hz, OCH_2CH_3), 10.53 (q, $^1J_{CH}$ = 124 Hz, C_5Me_5). $Cp^*_2YD(Et_2O)$: ^{1}H NMR (300 MHz, benzene-d_6) δ 3.37 (q, $^3J_{HH}$ = 7.0 Hz, 4H, OCH_2CH_3), 2.08 (s, 30H, C_5Me_5), 0.84 (t, $^3J_{HH}$ = 7.0 Hz, 6H, OCH_2CH_3).

Gas Analysis. On a vacuum line 10 mL of Et_2O was condensed on 0.129 g (0.18 mmol) of **1a** at −196 °C. The solution was allowed to warm to room temperature and stirred for 15 h. The gasses evolved were pumped off through a cold trap of −80 °C and analyzed as 0.35 mmol of ethane (GC and MS, 0.97 mol/mol of Y). The solvent was removed in vacuum, and the white residue was characterized as the diethyl ether adduct of Cp^*_2YOEt (**3a**) by ^{1}H NMR.[35]

Kinetic Measurements. NMR tubes (5 mm with Young valve) were filled with solutions of **1a** in methylcyclohexane-d_{14} of accurately determined concentration. At −196 °C known amounts of Et_2O were added and the NMR tubes were sealed under nitrogen atmosphere. The reaction mixtures were allowed to become homogeneous at −30 °C and were quickly inserted in the probe of an NMR spectrometer and warmed to 0 °C. The progress of the reaction was monitored by taking a ^{1}H-NMR spectrum (300 MHz) at constant intervals (at least three spectra per half-life) for more than 5 half-lives. The decrease in intensity of the Cp* and Y*H* signals of **7** were fitted to an exponential decay using a least-squares method. At the end of the measurement it was made sure that no insoluble material was present. **7**: ^{1}H NMR (300 MHz, methylcyclohexane-d_{14}) δ 5.62 (d, $^1J_{HY}$ = 83.1 Hz, 1H, YH), 1.92 (s, 30H, C_5Me_5).

NMR Tube Reaction of $(Cp^*_2LaH)_2$ (1b) with Et_2O. In an NMR tube 0.020 g (0.025 mmol) of **1b** was dissolved in 0.5 mL of benzene-d_6 and 16 μL (0.16 mmol) of Et_2O was added. ^{1}H NMR after 10 min at room temperature showed the quantitative formation of **3b** and ethane (δ 0.78). The NMR tube was opened, and volatiles were removed in vacuum. The residue was redissolved in benzene-d_6. **3b**: ^{1}H NMR (300 MHz, benzene-d_6) δ 4.15 (q, $^3J_{HH}$ = 6.8 Hz, 2H, $LaOCH_2CH_3$), 3.28 (q, $^3J_{HH}$ = 7.3 Hz, 4H, $O(CH_2CH_3)_2$), 2.08 (s, 30H, C_5Me_5), 1.27 (t, $^3J_{HH}$ = 6.8 Hz, 3H, $LaOCH_2CH_3$), 0.87 (t, $^3J_{HH}$ = 7.3 Hz, 6H, $O(CH_2CH_3)_2$).

$Cp^*_2YOMe(^t$BuOMe) (4a). To a solution of 0.58 g (0.80 mmol) of **1a** in 30 mL of pentane was added 0.40 mL (0.30 g, 3.4 mmol) of *tert*-butyl methyl ether. Immediately, a clear orange solution was formed and some gas evolution was observed. The reaction mixture was stirred for 15 h, concentrated to 20 mL, and filtered. Cooling at −80 °C afforded 0.42 g (0.90 mmol, 55%) of **4a**: IR (cm^{-1}) 2950(s), 2780(s), 2720(w), 2180(w), 1450(s), 1390(m), 1370(s), 1275(m), 1240(m), 1200(m), 1170(sh), 1145(vs), 1040(s), 1005(s), 835(s), 805(w), 710(s), 625(w), 590(w), 465(m), 430(s); ^{1}H NMR (90 MHz, benzene-d_6) δ 4.05 (s, 3H, YOMe), 2.79 (s, 3H, ^{t}BuO*Me*), 2.03 (s, 30H, C_5Me_5), 1.04 (s, 9H, ^{t}*Bu*OMe). Anal. Calcd for $C_{26}H_{45}O_2Y$: C, 65.25; H, 9.48. Found: C, 65.07; H, 9.45.

NMR Tube Reaction of 1a with ^{t}BuOEt. In an NMR tube 0.020 g (0.028 mmol) of **1a** was dissolved in a mixture of 7.6 μL (0.056 mmol) of ^{t}BuOEt and 0.5 mL of benzene-d_6. ^{1}H NMR showed the formation of a mixture of **2a** (49%) and **5a** (43%) together with a small amount of unidentified material (8%) over a period of 4 days at 50 °C. Resonances of isobutane (d, δ 0.85) and ethane (δ 0.78) were also observed. **5a**: ^{1}H NMR (300 MHz, benzene-d_6) δ 1.95 (s, 30H, C_5Me_5) 1.41 (s, 9H, ^{t}Bu); ^{13}C NMR (75.4 MHz, benzene-d_6) δ 118.36 (s, C_5Me_5), 72.50 (d, $^2J_{CY}$ = 6 Hz, CMe_3), 35.20 (qsept, $^1J_{CH}$ = 124 Hz, $^3J_{CH}$ = 4 Hz, CMe_3), 11.30 (q, $^1J_{CH}$ = 125 Hz, C_5Me_5).

NMR Tube Reaction of 1a with ^{n}BuOEt. In an NMR tube 0.021 g (0.029 mmol) of **1a** was dissolved in a mixture of 7.7 μL (0.056 mmol) of ^{n}BuOEt and 0.5 mL of benzene-d_6. ^{1}H NMR after 15 min at room temperature showed the formation of **6a** and resonances which were assigned to $Cp^*_2YD(^n$BuOEt) (3:1). After 1 h at room temperature, quantitative conversion to **6a** and ethane (δ 0.78) had taken place. **6a**: ^{1}H NMR (300 MHz, benzene-d_6) δ 4.23 (t, $^3J_{HH}$ = 7.0 Hz, 2H, OCH_2), 1.95 (s, 30 H, C_5Me_5), 1.68 (quint, $^3J_{HH}$ = 7.3 Hz, 2H, $YOCH_2CH_2$), 1.43 (sext, $^3J_{HH}$ = 7.3 Hz, 2H, $CH_2CH_2CH_3$), 1.05 (t, $^3J_{HH}$ = 7.3 Hz, 3H, $CH_2CH_2CH_3$); ^{13}C NMR (75.4 MHz, benzene-d_6) δ 117.86 (s, C_5Me_5), 67.24 (td, $^1J_{CH}$ = 135 Hz, $^2J_{CY}$ = 7 Hz, $YOCH_2$), 39.20 (t, $^1J_{CH}$ = 121 Hz, $YOCH_2CH_2$), 19.85 (t, $^1J_{CH}$ = 122 Hz, $CH_2CH_2CH_3$), 14.73 (q, $^1J_{CH}$ = 124 Hz, $CH_2CH_2CH_3$), 10.70 (q, $^1J_{CH}$ = 125 Hz, C_5Me_5).

NMR Tube Reaction of 1b with ^{t}BuOMe. In an NMR tube 0.016 g (0.019 mmol) of **1b** was dissolved in 0.5 mL of cyclohexane-d_{12} and 23 μL (0.19 mmol) of ^{t}BuOMe was added. ^{1}H NMR after 1 day at room temperature showed the quantitative formation of **4b**: ^{1}H NMR (300 MHz, benzene-d_6) δ 3.67 (s, 3H, LaOMe), 3.11 (s, ^{t}BuO*Me*), 1.94 (s, 30H, C_5Me_5), 1.15 (s, 9H, ^{t}*Bu*OMe). Also, resonances of isobutane (δ 0.89, d) were observed.

NMR Tube Reaction of 1b with ^{t}BuOEt. In an NMR tube 0.014 g (0.017 mmol) of **1b** was dissolved in 0.5 mL of benzene-d_6 and 25 μL (0.18 mmol) of ^{t}BuOEt was added. ^{1}H NMR showed that a mixture of **2b** (44%) and **5b** (56%) had been formed within 2 h at room temperature. Also, resonances of isobutane (doublet at δ 0.85) and ethane (δ 0.79) were observed. The NMR tube was opened, and volatiles were removed in vacuum. The residue was redissolved in benzene-d_6. **5b**: ^{1}H NMR (300 MHz, benzene-d_6) δ 3.95 (q, $^3J_{HH}$ = 7.3 Hz, 2H, $LaOCH_2CH_3$), 1.97 (s, overlapping C_5Me_5 resonances of Cp^*_2LaOEt and $Cp^*_2LaO^tBu$), 1.38 (s, 9H, ^{t}Bu), 1.25 (t, $^3J_{HH}$ = 7.3 Hz, 3H, $LaOCH_2CH_3$).

NMR Tube Reaction of 1b with ^{n}BuOEt. In an NMR tube 0.016 g (0.019 mmol) of **1b** was dissolved in 0.5 mL of benzene-d_6 and 25 μL (0.18 mmol) of ^{n}BuOEt was added. ^{1}H NMR after 10 min at room temperature showed that **6b** had been formed in 87% yield. Volatiles were removed in vacuum, and the residue was redissolved in benzene-d_6. **6b**: ^{1}H NMR (300 MHz, benzene-d_6) δ 4.11 (t, $^3J_{HH}$ = 7.3 Hz, 2H, $LaOCH_2$), 3.30 (m, 4H, ^{n}BuOEt), 2.10 (s, 30H, C_5Me_5), 1.67 (quint, $^3J_{HH}$ = 7.3 Hz, 2H, $LaOCH_2CH_2$), 1.44 (m, 4H, $LaO(CH_2)_2CH_2CH_3$ and ^{n}BuOEt), 1.13 (sext, $^3J_{HH}$ = 7.3 Hz, 2H, ^{n}BuOEt), 1.04 (t,

(35) Den Haan, K. H.; Wielstra, Y.; Teuben, J. H. *Organometallics* **1987**, *6*, 2053.
(36) Den Haan, K. H. Thesis, University of Groningen, Groningen, 1987.
(37) Wakefield, B. J. *Organolithium Methods*; Academic Press: London, 1988; p 38.

$^3J_{HH}$ = 7.3 Hz, 3H, $LaO(CH_2)_3CH_3$), 0.96 (t, $^3J_{HH}$ = 7.3 Hz, 3H, ^{n}BuOEt), 0.84 (t, $^3J_{HH}$ = 7.3 Hz, 3H, ^{n}BuOEt); ^{13}C NMR (75.4 MHz, benzene-d_6) δ 117.83 (s, C_5Me_5), 70.69, (t, $^1J_{CH}$ = 141 Hz, OCH_2 of ^{n}BuOEt), 68.00 (t, $^1J_{CH}$ = 135 Hz, $LaOCH_2$), 66.65 (t, $^1J_{CH}$ = 142 Hz, OCH_2 of ^{n}BuOEt), 39.30 (t, $^1J_{CH}$ = 124 Hz, $LaOCH_2CH_2CH_2Me$), 31.17 (t, $^1J_{CH}$ = 124 Hz, CH_2 of ^{n}BuOEt), 19.91 (t, $^1J_{CH}$ = 123 Hz, $LaO(CH_2)_2CH_2Me$), 19.14 (t, $^1J_{CH}$ = 123 Hz, Me of ^{n}BuOEt), 14.69 (q, $^1J_{CH}$ = 126 Hz, $LaO(CH_2)_3Me$), 14.58 (q, $^1J_{CH}$ = 126 Hz, Me of ^{n}BuOEt), 14.00 (q, $^1J_{CH}$ = 124 Hz, Me of ^{n}BuOEt), 11.28 (q, $^1J_{CH}$ = 124 Hz, C_5Me_5).

NMR Tube Reaction of 1a with THF. In an NMR tube 4.9 μL (0.060 mmol) of THF was added to a solution of 0.021 g (0.028 mmol) of **1a** in 0.5 mL of cyclohexane-d_{12}. ^{1}H NMR after 10 min at room temperature showed clean formation of $Cp^*_2YH(THF)$ which, upon warming to 85 °C, converted to **6a** (^{1}H and ^{13}C NMR, 60%) within 1 h along with some unidentified products. $Cp^*_2YH(THF)$: ^{1}H NMR (90 MHz, cyclohexane-d_{12}) δ 5.70 (d, $^1J_{HY}$ = 78 Hz, $\Delta\nu_{1/2}$ = 14 Hz, 1H, YH), 3.84 (m, 4H, α-THF), 1.94 (s, 30H, C_5Me_5), 1.88 (m, 4H, β-THF). **6a**: ^{1}H NMR (300 MHz, cyclohexane-d_{12}) δ 3.98 (t, $^3J_{HH}$ = 7.3 Hz, 2H, $YOCH_2$), 1.91 (s, 30H, C_5Me_5), 1.48 (quint, $^3J_{HH}$ = 7.3 Hz, 2H, OCH_2CH_2), 1.28 (sext, $^3J_{HH}$ = 7.3 Hz, 2H, $O(CH_2)_2CH_2$), 0.92 (t, $^3J_{HH}$ = 7.3 Hz, 3H, $O(CH_2)_3Me$).

$(Cp^*_2Y)_2(\mu\text{-}OCH_2CH_2O)(THF)_2$ (8). On a vacuum line, a bulb containing 0.242 g (0.336 mmol) of **1a** was evacuated. A mixture of 58 μL (0.68 mmol) of 1,4-dioxane and 5.0 mL of toluene was condensed onto the solid at −196 °C. The reaction mixture was allowed to warm to room temperature and stirred for 15 h. A white precipitate was formed. The gasses evolved were collected by Töpler pump and analyzed by GC to be ethane (0.34 mmol, 0.50 mol/mol of Y). Volatiles were removed in vacuum, and the white solid was redissolved in 10 mL of THF. Crystallization at −80 °C yielded 0.184 g (0.20 mmol, 59%) of **8** as white crystals: IR (cm^{-1}) 2900(s), 2799(sh), 2724(m), 2658(m), 2562(w), 1462(s), 1379(s), 1314(m), 1294(m), 1273(m), 1134(vs), 1074(m), 1061(m), 1020(s), 914(m), 872(s), 802(w), 723(m), 669(w), 635(vw), 590(w), 421(s); ^{1}H NMR (300 MHz, THF-d_8) δ 3.90 (s, 4H, $YOCH_2CH_2OY$), 1.88 (s, 60H, C_5Me_5); ^{13}C NMR (75.4 MHz, THF-d_8) δ 115.61 (s, C_5Me_5), 72.23 (tq, $^1J_{CH}$ = 136.0 Hz, $^3J_{CH}$ = 5 Hz, $^2J_{YC}$ = 5 Hz, $YOCH_2CH_2OY$), 11.28 (s, C_5Me_5). Anal. Calcd for $C_{50}H_{80}O_4Y_2(THF)$: C, 65.18; H, 8.91; Y, 17.87. Found: C, 65.08; H, 8.99; Y, 17.69.

X-ray Structure Determination of $(Cp^*_2Y)_2(\mu\text{-}OCH_2CH_2O)(THF)_2$ (8). A colorless, block-shaped crystal was glued to the tip of a glass fiber and transferred into the cold nitrogen stream on an Enraf-Nonius CAD4-Turbo diffractometer on rotating anode. Accurate unit cell parameters and an orientation matrix were determined by least-squares refinement of the setting angles of 25 well-centered reflections (SET4) in the range 10.6° < θ < 13.8°. The unit cell parameters were checked for the presence of higher lattice symmetry.[38] Crystal data and details on data collection and refinement are presented in Table 4. All data were collected in $\omega/2\theta$ scan mode. Data were corrected for *Lp* effects and the observed linear decay. An empirical absorption and extinction correction was applied (DIFABS[39]). The structure was solved by automated Patterson methods and subsequent difference Fourier techniques (DIRDIF-92[40]). Refinement on F^2 was carried out by full-matrix least-squares techniques (SHELXL-93[41]); no observance criterium was applied during refinement. Hydrogen atoms were included in the refinement on calculated positions (C−H = 0.98 Å) riding on their carrier atoms. The Cp* moiety containing atom C11 appeared to be disordered over two positions. The site occupation factor of the major component of the disorder model refined to a value of 0.677(9). All non-hydrogen atoms were refined with anisotropic thermal parameters, except for the minor component of the disordered Cp* moiety. The hydrogen atoms were refined with a fixed isotropic thermal parameter related to the value of the equivalent isotropic thermal parameter of their carrier atoms by a factors of 1.5 for the methyl hydrogen atoms and 1.2 for the other hydrogen atoms, respectively. Final positional parameters are listed in Table 5. Neutral atom scattering factors and anomalous dispersion corrections were taken from *International Tables of Crystallography*.[42] Geometrical calculations and illustrations were performed with PLATON.[43] All calculations were performed on a DECstation 5000/125.

Table 4. Details of the X-ray Structure Determinations of $(Cp^*_2Y)_2(\mu\text{-}OCH_2CH_2O)(THF)_2$ (8) and $(Cp^*_2Ce)_2(\mu\text{-}O)(THF)_2$ (12)

formula	$C_{50}H_{80}O_4Y_2{\cdot}C_4H_8O$ (**8**)	$C_{48}H_{76}Ce_2O_3{\cdot}(C_4H_8O)_2$ (**12**)
molecular weight	995.10	1125.59
crystal system	orthorhombic	triclinic
space group	*Pbcn* (no. 60)	$P\bar{1}$ (no. 2)
a, Å	21.7483(12)	13.399(2)
b, Å	14.2806(12)	14.864(4)
c, Å	16.726(2)	15.812(6)
α, deg		70.75(2)
β, deg		85.15(2)
γ, deg		63.78(2)
V, Å^3	5194.7(8)	2660(2)
D_{calc}, g cm^{-3}	1.272	1.405
Z	4	2
$F(000)$	2120	1168
μ, cm^{-1}	22.8	17.6
crystal size, mm	0.5 × 0.5 × 0.5	0.10 × 0.22 × 0.25
T, K	150	130
θ range, deg	0.94, 24.20	1.37, 23.0
wavelength (Mo Kα), Å	0.71073 (graphite monochromator)	0.71073 (graphite monochromator)
scan type	$\omega/2\theta$	$\omega/2\theta$
scan, deg	0.85 + 0.35 tan θ	0.90 + 0.35 tan θ
hor, ver aperture, mm	2.77, 4.00	3.2 + tan θ, 4.0
X-ray exposure time, h	22	169.6
linear decay, %	1	10
instability constant P		0.029
reference reflections	207, 521, 252	531, −5,1,−1
data set (*hkl*)	−25 to 0, −16 to 0, −19 to +19	−14 to +14, −15 to +16, −1 to +17
total data	8947	8379
unique data	4163, R_{int} = 0.08	7421, R_{int} = 0.04
DIFABS corr range	0.871, 1.153	
no. of refined parameters	332	797
R^a	0.063 for 2200, $F_o > 4\sigma(F_o)$	0.038 for 6294, $I > 2.5\sigma$
wR^b		0.049
$wR2^c$	0.144	
$w^{-1\,d}$	$\sigma^2(F^2) + (0.0488P)^2$	$\sigma(F^2)$
S	0.995	2.670
$(\Delta/\sigma)_{mean}$, $(\Delta/\sigma)_{max}$	0.005, −0.123	0.026, 0.403
min residual density, e Å^{-3}	−0.39	−1.43
max residual density, e Å^{-3}	0.43	1.27

^{a} $R = \sum||F_o| - |F_c||/\sum|F_o|$. ^{b} $R_w = [\sum[(w|F_o| - |F_c|^2)/\sum w|F_o|^2]]^{1/2}$. ^{c} $wR2 = [\sum[w(F^2_o - F^2_c)^2]/\sum[w(F^2_o)^2]]^{1/2}$. ^{d} $P = (\max(F^2_o, 0) + 2F^2_c)/3$.

NMR Tube Reaction of 1a with Furan. To a suspension of 0.019 g (0.026 mmol) of **1a** in 0.5 mL of cyclohexane-d_{12} was added 3.8 μL (0.053 mmol) of furan. Immediately evolution of a gas was observed and **1a** dissolved completely. The solution was transferred to an NMR tube, and ^{1}H NMR showed the complete conversion of **1a** to **9**: ^{1}H NMR (200 MHz,

(38) Spek, A. L. *J. Appl. Crystallogr.* **1988**, *21*, 578.
(39) Walker, N.; Stuart, D. *Acta Crystallogr.* **1983**, *A39*, 158.
(40) Beurskens, P. T.; Admiraal, G.; Beurskens, G.; Bosman, W. P.; García-Granda, S.; Gould, R. O.; Smits, J. M. M.; Smykalla, C. The DIRDIF program system. Technical report of the Crystallography Laboratory, University of Nijmegen, The Netherlands, 1992.
(41) Shelldrick, G. M. Program for crystal structure refinement. University of Göttingen, Germany, 1992.
(42) Wilson, A. J. C., Ed. *International Tables of Crystallography*; Kluwer Academic Publishers: Dordrecht, The Netherlands, 1992; Vol. C.
(43) Spek, A. L. *Acta Crystallogr.* **1990**, *A46*, C34.

Table 5. Final Fractional Atomic Coordinates and Equivalent Isotropic Thermal Parameters of the Non-Hydrogen Atoms for $(Cp^*_2Y)_2(\mu\text{-}OCH_2CH_2O)(THF)_2$ (8)

atom	x	y	z	U_{eq}[a] (Å^2)
Y(1)	0.12314(3)	0.19694(4)	0.09224(3)	0.0292(2)
O(1)	0.0524(2)	0.1611(3)	0.1665(2)	0.0333(17)
O(2)	0.1425(2)	0.3325(3)	0.1730(3)	0.0440(17)
C(1)	0.1674(3)	0.0360(5)	0.1477(4)	0.031(2)
C(2)	0.1964(3)	0.1043(5)	0.1918(4)	0.043(3)
C(3)	0.2384(3)	0.1525(5)	0.1413(5)	0.047(3)
C(4)	0.2337(3)	0.1127(5)	0.0662(4)	0.044(3)
C(5)	0.1903(3)	0.0404(5)	0.0687(4)	0.035(3)
C(6)	0.1233(4)	−0.0336(5)	0.1781(5)	0.067(3)
C(7)	0.1864(4)	0.1221(7)	0.2794(4)	0.085(4)
C(8)	0.2850(4)	0.2227(6)	0.1692(8)	0.116(6)
C(9)	0.2798(4)	0.1345(6)	−0.0006(6)	0.089(4)
C(10)	0.1754(5)	−0.0290(5)	0.0049(5)	0.087(4)
*C(11A)[b]	0.0257(7)	0.2328(12)	−0.0077(9)	0.062(7)
*C(11B)	0.1329(9)	0.2989(18)	−0.0404(13)	0.001(5)
*C(12A)	0.0622(11)	0.3158(13)	0.0037(10)	0.071(8)
*C(12B)	0.0966(16)	0.219(2)	−0.064(3)	0.09(2)
*C(13A)	0.1158(9)	0.3078(16)	−0.0386(13)	0.083(9)
*C(13B)	0.0450(12)	0.2149(19)	−0.0174(19)	0.021(8)
*C(14A)	0.1204(8)	0.2173(7)	−0.0678(6)	0.029(4)
*C(14B)	0.0356(9)	0.3028(16)	0.0162(16)	0.013(6)
*C(15A)	0.0654(5)	0.1766(7)	−0.0496(6)	0.033(4)
*C(15B)	0.0879(10)	0.3512(13)	0.0010(14)	0.019(7)
*C(16A)	−0.0349(6)	0.2179(16)	0.0188(8)	0.161(14)
*C(16B)	0.1839(11)	0.334(2)	−0.0841(17)	0.073(10)
*C(17A)	0.0391(12)	0.4077(13)	0.0417(12)	0.240(16)
*C(17B)	0.1117(16)	0.141(2)	−0.1249(19)	0.115(14)
*C(18A)	0.1689(9)	0.3797(11)	−0.0494(9)	0.130(9)
*C(18B)	−0.0067(13)	0.1411(18)	−0.0237(18)	0.083(10)
*C(19A)	0.1644(6)	0.1768(10)	−0.1286(6)	0.068(6)
*C(19B)	−0.0174(10)	0.3371(18)	0.0645(15)	0.057(8)
*C(20A)	0.0446(7)	0.0809(8)	−0.0821(7)	0.081(6)
*C(20B)	0.1007(10)	0.4527(13)	0.0258(13)	0.040(6)
C(21)	−0.0017(4)	0.1485(5)	0.2057(4)	0.049(3)
C(22)	0.1850(4)	0.4084(6)	0.1690(7)	0.095(5)
C(23)	0.1858(5)	0.4542(8)	0.2455(6)	0.117(6)
C(24)	0.1350(5)	0.4132(8)	0.2930(5)	0.106(5)
C(25)	0.1022(4)	0.3545(6)	0.2367(5)	0.069(3)
O(3)	0	0.5594(10)	1/4	0.293(15)
C(26)	0.0068(11)	0.6163(9)	0.1838(9)	0.242(15)
C(27)	0.0155(8)	0.7013(9)	0.2120(6)	0.157(8)

[a] U_{eq} = one-third of the trace of the orthogonalized U. [b] Starred atom sites have a population less than 1.0.

cyclohexane-d_{12}) δ 7.49 (m, 1H, H5), 6.27 (broad s, 2H, H3 and H4), 1.79 (s, 30H, C_5Me_5).

$Cp^*_2Y(2\text{-}OC_4H_3)(THF)_2$ (10). To a stirred suspension of 1.50 g (2.56 mmol) of $Cp^*_2Cl(LiCl)(Et_2O)_2$ in 35 mL of Et_2O was added 4.10 mL of a 0.620 M solution (2.54 mmol) of 2-lithiofuran in THF. The reaction mixture turned yellow within several minutes. After 1.5 h, volatiles were removed under vacuum and the solid was stripped with pentane. Extraction with 20 mL of pentane, concentration, and cooling to −30 °C gave 0.354 g (0.620 mmol, 24%) of yellow crystals: IR (cm^{-1}) 1543(w), 1173(m), 1117(m), 1045(s), 1003(s), 916(s), 891(s), 831(m), 795(m), 710(s), 590(s); ^{1}H NMR (300 MHz, benzene-d_6) δ 7.48 (m, 1H, H5), 6.51 (m, 1H, H3 or H4), (pseudo d, J = 2.9 Hz, 1H, H3, or H4), 3.41 (m, 8H, α-THF), 2.16 (s, 30H, C_5Me_5), 1.29 (m, 8H, β-THF); ^{13}C NMR (75.4 MHz, benzene-d_6) δ 210.09 (d, $^1J_{CY}$ = 62 Hz, C2), 142.35 (ddd, $^1J_{CH}$ = 193 Hz, J = 13 Hz, J = 6 Hz, C5), 119.55 (d, $^1J_{CH}$ = 166 Hz, C3), 116.50 (s, C_5Me_5), 110.05 (ddd, $^1J_{CH}$ = 170 Hz, J = 14 Hz, J = 6 Hz, C4), 68.21 (t, $^1J_{CH}$ = 147 Hz, α-THF), 25.32 (t, $^1J_{CH}$ = 133 Hz, β-THF), 11.89 (q, $^1J_{CH}$ = 126 Hz, C_5Me_5). It was not possible to obtain satisfactory elemental analysis data due to THF dissociation.

NMR Tube Reaction of 1a with Vinyl Ethyl Ether. In an NMR tube 0.030 g (0.042 mmol) of **1a** was added to a mixture of 8.0 μL (0.083 mmol) of vinyl ethyl ether and 0.5 mL of benzene-d_6. Upon addition of **1a** the solution turned yellow. ^{1}H NMR after 20 min at room temperature showed the formation of **2a** in quantitative yield.

Reaction of 1a with Vinyl Ethyl Ether: Gas Analysis and GC/MS Analysis. A mixture of 210 μL (2.20 mmol) of vinyl ethyl ether and 4.3 mL of toluene was condensed onto 0.270 g (0.375 mmol) of **1a** at −196 °C. The mixture was allowed to reach room temperature with stirring, during which the solution turned yellow. After stirring for 15 h, gasses were collected by Töpler pump and analyzed by GC: 0.03 mmol of ethylene (0.04 mol/mol of Y). The remaining volatiles were removed in vacuum and identified as toluene and vinyl ethyl ether by GC. The yellow residue was identified as **2a** by ^{1}H NMR. The solid was dissolved in 10 mL of toluene, and then 250 μL of methanol and 150 μL of water were added. The liquid was dried over $MgSO_4$ and filtrated. GC/MS analysis showed the presence of C_{16}−C_{22} alkanes with exclusively even numbers of carbon atoms.

NMR Tube Reaction of 1a with Allyl Ethyl Ether. 1a (18.0 mg, 0.025 mmol) was dissolved in 0.5 mL of benzene-d_6, and 64 μL (0.56 mmol) of allyl ethyl ether was added, upon which the solution turned yellow. After 5 min at room temperature, ^{1}H NMR showed that **1a** had completely been converted to the allyl ethyl ether adduct of **2a** (57%) and some unidentified products.

Reaction of 1a with Allyl Ethyl Ether: Gas Analysis. On a vacuum line 10 mL of toluene and 50 μL (0.44 mmol) of allyl ethyl ether were condensed onto 0.133 g (0.185 mmol) of **1a** at −196 °C. The reaction mixture was stirred at room temperature for 15 min, and the gasses evolved were pumped off through a cold trap at −80 °C and analyzed as 0.046 mmol of propane (0.12 mol/mol of Y) and 0.162 mmol of propene (0.44 mol/mol of Y) by GC.

$(Cp^*_2Y)_2(\mu\text{-}O)$ (11a). On a vacuum line, a bulb containing 0.986 g (1.37 mmol) of **1a** was evacuated. Next, 20 mL of cyclohexane and 140 μL (1.35 mmol) of Et_2O were condensed on the solid at −196 °C. After stirring for 0.5 h at room temperature, the gasses evolved were collected by Töpler pump and analyzed by GC: 1.34 mmol of ethane (0.49 mol/mol of Y). After stirring for 4 days at 80 °C, the gasses evolved were collected and analyzed: 1.29 mmol of ethane (0.47 mol/mol of Y). Volatiles were removed in vacuum, and crystallization from THF afforded 0.703 g (0.957 mmol, 70%) of colorless crystals. **11a**: IR (cm^{-1}) 2900(s), 2726(w), 1460(s), 1377(s), 1306(w), 1150(m), 1067(w), 1020(m), 723(m), 658(s), 625(m), 590(w); ^{1}H NMR (300 MHz, benzene-d_6) δ 2.02 (s, C_5Me_5); ^{13}C NMR (75.4 MHz, benzene-d_6) δ 117.6 (s, C_5Me_5), 12.06 (q, $^1J_{CH}$ = 124 Hz, C_5Me_5). Anal. Calcd for $C_{40}H_{60}OY_2$: C, 65.39; H, 8.23; Y, 24.20. Found: C, 65.05; H, 8.36; Y, 23.21. MS (EI, 70 eV): m/e 734 (M^+).

NMR Tube Reaction: $(Cp^*_2La)_2(\mu\text{-}O)$ (11b). In an NMR tube 0.014 g (0.017 mmol) of **1b** was dissolved in 0.5 mL of cyclohexane-d_{12}, and 1.8 μL (0.017 mmol) of Et_2O was added. In 24 h at 80 °C colorless crystals were formed. In the ^{1}H-NMR spectrum resonances of **11b** and ethane (δ 0.84) were observed. **11b**: ^{1}H NMR (300 MHz, cyclohexane-d_{12}) δ 1.95 (s, C_5Me_5); the NMR tube was opened, volatiles were removed in vacuum, and the residue was dissolved completely in THF-d_8; ^{1}H NMR (300 MHz, THF-d_8) δ 1.99 (s, C_5Me_5).

NMR Tube Reaction: $(Cp^*_2Ce)_2(\mu\text{-}O)(THF)_2$ (12). In an NMR tube 0.021 g (0.025 mmol) of **1c** was dissolved in 0.5 mL of cyclohexane-d_{12} and 3.5 μL (0.034 mmol) of Et_2O was added. The reaction was monitored by ^{1}H NMR spectroscopy. After 24 h at room temperature, the Et_2O was completely converted to **2c** and ethane (δ 0.84) was observed. **2c**: ^{1}H NMR (90 MHz, cyclohexane-d_{12}) δ 26.9 (s, $\Delta\nu_{1/2}$ = 150 Hz, 2H, $CeOCH_2$), 7.62 (s, $\Delta\nu_{1/2}$ = 100 Hz, 3H, $CeOCH_2CH_3$), 1.93 (s, $\Delta\nu_{1/2}$ = 50 Hz, 30 H, C_5Me_5). In 24 h at 80 °C green crystals were formed. Volatiles were removed in vacuum, and the residue was redissolved in THF-d_8, upon which a yellow solution formed. ^{1}H NMR showed resonances which were assigned to $Cp^*_2CeOEt(THF\text{-}d_8)$ and $(Cp^*_2Ce)_2(\mu\text{-}O)(THF\text{-}d_8)_2$ (1.1:1.0). $Cp^*_2CeOEt(THF\text{-}d_8)$: ^{1}H NMR (300 MHz, THF-d_8) δ 22.48 (s,

2H, $CeOCH_2$), 6.26 (s, 3H, $CeOCH_2CH_3$), 2.24 (s, 30H, C_5Me_5). $(Cp^*_2Ce)_2(\mu\text{-}O)(THF\text{-}d_8)_2$: ^1H NMR (300 MHz, THF-d_8) δ 3.54 (s, $\Delta\nu_{1/2}$ = 15 Hz, C_5Me_5); ^{13}C NMR (75.4 Mhz, THF-d_8) δ 128.45 (s, C_5Me_5), 5.01 (q, $^1J_{CH}$ = 121.5 Hz, C_5Me_5). Crystals of **12** were obtained by slow diffusion of pentane into a THF solution of **11c**.

X-ray Structure Determination of $(Cp^*_2Ce)_2(\mu\text{-}O)(THF)_2$ (12). A suitable yellow block-shaped crystal was glued on the top of a glass fiber in a drybox and transferred into the cold nitrogen stream of the low-temperature unit mounted on an Enraf-Nonius CAD-4F diffractometer interfaced to a PDP-11/23 computer. Unit cell dimensions and their standard deviations were determined from the setting angles of 21 reflections in the range $12.01° < \theta < 19.99°$. Reduced cell calculations did not indicate any higher lattice symmetry.[44] A search of a limited hemisphere of reciprocal space yielded a set of reflections that showed no evidence of symmetry or systematic extinction. The unit cell was identified as triclinic, space group $P\bar{1}$. This choice was confirmed by the solution and the successful refinement of the structure in this space group. Two reference reflections measured every 3 h of X-ray exposure indicated a linear decay of 10% over 169.6 h of X-ray exposure time. The net intensities of the data were corrected for the scale variation and Lorentz and polarization effects, but not for absorption. Standard deviation $\sigma(I)$ in the intensities was increased according to an analysis of the excess variance of the reference reflection: Variance was calculated based on counting statistics and the term (P^2I^2) where P (=0.029) is the instability constant[45] as derived from the excess variance in the reference reflections. The structure was solved by Patterson methods and subsequent partial structure expansion (SHELXS86[46]). Refinement with isotropic temperature factors and subsequent Fourier synthesis revealed the three remaining non-hydrogen atoms and the two solvent molecules. It was obvious from the Fourier synthesis that the THF solvent groups [O4–C52] and [O5–C56] show some degree of disorder. Refinement using anisotropic thermal parameters followed by difference Fourier synthesis resulted in the location of all the nonsolvent hydrogen atoms. The solvent hydrogen atoms were introduced on calculated positions by using sp^3 hybridization at the C atom as appropriate and a fixed C–H distance of 1.0 Å included in the refinement in the riding mode. The C1 atom converged to nonpositive definite thermal parameters when allowed to vary anisotropically. Weights were introduced in the final refinement cycles. Refinement on F_o by block-diagonal least-squares techniques with anisotropic thermal parameters for the non-hydrogen atoms and one common isotropic thermal parameter for the hydrogen atoms converged at $R = 0.038$ ($wR = 0.049$). A final difference Fourier synthesis reveals residual densities between −1.43 and 1.27 e/Å^3. Crystal data and experimental details of the structure determination are listed in Table 4. The final fractional atomic coordinates and equivalent isotropic thermal parameters for the non-hydrogen atoms are given in Table 6. Scattering factors were taken from Cromer and Mann.[47] Anomalous dispersion factors were taken from Cromer and Liberman.[48] All calculations were carried out on a CDC-Cyber 170/760 computer with the program packages XTAL,[49] EUCLID[50] (calculation of geometric data), and ORTEP[51] (preparation of illustrations).

(44) Le Page, Y. *J. Appl. Crystallogr.* **1982**, *15*, 255.
(45) McCandlish, L. E.; Stout, G. H.; Andrews, L. C. *Acta Crystallogr.* **1975**, *A31*, 245.
(46) Sheldrick, G. M. SHELXS86, Program for crystal structure solution. University of Göttingen, Germany, 1986.
(47) Cromer, D. T.; Mann, J. B. *Acta Crystallogr.* **1968**, *A24*, 321.
(48) Cromer, D. T.; Liberman, D. *J. Chem. Phys.* **1970**, *53*, 1891.
(49) Hall, S. R.; Stewart, J. H. *XTAL2.2 User's Manual*; Computer Science Center: University of Maryland, College Park, MD, 1987.
(50) Spek, A. L. In *Computational Crystallography*; Sayre, D., Ed.; Clarendon Press: Oxford, England, 1982; p 528.
(51) Johnson, C. K. ORTEP. Report ORNL-3794, Oak Ridge National Laboratory, Oak Ridge, TN, 1965.

Table 6. Final Fractional Atomic Coordinates and Equivalent Isotropic Thermal Parameters of the Non-Hydrogen Atoms for $(Cp^*_2Ce)_2(\mu\text{-}O)(THF)_2$ (12)

	x	y	z	U_{eq}[a] (Å^2)
		Residue 1		
Ce(1)	0.17242(3)	0.22134(2)	0.31961(2)	0.0125(1)
Ce(2)	0.27758(3)	0.47499(3)	0.24100(2)	0.0134(1)
O(1)	−0.0025(3)	0.2856(3)	0.4096(3)	0.022(1)
O(2)	0.1310(3)	0.6270(3)	0.1134(3)	0.022(1)
O(3)	0.2189(3)	0.3524(3)	0.2783(3)	0.017(1)
C(1)[b]	0.1139(5)	0.2854(5)	0.1349(4)	0.017(2)
C(2)	0.0090(5)	0.3132(5)	0.1735(4)	0.016(2)
C(3)	−0.0008(5)	0.2200(5)	0.2221(4)	0.019(2)
C(4)	0.0975(5)	0.1331(5)	0.2132(4)	0.020(2)
C(5)	0.1700(5)	0.1725(5)	0.1609(4)	0.017(2)
C(6)	0.1525(5)	0.3619(5)	0.0745(4)	0.020(2)
C(7)	−0.0802(5)	0.4239(5)	0.1636(4)	0.023(2)
C(8)	−0.1033(5)	0.2128(5)	0.2608(5)	0.028(2)
C(9)	0.1115(6)	0.0206(5)	0.2392(5)	0.032(3)
C(10)	0.2777(5)	0.1093(5)	0.1289(5)	0.026(2)
C(11)	0.2422(5)	0.0300(5)	0.4756(4)	0.020(2)
C(12)	0.3151(5)	−0.0019(5)	0.4104(4)	0.020(2)
C(13)	0.3828(5)	0.0517(5)	0.3930(4)	0.020(2)
C(14)	0.3546(5)	0.1148(5)	0.4494(4)	0.021(2)
C(15)	0.2660(5)	0.1024(5)	0.5006(4)	0.022(2)
C(16)	0.1675(5)	−0.0207(5)	0.5223(5)	0.029(3)
C(17)	0.3359(5)	−0.0954(5)	0.3829(5)	0.029(2)
C(18)	0.4816(5)	0.0293(5)	0.3363(5)	0.024(2)
C(19)	0.4148(5)	0.1758(5)	0.4572(5)	0.024(2)
C(20)	0.2149(5)	0.1483(5)	0.5728(5)	0.027(2)
C(21)	0.3940(5)	0.4630(5)	0.0836(4)	0.021(2)
C(22)	0.4413(5)	0.3570(5)	0.1438(4)	0.020(2)
C(23)	0.5049(5)	0.3516(5)	0.2137(4)	0.018(2)
C(24)	0.4990(5)	0.4534(5)	0.1983(4)	0.022(2)
C(25)	0.4297(5)	0.5222(5)	0.1173(4)	0.022(2)
C(26)	0.3276(5)	0.5021(5)	−0.0033(5)	0.026(2)
C(27)	0.4359(5)	0.2649(5)	0.1304(5)	0.025(2)
C(28)	0.5834(5)	0.2523(5)	0.2843(5)	0.030(2)
C(29)	0.5757(6)	0.4735(5)	0.2452(5)	0.030(2)
C(30)	0.4097(5)	0.6357(5)	0.0734(5)	0.029(2)
C(31)	0.2118(5)	0.4961(5)	0.4093(4)	0.017(2)
C(32)	0.3147(5)	0.5040(5)	0.4035(4)	0.022(2)
C(33)	0.2968(5)	0.6017(5)	0.3397(4)	0.022(2)
C(34)	0.1848(5)	0.6574(5)	0.3053(4)	0.021(2)
C(35)	0.1309(5)	0.5916(5)	0.3482(4)	0.019(2)
C(36)	0.1872(5)	0.4101(5)	0.4708(4)	0.020(2)
C(37)	0.4188(6)	0.4243(5)	0.4612(5)	0.029(2)
C(38)	0.3759(6)	0.6527(6)	0.3249(5)	0.034(3)
C(39)	0.1272(6)	0.7703(5)	0.2474(5)	0.034(3)
C(40)	0.0090(5)	0.6241(5)	0.3341(5)	0.026(2)
C(41)	−0.0655(5)	0.3953(5)	0.4064(5)	0.025(2)
C(42)	−0.1853(5)	0.4138(5)	0.4028(5)	0.030(2)
C(43)	−0.1801(6)	0.3087(6)	0.4642(5)	0.034(3)
C(44)	−0.0585(6)	0.2284(5)	0.4699(5)	0.030(2)
C(45)	0.0261(6)	0.6260(6)	0.0977(5)	0.032(3)
C(46)	−0.0578(5)	0.7394(5)	0.0749(5)	0.032(3)
C(47)	0.0056(6)	0.7985(6)	0.0200(5)	0.041(3)
C(48)	0.1263(6)	0.7241(5)	0.0479(5)	0.032(3)
		Residue 2		
O(4)	0.4632(9)	0.173(1)	0.8151(8)	0.171(6)
C(49)	0.3786(9)	0.259(1)	0.7382(9)	0.115(6)
C(50)	0.278(1)	0.306(1)	0.767(1)	0.22(1)
C(51)	0.313(1)	0.280(1)	0.862(1)	0.23(2)
C(52)	0.413(1)	0.205(1)	0.8914(9)	0.17(1)
		Residue 3		
O(5)	0.699(1)	−0.004(1)	0.085(1)	0.25(1)
C(53)	0.748(1)	−0.021(1)	0.1693(9)	0.16(1)
C(54)	0.796(1)	0.043(2)	0.158(1)	0.32(2)
C(55)	0.828(1)	0.066(1)	0.076(1)	0.24(1)
C(56)	0.749(1)	0.0636(9)	0.026(1)	0.16(1)

[a] $U_{eq} = 1/3\sum_i\sum_j U_{ij}a_ia_j\mathbf{a}_i\cdot\mathbf{a}_j$. [b] Nonpositive definite temperature factors.

NMR Tube Reaction of 1a with Me_2S. To a suspension of 30.4 mg (0.0422 mmol) of **1a** in 0.5 mL of cyclohexane-d_{12} was added 6.2 μL (0.085 mmol) of Me_2S. Immediately after addition, gas evolution was observed and **1a** dissolved. The reaction mixture was transferred to an NMR tube, and the

tube was sealed under vacuum. The ^{1}H NMR spectrum after 0.5 h at room temperature showed that **13** (75%) and an unidentified compound had been formed. When performed with an excess of Me_2S (Me_2S:Y = 10), this unidentified product was absent. **13**: ^{1}H NMR (200 MHz, cyclohexane-d_{12}) δ 2.21 (s, 3H, SMe), 1.91 (s, 30H, C_5Me_5), 1.33 (broad s, 2H, YCH_2). Unidentified compound: ^{1}H NMR (200 MHz, cyclohexane-d_{12}) δ 1.94 (s, C_5Me_5).

Cp*$_2$YCH$_2$SMe(THF) (14). To a stirred suspension of 0.53 g (0.74 mmol) of $(Cp^*_2YH)_2$ in 20 mL of pentane was added 108 μL (1.5 mmol) of Me_2S. Gas evolution was observed, and $(Cp^*_2YH)_2$ dissolved completely. After 10 min at room temperature, the orange solution was cooled to −30 °C, affording 0.50 g of pink crystals. The pink material was recrystallized from and washed with pentane:THF (2:1), affording 0.31 g (0.63 mmol, 43%) of white crystals. **14**: IR (in cm^{-1}) 2726(m), 2672(w), 1303(m), 1169(w), 1157(w), 1015(m), 970(w), 864(m), 839(m), 721(m); ^{1}H NMR (200 MHz, benzene-d_6) δ 3.44 (m, 4H, α-THF), 2.27 (s, 3H, SMe), 2.03 (s, 30H, C_5Me_5), 1.23 (m, 4H, β-THF), 1.19 (d, $^2J_{HY}$ = 2.6 Hz, 2H, YCH_2); ^{13}C NMR (75.4 MHz, benzene-d_6) δ 116.88 (s, C_5Me_5), 69.79 (t, $^1J_{CH}$ = 149 Hz, α-THF), 37.69 (td, $^1J_{CH}$ = 123 Hz, $^1J_{CY}$ = 46 Hz, YCH_2), 25.97 (q, SMe, overlaps with β-THF), 25.27 (t, $^1J_{CH}$ = 131 Hz, β-THF), 11.37 (q, $^1J_{CH}$ = 126 Hz, C_5Me_5). Anal. Calcd for $C_{26}H_{43}OSY$: C, 63.40; H, 8.80; Y, 18.05. Found: C, 63.40; H, 8.77; Y, 18.25.

NMR Tube Reaction of 1a with Benzyl Methyl Sulfide. To a solution of 0.015 g (0.020 mmol) of **1a** was added 5.5 μL (0.040 mmol) of benzyl methyl sulfide. Immediately gas evolution was observed as was a color change to yellow. ^{1}H NMR after 40 min at room temperature showed the essentially quantitative formation of **15**: ^{1}H NMR (300 MHz, cyclohexane-d_{12}) 7.21 (m, 1H, aryl H), 6.94 (m, 3H, aryl H), 6.64 (m, 1H, aryl H), 3.43 (d, $^2J_{HY}$ = 3.0 Hz, 1H, YCH), 2.19 (s, 3H, SMe), 2.03 (s, 15H, C_5Me_5), 1.74 (s, 15H, C_5Me_5).

Cp*$_2$YSEt(THF) (17). To a stirred suspension of 1.50 g (2.08 mmol) of **1a** in 50 mL of pentane was added 0.95 mL (8.8 mmol) of Et_2S. After 6 days at room temperature, a red solution with a yellow precipitate had been formed. The volatiles were removed in vacuum, and the solid was washed with 50 mL of pentane. The residue was dissolved in 5 mL of THF and cooling afforded 0.550 g (1.12 mmol, 27%) of **17** as white crystals: IR (cm^{-1}) 2724(w), 1244(s), 1014(s), 959(w), 918(w), 860(s), 766(w), 665(m), 592(w); ^{1}H NMR (200 MHz, THF-d_8) δ 2.70 (q, $^3J_{HH}$ = 7.3 Hz, 2H, SCH_2), 1.96 (s, 30H, C_5Me_5), 1.19 (t, $^3J_{HH}$ = 7.3 Hz, 3H, CH_2CH_3); ^{13}C NMR (75.4 MHz, THF-d_8) δ 119.09 (s, C_5Me_5), 24.99 (t, $^1J_{CH}$ = 136 Hz, SCH_2CH_3), 23.20 (q, $^1J_{CH}$ = 125 Hz, SCH_2CH_3), 12.85 (q, $^1J_{CH}$ = 125 Hz, C_5Me_5). Anal. Calcd for $C_{26}H_{43}OSY$: C, 63.40; H, 8.80; Y, 18.05. Found: C, 63.30; H, 8.81; Y, 18.14.

Cp*$_2$Y(2-SC$_4$H$_3$)(THF) (19). $(Cp^*_2YH)_2$ (0.876 g, 1.22 mmol) was suspended in 30 mL of pentane, and 200 μL (2.38 mmol) of thiophene was added with stirring. Immediately gas evolution was observed along with the formation of a white solid. Volatiles were removed in vacuum, and the pink residue was washed three times with 5 mL of pentane. Recrystallization from THF afforded 0.900 g (1.75 mmol, 72%) of white crystals. **19**: IR (cm^{-1}) 3084(m), 3050(s), 2957(s), 2926(s), 2917(s), 2857(s), 2722(m), 1759(w), 1559(w), 1458(s), 1377(s), 1343(m), 1316(w), 1294(m), 1246(w), 1188(m), 1144(w), 1063(m), 1017(s), 955(w), 920(m), 864(s), 843(sh), 820(m), 812(m), 729(m), 683(s), 615(w), 592(m), 476(m); ^{1}H NMR (300 MHz, THF-d_8) δ 7.38 (d, $^3J_{HH}$ = 4.4 Hz, 1H, H5), 7.04 (dd, $^3J_{HH}$ = 4.2 Hz, $^3J_{HH}$ = 3.1 Hz, 1H, H4), 6.81 (d, $^3J_{HH}$ = 2.9 Hz, 1H, H3), 1.79 (s, 30H, C_5Me_5); ^{13}C NMR (75.4 MHz, THF-d_8) δ 180.24 (d, $^1J_{CY}$ = 62 Hz, C2), 133.68 (ddd, $^1J_{CH}$ = 159 Hz, $^3J_{CH}$ = 12 Hz, $^2J_{CH}$ = 6 Hz, C3), 128.24 (dt, $^1J_{CH}$ = 180 Hz, $^2J_{CH}$ = $^3J_{CH}$ = 9 Hz, C5), 127.16 (dt, $^1J_{CH}$ = 143 Hz, $^2J_{CH}$ = 7 Hz, C4), 118.05 (s, C_5Me_5), 11.72 (q, $^1J_{CH}$ = 126 Hz, C_5Me_5). Anal. Calcd for $C_{28}H_{41}OSY$: C, 65.35; H, 8.03; S, 6.23; Y, 17.28. Found: C, 65.46; H, 8.08; S, 5.32; Y, 17.28.

NMR Tube Reaction of 1a with Allyl Methyl Sulfide. To a suspension of 0.016 g (0.022 mmol) of **1a** in 0.5 mL of cyclohexane-d_{12} was added 5.0 μL (0.046 mmol) of allyl methyl sulfide. ^{1}H NMR (300 MHz) after 5 min at room temperature showed that 53% of **20** had been formed along with some unidentified products and unreacted allyl methyl sulfide. For NMR data see text.

Hydrogenation of Allyl Methyl Sulfide. To a suspension of 0.016 g (0.022 mmol) of **1a** in 0.5 mL of cyclohexane-d_{12} under H_2 (1 bar) was added 50 μL (0.46 mmol) of allyl methyl sulfide. ^{1}H NMR after stirring for 4 days at room temperature showed that 30% of the allyl methyl sulfide had been converted to *n*-propyl methyl sulfide (3.1 mol/mol of Y), while the remaining allyl methyl sulfide was present unreacted.

Acknowledgment. This investigation was supported by the Netherlands Organization for Chemical Research (SON) with financial aid from the Netherlands Foundation for the Advancement of Scientific Research (NWO).

Supplementary Material Available: Lists of atom coordinates and U values, all bond lengths and angles, torsion angles, and thermal parameters for **8** and **12** (40 pages). Ordering information is given on any current masthead page.

OM940986J

Dicarbonyl and Tricarbonyl Adducts of $(W{\equiv}W)^{6+}$-Containing Complexes. Preparation and Structures of $W_2(OCMe_2CF_3)_6(CO)_2$ and $W_2(OCMe(CF_3)_2)_4(NMe_2)_2(CO)_3$

Theodore A. Budzichowski, Malcolm H. Chisholm,* Darin B. Tiedtke, John C. Huffman, and William E. Streib

Department of Chemistry and Molecular Structure Center, Indiana University, Bloomington, Indiana 47405

Received September 26, 1994[⊗]

Carbon monoxide adds reversibly to $W_2(OR)_6$ compounds to give $W_2(OR)_6(CO)_2$ complexes (R = Si^{t}BuMe$_2$, **1**; CMe$_2$CF$_3$, **2**; 2,6-Me$_2$C$_6$H$_3$, **3**) wherein the CO ligands bond to alternate tungsten atoms in a manner that allows mixing of WW π and W dπ to CO π^* bonding. In contrast to the homoleptic alkoxides above, the mixed amido–alkoxide complex $W_2(OCMe(CF_3)_2)_4(NMe_2)_2$ (**4**), which also takes up 2 equiv of CO, reacts further to give $W_2(OCMe(CF_3)_2)_4(NMe_2)_2(CO)_3$ (**6**), which has an unusual structure wherein three CO ligands are bonded to a single tungsten atom and the W–W bond is supported by one NMe_2 bridge. The formation of **6** is also reversible. **2** and **6** have been characterized by single-crystal X-ray crystallography, and all compounds have been characterized by ^{1}H and ^{13}C{^{1}H} NMR spectroscopy. The results are compared to earlier studies of the addition of CO to $M_2(OR)_6$ complexes such as $W_2(O^tBu)_6$, which give bridged monocarbonyl adducts, and that of Wolczanski *et al.* (Miller, R. L.; Wolczanski, P. T.; Rheingold, A. L. *J. Am. Chem. Soc.* **1993**, *115*, 10422) wherein CO and $W_2Cl_2(silox)_4$ (silox = ^{t}Bu$_3$SiO) react reversibly to give a bis(carbonyl) adduct with subsequent cleavage to give $(silox)_2(O)W(\mu\text{-}C)W(silox)_2Cl_2$. For **2**, $C_{26}H_{36}F_{18}O_8W_2$, FW = 1186.2; a = 11.256(4), b = 18.496(6), c = 17.789(7) Å; β = 97.97(1)°; monoclinic $P2_1/n$, Z = 4. For **6**, $C_{23}H_{24}F_{24}N_2O_7W_2$, FW = 1264.1; a = 14.053(3), b = 21.148(5), c = 12.789(3) Å; α = 106.11(1), β = 103.15(1), γ = 86.81(1)°; triclinic $P\bar{1}$, Z = 4.

Introduction

Prior work has established that carbon monoxide will add across the M≡M bond in $M_2(OR)_6$ (M = Mo, W) complexes[1] to give $M_2(OR)_6(\mu\text{-CO})$ compounds that exhibit extremely low C–O stretching frequencies, e.g., ν(CO) ~1575 cm^{-1} in $W_2(O^tBu)_6(\mu\text{-CO})$ and $W_2(O^iPr)_6(\mu\text{-CO})(py)_2$.[1c] The electronic structure of the carbonyl adducts has been investigated by molecular orbital calculations employing the method of Fenske and Hall, and an understanding of the bonding has been obtained.[2] They are inorganic analogues of cyclopropenones, and the C–O bond is thereby weakened relative to a simple ketone. The oxygen is nucleophilic, as is evidenced by the formation of the "dimer of dimers" $[W_2(O^iPr)_6(\mu\text{-CO})]_2$ and $[W_2(O^iPr)_6(\mu\text{-CO})(py)]_2$.[1c,3] We were therefore most intrigued to learn that the related compound $W_2Cl_2(silox)_4$, where silox = OSi^{t}Bu$_3$, reacts with carbon monoxide to form a bis(carbonyl) adduct of proposed structure **A** which exhibits relatively high

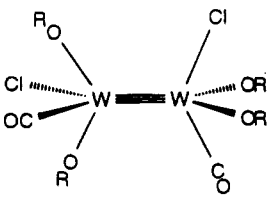

A

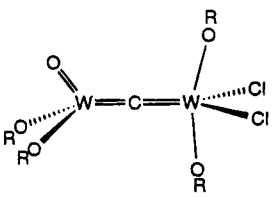

B

C–O stretching frequencies ν(CO) = 2035 and 2010 cm^{-1}.[4] Furthermore, upon heating $W_2Cl_2(silox)_4(CO)_2$ (120°, C_7D_8), 1 equiv of CO was lost (reversibly) and the remaining carbonyl ligand was cleaved to give $W_2(\mu\text{-}C)(O)_2Cl_2(silox)_4$ having the structure depicted by **B**.[4] This is an extremely rare example of the cleavage of C≡O (D = 256 kcal/mol) in coordination chemistry.[5]

Earlier attempts in this laboratory to prepare $W_2(OSi^tBuMe_2)_6(\mu\text{-CO})$ by the addition of HOSi^{t}BuMe$_2$ to $W_2(O^tBu)_6(\mu\text{-CO})$ resulted in failure.[6] Only $W_2(OSi^tBuMe_2)_6$ was isolated. The recent work by Wolczanski

[⊗] Abstract published in *Advance ACS Abstracts,* March 1, 1995.

(1) (a) Chisholm, M. H.; Cotton, F. A.; Extine, M. W.; Kelly, R. L. *J. Am. Chem. Soc.* **1979**, *61*, 7645. (b) Chisholm, M. H.; Huffman, J. C.; Leonelli, J.; Rothwell, I. P. *J. Am. Chem. Soc.* **1982**, *104*, 7030. (c) Chisholm, M. H.; Hoffman, D. M.; Huffman, J. C. *Organometallics* **1985**, *4*, 986.

(2) Blower, P. J.; Chisholm, M. H.; Clark, D. L.; Eichorn, B. W. *Organometallics* **1986**, *5*, 2127.

(3) Cotton, F. A.; Schwotzer, W. *J. Am. Chem. Soc.* **1983**, *105*, 4955.

(4) Miller, R. L.; Wolczanski, P. T.; Rheingold, A. L. *J. Am. Chem. Soc.* **1993**, *115*, 10422.

(5) (a) Chisholm, M. H.; Hammond, C. E.; Johnston, V. J.; Streib, W. E.; Huffman, J. C. *J. Am. Chem. Soc.* **1992**, *114*, 7056. (b) Chisholm, M. H. *J. Organomet. Chem.* **1987**, *334*, 77. (c) Neithamer, D. R.; LaPointe, R. E.; Wheeler, R. A.; Richeson, D. S.; Van Duyne, G. D.; Wolczanski, P. T. *J. Am. Chem. Soc.* **1989**, *111*, 9056. (d) Evans, W. J.; Grate, J. W.; Hughs, L. A.; Zhang, H.; Atwood, J. L. *J. Am. Chem. Soc.* **1985**, *107*, 3728. (e) Tachikawa, M.; Muetterties, E. L. *Prog. Inorg. Chem.* **1981**, *28*, 203.

(6) Dr. Cindy Cook, personal communication.

0276-7333/95/2314-2318$09.00/0

et al.[4] prompted us to reexamine the addition of CO to $(W{\equiv}W)^{6+}$ centers bearing less electron-donating ligands such as OSi^tBuMe_2, $OCMe_2CF_3$, and $O(2,6\text{-}Me_2C_6H_3)$. We report here the results of these initial investigations and the first structural characterizations of bis- and tris(carbonyl) adducts of $(W{\equiv}W)^{6+}$-containing compounds.

Results and Discussion

Carbon monoxide (≥2 equiv) was added by vacuum transfer to NMR tubes containing $W_2(OR)_6$ compounds where R = Si^tBuMe_2, CMe_2CF_3, and $2,6\text{-}Me_2C_6H_3$ in toluene-d_8 (0.03 M, −196 to 23 °C). By $^{13}C\{^1H\}$ and ^1H NMR spectroscopies, a reversible reaction occurred which favored the formation of bis(carbonyl) adducts, eq 1.

$$W_2(OR)_6 + 2CO \rightleftharpoons W_2(OR)_6(CO)_2 \quad (1)$$

1, R = Si^tBuMe_2
2, R = CMe_2CF_3
3, R = $2,6\text{-}Me_2C_6H_3$

The $^{13}C\{^1H\}$ NMR spectra clearly showed the presence of terminal carbonyl ligands based on their chemical shift (δ 217−241 ppm), $^1J_{^{183}W-^{13}C}$ coupling constants (106−124 Hz), and magnitude of the observed satellites (14%, ^{183}W; $I = {}^1/_2$, 14.3% natural abundance). Rather interestingly we have found no evidence for a monocarbonyl adduct (μ-CO) by NMR spectroscopy when R = Si^tBuMe_2 or CMe_2CF_3. When R = $2,6\text{-}Me_2C_6H_3$, the formation of a bis(CO) adduct is favored (≥80% of the product mixture) when 2 equiv of CO is added, but there was clear evidence for the formation of a mono(carbonyl) derivative. The latter apparently adopts a structure analogous to that observed for $[W_2(O^iPr)_6(\mu\text{-}CO)]_2$ based on the similarities of the spectroscopic data.[1c]

The reversibility of CO binding impedes the isolation of these adducts, but crystals may be obtained upon cooling hexane or toluene solutions of **1** and **2** under an atmosphere of CO. For **2**, the crystals were suitable for analysis by single-crystal X-ray diffraction (see Figure 1).

The fractional atomic coordinates from this study appear in Table 1, and pertinent bond distances and angles are summarized in Table 2. The striking features of the structure are the eclipsed geometry, the syn arrangement of the two CO ligands (C−W−W−C torsion angle, 100°) and the relatively small C−W−W angles of 81.7(6) and 84.4(5)°. The W−W distance of 2.4498(13) Å implies some loss of M−M bonding due to the presence of the π-acceptor carbonyl ligands. Pictorially the bonding can be described by **C** wherein it becomes

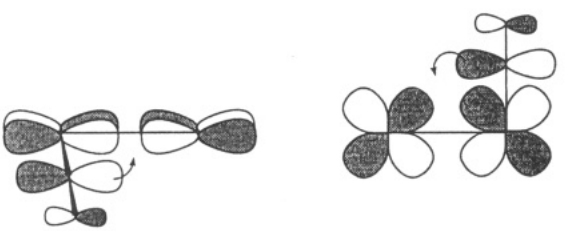

C

readily apparent that the CO ligands are involved in bonding to different M−M π-bonding orbitals. A mixing of M−M and M−CO π bonding is implied by **C**, and this presumably is responsible for the acute C−W−W angles observed in the solid state.

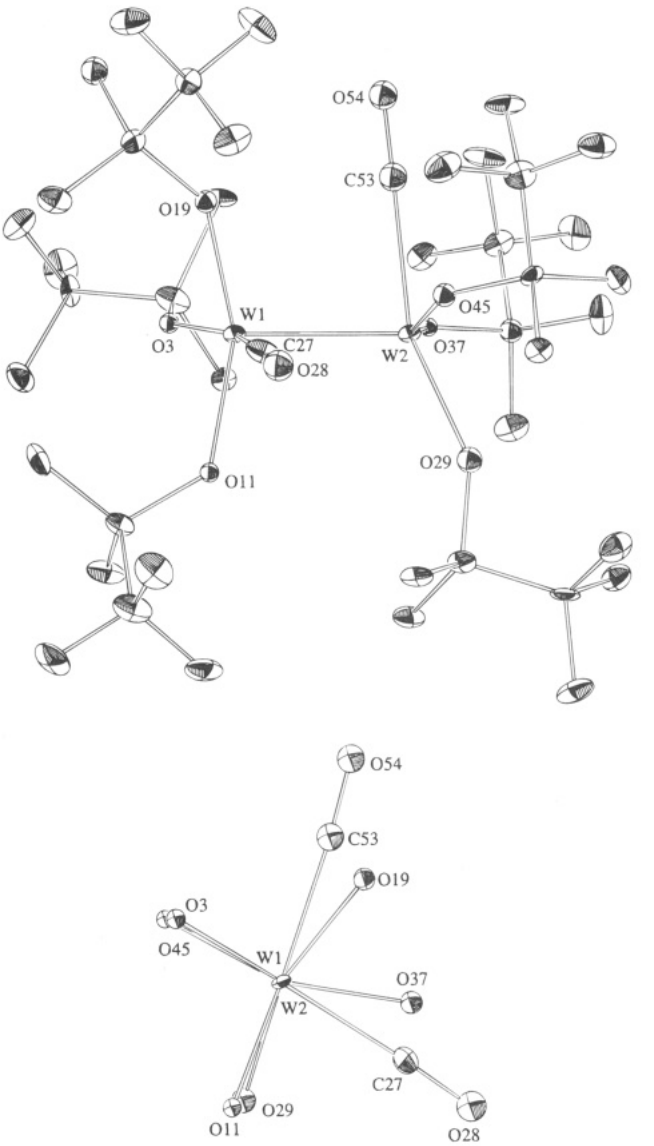

Figure 1. ORTEP view of the $W_2(OCMe_2CF_3)_6(CO)_2$ molecule giving the atom number scheme (top) and a view of the central $W_2O_6(CO)_2$ core looking down the W−W bond (bottom).

The observed structure cannot be favored by much over a structure where the two CO ligands are eclipsed and thus compete for the same M−M π-bonding orbital since only at low temperatures is rotation about the W−W bond frozen out on the NMR time scale. On the basis of the observed coalescence temperature (T_c = −20 °C), we estimate $\Delta G^{\ddagger}$ as ~11 kcal/mol.

A comparison of the infrared ν(CO) values for the two crystalline bis(carbonyl) adducts reported here and that of Wolczanski's compound is given in Table 3. These numbers provide an indication of the electron density at the metal, with lower ν(CO) values correlating with greater W dπ to CO π* donation, and presumably with alkoxide pπ to metal dπ donation, as was observed by Caulton and co-workers for a series of Ru(H)(X)(CO)-$(P^tBu_2Me)_2$ complexes.[7] We attribute the observation of three CO stretches in the IR spectrum of **2** to the

(7) Poulton, J. T.; Folting, K.; Streib, W. E.; Caulton, K. G. *Inorg. Chem.* **1992**, *31*, 3190.

Table 1. Fractional Coordinates (×10⁴) and Isotropic Thermal Parameters (×10) for 2

atom	*x*	*y*	*z*	B_{iso}
W(1)	9632(1)	2464.5(4)	665.6(4)	10
W(2)	7634(1)	2310.9(4)	1041.4(4)	9
O(3)	10881(10)	1895(6)	1230(6)	10
C(4)	11276(18)	1470(10)	1872(10)	19
C(5)	10686(17)	735(10)	1811(11)	17
C(6)	11030(17)	1885(9)	2583(9)	16
C(7)	12595(15)	1412(10)	1882(10)	16
F(8)	13124(10)	1010(7)	2472(6)	29
F(9)	12899(9)	1072(6)	1252(6)	24
F(10)	13174(10)	2033(6)	1910(6)	25
O(11)	9528(10)	1828(6)	−191(6)	11
C(12)	10428(17)	1632(9)	−650(10)	15
C(13)	10832(20)	873(11)	−446(11)	26
C(14)	11415(18)	2164(12)	−599(12)	25
C(15)	9777(21)	1611(11)	−1478(11)	27
F(16)	10530(11)	1458(7)	−1959(6)	31
F(17)	9295(11)	2263(6)	−1679(6)	30
F(18)	8878(11)	1137(6)	−1573(6)	28
O(19)	10175(11)	3336(6)	1159(6)	13
C(20)	11004(16)	3930(10)	1126(11)	17
C(21)	11937(17)	3871(10)	1851(11)	19
C(22)	11576(19)	3934(11)	419(11)	24
C(23)	10235(18)	4599(10)	1182(11)	19
F(24)	10886(11)	5200(6)	1153(6)	29
F(25)	9329(10)	4634(6)	606(6)	26
F(26)	9728(12)	4628(6)	1816(7)	32
C(27)	8675(20)	3166(11)	−141(12)	24
O(28)	8171(12)	3522(7)	−596(7)	23
O(29)	6571(11)	1702(6)	393(7)	18
C(30)	6307(17)	1320(10)	−304(10)	17
C(31)	6411(17)	1820(10)	−981(9)	16
C(32)	7077(18)	645(10)	−304(11)	20
C(33)	5006(17)	1137(10)	−333(11)	19
F(34)	4572(10)	745(6)	−945(6)	28
F(35)	4774(10)	737(5)	282(6)	21
F(36)	4285(10)	1715(6)	−327(7)	26
O(37)	6840(11)	3182(6)	659(6)	14
C(38)	5688(15)	3508(9)	662(10)	13
C(39)	5100(16)	3581(11)	−160(10)	18
C(40)	4920(17)	3087(11)	1127(11)	20
C(41)	5928(18)	4245(10)	986(11)	21
F(42)	4925(11)	4621(6)	1031(7)	29
F(43)	6547(10)	4232(6)	1696(6)	26
F(44)	6612(11)	4657(6)	581(7)	29
O(45)	7946(10)	1590(5)	1809(6)	12
C(46)	7217(16)	1191(9)	2252(9)	15
C(47)	7159(18)	415(11)	1985(10)	22
C(48)	6010(17)	1512(11)	2231(11)	23
C(49)	7857(17)	1247(9)	3074(10)	16
F(50)	8924(9)	915(6)	3157(5)	19
F(51)	7229(10)	942(6)	3566(6)	25
F(52)	8074(11)	1931(6)	3293(6)	26
C(53)	8287(19)	3029(9)	1950(11)	23
O(54)	8664(12)	3370(7)	2451(8)	22

Table 2. Selected Bond Distances and Angles for $W_2(OCMe_2CF_3)_6(CO)_2$ (2)

Bond Distances (Å)

W(1)−W(2)	2.4498(13)	W(1)−O(19)	1.896(11)	W(2)−O(37)	1.921(11)
W(1)−O(3)	1.925(11)	W(1)−C(27)	2.115(21)	W(2)−O(45)	1.906(10)
W(1)−O(11)	1.917(11)	W(2)−O(29)	1.910(11)	W(2)−C(53)	2.141(23)

Bond Angles (deg)

W(1)−C(27)−O(28)	177.1(16)	W(2)−C(53)−O(54)	175.7(15)
W(1)−W(2)−O(29)	115.2(4)	W(2)−W(1)−O(3)	115.2(3)
W(1)−W(2)−O(37)	101.9(4)	W(2)−W(1)−O(11)	100.9(4)
W(1)−W(2)−O(45)	101.1(4)	W(2)−W(1)−O(19)	102.8(4)
W(1)−W(2)−C(53)	84.4(5)	W(2)−W(1)−C(27)	81.7(6)
cis L−W−L	87.9 av	*trans* L−W−L	156.1 av

presence of rotamers in the Nujol mull at room temperature. Two absorptions may be readily assigned to the symmetric and asymmetric modes of the *syn* rotamer (C_2 symmetry), which was structurally characterized by single-crystal X-ray diffraction. Another rotamer with an *anti* 1,2-CO structure (C_{2h} symmetry) is

Scheme 1

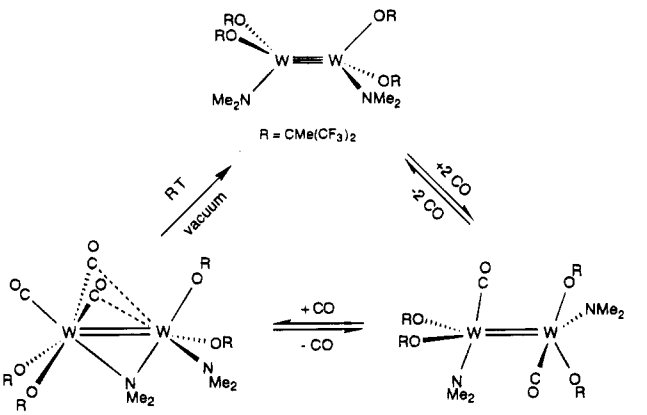

Table 3. Comparison of ν(CO) Values in Bis(carbonyl) Adducts of W_2^{6+}-Containing Compounds

compound	ν(CO) (cm⁻¹)	ref
$W_2(OSiMe_2{}^tBu)_6(CO)_2$	2029, 1995	this work
$W_2(OCMe_2CF_3)_6(CO)_2$	2081, 2064, 2050	this work
$W_2Cl_2(silox)_4(CO)_2$)	2055, 2035	4

postulated to account for the third absorption. For this species the symmetric (A_g) stretch is IR inactive, and only the asymmetric (B_u) stretch is observed.

The addition of a large excess of $(CF_3)_2MeCOH$ to $W_2(NMe_2)_6$ does not lead to complete replacement of all of the amido ligands, and $W_2(OCMe(CF_3)_2)_4(NMe_2)_2$ (**4**) is formed instead. This is presumably the result of a combination of steric and electronic factors. Partial replacement of the amido ligands by the more weakly π-donating hexafluoro-*tert*-butoxide ligands results in a significant strengthening of the remaining W−NMe_2 bonds due to enhanced N pπ to W dπ bonding, which renders this linkage less susceptible to attack by electrophiles. Partial replacement of amido groups for the more sterically demanding hexafluoro-*tert*-butoxide ligands also makes these linkages less accessible on steric grounds. Similar results have been observed by Cotton *et al.* for the reaction of $Mo_2(NMe_2)_6$ with $HOC(CF_3)_3$.[8]

Addition of CO to **4** leads to the formation of a bis(CO) adduct $W_2(OCMe(CF_3)_2)_4(NMe_2)_2(CO)_2$ (**5**). This complex also possesses terminally bound CO ligands on alternate W atoms, and these apparently are trans to each of the remaining amido ligands. Unlike the other bis(CO) adducts, however, **5** slowly reacts in a reversible manner with additional CO to form the tris(CO) adduct $W_2(OCMe(CF_3)_2)_4(NMe_2)_2(CO)_3$ (**6**) as shown in Scheme 1. This complex was initially believed to be a carbamoyl derivative, as had been previously observed in the reaction between $W_2Cl_2(NMe_2)_4$ and CO.[9] In the $^{13}C\{^1H\}$ NMR spectrum, there are three resonances arising from ^{13}CO at δ 231, 211, and 197 ppm and each is flanked by satellites due to ^{183}W coupling that indicate a terminal, rather than bridging mode of bonding. The low-field resonance appears as a doublet, and the high-field resonance is notably broader than the others. We propose that these signals are coupled with the high-field resonance, exhibiting significant quadrupolar broadening due to its proximity to ^{14}N ($I = 1$), which obscures

(8) Abbott, R. G.; Cotton, F. A.; Falvello, L. R. *Polyhedron* **1990**, *9*, 1821.
(9) Ahmed, K. J.; Chisholm, M. H. *Organometallics* **1986**, *5*, 185.

Table 4. Fractional Coordinates (×10^4) and Isotropic Thermal Parameters (×10) for 6

atom	*x*	*y*	*z*	B_{iso}	atom	*x*	*y*	*z*	B_{iso}
W(1)A	3116.1(5)	874.2(3)	1830(1)	13	W(1)B	6867.9(4)	3463.4(3)	6903(1)	11
W(2)A	2194.8(5)	1624.8(3)	665(1)	12	W(2)B	8010.2(4)	3299.9(3)	5556(1)	11
N(3)A	1520(9)	1081(7)	1407(11)	17	N(3)B	7599(9)	4217(7)	6418(11)	16
C(4)A	1124(12)	1378(9)	2411(15)	24	C(4)B	8290(12)	4636(9)	7399(14)	25
C(5)A	830(12)	528(8)	735(15)	21	C(5)B	7002(11)	4669(8)	5834(14)	17
N(6)A	1672(11)	1159(7)	−802(12)	21	N(6)B	7348(9)	3381(6)	4149(10)	13
C(7)A	1728(12)	470(9)	−1530(14)	24	C(7)B	6321(110	3410(8)	3511(13)	15
C(8)A	1025(13)	1567(9)	−1472(14)	22	C(8)B	8026(12)	3363(9)	3415(14)	20
C(9)A	3555(13)	741(8)	380(18)	28	C(9)B	6337(11)	2810(7)	5454(15)	18
O(10)A	3922(9)	639(6)	−359(10)	29	O(10)B	5962(8)	2418(6)	4675(10)	24
C(11)A	3639(13)	1818(9)	2593(14)	22	C(11)B	8083(11)	2979(8)	7515(14)	18
O(12)A	3951(8)	2327(6)	3004(9)	22	O(12)B	8734(7)	2690(5)	7828(9)	17
C(13)A	4592(15)	688(8)	2187(16)	30	C(13)B	6185(12)	2734(8)	7233(13)	19
O(14)A	5435(9)	627(7)	2306(12)	37	O(14)B	5857(9)	2274(6)	7334(10)	28
O(15)A	2950(8)	821(5)	3353(8)	15	O(15)B	7055(7)	4095(5)	8480(8)	15
C(16)A	3374(15)	1005(8)	4449(16)	30	C(16)B	7260(13)	4207(9)	9613(15)	24
C(17)A	4543(15)	1195(16)	4753(15)	71	C(17)B	6539(24)	4779(11)	10108(16)	71
C(18)A	2929(14)	1642(10)	5071(14)	30	C(18)B	8288(16)	4411(11)	10092(19)	41
F(19)A	2935(10)	2109(6)	4607(11)	53	F(19)B	8905(9)	4019(7)	9640(12)	51
F(20)A	2023(9)	1540(7)	5118(11)	54	F(20)B	8414(12)	5024(7)	9937(11)	63
F(21)A	3407(10)	1877(7)	6151(11)	59	F(21)B	8534(11)	4517(8)	11214(11)	66
C(22)A	3220(20)	413(17)	4916(18)	70	C(22)B	7017(14)	3620(10)	9945(15)	29
F(23)A	2305(12)	271(7)	4719(11)	62	F(23)B	7118(8)	3694(6)	11032(9)	36
F(24)A	3551(13)	594(8)	6076(11)	72	F(24)B	6137(7)	3378(6)	9465(9)	38
F(25)A	3747(11)	−92(6)	4547(11)	56	F(25)B	7619(7)	3095(5)	9646(8)	26
O(26)A	2622(7)	−77(5)	1339(9)	13	O(26)B	5682(8)	4033(5)	6619(9)	20
C(27)A	2898(12)	−722(8)	1181(13)	16	C(27)B	4709(11)	4094(8)	6635(15)	21
C(28)A	3944(12)	−809(8)	1739(15)	22	C(28)B	4374(12)	3803(10)	7468(17)	33
C(29)A	2234(13)	−1043(8)	1640(15)	24	C(29)B	4495(14)	4847(9)	6915(16)	28
F(30)A	1269(7)	−994(5)	1154(10)	33	F(30)B	4789(8)	5143(5)	6253(11)	40
F(31)A	2317(9)	−794(6)	2706(9)	40	F(31)B	5014(9)	5132(6)	7952(10)	46
F(32)A	2367(8)	−1703(5)	1472(10)	37	F(32)B	3564(7)	4994(5)	6915(10)	36
C(33)A	2761(12)	−1044(9)	−122(16)	27	C(33)B	4095(13)	3782(10)	5467(18)	35
F(34)A	2948(8)	−1681(5)	−351(9)	37	F(34)B	3131(7)	3849(7)	5412(10)	52
F(35)A	3386(9)	−745(5)	−502(9)	38	F(35)B	4261(8)	3132(6)	5228(12)	56
F(36)A	1867(8)	−958(5)	−667(8)	30	F(36)B	4291(8)	3998(8)	4677(9)	54
O(37)A	3059(8)	2221(6)	470(9)	22	O(37)B	8427(8)	2400(5)	5129(9)	20
C(38)A	3817(12)	2479(9)	152(14)	23	C(38)B	8375(12)	1722(8)	4751(14)	18
C(39)A	4796(15)	2152(9)	533(18)	36	C(39)B	7679(14)	1408(9)	5220(17)	29
C(40)A	3574(16)	2323(10)	−1105(17)	35	C(40)B	8035(14)	1534(8)	3493(16)	28
F(41)A	3460(8)	1679(6)	−1563(9)	37	F(41)B	7123(8)	1752(6)	3169(9)	40
F(42)A	4278(8)	2514(6)	−1500(10)	42	F(42)B	8023(10)	889(5)	3022(9)	44
F(43)A	2744(9)	2610(6)	−1466(10)	43	F(43)B	8575(9)	1805(5)	2984(9)	40
C(44)A	3922(12	3210(9)	734(15)	25	C(44)B	9415(14)	1463(10)	5079(16)	33
F(45)A	4616(8)	3488(5)	436(11)	45	F(45)B	9403(9)	784(6)	4819(12)	53
F(46)A	3098(8)	3541(6)	475(11)	44	F(46)B	10025(8)	1595(6)	4508(11)	47
F(47)A	4151(8)	3340(5)	1841(10)	40	F(47)B	9765(10)	1673(7)	6136(11)	58
O(48)A	1449(7)	2328(5)	1358(8)	14	O(48)B	9336(7)	3599(5)	6256(9)	18
C(49)A	966(11)	2926(7)	1491(14)	15	C(49)B	10304(11)	3642(8)	6235(14)	20
C(50)A	896(12)	3238(8)	562(15)	21	C(50)B	10683(14)	3087(10)	5422(18)	35
C(51)A	−68(13)	2820(9)	1617(15)	25	C(51)B	10457(13)	4291(9)	5973(19)	32
F(52)A	−644(8)	3332(6)	1588(10)	39	F(52)B	11367(8)	4357(6)	5865(12)	49
F(53)A	−494(8)	2315(6)	762(9)	36	F(53)B	9828(9)	4297(7)	5014(12)	55
F(54)A	−84(7)	2649(5)	2557(8)	26	F(54)B	10286(8)	4822(6)	6743(12)	50
C(55)A	1538(13)	3373(8)	2622(16)	25	C(55)B	10858(12)	3656(9)	7412(15)	25
F(56)A	1030(9)	3907(5)	2985(11)	43	F(56)B	11803(8)	3789(7)	7603(10)	49
F(57)A	1779(7)	3076(5)	3410(9)	32	F(57)B	10507(8)	4105(7)	8210(10)	50
F(58)A	2372(8)	3591(5)	2475(10)	38	F(58)B	10796(8)	3083(7)	7638(10)	46

the weak $J_{^{13}C-^{13}C}$ coupling of ~7 Hz. The ^{1}H NMR spectrum at low temperature (−40 °C, C_7D_8) showed that this complex was asymmetric and exhibited unique resonances for each of the four alkoxide ligands and two resonances for each amido group. Single crystals were grown from toluene solution under an atmosphere of CO and a single-crystal X-ray diffraction study was performed. Fractional atomic coordinates appear in Table 4, and pertinent bond distances and angles are summarized in Table 5. There were two unique molecules in the asymmetric unit, and these have been labeled A and B for convenience in comparing the metrical parameters for each. As is readily apparent, the two differ very little in structure. The molecular structure as determined from this experiment is shown in Figure 2, where a single molecule is shown for clarity. Quite remarkably there are three carbonyl ligands bonded to a single tungsten atom, two of which appear to be semibridging in the solid state. Note the acute W(2)−W(1)−C(9) and W(2)−W(1)−C(11) angles (68.0(5) and 72.2(5)°, respectively, for molecule A shown), as well as the long W(2)−C(9) and W(2)−C(11) distances (2.611(15) and 2.761(15) Å, respectively). There is also one bridging NMe_2 ligand which completes a distorted octahedral coordination geometry about the metal centers. It is evident from the disposition of the ligands that a valence disproportionation has occurred. Previously it was observed that, in the reaction of $M_2(OR)_6$ compounds with excess CO, $M(CO)_6$ is often formed (M = Mo, W),[1] and Cotton and co-workers isolated and structurally

Table 5. Selected Bond Distances and Angles for $W_2(OC(CF_3)_2Me)_4(NMe_2)_2(CO)_3$ (6)

Bond Distances (Å)					
Molecule A					
W(1)–W(2)	2.5734(10)	W(1)–O(26)	2.043(10)	W(2)–O(37)	1.900(11)
W(1)–C(13)	2.061(21)	W(1)–N(3)	2.233(13)	W(2)–O(48)	1.901(10)
W(1)–C(9)	2.027(22)	W(2)–N(3)	2.064(12)	W(2)–C(9)	2.611(15)
W(1)–C(11)	2.057(18)	W(2)–N(6)	1.860(14)	W(2)–C(11)	2.761(15)
W(1)–O(15)	2.047(9)				
Molecule B					
W(1)–W(2)	2.5551(10)	W(1)–O(26)	2.026(11)	W(2)–O(37)	1.926(10)
W(1)–C(13)	2.047(17)	W(1)–N(3)	2.235(12)	W(2)–O(48)	1.931(10)
W(1)–C(9)	1.991(17)	W(2)–N(3)	2.071(14)	W(2)–C(9)	2.584(15)
W(1)–C(11)	2.054(15)	W(2)–N(6)	1.877(13)	W(2)–C(11)	2.751(15)
W(1)–O(15)	2.056(10)				

Bond Angles (deg)			
Molecule A			
W(2)–W(1)–C(9)	68.0(5)	W(1)–C(13)–O(14)	172.0(16)
W(2)–W(1)–C(11)	72.2(5)	C(9)–W(1)–C(11)	98.0(6)
W(1)–C(9)–O(10)	170.4(16)	C(9)–W(1)–C(13)	74.1(8)
W(1)–C(11)–O(12)	178.0(16)	C(11)–W(1)–C(13)	80.3(7)
Molecule B			
W(2)–W(1)–C(9)	68.0(4)	W(1)–C(13)–O(14)	172.0(14)
W(2)–W(1)–C(11)	72.4(5)	C(9)–W(1)–C(11)	100.9(6)
W(1)–C(9)–O(10)	172.8(14)	C(9)–W(1)–C(13)	72.3(7)
W(1)–C(11)–O(12)	177.3(14)	C(11)–W(1)–C(13)	81.2(7)

characterized $(^iPrO)_4W(\mu\text{-}O^iPr)_2W(CO)_4$, a complex (shown schematically in **D**) with a $W(CO)_4$-d_6 moiety

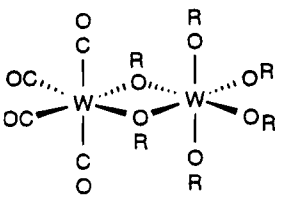

D

bridged to $W(O^iPr)_6$-d_0 center that lacked a W–W bond.[10] The formation of a tricarbonyl compound with a structure related to that shown in Figure 2 for $W_2(OCMe(CF_3)_2)_4(NMe_2)_2(CO)_3$ may be a precursor to $(^iPrO)_4W(\mu\text{-}O^iPr)_2W(CO)_4$ shown in **D**. While **6** clearly exhibits valence disproportionation, this process also is completely reversible, and complex **4** may be obtained simply by applying a vacuum to samples of **6**. Also, in contrast to the reactions of aliphatic W_2^{6+} alkoxide complexes with excess CO, which rapidly result in valence disproportionation, formation of the tris(CO) complex **6** from the bis(CO) complex **5** takes nearly 1 week to proceed to completion. We also note that the NMR spectroscopic data for **6** are consistent with the maintenance of the solid state structure in toluene solution at low temperature.

Since changing the electronic characteristics of the alkoxide ligands favored the formation of bis(CO) derivatives similar to $W_2(Cl)_2(silox)_4(CO)_2$, we were eager to thermolyze these new adducts to see if reductive cleavage of the C≡O bond would occur. To date all of these efforts have failed. If the bis(CO) adducts **1** and **2** are dissolved in toluene-d_8 at low temperature and then heated in a sealed NMR tube, the only reaction that occurs involves the reversible dissociation of the carbonyl ligands even after prolonged heating (100°, 12 h or more). When $W_2(OCMe_2CF_3)_6$ is pressurized with CO (large excess) and heated, a valence disproportionation reaction is apparent, as evidenced by the formation of $W(CO)_6$. The other tungsten-containing species have not been identified, but we are confident that a carbido cluster is not produced from reactions employing ^{13}CO which were monitored by $^{13}C\{^1H\}$ NMR spectroscopy.

(10) Cotton, F. A.; Schwotzer, W. *J. Am. Chem. Soc.* **1983**, *105*, 5639.

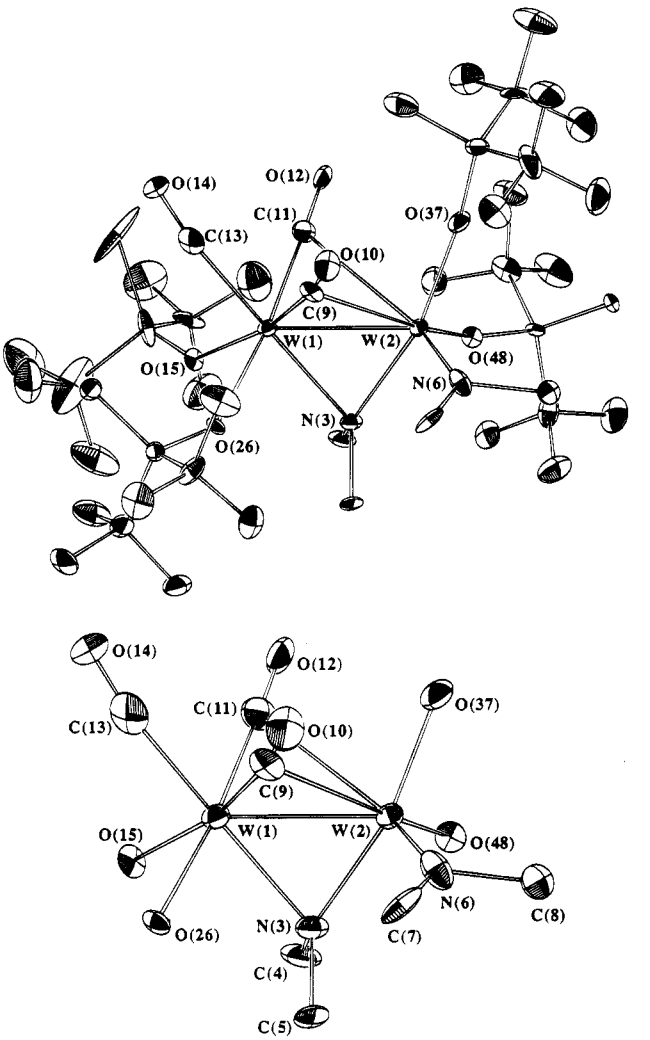

Figure 2. ORTEP view of the $W_2(OCMe(CF_3)_2)_4(NMe_2)_2(CO)_3$ molecule giving the atom number scheme (top) and a view of the central $W_2N_2O_4(CO)_3$ core showing the local geometry about each W atom (bottom). Two independent molecules were present in the asymmetric unit of the unit cell, but only one is shown for clarity.

Concluding Remarks

In summary, the following points are worthy of note. 1. The bis(carbonyl) complexes $W_2(OR)_6(CO)_2$ **1**, **2**, and **3** are thermodynamically favored relative to $W_2(OR)_6(\mu\text{-}CO)$ compounds, which are preferred when R = ^{t}Bu and ^{i}Pr. 2. The bis(carbonyl) compounds reported here are likely to be directly analogous to Wolczanski's compound $W_2Cl_2(silox)_4(CO)_2$, and though carbonyl binding is reversible, we have yet to observe any C≡O cleavage products even at elevated temperatures. We can only postulate that steric factors account for this disparity. When the extremely bulky OSi^tBu_3 ligand is a spectator, steric pressure may force the two tungsten centers apart and provide an additional thermo-

dynamic impetus (ground state destabilization of $W_2Cl_2(silox)_4$) for C≡O cleavage. It is quite clear that the electronic properties which favor reversible formation of bis(CO) adducts and inhibit valence disproportionation are similar to $W_2(OSi^tBuMe_2)_6$, $W_2(OCMe_2CF_3)_6$, $W_2(NMe_2)_2(OCMe(CF_3)_2)_4$, and $W_2Cl_2(OSi^tBu_3)_4$. Subtle electronic differences that enable the latter to reductively cleave C≡O are not easily identifiable. 3. The tris(carbonyl) compound $W_2(OCMe(CF_3)_2)_4(NMe_2)_2(CO)_3$ adopts a remarkable structure in the solid state and provides insight into the redox reactions that have been noted previously in the reaction between CO and $M_2(OR)_6$ complexes wherein $M(CO)_6$ is one of the ultimate products. In the presence of the less electron-donating groups $CMe(CF_3)_2$, $OCMe_2CF_3$, and OSi^tBuMe_2, the formation of $W(CO)_6$ is suppressed. A critical factor may be the inability of these ligands to stabilize the high oxidation state product which would be formed concomitantly. Steric factors may also play a role since bulky alkoxide(siloxide) ligands are less likely to occupy bridging sites and are therefore harder to transfer from one metal to the other as required for the valence disproportionation process (cf. the structure of **6**, Figure 2).

At this point it is worth mentioning that the corresponding molybdenum complexes have been prepared and their reactions with CO investigated. Adduct formation was not detected even at low temperatures for $Mo_2(OSi^tBuMe_2)_6$, $Mo_2(OCMe_2CF_3)_6$, or $Mo_2(NMe_2)_2(OCMe(CF_3)_2)_4$, consistent with the lower Lewis acidity of Mo versus W.[11]

Collectively these results provide further evidence of the rich chemistry associated with the central $(W{\equiv}W)^{6+}$ moiety that may be modified subtly or quite dramatically by the attendant ligands. Further studies are in progress.

Experimental Section

All operations were carried out in an inert atmosphere (nitrogen) using standard Schlenk and vacuum techniques. Aromatic and aliphatic hydrocarbon solvents were dried and distilled from sodium diphenyl ketyl and stored over 4 Å molecular sieves. The NMR solvent, toluene-d_8, was degassed with dry nitrogen and stored over 4 Å sieves. The fluoro alcohols were purchased from PCR Chemical Co., distilled, degassed with dry nitrogen, and dried over 4 Å sieves. The silanol was purchased from Aldrich Chemical Co., degassed with dry nitrogen, and dried over 4 Å sieves. $W_2(NMe_2)_6$,[12a] $W_2(OSi^tBuMe_2)_6$,[12b] and $W_2(O\text{-}2,6\text{-}Me_2C_6H_3)_6$[12c] were prepared according to the literature procedures. $W_2(OCMe_2CF_3)_6$ was prepared by the alcoholysis of $W_2(NMe_2)_6$ in a manner similar to the preparation of $W_2(OSi^tBuMe_2)_6$. In this case, the product is initially isolated as a black/brown bis($HNMe_2$) adduct, but the ammine ligands are liberated upon heating *in vacuo* (50 °C, 0.01 Torr). Red powdery $W_2(OCMe_2CF_3)_6$ produced in this manner may be recrystallized from toluene (75 to −34 °C).

^1H and ^{13}C NMR spectra were recorded on a Varian XL-300. Infrared spectra were recorded on a Perkin-Elmer 283 spectrometer working quickly with a Nujol mull between NaCl plates.

Preparation of $W_2(OSi^tBuMe_2)_6(CO)_2$ (1). $W_2(OSi^tBuMe_2)_6$ (25 mg, 0.0216 mmol) was dissolved in 0.6 mL of toluene-d_8 in an NMR tube equipped with a J. Young valve. One atmosphere of CO was added with the aid of a calibrated gas manifold at −196 °C. Upon thawing the solution, a reaction is evident based on the observation of a color change from deep burgundy to brownish black. The reaction was then monitored by NMR spectroscopy, which showed that the yield of **1** was >90% at −20 °C or lower but that the carbonyl ligands reversibly dissociated upon warming. Due to the lability of this complex, analytically pure samples have not been obtained and elemental analysis was not attempted. Crystalline material has been obtained from hexanes at −35 °C, but the crystals have thus far been unsuitable for study by X-ray diffraction. This material was used for analysis by IR spectroscopy by working quickly since the material loses CO even in the solid state. ^1H NMR (300 MHz, C_7D_8, −60 °C): δ 1.18 (s, 18H), 1.07 (s, 18H), 0.89 (s, 18H), 0.48 (s, 6H), 0.42 (s, 12H), 0.41 (s, 6H), 0.39 (s, 6H), 0.26 (s, 6H). $^{13}C\{^1H\}$ NMR (75 MHz, C_7D_8, −60 °C): δ 240.2 (*C*O, J_{W-C} = 103 Hz, 14%), 27.30, 26.83, 26.63 (1:1:1 for $C(CH_3)_3$), 0.69, −1.21, −1.59, −1.96, −2.54 (2:1:1:1:1 for $Si(CH_3)_2$); $SiC(CH_3)_3$ not observed.

Preparation of $W_2(OCMe_2CF_3)_6(CO)_2$ (2). $W_2(OCMe_2CF_3)_6$ (25 mg, 0.0221 mmol) was dissolved in 0.6 mL of toluene-d_8 in an NMR tube equipped with a J. Young valve. One atmosphere of CO was added with the aid of a calibrated gas manifold at −196 °C. Upon thawing, a reaction is clearly evident based on the observation of a color change from deep burgundy to brownish black. Analysis by NMR spectroscopy shows that the yield of **2** at −20 °C exceeds 95%, but the complex dissociates upon warming. Due to the lability of this complex, analytically pure samples have not been obtained and elemental analysis was not attempted. Crystalline material may be obtained from toluene at −35 °C. This material was used for analysis by IR spectroscopy by working quickly since the material loses CO even in the solid state. ^1H NMR (300 MHz, C_7D_8, −40 °C): δ 1.91, 1.88, 1.34, 1.22, 1.05, 0.96 (s, 6H). $^{13}C\{^1H\}$ NMR (75 MHz, C_7D_8, −40 °C): δ 217.6 (*C*O, J_{W-C} = 110 Hz, 13%).

Preparation of $W_2(O\text{-}2,6\text{-}Me_2C_6H_3)_6(CO)_2$ (3). $W_2(O\text{-}2,6\text{-}Me_2C_6H_3)_6$ (25 mg, 0.0229 mmol) was dissolved in 0.6 mL of toluene-d_8 in an NMR tube equipped with a J. Young valve. One atmosphere of CO was added with the aid of a calibrated gas manifold. The yield from NMR spectroscopy at −20 °C is ~80%. ^1H NMR (300 MHz, C_7D_8, −40 °C): δ 2.36, 2.27, 1.97 (s, 12H), 7.0−6.4 br m's (18H total). $^{13}C\{^1H\}$ NMR (75 MHz, C_7D_8, −40 °C): δ 228.6 (*C*O, J_{W-C} = 124 Hz, 14%). The remainder (~20%) is mostly $[W_2(O\text{-}2,6\text{-}Me_2C_6H_3)_6(CO)]_2$. ^1H NMR (300 MHz, C_7D_8, −40 °C): δ 2.90, 1.85, 1.72, 1.61 (6:12:12:6 for CH_3), 7.0−6.5 br m's (18H). $^{13}C\{^1H\}$ NMR (75 MHz, C_7D_8, −40 °C): δ 320.1 (J_{W-C} = 198, 157 Hz, 26.5% total satellite intensity). Crystalline samples of either species have not yet been obtained. In this case, it is quite apparent that the reaction proceeds beyond addition of 2 equiv of CO under mild conditions: $W(CO)_6$ is observed after 1 day under an atmosphere of CO at room temperature.

Preparation of $W_2(OC(CF_3)_2Me)_4(NMe_2)_2$ (4). $W_2(NMe_2)_6$ (2.20 g, 3.48 mmol) was dissolved in 25 mL of hexanes. The fluoro alcohol (4.3 g, 23.6 mmol) was then added to the solution with a syringe and the reaction stirred for several hours. An instantaneous reaction is evident based on the observation of a color change to a deep red and red microcrystals of the sparingly soluble product deposit over the course of the reaction. At the conclusion the solvent was evaporated *in vacuo* (23 °C, 0.01 Torr), and 2.49 g of **4** (61% yield) was crystallized from hexanes (65 to −35 °C). The crystalline material was dried *in vacuo* (23 °C, 2 h, 0.01 Torr) prior to use. ^1H NMR (300 MHz, C_7D_8, 23 °C): δ 4.22, 2.47, 1.54 (6:6:12 for *anti* rotamer), 4.30, 2.34, 2.07, 1.21 (septet, J_{H-F} = 1.5 Hz) (6:6:6:6 for *gauche* rotamer). $^{13}C\{^1H\}$ NMR (75 MHz, C_7D_8, 23 °C): δ 82.36, 60.42, 39.37, 19.42 (s, for *anti* rotamer), 82.60, 82.13, 60.11, 40.04, 20.24, 19.57 (s for *gauche* rotamer).

(11) Budzichowski, T. A.; Chisholm, M. H. *Polyhedron* **1994**, *13*, 2035, and references therein.

(12) (a) Chisholm, M. H.; Cotton, F. A.; Extine, M.; Stults, B. R. *J. Am. Chem. Soc.* **1976**, *98*, 4477. (b) Chisholm, M. H.; Cook, C. M.; Huffman, J. C.; Streib, W. E. *J. Chem. Soc., Dalton Trans.* **1991**, 929. (c) Latham, I. A.; Sita, L. R.; Schrock, R. R. *Organometallics* **1986**, *5*, 1508.

Table 6. Summary of Crystallographic Data

	2	6
empirical formula	$C_{26}H_{36}O_8F_{18}W_2$	$C_{23}H_{24}F_{24}N_2O_7W_2$
formula wt	1186.24	1264.12
color; habit	dark brown	black
cryst size (mm)	0.25 × 0.35 × 0.35	0.12 × 0.12 × 0.28
space group	$P2_1/n$	$P\bar{1}$
a (Å)	11.256(4)	14.053(3)
b (Å)	18.496(6)	21.148(5)
c (Å)	17.789(7)	12.789(3)
α (deg)		106.11 (1)
β (deg)	97.97(1)	103.15(1)
δ (deg)		86.81(1)
temp (°C)	−172	−169
vol (Å^3)	3668.01	3555.60
Z	4	4
D_{calcd} (g/cm^3)	2.148	2.362
radiation	Mo Kα (0.710 69)	Mo Kα (0.710 69)
scan range (ω, deg)	2.0 plus dispersion	2.0 plus dispersion
scan speed (deg/min)	8.0	6.0
abs coeff (mm^{-1})	65.336	67.701
2θ range (deg)	6−45	6−45
no. of reflctns collected	5110	11 317
no. of independent reflctns	4782 (R_{int} = 3.10%)	9325 (R_{int} = 4.70%)
no. of obsd reflctns	3946 ($F > 2.33\sigma F$)	7677 ($F > 3.0\sigma F$)
$R(F)$	0.0615	0.0599
$R_w(F)$	0.0612	0.0535
goodness of fit	2.346	1.383
largest Δ/σ	0.23	0.015

$^{19}F\{^1H\}$ NMR (340 MHz, C_7D_8, 23 °C): δ −78.75 (q, J_{F-F} = 10 Hz), −79.59 (q, J_{F-F} = 10Hz) (*anti* rotamer), −78.87 (q, 6F, J_{F-F} = 9 Hz), −79.04 (s, 12F), −79.96 (q, 6F, J_{F-F} = 9Hz) (*gauche* rotamer).

Preparation of $W_2(OC(CF_3)_2Me)_4(NMe_2)_2(CO)_2$ (5). $W_2(OC(CF_3)_2Me)_4(NMe_2)_2$ (25 mg, 0.0251 mmol) was dissolved in 0.6 mL of toluene-d_8 in an NMR tube equipped with a J. Young valve. One atmosphere of CO was added with the aid of a calibrated gas manifold at −196 °C. Upon thawing, a reaction is clearly evident based on the observation of a color change from deep burgundy to brownish black. The yield from NMR spectroscopy at −20 °C exceeds 90%, with the major contaminant (~10%) being **6**. Due to the lability of this complex, analytically pure samples have not been obtained and elemental analysis was not attempted. ^1H NMR (300 MHz, C_7D_8, −40 °C): δ 4.01, 1.99, 1.47, 1.41 (6:6:6:6). $^{13}C\{^1H\}$ NMR (75 MHz, C_7D_8, −40 °C): δ 208.6 (*CO*, J_{W-C} = 123 Hz, 14%).

Preparation of $W_2(OC(CF_3)_2Me)_4(NMe_2)_2(CO)_3$ (6). If the NMR tube equipped with a J. Young valve containing **5** and 1 atm of CO remains at −35 °C for 1 week, **6** is produced in greater than 90% yield by NMR spectroscopy. Crystalline material was obtained by reducing the volume of solvent *in vacuo* (0 °C, 0.01 Torr), pressurizing with an atmosphere of CO, and cooling to −35 °C for 1 week. This material was used for analysis by IR spectroscopy by working quickly since the material loses CO even in the solid state. Due to the lability of this complex, analytically pure samples have not yet been obtained and elemental analysis was not attempted. ^1H NMR (300 MHz, C_7D_8, −20 °C): δ 4.27, 4.07, 3.48, 2.92, 1.54, 1.50, 1.38, 1.25 (3:3:3:3:3:3:3:3). $^{13}C\{^1H\}$ NMR (75 MHz, C_7D_8, −20 °C): δ 230.46 (d, *CO*, J_{C-C} = 7 Hz, J_{W-C} = 133 Hz, 14%), 211.36 (*CO*, J_{W-C} = 131 Hz, 14%), 196.65 (br s, *CO*, J_{W-C} = 105 Hz, 14%). IR (Nujol, KBr plates): ν(CO) = 2064, 1964, 1875 cm^{-1}.

Crystal Structure Analyses. Crystal data for **2** and **6** appear in Table 6.

$W_2(OCMe_2CF_3)_6(CO)_2$. Crystals suitable for study by single-crystal X-ray diffraction were grown by cooling a toluene solution of **2** to −35 °C under an atmosphere of CO for several days. Working quickly at room temperature, a small well-formed crystal was cleaved from a larger specimen, affixed to the end of a glass fiber with silicone grease, and transferred to the goniostat where it was cooled to −172 °C for characterization and data collection. A systematic search of a limited hemisphere of reciprocal space located a set of reflections with monoclinic symmetry and systematic absences corresponding to the unique space group $P2_1/n$. Data were collected using a standard moving crystal, moving detector technique with fixed background counts at each extreme of the scan. The data were corrected for Lorentz and polarization effects, and equivalent data were averaged. The structure was solved by direct methods (SHELX-86) and Fourier techniques. Hydrogen atoms were not located but were placed in fixed idealized positions for the final cycles of refinement.

$W_2(OCMe(CF_3)_2)_4(NMe_2)_2(CO)_3$. Crystals suitable for study by single-crystal X-ray diffraction were grown by cooling a toluene solution of **6** to −35 °C under an atmosphere of CO for several days. Working quickly at room temperature, a small well-formed crystal was selected under an inert atmosphere in a glovebag and affixed to the end of a glass fiber with silicone grease. It was then transferred to the goniostat, where it was cooled to −169 °C for characterization and data collection. A systematic search of a limited hemisphere of reciprocal space revealed no symmetry among the observed intensities. An initial choice of $P\bar{1}$ was later proven correct by the successful solution of the structure. Data were collected using a standard moving crystal, moving detector technique with fixed background counts at each extreme of the scan. The data were corrected for Lorentz and polarization effects, and equivalent data were averaged. The structure was solved by initially locating the positions of the tungsten atoms from a Patterson map (SHELX-86). The positions of the remaining non-hydrogen atoms were obtained from subsequent iterations of least-squared refinement and difference Fourier calculations. Hydrogen atoms were not located but were placed in fixed idealized positions for the final cycles of refinement with thermal parameters fixed at 1 plus the thermal parameter of the atom to which they were bonded. All non-hydrogen atoms were refined anisotropically. There are two molecules of the complex in the asymmetric unit which were labeled A and B to facilitate comparison of the metrical parameters. The final difference map was somewhat noisier than usual possibly due to some disorder and/or thermal motion of the CH_3 and CF_3 groups. The largest difference peak was 2.9 e/Å^3 near the C(17)B methyl group and the deepest hole was −2.0 e/Å^3.

Acknowledgment. We thank the Department of Energy, Office of Basic Science, Chemistry Division for support of this work.

Supplementary Material Available: Complete tables of H-atom coordinates, bond distances and angles, and anisotropic thermal parameters and VERSORT/ORTEP drawings for **2** and **6** (MSC report numbers 93251 and 94017, respectively) (30 pages). Ordering information is given on any current masthead page.

OM940743R

Diiron–Hydride Complexes: Synthesis, Structure, and Reactivity of *trans*-[$Fe_2(CO)_4(\mu$-H)(μ-CO)(μ-PCy_2)(μ-$Ph_2PCH_2PPh_2$)]

Graeme Hogarth,* Mark H. Lavender, and Khalid Shukri

Chemistry Department, University College London, 20 Gordon Street, London WC1H 0AJ, U.K.

Received February 2, 1995[⊗]

The diphosphine-stabilized diiron complex [$Fe_2(CO)_6(\mu$-CO)(μ-dppm)] (dppm = $Ph_2PCH_2PPh_2$) reacts readily with dicyclohexylphosphine upon UV irradiation to give the phosphido–hydrido complex [$Fe_2(CO)_4(\mu$-H)(μ-CO)(μ-PCy_2)(μ-dppm)] (**1**) shown to contain a *trans* arrangement of phosphorus-containing ligands, which is maintained throughout reactions. Two general types of reactivity are noted for **1**, namely, insertion of unsaturated compounds into the diiron–hydride moiety with concomitant loss of carbon monoxide and hydride elimination reactions, which may or may not occur with carbonyl loss. Insertion of ethyne affords [$Fe_2(CO)_4(\mu$-HC=CH_2)(μ-PCy_2)(μ-dppm)] (**2**). With propyne, an inseparable mixture of isomers [$Fe_2(CO)_4(\mu$-MeC=CH_2)(μ-PCy_2)(μ-dppm)] (**3a**) and [$Fe_2(CO)_4(\mu$-HC=CHMe)(μ-PCy_2)(μ-dppm)] (**3b**) is formed in a 2.5:1 ratio, while with phenylethyne, regioselective insertion yields only the β-alkenyl complex [$Fe_2(CO)_4(\mu$-HC=CHPh)(μ-PCy_2)(μ-dppm)] (**4**). The "windshield-wiper" σ–π alkenyl fluxionality of these complexes has been monitored by both ^{1}H and ^{31}P NMR spectroscopy, the former revealing that the fluxional process does not interconvert the β-hydrogen atoms. The free energies of activation vary considerably between α- and β-substituted alkenyl complexes, an effect which is believed to be steric in origin. Unactivated disubstituted alkynes do not react with **1**; however, the activated alkyne dimethyl acetylenedicarboxylate (DMAD) readily inserts to afford the metallacyclic complex [$Fe_4(CO)_4\{\eta^2$-C(CO_2Me)=CH–C(OMe)=O}(μ-PCy_2)(μ-dppm)] (**5**) as a result of *cis–trans* vinyl isomerization and ester carbonyl coordination. Addition of allene to **1** affords **3a** via selective proton transfer to the external carbons. Carbon dioxide is unreactive toward **1**, but carbon disulfide readily inserts to yield the dithioformato complex [$Fe_2(CO)_4(\mu$-S_2CH)(μ-PCy_2)(μ-dppm)] (**6**). Organic isothiocyanates (RNCS) also insert into **1**, giving *N*-thioformamido [$Fe_2(CO)_4(\mu$-RNCHS)(μ-PCy_2)(μ-dppm)] (**7a–c**; R = allyl, Et, Ph) and formimidoyl [$Fe_2(CO)_4(\mu$-RN=CH)(μ-PCy_2)(μ-dppm)] (**8a,b**) complexes. Both result from selective hydride transfer to carbon, which occurs with sulfur loss in the case of the latter. Heating a toluene solution of **7b** leads to the formation of **8b** as a result of sulfur loss. Another formimidoyl complex [$Fe_2(CO)_4(\mu$-^{t}BuN=CH)(μ-PCy_2)(μ-dppm)] (**8d**) has been prepared as the only product from the reaction of **1** with *tert*-butyl isocyanide, while in contrast **1** is unreactive toward nitriles. Both *N*-thioformamido **7** and formimidoyl **8** complexes contain an sp^2-hybridized nitrogen and partial carbon–nitrogen double-bond character. Chromatography of **1** on alumina in the presence of dichloromethane affords [$Fe_2(CO)_4(\mu$-OH)(μ-PCy_2)(μ-dppm)] (**9**) together with chloro-bridged [$Fe_2(CO)_4(\mu$-Cl)(μ-PCy_2)(μ-dppm)] (**10**). The latter is more easily prepared upon reaction of **1** with hydrochloric acid. Addition of iodine to **1** yields the analogous iodo-bridged complex [$Fe_2(CO)_4(\mu$-I)(μ-PCy_2)(μ-dppm)] (**11**) in moderate yield. Thermolysis of **1** in the presence of diphenylphosphine affords mixtures of [$Fe_2(CO)_4(\mu$-PPh_2)(μ-PCy_2)(μ-dppm)] (**12**) and [$Fe_2(CO)_4(\mu$-$PPh_2)_2(\mu$-dppm)] (**13**). In a separate experiment, thermolysis of **12** with diphenylphosphine did not afford **13**, indicating that phosphido-bridge exchange occurs prior to the formation of the electron-precise bis(phosphido)-bridged species. Thermolysis of **1** alone results in benzene elimination to yield [$Fe_2(CO)_5(\mu$-PCy_2)(μ-PhPCH_2PPh_2)] (**14**). Complexes **1**, **2**, **4**, **7a**, **8a**, and **11** were characterized by single-crystal X-ray diffraction analyses. Crystal data: for **1**, space group $P\bar{1}$, a = 10.2577(34) Å, b = 13.0315(81) Å, c = 15.8986(71) Å, α = 81.902(43)°, β = 84.672(31)°, γ = 72.272(38)°, Z = 2, 4136 reflections, R = 0.068; for **2**, space group $P\bar{1}$, a = 11.7987(15) Å, b = 12.8813(16) Å, c = 17.0025(9) Å, α = 73.670(8)°, β = 77.770(8)°, γ = 64.870(8)°, Z = 2, 6506 reflections, R = 0.046; for **4**, space group $P\bar{1}$, a = 12.5326(15) Å, b = 12.5939(16) Å, c = 18.4748(25) Å, α = 105.240(10)°, β = 91.975(10)°, γ = 118.025(10)°, Z = 2, 7416 reflections, R = 0.051; for **7a**, space group $P\bar{1}$, a = 11.9777(39) Å, b = 13.5843(36) Å, c = 13.7530(51) Å, α = 88.912(26)°, β = 89.293(28)°, γ = 78.931(25)°, Z = 2, 4235 reflections, R = 0.061; for **8a**, space group $P2_1/c$, a = 11.8267(32) Å, b = 15.5264(29) Å, c = 27.1868(71) Å, α = 90°, β = 91.366(22)°, γ = 90°, Z = 4, 3252 reflections, R = 0.088; for **11**, space group $P\bar{1}$, a = 11.8975(20) Å, b = 12.9829(16) Å, c = 16.6072(25) Å, α = 72.937(12)°, β = 76.891(13)°, γ = 64.089(11)°, Z = 2, 5957 reflections, R = 0.069.

Introduction

As the simplest possible ligand system, the hydride moiety is of fundamental interest, while its involvement in a variety of important stoichiometric and catalytic processes has led to its extensive commercial exploitation. Not surprisingly then, transition metal hydride complexes have received considerable attention, with the synthesis, properties, and reactivity of the ligand bound to both mono- and polynuclear metal centers

* E-mail: uccaxgh@ucl.ac.uk.

⊗ Abstract published in *Advance ACS Abstracts,* May 1, 1995.

0276-7333/95/2314-2325$09.00/0

being extensively developed.[1] Among the most notable examples of this latter class of compounds are the formally unsaturated dihydride complexes $[Os_3(CO)_{10}(\mu\text{-}H)_2]$[2] and $[Mn_2(CO)_6(\mu\text{-dppm})(\mu\text{-}H)_2]$,[3] which display an extensive chemistry that is centered around the insertion of unsaturated organics into one or both of the hydride moieties.

Recently we have been concerned with the development of the chemistry of the hydride ligand when bound to low-valent diiron centers,[4-8] primarily since such complexes should be easy to prepare from relatively cheap and abundant starting materials and are anticipated to display high reactivity. Diiron complexes containing a metal–metal double bond are, however, extremely rare,[9] and to our knowledge no such hydride-containing species are known. In view of this, we have developed the synthesis of diiron–hydride complexes, which, while formally being electronically saturated, readily lose carbon monoxide and thus can be considered as "masked" iron–iron doubly bonded species.[6-8]

One such example of a complex of this type is $[Fe_2(CO)_4(\mu\text{-}H)(\mu\text{-}CO)(\mu\text{-}PPh_2)(\mu\text{-dppm})]$ **1-Ph**, which we have previously shown to readily lose a carbonyl and insert alkynes to afford $\sigma-\pi$ alkenyl complexes with high regio-[6] and stereoselectivity.[8] The phosphorus-containing ligands in the latter serve a dual purpose. Firstly, they hold the two metal atoms in close proximity, thus preventing fragmentation into mononuclear species (a reaction prevalant in low-valent diiron carbonyls), while allowing a large range of internuclear separations which can vary by up to 1 Å in order to accommodate the electronic and steric requirements of other metal-bound ligands. Their second role is one of practical importance; namely, they act as excellent NMR probes, allowing simple monitoring of reactions, often providing mechanistic insight and allowing simple structure elucidation on the basis of phosphorus–phosphorus coupling constants and signal structure. For example, reaction of ethyne with **1-Ph** affords the μ-ethenyl complex $[Fe_2(CO)_4(\mu\text{-}HC{=}CH_2)(\mu\text{-}PPh_2)(\mu\text{-dppm})]$ (**2-Ph**), shown to contain a *trans* configuration of phosphorus-containing ligands on the basis of the relatively large phosphorus–phosphorus coupling constants,[6] and a static vinyl moiety by the observation of two diphosphine signals at room temperature.[5] Complexities arise in this system, however, upon insertion of primary alkynes, since, while the process occurs with high regioselectivity associated with Markovnikov addition, mixtures of isomers arise differing in the relative orientation of the phosphorus-containing ligands, namely, *cis* and *trans*.[6] This appears to be a result of the preferred *cis* arrangement of these ligands in $[Fe_2(CO)_4(\mu\text{-}H)(\mu\text{-}CO)(\mu\text{-}PPh_2)(\mu\text{-dppm})]$ (**1-Ph**), while upon insertion the formation of the alkenyl moiety favors a *trans* configuration.

In order to carry out a full investigation of the reactivity of these hydride complexes, we sought to simplify possible products by developing the synthesis of a starting hydride complex in which the phosphorus-containing ligands adopt a relative *trans* disposition, anticipating that this would be retained in consequent products. In order to achieve this while minimizing changes to the electronic properties of the diiron center, we sought to replace the diphenylphosphido ligand by the bulkier dicyclohexylphosphido moiety, expecting that this would lead to a preferred *trans* orientation with respect to the diphosphine. Herein we describe the synthesis of $[Fe_2(CO)_4(\mu\text{-}H)(\mu\text{-}CO)(\mu\text{-}PCy_2)(\mu\text{-dppm})]$ (**1**), shown by X-ray crystallography to adopt the *trans* configuration, and extensive reactivity studies during which the *trans* configuration is always maintained. No aspects of this work have been previously communicated.

Results and Discussion

1. Synthesis and Structure of $[Fe_2(CO)_4(\mu\text{-}H)(\mu\text{-}CO)(\mu\text{-}PCy_2)(\mu\text{-dppm})]$ (1). The synthesis of a variety of binuclear phosphido–hydrido complexes has previously been achieved via the oxidative addition of secondary phosphines to bimetallic centers.[10] Addition of dicyclohexylphosphine to $[Fe_2(CO)_6(\mu\text{-}CO)(\mu\text{-dppm})]$ in the absence of UV irradiation does not lead to any appreciable reaction, which is in keeping with the general reactivity of the latter.[11-13] Upon photolysis however, a slow reaction takes place over approximately 16 h, which can be accelerated somewhat by the introduction of a slow nitrogen purge of the solution, to generate the phosphido–hydrido complex $[Fe_2(CO)_4(\mu\text{-}H)(\mu\text{-}CO)(\mu\text{-}PCy_2)(\mu\text{-dppm})]$ (**1**) in 60% yield (eq 1). Characterization initially appeared to be straightforward on the basis of a comparison of spectroscopic properties with the analogous diphenylphosphido-bridged complex[6] which contains a *cis* arrangement of phosphorus-containing ligands. In the ^{31}P NMR spectrum, a triplet at 192.2 and a doublet at 75.2 ppm in the ratio 1:2 were assigned to the phosphido bridge and equivalent phosphorus atoms of the diphosphine, respectively, the coupling constant of 41 Hz appearing to indicate a *cis* arrangement of phosphines, while in the ^1H NMR spectrum the hydride appeared as a doublet of triplets at δ −10.14 (J = 24.1, 45.3 Hz). Full spectroscopic data for **1** together with data for all new complexes described herein is given in Table 1.

(1) Hlatky, G. G.; Crabtree, R. H. *Coord. Chem. Rev.* **1985**, 65 1. Moore, D. S.; Robinson, S. D. *Chem. Soc. Rev.* **1983**, 415.
(2) Knox, S. A. R.; Koepke, J. W.; Andrews, M. A.; Kaesz, H. D. *J. Am. Chem. Soc.* **1975**, *97*, 3942. Deeming, A. J. *Adv. Organomet. Chem.* **1986**, *26*, 1.
(3) Riera, V.; Ruiz, M. A.; Tiripicchio, A.; Tiripicchio-Camellini, M. *J. Chem. Soc., Chem. Commun.* **1985**, 1505. Carreño, R.; Riera, V.; Ruiz, M. A.; Bois, C.; Jeannin, Y. *Organometallics* **1993**, *12*, 1946 and references given therein.
(4) Boothman, J.; Hogarth, G. *J. Organomet. Chem.* **1992**, *437*, 201.
(5) Hogarth, G. *J. Organomet. Chem.* **1991**, *407*, 91.
(6) Hogarth, G.; Lavender, M. H. *J. Chem. Soc., Dalton Trans.* **1992**, 2759.
(7) Hogarth, G.; Lavender, M. H. *J. Chem. Soc., Dalton Trans.* **1993**, 143.
(8) Hogarth, G.; Lavender, M. H. *J. Chem. Soc., Dalton Trans.* **1994**, 3389.
(9) Walther, B.; Hartung, H.; Reinhold, J.; Jones, P. G.; Mealli, C.; Böttcher, H.-C.; Baumeister, U.; Krug, A.; Möckel, A. *Organometallics* **1992**, *11*, 1542. Walther, B.; Hartung, H.; Bambirra, S.; Krug, A.; Böttcher, H.-C. *Organometallics* **1994**, *13*, 172. Adams, M. R.; Galluci, J.; Wojcicki, A. *Inorg. Chem.* **1991**, *31*, 2. Nicholas, K.; Bray, L. S.; Davis, R. E.; Pettit, R. *J. Chem. Soc., Chem. Commun.* **1971**, 608. Schmitt, H. J.; Ziegler, M. L. *Z. Naturforsch.* **1973**, *28B*, 508. Cotton, F. A.; Jamerson, J. D.; Stults, B. R. *J. Am. Chem. Soc.* **1976**, *98*, 1774. Calderon, J. L.; Fontana, S.; Frauendorfer, E.; Day, V. W.; Iske, S. D. A. *J. Organomet. Chem.* **1974**, *64*, C16. Seyferth, D.; Breuer, K. S.; Wood, T. G.; Cowie, M.; Hilts, R. W. *Organometallics* **1992**, *11*, 2570.
(10) Caffyn, A. J.; Mays, M. J.; Raithby, P. R. *J. Chem. Soc., Dalton Trans.* **1991**, 2329 and references given therein.
(11) Hogarth, G.; Kayser, F.; Knox, S. A. R.; Morton, D. A. V.; Orpen, A. G.; Turner, M. L. *J. Chem. Soc., Chem. Commun.* **1988**, 358.
(12) Doherty, N. M.; Hogarth, G.; Knox, S. A. R.; Macpherson, K. A.; Melchior, F.; Morton, D. A. V.; Orpen, A. G. *Inorg. Chim. Acta* **1992**, *198–200*, 257.
(13) Knox, S. A. R.; Morton, D. A. V.; Orpen, A. G.; Turner, M. L. *Inorg. Chem. Acta* **1994**, *220*, 201.

Table 1. Spectroscopic Data for New Complexes

no.	IR (ν_{CO}) (cm^{-1})[a]	^{31}P (δ), J (Hz)[b]	^{1}H (δ), J (Hz)[b]
1	1993.6 (m), 1970.1 (s), 1931.1 (s), 1710.0 (m)	192.2 (t, J = 41), 75.2 (d)	7.8–7.2 (20H, m, Ph), 2.60 (2H, br, CH_2), 2.4–0.9 (22H, m, Cy), −10.14 (1H, dt, J = 24.1, 45.3, μ-H)
2	1971.5(m), 1943.5 (m), 1909.5 (m), 1892.0 (sh)	242.8 (t, J = 84, 79), 87.7 (dd, J = 67, 78), 77.4 (dd, J = 67, 84)	8.2–6.7 (20H, m, Ph), 6.50 (1H, m, H_α), 3.74 (1H, q, J = 10.6, CH_3), 2.60 (1H, dd, J = 5.8, 2.5 $H_{\beta cis}$), 2.64 (1H, dt, J = 9.1, 7.8, $H_{\beta trans}$), 2.76 (1H, dt, J = 8.8, 14.3, CH_2), 2.7–1.1 (22H, m, Cy)
3a	1966.4 (m), 1938.9 (s), 1906.5 (m), 1888.0 (sh)	247.1 (dd, J = 74, 85), 79.3 (dd, J = 74, 117), 78.0 (dd, J = 117, 85)	7.7–7.0 (20H, m, Ph), 3.80 (1H, dt, J = 15.2, 9.3, CH_2), 3.48 (1H, q, J = 9.3, CH_2), 3.44 (1H, q, J = 9.3), 2.61 (1H, d, J = 12.7, $H_{\beta trans}$), 2.2–1.1 (22H, m, Cy), 0.83 (3H, d, J, Me)
3b	1966.4 (m), 1938.9 (s), 1906.5 (m), 1888.0 (sh)	242.8 (t, J = 79), 82.8 (t, J = 72), 79.4 (t, J = 74)[c]	8.2–7.0 (20, m, Ph), 6.05 (1H, ddt, J = 28.8, 12.0, 6.5, H_α), 3.91 (1H, M, H_β), 2.64 (1H, dt, J = 14.5, 9.4, CH_2), 2.32 (1H, q, J = 11.0, CH_2), 2.2–0.8 (22H, m, Cy), 0.45 (3H, d, J = 5.9, Me)
4	1970.8 (m), 1941.1 (s), 1909.1 (m), 1890.0 (sh)	242.0 (t, J = 78), 81.1 (t, J = 75), 77.6 (t, J = 80)[c]	7.7–6.5 (25H, m, Ph), 6.79 (1H, m, H_α), 3.93 (1H, m, CH_2), 2.63 (1H, dt, J = 9.4, 13.1), 2.40 (1H, br, H_β), 2.8–1.2 (22H, m, Cy)[c]
5	2002.5 (m), 1938.0 (s), 1891.7 (m), 1887.5 (m)	227.0 (dd, J = 87, 29), 64.0 (dd, J = 83, 29), 56.5 (t, J = 85)	7.8–7.0 (20H, m, Ph), 5.98 (1H, s, CH), 4.43 (1H, m, CH_2), 3.98 (1H, m, CH_2), 3.79 (3H, s, CO_2*Me*), 3.47 (3H, s, CO_2*Me*), 2.4–0.9 (22H, m, Cy)
6	1980.2 (m), 1950.1 (s), 1920.8 (m), 1902.5 (sh)	236.5 (t, J = 72), 58.0 (d)	10.66 (1H, J = 4.0, CH), 7.7–7.0 (20H, m, Ph), 4.40 (1H, q, J = 11.8, CH_2), 3.31 (1H, q, J = 11.5, CH_2), 2.3–0.9 (22H, m, Cy)
7a	1971.9 (m), 1939.2 (s), 1908.1 (m), 1887.4 (sh)	242.8 (t, J = 81), 59.5 (dd, J = 82, 134), 57.9 (dd, J = 80, 134)	8.21 (1H, q, J = 3.3, CH), 8.0–6.9 (20H, m, Ph), 5.24 (1H, dt, J = 10.0, 7.2, H_c), 4.92 (1H, d, J = 10.0, H_b), 4.74 (1H, d, J = 16.9, H_a), 4.34 (2H, t, J = 10.9, CH_2), 3.16 (1H, q, J = 7.2, H_d), 2.81 (1H, q, J = 6.9, H_d), 2.4–1.0 (22H, m, Cy)
7b	1971.3 (m), 1938.8 (s), 1907.5 (m), 1886.8 (sh)	242.0 (t, J = 81), 59.0 (dd, J = 82, 134), 57.5 (dd, J = 80, 134)	8.22 (1H, q, J = 3.4, CH), 7.9–6.9 (20H, m, Ph), 4.34 (2H, dt, J = 11.0, 4.5, t, CH_2), 2.31 (2H, m, CH_2, Et), 0.80 (3H, t, J = 7.0, Me) 2.4–0.8 (22H, m, Cy)
7c	1973.5 (m), 1940.0 (s), 1910.7 (m), 1889.8 (sh)	240.0 (t, J = 81), 57.6 (dd, J = 79, 130), 55.0 (dd, J = 82, 130)	8.28 (1H, q, J = 3.2, CH), 8.0–6.1 (25H, m, Ph), 4.53 (1H, q, J = 11.4, CH_2), 4.35 (1H, q, J = 12.8, CH_2), 2.5–0.8 (m, 22H, Cy)
8a	1968.1 (m), 1937.0 (s), 1901.0 (m)	263.2 (dd, J = 104, 72), 55.8 (dd, J = 72, 58), 52.6 (dd, J = 104, 58)	9.71 (1H, s, CH), 7.9–7.0 (20H, m, Ph), 5.30 (1H, q, J = 10.0, H_c), 4.93 (1H, d, J = 9.8, H_b), 4.71 (1H, d, J = 17.0, H_a), 3.88 (1H, q, J = 11.9, CH_2), 3.37 (1H, m, H_d), 3.10 (1H, dt, J = 9.8, 13.5, CH_2), 2.98 (1H, m, H_d), 2.3–0.8 (22H, m, Cy)
8b	1966.5 (m), 1934.8 (s), 1898.8 (m), 1885.2 (sh)	262.7 (dd, J = 72, 104), 55.9 (dd, J = 59, 72), 53.2 (dd, J = 59, 104)	9.73 (1H, t, J = 4.0, CH), 7.9–7.0 (20H, m, Ph), 3.89 (1H, m, CH_2), 2.99 (dt, J = 9.6, 13.8, CH_2), 2.79 (1H, m, CH_2, Et), 2.42 (1H, m, CH_2, Et), 2.30 (1H, t, J = 4.1, CH), 2.2–0.8 (22H, m, Cy), 0.61 (2H, t, J = 7.2, CH_3)
8d	1964.2 (m), 1932.9 (s), 1894.8 (m), 1883.9 (sh)	259.7 (dd, J = 70, 107), 54.3 (dd, J = 70, 61), 50.8 (dd, J = 61, 107)	8.04 (1H, t, J = 8.0, CH), 7.7–6.9 (20H, m, Ph), 4.11 (1H, q, J = 12.6 CH_2), 3.20 (1H, dt, J = 9.3, 13.2, CH_2), 2.4–0.8 (22H, m, Cy), 0.62 (9H, s, ^{t}Bu)
9	1970.0 (m), 1940.0 (s), 1900.0 (m)	195.5 (t, J = 107), 59.9 (d)	7.5–7.2 (20H, m, Ph), 3.46 (1H, q, J = 10.0, CH_2), 2.95 (1H, q, J = 10.4, CH_2), 2.3–0.8 (22H, m, Cy), −2.33 (1H, m, μ-OH)
10	1980.5 (m), 1950.5 (s), 1915.7 (m)	217.0 (t, J = 99), 60.7 (d)[d]	7.8–7.3 (20H, m, Ph), 3.51 (1H, q, J = 11.4, CH_2), 3.00 (1H, q, J = 10.4, CH_2), 2.3–1.1 (20H, m, Cy)
11	1979.0 (m), 1949.5 (s), 1915.7 (m), 1898.1 (sh)	195.4 (t, J = 108), 60.2 (d)[d]	7.8–7.2 (20H, m, Ph), 4.06 (1H, dt, J = 14.8, 9.9, CH_2), 3.69 (1H, dt, J = 14.7, 10.1, CH_2), 2.2–1.1 (22H, m, Cy)
14	3013.0 (s), 1962.0 (s), 1939.0 (s), 1907.0 (sh)	192.3 (dd, J = 135, 49), 96.5 (dd, J = 135, 103), 22.9 (dd, J = 49, 103)	7.8–6.7 (15H, m, Ph), 4.38 (2H, dt, J = 3.0, 12.2, CH_2), 1.8–1.3 (22H, m, Cy)

[a] In CH_2Cl_2. [b] In $CdCl_3$ (293 K). [c] In $CDCl_3/CH_2Cl_2$ (203 K). [d] In C_6D_6 (293 K). [e] In CD_2Cl_2 (293 K).

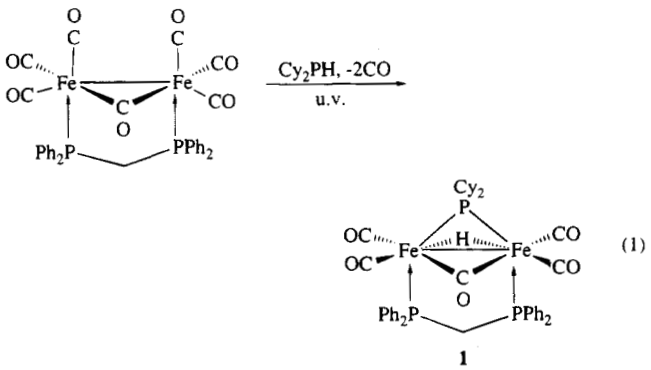

1

In order to fully elucidate the structure of **1** an X-ray crystallographic study was carried out, the results of which are summarized in Figure 1, while Table 2 gives selected bond lengths and angles. As expected, the molecule consists of two iron atoms in close contact with one another [Fe(1)–Fe(2), 2.579(2) Å] being bridged approximately symmetrically by dicyclohexylphosphido [Fe(1)–P(3), 2.241(3) Å; Fe(2)–P(3), 2.259(3) Å], diphosphine [Fe(1)–P(1), 2.234 Å; Fe(2)–P(2), 2.257(3) Å], and carbonyl [Fe(1)–C(1), 1.984(8) Å; Fe(2)–C(1), 1.967(7) Å] moieties. Each iron atom also carries two terminal carbonyls which are bent slightly out of the plane bisecting the two phosphorus ligands, lying closer to the dicyclohexylphosphido moiety. The most notable feature of the molecule in light of the spectroscopic data is the *trans* arrangement of the diphosphine and dicyclohexylphosphido ligands [P(1)–Fe(1)–P(3), 152.7(1)°; P(2)–Fe(2)–P(3), 152.6(1)°]. The hydride was not located, however, inspection of the molecule strongly

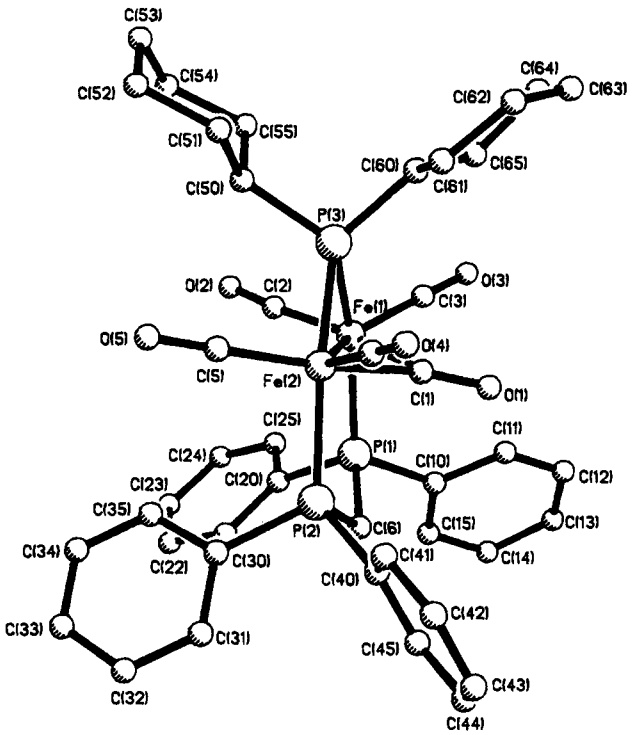

Figure 1. Molecular structure of **1**.

Table 2. Selected Bond Lengths (Å) and Angles (deg) for 1

Fe(1)–Fe(2)	2.579(2)	Fe(2)–C(1)	1.967(7)
Fe(1)–P(1)	2.234(3)	Fe(1)–C(2)	1.820(9)
Fe(2)–P(2)	2.257(3)	Fe(1)–C(3)	1.779(8)
Fe(1)–P(3)	2.241(3)	Fe(2)–C(4)	1.787(9)
Fe(2)–P(3)	2.259(3)	Fe(2)–C(5)	1.773(9)
Fe(1)–C(1)	1.984(8)	C(1)–O(1)	1.163(9)
P(1)–Fe(1)–P(3)	152.7(1)	Fe(2)–C(1)–O(1)	138.4(6)
P(2)–Fe(2)–P(3)	152.6(1)	Fe(2)–Fe(1)–C(2)	118.0(3)
Fe(1)–P(3)–Fe(2)	69.9(1)	Fe(2)–Fe(1)–C(3)	139.5(3)
P(3)–Fe(1)–C(1)	76.7(2)	Fe(1)–Fe(2)–C(4)	137.2(3)
P(3)–Fe(2)–C(1)	76.6(3)	Fe(1)–Fe(2)–C(5)	117.6(3)
Fe(1)–C(1)–O(1)	140.0(6)		

suggests that it resides between the two iron atoms, lying in the vacant coordination site *trans* to C(3) and C(4), since the site on the opposite side of the molecule is occupied by the bridging carbonyl that lies *trans* to C(2) and C(5) [C(1)–Fe(1)–C(2), 166.9(3)°; C(1)–Fe(2)–C(5), 167.0(4)°].

We were initially concerned that the apparent contradiction between the relatively small phosphorus–phosphorus coupling constant (41 Hz) and the *trans* arrangement of phosphines may be a consequence of *cis–trans* isomerization of the latter during the recrystallization process; however, NMR spectra of the recrystallized material were identical to those from crude samples. A further explanation, namely, that bulk samples of **1** contained the *cis* phosphine configuration while the crystal chosen for diffraction contained a *trans* arrangement, was easily ruled out on the basis that the crystal chosen was from a homogeneous sample and, more importantly, the observation that *all* complexes derived from **1** contain the *trans* phosphine configuration. The latter is in marked contrast to the diphenylphosphido analogue $[Fe_2(CO)_4(\mu\text{-H})(\mu\text{-CO})(\mu\text{-PPh}_2)(\mu\text{-dppm})]$ (**1-Ph**), which is shown to give mixtures of $\sigma-\pi$ alkenyl complexes with *cis* and *trans* phosphine configurations upon addition of alkynes.[6] Thus we believe that, while in **1**, the phosphines adopt a *trans* configuration, in **1-Ph** they are *cis*. The reason for this major structural difference is unlikely to be due to the differing electronic properties of the diphenyl- and dicyclohexylphosphido moieties and is almost certainly a consequence of the greater steric bulk of the latter. Thus, in adopting the *trans* phosphine configuration, adverse steric interactions between these relatively bulky ligands are minimized.

A recent report details the preparation of the unsubstituted phosphido–hydrido complexes $[HFe_2(CO)_7(\mu\text{-}PR_2)]$,[14] although none have been characterized by crystallography. The unsubstituted heptacarbonyl complexes almost certainly have a core geometry similar to that found in **1** since they have similar spectroscopic properties. For example, $[HFe_2(CO)_7(\mu\text{-}P^tBu_2)]$ shows a bridging carbonyl in the IR spectrum (1804 cm^{-1}), while the hydride appears at δ −10.7 (d, J = 51.0 Hz) in the ^1H NMR spectrum.[14] A related diruthenium phosphido–hydrido complex, namely, $[Ru_2(CO)_5(P^tBu_2H)(\mu\text{-H})(\mu\text{-CO})(\mu\text{-}P^tBu_2)]$, has recently been prepared,[15] but is only stable under an atmosphere of carbon monoxide. In solution, in the absence of CO and presence of $^tBu_2PH$, rapid formation of the unsaturated complex $[Ru_2(CO)_4(^tBu_2PH)_2(\mu\text{-H})(\mu\text{-}P^tBu_2)]$ occurs which contains a bridging carbonyl in the solid state.

2. Hydrodimetalation of Primary Alkynes and $\sigma-\pi$ Alkenyl "Windshield-Wiper" Fluxionality. The insertion of alkynes into metal–hydrogen bonds (hydrometalation) to afford alkenyl complexes is a well-known process. At binuclear centers this process is termed "hydrodimetalation", and Carty and co-workers have recently shown that the parent phosphido–hydrido complex $[HFe_2(CO)_7(\mu\text{-dppm})]$ readily inserts both alkynes and diynes to afford $\sigma-\pi$ alkenyl and $\sigma-\pi$ alkenyl–enyl complexes, respectively.[16] Indeed we have also recently shown that the insertion of primary alkynes into diiron–hydrido complexes is a facile process.[4,6]

Addition of ethyne to a toluene solution of **1** results in the exclusive formation of $[Fe_2(CO)_4(\mu\text{-HC=CH}_2)(\mu\text{-}PCy_2)(\mu\text{-dppm})]$ (**2**) in 69% yield (eq 2). Characterization

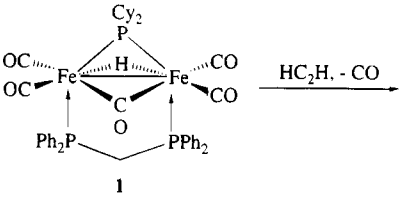

1

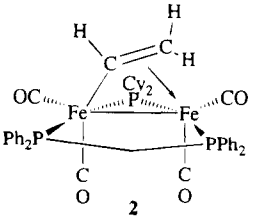

2 (2)

was easily made on the basis of spectroscopic data (Table 1). At room temperature the ethenyl group is static as shown by the inequivalent ends of the diphosphine which appear as doublets of doublets at 87.7 (J = 78, 67 Hz) and 77.4 (J = 84, 67) ppm in the ^{31}P NMR

(14) Walther, B.; Hartung, H.; Böttcher, H.-C.; Baumeister, U.; Böhland, U.; Reinhold, J.; Sider, J.; Ladriere, J.; Schiebel, H.-M. *Polyhedron* **1991**, *10*, 2423.
(15) Böttcher, H.-C.; Rheinwald, G.; Stoeckli-Evans, H.; Süss-Fink, G.; Walther, B. *J. Organomet. Chem.* **1994**, *469*, 163.
(16) McLaughlin, S. A.; Doherty, S.; Taylor, N. J.; Carty, A. J. *Organometallics* **1992**, *11*, 4315.

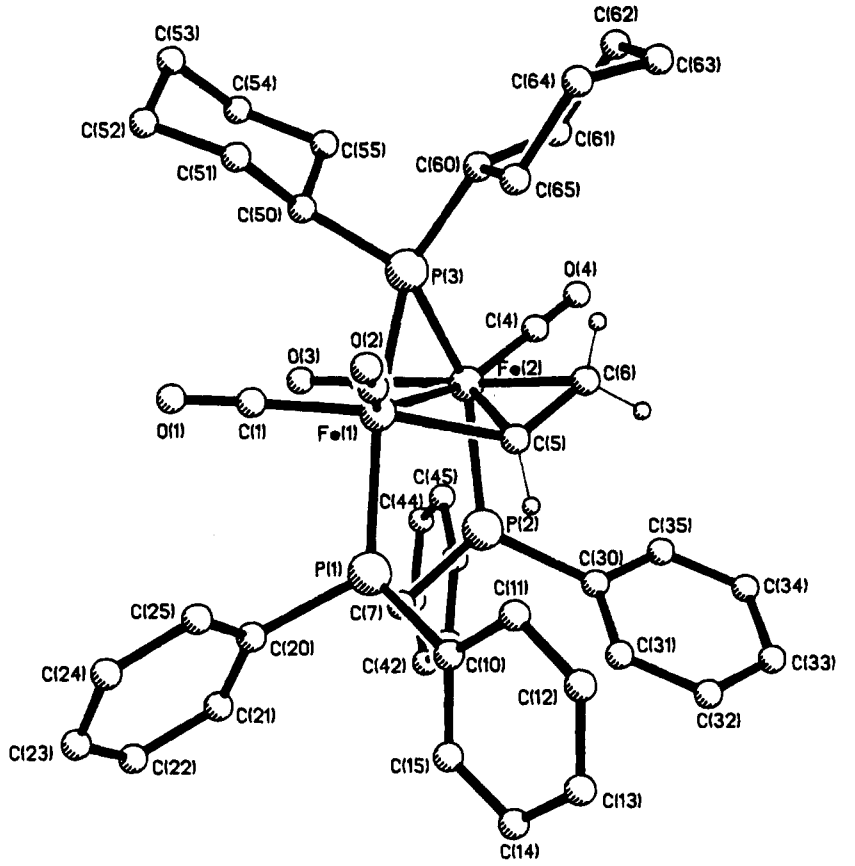

Figure 2. Molecular structure of **2**.

Table 3. Selected Bond Lengths (Å) and Angles (deg) for 2·CH_2Cl_2

Fe(1)–Fe(2)	2.577(1)	Fe(2)–C(3)	1.762(4)
Fe(1)–P(1)	2.225(1)	Fe(2)–C(4)	1.757(4)
Fe(2)–P(2)	2.221(1)	Fe(1)–C(5)	1.953(3)
Fe(1)–P(3)	2.224(1)	Fe(2)–C(5)	2.099(4)
Fe(2)–P(3)	2.249(1)	Fe(2)–C(6)	2.168(4)
Fe(1)–C(1)	1.744(5)	C(5)–C(6)	1.390(5)
Fe(1)–C(2)	1.774(4)		
P(1)–Fe(1)–P(3)	152.0(1)	Fe(1)–C(5)–Fe(2)	78.9(1)
P(2)–Fe(2)–P(3)	151.0(1)	Fe(2)–Fe(1)–C(1)	108.6(1)
Fe(1)–P(3)–Fe(2)	70.4(1)	Fe(2)–Fe(1)–C(2)	145.7(1)
P(3)–Fe(1)–C(5)	85.8(1)	Fe(1)–Fe(2)–C(3)	91.4(1)
P(3)–Fe(2)–C(5)	81.8(8)	Fe(1)–Fe(2)–C(4)	156.8(2)
P(3)–Fe(2)–C(6)	83.8(8)		

spectrum. That the *trans* arrangement of the phosphorus-containing ligands is maintained throughout the insertion process is readily ascertained from the magnitude of the coupling constants to the phosphido-bridge signal at 242.8 (J = 84, 78 Hz) ppm. The ^{1}H NMR spectrum was most informative, revealing, in addition to the phenyl, cyclohexyl, and inequivalent methylene protons of the diphosphine, signals at δ 6.50, 3.60, and 2.64, which were assigned on the basis of chemical shifts and coupling constants to H_α, $H_{\beta cis}$, and $H_{\beta trans}$, respectively. On the basis of the spectroscopic data, however, we were not able to assign the position of the vinyl group with respect to the phosphido moiety, that is, exo or endo. Thus an X-ray crystallographic study was carried out, the results of which are summarized in Figure 2, while Table 3 gives selected bond lengths and angles.

The molecule shows the main structural features as expected, namely, a short iron–iron vector [Fe(1)–Fe(2), 2.577(1) Å] bridged approximately symmetrically by diphosphine [Fe(1)–P(1), 2.225(1) Å; Fe(2)–P(2), 2.221(1) Å] and dicyclohexylphosphido [Fe(1)–P(3), 2.224(1) Å; Fe(2)–P(3), 2.249(1) Å] moieties. Each iron atom also carries two carbonyls, one approximately *trans* to the metal–metal vector, while the second lies *cis* to it and *trans* to the ethenyl ligand. The latter also bridges the diiron center, being σ-bound to Fe(1) [Fe(1)–C(5), 1.953(3) Å] and π-bound to Fe(2) [Fe(2)–C(5), 2.099(6) Å; Fe(2)–C(6), 2.168(4) Å]. As expected, the carbon–carbon bond of the ethenyl is elongated [C(5)–C(6), 1.390(5) Å] as a result of metal coordination. It adopts an endo position with respect to the dicyclohexylphosphido moiety, that is, the β-carbon lies above the C(1)–Fe(1)–Fe(2)–C(3) plane and toward the dicyclohexylphosphido moiety, while C_α lies below this plane.

While a number of structures have been elucidated in which the dimetal center is spanned by the ethenyl ligand,[16,17] it is most useful to compare the structure of **2** in the solid state with that of the closely related diiron hexacarbonyl complex $[Fe_2(CO)_6(\mu\text{-}HC{=}CH_2)(\mu\text{-}PPh_2)]$.[16] In the latter the ethenyl moiety also adopts an endo configuration with the phosphido bridge suggesting that the adoption of this arrangement in **2** is not a consequence of the relative steric bulk of the phosphorus-containing ligands, but rather is an electronic effect. Other major structural features of the two molecules are also similar. Thus no significant changes in the metal–metal, metal–phosphido, or metal–ethenyl bond lengths occur upon diphosphine coordination, and, while there is a slight increase in the C_α–C_β bond length [1.379(5) vs. 1.390(5) Å], it is not significant. The main structural change which occurs upon coordination of the

(17) See for example: Huang, Y.-H.; Stang, P. J.; Arif, A. M. *J. Am. Chem. Soc.* **1990**, *112*, 5648. Iggo, J. A.; Mays, M. J.; Raithby, P. R.; Hendrick, K. J. *J. Chem. Soc., Dalton Trans.* **1983**, 205. Orpen, A. G.; Pippard, D.; Sheldrick, G. M.; Rouse, K. D. *Acta Crystallogr., Sect. B* **1978**, *34*, 2466.

diphosphine is concerned with the relative orientations of the carbonyls on adjacent metal centers. Hence in **2**, the carbonyls that lie *cis* to the metal–metal bond, namely, CO(2) and CO(4), lie approximately in a plane with the metal–metal vector which lies perpendicular to the phosphido bridge, while in $[Fe_2(CO)_6(\mu\text{-}HC{=}CH_2)(\mu\text{-}PPh_2)]$ the appropriate carbonyls are staggered, with one lying above and the second lying below the plane. Thus coordination of the diphosphine has had the effect of twisting the two tricarbonyl fragments with respect to one another. This is also manifested in the coordination geometries about the metal atoms in both complexes which, ignoring the metal–metal bond, are approximately trigonal bipyramidal. The axial ligands at Fe(1) in **2** are best considered to be CO(2) and C(5) of the vinyl ligand, and the C(2)–Fe(1)–C(5) angle of 158.0(2)° varies by 8° from the corresponding angle in $[Fe_2(CO)_6(\mu\text{-}HC{=}CH_2)(\mu\text{-}PPh_2)]$ [166.1(1)°]. An even greater variation occurs at Fe(2), where P(3) and P(2) are best considered the axial ligands (taking the midpoint of the C_α–C_β vector as an equatorial site), the P(2)–Fe(2)–P(3) angle being 151.0(1)° as compared to 168.3(1)° in the unsubstituted complex. From this it is apparent that, while both trigonal centers are twisted upon diphosphine coordination, it is the π-bound center Fe(2) which is most affected.

The hydrodimetalation of other primary alkynes also proceeded smoothly upon reaction with **1**. Insertion of propyne affords an inseparable mixture of α- and β-substituted complexes $[Fe_2(CO)_4(\mu\text{-}MeC{=}CH_2)(\mu\text{-}PCy_2)(\mu\text{-}dppm)]$ **3a** with $[Fe_2(CO)_4(\mu\text{-}HC{=}CHMe)(\mu\text{-}PCy_2)(\mu\text{-}dppm)]$ **3b** in an approximate 2.5:1 ratio, while with phenylethyne the β-substituted isomer $[Fe_2(CO)_4(\mu\text{-}HC{=}CHPh)(\mu\text{-}PCy_2)(\mu\text{-}dppm)]$ **4** is formed exclusively (eq 3). Characterization of isomers proved relatively

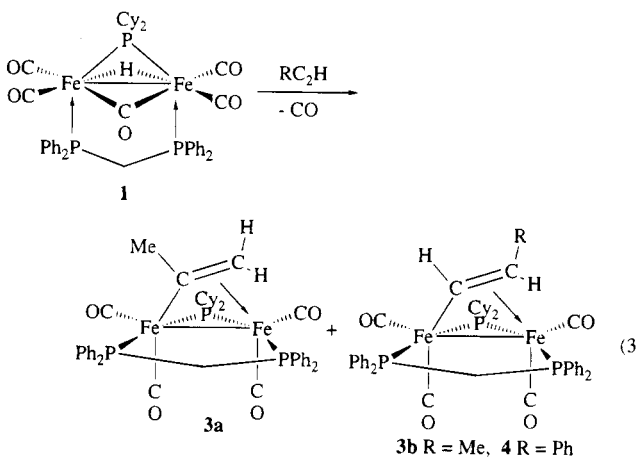

straightforward by ^1H NMR spectroscopy, with β-substituted complexes **3b** and **4** showing a relatively high field signal associated with H_α, while for the α-substituted complex **3a**, the alkenyl protons appeared between δ 3.5 and 2.5. That all complexes adopted the expected *trans* disposition of phosphorus-containing ligands was easily shown by the relatively large phosphorus–phosphorus coupling constants of between 90 and 70 Hz to the high-field phosphido-bridge resonance [213 K: **3a**, 247.1 (dd, J = 85, 74); **3b**, 242.8 (t, J = 79) ppm]. In order to confirm the assignment of **4** as the β-substituted isomer, an X-ray crystallographic study was carried out, the results of which are summarized in Figure 3, while Table 4 gives selected bond lengths and angles.

Table 4. Selected Bond Lengths (Å) and Angles (deg) for 4·CH_2Cl_2

Fe(1)–Fe(2)	2.564(1)	Fe(2)–C(3)	1.745(4)
Fe(1)–P(1)	2.229(1)	Fe(2)–C(4)	1.761(5)
Fe(2)–P(2)	2.234(1)	Fe(1)–C(5)	1.971(4)
Fe(1)–P(3)	2.222(1)	Fe(2)–C(5)	2.104(5)
Fe(2)–P(3)	2.256(1)	Fe(2)–C(6)	2.261(4)
Fe(1)–C(1)	1.768(4)	C(5)–C(6)	1.395(5)
Fe(1)–C(2)	1.738(5)		
P(1)–Fe(1)–P(3)	151.9(1)	Fe(1)–C(5)–Fe(2)	77.9(2)
P(2)–Fe(2)–P(3)	151.2(1)	Fe(2)–Fe(1)–C(1)	109.5(2)
Fe(1)–P(3)–Fe(2)	69.8(1)	Fe(2)–Fe(1)–C(2)	145.2(1)
P(3)–Fe(1)–C(5)	85.7(1)	Fe(1)–Fe(2)–C(3)	88.0(2)
P(3)–Fe(2)–C(5)	81.7(1)	Fe(1)–Fe(2)–C(4)	157.1(1)
P(3)–Fe(2)–C(6)	82.1(1)		

As expected, the main structural features are very similar to those found in **2**, the short iron–iron vector [Fe(1)–Fe(2), 2.564(1) Å] being bridged symmetrically by the phosphorus-containing ligands which adopt the relative *trans* disposition. The unsubstituted α-carbon of the alkenyl ligand bridges the diiron vector [Fe(1)–C(5), 1.971(4) Å; Fe(2)–C(5), 2.104(5) Å] while the β-carbon is bound only to a single iron center [Fe(2)–C(6), 2.261(4) Å], and again the alkenyl moiety adopts an endo position with respect to the dicyclohexylphosphido moiety. The most interesting feature of **4** is the orientation of the phenyl substituent, which is endo to the diphosphine ligand and lies over one of the phenyl rings of the latter. Thus, the distance between the ring centroid of this ring [C(70)–C(75)] and the phenyl substituent [C(30)–C(35)] of 3.683 Å is indicative of a weak π-stacking interaction. Indeed, while the orientation of the phenyl substituents on the diphosphine varies little for three of the rings between **2** and **4**, this latter has undergone a significant twist in order to accommodate the phenyl substituent.

The selectivity for α-substituted complexes during hydrometalation reactions constitutes a Markovnikov type addition process and is generally observed, for example, at diiron[4,6] and other binuclear metal centers.[18] In the case of **1**, the regioselectivity of the insertion process is strongly dependent upon the nature of the alkyne. Close inspection of the solid-state structure of **4** sheds light onto this. Substitution by a phenyl group at the α-carbon would lead to unfavorable steric interactions between it and the substituents on the phosphorus-containing ligands in either the endo or exo conformation. Hence it appears that the high regioselectivity for anti-Markovnikov addition in the case of the insertion of phenylethyne into **1** is sterically controlled. In contrast, the major product of the insertion of propyne is the α-substituted isomer **3a**. Here the methyl group is less sterically demanding and can be tolerated in either site. In terms of reducing unfavorable steric interactions, it is still the β-site that is favored since this removes the substituent away from the sterically congested diiron center. Thus it is tempting to suggest that Markovnikov addition which affords the α-substituted products is electronically favored, while the anti-Markovnikov hydrodimetalation which affords β-substituted isomers is sterically preferable.

We,[5] Carty,[16] and Seyferth[19] have noted that phosphido-bridged diiron alkenyl complexes show an unusu-

(18) Xue, Z.; Sieber, W. J.; Knobler, C. B.; Kaesz, H. D. *J. Am. Chem. Soc.* **1990**, *112*, 1825. Breckenridge, S. M.; McLaughlin, S. A.; Taylor, N. J.; Carty, A. J. *J. Chem. Soc., Chem. Commun.* **1991**, 1718.

(19) Seyferth, D.; Hoke, J. B.; Womack, G. B. *Organometallics* **1990**, *9*, 2662. Seyferth, D.; Archer, C. M.; Ruschke, D. P.; Cowie, M.; Hilts, R. W. *Organometallics* **1991**, *10*, 3363.

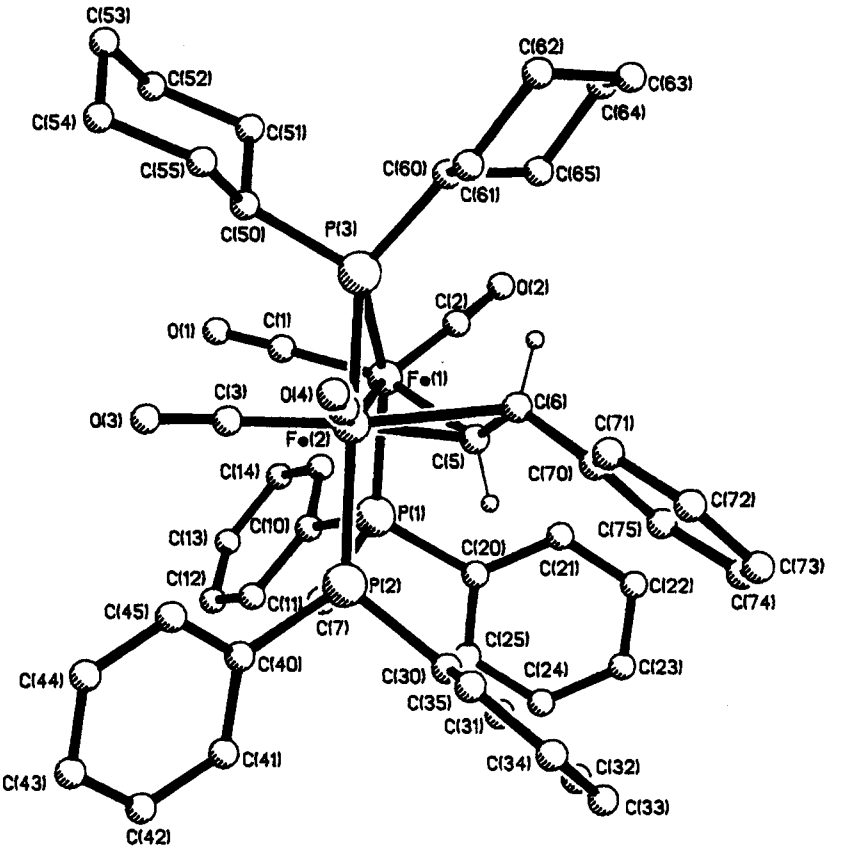

Figure 3. Molecular structure of **4**.

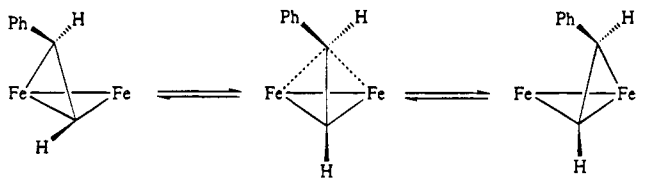

Figure 4. $\sigma-\pi$ Alkenyl fluxionality.

ally high barrier to exchange via the "windshield-wiper" process.[20] The four μ-alkenyl complexes described above are of two different types with respect to the size of the energy barrier to this exchange process, **2** and **3a** having relatively high energy barriers while for the β-substituted complexes **3b** and **4**, the energy barrier is lowered considerably. This is readily apparent from their room temperature ^{31}P NMR spectra, the former displaying inequivalent ends of the diphosphine indicative of a slow exchange regime, while for the latter the spectrum is simplified significantly such that the diphosphine appears as a single doublet in accord with fast alkenyl exchange (Figure 4).

In order to investigate this further, variable temperature ^{31}P NMR studies were performed. Warming a toluene-d_8 solution of **2** resulted in a gradual broadening of the diphosphine resonances; however, even at 100 °C coalescence was not observed. In an analogous experiment, warming a toluene-d_8 solution of **3a** also resulted in a broadening of the diphosphine signals at 70 °C. At temperatures above this, however, the spectrum changed radically, with a number of new species growing in at the expense of **3a**. Indeed, upon warming to 80 °C and cooling back to room temperature all traces of **3a** had disappeared. The precise details of these irreversible thermal transformations are currently under investigation. In related experiments, cooling $CH_2Cl_2/CDCl_3$ solutions of **3b** and **4** led to changes in the spectra in accord with the freezing out of the "windshield-wiper" fluxionality such that at 213 K three well-resolved signals were observed for each complex. From the separation of the inequivalent ends of the diphosphine when frozen out (**2**, 1652; **3a**, 233; **3b**, 556; **4**, 573 Hz) and the coalescence temperature (**2**, >378; **3a**, >353; **3b**, 253; **4**, 233 K), approximate free energies of activation for the process are calculated as $\geq 68\pm2$ (**2**), $\geq 68\pm2$ (**3a**), 47 ± 2 (**3b**), and 34 ± 2 (**4**) kJ mol^{-1}.

The nature of this pronounced difference in the free energies of activation between those complexes substituted in the β-position, **3b** and **4**, with respect to those not substituted in this position, **2** and **3a**, is open for debate. In view of the large difference between isomers **3a** and **3b** of ≥ 21 kJ mol^{-1} and the relative similarity of **3b** and **4** which have electron-releasing and electron-withdrawing substituents on the β-carbon, respectively, it is difficult to imagine that electronic effects alone can account for these observations. For example, one might imagine a development of charge in the transition state being stabilized either by a phenyl or a methyl group on the β-carbon, but not both. Instead we favor an explanation based primarily on steric factors. This necessitates that for the β-substituted complexes relief of unfavorable steric interactions must occur in the transition state, thus lowering the activation barrier for the fluxional process. This is easy to image for **4**, since in the ground state the phenyl substituent lies direct over one of the phenyl groups of the diphosphine while in the transition state it will lie between the two ends of the diphosphine since there is a plane of symmetry bisecting the iron–iron vector (Figure 4). For **3b**, a similar release of unfavorable steric interactions is envisaged; however, since the methyl group is smaller, then these will be smaller in the ground state, and thus

the effect will not be so pronounced. For **2** and **3a**, the steric nature of the alkenyl moiety will not vary significantly between the ground and transition state since the α-carbon (and hence its substituent) are fixed during the fluxional process. Hence we suggest that the high energy barriers noted for the exchange process in these and related phosphido-bridged diiron complexes[5,6,16,19] are electronic in origin.

As detailed above, ^{31}P NMR spectroscopy is a particularly convenient method for observing the $\sigma-\pi$ alkenyl fluxionality since in the slow-exchange region inequivalent diphosphine resonances are observed which are made equivalent in the fast-exchange regime. Conventionally this process has been studied by ^{13}C NMR spectroscopy, monitoring changes in the carbonyl signals. The latter approach is handicapped by a number of factors including the low natural abundance of carbon-13, long relaxation times of metal-bound carbonyls, and the occurrence of other carbonyl exchange mechanisms (e.g., trigonal rotation, bridge–terminal exchange) with similar energies to the "windshield-wiper" fluxionality. The ^{31}P NMR spectra, however, give no insight into the mechanistic details of the transformation, namely, whether the two β-protons interconvert during the fluxional process. Generally this is not found to be the case;[20] however, in a few instances, proton exchange has been found to be concomitant with the alkenyl fluxionality,[21] and we had reason to suspect that this may be the case for **2**–**4**.[8] Thus, the $\sigma-\pi$ alkenyl fluxionality in **2** was also monitored by ^1H NMR spectroscopy. At room temperature in toluene-d_8 signals assigned to the vinylic protons are broadened slightly, while those due to the cyclohexyl and phenylic hydrogens are sharp. Warming to 100 °C results in a gradual broadening of the latter, while in contrast, the vinylic protons sharpen and remain distinct. Hence we conclude that under these conditions, the "windshield-wiper" fluxionality does not occur with exchange of the β-hydrogens, indicating that rotation about the $C_\alpha-C_\beta$ vector cannot occur in the transition state and suggesting that the latter is not significantly zwitterionic in nature.[8]

3. Hydrodimetalation of the Activated Alkyne Dimethyl Acetylenedicarboxylate. While **1** does not react appreciably with unactivated disubstituted alkynes, addition of an excess of the activated alkyne, dimethyl acetylenedicarboxylate (DMAD), resulted in a rapid reaction at 50 °C. The compound isolated was not, however, the expected hydrodimetalation product, namely, *cis*-$[Fe_2(CO)_4\{\mu$-$C(CO_2Me)$=$CH(CO_2Me)\}(\mu$-$PCy_2)(\mu$-dppm)], but rather the metallacyclic complex $[Fe_2(CO)_4\{\eta^2$-$C(CO_2Me)$=CH-$C(OMe)$=$O\}(\mu$-$PCy_2)(\mu$-dppm)] (**5**) formed in 71% yield (eq 4).

Characterization was straightforward based on a comparison of spectroscopic data with that of the analogous diphenylphosphido complex which we have crystallographically characterized.[8] The most notable feature that distinguishes **5** from a simple hydrodimetalation product is the carbonyl region of the IR spectrum, which differs significantly from those containing two iron dicarbonyl units, indicating $Fe(CO)_3$ and $Fe(CO)$

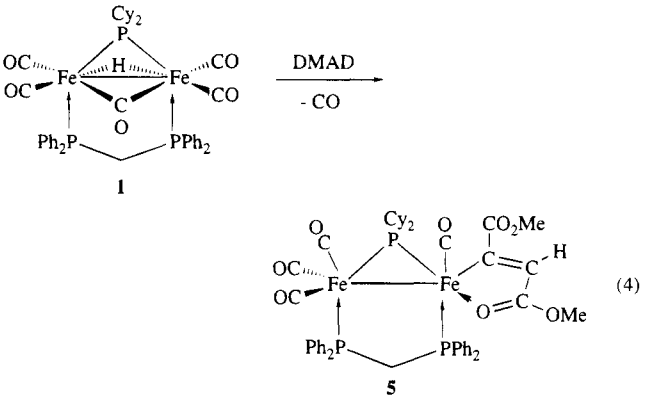

(4)

moieties. The most noteworthy features of **5** are the *trans* orientation of the vinyl substituents and the metal coordination of one of the carbonyl groups of the ester. A number of mononuclear complexes containing a metallacycle of this type have been reported previously.[22]

In the analogous diphenylphosphido chemistry, we were able to isolate and crystallographically characterize the *cis* hydrodimetalation product; however, monitoring the reaction between **1** and DMAD by IR and ^{31}P NMR spectroscopy did not reveal the formation of any species other than **5**. The reason for this difference becomes apparent when one considers the relative arrangements of the phosphorus-containing ligands in **1** and **1-Ph**, being *trans* and *cis*, respectively. Thus, insertion of DMAD into **1-Ph** affords *cis,cis*-$[Fe_2(CO)_4\{\mu$-$(MeCO_2)C$=$CH(CO_2Me)\}(\mu$-$PPh_2)(\mu$-dppm)] which contains a *cis* arrangement of phosphorus ligands and a *cis* alkenyl moiety, and it is only upon thermolysis in toluene that both *cis–trans* alkenyl and *cis–trans* phosphine rearrangements occur.[8] In contrast, since **1** already contains a *trans* arrangement of phosphines, then rearrangement of the initially formed insertion product *trans,cis*-$[Fe_2(CO)_4\{\mu$-$MeCO_2)C$=$CH(CO_2Me)\}$-$(\mu$-$PCy_2)(\mu$-dppm)] to **5** must be extremely facile under the reaction conditions employed, and thus we conclude that it is the *cis–trans* rearrangement of the phosphorus-containing ligands which is the high-energy process in the formation of **5-Ph**.

4. Hydrodimetalation of Cumulenes and Heterocumulenes. A wide range of compounds with cumulated double bonds have been shown to insert into metal–hydrogen bonds at mononuclear centers,[23] while in contrast, hydrodimetalation reactions of cumulenes have been studied to a far lesser extent.[24] Hydrodimetalation of allene can occur to give either $\sigma-\pi$ alkenyl or allyl complexes, resulting from the addition of the proton to the external and internal carbon centers, respectively. A number of reports have detailed such reactivity, and the selectivity of the transfer process appears to be highly dependent upon the nature of the dimetallic hydride complex itself. Thus selectivity toward the formation of $\sigma-\pi$ ethenyl[6,25] and allyl[26]

(20) Shapley, J. R.; Richter, S. I.; Tachikawa, M.; Keister, J. B. *J. Organomet. Chem.* **1975**, *94*, C43. Farrugia, L. J.; Chi, Y.; Tu, W.-C. *Organometallics* **1993**, *12*, 1616 and references given therein.

(21) Beck, J. A.; Knox, S. A. R.; Riding, G. H.; Taylor, G. E.; Winter, M. J. *J. Organomet. Chem.* **1980**, *202*, C49. Liu, J.; Deeming, A. J.; Donovan-Mtunzi, S. *J. Chem. Soc., Chem. Commun.* **1984**, 1182.

(22) Vessey, J. D.; Mawby, R. J. *J. Chem. Soc., Dalton Trans.* **1993**, 51. Vander Zeijden, A. A. H.; Bosch, H. W.; Berke, H. *Organometallics* **1992**, *11*, 563. Alt, H. G.; Engelhardt, H. E.; Thewalt, U.; Riede, J. *J. Organomet. Chem.* **1985**, *288*, 165. Werner, H.; Weinand, R.; Otto, H. *J. Organomet. Chem.* **1986**, *307*, 49.

(23) Jia, G.; Meek, D. W. *Inorg. Chem.* **1991**, *30*, 1953 and references given therein.

(24) García Alonso, F. J.; García-Sanz, M.; Riera, V. J. *J. Organomet. Chem.* **1991**, *421*, C12.

(25) Horton, A. D.; Mays, M. J.; *J. Chem. Soc., Dalton Trans.* **1990**, 155.

complexes has been reported, while in other examples, mixtures of products result from competitive hydrogen transfer reactions. Addition of allene to a toluene solution of **1** results in the exclusive formation of $[Fe_2(CO)_4(\mu\text{-MeC=CH}_2)(\mu\text{-PCy}_2)(\mu\text{-dppm})]$ **3a** in 55% yield, in an analogous fashion to that previously reported for the diphenylphosphido complex[6] and resulting from selective proton transfer to an external carbon of the allene.

In contrast, hydrodimetalation of carbon disulfide by **1** resulted in the exclusive formation of the dithioformato complex $[Fe_2(CO)_4(\mu\text{-S}_2\text{CH})(\mu\text{-PCy}_2)(\mu\text{-dppm})]$ (**6**) in 83% yield (eq 5). That transfer of the proton had

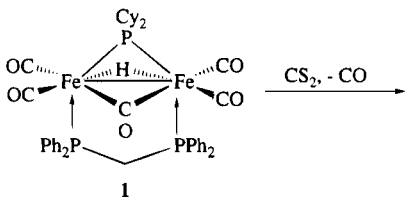

1

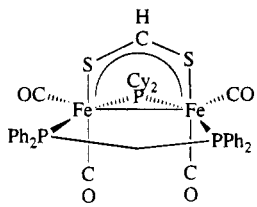

(5)

6

occurred exclusively at the central carbon atom was easily verified by the ^{31}P NMR spectrum, which showed a triplet at 236.5 and doublet at 58.0 ppm (J = 72 Hz) assigned to phosphido and diphosphine moieties respectively, indicating that the molecule contained a plane of symmetry bisecting the metal–metal vector. Other spectroscopic data also support this formulation; for example, there was an absence of any C=S and S–H absorptions in the IR spectrum. The dithioformato proton could not be assigned since it lay under the phenylic region in the ^1H NMR spectrum. In contrast to the facile insertion of carbon disulfide, carbon dioxide did not react with **1** even over prolonged periods. We have, however, synthesized the anticipated product of the latter, namely, $[Fe_2(CO)_4(\mu\text{-O}_2\text{CH})(\mu\text{-PCy}_2)(\mu\text{-dppm})]$ via an alternative route.[27] Thus, it appears that coordination of the heterocumulene to the binuclear center may be a necessary prerequisite for the insertion reaction. The insertion of carbon disulfide into mononuclear metal hydrides is again a well-established process, and proton transfer is generally selective to carbon.[28] While the hydrodimetalation of carbon disulfide appears to be quite rare, this is shown to occur with similar selectivity.

Hydrometalation of isocyanates and isothiocyanates can in theory result in the formation of three products via proton transfer to carbon, nitrogen, or the heteroatom. While organic isocyanates do not react with **1**, isothiocyanates readily insert with loss of carbon monoxide. The major insertion products in all cases were *N*-thioformamido complexes $[Fe_2(CO)_4(\mu_2\text{-RNCHS})(\mu\text{-}$

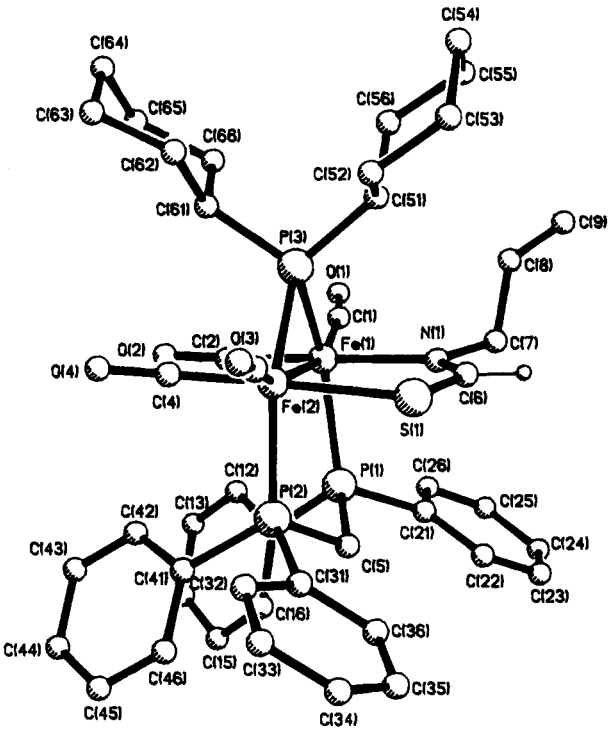

Figure 5. Molecular structure of **7a**.

$PCy_2)(\mu\text{-dppm})]$ (**7a–c**), formed in yields of 27–47% as a result of proton transfer to the central carbon atom (eq 6). These were identified on the basis of spectro-

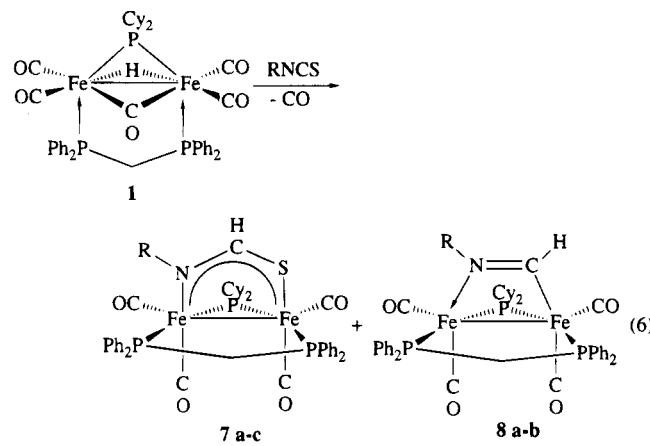

(6)

7 a-c 8 a-b

scopic data; notably all showed a resonance in the ^1H NMR spectrum around δ 8.2 assigned to the unique proton bound to the central carbon atom, while IR spectra did not contain absorptions assignable to nitrogen–hydrogen or sulfur–hydrogen moieties. In order to confirm this assignment, and elucidate structural features of the bridging *N*-thioamidate ligand, an X-ray crystallographic study was carried out on **7a**, the results of which are summarized in Figure 5, while Table 5 gives selected bond lengths and angles.

The structure of **7a** confirms the spectroscopic assignment, and major features are as expected. The diiron vector [Fe(1)–Fe(2), 2.741(2) Å] is significantly elongated with respect to those found in other complexes reported herein [Fe(1)–Fe(2), 2.577–2.580 Å]. The major structural change due to this elongation is as expected an opening up of the angle at the bridging phosphido ligand, Fe(1)–P(3)–Fe(2), 75.4(1)°, as compared to the range of 69.9–71.0° for the other complexes. The remaining coordination sites on the diiron center

(26) Hay, C. M.; Horton, A. D.; Mays, M. J.; Raithby, P. R. *Polyhedron* **1988**, *7*, 987.
(27) Corby, D.; Hogarth, G.; Lavender, M. H. Manuscript in preparation.
(28) (a) Robinson, S. D.; Sahajpal, A. *Inorg. Chem.* **1977**, *16*, 2718. (b) Adams, R. D.; Golembeski, N. M.; Selegue, J. P. *J. Am. Chem. Soc.* **1981**, *103*, 546.

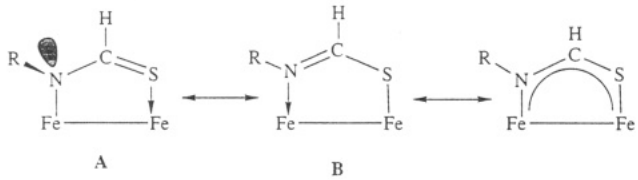

Figure 6. Canonical representations of **7**.

Table 5. Selected Bond Lengths (Å) and Angles (deg) for 7a

Fe(1)–Fe(2)	2.741(2)	Fe(2)–C(3)	1.767(8)
Fe(1)–P(1)	2.277(2)	Fe(2)–C(4)	1.727(8)
Fe(2)–P(2)	2.245(2)	Fe(1)–N(1)	2.031(6)
Fe(1)–P(3)	2.247(2)	Fe(2)–S(1)	2.324(2)
Fe(2)–P(3)	2.234(2)	N(1)–C(6)	1.274(10)
Fe(1)–C(1)	1.775(8)	S(1)–C(6)	1.695(7)
Fe(1)–C(2)	1.738(7)		
P(1)–Fe(1)–P(3)	146.6(1)	Fe(1)–Fe(2)–C(3)	161.9(2)
P(2)–Fe(2)–P(3)	144.9(1)	Fe(1)–Fe(2)–C(4)	101.7(3)
Fe(1)–P(3)–Fe(2)	75.4(1)	Fe(1)–N(1)–C(6)	124.8(5)
P(3)–Fe(1)–N(1)	90.8(2)	Fe(2)–S(1)–C(6)	109.2(3)
P(3)–Fe(2)–S(2)	92.0(1)	N(1)–C(6)–S(1)	127.6(6)
Fe(2)–Fe(1)–C(1)	161.8(3)	Fe(1)–N(1)–C(7)	120.8(5)
Fe(2)–Fe(1)–C(2)	86.4(2)	C(6)–N(1)–C(7)	114.4(6)

are occupied by the *N*-thioamidate ligand which is bound to Fe(1) through nitrogen [Fe(1)–N(1), 2.031(6) Å], while Fe(2) is sulfur-bound [Fe(2)–S(1), 2.324(2) Å]. The solid-state structure also reveals that the allyl substituent adopts a position endo to the phosphido bridge and exo to the diphosphine.

A number of possible resonance forms can be drawn for the diiron *N*-thioamidate core (Figure 6). In A, the nitrogen is pyramidal and there is a carbon–sulfur double bond, while in B it is planar and it is the carbon–nitrogen interaction that contains π-character. Scrutiny of the bond lengths and angles within the dimetalacyclic unit clearly shows that it is form B that is the predominant valence-bond representation. Thus, the central nitrogen–carbon bond N(1)–C(6) at 1.274(10) Å is a shortened considerably with respect to the external interaction to the allyl moiety [N(1)–C(7), 1.493(9) Å], which is a simple σ-interaction and within the range found for carbon–nitrogen single bonds. More importantly, the geometry about nitrogen is planar as evidenced by the sum of the bond angles about N(1) being 360° [Fe(1)–N(1)–C(6), 124.8(6)°; Fe(1)–N(1)–C(7), 120.8(5)°; C(6)–N(1)–C(7), 114.4(6)°]. In further support of the imine formulation, C(7) lies approximately in the plane of the metallacycle as expected for an sp^3-hybridized carbon. The carbon–sulfur bond [Fe(2)–S(1), 1.695(7) Å] is, however, also slightly shorter than would be expected for a simple σ-interaction, suggesting that A might play a small role; however, the bond angle at sulfur [Fe(2)–S(1)–C(6), 109.2(3)°] is clearly representative of sp^3 hybridization, being similar to that found in thioethers. Only a handful of related *N*-thioformamido complexes have been characterized,[29,30] and **7a** appears to be the first such binuclear complex crystallographically characterized. Most similar is the triosmium complex $[Os_3(CO)_9(PhPMe_2)(\mu\text{-H})(\mu\text{-}\eta^2\text{-PhNCHS})]$,[30] which shows similar carbon–nitrogen [1.32(1) Å] and carbon–sulfur [1.69(1) Å] bond lengths.

With both allyl and ethyl isothiocyanate, a second product was obtained from the hydrodimetalation of **1**,

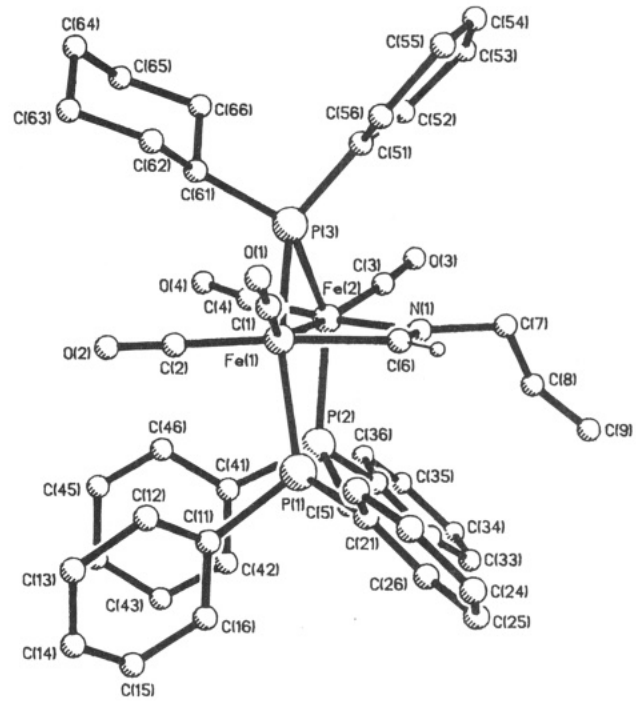

Figure 7. Molecular structure of **8a**.

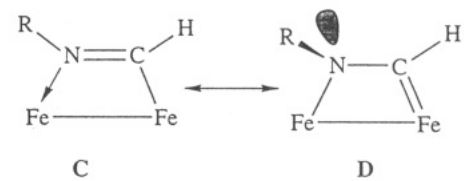

Figure 8. Canonical representations of **8**.

identified as $[Fe_2(CO)_4(\mu_2\text{-RN=CH})(\mu\text{-PCy}_2)(\mu\text{-dppm})]$ (**8a**,**b**) and resulting from proton addition to carbon and loss of sulfur (eq 6). Spectroscopic data for **8** were very similar to that for **7**; for example, IR spectra are virtually identical in the carbonyl region indicating that both new ligands have similar electron-donating abilities. Microanalytical results showed, however, that sulfur had been lost, while the unique proton is shifted downfield with respect to **7**, appearing as a triplet at about δ 9.7 in the ^{1}H NMR spectrum. In order to confirm this assignment and to gain more insight into the bonding within the dimetallacyclic ring, and X-ray crystallographic study was undertaken of **8a**, the results of which are summarized in Figure 7 and Table 6.

The structure of **8a** is very similar to that of **7a**, the diiron vector [Fe(1)–Fe(2), 2.680(3) Å] being bridged by the new formimidoyl ligand which is linked to Fe(1) through the carbon [Fe(1)–C(6), 1.975(16) Å] and to Fe(2) through nitrogen [Fe(2)–N(1), 2.015(13) Å]. While two resonance forms (C and D) can be drawn for the formimidoyl ligand (Figure 8), representation C, in which the there is a carbon–nitrogen double bond, predominates as shown by the relatively short carbon–nitrogen contact [C(6)–N(1), 1.210(23) Å] and the planar nature of the latter. Thus as in **7a**, the angles about nitrogen sum to 360°, while the methylene carbon of the allyl ligand, C(7), lies in the metallacyclic plane. Indeed, in a number of other crystallographically characterized formimidoyl complexes, similar short carbon–nitrogen distances are found[31] for example, in $[Os_3(CO)_9(\mu\text{-H})(\mu_2\text{-HC=NC}_6\text{H}_4\text{-}p\text{-F})(\mu_3\text{-S})]$ the carbon–nitrogen bond is 1.213(14) Å.[30] A further point of note in relation to a comparison of the two structures is the exo nature of

(29) Robinson, S. D.; Sahajpal, A. *Inorg. Chem.* **1977**, *16*, 2722.
(30) Adams, R. D.; Dawoodi, Z.; Foust, D. F.; Segmüller, B. E. *Organometallics* **1983**, *2*, 315.

Table 6. Selected Bond Lengths (Å) and Angles (deg) for 8a·C_5H_{12}

Fe(1)–Fe(2)	2.680(3)	Fe(1)–C(2)	1.783(17)
Fe(1)–P(1)	2.207(4)	Fe(2)–C(3)	1.779(20)
Fe(2)–P(2)	2.257(5)	Fe(2)–C(4)	1.771(17)
Fe(1)–P(3)	2.193(4)	Fe(2)–N(1)	2.015(13)
Fe(2)–P(3)	2.224(4)	Fe(1)–C(6)	1.975(16)
Fe(1)–C(1)	1.752(19)	N(1)–C(6)	1.210(23)
P(1)–Fe(1)–P(3)	152.6(2)	Fe(1)–Fe(2)–C(3)	155.8(6)
P(2)–Fe(2)–P(3)	138.1(2)	Fe(1)–Fe(2)–C(4)	108.8(5)
Fe(1)–P(3)–Fe(2)	74.7(1)	Fe(2)–N(1)–C(6)	110.1(11)
P(3)–Fe(2)–N(1)	83.3(4)	Fe(1)–C(6)–N(1)	113.2(12)
P(3)–Fe(1)–C(6)	84.2(4)	Fe(2)–N(1)–C(7)	130.6(12)
Fe(2)–Fe(1)–C(1)	152.6(5)	C(6)–N(1)–C(7)	119.3(15)

the allyl moiety with respect to the phosphido bridge. This is presumably a result of steric effects; in the smaller ring, positioning of the allyl group endo to the dicyclohexylphosphido ligand would result in considerable steric interactions with a cyclohexyl group, while in the larger ring it is moved further away, thus minimizing the latter.

The insertion of organic isothiocyanates into metal–hydrogen bonds has been reported in only a few instances previously and generally yields *N*-thioformamido complexes;[29,30] however, amido-substituted thioacyl complexes have also been noted.[32] Most relevant to this work is that of Adams and co-workers who have described the insertion of both aryl and alkyl isothiocyanates into $[Os_3(CO)_{10}(\mu\text{-H})_2]$.[30] Thus at 25 °C, insertion occurs to afford η^1-thioformamido complexes $[Os_3(CO)_{10}(\mu\text{-H})(\mu_2\text{-}\eta^1\text{-SCH=NR})]$ which rearrange with loss of CO when irradiated to give η^2-complexes $[Os_3(CO)_9(\mu\text{-H})(\mu_3\text{-}\eta^2\text{-SCHNR})]$. Interestingly, when octane solutions of the latter are refluxed, rapid carbon–sulfur bond cleavage occurs to afford sulfido–formimidoyl complexes $[Os_3(CO)_9(\mu\text{-H})(\mu\text{-HC=NR})(\mu_3\text{-S})]$. In light of these results, we considered that *N*-thioformamido complexes **7** may be precursors to formimidoyl complexes **8**. Indeed, thermolysis of a toluene solution of **7b** for 9 h afforded **8b** in 57% yield. We have previously found that carbon–sulfur bond cleavage in isothiocyanates at organometallic metal centers can be a very facile process.[33]

Robinson and co-workers in a series of papers have shown that the insertions of carbon disulfide,[28a] isothiocyanates,[29] and carbodiimides[34] at late transition metal mononuclear centers are directly comparable, the latter being a useful synthetic route toward the synthesis of *N,N'*-formamidinato complexes via selective proton transfer to carbon. Thus as a comparison, the hydrodimetalation of dicyclohexylcarbodiimide (CyN=C=NCy) by **1** was attempted. Warming a toluene solution to 60 °C, however, resulted in only a very slow reaction from which a number of low-yield products were observed, none of which displayed spectroscopic data consistent with the anticipated *N,N'*-formamidinato complex.

5. Other Insertion Reactions. In a recent publication, the unsubstituted phosphido–hydrido complex $[HFe_2(CO)_6(\mu\text{-CO})(\mu\text{-PPh}_2)]$ has been shown to react with oxygen to afford the corresponding hydroxide complex $[Fe_2(CO)_6(\mu\text{-OH})(\mu\text{-PPh}_2)]$, formally resulting from the insertion of an oxygen atom into the hydride;[14] indeed this type of oxygen insertion reaction has been known for some time.[35] We have also shown that a similar insertion process occurs for the diphosphine-substituted derivative **1-Ph**, albeit only very slowly and giving the corresponding hydroxide $[Fe_2(CO)_4(\mu\text{-OH})(\mu\text{-PPh}_2)(\mu\text{-dppm})]$ in low yield.[7] Bubbling dry air through a toluene solution of **1** for 48 h did not, however, result in the formation of the corresponding hydroxide complex $[Fe_2(CO)_4(\mu\text{-OH})(\mu\text{-PCy}_2)(\mu\text{-dppm})]$ (**9**); rather, slow decomposition of **1** was noted. In a similar attempt to synthesize a thiolate-bridged complex, toluene solutions of **1** were reacted with both elemental sulfur and propene sulfide, the latter being an excellent source of a sulfur atom. Both of these reactions, however, failed to yield the desired product; indeed **1** was recovered unchanged in both instances.

In view of the formation of formimidoyl complexes via sulfur loss from an isothiocyanate, the synthesis of one such complex was attempted via the hydrodimetalation of ^{t}BuNC by **1**. Warming a toluene solution of **1** with a slight excess of ^{t}Bu'NC at 60 °C resulted in the selective formation of $[Fe_2(CO)_4(\mu\text{-HC=N}^t\text{Bu})(\mu\text{-PCy}_2)(\mu\text{-dppm})]$ (**8d**) in 83% yield (eq 7). Characterization proved straightforward, spectroscopic data being in accord with the other formimidoyl derivatives.

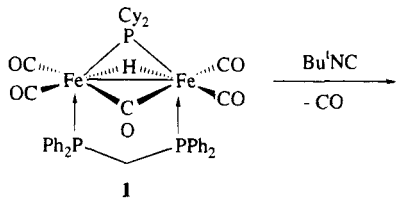

1

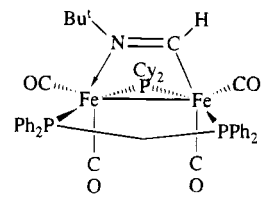

8c (7)

In light of the successful insertion of an isocyanide into **1**, insertion of nitriles was also attempted. Complex **1** proved to be sparingly soluble in acetonitrile at room temperature, but even upon warming to 60 °C, while the solubility increased, no spectroscopic changes resulted, indicating that insertion had not occurred. In an additional experiment, an excess of acrylonitrile was added to a toluene solution of **1**; however, again, no detectable reaction occurred.

6. Hydride Elimination Reactions. In a number of reactions of **1**, rather than insertion into the diiron–hydride moiety, elimination of the hydride occurs. For example, chromatography of **1** on an alumina support, eluting with dichloromethane–petroleum ether mixtures, results in the slow formation of two new complexes, $[Fe_2(CO)_4(\mu\text{-OH})(\mu\text{-PCy}_2)(\mu\text{-dppm})]$ (**9**) and $[Fe_2(CO)_4(\mu\text{-Cl})(\mu\text{-PCy}_2)(\mu\text{-dppm})]$ (**10**), the yields of which vary with exposure time on the column (eq 8). Hence, **1** can be eluted virtually unchanged on very short columns

(31) Adams, R. D.; Golembeski, N. M. *J. Am. Chem. Soc.* **1979**, *101*, 2579. Mays, M. J.; Prest, D. W.; Raithby, P. R. *J. Chem. Soc., Chem. Commun.* **1980**, 171. Aspinall, H. C.; Deeming, A. J. *J. Chem. Soc., Chem. Commun.* **1983**, 838. Beringhelli, T.; D'Alfonson, G.; Freni, M.; Giani, G.; Moret, M.; Sironi, A. *J. Organomet. Chem.* **1990**, *339*, 291. García Alonso, F. J.; García Sanz, M.; Riera, V.; Abril, A. A.; Tiripicchio, A.; Ugozzoli, F. *Organometallics* **1992**, *11*, 801.

(32) Seyferth, D.; Womack, G. B.; Archer, C. M.; Fackler, J. P., Jr.; Marler, D. O. *Organometallics* **1989**, *8*, 443.

(33) Hogarth, G.; Skordalakis, E. *J. Organomet. Chem.* **1993**, *458*, C8.

(34) Brown, L. D.; Robinson, S. D.; Sahajpal, A.; Ibers, J. A. *Inorg. Chem.* **1977**, *16*, 2728.

(35) Treichel, P. M.; Dean, W. K.; Calabrese, J. C. *Inorg. Chem.* **1973**, *12*, 2908.

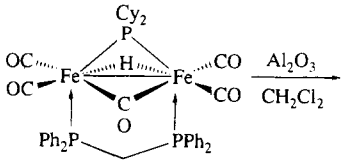

1

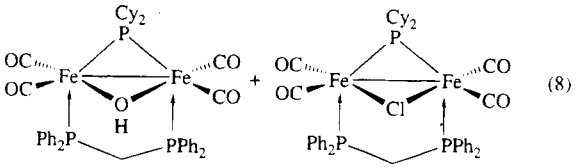

9 10 (8)

and short exposure times, while after approximately 2 h on a long column, complete conversion occurs. We have previously found that the diphenylphosphido complex **1-Ph** also reacts with an alumina support; however, in the case of the latter, the reaction occurs almost instantaneously upon alumina absorption, and the hydroxide complex $[Fe_2(CO)_4(\mu\text{-OH})(\mu\text{-PCy}_2)(\mu\text{-dppm})]$ is the only product. In an attempt to explore the role of the dichloromethane in the formation of **10**, chromatography of **1** was carried out on a similar alumina support while eluting with diethyl ether–petroleum ether mixtures. Under these conditions, **1** was eluted from the column unchanged, indicating that the presence of the chlorinated solvent is critical to both the formation of chloro- and hydroxide-bridged species. In separate experiments both of the latter were eluted unchanged from an alumina support by dichloromethane–petroleum ether mixtures, indicating that they are formed via different degradation routes but probably via a common intermediate. While the nature of such an intermediate remains unknown, it is tempting to speculate that it may result from a support-mediated carbonyl loss from **1** and undergoes competitive attack of chloride (from the solvent) and hydroxide (from the support).

Chloro-bridged **10** is more easily prepared via addition of HCl to **1**, either in gaseous or aqueous form. This reaction presumably results from hydride elimination with concomitant formation of hydrogen. Hydride elimination also occurs upon reaction of **1** with iodine, which affords the iodo-bridged complex $[Fe_2(CO)_4(\mu\text{-I})(\mu\text{-PCy}_2)(\mu\text{-dppm})]$ (**11**) in 60% yield (eq 9). Characterization was easily made on the basis of analytical and spectroscopic results; however, since iodo-bridged organometallic diiron complexes are relatively rare,[36] a crystallographic study was carried out, the results of which are shown in Figure 9 and Table 7.

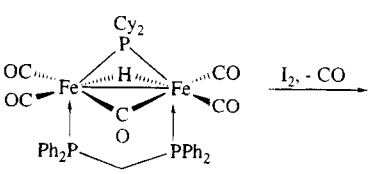

1

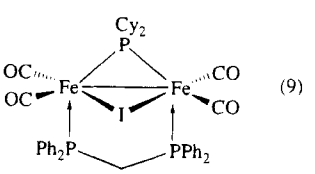

11 (9)

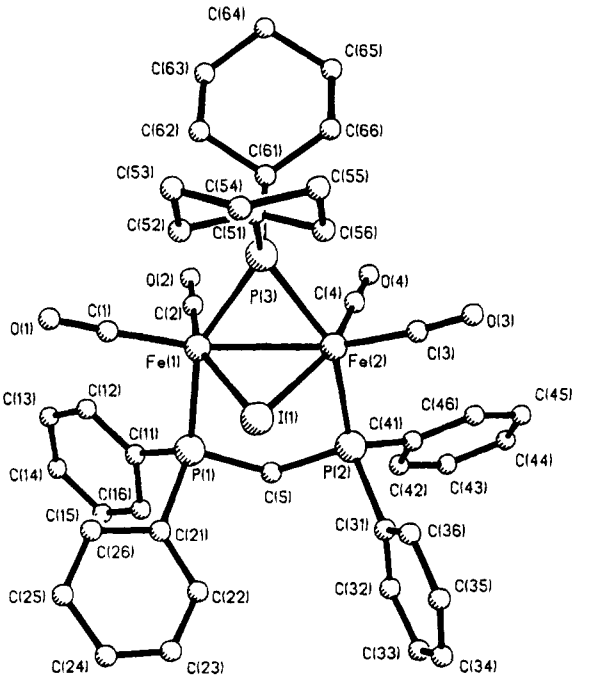

Figure 9. Molecular structure of **11**.

Table 7. Selected Bond Lengths (Å) and Angles (deg) for 11·CH_2Cl_2

Fe(1)–Fe(2)	2.580(2)	Fe(1)–C(2)	1.714(11)
Fe(1)–P(1)	2.235(3)	Fe(2)–C(3)	1.760(12)
Fe(2)–P(2)	2.245(3)	Fe(2)–C(4)	1.740(10)
Fe(1)–P(3)	2.219(3)	Fe(1)–I(1)	2.604(2)
Fe(2)–P(3)	2.224(2)	Fe(2)–I(2)	2.606(1)
Fe(1)–C(1)	1.783(10)		
P(1)–Fe(1)–P(3)	151.1(1)	Fe(2)–Fe(1)–C(1)	153.9(5)
P(2)–Fe(2)–P(3)	150.4(1)	Fe(2)–Fe(1)–C(2)	98.3(3)
Fe(1)–P(3)–Fe(2)	71.0(1)	Fe(1)–Fe(2)–C(3)	153.1(3)
P(3)–Fe(1)–I(1)	82.4(1)	Fe(1)–Fe(2)–C(4)	101.0(4)
P(3)–Fe(2)–I(1)	82.3(1)	Fe(1)–I(1)–Fe(2)	59.4(1)

In **11**, the short iron–iron vector [Fe(1)–Fe(2), 2.580(2) Å] is bridged approximately symmetrically by the iodide [Fe(1)–I(1), 2.604(2) Å; Fe(2)–I(1), 2.606(1) Å], the bond angle at the latter [Fe(1)–I(1)–Fe(2), 59.4(1)°] being relatively acute, and the metal–carbonyl interactions *trans* to the iodide are shortened [Fe(1)–C(2), 1.714(11) Å, Fe(2)–C(4), 1.740(10) Å] with respect to those *trans* to the metal–metal bond [Fe(1)–C(1), 1.783(10) Å; Fe(2)–C(3), 1.760(12) Å], indicating that the relative σ-inductive effects of the iodide and metal–metal bond are quite different.

We have previously shown that thermolysis of $[Fe_2(CO)_4(\mu\text{-H})(\mu\text{-CO})(\mu\text{-PPh}_2)(\mu\text{-dppm})]$ (**1-Ph**) in the presence of dicyclohexylphosphine results in loss of hydrogen to afford the mixed phosphido-bridged complex $[Fe_2(CO)_4(\mu\text{-PCy}_2)(\mu\text{-PPh}_2)(\mu\text{-dppm})]$ (**12**).[7] In an analogous experiment, heating a toluene solution of **1** in the presence of a slight excess of diphenylphosphine gave the expected mixed phosphido-bridged complex **12** in 60% yield, while also affording the bis(diphenyl)phosphido complex $[Fe_2(CO)_4(\mu\text{-PPh}_2)_2(\mu\text{-dppm})]$ (**13**) in 30% yield (eq 10). The formation of **13** was unexpected and

(36) See for example: Mott, G. N.; Carty, A. J. *Inorg. Chem.* **1979**, *18*, 2926. Kilner, M.; Midcalf, C. *J. Chem. Soc., Chem. Commun.* **1971**, 944. Koerner von Gustorf, E.; Grevels, F.-W.; Hogan, J. C. *Angew. Chem., Int. Ed. Eng.* **1969**, 8, 899.

Table 8. Crystallographic Data

	1	**2**·CH_2Cl_2	**4**·CH_2Cl_2	**7a**	**8a**·C_5H_{12}	**11**·CH_2Cl_2
formula	$Fe_2C_{42}H_{45}O_5P_3$	$Fe_2C_{44}H_{49}O_4P_3Cl_2$	$Fe_2C_{50}H_{53}O_4P_3Cl_2$	$Fe_2C_{45}H_{50}N_1O_4S_1P_3$	$Fe_2C_{50}H_{62}N_1O_4P_3$	$Fe_2C_{42}H_{46}O_4P_3I_1Cl_2$
color	orange	orange	orange	red	orange	orange
space group	$P\bar{1}$	$P\bar{1}$	$P\bar{1}$	$P\bar{1}$	$P2_1/c$	$P\bar{1}$
a, Å	10.2577(34)	11.7987(15)	12.5326(15)	11.9777(39)	11.8267(32)	11.8975(20)
b, Å	13.0315(81)	12.8813(16)	12.5939(16)	13.5848(36)	15.5264(29)	12.9829(16)
c, Å	15.8986(71)	17.0025(9)	18.4748(25)	13.7530(51)	27.1868(71)	16.6072(25)
α, deg	81.902(43)	73.670(8)	105.240(10)	88.912(26)	90	72.937(12)
β, deg	84.672(31)	77.770(8)	91.975(10)	89.293(28)	91.366(22)	76.891(13)
γ, deg	72.272(38)	64.870(8)	118.025(10)	78.931(25)	90	64.089(11)
V, Å^3	2001.30	2228.62	2440.43	2195.71	4990.80	2191.23
Z	2	2	2	2	2	2
$F(000)$	868	952	1032	944	1908	1028
d_{calcd}, g/cm^3	1.38	1.37	1.35	1.37	1.21	1.54
μ(Mo Kα), cm^{-1}	8.84	9.16	8.42	8.54	7.13	16.30
orientation reflns: no.; range (2θ), deg	37; 11–27	39; 19–30	30; 24–32	25; 13–26	30; 11–24	34; 19–30
no. of data measd	7542	8325	9344	8211	9933	8439
no. of unique data	7333	8287	9017	7924	9047	8175
no. of unique data with $I \geq 3.0\sigma(I)$	4395	6870	7815	4459	3449	6287
no. of params	469	484	535	505	497	472
R^a	0.068	0.046	0.051	0.061	0.088	0.069
R_w^b	0.076	0.053	0.064	0.052	0.093	0.074
largest shift/esd, final cycle	0.005	0.003	0.06	0.001	0.02	0.02
largest peak, e/Å^3	1.16	1.00	1.61	0.44	0.58	1.76

formally results from the substitution of a dicyclohexyl- for a diphenylphosphido moiety. In order to ascertain the point at which the substitution occurred, (i.e., before

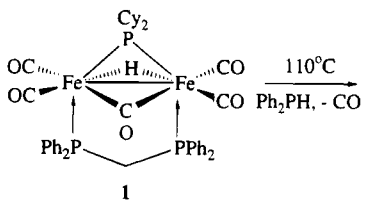

1

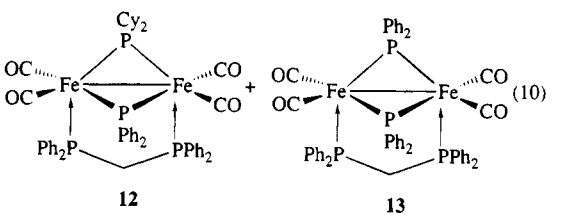

12 13

or after hydrogen loss), a toluene solution of **12** was heated in the presence of an excess of diphenylphosphine; however, even after a prolonged period, the starting material was recovered unchanged. Thus, it appears that phosphido-bridge exchange occurs prior to the formation of the electron-precise bis(phosphido) complexes.

Hydride elimination from **1** also occurs in the absence of external reagents. Thermolysis of a toluene solution of **1** for 2 h results in loss of benzene and the formation of [$Fe_2(CO)_5(\mu_2$-η^3-$Ph_2PCH_2PPh)(\mu$-$PCy_2)$] (**14**) in 71% yield (eq 11), characterization being made by comparison of spectroscopic data with that of the crystallographically characterized diphenylphosphido derivative.[7] The most interesting feature of the formation of **14** is that hydride elimination occurs without loss of carbon monoxide. This leads us to suggest that the pathway by which these elimination reactions occur may not be via initial loss of a carbonyl, but rather via metal–metal bond cleavage and retainment of the carbonyl. Thus in the formation of **14**, initial oxidative addition of the carbon–phosphorus bond may occur with cleavage of the metal–metal bond to form an intermediate [$Fe_2(CO)_5$(H)(Ph)(μ-PCy_2)(μ_2-η^3-Ph_2PCH_2PPh)] in which the new phenyl ligand is metal-bound, and this transforms rapidly via benzene loss into the observed

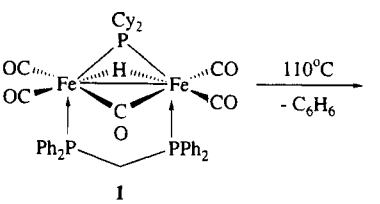

1

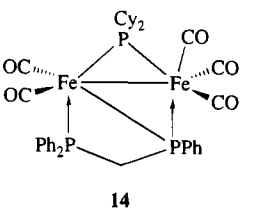

14 (11)

product. Addition of HCl is likely to occur via initial protonation at the metal–metal bond to give the dihydride [$Fe_2(CO)_5(\mu$-$H)_2(\mu$-$PCy_2)(\mu$-dppm)]$^+$, which leads to loss of H_2 and a carbonyl upon complexation of chloride; however, the precise sequence of events cannot be ascertained.

Experimental Section

General Procedures. All reactions were carried out under a nitrogen atmosphere using predried solvents. NMR spectra were recorded on a Varian VXR 400 spectrometer, and IR spectra were recorded on a Nicolet 205 FT-IR spectrometer. Column chromatography was carried out on columns of deactivated alumina (6% w/w water). Elemental analysis was performed within the chemistry department of University College. Ultraviolet photolysis was carried out using a Hanovia medium-pressure lamp. Dicyclohexylphosphine and propyne were purchased from Fluorochem; diphenylphosphine, phenylethyne, and isothiocyanates were purchased from Aldrich and used as supplied. Unless otherwise stated, all complexes were recrystallized upon slow diffusion of methanol into a dichloromethane solution.

Table 9. Positional Parameters ($\times 10^4$) and U_{eq} (Å^2 $\times$ 10^3) for 1

	x	y	z	U_{eq}
Fe(1)	3459(1)	2466(1)	1920(1)	28(1)
Fe(2)	3354(1)	1585(1)	3472(1)	31(1)
P(1)	3763(2)	4009(2)	2195(1)	28(1)
P(1)	3659(2)	2930(2)	4111(1)	31(1)
P(3)	3195(2)	817(2)	2312(1)	33(1)
O(1)	830(6)	3249(5)	2920(4)	46(2)
O(2)	6014(7)	1748(6)	856(5)	71(3)
O(3)	1723(8)	3312(6)	473(5)	69(3)
O(4)	1342(8)	910(7)	4657(4)	73(3)
O(5)	5767(8)	−178(6)	4076(5)	86(3)
C(1)	1964(8)	2729(6)	2822(5)	34(3)
C(2)	5058(9)	2029(7)	1288(6)	46(3)
C(3)	2383(8)	2974(7)	1046(5)	40(3)
C(4)	2117(9)	1173(7)	4197(5)	45(3)
C(5)	4812(10)	529(8)	3833(6)	52(4)
C(6)	3423(8)	4186(6)	3337(5)	35(3)
C(10)	2624(8)	5311(6)	1737(5)	34(3)
C(11)	1265(8)	5393(7)	1584(5)	40(3)
C(12)	370(9)	6357(7)	1217(6)	50(3)
C(13)	808(11)	7258(7)	1027(7)	62(4)
C(14)	2142(12)	7227(8)	1199(8)	73(5)
C(15)	3042(11)	6248(7)	1546(7)	58(4)
C(20)	5459(8)	4179(6)	1901(5)	34(3)
C(21)	6395(9)	4226(8)	2460(6)	53(4)
C(22)	7700(11))	4262(9)	2154(8)	66(5)
C(23)	8062(10)	4330(9)	1302(7)	63(4)
C(24)	7132(10)	4328(9)	746(7)	61(4)
C(25)	5834(9)	4257(7)	1023(6)	47(3)
C(30)	5339(8)	2730(6)	4536(5)	37(3)
C(31)	5486(10)	3109(8)	5301(6)	48(3)
C(32)	6752(11)	2943(9)	5609(7)	64(5)
C(33)	7932(9)	2383(9)	5150(7)	63(4)
C(34)	7825(11)	2010(11)	4409(8)	83(6)
C(35)	6555(10)	2170(9)	4113(7)	63(4)
C(40)	2474(8)	3469(6)	5000(4)	32(3)
C(41)	2006(9)	2764(7)	5602(5)	40(3)
C(42)	1129(10)	3155(8)	6283(6)	52(4)
C(43)	724(10)	4228(9)	6376(6)	59(4)
C(44)	1176(11)	4951(8)	5776(6)	60(4)
C(45)	2040(10)	4570(7)	5106(6)	51(3)
C(50)	4643(9)	−385(6)	2051(5)	42(3)
C(51)	4554(11)	−1445(7)	2569(6)	53(4)
C(52)	5859(12)	−2382(8)	2377(7)	68(4)
C(53)	6118(11)	−2484(8)	1450(7)	66(4)
C(54)	6169(11)	−1447(8)	925(7)	59(4)
C(55)	4849(10)	−525(7)	1101(6)	48(3)
C(60)	1621(11)	491(9)	2102(7)	61(4)
C(61)	882(12)	37(11)	2865(7)	74(5)
C(62)	−407(15)	−179(13)	2705(9)	98(7)
C(63)	−1166(13)	395(16)	2027(11)	135(10)
C(64)	−399(13)	731(11)	1224(8)	82(6)
C(65)	825(16)	1066(16)	1417(9)	128(10)

Table 10. Positional Parameters ($\times 10^4$) and U_{eq} (Å^2 $\times$ 10^3) for 2·CH_2Cl_2

	x	y	z	U_{eq}
Fe(1)	542(1)	2724(1)	7819(1)	34(1)
Fe(2)	2742(1)	2675(1)	7139(1)	35(1)
P(1)	−320(1)	4589(1)	7937(1)	33(1)
P(2)	2329(1)	4552(1)	7049(1)	35(1)
P(3)	2193(1)	1115(1)	7579(1)	37(1)
O(1)	−1579(3)	2203(3)	7737(2)	74(2)
O(2)	563(3)	1968(3)	9606(2)	71(2)
O(3)	5166(3)	1867(4)	6140(3)	104(2)
O(4)	3624(3)	2114(3)	8725(2)	61(1)
C(1)	−741(4)	2424(3)	7759(2)	46(2)
C(2)	569(3)	2250(3)	8903(2)	46(2)
C(3)	4213(4)	2186(4)	6535(3)	58(2)
C(4)	3255(3)	2340(3)	8107(2)	42(2)
C(5)	986(3)	3447(3)	6685(2)	38(1)
C(6)	1870(4)	2963(3)	6059(2)	46(2)
C(7)	912(3)	5185(3)	7765(2)	37(1)
C(10)	−1483(3)	5676(3)	7240(2)	40(1)
C(11)	−1886(3)	5342(3)	6682(2)	48(2)
C(12)	−2778(4)	6191(4)	6170(2)	58(2)
C(13)	−3214(4)	7346(5)	6197(3)	70(2)
C(14)	−2828(4)	7694(4)	6748(3)	70(2)
C(15)	−1971(4)	6855(3)	7284(3)	55(2)
C(20)	−1220(3)	4972(3)	8917(2)	35(1)
C(21)	−1108(3)	5749(3)	9280(2)	45(2)
C(22)	−1928(4)	6083(4)	9981(2)	53(2)
C(23)	−2833(4)	5638(3)	10306(2)	53(2)
C(24)	−2949(4)	4866(4)	9946(3)	58(2)
C(25)	−2143(4)	4531(3)	9252(2)	48(2)
C(30)	2088(3)	5563(3)	6045(2)	42(2)
C(31)	975(5)	6439(4)	5847(3)	75(2)
C(32)	875(6)	7163(5)	5072(3)	99(3)
C(33)	1874(6)	7027(5)	4489(3)	80(3)
C(34)	3008(6)	6150(5)	4664(3)	86(3)
C(35)	3112(5)	5422(4)	5437(3)	71(2)
C(40)	3461(3)	4937(3)	7373(2)	38(1)
C(41)	3123(4)	6065(3)	7484(3)	54(2)
C(42)	3940(4)	6359(4)	7748(3)	59(2)
C(43)	5131(4)	5539(4)	7888(3)	59(2)
C(44)	5486(4)	4436(4)	7776(3)	61(2)
C(45)	4659(3)	4132(3)	7509(2)	47(2)
C(50)	2840(3)	26(3)	8508(2)	43(2)
C(51)	2062(4)	−702(3)	8972(3)	54(2)
C(52)	2572(2)	−1443(4)	9788(3)	78(3)
C(53)	3963(6)	−2216(4)	9658(4)	87(3)
C(54)	4733(5)	−1509(4)	9177(3)	80(3)
C(55)	4239(4)	−775(3)	8355(3)	56(2)
C(60)	2308(4)	137(3)	6900(2)	49(2)
C(61)	3457(4)	−92(4)	6245(3)	57(2)
C(62)	3521(5)	−894(5)	5718(3)	79(3)
C(63)	2308(5)	−506(5)	5370(3)	86(3)
C(64)	1209(5)	−398(5)	6055(3)	73(3)
C(65)	1086(4)	455(4)	6566(3)	60(2)
C(100)	1734	10731	1445	259(413)
Cl(1)	320	11577	1828	242(413)
Cl(2)	2738	9900	2167	491(413)

Preparation of $[Fe_2(CO)_4(\mu\text{-H})(\mu CO)(\mu\text{-PCy}_2)(\mu\text{-dppm})]$ (1). UV irradiation of a toluene solution (150 cm^3) of $[Fe(CO)_6(\mu\text{-CO})(\mu\text{-dppm})]$ (1.0 g, 1.45 mmol) and dicyclohexylphosphine (0.30 g, 1.51 mmol) for 16 h while purging with a steady stream of nitrogen resulted in a color change from deep red to orange. Removal of the solvent under reduced pressure and washing with 40−60 °C petroleum ether afforded orange crystalline **1** (720 mg, 60%). Anal. Calcd for $C_{42}H_{45}O_5P_3Fe_2{\cdot}0.5CH_2Cl_2$: C, 58.18; H, 5.25. Found: C, 58.47; H, 5.23.

Preparation of $[Fe_2(CO)_4(\mu\text{-HC=CH}_2)(\mu\text{-PCy}_2)(\mu\text{-dppm})]$ (2). Slow purging of ethyne through a toluene solution (20 cm^3) of **1** (0.20 g, 0.24 mmol) for 10 min and stirring for an additional 4 h at 50 °C in a water bath resulted in a change in the carbonyl region of the IR spectrum. Removal of the solvent and chromatography gave upon elution with 40−60 °C petroleum ether−dichloromethane (4:1) a yellow-orange band which afforded **2** as a bright yellow solid (0.14 g, 69%). Anal. Calcd for $C_{43}H_{47}O_4P_3Fe_2{\cdot}CH_2Cl_2$: C, 57.58; H, 5.34. Found: C, 57.69; H, 5.41.

Preparation of $[Fe_2(CO)_4(\mu\text{-MeC=CH}_2)(\mu\text{-PCy}_2)(\mu\text{-dppm})]$ (3a) and $[Fe_2(CO)_4(\mu\text{-HC=CHMe})(\mu\text{-PCy}_2)(\mu\text{-dppm})]$ (3b). A toluene solution (50 cm^3) of **1** (0.30 g, 0.36 mmol) was saturated with propyne and stirred for 48 h. Removal of the solvent under reduced pressure and chromatography eluting with 40−60 °C petroleum ether−diethyl ether (9:1) afforded an orange band which gave a mixture of **3a** and **3b** (2.5:1 by ^{31}P NMR spectroscopy) (0.22 g, 72%). Crystallization upon cooling a saturated hexane solution of the mixture afforded an orange crystalline solid. Anal. Calcd for $C_{44}H_{49}O_4P_3Fe_2$: C, 62.41; H, 5.79. Found: C, 61.77; H, 6.32.

Slow purging of allene through a toluene solution (20 cm^3) of **1** (0.4 g, 0.48 mmol) for 10 min and stirring for an additional 12 h at room temperature resulted in a change in the carbonyl region of the infrared spectrum. Removal of the solvent and chromatography gave upon elution with 40−60 °C petroleum ether−dichloromethane (9:1) an orange band which afforded **3a** as an orange solid (0.23 g, 55%).

Preparation of $[Fe_2(CO)_4(\mu\text{-HC=CHPh})(\mu\text{-PCy}_2)(\mu\text{-dppm})]$ (4). A toluene solution (50 cm^3) of **1** (0.50 g, 0.61 mmol) and phenylethyne (0.12 g, 1.17 mmol) was stirred for 48 h. Removal of the solvent and chromatography gave upon

Table 11. Positional Parameters ($\times 10^4$) and U_{eq} (Å^2 $\times$ 10^3) for 4·CH_2Cl_2

	x	v	z	U_{eq}
Fe(1)	3413(1)	4053(1)	2097(1)	29(1)
Fe(2)	1977(1)	4808(1)	2700(1)	28(1)
P(1)	2241(1)	2002(1)	1967(1)	29(1)
P(2)	542(1)	2947(1)	2782(1)	28(1)
P(3)	3685(1)	5988(1)	2288(1)	31(1)
O(1)	2905(4)	3452(3)	441(2)	73(2)
O(2)	5902(3)	4467(4)	2229(3)	80(2)
O(3)	624(3)	4056(3)	1184(2)	55(2)
O(4)	1242(3)	6640(3)	3451(2)	61(2)
C(1)	3109(4)	3699(4)	1096(2)	43(2)
C(2)	4900(4)	4290(4)	2186(3)	45(2)
C(3)	1176(3)	4345(3)	1781(2)	35(2)
C(4)	1532(4)	5904(4)	3174(2)	38(2)
C(5)	3151(3)	4289(3)	3161(2)	32(2)
C(6)	3372(3)	5376(3)	3738(2)	34(2)
C(7)	666(3)	1653(3)	2102(2)	31(2)
C(10)	1973(3)	832(3)	1049(2)	32(2)
C(11)	829(4)	−227(4)	695(2)	43(2)
C(12)	718(5)	−1118(4)	18(2)	51(2)
C(13)	1725(5)	−968(4)	−302(2)	51(2)
C(14)	2852(5)	81(5)	36(3)	56(3)
C(15)	2993(4)	985(4)	711(3)	45(2)
C(20)	2645(3)	1286(3)	2599(2)	33(2)
C(21)	3693(4)	2009(4)	3171(2)	45(2)
C(22)	3926(5)	1454(5)	3678(3)	62(3)
C(23)	3124(5)	205(5)	3605(3)	60(3)
C(24)	2113(5)	−515(4)	3041(3)	55(2)
C(25)	1875(4)	18(4)	2529(2)	44(2)
C(30)	428(3)	2602(3)	3688(2)	33(2)
C(31)	647(4)	1701(4)	3841(2)	45(2)
C(32)	517(5)	1497(5)	4547(3)	56(3)
C(33)	193(5)	2183(5)	5084(3)	64(3)
C(34)	−20(5)	3096(5)	4945(3)	60(3)
C(35)	100(4)	3311(4)	4245(2)	46(2)
C(40)	−1076(3)	2438(4)	2459(2)	34(2)
C(41)	−1994(4)	1201(4)	2380(3)	50(2)
C(42)	−3196(4)	811(5)	2111(3)	57(2)
C(43)	−3534(4)	1605(5)	1933(3)	62(3)
C(44)	−2653(5)	2829(5)	2026(3)	56(3)
C(45)	−1423(4)	3257(4)	2285(2)	43(2)
C(50)	3469(4)	6393(4)	1417(2)	39(2)
C(51)	4566(4)	6735(4)	1001(3)	50(2)
C(52)	4225(6)	6907(6)	256(3)	69(3)
C(53)	3813(6)	7882(6)	367(3)	75(3)
C(54)	2759(6)	7555(6)	797(3)	67(3)
C(55)	3088(5)	7412(5)	1554(3)	51(2)
C(60)	5051(4)	7543(3)	2909(2)	40(2)
C(61)	4712(5)	8389(4)	3486(3)	51(2)
C(62)	5829(5)	9666(5)	3925(3)	69(3)
C(63)	6801(6)	9481(6)	4274(3)	93(3)
C(64)	7183(5)	8684(5)	3679(3)	73(3)
C(65)	6086(4)	7408(4)	3257(3)	53(2)
C(70)	3160(3)	5430(3)	4529(2)	35(2)
C(71)	2885(4)	6319(4)	4966(2)	45(2)
C(72)	2754(5)	6422(5)	5718(3)	57(2)
C(73)	2920(5)	5640(6)	6050(3)	67(3)
C(74)	3210(5)	4772(5)	5637(3)	60(3)
C(75)	3327(4)	4653(4)	4879(2)	45(2)
C(100)	8060(13)	6630(12)	1431(8)	182(5)
Cl(1)	8188(4)	7964(4)	1740(3)	212(2)
Cl(2)	9249(7)	6257(7)	1407(4)	321(3)

elution with 40–60 °C petroleum ether–dichloromethane (4:1) an orange band which afforded **4** as a bright orange solid (0.18 g, 33%). Anal. Calcd for $C_{49}H_{51}O_4P_3Fe_2{\cdot}CH_2Cl_2$: C, 60.42; H, 5.34. Found: C, 59.72; H, 5.04.

Preparation of [$Fe_2(CO)_4${η^2-C(CO_2Me)=CH–C(O-Me)=O}(μ-PCy_2)(μ-dppm)] (5). A toluene solution (20 cm^3) of **1** (0.50 g, 0.60 mmol) and DMAD (0.20 cm^3, 1.63 mmol) was stirred at room temperature for 96 h, resulting in dissolution of **1** and formation of a bright orange solution. Removal of the solvent under reduced pressure gave an orange solid, which was chromatographed on alumina. Elution with 40–60 °C petroleum ether–dichloromethane (4:1) gave an orange band which afforded **5** (0.40 g, 71%). Anal. Calcd for $C_{47}H_{51}O_8P_3Fe_2$: C, 59.49; H, 5.38. Found: C, 59.29; H, 5.81.

Table 12. Positional Parameters ($\times 10^4$) and U_{eq} (Å^2 $\times$ 10^3) for 7a

	x	y	z	U_{eq}
Fe(1)	1922(1)	3740(1)	2977(1)	27(1)
Fe(2)	3088(1)	2069(1)	1315(1)	30(1)
S(1)	1385(2)	3614(2)	504(1)	41(1)
P(1)	1110(2)	2365(1)	3182(1)	30(1)
P(2)	2565(2)	1571(1)	1441(1)	31(1)
P(3)	2984(2)	4556(1)	2013(1)	29(1)
N(1)	508(5)	4323(4)	2204(5)	34(2)
O(1)	1336(6)	4819(5)	4781(5)	75(3)
O(2)	3972(5)	2923(4)	4048(4)	46(2)
O(3)	4194(7)	2986(5)	−588(5)	87(3)
O(4)	5370(5)	2308(5)	1979(5)	72(3)
C(1)	1480(7)	4432(6)	4041(6)	39(3)
C(2)	3154(7)	3216(5)	3598(5)	33(3)
C(3)	3749(7)	3045(4)	158(6)	44(3)
C(4)	4436(8)	2616(6)	1757(6)	44(3)
C(5)	1175(6)	1667(5)	2052(5)	32(3)
C(6)	406(6)	4230(5)	1291(6)	37(3)
C(7)	−504(6)	4946(5)	2686(6)	43(3)
C(8)	−428(9)	6023(7)	2761(9)	94(5)
C(9)	−992(11)	6767(8)	2514(12)	151(9)
C(11)	1621(6)	1433(5)	4129(5)	36(3)
C(12)	2073(7)	1717(6)	4980(5)	47(3)
C(13)	2396(9)	1036(7)	5736(6)	70(4)
C(14)	2278(11)	71(8)	5644(8)	89(5)
C(15)	1826(11)	−234(7)	4814(8)	94(6)
C(16)	1502(8)	442(6)	4064(7)	63(4)
C(21)	−420(6)	2556(5)	3495(6)	35(3)
C(22)	−1240(7)	2332(6)	2875(7)	56(3)
C(23)	−2353(7)	2459(8)	3180(9)	76(5)
C(24)	−2674(9)	2785(7)	4091(10)	78(5)
C(25)	−1895(9)	3028(6)	4696(8)	66(4)
C(26)	−754(7)	2915(6)	4414(7)	55(4)
C(31)	2365(7)	1007(5)	274(5)	38(3)
C(32)	3293(8)	709(7)	−317(7)	65(4)
C(33)	3201(11)	267(8)	−1192(8)	81(5)
C(34)	2175(11)	157(8)	−1530(7)	80(5)
C(35)	1218(10)	458(7)	−966(7)	68(4)
C(36)	1300(8)	890(6)	−60(6)	52(3)
C(41)	3438(6)	503(5)	2090(5)	38(3)
C(42)	4003(7)	657(6)	2919(6)	49(3)
C(43)	4603(8)	−121(7)	3472(7)	67(4)
C(44)	4629(9)	−1086(7)	3186(8)	77(4)
C(45)	4112(10)	−1267(7)	2340(8)	87(5)
C(46)	3477(8)	−476(5)	1823(7)	65(4)
C(51)	2327(6)	5717(5)	1323(5)	33(3)
C(52)	2843(7)	5771(5)	293(5)	44(3)
C(53)	2199(8)	6680(6)	−285(6)	59(4)
C(54)	2125(8)	7649(6)	247(6)	63(4)
C(55)	1587(7)	7582(5)	1248(6)	52(3)
C(56)	2253(7)	6706(5)	1843(6)	46(3)
C(61)	4318(6)	4799(5)	2566(5)	31(3)
C(62)	5154(6)	5122(6)	1812(5)	40(3)
C(63)	6296(6)	5155(6)	2286(6)	46(3)
C(64)	6149(7)	5842(7)	3156(6)	55(3)
C(65)	5338(7)	5535(6)	3887(6)	49(3)
C(66)	4174(6)	5485(6)	3452(5)	40(3)

Preparation of [$Fe_2(CO)_4$(μ-S_2CH)(μ-PCy_2)(μ-dppm)] (6). Addition of carbon disulfide (0.10 g, 1.32 mmol) to a toluene solution (20 cm^3) of **1** (0.40 g, 0.48 mmol) and subsequent stirring for 6 h at 50 °C in a water bath resulted in dissolution of **1** and formation of an orange solution. The solvent was removed, and the resulting orange solid was adsorbed onto alumina and chromatographed. Elution with 40–60 °C petroleum ether–dichloromethane (9:1) afforded an orange band which on removal of the solvent yield **6** as an orange microcrystalline solid (0.35 g, 83%). Anal. Calcd for $C_{42}H_{45}O_4P_3S_2Fe_2{\cdot}0.5CH_2Cl_2$: C, 55.16; H, 4.98; S, 6.92. Found: C, 55.16; H, 4.92; S, 6.87.

Preparation of [$Fe_2(CO)_4$(μ-RNCHS)(μ-PCy_2)(μ-dppm)] (7a–c) and [$Fe_2(CO)_4$(μ-RN=CH)(μ-PCy_2)(μ-dppm)] (8a,b). Addition of allyl isothiocyanate (0.20 g, 2.04 mmol) to a toluene solution (20 cm^3) of **1** (0.40 g, 0.48 mmol) and subsequent stirring for 6 h at 50 °C in a water bath resulted in dissolution of **1** and formation of an orange solution. The solvent was removed, and the resulting orange solid was adsorbed onto

Table 13. Positional Parameters ($\times 10^4$) and U_{eq} ($Å^2 \times 10^3$) for 8a·C_5H_{12}

	x	y	z	U_{eq}
Fe(1)	3631(2)	7796(1)	1095(1)	37(1)
Fe(2)	2949(2)	8417(1)	1958(1)	45(1)
P(1)	4524(4)	6627(2)	1354(1)	41(1)
P(2)	4192(4)	7503(2)	2323(1)	43(1)
P(3)	2568(3)	8933(2)	1209(1)	40(1)
O(1)	3316(13)	7538(9)	45(5)	99(6)
O(2)	5660(11)	8859(7)	1013(5)	68(5)
O(3)	1308(14)	8992(10)	2570(6)	113(7)
O(4)	4159(13)	9989(8)	2223(5)	96(6)
N(1)	1975(12)	7428(8)	1724(6)	56(5)
C(1)	3449(13)	7602(10)	463(7)	57(7)
C(2)	4869(15)	8445(11)	1056(6)	49(6)
C(3)	1948(18)	8737(12)	2401(7)	68(8)
C(4)	3736(14)	9358(11)	2102(5)	50(6)
C(5)	4291(14)	6462(8)	2005(5)	46(5)
C(6)	2313(13)	7156(9)	1337(7)	47(6)
C(7)	937(16)	7039(12)	1940(9)	89(9)
C(8)	1106(22)	6580(25)	2351(13)	202(20)
C(9)	857(23)	5831(21)	2486(12)	182(18)
C(11)	6064(14)	6522(9)	1260(6)	49(6)
C(12)	6463(15)	6828(10)	851(6)	57(4)
C(13)	7623(19)	6736(12)	727(8)	82(9)
C(14)	8290(21)	6305(18)	1036(9)	108(12)
C(15)	7932(20)	6042(24)	1449(11)	170(19)
C(16)	6772(21)	6083(15)	1576(7)	102(10)
C(21)	4083(14)	5589(9)	1090(6)	52(6)
C(22)	3942(20)	5514(11)	595(7)	92(10)
C(23)	3648(22)	4726(13)	386(9)	115(12)
C(24)	3488(23)	4030(12)	662(9)	114(12)
C(25)	3687(27)	4081(13)	1143(10)	143(15)
C(26)	3931(18)	4864(11)	1360(8)	88(9)
C(31)	3864(12)	7163(11)	2949(6)	47(5)
C(32)	3695(15)	6330(11)	3094(6)	64(7)
C(33)	3446(16)	6117(14)	3578(6)	74(8)
C(34)	3409(15)	6743(16)	3914(7)	72(8)
C(35)	3614(18)	7578(15)	3789(7)	83(9)
C(36)	3823(16)	7803(12)	3305(7)	75(8)
C(41)	5691(15)	7786(10)	2404(5)	49(6)
C(42)	6398(18)	7279(12)	2686(7)	79(8)
C(43)	7546(22)	7441(16)	2737(7)	101(10)
C(44)	7954(17)	8150(16)	2507(9)	95(10)
C(45)	7256(22)	8662(14)	2253(8)	92(10)
C(46)	6129(16)	8507(12)	2190(7)	69(7)
C(51)	1068(15)	9019(14)	986(6)	71(7)
C(52)	256(14)	9383(10)	1344(7)	62(7)
C(53)	−952(22)	9390(26)	1178(10)	177(20)
C(54)	−1209(19)	9180(24)	750(12)	173(19)
C(55)	−535(18)	8780(15)	386(7)	92(9)
C(56)	683(20)	8738(31)	587(12)	316(35)
C(61)	3180(11)	9971(8)	1003(5)	38(5)
C(62)	3403(13)	10001(9)	454(5)	46(6)
C(63)	4077(15)	10774(10)	323(6)	58(6)
C(64)	3504(18)	11581(11)	488(7)	82(9)
C(65)	3262(15)	11564(10)	1024(6)	62(7)
C(66)	2571(13)	10807(9)	1175(5)	50(6)
C(101)	9827	2352	1247	157(23)
C(102)	9864	2860	936	222(34)
C(103)	10133	3713	1039	311(53)
C(104)	9437	3636	692	338(59)
C(105)	9359	3803	298	257(41)

alumina and chromatographed. Elution with 40–60 °C petroleumether–diethyl ether (9:1) afforded a yellow band which on removal of the solvent yielded a yellow solid, **8a** (0.10 g, 24%). Further elution with 40–60 °C petroleum ether–diethyl ether (4:1) gave an orange band which on removal of the solvent afforded an orange microcrystalline solid, **7a** (0.15 g, 35%). Anal. Calcd for $C_{45}H_{50}O_4N_1P_3S_1Fe_2{\cdot}0.5CH_2Cl_2$ (**7a**): C, 57.63; H, 5.38; S, 3.38; N, 1.48. Found: C, 57.09; H, 5.36; S, 3.34; N, 1.52. Anal. Calcd for $C_{45}H_{50}O_4N_1P_3Fe_2{\cdot}C_5H_{12}$ (**8a**): C, 62.69; H, 6.48; N, 1.46. Found: C, 62.46; H, 6.40; N, 1.22.

Addition of ethyl isothiocyanate (0.20 g, 2.30 mmol) to a toluene solution (20 cm^3) of **1** (0.40 g, 0.48 mmol) proceeded in an analogous manner. Chromatography eluting with 40–60 °C petroleum ether–diethyl ether (9:1) afforded a yellow band which on removal of the solvent yielded a yellow solid,

Table 14. Positional Parameters ($\times 10^4$) and U_{eq} ($Å^2 \times 10^3$) for 11·CH_2Cl_2

	x	y	z	U_{eq}
Fe(1)	2234(1)	2311(1)	2844(1)	28(1)
Fe(2)	4478(1)	2198(1)	2261(1)	27(1)
I(1)	3902(1)	1565(1)	3888(1)	45(1)
P(1)	2663(2)	417(2)	2975(1)	27(1)
P(2)	5344(2)	299(2)	2194(1)	27(1)
P(3)	2792(2)	3827(2)	2419(1)	31(1)
O(1)	−183(9)	3137(9)	3877(7)	93(6)
O(2)	1259(8)	2946(7)	1253(5)	57(4)
O(3)	6586(7)	2826(6)	2125(5)	58(4)
O(4)	4364(8)	2832(7)	465(5)	63(4)
C(1)	768(10)	2799(9)	3489(7)	46(5)
C(2)	1659(9)	2681(7)	1895(6)	36(4)
C(3)	5782(9)	2526(8)	2212(6)	38(4)
C(4)	4393(9)	2580(8)	1174(6)	38(4)
C(5)	4110(8)	−254(8)	2307(5)	30(4)
C(11)	1567(9)	40(8)	2616(5)	32(4)
C(12)	358(9)	833(9)	2485(6)	42(4)
C(13)	−441(10)	502(11)	2428(7)	56(6)
C(14)	−69(11)	−610(11)	2145(7)	52(6)
C(15)	1128(11)	−1407(9)	2286(7)	54(6)
C(16)	1933(10)	−1104(8)	2516(7)	46(5)
C(21)	2837(9)	−585(8)	4023(5)	36(4)
C(22)	3868(12)	−1557(10)	4240(7)	64(6)
C(23)	3903(15)	−2254(13)	5016(9)	86(8)
C(24)	2965(17)	−2070(13)	5603(8)	78(8)
C(25)	1875(18)	−1098(16)	5428(8)	99(11)
C(26)	1796(12)	−330(12)	4621(7)	69(6)
C(31)	6501(8)	−832(8)	2902(5)	35(4)
C(32)	6954(10)	−1999(9)	2862(7)	50(5)
C(33)	7861(12)	−2854(10)	3370(8)	68(6)
C(34)	8275(11)	−2526(12)	3913(7)	65(6)
C(35)	7871(11)	−1406(12)	3945(7)	62(6)
C(36)	6970(10)	−552(10)	3435(6)	49(5)
C(41)	6270(8)	−30(7)	1184(5)	27(3)
C(42)	6149(9)	−747(8)	766(6)	40(4)
C(43)	6963(10)	−1043(9)	46(6)	50(5)
C(44)	7866(10)	−612(9)	−261(6)	48(5)
C(45)	7964(10)	121(10)	144(6)	51(5)
C(46)	7169(9)	407(8)	859(6)	40(4)
C(51)	2650(9)	4779(8)	3127(6)	37(4)
C(52)	1720(10)	4724(9)	3912(6)	45(5)
C(53)	1597(11)	5571(10)	4438(7)	58(4)
C(54)	2830(12)	5347(11)	4662(7)	62(6)
C(55)	3571(11)	5441(10)	3885(7)	55(6)
C(56)	3920(10)	4593(9)	3338(7)	46(5)
C(61)	2197(9)	4911(7)	1457(6)	35(4)
C(62)	822(10)	5735(9)	1585(7)	50(5)
C(63)	358(13)	6535(11)	728(9)	76(7)
C(64)	1103(15)	7235(11)	307(9)	83(8)
C(65)	2494(15)	6458(11)	188(7)	73(7)
C(66)	2988(11)	5625(9)	1023(7)	51(5)
C(70)	7001(25)	5762(23)	1334(17)	180(11)
Cl(1)	5374(9)	6604(8)	1775(5)	194(3)
Cl(2)	7730(18)	4838(16)	2245(12)	404(9)

8b (0.10 g, 24%). Further elution with 40–60 °C petroleum ether–diethyl ether (4:1) gave an orange band which on removal of the solvent afforded an orange microcrystalline solid, **7b** (0.20 g, 47%). Anal. Calcd for $C_{44}H_{50}O_4N_1P_3S_1Fe_2{\cdot}CH_2Cl_2$ (**7b**): C, 55.21; H, 5.31; S, 3.27; N, 1.43. Found: C, 55.19; H, 5.40; S, 3.54; N, 1.49. Anal. Calcd for $C_{45}H_{50}O_4N_1P_3Fe_2{\cdot}C_5H_{12}$ (**8b**): C, 62.69; H, 6.48; N, 1.46. Found: C, 62.46; H, 6.40; N, 1.22.

Addition of phenyl isothiocyanate (0.30 g, 2.22 mmol) to a toluene solution (30 cm^3) of **1** (0.30 g, 0.36 mmol) proceeded in an analogous manner. Chromatography eluting with 40–60 °C petroleum ether–dichloromethane (4:1) gave an orange band which yielded **7c** as an orange solid (0.09 g, 27%). Anal. Calcd for $C_{48}H_{50}O_4N_1P_3S_1Fe_2{\cdot}0.5CH_2Cl_2$: C, 59.17; H, 5.19; S, 3.25; N, 1.42. Found: C, 59.56; H, 4.29; S, 3.06; N, 1.29.

Preparation of [$Fe_2(CO)_4(\mu$-^{t}BuN=CH)(μ-PCy$_2$)(μ-dppm)] (8d). Addition of *tert*-butyl isocyanide (0.10 g, 1.20 mmol) in a toluene solution (20 cm^3) of **1** (0.40 g, 0.48 mmol) and subsequent stirring for 6 h at 50 °C resulted in the gradual fading of the orange coloration. Removal of the solvent and

chromatography eluting with 40–60 °C petroleum ether–dichloromethane (9:1) gave a yellow band which afforded **8d** as a yellow powder (0.35 g, 83%). Anal. Calcd for $C_{46}H_{54}O_4N_1P_3Fe_2$: C, 62.09; H, 6.07; N, 1.57. Found: C, 62.86; H, 6.19; N, 1.14.

Preparation of $[Fe_2(CO)_4(\mu\text{-OH})(\mu\text{-PCy}_2)(\mu\text{-dppm})]$ (9). Complex **1** (1.00 g, 1.20 mmol) was adsorbed onto alumina and chromatographed. Elution with 40–60 °C petroleum ether produced an orange band. The solvent was subsequently removed to yield **10** as an orange solid (0.38 g, 38%). Further elution with 40–60 °C petroleum ether–dichloromethane (9:1) produced an orange band which changed to pink as it moved down the column. Removal of the solvent afforded **9** (0.4 g, 41%) as an orange solid. NMR spectra revealed that samples of **9** were contaminated with **10** (up to 10%), which proved difficult to remove. Anal. Calcd for $C_{41}H_{45}O_5P_3Fe_2$ (**9**): C, 59.85; H, 5.47. Found: C, 59.63; H, 5.26.

Preparation of $[Fe_2(CO)_4(\mu\text{-Cl})(\mu\text{-PCy}_2)(\mu\text{-dppm})]$ (10). Addition of 40% concentrated hydrochloric acid (0.1 cm^3) to a toluene solution (20 cm^3) of **1** (0.30 g, 0.36 mmol) and subsequent stirring for 12 h at room temperature followed by an additional 2 h at 50 °C in a water bath resulted in dissolution of **1** and formation of an orange solution. A color change to yellow-orange was noted. The solvent was removed, and the resulting orange solid was adsorbed onto alumina and chromatographed. Elution with 40–60 °C petroleum ether afforded an orange band which on removal of the solvent yielded an orange microcrystalline solid, **10** (0.20 g, 61%). Anal. Calcd for $C_{41}H_{44}O_4P_3Cl_1Fe_2{\cdot}CH_2Cl_2$: C, 54.45; H, 4.75. Found: C, 54.08; H 5.34.

Hydrogen chloride gas was bubbled through a toluene solution (20 cm^3) of **1** (0.30 g, 0.36 mmol) until a saturated solution was obtained (approximately 2 min), during which time an orange solution formed which rapidly faded to yellow-orange. The solution was left to stir for an additional 2 h, and the solvent was removed. Adsorption onto alumina and chromatography afforded **10** (0.19 g, 62%).

Preparation of $[Fe_2(CO)_4(\mu\text{-I})(\mu\text{-PCy}_2)(\mu\text{-dppm})]$ (11). Addition of a 2-fold excess of iodine (0.29 g, 0.79 mmol) to a toluene solution (20 cm^3) of **1** (0.30 g, 0.36 mmol) afforded a red-orange solution with a white precipitate after 12 h of stirring. Filtration and removal of the solvent afforded an orange solid. Chromatography eluting with 40–60 °C petroleum ether gave a pink band which afforded **11** (0.20 g, 60%) as an orange solid. Anal. Calcd for $C_{41}H_{44}O_4P_3I_1Fe_2$: C, 52.79; H, 4.72; I, 13.63. Found: C, 52.55; H, 4.88; I, 13.50.

Preparation of $[Fe_2(CO)_4(\mu\text{-PPh}_2)(\mu\text{-PCy}_2)(\mu\text{-dppm})]$ (12) and $[Fe_2(CO)_4(\mu\text{-PPh}_2)_2(\mu\text{-dppm})]$ (13). A toluene solution (40 cm^3) of **1** (1.00 g, 1.20 mmol) was refluxed with diphenylphosphine (0.30 g, 1.60 mmol) for 3 h. Removal of the solvent and chromatography afforded upon elution with 40–60 °C petroleum ether–dichloromethane (9:1) an orange band which afforded **13** (0.71 g, 60%) as an orange-yellow solid. Further elution with 40–60 °C petroleum ether–dichloromethane (4:1) gave a second orange band which afforded **12** (0.35 g, 30%) as an orange solid.

Preparation of $[Fe_2(CO)_5(\mu\text{-PCy}_2)(\mu\text{-PhPCH}_2\text{PPh}_2)]$ (14). A toluene solution (100 cm^3) of **1** (1.00 g, 1.20 mmol) was refluxed for 2 h, and color changes from orange to an intermediate green and then to orange-brown were noted. Removal of the solvent under reduced pressure gave an orange solid, which was chromatographed on alumina. Elution with light petroleum ether gave a yellow band which afforded **14** (0.65 g, 71%). Anal. Calcd for $C_{36}H_{39}O_5P_3Fe_2{\cdot}0.4CH_2Cl_2$: C, 55.29; H, 5.03. Found: C, 55.65; H, 4.09.

Thermolysis of $[Fe_2(CO)_4(\mu\text{-EtNCS})(\mu\text{-PCy}_2)(\mu\text{-dppm})]$ (7b). Thermolysis of a toluene solution (20 cm^3) of **7b** (0.07 g, 0.08 mmol) for 9 h led to the isolation of **7b** (0.015 g) and **8b** (0.03 g, 57%) (yield based on the amount of **7b** consumed) after chromatography.

Thermolysis of $[Fe_2(CO)_4(\mu\text{-PPh}_2)(\mu\text{-PCy}_2)(\mu\text{-dppm})]$ (12) with Diphenylphosphine. Thermolysis of a toluene solution (20 cm^3) of **12** (0.10 g, 0.10 mmol) with diphenylphosphine (0.10 g, 0.54 mmol) for 24 h did not lead to a color change, and **12** was recovered quantitatively.

Crystal Structure Determinations. Crystals of **1**, **2**, **4**, **7a**, and **11** were grown from the slow diffusion of methanol into dichloromethane solutions, while **8a** was crystallized upon concentration of a 40–60 °C petroleum ether solution. Crystals were mounted on a glass fiber. All geometric and intensity data were taken from this sample using an automated four-circle diffractometer (Nicolet R3mV) equipped with Mo Kα radiation (λ = 0.710 73 Å) at 19±1 °C. The lattice vectors were identified by application of the automatic indexing routine of the diffractometer to the positions of a number of reflections taken from a rotation photograph and centered by the diffractometer. For **1**, **2**, **4**, **7a**, and **11** the ω–2θ technique was used to measure reflections in the range $5° \le 2\theta \le 50°$, while for **8a** the ω technique was used. For **2**, **4**, **7a**, **8a**, and **11** three standard reflections (remeasured every 97 scans) showed no significant loss in intensity during data collection; however, for **1** a 10% loss of intensity was noted. The data were corrected for Lorentz and polarization effects, and **1**, **2**, **4**, **7a**, and **11** were corrected empirically for absorption. The unique data with $I \ge 3.0\sigma(I)$ were used to solve and refine the structures.

The structures were solved by direct methods and developed by using alternating cycles of least-squares refinement and difference-Fourier synthesis. All non-hydrogen atoms were refined anisotropically except those of the solvate in **4**, **8a**, and **11** and C(12) in **8a**. All hydrogens were placed in idealized positions (C–H, 0.96 Å) and assigned a common isotropic thermal parameter (U = 0.08 Å^2). Structure solution used the SHELXTL PLUS program package on a microVax II computer.[37] The final R and R_w values together with residual electron density levels and other important crystallographic parameters are given in Table 8. Positional parameters for **1**, **2**, **4**, **7a**, **8a**, and **11** are listed in Tables 9–14, respectively.

Note Added in Proof. The crystal structure of $[Fe_2(CO)_6(\mu\text{-H})(\mu\text{-PBu}^t_2)]$ has recently been reported: Böttcher, H.-C.; Hartung, W.; Krug, A.; Walther, B. *Polyhedron* **1994**, *13*, 2893.

Acknowledgment. We thank University College Access Fund for the award of a postgraduate scholarship (M.H.L.) and Dr. Glyn D. Forster and Mr. Simon P. Redmond for help with aspects of the crystallography.

Supplementary Material Available: For **1**, **2**, **4**, **7a**, **8a**, and **11**, text giving additional details of the structure determination, figures giving additional views of the structure, and tables of positional and thermal parameters and bond distances and angles (58 pages). Ordering information is given on any current masthead page.

OM9500883

(37) Sheldrick, G. M. *SHELXTL*; University of Göttingen: Göttingen, Germany, 1985.

Hydrodesulfurization (HDS) Model Systems. Opening, Hydrogenation, and Hydrodesulfurization of Dibenzothiophene (DBT) at Iridium. First Case of Catalytic HDS of DBT in Homogeneous Phase

Claudio Bianchini,*[1a] M. Victoria Jiménez,[1a] Andrea Meli,[1a] Simonetta Moneti,[1a] Francesco Vizza,[1a] Verónica Herrera,[1b] and Roberto A. Sánchez-Delgado*[1b]

Instituto per lo Studio della Stereochimica ed Energetica dei Composti di Coordinazione, ISSECC-CNR, Via J. Nardi 39, 50132 Firenze, Italy, and Instituto Venezolano de Investigaciones Cientificas, IVIC, Caracas 1020 A, Venezuela

Received January 23, 1995[⊗]

The kinetic selectivity for C−H vs C−S activation of dibenzothiophene (DBT) by the [(triphos)IrH] fragment has been observed upon either thermolysis of (triphos)Ir(H)$_2$(C$_2$H$_5$) in THF in the temperature range from 70 to 160 °C or dehydrohalogenation of (triphos)Ir(H)$_2$Cl with *t*-BuLi at room temperature [triphos = MeC(CH$_2$PPh$_2$)$_3$]. C−H bond cleavage already occurs at 20 °C to give as many as three isomeric DBTyl complexes of the formula (triphos)Ir(H)$_2$(DBTyl). The kinetic preference follows the order 3-DBTyl > 4-DBTyl ≥ 2-DBTyl, while the thermodynamic stability is in the order 4-DBTyl > 3-DBTyl > 2-DBTyl. Both C−H insertion and C−S insertion occur in the temperature range from 120 to 160 °C. Above the latter temperature, C−S insertion prevails over C−H insertion, and the complex (triphos)IrH(η^2-*C*,*S*-DBT) (**5**) is generated quantitatively. By reaction with H$_2$ (THF, 170 °C, 30 atm of H$_2$, 4 h), **5** is converted to a 31:69 mixture of the 2-phenylthiophenolate dihydride (triphos)Ir(H)$_2$(SC$_{12}$H$_9$) (**7**) and the trihydride (triphos)Ir(H)$_3$ (**8**) while free 2-phenylthiophenol, DBT, and biphenyl + H$_2$S are evolved in a relative ratio of 48:42:10. In the presence of an excess of DBT, the reaction is catalytic and converts 10 mol of DBT/mol of **5** in 24 h to both hydrogenation (60%) and desulfurization (40%) products. A rationale of the catalysis cycle is discussed in the light of the results of a study involving the use of isolated compounds in a variety of independent reactions. In accord with previous studies, the thiolate complex **7** is proposed as the intermediate species that undergoes desulfurization by action of H$_2$.

Introduction

Catalytic hydrodesulfurization (HDS) is of prime importance in the petroleum and coal industries because of the growing need to process feedstocks of high sulfur levels with the aim of producing fuels with the smallest possible sulfur content. Residual sulfur in fuels is present mainly in thiophenic forms and predominantly as benzo- and dibenzothiophene derivatives. The mechanisms of HDS of such heteroaromatic compounds has been a subject of continuing discussion over the years, since the understanding of the reaction pathways followed by these molecules is essential for the development of improved practical catalysts.[2]

Homogeneous modeling of the HDS reaction through the study of the coordination and reactivity of thiophenes on metal complexes has emerged as a powerful tool to help elucidate the main mechanistic pathways involved in this important heterogeneous process.[3] Although related studies have provided a wealth of information on the activation and HDS-related reactions of thiophene (T)[3−5] and benzo[*b*]thiophene (BT)[3,6] on transition metal complexes, much less is known about dibenzothiophene (DBT).[3] The latter is a particularly interesting substrate, since it represents a class of compounds present in heavy oils and distillates, which are among the most difficult to desulfurize.[2]

Several bonding modes of T and BT, as well as reactions leading to C−S bond cleavage, hydrogenation, and desulfurization, have been described in detail.[3−6] On the other hand, DBT has been much less studied. Coordination to metals through the sulfur atom (η^1-*S*)[7−12] or through one[10,13−15] or both[14,15] of the benzene rings (η^6) has been demonstrated in several cases; little

⊗ Abstract published in *Advance ACS Abstracts,* March 15, 1995.

(1) (a) ISSECC-CNR, Firenze. (b) IVIC, Caracas.

(2) (a) Mitchell, P. C. H. *The Chemistry of Some Hydrodesulphurisation Catalysts Containing Molybdenum*; Climax Molybdenum Co. Ltd.: London, 1967. (b) Schuman, S. C.; Shalit, H. *Catal. Rev.* **1970**, *4*, 245. (c) Weisser, O.; Landa, O. *Sulfide Catalysts. Their Properties and Applications*; Pergamon: Oxford, 1973. (d) Gates, B. C.; Katzer, J. R.; Schuit, G. C. A. *Chemistry of Catalytic Properties*; McGraw-Hill: New York, 1979. (e) Satterfield, C. N. *Heterogeneous Catalysis in Practice*; McGraw-Hill: New York, 1980. (f) *Geochemistry of Sulfur in Fossil Fuels*; Orr, W. L., White, C. M., Eds.; ACS Symposium Series 429; American Chemical Society: Washington, DC, 1990. (g) McCulloch, D. C. In *Applied Industrial Catalysis*; Leach, B. E., Ed.; Academic: New York, 1983; Vol. 1, p 69. (h) Lyapina, N. K. *Russ. Chem. Rev. (Engl. Transl.)* **1982**, *51*, 189. (i) Challenger, F. *Aspects of the Organic Chemistry of Sulfur*; Butterworths: London, 1959.

(3) (a) Sánchez-Delgado, R. A. *J. Mol. Catal.* **1994**, *86*, 287. (b) Rauchfuss, T. B. *Prog. Inorg. Chem.* **1991**, *39*, 259. (c) Angelici, R. J. *Coord. Chem. Rev.* **1990**, *105*, 61. (d) Angelici, R. J. *Acc. Chem. Res.* **1988**, *21*, 387.

(4) Bianchini, C.; Meli, A.; Peruzzini, M.; Vizza, F.; Frediani, P.; Herrera, V.; Sánchez-Delgado, R. A. *J. Am. Chem. Soc.* **1993**, *115*, 2731 and references therein.

(5) Jones, W. D.; Chin, R. M. *J. Am. Chem. Soc.* **1994**, *116*, 198.

(6) Bianchini, C.; Meli, A.; Peruzzini, M.; Vizza, F.; Moneti, S.; Herrera, V.; Sánchez-Delgado, R. A. *J. Am. Chem. Soc.* **1994**, *116*, 4370 and references therein.

(7) Benson, J. W.; Angelici, R. J. *Organometallics* **1993**, *12*, 680.

0276-7333/95/2314-2342$09.00/0

is known, however, about the reactivity of coordinated DBT. There is one example by Jones and Dong[16] of C–H and C–S activation by Rh to yield, respectively, the DBTyl complex $(C_5Me_5)Rh(PMe_3)H(SC_{12}H_7)$ and the ring-opened derivative $(C_5Me_5)Rh(PMe_3)(SC_{12}H_8)$; a recent report by Garcia and Maitlis[17] describes the insertion of Pt(0) to the C–S bond of DBT to yield the thia metallocycle $Pt(SC_{12}H_8)(PEt_3)_2$ which could be cleaved with protonic as well as hydridic reagents to yield free 2-phenylthiophenol and biphenyl, respectively.

Following our previous reports on HDS-related chemistry of T[4] and BT[6] promoted by Ir–triphos complexes [triphos = $MeC(CH_2PPh_2)_3$], in this paper we describe C–H and C–S activation reactions of DBT by the [(triphos)IrH] fragment leading to (triphos)$Ir(H)_2$(DBTyl) (DBTyl = dibenzothienyl) and (triphos)$IrH(\eta^2$-*C,S*-DBT), respectively; the selectivity for one or the other of these processes may be tuned by adjusting the reaction temperature. By treating the complex containing a ring-opened DBT with H_2 under appropriate reaction conditions, we have achieved the unprecedented *homogeneous catalytic HDS of DBT* to yield 2-phenylthiophenol and biphenyl + H_2S, which are the same primary products observed for the *heterogeneous* HDS of DBT;[2,18] furthermore, on the basis of independent reactions performed on isolated complexes, we have been able to identify a number of species and elementary steps involved in the hydrogenation and hydrodesulfurization reactions which allowed us to deduce an overall catalytic cycle for this important transformation. The chemistry herein described constitutes an excellent homogeneous model for one of the most commonly invoked mechanisms for HDS of DBT on solid catalysts.[18]

Experimental Section

General Procedure. All reactions and manipulations were routinely performed under a nitrogen atmosphere by using standard Schlenk techniques unless otherwise stated. Tetrahydrofuran (THF) and diethyl ether (Et_2O) were distilled from $LiAlH_4$, CH_2Cl_2 was distilled from CaH_2, and *n*-heptane was distilled from sodium. The solvents were stored over 4-Å molecular sieves and purged with nitrogen before use. Commerical benzo[*b*]thiophene and dibenzothiophene were sublimed prior to use. $HBF_4{\cdot}Et_2O$ (85% solution in Et_2O), CF_3SO_3D (98 atom % D), *n*-butyllithium (1.6 M solution in hexanes), *tert*-butyllithium (1.7 M solution in pentane), and $LiHBEt_3$ (1.0 M solution in THF) were purchased from Aldrich. 2-Phenylthiophenol was prepared following a literature method.[19] All other chemicals were commercial products and used as received without further purification. Literature methods were used for the preparation of (triphos)$Ir(H)_2(C_2H_5)$,[20] (triphos)$Ir(H)_3$,[21] [(triphos)$Ir(H)_2$(THF)]BPh_4,[22] and (triphos)$Ir(H)_2Cl$.[4] All metal complexes were collected on sintered glass frits and washed with appropriate solvents before being dried in a stream of nitrogen. Infrared spectra were recorded on a Perkin-Elmer 1600 Series FT-IR spectrophotometer using samples mulled in Nujol between KBr plates. Deuterated solvents for NMR measurements were dried over molecular sieves. ^1H NMR spectra were obtained on a Bruker ACP 200 (200.13 MHz) spectrometer. ^1H NMR shifts are recorded relative to residual ^1H resonance in the deuterated solvent: CD_2Cl_2, δ 5.32; $CDCl_3$, δ 7.23. The ^{13}C [^1H] NMR spectra were recorded on the Bruker ACP 200 instrument operating at 50.32 MHz. The $^{13}C[^1H]$ NMR shifts are given relative to the solvent resonance: CD_2Cl_2, δ 54.2; $CDCl_3$, δ 77.7. ^{31}P [^1H] NMR spectra were recorded on either a Varian VXR 300 or a Bruker ACP 200 spectrometer operating at 121.42 and 81.01 MHz, respectively. Chemical shifts are relative to external 85% H_3PO_4 with downfield values reported as positive. Broad band and selective ^1H [^{31}P] NMR experiments were carried out on the Bruker ACP 200 instrument equipped with a 5-mm inverse probe and a BFX-5 amplifier device. ^{13}C-DEPT, ^1H, ^{13}C 2D-HETCOR, and ^1H,^1H 2D-COSY NMR experiments were conducted on the Bruker ACP 200 spectrometer. Conductivities were measured with an Orion Model 990101 conductance cell connected to a Model 101 conductivity meter. The conductivity data were obtained at sample concentrations of ca. 10^{-3} M in nitroethane solutions at room temperature. GC analyses were performed on a Shimadzu GC-14 A gas chromatograph equipped with a flame ionization detector and a 30-m (0.25-mm i.d., 0.25-μm FT) SPB-1 Supelco fused silica capillary column. GC/MS analyses were performed on a Shimadzu QP 2000 apparatus equipped with a column identical to that used for GC analyses. Reactions at high temperature or under controlled pressure of hydrogen were performed with a Parr 4565 reactor (100 mL) equipped with a Parr 4842 temperature and pressure controller.

Reaction of (Triphos)$Ir(H)_2(C_2H_5)$ (1) with DBT. NMR Experiment. A. 70 °C. A solution of (triphos)$Ir(H)_2(C_2H_5)$ (**1**) (10 mg, 0.012 mmol) and DBT (13 mg, 0.071 mmol) in THF-d_8 (1 mL) was transferred under nitrogen into a 5-mm NMR tube, which was flame sealed and then introduced into a NMR probe preheated at a fixed temperature. The reaction occurred at ca. 70 °C and was followed by ^{31}P [^1H] NMR spectroscopy by determining the concentration of **1** and the other products as a function of time. Spectra (acquisition time 15 min) were recorded every 30 s during the first 2 h and then every 30 min for a further 14 h. After the first 30 min, three products were formed in a ratio of 28:40:32. These products were identified (*vide infra*) as arene C–H bond activation products of formulas (triphos)$Ir(H)_2$(2-DBTyl) (**2**), (triphos)$Ir(H)_2$(3-DBTyl) (**3**), and (triphos)$Ir(H)_2$(4-DBTyl) (**4**), respectively. The site of C–H activation in **2** and **3** could not be determined experimentally. The proposed structural assignment is essentially based on indirect evidence (*vide infra*). In contrast, the structure of **4** was unambiguously determined by labeling studies (see below). Conversion > 90% was achieved after ca. 11 h with the following product distribution: **2** (21%), **3** (40%), and **4** (39%). After ca. 16 h (quantitative conversion), these products were detected in a ratio of 18:38:42, respectively.

B. 100 °C. By working as above at 100 °C, a conversion > 90% was reached after ca. 2 h with the following product distribution: **2** (18%), **3** (40%), and **4** (42%). At the quantitative conversion (ca. 3 h), **2**–**4** were detected in a ratio of 10:

(8) Sánchez-Delgado, R. A.; Herrera, V.; Bianchini, C.; Masi, D.; Mealli, C. *Inorg. Chem.* **1993**, *32*, 3766.
(9) Benson, J. W.; Angelici, R. J. *Organometallics* **1992**, *11*, 922.
(10) Rao, K. M.; Day, C. L.; Jacobson, R. A.; Angelici, R. *J. Inorg. Chem.* **1991**, *30*, 5046.
(11) Goodrich, J. D.; Nickias, P. N.; Selegue, J. P. *Inorg. Chem.* **1987**, *26*, 3424.
(12) Choi, M.-G.; Angelici, R. J. *Organometallics* **1991**, *10*, 2436.
(13) Fischer, E. O.; Goodwin, H. A.; Kreiter, C. G.; Simmons, H. D., Jr.; Sonogashira, K.; Wild, S. B. *J. Organomet. Chem.* **1968**, *14*, 359.
(14) Lee, C. C.; Steele, B. R.; Sutherland, R. G. *J. Organomet. Chem.* **1980**, *186*, 265.
(15) Wang, C.-M. J.; Angelici, R. J. *Organometallics* **1990**, *9*, 1770.
(16) Jones, W. D.; Dong, L. *J. Am. Chem. Soc.* **1991**, *113*, 559.
(17) Garcia, J. J.; Maitlis, P. M. *J. Am. Chem. Soc.* **1993**, *115*, 12200.
(18) (a) Geneste, P.; Amblard, P.; Bonnet, M.; Graffin, P. *J. Catal.* **1980**, *61*, 115. (b) Kwart, H.; Schuit, G. C. A.; Gates, B. C. *J. Catal.* **1980**, *61*, 128. (c) Singhal, G. H.; Espino, R. L.; Sobel, J. E. *J. Catal.* **1981**, *67*, 446.
(19) Klemm, L. H.; Karchesy, J. J. *J. Heterocycl. Chem.* **1978**, *15*, 281.
(20) Barbaro, P.; Bianchini, C.; Meli, A.; Peruzzini, M.; Vacca, A.; Vizza, F. *Organometallics* **1991**, *10*, 2227.
(21) Janser, P.; Venanzi, L. M.; Bachechi, F. *J. Organomet. Chem.* **1985**, *296*, 229.
(22) Bianchini, C.; Caulton, K. G.; Folting, K.; Meli, A.; Peruzzini, M.; Polo, A.; Vizza, F. *J. Am. Chem. Soc.* **1992**, *114*, 7290.

39:51. Upon heating the NMR tube at 100 °C for a further ca. 2 h, **2** and **3** were quantitatively converted to **4**.

C. 120 °C. A 5-mm NMR tube was charged with a mixture of **1** (10 mg, 0.012 mmol) and DBT (13 mg, 0.071 mmol) in THF-d_8 (1 mL) under nitrogen, flame sealed, and kept at 120 °C (oil bath). After ca. 2 h, the tube was cooled to room temperature. The ^1H and ^{31}P [^1H] NMR spectra of this sample showed that the C−S bond cleavage product (triphos)IrH(η^2-*C,S*-DBT) (**5**) (see below) formed along with the C−H activation products with the following product distribution: **2** (4%), **3** (8%), **4** (80%), and **5** (8%). After 3 h, the products were present in a ratio of 2:6:72:20.

D. 160 °C. When the reaction was performed as above at 160 °C for 4 h, **5** was the only product detected in solution. For periods less than 4 h, variable amounts of **2**−**4** were also present in the reaction mixture.

Synthesis of (Triphos)Ir(H)$_2$(4-DBTyl) (4). A Parr reactor was charged with a solid sample of **1** (0.25 g, 0.30 mmol) and a solution of DBT (0.33 g, 1.80 mmol) in THF (50 mL) under nitrogen at room temperature and then heated at 100 °C. After 5 h, the bomb was cooled to room temperature and the contents were transferred into a Schlenk-type flask. Portionwise addition of *n*-heptane (40 mL) led to the precipitation of **4** as off-white microcrystals, which were collected by filtration and washed with diethyl ether; yield 85%. When the reaction was carried out for periods less than 5 h, variable amounts of **2** and **3** were detected in the reaction mixture. Compounds **2**−**4** are stable in solvents such as THF and acetone up to 60−70 °C. At higher temperatures (up to ca. 120 °C), the isomerization process of **2** and **3** to **4** is accompanied by some decomposition unless excess DBT is present in solution.

Compound 2. IR: ν(Ir-H) 2070 (s) cm^{-1}. ^{31}P [^1H] NMR (CD_2Cl_2, 20 °C, AM_2 spin system): −9.9 (P_A), −18.9 (P_V, $^2J(P_AP_M)$ = 15.0 Hz). ^1H NMR (CD_2Cl_2, 20 °C): δ 2.8−2.2 [CH_2 (triphos)], 1.54 [q, CH_3 (triphos)], −8.76 (second-order double of multiplets, AA′XX′Y spin system, $|^2J(HP_M) + {}^2J(HP_{M'})|$ = 124.0 Hz, $^2J(HP_A)$ = 14.0 Hz, IrH).

Compound 3. IR: ν(Ir-H) 2070 (s) cm^{-1}. ^{31}P [^1H] NMR (CD_2Cl_2, 20 °C, AM_2 spin system): −10.0 (P_A), −18.7 (P_M, $^2J(P_AP_M)$ = 15.0 Hz). ^1H NMR (CD_2Cl_2, 20 °C): δ 2.8−2.2 [CH_2 (triphos)] 1.55 [q, CH_3 (triphos)], −8.81 (second-order doublet of multiplets, AA′XX′Y spin system, $|^2J(HP_M) + {}^2J(HP_{M'})|$ = 123.0 Hz, $^2J(HP_A)$ = 13.9 Hz, IrH).

Compound 4. Anal. Calcd (found) for $C_{53}H_{48}IrP_3S$: C, 63.52 (63.01); H, 4.83 (4.73); Ir, 19.18 (19.06); S, 3.20 (3.09). IR: ν(Ir-H) 2070 (s) cm^{-1}. ^{31}P[^1H] NMR (CD_2Cl_2, 20 °C, AM_2 spin system): δ −11.3 (P_A), −18.7 (P_M, $^2J(P_AP_M)$ = 15.3 Hz). ^1H NMR (CD_2Cl_2, 20 °C): δ 2.8−2.2 [CH_2 (triphos)], 1.59 [q, CH_3 (triphos)], −8.55, (second-order doublet of multiplets, AA′XX′Y spin system, $|^2J(HP_M) + {}^2J(HP_{M'})|$ = 120.1 Hz, $^2J(HP_A)$ = 12.8 Hz, IrH). ^{13}C [^1H] NMR (CD_2Cl_2, 20 °C): δ 158.9 (br s, IrC), the other resonances of DBT were masked by those of the phenyl carbons of triphos ligand (120−140 ppm).

Reaction of (Triphos)Ir(H)$_2$Cl with (*n*-Butyllithium + DBT). *n*-Butyllithium (30.5 mL, 48.8 mmol, 1.6 M solution in hexanes) was added to a stirred solution of DBT (5.0 g, 27.2 mmol) in Et_2O (40 mL) at 0 °C over 15 min. The mixture was refluxed for 18 h and cooled to room temperature.[23] A sample of this solution (0.10 mL, 0.039 mmol, 0.388 M) was syringed into a solution of (triphos)Ir(H)$_2$Cl (20 mg, 0.02 mmol) in THF-d_8 (1 mL) at room temperature. The reaction mixture was transferred into a 5-mm NMR tube. The ^{31}P [^1H] NMR spectrum of this sample showed the quantitative formation of **2**−**4** in ca. 28:41:31 ratio.

Reaction of [(Triphos)Ir(H)$_2$Cl + *tert*-Butyllithium] with DBT. *tert*-Butyllithium (0.13 mL, 0.22 mmol, 1.7 M solution in pentane) was syringed into a stirred solution of (triphos)Ir(H)$_2$Cl (0.20 g, 0.20 mmol) in THF (50 mL) at 0 °C. An immediate reaction took place. Gas evolution accompanied by color change from pale yellow to red occurred. Solid DBT (0.23 g, 1.2 mmol) was then added to the reaction mixture. After ca. 10 min, the solution was allowed to reach room temperature, stirred for 2 h, and then concentrated to dryness under vacuum. The ^{31}P [^1H] NMR spectrum of the residue showed the quantitative formation of **2**−**4** in almost the same ratio as above.

Reaction of 4 with HBF$_4$·Et$_2$O. A stoichiometric amount of neat HBF$_4$·Et$_2$O (ca. 70 μL) was syringed into a solution of **4** (0.30 g, 0.30 mmol) in CH_2Cl_2 (30 mL) at room temperature. After 30 min, a solution of $NaBPh_4$ (0.14 g, 0.40 mmol) in ethanol (5 mL) followed by *n*-heptane (30 mL) was added to the reaction mixture. On partial concentration under a brisk flow of nitrogen, off-white crystals of [(triphos)Ir(H)$_2$(η^1-*S*-DBT)]BPh_4 (**6**) (see below) precipitated in 75% yield.

Independent Synthesis of [(Triphos)Ir(H)$_2$(η^1-*S*-DBT)]BPh_4 (6). A solid sample of [(triphos)Ir(H)$_2$(THF)]BPh_4 (0.20 g, 0.16 mmol) was dissolved into a solution of DBT (0.29 g, 1.6 mmol) in CH_2Cl_2 (20 mL). After ca. 15 min, ethanol (10 mL) and *n*-heptane (20 mL) were added to the reaction mixture. Partial evaporation of the solvents under a steady stream of nitrogen led to the precipitation of **6** as an off-white microcrystalline solid in 90% yield. Anal. Calcd (found) for $C_{77}H_{69}BIrP_3S$: C, 69.94 (69.21); H, 5.26 (5.11); Ir, 14.54 (14.00); S, 2.42 (2.23). Λ_M: 49 Ω^{-1} cm^2 mol^{-1}. IR: ν(Ir-H) 2092 (s) cm^{-1}. ^{31}P [^1H] NMR (CD_2Cl_2, 20 °C, AM_2 spin system): δ −1.8 (P_A) −17.0 (P_M, $^2J(P_AP_M)$ = 16.0 Hz). ^1H NMR (CD_2Cl_2, 20 °C): δ 2.7−2.3 [CH_2 (triphos)], 1.68 [q, CH_3 (triphos)], −9.46 (second-order doublet of multiplets, AA′XX′Y spin system, $|^2J(HP_M) + {}^2J(HP_{M'})|$ = 113.3 Hz, $^2J(HP_A)$ = 10.7 Hz, IrH).

Reaction of 6 with CO. Carbon monoxide was bubbled through a CH_2Cl_2 (20 mL) solution of **6** (0.20 g, 0.15 mmol) at room temperature for 2 h. After the solvent was removed under vacuum, a pale yellow solid was obtained which was characterized by IR and NMR spectroscopy as a 1:1 mixture of DBT and [(triphos)Ir(H)$_2$(CO)]BPh_4.[21]

Reaction of 4 with CF_3SO_3D under CO. A stoichiometric amount of neat CF_3SO_3D (ca. 25 μL) was syringed into a solution of **4** (0.30 g, 0.30 mmol) in CH_2Cl_2 (30 mL) under CO atmosphere at room temperature. After 3 h, the solution was concentrated to dryness in vacuo. ^1H and ^{31}P NMR spectra of a portion of the residue showed the quantitative conversion of **4** to [(triphos)Ir(H)$_2$(CO)](CF_3SO_3). The rest of the residue was chromatographed on a silica gel column with *n*-pentane as eluant. The eluate was concentrated to dryness and dissolved in CD_2Cl_2. The ^1H NMR spectrum of this sample showed that deuterium was incorporated exclusively in the 4-position of DBT. This was established by integrating the individual DBT peaks.[24] This finding confirmed the structure assigned to **4** where the DBTyl ligand binds iridium *via* the C_4 carbon atom.

Thermal Behavior of 4. A. At 120−160 °C in THF. A 5-mm NMR tube was charged with a THF-d_8 (0.7 mL) solution of **4** (30 mg, 0.03 mmol) under nitrogen, flame sealed, and kept at 120 °C (oil bath). After 3 h, the tube was cooled to room temperature. ^1H and ^{31}P [^1H] NMR spectra of this sample showed the partial conversion of **4** to both **5** (ca. 10%) and several unidentified triphos−iridium complexes (ca. 50%) (see text). Free DBT (^1H NMR resonances in the range 7.5−8.4 ppm) was also produced in concentration comparable with that of the unidentified iridium complexes. Analogous behavior was observed at reaction temperatures ranging from 120 to 160 °C. As an example, at 160 °C **5** was produced in ca. 25% yield whereas the extent of decomposition was ca. 70%.

B. At 70−100 °C in Benzene. A solution of **4** (0.10 g, 0.10 mmol) in benzene (30 mL) was heated at 100 °C in a Parr

(23) (a) Campaigne, E.; Hewitt, L.; Ashby, J. *J. Heterocycl. Chem.* **1969**, *6*, 753. (b) Gilman, H.; Esmay, D. L. *J. Am. Chem. Soc.* **1954**, *76*, 5786. (c) Gilman, H.; Jacoby, A. L. *J. Org. Chem.* **1938**, *3*, 108.

(24) Bartle, K. D.; Jones, D. W.; Matthews, R. S. *Tetrahedron* **1971**, *27*, 5177.

reactor. After 1 h, the bomb was cooled to room temperature, the contents were transferred into a Schlenk-type flask, and the volatiles were removed under vacuum. The residue was characterized by ^1H and ^{31}P [^1H] NMR spectroscopy as a 2:3 mixture of **4** and (triphos)Ir(H)$_2$(C$_6$H$_5$).[25] Quantitative formation of free DBT also occurred during the reaction. Further heating for 2 h led to the complete conversion of **4** to the phenyl dihydride complex and free DBT (^1H NMR and GC/MS). Though at a much lower rate, the reaction occurred already at 70 °C.

C. At 160 °C in THF in the Presence of BT. A 5-mm NMR tube was charged with a THF-d_8 (0.7 mL) solution of **4** (30 mg, 0.03 mmol) and a 10-fold excess of BT (40 mg, 0.30 mmol) under nitrogen, flame sealed, and heated to 160 °C (oil bath). After 3 h, it was cooled to room temperature and placed into an NMR spectrophotometer. The ^1H and ^{31}P [^1H] NMR spectra of this sample showed the quantitative conversion of **4** to the 2-vinylthiophenolate complex (triphos)Ir(η^3-S(C$_6$H$_4$)-CH=CH$_2$)[6] and DBT (^1H NMR and GC/MS).

D. At 160 °C in THF in the Presence of DBT. The reaction was worked up as above with **4** (30 mg, 0.03 mmol) and a 10-fold excess of DBT (55 mg, 0.30 mmol) and gave quantitative conversion of **4** to **5**.

Synthesis of (Triphos)IrH(η^2-*C,S*-DBT) (5). A Parr reactor was charged with solid (triphos)Ir(H)$_2$(C$_2$H$_5$) (**1**) (0.25 g, 0.30 mmol) and a solution of DBT (0.33 g, 1.80 mmol) in THF (40 mL) under nitrogen at room temperature and then heated at 160 °C. After 4 h, the bomb was cooled to room temperature and the contents were transferred into a Schlenk-type flask. Addition of *n*-heptane (30 mL) led to the precipitation of **5** as off-white microcrystals, which were collected by filtration and washed with diethyl ether; yield 85%. Anal. Calcd (found) for C$_{53}$H$_{48}$IrP$_3$S: C, 63.52 (62.86); H, 4.83 (4.79); Ir, 19.18 (19.00); S, 3.20 (3.06). IR: ν(Ir-H) 2098 (s) cm^{-1}. ^{31}P [^1H] NMR (CD$_2$Cl$_2$, 20 °C, AMQ spin system): δ −10.6 (P$_A$), −23.1 (P$_M$), −47.0 (P$_Q$, ^2J(P$_A$P$_M$) = 13.5 Hz, ^2J(P$_A$P$_Q$) = 14.4 Hz, ^2J(P$_M$P$_Q$) = 16.6 Hz). ^1H NMR (CD$_2$Cl$_2$, 20 °C): δ 2.7−2.1 [CH$_2$ (triphos)], 1.45 [q, CH$_3$ (triphos)], −8.01 (ddd, ^2J(HP) = 153.2, 12.3, 8.8 Hz, IrH). ^{13}C [^1H] NMR (CD$_2$Cl$_2$, 20 °C): δ 161.1 (br s, IrC), the other resonances of DBT were masked by those of the phenyl carbons of triphos (120−140 ppm).

Thermal Behavior of 5. A. At 170 °C in THF. A 5-mm NMR tube was charged with a THF-d_8 (0.7 mL) solution of **5** (30 mg, 0.03 mmol) under nitrogen, flame sealed, and kept at 170 °C (oil bath). After 3 h, the tube was cooled to room temperature. The ^1H and ^{31}P [^1H] NMR spectra of this sample showed the partial decomposition of **5** to the same unidentified triphos−iridium compounds (ca. 10%), and the formation of free DBT in a comparable amount (^1H NMR and GC/MS).

B. At 170 °C in THF in the Presence of BT. A 5-mm NMR tube was charged with a THF-d_8 (0.7 mL) solution of **5** (30 mg, 0.03 mmol) and a 10-fold excess of BT (40 mg, 0.30 mmol) under nitrogen, flame sealed, and heated to 170 °C (oil bath). After 3 h, the tube was cooled to room temperature and placed into an NMR spectrophotometer. The ^1H and ^{31}P [^1H] NMR spectra of this sample showed the partial conversion of **5** to (triphos)Ir(η^3-S(C$_6$H$_4$)CH=CH$_2$)[6] and DBT (43%).

Reaction of 5 with H$_2$. A. 100 °C, 5 atm; Synthesis of (Triphos)Ir(H)$_2$(SC$_{12}$H$_9$) (7). A solution of **5** (0.25 g, 0.25 mmol) in THF (30 mL) was pressurized with hydrogen to 5 atm at room temperature in a Parr reactor and then heated at 100 °C for 4 h. The bomb was then cooled to room temperature, and after it was depressurized and vented under a nitrogen stream, the contents were transferred into a Schlenk-type flask. Addition of ethanol (30 mL) followed by partial evaporation of the solvents led to the precipitation of the 2-phenylthiophenolate dihydride **7** as pale yellow microcrystals. They were filtered off and washed with *n*-pentane; yield 75%. Anal. Calcd (found) for C$_{53}$H$_{50}$IrP$_3$S: C, 63.39 (63.06); H, 5.02 (5.01); Ir, 19.14 (19.09); S, 3.19 (3.03). IR: ν(Ir-H) 2046 (s) cm^{-1}. ^{31}P [^1H] NMR (CD$_2$Cl$_2$, 20 °C, AM$_2$ spin system): δ −2.4, (P$_A$), −25.5 (P$_M$, ^2J(P$_A$P$_M$) = 14.1 Hz). ^1H NMR (CD$_2$Cl$_2$, 20 °C): δ 2.6−2.2 [CH$_2$ (triphos)], 1.49 [q, CH$_3$ (triphos)], −9.22 (second-order doublet of multiplets, AA'XX'Y spin system, $|^2J(HP_M) + {}^2J(HP_{M'})|$ = 132.3 Hz, ^2J(HP$_A$) = 12.2 Hz, IrH).

B. 170 °C, 5 atm. A solution of **5** (0.25 g, 0.25 mmol) in THF (30 mL) was pressurized with hydrogen to 5 atm at room temperature in a Parr reactor and then heated at 170 °C. After 4 h, the bomb was cooled to room temperature. After it was depressurized and vented under a nitrogen stream, the contents were transferred into a Schlenk-type flask. The volatiles were removed in vacuo, and the residue was characterized by ^1H and ^{31}P [^1H] NMR spectroscopy as a 96:4 mixture of **7** and (triphos)Ir(H)$_3$ (**8**).

C. 170 °C, 30 atm. A solution of **5** (0.25 g, 0.25 mmol) in THF (30 mL) was pressurized with hydrogen to 30 atm at room temperature in a Parr reactor and then heated at 170 °C. After 4 h, the bomb was cooled to room temperature and slowly depressurized by bubbling the gaseous phase through an aqueous solution of Pb(II) acetate. H_2S released during the reaction led to the formation of the characteristic black precipitate of PbS, which was authenticated as described in ref 26. The contents of the bomb were then transferred into a Schlenk-type flask. The volatiles were removed in vacuo, and the residue was dissolved in CD$_2$Cl$_2$. ^1H and ^{31}P [^1H] NMR spectra of this sample showed the presence of **7** and **8** in a ratio of 31:69. The sample was chromatographed over a silica gel column (5:1 mixture of *n*-pentane/CH$_2$Cl$_2$ as eluant) to remove the iridium complexes. The organic phase was evaporated to dryness in vacuo, and the residue, analyzed by ^1H NMR and GC/MS, was found to contain DBT (42%), 2-phenylthiophenol (48%), and biphenyl (10%). Quite similar organic product distribution was found by analyzing the reaction solution, after it was cooled to room temperature, by GC/MS.

2-Phenylthiophenol.[19] ^1H NMR (CDCl$_3$, 20 °C): δ 7.5−7.1 (m, 9H, CH), 3.36 (s, 1H, SH). GC/MS [EIMS, 70 eV, *m/e* (%)]: 186 (70) M$^+$, 185 (100) M − H$^+$, 152(42) M − H_2S^+.

Reaction of 5 with 2-Phenylthiophenol. A solution of **5** (0.25 g, 0.25 mmol) and 2-phenylthiophenol (93 mg, 0.5 mmol) in THF (30 mL) was introduced in a Parr reactor and heated at 170 °C. After 3 h, the bomb was cooled to room temperature. After it was depressurized and vented under a nitrogen stream, the contents were transferred into a Schlenk-type flask. The volatiles were removed in vacuo, and the residue was characterized as a 61:39 mixture of **7** and **5** (^1H and ^{31}P [^1H] NMR). The formation of DBT also occurred during the reaction (^1H NMR and GC/MS).

Reaction of (Triphos)Ir(H)$_3$ (8) with 2-Phenylthiophenol. A. A 5-mm NMR tube was charged with a mixture of (triphos)Ir(H)$_3$ (**8**) (20 mg, 0.025 mmol) and 2-phenylthiophenol (9 mg, 0.05 mmol) in THF-d_8 (0.7 mL) under nitrogen, flame sealed, and kept at 170 °C (oil bath). After 3 h, the tube was cooled to room temperature. The ^1H and ^{31}P [^1H] NMR spectra of this sample indicated the partial conversion of **8** to **7** (31%) and the formation of hydrogen (^1H NMR: singlet at 4.7 ppm).

B. 30 atm of H$_2$. A solution of **8** (0.20 g, 0.25 mmol) and 2-phenylthiophenol (93 mg, 0.5 mmol) in THF (30 mL) was introduced in a Parr reactor, pressurized with H_2 to 30 atm, and heated at 170 °C. After 3 h, the bomb was cooled to room temperature. After it was depressurized and vented under a nitrogen stream, the contents were transferred into a Schlenk-type flask. The volatiles were removed in vacuo, and the residue was characterized by ^1H and ^{31}P [^1H] NMR and GC/MS as a mixture of **8** (90%) and **7** (10%).

Thermal Behavior of 7. A. A 5-mm NMR tube, charged with a THF-d_8 (0.7 mL) solution of **7** (30 mg, 0.03 mmol) under nitrogen, was flame sealed and heated to 170 °C (oil bath).

(25) Bianchini, C.; Barbaro, P.; Meli, A.; Peruzzini, M.; Vacca, A.; Vizza, F. *Organometallics* **1993**, *12*, 2505.

(26) Koltoff, I. M.; Sandell, E. B. *Textbook of Quantitative Inorganic Analysis*; MacMillan Co.: New York, 1943.

After 14 h, it was cooled to room temperature and placed into an NMR spectrophotometer. the ^1H and ^{31}P [^1H] NMR spectra of this sample indicated the partial conversion of **7** to **5** (18%) and hydrogen evolution (^1H NMR: singlet at 4.7 ppm). Appreciable formation (12%) of unidentified iridium compounds also occurred (see text).

B. In the Presence of DBT. Workup as above starting with **7** (30 mg, 0.03 mmol) and a 10-fold excess of DBT (55 mg, 0.30 mmol) gave the partial conversion of **7** to **5** (46%) and the formation of hydrogen and 2-phenylthiophenol in an amount of ca. 15% based on **7** (^1H NMR and GC/MS).

Reaction of 7 with H_2. A. 170 °C, 5 atm. A solution of **7** (0.25 g, 0.25 mmol) in THF (30 mL) was pressurized with hydrogen to 5 atm at room temperature in a Parr reactor and then heated at 170 °C. After 14 h, the bomb was cooled to room temperature. After it was depressurized and vented under a nitrogen stream, the contents were transferred into a Schlenk-type flask. The volatiles were removed in vacuo, and the residue was characterized by ^1H and ^{31}P [^1H] NMR spectroscopy as a 90:4:6 mixture of **7**, **5**, and **8**. Free DBT was also detected in solution (ca. 5% based on **7**).

B. 170 °C, 30 atm. A solution of **7** (0.25 g, 0.25 mmol) in THF (50 mL) was pressurized with hydrogen to 30 atm at room temperature in a Parr reactor and then heated at 170 °C. After 14 h, the bomb was cooled to room temperature and depressurized by slowly bubbing the gaseous phase through an aqueous solution of Pb(II) acetate. H_2S released during the reaction led to the formation of the characteristic black precipitate of PbS. The contents of the bomb were then transferred into a Schlenk-type flask. The volatiles were removed in vacuo, and the residue was dissolved in CD_2Cl_2. ^1H and ^{31}P [^1H] NMR spectra of this sample showed the presence of **7** and **8** in a ratio of 64:36. The sample was then chromatographed on a silica gel column (5:1 mixture of *n*-pentane/CH_2Cl_2 as eluant) to eliminate the iridium complexes. The eluate was then concentrated to dryness in vacuo, and the residue was characterized by ^1H NMR and GC/MS as a mixture of DBT (2%), 2-phenylthiophenol (57%), and biphenyl (41%).

Synthesis of (Triphos)Ir(H)$_2$SH (9). A Parr reactor was charged with a solid sample of **1** (0.25 g, 0.30 mmol) and a H_2S-saturated THF (40 mL) solution at room temperature and then heated at 70 °C. After 6 h, the bomb was cooled to room temperature and depressurized and the contents were transferred into a Schlenk-type flask. Portionwise addition of *n*-heptane (40 mL) led to the precipitation of **9** as off-white microcrystals, which were collected by filtration and washed with *n*-pentane; yield 80%. Anal. Calcd (found) for $C_{41}H_{42}IrP_3S$: C, 57.80 (57.12); H, 4.97 (4.93); Ir, 22.56 (21.99); S, 3.76 (3.58). IR: ν(Ir-H) 2050 (s) cm^{-1}. ^{31}P [^1H] NMR (CD_2Cl_2, 20 °C, AM_2 spin system): δ −1.0 (P_A), −25.8 (P_M, $^2J(P_AP_M)$ = 14.0 Hz). ^1H NMR (CD_2Cl_2, 20 °C): δ 2.5−2.2 [CH_2 (triphos)], 1.51 [q, CH_3 (triphos)], −2.58 (m, IrSH), −9.28, (second-order doublet of multiplets, AA′XX′Y spin system, $|^2J(HP_M) + {}^2J(HP_{M'})|$ = 134.8 Hz, $^2J(HP_A)$ = 11.3 Hz, IrH).

Reaction of 9 with H_2. A solution of **9** (0.21 g, 0.25 mmol) in THF (50 mL) was pressurized with hydrogen to 30 atm at room temperature in a Parr reactor and then heated at 170 °C. After 14 h, the bomb was cooled to room temperature and depressurized by slowly bubbling the gaseous phase through an aqueous solution of Pb(II) acetate. H_2S released during the reaction led to the formation of the characteristic black precipitate of PbS. The contents of the bomb were then transferred into a Schlenk-type flask. The volatiles were removed in vacuo, and the residue was dissolved in CD_2Cl_2. ^1H and ^{31}P [^1H] NMR spectra of this sample showed the presence of **9** and **8** in a ratio of 80:20.

Catalytic Hydrogenation and Hydrodesulfurization Reaction of DBT. A solution of **5** (0.20 g, 0.20 mmol) and an 80-fold excess of DBT (0.44 g, 16 mmol) in THF (100 mL) was pressurized at 30 atm at room temperature into the Parr reactor and then heated at 170 °C. After 24 h, the bomb was cooled to room temperature and slowly depressurized by bubbling the gaseous phase through an aqueous solution of Pb(II) acetate. H_2S released during the reaction led to the formation of the characteristic black precipitate of PbS. The contents of the bomb were then transferred into a Schlenk-type flask. The volatiles were removed in vacuo, and the residue was dissolved in CD_2Cl_2. ^1H and ^{31}P [^1H] NMR spectra of this sample showed the presence of **7** and **8** in a ratio of 12:88. The sample was then chromatographed on a silica gel column (5:1 mixture of *n*-pentane/CH_2Cl_2 as eluant) to eliminate the iridium complexes. The eluate was then concentrated to dryness in vacuo, and the residue was characterized by ^1H NMR and GC/MS as a mixture of DBT (87%), 2-phenylthiophenol (8%), and biphenyl (5%). Almost identical conversions and product distribution were observed when an analogous reaction was carried out in the presence of an excess of elemental mercury.[27]

Results and Discussion

The preparations and the principal reactions of the complexes described in this paper are illustrated in Schemes 1−10. Selected IR and NMR spectral data for all products are reported in the Experimental Section. With the exception of the C−S bond cleavage product (triphos)IrH(η^2-*C*,*S*-DBT) (**5**), all the new iridium complexes adopt the same primary coordination geometry. This consists of an octahedral arrangement of six donor atoms about iridium comprising the three phosphorus atoms of a *fac* triphos molecule (^{31}P [^1H] NMR AM_2 pattern), two chemically but not magnetically equivalent terminal hydrides (^1H NMR AA′XX′Y spin system where X, X′, and Y are the phosphorus nuclei), and either a carbon or sulfur atom.[20,21,25] All complexes are stereochemically rigid in solution on the NMR time scale and air-stable in both the solid state and solution.

Thermolysis of (Triphos)Ir(H)$_2$(C$_2$H$_5$) (1) in the Presence of DBT in the Temperature Range from 70 to 100 °C. Thermolysis of the ethyl dihydride complex **1** in THF occurs already at 70 °C and produces ethane and the [(triphos)IrH] fragment.[25] In the absence of added substrates, this highly energetic 16-electron metal system activates the solvent to give several unidentified products, due to both primary and secondary insertion of iridium into C−H bonds from THF (for simplicity these products are reported as "decomposition products" in the schemes).[25] However, when the thermolytic reaction is carried out in the presence of a slight excess of DBT, oxidative addition of DBT C−H bonds at iridium prevails over THF activation. In the temperature range from 70 to 100 °C and within 5 h, the C−H bond cleavage is not regioselective as three DBTyl complexes are invariably formed (Scheme 1a). In contrast, after 5 h at 100 °C, a unique product is obtained in quantitative yield. This complex can safely be formulated as (triphos)Ir(H)$_2$(4-DBTyl) (**4**) in the light of the labeling experiment illustrated in Scheme 2. The experiment involves treatment of **4** in CH_2Cl_2 with CF_3SO_3D followed by addition of CO (1 atm) to give free DBT selectively deuterated in the 4 position. Prior to CO addition, an η^1-*S*-DBT adduct of the formula [(triphos)Ir(H)$_2$(η^1-*S*-DBT)]$^+$ can be isolated as the tetraphenylborate salt **6**. The present protonation reaction thus closely resembles that recently reported by Angelici for Cp(PMe$_3$)$_2$Ru(2-

(27) Lin, Y.; Finke, R. G. *Inorg. Chem.* **1994**, *33*, 4891.

Scheme 1

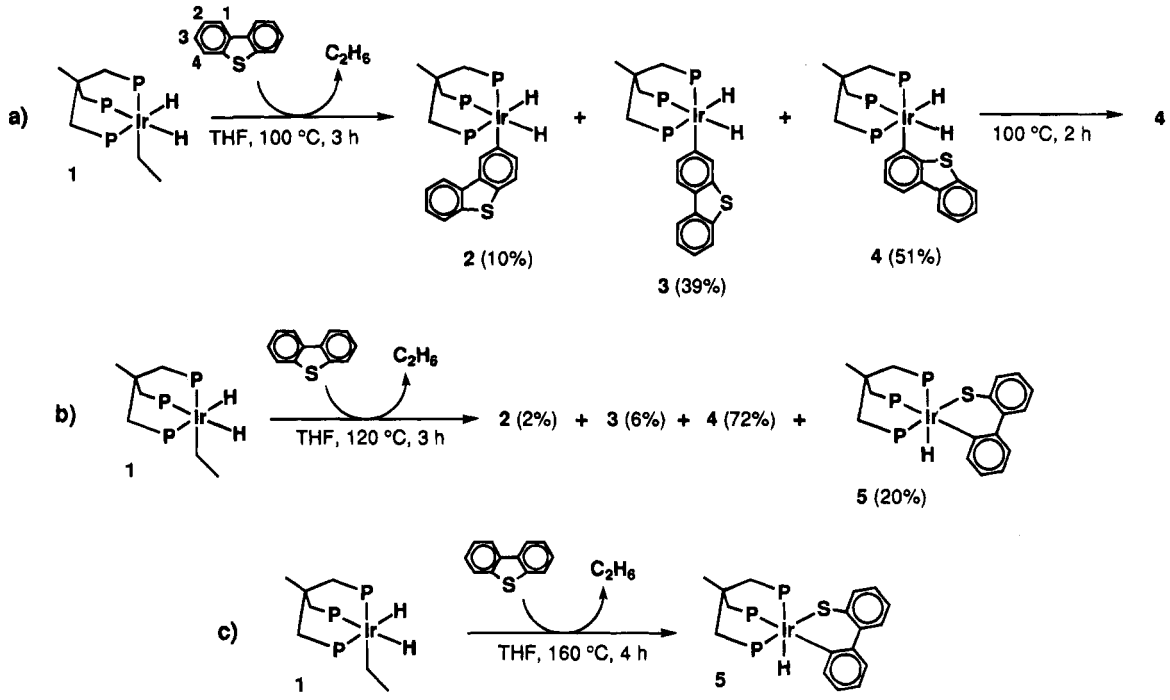

Scheme 2

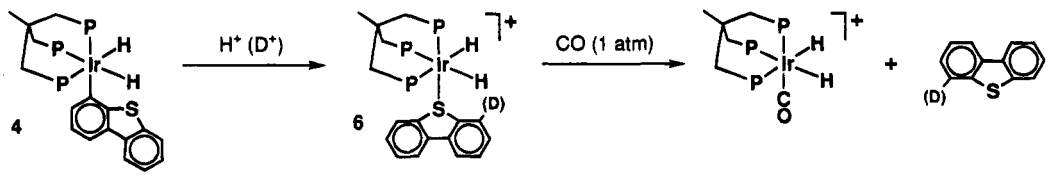

BTyl) (BTyl = benzothienyl).[28] η^1-*S*-Coordination is quite common for DBT; see, for example, $[Cp(CO)_2Ru(\eta^1\text{-}S\text{-DBT})]BF_4$,[7] $[IrH_2(\eta^1\text{-}S\text{-DBT})(PPh_3)_2]PF_6$,[8] $[Cp(CO)(PPh_3)Ru(\eta^1\text{-}S\text{-DBT})]BF_4$,[9] $Cp^*MCl_2(\eta^1\text{-}S\text{-DBT})$ (M = Rh, Ir),[10] $[Fe(\eta^1\text{-}S\text{-DBT})(CO)_2(Cp)]BF_4$,[11] and $Cp(CO)_2Re(\eta^1\text{-}S\text{-DBT})$.[12]

The structure of the other two DBTyl dihydride complexes, **2** and **3**, obtained at either temperatures below 100 °C or times shorter than 5 h at 100 °C is still ambiguous. Actually, it is possible that **2** may have the structure of **3** and *vice versa*. Our assignment as shown in Scheme 1a is essentially based on reasoning rather than on direct experiments. In no way, in fact, were we capable of preparing pure samples of either **2** or **3** to carry out labeling studies. Neither were helpful for structural assignments of the reactions of (triphos)Ir(H)$_2$Cl with (*n*-BuLi + DBT) or *t*-BuLi/DBT carried out at room temperature. In both cases, mixtures of **2**–**4** were invariably obtained. On the other hand, from a perusal of the variable-temperature thermolysis reactions as well as the metathetical and dehydrohalogenation[29] reactions of (triphos)Ir(H)$_2$Cl, one may draw out the following conclusions. (i) The barriers to insertion of iridium into the C_4–H, C_3–H, and C_2–H bonds of DBT are quite comparable in energy. (ii) The thermodynamic stability of the C–H bond cleavage products follows the order **4** > **3** > **2**. Just on the basis of this stability trend, compound **3** is suggested to contain a 3-DBTyl ligand as it is less sterically demanding than the 2-DBTyl one.

The greater stability of the 4-DBTyl isomer is not surprising in view of previous reports according to which metalation of DBT by RLi or RK compounds, followed by carbonation or bromination, affords DBTs substituted at the 4 position.[23] Metalation of DBT at the 3 position is also possible with the use of phenylcalcium iodide,[23c] while the direct substitution in the 2 position may be achieved *via* electrophilic attack.[30] There is no method for the direct introduction of substituents into the 1 position.[23c] In general, however, substitution reactions *via* metalation exhibit low yields (30–50% in the 4-substituted product), which suggests that the metalation reactions are not regioselective and that the isolation of the 4-substituted products is just due to the greater reactivity of metalated 4-DBTyl compounds toward electrophilic substitution. Indeed, we have the same evidence: the metalation reaction of DBT by [(triphos)IrH] is not regioselective, and the 4-DBTyl derivative is the thermodynamically most stable isomer.

DBTyl metal complexes obtained *via* C–H bond activation of DBT are much less numerous than η^1-*S*-DBT complexes. To the best of our knowledge, the only known complex is Jones' compound, $(C_5Me_5)Rh(PMe_3)H(SC_{12}H_7)$, prepared by thermolysis in hexane of $(C_5Me_5)Rh(PMe_3)(Ph)H$ in the presence of DBT.[16]

Thermolysis of (Triphos)Ir(H)$_2$(C$_2$H$_5$) (1) in the Presence of DBT at Temperatures Higher than 100 °C. When the thermolysis reaction of **1** in the

(28) Benson, J. W.; Angelici, R. *J. Inorg. Chem.* **1993**, *32*, 1871.
(29) Heyn, R. H.; Caulton, K. G. *J. Am. Chem. Soc.* **1993**, *115*, 3354.
(30) (a) Courtot, P.; Nicolas; Liang, Y. *Compt. Rend.* **1928**, *186*, 1624. (b) Courtot, P.; Pomonis. *Compt. Rend.* **1926**, *182*, 931. (c) Cullinane; Davies; Davies. *J. Chem. Soc.* **1936**, 1435. (d) Courtot, P.; Kelner. *Compt. Rend.* **1934**, *198*, 2003.

Scheme 3

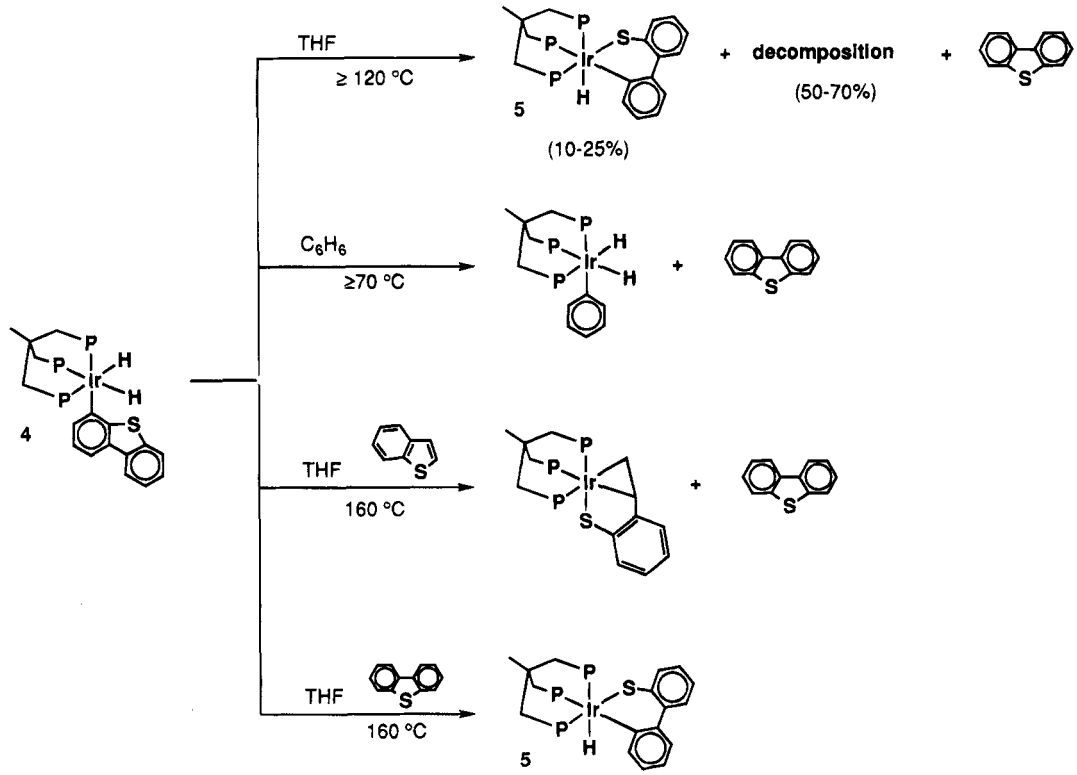

Scheme 4[a]

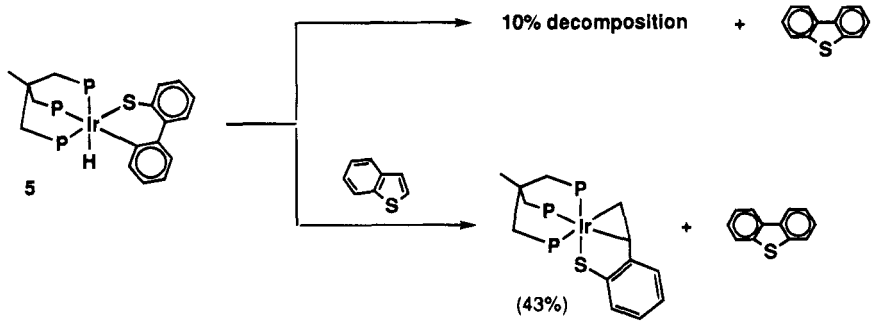

[a] Reaction conditions: THF, 170 °C, 3 h.

presence of DBT is carried out at temperatures higher than 100 °C, the 4-DBTyl complex becomes the largely predominant product among the C−H bond activation complexes and, more importantly, a new complex begins to form. An appreciable concentration (ca. 20%) of the latter product is observed when the mixture of **1** and DBT in THF is heated to 120 °C for 3 h (Scheme 1b). Selective and quantitative formation of this new species, isolable as off-white crystals, occurs as the reaction mixture is heated to 160 °C for 4 h (Scheme 1c).

Unambiguous identification of the new complex as the C−S insertion product (triphos)IrH(η^2-*C,S*-DBT) (**5**) is provided by NMR spectroscopy. ^{1}H NMR examination of the sample in CD_2Cl_2 shows the presence of a unique terminal hydride at −8.01 ppm lying *trans* to a phosphorus atom ($J(HP_{trans})$ = 153.2 Hz) and *cis* to two inequivalent phosphorus nuclei ($J(HP_{cis})$ = 12.3 and 8.8 Hz) (ν(Ir-H) = 2098 cm^{-1}). In accord with the inequivalence of the three phosphorus atoms of triphos, the ^{31}P [^{1}H] NMR spectrum consists of an AMQ spin system. Finally, the insertion of iridium into a C−S bond of DBT is clearly shown by the low-field shift of a DBT carbon resonance which moves to 161.1 ppm (Ir*C*). Indeed, almost identical ^{13}C NMR chemical shifts of the metalated carbon atom have been observed for the other two known examples of metal complexes containing an open DBT molecule: $(C_5Me_5)Rh(PMe_3)(SC_{12}H_8)$ [δ 159.9 (Rh*C*)][16] and $Pt(SC_{12}H_8)(PEt_3)_2$ [δ 158.0 (Pt*C*)].[17]

Thermolysis Reactions of the 4-DBTyl Complex In the Presence of Various Substrates. In an attempt to gain insight into the mechanism of conversion of the C−H bond insertion product **4** to the C−S insertion product **5**, a number of independent thermal reactions have been performed using isolated samples of both complexes (Schemes 3 and 4).

In THF. Heating a sample of **4** in THF at temperatures higher than 120 °C results in formation of **5** in concentrations that increase with temperature but never exceed 25% due to competitive C−H bond activation of the solvent by the [(triphos)IrH] fragment. Free DBT is also formed in an amount corresponding to that of THF activation products.

In C_6H_6. Thermolysis in benzene at 100 °C for 3 h quantitatively transforms **4** into the known phenyl dihydride complex (triphos)Ir(H)$_2$(C_6H_5)[25] and free DBT.

Though at a lower rate, this transformation occurs also at 70 °C.

In THF/BT. Stirring **4** in THF at 160 °C for 3 h in the presence of an excess of BT gives the 2-vinylthiophenolate complex (triphos)Ir(η^3-S(C_6H_4)CH=CH_2)[6] and DBT in quantitative yield.

In THF/DBT. Substitution of DBT for BT in the above reaction leads to quantitative conversion of **4** to **5**.

From these studies it is concluded that the C−H insertion product **4** is not a direct intermediate to the C−S insertion product **5**. As previously noted for similar activation reactions of T[4] and BT[31] at the [(triphos)IrH] system, also the DBTyl and η^2-*C,S*-DBT compounds form in parallel reactions over the temperature range from 120 to 160 °C; at the latter temperature the formation of the thermodynamically more stable C−S insertion product prevails over formation of the C−H cleavage product. Quantitative formation of **5**, however, occurs only when an excess of DBT is added. This suggests that the reductive coupling occurring at **4** is followed by either dissociation of DBT or formation of a labile η^2-*C,C*-DBT intermediate that, before slipping to η^1-*S*-coordination, is displaced by a competing substrate. Indeed, when there is no excess of DBT, other substrates in large concentration (the THF and C_6H_6 solvents or added BT) prevail over DBT for interaction with the [(triphos)IrH] fragment (Scheme 3).

Thermal Behavior of (Triphos)IrH(η^2-*C,S*-DBT). Once formed, the C−S insertion product **5** is thermally stable in THF up to 160 °C. This behavior apparently differs from that of the analogous thiophene (T) and benzo[*b*]thiophene (BT) derivatives (triphos)IrH(η^2-*C,S*-T)[4] and (triphos)IrH(η^2-*C,S*-BT)[6] which thermally undergo the reductive coupling of the terminal hydride with the vinyl moiety of the cleaved T and BT ligands. As a result, η^3-*C,C,S*-butadienethiolate and η^3-*C,C,S*-2-vinylthiophenolate complexes are formed as thermodynamically stable products. A similar reductive coupling process does occur when **5** is heated in THF at temperatures higher than 100 °C in the presence of a reagent capable of trapping the electronically and coordinatively unsaturated 2-phenylthiophenolate fragment [(triphos)Ir($SC_{12}H_9$)]. Appropriate trapping reagents may be either monodentate ligands such as CO to give (triphos)Ir(CO)($SC_{12}H_9$)[32] or binuclear molecules capable of oxidative addition such as H_2 (*vide infra*).

Above 160 °C in pure THF, **5** starts decomposing to give DBT and the above-mentioned products derived from C−H bond cleavage of the solvent. In comparison with the C−H activation product **4**, the reductive elimination of DBT from the C−S insertion product **5** is thus a process that occurs with a higher energy barrier. At 170 °C, only 10% of the starting complex disappears in 3 h. Under these conditions but in the presence of an excess of BT, the loss of DBT from **5** is faster (43%) and the 2-vinylthiophenolate complex is obtained (Scheme 4).

In view of these results we propose that, above 160 °C, **5** is in equilibrium with an η^1-*S*-DBT species. In the presence of an excess of BT,[33] the intact DBT ligand can be displaced by BT in excess, which is then opened and hydrogenated *via* hydride migration.[6] Hence, what we suggest for DBT is quite consistent with previous reports by Jones and co-workers who have proposed η^1-*S*-coordination of thiophenic molecules as a key step for C−S bond scission at 16-electron metal-d^8 fragments.[34] Interestingly, the overall picture of the interaction of [(triphos)IrH] with DBT closely resembles that recently reported for the reaction with ethene in refluxing THF: the vinyl hydride (triphos)Ir($H)_2$(CH=CH_2) and the thermodynamically more stable π-complex (triphos)IrH-(C_2H_4) form in parallel reactions *via* two different transition states.[25]

Hydrogenation and Hydrodesulfurization Reactions of (Triphos)IrH(η^2-*C,S*-DBT). The C−S insertion product **5** in THF quantitatively transforms into the 2-phenylthiophenolate dihydride complex (triphos)-Ir($H)_2$($SC_{12}H_9$) (**7**) by reaction with H_2 (5 atm) at 100 °C for 4 h. Increasing the temperature to 170 °C while keeping constant the H_2 pressure results in the formation of a 96:4 mixture of **7** and (triphos)Ir($H)_3$ (**8**). Free DBT is also produced most likely by displacement of η^1-DBT by H_2. Finally, both hydrogenation (formation of 2-phenylthiophenol) and hydrodesulfurization (formation of biphenyl + H_2S) of DBT occur when the H_2 pressure is increased to 30 atm (Scheme 5). After 4 h at 170 °C and 30 atm of H_2, all iridium of the starting complex **5** is incorporated into a 31:69 mixture of **7** and **8**, while the "open DBT" ligand is converted to a 10:48:42 mixture of biphenyl (+H_2S), 2-phenylthiophenol, and DBT. Under these conditions but in the presence of an excess of DBT (80 equiv), the reaction is catalytic even though with a low rate. In 24 h, 10 mol of DBT/mol of **5** is consumed to give 2-phenylthiophenol (60%) and biphenyl + H_2S (40%), while all iridium is incorporated into a 12:88 mixture of **7** and **8** (Scheme 6). After 48 h of reaction time, 15 mol of DBT/mol of Ir was consumed showing that the system is not deactivated within this time. Almost identical results were obtained when the reaction was carried out in the presence of excess elemental Hg, which indicates that the reaction is truly homogeneous.[27]

The very slow rate, the occurrence of several equilibria, the formation of several products, and the drastic reaction conditions, taken altogether, did not allow us to carry out a kinetic study of the catalytic hydrogenation and hydrodesulfurization of DBT described above. However, valuable mechanistic information was obtained with the use of isolated compounds in a variety of independent reactions carried out under conditions as close as possible to the catalytic ones.

Thermolysis of the 2-Phenylthiophenolate Dihydride Complex 7. In view of the results illustrated in Schemes 5 and 6, it is very likely that the 2-phenylthiophenolate complex **7** plays an intermediate role in both hydrogenation and hydrodesulfurization of DBT assisted by **5**. We have thus looked at the reactivity of **7** in THF at 170 °C.

In the absence of H_2, 30% of **7** converts in 14 h to the C−S insertion product **5** (18%) and to the products of

(31) Bianchini, C.; Meli, A. Manuscript in preparation. See also ref 6.

(32) Bianchini, C.; Meli, A. Unpublished results.

(33) An excess of BT is required for the substitution reaction as DBT is a better S-ligand than BT; see refs 7 and 9.

(34) Dong, L.; Duckett, S. B.; Ohman, K. F.; Jones, W. D. *J. Am. Chem. Soc.* **1992**, *114*, 151.

Scheme 5[a]

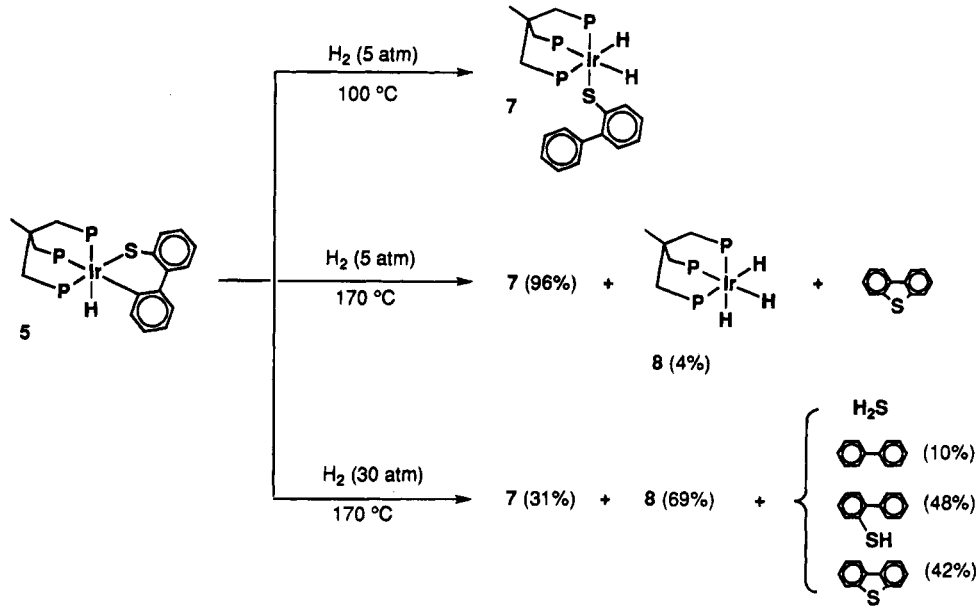

[a] Reaction conditions: THF, 4 h.

Scheme 6[a]

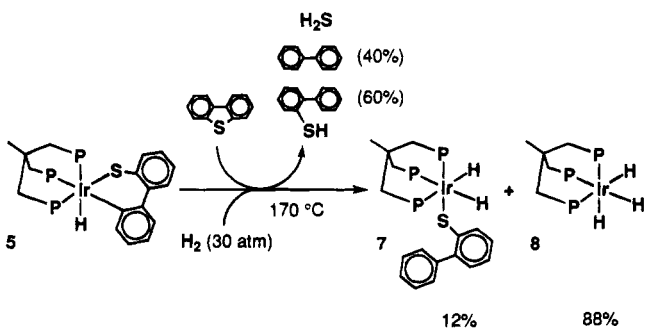

[a] Conversion: 24 h, 10 mol of DBT/mol of **5**.

C–H bond activation of THF (12%) (Scheme 7a). The concomitant evolution of both H_2 and DBT in comparable amounts rationalizes the thermolysis reaction of **7**. In particular, the formation of H_2 is consistent with the reductive elimination of H_2 from **7** occurring at 170 °C. As a result, the unsaturated fragment [(triphos)-Ir($SC_{12}H_9$)] forms which, in the absence of a trapping reagent (*vide infra*) and at 170 °C, undergoes intramolecualr insertion of iridium into an *ortho* C–H bond of the phenyl ring to give **5**. On the other hand, since the C–S insertion product **5** in THF at 170 °C is in equilibrium with an η^1-*S*-DBT species (reductive ring closure), displacement of DBT by THF can occur to give the unidentified C–H activation products. This reaction path is totally suppressed when the thermolysis of **7** at 170 °C is carried out in the presence of an excess of DBT. Notably, the latter substrate, besides prevailing over THF (see Schemes 1 and 3), is also capable of aiding the reductive elimination of 2-phenylthiophenol by stabilizing the 16-electron fragment (triphos)IrH (See Schemes 7 and 8). The amount of **5** formed upon thermolysis of **7** at 170 °C in the presence of excess DBT (46%) thus comes from two independent reactions. The major path (31%) involves the reductive elimination of H_2 followed by intramolecular insertion of iridium into a C–H bond of the phenyl substituent. The minor path (15%) involves the reductive elimination of 2-phenylthiophenol from **7** followed by coordination and then opening of a DBT molecule by the [(triphos)IrH] fragment. The complicated thermolysis pattern of **7** in THF at 170 °C is summarized in Scheme 8.

Reactions of the 2-Phenylthiophenolate Dihydride Complex 7 with H_2. Heating a sample of **7** dissolved in THF at 170 °C under 5 atm of H_2 for 4 h results in low conversion of **7** (10%) to **5** (4%), **8** (6%), and free DBT (Scheme 9a). Evidently, the pressure of H_2 slows down the reductive coupling of the two terminal hydrides in **7**. No trace of 2-phenylthiophenol was detected, which confirms the significant role of DBT in promoting the elimination of this thiol from **7**.

The elimination of 2-phenylthiophenol from **7** can also be achieved in the absence of an excess of DBT provided the H_2 pressure is increased to 30 atm (Scheme 9b). In this case, in fact, a larger amount of **7** is converted to **8** (36%), while the 2-phenylthiophenolate ligand is transformed into a 41:57:2 mixture of biphenyl (+H_2S), 2-phenylthiophenol, and DBT. These results are nicely consistent with those reported in Scheme 5 and clearly indicate that **7** can be an important intermediate for both hydrogenation and hydrodesulfurization of DBT at the [(triphos)IrH] fragment.

Reactions of (Triphos)Ir$(H)_3$ (8) with 2-Phenylthiophenol. To our surprise **8** was found to be fully stable when heated in THF at 170 °C in the presence of an excess of DBT. This evidence shows that DBT cannot enter the catalysis cycle *via* **8** and thus suggests that other reaction steps, besides hydrogenation of **7**, are necessary to accomplish the catalytic hydrodesulfurization of DBT.

One of these steps may be the reaction of **8** with 2-phenylthiophenol. The trihydride, in fact, reacts in THF at 170 °C with 2-phenylthiophenol to give **7** (31% conversion in 3 h) and H_2. Under a pressure of 30 atm of H_2, though disfavored (10% conversion), this reaction still takes place as it does not proceed *via* thermal elimination of H_2 from **8** followed by S–H oxidative addition. In fact, the trihydride complex is thermally stable in THF at 170 °C, while it is known to react with

Scheme 7[a]

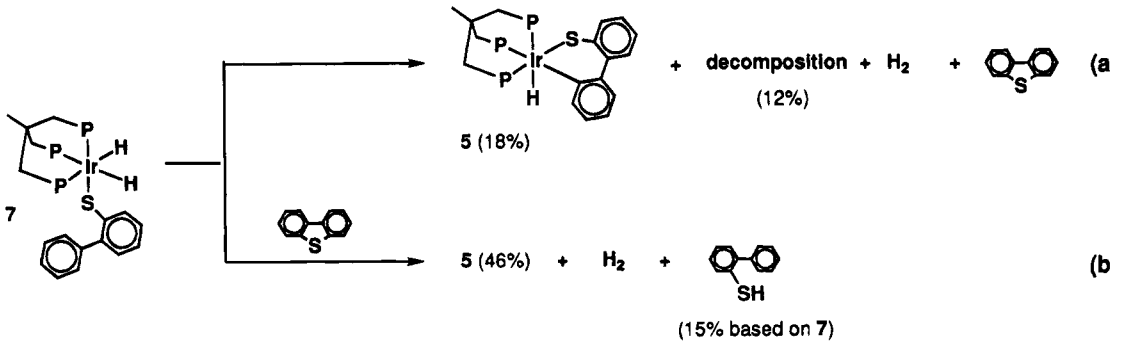

[a] Reaction conditions: THF, 170 °C, 14 h.

Scheme 8

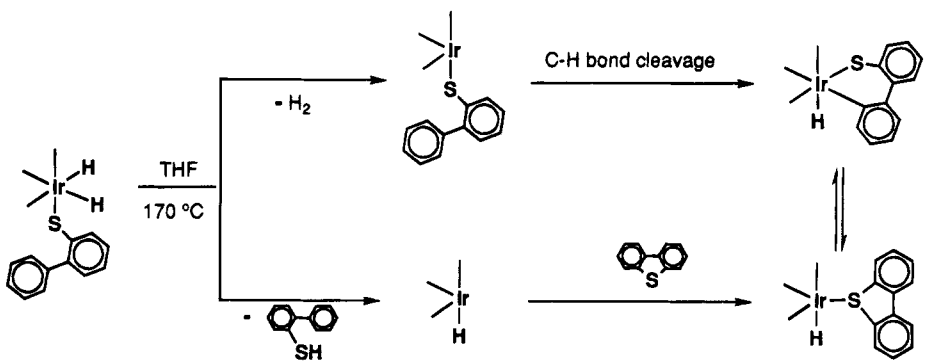

Scheme 9[a]

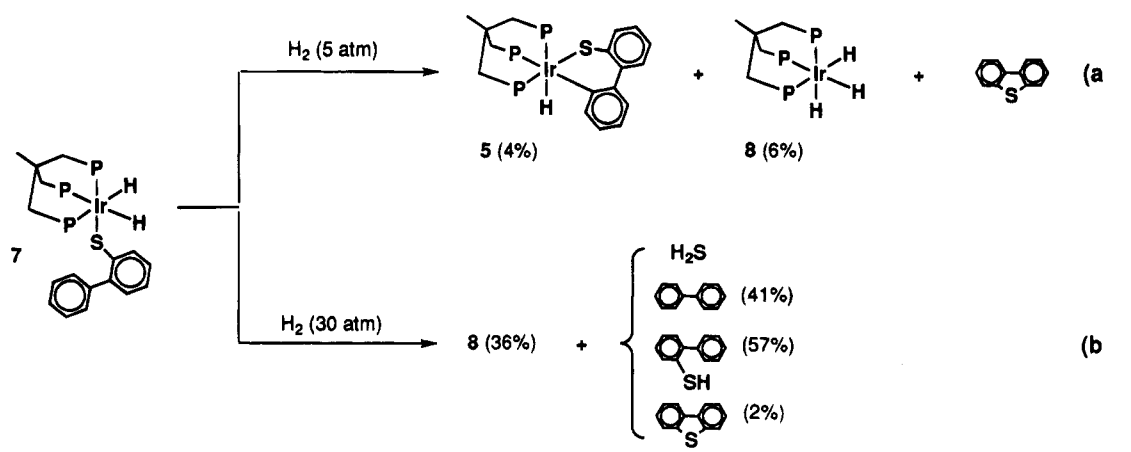

[a] Reaction conditions: THF, 170 °C, 14 h.

protic acids which generally attack a terminal hydride ligand.[21]

Reaction of (Triphos)IrH(η^2-*C,S*-DBT) (5) with 2-Phenylthiophenol. Having found that 2-phenylthiophenol reacts with **8** under the catalytic conditions, it was of interest to see whether other metal species participating in the catalysis cycle might be attacked by this thiophenol. Indeed, a reaction occurs between the C–S insertion product **5** and a slight excess of 2-phenylthiophenol in THF at 170 °C to give **7** (61% in 3 h) and free DBT. In view of the reactions of 2-phenylthiophenol with **8** and **5**, it is thus conceivable that also the 2-phenylthiophenol produced in the reactions shown in Schemes 5–7 and 9 is actually the result of a mass balance involving several equilibria.

In Search of a Mechanism for the Cleavage of the Ir–S–C Linkage in 7. The reactions of thiols with organometallic compounds have extensively been investigated in recent years. It is generally agreed that (i) metal thiolates are key intermediates in all cases where C–S bond scission is seen, (ii) desulfurization of thiols is aided greatly by the presence of either a hydride source in the reaction mixture or a hydride ligand directly on the complex, and (iii) the C–S bond cleavage occurs *via* migration of a hydride to the sulfur-bound carbon of the thiolate ligand.[35] After the hydrocarbon is eliminated, the remaining M-S moiety may be stabilized by either dimerization (*e.g.*, M(μ-S)$_2$M) or electronic redistribution within the complex (*e.g.*, M=S). In the presence of H_2 as in the case at hand, an M(SH)(H) species may eventually form. In this respect, it is worth mentioning an interesting case of hydrodesulfurization

(35) (a) Wiegand, B. C.; Friend, C. M. *Chem. Rev.* **1992**, *92*, 491 and references therein. (b) Tatsumi, K.; Sekiguchi, Y.; Nakamura, A. *J. Am. Chem. Soc.* **1986**, *108*, 1358. (c) Okasada, K.; Matsumoto, K.; Yamamoto, T.; Yamamoto, A. *Organometallics* **1985**, *4*, 857.

Scheme 10

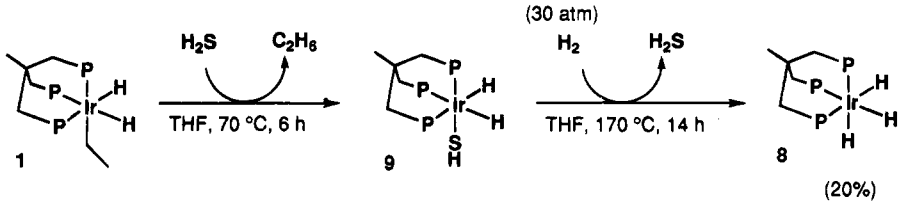

of DBT in homogeneous phase recently reported by Garcia and Maitlis for $Pt(SC_{12}H_8)(PEt_3)_2$.[17] The reaction of the latter complex with Et_3SiH leads to stoichiometric formation of biphenyl and *trans*-$Pt(PEt_3)_2(SH)(H)$, which is converted by HCl to H_2S and *trans*-$Pt(PEt_3)_2(H)(Cl)$.

Intrigued by Maitlis' discovery, we decided to look at the possible intermediacy of (triphos)Ir(SH)$(H)_2$ (**9**) in the hydrogenation of the 2-phenylthiophenolate ligand in **7** (30 atm of H_2, 170 °C). No experimental evidence was obtained for the formation of **9** through a direct study of this reaction on a preparative scale. Then **9** was independently synthesized by thermolysis of **1** in THF at 70 °C in the presence of an excess of H_2S.[36] Interestingly, this mercapto complex in THF does react, even though slowly, with a high pressure of H_2 (>30 atm, 170 °C) to give the trihydride **8** and H_2S (Scheme 10). In light of these precedents and experimental results, it is reasonable to propose that the C–S bond scission step in the HDS of DBT proceeds by reaction of H_2 with complex **7** to yield (triphos)Ir(SH)(H) (**9**) + biphenyl, conceivably via a heterolytic activation, followed by reaction of **9** with H_2 to produce the trihydride **8** + H_2S. However, high-pressure NMR studies would be needed in order to confirm the intermediacy of **9** in the catalytic cycle. In summary, the S–C bond in the Ir-S-$C_{12}H_9$ moiety is cleaved by H_2 to give H_2S and biphenyl, and this reaction occurs at a high pressure of H_2 (>30 atm).

The Catalysis Cycle. Incorporation of all the above experimental evidence leads to the mechanism shown in Scheme 11 for the hydrogenation and hydrodesulfurization of DBT catalyzed by the [(triphos)IrH] fragment. In the scheme, the skeleton of the tripodal ligand and the phosphorus donors are omitted for clarity.

After DBT has been cleaved, the C–S insertion product **5** reacts with H_2 to give the 2-phenylthiophenolate dihydride **7**. This complex has two reaction options: the reductive elimination of 2-phenylthiophenol promoted by interaction with DBT and the further hydrogenation to give 2-phenylthiophenol and biphenyl + H_2S. In the first case, compound **5** is regenerated for use in a following cycle. In the second case, **8** forms and the reaction would stop since the trihydride does not react with DBT. Fortunately, this does not occur as the 2-phenylthiophenol converts **8** to **7** which can reenter the catalysis cycle. Besides the intrinsic kinetic sluggishness of iridium compounds, the low tof of the catalytic reaction seems to be just the slowness with which **8** is converted to **7** by action of 2-phenylthiophenol. In fact, this transformation is disfavored at a high pressure of H_2.

Scheme 11. Proposed Mechanism for the Catalytic Hydrogenation and Hydrodesulfurization of DBT[a]

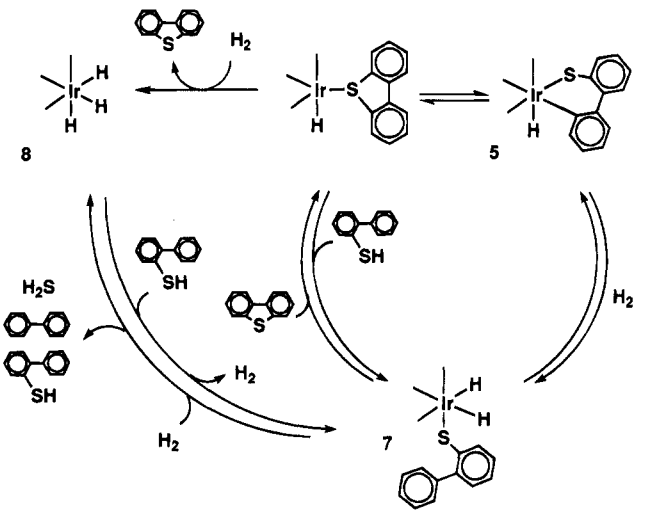

[a] Reaction conditions: THF, 170 °C, 30 atm of H_2.

Conclusions

The C–S insertion product (triphos)IrH(η^2-*C,S*-DBT) (**5**) is the ultimate thermodynamic sink for the system [(triphos)IrH]/DBT. Compound **5** is a catalyst precursor as well as an intermediate species in the homogeneous hydrogenation and hydrodesulfurization of DBT to 2-phenylthiophenol and biphenyl + H_2S. The catalysis reaction, which represents the first example for DBT in homogeneous phase, proceeds *via* several intermediate steps among which is the reaction of **5** with H_2 to give the 2-phenylthiophenolate complex (triphos)$Ir(H)_2(SC_{12}H_9)$ (**7**). Recent reactor and surface studies have provided evidence for a two-stage process involving a metal thiolate in the HDS of DBT.[19,37] This picture thus agrees quite well with that painted by the homogeneous modeling studies presented here. In particular, the present HDS of DBT reasonably accounts for one of the major modes of DBT reactivity on HDS catalysts, namely the direct sulfur extrusion to give biphenyl + H_2S.

Acknowledgment. A postdoctoral grant to M.V.J. from Ministerio de Educación y Ciencia (España) is gratefully acknowledged. Thanks are due also to CNR (Italy) and CONICIT (Venezuela) for financial support.

OM9500580

(36) Wander, S. A.; Reibenspies, J. H.; Kim, J. S.; Darensbourg, Y. M. *Inorg. Chem.* **1994**, *33*, 1421.

(37) (a) Girgis, M. J.; Gates, B. C. *Ind. Eng. Chem. Res.* **1991**, *30*, 2021 and references therein. (b) Topsøe, H.; Clausen, B. S. *Appl. Catal.* **1986**, *25*, 273. (c) Kasztelan, S. *Langmuir* **1990**, *6*, 590. (d) Brunier, T. M.; Drew, M. G. B.; Mitchell, P. C. H. *J. Chem. Soc., Faraday Trans.* **1992**, *88*, 3225.

Alkoxycarbonylation Reaction Involving a Tandem 1,3-Metal Shift across Conjugated Allyl and Alkyne Bonds

Kwei-Wen Liang,† Gene-Hsiang Lee,‡ Shie-Ming Peng,‡ and Rai-Shung Liu*,†

Departments of Chemistry, National Tsing-Hua University, Hsinchu 30043, Taiwan, Republic of China, and National Taiwan University, Taipei 10764, Taiwan, Republic of China

Received January 9, 1995®

The reaction between $CpW(CO)_3Na$ and 1-chlorohex-2-en-4-yne (**1**; *cis/trans* = 1/4) gave $CpW(CO)_3(\eta^1$-hex-2-en-4-yn-1-yl) (**2**) in good yield (*cis/trans* = 1/4). The *cis/trans* isomers of **2** were separated on a silica column at 0 °C. Treatment of the *trans* isomer **2a** with TCNE gave the [3 + 2] cycloaddition product exclusively to retain the η^1-allyl activity. Addition of CF_3SO_3H (1.1 equiv) to **2a** in cold diethyl ether in the presence of CH_3OH gave $CpW(CO)_3$-(η^1-*trans*-4-oxo-2-hexen-1-yl) (**5**) in 61% yield. Stirring of **2a** with RXH (RXH = H_2O, MeOH, $Me_2CHCH_2NH_2$) in THF over Florisil at 30 °C led to a new carbonylation to give $CpW(CO)_2$-(η^3-1-*syn*-COXR-1-*anti*-Me-3-*syn*-vinylallyl) compounds (RX = OH (**6**), MeO (**7**), Me_2CHCH_2-NH (**8**)) in 52–18% yields. The reaction of $CpW(CO)_3Na$ and 1-chloro-8-hydroxy-2-octen-4-yne gave the corresponding η^1-allyl compound which on a silica column produced the intramolecular alkoxycarbonylation product **13** in moderate yield. In the presence of $BF_3{\cdot}Et_2O$, compound **7** reacted with aldehydes and unsaturated enones to give η^4-diene salts, which after demetalation by Me_3NO liberated organic products in 40–55% isolated yields.

Introduction

Metal–η^1-allyl,[1] –η^1-propargyl,[2,3] and –η^1-allenyl compounds[2,3] are important in both organic and organometallic reactions. The reactions of these unsaturated η^1-hydrocarbyl ligands with electrophiles[2,3ab,4] are recognized to be useful processes for forming carbon–carbon bonds in organic synthesis. One important feature of these compound is the presence of a 1,3-metal shift (Scheme 1) that shows a significant influence on electrophilic regiochemistry.[1–3] Direct evidence of these metal shifts is well documented for both main-group-metal and transition-metal complexes.[1–3] The shift proceeds more rapidly for more electropositive metals according to experimental and theoretical evidence.[4,5]

Scheme 1

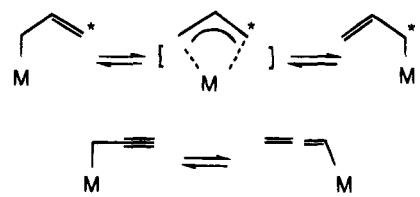

Metal-mediated alkoxylcarbonylation is a useful reaction in organic synthesis.[6,7] In the presence of acid catalysts, $CpW(CO)_3(\eta^1$-propargyl) reacted smoothly with alcohols to give allyl compounds in which alkoxycarbonylation occurred at the cental propargyl carbon.[8,9] In contrast, the reaction of $CpW(CO)_3(\eta^1$-allenyl)[8] with alcohols, under the same conditions, produced a 1-(alkox-

† National Tsing-Hua University.
‡ National Taiwan University.
® Abstract published in *Advance ACS Abstracts,* April 1, 1995.

(1) For the chemistry and application of metal–allyl compounds, see the review paper by: Yamamoto, Y.; Asao, N. *Chem. Rev.* **1993**, *93*, 2207.

(2) For main-group-metal allenyl and propargyl compounds, see the representative examples: (a) Seyferth, D.; Son, D. Y.; Shah S. *Organometallics* **1994**, *13*, 2105. (b) Brown, H. C.; Khire, U. R.; Racherla, U. S. *Tetrahedron Lett.* **1993**, *34*, 15. (c) Danheiser, R. L.; Carini, D. J. *J. Org. Chem.* **1980**, *45*, 3925. (d) Boaretto, A.; Marton, D.; Tagliavini, G. *J. Organomet. Chem.* **1985**, *297*, 149. (e) Marshall, J. A.; Wang, X.-J. *J. Org. Chem.* **1991**, *56*, 3212. (f) Marshall, J. A.; Wang, X. J. *J. Org. Chem.* **1991**, *56*, 6264.

(3) For transition-metal propargyl and allenyl compounds, see: (a) Bell, P. B.; Wojcicki, A. *Inorg. Chem.* **1981**, *20*, 1585. (b) Raghu, S.; Rosenblum, M. *J. Am. Chem. Soc.* **1973**, *95*, 3060. (c) Pu, J.; Peng, T. S.; Arif, A. M.; Gladysz, J. A. *Organometallics* **1992**, *11*, 3232. (d) Blosser, P. W.; Shimpff, D. G.; Gallucci, J. C.; Wojcicki, A. *Organometallics* **1993**, *12*, 1393. (e) Keng, R.-S.; Lin, Y.-C. *Organometallics* **1990**, *9*, 289. (g) Benaim, J.; Merour, J.-Y.; Roustan, J. L. *C. R. Acad. Sci. Paris, Ser. C* **1971**, *272*, 789.

(4) (a) Clark, T.; Rohde, C.; Schleyer, P. v. R. *Organometallics* **1983**, *2*, 1344. (b) Buhl, M.; Schleyer, P. v. R.; Ibrahim, M. A.; Clark, T. *J. Am. Chem. Soc.* **1991**, *113*, 2466.

(5) Gridnev, I. D.; Gurskii, M. E.; Ignatenko, A. V.; Bubnov, Y. N. *Organometallics* **1993**, *12*, 2487.

(6) (a) Heck, R. F.; Wu, G.; Tao, W.; Rheingold, A. L. In *Catalysis of Organic Reactions*; Blackburn, D. W., Ed.; Marcel Dekker: New York, 1990; p 169. (b) Heck, R. F. *Org. React.* **1982**, *27*, 345. (c) Collman, J. P.; Hegedus, L. S.; Norton, J. R.; Finke, R. G. *Principles and Application of Organotransition Metal Chemistry*; University Science Books: Mill Valley, CA, 1987; Chapter 12, p 619. (d) Hegedus, L. S. *Transition Metals in the Synthesis of Complex Organic Molecules*; University Science Books: Mill Valley, CA, 1994; Chapter 4, p 103.

(7) For representative examples of catalytic alkoxycarbonylation, see: (a) Murray, T. F.; Norton, J. R. *J. Am. Chem. Soc.* **1979**, *101*, 4107. (b) Semmelhack, M. F.; Brickner, S. J. *J Am. Chem. Soc.* **1981**, *103*, 3945. (c) Matsuda, I.; Ogiso, A.; Sato, S. *J. Am. Chem. Soc.* **1990**, *112*, 6120. (d) Negishi, E. I.; Sawada, H.; Tour, J. M.; Wei, Y. *J. Org. Chem.* **1988**, 53, 913. (e) Zhang, Y.; Negishi, E. I. *J. Am. Chem. Soc.* **1989**, *111*, 3454. (f) Tsuji, Y.; Kondo, T.; Watanabe, Y. *J. Mol. Catal.* **1987**, *40*, 295. (g) Jager, V.; Hummer, W. *Angew. Chem., Int. Ed. Engl.* **1990**, *29*, 1171.

(8) Tseng, T.-W.; Wu, I.-Y.; Lin, Y.-C.; Chen, C.-T.; Chen, M.-C.; Tsai, Y.-J.; Chen, M.-C.; Wang, Y. *Organometallics* **1991**, *10*, 43.

(9) (a) Collin, J.; Charrier, C.; Pouet, M. J.; Cadiot, P.; Roustan, J. L. *J. Organomet. Chem.* **1979**, *168*, 321. (b) Roustan, J. L.; Merour, J. Y.; Charrier, C.; Benaim, J.; Cadiot, P. *J. Organomet. Chem.* **1979**, *169*, 39. (c) Charrier, C.; Collin, J.; Merour, J. Y.; Roustan, J. L. *J. Organomet. Chem.* **1978**, *162*, 57. (d) Cheng, M.-H.; Ho, Y.-H.; Lee, G.-H.; Peng, S.-M.; Liu, R.-S. *J. Chem. Soc., Chem. Commun.* **1991**, 697.

0276-7333/95/2314-2353$09.00/0

Scheme 2[a]

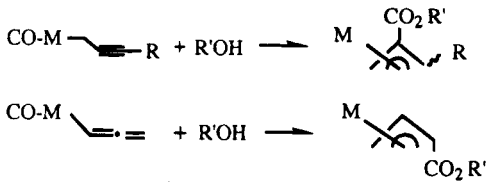

[a] M = $CpW(CO)_2$.

Scheme 3

Scheme 4[a]

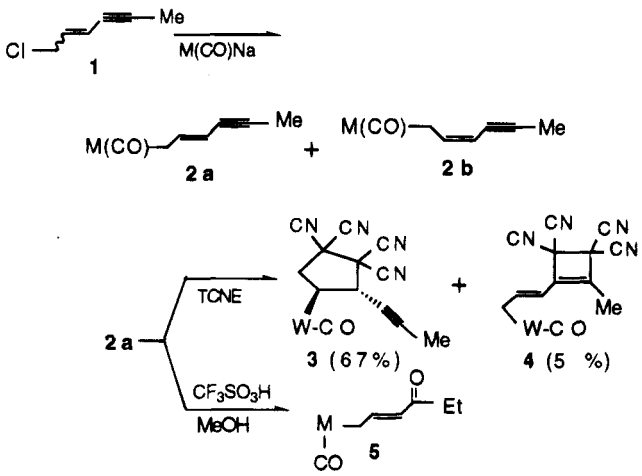

[a] M = $CpW(CO)_2$.

ycarbonyl)allyl compound as depicted in Scheme 2. In a continuing effort to explore the synthetic utility of tungsten–propargyl compounds,[10] we report[11] here a novel alkoxycarbonylation reaction, the mechanism of which is initiated by uncommon tandem 1,3-shifts of the metal fragment across conjugated allyl and alkyne bonds, as shown in Scheme 3. Although this process might be involved in the reaction of $BrCH_2CH{=}CHCCH$ with magnesium and zinc metals to give $CH_2{=}CHCH{=}C{=}CHMBr$ (M = Mg, Zn),[12] no corresponding η^1-pent-2-en-4-yn-1-yl compound was ever isolated.

Results and Discussion

Synthesis and Reaction Chemistry of η^1-Hex-2-en-4-yn-1-yl Species 2. Similar to the case for common transition-metal allyl compounds, the reaction of $CpW(CO)_3Na$ and 1-chlorohex-2-en-4-yne (**1**; *trans/cis* = 4/1) in cold THF (0 °C, 5 h) proceeded smoothly to give the corresponding η^1-allyl compound **2** in reasonable yields (78%) with a *trans* (**2a**)/*cis* (**2b**) ratio of 4/1. Two isomers were separated by chromatographic elution on a silica gel (diethyl ether/hexane, 1/1) column at 0 °C. Chromatographic elution of the mixtures on a silica column at 30 °C led to skeletal rearrangement of the η^1-*trans* isomer **2a** to a π-allyl compound (*vide infra*; Scheme 6).

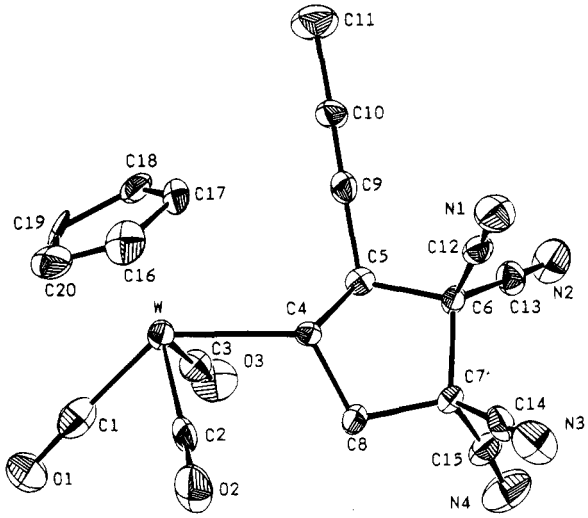

Figure 1. ORTEP drawing of compound **3**.

Table 1. Selected Bond Distances (Å) and Angles (deg) for 3

W–C1	1.919(13)	C6–C12	1.491(15)
W–C2	1.971(10)	C6–C13	1.480(13)
W–C3	1.987(11)	C7–C8	1.567(13)
W–C4	2.318(9)	C7–C14	1.500(14)
C1–O1	1.192(15)	C7–C15	1.455(15)
C2–O2	1.135(13)	C9–C10	1.153(14)
C3–O3	1.143(13)	C10–C11	1.454(15)
C4–C5	1.570(12)	C12–N1	1.118(14)
C4–C8	1.514(13)	C13–N2	1.142(13)
C5–C6	1.564(12)	C14–N3	1.120(14)
C5–C9	1.489(14)	C15–N4	1.128(15)
C6–C7	1.583(12)		
C1–W–C2	75.6(5)	C5–C6–C13	109.2(7)
C1–W–C3	76.9(5)	C7–C6–C12	111.4(7)
C1–W–C4	134.6(4)	C7–C6–C13	113.2(8)
C2–W–C3	107.8(5)	C12–C6–C13	110.0(8)
C2–W–C4	78.2(3)	C6–C7–C8	104.5(7)
C3–W–C4	76.8(4)	C6–C7–C14	112.4(8)
W–C1–O1	177.5(10)	C6–C7–C15	110.9(7)
W–C2–O2	173.4(10)	C8–C7–C14	110.1(7)
W–C3–O3	177.8(9)	C8–C7–C15	111.4(8)
W–C4–C5	119.4(6)	C14–C7–C15	107.6(8)
W–C4–C8	117.7(6)	C4–C8–C7	107.5(7)
C5–C4–C8	99.3(7)	C5–C9–C10	178.6(10)
C4–C5–C6	102.3(6)	C9–C10–C11	178.8(11)
C4–C5–C9	117.7(7)	C6–C12–N1	178.9(10)
C6–C5–C9	110.8(8)	C6–C13–N2	176.9(10)
C5–C6–C7	101.8(7)	C7–C14–N3	176.6(10)
C5–C6–C12	111.0(8)	C7–C15–N4	174.5(12)

The *trans* isomer **2a** retains the chemical reactivity of η^1-allyl compounds[13] and undergoes [3 + 2] cycloaddition with TCNE to give **3** as the major product (67%) with a small amount of **4** (5%) after separation by column chromatography. For **3**, only one stereoisomer was detected in the ^1H NMR spectra ($CDCl_3$), which was assumed to be the *trans* isomer according to the related chemistry of metal η^1-allyl compounds.[12,13] It is difficult to elucidate the stereochemistry from ^1H NOE difference spectra because the ^1H NMR chemical shifts of the four ring protons are close to each other. We determined the structure of **3** by means of X-ray diffraction measurements. Figure 1 shows the ORTEP drawing of **3**, with selected bond distances and angles being provided in Table 1. The ORTEP drawing con-

(10) Wang, S.-H.; Shu, L.-H.; Shu, H.-G.; Liao, Y.-L.; Wang, S.-L.; Lee, G.-H.; Peng, S.-M.; Liu, R.-S. *J. Am. Chem. Soc.* **1994**, *116*, 5967.

(11) Preliminary communication of this paper: Liang, K. W.; Lee, G. H.; Peng, S. H.; Liu, R. S. *J. Chem. Soc., Chem. Commun.* **1994**, 2705.

(12) (a) Gerard, F.; Miginiac, P. *J. Organomet. Chem.* **1978**, *155*, 271. (b) Dulcere, J. P.; Gore, J.; Roumestant, M. L. *Bull. Soc. Chim. Fr.* **1974**, 1119.

(13) (a) Watkins, J. C.; Rosenblum, M. *Tetrahedron Lett.* **1984**, *25*, 2097. (b) Buchester, A.; Klemarczyk, P.; Rosenblum, M. *Organometallics* **1982**, *1*, 1697. (c) Baker, R.; Morris, M. D.; Tunner, R. W. *J. Chem. Soc. Chem. Commun.* **1984**, 987.

Scheme 5[a]

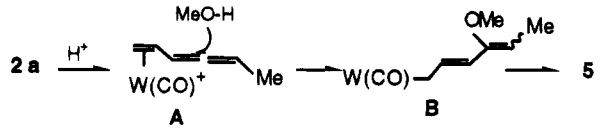

[a] W = $CpW(CO)_2$.

Scheme 6[a]

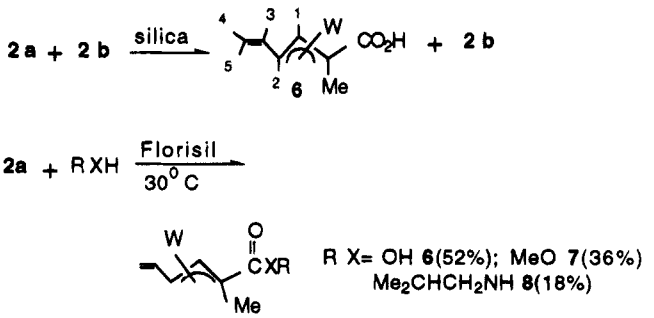

[a] W = $CpW(CO)_2$.

firms the formation of a five-membered ring with the $CpW(CO)_3$ and alkyne groups *trans* to each other. The five carbon–carbon bond distances of the five-membered ring lie within the range 1.489(14)–1.583(12) Å, consistent with single carbon–carbon bonds.

Compound **2a** is prone to hydrolysis to convert its alkyne group to methylene ketone. Treatment of **2a** with CF_3SO_3H (1.1 equiv) in cold diethyl ether (−40 °C) in the presence of excess MeOH delivered the η^1-*trans*-4-oxo-2-hexen-1-yl compound **5** in 65% yield; the reaction was complete within 1 h. During the workup, we did not find any cationic tungsten species as byproducts. In organic chemistry, acid-catalyzed hydration of an organic alkyne to a ketone is practical but requires severe conditions (concentrated H_2SO_4, 23 °C)[14] because the resulting vinyl cation intermediate is not energetically favorable.[15] The rapid hydration at low temperature in the present work is attributed to formation of the η^2-vinylallene cation **A** to further stabilize the resulting vinyl cation. Further attack of MeOH at **A** generates the η^1-4-methoxypenta-2,3-dien-1-yl species **B**, which is expected to give **5** after subsequent acid-catalyzed hydrolysis. Although the allyl group of **2a** reacted well with TCNE, the alkyne group is more reactive toward the proton than the allyl group.

Carbonylation Reaction through a Tandem 1,3-Metal Shift. We attempted first to separate the *cis* and *trans* isomers of **2** on a silica column at 30 °C but obtained the new organometallic compound **6** at the expense of the *trans* isomer; in this case compound **6** and the *cis* isomer **2b** were obtained in 38% and 11% yields, respectively. The fact that **2b** was inactive toward a silica column at 30 °C was confirmed in a separate test. ^{1}H NMR and IR spectra of **6** indicate that the compound has a $CpW(CO)_2(\pi$-allyl) structure with the presence of vinyl, methyl, and carboxylic acid groups. This information revealed a considerable structural rearrangement in the conversion of **2a** to **6**. The molecular structure of **6** was determined by X-ray diffraction measurements, and its ORTEP drawing is

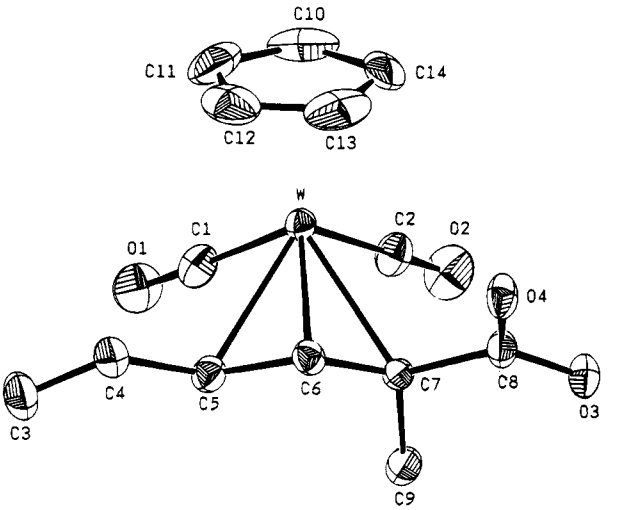

Figure 2. ORTEP drawing of compound **6**.

Table 2. Selected Bond Distances (Å) and Angles (deg) for 6

W–C1	1.959(8)	C4–C5	1.453(11)
W–C2	1.942(8)	C5–C6	1.418(9)
W–C5	2.391(8)	C6–C7	1.399(10)
W–C6	2.206(7)	C7–C8	1.482(9)
W–C7	2.354(7)	C7–C9	1.528(11)
C1–O1	1.140(9)	C8–O3	1.231(9)
C2–O2	1.155(10)	C8–O4	1.307(9)
C3–C4	1.301(11)		
C1–W–C2	80.0(3)	W–C5–C6	65.0(4)
C1–W–C5	72.4(3)	C4–C5–C6	123.5(7)
C1–W–C6	105.5(3)	W–C6–C5	79.3(4)
C1–W–C7	108.6(3)	W–C6–C7	78.0(4)
C2–W–C5	114.7(3)	C5–C6–C7	119.2(6)
C2–W–C6	108.3(3)	W–C7–C6	66.4(4)
C2–W–C7	74.1(3)	W–C7–C8	113.5(5)
C5–W–C6	35.65(23)	W–C7–C9	117.4(4)
C5–W–C7	61.59(24)	C6–C7–C8	119.3(6)
C6–W–C7	35.5(3)	C6–C7–C9	121.0(6)
W–C1–O1	178.4(8)	C8–C7–C9	111.7(6)
W–C2–O2	179.8(7)	C7–C8–O3	121.6(6)
C3–C4–C5	124.5(8)	C7–C8–O4	116.0(6)
W–C5–C4	118.8(6)	O3–C8–O4	122.5(6)

provided in Figure 2, with selected bond distances and angles being given in Table 2. The ORTEP drawing confirms the formation of a tungsten–π-allyl group with the vinyl and COOH groups in *syn* positions and the methyl group in an *anti* position. This structure may be envisaged by considering that one of the three carbonyls of **2a** has been attacked by H_2O to give W–η^1-CO_2H, which subsequently adds to the *C*Me carbon of the ligand; the remaining $CpW(CO)_2$ fragment migrates to the original alkyne fragment to form a π-allyl complex. Compound **6** has an *exo* conformation; i.e. the allyl mouth faces away from the cyclopentadienyl group. The W–C5 (2.391(8) Å), W–C6 (2.206(7) Å), and W–C7 (2.354(7) Å) bond lengths represent normal tungsten–π-allyl distances. The eight atoms including C3–C8, O3, and O4 were quite planar within a maximum deviation of 0.17(1) Å; this orientation is favorable for electron delocalization over the vinyl, carboxylate carbonyl, and allyl fragments.

We examined the carbonylation reaction of **2a** with alcohol and amine. Chromatographic elution of **2a** through a silica column (30 °C) with methanol and isobutylamine is ineffective at inducing carbonylation, and in each case **2a** was recovered exclusively. We found an effective method involving stirring of a THF

(14) (a) Crammer, P.; Tidwell, T. T. *J. Org. Chem.* **1981**, *46*, 2683. (b) Allen, A. D.; Chiang, Y.; Kresge, A. J.; Tidwell, T. T. *J. Org. Chem.* **1982**, *47*, 775.

(15) Kohler, H. J.; Lischka, H. *J. Am. Chem. Soc.* **1979**, *101*, 3479.

Scheme 7[a]

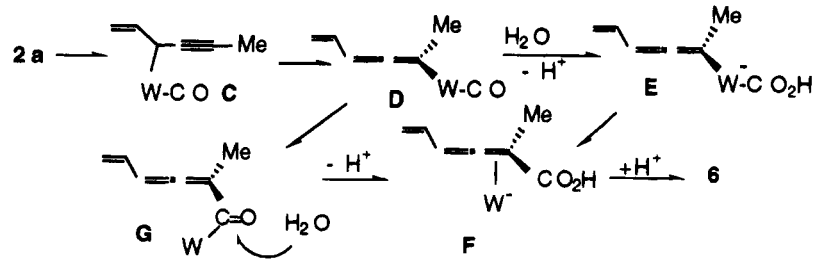

[a] W = $CpW(CO)_2$.

Scheme 8[a]

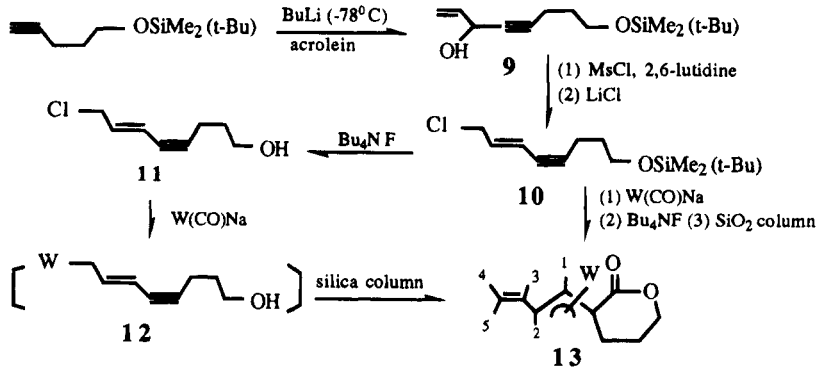

[a] W = $CpW(CO)_2$.

solution of **2a** with H_2O, MeOH, or isobutylamine over predried Florisil (250 °C, 12 h, 10^{-4} Torr) at 30 °C, to give **6**, **7**, and **8** in 52%, 36%, and 18% yields, respectively. The *cis* isomer **2b** was inactive under the same conditions. Spectral data for **7** and **8** are fully consistent with the attributed structure given in Scheme 6.

To account for the formation of **6**, we propose that, with Florisil as catalyst, the $CpW(CO)_3$ fragment of **2a** first undergoes 1,3-allyl migration to give η^1-1-hexen-4-yn-3-yl intermediate **C**, but this intermediate gives a 2-carboxylated allyl compound rather than **6** (*vide supra*; Scheme 2). Further 1,3-$CpW(CO)_3$ migration to the η^1-2,3,5-hexatrien-2-yl species **D** is necessary to achieve alkoxycarbonylation at the *C*Me carbon. Although alkoxycarbonylation of the η^1-allenyl compound has been previously reported, the mechanism was neglected.

In our proposal, formation of **6** is envisaged by considering that one of the three CO groups of **D** is attacked by H_2O to form **E**, which after reductive elimination produces the anion **F**. Further protonation of **F** will give the observed product. To achieve the most stable configuration, the structure is expected to have the COOH and vinyl groups in *syn* positions to minimize interligand steric hindrance. An alternative possibility for the formation of **F** involves insertion of CO into the W–σ-allenyl bond of **D**, followed by H_2O attack as depicted in Scheme 7.

This mechanism (Scheme 7) is operable only in the presence of Florisil and silica gel rather than basic alumina. Silica gel is commonly employed in organic reactions[16] as an acidic catalyst; its function is very specific such that it cannot be replaced by another catalyst.[17] We tested the above carbonylation with some acidic catalysts, including $BF_3{\cdot}Et_2O$, $TiCl_4$, and $ZnCl_2$, but **2a** was recovered exclusively in every case. Although the roles of Florisil and silica gel remain unclear, we believe that the carbonylation is a surface reaction which requires a widely acidic surface area to initiate the reaction.

The *cis* isomer **2b** was inactive toward H_2O, MeOH, and isobutylamine even when Florisil was employed. According to theoretical calculations, the first 1,3-metal shift across the allyl group involves a π-allyl-like intermediate (Scheme 1). Therefore, the inactivity of the *cis* isomer **2b** is attributed to increasing steric hindrance between $CpW(CO)_3$ and the methyl groups of this π-allyl transition structure.

Intramolecular Alkoxycarbonylation though a Tandem 1,3-Metal Shift. To achieve intramolecular carbonylation, we prepared 1-chloro-8-((*tert*-butyldimethylsilyl)oxy)-2-octen-4-yne (**10**; *trans*/*cis* = 5/1) according to Scheme 8. The *trans* isomer of **10** was isolated in pure form (62%) after chromatographic purification. Similar to **2**, the *cis* isomer of **10** is not a useful material for carbonylation. Treatment of **10** with Bu_4NF (2.0 equimolar) in THF at 23 °C for 1 h afforded the alcohol **11** in 57% yield. The reaction of $CpW(CO)_3Na$ and **11** proceeded smoothly under ambient conditions (23 °C, 4 h) to give the η^1-allyl compound **12** as monitored by ^1H NMR spectra. Attempts to purify **12** by chromatographic elution were unsuccessful even at 0 °C, due to its intrinstic tendency to undergo intramolecular cyclization. Therefore, the η^1-allyl intermediate was converted directly to **13** on elution through a silica column at 23 °C; the yield of **13** was 51%. Compound **13** could also be prepared directly from $CpW(CO)_3$ and **10** in THF (23 °C, 3 h), followed by treatment with Bu_4NF (1.8 equiv, 23 °C, 3 h) and column elution (23 °C); the yield was 35%. In the two

(16) (a) Hojo, M.; Masuda, R. *Synth. Commun.* **1975**, *5*, 169. (b) Hojo, M.; Masuda, R. *Tetrahedron Lett.* **1976**, 613.

(17) (a) Regen, S. L.; Koteel, C. *J. Am. Chem. Soc.* **1977**, *99*, 3837. (b) Mckillop, A.; Young, D. W. *Synthesis* **1979**, 401.

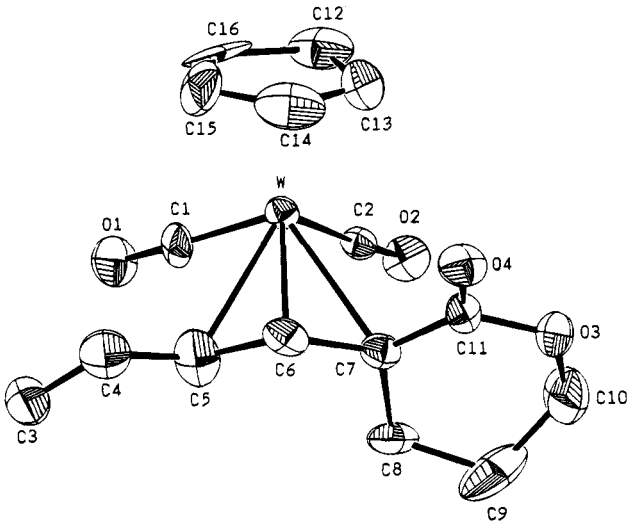

Figure 3. ORTEP drawing of compound **13**.

Table 3. Selected Bond Distances (Å) and Angles (deg) for 13

W–C1	1.934(14)	C5–C6	1.407(21)
W–C2	1.927(12)	C6–C7	1.498(19)
W–C5	2.409(15)	C7–C8	1.514(17)
W–C6	2.224(12)	C7–C11	1.431(17)
W–C7	2.422(13)	C8–C9	1.438(23)
C1–O1	1.166(17)	C9–C10	1.44(3)
C2–O2	1.161(15)	C10–O3	1.375(19)
C3–C4	1.303(23)	C11–O3	1.364(15)
C4–C5	1.392(23)	C11–O4	1.215(16)
C1–W–C2	80.6(5)	W–C6–C5	79.7(8)
C1–W–C5	69.9(5)	W–C6–C7	78.6(7)
C1–W–C6	104.3(5)	C5–C6–C7	118.8(12)
C1–W–C7	114.5(5)	W–C7–C6	64.1(6)
C2–W–C5	109.8(5)	W–C7–C8	118.4(9)
C2–W–C6	110.3(5)	W–C7–C11	107.6(8)
C2–W–C7	76.6(5)	C6–C7–C8	119.3(11)
C5–W–C6	35.1(5)	C6–C7–C11	113.1(11)
C5–W–C7	62.3(5)	C8–C7–C11	120.9(12)
C6–W–C7	37.3(5)	C7–C8–C9	109.2(12)
W–C1–O1	177.7(12)	C8–C9–C10	115.8(14)
W–C2–O2	178.2(10)	C9–C10–O3	113.0(14)
C3–C4–C5	122.9(17)	C7–C11–O3	117.9(11)
W–C5–C4	122.9(12)	C7–C11–O4	127.8(12)
W–C5–C6	65.3(8)	O3–C11–O4	114.3(11)
C4–C5–C6	123.1(15)	C10–O3–C11	120.1(11)

reactions above, we obtained no η^3-allyl acid compound from the intermolecular carboxylation of **12** with water from silica. The latter is slower than intramolecular alkoxycarbonylation reactions.

The molecular structure of **13** is presented in Figure 3, with selected bond distances and angles being provided in Table 3. Similar to **6**, compound **13** has an *exo* conformation with the allyl mouth opposite the cyclopentadienyl group; the vinyl and lactonyl carbonyl groups are in *syn* positions with respect to the allyl group. The six-membered lactone ring approaches a distorted-boat conformation with the C11–O4 (1.215(16) Å) and C11–O3 (1.364(15) Å) lengths representing carbon–oxygen double and single bonds, respectively. The allyl C5–C6 (1.407(21) Å) and C6–C7 (1.498(19) Å) bond lengths are asymmetric, whereas the C4–C5 length (1.392(23) Å) is significantly shorter than that of a normal carbon–carbon length (1.54 Å). This information demonstrates electron delocalization between the vinyl and allyl groups. The dihedral angles defined by the C7–C11–O4/allyl planes and C3–C4–C5/allyl planes are 13.7(15) and 19.5(19)°, respectively, indicative of electron delocalization through the C3–C11 and O4 unsaturated fragment.

BF_3-Promoted Addition of Aldehydes and Enones to 7. These alkoxycarbonylation products belong to the class of η^3-pentadienyl compounds; they are expected to be reactive toward electrophiles in the presence of a Lewis acid.[18,19] To demonstrate its synthetic utility, as shown in Scheme 9, we treated compound **7** with aldehydes RCHO (R = Ph, Me_2CH; 1.5 equiv) in the presence of $BF_3{\cdot}Et_2O$ (1.0 equiv) in cold diethyl ether, yielding an orange insoluble precipitate, presumably the η^4-diene salts **G**.[19,20] The salts were unstable above −40 °C, and organic compounds **14** and **15** were gradually liberated. Spectral characterization of the salts was unsuccessful due to their thermal instability. Complete demetalation of the salts was achieved with Me_3NO to liberate organic compounds **14** and **15** in 56% and 50% yields, respectively. The reactions between **7** and enones $RCOCH{=}CH_2$ (R = Me, Et) under the same conditions proceeded smoothly to give analogous diene salts **H**, which after demetalation gave ketone compounds **16** and **17** in 42% and 40% yields, respectively.

Experimental Section

All operations were carried out under argon in a Schlenk apparatus or in a glovebox. The solvents benzene, diethyl ether, tetrahydrofuran, and hexane were dried with sodium benzophenone and distilled before use. Dichloromethane was dried over calcium hydride and distilled. Organic ligands **1** and 5-((*tert*-butyldimethylsilyl)oxy)-1-pentyne were prepared according to the procedures in the literature.[21]

All ^1H NMR (400 and 300 Hz) and ^{13}C NMR (100 and 75 MHz) spectra were obtained on either a Bruker AM-400 or a Varian Gemini-300 spectrometer; the chemical shifts of ^1H and ^{13}C NMR are reported relative to tetramethylsilane (δ 0 ppm). Elemental analyses were performed at National Cheng Kung University, Tainan, Taiwan, Republic of China. Infrared spectra were recorded on a Perkin-Elmer 781 spectrometer. High-resolution mass spectra were recorded on a JEOL HX 110 spectrometer.

(a) Synthesis of $CpW(CO)_3(\eta^1$-hex-2-en-4-yn-1-yl) (2a (*trans* Isomer) and 2b (*cis* Isomer). To a THF solution (100 mL) of $W(CO)_6$ (5.0 g, 14.4 mmol) was added NaC_5H_5 (C_5H_6 (0.94 g, 14.2 mmol), Na (0.34 g, 14.4 mmol), THF (20 mL)), and the mixtures were heated under reflux for 3 days. To the yellow $CpW(CO)_3Na$ solution was added 1-chlorohex-2-en-4-yne (1.65 g, 14.5 mmol) at 0 °C, and the solution was stirred for 4 h before being warmed to 23 °C. After it was stirred for an additional 3 h at 23 °C, the solution was evaporated to dryness; the residues were eluted through a silica column at 0 °C with diethyl ether/hexane (1/2) as the eluting solvent. Two yellow bands were developed and collected to give **2a** (*trans* isomer; R_f = 0.65, yellow solid, 3.68 g, 8.90 mmol) and **2b** (*cis* isomer; R_f = 0.57, yellow oil, 0.95 g, 2.30 mmol, 16%), respectively.

Data for **2a:** IR (neat, cm^{-1}) ν(C≡C) 2189 (w), ν(CO) 2009 (s), 1914 (s), ν(C=C) 1635 (w); ^1H NMR (400 MHz, $CDCl_3$) δ 1.86 (d, J = 2.1 Hz, 3H, Me), 2.35 (d, 2H, J = 8.8 Hz, $W{-}CH_2$), 5.13 (dq, 1H, J = 15.2, 2.1 Hz, $=CHC{\equiv}$), 5.33 (s, 5H, Cp), 6.28 (dt, J = 15.2, 8.8 Hz, 1H, $W{-}CH_2CH{=}$); ^{13}C NMR (100 MHz, $CDCl_3$) δ −7.6 ($W{-}CH_2$), 4.4 (Me), 79.1 and 88.4 (C≡C), 92.4

(18) Lin, S. H.; Yang, Y. J.; Liu, R. S. *J. Chem. Soc., Chem. Commun.* **1991**, 1004.
(19) Cheng, M.-H.; Yang, G. M.; Chow, J. F.; Lee, G. H.; Peng, S. M.; Liu, R. S. *J. Chem. Soc., Chem. Commun.* **1992**, 934.
(20) Cheng, M. H.; Ho, Y. H.; Wang, S. L.; Peng, S. M.; Liu, R. S. *J. Chem. Soc. Chem. Commun.* **1992**, 45.
(21) Corey, E. J.; Venkateswarlu, A. *J. Am. Chem. Soc.* **1972**, *94*, 6190.

Scheme 9[a]

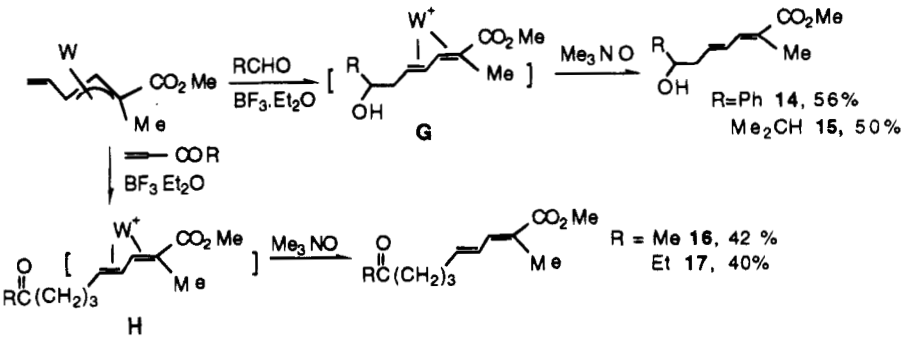

[a] W = $CpW(CO)_2$.

(Cp), 114.6 (=$CHCH_2$), 151.3 (=$CHC\equiv$), 216.7 and 228.1 (3 W—CO); mass (75 eV, *m/e*) 384 (M^+ − CO), 356 (M^+ − 2CO). Anal. Calcd for $C_{14}H_{12}WO_3$: C, 40.80; H, 2.94. Found: C, 40.48; H, 2.95.

Data for **2b:** IR (Nujol, cm^{-1}) ν(C≡C) 2179 (w), ν(CO) 2004 (s), 1920 (s), ν(C=C) 1631 (w); IR (neat, cm^{-1}) ν(CO) 2008 (s), 1918 (s); ^1H NMR (300 MHz, $CDCl_3$) δ 2.04 (d, J = 2.1 Hz, 3H, Me), 2.60 (d, J = 9.1 Hz, 2H, W—CH_2), 5.00 (dq, J = 10.4, 2.1 Hz, 1H, =C*H*C≡), 5.48 (s, 5H, Cp), 6.33 (dt, 1H, J = 10.4, 9.1 Hz, =C*H*CH_2); ^{13}C NMR (75 MHz, $CDCl_3$) δ −9.8 (W—CH_2), 4.7 (Me), 90.6 and 91.2 (C≡C), 92.4 (Cp), 100.6 (=*C*HCH_2), 151.6 (d, =*C*HC≡), 217.1 and 228.3 (3 W—CO); mass (75 eV, *m/e*) 384 (M^+ − CO), 356 (M^+ − 2CO). Anal. Calcd for $C_{14}H_{12}WO_3$: C, 40.80; H, 2.94. Found: C, 40.51; H, 3.02.

(b) Cycloaddition of 2a with TCNE. To **2a** (0.18 g, 0.45 mmol) in THF (5 mL) was slowly added a THF solution (3 mL) of TCNE (58 mg, 0.45 mmol) at 0 °C. After the mixture was stirred for 30 min, the resulting green solution was brought to dryness and chromatographed through a silica column with diethyl ether/hexane (1/1) as the eluting solvent. Two bands were developed and collected to give **3** (R_f = 0.42, yellow solid, 0.16 g, 0.30 mmol, 67%) and **4** (R_f = 0.21, red solid, 12 mg, 0.023 mmol, 5%), respectively.

Data for **3:** IR (Nujol, cm^{-1}) ν(C≡C) 2179 (w), ν(CN) 2250 (s), ν(CO) 2022 (s), 1919 (s); ^1H NMR (400 MHz, $CDCl_3$) δ 1.95 (d, J = 2.2 Hz, 3H, Me), 2.65 (dd, J = 14.1, 12.3 Hz, 1H, C*H*H′), 2.86 (ddd, J = 12.3, 12.0, 8.2 Hz, 1H, W—C*H*), 3.11 (dd, J = 14.1, 8.2 Hz, 1H, CH*H*′), 3.45 (dq, J = 12.0, 2.2 Hz, 1H, C*H*C≡C), 5.66 (s, 5H, Cp); ^{13}C NMR (100 MHz, $CDCl_3$) δ 1.4 (W—CH), 3.8 (Me), 45.0 and 52.6 (2 *C*—CN), 53.4 (CHH′), 55.9 (*C*HC≡), 73.5 and 87.3 (C≡C), 91.6 (Cp), 110.2 (CN), 110.5 (CN), 111.3 (CN), 111.5 (CN), 216.4 (W—CO), 216.6 (W—CO), 223.9 (W—CO). Anal. Calcd for $C_{22}H_{12}N_4WO_3$: C, 46.81; H, 2.14; N, 9.93. Found: C, 46.95; H, 2.08; N, 9.65.

Data for **4**: IR (neat, cm^{-1}) ν(CN) 2220 (m), ν(CO) 2019 (s), 1922 (s); ^1H NMR (300 MHz, C_6D_6) δ 1.05 (s, 3H, Me), 1.92 (d, J = 9.5 Hz, 2H, W—CH_2), 4.33 (s, 5H, Cp), 6.14 (d, J = 15.0 Hz, 1H, =C*H*C≡), 6.44 (dt, J = 15.0, 9.5 Hz, 1H, CH_2C*H*=). Anal. Calcd for $C_{22}H_{12}N_4WO_3$: C, 46.81; H, 2.14; N, 9.93. Found: C, 46.99; H, 2.23; N, 9.91. Attempts to record ^{13}C NMR spectra in d_8-toluene were unsuccessful due to the poor solubility and solution instability of **4** at 25 °C.

(c) Synthesis of $CpW(CO)_3$(η^1-*trans*-4-oxo-2-hexen-1-yl) (5). To a solution of **2a** (0.18 g, 0.45 mmol) in diethyl ether/CH_3OH (6 mL/3 mL) was added CF_3SO_3H (0.40 mL, 0.45 mmol) at −40 °C, and the solution was stirred for 1 h at the same temperature before addition of a saturated $NaHCO_3$ solution. The solution was concentrated to half its volume, and the organic layer was extracted with diethyl ether (2 × 10 mL). The residue was eluted through a silica column to produce a yellow band that yielded **5** as a yellow oil (0.12 g, 0.28 mmol, 61%). IR (neat, cm^{-1}) ν(CO) 2004 (s), 1924 (s), 1668 (s), ν(C=C) 1625 (m); ^1H NMR (400 MHz, $CDCl_3$) δ 1.05 (t, J = 7.2 Hz, 3H, Me), 2.36 (d, J = 8.1 Hz, 2H, W—CH_2), 2.48 (q, J = 7.2 Hz, 2H, $COCH_2$), 5.33 (s, 5H, Cp), 5.80 (d, J = 15.0 Hz, 1H, =CHCO), 7.13 (dt, J = 15.0, 8.1 Hz, 1H, CH_2C*H*=); ^{13}C NMR (100 MHz, $CDCl_3$) δ −8.9 (W—CH_2), 8.6 (CH_3), 33.6 ($COCH_2$), 92.1 (Cp), 121.7 (=*C*HCO), 156.6 (CH_2CH=), 200.9 (CO), 216.7 and 228.1 (3 W—CO); mass (75 eV, *m/e*) 402 (M^+ − CO). Anal. Calcd for $C_{14}H_{14}WO_4$: C, 39.07; H, 3.28. Found: C, 39.15; H, 3.35.

(d) Synthesis of $CpW(CO)_2$(η^3-1-*syn*-carboxy-1-*anti*-methyl-3-*syn*-vinylallyl) (6). Method A. A crude mixture of **2a** and **2b** (2.00 g, 4.80 mmol, **2a/2b** = 4/1) was chromatographed through a silica column at 30 °C with diethyl ether/hexane (1/2) as eluent. A yellow band was collected to produce **2b** (R_f 0.57) as a yellow oil (0.23 g, 0.53 mmol, 11%). After **2b** was eluted, the top immobile band was eluted with diethyl ether/hexane (2/1) to give a dark yellow band (R_f 0.31) that afforded **6** as a yellow solid (0.78 g, 1.82 mmol, 38%).

Method B. Florisil (8.5 g) was heated in vacuo (250 °C, 1.0×10^{-4} Torr) for 12 h, and this solid was treated with THF (20 mL) and H_2O (0.50 mL) after it was cooled to 23 °C. To this THF—Florisil mixture was added a THF solution (15 mL) of **2a** (0.25 g, 0.60 mmol); the resulting solution was stirred at 30 °C for 1 h. After removal of the solvent, the wet Florisil solid was placed on top of a silica column immersed with hexane. The column was first eluted with diethyl ether/hexane (1/2) to remove impurities and subsequently eluted with diethyl ether/hexane (2/1) to produce a dark yellow band of **6** (0.78 g, 1.82 mmol, 38%). IR (Nujol, cm^{-1}) ν(OH) 3300−2700 (br, s), ν(CO) 1932 (s), 1876 (s), 1652 (s), ν(C=C) 1625 (w); ^1H NMR (400 MHz, $CDCl_3$) δ 1.30 (s, 3H, Me), 3.10 (t, J = 10.0 Hz, 1H, H^2), 4.83 (d, J = 10.0 Hz, 1H, H^1), 4.89 (d, J = 10.0 Hz, 1H, H^4), 5.38 (d, J = 16.8 Hz, 1H, H^5), 5.41 (s, 5H, Cp), 5.83 (dt, J = 16.8, 10.0 Hz, 1H, H^3); ^{13}C NMR (100 MHz, $CDCl_3$) δ 16.7 (Me), 45.5 (*C*Me), 56.7 (CH^2), 67.2 (CH^1), 93.7 (Cp), 138.5 (=CH^3), 143.4 (=CH^4), 181.3 (C=O), 227.1 and 226.5 (2 W—CO); mass (75 eV, *m/e*) 430 (M^+), 402 (M^+ − CO), 374 (M^+ − 2CO). Anal. Calcd for $C_{14}H_{14}WO_4$: C, 39.10; H, 3.28. Found: C, 39.11; H, 3.35.

(e) Synthesis of $CpW(CO)_2$(η^3-1-*syn*-(methoxycarbonyl)-1-*anti*-methyl-3-*syn*-vinylallyl) (7). This compound was prepared from **2a** and MeOH over Florisil according to synthetic procedures described in method B for compound **6**; the yield of **7** was 36%: IR (neat, cm^{-1}) ν(CO) 1942 (s), 1860 (s), 1685 (m), ν(C=C) 1625 (w); ^1H NMR (300 MHz, $CDCl_3$) δ 1.28 (s, 3H, Me), 3.03 (t, J = 10.0 Hz, 1H, H^2), 3.66 (s, 3H, OMe), 4.82 (d, J = 10.0 Hz, 1H, H^4), 4.86 (d, J = 10.0 Hz, 1H, H^1), 5.37 (s, 5H, Cp), 5.36 (d, J = 16.2 Hz, 1H, H^5), 5.84 (dt, 1H, J = 16.2, 10.0 Hz, H^3); ^{13}C NMR (75 MHz, $CDCl_3$) δ 16.7 (Me), 46.6 (CCH_3), 51.8 (OMe), 56.2 (CH^2), 66.6 (CH^1), 93.4 (Cp), 112.9 (=CH^4H^5), 138.7 (=CH^3), 176.0 (C=O), 227.2 and 226.6 (2 W—CO); mass (75 eV) 444 (M^+), 416 (M^+ − CO), 388 (M^+ − 2CO). Anal. Calcd for $C_{15}H_{16}WO_4$: C, 40.57; H, 3.63. Found: C, 40.67; H, 3.62.

(f) Synthesis of $CpW(CO)_2$(η^3-1-*syn*-((isobutylamino)-carbonyl)-1-*anti*-methyl-3-*syn*-vinylallyl) (8). This compound was prepared from **2a** and isobutylamine over Florisil according to synthetic procedures described in method **B** for compound **6**; the yield of **8** was 18%: IR (Nujol, cm^{-1}) ν(NH) 3363 (m), ν(CO) 1935 (s), 1853 (s), 1630 (s); ^1H NMR (300 MHz,

$CDCl_3$) δ 0.91 (d, 6H, J = 6.6 Hz, 2 Me), 1.24 (s, 3H, Me), 1.77 (m, 1H, C*H*Me_2), 2.89 (t, 1H, J = 9.8 Hz H^2), 3.06 (m, 2H, NHC*HH'*), 4.82 (d, J = 9.8 Hz, 1H, H^1), 4.97 (d, J = 10.0 Hz, 1H, H^4), 5.37 (s, 5H, Cp), 5.35 (d, J = 16.8 Hz, 1H, H^5), 5.84 (ddd, J = 16.8, 10.0, 9.8 Hz, 1H, H^3); ^{13}C NMR (75 MHz, $CDCl_3$) δ 17.0 (Me), 19.9 (Me), 20.2 (Me), 28.5 (*C*HMe_2), 47.2 (NH—*C*H_2), 50.3 (*C*C=O), 55.4 (CH^2), 65.1 (CH^1), 93.7 (Cp), 112.5 (=CH^4H^5), 139.1 (=CH^3), 173.8 (C=O), 226.7 and 230.3 (2 W—CO); mass (75 eV, *m/e*) 485 (M^+), 457 (M^+ − CO), 429 (M^+ − 2CO). Anal. Calcd for $C_{18}H_{22}WO_3N$: C, 44.65; H, 4.58; N, 2.88. Found: C, 44.48; H, 4.86; N, 3.01.

(g) Synthesis of 3-Hydroxy-8-((*tert*-butyldimethylsilyl)oxy)-1-octen-4-yne (9). To 5-((*tert*-butyldimethylsilyl)-oxy)-1-pentyne (9.0 g, 48.0 mmol) in THF was added BuLi (2.50 M, 19.2 mL, 48.0 mmol) at −78 °C, and the mixture was stirred for 2 h before it was transferred to a THF (10 mL) solution of acrolein (3.40 g, 60.0 mmol) at −40 °C. After it was stirred for 2 h, the solution was quenched with a saturated NH_4Cl solution, concentrated, and extracted with diethyl ether (2 × 30 mL). The extract was concentrated, and flash chromatography (silica column, 1/1 diethyl ether/hexane) of the residues afforded **9** as a colorless oil (10.9 g, 45.1 mmol, 94.0%): IR (neat, cm^{-1}) ν(C≡C) 2128 (w), ν(C=C) 1645 (w); ^1H NMR (300 MHz, $CDCl_3$) δ 0.05 (s, 6H, Si*Me*$_2$), 0.86 (s, 9H, Si*Me*$_3$), 1.69 (m, 2H, *C*H_2 CH_2OSi), 1.93 (s, 1H, OH), 2.30 (t, J = 6.7 Hz, 2H, ≡CC*H*$_2$), 3.65 (t, J = 6.0 Hz, 2H, CH_2OSi), 4.82 (dd, J = 5.4, 1.9 Hz, 1H, C*H*OH), 5.16 (d, J = 10.1 Hz, 1H, =C*H*H'), 5.40 (d, J = 17.0 Hz, 1H, =CH*H'*), 5.95 (ddd, J = 17.0, 10.1, 5.4 Hz, 1H, =C*H*); ^{13}C NMR (75 MHz, $CDCl_3$) δ −5.4 (SiMe), 15.2 (CH_2), 18.3 (Si*C*Me_3), 25.9 (SiC*Me*$_3$), 31.7 (*C*H_2CH_2OSi), 61.6 (CH_2OSi), 63.4 (CHOH), 86.8 and 79.1 (C≡C), 115.9 (=CH_2), 137.4 (=CH). Anal. Calcd for $C_{14}H_{26}SiO_2$: C, 66.10; H, 10.31. Found: C, 66.08; H, 10.40.

(h) Synthesis of 1-Chloro-8-((*tert*-butyldimethylsilyl)-oxy)-2-octen-4-yne (10). To a mixture of **9** (2.24 g, 8.80 mmol) and 2,6-lutidine (2.10 mL, 13.2 mmol) was added a DMF solution (50 mL) containing LiCl (0.38 g, 8.80 mmol), and the mixture was stirred at 0 °C for 0.5 h before methanesulfonyl chloride (1.48 mL, 13.2 mmol) was added. After it was stirred for 20 min at 0 °C, the solution was heated at 80 °C for 10 min, cooled to 23 °C and then added to diethyl ether (150 mL) and water (50 mL). The organic layer was separated, washed with water (3 × 30 mL), and dried over $MgSO_4$. Removal of the solvent in vacuo afforded **10** as an oil (2.30 g, 8.40 mmol, *trans/cis* = 5/1). Chromatographic elution of the crude product through a silica column (diethyl ether/hexane, 1/5) yielded the desired *trans* isomer as a colorless oil (1.5 g, 5.50 mmol, 62%). Data for the *trans* isomer: IR (neat, cm^{-1}) ν(C≡C) 2158 (w), ν(C=C) 1639 (w); ^1H NMR (300 MHz, $CDCl_3$) δ 0.05 (s, 6H, Si*Me*$_2$), 0.89 (s, 9H, SiC*Me*$_3$), 1.72 (m, 2H, *C*H_2CH_2OSi), 2.30 (t, J = 6.5 Hz, 2H, ≡CCH_2), 3.65 (t, J = 6.0 Hz, 2H, CH_2OSi), 4.07 (d, J = 6.6 Hz, 2H, $ClCH_2$), 5.75 (d, J = 17.0 Hz, 1H, =CHC≡), 6.14 (dt, J = 17.0, 6.6 Hz, 1H, =C*H*CH_2Cl); ^{13}C NMR (75 MHz, $CDCl_3$) δ −5.4 (SiMe), 15.8 (≡*C*CH_2), 18.3 (Si*C*$(CH_3)_3$), 25.9 (SiC*Me*$_3$), 31.5 (*C*H_2CH_2OSi), 44.2 (CH_2Cl), 61.6 (CHOSi), 92.6 and 90.6 (C≡C), 114.7 (=*C*HCH_2Cl), 137.4 (=*C*HC≡). Anal. Calcd for $C_{14}H_{25}SiClO$: C, 61.73; H, 9.26. Found: C, 61.80; H, 9.30.

(i) Synthesis of 1-Chloro-8-hydroxy-2-octen-4-yne (11). To a THF (10 mL) solution of **10** (1.50 g, 5.50 mmol) was added Bu_4NF (2.87 g, 11.0 mmol), and the mixture was stirred at 1 h at 23 °C before addition of a saturated NaCl solution (10 mL). The organic layer was extracted with diethyl ether (3 × 20 mL), dried over $MgSO_4$, and concentrated in vacuo. Flash chromatography of the residues afforded **11** as a colorless oil (0.50 g, 3.14 mmol, 57%): IR (neat, cm^{-1}) ν(C≡C) 2158 (w), ν(C=C) 1639 (w); ^1H NMR (300 MHz, $CDCl_3$) δ 1.72 (m, 2H, *C*H_2CH_2OH), 1.84 (br s, 1H, OH), 2.30 (t, J = 6.5 Hz, 2H, C≡C*C*H_2), 3.65 (t, J = 6.0 Hz, 2H, *C*H_2OH), 4.07 (d, J = 6.6 Hz, 2H, *C*H_2Cl), 5.75 (d, J = 17.0 Hz, 1H, =*C*HC≡), 6.14 (dt, 1H, J = 17.0, 6.6 Hz, =C*H*CH_2Cl); ^{13}C NMR (75 MHz, $CDCl_3$) δ 15.8 (≡*C*CH_2), 31.5 (*C*H_2CH_2O), 44.0 (CH_2Cl), 61.2 (CHOH), 92.1 and 90.6 (C≡C), 114.5 (=*C*HCCl), 136.0 (=*C*HC≡); HRMS calcd for $C_8H_{11}ClO$ 158.0498, found 158.0503.

(j) Synthesis of 13. Method A. To a THF (30 mL) solution of $CpW(CO)_3Na$ (ca. 2.80 mmol) was added **11** (0.40 g, 2.84 mmol) at 23 °C; the mixture was stirred for 4 h. Sampling of the solution (ca. 5 mL) for NMR measurement (300 MHz, $CDCl_3$) showed the presence of the η^1-allyl compound **12** (δ 2.14, J = 7.0 Hz, W—CH_2). The solution was evaporated to dryness and chromatographed through a silica column (diethyl ether/hexane, 1/1) at 23 °C to produce an orange band (R_f 0.48) of **13** (0.65 g, 1.43 mmol, 51%): IR (neat, cm^{-1}) ν(CO) 1947 (s), 1866 (s), 1695 (s), ν(C=C) 1625 (m); ^1H NMR (400 MHz, $CDCl_3$) δ 1.94−1.49 (m, 4H, *C*$H_2CH_2CH_2O$), 3.19 (t, 1H, J = 10.1 Hz, H^2), 4.41−4.18 (m, 2H, *C*$HH'O$), 4.82 (d, J = 10.1 Hz, 1H, H^1), 5.03 (d, J = 10.1 Hz, 1H, H^4), 5.28 (d, J = 16.6 Hz, 1H, H^5), 5.36 (s, 5H, Cp), 5.84 (dt, 1H, J = 16.6, 10.1 Hz, H^3); ^{13}C NMR (100 MHz, $CDCl_3$) δ 23.5 (CH_2), 27.9 (CH_2), 44.6 (*C*CO), 57.7 (CH^2), 66.8 (CH^1), 71.8 (CHH'O), 94.2 (Cp), 113.9 (=CH^4H^5), 138.2 (=CH^3), 175.6 (CO_2), 231.8 and 227.1 (2 W—CO); mass (75 eV, *m/e*): 456 (M^+), 418 (M^+ − CO), 390 (M^+ − 2CO). Anal. Calcd for $C_{16}H_{16}WO_4$: C, 42.13; H, 3.54. Found: C, 42.17; H, 3.55.

Method B. To a THF (40 mL) solution of $CpW(CO)_3Na$ (ca. 10 mmol) was slowly added **10** (2.72 g, 10 mmol), and the resulting solution was stirred for 3 h at 23 °C before evaporation to dryness. The residues were extracted with diethyl ether (15 mL) and then added to a wet THF solution (30 mL) of Bu_4NF (4.70 g, 18 mmol). The mixture was stirred at 23 °C for 4 h, dried in vacuo, and finally chromatographed through a silica column to yield **13** as an orange solid (1.46 g, 3.5 mmol, 35%).

(k) Synthesis of Methyl 7-Phenyl-7-hydroxy-2-methyl-(*E,E*)-2,4-heptadienate (14). To **7** (0.10 g, 0.23 mmol) in toluene (7 mL) was added benzaldehyde (50 mg, 0.67 mmol) at −60 °C and then $BF_3{\cdot}Et_2O$ (0.050 mL, 0.39 mmol). The mixture was stirred at −60 °C for 5 h to produce a red glassy solid. The toluene was decanted, and to the red residue was added CH_2Cl_2 (5 mL) at −60 °C. To this solution was added Me_3NO (0.10 g, 1.30 mmol), and the mixture was stirred for 1 h at −60 °C before the temperature was raised to 23 °C. After it was stirred for an additional 7 h, the solution was concentrated, and the residues were chromatographed through a preparative TLC plate to afford **14** as an oil (31 mg, 0.13 mmol, 56%): IR (Nujol, cm^{-1}) ν(OH) 3422 (br, s), ν(C=O) 1700 (s), ν(C=C) 1638 (m); ^1H NMR (400 MHz, $CDCl_3$) δ 1.65 (s, 3H, Me), 2.59 (t, 2H, J = 7.2 Hz, *C*H_2CHOH), 3.66 (s, 3H, OMe), 4.72 (t, J = 6.2 Hz, 1H, C*H*OH), 5.98 (dt, 1H, J = 15.0, 7.2 Hz, =C*H*CH_2), 6.38 (dd, 1H, J =15.0, 11.5 Hz, =C*H*), 7.08 (d, 1H, J = 11.5 Hz, C*H*=CMe), 7.27 (s, 5H, Ph); ^{13}C NMR (100 MHz, $CDCl_3$) δ 12.6 (=C*Me*), 43.0 (*C*H_2CHOH), 51.8 (OMe), 73.6 (CHOH), 126.1 (*C*CO_2Me), 127.8 (=*C*HCH_2), 137.7 (*C*H=CMe), 138.7 (=*C*H), 125.8 (Ph), 128.6 (Ph), 128.9 (Ph), 143.6 (Ph), 168.9 (C=O); HRMS calcd for $C_{15}H_{18}O_3$: 246.1256, found 246.1253.

(l) Synthesis of Methyl 7-Hydroxy-2,8-dimethyl-(*E,E*)-2,4-nonadienate (15). This compound was similarly prepared from **7**, isobutyraldehyde, and $BF_3{\cdot}Et_2O$ in cold toluene according to the method described in section k; the yield of **15** was 50%: IR (neat, cm^{-1}) ν(OH) 3452 (br), ν(C=O) 1703 (s), ν(C=C) 1638 (m); ^1H NMR (400 MHz, $CDCl_3$) δ 0.90 (d, J = 5.1 Hz, 6H, C*H*Me_2), 1.64 (m, 1H, C*H*Me_2), 1.67 (s, 3H, Me), 2.28 (m, 2H, =CHC*HH'*), 3.36 (dt, J = 6.2, 5.0 Hz, 1H, C*H*OH), 3.69 (s, 3H, OCH_3), 6.05 (dt, J = 15, 5.6 Hz, 1H, =C*H*CH_2), 6.38 (dd, J = 15.0, 11.5 Hz, 1H, =C*H*—), 7.12 (d, J = 11.2 Hz, 1H, C*H*=CMe); ^{13}C NMR (100 MHz, $CDCl_3$) δ 12.6 (=C*Me*), 17.3 and 18.7 (CH*Me*$_2$), 33.2 (*C*HMe_2), 38.2 (=CH*C*H_2), 51.8 (OMe), 75.8 (CHOH), 125.8 (*C*CO_2Me), 128.2 (=CH), 138.2 (*C*H=CMe), 139.0 (=*C*H), 169.0 (C=O); HRMS calcd for $C_{12}H_{21}O_3$ 213.1490, found 213.1486.

(m) Synthesis of Methyl 2-Methyl-9-oxo-2,4-decadienate (16). This compound was similarly prepared from **7**, methyl vinyl ketone, and $BF_3{\cdot}Et_2O$ in cold toluene according

Table 4. Crystal Data and Conditions for Crystallographic Data Collection and Structure Refinement for 3, 6, and 13

	6	13	3
formula	$WO_4C_{14}H_{14}$	$WO_4C_{16}H_{16}$	$WC_{20}H_{12}N_4O_3$
FW	430.11	456.15	540.18
diffractometer used	Nonius	Nonius	Nonius
space group	monoclinic, $P2_1/n$	orthorhombic, $P2_12_12_1$	orthorhombic, $Pbca$
a (Å)	7.759(3)	6.830(4)	8.066(5)
b (Å)	14.201(5)	11.862(4)	25.917(6)
c (Å)	12.638(3)	18.122(8)	18.618(4)
β (deg)	101.074(24)		
V (Å^3)	1366.5(8)	1468.1(12)	3892(3)
Z	4	4	8
D_{calc} (g cm^{-3})	2.091	2.064	1.844
λ (Å)	0.7107	0.7107	0.7107
$F(000)$	816	892	2056
unit cell detn: no. (2θ range (deg))	25 (18.60−32.44)	25 (15.90−24.00)	25 (16.68−28.52)
scan type	$\theta/2\theta$	$\theta/2\theta$	$\theta/2\theta$
scan width (deg)	$2(0.65 + 0.35 \tan \theta)$	$2(0.80 + 0.35 \tan \theta)$	$2(0.75 + 0.35 \tan \theta)$
scan speed (deg min^{-1})	2.06−8.24	2.06−8.24	2.06−8.24
2θ(max) (deg)	50.0	50.0	45.0
hkl ranges	−9 to +9; 0−16; 0−15	0−8; 0−14; 0−21	0−8; 0−27; 0−20
μ (cm^{-1})	86.399	80.508	60.885
cryst size (mm)	0.40 × 0.50 × 0.60	0.05 × 0.10 × 0.35	0.30 × 0.40 × 0.45
transmissn	0.340; 1.000	0.914; 1.000	0.439; 1.000
temp (K)	298.00	298.00	298.00
no. of meas rflns	2390	1503	2541
no. of obs rflns ($I > 2.0\sigma(I)$)	2087	1333	1728
no. of unique rflns	2390	1503	2541
R_F; R_w[a]	0.032; 0.036	0.032; 0.032	0.032; 0.020
GOF[b]	2.88	1.55	1.59
refinement program	NRCVAX	NRCVAX	NRCVAX
no. of atoms	33	37	40
no. of refined params	193 (2087 out of 2390 rflns)	191 (1333 out of 1503 rflns)	253 (1728 out of 2541 rflns)
minimize function	$\Sigma(w\|F_o - F_c\|^2)$	$\Sigma(w\|F_o - F_c\|^2)$	$\Sigma(w\|F_o - F_c\|^2)$
wt scheme	$1/\sigma^2(F_o)$	$1/\sigma^2(F_o)$	$1/\sigma^2(F_o)$
wt modifier K (in KF_o^2)	0.000 040	0.000 070	0
g (2nd ext coeff) × 10^4	1.21(3)	2.67(25)	0
Δ/σ (max)	0.077	0.0508	0.0119
D-map (max; min) (e/Å^3)	−1.770; 1.810	−0.860; 1.560	−0.860; 1.010

[a] $R_F = \Sigma(F_o - F_c)/\Sigma(F_o)$; $R_w = [\Sigma(w(F_o - F_c)^2)/\Sigma(wF_o^2)]^{1/2}$. [b] GOF = $[\Sigma(w(F_o - F_c)^2)/((\text{no. of rflns}) - (\text{no. of params})]^{1/2}$.

to the method described in section k; the yield of **16** was 42%: IR (neat, cm^{-1}) ν(C=O) 1709 (s), ν(C=C) 1639 (m), 1610 (m); ^{1}H NMR (400 MHz, $CDCl_3$) δ 1.77 (m, 2H, CH_2), 1.90 (s, 3H, =C*Me*), 2.10 (s, 3H, *Me*CO), 2.19 (m, 2H, CH_2CH=), 2.46 (t, 2H, J = 5.0 Hz, CH_2CO), 3.72 (s, 3H, OMe), 6.00 (dt, J = 15.4, 7.1 Hz, 1H, =C*H*), 6.33 (dd, 1H, J = 15.4, 11.2 Hz, =C*H*), 7.15 (d, 1H, J = 11.2Hz, C*H*=CMe); ^{13}C NMR (100 MHz, $CDCl_3$) δ 12.5 (=C*Me*), 22.7 (*Me*CO), 30.0 and 32.3 (2 Me), 42.7 (CH_2C=O), 51.8 (OMe), 125.8 (CCO_2Me), 126.6 (=*C*H), 138.4 (CH=), 141.7 (=CH), 169.1 (CO), 208.6 (CO); HRMS calcd for $C_{12}H_{18}O_3$ 210.1256, found 210.1254.

(n) Synthesis of Methyl 2-Methyl-9-oxo-2,4-undecadienate (17). This compound was similarly prepared from **7**, ethyl vinyl ketone, and BF_3·Et_2O in cold toluene according to the method described in section k; the yield of **17** was 40%: IR (neat, cm^{-1}) ν(C=O) 1709 (s), ν(C=C) 1639 (m), 1610 (m); ^{1}H NMR (400 MHz, $CDCl_3$) δ 1.77 (m, 2H, CH_2), 1.90 (s, 3H, =C*Me*), 2.10 (s, 3H, MeCO), 2.19 (m, 2H, CH_2CH=), 2.46 (t, 2H, J = 5.0 Hz, CH_2CO), 3.72 (s, 3H, OCH_3), 6.00 (dt, J = 15.4, 7.1 Hz, 1H, =C*H*CH_2), 6.33 (dd, J = 15.4, 11.2 Hz, 1H, =CH), 7.15 (d, J = 11.2 Hz, 1H, =CH); ^{13}C NMR (100 MHz, $CDCl_3$) δ 12.5 (=C*Me*), 22.7 (*Me*C=O), 30.0 and 32.3 (2 CH_2), 42.7 (CH_2C=O), 51.8 (OMe), 125.8 (CCO_2Me), 126.6 (=CH), 138.4 (CH), 141.7 (=CH), 169.1 (CO), 208.6 (C=O); HRMS calcd for $C_{13}H_{20}O_3$ 224.1412, found 224.1413.

X-ray Diffraction of 3, 6, and 13. Single crystals of **3**, **6**, and **13** were sealed in glass capillaries under an inert atmosphere. Data were collected on a Nonius CAD 4 using graphite-monochromated Mo Kα radiation, and the structure was solved by the heavy-atom method; all data reduction and structure refinement were performed with the NRCCSDP package. Crystal data, details of the data collection, and the structure analysis are summarized in Table 4. For all structures, all non-hydrogen atoms were refined with anisotropic parameters, and all hydrogen atoms included in the structure factors were placed in idealized positions.

Acknowledgment. We wish to thank the National Science Council of the Republic of China for financial support of this work.

Supplementary Material Available: Tables of atom coordinates, all bond distances and angles, and thermal parameters for **3**, **6**, and **13** (9 pages). Ordering information is given on any current masthead page.

OM950013Z

Aluminum Chloride Catalyzed Regioselective Allylsilylation of Alkenes: Convenient Route to 5-Silyl-1-alkenes

Seung Ho Yeon, Bong Woo Lee, Bok Ryul Yoo, Mi-Yeon Suk, and Il Nam Jung*

Organometallic Chemistry Laboratory, Korea Institute of Science & Technology, P.O. Box 131, Cheongryang, Seoul 130-650, Korea

Received September 27, 1994[⊗]

Allyltriorganosilanes react regioselectively with terminal or cyclic alkenes in the presence of aluminum chloride catalyst under mild conditions to afford 5-silyl-1-alkenes in good yield. In the allylsilylation of terminal alkenes the silyl group adds to the terminal carbon and the allyl group to the inner carbon of the double bond and the reaction with cyclic olefins gives allylsilylated products having the silyl and allyl groups in the *trans* position. This allylsilylation is a convenient route to 5-silyl-1-alkenes. In the allylsilylations with the stereohomogeneous (*Z*)-crotyltrimethylsilane, an allylic inversion is observed indicating a stepwise process of allylsilylation.

Introduction

The allylation of carbonyl compounds using allyltrimethylsilane is an important carbon–carbon bond forming method.[1] In particular, the Lewis acid-promoted allylation, which proceeds in high regioselectivities, is versatile and broadly applicable to many organic reactions.[2] In the allylation reaction, the allyl group adds to the carbon atom and the silyl group to the oxygen atom of the carbonyl group. Subsequent hydrolysis of the allylsilylated products then gives the corresponding homoallyl alcohol. The allylation reaction also can be applied to α,β-enones to give δ,ε-enones.[3] The [3 + 2] cycloaddition of α,β-enones with allylsilanes to give silylcyclopentanes has been reported recently (eq 1).[4]

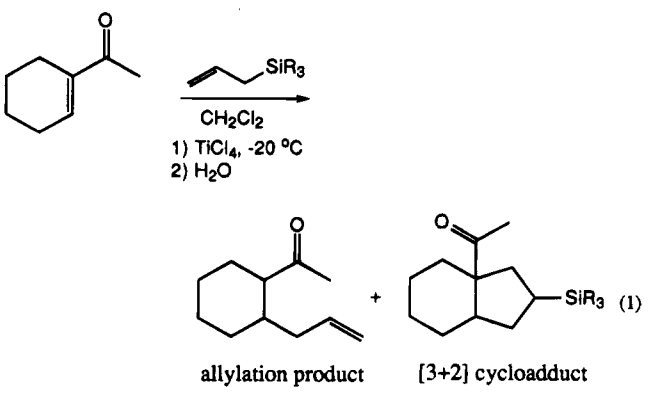

To our knowledge, however, allylsilane addition reactions to alkenes having no other functional groups have not been reported. We previously studied the direct synthesis[5] of allylchlorosilanes and the Friedel–Crafts alkylation[6] of substituted benzenes with allylsilanes in the presence of a Lewis acid catalyst. Considering the allylation, cycloaddition, and alkylation reactions of allylsilanes to unsaturated compounds, we attempted the addition of allylsilanes to olefins. In this paper, we wish to report the allylsilylation reactions of linear or cyclic alkenes and the probable reaction mechanism.

Results and Discussion

Allylsilylation of Linear Alkenes. The addition of allyltrimethylsilane, **1a**, to 1-hexene, **2a**, in *n*-hexane solution in the presence of anhydrous aluminum chloride as a catalyst at room temperature gave the allylsilylated 4-((trimethylsilyl)methyl)-1-octene, **3a**, as the major product in 78% yield based on **1a** used. The compound **3a** was presumably produced by addition of the silyl group to the terminal carbon atom and of the allyl group to the inner carbon atom of the double bond of **2a** as shown in eq 2. The other regio-isomer of **3a**

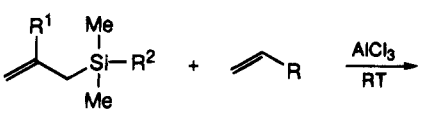

1a : R^1=H, R^2=Me
b : R^1, R^2=Me
c : R^1=H, R^2=Ph
d : R^1=H, R^2=CH_2Ph

2a : R=C_4H_9
b : R=C_6H_{13}
c : R=CH_2Ph

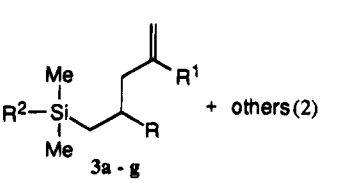

was not detected indicating that the allylsilylation is regioselective. In addition to **3a**, 4,6,6-trimethyl-6-

[⊗] Abstract published in *Advance ACS Abstracts,* April 15, 1995.

(1) For general review, see: (a) Colvin, E. W. *Silicon in Organic Synthesis*; Butterworths: London, 1981. (b) Weber, W. P. *Silicon Reagents for Organic Synthesis;* Springer: Berlin, 1983. (c) Fleming, I.; Dunoguès, J.; Smithers, R. *Organic Reactions*; Wiley: New York, 1989; Vol. 37.

(2) (a) Hosomi, A.; Sakurai, H. *Tetrahedron Lett.* **1976**, *17*, 1295. (b) Seyferth, D.; Pornet, J.; Weinstein, R. M. *Organometallics* **1982**, *1*, 1651.

(3) Hosomi, A.; Sakurai, H. *J. Am. Chem. Soc.* **1977**, *99*, 1675.

(4) (a) Knolker, H.-J.; Graf, R. *Tetrahedron Lett.* **1993,** *34*, 4765. (b) Knolker, H.-J.; Foitzik, N.; Goesmann, H.; Graf, R. *Angew. Chem., Int. Ed. Engl.* **1993**, *32*, 1081. (c) Knolker, H.-J.; Foitzik, N.; Graf, R.; Pannek, J.-B. Jones, P. G. *Tetrahedron* **1993**, *49*, 9955.

(5) Yeon, S. H.; Lee, B. W.; Kim, S.-I.; Jung, I. N. *Organometallics* **1993**, *12*, 4887.

(6) Lee, B. W.; Yoo, B. R.; Kim, S.-I.; Jung, I. N. *Organometallics* **1994**, *13*, 1312.

0276-7333/95/2314-2361$09.00/0

Table 1. Results on Allylsilylation of Linear Alkenes with Allylsilanes

entry no.	reacn conditions[a] allylsilane	alkene	solvent	time (h)	product	yield[b] (%)
1	**1a**	**2a**	*n*-hexane	1.5	**3a**	78
2	**1a**	**1a**	*n*-hexane	12	**3b**	48
			benzene	6	**3b**	44
3	**1a**	**2b**	*n*-hexane	3	**3c**	60
4	**1a**	**2c**	*n*-hexane	6	**3d**	20
5	**1b**	**2a**	none	8.5	**3e**	79
6	**1c**	**2a**	benzene	6	**3f**	42
7	**1d**	**2a**	*n*-hexane	1.5	**3g**	47

[a] Reactions were carried out at room temperature. [b] Based on allylsilane used.

silahept-1-ene (3%), **4a**, was obtained as a minor product. Several other minor byproducts also were obtained and identified as 4-((trimethylsilyl)methyl)-6-silahept-1-ene, **3b** (2%), hexamethyldisiloxane (7%), and unidentified high boilers and polymeric materials (10%).

Lewis acids such as titanium tetrachloride, stannic chloride, aluminum trichloride, boron trifluoride, etc., have been used as catalysts for the allylation of carbonyl compounds with allyltrimethylsilane.[1c,3,4] However, this allylsilylation of alkenes did not occur with Lewis acid catalysts other than aluminum chloride. About 10 mol % of aluminum chloride was sufficient to catalyze the allylsilylation, and the reaction proceeded at room temperature or below. In benzene solution, the reaction was observed to be more exothermic and generally proceeded faster than in *n*-hexane. This reactivity difference may be attributed to the higher solubility of aluminum chloride in benzene.

The allylsilylation of **2a** with 2-methyl-2-propenyltrimethylsilane, **1b**, instead of **1a** gave 2-methyl-4-((trimethylsilyl)methyl)-1-octene, **3e**, as expected, in 79% yield. This reaction proceeded at a slightly slower rate than that of **1a**. The allylsilylations of various linear alkenes with allylsilanes were carried out in the presence of aluminum chloride catalyst as represented in eq 2, and the results are summarized in Table 1.

As shown in Table 1, the isolated yields were good, ranging from 20% to 79% depending upon the nature of two reactants. Advantageously, the present allylsilylation can be carried out under mild conditions affording 5-silyl-1-alkenes in good yield and high regioselectivities also are attained in all the experiments. The allylsilylation of allylbenzene gave the lowest yield and a large amount of polymeric material.

The hexamethyldisiloxane byproduct, apparently produced by hydrolysis of trimethylchlorosilane, was obtained in the every allylsilylation reaction, indicating that the cleavage of allyl group from allyltrimethylsilane was involved. Protodesilylation of allyltrimethylsilane by acids has been reported.[7] In the Friedel–Crafts alkylation with alkenes in the presence of aluminum chloride, a small amount of hydrogen chloride resulting from the reaction of anhydrous aluminum chloride with adventitious water in the reaction mixture is responsible for this well-known[8] and well-understood[9,10] cleavage reaction. The stabilized carbocation intermediate **I** generated by the protonation of **1a** either undergoes desilylation to give propylene and the trimethylsilyl cation[7,11] or reacts with **1a** to give the cation adduct **II** which gives the byproduct **4a** by donating a trimethylsilyl cation to **1a**. Electrophilic attack on electron-rich systems by trialkylsilyl cations has been reported for other systems.[12] GC–MS analysis of the off-gas indeed showed the presence of propylene indicating the occurence of the desilylation of **1a**. This type of intermediate i.e., **II**, was proposed to be formed by protonation of 1,3-bis(trimethylsilyl)propene, which resulted in the desilylation to give allylsilane.[11] At the final stage of the allylsilylation, the cation intermediate **II** would interact with $AlCl_4^-$ to give trimethylchlorosilane which is hydrolyzed to hexamethyldisiloxane during the work-up. These results are consistent with the initial formation of trimethylsilyl cation intermediates by protodesilylation. The reaction pathways for the byproducts are proposed in Scheme 1.

Allylic Inversion. The stereohomogeneous (*Z*)-crotyltrimethylsilane, **1e**, was prepared[13] and reacted with **2a**. This allylsilylation gave 3-methyl-4-((trimethylsilyl)methyl)-1-octene, **3h**, as a mixture of two diastereomers in 25% yield (eq 3). The structural assignment

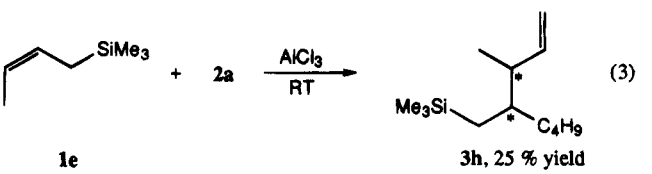

(3)

of diastereomers by ^{13}C NMR was reported for other system.[4] ^{13}C NMR studies of **3h** showed indeed the presence of two diastereomers. The products have a methyl group at the carbon α to the double bond which was moved from the terminal carbon of the starting allylsilane, indicating that an allylic inversion occured during the allylsilylation. This type of allylic inversion has been reported in the allylation of carbonyl compounds.[13b] This allylic inversion is consistent with the interaction of the cation intermediate **II** with the electron-rich double bond of the allylsilane and then elimination of a silyl cation from the incoming allylsilane to give the allylsilylated products.

Allylsilylation of Cycloalkenes. We extended the allylsilylation to cyclohexene, **2d**, and *trans*-1-(trimethylsilyl)-2-allylcyclohexane, **3i**, was obtained in 22% yield (eq 4). The NMR studies of **3i** show that the coupling

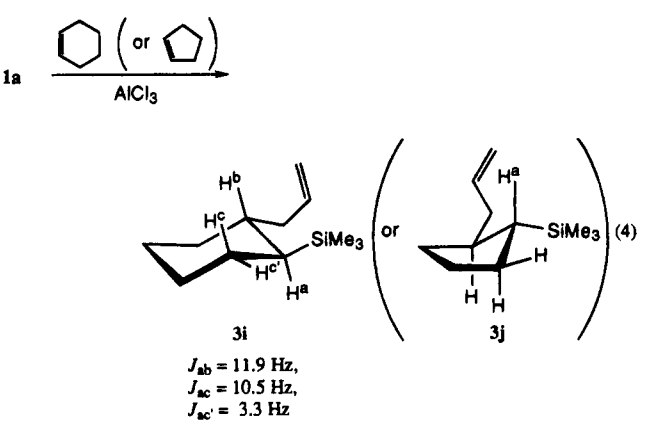

(4)

J_{ab} = 11.9 Hz,
J_{ac} = 10.5 Hz,
$J_{ac'}$ = 3.3 Hz

constant between the protons H^a and H^b at the carbons, to which the silyl and allyl groups are attached, respec-

(7) (a) Jenkins P. R.; Gut, R.; Wetter, H.; Eschenmoser, A. *Helv. Chim. Acta* **1979**, *62*, 1922. (b) Fleming, I.; Marchi, D.; Patel, K. *J. Chem. Soc., Perkin Trans. 1*, **1981**, 2518.

(8) Thomas, C. A. *Anhydrous Aluminum Chloride in Organic Chemistry*; Reinhold Publishing Co.: New York, 1941.

Scheme 1

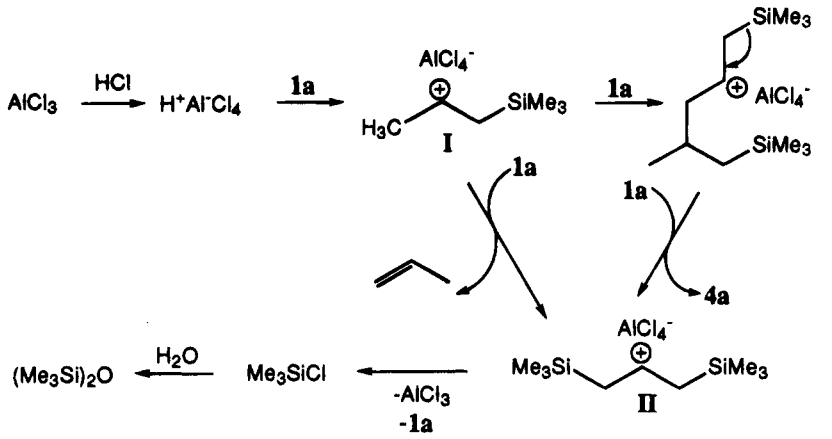

Scheme 2. Catalytic Cycle of Allylsilylation

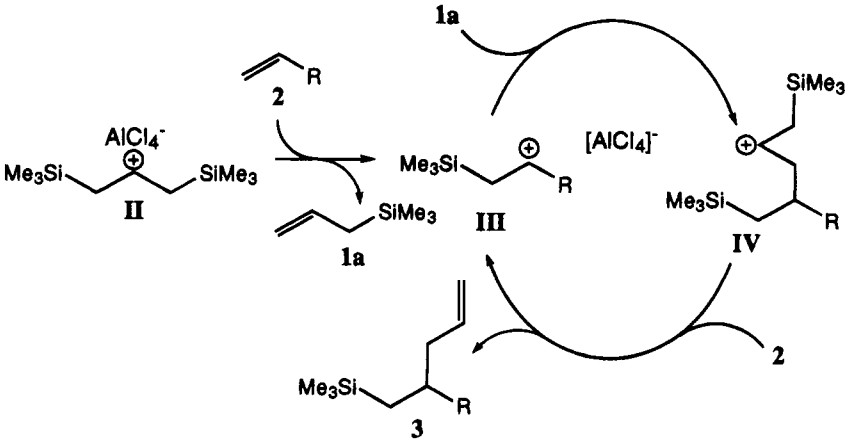

tively, is 11.9 Hz. Since the *cis* coupling constant is smaller than the *trans* coupling constant in general and usually smaller than 6 Hz,[14] it can be concluded that the two bulky groups are positioned *trans*. The allylsilylation of cyclopentene, **2e**, also gave *trans*-1-(trimethylsilyl)-2-allylcyclopentane, **3j**, in 39% yield. The stereochemistry of **3j** has been assigned analogously to be *trans*. The *trans* configurtion for the two bulky groups is consistent with a stepwise process of allylsilylation.

Reaction Mechanism. We propose a mechanism for the allylsilylation in which a cation intermediate, **II**, is formed at the begining stages of the reaction as illustrated in Scheme 1. The sterically hindered intermediate **II** is stabilized by the β stabilization effect from two silyl groups. This may be the reason for the slower self-allylsilylation reaction compared with the allylsilylation of alkenes. When intermediate **II** interacts with **2**, the trimethylsilyl cation would be transferred to the terminal carbon of **2** to generate a new intermediate **III**. The more stable secondary carbocation formation and the β stabilization effect in the intermediate **III** would be responsible for the regiochemistry of the products. When intermediate **III** interacts with the double bond of **1a** to form a new carbon–carbon bond, the carbenium ion center at the carbon β to silicon, **IV**, would be generated. When intermediate **IV** interacts with **2**, the allylsilylated products, **3**, would be obtained by transferring the trimethylsilyl cation to **2** to regenerate the intermediate, **III**. The allylic inversion could be best explained by forming a new double bond between the carbons α and β to silicon of the incoming allylsilane and eliminating trimethylsilyl cation as illustrated in Scheme 2.

The *trans* allylsilylation of **1a** to cyclic olefins could be explained by the approach of **1a** to the intermediate **III** type cation from the other side of trimethylsilyl group in order to minimize the steric repulsion between the bulky trimethylsilyl group and the incoming allyltrimethylsilane. All the results are consistent with a stepwise process of allylsilylation in the proposed mechanism above.

Experimental Section

The solvents *n*-hexane and benzene were dried over sodium benzophenone ketyl and distilled before use. Allyltrimethylsilane was purchased from Hüls America Inc. and used without further purification. 2-Methyl-2-propenyltrimethylsilane and

(9) Wierschke, S. G.; Chandrasekhar, J.; Jorgensen, W. L. *J. Am. Chem. Soc.* **1985**, *107*, 1496.
(10) Eaborn, C.; Bott, R. W. *Organometallic Compounds of the Group IV Elements*; MacDiarmid, A. G., Ed.; Dekker: New York, 1968; Vol. 1, Part 1, pp 359–437.
(11) Fleming, I.; Langley, J. A. *J. Chem. Soc., Perkin Trans. 1*, **1981**, 1421.
(12) (a) Olah, G. A.; Bach, T.; Surya Prakash, G. K. *J. Org. Chem.* **1989**, *54*, 3770. (b) Frick, U.; Simchen, G. *Synthesis* **1984**, 929. (c) Eaborn, C.; Jones, K. L.; Lickiss, P. D. *J. Chem. Soc., Perkin Trans. 2* **1992**, 489. (d) Fornarini, S. *J. Org. Chem.* **1988**, *53*, 1314.
(13) (a) Tsuji, J.; Hara, M.; Ohno, K. *Tetrahedron* **1974**, *30*, 2143. (b) Kira, M.; Hino, T; Sakurai, H. *Tetrahedron Lett.* **1989**, *30*, 1099.
(14) Pretsch, E.; Clerc, T.; Siebl, J.; Simon, W. *Spectral Data for Structure Determination of Organic Compounds*; Springer-Verlag: New York, 1983; p H185.

(*Z*)-crotyltrimethylsilane were prepared from literature methods.[12] Anhydrous aluminum chloride was obtained from Aldrich Chemical Co. Other simple chemicals were purchased and used without further purification.

Products obtained from the allylsilylation of various alkenes were analyzed by GLC using a capillary column (SE-54, 30-m) or a packed column (10% OV-101 on 80–100 mesh Chromosorb W/AW, 1.5 m × 1/8 in.) on a Varian 3300 gas chromatograph equipped with a flame ionization detector or a thermal conductivity detector, respectively. The samples for characterization were purified by a preparative GLC using a Varian Aerograph Series 1400 gas chromatograph with a thermal conductivity detector and a 2 m by 1/8 in. stainless steel column packed with 20% OV-101 on 80–100 mesh Chromosorb P/AW. NMR spectra were recorded using $CDCl_3$ ($CHCl_3$ taken as δ 7.26) on a Varian Gemini 300 spectrometer. Mass spectra were obtained using a Hewlett Packard 5890 Series II gas chromatograph equipped with a Model 5972 mass selective detector. Elemental analyses were performed by the Advanced Analysis Center of the Korea Institute of Science and Technology, Seoul, Korea. HRMS (high resolution mass (70 eV, EI) spectra) were performed by the Analytical Chemistry Laboratory of the Korea Research Institute of Chemical Technology, Daejon, Korea.

Typical Procedure for Allylsilylation Reaction. To a stirred solution of 0.52 g (4.0 mmol) of anhydrous aluminum chloride and 10.0 mL of dried *n*-hexane in a 50 mL three-necked round-bottomed flask equipped with an addition funnel, a reflux condenser, and a gas inlet tube at room temperature was added dropwise mixture of 4.6 g (40 mmol) of **1a** and 10.1 g (120 mmol) of **2a** under dry nitrogen. The mixture was stirred for 1.5 h at room temperature, and the solution was quenched with 5 mL of water. The upper layer was separated and dried over anhydrous magnesium sulfate. The solvent and low boilers were distilled, and the product mixture was distilled under vacuum to give 4-((trimethylsilyl)methyl)-1-octene, **3a** (6.2 g, bp 28–30 °C/0.6 Torr) in 78% yield based on **1a**. Several other byproducts also were obtained by vacuum distillation and identified as 4,6,6-trimethyl-6-silahept-1-ene (3%), **4a**, 6,6-dimethyl-4-((trimethylsilyl)methyl)-6-silahept-1-ene, **3b** (2%), hexamethyldisiloxane (7%), and unidentified high boilers and polymeric material (10%). Data for **3a**: ^{1}H-NMR δ 0.01 (s, 9H, SiC*H*$_3$), 0.51–0.60 (m, 2H, SiC*H*$_2$), 0.90 (t, J = 6.8 Hz, 3H, C*H*$_3$), 1.26 (br s, 6H, C*H*$_2$), 1.50–1.60 (br m, 1H, C*H*), 1.98–2.10 (m, 2H, C*H*$_2$), 4.99 (d, J = 12.3 Hz, 2H, C*H*$_2$=), 5.70–5.85 (m, 1H, –C*H*=); ^{13}C-NMR δ 0.54 (Si*C*H$_3$), 14.16 (*C*H$_3$), 21.63, 23.01, 28.91, 34.14, 36.10, 41.01 (*C*H, *C*H$_2$), 115.64 (*C*H$_2$=), 137.64 (–*C*H=); mass spectra: m/e (relative intensity) 157 (11, M$^+$ – $CH_2CH{=}CH_2$), 99 (12), 74 (9), 73 (100), 59 (8). HRMS (m/e): calcd for $C_{11}H_{23}Si$ (M$^+$ – CH_3), 183.1569; found, 183.1570. Anal. Calcd (found) for $C_{12}H_{26}Si$: C, 72.64 (72.71); H, 13.21 (13.42). Data for **4a**: ^{1}H-NMR δ 0.02 (s, 9H, SiC*H*$_3$), 0.40 (dd, J = 8.9, 14.7 Hz, 1H, SiC*H*^{a}H), 0.67 (dd, J = 4.9, 14.7 Hz, 1H, SiCH*H*^{b}), 0.92 (d, J = 6.6 Hz, 3H, C*H*$_3$), 1.61–1.74 (m, 1H, C*H*), 1.89–2.09 (m, 2H, C*H*$_2$), 4.96–5.03 (m, 2H, =C*H*$_2$), 5.72–5.87 (m, 1H, –C*H*=); ^{13}C-NMR δ –0.60 (Si*C*H$_3$), 22.59 (*C*H$_3$), 24.75, 45.04 (*C*H$_2$), 29.78 (*C*H), 115.52 (*C*H$_2$=), 137.85 (–*C*H=); mass spectra m/e (relative intensity) 115 (14, M$^+$ – $CH_2CH{=}CH_2$), 99 (13), 73 (100), 59 (10).

Self-Allylsilylation of 1a. Using the reaction procedure described above, 6,6-dimethyl-4-((trimethylsilyl)methyl)-6-silahept-1-ene, **3b**, 1.4 g (bp 30–32 °C/0.6 Torr, 48% yield), was obtained from the reaction of 3.0 g (26 mmol) of **1a** only using 0.35 g (2.6 mmol) of anhydrous aluminum chloride in *n*-hexane. Other byproducts were identified as hexamethyldisiloxane (13%) and **4a** (1%). Data for **3b**: ^{1}H-NMR δ 0.01 (s, 18H, SiC*H*$_3$), 0.68 (dd, J = 6.9 Hz, 14.7 Hz, 2H, SiC*H*^{a}H), 0.53 (dd, J = 6.4 Hz, 14.7 Hz, 2H, SiCH*H*^{b}), 1.77 (hep, J = 6.5 Hz, 1H, C*H*), 2.03 (t, J = 6.4 Hz, 2H, C*H*$_2$), 4.96–5.02 (m, 2H, C*H*$_2$=), 5.70–5.81 (m, 1H, –C*H*=); ^{13}C-NMR δ 0.40 (Si*C*H$_3$), 25.30 (Si*C*H$_2$), 31.02 (*C*H), 44.87 (*C*H$_2$), 117.15 (*C*H$_2$=), 137.65 (–*C*H=); mass spectra m/e (relative intensity) 187 (39, M$^+$ – $CH_2CH{=}CH_2$), 100 (14), 74 (17), 73 (100), 59 (18). HRMS (m/e): calcd for $C_9H_{23}Si_2$ (M$^+$ – $CH_2CH{=}CH_2$), 187.1338; found, 187.1337. Anal. Calcd (found) for $C_{12}H_{28}Si_2$: C, 63.07 (62.83); H, 12.35 (12.81).

Allylsilylation of 2b with 1a. Using the typical reaction procedure above, 4-((trimethylsilyl)methyl)-1-decene, **3c**, 3.5 g (bp 46–48 °C/0.6 Torr, 60% yield), was obtained from the reaction of 3.0 g (26 mmol) of **1a** and 8.8 g (78 mmol) of 1-octene, **2b**, using 0.35 g (2.6 mmol) of anhydrous aluminum chloride. Data for **3c**: ^{1}H-NMR δ 0.12 (s, 9H, SiC*H*$_3$), 0.48–0.62 (m, 2H, SiC*H*$_2$), 0.89 (t, J = 6.9 Hz, 3H, C*H*$_3$), 1.27 (br s, 10H, C*H*$_2$), 1.51–1.62 (br m, 1H, C*H*), 2.01–2.06 (m, 2H, C*H*$_2$), 4.99 (d, J = 12.4 Hz, 2H, C*H*$_2$=), 5.70–5.85 (m, 1H, –C*H*=); ^{13}C-NMR δ 0.54 (Si*C*H$_3$), 14.11 (*C*H$_3$), 21.63, 22.74, 26.62, 29.67, 31.98, 34.43, 36.43, 41.10 (*C*H, *C*H$_2$), 115.62 (*C*H$_2$=), 137.64 (–*C*H=); mass spectra m/e (relative intensity) 185 (4, M$^+$ – $CH_2CH{=}CH_2$), 99 (8), 73 (100), 59 (8). HRMS (m/e): calcd for $C_{14}H_{30}Si$ (M$^+$), 226.2116; found, 226.2115. Anal. Calcd (found) for $C_{14}H_{30}Si$: C, 74.25 (74.11); H, 13.35 (13.89).

Allylsilylation of 2c with 1a. 4-Benzyl-6,6-dimethyl-6-silahept-1-ene, **3d**, 1.2 g (bp 51–52 °C/0.6 Torr, 20% yield), was obtained from the reaction of 3.0 g (26 mmol) of **1a** and 9.3 g (79 mmol) of allylbenzene, **2c**, using 0.35 g (2.6 mmol) of anhydrous aluminum chloride. Data for **3d**: ^{1}H-NMR δ 0.04 (s, 9H, SiC*H*$_3$), 0.57 (dd, J = 6.6, 15.0 Hz, 1H, SiC*H*^{a}H), 0.67 (dd, J = 6.3, 15.0 Hz, 1H, SiCH*H*^{b}), 1.91 (hep, J = 6.5 Hz, 1H, C*H*), 1.98–2.10 (m, 2H, C*H*$_2$), 2.58 (d, 2H, C*H*$_2$), 5.00–5.12 (m, 2H, C*H*$_2$=), 5.74–5.88 (m, 1H, –C*H*=), 7.13–7.32 (Ar*H*); ^{13}C-NMR δ –0.57 (Si*C*H$_3$), 21.22, 36.36, 40.40, 43.28 (*C*H, *C*H$_2$), 116.37 (*C*H$_2$=), 125.74, 128.17, 129.31, 141.49 (*Ar*), 137.13 (–*C*H=); mass spectra m/e (relative intensity) 217 (0.8, M$^+$ – CH_3), 191 (3, M$^+$ – $CH_2CH{=}CH_2$), 141 (18), 99 (11), 91 (12), 73 (100), 59 (9). HRMS (m/e): calcd for $C_{14}H_{21}Si$ (M$^+$ – CH_3), 217.1413; found, 217.1416. Anal. Calcd (found) for $C_{15}H_{24}Si$: C, 77.51 (77.28); H, 10.44 (10.63).

Allylsilylation of 2a with 1b. 2-Methyl-4-((trimethylsilyl)methyl)-1-octene, **3e**, 2.3 g (bp 35–37 °C/0.6 Torr, 79% yield), was obtained from the reaction of 1.8 g (14 mmol) of **1b** and 3.4 g (40 mmol) of **2a** using 0.19 g (1.4 mmol) of anhydrous aluminum chloride in the absence of solvent at room temperature for 8.5 h. Other byproducts were identified as hexamethyldisiloxane (6%) and 2,4,4,6,6-pentamethyl-6-silahept-1-ene, **4b** (12%). Data for **3b**: ^{1}H-NMR δ 0.02 (s, 9H, SiC*H*$_3$), 0.52 (d, J = 6.5 Hz, 2H, SiC*H*$_2$), 0.90 (t, J = 6.3 Hz, 3H, C*H*$_3$), 1.18–1.34 (br m, 6H, C*H*$_2$), 1.58–1.66 (m, 1H, C*H*), 1.68 (s, 3H, C*H*$_3$), 1.88 (dd, J = 6.9, 13.4 Hz, 1H, C*H*^{a}H), 2.02 (dd, J = 7.3, 13.4 Hz, 1H, CH*H*^{b}), 4.65 (s, 1H, =C*H*^{a}H), 4.74 (s, 1H, =CH*H*^{b}); ^{13}C-NMR δ 0.52 (Si*C*H$_3$), 14.19, 22.21 (*C*H$_3$), 21.53, 23.05, 28.72, 36.08, 46.17, 31.94 (*C*H, *C*H$_2$), 111.56 (*C*H$_2$=), 144.94 (–*C*H=); mass spectra m/e (relative intensity) 157 (14, M$^+$ – $CH_2C(Me){=}CH_2$), 113 (8), 85 (4), 75 (4), 74 (9), 73 (100), 59 (9), 43 (3). HRMS (m/e): calcd for $C_{13}H_{28}Si$ (M$^+$), 212.1960; found, 212.1943. Anal. Calcd (found) for $C_{13}H_{28}Si$: C, 73.50 (74.32); H, 13.28 (13.46). Data for **4b**: ^{1}H-NMR δ 0.05 (s, 9H, SiC*H*$_3$), 0.72 (s, 2H, SiC*H*$_2$), 0.98 (s, 6H, C*H*$_3$), 1.79 (s, 3H, C*H*$_3$), 1.99 (s, 2H, C*H*$_2$), 4.62–4.65 (m, 1H, =C*H*^{a}H), 4.83–4.87 (m, 1H, =CH*H*^{b}); ^{13}C-NMR δ 1.03 (Si*C*H$_3$), 25.49, 55.69 (*C*H$_2$), 30.38, 33.02 (*C*H$_3$), 34.45 (*C*), 113.96 (*C*H$_2$=), 144.12 (=*C*–); mass spectra m/e (relative intensity) 169 (1, M$^+$ – CH_3), 129 (19, M$^+$ – $CH_2C(Me){=}CH_2$), 113 (11), 74 (10), 73 (100), 59 (12), 45 (16). HRMS (m/e): calcd for $C_7H_{17}Si$ (M$^+$ – $CH_2C(Me){=}CH_2$), 129.1099; found, 129.1099.

Allylsilylation of 2a with 1c. 4-((Dimethylphenylsilyl)-methyl)-1-octene, **3f**, 2.1 g (bp 72–74 °C/0.6 Torr, 47% yield), was obtained from the reaction of 3.0 g (7.0 mmol) of allyldimethylphenylsilane, **1c**, and 4.3 g (51 mmol) of **2a** using 0.10 g (0.7 mmol) of anhydrous aluminum chloride. Data for **3f**: ^{1}H-NMR δ 0.31 (s, 6H, SiC*H*$_3$), 0.73–0.87 (m, 2H, SiC*H*$_2$), 0.85 (t, J = 6.7 Hz, 3H, C*H*$_3$), 1.12–1.30 (br m, 6H, C*H*$_2$), 1.53–1.64 (m, 1H, C*H*), 1.92–2.08 (m, 2H, C*H*$_2$), 4.90–5.00 (m, 2H, C*H*$_2$=), 5.64–5.79 (m, 1H, –C*H*=), 7.30–7.55 (m, 5H, Ar*H*);

^{13}C-NMR δ −1.98 ($SiCH_3$), 14.13, 20.75, 22.94, 28.80, 34.02, 36.00, 41.00 (CH, CH_2), 115.80 (CH_2=), 127.72, 128.74, 133.57, 140.11 (*Ar*), 137.46 (−*C*H=); mass spectra *m/e* (relative intensity) 219 (4, $M^+ - CH_2CH{=}CH_2$), 161 (4), 136 (14), 135 (100), 121 (6), 119 (3), 107 (6), 105 (5). HRMS (*m/e*): calcd for $C_{14}H_{23}Si$ ($M^+ - CH_2CH{=}CH_2$), 219.1569; found, 219.1603. Anal. Calcd (found) for $C_{17}H_{28}Si$: C, 78.38 (78.62); H, 10.83 (11.23).

Allylsilylation of 2a with 1d. 4-((Benzyldimethylsilyl)-methyl)-1-octene, **3g**, 1.2 g (bp 78−80 °C/0.6 Torr, 42% yield), was obtained from the reaction of 2.0 g (10 mmol) of allylbenzyldimethylsilane, **1d**, and 2.6 g (31 mmol) of **2a** using 0.13 g (1.0 mmol) of anhydrous aluminum chloride. Data for **3g**: ^{1}H-NMR δ 0.00 (s, 6H, $SiCH_3$), 0.51−0.65 (m, 2H, $SiCH_2$), 0.91 (t, J = 6.7 Hz, 3H, CH_3), 1.20−1.33 (br m, 6H, CH_2), 1.53−1.62 (m, 1H, C*H*), 1.95−2.09 (m, 2H, CH_2), 2.10 (s, 2H, CH_2), 4.97−5.03 (m, 2H, CH_2=), 5.69−5.83 (m, 1H, −C*H*=), 7.00−7.28 (m, 5H, Ar*H*); ^{13}C-NMR δ −2.43 ($SiCH_3$), 14.17, 20.00, 23.01, 26.50, 28.93, 34.00, 36.16, 41.08 (CH, CH_2), 115.84 (CH_2=), 123.91, 128.13, 128.19, 140.43 (*Ar*), 137.44 (−*C*H=); mass spectra *m/e* (relative intensity) 259 (0.2, $M^+ - CH_3$), 233 (0.2, $M^+ - CH_2CH{=}CH_2$), 183 (32), 155 (7), 149 (29), 121 (27), 99 (100), 91 (9), 59 (15). HRMS (*m/e*): calcd for $C_{15}H_{25}Si$ ($M^+ - CH_2CH{=}CH_2$), 233.1726; found, 233.1719. Anal. Calcd (found) for $C_{18}H_{30}Si$: C, 78.76 (78.93); H, 11.01 (11.35).

Allylsilylation of 2a with 1e. 3-Methyl-4-((trimethylsilyl)-methyl)-1-octene, **3h**, 0.3 g (bp 32−34 °C/0.6 Torr, 25% yield), was obtained from the reaction of 0.7 g (5.5 mmol) of **1e** and 1.4 g (17 mmol) of **2a** using 0.08 g (0.6 mmol) of anhydrous aluminum chloride at room temperature for 4 h. Other byproducts were identified as hexamethyldisiloxane (7%) and 4-ethyl-3,6,6-trimethyl-6-silahept-1-ene, **4c** (5%). Data for **3h** (mixed diastereomers): ^{1}H-NMR δ 0.01 (s, 9H, $SiCH_3$), 0.30−0.39 (m, 1H, $SiCH^aH$), 0.51−0.63 (m, 1H, $SiCHH^b$), 0.86−0.95 (m, 6H, CH_3), 1.14−1.35 (m, 6H, CH_2), 1.39−1.53 (br m, 1H, C*H*), 2.28−2.60 (br m, 1H, C*H*), 4.93−4.99 (m, 2H, CH_2=), 5.70−5.81 (m, 1H, −C*H*=); ^{13}C-NMR δ (chemical shifts for the diastereomers are given in parentheses) −0.69 ($SiCH_3$), 14.15 (14.63), 16.49, 18.04 (17.77), 23.04, 29.51 (29.68), 33.31, 39.18 (38.96) (CH, CH_2), 40.78 (40.48) (CH_2), 113.51 (113.14) (CH_2=), 142.75 (143.65) (−*C*H=); mass spectra *m/e* (relative intensity) 157 (8, $M^+ - CH(Me)CH{=}CH_2$), 113 (5), 73 (100), 59 (8), 45 (8), 29 (5). HRMS (*m/e*): calcd for $C_9H_{21}Si$ ($M^+ - CH(Me)CH{=}CH_2$), 157.1413; found, 157.1425. Anal. Calcd (found) for $C_{13}H_{28}Si$: C, 73.50 (73.06); H, 13.28 (13.45). Data for **4c** (mixed diastereomers): ^{1}H-NMR δ 0.01 (s, 9H, $SiCH_3$), 0.30−0.63 (m, 2H, $SiCH_2$), 0.84−0.96 (m, 6H, CH_3), 1.21−1.43 (br m, 3H, C*H*, CH_2), 2.21−2.32 (br m, 1H, C*H*), 4.93−4.99 (m, 2H, CH_2=), 5.68−5.82 (m, 1H, −C*H*=); ^{13}C-NMR δ (chemical shifts for the diastereomers are given in parentheses) −0.70 ($SiCH_3$), 16.63 (14.72), 17.32 (17.62) (CH_3), 11.75 (11.61), 26.11 (CH_2), 40.26 (40.56), 40.48 (40.89) (CH), 113.10 (113.49) (CH_2=), 142.77 (143.70) (−*C*H=).

Allylsilylation of 2d with 1a. *trans*-1-(Trimethylsilyl)-2-allylcyclohexane, **3i**, 2.3 g (bp 38−41 °C/0.6 Torr, 31% yield), was obtained from the reaction of 4.2 g (37 mmol) of **1a** and 13.2 g (160 mmol) of **2d** using 0.49 g (3.7 mmol) of anhydrous aluminum chloride in benzene solution at room temperature for 1.5 h. Other byproducts were identified as hexamethyldisiloxane (8%), **3b** (29%), 3-(cyclohex-2-enyl)-1-(trimethylsilyl)propane (4%) and **4a** (5%). Data for **3i**: ^{1}H-NMR δ 0.02 (s, 9H, $SiCH_3$), 0.45−0.54 (ddd, $J(H^aH^b)$ = 11.9 Hz, $J(H^aH^c_{ax})$ = 10.5 Hz, $J(H^aH^c_{eq})$ = 3 .3 Hz, 1H, ring-C*H*Si), 0.85−0.98, 1.78−1.84 (m, 2H, ring-CH_2), 1.08−1.19, 1.67−1.69 (m, 2H, ring-CH_2), 1.20−1.25 (m, 2H, ring-CH_2), 1.31−1.42 (m, 1H, ring-C*H*), 1.70−1.77 (m, 2H, ring-CH_2), 1.85−1.92, 2.23−2.35 (m, 2H, CH_2), 4.96−5.01 (m, 2H, CH_2=), 5.74−5.83 (m, 1H, −C*H*=); ^{13}C-NMR δ 1.12 ($SiCH_3$), 26.27, 27.72, 28.02, 30.64, 33.17, 38.83, 40.98 (CH, CH_2), 115.45 (CH_2=), 137.69 (−*C*H=); mass spectra *m/e* (relative intensity) 155 (13, $M^+ - CH_2CH{=}CH_2$), 99 (3), 81 (5), 74 (9), 73 (100), 59 (9), 45 (7). HRMS (*m/e*): calcd for $C_{11}H_{21}Si$ ($M^+ - CH_3$), 181.1412; found, 181.1387. Anal. Calcd (found) for $C_{12}H_{24}Si$: C, 73.38 (73.12); H, 12.32 (12.67).

Allylsilylation of 2e with 1a. *trans*-1-(Trimethylsilyl)-2-allylcyclopentane, **3j**, 1.9 g (bp 23−25 °C/0.6 Torr, 39% yield), was obtained from the reaction of 3.0 g (26 mmol) of **1a** and 5.3 g (78 mmol) of **2e** using 0.35 g (2.6 mmol) of anhydrous aluminum chloride in benzene solution at room temperature for 5 h. Data for **3j**: ^{1}H-NMR δ 0.00 (s, 9H, $SiCH_3$), 0.64 (dt, J = 8.0, 9.2 Hz, 1H, SiC*H*), 1.25−1.43 (m, 2H, ring-CH_2), 1.47−1.56 (m, 2H, ring-CH_2), 1.60−1.70 (m, 1H, ring-C*H*), 1.72−1.85 (m, 2H, ring-CH_2), 1.78−1.95, 2.17−2.32 (m, 2H, CH_2), 4.94−5.03 (m, 2H, CH_2=), 5.73−5.88 (m, 1H, −C*H*=); ^{13}C-NMR δ −2.52 ($SiCH_3$), 26.39, 28.68, 31.35, 33.50, 41.10, 41.65 (CH, CH_2), 114.94 (CH_2=), 138.40 (−*C*H=); mass spectra *m/e* (relative intensity) 167 (1, $M^+ - CH_3$), 141 (16, $M^+ - CH_2CH{=}CH_2$), 99 (2), 79 (3), 73 (100), 67 (6), 59 (10). HRMS (*m/e*): calcd for $C_{10}H_{19}Si$ ($M^+ - CH_3$), 167.1256; found, 167.1243. Anal. Calcd (found) for $C_{11}H_{22}Si$: C, 72.44 (73.57); H, 12.16 (12.54).

Acknowledgment. This research was supported financially by the Ministry of Science and Technology of Korea (Project 2N11700). We thank Prof. H. Sakurai of Tohoku University for many valuable discussions on the mechanism of allylsilylation.

OM940749G

Photochemistry of Monosubstituted Manganese Carbonyl Compounds, $Mn_2(CO)_9L$, in 3-Methylpentane at Low Temperature. Flash Photolysis Studies in Hexane at Room Temperature

Shulin Zhang, Xiaoqing Song, and Theodore L. Brown*

School of Chemical Sciences and Beckman Institute for Advanced Science and Technology, 505 S. Mathews Avenue, University of Illinois at Urbana-Champaign, Urbana, Illinois 61801

Received December 27, 1994[⊗]

The photochemical behavior of monosubstituted manganese carbonyl dimers, $Mn_2(CO)_9L$ (L = PMe_3, $P(n\text{-}Bu)_3$, PPh_3, $P(CH_2Ph)_3$, and $P(i\text{-}Pr)_3$), in 3-methylpentane at 93 K has been studied. Loss of CO leads to formation of the semibridging structure $Mn_2(CO)_7L(\mu\text{-}\eta^1,\eta^2\text{-}CO)$. Because loss of CO might occur from either of the two nonequivalent metals, and because the phosphine exhibits positional isomerism, several isomeric semibridging structures are possible, depending on the steric requirements of the phosphine. Each gives rise to a unique semibridging CO stretching frequency. Upon warming of the low-temperature glass, recombination with CO and intramolecular rearrangements of the semibridging forms occur in competition. Recombination with CO occurs most readily at the least sterically hindered sites. Thus, recombination to form the parent carbonyl, $Mn_2(CO)_9L$, occurs most readily with $Mn_2(CO)_9PMe_3$ and most slowly with $Mn_2(CO)_9P(i\text{-}Pr)_3$. Studies of the PMe_3 and PPh_3 complexes show that recombination with CO leads to substantial quantities of the equatorial form, which isomerizes to the axial form as the solution is warmed. At room temperature the thermodynamic equilibrium between the equatorial and axial isomers of $Mn_2(CO)_9L$ lies heavily toward the axial form. Flash photolysis of hexane solutions of $Mn_2(CO)_9L$ compounds in hexane solutions at room temperature reveal a complex decay of absorbances due to CO loss products. Analysis of the transient behavior leads to three pseudo-first-order rate constants: one is due to recombination of CO with $Mn_2(CO)_9$, formed via photochemical loss of L. The other two correspond to recombination of CO with $Mn_2(CO)_8L$ intermediates in which the CO has been lost from either Mn center.

Introduction

Dinuclear metal carbonyl compounds are subject to two primary photochemical processes, metal–metal bond homolysis and CO dissociation.[1,2] This duality of photochemical processes was established early for $Mn_2(CO)_{10}$ in laser flash photolysis experiments, which revealed the presence of UV–visible absorptions attributable to both $Mn(CO)_5$ radicals and $Mn_2(CO)_9$.[3] Both $Mn(CO)_5$ and $Mn_2(CO)_9$ were observed in hydrocarbon solution at room temperature via direct IR detection of the transient species.[4] Shortly thereafter, Hepp and Wrighton[5] established that photolysis in 3-methylpentane (3MP) at 77 K leads to formation of a CO-loss product with an IR absorption at 1760 cm^{-1}, attributed to a linear semibridge bond analogous to that established in $Mn_2(CO)_5(dppm)_2$.[6] More recently we have discussed the nature and stability of the semibridge bond in manganese carbonyl dimers and in analogous dimers involving rhenium.[7] The kinetic stabilities of the semibridge structures formed from CO loss in $Mn_2(CO)_{10}$, $Mn_2(CO)_8L_2$, and $Mn_2(CO)_6(\mu\text{-}L\frown L)_2$ (where L is a phosphorus donor) toward reaction with nucleophiles or in oxidative addition reactions vary widely, largely because of variations in the steric requirements of the donor groups bound to the metals.

The study of CO dissociation from monosubstituted manganese carbonyl compounds, $Mn_2(CO)_9L$, at low temperature in a glass affords an opportunity to test various hypotheses regarding the properties of semibridge bonds formed following CO loss. If the semibridge bonds are unsymmetrical, as assumed, there should be evidence of isomers based on whether the metal from which CO has photodissociated is that to which the phosphorus ligand is bound. The kinetic stability of a given semibridge isomer should depend on the position and steric bulk of the phosphine. The relative stabilities of the various possible isomers formed from CO loss can be assessed from observations of the IR spectra as the low-temperature glass is warmed. However, interconversion among the isomers may compete with recombination with CO, affording a complex reaction system. Herein we report the photochemistry of $Mn_2(CO)_9L$ (L = PMe_3, P(n-Bu)$_3$, PPh_3, $P(CH_2Ph)_3$, and $P(i\text{-}Pr)_3$) in 3MP at 93 K and above, following xenon flash lamp and

[⊗] Abstract published in *Advance ACS Abstracts,* April 15, 1995.

(1) Geoffroy, G. L.; Wrighton, M. S. *Organometallic Photochemistry*; Academic Press: New York, 1978.

(2) Meyer, T. J.; Caspar, J. V. *Chem. Rev.* **1985**, *85*, 187.

(3) (a) Rothberg, J.; Cooper, N. J.; Peters, K. S.; Vaida, V. *J. Am. Chem. Soc.* **1982**, *104*, 3536. (b) Yesaka, H.; Kobayashi, T.; Yasufuku, K.; Nagakura, S. *J. Am. Chem. Soc.* **1983**, *105*, 6249.

(4) Church, S. P.; Hermann, H.; Grevels, F. W.; Schaffner, K. *J. Chem. Soc., Chem. Commun.* **1984**, 785.

(5) Hepp, A. F.; Wrighton, M. S. *J. Am. Chem. Soc.* **1983**, *105*, 5934.

(6) (a) Colton, R.; Commons, C. J.; Hoskins, B. F. *J. Chem. Soc., Chem. Commun.* **1975**, 363. (b) Commons, C. J.; Hoskins, B. F. *Aust. J. Chem.* **1975**, *28*, 1663.

(7) Brown, T. L.; Zhang, S. *Inorg. Chem.* **1995**, *34*, 1164.

0276-7333/95/2314-2366$09.00/0

Table 1. IR Data for $Mn_2(CO)_9L$ in Hexane at 25 °C

L	ν_{CO} (cm^{-1})
$P(n\text{-}Bu)_3$	2089, 2006, 1992, 1971, 1957, 1933
PPh_3	2091, 2011, 1996, 1974, 1962, 1939
PMe_3	2090, 2009, 1991, 1972, 1959, 1937
$P(CH_2Ph)_3$	2090, 2010, 1994, 1973, 1960, 1934
$P(i\text{-}Pr)_3$	2090, 2030, 1996, 1974, 1959, 1930

continuous sunlamp photolysis at 93 K, and flash photolysis in hexane under 1 atm of CO at room temperature.

Experimental Section

All experiments were carried out under an atmosphere of purified argon, employing Schlenk techniques. 3-Methylpentane (3MP, 99+%, Aldrich) was distilled over CaH_2, passed over activated silica, and stored over freshly activated 4 Å molecular sieves. It was subjected to three freeze–pump–thaw cycles before use. $Mn_2(CO)_{10}$ was purchased from Strem and sublimed before use. Hexane was purified as described previously.[7] CO (Matheson purity grade, minimum purity 99.99%) was obtained from Matheson Gas Products, Inc. Trace $Fe(CO)_5$ was removed by passing the CO through an activated charcoal trap in a sand bath at 180 °C, followed by passage through a second activated charcoal trap cooled in a dry ice–acetone bath, a column of activated 3 Å molecular sieves, and an oxygen trap purchased from American Scientific.

$Mn_2(CO)_9PPh_3$ was prepared from reaction of $Mn_2(CO)_{10}$ (0.56 mmol) and PPh_3 (0.62 mmol) in the presence of Me_3NO (0.65 mmol) in toluene (40 mL) overnight at room temperature.[8] $Mn_2(CO)_9P(CH_2Ph)_3$ was prepared from the photoreaction (sunlamp) of $Mn_2(CO)_{10}$ (1.1 mmol) with $P(CH_2Ph)_3$ (1.0 mmol) in 80 mL of hexane/30 mL of toluene mixed solvent for 2 days. The other monosubstituted dimers $Mn_2(CO)_9L$ (L = $P(n\text{-}Bu)_3$, PMe_3, and $P(i\text{-}Pr)_3$) were synthesized by "cross-coupling" photolysis of $Mn_2(CO)_{10}$ and the corresponding dimers $Mn_2(CO)_8L_2$ in hexane and/or toluene, using a sunlamp. The disubstituted dimers were prepared and fully characterized in these laboratories by Sullivan.[9]

All monosubstituted dimers were separated and purified by passing through columns packed with activated neutral alumina, using hexane as eluent. The compounds were characterized by their IR spectra, in particular noting the absence of bands due to the reactant metal carbonyl compounds. The CO IR stretching mode absorptions in hexane solution are listed in Table 1, and the IR spectra are displayed in Figure 1. The IR spectrum of $Mn_2(CO)_9PPh_3$ is consistent with that reported in the literature.[9,10] The other monosubstituted compounds are new, to our knowledge.

IR spectra were recorded on a Perkin-Elmer Model 1710 FTIR spectrophotometer. A sealable cell with CaF_2 windows and a 1.0 mm pathlength, capable of variable-temperature use, was used for the low-temperature measurements. The solution of the dinuclear metal carbonyl (~0.5 to 1.0 mM) in 3MP was loaded into the IR cell under Ar. A SPECAC Model 21500 variable-temperature system was employed. The cell was cooled to 93 K using liquid nitrogen. After a solution in the cell has been flash-photolyzed while at low temperature, using a xenon flash lamp source (broadband UV–visible), the assembly is quickly moved to the IR spectrometer to record spectra. To obtain the desired IR spectra at various temperatures, the solvent background spectra were subtracted. The reference spectra for this purpose were obtained by separately recording the solvent background at corresponding temperatures and saving them on a computer disk. Data analyses were performed using a combination of ASYST-based programs and SlideWrite Plus, version 5.0.

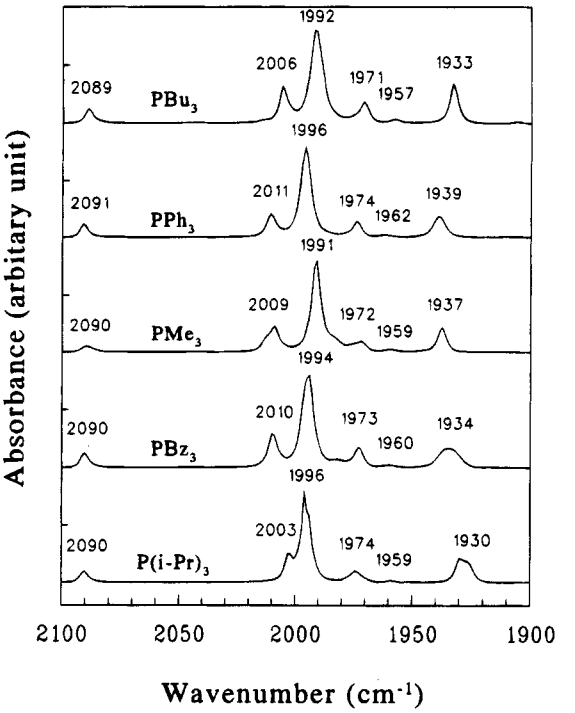

Figure 1. FTIR spectra of $Mn_2(CO)_9L$ compounds in hexane at 298 K.

In variable-temperature experiments, after the photoproducts have been generated by photolysis at 93 K in the cell, the liquid nitrogen is removed and the cell temperature allowed to increase. The temperature increase was determined to reproducibly obey the "natural" warmup function $T = \alpha - \beta \exp(-\gamma t)$, where $\alpha = 312$ K, $\beta = 220$ K, $\gamma = 2.7 \times 10^{-4}$ K s^{-1}, and t is time in seconds. The cell temperature was measured by a thermocouple located at the lower end of the cell.

The flash photolysis apparatus has been described previously.[11] The 10^{-4}–10^{-5} M solutions in hexane were prepared under an argon atmosphere and degassed by three freeze–pump–thaw cycles. After the degassed solution warmed to room temperature, purified CO was then added to the solution to a total of 1 atm with constant shaking of the flask for 10 min to ensure saturation by CO.

$Mn_2(CO)_7L_2$* is known to have a broad absorption around 510 nm with maximum of 500 nm for L = PMe_3 and 550 nm for L = $P(i\text{-}Pr)_3$.[11b] In the present study, transient absorbances were monitored at both 510 and 530 nm. The time-dependent transient absorbances are analyzed by fitting into three first-order processes. Except for slight differences in the relative amplitudes of the three processes, the kinetic behaviors are the same for both monitoring wavelengths. Since photolysis of $Mn_2(CO)_9L$ in solution at room temperature results in formation of $Mn_2(CO)_{10}$ and $Mn_2(CO)_8L_2$ in each experiment, only the trace from the first flash is used for kinetics analysis. The experiments are repeated with freshly prepared solutions. Reported rate constants are averages of three or more flash experiments.

Results and Discussion

Not a great deal of structural information is available for monosubstituted manganese carbonyl compounds.

(8) Koelle, U. *J. Organomet. Chem.* **1978**, *155*, 53.
(9) Sullivan, R. J.; Brown, T. L. *J. Am. Chem. Soc.* **1991**, *113*, 9155.
(10) (a) Fawcett, J. P.; Poë, A. J.; Twigg, M. V. *J. Organomet. Chem.* **1973**, *61*, 315. (b) Wawersik, H.; Basolo, F. *Inorg. Chim. Acta* **1969**, *3*, 113. (c) Jackson, R. A.; Poë, A. *Inorg. Chem.* **1978**, *17*, 997.
(11) (a) Sullivan, R. J.; Brown, T. L. *J. Am. Chem. Soc.* **1991**, *113*, 9162. (b) Herrick, R. S.; Brown, T. L. *Inorg. Chem.* **1984**, *23*, 4550. (c) Herrick, R. S.; Herrinton, T. R.; Walker, H. W.; Brown, T. L. *Organometallics* **1985**, *4*, 42.

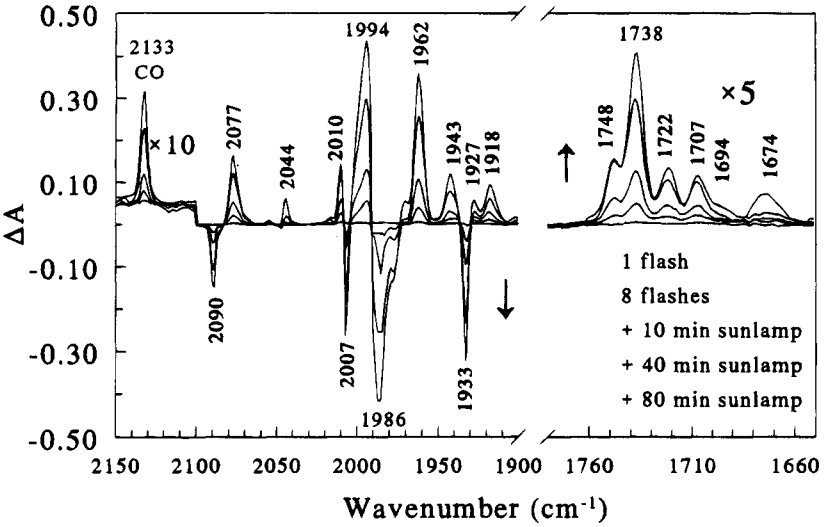

Figure 2. Difference FTIR spectra of a 1 mM solution of $Mn_2(CO)_9P(n\text{-}Bu)_3$ in 3MP at 93 K, before and following successive degrees of photoirradiation as listed.

The crystal structure of $Mn_2(CO)_9PPhMe_2$ reveals that the phosphine occupies an axial position on the manganese.[12] The IR spectrum in benzene,[13] with bands at 2094 (w), 2016 (s), 1993 (vs), 1969 (sh), and 1938 (m), is characteristic of axial monosubstitution.[12,14,15] In $Mn_2(CO)_9P(OCH)_3$ and related phosphite derivatives, the phosphite is assigned to an axial location on the basis of the IR spectra.[5]

Equatorial substitution was proposed for $Mn_2(CO)_9PH_3$,[17] on the basis of the small size of the PH_3 ligand and the concordance of the IR pattern (2094 (w), 2023 (s), 2012 (s), 1996–1990 (vs), 1970 (m), 1955 (m)) with that of $Mn_2(CO)_9$(nitrile) compounds, which are presumed to be equatorially substituted.[14] The crystal structure of $Mn_2(CO)_9PPh_2H$ reveals the ligand to be in an equatorial location. The P–H bond lies over the Mn–Mn bond, and the two metals are in a staggered configuration with respect to one another.[18]

The infrared spectra of five monosubstituted phosphine derivatives of $Mn_2(CO)_9$ are shown in Figure 1. The frequencies of the major observed IR bands are listed in Table 1. The strongest pattern of absorptions is that characteristic of axially-substituted derivatives.[15] On the other hand, nearly all the compounds exhibit weak absorptions associated with equatorial substitution. For example, the shoulder at about 2013 cm^{-1}, and the weak absorption at 1959 cm^{-1}, in the spectrum of $Mn_2(CO)_9PMe_3$ are attributable to the *eq*-isomer. A weak absorbance in the vicinity of 1960 cm^{-1}, characteristic of the *eq*-isomer, is seen in all the spectra. We conclude that the dominant isomer in solution is *ax*-$Mn_2(CO)_9L$ but that in most instances some *eq*-$Mn_2(CO)_9L$ is also present. (It should be noted that at room temperature the equilibrium between equatorial and axial isomers is expected to be facile.[19]) The fact that $Mn_2(CO)_9PMe_3$ exists to a large extent as the axial isomer is rather surprising, given that $Mn_2(CO)_8(PMe_3)_2$ exists largely in the *eq*,*eq*-form.[11b,19]

Photolysis of $Mn_2(CO)_9L$ in 3MP at 93 K results in loss of CO, with formation of a semibridge, yielding $Mn_2(CO)_7L(\mu\text{-}\eta^1,\eta^2\text{-}CO)$. Figure 2 shows the difference FTIR spectra obtained during photolysis of $Mn_2(CO)_9P(n\text{-}Bu)_3$, initially using a xenon flash lamp and then under continuous irradiation with a sunlamp. Loss of starting material is accompanied by the appearance of new bands, including one at 2133 cm^{-1} due to free CO. Of most interest is the band structure in the region of the semibridging CO stretch.

After several xenon lamp flashes there already is evident in the 1660–1760 cm^{-1} region a multiplet of absorptions. Since the multiplet structure appears early in the photolysis process, when only a low level of conversion of the starting dimer has occurred, the bands cannot be ascribed to a secondary photolysis step, such as loss of a second CO. Use of the sunlamp permits a higher degree of conversion to semibridge forms than can conveniently be obtained by repeated xenon lamp flashes, but it does not appear to give rise to significant secondary photoproduct formation.

The possibility exists that at least one of the observed IR bands might result from loss of a phosphine rather than CO in the photolysis process. However, aside from the much lower likelihood of the phosphine escaping from the solvent cage in the low temperature 3MP glass, this possibility can readily be ruled out because the resulting species, $Mn_2(CO)_8(\mu\text{-}\eta^1,\eta^2\text{-}CO)$, would give rise to an absorption at 1758 cm^{-1},[5,20] where no absorption is seen (Figure 2). It should also be noted that upon warming the 3MP glass following photolysis, there is eventually a recombination with CO to re-form the starting material with at least 95% efficiency.

Scheme 1 illustrates the various isomeric CO-loss products that might result from the photolysis process. CO might be lost from either of the two distinct metal centers, giving rise to two sets of isomers that are

(12) Liang, M.; Singleton, E.; Reimann, R. *J. Organomet. Chem.* **1973**, *56*, C21.
(13) Reimann, R.; Singleton, E. *J. Chem. Soc., Dalton Trans.* **1976**, 2109.
(14) Ziegler, M. L.; Haas, H.; Sheline, R. K. *Chem. Ber.* **1965**, *98*, 2454.
(15) Harris, G. W.; Coville, N. J. *J. Crystallogr. Spectroscopic Res.* **1989**, *19*, 451.
(16) Chan, H. S. O.; Hor, T. S. A.; Tan, K.-L.; Leong, Y.-P. *Inorg. Chim. Acta* **1991**, *184*, 23.
(17) Fischer, E. O.; Herrmann, W. *Chem. Ber.* **1972**, *105*, 286.
(18) Giordano, R.; Sappa, E.; Tiripicchio, A.; Camellini, M. T.; Mays, M. J.; Brown, M. P. *Polyhedron* **1989**, *8*, 1855.
(19) Zhang, H.-T.; Brown, T. L. *J. Am. Chem. Soc.* **1993**, *115*, 107.
(20) Zhang, S.; Zhang, H.-T.; Brown, T. L. *Organometallics* **1992**, *11*, 3929.

Scheme 1

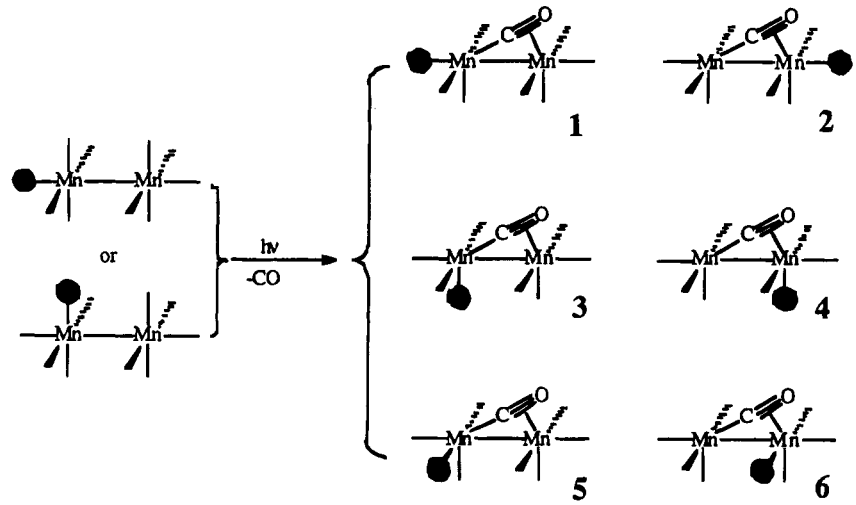

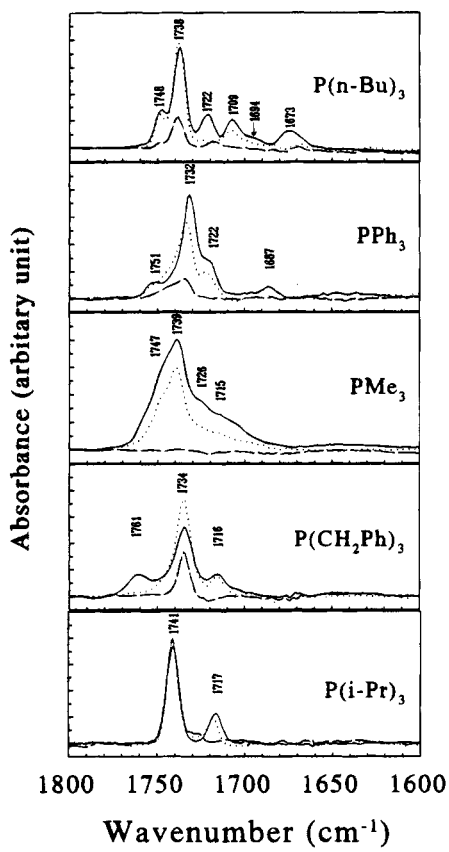

Figure 3. Difference FTIR spectra in the region of the semibridging CO stretch mode for $Mn_2(CO)_9L$ compounds in 3MP solution, before and following sunlamp irradiation at 93 K and upon subsequent warming. The spectra in each case were taken at 93 K (—), 143 K (···), and 183 K (- - -).

distinguished within each set by the location of the phosphine substituent relative to the semibridge. Because the photochemical event results in the deposition of excess energy in the system beyond that needed for CO dissociation, there is energy available to cause rearrangements of the dinuclear CO-loss products. Six distinct isomers, each with a characteristic semibridge stretching frequency, are possible.

From photolysis studies of disubstituted compounds in 3MP at low temperature, it can be expected that the different locations of the phosphine relative to the semibridge will give rise to frequency shifts on the order of 15–20 cm^{-1}.[19] Thus, it is reasonable to associate the pattern of semibridge stretching frequencies shown in Figure 2 with the existence of the various isomers shown in Scheme 1. Figure 3 shows the pattern of bands at 93 K for all five compounds studied and, upon warming, at 143 and 183 K. As seen, phosphines other than P(*n*-Bu)$_3$ also give rise to multiple bands, but in no case are the bands as well-distinguished as in Figure 2.

To assign the bands in Figure 2 to the possible isomeric forms, it is useful to begin with the question of whether the set of isomers based on loss of CO from the phosphine-bearing Mn (**2**, **4**, **6**) should differ as a class from those based on loss from the other Mn (**1**, **3**, **5**). We have recently shown that, in symmetrically-substituted manganese dimers, there is a remarkable constancy in the quantity Δ, defined as $\Delta = \nu_{ATCO} - \nu_{sb}$, where ν_{ATCO} is the average of the terminal CO stretching frequencies in the semibridging species $Mn_2(CO)_{8-n}L_n(\mu\text{-}\eta^1,\eta^2\text{-CO})$ ($n = 2, 4$) and ν_{sb} is the frequency of the semibridging CO stretch.[7] This constancy, which gives rise to a value for Δ in the range of 245 cm^{-1}, can be interpreted as resulting from a more or less constant degree of electronic stabilization of the semibridge bond with increasing degree of substitution at the metal centers. When substitution is unsymmetrical, as in $Mn_2(CO)_6(\alpha\text{-diimine})(\mu\text{-}\eta^1,\eta^2\text{-CO})$,[21] a smaller value for Δ is seen. In this case, CO photodissociates from the Mn bearing the α-diimine ligand. The smaller value for Δ arises because the center to which the semibridge CO is bound in η^2 fashion is a poorer Lewis acid by virtue of replacement of two CO groups by the diimine ligand. (Unsymmetrical substitution in the opposite sense, i.e., in which the substituting ligand is on the metal to which the semibridging CO is η^1 coordinated, might conversely result in a larger value for Δ. However, this instance has not yet been realized experimentally.)

The semibridging CO in isomer **1** in Scheme 1 will exhibit a value of ν_{sb} which, to first approximation, will be close to that seen in $ax,ax\text{-}Mn_2(CO)_6L_2(\mu\text{-}\eta^1,\eta^2\text{-CO})$, about 1700 cm^{-1}.[7,19] It could have a somewhat lower value because, by being coordinated to an $Mn(CO)_4$ rather than to an $Mn(CO)_3L$ center, it is bonded to a stronger Lewis acid. On the other hand, the terminal

(21) an der Graaf, T.; Stufkens, D. J.; Oskam, A.; Goubitz, K. *Inorg. Chem.* **1991**, *30*, 599.

CO groups on the Mn to which the semibridging CO is bonded in η^1 fashion should have an average stretching frequency slightly higher than those in $Mn_2(CO)_6L_2(\mu$-η^1,η^2-CO), because the other manganese center is less electron-donating than in the reference compound, by virtue of lacking a phosphine substituent. (The value of ν_{ATCO} for the CO groups on the $Mn(CO)_4L$ center is hypothetical; there is no way of distinguishing the CO stretching modes on the two metal centers, because of extensive coupling.) The first effect noted should be larger than the second. Thus, we expect that ν_{sb} for isomer **1** will be in the vicinity of 1690 cm^{-1}. Isomers **3** and **5** should exhibit frequencies on the order of 15−20 cm^{-1} on either side of this, as was observed for such isomerism in $Mn_2(CO)_6[P(n\text{-}Bu)_3]_2(\mu$-$\eta^1,\eta^2$-CO).[19]

The semibridging CO in isomer **2** in Scheme 1 will exhibit a value of ν_{sb} which, to first approximation, will be close to that seen in $Mn_2(CO)_8(\mu$-η^1,η^2-CO), about 1760 cm^{-1}. It could have a somewhat higher value than this because it is η^2 coordinated to a metal center that is a weaker Lewis acid than that in $Mn_2(CO)_8(\mu$-η^1,η^2-CO) by virtue of the presence of the phosphine on the metal center. On the other hand, the (hypothetical) value for ν_{ATCO} should be slightly lower for the CO groups on the metal bearing the five CO groups, because of the presence of the electron-releasing phosphine on the second metal center. Assuming that the first effect is more important than the second, we would predict a value of ν_{sb} for isomer **2** of about 1770 cm^{-1}. Isomers **4** and **6** should exhibit bands about 15 cm^{-1} on either side of this.

Comparison of these predictions with the observed bands for $Mn_2(CO)_7P(n\text{-}Bu)_3(\mu$-$\eta^1,\eta^2$-CO), Figure 2, reveals that, while the lower frequency bands are about where expected, the higher frequency bands are lower than predicted. Nevertheless, the general separation into bands spaced at about 15−20 cm^{-1} intervals is observed.

Further insight into the origins of the bands comes from consideration of their behavior as the glass is warmed. Previous work has established that steric factors play a major role in determining the relative kinetic stabilities of the semibridge structures toward recombination with CO. The presence of a phosphine on the metal center to which the CO group is bound in η^2 fashion results in a lower rate of recombination with CO, in proportion to the steric requirement of the phosphine. Thus, we expect that isomers **1**, **3**, and **5** will undergo recombination with CO at lower temperature than isomers **2**, **4**, and **6**.

A second aspect is the interconversion of the isomers. Isomers **2**, **4**, and **6** can interconvert during a momentary opening up of the semibridge, which renders the metal center coordinatively unsaturated and thus liable to intramolecular rearrangement. This process might be expected to occur at temperatures which are even lower than those at which isomers **1**, **3** and **5** undergo intermolecular reaction with CO. The same mode of interconversion is not available to isomers **1**, **3**, and **5**; a momentary opening of the semibridge does not change the coordination environment at the metal which bears the phosphine.

The changes in the IR bands due to semibridging CO groups in $Mn_2(CO)_7P(n\text{-}Bu)_3(\mu$-$\eta^1,\eta^2$-CO) upon warming are shown in greater detail in Figure 4. In the initial

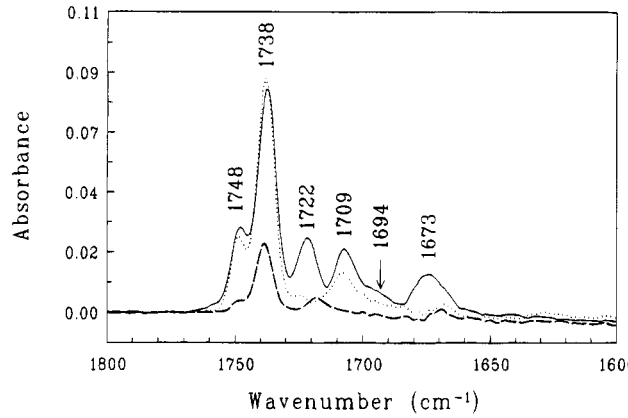

Figure 4. Difference FTIR spectra in the region of the semibridging CO stretch mode for $Mn_2(CO)_9P(n\text{-}Bu)_3$ following xenon flash lamp and sunlamp irradiation (see caption for Figure 1) at 93 K. The spectra were taken at 93 K (—), 143 K (···), and 183 K (- - -) as the glass was warmed.

stages of warming, as represented by the 143 K spectrum, there is a clear loss in total IR intensity, resulting from recombination with CO. As expected, the lower frequency bands disappear first, because these are associated with isomers **1**, **3**, and **5**. There is a question of the assignment of the 1709 and 1722 cm^{-1} bands. The 1722 cm^{-1} band disappears at a quite low temperature, even though it might be expected to belong to the **2**, **4**, **6** isomer set. However, there is in this temperature interval some conversion of isomers, as evidenced by a slight increase in intensity of the 1738 cm^{-1} band, in spite of the fact that there should be some, although a smaller, loss in all the higher frequency bands due to reaction with CO. Thus, the 1722 cm^{-1} band may disappear because of interconversion to the 1738 cm^{-1} (and possibly the 1748 cm^{-1}) band. Alternatively, the 1722 cm^{-1} band may belong to the **1**, **3**, **5** isomer set, and the 1709 cm^{-1} band to the **2**, **4**, **6** isomer set.

Although all the details of the changes in relative band intensities with temperature cannot be assigned with certainty, the general behavior of the system is in good accord with expectations. The changes occurring in the spectra of the other monosubstituted compounds, shown in Figure 3, reveal behavior that supports the interpretations given above. In $Mn_2(CO)_7P(i\text{-}Pr)_3(\mu$-$\eta^1,\eta^2$-CO), only two bands are seen. These can be ascribed to isomers **2** (1741 cm^{-1}) and **1** (1717 cm^{-1}), on the grounds that the large steric requirement of $P(i\text{-}Pr)_3$ precludes its location in an equatorial position. Indeed, upon recombination with CO with warming, only the axial isomer is seen, whereas the equatorial isomer is formed in substantial quantity when less bulky ligands are involved (*vide infra*). Consistent with the relative assignment of the two bands, the 1717 cm^{-1} band disappears at the lower temperature. If this assignment is correct, the close correspondence in frequencies argues for assignment of the 1722 cm^{-1} band in $Mn_2(CO)_7P(n\text{-}Bu)_3(\mu$-$\eta^1,\eta^2$-CO) to the isomer set {**1**, **3**, **5**}.

In each of the compounds studied there is an IR band in the 2077−2080 cm^{-1} interval due to a terminal CO stretch of the semibridging form, which is effectively invariant to the particular isomer. The intensity of this absorption thus can be used as a measure of the total amount of semibridging form present. A second mea-

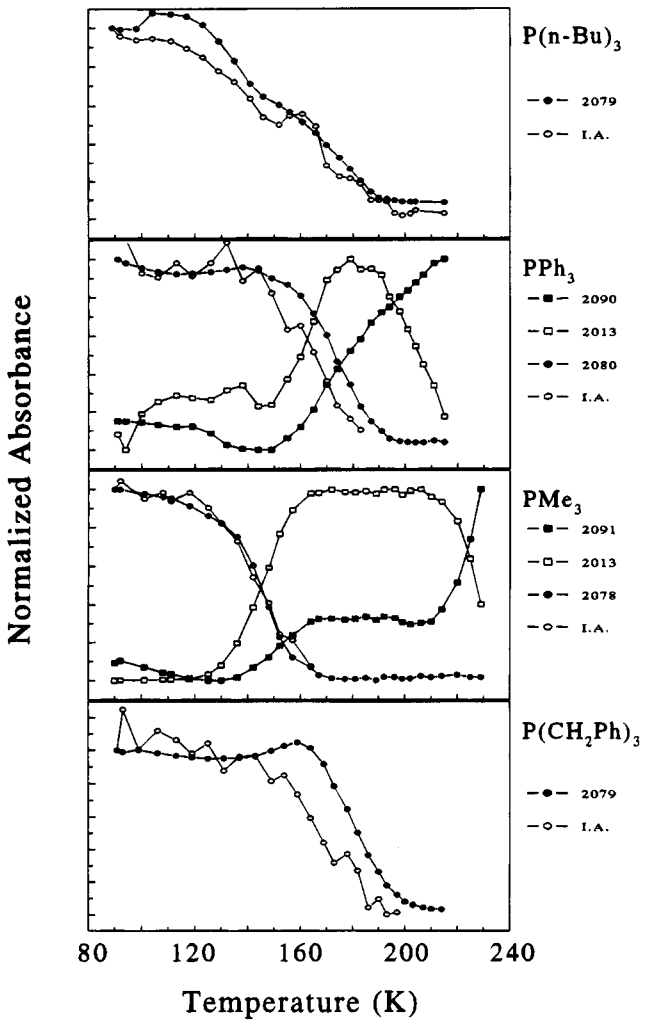

Figure 5. Variation with temperature of (a) the 2077–2080 cm^{-1} band, common to all states of the semibridge form, $Mn_2(CO)_8L(\mu\text{-}\eta^1,\eta^2\text{-CO})$, – ● –, (b) the integrated intensity of all semibridging CO stretch bands, – ○ –, and (c) normalized intensities of the bands due to *ax*-$Mn_2(CO)_9L$, – ■ –, and *eq*-$Mn_2(CO)_9L$, – □ – (L = CH_3, PPh_3).

sure, less precise because of uncertainties in the baseline as the temperature is varied, is the integrated intensity of all the semibridging CO absorptions. These two measures are shown as a function of temperature in Figure 5 for four of the compounds studied. In each case the 3MP glass was warmed at the same controlled rate, starting from 93 K. It is evident that steric factors are important in the reactivity toward CO. $Mn_2(CO)_9PMe_3$ is formed at the lowest temperature of any of the four compounds; $Mn_2(CO)_9P(n\text{-Bu})_3$ is formed at a lower rate, followed by $Mn_2(CO)_9PPh_3$ and $Mn_2(CO)_9P(CH_2Ph)_3$. The order of reactivity is roughly inversely related to the steric requirements of the phosphine ligand.[22]

Also shown are the normalized intensities of bands for the PMe_3 and PPh_3 derivatives that are characteristic of *ax*-$Mn_2(CO)_9L$ and *eq*-$Mn_2(CO)_9L$, the immediate products of recombination with CO. In these two cases, by careful use of difference spectra, it was possible to estimate the relative amounts of *eq*- and *ax*-isomeric products. We see initial formation of a relatively large quantity of the equatorial isomer upon formation of $Mn_2(CO)_9PMe_3$ or $Mn_2(CO)_9PPh_3$. The *eq*-form constitutes about 70% of the $Mn_2(CO)_9PMe_3$ formed initially upon reaction with CO, in the temperature range 120–160 K. This isomer is kinetically stable upon warming to about 210 K, at which point a substantial fraction of the *eq*-isomer converts to the *ax*-form. Analogous behavior was observed for $Mn_2(CO)_9PPh_3$, except that the *eq*- → *ax*-conversion occurs at a lower temperature. The fact that the axial/equatorial isomer distribution in the initial products of recombination with CO is different from the thermodynamic one supports the arguments for the presence of semibridging isomers in which the phosphine is located in an equatorial as well as axial position.

In summary, the present study has provided convincing evidence for formation of semibridging isomeric forms upon photodissociation of CO from $Mn_2(CO)_9L$ compounds in a low-temperature glass. The number and variety of these isomers for $Mn_2(CO)_9P(n\text{-Bu})_3$ is consistent with loss of CO from either metal center, with formation of linear semibridging structures. The smaller phosphines can apparently occupy equatorial sites in the photoproduct, $Mn_2(CO)_8L(\mu\text{-}\eta^1,\eta^2\text{-CO})$. Upon warming of the glass, recombination with CO is evident from the loss in absorbances in the semibridging CO stretch region of the IR. The reactivity of any given isomer toward recombination, for which the evidence suggests an associative process,[3] is clearly reduced by steric crowding at the metal center which the incoming CO must approach. Thus, recombination is observed to occur most readily for isomers **1**, **3**, and **5**. In general, reactivity is inversely related to the steric requirement of the phosphine.

Recombinations with CO of isomers in which the phosphine occupies an equatorial site, **3**, **5**, **4**, and **6**, appear to lead in substantial measure, if not exclusively, to the *eq*-$Mn_2(CO)_9L$ product, which isomerizes upon further warming largely to *ax*-$Mn_2(CO)_9L$.

The $Mn_2(CO)_8L(\mu\text{-}\eta^1,\eta^2\text{-CO})$ compounds, particularly for L = $P(n\text{-Bu})_3$, represent interesting examples, in a low molar mass system, of "rugged energy landscapes".[24] A given $Mn_2(CO)_8L(\mu\text{-}\eta^1,\eta^2\text{-CO})$ system is in principle capable of existing in a variety of energy states. These states can be categorized in a hierarchy with at least three distinct levels, as illustrated schematically in Figure 6: (a) The phosphine may be on either of the two nonequivalent metals, giving rise to the {**1**, **3**, **5**} and {**2**, **4**, **6**} isomer sets. (b) It may occupy any of three geometrically distinct positions at each metal. (c) The ligand may exist in a variety of conformational states in each location. This last level of complexity is potentially of interest for ligands such as $P(n\text{-Bu})_3$, $P(CH_2Ph)_3$, or PPh_3; the various conformational states could vary considerably in the degree of steric access they allow for an incoming reagent.

Recombinations with CO as well as possibly other reactions, such as oxidative addition of HX,[8] are associative processes characterized by smaller free energy barriers than those separating many of the possible states of the system. The reaction barriers are much lower than those for interconversion of the {**1**, **3**, **5**} and

(22) (a) Brown, T. L. *Inorg. Chem.* **1992**, *31*, 1286. (b) Brown, T. L.; Lee, K. J. *Coord. Chem. Rev.* **1993**, *128*, 89.
(23) Zhang, H.-T.; Zhang, S.; Brown, T. L. Unpublished kinetics studies, to be submitted for publication.
(24) Frauenfelder, H.; Sligar, S. G.; Wolynes, P. G. *Science* **1991**, *254*, 1598.

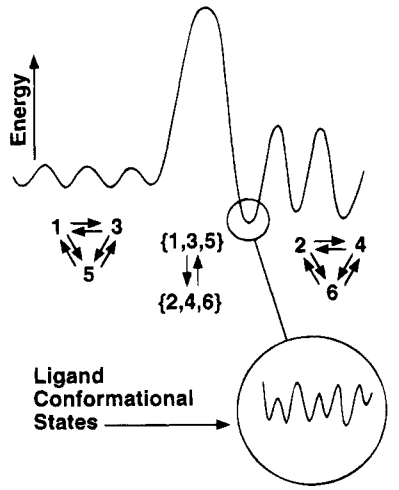

Figure 6. Schematic illustration of the energy surfaces connecting the various substates of $Mn_2(CO)_8L(\mu\text{-}\eta^1,\eta^2\text{-CO})$. The illustration is meant to show the multilevel character of the energy surface. It further illustrates the lower energy barriers to interconversions of isomers **1**, **3**, and **5** as compared with isomers **2**, **4**, and **6**, the large barrier to interconversion of the two sets of isomers, and the existence of ligand conformational states for each isomer.

{**2**, **4**, **6**} isomer sets and possibly also than those for interconversion among isomers **1**, **3**, and **5**. It appears that interconversions among isomers **2**, **4**, and **6** occur at about the rates of recombination of those isomers with CO or slower. It is likely that interconversion of conformational states of the ligand occur more rapidly than intermolecular reaction processes, although there is no experimental evidence on this point. Thus there may exist a Boltzmann population distribution of ligand conformational states for each of the six isomers that may exist. Whether this distribution is of significance for the reactivities of the isomers will depend on the particular ligand and attacking reagent.

The various states of $Mn_2(CO)_8L(\mu\text{-}\eta^1,\eta^2\text{-CO})$ are formed in a nonequilibrium distribution under irradiation at low temperature. Thus the overall reactivity at low temperature or upon warming will be a complex function of the distribution of substates and the barriers to interconversion among them in comparison with the barriers to reaction. Recombination with CO, for example, is not characterized by a single exponential decay but rather by a sum of such decays, each characteristic of a distinct species that does not readily interconvert with other substates under reaction conditions.

When $Mn_2(CO)_9L$ is flash-photolyzed at room temperature, many of the interconversions between substates will occur rapidly with respect to bimolecular reaction with a subtrate, e.g. CO. In this case, the number of characteristic reaction rates will be smaller but still not reduced to a single characteristic rate constant. The complexity of the reaction system should be discernible from analysis of the absorbance decay following flash photolysis, in which all the substates of the system contribute more or less equally to a single UV–visible absorption which is monitored in following the decay.

We have studied the transient behavior of four $Mn_2(CO)_9L$ compounds in hexane at room temperature, under 1 atm CO pressure. The absorbance at either 510 or 530 nm was monitored to provide information on the transient concentration of the CO-loss product, denoted as $Mn_2(CO)_8L^*$ or $Mn_2(CO)_9{}^*$, following flash photolysis. A representative decay curve, for $Mn_2(CO)_8P(i\text{-}Pr)_3{}^*$, is shown in Figure 7. Analysis of this and other decay curves as a sum of exponential terms reveals that there are three components. The solid line in Figure 7 shows the fit of the calculated decay to the observed data. Similar results were obtained for L = PMe_3, $P(n\text{-}Bu)_3$, and PPh_3.

Table 2 lists the calculated second-order rate constants corresponding to each component of the decay, assuming that each process is pseudo-first-order, first order each in metal carbonyl intermediate and CO, with the latter present in excess concentration of 13.5 mM.[25] Also listed are second-order rate constants taken from the literature for related processes[11b] and corrected as necessary to reflect the newer assumed value of CO concentration in hexane under 1 atm pressure.

The largest of the rate constants has essentially the same value for all four compounds studied. It matches well the value previously determined for recombination of CO with $Mn_2(CO)_9{}^*$.[11b] This process, which corresponds to only a small fraction of the total change in absorbance, is apparently due to reaction 1. The $Mn_2(CO)_9{}^*$ arises from photochemical loss of phosphine rather than CO from the parent compound. Our results contrast with those of Banister et al.,[26] who observed relatively more extensive phosphine ligand loss on room-temperature photolysis of some $CpMn(CO)_2PR_3$ compounds.

$$Mn_2(CO)_9{}^* + CO \xrightarrow{k_1} Mn_2(CO)_{10} \quad (1)$$

The other two decays we ascribe to recombination of CO with $Mn_2(CO)_8L^*$, according to eqs 2 and 3. The

$$Mn^*(CO)_4{-}Mn(CO)_4L + CO \xrightarrow{k_2} Mn_2(CO)_9L \quad (2)$$

$$Mn(CO)_5{-}Mn^*(CO)_3L + CO \xrightarrow{k_3} Mn_2(CO)_9L \quad (3)$$

faster process is associated with recombination of CO with the isomer in which L is on the Mn center to which the semibridging CO is η^1-bonded, i.e., the {**1**, **3**, **5**} set, eq 2. The slower rate process corresponds to recombination at the other, more crowded Mn center, represented by the {**2**, **4**, **6**} isomer set, eq 3. The fact that the fit to a three-component decay is essentially exact indicates that each of the three components is precisely a single exponential decay. Thus, reactions 2 and 3 represent effectively single processes, suggesting that the equilibration among the equatorial and axial isomers in each of the two sets is rapid at room temperature with respect to the rate of recombination with CO. Although at equilibrium there may be small amounts of the equatorial isomer present in the $Mn_2(CO)_8L^*$ intermediates, as suggested by the spectra of Figure 1 for the products, the axial isomer probably predominates in each case, resulting in the appearance of only a single decay process.

(25) *Carbon Monoxide*; Cargill, R. W., Ed.; Solubility Data Series; Pergamon Press: New York, 1990; pp 51–52.
(26) Banister, J. A.; George, N. W.; Grubert, S.; Howdle, S. M.; Jobling, M.; Johnson, F. P. A.; Morrison, S. L.; Poliakoff, M.; Schubert, U.; Westwell, J. R. *J. Organomet. Chem.* **1994**, *484*, 129.

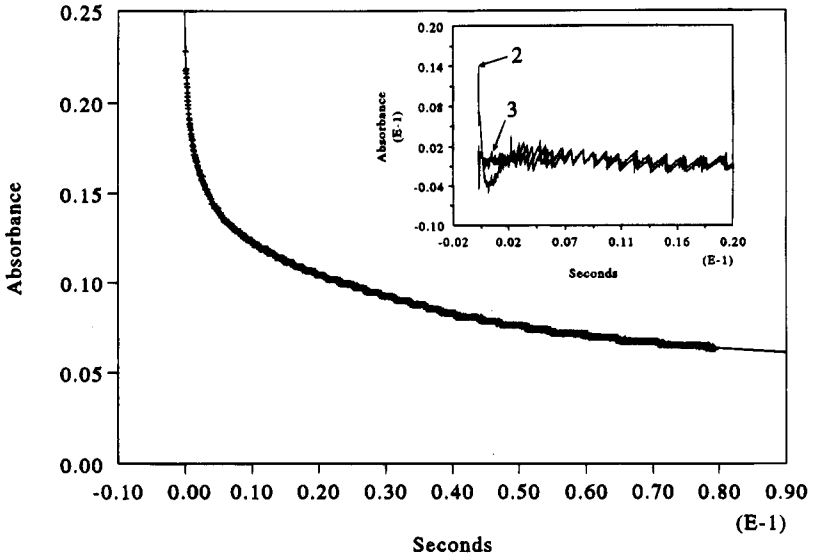

Figure 7. Transient decay of the absorbance at 510 nm following xenon flash lamp photolysis of a 2.0×10^{-5} M hexane solution of $Mn_2(CO)_9P(i\text{-}Pr)_3$ at 296 K. The continuous solid line represents a computed fit to the experimental results. The insert shows the residuals for two- or three-parameter least-squares fits. The two-parameter fit is noticeably poorer at short times.

Table 2. Second-Order Rate Constants under 1 atm CO ([CO] = 13.5 mM)[a]

L	k_1[b]	$10^{-4}k_2$[c]	$10^{-3}k_3$[c]
PMe_3	1.9×10^5	6.1	7.3
$P(n\text{-}Bu)_3$	2.0×10^5	3.1	5.0
PPh_3	2.1×10^5	4.2	4.1
$P(i\text{-}Pr)_3$	1.8×10^5	2.5	1.6
CO	2.1×10^5 [d,f]		
PMe_3	3.5×10^4 [e,f]		
$P(n\text{-}Bu)_3$	6.7×10^3 [e,f]		
$P(i\text{-}Pr)_3$	1.0×10^2 [e,f]		

[a] $M^{-1}\ s^{-1}$. [b] ±15%. [c] ±10%. [d] For $Mn_2(CO)_9$*.[11b] [e] For $Mn_2(CO)_7L_2$*.[11b] [f] Corrected to [CO] = 13.5 mM.

The k_2 values are larger than the k_3 in each case, as expected. The variation among the four compounds studied represents only a 3-fold variation. The k_3 values are approximately 1 order of magnitude smaller than k_2 in each case. One might expect that an increasing steric requirement of the phosphine would be reflected more strongly in the isomer in which the phosphine is bound to the metal center at which CO is recombining. While this is true to a limited degree, the effect is not large; the k_3 values span slightly less than a 5-fold range.

When the k_3 values are compared with the corresponding rate constants for recombination of CO with $Mn_2(CO)_7L_2$*, listed in Table 1, a curious pattern emerges. While k_3 for L = $P(i\text{-}Pr)_3$ is larger than for the disubstituted compound, as expected, k_3 for L = PMe_3 is smaller than for the disubstituted analog, and k_3 for L = $P(n\text{-}Bu)_3$ is essentially the same. The PMe_3 comparison may be related to the fact that in $Mn_2(CO)_8(PMe_3)_2$ the PMe_3 ligands are predominantly in the equatorial positions, whereas PMe_3 is predominantly in the axial position in $Mn_2(CO)_9PMe_3$. Thus, the PMe_3 substituents may be located in equatorial positions in $Mn_2(CO)_7(PMe_3)_2$* and in the axial position in $Mn_2(CO)_8PMe_3$*.

The dinuclear compounds which are the subject of this study are not the only examples in which complexity can arise. In reactions proceeding via thermal or photodissociation of a CO or other ligand from heterodinuclear compounds, or from cluster compounds in which internal rearrangement reactions compete with intermolecular processes, and in various ligand-substituted systems similar considerations might apply.

Acknowledgment. This research was supported by the National Science Foundation through Grant NSFCHE92-13531.

OM940984Z

Bridging Vinylidene Complexes of RhMn and Evidence for Migratory Insertions To Give Terminal Vinyl Groups

Li-Sheng Wang and Martin Cowie*

Department of Chemistry, University of Alberta, Edmonton, Alberta, Canada T6G 2G2

Received November 23, 1994[⊗]

The reaction of the heterobinuclear complex $[RhMn(CO)_4(dppm)_2]$ (**1**) (dppm = $Ph_2PCH_2PPh_2$) with 3-butyn-2-one at −40 °C yields the alkyne-bridged product $[RhMn(CO)_4(\mu\text{-}HC_2C(O)Me)(dppm)_2]$ (**3**), which undergoes a 1,2-hydrogen shift, yielding two isomers of the vinylidene-bridged species $[RhMn(CO)_4(\mu\text{-}CC(H)C(O)Me)(dppm)_2]$ (**4**) as the temperature is raised. Compound **4** undergoes facile CO loss to give $[RhMn(CO)_3(\mu\text{-}\eta^1\text{:}\eta^2\text{-}CC(H)C(O)Me)(dppm)_2]$ (**5**) in which the ketonic moiety of the bridging vinylidene group coordinates to Mn, filling the open coordination site left vacant by the departing CO. Protonation of the alkyne- or vinylidene-bridged species **3**–**5** yields a series of vinyl complexes. Addition of methyl triflate to **4** and **5** yields the respective methyl-substituted vinyl complexes, analogous to the protonation products. In the alkylation of **5** at low temperature an intermediate, $[RhMn(CH_3)(CO)_3(\mu\text{-}\eta^1\text{:}\eta^2\text{-}CC(H)C(O)Me)(dppm)_2][SO_3CF_3]$ (**12**), having a vinylidene bridge and a methyl group terminally bound to Rh, is obtained. The rearrangement of **12** to a vinyl complex upon warming presents evidence for a migratory insertion involving these groups. The structure of **5** was determined by X-ray crystallography. This compound crystallizes in the monoclinic space group $P2_1/n$ (nonstandard setting of $P2_1/c$ [No. 14]) with $a = 14.489(1)$ Å, $b = 15.754(2)$ Å, $c = 24.104(2)$ Å, $\beta = 91.41(1)$ Å, $V = 5500(1)$ Å^3, and $Z = 4$. On the basis of 3980 observations the structure has refined to $R = 0.058$ and $R_w = 0.063$.

Introduction

The coordination and activation of alkynes at two metal centers and subsequent transformations involving these substrates have attracted considerable attention.[1] Our recent interest in such chemistry has been aimed at transformations in which vinyl[2–5] and vinylidene ligands[6–8] are generated. Vinyl complexes can be prepared from the insertion of alkynes into metal–hydrogen bonds, a fundamental process in organometallic chemistry,[9] or they can be generated from the related vinylidene complexes (vide infra).[10] Recent interest in vinyl complexes stems from a proposal suggesting the intermediacy of surface-vinyl species in Fischer–Tropsch chemistry.[11] Vinylidene complexes can be prepared from 1-alkynes via a 1,2-hydrogen shift occurring at the metals.[10,12] It has been suggested that, like vinyl groups, the vinylidene units may also play a key role in Fischer–Tropsch chemistry,[13] as well as in alkyne polymerization[14] and in C–C bond formation in the condensation of alkynes with a number of substrates.[15–23]

The similarity of the vinylidene unit to the isoelectronic carbonyl ligand has been noted,[12] and evidence suggests that a vinylidene group can be an even better π acceptor than CO.[15] Like the CO ligand, the vinylidene group can function as a terminal group bound to one metal or can bridge two or more metals.[10] Furthermore, like CO, the vinylidene bridge can be symmetric[10] or side-on-bound,[24,25] in which case it is σ-bound to one metal and π-bound to another.

In spite of the carbonyl–vinylidene analogy and the suggested role of vinylidene units in C–C bond-forming

[⊗] Abstract published in *Advance ACS Abstracts,* March 15, 1995.

(1) See, for example: (a) Hoffman, D. M.; Hoffmann, R.; Fisel, C. R. *J. Am. Chem. Soc.* **1982**, *104*, 3858 and references therein. (b) Dickson, R. S.; Gatehouse, B. M.; Nesbit, M. C.; Pain, G. N. *J. Organomet. Chem.* **1981**, *215*, 97. (c) Johnson, K. A.; Gladfelter, W. L. *Organometallics* **1992**, *11*, 2534. (d) Dyke, A. F.; Knox, S. A. R.; Naish, P. J.; Taylor, G. E. *J. Chem. Soc., Dalton Trans.* **1982**, 1297. (e) Knox, S. A. R. *J. Organomet. Chem.* **1990**, *400*, 255. (f) Knox, S. A. R. *Pure Appl. Chem.* **1984**, *56*, 81. (g) Casey, C. P.; Meszaros, M. W.; Fagan, P. J.; Bly, R. K.; Marder, S. R.; Austin, E. A. *J. Am. Chem. Soc.* **1986**, *108*, 4043. (h) Casey, C. P.; Fagan, P. J. *J. Am. Chem. Soc.* **1982**, *104*, 4950. (i) Casey, C. P.; Audett, J. D. *Chem. Rev.* **1986**, *86*, 339 and references therein. (j) Takats, J. *J. Cluster Sci.* **1992**, *3*, 479. (k) Dickson, R. S. *Polyhedron* **1991**, *10*, 1995.

(2) Vaartstra, B. A.; Cowie, M. *Organometallics* **1990**, *9*, 1594.

(3) Jenkins, J. A.; Cowie, M. *Organometallics* **1992**, *11*, 2767 and references therein.

(4) Sterenberg, B. T.; Hilts, R. W.; Moro, G.; McDonald, R.; Cowie, M. *J. Am. Chem. Soc.* **1995**, *117*, 245.

(5) Wang, L. S.; Cowie, M. *Can. J. Chem.*, in press.

(6) Xiao, J.; Cowie, M. *Organometallics* **1993**, *12*, 463.

(7) Antwi-Nsiah, F.; Cowie, M. Manuscript in preparation.

(8) Wang, L. S.; Cowie, M. *Organometallics*, in press.

(9) (a) Otsuka, S.; Nakamura, A. *Adv. Organomet. Chem.* **1976**, *14*, 245. (b) Nakamura, A.; Otsuka, S. *J. Mol. Catal.* **1975/76**, *1*, 285.

(10) Bruce, M. I. *Chem. Rev.* **1991**, *91*, 197.

(11) Maitlis, P. M. *Pure Appl. Chem.* **1989**, *61*, 1747.

(12) Werner, H. *Angew. Chem., Int. Ed. Engl.* **1990**, *29*, 1077.

(13) McCandlish, L. E. *J. Catal.* **1983**, *83*, 362.

(14) Alta, H. G.; Engelhardt, H. E.; Rausch, M. D.; Kool, L. B. *J. Organomet. Chem.* **1987**, *329*, 61.

(15) Kolobova, N. E.; Antonova, A. B.; Khitrova, O. M.; Antipin, M. Yu.; Struchkov, Yu. T. *J. Organomet. Chem.* **1977**, *137*, 69.

(16) Moran, G.; Green, M.; Orpen, A. G. *J. Organomet. Chem.* **1983**, *250*, C15.

(17) Casey, C. P.; Miles, W. H.; Fagan, P. J.; Haller, K. J. *Organometallics* **1985**, *4*, 559.

(18) Landon, S. J.; Shulman, P. M.; Geoffroy, G. L. *J. Am. Chem. Soc.* **1985**, *107*, 6739.

(19) Berry, D. H.; Eisenberg, R. *Organometallics* **1987**, *6*, 1796.

(20) Gamble, A. S.; Birdwhistell, K. R.; Templeton, J. L. *Organometallics* **1988**, *7*, 1046.

(21) Etienne, M.; Guerchais, J. E. *J. Chem. Soc., Dalton Trans.* **1989**, 2187.

(22) Trost, B. M.; Dyker, G.; Kulawiec, R. J. *J. Am. Chem. Soc.* **1990**, *112*, 7809.

(23) Selnau, H. E.; Merola, J. S. *J. Am. Chem. Soc.* **1991**, *113*, 4008.

(24) Doherty, N. M.; Elschenbroich, C.; Kneuper, H.-J.; Knox, S. A. R. *J. Chem. Soc., Chem. Commun.* **1985**, 170.

(25) Mercer, R. J.; Green, M.; Orpen, A. G. *J. Chem. Soc., Chem. Commun.* **1986**, 567.

0276-7333/95/2314-2374$09.00/0

reactions, the migratory insertion of a hydrocarbyl ligand and vinylidene unit had until recently[26,27] *not* been clearly demonstrated, although evidence for these insertions had been obtained.[28-30] In fact, it has been noted[26] that complexes containing both a hydrocarbyl and a vinylidene unit are conspicuously lacking. This is surprising when it is recalled that migratory insertions involving CO and other unsaturated substrates are well documented and occupy a position of fundamental importance in the formation of C–C bonds.[31] Although little is known about the migratory-insertion reactions involving terminal vinylidenes, even less is known about the less studied bridging vinylidene unit.

Among the reactions typical of vinylidenes are nucleophilic attack at the α-carbon or electrophilic attack at the β-carbon.[32] While protonation usually occurs at the β-carbon, generating a carbyne moiety,[10] metal basicity can dominate in square-planar iridium(I) complexes to give hydrido–vinylidene complexes via protonation at the metal.[29,33] On the assumption that binuclear complexes containing a bridging vinylidene adjacent to a Rh(I) center could also have Rh as the most basic site, we have investigated the protonation and alkylation (using CH_3^+) reactions of such species in hopes of obtaining hydrido–vinylidene and alkyl–vinylidene complexes, which could be induced to undergo migratory insertions yielding vinyl complexes. The results of this study are reported herein.

Experimental Section

General Procedures. Purified argon and carbon monoxide were obtained from Linde. The 99% carbon-13-enriched carbon monoxide was purchased from Isotec Inc. All gases were used as received. Diethyl ether, hexane, and tetrahydrofuran were dried over Na/benzophenone ketyl, and methylene chloride was dried over P_2O_5. All solvents were distilled under argon before use. The perdeuterated methylene chloride was dried over molecular sieves and deoxygenated by repeated freeze–pump–thaw cycles. The compounds tetrafluoroboric acid–diethyl etherate, triflic acid, trifluoroacetic acid, 3-butyn-2-one, and methyl triflate were used as received from Aldrich. Hydrated rhodium trichloride was received from Johnson Matthey, and $Mn_2(CO)_{10}$ from Strem Chemicals Inc. Compounds $[RhMn(CO)_4(dppm)_2]$ (**1**)[34] and $[RhMn(CO)_4(\mu\text{-}H)(dppm)_2][BF_4]$ (**2**)[35] (dppm = $Ph_2PCH_2PPh_2$) were prepared by the reported procedures. Reactions were routinely carried out under Schlenk conditions.

All routine NMR experiments were conducted on a Bruker AM-400 spectrometer, whereas the $^{13}C\{^{31}P\}$ NMR experiments were run on a Bruker AM-200 spectrometer. For all NMR experiments CD_2Cl_2 (except ^2H experiments for which CH_2Cl_2 was used) was used as solvent. IR spectra were recorded on either a Nicolet 7199 Fourier transform interferometer or a Perkin-Elmer 883 spectrophotometer as solids (Nujol mull or CH_2Cl_2 cast) or CH_2Cl_2 solutions. Elemental analyses were performed by the microanalytical service within the department. The spectral data for all compounds are given in Tables 1 and 2. All compounds were moderately air sensitive in solution and so were routinely handled under dinitrogen or argon.

Preparation of Compounds. (a) $[RhMn(CO)_4(\mu\text{-}HC{=}CC(O)Me)(dppm)_2]$ (3). At −78 °C 10 μL of 3-butyn-2-one (128 μmol) was added to a CD_2Cl_2 solution of $[RhMn(CO)_4(dppm)_2]$ (**1**) (10 mg, 10 μmol in 0.5 mL) in an NMR tube. The compound was characterized by NMR experiments at −40 °C.

(b) $[RhMn(CO)_3(\mu\text{-}C{=}CHC(O)Me)(\mu\text{-}CO)(dppm)_2]$ (4a and 4b). To a CH_2Cl_2 solution of compound **1** (50 mg, 48 μmol in 5 mL) was added 8 μL of 3-butyn-2-one (102 μmol). The solution was stirred under CO for 1 h, causing the color to change from light yellow to red. The solvent was reduced under a rapid flow of CO. The residue was recrystallized from CH_2Cl_2/Et_2O under a CO atmosphere and washed with 5 mL of Et_2O, yielding a red solid (86%). Anal. Calcd for $RhMnP_4C_{58}O_5H_{48}$: C, 62.93; H, 4.34. Found: C, 62.02; H, 4.61.

(c) $[RhMn(CO)_3(\mu\text{-}\eta^1{:}\eta^2\text{-}C{=}CHC(O)Me)(dppm)_2]$ (5). To a suspension of compound **1** (50 mg, 48 μmol in 5 mL of THF) was added 8 μL of 3-butyn-2-one (102 μmol), and the mixture was refluxed for 1 h. Removal of the solvent in vacuo and recrystallization from THF/hexane gave a red-brown crystalline solid (yield 90%). Anal. Calcd for $RhMnP_4C_{57}O_4H_{48}$: C, 63.45; H, 4.45. Found: C, 63.46; H, 4.64.

(d) $[RhMn(trans\text{-}CH{=}CHC(O)Me)(CO)_2(\mu\text{-}CO)_2(dppm)_2][SO_3CF_3]$ (6a). To a CH_2Cl_2 solution of isomers **4a** and **4b** (50 mg, 45 μmol in 5 mL under CO) was added 4.0 μL of CF_3SO_3H (1 equiv) followed by stirring for 0.5 h. The color changed from red to light yellow. Removal of the solvent and recrystallization from CH_2Cl_2/Et_2O gave a yellow solid (70%). Satisfactory elemental analyses could not be obtained owing to sample decomposition.

(e) $[RhMn(trans\text{-}CH{=}CHC(O)Me)(CO)_2(\mu\text{-}CO)_2(dppm)_2][BF_4]$ (6b). To a CH_2Cl_2 solution of isomers **4a** and **4b** (50 mg, 45 μmol in 5 mL under CO) was added 7.8 μL of $HBF_4{\cdot}Et_2O$ (85%, 1 equiv). The color changed from red to light yellow immediately. The solution was stirred for 0.5 h, followed by removal of the solvent and recrystallization from CH_2Cl_2/Et_2O to give a yellow solid (74%).

(f) $[RhMn(CO)_3(\mu\text{-}CCH{=}C(OH)Me)(\mu\text{-}CO)(dppm)_2][BF_4]$ (7). To a CD_2Cl_2 solution of compound **1** (15 mg, 15 μmol in 0.5 mL in an NMR tube) under CO (10 psi) was added 3 μL of 3-butyn-2-one (38 μmol). The color changed from light yellow to red. The NMR tube was left for 3 h; then to this solution was added 3 μL of $HBF_4{\cdot}Me_2O$ (25 μmol) at −78 °C. The compound was characterized by variable-temperature NMR experiments.

(g) $[RhMn(cis\text{-}CH{=}CHC(O)Me)(CO)_2(\mu\text{-}CO)_2(dppm)_2][SO_3CF_3]$ (8a). A 50 mg amount of $[RhMn(\eta^2\text{-}CHCHC(O)Me)(CO)_2(\mu\text{-}CO)(dppm)_2][SO_3CF_3]$ (**9a**) (41 μmol) was dissolved in 5 mL of CH_2Cl_2 and stirred overnight under CO (10 psi). Removal of the solvent and recrystallization from CH_2Cl_2/Et_2O gave an orange solid (86%). Satisfactory elemental analyses could not be obtained owing to sample decomposition.

(h) $[RhMn(cis\text{-}CD{=}CHC(O)Me)(CO)_2(\mu\text{-}CO)_2(dppm)_2][CO_2CF_3]$ (8b). To a CD_2Cl_2 solution of compound **5** (10 mg, 9 μmol in 0.5 mL) in an NMR tube was added 4 μL of CF_3CO_2D (52 μmol). The color changed from deep red-orange to orange immediately. The solution was put under CO (10 psi) for 12 h, followed by characterization by NMR.

(i) $[RhMn(cis\text{-}CH{=}CDC(O)Me)(CO)_2(\mu\text{-}CO)_2(dppm)_2][CO_2CF_3]$ (8c). To a CD_2Cl_2 solution of compound **1** (15 mg, 15 μmol in 0.5 mL) in an NMR tube was added 50 μL of 3-butyn-2-one (639 μmol, excess) at −78 °C. After 1 h, a yellow suspension appeared. The ^{31}P NMR spectrum was run at −40 °C and showed the presence of only compound **3**. A 15 μL

(26) Fryzuk, M. D.; Huang, L.; McManus, N. T.; Paglia, P.; Rettig, S. J.; White, G. S. *Organometallics* **1992**, *11*, 2979.
(27) Wiechemann, R.; Steinert, P.; Schäfer, M.; Werner, H. *J. Am. Chem. Soc.* **1993**, *115*, 9864.
(28) Beevor, R. G.; Freeman, M. J.; Green, M.; Morton, C. E.; Orpen, A. G. *J. Chem. Soc., Chem. Commun.* **1985**, 68.
(29) Höhn, A.; Werner, H. *J. Organomet. Chem.* **1990**, *382*, 255.
(30) Proulx, G.; Bergman, R. G. *J. Am. Chem. Soc.* **1993**, *115*, 9802.
(31) Collman, J. P.; Hegedus, L. S.; Norton, J. R.; Finke, R. G. *Principles and Applications of Organotransition Metal Chemistry*; University Science Books: Mill Valley, CA, 1987.
(32) Kostic, N. M.; Fenske, R. F. *Organometallics* **1982**, *1*, 974.
(33) Höhn, A.; Werner, H. *Angew. Chem., Int. Ed. Engl.* **1986**, *8*, 737.
(34) Antonelli, D. M.; Cowie, M. *Organometallics* **1990**, *9*, 1818.
(35) Wang, L.-S.; McDonald, R.; Cowie, M. *Inorg. Chem.* **1994**, *33*, 3735.

Table 1. Spectroscopic Data for the Compounds

compd	IR, cm^{-1} [a]	NMR[a] δ ($^{31}P\{^1H\}$)	NMR[a] δ (^1H)	NMR[a] δ (^{13}C)
$RhMn(CO)_4(\mu\text{-}HC{\equiv}CC(O)Me)(dppm)_2$ (**3**)		56.7 (m),[e] 15.7 (dm, $^1J_{RhP}$ = 157 Hz)	9.99 (b, 1H, HC≡C),[e] 3.87 (b, 2H, PCH_2P), 2.85 (b, 2H, PCH_2P), 0.59 (s, 3H, CH_3)	228.3 (b, 1CO),[e] 221.3 (b, 1CO), 220.5 (b, 1CO), 195.6 (dt, $^1J_{RhC}$ = 58 Hz, $^2J_{P(Rh)C}$ = 12 Hz, 1CO)
$RhMn(CO)_3(\mu\text{-}CCHC(O)Me)(\mu\text{-}CO)(dppm)_2$ (**4a**)		67.7 (m),[e] 35.2 (dm, $^1J_{RhP}$ = 170 Hz)	6.59 (t, 1H$_\beta$, $^4J_{P(Rh)CCH}$ = 12 Hz),[e] 2.98 (m, 2H, PCH_2P), 2.19 (m, 2H, PCH_2P), 1.55 (s, 3H, CH_3)	244.9 (dt, $^1J_{RhC}$ = 15 Hz, $^2J_{P(Mn)C}$ = 21 Hz, 1CO),[e] 229.5 (t, $^2J_{P(Mn)C}$ = 13 Hz, 1CO), 223.4 (t, $^2J_{P(Mn)C}$ = 18 Hz, 1CO), 206.2 (dt, $^1J_{RhC}$ = 59 Hz, $^2J_{P(Mn)C}$ = 20 Hz, 1CO)
$RhMn(CO)_3(\mu\text{-}CCHC(O)Me)(\mu\text{-}CO)(dppm)_2$ (**4b**)	1964 (w),[d] 1907 (st), 1857 (vs), 1788 (m), 1597 (st); 2002 (sh),[c] 1946 (vs), 1887 (st), 1801 (m), 1600 (w)	64.1 (m),[d] 23.1 (dm, $^1J_{RhP}$ = 163 Hz)	8.09 (t, 1H$_\beta$, $^4J_{P(Rh)CCH}$ = 7 Hz),[d] 3.28 (m, 2H, PCH_2P), 2.46 (m, 2H, PCH_2P), 0.62 (s, 3H, CH_3)	242.0 (dt, $^1J_{RhC}$ = 10 Hz, $^2J_{P(Mn)C}$ = 18 Hz, 1CO),[d] 226.6 (t, $^2J_{P(Mn)C}$ = 17 Hz, 1CO), 223.8 (t, $^2J_{P(Mn)C}$ = 20 Hz, 1CO), 207.6 (dt, $^1J_{RhC}$ = 56 Hz, $^2J_{P(Rh)C}$ = 20 Hz, 1CO), 193.8 (s, 1C, $C(O)CH_3$), 146.8 (s, 1C$_\beta$), 137.4 (dtt, $^1J_{RhC}$ = 4 Hz, $^2J_{P(M)C}$ = 19 Hz, $^2J_{P(M')C}$ = 4 Hz, 1C$_\alpha$), 22.0 (s, 1C, CH_3)
$RhMn(CO)_3(\mu\text{-}\eta^1\text{:}\eta^2\text{-}CCHC(O)Me)(dppm)_2$ (**5**)	1937 (st),[b] 1876 (vs), 1790 (m); 1942 (st),[c] 1893 (vs), 1808 (m)	73.1 (m),[d] 29.6 (dm, $^1J_{RhP}$ = 175 Hz)	3.08 (m, 2H, PCH_2P),[d] 2.68 (m, 2H, PCH_2P), 0.99 (t, 3H, CH_3, $^5J_{P(Mn)OCCH}$ = 2 Hz)	230.1 (t, $^2J_{P(Mn)C}$ = 14 Hz, 1CO),[d] 228.7 (t, $^2J_{P(Mn)C}$ = 20 Hz, 1CO), 206.2 (dt, $^1J_{RhC}$ = 57 Hz, $^2J_{P(Rh)C}$ = 15 Hz, 1CO), 190.8 (s, 1C, $C(O)CH_3$), 140.1 (s, 1C$_\beta$), 138.3 (tt, $^2J_{P(Mn)C}$ = 14.4 Hz, $^2J_{P(Rh)C}$ = 4 Hz, 1C$_\alpha$), 23.8 (s, 1C, CH_3)
$[RhMn(trans\text{-}CH{=}CHC(O)Me)(CO)_2(\mu\text{-}CO)_2(dppm)_2][SO_3CF_3]$ (**6a**)	2036 (st),[b] 1974 (vs), 1845 (w), 1815 (st), 1654 (m); 2026 (vs),[c] 1984 (st), 1838 (sh), 1809 (st), 1654 (m)	58.8 (m),[d] 24.3 (dm, $^1J_{RhP}$ = 134 Hz)	7.99 (dt, 1H$_\alpha$, $^3J_{HCCH}$ = 17 Hz, $^3J_{P(Rh)CH}$ = 7 Hz),[d] 5.32 (d, 1H$_\beta$, $^3J_{HCCH}$ = 17 Hz), 3.16 (m, 4H, PCH_2P), 1.05 (s, 3H, CH_3)	244.1 (dt, $^1J_{RhC}$ = 22 Hz, $^2J_{P(Mn)C}$ = 11 Hz, 2CO),[d] 217.4 (t, $^2J_{P(Mn)C}$ = 17 Hz, 2CO)
$[RhMn(trans\text{-}CH{=}CHC(O)Me)(CO)_2(\mu\text{-}CO)_2(dppm)_2][BF_4]$ (**6b**)	2026 (vs),[c] 1982 (st), 1830 (sh), 1807 (st) 1652 (m)	58.8 (m),[d] 24.3 (dm, $^1J_{RhP}$ = 134 Hz)	8.00 (dt, 1H$_\alpha$, $^3J_{HCCH}$ = 17 Hz, $^3J_{P(Rh)CH}$ = 7 Hz),[d] 5.32 (d, 1H$_\beta$, $^3J_{HCCH}$ = 17 Hz), 3.16 (m, 4H, PCH_2P), 1.04 (s, 3H, CH_3)	244.1 (dt, $^1J_{RhP}$ = 21 Hz, $^2J_{P(Mn)C}$ = 12 Hz, 2CO),[d] 217.4 (t, $^2J_{P(Mn)C}$ = 16 Hz, 2CO)
$[RhMn(CO)_3(\mu\text{-}CCHC(OH)Me)(\mu\text{-}CO)(dppm)_2][BF_4]$ (**7**)		61.3 (m),[h] 23.6 (m)	9.30 (b, 1H, OH),[f] 2.62 (b, 2H, PCH_2P), 0.81 (s, 3H, Me)	236.0 (dt, $^1J_{RhC}$ = 20 Hz, $^2J_{P(Mn)C}$ = 16 Hz, 1CO),[h] 227.4 (t, $^2J_{P(Mn)C}$ = 18 Hz, 1CO) 220.9 (t, $^2J_{P(Mn)C}$ = 20 Hz, 1CO), 206.8 (dt, $^1J_{RhC}$ = 56 Hz, $^2J_{P(Mn)C}$ = 19 Hz, 1CO)
$[RhMn(cis\text{-}CH{=}CHC(O)Me)(CO)_2(\mu\text{-}CO)_2(dppm)_2][SO_3CF_3]$ (**8a**)	2015 (st),[b] 1972 (st), 1857 (m), 1751 (m), 1617 (w); 2014 (vs),[c] 1966 (st), 1859 (st), 1736 (st), 1613 (w)	58.0 (m),[d] 25.3 (dm, $^1J_{RhP}$ = 124 Hz)	9.20 (ddt, 1H$_\alpha$, $^3J_{HCCH}$ = 7.5 Hz, $^2J_{RhCH}$ = 5 Hz, $^3J_{P(Rh)CH}$ = 6 Hz),[d] 6.42 (dd, 1H$_\beta$, $^3J_{HCCH}$ = 7.5 Hz, $^3J_{RhCCC}$ = 2.5 Hz), 3.34 (m, 2H, PCH_2P), 3.15 (m, 2H, PCH_2P), 1.03 (s, 3H, Me)	259.8 (dqui, $^1J_{RhC}$ = 41 Hz, $^2J_{P(Rh)C}$ = $^2J_{P(Mn)C}$ = 9 Hz, 1CO),[d] 231.9 (dt, $^1J_{RhC}$ = 12 Hz, $^2J_{P(Mn)C}$ = 13 Hz, 1CO), 219.7 (t, $^2J_{P(Mn)C}$ = 22 Hz, 1CO), 218.0 (t, $^2J_{P(Mn)C}$ = 15 Hz, 1CO)
$[RhMn(cis\text{-}CD{=}CHC(O)Me)(CO)_2(\mu\text{-}CO)_2(dppm)_2][CO_2CF_3]$ (**8b**)		57.6 (m),[d] 25.1 (dm, $^1J_{RhP}$ = 126 Hz)	6.42 (d, 1H$_\beta$, $^3J_{RhCCH}$ = 2.5 Hz),[d] 3.35 (m, 2H, PCH_2P), 3.13 (m, 2H, PCH_2P), 1.03 (s, 3H, CH_3)	
$[RhMn(cis\text{-}CH{=}CDC(O)Me)(CO)_2(\mu\text{-}CO)_2(dppm)_2][CO_2CF_3]$ (**8c**)		57.8 (m),[d] 25.2 (dm, $^1J_{RhP}$ = 126 Hz)	9.20 (m, 1H$_\alpha$),[d] 3.35 (m, 2H, PCH_2P), 3.13 (m, 2H, PCH_2P), 1.04 (s, 3H, CH_3)	
$[RhMn(\eta^2\text{-}CH{=}CHC(O)Me)(CO)_3(dppm)_2][SO_3CF_3]$ (**9a**)	1981 (vs),[b] 1934 (st), 1820 (st); 1987 (st),[c] 1939 (st), 1818 (m)	67.1 (m),[d] 25.7 (dm, $^1J_{RhP}$ = 107 Hz)	8.04 (dt, $^3J_{HCCH}$ = 10 Hz, $^3J_{P(Mn)CH}$ = 2.5 Hz, 1H$_\beta$),[d] 3.24 (m, 2H, PCH_2P), 2.94 (m, 2H, PCH_2P), 0.98 (t, 3H, CH_3, $^5J_{P(Mn)OCCH}$ = 3 Hz)	228.8 (t, $^2J_{P(Mn)C}$ = 23 Hz, 1CO),[d] 225.0 (t, $^2J_{P(Mn)C}$ = 17 Hz, 1CO), 186.7 (dt, $^1J_{RhC}$ = 80 Hz, $^2J_{P(Rh)C}$ = 18 Hz, 1CO)

Table 1 (Continued)

compd	IR, cm^{-1} [a]	NMR[a] δ ($^{31}P\{^1H\}$)	NMR[a] δ (^1H)	NMR[a] δ (^{13}C) *
[RhMn(η^2-CD=CHC(O)Me)(CO)$_3$-(dppm)$_2$][CO_2CF_3] (**9b**)		67.0 (m,),[d] 25.6 (dm, $^1J_{RhP}$ = 107 Hz)	7.91 (t, $^3J_{P(Mn)CH}$ = 2.5 Hz, 1H$_\beta$),[d] 3.24 (m, 2H, PCH_2P), 2.83 (m, 2H, PCH_2P), 0.92 (t, $^5J_{P(Mn)OCCH}$ = 3 Hz, 3H, CH_3)	
[RhMn(CH_2=CC(O)Me)(CO)$_2$(μ-CO)$_2$-(dppm)$_2$][SO_3CF_3] (**10**)		57.7 (m),[d] 22.4 (dm, $^1J_{RhP}$ = 134 Hz)	5.89 (dt, $^3J_{RhCCH}$ = 3 Hz, $^4J_{PRhCCH}$ = 2 Hz, 1H, CH_2=C),[d] 5.42 (t, $^4J_{PRhCCH}$ = 2 Hz, 1H, CH_2=C), 3.22 (m, 2H, PCH_2P), 3.10 (m, 2H, PCH_2P), 1.20 (s, 3H, CH_3)	249.7 (dm, $^1J_{RhC}$ = 32 Hz, 1CO),[d] 237.8 (dt, $^1J_{RhC}$ = 13 Hz, $^2J_{P(Mn)C}$ = 15 Hz, 1CO), 218.5 (t, $^2J_{P(Mn)C}$ = 19 Hz, 1CO), 217.4 (t, $^2J_{P(Mn)C}$ = 18 Hz, 1CO)
[RhMn(Z-C(Me)=CHC(O)Me)(CO)$_2$-(μ-CO)$_2$(dppm)$_2$][SO_3CF_3] (**11**)	2006 (st),[b] 1953 (st), 1864 (m), 1728 (m), 1605 (w); 2016 (st),[c] 1957 (st), 1869 (st), 1723 (m), 1603 (w)	58.1 (m),[d] 20.0 (dm, $^1J_{RhP}$ = 125 Hz)	6.30 (s, 1H, H$_\beta$),[d] 3.30 (m, 2H, PCH_2P), 3.15 (m, 2H, PCH_2P), 1.57 (s, 3H, CH_3), 1.41 (s, 3H, CH_3)	260.7 (dtt, $^1J_{RhC}$ = 45 Hz, $^2J_{P(Rh)C}$ = $^2J_{P(Mn)C}$ = 8 Hz, 1CO),[d] 230.1 (dt, $^1J_{RhC}$ = 5 Hz, $^2J_{P(Mn)C}$ = 15 Hz, 1CO), 220.0 (t, $^2J_{P(Mn)C}$ = 17 Hz, 1CO), 218.9 (t, $^2J_{P(Mn)C}$ = 20 Hz, 1CO)
[RhMn(Me)(CO)$_3$(μ-η^1:η^2-C=CHC(O)Me)-(dppm)$_2$][SO_3CF_3] (**12**)		62.9 (m),[e] 26.0 (dm, $^1J_{RhP}$ = 101 Hz)	3.40 (b, 2H, PCH_2P),[e] 2.89 (b, 2H, PCH_2P), 1.43 (b, 3H, CH_3), 0.04 (b, 3H, CH_3)	227.6 (t, $^2J_{P(Mn)C}$ = 17 Hz, 1CO),[e] 225.8 (t, $^2J_{P(Mn)C}$ = 13 Hz, 1CO), 193.2 (dt, $^1J_{RhC}$ = 47 Hz, $^2J_{P(Rh)C}$ = 16 Hz, 1CO); 26.0 (s, 1C, CH_3),[i] 20.4 (m, 2C, PCH_2P), 9.0 (db, $^1J_{RhC}$ = 27 Hz, 1C, CH_3)
[RhMn(η^2-MeC=CHC(O)Me)(CO)$_3$-(dppm)$_2$][SO_3CF_3] (**13**)		57.7 (m),[i] 29.1 (dm, $^1J_{RhP}$ = 127 Hz)	6.04 (b, 1H$_\beta$),[i] 3.70 (b, 2H, PCH_2P), 3.44 (b, 2H, PCH_2P), 1.44 (b, 3H, CH_3), 0.72 (b, 3H, CH_3)	231.0 (t, $^2J_{P(Mn)C}$ = 27 Hz, 1CO),[i] 229.7 (t, $^2J_{P(Mn)C}$ = 15 Hz, 1CO), 192.4 (dt, $^1J_{RhC}$ = 49 Hz, $^2J_{P(Rh)C}$ = 14 Hz, 1CO); 29.6 (s, 1C, CH_3),[f] 29.1 (s, 1C, CH_3), 28.5 (m, 2C, PCH_2P)
[RhMn(CO)$_3$(μ-η^1:η^1-MeC=CHC(O)Me)-(dppm)$_2$][SO_3CF_3] (**14**)	1993 (st),[b] 1979 (st), 1910 (st), 1846 (st); 1992 (st),[c] 1926 (st), 1862 (vs)	58.2 (m),[d] 24.2 (dm, $^1J_{RhP}$ = 128 Hz)	6.77 (s, 1H$_\beta$),[d] 3.17 (m, 2H, PCH_2P), 2.43 (m, 2H, PCH_2P), 1.97 (t, 3H, CH_3, $^5J_{P(Mn)OCCH}$ = 3 Hz), 1.27 (s, 3H, CH_3)	231.3 (t, $^2J_{P(Mn)C}$ = 20 Hz, 1CO),[d] 222.2 (t, $^2J_{P(Mn)C}$ = 19 Hz, 1CO), 190.4 (dt, $^1J_{RhC}$ = 77 Hz, $^2J_{P(Rh)C}$ = 15 Hz, 1CO), 202.1 (s, 1C, $C(O)CH_3$), 138.7 (m, 1C$_\alpha$), 36.0 (s, 1C, CH_3), 25.7 (s, 1C, CH_3)

[a] Abbreviations used: IR, w = weak, m = medium, st = strong, vs = very strong; NMR, s = singlet, d = doublet, t = triplet, q = quartet, qui = quintet, m = multiplet, b = broad, or any combination. [b] Nujol mull. [c] CH_2Cl_2 solution. [d] 22 °C. [e] −40 °C. [f] −60 °C. [g] −70 °C. [h] −80 °C. [i] −20 °C. [j] 0 °C.

amount of CF_3CO_2D (195 μmol, excess) was added, causing the solution to turn clear yellow. The NMR spectroscopic characterization was carried out at both −40 °C and room temperature. For the ^2H NMR spectrum 0.5 mL of CH_2Cl_2 was used as solvent instead of CD_2Cl_2.

(j) [RhMn(η^2-CH=CHC(O)Me)(CO)$_2$(μ-CO)(dppm)$_2$][SO_3CF_3] (9a). To a CH_2Cl_2 solution of compound **5** (50 mg, 46 μmol in 5 mL) was added 4.1 μL of CF_3SO_3H (1 equiv). The color changed to orange from deep red-orange immediately. Removal of the solvent and recrystallization from CH_2Cl_2/Et_2O gave an orange compound (96%). Anal. Calcd for $RhMnSP_4F_3O_7C_{58}H_{49}$: C, 56.68; H, 3.99. Found: C, 56.34; H, 3.85.

(k) [RhMn(η^2-CD=CHC(O)Me)(CO)$_2$(μ-CO)(dppm)$_2$][CO_2CF_3] (9b). To a CD_2Cl_2 solution of compound **5** (10 mg, 9 μmol in 0.5 mL) in an NMR tube was added 4 μL of CF_3CO_2D (52 μmol). The color changed from deep red-orange to orange immediately. Characterization was by NMR. To obtain the ^2H NMR spectrum 0.5 mL of CH_2Cl_2 was used as solvent instead of CD_2Cl_2.

(l) [RhMn(C(C(O)Me)=CH_2)(CO)$_2$(μ-CO)$_2$(dppm)$_2$][SO_3CF_3] (10). To a CH_2Cl_2 solution of [RhMn(μ-H)(CO)$_4$(dppm)$_2$]-[SO_3CF_3] (**2**) (50 mg, 42 μmol in 5 mL) was added 100 μL of 3-butyn-2-one (1279 μmol), and the solution was stirred for 5 days. Recrystallization from CH_2Cl_2/Et_2O gave a yellow mixture (86%) which contained [RhMn(*trans*-CH=CHC(O)-Me)(CO)$_2$(μ-CO)$_2$(dppm)$_2$][SO_3CF_3] (**6a**) and [RhMn(C(C(O)-Me)=CH_2)(CO)$_2$(μ-CO)$_2$(dppm)$_2$][SO_3CF_3] (**10**) in a 1:1 ratio, as characterized by NMR experiments.

(m)[RhMn(Z-C(Me)=CHC(O)Me)(CO)$_2$(μ-CO)$_2$(dppm)$_2$]-[SO_3CF_3] (11). To a CH_2Cl_2 solution of isomers **4a** and **4b** (50 mg, 45 μmol in 5 mL under CO) was added 5.0 μL of CF_3-SO_3CH_3 (1 equiv) followed by stirring for 1 h. Removal of the solvent in vacuo and recrystallization from CH_2Cl_2/Et_2O gave a yellow solid (72%). Anal. Calcd for $RhMnP_4SF_3C_{60}H_{51}O_8$: C, 56.69; H, 4.02. Found: C, 56.66; H, 3.82.

(n) [RhMn(CH_3)(CO)$_3$(μ-η^1:η^2-CCHC(O)Me)(dppm)$_2$][SO_3CF_3] (12). To a CD_2Cl_2 solution of [RhMn(CO)$_3$(μ-η^1:η^2-CCHC-(O)Me)(dppm)$_2$] (**5**) (10 mg, 9 μmol in 0.5 mL) in an NMR tube was added 2 μL of $CF_3SO_3CH_3$ (17 μmol) at −78 °C, causing the solution to turn from maroon to red. The compound was characterized by NMR experiments at −40 °C.

(o) [RhMn(CO)$_3$(η^2-MeC=CHC(O)Me)(dppm)$_2$][SO_3CF_3] (13). To a CD_2Cl_2 solution of [RhMn(CO)$_3$(μ-η^1:η^2-CCHC(O)-Me)(dppm)$_2$] (**5**) (10 mg, 9 μmol in 0.5 mL) in an NMR tube was added 2 μL of $CF_3SO_3CH_3$ (17 μmol) at −78 °C. The solution turned black after the solution was warmed up to −20 °C. The compound was characterized by NMR experiments at −20 °C.

(p) [RhMn(CO)$_3$(μ-η^1:η^1-MeC=CHC(O)Me)(dppm)$_2$][SO_3CF_3] (14). To a CH_2Cl_2 solution of compound **5** (50 mg, 46 μmol in 5 mL) was added 5.2 μL of $CF_3SO_3CH_3$ (1 equiv) followed by stirring for 1 h. Removal of the solvent in vacuo and recrystallization from CH_2Cl_2/Et_2O gave a red crystalline

Table 2. Crystallographic Data for Compound 5

formula	$C_{60}H_{54}MnO_5P_4Rh$
formula wt	1136.84
space group	$P2_1/n$ (a non standard setting of $P2_1/c$ [No. 14])
unit cell params	
a (Å)	14.489(1)
b (Å)	15.754(2)
c (Å)	24.104(2)
β (deg)	91.41(1)
V (Å^3)	5500(1)
Z	4
D_{calcd} (g cm^{-3})	1.373
μ (cm^{-1})	6.756
diffractometer	Enraf-Nonius CAD4
temp (°C)	23
radiation (λ (Å))	graphite-monochromated Mo Kα (0.710 69)
cryst–detector distance (mm)	173
scan type	$\theta/2\theta$
scan rate (deg min^{-1})	1.73–6.71
scan width (deg)	0.80 + 0.344 tan θ
max 2θ (deg)	50.0
total unique rflns	9709 ($\pm h+k+l$)
total obs (NO)	3980 ($F_o^2 \geq 3.0\sigma(F_o^2)$)
range of abs cor factors	0.7792–1.1061
final no. of param varied (NV)	404
R^a	0.058
R_w^b	0.063
error in obs of unit wt (GOF)^c	1.615

$^a R = \sum||F_o| - |F_c||/\sum|F_o|$. $^b R_w = [\sum w(|F_o| - |F_c|)^2/\sum wF_o^2]^{1/2}$. ^{c} GOF $= [\sum w(|F_o| - |F_c|)^2/(NO - NV)]^{1/2}$.

solid (84%). Anal. Calcd for $RhMnSP_4F_3O_7C_{59}H_{51}$: C, 57.00; H, 4.11. Found: C, 56.82; H, 4.25.

Reactions. (a) Reaction of Compound 12 with CO. A 50 mg amount of compound **5** (46 μmol) was dissolved in 10 mL of CH_2Cl_2 at −78 °C to which 10 μL of $CF_3SO_3CH_3$ (85 μmol) was added, followed by stirring at −78 °C for 1 h. The color changed to red from maroon. The solution was partially evacuated and put under CO (10 psi). The sample was left in the acetone–dry ice bath overnight and allowed to slowly warm to room temperature. A yellow powder was obtained after recrystallization from Et_2O/CH_2Cl_2 (80% yield). It was shown to be compound **11** by ^{31}P and ^1H NMR spectra.

(b) Reaction of Compound 13 with CO. To a CD_2Cl_2 solution of compound **5** (10 mg, 9 μmol in 0.5 mL) in an NMR tube was added 2 μL of $CF_3SO_3CH_3$ (17 μmol) at −78 °C. The ^{31}P and ^1H NMR spectra showed the formation of compound **13** at −20 °C (black solution). To the solution was added 1 mL of CO by syringe. The sample was left in the acetone–dry ice bath overnight and allowed to slowly warm to room temperature. The ^{31}P and ^1H NMR spectra showed the presence of only compound **11**.

X-ray Data Collection. Red crystals of $[RhMn(CO)_3(\mu\text{-}\eta^1\text{:}\eta^2\text{-}C{=}C(H)C(O)CH_3)(dppm)_2]\cdot(CH_3)_2CO$ (**5**·$(CH_3)_2CO$) were grown by diffusion of Et_2O into an acetone solution of the complex. Several of these were mounted and flame sealed in glass capillaries under an atmosphere of the solvent vapor to minimize solvent loss. Data were collected on an Enraf-Nonius CAD4 diffractometer using Mo Kα radiation. Unit cell parameters were obtained from a least-squares refinement of the setting angles of 25 reflections in the range $20.0° < 2\theta < 23.8°$. The monoclinic diffraction symmetry and the systematic absences ($h0l$, $h + l \neq 2n$; $0k0$, $k \neq 2n$) defined the space group as $P2_1/n$ (a nonstandard setting of $P2_1/c$ [No. 14]).

Intensity data were collected at 22 °C by using the $\theta/2\theta$ scan technique, covering reflections having indices of the form $\pm h,+k,+l$ to a maximum of $2\theta = 50°$. Of the 10 259 data collected, 9709 were unique, and of these, 3980 were observed ($I \geq 3\sigma(I)$). Backgrounds were scanned for 25% of the scan width on either side of the scan. Three reflections were chosen as intensity standards and were remeasured after every 120 min of X-ray exposure. The intensities of these standards dropped by *ca* 7.5% over the duration of data collection, so a linear correction was applied to the data. The data were processed in the usual way, with a value of 0.04 for p employed to downweight intense reflections.[36,37] Absorption corrections were applied to the data according to the method of Walker and Stuart.[38] See Table 2 for crystal data and additional information on X-ray data collection.

Structure Solution and Refinement. The structure of $RhMn(CO)_3(\mu\text{-}\eta^1\text{:}\eta^2\text{-}C{=}C(H)C(O)CH_3)(dppm)_2]\cdot(CH_3)_2CO$ was solved in space group $P2_1/n$ using standard Patterson and Fourier techniques. Full-matrix, least-squares refinements minimized the function $\sum w(|F_o| - |F_c|)^2$, where the weighting factor $w = 4F_o^2/\sigma^2(F_o)^2$. Atomic scattering factors[39] and anomalous dispersion terms[40] were taken from the usual tabulations. All hydrogen atoms were observed but were generated at idealized calculated positions by assuming a C–H bond length of 0.95 Å and the appropriate sp^2 or sp^3 geometry, except for the acetone hydrogens, which were not included. All hydrogens within the complex molecule were included in calculations with fixed, isotropic thermal parameters 20% greater than those of the attached atoms. Their positions were recalculated after every few cycles of refinement. In the final cycles of refinement the vinylidene hydrogen atom was allowed to refine and was shown to be well-behaved. There was no evidence of secondary extinction; therefore no correction was applied.

The final model with 404 parameters varied converged to $R = 0.058$ and $R_w = 0.063$. In the final difference Fourier map the highest residuals (0.47–0.65 e/Å^3) were found in the vicinities of Rh and the phenyl groups. The atomic coordinates and thermal parameters for selected atoms of compound **5** are given in Table 3, and selected bond lengths and angles are given in Table 4.

Results and Discussion

(a) Vinylidene Complexes. As a continuation of our studies into the reactivities of alkynes at two metal centers we have investigated reactions of $[RhMn(CO)_4(dppm)_2]$ (**1**) with terminal alkynes, with the goal of inducing alkyne-to-vinylidene transformations. Those alkynes not having strongly electron-withdrawing substituents, such as acetylene, phenylacetylene, and propyne, do not react with **1**, even when present in a large excess for extended periods of time. However, 3-butyn-2-one, having an electron-withdrawing C(O)Me substituent, reacts readily with **1**, even at −40 °C. The first species observed at this temperature is the alkyne-bridged product, $[RhMn(CO)_4(\mu\text{-}HC{\equiv}CC(O)Me)(dppm)_2]$ (**3**). All the NMR spectroscopic data (^1H, ^{13}C, ^{31}P) are very similar to those of $[RhMn(CO)_4(\mu\text{-}RC_2R)(dppm)_2]$ (R = CO_2Me, CF_3), which have recently been characterized;[5] therefore **3** is assigned an analogous structure, having a conventional alkyne bridge as shown in Scheme 1. The $^{13}C\{^1H\}$ NMR spectrum of **3** shows three terminal carbonyls on Mn (δ 220–228) and one on Rh (δ 195.6), with only the last one showing Rh-coupling

(36) Doedens, R. J.; Ibers, J. A. *Inorg. Chem.* **1967**, *6*, 204.
(37) Programs used were those of the Enraf-Nonius Structure Determination Package by B. A. Frenz, in addition to local programs by R. G. Ball.
(38) Walker, N.; Stuart, D. *Acta Crystallogr., Sect. A: Found. Crystallogr.* **1983**, *39*, 158.
(39) (a) Cromer, D. T.; Waber, J. T. *International Tables for Crystallography*; Kynoch Press: Birmingham, England, 1974; Vol. IV, Table 2.2A. (b) Stewart, R. F.; Davidson, E. R.; Simpson, W. T. *J. Chem. Phys.* **1965**, *42*, 3175.
(40) Cromer, D. T.; Liberman, D. *J. Chem. Phys.* **1970**, *53*, 1891.
(41) Werner, H.; Alonso, F. J. G.; Otto, H.; Peters, K.; von Schnering, H. G. *Chem. Ber.* **1988**, *121*, 1565.

Table 3. Atomic Coordinates and Equivalent Isotropic Thermal Parameters for the Core Atoms of 5[a]

atom[a]	*x*	*y*	*z*	*B*, Å^2 [b]
Rh	0.12279(5)	0.22450(5)	−0.08839(3)	2.89(2)*
Mn	0.1503(1)	0.34558(9)	−0.18423(6)	2.63(4)*
P(1)	0.2693(2)	0.1729(2)	−0.0932(1)	2.86(7)*
P(2)	0.3022(2)	0.3075(2)	−0.1827(1)	2.87(7)*
P(3)	−0.0338(2)	0.2241(2)	−0.1021(1)	3.17(7)*
P(4)	−0.0064(2)	0.3598(2)	−0.1923(1)	3.15(7)*
O(1)	0.1179(5)	0.2338(5)	0.0366(3)	5.9(2)*
O(2)	0.1604(5)	0.4233(4)	−0.0739(3)	4.3(2)*
O(3)	0.1902(5)	0.5187(4)	−0.2235(3)	5.4(2)*
O(4)	0.1438(4)	0.2967(4)	−0.2637(2)	3.5(2)*
C(1)	0.1205(7)	0.2327(6)	−0.0105(4)	3.6(3)*
C(2)	0.1547(6)	0.3825(6)	−0.1156(4)	3.5(3)*
C(3)	0.1741(7)	0.4495(6)	−0.2095(4)	3.5(3)*
C(4)	0.1251(6)	0.2231(6)	−0.1701(3)	2.6(2)*
C(5)	0.1166(7)	0.1732(6)	−0.2162(4)	3.8(3)*
C(6)	0.1272(6)	0.2185(7)	−0.2660(4)	3.8(3)*
C(7)	0.1203(8)	0.1777(8)	−0.3230(4)	5.7(4)*
C(8)	0.3251(6)	0.1983(6)	−0.1590(4)	2.7(3)*
C(9)	−0.0728(7)	0.2671(6)	−0.1701(4)	3.7(3)*
H(5)	0.098(6)	0.110(6)	−0.207(4)	2.8(24)

[a] Phenyl carbons and solvent atoms are given in the supplementary material. [b] Anisotropically refined atoms are marked with an asterisk (*). Displacement parameters for the anisotropically refined atoms are given in the form of the equivalent isotropic Gaussian displacement parameter, B_{eq}, defined as $^4/_3[a^2\beta_{11} + b^2\beta_{22} + c^2\beta_{33} + ab(\cos\gamma)\beta_{12} + ac(\cos\beta)\beta_{13} + bc(\cos\alpha)\beta_{23}]$.

Table 4. Selected Bond Lengths (Å) and Angles (deg) for 5

	Distances		
Rh−P(1)	2.278(2)	Mn−C(4)	1.995(8)
Rh−P(3)	2.285(2)	O(1)−C(1)	1.138(8)
Rh−C(1)	1.883(9)	O(2)−C(2)	1.196(9)
Rh−C(4)	1.971(7)	O(3)−C(3)	1.167(9)
Mn−P(2)	2.282(2)	O(4)−C(6)	1.26(1)
Mn−P(4)	2.284(3)	C(4)−C(5)	1.36(1)
Mn−O(4)	2.065(5)	C(5)−C(6)	1.41(1)
Mn−C(2)	1.752(9)	C(5)−H(5)	1.05(8)
Mn−C(3)	1.783(9)	C(6)−C(7)	1.52(1)
	Angles		
P(1)−Rh−P(3)	156.17(9)	O(4)−Mn−C(4)	78.1(3)
P(1)−Rh−C(1)	96.6(3)	C(2)−Mn−C(3)	90.9(4)
P(1)−Rh−C(4)	84.7(2)	C(2)−Mn−C(4)	99.4(3)
P(3)−Rh−C(1)	95.9(3)	C(3)−Mn−C(4)	169.8(4)
P(3)−Rh−C(4)	84.0(2)	Mn−O(4)−C(6)	114.3(6)
C(1)−Rh−C(4)	176.7(4)	Rh−C(1)−O(1)	176.8(9)
P(2)−Mn−P(4)	169.6(1)	Mn−C(2)−O(2)	166.6(7)
P(2)−Mn−O(4)	86.5(2)	Mn−C(3)−O(3)	176.9(8)
P(2)−Mn−C(2)	93.4(3)	Rh−C(4)−Mn	99.6(4)
P(2)−Mn−C(3)	93.0(3)	Rh−C(4)−C(5)	144.8(7)
P(2)−Mn−C(4)	85.6(2)	Mn−C(4)−C(5)	115.6(6)
P(4)−Mn−O(4)	86.3(2)	C(4)−C(5)−C(6)	113.1(8)
P(4)−Mn−C(2)	93.5(3)	C(4)−C(5)−H(5)	113(4)
P(4)−Mn−C(3)	94.7(3)	C(6)−C(5)−H(5)	134(4)
P(4)−Mn−C(4)	85.6(2)	O(4)−C(6)−C(5)	118.9(8)
O(4)−Mn−C(2)	177.4(3)	O(4)−C(6)−C(7)	117.7(9)
O(4)−Mn−C(3)	91.7(3)	C(5)−C(6)−C(7)	123.4(9)

(58 Hz). In the ^{1}H NMR spectrum the acetylenic hydrogen appears at δ 9.99, but shows no coupling to either Rh or the phosphorus nuclei. The absence of coupling involving this hydrogen makes it impossible to unambiguously determine whether the alkyne unit is bound as shown in Scheme 1, or whether it has the opposite orientation in which the C(O)Me moiety is adjacent to Mn. The orientation shown should be sterically favored, having the less encumbered end of the alkyne adjacent to the more crowded $Mn(CO)_3P_2$ end of the complex, but would be less favorable for the subsequent oxidative addition into the alkyne C−H bond, a presumed step in the conversion to vinylidene-bridged species.[12,29] Upon warming solutions of **3**, two new compounds, **4a**and **5**, start to appear at *ca.* −20 °C, while warming to *ca.* 0 °C results in the appearance of a third species, **4b**. When ambient temperature is reached, compounds **4b** and **5** are the major species, with **4a** being present at only *ca.* 10% of the amount of **4b**. Compounds **4a** and **4b** are isomers of the vinylidene-bridged species $[RhMn(CO)_4(\mu\text{-}CC(H)C(O)Me)(dppm)_2]$, differing only in the orientations of the substituents on the vinylidene β-carbon. The major isomer (**4b**) shows four carbonyl resonances in the ^{13}C-{^{1}H} NMR; the high-field signal corresponds to a carbonyl which is terminally bound to Rh ($^1J_{Rh-C}$ = 56 Hz), the intermediate two are terminally bound to Mn, and the low-field carbonyl is bound primarily to Mn with a semibridging interaction with Rh ($^1J_{Rh-C}$ = 10 Hz). For this isomer the ^{13}C resonances for the carbons within the vinylidene unit could be obtained using unenriched alkyne. The α-carbon appears at δ 137.4 and displays coupling to Rh (4 Hz) and to all phosphorus nuclei (one pair with 19 Hz coupling and one pair with 4 Hz coupling). Since overnight data acquisition on a 400 MHz instrument (for which we do not have appropriate heteronuclear decoupling capabilities) was necessary to observe these signals, no ^{31}P-decoupling experiments could be carried out, so we do not know whether the larger coupling is to the Rh- or the Mn-bound phosphorus nuclei. However, the surprisingly small coupling to Rh suggests that the Rh−C_α interaction may be weak, leading us to propose that coupling to the Rh-bound phosphines will also be weak. The chemical shift for C_α in our RhMn compounds appears to be anomalous compared to other bridging vinylidenes,[10] in which these carbons typically resonate *downfield* from δ 230. Even the complex $[Cp(P^iPr_3)Rh(\mu\text{-}CO)(\mu\text{-}CCH_2)Mn(CO)Cp]$,[41] having the same metal combination as our compounds, has the C_α resonance at δ 279, in the typical region. However, in related vinylidene-bridged complexes of Rh and Ir, we routinely observe chemical shifts for C_α *upfield* of δ 150,[5,7] with some even as high-field as δ 100. In addition compound **5**, which also has a high-field shift for C_α, has been structurally characterized, confirming the vinylidene formulation (vide infra). The ^{13}C signals for C_β, the ketonic carbonyl, and the methyl group appear at δ 146.8, 193.8, and 22.0, respectively, and ^{13}C APT experiments support these assignments. The ^{1}H resonance for the methyl group of **4b** appears as a singlet at δ 0.62, and the vinylidene hydrogen appears as a triplet at δ 8.09, displaying coupling to the Rh-bound phosphorus nuclei of 7 Hz, as shown by the appropriate heteronuclear decoupling experiments. The minor isomer (**4a**) has very similar spectroscopic properties to **4b**, with the major difference being in the ^{1}H NMR resonance for the vinylidene hydrogen which appears at δ 6.59, again showing coupling (12 Hz) to the Rh-bound phosphorus nuclei. It appears that **4b** is the thermodynamically favored isomer owing to steric considerations, with the more bulky C(O)Me substituent being directed away from the more crowded Mn center. In the IR spectrum the ketonic carbonyl stretch is observed at 1600 cm^{-1}.

The third species present (**5**) is shown (vide infra) to be a tricarbonyl species resulting from carbonyl loss from **4**. With this is mind, an equilibrium mixture of only **4a** and **4b** (in *ca.* 10:90 molar ratio) can be prepared by allowing **3** to warm up in the presence of CO, and

Scheme 1

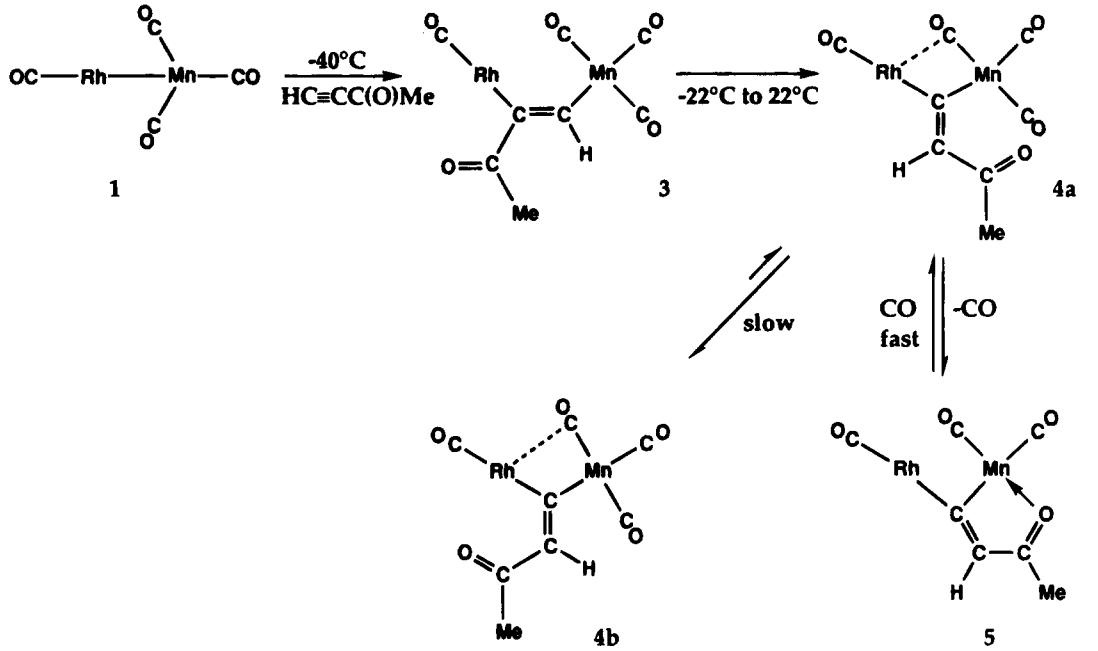

conversely **5** results as the sole species by refluxing **4a** and **4b** in THF under an N_2 flush. Rearrangement of **4a** to **4b** is shown to be slow compared to CO attack on **5**, the former appearing as the only species at −40 °C under CO with slow equilibration to the 10:90 mix of isomers as the temperature is raised to 20 °C. On the basis of the structure established for **5** (vide infra), the structure of isomer **4a**, which is formed rapidly upon reaction of **5** with CO, can be assigned as shown, with rearrangement by rotation about the vinylidene unit, to give the thermodynamic product, being slow. Although rotation about the C=C bond in terminal vinylidenes is apparently facile,[12] a similar rotation in vinylidene-bridged complexed appears less common, but has been observed.[7,42]

The $^{13}C\{^1H\}$ NMR spectrum of **5** confirms the tricarbonyl formulation, displaying three equal intensity carbonyl resonances, with one bound terminally to Rh and two bound terminally to Mn. The C_α resonance of the bridging vinylidene unit appears at δ 138.3 and is coupled to all four phosphorus nuclei. Surprisingly no coupling to Rh is observed (although it should be recalled that this coupling in **4b** was only 4 Hz). Resonances for C_β, the ketonic carbon, and the methyl carbon appear as singlets at δ 140.1, 190.8, ad 23.8, respectively. Again, ^{13}C APT experiments support these assignments. The ^1H NMR spectrum is unexceptional, apart from the methyl resonance which shows 2 Hz coupling to the Mn-bound phosphorus nuclei; the vinylidene-proton resonance was not observed and is presumably obscured by phenyl resonances. It is also significant that no stretch for the ketone carbonyl was observed in the IR spectrum. This fact and the ^{31}P-coupling to the methyl protons in the ^1H NMR suggests that coordination of the ketonic oxygen to Mn occurs to occupy the coordination site vacated by CO in the transformation from **4a**. This coordination mode has previously been noted in related vinylidene-bridged compounds of manganese,[43-45] and has been confirmed in the present study by the X-ray structure determination of **5**, as shown in Figure 1.

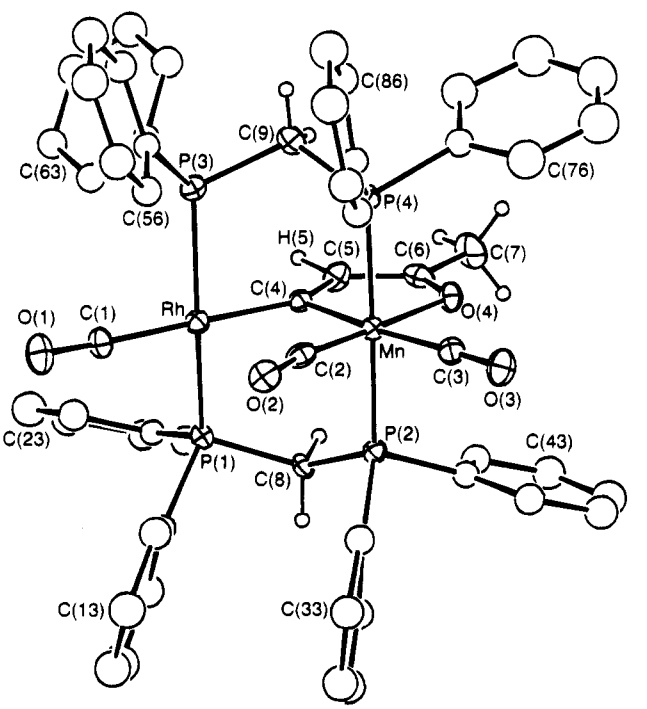

Figure 1. A perspective view of $[RhMn(CO)_3(\mu\text{-}\eta^1{:}\eta^2\text{-}CC(H)C(O)Me)(dppm)_2]$ (**5**) showing the numbering scheme. Thermal ellipsoids are shown at the 20% level except for hydrogens, which are shown artificially small or are omitted for phenyl groups. The numbering of the phenyl carbons starts at the ipso carbon and works sequentially around the ring.

Compound **5** crystallizes with 1 equiv of acetone, which has the expected geometry and displays no unusual contacts with the complex molecule. The bridging diphosphines have the common trans geometry at both

(42) Afzol, D.; Lukehart, C. M. *Organometallics* **1987**, *6*, 546.

metal centers, and all parameters within these units are normal. At rhodium the geometry is square planar, having the vinylidene bridge opposite a carbonyl, whereas at Mn the geometry is distorted octahedral, having the carbonyls opposite the vinylidene unit and the dative bond from the ketonic carbonyl group. The major distortions from an idealized octahedral geometry result from the bite of the bidentate ligand, which gives rise to a C(4)–Mn–O(4) angle of 78.1(3)° within the five-membered metallacycle. Within this metallacycle the bond lengths suggest delocalized bonding. Although no single parameter is substantially different from that expected for a localized bonding model, all differ in the direction expected for delocalization. Therefore, the C(4)–C(5) distance (1.36(1) Å) is slightly longer than that expected (1.34 Å) when conjugated with a ketone group, the C(5)–C(6) distance (1.41(1) Å) is shorter than expected (1.464 Å) for a single bond between conjugated olefin and ketone moieties, and the C(6)–O(4) distance (1.26(1) Å) is also longer than expected for a C=O bond in this environment (1.22 Å).[46] By contrast the C(6)–C(7) distance is exactly as expected for a $C(sp^2)$–$C(sp^3)$ bond in a ketone.[46] In addition all angles within the metallacycle are consistent with sp^2 hybridization of the carbon and oxygen atoms, keeping in mind the slight strain within the ring. The Mn–C(4) and Mn–O(4) distances are essentially as expected.[41,43–45]

Although the lack of coupling of the vinylidene C_α nucleus to Rh, together with the smaller coupling of C_α to the Rh-bound phosphorus nuclei than to those on Mn, suggests a weaker interaction of the vinylidene unit with Rh, this does not manifest itself in the structural parameters. Therefore the Rh–C(4) distance is actually shorter than Mn–C(4) (1.971(7) *vs* 1.995(8) Å), in spite of an opposite prediction based on the covalent radii of the metals. The Rh–Mn separation (3.030(1) Å) is significantly longer than the single bond (2.667(1) Å) in $[Cp(P^iPr_3)Rh(\mu\text{-}CO)(\mu\text{-}CCH_2)Mn(CO)Cp]$,[41] consistent with the absence of a metal–metal bond. However, the Rh–C(4)–Mn angle of 99.6(4)° is more acute than expected, and there seems to be no reason that the Rh–Mn distance could not expand to allow an undistorted sp^2 geometry at C(4). This suggests that the two metals are drawn together. Such a compression of the nominally nonbonded metal–metal separation has been noted in a related system, induced by a weak semibridging carbonyl interaction.[35] The carbonyl group C(2)O(2) in **5** is bent away from Rh slightly, consistent with a semibridging interaction, giving a Mn–C(2)–O(2) angle of 166.6(7)°, but the long Rh–C(2) contact (2.618(8) Å) suggests a weak interaction at best.

The vinylidene unit is not perpendicular to the Rh–Mn vector but is tilted substantially toward Mn, as shown by the Rh–C(4)–C(5) and Mn–C(4)–C(5) angles of 144.8(7)° and 115.6(6)°, respectively. Presumably this tilting occurs to accommodate coordination of the ketonic oxygen at the sixth site, giving Mn the octahedral geometry. This offers further support that Rh is being drawn in the direction of C(2) since movement in the opposite direction would give less distortion at C(4). A similar tilting of a bridging vinylidene unit has been observed in related complexes in which the vinylidene forms part of a five-membered metallacycle ring.[41,43–45]

In an attempt to detect the interconversion of compounds **4a** and **4b**, spin-saturation transfer experiments were attempted by irradiating the ^{31}P resonance corresponding to the Mn-bound phosphines in **4b**. No change in the resonances of **4a** was noted, presumably because exchange is too slow. However, when this experiment was carried out by irradiating the corresponding resonance (δ 73.1) of compound **5**, a decrease in intensity of 80% was noted in the appropriate resonance (δ 67.7) of **4a**. This indicates that reversible CO loss from **4a** and concomitant coordination of the ketonic carbonyl is occurring readily in solution.

(b) Vinylidene Reactivity. (i) Protonation. Having isolated and characterized the vinylidene-bridged complexes **4** and **5**, it was of interest to investigate their reactivities. In particular we were interested in the transformation of the vinylidene bridges to substituted vinyl moieties, either by protonation or alkylation. It was felt that the square planar Rh(I) center could be basic enough to react with electrophiles such as H^+ and CH_3^+, and that the resulting rhodium–hydride and rhodium–alkyl moieties might undergo migratory insertion with the bridging vinylidene units. Protonation of a mixture of **4a** and **4b** gives only one species at ambient temperature, the vinyl complex $[RhMn(trans\text{-}CH{=}C(H)C(O)Me)(CO)_2(\mu\text{-}CO)_2(dppm)_2][SO_3CF_3]$ (**6a**), as shown in Scheme 2. This product is analogous to the vinyl compounds $[RhMn(CR{=}C(H)R)(CO)_2(\mu\text{-}CO)_2(dppm)_2]^+$ (R = CO_2Me, CF_3) described earlier,[5] in which the vinyl groups were terminally bound to Rh. The trans geometry for **6a** (in which the C(O)Me group is opposite Rh) is as expected if the initial protonation were to occur at the vacant site on Rh, adjacent to the vinylidene unit in isomer **4b**. Significantly no species corresponding to a cis arrangement of vinyl hydrogens is observed, even though both isomers **4a** and **4b** were initially present.

At temperatures between −80 and −40 °C protonation of **4** yields an intermediate **7** in between 5% and 20% yield, transforming to **6**, even at these low temperatures. Owing to the presence of **4a**, **4b**, and **6**, together with impurities (ether, excess acid, etc.), not all the proton resonances of **7** could be identified. In the ^1H NMR spectrum, a low-field signal at δ 9.30, one of the dppm-methylene resonances at δ 2.62, and the methyl resonance at δ 0.81 were observed. The vinyl-hydrogen resonance and the second dppm-methylene resonance were not identified. Significantly, no evidence of a hydride resonance was observed. Compound **7** is assigned as the enol intermediate $[RhMn(CO)_3(\mu\text{-}CC(H){=}C(OH)Me)(\mu\text{-}CO)(dppm)_2][BF_4]$ on the basis of the broad low-field ^1H signal which appears to be typical for an enol proton.[47] Keto–enol tautomerism generally occurs via deprotonation and reprotonation at an alternative site.[48] Whether the Rh center or the anion of the acid functions as the base is not known, although

(43) García Alonso, F. J.; Riera, V.; Ruiz, M. A.; Tiripicchio, A.; Tiripicchio Camellini, M. *Organometallics* **1992**, *11*, 370.
(44) Adams, R. D.; Chen, G.; Chen, L.; Yin, J. *Organometallics* **1993**, *12*, 2644.
(45) Kolobova, N. E.; Ivanov, L. L.; Zhvanko, O. S.; Batsanov, A. S.; Struchkov, Yu. T. *J. Organomet. Chem.* **1985**, *279*, 419.
(46) Allen, F. H.; Kennard, O.; Watson, D. G.; Brammer, L.; Orpen, A. G.; Taylor, R. *J. Chem. Soc., Perkin Trans. 2* **1987**, 51.
(47) (a) Silverstein, R. M.; Bassler, G. C. *Spectrometric Identification of Organic Compounds*, 2nd ed.; John Wiley and Sons: New York, NY, 1981; Ch. 4. (b) Bergens, S. H.; Bosnich, B. *J. Am. Chem. Soc.* **1991**, *113*, 958.
(48) Marsh, J. *Advanced Organic Chemistry*, 4th ed.; John Wiley and Sons: New York, NY, 1992; p 585.

Scheme 2

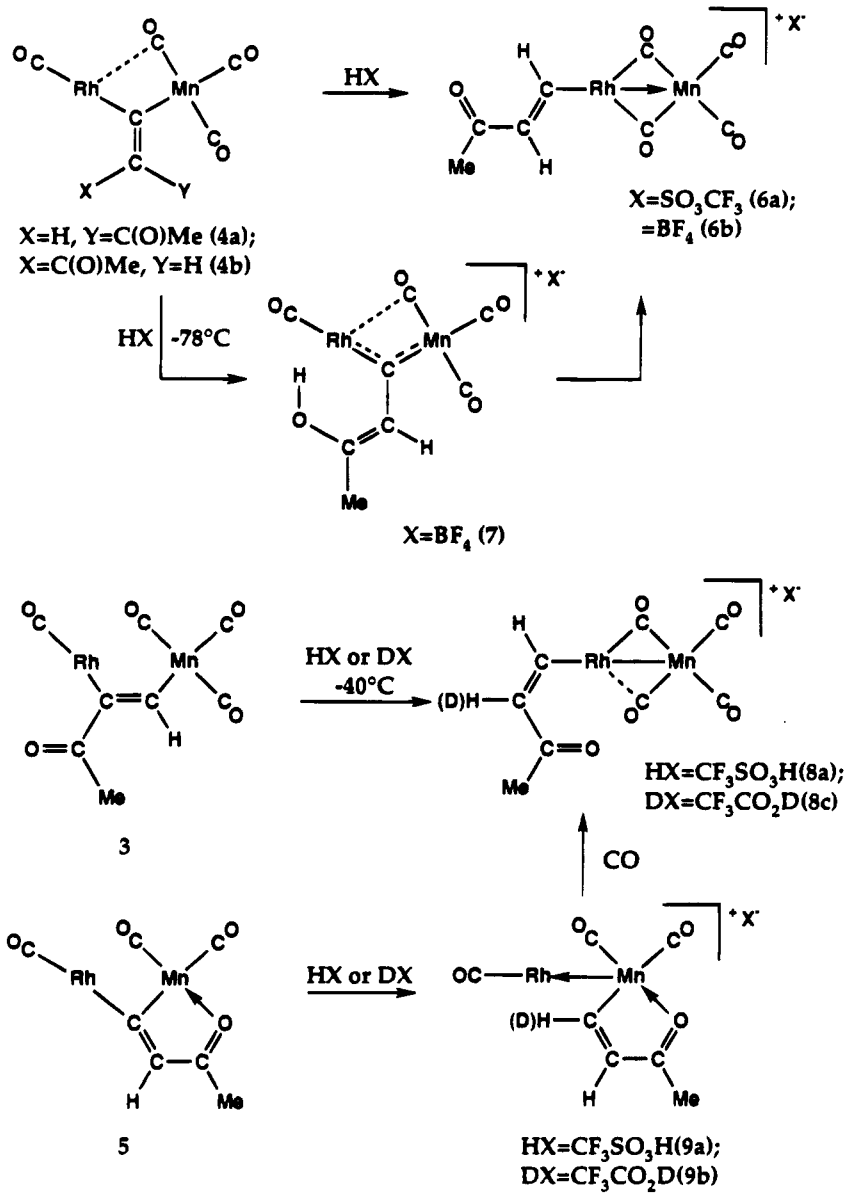

as noted, no high-field ^1H signals, which would indicate proton transfer to the metal, was observed. If we assume the involvement of a rhodium–hydride intermediate in the protonation of **4a** and **4b**, the observation of only one isomer of **6** can be rationalized by the transfer of the enol proton to Rh, followed by rapid migratory insertion of the resulting hydride and vinylidene groups; only the orientation in which the enol oxygen is adjacent to Rh will favor proton transfer to this metal. We suggest that both isomers **4a** and **4b** are protonated to yield the respective enols but that their interconversion is facile by rotation about $C_\alpha-C_\beta$ single bond, yielding **7** which can then yield the vinyl product **6**.

Protonation of the alkyne-bridged precursor (**3**) yields the vinyl species **8**, in which the major difference to **6** is a cis arrangement of vinyl hydrogens in the new product. The ^1H NMR spectrum of **8** shows the vinyl protons at δ 9.20 (H_α) and 6.42 (H_β) with mutual coupling of 7.5 Hz, consistent with the cis arrangement shown in Scheme 2. Additional coupling of H_α to Rh ($^2J_{Rh-H}$ = 5 Hz) and to the Rh-bound phosphorus nuclei of 6 Hz is also observed. In addition, the β-hydrogen also shows coupling to Rh of 2.5 Hz. Subtle differences in the $^{13}C\{^1H\}$ NMR spectrum, compared to **6**, show a carbonyl resonance at δ 259.8 with relatively strong coupling to Rh (41 Hz) as well as equal coupling to all four phosphorus nuclei, indicating a conventionally bridged CO, another at δ 231.9 coupling weakly to Rh (12 Hz), and two other higher field resonances for the terminal carbonyls on Mn. The difference in the two bridged carbonyls of **8** may result from steric interactions, in which the mutually cis arrangement of the C(O)Me group and Rh forces one of the bridged carbonyls away from Rh. A similar affect was noted in related vinyl compounds of RhMn.[5] Confirmation of the vinyl hydrogen assignments comes from reaction of **3** with CF_3CO_2D to give [RhMn(*cis*-CH=C(D)C(O)Me)-$(CO)_2(\mu\text{-}CO)_2$(dppm)$_2$][CF_3CO_2]; as expected the signal for the β-hydrogen is absent in the ^1H NMR spectrum, but appears in the ^2H NMR. Similarly species **8** having deuterium incorporated into the α position can be prepared (vide infra) giving the expected NMR results. The generation of a *cis*-vinyl species **8** from the *cis*-

Scheme 3

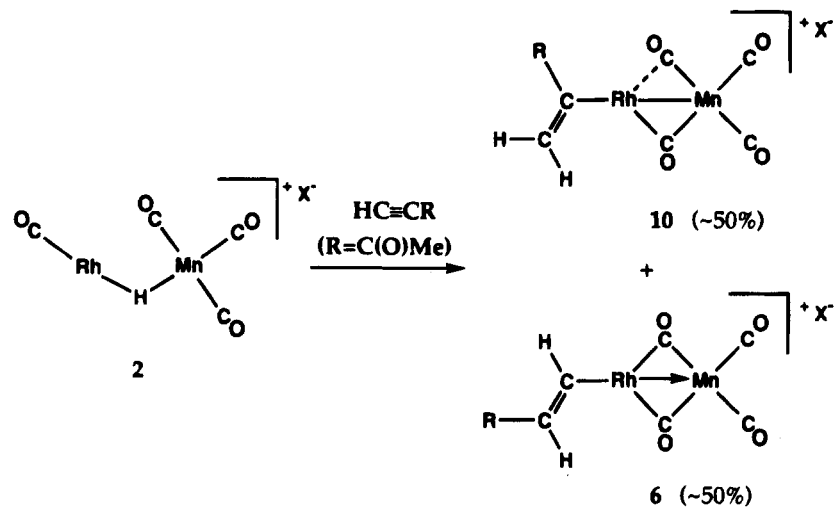

dimetalated olefinic precursor **3** is unexpected since rotation about the C=C bond has apparently occurred, such that the originally cis H_α and C(O)Me groups are now in a mutually trans arrangement. It is not clear how this occurs.

Protonation of the vinylidene species **5** yields the vinyl product $[RhMn(\eta^2\text{-}CH{=}C(H)C(O)Me)(CO)_3(dppm)_2][SO_3CF_3]$ (**9**), in which the vinyl group chelates the Mn atom, binding through C_α and the ketone oxygen. Although no metal–hydride species was observed, **9** is the anticipated product of protonation of **5** at Rh followed by hydrogen transfer to C_α accompanied by cleavage of the $Rh-C_\alpha$ bond. As was observed in **5**, which also has a five-membered metallacycle involving Mn, the methyl resonance in the ^1H NMR spectrum of **9** displays coupling to the Mn-bound ^{31}P nuclei ($^5J_{P-H}$ = 3 Hz). The resonance for H_α is not observed, being obscured by phenyl resonances; however, H_β appears at δ 8.04, showing 10 Hz coupling to H_α and 2.5 Hz coupling to the phosphorus nuclei on Mn. The magnitude of $H_\alpha H_\beta$ coupling is in line with a cis arrangement, which is also required by the chelated structure. If the protonation is carried out using CF_3CO_2D, the product having deuterium in the α position is obtained, and this signal is observed in the ^2H NMR spectrum at δ 7.66 (confirming the proposal that this resonance in the ^1H NMR spectrum is obscured by phenyl protons). As expected, no deuterium–hydrogen coupling is observed between the vinylic H and D atoms; H_β displays coupling (2.5 Hz) to only the ^{31}P nuclei on Mn. Unlike all species in which the ketonic carbonyl is not coordinated, but like the precursor (**5**), the IR spectrum of **9** shows no ketonic carbonyl stretch. Compound **9** can be transformed to **8** under CO, so replacing the donor bond from the ketone oxygen by a carbonyl group is also accompanied by migration of the vinyl group from Mn to Rh with concomitant transfer of the CO from Rh to Mn. This was the route used to generate **8** having deuterium incorporation at the α position (vide supra).

It is significant that protonation of the vinylidene-bridged species **4** and **5** has *not* yielded carbyne-bridged products as frequently occurs by attack of electrophiles at the β-carbon.[10] Instead the products obtained are consistent with the intervention of a Rh-hydride intermediate (although no such intermediate was observed). The formation of vinyl products via protonation of vinylidene complexes parallels an earlier study by Werner,[49] in which no metal–hydride species were detected, and is an interesting contrast to other work by the Werner group in which metal–hydride species rearranged by 1,3-hydride transfer to give carbynes.[29,33] Even though no metal–hydride species were observed in this part of our study, the formation of vinyl rather than carbyne products leads us to propose that they result from migratory insertion involving the vinylidene and hydride groups.

Vinyl species can also be generated by the insertion of alkynes into the metal–hydride bonds of $[RhMn(CO)_4(\mu\text{-}H)(dppm)_2][SO_3CF_3]$ (**2**).[5] Therefore **2** reacts with 3-butyn-2-one to give two isomers of the vinyl compound $[RhMn(C_2H_2C(O)Me)(CO)_4(dppm)_2][SO_3CF_3]$ (**6** and **10**) in approximately equal proportions, as shown in Scheme 3. These isomers differ mainly in the stereochemistry of the vinyl C=C bond, depending on whether alkyne insertion yields the products having a geminal (**10**) or trans arrangement (**6**) of vinyl hydrogens. In isomer **6** the trans vinyl hydrogens resonate at δ 7.99 and 5.32 for H_α and H_β, respectively, in the ^1H NMR spectrum. The 17 Hz coupling between these protons is consistent with a trans arrangement, and in addition H_α shows additional coupling ($^3J_{P(Rh)-H}$ = 7 Hz) to the two Rh-bound phosphorus nuclei. The $^{13}C\{^1H\}$ NMR spectrum for this isomer shows two carbonyl resonances, one corresponding to two bridging groups (δ 244.1, $^1J_{Rh-C}$ = 22 Hz) and the other corresponding to two terminal groups (δ 217.4) bound to Mn. The slightly smaller Rh–C coupling observed for the bridging carbonyls (compared to that for the symmetrically bridged CO in **10**) suggests asymmetric bridges for these groups, with stronger binding to Mn. In addition to the four carbonyl stretches (two terminal, two bridging) in the IR spectrum, the ketonic stretch is observed at 1654 cm^{-1}. For the other isomer (**10**) the geminal protons on the β-carbon of the vinyl group appear at δ 5.89 and 5.42 in the ^1H NMR spectrum. Both protons show coupling of 2 Hz to the Rh-bound phosphorus nuclei, and the lower-field signal also displays 3 Hz coupling to Rh. No coupling between the geminal protons is observed. Isomer **10** differs subtly from **6** in the natures of the carbonyl groups, displaying four carbonyl resonances in

(49) Wolf, J.; Werner, H. *J. Organomet. Chem.* **1987**, 413.

Scheme 4

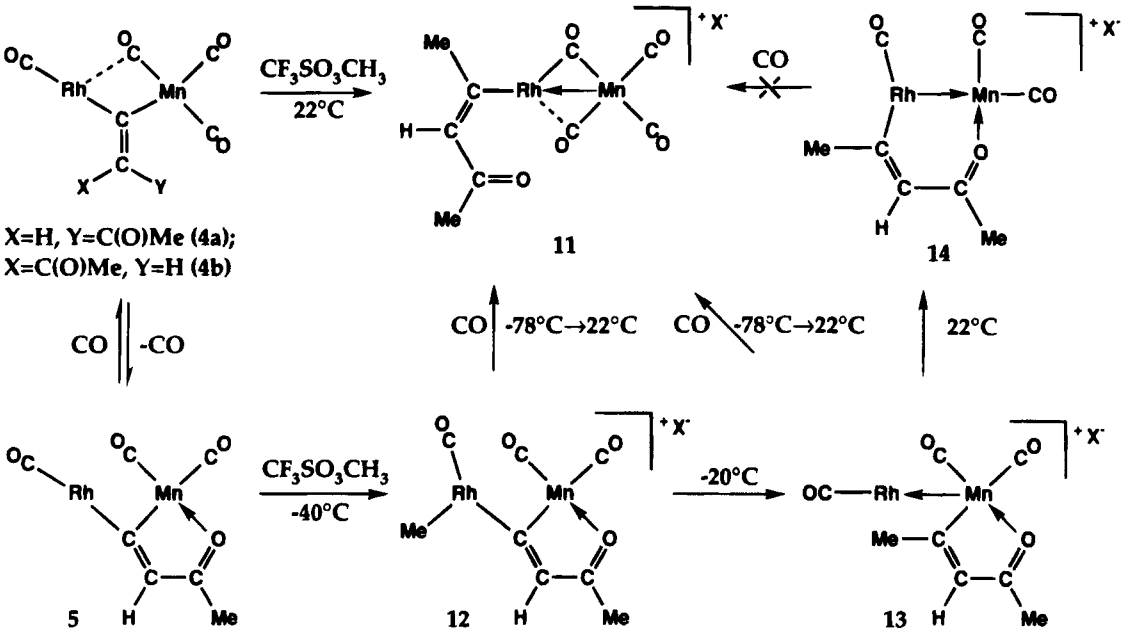

the $^{13}C\{^1H\}$ NMR spectrum. The lowest-field signal (δ 249.7) shows coupling of 32 Hz with Rh, suggesting a conventional, bridged geometry, whereas the signal at δ 237.8 displays coupling to Rh of only 13 Hz, indicating that it is semibridging. Again we suggest that this difference is steric in origin, in which the bulkier C(O)Me group on the α-carbon forces the adjacent carbonyl away from Rh, weakening the Rh–CO interaction. This is compensated for by a stronger interaction between Rh and the other carbonyl, as reflected in the larger $^1J_{Rh-C}$ value for this carbonyl.

These subtle structural differences between **10** and **6** demonstrate how adjacent metal centers can "tune" the electron distributions within the complex to changes in ligand binding modes. In **10** one carbonyl is semibridging while the other is symmetrically bridging, having weak and strong interactions with Rh, respectively. In **6** the strengthening of the semibridging interaction with Rh is compensated for by a weakening of the other Rh–CO interaction such that both bridging carbonyls are asymmetrically bound. These changes in carbonyl binding modes, with each carbonyl being a one-electron donor to each metal for the symmetrically or asymmetrically bridged CO's or a two-electron donor to Mn in the semibridging CO,[50] are accompanied by a change in the nature of the Rh–Mn bond as shown in Scheme 3. Although such bonding descriptions are formalisms, they do demonstrate how the polarity of a metal–metal bond can change to compensate for changes in ligand binding.

(ii) Alkylation. Reaction of the vinylidene-bridged isomers **4a** and **4b** with methyl triflate yields [RhMn(MeC=C(H)C(O)Me)(CO)$_2$(μ-CO)$_2$(dppm)$_2$][SO_3CF_3] (**11**) as the sole observed product over the temperature range from −80 to 22 °C. Unlike protonation, which yields a vinyl group in which the proton ends up on the α-carbon *cis* to the C(O)Me group, the methyl carbocation ends up trans to C(O)Me to give a product that is analogous to **8** rather than **6** (see Scheme 4). This analogy to **8** carries through to the binding of the bridging CO's, in which one is semibridging while the other is conventionally bridging, presumably for the reasons discussed earlier. The ^1H NMR spectrum of **11** shows the methyl signals as singlets at δ 1.57 and 1.41 and the vinyl hydrogen at δ 6.30. The arrangement shown about the vinyl C=C bond is supported by proton NOE experiments which indicate that the vinyl proton has a positive NOE effect with both sets of methyl protons, whereas the two methyl groups show no NOE effect with each other. If **11** results from an undetected Rh–methyl intermediate followed by migratory insertion with the vinylidene group, it would appear that isomer **4a** is the favored target, since this isomer would yield the appropriate stereochemistry at the double bond. Attack at Rh in this isomer, as opposed to the more predominant **4b**, would appear to be steric in origin with the larger C(O)Me substituent blocking attack at Rh in the latter.

The tricarbonyl, vinylidene-bridged **5** also reacts with methyl triflate, but in this case a couple of key intermediates can be detected at low temperature. At −40 °C the first intermediate observed, [RhMnCH_3(CO)$_3$(μ-CC(H)C(O)Me)(dppm)$_2$][SO_3CF_3] (**12**), is a metal–alkyl species having the methyl group bound to Rh as shown in Scheme 4. This is the first complex in this study in which an alkyl unit is adjacent to a vinylidene unit, and as suggested earlier,[26] such species are unusual. In the ^1H NMR spectrum of **12** the resonance for the Rh-bound methyl group is broad, obscuring the expected 2–3 Hz coupling to Rh. However, the $^{13}C\{^1H\}$ NMR study shows the broad methyl resonance at δ 9.0 with coupling of 27 Hz to Rh, clearly indicating a direct bond between the two. In addition, the ^{13}C chemical shift for this methyl group is at higher field than the alkyne-bound methyl group, falling in the range observed for other Rh–methyl complexes.[51] The methyl group of the C(O)Me moiety appears as a broad singlet at δ 26.0 in the $^{13}C\{^1H\}$ NMR spectrum with no obvious coupling to the Mn-bound phosphines, as was noted in the related

(50) Colton, R.; McCormick, M. J. *Coord. Chem. Rev.* **1980**, *31*, 1.

(51) Mann, B. E.; Taylor, B. F. *^{13}C NMR Data for Organometallic Compounds*; Academic Press: London, 1981; p 44.

metallacycles (**5**, **9**). It is noteworthy that upon reaction with CH_3^+ the value of $^1J_{Rh-P}$ drops from 175 Hz in **5** to 101 Hz in **12**, consistent with an increase in oxidation state from +1 to +3.[52] An analogous drop (from 155 to 104 Hz) was previously observed upon protonation of $[RhMn(CO)_4(\mu\text{-}RC_2R)(dppm)_2]$ to give $[RhMnH(CO)_4(\mu\text{-}RC_2R)(dppm)_2]^+$,[5] a product that is rather similar in formulation to **12**, except having a bridging alkyne (R = CO_2Me, CF_3) rather than vinylidene unit.

Upon warming a solution of **12** to −20 °C, a transformation to $[RhMn(CO)_3(\eta^2\text{-}MeC{=}C(H)C(O)Me)(dppm)_2][SO_3CF_3]$ (**13**) occurs in which migration of the methyl group from Rh to the vinylidene ligand occurs, apparently yielding the chelated vinyl complex. The $^{13}C\{^1H\}$ NMR spectrum shows two Mn-bound (δ 231.0, 229.7) and one Rh-bound (δ 192.4, $^1J_{Rh-C}$ = 49 Hz) carbonyls, in addition to singlets for the methyl groups at δ 29.6 and 29.1. The lack of coupling of these methyl groups to phosphorus or Rh and the downfield shift from that observed for the $Rh-CH_3$ group in **12** suggests that the methyl group now resides on the transformed vinyl moiety. Unfortunately, attempts to verify the geometry of the vinyl group in **13** by NOE experiments failed. The migratory insertion of the bridged vinylidene and methyl groups in **12** to give the vinyl moiety in **13** is unprecedented. This transformation can be regarded as reductive elimination from the Rh^{3+} center in **12** to give Rh^+ in **13**, and is supported by the increase in the value of $^1J_{Rh-P}$ that is observed (to 127 Hz in **13**). In the ^1H NMR spectrum, the methyl resonances appear as singlets at δ 1.44 and 0.72 and the vinyl proton appears at δ 6.04.

Under a CO atmosphere both **12** and **13** transform to **11**. This product was well characterized and offers support for the formulation of **13**. Furthermore, the transformation of **12** to **11** offers an additional example of migratory insertion of the bridging vinylidene group and the methyl group to give a substituted vinyl species. It may be that alkylation of **4** proceeds via intermediate **12**, since compounds **4a** and **5** were shown earlier to be in equilibrium. Alkylation to yield **12** would then be followed by attack of the CO initially lost from **4a**.

At ambient temperature compound **13** is unstable, even in the absence of CO, and gives a new species, $[RhMn(CO)_3(\mu\text{-}\eta^1{:}\eta^1\text{-}MeC{=}C(H)C(O)Me)(dppm)_2][SO_3CF_3]$ (**14**) in which the chelated vinyl moiety appears to adopt a bridging arrangement. In the $^{13}C\{^1H\}$ NMR spectrum the three carbonyl resonances are not unlike those of **13**, apart from the larger $^1J_{Rh-C}$ value (77 Hz) for **14**. The ketonic carbon is observed at δ 202.1, the vinyl C_α carbon is a complex multiplet at δ 138.7, and the methyl singlets appear at δ 36.0 and 25.7. Since the alkyne used was not isotopically enriched, overnight data acquisition was required, ruling out heteronuclear decoupling experiments. For this reason we were unable to resolve coupling of C_α to Rh. In the ^1H NMR spectrum one methyl group (δ 1.97) displays 3 Hz coupling to the Mn-bound phosphines, reminiscent of the coupling observed in **5** and **9** in which the ketone oxygen is coordinated to Mn. Although compound **13**, containing the chelating vinyl ketone group, reacts with CO to displace the ketone oxygen and cause migration of the vinyl group to Rh, compound **14** is inert to CO. Presumably in **13** the ketone oxygen is labile owing to the strain within the five-membered metallacycle. Migration of the vinylic carbon to Rh in **14** generates a six-membered metallacycle in which the intraligand strain is much less, resulting in decreased lability of the ketone oxygen.

(52) Nixon, J. F.; Pidcock, A. *Annu. Rev. NMR Spectrosc.* **1969**, *2*, 345.

Summary and Conclusions

When reaction of $[RhMn(CO)_4(dppm)_2]$ (**1**) with the terminal alkyne 3-butyn-2-one is monitored at low temperature, the expected product having the alkyne coordinated in a bridging position, parallel to the metals, is observed. However, upon warming to ambient temperature this species undergoes a 1,2-hydrogen shift to give a vinylidene-bridged product, $[RhMn(CO)_4(\mu\text{-}CC(H)C(O)Me)(dppm)_2]$ (**4**). Compound **4** is observed as two isomers which are related by apparent rotation about the C=C bond of the bridging vinylidene unit. Transformation of one isomer to the other occurs readily at ambient temperature, requiring less than $^1/_2$ h to reach an equilibrium mixture. Loss of one carbonyl from the Mn center is facile, assisted by the formation of a donor bond from the ketone oxygen of the vinylidene group to yield $[RhMn(CO)_3(\mu\text{-}\eta^1{:}\eta^2\text{-}CC(H)C(O)Me)(dppm)_2]$ (**5**).

Although protonation of a vinylidene ligand generally occurs at the β-carbon, the C(O)Me substituent on this carbon appears to lower its nucleophilicity so bridging alkylidyne species are not obtained. In compound **4** the initial site of protonation appears to be at the ketone oxygen of the bridging vinylidene group, with subsequent proton transfer to the α-carbon. No metal−hydride species was observed, so it is not clear whether such an intermediate was present. Protonation of the tricarbonyl species **5** again yields a vinyl product in which the vinyl group is chelating Mn, bound through the α-carbon and the ketone oxygen, and reaction of this product with CO results in replacement of the ketone-to-Mn dative interaction by a carbonyl group and also in migration of the vinyl group from Mn to Rh. The isomer observed has the two vinyl hydrogens in a mutually cis arrangement, in contrast to the protonation product of **4**, in which the vinylic hydrogens are trans. These vinyl products are consistent with protonation at Rh at some stage in the reaction, followed by a migratory insertion of the vinylidene group.

The reaction of the vinylidene-bridged species **4** and **5** with methyl triflate yields the corresponding vinyl products in which the carbocation has again ended up on the α-carbon, again suggesting primary attack at Rh, followed by migration to the vinylidene groups. In the case of the tricarbonyl species **5**, the unusual vinylidene-bridged methyl complex $[RhMn(CH_3)(CO)_3(\mu\text{-}\eta^1{:}\eta^2\text{-}CC(H)C(O)Me)(dppm)_2][SO_3CF_3]$ is observed at −40 °C and is shown to have the methyl group coordinated to Rh. Upon warming, this species undergoes a migratory insertion of the methyl and vinylidene ligands to give a tricarbonyl vinyl species in the absence of CO or a tetracarbonyl vinyl species in the presence of CO. These appear to be the only clearly defined examples involving the migratory insertion of a bridged vinylidene group; even examples involving terminal vinylidenes are not common.

It is significant that attack by the electrophiles H^+ and CH_3^+ on an equilibrium mixture of **4a** and **4b** yields

only one product in each case, and it is even more significant that these products differ in their geometries about the vinyl C=C bond. In both cases the observations can be rationalized by the intervention of a rhodium–hydride or a rhodium–alkyl intermediate with subsequent migratory insertion involving the vinylidene group. Protonation appears to occur initially at the ketonic oxygen to give an enol product for which only one isomer can give facile proton transfer to Rh giving the vinyl product observed. Alkylation of a **4a**/**4b** mixture apparently occurs directly at Rh, with attack being favored in isomer **4a**, in which there is better access to Rh. Again, subsequent migratory insertion of this product would yield the observed product.

Acknowledgment. We thank the Natural Sciences and Engineering Research Council of Canada and the University of Alberta for financial support and Dr. R. McDonald of the departmental Structure Determination Laboratory for technical assistance.

Supplementary Material Available: Tables of positional and thermal parameters for the phenyl carbons and solvent atoms, anisotropic thermal parameters, idealized hydrogen parameters, and bond distances and angles for the dppm ligands and solvent molecule (6 pages). Ordering information is given on any current masthead page.

OM940895M

Synthesis, Redox Reactivity, and X-ray Diffraction Structures of the Rhenium Carbonyl Complexes *fac*-ReBr(CO)$_3$(bma) and [*fac*-ReBr(CO)$_3$(bma)][Cp$_2$Co]. Structural Consequences of Electron Accession in *fac*-ReBr(CO)$_3$(bma)

Kaiyuan Yang, Simon G. Bott,* and Michael G. Richmond*

Center for Organometallic Research and Education, Department of Chemistry, University of North Texas, Denton, Texas 76203

Received December 29, 1994[⊗]

Solvent displacement in the rhenium complex ReBr(CO)$_3$(THF)$_2$ (**2**) by the redox-active diphosphine ligand 2,3-bis(diphenylphosphino)maleic anhydride (bma) affords the corresponding bma-substituted complex *fac*-ReBr(CO)$_3$(bma) (**3**) in near quantitative yield. The same product is also obtained, albeit in lower yield, from BrRe(CO)$_5$ (**1**) and bma in refluxing 1,2-dichloroethane. *fac*-ReBr(CO)$_3$(bma) has been isolated and characterized in solution by IR and NMR (^{31}P and ^{13}C) spectroscopies. The oxidation/reduction chemistry of *fac*-ReBr(CO)$_3$(bma) was explored by cyclic and rotating disk electrode voltammetric techniques. Two diffusion-controlled one-electron reduction processes at $E_{1/2} = -0.33$ V and $E_{1/2} = -1.23$ V and an irreversible oxidation at $E_{pa} = 1.58$ V are observed in CH_2Cl_2/TBAP at a platinum electrode. The reductive electrochemistry is discussed in the context of a scheme involving the formal reduction of the bma ligand, a property that is common with other known 18 + δ paramagnetic compounds containing an ancillary bma ligand. Reductive bulk electrolyses have been carried out on **3**, and the product of one-electron reduction, [fac-ReBr(CO)$_3$(bma)]$^{\bullet-}$ (**4**), has been characterized by IR and UV–vis spectroscopies. Large infrared frequency shifts in the carbonyl stretching bands of the bma ligand in [*fac*-ReBr(CO)$_3$(bma)]$^{\bullet-}$ are observed, as expected for a reduction process confined to the electron-accepting bma ligand. The unequivocal identity of [*fac*-ReBr(CO)$_3$(bma)]$^{\bullet-}$ was independently established by the isolation and structural characterization of the product formed from the cobaltocene reduction of *fac*-ReBr(CO)$_3$(bma). The molecular structures of compounds **3** and **4** have been determined by single-crystal X-ray diffraction analysis. *fac*-ReBr(CO)$_3$(bma) crystallizes in the triclinic space group $P\bar{1}$: $a = 9.855(1)$ Å, $b = 12.1153(4)$ Å, $c = 13.7751(8)$ Å, $\alpha = 85.322(4)°$, $\beta = 73.828(6)°$, $\gamma = 75.812(6)°$, $V = 1531.3(2)$ Å^3, $Z = 2$, $d_{calc} = 1.771$ g·cm^{-3}; $R = 0.0552$, $R_w = 0.0771$ for 3342 observed reflections. The radical anion [*fac*-ReBr(CO)$_3$(bma)][Cp$_2$Co], as the CH_2Cl_2 solvate, crystallizes in the monoclinic space group $C2/c$: $a = 39.600(3)$ Å, $b = 10.2625(2)$ Å, $c = 23.253(2)$ Å, $\beta = 120.278(7)°$, $V = 8161(1)$ Å^3, $Z = 8$, $d_{calc} = 1.793$ g·cm^{-3}; $R = 0.0511$, $R_w = 0.0598$ for 3811 observed reflections. These two structures permit a direct comparison regarding the consequences of electron accession in *fac*-ReBr(CO)$_3$(bma). Extended Hückel calculations have been performed on the model compound *fac*-ReBr(CO)$_3$(H$_4$bma), the results of which are used to support the electrochemical data and the proposed reduction pathway involving electron addition to the bma ligand.

Introduction

The photochemical and photophysical study of compounds based on XRe(CO)$_3$(N–N) (where X = halide; N–N = diimine ligand) has played a prominent role in the elucidation of the mechanistic details related to intramolecular energy-transfer processes[1] and in the catalytic reduction of carbon dioxide.[2] Such diimine-substituted complexes are attractive as starting compounds in these studies because of the fact that the lowest unoccupied molecular orbital belongs to the π^* system of the diimine ligand.[3] The use of mono- and

⊗ Abstract published in *Advance ACS Abstracts*, April 15, 1995.

(1) (a) Geoffroy, G. L.; Wrighton, M. S. *Organometallic Photochemistry*; Academic Press: New York, 1979. (b) Wrighton, M. S.; Morse, D. L. *J. Am. Chem. Soc.* **1974**, *96*, 998. (c) Worl, L. A.; Duesing, R.; Chen, P.; Ciana, L. D.; Meyer, T. J. *J. Chem. Soc., Dalton Trans.* **1991**, 849 and references therein.

(2) (a) Hawecker, J.; Lehn, J.-M.; Ziessel, R. *J. Chem. Soc., Chem. Commun.* **1983**, 536; **1984**, 328. (b) Kutal, C.; Weber, M. A.; Ferraudi, G.; Geiger, D. *Organometallics* **1985**, *4*, 2161. (c) Hawecker, J.; Lehn, J.-M.; Ziessel, R. *Helv. Chim. Acta* **1986**, *69*, 1990.

(3) For reports dealing with diimine ligand reduction, see: (a) van Outersterp, J. W. M.; Hartl, F.; Stufkens, D. J. *Inorg. Chem.* **1994**, *33*, 2711. (b) Duesing, R.; Tapolsky, G.; Meyers, T. J. *J. Am. Chem. Soc.* **1990**, *112*, 5378. (c) Sahai, R.; Rillema, D. P.; Shaver, R.; Van Wallendale, S.; Jackman, D. C.; Boldaji, M. *Inorg. Chem.* **1989**, *28*, 1022. (d) Baiano, J. A.; Carlson, D. L.; Wolosh, G. M.; DeJesus, D. E.; Knowles, C. F.; Szabo, E. G.; Murphy, W. R., Jr. *Inorg. Chem.* **1990**, *29*, 2327. (e) Tapolsky, G.; Duesing, R.; Meyer, T. J. *Inorg. Chem.* **1990**, *29*, 2285. (f) Glyn, P.; George, M. W.; Hodges, P. M.; Turner, J. J. *J. Chem. Soc., Chem. Commun.* **1989**, 1655.

0276-7333/95/2314-2387$09.00/0

bidentate phosphine-substituted compounds derived from the *fac*-$ReX(CO)_3$ fragment would not function as suitable probe compounds for such studies since the LUMO is not predicted to be a ligand-based orbital but rather a much higher lying Re−CO antibonding orbital.[4]

Given the dearth of *fac*-$XRe(CO)_3(PR_3)_2$ compounds possessing an accessible π^* phosphine-based orbital,[5] we set out to prepare such a compound using the redox-active ligand 2,3-bis(diphenylphosphino)maleic anhydride (bma). This ligand displays unique electronic properties in comparison to the common diphosphine ligands such as dppm, dppe, and (*Z*)-$Ph_2PCH{=}CHPPh_2$ because it possesses a low-lying π^* orbital that is delocalized over the maleic anhydride ring. An organometallic compound with this type of LUMO is expected to serve as an efficient electron reservoir by stabilizing electron counts in excess of 18-electrons. In the case of a one-electron reduction, the resulting radical is expected to exhibit significant unpaired spin density on the bma ligand, which leads to the preferred $18 + \delta$ description for this genre of compound.[6] Elegant spectroscopic and structural studies that demonstrate this principle have been presented by the groups of Fenske[7,8] and Tyler[9,10] for a variety of mononuclear compounds bearing a bma ligand. Recently, we have presented data showing this same trend in the binuclear complex $Co_2(CO)_4(\mu\text{-PhC}{\equiv}\text{CPh})$(bma) (chelating and bridging isomers).[11,12] Electrochemical reduction of either isomer affords the corresponding radical anion $Co_2(CO)_4(\mu\text{-PhC}{\equiv}\text{CPh})(\text{bma})^{\bullet-}$, which was shown to contain a reduced bma ligand. We are currently investigating bma-substituted polynuclear complexes with the goal of obtaining a compound whose LUMO is formed from bma/cluster framework orbitals. It is hoped that this type of composite LUMO would yield compounds possessing superior electron reservoir properties.

Herein we report our results on the synthesis, characterization, and redox properties of *fac*-$ReBr(CO)_3$(bma). A study on the effects of electron accession in *fac*-$ReBr(CO)_3(\text{bma})^{0/1-}$ is facilitated by the isolation and structural characterization of the corresponding neutral and paramagnetic compounds. The bond length alterations observed in going from **3** to **4** are consistent with the known properties of the bma ligand and are validated by extended Hückel MO calculations.

Results and Discussion

I. Synthesis and Spectroscopic Data for *fac*-$ReBr(CO)_3$(bma). *fac*-$ReBr(CO)_3$(bma) was initially prepared from the direct thermolysis reaction between $BrRe(CO)_5$[13] (**1**) and bma[8] in 1,2-dichloroethane solvent. The reaction proceeded easily and gave a good yield of the desired product, as determined by IR spectroscopy. Extensive decomposition of *fac*-$ReBr(CO)_3$(bma) was observed when chromatographic purification over silica gel was attempted. Performing the chromatography at a low temperature (−78 °C) did not significantly improve the isolated yields of **3**, which stands in contrast to the other bma-substituted compounds worked with by our groups.[11,12] Silica gel promoted hydrolysis of the anhydride ring is presumed to be responsible for the decomposition of **3** during workup. Alternatively, the quantitative formation of *fac*-$ReBr(CO)_3$(bma) was observed in the reaction between the bis(solvent) compound $ReBr(CO)_3(THF)_2$ (**2**) and an equimolar amount of bma at room temperature.[14] Compound **2**, with its exceptionally labile THF ligands, has been employed in the preparation of a variety of substituted-rhenium compounds under mild reaction conditions. Here the isolated product was pure enough for our purposes and eliminated the need for a purification step. Scheme 1 illustrates the two methods that we employed in the preparation of **3**.

3 exhibits three terminal carbonyl bands at 2045 (vs), 1975 (vs), and 1920 (vs) cm^{-1} in CH_2Cl_2 consistent with the proposed facial stereochemistry about the rhenium center. The latter two ν(CO) bands derive from a splitting of the e mode in a *fac*-$M(CO)_3L_3$ (where L = symmetrical ligand) complex.[15] The vibrationally coupled carbonyl bands belonging to the bma ligand are found at 1848 (w) and 1778 (s) cm^{-1} and are assigned to the asymmetric and symmetric carbonyl stretches, respectively.[16] The $^{31}P\{^1H\}$ NMR spectrum of **3** in $CDCl_3$ at room temperature displays a single, sharp ^{31}P resonance at δ 19.2. The high-field frequency associated with the chelating bma ligand is comparable to the chelating diphosphine ligands in other third-row metal complexes.[17,18] Two terminal carbonyl resonances were recorded for **3** in the $^{13}C\{^1H\}$ NMR spectrum. The slightly overlapping doublet of doublets centered at δ 188.5 ($2C_b$, $J_{P_{cis}-C}$ = 11.9 Hz, $J_{P_{trans}-C}$ = 67.1 Hz) and the triplet at δ 187.6 ($1C_a$, J_{P-C} = 6.2 Hz) support the facial orientation of the rhenium carbonyl groups shown

(4) Albright, T. A.; Burdett, J. K.; Whangbo, M. H. *Orbital Interactions in Chemistry*; Wiley-Interscience: New York, 1985.
(5) (a) Reimann, R. H.; Singleton, E. *J. Organomet. Chem.* **1973**, *59*, 309. (b) Singleton, E.; Moelwyn-Hughes, J. T.; Garner, A. W. B. *J. Organomet. Chem.* **1970**, *21*, 449. (c) Freni, M.; Valenti, V.; Giusto, D. *J. Inorg. Nucl. Chem.* **1965**, *27*, 2635. (d) Freni, M.; Giusto, D.; Romiti, P. *J. Inorg. Nucl. Chem.* **1971**, *33*, 4093. (e) Zingales, F.; Sartorelli, U.; Trovati, A. *Inorg. Chem.* **1967**, *6*, 1246. (f) Chatt, J.; Dilworth, J. R.; Gunz, H. P.; Leigh, G. J. *J. Organomet. Chem.* **1974**, *64*, 245. (g) Miller, T. M.; Ahmed, K. J.; Wrighton, M. S. *Inorg. Chem.* **1989**, *28*, 2347. (h) Lorkovic, I. M.; Wrighton, M. S.; Davis, W. M. *J. Am. Chem. Soc.* **1994**, *116*, 6220.
(6) Brown, T. L. In *Organometallic Radical Processes*; Trogler, W. C., Ed.; Elsevier: New York, 1990; Chapter 3 (see also references therein).
(7) (a) Fenske, D. *Chem. Ber.* **1979**, *112*, 363. (b) Fenske, D. *Angew. Chem., Int. Ed. Engl.* **1976**, *15*, 381. (c) Bensmann, W.; Fenske, D. *Angew. Chem., Int. Ed. Engl.* **1978**, *17*, 462; **1979**, *18*, 677. (d) Fenske, D.; Christidis, A. *Angew. Chem., Int. Ed. Engl.* **1981**, *20*, 129.
(8) See also: (a) Fenske, D.; Becher, H. J. *Chem. Ber.* **1974**, *107*, 117; **1975**, *108*, 2115. (b) Becher, H. J.; Bensmann, W.; Fenske, D. *Chem. Ber.* **1977**, *110*, 315.
(9) (a) Mao, F.; Tyler, D. R.; Keszler, D. *J. Am. Chem. Soc.* **1989**, *111*, 130. (b) Mao, F.; Philbin, C. E.; Weakley, T. J. R.; Tyler, D. R. *Organometallics* **1990**, *9*, 1510. (c) Mao, F.; Tyler, D. R.; Rieger, A. L.; Rieger, P. H. *J. Chem. Soc., Dalton Trans.* **1991**, *87*, 3113. (d) Fei, M.; Sur, S. K.; Tyler, D. R. *Organometallics* **1991**, *10*, 419. (e) Mao, F.; Tyler, D. R.; Bruce, M. R. M.; Bruce, A. E.; Rieger, A. L.; Rieger, P. H. *J. Am. Chem. Soc.* **1992**, *114*, 6418.
(10) For review articles, see: (a) Tyler, D. R.; Mao, F. *Coord. Chem. Rev.* **1990**, *97*, 119. (b) Tyler, D. R. *Acc. Chem. Res.* **1991**, *24*, 325.
(11) (a) Yang, K.; Bott, S. G.; Richmond, M. G. *Organometallics* **1994**, *13*, 3788. (b) See also ref 12.
(12) (a) Yang, K.; Smith, J. M.; Bott, S. G.; Richmond, M. G. *Organometallics* **1993**, *12*, 4779. (b) Yang, K.; Bott, S. G.; Richmond, M. G. *Organometallics* **1994**, *13*, 3767.
(13) Schmidt, S. P.; Trogler, W. C.; Basolo, F. *Inorg. Synth.* **1990**, *28*, 160.
(14) (a) Vitali, D.; Calderazzo, F. *Gazz. Chim. Ital.* **1972**, *102*, 587. (b) Calderazzo, F.; Mavani, I. P.; Vitali, D.; Bernal, I.; Korp, J. D.; Atwood, J. L. *J. Organomet. Chem.* **1978**, *160*, 207.
(15) Lukehart, C. M. *Fundamental Transition Metal Organometallic Chemistry*; Brooks/Cole Publishing Co.: Monterey, CA, 1985.
(16) Dolphin, D.; Wick, A. *Tabulation of Infrared Spectral Data*; Wiley-Interscience: New York, 1977.
(17) Garrou, P. E. *Chem. Rev.* **1981**, *81*, 229 and references therein.
(18) Simpson, R. D.; Bergman, R. G. *Organometallics* **1993**, *12*, 781 and references therein.

Scheme 1

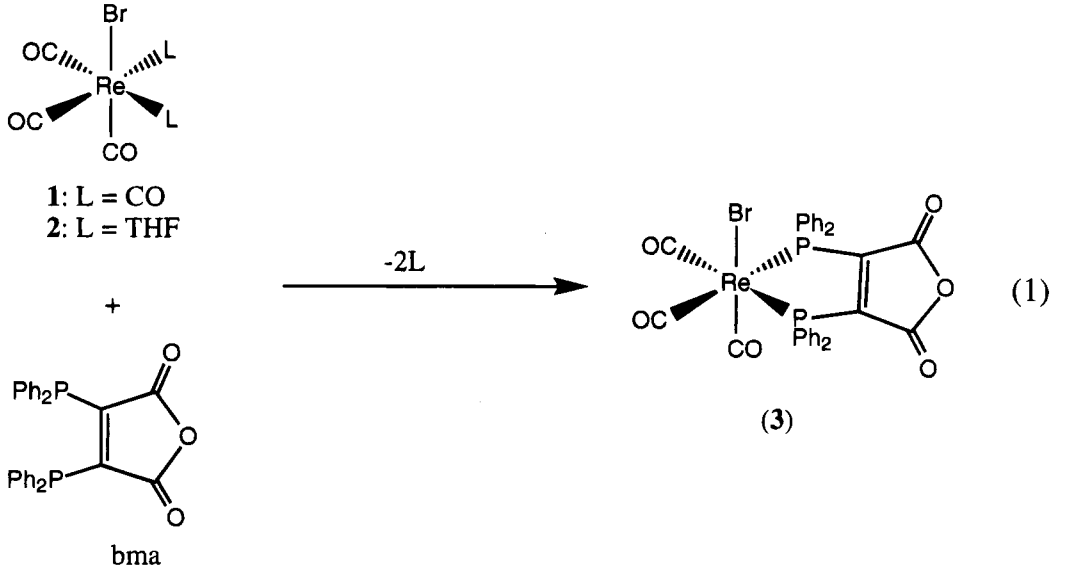

below. Our ^{13}C NMR data are similar to those reported by Bergman for a large variety of *fac*-ReX(CO)$_3$(L−L) compounds.[18]

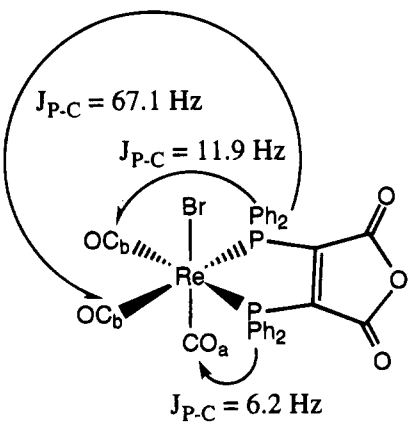

II. Electrochemical Studies. Cyclic voltammetric data were collected at a platinum electrode in solutions containing 0.2 M tetra-*n*-butylammonium perchlorate (TBAP) as the supporting electrolyte. **3** was examined in the solvents CH_2Cl_2, THF, and MeCN. Aside from minor potential shifts observed in the redox couples, the nature of the solvent did not affect the redox process, and we report only the data obtained in CH_2Cl_2. Compound **3** displays two well-defined, diffusion-controlled reductions at $E_{1/2} = -0.33$ and $E_{1/2} = -1.23$ V, assignable to the 0/1− and 1−/2− redox couples, as shown by the cyclic voltammogram (CV) in Figure 1a. Both couples are chemically reversible on the basis of the near unity current ratios (I_{pa}/I_{pc}) and the linear plots of the current function (I_p) vs the square root of the scan rate (ν) observed over the scan rates investigated (0.05−1.0 V/s).[19] The peak-to-peak separation of each couple at 0.1 V/s was calculated to be 68 and 86 mV and, when compared with the value of 84 mV found for internally added ferrocene, supports a fast electron transfer for each redox couple. The assumed one-electron stoichiometry of each redox couple of the CV was verified by application of Walden's rule using added ferrocene. Not shown in the CV of Figure 1 is the irreversible multi-electron oxidation at $E_{pa} = 1.58$ V recorded for **3**, an observation that has been reported by others.[5g]

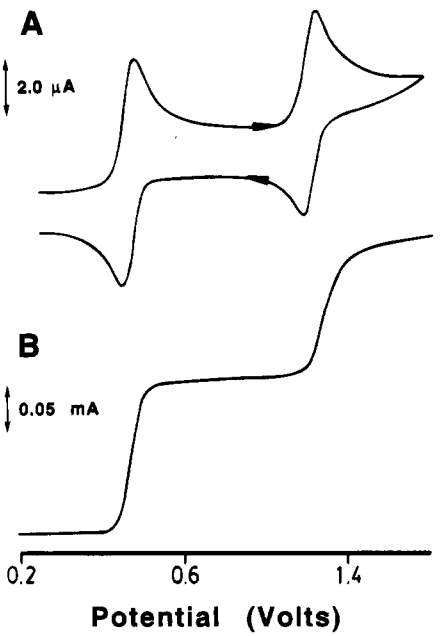

Figure 1. (A) Cathodic scan cyclic voltammogram of *fac*-ReBr(CO)$_3$(bma) (ca. 10^{-3} M) in CH_2Cl_2 containing 0.2 M TBAP at 0.1 V/s and (B) RDE voltammogram of *fac*-ReBr(CO)$_3$(bma) (ca. 10^{-3} M) in CH_2Cl_2 at 273 K containing 0.2 M TBAP at 50 mV/s.

The rotating disk electrode (RDE) voltammogram of the two reductions in **3** (Figure 1B) was also recorded in the same solvent as the CV, as an independent check of the electron stoichiometry for these two couples and the assumption concerning rapid heterogeneous electron transfer (k_{het}) in **3**. The RDE voltammogram yields half-wave potentials of $E_{1/2} = -0.34$ V and $E_{1/2} = -1.29$ V in close agreement with the CV data. Since both reduction waves give identical limiting currents ($|i_d|$) it may be concluded that the number of electrons transferred in each step is the same. The Nernstian nature of the 0/1− redox couple is revealed by a plot of E vs

(19) (a) Rieger, P. H. *Electrochemistry*; Chapman & Hall: New York, 1994. (b) Bard, A. J.; Faulkner, L. R. *Electrochemical Methods*; Wiley: New York, 1980.

$\log[(i_d - i)/i]$, which gave a slope close to the theoretically predicted value of 54.2 mV for a reversible one-electron transfer, while data analysis using Tomes' criterion for reversibility ($|E_{3/4} - E_{1/4}|$) affords values of 60 and 80 mV for the 0/1− and 1−/2− redox couples, respectively.[20] No kinetic complications were observed with these redox couples when the RDE data were analyzed by the relationship developed by Levich.[21] Here plots of i_d vs $\omega^{1/2}$ all displayed intercepts of zero within experimental error. This rules out the possibility of a rate-limiting heterogeneous electron transfer (k_{het}) in each of the reduction steps reported for **3**. Finally, using the Levich data we have determined the diffusion coefficient (D_o) of **3** to be 4.9×10^{-6} cm^2/s, which appears reasonable given the overall size of **3** with its large ancillary bma ligand (*vide supra*).[22]

We next examined **3** by constant-potential coulometry in an effort to more fully characterize [*fac*-ReBr(CO)$_3$(bma)]$^{\bullet-}$ (**4**), the product of one-electron reduction. The reduction of **3** was carried out at −0.60 V in CH_2Cl_2 containing 0.1 M TBAP at 273 K, and the total charge passed upon completion of the reduction was calculated to be $Q = 1.05$ C/mol of **3**. IR analysis of the catholyte allowed us to assess the effect of electron accession on the carbonyl stretching bands of **4**. Compound **4** exhibits ν(CO) bands at 2026 (vs), 1943 (vs), 1905 (vs), 1730 (s), and 1649 (vs) cm^{-1}, the first three bands represent the Re−CO groups that have shifted from 15 to 32 cm^{-1} to lower energy. The magnitude of these frequency shifts indicates that little of the odd-electron density is associated with these carbonyl groups. The existence of a reduced bma ligand in **4** is readily seen by the large frequency shifts in the latter two bma bands of 118 and 129 cm^{-1} relative to neutral **3**. The IR data for **4** are in total agreement with the 18 + δ nature of this and related compounds, as originally put forth by Tyler.[9,10] Further proof regarding the nature of **4** was obtained from the chemical reduction of **3** using the one-electron reducing agent cobaltocene. In this experiment, we isolated [**4**][Cp_2Co] and were able to characterize the radical anion by IR and X-ray diffraction analysis (*vide infra*). The IR spectrum of [**4**][Cp_2Co] in CH_2Cl_2 was identical to that recorded from the bulk electrolysis experiment, removing any doubt as to the identity of **4**.

III. X-ray Diffraction Structures of *fac*-ReBr(CO)$_3$(bma) and [*fac*-ReBr(CO)$_3$(bma)][Cp_2Co]. The structural consequences resulting from electron transfer in the redox pair of **3** and **4** were established by X-ray crystallography. Both complexes exist as discrete molecules in the unit cell with no unusually short inter- or intramolecular contacts. The X-ray data collection and processing parameters may be found in Table 1, while Tables 2 and 3 give the listings of the final fractional coordinates and selected bond lengths and angles, respectively. The ORTEP diagrams are depicted in Figure 2.

The six-coordinate rhenium center in **3** and **4** confirms the idealized octahedral geometry for each of these compounds, and the presence of three cis carbonyl groups is in agreement with the proposed facial stereochemistry. The Re−Br, Re−CO, and Re−P distances found for both structures are unexceptional in comparison with other structurally characterized rhenium complexes.[23] The cobaltocenium cation in **4** exhibits no unusual structural perturbations requiring any comment.[24]

Table 1. X-ray Crystallographic Data and Processing Parameters for *fac*-ReBr(CO)$_3$(bma) (3) and [*fac*-ReBr(CO)$_3$(bma)][Cp_2Co] (4)

	3	**4**
space group	$P\bar{1}$, triclinic	$C2/c$, monoclinic
a, Å	9.855(1)	39.600(3)
b, Å	12.1153(4)	10.2625(2)
c, Å	13.7751(8)	23.253(2)
α, deg	85.322(4)	
β, deg	73.828(6)	120.278(7)
γ, deg	75.812(6)	
V, Å^3	1531.3(2)	8161(1)
mol formula	$C_{31}H_{20}BrO_6P_2Re$	$C_{42}H_{32}BrCl_2CoO_6P_2Re$
fw	816.56	1101.70
formula units per cell (Z)	2	8
ϱ, g·cm^{-3}	1.771	1.793
abs coeff (μ), cm^{-1}	54.56	46.36
λ(Mo Kα), Å	0.710 73	0.710 73
collecn range, deg	$2.0 \le 2\theta \le 44.0$	$2.0 \le 2\theta \le 44.0$
max scan time, s	120	120
scan speed range, deg·min^{-1}	0.87−8.0	0.67−8.0
tot. no. of data collcd	3750	5399
no. of ind data, $I > 3\sigma(I)$	3342	3811
R	0.0552	0.0511
R_w	0.0771	0.0598
weights	$[0.04F^2 + (\sigma F)^2]^{-1}$	$[0.04F^2 + (\sigma F)^2]^{-1}$

Important differences are observed in the bond lengths of the C−C and C−P bonds of the coordinated bma ligand in each compound. Here bond length decreases of 0.07, 0.06, 0.04, and 0.04 Å in the C(11)−C(12), C(14)−C(15), P(1)−C(11), and P(2)−C(15) bonds, respectively, and the C(11)−C(15) bond length increase of 0.07 Å in going from **3** to **4** reveal the principal site of electron localization in the latter complex. Analogous bond alterations in other 18- and 19-electron complexes have been discussed by Tyler in terms of the bma-based canonical resonance contributors (Scheme 2),[9b] and fully support the contention that the vast amount of odd-electron density in **4** occurs on the bma ligand. **3** and **4** represent the first neutral/anionic redox state isomers of a bma-substituted compound. Structural alterations in the core of the reduced bma ligand are reminiscent of the M−M bond length elongations reported for polynuclear cluster compounds during reduction, where the geometrical changes demonstrate the antibonding M−M character of the LUMO.[25]

IV. Extended Hückel Calculations. The model compound *fac*-ReBr(CO)$_3$(H$_4$bma) was examined by extended Hückel molecular orbital calculations in order to establish the composition of the HOMO and LUMO in *fac*-ReBr(CO)$_3$(bma). Here the phenyl groups have been replaced by hydrogens. Figure 3 shows the three-

(20) Tomes, J. *Collect. Czech. Chem. Commun.* **1937**, *9*, 12, 81, 150.
(21) Levich, V. G. *Physicochemical Hydrodynamics*; Prentice Hall: Englewood Cliffs, NJ, 1962.
(22) Cf.: The calculated D_o value of 7.1×10^{-6} cm^2/s obtained from the X-ray data on *fac*-ReBr(CO)$_3$(bma) and application of the Stokes−Einstein relationship.

(23) (a) Nunn, C. M.; Cowley, A. H.; Lee, S. W.; Richmond, M. G. *Inorg. Chem.* **1990**, *29*, 2105. (b) Stack, J. G.; Simpson, R. D.; Hollander, F. J.; Bergman, R. G.; Heathcock, C. H. *J. Am. Chem. Soc.* **1990**, *112*, 2716. (c) Drew, M. G. B.; Brisdon, B. J.; Watts, A. M. *Polyhedron* **1984**, *3*, 1059. (d) Carriedo, G. A.; Rodriguez, M. L.; García-Granda, S. *Inorg. Chim. Acta* **1990**, *178*, 101.
(24) Riley, P. E.; Davis, R. E. *J. Organomet. Chem.* **1978**, *152*, 209.
(25) (a) Beurich, H.; Madach, T.; Richter, F.; Vahrenkamp, H. *Angew. Chem., Int. Ed. Engl.* **1979**, *18*, 690. (b) Kubat-Martin, K. A.; Barr, M. E.; Spencer, B.; Dahl, L. F. *Organometallics* **1987**, *6*, 2570. (c) Bedard, R. L.; Dahl, L. F. *J. Am. Chem. Soc.* **1986**, *108*, 5942. (d) Kubat-Martin, K. A.; Spencer, B.; Dahl, L. F. *Organometallics* **1987**, *6*, 2580.

Table 2. Positional Parameters for the Non-Hydrogen Atoms in *fac*-ReBr(CO)$_3$(bma) (3) and [*fac*-ReBr(CO)$_3$(bma)][Cp$_2$Co] (4) with Estimated Standard Deviations in Parentheses[a]

atom	x	y	z	B, Å^2	atom	x	y	z	B, Å^2
				fac-ReBr(CO)$_3$(bma) (**3**)					
Re	0.73911(7)	0.08869(6)	0.82953(5)	2.50(1)	C(115)	0.659(2)	0.526(2)	0.574(2)	4.9(6)
Br	0.9853(2)	0.0567(2)	0.6855(2)	3.88(4)	C(116)	0.610(2)	0.428(1)	0.611(1)	3.9(5)
P(1)	0.6323(5)	0.2142(4)	0.7089(3)	2.6(1)	C(117)	0.437(2)	0.270(1)	0.751(1)	3.0(4)
P(2)	0.6989(5)	−0.0608(4)	0.7378(3)	2.7(1)	C(118)	0.387(2)	0.347(2)	0.830(2)	5.0(5)
O(1)	0.890(2)	−0.091(1)	0.961(1)	5.7(4)	C(119)	0.239(3)	0.384(2)	0.873(2)	6.5(7)
O(2)	0.829(2)	0.272(1)	0.926(1)	6.2(4)	C(120)	0.140(2)	0.347(2)	0.837(2)	6.3(7)
O(3)	0.451(1)	0.136(1)	0.991(1)	4.4(3)	C(121)	0.189(2)	0.273(2)	0.759(2)	6.1(6)
O(12)	0.597(2)	0.238(1)	0.4642(9)	4.9(3)	C(122)	0.336(2)	0.233(2)	0.717(2)	4.4(5)
O(13)	0.647(1)	0.045(1)	0.4572(8)	3.7(3)	C(211)	0.847(2)	−0.188(1)	0.714(1)	3.2(4)
O(14)	0.697(1)	−0.139(1)	0.5014(9)	4.3(3)	C(212)	0.955(2)	−0.208(2)	0.624(1)	3.5(4)
C(1)	0.832(2)	−0.025(2)	0.912(1)	3.8(5)	C(213)	1.071(2)	−0.301(2)	0.617(2)	4.1(5)
C(2)	0.797(2)	0.205(2)	0.888(1)	3.5(4)	C(214)	1.078(2)	−0.372(2)	0.699(2)	5.2(6)
C(3)	0.561(2)	0.115(1)	0.930(1)	3.0(4)	C(215)	0.973(2)	−0.353(2)	0.790(2)	4.8(5)
C(11)	0.654(2)	0.120(1)	0.606(1)	2.7(4)	C(216)	0.855(2)	−0.260(2)	0.797(1)	4.0(5)
C(12)	0.628(2)	0.148(2)	0.503(1)	3.8(4)	C(217)	0.532(2)	−0.113(1)	0.771(1)	2.7(4)
C(14)	0.681(2)	−0.043(1)	0.523(1)	3.2(4)	C(218)	0.534(2)	−0.221(2)	0.747(2)	4.2(5)
C(15)	0.686(2)	0.006(1)	0.616(1)	2.6(4)	C(219)	0.406(2)	−0.257(2)	0.767(2)	4.9(5)
C(111)	0.696(2)	0.341(1)	0.653(1)	3.1(4)	C(220)	0.277(2)	−0.183(2)	0.809(2)	5.3(5)
C(112)	0.829(2)	0.352(2)	0.660(1)	4.0(5)	C(221)	0.275(2)	−0.072(2)	0.832(1)	4.3(5)
C(113)	0.876(2)	0.452(2)	0.623(2)	5.2(5)	C(222)	0.401(2)	−0.041(2)	0.815(1)	3.6(4)
C(114)	0.788(2)	0.537(2)	0.581(2)	5.2(6)					
				[*fac*-ReBr(CO)$_3$(bma)][Cp$_2$Co] (**4**)					
Re	0.08743(1)	0.09612(6)	0.28283(2)	2.45(1)	C(111)	0.1524(3)	−0.086(1)	0.4346(5)	2.9(3)*
Br	0.14396(6)	0.2238(2)	0.38305(9)	7.00(6)	C(112)	0.1922(3)	−0.068(1)	0.4641(6)	3.3(3)*
Co	0.31600(5)	0.0330(2)	0.44090(9)	3.99(5)	C(113)	0.2146(4)	−0.047(2)	0.5311(7)	4.8(4)*
P(1)	0.12120(8)	−0.1031(4)	0.3444(1)	2.44(7)	C(114)	0.1977(4)	−0.039(2)	0.5705(7)	5.0(4)*
P(2)	0.12628(8)	0.0657(3)	0.2280(1)	2.44(8)	C(115)	0.1590(4)	−0.056(2)	0.5424(7)	5.0(4)*
O(1)	0.0431(3)	0.330(1)	0.1936(5)	5.8(3)	C(116)	0.1358(4)	−0.081(2)	0.4744(6)	4.0(3)*
O(2)	0.0422(3)	0.141(1)	0.3576(5)	7.0(3)	C(117)	0.0905(3)	−0.241(1)	0.3378(5)	2.5(2)*
O(3)	0.0267(2)	−0.0763(6)	0.1768(3)	5.7(1)*	C(118)	0.1011(4)	−0.370(1)	0.3377(6)	3.7(3)*
O(12)	0.1906(3)	−0.339(1)	0.3742(4)	4.3(3)	C(119)	0.0795(4)	−0.471(2)	0.3378(7)	4.7(4)*
O(13)	0.1930(2)	−0.2588(9)	0.2864(4)	3.4(2)	C(120)	0.0445(5)	−0.448(2)	0.3352(8)	5.8(4)*
O(14)	0.1840(2)	−0.144(1)	0.1974(4)	4.2(2)	C(121)	0.0332(5)	−0.322(2)	0.3363(8)	6.4(5)*
C(1)	0.0602(4)	0.241(2)	0.2280(6)	4.0(4)	C(122)	0.0554(4)	−0.219(2)	0.3339(7)	4.9(4)*
C(2)	0.0587(4)	0.119(2)	0.3294(6)	4.2(4)	C(211)	0.0974(3)	0.056(1)	0.1380(6)	3.0(3)*
C(3)	0.0491(3)	−0.013(1)	0.2157(5)	5.5(2)*	C(212)	0.0827(4)	0.169(2)	0.1020(7)	5.2(4)*
Cp(1)	0.3369(5)	0.076(2)	0.3811(7)	6.2(5)	C(213)	0.0579(5)	0.163(2)	0.0317(8)	6.2(4)*
Cp(2)	0.3505(5)	0.166(2)	0.4329(8)	6.6(5)	C(214)	0.0483(5)	0.051(2)	0.0011(8)	6.2(5)*
Cp(3)	0.3716(5)	0.097(2)	0.4919(8)	6.1(5)	C(215)	0.0623(5)	−0.062(2)	0.0338(8)	6.1(4)*
Cp(4)	0.3705(5)	−0.032(2)	0.4782(8)	5.6(5)	C(216)	0.0880(4)	−0.061(2)	0.1050(7)	4.6(4)*
Cp(5)	0.3499(5)	−0.046(2)	0.4093(8)	6.6(5)	C(217)	0.1639(3)	0.184(1)	0.2405(6)	2.8(3)*
Cp(6)	0.2588(5)	0.054(3)	0.3885(8)	15.4(9)	C(218)	0.1657(4)	0.305(2)	0.2670(7)	4.1(3)*
Cp(7)	0.2730(6)	0.122(2)	0.448(1)	13.4(8)	C(219)	0.1953(4)	0.395(2)	0.2792(7)	5.1(4)*
Cp(8)	0.2916(4)	0.043(2)	0.4975(8)	8.7(5)	C(220)	0.2230(4)	0.361(2)	0.2636(7)	4.7(4)*
Cp(9)	0.2874(5)	−0.076(2)	0.4742(9)	7.4(5)	C(221)	0.2205(4)	0.244(2)	0.2337(6)	3.9(3)*
Cp(10)	0.2687(5)	−0.071(3)	0.4097(8)	9.4(7)	C(222)	0.1913(4)	0.156(1)	0.2222(6)	3.3(3)*
C(11)	0.1520(3)	−0.151(1)	0.3122(5)	2.5(3)	Cl(1s)	0.3969(2)	0.0755(8)	0.3158(3)	9.4(2)*
C(12)	0.1789(4)	−0.258(1)	0.3308(6)	3.5(3)	Cl(2s)	0.4720(4)	0.087(2)	0.4208(6)	8.7(3)*
C(14)	0.1758(3)	−0.156(1)	0.2408(6)	3.2(3)	C(1s)	0.4418(7)	0.122(3)	0.349(1)	10.3(8)*
C(15)	0.1513(3)	−0.086(1)	0.2582(5)	2.3(3)					

[a] Starred values refer to atoms that were refined isotropically. Anisotropically refined atoms are given in the form of the isotropic equivalent displacement parameter defined as $(4/3)[a^2B(1,1) + b^2B(2,2) + c^2B(3,3) + ab(\cos\gamma)B(1,2) + ac(\cos\beta)B(1,3) + bc(\cos\alpha)B(2,3)]$.

dimensional CACAO drawings of these orbitals along with the calculated energy for each orbital.[26]

The HOMO in *fac*-ReBr(CO)$_3$(H$_4$bma) is best described as a Re−Br π bond formed from an out-of-phase overlap of rhenium d_{yz} (29%) and bromine p_y (52%) orbitals, with minor in-phase contributions to the rhenium d_{yz} orbital from the facial carbonyl groups being observed. The energy level of the HOMO occurs at −12.38 eV and is only slightly lower in energy than the corresponding symmetry-related orbital derived from overlap of the rhenium d_{xz} (32%) and bromine p_x (55%) orbitals, which is found at ca. −12.41 eV. Given the large bromine (p_y) contribution to the HOMO it is not surprising that an irreversible oxidation at $E_{pa} = 1.58$ V was observed in the CV of **3**. Typically, a metal-based HOMO should yield a relatively stable radical cation upon oxidation.

The nodal pattern of the LUMO, which occurs exclusively on the bma ligand and at ca. −10.74 eV bears resemblance to Ψ_4 of maleic anhydride and other six-π-electron systems.[27] This low-energy π^* orbital results from an overlap of p_z orbitals and nicely accounts for the above canonical resonance structures for [*fac*-ReBr(CO)$_3$(bma)]$^{\bullet-}$. Our calculations on *fac*-ReBr(CO)$_3$(H$_4$bma) at the extended Hückel level are in good agreement with analogous SCF−Xα−SW calculations performed on the neutral compound Co(CO)$_3$(bma) by Tyler.[9e] Finally, we examined the HOMO and LUMO in the phosphine complex *fac*-ReBr(CO)$_3$(PH$_3$)$_2$. Here the two PH$_3$ ligands are not expected to afford a low-

(26) Mealli, C.; Proserpio, D. M. *J. Chem. Educ.* **1990**, *67*, 399.

(27) Hayakawa, K.; Mibu, N.; Osawa, E.; Kanematsu, K. *J. Am. Chem. Soc.* **1982**, *104*, 7136.

Table 3. Selected Bond Distances (Å) and Angles (deg) in *fac*-ReBr(CO)$_3$(bma) (3) and [*fac*-ReBr(CO)$_3$(bma)][Cp$_2$Co] (4)[a]

fac-ReBr(CO)$_3$(bma) (**3**)

Bond Distances

Re–Br	2.638(2)	Re–P(1)	2.441(4)
Re–P(2)	2.457(5)	Re–C(1)	1.93(2)
Re–C(2)	1.95(2)	Re–C(3)	1.88(1)
P(1)–C(11)	1.83(2)	P(2)–C(15)	1.82(2)
O(1)–C(1)	1.15(2)	O(2)–C(2)	1.15(3)
O(3)–C(3)	1.16(2)	O(12)–C(12)	1.19(2)
O(13)–C(12)	1.40(2)	O(13)–C(14)	1.38(2)
C(11)–C(12)	1.50(3)	C(11)–C(15)	1.34(2)
C(14)–C(15)	1.48(3)	O(14)–C(14)	1.18(2)

Bond Angles

Br–Re–P(1)	86.2(1)	Br–Re–P(2)	82.0(1)
Br–Re–C(1)	89.5(5)	Br–Re–C(2)	90.0(5)
Br–Re–C(3)	178.5(5)	P(1)–Re–P(2)	83.1(2)
P(1)–Re–C(1)	172.9(6)	P(1)–Re–C(2)	96.7(5)
P(1)–Re–C(3)	92.3(5)	P(2)–Re–C(1)	90.7(7)
P(2)–Re–C(2)	172.0(5)	P(2)–Re–C(3)	98.2(6)
C(1)–Re–C(2)	89.0(8)	C(1)–Re–C(3)	92.0(7)
C(2)–Re–C(3)	89.8(7)	Re–P(1)–C(11)	103.9(5)
Re–P(2)–C(15)	103.7(6)	Re–C(1)–O(1)	178(2)
Re–C(2)–O(2)	177(2)	Re–C(3)–O(3)	177(1)
C(12)–O(13)–C(14)	109(1)	P(1)–C(11)–C(12)	130(1)
P(1)–C(11)–C(15)	122(1)	C(12)–C(11)–C(15)	108(2)
O(12)–C(12)–O(13)	124(2)	O(12)–C(12)–C(11)	129(2)
O(13)–C(12)–C(11)	107(1)	O(13)–C(14)–O(14)	121(2)
O(13)–C(14)–C(15)	109(1)	O(14)–C(14)–C(15)	130(2)
P(2)–C(15)–C(11)	121(1)	P(2)–C(15)–C(14)	130(1)
C(11)–C(15)–C(14)	108(1)		

[*fac*-ReBr(CO)$_3$(bma)][Cp$_2$Co] (**4**)

Bond Distances

Re–Br	2.626(2)	Re–P(1)	2.467(3)
Re–P(2)	2.463(4)	Re–C(1)	1.90(1)
Re–C(2)	1.94(2)	Re–C(3)	1.899(9)
P(1)–C(11)	1.79(2)	P(2)–C(15)	1.78(1)
O(1)–C(1)	1.18(2)	O(2)–C(2)	1.16(2)
O(3)–C(3)	1.10(1)	O(12)–C(12)	1.20(2)
O(13)–C(12)	1.40(2)	O(13)–C(14)	1.41(2)
C(11)–C(12)	1.43(2)	C(11)–C(15)	1.41(2)
C(14)–C(15)	1.42(2)	O(14)–C(14)	1.21(2)

Bond Angles

Br–Re–P(1)	85.89(8)	Br–Re–P(2)	92.69(9)
Br–Re–C(1)	98.4(4)	Br–Re–C(2)	85.6(4)
Br–Re–C(3)	173.8(3)	P(1)–Re–P(2)	84.2(1)
P(1)–Re–C(1)	174.7(4)	P(1)–Re–C(2)	94.3(4)
P(1)–Re–C(3)	87.9(3)	P(2)–Re–C(1)	92.5(5)
P(2)–Re–C(2)	177.7(3)	P(2)–Re–C(3)	87.1(3)
C(1)–Re–C(2)	89.2(6)	C(1)–Re–C(3)	87.8(5)
C(2)–Re–C(3)	94.5(5)	Re–P(1)–C(11)	105.6(4)
Re–P(2)–C(15)	106.0(5)	Re–C(1)–O(1)	179(1)
Re–C(2)–O(2)	175(1)	Re–C(3)–O(3)	180(1)
C(12)–O(13)–C(14)	109(1)	P(1)–C(11)–C(12)	130(1)
P(1)–C(11)–C(15)	121.8(9)	C(12)–C(11)–C(15)	108(1)
O(12)–C(12)–O(13)	119(1)	O(12)–C(12)–C(11)	134(2)
O(13)–C(12)–C(11)	107(1)	O(13)–C(14)–O(14)	118(1)
O(13)–C(14)–C(15)	108(1)	O(14)–C(14)–C(15)	134(1)
P(2)–C(15)–C(11)	121(1)	P(2)–C(15)–C(14)	131(1)
C(11)–C(15)–C(14)	107(1)		

[a] Numbers in parentheses are estimated standard deviations in the least significant digits.

lying acceptor LUMO, as was observed with the bma ligand in **3**. While the HOMO in this compound mimics that in **3**, the LUMO was found at much higher energy (ca. −8.73 eV), consisting of primarily carbonyl π^* interactions.

Experimental Section

General Procedures. Re$_2$(CO)$_{10}$ was prepared from [ReO$_4$]-[NH$_4$] according to the method of Heinekey,[28] and BrRe(CO)$_5$ was obtained from the published bromination procedure using Re$_2$(CO)$_{10}$.[13] Cobaltocene was prepared by the known method.[29] The solvent complex ReBr(CO)$_3$(THF)$_2$[14] and bma[9b] were synthesized by using published methods. THF was distilled from Na/benzophenone, while CH_2Cl_2, $CDCl_3$, and 1,2-$C_2H_4Cl_2$ were all distilled from P_2O_5. The MeCN solvent used in the electrochemical studies was distilled from CaH_2. All purified solvents were transferred to storage vessels equipped with Teflon stopcocks using Schlenk techniques.[30] TBAP (caution: strong oxidant) was purchased from Johnson Matthey Electronics and recrystallized from ethyl acetate/petroleum ether, after which it dried under vacuum for at least 48 h. Microanalyses were performed by Atlantic Microlab, Atlanta, GA.

All infrared spectra were recorded on a Nicolet 20SXB FT-IR in 0.1-mm NaCl cells. The ^{13}C and ^{31}P NMR spectra were recorded on a Varian 300-VXR spectrometer at 75 and 121 MHz, respectively. The ^{31}P NMR data were referenced to external H_3PO_4 (85%), taken to have $\delta = 0$. The reported positive chemical shift for **3** signifies a resonance that is low field to the external standard. A Hewlett-Packard 8425A diode array spectrometer was used to record the quoted UV–visible data on compounds **3** and **4**. All UV–visible data were obtained in specially designed 1.0-cm quartz cells that were equipped with a Teflon stopcock.

Synthesis of *fac*-ReBr(CO)$_3$(bma). To a Schlenk tube containing 0.10 g (0.20 mmol) of ReBr(CO)$_3$(THF)$_2$ in 20 mL of THF was added 0.10 g (0.23 mmol) of bma, after which the reaction was stirred at room temperature for 2 h. IR analysis at this point revealed only the presence of the desired product *fac*-ReBr(CO)$_3$(bma). The solvent was removed and the crude material was extracted with petroleum ether in order to remove the excess bma. The analytical sample and crystals of **3** suitable for X-ray diffraction analysis were obtained from a CH_2Cl_2 solution of **3** that had been layered with heptane. Yield: 0.15 g (92%). IR (CH_2Cl_2): ν(CO) 2045 (vs), 1975 (vs), and 1920 (vs), 1848 (w, asymm bma C=O), 1778 (s, symm bma C=O) cm^{-1}. UV–vis (CH_2Cl_2): λ_{max} 306 (ϵ = 7345), 338 (ϵ = 3563). $^{13}C\{^1H\}$ NMR ($CDCl_3$, room temperature): δ 188.5 (2C, equatorial, $J_{P_{cis}-C}$ = 11.9 Hz, $J_{P_{trans}-C}$ = 67.1 Hz), 187.6 (1C, axial, J_{P-C} = 6.2 Hz). $^{31}P\{^1H\}$ NMR ($CDCl_3$, room temperature): δ 19.2. Anal. Calcd (found) for $C_{31}H_{20}BrO_6P_2Re$: C, 45.60 (45.08); H, 2.47 (2.42).

Synthesis of [*fac*-ReBr(CO)$_3$(bma)][Cp$_2$Co]. To a Schlenk tube containing 0.1 g (0.12 mmol) of *fac*-ReBr(CO)$_3$(bma) in 20 mL of CH_2Cl_2 at −20 °C was added 25.0 mg (0.13 mmol) of Cp_2Co. Stirring was continued for 20 min, and then the solution was examined by IR spectroscopy, which revealed only the product of electron transfer, [*fac*-ReBr(CO)$_3$(bma)][Cp$_2$Co]. The solvent was concentrated under vacuum to ca. 5 mL, and excess petroleum ether was added to precipitate the product. The analytical sample and single crystals of **4** suitable for X-ray diffraction analysis were obtained from a CH_2Cl_2 solution of **4** that was layered with heptane. Yield: 0.11 g (92%). IR (CH_2Cl_2): ν(CO) 2026 (vs), 1943 (vs), 1905 (vs), 1730 (s, asymm bma C=O), 1649 (s, symm bma C=O) cm^{-1}. UV–vis (CH_2Cl_2): λ_{max} 310 (ϵ = 8943), 340 (ϵ = 7317), 364 (ϵ = 6498). Anal. Calcd (found) for $C_{41}H_{30}BrCoO_6P_2Re^2/_3CH_2Cl_2$: C, 47.05 (47.02); H, 3.08 (3.18).

X-ray Crystal Structure of *fac*-ReBr(CO)$_3$(bma). A yellow crystal, of dimensions 0.2 × 0.3 × 0.5 mm^3, was sealed inside a Lindemann capillary and then mounted on an Enraf-Nonius CAD-4 diffractometer. Cell constants were obtained from a least-squares refinement of 25 reflections with $2\theta > 34°$. Intensity data in the range $2.0 \le 2\theta \le 44°$ were collected at 298 K using the $\theta/2\theta$-scan technique in the variable scan

(28) Crocker, L. S.; Gould, G. L.; Heinekey, D. M. *J. Organomet. Chem.* **1988**, *342*, 243.
(29) King, R. B. *Organometallic Syntheses*; Academic Press: New York, 1965; Vol. 1.
(30) Shriver, D. F. *The Manipulation of Air-Sensitive Compounds*; McGraw-Hill: New York, 1969.

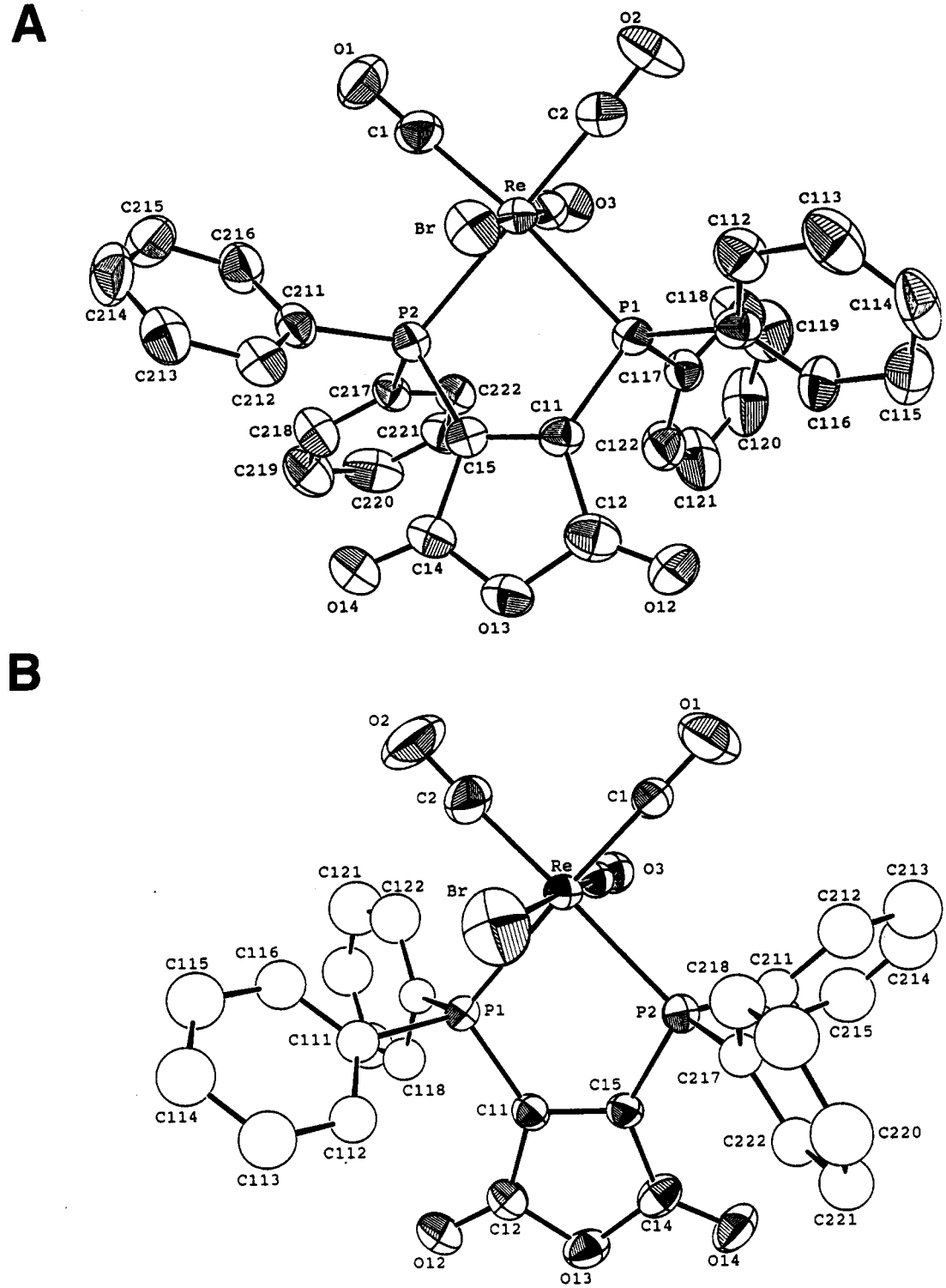

Figure 2. ORTEP diagrams of the non-hydrogen atoms of (A) *fac*-ReBr(CO)$_3$(bma) (**3**) and (B) [*fac*-ReBr(CO)$_3$(bma)][Cp$_2$Co] (**4**) showing the thermal ellipsoids at the 50% probability level. The gegencation has been omitted from the latter ORTEP diagram for clarity.

speed mode and were corrected for Lorentz, polarization, and absorption (DIFABS). Three reflections (600, 060, 007) were measured after every 3600 s of exposure time in order to monitor crystal decay (<2%). The structure was solved by using standard Patterson techniques, which revealed the position of the rhenium atom. All remaining non-hydrogen atoms were located with difference Fourier maps and full-matrix least-squares refinement and were refined anisotropically. Refinement converged at $R = 0.0552$ and $R_w = 0.0771$ for 3342 unique reflections with $I > 3\sigma(I)$.

X-ray Structure of [*fac*-ReBr(CO)$_3$(bma)][Cp$_2$Co]•CH$_2$Cl$_2$. A suitable black crystal, of dimensions 0.08 × 0.22 × 0.34 mm^3, was sealed inside a Lindemann capillary and then mounted on an Enraf-Nonius CAD-4 diffractometer. Cell constants were obtained from a least-squares refinement of 25 reflections with $2\theta > 25°$. Intensity data in the range $2.0 \leq 2\theta \leq 44°$ were collected at 298 K using the ω-scan technique in the variable scan speed mode and were corrected for Lorentz, polarization, and absorption (DIFABS). Three reflections (−5,−5,0, 20,0,−10, 0,0,12) were measured after every 3600 s of exposure time in order to monitor crystal decay (<1%). The structure was solved by using standard Patterson

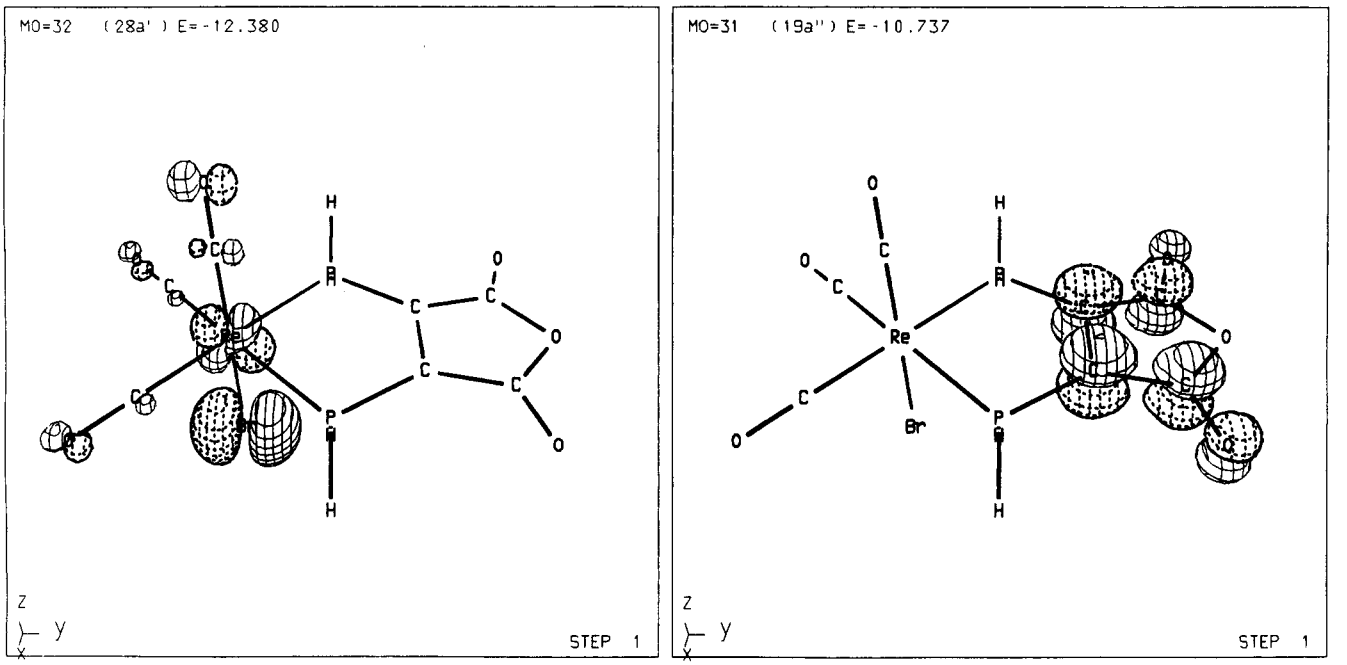

Figure 3. CACAO drawings of the HOMO (left) and the LUMO (right) for *fac*-$ReBr(CO)_3(bma)$.

Scheme 2

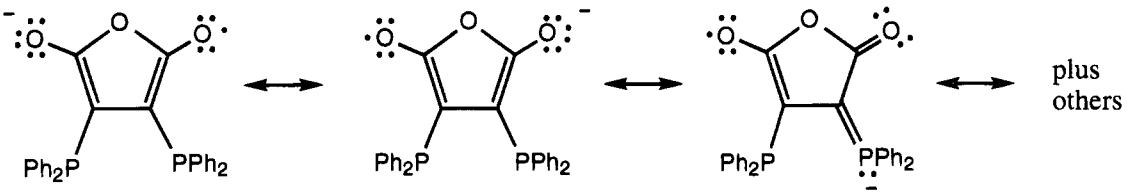

techniques, which revealed the position of the rhenium atom. All remaining non-hydrogen atoms were located with difference Fourier maps and full-matrix least-squares refinement. With the exception of the phenyl groups, the solvent molecule, and the axial carbonyl C(3)–O(3) group, all non-hydrogen atoms were refined anisotropically. Refinement converged at $R = 0.0511$ and $R_w = 0.0598$ for 3811 unique reflections with $I > 3\sigma(I)$.

Electrochemical Studies. Cyclic and rotating disk electrode voltammograms were obtained with a PAR Model 273 potentiostat/galvanostat, equipped with positive feedback circuitry to compensate for *iR* drop. The airtight cyclic voltammetry cell was based on a three-electrode design. All electrochemical experiments employed a platinum disk as the working and auxiliary electrodes. The RDE studies were conducted in a Vacuum Atmospheres Dribox at 273 K using a PAR Model 616 RDE unit. The reference electrode in all experiments consisted of a silver wire quasi-reference electrode, with all potential data reported relative to the formal potential of the Cp_2Fe/Cp_2Fe^+ (internally added) redox couple, taken to have $E_{1/2} = 0.307$ V.[19b]

MO Calculations. The extended Hückel calculations on *fac*-$ReBr(CO)_3(H_4bma)$ were carried out with the original program developed by Hoffmann,[31] as modified by Mealli and Proserpio,[26] with weighted H_{ij}'s.[32] The input **Z** matrix was constructed on a model possessing an octahedral rhenium center, using a distance of 1.42 Å for each P–H bond.[33] Other distances and angles were taken from the X-ray data.

Acknowledgment. We thank the Cyprus Sierrita Corp. for a gift of ammonium perrhenate and Prof. Carlo Mealli for providing us with a copy of his CACAO drawing program. Financial support from the Robert A. Welch Foundation (Grant B-1202-SGB and B-1039-MGR) and the UNT Faculty Research Program is appreciated.

Supplementary Material Available: Packing diagrams, ORTEP diagram, and listings of crystallographic data, bond distances, bond angles, and positional and thermal parameters for *fac*-$ReBr(CO)_3(bma)$ and [*fac*-$ReBr(CO)_3(bma)$][Cp_2Co]-CH_2Cl_2 (33 pages). Ordering information is given on any current masthead page.

OM940995S

(31) (a) Hoffmann, R.; Libscomb, W. N. *J. Chem. Phys.* **1962**, *36*, 3179. (b) Hoffmann, R. *J. Chem. Phys.* **1963**, *39*, 1397.
(32) Ammeter, J. H.; Bürgi, H.-B.; Thibeault, J. C.; Hoffmann, R. *J. Am. Chem. Soc.* **1978**, *100*, 3686.
(33) Weast, R. C., Ed. *Handbook of Chemistry and Physics*, 56th ed.; CRC Press: Cleveland, OH, 1975.

Matrix Photochemistry of $Mn_2(CO)_{10}$: Reversible Formation of $Mn_2(CO)_8$ from $Mn_2(CO)_8(\mu\text{-}\eta^1\text{:}\eta^2\text{-CO})$

Frank A. Kvietok and Bruce E. Bursten*

Department of Chemistry, The Ohio State University, Columbus, Ohio 43210

Received January 18, 1995[⊗]

The CO-loss photochemistry of $Mn_2(CO)_{10}$ (**1**) has been investigated using frozen-matrix photochemical techniques. A solution of **1** (0.6 mM) in neat 3-methylpentane is cooled to 96 K to form a frozen matrix. Initial irradiation of the matrix with broad-band light from a medium-pressure Hg lamp produces the known single-CO-loss product $Mn_2(CO)_8(\mu\text{-}\eta^1\text{:}\eta^2\text{-CO})$ (**3**). Continued irradiation leads to additional loss of CO and the formation of new IR bands. When thermal back-reactions in the matrix at 96 K are monitored, two additional products are identified. One is $Mn_2(CO)_8$ (**8**), a double-CO-loss product from **1** that has only terminal CO ligands and may possess a Mn–Mn triple bond. The other product is an isomer of **3**, $Mn_2(CO)_9'$ (**9**), which likely has a semibridging CO (ν_{CO} 1728 cm^{-1}). Under thermal conditions at 96 K, **8** and **9** reversibly reconvert to **3**.

The photochemistry of dinuclear organometallic complexes generally exhibits two distinct photochemical channels, namely cleavage into mononuclear radicals and loss of a single ligand while maintaining a dinuclear framework.[1] The dinuclear metal carbonyl complex $Mn_2(CO)_{10}$ (**1**) is a prototypical member of this class of compounds, and its air stability, high symmetry, and incontrovertible metal–metal bond have contributed to the interest in its photochemistry.

Early photochemical studies of **1** elegantly developed an understanding of the various products generated upon irradiation. Initially, much attention was focused on homolysis of the Mn–Mn bond, a process that yields $\cdot Mn(CO)_5$ radicals (**2**).[2] Later, transient absorption experiments by Vaida et al. provided evidence for the existence of an alternative photochemical product, which was suggested to be a dinuclear CO-loss species.[3] Kobayashi et al. used solution laser flash photolysis to explore the nature of this dinuclear species and proposed it to be $Mn_2(CO)_9$ (**3**), which reacts rapidly with various substrates to form $Mn_2(CO)_9L$ species.[4] Detail concerning the structure of **3** was provided by matrix isolation studies,[5] which demonstrated that irradiation of **1** leads to a CO-loss complex containing a semibridging CO, formulated as $Mn_2(CO)_8(\mu\text{-}\eta^1\text{:}\eta^2\text{-CO})$ (**3**). More recent studies have continued exploring the formation and reactivity of the CO-loss species **3** and related species using fast[6] and ultrafast[7] spectroscopy in solution. Gas-phase experiments have also richly contributed to our present understanding of possible CO-loss pathways and species.[8]

Very recently, Brown and co-workers have reported new photochemical studies of **1** in a matrix of 3-methylpentane (3-MP) at 93 K.[9] They provided evidence for the formation of the solvento species $Mn_2(CO)_9{\cdot}S$ (**4**; S = 3-MP) upon photodissociation of CO in the matrix. Species **4** decays into the semibridged species **3** by a first-order process with a half-life of ca. 140 s at 93 K.

Our current interest in the matrix photochemistry of **1** stems from recent studies in our laboratories on photochemical double CO loss from dinuclear organometallic complexes. For example, we have reported that the well-known complex $Cp_2Fe_2(CO)_2(\mu\text{-CO})_2$ (**5**; Cp = $\eta^5\text{-}C_5H_5$) undergoes two stepwise CO losses in a 3-MP matrix at 98 K.[10] Loss of the first CO generates the triply bridged intermediate $Cp_2Fe_2(\mu\text{-CO})_3$ (**6**).[11] Continued irradiation of **6** leads to loss of a second CO and the formation of $[CpFe(CO)]_2$ (**7**), an unusual species inasmuch as it contains two terminal CO ligands and apparently an unsupported Fe–Fe triple bond. We have found similar behavior in the matrix photochemistry of a methylene-bridged analogue of **5**, namely $[Cp^*Fe(CO)]_2(\mu\text{-CO})(\mu\text{-}CH_2)$, although in this case, the double-CO-loss product contains a methylene bridge and a semibridging CO ligand.[12]

[⊗] Abstract published in *Advance ACS Abstracts,* April 15, 1995.

(1) (a) Geoffroy, G. L.; Wrighton, M. S. *Organometallic Photochemistry*, Academic Press: New York, 1979. (b) Meyer, T. J.; Caspar, J. V. *Chem. Rev.* **1985**, *85*, 187–218.

(2) (a) Wrighton, M. S.; Ginley, D. S. *J. Am. Chem. Soc.* **1975**, *97*, 2065–2072. (b) Wrighton, M. S.; Abrahamson, H. B. *J. Am. Chem. Soc.* **1977**, *99*, 5510–5512. (c) Hughey, J. L., IV; Anderson, C. P.; Meyer, T. J. *J. Organomet. Chem.* **1977**, *125*, C49–C52. (d) Waltz, W. L.; Hackelberg, O.; Dorfman, L. M.; Wojcicki, A. *J. Am. Chem. Soc.* **1978**, *100*, 7259–7264. (e) Church, S. P.; Poliakoff, M.; Timney, J. A.; Turner, J. J. *J. Am. Chem. Soc.* **1981**, *103*, 7515–7520. (f) Wegman, R. W.; Olsen, R. J.; Gard, D. R.; Faulkner, L. R.; Brown, T. L. *J. Am. Chem. Soc.* **1981**, *103*, 6089–6092. (g) Walker, H. W.; Herrick, R.; Olsen, R. J.; Brown, T. L. *Inorg. Chem.* **1984**, *23*, 3748–3752.

(3) Rothberg, L. J.; Cooper, N. J.; Peters, K. S.; Vaida, V. *J. Am. Chem. Soc.* **1982**, *104*, 3536–3537.

(4) Yesaka, H.; Kobayashi, T.; Yasufuku, K.; Nagakura, S. *J. Am. Chem. Soc.* **1983**, *105*, 6249–6252.

(5) (a) Hepp, A. F.; Wrighton, M. S. *J. Am. Chem. Soc.* **1983**, *105*, 5934–5935. (b) Dunkin, I. R.; Härter, P.; Shields, C. J. *J. Am. Chem. Soc.* **1984**, *106*, 7248–7249.

(6) Church, S. P.; Hermann, H.; Grevels, F.-W.; Schaffner, K. *J. Chem. Soc., Chem. Commun.* **1984**, 785–786.

(7) (a) Zhang, J. Z.; Harris, C. B. *J. Chem. Phys.* **1991**, *95*, 4024–4032. (b) Waldman, A.; Ruhman, S.; Shaik, S.; Sastry, G. N. *Chem. Phys. Lett.* **1994**, *230*, 110–116.

(8) (a) Leopold, D. G.; Vaida, V. *J. Am. Chem. Soc.* **1984**, *106*, 3720–3722. (b) Seder, T. A.; Church, S. P.; Weitz, E. *J. Am. Chem. Soc.* **1986**, *108*, 1084–1086. (c) Seder, T. A.; Church, S. P.; Weitz, E. *J. Am. Chem. Soc.* **1986**, *108*, 7518–7524. (d) Prinslow, D. A.; Vaida, V. *J. Am. Chem. Soc.* **1987**, *109*, 5097–5100.

(9) (a) Zhang, S.; Zhang, H.-T.; Brown, T. L. *Organometallics* **1992**, *11*, 3929–3931. (b) Zhang, H.-T.; Brown, T. L. *J. Am. Chem. Soc.* **1993**, *115*, 107–117.

(10) Kvietok, F. A.; Bursten, B. E. *J. Am. Chem. Soc.* **1994**, *116*, 9807–9808.

(11) (a) Caspar, J. V.; Meyer, T. J. *J. Am. Chem. Soc.* **1980**, *102*, 7794–7795. (b) Hooker, R. H.; Mahmoud, K. A.; Rest, A. *J. Chem. Soc., Chem. Commun.* **1983**, 1022–1024. (c) Hepp, A. F.; Blaha, J. P.; Lewis, C.; Wrighton, M. S. *Organometallics* **1984**, *3*, 174–177.

0276-7333/95/2314-2395$09.00/0

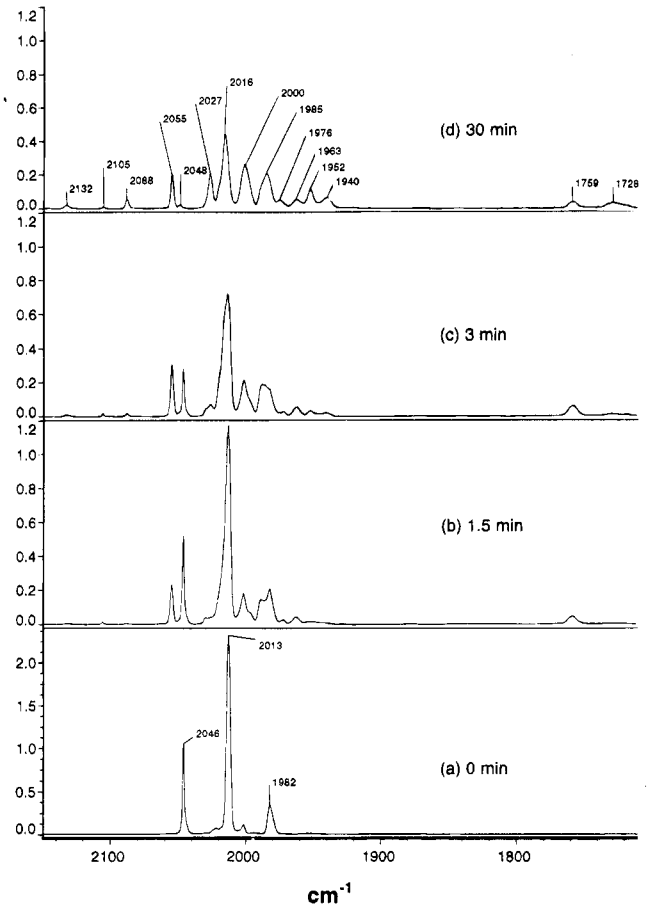

Figure 1. Progressive IR spectra during the irradiation of $Mn_2(CO)_{10}$ (**1**) in 3-methylpentane at 96 K (all abscissas are in cm^{-1}; the ordinates are absorbance): (a) spectrum obtained after 0 min of irradiation; (b) spectrum obtained after 1.5 min of irradiation; (c) spectrum obtained after 3.0 min of irradiation; (d) spectrum obtained after 30 min of irradiation. Note that the scale of absorbance for (a) is different from that for (b), (c), and (d).

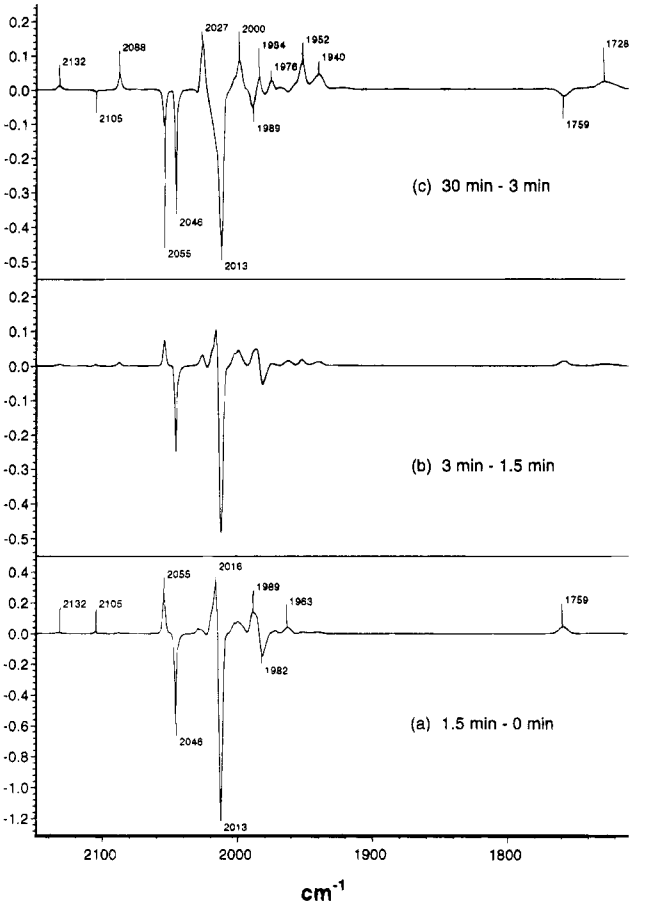

Figure 2. Progressive differences of the IR spectra presented in Figure 1 (all abscissas are in cm^{-1}; the ordinates are Δ(absorbance)): (a) difference between spectra obtained after 1.5 and 0 min of irradiation (Figure 1b − Figure 1a); (b) difference between spectra obtained after 3.0 and 1.5 min of irradiation (Figure 1c − Figure 1b); (c) difference between spectra obtained after 30 and 3.0 min of irradiation (Figure 1d − Figure 1c). Note that the scale of Δ(absorbance) for (a) is different from that for (b) and (c).

We were curious as to what similarities there might be between **5** and its trichoric[13] cousin **1**, particularly with respect to multiple photochemical CO loss. Previous studies of **1** have discussed the existence of secondary photolytic processes, although detailed characterization data of the resulting species have been scarce.[8c,d,14] We present here new matrix photochemistry that indicates the formation of new species from the secondary photolysis of the CO-loss product **3**, including a double-CO-loss product, $Mn_2(CO)_8$, that contains only terminal CO ligands.

Experimental Section

Standard Schlenk and inert-atmosphere techniques for handling air- and water-sensitive compounds were employed in these studies. $Mn_2(CO)_{10}$ (Strem Chemicals, Inc.) was purified by sublimation and stored under an Ar atmosphere in a refrigerator prior to use. 3-Methylpentane (Aldrich) was dried over Na/K alloy and stored under an Ar atmosphere. The matrix studies were performed with a Specac P/N 21500 variable temperature cell equipped with CaF_2 windows. The apparatus consists of a sample cell held inside a vacuum jacket by a compartment that also serves as the refrigerant holder. The path length of the cell is 1 mm. Liquid N_2 was used as the refrigerant for all experiments. The irradiation source was a 200-W broad-spectrum, medium-pressure Hg-vapor UV/vis lamp (Oriel) filtered with water. All IR spectra were collected on a Nicolet Magna 550 FT-IR spectrophotometer (32 scans, 1.0 cm^{-1} resolution). Difference spectra were generated using a scaling factor of 1; i.e., each difference spectrum represents the exact subtraction of two spectra, with no additional scaling.

Slow warming of the matrix was achieved through thermal contact with ambient conditions (room temperature) following removal of the refrigerant from the apparatus. The warming and recooling process did not affect the band shape or intensity of stable species or generate any spurious signals in a matrix-solvent-only control experiment. Comparative peak heights were measured from unsubtracted spectra at a constant temperature.

Results and Discussion

When a matrix of 0.6 mM **1** in 3-methylpentane (3-MP) at 96 K is irradiated with an unfiltered medium-pressure Hg lamp, we observe significant changes in the IR spectrum of the matrix. Figure 1 presents the IR spectra prior to irradiation and after 1.5, 3, and 30 min

(12) Spooner, Y. H.; Mitchell, E. M.; Bursten, B. E. Submitted for publication.
(13) King, R. B. *Inorg. Chem.* **1966**, *5*, 2227−2230.
(14) Kobayashi, T.; Ohtani, H.; Noda, H.; Teratani, S.; Yamazaki, H.; Yasufuku, K. *Organometallics* **1986**, *5*, 110−113.

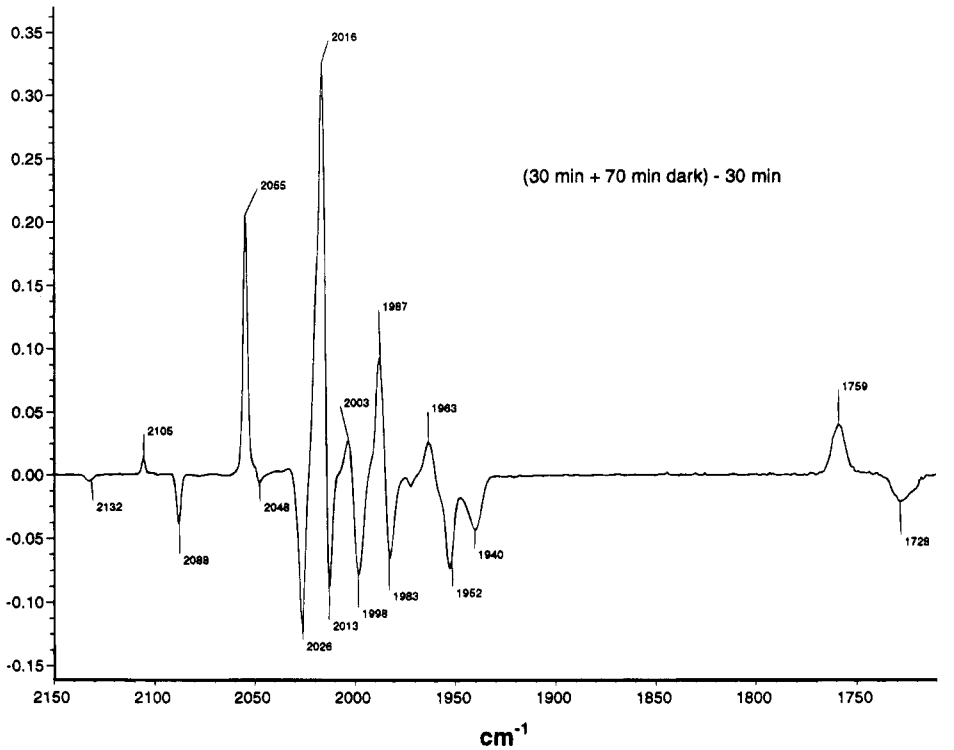

Figure 3. Difference IR spectrum from the irradiation and thermal back-reaction of 1 in 3-methylpentane at 96 K. The spectrum shown is the difference A − B, where A and B are defined as follows: (A) the spectrum obtained after irradiation of the matrix for 30 min followed by 70 min of thermal (dark) reaction at 96 K; (B) the spectrum obtained immediately after irradiation of the matrix for 30 min.

of irradiation. The progressive changes in the species in the matrix are clarified by the difference spectra presented in Figure 2. After 1.5 min of irradiation, the difference IR spectrum reveals the conversion of **1** to **3** and the evolution of CO, consistent with previous findings (Figure 2a).[5] Additional illumination (3 min) leads to the continued production of **3** and CO at the expense of **1**, along with the emergence of several new peaks, most notably at 2088, 2027, 1952, 1940, and 1728 cm^{-1} (Figure 2b). Further irradiation for a total time of 30 min leads to enhancement of the new peaks and of the signal for free CO with concurrent consumption of **1** and a decrease in the peaks for **3** (Figure 2c). Because there continues to be a loss of **1**, it was not initially clear if the new peaks derive from species produced by the photolysis of **1** or of **3**. We see no evidence for the production of radicals **2** in the matrix.

The above photochemical processes are thermally reversible: when 70 min is allowed for thermal reactions to occur while the matrix is kept 96 K, **3** is regenerated at the expense of species associated with the new peaks and free CO (Figure 3). These photochemical/thermal conversions are reversible upon further irradiation/dark cycles. In order to effect complete thermal conversion of the new species to **3**, it was necessary to warm the matrix to ca. 120 K in the continued absence of light, presumably to improve the diffusion of CO through the matrix.

To gauge the stoichiometry of the thermal back-reaction that forms **3**, we have used a comparison of the intensities of the absorptions for free CO at 2132 cm^{-1} and for **3** at 2055 cm^{-1}, as based on their peak heights. We find that the intensity ratio [free CO consumed]:[**3** produced] = 0.024 during the thermal reaction (Figure 3) is nearly the same as the ratio [free CO produced]:[**3** produced] = 0.026 during the early (1.5 min) stages of photolysis. The latter ratio provides us with a measure of the intensity ratio in a 1:1 mixture of **3** and free CO. This result therefore leads us to conclude that 1 equiv of CO is consumed in regenerating **3** from the new species. These observations provide support for the formation of $Mn_2(CO)_8$ (**8**) as a secondary photolysis product.

Greater detail concerning the number of new species and their associated CO stretching frequencies was ascertained by monitoring the IR spectrum after shorter periods of thermal back-reaction. The difference spectrum in Figure 4 was obtained by irradiating the matrix for 40 min and then allowing it to react thermally for 20.5 min. The new IR peaks evident in Figure 2 segregate into two sets under these conditions. The peaks at 2088, 2027, and 1728 cm^{-1} increase in intensity at the expense of the peaks at 2048, 1952, and 1940 cm^{-1} and of free CO. Note that the first set of peaks show a *decrease* in intensity under the longer thermal reaction time used in Figure 3. These observations imply the existence of another new species **9**, in addition to **8**, among the new species observed in Figure 2. Peaks associated with the formation of **3** are also present in Figure 4, most clearly at 2055 cm^{-1}, and over longer periods of thermal back-reaction the peaks for both **8** and **9** decrease in intensity while those for **3** increase. Because of the potential for overlap with peaks of either **1** or **3**, the peaks at 2013, 2001, and 1984 cm^{-1} are only tentatively assigned to **9**. Similarly, the negative peak at 1977 cm^{-1} is guardedly assigned to **8**. A summary of peak assignments is given in Table 1.

Another species is present during initial thermal back-reactions when the photolysis is carried out for shorter periods of time, namely the known solvento

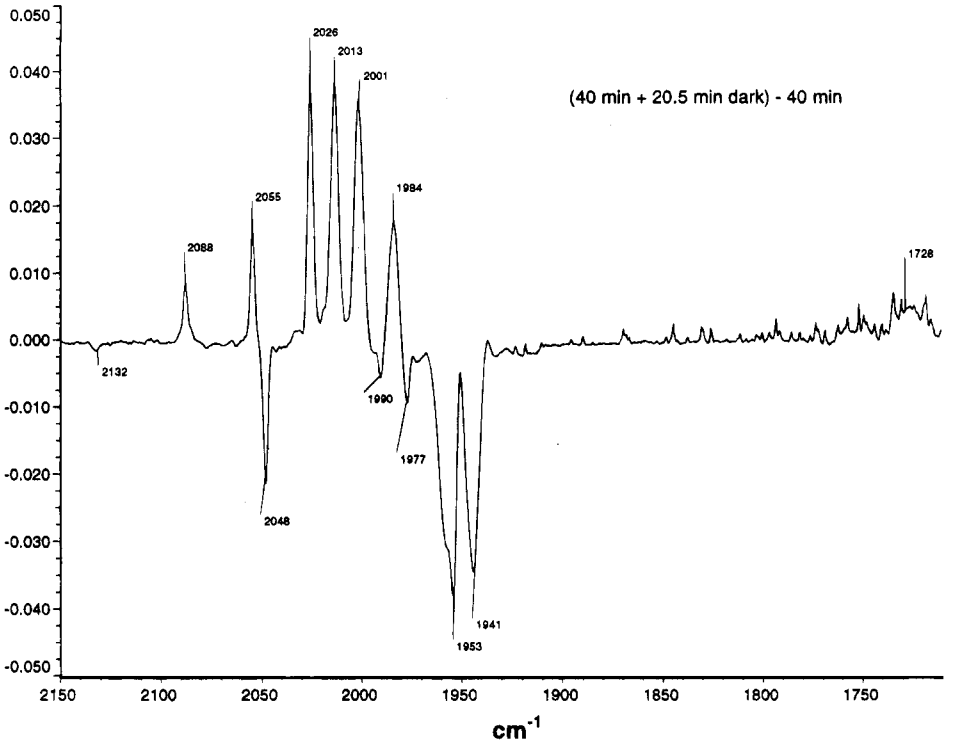

Figure 4. Difference IR spectrum from the irradiation and thermal back-reaction of **1** in 3-methylpentane at 96 K. The spectrum shown is the difference A − B, where A and B are defined as follows: (A) the spectrum obtained after irradiation of the matrix for 40 min followed by 20.5 min of thermal (dark) reaction at 96 K; (B) the spectrum obtained immediately after irradiation of the matrix for 40 min.

Table 1. IR Stretching Frequencies for Photoproducts of $Mn_2(CO)_{10}$

complex	ν_{CO} (cm^{-1})[a]
$Mn_2(CO)_8(\mu\text{-}\eta^1{:}\eta^2\text{-CO})$ (**3**)[b]	2105, 2055, 2016, 2003, *2000*, 1986, 1963, 1759
$Mn_2(CO)_8$ (**8**)	2048, *1977*, 1952, 1940
$Mn_2(CO)_9'$ (**9**)	2088, 2027, *2013*, *2001*, *1984*, 1728

[a] Values in italics are only tentatively assigned due to overlapping signals. [b] Reference 5.

complex **4** that was proposed by Brown et al.[9] Complex **4** was readily identified by its CO stretching frequencies at 2029, 1996, 1990, 1972, and 1948 cm^{-1}. Although species **4** rapidly decayed with concomitant growth of **3** during thermal reaction periods, as previously reported, it was found to be a relatively minor component of the sample when longer irradiation times were employed (cf. the relatively small peak at 1990 cm^{-1} in Figure 4 as an indicator of consumed **4**).

Although a detailed kinetic analysis of the thermal reactions of **8** and **9** with CO to give **3** was not warranted on the basis of the complexity of the system, the potential for overlapping signals, and the viscous nature of the matrices, a plot of normalized spectral peak heights vs thermal reaction time is informative in several respects (Figure 5). First, the close match of the growth and decay behavior for the signals associated with each species is reassuring corroboration of their assignments. Second, the rapid decay of the peaks related to complex **4** reflects the relatively small influence this species has on the system once secondary photolysis products have been produced. Third, the general appearance of the plot suggests the intermediacy of **9** in the thermal conversion of **8** to **3**. The relative amounts of complexes **3**, **8**, and **9** present at the beginning of thermal reaction periods were somewhat variable due to minor differences in concentration and the extent of photolysis. Nevertheless, plots from other runs reveal the same general features shown in Figure 5.

On the basis of the above data, we propose that complex **8** combines with CO to form **9**, which thermally isomerizes to the known species **3**.[15] We therefore propose that **9** is an isomer of **3** that we will denote $Mn_2(CO)_9'$ (eq 1). The most intriguing feature in the IR

$$\underset{\mathbf{8}}{Mn_2(CO)_8} + CO \rightarrow \underset{\mathbf{9}}{Mn_2(CO)_9'} \rightarrow \underset{\mathbf{3}}{Mn_2(CO)_8(\mu\text{-}\eta^1{:}\eta^2\text{-CO})} \quad (1)$$

spectrum of **9** is the observation of the CO stretch at 1728 cm^{-1}. The position of this peak, like the peak at 1759 cm^{-1} for complex **3**, suggests the presence of a semibridging carbonyl in **9**.[16] If this conclusion is correct, **9** represents yet another photochemical intermediate that possesses a semibridging carbonyl, as has been seen for **3** and for several dinuclear complexes of Fe.[12,17] The findings that species **3** and **9** are both isomers of $Mn_2(CO)_9$, that both apparently contain at least one semibridging carbonyl, and that there is a ca. 30 cm^{-1} difference in the stretching frequencies of these species in the semibridging region of the spectrum is very striking. We shall be investigating further the structures of these two isomers. Interestingly, two

(15) On the basis of the data in Figure 5, we cannot rule out the possibility that **8** reacts with CO to form **3** directly in addition to forming **9**.

(16) Crabtree, R. H.; Lavin, M. *Inorg. Chem.* **1986**, *25*, 805–812.
(17) Zhang, S.; Brown, T. L. *J. Am. Chem. Soc.* **1993**, *115*, 1779–1789.

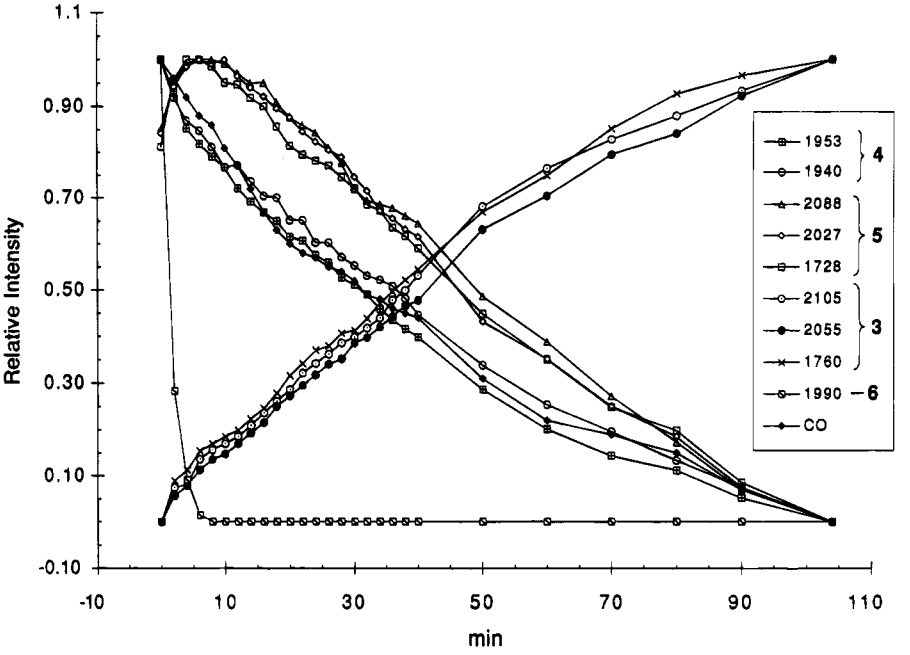

Figure 5. Temporal behavior of the product IR bands following the irradiation of **1** for 30 min in 3-methylpentane at 96 K. The abscissa shows the time of thermal (dark) reaction after the irradiation. Compound numbers in the legend are referenced in the text. Peak intensities were approximated by IR peak heights, and all spectra were recorded at 96 K. For each frequency, the intensity was renormalized so that its maximum relative intensity was unity.

isomers of $Re_2(CO)_9$ have also been proposed, although both of these contain only terminal carbonyl ligands.[18]

Compound **8** exhibits no peaks below 1940 cm^{-1}, an indication that there are no bridging or semibridging CO ligands in $Mn_2(CO)_8$. The apparent absence of bridging carbonyls in the structure of **8** is reminiscent of the double-CO-loss product $[CpFe(CO)]_2$ (**7**) detected in our earlier matrix photochemical studies of **5**.[10] Compound **7** exhibited only two CO stretching frequencies (1958 and 1904 cm^{-1}), which clearly indicated terminal configurations for the carbonyl ligands and, when coupled with MO calculations, led to the proposition of an Fe–Fe triple bond. Because $[CpFe(CO)]_2$ and $Mn_2(CO)_8$ are isovalent, it is possible that **8** contains an unsupported Mn–Mn triple bond.[19] In support of this notion, gas-phase studies suggest a strengthening of the Mn–Mn bond upon stepwise decarbonylation of **1**.[14] We are currently undertaking additional characterization experiments and *ab initio* calculations[20] to explore further the structure of **8**.

Acknowledgment. We gratefully acknowledge the National Science Foundation (Grant CHE-9208703) for support of this research. We are also grateful to Drs. T. L. Brown and M. Poliakoff for helpful reviewer comments.

OM9500329

(18) (a) Firth, S.; Hodges, P. M.; Poliakoff, M.; Turner, J. J. *Inorg. Chem.* **1986**, *25*, 4608–4610. (b) Firth, S.; Klotzbücher, W. E.; Poliakoff, M.; Turner, J. J. *Inorg. Chem.* **1987**, *26*, 3370.

(19) Brown has suggested to us that **8** could contain two molecules of coordinated 3-MP, in analogy to **4** (Brown, T. L., personal communication). Additionally, he has suggested that the 1728 cm^{-1} peak could be due to a monosolvento complex, $Mn_2(CO)_8$·S, that contains a semibridging CO, which could be generated by loss of solvent from the disolvento species. We believe that these proposals are unlikely. First, we do not see the formation of **4** in the reaction of **8** with CO, as might be expected upon the addition of CO to a disolvento species. Second, the uptake of CO in the thermal reaction of **8** with CO to form **9** is inconsistent with the formulation of **9** as having only eight CO ligands. Nevertheless, this possibility will be examined by exploring this photochemistry in matrices of differing Lewis basicity.

(20) Preliminary results: Barckholtz, T. A.; Lavender, H. B.; Kvietok, F. A.; Bursten, B. E. *Abstracts of Papers*, 209th National Meeting of the American Chemical Society, Anaheim, CA; American Chemical Society: Washington, DC, 1995; INOR 128.

Group 13 Halides and Hydrides with *o*-(Aminomethyl)phenyl Substituents

Harold S. Isom, Alan H. Cowley,* Andreas Decken, Frankwin Sissingh, Siegfried Corbelin, and Richard J. Lagow

Department of Chemistry and Biochemistry, The University of Texas at Austin, Austin, Texas 78712

Received December 19, 1994[⊗]

Two new group 13 dihalides of the type $ArMX_2$ (Ar = *o*-[(dimethylamino)methyl]phenyl; MX_2 = $AlBr_2$ (**4**), $GaCl_2$ (**5**)) have been prepared *via* the salt-elimination reactions of *o*-$(Me_2NCH_2)C_6H_4Li$ with MX_3. The reaction of **4** or **5** with $LiAlH_4$ afforded the corresponding aluminum dihydride dimer $[Ar(H)Al(\mu\text{-}H)]_2$ (**6**). Treatment of **5** with $LiGaH_4$ resulted in the monomeric gallium dihydride $ArGaH_2$ (**7**), which rearranged to the monohydride Ar_2GaH (**8**) upon standing in toluene solution at −20 °C. Compounds **4**–**8** have been characterized by X-ray crystallography, elemental analysis, NMR, and mass spectroscopy. Crystal data for **4**: monoclinic, space group $P2_1/c$, a = 9.535(3) Å, b = 10.209(4) Å, c = 12.622(5) Å, β = 92.70(2)°, V = 1227.3(4) Å^3, Z = 4, R = 0.0491. Crystal data for **5**: monoclinic, space group $P2_1/c$, a = 9.371(1) Å, b = 13.143(2) Å, c = 10.286(1) Å, β = 116.38(1)°, V = 1134.9(2) Å^3, Z = 4, R = 0.0311. Crystal data for **6**: monoclinic, space group $P2_1/n$, a = 9.007(1) Å, b = 11.131(1) Å, c = 10.279(1) Å, β = 105.64(1)°, V = 992.3(5) Å^3, Z = 4, R = 0.0684. Crystal data for **7**: monoclinic, space group $P2_1/c$, a = 9.511(3) Å, b = 12.588(3) Å, c = 16.92(1) Å, β = 102.73(3)°, V = 1976(1) Å^3, Z = 8, R = 0.086. Crystal data for **8**: orthorhombic, space group $P2_12_12_1$, a = 9.615(1) Å, b = 10.050(1) Å, c = 17.856(2) Å, V = 1717.9(9) Å^3, Z = 4, R = 0.052.

Introduction

Although organoaluminum hydrides are well-known,[1] such compounds generally involve hydride-bridged structures, and it is only recently that a monomeric aluminum dihydride has been reported.[2] Information on neutral gallium mono- and dihydrides is considerably more sparse and, until 1993, the compounds with known structures comprised the dimers $[H_2Ga(\mu\text{-}X)]_2$ (X = Cl,[3] NMe_2[4]), $[Me_2Ga(\mu\text{-}H)]_2$,[5] and $[H_2Ga(\mu\text{-}H)BH_2]_2$[6] and the unusual trinuclear species $[HGa(BH_4)_2]$.[7,8] Since that time, [2,6-$(Me_2N)_2C_6H_3$]GaH_2 (**1**),[9] [2,4,6-*t*-$Bu_3C_6H_2$]-GaH_2 (**2**),[10] and [(3,5-*t*-$Bu_2C_6H_3Me_2CH_2$)(2,4,6-*t*-$Bu_3C_6H_2$)]-GaH,[10] the first examples of terminal gallium mono- and dihydrides, have been reported. Species with indium–hydrogen bonds are extremely rare. Apart from the very short-lived species InH_3, In(III) hydrides are of the indate type, namely $M[InR_3H]$ (M = Na, K; R = Me,[11] Et,[11] Me_3SiCH_2[12]), $Na[InEt_2H_2]$,[11] and $[Li(THF)_2[\{(Me_3Si)_3C\}_2In_2H_5]$.[13] The polymeric ether adduct $(InH_3)_x \cdot n Et_2O$ is unstable and decomposes to a polymeric indium(I) hydride of unknown structure.[14]

Our interest in preparing terminal hydrides of the heavier group 13 elements has arisen for several reasons. First, aluminum and gallium hydride moieties have been detected on surfaces during thin-film growth from organoaluminum[15] or organogallium sources.[16] In principle, therefore, monomeric organoaluminum or organogallium hydrides could serve as useful models for enhanced understanding of the reaction chemistry of surface-bound MH_n entities. Second, monomeric organoaluminum or organogallium dihydrides are potentially attractive candidates for gaining access to the +1 oxidation states of these elements *via* thermal or photochemical elimination of molecular hydrogen. A third reason relates to the possibility that, by appropriate choice of ligand, it might be possible to stabilize a neutral organoindium hydride.

The stabilization of the gallium dihydrides **1** and **2** has been achieved by the use of intramolecular base

⊗ Abstract published in *Advance ACS Abstracts,* March 15, 1995.

(1) *Comprehensive Organometallic Chemistry*; Wilkinson, G., Stone, F. G. A., Abel, E. W., Eds.; Pergamon: Oxford, U.K., 1982; Vol. 1, Chapter 6.

(2) Contreras, L.; Cowley, A. H.; Gabbaï, F. P.; Jones, R. A.; Carrano, C. J.; Bond, M. R. *J. Organomet. Chem.* **1995**, *489*, C1.

(3) Goode, M. J.; Downs, A. J.; Pulham, C. R.; Rankin, D. W. H.; Robertson, H. E. *J. Chem. Soc., Chem. Commun.* **1988**, 768.

(4) Baxter, P. L.; Downs, A. J.; Goode, M. J.; Rankin, D. W. H.; Robertson, H. E. *J. Chem. Soc., Dalton Trans.* **1985**, 807.

(5) Baxter, P. L.; Downs, A. J.; Goode, M. J.; Rankin, D. W. H.; Robertson, H. E. *J. Chem. Soc., Chem. Commun.* **1986**, 805.

(6) Pulham, C. R.; Brain, P. T.; Downs, A. J.; Goode, M. J.; Rankin, D. W. H.; Robertson, H. E. *J. Chem. Soc., Chem. Commun.* **1990**, 177.

(7) Barlow, M. T.; Dain, C. J.; Downs, A. J.; Laurensen, G. S.; Rankin, D. W. H. *J. Chem. Soc., Dalton Trans.* **1982**, 597.

(8) For other interesting systems with gallium hydride moieties, see: Atwood, J. L.; Bennett, F. R.; Elms, F. M.; Jones, C.; Raston, C. L.; Robinson, K. D. *J. Am. Chem. Soc.* **1991**, *113*, 8183. Henderson, M. J.; Kennard, C. H.; Raston, C. L.; Smith, G. *J. Chem. Soc., Chem. Commun.* **1990**, 1203. Atwood, J. L.; Bott, S. G.; Jones, C.; Raston, C. L. *Inorg. Chem.* **1991**, *30*, 4868.

(9) Cowley, A. H.; Gabbaï, F. P.; Atwood, D. A.; Carrano, C. J.; Mokry, L. M.; Bond, M. A. *J. Am. Chem. Soc.* **1994**, *116*, 1559.

(10) Cowley, A. H.; Gabbaï, F. P.; Isom, H. S.; Carrano, C. J.; Bond, M. R. *Angew. Chem., Int. Ed. Engl.* **1994**, *33*, 1253.

(11) Gavrilenko, V. V.; Kolesov, V. S.; Zakharkin, L. I. *Zh. Obshch. Khim.* **1977**, *47*, 964; **1979**, *49*, 1845.

(12) Hallock, R. B.; Beachley, O. T.; Li, Y.-J.; Sanders, W. M.; Churchill, M. R.; Hunter, W. E.; Atwood, J. L. *Inorg. Chem.* **1983**, *22*, 3683.

(13) Avent, A. G.; Eaborn, C.; Hitchcock, P. B.; Smith, J. D.; Sullivan, A. C. *J. Chem. Soc., Chem. Commun.* **1986**, 988.

(14) Wiberg, E.; Amberger, E. *Hydrides of the Elements of Main Groups I-IV*; Elsevier: Amsterdam, 1971; p 454.

(15) Bart, B. E.; Nuzzo, R. G.; DuBois, L. H. *J. Am. Chem. Soc.* **1989**, *111*, 1634.

(16) Zanella, P.; Rossetto, G.; Brianses, N.; Ossola, F.; Porchia, M.; Williams, J. O. *Chem. Mater.* **1991**, *3*, 275. Butz, K. W.; Elms, F. M.; Raston, C. L.; Lamb, R. N.; Pigram, P. J. *Inorg. Chem.* **1993**, *32*, 3985.

0276-7333/95/2314-2400$09.00/0

stabilization and steric bulk, respectively. Compound **1**

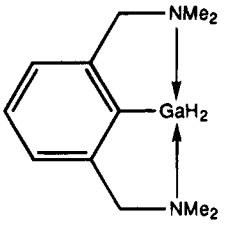

1

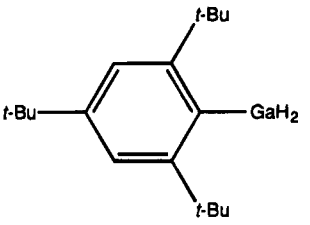

2

is surprisingly stable and is resistant to vapor-phase heating at 350 °C or irradiation with 254 nm light (toluene solution, 25 °C). In contrast, **2** undergoes facile photolysis to produce elemental gallium and 1,3,5-*t*-$Bu_3C_6H_3$. With the hope of preparing hydrides with intermediate stability, we decided to employ the "one-arm" ligand system **3**.

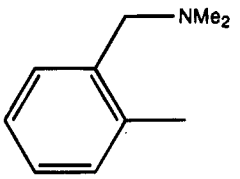

3

Herein we report the syntheses of aluminum and gallium halides featuring ligand **3** along with their reactions with $[AlH_4]^-$ and $[GaH_4]^-$ anions. Similar reactions were attempted with the recently prepared[17] indium iodide $[2\text{-}(Me_2NCH_2)C_6H_4]InI_2$.

Results and Discussion

The colorless crystalline dihalides **4** and **5** were prepared by treatment of [*o*-[(dimethylamino)methyl]-phenyl]lithium with the appropriate group 13 trihalide in toluene or Et_2O solution. The choice of trihalide was dictated by solubility considerations. A satisfactory

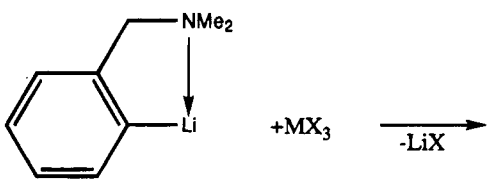

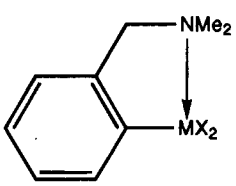

4 $MX_2 = AlBr_2$

5 $MX_2 = GaCl_2$

elemental analysis was obtained for both compounds, and the ^1H and ^{13}C NMR spectral data were consistent with the presence of the one-arm aryl ligand **3** (see

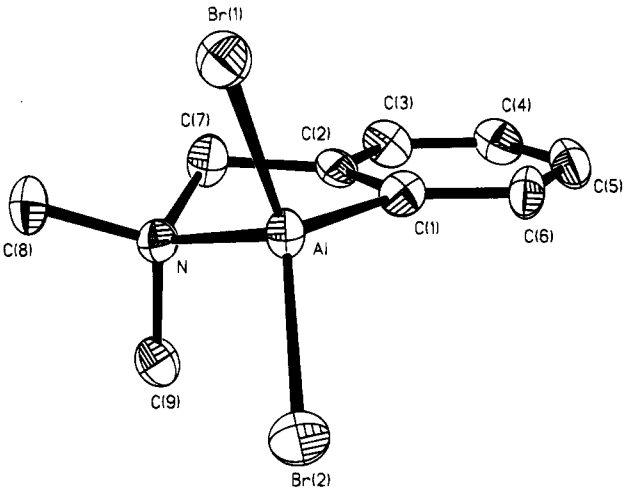

Figure 1. View of $[o\text{-}(Me_2NCH_2)C_6H_4]AlBr_2$ (**4**) showing the atom-labeling scheme. Thermal ellipsoids are scaled to the 50% probability level.

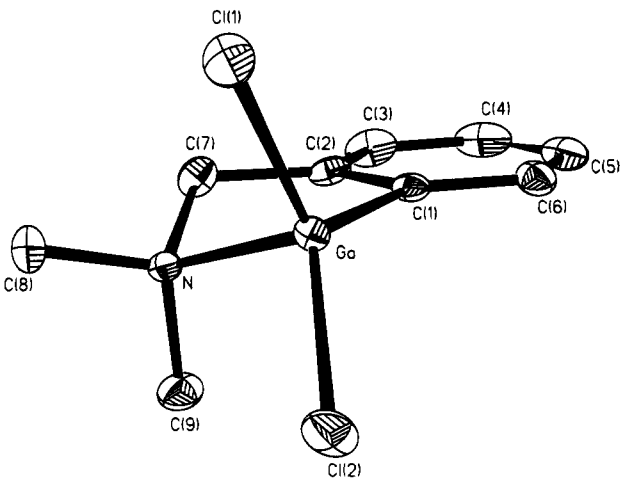

Figure 2. View of $[o\text{-}(Me_2NCH_2)C_6H_4]GaCl_2$ (**5**) showing the atom-labeling scheme. Thermal ellipsoids are scaled to the 50% probability level.

Experimental Section). It was not clear, however, whether the amine arm is coordinated; moreover, it was of interest to determine the extent of any intermolecular interactions in the solid state. For these reasons X-ray crystallographic studies of **4** and **5** were undertaken. The X-ray crystal structures reveal that **4** and **5** are isolated molecules with no abnormally short intermolecular contacts (Figures 1 and 2). The amine arm is coordinated to the group 13 element in both molecules, and the resulting N→metal–C–C–C ring is nonplanar. In each case it is the nitrogen atom that experiences the largest deviation from the least-squares aryl reference plane, and this is larger for **5** (0.65 Å) than for **4** (0.47 Å). The reverse order is observed for the C(7)–N–metal and C(1)–metal–N bond angles. In **4** and **5** the metal atom is four-coordinate; however, there is considerable departure from the tetrahedral angle. For **4**, the bond angles at aluminum range from 89.3(3)° (C(1)–Al–N) to 120.6(2)° (C(1)–Al–Br(2)), while for **5** the range is 87.44(7)° (C(1)–Ga–N) to 125.91(6)° (C(1)–Ga–Cl(2)). Another way to consider these bond angles is to think in terms of the distortive effect of intramolecular Lewis base coordination. In the absence of such an interaction, the sum of C–metal–X and X–metal–X bond angles is 360°; in **4** and **5** these

(17) Cowley, A. H.; Gabbaï, F. P.; Isom, H. S.; Decken, A.; Culp, R. D. *Main Group Chem.*, in press.
(18) Cowley, A. H.; Jones, R. A.; Mardones, M. A.; Ruiz, J.; Atwood, J. L.; Bott, S. G. *Angew. Chem., Int. Ed. Engl.* **1990**, *29*, 1150.

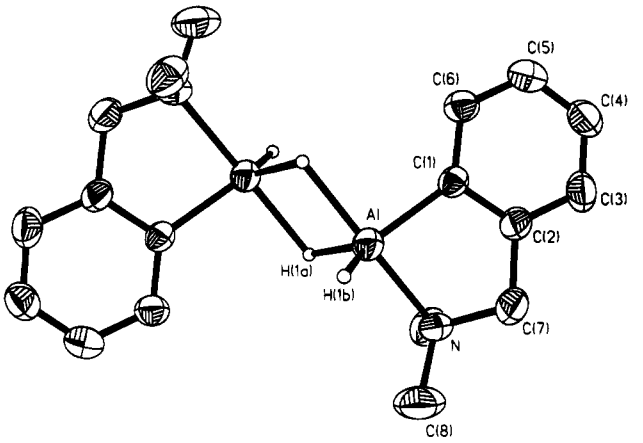

Figure 3. View of $[\{o\text{-}(Me_2NCH_2)C_6H_4\}(H)Al(\mu\text{-}H)]_2$ (**6**) showing the atom-labeling scheme. Thermal ellipsoids are scaled to the 30% probability level.

sums are 347.0(8)° and 354.5(6)°, respectively. The metal–N bond distances in **4** (2.003(5) Å) and **5** (2.071(2) Å) are considerably shorter than those in the corresponding two-arm ligated systems $[(2,6\text{-}Me_2NCH_2)_2C_6H_3]AlCl_2$ (2.261(3) Å)[2] and $[(2,6\text{-}Me_2NCH_2)_2C_6H_3]GaCl_2$ (2.355(4) Å).[17] The trend in the C(aryl)–metal bond lengths C–Al > C–Ga is consistent with the covalent radii of Al and Ga.

Upon reduction with $LiAlH_4$, **4** affords an 85% yield of the corresponding hydride, **6**. Compound **6** also resulted from the transmetalation reaction of **5** with $LiAlH_4$. The dimeric nature of **6** was implied both from

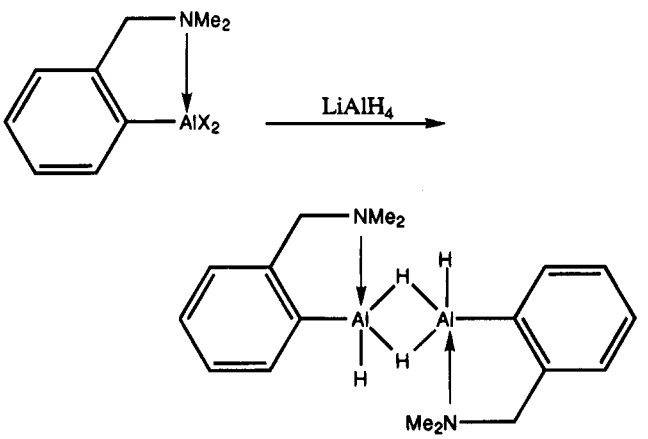

6

the detection of a peak corresponding to $M_2^+ - CH_3$ in the CI mass spectrum (*m/z* 295) and also from the presence of terminal (1775 cm^{-1}) and bridging (1622 cm^{-1}) Al–H stretching frequencies in the IR spectrum. Confirmation was provided by X-ray crystallography. Compound **6** crystallizes in the monoclinic space group $P2_1/n$ with two pairs of dimers in the unit cell. The structure was of sufficient quality to locate the hydride ligands. Each dimer resides on an inversion center, and as a consequence, the bridging Al_2H_2 moiety is required to be planar (Figure 3). Note, however, that the two Al–H bridge bonds differ in length by 0.24 Å. The amine arm of the aryl ligand is coordinated, and the Al–N bond distance (2.102(4) Å) is ~0.1 Å longer than that in the precursor bromide complex **4**. The geometry at the pentacoordinate aluminum atoms in **6** is close to trigonal bipyramidal, while that in **4** is approximately tetrahedral. Thus, for the C(1)H(1b)H(1a)Al plane the sum of bond angles is 359.1(1)° and the angle of the N–Al–H(1aa) axis is 170.4(2)°. As expected, the terminal Al–H bonds (1.521 Å) are shorter than the bridge bonds and are similar in length to those in the dihydride $[2,6\text{-}(Me_2NCH_2)_2C_6H_3]AlH_2$ (1.50(4) Å).[2] The monomeric nature of the latter is clearly a consequence of the coordination of the two amine arms.

The initial product of the reaction of **5** with $LiGaH_4$ is the gallium dihydride **7**. On account of the facile redistribution reaction of **7** (*vide infra*), it was necessary to develop a special procedure for the isolation of this compound (see Experimental Section). The monomeric

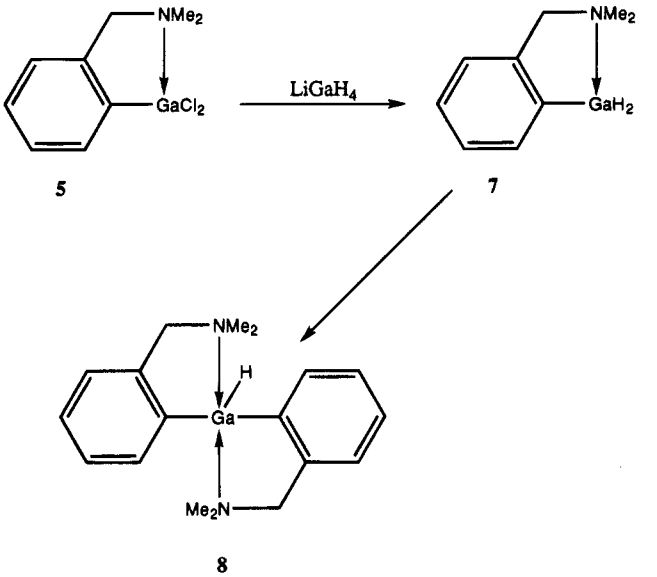

8

nature of the product was indicated by the presence of a sharp cutoff at *m/z* 206 in the CI mass spectrum and the detection of symmetric (1856 cm^{-1}) and antisymmetric (1837 cm^{-1}) stretching frequencies in the IR spectrum. When allowed to stand at −20 °C for several days, solutions of **7** undergo a ligand redistribution reaction to form the monohydride **8**. The composition of **8** was indicated by the presence of the $M^+ + H$ ion in the CI mass spectrum (*m/z* 339). Moreover, only a single Ga–H stretching frequency (1805 cm^{-1}) was evident in the IR spectrum. The structures of both **7** and **8** were confirmed by X-ray crystallography. Compound **7** crystallizes in the monoclinic space group $P2_1/c$ with eight molecules per unit cell. The crystalline state comprises monomers of **7**, and there are no unusually short intermolecular contacts (Figure 4). The amine arm of the aryl ligand is coordinated, and since the coordination numbers at gallium are the same, the Ga–N bond distance of 2.087(7) Å is very similar to that in **5** (2.071(2) Å). Unfortunately, the quality of the crystal structure was such that it was not possible to locate the hydride ligands. Nevertheless, the presence of the GaH_2 moiety was established unequivocally by IR spectral data (see above) and the presence of a proton resonance at δ 5.49, which is in the region reported for other molecules with a terminal GaH_2 moiety.[9,10] Compound **8** crystallizes in the orthorhombic space group $P2_12_12_1$ with four molecules in the unit cell. There are no unusually short intermolecular contacts between the individual molecules of **8**. The overall geometry of **8**

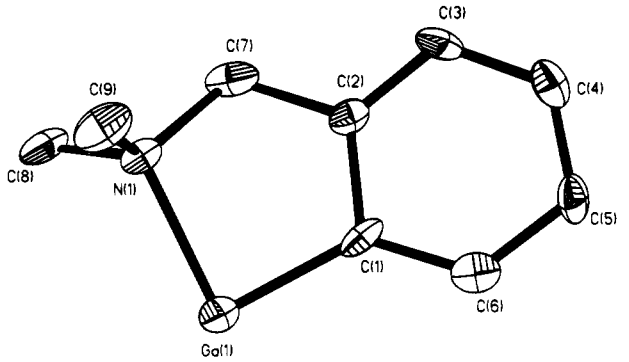

Figure 4. View of $[o\text{-}(Me_2NCH_2)C_6H_4]GaH_2$ (**7**) showing the atom-labeling scheme. Thermal ellipsoids are scaled to the 30% probability level.

resembles that of the corresponding chloride complex $(Ar)_2GaCl$ (Ar = 2-$(Me_2NCH_2)C_6H_4$) (Figure 5).[19] The amine "arms" of both aryl ligands are involved in donor–acceptor interactions with gallium, and the geometry at this pentacoordinate center is approximately that of a trigonal bipyramid with a HGaC(1)C(10) plane (sum of bond angles 357.3(4)°) and a N(1)–Ga–N(2) axis (angle 177.0(3)°). Not unexpectedly, the Ga–N bond distances in **8**, which average 2.390(8) Å, are longer than those in **7** due to the fact that two N–Ga donor interactions are in competition. The hydride ligand in **8** was located, and the Ga–H bond distance (1.150 Å) is slightly longer than that in $[2,6\text{-}(Me_2NCH_2)_2C_6H_3]GaH_2$ (average 1.42(8) Å),[9] the only other experimental value for a terminal Ga–H bond distance of which we are aware.

Our attempts to prepare compounds with In–H bonds have not been successful thus far. As indicated below, the reaction of $ArInI_2$ (Ar = 2-$(Me_2NCH_2)C_6H_4$) with $LiAlH_4$ or $LiGaH_4$ resulted in the formation of **6**, **7**, or **8**:

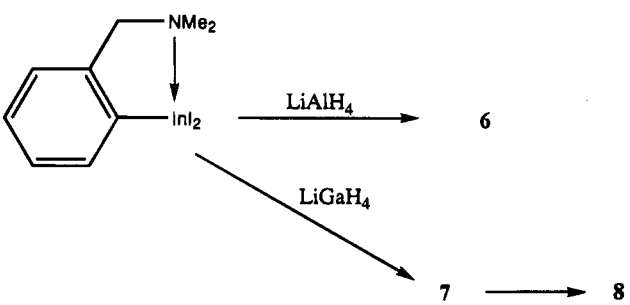

Finally, we note that, like the two-armed hydride **1**, the new one-armed hydrides **6**–**8** are unchanged after prolonged irradiation (18 h, toluene) with 254 nm light. The appreciable thermal stability of **6**–**8** is evident from the fact that all three compounds sublime without decomposition.

Experimental Section

General Procedures. All manipulations were performed under a dry, oxygen-free dinitrogen or argon atmosphere using standard Schlenk techniques or an HE-493 Vacuum Atmospheres drybox. Unless otherwise stated, all solvents were dried over sodium and distilled from sodium benzophenone ketyl under argon prior to use. The reagents $o\text{-}(Me_2NCH_2)C_6H_4Li$[20] and $LiGaH_4$[21] were prepared according to literature methods. Photolysis experiments were carried out using a 450 W Immer type lamp. Elemental analyses were performed by Atlantic Microlab, Inc., Norcross, GA.

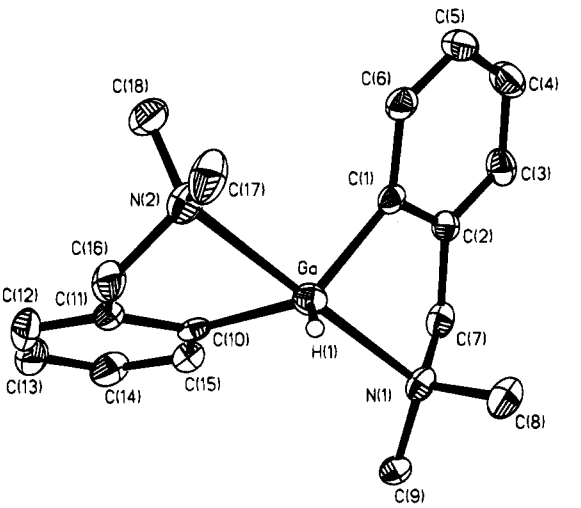

Figure 5. View of $[o\text{-}(Me_2NCH_2)C_6H_4]_2GaH$ (**8**) showing the atom-labeling scheme. Thermal ellipsoids are scaled to the 30% probability level.

Physical Measurements. IR spectra were obtained on a Digilab FTS-40 spectrophotometer. CIMS measurements were made on a Finnagan MAT 4023 instrument, and NMR spectra were recorded on a GE QE-300 spectrometer (^1H, 300.15 MHz; ^{13}C, 75.48 MHz). NMR spectra are referenced to C_6D_6, which was dried over sodium–potassium alloy and distilled prior to use; ^1H and ^{13}C chemical shifts are reported relative to $Si(CH_3)_4$ (0.00 ppm). Melting points were obtained in sealed glass capillaries under argon (1 atm) and are uncorrected.

Synthesis of 4. A slurry of $o\text{-}(Me_2NCH_2)C_6H_4Li$ (1.41 g, 10 mmol) in 50 mL of toluene was added *via* cannula to a stirred solution of $AlBr_3$ (2.67 g, 10 mmol) in 20 mL of toluene. The reaction temperature was maintained at −78 °C for 1 h, following which the reaction mixture was warmed slowly to ambient temperature. After being stirred for an additional 12 h, the reaction mixture was filtered and the volume of the filtrate reduced by evacuation until it became viscous. Cooling of the resulting solution to −20 °C overnight afforded a 69% yield (2.20 g) of colorless crystalline **4** (mp 103–105 °C). Anal. Calcd for $C_9H_{12}NAlBr_2$: C, 33.65; H, 3.73; N, 4.36. Found: C, 33.39; H, 3.84; N, 4.25. CIMS (CH_4): *m/z* 322 ($M^+ + H$), 240 ($M - Br^-$), 136 (ligand + H). ^1H NMR (C_6D_6): δ 1.83 (s, 3H, $N(CH_3)_2$), 2.96 (s, 2H, CH_2), 6.63 (d, ^3J = 7.45 Hz, 1H, ring), 7.07 (m, 2H, ring), 7.63 (d, ^3J = 7.50 Hz, 1H, ring). $^{13}C\{^1H\}$ NMR (C_6D_6): δ 45.69 (s, CH_3), 65.21 (s, CH_2), 125.10 (s, CH, ring), 128.72 (s, CH, ring), 129.42 (s, CH, ring), 136.75 (s, CH, ring), 142.31 (s, C, ring), *ipso* carbon not detected.

Synthesis of 5. A slurry of $o\text{-}(Me_2NCH_2)C_6H_4Li$ (1.41 g, 10 mmol) in 50 mL of toluene was added *via* cannula to a stirred solution of $GaCl_3$ (1.76 g, 10 mmol) in 20 mL of toluene. The reaction temperature was maintained at −78 °C for 1 h, following which the reaction mixture was warmed slowly to ambient temperature. After being stirred for an additional 12 h, the reaction mixture was filtered and the volume of the filtrate reduced by evacuation until it became viscous. Cooling of the resulting solution to −20 °C overnight afforded a 65% yield (1.80 g) of colorless, crystalline **5** (mp 95–97 °C). Anal. Calcd for $C_9H_{12}NGaCl_2$: C, 39.33; H, 4.40; N, 5.10. Found: C, 39.59; H, 4.26; N, 5.13. CIMS (CH_4): *m/z* 274 ($M^+ + H$), 238 ($M - Cl^-$), 136 (ligand + H). ^1H NMR (C_6D_6): δ 1.85 (s, 3H, $N(CH_3)_2$), 2.89 (s, 2H, CH_2), 6.62 (d, ^3J = 7.48 Hz, 1H,

(19) Coggin, D. A.; Fanwick, P. E.; Green, M. A. *J. Chem. Soc., Chem. Commun.* **1993**, 1127. Schumann, H.; Seuss, T. D.; Just, O.; Weimann, R.; Hemling, H.; Gorlitz, F. H. *Organomet. Chem.* **1994**, *479*, 171.

(20) Manzer, L. E. *J. Am. Chem. Soc.* **1978**, *100*, 8068.

(21) Shirk, A. E.; Shriver, D. F. *Inorg. Synth.* **1977**, *17*, 45.

Table 1. Summary of Crystallographic Data for [*o*-(Me_2NCH_2)C_6H_4]$AlBr_2$ (4), [*o*-(Me_2NCH_2)C_6H_4]$GaCl_2$ (5), [{*o*-(Me_2NCH_2)C_6H_4}(H)Al(μ-H)]$_2$ (6), [*o*-(Me_2NCH_2)C_6H_4]GaH_2 (7), and [*o*-(Me_2NCH_2)C_6H_4]$_2$GaH (8)

	4	5	6	7	8
emp formula	$C_9H_{12}AlBr_2N$	$C_9H_{12}Cl_2GaN$	$C_9H_{14}AlN$	$C_9H_{14}GaN$	$C_{18}H_{25}GaN_2$
fw	321.16	274.82	163.20	205.93	339.10
cryst syst	monoclinic	monoclinic	monoclinic	monoclinic	orthorhombic
space group	$P2_1/c$	$P2_1/c$	$P2_1/n$	$P2_1/c$	$P2_12_12_1$
a, Å	9.535(3)	9.371(1)	9.007(1)	9.511(3)	9.615(1)
b, Å	10.209(4)	13.143(2)	11.131(1)	12.588(3)	10.050(1)
c, Å	12.622(5)	10.286(1)	10.279(1)	16.92(1)	17.856(2)
α, deg	90	90	90	90	90
β, deg	92.70(2)	116.38(1)	105.64(1)	102.72(3)	90
γ, deg	90	90	90	90	90
V, Å^3	1227.3(4)	1134.9(2)	992.3(5)	1976(1)	1717.9(9)
Z	4	4	4	8	4
d(calcd), g cm^{-3}	1.737	1.608	1.092	1.384	1.311
μ, cm^{-1}	66.4	28.5	1.45	27.25	15.98
F(000)	624	552	352	848	712
no. of rflns collected	2226	3416	2558	4376	2943
no. of rflns obsd.	1568	2574	988	3390	1355
temp, K	173 ± 1	173 ± 1	298 ± 2	298 ± 2	298 ± 2
ref params	131	131	102	200	193
R/R_w, %			6.84/7.42		5.20/5.15
$R1$/wR2, %	4.91/11.91	3.11/7.94		8.60/12.71	
GOF	1.05	1.08	1.80	1.29	0.99
w^{-1} [a]	a	b	c	d	e
ref based on	F^2	F^2	F	F^2	F

[a] $\sigma(F_o^2) + (0.0876P)^2$; (b) $\sigma^2(F_o^2) + (0.0363P)^2 + 0.1598P$; (c) $\sigma(F) + 0.0005F^2$; (d) $\sigma^2(F_o^2) + (0.03P)^2$; (e) $\sigma^2(F) + 0.001F^2$; $P = (\mathrm{Max}(F_o^2,0) + 2F_c^2)/3$.

Table 2. Fractional Coordinates and Equivalent Isotropic Thermal Parameters[a] for the Non-Hydrogen Atoms of 4

atom	x/a	y/b	z/c	U, Å^2
Br(1)	0.0725(1)	0.0848(1)	0.6797(1)	0.030(1)
Br(2)	0.4640(1)	0.0428(1)	0.7010(1)	0.038(1)
Al	0.2627(2)	0.0439(2)	0.7960(2)	0.023(1)
N	0.2717(5)	0.1879(5)	0.9038(4)	0.028(1)
C(1)	0.2381(6)	−0.0835(6)	0.9106(5)	0.026(2)
C(2)	0.2483(6)	−0.2208(6)	0.9173(5)	0.028(1)
C(3)	0.2245(6)	−0.2860(7)	1.0124(6)	0.034(2)
C(4)	0.1948(6)	−0.2153(7)	1.1029(5)	0.033(2)
C(5)	0.1863(7)	−0.0786(6)	1.0971(5)	0.033(2)
C(6)	0.2076(6)	−0.0139(6)	1.0023(5)	0.027(2)
C(7)	0.1857(6)	0.1339(6)	0.9930(5)	0.032(2)
C(8)	0.2161(7)	0.3187(6)	0.8698(6)	0.036(2)
C(9)	0.4217(7)	0.2046(7)	0.9451(6)	0.036(2)

[a] For anisotropic atoms, the U value is U_{eq}, defined as one-third of the trace of the orthogonalized $\mathbf{U}_{ij}$ tensor.

Table 3. Fractional Coordinates and Equivalent Isotropic Thermal Parameters[a] for the Non-Hydrogen Atoms of 5

atom	x/a	y/b	z/c	U, Å^2
Ga	0.3599(1)	0.9584(1)	0.7677(1)	0.012(1)
Cl(1)	0.5895(1)	0.8979(1)	0.9251(1)	0.024(1)
Cl(2)	0.3906(1)	1.1090(1)	0.6978(1)	0.028(1)
N	0.3042(2)	0.8694(1)	0.5853(2)	0.014(1)
C(1)	0.1665(2)	0.9064(2)	0.7709(2)	0.014(1)
C(2)	0.1149(2)	0.8204(1)	0.6805(2)	0.016(1)
C(3)	−0.0256(2)	0.7705(2)	0.6586(2)	0.025(1)
C(4)	−0.1139(2)	0.8060(2)	0.7271(3)	0.029(1)
C(5)	−0.0661(2)	0.8899(2)	0.8144(2)	0.026(1)
C(6)	0.0741(2)	0.9411(2)	0.8372(2)	0.019(1)
C(7)	0.2188(2)	0.7821(2)	0.6127(2)	0.019(1)
C(8)	0.4400(3)	0.8328(2)	0.5614(2)	0.025(1)
C(9)	0.1913(3)	0.9257(2)	0.4539(2)	0.024(1)

[a] For anisotropic atoms, the U value is U_{eq}, defined as one-third of the trace of the orthogonalized $\mathbf{U}_{ij}$ tensor.

ring), 7.04 (m, 2H, ring), 7.43 (d, ^3J = 7.49 Hz, 1H, ring). $^{13}C\{^1H\}$ NMR (C_6D_6): δ 45.32 (s, CH_3), 64.64 (s, CH_2), 125.39 (s, CH, ring), 128.57 (s, CH, ring), 129.64 (s, CH, ring), 135.63 (s, CH, ring), 140.92 (s, C, ring), *ipso* carbon not detected.

Synthesis of 6. A mixture of 100 mg (0.36 mmol) of **5** and 38 mg of $LiAlH_4$ (1.0 mmol) was treated with 25 mL of Et_2O at −78 °C and immediately warmed to room temperature while good stirring was maintained. After a few minutes at room temperature, a gray solid precipitated from the reaction mixture. The reaction mixture was stirred for an additional 1 h, and the volatiles were removed *in vacuo*. The residue was extracted with toluene (3 × 10 mL) and filtered. The volume of the filtrate was reduced by ~75%. Cooling of the resulting solution to −20 °C overnight afforded an 85% yield (50 mg) of colorless, crystalline **6** (mp 102−104 °C). Anal. Calcd for $C_9H_{14}NAl$: C, 66.24; H, 8.65; N, 8.58. Found: C, 65.86; H, 8.37; N, 8.27. CIMS (CH_4): m/z 295 ($M_2 - CH_3$), 162 ($M^+ - H$), 136 (ligand + H). ^1H NMR (C_6D_6): δ 1.98 (s, 3H, $N(CH_3)_2$), 3.18 (s, 2H, CH_2), 4.57 (s, 2H, AlH_2), 6.78 (d, ^3J = 7.52 Hz, 1H, ring), 7.21 (m, 2H, ring), 7.88 (d, ^3J = 7.50 Hz, 1H, ring). $^{13}C\{^1H\}$ NMR (C_6D_6): δ 45.19 (s, CH_3), 65.63 (s, CH_2), 124.22 (s, CH, ring), 126.85 (s, CH, ring), 129.20 (s, CH, ring), 138.52 (s, CH, ring), 145.14 (s, C, ring), *ipso* carbon not detected. IR: ν 1775 (terminal), 1622 cm^{-1} (bridge).

Synthesis of 7. A freshly prepared solution of $LiGaH_4$ (10 mmol, 25 mL of Et_2O), which had been precooled to −78 °C, was added *via* cannula to a stirred solution of **5** (87 mg, 0.32 mmol) in 25 mL of Et_2O at −78 °C. The reaction mixture was warmed immediately to room temperature. After a few minutes at room temperature, a gray solid precipitated from the reaction mixture. The reaction mixture was stirred for an additional 1 h, and the volatiles were removed *in vacuo*. Slow (~12 h) sublimation of the residue with a thermal gradient sublimator (maximum temperature 50 °C) resulted in a 62% yield (40 mg) of colorless crystalline **7** (mp 49−51 °C). Anal. Calcd for $C_9H_{14}NGa$: C, 52.49; H, 6.85; N, 6.80. Found: C, 52.38; H, 6.86; N, 6.71. CIMS (CH_4): m/z 204 ($M^+ - H$), 136 (ligand + H). ^1H NMR (C_6D_6): δ 1.90 (s, 3H, $N(CH_3)_2$), 3.09 (s, 2H, CH_2), 5.49 (s, 2H, GaH_2), 6.86 (d, ^3J = 7.50 Hz, 1H, ring), 7.18 (m, 2H, ring), 7.75 (d, ^3J = 7.51 Hz, 1H, ring). $^{13}C\{^1H\}$ NMR (C_6D_6): δ 46.92 (s, CH_3), 67.62 (s, CH_2), 124.29 (s, CH, ring), 127.03 (s, CH, ring), 127.50 (s, CH, ring), 136.55 (s, CH, ring), 143.55 (s, C, ring), *ipso* carbon not detected. IR: ν 1856 (sym), 1837 cm^{-1} (asym).

Synthesis of 8. A freshly prepared solution of $LiGaH_4$ (10 mmol, 25 mL of Et_2O), which had been precooled to −78 °C, was added *via* cannula to a stirred solution of Ar_2GaCl (370 mg, 1.0 mmol) in 25 mL of Et_2O at −78 °C. The reaction

Table 4. Fractional Coordinates and Equivalent Isotropic Thermal Parameters[a] for the Non-Hydrogen Atoms for 6

atom	x/a	y/b	z/c	U, Å²
Al	0.1579(2)	0.9795(1)	0.0245(1)	0.062(1)
N	0.3105(4)	0.8389(3)	0.1058(3)	0.062(2)
C(1)	0.2053(5)	0.937(4)	−0.1464(4)	0.055(2)
C(2)	0.334(6)	0.8611(4)	−0.123(5)	0.073(2)
C(3)	0.387(7)	0.8155(5)	−0.2303(6)	0.091(3)
C(4)	0.3146(7)	0.8502(5)	−0.3591(5)	0.086(3)
C(5)	0.1952(6)	0.9291(5)	−0.3838(5)	0.079(2)
C(6)	0.1391(5)	0.9717(4)	−0.2794(5)	0.069(2)
C(7)	0.4254(7)	0.8401(5)	0.0246(6)	0.093(3)
C(8)	0.3884(8)	0.8509(6)	0.2507(6)	0.128(4)
C(9)	0.2279(7)	0.7235(5)	0.0896(6)	0.093(3)

[a] For anisotropic atoms, the U value is U_{eq}, defined as one-third of the trace of the orthogonalized $\mathbf{U}_{ij}$ tensor.

Table 5. Fractional Coordinates and Equivalent Isotropic Thermal Parameters[a] for the Non-Hydrogen Atoms of 7

atom	x/a	y/b	z/c	U, Å²
Ga(1)	0.2840(1)	0.0544(1)	0.6010(1)	0.040(1)
N(1)	0.1315(8)	0.1759(6)	0.5888(5)	0.035(2)
C(1)	0.2514(9)	0.0566(7)	0.4848(6)	0.030(3)
C(2)	0.1282(10)	0.1200(7)	0.4475(7)	0.031(3)
C(3)	0.0891(11)	0.1360(8)	0.3661(7)	0.041(3)
C(4)	0.1620(11)	0.0882(8)	0.3147(6)	0.043(3)
C(5)	0.2783(11)	0.0246(8)	0.3434(6)	0.041(3)
C(6)	0.3192(10)	0.0108(7)	0.4289(7)	0.038(3)
C(7)	0.0417(10)	0.1600(7)	0.5056(7)	0.045(3)
C(8)	0.0442(11)	0.1720(8)	0.6505(7)	0.053(3)
C(9)	0.2040(11)	0.2798(7)	0.5933(7)	0.055(3)
Ga(2)	0.7427(1)	0.0876(1)	0.8858(1)	0.043(1)
N(2)	0.5667(8)	0.1879(7)	0.8859(5)	0.040(2)
C(11)	0.7713(10)	0.0890(7)	1.0004(6)	0.032(3)
C(12)	0.6942(10)	0.1684(9)	1.0294(7)	0.041(3)
C(13)	0.6859(12)	0.1837(10)	1.1099(7)	0.051(3)
C(14)	0.7660(12)	0.1198(10)	1.1671(7)	0.051(3)
C(15)	0.8518(12)	0.0381(10)	1.1462(7)	0.053(3)
C(16)	0.8516(11)	0.0273(9)	1.0629(8)	0.056(4)
C(17)	0.6101(11)	0.2416(8)	0.9662(6)	0.047(3)
C(18)	0.5362(11)	0.2628(8)	0.8196(6)	0.051(3)
C(19)	0.4390(10)	0.1232(8)	0.8853(7)	0.054(3)

[a] For anisotropic atoms, the U value is U_{eq}, defined as one-third of the trace of the orthogonalized $\mathbf{U}_{ij}$ tensor.

mixture was warmed immediately to room temperature. After a few minutes at room temperature, a gray solid precipitated from the reaction mixture. The reaction mixture was stirred for an additional 1 h, and the volatiles were removed *in vacuo*. The residue was extracted with toluene (3 × 10 mL) and filtered. The volume of the filtrate was reduced by ~75%. Cooling of the resulting solution to −20 °C overnight afforded an 84% yield (313 mg) of colorless, crystalline **8** (mp 144−145 °C). Anal. Calcd for $C_{18}H_{25}NGa$: C, 63.75; H, 7.43; N, 8.26. Found: C, 63.29; H, 7.25; N, 8.22. CIMS (CH_4): *m/z* 339 (M^+ − H), 136 (ligand + H). ^{1}H NMR (C_6D_6): δ 2.13 (s, 3H, $N(CH_3)_2$), 3.45 (s, 2H, CH_2), 5.12 (s, 2H, GaH_2), 7.05 (d, ^3J = 7.53 Hz, 1H, ring), 7.25 (m, 2H, ring), 7.69 (d, ^3J = 7.51 Hz, 1H, ring). $^{13}C\{^1H\}$ NMR (C_6D_6): δ 45.40 (s, CH_3), 66.72 (s, CH_2), 126.14 (s, CH, ring), 126.37 (s, CH, ring), 126.69 (s, CH, ring), 136.92 (s, CH, ring), 144.56 (s, C, ring), *ipso* carbon not detected. IR: ν 1805 cm^{-1} (terminal).

X-ray Crystallography. Details of the crystal data and a summary of intensity data collection parameters for **4**−**8** are given in Table 1. Fractional atomic coordinates and equivalent isotopic thermal parameters for **4**−**8** are presented in Tables 2−6, respectively. Crystals of **4**−**6** and **8** were grown from toluene solutions stored at −20 °C. Crystals of **7** were grown by thermal gradient sublimation. Crystals of **4** and **5** were mounted on thin glass fibers, and crystals of **6**−**8** were mounted in thin-walled glass capillaries and sealed under argon (1 atm). Data sets for **4** and **5** were collected on a

Table 6. Fractional Coordinates and Equivalent Isotropic Thermal Parameters[a] for the Non-Hydrogen Atoms of 8

atom	x/a	y/b	z/c	U, Å²
Ga	0.0567(1)	1.0030(2)	0.0792(1)	0.037(1)
N(1)	0.2651(7)	1.1201(8)	0.0775(5)	0.038(3)
C(1)	−0.0013(10)	1.1673(9)	0.1302(5)	0.030(3)
C(2)	0.0864(10)	1.2776(10)	0.1185(5)	0.035(3)
C(3)	0.0584(13)	1.4031(9)	0.1507(5)	0.045(3)
C(4)	−0.0568(13)	1.4167(11)	0.1953(6)	0.054(4)
C(5)	−0.1425(12)	1.3151(12)	0.2076(6)	0.054(4)
C(6)	−0.1167(11)	1.1898(12)	0.1773(6)	0.039(4)
C(7)	0.2154(10)	1.2585(10)	0.0703(6)	0.042(4)
C(8)	0.3285(11)	1.1008(11)	0.1507(6)	0.051(4)
C(9)	0.3680(10)	1.0909(11)	0.0191(5)	0.044(4)
N(2)	−0.1591(8)	0.8727(8)	0.0865(6)	0.042(3)
C(10)	0.0164(8)	0.9723(8)	−0.0290(5)	0.029(3)
C(11)	−0.0722(11)	0.8652(9)	−0.0424(6)	0.039(3)
C(12)	−0.1158(13)	0.8328(12)	−0.1143(8)	0.062(5)
C(13)	−0.0703(13)	0.9064(14)	−0.1737(7)	0.065(5)
C(14)	0.0167(9)	1.0127(17)	−0.1640(5)	0.055(4)
C(15)	0.0602(11)	1.0453(9)	−0.0915(5)	0.049(4)
C(16)	−0.1202(12)	0.7847(10)	0.0243(7)	0.051(4)
C(17)	−0.1755(13)	0.7976(13)	0.1557(7)	0.058(5)
C(18)	−0.2894(9)	0.9384(10)	0.0669(7)	0.049(4)

[a] For anisotropic atoms, the U value is U_{eq}, defined as one-third of the trace of the orthogonalized $\mathbf{U}_{ij}$ tensor.

Table 7. Selected Bond Lengths (Å) and Angles (deg) for [*o*-(Me_2NCH_2)C_6H_4]$AlBr_2$ (4), [*o*-(Me_2NCH_2)C_6H_4]$GaCl_2$ (5), [{*o*-(Me_2NCH_2)C_6H_4}(H)Al(μ-H)]$_2$ (6), [*o*-(Me_2NCH_2)C_6H_4]GaH_2 (7), and [*o*-(Me_2NCH_2)C_6H_4]$_2$GaH (8)

Bond Lengths for Compound **4**			
Al−Br(1)	2.316(2)	Al−N	2.003(5)
Al−Br(2)	2.310(2)	Al−C(1)	1.967(6)
Bond Angles for Compound **4**			
Br(1)−Al−Br(2)	108.45(8)	C(1)−Al−Br(2)	120.6(2)
C(1)−Al−N	89.3(3)	C(1)−Al−Br(1)	117.9(2)
Bond Lengths for Compound **5**			
Ga−Cl(1)	2.1886(6)	Ga−N	2.071(2)
Ga−Cl(2)	2.1682(6)	Ga−C(1)	1.951(2)
Bond Angles for Compound **5**			
Cl(1)−Ga−Cl(2)	110.21(2)	C(1)−Ga−Cl(2)	125.91(6)
C(1)−Ga−N	87.44(7)	C(1)−Ga−Cl(1)	118.38(6)
Bond Lengths for Compound **6**			
Al−H(1A)	1.688	A−N	2.102(4)
Al−H(1AA)	1.928(3)	Al−H(1B)	1.521
Al−C(1)	1.974(5)		
Bond Angles for Compound **6**			
N−Al−H(1AA)	170.42	C(1)−Al−H(1B)	124.9(1)
C(1)−Al−H(1A)	118.6(1)	H(1A)−Al−H(1B)	115.6(1)
Bond Lengths for Compound **7**			
Ga−C(1)	1.92(1)	Ga−N	2.087(7)
Bond Angles for Compound **7**			
C(1)−Ga−N	86.3(4)		
Bond Lengths for Compound **8**			
Ga−C(1)	1.966(9)	Ga−N(1)	2.324(7)
Ga−C(10)	1.993(9)	Ga−N(2)	2.457(8)
Ga−H	1.150		
Bond Angles for Compound **8**			
N(1)−Ga−N(2)	177.0(3)	C(1)−Ga−C(10)	121.6(4)
C(1)−Ga−H	120.3(3)	C(10)−Ga−H	115.4(2)

Siemens P4 diffractometer at −100 °C, and an Enraf-Nonius CAD4 diffractometer was used for the collection of data for compounds **6**−**8** at 25 °C. Mo Kα radiation (λ = 0.710 73 Å) was used for all structures. The structures were solved by direct methods and refined with the SHELXTL Plus (PC)

[4.2][22] software package for compounds **6** and **8** and SHELXTL-93[23] for compounds **4**, **5**, and **7**. The hydride ligands in **6** and **8** were located in the difference map and refined as a riding model.

Acknowledgment. We are grateful to the National Science Foundation (Grant No. CHE-9108228), the Science and Technology Center Program of the National Science Foundation (Grant No. CHE-08920120), and the Robert A. Welch Foundation for generous financial support.

(22) Sheldrick, G. M. SHELXTL-PC [4.2]; Siemens Analytical X-ray Instruments, Inc., 1990.
(23) Sheldrick, G. M. SHELXL-93; University of Göttingen, 1993.

Supplementary Material Available: Tables of crystal data and refinement details, bond lengths, bond angles, H atom coordinates, and thermal parameters for **4**–**8** (27 pages). Ordering information is given on any current masthead page.

OM9409635

Synthesis and Molecular Structure of the First Example of an η^4-Complex of Hexafluorobutadiene: $[RuCl(\eta^5\text{-}C_5Me_5)(\eta^4\text{-}C_4F_6)]$. Structural Comparison of Coordinated Butadiene and Its Perfluorinated Analogue

Russell P. Hughes,*[1a] Peter R. Rose,[1a] Xiaoming Zheng,[1a] and Arnold L. Rheingold[1b]

Chemistry Departments, Burke Chemistry Laboratory, Dartmouth College, Hanover, New Hampshire 03755-3564, and University of Delaware, Newark, Delaware 19716

Received November 10, 1994[⊗]

Hexafluorobutadiene reacts with $[RuCp^*Cl]_4$ ($Cp^* = C_5Me_5$) to give the first example of an η^4-hexafluorobutadiene transition metal complex, $[RuCp^*Cl(\eta^4\text{-}C_4F_6)]$ (**9**), which has been characterized by a single crystal X-ray diffraction study: orthorhombic, *Pnma*, $a = 13.360(3)$ Å, $b = 12.919(3)$ Å, $c = 8.600(3)$ Å, $V = 1484.3(7)$ Å^3, and $Z = 4$. The structure of **9** reveals significant differences in ruthenium–carbon and carbon–carbon distances compared to a previously reported hydrocarbon analogue $[RuCp^*I(\eta^4\text{-}C_4H_6)]$ (**7b**). The fluorocarbon ligand in **9** shows a long–short–long pattern of C–C distances, contrasting with the short–long–short pattern previously observed for **7b**. Significant pyramidalization is observed at the CF_2 groups in **9**. A detailed analysis of the ^{19}F NMR spectrum of **9** reveals an unusually large five-bond coupling between two fluorines, consistent with these fluorines being forced closer together on coordination of hexafluorobutadiene. The data are compared with those for the free diene which exists in a skewed ground state conformation. An intermediate en route to **9** has also been observed, although it could not be obtained pure. ^1H and ^{19}F NMR spectroscopic analysis indicates the intermediate is $[(RuCp^*Cl)_2(\mu\text{-}C_4F_6)]$, and a detailed analysis of the ^{19}F NMR coupling constants suggests that the μ-hexafluorobutadiene ligand adopts the *s-trans* conformation to give structure **11**.

Introduction

Transition metal complexes containing the 1,3-butadiene ligand and its substituted analogues are numerous. The prototype, $[Fe(\eta^4\text{-}C_4H_6)(CO)_3]$ (**1**), was prepared in 1930 by the reaction of iron carbonyl with butadiene,[2] and the organic chemistry of iron complexes of conjugated dienes is now quite elaborate.[3] Conjugated diene complexes of transition metals in all the transition metal groups (3–10) have been reported, and a variety of coordination modes have been observed, as summarized in Figure 1. While the vast majority of complexes containing middle and late transition metals adopt the η^4-*s-cis*-1,3-diene structure **A**, it is now apparent from X-ray and NMR data that the mononuclear diene complexes of early transition metals of groups 3–5 prefer the bent σ^2-bonded η^4-metallacyclo-3-pentene structure **B**, the planar σ^2-bonded η^2-metallacyclo-3-pentene structure **C**, or the η^4-*s-trans*-1,3-diene structure **D**.[4] In dinuclear complexes *s-trans*-dienes can bridge two metal fragments as in complexes $[(Pt_2Cl_6)_2(butadiene)]^{2-}$ (type **E**)[5] and $[Mn_2(CO)_8(butadiene)]$ (type **F**),[6] or *s-cis*-dienes can span two metal centers (**G** and **H**) as in complexes $[Rh_2(iPr_2PCH_2CH_2$-

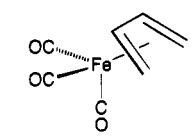

1

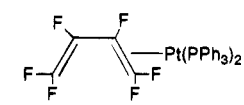

2

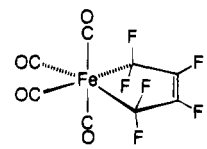

3

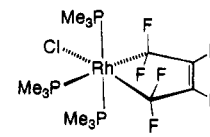

4

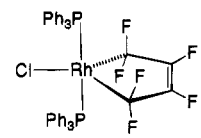

5

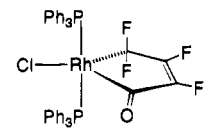

6

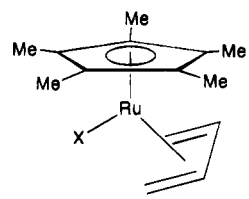

7 a. X = Cl
b. X = I

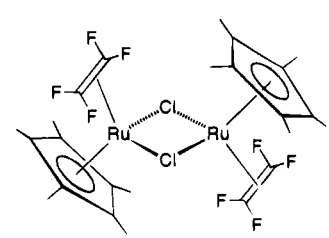

8

[⊗] Abstract published in *Advance ACS Abstracts,* February 1, 1995.

(1) (a) Dartmouth College. (b) University of Delaware.

(2) Reihlen, H.; Gruhl, A.; von Hessling, G.; Pfrengle, O. *Justus Liebigs Ann. Chem.* **1930**, *482*, 161.

(3) Collman, J. P.; Hegedus, L. S.; Norton, J. R.; Finke, R. G. *Principles and Applications of Organotransition Metal Chemistry*; University Science: Mill Valley, CA, 1987; Chapter 17.

(4) Yasuda, H.; Nakamura, A. *Angew. Chem., Int. Ed. Engl.* **1987**, *26*, 723.

(5) Adam, V. C.; Jarvis, J. A. J.; Kilbourn, B. T.; Owston, P. G. *J. Chem. Soc., Chem. Commun.* **1971**, 467.

0276-7333/95/2314-2407$09.00/0

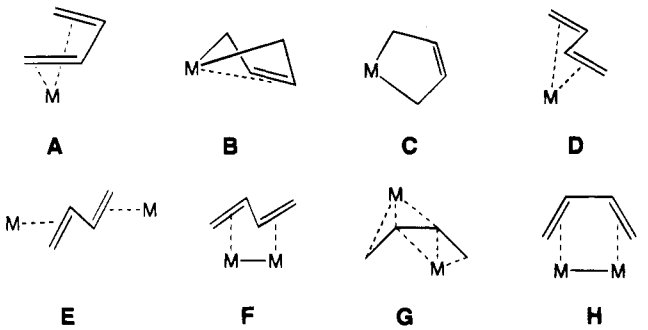

Figure 1. Various coordination modes for 1,3-dienes.

$CH_2PiPr_2)_2$(butadiene)] (type **G**)[7] and [$Co_2Cp_2(CO)$(butadiene)] (type **H**).[8]

In contrast to the abundance of hydrocarbon examples, transition metal complexes of 1,3-hexafluorobutadiene are remarkably rare. Only four well-characterized complexes have been reported prior to this work. A single example of η^2-coordination is found in complex **2**, as evidenced by NMR spectroscopy.[9] Instead of forming an η^4-*s*-*cis*-diene complex (type **A**), as does 1,3-butadiene in complex **1**, hexafluorobutadiene reacts with iron carbonyl to give a σ^2-bonded η^2-metallacyclo-3-pentene complex **3** (type **C**),[10] which has been characterized unambiguously by X-ray crystallography.[11] An analogous oxidative addition reaction of hexafluorobutadiene with [$RhCl(PMe_3)_3$] and [$RhCl(PPh_3)_3$] affords complexes **4** and **5**, respectively, both of which contain type **C** structures based on the X-ray crystallographic determinations of **4** and **6**, the product of hydrolysis of **5**.[12] The harmonious conspiracy of circumstances that drive this mode of coordination probably include formation of stronger metal−carbon σ-bonds to fluorinated carbon atoms,[13] the *gem*-difluoro effect arising from the exothermicity associated with the pyramidalization of a planar CF_2 group,[14] and the ability of the metal [Fe(0) or Rh(I)] to undergo the formally required two-electron oxidation. A poorly characterized complex of apparent formula [$Co_2(CO)_6(C_4F_6)$], presumably containing a bridging hexafluorobutadiene ligand, has been reported,[10] and the insertion reaction of hexafluorobutadiene into a Co−H bond has also been observed.[15]

Intrigued by the notable absence of η^4-*cis*-hexafluorobutadiene complexes, we set out to synthesize an unambiguous example for structural comparison with a hydrocarbon analogue. Recent reports of η^4-*s*-*cis*-1,3-butadiene complexes of ruthenium(II) (**7a,b**)[16] and the knowledge that the [RuCp*Cl] (Cp* = C_5Me_5) fragment

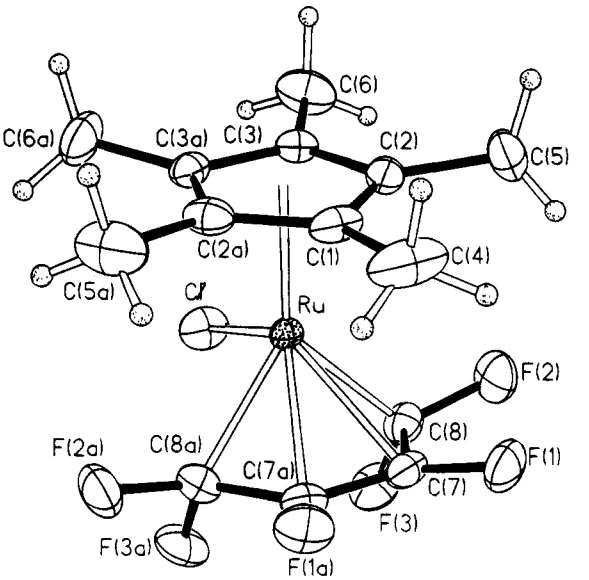

Figure 2. Molecular structure and atom numbering scheme for **9**. Thermal ellipsoids are drawn at the 40% probability level.

was capable of binding fluoroolefins, as in **8**,[17] led us to investigate the reaction of hexafluorobutadiene with the tetrameric complex [RuCp*Cl]$_4$.

Results and Discussion

Treatment of [RuCp*Cl]$_4$ with excess hexafluorobutadiene in methylene chloride led to a mixture of two compounds, according to ^{19}F NMR spectroscopic evidence. The principal, and thermodynamically favored, component of the mixture could be crystallized and was unambiguously identified as **9** by a single crystal X-ray

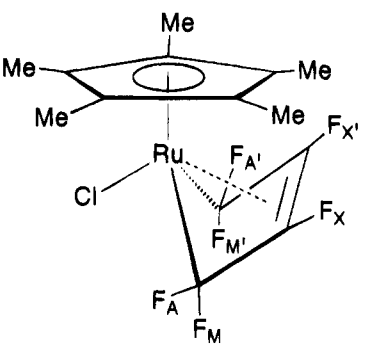

9

diffraction study. An ORTEP of **9**, along with key bond distances and angles, is shown in Figure 2. Table 1 summarizes details of the structure determination, and fractional coordinates are presented in Table 2. A crystallographic plane includes the Ru−Cl bond and relates the two halves of the diene ligand. The C_4F_6 ligand is η^4-*cis* coordinated, in an *endo* conformation with the two terminal CF_2 groups pointing to the chloride ligand. The overall *endo* conformation of the diene is identical with that found in the hydrocarbon analogue **7b**.[16]

(6) Sasse, H. E.; Ziegler, M. L. *Z. Anorg. Allg. Chem.* **1972**, *392*, 167.
(7) Fryzuk, M. D.; Piers, W. E.; Rettig, S. J. *J. Am. Chem. Soc.* **1985**, *107*, 8259.
(8) Vollhardt, K. P. C.; King, J. A. *Organometallics* **1983**, *2*, 684.
(9) Green, M.; Osborn, A. J.; Stone, F. G. A. *J. Chem. Soc. A* **1968**, 2525.
(10) Hunt, R. L.; Roundhill, D. M.; Wilkinson, G. *J. Chem. Soc. A* **1967**, 982.
(11) Hitchcock, P. B.; Mason, R. *J. Chem. Soc., Chem. Commun.* **1967**, 242.
(12) Hughes, R. P.; Rose, P. R.; Rheingold, A. L. *Organometallics* **1993**, *12*, 3109.
(13) Hughes, R. P. *Adv. Organomet. Chem.* **1990**, *31*, 183 and references cited therein.
(14) Smart, B. E. In *The Chemistry of Functional Groups;* Patai, S., Rappoport, Z., Eds.; John Wiley & Sons: New York, 1983; Suppl. D, Chapter 14.
(15) Sasaoka, S.-I.; Joh, T.; Tahara, T.; Takahashi, S. *Chem. Lett.* **1989**, 1163.
(16) Fagan, P. J.; Mahoney, W. S.; Calabrese, J. C.; Williams, I. D. *Organometallics* **1990**, *9*, 1843.
(17) Curnow, O. J.; Hughes, R. P.; Mairs, E. N.; Rheingold, A. L. *Organometallics* **1993**, *12*, 3102.
(18) Churchill, M. R.; Mason, R. *Proc. R. Soc. A* **1967**, *301*, 433.

Table 1. X-ray Crystallographic Structure Determination Summary for 9

Crystal Data	
empirical formula	$C_{14}H_{15}ClF_6Ru$
color; habit	amber block
cryst size (mm)	0.28 × 0.30 × 0.30
cryst syst	orthorhombic
space group	*Pnma*
unit cell dimens	
a (Å)	13.360(3)
b (Å)	12.919(3)
c (Å)	8.600(3)
volume (Å³)	1484.3(7)
Z	4
fw	433.8
density(calc) (g/cm³)	1.941
abs coeff (cm^{-1})	12.73
F(000)	856
Data Collection	
diffractometer used	Siemens P4
radiation, λ (Å)	Mo Kα, 0.710 73
temp (K)	239
monochromator	highly oriented graphite crystal
2θ range (deg)	4.0−52.0
scan type	Wyckoff
scan speed (deg/min)	variable; 7.00−20.00 in ω
scan range, ω (deg)	1.00
bckgd measurement	Stationary crystal and stationary counter at beginning and end of scan, each for 50.0% of total scan time
no. of std reflns	3 measured every 197 reflections
index ranges	$0 \le h \le 16, 0 \le k \le 15, 0 \le l \le 10$
no. of reflns collcd	1522
no. of ind reflns	1522 (R_{int} = 0.00%)
no. of obsd reflns	1317 ($F > 5.0\sigma(F)$)
abs corr	N/A
Solution and Refinement	
system used	Siemens SHELXTL PLUS (PC Version)
solution	direct methods
refinement method	full-matrix least-squares
quantity minimized	$\sum w(F_o - F_c)^2$
absolute structure	N/A
ext corr	$\chi = 0.0018(2)$, where $F^* = F[1 + 0.002\chi F^2/\sin(2\theta)]^{-1/4}$
hydrogen atoms	riding model, fixed isotropic *U*
weighting scheme	$w^{-1} = \sigma^2(F) + 0.0005F^2$
no. of params refined	107
final *R* indices (obsd data) (%)	R = 2.44, R_w = 3.69
R indices (all data) (%)	R = 2.94, R_w = 3.87
goodness-of-fit	1.26
largest and mean Δ/σ	0.016, 0.002
data to param ratio	12.3:1
largest diff peak (e Å⁻³)	0.36
largest diff hole (e Å⁻³)	−0.44

A comparison of bond lengths in η^4-coordinated butadiene (complex **7b**),[16] η^4-coordinated hexafluorobutadiene (complex **9**), and η^4-coordinated hexafluorobutadiene (complex **4**)[12] is presented in Figure 3. An analogous comparison of bond angles is presented in Figure 4. Unlike **9**, complex **4** does not have any crystallographically imposed symmetry; data are available for the two halves of the fluorinated ligand in two crystallographically independent molecules.[12] Before comparing the structures of these transition metal complexes, a brief discussion of the structural parameters of the free ligands is worthwhile, as we will also make comparisons between the metal-bound ligands and their uncoordinated forms.

The question of how significantly the structural parameters of the coordinated ligands differ from those in their uncoordinated forms must be approached with some caution. The structure of the *s-cis* conformation of each diene clearly represents the most valid comparison with that of the coordinated ligand, but *s-cis* is in fact the least stable conformation for either diene. In addition, the significantly different properties of hydrogen and fluorine also lead to different ground state structures for butadiene and its perfluorinated analogue. Before continuing, we must consider what available structural data for the free ligands provide the most useful and meaningful comparisons.

Table 2. Fractional Atomic Coordinates (×10⁴) and Equivalent Isotropic Displacement Coefficients (Å² ×10³) for 9

	x	*y*	*z*	*U*(eq)[a]
Ru	7128(1)	7500	678(1)	23(1)
Cl	6936(1)	7500	−2065(1)	46(1)
F(1)	5975(1)	6473(1)	3470(2)	49(1)
F(2)	6239(2)	5385(2)	890(2)	53(1)
F(3)	5267(1)	6425(2)	−389(2)	53(1)
C(1)	8251(3)	7500	2581(4)	37(1)
C(2)	8453(2)	6597(2)	1665(3)	37(1)
C(3)	8719(2)	6937(2)	179(3)	32(1)
C(4)	8042(4)	7500	4309(5)	71(3)
C(5)	8444(3)	5505(3)	2222(6)	71(2)
C(6)	9069(3)	6295(3)	−1147(5)	59(1)
C(7)	5892(2)	6959(2)	2094(3)	35(1)
C(8)	6012(2)	6394(2)	671(3)	37(1)

[a] Equivalent isotropic *U* defined as one-third of the trace of the orthogonalized U_{ij} tensor.

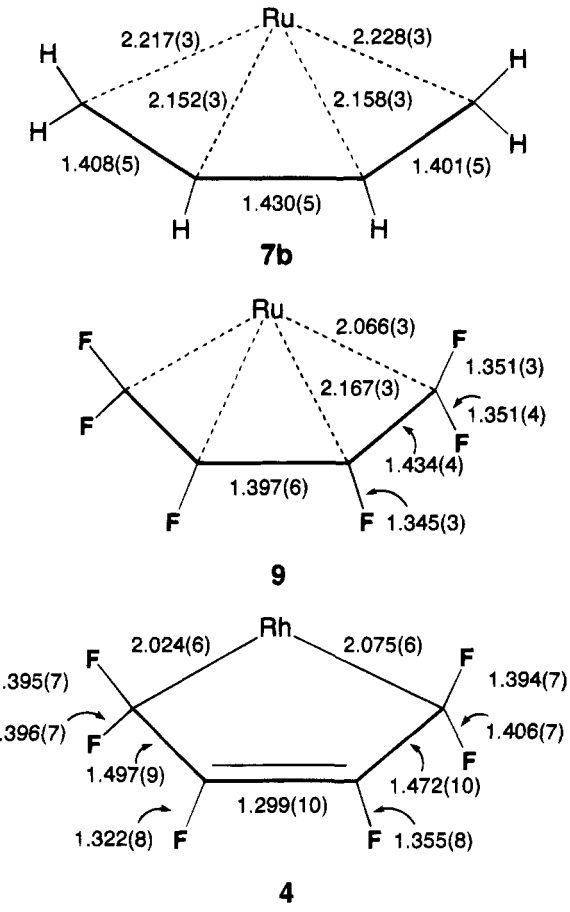

Figure 3. Comparison of bond lengths (Å) of coordinated butadiene in **7b**[16] and hexafluorobutadiene in **9** and **4**.[12]

The ground state conformation of butadiene is *s-trans*; in this conformation the torsion angle (ϕ) between the two double bonds is 180°, by definition.[19] A less stable *gauche*, or *skew-cis*, conformer is calculated by SCF ab initio methods to have ϕ = 37.8°[20] and lies 3.15 kcal mol^{-1} above the *s-trans* conformation.[21] The *s-cis*

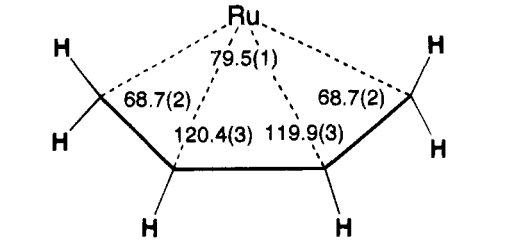

7b

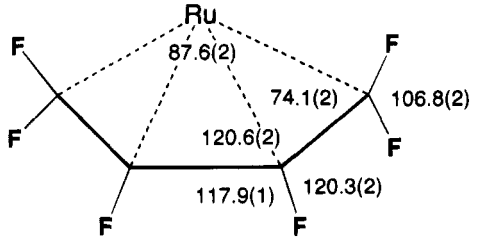

9

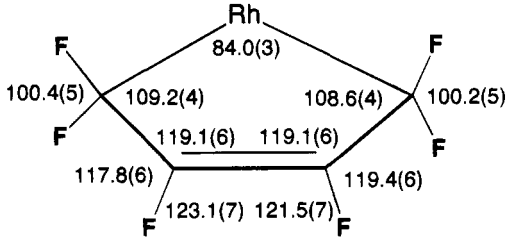

4

Figure 4. Comparison of bond angles (deg) of coordinated butadiene in **7b**[16] and hexafluorobutadiene in **9** and **4**.[12]

conformation ($\phi = 0°$) is calculated to be a transition state for interconversion of the two enantiomeric *skew-cis* conformations, with a barrier calculated to be between 0.4 and 0.7 kcal mol^{-1}.[20] The structural parameters for the *s-cis* and *skew-cis* conformers of butadiene have been calculated by ab initio methods.[20] A summary of C−C distances in these two conformers is presented in Table 3; the bond lengths and angles calculated for the *s-cis* conformer are also presented in Figure 5A.[20] At this level of theory there are no significant differences between the two structures.

In contrast, the ground state structure of hexafluorobutadiene is not planar, but has been shown by gas phase electron diffraction methods to be *skew-cis*, with an estimated $\phi = 47.4(8)°$.[22] Hexafluorobutadiene has recently been subjected to ab initio calculations[23] at a level of theory closely comparable with that applied[20] to butadiene. The *skew-cis* conformer is calculated to be the ground state, with an optimized structure having $\phi = 58.4°$. The optimized structures for the *s-trans* and *s-cis* conformers lie, respectively, 1.8 and 5.7 kcal mol^{-1} above the ground state.[23] It has been noted[23] that application of this level of calculation to unsaturated fluorocarbons invariably results in C−C and C−F distances that are too short; a correction factor[24] should be applied to elongate each C−C bond by 0.016 Å and each C−F bond by 0.011 Å. Addition of this factor brings the calculated distances for the *skew-cis* conformer[23] in line with the experimental ones (see Table 3).[22,25]

The *skew-cis* conformation is preferred over the *s-trans* because it minimizes repulsive 1,3-interactions between fluorines [e.g. F_M and $F_{X'}$ in Figure 5D]. The van der Waals radius of fluorine bound to carbon is 1.45−1.50 Å.[14,23] In the *s-trans* conformer the F_M···$F_{X'}$ distance is 2.62 Å, resulting in a strong destabilization of this conformer.[23] Notably 1,1,4,4-tetrafluorobutadiene, in which these destabilizing interactions are absent, has an *s-trans* ground state like butadiene itself.[22] The *s-cis* conformer is even more strongly disfavored due to strong repulsive interactions between F_M and $F_{M'}$ and between F_X and $F_{X'}$; in this conformation the F_M···$F_{M'}$ and F_X···$F_{X'}$ distances are each 2.54 Å.[23,25] In the *skew-cis* conformer ($\phi = 58.4°$), the corresponding distances relax to 3.04 and 2.84 Å, respectively.[23] The distances and angles calculated for the *s-cis* conformer of hexafluorobutadiene are presented in Figure 5B (see also Table 3).

These calculations reveal small, though significant, differences in structure between the *s-cis* conformations of butadiene and its perfluorinated analogue. The F−C−F angle in the CF_2 groups is more acute than the corresponding angle for the CH_2 groups; this phenomenon is well known in fluorolefins.[14,23,24] The fluorinated diene has a longer internal C−C bond (1.499 Å) than does butadiene (1.484 Å), and while the C=C−C angles in both compounds are significantly larger than 120°, that in the fluorocarbon (130.0°) is larger than that in butadiene (127.2°). Presumably, repulsions between F_M···$F_{M'}$ in the fluorinated diene cause it to splay out more significantly.

Ligation of butadiene to the [RuCp*I] fragment in **7b** results in elongation of the terminal C−C bonds to an average of 1.405(5) Å [Δ(C−C) = +0.077(5) Å] and contraction of the internal C−C bond to 1.430(5) Å [Δ(C−C) = −0.054(5) Å]. A summary of Δ(C−C) values is presented in Table 3. Hydrogen atoms were not located in this structure, so any pyramidalization of the CH_2 groups is not revealed, but the relaxation of the internal C−C−C angle to an average of 120.1(3)° indicates that intramolecular repulsions between the CH_2 groups may have been diminished significantly upon coordination. Examination of the structure of **9** reveals similar, though more significant, trends. Compared to its hydrocarbon analogue, η^4-ligation of hexafluorobutadiene results in a more significant elongation of the terminal C−C bonds to 1.434(4) Å [Δ(C−C) = +0.104(4) Å], and a more significant contraction of the internal C−C bond to 1.397(6) Å [Δ(C−C) = −0.102(6) Å]. As with butadiene, ligation results in relaxation of the C−C−C angle to 120.6(2)°. The CF_2 groups are significantly pyramidalized, with a significant contrac-

(19) (a) Kuchitsu, K.; Fukuyama, T.; Morino, Y. *J Mol. Struct.* **1967–1968**, *1*, 463. (b) Almenningen, A.; Traetteberg, M. *Acta Chem. Scand.* **1958**, *12*, 1221.
(20) Breulet, J.; Lee, T. J.; Schaeffer, H. F. *J. Am. Chem. Soc.* **1984**, *106*, 6250.
(21) Bock, C. W.; George, P.; Trachtman, M. *Theor. Chim. Acta* **1984**, *64*, 293.
(22) Chang, C. H.; Andreassen, A. L.; Bauer, S. H. *J. Org. Chem.* **1971**, *36*, 920.
(23) Dixon, D. A. *J. Phys. Chem.* **1986**, *90*, 2038.
(24) Dixon, D. A.; Fukunaga, T.; Smart, B. E. *J. Am. Chem. Soc.* **1986**, *108* , 1585.
(25) The distances given for the *s-cis* and *s-trans* conformers in ref 23 do not include the correction factors applied to the *skew-cis* conformer: Dixon, D. A. Private communication. Values quoted in this paper are slightly larger because the corrected (longer) C−C and C−F distances have been used.

Table 3. Changes in C−C Bond Distances [Δ(C−C) = [(C−C)$_{coord}$ − (C−C)$_{uncoord}$] on η^4-Coordination of Butadiene (C_4H_6) in Complex 7b,[12] η^4-Coordination of Hexafluorobutadiene (C_4F_6) in 9, and η^2-Coordination of Hexafluorobutadiene in 4[12]

	C_4H_6 (*s-cis*)	C_4H_6 (*skew-cis*)[a]	C_4F_6 (*s-cis*)	C_4F_6 (*skew-cis*)[b]	**7b**	Δ(C−C)[c]	**9**	Δ(C−C)[c]	**4**	Δ(C−C)[c]
terminal C−C	1.328[d]	1.328[d]	1.314[e]	1.311[e]	1.405(5)	+0.077(5)				
			1.330[f]	1.327[f]			1.434(4)	+0.104(4)	1.485(10)[h]	+0.155(10)[h]
				1.336(6)[g]						
internal C−C	1.484[d]	1.482[d]	1.483[b]	1.462[b]	1.430(5)	−0.054(5)				
			1.499[f]	1.478[f]			1.397(6)	−0.102(6)	1.297(10)[i]	−0.202(10)[i]
				1.488(6)[g]						

[a] Dihedral angle between double bonds (ϕ) is calculated to be 33.2 °.[20] [b] Dihedral angle between double bonds (ϕ) is calculated to be 65.5°. After inclusion of bond length correction factors to account for configuration interactions, and subsequent reoptimization, ϕ decreases to 58.4°.[23] [c] Difference between experimentally observed distance and that calculated for the *s-cis* structure. See text for further discussion. [d] Calculated at the SCF level using a double-ζ basis set plus polarization functions C(3d) and H(2p).[20] [e] Calculated at the SCF level using a double-ζ basis set plus polarization function on C(3d) only.[23] See text for further discussion. [f] After inclusion of a correction factor of +0.016 Å per C−C bond.[23] [g] Distances from gas phase electron diffraction experiments; dihedral angle between double bonds is 47.4(8)°.[22] [h] Average of four distances in two independent molecules.[12] [i] Average of two distances in two independent molecules.[12]

tion of the F−C−F angle to 106.8(2)°. Pyramidalization is accompanied by significant lengthening of the CF bonds in the CF_2 groups from 1.311 Å in the free diene to 1.351(3) Å in **9**. Relief of intramolecular repulsions between F_M···$F_{M'}$ is also quite clear; the distance between these fluorines is increased from 2.54 Å in the free diene to 2.78 Å in **9**. Contraction of the internal C−C bond might be expected to lead to a corresponding increase in repulsions between F_X···$F_{X'}$, but the distance between these fluorines actually increases from 2.54 Å in the free diene to 2.64 Å in **9**. This results not from any significant change in the individual C−F bond distances but from an opening of the F−C−CF bond angle from 112.8 to 117.9(1)°. The carbon atoms at each CF group are not pyramidalized; within experimental error the three angles at each carbon atom sum to 360°.

The Ru−C interactions in **9** are also significantly different from those in its hydrocarbon analogue **7b**. The distance from Ru to the terminal diene carbon atoms in **9** [2.066(3) Å] is shorter than the average of the corresponding distances in **7b** [2.223(3) Å], while the distances from Ru to the internal diene carbon atoms are identical within experimental error. The larger "bite-angle" at the metal found for **9** [angle (CF_2−Ru−CF_2) = 87.6(2)°] compared to **7b** [angle (CH_2−Ru−CH_2) = 79.5(1)°] reflects the longer terminal C−C distances in the former complex.

To summarize thus far, while structure type **A** (Figure 1) is clearly that preferred in **7b**, as illustrated by the alternation pattern (short−long−short) of the diene carbon−carbon distances, structure type **B** is clearly the preferred coordination mode in **9**, as indicated by the long−short−long pattern of the C−C bond lengths of the diene ligand. This type of internal bond length alternation and rehybridization at the terminal carbon atoms is analogous to that found previously in the tricarbonyliron compound containing η^4-bound perfluoro-1,3-cyclohexadiene (**10**),[18] and in related metal complexes of fluorinated cyclodienes.[13] The η^4-metallacyclo-3-pentene description for **9** is also supported by observation of extensive pyramidalization at the terminal CF_2 groups.

Comparison of the η^4-metallacyclo-3-pentene structure of the hexafluorobutadiene ligand in **9** with that of the η^2-metallacyclo-3-pentene form of ligation in **4** is also instructive. The ruthenium−CF_2 distance of 2.066(3) Å in **9** is similar to the rhodium−CF_2 distances in **4** [2.075(6) Å for Rh−CF_2 *trans* to PMe_3; 2.024(6) Å for Rh−CF_2 *trans* to Cl].[12] The internal carbon atoms of the

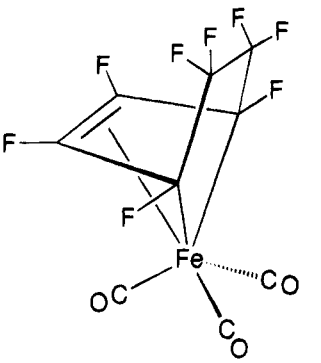

10

fluorinated ligand in **4** are folded away from the metal so that the metallacyclic structure is planar, reflected by a large increase in the Rh−C−C bond angles compared to the corresponding angles in the ruthenium complex **9**. The bond distances and angles within the fluorinated ligand in **4** continue the trends observed on going from free ligand to complex **9**. The terminal C−C bonds undergo further elongation to an average of 1.485(10) Å [Δ(C−C) = +0.155(10) Å], consistent with a CF−CF_2 single bond, and the internal C−C interaction shrinks to a value of 1.297(10) Å [Δ(C−C) = −0.202(10) Å], typical of a CF=CF double bond. The internal C−C−C angle in **4** is no different from that in **9**, nor do the C−F bond lengths involving the internal carbon atoms change significantly. However, the C−F bond distances within the CF_2 groups in **4** are significantly longer than those in **9**, and the F−C−F angle is contracted further to 100.2(5)°, consistent with a CF_2 group in a saturated fluorocarbon.[14]

This comparison of the structure of uncoordinated *s-cis* hexafluorobutadiene with those of its complexes **9** and **4** illustrates stepwise progressions: (a) from short−long−short to long−short−long in the C−C distances and (b) contraction of the F−C−F angle and elongation of the C−F bonds in the CF_2 groups. Changes in distances and angles at the internal CF centers is much less significant. Comparison of the structures of **9** and **7b** illustrates that the changes observed on coordination of the fluorinated diene to Ru are much larger than those observed for butadiene itself. Whether these differences are due primarily to differences in metal−diene orbital interactions remains unclear, but it does seem likely that the driving force of minimizing repulsions between fluorine atoms also probably plays a significant role in the structure of **9**.

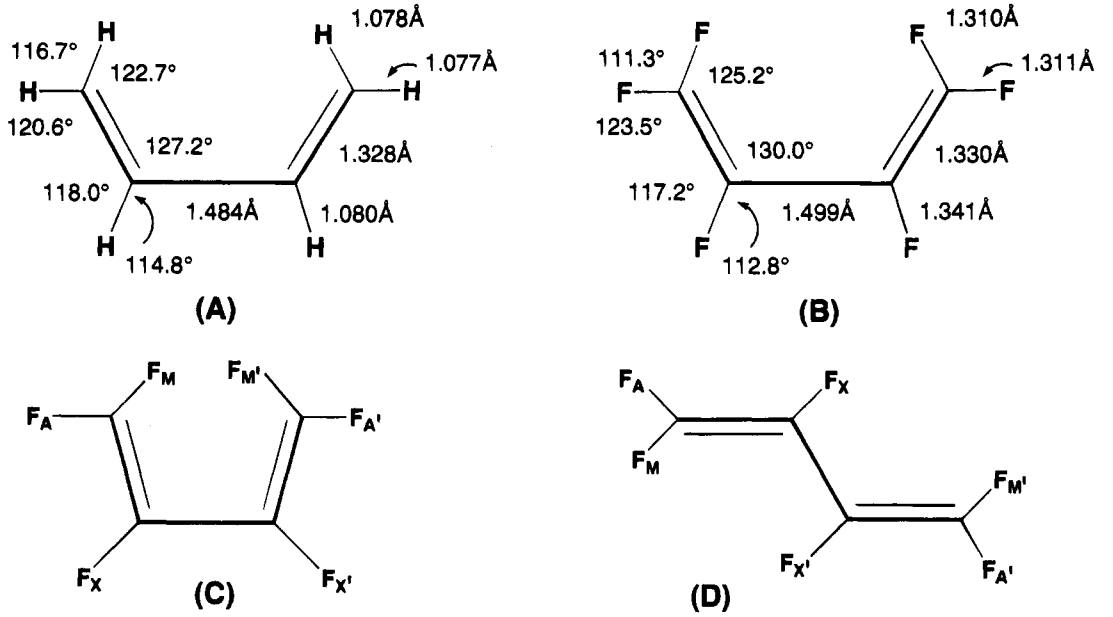

Figure 5. Calculated bond lengths (Å) and angles (deg) for the *s-cis* conformations of (A) butadiene[20] and (B) hexafluorobutadiene.[23] Fluorine atom labeling for hexafluorobutadiene in (C) the *s-cis* and (D) the *s-trans* conformations.

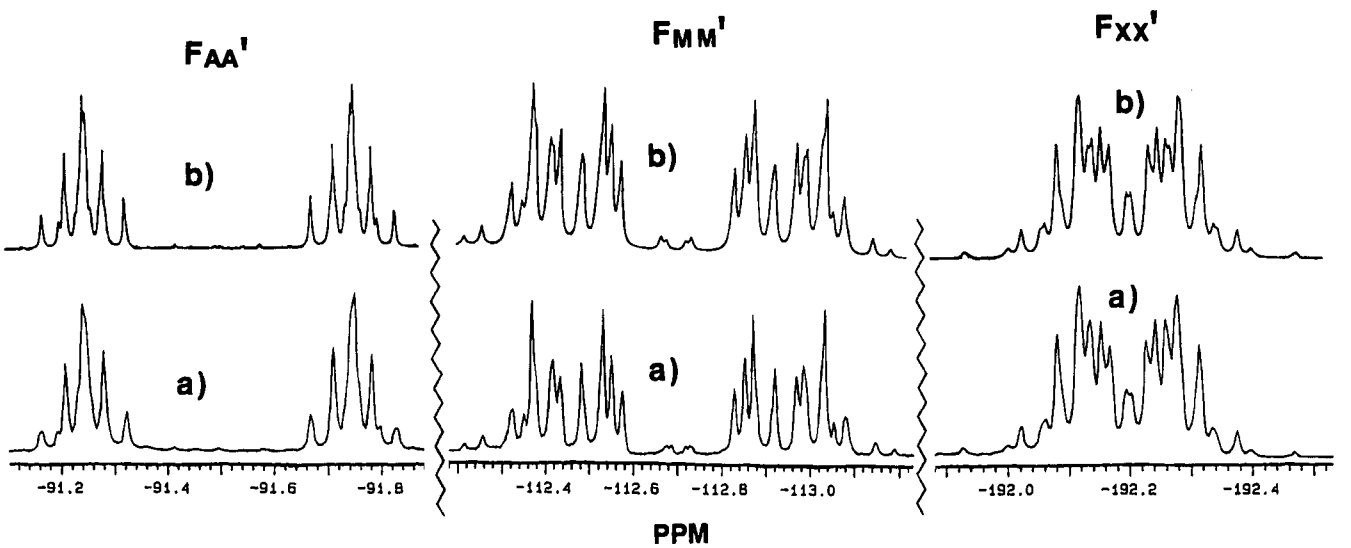

Figure 6. Observed (a) and simulated (b) ^{19}F NMR resonances for **9**. See Figure 5 for labeling of AA'MM'XX'.

Table 4. ^{19}F NMR Data[a] for Free Hexafluorobutadiene (C_4F_6)[28] and Coordinated Hexafluorobutadiene in Complexes 9 and 11[a]

	$\delta_{A,A'}$	$\delta_{M,M'}$	$\delta_{X,X'}$	J_{AM}	J_{AX}	$J_{AA'}$	$J_{AM'}$	$J_{AX'}$	J_{MX}	$J_{MX'}$	$J_{MM'}$	$J_{XX'}$
C_4F_6	−93.4	−107.9	−179.7	50.7	31.9	4.8	2.5	2.4	−118.6	14.2	11.31	−30.3
9	−92.6	−113.5	−192.2	141.2	5.0	0.5	0.8	15.0	−47.0	1.1	24.0	−32.0
11	−93.3	−106.6	−162.2	117.0	2.3	1.0	0.2	−1.0	−30.5	5.0	0.5	−30.5

[a] δ: chemical shift in ppm. Reference: $CFCl_3$. J: coupling constant in Hz. Solvent: $CDCl_3$. See Figure 5 for numbering scheme.

Spectroscopic evidence indicates that the solution structure of **9** is analogous to that observed in the solid state. The absence of any IR bands in the region of $\nu_{C=C}$ stretching rules out a σ^2-metallacyclopentene structure **C** (Figure 1) or simple η^2-coordination. The ^1H NMR spectrum shows a sharp singlet at 1.78 ppm corresponding to the Cp* ligand, and the ^{19}F NMR spectrum is composed of three symmetric multiplets of equal intensity. The $^{19}F-^{19}F$ coupling constants were obtained by analyzing the spectrum following the general procedures for AA'MM'XX' spin systems,[26] knowledge of coupling constants in trifluorovinyl groups,[27] and subsequent simulation of the spectrum to obtain the best fit with experiment. The observed and simulated spectra are shown in Figure 6, and the values of chemical shifts and coupling constants for **9** and those for free hexafluorobutadiene[28] are presented in Table 4. Coordination to ruthenium causes the coupling constants (J_{AM}, J_{MX}, and J_{AX}) within each vinyl group of hexafluorobutadiene to change dramatically, reflecting loss of planarity of the vinyl groups. Similar changes in coupling constants consistent with pyramidalization of CF_2 groups have been noted for tetrafluoroethylene complexes.[17] The large value of the long range coupling constant $^5J_{MM'} = 24$ Hz is most notable

(26) Abraham, R. J. *The Analysis of High Resolution NMR Spectra*; Elsevier: Amsterdam-London-New York, 1971; pp 218–221.
(27) Emsley, J. W.; Phillips, L.; Wray, V. *Fluorine Coupling Constants*, 1st ed.; Pergamon: New York, 1977; pp 341.
(28) Manatt, S. L.; Bowers, M. T. *J. Am. Chem. Soc.* **1969**, *91*, 4381.

when compared with the corresponding value of 11.31 Hz for the free diene.[28] As mentioned earlier, the ground state of uncoordinated hexafluorobutadiene is *s-skew*, with a dihedral angle between the vinyl groups of about 58° and a distance between F_M and $F_{M'}$ of 3.04 Å.[23] Coordination forces the carbon skeleton to be planar, with pyramidalization at the CF_2 termini allowing relaxation of the otherwise unacceptable repulsions between F_M and $F_{M'}$. Nevertheless, in complex **9** the two fluorines $F_{M,M'}$ are in closer proximity than in the free *skew-cis* diene, with the distance between F(3)–F(3a) in the solid state being 2.78 Å. Consequently, the increased spin–spin coupling may arise from enhanced through space interactions resulting from the shorter distance between these F substituents.

We turn now to the kinetic product of the reaction of hexafluorobutadiene with [RuCp*Cl]$_4$. NMR monitoring of the reaction of hexafluorobutadiene with [RuCp*Cl]$_4$ at −25 °C in CD_2Cl_2 as the solvent showed initial formation of this kinetic product, which slowly converted to **9**. Unfortunately, this product could not be obtained free of **9** and, on standing, was converted to the thermodynamic product **9**, even in the absence of additional hexafluorobutadiene. Inability to acquire a pure sample of this material precluded suitable microanalysis, and the structural identification of this compound is based on spectroscopic methods. The ^{1}H NMR spectrum shows a singlet at δ 1.55 and the ^{19}F NMR spectrum shows three equal intensity multiplets at δ −92.7, −106.6, and −162.0 ppm. These multiplets were analyzed and simulated, and the resultant J values are shown in Table 4. The ratio of C_4F_6 to Cp* in the kinetic product was revealed by inspection of a sample containing both compounds, in which the ^{19}F resonances were of equal intensity, but the ^{1}H resonance due to the Cp* ligand of **9** was exactly half the intensity of that of the other Cp* resonance. Therefore the compound contains two Cp* rings for every hexafluorobutadiene. The most plausible molecular formula of the kinetic product must be [(RuCp*Cl)$_2$(C_4F_6)]. The number of ^{1}H and ^{19}F resonances are consistent either with structure **11** of C_2 symmetry or structure **12** of C_s symmetry. Inspection of the ^{19}F–^{19}F coupling constants in Table 4 reveals a value for $J_{MM'}$ of almost zero. Comparison with the corresponding value of 24 Hz for **9**, in which the diene conformation is unambiguously *cis*, and the value of 11 Hz in the free diene with a *skew-cis* conformation allows the reasonable choice of **11** for the structure of the kinetic product. The smaller geminal ^{19}F–^{19}F coupling (J_{AM}) in **11** compared to that in **9** (117.0 Hz vs 141.2 Hz) suggests less pyramidalization at the terminal carbon atoms of the coordinated diene in the former compound.

Therefore the mechanism of formation of these compounds probably involves partial breakup of the tetrameric structure of [RuCp*Cl]$_4$, with initial coordination of a fluoroolefin to ruthenium followed by coordination of the second olefin function to another ruthenium to give **11**. Subsequent reaction of **11** to afford **9** is slow but does occur, even in the absence of free hexafluorobutadiene.

We commented earlier that the observed formation of metallacycles **3**–**5** resulted in part from the facility of formal two-electron oxidation of the metal center. Attempts to convert the fluorinated ligand in **9** into an analogous fully opened metallacyclopentene of Ru(IV) were unsuccessful. Attempts to add phosphine ligands resulted in complex mixtures of products. Addition of CO proceeded smoothly in methylene chloride at room temperature and under 1 atm pressure of CO but resulted in clean displacement of hexafluorobutadiene. The ruthenium product was identified as [RuCp*Cl(CO)$_2$] by ^{1}H NMR and IR spectroscopy. We appear to have chosen fortuitously a set of conditions in which a formal oxidative addition of the diene to give a metallacycle of Ru(IV) is disfavored, thus allowing isolation of the first example of the η^4-species.

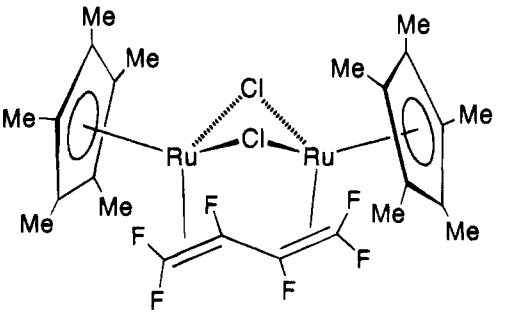

11

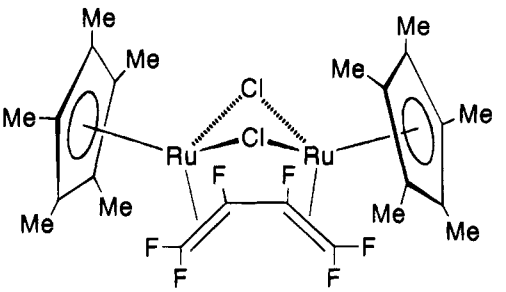

12

Experimental Section

General Considerations. All reactions were performed in oven-dried glassware, using standard Schlenk techniques, under an atmosphere of nitrogen which had been deoxygenated over BASF catalyst and dried using Aquasorb. All solvents were obtained from Fisher Scientific and distilled under nitrogen over one of the following drying agents: petroleum ether (35–60 °C) and methylene chloride over calcium hydride; diethyl ether over an alloy of sodium and potassium; THF over potassium. ^{1}H (300 MHz) and ^{19}F (282 MHz) NMR spectra were recorded on a Varian Associates XL-300 spectrometer or a Varian Unity Plus 300 System in the solvents indicated. Chemical shifts are reported as ppm downfield of internal TMS for ^{1}H and upfield of external $CFCl_3$ for ^{19}F NMR. Infrared spectra were recorded on a Perkin-Elmer 1600 series FTIR, calibrated against the 1601 cm^{-1} peak of polystyrene. Melting points were measured using an Electrothermal capillary melting point apparatus and are uncorrected.

[RuCp*Cl]$_4$ was prepared following the literature procedure.[29] 1,3-Hexafluorobutadiene was purchased from PCR Research Chemicals, Gainesville, FL. $RuCl_3$•$3H_2O$ was obtained from Johnson Matthey Aesar/Alfa; carbon monoxide from Matheson; PMe_3 from Aldrich.

Synthesis of [RuCp*(η^4-*cis*-C_4F_6)Cl] (9). A Schlenk flask containing a suspension of [RuCp*Cl]$_4$ (0.29 g, 1.07 mmol of

(29) Fagan, P. J.; Ward, M. D.; Calabrese, J. C. *J. Am. Chem. Soc.* **1989**, *111*, 1698.

Ru) in methylene chloride (5 mL) was cooled in liquid nitrogen. 1,3-Hexafluorobutadiene (2.70 mmol) was collected in a 60 mL gas bulb and condensed into the flask. The mixture was warmed to −78 °C and then slowly to room temperature. After 4 days the solvent and excess hexafluorobutadiene were removed under reduced pressure from the deep red solution. The resultant deep red solid was washed with warm petroleum ether (2 × 15 mL), and the resultant brown solid was extracted with methylene chloride (8 mL). Cooling the concentrated extract led to the precipitation of an orange-brown solid **9** (0.18 g, 0.41 mmol; 38%). Light orange crystals suitable for X-ray crystallography were obtained by recrystallization from methylene chloride. Mp: 98 °C dec. ^{1}H NMR ($CDCl_3$): δ 1.77 (s, Cp*). ^{19}F NMR ($CDCl_3$): see Table 4.

Synthesis of [(RuCp*Cl)$_2$(μ-C$_4$F$_6$)] (11). A solution of [RuCp*Cl]$_4$ (0.23 g, 0.84 mmol of Ru) in methylene chloride (10 mL) was cooled to −60 °C, and hexafluorobutadiene (2.2 mmol, collected on the vacuum line) was condensed into the reaction flask. The mixture was stirred for 2 h during which time the temperature of the cooling bath rose from −60 to −15 °C. The resultant deep red solution was stripped of volatiles to yield a deep red solid (0.30 g). ^{1}H and ^{19}F NMR spectra of the products recorded immediately after the isolation of the sample indicated a 1:23 mixture of **9** and **11**. Attempts to isolate pure **11** by crystallization from methylene chloride or petroleum ether at −78 °C was unsuccessful. **11**: ^{1}H NMR ($CDCl_3$): δ 1.55 (s, Cp*). ^{19}F NMR ($CDCl_3$): see Table 4.

NMR Observation of the Reaction between [RuCp*Cl]$_4$ and Hexafluorobutadiene. A 5 mm NMR tube was charged with [RuCp*Cl]$_4$ (5 mg, 1.84 × 10^{-3} mmol of Ru) and CD_2Cl_2 (1 g). Hexafluorobutadiene (5.52 × 10^{-3} mmol) was collected in a 15 mL Schlenk flask on a vacuum line and condensed into the NMR tube. The tube was then sealed, placed in a −78 °C refrigerator overnight, and then transferred into a −25 °C refrigerator. After 1 day the sample was examined by ^{1}H and ^{19}F NMR spectra at −25 °C and found to contain mostly **11**. Further standing of the sample at room temperature led to the gradual transformation of **11** to **9**.

X-ray Structural Determination of 9. Crystallographic data are collected in Table 1. The Laue group was determined photographically, and the systematic absences in the diffraction data indicated either of the orthorhombic space groups *Pnma* or *Pna*2$_1$. The presence of a molecular mirror plane perpendicular to the unit cell *b* axis, containing C(1), Cl, Ru, and the midpoint of the C(7)−C(7a) bond, indicated that the former, centrosymmetric space group was correct. No correction for absorption was applied; the azimuthal-scan variation in transmission was less than 10%. The locations of all non-hydrogen atoms were provided by direct methods. All the hydrogen atoms of the Cp* ring were idealized following location of at least one hydrogen atom on each carbon atom to fix the rotational assignment. All non-hydrogen atoms were refined with anisotropic thermal parameters. All computations used SHELXTL-PLUS software (G. Sheldrick, Siemens Corp., Madison, WI).

Reaction of 9 with Carbon Monoxide. Compound **9** (0.17 g, 0.44 mmol) was dissolved in methylene chloride (8 mL). Carbon monoxide was bubbled through the solution for 2 h. Evaporation of the solution afforded a yellow solid identified as [RuCp*Cl(CO)$_2$] by comparing its ^{1}H NMR and IR spectra with the literature data[16] (0.13 g, 0.4 mmol; 91%). Inspection of the volatiles by ^{19}F NMR spectroscopy revealed the presence of hexafluorobutadiene.

Acknowledgment. We are grateful to the National Science Foundation and to the U.S. Air Force Office of Scientific Research for generous financial support of this work and to Johnson Matthey Aesar/Alfa for a loan of ruthenium chloride.

Supplementary Material Available: Bond distances (Table 1S), bond angles (Table 2S), anisotropic displacement coefficients (Table 3S), and H-atom coordinates and isotropic displacement coefficients (Table 4S) (2 pages) for **9**. Ordering information is given on any current masthead page.

OM940855I

Dehydrohomopolymerization and Dehydrocopolymerization of New Alkylsilanes: Synthesis of Poly(3-aryl-1-silabutanes)

Hee-Gweon Woo,*,† Sook-Yeon Kim,† Mi-Kyung Han,† Eun Jeong Cho,‡ and Il Nam Jung‡

Department of Chemistry, Chonnam National University, Kwangju 500-757, Korea, and Organometallic Chemistry Laboratory, Korea Institute of Science & Technology, P.O. Box 131 Cheongryang, Seoul 130-650, Korea

Received November 7, 1994®

3-Aryl-1-silabutanes such as 3-phenyl-1-silabutane (**1**), 3-tolyl-1-silabutane (**2**), 3-(2,5-dimethylphenyl)-1-silabutane (**3**), 3-chlorophenyl-1-silabutane (**4**), 3-(chloro-*p*-tolyl)-1-silabutane (**5**), 3-(phenoxyphenyl)-1-silabutane (**6**), 3-naphthyl-1-silabutane (**7**), and bis(1-sila-3-butyl)benzene (**8**) were prepared in 62–98% yields by reduction of the corresponding 3-aryl-1,1-dichloro-1-silabutanes with $LiAlH_4$. The dehydrohomopolymerization and dehydrocopolymerization of the monomer silanes were carried out with the Cp_2MCl_2/Red-Al (M = Ti, Hf) combined catalyst system. The molecular weight of the polymers produced ranged from 600 to 1300 (vs polystyrene) with degree of polymerization (DP) equal to 3–16 and with polydispersity index (PDI) equal to 1.1–3.8. A set of the monomer silanes dehydrocoupled to produce a copolymer. The polymerization of bis(silabutyl)benzene (**8**) seemed to initially produce a low molecular weight of polymer, which then underwent an extensive cross-linking reaction of backbone Si–H bonds, leading to insoluble polymer.

Introduction

Polysilanes with unusual optical and electronic properties due to σ-conjugation along the silicon backbone have received a copious amount of attention as ceramic precursors, third-order NLO materials, deep-UV photoresists, photoconductors, and photoinitiators.[1-3] The conventional synthetic method to get high-molecular-weight polysilanes to date has been the Wurtz coupling reaction of dichlorosilanes, which are intolerant of some functional groups and have other limitations for controlling stereochemistry and molecular weight.

Harrod's recent discovery of group 4 metallocene catalyzed dehydropolymerization made great progress in poly(organosilane) synthesis.[4] Two mechanisms have been suggested: (1) oxidative-addition/reductive-elimination sequences via the intermediacy of transition-metal silylene complexes[4] and (2) four-center σ-bond metathesis processes among silicon, hydrogen, and a d^0 metal center via the intermediacy of transition-metal silyl and hydride complexes.[5] While theoretical calculation backs up the first mechanism,[4d] the second mechanism is supported by many model reactions[4e,f,5,13b] and thermochemical results.[6] A major disadvantage of the metallocene-catalyzed dehydrocoupling method is the production of low molecular weights of polysilanes.[4,5] Considerable efforts have been made to increase the molecular weight of the polysilanes.[7-10]

The ^{29}Si NMR technique has been useful in analyzing polysilane chain microstructure.[11] The structures of all polysilanes synthesized via the dehydrocoupling method are predominantly random atactic ones, although some diastereomeric selection was observed in certain cases.[12] To date, silanes which have been employed in the literature have been mostly arylsilanes. There are few reports on the dehydrocoupling of alkylsilanes.[8,13] To

† Chonnam National University.
‡ Korea Institute of Science & Technology.
® Abstract published in *Advance ACS Abstracts,* April 1, 1995.

(1) Miller, R. D.; Michl, *J. Chem. Rev.* **1989**, *89*, 1359.
(2) West, R. *J. Organomet. Chem.* **1986**, *300*, 327.
(3) Ziegler, J. M.; Fearon, F. W. G. *Silicon-Based Polymer Science*; American Chemical Society: Washington, DC, 1990.
(4) (a) Aitken, C.; Harrod, J. F.; Gill, U. S. *Can. J. Chem.* **1987**, *65*, 1804. (b) Harrod, J. F.; Yun, S. S. *Organometallics* **1987**, *6*, 1381. (c) Aitken, C.; Barry, J.-P.; Gauvin, F.; Harrod, J. F.; Malek, A.; Rousseau, D. *Organometallics* **1989**, *8*, 1732. (d) Harrod, J. F.; Ziegler, T.; Tschinke, V. *Organometallics* **1990**, *9*, 897. (e) Woo, H.-G.; Harrod, J. F.; Hénique, J.; Samuel, E. *Organometallics* **1993**, *12*, 2883. (f) Britten, J.; Mu, Y.; Harrod, J. F.; Polowin, J.; Baird, M. C.; Samuel, E. *Organometallics* **1993**, *12*, 2672.
(5) (a) Woo, H.-G.; Tilley, T. D. *J. Am. Chem. Soc.* **1989**, *111*, 3757. (b) Woo, H.-G.; Tilley, T. D. *J. Am. Chem. Soc.* **1989**, *111*, 8043. (c) Woo, H.-G.; Heyn, R. H.; Tilley, T. D. *J. Am. Chem. Soc.* **1992**, *114*, 5698. (d) Woo, H.-G.; Walzer, J. F.; Tilley, T. D. *J. Am. Chem. Soc.* **1992**, *114*, 7047. (e) Banovetz, J. P.; Suzuki, H.; Waymouth, R. M. *Organometallics* **1993**, *12*, 4700.
(6) (a) Nolan, S. P.; Porchia, M.; Marks, T. J. *Organometallics* **1991**, *10*, 1450. (b) Forsyth, C. M.; Nolan, S. P.; Marks, T. J. *Organometallics* **1991**, *10*, 2543.
(7) (a) Woo, H.-G.; Walzer, J. F.; Tilley, T. D. *Macromolecules* **1991**, *24*, 6863. (b) Imori, T.; Woo, H.-G.; Walzer, J. F.; Tilley, T. D. *Chem. Mater.* **1993**, *5*, 1487.
(8) (a) Harrod, J. F. In *Transformation of Organometallics into Common and Exotic Materials: Design and Activation*; Laine, R. M., Ed.; NATO ASI Series E: Appl. Sci. No. 141; Martinus Nijhoff: Amsterdam, 1988; p 103. (b) Mu, Y.; Harrod, J. F. In *Inorganic and Organometallic Polymers and Oligomers*; Harrod, J. F., Laine, R. M., Eds.; Kluwer Academic: Dordrecht, The Netherlands, 1991; p 23.
(9) Woo, H.-G.; Harrod, J. F. Manuscript in preparation.
(10) Tilley, T. D. *Acc. Chem. Res.* **1993**, *26*, 22.
(11) (a) Wolff, A. R.; Nozue, I.; Maxka, J.; West, R. *J. Polym. Sci., Part A: Polym. Chem.* **1988**, *26*, 701. (b) Maxka, J.; Mitter, F. K.; Powell, D. R.; West, R. *Organometallics* **1991**, *10*, 660.
(12) (a) Banovetz, J. P.; Stein, K. M.; Waymouth, R. M. *Organometallics* **1991**, *10*, 3430. (b) Corey, J. Y.; Huhmann, J. L.; Zhu, X.-H. *Organometallics* **1993**, *12*, 1121. (c) Woo, H.-G.; Harrod, J. F. Manuscript in preparation.
(13) (a) Campbell, W. H.; Hilty, T. K. *Organometallics* **1989**, *8*, 2615. (b) Hengge, E.; Weinberger, M.; Jammegg, C. *J. Organomet. Chem.* **1991**, *410*, C1. (c) Hengge, E.; Weinberger, M. *J. Organomet. Chem.* **1992**, *433*, 21.

0276-7333/95/2314-2415$09.00/0

our knowledge, the dehydrocopolymerization of aryl-substituted alkylsilanes has not been reported to date.

The transition-metal-mediated dehydrocoupling route of 3-(substituted aryl)-1-silabutanes may provide the possibility of controlling the molecular weight distribution and stereochemistry of polymer due to the presence of 3-methyl and 3-aryl groups as well as the introduction of functionality into the polymer. Here we report the dehydrohomopolymerization and dehydrocopolymerization of 3-aryl-1-silabutanes to give poly(3-aryl-1-silabutanes) catalyzed by metallocene complexes generated *in situ* from Cp_2MCl_2 (M = Ti, Hf)/Red-Al.

Experimental Section

General Considerations. All reactions and manipulations were performed under prepurified nitrogen using Schlenk techniques. Dry, oxygen-free solvents were employed throughout. Glassware was flame-dried or oven-dried before use. Elemental analyses were performed by the Advanced Analysis Center of the Korea Institute of Science and Technology, Seoul, Korea. Infrared spectra were obtained using a Perkin-Elmer 1600 Series FT-IR or a Nicolet 520P FT-IR spectrometer. Electronic spectra were acquired using an IBM 9420 UV−vis spectrophotometer. Proton NMR spectra were recorded on a Varian Gemini 300 spectrometer using $CDCl_3/CHCl_3$ as a reference at 7.24 ppm downfield from TMS. Carbon-13 NMR spectra were obtained using a Varian Gemini 300 (operating at 75.5 MHz) spectrometer with $CDCl_3$ as a reference at 77.0 ppm. Gas chromatography (GC) analyses were performed using a Varian 3300 chromatograph equipped with a packed column (10% OV-101 on Chromosorb, W/AW-DMCS 1.5 m × $^1/_8$ in. o.d.) in conjunction with a flame ionization detector. GC/MS data were obtained using a Hewlett-Packard 5890II chromatograph (HP-5, 5% phenylmethylsiloxane, 0.25 mm i.d. × 30.0 m, film thickness 0.25 μm) connected to a Hewlett-Packard 5972A mass selective detector. Gel permeation chromatography (GPC) was carried out on a Waters Millipore GPC liquid chromatograph. The calibrant (monodisperse polystyrene) and the sample were dissolved in toluene and separately eluted from an Ultrastyragel GPC column series (sequence 500, 10^3, 10^4 Å columns). Molecular weights were extrapolated from the calibration curve derived from the polystyrene standard. Data analyses were carried out using a Waters Data Module 570. An approximate estimate for the average degree of polymerization (DP) for the polysilane chains was made by simply calculating the differences in molecular weight between styrene and silylene monomer units. Thermogravimetric analysis (TGA) of the polymer sample was performed on a Perkin-Elmer 7 Series thermal analysis system under an argon flow. The polymer sample was heated from 25 to 800 °C at a rate of 20 °C/min. Ceramic residue yield is reported as the percentage of the sample remaining after completion of the heating cycle. Differential scanning calorimetry (DSC) of the polymer sample was performed on a Perkin-Elmer 7 Series thermal analysis system under an argon flow. Polymer sample was heated at 20 °C/min. Melting points were determined on a Thomas-Hoover Unimelt apparatus and are uncorrected. Cp_2TiCl_2, Cp_2HfCl_2, Red-Al (3.4 M in toluene), and $LiAlH_4$ were purchased from Aldrich Chemical Co. and were used without further purification.

Monomer Synthesis.[14a] 3-Aryl-1,1-dichloro-1-silabutanes[14b] and bis(1,1-dichloro-1-sila-3-butyl)benzene[14c] were prepared according to the literature procedure. The following reduction procedure is representative of the other monomers. (***Warning!*** *In the absence of diethyl ether solvent, $AlCl_3$ can catalyze silane redistribution reactions to produce SiH_4, which is an explosive gas upon contact with air. Therefore, the $LiAlH_4$ reduction of the silicon chlorides should be performed in ether and quenched properly with an isopropyl alcohol solution of aqueous HCl and then with water.*) All the silanes obtained here are stereoisomeric mixtures.

Synthesis of 3-Phenyl-1-silabutane (1). To a diethyl ether suspension of lithium aluminum hydride (3.07 g, 0.08 mol) in 70 mL of diethyl ether in a 250 mL three-necked, round-bottomed flask equipped with a reflux condenser topped with an inlet/outlet tube was slowly added 3-phenyl-1,1-dichloro-1-silabutane (10.1 g, 0.04 mol) in 70 mL of diethyl ether in a pressure-equalizing addition funnel. After addition was completed, the mixture was stirred at room temperature for 3 h. The reaction mixture was filtered, cooled to 0 °C, slowly quenched with an HCl/isopropyl alcohol solution (20 mL/150 mL), and then poured into ice−water. The resulting slurry was extracted with diethyl ether. The combined ether phases were washed twice with water, dried over anhydrous $MgSO_4$, and concentrated on a rotary vacuum evaporator. The solution was then fractionally distilled at 74−76 °C/20 mmHg to yield **1** (3.70 g, 62%). Anal. Calcd for SiC_9H_{14}: C, 71.92; H, 9.31. Found: C, 71.72; H, 9.42. IR (neat, KBr, cm^{-1}): 2155 s (ν_{SiH}), 910 s (δ_{SiH}). ^1H NMR (δ, $CDCl_3$, 300 MHz): 1.14−1.20 (m, 2 H, CH_2), 1.36 (d, J = 3.5 Hz, 3 H, CH_3), 2.92 (sextet, J = 3.6 Hz, 1 H, CH), 3.43 (t, J = 3.9 Hz, 3 H, SiH), 7.19−7.35 (m, 5 H, ArH). $^{13}C\{^1H\}$ NMR (δ, $CDCl_3$, 75.5 MHz): 16.16 ($SiCH_2$), 24.54 (CH_3), 37.77 (CH), 126.13, 126.55, 128.43, 148.26 (ArC). GC/MS (m/e (relative intensity)): 150 (23) (M^+), 135 (18), 119 (5), 109 (4), 108 (17), 107 (66), 105 (100), 91 (16), 79 (12), 77 (18), 72 (13), 65 (4), 51 (8).

Synthesis of 3-tolyl-1-silabutane (2): 98% yield; bp 36−38 °C/0.6 mmHg. Anal. Calcd for $SiC_{10}H_{16}$: C, 73.09; H, 9.81. Found: C, 73.22; H, 9.99. IR (neat, KBr, cm^{-1}): 2150 s (ν_{SiH}), 910 s (δ_{SiH}). ^1H NMR (δ, $CDCl_3$, 300 MHz): 1.00−1.19 (m, 2 H, CH_2), 1.32, 1.31, 1.32 (d, J = 7.0 Hz, 3 H, CH_3), 2.33, 2.34, 2.35 (s, 3 H, Ar−CH_3), 3.17, 2.86, 2.87 (sextet, J = 7.0 Hz, 1 H, CH), 3.44, 3.40, 3.41 (t, J = 4.0 Hz, 3 H, SiH), 7.00−7.27 (m, 4 H, ArH) (isomer ratio ortho:meta:para = 23:35:42). $^{13}C\{^1H\}$ NMR (δ, $CDCl_3$, 75.5 MHz): 15.31, 16.11, 16.12 ($SiCH_2$), 19.46, 21.48, 20.98 (CH_3), 23.71, 24.45, 24.63 (CH_3), 32.31, 37.28, 37.61 (CH), 123.46, 124.96, 125.68, 126.25, 126.36, 126.80, 127.29, 128.25, 129.03, 130.23, 135.51 (Ar C). GC/MS (m/e (relative intensity)): 164 (16) (M^+), 122 (43), 121 (66), 120 (16), 119 (100), 117 (30), 115 (26), 105 (28), 103 (11), 93 (14), 91 (69), 77 (25), 72 (12), 65 (19), 51 (12).

Synthesis of 3-(2,5-dimethylphenyl)-1-silabutane (3): 96% yield; bp 62−65 °C/0.6 mmHg. Anal. Calcd for $SiC_{11}H_{18}$: C, 74.08; H, 10.17. Found: C, 74.21; H, 10.22. IR (neat, KBr, cm^{-1}): 2150 s (ν_{SiH}), 905 s (δ_{SiH}). ^1H NMR (δ, $CDCl_3$, 300 MHz): 1.11−1.16 (m, 2 H, CH_2), 1.29 (d, J = 7.0 Hz, 3 H, CH_3), 2.29, 2.32 (s, 3 H, CH_3), 3.13 (sextet, J = 7.0 Hz, 1 H, CH), 3.44 (t, J = 3.5 Hz, 3 H, SiH), 6.89−7.04 (m, 3 H, ArH) (isomer ratio 3:2). $^{13}C\{^1H\}$ NMR (δ, $CDCl_3$, 75.5 MHz): 15.35 ($SiCH_2$), 19.35, 21.26, 23.77 (CH_3), 32.44 (CH), 125.72, 126.50, 130.13, 131.92, 135.96, 146.15 (Ar C). GC/MS (m/e (relative intensity)): 178 (22) (M^+), 163 (10), 136 (31), 135 (55), 133 (100), 131 (20), 119 (15), 117 (18), 115 (22), 105 (38), 91 (27), 77 (14).

Synthesis of 3-(chlorophenyl)-1-silabutane (4): 68% yield; bp 64−67 °C/0.6 mmHg. Anal. Calcd for $SiC_9H_{13}Cl$: C, 58.51; H, 7.09. Found: C, 58.50; H, 7.38. IR (neat, KBr, cm^{-1}): 2160 s (ν_{SiH}), 910 s (δ_{SiH}). ^1H NMR (δ, $CDCl_3$, 300 MHz): 1.09−1.27 (m, 2 H, CH_2), 1.32 (1.31) (d, J = 7.0 Hz, 3 H, CH_3), 3.43 (2.88) (sextet, J = 7.0 Hz, 1 H, CH), 3.46 (3.41) (t, J = 4.0 Hz, 3 H, SiH), 7.10−7.36 (m, 4 H, Ar H) (isomer ratio ortho:meta:para = 15:1:34). $^{13}C\{^1H\}$ NMR (δ, $CDCl_3$, 75.5 MHz): 14.86, 15.95, 16.03 ($SiCH_2$), 22.77, 24.18, 24.40 (CH_3), 33.22, 37.24, 37.58 (CH), 124.76, 126.30, 126.91, 126.99, 127.09, 127.88, 128.53, 129.66, 131.76, 146.67, 150.40 (Ar C). GC/MS (m/e (relative intensity)): 184 (19) (M^+), 169 (12), 143 (32),

(14) (a) There is a previous report; a series of analogous aryl-substituted alkylsilanes $Ph(CH_2)_3SiH_3$, (p-chloromethyl)phenethylsilane, etc. were reported: Chang, V. S. C. Ph.D. Thesis, University of Akron, 1981; *Chem. Abstr.* **1982**, *95*, 220380a. (b) Lee, B. W.; Yoo, B. R.; Kim, S.-I.; Jung, I. N. *Organometallics* **1994**, *13*, 1312. (c) Park, S. K., Master's Thesis, Chosun University, 1995.

141 (100), 139 (84), 125 (11), 115 (21), 105 (19), 103 (60), 102 (13), 91 (20), 78 (12), 77 (43), 75 (11), 65 (19), 63 (32), 51 (17).

Synthesis of 3-(chloro-*p*-tolyl)-1-silabutane (5): 93% yield; bp 50–52 °C/0.6 mmHg. Anal. Calcd for $SiC_{10}H_{15}Cl$: C, 60.42 H, 7.61. Found: C, 60.70; H, 7.89. IR (neat, KBr, cm^{-1}): 2160 s (ν_{SiH}), 910 s (δ_{SiH}). ^1H NMR (δ, $CDCl_3$, 300 MHz): 1.10–1.17 (m, 2 H, CH_2), 1.33 (1.31) (d, J = 7.0 Hz, 3 H, CH_3), 2.34 (2.31) (s, 3 H, CH_3), 3.44 (3.13) (sextet, J = 7.0 Hz, 1 H, CH), 3.48 (3.47) (t, J = 4.0 Hz, 3 H, SiH), 6.93–7.27 (m, 3 H, ArH) (isomer ratio 4:1). $^{13}C\{^1H\}$ NMR (δ, $CDCl_3$, 75.5 MHz): 14.86 (15.23) ($SiCH_2$), 22.10 (18.90) (CH_3), 22.79 (22.52) (CH_3), 33.05 (32.56) (CH), 125.29, 125.72, 127.51, 127.84, 129.16, 130.16, 131.51, 133.10, 136.66, 144.90, 148.36 (Ar C). GC/MS (*m*/*e* (relative intensity)): 198 (26) (M^+), 157 (27), 156 (16), 155 (100), 154 (11), 153 (93), 145 (12), 121 (18), 119 (18), 117 (34), 116 (18), 115 (64), 105 (10), 93 (10), 92 (10), 91 (51), 89 (11), 77 (14), 65 (21), 63 (29).

Synthesis of 3-(phenoxyphenyl)-1-silabutane (6): 85% yield; bp 90–100 °C/0.5 mmHg. Anal. Calcd for $SiC_{15}H_{18}O$: C, 74.32; H, 7.43. Found: C, 74.10; H, 7.42. IR (neat, KBr, cm^{-1}): 2147 s (ν_{SiH}), 918 s (δ_{SiH}). ^1H NMR (δ, $CDCl_3$, 300 MHz): 1.18–1.37 (m, 2 H, CH_2), 1.42 (1.43) (d, J = 3.3 Hz, 3 H, CH_3), 3.44 (2.99) (sextet, J = 3.6 Hz, 1 H, CH), 3.52 (3.50) (t, J = 3.9 Hz, 3 H, SiH), 6.96–7.44 (m, 9 H, Ar H) (isomer ratio ortho:meta:para = 71:2:27). $^{13}C\{^1H\}$ NMR (δ, $CDCl_3$, 75.5 MHz): 15.10 (16.44) ($SiCH_2$), 23.47 (24.79) (CH_3), 30.61 (37.23) (CH), 117.98, 118.68, 119.14, 119.69, 122.69, 123.05, 124.15, 127.23, 127.42, 127.83, 129.79, 130.16, 139.46, 143.30, 153.86, 155.38, 158.17 (Ar C). GC/MS (*m*/*e* (relative intensity)): 242 (34) (M^+), 227 (15), 197 (100), 181 (17), 165 (5), 149 (9), 120 (9), 103 (10), 91 (17), 77 (23), 65 (5), 51 (9).

Synthesis of 3-Naphthyl-1-silabutane (7): 66% yield; bp 72–75 °C/0.6 mmHg. Anal. Calcd for $SiC_{13}H_{16}$: C, 77.93; H, 7.98. Found: C, 77.83; H, 7.99. IR (neat, KBr, cm^{-1}): 2145 s (ν_{SiH}), 918 s (δ_{SiH}). ^1H NMR (δ, $CDCl_3$, 300 MHz): 1.26–1.45 (m, 2 H, CH_2), 1.58 (1.52) (d, J = 3.5 Hz, 3 H, CH_3), 3.61 (3.56) (t, J = 3.9 Hz, 3 H, SiH), 3.91 (3.17) (sextet, J = 3.9 Hz, 1 H, CH), 7.41–8.18 (m, 7 H, Ar H) (isomer ratio 3:1). $^{13}C\{^1H\}$ NMR (δ, $CDCl_3$, 75.5 MHz): 15.64 (16.10) ($SiCH_2$), 23.55 (24.63) (CH_3), 31.75 (37.99) (CH), 122.57, 123.21, 124.67, 125.36, 125.46, 125.70, 125.94, 126.04, 126.71, 127.75, 128.23, 129.16, 131.32, 132.42, 133.75, 134.12, 144.35, 145.75 (Ar C). GC/MS (*m*/*e* (relative intensity)): 200 (37) (M^+), 185 (7), 183 (6), 169 (5), 158 (30), 157 (41), 156 (16), 155 (100), 153 (27), 152 (20), 141 (8), 129 (9), 128 (18), 115 (7), 63 (2), 53 (1).

Synthesis of bis(1-sila-3-butyl)benzene (8): 98% yield; bp 65–66 °C/0.6 mmHg. Anal. Calcd for $Si_2C_{12}H_{22}$: C, 64.80; H, 9.97. Found: C, 64.90; H, 10.20. Isomer ratio (by GLC): meta:para = 2:3. IR (neat, KBr, cm^{-1}): 2147 s (ν_{SiH}), 932 s (δ_{SiH}). ^1H NMR (δ, $CDCl_3$, 300 MHz): 1.14–1.25 (m, 2 H, $SiCH_2$), 1.38 (1.39) (d, J = 6.9 Hz, 3 H, CH_3), 2.63 (sextet, J = 7.2 Hz, 2 H, CH), 3.46 (t, J = 3.6 Hz, 6 H, SiH), 7.07–7.30 (m, 4 H, Ar H). $^{13}C\{^1H\}$ NMR (δ, $CDCl_3$, 75.5 MHz): 16.30 (CH_3), 24.50 ($SiCH_2$), 37.40 (37.90) (CH), 122.00, 125.00, 126.50, 128.50, 146.0, 148.30 (Ar C). GC/MS (*m*/*e* (relative intensity)): meta isomer 222 (M^+) (22), 177 (47), 163 (5), 149 (100), 147 (50), 135 (33), 133 (61), 131 (16), 107 (54), 105 (20), 91 (13), 73 (17); para isomer 222 (M^+) (19), 207 (6), 177 (100), 149 (21), 147 (24), 133 (41), 131 (14), 107 (21), 105 (12), 91 (10), 73 (18).

Homopolymerization Catalyzed by Cp_2TiCl_2/Red-Al: Polymerization of 1. The following procedure is representative of the polymerization reactions. To a Schlenk flask charged with Cp_2TiCl_2 (0.20 g, 0.80 mmol) and Red-Al (24 mL, 0.80 mmol) was slowly added **1** (1.20 g, 8.00 mmol). The reaction mixture immediately turned dark green, and the reaction medium became rapidly viscous with strong gas evolution. The mixture was stirred under a stream of nitrogen for 24 h and then heated at 90 °C until the mixture became rigid. The catalyst was allowed to oxidize by exposure to the air for a few seconds, and the solution was then passed rapidly through a silica gel column (70–230 mesh, 20 cm × 2 cm). The column was rinsed with 200 mL of toluene. The removal of volatiles at reduced pressure yielded 1.00 g (83% yield) of off-white tacky product: IR (neat, KBr, cm^{-1}) 2150 s (ν_{SiH}); ^1H NMR (δ, $CDCl_3$, 300 MHz) 0.68–1.96 (m, 5 H, $SiCH_2$, CH_3), 2.56–3.10 (m, 1 H, CH), 3.10–3.85 (m, SiH), 6.88–7.47 (m, 5 H, ArH); GPC M_w = 821, M_n = 455 (approximate DP = 6), M_w/M_n = 1.78.

Polymerization of 2: 91% yield; IR (neat, KBr, cm^{-1}) 2105 s (ν_{SiH}); ^1H NMR (δ, $CDCl_3$, 300 MHz) 1.00–1.30 (m, 5 H, $SiCH_2$, CH_3), 2.35–2.39 (m, 3 H, Ar–CH_3), 2.80–2.96 (m, 1 H, CH), 3.37–3.53 (m, SiH), 7.02–7.27 (m, 4 H, ArH); GPC M_w = 1088, M_n = 564 (approximate DP = 8), M_w/M_n = 1.93.

Polymerization of 3: 79% yield; IR (neat, KBr, cm^{-1}) 2105 s (ν_{SiH}); ^1H NMR (δ, $CDCl_3$, 300 MHz) 0.80–1.50 (m, 5 H, $SiCH_2$, CH_3), 2.10–2.40 (m, 6 H, Ar–CH_3), 2.92–3.26 (m, 1 H, CH), 3.26–3.72 (m, SiH), 6.77–7.40 (m, 3 H, Ar H); GPC M_w = 1292, M_n = 1162 (approximate DP = 16), M_w/M_n = 1.11.

Polymerization of 4: 99% yield; IR (neat, KBr, cm^{-1}) 2100 s (ν_{SiH}); ^1H NMR (δ, $CDCl_3$, 300 MHz) 0.82–1.58 (m, 5 H, $SiCH_2$, CH_3), 2.75–2.97 (m, 1 H, CH), 3.29–3.55 (m, SiH), 6.93–7.26 (m, 4 H, Ar H); GPC M_w = 1050, M_n = 497 (approximate DP = 7), M_w/M_n = 2.11.

Polymerization of 5: 81% yield; IR (neat, KBr, cm^{-1}) 2108 s (ν_{SiH}); ^1H NMR (δ, $CDCl_3$, 300 MHz) 0.78–1.49 (m, 5 H, $SiCH_2$, CH_3), 2.09–2.49 (m, 3 H, Ar–CH_3), 3.31–3.43 (m, 1 H, CH), 3.43–3.62 (m, SiH), 6.78–7.38 (m, 3 H, Ar H); GPC M_w = 851, M_n = 715 (approximate DP = 10), M_w/M_n = 1.19.

Polymerization of 6: 79% yield; IR (neat, KBr, cm^{-1}) 2140 s (ν_{SiH}); ^1H NMR (δ, $CDCl_3$, 300 MHz) 0.96–1.46 (m, 5 H, $SiCH_2$, CH_3), 2.77–2.94 (m, 1 H, CH), 3.20–3.54 (m, SiH), 6.85–7.36 (m, 9 H, ArH); GPC M_w = 887, M_n = 490 (approximate DP = 7), M_w/M_n = 1.81; UV–vis (hexane): $\lambda_{\sigma\rightarrow\sigma^*}$ 285 nm (ϵ = 2500).

Polymerization of 7: 83% yield; IR (neat, KBr, cm^{-1}) 2106 s (ν_{SiH}); ^1H NMR (δ, $CDCl_3$, 300 MHz) 0.79–1.73 (m, 5 H, $SiCH_2$, CH_3), 2.71–3.08 (m, 1 H, CH), 3.08–3.80 (m, SiH), 7.00–8.24 (m, 7 H, Ar H); GPC M_w = 831, M_n = 699 (approximate DP = 9), M_w/M_n = 1.19; UV–vis (hexane) $\lambda_{\sigma\rightarrow\sigma^*}$ 290 nm (ϵ = 2800).

Homopolymerization Catalyzed by Cp_2HfCl_2/Red-Al: Polymerization of 1. The following procedure is representative of the polymerization reactions. **1** (0.14 g, 0.92 mmol) was slowly added to a Schlenk flask charged with Cp_2HfCl_2 (24 mg, 0.06 mmol) and Red-Al (18 μL, 0.06 mmol). The reaction mixture immediately turned light yellow, and the reaction medium became slowly viscous with moderate gas evolution. The mixture was stirred under a stream of nitrogen for 30 min and then heated at 90 °C until the mixture became rigid. The catalyst was inactivated by exposure to the air for a few minutes, and the solution was then passed rapidly through a silica gel column (70–230 mesh, 20 cm × 2 cm). The column was rinsed with 200 mL of toluene. The removal of volatiles at reduced pressure yielded 0.043 g (31% yield) of off-white tacky product: IR (neat, KBr, cm^{-1}) 2150 s (ν_{SiH}); ^1H NMR (δ, $CDCl_3$, 300 MHz) 1.01–1.48 (m, 5 H, $SiCH_2$, CH_3), 2.70–2.90 (m, 1 H, CH), 3.15–3.56 (m, SiH), 7.08–7.39 (m, 5 H, Ar H); GPC M_w = 807, M_n = 410 (approximate DP = 5), M_w/M_n = 1.97.

Polymerization of 2: 32% yield; IR (neat, KBr, cm^{-1}) 2105 s (ν_{SiH}); ^1H NMR (δ, $CDCl_3$, 300 MHz) 0.85–1.46 (m, 5 H, $SiCH_2$, CH_30, 2.23–2.47 (m, 3 H, Ar–CH_3), 2.61–2.90 (m, 1 H, CH), 3.18–3.60 (m, SiH), 6.82–7.37 (m, 4 H, ArH); GPC M_w = 954, M_n = 251 (approximate DP = 3), M_w/M_n = 3.80.

Polymerization of 3: 46% yield; IR (neat, KBr, cm^{-1}) 2105 s (ν_{SiH}); ^1H NMR (δ, $CDCl_3$, 300 MHz) 1.01–1.36 (m, 5 H, $SiCH_2$, CH_3), 2.17–2.36 (m, 6 H, Ar–CH_3), 2.98–3.19 (m, 1 H, CH), 3.32–3.54 (m, SiH), 6.83–7.14 (m, 3 H, ArH); GPC M_w = 948, M_n = 488 (approximate DP = 7), M_w/M_n = 1.94.

Polymerization of 4: 53% yield; IR (neat, KBr, cm^{-1}) 2150 s (ν_{SiH}); ^1H NMR (δ, $CDCl_3$, 300 MHz) 0.63–1.02 (m, 5 H, $SiCH_2$, CH_3), 2.47–2.98 (m, 1 H, CH), 3.06–3.75 (m, SiH),

6.87–7.48 (m, 4 H, Ar H); GPC M_w = 1028, M_n = 445 (approximate DP = 6), M_w/M_n = 2.31.

Polymerization of 6: 67% yield; IR (neat, KBr, cm^{-1}) 2108 s (ν_{SiH}); ^1H NMR (δ, $CDCl_3$, 300 MHz) 0.84–1.64 (m, 5 H, $SiCH_2$, CH_3), 2.62–2.97 (m, 1 H, CH), 3.15–3.64 (m, SiH), 6.68–7.57 (m, 9 H, Ar H); GPC M_w = 900, M_n = 428 (approximate DP = 6), M_w/M_n = 2.10.

Polymerization of 7: 84% yield; IR (neat, KBr, cm^{-1}) 2106 s (ν_{SiH}); ^1H NMR (δ, $CDCl_3$, 300 MHz) 0.97–1.59 (m, 5 H, $SiCH_2$, CH_3), 2.89–3.06 (m, 1 H, CH), 3.27–3.79 (m, SiH), 7.16–8.21 (m, 7 H, Ar H); GPC M_w = 738, M_n = 400 (approximate DP = 5), M_w/M_n = 1.85.

Copolymerization Catalyzed by Cp_2TiCl_2/Red-Al: Copolymerization of 2 and 4. The following procedure is representative of the polymerization reactions. To a Schlenk flask charged with Cp_2TiCl_2 (20 mg, 0.085 mmol) and Red-Al (25 μL, 0.085 mmol) was slowly added **1** (0.28 g, 1.70 mmol) and **2** (0.31 g, 1.70 mmol). The reaction mixture immediately turned dark green, and the reaction medium became rapidly viscous with strong gas evolution. The mixture was stirred under a stream of nitrogen for 20 h and then heated at 90 °C until the mixture became rigid. The catalyst was allowed to oxidize by exposure to the air for a few seconds, and the solution was then passed rapidly through a silica gel column (70–230 mesh, 20 cm × 2 cm). The column was rinsed with 200 mL of toluene. The removal of volatiles at reduced pressure afforded 0.30 g (51% yield) of off-white tacky product: IR (neat, KBr, cm^{-1}) 2110 s (ν_{SiH}); ^1H NMR (δ, $CDCl_3$, 300 MHz) 0.91–1.68 (m, 10 H, $SiCH_2$, CH_3), 2.33 (m, 3 H, Ar–CH_3), 2.78–2.82 (m, 2 H, CH), 3.36–3.43 (m, SiH), 7.00–7.27 (m, 8 H, Ar H); GPC M_w = 813, M_n = 407 (approximate DP = 5), M_w/M_n = 2.00.

Copolymerization of 2 and 6: 86% yield; Ir (neat, KBr, cm^{-1}) 2110 s (ν_{SiH}); ^1H NMR (δ, $CDCl_3$, 300 MHz) 1.60–1.89 (m, 10 H, $SiCH_2$, CH_3), 2.32 (m, 3 H, Ar–CH_3), 2.73–2.76 (m, 2 H, CH), 3.28–3.50 (m, SiH), 6.92–7.27 (m, 13 H, Ar H); GPC M_w = 904, M_n = 538 (approximate DP = 7), M_w/M_n = 1.68.

Copolymerization of 4 and 6: 71% yield; IR (neat, KBr, cm^{-1}) 2120 s (ν_{SiH}); ^1H NMR (δ, $CDCl_3$, 300 MHz) 0.97–1.52 (m, 10 H, $SiCH_2$, CH_3), 2.75–2.82 (m, 2 H, CH), 3.30–3.47 (m, SiH), 6.85–7.32 (m, 13 H, Ar H); GPC M_w = 678, M_n = 405 (approximate DP = 5), M_w/M_n = 1.68.

Polymerization of 8 Catalyzed by Cp_2TiCl_2/Red-Al. To a Schlenk flask charged with Cp_2TiCl_2 (16 mg, 0.04 mmol) and Red-Al (8.8 μL, 0.034 mmol) was slowly added **8** (0.33 g, 1.48 mmol). The reaction mixture immediately turned dark green, and the reaction medium became rapidly gelatinous with violent gas evolution. The mixture remained undisturbed under a stream of nitrogen for 2 days. The catalyst was destroyed by exposure to the air for a few hours. The yellow gelatinous material was washed several times with toluene and diethyl ether and dried at reduced pressure to give 0.18 g (55% yield) of off-white solid (mp >300 °C; TGA ceramic residue yield 64% (black solid)) which was insoluble in most organic solvents. The combined washing solutions were concentrated on a rotary vacuum evaporator and then passed rapidly through a silica gel column (70–230 mesh, 15 cm × 2 cm) with 200 mL of toluene used as the eluent. The colorless effluent was evaporated to dryness to yield 0.12 g (36% yield) of a very viscous clear oil which was soluble in most organic solvents. IR (KBr pellet, cm^{-1}): 2140 s (ν_{SiH}) for solid. For the very viscous clear oil: IR (neat, KBr, cm^{-1}) 2148 s (ν_{SiH}); ^1H NMR (δ, $CDCl_3$, 300 MHz) 1.08–1.23 (m, 4 H, $SiCH_2$), 1.24–1.38 (m, 6 H, CH_3), 2.85–2.95 (m, 2 H, CH), 3.37–3.48 (m, SiH), 6.98–7.32 (m, 4 H, Ar H); GPC M_w = 1046, M_n = 819 (approximate DP = 11), M_w/M_n = 1.28.

Results

Monomer Synthesis.[14a] 3-Aryl-1,1-dichloro-1-silabutanes[14b] and bis(1,1-dichloro-1-sila-3-butyl)benzene[14c] were prepared by $AlCl_3$-catalyzed Friedel–Crafts reactions of allyldichlorosilane with substituted aryl compounds. The monomeric silanes, 3-aryl-1-silabutanes and bis(1-sila-3-butyl)benzene, were prepared in 62–98% yields by reaction of the corresponding 3-aryl-1,1-dichloro-1-silabutanes and bis(1,1-dichloro-1-sila-3-butyl)benzene, respectively, with $LiAlH_4$ (eq 1). The

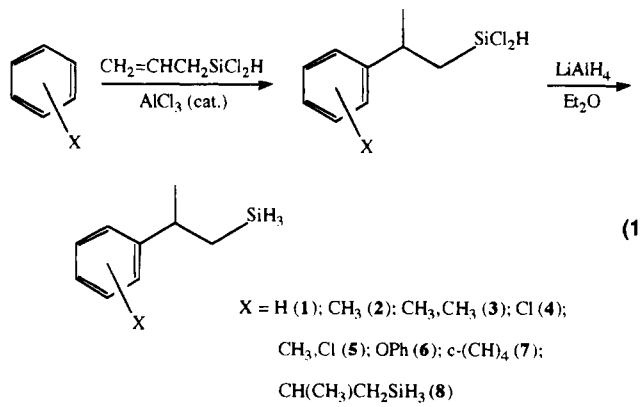

(1)

monomeric silanes 3-phenyl-1-silabutane (**1**), 3-tolyl-1-silabutane (**2**), 3-(2,5-dimethylphenyl)-1-silabutane (**3**), 3-(chlorophenyl)-1-silabutane (**4**), 3-(chloro-*p*-tolyl)-1-silabutane (**5**), 3-(phenoxyphenyl)-1-silabutane (**6**), 3-naphthyl-1-silabutane (**7**), and bis(1-sila-3-butyl)benzene (**8**) were purified by fractional distillation. All the silanes obtained here are stereoisomeric mixtures and were used without further attempts to separate them. The spectroscopic data for the monomeric silanes are summarized in Table 1.

Table 1. Spectroscopic Characterization of Monomeric Silanes

monomer	yield (%)	bp (°C)/ *p* (mmHg)	^1H NMR[a] (Si–H, ppm)	IR[b] (Si–H, cm^{-1})
1	62	74–76/20	3.43	2155
2	98	36–38/0.6	3.40, 3.41, 3.44	2150
3	96	62–65/0.6	3.44	2150
4	68	64–67/0.6	3.41, 3.46	2160
5	93	50–52.0.6	3.48	2160
6	85	90–100/0.5	3.50, 3.52	2147
7	66	72–75/0.6	3.61	2145
8	98	65–66/0.6	3.46	2147

[a] All measurements were carried out in $CDCl_3$ solvent. [b] All measurements were performed neat in a KBr cell.

Homopolymerization of Monomer Silanes. Polymerization of the monomeric silanes **1**–**7** with the Cp_2TiCl_2/Red-Al catalyst system was initiated immediately, as evidenced by the immediate release of hydrogen gas, and the reaction medium became rapidly viscous (eq 2).

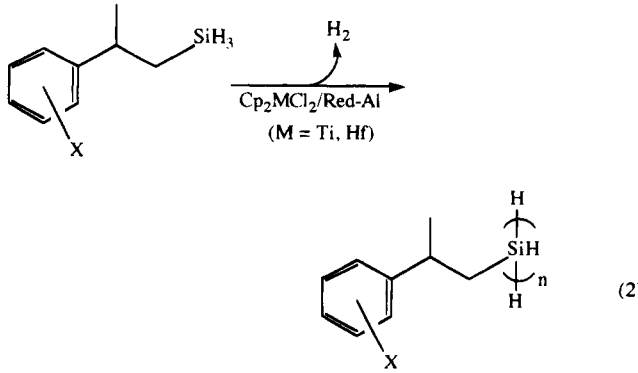

(2)

To drive the reaction toward completion, the mixture

Table 2. GPC Characterization of Homopolymerization of Monomeric Silanes with Cp_2TiCl_2/Red-Al[a]

monomer	yield (%)	mol wt[b] M_w	mol wt[b] M_n (DP)[c]	PDI
1	83	821	455 (6)	1.78
2	91	1088	564 (8)	1.93
3	79	1292	1162 (16)	1.11
4	99	1050	497 (7)	2.11
5	81	851	715 (10)	1.19
6	79	887	490 (7)	1.81
7	83	831	699 (9)	1.19

[a] [Ti]/[Si] = 0.10. [b] GPC vs polystyrene. [c] Approximate estimate for DP made by simply calculating the differences in molecular weight between styrene and silylene monomer units.

Table 3. GPC Characterization of Homopolymerization of Monomeric Silanes with Cp_2HfCl_2/Red-Al[a]

monomer	yield (%)	mol wt[b] M_w	mol wt[b] M_n (DP)[c]	PDI
1	31	807	410 (5)	1.97
2	32	954	251 (3)	3.80
3	46	948	488 (7)	1.94
4	53	1028	445 (6)	2.31
6	79	900	428 (6)	2.10
7	84	738	400 (5)	1.85

[a] [Hf]/[Si] = 0.065. [b] GPC vs polystyrene. [c] Approximate estimate for DP made by simply calculating the differences in molecular weight between styrene and silylene monomer units.

was stirred at room temperature for 24 h and then heated at 90 °C until the mixture became rigid. The polymers were isolated in 79–99% yields after workup including column chromatography as off-white tacky materials which were soluble in most organic solvents. The polymerization results are shown in Table 2.

Polymerization of the monomer silanes **1**–**7** with the Cp_2HfCl_2/Red-Al catalyst system commenced slowly, as monitored by the moderate release of hydrogen gas, and the reaction medium became slowly viscous (eq 2). To bring the reaction toward completion, the mixture was stirred at room temperature for 30 min and then heated at 90 °C until the mixture became rigid. The polymers were obtained in 31–84% yields after workup including column chromatography as off-white tacky materials which were soluble in most organic solvents. The polymerization results are given in Table 3.

Copolymerization of Monomer Silanes. Copolymerization of the monomeric silanes with the Cp_2TiCl_2/Red-Al catalyst system started immediately, as monitored by the immediate release of hydrogen gas, and the reaction medium became rapidly viscous (eq 3).

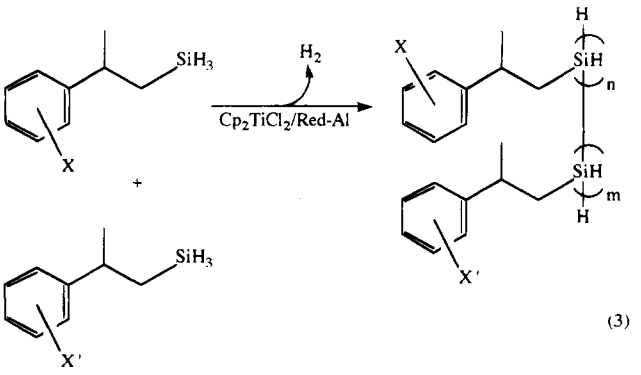

(3)

Table 4. GPC Characterization of Copolymerization of Monomeric Silanes with Cp_2TiCl_2/Red-Al[a]

monomer[b]	yield (%)	mol wt[c] M_w	mol wt[c] M_n (DP)[d]	PDI
2 and **4**	51	813	407 (5)	2.00
2 and **6**	86	904	538 (7)	1.68
4 and **6**	71	678	405 (5)	1.68

[a] [Ti]/[Si] = 0.025. [b] 1:1 mole ratio. [c] GPC vs polystyrene. [d] Approximate estimate for DP made by simply calculating the differences in molecular weight between styrene and silylene monomer units.

To reach completion, the mixture was stirred at room temperature for 24 h and then heated at 90 °C until the mixture became rigid. The polymers were acquired in 51–86% yields after workup including column chromatography as off-white tacky materials which were soluble in most organic solvents. The polymerization results are shown in Table 4.

Polymerization of Bis(1-sila-3-butyl)benzene (8). Polymerization of **8** with the Cp_2TiCl_2/Red-Al catalyst system began immediately, as monitored by the immediate release of hydrogen gas, and the reaction medium became rapidly gelatinous (eq 4). The polymer

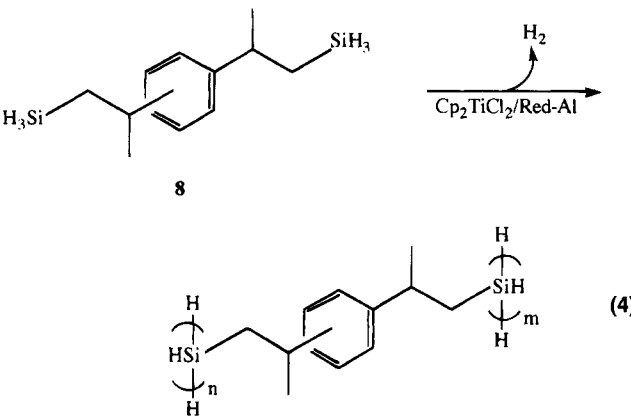

(4)

was acquired in ≥90% total yield as two phases after workup including washing and column chromatography. The first part of the polymer was obtained in 55% yield as an off-white solid (mp >300 °C) which was insoluble in most organic solvents. Its TGA ceramic residue yield was 64%. The second part of the polymer was acquired in 36% yield as a very viscous clear oil which was soluble in most organic solvents. The weight-average molecular weight (M_w) and number-average molecular weight (M_n) of the oily polymer were 1046 and 819, respectively. The approximate estimate for the average degree of polymerization (DP) was 11.

Discussion

The chemical shifts and coupling constants associated with the protons of the Si–H bonds in the ^1H NMR spectra of the monomer silanes are in the ranges of 3.4–3.6 ppm and 3.5–4.0 Hz, respectively. The variation of chemical shifts of the Si–H bonds with change of substituents was minor, albeit the aryl substitution on the 3-phenyl group as in **6** and **7** resulted in a downfield shift. The Si–H stretching bands in the IR spectra of the silanes are in the 2140–2160 cm^{-1} range. The spectral data appear to be little affected by the substituents on the aryl ring, due probably to the separation

of the silicon center from the aryl ring by an ethylene spacer, and were in good agreement with those for other alkylsilanes reported in the literature. Thus, one may expect that the dehydrocoupling of 3-aryl-substituted alkylsilanes should closely resemble the dehydrocoupling of other alkylsilanes.

While the molecular weights of polysilanes produced via the dehydrocoupling reaction are lower than those produced via Wurtz coupling of dichlorosilanes, the dehydrocoupling method is more tolerant of functional groups. The Wurtz coupling method cannot be used to polymerize chlorine-substituted arylsilanes due to cross-linking.[1] Organo rare-earth-metal complexes have been used as catalysts to dehydrocouple silanes to give low-molecular-weight oligomers.[4c,15] Although Cp_2MMe_2 (M = Ti, Zr),[4] $Cp_2Zr[Si(SiMe_3)_3]Me$,[5] and Cp_2ZrCl_2/*n*-BuLi[12b] are known to be the active catalysts for the dehydropolymerization of primary silanes and CpCp*Zr-[Si(SiMe$_3$)$_3$]Me and $(CpCp^*ZrH_2)_2$ were the most active catalysts previously examined,[5] we wanted to employ a new catalyst system, Cp_2MCl_2/Red-Al (M = Ti, Hf),[9] which was recently found to give predominantly linear, higher molecular weight polysilanes than for any other catalyst system, because the monomeric silanes 3-aryl-1-silabutanes are sterically hindered. Sterically hindered silanes were known to be very slow to polymerize and to give low-molecular-weight oligosilanes.[5] Thus, in order to accelerate the rate of polymerization, both higher catalyst concentration (i.e., 10 mol % for Ti and 6.5 mol % for Hf in the homopolymerization; 2.5 mol % for Ti in the copolymerization) than the usual concentration range of 0.5−1.0 mol % and heating to 90 °C were employed in these polymerization reactions.

The ^{1}H NMR spectra of all of the polysilanes prepared apparently show only one broad unresolved mountain-like resonance centered at ca. 4.4 ppm, unlike poly(phenylsilane), which shows a set of broad resonances centered at 4.5 and 5.1 ppm corresponding to linear and cyclic polymers.[4a] The IR spectra of all of the polysilanes produced here exhibit an intense ν_{SiH} band at ca. 2100 cm^{-1} and a weak or nearly absent δ_{SiH} band at ca. 910 cm^{-1}. The weak intensity of the δ_{SiH} IR band and ^{1}H NMR spectra imply that the polysilanes could be mostly cyclic.[4a] However, one should note that the decrease of polydispersity index in GPC is not always proportional to the increase of percent of cyclic product.[5e] We expect some degree of diastereomeric selection in the polymerization, especially at the Si−Si coupling step via σ-bond metathesis,[5] due to the presence of asymmetric center by the 2-methyl group of the 3-aryl-1-silabutanes, although the monomeric silanes are used as a mixture of stereoisomers. An investigation of percentage of cyclic and linear oligomers in the polymers and the degree of diastereomeric selection in the polymerization in detail by using ^{29}Si NMR and GC/mass/FT-IR techniques is currently in progress and will be the subject of a future paper. The polymers reported here apparently show no sign of cross-linking due to coupling of the substituted chlorine and of the backbone Si−H bonds of the polymer chains, evidenced by ^{1}H NMR, IR, and GPC. UV−vis spectra in hexane of poly(3-(phenoxyphenyl)-1-silabutane) and poly(3-naphthyl-1-silabutane) showed $\lambda_{\sigma\to\sigma^*}$ 285 (ϵ = 2500) and 290 (ϵ = 2800), respectively, which are in the normal range for polysilanes.[1] The polysilanes did not exhibit a significant photobleaching behavior upon irradiation by room light under an atmosphere of nitrogen within several hours.

Although the molecular weights determined by GPC (vs polystyrene standard) are not directly comparable for various substituted polysilanes,[1] it appears that the polymers of 3-aryl-1-silabutanes have a lower degree of polymerization than those obtained from phenylsilane but have an approximately similar degree of polymerization as those obtained from benzylsilane[8] or *n*-butylsilane.[13a] An approximate estimate for the average degree of polymerization (DP) for these polysilanes, made by simply calculating the differences in molecular weight between styrene and silylene monomer units, can be made. As shown in Tables 2−4, polymers with degrees of polymerization (DP) of 6−16 and with polydispersity indexes (PDI) of 1.1−2.1 were obtained by the Cp_2TiCl_2/Red-Al system, and polymers with DP values of 3−7 and with PDI values of 1.8−3.8 were obtained by the Cp_2HfCl_2/Red-Al system. For comparison, the dehydropolymerization of the monomeric silanes with the Cp_2MCl_2 (M = Ti, Hf)/*n*-BuLi catalyst system is currently underway.

As seen in Table 4, copolymers with DP values of 5−7 and with PDI values of 1.6−2.0 were obtained. Although the homopolymers of each component monomer along with the copolymer may be formed, the possibility is slim due to the similar reactivity of each monomeric silane. However, it is currently uncertain whether the copolymers are random or not. ^{1}H NMR, IR, and GPC for these copolymers are relatively uninformative. Differential scanning calorimetry (DSC) for these copolymers did not give us much information either: it did not show the existence of a glass transition temperature (T_g) between 25 and 200 °C.

Dehydropolymerization of **8** produced two phases of polymers. One is a very viscous oil (M_w = 1046, M_n = 819 (approximate DP = 11)) which seems to be non-cross-linked or slightly cross-linked and thus soluble in most organic solvents. The other is an off-white solid which appears to be extensively cross-linked and thus insoluble in most organic solvents. The solid polymer did not melt or decompose upon heating to 300 °C. Thermogravimetric analysis (TGA) shows that only 10% of the initial weight of the polymer is lost by 400 °C and the TGA ceramic residue yield is 64% at 800 °C. Differential scanning calorimetry (DSC) for these polymers did not show the existence of a glass transition temperature (T_g) between 25 and 350 °C. X-ray powder pattern analysis (2θ = 5−80°) of the solid polymer was featureless, which suggests that the polymer adopts an amorphous, glasslike structure. One might naturally think that the polymerization first produced a low-molecular-weight polymer which then underwent an extensive cross-linking reaction of backbone Si−H bonds, leading to an insoluble polymer. The dehydropolymerizability of two isomers (meta:para = 2:3) of **8** seems to be similar by judging from the ^{1}H NMR spectrum of the oily product. The monomer **8** can be used as a cross-linking agent in the dehydropolymerization of 3-aryl-1-silabutanes. Details on the dehydropolymerization of multi(silylalkyl)-substituted arenes will be reported in

(15) (a) Watson, P. L.; Tebbe, F. N. U.S. Patent 4965386 Oct 23 1990; *Chem. Abstr.* **1991**, *114*, 123331p. (b) Sakakura, T.; Lautenschlager, H.-J.; Tanaka, M. *J. Chem. Soc., Chem. Commun.* **1991**, 40.

the near future. One of us reported the dehydropolymerization of multisilanylenearylenes.[7]

Conclusion

This work describes the preparation, dehydrohomopolymerization, and dehydrocopolymerization of new aryl-substituted alkylsilanes, 3-aryl-1-silabutanes, catalyzed by the Cp_2MCl_2 (M = Ti, Hf)/Red-Al combined system. While polymers produced by the Cp_2TiCl_2/Red-Al system with degrees of polymerization (DP) of 6−16 and with polydispersity indexes (PDI) of 1.1−2.1 were obtained, polymers produced by the Cp_2HfCl_2/Red-Al system with DP values of 3−7 and with PDI values of 1.8−3.8 were obtained. The dehydrocopolymerization of the silanes gave copolymers with DP = 5−7 and with PDI = 1.6−2.0. Bis(silabutyl)benzene (**8**) dehydrocoupled to produce two phases of polymers: one is a highly cross-linked solid, and the other is a non-cross-linked or slightly cross-linked oil and could be a precursor for the solid. X-ray powder pattern analysis suggests the solid polymer adopts amorphous structure.

Acknowledgment. This research was supported in part by the Non-directed Research Fund, Korea Research Foundation (1994), in part by the Korea Science and Engineering Foundation (1994), and in part by the Ministry of Science and Technology of Korea.

OM940844P

Bis(2-pyridyl)phosphides and -arsenides of Group 13 Metals: Substituent-Separated Contact Ion Pairs

Alexander Steiner and Dietmar Stalke*

Institut für Anorganische Chemie der Universität Göttingen, Tammannstrasse 4, D-37077 Göttingen, Germany

Received January 23, 1995[⊗]

Tris(2-pyridyl)phosphine reacts with lithium metal in THF with cleavage of a P−aryl bond and ligand coupling to give 2,2′-bipyridyl and lithium bis(2-pyridyl)phosphide. Hydrolysis of this solution leads to bis(2-pyridyl)phosphine **1**. Deprotonation of **1** with *n*-butyllithium yields $(THF)_2Li(\mu\text{-}Py)_2P$, **2**, (Py = 2-pyridyl). Addition of trimethylaluminum to tris(2-pyridyl)phosphine gives the $Me_3Al(\mu\text{-}Py)PPy_2$ adduct complex **3**, while deprotonation of **1** and elimination of methane forms $Me_2Al(\mu\text{-}Py)_2P$, **4**. **4** is also obtained by a transmetalation reaction of **2** with Me_2AlCl. Lithium metal also cleaves one As−aryl bond in tris(2-pyridyl)-arsine to give lithium bis(2-pyridyl)arsenide, which is directly treated with Me_2AlCl and Me_2GaCl, yielding $Me_2Al(\mu\text{-}Py)_2As$, **5**, and $Me_2Ga(\mu\text{-}Py)_2As$, **6**, respectively. While in **1** the hydrogen atom is located at the phosphorus atom, as indicated by IR and NMR spectroscopy, X-ray structure analyses of **2**−**5** prove that there is no contact between the metal center and the central phosphorus or arsenic atoms of the ligand. The $[Py_2E]^-$ ligands (E = P, As) chelate the metal centers exclusively by both pyridyl nitrogen atoms, leaving the central E atom two-coordinated. The negative charge in the monoanionic $[Py_2E]^-$ ligands of **2**−**6** is largely delocalized from the central E atom to both pyridyl ring systems. The correspondence in spectroscopic data of **5** and **6** suggests the same structure type in the gallium arsenide complex **6**.

Introduction

N-Heteroaryl ring systems are well-known as bridging functions between transition metal centers, but related complexes in main group chemistry are hardly known up to now.[1] Recently we described the replacement of the central BH unit in the widely used tris(pyrazol-1-yl)borates[2] with tin(II) or germanium(II) atoms leading to monoanionic ligands of the composition $[Pz_3E]^-$ (Pz = pyrazol-1-yl, E = Ge, Sn).[3] We studied their coordination behavior toward s-block metal centers such as sodium and barium and also toward further Ge(II) and Sn(II) units. In all of these complexes pyrazol-1-yl acts almost exclusively in an *exo*-bidentate bridging manner via both N-donor functions. Surprisingly, one of the pyrazol-1-yl ligands in these substituents coordinates *side on* to a barium center.

Recently we reported complexes in which group 13 and 15 elements are connected via two pyridyl ring systems.[4] Low molecular aggregates containing group 13 and 15 elements are of great interest as precursors for III/V semiconductors.[5] Monomeric group 13/15 compounds are commonly obtained only with extremely bulky substituents, so the low valence metal centers are protected against nucleophilic attack.[6] However, we showed that pyridyl substituents at the phosphorus atom inhibit oligomerization by donation to the group 13 metals exclusively by their nitrogen atoms, leaving the phosphorus atom two-coordinated. This paper is concerned with a more detailed discussion of the structural and electronic aspects of the $[Py_2P]^-$ ligand and the investigation of analogous arsenic derivates.

Results and Discussion

Preparations of 1−6 (Scheme 1). Tris(2-pyridyl)-phosphine[7] and tris(2-pyridyl)arsine,[8] respectively, react with an equimolar amount of lithium metal in THF, yielding deep crimson solutions containing $LiPy_2E$ (Py = 2-pyridyl; E = P, As) and 2,2′-bipyridyl in a 2:1 molar ratio (eq i).

The cleavage of an E−aryl bond seems to be the initial step leading to $LiPy_2E$ and 2-pyridyllithium. The latter product undergoes a ligand coupling reaction and a metal transfer to excess Py_3E to give $LiPy_2E$ and 2,2′-bipyridyl. Uchida, Oae et al. describe ligand coupling reactions of heteroaryl-substituted phosphines with organolithium compounds[9] assuming a hypervalent transition state $[R_4PLi]$, which is related to phosphoranides[10] $[PX_4]^-$. Decomposition yields the R_2PLi spe-

[⊗] Abstract published in *Advance ACS Abstracts,* April 15, 1995.

(1) (a) Steel, P. J. *Coord. Chem. Rev.* **1990**, *106*, 227. (b) Trofimenko, S. *Prog. Inorg. Chem.* **1986**, *34*, 115.

(2) (a) Trofimenko, S. *Chem. Rev.* **1972**, *72*, 497; (b) **1993**, *93*, 943. (c) Byers, P. K.; Canty, A. J.; Honeyman, R. T. *Adv. Organomet. Chem.* **1992**, *34*, 1.

(3) (a) Steiner, A.; Stalke, D. *J. Chem. Soc., Chem. Commun.* **1993**, 1702. (b) Steiner, A.; Stalke, D. *Inorg. Chem.* submitted for publication.

(4) Steiner, A.; Stalke, D. *J. Chem. Soc., Chem. Commun.* **1993**, 444.

(5) (a) Cowley, A. H.; Jones, R. A. *Angew. Chem.* **1989**, *101*, 1235; *Angew. Chem., Int. Ed. Engl.* **1989**, *28*, 1208. (b) Heaton, D. E.; Jones, R. A.; Kidd, K. B.; Cowley, A. H.; Nunn, C. M. *Polyhedron* **1988**, *7*, 1901. (c) Cowley, A. H.; Jones, R. A. *Polyhedron* **1994**, *13*, 1149. (d) Buhro, W. E. *Polyhedron* **1994**, *13*, 1131.

(6) (a) Higa, K. T.; George, C. *Organometallics* **1990**, *9*, 275. (b) Byrne, E. K.; Parkanyi, L.; Theopold, K. H. *Science* **1988**, *241*, 332. (c) Petrie, M. A.; Power, P. P. *J. Chem. Soc., Dalton Trans.* **1993**, 1737. (d) Petrie, M. A.; Ruhlandt-Senge, K.; Power, P. P. *Inorg. Chem.* **1992**, *31*, 4038. (e) Wehmschulte, R. J.; Ruhlandt-Senge, K.; Power, P. P. *Inorg. Chem.* **1994**, *33*, 3205.

(7) Keene, F. R.; Snow, M. R.; Stephenson, P. J.; Tiekink, E. R. T. *Inorg. Chem.* **1988**, *27*, 2040.

(8) Plazek, E.; Tyka, R. *Zesz. Nauk Politech. Wroclaw., Chem.* **1957**, *4*, 79.

0276-7333/95/2314-2422$09.00/0

Scheme 1

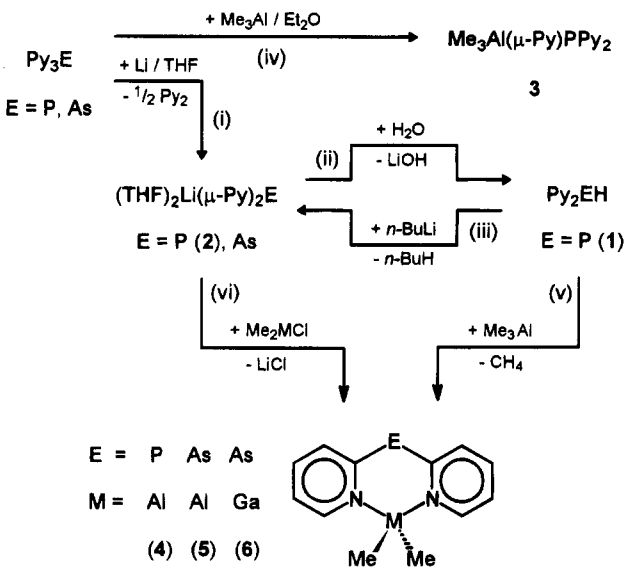

cies and biaryls. Although there are a lot of investigations concerning the biaryl coupling products, up to now only very little attention has been paid to the resulting phosphorus components.

Hydrolysis of the reaction mixture from eq i leads to bis(2-pyridyl)phosphine **1** (eq ii). After filtration and extraction with diethyl ether, it can be separated from 2,2′-bipyridyl by distillation under reduced pressure. While 2,2′-bipyridyl boils at 73 °C/0.01 Torr, **1** is obtained at 110 °C/0.01 Torr as a dark crimson oil. Bis(2-pyridyl)arsine is not available via this route, probably because of thermal decomposition during distillation. In contrast to diacylphosphines, which are *keto–enol* tautomers in solution and crystallize exclusively in the *enol* form in the solid state without P–H contacts,[11] the hydrogen atom in **1** is entirely bound to the phosphorus atom, indicated in the ^{1}H and ^{31}P NMR ($^1J_{P-H}$ = 225 Hz) and IR (ν_S(P–H) = 2312 cm^{-1}) spectra.

Addition of *n*-butyllithium to a solution of **1** in THF leads to the pure corresponding lithium compound (eq iii). Slow evaporation of the solvent yields dark red crystals of the THF adduct **2**. In contrast, the isolation of **2** by direct crystallization from the reaction mixture of tris(2-pyridyl)phosphine and lithium metal (eq i) is impossible because of the presence of 2,2′-bipyridyl.

When tris(2-pyridyl)phosphine is treated directly with trimethylaluminum in diethyl ether, the adduct complex **3** is obtained (eq iv). Different from analogous reactions with organolithium compounds, the reaction stops with the adduct species rather than undergoing ligand coupling to the corresponding aluminum phosphide. The saturated coordination sphere of the aluminum atom in **3** and the strong Al–C bonds presumably prevent methyl transfer to the phosphorus atom.

The dimethylaluminum derivative **4** can be obtained either by treating **1** with trimethylaluminum in *n*-hexane (eq v) or by transmetalation reaction of **2** with dimethylaluminum chloride in diethyl ether/*n*-hexane (eq vi). **4** crystallizes from a diethyl ether/*n*-hexane mixture at 3 °C.

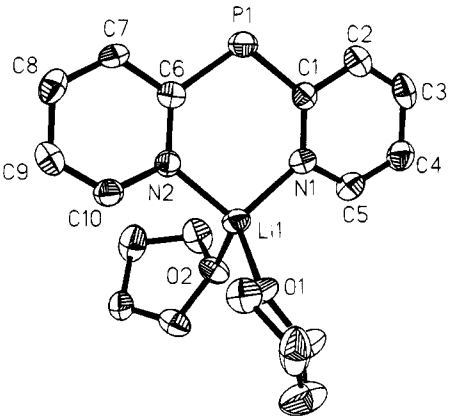

Figure 1. Molecular structure of **2** in the solid state, selected bond lengths (pm) and angles (deg); see also Table 1: P1–C1 179.4(4), P1–C6 179.8(4), Li1–N1 196.9(8), Li1–N2 196.9(7), Li1–O1 193.2(7), Li1–O2 193.7(7); C1–P1–C6 110.4(2), N1–Li1–N2 102.1(3), P1–C1–N1 127.0(3), P1–C6–N2 127.1(3), C1–N1–Li1 126.4(3), C6–N2–Li1 126.3(3), O1–Li1–O2 99.9(3).

The bis(2-pyridyl)arsenides $Me_2Al(\mu\text{-}Py)_2As$, **5**, and $Me_2Ga(\mu\text{-}Py)_2As$, **6**, are synthesized directly by using the reaction mixtures of tris(2-pyridyl)arsine and lithium metal (eq i). After the reaction is complete and THF replaced by toluene, Me_2MCl (M = Al, Ga) is added at −40 °C (eq vi). Lithium chloride is filtered off and the resulting 2,2′-bipyridyl can be separated by washing with *n*-pentane. Spectroscopic data show pure products. **5** crystallizes as dark violet needles from a diethyl ether/*n*-hexane solution.

Crystal Structure of 2. Figure 1 illustrates the tetrahedral environment of the central lithium atom, which is coordinated by both pyridyl nitrogen and two THF oxygen atoms. The Li–N distances are identical (196.9(8) and 196.9(7) pm). They are comparable to corresponding Li–N distances in lithium salts of 2-pyridyl-substituted carbanions.[12] The molecule is almost planar with the exception of the THF ligands, which are arranged above and below the main plane (Figure 5). The bond angle at the phosphorus atom is 110.4(2)°, and the P–C bond length is 179.6 pm on average. In contrast to P–C single bonds, which are about 185 pm long, values for P–C double bonds in phosphaalkenes range from 161 to 171 pm.[13] While in **2** the planes of the pyridyl rings intersect at an angle of 7°, the corresponding value for both phenyl rings in the solvent-separated ion pair of $[Li(12\text{-crown-}4)_2][Ph_2P]$ is 43°.[14] The negative charge of the sp^2-hybridized phosphorus atom in **2** is highly delocalized throughout the whole ligand because of the good π-acceptor capacity of the 2-pyridyl substituents. The consequence is a partial P–C double bond character. Compounds containing a phosphorus atom in a delocalized carbon ring system

(9) (a) Uchida, Y.; Takaya, Y.; Oae, S. *Heterocycles* **1990**, *30*, 347. (b) Uchida, Y.; Kawai, M.; Masauji, H.; Oae, S. *Heteroatom Chem.* **1993**, *4*, 421. (c) Oae, S. *Croat. Chem. Acta* **1986**, *59*, 129.

(10) Dillon, K. B. *Chem. Rev.* **1994**, *94*, 1441.

(11) (a) Becker, G.; Beck, H. P. *Z. Anorg. Allg. Chem.* **1977**, *430*, 77. (b) Becker, G.; Becker, W.; Schmidt, M.; Schwarz, W.; Westerhausen, M. *Z. Anorg. Allg. Chem.* **1991**, *605*, 7. (c) Becker, G.; Schmidt, M.; Schwarz, W.; Westerhausen, M. *Z. Anorg. Allg. Chem.* **1992**, *608*, 33.

(12) (a) Pieper, U.; Stalke, D. *Organometallics* **1993**, *12*, 1201. (b) Engelhardt, L. M.; Jacobsen, G. E.; Junk, P. C.; Raston, C. L.; Skelton, B. W.; White, A. H. *J. Chem. Soc., Dalton Trans.* **1988**, 1011.

(13) (a) Appel, R.; Knoll, F.; Ruppert, I. *Angew. Chem.* **1981**, *93*, 771; *Angew. Chem., Int. Ed. Engl.* **1981**, *20*, 731. (b) Appel, R.; Knoll, F. *Adv. Inorg. Chem.* **1989**, *33*, 259.

(14) Hope, H.; Olmstead, M. M.; Power, P. P.; Xu, X. *J. Am. Chem. Soc.* **1984**, *106*, 819.

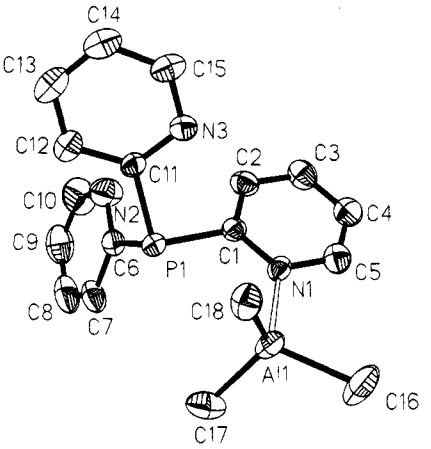

Figure 2. Molecular structure of **3** in the solid state, selected bond lengths (pm) and angles (deg); see also Table 1: P1–C1 184.2(2), P1–C6 184.2(2), P1–C11 183.2(2), Al1–N1 205.7(2), Al1–C16 197.8(3), Al1–C17 197.3(3), Al1–C18, 196.6(2); C1–P1–C6 99.88(9), C1–P1–C11 100.08(9), C6–P1–C11 101.9(1), P1–C1–N1 116.2(1), C1–N1–Al1 124.4(1), av N–Al–C 105.1, av C–Al–C 113.4.

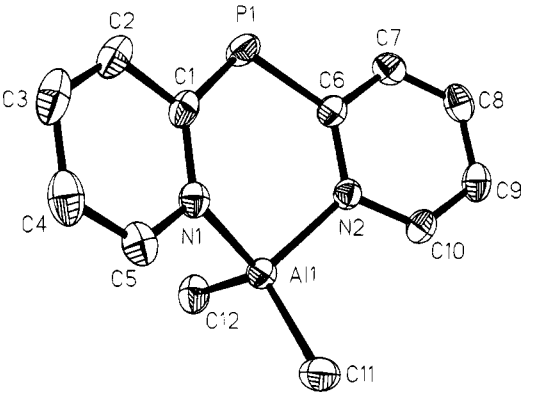

Figure 3. Molecular structure of **4** in the solid state, selected bond lengths (pm) and angles (deg); see also Table 1: P1–C1 178.6(2), P1–C6 178.2(2), Al1–N1 192.4(1), Al1–N2 191.9(1), Al1–C11 195.5(2), Al1–C12 195.2(2); C1–P1–C6 106.60(7), P1–C1–N1 127.1(1), P1–C6–N2 126.9(1), C1–N1–Al1 123.2(2), C6–N2–Al1 123.2(1), N1–Al1–N2 98.98(6), C11–Al1–C12 119.47(9).

are neutral phosphabenzenes[15] (P–C 174 pm in 2,6-dimethyl-4-phenylphosphabenzene)[16] and η^5-coordinated phospholides[17] (P–C 179 pm in (η^5-Cp*)Ru(η^5-*t*-$Bu_2C_4H_2P$)).[18] The latter resembles the main structural features of **2** regarding the P–C bond length and ^{31}P NMR spectroscopic shift. In both systems the phosphorus atom is part of a delocalized π-excess monoanion. Two-coordinated phosphorus atoms are also found in the $[(CN)_2P]^-$ anion of the crown ether-solvated sodium salt[19] and in the DME-saturated lithium dibenzoylphosphide.[20] This compound shows a structural pattern related to **2**. Both benzoyl substituents donate the lithium atom via their oxygen atoms. Lithium diphenylphosphide is isoelectronic to **2** and often used as a transfer reagent for the diphenylphosphide group.[21] With exception of the solvent-separated [Li(12-crown-4)$_2$][Ph_2P] ion pair, all known structures show Li–P contacts. The P–C bond lengths in these systems are 185 pm on average and therefore about 5 pm longer than in **2**. While the THF adduct gives a polymer in the solid state, dimeric and monomeric complexes are formed in the presence of the chelating nitrogen donor bases TMEDA ($Me_2NCH_2CH_2NMe_2$) and PMDETA (($Me_2NCH_2CH_2)_2NMe$), respectively.[22] The formal replacement of the *o*-phenyl-CH positions by N functions converts the monodentate diphenylphosphide into a chelating system. As a consequence, the metal cation is separated from the phosphorus ligand center and oligomerization is prevented.

Crystal Structure of 3. Just one of the three pyridyl substituents donates to the aluminum atom via its nitrogen function (Figure 2). The "hard" aluminum atom prefers the "hard" nitrogen donor rather than the "soft" phosphine function. Three methyl groups and the single N-donor atom leave the central aluminum atom tetrahedrally-coordinated. The Al–N-donor bond length of 205.7(2) pm corresponds with bond lengths in related donor-acceptor complexes. Three neutral pyridine molecules donate to the central aluminum atom in the octahedral complex $(PyH)_3AlCl_3$ with Al–N distances between 206.7 and 209.6 pm.[23] A slightly longer distances is observed in the adduct $Me_3Al–NMe_3$ (209.9 pm) in the gas phase.[24] The Al–C distance in **3** is on average 197.2 pm long and comparable with that in $Me_3Al–NMe_3$ (198.7 pm). The average C–Al–N angle is about 8° more acute than the average C–Al–C-angle, indicating the higher sterical demand of the more covalent-bound methyl groups in the coordination sphere of the aluminum atom rather than the loosely donating nitrogen atom.[25] There is no significant difference in the P–C bond lengths of the single ring coordinated to the aluminum atom and the two noncoordinated pyridyl substituents, respectively. On average, the C–P–C angle is 100.6° and comparable with those in noncomplexing tris(2-pyridyl)phosphine.[26] Transition metal complexes containing tris(2-pyridyl)phosphine as a neutral ligand are structurally well-known.[27] Toward zinc[28] and ruthenium[7] it coordinates as a tripod ligand via all three ring nitrogen atoms, while in the linear gold complex Py_3PAuCl, it coordinates the softer gold center exclusively with the phosphorus atom.[29]

Crystal Structure of 4. In the monomeric complex **4** the aluminum and phosphorus atoms are μ_2-bridged by two pyridyl ring systems (Figure 3). The $(THF)_2Li$ unit in **2** is replaced by a Me_2Al unit. As in **4**, the

(15) Ashe, A. J., III. *Top. Curr. Chem.* **1982**, *105*, 125.
(16) Fluck, E. *Top. Phosphorus Chem.* **1980**, *10*, 193.
(17) Nixon, J. F. *Chem. Rev.* **1988**, *88*, 1327.
(18) Carmichael, D.; Ricard, L.; Mathey, F. *J. Chem. Soc., Chem. Commun.* **1994**, 1167.
(19) Sheldrick, W. S.; Kroner, J.; Zwaschka, F.; Schmidpeter, A. *Angew. Chem.* **1979**, *91*, 998; *Angew. Chem., Int. Ed. Engl.* **1979**, *18*, 934.
(20) Becker, G.; Birkhahn, M.; Massa, W.; Uhl, W. *Angew. Chem.* **1980**, *92*, 756; *Angew. Chem., Int. Ed. Engl.* **1980**, *19*, 741.
(21) Issleib, K.; Wenschuh, E. *Chem. Ber.* **1964**, *97*, 715.
(22) Mulvey, R. E.; Wade, K.; Armstrong, D. R.; Walker, G. T.; Snaith, R.; Clegg, W.; Reed, D. *Polyhedron* **1987**, *6*, 987.
(23) Pullmann, P.; Hensen, K.; Bats, J. W. *Z. Naturforsch.* **1982**, *B37*, 1312.
(24) Andersen, G. A.; Forgaard, F. R.; Haaland, A. *Acta Chem. Scand.* **1972**, *26*, 1947.
(25) (a) Gillespie, R. J.; Hargittai, I. *The VSEPR Model of Molecular Geometry*; Allyn and Bacon: Boston, 1991. (b) Haaland, A. *Angew. Chem.* **1989**, *101*, 1017; *Angew. Chem., Int. Ed. Engl.* **1989**, *28*, 992.
(26) Keene, F. R.; Snow, M. R.; Tiekink, E. R. T. *Acta Crystallogr. Sect. C* **1988**, *44*, 757.
(27) Newkome, G. R. *Chem. Rev.* **1993**, *93*, 2067.
(28) Gregorzik, R.; Wirbser, J.; Vahrenkamp, H. *Chem. Ber.* **1992**, *125*, 1575.
(29) Lock, C. L. J.; Turner, M. A. *Acta Crystallogr. Sect. C* **1987**, *43*, 2096.

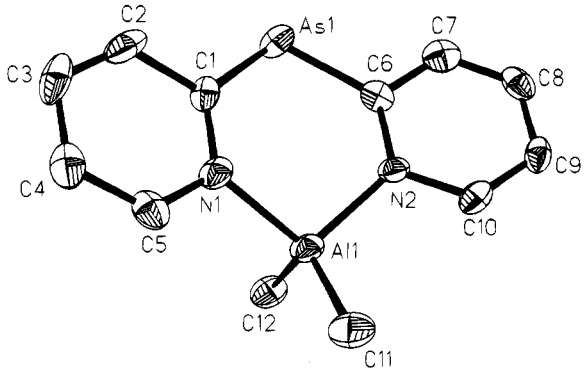

Figure 4. Molecular structure of **5** in the solid state, selected bond lengths (pm) and angles (deg); see also Table 1: As1–C1 191.9(7), As1–C6 189.3(8), Al1–N1 193.4(6), Al1–N2 192.3(6), Al1–C11 194.5(9), Al1–C12 194.0(8); C1–As1–C6 103.0(3), As1–C1–N1 126.9(5), As1–C6–N2 127.3(5), C1–N1–Al1 123.6(5), C6–N2–Al1 122.9(5), N1–Al1–N2 101.2(3), C11–Al1–C12 119.4(4).

phosphorus atom is two-coordinated and the two P–C bond lengths are very similar (P1–C1 178.6(2) pm; P1–C6 178.2(2) pm), indicating delocalization of the negative charge throughout the anion. Al1 shows a distorted tetrahedral coordination sphere. Both Al–N bonds are of the same length (av 192.2 pm). While an Al–N single bond in the three-coordinated triamide $Al[N(SiMe_3)_2]_3$[30] is 14 pm shorter than in **4**, the Al–N-donor bond in **3** is about 13 pm longer. Consequently, the Al–N bond order in **4** ranges between a single bond and a donor bond. A comparable Al–N bond distance is observed in the cationic bis[(2-pyridyl)bis(trimethylsilyl)methyl]-aluminum complex (av 192 pm).[31] As in **4**, the phosphorus atom in $Me_2Al(\mu\text{-}NMes^*)_2P$ is only two-coordinated. The Al–N distance in the AlN_2P ring system is 6 pm longer than in **4**.[32] The Al–C bond lengths (av 195.4 pm) are in accordance with those in related systems.[33]

Figure 5 illustrates the deviation from planarity in contrast to the lithium derivative **2**. Both pyridyl ring planes intersect at an angle of 155°. Therefore, the methyl groups are chemically nonequivalent in the solid state. Nevertheless, ^1H and ^{13}C NMR spectra from solution show only a single signal at room temperature for both methyl groups. Not even cooling the solution to −80 °C reveals two different signals in the NMR spectrum. The C–P–C angle in **4** is 4° more acute than in **2**. The intramolecular N···N distance (the "bite") of the ligand differs in both compounds (**2**, 306.4 pm; **4**, 292.2 pm). Hence, the ligand shows coordination flexibility toward different metal centers, while not giving up the full conjugation.

Crystal Structure of 5. Replacement of the phosphorus atom by an arsenic atom does not change the basic structural features. **5** is isostructural with **4** in the solid state (Figure 4). Like the phosphorus atom in **4**, the arsenic atom in **5** is two-coordinated. The As–C bonds (av 190.1 pm) are very short compared to

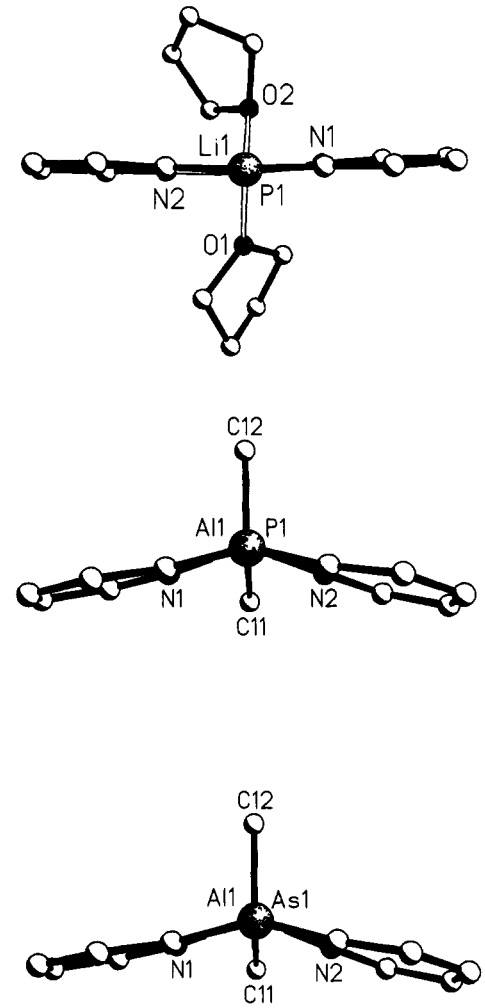

Figure 5. View along the E–M axes of **2**, **4**, and **5** illustrating the deviation from planarity.

the 8 pm longer As–C bonds in dioxane-solvated sodium diphenylarsenide.[34] Two-coordinated arsenic atoms in delocalized carbon ring systems are known from arsabenzenes[35] (av As–C 185 pm) and the Cp-analogous arsolide anions[36] (av As–C 190 pm). The partial E–C double bond character in **5** corresponds to that in the phosphorus derivative **4**. In comparison to that, the As–C double bond distances in arsaalkenes on average are 182 pm.[37] The aluminum atom in **5** shows the same coordination pattern as in **4** (av Al–N 192.8 pm; Al–C 194.3 pm). There is also a noticeable deviation from planarity of the ligand (Figure 5). Both planes of the pyridyl rings intersect at the same value as in **4** (155°). The N···N distance of the ligand is 298 pm. As in **4**, the ligand shows coordination flexibility toward the metal center.

Comparison of Structural and Spectroscopical Data. Average values of equivalent bond lengths in the

(30) Sheldrick, G. M.; Sheldrick, W. S. *J. Chem. Soc. A* **1969**, 2279.
(31) Engelhardt, L. M.; Kynast, U.; Raston, C. L.; White, A. H. *Angew. Chem.* **1987**, *99*, 702; *Angew. Chem., Int. Ed. Engl.* **1987**, *26*, 681.
(32) Hitchcock, P. B.; Jasim, H. A.; Lappert, M. F.; Williams, H. D. *J. Chem. Soc., Chem. Commun.* **1986**, 1634.
(33) Kumar, R.; de Mel, S. J.; Oliver, J. P. *Organometallics* **1989**, *8*, 2488.
(34) (a) Belforte, A.; Calderazzo, F.; Morvillo, A.; Pelizzi, G.; Vitali, D. *Inorg. Chem.* **1984**, *23*, 1504. (b) Doak, G. O.; Freedman, D. *Synthesis* **1974**, 328.
(35) (a) Sanz, F.; Daly, J. J. *J. Chem. Soc., Dalton Trans.* **1973**, 511. (b) Wong, T. C.; Bartell, L. S. *J. Mol. Struct.* **1978**, *44*, 169.
(36) (a) Abel, E. W.; Nowell, I. W.; Modinos, G. J.; Towers, C. *J. Chem. Soc., Chem. Commun.* **1973**, 258. (b) Chiche, P. L.; Galy, J.; Thiollet, G.; Mathey, F. *Acta Crystallogr. Sect. B* **1980**, *36*, 1344.
(37) (a) Weber, L.; Meine, G.; Boese, R. *Angew. Chem.* **1986**, *98*, 463; *Angew. Chem., Int. Ed. Engl.* **1986**, *25*, 469. (b) Driess, M.; Pritzkow, H.; Sander, M. *Angew. Chem.* **1993**, *105*, 273; *Angew. Chem., Int. Ed. Engl.* **1993**, *32*, 283.

Table 1. Selected Bond Lengths (pm) of 2–5 [Chemically Equivalent Bonds Are Averaged (See Also Figure Captions)]

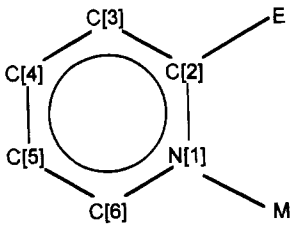

E = P, As

M = Li, Al

bond	2 (E = P, M = Li)	3 (E = P, M = Al) μ-Py	3 (E = P, M = Al) Py	4 (E = P, M = Al)	5 (E = As, M = Al)
E–C[2]	179.6	184.2	183.7	178.4	190.1
N[1]–C[2]	135.7	135.3	133.4	136.8	135.5
C[2]–C[3]	141.2	138.4	138.5	141.5	142.0
C[3]–C[4]	136.5	138.4	138.6	136.2	135.0
C[4]–C[5]	138.8	137.4	136.5	139.8	140.0
C[5]–C[6]	136.9	136.9	136.3	135.8	134.9
C[6]–N[1]	135.7	135.4	134.0	136.2	138.2
N[1]–M	196.9	205.7		192.1	192.8

Scheme 2

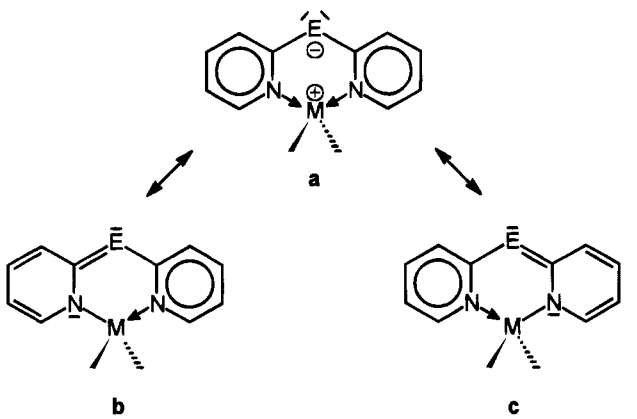

E = P, As

M = Li, Al, Ga

ligands of **2**, **4**, and **5** and in the coordinating and noncoordinating substituents of **3** are listed in Table 1. The pyridyl rings of **2**, **4**, and **5** exhibit alternating bond lengths. The C[3]–C[4] and C[5]–C[6] bond distances are significantly shorter than the C[2]–C[3] and C[4]–C[5] bond distances, indicating partial double bond localization in these positions.

In contrast to this, the corresponding values in **3** are almost alike, even in the ring coordinated to aluminum, demonstrating full conjugation. The C–N bond lengths are marginally longer in the $[Py_2E]^-$ anions than in the neutral donor molecule of **3**, indicating charge accumulation at the ring nitrogen atoms. As described above, the E–C bond lengths in the $[Py_2E]^-$ anions are almost halfway between the value of the E–C single bonds (as in **3**) and an E–C bond in heterobenzenes, with a formal bond order of 1.5. These observations permit a description of the bond situation in the $[Py_2E]^-$ ligands as illustrated in Scheme 2.

The partial negative charge at the central E atom (**a**) is partly delocalized from the p orbital of the sp^2-hybridized E atom onto both π-accepting pyridyl substituents (**b**, **c**). This delocalization is even more pronounced in the isoelectronic and isostructural complexes of $Me_2M(\mu\text{-}Py)_2CH$ (M = Al, Ga).[38] The central carbon atom is also regarded as sp^2-hybridized without any negative charge, whereas it is almost entirely located at both ring nitrogen atoms. Due to the even more striking delocalization in the $[HCPy_2]$ anion, it shows a quite rigid coordinational behavior toward different metals.

Table 2 compares the ^{13}C NMR shifts of **1**, **3**, **4**, **5** and **6**, and the corresponding $^nJ_{C-P}$ coupling constants of **1**, **3**, and **4**. It is worth noting the downfield shift of the C[2] nucleus in the monoanionic ligand of **4**–**6** relative to that in the neutral phosphine derivatives **1** and **3**. The partially negatively charged E and N atoms shield the C[2] position, while the inductive effect of the phosphorus atom in the neutral molecules causes a high field shift. In addition, the $^nJ_{C-P}$ coupling constants in **4** are much larger than in **1** and **3**, demonstrating an extensive delocalization of the negative charge throughout the whole $[Py_2E]^-$ unit and a partial double-bond character of the P–C bonds.

We could not succeed in preparing crystals of **6** suitable for X-ray structure analysis. However, it can be assumed that **5** and **6** have similar structures because their spectroscopic properties are very similar. Compared to the starting material, the highest energetic pyridyl ring deformation vibration in the IR spectrum of **5** and **6** is shifted to lower frequencies by coordination toward the metal centers (ν = 1570 (Py_3As), 1600 (**5**), 1595 (**6**) cm^{-1}).[28,39] The metal coordination causes also a high field shift of the [6]-H signal in the ^1H NMR spectrum of more than 1 ppm (δ 8.67 (Py_3As), 7.61 (**5**), 7.49 (**6**)).

Conclusion

The reaction of tris(2-pyridyl)phosphine and tris(2-pyridyl)arsine, respectively, with lithium metal leads to $(THF)_2Li(\mu\text{-}Py)_2E$ via cleavage of one E–aryl bond and ligand coupling yielding bipyridyl. Transmetalation reactions yield complexes of the composition $Me_2M(\mu$-

(38) (a) Gornitzka, H.; Stalke, D. *Organometallics* **1994**, *13*, 4398. (b) Gornitzka, H.; Stalke, D. *Angew. Chem.* **1994**, *106*, 695; *Angew. Chem., Int. Ed. Engl.* **1994**, *33*, 693.

(39) Anderegg, G.; Hubmann, E.; Wenk, F. *Helv. Chim. Acta* **1977**, *60*, 123.

Table 2. ^{13}C NMR Spectroscopic Shifts of 1–6 and J_{C-P} Coupling Constants (Hz) of 1, 3, and 4

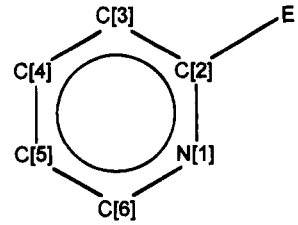

	$^nJ_{C-P}$ (Hz)	C[2], $n = 1$	C[3], $n = 2$	C[4], $n = 3$	C[5], $n = 4$	C[6], $n = 3$
1	δ	128.7	150.1	135.6	122.3	160.1
	($^nJ_{C-P}$)	(18.5)	(10.3)	(3.4)	(0)	(2.1)
3	δ	129.8	150.2	135.3	122.5	163.1
	($^nJ_{C-P}$)	(20.7)	(11.3)	(4.1)	(0)	(0)
4	δ	179.0	129.4	133.4	115.6	143.1
	($^nJ_{C-P}$)	(74.1)	(53.0)	(18.3)	(0)	(4.5)
5	δ	186.5	130.6	132.8	116.4	144.6
6	δ	185.7	130.6	132.8	116.7	144.6

$Py)_2E$ (M = Al, Ga). The hard metal centers are exclusively chelated by the pyridyl N atoms, leaving the E atom two-coordinated. The negative charge is largely delocalized throughout the whole $[Py_2E]^-$ anion. Nevertheless, this delocalization permits coordinational flexibility and deviation from planarity. It would be interesting to see what coordination properties these new $[Py_2P]^-$ ligands and also the mixed group 13/15 complexes **2** and **4–6** have toward soft *d*-block metal centers. This might prevent a route to hard–soft bimetallic reagents due to coordination site selective behavior.

Experimental Section

All manipulations were performed under an inert atmosphere of dry nitrogen gas with Schlenk techniques or in an argon drybox. Solvents were dried over Na/K alloy and distilled prior to use.

NMR spectra were obtained with a Bruker MSL 400 or AM 250 instrument. All NMR spectra were recorded in benzene-d_6 or $CDCl_3$ with $SiMe_4$, LiCl, and H_3PO_4 (85%) as external standards. EI and FI mass spectra were measured on Finnigan MAT 8230 or Varian MAT CH 5 instruments. Elemental analyses were obtained from the Analytische Labor des Instituts für Anorganische Chemie der Universität Göttingen.

1 (Py_2PH). Freshly rolled lithium wire (0.7 g, 100 mmol) is added to a solution of 12.8 g (50 mmol) of tris(2-pyridyl)-phosphine in 100 mL of THF. The deep crimson reaction mixture is stirred for 3 h at room temperature and filtered from the unreacted lithium metal. The THF is removed under vacuum, and the precipitate is redissolved in 100 mL of ether. Under ice cooling the solution is hydrolyzed with 50 mL of degassed water. The organic layer is separated, and the water phase is extracted twice with 50 mL of ether. From the joint organic phases the ether is removed under vacuum. The product is purified by distillation at reduced pressure (10^{-2} Torr). After the first runnings at 73 °C (2,2′-bipyridyl), the product is obtained at 110 °C as a crimson oil: yield 6.2 g, 66%; IR(film) ν (cm^{-1}) 3041 st, 2988, m, 2930 m, 2854 m, 2312 st, 1572 vst, 1559 st, 1450 vst, 1419 vst, 1278 m, 1152 st, 1946 st, 988 st, 883 m, 752 sst, 620 st, 519 st; ^1H NMR ($CDCl_3$) δ 5.44 (d, $^1J_{H-P}$ = 225 Hz, 1H, P-H), 7.0–8.6 (m, 8H, Py); ^{13}C NMR ($CDCl_3$) δ 122.3 (s, C[5]), 128.7 (d, $^1J_{C-P}$ = 18.5 Hz, C[2]), 135.6 (d, $^3J_{C-P}$ = 3.4 Hz, C[4]), 150.1 (d, $^2J_{C-P}$ = 10.3 Hz, C[3]), 160.1 (d, $^3J_{C-P}$ = 2.1 Hz, C[6]); ^{31}P NMR ($CDCl_3$) δ −34.1; MS(EI) *m/z* 188 (M^+, 100%), 109 (PyP, 92%); MS(FI) *m/z* 188 (M^+, 100%). Anal. Calcd (Found): C, 63.83 (64.42); H, 4.82 (4.60); N, 14.89 (14.41).

2 [$(THF)_2Li(\mu$-$Py)_2P$]. A solution of 2.2 mL of 2.3 M (5 mmol) *n*-butyllithium in *n*-hexane is added dropwise to 0.94 g (5 mmol) of **1** in 15 mL of THF. Slowly evaporating the solvent gives red crystals: yield 1.11 g (66%); decomposition > 50 °C; ^1H NMR (C_6D_6) δ 1.36 (8H, thf), 3.52 (8H, thf), 6.0–8.0 (m, 8H, ArH); ^7Li NMR (C_6D_6) δ 2.5; ^{31}P NMR (C_6D_6) δ 13.0.

3 ($Me_3Al(\mu$-$Py)PPy_2$). One gram (3.8 mmol) of tris(2-pyridyl)phosphane is dissolved in 15 mL of ether. To this solution is added 1.9 mL of 2.0 M trimethylaluminum solution in *n*-hexane (3.8 mmol) at room temperature. The pink reaction mixture is stirred for 3 days and filtered subsequently through a glass frit. Light red single crystals are obtained after storage of the filtrate for 1 day at −38 °C. The crystals are thermolabile and decompose instantaneously at ambient conditions. They were handled and transferred to the diffractometer at about −20 °C.[40] ^1H NMR (C_6D_6) δ 0.08 (s, 9H, Me), 6.52 (m, 3H, Py), 6.94 (m, 3H, Py), 7.46 (m, 3H, Py), 8.48 (m, 3H, Py); ^{13}C NMR (C_6D_6) δ 122.8 (s, C[5]), 129.8 (d, $^1J_{C-P}$ = 20.7 Hz, C[2]), 135.3 (d, $^3J_{C-P}$ = 4.1 Hz, C[4]), 150.2 (d, $^2J_{C-P}$ = 11.3 Hz, C[3]), 163.1 (s, C[6]); ^{31}P NMR (C_6D_6) δ −0.4.

4 ($Me_2Al(\mu$-$Py)_2P$). (a) First Route. **1** (1.13 g, 6 mmol) is dissolved in 10 mL of diethyl ether. A solution of 2.6 mL of 2.3 M (6 mmol) *n*-butyllithium in *n*-hexane is added at room temperature over a period of 30 min. After stirring for 2 h, the dark red reaction solution is cooled to −40 °C, and a solution of 6 mL of 1 M (6 mmol) dimethylaluminum chloride in *n*-hexane is added over a period of 1 h. The reaction solution is warmed to room temperature and stirred overnight. Lithium chloride is filtered off and 3 days of storage of the clear solution at 3 °C yielded dark red crystals.

(b) Second Route. **1** (3.76 g, 20 mmol) is suspended in 30 mL of *n*-hexane. After the mixture is cooled to −40 °C, a solution of 10 mL of 2 M trimethylaluminum in *n*-hexane (20 mmol) is added over a period of 30 min. The reaction solution is allowed to warm to room temperature and stirred overnight. After the organic solvent is evaporated, **3** is obtained as a crude product in a yield of 90%, which can be purified by recrystallization in a solution of *n*-hexane/diethyl ether at 3 °C: mp 105 °C; ^1H NMR (C_6D_6) δ −0.36 (s, 6H, CH_3), 5.94 (dddd, $^3J_{5,4}$ = 7.0, $^3J_{5,6}$ = 6.1, $^4J_{5,3}$ = 1.3, $^5J_{5,P}$ = 0.5 Hz, 2H, 5-H), 6.37 (dddd, $^3J_{4,3}$ = 8.6, $^3J_{4,5}$ = 7.0, $^4J_{4,6}$ = 1.6, $^4J_{4,P}$ = 1.0 Hz, 2H, 4-H), 7.30 (dddd, $^3J_{3,P}$ = 10.0, $^3J_{3,4}$ = 8.6, $^4J_{3,5}$ = 1.3, $^5J_{3,6}$ = 1.0 Hz, 2H, 3-H), 7.49 (dddd, $^3J_{6,5}$ = 6.1, $^4J_{6,4}$ = 1.6, $^4J_{6,P}$ = 1.0, $^5J_{6,3}$ = 1.0 Hz, 2H, 6-H); ^{13}C NMR (C_6D_6) δ −12.1 (s, CH_3), 115.6 (s, C[5]), 129.4 (d, $^2J_{C-P}$ = 53.0 Hz, C[3]), 133.4 (d, $^3J_{C-P}$ = 18.3 Hz, C[4]), 143.1 (d, $^3J_{C-P}$ = 4.5 Hz, C[6]), 179.0 (d, $^1J_{C-P}$ = 74.1 Hz, C[2]); ^{31}P NMR (C_6D_6) δ 25.7; MS(EI) *m/z* 244 (M^+, 85%). Anal. Calcd (Found): 59.02 (58.79); H, 5.78 (5.43); N, 11.47 (11.89).

5 ($Me_2Al(\mu$-$Py)_2As$). To a solution of 3.3 g (10.7 mmol) of $AsPy_3$ in 100 mL of THF is added 0.15 g (21.4 mmol) of freshly rolled lithium wire. The deep purple reaction mixture is

(40) Kottke, T.; Stalke, D. *J. Appl. Crystallogr.* **1993**, *26*, 615.

Table 3. Crystal Data of 2–5

	2	3	4	5
formula	$C_{18}H_{24}LiN_2O_2P$	$C_{18}H_{21}AlN_3P$	$C_{12}H_{14}AlN_2P$	$C_{12}H_{14}AlAsN_2$
fw	338.3	337.3	244.2	288.2
cryst size (mm)	0.4 × 0.3 × 0.2	0.6 × 0.5 × 0.4	0.5 × 0.3 × 0.3	0.5 × 0.5 × 0.2
space group	$Pna2_1$	$P2_1/c$	$P2_1/c$	$P2_1/c$
a (pm)	1791.7(1)	1282.3(3)	1060.08(7)	1065.7(5)
b (pm)	935.69(7)	1877.6(5)	864.42(6)	863.6(5)
c (pm)	1085.0(1)	788.3(2)	1414.91(9)	1423.8(7)
β (deg)	90	102.26(3)	104.968(5)	104.56(4)
V (nm^3)	1.8191(1)	1.8547(8)	1.2526(1)	1.268(1)
Z	4	4	4	4
temp (K)	153(2)	153(2)	153(2)	153(2)
ϱ_c (Mgm^{-3})	1.235	1.208	1.295	1.509
μ (mm^{-1})	0.162	0.198	0.263	2.723
F(000)	720	712	512	584
2θ range (deg)	8–45	8–55	8–60	8–45
no. of reflns measd	2628	5799	6370	3241
no. of unique reflns	2386	4276	3676	1624
no. of restraints	70	0	0	0
refined param	259	208	201	147
R1 [$I > 2\sigma(I)$]	0.045	0.057	0.040	0.061
wR2[a] (all data)	0.100	0.162	0.111	0.177
g_1; g_2[b]	0.022; 1.959	0.094; 0.833	0.059; 0.175	0.112; 2.552
highest diff peak (10^{-6} e pm^{-3})	0.17	0.41	0.47	0.75

[a] $wR2 = \{[\sum w(F_c^2 - F_o^2)^2]/[\sum w(F_o^2)^2]\}^{1/2}$. [b] $w^{-1} = \sigma^2(F_o^2) + (g_1P)^2 + g_2P$; $P = [F_o^2 + 2F_c^2]/3$.

Table 4. Atomic Coordinates (×10^4) and Equivalent Isotropic Displacement Parameters (pm^2 × 10^{-1}) for 2

	x	y	z	U(eq)[a]
P(1)	8400(1)	654(1)	8727(1)	34(1)
Li(1)	9446(4)	−1788(7)	10640(7)	33(4)
N(1)	8773(2)	−2216(4)	9253(3)	30(2)
N(2)	9325(2)	293(4)	10820(3)	30(2)
C(1)	8421(2)	−1249(4)	8526(4)	29(2)
C(2)	8018(3)	−1734(5)	7491(4)	41(3)
C(3)	7953(3)	−3152(6)	7225(4)	45(3)
C(4)	8308(3)	−4140(5)	7984(5)	44(3)
C(5)	8696(2)	−3618(5)	8968(5)	36(3)
C(6)	8906(2)	1156(4)	10090(4)	27(2)
C(7)	8859(2)	2628(5)	10371(4)	34(3)
C(8)	9224(3)	3203(5)	11338(4)	39(3)
C(9)	9665(3)	2332(5)	12070(4)	39(3)
C(10)	9691(3)	900(5)	11783(4)	36(3)
O(1)	10481(2)	−2319(3)	10441(3)	36(2)
C(11)	11068(2)	−1321(5)	10193(5)	42(3)
C(12)	11710(5)	−2187(9)	9728(16)	60(8)
C(13)	11614(4)	−3547(10)	10447(19)	66(8)
C(14)	10776(3)	−3734(5)	10413(6)	57(3)
C(12′)	11779(3)	−2182(7)	10300(9)	60(4)
C(13′)	11534(3)	−3626(3)	9856(8)	63(5)
O(2)	9185(2)	−2967(3)	12042(3)	38(2)
C(15)	9633(3)	−3048(5)	13134(4)	42(3)
C(16)	9174(3)	−2442(6)	14162(4)	56(4)

[a] U(eq) is defined as one-third of the trace of the orthogonalized U_{ij} tensor.

Table 5. Atomic Coordinates (×10^4) and Equivalent Isotropic Displacement Parameters (pm^2 × 10^{-1}) for 3

	x	y	z	U(eq)[a]
P(1)	6806(1)	9692(1)	1738(1)	31(1)
Al(1)	7962(1)	11288(1)	2187(1)	36(1)
N(1)	8234(1)	10489(1)	4014(2)	30(1)
N(2)	5770(2)	8645(1)	3224(4)	54(1)
N(3)	8441(1)	8833(1)	1340(2)	35(1)
C(1)	7786(2)	9834(1)	3784(3)	29(1)
C(2)	8051(2)	9308(1)	5030(3)	38(1)
C(3)	8798(2)	9446(1)	6538(3)	42(1)
C(4)	9266(2)	10108(1)	6762(3)	40(1)
C(5)	8964(2)	10612(1)	5499(3)	37(1)
C(6)	5701(2)	9305(1)	2593(3)	35(1)
C(7)	4811(2)	9729(2)	2543(3)	44(1)
C(8)	3958(2)	9452(2)	3160(4)	59(1)
C(9)	4021(2)	8777(2)	3780(4)	64(1)
C(10)	4930(2)	8400(2)	3812(5)	69(1)
C(11)	7378(2)	8901(1)	923(3)	31(1)
C(12)	6733(2)	8450(1)	−244(3)	48(1)
C(13)	7202(2)	7902(1)	−987(4)	57(1)
C(14)	8293(2)	7826(1)	−553(4)	50(1)
C(15)	8869(2)	8296(1)	602(3)	42(1)
C(16)	8882(3)	12068(2)	3340(4)	68(1)
C(17)	6436(2)	11548(2)	1722(4)	58(1)
C(18)	8504(2)	10886(1)	238(3)	42(1)
C(17)	8438(3)	−2021(5)	13585(5)	55(3)
C(18)	8423(2)	−2866(6)	12418(4)	49(3)

[a] U(eq) is defined as one-third of the trace of the orthogonalized U_{ij} tensor.

stirred for 3 h at room temperature and subsequently filtered from the not reacted lithium metal through a glass frit. THF is removed under vacuum and replaced by the equivalent amount of toluene. At −78 °C 10.7 mL of a 1 M solution of dimethylaluminum chloride in *n*-hexane (10.7 mmol) is added dropwise. The deep purple solution is warmed to room temperature overnight. The solution is filtered over Celite and separated from lithium chloride. Toluene is removed in vacuum, and the precipitate is washed twice with 10 mL of pentane. The product is recrystallized from an ether/*n*-hexane solution. X-ray suitable single crystals were obtained as needles: mp 125 °C; yield 23.1 g (75%); IR(Nujol) ν (cm^{-1}) 1600 st, 1533 m, 1511 st, 1453 st, 1399 st, 1129 st, 1076 m, 1054 m, 1015 m, 972 st, 749 st, 697 st, 572 m; ^{1}H NMR (C_6D_6) δ −0.32 (s, 6H, Me), 5.95 (ddd, $^3J_{H-[4]H}$ = 7.0, $^3J_{H-[6]H}$ = 6.1, $^4J_{H-[3]H}$ = 1.3 Hz, 2H, [5]H), 6.28 (ddd, $^3J_{H-[3]H}$ = 8.5, $^3J_{H-[5]H}$ = 7.0, $^4J_{H-[6]H}$ = 1.7 Hz, 2H, [4]H), 7.39 (ddd, $^3J_{H-[4]H}$ = 8.5, $^4J_{H-[5]H}$ = 1.3, $^5J_{H-[6]H}$ = 1.0 Hz, 2H, [3]H), 7.61 (ddd, $^3J_{H-[5]H}$ = 6.1, $^4J_{H-[4]H}$ = 1.7, $^5J_{H-[3]H}$ = 1.0 Hz, 2H, [6]H); ^{13}C NMR (C_6D_6) δ −12.2 (s, Me), 116.4 (s, C[5]), 130.6 (s, C[3]), 132.8 (s, C[4]), 144.6 (s, C[6]), 186.5 (s, C[2]); MS(EI) *m/z* 288 (M^+, 19%), 273 (M^+ − Me, 100%), 258 (M^+ − 2Me, 12%). Anal. Calcd (Found): C, 50.02 (49.28); H, 4.90 (4.76); N, 9.72 (10.04).

6 ($Me_2Ga(\mu$-Py$)_2As$). To a solution of 1.0 g (3.2 mmol) of $AsPy_3$ in 100 mL of THF is added 50 mg (6.4 mmol) of freshly rolled lithium wire. The deep purple reaction mixture is stirred for 3 h at room temperature and filtered from the remaining lithium metal. THF is removed under vacuum and replaced by the equivalent amount of toluene. At −78 °C a solution of 600 mg (3.2 mmol) of dimethylgallium chloride in 10 mL of *n*-hexane is added dropwise. The deep purple solution is warmed to room temperature overnight under stirring. Then the solution is filtered over Celite and separated

Table 6. Atomic Coordinates (×10⁴) and Equivalent Isotropic Displacement Parameters (pm² × 10⁻¹) for 4

	x	y	z	U(eq)[a]
P(1)	2701(1)	2064(1)	9020(1)	31(1)
Al(1)	2691(1)	4698(1)	7123(1)	24(1)
N(1)	2920(1)	5188(2)	8483(1)	25(1)
N(2)	1619(1)	2890(1)	7046(1)	24(1)
C(1)	3017(1)	4088(2)	9194(1)	26(1)
C(2)	3410(2)	4574(2)	10184(1)	33(1)
C(3)	3679(2)	6083(2)	10425(1)	39(1)
C(4)	3542(2)	7191(2)	9686(1)	37(1)
C(5)	3164(2)	6698(2)	8742(1)	32(1)
C(6)	1788(1)	1822(2)	7781(1)	25(1)
C(7)	1142(2)	387(2)	7568(1)	30(1)
C(8)	294(2)	103(2)	6681(1)	33(1)
C(9)	68(2)	1254(2)	5967(1)	32(1)
C(10)	751(2)	2594(2)	6167(1)	29(1)
C(11)	1642(2)	6284(2)	6294(1)	35(1)
C(12)	4389(2)	4136(2)	6927(1)	35(1)

[a] U(eq) is defined as one-third of the trace of the orthogonalized U_{ij} tensor.

Table 7. Atomic Coordinates (×10⁴) and Equivalent Isotropic Displacement Parameters (pm² × 10⁻¹) for 5

	x	y	z	U(eq)[a]
As(1)	2264(1)	1924(1)	5952(1)	34(1)
Al(1)	2314(2)	4658(3)	7851(2)	27(1)
N(1)	2076(6)	5178(7)	6496(4)	29(2)
N(2)	3406(6)	2861(7)	7961(4)	24(1)
C(1)	1981(7)	4113(8)	5789(5)	23(2)
C(2)	1578(7)	4626(11)	4805(6)	38(2)
C(3)	1301(7)	6121(11)	4580(6)	37(2)
C(4)	1456(7)	7215(10)	5333(6)	35(2)
C(5)	1835(7)	6725(9)	6258(6)	32(2)
C(6)	3246(7)	1759(8)	7256(5)	22(2)
C(7)	3929(7)	356(9)	7501(6)	33(2)
C(8)	4761(7)	105(9)	8388(6)	32(2)
C(9)	4967(7)	1304(9)	9069(5)	29(2)
C(10)	4285(8)	2631(10)	8842(5)	30(2)
C(11)	3321(8)	6258(10)	8665(6)	38(2)
C(12)	637(8)	4074(10)	8040(6)	36(2)

[a] U(eq) is defined as one-third of the trace of the orthogonalized U_{ij} tensor.

from lithium chloride. Toluene is removed in vacuum. The precipitate is washed twice with 5 mL of *n*-pentane. The product is a black violet solid: mp 65 °C; yield 0.70 g (66%); IR(Nujol) ν (cm^{-1}) 1595 st, 1534 m, 1516 st, 1399 st, 1160 m, 1111 st, 1071 m, 1053 m, 1010 m, 980 st, 749 st, 717 st, 690 m, 580 m; ^1H NMR (C_6D_6) δ −0.03 (s, 6H, Me), 5.98 (dd, $^3J_{H-[4]H}$ = 7.0, $^3J_{H-[6]H}$ = 5.5 Hz, 2H, [5]H), 6.34 (dd, $^3J_{H-[3]H}$ = 8.3, $^3J_{H-[5]H}$ = 7.0 Hz, 2H, [4]H), 7.40 (d, $^3J_{H-[4]H}$ = 5.5 Hz, 2H, [6]H), 7.49 (d, $^3J_{H-[5]H}$ = 8.3 Hz, 2H, [3]H); ^{13}C NMR (C_6D_6) δ −10.1 (s, Me), 116.7 (s, C[5]), 130.6 (s, C[3]), 132.8 (s, C[4]), 144.6 (s, C[6]), 185.7 (s, C[2]); MS(EI) *m/z* 330 (M^+, 26%), 315 (M^+ − Me, 100%), 300 (M^+ − 2Me, 25%). Anal. Calcd (Found): C, 43.56 (43.23); H, 4.26 (3.91); N, 8.47 (8.64).

X-ray Measurements of 2−5. All data were collected at low temperature using an oil-coated shock-cooled crystal[40] on a Stoe-Siemens AED with MoKα (λ = 71.073 pm) radiation. The structures were solved by direct methods using SHELXS-90[41] and refined with all data on F^2 with a weighting scheme of $w^{-1} = \sigma^2(F_o^2) + (g_1P)^2 + g_2P$ with $P = (F_o^2 + 2F_c^2)/3$ using SHELXL-93.[42] Refinement of the Flack x parameter[43] [x = −0.09(18), where x = 0 for the correct absolute structure and +1 for the inverted structure] confirmed the absolute structure of **2**. The *twist* disorder of the β-carbon atoms of the THF molecule around O1 was successfully defined to two positions using distance and ADP similarity restraints. The site occupation factor of the main component refined to 68%. Selected bond lengths and angles of **2−5** can be found in Table 1, relevant crystallographic data for **2−5** in Table 3, and fractional coordinates of **2−5** in Tables 4−7.

Acknowledgment. We thank the Deutsche Forschungsgemeinschaft and the Fonds der Chemischen Industrie for financial support.

Supplementary Material Available: Tables of crystal data, fractional coordinates, and bond lengths and angles, fully labeled figures of 50% anisotropic displacement parameters of the structures **2−5**, and tables of anisotropic displacement parameters and hydrogen atom coordinates of **2−5** (27 pages). Ordering information is given on any current masthead page.

OM9500578

(41) Sheldrick, G. M. *Acta Crystallogr. Sect. A* **1990**, *46*, 467.
(42) Sheldrick, G. M. SHELXL-93 program for crystal structure refinement, 1993, Universität Göttingen.
(43) Flack, H. D. *Acta Crystallogr. Sect. A* **1983**, *39*, 876.

Heterobimetallic Indenyl Complexes. The *trans*–*cis* Isomerization of $Cr(CO)_3(\mu,\eta{:}\eta$-indenyl)Rh(NBD)

Chiara Bonifaci, Alberto Ceccon,* Alessandro Gambaro, Paolo Ganis,† and Saverio Santi

Dipartimento di Chimica Fisica, Università di Padova, Via Loredan 2, 35131 Padova, Italy

Alfonso Venzo

CNR, Centro di Studio sugli Stati Molecolari, Radicalici ed Eccitati, Via Loredan 2, 35131 Padova, Italy

Received October 11, 1994®

Reaction of *trans*-[$Cr(CO)_3(\mu,\eta{:}\eta$-indenyl)$Rh(CO)_2$] at room temperature in CH_2Cl_2 with norbornadiene (NBD) yields *trans*-[$Cr(CO)_3(\mu,\eta{:}\eta$-indenyl)Rh(NBD)], **3**. X-ray analysis for **3** shows a = 8.200(5) Å, b = 11.388(5) Å, c = 17.868 Å, β = 92.1°, space group $P2_1/c$. In contrast with the *cis*-[$Cr(CO)_3(\mu,\eta{:}\eta$-indenyl)Rh(NBD)], **2**, isomer, the indenyl moiety in **3** is far less distorted, and the planes defined by [C_1, C_2, C_3] of the indenyl frame and by [C_{11}, C_{12}, C_{14}, C_{15}] of NBD are almost exactly parallel to each other, showing an undistorted coordination about the rhodium atom. Under suitable conditions (THF as solvent in the presence of the tetrafluoroborate salt of $[Rh(NBD)]^+$, or a similar cation species) **3** undergoes a fast intramolecular rearrangement to give the isomer *cis*-[$Cr(CO)_3(\mu,\eta{:}\eta$-indenyl)Rh(NBD)], **2**. The process exhibits a relatively low activation enthalpy ($\Delta H^{\ddagger}$ = 11.7 ± 0.9 kcal mol^{-1}) and a very negative activation entropy ($\Delta S^{\ddagger}$ = −30 ± 3 cal mol^{-1} K^{-1}).

Introduction

The synthesis of dinuclear complexes in which two inorganic units are coordinated to the same ligand ("bridging ligand") has been achieved successfully in recent years. Usually, the two metals reside on the same side of the ligand plane (*i.e.* in a *cis* stereochemistry) that often results in the formation of a metal–metal bond.[1] Some binuclear complexes of *trans* stereochemistry were also obtained, with either monocyclic[1a,1b,2] or bicyclic[2–4] bridging ligands.

Recently, we were able to synthesize *trans*-[$Cr(CO)_3$-($\mu,\eta{:}\eta$-indenyl)Rh(COD)], **1**, by reacting the (η^6-indenyl)-$Cr(CO)_3$ potassium salt with [$Rh(\mu$-Cl)$COD]_2$ in THF at −30 °C.[4] Surprisingly, when the same anion was quenched with [$Rh(\mu$-Cl)$NBD]_2$ under identical conditions, the only product isolated was *cis*-[$Cr(CO)_3(\mu,\eta{:}\eta$-indenyl)Rh(NBD)], **2**,[5] showing that the structure of the ancillary ligand at rhodium plays an important role in determining the stereochemistry of the reaction product. Compounds **1** and **2** may now serve as starting materials for the preparation of other *trans* and *cis* complexes, respectively, as ligand exchange at rhodium occurs without changing the molecular stereochemistry.[5,6]

In this paper we report the preparation of the new complex *trans*-[$Cr(CO)_3(\mu,\eta{:}\eta$-indenyl)Rh(NBD)], **3**, *i.e.*, the *trans* isomer of **2**. The availability of this compound allowed us to make a direct comparison between the structural characteristics of the *trans* and those of the *cis* isomer. In addition, we found that the *trans* isomer rearranges intramolecularly to the *cis* isomer, and we have studied the kinetics of this rearrangement. The results are reported below.

Results and Discussion

Bubbling CO through a CH_2Cl_2 solution of **1** at room temperature produced *trans*-[$Cr(CO)_3(\mu,\eta{:}\eta$-indenyl)Rh-$(CO)_2$] in quantitative yield.[6] This compound was converted quantitatively into **3** within a few minutes by treating a CH_2Cl_2 solution with excess NBD at room temperature, as indicated by IR, NMR, and mass spectrometric measurements (see Experimental Sec-

* To whom correspondance should be addressed.
† On sabbatical leave from University of Napoli, Italy.
® Abstract published in *Advance ACS Abstracts,* March 15, 1995.

(1) (a) Geiger, W. E.; Salzer, A.; Edwin, J.; von Philipsborn, W.; Piantini, U.; Rheingold, A. L. *J. Am. Chem. Soc.* **1990**, *112*, 7113. (b) Bieri, J. H.; Egolf, T.; von Philipsborn, W.; Piantini, U.; Prewo, R.; Ruppli, U.; Salzer, A. *Organometallics*, **1986**, *5*, 2413. (c) Heck, J.; Rist, G. *J. Organomet. Chem.* **1985**, *286*, 183. (d) Astley, S. T.; Takats, J. *J. Organomet. Chem.* **1989**, *363*, 167. (e) Edelmann, F.; Kiel, G.-Y.; Takats, J.; Vasudevamurthy, A.; Yeung, M.-Y. *J. Chem. Soc., Chem. Commun.* **1988**, 296. (f) Edelmann, F.; Takats, J. *J. Organomet. Chem.* **1988**, *344*, 351. (g) Ball, R. G.; Edelmann, F.; Kiel, G.-Y.; Takats, J.; Drwes, R. *Organometallics* **1986**, *5*, 829. (h) Bennet, M. J.; Prat, J. L.; Simpson, K. A.; LiShing Man, L. K. K.; Takats, J. *J. Am. Chem. Soc.* **1976**, *98*, 4810. (i) Jonas, K.; Koepe, G.; Schieferstein, L.; Mynott, R.; Krüger, C.; Tasy, Y.-H. *Angew. Chem., Int. Ed. Engl.* **1983**, *22*, 620. *Angew. Chem. Suppl.* **1983**, 920. (j) Duff, A. W.; Jonas, K.; Goddard, R.; Kraus, H.-J.; Krüger, C. *J. Am. Chem. Soc.* **1983**, *105*, 5479. (k) Jonas, K.; Wiskamp, V.; Tsay, Y.-H.; Krüger, C. *J. Am. Chem. Soc.* **1983**, *105*, 5480. (l) Jonas, K.; Rüsseler, W.; Angermund, K.; Krüger, C. *Angew. Chem., Int. Ed. Engl.* **1986**, *25*, 927. (m) Behrens, U.; Heck, J.; Maters, M.; Frenzen, G.; Roelofsen, A.; Sommerdijk, H. T. *J. Organomet. Chem.* **1994**, *475*, 233. (n) Airoldi, M.; Deganello, G.; Gennaro, G.; Moret, M.; Sironi, A. *Organometallics* **1993**, *12*, 3964.
(2) Jonas, K. *Pure Appl. Chem.* **1990**, *62*, 1169 and references therein.
(3) (a) Green, M. L. H.; Lowe, N. D.; O'Hare, D. J. *J. Chem. Soc., Chem. Commun.* **1986**, 1547. (b) Bennett, M. A.; Neumann, H.; Thomas, M.; Wang, X. *Organometallics* **1991**, *10*, 3237. (c) Schulz, H.; Pritzkow, H.; Siebert, W. *Chem. Ber.* **1992**, *125*, 987. (d) Klein, H. F.; Hammerschmitt, B.; Lull, G.; Flörke, U.; Haupt, H. J., *Inorg. Chim. Acta* **1994**, *218*, 143. (e) Kudinov, A. R.; Petrovskii, P. V.; Struchkov, Yu. K.; Yanovskii, A. I.; Rybinskaya, M. I. *J. Organomet. Chem.* **1991**, *412*, 91.
(4) Ceccon, A.; Gambaro, A.; Santi, S.; Valle, G.; Venzo, A. *J. Chem. Soc., Chem. Commun.* **1989**, 51.
(5) Bonifaci, C.; Ceccon, A.; Gambaro, A.; Ganis, P.; Santi, S.; Valle, G.; Venzo, A. *Organometallics* **1993**, *12*, 4211.
(6) Ceccon, A.; Gambaro, A.; Santi, S.; Venzo, A. *J. Mol. Catal.* **1991**, *69*, L1-L6.

0276-7333/95/2314-2430$09.00/0

Table 1. Selected Bond Distances (Å) and Angles (deg) of *cis*-[Cr(CO)$_3$IndRh(NBD)], 2, *trans*-[Cr(CO)$_3$IndRh(NBD)], 3, and IndRh(NBD), 4

	Rh−C$_{1,3}$[a]	Rh−C$_2$[a]	Rh−C$_{3a,7a}$[a]	Cr−C$_{4,7}$[a]	Cr−C$_{5,6}$[a]	Cr−C$_{3a,7a}$	C$_{3a}$−C$_{7a}$	$\Delta\overline{MC}$[b]	$\Delta\overline{MC}$*[c]	HA (Cp)[d]	HA (Bz)[e]	θ[f]
2[g]	2.244	2.164	2.560	2.264	2.202	2.468	1.456	0.316	0.342	≃12	≃11	≃23
3[h]	2.253	2.248	2.339	2.246	2.226	2.320	1.469	0.087	0.088	≃6	≃6	≃3
4[g]	2.226	2.240	2.395				1.42	0.169	0.164	≃10	≃1	≃1

[a] Mean values of the distances between the metal and the indicated carbon atoms. [b] $\Delta\overline{M-C}$ = {[(Rh−C$_{3a}$) + (Rh−C$_{7a}$)]/2 − [(Rh−C$_1$) + (Rh−C$_3$)]/2} (Å). [c] $\Delta\overline{M-C}$* = {[(Rh−C$_{3a}$) + (Rh−C$_{7a}$)]/2 − [(Rh−C$_1$) + (Rh−C$_2$) + (Rh−C$_3$)]/3} (Å). [d] HA (Cp) = [C$_1$, C$_2$, C$_3$]∠[C$_3$, C$_{3a}$, C$_4$, C$_7$, C$_{7a}$, C$_1$] (deg). [e] HA (Bz) = [C$_4$, C$_5$, C$_6$, C$_7$]∠[C$_3$, C$_{3a}$, C$_4$, C$_7$, C$_{7a}$, C$_1$] (deg). [f] θ = [C$_1$, C$_2$, C$_3$]∠[C$_{11}$, C$_{12}$, C$_{14}$, C$_{15}$] (deg). [g] Data from ref 5. [h] Data of this work.

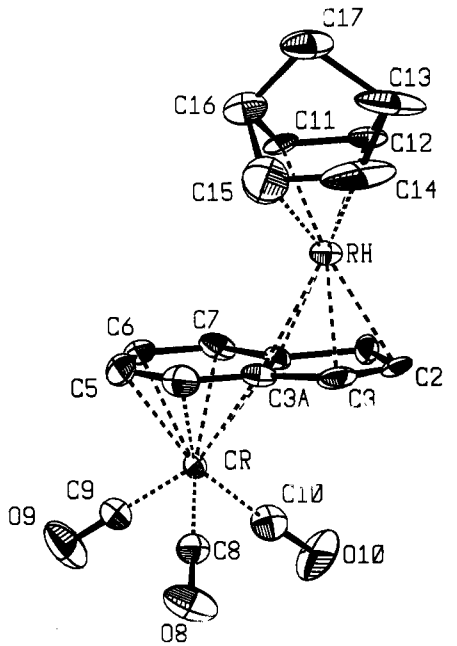

Figure 1. ORTEP view of **3**. Selected bond lengths (Å): Rh−C$_1$ 2.270(4), Rh−C$_2$ 2.248(5), Rh−C$_3$ 2.235(5), Rh−C$_{3a}$ 2.334(5), Rh−C$_{7a}$ 2.344(4), Cr−C$_{3a}$ 2.351(5), Cr−C$_4$ 2.237(5), Cr−C$_5$ 2.214(5), Cr−C$_6$ 2.197(5), Cr−C$_7$ 2.255(4), Cr−C$_{7a}$ 2.359(4), C$_1$−C$_2$ 1.397(7), C$_2$−C$_3$ 1.425(7), C$_3$−C$_{3a}$ 1.446(7), C$_{3a}$−C$_{7a}$ 1.469(6), C$_1$−C$_{7a}$ 1.454. Bond angles (deg): C$_8$−Cr−C$_9$ 88.2(2), C$_8$−Cr−C$_{10}$ 87.9(2), C$_9$−Cr−C$_{10}$ 89.3(2), Cr−C$_8$−O$_8$ 178.7(4), Cr−C$_9$−O$_9$ 178.9(6), Cr−C$_{10}$−O$_{10}$ 178.0(5). Torsion angles (deg): C$_9$−Cr−*P*−C$_6$ 11.8, C$_8$−Cr−*P*−C$_4$ 14.0, C$_{10}$−Cr−*P*−C$_{7a}$ 10.7 (*P* designates the location of the center of the benzene ring).

tion). Orange crystals suitable for X-ray analysis were obtained from CH_2Cl_2−pentane solutions.

Figure 1 shows the molecular structure of complex **3**, together with some relevant geometrical parameters. The distances from rhodium to the carbon atoms of the five-membered ring of the indenyl ligand indicate a distorted η^5-coordination of rhodium similar to that found for several monometallic (η-indenyl)RhL$_2$ complexes.[7] This distortion arises from the puckering of the [C$_1$, C$_2$, C$_3$] plane with respect to the remainder of the indenyl group, the corresponding hinge angle being *ca.* 6°. The distances Rh−C$_{3a}$ = 2.334(5) Å and Rh−C$_{7a}$ = 2.344(4) Å are about 0.1 Å longer than the distances Rh−C$_1$ = 2.270(4) Å, Rh−C$_2$ = 2.248(5) Å, and Rh−C$_3$ = 2.235(5) Å. As a consequence, the $\Delta\overline{M-C}$ parameter[7c,d,i] ($\Delta\overline{M-C}$ = {[(Rh−C$_{3a}$) + (Rh−C$_{7a}$)]/2 − [(Rh−C$_1$) + (Rh−C$_3$)]/2}, Å) amounts to 0.087 Å, and most of the distortion can be traced to ring folding rather than "slippage".

The planes defined by [C$_1$, C$_2$, C$_3$] of the indenyl frame and by [C$_{11}$, C$_{12}$, C$_{14}$, C$_{15}$] of NBD are approximately parallel to each other, showing an undistorted coordination about the Rh atom. Also, the distances from chromium to the ring-junction carbons C$_{3a}$ and C$_{7a}$ are longer than those from chromium to the other carbon atoms of the benzene ring. The plane defined by [C$_4$, C$_5$, C$_6$, C$_7$] forms a hinge angle of *ca.* 6° with the planar frame [C$_3$, C$_{3a}$, C$_4$, C$_7$, C$_{7a}$, C$_1$], showing, therefore, that the puckering of the benzene ring due to its coordination with Cr(CO)$_3$ is comparable in magnitude with that induced by rhodium coordination to the five-membered ring.

The comparison between the structural characteristics of *cis* and *trans* isomers is instructive. Selected parameters and bond distances of **2** and **3** are listed in Table 1, together with the corresponding data for monometallic IndRh(NBD), **4**. The data in Table 1 show that (*i*) the Rh−C$_1$ and Rh−C$_3$ distances in the three complexes are quite similar; on the other hand, the Rh−C$_2$ distance, which is almost equal for **3** and **4**, appears to be markedly shorter in the case of the *cis* isomer **2**. The slippage of rhodium toward the C$_2$ carbon atom is, therefore, more pronounced when the two metals are coordinated to the same side of the ligand plane. The *cis* arrangement of the metals is also responsible for the longer average distance of rhodium from the C$_{3a}$ and C$_{7a}$ atoms observed (2.560(5) Å) in comparison with that found in the *trans* isomer **3** (2.350(6) Å) and in the monometallic complex **4** (2.394(9) Å). The ring slippage parameter $\Delta\overline{M-C}$ describes well these structural differences in the indenyl complexes. It can be seen from the data reported in column 9 of Table 1 that the $\Delta\overline{M-C}$ values change in the order **2** ≫ **4** > **3**, indicating that rhodium coordination to the Cp ring is the least distorted in the *trans* complex and that the distortion is noticeably increased in the case of the *cis* isomer, as confirmed by the values of the hinge angles (columns 11 and 12). Taking into account also the Rh−C$_2$ bond distance, the new parameter can be defined $\Delta\overline{M-C}$* = {[(Rh−C$_{3a}$) + (Rh−C$_{7a}$)]/2 − [(Rh−C$_1$) + (Rh−C$_2$) + (Rh−C$_3$)]/3} (Å); it exhibits practically the same value of $\Delta\overline{M-C}$ in the case of **3** and **4**, while it is noticeably greater in the case of **2** ($\Delta\overline{M-C}$* = 0.342, $\Delta\overline{M-C}$ = 0.316) because of the higher sensitivity of $\Delta\overline{M-C}$* to

(7) (a) Al-Obaidi, Y. N.; Baker, P. K.; Green, M.; White, N. D.; Taylor, G. E. *J. Chem. Soc., Dalton Trans.* **1981**, 2321. (b) Barr, R. D.; Green, M.; Marder, T. B.; Stone, F. G. A. *J. Chem. Soc., Dalton Trans.* **1984**, 1261. (c) Baker, R. T.; Tulip, T. H. *Organometallics* **1986**, *5*, 839. (d) Mlekuz, M.; Bougeard, P.; Sayer, B. G.; McGlinchey, M. J.; Rodger, C. A.; Churchill, M. R.; Ziller, J. W.; Kanz, S. W.; Albright, T. A. *Organometallics* **1986**, *5*, 1656. (e) O'Connor, J. M.; Casey, C. P. *Chem. Rev.* **1987**, *87*, 307 and references therein. (f) Marder, T. B.; Calabrese, J. C.; Roe, D. C.; Tulip, T. H. *Organometallics* **1987**, *6*, 2012. (g) Carl, R. T.; Hughes, R. P.; Rheingold, A. L.; Marder, T. B.; Taylor, N. J. *Organometallics* **1988**, *7*, 1613. (h) Kakkar, A. K.; Taylor, N. J.; Calabrese, J. C.; Nugent, W. A.; Roe, D. C.; Connaway, E. A.; Marder, T. B. *J. Chem. Soc., Chem. Commun.* **1989**, 990. (i) Kakkar, A. K.; Jones, S.; Taylor, N. J.; Collins, S.; Marder, T. B. *J. Chem. Soc., Chem. Commun.* **1989**, 1454. (j) Merola, S.; Kacmarcik, R. T. *Organometallics* **1989**, *8*, 778.

the slippage of the metal toward C_2. Table 1 also shows that (*ii*) the distortion of the coordination about rhodium evidenced in **2** by the large dihedral angle (23°) between the planes [C_1, C_2, C_3] of the indenyl frame and [C_{11}, C_{12}, C_{14}, C_{15}] of NBD is practically absent in the case of the *trans* isomer **3** as well as in the monometallic complex **4** and (*iii*) the coordination with $Cr(CO)_3$ of IndRh(NBD) causes the bending of the benzene ring which is larger in the *cis* complex (11°) than in the *trans* one (6°). Analogously to the $\Delta\overline{M-C}$ parameter defined for the Cp ring, we have calculated the $\Delta\overline{M-C}_{benzene}$ parameter ($\Delta\overline{M-C}_{benzene}$ = {[(Cr−C_{3a}) + (Cr−C_{7a})]/2 − [(Cr−C_4) + (Cr−C_7)]/2}, Å) which is much higher for **2** (0.184 Å) than for **3** (0.109 Å). Again, the distortion in the *cis* species is substantially larger than that in the *trans* isomer, indicating a pronounced shift of chromium from the ideal η^6 hapticity toward an η^4 one.

This conclusion is corroborated by the NMR results which indicate that the difference between the structural features of **2** and **3** also persists in solution. As reported previously,[5] the most relevant effects caused by the coordination of the benzene ring with $Cr(CO)_3$ to form the *cis* isomers, $\Delta\delta(^{13}C)$, are the tetrahedralization of the C_1,C_3 and C_4,C_7 carbon atoms as indicated by their very high upfield shifts and the low coordinative engagement of C_{3a} and C_{7a} as suggested by the low-field position of their resonance. Conversely, the complexation effects observed for the same carbon nuclei in the *trans* isomer **3** are quite different, *i.e.*, lower $\Delta\delta(^{13}C)$ values for C_1, C_3, C_4, and C_7, and higher for C_{3a} and C_{7a}, and they are very close to those previously reported for a series of *trans*-[$Cr(CO)_3$(indenyl)Rh(COD)] derivatives.[8]

These features indicate that the structure of the *cis* isomer is characterized by severe molecular constraints which could make this isomer less stable than the *trans* one. In fact, we have found that the reaction between the (η^6-indenyl)$Cr(CO)_3$ potassium salt and [Rh(μ-Cl)(NBD)]$_2$ in THF affords quantitatively the *trans* isomer which, however, is stable only at temperatures below −30 °C. The stereochemistry of this product was established by ^{1}H (see Figure 2A) and ^{13}C NMR measurements, as the spectra of the reaction mixture proved to be identical to those recorded for solutions of the authentic *trans* complex, **3**. When the temperature was raised above −20 °C, the IR, NMR, and TLC analyses indicated that the *trans* species isomerizes quantitatively to the *cis* one (see Figure 2C), which is the sole product isolated at room temperature after the workup of the crude reaction mixture. Thus, in contrast to what would be anticipated on the basis of the structural evidence, the *cis* isomer **2** is thermodynamically more stable than the *trans* isomer **3**, the formation of which is in turn kinetically favored under preparative conditions. The unexpected stability of the *cis* isomer **2** seems to trace both to Rh−Cr bond interaction and to important stabilizing interactions between the NBD hydrogen atoms H_{11} and H_{15} and the facing carbonyl groups, as suggested by the experimental evidences reported and discussed in a previous paper.[5]

Attempts to accomplish the *trans* → *cis* isomerization starting from a pure sample of complex **3** in THF, with added KCl and [Rh(μ-Cl)NBD]$_2$ in order to simulate the preparative conditions, failed. As a matter of fact, we found that *trans*-**3** isomerizes to *cis*-**2** at room temperature in THF only in the presence of [Rh(NBD)]$^+$BF$_4^-$. The process takes place at a reasonable rate only when the amount of the salt overcomes a threshold value (*ca.* 5%), and a strong dependence of the isomerization rate on the catalyst concentration was qualitatively observed. The catalytic effect is not peculiar only to the [Rh(NBD)]$^+$ species, but it was observed with other cations as well, *viz.*, [Rh(COD)]$^+$, [Rh(COD)$_2$]$^+$, [Ir(COD)]$^+$, or [Rh(NBD-d_8)]$^+$. Both with deuterated [Rh(NBD-d_8)]$^+$ and with the other cations, careful ^{1}H NMR analysis of the well-resolved signals of the CH_2 protons of NBD allowed us to rule out the occurrence of scrambling between the coordinated Rh(NBD) group and the cation used as catalyst. These results seem to favor a concerted intramolecular rather than a dissociative pathway for the rearrangement. As [Rh(μ-Cl)NBD]$_2$ induces the isomerization in the preparative and not in the simulated conditions, we believe that only in the former medium is a sufficient catalyst concentration produced.

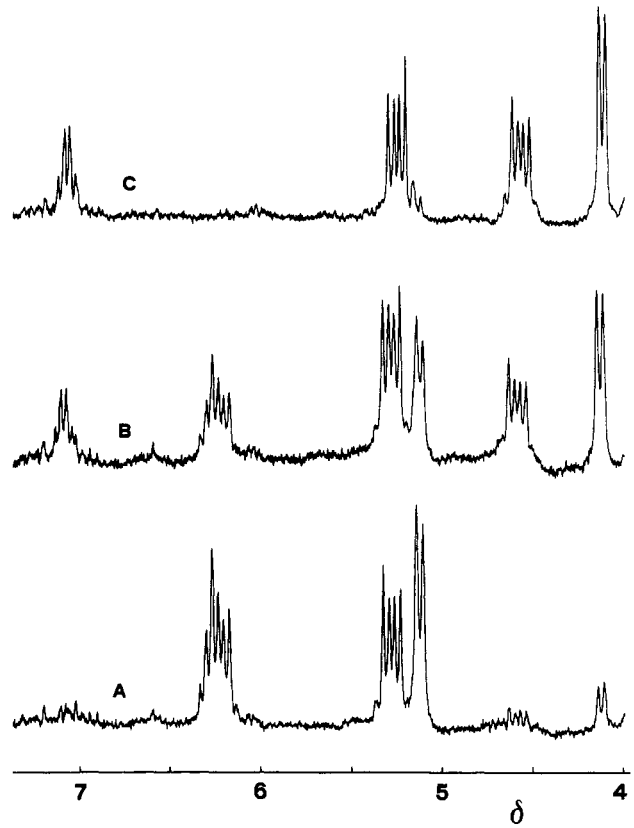

Figure 2. Changes in the ^{1}H NMR spectrum of complex **3** in THF-d_8 at 268 K in the presence of 16.8% [Rh(NBD)]BF$_4$ (Me_4Si as internal standard, ν_0 80.13 MHz): (A) spectrum after 3 min; (B) spectrum after *ca.* 24 min; (C) final spectrum (*t ca.* 90 min).

In a quantitative study, the kinetics of the **3** → **2** isomerization in THF-d_8 in the presence of 16.8% [Rh(NBD)]$^+$BF$_4^-$ was monitored by ^{1}H NMR spectroscopy between 248 and 267 K, and an intermediate situation of the experiment carried out at 267 K is shown in Figure 2B. Use of the first-order kinetic equation for an irreversible process gave satisfactory plots ($r \geq 0.998$) up to 95% reaction, and the calculated values (±5%) of the rate constants are $10^4 k_{obs}$ = 0.75 (at 248 K), 1.03 (253 K), 1.70 (258 K), and 4.64 (267 K) s^{-1}. The activation parameters $\Delta H^{\ddagger}$ = 11.7 ± 0.9 kcal

(8) Ceccon, A.; Elsevier, C. J.; Ernsting, J. M.; Gambaro, A.; Santi, S.; Venzo, A. *Inorg. Chim. Acta* **1993**, *204*, 15.

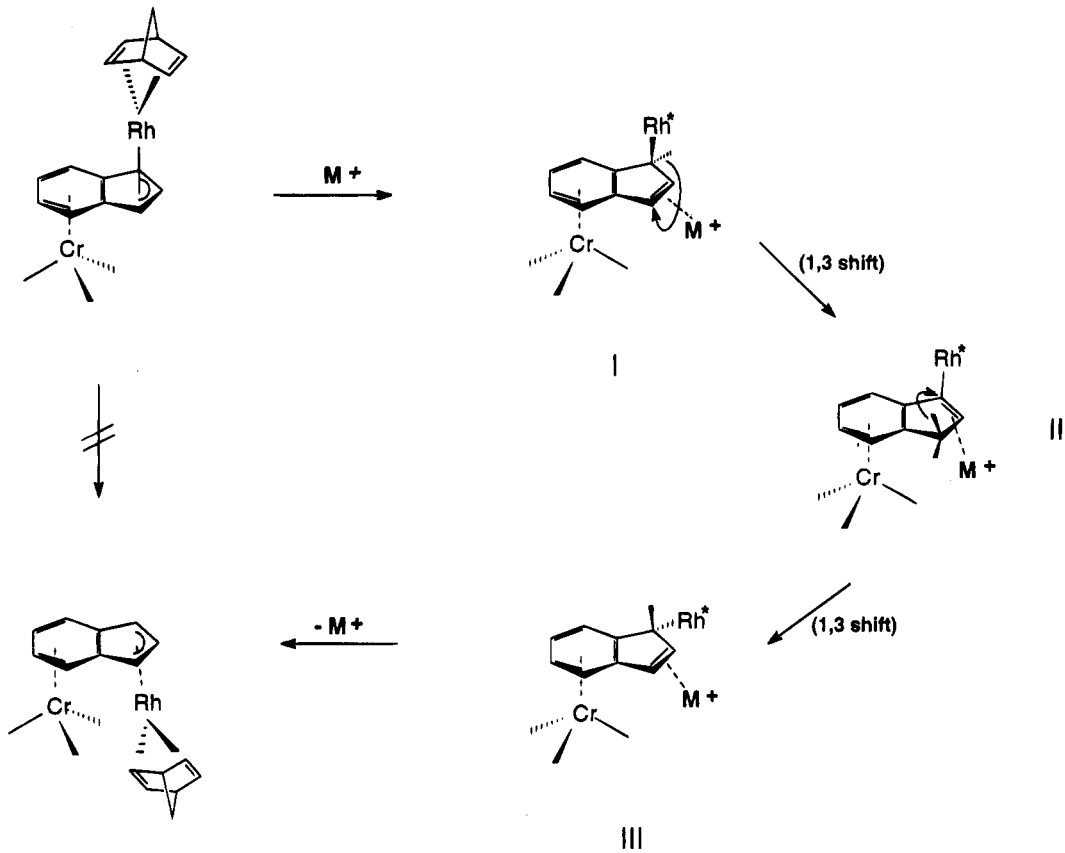

Figure 3. Proposed mechanism of *trans*-**3** → *cis*-**2** isomerization (Rh* ≡ Rh(NBD)).

mol^{-1} and $\Delta S^{\ddagger} = -30 \pm 3$ cal mol^{-1} K^{-1} were calculated from the Eyring plot.

A likely reaction pathway involving an intramolecular isomerization process assisted by rhodium– or iridium–olefin cations is presented in Figure 3. The rate-determining step is proposed to be the interaction of the incoming cation M^+ (the catalyst) with the π electron cloud of the Cp ring to produce species **I** involving a crowded transition state. The Rh(NBD) and the Cr(CO)$_3$ units are still in the *trans* arrangement and the rhodium atom is σ-bonded to the indene frame. This associative step is in agreement with the strongly negative activation entropy value; moreover, the low enthalpy barrier allows us to rule out a dissociative route. A *cis* stereochemistry of Rh(NBD) and Cr(CO)$_3$ can be achieved through two fast [1,3]-hydrogen shifts **I** → **II** and **II** → **III** necessary to invert the configuration at the indene carbon atom σ-bonded to Rh(NBD). Removal of M^+ restores the π coordination of rhodium to the five-membered ring, giving **2**.

The proposed mechanism is based on the stepwise formation of several η^1-indenyl rhodium(I) intermediates. Even though this kind of coordination of rhodium to a cyclopentadienyl residue is very scarcely documented (we are aware of the existence of only a few (η^1-indenyl)Rh(CNR)$_4$ complexes[9]), we believe that for metals of d^8 electronic configuration the existence of species such as **I**–**III** is reasonable. For example, we have demonstrated the remarkable ability of Ir(I) to form rather stable η^1-indenyl complexes in the reaction between carbon monoxide and the closely related (indenyl)Ir(COD)[10a] and Cr(CO)$_3$–(indenyl)Ir(COD) species.[10b] The formation of (η^1-indenyl)Ir^{III} intermediates was recently reported by Foo and Bergman.[11] Moreover, it is worth noting that the isomerization must be carried out in a coordinating solvent such as THF, which seems to be necessary to stabilize the intermediates with coordinatively unsaturated rhodium centers of low hapticity.

As far as we are aware, this kind of isomerization in which the metal moves through the Cp plane of the bridging ligand is unprecedented. A nondissociative exchange of the C=C enantioface bound to the metal has been recently reported,[12] where the metal is suggested to traverse through the alkene π nodal plane *via* a carbon–hydrogen σ bond complex.

Finally, the occurrence of the [1,3]-hydrogen shifts **I** → **II** and **II** → **III** as fast steps is in agreement with the previous finding that such processes in indene derivatives are strongly favored when inorganic units such as Cr(CO)$_3$ are present.[13]

Experimental Section

General Comments. All reactions were carried out under a blanket of purified argon, and oxygen-free solvents and reagents were used. Solvents were purified according to standard procedures,[14] distilled, and purged with argon before use. Commercial grade norbornadiene (Aldrich) was dried over $MgSO_4$ and distilled just before use. [Rh(NBD)]$^+BF_4^-$ and

(9) Caddy, P.; Green, M.; O'Brien, E.; Smart, L. E.; Woodward, P. *Angew. Chem., Int. Ed. Engl.* **1977**, *16*, 648.

(10) (a) Bellomo, S.; Ceccon, A.; Gambaro, A.; Santi, S.; Venzo, A. *J. Organomet. Chem.* **1993**, *453*, C4. (b) Bonifaci, C.; Ceccon, A.; Gambaro, A.; Manoli, F.; Santi, S.; Venzo, A. *Abstracts of XVIth International Conference on Organometallic Chemistry*, Brighton (U.K.), July 10–15, 1994; OA.9.

(11) Foo, T.; Bergman, R. G. *Organometallics* **1992**, *11*, 1811 and references therein.

(12) Peng, T.-S.; Gladysz, J. A. *J. Am. Chem. Soc.* **1992**, *114*, 4174.

(13) Berno, P.; Ceccon, A.; Gambaro, A.; Daprà, F.; Venzo, A. *Tetrahedron Lett.* **1988**, *29*, 3489.

(14) Perrin, D. D.; Armageo, W. L. F. *Purification of Laboratory Chemicals*, 3rd ed.; Pergamon Press: Oxford, England, 1988.

Table 2. Summary of Crystal Data and Intensity Data Collection for *trans*-3

formula	$C_{19}H_{15}CrO_3Rh$
M	446.22
a/Å	8.200(5)
b/Å	11.388(5)
c/Å	17.868(5)
β/deg	92.1
V/Å^3	1667.4
Z	4
D_c/g cm^{-3}	1.78
$F(000)$	888
space group	$P2_1/c$
cryst dimens/mm	0.15 × 0.20 × 0.20
T/K	298
radiation (λ/Å)	graphite monochromated Mo Kα (0.710 73)
μ/cm^{-1}	17.42
scan speed/deg min^{-1}	2.0 in the 2θ scan mode
takeoff angle/deg	3
2θ range/deg	$3.0 \le \theta \le 45$
unique reflns	3086
used reflns (with $F_o^2 > 2\sigma(F_o^2)$)	2904
soln method	Patterson
R_o (on F_o)[a]	0.044
R_w[b]	0.045
GOF[c]	0.059
residual ϱ/e Å^{-3}	0.68

[a] $R_o = \sum||F_o| - |F_c||/\sum|F_o|$. [b] $R_w = [\sum w(|F_o| - |F_c|)^2/\sum wF_o^2]^{1/2}$. [c] GOF $= [\sum w(|F_o| - |F_c|)^2/(NO - NV)^2]^{1/2}$.

the other used salts were obtained from the corresponding dimers according to literature methods.[15] Instruments: mass spectrum, 70 eV-EI, VG-16 MicroMass; IR, Perkin-Elmer 1600 FT-IR; NMR, Bruker AM-400 (^{1}H, 400.133 MHz; ^{13}C, 100.614 MHz) and UP-80 SY (^{1}H, 80.13 MHz). The ^{1}H and ^{13}C NMR spectra were recorded in CD_2Cl_2 solution at 298 K and are in units of ppm referenced to internal Me_4Si. IR spectra were run as CH_2Cl_2 solutions within CaF_2 windows.

Preparation of 3. Complex **3** was obtained in quantitative yield by reacting a solution of *trans*-[Cr(CO)$_3$(indenyl)Rh(CO)$_2$][6] in CH_2Cl_2 with a large excess of NBD for 10 min at room temperature. Removal of the solvent and excess NBD *in vacuo* gave an orange-brown residue which was crystallized from CH_2Cl_2/pentane. Mp = 168−172 °C dec. Anal. Calcd for $C_{19}H_{15}CrO_3Rh$: C, 51.14; H, 3.39. Found: C, 51.01; H, 3.52. MS: m/z 446, M$^+$ (calcd: 446). IR ν(C≡O) 1949 (vs) and 1872 (vs) cm^{-1}. ^{1}H NMR (CD_2Cl_2, 25 °C, assignments confirmed by {^{1}H}−^{1}H NOE): δ = 6.29 (m, 1H, $J(^{103}Rh-^1H)$ = 2.1 Hz, H_2), 5.22 and 6.12 (m, 2H each, AA′BB′, $H_{5,6}$ and $H_{4,7}$, respectively), 5.05 (m, 2H, $H_{1,3}$); (NBD resonances) δ = 3.69 (m, 4H, olefin protons), 3.26 (m, 2H, bridgehead protons), 0.99 (m, 2H, CH_2). ^{13}C NMR (CD_2Cl_2, 25 °C, assignments made by selective ^{1}H-decoupling): δ = 234.84 (Cr−C≡O), 85.51 (d, $J(^{103}Rh-^{13}C)$ = 2.3 Hz, $C_{3a,7a}$), 102.36 ($J(^{13}C-^1H)$ = 176 Hz, $J(^{103}Rh-^{13}C)$ = 6.3 Hz, C_2), 90.37 ($J(^{13}C-^1H)$ = 173 Hz, $C_{5,6}$), 83.33 ($J(^{13}C-^1H)$ = 176 Hz, $C_{4,7}$, 73.29 ($J(^{13}C-^1H)$ = 175 Hz, $J(^{103}Rh-^{13}C)$ = 4.0 Hz, $C_{1,3}$); (NBD resonances) δ = 59.91 ($J(^{13}C-^1H)$ = 134 Hz, $J(^{103}Rh-^{13}C)$ = 7.2 Hz, methylene carbon), 48.58 ($J(^{13}C-^1H)$ = 152 Hz, $J(^{103}Rh-^{13}C)$ = 2.0 Hz, bridgehead carbons), 43.621 ($J(^{13}C-^1H)$ = 176 Hz, $J(^{103}Rh-^{13}C)$ = 9.0 Hz, olefin carbons).

Crystallography. Crystal data, intensity data collection, and processing details for **3** are presented in Table 2. The data were obtained with a Philips PW-100 four-cycle diffractometer with graphite monochromator. Intensity data were collected at 25 °C using the 2θ scan method. Two reference reflections, monitored periodically, showed no significant variation in intensity. Data were corrected for Lorentz and polarization effects and an empirical absorption correction was applied to the intensities. The positions of Cr and Rh atoms were determined from the three-dimensional Patterson function. All the remaining atoms, including hydrogens, were located from successive Fourier maps using SHELX-76.[16] Anisotropic thermal parameters were used for all the non-hydrogen atoms. Blocked-cascade least-squares refinements converged to R 0.043. The positional parameters of the non-hydrogen atoms are listed in Table 3. The anisotropic thermal parameters of the non-hydrogen atoms, the positional parameters of the hydrogen atoms, and full lists of bond lengths and angles are available as supplementary material.

(15) Schrock, R. R.; Osborn, J. A. *J. Am. Chem. Soc.* **1971**, *93*, 3089.

Table 3. Fractional Coordinates with Equivalent Isotropic Thermal Parameters (Å^2) for the Complex *trans*-[Cr(CO)$_3$IndRh(NBD)][a]

atom	x	y	z	U_{equiv}
Rh	0.40742(4)	0.17322(3)	0.12896(2)	0.0362(1)
Cr	0.08838(7)	0.23993(5)	0.31992(4)	0.0307(2)
C_8	−0.1295(5)	0.2025(4)	0.3056(3)	0.039(1)
C_9	0.0350(6)	0.3189(4)	0.4046(3)	0.043(1)
C_{10}	0.1117(5)	0.1049(4)	0.3754(2)	0.042(1)
O_8	−0.2661(4)	0.1795(4)	0.2981(2)	0.062(2)
O_9	0.0039(6)	0.3692(4)	0.4580(2)	0.071(2)
O_{10}	0.1216(6)	0.0195(4)	0.4103(3)	0.077(2)
C_1	0.3803(5)	0.0643(4)	0.2341(3)	0.040(1)
C_2	0.2809(7)	0.0165(4)	0.1767(3)	0.051(2)
C_3	0.1612(5)	0.0982(5)	0.1496(3)	0.047(1)
C_{3a}	0.1747(5)	0.1991(4)	0.1986(2)	0.036(1)
C_4	0.0876(6)	0.3081(4)	0.2025(3)	0.047(1)
C_5	0.1442(6)	0.3965(4)	0.2521(3)	0.052(2)
C_6	0.2758(6)	0.3740(4)	0.3025(3)	0.050(2)
C_7	0.3581(5)	0.2666(4)	0.3059(2)	0.038(1)
C_{7a}	0.3137(5)	0.1791(3)	0.2513(2)	0.031(1)
C_{11}	0.6131(5)	0.2902(4)	0.1244(3)	0.038(1)
C_{12}	0.6578(7)	0.1792(4)	0.0988(4)	0.055(2)
C_{13}	0.6270(9)	0.1800(6)	0.0143(4)	0.079(3)
C_{14}	0.4400(9)	0.1812(7)	0.0115(3)	0.078(3)
C_{15}	0.3931(7)	0.2940(8)	0.0373(3)	0.073(2)
C_{16}	0.5535(7)	0.3598(5)	0.0547(3)	0.054(2)
C_{17}	0.6652(9)	0.3088(7)	−0.0057(3)	0.075(2)

[a] U_{equiv} is defined as one-third of the trace of the orthogonalized U_{ij} tensor.

Kinetic Measurements. A 3 mL aliquot of a THF-d_8 solution prepared by dissolving 52.2 mg of **3** (1.17 × 10^{-4} mol) in 0.2 mL of a THF-d_8 solution containing 0.39 × 10^{-4} mol of [Rh(NBD)]$^+$BF$_4^-$ (obtained from 4.63 mg of [Rh(μ-Cl)NBD]$_2$ and 3.83 mg of $AgBF_4$ as reported in ref 14) were mixed at −70 °C. The resulting mixture (3.65 × 10^{-2} M in **3** and 6.14 × 10^{-3} M in [Rh(NBD)]$^+$BF$_4^-$, *i.e.* (mol catalyst)/(mol **3**) = 0.168) was stored at liquid nitrogen temperature. Aliquots of the solution were transferred into precooled 5 mm NMR sample tubes for the kinetic runs. The isomerization reaction was followed at different temperatures by 80 MHz ^{1}H NMR spectroscopy, the time variation of the concentration of the two isomers being estimated by integration of the corresponding signals. Rate constants, k_{obs}, were obtained by plotting the function $\ln([\mathbf{3}]/[\mathbf{3}]_0)$ *vs* time. It was possible to use directly the ratio $[I]/[I]_0$ of the signal integrals instead of the concentration ratio, $[\mathbf{3}]/[\mathbf{3}]_0$, since it was verified that at the end of the reaction $[\mathbf{3}]_\infty = [I]_\infty = 0$. The sample kinetic plots obtained at four temperatures and the Eyring plot are available as supplementary material.

Acknowledgment. This work was supported in part by CNR through its Centro di Studi sugli Stati Molecolari Radicalici ed Eccitati, Padova, Italy, and through its Progetto Finalizzato Chimica Fine II.

Supplementary Material Available: Full lists of bond distances and bond angles, anisotropic thermal parameters, and fractional coordinates of the H atoms and sample kinetic plot at different temperatures and the Eyring plot (7 pages). Ordering information is given on any current masthead page.

OM940781A

(16) Sheldrick, G. M. SHELX-76, A System of Computer Programs for X-ray Crystal Structure Determination. Cambridge University, England, 1976.

Intra- vs Intermolecular α-Hydrogen Abstraction in the Generation of Multiple Imido Complexes: Synthesis, Reactivity, and Structural Studies of the d^0 Tris(imido) Functional Group of Tungsten

Donald L. Morrison,[†,‡] Paula M. Rodgers,[†] Yuan-Wei Chao,[†] Michael A. Bruck,[†] Carina Grittini,[†] Tracey L. Tajima,[†,§] Steven J. Alexander,[‖] Arnold L. Rheingold,[‖] and David E. Wigley*,[†]

Carl S. Marvel Laboratories of Chemistry, Department of Chemistry, University of Arizona, Tucson, Arizona 85721, and Department of Chemistry and Biochemistry, University of Delaware, Newark, Delaware 19716

Received January 11, 1995[⊗]

The synthesis, reactivity, and structural characterization of the d^0 tris(imido) complex $[Li(THF)_4][W(NAr)_3Cl]$ (**2**, Ar = 2,6-C_6H_3-*i*-Pr_2) are reported. When $W(NAr)Cl_4(THF)$ reacts with 2 equiv of $Me_3SiNHAr$ in THF, the bis(imido) compound $W(NAr)_2Cl_2(THF)_2$ (**1**) is isolated. Reacting $W(NAr)_2Cl_2(THF)_2$ with 2 equiv of LiNHAr in THF affords the yellow, crystalline tris(imido) complex $[Li(THF)_4][W(NAr_3)Cl]$ (**2**). Complex **2** is shown to be the kinetic product of this reaction since it reacts with byproduct H_2NAr to afford $W(NAr)_2(NHAr)_2$ (**3**). Experiments are described that support the d^0 $W(=NR)_2$ functional group in $W(NAr)_2Cl_2(THF)_2$ (**1**) arising by an *intra*molecular α-H abstraction in $[W(NAr)(NHAr)_2Cl_2(THF)_n]$ (with loss of H_2NAr), while the formation of $[W(NAr)_3Cl]^-$ (**2**) from $W(NAr)_2Cl_2(THF)_2$ (**1**) most likely proceeds by an *inter*molecular deprotonation of nascent $W(NAr)_2(NHAr)Cl$ by the second equivalent of $[NHAr]^-$. These experiments include synthesis and reactivity studies of $W(NAr)_2Cl_2(NH_2Ar)$ (**4**), $W(NAr)(NEt_2)Cl_3(THF)$ (**5**), and $W(NAr)_2(NEt_2)Cl$ (**6**). The d^0 metal center in $[W(NAr)_3Cl]^-$ (**2**) is susceptible to nucleophilic attack as seen in its reactions with $PMePh_2$, PMe_3, $[n\text{-}Bu_4N]Br$, MeLi, and $LiCH_2SiMe_3$ to afford the substitution products $W(NAr)_3(PMePh_2)$ (**7**), $W(NAr)_3(PMe_3)$ (**8**), $[n\text{-}Bu_4N][W(NAr)_3Br]$ (**9**), $[Li(THF)_4][W(NAr)_3Me]$ (**10**), and $[Li(THF)_4][W(NAr)_3(CH_2SiMe_3)]$ (**11**), respectively. Kinetic and mechanistic evidence is presented that suggests these reactions proceed by a bimolecular, S_N2 attack at the d^0 tungsten center. $[Li(THF)_4][W(NAr)_3Cl]$ (**2**) crystallizes in the monoclinic space group $P2_1/n$ (No. 14) with a = 13.787(4), Å, b = 17.348(5) Å, c = 22.781(8) Å, β = 90.426(28)°, and V = 5448.5(30) Å^3, with Z = 4 and D(calc) = 1.268 g cm^{-3}. $W(NAr)_3(PMe_3)$ (**8**) crystallizes in the orthorhombic space group *Pbca* (No. 61) with a = 18.572(3) Å, b = 25.966(4) Å, c = 16.819(3) Å, and V = 8111(4) Å^3, with Z = 8 and D(calc) = 1.29 g cm^{-3}. The tungsten atom of $[Li(THF)_4][W(NAr)_3Cl]$ (**2**) is tetrahedrally coordinated with three virtually identical imido ligands with an average W–N bond length of 1.78 Å and an average W–N–C_{ipso} bond angle of 171°. $W(NAr)_3(PMe_3)$ (**8**) is also tetrahedrally coordinated and displays an average imido W–N bond length of 1.79 Å and slightly bent W–N–C_{ipso} bond angles (av 167°), though one imido ligand is more strongly bent than the other two. The electronic structure of the C_{3v} $W(NAr)_3L$ compounds suggests a ligand-based, nonbonding a_2 HOMO comprised of a N(pπ) orbital combination oriented perpendicular to the molecule's C_3 axis. Accordingly, an imido nitrogen is subject to electrophilic attack, as seen in the reactions of $W(NAr)_3(PMe_3)$ (**8**) with HOAr′ (Ar′ = 2,6-$C_6H_3Me_2$), Me_3SiI, MeI, and PhNCO that afford $W(NAr)_2(NHAr)(OAr')$ (**12**), $W(NAr)_2[N(SiMe_3)Ar]I$ (**13**), $W(NAr)_2(NMeAr)I$ (**14**), and $W[NArC(O)NPh](NAr)_2(PMe_3)$ (**15**), respectively. Similarly, the reaction of $[Li(THF)_4][W(NAr)_3Me]$ (**10**) with $[HNMe_3]BPh_4$ does not protonate the W–Me bond but rather attacks the imido nitrogen to afford $W(NAr)_2(NHAr)Me$ (**16**). $W(NAr)_2(NHAr)Me$ (**16**) does not eliminate CH_4 upon thermolysis to afford base-free $[W(NAr)_3]$; other attempts to generate this species are described.

Introduction

Transition metal organoimido complexes[1,2] have been applied to catalytic and synthetic methodologies involving net [NR] transfer chemistry,[3] as in the amination[4] and aziridination[5] of olefins or the ammoxidation of propylene.[6] Organoimido ligands have also been implicated in nitrile reduction[7] and have seen increasing utility as ancillary groups to support high oxidation

† University of Arizona.
‡ Carl S. Marvel Fellow, 1994–1995.
§ Participant, NSF-REU Program, University of Arizona.
‖ University of Delaware.
⊗ Abstract published in *Advance ACS Abstracts,* April 15, 1995.

(1) Wigley, D. E. *Prog. Inorg. Chem.* **1994,** *42,* 239.
(2) Nugent, W. A.; Mayer, J. M. *Metal–Ligand Multiple Bonds*; John Wiley and Sons: New York, 1988.

0276-7333/95/2314-2435$09.00/0

state metals.[8] Recent advances in metal imido chemistry include the generation of compounds containing reactive $L_nM{=}NR$ ligands that can activate the C−H bonds of methane[9] or engage in cycloaddition chemistry.[3d,10] Various strategies employed to activate imido ligands include coordinating these ligands to late transition elements or using mid- to low-valent metals in an effort to destabilize the strong $d\{\pi\} \leftarrow p\{\pi\}$ interactions that often make imido complexes inert. One aspect of many early transition metal compounds with reactive $L_nM{=}NR$ ligands is a coordination sphere containing *multiple* π donor ligands,[11,12] a feature that has aroused interest in "π-loaded" multiple imido complexes as another potential means to activate M=NR bonds.[12-17]

We recently reported[12] the preparation and properties of d^0 tris(imido) complexes of tungsten, thereby completing the series of d^0 $W(NR)_n$ imido−metal functional groups for $n = 1$,[18] 2,[19] 3,[12] and 4.[20] Prior to our initial report, tris(imido) complexes were restricted to select metals in groups 7 and 8.[1] Given the potential utility of imido complexes such as $Mn(N\text{-}t\text{-}Bu)_3X$[21] in oxidation chemistry and $Tc(NAr)_3X$[22] in radiopharmaceutical applications, delineating the properties of this class of compound constitutes a significant goal. In this paper, we report the synthesis, reactivity, and structural properties of the d^0 $W(=NR)_3$ functional group, describe experiments that address how multiple imido complexes arise, and demonstrate an electronic analogy of $W(=NR)_3$ to related $M(1\sigma,2\pi)_3$ complexes.

Results

Formation of the d^0 $W(=NR)_2$ and d^0 $W(=NR)_3$ Functional Groups. Upon reacting $W(NAr)Cl_4(THF)$[23] with 2 equiv of $Me_3SiNHAr$ in THF (Ar = 2,6-C_6H_3-*i*-Pr_2), red-orange $W(NAr)_2Cl_2(THF)_2$ (**1**) is isolated in 81% yield. NMR data for **1** reveal equivalent imido and THF ligands; thus, a structure analogous to the chelate adducts $W(NR)_2Cl_2(L{-}L)$ is proposed, i.e., with *cis*-imido and *trans*-chloride ligands, as suggested in Scheme 1.[19c,23,24] When $W(NAr)_2Cl_2(THF)_2$ is reacted with 2 equiv of LiNHAr in THF, the yellow, crystalline tris(imido) complex $[Li(THF)_4][W(NAr)_3Cl]$ (**2**) is obtained in ~75% yield. This formulation of **2** is consistent with the absence of a $\nu(N{-}H)$ mode in its IR spectrum, the lack of N*H* resonances in its ^1H NMR spectrum, its elemental analysis, and its X-ray structural determination (vide infra). Under prolonged vacuum, $[Li(THF)_4][W(NAr)_3Cl]$ slowly loses THF; thus, $[Li(THF)_4]^+$ is considered the maximum THF coordination in this complex. The solid state structure of **2** reveals the plane of the imido phenyl rings oriented roughly parallel with the molecule's *z* axis (the W−Cl bond), but ^1H and ^{13}C NMR spectra of the equivalent NAr ligands exhibit one C*H*Me_2 septet and a single CH*Me*$_2$ doublet, implying free rotation about the $W{-}N{-}C_{ipso}$ bond and a threefold axis of symmetry.

$[Li(THF)_4][W(NAr)_3Cl]$ (**2**) is observed to be the kinetic product of the reaction between $W(NAr)_2Cl_2(THF)_2$ (**1**) and LiNHAr, since byproduct H_2NAr reacts with $[W(NAr)_3Cl]^-$ over a period of 1−2 days to convert it to the more stable $W(NAr)_2(NHAr)_2$ (**3**). This reactivity feature is confirmed by reacting isolated $[Li(THF)_4][W(NAr)_3Cl]$ with 1 equiv of H_2NAr, which affords yellow $W(NAr)_2(NHAr)_2$ in high yield; therefore, reaction time is important for the successful isolation of complex **2**. A similar reactivity feature has been established in

(3) For examples of [NR] transfer reactions, see: (a) Harlan, E. W.; Holm, R. H. *J. Am. Chem. Soc.* **1990**, *112*, 186. (b) Elliot, R. L.; Nichols, P. J.; West, B. O. *Polyhedron* **1987**, *6*, 2191. (c) Walsh, P. J.; Baranger, A. M.; Bergman, R. G. *J. Am. Chem. Soc.* **1992**, *114*, 1708. (d) Glueck, D. S.; Wu, J.; Hollander, F. J.; Bergman, R. G. *J. Am. Chem. Soc.* **1991**, *113*, 2041.

(4) (a) Sharpless, K. B.; Patrick, D. W.; Truesdale, L. K.; Biller, S. A. *J. Am. Chem. Soc.* **1975**, *97*, 2305. (b) Chong, A. O.; Oshima, K.; Sharpless, K. B. *J. Am. Chem. Soc.* **1977**, *99*, 3420. (c) Patrick, D. W.; Truesdale, L. K.; Biller, S. A.; Sharpless, K. B. *J. Org. Chem.* **1978**, *43*, 2628. (d) Hentges, S. G.; Sharpless, K. B. *J. Org. Chem.* **1980**, *45*, 2257.

(3) (a) Groves, J. T.; Takahashi, T. *J. Am. Chem. Soc.* **1983**, *105*, 2073. (b) Mansuy, D.; Mahy, J.-P.; Dureault, A.; Bedi, G.; Battioni, P. *J. Chem. Soc., Chem. Commun.* **1984**, 1161.

(3) (a) Maatta, E. A.; Du, Y.; Rheingold, A. L. *J. Chem. Soc., Chem. Commun.* **1990**, 756. (b) Maatta, E. A.; Du, Y. *J. Am. Chem. Soc.* **1988**, *110*, 8249. (c) Chan, D. M.-T.; Fultz, W. C.; Nugent, W. A.; Roe, D. C.; Tulip, T. H. *J. Am. Chem. Soc.* **1985**, *107*, 251. (d) Chan, D. M.-T.; Nugent, W. A. *Inorg. Chem.* **1985**, *24*, 1422.

(3) (a) Bakir, M.; Fanwick, P. E.; Walton, R. A. *Inorg. Chem.* **1988**, *27*, 2016. (b) Rhodes, L. F.; Venanzi, L. M. *Inorg. Chem.* **1987**, *26*, 2692. (c) Han, S. H.; Geoffroy, G. L. *Polyhedron* **1988**, *7*, 2331.

(8) (a) Murdzek, J. S.; Schrock, R. R. *Organometallics* **1987**, *6*, 1373. (b) Schrock, R. R.; Krouse, S. A.; Knoll, K.; Feldman, J.; Murdzek, J. S.; Yang, D. C. *J. Mol. Catal.* **1988**, *46*, 243. (c) Feldman, J.; Davis, W. M.; Thomas, J. K.; Schrock, R. R. *Organometallics* **1990**, *9*, 2535. (d) Schrock, R. R.; Crowe, W. E.; Bazan, G. C.; DiMare, M.; O'Regan, M. B.; Schofield, M. H. *Organometallics* **1991**, *10*, 1832.

(9) (a) Cummins, C. C.; Baxter, S. M.; Wolczanski, P. T. *J. Am. Chem. Soc.* **1988**, *110*, 8731. (b) Cummins, C. C.; Van Duyne, G. D.; Schaller, C. P.; Wolczanski, P. T. *Organometallics* **1991**, *10*, 164. (c) For a theoretical treatment of methane activation by group 4 imido complexes, see: Cundari, T. R. *J. Am. Chem. Soc.* **1992**, *114*, 10557. (d) Schaller, C. P.; Bonanno, J. B.; Wolczanski, P. T. *J. Am. Chem. Soc.* **1994**, *116*, 4133.

(10) (a) McGrane, P. L.; Jensen, M.; Livinghouse, T. *J. Am. Chem. Soc.* **1992**, *114*, 5459. (b) Walsh, P. J.; Hollander, F. J.; Bergman, R. G. *Organometallics* **1993**, *12*, 3705.

(11) (a) Williams, D. S.; Schrock, R. R. *Organometallics* **1993**, *12*, 1148. (b) Williams, D. N.; Mitchell, J. P.; Poole, A. D.; Siemeling, U.; Clegg, W.; Hockless, D. C. R.; O'Neil, P. A., Gibson, V. C. *J. Chem. Soc., Dalton Trans.* **1992**, 739. (c) Huber, S. H.; Baldwin, T. C.; Wigley, D. E. *Organometallics* **1993**, *12*, 91.

(12) Chao, Y.-W.; Rodgers, P. M.; Wigley, D. E.; Alexander, S. J.; Rheingold, A. L. *J. Am. Chem. Soc.* **1991**, *113*, 6326.

(13) Cundari, T. R. *J. Am. Chem. Soc.* **1992**, *114*, 7879.

(14) Burrell, A. K.; Bryan, J. C. *Organometallics* **1992**, *11*, 3501.

(15) Wolf, J. R.; Bazan, G. C.; Schrock, R. R. *Inorg. Chem.* **1993**, *32*, 4155.

(16) Williams, D. S.; Anhaus, J. T.; Schofield, M. H.; Schrock, R. R.; Davis, W. M. *J. Am. Chem. Soc.* **1991**, *113*, 5480.

(17) Smith, D. P.; Allen, K. D.; Carducci, M. D.; Wigley, D. E. *Inorg. Chem.* **1992**, *31*, 1319.

(18) Examples of $W^{VI}{=}NR$: (a) Bradley, D. C.; Errington, R. J.; Hursthouse, M. B.; Short, R. L. *J. Chem. Soc., Dalton Trans.* **1990**, 1043. (b) Bradley, D. C.; Hursthouse, M. B.; Malik, K. M. A.; Nielson, A. J.; Short, R. L. *J. Chem. Soc., Dalton Trans.* **1983**, 2651. (c) Schrock, R. R.; DePue, R. T.; Feldman, J.; Schaverien, C. J.; Dewan, J. C.; Liu, A. H. *J. Am. Chem. Soc.* **1988**, *110*, 1423.

(19) Examples of $W^{VI}(=NR)_2$: (a) Nugent, W. A. *Inorg. Chem.* **1983**, *22*, 965. (b) Nielson, A. J. *Polyhedron* **1987**, *6*, 1657. (c) Ashcroft, B. R.; Nielson, A. J.; Bradley, D. C.; Errington, R. J.; Hursthouse, M. B.; Short, R. L. *J. Chem. Soc., Dalton Trans.* **1987**, 2059.

(20) Examples of $[W^{VI}(=NR)_4]^{2-}$: (a) Danopoulos, A. A.; Wilkinson, G.; Hussain, B.; Hursthouse, M. B. *Polyhedron* **1989**, *9*, 2947. (b) Danopoulos, A. A.; Wilkinson, G.; Hussain-Bates, B.; Hursthouse, M. B. *J. Chem. Soc., Dalton Trans.* **1990**, 2753.

(21) (a) Danopoulos, A. A.; Wilkinson, G.; Sweet, T.; Hursthouse, M. B. *J. Chem. Soc., Chem. Commun.* **1993**, 495. (b) Danopoulos, A. A.; Wilkinson, G.; Sweet, T. K. N.; Hursthouse, M. B. *J. Chem. Soc., Dalton Trans* **1994**, 1037.

(22) (a) Bryan, J. C.; Burrell, A. K.; Miller, M. M.; Smith, W. H.; Burns, C. J.; Sattelberger, A. P. *Polyhedron* **1993**, *12*, 1769. (b) Bryan, J. C.; Burns, C. J.; Sattelberger, A. P. *Isotope and Nuclear Chemistry Division Annual Report FY 1990*; Report No. LA-12143-PR; National Technical Information Service, U.S. Department of Commerce: Washington, DC, 1990; pp 40−41.

(23) Schrock, R. R.; DePue, R. T.; Feldman, J.; Yap, K. B.; Yang, D. C.; Davis, W. M.; Park, L.; DiMare, M.; Schofield, M.; Anhaus, J.; Walborsky, E.; Evitt, E.; Krüger, C.; Betz, P. *Organometallics* **1990**, *9*, 2262.

(24) Bradley, D. C.; Errington, R. J.; Hursthouse, M. B.; Short, R. L.; Ashcroft, B. R.; Clark, G. R.; Nielson, A. J.; Rickard, C. E. F. *J. Chem. Soc., Dalton Trans.* **1987**, 2067.

Scheme 1

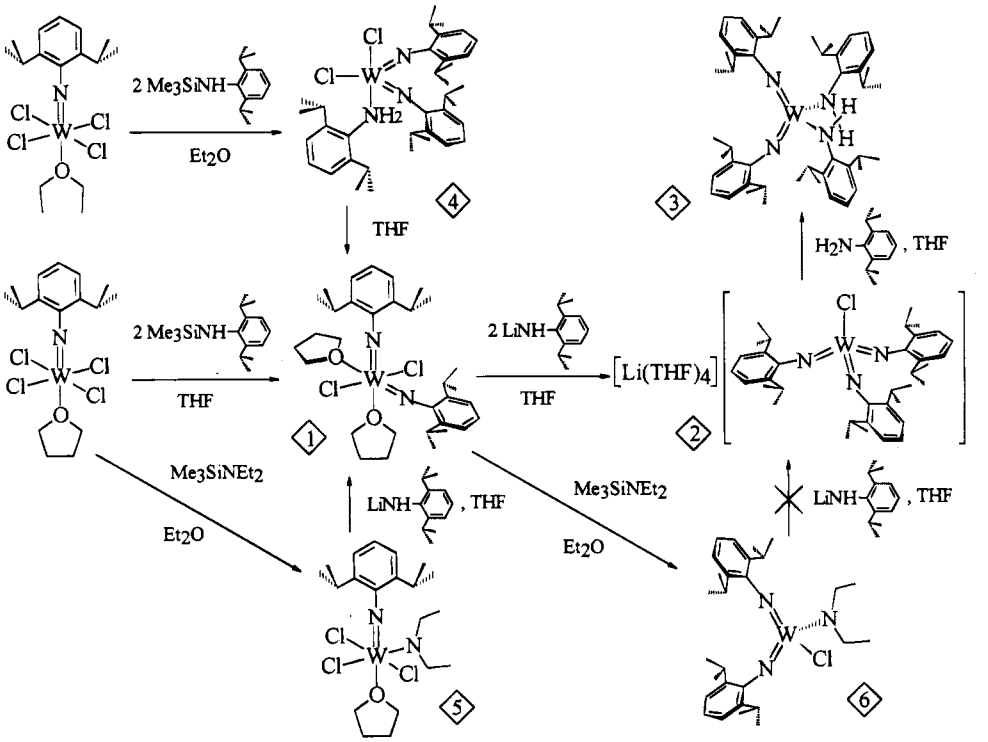

the preparation of the molybdenum analog, $[Li(THF)_4][Mo(NAr)_3Cl]$, except that $[Mo(NAr)_3Cl]^-$ reacts with H_2NAr even faster than $[W(NAr)_3Cl]^-$.[25]

The conversion of the d^0 W=NR functional group in $W(NAr)Cl_4(THF)$ to the d^0 $W(=NR)_2$ functional group in $W(NAr)_2Cl_2(THF)_2$ (**1**) could conceivably proceed by two pathways: (i) the formation of intermediate $W(NAr)(NHAr)_2Cl_2(THF)_n$ that undergoes an *intra*molecular α-H transfer to afford $W(NAr)_2Cl_2(NH_2Ar)$, followed by THF displacement of diisopropylaniline, or (ii) the intermediacy of $W(NAr)(NHAr)Cl_3(THF)$ that undergoes an *inter*molecular deprotonation by the second equivalent of base ($Me_3SiNHAr$), followed by THF displacement of Cl^- from presumed $[W(NAr)_2Cl_3(THF)]^-$. The formation of the d^0 $W(=NR)_2$ group in $W(NAr)_2Cl_2(THF)_2$ (**1**) is examined in the following experiments.

(i) When $W(NAr)Cl_4(OEt_2)$[23] reacts with 2 equiv of $Me_3SiNHAr$ in a weakly coordinating solvent, viz. Et_2O, the five-coordinate adduct $W(NAr)_2Cl_2(NH_2Ar)$ (**4**) is isolated as an orange solid in moderate yield, presumably via the unobserved bis(amide) $[W(NAr)(NHAr)_2Cl_2]$. Adding THF to **4** results in the rapid displacement of the coordinated aniline and formation of **1**. The structure proposed for **4** is analogous to the related five-coordinate $W(NSiMe_3)_2Cl_2(PMePh_2)$[26] and $Ta(NAr)_2Cl(py)_2$,[27] i.e., trigonal bipyramidal with two equatorial imides and an axial H_2NAr ligand. (Note that many imides of this stiochiometry are dimeric in the solid state.[1])

(ii) Orange, crystalline $W(NAr)(NEt_2)Cl_3(THF)$ (**5**) can be obtained in 77% yield from the reaction of $W(NAr)Cl_4(THF)$ with Me_3SiNEt_2 in Et_2O. The structure of $W(NAr)(NEt_2)Cl_3(THF)$ presented in Scheme 1 allows for the maximum number of $M(d\pi) \leftarrow N(p\pi)$ interactions since the $[NAr]^{2-}$ ligand will engage the d_{xz} and d_{yz} orbitals (with the $M-N_{imido}$ linkage defining the z axis), leaving the d_{xy} orbital available for π bonding with the amido $[NEt_2]^-$ ligand. This notion is consistent with the NMR data that reveal inequivalent ethyl groups in the NEt_2 ligand. $W(NAr)_2Cl_2(THF)_2$ (**1**) is generated in quantitative yield upon reacting $W(NAr)(NEt_2)Cl_3(THF)$ (**5**) with 1 equiv of LiNHAr (in THF), most likely via incipient $[W(NAr)(NHAr)(NEt_2)Cl_2(THF)_n]$. When this reaction is monitored in THF-d_8 (over 48 h, room temperature, ^1H NMR), exactly 1 equiv of $HNEt_2$ is produced per equiv of $W(NAr)_2Cl_2(THF)_2$ formed. Based on these experiments, the d^0 $W(=NR)_2$ group in $W(NAr)_2Cl_2(THF)_2$ (**1**) is proposed to arise through an *intra*molecular α-H abstraction sequence in an intermediate of the type $W(NAr)(NHAr)_2Cl_2(THF)_n$, with the concomitant loss of H_2NAr.

Similarly, the question of how the tris(imido) complex **2** arises from $W(NAr)_2Cl_2(THF)_2$ (**1**) and LiNHAr is also significant. One can envision the **1** + 2LiNHAr → **2** reaction proceeding either by (i) the formation of intermediate $W(NAr)_2(NHAr)_2$ that transfers an amido α-H *intra*molecularly to afford $W(NAr)_3(NH_2Ar)$, followed by displacement of aniline by Cl^-, or (ii) the intermediacy of nascent $W(NAr)_2(NHAr)Cl$ (cf. $W(NAr)_2(NEt_2)Cl$) that undergoes an *inter*molecular deprotonation by the second equivalent of $[NHAr]^-$. The formation of the d^0 $W(=NR)_3$ functional group in $[W(NAr)_3Cl]^-$ is examined in the following experiments.

(i) $W(NAr)_2Cl_2(THF)_2$ is readily functionalized using excess Me_3SiNEt_2 (in Et_2O) to provide orange crystals of the base-free amido complex $W(NAr)_2(NEt_2)Cl$ (**6**). However, upon reacting $W(NAr)_2(NEt_2)Cl$ with LiNHAr, *no* $[Li(THF)_4][W(NAr)_3Cl]$ could be identified in the reaction mixture.

(ii) As described above, byproduct H_2NAr (from the **1** + 2LiNHAr → **2** reaction) is observed to react with

(25) Morrison, D. L.; Wigley, D. E. *J. Chem. Soc., Chem. Commun.* **1995**, 79.
(26) Lichtenhan, J. D.; Critchlow, S. C.; Doherty, N. M. *Inorg. Chem.* **1990**, *29*, 439.
(27) Chao, Y.-W.; Wexler, P. A.; Wigley, D. E. *Inorg. Chem.* **1990**, *29*, 4592.

$[W(NAr)_3Cl]^-$ over a period of 1−2 days to convert it to more stable $W(NAr)_2(NHAr)_2$ (**3**) and LiCl. This reaction proceeds even in solvents in which LiCl is soluble, clearly demonstrating the thermodynamics of the $[W(NAr)_3Cl]^- + H_2NAr \rightleftarrows W(NAr)_2(NHAr)_2 + Cl^-$ system.

(iii) Accordingly, prolonged heating of solutions of $W(NAr)_2(NHAr)_2$ (**3**) in the presence of PMe_3 or $PMePh_2$ does not produce any detectable amount of either H_2NAr or the tris(imido) complexes $W(NAr)_3(PR_3)$ (^1H NMR, C_6D_6).

Thus, while the d^0 $W(=NR)_2$ group in $W(NAr)_2Cl_2(THF)_2$ (**1**) appears to arise by an *intra*molecular α-H abstraction in $[W(NAr)(NHAr)_2Cl_2(THF)_n]$, the formation of $[W(NAr)_3Cl]^-$ (**2**) from $W(NAr)_2Cl_2(THF)_2$ most likely proceeds by an *inter*molecular deprotonation of nascent $W(NAr)_2(NHAr)Cl$ by the second equivalent of $[NHAr]^-$. These results provide precedent for each step of the proposed sequence illustrated in eqs 1−7 for the sequential formation of the d^0 $W(=NR)_2$ and d^0 $W(=NR)_3$ functional groups, followed by conversion of the *kinetic* product of the $W(NAr)_2Cl_2(THF)_2$ + 2LiNHAr system, $[W(NAr)_3Cl]^-$, to the *thermodynamic* product $W(NAr)_2(NHAr)_2$. We note that the influence of a bulky aryl substituent such as 2,6-C_6H_3-*i*-Pr_2 is paramount in determining both the course of these reactions and the kinetic stability of **2**, since attempts to prepare stable $[W(NR)_3Cl]^-$ with less-hindered substituents have not yet proven fruitful.

$$W(=NR)Cl_4 + 2[NHR]^- \rightarrow W(=NR)(NHR)_2Cl_2 \quad (1)$$

$$W(=NR)(NHR)_2Cl_2 \rightarrow W(=NR)_2(NH_2R)Cl_2 \quad (2)$$

$$W(=NR)_2(NH_2R)Cl_2 + nL \rightleftarrows W(=NR)_2Cl_2L_n + H_2NR \quad (3)$$

$$W(=NR)_2(NH_2R)Cl_2 \text{ or } W(=NR)_2Cl_2L_n + [NHR]^- \rightarrow W(=NR)_2(NHR)Cl + Cl^- \quad (4)$$

$$W(=NR)_2(NHR)Cl + [NHR]^- \rightarrow [W(=NR)_3Cl]^- + H_2NR \quad (5)$$

$$[W(=NR)_3Cl]^- + H_2NR \rightarrow W(=NR)_3(NH_2R) + Cl^- \quad (6)$$

$$W(=NR)_3(NH_2R) \rightarrow W(=NR)_2(NHR)_2 \quad (7)$$

Reactions of the d^0 $W(=NR)_3$ Functional Group with Nucleophiles. $[Li(THF)_4][W(NAr)_3Cl]$ (**2**) affords a convenient source of the d^0 tris(imido) functional group of tungsten since the metal center in $[W(NAr)_3Cl]^-$ is susceptible to attack by nucleophiles, Scheme 2. Upon adding excess $PMePh_2$ to a benzene solution of $[Li(THF)_4][W(NAr)_3Cl]$, red $W(NAr)_3(PMePh_2)$ (**7**) readily forms in >90% yield. Similarly, the chloride ligand in $[Li(THF)_4][W(NAr)_3Cl]$ is smoothly displaced by PMe_3 to afford red crystals of $W(NAr)_3(PMe_3)$ (**8**) in high yield. ^1H and ^{13}C NMR spectra for **7** and **8** reveal symmetric compounds in which all of the imido ligands are equivalent, consistent with free rotation around the W−N−C_{ipso} linkage and a three-fold axis of symmetry.

Treatment of **2** with $[n\text{-}Bu_4N]Br$ also results in the loss of LiCl and the formation of $[n\text{-}Bu_4N][W(NAr)_3Br]$ (**9**) as an orange solid in 90% yield, Scheme 2. Alkylation reactions also proceed smoothly at low temperatures; reacting **2** with MeLi in THF at −35 °C cleanly yields $[Li(THF)_4][W(NAr)_3Me]$ (**10**) as a yellow solid in good yield. Complex **10** exhibits coupling of the methyl resonance to ^{183}W [14% abundance, $^2J(^{183}W-^1H) = 11$ Hz] in its ^1H NMR spectrum. The analogous reaction between **2** and $LiCH_2SiMe_3$ affords $[Li(THF)_4][W(NAr)_3(CH_2SiMe_3)]$ (**11**) as a yellow solid in moderate yield. One significant question concerning these nucleophilic displacements is whether they proceed via a binuclear, S_N2 attack on $[W(NAr)_3Cl]^-$ or via an S_N1 loss of chloride ion and generation of the short-lived intermediate $[W(NAr)_3]$. The displacement reactions described above are observed to proceed at rates that are *nucleophile dependent*, suggesting the former, bimolecular pathway. Attempts to form base-free $[W(NAr)_3]$ are described below.

Molecular and Electronic Structures of Complexes Containing the d^0 $W(=NR)_3$ Functional Group. Yellow single crystals of $[Li(THF)_4][W(NAr)_3Cl]$ suitable for a structural determination were grown from THF/pentane solution at −35 °C. A summary of the crystal data and the structural analysis is given in Table 1, and relevant bond distances and angles are given in Table 2. Figure 1 presents the molecular structure of the $[W(NAr)_3Cl]^-$ anion in $[Li(THF)_4][W(NAr)_3Cl]$, in which the tungsten atom is tetrahedrally coordinated with three virtually identical imido ligands. The W−N−C_{ipso} bond angles are close to linear at 171° (av), and the average W−N bond length is 1.78 Å. Some tilting of the phenyl rings in a propeller arrangement is evident since a more favorable orientation of the isopropyl groups about the metal−chloride bond is attained.

Red single crystals of $W(NAr)_3(PMe_3)$ (**8**) suitable for a structural determination were grown from toluene/pentane solution at −35 °C. A summary of the crystal data and the structural analysis is given in Table 1, and key bond distances and angles are given in Table 3. Figure 2 presents the molecular structure $W(NAr)_3(PMe_3)$ and reveals a tetrahedrally coordinated tungsten atom with the P−C bonds of PMe_3 staggering the W−N bonds of the $W(NAr)_3$ moiety. Also evident are some slight differences in the local coordination geometry as compared to $[W(NAr)_3Cl]^-$. The average imido W−N bond length is 1.79 Å, and the W−N−C_{ipso} bond angles are slightly bent (av 167°), though one imido ligand is more strongly bent than the other two. Thus, the W−N(2)−C(21) angle of 161.4(9)° is roughly 10° more acute than the other two imido bond angles. It seems likely that solid state effects are responsible for the slight distortion of this one imido ligand, as well as the resultant deviation from C_{3v} symmetry, since there appears to be no electronic constraints that might induce such a bend (vide infra).

Table 4 compares average bond angles and lengths for the imido ligands in **2** and **8**, as well as their local tetrahedral geometries, and includes the results of Cundari's ab initio calculations on hypothetical $[W(NH)_3Cl]^-$.[13,28] Aside from the somewhat bent W−N(2)−C(21) angle in $W(NAr)_3(PMe_3)$ (**8**), the imido ligand geometries in the two structurally characterized complexes are nearly identical. However, an examina-

Scheme 2

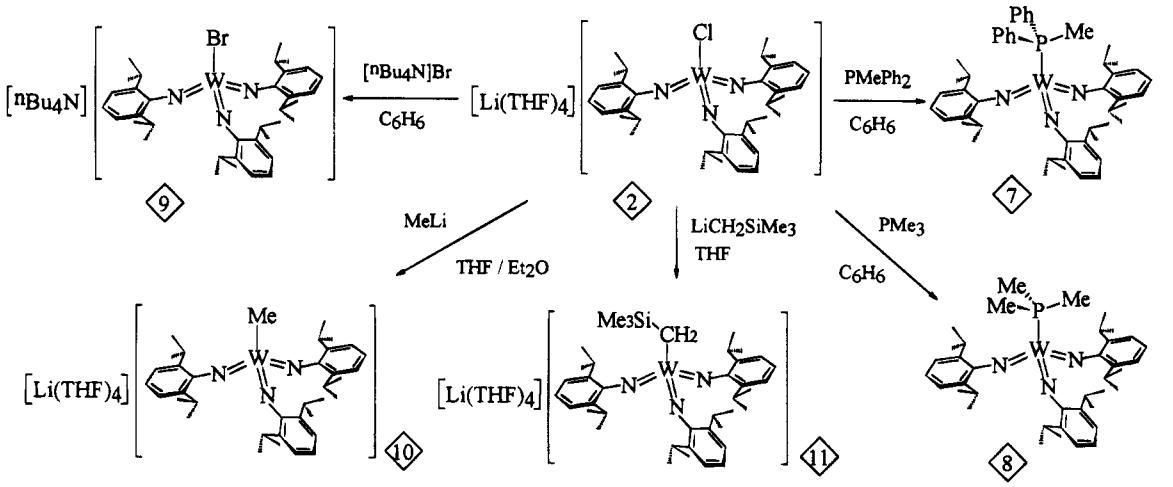

Table 1. Details of the X-ray Diffraction Studies for [Li(THF)$_4$][W(NAr)$_3$Cl] (2) and W(NAr)$_3$(PMe$_3$) (8)

parameter	[Li(THF)$_4$][W(NAr)$_3$Cl]	W(NAr)$_3$(PMe$_3$)
	Crystal Parameters	
molecular formula	$C_{52}H_{83}ClLiN_3O_4W$	$C_{39}H_{60}N_3PW$
molecular weight	1040.49	785.76
F(000)	2168	3232
crystal color	yellow	red
space group	monoclinic $P2_1/n$ (No. 14)	orthorhombic $Pbca$ (No. 61)
unit cell volume, Å^3	5449(3)	8111(4)
a, Å	13.787(4)	18.572(3)
b, Å	17.348(5)	25.966(4)
c, Å	22.781(8)	16.819(3)
β, deg	90.43(3)	
Z	4	8
D(calc), g cm^{-3}	1.27	1.29
crystal dimens, mm	0.46 × 0.32 × 0.06	0.23 × 0.23 × 0.47
absorpt coeff, cm^{-1}	23.3	29.7
data collctn temp, °C	23 ± 1	19 ± 1
	Data Collection	
diffractometer	Nicolet R3m	Syntex P2$_1$, Crystal Logics
monochromator	graphite crystal	graphite crystal, incident beam
Mo Kα radiation, λ, Å	0.710 73	0.710 73
2θ range, deg	4–45	2–50
octants collected	$\pm h+k+l$	$+h+k+l$
scan type	$\omega-2\theta$	$\omega-2\theta$
scan speed, deg min^{-1}	5.0–20.0	3.0
total no. of reflns measd	6967 (6532 unique)	7839 (7141 unique)
corrections	Lorentz-polarization, Ψ-scan absorption	Lorentz-polarization, Ψ-scan absorption
	Solution and Refinement	
solution	Patterson method	Patterson method
refinement	blocked-matrix least-squares	full-matrix least-squares
reflns used in refinement	2938 with $F > 5\sigma(F)$	2907 with $I > 3\sigma(I)$
parameters refined	359	397
R	0.068	0.036
R_w	0.064	0.048
esd of obs of unit weight (GOF)	1.23	1.28
Δ/σ(max), e^{-1}/Å^3	0.822	0.65(10)
Δ/σ(min), e^{-1}/Å^3	0.943	−0.30(10)
computer hardware	Data General Eclipse S-30	VAX
computer software	SHELXTL (4.2)	MolEN (Enraf-Nonius)

tion of the local tetrahedral geometries is instructive. As indicated in Table 4, the tetrahedron of the PMe$_3$ adduct W(NAr)$_3$(PMe$_3$) (**8**) is more "flattened" toward a trigonal pyramidal structure as compared to the more nearly tetrahedral [W(NAr)$_3$Cl]$^-$ (**2**). Thus, the tungsten atom in [W(NAr)$_3$Cl]$^-$ lies 0.72 Å out of the imido N$_3$ plane, while the tungsten atom in W(NAr)$_3$(PMe$_3$) is only 0.39 Å out of this molecule's N$_3$ plane. Bryan and co-workers[22b] have taken such parameters to indicate increased imido ligand π donation in the flattened, more pyramidal complexes in comparing technetium tris(imido) complexes. Indeed, in the molecular π *framework*, the chloride ion can engage in π bonding, whereas PMe$_3$ cannot; however, we hasten to add that the structural differences deliberated by this possible effect are slight. We note that in both complexes, the X–W–N angles are all less than 109° and the N–W–N angles are all greater than 109°.

In describing the electronic structure of C_{3v} M(NR)$_3$L complexes, as well as their D_{3h} M(NR)$_3$ relatives such as Os(NAr)$_3$,[29] it is convenient to consider these species

(28) For an analysis of methane binding by base-free W(=NH)$_3$, see: Cundari, T. R. *Organometallics* **1993**, *12*, 1998.

Table 2. Selected Bond Distances (Å) and Bond Angles (deg) in $[Li(THF)_4][W(NAr)_3Cl]$ (2)[a]

	Bond Distances		
W–Cl	2.342(6)	N(1)–C(16)	1.398(25)
W–N(1)	1.777(15)	N(2)–C(36)	1.415(26)
W–N(2)	1.763(15)	N(3)–C(56)	1.430(29)
W–N(3)	1.805(18)		
	Bond Angles		
Cl–W–N(1)	106.0(6)	N(2)–W–N(3)	112.1(7)
Cl–W–N(2)	104.7(5)	W–N(1)–C(16)	173.4(16)
Cl–W–N(3)	107.2(6)	W–N(2)–C(36)	167.7(14)
N(1)–W–N(2)	112.5(7)	W–N(3)–C(56)	171.4(15)
N(1)–W–N(3)	113.5(7)		

[a] Numbers in parentheses are estimated standard deviations in the least significant digits.

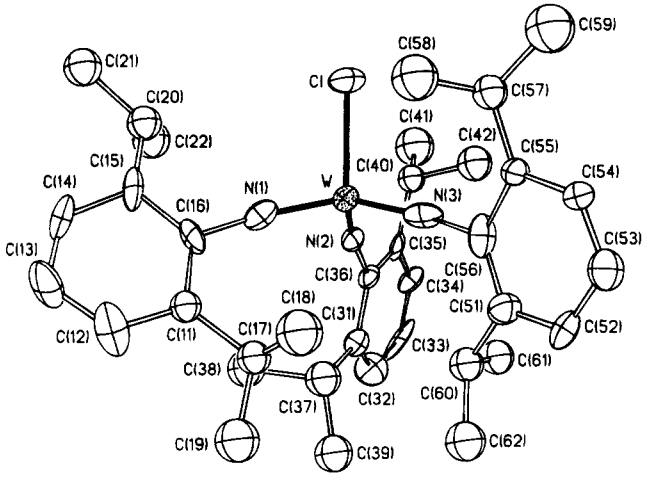

Figure 1. Molecular structure of the $[W(NAr)_3Cl]^-$ anion in $[Li(THF)_4][W(NAr)_3Cl]$ (2) with atoms represented as 35% ellipsoids.

Table 3. Selected Bond Distances (Å) and Bond Angles (deg) in $W(NAr)_3(PMe_3)$ (8)[a]

	Bond Distances		
W–P	2.466(4)	N(1)–C(11)	1.40(1)
W–N(1)	1.78(1)	N(2)–C(21)	1.38(1)
W–N(2)	1.80(1)	N(3)–C(31)	1.38(1)
W–N(3)	1.79(1)		
	Bond Angles		
P–W–N(1)	97.3(3)	N(2)–W–N(3)	112.8(4)
P–W–N(2)	104.8(3)	W–N(1)–C(11)	172.5(8)
P–W–N(3)	105.9(3)	W–N(2)–C(21)	161.4(9)
N(1)–W–N(2)	117.3(5)	W–N(3)–C(31)	169(1)
N(1)–W–N(3)	115.9(4)		

[a] Numbers in parentheses are estimated standard deviations in the least significant digits.

as "$M(1\sigma,2\pi)_3$" complexes, characterizing the symmetries of the $[NAr]^{2-}$ donor orbitals. Thus, tris(imido) complexes such as $W(NAr)_3L$ ($L = X^-$ or PR_3) and $Os(NAr)_3$ have been characterized by a ligand-based, nonbonding a_2 (C_{3v}) or a_2' (D_{3h}) MO comprised of a set of ligand π orbitals oriented perpendicular to the molecule's C_3 axis, Figure 3. Therefore, while each of these compounds may be considered a 20 electron species if the ligands donate their full complement of electrons to the metal, it has been established[11c,12,29] (in three-fold symmetry) that occupation of this nonbonding MO results in these compounds being more accurately

(29) (a) Anhaus, J. T.; Kee, T. P.; Schofield, M. H.; Schrock, R. R. *J. Am. Chem. Soc.* **1990**, *112*, 1642. (b) Schofield, M. H.; Kee, T. P.; Anhaus, J. T.; Schrock, R. R.; Johnson, K. H.; Davis, W. M. *Inorg. Chem.* **1991**, *30*, 3595.

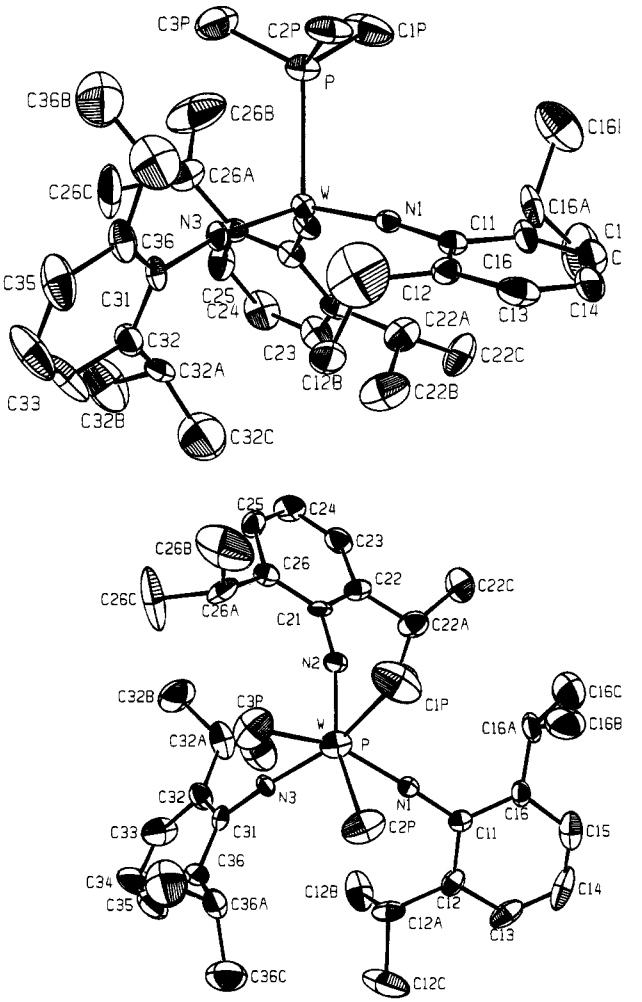

Figure 2. Molecular structure of $W(NAr)_3(PMe_3)$ (8) with atoms represented as 20% ellipsoids.

Table 4. Comparison of Structural Data[a] for $[W(NAr)_3Cl]^-$ (2) and $W(NAr)_3(PMe_3)$ (8)

	$[W(NAr)_3Cl]^-$	$W(NAr)_3(PMe_3)$	$[W(NH)Cl]^-$ [b]
W=N (Å)	1.78	1.79	1.79
∠W–N–C_{ipso} (deg)	170.8	167.6	
∠X–W–N (deg)	106.0	102.7	
∠N–W–N (deg)	112.7	115.3	112

[a] Average values. [b] Ab initio calculations from ref 13.

described as 18 electron complexes.[30] There is now a significant number of d^0 tris(imido) species characterized by this same orbital description, including $Re(NR)_3X$,[31] $Tc(NAr)_3X$,[14,22] $Mo(NAr)_3(PMe_3)$,[25] and $Mn(N\text{-}t\text{-}Bu)_3X$.[21] A simple, qualitative orbital interaction diagram for complexes of the form $W(NAr)_3L$ ($L = X^-$ or PR_3) is presented in Figure 3. The bonding description in C_{3v} symmetry of complexes of the type $M(NR)_3L$ (where L is a σ donor only) is illustrated by ligand and metal orbitals of the following symmetries: ligand σ ($2a_1 + e$), ligand π ($a_1 + 2e + a_2$), metal s + p ($2a_1 + e$), and

(30) See also: (a) Maher, J. M.; Fox, J. R.; Foxman, B. M.; Cooper, N. J. *J. Am. Chem. Soc.* **1984**, *106*, 2347. (b) Laine, R. M.; Moriarty, R. E.; Bau, R. *J. Am. Chem. Soc.* **1972**, *94*, 1402. (c) King, R. B. *Inorg. Chem.* **1968**, *7*, 1044.

(31) (a) Herrmann, W. A.; Weichselbaumer, G.; Paciello, R. A.; Fischer, R. A.; Herdtweck, E.; Okuda, J.; Marz, D. *Organometallics* **1990**, *9*, 489. (b) Longley, C. J.; Savage, P. D.; Wilkinson, G.; Hussain, B.; Hursthouse, M. B. *Polyhedron* **1988**, *7*, 1079. (c) Gutierrez, A.; Wilkinson, G.; Hussain-Bates, B.; Hursthouse, M. B. *Polyhedron* **1990**, *9*, 2081. (d) Horton, A. D.; Schrock, R. R. *Polyhedron* **1988**, *7*, 1841.

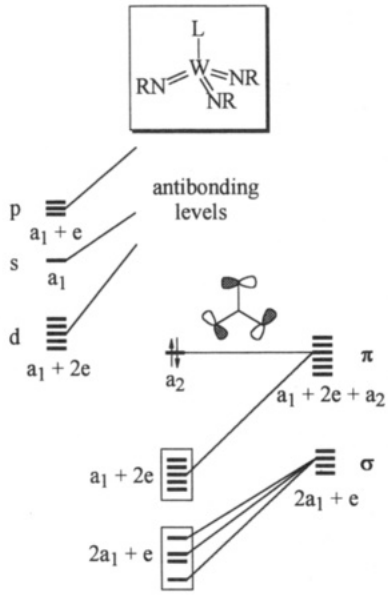

Figure 3. Qualitative orbital interaction diagram for $W(NAr)_3L$ complexes (L = σ donor only) in C_{3v} symmetry.

metal d ($a_1 + 2e$).[1,32] Thus, one of the ligand π orbitals, the a_2, is necessarily nonbonding. An analogous electronic structure also appears to describe certain d^1 complexes, such as $Tc_2(NAr)_6$.[33]

Reactions of the d^0 W(=NR)$_3$ Functional Group with Electrophiles. The presence of a nonbonding a_2 MO situated on the imido nitrogens in $W(NR)_3L$, which appears to be the HOMO of these complexes, suggests that this orbital might be subject to electrophilic attack. Thus, the reaction of $W(NAr)_3(PMe_3)$ (**8**) with 1 equiv of HOAr′ (Ar′ = 2,6-$C_6H_3Me_2$) affords yellow crystals of $W(NAr)_2(NHAr)(OAr')$ (**12**) in low to moderate yield, Scheme 3. The low yield of this complex can be attributed in part to its extreme solubility. Other electrophiles also attack the imido nitrogens with formation of a compound of the form $W(NAr)_2(NEAr)X$. For example, excess Me_3SiI can be added to a pentane solution of $W(NAr)_3(PMe_3)$ to provide a moderate yield of $W(NAr)_2[N(SiMe_3)Ar]I$ (**13**). Similarly, excess methyl iodide reacts with $W(NAr)_3(PMe_3)$ in benzene, forming yellow $W(NAr)_2(NMeAr)I$ (**14**) and byproduct $[Me_4P]I$. The broad resonances observed in the ^1H NMR spectra of these species at room temperature are consistent with rotation about the $W-N_{amide}$ bond on the order of the NMR time scale. However, at lower temperatures, rotation about $W-N_{amide}$ is slowed, and spectra consistent with the structures presented in Scheme 3 are observed. A cycloaddition reaction occurs between PhNCO and a W=NAr bond in $W(NAr)_3(PMe_3)$ to afford the metallacyclic complex $W[NArC(O)NPh](NAr)_2(PMe_3)$ (**15**). ^1H and ^{13}C NMR data for **15** indicate that only one imido ligand has reacted with isocyanate, even though excess PhNCO is present. The proposed regiochemistry is that expected from the polarity of the $W^{\delta+}-N^{\delta-}$ bond and the highly electropositive carbon in PhNCO and is consistent with the strong mode at 1654 cm^{-1} (Nujol mull) in the IR spectrum of 15 that is assigned as ν(C=O), Scheme 3. Accordingly, similar metallacyclic structures have been reported with this same regiochemistry.[34]

Since metal–carbon bonds in early metal alkyl complexes are typically subject to electrophilic attack, the question arises whether $[Li(THF)_4][W(NAr)_3R]$ compounds will be protonated at the alkyl or the imido ligand. Thus, $[Li(THF)_4][W(NAr)_3Me]$ (**10**) is found to react with $[HNMe_3]BPh_4$ in Et_2O to form yellow crystals of $W(NAr)_2(NHAr)Me$ (**16**), as indicated in eq 8.

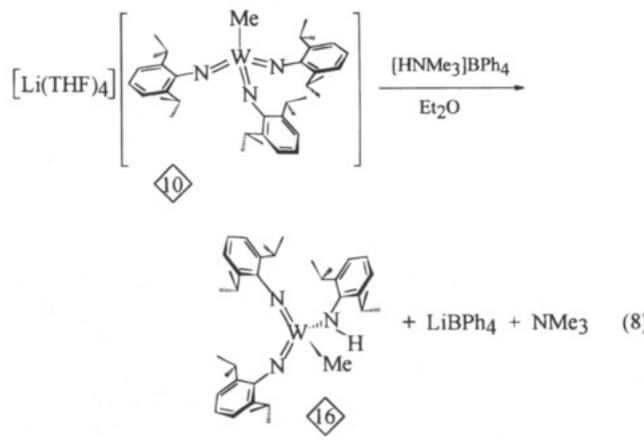

(8)

Attempts To Generate Base-Free [W(NAr)$_3$]. $W(NAr)_3L$ derivatives are characterized as saturated compounds, and highly polar $W^{\delta+}-N^{\delta-}$ bonds are a feature of this π-loaded system; therefore, we considered whether generating base-free, 16 electron $[W(NAr)_3]$ would provide a highly reactive species that might be capable of, inter alia, activating C–H bonds. Such a notion is supported by Cundari's ab initio calculations on base-free $[W(NH)_3]$ that suggest a *pyramidal* ground state, a highly distended d_{z^2} LUMO, and extremely polar $W^{\delta+}-N^{\delta-}$ bonds.[13] These features have led to calculations of hypothetical $[W(NH)_3]$ that coordinates methane [as the adduct $W(NH)_3(\eta^2\text{-}CH_4)$] with the highest binding energy of all the imido complexes examined[28] and suggest that C–H activation by base-free $[W(NAr)_3]$ should be facile. In the event that base-free, nascent $[W(NAr)_3]$ could be generated, either a solvent C–H bond activation product, a stable dinuclear species, or some other product that arises from $[W(NAr)_3]$ might be isolated. The following experiments were carried out in attempts to form transient $[W(NAr)_3]$.

(i) Attempts to precipitate chloride ion from solutions of $[W(NAr)_3Cl]^-$ by addition of $AgBPh_4$ in THF resulted in no reaction, even under forcing conditions.

(ii) Attempts to remove PMe_3 from $W(NAr)_3(PMe_3)$ under high-vacuum and high-temperature conditions (e.g., 10^{-6} Torr and >100 °C) resulted in no reaction; starting material was recovered.

(iii) The gradual (over several days) precipitation of LiCl is observed from solutions of $[Li(THF)_4][W(NAr)_3Cl]$ (**2**) in benzene, and the formation of a complex formulated as $W(NAr)_3(THF)\cdot n$THF (n = 2–3) by ^1H NMR is observed. Attempts to remove THF from $W(NAr)_3$-

(32) Lin, Z.; Hall, M. B. *Coord. Chem. Rev.* **1993**, *123*, 149.

(33) (a) Burrell, A. K.; Bryan, J. C. *Angew. Chem., Int. Ed. Engl.* **1993**, *32*, 94. (b) Burrell, A. K.; Bryan, J. C.; Clark, D. L.; Smith, W. H.; Burns, C. J.; Sattelberger, A. P. *Abstracts of Papers*, 205th National Meeting of the American Chemical Society, Denver, CO, Spring 1993; American Chemical Society: Washington, DC, 1993; INOR 391.

(34) (a) Leung, W.-H.; Wilkinson, G.; Hussain-Bates, B.; Hursthouse, M. B. *J. Chem. Soc., Dalton Trans.* **1991**, 2791. (b) Hasselbring, R.; Roesky, H. W.; Noltemeyer, M. *Angew. Chem., Int. Ed. Engl.* **1992**, *31*, 601. (c) Legzdins, P.; Phillips, E. C.; Rettig, S. J.; Trotter, J.; Veltheer, J. E.; Yee, V. C. *Organometallics* **1992**, *11*, 3104.

Scheme 3

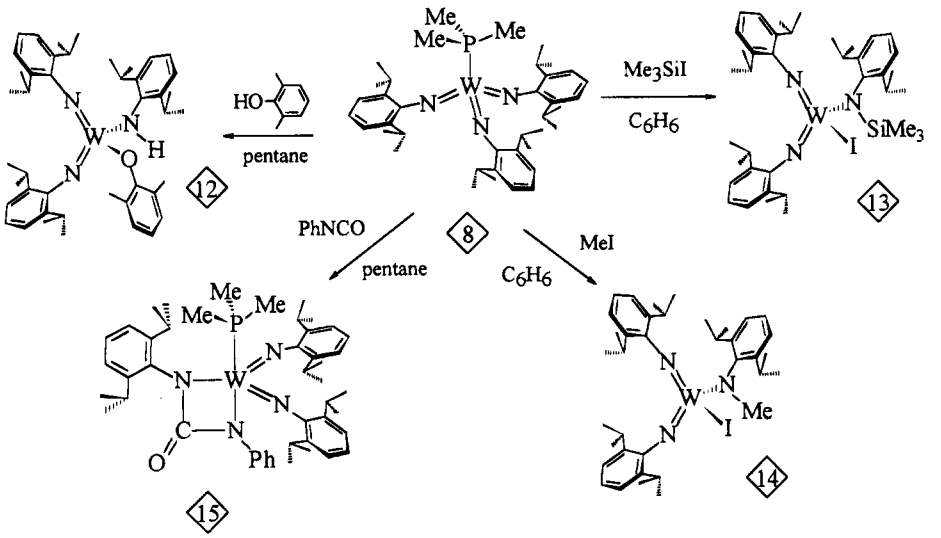

(THF)·*n*THF under high-vacuum and high-temperature conditions resulted in the loss of some THF, with the analysis of the residue approaching a minimum THF component of $W(NAr)_3(THF)$·THF (i.e., $n = 1$). NMR data for this compound reveal equivalent though broad THF resonances, suggesting exchange between free and bound THF. ($W(NAr)_3(THF)$·*n*THF has rarely been induced to crystallize.) In no case was evidence for base-free $[W(NAr)_3]$ or the solvent C−H activation product $W(NAr)_2(NHAr)Ph$ observed.

(iv) Extended thermolysis of $W(NAr)_2(NHAr)Me$ (**16**) (vide supra) in refluxing benzene affords no evidence for the elimination of CH_4 and the formation of either a C−H bond activation product $W(NAr)_2(NHAr)Ph$ that might arise via the formation of base-free $[W(NAr)_3]$ or any other product that might arise from $[W(NAr)_3]$ under these conditions.

These experiments are consistent with the mechanistic studies described above, suggesting that ligand dissociation from $W(NAr)_3L$ ($L = X^-$ or PR_3) to generate $[W(NAr)_3]$ in the absence of a nucleophile is unlikely. Furthermore, the fact that $W(NAr)_2(NHAr)Me$ does not eliminate methane is most likely a reflection of the thermodynamic differences between $[W(NAr)_3] + CH_4$ and $W(NAr)_2(NHAr)(CH_3)$ as predicted from the high-energy, *pyramidal* ground state calculated for $[W(NAr)_3]$.[13]

Discussion

When the reaction of $W(NAr)_2Cl_2(THF)_2$ with LiNHAr is allowed to proceed for more than several hours, significant amounts of $W(NAr)_2(NHAr)_2$ are isolated from the reaction mixture. After prolonged reaction time, most of the kinetic product $[Li(THF)_4][W(NAr)_3Cl]$ has converted to the more stable $W(NAr)_2(NHAr)_2$. This feature is also established by reacting isolated $[Li(THF)_4][W(NAr)_3Cl]$ with H_2NAr, which affords $W(NAr)_2(NHAr)_2$ in near quantitative yield; therefore, reaction time is crucial for the successful isolation of $[Li(THF)_4][W(NAr)_3Cl]$. This reaction probably proceeds through the intermediacy of unstable $[W(NAr)_3(NH_2Ar)]$, as suggested in Scheme 4, and, consistent with the experiments described above, clearly demonstrates the thermodynamic preferences of this system.

Scheme 4

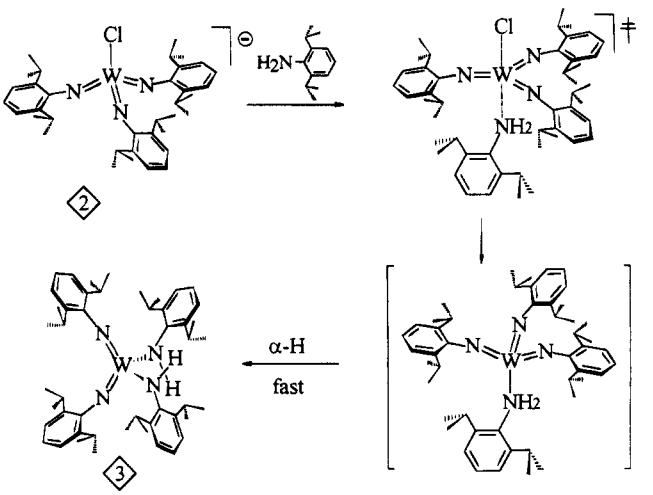

The polarity of the $W^{\delta+}-N^{\delta-}$ bonds of the imido ligands in the d^0 tris(imido) complexes make them subject to both nucleophilic and electrophilic attack, as described above. Reactions with electrophiles underscore the stability of four-coordinate bis(imido) complexes of W^{VI} of the form $W(NAr)_2X_2$ and five-coordinate bis(imido) metallacyclic compounds, relative to the higher energy $W(NAr)_3L$ derivatives.

Since the cyclopentadienyl anion $[C_5R_5]^-$, the acetylene dianion $[RC{\equiv}CR]^{2-}$, and oxo O^{2-}, nitrido N^{3-}, and alkylidyne $[CR]^{3-}$ ligands may all be described as $1\sigma,2\pi$ donors,[11a,c,16,35] one might expect analogies in the stoichiometries and structures of their compounds. Therefore, other C_{3v} or D_{3h} compounds that are intimately related by analogous orbital descriptions include tris(alkyne) compounds, such as $Re(RC{\equiv}CR)_3X$ (X = I, Me, or $OSiMe_3$),[36] $[W(RC{\equiv}CR)_3]^{2-}$,[30a] and $W(RC{\equiv}CR)_3L$.[30b,c] An argument has been made regarding the application of such an orbital description to mixed-ligand species

(35) Williams, D. S.; Schofield, M. H.; Anhaus, J. T.; Schrock, R. R. *J. Am. Chem. Soc.* **1990**, *112*, 6728.

(36) (a) Manion, A. B.; Erikson, T. K. G.; Spaltenstein, E.; Mayer, J. M. *Organometallics* **1989**, *8*, 1871. (b) Spaltenstein, E.; Conry, R. R.; Critchlow, S. C.; Mayer, J. M. *J. Am. Chem. Soc.* **1989**, *111*, 8741. (c) Mayer, J. M.; Atagi, L. M.; Conry, R. R.; Brown, S. N. *Abstracts of Papers*, 201st National Meeting of the American Chemical Society, Atlanta, GA, Spring, 1991; American Chemical Society: Washington, DC, 1991; INOR 468.

with $1\sigma,2\pi$ *orbital* symmetry, such as $Re(RC{\equiv}CR)_2(NR)X$[11a] and $(\eta^5\text{-}C_5Me_5)W(NAr)_2Cl$.[11c]

These experiments reported here suggest one way to attain reactive imido ligands: π-loading appears to encourage *highly polar* $M^{\delta+}-N^{\delta-}$ linkages and renders the imido ligand especially susceptible to electrophilic attack. Since factors that favor C−H bond activation by imido ligands include (i) an imido nitrogen bearing a large negative charge and (ii) an empty metal orbital of σ symmetry,[9,28] ligand loss from $W(NAr)_3L$ to generate transient, 16 electron $W(NAr)_3$ would presumably form a species capable of such reactivity. However, we have found no indication that a ligand coordinated to $[W(NAr)_3]$ is labile, nor have attempts to eliminate alkane RH upon thermolyzing $W(NAr)_2(NHAr)R$ been successful. Since base-free $[W(NAr)_3]$ is not required for any of the reactions reported here, we conclude that it is highly energetic and does not form if a lower energy pathway is accessible. The preparation and reactivity of such species are areas of our continued interest.

Experimental Section

General Details. All experiments were performed under a nitrogen atmosphere either by standard Schlenk techniques[37] or in a Vacuum Atmospheres HE-493 drybox at room temperature (unless otherwise indicated). Solvents were distilled under N_2 from an appropriate drying agent[38] and were transferred to the drybox without exposure to air. The "cold" solvents used to wash isolated solid products were typically cooled to ~−35 °C before use. NMR solvents were passed down a short (5−6 cm) column of activated alumina prior to use. In all preparations, Ar = 2,6-C_6H_3-*i*-Pr_2 and Ar′ = 2,6-$C_6H_3Me_2$.

Starting Materials. $WOCl_4$ was obtained from Hermann C. Stark (Berlin), sublimed (~80 °C, 10^{-2} Torr) prior to use, and converted to $W(NAr)Cl_4$ and then to $W(=NAr)Cl_4(THF)$ or $W(=NAr)Cl_4(Et_2O)$ according to the literature procedures.[23] 2,6-Diisopropylaniline was obtained from Aldrich, vacuum distilled before use, and converted to LiNHAr[39] according to the literature procedure. $Me_3SiNHAr$ was prepared from LiNHAr and Me_3SiCl as previously described.[39] Me_3SiI and Me_3SiNEt_2 were obtained from Petrarch and used as received. Methyl iodide was obtained from EM Sciences and distilled prior to use. Alkyllithium solutions (used as received), $[HNMe_3]BPh_4$ (used as received), phenyl isocyanate (distilled), and HO-2,6-$C_6H_3Me_2$ (sublimed) were obtained from Aldrich. Trimethylphosphine was prepared and purified according to the literature procedure,[40] with the modification of using MeMgI rather than MeMgBr in the preparation. $PMePh_2$ was obtained from Strem and used as received. Tetraalkylammonium bromide was dried by heating to ~120 °C under high vacuum (>10^{-6} Torr), followed by recrystallization from minimal THF at −35 °C. $AgBPh_4$ was prepared according to the literature procedure.[41]

Physical Measurements. ^1H (250 MHz) and ^{13}C (62.9 MHz) NMR spectra were recorded at probe temperature (unless otherwise specified) on a Brucker WM-250 or AM-250 spectrometer in C_6D_6, $CDCl_3$, CD_2Cl_2, or toluene-d_8 solvent. Chemical shifts are referenced to protio impurities (δ 7.15, C_6D_6; 7.24, $CDCl_3$; 5.32, CD_2Cl_2; 2.09, toluene-d_8) or solvent ^{13}C resonances (δ 128.0, C_6D_6; 77.0, $CDCl_3$; 53.8, CD_2Cl_2; 20.4, toluene-d_8) and are reported downfield of Me_4Si. ^{13}C NMR assignments were assisted by APT spectra. Infrared spectra were recorded as Nujol mulls (NaCl plates) between 4000 and 600 cm^{-1} using a Perkin-Elmer 1310 spectrometer. Microanalytical samples were stored cold, handled under N_2, and combusted with WO_3 (Texas Analytical Laboratories, Inc., Stafford, TX, or Desert Analytics, Tucson, AZ).

Preparations. $W(NAr)_2Cl_2(THF)_2$ (1). Neat $Me_3SiNHAr$ (4.33 g, 17.4 mmol) was added dropwise to a stirred solution of 5.00 g (8.69 mmol) of $W(NAr)Cl_4(OEt_2)$ in ~85 mL of THF. (The solution of $W(NAr)Cl_4(OEt_2)$ in THF immediately forms $W(NAr)Cl_4(THF)$.) This mixture was heated to 60 °C for 48 h, over which time its color changed from dark green to bright red. The reaction volatiles were then removed in vacuo to provide the product as a microcrystalline, red solid. This solid was washed with cold heptane, collected by filtration, and dried in vacuo. Additional product was obtained upon concentrating the heptane filtrate and cooling to −35 °C; yield (two crops) 5.28 g (7.04 mmol, 81%). Analytically pure samples were obtained from pentane/Et_2O solutions at −35 °C. Either $W(NAr)Cl_4$ or (isolated) $W(NAr)Cl_4(THF)$ can also be used in this preparation, although $W(NAr)Cl_4(OEt_2)$ is preferred since it can be obtained purer than $W(NAr)Cl_4$. If this reaction is run under more dilute conditions, the product is contaminated with varying amounts of $W(NAr)_2Cl_2(NH_2Ar)$, and heating must be prolonged for several more days for $W(NAr)_2Cl_2(THF)_2$ to form completely. ^1H NMR (C_6D_6): δ 7.13−6.81 (A_2B mult, 6 H, H_{aryl}), 4.09 (spt, 4 H, C*H*Me_2), 3.87 (br, 8 H, $C_\alpha H$, THF), 1.34 (br, 8 H, $C_\beta H$, THF), 1.26 (d, 24 H, CH*Me*$_2$). ^{13}C NMR (C_6D_6): δ 151.2 (C_{ipso}), 144.9 (C_o), 126.6 (C_p), 122.5 (C_m), 71.2 (C_α, THF), 27.8 (*C*HMe$_2$), 25.6 (C_β, THF), 24.7 (CH*Me*$_2$). Anal. Calcd for $C_{32}H_{50}Cl_2N_2O_2W$: C, 51.28; H, 6.72; N, 3.74. Found: C, 51.68; H, 6.95; N, 3.97.

[Li(THF)$_4$][W(NAr)$_3$Cl] (2). A solution of LiNHAr (0.977 g, 5.33 mmol) in 15 mL of THF was added dropwise to a rapidly stirred solution of $W(NAr)_2Cl_2(THF)_2$ (**1**) (2.00 g, 2.67 mmol) in ~50 mL of THF. The reaction was allowed to stir at room temperature for 2 h, over which time its color changed from red to yellow. The reaction volatiles were then removed in vacuo to provide a yellow oil. The product was extracted from the oil with Et_2O (~20 mL), the extract was filtered through Celite, and the solvent was removed from the filtrate in vacuo to yield a waxy, yellow solid. This solid was transferred to a frit, pumped on for ~1 h to remove H_2NAr, washed with cold pentane (3 × 10 mL), and dried in vacuo, yielding a yellow, microcrystalline solid. Additional product was obtained by concentrating the pentane wash and cooling to −35 °C; yield (two crops) 2.074 g (1.99 mmol, 75%). Analytically pure samples were obtained by recrystallization from THF/pentane solutions at −35 °C. ^1H NMR (CD_2Cl_2): δ 6.97−6.65 (A_2B mult, 9 H, H_{aryl}), 3.71 (m, 16 H, $C_\alpha H$, THF), 3.57 (spt, 6 H, C*H*Me_2), 1.90 (m, 16 H, $C_\beta H$, THF), 1.06 (d, 36 H, CH*Me*$_2$). ^1H NMR (C_6D_6): δ 7.17−6.91 (A_2B mult, 9 H, H_{aryl}), 3.81 (spt, 6 H, C*H*Me_2), 3.35 (m, 16 H, $C_\alpha H$, THF), ~1.3 (obscured m, 16 H, $C_\beta H$, THF), 1.26 (d, 36 H, CH*Me*$_2$). ^{13}C NMR (CD_2Cl_2): δ 140.4 (C_0), 125.1 (C_{ipso}), 122.0 (overlapping C_m and C_p), 68.7 (C_α, THF), 28.3 (*C*HMe$_2$), 25.8 (C_β, THF), 23.8 (CH*Me*$_2$). ^{13}C NMR (C_6D_6): δ 154.7 (C_{ipso}), 140.3 (C_o), 122.9 (C_p), 122.4 (C_m), 68.4 (C_α, THF), 28.3 (*C*HMe$_2$), 25.4 (C_β, THF), 24.2 (CH*Me*$_2$). Anal. Calcd for $C_{52}H_{83}ClLiN_3O_4W$: C, 60.03; H, 8.04; N, 4.04; Cl, 3.41. Found: C, 59.54; H, 8.44; N, 4.15; Cl, 2.81. This complex loses THF under prolonged vacuum.

W(NAr)$_2$(NHAr)$_2$ (3). To a solution of 0.20 g (0.192 mmol) of $[Li(THF)_4][W(NAr)_3Cl]$ (**2**) in 20 mL of benzene was added a solution of 1 equiv of H_2NAr (0.034 g, 0.192 mmol) in 5 mL of benzene. This mixture was stirred at room temperature for 36 h, over which time a white solid (presumably LiCl) precipitated, but little change in solution color was observed. The solution was then filtered through Celite, and the volatile components were removed from the filtrate in vacuo to afford a sticky, yellow solid. This solid was washed with cold

(37) Shriver, D. F.; Drezdzon, M. A. *The Manipulation of Air-Sensitive Compounds*, 2nd ed.; John Wiley and Sons: New York, 1986.
(38) Perrin, D. D.; Armarego, W. L. F. *Purification of Laboratory Chemicals*, 3rd ed.; Pergamon Press: Oxford, 1988.
(39) Chao, Y.-W.; Wexler, P. A.; Wigley, D. E. *Inorg. Chem.* **1989**, *28*, 3860.
(40) Luetkens, M. L., Jr.; Sattelberger, A. P.; Murray, H. H.; Basil, J. D.; Fackler, J. P., Jr. *Inorg. Synth.* **1990**, *28*, 305.
(41) Jordan, R. F.; Bajgur, C. S.; Dasher, W. E.; Rheingold, A. L. *Organometallics* **1987**, *6*, 1041.

pentane, collected on a frit, and dried in vacuo; yield 0.12 g (1.37) mmol, 71%). Analytically pure samples were obtained by recrystallization from minimal Et_2O/pentane solutions at −35 °C. ^1H NMR (C_6D_6): δ 7.44 (s, 2 H, N*H*Ar), 7.12−6.87 (overlapping A_2B mult, 12 H total, H_{aryl}, NAr and NHAr), 3.82 and 3.37 (spt, 4 H each, C*H*Me$_2$, NAr and NHAr), 1.27 and 1.03 (d, 24 H each, CH*Me*$_2$, NAr and NHAr). ^{13}C NMR (C_6D_6): δ 151.9 and 146.7 (C_{ipso}, NAr and NHAr), 142.8 and 141.5 (C_o, NAr and NHAr), 125.2 and 124.9 (C_p, NAr and NHAr), 123.7 and 122.3 (C_m, NAr and NHAr), 29.1 and 28.3 (*C*HMe$_2$, NAr and NHAr), 24.4 and 23.6 (CH*Me*$_2$, NAr and NHAr). Anal. Calcd for $C_{48}H_{70}N_4W$: C, 65.00; H, 7.95. Found: C, 64.82; H, 8.07.

W(NAr)$_2$Cl$_2$(NH$_2$Ar) (4). A solution of 0.31 g (1.21 mmol) of $Me_3SiNHAr$ in 5 mL of Et_2O was added to a stirred solution of 0.35 g (0.608 mmol) of W(NAr)Cl$_4$(OEt$_2$) in 15 mL of Et_2O. This mixture was stirred at room temperature for 24 h, during which time the solution color slowly changed to red. The reaction volatiles were then removed in vacuo to afford an orange oil. Upon trituration of the oil with cold pentane, an orange, fluffy solid was obtained which was filtered off and dried in vacuo; yield 0.28 g (0.34 mmol, 56%). Analytically pure samples were obtained by recrystallization from pentane at −35 °C. ^1H NMR (C_6D_6): δ 7.10−6.82 (m, 9 H, H_{aryl}), 5.28 (br, 2 H, N*H*$_2$Ar), 3.92 (spt, 4 H, C*H*Me$_2$, NAr), 3.20 (spt, 2 H, C*H*Me$_2$, NH$_2$Ar), 1.195 (d, 24 H, CH*Me*$_2$, NAr), 1.17 (d, 12 H, CH*Me*$_2$, NH$_2$Ar). ^{13}C NMR ($CDCl_3$): δ 150.5, 145.4, 138.5, and 135.1 (C_{ipso} and C_o, NH$_2$Ar and NAr), 127.4, 125.3, 123.2, and 121.9 (C_m and C_p, NAr and NH$_2$Ar), 28.7 (*C*HMe$_2$, NH$_2$Ar), 27.9 (*C*HMe$_2$, NAr), 23.9 (CH*Me*$_2$, NH$_2$Ar), 23.2 (CH*Me*$_2$, NAr). Anal. Calcd for $C_{36}H_{53}Cl_2N_3W$: C, 55.25; H, 6.83; N, 5.37. Found: C, 55.54; H, 7.10; N, 5.24.

W(NAr)(NEt$_2$)Cl$_3$(THF) (5). To a stirred solution of 0.66 g (1.14 mmol) of W(NAr)Cl$_4$(THF) in 10 mL of diethyl ether was added 0.35 g (2.29 mmol) of Me_3SiNEt_2 (neat). After the solution was stirred at room temperature for 16 h, the volatile components were removed from the resulting orange solution in vacuo to afford an orange solid. Redissolving this solid in minimal Et_2O (~2 mL) and cooling the solution to −30 °C provided orange crystals of product which were filtered off and dried in vacuo; yield 0.54 g (0.88 mmol, 77%). Analytically pure compound was obtained by recrystallization from Et_2O solutions at −35 °C. ^1H NMR (C_6D_6): δ 7.12−6.74 (A_2B mult, 3 H, H_{aryl}), 4.94 and 4.83 (q, 2 H each, NC*H*$_2$CH$_3$), 4.75 (spt, 2 H, C*H*Me$_2$), 4.06 (br, 4 H, C_αH, THF), 1.34 (d, 12 H, CH*Me*$_2$), 1.14 (br, 4 H, C_βH, THF), 1.26 and 1.00 (t, 3 H each, NCH$_2$C*H*$_3$). ^{13}C NMR (C_6D_6): δ 153.4 (C_o), 145.8 (C_{ipso}), 130.6 (C_p), 123.6 (C_m), 72.5 (C_α, THF), 66.1 and 59.0 (N*C*H$_2$CH$_3$), 27.9 (*C*HMe$_2$), 25.3 (CH*Me*$_2$), 15.7 and 14.0 (NCH$_2$*C*H$_3$). The C_β THF peak was not observed and is presumably coincident with another resonance. Anal. Calcd for $C_{20}H_{35}Cl_3N_2OW$: C, 39.40; H, 5.79; N, 4.59. Found: C, 39.58; H, 5.87; N, 4.58.

W(NAr)$_2$(NEt$_2$)Cl (6). To a solution of 0.58 g (0.77 mmol) of W(NAr)$_2$Cl$_2$(THF)$_2$ (**1**) in 15 mL of Et_2O was added 0.14 g (0.91 mmol) of neat Me_3SiNEt_2. This mixture was allowed to stir with gentle heating (~35 °C) for 7 days, over which time the solution color changed from red to yellow-orange. The volatile components were then removed from the reaction in vacuo, and the yellow orange solid which remained was redissolved in minimal Et_2O. Upon cooling of this ether solution to −35 °C for 2 days, orange crystals of product formed. The crystals were filtered off and dried in vacuo; yield 0.26 g (0.40 mmol, 52%). Analytically pure samples were obtained by recrystallization from Et_2O solution at −35 °C. ^1H NMR (C_6D_6): δ 7.12−6.83 (A_2B mult, 6 H, H_{aryl}), 4.04 (spt, 4 H, C*H*Me$_2$), 3.21 and 2.60 (mult, 2 H each, NC*H*$_2$CH$_3$), 1.23 (d, 24 H, CH*Me*$_2$) 0.98 (t, 6 H, NCH$_2$C*H*$_3$). ^{13}C NMR (C_6D_6): δ 151.0 (C_{ipso}), 146.1 (C_o), 127.9 (C_m), 122.5 (C_p), 46.4 (N*C*H$_2$CH$_3$), 28.3 (*C*HMe$_2$), 24.6 (CH*Me*$_2$), 14.5 (NCH$_2$*C*H$_3$). Anal. Calcd for $C_{28}H_{44}ClN_3W$: C, 52.39; H, 6.91; N, 6.55. Found: C, 52.23; H, 6.95; N, 6.53.

W(NAr)$_3$(PMePh$_2$) (7). A 0.053 g (0.526 mmol) sample of $PMePh_2$ was added directly (neat) to a solution of 0.25 g (0.245 mmol) of [Li(THF)$_4$][W(NAr)$_3$Cl] (**2**) in ~15 mL of benzene. The reaction was stirred at room temperature for 4 h, during which time the yellow solution developed a dark red color. The reaction volatiles were removed in vacuo to afford a red solid. The product was extracted with pentane, the extract filtered through Celite, and the filtrate concentrated in vacuo and cooled to −35 °C. The analytically pure, red crystals which formed overnight were filtered off and dried in vacuo; yield 0.198 g (0.218 mmol, 91%). ^1H NMR (C_6D_6): δ 7.69 (dd, 4 H, H_o, PMePh$_2$), 7.18−6.95 (A_2B mult, 9 H, H_{aryl}, NAr), 6.87 (m, 6 H, H_m and H_p, PMePh$_2$), 3.87 (spt, 6 H, C*H*Me$_2$), 2.04 (d, $^2J_{H-P}$ = 9.8 Hz, 3 H, P*Me*Ph$_2$), 1.12 (d, 36 H, CH*Me*$_2$). ^{13}C NMR (C_6D_6): δ 154.9 (C_{ipso}, NAr), 140.8 (C_o, NAr), 133.6 (d, C_{ipso}, PMe*Ph*$_2$), 132.0, 129.6, and 129.4 (PMe*Ph*$_2$), 123.0 (C_p, NAr), 122.2 (C_m, NAr), 28.3 (*C*HMe$_2$), 23.9 (CH*Me*$_2$), 16.6 (d, P*Me*-Ph$_2$). Anal. Calcd for $C_{49}H_{64}N_3PW$: C, 64.68; H, 7.09; N, 4.62. Found: C, 64.37; H, 7.18; N, 4.60.

W(NAr)$_3$(PMe$_3$) (8). A solution of 2.00 g (1.92 mmol) of [Li(THF)$_4$][W(NAr)$_3$Cl] (**2**) in ~50 mL of benzene was prepared and cooled to −78 °C. A 0.44 g (5.80 mmol) sample of PMe_3 was then added dropwise (neat) to the stirred [Li(THF)$_4$]-[W((NAr)$_3$Cl] solution. The reaction was allowed to warm to room temperature over several hours, during which time the yellow solution developed a cherry red color. After the solution was stirred for 15 h, the reaction volatiles were removed in vacuo to afford a red oil. The product was extracted with Et_2O, the extract filtered through Celite, and the solvent removed from the filtrate in vacuo to afford a red solid. The product was washed with cold pentane and dried in vacuo; yield 1.40 g (1.78 mmol, 92%) of W(NAr)$_3$(PMe$_3$) sufficiently pure for further reactions. Analytically pure compound was obtained by recrystallization from pentane solutions at −35 °C. ^1H NMR (C_6D_6): δ 7.18−6.94 (A_2B mult, 9 H, H_{aryl}, NAr), 3.95 (spt, 6 H, C*H*Me$_2$), 1.24 (d, 36 H, CH*Me*$_2$), 1.21 (d, overlapping with δ 1.24 signal, 9 H, P*Me*$_3$). ^{13}C NMR (C_6D_6): δ 155.0 (C_{ipso}, NAr), 140.4 (C_o, NAr), 122.9 (C_p, NAr), 122.1 (C_m, NAr), 28.2 (*C*HMe$_2$), 23.9 (CH*Me*$_2$), 16.7 (d, P*Me*$_3$). Anal. Calcd for $C_{39}H_{60}N_3PW$: C, 59.62; H, 7.70. Found: C, 59.54; H, 7.61.

[*n*-Bu$_4$N][W(NAr)$_3$Br] (9). A 0.309 g (0.96 mmol) sample of solid [*n*-Bu$_4$N]Br was added directly to a solution of 1.00 g (0.96 mmol) of [Li(THF)$_4$][W(NAr)$_3$Cl] (**2**) in 20 mL of benzene. This mixture was stirred at room temperature for 15 h, over which time an orange color developed and a white precipitate formed. The reaction solution was filtered through Celite, and the volatile components were removed from the filtrate in vacuo to afford an orange solid. This product was washed with cold pentane, collected by filtration, and dried in vacuo; yield 0.89 g (0.87 mmol, 90%). Analytically pure compound was obtained by recrystallization from Et_2O solution at −35 °C. ^1H NMR (C_6D_6): δ 7.21−6.85 (A_2B mult, 9 H, H_{aryl}), 4.19 (spt, 6 H, C*H*Me$_2$), 2.31 (br m, 8 H, NC*H*$_2$CH$_2$CH$_2$CH$_3$), 1.42 (d, 36 H, CH*Me*$_2$), 1.09−0.93 (br m, 16 H total, NCH$_2$C*H*$_2$C*H*$_2$CH$_3$), 0.80 (pseudo t, 12 H, NCH$_2$CH$_2$CH$_2$C*H*$_3$). ^{13}C NMR (C_6D_6): δ 156.6 (C_{ipso}), 140.0 (C_o), 121.5 (C_m), 119.6 (C_p), 58.4 (N*C*H$_2$-CH$_2$CH$_2$CH$_3$), 28.5 (*C*HMe$_2$), 24.1 (CH*Me*$_2$), 23.8 and 19.7 (NCH$_2$*C*H$_2$*C*H$_2$CH$_3$), 13.8 (NCH$_2$CH$_2$CH$_2$*C*H$_3$). Anal. Calcd for $C_{52}H_{87}BrN_4W$: C, 60.52; H, 8.50; N, 5.43. Found: C, 60.44 (60.61); H, 9.02 (8.87); N, 5.28 (5.15). (Duplicate analyses reported.)

[Li(THF)$_4$][W(NAr)$_3$Me] (10). To a cold (−35 °C) solution of 1.00 g (0.96 mmol) of [Li(THF)$_4$][W(NAr)$_3$Cl] in 30 mL of THF was added 1 equiv of MeLi (0.68 mL of a 1.4 M Et_2O solution) dropwise. This reaction mixture was stirred at room temperature for 18 h, after which the solvent was removed in vacuo to afford a yellow, oily residue. The product was extracted with Et_2O, the ether extract filtered through Celite, and the solvent removed from the filtrate in vacuo to provide a yellow solid. The solid was washed with minimal cold

pentane, collected on a frit, and dried in vacuo; yield 0.60 g (0.59 mmol, 61%). Analytically pure compound was obtained by recrystallization from THF/pentane solutions at −35 °C. ^{1}H NMR (C_6D_6): δ 7.17−6.92 (A_2B mult, 9 H, H_{aryl}), 3.79 (spt, 6 H, C*H*Me$_2$), 3.22 (m, C_αH, THF), 1.20 (m, C_βH, THF), 1.51 (s, 3 H, WMe), 1.27 (d, 36 H, CH*Me*$_2$). ^{13}C NMR (C_6D_6): δ 155.3 (C_{ipso}), 139.3 (C_o), 122.3 (C_m), 121.6 (C_p), 68.4 (C_α, THF), 28.3 (*C*HMe$_2$), 25.3 (C_β, THF), 24.1 (CH*Me*$_2$), 15.2 (WMe). Anal. Calcd for $C_{53}H_{86}N_3O_4W$: C, 62.40; H, 8.50; N, 4.12. Found: C, 62.24; H, 8.71; N, 4.01.

[Li(THF)$_4$][W(NAr)$_3$(CH$_2$SiMe$_3$)] (11). To a cold (−35 °C) solution of 0.127 g (0.12 mmol) of [Li(THF)$_4$][W(NAr)$_3$Cl] in 25 mL of THF was added 1 equiv of solid LiCH$_2$SiMe$_3$ (0.011 g, 0.12 mmol). This reaction mixture was allowed to stir at room temperature for 15 h, after which the solvent was removed in vacuo to afford a yellow, oily residue. The product was extracted with Et$_2$O, the ether extract filtered through Celite, and the solvent removed from the filtrate in vacuo to provide an oily, yellow solid. This solid was dissolved in ~10 mL of pentane and cooled to −35 °C for 24 h, whereupon a yellow solid precipitated. This solid was filtered off and dried in vacuo; yield 0.058 g (0.053 mmol, 44%). Analytically pure compound was obtained by recrystallization from THF/pentane solutions at −35 °C. ^{1}H NMR (C_6D_6): δ 7.15−6.90 (A_2B mult, 9 H, H_{aryl}), 3.83 (spt, 6 H, C*H*Me$_2$), 3.19 (m, 16 H, C_αH, THF), 1.44 (br, 2 H, C*H*$_2$SiMe$_3$), 1.26 (d, 36 H, CH*Me*$_2$), 1.14 (m, 16 H, C_βH, THF), 0.31 (s, 9 H, CH$_2$Si*Me*$_3$). ^{13}C NMR (C_6D_6): δ 122.5 (C_m), 122.2 (C_p), 68.2 (C_α, THF), 28.2 (*C*HMe$_2$), 25.3 (C_β, THF), 24.2 (CH*Me*$_2$), 3.0 (CH$_2$Si*Me*$_3$). Several attempts were made to locate the signals for C_{ipso} (NAr), C_o (NAr), and *C*H$_2$SiMe$_3$; C_o (NAr) is possibly obscured by the C_6D_6 signal. Anal. Calcd for $C_{56}H_{94}N_3O_4LiSiW$: C, 61.58; H, 8.68; N, 3.85. Found: C, 61.40; H, 8.72; N, 3.81.

W(NAr)$_2$(NHAr)(OAr′) (12). A solution of 2,6-dimethylphenol (0.081 g, 0.67 mmol) in 10 mL of pentane was added dropwise to a stirred solution of W(NAr)$_3$(PMe$_3$) (**8**, 0.52, 0.66 mmol) in 40 mL of pentane. The reaction was stirred at room temperature for 15 h, over which time the solution color had changed from red to yellow-orange. After this time, the solvent was removed in vacuo to afford a clear, pale orange oil which was dissolved in minimal pentane and stored at −35 °C for ~24 h. The yellow block crystals which had formed were filtered off and dried in vacuo; yield 0.230 g (0.28 mmol, 42%). Analytically pure samples were obtained by recrystallization from a minimal volume of pentane at −35 °C. ^{1}H NMR (C_6D_6): δ 7.88 (s, 1 H, N*H*Ar), 7.10−6.74 (overlapping mult, 12 H total, H_{aryl}; NAr, NHAr, and OAr′), 3.76 (spt, 2 H, C*H*Me$_2$, NHAr), 3.45 (spt, 4 H, C*H*Me$_2$, NAr), 2.44 (s, 6 H, Me, OAr′), 1.17, 1.05, and 0.98 (d, 12 H each, CH*Me*$_2$, NAr and NHAr). ^{13}C NMR (C_6D_6): δ 160.6, 151.4, and 145.0 (C_{ipso}, NAr, NHAr, and OAr′), 143.2 and 142.9 (C_o, NAr and NHAr), 128.8, 127.3, 126.4, 125.6, 123.8, 122.4, and 122.2 (C_o, OAr′; C_p and C_m, NAr, NHAr, and OAr′), 28.9 (*C*HMe$_2$, NHAr), 28.4 (*C*HMe$_2$, NAr), 24.1, 23.8, and 23.5 (CH*Me*$_2$, NAr and NHAr), 17.3 (Me, OAr′). Anal. Calcd for $C_{44}H_{61}N_3OW$: C, 63.53; H, 7.39; N, 5.05. Found: C, 63.48; H, 7.42; N, 5.02.

W(NAr)$_2$[N(SiMe$_3$)Ar]I (13). Neat Me$_3$SiI (0.224 g, 1.11 mmol, ~0.16 mL) was added dropwise to a stirred solution of 0.15 g (0.19 mmol) of W(NAr)$_3$(PMe$_3$) (**8**) in 20 mL of pentane. This mixture was stirred at room temperature for 24 h, over which time the solution had become cloudy, red-orange in color. The reaction mixture was filtered (fine porosity frit), and the volatile components were removed from the filtrate in vacuo to afford an orange oil which, upon trituration with cold pentane, formed an orange powder. This powder was collected by filtration and dried in vacuo; yield 0.09 g (0.0989 mmol), 52%). Analytically pure compound was obtained by recrystallization from pentane solution at −35 °C. ^{1}H NMR (C_6D_6): δ 7.06−6.91 (overlapping A_2B m, 9 H total, H_{aryl}), 3.63 and 3.47 (overlapping br, 6 H total, C*H*Me$_2$, NAr and N(SiMe$_3$)Ar), 1.30 (br, 6 H, CH*Me*$_2$, Ar), 1.18−1.06 (br, 30 H, CH*Me*$_2$, NAr and N(SiMe$_3$)Ar), 0.35 (s, 9 H, N (Si*Me*$_3$)Ar). ^{13}C NMR (C_6D_6): δ 151.9, 148.5, and 142.0 (C_{ipso} and C_o, NAr and N(SiMe$_3$)Ar; one signal not observed), 126.8 (C_p, NAr), 126.5 (C_p, N(SiMe$_3$)Ar), 124.8 (C_m, NAr), 122.8 (C_m, N(SiMe$_3$)Ar), 29.0 and 28.2 (*C*HMe$_2$, NAr and N(SiMe$_3$)Ar), 26.2, 25.2, 24.7, and 24.2 (CH*Me*$_2$, NAr and N(SiMe$_3$)Ar), 2.6 (N(Si*Me*$_3$)Ar). Anal. Calcd for $C_{39}H_{60}N_3ISiW$: C, 51.49; H, 6.65. Found: C, 51.36; H, 6.73.

W(NAr)$_2$(NMeAr)I (14). An ampule (Teflon stopcock) was charged with 0.25 g (0.319 mmol) of W(NAr)$_3$(PMe$_3$), 20 mL of benzene, and excess MeI (0.50 g, 3.50 mmol). The reaction vessel was closed, placed in an oil bath maintained at ~70 °C, and allowed to stir for 15 h. Over this time, the solution's red color turned to pale yellow, and a white precipitate ([Me$_4$P]I by ^{1}H NMR) formed. The reaction mixture was filtered through Celite, concentrated in vacuo, and filtered again, and the solution was further stripped to afford the product as a yellow powder. Analytically pure samples of W(NAr)$_2$(NMeAr)I, obtained by recrystallization from pentane at −35 °C, were collected by filtration and dried in vacuo; yield 0.20 g (0.247 mmol, 77%). ^{1}H NMR (C_6D_6): δ 7.07−6.93 (overlapping A_2B mult, 9 H total, H_{aryl}), 3.83 (s, 3 H, N*Me*Ar), 3.58 (br, overlapping spt, 6 H total, C*H*Me$_2$, NAr and NMeAr), 1.20−1.05 (overlapping br, 36 H total, CH*Me*$_2$, NAr and NMeAr). Anal. Calcd for $C_{37}H_{59}N_3IW$: C, 52.18; H, 6.39. Found: C, 52.13; H, 6.48.

W[NArC(O)NPh](NAr)$_2$(PMe$_3$) (15). Neat phenyl isocyanate (0.192 g, 1.61 mmol, ~0.17 mL) was added dropwise to a stirred solution of 0.15 g (0.19 mmol) of W(NAr)$_3$(PMe$_3$) (**8**) in 15 mL of pentane at room temperature. Reaction occurred quickly as this mixture was stirred for 15−20 min, over which time an orange powder precipitated. The powder was collected by filtration, washed with minimal cold pentane, and dried in vacuo; yield 0.15 g (0.16 mmol, 82%). Analytically pure compound was obtained by recrystallization from a pentane solution at −35 °C. ^{1}H NMR (C_6D_6): δ 8.01 (d, 2 H, H_o, C_6H_5), 7.20−6.72 (m, 12 H total, H_{aryl}), 3.733 and 3.725 (overlapping spt, 6 H total, C*H*Me$_2$, NAr and WNArC(O)NPh), 1.60 and 1.27 (d, 6 H each, CH*Me*$_2$, WNArC(O)NPh), 1.17 and 1.03 (d, 12 H each, CH*Me*$_2$, NAr), 0.86 (d, 9 H, PMe$_3$). ^{13}C NMR (C_6D_6): δ 152.6, 146.7, 145.0, 140.4, 133.3, 133.1, 129.3, 129.2, 126.8, 126.7, 123.7, and 122.9 (C_{aryl}, *C*O, and C_6H_5), 28.8, 28.0, 25.3, 25.0, and 23.9 (*C*HMe$_2$ and CH*Me*$_2$, imide and amide), 13.5 (PMe$_3$). One resonance from the *C*HMe$_2$ and CH*Me*$_2$ set was not located. Anal. Calcd for $C_{46}H_{65}N_4OPW$: C, 61.06; H, 7.24; N, 6.19. Found: C, 61.53; H, 7.52; N, 5.77. IR (Nujol mull), cm^{-1}: 1654 s [ν(C=O)].

W(NAr)$_2$(NHAr)Me (16). A slurry of 0.18 g (0.47 mmol) of [HNMe$_3$]BPh$_4$ in ~20 mL of Et$_2$O was added to a stirred solution of 0.50 g (0.47 mmol) of [Li(THF)$_4$][W(NAr)$_3$Me] in 20 mL of Et$_2$O. This mixture was stirred at room temperature for 12 h, after which the solution was filtered through Celite and the solvent removed under reduced pressure to afford a yellow to brown oil. This oil was dissolved in a minimal volume of pentane and cooled to −35 °C to provide yellow crystals, which were collected by filtration and dried in vacuo. Additional product was obtained from the pentane filtrate (−35 °C), for a total yield of 0.14 g (0.21 mmol, 45%). Analytically pure product was obtained from Et$_2$O/pentane solutions at −35 °C. ^{1}H NMR (C_6D_6): δ 8.36 (s, 1 H, N*H*Ar), 7.08−6.91 (m, 9 H total, H_{aryl}), 3.63−3.50 (overlapping spt, 6 H total, C*H*Me$_2$, NAr and NHAr), 1.73 (s, 3 H, WCH$_3$), 1.17, 1.13, and 1.10 (overlapping d, 12 H each, CH*Me*$_2$, NAr and NHAr). ^{13}C NMR (C_6D_6): δ 152.4 (C_{ipso}, NAr), 146.0 (C_{ipso}, NHAr), 142.7 (C_o, NAr), 141.1 (C_o, NHAr), 125.1 and 123.6 (C_p, NAr and C_m, NHAr), 125.7 (C_p, NHAr), 122.4 (C_m, NAr), 29.2, 28.6, 23.8, 23.7, and 23.4 (*C*HMe$_2$ and CH*Me*$_2$, NAr and NHAr; WCH$_3$). Anal. Calcd for $C_{37}H_{55}N_3W$: C, 61.23; H, 7.64; N, 5.79. Found: C, 61.15; H, 7.71; N, 5.73.

Structural Determinations. [Li(THF)$_4$][W(NAr)$_3$Cl] (2). Crystallographic data for **2** are collected in Table 1. Data were collected on a specimen sealed in a Lindemann capillary.

Photographic evidence and systematic absences in the diffraction data uniquely identified the space group. The structure was solved by direct methods. All non-hydrogen atoms were anisotropically refined, and hydrogen atoms were treated as idealized contributions.

$W(NAr)_3(PMe_3)$ (8). Crystallographic data for **8** are collected in Table 1. A red, irregular block crystal of **8** was mounted in a glass capillary in a random orientation. The space group was determined from the systematic absences and the subsequent least-squares refinement, and the structure was solved by the Patterson method. All non-hydrogen atoms were refined anisotropically. All hydrogen atoms were placed in idealized positions and were included in the refinement. Methyl group hydrogens were initially located from a difference map and then idealized.

Acknowledgment is made to the Division of Chemical Sciences, Office of Basic Energy Sciences, Office of Energy Research, U.S. Department of Energy (DE-FG03-93ER14349), for support of this research.

Supplementary Material Available: Details of the structure solution and refinement, including tables of crystal data and data collection parameters, atomic positional and thermal parameters, bond distances, bond angles, least-squares planes, and ORTEP figures for $[Li(THF)_4][W(NAr)_3Cl]$ and $W(NAr)_3(PMe_3)$ (19 pages). Ordering information is given on any current masthead page.

OM9500228

Organic Syntheses via Transition Metal Complexes. 78.[1] Hydrazinolysis of Alkynylcarbene Complexes of Chromium and Tungsten. Formation of Hydrazinocarbene, Imidate, Pyrazolidinylidene, and Nitrile Complexes

Rudolf Aumann,* Beate Jasper, and Roland Fröhlich

Organisch-Chemisches Institut der Universität Münster, Orléans-Ring 23, D-48149 Münster, Germany

Received December 21, 1994[⊗]

Hydrazinolysis of alkynylcarbene complexes $(CO)_5M{=}C(OEt)C{\equiv}Ph$ (**1**, M = W; **1′**, M = Cr) with mono- and 1,2-dimethylhydrazine MeHNNHR (**2a,b**) (R = Me, H) affords three different-type compounds: hydrazinocarbene complexes $(CO)_5M{=}C(NMe\text{-}NHR)C{\equiv}CPh$ [(*E*/*Z*)-**3a,b**], imidate complexes $(CO)_5M[MeN{=}C(OEt)\text{-}C{\equiv}CPh]$ [(*E*/*Z*)-**4a**], and pyrazolidinylidene complexes **5a,b**. Hydrazinolysis of **1**/**1′** with 1,1-dimethylhydrazine or (unsubstituted) hydrazine H_2NNR_2 (**2c,d**) (R = Me, H) yields hydrazinocarbene complexes $(CO)_5M{=}C(NH\text{-}NR_2)C{\equiv}CPh$ [(*E*/*Z*)-**3c**], imidate complexes $(CO)_5M[HN{=}C(OEt)C{\equiv}CPh]$ [(*E*/*Z*)-**4a**], and benzonitrile complexes $(CO)_5M(N{\equiv}CPh)$ (**8**). Hydrazinolysis of **1** with H_2NNHR (**2e,f**) (R = COMe, Ph) gives pyrazoles **12e,f** as the only products. The product composition of the reactions of **2a–d** with **1** is markedly influenced by the reaction temperature. Reaction of **1** with *N*- and *O*-methylhydroxylamines (**13**, **14**) affords imidate complexes **4** only. The hydrazinocarbene complexes (*E*)-**3a** and (*Z*)-**3c** were characterized by X-ray diffraction. Both compounds crystallize in space group $P\bar{1}$ (No. 2): (*E*)-**3a**, $C_{16}H_{12}N_2O_5W$, cell parameters a = 8.501(2) Å, b = 9.645(2) Å, c = 11.860(2) Å, α = 103.56(2)°, β = 95.59(2)°, γ = 111.76(2)°, Z = 2, R_1 = 0.043, and wR^2 = 0.083; (*Z*)-**3c**, $C_{16}H_{12}N_2O_5W$, cell parameters a = 9.380(3) Å, b = 9.685(4) Å, c = 10.804(3) Å, α = 84.77(5)°, β = 80.74(3)°, γ = 66.47(3)°, Z = 2, R_1 = 0.036, and wR^2 = 0.086.

The hydrazinolysis of alkoxycarbene complexes $(CO)_5M{=}C(OR)R^1$ (M = Cr, Mo, W) has been studied to a much less an extent than the aminolysis of such compounds. Usually the hydrazinolysis takes a nonuniform course and yields several and also seemingly different-type products. Some features of the hydrazinolysis of carbene complexes have been unraveled so far.[2,3] To date, four main reaction paths have been distinguished, which consist in the formation of hydrazinocarbene complexes (by 1-substitution at the carbene carbon atom), imidate complexes (by insertion of a =NR group into the M=C bond),[2] pyrazinylidene complexes (by retaining of the N–N bridge), and nitrile complexes (by fragmentation of the ligand). We wish to report on our studies of reactions of hydrazines **2a–f** as well as of hydroxylamines **13** and **14** with alkynylcarbene complexes $(CO)_5M{=}C(OEt)\text{-}C{\equiv}CPh$ (**1**, M = W; **1′**, M = Cr). A great diversity of parallel reactions has been anticipated as a consequence of the ambident character of both the reagent and the substrate: compounds **1** are prone to both electrophilic 1-addition and 3-addition reactions and compounds **2**, **13**, and **14** on the other hand possesses two different nucleophilic centers. By probing the influence of substituents as well as the reaction temperature on the product distribution, we could obtain some insight into the mechanism of the hydrazinolysis of carbene complexes.

Substitution and Fragmentation of 1 on Reaction with (Symmetrical) 1,2-Dimethylhydrazine (2a)

The basic features of the hydrazinolysis of carbene complexes can be derived from the reaction of (symmetrical) 1,2-dimethylhydrazine (**2a**) with alkynylcarbene complexes **1** (M = W; **1′**, M = Cr). This reaction affords three different-type products: hydrazinocarbene complexes (*E*/*Z*)-**3a**, imidate complexes (*E*/*Z*)-**4a**, and pyrazinylidene complexes **5a** (Scheme 1). It has been demonstrated by ^{1}H NMR measurements that compounds **3**–**5** are not interconverted under the reaction conditions and therefore appear to be formed in parallel reactions. Most strikingly, a strong influence of the temperature on the product distribution is observed (Table 1). Although complexes (*E*/*Z*)-**3a** are generated on reaction of **1** with **2a** at −78 °C in 27% yield, they are formed in only trace amounts at 20 °C. Since compounds (*E*/*Z*)-**3a** are quite stable at 20 °C, its appears that the 1-addition of **2a** to **1** becomes favored at −78 °C over the 3-addition (Scheme 1).[4]

Both, compounds **3a** and **4a** are generated *via* 1-addition of **2a** to the carbene complex **1**. Zwitterionic

[⊗] Abstract published in *Advance ACS Abstracts,* April 15, 1995.

(1) Part 77: Aumann, R.; Jasper, B. *Organometallics* **1995**, *14*, 1461.

(2) (a) Fischer, E. O.; Aumann, R. *Angew. Chem.* **1967**, *79*, 191; *Angew. Chem., Int. Ed. Engl.* **1967**, *6*, 181. (b) Fischer, E. O.; Aumann, R. *Chem. Ber.* **1968**, *101*, 963.

(3) Fischer, H.; Roth, G.; Reindl, G.; Troll, C. *J. Organomet. Chem.* **1993**, *454*, 133–149.

(4) Similar effects are observed with the aminolysis of **1**. See e.g.: Werner, H.; Fischer, E. O.; Heckl, B.; Kreiter, C. G. *J. Organomet. Chem.* **1971**, *28*, 367–389.

0276-7333/95/2314-2447$09.00/0

Scheme 1

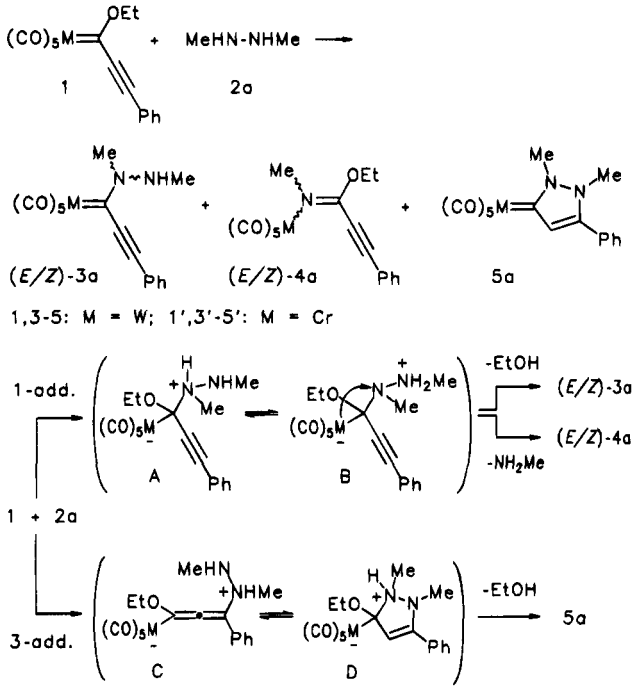

Table 1. Influence of Temperature on Product Composition in the Reaction of 2a with 1 (1')

	M	(*E*)-**3**/(*Z*)-**3**/(*E*)-**4**/(*Z*)-**4**/**5**[a]	*b*	*c*
a	W	17/11/22/12/23	85	−78
a	W	0/0/3/5/80	88	20
a'	Cr	0/0/0/0/81	81	20

[a] Product ratio. [b] Total yield in %. [c] Reaction temperature in °C.

species **A** and **B** are assumed to be key intermediates in this addition. The elimination of EtOH from **A** is expected to yield hydrazinocarbene complexes (*E*/*Z*)-**3a**, while the elimination of $MeNH_2$ from **B** should result in the formation of imidate complexes (*E*/*Z*)-**4a** (Scheme 1).[2,5,6] $MeNH_2$ is trapped by the alkynylcarbene complex **1** in a Michael-type addition with formation of 1-amino and (2-aminoethenyl)carbene complexes in competing (high-yield) reaction paths.[4,12] In line with expectation, the latter products are obtained in amounts equivalent to those of the imidate complexes **4** (see Table 3 and Scheme 5). For the present case, this side reaction may be suppressed, if a (local) excess of hydrazine **2a** *vs* carbene complex **1** is guaranteed by proper reaction conditions.

Compounds **3a** and **4a** are each obtained as mixtures of stereoisomers (Scheme 1). The formation of an *anti* stereoisomer (*E*)-**4a** is slightly favored kinetically at −78 °C over the formation of the *syn* product (*Z*)-**4a**. The latter proves to be more stable thermally than the former. It has been demonstrated by NMR measurements that the chromium complex (*E*)-**4a'** smoothly rearranges to (*Z*)-**4a'** within 2 h at 40 °C in C_6D_6. Interestingly, the pyrazinylidene complex **5a** does not result from cyclization of the hydrazine complex (*E*)-**3a**. This is easily explained by consideration of sterical restrictions implied to the transition state geometry for such a reaction. Therefore, not unexpectedly, a solution of (*E*)-**3a** in C_6D_6 according to ^1H NMR measurements remains unchanged for several hours at 40 °C. Apparently, the pyrazinylidene complex **5a** is formed by 3-addition of **2a** to **1** *via* zwitterionic intermediates[7] **C** and **D**.

Scheme 2

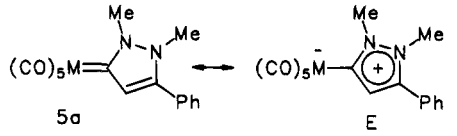

Spectroscopy of 3a, 4a, and 5a

The signals of the carbene carbon atoms in the ^{13}C NMR spectra of the hydrazinocarbene complexes (*E*/*Z*)-**3a** are shifted upfield [(*E*)-**3a**, δ(W=*C*) 212.3; (*Z*)-**3a**, 212.1] relative to those of aminocarbene complexes {e.g. δ[$(CO)_5W$=*C*(NHMe)-C≡CPh] 233.0}.[8] This is attributed to a strong resonance contribution of the dipolar iminium structure $(CO)_5WC(=NMe^+NHMe)C{\equiv}CPh$. In line with this assumption, a bathochromic shift of the [ν(C≡O)] E-band in the IR spectrum [(*E*)-**3a**, 1930.2 cm^{-1}, *vs* $(CO)_5W{=}C(NHMe)C{\equiv}CPh$, 1943.3] is also observed.

The configuration assignment of the stereoisomers (*E*/*Z*)-**3a** is based on the *de*shielding of the hydrogen as well as of the carbon atom of the 1-NCH_3 group by the *syn* $(CO)_5M$ group of compound (*E*)-**3a** [δ(1-N*CH*$_3$) 3.20, δ-(1-N*C*H$_3$) 46.6 as compared to (*Z*)-**3a** δ(1-N*CH*$_3$) 2.70, δ(1-N*C*H$_3$) 40.7]. The configuration of (*E*/*Z*)-**4a** was determined by NOE experiments which indicated a positive interaction between the N*CH*$_3$ and the O*CH*$_2$ signals in (*E*)-**4a** but not in (*Z*)-**4a**. This is in line with the highfield shift of the signals of the N*CH*$_3$ (by 0.25 ppm) and the O*CH*$_2$ group (by 0.20 ppm) in (*E*)-**4a**, compared to (*Z*)-**4a**, due to mutual anisotropic shielding of these groups.

The strong upfield shift of the carbene carbon signal of **5a** (**5a**, δ = 176.9; **5a'**, δ = 190.8) and the bathochromic shift of the [ν(C≡O)] A_1- and E-bands in the IR spectrum of **5a** [**5a**, 2059.0 cm^{-1} (10%), 1917.8 (100); **5a'**, 2049.3 (20), 1925.9 (100)] relative to those of aminocarbene complexes indicate a strong influence of the zwitterionic structure **E** (Scheme 2).

Since only few examples of hydrazinocarbene complexes are known so far,[3,9] an X-ray structure analysis was carried out for (*E*)-**3a** and (*Z*)-**3c**. Figure 1 shows the molecular structure and Tables 5−7 give the experimental data for the crystal structure of the hydrazino alkynylcarbene complexes (*E*)-**3a**. The plane defined by N(2)−C(1)−C(6) approximately bisects the angle between two *cis*-CO groups at tungsten [C(16)−W−C(1)−N(2) = 41.3°]. The coordination geometry at N(2) is planar (sum of bond angles 360.0°). The lone

(5) The reaction of zwitterions $(CO)_5W^-N(Ph)N^+(Ph){=}C(OMe)Ph$ with iodine has been recently reported to give imidates: McGowan, P. C.; Massey, S. T.; Abboud, K. A.; McElwee-White, L. *J. Am. Chem. Soc.* **1994**, *116*, 7419−7420.

(6) Imidates were obtained from photochemical reactions of Fischer carbene chromium complexes and sulfilimines: Alcaide, B.; Cassarubios, L.; Domínguez, G.; Sierra, M. *J. Org. Chem.* **1993**, *58*, 3886−3894. Imidates were also obtained from reactions of Fischer carbene complexes with nitrosobenzene: Herndon, J. W.; McMullen, L. A. *J. Organomet. Chem.* **1989**, *368*, 83.

(7) Compounds of related type have been isolated and characterized by an X-ray analysis; see: Aumann, R.; Jasper, B.; Läge, M.; Krebs, B. *Chem. Ber.* **1994**, *27*, 2475.

(8) Aumann, R.; Hinterding, P. *Chem. Ber.* **1993**, *126*, 421−427.

(9) Ito, Y.; Hirao, T.; Saegusa, T. *J. Organomet. Chem.* **1977**, *131*, 121.

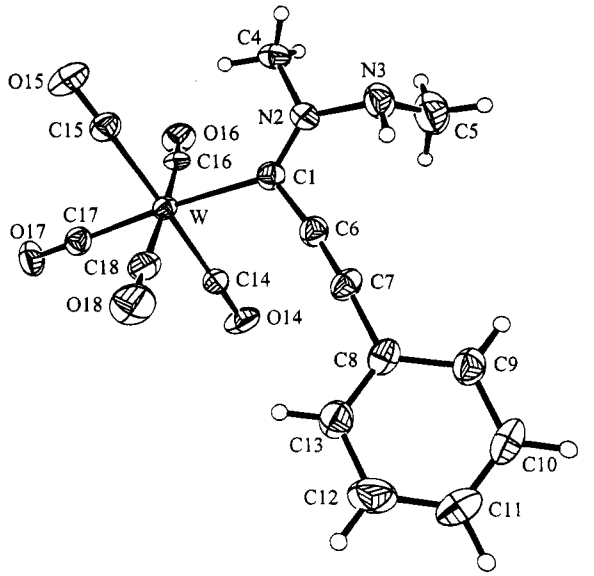

Figure 1. Molecular structure of hydrazinocarbene complex (*E*)-**3a**.

pair at N(2) is delocalized by virtue of the small interplanar angle C(6)−C(1)−N(2)−N(3) = −4.1(10)° and the short distance C(1)−N(2) = 1.307(9) Å. Due to the repulsive interaction of the lone pairs at the nitrogen atom N(3) with the adjacent delocalized π system, the interplanar angle C(1)−N(2)−N(3)−C(5) amounts to 96.3(10)°. A geometry similar to that of the hydrazino alkynylcarbene complexes (*E*)-**3a** has been found for a hydrazino alkenylcarbene complex.[3]

Regioselectivity of (Unsymmetrical) Methylhydrazine (2b)

The site of alkylation in methylhydrazine (**2b**) with most alkylating agents is the (more nucleophilic) substituted nitrogen atom,[10] while the position of acylation is very sensitive to the nature of the reagent used.[11] The addition of the ambident electrophile **1** to **2b** is very selective and occurs preferentially at the substituted nitrogen atom. Minor products (<10%) resulting from an attack of the unsubstituted nitrogen atom at **1** have been detected by NMR measurements, but they have not been fully characterized. Complexes (*E*/*Z*)-**3b**, (*E*/*Z*)-**4a**, **5b**, and **6b** are obtained as the main products (Scheme 3).

The reaction of **2b** with **1** (Scheme 3) follows a similar pattern as outlined in Scheme 1 for the reaction of **2a** with **1**. The product composition varies with the reaction temperature (Table 2). At −78 °C the 1-addition is favored over the 3-addition and leads to the formation of (*E*/*Z*)-**3b** and (*E*/*Z*)-**4a** *via* intermediates **F** and **G**. Cyclization to **5b** may involve the formation of intermediates **H** and **I**. Interestingly, the pyrazolinylidene complexes **5a**/**5a′** are stable thermally in C_6D_6 for at least 24 h at 80 °C, whereas the corresponding (*NH*) aminocarbene derivative **5b** rearranges quickly (*via* an intermediate **K**) to the pyrazole complex **6b** (Scheme 4). Furthermore, the tungsten compound **6b** is stable at 60 °C for several hours, but the corresponding chromium complex **6b′** is demetalated in C_6D_6 at 60 °C in 10 h to give the pyrazole **7b** together with $Cr(CO)_6$. The configurational assignment of **6b** and **6b′** is based on NOE experiments, which for each compound indicate a strong interaction between the NCH_3 group and the *o*-H's of the phenyl group.

Scheme 3

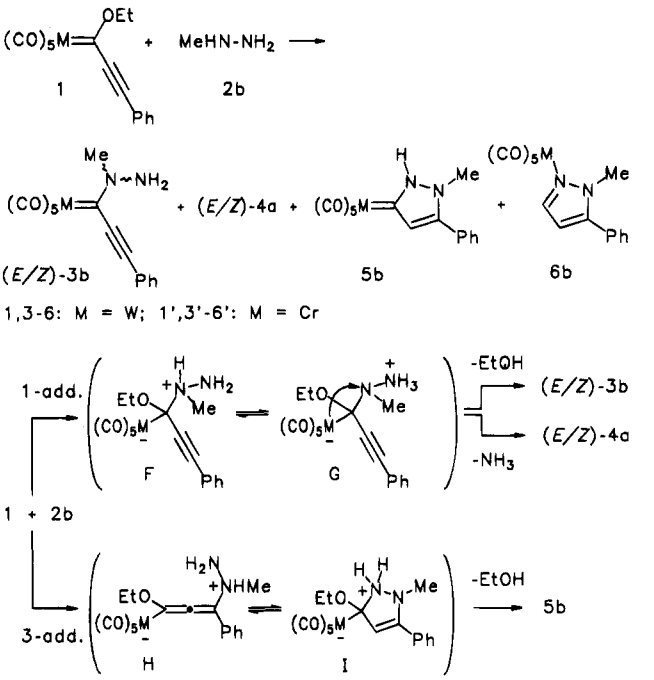

Table 2. Influence of Temperature on Product Composition in the Reaction of 2b with 1 (1′)

	M	(*E*)-**3**/(*Z*)-**3**/(*E*)-**4**/(*Z*)-**4**/**5**/**6**[a]	*b*	*c*
b	W	22/14/21/9/7/8	81	−78
b	W	0/0/8/3/26/39	76	20
b′	Cr	0/0/0/0/0/74	74	20

[a] Product ratio. [b] Total yield in %. [c] Reaction temperature in °C.

Table 3. Influence of Temperature on Product Composition in the Reaction of 2c with 1 (1′)

	M	(*Z*)-**3**/(*E*)-**3**/(*E*)-**4**/(*Z*)-**4**/**8**/**10**/**11**[a]	*b*	*c*
c	W	26/0/25/15/0/21/5	92	−78
c	W	0/0/33/7/5/3/39	84	20
c′	Cr	0/0/25/15/5/3/40	85	20

[a] Product ratio. [b] Total yield in %. [c] Reaction temperature in °C.

Table 4. Product Composition of the Reaction of 2d with 1′

	M	(*E*)-**3**/(*Z*)-**3**/(*E*)-**4**/(*Z*)-**4**/**8**/**10**/**11**[a]	*b*	*c*
d′	Cr	0/0/24/16/7/25/10	82	20

[a] Product ratio. [b] Total yield in %. [c] Reaction temperature in °C.

Fragmentation of (Unsymmetrical) 1,1-Dimethylhydrazine (2c)

All products from the reaction of 1,1-dimethylhydrazine (**2c**) with **1** seem to result from addition of the unsubstituted nitrogen atom. A hydrazinocarbene complexes (*Z*)-**3c** and imidates (*E*/*Z*)-**4c** are obtained, most probably, *via* intermediates **L** and **M** (Scheme 5). Interestingly, a benzonitrile complex **8** is formed instead

(10) Butler, D. E.; Alexander, S. M.; McLean, J. M.; Strand, L. B. *J. Med. Chem.* **1971**, *14*, 1052.
(11) (a) Hinman, R. L.; Fulton, D. *J. Am. Chem. Soc.* **1958**, *80*, 1895. (b) Condon, F. E. *J. Org. Chem.* **1972**, *37*, 3615.

Scheme 4

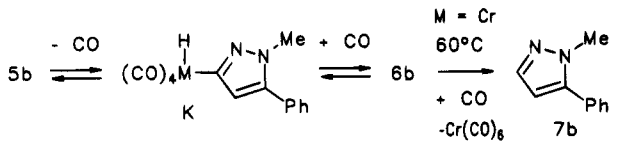

Scheme 5

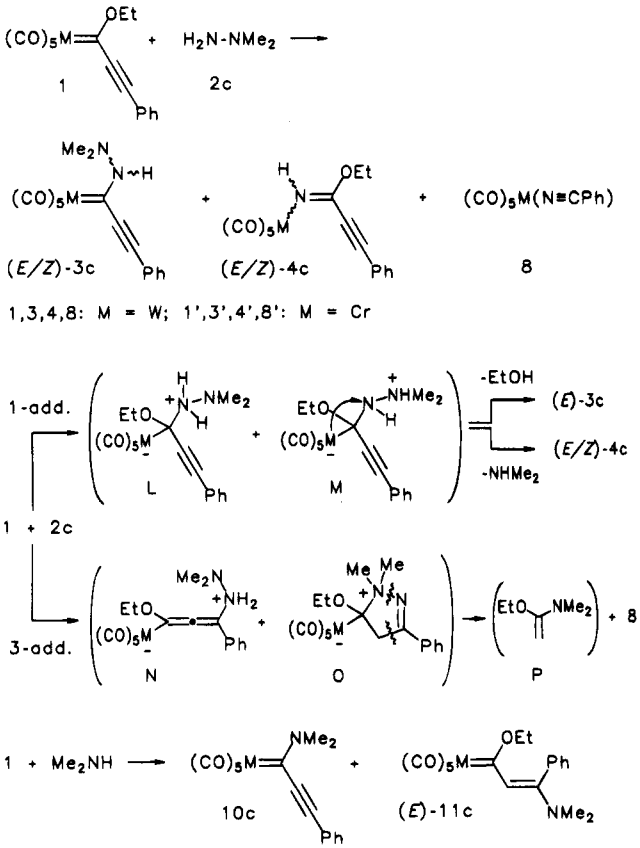

of a zwitterionic cyclization product related to **5**. Compound **8** is thus obtained from **2c** and **1** at 20 °C but not at −78 °C. The generation of a benzonitrile complex **8** is quite unexpected. It may result from 3-addition *via* intermediates **N** and **O**. A cycloreversion of **O** could possibly lead to formation of **8** together with a ketene semiaminal **P**. As a further peculiarity of the reaction of **2c** with **1** high amounts of (dimethylamino)carbene complexes **10c** and (*E*)-**11c** are obtained by 1- and 3-addition, respectively, of dimethylamine to **1**. Dimethylamine, which is eliminated from **M** while compound **4c** is formed, apparently reacts faster with **1** than does **2c**.

Figure 2 shows the molecular structure of (*Z*)-**3c**, and Tables 5, 6, and 8 give the experimental details of the crystal structure of this compound. The plane defined by N(2)−C(1)−C(6) approximately bisects the angle between two *cis*-CO groups at tungsten [C(24)−W−C(1)−N(2) = 46.6°], and the lone pair at N(2) is delocalized as indicated by the interplanar angle C(6)−C(1)−N(2)−N(3) = 176.9(6)° and the short distance C(1)−N(2) = 1.304(9) Å. N(3) has a tetrahedral configuration (sum of bond angles 329.5°).

A stereoisomer (*E*)-**3c** has not been detected in the reaction mixture of **1** with **2c**. This is possibly due to the thermal instability of such a compound.[2,3] From earlier studies (*E*)-**3c** is expected to afford the complex

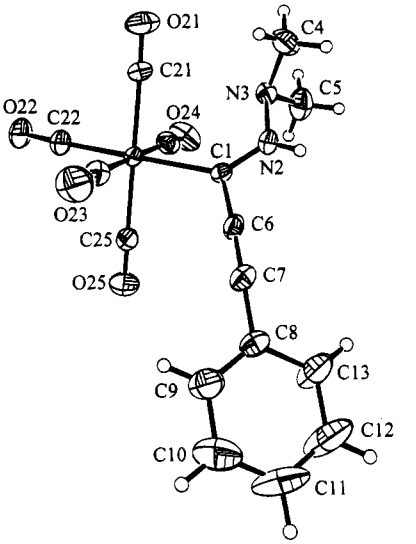

Figure 2. Molecular structure of hydrazinocarbene complex (*Z*)-**3c**.

Table 5. Selected Bond Lengths (Å) and Angles (deg) of (*E*)-3a and (*Z*)-3c

	(*E*)-**3a**		(*Z*)-**3c**
W−C(1)	2.239(7)		2.210(6)
C(1)−N(2)	1.307(9)		1.304(9)
N(2)−N(3)	1.430(8)		1.409(8)
N(2)−C(4)	1.460(9)	N(3)−C(4)	1.463(10)
N(3)−C(5)	1.453(11)		1.446(11)
C(1)−C(6)	1.439(10)		1.427(9)
C(6)−C(7)	1.186(10)		1.197(10)
C(7)−C(8)	1.451(10)		1.433(10)
W−C(1)−N(2)	132.1(5)		128.6(5)
W−C(1)−C(6)	113.8(5)		118.7(5)
C(6)−C(1)−N(2)	114.1(6)		112.7(7)
C(1)−N(2)−N(3)	123.7(6)		123.2(6)
C(1)−N(2)−C(4)	124.6(6)	C(4)−N(3)−C(5)	111.3(7)
C(4)−N(2)−N(3)	111.7(6)	N(2)−N(3)−C(4)	109.3(6)
N(2)−N(3)−C(5)	111.1(6)		108.9(6)
C(1)−C(6)−C(7)	173.9(8)		172.5(8)
C(6)−C(7)−C(8)	175.2(8)		177.7(8)
C(1)−N(2)−N(3)−C(5)	96.3(10)		−120.9(8)
C(6)−C(1)−N(2)−N(3)	−4.1(10)		176.9(6)
C(16)−W−C(1)/ W−C(1)−N(2)	41.3	C(24)−W−C(1)/ W−C(1)−N(2)	46.6

Q by elimination of Me_2NH in a Beckmann-type rearrangement. Experimental evidence for the formation of **Q** is yet to be obtained.

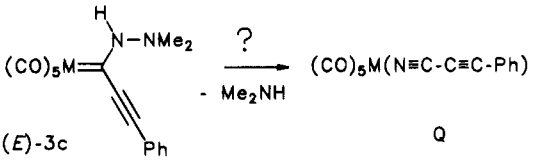

(Unsubstituted) Hydrazine (2d)

The reaction of hydrazine (**2d**) with the chromium complex **1'** (Scheme 6) also corresponds to the reaction scheme outlined above. It leads to the formation of imidate complexes (*E*/*Z*)-**4c'** and of aminocarbene complexes **10d'** and (*Z*)-**11d'** as main reaction products. Small amounts of the (benzonitrile)$Cr(CO)_5$ (**8'**) are also obtained.

(Electron-Deficient) Acetylhydrazine (2e)

The smooth reaction of acetylhydrazine (**2e**) with chromium complex **1'** leads to formation of the *N*-

Table 6. Details of the X-ray Crystal Structures Analyses of (*E*)-3a and (*Z*)-3c: Data Collection and Structures Solution

	(*E*)-3a	(*Z*)-3c
formula	$C_{16}H_{12}N_2O_5W$	$C_{16}H_{12}N_2O_5W$
mol wt	496.13	496.13
cryst color	orange	red-orange
cryst system	triclinic	triclinic
space group (No.)	$P\bar{1}$ (No. 2)	$P\bar{1}$ (No. 2)
a (Å)	8.501(2)	9.380(3)
b (Å)	9.645(2)	9.685(4)
c (Å)	11.860(2)	10.804(3)
α (deg)	103.56(2)	84.77(5)
β (deg)	95.59(2)	80.74(3)
γ (deg)	111.76(2)	66.47(3)
V (Å^3)	859.5(3)	887.8(5)
Z	2	2
D_{calc} (g cm^{-3})	1.917	1.856
μ (cm^{-1})	67.5	65.3
wavelength (Å)	0.710 73	0.710 73
F(000) (e)	472	472
diffractometer	Enraf-Nonius MACHIII	Enraf-Nonius MACHIII
scan mode	$\omega-2\theta$	$\omega-2\theta$
$[(\sin\theta)/\lambda]_{max}$ (Å^{-1})	0.62	0.62
T (°C)	−50	−50
abs corr	ψ-scan (empirical)	ψ-scan (empirical)
transm	69.2 ↔ 99.9%	71.1 ↔ 99.9%
no. of measd reflcns	3648 ($\pm h,\pm k,-l$)	3818 ($\pm h,+k,\pm l$)
no. of indep reflcns	3474	3596
no. of obsd reflcns [$>2\sigma(I)$]	3.49	3213
R_{av}	0.027	0.021
no. of refined params	222	222
R (all data)	0.043	0.036
wR^2 (all data)	0.083	0.086
resid elec dens (e Å^{-3})	2.11 (−1.84)	1.15 (−1.23)
H atoms	calculated	calculated
programs used	EXPRESS, MolEN, SHELX-86, SHELXL-93, ORTEX	

Table 7. Atomic Coordinates (×10^4) and Equivalent Isotropic Displacement Parameters (Å^2 × 10^3) of (*E*)-3a[a]

	x	y	z	U(eq)
W	7262(1)	4157(1)	1433(1)	31(1)
C(1)	6879(9)	3330(8)	3039(6)	37(2)
N(2)	6132(8)	1938(7)	3164(5)	42(1)
N(#)	6091(10)	1638(9)	4288(6)	50(2)
C(4)	5321(12)	497(9)	2186(7)	55(2)
C(5)	4484(14)	545(14)	4657(9)	75(3)
C(6)	7566(9)	4569(9)	4138(6)	40(2)
C(7)	8149(10)	5684(9)	4981(6)	40(2)
C(8)	8848(9)	7124(9)	5948(6)	40(2)
C(9)	8322(11)	7155(10)	7027(6)	47(2)
C(10)	8899(12)	8549(12)	7903(7)	59(2)
C(11)	10009(12)	9888(11)	7724(8)	60(2)
C(12)	10565(12)	9859(11)	6677(9)	67(3)
C(13)	9980(10)	8471(10)	5788(7)	52(2)
C(14)	6304(9)	5741(8)	2136(6)	39(2)
O(14)	5752(8)	6621(7)	2506(6)	60(2)
C(15)	8089(10)	2519(9)	601(7)	42(2)
O(15)	8469(8)	1615(7)	54(5)	62(2)
C(16)	4851(9)	2700(7)	463(6)	37(2)
O(16)	3561(7)	1918(7)	−148(5)	59(2)
C(17)	7683(9)	5060(9)	74(7)	42(2)
O(17)	7905(8)	5564(8)	−706(5)	60(2)
C(18)	9714(10)	5668(9)	2338(7)	44(2)
O(18)	11062(8)	6528(8)	2851(6)	71(2)

[a] U(eq) is defined as one-third of the trace of the orthogonalized U_{ij} tensor.

acetylpyrazole (12e) (75%) as the only organic product (Scheme 7). Since the nucleophilicity of the substituted nitrogen atom of **2e** is amide-like and therefore low, the addition of the NH_2 group of **2e** to **1′** becomes the main reaction pathway. It is initiated by a Michael-type addition and follows the principles outlined above.

The configurational assignment of **12e** is based on the deshielding of 5-H (δ 8.10) by the anisotropic effect of the (N)C=O group and also on the deshielding of the *o*-H's of the phenyl group by the C=N unit. As expected, an NOE between the $COCH_3$ and the phenyl group was not observed.

Table 8. Atomic Coordinates (×10^4) and Equivalent Isotropic Displacement Parameters (Å^2 × 10^3) of (*Z*)-3c[a]

	x	y	z	U(eq)
W	550(1)	1616(1)	1886(1)	32(1)
C(1)	2943(7)	1392(7)	2079(6)	31(1)
N(2)	3766(7)	2103(7)	1450(6)	39(1)
N(3)	3219(7)	3175(7)	482(6)	40(1)
C(4)	3102(11)	4643(10)	837(9)	58(2)
C(5)	4287(11)	2681(12)	−664(9)	66(3)
C(6)	3780(7)	307(8)	2966(7)	36(2)
C(7)	4484(8)	−725(8)	3623(7)	41(2)
C(8)	5347(9)	−1998(9)	4368(7)	43(2)
C(9)	4613(12)	−2639(11)	5286(10)	66(3)
C(10)	5456(17)	−3914(13)	5961(11)	91(4)
C(11)	7053(17)	−4538(12)	5686(11)	95(5)
C(12)	7719(14)	−3891(16)	4772(12)	111(5)
C(13)	6958(11)	−2627(13)	4120(10)	79(3)
C(21)	−184(9)	3905(8)	1733(8)	44(2)
O(21)	−642(8)	5171(7)	1631(7)	75(2)
C(22)	−1595(9)	1819(9)	1690(9)	50(2)
O(22)	−2850(6)	1983(8)	1548(7)	70(2)
C(23)	42(9)	1712(9)	3791(8)	48(2)
O(23)	−227(9)	1756(8)	4861(6)	77(1)
C(24)	1167(10)	1512(9)	−14(8)	46(2)
O(24)	1499(9)	1443(8)	−1069(6)	71(2)
C(25)	1294(9)	−679(8)	2055(8)	43(2)
O(25)	1717(8)	−1948(6)	2157(7)	66(2)

[a] U(eq) is defined as one-third of the trace of the orthogonalized U_{ij} tensor.

Scheme 6

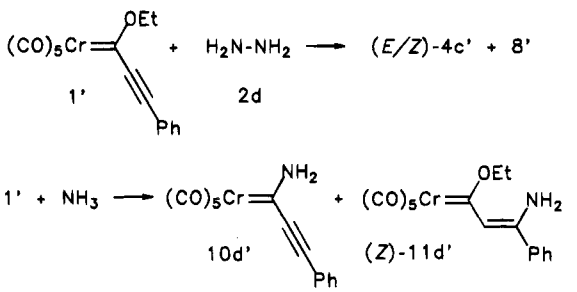

Scheme 7

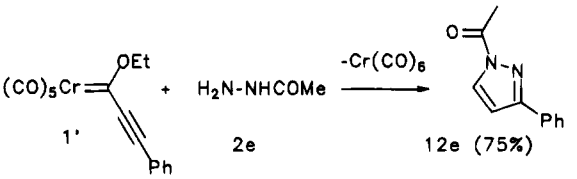

Scheme 8

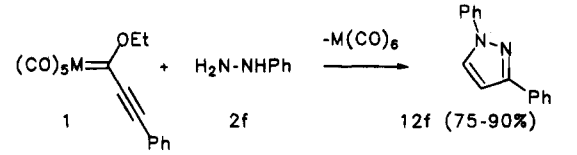

Phenylhydrazine (2f)

The hydrazinolysis of **1** (or **1′**) with phenylhydrazine (**2f**) at 80 °C for 4 h affords the *N*-phenylpyrazole (**12f**)

Scheme 9

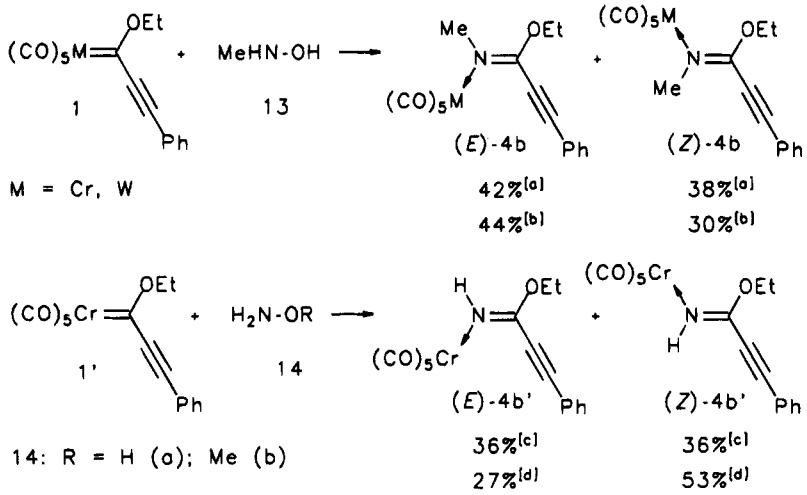

[a] obtained from 1, [b] obtained from 1', [c] obtained from 14a, [d] obtained from 14b

(Scheme 8) as the only isolated product. The reaction is initiated by a 3-addition of the unsubstituted nitrogen atom of **2f** to **1** and followed by a cyclization as outlined above.

Imidates 4 from Hydroxylamines 13 and 14

The formation of imidate complexes **4** from the reaction of hydrazines **2** with carbene complexes **1** involves the insertion of a NH fragment into the M=C bond of the carbene complexes. An insertion of similar type is also observed in reactions of hydroxylamines **13** or **14** with **1** (Scheme 9).[2] Apparently these reactions follow a similar pattern as is outlined above, but they give better yields of imidate complexes **4** than obtained with hydrazines **2**.

Experimental Section

All operations were performed under argon. Solvents were dried by distillation from sodium/benzophenone. Melting points are uncorrected. Instrumentation: ^{1}H NMR and ^{13}C NMR spectra were obtained with Bruker WM 300 and WP 360 spectrometers. Multiplicities were determined by DEPT. Chemical shifts refer to $\delta_{TMS} = 0.00$ (ppm). Other analyses: IR Digilab FTS 45; MS Finnigan MAT 312; elemental analysis, Perkin-Elmer 240 elemental analyser; column chromatography, Merck-Kieselgel 100; TLC, Merck DC-Alufolien Kieselgel 60 F 254. R_f values refer to TLC tests.

Pentacarbonyl[1-(1,2-dimethylhydrazino)-3-phenylpropynylidene]tungsten [(*E*)-3a and (*Z*)-3a], Pentacarbonyl(ethyl *N*-methyl-3-phenylpropiolimidato-*N*)tungsten [(*E*)-4a and (*Z*)-4a], and Pentacarbonyl(1,2-dimethyl-3-phenyl-3-pyrazolin-5-ylidene)tungsten (5a). Pentacarbonyl(1-ethoxy-3-phenyl-2-propynylidene)tungsten (**1**) (482 mg, 1.00 mmol) is added to a precooled solution of 1,2-dimethylhydrazine (**2a**) in 3 mL of diethyl ether [generated from 1,2-dimethylhydrazine dihydrochloride, 266 mg (2.00 mmol) and concentrated KOH/H_2O in diethyl ether/H_2O] with vigorous stirring at −78 °C within 5 min. After a few minutes a yellow solution is obtained, from which the solvent is removed in vacuo (20 °C, 15 Torr). According to the ^{1}H NMR spectrum (integration of the NCH_3 and OCH_2 groups) in C_6D_6 a mixture of (*E*)-**3a**:(*Z*)-**3a**:(*E*)-**4a**:(*Z*)-**4a**:**5a** = 3:2:4:2:4 is formed. Chromatography on silica gel with pentane/diethyl ether (2:1) affords a yellow band of (*E*/*Z*)-**4a** [173 mg, 34%, R_f = 0.8 in pentane/diphenyl ether (2:1), (*E*)-**4a**:(*Z*)-**4a** = 2:1; separation by fractional crystallization from 10 mL of pentane at −15 °C], a red band of (*E*/*Z*)-**3a** [139 mg, 28%, R_f = 0.4 in pentane/diethyl ether (2:1), (*E*)-**3a**:(*Z*)-**3a** = 3:2; fractional crystallization from 10 mL of pentane at −15 °C yields red platelets of the (*E*) isomer and red needle of the (*Z*) isomer (mp 112 °C)], and a pale yellow band of **5a** [114 mg, 23%, R_f = 0.2 in pentane/diethyl ether (2:1); yellowish crystals from pentane at −15 °C, mp 150 °C]. The reaction of **1** with **2a** at 20 °C yields (*E*)-**3a**:(*Z*)-**3a**:(*E*)-**4a**:(*Z*)-**4a**:**5a** = 3:2:0:0:48 according to the ^{1}H NMR spectrum. Chromatography affords **5a** [397 mg, 80%].

(*E*)-3a. ^{1}H NMR (C_6D_6): δ 7.40, 7.00 and 6.95 (2:1:2 H, *o*-:*m*-:*p*-H, Ph), 5.66 (1 H, q, ^2J = 6 Hz, NH), 3.20 (3 H, s, 1-NCH_3), 1.95 (3 H, d, ^2J = 6 Hz, 2-$NHCH_3$). ^{13}C NMR ($CDCl_3$): δ 212.3 (W=C), 202.9 and 198.9 [1:4, *trans*- and *cis*-CO, $W(CO)_5$], 131.8, 130.4, 129.0 (2:1:2, CH each, *o*-:*m*-:*p*-C, Ph), 123.1 and 121.4 [C(q) each, *i*-C Ph and C3], 89.1 [C(q), C2], 46.6 (1-NCH_3), 36.9 (2-NCH_3). IR (diffuse reflection) (cm^{-1}) (%): $\tilde{\nu}$ = 3304.3 (10) [ν(N−H)], 2171.8 (ν(C≡C)], 2060.0 (20), 1895.0 (100) [ν(C≡O)]. IR (hexane): 2063.5 (20), 1975.4 (10), 1930.2 (100). MS (70 eV) [*m*/*z* (%)] (^{184}W): 496 (20), 468 (20), 440 (30), 412 (50), 384 (30), 356 (70) [M^+ − 5CO], 328 (100). Anal. Calcd for $C_{16}H_{12}N_2O_5W$ (496.1): C, 38.73; H, 2.44; N, 5.65. Found: C, 38.86; H, 2.56; N, 2.76.

(*Z*)-3a. ^{1}H NMR (C_6D_6): δ 7.35, 7.00 and 6.97 (2:1:2 H, *o*-:*m*-:*p*-H, Ph), 6.02 (1 H, q, ^2J = 6 Hz, NH), 2.70 (3 H, s, 1-NCH_3), 2.10 (3 H, d, ^2J = 6 Hz, 2-$NHCH_3$). ^{13}C NMR ($CDCl_3$): δ 212.1 (W=C), 203.8 and 197.0 [1:4, *trans*- and *cis*-CO, $W(CO)_5$], 131.7, 130.2, 129.0 (2:1:2, CH each, *o*-:*m*-:*p*-C, Ph), 122.5 and 122.0 [C(q) each, *i*-C Ph and C3], 91.6 [C(q), C2], 40.7 (1-NCH_3), 36.1 (2-NCH_3). IR (diffuse reflection) (cm^{-1}) (%): $\tilde{\nu}$ = 3295.3 (5) [ν(N−H)], 2172.7 [ν(C≡C)], 2061.3 (40), 1901.8 (100) [ν(C≡O)]. MS (70 eV) [*m*/*e* (%)] (^{184}W): 496 [M^+].

(*E*)-4a. ^{1}H NMR (C_6D_6): δ, 7.50, 6.90 and 6.85 (2:1:2 H, *o*-:*m*-:*p*-H, Ph), 3.55 (2 H, q, OCH_2), 3.00 (3 H, s, NCH_3), 0.75 (3 H, t, OCH_2CH_3). ^{13}C NMR (C_6D_6): δ 202.4 and 199.3 [1:4, *trans*- and *cis*-CO, $W(CO)_5$], 153.9 [C(q), C=N]; 132.3, 131.0, 128.9 (2:2:1, CH each, *o*-:*m*-:*p*-C, Ph); 119.5 [C(q), *i*-C, Ph], 102.0 [C(q), C3], 80.2 [C(q), C2], 68.2 (OCH_2), 46.5 (NCH_3), 14.3 (CH_3, Et). IR (hexane) (cm^{-1}) (%): $\tilde{\nu}$ = 2068.3 (10), 1972.9 (10), 1928 (100), 1897.0 (30) [ν(C≡O)]. IR (diffuse reflection): 3309.6 (10) [ν(N−H)], 2217.9 [ν(C≡C], 2067.7 (20), 1973.3 (20), 1905.0 (100) [ν(C≡O)], 1603.3 (30) [ν(C=N)]. MS (70 eV) [*m*/*e* (%)] (^{184}W): 511 (10) [M^+], 483 (5), 455 (20), 427 (40), 399 (30), 371 (40) [M^+ − 5CO], 343 (50), 187 (100). Anal. Calcd for $C_{17}H_{13}NO_6W$ (511.1): C, 39.95; H, 2.56; N. 2.74. Found: C, 39.85; H, 2.67; N, 2.96.

(*Z*)-4a. ^{1}H NMR (C_6D_6): δ 7.05, 7.00 and 6.90 (2:1:2 H, *o*-:*m*-:*p*-H, Ph), 3.75 (2 H, q, OCH_2), 3.25 (3 H, s, NCH_3), 1.05 (3

H, t, OCH_2CH_3). ^{13}C NMR (C_6D_6): δ 204.3 and 199.2 [1:4, *trans*- and *cis*-CO, $W(CO)_5$], 155.6 [C(q), C=N]; 132.2, 131.0, 128.9 (2:2:1, CH each, *o*-:*m*-:*p*-C, Ph); 119.0 [C(q), *i*-C, Ph], 102.0 [C(q), C3], 80.2 [C(q), C2], 67.8 (OCH_2), 50.2 (NCH_3), 14.3 (CH_3, Et). IR (hexane) (cm^{-1}) (%): $\bar{\nu}$ = 2068.4 (10), 1972.6 (10), 1928.9 (100), 1894.0 (30) [ν(C≡O)]. IR (diffuse reflection): 3343.8 (10) [ν(N−H)], 2209.0 [ν(C≡C)], 2067.8 (20), 1973.8 (20), 1907.8 (100) [ν(C≡O)], 1587.7 (30) [ν(C=N)]. Anal. Calcd for $C_{17}H_{13}NO_6W$ (511.1): C, 39.95; H, 2.56; N, 2.74. Found: C, 39.89; H, 2.74; N, 3.02

5a. ^1H NMR (C_6D_6): δ 7.05 and 6.85 (3:2 H, Ph), 6.60 (1 H, s, 4-H), 3.20 (3 H, s, 1-NCH_3), 2.30 (3 H, s, 2-NMe). ^{13}C NMR ($CDCl_3$): δ 203.5 and 200.1 [1:4, *trans*- and *cis*-CO, $W(CO)_5$], 176.9 [C(q), C5], 145.9 [C(q), C3]; 130.0, 129.2 and 128.9 (1:2:2 C, CH each, Ph), 128.5 [C(q), *i*-C, Ph], 123.1 (CH, C4), 38.6 (1-NCH_3), 33.5 (2-NCH_3). IR (hexane) (%): $\bar{\nu}$ = 2057.5 (10), 1978.7 (10), 1963.3 (5), 1917.8 (100) [ν(C≡O)]. MS (70 eV) [*m/e* (%)] (^{184}W): 496 (50) [M^+], 468 (40), 440 (40), 412 (20), 384 (50), 356 (80) [M^+ − 5CO], 91 (70), 86 (80), 51 (100). Anal. Calcd for $C_{16}H_{12}N_2O_5W$ (496.1): C, 38.73; H, 2.44; N, 5.65. Found: C, 39.01; H, 2.52; N, 5.66.

Pentacarbonyl(1,2-dimethyl-3-phenyl-3-pyrazolin-5-ylidene)chromium (5a′). Pentacarbonyl(1-ethoxy-3-phenyl-2-propynylidene)chromium (**1′**) (350 mg, 1.00 mmol) is added to 1,2-dimethylhydrazine (**2a**) in 3 mL of diethyl ether [generated from 1,2-dimethylhydrazine dihydrochloride, 266 mg (2.00 mmol), and concentrated KOH/H_2O in diethyl ether/H_2O] with vigorous stirring at −20 °C within 5 min. The reaction is slightly exothermic and yields a yellow solution, from which the solvent is removed in vacuo (20 °C, 15 Torr). Chromatography on silica gel with pentane/dichloromethane (10:1) affords a pale yellow band of **5a′** [299 mg, 81%, R_f = 0.3 in pentane/dichloromethane (2:1), yellowish crystals from pentane at −15 °C, mp 160 °C, dec]. ^1H NMR (C_6D_6): δ 7.15 and 6.95 (3:2 H, Ph), 6.50 (1 H, s, 4-H), 3.50 (3 H, s, 1-NCH_3), 2.35 (3, H, s, 2-NMe). ^{13}C NMR (C_6D_6): δ 224.3 and 220.5 [1:4, *trans*- and *cis*-CO, $Cr(CO)_5$], 190.8 [C(q), C5], 145.5 [C(q), C3]; 129.9, 129.2 and 128.8 (1:2:2 C, CH each, Ph), 128.6 [C(q), *i*-C, Ph], 121.9 (CH, C4), 37.8 (1-NCH_3), 33.9 (2-NCH_3). IR (hexane) (%): $\bar{\nu}$ = 2049.3 (20), 1937.9 (10), 1925.9 (100) [ν(C≡O)]. MS (70 eV) [*m/e* (%)]: 364 (50) [M^+], 336 (40), 308 (40), 280 (30), 252 (50), 224 (80) [M^+ − 5CO], 172 (50) [224 − Cr], 171 [ligand − H], 93 (100), 91 (100). Anal. Calcd for $C_{16}H_{12}CrN_2O_5$ (364.3): C, 52.76; H, 3.32; N, 7.69. Found: C, 52.59; H, 3.47; N, 7.69.

Pentacarbonyl[1-(1-methylhydrazino)-3-phenylpropynylidene]tungsten [(*E*)-3b and (*Z*)-3b], Pentacarbonyl(ethyl *N*-methyl-3-phenylpropiolimidato-*N*)tungsten [(*E*)-4a and (*Z*)-4a], Pentacarbonyl(2-methyl-3-phenyl-3-pyrazolin-5-ylidene)tungsten (5b), and Pentacarbonyl(1-methyl-5-phenylpyrazole-*N*)tungsten (6b) from 1 and 2b. Pentacarbonyl(1-ethoxy-3-phenyl-2-propynylidene)tungsten (**1**) (482 mg, 1.00 mmol) is added to a precooled solution of methylhydrazine (**2a**) (138 mg, 3.00 mmol) in 3 mL of diethyl ether at −78 °C with vigorous within 5 min. A yellow solution is obtained, from which the solvent is removed (15 Torr, 20 °C). The ^1H NMR spectrum in C_6D_6 (360 MHz, integration of the NCH_3 and OCH_2 signals) shows (*E*)-**3b**:(*Z*)-**3b**:(*E*)-**4a**:(*E*)-**4a**:**5b**:**6b** = 3:2:3:1:1:1. Chromatography on silica gel with pentane/dichloromethane (10:1 to 2:1) affords a pale yellow band of **6b** [39 mg, 8%, R_f = 0.3 in pentane/dichloromethane (2:1), yellowish crystals from pentane at −15 °C], a yellow band with (*E*/*Z*)-**4a** [153 mg, 30%, R_f = 0.8 in pentane/diethyl ether (2:1), see above], a red band with (*E*/*Z*)-**3b** [174 mg, 36%, R_f = 0.4 in pentane/diethyl ether (2:1)], and a pale yellow band of **5b** [34 mg, 7%, R_f = 0.2 in pentane/diethyl ether (2:1)]. The reaction of **1** with **2b** at 20 °C affords (*E*)-**3b**:(*Z*)-**3b**:(*E*)-**4a**:(*Z*)-**4a**:**5b**:**6b** = 0:0:3:1:10:15, total yield 76%.

(*E*)-3b. ^1H NMR (C_6D_6): δ 7.35, 7.00 and 6.95 (2:1:2 H, *o*-:*m*-:*p*-H, Ph), 4.55 (2 H, s, NH_2), 2.95 (3 H, q, NCH_3). ^{13}C NMR ($CDCl_3$): δ 203.6 and 198.8 [1:4, *trans*- and *cis*-CO, $W(CO)_5$], 203.3 (W=C); 131.9, 130.5, 129.0 (2:1:2, CH each, *o*-:*m*-:*p*-C, Ph), 123.0 and 121.5 [C(q) each, *i*-C Ph and C3], 89.6 [C(q), C2], 49.4 (NCH_3). IR (diffuse reflection): $\bar{\nu}$ = 3352.0 (10) [ν(N−H)], 2174.8 [ν(C≡C)], 2060.8 (20), 1972.2 (20), 1888.0 (100) [ν(C≡O)]. MS (70 eV) [*m/e* (%)] (^{184}W): 482 (20) [M^+], 454 (5), 426 (50), 398 (10), 370 (30), 342 (100). Anal. Calcd for $C_{15}H_{10}N_2O_5W$ (482.1): C, 37.37; H, 2.09; N, 5.81. Found: C, 37.51; H, 2.02; N, 6.07.

(*Z*)-3b. ^1H NMR (C_6D_6): δ 7.40, 7.00 and 6.98 (2:1:2 H, *o*-:*m*-:*p*-H, Ph), 4.80 (2 H, s, NH_2), 2.55 (3 H, q, NCH_3). ^{13}C NMR ($CDCl_3$): δ 202.2 and 198.2 [1:4, *trans*- and *cis*-CO, $W(CO)_5$], 203.6 (W=C); 131.7, 130.2, 128.9 (2:1:2, CH each, *o*-:*m*-:*p*-C, Ph), 124.5 and 122.0 [C(q) each, *i*-C Ph and C3], 91.2 [C(q), C2], 43.9 (NCH_3). IR (diffuse reflection): $\bar{\nu}$ = 3354.3 (5) and 3278.8 (2) [ν(N−H)], 2175.6 [ν(C≡C)], 2060.9 (40), 1970.3 (50), 1940.0 (60), 1889.8 (100) [ν(C≡O)]. MS (70 eV) [*m/e* (%)] (^{184}W): 482 [M^+]. Anal. Calcd for $C_{15}H_{10}N_2O_5W$ (482.1): C, 37.37; H, 2.09; N, 5.81. Found: C, 37.43; H, 2.20; N, 5.93.

5b. ^1H NMR (C_6D_6): δ 7.05 and 6.98 (3:2 H, m and "d", Ph), 6.80 (1 H, s, 4-H), 6.60 (1 H, s, broad, NH), 2.20 (3 H, 2, 2-NMe).

6b. ^1H NMR (C_6D_6): δ 7.33 (1 H, d, ^3J = 2.5 Hz, 3-H), 7.05 and 6.75 (3:2 H, m and "d", Ph), 5.70 (1 H, d, ^3J = 2.5 Hz, 4-H), 3.32 (3 H, s, 1-NCH_3). ^{13}C NMR (C_6D_6): δ = 203.1 and 200.0 [1:4, *trans*- and *cis*-CO, $W(CO)_5$], 149.0 (CH, C3), 148.0 [C(q), C5], 131.0 [C(q), *i*-C, Ph]; 130.8, 130.3, 130.1 (2:2:1, CH each, *o*-:*m*-:*p*-C, Ph), 109.0 [C(q), C4], 39.6 (NCH_3). IR (diffuse reflection) (cm^{-1}) (%): $\bar{\nu}$ = 2070.8 (50), 1975.1 (50), 1892.5 (100) [ν(C≡O)]. Anal. Calcd for $C_{15}H_{10}N_2O_5W$ (482.1): C, 37.37; H, 2.09; N, 5.81. Found: C, 37.54; H, 2.15; N, 6.02.

Pentacarbonyl(1-methyl-5-phenylpyrazole-N)chromium (6b′) from 1′ and 2b. Pentacarbonyl(1-ethoxy-3-phenyl-2-propynylidene)chromium (**1′**) (350 mg, 1.00 mmol) in 4 mL of ethanol is added to methylhydrazine (**8b**) (138 mg, 3.00 mmol) in 1 mL of ethanol with vigorous stirring at 20 °C within 5 min. The reaction is slightly exothermic and yields a yellow solution. The ^1H NMR spectrum in C_6D_6 (360 MHz, integration of the OCH_2 signals) shows **6b′** as the main product. The solvent is removed in vacuo (20 °C, 15 Torr), and the yellow oily residue is crystallized from 10 mL of pentane at −78 °C [259 mg, 74%, R_f = 0.3 in pentane/dichloromethane (2:1), yellowish crystals from pentane at −15 °C].

6b. ^1H NMR (C_6D_6): δ 7.35 (1 H, d, ^3J = 2.5 Hz, 3-H), 7.03 and 6.72 (3:2 H, m and "d", Ph), 5.70 (1 H, d, ^3J = 2.5 Hz, 4-H), 3.13 (3 H, s, 1-NCH_3). IR (diffuse reflection) (cm^{-1}) (%): $\bar{\nu}$ = 2067.5 (50), 1981.4 (50), 1898.5 (100) [ν(C≡O)]. Anal. Calcd for $C_{15}H_{10}CrN_2O_5$ (350.3): C, 51.44; H, 2.88; N, 8.00. Found: C, 51.65; H, 3.00; N, 8.13.

1-Methyl-5-phenylpyrazole (7b). Pentacarbonyl(1-methyl-5-phenylpyrazole-N)chromium (**6b′**) in C_6D_6 is heated to 60 °C for 10 h. The ^1H NMR of the solution shows signals of **6b′** and **7b** in a ratio of 1:5, but after 20 h at 60 °C signals of **7b** only are detected. ^1H NMR (C_6D_6): δ 7.53 (1 H, s, broad, 3-H), 7.05 (5 H, m, Ph), 6.10 (1 H, s broad, 4-H), 3.40 (N-CH_3).

Pentacarbonyl[1-(2′,2′-dimethylhydrazino)-3-phenylpropynylidene]tungsten [(*Z*)-4c and (*Z*)-4c], (Benzonitrile)pentacarbonyltungsten (8), Pentacarbonyl[(2*E*)-1-ethoxy-3-(dimethylamino)-3-phenyl-2-propenylidene]tungsten (10c), and Pentacarbonyl[(2*E*)-1-(dimethylamino)-3-phenyl-2-propynylidene]tungsten (11c) from 1 and 2c. Pentacarbonyl(1-ethoxy-3-phenyl-2-propynylidene)tungsten (**1**) (482 mg, 1.00 mmol) is added to a precooled solution of 1,1-dimethylhydrazine (**2c**) (180 mg, 3.00 mmol) in 3 mL of diethyl ether with vigorous stirring at −78 °C within 5 min. After a few minutes a yellow solution is obtained, from which the solvent is removed in vacuo (20 °C, 15 Torr). According to the ^1H NMR spectrum (integration of the NCH_3 and OCH_2 groups) in C_6D_6 a mixture of (*Z*)-**3c**:(*E*)-**3c**:(*E*)-**4c**:(*Z*)-**4c**:**8**:**10c**:**11c** = 6:0:6:4:0:5:1 is formed. Chromatography on silica gel with pentane/diethyl ether (2:1) affords a yellow band of (*E*/*Z*)-**4c** [169 mg, 34%, R_f = 0.8 in pentane/diethyl ether (2:1), (*E*)-**4c**:(*Z*)-**4c** = 6:1; separation by fractional crystallization from 10 mL of pentane at −15 °C], a red band of (*Z*)-**3c** [199 mg, 40%, R_f = 0.4 in pentane/diethyl ether (2:

1); red platelets from 10 mL of pentane at −15 °C, mp 88 °C], and a pale yellow band of **10c** [110 mg, 21%, R_f = 0.3 in pentane/diethyl ether (1:1)].[12] The reaction of **1** with **2c** at 20 °C yields (*Z*)-**3c**:(*e*)-**3c**:(*E*)-**4c**:(*Z*)-**4c**:**8**:**10c**:(*E*)-**11c** = 0:0:6:1:1:1:7 according to the ^{1}H NMR spectrum. Chromatography affords **8** [38 mg, 9%, R_f = 0.80 in pentane/dichloromethane (4:1), yellow crystals][13] and (*E*)-**11c** [205 mg, 39%, R_f = 0.2 in pentane/diethyl ether (1:1)].[12]

(*Z*)-3c. ^{1}H NMR (C_6D_6): δ 7.85 (1 H, s broad, NH), 7.60 and 6.95 (2:3 H, "d" and m, Ph), 2.00 [6 H, s, $N(CH_3)_2$]. ^{13}C NMR ($CDCl_3$): δ 229.9 (W=C); 206.4 and 199.6 [1:4, *trans*- and *cis*-CO, $W(CO)_5$], 132.3, 130.5, 129.1 (2:1:2, CH each, *o*-:*m*-:*p*-C, Ph), 122.6 and 118.5 [C(q) each, *i*-C Ph and C3], 93.3 [C(q), C2], 46.9 (NCH_3). IR (diffuse reflection): $\tilde{\nu}$ = 3226.0 (10), [ν(N−H)], 2182.4 [ν(C≡C)], 2061.3 (20), 1975.7 (20), 1911.7 (100) [ν(C≡O)]. MS (70 eV) [*m/e* (%)] (^{184}W): 496 (20) [M^+], 468 (25), 440 (30), 412 (30), 384 (30), 356 (80), 127 (100). Anal. Calcd for $C_{16}H_{12}N_2O_5W$ (496.1): C, 38.73; H, 2.44; N, 5.65. Found: C, 38.85; H, 2.39; N, 5.67.

(*E*)-4c. ^{1}H NMR (C_6D_6): δ 7.60, 7.15 and 7.05 (2:1:2 H, *o*-:*m*-:*p*-H, Ph), 6.50 (1 H, s broad, NH), 3.30 (2 H, q, OCH_2), 0.90 (3 H, t, OCH_2CH_3). ^{13}C NMR ($CDCl_3$): δ 202.4 and 197.9 [1:4, *trans*- and *cis*-CO, $W(CO)_5$], 158.8 [C(q), C=N]; 132.9, 131.4, 129.9 (2:2:1, CH each, *o*-:*m*-:*p*-C, Ph); 118.9 [C(q), *i*-C, Ph], 102.0 [C(q), C3], 78.4 [C(q), C2], 67.7 (OCH_2), 15.1 (CH_3). IR (hexane) (cm^{-1}) (%): $\tilde{\nu}$ = 2068.3 (10), 1972.9 (10), 1928.1 (100), 1897.0 (30) [ν(C≡O)]. IR (diffuse reflection): 3309.6 (10) [ν(N−H)], 2217.9 [ν(C≡C)], 2067.7 (20), 1973.3 (20), 1905.0 (100) [ν(C≡O)], 1603.3 (30) [ν(C=N)]. MS (70 eV) [*m/e* (%)] (^{184}W): 497 (10) [M^+], 469 (5), 441 (20), 413 (20), 385 (20), 357 (20) [M^+ − 5CO], 127 (100) [N≡CC≡CPh$^+$]. Anal. Calcd for $C_{16}H_{11}NO_6W$ (497.1): C, 38.66; H, 2.23; N, 2.82. Found: C, 38.94; H, 2.38; N, 3.10.

(*Z*)-4c. ^{1}H NMR (C_6D_6): δ 7.20, 7.10 and 7.08 (2:1:2 H, *o*-:*m*-:*p*-H, Ph), 7.05 (1 H, s broad, NH), 3.80 (2 H, q, OCH_2), 1.05 (3 H, t, OCH_2CH_3). ^{13}C NMR ($CDCl_3$): δ 208.6 and 197.6 [1:4, *trans*- and *cis*-CO, $W(CO)_5$], 159.6 [C(q), C=N]; 132.6, 131.4, 128.8 (2:1:2, CH each, *o*-:*m*-:*p*-C, Ph); 118.6 [C(q), *i*-C, Ph], 98.1 [C(q), C3], 76.3 [C(q), C2], 68.8 (OCH_2), 14.6 (CH_3). IR (hexane) (cm^{-1}) (%): $\tilde{\nu}$ = 2068.4 (10), 1972.6 (10), 1928.9 (100), 1894.0 (30) [ν(C=O)]. IR (diffuse reflection): 3343.8 (10) [ν(N−H)], 2209.0 [ν(C≡C)], 2067.8 (20), 1973.8 (20), 1907.8 (100) [ν(C≡O)], 1587.7 (30) [ν(C=N)]. Anal. Calcd for $C_{16}H_{11}NO_6W$ (497.1): C, 38.66; H, 2.23; N, 2.82. Found: C, 38.85; H, 2.27; N, 3.05. Found: C, 38.89; H, 2.34; N, 3.12.

Pentacarbonyl(ethyl 3-phenylpropiolimidato-*N*)chromium [(*E*)-4c′ and (*Z*)-4c′], Pentacarbonyl[(2E)-1-ethoxy-3-(dimethylamino)-3-phenyl-2-propenylidene]chromium (10′), and (Benzonitrile)(pentacarbonyl)chromium (8′) from 1′ and 2c. Pentacarbonyl(1-ethoxy-3-phenyl-2-propynylidene)chromium (**1′**) (350 mg, 1.00 mmol) in 3 mL of dichloromethane is added dropwise to 1,1-dimethylhydrazine (**2c**) (180 mg, 3.00 mmol) in 1 mL of ethanol at 20 °C within 5 min with vigorous stirring. The reaction is slightly exothermic and yields a yellow solution. After the solvent has been removed in vacuo (20 °C, 15 Torr), a yellow oil is obtained. The ^{1}H NMR spectrum in C_6D_6 (360 MHz, integration of the OCH_2 signals) shows (*E*)-**4c′**:(*Z*)-**4c′**:**8′** = 5:3:8. Chromatography on silica gel with pentane/dichloromethane (10:1) affords a small bright yellow band with **8′** [15 mg, 5%, R_f = 0.80 in pentane/dichloromethane (4:1), yellow crystals].[13] The second yellow band contains (*E*)-**4c′** [91 mg, 25%, R_f = 0.50 in pentane/dichloromethane (4:1), yellow spherical crystals from pentane at −15 °C] and (*Z*)-**4c′** [55 mg, 15%, R_f = 0.55 in pentane/dichloromethane (4:1), yellow needles from pentane at −15 °C, mp 81 °C]. The compounds (*E*)-**4c′** and (*Z*)-**4c′** are separated by fractional crystallization from pentane at −15 °C. A third yellow fraction contains **10′** [160 mg, 40%, R_f = 0.3 in pentane/diethyl ether (1:1), yellow crystals].[12]

(*E*)-4c′. ^{1}H NMR (C_6D_6): δ 7.50, 7.15 and 7.10 (2:1:2 H, *o*-:*m*-:*p*-H, Ph), 6.40 (1 H, s broad, NH), 3.80 (2 H, q, OCH_2), 1.10 (3 H, t, OCH_2CH_3). ^{13}C NMR (C_6D_6): δ 220.8 and 214.9 [1:4, *trans*- and *cis*-CO, $Cr(CO)_5$], 165.6 [C(q), C=N]; 132.7, 131.3, 129.0 (2:2:1, CH each, *o*-:*m*-:*p*-C, Ph); 119.5 [C(q), *i*-C, Ph], 100.2 [C(q), C3], 78.8 [C(q), C2], 66.9 (OCH_2), 14.6 (CH_3). IR (hexane) (cm^{-1}) (%): $\tilde{\nu}$ = 2219.2 (5) [ν(C≡C)], 2064.3 (10), 1975.2 (10), 1936.9 (100), 1912.5 (30) [ν(C≡O)]. IR (diffuse reflection): 3308.5 (10) [ν(N−H)], 2221.1 [ν(C≡C)], 2065.7 (20), 1982.1 (20), 1917.6 (100) [ν(C≡O)], 1608.4 (30) [ν(C=N)]. MS (70 eV) [*m/e* (%)]: 365 (50) [M^+], 337 (30), 309 (20), 281 (40), 253 (50), 225 (60) [M^+ − 5CO], 196 (50), 173 (30) [225 − Cr], 172 [ligand − H], 153 (70), 128 (80), 127 (80), 123 (70), 101 (80), 77 (100). Anal. Calcd for $C_{16}H_{11}CrNO_6$ (365.3): C, 52.61; H, 3.04; N, 3.83. Found: C, 52.94; H, 3.23; N, 4.05.

(*Z*)-4c′. ^{1}H NMR (C_6D_6): δ 7.35, 7.18 and 7.15 (2:2:1 H, *o*-:*m*-:*p*-H, Ph), 7.00 (2 H, s broad, NH), 4.10 (2 H, q, OCH_2), 135 (3 H, t, OCH_2CH_3). ^{13}C NMR (C_6D_6): δ 222.0 and 215.4 [1:4, *trans*- and *cis*-CO, $Cr(CO)_5$], 166.1 [C(q), C=N]; 132.4, 131.3, 128.3 (2:1:2, CH each, *o*-:*m*-:*p*-C, Ph); 119.2 [C(q), *i*-C, Ph], 96.9 [C(q), C3], 77.0 [C(q), C2], 66.4 (OCH_2), 14.6 (CH_3). IR (hexane) (cm^{-1}) (%): $\tilde{\nu}$ = 2209.4 (5) [ν(C≡C)], 2064.6 (10), 1978.3 (10), 1938.3 (100), 1911.2 (30) [ν(C≡O)]. IR (diffuse reflection): 3350.3 (10) [ν(N−H)], 2215.7 [ν(C≡C)], 2064.2 (20), 1979.5 (30), 1930.1 (100) [ν(C≡O)], 1591.8 (20) [ν(C=N)]. Anal. Calcd for $C_{16}H_{11}CrNO_6$ (365.3): C, 52.61; H, 3.04; N, 3.83. Found: C, 52.78; H, 3.12; N, 3.76.

8′. ^{1}H NMR (C_6D_6/CS_2 1:1, 25 °C): δ 7.30 and 6.90 (3:2 H, m each, C_6H_5), 6.60 (1 H, s, 2-H), 4.40 (2H, q broad, OCH_2), 2.80 and 2.20 (3 H each, s broad each, NMe_2), 0.60 (3 H, t, CH_2CH_3). ^{13}C NMR ($CDCl_3$, 20 °C): δ 293.7 (Cr=C), 224.8 and 219.5 [1:4C, *trans*- and *cis*-CO $Cr(CO)_5$], 156.2 [C(q), C3), 137.7 [C(q), *i*-C, Ph]; 128.9, 128.8 and 128.6 (1:2:2 C, CH each, Ph), 118.8 (CH, C2), 73.2 (OCH_2), 41.4 (2 C, broad, NMe_2), 14.2 (CH_3, Et). IR (hexane) (cm^{-1}) (%): $\tilde{\nu}$ = 2048.0 (20), 1982.1 (5), 1928.2 (100) [ν(C≡O)]. MS (70 eV) [*m/e* (%)]: 395 (20) [M^+], 367 (20), 339 (10), 311 (50), 283 (30), 255 (100) [M^+ − 5CO], 227 (80), 184 (60), 158 (80), 155 (60).

Pentacarbonyl(ethyl 3-phenylpropiolimidato-*N*)chromium [(*E*)-4c′ and (*Z*)-4c′], Pentacarbonyl[1-amino-3-phenyl-2-propynylidene]chromium (10d′), Pentacarbonyl-[(2*Z*)-1-ethoxy-3-amino-3-phenyl-2-propenylidene]-chromium [(*Z*)-11d′], and (Benzonitrile)(pentacarbonyl)-chromium (8′) from 1′ and 2d. Pentacarbonyl(1-ethoxy-3-phenyl-2-propynylidene)chromium (**1′**) (350 mg, 1.00 mmol) and hydrazine monohydrate (**2d**) (150 mg, 3.00 mmol) are reacted as described above in EtOH at 20 °C. The ^{1}H NMR spectrum in C_6D_6 (360 MHz, integration of the OCH_2 signals) shows (*E*)-**4c**:(*Z*)-**4c**:**8′**:**10d′**:(*Z*)-**11d′** = 3:2:1:2:1. Chromatography on silica gel yields **8′** [20 mg, 7%, R_f = 0.80 in pentane/dichloromethane (4:1), yellow crystals, literature ref 8], (*E*)-**4c′** (88 mg, 24%, see above) together with (*Z*)-**4c′** (58 mg, 16%, see above), **10d′** (92 mg, 25%, red crystals),[8] and **11d′** (37 mg, 10%, yellow crystals).[8]

1-Acetyl-3-phenylpyrazole (12e) from 1′ and 2e. Pentacarbonyl(1-ethoxy-3-phenyl-2-propynylidene)chromium (**1′**) (350 mg, 1.00 mmol) and acetylhydrazine (**2e**) (74 mg, 1.00 mmol) are reacted in 3 mL of dichloromethane for 2 h at 20 °C. After the mixture has turned yellow the solvent is removed in vacuo (20 °C, 15 Torr). Chromatography on silica gel with pentane/dichloromethane (10:1) affords colorless $Cr(CO)_6$ and a pale yellow band of **12e** [140 mg, 75%, R_f = 0.2 in pentane/dichloromethane (2:1), yellowish crystals from pentane at −15 °C, mp 58 °C]. ^{1}H NMR (C_6D_6): δ 8.10 (1 H, d, ^3J = 3 Hz, 5-H), 7.80 and 7.10 (2:3 H, "d" and m, Ph), 6.20 (1 H, d, ^3J = 3 Hz, 4-H), 2.50 (3 H, s, $COCH_3$). ^{13}C NMR ($CDCl_3$): δ 169.3 [C(q), NC=O], 155.6 [C(q), C3], 133.0 [C(q), *i*-C, Ph]; 129.7, 129.4 and 128.7 (1:2:2 C, CH each, Ph), 107.9 and 107.3 (CH each, C4 and C5), 21.7 (CH_3). IR (diffuse reflection (cm^{-1})

(12) For spectroscopic data see: (a) Fischer, E. O.; Kreissl, F. R. *J. Organomet. Chem.* **1972**, *35*, C47−C52. (b) Aumann, R. *Chem. Ber.* **1993**, *126*, 1867−1872. (c) Duetsch, M.; Stein, F.; Pohl, E.; Herbst-Irmer, R.; de Meijere, A. *Chem. Ber.* **1993**, *126*, 2535−2541.

(13) Aumann, R.; Althaus, S.; Krüger, C.; Betz, P. *Chem. Ber.* **1989**, *122*, 357−364.

(%): ν = 1732.6 (90) [ν(NC=O)], 1539.3 (30) and 1503.8 (20) [ν(C=N)] and [ν(C=C)]. MS (70 eV) [*m/e* (%)]: 186 (60) [M^+], 145 (60), 144 (100) [$M^+ - O{=}C{=}CH_2$], 117 (60), 115 (60). Anal. Calcd for $C_{11}H_{10}N_2O$ (186.2): C, 70.95; H, 5.41; N, 15.04. Found: C, 70.65; H, 5.38; N, 14.96.

1-Phenyl-3-phenylpyrazole (12f) from 1 or 1′ and 2f. Pentacarbonyl(1-ethoxy-3-phenyl-2-propynylidene)tungsten (**1**) (482 mg, 1.00 mmol) [or pentacarbonyl(1-ethoxy-3-phenyl-2-propynylidene)chromium (**1′**) (350 mg, 1.00 mmol)] and phenylhydrazine (**2f**) (108 mg, 1.00 mmol) in 3 mL of toluene are heated for 4 h at 80 °C. It is shown by TLC that **1** has been consumed completely. Chromatography on silica gel with pentane/dichloromethane (10:1) affords colorless $W(CO)_6$ [$Cr(CO)_6$] and a pale yellow band of **12f** [165 (198) mg, 75 (90)%, R_f = 0.5 in pentane/dichloromethane (3:1), colorless felty crystals from pentane at −15 °C, mp 80 °C]. ^{1}H NMR (C_6D_6): δ 8.05 and 7.60 (2:2 H, "d" each, *o*-H of Ph each), 7.33 (1 H, d, ^3J = 3 Hz, 3-H), 7.20 and 7.05 (2:2 H, "t" each, *m*-H of Ph each), 7.12 and 6.85 (1:1 H, "t" each, *p*-H of Ph each), 6.40 (1 H, d, ^3J = 3 Hz, 4-H). ^{13}C NMR (C_6D_6): δ 152.9 [C(q), C3], 140.4 [C(q), *i*-C, 1-Ph], 133.7 [C(q), *i*-C, 3-Ph]; 129.7, 129.0 and 128.6 (2:2:1 C, CH each, 3-Ph); 126.1, 126.0 and 119.1 (2:1:2 C, CH each, 1-Ph); 118.9 and 105.0 (CH each, C4 and C5). MS (70 eV) [*m/e* (%)]: 220 (100) [M^+], 192 (20), 178 (5), 165 (10), 143 (5), 116 (10), 89 (30), 77 (50). Anal. Calcd for $C_{15}H_{12}N_2$ (220.3): C, 81.79; H, 5.49; N, 12.72. Found: C, 82.00; H, 5.64; N, 13.01.

Pentacarbonyl(ethyl *N*-methyl-3-phenylpropiolimidato-*N*)tungsten [(*E*)-4a and (*Z*)-4a] from 1 and 13. Triethylamine (101 mg, 1.00 mmol) in 2 mL of ethanol is added to pentacarbonyl(1-ethoxy-3-phenyl-2-propynylidene)tungsten (**1**) (482 mg, 1.00 mmol) and *N*-methylhydroxylamine hydrochloride (166 mg, 2.00 mmol) in 3 mL of ethanol with vigorous stirring at 20 °C within 5 min. A yellow solution is obtained from which the solvent is removed in vacuo (20 °C, 15 Torr). According to the ^{1}H NMR spectrum in C_6D_6 of the pentane extract, (*E*)-**4a**:(*Z*)-**4a** = 1:1 is obtained. Fractional crystallization from 10 mL of pentane at −15 °C yields (*E*)-**4a** (215 mg, 42%) and (*Z*)-**4a** (194 mg, 38%).

Pentacarbonyl(ethyl *N*-methyl-3-phenylpropiolimidato-*N*)chromium [(*E*)-4a′ and (*Z*)-4a′] from 1′ and 13. Triethylamine (101 mg, 1.00 mmol) in 2 mL of ethanol is added to a solution of pentacarbonyl(1-ethoxy-3-phenyl-2-propynylidene)chromium (**1′**) (350 mg, 1.00 mmol) and *N*-methylhydroxylamine hydrochloride (166 mg, 2.00 mmol) in 3 mL of ethanol with vigorous stirring at 20 °C within 5 min. A yellow solution is obtained from which the solvent is removed in vacuo (20 °C, 15 Torr). According to the ^{1}H NMR spectrum in C_6D_6 of the pentane extract, (*E*)-**4a′**:(*Z*)-**4a′** = 3:2 is obtained. Fractional crystallization from 10 mL of pentane at −15 °C yields (*E*)-**4a′** (168 mg, 44%) and (*Z*)-**4a′** (112 mg, 30%).

Pentacarbonyl(ethyl 3-phenylpropiolimidato-*N*)chromium [(*E*)-4c′ and (*Z*)-4c′] from 1′ and 14a. Triethylamine (101 mg, 1.00 mmol) in 2 mL of ethanol is added to a solution of pentacarbonyl(1-ethoxy-3-phenyl-2-propynylidene)chromium (**1′**) (350 mg, 1.00 mmol) and hydroxylamine hydrochloride (138 mg, 2.00 mmol) in 3 mL of ethanol with vigorous stirring at 20 °C within 5 min. A yellow solution is obtained from which the solvent is removed in vacuo (20 °C, 15 Torr). The residue is extracted with pentane. It is shown by TLC and a ^{1}H NMR spectrum in C_6D_6 that a mixture of (*E*)-**4c′**:(*Z*)-**4c′** = 1:1 is obtained, which can be crystallized from 10 mL of pentane to give yellow crystals (263 mg, 72%).

Pentacarbonyl(ethyl 3-phenylpropiolimidato-*N*)chromium [(*E*)-4c′ and (*Z*)-4c′] from 1′ and 14b. Triethylamine (101 mg, 1.00 mmol) in 2 mL of ethanol is added to a solution of pentacarbonyl(1-ethoxy-3-phenyl-2-propynylidene)chromium (**1′**) (350 mg, 1.00 mmol) and *O*-methylhydroxylamine hydrochloride (83 mg, 1.00 mmol) in 3 mL of ethanol with vigorous stirring at 20 °C within 5 min. A yellow solution is obtained from which the solvent is removed in vacuo (20 °C, 15 Torr). The residue is extracted with pentane. It is shown by TLC and a ^{1}H NMR spectrum in C_6D_6 that a mixture of (*E*)-**4c′**:(*Z*)-**4c′** = 1:2 is obtained, which can be crystallized from 10 mL of pentane to give yellow crystals (292 mg, 80%).

Acknowledgment. This work was supported by the *Volkswagen-Stiftung* and by the *Fonds der Chemischen Industrie*.

Supplementary Material Available: Tables of positional and displacement parameters and bond distances and angles (5 pages). Ordering information is given on any current masthead page.

OM9409682

Synthesis and Reactivity of New Mono(cyclopentadienyl)zirconium and -hafnium Alkyl Complexes. Crystal and Molecular Structure of $[\{C_5H_3(SiMe_3)_2\}HfMe_2(\eta^6\text{-toluene})][BMe(C_6F_5)_3]$

Simon J. Lancaster, Oliver B. Robinson, and Manfred Bochmann*

School of Chemical Sciences, University of East Anglia, Norwich NR4 7TJ, U.K.

Simon J. Coles and Michael B. Hursthouse

School of Chemistry and Applied Chemistry, University of Wales Cardiff, P.O. Box 912, Cardiff CF1 3TB, U.K.

Received December 22, 1994[⊗]

The reaction of $Cp''MCl_3$ with LiMe affords $Cp''MMe_3$ [M = Zr, Hf; Cp'' = 1,3-$C_5H_3(SiMe_3)_2$]. In the case of M = Hf the ethyl and *n*-butyl complexes $Cp''HfR_3$ (R = C_2H_5, C_4H_9) are similarly accessible in good yields. The ethyl complex is stable at room temperature. The reaction of $Cp''MR_3$ (M = Zr, R = Me; M = Hf, R = Me, Et) with $B(C_6F_5)_3$ in toluene affords the ionic compounds $[Cp''MR_2(toluene)][BR(C_6F_5)_3]$. The structure of the hafnium methyl complex was determined by X-ray diffraction. The cation $[Cp''HfMe_2(toluene)]^+$ possesses a bent-sandwich structure with an η^6-coordinated toluene ligand. There is no close contact between the metal and the anion. The Hf–CH_3 bonds are significantly shorter than the corresponding distances in the isoelectronic neutral complex Cp_2HfMe_2, while the Hf–Cp distances are comparable. The ethyl compound $[Cp''HfEt_2(toluene)]^+$ eliminates ethane on warming to give an ethene-bridged species, $[\{Cp''HfEt(toluene)\}(\mu\text{-}C_2H_4)]^{2+}$, a process indicative of a possible deactivation pathway in olefin polymerization reactions.

While much work has been devoted to 14-electron group 4 metallocene cations $[Cp_2MR]^+$ (R = alkyl) as polymerization catalysts,[1,2] electronically more deficient and potentially more reactive cationic mono(cyclopentadienyl)metal dialkyl complexes $[CpMR_2]^+$ have attracted less attention. Cationic complexes stabilized by donor ligands such as ethers and phosphines are inactive.[3] Active catalysts have been generated in-situ in hydrocarbon solution from $Cp'MR_3$ (M = Ti, Zr; Cp' = Cp, C_5Me_5; R = CH_3, CH_2Ph, $CH_2C_6H_4NMe_2$) and either $B(C_6F_5)_3$, $[NHMe_2Ph][B(C_6F_5)_4]$, or $[CPh_3]B(C_6F_5)_4]$ for the polymerization of ethene and styrene and the copolymerization of ethene with 1-hexene,[4] and several zirconium benzyl half-sandwich complexes have been isolated.[5] Recently, Baird et al. found that treatment of zirconium and hafnium methyls with $B(C_6F_5)_3$ in aromatic solvents gives cationic arene complexes of the type $[\{C_5Me_5\}MMe_2(arene)][BMe(C_6F_5)_3]$ (arene = benzene, toluene, mesitylene, styrene).[6] As part of our investigations of the reactivity and structure of polymerization catalysts based on cationic group 4 metal alkyl complexes,[2,7,8] we have become interested in the behavior of complexes with long chain alkyl ligands and report here the syntheses of some neutral and cationic mono(cyclopentadienyl)zirconium and -hafnium methyl, ethyl, and *n*-butyl derivatives stabilized by the bulky bis(trimethylsilyl)cyclopentadienyl ligand.

Results and Discussion

The reaction of $Cp''ZrCl_3$ [Cp'' = 1,3-$C_5H_3(SiMe_3)_2$] with 3 equiv of methyllithium in diethyl ether gives $Cp''ZrMe_3$ (**1**) as colorless crystals. The analogous hafnium complex $Cp''HfMe_3$ (**2**) is obtained similarly. Whereas the reaction of $(C_5Me_5)HfCl_3$ with EtMgBr leads to decomposition, the alkylation of $Cp''HfCl_3$ with EtMgBr or *n*-BuLi affords $Cp''HfEt_3$ (**3**) and $Cp''HfBu^n_3$ (**4**), respectively. The ethyl complex **3** is highly air-sensitive but thermally stable at room temperature; it

⊗ Abstract published in *Advance ACS Abstracts,* April 15, 1995.

(1) Reviews: Jordan, R. F. *Adv. Organomet. Chem.* **1991**, *32*, 325. Marks, T. J. *Acc. Chem. Res.* **1992**, *25*, 57. Bochmann, M. *Nachr. Chem. Lab. Techn.* **1993**, *41*, 1220.

(2) Bochmann, M; Lancaster, S. J. *Organometallics* **1993**, *12*, 633 and references cited therein.

(3) (a) Bochmann, M; Karger, G; Jaggar, A. J *J. Chem. Soc., Chem. Commun.* **1990**, 1038. (b) Crowther, D. J.; Jordan, R. F.; Baenziger, N. J.; Verna, A. *Organometallics* **1990**, *9*, 2574.

(4) (a) Stevens, J. C.; Neithamer, D. R. Eur. Pat. Appl. 418 044, 1991 (to Dow Chemical Co.). (b) Campbell, R. E. Eur. Pat. Appl. 421 659, 1991 (to Dow Chemical Co.). (c) LaPointe, R. E.; Rosen, R. K.; Nickias, P. N. Eur. Pat. Appl. 495 375, 1992 (to Dow Chemical Co.). (d) Pellecchia, C.; Proto, A.; Longo, P.; Zambelli, A. *Makromol. Chem. Rapid Commun.* **1991**, *12*, 663. (e) Pellecchia, C.; Longo, P.; Proto, A.; Zambelli, A. *Makromol. Chem. Rapid Commun.* **1992**, *13*, 265. (f) Quyoum, R.; Wang, Q.; Tudoret, M. J.; Baird, M. C.; Gillis, D. J. *J. Am. Chem. Soc.* **1994**. *116*, 6435.

(5) (a) Pellecchia, C.; Grassi, A.; Zambelli, A. *J. Chem. Soc., Chem. Commun* **1993**, 947. (b) Pellecchia, C.; Immirzi, A.; Grassi, A.; Zambelli, A. *Organometallics* **1993**, *12*, 4473. (c) Pellecchia, C.; Grassi, A.; Zambelli, A. *Organometallics* **1994**, *13*, 298. (d) Pellecchia, C.; Immirzi, A.; Zambelli, A. *J. Organomet. Chem.* **1994**, *479*, C9. (e) Pellecchia, C.; Immirzi, A.; Pappalardo, D.; Peluso, A. *Organometallics* **1994**, *13*, 3773.

(6) Gillis, D. J.; Tudoret, M. J.; Baird, M. C. *J. Am. Chem. Soc.* **1993**, *115*, 2543.

(7) (a) Bochmann, M.; Jaggar, A. J.; Nicholls, J. C. *Angew. Chem.* **1990**, *102*, 830; *Angew. Chem., Int. Ed. Engl.* **1990**, *29*, 780. (b) Bochmann, M.; Jaggar, A. J. *J. Organomet. Chem.* **1992**, *424*, C5. (c) Bochmann, M.; Lancaster, S. J. *J. Organomet. Chem.* **1992**, *434*, C1. (d) Bochmann, M.; Lancaster, S. J. *Angew. Chem.* **1994**, *106*, 1715; *Angew. Chem., Int. Ed. Engl.* **1994**, *33*, 1634. (e) Bochmann, M.; Lancaster, S. J. *J. Organomet. Chem.*, in press.

(8) Bochmann, M.; Lancaster, S. J.; Hursthouse, M. B.; Malik, K. M. A. *Organometallics* **1994**, *13*, 2235.

0276-7333/95/2314-2456$09.00/0

Scheme 1

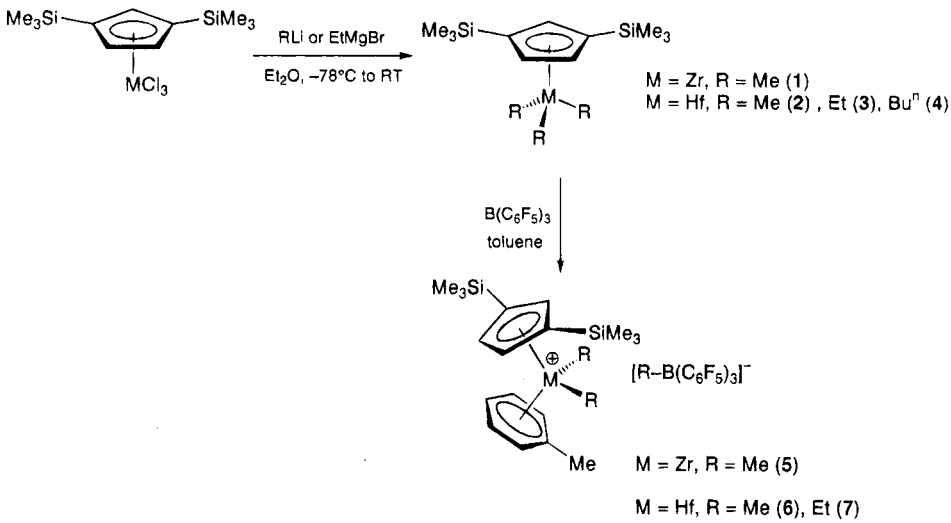

is very soluble in hydrocarbons and melts at about 0 °C to give a yellow oil. Compound **4** is isolated as a light brown but spectroscopically pure oil; it is thermally less stable and decomposes above 0 °C. The relatively high thermal stability of these trialkyl complexes is thought to be due to the kinetic stabilization provided by the bulky Cp″ ligand which has higher steric requirements than the more widely used C_5Me_5.[9]

The addition of $B(C_6F_5)_3$ to toluene solutions of **1** or **2** at −78 °C, followed by slow warming to room temperature, leads to the formation of the toluene complexes $[Cp''MMe_2(toluene)][BMe(C_6F_5)_3]$ (**5**, M = Zr; **6**, M = Hf). The compounds form yellow oils initially but solidify on removal of excess toluene in vacuo or by washing with petroleum ether. The reactions are summarized in Scheme 1. The spectroscopic data for all new compounds are collected in Table 1.

NMR studies confirm that the toluene ligands in **5** and **6** are strongly bound and do not readily exchange with either free toluene or moderately coordinating solvents such as dichloromethane. The crystal structure of **6** confirms that the toluene ligand is bonded quite strongly, even though back-bonding is not expected to play a significant role with d^0 metals. There is however rapid displacement of toluene on addition of donor ligands such as THF.

The reaction of toluene solutions of **3** with $B(C_6F_5)_3$ leads to the formation of the diethyl complex, $[Cp''HfEt_2(toluene)][BEt(C_6F_5)_3]$ (**7**). The compound was characterized spectroscopically at −60 °C. The signals for the cyclopentadienyl ligand, and in particular for the coordinated toluene, are very similar to that of **6**, in agreement with an analogous structure. The spectroscopic data for the ethyl groups in **7** resemble closely those for Cp_2HfEt_2;[7e,9f,k] there is no evidence for unusual bonding modes such as agostic interactions. Complex **7** is less stable in CD_2Cl_2 solution than **6** and slowly decomposes on warming to −20 °C under chloride abstraction from the solvent to give $Cp''HfCl_3$.

Attempts to isolate **7** from toluene solutions by evaporating the solvent at −10 to 0 °C led to the formation of a viscous oil which darkened slowly. Gas evolution was observed, even at −20 °C. The NMR spectra of the product obtained after storing **7** for 2 days at −20 °C are consistent with the formation of an ethene-bridged dinuclear complex (**8**) as the result of the loss of ethane (eq 1). The μ-C_2H_4 moiety is indicated

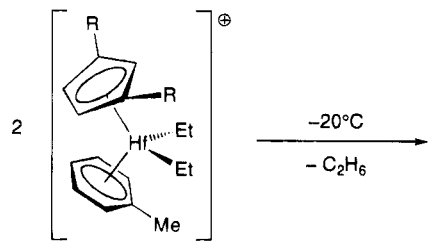

7, R = $SiMe_3$

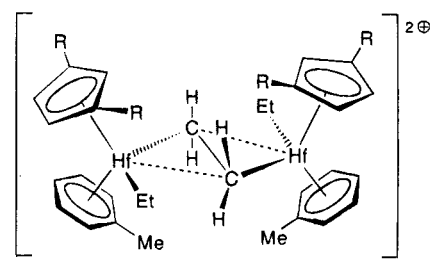

(1)

8

in the ^1H NMR spectrum by two doublets at $\delta = -2.686$ and −0.492 ppm. **8** decomposes in CD_2Cl_2 on warming −20 °C to a mixture of unidentified products. The NMR spectra recorded at −60 and −20 °C are essentially identical and do not provide any indication of fluxionality. The thermal instability of **8** in chlorocarbons prevented studies at higher temperatures. Interestingly, the observed ^1H NMR pattern for the methylene hydrogens is consistent with the formation of only one

(9) For other isolable zirconium and hafnium alkyls with β-hydrogens see for example: (a) Andersen, R. A. *Inorg. Chem.* **1979**, *18*, 2928. (b) Andersen, R. A. *J. Organomet. Chem.* **1980**, *192*, 189. (c) Roddick, D. M.; Santarsiero, B. D.; Bercaw, J. E. *J. Am. Chem. Soc.* **1985**. *107*, 4670. (d) Roddick, D. M.; Bercaw, J. E. *Chem. Ber.* **1989**. *122*, 1579. (e) Bercaw, J. E.; Moss, J. R. *Organometallics* **1992**. *11*, 639. (f) Erker, G.; Schlund, R.; Krüger, C. *Organometallics* **1989**, *8*, 2349. (g) Alt, H. G.; Denner, C. E. *J. Organomet. Chem.* **1990**, *391*, 53. (h) Alt, H. G.; Denner, C. E. *J. Organomet. Chem.* **1990**, *398*, 91. (i) Van den Hende, J. R.; Hessen, B.; Meetsma, A.; Teuben, J. H. *Organometallics* **1990**, *9*, 537. (j) Wielstra, Y.; Gambarotta, S.; Spek, A. L. *Organometallics* **1990**, *9*, 572. (k) Siedle, A. R.; Newmark, R. A.; Schroepfer, J. N.; Lyon, P. A. *Organometallics* **1991**, *10*, 400. (l) Brand, H.; Arnold, J. *J. Am. Chem. Soc.* **1992**, *114*, 2266. (m) Fryzuk, M. D.; Mylvaganam, M.; Zaworotko, M. J.; MacGillivray, L. R. *J. Am. Chem. Soc.* **1993**, *115*, 10360.

Table 1. ^{1}H and ^{13}C NMR Data for Zirconium and Hafnium Complexes

compd	^{1}H NMR (ppm)	assgnt	^{13}C NMR (ppm)	assgnt
Cp″$ZrMe_3$ (**1**)	0.20 (s, 18 H)[a]	Si−CH_3	−0.09[a]	Si−CH_3
	0.24 (s, 9 H)	Zr−CH_3	45.19	Zr−CH_3
	6.58 (s, 3 H)	C_5H_3	119.39	C4 and C5 of Cp″
			120.48	C2 of Cp″
			130.08	C1 and C3 of Cp″
Cp″$HfMe_3$ (**2**)	0.068 (s, 9 H)	Hf−CH_3	0.018	Si−CH_3
	0.29 (s, 18 H)	Si−CH_3	56.77 (q, $^1J_{CH}$ = 113.53 Hz)	Hf−CH_3
	6.61 (d, 2 H, $^4J_{HH}$ = 2.02 Hz)	H4,5 of Cp″	119.94	C4 and C5 of Cp″
	6.64 (t, 1 H)	H2 of Cp″	121.33	C2 of Cp″
			130.01	C1 and C3 of Cp″
Cp″$HfEt_3$ (**3**)	0.30 (s, 18 H)	Si−CH_3	0.018	Si−CH_3
	0.43 (q, 6 H, $^3J_{HH}$ = 8.2 Hz)	$HfCH_2$	12.22	$HfCH_2CH_3$
	1.53 (t, 9 H)	$HfCH_2CH_3$	69.34 (t, $^1J_{CH}$ = 111.85 Hz)	$HfCH_2CH_3$
	6.49−6.53 (m, 3 H)	Cp″	119.96	C4 and C5 of Cp″
			121.47	C2 of Cp″
			129.97	C1 and C3 of Cp″
Cp″$HfBu^n_3$ (**4**)	0.19 (s, 18 H)[b]	Si−CH_3	0.22[b]	Si−CH_3
	0.28−0.35 (m, 6 H)	$HfCH_2CH_2CH_2CH_3$	13.78 ($^1J_{CH}$ = 123 Hz)	δ-C of Bu
	0.78−0.90 (m, 9 H)	$CH_2CH_2CH_2CH_3$	29.97 ($^1J_{CH}$ = 122 Hz)	γ-C of Bu
	1.10−1.31 (m, 6 H)	$CH_2CH_2CH_2CH_3$	31.02 ($^1J_{CH}$ = 126 Hz)	β-C of Bu
	1.57−1.69 (m, 6 H)	$CH_2CH_2CH_2CH_3$	78.47 ($^1J_{CH}$ = 110 Hz)	α-C of Bu
	6.42 (s, 3 H)	Cp″	119.48	C4 and C5 of Cp″
			121.00	C2 of Cp″
			129.47	C1 and C3 of Cp″
[Cp″$ZrMe_2$(η^6-toluene)]-[$BMe(C_6F_5)_3$] (**5**)[a,c]	0.23 (s, 6 H)[a]	Zr−CH_3	−0.07	Si−CH_3
	0.26 (s, 18 H)	Si−CH_3	21.51	$PhCH_3$
	0.48 (br, 3 H)	B−CH_3	45.39	Zr−CH_3
	2.74 (s, 3 H)	$PhCH_3$	124.28	C2 of Cp″
	6.28 (t, 1 H)	C2 of Cp″	125.62	C4 and C5 of Cp″
	6.78 (d, 2 H)	C4 and C5 of Cp″	124.58	*p*-C of PhMe
	7.43 (t, 1 H)	*p*-H of PhMe	128.55	*m*-C of PhMe
	7.63 (t, 2 H)	*m*-H of PhMe	130.40	*o*-C of PhMe
	7.81 (d, 2 H)	*o*-H of PhMe		
[Cp″$HfMe_2$(η^6-toluene)]-[$BMe(C_6F_5)_3$] (**6**)[a,c]	−0.11 (s, 6 H)[b]	Hf−CH_3	−0.36	Si−CH_3
	0.22 (s, 18 H)	Si−CH_3	10.0 (br)	B−Me
	0.44 (br, 3 H)	B−CH_3	22.79	$PhCH_3$
	2.70 (s, 3 H)	$PhCH_3$	48.88 ($^1J_{CH}$ = 117.8 Hz)	Hf−CH_3
	6.18 (t, 1 H)	C2 of Cp″	123.59	*p*-C of PhMe
	6.71 (d, 2 H, $^4J_{HH}$ = 2.02 Hz)	C4 and C5 of Cp″	124.06	C2 of Cp″
	7.42 (t, 1 H, $^3J_{HH}$ = 7.26 Hz)	*p*-H of PhMe	125.52	C4 and C5 of Cp″
	7.62 (t, 2 H, $^3J_{HH}$ = 6.27 Hz)	*m*-H of PhMe	129.70	C1 and C3 of Cp″
	7.80 (d, 2 H, $^3J_{HH}$ = 6.6 Hz)	*o*-H of PhMe	130.08	*m*-C of PhMe
			134.57	*o*-C of PhMe
			147.96	*ipso*-C of PhMe
[Cp″$HfEt_2$(η^6-toluene)]-[$BEt(C_6F_5)_3$] (**7**)[d,g]	0.29 (s, 18 H)	Si−CH_3	−0.54	Si−CH_3
	0.56 (t, 3 H, $^3J_{HH}$ = 7.82 Hz)	B−CH_2CH_3	11.82	B−CH_2CH_3
	1.1−1.2 (br, 2 H)	B−CH_2CH_3	13.8 (br)	B−CH_2CH_3
	1.43 (t, 6 H, $^3J_{HH}$ = 7.26 Hz)[e]	Hf−CH_2CH_3	16.96 ($^1J_{CH}$ = 125.7 Hz)	Hf−CH_2CH_3
	2.71 (s, 3 H)	$PhCH_3$	22.32	$PhCH_3$
	6.26 (s, 1H)	C2 of Cp″	64.13 ($^1J_{CH}$ = 112.3 Hz)	Hf−CH_2CH_3
	6.86 (s, 2 H)	C4 and C5 of Cp″	123.59	C2 of Cp″
	7.41 (t, 1 H, $^3J_{HH}$ = 7.26 Hz)	*p*-H of PhMe	123.54	*p*-C of PhMe
	7.72 (t, 2 H, $^3J_{HH}$ = 7.59 Hz)	*m*-H of PhMe	125.14	C4 and C5 of Cp″
	7.83 (d, 2 H, $^3J_{HH}$ = 6.93 Hz)	*o*-H of PhMe	128.89	C1 and C3 of Cp″
			129.90	*m*-C of PhMe
			132.29	*o*-C of PhMe
			147.96	*ipso*-C of PhMe
[{Cp″HfEt(η^6-toluene)}$_2$(μ-C_2H_4)]-[$BEt(C_6F_5)_3]_2$ (**8**)[d,g]	−2.69 (d, 2 H, $^2J_{HH}$ = 14.0 Hz)	μ-CH_2CH_2	−0.61	Si−CH_3
	−0.49 (d, 2 H, $^2J_{HH}$ = 14.0 Hz)	μ-CH_2CH_2	11.88	B−CH_2CH_3
	0.29 (s, 36 H)	Si−CH_3	13.8 (br)	B−CH_2CH_3
	0.61 (t, br, 6 H)	B−CH_2CH_3	17.50 ($^1J_{CH}$ = 125.7 Hz)	Hf−CH_2CH_3
	1.18 (br, 4 H)	B−CH_2CH_3	22.52	$PhCH_3$
	1.35 (t, 6 H, $^3J_{HH}$ = 7.59 Hz)[e]	Hf−CH_2CH_3	34.52 ($^1J_{CH}$ = 119.9 Hz)	μ-CH_2CH_2
	2.64 (s, 6 H)	$PhCH_3$	60.25 ($^1J_{CH}$ = 115.4 Hz)	Hf−CH_2CH_3
	5.81 (s, 2 H)	C4 or C5 of Cp″	116.67	C4 or C5 of Cp″
	6.06 (s, 2 H)	C4 or C5 of Cp″	120.16	C4 or C5 of Cp″
	6.84 (s, 1 H)	C2 of Cp″	128.48	C2 of Cp″
	7.78 (t, 4 H, $^3J_{HH}$ = 7.26 Hz)	*m*-H of PhMe	132.24	*m*-C of PhMe
	7.96 (d, 4 H, $^3J_{HH}$ = 7.26 Hz)	*o*-H of PhMe[f]	134.48	*o*-C of PhMe
			146.16	*ipso*-C of PhMe

[a] CD_2Cl_2, 25 °C. [b] CD_2Cl_2, −20 °C. [c] Resonances of C_6F_5 substituents are identical to those given in ref 5 and have been omitted. [d] At −60 °C. [e] The Hf−CH_2 signal in the ^{1}H NMR spectrum is obscured under the $SiMe_3$ region according to ^{1}H−^{1}H COSY. [f] Signals for *p*-H obscured by excess toluene. [g] ^{13}C NMR data for C_6F_5 of [$BEt(C_6F_5)_3$]$^-$: 126−128 (v br, *ipso*-C), 135.8 (d, br, J_{CF} = 244 Hz, *o*-C), 137.3 (d, br, J_{CF} = 198.9 Hz, *m*-C), 147.9 (d, br, J_{CF} = 231.9 Hz, *p*-C).

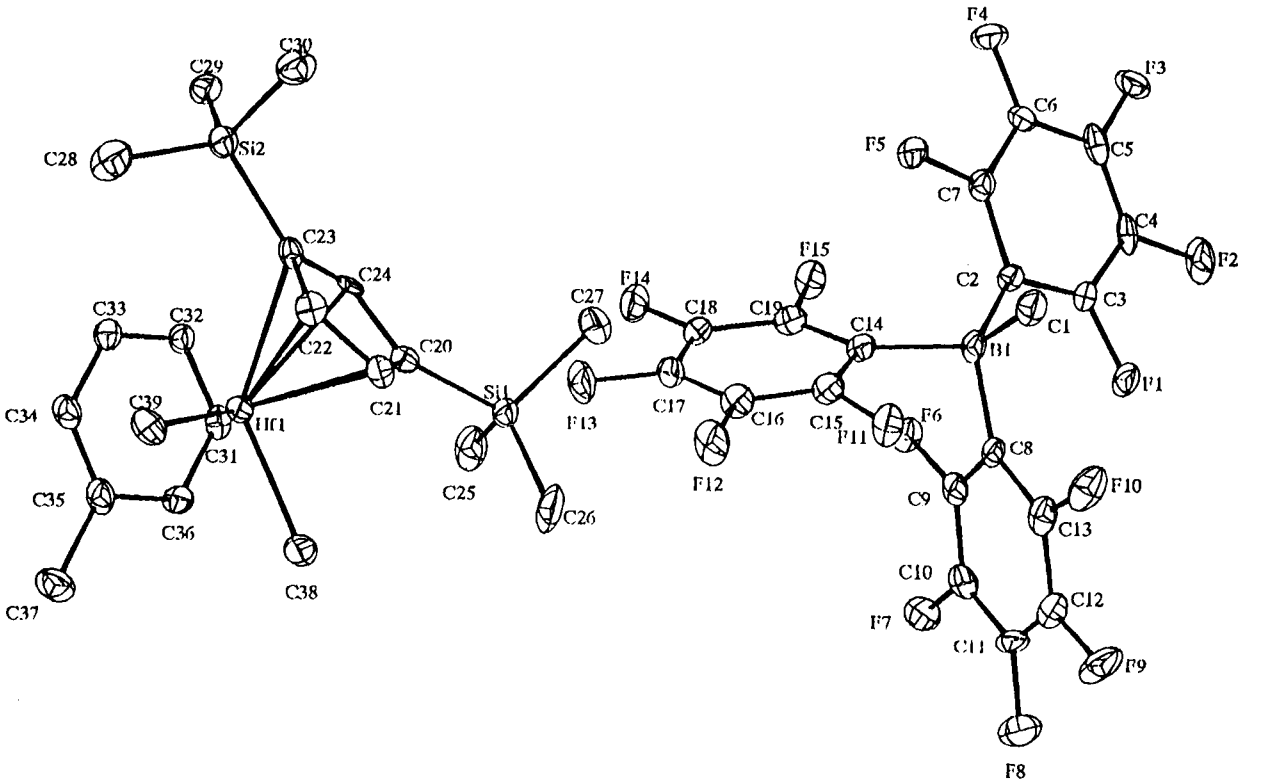

Figure 1. Structure of [Cp″$HfMe_2$(η^6-toluene)][$BMe(C_6F_5)_3$] (**6**), showing the atomic numbering scheme. Ellipsoids are drawn at 30% probability.

Table 2. Selected Bond Lengths (Å) and Angles (deg) of [Cp″$HfMe_2$(η^6-toluene)][$BMe(C_6F_5)_3$] (6)

Hf–C(38)	2.245(7)	Hf–C(39)	2.244(7)
Hf–C(20)	2.512(6)	Hf–C(21)	2.482(6)
Hf–C(22)	2.464(6)	Hf–C(23)	2.482(6)
Hf–C(24)	2.496(6)	Hf–C(31)	2.684(6)
Hf–C(32)	2.681(6)	Hf–C(33)	2.651(6)
Hf–C(34)	2.676(6)	Hf–C(35)	2.749(6)
Hf–C(36)	2.691(6)	B(1)–C(1)	1.630(9)
B(1)–C(2)	1.661(9)	C(31)–C(32)	1.401(9)
C(32)–C(33)	1.373(9)	C(33)–C(34)	1.394(9)
C(34)–C(35)	1.393(9)	C(35)–C(36)	1.394(9)
C(35)–C(37)	1.506(9)		
C(38)–Hf–C(39)	93.5(3)	C(39)–Hf–C(22)	77.6(2)
C(38)–Hf–C(22)	110.5(2)	C(39)–Hf–C(23)	97.1(2)
C(38)–Hf–C(34)	111.8(2)	C(39)–Hf–C(34)	74.5(2)
C(1)–B(1)–C(2)	101.6(5)	C(1)–B(1)–C(8)	116.5(5)
C(1)–B(1)–C(14)	112.8(5)	C(2)–B(1)–C(8)	109.6(5)

of four possible isomers, although the data do not allow us to make an unambiguous assignment.

The formation of C_2H_4-bridged dinuclear compounds as decomposition products of ethyl complexes of early transition metals was observed some time ago by Kaminsky et al. for the reaction of Cp_2ZrCl_2 with $AlEt_3$ to give compounds such as $Et_3Al(\mu\text{-Cl})ZrCp_2(\mu\text{-}CH_2CH_2)\text{-}ZrCp_2(\mu\text{-Cl})AlEt_3$.[10] The same structural motif was recently found in the complex [$(Cp_2ZrMe)_2(\mu\text{-}\eta^2\text{:}\eta^2\text{-}C_2H_4)$];[11] related scandium compounds have also been reported.[12,13] It is evident that in electron-deficient complexes of early transition metals the ethylene moiety is generally η^2:η^2-bridging, whereas 18-electron complexes such as $[Re(CO)_5CH_2]_2$ contain η^1-ethanediyl units. On this basis it is likely that the C_2H_4 ligand in **8** adopts a bridging structure. On the other hand, η^2:η^2-bridged C_2H_4 ligands usually exhibit C–H coupling constants of about 140 Hz, as expected for sp^2-hybridized carbons, whereas the corresponding value for **8** is significantly smaller. Clarification of this point awaits further structural evidence.

Mülhaupt et al. found that the kinetics of the deactivation of zirconocene-based polymerization catalysts is second order in the transition metal, suggestive of a binuclear deactivation product.[14] The structure of this deactivated species formed under real polymerization conditions is not known. We found earlier that certain zirconium methyl complexes undergo α-H eliminations very readily to give μ-CH_2 complexes which exhibit only low catalytic activity.[15] The conversion of **7** into **8** illustrates the possible participation of β-H elimination reactions in binuclear deactivation processes, in this case involving cationic mono(cyclopentadienyl) complexes.

Structure of [Cp″$HfMe_2$(toluene)][$BMe(C_6F_5)_3$] (6). X-ray quality crystals of **6** are obtained by recrystallization from dichloromethane at −16 °C. The structure of the complex is shown in Figure 1. Important

(10) Kaminsky, W.; Sinn, H. *Liebigs Ann.* **1975**, 424. Kaminsky, W.; Vollmer, H. J. *Liebigs Ann.* **1975**, 438. Kaminsky, W.; Kopf, J.; Sinn, H.; Vollmer, H. J. *Angew. Chem.* **1976**, *88*, 688; *Angew. Chem., Int. Ed. Engl.* **1976**, *15*, 629.

(11) Takahashi, T.; Kasai, K.; Suzuki, N.; Nakajima, K.; Negishi, E. *Organometallics* **1994**. *13*, 3413.

(12) Shapiro, P. J.; Cotter, W. D.; Schaefer, W. P.; Labinger, J. A.; Bercaw, J. E. *J. Am. Chem. Soc.* **1994**. *116*, 4623.

(13) For examples of C_2H_4-bridged complexes see: King, R. B.; Bisnette, M. B. *J. Organomet. Chem.* **1964**, *2*, 15. Beck, W.; Olgemoller, B. *J. Organomet. Chem.* **1977**, *127*, C45. Olgemoller, B.; Beck, W. *Chem Ber.* **1981**, *114*, 867. Raab, K.; Nagel, U.; Beck, W. *Z. Naturforsch. B* **1983**, *38b*, 1466. Wengrovius, J. H.; Schrock, R. R.; Day, C. S. *Inorg. Chem.* **1981**, *20*, 1844. Cotton, F. A.; Kibala, P. A. *Inorg. Chem.* **1990**, *29*, 3192. Bullock, R. M.; Lemke, F. R.; Szalda, D. J. *J. Am. Chem. Soc.* **1990**. *112*, 3244.

(14) Fischer, D.; Mülhaupt, R. *J. Organomet. Chem.* **1991**, *417*, C7. Fischer, D.; Jüngling, S.; Mülhaupt, R. *Makromol. Chem. Macromol. Symp.* **1993**, *66*, 191.

(15) Bochmann, M.; Cuenca, T.; Hardy, D. T. *J. Organomet. Chem.* **1994**, *484*, C10.

Table 3. Crystal Data for Compound 6

formula	$C_{39}H_{38}BF_{15}HfSi_2$
fw	1037.17
cryst system	triclinic
space group	$P\bar{1}$
cell dimens	
a, Å	11.289(7)
b, Å	12.891(8)
c, Å	14.531(8)
α, deg	95.06(4)
β, deg	95.64(5)
γ, deg	105.50(3)
V, Å^3	2013(2)
Z	2
D_{calcd}, g cm^{-3}	1.711
abs coeff, mm^{-1}	2.749
$F(000)$	1024
θ range, deg	$2.21 \le \theta \le 24.96$
index range	$-12 \le h \le 12$, $-14 \le k \le 13$, $-16 < l < 12$
no. of reflns collcd	8741
no. of ind reflns	5686 [$R_{int} = 0.0714$]
no. of params	533
goodness of fit on F^2	1.015
final R indices[a] [$I > 2\sigma(I)$]	$R_1 = 0.0395$, $wR_2 = 0.0956$
R indices (all data)	$R_1 = 0.0461$, $wR_2 = 0.1071$
largest diff peak and hole, e Å^{-3}	1.513 and −1.234

[a] $R_1 = \sum(\Delta F)/\sum(F_o)$; $wR_2 = [\sum\{w(\Delta(F^2)^2\}/\sum\{w(F_o^2)^2]^{1/2}$; $w = 1/[\sigma^2(F_o)^2 + (0.068P)^2]$, where $P = [\max((F_o)^2,0) + 2(F_c)^2]/3$.

bond lengths and angles are collected in Table 2. As expected for a 16-electron complex isoelectronic to Cp_2HfMe_2, the cation $[Cp''HfMe_2(toluene)]^+$ possesses a bent-sandwich structure, with an η^6-coordinate toluene ligand. The $SiMe_3$ substituents of the Cp″ ligand, the hafnium–methyl ligands, and the methyl group of toluene are oriented so as to minimize steric interactions. Most notably, the cation and the anion in **6** are well separated, in contrast to the bis(cyclopentadienyl) complexes $Cp'_2ZrMe(\mu\text{-}Me)B(C_6F_5)_3$ (Cp′ = C_5H_5, $C_5H_3Me_2$, Cp″)[8,16] where the $[BMe(C_6F_5)_3]^-$ anions form methyl bridges to the metal center. The Hf–CH_3 bond length of 2.244(7) Å is significantly shorter than those found in the neutral compound $Cp_2Hf(CH_3)_2$ [2.318(8) and 2.382(7) Å],[17] while the distances to the cyclopentadienyl carbons (ca. 2.5 Å) are almost identical in both cases. By comparison, the Hf–C distances to the coordinated toluene are somewhat longer, with an average bond length to the hydrogen-carrying phenyl carbons of 2.676 Å, while the distance to the *ipso*-carbon C(35) is rather longer, 2.749(6) Å. This bond lengths distribution is consistent with a distorted η^6-coordination of the arene ligand. A very similar bond lengths distribution was found recently for the η^6-coordinated benzyl group in $Zr(CH_2Ph)_3\{\eta^6\text{-}C_6H_5CH_2B(C_6F_5)_3\}$.[18] By contrast, the Hf–C distances in the toluene-bridged Hf(II) complex $\{HfI_2(PMe_2Ph)_2\}_2(\mu\text{-}C_7H_8)$ are very much shorter, ranging from 2.28 to 2.55 Å.[19] The Cp–Hf–toluene (ring centroids) angle in **6** is 134.2(2)°, very similar to the Cp–Hf–Cp angle in Cp_2HfMe_2 (132.1°).[17]

Arene complexes to d^0 metals are rare. Isolable examples reported so far are typically cationic, and in several cases the π-bonded arene is part of an anionic ligand. Apart from the recently described compounds $[\{C_5Me_5\}MMe_2(arene)][BMe(C_6F_5)_3]$ (M = Zr, Hf)[6] and $Zr(CH_2Ph)_3\{\eta^6\text{-}C_6H_5CH_2B(C_6F_5)_3\}$[18] mentioned above, examples include $[(C_6Me_6)TiCl_3][Ti_2Cl_9]$,[20] $Zr(CH_2Ph)_3(\eta^6\text{-}C_6H_5BPh_3)$,[3a] and $Zr(CH_2Ph)_2Cp\{\eta^6\text{-}C_6H_5CH_2B(C_6F_5)_3\}$.[5b,8] There are also the mixed-valence clusters $[M_3(\mu\text{-}Cl)_6(C_6Me_6)_3]^{n+}$ (M = Ti, Zr; n = 1, 2)[21] and a

Table 4. Atomic Coordinates (×10^4) and Equivalent Displacement Parameters (Å^2 × 10^3) for Compound 6[a]

	x	y	z	U(eq)
Hf(1)	808(1)	2627(1)	3323(1)	18(1)
Si(1)	3261(2)	959(2)	3773(1)	22(1)
Si(2)	3277(2)	5473(2)	3315(1)	22(1)
F(1)	9672(3)	−4484(3)	1300(2)	26(1)
F(2)	11616(3)	−4290(3)	402(2)	31(1)
F(3)	12734(3)	−2355(3)	−193(2)	30(1)
F(4)	11847(3)	−628(3)	144(3)	31(1)
F(5)	9882(3)	−795(3)	1044(2)	23(1)
F(6)	7117(3)	−4090(3)	219(2)	25(1)
F(7)	5545(3)	−6071(3)	89(3)	33(1)
F(8)	5191(4)	−7106(3)	1654(3)	41(1)
F(9)	6477(4)	−6102(3)	3328(3)	42(1)
F(10)	8055(4)	−4154(3)	3459(2)	36(1)
F(11)	6822(3)	−2259(3)	3119(2)	31(1)
F(12)	4998(4)	−1375(3)	2786(3)	37(1)
F(13)	4499(3)	−734(3)	1100(3)	34(1)
F(14)	5890(3)	−1060(3)	−290(2)	31(1)
F(15)	7764(3)	−1904(3)	21(2)	24(1)
B(1)	8523(7)	−2720(6)	1893(5)	19(2)
C(1)	9374(6)	−2188(5)	2881(4)	26(2)
C(2)	9592(5)	−2675(5)	1177(4)	16(1)
C(3)	10132(6)	−3496(5)	996(4)	20(1)
C(4)	11171(6)	−3426(5)	539(4)	20(2)
C(5)	11760(6)	−2470(5)	243(4)	22(2)
C(6)	11296(5)	−1582(5)	415(4)	21(2)
C(7)	10240(6)	−1708(5)	871(4)	19(1)
C(8)	7642(5)	−3995(5)	1848(4)	19(1)
C(9)	6974(5)	−4554(5)	1026(4)	20(1)
C(10)	6175(6)	−5580(5)	922(4)	23(2)
C(11)	5999(6)	−6100(5)	1716(5)	28(2)
C(12)	6632(6)	−5603(5)	2552(4)	24(2)
C(13)	7430(6)	−4574(5)	2606(4)	23(2)
C(14)	7463(6)	−2090(5)	1608(4)	19(1)
C(15)	6690(6)	−1920(5)	2263(4)	24(2)
C(16)	5712(6)	−1491(5)	2109(5)	26(2)
C(17)	5433(6)	−1183(5)	1252(5)	26(2)
C(18)	6155(6)	−1323(5)	563(4)	22(2)
C(19)	7125(6)	−1765(5)	760(4)	22(2)
C(20)	2831(6)	2281(5)	3878(4)	22(2)
C(21)	2424(5)	2757(5)	4650(4)	22(2)
C(22)	2404(6)	3827(5)	4517(4)	21(2)
C(23)	2817(5)	4055(5)	3644(4)	18(1)
C(24)	3090(5)	3100(5)	3264(4)	19(1)
C(25)	2658(7)	180(6)	2607(5)	34(2)
C(26)	2659(7)	168(6)	4724(5)	40(2)
C(27)	4982(6)	1306(6)	3910(6)	43(2)
C(28)	2026(7)	6146(6)	3434(5)	38(2)
C(29)	3720(6)	5477(5)	2121(4)	25(2)
C(30)	4644(7)	6193(6)	4169(5)	37(2)
C(31)	600(6)	1678(5)	1572(4)	20(1)
C(32)	1097(6)	2789(5)	1527(4)	19(1)
C(33)	417(6)	3486(5)	1769(4)	21(2)
C(34)	−760(6)	3110(5)	2037(4)	24(2)
C(35)	−1291(6)	2005(5)	2049(4)	23(2)
C(36)	−577(5)	1304(5)	1844(4)	21(2)
C(37)	−2586(6)	1578(6)	2292(5)	33(2)
C(38)	−41(6)	1046(6)	3852(5)	34(2)
C(39)	−295(6)	3520(6)	4121(5)	32(2)

[a] Ueq is defined as one-third of the trace of the orthogonalized U_{ij} tensor.

(16) (a) Yang, X.; Stern, C. L.; Marks, T. J. *J. Am. Chem. Soc.* **1991**, *113*, 3623. (b) Yang, X.; Stern, C. L.; Marks, T. J. *J. Am. Chem. Soc.* **1994**, *116*, 10015.

(17) Fronczek, F. R.; Baker, E. C.; Sharp, P. R.; Raymond, K. N.; Alt, H. G.; Rausch, M. D. *Inorg. Chem.* **1976**, *15*, 2284.

(18) Pellecchia, C.; Grassi, A.; Immirzi, A. *J. Am. Chem. Soc.* **1993**, *115*, 1160.

(19) Cotton, F. A.; Kibala, P. A.; Wojtczak, W. A. *J. Am. Chem. Soc.* **1991**, *113*, 1462.

(20) Solari, E.; Floriani, C.; Chiesi-Villa, A.; Guastini, C. *J. Chem. Soc., Chem. Commun.* **1989**, 1747.

(21) Fischer, E. O.; Röhrscheid, F. *J. Organomet. Chem.* **1966**, *6*, 53. Stollmeier, F.; Thewalt, U. *J. Organomet. Chem.* **1981**, *208*, 327.

series of arene complexes of zerovalent and divalent titanium, zirconium, and hafnium.[19,22]

Conclusion

Given a suitably bulky Cp ligand, even trialkyl complexes $Cp''HfR_3$ with alkyl ligands carrying β-hydrogens become readily isolable. The abstraction of R^- in aromatic solvents such as toluene leads to mono(cyclopentadienyl)hafnium dialkyl cations which coordinate a toluene molecule, in favor of coordination to the anion. The driving force appears the be the formation of a 16-electron sandwich complex, rather than a 12-electron zwitterionic structure of the type $Cp''HfR_2(\mu\text{-}R)B(C_6F_5)_3$. The apparent fairly strong coordination of toluene in **6** underlines the importance of defining the role a solvent might play in understanding the chemistry of such electron-deficient cationic polymerization catalysts.

Experimental Section

General Procedures. All reactions were carried out under inert gas using standard vacuum line techniques. Solvents were distilled under nitrogen from sodium–benzophenone [diethyl ether, thf, petroleum ether (bp 40–60 °C)], sodium (toluene), or calcium hydride (dichloromethane). The NMR solvents were stored over 4A molecular sieves under nitrogen or argon and degassed by several freeze–thaw cycles. $B(C_6F_5)_3$ was prepared following the literature procedure.[23] NMR spectra were recorded on a JEOL EX270 instrument. The NMR assignments of the hafnium ethyl and butyl complexes were confirmed by $^1H-^1H$ and $^1H-^{13}C$ correlation experiments.

Synthesis of $Cp''ZrMe_3$ (1). To a solution of $Cp''ZrCl_3$ (2.09 g, 5.12 mmol) in 100 mL of diethyl ether at −78 °C was added 11 mL of a 1.4 M solution of LiMe (15.4 mmol). The mixture was allowed to slowly warm to room temperature. Stirring was continued for 1 h before the solvent was removed in vacuo and the product extracted with petroleum ether. Cooling to −78 °C gave **1** as colorless crystals (1.39 g, 80%). Anal. Calcd for $C_{14}H_{30}Si_2Zr$: C, 48.6; H, 8.8. Found: C, 46.0; H, 8.1.

$Cp''HfMe_3$ (2). To 7.0 g of $Cp''HfCl_3$ (15 mmol) suspended in 100 mL of THF at −78 °C was added 15 mL of a 3.0 M solution of MeMgCl in THF (45 mmol). The mixture was slowly warmed to room temperature and stirred for 4 h. After removal of the THF in vacuo the residue was extracted with petroleum ether (80 mL), and the extract was filtered. The filtrate was evaporated and the residue recrystallized from cyclopentane at −30 °C to give very hydrolysis sensitive colorless crystals of **2** (4.0 g, 61%). Anal. Calcd for $C_{14}H_{30}HfSi_2$: C, 38.8; H, 7.0. Found: C, 38.2; H, 6.8.

$Cp''HfEt_3$ (3). To 4.6 g of $Cp''HfCl_3$ (9.3 mmol) cooled to −78 °C was added 130 mL of a 0.3 M solution of EtMgBr in diethyl ether. The reaction was stirred at −30 °C for 1 h, followed by 1 h at 0 °C and 2 h at room temperature. The ether was removed in vacuo. The solution darkened slightly to yellow. The residue was extracted with 50 mL of petroleuem ether and cooled to −20 °C for 48 h to precipitate the remaining Grignard reagent. Filtration and cooling to −78 °C yielded crystals of **3** which were filtered off and dried in vacuo; they melted on warming < 0 °C to give a yellow oil which readily crystallized on cooling. Yield: 2.5 g (53%). The low melting point made it impossible to obtain a reliable elemental analysis.

$Cp''HfBu^n_3$ (4). To 9.6 g of $Cp''HfCl_3$ (19.4 mmol) dissolved in 150 mL of diethyl ether at −60 °C was added via syringe 36.4 mL of a 1.6 M solution of Bu^nLi in hexanes. A clear orange-yellow solution formed rapidly, with precipitation of LiCl. The reaction was allowed to warm to 0 °C over 4 h. The ether was removed in vacuo below 0 °C, the residue was extracted with cold (0 °C) petroleum ether (200 mL), and the extract was filtered. The filtrate was taken to dryness < 0 °C to give a light brown oil which decomposes above 0 °C. Yield: 5.0 g (46%).

Synthesis of $[Cp''ZrMe_2(\eta^6\text{-toluene})][BMe(C_6F_5)_3]$ (5). A solution of 0.350 g (0.684 mmol) of $B(C_6F_5)_3$ in 10 mL of toluene at −78 °C was added to a stirred cold (−78 °C) solution of 0.234 g (0.675 mmol) of **1** in 30 mL of toluene. The mixture was slowly warmed to room temperature to give a yellow solution. The solvent was removed under reduced pressure to leave a yellow oil which was washed with 5 mL of petroleum ether. On drying in vacuo a yellow solid resulted (0.520 g, 89%). Anal. Calcd for $C_{39}H_{38}BF_{15}Si_2Zr$: C, 49.3; H, 4.0. Found: C, 48.3; H, 4.0.

Synthesis of $[Cp''HfMe_2(\eta^6\text{-toluene})][BMe(C_6F_5)_3]$ (6). A mixture of 0.55 g of $B(C_6F_5)_3$ (1.07 mmol) and 0.40 g of $Cp''HfMe_3$ (0.92 mmol) was cooled to −78 °C, and 20 mL of precooled toluene was added. The mixture was warmed to −30 °C and stirred for 1 h before being allowed to warm slowly to room temperature. The supernatant was decanted from the resulting yellow oil. This oil crystallized when dried in vacuo. Crystals suitable for X-ray diffraction were grown from dichloromethane at −16 °C. Anal. Calcd for $C_{39}H_{38}BF_{15}HfSi_2$: C, 45.3; H, 3.4. Found: C, 44.8; H, 3.4.

Synthesis of $[Cp''HfEt_2(\eta^6\text{-toluene})][BEt(C_6F_5)_3]$ (7). A 0.102 g amount of $B(C_6F_5)_3$ (0.2 mmol) was dissolved in 0.6 mL of CD_2Cl_2, and the solution was transferred to an NMR tube and cooled to −78 °C. To this was added 0.1 mL of a cold CD_2Cl_2 solution which was 2 M in both $Cp''HfEt_3$ and toluene. An orange solution formed on mixing. The product was characterized spectroscopically at −60 °C.

Formation of $[\{Cp''HfEt(\eta^6\text{-toluene})\}_2(\mu\text{-}C_2H_4)][BEt(C_6F_5)_3]_2$ (8). To 0.6 g of $B(C_6F_5)_3$ (1.17 mmol) dissolved in 10 mL of toluene and cooled to −78 °C was added via syringe 2.4 mL of a 0.56 M solution of $Cp''HfEt_3$ (1.34 mmol) in toluene. The color changed to yellow on warming to −60 °C. The reaction was warmed to −20 °C, and the finely suspended yellow oil was allowed to settle. The solvent was decanted and the residue dried in vacuo <0 °C. The oily residue was stored at −20 °C under argon, and gas bubbles were seen to form. The NMR spectrum of the product in CD_2Cl_2 after 2 d at −20 °C showed the formation of **8** in essentially quantitative yield. The compound decomposes in CD_2Cl_2 at higher temperatures.

X-ray Crystallography. Crystals of **5** were grown from dichloromethane at −16 °C as colorless blocks. X-ray measurements were made using a crystal of dimensions 0.36 × 0.29 × 0.29 mm mounted in a sealed capillary tube under argon. Crystal data are given in Table 3. Data were collected at 120 ± 2 K on an Enraf-Nonius FAST TV area detector diffractometer using graphite-monochromated Mo Kα radiation (λ = 0.710 69 Å) using a procedure described elsewhere.[24] The structure was solved by direct methods of phase determination using the SHELX-S package[25] and refined on F_o^2 by

(22) Martin, H.; Vohwinkel, F. *Chem. Ber.* **1961**, *94*, 2416. Giezynski, R.; Dzierzgowski, S.; Pasynkiewicz, S. *J. Organomet. Chem.* **1975**, *87*, 295. Anthony, M. T.; Green, M. L. H.; Young, D. *J. Chem. Soc., Dalton Trans.* **1975**, 1419. Dzierzgowski, S.; Giezynski, R.; Jarosz, M.; Pasynkiewicz, S. *J. Organomet. Chem.* **1978**, *152*, 281. Cloke, F. G. N.; Green, M. L. H. *J. Chem. Soc., Chem. Commun.* **1979**, 127. Cloke, F. G. N.; Green, M. L. H. *J. Chem. Soc., Dalton Trans.* **1981**, 1938. Cloke, F. G. N.; Lappert, M. F.; Lawless, G. A.; Swain, A. C. *J. Chem. Soc., Chem Commun.* **1987**, 1667. Biagini, P.; Calderazzo, F.; Pampaloni, G. *J. Organomet. Chem.* **1988**, *355*, 99. Diamond, G. M.; Green, M. L. H.; Walker, N. M.; Howard, J. A. K.; Mason, S. A. *J. Chem. Soc., Dalton Trans.* **1992**, 2641. Blackburn, D. W.; Britton, D.; Ellis, J. E. *Angew. Chem.* **1992**, *104*, 1520; *Angew. Chem., Int. Ed. Engl.* **1992**, *31*, 1495. Green, M. L. H.; Morise, X. *J. Organomet. Chem.* **1993**, *462*, 209.

(23) Pohlmann, J. L.; Brinckmann, F. E. *Z. Naturforsch. B* **1965**, *20b*, 5.

(24) Drake, S. M.; Hursthouse, M. B.; Malik, K. M. A.; Miller, S. A. S. *Inorg. Chem.* **1993**, *32*, 4653.

full-matrix least squares techniques using SHELXL-93[26] with data corrected for absorptions by DIFABS.[27] Hydrogens were allowed to ride on their parents with fixed isotropic U. Atomic coordinates are given in Table 4.

Acknowledgment. This work was supported by the Innovative Polymer Synthesis Initiative of the U.K. Engineering and Physical Sciences Research Council.

(25) Sheldrick, G. M. *Acta Crystallogr.* **1990**, *A46*, 467.
(26) Sheldrick, G. M. University of Göttingen, 1993.

Supplementary Material Available: Tables of bond lengths and angles, anisotropic displacement parameters, and hydrogen coordinates and U values for **6** (4 pages). Ordering information is given on any current masthead page.

OM940980U

(27) Walker, N.; Stuart, D. *Acta Crystallogr.* **1983**, *A39*, 158 (adapted for FAST geometry by A. Karaulov, University of Cardiff, 1990).

(1,2-Bis(diphenylphosphino)ethane)(η^3-1-arylallyl)palladium Tetrafluoroborates. Distribution of the Positive Charge Density by Correlation of NMR Chemical Shifts with Hammett Substituent Constants

Ramón Malet, Marcial Moreno-Mañas,* Teodor Parella, and Roser Pleixats

Department of Chemistry, Universitat Autònoma de Barcelona, Bellaterra, 08193-Barcelona, Spain

Received February 3, 1995[⊗]

^{13}C NMR differences of chemical shifts ($\delta_X - \delta_H$) of allyl carbon atoms in a series of (1,2-bis(diphenylphosphino)ethane)(η^3-1-(4-X-phenyl)allyl)palladium tetrafluoroborates, X ranging from NO_2 to OMe, correlate very well ($r > 0.994$) with σ Hammett constants. However, ^{31}P NMR differences of the ligand *cis* and *trans* phosphorus atoms correlate well with σ and with σ^+, respectively. These data indicate that the positive charge density of the cation is localized mainly in the P–Pd–P region.

Introduction

Palladium(0)-catalyzed allylation of nucleophiles is a powerful synthetic methodology that has attracted enormous interest because of its broad scope and versatility.[1] Many fine details of this well-accepted alkylation method have been studied: for instance, the generation of enantioselectivity at the allylic framework and the factors governing the regioselectivity when both termini of the allylic system are different.

Despite the enormous effort devoted to the generation of enantioselectivity at the electrophile,[2] a general solution to this problem has yet to be found. Let us consider a symmetrical allylic framework; the differentiation of both termini of the cationic (η^3-allyl)-palladium intermediate depends on the asymmetry of the ligand which renders them diastereotopic. However, the mechanism of the second step of the palladium(0)-catalyzed allylation of most nucleophiles (amines and carbon nucleophiles with $pK_a < 20$) occurs with inversion of configuration; that is, the attack of the nucleophile occurs from the side opposite to the ligand. Under these circumstances steric effects by the ligand do not, in general, sufficiently differentiate both ends of the allylic moiety. Exceptions are based on the generation of severe but different distortions at both termini of the allylic system by means of chiral ligand propellers[3] or bulky ligands possessing C_2 symmetry.[4] Otherwise, any differentiation must rely upon the different transmission of electronic effects from the ligands toward both termini, thus rendering them different in electrophilicity. This is normally accomplished by chiral bidentate asymmetric ligands featuring two coordinating sites based on atoms of the same[5] or different nature, such as phosphorus and nitrogen and other combinations.[6] Therefore, to know how electronic effects are transmitted from the asymmetric ligand to the allylic carbon atoms through the palladium atom is a problem of great importance.[7] Isomerization of the intermediate (η^3-allyl)palladium complexes renders the problem still more complicated. Thus, three isomerization mechanisms have been identified: (1) $\pi-\sigma-\pi$ mechanisms interconverting *syn* and *anti* isomers,[8] (2) S_N2-type PdL_2 displacement by PdL_2,[9] and (3) apparent π-allyl–Pd rotation.[10] NMR spectroscopy is a useful technique to study these equilibria in solution.[8d,10a,11]

It is generally accepted that regioselectivity of the palladium(0)-catalyzed allylation of nucleophiles is governed by the difference in steric requirements of both

[⊗] Abstract published in *Advance ACS Abstracts,* March 15, 1995.

(1) For useful reviews see: (a) Trost, B. M.; Verhoeven, T. R. Organopalladium Compounds in Organic Synthesis and in Catalysis. In *Comprehensive Organometallic Chemistry*; Wilkinson, G., Stone, F. G. A., Abel, E. W., Eds.; Pergamon Press: Oxford, U.K., 1982; Vol. 8, Chapter 57. (b) Heck, R. F. *Palladium Reagents in Organic Synthesis*; Academic: London, 1985; Chapter 5. (c) Godleski, S. A. Nucleophiles with Allyl-Metal Complexes. In *Comprehensive Organic Synthesis*; Trost, B. M., Fleming, I., Eds.; Pergamon Press: Oxford, U.K., 1991; Vol. 4, Chapter 3.3. (d) Frost, C. G.; Howarth, J.; Williams, J. M. J. *Tetrahedron: Asymmetry* **1992,** *3,* 1089.

(2) For a review see: Reiser, O. *Angew. Chem., Int. Ed. Engl.* **1993,** *32,* 547.

(3) Trost, B. M.; Breit, B.; Organ, M. G. *Tetrahedron Lett.* **1994,** *35,* 5817.

(4) (a) Trost, B. M.; Van Vranken, D. L. *Angew. Chem., Int. Ed. Engl.* **1992,** *31,* 228. (b) Trost, B. M.; Van Vranken, D. L.; Bingel, C. *J. Am. Chem. Soc.* **1992,** *114,* 9327. (c) Leutenegger, U.; Umbricht, G.; Fahrni, C.; von Matt, P.; Pfaltz, A. *Tetrahedron* **1992,** *48,* 2143. (d) Gamez, P.; Dunjic, B.; Fache, F.; Lemaire, M. *J. Chem. Soc., Chem. Commun.* **1994,** 1417.

(5) (a) Togni, A. *Tetrahedron: Asymmetry* **1991,** *2,* 683. (b) Togni, A.; Breutel, C.; Schnyder, A.; Spindler, F.; Landert, H.; Tijani, A. *J. Am. Chem. Soc.* **1994,** *116,* 4062. (c) Kang, J.; Cho, W. O.; Cho, H. G. *Tetrahedron: Asymmetry* **1994,** *5,* 1347.

(6) (a) Hayashi, T.; Yamamoto, A.; Ito, Y.; Nishioka, E.; Miura, H.; Yanagi, K. *J. Am. Chem. Soc.* **1989,** *111,* 6301. (b) von Matt, P.; Pfaltz, A. *Angew. Chem., Int. Ed. Engl.* **1993,** *32,* 566. (c) Sprinz, J.; Helmchen, G. *Tetrahedron Lett.* **1993,** *34,* 1769. (d) Dawson, G. J.; Frost, C. G.; Williams, J. M. J.; Coote, S. J. *Tetrahedron Lett.* **1993,** *34,* 3149. (e) Von Matt, P.; Loiseleur, O.; Koch, G.; Pfaltz, A.; Lefeber, C.; Feucht, T.; Helmchen, G. *Tetrahedron: Asymmetry* **1994,** *5,* 573. (f) Allen, J. V.; Coote, S. J.; Dawson, G. J.; Frost, C. G.; Martin, C. J.; Williams, J. M. J. *J. Chem. Soc., Perkin Trans. 1* **1994,** 2065.

(7) Yang, H.; Khan, M. A.; Nicholas, K. M. *Organometallics* **1993,** *12,* 3485.

(8) (a) Faller, J. W.; Thomsen, M. E.; Mattina, M. J. *J. Am. Chem. Soc.* **1971,** *93,* 2642. (b) Faller, J. W.; Tully, M. T. *J. Am. Chem. Soc.* **1972,** *94,* 2676. (c) Cesarotti, E.; Grassi, M.; Prati, L.; Demartin, F. *J. Organomet. Chem.* **1989,** *370,* 407. (d) Breutel, C.; Pregosin, P. S.; Salzmann, R.; Togni, A. *J. Am. Chem. Soc.* **1994,** *116,* 4067.

(9) Granberg, K. L.; Bäckvall, J.-E. *J. Am. Chem. Soc.* **1992,** *114,* 6858.

(10) (a) Hansson, S.; Norrby, P.-O.; Sjögren, M. P. T.; Åkermark, B.; Cucciolito, M. E.; Giordano, F.; Vitagliano, A. *Organometallics* **1993,** *12,* 4940. (b) Gogoll, A.; Örnebro, J.; Grennberg, H.; Bäckvall, J.-E. *J. Am. Chem. Soc.* **1994,** *116,* 3631.

(11) (a) Oslinger, M.; Powell, J. *Can. J. Chem.* **1973,** *51,* 274. (b) Ohkita, K.; Kurosawa, H.; Hasegawa, T.; Hirao, T.; Ikeda, I. *Organometallics* **1993,** *12,* 3211. (c) Pregosin, P. S.; Salzmann, R. *Magn. Reson. Chem.* **1994,** *32,* 128.

0276-7333/95/2314-2463$09.00/0

allylic termini; i.e., the reactions occur in general at the less hindered side. However, the number of exceptions is so high that some hypotheses have been advanced to explain them. Thus, Trost and co-workers found that the regiochemical outcome of some allylations of stabilized carbanions depends on the nature of the ligand.[12] If due to the ligand effects the palladium atom is more bound to the less substituted allylic terminus than to the more heavily substituted one, the carbocationic character of the latter terminus is enhanced, thus being preferentially attacked by a charged nucleophile. This possible partial carbocationic character of the more substituted terminus is reminiscent of the well-known order of stability of carbocations, and it has been invoked as a hypothesis to explain preferential attack in spite of the steric hindrance.[12,13] Electronic and steric effects are important in governing the regiochemistry of the palladium(0)-catalyzed allylation of nucleophiles, and both factors normally operate together. In order to evaluate the influence of the electronic factors in the absence of any steric influence, we studied previously the regiochemistry of attack at some (1,3-diaryl-η^3-allyl)-palladium complexes with different substituents at the *para* positions. These systems offer the same steric requirements but different electronic requirements at both termini of the allylic system. The conclusion was that the attack occurs preferentially at the terminus most remote from the more electron-withdrawing substituent.[14]

There is a question that, to the best of our knowledge, has never been addressed and whose answer has some bearing on both enantioselectivity and regioselectivity and, in short, on the mechanisms of transmission of electronic effects from the ligands to the allylic termini. The question is as follows: *what is the actual distribution of the positive charge density in cationic η^3-allylic complexes?*

(η^3-Allyl)palladium cations are square-planar and can be represented as in the upper part of Figure 1. Some possible canonical formulas (for aryl-substituted cations and 1,2-bis(diphenylphosphino)ethane as ligand) are represented also in Figure 1. In order to conform to the more uncomfortable but more informative organic style, we have represented double bonds Pd=P to account for both donation and back-donation. Formula A features the usual representation of the η^3 type. The η^2 type is represented as in formulas B and C with a Pd–C single bond and a metal–olefin interaction which could also be represented as a palladacyclopropane. Formulas A–C require that the positive charge be on the coordinatively unsaturated (16 electrons) Pd atom. The extreme cases of the η^2 type, coming from B and C, are D and E. In them, the Pd–C bond is so strongly polarized that the electrons lie on the Pd atom, which is now neutral, the positive charge being concentrated on one or the other of the allylic termini. Formulas A–E are not the only possible ones; thus, the positive charge can be accommodated on the phosphorus atoms, as represented in F and G. We thought that NMR data could be informative with respect to the distribution of the positive charge density.[15]

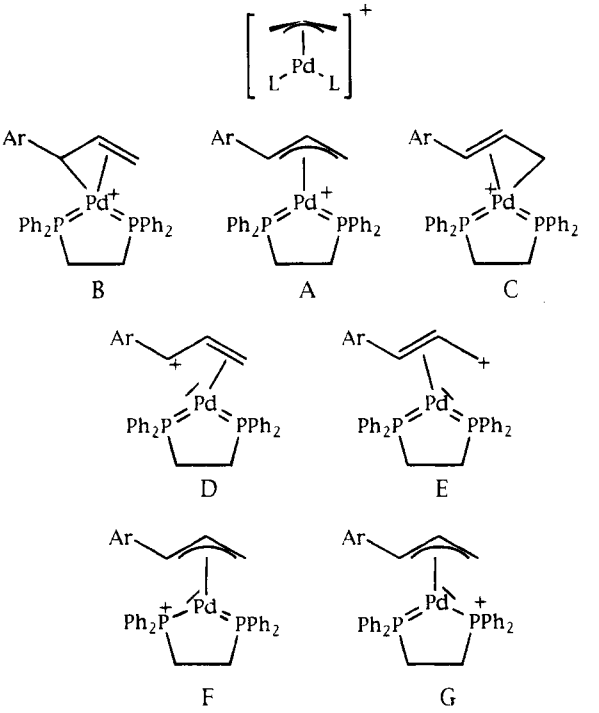

Figure 1.

Äkermark, Vitagliano, et al. reported the effects of different ligands on the ^{13}C NMR chemical shifts of the carbon atoms of the allylic framework.[16] They prepared complexes with two different ligands on the Pd atom and concluded that a donor–acceptor ligand (phosphines) induced a lower field signal to its *trans* carbon atom with respect to a pure donor ligand (amines). Thus, the chemical shifts could be considered as a measure of the positive charge density on the terminal carbon atoms in the allyl part of the complexes and their results indicate that the electronic effects are transmitted in a *trans* direction. Similar results have been reported by Nicholas et al.[7]

Linear free energy relationships (LFER) correlating NMR data with Hammett constants are a useful technique for determining the transmission of inductive and resonant electronic effects, through benzene rings, and some reviews are available.[17,18] Good linear correlations have been found between differences in chemical shifts with σ constants or with dual substituent parameters ($\Delta\delta$ *vs* $\rho_I\sigma_I + \rho_R\sigma_R$) for atoms directly linked to a benzene ring: ^1H in *para* and in *meta* positions in monosubstituted benzenes (dual correlation),[19] ^{19}F in *meta*- and *para*-substituted fluorobenzenes (dual correlation),[17,20] and ^{13}C (methyl group carbon atom) in *para*-substituted

(12) Trost, B. M.; Lautens, M.; Hung, M.-H.; Carmichael, C. S. *J. Am. Chem. Soc.* **1984**, *106*, 7641.

(13) (a) Äkermark, B.; Hansson, S.; Krakenberger, B.; Vitagliano, A.; Zetterberg, K. *Organometallics* **1984**, *3*, 679. (b) Äkermark, B.; Vitagliano, A. *Organometallics* **1985**, *4*, 1275.

(14) Prat, M.; Ribas, J.; Moreno-Mañas, M. *Tetrahedron* **1992**, *48*, 1695.

(15) Pd has only one natural isotope with spin different from zero, Pd^{105} (spin $^5/_2$, natural abundance 22.33%), and ^{105}Pd NMR seems to be a nonroutine affair.

(16) Äkermark, B.; Krakenberger, B.; Hansson, S.; Vitagliano, A. *Organometallics* **1987**, *6*, 620.

(17) Hehre, W. J.; Taft, R. W.; Topsom, R. D. *Prog. Phys. Org. Chem.* **1976**, *12*, 159.

(18) Ewing, D. F. Correlation of nmr Chemical Shifts with Hammett σ Values and Analogous Parameters. In *Correlation Analysis in Chemistry: Recent Advances*; Chapman, N. B., Shorter, J., Eds.; Plenum Press: New York, 1978.

(19) Brownlee, R. T. C.; Taft, R. W. *J. Am. Chem. Soc.* **1968**, *90*, 6537.

(20) (a) Taft, R. W.; Price, E.; Fox, I. R.; Lewis, I. C.; Andersen, K. K.; Davis, G. T. *J. Am. Chem. Soc.* **1963**, *85*, 709. (b) Taft, R. W.; Price, E.; Fox, I. R.; Lewis, I. C.; Andersen, K. K.; Davis, G. T. *J. Am. Chem. Soc.* **1963**, *85*, 3146. (c) Brownlee, R. T. C.; Dayal, S. K.; Lyle, J. L.; Taft, R. W. *J. Am. Chem. Soc.* **1972**, *94*, 7208.

Scheme 1[a,b]

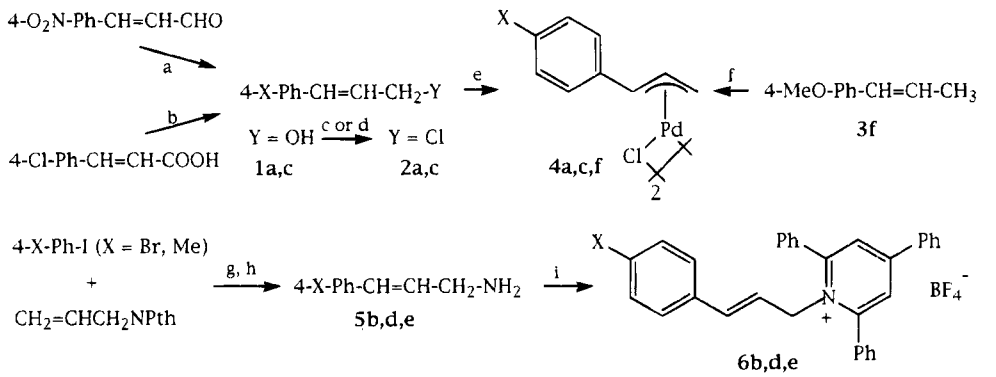

[a] X = NO_2 (**a**), Br (**b**), Cl (**c**), H (**d**), Me (**e**), MeO (**f**).[b] Legend: (a) $NaBH_4$, EtOH, room temperature; (b) $LiAlH_4$, THF, room temperature; (c) $SOCl_2$, Cl_2CH_2 (for **2a**); (d) $SOCl_2$, PhH (for **2c**); (e) $Pd_2(dba)_3{\cdot}HCCl_3$, PhH; (f) $Pd(OCOCF_3)_2$, $ClNBu_4$, acetone; (g) $Pd(OAc)_2$, P(*o*-Tol)$_3$, Et_3N, MeCN, 100 °C, sealed reactor; (h) hydrazine hydrate, EtOH, reflux; (i) 2,4,6-triphenylpyrilium tetrafluoroborate, Cl_2CH_2, first cat. Et_3N, then cat. AcOH.

toluenes (correlation with σ).[21] It can be concluded that in systems of the type 4-X-C_6H_4-(nucleus) fairly good linear correlations exist between $\Delta\delta$ for the NMR-active nucleus and σ, $\varrho_I\sigma_I + \varrho_R\sigma_R$, or both.[18] Data on carbenium ion systems are, of course, more scarce. However, good linear correlations have been described for $\Delta\delta$ (for the charged carbon atom) and σ^+ in the systems 4-X-C_6H_4–C^+(R)(CH_3).[22]

Results and Discussion

With these ideas in mind, we prepared a series of (1,2-bis(diphenylphosphino)ethane)(η^3-1-arylallyl)palladium tetrafluoroborates, **7a–f**, having the same symmetric bidentate ligand but featuring different substituents at the *para* position of the aryl ring embracing a broad selection of electronic effects (attempts to prepare the compound with the NMe_2 substituent failed). The preparation of the required precursors is represented in Scheme 1; the bis(μ-chloro)bis(1-(4-X-aryl)-η^3-allyl)palladium complexes **4a,c,f** were prepared either by the classical treatment of the corresponding allylic chlorides with $Pd_2(dba)_3(HCCl_3)$ (for **4a,c**) or by reaction of **3f** with $Pd(OCOCF_3)_2/Bu_4NCl$ following a general method modified by Trost.[23] Compounds **4a,c,f** were converted into the cationic complexes **7a,c,f** by reaction with AgF_4B and 1,2-bis(diphenylphosphino)ethane (dppe) as indicated in Scheme 2. Salts **7b,d,e** were prepared by a method recently reported by us[24] requiring allylamines **5b,d,e** as starting materials, which were converted into the 1-cinnamyl-2,4,6-triphenylpyridinium tetrafluoroborates **6b,d,e.** The pyridinium salts were treated with $Pd(dba)_2$/dppe to afford **7b,d,e**.

Tables 1 and 2 contain the ^{13}C and ^{31}P NMR chemical shifts for the allylic carbon atoms and the ligand phosphorus atoms as well as the differences in chemical shifts with respect to product **7d** (X = H). Signals were assigned to each nucleus as indicated in the Experimental Section. All *trans* $^1H-^1H$ coupling constants ($J_{H\text{-}1anti/H\text{-}2}$ and $J_{H\text{-}2/H\text{-}3anti}$) are in the range 11–13 Hz,

Scheme 2[a,b]

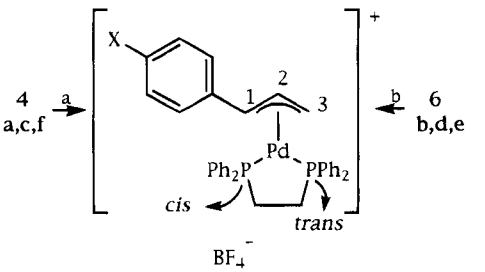

7a-f

[a] See footnote *a* in Scheme 1.[b] Legend: (a) $AgBF_4$, acetone, then DPPE; (b) $Pd(dba)_2$, DPPE, PhH, room temperature.

whereas *cis* coupling constants ($J_{H\text{-}2/H\text{-}3syn}$) are smaller: 7–8 Hz. $^1H-^{31}P$ coupling constants are in the ranges 11–13 Hz ($J_{H\text{-}1anti/Ptrans}$ and $J_{H\text{-}3anti/Pcis}$) and 6–7 Hz ($J_{H\text{-}3syn/Pcis}$). The $^{13}C-^{31}P$ coupling constants are as follows: 25.9–27.7 ($J_{C\text{-}1/Ptrans}$), 6.5–6.6 ($J_{C\text{-}1/Pcis}$), 6.5–6.9 ($J_{C\text{-}2/Ptrans}$ and $J_{C\text{-}2/Pcis}$), 4.6–6.5 ($J_{C\text{-}3/Ptrans}$), and 24.6–27.7 Hz ($J_{C\text{-}3/Pcis}$). The coupling constant data indicate that equilibria ($\pi-\sigma-\pi$ mechanisms and apparent π-allyl–Pd rotation are *a priori* possible) are slow on the NMR time scale.

Hammett correlations have been performed using several different constants or combinations of constants (σ, σ^+, dual σ/σ^+ and dual σ_I/σ_R) and refined by least-squares methods. The results are summarized in Table 3. For the carbon atoms of the allylic framework excellent linear correlations have been found between $\Delta\delta$ and σ (eqs 1, 4, and 7), although dual substituent parameter correlations ($\Delta\delta$ *vs* $\varrho_I\sigma_I + \varrho_R\sigma_R$) are also good (eqs 3, 6, and 9). Any of these correlations is clearly superior to those in eqs 2, 5, and 8 involving σ^+ values. The obvious interpretation of these data is that *the positive charge density is mainly concentrated outside the allylic carbon atom framework.*

Both phosphorus atoms behave differently. Thus, $\Delta\delta$ values for P *cis* to the aryl ring correlate fairly well with σ (eq 10), and in any case much better than with σ^+ (eq 11). A dual substituent parameter correlation (σ and σ^+) (eq 12) was as good as that found with only σ, the absolute ϱ value (in eq 12) being much larger than ϱ^+ (+4.72 and −0.30). A different combination of substituent constants (σ_I and σ_R) (eq 13) gave a correlation similar in quality to that in eq 10, where only σ values were introduced.

(21) Malet, R.; Moreno-Mañas, M.; Pleixats, R.; Parella, T., submitted for publication.
(22) Olah, G. A.; Porter, R. D.; Jeuell, C. L.; White, A. M. *J. Am. Chem. Soc.* **1972**, *92*, 2044.
(23) Trost, B. M.; Metzner, P. J. *J. Am. Chem. Soc.* **1980**, *102*, 3572.
(24) Malet, R.; Moreno-Mañas, M.; Pleixats, R. *Organometallics* **1994**, *13*, 397.

Table 1. ^{13}C NMR Chemical Shifts in δ Units ($CDCl_3$) and in Hz (at 62.50 MHz) of Allyl Carbon Atoms in Compounds 7a–f

		C-1			C-2			C-3		
compd	X	δ	ν_X	$\nu_X - \nu_H$	δ	ν_X	$\nu_X - \nu_H$	δ	ν_X	$\nu_X - \nu_H$
7a	NO_2	89.84	5615	−335	120.00	7500	+191	69.27	4329	+183
7b	Br	93.09	5818	−132	117.56	7348	+39	67.15	4197	+51
7c[a]	Cl									
7d	H	95.20	5950	0	116.95	7309	0	66.35	4146	0
7e	Me	95.83	5989	+39	116.20	7262	−47	65.77	4110	−36
7f	MeO	96.66	6041	+91	114.11	7208	−101	65.25	4078	−68

[a] Insufficient solubility prevented reliable determinations.

Table 2. ^{31}P NMR Chemical Shifts in δ Units ($CDCl_3$) and in Hz (H_3PO_4 as External Standard and at 101 MHz) for P Atoms in Compounds 7a–f

		P-*cis*			P-*trans*		
compd	X	δ	ν_X	$\nu_X - \nu_H$	δ	ν_X	$\nu_X - \nu_H$
7a	NO_2	50.44	5108	+334	51.97	5263	+110
7b	Br	48.57	4918	+144	50.97	5161	+8
7c	Cl	47.46	4806	+32	50.90	5155	+2
7d	H	47.14	4774	0	50.89	5153	0
7e	Me	45.93	4651	−123	49.99	5062	−91
7f	MeO	45.95	4653	−121	49.48	5011	−142

Table 3. Equations Relating $\Delta\delta$ ($\delta_X - \delta_H$) from ^{13}C NMR and ^{31}P NMR Data with Hammett Constants

atom	eq	r	eq no.
C-1	$\Delta\delta = -0.25 - 6.07\sigma$	0.998	1
	$\Delta\delta = -1.21 - 4.49\sigma^+$	0.952	2
	$\Delta\delta = -0.08 - 6.58\sigma_I - 7.82\sigma_R$	0.995	3
C-2	$\Delta\delta = -0.27 + 4.10\sigma$	0.994	4
	$\Delta\delta = +0.35 + 3.00\sigma^+$	0.982	5
	$\Delta\delta = -0.06 + 3.53\sigma_I + 5.96\sigma_R$	0.998	6
C-3	$\Delta\delta = -0.06 + 3.66\sigma$	0.999	7
	$\Delta\delta = +0.49 + 2.62\sigma^+$	0.966	8
	$\Delta\delta = -0.03 + 3.52\sigma_I + 4.87\sigma_R$	0.998	9
P-*cis*	$\Delta\delta = -0.20 + 4.33\sigma$	0.974	10
	$\Delta\delta = +0.46 + 3.07\sigma^+$	0.932	11
	$\Delta\delta = -0.26 + 4.72\sigma - 0.30\sigma^+$	0.974	12
	$\Delta\delta = -0.31 + 4.58\sigma_I + 5.30\sigma_R$	0.976	13
P-*trans*	$\Delta\delta = -0.50 + 2.13\sigma$	0.949	14
	$\Delta\delta = -0.18 + 1.64\sigma^+$	0.989	15
	$\Delta\delta = -0.15 - 0.15\sigma + 1.75\sigma^+$	0.989	16
	$\Delta\delta = -0.26 + 1.64\sigma_I + 3.29\sigma_R$	0.951	17

In contrast, $\Delta\delta$ values for P *trans* to the aryl ring correlate well with σ^+ (eq 15) and, in any case, much better than with σ (eq 14). A dual substituent parameter correlation (σ and σ^+) (eq 16) was as good as that found with only σ^+, the absolute value of the ϱ value (in eq 16) being much smaller than that for ϱ^+ (−0.15 and +1.75). A different combination of substituent constants (σ_I and σ_R) (eq 17) gave a correlation similar in quality to that in eq 14, where only σ values were introduced.

The interpretation of these results is that *the positive charge density is mostly concentrated in the phosphorus atoms and possibly in the palladium atom in compounds* **7**. We cannot conclude from our correlations that the charge density in the *trans* phosphorus atom is higher than in the *cis* atom, since the transmission of electronic effects in a *trans* fashion (but not in a *cis* fashion) would render the *cis* phosphorus atom quite insensitive to conjugative effects having their origin in the *cis* region (however, see comment 3 below). Since the best linear correlations for phosphorus atoms, those in eqs 12 and 16, are not as good as the best linear correlations for carbon atoms, it seems reasonable to admit that a part of the positive charge could be on the palladium atom. This cannot be proved at present with NMR techniques.[15] In summary, we conclude that *the positive charge density is in the P–Pd–P region.*

Some fine details of the best equations deserve further comment.

1. The absolute values of the slopes (correlations with σ values, eqs 1, 4, and 7) for carbon atoms in the allylic framework decrease with the distance to the aryl ring, from C-1 to C-3.

2. The slope for C-1, directly attached to the aryl ring, is negative (eq 1) which means that an electron-withdrawing substituent (i.e. nitro, $\sigma = +0.81$) induces a high-field signal for C-1 with respect to an electron-releasing group (see Table 1). This phenomenon has been observed for the C-1 carbon atom in 1-arylbutadienes and 1-arylacetylenes and for the terminal carbon atom in aryl vinyl ethers and sulfides.[18] In our compounds **7** this could be attributed to an overcompensation by electron donation from a strong electron donor suitably placed, e.g. the phosphorus atom in a *trans* position.

3. The chemical shifts for *trans* P atoms appear always at lower fields with respect to their *cis* counterparts, indicating a lower electron density at P-*trans*, which is therefore more positive.

4. When the dual substituent parameter correlations with σ and σ^+ are examined (eqs 12 and 16), the relative importance of σ and σ^+ can be evaluated in each case. The simple σ value is decisive in determining the chemical shifts in P-*cis* (ϱ value +4.72 in front of −0.30 for ϱ^+), and the reverse occurs for P-*trans* ($\varrho = -0.15$ and $\varrho^+ = +1.75$).

5. Another conclusion can be drawn by examining the dual substituent parameter correlations with σ_I and σ_R (eqs 13 and 17), despite the bad quality of the correlation of eq 17. The ϱ_I and ϱ_R values for P-*cis* (eq 13) are similar (4.58 and 5.30), but for P-*trans* ϱ_R is twice as much as ϱ_I, thus indicating once more the relative importance of the inductive and the resonance mechanisms of transmission to and from P-*cis* (important inductive transmission) and to and from P-*trans* (major resonance transmission).

The above conclusions on the localization of the positive charge density hold only for the series of compounds **7**, but in spite of the dangers of precipitate generalizations, we wish to conclude that in similar cationic (η^3-allyl)palladium complexes stabilized by phosphine ligands, the positive charge density is probably concentrated in the P–Pd–P region.

We have performed allylations of dimethyl malonate with 4-nitrocinnamyl and 4-methoxycinnamyl acetates (**8a,f**) under Pd(0) catalysis. Both reactions present the same regioselectivity, the allylations taking place at the less substituted terminus of the cinnamyl framework

Scheme 3 [a,b]

4-X-Ph-CH=CH-CH_2OAc

↓ a

(4-X-Ph-CH=CH-CH_2)$_2$C(COOMe)$_2$

9a: NO_2; 9f: MeO

[a] X = NO_2 (**a**), MeO (**f**). [b] Legend: (a) $(MeOCO)_2CHNa$, $Pd(PPh_3)_4$, THF, 60–65 °C.

to afford compounds **9a,f** (Scheme 3). These results are in agreement with our hypothesis of the positive charge density being concentrated in the P–Pd–P region, although steric effects militate in both cases in favor of the observed regioselectivity. Studies on the (1,3-diaryl-η^3-allyl)palladium series are in progress in order to cancel steric effects at both sides.

Experimental Section

NMR Experiments. Structural studies were performed on a Bruker ARX400 spectrometer equipped with an inverse broad-band probe head incorporating a shielded Z-gradient coil. The exact carbon and phosphorus shifts were measured from a conventional decoupled 1D spectrum acquired on a Bruker AC250 spectrometer equipped with a triple $^1H-^{13}C-^{31}P$ probe head. Proton and carbon chemical shifts were referenced to the $CDCl_3$ signals at 7.24 and 77.0 ppm, respectively. Phosphorus chemical shifts were referenced to the phosphoric acid signal at 0.00. ^1H, ^{13}C, and ^{31}P assignments were made for compounds **4c** and **7e** by concerted use of a gradient-enhanced COSY experiment, phase-cycled ROESY experiment, gradient-enhanced $^1H-^{13}C$ HMQC experiment, and gradient-enhanced $^1H-^{31}P$ HMBC experiment. In (η^3-allyl)palladium complexes the rule is that coupling constant values between protons on a certain terminal allylic carbon atom and the phosphorus atom *cis* to that carbon atom are ca. 0 Hz, whereas coupling constants of the same protons with the phosphorus atom *trans* to the same carbon atom have significant values.[25] For the rest of complexes **4** and **7** assignments have been made by analogy to **4c** and **7e**. The signals of the allylic moieties in the NMR spectra for all the compounds of the same series are very similar (see below and supplementary material).

Magnitude-mode gradient-enhanced COSY spectra[26] resulted from a 512 × 1024 data matrix size with 2 scans per t_1 value. The recycle time was 1 s, and a 1:1 gradient combination was used. The data were zero-filled once in the t_1 dimension, and a sine bell filter was used before Fourier transformation in both dimensions.

Phase-sensitive ROESY experiments[27] resulted from a 2 × 512 × 1024 data matrix size with 32 scans per t_1 value. The recycle time was 1 s. As a mixing time, a continuous off-resonance low-power pulse (2.6-KHz rf field strength) lasting 400 ms was used. Quadrature detection in the t_1 dimension was achieved by the TPPI method. The data were zero-filled once in the t_1 dimension, and a cosine bell filter was used before Fourier transformation in both dimensions.

Magnitude-mode gradient-enhanced one-bond $^1H-^{13}C$ correlation (HMQC) spectra[28] resulted from a 128 × 1024 data matrix size with 2 scans per t_1 value (no dummy scans). The delay was set to 3.5 ms, and the recycle time was 1 s. A 2:2:1 gradient combination was used. Broad-band ^{13}C decoupling with GARP-1[29] was applied during acquisition. A sine bell filter function was used prior to Fourier transformation in the t_2 and t_1 dimensions.

Magnitude-mode gradient-enhanced multiple-bond $^1H-^{31}P$ shift correlation (HMBC) spectra[28] resulted from a 64 × 512 data matrix size with 8 scans (no dummy scans) per t_1 value and a recycle time of 1 s. The delay was set to 50 ms. The data were zero-filled once in the t_1 dimension, and a sine bell filter was used before Fourier transformation in both dimensions. A gradient combination of 1.238:1.238:1 was used to select the desired coherence.

All B_0 field gradient pulses had a Gaussian shape truncated at 5% and a length of 1 ms. Only peak amplitudes were varied according to the required ratios described above.

Saturated solutions of compounds **7** in $CDCl_3$ were used throughout.

Substituent Constants. Substituent constant values were taken from the textbook by March.[30]

4-Nitrocinnamyl alcohol (1a) was prepared in 87% yield by reduction of 4-nitrocinnamaldehyde with sodium borohydride in ethanol at room temperature: mp 125–127 °C (lit.[31] mp 124.5–126.5 °C); IR (KBr) 3528 (broad), 1510, 1342, 969 cm^{-1}; ^1H NMR (250 MHz, $CDCl_3$) δ 1.67 (broad s, 1H, OH), 4.38 (dd, J = 5.0 and 1.3 Hz, 2H), 6.52 (dt, J = 15.9 and 5.1 Hz, 1H), 6.70 (d, J = 15.9 Hz, 1H), 7.49 (d, J = 8.8 Hz, 2H), 8.17 (d, J = 8.8 Hz, 2H).

4-Chlorocinnamyl alcohol (1c) was prepared in 59% yield by reduction of 4-chlorocinnamic acid with lithium aluminum hydride in THF at room temperature: mp 42–43 °C; IR (KBr) 3332 (broad), 969 cm^{-1}; ^1H NMR (250 MHz, $CDCl_3$) δ 1.61 (broad s, 1H, OH), 4.29 (d, J = 5.3 Hz, 2H), 6.30 (dt, J = 15.7 and 5.3 Hz, 1H), 6.54 (d, J = 15.7 Hz, 1H), 7.25 (m, 4H).

4-Nitrocinnamyl chloride (2a) was prepared in 40% yield by reaction of **1a** with thionyl chloride in dichloromethane: mp 49–51 °C (lit.[32] mp 56–56.5 °C); IR (KBr) 1510, 1342, 969 cm^{-1}; ^1H NMR (250 MHz, $CDCl_3$) δ 4.24 (dd, J = 6.9 and 1.1 Hz, 2H), 6.46 (dt, J = 15.7 and 6.9 Hz, 1H), 6.71 (d, J = 15.7 Hz, 1H), 7.50 (d, J = 8.8 Hz, 2H), 8.17 (d, J = 8.8 Hz, 2H).

4-Chlorocinnamyl chloride (2c) was prepared in 63% yield by reaction of **1c** with thionyl chloride in benzene at room temperature, mp 42–44 °C (lit.[32] mp 41.0–41.5 °C); IR (KBr) 969 cm^{-1}; ^1H NMR (250 MHz, $CDCl_3$) δ 4.20 (dd, J = 7.3 and 1.1 Hz, 2H), 6.26 (dt, J = 15.7 and 6.9 Hz, 1H), 6.58 (d, J = 15.7 Hz, 1H), 7.11–7.39 (m, 4H).

Bis(μ-chloro)bis(1-(4-nitrophenyl)-η^3-allyl)dipalladium (4a). A degassed solution of **2a** (61 mg, 0.308 mmol) in anhydrous benzene (8 mL) was added under an argon atmosphere over a degassed suspension of $Pd_2(dba)_3(HCCl_3)$ (125 mg, 0.116 mmol) in anhydrous benzene (7 mL). The mixture was kept under vigorous magnetic stirring at room temperature for 17 h. During this time the color changed from dark red to yellow at the initial stages of the reaction and then to cream. The precipitate was filtered off to give product **4a** as a very insoluble solid that was washed several times with benzene (62 mg, 88%): mp 225–228 °C; IR (KBr) 3071, 1595, 1518, 1342, 1110, 850, 814, 751 cm^{-1}; ^1H NMR (250 MHz, $CDCl_3$) δ 3.16 (d, J = 12.1 Hz, H-3a), 4.08 (d, J = 6.2 Hz, H-3s), 4.50 (d, J = 11.3 Hz, H-1a), 5.85 (apparent dt, J = 11.4 and 6.7 Hz, H-2), 7.59 (d, J = 8.4 Hz, 2H), 8.10 (d, J = 8.4 Hz, 2H); ^{13}C NMR (62.5 MHz, C_2D_6SO) δ 66.33 (C-3), 83.16 (C-1), 115.12 (C-2), 123.85 (2C), 129.12 (2C), 145.19 (1C), 146.36 (1C). Anal. Calcd for $C_{18}H_{16}Cl_2N_2O_4Pd_2$: C, 35.56; H, 2.65; N, 4.61. Found: C, 34.62; H, 2.48; N, 4.24.

Bis(μ-chloro)bis(1-(4-chlorophenyl)-η^3-allyl)dipalladium (4c) was prepared as for **4a**, in 79% yield from **2c**: mp

(25) (a) Powell, J.; Shaw, B. L. *J. Chem. Soc. A* **1967**, 1839. (b) Vrieze, K.; Praat, A. P.; Cossee, P. *J. Organomet. Chem.* **1968**, *12*, 533. (c) Tibbetts, D. L.; Brown, T. L. *J. Am. Chem. Soc.* **1970**, *92*, 3031.
(26) Hurd, R. E. *J. Magn. Reson.* **1990**, *87*, 422.
(27) (a) Bothner-By, A. A.; Stephens, R. L.; Lee, J.-M.; Warren, C. D.; Jeanloz, R. W. *J. Am. Chem. Soc.* **1984**, *106*, 811. (b) Bax, A.; Davis, D. G. *J. Magn. Reson.* **1985**, *63*, 207.
(28) Hurd, R. E.; John, B. K. *J. Magn. Reson.* **1991**, *91*, 648.
(29) Shaka, A. J.; Barker, P. B.; Freeman, R. *J. Magn. Reson.* **1985**, *64*, 547.
(30) March, J. *Advanced Organic Chemistry: Reactions, Mechanisms and Structure*, 4th ed.; Wiley: New York, 1992.
(31) White, W. N.; Fife, W. K. *J. Am. Chem. Soc.* **1961**, *83*, 3846.
(32) Hayami, J.; Tanaka, N.; Kaji, A. *Bull. Chem. Soc. Jpn.* **1973**, *46*, 954.

210–215 °C; IR (KBr) 3071, 2938, 1595, 1482, 1398, 1089, 1011, 969, 814 cm^{-1}; ^1H NMR (250 MHz, $CDCl_3$) δ 3.02 (d, J = 12.1 Hz, H-3a), 3.96 (d, J = 6.9 Hz, H-3s), 4.52 (d, J = 11.3 Hz, H-1a), 5.73 (apparent dt, J = 11.7 and 6.6 Hz, H-2), 7.21 (d, J = 8.6 Hz, 2H), 7.38 (d, J = 8.6 Hz, 2H); ^{13}C NMR (62.5 MHz, C_2D_6SO) δ 64.86 (C-3), 85.61 (C-1), 113.57 (C-2), 128.80 (2C), 129.88 (2C), 132.53 (1C), 136.28 (1C). Anal. Calcd for $C_{18}H_{16}Cl_4Pd_2$: C, 37.00; H, 2.76. Found: C, 38.02; H, 2.88.

Bis(μ-chloro)bis(1-(4-methoxyphenyl)-η³-allyl)dipalladium (4f). A mixture of 4-propenylanisole (anethole; 0.148 g, 1.0 mmol), palladium(II) trifluoroacetate (0.308 g, 1.0 mmol), and anhydrous acetone (6 mL) was stirred under argon for 30 min. Then, a solution of tetrabutylammonium chloride (0.250 g, 1.1 mmol) in anhydrous acetone (2.5 mL) was added and the mixture was stirred 10 min more and filtered through Celite. The filtrare was evaporated at reduced pressure, and the resulting oil was chromatographed through a silica gel column using hexanes–ethyl acetate (60:40). Compound **4f** was obtained as a yellowish solid (50% yield): mp 155–158 °C; IR (KBr) 1602, 1496, 1454, 1257, 1174, 1032, 828 cm^{-1}; ^1H NMR (250 MHz, $CDCl_3$) δ 2.94 (d, J = 11.7 Hz, H-3a), 3.75 (s, 3H), 3.88 (d, J = 6.6 Hz, H-3s), 4.64 (d, J = 11.3 Hz, H-1a), 5.69 (apparent dt, J = 11.7 and 6.8 Hz, H-2), 6.78 (d, J = 8.8 Hz, 2H), 7.41 (d, J = 8.8 Hz, 2H); ^{13}C NMR (62.5 MHz, $CDCl_3$) δ 55.18 (OCH_3), 58.47 (C-3), 82.54 (C-1), 104.42 (C-2), 114.61 (2C), 129.17 (1C), 129.32 (2C), 159.77 (1C). Anal. Calcd for $C_{20}H_{22}Cl_2O_2Pd_2$: C, 41.55; H, 3.83. Found: C, 40.78; H, 3.37.

(4-Bromocinnamyl)amine (5b). *N*-(4-Bromocinnamyl)-phthalimide was prepared (42% yield after column chromatography through silica gel) by the Heck reaction between 4-bromo-1-iodobenzene and *N*-allylphthalimide, according to the method described by Malek and Moormann:[33] mp 169–173 °C; IR (KBr) 1766, 1700, 955 cm^{-1}; ^1H NMR (250 MHz, $CDCl_3$) δ 4.39 (dd, J = 6.2 and 1.1 Hz, 2H), 6.20 (dt, J = 15.7 and 6.2 Hz, 1H), 6.55 (d, J = 15.7 Hz, 1H), 7.18 (d, J = 6.6 Hz, 2H), 7.37 (d, J = 6.6 Hz, 2H), 7.67–7.74 (m, 2H), 7.81–7.86 (m, 2H).

The free amine **5b** was prepared (67%) from the above phthalimide by treatment with hydrazine hydrate in ethanol. Amine **5b** was an oil: IR (film) 3371, 3272, 971 cm^{-1}; ^1H NMR (250 MHz, $CDCl_3$) δ 1.34 (broad s, NH_2), 3.44 (dd, J = 5.5 and 1.1 Hz, 2H), 6.28 (dt, J = 15.9 and 5.1 Hz, 1H), 6.42 (d, J = 15.9 Hz, 2H), 7.20 (d, J = 8.4 Hz, 2H), 7.40 (d, J = 8.4 Hz, 2H).

Cinnamylamine (5d). *N*-cinnamylphthalimide was prepared in 84% yield by reaction of cinnamyl chloride with potassium phthalimide in anhydrous DMF at 100 °C: mp 149–151 °C (lit.[34] mp 150–150.5 °C); IR (KBr) 1771, 1707, 955 cm^{-1}; ^1H NMR (400 MHz, $CDCl_3$) δ 4.40 (dd, J = 6.4 and 1.2 Hz, 2H), 6.21 (dt, J = 15.9 and 6.4 Hz, 1H), 6.62 (d, J = 15.9 Hz, 1H), 7.21–7.37 (m, 5H), 7.69–7.86 (m, 4H).

The free amine **5d** was prepared (79%) from the above phthalimide by treatment with hydrazine hydrate in ethanol. Amine **5d** was an oil: IR (film) 3336, 3261, 969 cm^{-1}; ^1H NMR (400 MHz, $CDCl_3$) δ 1.71 (broad s, NH_2), 3.41 (dd, J = 5.8 and 1.5 Hz, 2H), 6.26 (dt, J = 15.9 and 6.1 Hz, 1H), 6.44 (d, J = 15.9 Hz, 1H), 7.15–7.33 (m, 5H).

(4-Methylcinnamyl)amine (5e). *N*-(4-Methylcinnamyl)-phthalimide was prepared by the Heck reaction between 4-methyl-1-iodobenzene and *N*-allylphthalimide, according to the general method described by Malek and Moormann:[33] mp 155–160 °C (lit.[35] mp 165–166 °C); IR (KBr) 1771, 1707, 955 cm^{-1}; ^1H NMR (250 MHz, $CDCl_3$) δ 2.27 (s, 3H), 4.39 (d, J = 6.6 Hz, 2H), 6.16 (dt, J = 15.7 and 6.4 Hz, 1H), 6.59 (d, J = 15.7 Hz, 1H), 7.05 (d, J = 8.0 Hz, 2H), 7.21 (d, J = 8.2 Hz, 2H), 7.66–7.74 (m, 2H), 7.81–7.86 (m, 2H).

The free amine **5e** was prepared (82%) from the above phthalimide by treatment with hydrazine hydrate in ethanol. Amine **5e** was an oil: IR (film) 3268, 969 cm^{-1}; ^1H NMR (400 MHz, $CDCl_3$) δ 1.44 (broad, 2H), 2.30 (s, 3H), 3.43 (dd, J = 5.8 and 1.5 Hz, 2H), 6.24 (dt, J = 15.9 and 5.8 Hz, 1H), 6.44 (d, J = 15.9 Hz, 1H), 7.09 (d, J = 8.1 Hz, 2H), 7.25 (d, J = 8.1 Hz, 2H).

1-(4-Bromocinnamyl)-2,4,6-triphenylpyridinium tetrafluoroborate (6b) was prepared by the general method reported by Katritzky and co-workers.[36] Amine **5b** (0.200 g, 0.943 mmol) and triethylamine (0.095 g, 0.943 mmol) were added to a solution of 2,4,6-triphenylpyrilium tetrafluoroborate (0.373 g, 0.943 mmol) in dichloromethane (20 mL). The mixture was magnetically stirred at room temperature for 10 min, acetic acid (0.113 g, 1.886 mmol) was then added, and the mixture was refluxed with stirring for 1 h. After it was cooled to room temperature, the mixture was poured upon diethyl ether. The solid formed was filtered and dissolved in chloroform. The solution was washed with saturated aqueous sodium hydrogencarbonate and with water, dried, and evaporated. The oily residue was digested with diethyl ether to afford **6b** as a solid (56%): mp 112–116 °C (dichloromethane–diethyl ether); IR (KBr) 1060 cm^{-1}; ^1H NMR (250 MHz, $CDCl_3$) δ 5.14 (d, J = 6.2 Hz, 2H), 5.49 (d, J = 16.1 Hz, 1H), 5.76 (dt, J = 16.1 and 6.2 Hz, 1H), 6.91 (d, J = 8.4 Hz, 2H), 7.31 (d, J = 8.4 Hz, 2H), 7.44–7.74 (m, 9H), 7.67–7.74 (m, 6H), 7.83 (s, 2H); ^{13}C NMR (62.5 MHz, $CDCl_3$) δ 57.12, 120.91, 122.61, 126.64, 128.10, 129.13, 129.18, 129.67, 131.07, 131.77, 132.16, 132.67, 133.76, 133.88, 134.88, 156.11, 156.83. Anal. Calcd for $C_{32}H_{25}BBrF_4N$: C, 65.12; H, 4.27; N, 2.37. Found: C, 65.51; H, 3.77; N, 2.44.

Compounds **6d** (57%) and **6e** (84%) were prepared by the same method as for **6b**.

1-Cinnamyl-2,4,6-triphenylpyridinium tetrafluoroborate (6d): mp 138–142 °C; IR (KBr) 1060 cm^{-1}; ^1H NMR (400 MHz, $CDCl_3$) δ 5.20 (d, J = 6.4 Hz, 2H), 5.60 (d, J = 15.8 Hz, 1H), 5.74 (dt, J = 15.8 and 6.4 Hz, 1H), 7.04–7.06 (m, 2H), 7.22–7.23 (m, 3H), 7.47–7.57 (m, 9H), 7.74–7.78 (m, 6H), 7.89 (s, 2H); ^{13}C NMR (62.5 MHz, $CDCl_3$) δ 57.63, 120.57, 127.03, 127.16, 128.51, 128.65, 128.95, 129.05, 129.58, 130.08, 131.45, 132.53, 133.15, 134.30, 135.26, 136.56, 156.39, 157.25. Anal. Calcd for $C_{32}H_{26}BF_4N$: C, 73.94; H, 5.38; N, 2.87. Found: C, 73.81; H, 5.39; N, 2.96.

1-(4-Methylcinnamyl)-2,4,6-triphenylpyridinium tetrafluoroborate (6e): mp 108–112 °C (acetone–diethyl ether); IR (KBr) 1053 cm^{-1}; ^1H NMR (250 MHz, $CDCl_3$) δ 2.33 (s, 3H), 5.25 (d, J = 6.2 Hz, 2H), 5.61 (d, J = 15.7 Hz, 1H), 5.74 (dt, J = 15.7 and 6.0 Hz, 1H), 7.01 (d, J = 8.0 Hz, 2H), 7.11 (d, J = 8.4 Hz, 2H), 7.48–7.67 (m, 9H), 7.72–7.86 (m, 6H), 7.96 (s, 2H); ^{13}C NMR (62.5 MHz, $CDCl_3$) δ 21.05, 51.18, 118.82, 125.33, 126.42, 127.93, 128.98, 129.04, 129.18, 129.51, 130.83, 131.90, 132.21, 132.63, 133.73, 135.98, 138.55, 155.73, 156.64. Anal. Calcd for $C_{33}H_{28}BF_4N$: C, 75.44; H, 5.37; N, 2.67. Found: C, 75.23; H, 5.40; N, 2.75.

(1,2-Bis(diphenylphosphino)ethane)(η³-1-(4-nitrophenyl)allyl)palladium Tetrafluoroborate (7a). A solution of **4a** (112 mg, 0.184 mmol) in anhydrous acetone (7 mL) was added over a solution of silver tetrafluoroborate (71 mg, 0.368 mmol) in anhydrous acetone (5 mL). The mixture was magnetically stirred in the dark at room temperature. The formed precipitate was filtered off and 1,2-bis(diphenylphosphino)ethane (146 mg, 0.368 mmol) was added to the solution. The mixture was stirred for 10 h at room temperature and filtered, and the solvent was evaporated to give a foam that was digested with diethyl ether to afford **7a** (70%): mp 209–216 °C (acetone–diethyl ether–pentane); IR (KBr) 1060 cm^{-1}; ^1H NMR (250 MHz, $CDCl_3$) δ 2.28–2.75 (m, CH_2CH_2), 3.53–3.68 (m, H-3a), 4.65–4.81 (m, H-3s), 5.41 (apparent t, J *ca.* 11.2 Hz, H-1a), 6.37–6.51 (m, H-2), 6.66–7.62 (m, 24H); ^{13}C NMR (62.5 MHz, $CDCl_3$) δ 27.28 (dd, $J_{C/P}$ = 31.4 and 13.9 Hz, one ligand CH_2), 28.52 (dd, $J_{C/P}$ = 31.4 and 13.9 Hz, another

(33) Malek, N. J.; Moormann, A. E. *J. Org. Chem.* **1982**, *47*, 5395.
(34) Meyers, A. I.; Lawson, J. P.; Carver, R. *J. Org. Chem.* **1981**, *46*, 3119.
(35) Brewbaker, J. L.; Hart, H. *J. Am. Chem. Soc.* **1969**, *91*, 711.
(36) Katritzky, A. R.; Marson, C. M. *Angew. Chem., Int. Ed. Engl.* **1984**, *23*, 420.

ligand CH_2), 69.27 (dd, $J_{C\text{-}3/Pcis}$ = 25.5 Hz, $J_{C\text{-}3/Ptrans}$ = 5.0 Hz, C-3), 89.84 (dd, $J_{C\text{-}1/Ptrans}$ = 27.7 Hz, $J_{C\text{-}1/Pcis}$ = 6.5 Hz, C-1), 120.00 (apparent t, $J_{C\text{-}2/Pcis}$ and $J_{C\text{-}2/Ptrans}$ = 6.5 Hz, C-2), 123.63–145.83 (30C); ^{31}P NMR (101 MHz, $CDCl_3$) δ 51.97 (d, J_{PP} = 42.5 Hz, P-*trans*), 50.44 (d, J_{PP} = 42.5 Hz, P-*cis*). Anal. Calcd for $C_{35}H_{32}BF_4NO_2P_2Pd$: C, 55.77; H, 4.28; N, 1.86. Found: C, 55.18; H, 4.11; N, 1.92.

Compounds **7c** (59%) and **7f** (65%) were prepared by the same method as for **7a**.

(1,2-Bis(diphenylphosphino)ethane)(η^3-1-(4-chlorophenyl)allyl)palladium tetrafluoroborate (7c): mp 175–180 °C (acetone–pentane); IR (KBr) 1053 cm^{-1}; ^{1}H NMR (250 MHz, $CDCl_3$) δ 2.39–2.59 (m, CH_2CH_2), 3.49 (apparent t, $J_{H\text{-}2/H\text{-}3a}$ and $J_{H\text{-}3a/Pcis}$ *ca.* 12–13 Hz, H-3a), 4.64 (apparent t, $J_{H\text{-}2/H\text{-}3s}$ and $J_{H\text{-}3s/Pcis}$ *ca.* 6–8 Hz, H-3s), 5.38 (apparent t, $J_{H\text{-}1a/H\text{-}2}$ and $J_{H\text{-}1a/Ptrans}$ *ca.* 11.3 Hz, H-1a), 6.23 (apparent dt, $J_{H\text{-}1a/H2}$ and $J_{H\text{-}2/H\text{-}3a}$ *ca.* 13 Hz, $J_{H\text{-}2/H\text{-}3s}$ *ca.* 8 Hz, H-2), 6.69–7.66 (m, 24H); ^{13}C NMR (62.5 MHz, $CDCl_3$), compound too insoluble for this spectrum to be registered; ^{31}P NMR (101 MHz, $CDCl_3$) δ 50.90 (d, J_{PP} = 41.2 Hz, P-*trans*), 47.46 (d, J_{PP} = 41.2 Hz, P-*cis*). Anal. Calcd for $C_{35}H_{32}BClF_4P_2Pd$: C, 56.56; H, 4.34. Found: C, 56.02; H, 4.14.

(1,2-Bis(diphenylphosphino)ethane)(η^3-1-(4-methoxyphenyl)allyl)palladium tetrafluoroborate (7f): mp 204–208 °C (acetone–diethyl ether); IR (KBr) 1053 cm^{-1}; ^{1}H NMR (250 MHz, $CDCl_3$) δ 2.39–2.64 (m, CH_2CH_2), 3.32 (apparent t, $J_{H\text{-}2/H\text{-}3a}$ and $J_{H\text{-}3a/Pcis}$ *ca.* 11.5 Hz; H-3a), 3.67 (s, OCH_3), 4.53 (apparent t, $J_{H\text{-}2/H\text{-}3s}$ and $J_{H\text{-}3s/Pcis}$ *ca.* 7 Hz, H-3s), 5.39 (apparent t, $J_{H\text{-}1a/H\text{-}2}$ and $J_{H\text{-}1a/Ptrans}$ *ca.* 11 Hz, H-1a), 6.16 (apparent dt, $J_{H\text{-}1a/H2}$ and $J_{H\text{-}2/H\text{-}3a}$ *ca.* 13 Hz, $J_{H\text{-}2/H\text{-}3s}$ *ca.* 8 Hz, H-2), 6.46 (d, J = 8.8 Hz, 2H), 6.71–6.82 (m, 2H), 6.96 (d, J = 8.8 Hz, 2H), 7.10–7.58 (m, 18H); ^{13}C NMR (62.5 MHz, $CDCl_3$) δ 27.31 (dd, $J_{C/P}$ = 25.0 and 13.9 Hz, one ligand CH_2), 27.75 (dd, $J_{C/P}$ = 25.0 and 13.9 Hz, another ligand CH_2), 55.27 (OCH_3), 65.25 (dd, $J_{C\text{-}3/Pcis}$ = 27.7 Hz, $J_{C\text{-}3/Ptrans}$ = 4.6 Hz, C-3), 96.66 (dd, $J_{C\text{-}1/Ptrans}$ = 25.9 Hz, $J_{C\text{-}1/Pcis}$ = 6.5 Hz, C-1), 114.11 (s, 2C), 115.33 (apparent t, $J_{C\text{-}2/Pcis}$ and $J_{C\text{-}2\text{-}Ptrans}$ = 7 Hz, C-2), 126.71–133.24 (27C), 159.58 (s, 1C); ^{31}P NMR (101 MHz, $CDCl_3$) δ 49.48 (d, J_{PP} = 40.7 Hz, P-*trans*), 45.95 (d, J_{PP} = 40.7 Hz, P-*cis*). Anal. Calcd for $C_{36}H_{35}BF_4OP_2Pd$: C, 58.52; H, 4.77. Found: C, 57.82; H, 4.53.

(1,2-Bis(diphenylphosphino)ethane)(η^3-1-(4-bromophenyl)allyl)palladium Tetrafluoroborate (7b). A solution of bis(dibenzylideneacetone)palladium(0) (0.172 g, 0.3 mmol) and 1,2-bis(diphenylphosphino)ethane (0.120 g, 0.3 mmol) in anhydrous benzene (10 mL) was added to a solution of pyridinium salt **6b** (0.177 g, 0.3 mmol) in anhydrous benzene (10 mL). The mixture was kept at room temperature for 4 h 30 min, and the formed solid was filtered off and washed several times with benzene to afford pure **7b** (0.229 g, 97%): mp 165–170 °C; IR (KBr) 1053 cm^{-1}; ^{1}H NMR (250 MHz, $CDCl_3$) δ 2.29–2.83 (m, CH_2CH_2), 3.45–3.66 (m, H-3a), 4.57–4.80 (m, H-3s), 5.29–5.52 (m, H-1a), 6.10–6.35 (m, H-2), 6.62–7.68 (m, 24H); ^{13}C NMR (62.5 MHz, $CDCl_3$) δ 27.54 (dd, $J_{C/P}$ = 30.5 and 14.2 Hz, one ligand CH_2), 28.12 (dd, $J_{C/P}$ = 30.5 and 14.2 Hz, another ligand CH_2), 67.15 (dd, $J_{C\text{-}3/Pcis}$ = 24.6 Hz, $J_{C\text{-}3/Ptrans}$ = 5.2 Hz, C-3), 93.09 (dd, $J_{C\text{-}1/Ptrans}$ = 26.5 Hz, $J_{C\text{-}1/Pcis}$ = 6.6 Hz, C-1), 117.56 (apparent t, $J_{C\text{-}2/Pcis}$ and $J_{C\text{-}2/Ptrans}$ = 6.6 Hz, C-2), 121.14–135.58 (30C); ^{31}P NMR (101 MHz, $CDCl_3$) δ 50.97 (d, J_{PP} = 40.7 Hz, P-*trans*), 48.57 (d, J_{PP} = 40.7 Hz, P-*cis*). Anal. Calcd for $C_{35}H_{32}BBrF_4P_2Pd$: C, 53.37; H, 4.09. Found: C, 53.79; H, 4.31.

Compounds **7d** (65%) and **7e** (96%) were prepared by the same method as for **7b**.

(1,2-Bis(diphenylphosphino)ethane)(η^3-1-phenylallyl)-palladium tetrafluoroborate (7d): mp 195–200 °C (lit.[24] mp 195–200 °C); IR (KBr) 1055 cm^{-1}; ^{1}H NMR (250 MHz, $CDCl_3$) δ 2.49–2.65 (m, CH_2CH_2), 3.42 (apparent t, $J_{H\text{-}2/H\text{-}3a}$ and $J_{H\text{-}3a/Pcis}$ *ca.* 13 Hz; H-3a), 4.60 (apparent t, $J_{H\text{-}2/H\text{-}3s}$ and $J_{H\text{-}3s/Pcis}$ *ca.* 7 Hz, H-3s), 5.32 (apparent t, $J_{H\text{-}1a/H\text{-}2}$ and $J_{H\text{-}1a/Ptrans}$ *ca.* 12 Hz, H-1a), 6.27 (apparent dt, $J_{H\text{-}1a/H2}$ and $J_{H\text{-}2/H\text{-}3a}$ *ca.* 13 Hz, $J_{H\text{-}2/H\text{-}3s}$ *ca.* 8 Hz, H-2), 6.65–7.80 (m, 25H); ^{13}C NMR (62.5 MHz, $CDCl_3$) δ 27.27 (dd, $J_{C/P}$ = 27.7 and 13.9 Hz, one ligand CH_2), 27.77 (dd, $J_{C/P}$ = 28.7 and 13.0 Hz, another ligand CH_2), 66.35 (dd, $J_{C\text{-}3/Pcis}$ = 26.8 Hz, $J_{C\text{-}3/Ptrans}$ = 6.5 Hz, C-3), 95.20 (dd, $J_{C\text{-}1/Ptrans}$ = 26.8 Hz, $J_{C\text{-}1/Pcis}$ = 6.5 Hz, C-1), 116.95 (apparent t, $J_{C\text{-}2/Pcis}$ and $J_{C\text{-}2\text{-}Ptrans}$ = 6.9 Hz, C-2), 126.52–133.17 (30C); ^{31}P NMR (101 MHz, $CDCl_3$) δ 50.89 (d, J_{PP} = 41.5 Hz, P-*trans*), 47.14 (d, J_{PP} = 41.5 Hz, P-*cis*).

(1,2-Bis(diphenylphosphino)ethane)(η^3-1-(4-methylphenyl)allyl)palladium Tetrafluoroborate (7e): mp 206–212 °C; IR (KBr) 1060 cm^{-1}; ^{1}H NMR (250 MHz, $CDCl_3$) δ 2.19 (s, 3H), 2.44–2.64 (m, CH_2CH_2), 3.37 (apparent t, $J_{H\text{-}2/H\text{-}3a}$ and $J_{H\text{-}3a/Pcis}$ *ca.* 12 Hz; H-3a), 4.57 (apparent t, $J_{H\text{-}2/H\text{-}3s}$ and $J_{H\text{-}3s/Pcis}$ *ca.* 7 Hz, H-3s), 5.36 (apparent t, $J_{H\text{-}1a/H\text{-}2}$ and $J_{H\text{-}1a/Ptrans}$ *ca.* 12 Hz, H-1a), 6.20 (apparent dt, $J_{H\text{-}1a/H2}$ and $J_{H\text{-}2/H\text{-}3a}$ *ca.* 13 Hz, $J_{H\text{-}2/H\text{-}3s}$ *ca.* 7.5 Hz, H-2), 6.65–7.60 (m, 24H); ^{13}C NMR (62.5 MHz, $CDCl_3$) δ 21.20 (s, CH_3), 27.15 (dd, $J_{C/P}$ = 25.9 and 13.9 Hz, one ligand CH_2), 27.65 (dd, $J_{C/P}$ = 26.8 and 13.9 Hz, another ligand CH_2), 65.77 (dd, $J_{C\text{-}3/Pcis}$ = 27.7 Hz, $J_{C\text{-}3/Ptrans}$ = 4.6 Hz, C-3), 95.83 (dd, $J_{C\text{-}1/Ptrans}$ = 25.9 Hz, $J_{C\text{-}1/Pcis}$ = 6.5 Hz, C-1), 116.20 (apparent t, $J_{C\text{-}2/Pcis}$ and $J_{C\text{-}2\text{-}Ptrans}$ = 6.5 Hz, C-2), 125.32–133.10 (30C); ^{31}P NMR (101 MHz, $CDCl_3$) δ 49.99 (d, J_{PP} = 40.7 Hz, P-*trans*), 45.93 (d, J_{PP} = 40.7 Hz, P-*cis*). Anal. Calcd for $C_{36}H_{35}BF_4P_2Pd$: C, 59.82; H, 4.88. Found: C, 59.00; H, 5.19.

Dimethyl Bis(4-methoxycinnamyl)malonate (9f). To the sodium salt of dimethyl malonate (from the diester (96 mg, 0.727 mmol) and sodium hydride (32 mg of 60% suspension, 791 mmol)) in anhydrous THF (10 mL) were added 4-methoxycinnamyl acetate (**8f**; 150 mg, 0.727 mmol) in anhydrous THF (7 mL) and tetrakis(triphenylphosphine)palladium(0) (84 mg, 0.073 mmol). The mixture was heated to 60 °C for 4.5 h. The solvent was evaporated, and the oily residue was chromatographed through a silica gel column using hexanes–diethyl ether (80:20) to afford **9f** (81 mg, 53%); mp 106–109 °C; IR (KBr) 1735, 969 cm^{-1}; ^{1}H NMR (250 MHz, $CDCl_3$) δ 2.77 (d, J = 7.3 Hz, 4H), 3.69 (s, 6H), 3.77 (s, 6H), 5.87 (dt, J = 15.7 and 7.7 Hz, 2H), 6.36 (d, J = 15.7 Hz, 2H), 6.79 (d, J = 11.7 Hz, 4H), 7.21 (d, J = 11.6 Hz, 4H); ^{13}C NMR (62.5 MHz, $CDCl_3$) δ 36.6, 52.4, 55.2, 58.3, 113.8, 121.5, 127.3, 129.9, 133.4, 159.0, 171.3. Anal. Calcd for $C_{25}H_{28}O_6$: C, 70.74; H, 6.65. Found: C, 70.79; H, 6.37.

Dimethyl Bis(4-nitrocinnamyl)malonate (9a). This compound was prepared by the same method as for **9f** (58% yield): mp 163–165 °C; IR (KBr) 1735, 1518, 1342, 962 cm^{-1}; ^{1}H NMR (250 MHz, $CDCl_3$) δ 2.86 (d, J = 7.5 Hz, 4H), 3.76 (s, 6H), 6.27 (dt, J = 15.8 and 7.5 Hz, 2H), 6.51 (d, J = 15.8 Hz, 2H), 7.43 (d, J = 8.8 Hz, 4H), 8.15 (d, J = 8.8 Hz, 2H); ^{13}C NMR (62.5 MHz, $CDCl_3$) δ 37.2, 52.7, 57.9, 124.0, 126.7, 128.9, 132.3, 143.1, 146.9, 170.7.

Acknowledgment. Financial support from the DGICYT (Ministry of Education and Science of Spain) through projects PB90-0063 and PB93-0896 and a predoctoral scholarship (to R.M.) is gratefully acknowledged.

Supplementary Material Available: Figures giving IR, ^{1}H NMR, and ^{13}C NMR spectra for compounds **4**, **6**, **7**, and **9** and plots of chemical shifts vs σ and σ^+ for C-1, C-2, and C-3 (59 pages). Ordering information is given on any current masthead page.

OM950089V

Synthesis, Structures, and Properties of Strained, Silicon-Bridged [1]Ferrocenophanes with Methylated Cyclopentadienyl Rings

John K. Pudelski, Daniel A. Foucher, Charles H. Honeyman, Alan J. Lough, and Ian Manners*

Department of Chemistry, University of Toronto, 80 St. George Street, Toronto M5S 1A1, Ontario, Canada

Stephen Barlow and Dermot O'Hare*

Inorganic Chemistry Laboratory, University of Oxford, South Parks Road, Oxford OX1 3QR, U.K.

Received December 15, 1994[⊗]

A series of strained, silicon-bridged [1]ferrocenophanes with methylated cyclopentadienyl rings, which are prospective monomeric precursors of poly(ferrocenylsilanes) via ring-opening polymerization, has been synthesized and characterized. The dimethylated silicon-bridged [1]ferrocenophanes Fe(η-$C_5H_3Me)_2SiMe_2$ (**4**) were prepared as a mixture of isomers via the reaction of Fe(η-$C_5H_3MeLi)_2$·TMEDA (TMEDA = tetramethylethylenediamine) with Me_2SiCl_2. The 3,3′-syn isomer **4a** was cleanly isolated via low-temperature crystallization. The tetramethylated silicon-bridged [1]ferrocenophane Fe(η-C_5Me_4)(η-C_5H_4)$SiMe_2$ (**6**) and the octamethylated silicon-bridged [1]ferrocenophane Fe(η-$C_5Me_4)_2SiMe_2$ (**8**) were prepared via the reaction of $FeCl_2$ with $Li_2[(C_5Me_4)(C_5H_4)SiMe_2]$ and $Li_2[(C_5Me_4)_2SiMe_2]$, respectively. X-ray diffraction studies of **4a** and **8** revealed that these molecules possess highly strained ring-tilted structures. Comparison with the previously determined structure of Fe(η-$C_5H_4)_2SiMe_2$ (**1**) revealed that, with increasing ring methylation, the tilt angle between the planes of the cyclopentadienyl ligands decreases significantly (**1**, 20.8(5)°; **4a**, 18.6(3)°; **8**, 16.1(3)°), the angle between the cyclopentadienyl ligand and the ipso cyclopentadienyl carbon–silicon bond increases (**1**, 37.0(6)°; **4a**, 39.1(2)°; **8**, 40.3(2)°), and the Fe–Si distance decreases (**1**, 2.690(3) Å; **4a**, 2.6767(8) Å; **8**, 2.652(1) Å). Cyclic voltammetric analysis of **1**, **4a**, **6**, and **8** in CH_2Cl_2 revealed that each ferrocenophane exhibits a reversible, one-electron oxidation. Analysis of **1** and **8** by ^{57}Fe Mössbauer spectroscopy in conjunction with the crystallographically determined trend in Fe–Si distances provided evidence for the presence of a weak dative Fe–Si interaction which is more substantial in the latter species than the former. Crystals of **4a** ($C_{14}H_{18}FeSi$) are orthohombic, space group *Pbca*, with a = 14.775(2) Å, b = 10.655(2) Å, c = 16.882(2) Å, V = 2657.7(7) Å^3, and Z = 8. Crystals of **8** ($C_{20}H_{30}FeSi$) are monoclinic, space group *C*2/*c*, with a = 15.687(3) Å, b = 9.194(1) Å, c = 26.612(5) Å, β = 98.65(2)°, V = 3653(6) Å^3, and Z = 8.

Introduction

Metallocenes are attracting growing attention as components of solid state, oligomeric, and high polymeric materials with novel physical properties.[1–11] Strained, ring-tilted ferrocenophanes are of interest as a result of their unusual structures and the recent discovery that these species readily undergo thermally[12] and anionically induced[13,14] ring-opening polymerization (ROP) reactions.[10] Thus, in 1992 we reported that, when heated in the melt at 130 °C, silicon-bridged [1]-ferrocenophane **1** polymerized affording high molecular weight, soluble poly(ferrocenylsilane) **2** in quantitative yield (Scheme 1).[12] Subsequent papers have reported the synthesis and ROP of a variety of silicon-bridged [1]ferrocenophanes analogous to **1** with different organic substituents at silicon.[15–17] Furthermore, we have recently prepared and polymerized [1]ferrocenophanes

[⊗] Abstract published in *Advance ACS Abstracts,* March 15, 1995.

(1) Nugent, H. M.; Rosenblum, M.; Klemarczyk, P. *J. Am. Chem. Soc.* **1993**, *115*, 3848–3849.
(2) Fritz, M.; Hiermeier, J.; Herktorn, N.; Köhler, F. H.; Muller, G.; Reber, G.; Steigelmann, O. *Chem. Ber.* **1991**, *124*, 1531–1539.
(3) Bergerat, P.; Blumel, J.; Fritz, M.; Hiermeier, J.; Hudeczek, P.; Kahn, O.; Köhler, F. H. *Angew. Chem., Int. Ed. Engl.* **1992**, *31*, 1258–1260.
(4) Atzkern, H.; Bergerat, P.; Fritz, M.; Hiermeier, J.; Hudeczek, P.; Kahn, O.; Kanellakopulos, B.; Köhler, F. H.; Ruhs, M. *Chem. Ber.* **1994**, *127*, 277–286.
(5) Brandt, P. F.; Rauchfuss, T. B. *J. Am. Chem. Soc.* **1992**, *114*, 1926–1927.
(6) Galloway, C. P.; Rauchfuss, T. B. *Angew. Chem., Int. Ed. Engl.* **1993**, *32*, 1319–1321.
(7) O'Hare, D. *Chem. Soc. Rev.* **1992**, 121–126.
(8) Hughes, A. K.; Murphy, V. J.; O'Hare, D. *J. Chem. Soc., Chem. Commun.* **1994**, 163–164.
(9) Miller, J. S.; Epstein, A. J.; Reiff, W. M. *Acc. Chem. Res.* **1988**, *21*, 114–120.
(10) Manners, I. *Adv. Organomet. Chem.* **1995**, *37*, 131–168.
(11) Wright, M. E.; Toplikar, E. G. *Contemp. Top. Polym. Sci.* **1992**, *7*, 285–292.
(12) Foucher, D. A.; Tang, B.-Z.; Manners, I. *J. Am. Chem. Soc.* **1992**, *114*, 6246–6248.
(13) Rulkens, R.; Lough, A. J.; Manners, I. *J. Am. Chem. Soc.* **1994**, *116*, 797–798.
(14) Rulkens, R.; Ni, Y.; Manners, I. *J. Am. Chem. Soc.* **1994**, *116*, 12121–12122.

0276-7333/95/2314-2470$09.00/0

Scheme 1

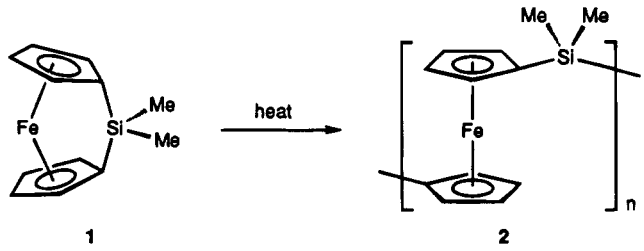

1 2

with other elements in the bridge, and also hydrocarbon-bridged [2]metallocenophanes.[18-22] The transition metal containing polymeric products that result from these ROP reactions exhibit a variety of interesting electrochemical, morphological, and (when oxidized) magnetic properties and serve as precursors to novel ceramics.[12,13,15,16,23-25]

As part of our continuing studies of strained metallocenophanes and their ring-opening polymerization reactions, we now report the synthesis, structure, and properties of a series of strained silicon-bridged [1]-ferrocenophanes with partial and full methyl substitution of the cyclopentadienyl (Cp) rings. Methyl substitution of metallocene Cp rings represents a well-established method of modifying the magnetic, electronic, chemical, solubility, and optical properties of metallocene-based molecules and materials.[9,26-30] For example, decamethylmanganocene is found to be a low-spin molecule, whereas manganocene has $S = {}^5/_2$, illustrating the much stronger ligand field of the pentamethylated ligand.[31] Methylation also notably increases the susceptibility of metallocenes to oxidation. Thus, for example, the decamethylcobaltocenium/decamethylcobaltocene couple is 0.56 V more negative than that of cobaltocenium/cobaltocene.[32] Furthermore, a range of decamethylmetallocenes, $M(C_5Me_5)_2$ (M = Cr, Mn, Fe, Ni), are found to form salts with tetracyanoethylene which are low-temperature ferromagnets.[33]

While we have previously approached the control of the structure and properties of silicon-bridged [1]ferrocenophanes and their corresponding ring-opened polymers via manipulation of the substituents at silicon, this work describes our first studies of the effects of systematic methyl substitution of the Cp rings. Studies of the polymerization reactions of the methylated ferrocenophanes which are described herein, together with studies of the properties of the resulting materials, will be reported elsewhere.[34]

Results and Discussion

1. Synthesis and Characterization of Dimethylated Ferrocenophanes 4. We have employed two synthetic strategies to prepare ferrocenophanes with methyl substitution of the Cp rings. A strategy similar to the route which we have used to prepare nonmethylated, silicon-bridged [1]ferrocenophanes was employed for the synthesis of methylated ferrocenophanes in which each Cp ring has a single methyl substituent (Scheme 2).[15,16,35,36] Reaction of 1,1′-dimethylferrocene with 2 equiv of BuLi and 2 equiv of tetramethylethylenediamine (TMEDA) in hexanes at room temperature for 2 days, followed by addition of Me_2SiCl_2 at −78 °C, afforded a red liquid. Fractional distillation of this liquid under high vacuum afforded a 59% yield of dimethylated ferrocenophanes **4** as a viscous red oil. Analysis of this oil by NMR and mass spectrometry revealed that it was composed of a complex mixture of isomers. The ^{1}H NMR spectrum (C_6D_6) of the isomer mixture consisted of multiple resonances in the Cp (4.6−3.7 ppm), Cp−Me (2.2−1.7 ppm), and Si−Me (0.6−0.2 ppm) regions. The ^{29}Si NMR spectrum of the mixture consisted of four intense resonances between −3.5 and −4.6 ppm, suggesting that four major isomers were present in the mixture. Mass spectrometric analysis of the mixture found the parent ion (*m/e* 270) as the base peak. Previous studies have demonstrated that the bulky trimethylsilyl groups of 1,1′-bis(trimethylsilyl)-ferrocene exert high regiocontrol in the lithiation of this compound under conditions similar to those which we have employed for lithiation of 1,1′-dimethylferrocene.[37] When electrophiles are added to the dilithio derivative of 1,1′-bis(trimethylsilyl)ferrocene, a product mixture consisting of mainly one tetrasubstituted isomer is obtained. The reduced steric demand of the methyl group relative to the trimethylsilyl group may explain the absence of this type of regiocontrol in the lithiation of 1,1′-dimethylferrocene.

Upon standing at room temperature for several days, the appearance of crystalline material in the isomer mixture was noted. While clean recovery of the crystalline material could not be directly accomplished, when

(15) Foucher, D. A.; Ziembinski, R.; Tang, B.-Z.; Macdonald, P. M.; Massey, J.; Jaeger, C. R.; Vancso, G. J.; Manners, I. *Macromolecules* **1993**, *26*, 2878−2884.
(16) Foucher, D.; Ziembinski, R.; Petersen, R.; Pudelski, J.; Edwards, M.; Ni, Y.; Massey, J.; Jaeger, C. R.; Vancso, G. J.; Manners, I. *Macromolecules* **1994**, *27*, 3992−3999.
(17) For the work of other groups on poly(ferrocenylsilanes) and related materials, see: (a) Rosenberg, H. U.S. Patent 3,426,053, 1969. (b) Tanaka, M.; Hayashi, T. *Bull. Chem. Soc. Jpn.* **1993**, *66*, 334. (c) Nguyen, M. T.; Diaz, A. F.; Dement'ev, V. V.; Pannell, K. H. *Chem. Mater.* **1993**, *5*, 1389.
(18) Foucher, D. A.; Manners, I. *Makromol. Chem., Rapid Commun.* **1993**, *14*, 63−66.
(19) Foucher, D. A.; Edwards, M.; Burrow, R. A.; Lough, A. J.; Manners, I. *Organometallics* **1994**, *13*, 4959−4966.
(20) Manners, I. *Adv. Mater.* **1994**, *6*, 68−71.
(21) Nelson, J. M.; Rengel, H.; Manners, I. *J. Am. Chem. Soc.* **1993**, *115*, 7035−7036.
(22) Nelson, J. M.; Lough, A. J.; Manners, I. *Angew. Chem., Int. Ed. Engl.* **1994**, *33*, 989−991.
(23) Foucher, D. A.; Honeyman, C. H.; Nelson, J. M.; Tang, B.-Z.; Manners, I. *Angew. Chem., Int. Ed. Engl.* **1993**, *32*, 1709−1711.
(24) Tang, B.-Z.; Petersen, R.; Foucher, D. A.; Lough, A. J.; Coombs, N.; Sodhi, R.; Manners, I. *J. Chem. Soc., Chem. Commun.* **1993**, 523−525.
(25) Hmyene, M.; Yassar, A.; Escorne, M.; Percheron-Guegan, A.; Garnier, F. *Adv. Mater.* **1994**, *6*, 564−568.
(26) Miller, J. S.; Glatzhofer, D. T.; O'Hare, D. M.; Reiff, W. M.; Chakraborty, A.; Epstein, A. J. *Inorg. Chem.* **1989**, *28*, 2930−2939.
(27) Gassman, P. G.; Macomber, D. W.; Hershberger, J. W. *Organometallics* **1983**, *2*, 1470−1472.
(28) Gassman, P. G.; Winter, C. H. *J. Am. Chem. Soc.* **1988**, *110*, 6130−6135.
(29) Gassman, P. G.; Mickelson, J. W.; Sowa, J. R. J. *J. Am. Chem. Soc.* **1992**, *114*, 6942−6944.
(30) Pudelski, J. K.; Callstrom, M. R. *Organometallics* **1994**, *13*, 3095−3109.
(31) Robbins, J. L.; Edelstein, N. M.; Cooper, S. R.; Smart, J. C. *J. Am. Chem. Soc.* **1979**, *101*, 3853−3857.
(32) Robbins, J. L.; Edelstein, N.; Spencer, B.; Smart, J. C. *J. Am. Chem. Soc.* **1982**, *104*, 1882−1893.
(33) For example, see: Miller, J. S.; Epstein, A. J. *Chem. Br.* **1994**, 477−480 and references cited therein.
(34) Pudelski, J. K.; Foucher, D. A.; MacDonald, P.; Manners, I.; Barlow, S.; O'Hare, D. Manuscript in preparation.
(35) Osborne, A. G.; Whiteley, R. H. *J. Organomet. Chem.* **1975**, *101*, C27.
(36) Fischer, A. B.; Kinney, J. B.; Staley, R. H.; Wrighton, M. S. *J. Am. Chem. Soc.* **1979**, *101*, 6501−6506.
(37) Brown, R. A.; Houlton, A.; Roberts, R. M. G.; Silver, J.; Frampton, C. S. *Polyhedron* **1992**, *11*, 2611−2619.

Scheme 2

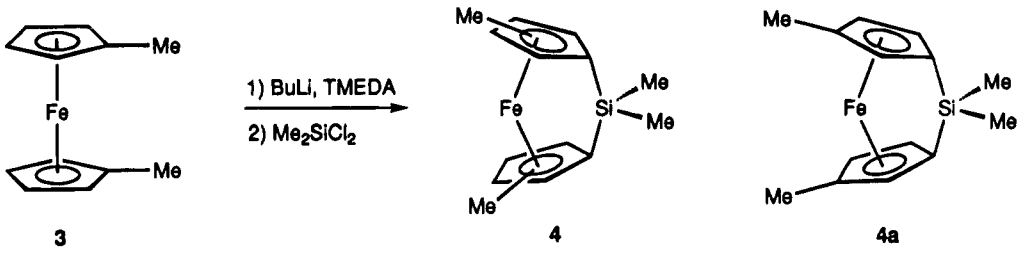

Scheme 3

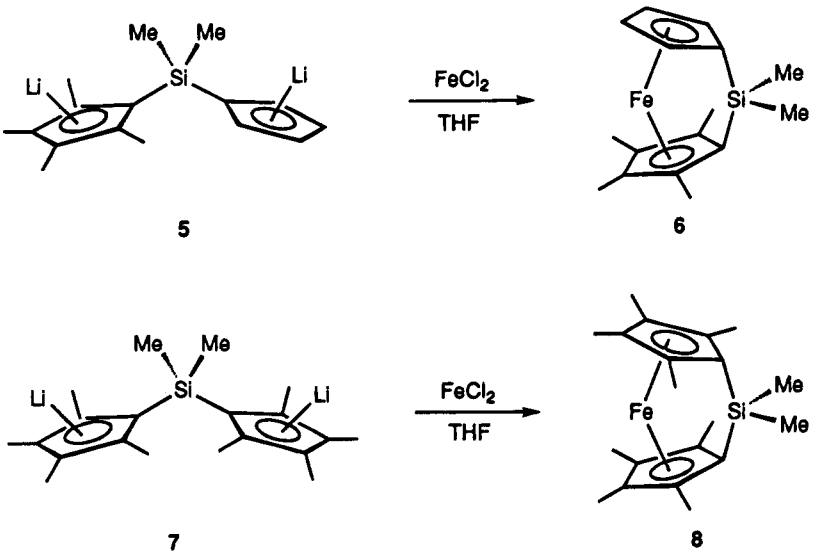

the sample was dissolved in hexanes and cooled to −30 °C a red solid readily crystallized out of solution. Filtration followed by recrystallization from hexanes afforded a 3% yield of a red crystalline solid. Remarkably, a single resonance at −4.5 ppm was observed in the ^{29}Si NMR spectrum (C_6D_6) of the material, indicating that the solid consisted of a single dimethylated ferrocenophane isomer. Interestingly, the ^{1}H NMR spectrum of the material in C_6D_6 contained a single Cp−Me resonance at 1.76 ppm but two Si−Me resonances at 0.39 and 0.34 ppm in a 1:1 ratio indicating that, while the Cp−Me groups of this isomer are equivalent, the Si−Me groups are inequivalent. Consistent with ^{1}H NMR findings was the ^{13}C NMR spectrum (C_6D_6) of the compound, which contained a single Cp−Me resonance at 13.0 ppm and two Si−Me resonances at −2.9 and −3.3 ppm. Also observed in the ^{13}C NMR spectrum were five distinct Cp resonances. The ipso Cp carbons exhibited the unusually high field chemical shift, relative to nonbridged ferrocenes, of 32.2 ppm typical of strained ferrocenophanes.[38] On the basis of the NMR findings, the possible identity of the compound was reduced to the 2,2′-syn isomer or the 3,3′-syn isomer. Indeed, an X-ray crystallographic study (see subsequent section) confirmed that the compound was the 3,3′-syn isomer **4a**. Concentration of filtrate remaining from the initial crystallization of **4a** followed by ^{1}H NMR analysis revealed that a substantial quantity of this species remained and thus that crystallization was not quantitative. Access to ferrocenophanes such as **4a**, in which placement of the methyl substituents is specific, is attractive, since ROP would then afford a well-defined polymeric material which would be expected to exhibit different properties from those arising from ROP of an isomeric mixture. All subsequent experiments employing **4** were carried out using the 3,3′-syn isomer **4a**.

2. Synthesis and Characterization of Tetra- and Octamethylated Ferrocenophanes 6 and 8. The second strategy which we have employed to prepare ferrocenophanes with methylated Cp rings is shown in Scheme 3; this illustrates the syntheses of tetramethylated ferrocenophane **6** and octamethylated ferrocenophane **8**. Reaction of the known salt $Li_2[(C_5Me_4)(C_5H_4)SiMe_2]$[39] (**5**) with $FeCl_2$ in THF afforded **6** in 27% yield. The highest yields of this compound were obtained by addition of **5** to a slight excess of $FeCl_2$ at room temperature. After removal of LiCl by filtration and removal of solvent in vacuo, **6** was obtained as a red-orange crystalline solid by sublimation at 60−90 °C (0.01 mmHg).

The identity of **6** was confirmed by ^{1}H, ^{13}C, and ^{29}Si NMR in addition to mass spectrometry and elemental analysis. The α and β Cp protons of **6** are found as the expected pseudotriplets at 3.41 and 4.30 ppm in the ^{1}H NMR spectrum (C_6D_6) of this compound. Significant separation of the α and β Cp proton resonances of ring-tilted ferrocenophanes is common (i.e., for the non-methylated ferrocenophane **1** with ring tilting of 20.8(5)° these triplets are found at 3.95 and 4.41 ppm[40]), and one explanation for this phenomenon is that the α protons are brought closer to the Fe center than the β

(38) Osborne, A. G.; Whiteley, R. H.; Meads, R. E. *J. Organomet. Chem.* **1980**, *193*, 345.

(39) Stern, D.; Sabat, M.; Marks, T. J. *J. Am. Chem. Soc.* **1990**, *112*, 9558−9575.

(40) Finckh, W.; Tang, B.-Z.; Foucher, D. A.; Zamble, D. B.; Ziembinski, R.; Lough, A.; Manners, I. *Organometallics* **1993**, *12*, 823−829.

protons by ring tilting and are thus more shielded.[41] Nonetheless, the separation of the α and β Cp protons of **6** is unusually wide. This increase probably results from more pronounced shielding of the α Cp protons by an Fe center which is more electron rich due to methylation of the opposite Cp ring and additional shielding of these protons by the α methyl groups of the opposite Cp ring which are brought close by ring tilting. Indeed, the chemical shifts of both the α and β Cp protons of **6** are upfield of the corresponding shifts of **1**. Analysis of **6** by ^{13}C NMR (C_6D_6) also proved revealing. The ipso Cp carbon atoms exhibited high-field chemical shifts of 33.5 and 27.5 ppm, typical of a strained ferrocenophane.[38] The 33.5 ppm shift is identical to that exhibited by nonmethylated analog **1** and is thus assigned to the ipso carbon of the nonmethylated Cp ring.[40] Similarly, the 27.5 ppm shift is similar to that exhibited by fully methylated analog **8** (see below) and is thus assigned to the ipso carbon of the methylated Cp ring.

The major side product in the synthesis of **6**, obtained in yields as high as 50%, is low molecular weight oligomeric material which is soluble in THF and can be isolated as an orange powdery solid by precipitation into methanol. Analysis of this material by ^1H and ^{29}Si NMR and mass spectrometry are consistent with structure **9**. GPC analysis of this oligomeric material vs

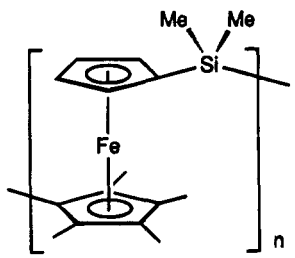

9

polystyrene standards yielded an average molecular weight (M_w = 1550) corresponding to 4–5 repeat units. In contrast, thermal ROP reactions of [1]ferrocenophanes generally afford materials with M_w in the 10^5–10^6 range. Given its low molecular weight, the oligomeric side product obtained in the synthesis of **6** probably forms via condensation type processes which are competitive with the ferrocenophane annulation reaction.

In a fashion similar to the preparation of **6**, reaction of the known salt $Li_2[(C_5Me_4)_2SiMe_2]$[42,43] (**7**) with a slight excess of $FeCl_2$ in THF at room temperature afforded the fully methylated ferrocenophane **8** in 46% yield (Scheme 3). Highly pure **8** is obtained as an orange crystalline solid from sublimation of the crude reaction mixture at 80–95 °C (0.01 mmHg) after removal of LiCl by filtration and solvent removal in vacuo. The identity of **8** was confirmed by ^1H, ^{13}C, and ^{29}Si NMR in addition to mass spectral analysis. Significantly, the high-field ^{13}C NMR chemical shift of 25.6 ppm found for the ipso Cp carbons of **8** is characteristic of a strained ferrocenophane structure.[38]

3. X-ray Crystallographic Analysis of Methylated Ferrocenophanes 4a and 8. X-ray crystallographic studies of **4a** and **8** were carried out in order to determine structural changes in these species brought about by increasing methyl substitution of the Cp rings. In this regard, comparison with the previously determined structure of nonmethylated ferrocenophane **1** is instructive.[40] Additionally, X-ray analysis confirmed the identity of **4a** as the 3,3′-syn isomer. Table 1 contains data collection details for the X-ray analyses of **4a** and **8**. Tables 2 and 3 contain atomic coordinates, equivalent isotropic displacement parameters, and selected bond lengths and bond angles for **4a**. Tables 4 and 5 contain atomic coordinates, equivalent isotropic displacement parameters, and selected bond lengths and bond angles for **8**. Figure 1 shows two ORTEP views of **4a**, and Figure 2 shows two ORTEP views of **8**. For comparison purposes, Table 6 summarizes important bond angles and bond lengths for **1**, **4a**, and **8**, and Figure 3 defines important bond angles used in the structural comparison of the ferrocenophanes.

Ferrocenophanes **1**, **4a**, and **8** are all characterized by strained, ring-tilted structures. A major structural effect of increased methyl substitution of the Cp rings in these ferrocenophanes, however, is a reduction of Cp ring tilting (defined as angle α in Figure 4). As the number of methyl Cp substituents in **1**, **4a**, and **8** increases from zero to two to eight, the ring tilt is reduced from 20.8(5)° to 18.6(3)° to 16.1(3)°. Reduction of Cp ring tilt with increasing methyl substitution is important since ring tilt in ferrocenophanes is a clear indication of strain in these species.[44] The reduced ring tilt of **8**, relative to **1**, is possibly a response to unfavorable steric interactions between the methyl groups at the α positions of opposing Cp rings which are brought close by ring tilting. Steric considerations cannot be used to explain the reduced ring tilt in **4a** relative to **1**, however, since Cp methyl groups of the former compound are at β positions and are moved further apart by ring tilting. An explanation for the reduced tilt of **4a** relative to **1**, and perhaps for the trend of reduced ring tilt with increasing methylation in general, lies in the observation that Fe–Cp bonding is strengthened by methylation.[32,45] With stronger Fe–Cp bonding, deviation of the Cp rings from planarity leads to greater bond energy losses; thus, increasingly methylated ferrocenophanes adopt less tilted Cp rings.

Numerous structural features of the bridging group in these ferrocenophanes vary in a smooth, consistent manner in response to increased methyl substitution. For example, the angle β between the Cp ring plane and the exocyclic Cp_{ipso}–Si bond increases as methyl substitution increases and ring tilt decreases. Increases in β are important since they are also indicative of increased strain in ferrocenophanes.[44] Along with increases in β, reduced ring tilt and increasing methyl substitution are accompanied by a lengthening of the exocyclic Cp_{ipso}–Si bonds. Furthermore, as the ring tilt decreases, the angle θ between the ipso Cp carbon atoms and the Si atom of the bridge increases, and a scissoring effect is observed as the angle between the Si bridging

(41) Rinehart, K. L. J.; Frerichs, A. K.; Kittle, P. A.; Westman, L. F.; Gustafson, D. H.; Pruett, R. L.; McMahon, J. E. *J. Am. Chem. Soc.* **1960**, *82*, 4111–4112.
(42) Fendrick, C. M.; Mintz, E. A.; Schertz, L. D.; Marks, T. J.; Day, V. W. *Organometallics* **1984**, *3*, 819–821.
(43) Fendrick, C. M.; Schertz, L. D.; Day, V. D.; Marks, T. J. *Organometallics* **1988**, *7*, 1828–1838.
(44) Stoeckli-Evans, H.; Osborne, A. G.; Whiteley, R. H. *Helv. Chim. Acta* **1976**, *59*, 2402–2406.
(45) Cauletti, C.; Green, J. C.; Kelley, M. R.; Powell, P.; Van Tilborg, J.; Robbins, J.; Smart, J. *J. Electron Spectrosc. Relat. Phenom.* **1980**, *19*, 327–353.

Table 1. Crystal Data, Data Collection, and Least-Squares Parameters for Crystallographic Analysis of 4a and 8

	4a	8
empirical formula	$C_{14}H_{18}FeSi$	$C_{20}H_{30}FeSi$
M_r	270.2	354.4
cryst size, mm^3	0.36 × 0.22 × 0.19	0.30 × 0.22 × 0.26
cryst class	orthorhombic	monoclinic
space group	*Pbca*	*C2/c*
a, Å	14.775(2)	15.687(3)
b, Å	10.655(2)	9.194(1)
c, Å	16.882(2)	26.612(5)
β, deg	90	98.65(2)
vol, Å^3	2657.7(7)	3653(6)
Z	8	8
D_{calcd}, g cm^{-3}	1.351	1.289
μ(Mo Kα), cm^{-1}	0.12	0.09
T, K	173	150
F(000)	1136	1520
scan range (ω), deg	0.64	0.58
range of θ collected, deg	3.4−28.0	2.0−28.0
min/max trans. coeff	0.6464/0.9363	0.5872/0.9147
total no. of rflns	3193	4825
unique reflns	3193	4383
R_{int}		0.0254
no. of data used	3193	3408
refinement method	full matrix least-squares on F^2 (SHELXL)	full matrix least-squares on *F*(SHELXTL-PC)
R indices (obs data)	$R = 0.035$, wR2 = 0.066 [$I > 2\sigma(I)$]	$R = 0.031$, $R_w = 0.043$ [$I > 3\sigma(I)$]
R indices (all data)[a]	$R = 0.069$, wR2 = 0.071	$R = 0.041$, $R_w = 0.046$
weighting scheme	$w = 1/[\sigma^2(F_o) + (0.061P)^2]$[b]	$w = 1/(\sigma^2(F_o) + 0.0008(F_o)^2)$
GOF	1.005	1.10
$(\Delta/\sigma)_{max}$ in last cycle	<0.01	0.01
no. of params refined	217	319
$\Delta\rho$(max) in final ΔF map, e Å^{-3}	0.37	0.39

[a] $R = \Sigma(F_o - F_c)/\Sigma F_o$, $R_w = \{\Sigma[w(F_o - F_c)]^2/\Sigma[w(F_o)^2]\}^{1/2}$, $R_s2 = \{\Sigma[w(F_o^2 - F_c^2)^2/\Sigma[w(F_o^2)^2]\}^{1/2}$ [b] $P = \text{Max}(F_o^2,0) + 2F_0^2/3$.

Table 2. Final Fractional Coordinates and Thermal Parameters for the Non-Hydrogen Atoms of 4a

atom	*x*	*y*	*z*	*U*(eq)
Fe	0.6311(1)	0.1625(1)	0.2911(1)	0.021(1)
Si	0.6352(1)	0.1832(1)	0.1332(1)	0.030(1)
C(1)	0.7054(2)	0.0866(2)	0.2038(2)	0.027(1)
C(2)	0.7630(2)	0.1484(3)	0.2612(2)	0.028(1)
C(3)	0.7512(2)	0.0925(3)	0.3370(2)	0.028(1)
C(4)	0.6866(2)	−0.0058(2)	0.3303(2)	0.028(1)
C(5)	0.6590(2)	−0.0101(2)	0.2490(2)	0.027(1)
C(6)	0.5609(2)	0.2592(2)	0.2098(2)	0.030(1)
C(7)	0.6022(2)	0.3443(3)	0.2666(2)	0.031(1)
C(8)	0.5706(2)	0.3155(3)	0.3438(2)	0.036(1)
C(9)	0.5076(2)	0.2144(3)	0.3386(2)	0.036(1)
C(10)	0.5015(2)	0.1830(3)	0.2572(2)	0.033(1)
C(11)	0.7023(2)	0.3013(3)	0.0722(2)	0.041(1)
C(12)	0.5699(3)	0.0785(4)	0.0670(2)	0.054(1)
C(13)	0.6559(3)	−0.0907(3)	0.3950(2)	0.043(1)
C(14)	0.4558(3)	0.1536(5)	0.4044(2)	0.059(1)

atom and its two methyl substituents decreases. Steric interactions between the α Cp methyl groups and the silyl methyl groups of **8** possibly contribute to the scissoring observed in this compound. Thus, as the ring tilt in these species decreases with methyl substitution of the Cp rings, strain is manifested by increasing structural distortion about the bridging group.

In addition to distortions of the bridging group, other structural features of these ferrocenophanes smoothly vary with increased methyl substitution and reduced ring tilt. For example, as ring tilt decreases, the angle δ between the Cp ring centroids and the iron atom increases from 164.74(8)° in **1** to 168.6(1)° in **8**. Furthermore, as δ increases, the displacement of the iron atom from the line joining the two Cp ring centroids decreases. A similar increase of δ is observed for titanocene dichlorides, where δ increases from 131.0° in $(C_5H_5)_2TiCl_2$ to 137.4(1)° in $(C_5Me_5)_2TiCl_2$.[46,47] The increase in δ with increasing methyl substitution observed in the titanocene dichlorides has been attributed to inter-ring methyl−methyl contacts.[47]

One of the most intriguing consequences of increasing methyl substitution involves the Fe−Si distance. As methyl substitution increases, the Fe−Si distance is reduced from 2.690(3) Å in **1** to 2.6767(8) Å in **4a** to 2.652(1) Å in **8**, possibly in response to the reduced ring tilt which accompanies increasing methylation. While all of these Fe−Si distances are greater than the sum of the covalent radii (2.37 Å) and greater than representative Fe−Si bond lengths (2.30−2.36 Å), the decreasing Fe−Si distance may result in increased Fe- - -Si dative interactions (See Mössbauer section) on the basis of work by Silver.[48]

4. Electronic Properties of Methylated Ferrocenophanes. We have probed the electronic effect of the methyl substituents of **4a**, **6**, and **8** via cyclic voltammetry, UV/vis analysis, and Mössbauer spectroscopic analysis. The use of the nonmethylated ferrocenophane **1** as a reference compound in these studies proved instructive.

(a) Cyclic Voltammetric Analysis of Methylated Ferrocenophanes. The methylated ferrocenophanes **4a**, **6**, and **8** were studied by cyclic voltammetry in order to determine if the transmission of electronic effects or the reversibility of the ferrocene/ferrocenium couple would be significantly disrupted as a consequence of their strained, ring-tilted structures. The nonmethylated ferrocenophane **1** was included in this study as a logical reference compound. We are aware of only one previous voltammetric study of [*n*]metallocenophanes which probes transmission of electronic effects from the

(46) Petersen, J. L.; Dahl, L. F. *J. Am. Chem. Soc.* **1975**, *97*, 6422−6433.
(47) McKenzie, T. C.; Sanner, R. D.; Bercaw, J. E. *J. Organomet. Chem.* **1975**, *102*, 457−466.
(48) Silver, J. *J. Chem. Soc., Dalton Trans.* **1990**, 3513−3516.

Table 3. Selected Bond Lengths (Å) and Angles (deg) for 4a

		Distances			
Fe–Si	2.6767(8)	Fe–C9	2.068(3)	C4–C5	1.433(3)
Fe–C1	2.009(2)	Fe–C10	2.101(3)	C1–C5	1.454(4)
Fe–C2	2.019(2)	Si–C1	1.887(3)	C4–C13	1.488(4)
Fe–C3	2.075(3)	Si–C6	1.881(3)	C6–C7	1.454(4)
Fe–C4	2.081(3)	Si–C11	1.859(3)	C7–C8	1.418(4)
Fe–C5	2.015(3)	Si–C12	1.850(3)	C8–C9	1.426(4)
Fe–C6	2.006(3)	C1–C2	1.448(3)	C9–C10	1.419(4)
Fe–C7	2.026(3)	C2–C3	1.422(4)	C6–C10	1.439(4)
Fe–C8	2.061(3)	C3–C4	1.422(4)	C9–C14	1.497(4)
		Angles			
C1–Si–C6	96.96(11)	C7–C8–C9	108.7(3)	C5–C1–Si	117.3(2)
C12–Si–C6	111.7(2)	C8–C9–C10	106.3(3)	C3–C4–C13	126.4(3)
C11–Si–C6	111.65(14)	C9–C10–C6	111.5(3)	C5–C4–C13	126.6(3)
C10–C6–Si	119.7(2)	C10–C6–C7	104.0(3)	C1–C2–C3	109.8(2)
C7–C6–Si	118.5(2)	C12–Si–C11	112.3(2)	C2–C3–C4	108.6(2)
C10–C9–C14	125.7(3)	C12–Si–C1	109.9(2)	C3–C4–C5	106.9(2)
C8–C9–C14	128.0(3)	C11–Si–C1	113.42(14)	C4–C5–C1	110.2(2)
C6–C7–C8	109.5(2)	C2–C1–Si	119.9(2)	C5–C1–C2	104.4(2)

Table 4. Final Fractional Coordinates and Thermal Parameters for the Non-Hydrogen Atoms of 8

atom	*x*	*y*	*z*	*U*(eq)
Fe	0.31549(2)	0.02769(3)	0.38367(1)	0.01790(8)
Si	0.16556(3)	0.06214(6)	0.32166(2)	0.02206(16)
C1	0.2551(1)	−0.0751(2)	0.3194(1)	0.021(1)
C2	0.3392(1)	−0.0209(2)	0.3096(1)	0.021(1)
C3	0.4053(1)	−0.0830(2)	0.3471(1)	0.023(1)
C4	0.3663(1)	−0.1803(2)	0.3800(1)	0.023(1)
C5	0.2750(1)	−0.1782(2)	0.3629(1)	0.022(1)
C6	0.2176(1)	0.1698(2)	0.3821(1)	0.022(1)
C7	0.2981(1)	0.2471(2)	0.3790(1)	0.023(1)
C8	0.3594(1)	0.2134(2)	0.4248(1)	0.022(1)
C9	0.3183(1)	0.1193(2)	0.4578(1)	0.023(1)
C10	0.2321(1)	0.0950(2)	0.4329(1)	0.023(1)
C11	0.3570(2)	0.0735(3)	0.2465(1)	0.027(1)
C12	0.5007(2)	−0.0581(3)	0.3493(1)	0.034(1)
C13	0.4132(2)	−0.2755(3)	0.4223(1)	0.033(1)
C14	0.2130(2)	−0.2776(3)	0.3845(1)	0.031(1)
C15	0.3154(2)	0.3550(3)	0.3378(1)	0.027(1)
C16	0.4996(1)	0.2702(3)	0.4364(1)	0.030(1)
C17	0.3571(2)	0.0630(3)	0.5113(1)	0.031(1)
C18	0.1666(2)	0.0159(3)	0.4596(1)	0.033(1)
C19	0.1382(1)	0.1684(3)	0.2595(1)	0.028(1)
C20	0.0604(2)	−0.0243(3)	0.3301(1)	0.036(1)

Table 5. Selected Bond Lenghts (Å) and Angles (deg) for 8

		Distances			
Fe–Si	2.652(1)	C1–C2	1.467(3)	Si–C6	1.913(2)
Fe–C1	2.008(2)	C2–C3	1.424(3)	Si–C19	1.862(2)
Fe–C2	2.038(2)	C3–C4	1.428(3)	Si–C20	1.872(3)
Fe–C3	2.072(2)	C4–C5	1.433(3)	C2–C11	1.504(3)
Fe–C4	2.079(2)	C5–C1	1.460(3)	C3–C12	1.506(3)
Fe–C5	2.042(2)	C6–C7	1.461(3)	C4–C13	1.497(3)
Fe–C6	2.012(2)	C7–C8	1.433(3)	C5–C14	1.500(3)
Fe–C7	2.036(2)	C8–C9	1.429(3)	C7–C15	1.504(3)
Fe–C8	2.069(2)	C9–C10	1.424(3)	C8–C16	1.496(3)
Fe–C9	2.071(2)	C10–C6	1.459(3)	C9–C17	1.505(3)
Fe–C10	2.044(2)	Si–C1	1.895(2)	C10–C18	1.505(3)
		Angles			
C1–Si–C6	98.1(1)	C1–C2–C11	127.1(2)	C9–C8–C16	126.2(2)
C1–C2–C3	109.3(2)	C3–C2–C11	123.4(2)	C8–C9–C17	126.2(2)
C2–C3–C4	108.5(2)	C2–C3–C12	125.6(2)	C10–C9–C17	125.5(2)
C3–C4–C5	107.9(2)	C4–C3–C12	125.8(2)	C9–C10–C18	122.7(2)
C4–C5–C1	109.4(2)	C3–C4–C13	125.8(2)	C6–C10–C18	127.4(2)
C5–C1–C2	104.9(2)	C5–C4–C13	126.1(2)	C1–Si–C19	113.5(1)
C6–C7–C8	109.3(2)	C4–C5–C14	123.5(2)	C1–Si–C20	113.0(1)
C7–C8–C9	107.9(2)	C1–C5–C14	127.0(2)	C6–Si–C19	115.8(1)
C8–C9–C10	108.2(2)	C6–C7–C15	127.4(2)	C6–Si–C20	113.7(1)
C9–C10–C6	109.6(2)	C8–C7–C15	123.1(2)	C19–Si–C20	103.2(1)
C10–C6–C7	104.9(2)	C7–C8–C16	125.9(2)		

Cp substituents to the metal center rather than focusing on electronic effects associated with the bridging group.[30] Furthermore, we are aware of only two cases in which the cyclic voltammetric behavior of silicon-bridged [1]-ferrocenophanes has been investigated.[49,50] Under the conditions of these studies, $Fe(\eta\text{-}C_5H_4)_2SiMeFc$[16] (Fc = $Fe(\eta\text{-}C_5H_4)(\eta\text{-}C_5H_5)$) was shown to undergo reversible oxidation while oxidation of **1** was reported to be irreversible.

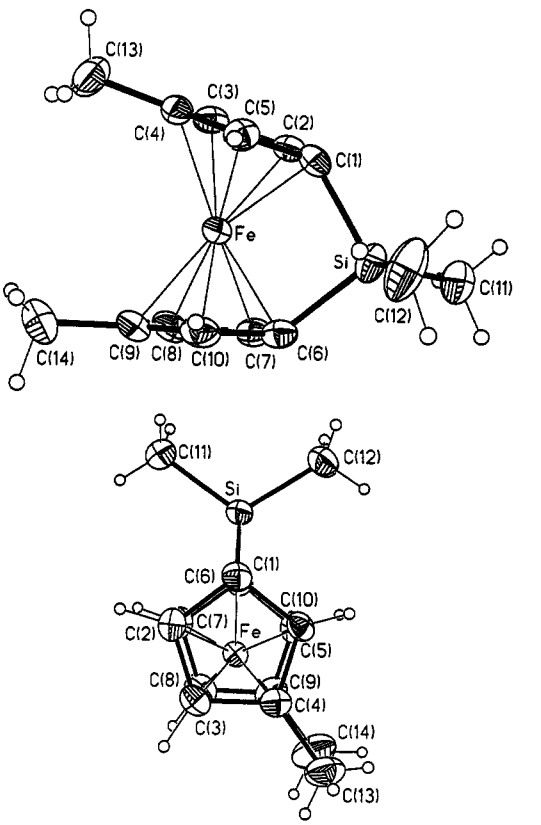

Figure 1. ORTEP views (with thermal ellipsoids drawn at the 50% probability level) and crystallographic numbering scheme for **4a**.

Cyclic voltammetric analysis of silicon-bridged [1]-ferrocenophanes is complicated by the sensitivity of these compounds to moisture or other nucleophilic species. Great care was therefore taken during the analyses to exclude such impurities (see Experimental Section). Figure 4 shows the cyclic voltammograms obtained from analyses of 5×10^{-3} M methylene chloride solutions of **1**, **4a**, **6**, and **8** which were 0.1 M

(49) Dement'ev, V. V.; Cervantes-Lee, F.; Parkanyi, L.; Sharma, H.; Pannell, K. H. *Organometallics* **1993**, *12*, 1983–1987.
(50) Pannell, K. H.; Dementiev, V. V.; Li, H.; Cervantes-Lee, F.; Nguyen, M. T.; Diaz, A. F. *Organometallics* **1994**, *13*, 3644–3650.

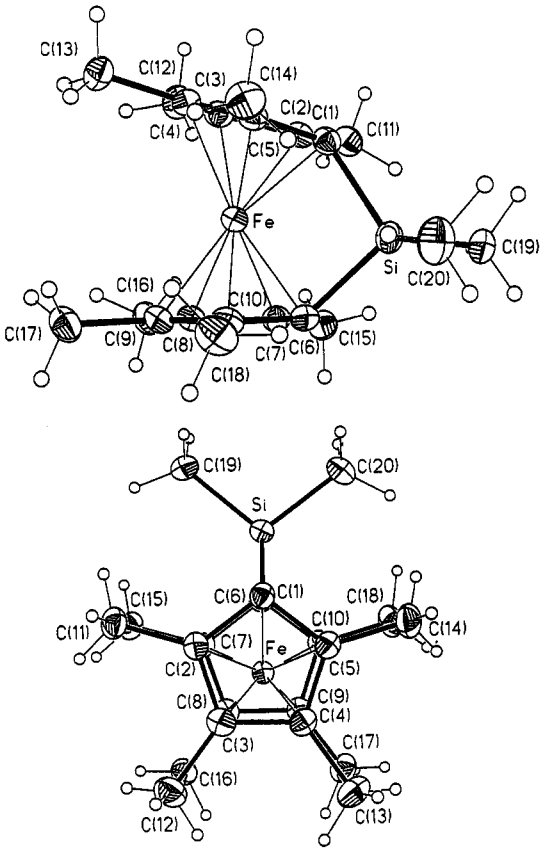

Figure 2. ORTEP views (with thermal ellipsoids drawn at the 50% probability level) and crystallographic numbering scheme for **8**.

Table 6. Summary of Critical Structural Data for Ferrocenophanes 1, 4a, and 8

	1	4a	8
ring tilt, α (deg)	20.8(5)	18.6(3)	16.1(3)
Cp–Si/Cp, β (deg)	37.0(6)	39.1(2)	40.3(2)
Si–C1 (Å)	1.851(9)	1.887(3)	1.895(2)
Si–C6 (Å)	1.865(9)	1.881(3)	1.913(2)
C1–Si–C6, θ (deg)	95.7(4)	96.96(11)	98.1(1)
C11–Si–C12 (deg)[a]	114.8(6)	112.3(2)	103.2(1)[a]
RC1–Fe–RC2, δ (deg)	164.74(8)	166.5(1)	168.6(1)
Fe displacement (Å)[b]	0.2164(11)	0.192(2)	0.164(2)
Fe---Si (Å)	2.690(3)	2.6767(8)	2.652(1)

[a] This angle is C19–Si–C20 in **8**. [b] The displacement of the Fe atom from the line that joins the cyclopentadienyl ring centroids.

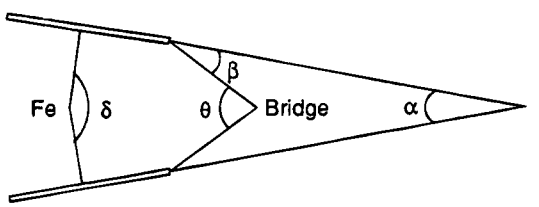

Figure 3. Important structural angles in silicon-bridged [1]ferrocenophanes.

in $[Bu_4N][PF_6]$. The voltammograms were obtained at room temperature with a scan rate of 250 mV/s and are referenced to the ferrocene/ferrocenium ion couple at 0.0 V. Additionally, Table 7 lists I_{red}/I_{ox} ratios as a function of scan rate for ferrocenophanes **1**, **4a**, **6**, and **8** and includes data for ferrocene which was obtained under identical experimental conditions.

A notable feature of these ferrocenophane cyclic voltammograms is the expected shift to more negative

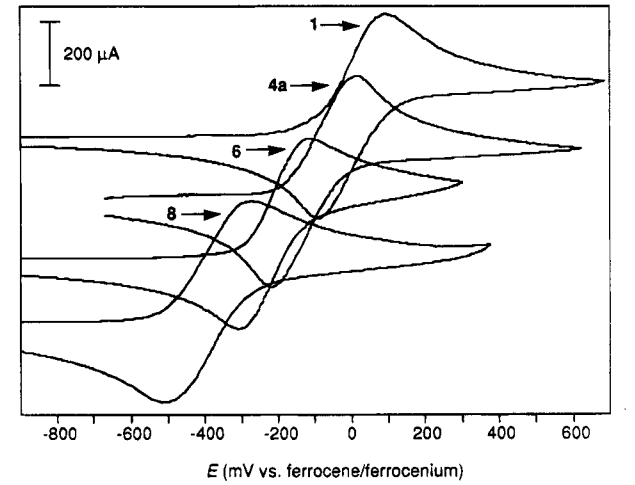

Figure 4. Cyclic voltammograms of methylene chloride solutions of **1**, **4a**, **6**, and **8** obtained at a scan rate of 250 mV/s and referenced to the ferrocene/ferrocenium ion couple at $E = 0.0$ V.

Table 7. I_{red}/I_{ox} Data from Cyclic Voltammetric Analysis of 1, 4a, 6, and 8

	I_{red}/I_{ox}[a]				
scan rate (mV/s)	ferrocene	1	4a	6	8
25	0.75	0.74	0.74	0.72	0.76
50	0.80	0.81	0.90	0.81	0.91
100	0.86	0.93	0.97	0.90	0.95
250	0.96	0.98	1.04	1.00	1.01
500	0.98	0.98	1.05	1.03	1.05
1000	1.00	0.98	1.06	1.02	1.05

[a] Bard, A. J.; Faulkner, L. R. *Electrochemical Methods*; Wiley: New York, 1980; p 229.

oxidation potentials with increasing methylation of the Cp rings. Gassman has reported that methyl substituents reduce the oxidation potential of substituted ferrocene derivatives by 55 mV per methyl group.[27] Half-wave oxidation potentials of 0.00, −0.10, −0.21, and −0.39 V vs the ferrocene/ferrocenium ion couple were found for **1**, **4a**, **6**, and **8**, respectively, at a scan rate of 250 mV/s. These values indicate that the methyl groups in **4a**, **6**, and **8** reduce the oxidation potential of these ferrocenophanes by ca. 50 mV per methyl group, close to the expected value. Thus, the electron-donating effect of the methyl substituents in these ferrocenophanes is effectively transmitted to the iron centers despite the distorted, ring-tilted structures.

A second notable feature of the voltammograms is the reversible nature of the redox couple exhibited by each ferrocenophane. It might be anticipated that monoatom-bridged [1]ferrocenophanes would exhibit nonreversible redox behavior due to the inability of the single-atom bridge to incorporate the slightly expanded Fe–Cp distances (ca 0.04 Å) which accompany oxidation.[49,50] Moreover, Watts and co-workers have noted that ring tilting leaves the metal centers of ferrocenophanes in a more accessible environment relative to nonbridged ferrocene derivatives.[51] This accessibility, which might be increased upon oxidation, could leave the corresponding electron-deficient ferrocenium metal centers extremely vulnerable to processes such as attack by solvent or electrolyte.[52] These factors clearly do not

(51) Gorton, J. E.; Lentzner, H. L.; Watts, W. E. *Tetrahedron* **1971**, *27*, 4353–4360.

Table 8. UV/vis Data for Methylated Ferrocenes and Ferrocenophanes

compd	solvent	λ_{max} band II (nm)	ϵ band II ($L \cdot mol^{-1} \cdot cm^{-1}$)
$Fe(\eta\text{-}C_5H_5)_2$	THF	440	99
$Fe(\eta\text{-}C_5H_4Me)_2$	THF	438	161
$Fe(\eta\text{-}C_5H_5)(\eta\text{-}C_5Me_5)$[a]	isooctane	430	120
$Fe(\eta\text{-}C_5HMe_4)_2$	THF	430	156
$Fe(\eta\text{-}C_5Me_5)_2$[b]	cyclohexane	420	120
1	THF	482	375
4a	THF	476	372
6	THF	473	337
8	THF	464	233

[a] Chao, S.; Robbins, J. L.; Wrighton, M. S. *J. Am. Chem. Soc.* **1983**, *105*, 181. [b] King, R. B.; Bisnette, M. B. *J. Organomet. Chem.* **1967**, *8*, 287.

have a dramatic influence on stability, as we have found the oxidations of **1**, **4a**, **6**, and **8** to be reversible. Indeed, as the data in Table 7 indicate, the ferrocenophane ferrocenium species appear to be as stable as ferrocenium itself under the conditions of our study.[53,54]

(b) UV/vis Analysis of Methylated Ferrocenophanes. The UV/vis spectroscopy of ferrocene and its derivatives has been studied extensively.[55] Briefly, six bands are found in the spectra of these compounds, and much attention has been focused on bands III and II found at *ca.* 330 and 440 nm, respectively.[56] These bands have been assigned to spin-allowed d−d transitions. Our UV/vis study of ferrocenophanes **1**, **4a**, **6**, and **8** focused only on visible absorption band II since band III appeared as a poorly resolved shoulder on an intense, higher energy band in the spectra of these compounds. The primary objectives of our study were to determine the effect on band II of methyl substitution among **1**, **4a**, **6**, and **8** and to compare the spectra of these ferrocenophanes with the spectra of electronically similar, nonbridged ferrocene derivatives obtained under identical conditions. Listed in Table 8 are UV/vis data for a number of methylated ferrocenes. Although care must be taken when assessing these data due to the variance of solvent, entries 1−5 reveal that increasing methyl substitution of ferrocene results in a blue shift of band II with an accompanying modest increase in extinction coefficient.

Table 8 also contains band II UV/vis data obtained from analysis of THF solutions of ferrocenophanes **1**, **4a**, **6**, and **8**. Significantly, as was observed for the series of methylated ferrocenes, a blue shift of band II was found upon increasing methyl substitution of the ferrocenophanes. These results suggest that methyl substitution exerts similar electronic effects in the ferrocene and ferrocenophane systems despite the ring-tilted structures of the latter. In the ferrocenophane series, increased methyl substitution (and decreased ring tilt) was accompanied by a decrease in the band II extinction coefficient. Barr and Watts also observed a decrease in band II intensity with decreasing ring tilt in their UV/vis studies of alkyl-bridged ferrocenophanes.[57]

Table 9. Room-Temperature Mössbauer Data for Selected Ferrocenes and Silicon-Bridged [1]Ferrocenophanes

compd	δ (mm s^{-1})	ΔE_q (mm s^{-1})	T (K)	Fe---Si (Å)
$Fe(\eta\text{-}C_5H_5)_2$[a]	0.44	2.37	295	
1	0.38	1.92	298	2.690(3)
$Fe(\eta\text{-}C_5HMe_4)_2$[b]	0.44	2.51	293	
8	0.36	1.85	298	2.652(1)

[a] See ref 38. [b] See ref 26.

Comparison of the ferrocenophane band II data with the data obtained from analysis of nonbridged, electronically similar ferrocenes proves revealing. Relative to the analogous nonbridged models, band II of the ferrocenophanes shows a substantial red shift. This shift is not very likely to be due to the electronic effect of the dimethylsilyl bridging groups, but is more likely to result from the ring-tilted structure of these compounds.[57] Further, the red shift of band II of the ferrocenophanes is accompanied by an increase in band intensity relative to the nonbridged models. A similar ferrocenophane red shift and intensity increase of band II was observed by Barr and Watts for the hydrocarbon-bridged [2]ferrocenophane $Fe(\eta\text{-}C_5H_4)_2(CMe_2)_2$ compared to the nonbridged model 1,1′-diisopropylferrocene.[57] It should also be noted that these workers found insignificant differences between the band II data for the [4]-ferrocenophane $Fe(\eta\text{-}C_5H_4)_2(CH_2)_4$ and the analogous nonbridged model 1,1′-diethylferrocene, presumably due to the unstrained nature of the former compound which does not suffer significant ring tilt.

(c) Mössbauer Spectra of Nonmethylated and Methylated Ferrocenophanes. A Mössbauer study of ferrocenophanes **1** and **8** was undertaken in order to probe the changes in the electronic environment at the iron nucleus that would be expected to occur with increasing methyl substitution of the cyclopentadienyl rings. The Mössbauer data for these ferrocenophanes along with the previously reported data for nonbridged analogs octamethylferrocene[26] and ferrocene[38] are compiled in Table 9.

Comparison of the room-temperature Mössbauer data reveals that, while ferrocene and octamethylferrocene show identical δ shift values, a substantially larger quadrupolar splitting (ΔE_q) value is observed for octamethylferrocene. It is believed that changes in ΔE_q are governed by the relative populations of the essentially nonbonding Fe 3d orbitals with e_2 (back-bonding) and e_1 (forward donation) symmetry.[48,58] Silver has noted that increased ΔE_q values for ferrocenes containing donor substituents are primarily due to reduction in the back-bonding component in these species.[59]

The room-temperature Mössbauer spectra for ferrocenophanes **1** and **8** show significant differences in both the δ and ΔE_q values compared to the nonbridged ferrocenes. While the δ shifts of the ferrocenophanes

(52) Churchill, M. R.; Landers, A. G.; Rheingold, A. L. *Inorg. Chem.* **1981**, *20*, 849−853.

(53) It is instructive to note that, contrary to popular belief, the ferrocene/ferrocenium couple does not exhibit perfect chemical or electrochemical reversibility. For example, see: Connelly, N. G.; Geiger, W. E. *Adv. Organomet. Chem.* **1984**, *23*, 1−93 and references cited therein.

(54) We thank a reviewer for calling to our attention the fact that I_{red}/I_{ox} ratios are usually less than unity at slow scan rates (<*ca.* 100 mV/s) due to convective mixing of the solution.

(55) Sohn, Y. S.; Hendrickson, D. N.; Gray, H. B. *J. Am. Chem. Soc.* **1971**, *93*, 3603.

(56) The UV/vis band II system of ferrocene has been shown to consist of two spin-allowed d−d transitions. See ref 55 and references cited therein.

(57) Barr, T. H.; Watts, W. E. *J. Organomet. Chem.* **1968**, *15*, 177−185.

(58) Clemance, M.; Roberts, R. M. G.; Silver, J. *J. Organomet. Chem.* **1983**, *243*, 461−467.

(59) Houlton, A.; Miller, J. R.; Roberts, R. M. G.; Silver, J. *J. Chem. Soc., Dalton Trans.* **1990**, 2181−2184.

are similar, both values are smaller than values reported for the analogous nonbridged ferrocenes, suggesting that there may be significant back-bonding from the Fe center to the silicon bridge.[48] Much more distinctive in the ferrocenophane Mössbauer spectra are the small ΔE_q values relative to the nonbridged ferrocenes. The presence of a weak dative interaction between the Fe and Si atoms in these species, as Silver concluded from studies of silicon- and germanium-bridged [1]ferrocenophanes, would cause substantial changes in the electron populations of the metal-centered orbitals of e_2 symmetry, causing smaller ΔE_q values.[48,58] The slightly smaller ΔE_q value observed for fully methylated **8**, relative to nonmethylated **1**, was unexpected on the basis of trends observed for nonbridged ferrocenes,[59] particularly since our cyclic voltammetry and UV/vis studies showed that communication of the methyl group electronic effect in the ferrocenophanes was identical to that in nonbridged models. A possible explanation for this unexpected ΔE_q trend lies in the crystallographic finding of a smaller Fe−Si distance and thus a stronger Fe- - -Si interaction for **8** relative to **1**. Our data are therefore consistent with Silver's suggestion that the smaller ΔE_q values result from dative Fe- - -Si interactions.[48,58]

While the increased Fe- - -Si interaction may be due to shorter Fe−Si distances which result from reduced ring tilt vis-à-vis bonding and steric arguments, it is possible that the increase in electron density at iron which results from increasing Cp methylation strengthens the Fe- - -Si interaction. Thus, although steric and bonding arguments can be used to explain the reduction in ferrocenophane ring tilt which is observed with increased methylation, we cannot rule out the interesting possibility that stronger Fe- - -Si interactions contribute to the reduction in ring tilt.

Summary

We have demonstrated two synthetic routes to strained, silicon-bridged [1]ferrocenophanes with methylated Cp rings. Increasing methylation of the Cp rings leads to interesting structural changes in the ferrocenophanes including decreased ring tilt, increased angles between the Cp ring planes and the exocyclic Cp−Si bonds, and decreased Fe−Si distances. Analysis of the ferrocenophanes **1**, **4a**, **6**, and **8** by cyclic voltammetry and UV/vis indicates that communication of the electron-donating effect of the methyl Cp substituents to the Fe centers is completely unhindered despite the structural distortion. In addition, electrochemical oxidation of these ferrocenophanes was found to be reversible, nearly identical to the response of ferrocene under the same conditions. The results of Mössbauer spectroscopic studies of the octamethylated species **8** are consistent with the presence of a weak dative Fe−Si interaction which is more substantial than that in **1**. Studies of the ROP reactions of these methylated ferrocenophanes are in progress, and results will be reported in due course.

Experimental Section

All reactions were performed under an inert atmosphere (prepurified N_2) using either standard Schlenk techniques or a Vacuum Atmospheres glovebox. THF and TMEDA were distilled from Na/benzophenone immediately prior to use. Hexanes were distilled from Na immediately prior to use. Me_2SiCl_2 was distilled immediately prior to use. Octamethylferrocene,[60] $Li_2[(C_5Me_4)(C_5H_4)Si(CH_3)_2]$, $Li_2[(C_5Me_4)_2Si(CH_3)_2]$,[42,43] and ferrocenophane **1**[35,36,40] were prepared according to literature procedures. Ferrocene, 1,1′-dimethylferrocene, $FeCl_2$, TMEDA, and BuLi (1.6 M in hexanes) were obtained from Aldrich Chemical Co.

Melting points were obtained with a Perkin Elmer DSC 7 differential scanning calorimeter under N_2. ^1H NMR spectra were recorded on a Varian Gemini 200 instrument and were referenced to residual protonated C_6D_6 at 7.15 ppm. ^{13}C NMR spectra were recorded on either Varian Gemini 200 or Varian Gemini 400 XL instruments and were referenced to C_6D_6 at 128.0 ppm. ^{29}Si NMR spectra were recorded on a Varian Gemini 400 instrument utilizing a proton-decoupled DEPT pulse sequence and were referenced externally to TMS. Mass spectra were obtained with the use of a VG 70-250S instrument operating in electron impact (EI) mode. UV/vis spectra were recorded in anhydrous THF on a Hewlett-Packard 6452A diode array instrument using a 1-cm cell. Elemental analyses were performed by Quantitative Technologies Inc., Whitehouse, NJ.

Room-temperature ^{57}Fe Mössbauer spectra were obtained using a Ranger Scientific Inc. Vt-1200 instrument with a MS-1200 digital channel analyzer. The γ-ray source was a 6-mCi ^{57}Co sample supplied by Amersham. The data were collected in a −15.8 to +15.8 mm s^{-1} range and referenced to Fe foil.

Cyclic voltammograms were recorded with a PAR model 273 potentiostat. A Pt working electrode was used in conjunction with a W auxiliary electrode and a Ag wire reference electrode in a Luggin capillary. All potentials are relative to the ferrocene/ferrocenium ion couple at 0.00 V, which was used as an internal reference. Methylene chloride solvent was freshly distilled from P_2O_5, anhydrous grade $[Bu_4N][PF_6]$ electrolyte (Aldrich) from a freshly opened bottle was used, and the analyses were carried out under argon after rigorous deoxygenation of the analyte solutions.

X-ray Structural Determinations of 4a and 8. Intensity data for both compounds were collected on a Siemens P4 diffractometer, using graphite-monochromated Mo Kα radiation (λ = 0.710 73 Å) with ω scans. In each case the intensities of three standard reflections measured every 97 reflections showed no decay. Data were corrected for Lorentz and polarization effects and for absorption. The absorption corrections for both **4a** and **8** were carried out using the SHELXA-90 routine in SHELXL.[61] The structures were solved by direct methods. All non-hydrogen atoms were refined with anisotropic thermal parameters. For both structures the hydrogen atoms were located from difference Fourier maps and refined with isotropic thermal parameters. Crystal data, data collection, and least squares parameters are listed in Table 1. All calculations were performed and all diagrams were created using SHELXTL PC[62] and SHELXL-93[61] on a 486-66 personal computer. The structures of **4a** and **8**, including the crystallographic labeling schemes, are shown in Figures 1 and 3.

Fe(η-$C_5H_3Me)_2SiMe_2$ (4). A solution of 6.68 g (31.2 mmol) of 1,1′-dimethylferrocene in 300 mL of hexanes was treated with a solution of 10.0 mL (7.70 g, 66.3 mmol) of TMEDA in 40.5 mL (1.6 M, 64.8 mmol) of a hexanes solution of BuLi at room temperature. The resulting mixture was stirred at room temperature for 42 h, cooled to −78 °C, and treated dropwise with 4.2 mL (35 mmol) of Me_2SiCl_2. After stirring at −78 °C for 15 min the resulting mixture was allowed to warm to room temperature and was filtered. The filtrate was concentrated in vacuo, and the resulting red liquid was distilled under

(60) Schmitt, V. G.; Ozman, S. *Chem. Ztg.* **1976**, *100*, 143.
(61) Sheldrick, G. M. *SHELXL-93, Program for the Refinement of Crystal Structures*; University of Göttingen: Göttingen, Germany, 1994.
(62) Sheldrick, G. M. *SHELXTL-PC*; Siemens Analytical X-ray Instruments Inc.: Madison, WI, 1990.

reduced pressure to afford 5.0 g (59%) of isomer mixture **4** as a viscous red oil: bp 35–40 °C (0.01 mmHg). The red oil was taken up in *ca.* 20 mL of hexanes and cooled to −30 °C, resulting in deposition of a red crystalline solid. The liquid was decanted, and the solid was recrystallized from hexanes at −30 °C to afford 0.24 g (3%) of 3,3′-syn isomer **4a** as a red crystalline solid: mp (DSC) 113 °C; ^{1}H NMR (200.0 MHz, C_6D_6) δ 4.39 (t, J = 2 Hz, 2H, Cp), 3.82–3.80 (m, 4H, Cp), 1.76 (s, 6H, CpCH_3), 0.39 (s, 3H, SiCH_3), 0.34 (s, 3H, SiCH_3); ^{13}C NMR (100.6 MHz, C_6D_6) δ 92.9 (*Cp*CH_3), 79.4, 76.8, 74.8 (*Cp*H), 32.2 (Cp ipso), 13.0 (CpCH_3), −2.9 (SiCH_3), −3.3 (SiCH_3); ^{29}Si NMR (79.5 MHz, C_6D_6) δ −4.5; HRMS calcd for $C_{14}H_{18}{}^{56}$FeSi 270.0527, found 270.0521. Anal. Calcd for $C_{14}H_{18}$FeSi: C, 62.23; H, 6.71. Found: C, 61.73; H, 6.78.

Fe(η-C_5Me_4)(η-C_5H_4)$SiMe_2$ (6). A slurry of 1.04 g (4.06 mmol) of Li_2[(C_5Me_4)(C_5H_4)$SiMe_2$] in 50 mL of THF was added to a slurry of 0.52 g (4.10 mmol) of $FeCl_2$ in 50 mL of THF at room temperature. The resulting mixture was stirred at room temperature for 4 h and then concentrated in vacuo, affording an oily, red residue, which was taken up in 50 mL of hexanes and filtered. The filtrate was concentrated in vacuo to give a red solid, which was sublimed at 60–90 °C (0.01 mmHg) to afford 0.32 g (27%) of **6** as a red crystalline solid: mp 131 °C (DSC); ^{1}H NMR (200.0 MHz, C_6D_6) δ 4.30 (pt, J = 2 Hz, 2H, Cp), 3.41 (pt, J = 2 Hz, 2H, Cp), 1.83 (s, 6H, CpCH_3), 1.80 (s, 6H, CpCH_3), 0.59 (s, 6H, SiCH_3); ^{13}C NMR (50.3 MHz, C_6D_6) δ 90.9, 88.3 (*Cp*Me), 80.8, 78.4 (*Cp*H), 33.5 (*Cp*Me ipso), 27.5 (*Cp*H ipso), 14.2 (CpCH_3), 12.1 (CpCH_3), 1.3 (SiCH_3); ^{29}Si NMR (79.5 MHz, C_6D_6) δ −3.10; HRMS calcd for $C_{16}H_{22}{}^{56}$FeSi 298.0840, found 298.0839. Anal. Calcd for $C_{16}H_{22}$FeSi: C, 64.43; H, 7.43. Found: C, 64.51; H, 7.57.

The material which remained after sublimation was dissolved in THF and precipitated by addition to methanol. Filtration followed by drying in vacuo afforded 0.45 g (37 %) of **9** as a powdery, orange solid: ^{1}H NMR (200.0 MHz, C_6D_6) δ 4.34–3.71 (br m, Cp), 1.93–1.57 (br m, CpCH_3), 0.80 (br s, SiCH_3); ^{29}Si NMR (79.5 MHz, C_6D_6) δ −6.1 to −6.8; MS (EI) 1789 (0.4, (n = 6) + 1), 1491 (1.5, (n = 5) + 1), 1192 (6.9, n = 4), 894 (23.8, n = 3), 596 (100, n = 2), 298 (41, n = 1); GPC (in THF vs polystyrene standards) M_w = 1550, M_n = 1270, PDI = 1.2.

Fe(η-C_5Me_4)$_2SiMe_2$ (8). A slurry of 1.06 g (3.39 mmol) of Li_2[(C_5Me_4)$_2SiMe_2$] in 25 mL of THF was treated dropwise at room temperature with a slurry of 0.50 g (4.0 mmol) of $FeCl_2$ in 25 mL of THF. The resulting mixture was stirred at room temperature for 6 h and then concentrated in vacuo to afford a red-brown residue, which was taken up in 60 mL of hexanes and filtered. The filtrate was concentrated in vacuo, yielding a red-brown solid, which was sublimed at 80–95 °C (0.01 mmHg) to afford 0.55 g (46%) of **8** as an orange crystalline solid: mp (DSC) 156 °C; ^{1}H NMR (200.0 MHz, C_6D_6) δ 1.68 (s, 12H, CpCH_3), 1.59 (s, 12H, CpCH_3), 0.65 (s, 6H, SiCH_3); ^{13}C NMR (100.6 MHz, C_6D_6) δ 90.2, 89.2 (Cp), 25.6 (Cp ipso), 12.3, 10.4 (CpCH_3), 4.1 (SiCH_3); ^{29}Si NMR (79.5 MHz, C_6D_6) δ −4.8; HRMS calcd for $C_{20}H_{30}{}^{56}$FeSi 354.1466, found 354.1459. Anal. Calcd for $C_{20}H_{30}$FeSi: C, 67.78; H, 8.53. Found: C, 67.55; H, 8.63.

Acknowledgment. We thank Dr. Jenny Green for helpful discussions. D.O'H. would like to acknowledge EPSRC for financial support and a studentship (S.B.). I.M. thanks NSERC and the Petroleum Research Fund (PRF) administered by the American Chemical Society for funding and the Alfred P. Sloan Foundation for a research fellowship (1994–1996).

OM9409581

Neutral Rhodium(I) Aminophosphine–Phosphinite Complexes: Synthesis, Structure, and Use in Catalytic Asymmetric Hydrogenation of Activated Keto Compounds. Crystal Structure of [(*S*)-1-(Dicyclohexylphosphino)-2-(((dicyclohexylphosphino)oxy)methyl)pyrrolidine](2,4-pentanedionato-*O*,*O*′)rhodium(I)

Francine Agbossou, Jean-François Carpentier,* Corinne Hatat, Nicolas Kokel, and André Mortreux*

Laboratoire de Catalyse Hétérogène et Homogène, Groupe de Chimie Organique Appliquée, URA CNRS 402, Ecole Nationale Supérieure de Chimie de Lille, B.P. 108, 59652 Villeneuve d'Ascq Cedex, France

Peter Betz, Richard Goddard, and Carl Krüger

Max-Planck-Institut für Kohlenforschung, Röntgenlaboratorium, D-45470 Mülheim/Ruhr, Germany

Received December 29, 1994[⊗]

Aminophosphine–phosphinite ligands (AMPP) derived from (*S*)-2-(hydroxymethyl)pyrrolidine ((*S*)-R,R′-ProNOP; **1a–c**, **5a–f** (R, R′ = cyclohexyl, cyclopentyl, 2-propyl, phenyl)) and (*S*)-1-(methylamino)-2-propanol ((*S*)-R,R′-isoAlaNOP; **2a,b**, **6a–c** (R, R′ = cyclohexyl, cyclopentyl, phenyl)) have been prepared in high yields and reacted with rhodium precursors to prepare neutral AMPP–rhodium(I) complexes **7–10** of the general formula $[RhX(AMPP)]_n$, where X = Cl, $n = 2$ or X = acac, η^5-C_5H_5, $n = 1$. The crystal structure of [Rh(acac){(*S*)-Cy,Cy-ProNOP}] ((*S*)-**10**) has been determined. The compound crystallizes in the triclinic space group $P1$ with $a = 11.459(3)$ Å, $b = 15.980(4)$ Å, $c = 21.684(7)$ Å, $\alpha = 75.17(2)°$, $\beta = 81.73(2)°$, $\gamma = 69.15(2)°$, and $Z = 4$. The rhodium atom has a *cis* square-planar coordination, and the seven-membered metallacycle is in a distorted λ boat-type conformation with the nitrogen atom in the mean plane RhP_2. Complexes **7–10** have been used as catalyst precursors for the asymmetric hydrogenation of dihydro-4,4-dimethyl-2,3-furandione and *N*-benzylbenzoylformamide, giving the corresponding hydrogenated products in excellent yields and with fair to good enantiomeric excess (20–89% and 39–88% ee, respectively). Catalytic activities (TOF at 50% conversion at room temperature up to 850 and 1500 h^{-1}, respectively) as well as enantioselectivities depended strongly on the nature of the substituents at the phosphorus atoms. The dinuclear chlororhodium complex of (*S*)-Cp,Cp-isoAlaNOP afforded (*S*)-pantolactone in 89% ee, whereas the corresponding (*S*)-Ph,Cp-isoAlaNOP rhodium complex yielded the *R* enantiomer in 81% ee. A similar inversion of the configuration of the hydrogenated product of *N*-benzylbenzoylformamide was also observed with these complexes. By varying the nonchiral ligand bound to rhodium as well as the reaction temperature, we observed marked effects on the efficiency of the catalysis. The results suggest that both catalytic activity and enantioselectivity of the $[RhX(AMPP)]_n$ complexes are mainly governed by the aminophosphine moiety of the ligand.

Introduction

The preparation of optically active hydroxy compounds by catalytic asymmetric hydrogenation of prochiral ketones is of great significance for research in enantioselective organometallic catalysis.[1] Accordingly, considerable attention has been directed toward the synthesis of bisphosphine ligands for the catalytic asymmetric hydrogenation of various functionalized ketones.[1] Hence, numerous chelating phosphines possessing a C_2 symmetry axis and the corresponding catalysts have been prepared.[1,2] Noteworthy in this regard are the BINAP ligands used to prepare rhodium, ruthenium, and recently iridium catalysts, exhibiting high to almost complete enantioselectivity for hydrogenation, isomerization, and hydroformylation.[3] Most of the chiral phosphines bear at least two aryl substituents on their phosphorus atoms, leading to relatively electron poor chelates. In addition, the syntheses of these phosphines often involve tedious routes, including a resolution step. Thus, much could be expected from

* To whom correspondence should be addressed.

⊗ Abstract published in *Advance ACS Abstracts,* April 15, 1995.

(1) See for example: (a) Takaya, H.; Ohta, T.; Noyori, R. In *Catalytic Asymmetric Synthesis*; Ojima, I., Ed.; VCH: New York, 1993; Chapter 1. (b) Noyori, R. In *Asymmetric Catalysis in Organic Synthesis*; Wiley: New York, 1994; Chapter 2, p 16.

(2) (a) Brunner, H. In *Topics in Stereochemistry*; Eliel, E. L., Wilen, S. H., Eds.; Wiley: New York, 1988; p 129. (b) Ojima, I.; Clos, N.; Bastos, C. *Tetrahedron* **1989**, *45*, 6901. (c) Kagan, H. B.; Sasaki, M. In *The Chemistry of Organophosphorus Compounds*; Hartley, F. R., Ed.; Wiley: New York, 1990; Vol. 1, p 53.

0276-7333/95/2314-2480$09.00/0

chiral electron-rich and easily accessible bisphosphines in terms of stereocontrol and catalytic activity. Recent reports have proven the capabilities of such ligands, especially for the asymmetric hydrogenation of ketones and olefins.[4] Moreover, a recent method for the respective control of electronic and steric effects of the phosphino groups on the chiral bisphosphine ligands has been developed.[4d]

We have extensively studied the synthesis and the catalytic applications of easily accessible ligands, the aminophosphine–phosphinites (abbreviated AMPP).[5] Particularly, we have demonstrated the efficiency of such ligands for asymmetric hydrogenation of activated ketones over rhodium and ruthenium catalysts.[6] Thus, by consideration of the electronic and steric effects of the phosphino groups on the chiral bisphosphines, several improvements were made in various AMPP chelates and many such amino alcohol based ligands became particularly efficient for rhodium-catalyzed asymmetric hydrogenation of activated ketones.[6b]

In this paper, we describe the synthesis and characterization of alkyl-substituted diphosphines and their corresponding neutral rhodium(I) complexes, their use in asymmetric hydrogenation, and a crystal structure that established the conformation of the chiral backbone.[7]

Results and Discussion

Synthesis and Characterization of Alkyl-Substituted Diphosphines. In order to investigate the electronic and steric effects of substituents at the aminophosphine and phosphinite functions on asymmetric hydrogenation, we have synthesized diphosphines with identical and different substituents at phosphorus. The "symmetrical" dialkylphosphino derivatives of (*S*)-2-(hydroxymethyl)pyrrolidine ((*S*)-R,R-ProNOP; (*S*)-**1a–c**) and of (*S*)-1-(methylamino)-2-propanol ((*S*)-R,R-isoAlaNOP; (*S*)-**2a,b**), were prepared as previously reported[6a] in one step as shown in Scheme 1. The full characterization of these ligands is given in the Experimental Section. In particular, their $^{31}P\{^1H\}$ NMR spectra exhibited two signals and the more deshielded was attributed to the phosphinite (PO) moiety on the basis of the electronegativities of oxygen and nitrogen.[8]

Scheme 1

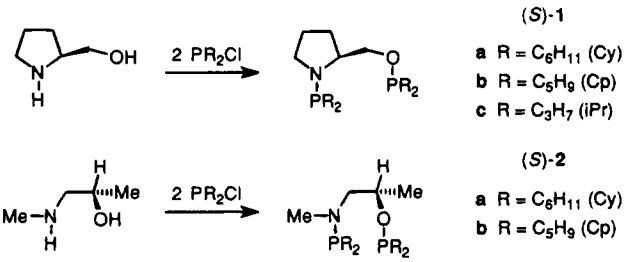

Scheme 2

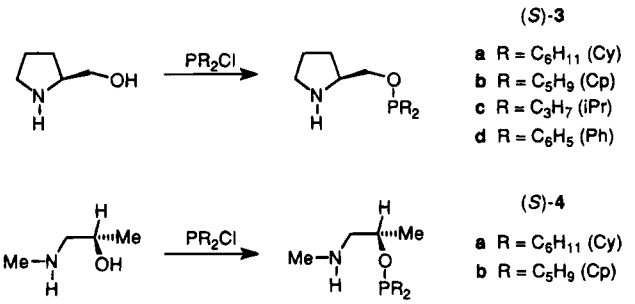

New mixed alkyl-substituted diphosphines were synthesized in two steps on the basis of the procedure employed for the synthesis of ligands (*S*)-**1** and (*S*)-**2**. Thus, in the first step, 1 equiv of chlorodialkylphosphine was reacted with either (*S*)-2-(hydroxymethyl)pyrrolidine or (*S*)-1-(methylamino)-2-propanol to produce the corresponding aminophosphinite intermediate, (*S*)-R-ProNHOP ((*S*)-**3a–d**) and (*S*)-R-isoAlaNHOP ((*S*)-**4a,b**) respectively (Scheme 2). The reaction was conducted at room temperature in diethyl ether in the presence of an excess of triethylamine and was monitored by $^{31}P\{^1H\}$ NMR. According to the number of signals observed in the $^{31}P\{^1H\}$ NMR spectra at the beginning of the reaction and to the evolution of the reaction mixture, we were able to define the mechanism of the synthesis of the monophosphine derivatives. Thus, two cases could be distinguished when four or three signals were detected at the beginning of the reaction, depending on the nature of the chlorodialkylphosphine and the amino alcohol used. In the first case, when 1 equiv of chlorodicyclohexylphosphine was reacted with (*S*)-1-(methylamino)-2-propanol for 2 h, the four observed signals were attributed to the expected amino–phosphinite intermediate "PO–NH" ((*S*)-**4a**; δ 137.9 ppm), the aminophosphine–phosphinite "PO–NP" ((*S*)-**2a**; δ(P(O)) 138.4 ppm, δ(P(N)) 81.8 ppm), and unreacted chlorodicyclohexylphosphine (δ 121.0 ppm).[9] After 4 h of reaction, only the signal of the expected compound (*S*)-**4a** was observed. This indicated that a portion of (*S*)-**4a** was formed through reaction of the starting amino alcohol with the bisphosphine (*S*)-**2a**. In the second case, during the reaction between chlorodicyclopen-

(3) (a) Noyori, R.; Kitamura, M. In *Modern Synthetic Methods*; Scheffold, R., Ed.; Springer-Verlag: Berlin, 1989; Vol. 5, p 116. (b) Noyori, R. *Chem. Soc. Rev.* **1989**, *18*, 187. (c) Noyori, R.; Takaya, H. *Acc. Chem. Res.* **1990**, *23*, 345. (d) Noyori, R. *CHEMTECH* **1992**, 360. (e) Zhang, X.; Taketomi, T.; Yoshizumi, T.; Kumobayashi, H.; Akutagawa, S.; Mashima, K.; Takaya, H. *J. Am. Chem. Soc.* **1993**, *115*, 3318. (f) Sakai, N.; Mano, S.; Nozaki, K.; Takaya, H. *J. Am. Chem. Soc.* **1993**, *115*, 1993. (g) Sakai, N.; Nozaki, K.; Takaya, H. *J. Chem. Soc., Chem. Commun.* **1994**, 395.

(4) (a) Miyashita, A.; Karino, H.; Shimamura, J. I.; Chiba, T.; Nagano, K.; Nohira, H.; Takaya, H. *Chem. Lett.* **1989**, 1849. (b) Tani, K.; Suwa, K.; Tanigawa, E.; Ise, T.; Yamagata, T.; Tatsuno, Y.; Otsuka, S. *J. Organomet. Chem.* **1989**, *370*, 203. (c) Burk, M. J.; Feaster, J. E.; Harlow, R. L. *Tetrahedron: Asymmetry* **1991**, *2*, 569. (d) Inoguchi, K.; Sakuraba, S.; Achiwa, K. *Synlett* **1992**, 169.

(5) (a) Mortreux, A.; Petit, F.; Buono, G.; Peiffer, G. *Bull. Soc. Chim. Fr.* **1987**, *4*, 631. (b) Hatat, C.; Karim, A.; Kokel, N.; Mortreux, A.; Petit, F. *Tetrahedron Lett.* **1988**, *29*, 3675. (c) Mutez, S.; Mortreux, A.; Petit, F. *Tetrahedron Lett.* **1988**, *29*, 1911. (d) Denis, P.; Jean, A.; Croisy, J.-F.; Mortreux, A.; Petit, F. *J. Am. Chem. Soc.* **1990**, *112*, 1292. (e) Suisse, I.; Bricout, H.; Mortreux, A. *Tetrahedron Lett.* **1994**, *35*, 413. (f) Naïli, S.; Carpentier, J.-F.; Agbossou, F.; Mortreux, A.; Nowogrocki, G.; Wignacourt, J.-P. *Organometallics* **1995**, *14*, 401.

(6) (a) Hatat, C.; Karim, A.; Kokel, N.; Mortreux, A.; Petit, F. *New J. Chem.* **1990**, *14*, 141. (b) Roucoux, A.; Agbossou, F.; Mortreux, A.; Petit, F. *Tetrahedron: Asymmetry* **1993**, *4*, 2279. (c) Hapiot, F.; Agbossou, F.; Mortreux, A. *Tetrahedron: Asymmetry* **1994**, *5*, 515. (d) Hapiot, F.; Agbossou, F.; Mortreux, A. *Tetrahedron: Asymmetry* **1995**, *6*, 11. (e) Carpentier, J.-F.; Agbossou, F.; Mortreux, A. *Tetrahedron: Asymmetry* **1995**, *6*, 39.

(7) A preliminary account of this work has been reported: Hatat, C.; Kokel, N.; Mortreux, A.; Petit, F. *Tetrahedron Lett.* **1990**, *31*, 4139.

(8) Cesarotti, E.; Grassi, M.; Prati, L. *J. Chem. Soc., Dalton Trans.* **1989**, 161.

(9) Assignment of the signals was made by comparison with an authentic sample. In particular, it was shown that, in the second case, the two singlets at δ 134.7 and 82.0 ppm did not correspond to (*S*)-Cp,Cp-isoAlaNOP ((*S*)-**2b**).

Scheme 3

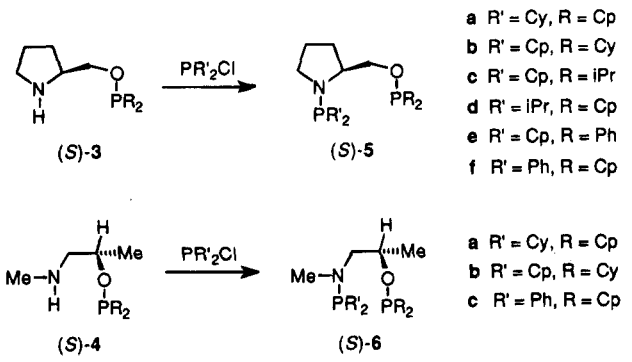

tylphosphine and (*S*)-1-(methylamino)-2-propanol, the three signals observed were assigned to the expected aminophosphinite intermediate "PO–NH" ((*S*)-**4b**; δ 134.4 ppm), unreacted chlorodicyclopentylphosphine (δ 121.7 ppm), and the aminophosphine HO–NP intermediate (δ 82.0 ppm).[9] Similarly, after a few hours, the two upfield signals disappeared, thus indicating the selective formation of the thermodynamically favored aminophosphinite product (*S*)-**4b** through the kinetic aminophosphine intermediate. Similar behavior was observed during the preparation of the (*S*)-R-ProNHOP (*S*)-**3a–d** compounds. Various amino–phosphinite derivatives were prepared successfully using this procedure through either pathway, except (*S*)-Ph-isoAlaNHOP. In this case, the reaction of chlorodiphenylphosphine with (*S*)-1-(methylamino)-2-propanol led predominantly to the formation of (*S*)-1-((diphenylphosphino)methylamino)-2-propanol, *i.e.* the aminophosphine (*S*)-Ph-isoAlaNPOH product. Nevertheless, even after 8 days, the conversion to the aminophosphinite derivative (*S*)-Ph-isoAlaNHOP remained incomplete, and heating of the reaction mixture resulted in the decomposition of the products.

In the second step, derivatives (*S*)-**3a–d** and (*S*)-**4a,b** were reacted under similar conditions with a different chlorodialkylphosphine to afford the expected mixed aminophosphine–phosphinites (*S*)-**5a–f** and (*S*)-**6a–c** in 76–92% yield. The characterization of these ligands (see Experimental Section) confirmed their "mixed" structures and showed that no exchange occurred between the $-PR_2$ and $-PR'_2$ functions located at the N- and O-positions. All the AMPP species described here are white solids or colorless oils which are quite air-sensitive, but they can be stored under nitrogen at −20 °C over long periods of time without appreciable alteration. From a practical point of view, $^{31}P\{^1H\}$ NMR analysis allows a fast and efficient technique for evaluation of their purity. The AMPP ligands (*S*)-**5a–f** and (*S*)-**6a–c** displayed two singlets of equal intensity due to the aminophosphine and phosphinite residues. The ^1H and $^{13}C\{^1H\}$ NMR spectra are by far more complex, particularly in the case of the (*S*)-R,R′-ProNOP derivatives (*S*)-**5a–f**, because of the strongly coupled systems.[8] Nevertheless, an almost complete assignment of all resonances on the basis of 2D NMR (^1H,^1H and ^{13}C,^1H COSY) was possible and is reported in the Experimental Section.

Synthesis and Characterization of Neutral AMPP–Rh(I) Complexes. Treatment of [Rh(COD)Cl]$_2$ (COD = 1,5-cyclooctadiene) with 2 equiv of (*S*)-AMPP ligands ((*S*)-**1a–c**, (*S*)-**2a,b**, (*S*)-**5a–f**, and (*S*)-**6a–c**) in toluene at room temperature afforded complexes (*S*)-**7a–e** and (*S*)-**8a–d** as red-orange solids in nearly quantitative yields (Scheme 4). In contrast to the free ligands, these AMPP–Rh complexes are relatively air-stable but are best stored under an inert atmosphere. Mass spectrometry studies of complexes (*S*)-**7a–e** and (*S*)-**8a–d** revealed the presence of the dimeric ion, thus indicating the conservation of the dinuclear structure in the solid state through chloro bridging. In toluene solution, the $^{31}P\{^1H\}$ NMR spectra of all these complexes exhibited the eight-line AB parts of ABX (X = ^{103}Rh) spin systems, due to the nonequivalence of the phosphorus atoms (see Experimental Section). Variable-temperature $^{31}P\{^1H\}$ NMR studies showed the existence of a dynamic phenomenon. Thus, by lowering the temperature, we could observe the coexistence of two species. Above a certain temperature, ranging from 290 to 320 K and characteristic of the nature of the ligand, the minor species disappeared.[10]

Scheme 4

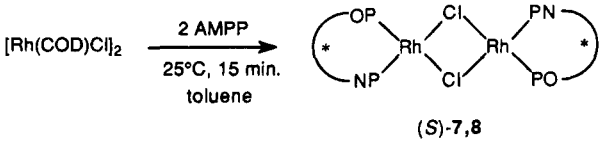

Scheme 5

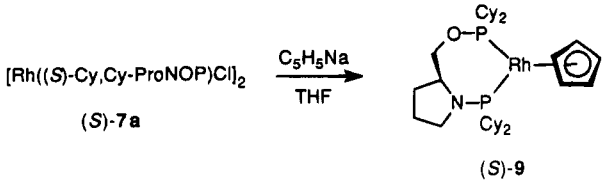

Scheme 6

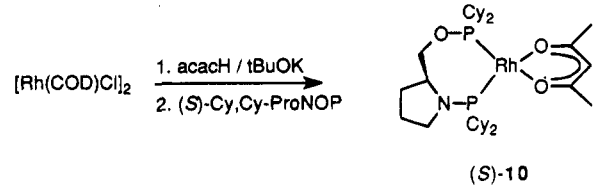

For comparison, other neutral rhodium derivatives of (*S*)-**1a** were synthesized. The cyclopentadienyl complex (*S*)-**9** was prepared in 93% yield by the reaction of (*S*)-**7a** and sodium cyclopentadienate in THF. This complex was fully characterized (see Experimental Section). When (acetylacetonato)(1,5-cyclooctadiene)rhodium(I) was used as the starting complex, the reaction with (*S*)-**1a** afforded complex (*S*)-**10**, which was isolated in 86% yield (56% yield after recrystallization, *vide infra*). The $^{31}P\{^1H\}$ NMR spectrum of the mononuclear species (*S*)-**9** revealed significant shifts of the P(N) (δ 110.2) and P(O) (δ 186.5) signals compared to those of the corresponding dinuclear halogeno complexes of (*S*)-**1a** (X = Cl, Br, I; δ(P(N)) 100.0–105.0; δ(P(O)) 178.0–179.6).[6a] In contrast, the ^{31}P NMR spectra of (*S*)-**10** (δ(P(N)) 103.6; δ(P(O)) 177.8) were quite similar. Moreover, the Rh–P coupling constants of the cyclopentadienyl complex (*S*)-**9** (J(Rh–P(N) = 238 Hz; J(Rh–P(O) = 243 Hz) were much higher than those of the corresponding dinuclear halo-

(10) The nature of the two rhodium species has not been determined so far. Nevertheless, the fact that this phenomenon is unique to complexes **7** and **8** suggests that it is a syn-dimer/anti-dimer isomerization equilibrium.

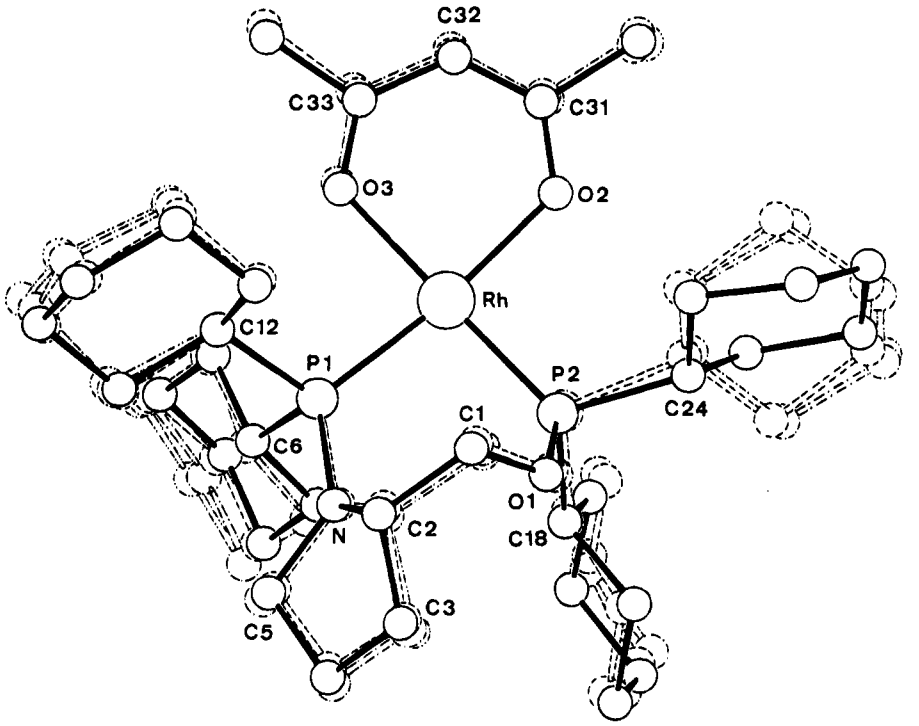

Figure 1. Molecular structure of [Rh(acac){(*S*)-Cy,Cy-ProNOP}] ((*S*)-**10**) showing superposition of the four independent molecules in the unit cell.

Table 1. Selected Bond Distances (Å) and Bond Angles and Torsion Angles (deg) for [Rh(acac){(*S*)-Cy,Cy-ProNOP}] ((*S*)-10)

	molecule			
	1	2	3	4
(a) Bond Distances				
Rh–P(1)	2.211(3)	2.203(3)	2.209(3)	2.212(3)
Rh–P(2)	2.188(3)	2.182(3)	2.189(3)	2.182(3)
Rh–O(2)	2.104(7)	2.091(8)	2.078(7)	2.083(7)
Rh–O(3)	2.107(7)	2.093(7)	2.090(7)	2.097(7)
P(1)–N	1.687(9)	1.700(9)	1.694(9)	1.698(9)
P(1)–C(6)	1.86(1)	1.87(1)	1.86(1)	1.846(9)
P(1)–C(12)	1.86(1)	1.86(1)	1.88(1)	1.87(1)
P(2)–O(1)	1.654(8)	1.638(8)	1.651(7)	1.652(8)
P(2)–C(18)	1.85(1)	1.84(1)	1.82(1)	1.86(1)
P(2)–C(24)	1.86(1)	1.88(1)	1.85(1)	1.88(1)
O(1)–C(1)	1.41(1)	1.42(1)	1.41(1)	1.40(1)
O(2)–C(31)	1.27(1)	1.29(1)	1.30(1)	1.29(1)
O(3)–C(33)	1.27(1)	1.28(1)	1.30(1)	1.26(1)
N–C(2)	1.49(1)	1.47(1)	1.48(1)	1.47(1)
N–C(5)	1.48(2)	1.43(2)	1.49(2)	1.48(1)
C(1)–C(2)	1.54(1)	1.53(2)	1.55(1)	1.50(1)
C(2)–C(3)	1.52(2)	1.57(2)	1.57(2)	1.55(2)
C(31)–C(32)	1.33(2)	1.35(2)	1.38(2)	1.38(1)
C(32)–C(33)	1.40(2)	1.39(2)	1.39(2)	1.38(2)
(b) Bond and Torsion Angles				
P(1)–Rh–P(2)	94.8(1)	94.7(1)	95.2(1)	95.3(1)
P(1)–N–C(2)	124.8(7)	122.4(7)	123.5(7)	124.5(7)
P(1)–N–C(5)	125.0(7)	124.4(7)	125.3(7)	126.4(7)
C(2)–N–C(5)	104.4(8)	106.8(9)	104.8(8)	104.0(8)
N–C(2)–C(1)	113.1(9)	114.9(9)	114.7(8)	115.1(9)
N–C(2)–C(3)	104.1(9)	103.5(9)	101.5(8)	104.3(8)
C(1)–C(2)–C(3)	113.5(9)	114.1(9)	113.6(8)	115.1(9)
P(1)–N–C(2)–C(1)	−42.6	−44.5	−41.9	−39.4
Rh–P(2)–C(18)–C(23)	61.2	68.7	64.4	64.6
Rh–P(2)–C(18)–C(19)	−171.3	−164.2	−166.5	−167.8
P(2)–C(18)–C(19)–C(20)	168.5	170.6	175.4	173.8
P(2)–C(18)–C(23)–C(22)	−167.7	−168.1	−170.5	−170.5

geno and acetylacetonato complexes (J(Rh–P(N) = 211–217 Hz; J(Rh–P(O) = 220–225 Hz), thus indicating that the cyclopentadienyl ligand induces stronger modifications at rhodium than acac does.[11] It is noteworthy that in contrast to the case for the chloro–rhodium complexes (*S*)-**7a–e** and (*S*)-**8a–d**, no dynamic phenomenon was observed by $^{31}P\{^1H\}$ NMR spectroscopy with complexes (*S*)-**9** and (*S*)-**10** in the temperature range 250–350 K.[10]

Crystal Structure of Rh(acac){(*S*)-Cy,Cy-ProNOP} ((*S*)-10). Slow recrystallization of (*S*)-**10** from a dichloromethane–diethyl ether–methanol mixture afforded lemon yellow crystals which proved to be suitable for X-ray investigation. A view of the molecule (*S*)-**10** is depicted in Figure 1, together with the labeling scheme adopted. Selected bond distances and angles are given in Table 1. The crystal structure revealed the existence of four independent molecules in the unit cell, essentially differentiated by the orientation of cyclohexyl substituents at phosphorus. In all cases, the rhodium atom has a square-planar coordination typical of 16-electron complexes. The distortion of this geometry is very low; that is, the dihedral angle between the RhP_2 and RhO_2 planes ranges from 1.27 to 3.27°. Nevertheless, an important widening of the P(N)–Rh–P(O) bond angle (94.7(1)–95.3(1)°), ascribed to the rigidity of the seven-membered metallacycle fused with the proline cycle, is observed. One of the most interesting feature is the conformation of this metallacycle. It is a distorted λ boat-type conformation with the nitrogen atom in the mean plane RhP_2, in contrast to the case for the previously reported rhodium,[12] ruthenium,[13] palladium,[14] and platinum[5f] complexes of (*S*)-Ph,Ph-ProNOP

(11) For a discussion of the influence of ligands on chemical shifts and J(RhP) values of (bisphosphine)rhodium complexes, see: Slack, D. A.; Greveling, I.; Baird, M. C. *Inorg. Chem.* **1979**, *18*, 3125.

(12) Cesarotti, E.; Chiesa, A.; Ciani, G.; Sironi, A. *J. Organomet. Chem.* **1983**, *251*, 79.

(13) (a) Cesarotti, E.; Prati, L.; Sironi, A.; Ciani, G.; White, C. *J. Chem. Soc., Dalton Trans.* **1987**, 1149. (b) Baldovino, C.; Cesarotti, E.; Prati, L.; Demartin, F. *Gazz. Chim. Ital.* **1992**, *122*, 475.

(14) (a) Cesarotti, E.; Grassi, M.; Prati, L.; Demartin, F. *J. Organomet. Chem.* **1989**, *370*, 407. (b) Cesarotti, E.; Grassi, M.; Prati, L.; Demartin, F. *J. Chem. Soc., Dalton Trans.* **1991**, 2073.

Scheme 7

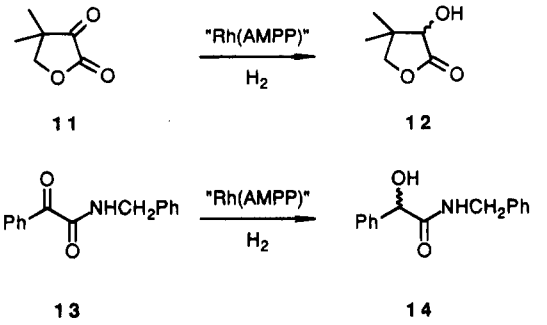

and the rhodium complex of (*R*)-Ph,Ph-PheNOP,[15] which show an opposite conformation (oxygen atom in the mean plane P(N)–metal–P(O)). This fact suggests that a number of similar conformational energy minima related to seven-ring chelates with either nitrogen or oxygen in the plane RhP_2 are readily accessible to this aminophosphine–phosphinite family. The rhodium–phosphorus bonds (Rh–P(O) = 2.182(3)–2.188(3) Å; Rh–P(N) = 2.203(3)–2.212(3) Å) are also somewhat shortened compared to those found in the rhodium complex of (*S*)-Ph,Ph-ProNOP[12] (Rh–P(O) = 2.271(3) Å; Rh–P(N) = 2.283(3) Å). The C(1)···Rh distances range from 3.404(8) to 3.438(9) Å for the methylene C atom C(1) in spite of the different environments of the four molecules, and this suggests there might be a weak interaction between the methylene H atom and the metal. The distances are significantly smaller than the shortest CH_3–Rh distances in (2,4-pentanedionato-*O,O'*)bis(phenyl 3,3',5,5'-tetra-*tert*-butyl-1,1'-biphenyl-2,2'-diyl phosphite-*P*)rhodium[16] (3.71 and 3.73 Å), which contains two bulky phosphite groups and a tetrahedrally distorted Rh coordination plane. There is a brief report in the literature of the crystal structure of (acac)Rh-($Ph_2P(CH_2)_4PPh_2$) containing a chelating diphosphine ligand where such an interaction is also possible, but no further details are available.[17]

Asymmetric Hydrogenation of Activated Keto Compounds with Neutral AMPP–Rh(I) Complexes as Catalyst Precursors. The catalytic behavior of the synthesized neutral AMPP–Rh(I) complexes has been investigated during asymmetric hydrogenation of two activated keto compounds, dihydro-4,4-dimethyl-2,3-furandione (**11**) and *N*-benzyl benzoylformamide (**13**). The hydrogenated products of these substrates are important synthetic intermediates for the production of pharmaceuticals, principally the *R* enantiomer of pantolactone (**12**) which is the key compound for the preparation of biologically important pantothenic acid, pantetheine, and coenzyme A.[18] The results are summarized in Table 2 (entries 1–16) and Table 3 (entries 17–31).

For both substrates, quantitative hydrogenation could be readily achieved under smooth conditions (room temperature, 1 atm of H_2, toluene) with all the chloro–rhodium complexes tested. When hydrogenation of **11** was carried out with the acetylacetonato–rhodium complex of (*S*)-Cy,Cy-ProNOP (*S*)-**10**, the reaction proceeded rather slowly (entry 16), whereas the use of the corresponding cyclopentadienyl complex (*S*)-**9** required 70 °C to go to completion (entry 15). This trend was even more marked for the reduction of **13** by (*S*)-**10**, since only 65% conversion was obtained after 48 h reaction at room temperature (entry 31). These differences in activity can be attributed to the existence of different catalytic species according to the nature of the nonchiral ligand present in the rhodium precursor introduced.

The catalytic activities of the chloro rhodium complexes (*S*)-**7a–e** and (*S*)-**8a–i** were greatly affected by the nature of the phosphine and, moreover, by the nature of the substituents at the phosphorus atoms. Thus, the best catalytic activities[19] for hydrogenation of **11** were observed with (*S*)-**7e** and (*S*)-**8h** ($TOF_{50\%}$ = 800 and 860 h^{-1}, respectively) (entries 11 and 13). Use of these last two complexes also afforded very good results for hydrogenation of **13** ($TOF_{50\%}$ = 1500 and 925 h^{-1}, respectively) (entries 27 and 29). We could observe for this substrate that the (*S*)-R,R'-ProNOP derivatives bearing the same phosphino substituents, *i.e.* R = Cp, R' = Cp ((*S*)-**7b**) and R = Cp, R' = Cy ((*S*)-**8b**) led to high activities ($TOF_{50\%}$ = 1200 and 630 h^{-1}, respectively) (entries 18 and 21). In fact, the results presented in Tables 2 and 3 indicate that, in most cases, ligands bearing an identical aminophosphine residue led to similar reaction rates. For instance, during hydrogenation of **13**, almost all half-reaction times of complexes substituted by an amino(dicyclohexylphosphino) group range from 13.5 to 19 min, whereas those bearing an amino(dicyclopentylphosphino) moiety range from 4 to 10 min (except for (*S*)-**8c** and (*S*)-**8e**). Nevertheless, the phosphinite group also affected the catalytic activity of the complexes. Actually, hydrogenation of **11** and **13** could be carried out in the presence of the Ph,Cp-derived complexes (*S*)-**8f** and (*S*)-**8i** at room temperature and under atmospheric pressure in reasonable times (entries 9, 14, 25 and 30), whereas (*S*)-Ph,Ph-ProNOP and (*S*)-Ph,Ph-isoAlaNOP chloro–rhodium complexes required 40 atm and 30 °C for significant rates.[21]

Stereoselectivities depended strongly on the nature of the substituents at the phosphorus atoms. Thus, the best enantioselectivities for hydrogenation of **11** were observed with (*S*)-**7e** and (*S*)-**8h**, both giving (*S*)-**12** in 89% ee (entries 11 and 13). The product of opposite configuration (*R*)-**12** could be obtained with all the (*S*)-R,R'-ProNOP-based complexes. The best ee was obtained with (*S*)-**8f** (85% ee, entry 9). Once again, enantioselectivity of the product was mainly dependent on the nature of the aminophosphine group. For instance, all prolinol derivatives substituted by an amino(dicyclopentylphosphino) residue afforded almost

(15) (*R*)-Ph,Ph-PheNOP: (2*R*)-3-phenyl-2-(methyl(diphenylphosphino)amino)-1-((diphenylphosphino)oxy)propane. Pavlov, V. A.; Klabunovskii, E. I.; Struchkov, Y. T.; Voloboev, A. A.; Yanovsky, A. I. *J. Mol. Catal.* **1988**, *44*, 217.

(16) Meetsma, A.; Jongsma, T.; Challa, G.; Van Leeuwen, P. W. N. M. *Acta Crystallogr.* **1993**, *C49*, 1160.

(17) Stults, B. R.; Knowles, W. S. *Abstracts of Papers*, Winter Meeting of the American Crystallographic Association, University of Oklahoma, Norman, OK, March 19–24, 1978; American Crystallographic Association: New York, 1978.

(18) See for example: *The Merck Index*, ed.; Budavari, S., Ed.; Merck: Rahway, NJ, 1994; p 1110.

(19) All reactions were carried out under 1 atm of H_2 with the same stirring. We did not check the rate-determining step. However, recent results obtained under identical reaction conditions with other Rh–AMPP type complexes exhibited higher turnover frequencies (up to 3300 h^{-1} for the hydrogenation of **11**). This indicates that, in the present case, mass transfer of hydrogen is not the rate-determining step. Roucoux, A.; Devocelle, M.; Carpentier, J.-F.; Agbossou, F.; Mortreux, A. *Synlett*, in press.

(20) Stiller, E. T.; Hanis, S. A.; Finkelstein, J.; Keresztesy, J. C.; Folkers, K. *J. Am. Chem. Soc.* **1940**, *62*, 1785.

(21) Karim, A.; Mortreux, A.; Petit, F.; Buono, G.; Peiffer, G.; Siv, C. *J. Organomet. Chem.* **1986**, *317*, 93.

Table 2. Asymmetric Hydrogenation of Dihydro-4,4-dimethyl-2,3-furandione (11)[a]

entry no.	complex	chiral ligand	X	$t_{1/2}$[b] (min)	time[c] (h)	ee[d] (%) (confign)
1[e]	(*S*)-**7a**	(*S*)-Cy,Cy-ProNOP	Cl	27	12	47 (*R*)
2[e]	(*S*)-**7b**	(*S*)-Cp,Cp-ProNOP	Cl	19	1	76 (*R*)
3	(*S*)-**7c**	(*S*)-*i*Pr,*i*Pr-ProNOP	Cl	19	1.7	56 (*R*)
4	(*S*)-**8a**	(*S*)-Cy,Cp-ProNOP	Cl	15	1.3	41 (*R*)
5	(*S*)-**8b**	(*S*)-Cp,Cy-ProNOP	Cl	10	1	81 (*R*)
6	(*S*)-**8c**	(*S*)-Cp,*i*Pr-ProNOP	Cl	16	1.2	78 (*R*)
7	(*S*)-**8d**	(*S*)-*i*Pr,Cp-ProNOP	Cl	9	2	45 (*R*)
8	(*S*)-**8e**	(*S*)-Cp,Ph-ProNOP	Cl	20	1	75 (*R*)
9	(*S*)-**8f**	(*S*)-Ph,Cp-ProNOP	Cl	*f*	48	85 (*R*)
10[e]	(*S*)-**7d**	(*S*)-Cy,Cy-isoAlaNOP	Cl	13.5	1.3	80 (*S*)
11[e]	(*S*)-**7e**	(*S*)-Cp,Cp-isoAlaNOP	Cl	7.5	2	89 (*S*)
12	(*S*)-**8g**	(*S*)-Cy,Cp-isoAlaNOP	Cl	12	1.3	78 (*S*)
13	(*S*)-**8h**	(*S*)-Cp,Cy-isoAlaNOP	Cl	7	0.5	89 (*S*)
14	(*S*)-**8i**	(*S*)-Ph,Cp-isoAlaNOP	Cl	f	18	81 (*R*)
15	(*S*)-**9**	(*S*)-Cy,Cy-ProNOP	η^5-C_5H_5[g]	16	1.3	20 (*R*)
16	(*S*)-**10**	(*S*)-Cy,Cy-ProNOP	acac	120	14	34 (*R*)

[a] Hydrogenation was carried out in a 200-mL flask in toluene at room temperature under 1 atm of hydrogen unless otherwise stated; substrate/Rh = 200. See Experimental Section. [b] Time for 50% conversion. [c] Time for total conversion. [d] Enantiomeric excess was determined by GC analysis (FS-CYCLODEX β-I/P 25 m × 0.32 mm column, 130 °C) and controlled on the basis of the optical rotation value (*c* 2.05, H_2O) in comparison with the reported one ($[\alpha]_D^{25} = -50.7°$).[20] [e] Results taken from ref 6a. [f] The time of half-reaction was not determined. [g] Temperature 70 °C.

Table 3. Asymmetric Hydrogenation of *N*-Benzylbenzoylformamide (13)[a]

entry no.	complex	chiral ligand	X	$t_{1/2}$[b] (min)	time[c] (h)	ee[d] (%) (confign)
17[e]	(*S*)-**7a**	(*S*)-Cy,Cy-ProNOP	Cl	19	1.5	74 (*S*)
18[e]	(*S*)-**7b**	(*S*)-Cp,Cp-ProNOP	Cl	5	0.5	79 (*S*)
19	(*S*)-**7c**	(*S*)-*i*Pr,*i*Pr-ProNOP	Cl	13.5	1.4	74 (*S*)
20	(*S*)-**8a**	(*S*)-Cy,Cp-ProNOP	Cl	15.5	2	74 (*S*)
21	(*S*)-**8b**	(*S*)-Cp,Cy-ProNOP	Cl	9.5	1.3	77 (*S*)
22	(*S*)-**8c**	(*S*)-Cp,*i*Pr-ProNOP	Cl	16	1	69 (*S*)
23	(*S*)-**8d**	(*S*)-*i*Pr,Cp-ProNOP	Cl	10	1.2	55 (*S*)
24	(*S*)-**8e**	(*S*)-Cp,Ph-ProNOP	Cl	*f*	18	74 (*S*)
25	(*S*)-**8f**	(*S*)-Ph,Cp-ProNOP	Cl	*f*	18	82 (*S*)
26[e]	(*S*)-**7d**	(*S*)-Cy,Cy-isoAlaNOP	Cl	15	1.5	75 (*R*)
27[e]	(*S*)-**7e**	(*S*)-Cp,Cp-isoAlaNOP	Cl	4	0.5	71 (*R*)
28	(*S*)-**8g**	(*S*)-Cy,Cp-isoAlaNOP	Cl	15	2.3	72 (*R*)
29	(*S*)-**8h**	(*S*)-Cp,Cy-isoAlaNOP	Cl	6.5	0.5	77 (*R*)
30	(*S*)-**8i**	(*S*)-Ph,Cp-isoAlaNOP	Cl	*f*	18	88 (*S*)
31	(*S*)-**10**	(*S*)-Cy,Cy-ProNOP	acac	*f*	48[g]	39 (*S*)

[a] Hydrogenation was carried out in a 200-mL flask in toluene at room temperature under 1 atm of hydrogen; substrate/Rh = 200. See Experimental Section. [b] Time for 50% conversion. [c] Time for total conversion unless otherwise stated. [d] Enantiomeric excess was determined on the basis of the optical rotation value (*c* 1.09, $CHCl_3$) in comparison with the reported one ($[\alpha]_D^{26} = +82.2°$).[6a] [e] Results taken from ref 6a. [f] The time of half-reaction was not determined. [g] Conversion 65%.

identical ee values, *i.e.* 78 ± 3% (entries 2, 5, 6, and 8). This phenomenon is still more pronounced for the isoalaninol derivatives which gave two sets of identical values totally independent of the nature of the phosphinite substituent (entries 10–13). The predominant influence of the aminophosphine moiety can also be observed for the hydrogenation of **13**, but the ee values are more narrow. In this case, the best enantioselectivity (88% ee) was observed with complex (*S*)-**8i** (entry 30).[22] This last complex, derived from (*S*)-Ph,Cp-isoAlaNOP, presents one of the most interesting features. Its use for hydrogenation of **11** and **13** brought about remarkable changes in enantioselectivity, since we obtained the products of the opposite configuration compared to the other (*S*)-R,R′-isoAlaNOP ligands (compare entries 10–14 and entries 26–30). This clearly shows that only changing cyclohexyl by phenyl groups at the amino phosphorus residue can induce major changes. However, the application of that principle to the prolinol skeleton did not result in the same effect, as (*R*)-**12** and (*S*)-**14** hydrogenated products were obtained alike with all (*S*)-R,R′-ProNOP-derived catalysts.

The results of the influence of temperature on the hydrogenation of **11** catalyzed by cyclohexyl- and cyclopentyl-substituted [RhCl((*S*)-R,R′-ProNOP)]$_2$ complexes are presented in Table 4. When amino(dicyclohexylphosphino)-substituted ligands were present (catalyst precursors (*S*)-**7a** and (*S*)-**8a**), the enantioselectivity increased moderately with temperature and a rather low apparent activation energy (4.8 and 5.6 kcal, respectively) was observed.[23] In contrast, in the presence of ligands bearing amino(dicyclopentylphosphino) groups (catalyst precursors (*S*)-**7b** and (*S*)-**8b**), there was no change in stereoselectivity and a higher apparent activation energy (9.6 and 10.9 kcal, respectively) was calculated. Interestingly, we notice that this behavior follows the dynamic phenomenons presented above. Actually, for the catalyst precursors (*S*)-**7a** and (*S*)-**8a**, which proved to be temperature dependent during catalysis, the minor species observed by $^{31}P\{^1H\}$ NMR disappeared at 320 and 315 K, respectively, whereas for complexes (*S*)-**7b** and (*S*)-**8b** these temperatures were 290 and 300 K, respectively.

(22) The highest ee (96%) obtained so far for the hydrogenation product of **13** was reported by: Chiba, T.; Miyashita, A.; Nohira, H.; Takaya, H. *Tetrahedron Lett.* **1993**, *34*, 2351.

(23) Relative apparent activation energies were obtained from the temperature dependence of initial turnover frequencies by using an Arrhenius plot.

Table 4. Asymmetric Hydrogenation of Dihydro-4,4-dimethyl-2,3-furandione (11): Temperature Effects[a]

entry no.	complex	chiral ligand	T (°C)	$t_{1/2}$[b] (min)	TOF[c] (min^{-1})	ee[d] (%) (confign of **12**)
1[e]	(*S*)-**7a**	(*S*)-Cy,Cy-ProNOP	20	27	4.2	47 (*R*)
32			45	13	8.2	51 (*R*)
33			70	8	13.9	53 (*R*)
2[e]	(*S*)-**7b**	(*S*)-Cp,Cp-ProNOP	20	19	4.3	76 (*R*)
34			50	3.3	34	77 (*R*)
35			70	2	43	77 (*R*)
4	(*S*)-**8a**	(*S*)-Cy,Cp-ProNOP	20	15	6.2	41 (*R*)
36			50	7.3	16.6	45 (*R*)
37			70	4.3	25	54 (*R*)
5	(*S*)-**8b**	(*S*)-Cp,Cy-ProNOP	20	10	2.8	81 (*R*)
38			50	3	30.5	80 (*R*)
39			70	2.3	37.5	80 (*R*)

[a] Conditions and notes: see Table 2, except [c]initial turnover frequency.

Conclusion

We have synthesized a series of new aminophosphine–phosphinite ligands bearing identical or different dialkylphosphino substituents. These chelates were used to prepare neutral AMPP–Rh(I) complexes which proved to be quite efficient catalysts for asymmetric hydrogenation of potentially important activated keto compounds. These complexes were principally used for the elucidation of various factors controlling the catalytic activities and stereoselectivities, and we assumed that the latter are mainly governed by the nature of the aminophosphine moiety.

Experimental Section

General Considerations. Nuclear magnetic resonance (^1H (300 and 200 MHz), ^{13}C (75 and 51 MHz), and ^{31}P (121, 81, and 32 MHz) NMR) spectra were recorded on Bruker AM-300, Bruker AC-200, and Bruker WP-80 spectrometers. Proton and carbon chemical shifts were referenced internally using the residual solvent resonances relative to tetramethylsilane (δ 0 ppm). Phosphorus chemical shifts were referenced to external 85% H_3PO_4 in D_2O (δ 0 ppm). Mass spectra were recorded on Finnigan MAT 311 A (70 eV) and on Kratos Concept II H-H (FAB^+, 3-nitrobenzyl alcohol/1,3,5-trichlorobenzene 80/20 v/v matrices) spectrometers. The compositions of the catalytic reaction mixtures were determined by GC analysis with a Delsi 30 gas instrument equipped with a flame ionization detector using a 25 m × 0.32 mm FS-CYCLODEX β-I/P capillary column. Optical rotations were measured on a Perkin-Elmer 241 polarimeter. Elemental analyses were performed by Laboratories Dornis & Kolbe, Mulheim, Germany, and by Laboratories Wolff, Clichy, France. All melting points were measured in sealed tubes and were not corrected.

(*S*)-2-(Hydroxymethyl)pyrrolidine (98.2% optical purity) was obtained from Aldrich Chemical Co. and used as received. (*S*)-(+)-1-(Methylamino)-2-propanol was synthesized by the method previously described.[6a] Chlorodicyclopentylphosphine and chlorodiisopropylphosphine were prepared by a modification of the literature method.[24] Chlorodicyclohexylphosphine and chlorodiphenylphosphine were purchased from Strem Chemical Inc. and used as received. The complex $[Rh(COD)Cl]_2$ was prepared according to the known procedure.[25] Dihydro-4,4-dimethyl-2,3-furandione was obtained from Aldrich Chemical Co. and recrystallized in diethyl ether prior to catalysis. *N*-benzylbenzoylformamide was synthesized according to the literature.[26] Basic alumina (grade 1) was obtained from Woelm Co., dried under vacuum, and stored at 80 °C prior to use. All reactions involving air- and moisture-sensitive compounds were carried out under a dry dinitrogen atmosphere using standard Schlenk techniques. Benzene, toluene, THF, and diethyl ether were distilled from sodium benzophenone ketyl. Pentane and dichloromethane were distilled over calcium hydride. Methanol and ethanol were dried over magnesium alkoxide. Triethylamine was dried over potassium hydroxide and distilled in the presence of 2% phenyl isocyanate. Dried solvents were degassed by freeze–thaw cycles prior to use.

Preparation of (*S*)-R,R-ProNOP Ligands ((*S*)-1a–c). In a typical experiment, in a 200-mL Schlenk tube (*S*)-2-(hydroxymethyl)pyrrolidine (1.01 g, 10 mmol) was reacted with a solution of chlorodialkylphosphine (22 mmol) in triethylamine (50 mL). The mixture was stirred under reflux, and the reaction was monitored by $^{31}P\{^1H\}$ NMR ($C_6D_5CD_3$). After the disappearance of reaction intermediates, the volatiles were evacuated *in vacuo* and excess chlorodialkylphosphine, ammonium chlorhydrate, and phosphorus impurities were removed by elution through basic alumina (1 × 20 cm) with diethyl ether (3 × 50 mL). The solvents were removed from the filtrate under reduced pressure to afford (*S*)-**1** as a solid or an oil.

(*S*)-Cy,Cy-ProNOP ((*S*)-1a): 30 h, 94% yield, white powder; mp 75–80 °C. $^{31}P\{^1H\}$ NMR ($C_6D_5CD_3$): δ 53.9 (s, P(N)) and 146.5 (s, P(O)). ^1H NMR ($CDCl_3$): δ 0.9–1.9 (m, 48H), 2.89 (m, 2H, NCH_2), 3.15 (m, 1H, OC*H*H), 3.27 (m, 1H, NCH), 3.61 (m, 1H, OCH*H*). $^{13}C\{^1H\}$ NMR ($CDCl_3$): δ 25.4 (s, CH_2 prol), 26.4–30.1 (m, CH_2), 34.5 (d, CH Cy, J(CP) = 16.5 Hz), 35.7 (d, CH Cy, J(CP) = 8.5 Hz), 38.0 (d, CH Cy, J(CP) = 17.1 Hz), 38.0 (d, CH Cy, J(CP) = 17.1 Hz), 47.1 (d, CH_2N, J(CP) = 9.8 Hz), 64.3 (dd, NCH, J(CP) = 8.6 and 26.3 Hz), 75.4 (dd, OCH_2, J(CP) = 4.9 and 16.5 Hz). MS (m/z, relative intensity): 493 (<1%, M^+), 410 (100%, M^+ − Cy), 280 (10%, M^+ − $OPCy_2$), 197 (20%, M^+ − $OPCy_2$ − Cy), 196 (35%, M^+ − $OPCy_2$ − CyH). Anal. Calcd for $C_{29}H_{53}NOP_2$: C, 70.55; H, 10.82; N, 2.84; P, 12.55. Found: C, 70.68; H, 11.11; N, 3.20; P, 10.95.

(*S*)-Cp,Cp-ProNOP ((*S*)-1b): 8 h, 91% yield, colorless oil. $^{31}P\{^1H\}$ NMR ($C_6D_5CD_3$): δ 57.0 (s, P(N)) and 142.0 (s, P(O)). ^1H NMR ($CDCl_3$): δ 1.2–2.2 (m, 40H), 2.90 (m, 2H, NCH_2), 3.23 (m, 1H, OC*H*H), 3.37 (m, 1H, NCH), 3.68 (m, 1H, OCH*H*). $^{13}C\{^1H\}$ NMR ($CDCl_3$): δ 24.9–30.7 (m, CH_2), 37.4 (d, CH Cp, J(CP) = 14.8 Hz), 38.6 (d, CH Cp, J(CP) = 4.3 Hz), 40.6 (2d, CH Cp, J(CP) = 15.8 Hz), 46.0 (d, CH_2N, J(CP) = 7.5 Hz), 63.4 (dd, NCH, J(CP) = 7.3 and 23.3 Hz), 73.8 (d broad, OCH_2, J(CP) ≈ 13 Hz).

(*S*)-*i*Pr,*i*Pr-ProNOP ((*S*)-1c): 30 h, 88% yield, colorless oil. $^{31}P\{^1H\}$ NMR ($C_6D_5CD_3$): δ 63.7 (s, P(N)) and 151.3 (s, P(O)). ^1H NMR ($CDCl_3$): δ 0.9–2.0 (m, 32H), 2.88 (m, 2H, NCH_2), 3.20 (m, 1H, OC*H*H), 3.32 (m, 1H, NCH), 3.67 (m, 1H, OCH*H*). $^{13}C\{^1H\}$ NMR ($CDCl_3$): δ 14.9–19.7 (m, CH_3 *i*Pr), 24.2 (d, CH *i*Pr, J(CP) = 15.9 Hz), 25.3 (s, CH_2 prol), 25.5 (d, CH *i*Pr, J(CP) = 4.8 Hz), 27.9 (d, CH *i*Pr, J(CP) = 16.7 Hz), 29.1 (d, CH_2CH, J(CP) = 5.2 Hz), 46.6 (d, CH_2N, J(CP) = 9.5 Hz), 64.3 (dd, NCH, J(CP) = 7.9 and 26.3 Hz), 75.0 (dd, OCH_2, J(CP) = 4.6 and 15.6 Hz). MS (m/z, relative intensity): 306 (50%), 290 (20%, M^+ − *i*Pr), 200 (25%, M^+ − $OPiPr_2$), 181 (40%), 156 (50%, M^+ − $OPiPr_2$ − *i*PrH), 84 (100%).

Physical Data for (*S*)-R,R-isoAlaNOP ligands [(*S*)-2a,b]. (*S*)-Cy,Cy-isoAlaNOP ((*S*)-2a): 30 h, 96% yield, white solid. $^{31}P\{^1H\}$ NMR ($C_6D_5CD_3$): δ 80.5 (s, P(N)) and 138.4 (s, P(O)). ^1H NMR ($CDCl_3$): δ 1.18 (d, 3H, CH_3, J(HH) = 6.1 Hz), 1.1–2.1 (m, 44H, Cy), 2.55 (d, 3H, NCH_3, J(HP) = 4.1 Hz), 2.83 (m, 1H, NC*H*H), 3.09 (m, 1H, NCH*H*), 3.62 (m, 1H, OCH). $^{13}C\{^1H\}$ NMR ($CDCl_3$): δ 20.3 (d, CH_3, J(CP) = 5.2 Hz), 26.3–

(24) Voskuil, W.; Arens, J. F. *Recl. Trav. Chim. Pays-Bas* **1963**, *82*, 302.
(25) Van Der Ant, A.; Onderdelinden, A. L. *Inorg. Synth.* **1973**, *14*, 92.
(26) Tani, K.; Tanigawa, E.; Tatsuno, Y.; Otsuka, S. *J. Organomet. Chem.* **1985**, *279*, 87.

29.8 (m, CH_2 Cy), 36.4–37.9 (4d, CH Cy, J(CP) ≈ 17 Hz), 64.0 (d broad, NCH_2, J(CP) ≈ 25 Hz), 76.4 (dd, OCH, J(CP) = 7 and 16 Hz).

(*S*)-Cp,Cp-isoAlaNOP ((*S*)-2b): 30 h, 70% yield, white oily solid. $^{31}P\{^1H\}$ NMR ($C_6D_5CD_3$): δ 81.9 (s, P(N)) and 135.8 (s, P(O)). ^1H NMR ($CDCl_3$): δ 1.14 (d, 3H, CH_3, J(HH) = 6.1 Hz), 1.2–2.1 (m, 36H, Cp), 2.47 (d, 3H, NCH_3, J(HP) = 4.9 Hz), 2.79 (m, 1H, NC*H*H), 3.09 (m, 1H, NCH*H*), 3.71 (m, 1H, OCH). $^{13}C\{^1H\}$ NMR ($CDCl_3$): δ 20.2 (d, CH_3, J(CP) = 4.5 Hz), 25.6–30.7 (m, CH_2 Cp), 36.5 (s broad, NCH_3), 38.7 (d, CH Cp, J(CP) = 22.7 Hz), 39.0 (d, CH Cp, J(CP) = 19.0 Hz), 40.5 (d, CH Cp, J(CP) = 15.5 Hz), 40.7 (d, CH Cp, J(CP) = 15.7 Hz), 63.9 (d broad, NCH_2, J(CP) = 25.1 Hz), 76.0 (dd, OCH, J(CP) = 7.3 and 16.4 Hz).

Preparation of (*S*)-R-ProNHOP Derivatives ((*S*)-3a–d). A solution of PR_2Cl (5 mmol) in triethylamine (5 mL) was added to a solution of (*S*)-2-(hydroxymethyl)pyrrolidine (0.505 g, 5 mmol) in diethyl ether (40 mL). The reaction mixture was stirred at room temperature and monitored by $^{31}P\{^1H\}$ NMR ($C_6D_5CD_3$). When only one signal remained ((*S*)-**3a** (R = Cy), 6 h, δ 146.2; (*S*)-**3b** (R = Cp), 16 h, δ 141.9; (*S*)-**3c** (R = *i*Pr), 20 h, δ 150.8; (*S*)-**3d** (R = Ph), 72 h, δ 113.3), the crude reaction mixture was directly used for the synthesis of the mixed ligands (*S*)-**5a–f**.

Preparation of (*S*)-R-isoAlaNHOP Derivatives ((*S*)-4a,b). The aminophosphinites (*S*)-**5a,b** were prepared in a manner similar to that described for (*S*)-R-ProNHOP derivatives [(*S*)-**3a–d**] by starting from (*S*)-(+)-1-(methylamino)-2-propanol (5 mmol). Reaction times and $^{31}P\{^1H\}$ NMR ($C_6D_5CD_3$) data were as follows: (*S*)-**4a** (R = Cy), 4 h, δ 137.9; (*S*)-**4b** (R = Cp), 48 h, δ 134.4. The crude reaction mixtures of (*S*)-**4a,b** were directly used for the synthesis of the mixed ligands (*S*)-**6a–c**.

Preparation of (*S*)-R,R′-ProNOP Ligands ((*S*)-5a–f). To a mixture of (*S*)-R-ProNHOP ((*S*)-**3**) prepared as described above was added dropwise a solution of PR'_2Cl (4.8 mmol) in diethyl ether (20 mL). The mixture was stirred at room temperature and monitored by $^{31}P\{^1H\}$ NMR ($C_6D_5CD_3$) until total conversion of (*S*)-**3**. After removal of solvents under vacuum, the crude product was filtered on alumina to remove excess chlorodialkylphosphine and triethylamine chlorhydrate and eluted with diethyl ether (30 mL). Evaporation to dryness of the filtrate afforded (*S*)-**4**.

(*S*)-Cy,Cp-ProNOP ((*S*)-5a): 12 h, 86% yield, white powder; mp 70 °C. $^{31}P\{^1H\}$ NMR ($C_6D_5CD_3$): δ 53.9 (s, P(N)) and 141.7 (s, P(O)). ^1H NMR (C_6D_6): δ 1.0–2.1 (m, 40H), 2.82 (m, 2H, NCH_2), 3.58 (m, 2H, OC*H*H and NCH), 4.14 (m, 1H, OC*H*H). $^{13}C\{^1H\}$ NMR (C_6D_6): δ 25.5–31.0 (m, CH_2), 35.3 (d, CH, J(CP) = 18.9 Hz), 36.2 (d, CH, J(CP) = 10.4 Hz), 41.3 (d, CH, J(CP) = 17.1 Hz), 41.4 (d, CH, J(CP) = 18.3 Hz), 47.5 (d, CH_2N, J(CP) = 9.2 Hz), 65.2 (dd, NCH, J(CP) = 7.9 and 27.5 Hz), 74.8 (dd, OCH_2, J(CP) = 5.5 and 14.7 Hz). MS (*m*/*z*, relative intensity): 396 (100%, M^+ – Cp), 382 (80%, M^+ – Cy), 280 (25%, M^+ – $OPCp_2$), 197 (40%, M^+ – $OPCp_2$ – Cy), 196 (60%, M^+ – $OPCp_2$ – CyH).

(*S*)-Cp,Cy-ProNOP ((*S*)-5b): 12 h, 92% yield, white powder; mp 70 °C. $^{31}P\{^1H\}$ NMR ($C_6D_5CD_3$): δ 57.0 (s, P(N)) and 146.6 (s, P(O)). ^1H NMR (C_6D_6): δ 1.0–2.2 (m, 40H), 2.81 (m, 2H, NCH_2), 3.57 (m, 1H, OCHH), 3.68 (m, 1H, NCH), 4.14 (m, 1H, OCHH). $^{13}C\{^1H\}$ NMR (C_6D_6): δ 25.4 (s, CH_2 prol), 26.0–31.5 (m, CH_2), 38.2 (d, CH, J(CP) = 17.1 Hz), 38.7 (d, CH, J(CP) = 18.3 Hz), 38.8 (d, CH, J(CP) = 18.3 Hz), 39.3 (d, CH, J(CP) = 7.3 Hz), 46.3 (d, CH_2N, J(CP) = 9.2 Hz), 64.2 (dd, NCH, J(CP) = 7.9 and 24.4 Hz), 76.2 (dd, OCH_2, J(CP) = 4.9 and 17.1 Hz). MS (*m*/*z*, relative intensity): 396 (25%, M^+ – Cp), 382 (100%, M^+ – Cy), 252 (20%, M^+ – $OPCy_2$), 183 (35%, M^+ – $OPCy_2$ – Cp), 182 (40%, M^+ – $OPCy_2$ – CpH). Anal. Calcd for $C_{27}H_{49}NOP_2$: C, 69.64; H, 10.61; N, 3.01. Found: C, 69.47; H, 10.46; N, 2.64.

(*S*)-Cp,*i*Pr-ProNOP ((*S*)-5c): 48 h, 89% yield, colorless oil. $^{31}P\{^1H\}$ NMR ($C_6D_5CD_3$): δ 57.1 (s, P(N)) and 151.0 (s, P(O)). ^1H NMR ($CDCl_3$): δ 0.9–2.2 (m, 32H), 2.91 (m, 2H, NCH_2), 3.21 (m, 1H, OC*H*H), 3.38 (m, 1H, NCH), 3.69 (m, 1H, OCH*H*). $^{13}C\{^1H\}$ NMR (C_6D_6): δ 16.9 (d, CH_3, J(CP) = 8.0 Hz), 17.1 (d, CH_3, J(CP) = 8.5 Hz), 17.8 (d, CH_3, J(CP) = 5.5 Hz), 18.1 (d, CH_3, J(CP) = 5.5 Hz), 24.8 (s, CH_2 prol), 25.5–30.8 (m, CH_2), 37.5 (d, CH, J(CP) = 14.7 Hz), 38.6 (d, CH, J(CP) = 4.9 Hz), 46.0 (d, CH_2N, J(CP) = 7.9 Hz), 63.5 (dd, NCH, J(CP) = 7.9 and 23.5 Hz), 75.0 (dd, OCH_2, J(CP) = 4.3 and 15.9 Hz). Anal. Calcd for $C_{21}H_{41}NOP_2$: C, 65.43; H, 10.72; N, 3.63. Found: C, 62.02; H, 10.39; N, 3.27.

(*S*)-*i*Pr,Cp-ProNOP ((*S*)-5d): 48 h, 90% yield, colorless oil. $^{31}P\{^1H\}$ NMR ($C_6D_5CD_3$): δ 62.7 (s, P(N)) and 142.0 (s, P(O)). ^1H NMR ($CDCl_3$): δ 0.9–1.8 (m, 32H), 2.90 (m, 2H, NCH_2), 3.24 (m, 1H, OC*H*H), 3.31 (m, 1H, NCH), 3.69 (m, 1H, OC*H*H). $^{13}C\{^1H\}$ NMR (C_6D_6): δ 18.3–19.3 (d, CH_3), 24.0–29.0 (m), 40.5 (d, CH, J(CP) = 15.9 Hz), 40.5 (d, CH, J(CP) = 16.5 Hz), 46.5 (d, CH_2N, J(CP) = 9.8 Hz), 64.3 (dd, NCH, J(CP) = 7.9 and 26.3 Hz), 73.8 (dd, OCH_2, J(CP) = 4.6 and 13.7 Hz).

(*S*)-Cp,Ph-ProNOP ((*S*)-5e): 96 h, 72% yield, colorless oil. $^{31}P\{^1H\}$ NMR ($C_6D_5CD_3$): δ 57.2 (s, P(N)) and 113.6 (s, P(O)).

(*S*)-Ph,Cp-ProNOP ((*S*)-5f): 48 h, 90% yield, colorless oil. $^{31}P\{^1H\}$ NMR ($C_6D_5CD_3$): δ 46.2 (s, P(N)) and 142.8 (s, P(O)).

Preparation of (*S*)-R,R′-isoAlaNOP Ligands ((*S*)-6a–c). The aminophosphine–phosphinites (*S*)-**6a–c** were prepared in a manner similar to that described for (*S*)-R,R′-ProNOP ligands ((*S*)-**5a–d**) by starting from the (*S*)-R-ProNHOP derivatives ((*S*)-**4a,b**).

(*S*)-Cy,Cp-isoAlaNOP ((*S*)-6a): 96 h, 82% yield, white solid. $^{31}P\{^1H\}$ NMR ($C_6D_5CD_3$): δ 80.4 (s, P(N)) and 135.2 (s, P(O)).

(*S*)-Cp,Cy-isoAlaNOP ((*S*)-6b): 48 h, 76% yield, white solid. $^{31}P\{^1H\}$ NMR ($C_6D_5CD_3$): δ 79.5 (s, P(N)) and 136.0 (s, P(O)).

(*S*)-Ph,Cp-isoAlaNOP ((*S*)-6c): 48 h, 85% yield, colorless oil. $^{31}P\{^1H\}$ NMR ($C_6D_5CD_3$): δ 46.1 (s, P(N)) and 142.7 (s, P(O)). ^1H NMR ($CDCl_3$): δ 1.21 (d, 3H, CH_3, J(HH) = 6.1 Hz), 1.2–2.0 (m, 18H, Cp), 2.54 (d, 3H, NCH_3, J(HP) = 5.1 Hz), 3.09 (m, 1H, NC*H*H), 3.25 (m, 1H, NCH*H*), 3.89 (m, 1H, OCH), 7.2–7.5 (m, 10H, H aro). $^{13}C\{^1H\}$ NMR ($CDCl_3$): δ 20.3 (d, CH_3, J(CP) = 4.7 Hz), 26.2–28.9 (m, CH_2 Cp), 37.8 (d, NCH_3, J(CP) = 3.4 Hz), 40.5 (d, CH Cp, J(CP) = 14.1 Hz), 40.7 (d, CH Cp, J(CP) = 14.4 Hz), 63.3 (dd, NCH_2, J(CP) = 4.7 and 30.9 Hz), 75.9 (dd, OCH, J(CP) = 6.7 and 16.6 Hz).

Preparation of [RhCl{(*S*)-Cy,Cy-ProNOP}]$_2$ ((*S*)-7a). To a solution of $[Rh(COD)Cl]_2$ (0.246 g, 0.5 mmol) in toluene (10 mL) was slowly added a solution of (*S*)-Cy,Cy-ProNOP ((*S*)-**1a**; 0.544 g, 1.1 mmol) in toluene (15 mL). After 15 min of stirring at room temperature, the solution was concentrated under reduced pressure and the resulting orange powder was washed with a small amount of ethanol to remove excess phosphine. Complex (*S*)-**7a** was obtained in a nearly quantitative yield: mp 235–237 °C. $^{31}P\{^1H\}$ NMR ($C_6D_5CD_3$): δ 105.0 (dd, J(PP) = 31 Hz, J(Rh–P(N)) = 217 Hz), 179.5 (dd, J(Rh–P(O)) = 225 Hz); ^{13}C NMR ($C_6D_5CD_3$): δ 23.6, 27.1 (2t, NCH_2CH_2 and $NCHCH_2$, J(CH) = 132 Hz), 27.3–33.4 (m, CH_2 cyclohexyl), 38.4 (dd, P–*C*H; J(CH) = 122 Hz, J(CP) = 36.7 Hz), 42.0 (dd, P–*C*H), 43.6 (dd, P–*C*H, J(CP) = 22.6 Hz), 44.2 (dd, P–*C*H, J(CP) = 30 Hz), 49.3 (t, N–CH_2, J(CH) = 139 Hz), 60.8 (d, N–*C*H, J(CH) = 135 Hz), 65.4 (t, O–CH_2, J(CH) = 143 Hz). Anal. Calcd for $C_{58}H_{106}N_2O_2P_4Cl_2Rh_2$: C, 55.11; H, 8.45; N, 2.22; P, 9.80; Cl, 5.61; Rh, 16.28. Found: C, 55.14; H, 8.54; N, 2.36; P, 9.72; Cl, 5.62; Rh, 16.21. MS (FAB$^+$; *m*/*z*, relative intensity): 1262 (20%, M^+), 631 (100%, M^+/2).

Synthesis and Physical Data for [RhCl{AMPP}]$_2$ Complexes ((*S*)-7b–e and (*S*)-8a–d). Complexes (*S*)-**7b–e** and (*S*)-**8a–d** were synthesized in a procedure similar to that employed for [RhCl{(*S*)-Cy,Cy-ProNOP}]$_2$ by using 1.0 equiv of $[Rh(COD)Cl]_2$ and 2.2 equiv of the appropriate ligand.

[RhCl{(*S*)-Cp,Cp-ProNOP}]$_2$ ((*S*)-7b): mp 190–205 °C dec. $^{31}P\{^1H\}$ NMR ($C_6D_5CD_3$): δ 99.9 (dd, J(PP) = 33 Hz, J(Rh-P(N)) = 219 Hz), 172.4 (dd, J(Rh–P(O)) = 227 Hz). MS

(FAB$^+$; *m/z*, relative intensity): 1151.3 (80%, isotopic mass for $C_{50}H_{90}N_2O_2Cl_2P_4Rh_2$).

[RhCl{(*S*)-*i*Pr,*i*Pr-ProNOP}]$_2$ ((*S*)-7c): $^{31}P\{^1H\}$ NMR ($C_6D_5CD_3$): δ 111.4 (dd, J(PP) = 32 Hz, J(Rh−P(N)) = 219 Hz), 178.7 (dd, J(Rh-P(O)) = 225 Hz).

[RhCl{(*S*)-Cy,Cy-isoAlaNOP}]$_2$ ((*S*)-7d): $^{31}P\{^1H\}$ NMR ($C_6D_5CD_3$): δ 117.1 (dd, J(PP) = 33 Hz, J(Rh-P(N)) = 224 Hz), 158.9 (dd, J(Rh-P(O)) = 218 Hz). Anal. Calcd for $C_{56}H_{106}N_2O_2P_4Cl_2Rh_2$: C, 54.24; H, 8.62; N, 2.26. Found: C, 53.19; H, 8.84; N, 1.72.

[RhCl{(*S*)-Cp,Cp-isoAlaNOP}]$_2$ ((*S*)-7e): $^{31}P\{^1H\}$ NMR ($C_6D_5CD_3$): δ 117.1 (dd, J(PP) = 33 Hz, J(Rh−P(N)) = 225 Hz), 158.8 (dd, J(Rh−P(O)) = 218 Hz).

[RhCl{(*S*)-Cy,Cp-ProNOP}]$_2$ ((*S*)-8a): mp 120 °C dec. $^{31}P\{^1H\}$ NMR ($C_6D_5CD_3$, 323 K): δ 104.7 (dd, J(PP) = 30 Hz, J(Rh−P(N)) = 221 Hz), 169.8 (dd, J(Rh-P(O)) = 223 Hz). MS (FAB$^+$; *m/z*, relative intensity): 1206 (25%, M$^+$), 849 (25%), 603 (100%, M$^+$/2).

[RhCl{(*S*)-Cp,Cy-ProNOP}]$_2$ ((*S*)-8b): mp 120 °C dec. $^{31}P\{^1H\}$ NMR ($C_6D_5CD_3$): δ 97.0 (dd, J(PP) = 31 Hz, J(Rh−P(N)) = 214 Hz), 176.5 (dd, J(Rh−P(O)) = 232 Hz).

[RhCl{(*S*)-Cp,*i*Pr-ProNOP}]$_2$ ((*S*)-8c): $^{31}P\{^1H\}$ NMR ($C_6D_5CD_3$): δ 96.7 (dd, J(PP) = 32 Hz, J(Rh−P(N)) = 216 Hz), 182.5 (dd, J(Rh−P(O)) = 227 Hz).

[RhCl{(*S*)-*i*Pr,Cp-ProNOP}]$_2$ ((*S*)-8d): $^{31}P\{^1H\}$ NMR ($C_6D_5CD_3$): δ 114.6 (dd, J(PP) = 33 Hz, J(Rh−P(N)) = 222 Hz), 166.4 (dd, J(Rh−P(O)) = 225 Hz). MS (FAB$^+$; *m/z*, relative intensity): 1047.3 (50%, isotopic mass for $C_{42}H_{83}N_2O_2Cl_2P_4Rh_2$).

[RhCl{(*S*)-Cp,Ph-ProNOP}]$_2$ [((*S*)-8e): $^{31}P\{^1H\}$ NMR ($C_6D_5CD_3$): δ 97.4 (dd, J(PP) = 41 Hz, J(Rh−P(N)) = 214 Hz), 142.3 (dd, J(Rh−P(O)) = 227 Hz).

[RhCl{(*S*)-Ph,Cp-ProNOP}]$_2$ ((*S*)-8f): $^{31}P\{^1H\}$ NMR ($C_6D_5CD_3$): δ 99.5 (dd, J(PP) = 39 Hz, J(Rh−P(N)) = 223 Hz), 160.8 (dd, J(Rh−P(O)) = 209 Hz).

[RhCl{(*S*)-Cy,Cp-isoAlaNOP}]$_2$ ((*S*)-8g): $^{31}P\{^1H\}$ NMR ($C_6D_5CD_3$): δ 125.2 (dd, J(PP) = 29 Hz, J(Rh−P(N)) = 234 Hz), 155.7 (dd, J(Rh−P(O)) = 220 Hz).

[RhCl{(*S*)-Cp,Cy-isoAlaNOP}]$_2$ ((*S*)-8h): $^{31}P\{^1H\}$ NMR ($C_6D_5CD_3$): δ 114.1 (dd, J(PP) = 33 Hz, J(Rh−P(N)) = 224 Hz), 162.4 (dd, J(Rh−P(O)) = 218 Hz).

[RhCl{(*S*)-Ph,Cp-isoAlaNOP}]$_2$ ((*S*)-8i): $^{31}P\{^1H\}$ NMR ($C_6D_5CD_3$): δ 99.5 (dd, J(PP) = 41 Hz, J(Rh−P(N)) = 222 Hz), 160.7 (dd, J(Rh−P(O)) = 208 Hz).

Preparation of [Rh(η^5-C_5H_5){(*S*)-Cy,Cy-ProNOP}] ((*S*)-9). To a solution of [RhCl{(*S*)-Cy,Cy-ProNOP}]$_2$ (2.01 g, 1.59 mmol) in THF (5 mL) was added dropwise a solution of C_5H_5-Na (0.294 g, 3.34 mmol) in THF (5 mL). Then, the resulting deep orange suspension was concentrated under reduced pressure and the residue was dissolved in a minimum of hot benzene and reprecipitated by addition of acetone. The mixture was kept at −20 °C for 2 days and filtered. The precipitate was then washed with acetone and dried under vacuum to afford (*S*)-**9** as a brown-orange powder (1.96 g, 93% yield): mp 209−210 °C. $^{31}P\{^1H\}$ NMR ($C_6D_5CD_3$): δ 110.2 (dd, J(PP) = 42 Hz, J(Rh−P(N)) = 238 Hz), 186.5 (dd, J(Rh−P(O)) = 243 Hz). ^1H NMR ($C_6D_5CD_3$): δ 1.0−2.2 (m, 48H), 2.45 (m, 1H), 2.85−3.45 (m, 5H), 5.35 (s, 5H, C_5H_5). Anal. Calcd for $C_{34}H_{58}NOP_2Rh$: C, 61.72; H, 8.84; N, 2.12; Rh, 15.55. Found: C, 62.29; H, 9.31; N, 2.28; Rh, 16.26. MS (FAB$^+$; *m/z*, relative intensity): 661 (75%, M$^+$), 578 (25%), 447 (100%). Complex (*S*)-**9** decomposes in chlorinated solvents.

Preparation of [Rh(acac){(*S*)-Cy,Cy-ProNOP}] ((*S*)-10). To a suspension of potassium *tert*-butoxide (0.577 g, 5.14 mmol) in cold (−30 °C) diethyl ether (15 mL) was added dropwise under magnetic stirring 2,4-pentanedione (0.6 mL, 5.84 mmol). The reaction mixture was kept at −30 °C, and a solution of [Rh(COD)Cl]$_2$ (1.26 g, 2.56 mmol) in THF (15 mL) was added. The solution was warmed to room temperature, and a solution of (*S*)-Cy,Cy-ProNOP ((*S*)-**1a**; 2.73 g, 5.54 mmol) in THF (5 mL) was added. The resulting yellow solution was stirred for 24 h, filtered, and evaporated to dryness. The residue was dried under vacuum at 50 °C for 2 h and finally washed with methanol (2 × 50 mL) to give a yellow powder. Crystallization from a dichloromethane−diethyl ether−methanol mixture for 5 days at 5 °C and 1 week at −30 °C afforded yellow crystals of (*S*)-**10**, which were washed with methanol and dried under nitrogen (1.98 g, 56%). The mother solution and washings were then concentrated and submitted to further crystallization at 0 °C (1.10 g, 31%): overall yield 86%; mp 193−195 °C. $^{31}P\{^1H\}$ NMR ($C_6D_5CD_3$): δ 103.6 (dd, J(PP) = 53 Hz, J(Rh−P(N)) = 211 Hz), 177.8 (dd, J(Rh−P(O)) = 220 Hz). Anal. Calcd for $C_{34}H_{60}NO_3P_2Rh$: C, 58.70; H, 8.69; N, 2.01; P, 8.90; Rh, 14.79. Found: C, 58.88; H, 8.78; N, 2.11; P, 8.77; Rh, 14.71. MS (FAB$^+$; *m/z*, relative intensity): 695 (100%, M$^+$), 612 (15%), 481 (35%).

Table 5. Crystal Data and Data Collection Parameters for [Rh(acac){(*S*)-Cy,Cy-ProNOP}] ((*S*)-10)

formula	$C_{34}H_{60}NO_3P_2Rh$
mol wt	695.72
cryst syst	triclinic
space group	*P*1
a, Å	11.459(3)
b, Å	15.980(4)
c, Å	21.684(7)
α, deg	75.17(2)
β, deg	81.73(2)
γ, deg	69.15(2)
Z	4
V, Å^3	3581(2)
d_{calcd}, g cm^{-3}	1.29
μ(Mo K$_\alpha$), cm^{-1}	5.87
temp, K	298
θ range, deg	1.4−27.4
scan type	$\omega/2\theta$
cryst size, mm	0.22 × 0.40 × 0.36
no. of unique data	16 338
no. of data in refinement ($I > 2\sigma(I)$)	14 293
no. of refined params	717
R	0.058
R_w	0.069
ϱ, e·Å^{-3}	0.77

X-ray Structure Determination of [Rh(acac){(*S*)-Cy,Cy-ProNOP}] ((*S*)-10). Lemon yellow crystals were grown from a mixture of dichloromethane, diethyl ether, and methanol. Intensity data for (*S*)-**10** were collected on an Enraf-Nonius CAD4 diffractometer using graphite-monochromated Mo Kα radiation (λ = 0.710 69 Å). Intensities were corrected for Lorentz and polarization effects but not for those of absorption. The pertinent details of data collection and the final cell dimensions are given in Table 5. The structure was solved using the SHELX-86 program[27] and refined by least-squares ($\Sigma w(F_o - F_c)^2$ minimized, $w = 1/\sigma^2(F_o)$].[28] Rh and P atoms were refined anisotropically and the remaining atoms isotropically, and H atoms were not included in the refinement. Atomic coordinates and bond lengths and angles have been deposited with the Cambridge Crystallographic Data Centre, 12 Union Road, Cambridge CB2 1EZ, U.K. Selected bond distances and angles are listed in Table 1.

Asymmetric Hydrogenation of Dihydro-4,4-dimethyl-2,3-furandione (11). A solution of dihydro-4,4-dimethyl-2,3-furandione (**11**; 0.512 g, 4 mmol) in toluene (10 mL) was degassed by freeze−thaw cycles and then was transferred to a Schlenk tube containing (*S*)-**7a** (12.6 mg, 0.01 mmol). The resulting solution was charged in a flask, hydrogen (1 atm) was introduced, and the reaction mixture was stirred at 25 °C for 12 h. Evolution of the reaction was monitored by the consumption of hydrogen. After evaporation of the solvent, the resulting residue was dissolved in water. The catalyst was then removed by filtration through alumina, and the filtrate

(27) Sheldrick, G. M. *Acta Crystallogr.* **1990**, *A46*, 467.
(28) GFMLX, a modified version of ORFLS: Busing, W. R.; Martin, K. O.; Levy, H. A. Report ORNL-TM-305; Oak Ridge National Laboratory: Oak Ridge, TN, 1962.

was evaporated to dryness, affording (*R*)-(−)-pantolactone ((*R*)-**12**) in a nearly quantitative yield. Enantioselectivity (47% ee) of the product was determined by GC analysis (FS-CYCLODEX β-I/P, 130 °C) and controlled on the basis of the optical rotation value (*c* 2.05, H_2O) in comparison with the reported one ($[\alpha]_D^{25} = -50.7°$).[20]

Asymmetric Hydrogenation of *N*-benzylbenzoylformamide (13). This process was carried out under the same conditions as employed for dihydro-4,4-dimethyl-2,3-furandione (**11**) by starting from 0.957 g (4 mmol) of *N*-benzylbenzoylformamide (**13**). At the end of the reaction, after evaporation of the solvent, the resulting powder was washed with a small amount of cold ether and dried under vacuum to afford (*S*)-(+)-*N*-benzylmandelamide ((*S*)-**14**) as a white powder. Chemoselectivity of the product was controlled by ^1H NMR analysis. Enantioselectivity was determined on the basis of the optical rotation value (*c* 1.09, $CHCl_3$) in comparison with the reported one ($[\alpha]_D^{26} = +82.2°$).[10]

Acknowledgment. This study was supported by the Centre National de la Recherche Scientifique and the Ministere de la Recherche et de la Technologie. We thank Dr. G. Ricart for skillful assistance in obtaining mass spectra.

Supplementary Material Available: Tables of atomic positional parameters, Rh and P atom anisotropic thermal parameters, isotropic thermal parameters for other atoms, and all bond distances and angles for (*S*)-**10** (18 pages). Ordering information is given on any current masthead page.

OM940996K

ortho- and *meta*-(Diethynylcyclopentadienyl)tricarbonylmanganese: Building Blocks toward the Construction of Metal Fragment Supported Fullerenynes?

Uwe H. F. Bunz,* Volker Enkelmann, and Frank Beer

Max-Planck-Institut für Polymerforschung, Ackermannweg 21, 55021 Mainz, FRG

Received November 22, 1994[⊗]

Starting from [(trimethylsilyl)ethynyl]cymantrene (**1**), the two isomeric 1,2- and 1,3-[bis-(trimethylsilyl)ethynyl]cymantrenes (**3a**, **4a**) were prepared by a deprotonation/iodination/coupling sequence. The coupling reaction was performed on the mixed *ortho-/meta*-iodo[(trimethylsilyl)ethynyl]cymantrenes (**2**) by using Stille methodology (tin alkynes and $PdCl_2(CH_3CN)_2$ as catalyst in ethyl ether/DMF). Separation of the isomers (**3a**, **4a**) is achieved by chromatography over flash silica gel. The *ortho*-diethynylcymantrene **3a** is isolated in 42%, while the corresponding *meta* compound **4a** is formed in 26%. If the deprotonation reaction of **1** in pentane/TMEDA is performed under carefully controlled conditions (−78 °C), the formation of only *ortho* **2** is observed in 67% yield. Coupling with trimethylstannyl(trimethylsilyl)acetylene furnished **3a** in 57%. Crystal structures have been carried out for complexes **3a** ($C2/c$; a = 29.923(1), b = 15.9145(7), c = 9.327(1) Å, α = 90, β = 102.920(7), γ = 90°; V = 4329.1(6) Å^3; Z = 8; 2948 reflections with $F > 3\sigma(F)$; R = 0.071, R_w = 0.074) and **4a** ($P2_12_12_1$; a = 17.027(3), b = 12.339(4), c = 10.235(2) Å; $\alpha = \beta = \gamma$ = 90°; V = 2150(1) Å^3; Z = 4; 1392 reflections with $F > 3\sigma(F)$; R = 0.059, R_w = 0.058). Removal of the alkyne-bound trimethylsilyl groups is achieved in yields of >80% by treatment of **3a** and **4a** with potassium carbonate in methanol. The parent diethynylcymantrenes (**3b**, **4b**) are stable compounds. Treatment of 1,2-diethynylcymantrene **3b** under Hay conditions gives coupled material, a polymer poly[(*ortho*-cymantrene)butadiynylene] (**6**) in 68% yield (M_n = 9300). If the Hay reaction is conducted with **3b** and an added capping reagent (ethynylcymantrene), a series of oligomeric butadiynylenecymantrenes is isolated starting from the dimer up to the heptamer (dimer **7a**, 8.2%; trimer **7b**, 12.5%; tetramer **7c**, 7.7%; pentamer **7d**, 5.5%; hexamer **7e**, 3.6%; heptamer **7f**, 2.5%; Σ = 40%). The compounds were separated by chromatography over flash silica gel or preparative HPLC. The oligomers **7** are unstable lemon yellow powders.

Introduction

Research on "all-carbon molecules", carbon allotropes, and carbon-rich networks has exploded[1a] since the isolation and characterization of C_{60} and C_{70} by Krätschmer, Fostiropolous, and Huffmann[1b] in 1990 and the observation of cyclocarbons in 1991 by Rubin and Diederich.[1a] Substantial progress has been made in the synthesis of segments of C_{60}. While Scott *et al.* and Siegel *et al.* prepared corannulene[1c] in preparative quantities, Schlüter[1d] was able to synthesize belt-shaped segments of C_{60}, coined "buckypeels".

An almost ubiquitous feature of two- and three-dimensional carbon nets (with exception of the fullerenes) is the alkyne unit as versatile and reactive functional group of sufficient shape stability. Very recently a novel type of "exploded fullerenes", the fullerenynes, was proposed by the Allied-Signal group.[2] These carbon allotropes can be envisioned by introducing two or four sp-hybridized carbon atoms between the original fullerene

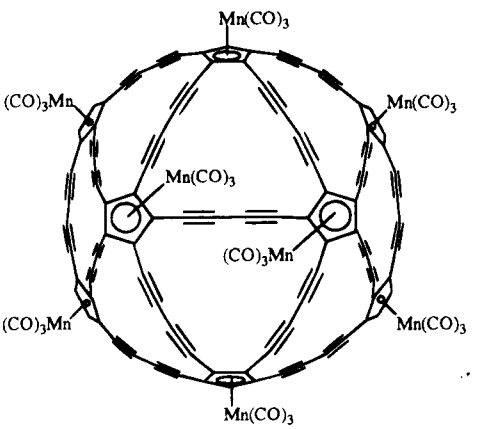

Figure 1. C_{180}-fullerenyne consisting of five-membered $Mn(CO)_3$-supported rings and butadiyne units.

[⊗] Abstract published in *Advance ACS Abstracts,* April 1, 1995.

(1) (a) Bunz, U. H. F. *Angew. Chem., Int. Ed. Engl.* **1994**, *33*, 1073. Diederich, F. *Nature* **1994**, *369*, 199. Diederich, F.; Rubin, Y. *Angew. Chem., Int. Ed. Engl.* **1992**, *31*, 1101. Gleiter, R.; Kratz, D. *Angew. Chem., Int. Ed. Engl.* **1993**, *32*, 842. (b) Krätschmer, W.; Lamb, L. D.; Fostiropoulos, K.; Huffmann, D. R. *Nature* **1990**, *347*, 354. Hammond, G. S., Kuck, V. J., Eds. *Fullerenes, ACS Symposium Series 481*; American Chemical Society: Washington, DC, 1992. (c) Scott, L. T.; Hashemi, M. M.; Meyer, D. T.; Warren, H. B. *J. Am. Chem. Soc.* **1991**, *113*, 7082. Borchardt, A.; Fuchicello, A.; Kilway, A. V.; Baldridge, K. K.: Siegel, J. S. *J. Am. Chem. Soc.* **1992**, *114*, 1921. (d) Schlüter, A. D.; Löffler, M.; Enkelmann, V. *Nature* **1994**, *368*, 831. (e) Expanded pentafulvenes with a pentatetraene linkage: Hafner, K. *Pure Appl. Chem.* **1990**, *62*, 531.

(2) Baughman, R. H.; Galvão, D. S.; Cui, C.; Wang, Y.; Tománek, D. *Chem. Phys. Lett.* **1993**, *204*, 8.

0276-7333/95/2314-2490$09.00/0

Scheme 1

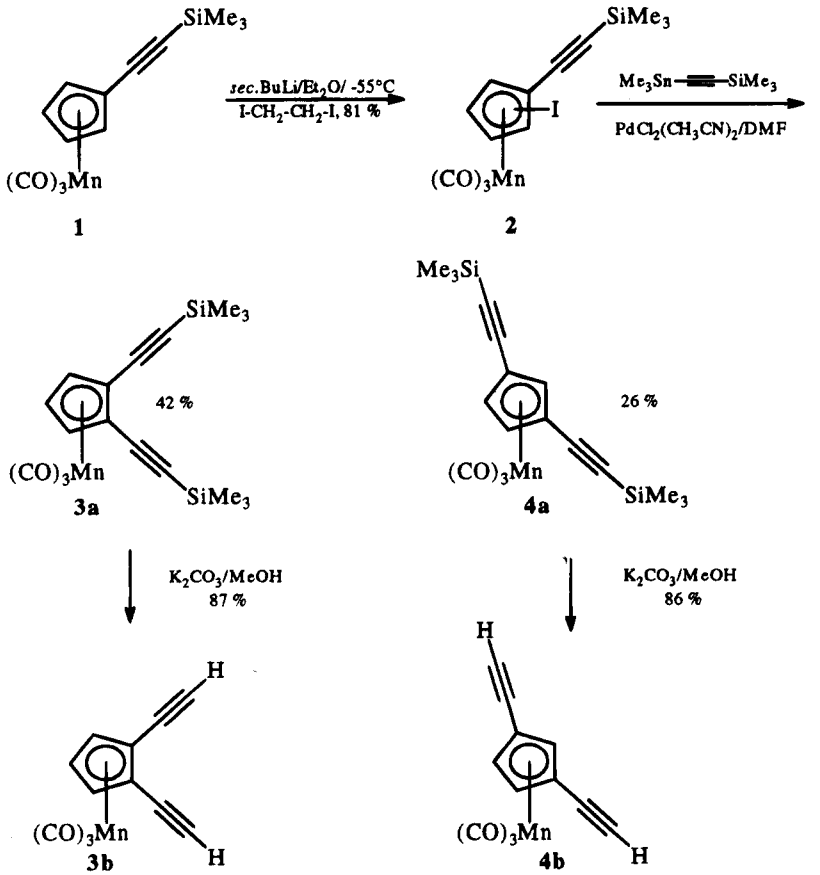

carbons. Some of the proposed species consist *of merely allene-type structures* where every six-membered ring is blown up and the five-membered rings of C_{60} are still intact. Containing merely allene structures will hamper the isolation of macroscopic amounts of these species (if formed) severely, due to their expected instability toward polymerization.[1e] Stabilization might be possible though by selective complexation of the five-membered rings by the $Mn(CO)_3$ group or a similar fragment (see Figure 1) to yield an isolable organometallic fullerenyne. It seemed an attractive goal to us to synthesize segments of these species. In this publication we wish to report on the synthesis of linear segments of an organometallic fullerenyne depicted in Figure 1.

When we started our investigation, only one example of a Cp ring carrying five ethynyl groups[3] was known. Cp complexes with two ethynyl groups on one ring (the necessary building blocks for fullerenyne segments) were not described in the literature. This is different for the well-known 1,1′-diethynyls derived from ferrocene,[4] the fair number of published monoethynyl substituted sandwich and half-sandwich complexes,[5] and the increasing number of diethynylated cyclobutadiene complexes.[6,7]

Results and Discussion

Synthesis of the Monomers 3b and 4b. Our strategy to build the desired monomers, the diethynyls **3** and **4**, rests on a reaction sequence already employed by Stille[5] for the synthesis of monoethynyl cymantrenes. Compound **1**, available in 10-g quantities, was treated with 1.2 equiv of *sec*-BuLi in ethyl ether at −55 °C (Scheme 1) and reacted with a slight excess of 1,2-diiodoethane. During the course of the functionalization a vigorous evolution of gas took place, presumably ethylene. After aqueous workup a mixture of compounds **2** was obtained as a yellow oil by filtration over flash silica gel. A proton NMR spectrum taken from a sample of this oil showed considerable broadening of the displayed signals. Attempts to further separate the mixture by thin layer or column chromatography were not met by success, so the material was used without further characterization in the following coupling step utilizing (trimethylstannyl)(trimethylsilyl)ethyne (**5**) as reaction partner and Beletskaya's catalyst[8] ($PdCl_2(CH_3CN)_2$) in a DMF/ethyl ether mixture (1 h reaction time, 5 mol % catalyst, −20 °C → +21 °C). After removal of the solvent the dark residue was filtered over a plug of flash silica gel to give a waxy yellow solid which was repeatedly chromatographed (flash silica gel, pentane/

(3) Bunz, U. H. F.; Enkelmann, V.; Räder, J. *Organometallics* **1993**, *12*, 4745.

(4) Schlögl, K.; Steyrer, W. *Monatsh. Chemie*, **1965**, *96*, 1520. Buchmeiser, M.; Schottenberger, H. *J. Organomet. Chem.* **1992**, *441*, 457. Buchmeiser, M.; Schottenberger, H. *J. Organomet. Chem.* **1992**, *436*, 223. Pudelski, J. K.; Callstrom, M. R. *Organometallics* **1992**, *11*, 2757. Doisneau, G.; Balvoine, G.; Fillebeen-Khan, T. *J. Organomet. Chem.* **1992**, *425*, 113.

(5) Bunel, E. E.; Valle, L.; Jones, N. L.; Caroll, P. J.; Gonzalez, M.; Munoz, N.; Manriquez, J. M. *Organometallics* **1988**, *7*, 789. Rausch, M. D.; Siegel, A.; Kleman, L. P. *J. Org. Chem.* **1969**, *31*, 2703. Lo Sterzo, C.; Stille, J. K. *Organometallics* **1990**, *9*, 687.

(6) Altmann, M.; Bunz, U. H. F. *Makromol. Chem. Rapid Commun.* **1994**, *15*, 785. Bunz, U. H. F.; Enkelmann, V. *Angew. Chem., Int. Ed. Engl.* **1993**, *32*, 1653.

(7) Fritch, J. R.; Vollhardt, K. P. C. *Organometallics* **1982**, *1*, 590.

(8) Beletskaya, I. P. *J. Organomet. Chem.* **1983**, *250*, 551.

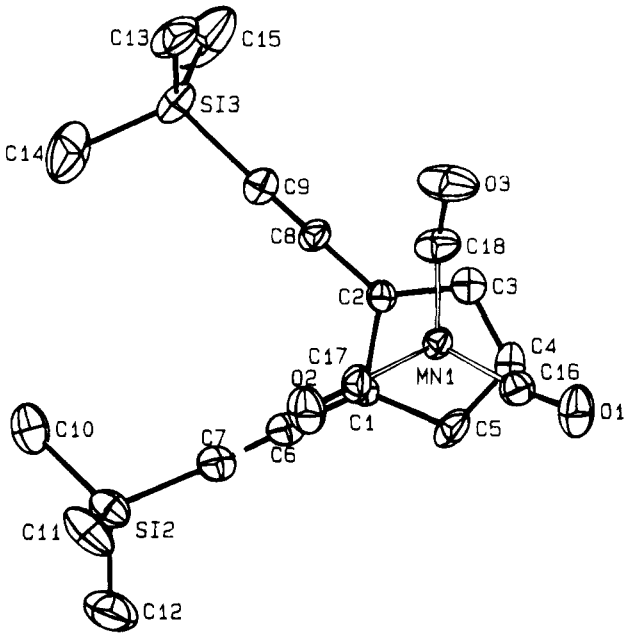

Figure 2. ORTEP drawing of **3a** with the numbering scheme. Hydrogen atoms were omitted for clarity. Selected bond lengths (Å) and angles (deg): C1–C6 1.42(1), C6–C7 1.19(1), C8–C9 1.19(1), C1–C2 1.44(1), C2–C3 1.43(1), C3–C4 1.43(1), C4–C5 1.38(1), C1–C5 1.42(1); C1–C6–C7 179.4(11), C2–C8–C9 179.6(1), C2–C1–C5 106.0 (8).

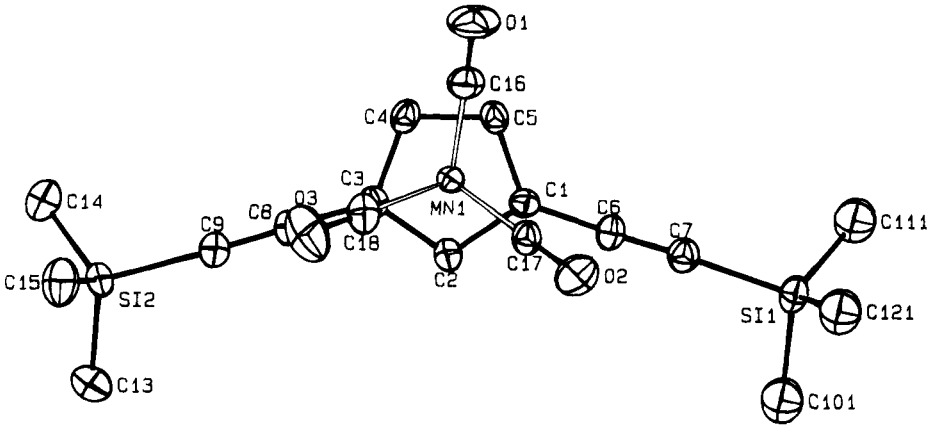

Figure 3. ORTEP drawing of **4a** with the numbering scheme. Hydrogen atoms were omitted for clarity. Selected bond lengths (Å) and angles (deg): C6–C7 1.19(1), C8–C9 1.19 (1), C1–C6 1.42(1), C3–C8 1.40(1), C1–C2 1.44(1), C1–C5 1.42(1), C2–C3 1.43(1), C3–C4 1.43(1), C4–C5 1.38(1); C6–C1–C2 126.2(8), C6–C1–C5 127.6(8), C3–C2–C1 109.2(8), C8–C3–C2 126.9(9). The trimethylsilyl groups are rotationally disordered, and for clarity only the major occupied site (62%) is shown.

ethyl ether as eluent) leading to the isolation of two fractions from which the latter unequivocally was identified by X-ray crystallography to be **3a** (Figure 2) and the forerun being a mixture of two compounds. Distillation of the forerun (0.1 mmHg) yielded as a first reaction **1**, unchanged starting material, and as second fraction (130 °C bath) a compound which was identified by its nuclear magnetic resonance spectra and its IR spectrum to be the *meta* isomer **4a**.[9] This structural assignment of **4a** was corroborated by a crystallographic study (see Figure 3).

In a second experiment the metalation reaction was carried out in pentane at −78 °C. After 5 min tetramethylethylenediamine (12 equiv) was introduced into the reaction mixture. After 1 h at −78 °C, addition of 1,2diiodoethane lead to vigorous evolution of ethylene. After workup and chromatography a yellow oil, *ortho* **2**, was isolated in 67% yield showing very broad resonances in the proton NMR, probably due to the occurrence of a paramagnetic trace impurity, so the palladium-catalyzed coupling with tin alkyne **5** was performed without further characterization of the obtained material (*vide supra*, Scheme 1). Workup and chromatography (flash silica gel, pentane removes unreacted **1**; 92:8 pentane/dichloromethane) affords light yellow crystals of **3a** (57%). No detectable amounts of **4a** were isolated.

It is known for the examples of ethynylbenzene,[9] ethynylthiophene,[10] and tricarbonyl(ethynylcyclobutadiene)iron[11] that deprotonation with excess KO*t*Bu/BuLi or *sec*-BuLi, respectively, preferably occurs in the *ortho*

(9) Brandsma, L.; Hommes, H.; Verkruijsse, H. D.; de Jong, R. C. P. *Recl. Trav. Chim. Pays-Bas* **1985**, *104*, 226.

(10) Soloki, D.; Bradshaw, J. D.; Tessier, C. A.; Youngs, W. J. *Organometallics* **1994**, *13*, 451.

(11) (a) Wiegelmann, J. E. C.; Bunz, U. H. F.; Schiel, P. *Organometallics* **1994**, *13*, 4649. Bunz, U. *Organometallics* **1993**, *12*, 3594. (b) Independently Hafner and Appel discovered that the deprotonation of tricarbonyl(cyclobutadiene)iron also takes place with lithium tetramethylpiperidide: Appel, R. Ph.D. Thesis, Darmstadt, 1991.

Scheme 2

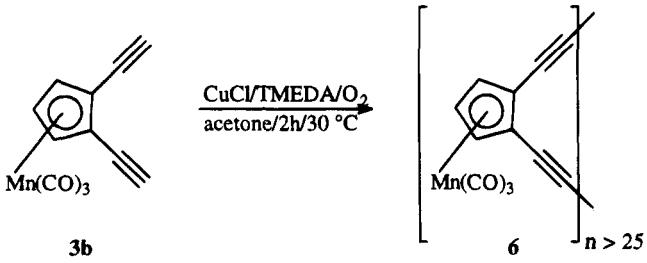

3b 6

position to the triple bond giving access to the corresponding *ortho*-substituted benzenes, thiophenes, and cyclobutadiene metal complexes. Exactly the same behavior is observed here; under suitable conditions merely *ortho* lithiation takes place, while at higher temperature and in ethyl ether as solvent the *meta* position in **1** is attacked as well.

The bond lengths and bond angles in both structures are in good agreement with the expected values. In **3a** the distance C7–C9 is 4.43 Å, which is ca. 0.3 Å more than in the parent *cis*-1,2-diethynylethylene, indicating that a Bergman type rearrangement[12] should be possible only at temperatures >250 °C. In **4a** the angle between the two alkyne arms is 143° and additionally the two trimethylsilyl groups are rotationally disordered.

The two isomers **3a**, **4a** do not show signs of decomposition during storage at ambient conditions for several days and are completely stable for an indefinite period of time when kept at −18 °C.

Deprotection of the silylated diethynyls is achieved in 87 and 86% yields by stirring **3a**, **4a** with potassium carbonate in methanol at 20 °C for 15 min. The deprotected diethynyls **3b** and **4b** are obtained analytically pure and are stable under atmospheric conditions for several hours. They can be stored at −30 °C indefinitely.

Hay Coupling Experiments with 3a. Synthesis of 6 and 7. In order to gain access to the desired fullerenyne segments, we subjected **3b** to the conditions of the oxidative Hay coupling[13] in acetone for 2 h at 30 °C at relatively high concentration (ca. 0.3 mol/L). To our surprise we were able to detect the formation of a polymer (Scheme 2) after double precipitation from pentane/dichloromethane (80:20) in 68% which we unequivocally can assign structure **6** by NMR and IR spectroscopy (see Figure 4). The polymer **6** should consist of stereoisomers. The ^{13}C NMR spectrum of **6** shows six broadened lines (five between δ 70 and 90; Table 1, Figure 4) indicating that the stereoisomers have very similar spectroscopic properties. Analytical GPC suggests that the number average degree of polymerization is ca. 38.[14] The small amount of formed oligomeric material consisted of a mixture of different compounds which we have not been able to separate by chromatography. The mixture was sensitive and decomposed immediately under considerable darkening. We presume that these species are cyclic oligomers.

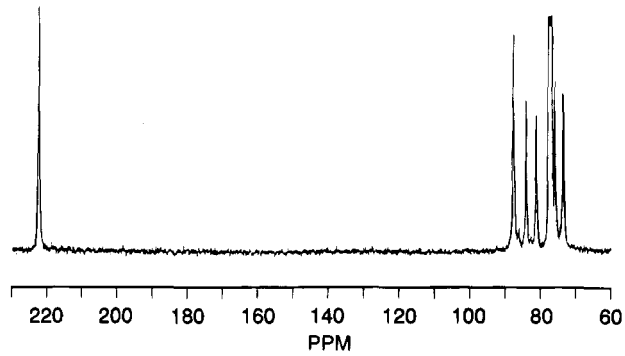

Figure 4. ^{13}C NMR spectrum of polymer **6** in $CDCl_3$.

Table 1. ^{13}C NMR Spectroscopic Data (δ) for the Compounds 6 and 7

	Cp						butadiyne C		CO
	end		inner		quaternary				
6			80.96	87.50	83.82		73.36	75.73	222.49
7a	82.07	88.13			78.60		72.67	73.95	223.47
7b	82.10	88.33	80.86	86.91	78.14	84.35	71.91	72.57	222.63
							75.29	75.82	223.47
7c	82.10	88.29	80.88	87.03	78.30	84.51	71.91	72.64	222.56
			87.28		83.90	83.95	73.29	75.38	223.43
							75.74	75.97	
7d	82.09	88.34	80.81	87.06	78.20	83.98	71.87	72.60	223.43
			87.35	87.44	84.44		73.20	73.30	222.55
							75.36	75.71	
							75.79	75.94	
7e	82.13	88.35	80.84	87.07	78.15	83.90	71.89	72.56	223.46
			87.46		84.41		73.28	75.40	222.54
							75.79	75.94	
7f	82.13	88.36	80.84	87.07	78.16	83.96	71.89	72.59	222.52
			87.46		84.43		73.29	75.40	223.47
							75.71	75.81	
							75.94		

Surprisingly the same experiment conducted at a much lower concentration of monomer did not seem to favor the formation of cycles either. In order to gain access to linear oligomers, we performed a co-oligomerization of **3b** with ethynylcymantrene[5,15] (Scheme 3). Aqueous workup resulted in the isolation of a 85% yield of coupled products. TLC of the raw product with ethyl ether as eluent showed that a whole series of compounds **7** must have formed in this reaction. Repeated chromatography and preparative HPLC made **7a**–**f** accessible in relatively low yields (**7a**, 8.2%; **b**, 12.5%; **c**, 7.7%; **d**, 5.5%; **e**, 3.6%; **f**, 2.5%; Σ = 40%). While it was possible to purify **7a**–**d** by chromatography over flash silica gel with 70:30 pentane/ethyl ether, the higher oligomers had to be separated by preparative HPLC. The low yields of the purified products in comparison to the 85% yield of the raw products is due to heavy losses during chromatography. While in the case of **7a**,**b** the occurrence of only one isomer is possible, the higher oligomers **7c**–**f** should form mixtures of stereoisomers which we have been able to resolve neither by column chromatography nor by HPLC. The ^{13}C NMR spectra of **7b**–**f** do not show a split of the lines (Table 1); the same behavior is observed here as it is in polymer **6** (exception is observed in **7c**), but some of the signals of the oligomers are considerably broadened (Table 1) indicating the (expected) formation of mixtures of stereoisomers.

(12) Nicolaou, K. C.; Dai, W.-M. *Angew. Chem., Int. Ed. Engl.* **1991**, *30*, 1387. Bergman, R. G. *Acc. Chem. Res.* **1973**, *6*, 25.

(13) Hay, A. S. *J. Org. Chem.* **1960**, *27*, 3320. Glaser, C. *Chem. Ber.* **1869**, *2*, 422.

(14) Gel permeation chromatography of **6** was performed using polystyrene as standard. The obtained molecular weights were multiplied by the factor of 2.42 to correct for the different molecular weights of the two monomers: M_n = 9300; M_w = 15200; M_w/M_n = 1.58.

(15) Lo Sterzo, C.; Miller, M. M.; Stille, J. K. *Organometallics* **1989**, *8*, 2331.

Scheme 3

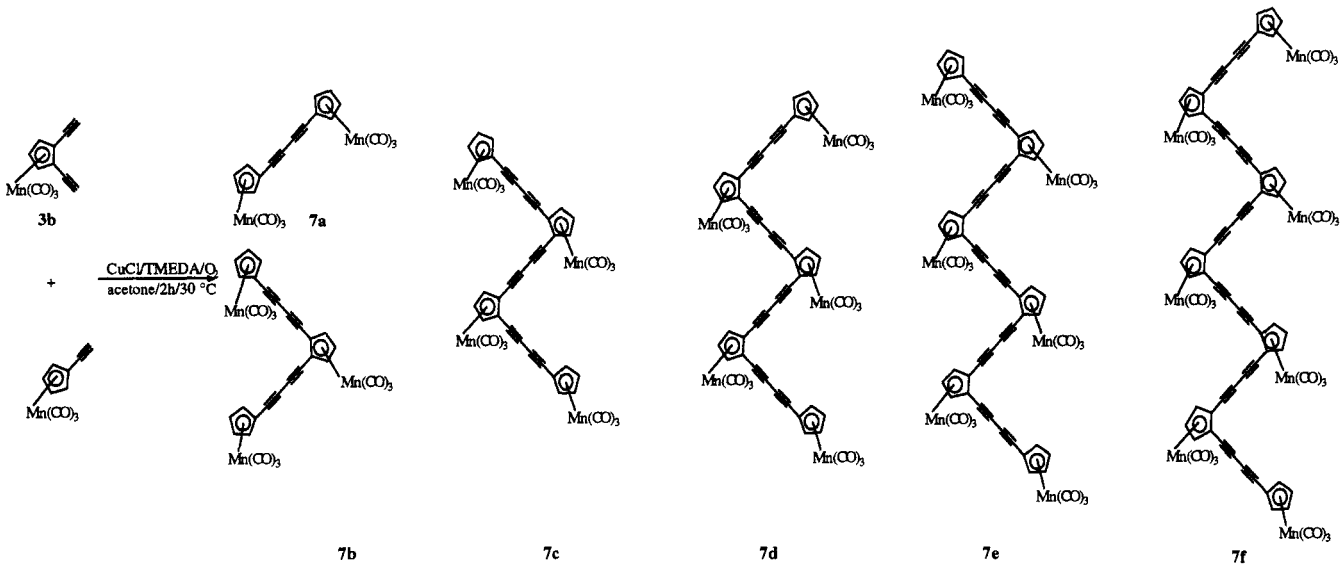

Conclusions

In conclusion we have been able to show that the facile preparation of the hitherto unknown tricarbonyl(diethynylcyclopentadienyl)manganese complexes **3** and **4** can be achieved utilizing Stille–Beletskaya methodology. Diethynyl **3b** can be used in a Hay-type reaction to either polymerize to **6** or by addition of an end capping reagent oligomerize this novel building block to **7a–f**. The formed linear oligomers **7** represent tricarbonylmanganese-supported linear segments out of a hitherto unknown member of the fullerenyne family.

Experimental Section

Ethyl ether and tetrahydrofuran (THF) were distilled from benzophenone/potassium under nitrogen. Dimethylformamide was distilled from calcium hydride *in vacuo*. Pentane and methanol were used as received from Riedel de Haen. *N,N,N′,N′*-Tetramethylethylenediamine (TMEDA), 1,2-diiodethane, triphenylarsine, $PdCl_2(CH_3CN)_2$, tris(dibenzylidene)-dipalladium, and *sec*-BuLi were purchased from Aldrich. (Trimethylsilyl)(trimethylstannyl)acetylene (**5**) was prepared by deprotonation of (trimethylsilyl)acetylene with BuLi in ethyl ether and functionalization with trimethyltin chloride. All reactions were carried out under an atmosphere of nitrogen in flame-dried glassware using standard inert-gas and Schlenk techniques. ^1H NMR spectra are recorded at 300 MHz, and ^{13}C NMR spectra, at 75 MHz at ambient temperature. For preparative HPLC a Gilson Abimed 305 with a Merck LiCroSorb CN (10 μm) column (21 cm × 5 cm) was used with pure ethyl ether (Riedel de Haen, pa quality) as eluent (flow rate 20 mL/min).

Tricarbonyl[((trimethylsilyl)ethynyl)cyclopentadienyl]-manganese (1). A 20.0 g (60.6 mmol) amount of iodocymantrene,[15] 17.0 g (65.1 mmol) of **5**, and 500 mg (1.93 mmol) of $PdCl_2(CH_3CN)_2$ are stirred at 0 °C in ca. 50 mL of DMF for 2 h. The reaction mixture is allowed to warm to 21 °C and is stirred at this temperature for another 14 h. Removal of DMF (oil pump vacuum, 21 °C) and sublimation of the dark residue (50 °C/0.05 mmHg) yields 13.7 g (75%, mp 55 °C) of **1** as yellow crystals. IR (KBr, cm^{-1}): ν 3119, 2963, 2161, 2025, 1938, 1468, 1251. ^1H ($CDCl_3$): 0.21 (s, 9 H), 4.66 (t, J = 2.1 Hz; 2 H), 4.97 (t, J = 2.1 Hz; 2 H). ^{13}C NMR ($CDCl_3$): δ 0.30, 81.92, 82.80, 86.21, 94.88, 96.94, 224.01. MS (EI; *m/z* (relative intensity)): 300 (M^+, 12%), 244 (M^+ − 2CO, 20%), 216 (M^+ − 3CO, 100%). Anal. Calcd: C, 52.01; H, 4.36. Found: C, 52.05; H, 4.33.

***Ortho* Metalation Experiment with TMEDA in Pentane at 78 °C.** An amount of 2.00 g (6.66 mmol) of **1** in 50 mL of pentane is cooled to −78 °C; *sec*-BuLi (5.0 mL, 7.0 mmol) is added by syringe, and the formed solution is stirred for 5 min. A precooled solution of TMEDA (9.76 g, 84.0 mmol, −78 °C) in 20 mL of pentane is added slowly. The resulting solution is stirred for 1 h at −78 °C whereupon a thick suspension forms. To this suspension 1,2-diiodoethane (2.11 g, 7.49 mmol) dissolved in the minimum amount of pentane is added quickly. Warming to 21 °C, aqueous workup, and filtration (flash silica gel, 3 cm × 2 cm, pentane) yields 1.56 g (55%) of *ortho* **2** which shows very broad resonances in the NMR and is used without further purification and characterization.

Metalation Experiment in Ethyl Ether at −55 °C. An amount of 5.00 g (16.7 mmol) of **1** in 200 mL of ethyl ether is treated with 15.0 mL (21.0 mmol) *sec*-BuLi at −55 °C for 20 min. Diiodoethane (6.00 g, 21.3 mmol) in ca. 20 mL of ethyl ether is added. Workup (*vide supra*) yields 5.84 g (81%) of **2** as a yellow oil.

Tricarbonyl{1,2-bis[(trimethylsilyl)ethynyl]cyclopentadienyl}manganese (3a). An amount of 1.56 g (3.62 mmol) of *ortho* **2**, 1.60 g (6.13 mmol) of **5**, and 20 mg (77 μmol) of $PdCl_2(CH_3CN)_2$ are dissolved at −20 °C in 2 mL of DMF and ca. 10 mL of ethyl ether. After removal of the cooling bath, the reaction mixture is stirred for 0.5 h. An additional 20 mg (77 μmol) of catalyst is added at 21 °C, and the stirring is continued for another 0.5 h. The solvent is removed at 0.1 mm/Hg at 21 °C. Repeated chromatography of the residue (flash silica gel, 18 cm × 2 cm; 19:1 pentane/dichloromethane) yields as first fraction 247 mg of **1** and as second fraction 821 mg (57%, mp 82 °C) of **3a**. IR (KBr, cm^{-1}): ν 3122, 3114, 2962, 2169, 2027, 1950, 1454. ^1H NMR ($CDCl_3$): δ 0.24 (s, 18 H), 4.56 (t, 1 H, J = 2.8 Hz), 4.91 (d, 2 H, J = 2.8 Hz). ^{13}C NMR ($CDCl_3$): δ −0.27, 80.33, 84.75, 86.20, 95.54, 97.75, 223.53. MS (EI; *m/z* (relative intensity)): 396 (M^+, 1%), 312 (M − 3CO, 100%). Anal. Calcd: C, 54.52; H, 5.33. Found: C, 54.44; H, 5.10.

Tricarbonyl{1,3-bis[(trimethylsilyl)ethynyl]cyclopentadienyl}manganese (4a). An amount of 5.84 g (13.6 mmol) of **2** (*ortho*–*para* mixture), 5.00 g (19.1 mmol) of **5**, and 2 × 90 mg (2 × 347 μmol) of $PdCl_2(CH_3CN)_2$ in 5 mL of DMF and 25 mL of ethyl ether are treated as described for **3a**. Repeated chromatography (*vide supra*; 20 cm × 4 cm) yields as first fraction a mixture of **4a** and **1**. Short path distillation of this mixture leads to the isolation of 432 mg of **1** (80 °C/0.01 mmHg) and 1.38 g (26%; 130–150 °C/0.01 mmHg; mp 51 °C) of **4a** as a light yellow solid. The second fraction of the

chromatography yields 2.27 g (42%) of **3a**. Data for **4a** are as follows. IR (KBr, cm^{-1}): ν 3118, 2968, 2169, 2020, 1944, 1250. ^1H NMR ($CDCl_3$): δ 0.17 (s, 18 H), 4.85 (d, 2 H, J = 1.7 Hz), 5.14 (t, 1 H, J = 1.7 Hz). ^{13}C NMR ($CDCl_3$): δ −0.33, 81.92, 85.19, 88.93, 95.28, 96.22, 223.47. MS (EI; *m/z* (relative intensity)): 396 (M^+ 6%), 340 (M − 2CO, 20%), 312 (M − 3CO, 80%). Anal. Calcd: C, 54.52; H, 5.34. Found: C, 54.72; H, 5.33.

Tricarbonyl(1,2-diethynylcyclopentadienyl)manganese (3b). An amount of 974 mg (2.44 mmol) of **3a** and 500 mg (5.00 mmol) of K_2CO_3 are dissolved in 20 mL of methanol, and the solution is stirred for 15 min. Partition between pentane and water yields 535 mg (87%; yellow powder, mp 51 °C) of analytically pure **3b**. IR (KBr, cm^{-1}): ν 3294, 3136, 3112, 2123, 2019, 1939, 1913. ^1H NMR ($CDCl_3$): δ 3.04 (s, 2 H), 4.62 (t, 1 H, J = 2.8 Hz), 4.98 (d, 2 H, J = 2.8 Hz). ^{13}C NMR ($CDCl_3$): δ 74.60, 79.93, 80.58, 84.80, 85.63, 223.20. MS (FD; *m/z*): 252 (M^+). Anal. Calcd: C, 57.17; H, 1.99. Found: C, 57.06; H, 1.94.

Tricarbonyl(1,3-diethynylcyclopentadienyl)manganese (4b). An amount of 991 mg (2.49 mmol) of **4a** is treated as described for **3b** to give 543 mg (86%; yellow powder, mp 53 °C) of analytically pure **4b**. IR (KBr, cm^{-1}): ν 3300, 2124, 2028, 1937. ^1H NMR ($CDCl_3$): δ 2.83 (s, 2 H), 4.96 (d, 2H, J = 1.5 Hz), 5.29 (t, 1H, J = 1.5 Hz). ^{13}C NMR ($CDCl_3$): δ 75.33, 77.56, 79.69, 85.83, 90.37, 223.12. Anal. Calcd: C, 57.17; H, 1.99. Found: C, 57.03; H, 1.78.

Poly{tricarbonyl(1,2-diethyndiylcyclopentadienyl)manganese} (6). An amount of 1.12 g (4.44 mmol) of **3b**, 500 mg of CuCl (5.05 mmol), and 600 mg (5.16 mmol) of TMEDA are dissolved in ca. 50 mL of acetone, and the solution is warmed to 30 °C. Under stirring, oxygen is bubbled through the solution for 2.5 h. After removal of the acetone *in vacuo* the residue is dissolved in dichloromethane and washed thoroughly with water to remove copper salts and amine. After evaporation of the solvent the crude product is dissolved in the minimum amount of dichloromethane and precipitated twice into a 85:15 mixture of pentane and dichloromethane to remove oligomers. Polymer **6** is isolated in 68% yield (767 mg) as a sensitive brownish film-forming and transparent material which decomposes in the laboratory atmosphere during several hours under darkening. IR (KBr, cm^{-1}): ν 3124, 2227, 2163, 2028, 1945, 1938. ^1H NMR ($CDCl_3$): δ 4.75 (bs, 2 H), 5.08 (bs, 1 H).

Hay-Coupling of Ethynylcymantrene with 3b in Acetone. An amount of 1.62 g (6.42 mmol) of **3b**, 0.910 g (3.99 mmol) of ethynylcymantrene, 2.00 g (20.2 mmol) of CuCl, and 2.00 g (17.2 mmol) of TMEDA in 100 mL of acetone are treated as described for the synthesis of **6** to isolate 2.11 g (84%) of the crude coupling product. Chromatography over flash silica with a pentane/ethyl ether gradient (0%−100% ethyl ether) yields two fractions (I, 497 mg; II, 1.05 g). Methanol/ethyl ether (1:1) yields 558 mg of a third fraction. We were able to separate **7a−d** from fraction I after repeated chromatography (pentane/ethyl ether variable ratio) involving heavy losses. Fraction II was separated by preparative HPLC and shown to contain **7a−f**. The HPLC-separated oligomers were dissolved in the minimum amount of dichloromethane and precipitated into pentane to remove traces of stabilizer added to the used eluent ethyl ether. The combined yields from I and II were as follows.

1,4-Bis(cymantrenyl)butadiyne (7a): 194 mg, 8.2%, retention time 16.1 min; mp 151 °C; ^1H NMR ($CDCl_3$) δ 4.10 (bs, 4 H), 5.11 (bs, 4 H).

(α-Cymantrenylbutadiynyl)-ω-cymantrenyl[1,2-cymantrenylene(4,1-butadiynediyl)] (7b): 306 mg, 12.5%, retention time 17.5 min; mp 169 °C; IR (KBr, cm^{-1}) ν 3124, 2226, 2162, 2024, 1940, 836; ^1H NMR ($CDCl_3$) δ 4.63 (bs, 1 H), 4.70 (bs, 4 H), 5.04 (bs, 2 H), 5.12 (bs, 4 H); MS (FD; *m/z*) 705 (M^+).

(α-Cymantrenylbutadiynyl)-ω-cymantrenylbis[1,2-cymantrenylene(4,1-butadiynediyl)] (7c): 192 mg, 7.7%, retention time 19.2 min; dec 115 °C; IR (KBr, cm^{-1}) ν 3123, 2228, 2162, 2026, 1941, 848, 836; ^1H NMR ($CDCl_3$) δ 4.66 (bs, 2 H), 4.71 (bs, 4 H), 5.08 (m, 4 H), 5.12 (bs, 4 H); MS (FD; *m/z*) 955 (M^+).

(α-Cymantrenylbutadiynyl)-ω-cymantrenyltris[1,2-cymantrenylene(4,1-butadiynediyl)] (7d): 139 mg, 5.5%, retention time 20.5 min; dec 123 °C; IR (KBr, cm^{-1}) ν 3124, 2227, 2162, 2025, 1939, 848, 834; ^1H NMR ($CDCl_3$) δ 4.64 (bs, 3 H), 4.70 (bs, 4 H), 5.05 (bs, 2 H), 5.10 (bs, 4 H), 5.13 (s, 4 H); MS (FD; *m/z*) 1205 (M^+).

(α-Cymantrenylbutadiynyl)-ω-cymantrenyltetrakis[1,2-cymantrenylene(4,1-butadiynediyl)] (7e): 93 mg, 3.6%, retention time 22.5 min; ^1H NMR ($CDCl_3$) δ 4.64 (bs, 4 H), 4.71 (bs, 4 H), 5.08 (bs, 12 H).

(α-Cymantrenylbutadiynyl)-ω-cymantrenylpentakis[1,2-cymantrenylene(4,1-butadiyne-diyl)] (7f): 65 mg, 2.5%, retention time 25.0 min; ^1H NMR ($CDCl_3$) δ 4.64 (bs, 5 H), 4.71 (bs, 4 H), 5.05 (bs, 2 H), 5.06 (bs, 8 H), 5.15 (bs, 4 H).

Crystallographic Data for 3a. $C_{18}H_{21}O_3Si_2Mn$: M = 396.4; light yellow, air stable blocks (0.30 × 0.25 × 0.40 mm^3); space group $C2/c$; a = 29.923(1), b = 15.9145(7), c = 9.327(1) Å; α = 90, β = 102.920(7), γ = 90°; V = 4329.1(6) $Å^3$; Z = 8; D_c = 1.217 g cm^{-3}; μ = 61.65 cm^{-1}; 3150 reflections, 2948 observed ($F > 3\sigma(F)$); R = 0.071, R_w = 0.074.

Crystallographic Data for 4a. $C_{18}H_{21}O_3Si_2Mn$: M = 396.4; light yellow, air stable blocks (0.20 × 0.25 × 0.50 mm^3); space group $P2_12_12_1$; a = 17.027(3), b = 12.339(4), c = 10.235(2) Å; $\alpha = \beta = \gamma$ = 90°; V = 2150(1) $Å^3$; Z = 4; D_c = 1.225 g cm^{-3}; μ = 62.06 cm^{-1}; 1585 reflections, 1392 observed ($F > 3\sigma(F)$); R = 0.059, R_w = 0.058.

Data collection was carried out in both cases at 298 K with an Enraf-Nonius-CAD4 automatic diffractometer (Cu Kα radiation, λ = 1.5405 Å). The structures were solved by the heavy atom method (Patterson), and the non-hydrogen atoms were refined anisotropically. Programs used were CRYSTALS and MOLEN. An empirical absorption correction was applied. Refinement was done by full matrix least squares analyses with anisotropic temperature factors for all non-hydrogen atoms. The hydrogen atoms were refined with fixed isotropic temperature factors in the riding mode.

Acknowledgment. U.H.F.B. is a Liebig scholar (1992−1994) and DFG scholar (1994−1996) and wishes to thank Prof. K. Müllen and Mrs. Addy Bunz for generous support and the Fonds der Chemischen Industrie, the Stiftung Volkswagenwerk, the Deutsche Forschungsgemeinschaft, and the BASF for financial aid. We thank also Jutta Wiegelmann for helpful discussions.

Supplementary Material Available: Tables of crystallographic parameters, positional and thermal parameters, and bond distances and angles for **3a** and **4a** (11 pages). Ordering information is given on any current masthead page.

OM940890P

Synthesis, X-ray Structure, and Protonation of $[Os(C_2Ph)\{NH{=}C(Ph)C_6H_4\}(CO)(PiPr_3)_2]$

Miguel A. Esteruelas,* Fernando J. Lahoz, Ana M. López, Enrique Oñate, and Luis A. Oro

Departamento de Química Inorgánica, Instituto de Ciencia de Materiales de Aragón, Universidad de Zaragoza-CSIC, 50009 Zaragoza, Spain

Received December 8, 1994[⊗]

The bis(alkynyl) complex $[Os(C_2Ph)_2(CO)(PiPr_3)_2]$ (**1**) reacts with benzophenone imine to give $[Os(C_2Ph)_2(CO)(NH{=}CPh_2)(PiPr_3)_2]$ (**2**) as a mixture of two isomers, *cis*-bis(alkynyl) (**2a**) and *trans*-bis(alkynyl) (**2b**). In toluene under reflux, this mixture is converted into $[Os(C_2Ph)\{NH{=}C(Ph)C_6H_4\}(CO)(PiPr_3)_2]$ (**3**) and phenylacetylene. The X-ray crystal structure of **3** has been determined (triclinic, space group $P\bar{1}$ with $a = 11.078(1)$ Å, $b = 18.910(2)$ Å, $c = 20.290(2)$ Å, $\alpha = 67.562(7)°$, $\beta = 89.427(9)°$, $\gamma = 87.289(9)°$, and $Z = 4$). **3** reacts with HBF_4 in diethyl ether to give phenylacetylene and $[Os\{NH{=}C(Ph)C_6H_4\}(CO)(OH_2)(PiPr_3)_2]BF_4$ (**4**), which by reaction with CH_3Li affords $[Os(CH_3)\{NH{=}C(Ph)C_6H_4\}(CO)(PiPr_3)_2]$ (**5**).

Introduction

Transition metal alkynyl complexes have received increasing attention in recent years.[1–4] The interest of these compounds stems from their potential applications in the materials science field[2] and from the fact that they have been found to be key intermediates in the oligomerization of alkynes.[3] Recently, it has also been suggested that these types of compounds can play a main role in the reduction of terminal alkynes by hydrogen transfer reactions and hydrogenation with molecular hydrogen.[4]

We recently reported that the tetrahydrido complex $[OsH_4(CO)(PiPr_3)_2]$ reacts with a stoichiometric amount of phenylacetylene to give the alkynyl–hydrido–dihydrogen derivative $[OsH(C_2Ph)(\eta^2\text{-}H_2)(CO)(PiPr_3)_2]$, which by reaction with a second molecule of phenylacetylene affords the bis(alkynyl) derivative $[Os(C_2Ph)_2(CO)(PiPr_3)_2]$ (**1**).[5] At room temperature, **1** undergoes addition of Lewis bases that are not too bulky (e.g. CO, $P(OMe)_3$, PMe_3) to form octahedral compounds of formula $[Os(C_2Ph)_2(CO)L(PiPr_3)_2]$.[6] In the presence of acetic acid, complex **1** gives the vinylacetato derivative $[Os(C_2Ph)\{C(=CHPh)OC(O)CH_3\}(CO)(PiPr_3)_2]$, which by protonation with HBF_4 in diethyl ether leads to the carbene compound $[Os(C_2Ph)\{=C(CH_2Ph)OC(O)CH_3\}(CO)(PiPr_3)_2]BF_4$.[7]

Continuing with our study on the chemical properties of **1**, we have now investigated its reactivity toward benzophenone imine. During this study, we have observed that one of the two alkynyl groups of **1** is displaced by the benzophenone imine ligand, to give the ortho-metalated compound $[Os(C_2Ph)\{NH{=}C(Ph)C_6H_4\}(CO)(PiPr_3)_2]$. Although ortho-metalated compounds of Schiff bases and other nitrogen-donor ligands related to benzophenone imine are known,[8] as far as we know, the displacement of an alkynyl group by this type of ligands has no precedent.

In this note, we report the synthesis, X-ray structure, and protonation of the ortho-metalated complex $[Os(C_2Ph)\{NH{=}C(Ph)C_6H_4\}(CO)(PiPr_3)_2]$.

⊗ Abstract published in *Advance ACS Abstracts,* April 1, 1995.

(1) Nast, R. *Coord. Chem. Rev.* **1982,** *47,* 89.

(2) (a) Hagihara, N.; Sonogashira, K.; Takahashi, S. *Adv. Poly. Sci.* **1981,** *41,* 149. (b) Wynne, K. J.; Rice, R. *Annu. Rev. Mater. Sci.* **1984,** *14,* 297. (c) Takahashi, S.; Takai, Y.; Morimoto, H.; Sonogashira, K. *J. Chem. Soc., Chem. Commun.* **1984,** 3. (d) Guha, S.; Frazier, C. C.; Kang, K.; Finberg, S. E. *Opt. Lett.* **1989,** *14,* 952. (e) Blau, W. J. ; Byrne, H. J. ; Cardin, D. J.; Davey, A. P. *J. Mater. Chem.* **1991,** *1,* 245. (f) Sun, Y.; Taylor, N. J.; Carty, A. J. *Organometallics* **1992,** *11,* 4293. (g) Espinet, P.; Esteruelas, M. A.; Oro, L. A.; Serrano, J. L.; Sola, E. *Coord. Chem. Rev.* **1992,** *117,* 215.

(3) (a) Field, L. D.; George, A. V.; Hambley, T. W. *Inorg. Chem.* **1990,** *29,* 4565. (b) Bianchini, C.; Peruzzini, M.; Zanobini, F.; Frediani, P.; Albinati, A. *J. Am. Chem. Soc.* **1991,** *113,* 5453. (c) Wakatsuki, Y.; Yamazaki, H.; Kumegawa, N.; Satoh, T.; Satoh, J. *J. Am. Chem. Soc.* **1991,** *113,* 9604. (d) Jia, G.; Galluci, J. C.; Rheingold, A. L.; Haggerty, B. S.; Meek, D. W. *Organometallics* **1991,** *10,* 3459. (e) Field, L. D.; George, A. V.; Malouf, E. Y.; Slip, I. H. M.; Hambley, T. W. *Organometallics* **1991,** *10,* 3842. (f) McMullen, A. K.; Selegue, J. P.; Wang, J. G. *Organometallics* **1991,** *10,* 3421. (g) Field, L. D.; George, A. V.; Purches, G. R.; Slip, I. H. M. *Organometallics* **1992,** *11,* 3019. (h) Santos, A.; López, J.; Matas, L.; Ros, J.; Galán, A.; Echavarren, A. M. *Organometallics* **1993,** *12,* 4215. (i) Schäfer, M.; Mahr, N.; Wolf, J.; Werner, H. *Angew. Chem., Int. Ed. Engl.* **1993,** *32,* 1315. (j) Wiedermann, R.; Steinert, P.; Schäfer, M.; Werner, H. *J. Am. Chem. Soc.* **1993,** *115,* 9864. (k) Barbaro, C.; Bianchini, C.; Peruzzini, M.; Polo, A.; Zanobini, F.; Frediani, P. *Inorg. Chim. Acta* **1994,** *220,* 5.

(4) Chaloner, P. A.; Esteruelas, M. A.; Joó, F.; Oro, L. A. *Homogeneous Hydrogenation*; Kluwer Academic Publishers: Boston, MA, 1994; Chapters 2 and 3.

(5) Espuelas, J.; Esteruelas, M. A.; Lahoz, F. J.; Oro, L. A.; Valero, C. *Organometallics* **1993,** *12,* 663.

(6) Werner, H.; Meyer, U.; Esteruelas, M. A.; Sola, E.; Oro, L. A.; Valero, C. *J. Organomet. Chem.* **1989,** *366,* 187.

(7) Esteruelas M. A.; Lahoz, F. J.; López, A. M.; Oñate, E.; Oro, L. A. *Organometallics* **1994,** *13,* 1669.

(8) (a) Gallop, M. A.; Rickard, C. E. F.; Roper, W. R. *J. Organomet. Chem.* **1990,** *395,* 333. (b) Martin, G. C.; Boncella, J. M.; Wucherer, E. J. *Organometallics* **1991,** *10,* 2804. (c) Anderson, C. M.; Crespo, M.; Jennings, M. C.; Lough, A. J.; Ferguson, G.; Puddephat, R. J. *Organometallics* **1991,** *10,* 2672. (d) Forniés, J.; Menjón, B.; Gómez, N.; Tomás, M. *Organometallics* **1992,** *11,* 1187. (e) Crespo, M.; Martínez, M.; Sales, J.; Solans, X.; Font-Bardía, M. *Organometallics* **1992,** *11,* 1288. (f) Ryabov, A. D.; Kazankov, G. M.; Yatsimirsky, A.; Kuz'mina, L. G.; Bursteva, O. Y.; Dvorstova, N. V.; Polyakow, V. A. *Inorg. Chem.* **1992,** 31, 3083.

0276-7333/95/2314-2496$09.00/0

Scheme 1

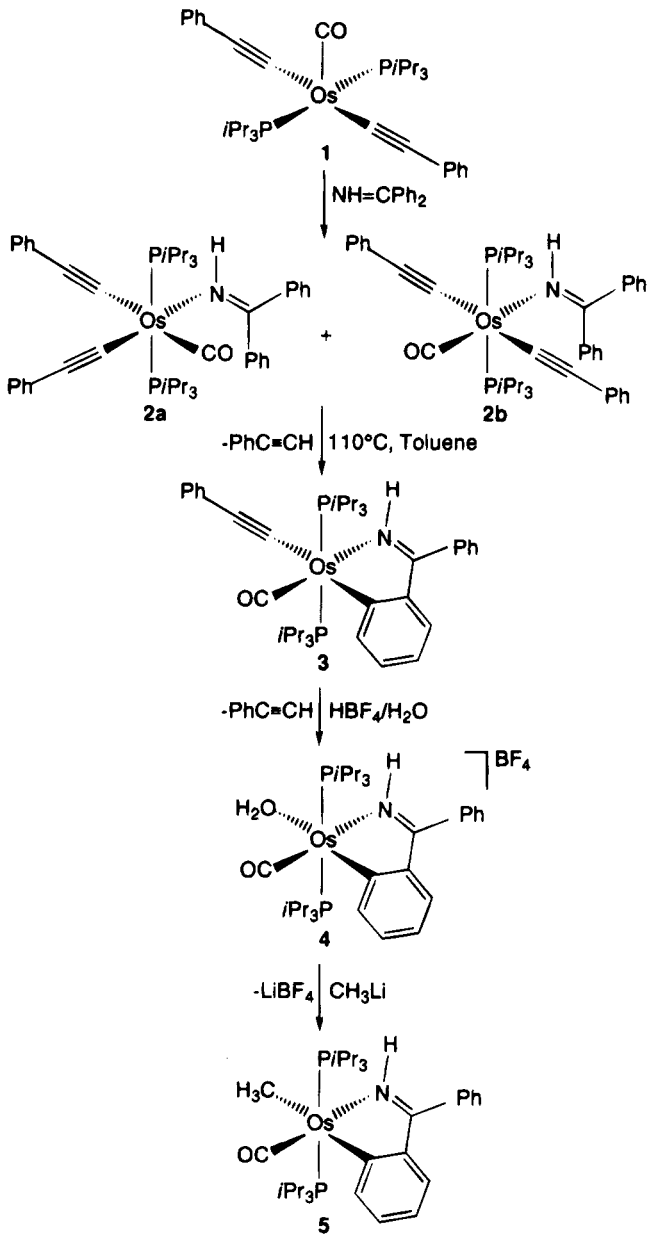

Results and Discussion

Although monodentate nitrogen-bound imine complexes are rare as a result of the weak Lewis basicity of the imine nitrogen atom,[9] the addition of benzophenone imine to an hexane suspension of **1** leads to the orange imine complex **2** in 85% yield. According to ^{1}H, ^{13}C{^{1}H}, and ^{31}P{^{1}H} NMR spectra, this complex is a mixture of the isomers **2a** and **2b** in a 1:3 molar ratio (Scheme 1).

The presence of the imine ligand in **2** is supported by the ^{1}H NMR spectrum in benzene-d_6, which shows two resonances due to the NH protons at 12.2 ppm for **2a** and 11.5 for **2b**. In the ^{13}C{^{1}H}NMR spectrum the C=N resonances appear as singlets at 174.84 (**2a**) and 180.87 (**2b**) ppm. This spectrum also shows six alkynyl resonances, four due to **2a** and two to **2b**. The α-carbon atoms of the alkynyl ligands of **2a** appear as triplets at 121.40 and 93.02 ppm with P−C coupling constants of 15.5 and 14.0 Hz, respectively, while the β-carbon atoms appear as singlets at 115.39 and 111.51 ppm. The α-carbon atoms of the alkynyl ligands of **2b** are observed as a single triplet at 117.67 ppm with a P−C coupling constant of 12.1 Hz, and the β-carbon atoms as a singlet at 114.06 ppm. The ^{31}P{^{1}H} NMR spectrum contains two singlets at −2.5 and 3.7 ppm, which are assigned to **2a** and **2b**, respectively.

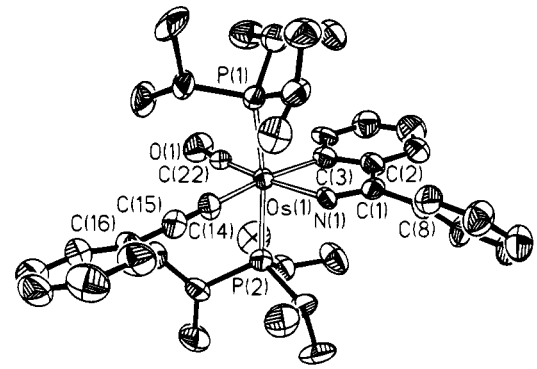

Figure 1. Molecular representation of [Os(C$_2$Ph){NH=C(Ph)C$_6$H$_4$}(CO)(P*i*Pr$_3$)$_2$] (**3**).

In toluene under reflux, the mixture is converted into the ortho-metalated complex **3**, which was isolated as a pink-red solid in 73% yield. The most noticeable absorptions in the IR spectrum of **3**, in Nujol, are three bands at 3329, 2091, and 1902 cm^{-1}, which are assigned to the ν(NH), ν(C≡C), and ν(CO) vibrations, respectively. The ^{1}H NMR spectrum in chloroform-*d* shows a broad singlet at 8.97 ppm, which was assigned to the NH proton, along with the resonances due to the phenyl groups and triisopropylphosphine ligands. In the region δ 195−180 the ^{13}C{^{1}H} NMR spectrum contains three triplets, at 193.90 (J_{P-C} = 10.2 Hz), 185.71 (J_{P-C} = 2.9 Hz), and 183.77 (J_{P-C} = 5.7 Hz). The triplet at 185.71 ppm was assigned to the carbon atom of the C=N group by comparison of this spectrum with those previously reported for the complexes [Ru{N(Ph)=C(R)C$_6$H$_4$}(η^6-C$_6$Me$_6$)(PMe$_3$)]BF$_4$ (R = H (175.3 ppm), CH$_3$ (180.4 ppm)),[10] [Os{NH=C(Ph)C$_6$H$_4$}(η^6-C$_6$H$_3$Me$_3$)(P*i*Pr$_3$)]PF$_6$ (191.72 ppm, d, J_{P-C} = 1.5 Hz),[11a] [Ru(η^5-C$_5$H$_5$){NH=C(Ph)C$_6$H$_4$}(PPh$_3$)] (183.24 ppm, d, J_{P-C} = 2.0 Hz),[12] and [OsH{NH=C(Ph)C$_6$H$_4$}(CO)(P*i*Pr$_3$)$_2$] (181.15 ppm).[13] The other two triplets, which are due to the carbonyl ligand and to the carbon atom of the aryl group directly linked to the metallic center, could not be clearly correlated. At 110.59 ppm the spectrum also contains a triplet with a P−C coupling constant of 15.5 Hz. This signal was

(9) Mehrota, R. C. In *Comprehensive Coordination Chemistry*; Wilkinson, G., Gillard, R. D., McCleverty, J. A., Eds.; Pergamon: Oxford, England, 1987; Vol. 2, pp 269−287. For examples of N-bound imine complexes see: (a) Elsbernd, H.; Beattie, J. K. *J. Chem. Soc. A* **1970**, 2598. (b) Lane, B. C.; Lester, J. E.; Basolo, F. *J. Chem. Soc., Chem. Commun.* **1971**, 1618. (c) Joss, S.; Bigler, P.; Ludi, A. *Inorg. Chem.* **1985**, 24, 3487. (d) Harman, W. D.; Taube, H. *Inorg. Chem.* **1988**, 27, 3261.

(10) Martin, G. C.; Boncella, J. M. *Organometallics* **1989**, *8*, 2968.

(11) (a) Daniel, T.; Müller, M.; Werner, H. *Inorg. Chem.* **1991**, *30*, 3118. (b) Daniel, T.; Knaup, W.; Dziallas, M.; Werner, H. *Chem. Ber.* **1993**, *126*, 1981. (c) Werner, H.; Daniel, T.; Braun, T.; Nürnberg, O. *J. Organomet. Chem.* **1994**, *480*, 145.

(12) Werner, H.; Daniel, T.; Knaup, W.; Nürnberg, O. *J. Organomet. Chem.* **1993**, *462*, 309.

(13) Daniel, T.; Werner, H. *Z. Naturforsch. B* **1992**, *4*, 1707.

Table 1. Selected Bond Lengths (Å) and Angles (deg) for the Complex $[Os(C_2Ph)\{NH=C(Ph)C_6H_4\}(CO)(PiPr_3)_2]$ (3)[14]

Os(1)–P(1)	2.412(2)	C(1)–C(2)	1.459(12)
Os(1)–P(2)	2.406(2)	C(1)–C(8)	1.516(14)
Os(1)–N(1)	2.106(7)	C(2)–C(3)	1.416(14)
Os(1)–C(3)	2.089(7)	C(14)–C(15)	1.224(11)
Os(1)–C(14)	2.074(7)	C(15)–C(16)	1.420(11)
Os(1)–C(22)	1.816(9)	C(22)–O(1)	1.196(12)
N(1)–C(1)	1.305(9)		
P(1)–Os(1)–P(2)	168.90(9)	C(3)–Os(1)–C(14)	167.7(3)
P(1)–Os(1)–N(1)	89.5(2)	C(3)–Os(1)–C(22)	93.8(4)
P(1)–Os(1)–C(3)	94.9(2)	C(14)–Os(1)–C(22)	98.5(3)
P(1)–Os(1)–C(14)	84.5(2)	Os(1)–N(1)–C(1)	119.3(5)
P(1)–Os(1)–C(22)	91.3(2)	N(1)–C(1)–C(2)	114.7(7)
P(2)–Os(1)–N(1)	90.5(2)	N(1)–C(1)–C(8)	120.8(7)
P(2)–Os(1)–C(3)	95.9(2)	C(1)–C(2)–C(3)	114.0(7)
P(2)–Os(1)–C(14)	84.4(2)	Os(1)–C(3)–C(2)	115.8(6)
P(2)–Os(1)–C(22)	90.6(3)	Os(1)–C(14)–C(15)	178.1(8)
N(1)–Os(1)–C(3)	76.0(3)	C(14)–C(15)–C(16)	176.8(9)
N(1)–Os(1)–C(14)	91.7(3)	Os(1)–C(22)–O(1)	173.6(7)
N(1)–Os(1)–C(22)	169.8(3)		

assigned to the α-carbon of the alkynyl group. The $^{31}P\{^1H\}$ NMR spectrum shows a singlet at 5.1 ppm, indicating the two phosphine ligands are equivalent and are mutually *trans* disposed.

The definitive characterization of **3** as an ortho-metalated imine complex is derived from an X-ray diffraction experiment on a single crystal. Figure 1 shows an ORTEP drawing of the molecule. Selected bond distances and angles are listed in Table 1.[14]

The coordination geometry around the osmium atom could be rationalized as derived from a distorted octahedron with the two phosphorus atoms of the triisopropylphosphine ligands occupying *trans* positions (P(1)–Os(1)–P(2) = 168.90(9)°). The perpendicular plane is formed by the atoms C(3) and N(1) of the ortho-metalated benzophenoneimine (N(1)–Os(1)–C(3) = 76.0(3)°), defining a five-membered ring with the osmium atom, the C(14) atom of the alkynyl group disposed *trans* to C(3) (C(3)–Os(1)–C(14) = 167.7(3)°), and the CO ligand located *trans* to the nitrogen atom (N(1)–Os(1)–C(22) = 169.8(3)°).

The Os(1)–N(1) bond length of 2.106(7) Å and the Os(1)–C(3) bond distance of 2.089(7) Å are typical for Os–N and Os–C(aryl) single bonds, respectively, and are in agreement with the values previously found for the complexes $[Os\{NH=C(Ph)C_6H_4\}(\eta^6\text{-}C_6H_3Me_3)(PiPr_3)]PF_6$ (2.083(4) and 2.072(4) Å),[11c] $[OsH\{(C_6H_3\text{-}p\text{-}Me)(p\text{-tolyl})CNNC(p\text{-tolyl})_2\}(CO)_2(PPh_3)]$ (2.119(5) and 2.100(7) Å),[8a] and *fac*-$Os\{C,N\text{-}3\text{-}Me[2\text{-}C(2\text{-}MeC_6H_4)NCMe_3]C_6H_3\}(2\text{-}MeC_6H_4)(CN\text{-}t\text{-}Bu)_3$ (2.193(24) and 2.077(20) Å).[15]

The Os(1)–C(14) bond length of 2.074(7) Å is consistent with a single bond from Os(II) to a C(sp) atom and indicates a low degree of metal to ligand back-bonding.[1] The C(14)–C(15) distance and the C(14)–C(15)–C(16) angle are 1.224(11) Å and 176.8(9)°, respectively. Similar values have been found for related complexes containing terminal alkynyl groups.[3h,5,16]

Ortho-metalated benzophenone imine complexes of osmium are rare. They have been generally prepared from azavinylidene derivatives, by treatment with carboxylic acids or methanol.[11,13] The presence of the electrophilic reagent in these transformations suggests that the reactions involve the initial electrophilic attack of a proton at the nitrogen atom of the azavinylidene group, to give an imine intermediate which evolves by C–H activation into the ortho-metalated benzophenone imine complex. The replacement of an alkynyl group in **1** by an ortho-metalated benzophenone imine ligand most probably involves a hydrido–bis(alkynyl) intermediate of osmium(IV), which could be generated by C–H activation of one of the phenyl groups of the imine. This intermediate should, thus, afford **3** by reductive elimination of phenylacetylene.

Interestingly, **3** reacts with the stoichiometric amount of a HBF_4 diethyl ether solution to give phenylacetylene and the cationic species **4** (Scheme 1). Coordination of $[RC{\equiv}C]^-$ to a metal center transfers the nucleophilicity from the α-carbon atom to the β-carbon atom. Thus, the addition of electrophiles to alkynyl complexes has been described on many occasions and is considered the most convenient method for the synthesis of vinylidene derivatives.[17] The formation of phenylacetylene from the reaction of **3** with HBF_4 implies acceptance of the fact that when the alkynyl group is coordinated to the $Os\{NH=C(Ph)C_6H_4\}(CO)(PiPr_3)_2$ fragment, the transfer of nucleophilicity from C_α to C_β is not efficient or, alternatively, that the H^+ attack takes place at the osmium atom of **3**. In the latter case, the formation of **4** should involve an osmium(IV) hydrido–alkynyl intermediate. A similar behavior to that described for **3** has been previously observed for some alkynylruthenium(II) complexes,[7] for anionic acetylide complexes of high-spin d^5 manganese(II), and for metals of groups 11 and 12, where the reactions with acids lead to the quantitative liberation of alkynes $RC{\equiv}CH$.[1]

Complex **4** was isolated as an orange solid in 67% yield. The presence of a coordinate water molecule, which most probably comes from the HBF_4 diethyl ether solution, is supported by the IR and ^1H NMR spectra. The IR spectrum of **4** in Nujol shows absorptions at 3440, 3310, and 1905 cm^{-1}, which were assigned to ν(OH), ν(NH), and ν(CO) vibrations, respectively. Furthermore, it contains a broad absorption centered at 1050 cm^{-1} due to the $[BF_4]^-$ group with T_d symmetry, an indication that the anion is not coordinated to the osmium metal center. The ^1H NMR spectrum in chloroform-*d* contains the resonances due to the triisopropylphosphine ligands and the phenyl groups, along with two broad signals at 10.33 and 3.08 ppm, which were assigned to the NH and OH protons, respectively. The $^{31}P\{^1H\}$ NMR spectrum shows a singlet at 9.7 ppm.

Complex **4** reacts with 2 equiv of methyllithium in toluene to afford the methyl derivative **5**, which was isolated as a pink solid in 72% yield on the addition of methanol, in which the complex is stable. The most noticeable absorption of the IR spectrum of **5** in Nujol is the vibration ν(NH), which appears at 3325 cm^{-1}. In

(14) The structure exhibits two chemically equivalent, but crystallographically independent, molecules in the asymmetric unit. The values given in Table 1 correspond to one molecule. All parameters for the second molecule are deposited as supplementary material.

(15) Arnold, J.; Wilkinson, G.; Hussain, B.; Hurthouse, M. B. *Organometallics* **1989**, *8*, 1362.

(16) (a) Fernández, M. J.; Esteruelas, M. A.; Covarrubias, M.; Oro, L. A.; Apreda, M. C.; Foces-Foces, C.; Cano, F. H. *Organometallics* **1989**, *8*, 1158. (b) Echavarren, A. M.; López, J.; Santos, A.; Romero, A.; Hermoso, J. A.; Vegas, A. *Organometallics* **1991**, *10*, 2371.

(17) Bruce, M. I. *Chem. Rev.* **1991**, *91*, 197.

the ^1H NMR spectrum in benzene-d_6, the NH proton is observed as a broad resonance at 8.71 ppm, and a triplet at 0.65 ppm, with a P−H coupling constant of 6.5 Hz, was assigned to the protons of the methyl ligand. The resonance due to the carbon atom of this group appears in the $^{13}C\{^1H\}$ NMR spectrum at −27.66 ppm as a triplet with a P−C coupling constant of 9.8 Hz. The $^{31}P\{^1H\}$ NMR spectrum shows a singlet at 0.3 ppm.

In conclusion, the reaction of the bis(alkynyl) complex $[Os(C_2Ph)_2(CO)(PiPr_3)_2]$ with benzophenone imine gives rise to the replacement of an alkynyl group by an ortho-metalated benzophenone imine ligand, to afford $[Os(C_2Ph)\{NH{=}C(Ph)C_6H_4\}(CO)(PiPr_3)_2]$. This reaction, which has no precedent, occurs via a bis(alkynyl)−imine intermediate. Interestingly the protonation of $[Os(C_2Ph)\{NH{=}C(Ph)C_6H_4\}(CO)(PiPr_3)_2]$ does not afford a vinylidene derivative but produces phenylacetylene, in contrast to previous observations in osmium alkynyl chemistry.

Experimental Section

All reactions were carried out under an argon atmosphere using standard Schlenk techniques. Solvents were dried using appropiate drying agents and freshly distilled under argon before use. Complex $[Os(C_2Ph)_2(CO)(PiPr_3)_2]$ (**1**) was prepared by a published method.[5]

^1H, $^{31}P\{^1H\}$, and $^{13}C\{^1H\}$ NMR spectra were recorded on either a Varian UNITY 300 or on a Bruker 300 AXR spectrophotometer. Chemical shifts are expressed in ppm upfield from Me_4Si (^1H and ^{13}C) and 85% H_3PO_4 (^{31}P). Coupling constants (J and N [$N = J(PH) + J(P'H)$ or $J(CP) + J(CP')$] are given in hertz. IR data were recorded on a Perkin-Elmer 783 or on a Nicolet 550 spectrophotometer. Elemental analyses were carried out with a Perkin-Elmer 240C microanalyzer.

Preparation of $[Os(C_2Ph)_2(CO)(NH{=}CPh_2)(PiPr_3)_2]$ (2). A stirred suspension of complex **1** (105 mg, 0.14 mmol) in 10 mL of hexane was treated with the stoichiometric amount of $NH{=}CPh_2$ (24 μL, 0.14 mmol). Immediately a red solution was observed, from which an orange solid precipitated. The suspension was stirred for a further 1 h at room temperature. The solution was decanted, and the orange solid was washed with hexane and dried in vacuo. Yield: 110 mg (85%). Anal. Calcd for $C_{48}H_{63}NOOsP_2$: C, 62.52; H, 6.89; N, 1.52. Found: C, 62.83; H, 6.98; N, 1.60. IR (Nujol): ν(NH) 3260 (m), ν(C≡C) 2070 (s), ν(C≡O) 1915 (br, vs) cm^{-1}. A mixture of two isomers was observed in solution, **2a** and **2b**, in a 1:3 ratio. Selected data for **2a** are as follows. ^1H NMR (300 MHz, C_6D_6): δ 12.2 (s, br, 1 H, NH). $^{31}P\{^1H\}$ NMR (121.4 MHz, C_6D_6): δ −2.5 (s). $^{13}C\{^1H\}$ NMR (75.43 MHz, C_6D_6): δ 188.53 (t, J(CP) = 7.9, CO), 174.84 (s, C=N), 121.40 (t, J(CP) = 15.5, OsC≡), 115.39 (s, ≡CPh), 111.51 (s, ≡CPh), 93.02 (t, J(CP) = 14.0, OsC≡). Selected data for **2b** are as follows. ^1H NMR (300 MHz, C_6D_6): δ 11.5 (s, br, 1 H, NH). $^{31}P\{^1H\}$ NMR (121.4 MHz, C_6D_6): δ 3.7 (s). $^{13}C\{^1H\}$ NMR (75.43 MHz, C_6D_6): δ 187.56 (t, J(CP) = 10.6, CO), 180.87 (s, br, C=N), 117.67 (t, J(CP) = 12.1, OsC≡), 114.06 (s, br, ≡CPh).

Preparation of $[Os(C_2Ph)\{NH{=}C(Ph)C_6H_4\}(CO)(PiPr_3)_2]$ (3). A solution of complex **1** (300 mg, 0.40 mmol) in 15 mL of toluene was treated with the stoichiometric amount of $NH{=}CPh_2$ (69 μL, 0.40 mmol). The mixture was stirred for 90 min at reflux temperature. The resulting dark red solution was concentrated to dryness, and the residue was treated with 5 mL of methanol to yield a pink-red solid. The solution was decanted, and the solid was washed with methanol and dried in vacuo. Yield: 240 mg (73%). Anal. Calcd for $C_{40}H_{57}NOOsP_2$: C, 58.59; H, 7.01; N, 1.71. Found: C, 58.63; H, 7.10; N, 1.61. IR (Nujol): ν(NH) 3329 (w), ν(C≡C) 2091 (m), ν(C≡O) 1902 (vs) cm^{-1}. ^1H NMR (300 MHz, $CDCl_3$): δ 8.97 (s, br, 1 H, NH); 8.57 (d, J(HH) = 7.6, 1 H), 7.6−7.2 (m, 10 H), 7.10 (m, 1 H), 7.01 (td, J(HH) = 7.5, J(HH) = 1.6, 1 H), 6.86 (td, J(HH) = 7.5, J(HH) = 1.2, 1 H) [C_6H_4 and Ph]; 2.49 (m, 6 H, PCH), 1.47 (dvt, J(HH) = 7.1, N = 14.0, 18 H, $PCCH_3$), 0.96 (dvt, J(HH) = 6.9, N = 12.1, 18 H, $PCCH_3$). $^{31}P\{^1H\}$ NMR (121.4 MHz, $CDCl_3$): δ 5.1 (s). $^{13}C\{^1H\}$ NMR (75.43 MHz, $CDCl_3$): δ 185.71 (t, J(CP) = 2.9, N=C), 193.90 (t, J(CP) = 10.2), 183.77 (t, J(CP) = 5.7) [CO and OsC], 144.57, 144.07, 138.40, 131.71, 130.46, 130.01, 129.87, 129.09, 128.91, 127.83, 127.54, 123.35, 118.90, 116.53 (all s, C_6H_4, Ph and ≡CPh), 110.59 (t, J(CP) = 15.5, OsC≡), 24.55 (vt, N = 25.0, PCH), 20.56 and 18.71 (both s, $PCCH_3$).

Preparation of $[Os\{NH{=}C(Ph)C_6H_4\}(CO)(OH_2)(PiPr_3)_2]BF_4$ (4). A solution of **3** (140 mg, 0.17 mmol) in 10 mL of diethyl ether was treated with a diethyl ether solution of HBF_4 ($HBF_4{\cdot}Et_2O$; 23 μL, 0.17 mmol) and stirred for 3 h at room temperature. The solvent was removed under vacuo, and the oily residue was dissolved in 2 mL of acetone. Concentration to ca. 0.5 mL followed by the addition of diethyl ether yielded an orange precipitate. The solution was decanted, and the solid was washed with diethyl ether and dried in vacuo. Yield: 94 mg (67%). Anal. Calcd for $C_{32}H_{54}BF_4NO_2OsP_2$: C, 46.66; H, 6.61; N, 1.70. Found: C, 46.30; H, 6.31; N, 1.67. IR (Nujol): ν(OH) 3440 (w), ν(NH) 3310 (w), ν(C≡O) 1905 (vs), $\nu(BF_4)$ 1050 (br, s) cm^{-1}. ^1H NMR (300 MHz, $CDCl_3$): δ 10.33 (s, br, 1 H, NH); 7.83 (d, J(HH) = 7.9, 1H), 7.55 (m, 5 H), 7.34 (dd, J(HH) = 7.9, J(HH) = 1.5, 1 H), 6.83 (td, J(HH) = 7.5, J(HH) = 1.5, 1 H), 6.70 (t, J(HH) = 7.7, 1 H) [C_6H_4 and Ph]; 3.08 (s, br, 2H, H_2O), 2.37 (m, 6 H, PCH), 1.15 (dvt, J(HH) = 7.2, N = 14.0, 18 H, $PCCH_3$), 1.10 (dvt, J(HH) = 7.1, N = 13.1, 18 H, $PCCH_3$). $^{31}P\{^1H\}$ NMR (121.4 MHz, $CDCl_3$): δ 9.7 (s). $^{13}C\{^1H\}$ NMR (75.43 MHz, $CDCl_3$): δ 189.02 (t, J(CP) = 9.4, CO), 184.54 (t, J(CP) = 3.1, N=C), 160.50 (br, OsC), 141.11, 141.04, 135.89, 132.16, 130.90, 130.45, 129.13, 128.33, 119.86 (all s, C_6H_4 and Ph), 24.58 (vt, N = 24.4, PCH), 19.44 and 18.90 (both s, $PCCH_3$).

Preparation of $[Os(CH_3)\{NH{=}C(Ph)C_6H_4\}(CO)(PiPr_3)_2]$ (5). A hexane solution of CH_3Li (0.15 mL, 0.24 mmol) was added to a solution of **4** (94 mg, 0.11 mmol) in 10 mL of toluene. An immediate color change from brown to red occurred. The reaction mixture was filtered, the filtrate was concentrated to ca. 0.5 mL, and the addition of methanol precipitated a pink-red solid. The solution was decanted, and the solid was washed with methanol and dried in vacuo. Yield: 60 mg (72%). Anal. Calcd for $C_{33}H_{55}NOOsP_2$: C, 54.00; H, 7.55; N, 1.91. Found: C, 53.53; H, 7.55; N, 1.81. IR (Nujol): ν(NH) 3325 (m), ν(C≡O) 1866 (s) cm^{-1}. ^1H NMR (300 MHz, C_6D_6): δ 8.92 (d, J(HH) = 7.8, 1 H), 8.71 (s, br, 1 H, NH); 7.54 (d, J(HH) = 7.9, 1 H), 7.45 (m, 2 H), 7.17 (m, 3 H), 7.09 (t, J(HH) = 7.3, 1 H), 6.85 (t, J(HH) = 7.4, 1 H) [C_6H_4 and Ph]; 2.28 (m, 6 H, PCH), 1.27 (dvt, J(HH) = 6.8, N = 13.3, 18 H, $PCCH_3$), 0.91 (dvt, J(HH) = 6.2, N = 12.0, 18 H, $PCCH_3$), 0.65 (t, 3H, J(HP) = 6.5, $OsCH_3$). $^{31}P\{^1H\}$ NMR (121.4 MHz, C_6D_6): δ 0.3 (s). $^{13}C\{^1H\}$ NMR (75.43 MHz, C_6D_6): δ 197.86 (t, J(CP) = 11.5), 188.78 (t, J(CP) = 5.7) [CO and OsC], 186.10 (t, J(CP) = 3.1, N=C), 145.23, 144.29, 139.27, 129.72, 129.47, 129.03, 127.34, 118.63 (all s, C_6H_4 and Ph), 24.60 (vt, N = 23.5, PCH), 20.50 and 18.97 (both s, $PCCH_3$), −27.66 (t, J(CP) = 9.8, $OsCH_3$).

X-ray Structure Analysis of $[Os(C_2Ph)\{NH{=}C(Ph)C_6H_4\}(CO)(PiPr_3)_2]$ (3). Single crystals were grown from $CDCl_3$/methanol. Crystal and collection data (from 50 reflections $10 < 2\theta < 25°$): triclinic space group $P\bar{1}$ (No. 2); a = 11.078(1) Å, b = 18.910 (2) Å, c = 20.290(2) Å, α = 67.562(7)°, β = 89.427(9)°, γ = 87.289(9)°, V = 3924.1(7) Å^3, Z = 4, d_{calcd} = 1.388 g cm^{-3}, μ(Mo Kα) = 3.36 mm^{-1}; crystal size 0.45 × 0.38 × 0.08 mm; 4-circle Siemens-P4 diffractometer, Mo Kα radiation (0.710 73 Å), graphite-oriented monochromator; T = 293 K;

$\theta/2\theta$ scan, max $2\theta = 45°$; 11 909 reflections measured, 9750 independent reflections, 6385 reflections with $F_o > 4.0\sigma(F_o)$. Intensity data were corrected for Lorentz and Polarization effects, and a semiempirical absorption correction (Ψ-scan method)[18] was applied. The structure was solved by Patterson and conventional Fourier techniques. Atomic coordinates and anisotropic thermal parameters of the non-hydrogen atoms were refined by full-matrix least-squares. The positions of hydrogen atoms were calculated according to ideal geometry (distance C–H = 0.96 Å). R values: $R_1(F_o > 4.0\sigma(F_o)) = 0.0355$; R_2 (all data) = 0.0781; $R_1(F) = \sum||F_o| - |F_c||/\sum|F_o|$, $R_2(F^2) = [\sum\{w(F_o^2 - F_c^2)^2\}/\sum\{w(F_o^2)^2\}]^{0.5}$; $w^{-1} = \sigma^2(F_o^2) + (0.0351P)^2$, where $P = [F_o^2 + 2F_c^2]/3$; reflex/parameter ratio 12.2:1. All calculations were performed by using the SHELXTL-PLUS[19] and SHELXL-93[20] systems of computer programs.

Acknowledgment. We thank the DGICYT (Project PB 92-0092, Programa de Promoción General del Conocimiento) and EU (Project: Selective Processes and Catalysis Involving Small Molecules) for financial support. E.O. thanks Diputación General de Aragón (DGA) for a grant.

Supplementary Material Available: Tables of atomic coordinates and thermal parameters, anisotropic thermal parameters, experimental details of the X-ray study, and complete bond distances and angles (21 pages). Ordering information is given on any current masthead page.

OM940936E

(18) North, A. C. T.; Phillips, D. C.; Mathews, F. S. *Acta Crystallogr.* **1968**, *A24*, 351.

(19) Sheldrick, G. M. *SHELXTL-PLUS*; Siemens Analytical X-Ray Instruments, Inc.: Madison, WI, 1990.

(20) Sheldrick, G. M. *SHELXL-93, Program for Crystal Structure Refinement*; University of Göttingen: Göttingen, Germany, 1993.

Electrochemical Behavior and Electron-Transfer Chain (ETC) Reactions of $H_4Ru_4(CO)_{12}$

Domenico Osella,* Carlo Nervi, and Mauro Ravera

Dipartimento di Chimica Inorganica, Chimica Fisica e Chimica dei Materiali, Università di Torino, Via P. Giuria 7, 10125 Torino, Italy

Jan Fiedler

The J. Heyrovsky Institute of Physical Chemistry, The Academy of Sciences of the Czech Republic, Dolejskova 3, 182 23 Prague 8, Czech Republic

Vladimir V. Strelets

Russian Academy of Sciences, Institute of Chemical Physics in Chernogolovka, Moscow Region, Chernogolovka 142432, Russian Federation

Received November 15, 1994[⊗]

The electrochemical reduction of $H_4Ru_4(CO)_{12}$ in tetrahydrofuran (THF) is studied by means of dc and ac polarography, cyclic voltammetry, and FT-IR spectroscopy following electrolysis in a optically transparent thin-layer electrochemical (OTTLE) cell. The reduction of the title complex generates a transient radical anion, $[H_4Ru_4(CO)_{12}]^-$, which produces the stable anion $[H_3Ru_4(CO)_{12}]^-$ on a longer time scale. In the presence of triphenylphosphine, nucleophilic substitutions readily take place by electrochemical initiation and produce mono- and bisubstituted derivatives in yields depending on PPh_3 concentration. The termination side chain reaction is the loss of a hydrido ligand, to give the above-mentioned anion, which is inert to substitution even in the presence of a large excess of Lewis base.

Introduction

$Ru_3(CO)_{12}$ and $H_4Ru_4(CO)_{12}$ are known to be excellent substrates for radical-anion-initiated reactions, in which nucleophilic substitutions occur very easily.[1] When a catalytic amount of sodium benzophenone ketyl (BPK) is added to a THF solution of phosphine ligand and $Ru_3(CO)_{12}$ or $H_4Ru_4(CO)_{12}$, the substitution of the Lewis bases for CO is fast, selective, and efficient.[1] In contrast, thermally activated nucleophilic substitutions take place producing mixtures of derivatives, with $Ru_3(CO)_9L_3$ being the major product in the former case.[2] The excellent results obtained by employing chemical reducing agents for both $Ru_3(CO)_{12}$ and $H_4Ru_4(CO)_{12}$ should imply the existence of reasonably stable radical anions as intermediates of electron-transfer chain (ETC) reactions. Surprisingly, chemical and electrochemical initiation of Lewis base substitution on $Ru_3(CO)_{12}$ did not give equivalent results.[3] The redox behavior of the clusters $M_3(CO)_{12}$ (M = Fe, Ru, Os) has been extensively studied and this apparent conflict tentatively explained.[3] To our knowledge, no data on the electrochemical behavior of $H_4Ru_4(CO)_{12}$ have been reported, and furthermore, in a recent review the tetrahydro cluster is reported to be redox inactive![4] Since ETC reactions are strictly correlated with electrochemical properties, electrochemical and spectroelectrochemical methods are employed here in order to elucidate this aspect of $H_4Ru_4(CO)_{12}$ reactivity.

Results and Discussion

Electrochemical Behavior of $H_4Ru_4(CO)_{12}$ (1). The dc polarographic response of a THF solution of **1** (Figure 1) exhibits a reduction wave (A) at $E_{1/2}(A) = -1.58$ V *vs* the ferrocene/ferrocenium (Fc/Fc^+) couple. The slope of the logarithmic plot analysis is 60 mV, near the value expected for a 1e Nernstian process.[5] However, comparison with the 1e oxidation wave of Fc (added in equimolar concentration as an internal standard)[6] gives a limiting current ratio, $i_l(A)/i_l(Fc)$, corrected for the different diffusion coefficients, equal to 1.6. The diffusion coefficients of **1** and Fc have been estimated from their molecular sizes by using the Stokes–Einstein equation.[7] The molecular radii have been calculated from the crystallographic volumes of the molecules[8,9] assuming a spherical shape. A dc polarographic limiting current ratio higher than that expected for a 1e process indicates that chemical complications

[⊗] Abstract published in *Advance ACS Abstracts,* April 1, 1995.

(1) (a) Bruce, M. I.; Kehoe, D. C.; Matisons, J. G.; Nicholson, B. K.; Rieger, P. H.; Williams, M. L. *J. Chem. Soc., Chem. Commun.* **1982**, 442. (b) Bruce, M. I.; Matison, J. G.; Nicholson, B. K.; Williams, M. L. *J. Organomet. Chem.* **1982**, *236*, C57. (c) Bruce, M. I.; Matison, J. G.; Nicholson, B. K. *J. Organomet. Chem.* **1983**, *247*, 321.

(2) Bruce, M. I. In *Comprehensive Organometallic Chemistry,* Wilkinson, G., Stone, F. G. A., Abel, E. W., Eds.; Pergamon Press: Oxford, U.K., 1982.

(3) (a) Cyr, J. C.; DeGray, J. A.; Gosser, D. K.; Lee, E. S.; Rieger, P. H. *Organometallics* **1985**, *4*, 950. (b) Downard A. J.; Robinson, B. H.; Simpson J. *J. Organomet. Chem.* **1987**, *320*, 363. (c) Cyr, J. E.; Rieger, P. H. *Organometallics* **1991**, *10*, 2153. (d) Osella D.; Hanzlik, J. *Inorg. Chim. Acta* **1993**, *213*, 311.

(4) Drake, S. R. *Polyhedron* **1990**, *9*, 455.

(5) (a) Bard, A. J.; Faulkner, L. L. *Electrochemical Methods*; Wiley: New York, 1980. (b) Brown, E. R. Sandifer, J. R. In *Physical Methods of Chemistry*; Rossiter, B. W., Hamilton, G. F., Eds.; Wiley: New York, 1986; Vol. II, Chapter IV.

(6) Adams, R. N.; *Electrochemistry at Solid Electrodes*; Marcel Dekker: New York, 1969; p 214.

(7) Bockris, J. O'M.; Reddy, A. K. M. *Modern Electrochemistry*; Plenum: New York, 1970; Chapter IV, p 380.

(8) Seiler, P.; Dunitz, J. D. *Acta Crystallogr.* **1979**, *B35*, 2020.

(9) Wilson, R. D.; Wu, S. M.; Love, R. A.; Bau, R *Inorg. Chem.* **1978**, *17*, 1271.

0276-7333/95/2314-2501$09.00/0

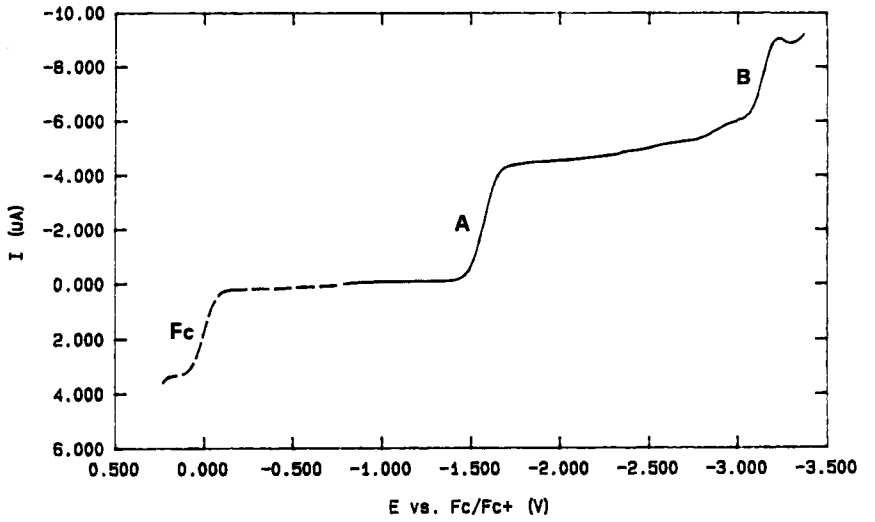

Figure 1. Sampled dc polarographic responses of a THF solution of **1** (5×10^{-4} M) containing $[Bu_4N][PF_6]$ as supporting electrolyte (0.1 M) at a mercury electrode, drop time 1 s. The oxidation wave of an equimolar amount of ferrocene (Fc) is reported as dashed line.

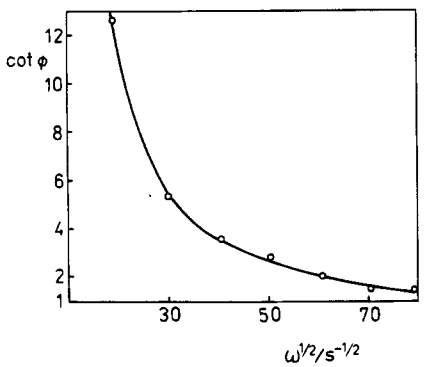

Figure 2. Frequency ($\omega = 2\pi f$) dependence of the cotangent of the phase angle ($\cot \phi = Z_F'/Z_F''$) of the ac signal measured at dc half-wave potential, $E_{1/2}(A) = -1.58$ V. The amplitude of applied ac voltage is 10 mV.

are associated with the electron-transfer process. A second wave (B) is also observed near the solvent discharge where the stability of the mercury drop becomes problematic, $E_{1/2}(B) = -3.14$ V.

Cyclic voltammetric (CV) response of a THF solution of **1** at a hanging mercury drop electrode (HMDE) provides similar results. A first reduction peak (A) at $E_p(A) = -1.61$ V is observed without any directly associated reoxidation peak, indicating the chemical irreversibility of this reduction process, followed by a second, irreversible reduction (peak B) at $E_p(B) = -3.16$ V, scan rate 0.2 V s^{-1}. In addition, CV response at a glassy carbon (GC) electrode shows in the anodic region a broad, irreversible oxidation peak (C) at $E_p \approx +0.6$ V, scan rate 0.2 V s^{-1}. Since the first reduction process is suitable to be involved in ETC reactions, only its electrochemical behavior is studied in detail.

Ac polarographic measurements provide the most conclusive view into the mechanism of the first reduction of **1**. Figure 2 shows the frequency dependence of cotangents of the phase angle (ϕ) of the ac signal measured at dc half-wave (A) potential. The high-frequency limit of cot ϕ is unity indicating the electrochemical reversibility of the process (fast electron transfer); on the other hand, infinite growing of cot ϕ at low frequencies is typical for regeneration of depolarizer **1** by catalytic reaction[10] or by disproportionation following the charge-transfer step.[11]

Further attempts of identifying the products of reduction of **1** were performed by combining coulometric and spectroelectrochemical investigations. Reduction of a THF solution of **1** in an OTTLE cell provides different results depending on the regime employed for the electrolysis. When the applied potential is held at the foot of peak A, the electrolysis proceeds very slowly with the growing of band maxima at 2037 s, 2031 s (sh), 2017 s, 1999 vs, 1976 m, 1949 w, 1931 w cm^{-1} (Figure 3). Two isosbestic points indicate a neat transformation. The reduction product is unambiguously identified as $[H_3Ru_4(CO)_{12}]^-$ by comparison with the spectrum of an authentic sample of $[Ph_4As][H_3Ru_4(CO)_{12}]$,[12] recorded under the same experimental conditions. Figure 4 shows the infrared spectra obtained during a fast electrolysis in OTTLE at potential well beyond the voltammetric peak A. The spectrum at the end of electrolysis exhibits different band maxima at 2031 w, 1991 s, 1952 s (br), 1905 m, 1886 m, 1811 w, 1757 m, and 1745 m cm^{-1}. The additional shoulders at 2037, 2017, and 1999 cm^{-1} are due to small amount of $[H_3Ru_4(CO)_{12}]^-$.

Polarographic responses recorded *in situ* during exhaustive electrolysis at a mercury-pool electrode are shown in Figure 5. The original wave A completely disappears when 1 F/mol is consumed, and a new, more cathodic wave D ($E_{1/2}(D) = -2.33$ V grows with a height approximately equal to that of Fc oxidation. The IR spectrum corresponds to that obtained in OTTLE cell when a "slow" electrolysis regime is employed. The final 1e reduction product is further identified as $[H_3Ru_4(CO)_{12}]^-$ by comparison of the polarographic halfwave $E_{1/2}(D)$ with that of an authentic sample of $[Ph_4As][H_3Ru_4(CO)_{12}]$[12] recorded in the same experimental conditions. If the applied potential is set at that of the limiting current of the wave D ($E_{appl} = -2.50$ V *vs* Fc/Fc^+), a further 1 F/mol is consumed. A sample at

(10) Smith, D. E. *Anal. Chem.* **1963**, *35*, 602; **1963**, *35*, 610.
(11) Hayes, J. W.; Ruzic, I.; Smith, D. E.; Booman, G. L.; Delmastro J. R. *J. Electroanal. Chem.* **1974**, *51*, 245.
(12) Koepke, J. W.; Johnson J. R.; Knox, S. A. R.; Kaesz, H. D. *J. Am. Chem. Soc.* **1975**, *97*, 3947.

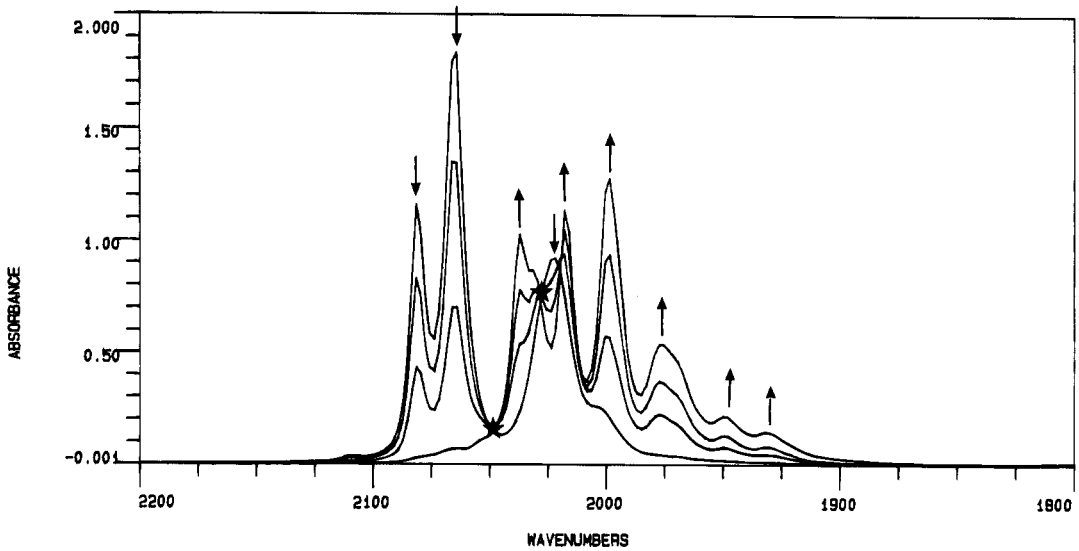

Figure 3. IR OTTLE spectra of a THF solution of **1** during the exhaustive reduction at $E_{appl} \approx -1.5$ V ("slow" regime).

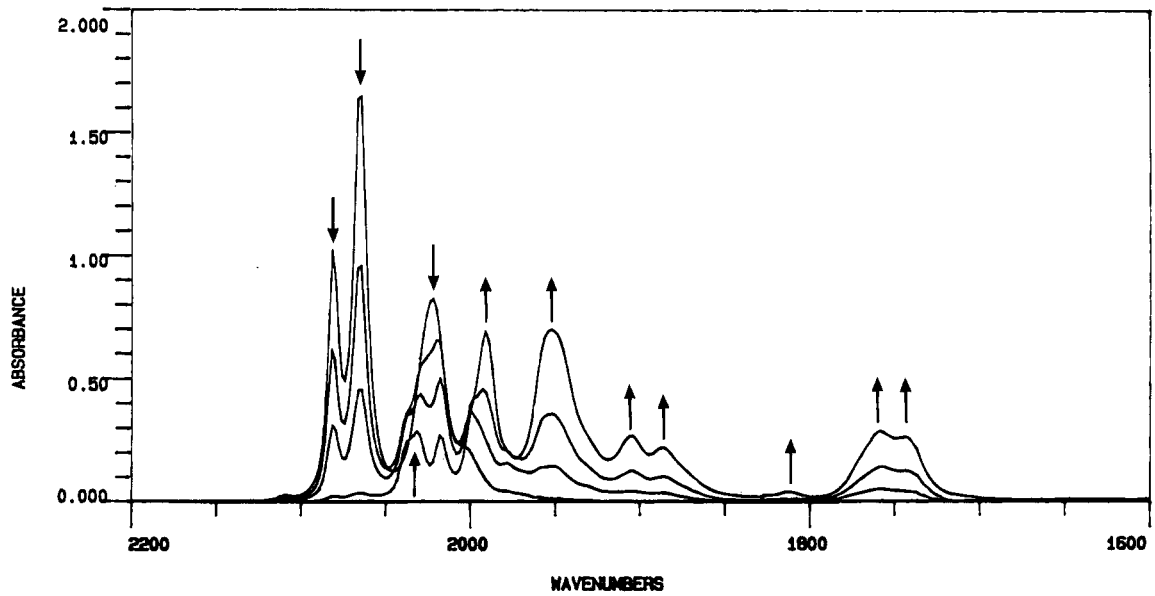

Figure 4. IR OTTLE spectra of a THF solution of **1** during the exhaustive reduction at $E_{appl} \approx -1.8$ V ("fast" regime).

the end of the 2e reduction gives an IR spectrum identical to that recorded in OTTLE during the "fast" electrolysis. The 2e reduction product shows a further reduction at a potential near $E_{1/2}$(B). We identified this product as $[H_2Ru_4(CO)_{12}]^{2-}$ since its spectrum is similar to that reported for $[(Ph_3P)_2N]_2[H_2Ru_4(CO)_{12}]$.[13]

Deliberate addition of an equimolar amount of parent compound **1** to the 2e reduced solution quantitatively regenerates the monoanion $[H_3Ru_4(CO)_{12}]^-$, according to the following equation:

$$[H_4Ru_4(CO)_{12}] + [H_2Ru_4(CO)_{12}]^{2-} \rightarrow 2[H_3Ru_4(CO)_{12}]^-$$

The bulk of the data suggests the reduction mechanism of **1** depicted in Figure 6: generation of $\mathbf{1}^-$ and its fast disproportionation to **1** (which increases the polarographic wave A) and $\mathbf{1}^{2-}$ followed by fast conversion to $[H_2Ru_4(CO)_{12}]^{2-}$ (by loss of hydrogen), which in turn can be reduced at a more cathodic potential (wave B). On the contrary, several slow reactions are able to generate the stable anion $[H_3Ru_4(CO)_{12}]^-$, further reducible at $E_{1/2}$(D) potential.

Electron-Transfer Chain (ETC) Reaction of $H_4Ru_4(CO)_{12}$ with PPh_3. Figure 7 shows the polarograms obtained when a THF solution of **1** (curve 1) is added with an equimolar amount of PPh_3 (curve 2) and then gradually electrolyzed at a mercury-pool electrode, $E_{appl} = -1.55$ V (curves 3 and 4). The original polarographic wave A decreases and after consumption of 0.25 F/mol (curve 4) totally disappears. Two well-resolved waves are observed at $E_{1/2}(E) = -1.73$ and $E_{1/2}(F) = -1.98$ V, respectively, in addition to wave D due to reduction of $[H_3Ru_4(CO)_{12}]^-$. The new waves are unambiguously assigned to reduction of $H_4Ru_4(CO)_{11}PPh_3$ and $H_4Ru(CO)_{10}(PPh_3)_2$, respectively, on the basis of polarographic results on authentic samples,[2] recorded in the same experimental conditions. The composition of the solution after 0.25 F/mol electrolysis can be estimated from the heights of the polarographic waves in the likely hypothesis that the diffusion coefficients of the products are the same: $H_4Ru_4(CO)_{11}PPh_3$ (60%),

(13) Inkrott, K. E.; Shore, S. G. *Inorg. Chem.* **1979**, *18*, 2817.

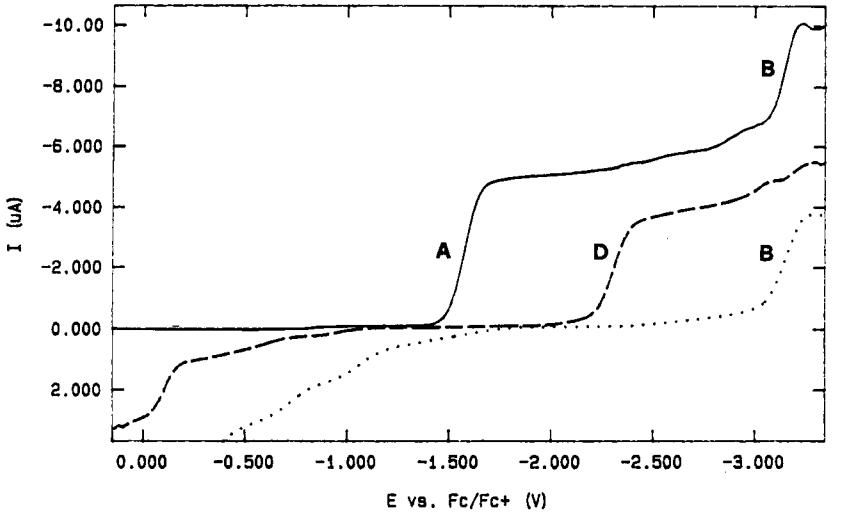

Figure 5. Polarographic responses of a THF solution of **1** recorded *in situ* during exhaustive electrolysis at a mercury-pool electrode. The bold curve corresponds to the initial solution, and the dashed curve is recorded after 1 F/mol is consumed at $E_{appl} = -1.75$ V. The dotted curve is recorded after a further 1 F/mol is passed at $E_{appl} = -2.50$ V.

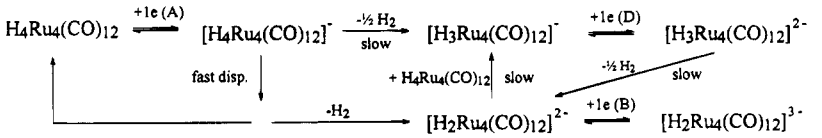

Figure 6. Proposed mechanism for the electrochemical reduction of **1**.

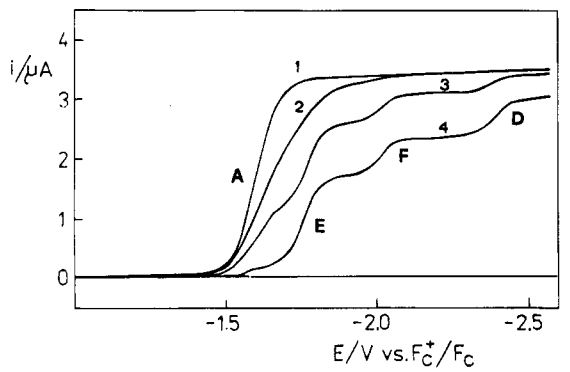

Figure 7. Polarograms of a THF solution of **1** (1×10^{-3} M). Curve 1 corresponds to the polarogram of the initial solution, curve 2 corresponds to the polarogram obtained after addition of PPh_3 (molar ratio 1:1), and curves 3 and 4 correspond to polarograms obtained for the above-mentioned mixture during exhaustive electrolysis at a mercury-pool electrode, $E_{appl} = -1.55$ V, when 0.10 and 0.25 F/mol are consumed, respectively.

$H_4Ru_4(CO)_{10}(PPh_3)_2$ (20%), $[H_3Ru_4(CO)_{12}]^-$ (20%). The electrolyzed residue, extracted with hot cyclohexane, gives TLC and IR results qualitatively and quantitatively consistent with the electrochemical ones, as far as the neutral substituted products are concerned. An analogous experiment ($E_{appl} = -1.55$ V) with 5-fold excess of PPh_3 leads, after 0.25 F/mol, to an electrolyzed solution containing $H_4Ru_4(CO)_{11}PPh_3$ (20%), $H_4Ru_4(CO)_{10}(PPh_3)_2$ (70%), and $[H_3Ru_4(CO)_{12}]^-$ (10%). In both experiments, the current yield of substitution is more than 100%, as expected for an ETC process.

It is noteworthy to recall that the electrochemical initiation must be always performed at a potential corresponding to the foot of the polarographic wave A in order to produce the reactive radical anion $\mathbf{1}^-$. When more cathodic potentials are applied, the efficiency of the process strongly decreases since an enhanced amount of the stable anion $[H_3Ru_4(CO)_{12}]^-$ is obtained, which proved to be totally inert toward PPh_3 substitution. This makes the electrochemical activation poorly selective, since one can pilot the reaction only by means of the phosphine/substrate ratio and not by the applied potential.

Interestingly, Bruce in his comprehensive work[1c] on BPK-initiated nucleophilic substitutions proposed that the minor efficiency found for $H_4Ru_4(CO)_{12}$ with respect to $Ru_3(CO)_{12}$ would be ascribed to a chain-termination process, the likely loss of hydride ligands. Indeed, BPK initiation was not able to produce tri- and tetrasubstituted derivatives with PPh_3; however, trisubstituted derivatives could have been obtained with phosphites.[1c]

Multiscan CV responses at a HMDE electrode of a THF solution of **1** are in agreement with the polarographic results: the original reduction peak A decreases in height when PPh_3 is added, and two new peaks appear in correspondence of the reduction of $H_4Ru_4(CO)_{11}(PPh_3)$ ($E_p(E) = -1.76$ V) and $H_4Ru_4(CO)_{10}(PPh_3)_2$ ($E_p(F) = -1.99$ V). A very weak peak is further observed only when a 10 times excess of PPh_3 is employed: it corresponds to $H_4Ru_4(CO)_9(PPh_3)_3$ reduction as verified on an authentic sample ($E_p = -2.31$ V, 0.2 V s^{-1}).[2] As usual in ETC reactions,[14] the increases of scan rate (which shortens the time scale available for the chemical reaction) decreases the height of peaks due to PPh_3-substituted derivatives.

Experimental Section

$H_4Ru_4(CO)_{12}$ (**1**) was synthesized from $Ru_3(CO)_{12}$ according to the literature method.[15] Triphenylphosphine was used as purchased from Aldrich. THF was distilled from sodium benzophenone ketyl just before use. Tetrabutylammonium

(14) Kochi, J. K. *J. Organomet. Chem.* **1986**, *300*, 139.
(15) Knox, S. A. R.; Koepke, J. W.; Andrews, M. A.; Kaesz, H. D. *J. Am. Chem. Soc.* **1975**, *97*, 3942.

hexafluorophosphate (Aldrich) was recrystallized three times from 95% ethanol and dried in a vacuum oven at 110 °C overnight.

Electrochemistry was performed with an EG&G PAR 273 electrochemical analyzer connected to an interfaced personal computer and to an EG&G PAR Model 5210 lock-in amplifier (for ac measurements). A standard three-electrode cell was designed to allow the tip of the reference electrode to closely approach the working electrode. The *pseudo*-reference electrode was a silver wire dipped in a 0.1 M solution of $[Bu_4N][PF_6]$ in THF and separated from the cell solution by a Vycor frit. At the end of each experiment the potential of the ferrocene(0/1+) couple was measured, to which all data are referred. The working electrode for CV was a HMDE (Metrohm Model 6.0335); for polarography a dropping mercury electrode (DME) with flow rate of 1.22 mg s^{-1} at a reservoir height of 0.5 m was employed. Drop time was controlled by an electromechanical hammer. The auxiliary electrode was a platinum wire sealed in glass. Positive feedback *iR* compensation was applied routinely. All measurements were carried out under Ar in anhydrous deoxygenated THF; solutions were 5×10^{-4} M with respect to the compounds under study and 1×10^{-1} M with respect to the supporting electrolyte, $[Bu_4N][PF_6]$. The temperature of the solution was kept constantly at 25 ± 1 °C, by circulation of a thermostated water–ethanol mixture through the double wall of the cell. Spectroelectrochemistry was performed in an optically transparent thin-layer electrochemical (OTTLE) cell assembled as previously described.[16] The corresponding IR spectra were measured on a Philips 9800 FT-IR spectrometer.

Acknowledgments. We thank the Ministero dell'Università e della Ricerca Scientifica e Tecnologica (MURST, Rome) for a fellowship (to J.F.) and the Council of National Research (CNR, Rome) for financial support. Johnson Matthey Ltd. is acknowledged for a generous loan of $RuCl_3$, and Mr. P. A. Loveday (University Chemical Laboratory, Cambridge, U.K.) for high-pressure synthesis of $Ru_3(CO)_{12}$. We are indebted to Professor M. I. Bruce (University of Adelaide) for his interest in this work.

OM940870N

(16) Krejcik, M.; Danek, M.; Hartl, F. *J. Electroanal. Chem.* **1991**, *317*, 179.

Electrochemical Polymerization of Hydrosilane Compounds

Yoshinori Kimata,* Hiroshi Suzuki, Shin Satoh, and Akira Kuriyama*

Tsukuba Research Laboratory, Toagosei Co., Ltd., 2 Ohkubo, Tsukuba, Ibaraki 300-33, Japan

Received November 16, 1994[⊗]

The electrolytic reactions of hydrosilane compounds were studied for the synthesis of polysilanes. Di- and trihydric substituted monosilanes, such as methylphenylsilane, phenylsilane, and *n*-hexylsilane, were electrolyzed under constant-current conditions with platinum electrodes in an undivided cell containing Bu_4NBF_4/DME as the electrolyte and solvent. In each case, polymerized products were obtained and the formation of silicon catenation was definitely confirmed by UV absorption, mass, and Raman spectroscopies.

Introduction

Polysilanes are interesting polymers possessing curious properties based on the delocalized σ electrons of the silicon–silicon bonds along the backbone. They have been intensely investigated for practical applications such as precursors for silicon carbide ceramics,[1] photoresists,[2] and electroconducting[3] and luminescent materials.[4] The most general synthetic pathway of polysilanes is the Wurtz coupling reaction of organodichlorosilane compounds with a sodium dispersion in toluene at refluxing temperature.[5–8] However, there are obvious problems such as the dangerous reaction conditions due to the treatment of moisture-sensitive alkali metals as well as the formation of large amounts of metal chlorides as byproducts. In addition, when monomers having functional groups such as fluoroalkyls were subjected to the Wurtz type condensation, the corresponding polysilanes were produced in extremely low yield.[9] Therefore, other synthetic methods have been successively investigated. For example, anionic polymerization of masked disilenes,[10,11] ring-opening polymerization of cyclosilanes,[12] the dehydrogenative coupling reaction of hydrosilanes using a transition metal catalyst,[13–24] and electroreductive polymerization of chlorosilanes[25–36] have been reported over the past several years. The electrochemical process, first studied by Hengge and Litscher,[25] is worthy of note since the electrolysis of chlorosilanes can be carried out under very mild conditions at room temperature. In this method, the practical problem is the anodic oxidation of the electrode itself with chlorine removed from the monomers to form quantitative amounts of metal chloride or corrosive hydrogen chloride.[36]

Recently, we have found an epoch-making electrochemical pathway for the preparation of Si–Si bonds from methylphenylsilane[37] without using any catalysts as investigated by Aitken et al.[14] In this paper, we report the novel synthesis of polysilanes from di- and trihydric substituted monosilanes using an electrolytic technique.

Results and Discussion

Electrolysis of Hydrosilanes. The electrochemical properties of some hydrosilanes were examined by Kunai et al.[38] An Si–H bond of dimethylphenylsilane is effectively chlorinated to form dimethylphenylchlorosilane by electro-oxidation in the presence of CuCl using platinum electrodes, and the resulting chlorosilanes were subsequently reduced and 1,2-diphenyltetramethyldisilane was produced in a one-pot reaction, if a copper anode was used instead of platinum.[38] Using this method, a sacrificial electrode is ultimately necessary to form an Si–Si bond in the same manner as the usual electroreductive polymerization of chlorosilanes, although hydrosilane was used as the starting material. It is obviously unfavorable for a practical electrolysis system to consume the electrode itself.

⊗ Abstract published in *Advance ACS Abstracts,* April 1, 1995.

(1) Yajima, S.; Omori, M.; Hayashi, J.; Okamura, K.; Matsuzawa, T.; Liaw, C. F. *Chem. Lett.* **1976**, 551.
(2) Griffing, B. F.; West, R. *Polym. Eng. Sci.* **1983**, *23*, 947.
(3) West, R.; David, L. D.; Djurovich, P. I.; Stearley, K. S. V.; Srinivasan, H. Y. *J. Am. Chem. Soc.* **1981**, *103*, 7352.
(4) Bianconi, P. A.; Weidman, T. W. *J. Am. Chem. Soc.* **1988**, *110*, 2342.
(5) Trujillo, R. E. *J. Organomet. Chem.* **1980**, *198*, C27.
(6) Trefonas, P., III; Damewood, J. R., Jr.; West, R.; Miller, R. D. *Organometallics* **1985**, *4*, 1318.
(7) West, R. *J. Organomet. Chem.* **1986**, *300*, 327.
(8) Harrah, L. A.; Zeigler, J. M. *Macromolecule* **1987**, *20*, 601.
(9) Fujino, M.; Hisaki, T.; Fujiki, M.; Matsumoto, N. *Macromolecules* **1992**, *25*, 1079.
(10) Sakamoto, K.; Obata, K.; Hirata, H.; Nakajima, M.; Sakurai, H. *J. Am. Chem. Soc.* **1989**, *111*, 7641.
(11) Sakamoto, K.; Yoshida, M.; Sakurai, H. *Macromolecules* **1990**, *23*, 4494.
(12) Matyjaszewski, K.; Cypryk, M.; Frey, H.; Hrkach, J.; Kim, H. K.; Moeller, M.; Ruehl, K.; White, M. *J. Macromol. Sci.-Chem.* **1991**, *A28* (11 & 12), 1151.
(13) Aitken, C.; Harrod, J. F.; Samuel, E. *J. Organomet. Chem.* **1985**, *269*, C11.
(14) Aitken, C.; Harrod, J. F.; Samuel, E. *J. Am. Chem. Soc.* **1986**, *108*, 4059.
(15) Aitken, C.; Harrod, J. F.; Gill, U. S. *Can. J. Chem.* **1987**, *65*, 1804.
(16) Harrod, J. F.; Yun, S. S. *Organometallics* **1987**, *6*, 1381.
(17) Harrod, J. F. *Inorganic and Organometallic Polymers*; ACS Symposium Series 360; Zeldin, M., Wynne, K. J., Allcock, H. R., Eds.; American Chemical Society: Washington, DC, 1988; Chapter 7.
(18) Aitken, C.; Barry, J. P.; Gauvin, F.; Harrod, J. F.; Malek, A.; Rousseau, D. *Organometallics* **1989**, *8*, 1732.
(19) Nakano, T.; Nakamura, H.; Nagai, Y. *Chem. Lett.* **1989**, 83.
(20) Corey, J. Y.; Zhu, X. H.; Bedard, T. C.; Lange, L. D. *Organometallics* **1991**, *10*, 924.
(21) Corey, J. Y.; Zhu, X. H. *J. Organomet. Chem.* **1992**, *439*, 1.
(22) Woo, H. G.; Heyn, R. H.; Tilley, T. D. *J. Am. Chem. Soc.* **1992**, *114*, 5698.
(23) Woo, H. G.; Walzer, J. F.; Tilley, T. D. *J. Am. Chem. Soc.* **1992**, *114*, 7047.
(24) Banovetz, J. P.; Suzuki, H.; Waymouth, R. M. *Organometallics* **1993**, *12*, 4700.
(25) Hengge, E.; Litscher, G. K. *J. Angew. Chem., Int. Ed. Engl.* **1976**, *15*, 370.
(26) Corriu, R. J. P.; Dabosi, G.; Martineau, M. *J. Organomet. Chem.* **1981**, *222*, 195.

0276-7333/95/2314-2506$09.00/0

Table 1. Electrochemical Polymerization of Hydrosilanes

monomer	electricity (F/mol)	product	yield (%)	mol wt[a] M_w	M_w/M_n	UV abs[b] λ_{max} (nm)	ϵ/SiSi
$MePhSiH_2$	2.0	$-(MePhSi)_n-$	60	477	1.05	240[c]	5300
$PhSiH_3$	3.0	$-(PhSiH)_n-$	32	640	1.42	240[c]	5700
$^nHexSiH_3$	3.0	$-(^nHexSiH)_n-$	70	1240	1.09	252	7700

[a] GPC vs polystyrene. [b] Solvent cyclohexane. [c] Shoulder.

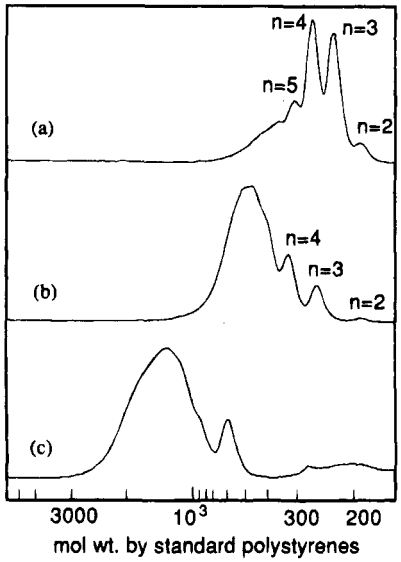

Figure 1. GPC profiles of electrolyzed (a) methylphenylsilane, (b) phenylsilane, and (c) *n*-hexylsilane.

We have found that di- and trihydric substituted monosilanes are suitable for electrochemical polymerization without using sacrificial electrodes. The electrolysis of methylphenylsilane was at first carried out in THF containing lithium perchlorate as the supporting electrolyte. However, reductive formation of metallic lithium occurred on the cathode and no compound having an Si–Si bond was obtained. When tetrabutylammonium tetrafluoroborate (TBAF) was used instead of lithium perchlorate as the electrolyte, the solvent decomposed to form poly(THF) during electrolysis. Therefore, we examined the electrolysis in 1,2-dimethoxyethane (DME)/TBAF as the solvent/electrolyte system. In this case, the electrochemical polymerization of methylphenylsilane occurred satisfactorily (Table 1).

The product was obtained as a mixture of oligomers containing more than five components (Figure 1a). The FT-IR spectrum indicates that the polymerized methylphenylsilane has Si–CH_3 (1250 cm^{-1}), Si–Ph (1428 cm^{-1}), and Si–H (2106 cm^{-1}) groups. Since the strength of the absorption band between 1000 and 1100 cm^{-1} was very weak, few siloxane bonds were present in the backbone. The complete separation of the oligomers into compounds ranging from dimers to pentamers was successfully carried out by HPLC. The isolation yield, molecular weight, and maximum wavelength of the UV absorption (λ_{max}) are summarized in Table 2. Obviously, the λ_{max} shows a remarkable red shift with increasing molecular weight. Furthermore, 1,2-dimethyl-1,2-diphenyldisilane (m/z = 242) and 1,2,3-trimethyl-1,2,3-triphenyltrisilane (m/z = 362) were detected by mass analysis corresponding to fractions no. 1 and 2, respectively (Figure 2). We can now conclude that the

Table 2. Characterization of the Oligomers $-[MePhSi]_n-$ Fractionated by HPLC

fraction no.	mol wt GPC[a]	mol wt MS	UV abs[b] λ_{max} (nm)	degree of polymerization	yield[c] (%)
1	219	242	230	2	10
2	304	362	243	3	14
3	378		251	4	16
4	427		257	5	6

[a] Polystyrene standards, peak top. [b] Solvent acetonitrile. [c] Based on the weight of isolated fraction by HPLC.

electrolysis product of methylphenylsilane in the present work is poly(methylphenylsilane) as shown by eq 1.

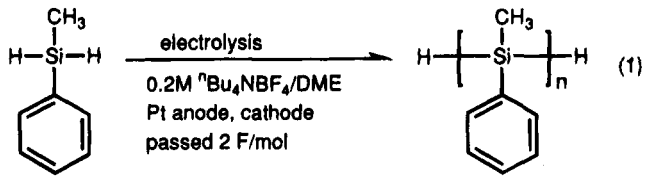

(1)

According to these results, the Si–Si bond can be electrochemically formed by condensation of monosilanes having Si–H bonds. In order to confirm the generality of this polymerization method, we examined the electrolysis of other hydrosilanes in a similar manner to methylphenylsilane.

The mean degree of polymerization of the obtained product from phenylsilane was estimated to be about 6 based on the molecular weight by GPC. The di-, tri- and tetramers, which corresponded to the components from n = 2 to 4 in Figure 1b, were purified and eluted by HPLC. Each of them exhibited obvious UV absorption maximums which red-shifted with increasing degree of polymerization (Figure 3), while the oligomer mixture showed a λ_{max} at 240 nm as a shoulder shape (Table 1). This is distinct evidence for the formation of silicon catenation. It is necessary to determine not only if the products have Si–Si bonds but also if the backbone structure is linear, cyclic, or branched, because phenylsilane has three reactive Si–H bonds. The FT-IR spectra, shown in Figure 4, indicate that although the intensity ratio of ($I(\delta_{SiH})/I(\nu_{SiH})$) in monomers was 1.2, it certainly decreased to 0.60 after electrolysis. This result suggests the formation of the $-(PhSiH)-$ structure from phenylsilane by the polymerization process.[15] The ^{29}Si-NMR spectrum was measured by a single pulse without decoupling in order to obtain information about the number of hydrogens directly bonded on the silicon

(27) Hengge, E.; Firgo, H. *J. Organomet. Chem.* **1981**, *212*, 155.
(28) Shono, T.; Kashimura, S.; Ishifune, S.; Nishida, R. *J. Chem. Soc., Chem. Commun.* **1990**, 1160.
(29) Umezawa, M.; Takeda, M.; Ichikawa, H.; Ishikawa, T.; Koizumi, T.; Fuchigami, T.; Nonaka, T. *Electrochim. Acta* **1990**, *35*, 1867.
(30) Bordeau, M.; Biran, C.; Lambert, M. P. L.; Dunogues, J. *J. Chem. Soc., Chem. Commun.* **1991**, 1476.
(31) Kunai, A.; Kawakami, T.; Toyoda, E.; Ishikawa, M. *Organometallics* **1991**, *10*, 893.
(32) Kunai, A.; Kawakami, T.; Toyoda, E.; Ishikawa, M. *Organometallics* **1991**, *10*, 2001.
(33) Biran, C.; Bordeau, M.; Leger, M. P. *Inorg. Organomet. Polym. Special Prop.* **1992**, *206*, 79.
(34) Shono, T.; Kashimura, S.; Murase, H. *J. Chem. Soc., Chem. Commun.* **1992**, *12*, 896.
(35) Aeiyach, S.; Lacaze, P. C.; Satge, J. *Synth. Met.* **1993**, *58*, 267.
(36) Jammegg, C.; Graschy, S.; Hengge, E. *Organometallics* **1994**, *13*, 2397.
(37) Kimata, Y.; Suzuki, H.; Satoh, S.; Kuriyama, A. *Chem. Lett.* **1994**, 1163.
(38) Kunai, A.; Kawakami, T.; Toyoda, E.; Sakurai, T.; Ishikawa, M. *Chem. Lett.* **1993**, 1945.

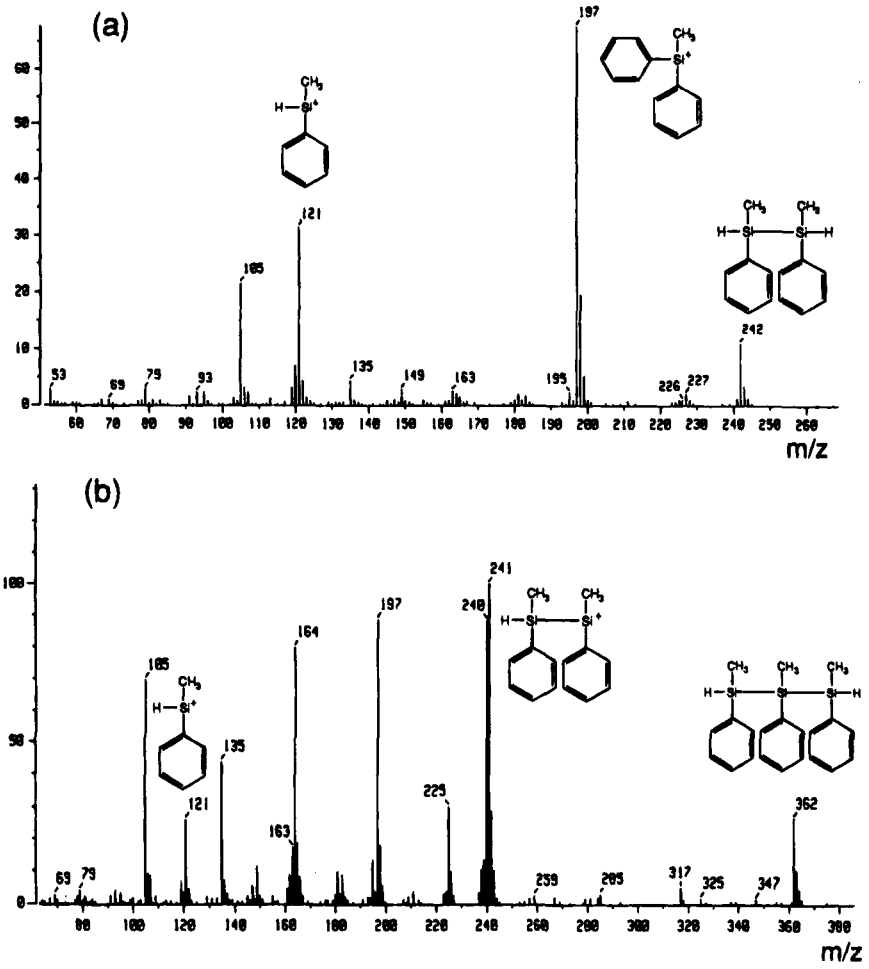

Figure 2. Mass spectra of (a) 1,2-dimethyl-1,2-diphenyldisilane and (b) 1,2,3-trimethyl-1,2,3-triphenyltrisilane obtained by the electrolysis of methylphenylsilane.

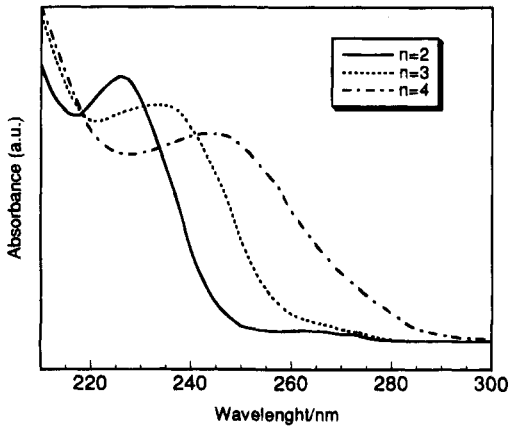

Figure 3. UV absorption spectra of phenylsilane oligomers eluted with acetonitrile by HPLC.

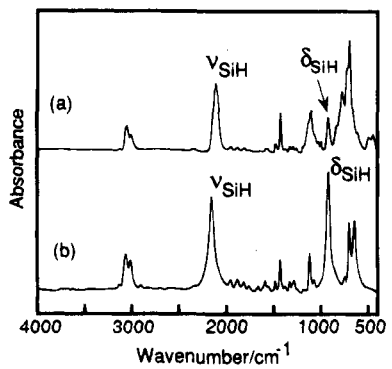

Figure 4. FT-IR spectra of (a) phenylsilane oligomer and (b) $PhSiH_3$ (KBr method).

atoms. As shown in Figure 5, resonances due to the linear main chain were observed in the range of −60 to −70 ppm, and two doublet peaks assigned to silicon nuclears possessing one hydrogen distinctly appeared with reasonable coupling constants (J_{SiH}). Waymouth synthesized stereoregular poly(phenylsilane) by the catalytic dehydrogenative coupling reaction of phenylsilane and reported that the resonance of ^{29}Si-NMR due to the SiH_2 end groups appeared sharply at −58 ppm.[39]

We also observed at −58.56 ppm the terminal SiH_2 as a triplet signal. No peak due to branched silicon atoms appeared in the high magnetic field. The ^{1}H-NMR spectrum also supported the presence of a linear silicon backbone, since the existing ratio of Si−H to phenyl groups was 1.1 which is slightly lower than the theoretical ratio of 1.3 calculated as a hexamer. It is considered that the electrochemically synthesized oligo(phenylsilane) consisted of −PhSiH− in the main chain and H_2PhSi− as the end groups.

On the other hand, *n*-hexylsilane, a typical hydrosilane possessing a non-aryl substituent, was also subjected to electrolysis, and a transparent liquid polymer was obtained in 70% yield. In Figure 1c, a simple

(39) Banovetz, J. P.; Stein, K. M.; Waymouth, R. M. *Organometallics* **1991**, *10*, 3430.

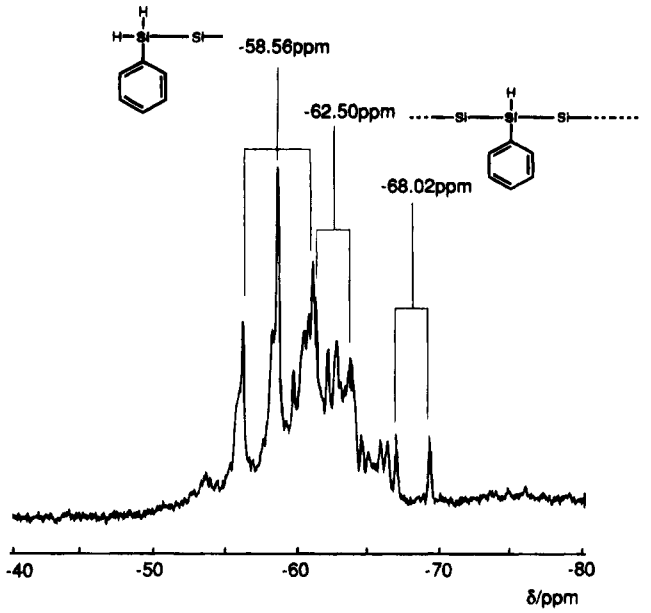

Figure 5. ^{29}Si-NMR spectrum of phenylsilane oligomer in benzene-d_6.

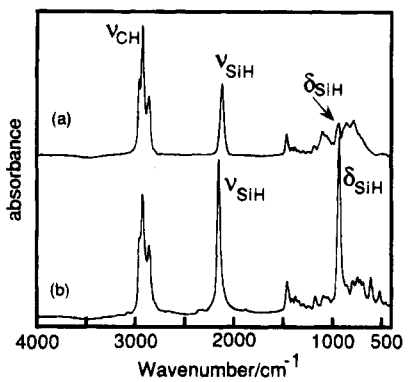

Figure 6. FT-IR spectra of (a) poly(n-hexylsilane) and (b) ^{n}HexSiH$_3$ (KBr method).

molecular weight distribution in the range 500−3000 was observed by GPC and the mean degree of polymerization reached 10. The intensity ratio of ($I(\delta_{SiH})$/$I(\nu_{SiH})$) in the FT-IR spectrum (Figure 6) of the polymer was drastically reduced to 0.28 in comparison to the value of 1.1. in the monomer, which obviously indicates the progress of an electrochemical dehydrogenative coupling reaction. We successfully confirmed the formation of silicon catenation by both UV and Raman spectroscopies. The polymer has a maximum UV absorption at 252 nm (ϵ = 7700, per Si unit), which is one of the characteristic properties of linear polysilanes. As reported in the literature,[40] alkyl-substituted polysilanes exhibit a Raman shift in the region around 400−500 cm^{-1}. In the Raman spectra of hexylsilane before and after polymerization, the signal assigned to the stretching vibrations of the Si−Si frame was certainly observed at 410 cm^{-1} as well as diminution of δ_{SiH} at 950 and 615 cm^{-1} (Figure 7). Similar to the phenylsilane oligomers, the ^{29}Si-NMR spectrum revealed that the electrochemically synthesized poly(n-hexylsilane) consisted of −HexSiH− in the main chain and H_2HexSi− as the end groups. The result of elemental analysis was also

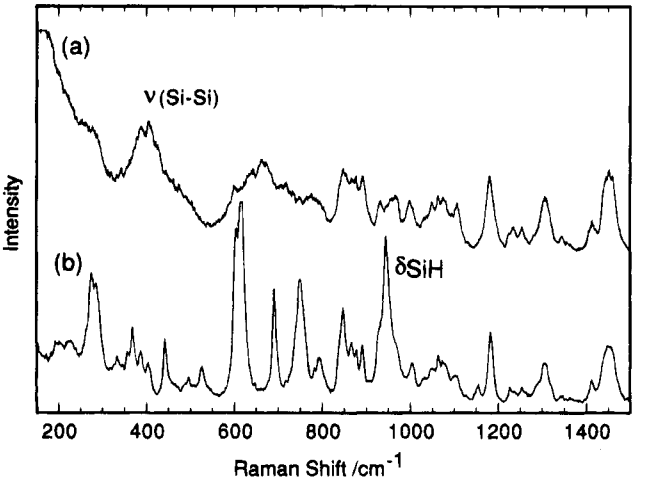

Figure 7. Raman spectra of (a) poly(n-hexylsilane) and (b) ^{n}HexSiH$_3$ obtained with 647.09 nm excitation.

Table 3. Reduction and Oxidation Potentials[a] of Hydrosilane Compounds

hydrosilane	E_{red} (V)	E_{ox} (V)
MePhSiH$_2$	<−3	+0.7
PhSiH$_3$	<−3	+0.7
^{n}HexSiH$_3$	<−3	+0.6

[a] Reference saturated Ag/AgCl.

consistent with the proposed linear structure. In addition, volatile components, which could not be detected by GPC, were identified by GC/MS and it was found that 1,2-dihexyldisilane (m/z = 230) and 1,2,3-trihexyltrisilane (m/z = 344) chiefly existed in the products. It is concluded that the electrochemical polymerization of trihydric substituted monosilanes affords linear polysilanes as shown in eq 2.

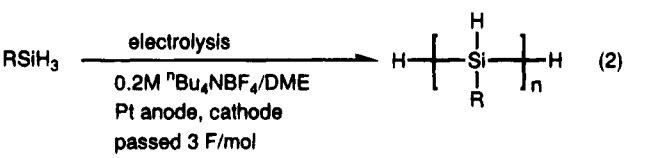

where R=Ph, ^{n}Hex

Voltammetry. The reduction and oxidation potentials of hydrosilanes were measured in order to predict the electrochemical reaction mechanism (Table 3). In all compounds, no reduction occurred until E_{red} = −3 V where solvent and/or electrolyte were forced to decompose. On the other hand, fairly low oxidation potentials were observed in the 0.6−0.7 V region. These results indicate that hydrosilanes can easily undergo an electro-oxidative reaction, while they have a strong resistance to reduction. Interestingly, this property was also common regardless of phenyl substitution. As reported by Diaz and Miller,[41] high molecular weight polysilanes are electrochemically oxidized to cut the silicon linkage. If the oxidation potential of a hydrosilane was higher than that of forming polysilane, it would be impossible to obtain polymerized products because of the prior decomposition. We confirmed the difference in the oxidation potential between the monomer and polymer of methylphenylsilane (Figure 8). The anodic current

(40) Bukalov, S. S.; Leites, L. A.; Morozov, V. A.; West, R.; Menescai, R. *Mendeleev Commun.* **1994**, 41.

(41) Diaz, A.; Miller, R. D. *J. Electrochem. Soc.* **1985**, *132*, 834.

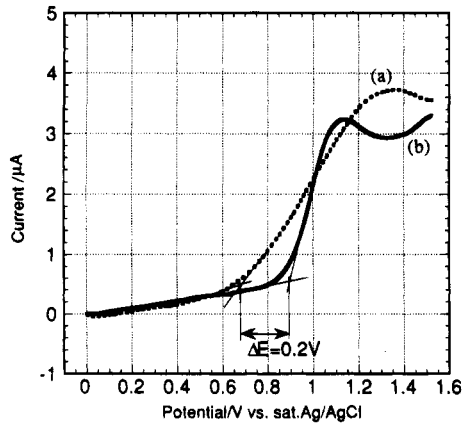

Figure 8. Anodic polarization curves of (a) $MePhSiH_2$ and (b) poly(methylphenylsilane) ($M_w = 2 \times 10^4$) on platinum measured in 0.1 M TBAF/acetonitrile.

of poly(methylphenylsilane) suddenly increased from E_{ox} = 0.9 V, which is 0.2 V more noble than the E_{ox} of monosilane. It should be expected that the oxidative reaction of hydrosilane monomers should prevent polymers from decomposing.

On the basis of the oxidative activity of hydrosilanes, silyl radical cations generated by the one-electron oxidation on the anode might attack another monomer to form an Si–Si bond for propagation while reductive generation of hydrogen gas is occurring on the cathode. A limitation of the molecular weight of electrochemically formed polymers is considered to be caused by the oxidative scission of the main chain. Polysilanes with aryl groups directly attached to the silicon backbone were more easily oxidized than the alkyl-substituted polymers.[41] In this study, the molecular weight of the poly(*n*-hexylsilane) was about two times higher than that of oligomers obtained from methylphenylsilane or phenylsilane. This result might be due to the stability of the polymers toward oxidation rather than the reactivity of the hydrosilanes, because the oxidation potential of each monomer was similar.

Experimental Section

Materials. 1,2-Dimethoxyethane (DME) and tetrahydrofuran (THF) were refluxed over sodium–benzophenone for 24 h and distilled into a vessel containing Molecular Sieves 4A and then kept overnight under argon. Acetonitrile was freshly distilled over P_2O_5 before use. Lithium perchlorate and tetrabutylammonium tetrafluoroborate (TBAF) were dried in vacuo at 60 and 100 °C for 1 day, respectively. Methylphenylsilane, phenylsilane (Shin-Etsu Chemical Co., Ltd.), and *n*-hexylsilane, prepared by the reduction of *n*-hexyltrichlorosilane with $LiAlH_4$ according to the literature,[42] were distilled over calcium hydride before use. Poly(methylphenylsilane) ($M_w = 2 \times 10^4$, $M_w/M_n = 1.42$) was synthesized by the Wurtz coupling reaction.[7] A platinum electrode was assembled with a plate (25 mm × 20 mm × 0.05 mm) welded to a Pt wire (1 mm o.d. × 17 cm).

Instrumental Analysis. Molecular weights were determined by gel permeation chromatography using a Toso 8020 multisystem with TSKgel H_{HR} type columns calibrated by standard polystyrenes. GPC profiles were recorded on a UV detector at 254 nm using chloroform as the eluent.

(42) Benkeser, R. A.; Landesman, H.; Foster, D. *J. Am. Chem. Soc.* **1952**, *74*, 648.

The NMR spectra were measured using a JEOL JNM-EX400-MHz FT-NMR spectrometer with a 5 mm diameter glass sample tube. A single pulse without decoupling was employed for observing ^{29}Si-NMR. Tetramethylsilane (TMS) was used as the internal standard for the determination of chemical shifts. The IR spectra were recorded on a Jasco IR-7300 FT-IR spectrometer using the KBr disk method. Mass analyses were performed using a JEOL JMS-AX505HA spectrometer equipped with a Hewlet Packard 5890 series II gas chromatograph with a TC-1 capillary column (GL Sciences Inc., 0.25 mm o.d. × 30 m), and the electron impact (70 eV) method was used for ionization. The UV absorption spectra were measured using a Simazu UV-2200 UV–vis spectrometer in spectroscopic grade cyclohexane or acetonitrile as the solvent. The Raman spectrum was recorded on a Jasco NR-1800 type laser Raman spectrometer. The wavelength for excitation was 647.09 nm (Kr, 300 mW). Elemental analyses were obtained on a Yanagimoto Seisakusyo MT-5 type CHN recorder.

General Procedure for the Electrolytic Polymerization. The electrolysis of hydrosilanes was performed under argon in an undivided cell with a constant current using a Model PAB 110-0.6A regulated power supply (Kikusui Denshi Kogyo Co., Ltd.). In a sealed glovebox with a pure argon atmosphere, TBAF was dissolved in DME at a concentration of 0.2 mol/L, and a 10 mL portion of the solution was then poured into the cell. Following the addition of 5 mmol of a hydrosilane, the platinum anode and cathode were installed parallel to each other at a distance of 5 mm. The electrolysis was continued with magnetic stirring until 2-3 F/mol was passed through the cell at room temperature. The resulting solution was then concentrated in vacuo, introduced onto the silica gel column (Varian, Mega Bond Elute Si), and eluted with toluene to remove TBAF. The product was obtained after evaporation of the solvent and dried in vacuum at 50 °C for 3 h.

Voltammetry. The voltammetry was carried out using a HZ-1A type automatic polarization system (Hokuto Denko Co., Ltd.). In a cylindrical glass cell, platinum wires (0.1 mm o.d.) as the working and counter electrodes and a double-junction reference electrode (saturated Ag/AgCl, HS-305DS, Toa Electrics Co., Ltd.) were fixed through a Teflon cap. A 20 mL portion of 0.1 M $LiClO_4$/THF (for cathodic polarization) or 0.1 M TBAF/acetonitrile (for anodic polarization) solution was placed in the cell, and then dry nitrogen gas was passed to remove oxygen and the silane was then injected at a concentration of 5 mM. The polarization curves were recorded from a rest potential to the prescribed voltage at a sweep rate of 50 mV s^{-1}.

Methylphenylsilane. A 0.61 g amount of methylphenylsilane was electrolyzed by passing a 20 mA constant current for 13.5 h (2 F/mol). A transparent oil was obtained in 60% yield. Molecular weight by GPC: M_n = 454, M_w = 477 (M_w/M_n = 1.05). IR (KBr): 2106 (ν(SiH)), 1250, 870 (Si–CH_3), 1110, 1428 (Si–Ph) cm^{-1}. ^{1}H-NMR (δ; C_6D_6): 0.1–0.7 (br, 3H (Si–CH_3)), 4.9–5.3 (m, 0.13H (terminal Si–H)), 7.2–7.8 (m, 5H (Si–C_6H_5)) ppm. UV (cyclohexane): λ_{max} 240 nm (shoulder, ϵ = 5300/SiSi). The oligomers were also fractionated by HPLC (eluent, acetonitrile; column, TSK gel ODS-80Ts (20 mm i.d. × 25 cm)) into 2–5mers as shown in Table 2.

Phenylsilane. The electrolysis of a 0.54 g amount of phenylsilane was performed for 20.1 h under a 20 mA constant current (3 F/mol), and the product was obtained as a viscous liquid in 32% yield. Molecular weight based on GPC: M_n = 450, M_w = 640 (M_w/M_n = 1.42). IR (KBr): 2121 (ν(SiH)), 1428, 1109 (Si–Ph), 917 (δ(SiH)) cm^{-1}. ^{1}H-NMR (δ; C_6D_6): 4.4–5.1 (m, 1.1H (Si–H)), 6.6–7.9 (m, 5H (Si–C_6H_5)) ppm. ^{29}Si-NMR (δ; C_6D_6): −58.56 (t, J_{SiH} = 192 Hz (H_2SiPh–)), −62.50 (d, J_{SiH} = 186 Hz (–PhSiH–)), −68.02 (d, J_{SiH} = 185 Hz (–PhSiH–)) ppm. UV (cyclohexane): λ_{max} 240 nm (shoulder, ϵ = 5700/SiSi). Anal. Calcd for H–(PhSiH)$_6$–H: C, 67.6; H, 6.0. Found: C, 65.0; H, 5.9. The lowest homolog (1,2-diphenyldisilane) was identified by MS: m/z = 214 (M^+).

***n*-Hexylsilane.** The electrolysis of a 0.57 g of *n*-hexylsilane was performed for 20.1 h under a 20 mA constant current (3 F/mol), and the product was obtained as a colorless oil in 70% yield. Molecular weight based on GPC: $M_n = 1120$, $M_w = 1240$ ($M_w/M_n = 1.09$). IR (KBr): 2959, 2942, 2873, 2856 (ν(CH)), 2117 (ν(SiH)), 930 (δ(SiH)) cm^{-1}. Raman: 410 (ν(SiSi)) cm^{-1}. ^{1}H-NMR (δ; C_6D_6): 0.6–0.9 (m, 5H (Si–CH_2(CH_2)$_4$CH_3)), 1.2–1.5 (m, 8H (Si–CH_2(CH_2)$_4$$CH_3$)), 3.3–3.8 (m, 1.1H (Si–H)) ppm. ^{29}Si-NMR (δ; C_6D_6): −25.47 (t, J_{SiH} = 186 Hz (H_2HexSi–)), −56.91 (t, J_{SiH} = 180 Hz (H_2HexSi–)), −60.29 (t, J_{SiH} = 185 Hz (H_2HexSi–)), −63.56 (t, J_{SiH} = 183 Hz (H_2HexSi–)), −69.30 (d, J_{SiH} = 167 Hz (–HexSiH–)), −72.97 (d, J_{SiH} = 173 Hz (–HexSiH–)) ppm. UV (cyclohexane): λ_{max} 252 nm (ϵ = 7700/SiSi). Anal. Calcd for H–(HexSiH)$_{10}$–H: C, 62.9; H, 12.5. Found: C, 63.0; H, 12.2.

Acknowledgment. This research was performed by Toagosei Co., Ltd., under the management of the Japan High Polymer Center as part of the Industrial Science and Technology Frontier Program supported by the New Energy and Industrial Technology Development Organization.

OM9408730

Bis(halodiphenylstannyl)alkanes as Bidentate Lewis Acids toward Halide Ions†

Dainis Dakternieks,* Klaus Jurkschat,*,‡ and Hongjian Zhu

School of Biological and Chemical Sciences, Deakin University, Geelong, Victoria 3217, Australia

Edward R. T. Tiekink

Department of Chemistry, The University of Adelaide, Adelaide, S.A. 5005, Australia

Received August 10, 1994®

^{119}Sn and ^{19}F NMR spectroscopies were used to study reaction of bis(halodiphenylstannyl)-alkanes $(Ph_2XSn)_2(CH_2)_n$ (X = F, Cl, Br, I; n = 1, 2, 3) with various halide ions in dichloromethane solution. All three series of bis(halodiphenylstannyl)alkanes, $(Ph_2XSn)_2(CH_2)_n$ (X = F, Cl, Br, I; n = 1, 2, 3), exhibit chelate ability toward halide, forming anionic 1:1 adducts $[(Ph_2XSn)_2(CH_2)_nX]^-$ which are static at −100 °C on the NMR time scale. The bis(halodiphenylstannyl)alkanes always preferentially chelate fluoride ion over chloride or bromide. Endocyclic Sn−CH_2 rotation brings about intramolecular exchange between bridging and terminal fluorine atoms at higher temperature. For n = 1, and 1:1 adducts $[(Ph_2XSn)_2(CH_2)X]^-$ react with additional fluoride (but not chloride or bromide) eventually to give $[(Ph_2F_2Sn)_2(CH_2)]^{2-}$ in which both tin atoms are five-coordinated. For n = 2, the 1:1 adducts $[(Ph_2XSn)_2(CH_2)_2X]^-$ appear particularly stable and there is no evidence for formation of 1:2 adducts $[(Ph_2X_2Sn)_2(CH_2)_2]^{2-}$. Propylene-bridged 1:1 adducts, $[(Ph_2XSn)_2(CH_2)_3X]^-$, react with both fluoride and chloride to give 1:2 adducts, $[(Ph_2F_2Sn)_2(CH_2)_3]^{2-}$ and $[(Ph_2Cl_2Sn)_2(CH_2)_3]^{2-}$, respectively, in which the tin atoms remain five-coordinated. The crystal structures of $[(Ph_2FSn)_2CH_2F]^-$ (**1**), $[(Ph_2BrSn)_2CH_2F]^-$ (**4**), $[(Ph_2ISn)_2CH_2F]^-$ (**8**), and $[(Ph_2ClSnCH_2)_2F]^-$ (**11**), as their tetraethylammonium salts (**1a**, **4a**, **8a**, and **11a**, respetively), are described. Colorless crystals of **1a** are monoclinic, space group $P2_1/n$, with a = 11.695(4) Å, b = 14.667(2) Å, c = 18.956(2) Å, β = 103.33(1)°, V = 3164(1) Å^3, and Z = 4. Colorless crystals of **4a** are monoclinic, space group Cc, with a = 11.758(1) Å, b = 14.880(2) Å, c = 19.316(2) Å, β = 93.981(9)°, V = 3371.3(6) Å^3, and Z = 4. Colorless crystals of **8a** are monoclinic, space group $P2_1/n$, with a = 10.032(1) Å, b = 16.923(3) Å, c = 20.523(3) Å, β = 99.65(1)°, V = 3434.9(8) Å^3, and Z = 4. Colorless crystals of **11a** are monoclinic, space group $P2_1$, with a = 9.562(2) Å, b = 15.529(4) Å, c = 11.359(4) Å, β = 95.51(2)°, V = 1678.9(9) Å^3, and Z = 2. The structures were refined to final R = 0.027, 0.029, 0.033, and 0.029 for 4661, 2647, 3843, and 3457 reflections with $I \geq 3.0\sigma(I)$, respectively.

Introduction

Organotin(IV) halides exhibit strong Lewis acidity, and the complexation chemistry of organotin(IV) halides has been the subject of study for many years.[1] Compounds containing two tin atoms which are bridged through carbon behave as bifunctional Lewis acids, and derivatives with Lewis bases such as chloride ion, dimethyl sulfoxide, and hexamethylphosphonic amide have been described.[2-13] Most earlier studies were concerned with the solid state properties of these complexes, there being only a few ^{119}Sn NMR investigations[11,12] on the chelating ability of bis(haloorganostannyl)alkanes toward chloride ion in solution. We now report on the reaction of bidentate Lewis acids bis(halodiphenylstannyl)alkanes $(Ph_2XSn)_2(CH_2)_n$ (X = F, Cl, Br, I; n = 1, 2, 3) with fluoride, chloride, and bromide ions in dichloromethane solution. Also reported are the crystal structures of $[(Ph_2FSn)_2CH_2F]^-$, $[(Ph_2BrSn)_2CH_2F]^-$, $[(Ph_2ISn)_2CH_2F]^-$, and $[(Ph_2ClSnCH_2)_2F]^-$ as their tetraethylammonium salts.

† Dedicated to Professor Frido Huber on the occasion of his retirement from the University of Dortmund.

‡ Current address: Fachbereich Chemie der Universität, Institut für Anorganische Chemie, D-44221 Dortmund, Germany.

® Abstract published in *Advance ACS Abstracts,* March 15, 1995.

(1) Nicholson, J. W. *Coord. Chem. Rev.* **1982**, *47*, 263.
(2) Newcomb, M.; Horner, J. H.; Blanda, M. T.; Squattrito, P. J. *J. Am. Chem. Soc.* **1989**, *111*, 6294.
(3) Swami, K.; Hutchinson, J. P.; Kuivila, H. G. *Organometallics* **1984**, *3*, 1687.
(4) Hyde, J. R.; Karol, T. J.; Hutchinson, J. P.; Kuivila, H. G.; Zubieta, J. A. *Organometallics* **1982**, *1*, 404.
(5) (a) Karol, T. J.; Hutchinson, J. P.; Hyde, J. R.; Kuivila, H. G.; Zubieta, J. A. *Organometallics*, **1983**, *2*, 106. (b) Kuivila, H. G.; Karol, T. J.; Swami, K. *Organometallics* **1983**, *2*, 909.
(6) Mitchell, T. N.; Amamria, A.; Fabisch, B.; Kuivila, H. G.; Karol, T. J.; Swami, K. *J. Organomet. Chem.* **1983**, *259*, 157.
(7) Gielen, M.; Jurkschat, K. *J. Organomet. Chem.* **1984**, *273*, 303.
(8) Gielen, M.; Jurkschat, K.; Meunier-Piret, J.; van Meerssche, M. *Bull. Soc. Chim. Belg.* **1984**, *93*, 379.
(9) Meunier-Piret, J.; van Meerssche, M.; Jurkschat, K.; Gielen, M. *J. Organomet. Chem.* **1985**, *288*, 139.
(10) Austin, M.; Gebreyes, K.; Kuivila, H. G.; Swami, K.; Zubieta, J. A. *Organometallics* **1987**, *6*, 834.
(11) Blanda, M. T.; Newcomb, M. *Tetrahedron Lett.* **1989**, *30*, 3501.
(12) Jurkschat, K.; Hesselbarth, F.; Dargatz, M.; Lehmann, J.; Kleinpeter, E.; Tzschach, A.; Meunier-Piret, J. *J. Organomet. Chem.* **1990**, *388*, 259.
(13) Horner, J. H.; Squatritto, P. J.; McGuire, N.; Riebenspies, J. P.; Newcomb, M. *Organometallics* **1991**, *10*, 1741.

0276-7333/95/2314-2512$09.00/0

Table 1. NMR Data (at −100 °C in Dichloromethane Solution) for Species Formed by Reaction of Bis(haloorganoyl)alkanes, $(Ph_2SnXSn)_2(CH_2)_n$, with Halide Ion

species	$\delta(^{119}Sn)$	$\delta(^{19}F)$	$J(^{119}Sn-^{19}F)$	$J(F-F)$	$^2J(^{119}Sn-^{117}Sn)$
		$n = 1$			
$(Ph_2ClSn)_2CH_2$	21.0				220
$(Ph_2BrSn)_2CH_2$	3.2				223
1[a]	−184.8	−172.1 (F_a)	2178	62	325
		−97.4 (F_b)	879	62	
2	−244.4	−141.9	1840		
3	−137.0				
4	−152.1	−98.1	787		288
5[b]	−188.6 (Sn_a)	−175.3 (F_a)	2211	59	271
	−147.4 (Sn_b)	−98.7 (F_b)	852	59	271
6	−154.8	−96.8	806		276
7[c]	−190.0 (Sn_a)	−174.4 (F_a)	2202	59	273
	−149.8 (Sn_b)	−97.6 (F_b)	850	59	273
8	−100.1		780		
		$n = 2$			
$(Ph_2ClSnCH_2)_2$	1.8				
$(Ph_2ISnCH_2)_2$	−40.4				
9	−230.0	−165.1[f] (F_a)	2100	81	350
		−159.3[f] (F_b)	1260	81	
10	−177.8	−153.2[g]	1128		
11	−191.2	−155.3	1180		
12[d]	−222.8 (Sn_a)	−169.7 (F_a)	2080	80	
	−199.8 (Sn_b)	−159.0 (F_b)	1251		
		$n = 3$			
$(Ph_2ClSnCH_2)_2CH_2$	10.3				
13	−142.8				
14	−200.0				
15	−172.7	−142.3	1204		
16[e]	−209.6 (Sn_a)	−168.8 (F_a)	2042	79	
	−180.7 (Sn_b)	−140.2 (F_b)	1250	79	
17	−214.9	−164.9 (F_a)	2030	88	
		−139.4 (F_b)	1264	88	
18	−267.8	−152.0	1880		

[a] $^3J(Sn-F_b-Sn-F_a)$ = 140 Hz. [b] $^3J(Sn_b-F_a)$ = 144 Hz; $J(Sn_a-F_b)$ = 815 Hz. [c] $^3J(Sn_b-F_a)$ = 145 Hz; $J(Sn_a-F_b)$ = 827 Hz. [d] $J(Sn_a-F_b)$ = 1204 Hz. [e] $J(Sn_a-F_b)$ = 1204 Hz. [f] Measured at −55 °C. [g] Measured at −80 °C. [h] Measured at −35 °C.

Results and Discussion

Reaction of Bis(halodiphenylstannyl)methane with Halide Ion. The compound $(Ph_2FSn)_2CH_2$ has too low solubility in common organic solvents to allow measurement of its ^{119}Sn or ^{19}F NMR spectrum. However, addition of 1 mol equiv of fluoride ion ($Bu_4NF{\cdot}3H_2O$) to $(Ph_2FSn)_2CH_2$ in dichloromethane solubilizes the system and gives rise to a doublet of doublets of doublets resonance at −184.8 ppm, accompanied by ^{117}Sn satellites, in the ^{119}Sn NMR spectrum recorded at −100 °C. The corresponding ^{19}F NMR spectrum comprises a doublet and a triplet resonance, of relative intensity 2:1, at −172.1 and −97.4 ppm, $J(F-F)$ = 62 Hz. These data (Table 1) are consistent with formation of the anionic species $[(Ph_2FSn)_2CH_2F]^-$ (**1**) (Chart 1) which contains two apical fluorine atoms and a fluorine atom chelated by two tin atoms to form a four-membered SnCSnF ring. The ^{19}F NMR chemical shift of the bridging fluorine atom is at considerably higher frequency than that for the two apical fluorine atoms, in line with the trend reported for comparable silicon systems.[14,15] The magnitude of $J(Sn-F)$ coupling of the terminal fluorides (2178 Hz) is appreciably larger than that of the bridging fluoride (879 Hz) similar to the trend observed in $[(Me_3SnF)_2F]^-$ and in a ditin macrocycle.[2,16,17]

Variable-temperature NMR spectra indicate that **1** is labile above −100 °C. The two ^{19}F resonances show loss of $J(F-F)$ coupling at −30 °C although coupling to $^{117/119}Sn$ is still evident. Raising the temperature causes the two ^{19}F resonances to broaden, and at about 0 °C coupling to $^{117/119}Sn$ is no longer evident. Lack of solubility in an appropriate solvent precluded measurements at significantly higher temperature.

These data are consistent with an intramolecular exchange of the terminal and chelated fluorine atoms resulting from rotation about a $Sn-CH_2$ bond in the methylene bridge. At −30 °C the rate of intramolecular fluorine atom exchange is sufficient such that observation $J(F-F)$ is no longer possible. At 24 °C the two ^{19}F resonances coalesce, presumably because the rate of rotation about each $Sn-CH_2$ has increased sufficiently to effectively exchange all three fluorine atoms within structure **1**. A similar intramolecular exchange process has been reported recently for some related organosilicon systems.[14]

The variable-temperature ^{119}Sn NMR spectra (Figure 1) appear more complex but nevertheless consistent with this intramolecular exchange process. At −30 °C the spectrum appears as a doublet of doublets in which the central two components are significantly broader than the outer two lines. Raising the temperature to 24 °C causes further broadening of all the components. This somewhat complex spectral pattern appears to be

(14) Tamao, K.; Hayashi, T.; Ito, Y. *Organometallics* **1992**, *11*, 2099.
(15) Harland, J. J.; Payne, J. S.; Day, R. O.; Holmes, R. R. *Inorg. Chem.* **1987**, *26*, 760.
(16) Dakternieks, D.; Zhu, H. *Organometallics* **1992**, *11*, 3820.
(17) Blunden, S. J.; Hill, R. *J. Organomet. Chem.* **1989**, *371*, 145.

Chart 1

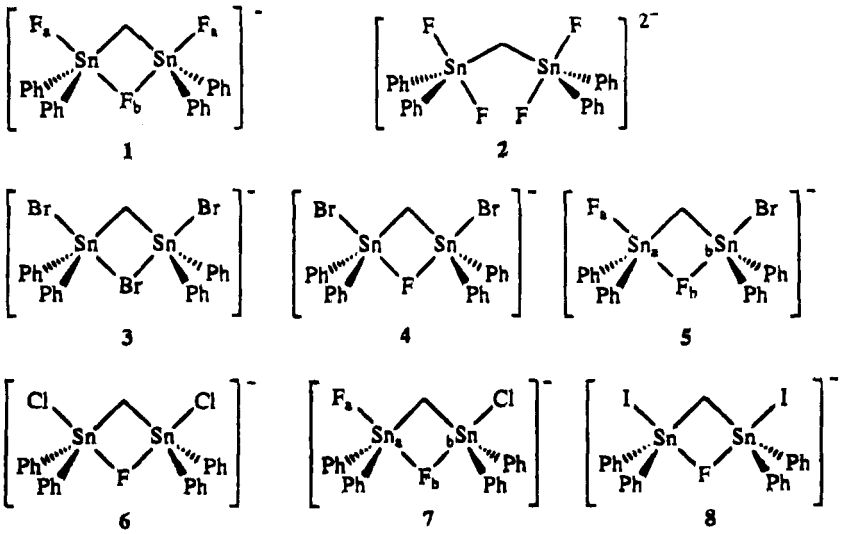

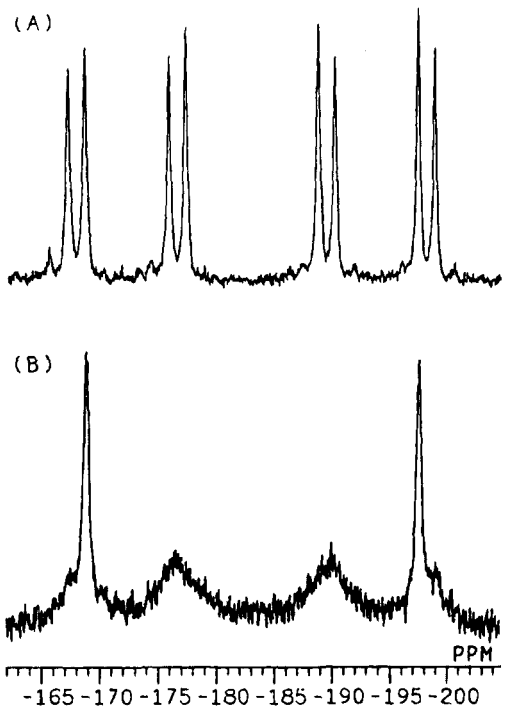

Figure 1. Tin-119 NMR spectrum of $[(Ph_2SnFSn)_2CH_2F)]^-$ in dichloromethane solution at (A) −100 °C and (B) at −30 °C.

on the pathway to becoming a triplet resonance where the two broad central resonances will eventually collapse to form the central component.

The ^{19}F NMR spectra at −15 °C show no variation as a function of concentration, which suggests that the observed exchange process is not intermolecular in nature.

As a comparison, the monodentate Lewis acid $Ph_2FSnCH_2SiMe_3$ was synthesized and its reaction with fluoride examined. The ^{19}F NMR spectrum at −75 °C of a 1:1 solution of $Ph_2FSnCH_2SiMe_3$ and $Bu_4NF{\cdot}3H_2O$ in dichloromethane solution shows a single sharp resonance at −145.5 ppm, accompanied by $^{117/119}Sn$ satellites (1897 and 1823 Hz, respectively). The ^{119}Sn spectrum at the same temperature shows a triplet at −260.2 ppm with $J(Sn-F)$ = 1897 Hz. Raising the temperature to −35 °C causes the ^{19}F resonance to broaden, but an average coupling to $^{117/119}Sn$ is still observed. Coupling is lost at −15 °C indicating that the rate of intermolecular fluorine exchange is now rapid on the NMR time scale. Comparison of the data from this system imply that the exchange process observed for **1** is indeed intramolecular in nature.

Addition of a second 1 mol equiv of fluoride to $(Ph_2FSn)_2CH_2$ results in the appearance of a triplet resonance at −244.4 ppm in the ^{119}Sn NMR spectrum at −100 °C. This resonance is assigned to the doubly-charged anionic species $[(Ph_2F_2Sn)_2CH_2]^{2-}$ (**2**) (Chart 1). The corresponding ^{19}F NMR spectrum is consistent with this assignment. Furthermore, the ^{19}F NMR spectrum this doubly-charged anionic species is intact at 24 °C. It appears that $(Ph_2FSn)_2CH_2$ may behave either as a bidentate or as a bismonodentate ligand toward fluoride ion, depending on the concentration of fluoride ion. NMR data are summarized in Table 1. Identical NMR spectra are obtained when $Bu_4NF{\cdot}3H_2O$ was replaced by the anhydrous fluoride source $[Ph_3SnF_2]^-[Bu_4N]^+$.

The reaction of $(Ph_2ClSn)_2CH_2$ with chloride ion to give a solid 1:1 adduct $[(Ph_2ClSn)_2CH_2{\cdot}Cl]^-$ has been described previously.[12] Similarly, we find that reaction of chloride with $(Ph_2ClSn)_2CH_2$ in 1:1 or 2:1 molar ratio leads only to formation of $[(Ph_2ClSn)_2CH_2{\cdot}Cl]^-$ in dichloromethane solution. Reaction of 1 mol equiv of bromide ion (Bu_4NBr) with $(Ph_2BrSn)_2CH_2$ in dichloromethane solution gives rise to a ^{119}Sn NMR singlet at −137.0 ppm in the temperature range −100 to 24 °C which is assigned to the bromide chelated anionic species $[(Ph_2BrSn)_2CH_2{\cdot}Br]^-$ (**3**). Addition of a second 1 mol equiv of bromide causes no apparent change in the ^{119}Sn NMR spectrum at −100 °C, and apparently no new species is formed. In contrast to the case for X = F where a dianion is formed, it appears that $[(Ph_2XSn)_2CH_2]$ (for X = Cl or Br) are not sufficiently acidic to add two additional halides.

The addition of 1 mol equiv of fluoride ion to $(Ph_2BrSn)_2CH_2$ in dichloromethane solution leads to a doublet at −152.1 ppm in the ^{119}Sn NMR spectrum and a singlet, with $^{117/119}Sn$ satellites, at −98.11 ppm in the ^{19}F NMR spectrum at −100 °C. These spectra are assigned to formation of a fluoride-chelated species $[(Ph_2BrSn)_2CH_2{\cdot}F]^-$ (**4**). It appears that fluoride is preferentially chelated by the two tin atoms of

Scheme 1

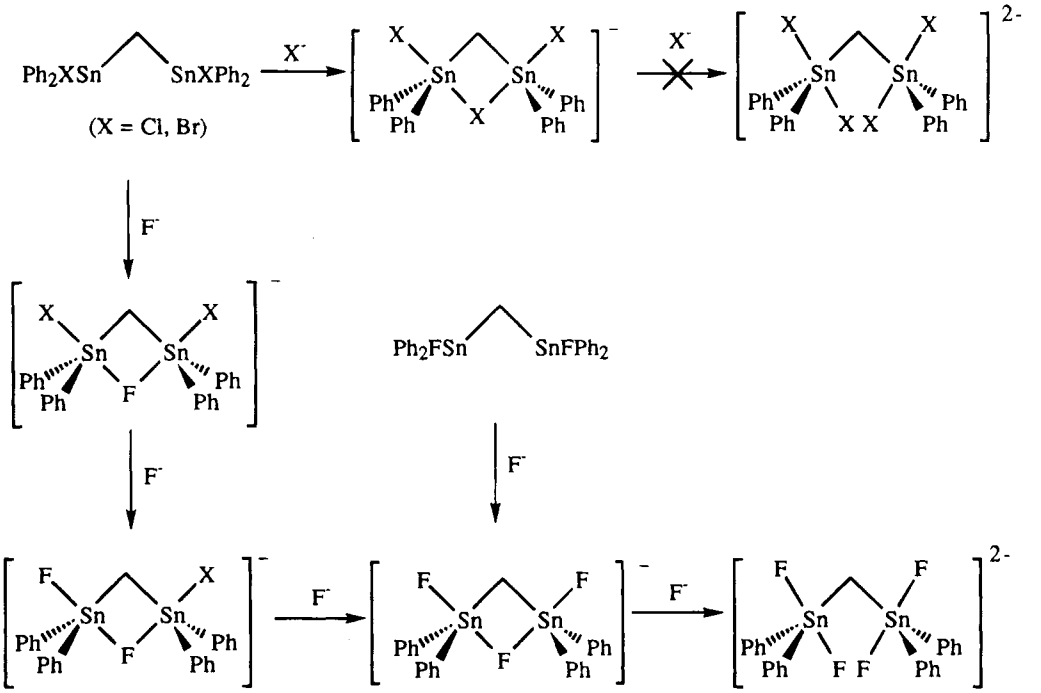

$(Ph_2BrSn)_2CH_2$. Significantly, the ^{119}Sn doublet resonance and the ^{19}F singlet resonance (with $^{117/119}Sn$ satellites) of **4** remain unchanged as the temperature is raised from −100 to 24 °C, indicating no appreciable exchange between Br and F thereby indicating that fluoride is a better bridging ligand than is bromide.

Addition of 2 mol equiv of fluoride ion to $(Ph_2BrSn)_2CH_2$ in dichloromethane results in a complex ^{119}Sn NMR spectrum at −100 °C. In addition to the resonances attributed to **4** and **1**, there are two doublets of doublets at −147.4 and −188.6 ppm, respectively. The corresponding ^{19}F spectrum contains two doublets at −98.72 and −175.31 ppm (J(F−F) = 59 Hz). These resonances are assigned to the mixed halide species $[(Ph_2FSn)CH_2(Ph_2BrSn)\cdot F]^-$ (**5**) in which one fluoride is chelated and the other is termianlly bound to tin. Variable-temperature ^{19}F NMR spectra indicate the onset of exchange between bridging and terminal fluorine atoms in **5** at about −30 °C. The reaction of 3 mol equiv of fluoride ion with $(Ph_2BrSn)_2CH_2$ results in displacement of all the bromide, and only species **1** is observed in the ^{119}Sn and ^{19}F spectra at −100 °C.

Addition of 1 mol equiv of fluoride ion to $[(Ph_2BrSn)_2CH_2\cdot Br]^-$ (**3**) results in identical ^{19}F and ^{119}Sn spectra as were observed for $[(Ph_2BrSn)_2CH_2\cdot F]^-$ (**4**); i.e. the fluoride displaces the bromide as bridging ligand, demonstrating the superior bridging capacity of the fluoride ion.

The reactions of fluoride ion with $(Ph_2ClSn)_2CH_2$ at molar ratios 1:1, 2:1, and 3:1 give very similar results to those observed for reactions of the bromo analogue. The ^{119}Sn NMR spectrum measured at −100 °C of a dichloromethane solution containing fluoride and $(Ph_2ClSn)_2CH_2$ at molar ratio 2:1 shows the presence of two chloride-fluoride mixed species $[(Ph_2ClSn)_2CH_2\cdot F]^-$ (**6**) and $[(Ph_2FSn)CH_2(Ph_2ClSn)\cdot F]^-$ (**7**) as well as **1**. The dynamic behavior of species **6** in solution is similar to that of its bromide analogue, **4**; i.e. the ^{19}F and ^{119}Sn spectra do not change significantly in the temperature range −100 to 24 °C.

Addition of 1 mol equiv of fluoride to $(Ph_2ISn)_2CH_2$ gives rise to a ^{19}F spectrum consistent with the formation of $[(Ph_2ISn)_2CH_2F]^-$ (**8**) in which the fluoride is chelated by the two tin atoms (Table 1). Compound **8** is not sufficiently soluble to allow determination of its ^{119}Sn spectrum. Addition of further mole equivalents of fluoride causes extensive precipitation.

The chelating reactions of bis(halodiphenylstannyl)methane with halide ion are summarized in Scheme 1.

Reaction of Bis(halodiphenylstannyl)ethane with Halide Ion. The compound $(Ph_2FSnCH_2)_2$ is not sufficiently soluble in common solvents to allow determination of its ^{19}F or ^{119}Sn spectra. However, addition of 1 mol equiv of fluoride ion to $(Ph_2FSnCH_2)_2$ in dichloromethane solubilizes the system and gives rise to a doublet of doublets resonance at −230 ppm in the ^{119}Sn NMR spectrum at −100 °C. The ^{19}F NMR resonances at −100 °C are a little broad but sharpen at −55 °C, and a doublet at −165.1 ppm and a triplet at −159.3 ppm with relative intensity of 2:1 are clearly observed. The above data are consistent with formation of an anionic fluoride-chelated species $([Ph_2FSnCH_2)_2\cdot F]^-$ (**9**) which contains a five-membered SnCCSnF ring. The one-bond coupling due to the bridging fluorine is larger than that observed for $[(Ph_2FSn)_2CH_2\cdot F]^-$ (**1**). These differences appear to result from steric strain in the four-membered ring of **1** (Sn−F−Sn = 97.4°) compared to the more suitable geometry possible in the five-membered ring of **9** (Sn−F−Sn = 120.5°).

Variable-temperature ^{19}F NMR spectra of $[(Ph_2FSnCH_2)_2\cdot F]^-$ (**9**) indicate an endocyclic Sn−C rotation resulting in intramolecular ligand exchange between bridging and terminal fluorine atoms. The ^{19}F NMR triplet and doublet resonances lose their J(F−F) coupling at about 10 °C, but coupling to tin is still evident for both resonances at 30 °C. It appears that the energy barrier of endocyclic Sn−C bond rotation is higher for $[(Ph_2FSnCH_2)_2\cdot F]^-$ (**9**) than for $[(Ph_2FSn)_2CH_2\cdot F]^-$ (**1**) indicating that the five-membered SnFSnCC ring is more stable than the four-membered SnFSnC ring.

Addition of a second 1 mol equiv of fluoride ion to a solution of $[(Ph_2FSnCH_2)_2{\cdot}F]^-$ (**9**) gives rise to additional, somewhat broad ($W_{1/2}$ = 120 Hz), ^{119}Sn resonance at −263.3 ppm. This resonance is only observed in the narrow temperature range of −40 to 10 °C where it appears as a triplet (J(Sn−F) = 1890 Hz) with some additional fine structure. Also present is a weak doublet resonance at −261 ppm, J(Sn−F) = 1980 Hz. The ^{19}F spectrum of this solution shows a sharp ^{19}F resonance at −151.2 ppm with very sharp $^{117/119}$Sn satelites, J(Sn−F) = 1890 Hz. It was subsequently shown that these additional peaks arose from interactions of the water from the fluoride source, $Bu_4NF{\cdot}3H_20$. Both ^{19}F and ^{119}Sn spectra of a solution made from the addition of 2 mol equiv of the anhydrous fluoride source $[Ph_3SnF_2]Bu_4N$ show only formation of **9** and unreacted $[Ph_3SnF_2]Bu_4N$. There was some precipitation which was subsequently identified as Ph_3SnF by elemental analysis. We are continuing work on the hydrolysis products of these and other related systems.

Apparently species **9** is particularly stable, there being no evidence for formation of the dianion $[(Ph_2FSnCH_2)_2F_2]^{2-}$. Earlier work[12] reported that the addition of chloride ion to $[(Ph_2ClSnCH_2)_2{\cdot}Cl]^-$ does not change the value of ^{119}Sn chemical shift of the complex, indicating that the doubly-charged anionic complex $[(Ph_2Cl_2SnCH_2)_2]^{2-}$ is probably not formed to any appreciable degree in solution. These results indicate the particular stability of 1:1 halide adducts of bis(halodiphenylstannyl)ethane, possibly due to the favorable formation of five-membered $SnCH_2CH_2SnX$ rings.

Addition of 1 mol equiv of fluoride to $(Ph_2ISnCH_2)_2$ results in formation of the fluoride-chelated species $[(Ph_2ISnCH_2)_2{\cdot}F]^-$ (**10**) (Chart 2), which is identified by the appearance of a doublet at −177.8 ppm in the ^{119}Sn NMR spectrum and a singlet, with $^{119/117}$Sn satellites, at −153.22 ppm in the ^{19}F NMR spectrum at −80 °C. There is no evidence for ligand exchange between fluoride and iodide at room temperature. Addition of a second 1 mol equiv of fluoride to $(Ph_2ISnCH_2)_2$ results in a precipitate which may be due to the formation of $(Ph_2FSnCH_2)_2$. However, the addition of a third mole of fluoride dissolves the precipitate and forms $[(Ph_2FSnCH_2)_2{\cdot}F]^-$ (**9**) which is identified by both ^{119}Sn and ^{19}F NMR spectra at −80 °C.

Addition of 1 mol equiv of chloride ion to $(Ph_2FSnCH_2)_2$ in dichloromethane results in formation of mixed chloro−fluoro complexes, $[(Ph_2ClSnCH_2)_2{\cdot}F]^-$ (**11**) and $[(Ph_2FSnCH_2CH_2SnClPh_2){\cdot}F]^-$ (**12**), as well as $[(Ph_2FSnCH_2)_2{\cdot}F]^-$ (**9**). The ^{19}F resonances which arise from the bridging and the terminal fluorine atoms of $[(Ph_2FSnCH_2CH_2SnClPh_2){\cdot}F]^-$ (**12**) do not collapse until 24 °C, again indicating that the barrier to intramolecular exchange of fluorides as a result of rotation about the Sn−C bond is higher in a five-membered SnC_2SnF ring than in a four-membered SnCSnF ring. On the other hand, the ^{19}F resonance due to $[(Ph_2ClSnCH_2)_2{\cdot}F]^-$ (**11**) remains sharp, with $^{119/117}$Sn satellites, at 24 °C which indicates that exchange between chloride and bridging fluoride does not occur on the NMR time scale. Addition of a second chloride to $(Ph_2FSnCH_2)_2$ does not change either the ^{119}Sn or the ^{19}F NMR spectrum. That the chelated halide ion is always fluoride indicates the superior bridging capability of fluoride ion over chloride ion.

Chart 2

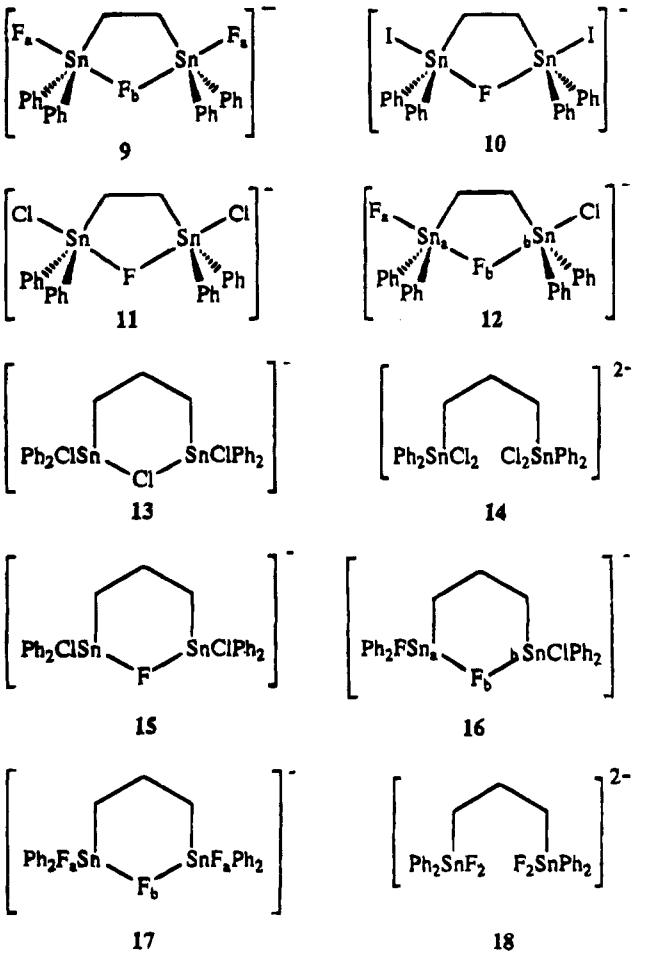

Reaction of Bis(chlorodiphenylstannyl)propane with Halide Ion. The reaction of chloride ion with $(Ph_2ClSnCH_2)_2CH_2$ at molar ratio 1:1 in dichloromethane solution at −100 °C gives rise to a ^{119}Sn NMR singlet at −142.8 ppm and at molar ratio 2:1 a singlet at −200.0 ppm. These data are assigned to the chloride chelated species $[(Ph_2ClSnCH_2)_2CH_2{\cdot}Cl]^-$ (**13**) and the doubly-charged species $[(Ph_2Cl_2SnCH_2)_2CH_2]^{2-}$ (**14**).

Addition of 1 mol equiv of fluoride to $(Ph_2ClSnCH_2)_2CH_2$ in dichloromethane gives rise to two doublets of relative intensity of approximately 5:1, at −172.7 and −156.7 ppm, in the ^{119}Sn NMR spectrum recorded at −100 °C. The major resonance is assigned to $[(Ph_2ClSnCH_2)_2CH_2{\cdot}F]^-$ (**15**). The addition of a second 1 mol equiv of fluoride to $(Ph_2ClSnCH_2)_2CH_2$ does not cause precipitation but results in formation of the two new species $[Ph_2FSn(CH_2)_3SnClPh_2{\cdot}F]^-$ (**16**) and $[(Ph_2FSnCH_2)_2CH_2{\cdot}F]^-$ (**17**), in addition to $[(Ph_2ClSnCH_2)_2CH_2{\cdot}F]^-$ (**15**). Variable-temperature ^{19}F NMR spectra of **17** indicate the onset of endocyclic Sn−C rotation, bringing about intramolecular exchange between bridging and terminal fluorine atoms at about −30 °C.

As expected, the addition of a third 1 mol equiv of fluoride to $(Ph_2ClSnCH_2)_2CH_2$ results only in the formation of $[(Ph_2FSnCH_2)_2CH_2{\cdot}F]^-$ (**17**) and the addition of fourth fluoride gives rise to both $[(Ph_2FSnCH_2)_2CH_2{\cdot}F]^-$ (**17**) and doubly-charged $[(Ph_2F_2SnCH_2)_2CH_2]^{2-}$ (**18**), in the ratio of approximately 1:4. NMR data are summarized in Table 1.

Table 2. Selected Interatomic Bond Distances (Å) and Angles (deg) for 1a, 4a, 8a, and 11a

	1a (X = F(2), Y = F(3))	**4a** (X = Br(1), Y = Br(2))	**8a** (X = I(1), Y = I(2))	**11a** (X = Cl(1), Y = Cl(2))
Sn(1)–F(1)	2.204(2)	2.274(5)	2.248(4)	2.197(4)
Sn(1)–X	2.004(2)	2.609(1)	2.8558(8)	2.5044(9)
Sn(1)–C(1)	2.095(4)	2.09(1)	2.103(7)	2.107(7)
Sn(1)–C(11)	2.104(4)	2.125(9)	2.115(7)	2.114(7)
Sn(1)–C(21)	2.114(4)	2.128(9)	2.117(7)	2.100(6)
Sn(2)–F(1)	2.249(2)	2.212(5)	2.231(4)	2.178(4)
Sn(2)–Y	1.995(2)	2.613(1)	2.8604(8)	2.511(2)
Sn(2)–C(1)	2.097(4)	2.08(1)	2.114(7)	2.109(7)[a]
Sn(2)–C(31)	2.112(4)	2.125(8)	2.097(7)	2.106(7)
Sn(2)–C(41)	2.097(4)	2.09(1)	2.126(7)	2.113(7)
F(1)–Sn(1)–X	175.51(9)	171.5(1)	169.6(1)	174.5(1)
F(1)–Sn(1)–C(1)	78.9(1)	76.1(3)	77.8(2)	82.9(3)
F(1)–Sn(1)–C(11)	87.8(1)	85.5(3)	85.8(2)	88.9(2)
F(1)–Sn(1)–C(21)	89.1(1)	87.3(3)	89.1(2)	88.1(2)
X–Sn(1)–C(1)	97.0(1)	95.5(3)	92.7(2)	91.9(2)
X–Sn(1)–C(11)	92.8(1)	97.2(2)	96.0(2)	95.4(2)
X–Sn(1)–C(21)	94.4(1)	98.4(3)	99.1(2)	92.9(2)
C(1)–Sn(1)–C(11)	119.0(2)	115.9(4)	121.9(3)	122.5(3)
C(1)–Sn(1)–C(21)	118.6(2)	121.3(4)	117.1(3)	118.2(3)
C(11)–Sn(1)–C(21)	120.4(1)	118.3(3)	117.9(3)	118.2(3)
F(1)–Sn(2)–Y	176.27(9)	172.1(1)	172.0(1)	173.5(1)
F(1)–Sn(2)–C(1)	77.8(1)	77.7(3)	77.9(2)	82.8(2)[a]
F(1)–Sn(2)–C(31)	87.7(1)	88.4(3)	89.5(2)	88.6(2)
F(1)–Sn(2)–C(41)	86.8(1)	88.6(3)	87.4(2)	88.8(2)
Y–Sn(2)–C(1)	98.7(1)	94.4(3)	94.2(2)	91.1(2)[a]
Y–Sn(2)–C(31)	95.2(1)	96.3(2)	95.2(2)	93.0(2)
Y–Sn(2)–C(41)	93.9(1)	95.4(3)	95.9(2)	96.1(2)
C(1)–Sn(2)–C(31)	118.9(2)	124.5(4)	114.3(3)	122.1(3)[a]
C(1)–Sn(2)–C(41)	119.4(2)	119.9(4)	124.5(3)	121.4(3)[a]
C(31)–Sn(2)–Sn(41)	118.5(2)	113.1(4)	118.8(3)	115.5(3)

[a] For C(1) substitute C(2).

Molecular Structures of 1a, 4a, 8a, and 11a. The X-ray crystal structures of **1**, **4**, **8**, and **11**, characterized as their NEt_4^+ salts (**1a**, **4a**, **8a**, and **11a**), confirm the stoichiometries of the compounds and provide detailed information on the molecular geometries; Table 2 lists pertinent interatomic parameters. The lattice of **1a** comprises discrete anions of **1** and NEt_4^+ cations, there being no significant interionic contacts; the closest contact in the lattice of 3.271(6) Å occurs between the F(2) and C(62) atoms. The structure of the anion in **1a** is shown in Figure 2 and comprises two Sn atoms linked by a F and a CH_2 bridge leading to the formation of a skewed rhombus; the deviations of the Sn(1), Sn(2), F(1), and C(1) atoms from the four-membered ring are 0.0002(3), 0.0003(3), −0.013(2), and −0.060(4) Å, respectively. Whereas the two Sn–C(1) bond distances are equivalent within experimental error, there is a significant difference between the Sn–F(1) distances, i.e. 2.204(2) *cf.* 2.249(2) Å. Each Sn atom is also coordinated by a terminal F atom and two phenyl groups. The Sn(1)...Sn(2) separation of 3.3446(6) Å is too long to be considered a significant interaction. The geometry about each of the Sn atoms is distorted trigonal bipyramidal with the equatorial plane being defined by the C atoms in each case; the F(1)–Sn–F(2) and F(1)–Sn(2)–F(3) axial angles are 175.51(9) and 176.27(9)°, respectively. Sn(1) and Sn(2) lie respectively 0.1733(3) and −0.2170(3) Å out of the trigonal planes in the direction of the terminal F atoms which form the shorter of the Sn–F interactions as expected. The gross geometric features found in the structure of **1a** are also observed in the structures of **4a** and **8a**.

The closest non-H contact in the lattice of **4a** is 3.19(1) Å found between the F(1) and C(61)′ atoms (symmetry operation: x, $1 - y$, $-0.5 + z$). The deviations of the

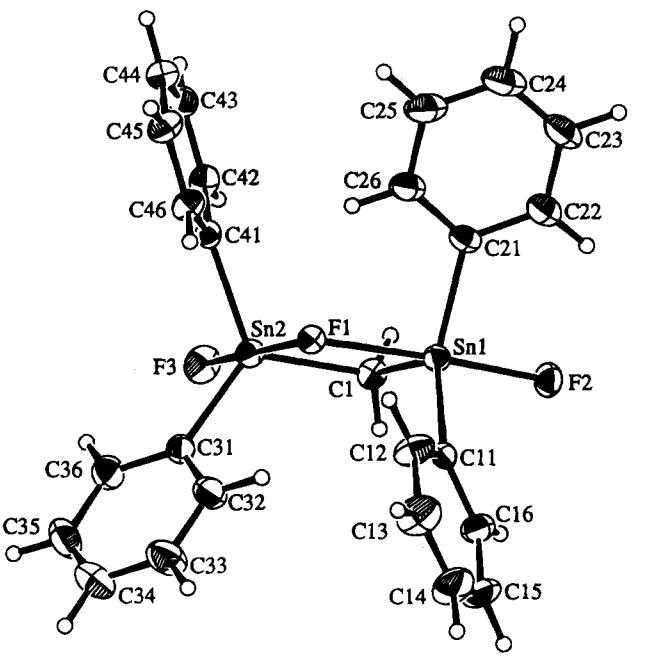

Figure 2. Molecular structure and crystallographic numbering scheme for **1a**.

Sn(1), Sn(2), F(1), and C(1) atoms from the central four-membered ring (see Figure 3) are 0.0000(1), 0.0000(1), 0.031(6), and 0.12(1) Å, respectively. As for **1a**, the Sn–C(1) bridges are symmetrical and the F(1) bridges are not; the Sn(1)...Sn(2) separation is 3.3777(8) Å. The Sn(1) lies 0.2593(1) Å out of the trigonal plane defined by the three C donors in the direction of the Br(1) atom, and the corresponding value for the Sn(2) atom is 0.1949(1) Å (i.e. in the direction of the Br(2) atom). In the lattice of **8a**, the closest non-H contact occurs

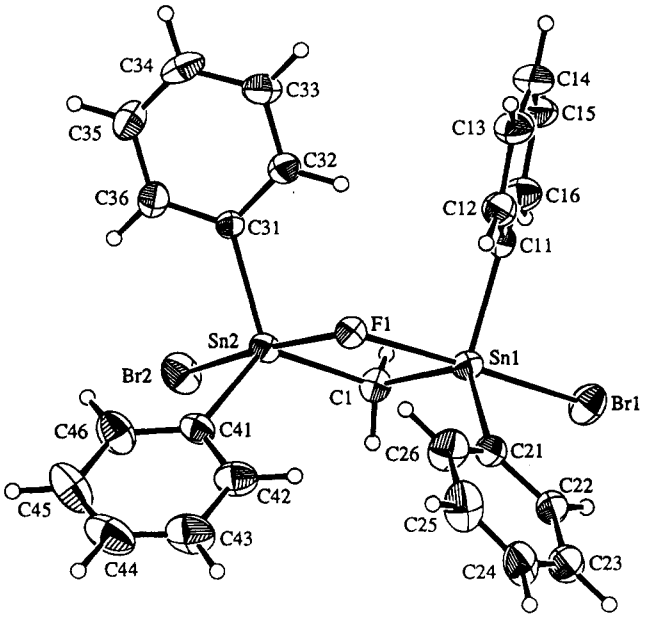

Figure 3. Molecular structure and crystallographic numbering scheme for **4a**.

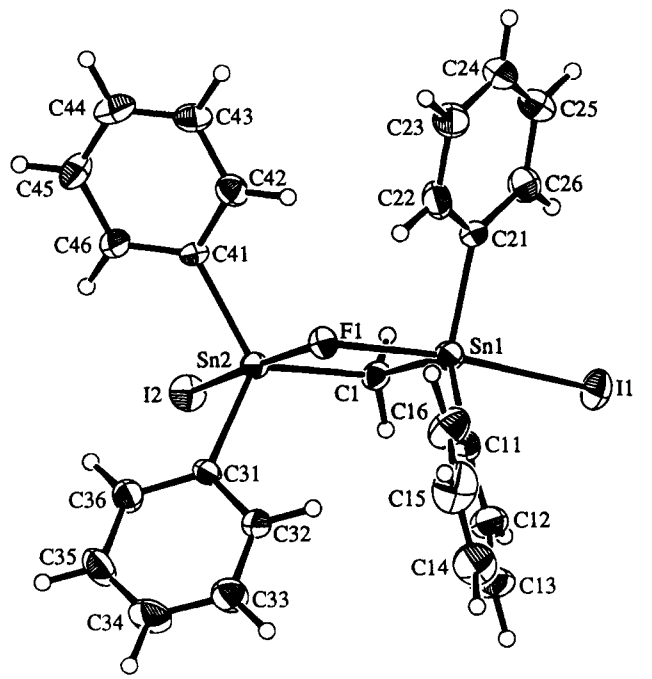

Figure 4. Molecular structure and crystallographic numbering scheme for **8a**.

between the F(1) and C(71)′ atoms (symmetry operation: $-x, 1-y, 1-z$); the molecular structure of the anion in **8a** is shown in Figure 4. The deviations from the four-membered ring of the Sn(1), Sn(2), F(1), and C(1) atoms are 0.0000(5), 0.0000(5), 0.001(4), and 0.005(7) Å, respectively. In contrast to that observed in **1a** and **4a**, both the methylene and F(1) bridges are symmetrical in **8a**; the Sn(1)...Sn(2) separation is 3.3776(7) Å. As with **1a** and **4a**, the Sn atoms lie out of the trigonal planes in the directions of the iodide to which they are bonded; the deviations out of the planes for the Sn(1) and Sn(2) atoms are 0.2155(5) and 0.1888(5) Å, respectively. Crystals were not obtained for the analogous Cl structure; however, those for the derivative in which the Sn atoms are linked by a ethylene bridge were obtained and subjected to an X-ray study.

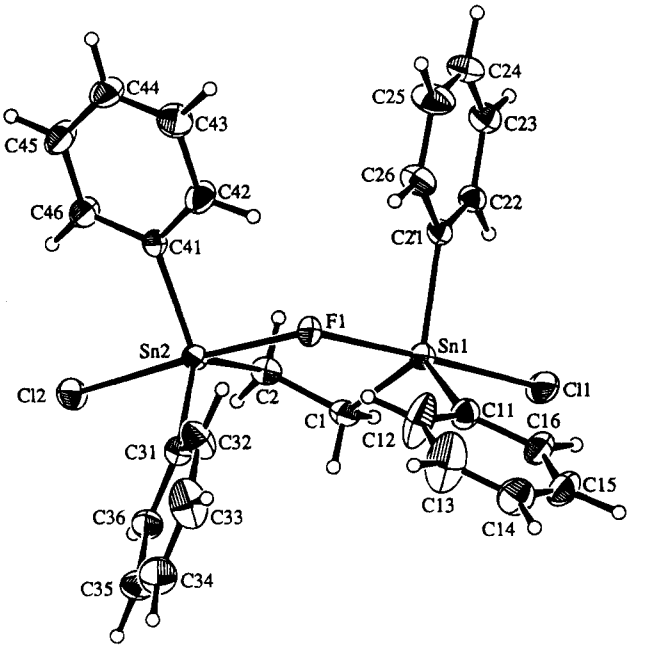

Figure 5. Molecular structure and crystallographic numbering scheme for **11a**.

Table 3. Analytical and Melting Point Data for Compounds 1a, 4a, 6a, 8a, 9a, and 11a[a]

			anal. (%): found (calcd)		
compd	formula	mp (°C)	C	H	N
1a	$C_{33}H_{42}F_3NSn_2$	192–193	53.10 (53.05)	5.76 (5.67)	1.80 (1.87)
4a	$C_{33}H_{42}Br_2FNSn_2$	165–167	45.77 (45.62)	4.90 (4.87)	1.40 (1.61)
6a	$C_{33}H_{42}Cl_2FNSn_2$	155	50.84 (50.81)	5.46 (5.43)	1.71 (1.80)
8a	$C_{33}H_{42}FI_2NSn_2$	192–196	41.25 (41.16)	4.43 (4.40)	1.41 (1.45)
9a	$C_{34}H_{44}F_3NSn_2$	198–200	53.64 (53.65)	5.80 (5.83)	1.84 (1.84)
11a	$C_{34}H_{44}Cl_2FNSn_2$	192–196	51.48 (51.43)	5.52 (5.58)	1.72 (1.76)

[a] $(Ph_2XSn)_2CH_2{\cdot}F^-Et_4N^+$: **1a**, X = F; **6a**, X = Cl; **4a**, X = Br; **8a**, X = I. $(Ph_2XSnCH_2)_2{\cdot}F^-Et_4N^+$: **9a**, X = F; **11a**, X = Cl.

The structure of the anion in **11a** is illustrated in Figure 5. The closest intermolecular contact in the lattice occurs between the C(13) and C(82) atoms (symmetry operation: $-1+x, y, z$) at 3.21(4) Å. The essential features of the anion in **11a** are as described above for **1a**, **4a**, and **8a** except that, as a result of a bridging ethylene group, the molecule is constructed about a central five-membered ring. This ring is puckered somewhat as seen in the F(1)/Sn(1)/C(1)/C(2) and F(1)/Sn(2)/C(2)/C(1) torsion angles of 38.1(5) and 40.5(5)°, respectively. The Sn atoms exist in distorted trigonal bipyramidal geometries and lie 0.1250(1) and 0.1232(4) Å out of their respective trigonal planes in the directions of the terminal Cl atoms. In **11a**, the F(1) bridge is symmetrical within experimental error as are the two Sn–C(ethylene) separations and the Sn(1)...Sn(2) separation is the longest of the four anions at 3.799(1) Å. Of the four structures investigated, the shortest Sn–F(1) bond distances are found in **11a**, although it is noted the errors associated with some of these distances are relatively high. The availability of several closely related structures enables a systematic comparison of their derived interatomic parameters.

As noted above, each of the Sn atoms exists in a distorted trigonal bipyramidal geometry and the distortion of the axial F(1)–Sn–X angles increases in the sequence F < Br < I for the methylene-bridged compounds; the distortion for X = Cl species, for which there

Table 4. Crystallographic Data

	compd			
	1a	**4a**	**8a**	**11a**
formula	$C_{33}H_{42}F_3NSn_2$	$C_{33}H_{42}Br_2FNSn_2$	$C_{33}H_{42}FI_2NSn_2$	$C_{34}H_{44}Cl_2FNSn_2$
fw	747.1	868.9	962.9	794.0
cryst size, mm	0.37 diameter	0.32 × 0.32 × 0.40	0.05 × 0.15 × 0.15	0.10 × 0.27 × 0.42
cryst syst	monoclinic	monoclinic	monoclinic	monoclinic
space group	$P2_1/n$	Cc	$P2_1/n$	$P2_1$
a, Å	11.695(4)	11.758(1)	10.032(1)	9.562(2)
b, Å	14.667(2)	14.880(2)	16.923(3)	15.529(4)
c, Å	18.956(2)	19.316(2)	20.523(3)	11.359(4)
β, deg	103.33(1)	93.981(9)	99.65(1)	95.51(2)
V, Å^3	3164(1)	3371.3(6)	3434.9(8)	1678.9(9)
Z	4	4	4	2
ϱ_{calcd}, g cm^{-3}	1.568	1.712	1.862	1.571
$F(000)$	1496	1704	1848	796
μ, cm^{-1}	16.18	38.86	32.79	16.75
transm factors	0.938−1.033	0.956−1.035	0.973−1.043	0.899−1.063
data collcd	$+h,+k,\pm l$	$+h,+k,\pm l$	$+h,+k,\pm l$	$+h,+k,\pm l$
no. of data collcd	6322	3391	6919	4394
no. of unique data	6013	3223	6528	4161
no. of unique data with $I \geq 3.0\sigma(I)$	4661	2647	3843	3457
R	0.027	0.029	0.033	0.029
R_w	0.032	0.032	0.032	0.033
residual density, e Å^{-3}	0.43	0.47	0.57	0.40

Table 5. Fractional Atomic Coordinates and Their Estimated Standard Deviations for 1a

atom	x	y	z
Sn(1)	−0.03538(2)	0.28032(2)	0.13340(2)
Sn(2)	−0.07784(3)	0.07290(2)	0.19610(2)
F(1)	−0.0850(2)	0.1431(1)	0.0897(1)
F(2)	0.0049(2)	0.4024(2)	0.1800(1)
F(3)	−0.0652(2)	0.0175(2)	0.2937(1)
N(1)	−0.0307(3)	0.6687(2)	0.1842(2)
C(1)	−0.0378(4)	0.2081(3)	0.2284(2)
C(11)	−0.1949(3)	0.3279(3)	0.0684(2)
C(12)	−0.2345(4)	0.3001(3)	−0.0015(3)
C(13)	−0.3395(5)	0.3310(4)	−0.0432(3)
C(14)	−0.4057(5)	0.3895(4)	−0.0140(4)
C(15)	−0.3695(5)	0.4158(4)	0.0554(4)
C(16)	−0.2638(4)	0.3861(3)	0.0958(3)
C(21)	0.1168(3)	0.2731(3)	0.0914(2)
C(22)	0.1922(4)	0.3462(3)	0.0981(2)
C(23)	0.2940(4)	0.3413(4)	0.0741(3)
C(24)	0.3225(5)	0.2634(5)	0.0447(3)
C(25)	0.2495(5)	0.1903(4)	0.0366(3)
C(26)	0.1474(4)	0.1959(3)	0.0608(3)
C(31)	−0.2554(4)	0.0359(3)	0.1555(2)
C(32)	−0.3268(4)	0.0870(3)	0.1025(3)
C(33)	−0.4435(5)	0.0650(4)	0.0794(3)
C(34)	−0.4091(5)	−0.0061(5)	0.1077(3)
C(35)	−0.4207(5)	−0.0570(4)	0.1597(3)
C(36)	−0.3035(4)	−0.0356(3)	0.1835(3)
C(41)	0.0533(3)	−0.0104(3)	0.1714(2)
C(42)	0.1487(4)	−0.0378(3)	0.2234(2)
C(43)	0.2372(4)	−0.0881(3)	0.2059(3)
C(44)	0.2307(4)	−0.1117(3)	0.1357(3)
C(45)	0.1365(4)	−0.0861(3)	0.0829(2)
C(46)	0.0494(4)	−0.0360(3)	0.1010(2)
C(51)	−0.1387(5)	0.6137(3)	0.1869(3)
C(52)	−0.2498(5)	0.6467(5)	0.1395(3)
C(61)	−0.0130(4)	0.6703(3)	0.1082(3)
C(62)	0.0040(6)	0.5807(4)	0.0762(3)
C(71)	0.0710(5)	0.6235(3)	0.2356(3)
C(72)	0.1867(6)	0.6668(4)	0.2406(4)
C(81)	−0.0433(4)	0.7660(3)	0.2047(3)
C(82)	−0.0657(5)	0.7803(4)	0.2785(3)

Table 6. Fractional Atomic Coordinates and Their Estimated Standard Deviations for 4a

atom	x	y	z
Sn(1)	0.4276(−)	0.28438(4)	0.1766(−)
Sn(2)	0.35522(6)	0.30725(4)	0.34188(4)
Br(1)	0.4519(1)	0.14142(8)	0.10078(8)
Br(2)	0.3117(1)	0.18531(8)	0.43375(7)
F(1)	0.3978(5)	0.3947(3)	0.2548(3)
N(1)	0.3742(7)	0.3392(5)	0.8439(5)
C(1)	0.3977(11)	0.2145(6)	0.2673(6)
C(11)	0.2808(7)	0.3366(6)	0.1199(5)
C(12)	0.2722(9)	0.4237(7)	0.1051(5)
C(13)	0.1737(10)	0.4600(8)	0.0743(7)
C(14)	0.0833(10)	0.4047(11)	0.0572(7)
C(15)	0.0907(9)	0.3172(9)	0.0722(7)
C(16)	0.1901(9)	0.2817(7)	0.1029(6)
C(21)	0.5880(7)	0.3455(6)	0.1628(5)
C(22)	0.6678(8)	0.3036(8)	0.1260(5)
C(23)	0.7714(10)	0.3405(11)	0.1183(6)
C(24)	0.7965(11)	0.4227(12)	0.1457(7)
C(25)	0.7174(12)	0.4666(9)	0.1787(7)
C(26)	0.6127(9)	0.4272(8)	0.1877(7)
C(31)	0.1955(7)	0.3741(5)	0.3421(5)
C(32)	0.1429(8)	0.4063(7)	0.2822(5)
C(33)	0.0434(9)	0.4545(8)	0.2818(6)
C(34)	−0.0049(9)	0.4665(8)	0.3440(8)
C(35)	0.0422(11)	0.4337(8)	0.4021(6)
C(36)	0.1428(8)	0.3873(7)	0.4013(5)
C(41)	0.4842(8)	0.3711(6)	0.4040(6)
C(42)	0.5822(9)	0.4005(8)	0.3753(7)
C(43)	0.6685(12)	0.4418(10)	0.4178(10)
C(44)	0.6542(15)	0.4568(10)	0.4842(10)
C(45)	0.5618(15)	0.4291(11)	0.5131(7)
C(46)	0.4751(10)	0.3875(8)	0.4716(7)
C(51)	0.2879(14)	0.2750(9)	0.8685(8)
C(52)	0.1953(13)	0.3206(14)	0.9060(11)
C(61)	0.3208(12)	0.4104(9)	0.8010(8)
C(62)	0.2658(15)	0.3761(12)	0.7305(9)
C(71)	0.4489(13)	0.2836(10)	0.8061(9)
C(72)	0.5533(14)	0.3394(12)	0.7790(9)
C(81)	0.4304(11)	0.3883(9)	0.9037(8)
C(82)	0.4791(14)	0.3212(13)	0.9611(8)

is an ethylene bridge between the Sn atoms, falls neatly between X = F and Br compounds, but this may be coincidental. Estimates of the Sn−X single bond distances have been listed in literature and are 1.96, 2.345, 2.49, and 2.72 Å for X = F to I, respectively.[18] The average differences between Sn−X(axial) observed in the present study and the ideal values follow the sequence F ≪ Br < I < Cl. For the first three compounds, this sequence follows the order found for the series of $Me_2SnX(C_6H_4-2-C(O)OMe)$ structures,[18] and the result for **11a** reflects, again, the steric relieving effect of the five-membered ring.

(18) Kolb, U.; Dräger, M.; Jousseaume, B. *Organometallics* **1991**, *10*, 2737.

Table 7. Fractional Atomic Coordinates and Their Estimated Standard Deviations for 8a

atom	*x*	*y*	*z*
Sn(1)	0.06294(5)	0.73970(3)	0.90483(2)
Sn(2)	0.01233(5)	0.74580(3)	0.73801(2)
I(1)	0.22443(6)	0.63344(4)	0.99310(3)
I(2)	0.13729(6)	0.65920(4)	0.64480(3)
F(1)	−0.0627(4)	0.8061(2)	0.8215(2)
N(1)	0.4445(6)	0.0941(4)	0.2661(3)
C(1)	0.1242(7)	0.6886(4)	0.8212(3)
C(11)	−0.1230(7)	0.7102(5)	0.9343(3)
C(12)	−0.1604(9)	0.6358(5)	0.9428(4)
C(13)	−0.2875(11)	0.6178(7)	0.9560(5)
C(14)	−0.3741(11)	0.6758(9)	0.9635(5)
C(15)	−0.3370(10)	0.7511(8)	0.9580(5)
C(16)	−0.2131(10)	0.7692(6)	0.9424(5)
C(21)	0.1560(8)	0.8475(5)	0.9396(3)
C(22)	0.0851(9)	0.9172(6)	0.9305(4)
C(23)	0.1420(11)	0.9881(5)	0.9520(4)
C(24)	0.2731(11)	0.9896(6)	0.9812(4)
C(25)	0.3447(10)	0.9222(7)	0.9906(5)
C(26)	0.2871(8)	0.8515(5)	0.9705(4)
C(31)	−0.1814(7)	0.6990(4)	0.7070(3)
C(32)	−0.2538(8)	0.6694(5)	0.7534(4)
C(33)	−0.3794(9)	0.6368(6)	0.7366(4)
C(34)	−0.4382(8)	0.6354(6)	0.6721(5)
C(35)	−0.3702(9)	0.6641(6)	0.6254(4)
C(36)	−0.2417(8)	0.6951(5)	0.6428(4)
C(41)	0.0578(7)	0.8598(4)	0.7041(3)
C(42)	0.0948(8)	0.9207(5)	0.7472(4)
C(43)	0.1239(8)	0.9944(5)	0.7253(4)
C(44)	0.1120(8)	1.0084(5)	0.6604(5)
C(45)	0.0751(9)	0.9493(5)	0.6167(4)
C(46)	0.0492(8)	0.8750(5)	0.6382(4)
C(51)	0.4475(12)	0.0261(6)	0.2232(5)
C(52)	0.3396(14)	0.0249(7)	0.1629(5)
C(61)	0.4520(10)	0.1700(6)	0.2290(5)
C(62)	0.5715(12)	0.1799(9)	0.1971(6)
C(71)	0.3132(9)	0.0979(6)	0.2920(5)
C(72)	0.2847(11)	0.0309(7)	0.3339(5)
C(81)	0.5615(10)	0.0865(7)	0.3202(5)
C(82)	0.5762(10)	0.1492(8)	0.3699(5)

Experimental Section

NMR Spectroscopy. NMR spectra were recorded on a JEOL GX270 FT NMR spectrometer with broad band proton decoupling of ^{119}Sn at 100.75 MHz and ^{19}F at 254.19 MHz, using an external deuterium lock, and referenced against external Me_4Sn and $CFCl_3$, respectively. Temperatures were maintained using a JEOL GTV3 control system. Complexes for NMR investigation were generally prepared in situ by reaction of bis(halodiorganostannyl)alkanes with appropriate mole ratios of tetrabutylammonium halide in dichloromethane solution. The concentration of bis(halodiorganostannyl)-alkanes was typically about 0.1 M.

General Methods. Tetrabutylammonium fluoride trihydrate, $Bu_4NF{\cdot}3H_2O$, tetrabutylammonium chloride, Bu_4NCl, tetrabutylammonium bromide, Bu_4NBr, and tetraethylammonium fluoride dihydrate, $Et_4NF{\cdot}2H_2O$, were obtained from Aldrich, Sigma, and Fluka, respectively. The bis(haloorganostannyl)alkanes and $[Ph_3SnF_2]^-[Bu_4N]^+$ were synthesized as described elsewhere.[7,8,12,19]

Synthesis of Diphenyl(trimethylsilylmethyl)fluorostannane, $Ph_2FSnCH_2SiMe_3$. Ph_3SnCl (70.0 g, 0.18 mol) dissolved in 150 mL of thf was added dropwise to a magnetically stirred solution of Me_3SiCH_2MgCl prepared from Me_3SiCH_2Cl (27.50 g, 0.20 mol) and Mg (4.80 g, 0.20 mol) in 150 mL of thf. The reaction mixture was refluxed for 3 h. Two-thirds of the thf was distilled off, and 150 mL of ether was added. The reaction mixture was then hydrolyzed under ice cooling with diluted HCl. The organic layer was separated, washed with water, and dried over Na_2SO_4. Filtration and evaporation of solvent yielded 63 g of crude $Ph_3SnCH_2SiMe_3$ as an oil which was not further analyzed. It was dissolved in 150 mL of CH_2Cl_2. Iodine (36.5 g, 0.14 mol) was added in small portions to this magnetically stirred solution, and stirring was continued over night. The solvent was then removed in vacuo and the oily residue dissolved in 50 mL of acetone. This solution was added dropwise to a magnetically stirred solution of KF (21.00 g, 0.36 mol) in water. Immediate precipitation took place. Stirring was continued overnight. The precipitate was filtered off, washed twice with water, and dried. Recrystallization from hot acetone yielded 49 g (72% with respect to Ph_3SnCl) of $Ph_2FSnCH_2SiMe_3$ as colorless crystals, mp 225 °C.

^{1}H NMR ($CDCl_3$): 0.12 (s, 9 H, $SiMe_3$), 0.67, $^2J(^{119}Sn-^1H)$ = 83.9 Hz (2 H, $SnCH_2$), 7.60 (m, 4 H, o-Ph), 7.45 ppm (m, 6 H, m,p-Ph). ^{119}Sn NMR ($CDCl_3$) 24.9 ppm, $^1J(^{119}Sn-^{19}F)$ = 2380 Hz. Anal. Found: C, 50.43; H, 5.30. Calcd for $C_{16}H_{21}FSiSn$ (MW 379.14): C, 50.69; H, 5.58.

Synthesis of Bis(diphenylfluorostannyl)methane, $(Ph_2FSn)_2CH_2$. $(Ph_2BrSn)_2CH_2$ (3 g, 4.2 mmol) and potassium fluoride (0.6 g, 10.3 mmol) were stirred in 20 mL of acetone and 5 mL of water for 24 h. The colorless precipitate formed was filtered off, washed with water, methanol, and diethyl ether, and then dried to give 2.3 g (92%) of $(Ph_2FSn)_2CH_2$ as a colorless amorphous solid, mp >360 °C dec. Anal. Found: C, 49.67; H, 3.78. Calcd for $C_{25}H_{22}F_2Sn_2$: C, 50.22; H, 3.71.

Table 8. Fractional Atomic Coordinates and Their Estimated Standard Deviations for 11a[a]

atom	*x*	*y*	*z*
Sn(1)	0.07970(5)	1/4	0.38261(4)
Sn(2)	0.19871(4)	0.06704(4)	0.19393(4)
Cl(1)	0.1040(2)	0.4074(2)	0.4280(2)
Cl(2)	0.3591(2)	0.0293(2)	0.0392(2)
F(1)	0.0703(4)	0.1141(2)	0.3286(3)
N(1)	0.6451(7)	0.1801(5)	0.7778(6)
C(1)	0.2495(7)	0.2531(6)	0.2775(6)
C(2)	0.2294(7)	0.1997(5)	0.1659(6)
C(11)	0.1022(8)	0.2095(6)	0.5611(6)
C(12)	0.1070(16)	0.1258(7)	0.5898(8)
C(13)	0.1281(20)	0.0978(9)	0.7082(10)
C(14)	0.1454(13)	0.1542(10)	0.7930(9)
C(15)	0.1361(10)	0.2370(8)	0.7688(8)
C(16)	0.1161(9)	0.2669(6)	0.6519(7)
C(21)	−0.1243(6)	0.2647(5)	0.2985(6)
C(22)	−0.1646(7)	0.3380(5)	0.2388(7)
C(23)	−0.2993(8)	0.3483(6)	0.1863(7)
C(24)	−0.3958(8)	0.2859(7)	0.1925(8)
C(25)	−0.3599(9)	0.2137(7)	0.2500(10)
C(26)	−0.2241(8)	0.1999(6)	0.3031(9)
C(31)	0.3199(7)	−0.0021(5)	0.3268(6)
C(32)	0.2559(9)	−0.0450(7)	0.4123(7)
C(33)	0.3387(14)	−0.0894(8)	0.5000(9)
C(34)	0.4814(14)	−0.0903(8)	0.5001(10)
C(35)	0.5415(10)	−0.0505(7)	0.4175(8)
C(36)	0.4640(9)	−0.0062(5)	0.3298(7)
C(41)	0.0205(7)	0.0018(4)	0.1135(6)
C(42)	−0.1002(9)	−0.0004(7)	0.1663(9)
C(43)	−0.2206(9)	−0.0415(8)	0.1119(11)
C(44)	−0.2178(9)	−0.0766(6)	0.0072(8)
C(45)	−0.0991(9)	−0.0766(7)	−0.0459(8)
C(46)	0.0187(9)	−0.0377(6)	0.0075(7)
C(51)	0.6220(30)	0.2838(18)	0.7878(25)
C(51′)	0.5351(23)	0.1974(16)	0.8652(19)
C(52)	0.5169(47)	0.3050(29)	0.8496(36)
C(52′)	0.4949(32)	0.2902(21)	0.8817(27)
C(61)	0.7750(24)	0.2389(18)	0.8085(19)
C(61′)	0.6913(26)	0.1477(17)	0.9065(21)
C(62)	0.8430(25)	0.2228(18)	0.9419(22)
C(62′)	0.8144(22)	0.1782(15)	0.9606(19)
C(71)	0.5673(35)	0.2094(24)	0.6611(30)
C(71′)	0.5043(30)	0.1376(21)	0.7361(24)
C(72)	0.4759(28)	0.1759(18)	0.5893(22)
C(72′)	0.5628(21)	0.0241(14)	0.7702(17)
C(81)	0.6836(30)	0.0868(21)	0.7735(25)
C(81′)	0.7591(34)	0.1789(24)	0.6982(30)
C(82)	0.7905(34)	0.0988(23)	0.6820(28)
C(82′)	0.6761(37)	0.1734(26)	0.5764(33)

[a] Atoms C(51)−C(82′) have 50% site occupancy factors.

(19) Gringas, M. *Tetrahedron Lett.* **1991**, *32*, 7381.

Synthesis of 1,2-Bis(diphenylfluorostannyl)ethane, $(Ph_2FSnCH_2)_2$. $(Ph_3SnCH_2)_2$ (11 g, 0.015 mol) was dissolved in 150 mL of CH_2Cl_2. Iodine (7.6 g, 0.03 mol) was added in small portions to the magnetically stirred solution. The iodine color disappeared. The reaction mixture was stirred over night followed by evaporation of the solvent. The residue was dissolved in 150 mL of ether and dropped under magnetic stirring into a solution of 5.3 g of potassium fluoride in 20 mL of water. Immediate precipitation took place. Stirring was continued for a further 4 h. The precipitate was filtered off and washed with water, methanol, and ether to give 7 g (76%) of $(Ph_2FSnCH_2)_2$ as a colorless amorphous solid, mp >250 °C dec. Anal. Found: C, 51.10, H, 3.86. Calcd for $C_{26}H_{24}F_2Sn_2$: C, 51.05, H, 3.92.

Synthesis of Fluoride Complexes (as Tetraethylammonium Salts) 1a, 4a, 6a, 8a, 9a, and 11a. Bis(halogenodiphenyl)methanes or -ethanes, respectively (0.3 mmol), and tetraethylammonium fluoride dihydrate (0.3 mmol) were refluxed in 10 mL of methylene chloride under magnetic stirring for 5 min. The resulting solution was carefully filtered. Hexane was added, and the reaction mixture was slowly evaporated to yield the complexes **1a**, **4a**, **6a**, **8a**, **9a**, and **11a** almost quantitatively as colorless crystals. Elemental analyses and melting points are given in Table 3.

Crystallography. Crystals of **1a**, **4a**, **8a**, and **11a** were grown from CH_2Cl_2/hexane solutions by slow evaporation. Intensity data for the colorless crystals were measured at room temperature (20 °C) on a Rigaku AFC6R diffractometer fitted with graphite-monochromatized Mo Kα radiation, $\lambda = 0.710\ 73$ Å. The $\omega-2\theta$ scan technique was employed to measure data in each case up to a maximum Bragg angle of 25.0° (27.5° for **11a**) in each case. The data sets were corrected for Lorentz and polarization effects,[20] and an empirical absorption correction was applied.[21] Relevant crystal data are given in Table 4.

The structures were solved by direct methods[22] and refined by a full-matrix least-squares procedure based on F.[20] Non-H atoms were refined with anisotropic thermal parameters, and H atoms were included in the models in their calculated positions (C–H = 0.97 Å) for **1a**, **4a**, and **8a**. In the refinement of **11a**, the anion atoms were refined as for the remaining structures and with H atoms in calculated positions; however, the NEt_4^+ cation was found to be disordered. The disorder was modeled by assigning two sites for each of the eight C atoms, and these were refined isotropically with 50% site occupancy factors; H atoms were not included for the disordered atoms. The refinements were continued until convergence employing σ weights; the analysis of variance showed no special features indicating that an appropriate weighting scheme had been applied in each case. The absolute configurations of both **4a** and **11a** were determined by reversing the signs of the reflections in each data set and comparing the refinements. Final refinement details are collected in Table 4. Fractional atomic coordinates are listed in Table 5–8, and the numbering schemes employed are shown in Figures 2–5 (drawn with ORTEP[23] at 25, 25, 30, and 20% probability ellipsoids, respectively). The teXsan[20] package, installed on an Iris Indigo workstation, was employed for all calculations.

Acknowledgment. We are grateful to the Australian Research Council (ARC) for financial assistance. K.J. thanks the Stiferverband für die Deutsche Wissenschaft and the Fonds der Chemischen Industrie for support.

Supplementary Material Available: Tables of anisotropic thermal parameters, H positional and thermal parameters, and bond distances and angles (23 pages). Ordering information is given on any current masthead page.

OM940639+

(20) teXsan: Structure Analysis Software. Molecular Structure Corp., The Woodlands, TX.

(21) Walker, N.; Stuart, D. *Acta Crystallogr., Sect. A* **1983**, *39*, 158.

(22) Sheldrick, G. M. SHELXS86, Program for the Automatic Solution of Crystal Structure, University of Göttingen, Germany, 1986.

(23) Johnson, C. K. *ORTEP*. Report ORNL-5138; Oak Ridge National Laboratory: Oak Ridge, TN, 1976.

Group 6 Pyrrolocarbene Complexes as Alkoxycarbene Complex Analogs

Isabel Merino and Louis S. Hegedus*

Department of Chemistry, Colorado State University, Fort Collins, Colorado 80523

Received December 22, 1994[⊗]

Chromium, molybdenum, and tungsten carbene complexes having the pyrrole group as the heteroatom-containing substituent were synthesized and characterized. Their thermal and photochemical reactivity more nearly resembled that of alkoxycarbene complexes than that of aminocarbene complexes. Thus, they cyclopropanated electron deficient olefins, produced hydroquinones rather than indenes in the Dötz annulation process, and underwent photochemical 2 + 2 cycloaddition with alkenes to produce cyclobutanones and with imines to produce β-lactams. With cyclohexadiene and cycloheptadiene, an unusual 4 + 2 cycloaddition of the diene across the ketene carbonyl group was observed. The pyrrole group was oxidatively cleaved to the corresponding formamide, the hydrolysis of which gave the free NH_2 group, making the pyrrole group functionally equivalent to the amino group.

Introduction

Group 6 alkoxycarbene complexes have recently found extensive use in organic synthesis,[1] both in their thermal reactions with alkenes to form cyclopropanes[2] and with alkynes to form quinone derivatives (Dötz benzannulation reaction)[3] and in their photochemical reactions to produce ketene-derived products, such as β-lactams,[4] cyclobutanones,[5] amino acids and peptides,[6] allenes,[7] and, with dienyl carbene complexes, benzannulation products.[8] Chromium aminocarbene complexes differ substantially from alkoxycarbene complexes in their reactivity.[9] They tend to undergo C–H insertion into alkenes, rather than to cyclopropanate them;[2b] they undergo benzannulation with alkynes to give indenes, rather than quinones;[10] and they fail to undergo photochemical 2 + 2 cycloaddition to alkenes to produce cyclobutanones.[5] This difference in reactivity can be somewhat mitigated by placing electron-withdrawing groups (e.g., aryl[11] or acyl[12] groups), on the nitrogen, reducing the electron-donating ability of the amino groups, although no systematic study of this phenomenon has been reported.

Pyrrole is a nitrogen heterocycle that has roughly the pK_a of methanol (≈17),[13] and can be converted to the NH_2 group after oxidative cleavage,[14] making this heterocycle functionally equivalent to the amino group.[15] Since the basicity of the heteroatom in chromium carbene complexes affects both the stability and the mode of reactivity, it seemed possible that chromium pyrrolocarbene complexes might have the reactivity profile of alkoxycarbene complexes, but would introduce an amino functionality in their reaction products. Experiments addressing these questions are described below.

Results and Discussion

The requisite pyrrolocarbene complexes **2a–d** were synthesized from the corresponding alkoxycarbene complexes **1a–d** by exchange with the lithium or potassium salt of pyrrole (eq 1). The resulting pyrrolocarbene

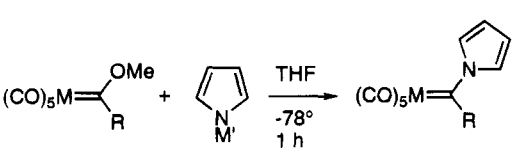

(Eq. 1)

M' = Li, K

M = Cr, R = Ph **1a**	**2a** 88%
M = Mo, R = Ph **1b**	**2b** 78%
M = W, R = Ph **1c**	**2c** 89%
M = W, R = Me **1d**	**2d** 39%

complexes **2a–d** were stable solids which could be stored in the freezer and handled without decomposition. The phenyl carbene complexes **2a–c** were obtained from the lithium salt of pyrrole in good yields.

[⊗] Abstract published in *Advance ACS Abstracts,* April 15, 1995.

(1) For reviews see: (a) Schmaltz, H. G. *Angew. Chem., Int. Ed. Engl.* **1994**, *33*, 303. (b) Reissig, H. U. *Org. Synth. Highlights* **1991**, *186*. (c) Wulff, W. D. Metal Carbene Cycloadditions. In *Comprehensive Organic Synthesis*; Trost, B. M., Ed.; Pergamon Press: Oxford, U.K., 1991; Vol. 5, pp 1065–1114. (d) Dötz, K. H. *New J. Chem.* **1990**, *14*, 433. (e) Dötz, K. H. *Angew. Chem., Int. Ed. Engl.* **1984**, *23*, 587.

(2) For a review see: Reissig, H. U. Organometallics in Organic Synthesis; Werner, H., Erker, G., Eds.; Springer-Verlag: Berlin, 1989, Vol. 2, p 311. (b) Weinand, A.; Reissig, H. U. *Organometallics* **1990**, *9*, 3133 and references therein.

(3) Wulff, W. D.; Bax, B. M.; Brandvold, T. A.; Chan, K. S.; Gilbert, A. M.; Hsung, R. P. *Organometallics* **1994**, *13*, 102 and references therein.

(4) Narukawa, Y.; Juneau, K. N.; Snustad, D.; Miller, D. B.; Hegedus, L. S. *J. Org. Chem.* **1992**, *57*, 5453 and references therein.

(5) Hegedus, L. S.; Bates, R. W.; Söderberg, B. C. *J. Am. Chem. Soc.* **1991**, *113*, 923.

(6) (a) Pulley, S. R.; Hegedus, L. S. *J. Am. Chem. Soc.* **1993**, *115*, 9037. (b) Hegedus, L. S. *Acc. Chem. Res.*, submitted.

(7) Sestrick, M. R.; Miller, M.; Hegedus, L. S. *J. Am. Chem. Soc.* **1992**, *114*, 4079.

(8) Merlic, C. A.; Xu, D.; Gladstone, B. G. *J. Org. Chem.* **1993**, *58*, 538.

(9) For a review see: Schwindt, M. A.; Miller, J. R.; Hegedus, L. S. *J. Organomet. Chem.* **1991**, *413*, 143. (b) Grotjahn, D. B.; Dötz, K. H. *Synlett* **1991**, 381.

(10) Yamashita, A.; Toy, A.; Watt, W.; Muchmore, C. R. *Tetrahedron Lett.* **1988**, *29*, 3403.

(11) Söderberg, B. C.; Hegedus, L. S. *J. Org. Chem.* **1991**, *56*, 2209.

(12) (a) Anderson, B. A.; Wulff, W. D.; Powers, T. S.; Tribbitt, S.; Rheingold, A. L. *J. Am. Chem. Soc.* **1992**, *114*, 10784. (b) Grotjahn, D. B.; Kroll, F. E. K.; Schäfer, T.; Harms, K.; Dötz, K. H. *Organometallics* **1992**, *11*, 298.

(13) Yagil, G. *Tetrahedron* **1967**, *23*, 2855.

(14) Kashima, C.; Maruyama, T.; Fujioka, Y.; Harada, K. *J. Chem. Soc., Perkin Trans. 1* **1989**, 1041.

(15) Davis, A. P.; Egan, T. J. *Tetrahedron Lett.* **1992**, *33*, 8125.

0276-7333/95/2314-2522$09.00/0

The tungsten methoxymethyl carbene complex **1d** was inert to pyrrol-1-yl lithium, and the corresponding pyrrolocarbene complex **2d** was formed from pyrrol-1-yl potassium, although in lower yield. The corresponding methyl chromium carbene complex could not be prepared.

The ^{13}C chemical shift of the carbene carbon is characteristic for Group 6 carbene complexes, with these signals for alkoxycarbene complexes appearing in the 330–360 ppm region, while those for aminocarbene complexes are seen substantially upfield, in the 250–290 ppm region.[16] Pyrrolocarbene chromium complex **2a** had this signal at δ 320 (vs δ 352 for the corresponding methoxycarbene and δ 275 for the dimethylaminocarbene complex).[16] Pyrrolocarbene tungsten complex **2c** similarly had the ^{13}C-signal for the carbene carbon intermediate (δ 291) between the corresponding (methoxy)(phenyl)carbene complex,[17] (δ 322.0), and the (dibenzylamino)(phenyl)carbene complex (δ 262.1),[18] while the signal for the carbene carbon of the molybdenum complex **2c** appeared at δ 309.4 vs δ 349.9 for the (benzyloxy)(methyl)carbene complex[18] and δ 275.0 for the (methylamino)(phenyl)carbene complex.[12b]

The reactivity of these complexes was next addressed, starting with the thermal cyclopropanations of electron deficient alkenes (eq 2). In contrast to carbene com-

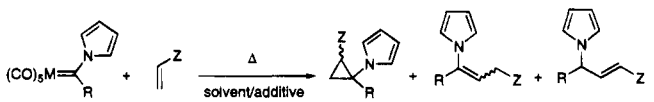

		solvent/additive, % yield			
2b	Z = CO_2Me	100°/THF/DBHT 90%	**3a** (66) ds 1:3.4	**4a** (4)	**5a** (30)
2c	Z = CO_2Me	100°/THF/DBHT 88%	**3a** (70) ds 1:2.3	**4a** (22)	**5a** (8)
2c	Z = CN	100°/THF/DBHT 72%	**3b** (93) ds 1:2.1	**4b** (7)	**5b** (0)
2d	Z = CO_2Me	100°/THF/DBHT 65%	**6a** (95) ds 1:1.6	**7a** (5)	**8a** (0)
2d	Z = CN	100°/THF/DBHT 42%	**6b** (98) ds 1:1.6	**7b** (2)	**8b** (0)

(Eq. 2)

plexes of saturated amines, which are far less reactive in the cyclopropanation process than are alkoxycarbene complexes and result in only formal C–H insertion products such as **4**, **7**, **5**, and **8**,[2b] the pyrrolocarbene complexes **2a–d** underwent reaction with electron deficient alkenes to give cyclopropanes (as a *cis/trans* mixture) as the major products, accompanied by varying amounts of C–H insertion products. The reaction of the carbene chromium complex **2a** with methyl acrylate in cyclohexane at reflux gave cyclopropane **3a** and olefin **4a** in a 36:64 ratio. The presence of DMAP inverted this ratio, and **3a** was obtained as the major product (61:39), although the reaction was not efficient (~25% yield), and pure products were not obtained. Molybdenum and tungsten carbene complexes were more efficient than the chromium complex, with tungsten strongly favoring cyclopropanation over insertion. THF was the better solvent for cyclopropanation selectivity, compared to cyclohexane or acetonitrile, which favored the insertion reaction. (A free-radical scavenger, DBHT, was added to suppress polymerization of the olefin substrates.) The pyrrole group was readily converted to the formamide group by ozonolysis (eq 3).[14] Further hydrolysis to the free amino group resulted in cleavage of the cyclopropane ring, a common occurrence with 2-aminocyclopropane carboxylic acids.[19]

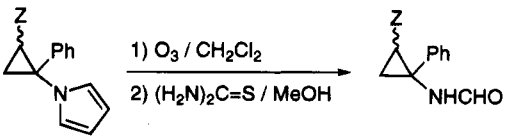

(Eq. 3)

Z = CO_2Me **3a** **9a** 73%
Z = CN **3b** **9b** 71%

Chromium pyrrolocarbene complex **2a** was subjected to Dötz benzannulation conditions with diphenyl acetylene, resulting in the production of a crude product consisting of a 2.5/1 mixture of CO-insertion product **10** and indene **11**, in moderate yield (eq 4). Aminonaphthol

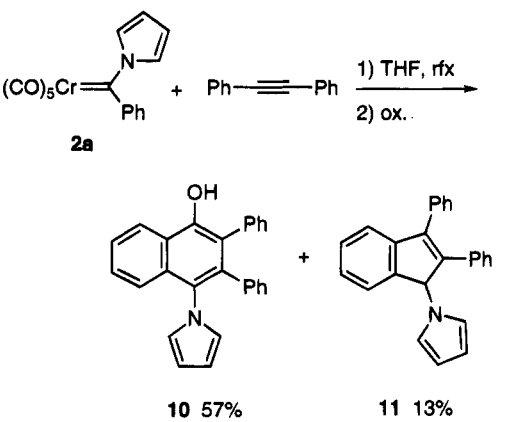

(Eq. 4)

10 was rather unstable and underwent air oxidation to produce 3,4-diphenylnaphthoquinone. Because of this and because of the low selectivity of this process, benzannulation reactions with pyrrolocarbene complexes **2** were not further pursued.

Although alkylaminocarbene chromium complexes failed to react with alkenes under photochemical conditions, the less electron rich arylaminocarbene complexes did react to form cyclobutanones, albeit in modest yield.[11] Similarly, chromium carbene complex **2a** underwent photochemical cycloaddition to a number of alkenes to give cyclobutanones in modest yield, and as only one diastereoisomer (eqs 5–10). The reactions were quite slow, requiring 40–60 h to go to completion. The stereoselectivity (both large groups *syn*) was typical of ketene olefin cycloadditions.[20] With ethyl vinyl ether, metathesis was a competitive reaction, and when the reaction was performed at room temperature, olefin was the major product (57% yield vs 6% of cyclobutanone).

(16) It has been noted that there is no *direct* correlation between electron density at the carbene carbon and its ^{13}C chemical shift value. See: Hafner, A.; Hegedus, L. S.; deWeck, G.; Hawkins, B.; Dötz, K. H. *J. Am. Chem. Soc.* **1988**, *110*, 8413.

(17) $(CO)_5W{=}C(OMe)(Ph)$ δ (ppm) ($CDCl_3$, 300 MHz): 322.0 (W=C), 203.4 (*cis* CO), 197.1 (*trans* CO), 155.1 (ipso), 131.7, 128.0, 126.2 (Ph), 70.0 (OMe).

(18) Wieber, G. M. Ph.D. Dissertation, Colorado State University, Fort Collins, CO, 1990.

(19) Burgess, K.; Ho, K.-K.; Moye-Sherman, D. *Synlett* **1994**, 575.

(20) Valentí, E.; Pericas, M. A.; Moyano, A. *J. Org. Chem.* **1990**, *55*, 3582.

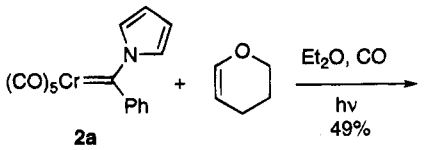

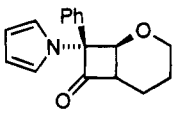

(Eq. 5)

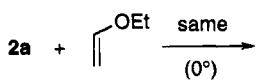

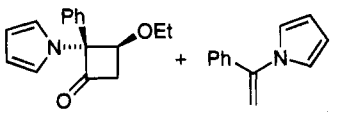

(Eq. 6)

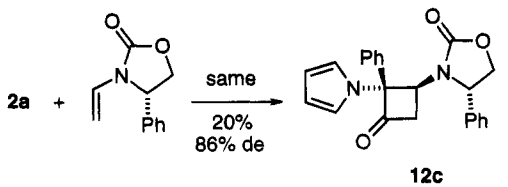

(Eq. 7)

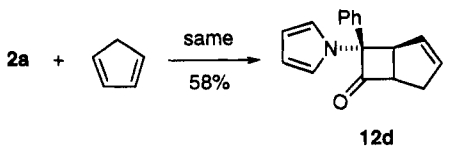

(Eq. 8)

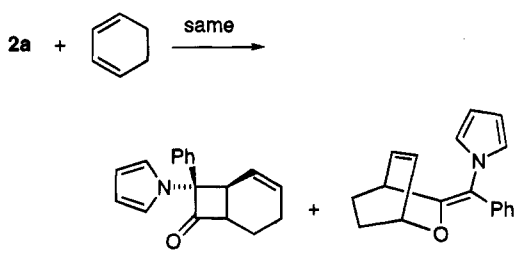

(Eq. 9)

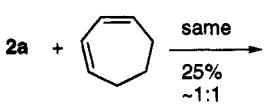

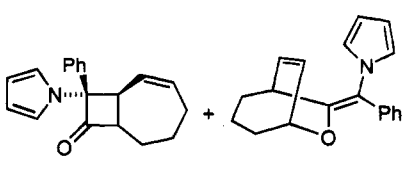

(Eq. 10)

This metathesis reaction was suppressed by carrying out photolysis at 0 °C. Remarkably, with cyclohexadiene (eq 9) and cycloheptadiene (eq 10), a second cycloaddition product corresponding to 4 + 2 cycloaddition of the diene across the ketene carbonyl group was observed. The reaction was also diastereoselective in the formation of the 4 + 2 adducts, which were obtained as single diastereoisomers. The disposition of the groups in compound **12e'** was determined by X-ray crystallography. Although precedented,[21] this mode of reactivity is rare.

The pyrrole group in **12a** was converted to the formamide **14a** in excellent yield (88%) by ozonolysis. The same process with **12d** resulted in ozonolysis of the alkene. Reduction of the double bond followed by ozonolysis gave the saturated bicyclic cyclobutanone **14d** with a pendant formamide group in good (72%) yield. The formamido group was hydrolyzed under acidic conditions to give the corresponding α-aminocyclobutanones **15a** and **15d** in ~60% yield. These products were converted to their *t*-BOC derivatives **16a** and **16d** (eqs 11 and 12).

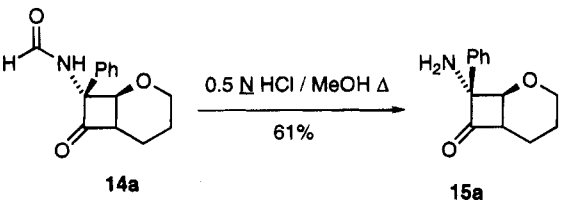

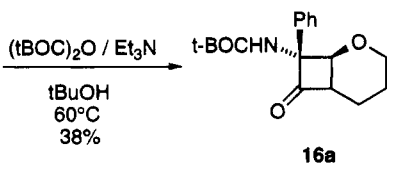

(Eq. 11)

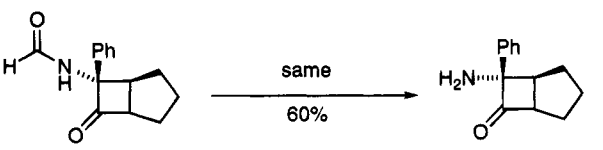

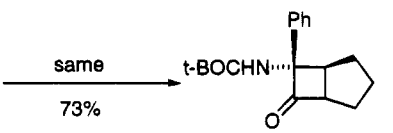

(Eq. 12)

Both chromium (aryl)(alkoxy)carbene complexes and (hydrido)(amino)carbene complexes undergo facile photocycloadditions to imines to produce β-lactams,[4] but (aryl)(amino)carbene complexes undergo this reaction little if at all.[16] Chromium pyrrolocarbene complex **2a** underwent photocycloaddition to imines to give β-lactams in modest yields (eqs 13 and 14). The stereoselectivity observed was similar to that observed with other classes of carbene complexes.[22] The pyrrole group in compounds **17a** and **17b** was converted to the formamido group in 86% and 63% yield, respectively, by ozonolysis. Deprotection of the 3-amino group in β-lactam **18a** was accomplished by hydrolysis of the forma-

(21) (a) Pittol, C. A.; Roberts, S. M.; Sutton, P. W.; Williams, J. O. *J. Chem. Soc., Chem. Commun.* **1994**, 803. (b) Mayr, H.; Heigl, U. W. *J. Chem. Soc., Chem. Commun.* **1987**, 1804 and references therein. (c) For a review on ketene cycloadditions see: Hyatt, J.; Raynolds, R. W. *Org. React.* **1994**, *45*, 159.

(22) For an extensive compilation see: Dumas, S.; Hegedus, L. S. *J. Org. Chem.* **1994**, *59*, 4967.

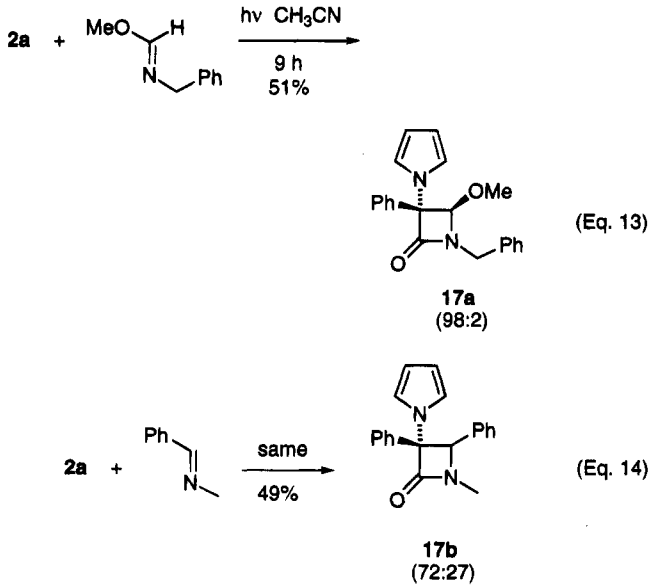

mido group with PBr_3 in MeOH,[23] followed by treatment with Et_3N (eq 15).

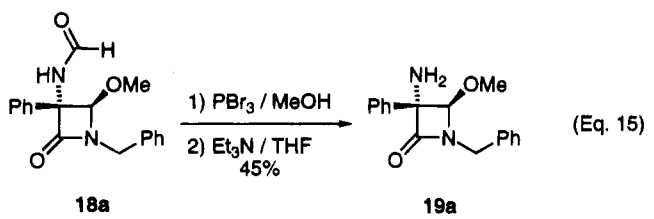

In summary, group 6 pyrrolocarbene complexes resemble alkoxycarbene complexes more than aminocarbene complexes in their reactivity pattern, but generate amino substituted products.

Experimental Section

General Methods. Melting points were taken on a Mel-Temp apparatus and are uncorrected. ^{1}H-NMR (300 MHz) and ^{13}C-NMR (75 MHz) spectra were obtained on Bruker ACE-300, Bruker ACP-300, or Bruker AM-500 MHz spectrometers. NMR were recorded in $CDCl_3$, and chemical shifts are given in ppm relative to tetramethylsilane (0 ppm, ^{1}H) and $CDCl_3$ (76.95 ppm, ^{13}C). Infrared spectra were recorded on a Perkin-Elmer 1600 Series FTIR. Mass spectra were obtained on a VG Quattro-SQ or VG Autospec (Fisons Instruments). Optical rotations were recorded on a Rudolph Research automatic polarimeter Autopol III. Elemental analyses were performed by M-H-W Laboratories, Phoenix, AZ.

Flash chromatography was performed on Merck silica gel (230–400 mesh). Radial chromatography was performed on a Chromatotron Model 7924, and the plates were prepared with silica gel 60 PF_{254} (EM Science). THF (Mallinckrodt) and Et_2O (Mallinckrodt) were distilled from sodium/benzophenone under a nitrogen atmosphere. MeOH (Mallinckrodt) and CH_2Cl_2 (technical grade) were distilled from CaH_2 and stored over 4 Å molecular sieves. Acetonitrile was distilled from P_2O_5 and stored under argon. Hexane (technical grade) was distilled at atmospheric pressure. Photoreactions were performed with dry degassed solvents (freeze–thaw method).

The following chemicals were prepared according to literature procedures: pentacarbonyl[(methoxy)(phenyl)carbene]-chromium(0),[24] pentacarbonyl[(methoxy)(phenyl)carbene]-molybdenum(0),[24] pentacarbonyl[(methoxy)(phenyl)carbene]-tungsten(0),[24] 3-vinyl-(*S*)-4-phenyl-2-oxazolidinone,[25] cyclopentadiene,[26] methyl *N*-benzylformimidate,[27] and *N*-methylbenzilidineimine.[28] Palladium on carbon was purchased from Lancaster, and the rest of the chemicals from Aldrich and were used as received.

General Procedure for the Synthesis of (Phenyl)(pyrrol-1-yl)carbene Complexes 2. All of the operations were carried out under an argon atmosphere. Pyrrol-1-yl lithium was prepared by adding *n*-BuLi (2 equiv) to a solution of pyrrole (2 equiv) in THF at 0 °C. The resulting faint yellow solution was stirred for 10 min at 0 °C and for 30 min at room temperature. The lithium reagent was added via canula to an Airless flask containing a solution of the corresponding (methoxy)(phenyl)carbene complex **1** (1 equiv) in THF at −78 °C. The initial red solution turned to yellow after the addition was concluded. The reaction mixture was stirred at −78 °C for 1 h and then quenched with water. After warming to room temperature, THF was evaporated under reduced pressure and the residue was extracted with hexane (**2a**) or ether (**2b,c**) several times until the aqueous phase no longer remained brown in color. The resulting dark brown organic layer was dried ($MgSO_4$), filtered through Celite, and concentrated under reduced pressure to afford the crude carbenes **2a–c** as brown-black solids. Purification via flash chromatography on silica using a 9/1 mixture of hexane/CH_2Cl_2 as eluent gave the pure carbenes **2a–c**.

Pentacarbonyl[(phenyl)(pyrrol-1-yl)carbene]chromium(0) (2a). Pentacarbonyl[(methoxy)(phenyl)carbene]-chromium(0) (**1a**) (2.714 g, 8.70 mmol) in THF (45 mL) was treated with pyrrol-1-yl lithium, prepared from pyrrole (1.21 mL, 17.40 mmol) and *n*-BuLi (8.50 mL, 17.40 mmol) in THF (10 mL), according to the general procedure. Purification of the crude reaction product afforded 2.680 g (7.72 mmol, 88% yield) of carbene **2a** as bright black needles: mp 80–82 °C; ^{1}H-NMR δ 7.39 (m, 3H), 7.24 (m, 3H), 6.86 (m, 2H), 6.56 (bs, 2H); ^{13}C-NMR δ 320.8 (Cr=C), 225.7 (*trans* CO), 215.9 (*cis* CO), 154.8 (ipso), 127.5, 127.2, 120.3 (Ph), ≈120 (b, pyrrole ring); IR (film) ν 2063, 1991, 1966, 1936, 1911 cm^{-1}; MS (EI) *m/z* 155 ($M^+ - (CO)_5Cr$, 41%), 105 (100%), 77 (Ph, 75%), 67 (pyrrole, 55%). Anal. Calcd for $C_{16}H_9CrNO_5$: C, 55.34; H, 2.61; N, 4.03. Found: C, 55.20; H, 2.84; N, 3.83.

Pentacarbonyl[(phenyl)(pyrrol-1-yl)carbene]molybdenum(0) (2b). Pentacarbonyl[(methoxy)(phenyl)carbene]-molybdenum(0) (**1b**) (0.579 g, 1.63 mmol) in THF (12 mL) was treated with pyrrol-1-yl lithium, prepared from pyrrole (0.23 mL, 3.26 mmol) and *n*-BuLi (2.05 mL, 3.26 mmol) in THF (4 mL), according to the general procedure. Purification of the crude reaction product afforded 0.497 g (1.27 mmol, 78% yield) of carbene **2b** as a brown solid: mp 180–181 °C; ^{1}H-NMR δ 7.37 (m, 3H), 7.23 (m, 2H), 6.90 (m, 2H), 6.6 (b, 2H); ^{13}C-NMR δ 309.4 (Mo=C), 215.3 (*trans* CO), 205.3 (*cis* CO), 154.6 (ipso), 127.5, 127.3, 120.7 (Ph), ≈120 (b); IR (film) ν 2068 (*trans* CO), 1944 (*cis* CO) cm^{-1}. Anal. Calcd for $C_{16}H_9MoNO_5$: C, 49.12; H, 2.31; N, 3.58. Found: C, 48.86; H, 2.13; N, 3.48.

Pentacarbonyl[(phenyl)(pyrrol-1-yl)carbene]tungsten(0) (2c). Pentacarbonyl[(methoxy)(phenyl)carbene]tungsten-(0) (**1c**) (0.888 g, 2.00 mmol) in THF (8 mL) was treated with pyrrol-1-yl lithium, prepared from pyrrole (0.28 mL, 4.00

(23) Cowley, B. R.; Humber, D. C.; Laundon, B.; Long, A. G.; Lynd, A. L. *Tetrahedron* **1983**, *39*, 461.

(24) Fischer, E. O.; Aumann, R. *Chem. Ber.* **1968**, *101*, 963. The method for the preparation of pentacarbonyl[(methoxy)(methyl)carbene]-chromium(0) was used for the phenyl-substituted chromium, molybdenum, and tungsten complexes. PhLi was prepared *in situ* from ^{n}BuLi and bromobenzene in Et_2O at −20 °C (1 h).

(25) Miller, M.; Hegedus, L. S. *J. Org. Chem.* **1993**, *58*, 6779.

(26) *Organic Synthesis*; Wiley: New York, 1963; Collect. Vol. 4, p 242.

(27) Guzman, A.; Muchowski, J. M.; Naal, N. T. *J. Org. Chem.* **1981**, *46*, 1224. The method for the preparation of methyl *N*-(2-phenylethyl)-formimidate was used for this benzyl derivative: bp 45–50 °C (0.4 mmHg).

(28) Hegedus, L. S.; McGuire, M. A.; Schultze, L. M.; Yijun, C.; Anderson, O. P. *J. Am. Chem. Soc.* **1984**, *106*, 2680.

mmol) and *n*-BuLi (1.95 mL, 4.00 mmol) in THF (4 mL), according to the general procedure. Purification of the crude reaction product afforded 0.857 g (1.79 mmol, 89% yield) of carbene **2c** as a crystalline black solid: mp 98–99 °C (d); ^{1}H-NMR δ 7.40 (m, 3H), 7.27 (m, 2H), 6.96 (m, 2H), 6.62 (bs, 2H); ^{13}C–NMR δ 291.7 (W=C), 205.9 (*trans* C=O), 197.1 (*cis* C=O), 155.7 (ipso), 127.6, 127.4, 120.7 (Ph), ≈120 (b, pyrrole); IR (film) ν 2068, 1987, 1947 cm^{-1}. Anal. Calcd for $C_{16}H_9NO_5W$: C, 40.11; H, 1.89; N, 2.92. Found: C, 39.93; H, 2.01; N, 2.86.

Synthesis of Pentacarbonyl[(methyl)(pyrrol-1-yl)carbene]tungsten(0) (2d). Airless flasks (50 and 200 mL) were flame dried and filled with argon. A 35% oil dispersion of KH (1.146 g) was placed into the 50 mL flask, and the oil was removed by washing with freshly distilled hexane (3 × 10 mL) and removing via syringe. After drying the clean KH under vacuum to produce 0.402 g (10.00 mmol), 22 mL of dry THF was introduced into the flask, which was cooled to 0 °C. Pyrrole (0.69 mL, 10.00 mmol) was added to the suspension, and the reaction mixture was stirred for 10 min at 0 °C and for 2 h at room temperature, until evolution of H_2 stopped. The resulting suspension of pyrrol-1-yl potassium was transferred via cannula into an addition funnel attached to the 200 mL Airless flask, which contained a solution of pentacarbonyl-[(methoxy)(methyl)carbene]tungsten(0) **1d** (3.51 g, 9.19 mmol) in 80 mL of THF, and then the suspension was added dropwise at −78 °C. The reaction mixture was stirred for 3 h and quenched with water. After warming to room temperature, THF was removed under reduced pressure and the brown residue was extracted with ether several times, until the aqueous layer lost its red color. The resulting dark red organic layer was dried ($MgSO_4$), filtered through Celite, and evaporated to give a garnet solid. Purification of this crude material was performed by chromatography on silica (hexane/CH_2Cl_2, 95/5). Contamination of $W(CO)_6$ that could not be removed in the column was eliminated by precipitation in MeOH, giving 1.400 g (3.36 mmol, 39% yield) of pure carbene **2d** as a garnet solid: mp 90–91 °C; ^{1}H-NMR δ 7.69 (bs, 1H), 7.18 (bs, 1H), 6.61 (bs, 2H), 3.22 (s, 3H, CH_3); ^{13}C-NMR δ 295.2 (W=C), 205.0 (*trans* CO), 197.5 (*cis* C=O), 134.3, 119.8, 118.8, 116.4, 46.8; IR (film) ν 2067, 1938 cm^{-1}. Anal. Calcd for $C_{11}H_7NO_5W$: C, 31.68; H, 1.69; N, 3.35. Found: C, 31.75; H, 1.46; N, 3.28.

General Procedure for the Synthesis of Cyclopropanes 3 from Pentacarbonyl[(phenyl)(pyrrol-1-yl)carbene]molybdenum(0) (2b) and Pentacarbonyl[(phenyl)-(pyrrol-1-yl)carbene]tungsten(0) (2c). A pressure tube was sealed with a rubber septum, flame dried, evacuated, and filled with Ar. The carbene complex was added in one portion followed by THF to produce a 0.02–0.03 M solution. To this solution were added 0.2 equiv of 2,6-di-*tert*-butyl-4-methylphenol (DBHT) and 1.1 equiv of the corresponding olefin. The tube was sealed with a pressure cap and heated at 100 °C behind a blast shield for 3–5 h. At this point, the initial brown (carbenes **2b** and **2c**) or red (carbene **2d**) transparent solution turned into a dark brown suspension, and the carbene complex was completely consumed as evidenced by TLC analysis. After cooling to room temperature, the reaction mixture was transferred to a round-bottomed flask and THF was removed by rotary evaporation. The residue was taken up in EtOAc, air was bubbled into the suspension for a few minutes, and then the suspension was filtered through Celite. The filtrate was concentrated under reduced pressure to give a crude material, which was purified by flash chromatography on silica to separate molybdenum or tungsten hexacarbonyl and DBHT from the reaction products. These organic reaction products were further purified as described in each synthesis.

Synthesis of Cyclopropane 3a from Pentacarbonyl-[(phenyl)(pyrrol-1-yl)carbene]molybdenum(0) (2b). Carbene complex **2b** (0.156 g, 0.40 mmol), methyl acrylate (36 μL, 0.40 mmol), and DBHT (18 mg, 0.08 mmol) in THF (15 mL) were allowed to react according to the general procedure for 3 h. Flash chromatography (hexane/AcOEt, 9/1) of the crude reaction mixture separated $Mo(CO)_6$ and DBHT and gave 88.3 mg (0.36 mmol, 90% crude yield) of an oil containing a mixture of cyclopropane **3a** and olefins **4a** and **5a** in a ratio of 66:4:30. Purification of this mixture by radial-layer chromatography (hexane/AcOEt, 70/1, 40/1, and 95/5) separated **4a** and gave 72.8 mg of an oil formed by **3a** and **5a** in a ratio of 74:26, indicating a 56% yield in cyclopropane. Separation of this mixture could not be accomplished quantitatively.[29] Compound **3a** was obtained as a 1/3.4 mixture of diastereoisomers.

Synthesis of Cyclopropane 3a from Pentacarbonyl-[(phenyl)(pyrrol-1-yl)carbene]tungsten(0) (2c). Carbene complex **2c** (0.144 g, 0.30 mmol), methyl acrylate (27 μL, 0.30 mmol), and DBHT (13.2 mg, 0.06 mmol) in THF (12 mL) were allowed to react according to the general procedure for 5 h. Flash chromatography (hexane/AcOEt, 9/1) of the crude reaction mixture separated $W(CO)_6$ and DBHT and gave 63.6 mg (0.26 mmol, 88% crude yield) of an oil containing a mixture of cyclopropane **3a** and olefins **4a** and **5a** in a ratio of 70:22:8. Purification of this mixture by radial chromatography (2 mm plate; hexane/AcOEt, 70/5, 40/5, and 95/5) separated **4a** and gave 45.70 mg of an oil formed by **3a** and **5a** in a ratio of 90:10, indicating a 57% yield in cyclopropane. Separation of this mixture could not be accomplished quantitatively,[29] but a sample of **3a** could be obtained for complete characterization of the product. Compound **3a** was produced as a 2.3/1 mixture of diastereoisomers: R_f = 0.25 (hexane/EtOAc, 4/1); ^{1}H-NMR (2 diastereoisomers, a/b = 2.3/1) δ 7.32–7.20 (m, 4H, Ph), 6.81 (m, 1H, Ph), 6.88 (b), 6.73 (a) (t, 2H, J = 2.2 Hz), 6.16 (a), 6.09 (b) (t, 2H, J = 2.2 Hz), 3.58 (a), 3.50 (b) (s, 3H, OMe), 2.76 (b), 2.65 (a) (dd, 1H, J = 9.2, 6.6 Hz), 2.47 (a), 2.21 (b) (dd, 1H, J = 6.8, 5.7 Hz), 1.86 (b), 1.74 (a) (dd, 1H, J = 9.2, 5.7 Hz); ^{13}C-NMR δ 169.4 (C=O, b), 168.7 (C=O, a), 141.9 (ipso, a), 137.0 (ipso, b), 128.5, 128.3, 128.0, 127.8, 127.2, 124.4 (Ph), 121.5, (pyrrole, a), 120.3 (pyrrole, b), 108.8 (pyrrole, b), 108.7 (pyrrole, a), 52.2 (OMe, a), 51.9 (OMe, b), 50.1 (Ph*C*N, b), 48.5 (Ph*C*N, a), 30.8 (CH, a), 29.1 (CH, b), 22.6 (CH_2, a), 18.8 (CH_2, b); IR (film) ν 1739 (CO_2Me) cm^{-1}. Anal. Calcd for $C_{15}H_{15}NO_2$: C, 74.67; H, 6.26; N, 5.80. Found: C, 74.80; H, 6.33; N, 5.78.

Synthesis of Cyclopropane 3b. Carbene **2c** (0.335 g, 0.70 mmol), acrylonitrile (46 μL, 0.70 mmol), and DBHT (46 mg, 0.21 mmol) in THF (22 mL) were allowed to react according to the general procedure for 4.5 h. Flash chromatography (hexane/AcOEt, 9/1) of the crude reaction mixture separated $W(CO)_6$ and DBHT and gave the products as a yellow oil due to complexation with chromium. This oil was taken up in hexane/AcOEt (4/1). Air was bubbled into the solution, and then the solution was air oxidized in sunlight and in a light box (6 × 20 Vitalite fluorescent bulbs). After 2–3 h, the resulting brown suspension was filtered through Celite and the filtrate was air oxidized again. These operations were successively repeated until a clear colorless solution was obtained (12–15 h).[30] Solvent removal on a rotary evaporator gave 105 mg (0.50 mmol, 72% crude yield) of an oil containing a mixture of cyclopropane **3b** and olefin **4b** in a ratio of 93:7. Cyclopropane **3b** was produced as a 1/2.1 mixture of diastereoisomers. Purification by radial layer chromatography (hexane/EtOAc, 70/1, 40/1, and 95/5) gave 88 mg (0.42 mmol, 61% yield) of cyclopropane **3b**. First diastereoisomer: R_f = 0.31 (hexane/EtOAc, 4/1); mp 86–7 °C; ^{1}H-NMR δ 7.38–7.31 (m, 3H, Ph), 7.18 (m, 2H, Ph), 6.83 (t, J = 2.2 Hz, 2H, pyrrole), 6.17 (t, J = 2.2 Hz, 2H, pyrrole), 2.51 (dd, J = 10.0, 6.8 Hz, 1H), 2.14 (dd, 1H, J = 6.8, 6.1 Hz), 2.11 (dd, 1H, J = 10.0, 6.1 Hz); ^{13}C-NMR δ 136.0 (ipso), 128.8, 128.7, 126.6 (Ph), 120.7 (pyrrole), 117.4 (CN), 109.6 (pyrrole), 48.3 (C(Ph)(N)), 21.2 (CH_2), 14.2 (CH); IR (film) ν 2243 (CN) cm^{-1}. Second diastereoisomer: R_f = 0.23 (hexane/EtOAc, 4/1); mp 90–91 °C;

(29) This was not an inconvenience for the next step, since ozonolysis could be performed with the contaminated cyclopropane. The α-formamidocyclopropanes were easily purified and isolated via chromatography.

(30) Air oxidation of the crude reaction mixture without separation of DBHT and $W(CO)_6$ resulted in decomposition of the products and lower yields.

^{1}H-NMR δ 7.32−7.25 (m, 3H, Ph), 6.89 (t, J = 2.1 Hz, 2H, pyrrole), 6.80 (m, 2H, Ph), 6.25 (t, J = 2.1 Hz, 2H, pyrrole), 2.34 (dd, J = 8.7, 6.5 Hz, 1H), 2.29 (dd, 1H, J = 6.5, 5.2 Hz), 1.95 (dd, 1H, J = 8.7, 5.2 Hz); ^{13}C-NMR δ 139.3 (ipso), 128.8, 128.1, 124.6 (Ph), 121.4 (pyrrole), 117.4 (CN), 109.8 (pyrrole), 47.4 (PhCN), 23.5 (CH_2), 14.5 (CH); IR (film) ν 2243 (CN) cm^{-1}. Anal. Calcd for $C_{14}H_{12}N_2$: C, 80.74; H, 5.80; N, 13.45. Found: C, 80.92; H, 5.71; N, 13.49.

Synthesis of Cyclopropane 6a. Carbene complex **2d** (0.333 g, 0.80 mmol), methyl acrylate (72 μL, 0.80 mmol), and DBHT (35.2 mg, 0.16 mmol) in THF (22 mL) were allowed to react according to the general procedure for 5 h. Flash chromatography of the crude reaction mixture (silica; hexane/EtOAc, 9/1) separated $W(CO)_6$ and DBHT and gave 94.0 mg (0.52 mmol, 65% crude yield) of an oil containing a mixture of cyclopropane **6a** and olefin **7a** in a ratio of 95:5. This mixture was purified by radial chromatography (2 mm plate; hexane/AcOEt, 40/1 and 95/5) to afford 42.5 and 27.1 mg of the two diasteromeric cyclopropanes: 69.6 mg, 0.39 mmol, 48% yield. Data for the major isomer: R_f = 0.34 (hex/EtOAc, 9/1); ^{1}H-NMR δ 6.76 (t, 2H, J = 2.1 Hz, pyrrole), 6.11 (t, 2H, J = 2.1 Hz, pyrrole), 3.76 (s, 3H, CO_2Me), 2.23 (dd, 1H, J = 9.5, 6.5 Hz), 1.65 (dd, 1H, J = 9.6, 5.5 Hz), 1.63 (s, 3H, CH_3), 1.50 (dd, 1H, J = 6.5, 5.5 Hz); ^{13}C-NMR δ 171.1 (C=O), 119.8 (pyrrole), 108.4 (pyrrole), 51.9 (OCH_3), 43.8 (MeCN), 27.5 ($CHCO_2Me$), 20.4 (CH_2), 20.2 (CH_3); IR (film) ν 1732 cm^{-1}. Anal. Calcd for $C_{10}H_{13}NO_2$: C, 67.01; H, 7.31; N, 7.81. Found: C, 66.97; H, 7.39; N, 7.69. Data for the minor isomer: R_f = 0.29 (hexane/EtOAc, 9/1); ^{1}H-NMR δ 6.68 (t 2H, J = 2.1 Hz, pyrrole), 6.09 (t, 2H, J = 2.1 Hz, pyrrole), 3.50 (s, 3H, CO_2Me), 2.09−1.99 (m, 2H), 1.63 (s, 3H, CH_3), 1.31 (dd, 1H, J = 7.6, 5.1 Hz); ^{13}C-NMR δ 169.5 (C=O), 120.2 (pyrrole), 108.2 (pyrrole), 51.9 (OCH_3), 43.5 (MeCN), 28.3 ($CHCO_2Me$), 26.7 (CH_3), 19.8 (CH_2); IR (film) ν 1732 cm^{-1}.

Synthesis of Cyclopropane 6b. Carbene **2d** (0.372 g, 0.89 mmol), acrylonitrile (58 μL, 0.80 mmol), and DBHT (49 mg, 0.22 mmol) in THF (22 mL) were allowed to react according to the general procedure for 5 h. Flash chromatography (hexane/AcOEt, 9/1) of the crude reaction mixture separated $W(CO)_6$ and DBHT and gave the products as a yellow oil due to complexation with chromium. This oil was taken up in hexane/AcOEt (4/1) and air oxidized as described above. Solvent removal of the colorless resulting solution gave a crude product formed by cyclopropane **6b** and olefin **7b** in 98:2 ratio. Purification of this material by flash chromatography afforded 14.2 and 34.5 mg of the two diastereomeric cyclopropanes: 48.8 mg, 0.33 mmol, 42% yield. Data for the first diastereoisomer: R_f = 0.45 (hexane/EtOAc, 4/1); ^{1}H-NMR δ 6.72 (t, 2H, pyrrole), 6.13 (t, 2H, pyrrole), 1.98 (dd, 1H, J = 10.0, 6.1 Hz), 1.83 (dd, 1H, J = 10.0, 5.7 Hz), 1.78 (s, 3H, CH_3), 1.44 (t, 1H, J = 5.9 Hz); ^{13}C-NMR δ 119.7 (pyrrole), 118.4 (CN), 109.3 (pyrrole), 41.8 (MeCN), 22.8 (CH_3), 21.0 (CH_2), 11.8 (CH); IR (film) ν 2241 (CN) cm^{-1}. Anal. Calcd for $C_9H_{10}N_2$: C, 73.94; H, 6.89; N, 19.16. Found: C, 73.81; H, 7.04; N, 19.02. Data for the second diastereoisomer: R_f = 0.13 (hexane/EtOAc, 4/1); ^{1}H-NMR δ 6.80 (t, 2H, J = 2.1 Hz, pyrrole), 6.20 (t, 2H, J = 2.1 Hz, pyrrole), 1.92 (t, 1H, J = 5.9 Hz), 1.74 (dd, 1H, J = 9.2, 5.9 Hz), 1.61 (s, 3H, CH_3), 1.50 (dd, 1H, J = 9.2, 5.9 Hz); ^{13}C-NMR δ 120.0 (pyrrole), 117.9 (CN), 109.5 (pyrrole), 42.2 (MeCN), 25.3 (CH_3), 21.0 (CH_2), 12.1 (CH); IR (film) ν 2244 (CN) cm^{-1}.

General Procedure for the Formamidocyclopropane Derivatives 9. The cyclopropanes **3** were placed in a round-bottomed flask equipped with a stir bar, followed by addition of CH_2Cl_2. The resulting colorless solution was ozonized at −78 °C (1 L per min) until the color of the solution turned blue (5−10 min). Then Ar was bubbled into the solution until the blue color disappeared (3−6 min), and a solution of thiourea (1 equiv) in MeOH was added. The reaction mixture was stirred at −78 °C for 15 min and at 0 °C for 1 h. Thiourea dioxide precipitated from the solution as a white solid, and the mixture was filtered through Celite. The filtrate was concentrated on a rotary evaporator, and the residue was taken up in CH_2Cl_2, washed with 1% $NaHCO_3$ aqueous solution (× 2), H_2O (× 1), and brine (× 2). The organic layer was dried ($MgSO_4$) and evaporated under reduced pressure to give a crude material whose ^{1}H-NMR and TLC showed that these compounds exist as a mixture of two rotamers about the formamide. Purification by column chromatography gave the pure compounds.

Synthesis of Formamidocyclopropane 9a. A 91 mg (0.38 mmol) amount of a mixture consisting of cyclopropane **3a** (2.5:1 diasteromeric ratio) and olefin **5a** in a 97:3 ratio, was ozonized in CH_2Cl_2 (7 mL) according to the general procedure. Addition of thiourea (30 mg, 0.39 mmol) in MeOH (3 mL) and workup of the reaction as described above gave 71 mg of the crude compound as a 98/2 mixture of two conformers. This material was purified by flash chromatography on silica (hexane/AcOEt, 1/1) to afford 58.2 mg (0.265 mmol, 73% yield) of cyclopropane **9a** (2.4:1 diastereomeric ratio) as the major conformer. Further separation (radial chromatography) of the two diastereoisomers furnished them as white solids. Data for the minor diastereoisomer: mp 69−70 °C; ^{1}H-NMR δ 8.84 (bs, 1H), 8.68 (bs, 1H), 7.50 (bs, 2H, Ph), 7.34−7.28 (m, 3H, Ph), 3.71 (s, 3H, CH_3), 2.60 (dd, 1H, J = 8.7, 7.3 Hz), 1.98 (t, 1H, J = 6.9 Hz), 1.92 (dd, 1H, J = 8.9, 6.4 Hz); ^{13}C-NMR δ 170.9 (CO_2Me), 163.8 (NHCHO), 138.1 (ipso), 128.6, 128.4 (Ph), 52.2 (CH_3), 41.9 (C(Ph)(N)), 26.5 (CH), 21.4 (CH_2); IR (film) ν 1728 (CO_2Me), 1681 (NHCHO) cm^{-1}. Data for the major diastereoisomer: mp 116−117 °C; ^{1}H-NMR δ 8.75 (bs, 2H, NHCHO), 7.53 (bs, 2H, Ph), 7.33−7.27 (m, 3H, Ph), 3.57 (s, 3H, OCH_3), 2.45 (dd, 1H, J = 9.2, 7.2 Hz), 2.23 (t, 1H, J = 6.9 Hz), 1.60 (dd, 1H, J = 9.2, 6.5 Hz); ^{13}C-NMR δ 169.5 (CO_2Me), 163.2 (NHCHO), 135.2 (ipso), 129.9, 128.8 (Ph), 52.1 (CH_3), 41.5 (PhCN), 27.6 (CH), 18.8 (CH_2); IR (film) ν 1731 (CO_2Me), 1681 (NHCHO) cm^{-1}. High-resolution exact mass spectrum (FAB) M + 1 calcd for $C_{12}H_{14}NO_3$: 220.0973. Found: 220.0972.

Synthesis of Formamidocyclopropane 9b. Cyclopropane **3b** (44 mg, 0.21 mmol, one diastereoisomer) was ozonized in CH_2Cl_2 according to the general procedure. Addition of thiourea (17 mg, 0.21 mmol) in MeOH (1.5 mL) and workup of the reaction as described above gave 35 mg of the crude product as a 98/2 mixture of two conformers. Flash chromatography of this material (hex/AcOEt, 1/1) gave a solid, which was washed with hexane to produce 28 mg (0.15 mmol, 71% yield) of pure cyclopropane **9b** as the major conformer: mp 138−139 °C; ^{1}H-NMR δ 8.88 (bs, 2H), 7.54−7.32 (m, 5H, Ph), 2.41 (t, 1H, J = 8.2 Hz), 1.99 (m, 2H); ^{13}C-NMR δ 163.1 (CO), 136.0 (ipso), 129.2, 128.8 (Ph), 118.1 (CN), 40.6 (PhCNHCHO), 21.4 (CH_2), 11.6 (CH); IR (film) ν 2246 (CN), 1685 (NHCHO) cm^{-1}. MS (EI) m/z 186 (M^+, 18%), 158 (M^+ − CO, 63%), 104 (PhCNH, 100%). High-resolution mass measurement (EI) calcd for $C_{11}H_{10}N_2O$: 186.0793. Found: 186.0785±0.000 18 (n = 4).

Procedure for the Benzannulation Reaction. Synthesis of Aminonaphthol 10. A 25 mL Airless flask was flame dried, evacuated, and filled with Ar. Pentacarbonyl[(phenyl)-(pyrrol-1-yl)carbene]chromium(0) (**2a**) (0.114 g, 0.33 mmol) was added into the flask, followed by the addition of THF (10 mL) and diphenylacetylene (53 mg, 0.30 mmol) to produce a dark brown solution that was heated at reflux temperature for 1 h and 40 min. The resulting clear red solution, which did not contain carbene (by TLC), was concentrated on a rotary evaporator, and the residue was taken up in hexane/AcOEt, 7/3, and filtered through Celite. Air was bubbled into the yellow filtrate for 30−40 min, and the resulting suspension was filtered through Celite. This operation was repeated two more times until the solution lost most of its yellow color.[31] Evaporation of the solvents under reduced pressure gave a crude product consisting in a 2.5/1 mixture of compounds **10**/**11**. This material was purified by flash chromatography on

(31) The use of light in the oxidation step led to oxidation of aminonaphthol **10** in 3,4-diphenylnaphthoquinone.

silica (hexane/AcOEt, 95/5) to afford 62 mg (0.17 mmol, 57% yield) of aminonaphthol **10** as a white solid. An analytical sample was recrystallized from hexane/CH_2Cl_2: mp 161–162 °C; ^{1}H-NMR δ 8.33 (dd, 1H, J = 9.0, 1.5 Hz), 7.55–7.44 (m, 2H), 7.36–7.14 (m, 6H), 6.97–6.87 (m, 5H), 6.63 (t, 2H, J = 2.1 Hz, pyrrole), 6.09 (t, 2H, J = 2.1 Hz, pyrrole), 5.67 (s, 1H, OH); ^{13}C-NMR δ 148.1 (C–OH), 137.6 (ipso), 137.1 (ipso), 134.6 (ipso), 131.8 (ipso), 131.0, 129.4, 129.0, 128.8 (ipso), 127.8, 127.0, 126.3, 125.9, 124.1 (pyrrole), 123.4, 123.3 (ipso), 122.3, 121.3 (ipso), 107.9 (pyrrole); IR (film) ν 3526 (OH) cm^{-1}. MS (EI) m/z 361 (M^+, 100%). High-resolution mass measurement calcd for $C_{26}H_{19}NO$: 361.1467. Found: 361.1465±0.0029 (n = 6).

General Procedure for the Synthesis of Cyclobutanones 12. An Ace pressure tube was sealed with a rubber septum, flame dried, evacuated, and filled with Ar twice. Pentacarbonyl[(phenyl)(pyrrol-1-yl)carbene]chromium(0) (**2a**) was added into the tube, followed by dry degassed ether (CH_2Cl_2 for **12c**) and an excess (5–7 equiv) of the corresponding olefin (for **12c** the carbene was used in excess) to produce a deep brown solution. Glass beads were added into the pressure tube to increase the light transmission of the reacting solution. The tube was equipped with a pressure head, and it was saturated with CO (3 cycles to 80 psi) and irradiated (450 W Conrad-Hanovia 7825 medium-pressure mercury lamp, Pyrex well) until the brown solution turned yellow (40–60 h) indicating complete consumption of the carbene. The solution was filtered through Celite and concentrated under reduced pressure to give a brown residue from which $Cr(CO)_6$ was recovered via sublimation (45 °C, 1 mmHg). The residue containing the crude cyclobutanone was purified by flash chromatography or by radial chromatography.

Synthesis of Cyclobutanone 12a. Pentacarbonyl[(phenyl)(pyrrol-1-yl)carbene]chromium(0) **2a** (0.590 g, 1.70 mmol) and dihydropyran (1.2 mL, 13 mmol) in ether (40 mL) were allowed to react according to the general procedure for 40 h. Flash chromatography of the crude reaction product (hexane/AcOEt, 9/1) yielded 222 mg (0.83 mmol, 49% yield) of cyclobutanone **12a** as a white solid: mp 90–92 °C; ^{1}H-NMR δ 7.29–7.16 (m, 5H, Ph), 6.83 (t, 2H, J = 2.2 Hz, pyrrole), 6.25 (t, 2H, J = 2.2 Hz, pyrrole), 4.91 (d, 1H, J = 5.9 Hz, C*H*–OCH_2), 3.88 (m, 1H), 3.65 (m, 1H, OC–C*H*–CH_2), 3.37 (m, 1H), 2.22 (m, 1H), 1.80–1.52 (m, 3H); ^{13}C-NMR δ 202.2 (CO), 134.8 (ipso), 128.1, 127.8, 127.5 (Ph), 119.0 (pyrrole), 109.7 (pyrrole), 85.3 (Ph*C*N), 70.8 (*C*H–OCH_2), 65.0 (CH–*O*CH_2), 55.1 (OC–*C*H–CH_2), 21.6 (CH_2), 18.5 (CH_2); IR (film) ν 1789 (CO) cm^{-1}; MS (EI) m/z 267 (M^+, 33%), 183 (M^+ – dihydropyran, 50%), 155 (PhCPyrrole, 100%). Anal. Calcd for $C_{17}H_{17}NO_2$: C, 76.38; H, 6.40; N, 5.24. Found: C, 76.34; H, 6.39; N, 5.25.

Synthesis of Cyclobutanone 12b. Pentacarbonyl[(phenyl)(pyrrol-1-yl)carbene]chromium(0) **2a** (0.213 g, 0.61 mmol) and ethyl vinyl ether (0.3 mL, 3.1 mmol) in ether (12 mL) at 0 °C were allowed to react according to the general procedure for 40 h to give a crude product consisting of a 2.1/1 mixture of cyclobutanone **12b** and the methathesis product **12b′**. This material was purified by filtration through a short column of silica (hexane/AcOEt, 7/3) followed by radial chromatography (2 mm plate; hex/AcOEt) to give 18 mg (0.11 mmol, 17% yield) of **12b′** followed by 55 mg (0.216 mmol, 35% yield) of cyclobutanone **12b** as a white solid. An analytical sample was recrystallized from hexane: mp 55–56 °C; ^{1}H-NMR δ 7.28 (m, 3H, Ph), 6.96 (m, 2H, Ph), 6.86 (t, 2H, J = 2.1 Hz, pyrrole), 6.25 (t, 2H, J = 2.1 Hz, pyrrole), 4.78 (dd, 1H, J = 8.4, 6.5 Hz, C*H*–OEt), 3.55 (dd, 1H, J = 18.7, 8.4 Hz, CH_2), 3.31 (dd, 1H, J = 18.7, 6.5 Hz, CH_2), 3.49, 3.28 (m, 2H, OCH_2), 1.00 (t, 3H, J = 7.0 Hz, CH_3); ^{13}C-NMR δ 201.6 (CO), 134.9 (ipso), 128.2, 128.1, 126.9 (Ph), 119.6 (pyrrole), 109.2 (pyrrole), 86.0 (Ph*C*N), 74.5 (*C*H–OEt), 65.9 (OCH_2CH_3), 51.5 (CH_2), 14.6 (CH_3); IR (film) ν 1789 (CO) cm^{-1}; MS (EI) m/z 255 (M^+, 23%), 183 (M^+ – ethyl vinyl ether, 37%), 155 (PhCPyrrole, 100%). Anal. Calcd for $C_{16}H_{17}NO_2$: C, 75.27; H, 6.71; N, 5.48. Found: C, 75.29; H, 6.72; N, 5.44. Data for compound **12b′**: semisolid that melts at room temperature; R_f = 0.66 (hexane/EtOAc, 4/1); ^{1}H-NMR δ 7.35 (s, 5H, Ph), 6.78 (t, 2H, J = 2.3 Hz, pyrrole), 6.22 (t, 2H, J = 2.3 Hz, pyrrole), 5.14 (s, 1H), 5.05 (s, 1H); ^{13}C-NMR δ 146.3 (Ph*C*N), 136.9 (ipso), 129.0, 128.2, 127.8 (Ph), 121.0 (pyrrole), 109.2 (pyrrole), 103.1 (CH_2). When the reaction was performed at room temperature, olefin **12b′** was the major product (57% yield) and cyclobutanone **12b** was the minor product (6% yield).

Synthesis of Cyclobutanone 12c. Pentacarbonyl[(phenyl)(pyrrol-1-yl)carbene] chromium(0) **2a** (302 mg, 0.87 mmol, 1.5 equiv) and 3-vinyl-(*S*)-4-phenyl-2-oxazolidinone (109 mg, 0.58 mmol, 1 equiv) in CH_2Cl_2 (13 mL) were allowed to react according to the general procedure for 60 h. Flash chromatography (hexane/AcOEt, 7/3) of the crude product followed by radial chromatography (2 mm plate; hexane/AcOEt, 95/1, 70/1, 40/1, and 9/1) gave recovered ene–carbamate and a minor diastereoisomer of product as an inseparable mixture (5.5 mg, 0.015 mmol, 2.5%) and cyclobutanone **12c** (42 mg, 0.12 mmol, 20% yield) as a white solid. An analytical sample was recrystallized from hexane/AcOEt/CH_2Cl_2: mp 134–135 °C; $[\alpha]_D$ = +28.39 (c = 1, CH_2Cl_2); ^{1}H-NMR δ 7.45 (m, 2H, Ph), 7.32 (m, 2H, Ph), 7.18 (m, 4H, Ph), 6.99 (m, 12H, Ph), 6.19 (t, 2H, J = 2.2 Hz, pyrrole), 5.54 (t, 1H, J = 9.8 Hz), 3.96 (t, 1H, J = 8.5 Hz), 3.83 (dd, 1H, J = 8.5, 2.8 Hz), 3.52 (dd, 1H, J = 8.5, 2.8 Hz), 3.03 (dd, 1H, J = 18.8, J = 9.4 Hz), 2.94 (dd, 1H, J = 18.8, J = 9.9 Hz); ^{13}C-NMR δ 200.5 (cyclobutanone CO), 158.1 (carbamate CO), 139.8 (ipso), 135.8 (ipso), 129.5, 129.3, 129.0, 126.2, 125.3 (Ph), 119.9 (pyrrole), 109.1 (pyrrole), 87.2 (Ph*C*N), 70.6 (CH_2), 57.8 (CH), 49.2 (CH), 46.9 (CH_2); IR (film) ν 1796, 1750 cm^{-1}. Anal. Calcd for $C_{23}H_{20}N_2O_3$: C, 74.17; H, 5.41; N, 7.52. Found: C, 74.15; H, 5.63; N, 7.55. Data for the minor diastereoisomer: R_f = 0.37 (hexane/EtOAc, 7/3); ^{1}H-NMR δ 7.73 (m, 2H, Ph), 7.42–7.29 (m, 6H, Ph), 7.11 (m, 2H, Ph), 6.65 (t, 2H, J = 2.1 Hz, pyrrole), 6.29 (t, 2H, J = 2.1 Hz, pyrrole), 5.63 (t, 1H, J = 8.9 Hz), 4.20 (t, 1H, J = 8.5 Hz), 3.90 (dd, 1H, J = 8.3, 3.2 Hz), 3.51 (dd, 1H, J = 8.7, 3.2 Hz), 3.07 (dd, 1H, J = 19.3, J = 9.6 Hz), 2.99 (dd, 1H, J = 19.3, J = 8.4 Hz).

Synthesis of Cyclobutanone 12d. Pentacarbonyl[(phenyl)(pyrrol-1-yl)carbene]chromium(0) **2a** (0.358 g, 1.03 mmol) and cyclopentadiene (0.58 mL, 7.10 mmol) in ether (12 mL) were allowed to react according to the general procedure for 60 h. Flash chromatography of the crude product (hexane/AcOEt, 9/1) followed by radial chromatography (2 mm plate; hexane/AcOEt, 40/1 and 9/1) yielded 144 mg (0.57 mmol, 58% yield) of **12d** as a white solid: mp 72–73 °C; ^{1}H-NMR δ 7.27, 7.01 (m 5H, Ph), 6.87 (t, 2H, J = 2.2 Hz, pyrrole), 6.24 (t, 2H, J = 2.2 Hz, pyrrole), 5.90 (m, 1H, =CH), 5.40 (m, 1H, =CH), 4.37 (m, 1H, C*H*–CH=), 4.18 (ddd, 1H, J = 9.1, 9.1, 1.3 Hz, CH_2), 2.86 (m, 1H, CH_2), 2.57 (dddd, 1H, J = 17.4, 9.1, 4.4, 4.3 Hz, CH_2); ^{13}C-NMR δ 206.9 (C=O), 137.0 (ipso), 135.4 (CH=), 129.2, 128.1, 128.0, 126.5 (Ph + CH=), 119.5, 109.4 (pyrrole), 86.7 (Ph*C*N), 59.7 (CH), 51.3 (CH), 35.0 (CH_2); IR (film) ν 1782 cm^{-1}. MS (EI) m/z 249 (M^+, 28%), 194 (M^+ – cyclopentadiene, 100%). Anal. Calcd for $C_{17}H_{15}NO$: C, 81.90; H, 6.06; N, 5.61. Found: C, 81.74, H, 6.04; N, 5.44.

Synthesis of Cyclobutanone 12e. Pentacarbonyl[(phenyl)(pyrrol-1-yl)carbene]chromium(0) **2a** (0.347 g, 1.00 mmol) and cyclohexadiene (47 mL, 5 mmol) in ether (12 mL) were allowed to react according to the general procedure for 60 h. Flash chromatography (hexane/AcOEt, 4/1) of the crude product followed by radial chromatography (2 mm plate; hexane/AcOEt, 50/1) gave 47 mg (0.18 mmol, 18%) of compound **12e′** as a white solid, followed by 63 mg (0.24 mmol, 24% yield) of cyclobutanone **12e** as a colorless oil. Data for cyclobutanone **12e**: ^{1}H-NMR δ 7.25 (m, 3H, Ph), 7.00 (m, 2H, Ph), 6.90 (t, 2H, J = 2.2 Hz, pyrrole), 6.25 (t, 2H, J = 2.2 Hz, pyrrole), 5.93 (m, 1H, =C*H*–CH_2), 5.48 (m, 1H, CH–C*H*=), 3.97 (m, 1H, C*H*–CH_2), 3.77 (m, 1H, C*H*–CH=), 2.19–2.03 (m, 3H), 1.65 (m, 1H); ^{13}C-NMR δ 204.6 (C=O), 136.6 (ipso), 131.3, 127.9, 127.8, 126.7, 124.6, 119.5 (pyrrole), 109.3 (pyrrole), 83.8 (ipso), 54.7 (CH), 36.8 (CH), 20.9 (CH_2), 18.3 (CH_2); IR (film)

ν 1778 (C=O) cm^{-1}. MS (EI) *m/z* 263 (M^+, 50%), 183 (M^+ − cyclohexadiene, 18%), 155 (PhCPyrrole, 100%). Anal. Calcd for $C_{18}H_{17}NO$: C, 82.09; H, 6.51; N, 5.31. Found: C, 81.96; H, 6.55; N, 5.22. Data for the [4 + 2] adduct **12e'** (this compound was identified by its X-ray structure): mp 85−86 °C (from hexane/CH_2Cl_2); ^{1}H-NMR δ 7.25 (m, 4H), 7.09 (m, 1H), 6.67 (t, 2H, J = 2.1 Hz), 6.49 (m, 2H), 6.28 (t, 2H, J = 2.1 Hz), 5.17 (m, 1H), 3.09 (m, 1H), 2.20 (m, 1H), 1.71 (m, 1H), 1.55 (m, 1H), 1.37 (m, 1H); ^{13}C-NMR δ 154.4, 137.1 (ipso), 133.3, 131.5, 127.9, 125.5, 125.4, 123.6, 112.0, 108.3, 71.5, 33.7, 25.8 (CH_2), 21.1 (CH_2); IR (film) ν 1636, 1613 cm^{-1}; MS (EI) *m/z* 263 (M^+, 45%), 155 (PhCPyrrole, 100%).

Synthesis of Cyclobutanone 12f. Pentacarbonyl[(phenyl)(pyrrol-1-yl)carbene]chromium(0) **2a** (0.175 g, 0.50 mmol) and 1,3-cycloheptadiene (0.27 mL, 2.52 mmol) in ether (13 mL) were allowed to react according to the general procedure for 72 h. The crude reaction product was purified by filtration through a short column on silica (hexane/AcOEt, 7/3) followed by radial chromatography (1 mm plate; hexane/AcOEt, 70/1, 40/1, and 9/1) to give 31 mg (0.108 mmol, 25% yield) of a mixture of products **12f** and **12f'** in a 46:54 ratio. With further purification by radial chromatography analytically pure samples of both isomers could be obtained. Data for cyclobutanone **12f**: white solid, mp 104−105 °C; ^{1}H-NMR δ 7.25 (m, 3H, Ph), 6.88−6.83 (m, 4H, Ph + pyrrole), 6.24 (t, 2H, pyrrole), 5.62−5.54 (m, 1H, =CH), 5.21 (bd, 1H, =CH), 4.26 (d, 1H, J = 11.3 Hz), 3.78 (dt, 1H, J = 11.2, 5.3 Hz, C*H*−CH_2), 2.23−1.94 (m, 4H), 1.67−1.52 (m, 2H); ^{13}C-NMR δ 207.4 (CO), 137.1 (ipso), 129.6, 128.3, 126.7, 125.7 (Ph + 2 =CH), 119.7 (pyrrole), 109.1 (pyrrole), 84.9 (Ph*C*N), 58.7 (CH), 42.5 (CH), 27.7 (CH_2), 23.6 (CH_2), 21.7 (CH_2); IR (film) ν 1777 (CO) cm^{-1}. Anal. Calcd for $C_{19}H_{19}NO$: C, 82.27; H, 6.90; N, 5.05. Found: C, 74.03; H, 7.04; N, 3.98. Data for the [4 + 2] adduct **12f'**: white solid, mp 78−79 °C; ^{1}H-NMR δ 7.31−7.19 (m, 4H, Ph), 7.11−7.05 (m, 1H, Ph), 6.63 (t, 2H, pyrrole), 6.29−6.14 (m, 4H, pyrrole + 2 =CH), 4.99 (m, 1H, CH), 2.91 (t, 1H, J = 6.8 Hz, CH), 1.82−1.53 (m, 6H); ^{13}C-NMR δ 156.6, 137.5 (ipso), 129.2, 129.2, 127.8, 125.9, 125.6 (Ph + 2 =CH), 123.7 (pyrrole), 112.9, 108.3 (pyrrole), 75.3 (CH), 35.0 (CH), 28.9 (CH_2), 28.8 (CH_2), 19.9 (CH_2); IR (film) ν 1627 cm^{-1}. High-resolution mass measurement (EI) calcd for $C_{19}H_{19}NO$: 277.1467. Found: 277.1474±0.0010.

Procedure for Hydrogenation of Cyclobutanone 12d. A pressure tube was sealed with a rubber septum, flame dried, evacuated, and filled with Ar. To the tube was added 10% Pd/C (27 mg), followed by a solution of cyclobutanone **12d** (0.103 g, 0.41 mmol) in EtOAc (5 mL). The tube was equipped with a pressure head and charged with H_2 (3 cycles to 45 psi). The reaction mixture was stirred for 30 min; H_2 was released, and the mixture was filtered through a bed of Celite. The filtrate was concentrated under reduced pressure to give the reduced cyclobutanone. This crude product was further purified by radial chromatography (2 mm plate; hexane/AcOEt, 50/1 and 95/5) to give 91.5 mg (0.36 mmol, 88% yield) of compound **13d** as a white solid. An analytical sample was recrystallized from hexane/CH_2Cl_2: mp 112−113 °C; ^{1}H-NMR δ 7.29 (m, 5H, Ph), 6.85 (t, J = 2.2 Hz, 2H, pyrrole), 6.18 (t, 2H, J = 2.2 Hz, pyrrole), 3.95 (dd, 1H, J = 8.2, 8.1 Hz), 3.72 (ddd, 1H, J = 8.6, 8.2, 1.6 Hz), 2.20 (m, 1H), 2.03−1.59 (m, 4H), 1.38−1.25 (m, 1H); ^{13}C-NMR δ 208.6 (CO), 136.0 (ipso), 128.4 (ipso), 128.0, 126.6 (Ph), 119.0 (pyrrole), 109.1 (pyrrole), 83.3 (Ph*C*N), 62.7 (CH), 43.1 (CH), 29.6 (CH_2), 29.3 (CH_2), 26.3 (CH_2); IR (film) ν 1772 (CO) cm^{-1}. Anal. Calcd for $C_{17}H_{17}NO$: C, 81.24; H, 6.82; N, 5.57. Found: C, 81.14; H, 6.76; N, 5.62.

General Procedure for the Ozonolysis of Cyclobutanones. Cyclobutanones **12a** and **13d** were ozonized following the same procedure described for cyclopropanes **3**. ^{1}H-NMR spectra of the crude reaction products for these reactions revealed that the α-formamidocyclobutanones existed in two conformeric structures (~95/5). The crude products were quite clean and could be used in the next step without purification. However, for characterization purposes, the compounds were chromatographed on silica or purified by radial chromatography, and the major conformers were isolated and characterized.

Synthesis of Compound 14a. Ozonolysis of compound **12a** (138 mg, 0.52 mmol) in CH_2Cl_2 (22 mL) followed by treatment with thiourea (40 mg, 0.52 mmol) in MeOH (3 mL) and workup as described above gave 111 mg (0.45 mmol, 88% yield) of pure α-formamidocyclobutanone as a mixture of two conformers (~95/5). Data for the major conformer after purification by radial chromatography (hexane/AcOEt, 4/1 and 1/1): white solid, mp 133−134 °C; ^{1}H-NMR δ 8.85 (s, 2H), 7.65, 7.35 (m, 5H, Ph), 4.95 (d, 1H, J = 6.5 Hz), 3.78 (m, 1H), 3.65 (m, 1H), 3.30 (m, 1H), 2.18 (m, 1H), 1.8−1.5 (m, 3H), 1.40 (m, 1H); ^{13}C-NMR δ 162.8 (CO, NHCHO), 132.4 (ipso), 129.5, 128.5, 127.9 (Ph), 81.8 (Ph*C*N), 68.9 (CH), 64.9 (CH_2), 54.8 (CH), 20.6 (CH_2), 18.1 (CH_2). IR (film) ν 1780 (CO), 1679 (NHCHO) cm^{-1}. MS (EI) *m/z* 245 (M^+, 16%), 216 (M^+ − HCO, 7%), 104 (PhCNH, 100%).

Synthesis of Compound 14d. Ozonolysis of compound **13d** (52 mg, 0.21 mmol) in CH_2Cl_2 (7 mL) followed by treatment with thiourea (18 mg, 0.24 mmol) in MeOH (1.5 mL) and workup of the reaction as described above gave 34 mg (0.15 mmol, 72% crude yield) of compound **14d** as an oil (92:8), which was chromatographed on silica (hexane/AcOEt, 1/1) to give 31 mg (0.14 mmol, 66% yield) of a white solid. An analytical sample was recrystallized from hexane/CH_2Cl_2. Data for the major conformer: mp 92−93 °C: ^{1}H-NMR δ 9.0 (bs, 2H, NHCHO), 7.52−7.20 (m, 5H, Ph), 3.98 (ddd, 1H, J = 9.4, 9.3, 2.2 Hz), 3.78 (m, 1H), 2.12−1.92 (m, 2H), 1.78−1.52 (m, 3H), 1.25 (m, 1H); ^{13}C-NMR δ 163.1 (CO, NHCHO), 134.7 (ipso), 128.6, 128.3 (Ph), 80.5 (Ph*C*NHCHO), 63.1 (CH), 41.5 (CH), 30.2 (CH_2), 28.3 (CH_2), 26.9 (CH_2); IR (film) ν 1774 (CO), 1681 (NHCHO) cm^{-1}. MS (EI) *m/z* 229 (M^+, 9%), 200 (M^+ − HCO, 100%). High-resolution mass measurement (EI) calcd for $C_{14}H_{15}NO_2$: 229.1103. Found: 229.1103.

General Procedure for the Hydrolysis of α-Formamidocyclobutanones.[14] The formamido group in α-formamidocyclobutanones was hydrolyzed by heating at reflux temperature a solution of the compound in HCl/MeOH (0.5−1 N) for 1−2.5 h. After cooling to room temperature, the solvent was evaporated under reduced pressure and the residue was diluted with water and four drops of concentrated hydrochloric acid. The solution was washed with CH_2Cl_2, and the aqueous layer was basified with NaOH (3 N aqueous solution) until pH 10−11 and extracted with CH_2Cl_2 (×2). The organic layer was washed with 5% $NaHCO_3$ aqueous solution (×2), water, and brine (×2), dried over $MgSO_4$, and concentrated on a rotary evaporator to give pure α-aminocyclobutanones.

Synthesis of Compound 15a. α-Formamidocyclobutanone **14a** (60 mg, 0.25 mmol) was dissolved in 15 mL of 1 N HCl/MeOH, and the solution was heated at reflux temperature for 1 h. Evaporation of the solvents and treatment of the residue according to the general procedure afforded 34 mg (0.16 mmol, 61% yield) of pure α-aminocyclobutanone **15a** as a colorless oil. This material was filtered through a small plug of silica before characterization: R_f = 0.29 (hexane/EtOAc, 1/2); ^{1}H-NMR (500 MHz, $CDCl_3$) δ 7.50−7.46 (m, 2H, Ph), 7.37−7.25 (m, 3H, Ph), 4.25 (d, 2H, J = 5.9 Hz, CH(O)), 3.88 (ddd, 1H, J = 7.9, 5.9, 2.0 Hz CH(CO)), 3.70 (d, 1H, J = 11.4 Hz, H-3), 3.25 (ddd, 1H, J = 11.2, 8.6, 2.6 Hz, H-3'), 2.14 (m, 1H, H-5), 1.90 (s, 2H, NH_2), 1.67−1.75 (m, 1H, H-5'), 1.57−1.24 (m, 2H, H4, 4'); ^{13}C-NMR δ 209.6 (CO), 138.6 (ipso), 128.0, 127.4, 127.0 (Ph), 79.4 (Ph*C*N), 73.1 (HCO), 64.7 (CH_2(O)), 53.5 (CH), 21.9 (CH_2), 18.6 (CH_2); IR (film) ν 3372, 3310 (NH_2), 1776 (CO) cm^{-1}. This material was used without further purification.

Synthesis of Compound 15d. α-Formamidocyclobutanone **14d** (55 mg, 0.24 mmol) was dissolved in 10 mL of 0.5 N HCl/MeOH, and the solution was heated at reflux temperature for 2.5 h. Evaporation of the solvents and treatment of the residue according to the general procedure afforded 29 mg

(0.14 mmol, 60% yield) of pure α-aminocyclobutanone **15d** as a colorless oil that became a white solid upon refrigeration overnight: mp 36–37 °C; ^{1}H-NMR δ 7.38–7.22 (m, 5H, Ph), 3.84 (t, 1H, J = 8.3 Hz), 2.80 (dd, 1H, J = 7.9, 6.7 Hz), 2.08 (dd, 1H, J = 12.9, 7.3 Hz), 2.00 (bs, 2H, NH_2), 1.69–1.45 (m, 4H), 1.22–1.07 (m, 1H); ^{13}C-NMR δ 216.8 (CO), 138.6 (ipso), 128.2, 127.5, 126.8 (Ph), 78.0 (Ph*C*N), 60.9 (CH), 46.6 (CH), 29.6 (CH_2), 29.5 (CH_2), 26.0 (CH_2); IR (film) ν 3360 (NH_2), 3290 (NH_2), 1766 (CO) cm^{-1}. This was used without further purification.

Preparation of α-(*tert*-Butoxycarbonylamino)cyclobutanone 16a. α-Aminocyclobutanone **15a** (11 mg, 0.05 mmol) was dissolved in *t*-BuOH (10 mL) under Ar, and di-*tert*-butyl dicarbonate (34 mg, 0.16 mmol) and Et_3N (22 μL, 0.16 mmol) were added to the solution. The reaction mixture was heated at 60 °C for 8.5 h. After removal of the solvent on a rotary evaporator, the residue was purified by flash chromatography on silica (hex/AcOEt, 1/1) followed by radial chromatography (hex/AcOEt, 95/5 and 9/1) to afford 6 mg (0.02 mmol, 38% yield) of compound **16a** as a white solid: mp 120–121 °C; ^{1}H-NMR δ 7.68 (s, 1H), 7.27 (m, 5H, Ph), 5.95 (bd, 1H, J = 7.5 Hz), 5.71 (d, 1H, J = 7.7 Hz), 4.00 (m, 2H), 2.28 (dt, 1H, J = 16.8, 6.4 Hz), 2.13 (dt, 1H, J = 16.8, 6.4 Hz), 1.79 (m, 2H), 1.38 (s, 9H), 1.23 (bs, 1H); ^{13}C-NMR δ 194.3 (CO), 158.8 (CH), 154.9 ($NHCO_2$), 138.8 (ipso), 128.9, 127.9, 127.5 (Ph), 114.0 (Ph*C*N), 79.6 (*C*(CH_3)), 67.1 (CH_2), 58.0 (CH), 28.2 (CH_3), 20.7 (CH_2), 18.3 (CH_2); IR (film) ν 3421, 3364 (NH), 1711 (CO), 1656, 1616 ($NHCO_2$) cm^{-1}. Anal. Calcd for $C_{18}H_{23}NO_4$: C, 68.11; H, 7.30; N, 4.41. Found: C, 67.93; H, 7.49; N, 4.13.

Preparation of α-(*tert*-Butoxycarbonylamino)cyclobutanone 16d. α-Aminocyclobutanone **15d** (28 mg, 0.14 mmol) was dissolved in *t*-BuOH (10 mL) under Ar, and di-*tert*-butyl dicarbonate (67 mg, 0.31 mmol) and Et_3N (43 μL, 0.31 mmol) were added to the solution. The reaction mixture was stirred at room temperature for 48 h and at 60 °C for 6 h. After removal of the solvents on a rotary evaporator, the residue was purified by flash chromatography on silica (hexane/AcOEt, 1/1) followed by radial chromatography (hexane/AcOEt, 95/5 and 9/1) to afford 31 mg (0.10 mmol, 73% yield) of compound **16d** as a colorless oil, which became a white solid upon refrigeration: mp 58–59 °C; ^{1}H-NMR δ 7.33–7.27 (m, 5H, Ph), 4.93 (bs, 1H, NH), 3.97 (t, 1H, J = 8.9 Hz), 3.45 (bs, 1H), 1.97 (dd, 1H, J = 13.3, 7.4 Hz), 1.68–1.44 (m, 3H), 1.36 (s, 10H, ^{t}Bu + CH), 0.94–0.83 (m, 1H); ^{13}C-NMR δ 154.1 (CO, $NHCO_2$), 136.1 (ipso), 128.6, 128.1, 127.1 (Ph), 80.3, 78.3, 62.4 (CH), 45.7 (CH), 29.9 (CH_2), 28.7 (CH_2), 28.1 (CH_3), 26.4 (CH_2); IR (film) ν 3348, 3262 (NH), 1778 (CO), 1694 ($NHCO_2$) cm^{-1}. Anal. Calcd for $C_{18}H_{23}NO_3$: C, 71.73; H, 7.69; N, 4.65. Found: C, 71.59; H, 7.63; N, 4.61.

General Procedure for the Synthesis of β-Lactams 17. An Ace pressure tube was sealed with a rubber septum, flame dried, evacuated, and filled with Ar. Carbene **2a** was added into the tube, followed by dry degassed acetonitrile (10–15 mL) and 0.9–1.1 equiv of the corresponding imine to produce a deep brown solution. Glass beads were added to the solution, and the tube was sealed with a pressure cap and irradiated (450 W Conrad-Hanovia 7825 medium-pressure Hg lamp, Pyrex well) until the brown solution turned bright yellow (9–15 h), which indicated complete consumption of the carbene. The yellow solution was filtered through Celite and concentrated under reduced pressure to give a solid residue, which was taken up in EtOAc. Air was bubbled into the solution, and the resulting suspension was filtered through Celite. The yellow filtrate was diluted 1:1 by volume with hexane and air oxidized either on the rooftop in sunlight or in a light box (6 × 20 W Vitalite fluorescent bulbs). After 2–3 h, the resulting brown suspension was filtered through Celite and the filtrate was air oxidized again. These operations were successively repeated until a clear colorless solution was obtained (12–36 h). Solvent removal on a rotary evaporator gave the crude β-lactam that was purified by column or radial chromatography.

Synthesis of β-Lactam 17a. Pentacarbonyl[(phenyl)(pyrrol-1-yl)carbene]chromium(0) **2a** (0.215 g, 0.62 mmol) and methyl *N*-benzylformimidate (89 mg, 0.60 mmol) were photolyzed in CH_3CN (14 mL) for 9 h according to the general procedure. Air oxidation of the reaction mixture as described above gave a crude product, which was purified by flash chromatography (hexane/AcOEt, 4/1) to afford 102 mg of β-lactam **17a** (0.31 mmol, 51% yield) in a 98:2 ratio of diastereomers as a white solid: mp 110–111 °C; ^{1}H-NMR δ 7.37–7.23 (m, 8H, Ph), 7.07–7.03 (m, 2H, Ph), 6.90 (t, 2H, J = 2.2 Hz, pyrrole), 6.27 (t, 2H, J = 2.2 Hz, pyrrole), 5.09 (s, 1H), 4.78 (d, 2H, J = 15.1 Hz, CH_2Ph), 4.33 (d, 2H, J = 15.1 Hz, CH_2Ph), 3.11 (s, 3H, OCH_3); ^{13}C-NMR δ 164.1 (C=O), 134.4 (ipso), 133.9 (ipso), 128.9, 128.5, 128.2, 128.1, 127.9, 126.9 (2Ph), 120.2, 109.2 (pyrrole), 91.1 (HC(OMe)), 80.1 (PhCN), 56.1 (OCH_3), 44.3 (CH_2); IR (film) ν 1772 cm^{-1}. Anal. Calcd for $C_{21}H_{20}N_2O_2$: C, 75.88; H, 6.06; N, 8.42. Found: C, 76.03; H, 5.89; N, 8.30.

Synthesis of β-Lactam 17b. Pentacarbonyl[(phenyl)(pyrrol-1-yl)carbene]chromium(0) **2a** (0.243 g, 0.70 mmol) and *N*-methylbenzaldimine (91 mg, 0.77 mmol) were photolyzed in CH_3CN (13 mL) for 14 h according to the general procedure. Air oxidation of the reaction mixture as described above gave a crude product, which was purified by radial chromatography (2 mm plate; hexane/AcOEt, 95/5 and 9/1) to afford 103 mg (0.34 mmol, 49% yield) of β-lactam **17b** in a 72:27 ratio of diastereomers as a white solid: mp 109–110 °C; ^{1}H-NMR δ 7.46–7.03 (m, 10H, Ph), 7.02 (b), 6.48 (a) (t, 2H, pyrrole), 6.24 (b), 5.85 (a) (t, 2H, pyrrole), 5.31 (b), 5.30 (a) (s, 1H), 2.92 (b), 2.91 (a) (s, 3H, CH_3). ^{13}C-NMR δ 166.0 (CO), 165.6 (CO), 137.4 (ipso), 134.1 (ipso), 133.2 (ipso), 133.0 (ipso), 128.8, 128.5, 128.4, 128.3, 128.0, 127.8, 127.6, 127.4, 126.9, 126.5 (Ph), 119.8 (pyrrole), 119.6 (pyrrole), 109.0 (pyrrole), 108.1 (pyrrole), 81.1 (Ph*C*N), 80.4 (Ph*C*N), 69.9 (CH), 69.0 (CH), 27.1 (CH_3), 26.9 (CH_3); IR (film) ν 1760 (CO) cm^{-1}. Anal. Calcd for $C_{20}H_{18}N_2O$: C, 79.44; H, 5.99; N, 9.26. Found: C, 77.80; H, 5.89; N, 9.16.

Ozonolysis of β-Lactams. β-Lactams **17a** and **17b** were ozonized following the same procedure described for cyclopropanes **3**. As in the case of cyclobutanones, the α-formamido-β-lactams were obtained in two rotameric forms (~95:5 ratio) and the crude reaction materials could be used in the next step without further purification; however, in some reactions these crude products were purified by chromatography prior to characterization.

Synthesis of Compound 18a. Ozonolysis of compound **15a** (67 mg, 0.20 mmol) in CH_2Cl_2 (8 mL) followed by treatment with thiourea (15 mg, 0.2 mmol) in MeOH (2 mL) and workup of the reaction as described above gave 54 mg (0.17 mmol, 86% yield) of α-formamido-β-lactam **18a** as a mixture of two rotamers (91:9 ratio). Data for the major conformer after separation by column chromatography (hexane/AcOEt, 1/1): R_f = 0.56 (hexane/EtOAc, 1/1); ^{1}H-NMR δ 9.33 (bs, 2H, NHCHO), 7.41–7.25 (m, 10H, Ph), 5.16 (s, 1H), 4.76 (d, 1H, J = 14.9 Hz, CH_2), 4.25 (d, 1H, J = 14.9 Hz, CH_2), 3.28 (s, 3H, OCH_3); ^{13}C-NMR δ 162.4 (NCO, NHCHO), 133.8 (ipso), 133.2, 129.0, 128.9, 128.5, 128.4, 128.2, 127.3 (Ph), 87.7 (CH), 76.4 (Ph*C*NHCHO), 57.3 (OCH_3), 44.1 (CH_2); IR (film) ν 1768, 1734, 1699 cm^{-1}. High-resolution mass measurement (FAB, M + 1) calcd for $C_{18}H_{19}N_2O_3$: 311.1396. Found: 311.1398±0.0010.

Synthesis of Compound 18b. Ozonolysis of compound **17b** (97 mg, 0.32 mmol) in CH_2Cl_2 (10 mL) followed by treatment with thiourea (27 mg, 0.35 mmol) in MeOH (3 mL) and workup of the reaction as described above gave 57 mg (0.20 mmol, 63% yield) of α-formamido-β-lactam **18b** as a mixture of two diastereoisomers (79:21 ratio) and in two rotamers (91/9). During purification by radial chromatography the two rotamers underwent interconversion, and the initially minor product was isolated as the major product (2:1 ratio of a/b) (2 mm plate; hexane/AcOEt, 4/1, 1/1, and 1/2): mp 108–109 °C (hex/CH_2Cl_2); ^{1}H-NMR (300 MHz, $CDCl_3$) δ 8.08 (a), 7.70 (b) (d, 1H, J = 11.9 Hz, HCO), 7.64–7.26 (m, 10H, Ph), 6.31

(b) (s, 1H, NH), 5.77 (a) (d, 1H, NH), 5.13 (b), 4.86 (a) (s, 1H, CH), 2.95 (a), 2.89 (b) (s, 3H, CH_3); ^{13}C-NMR δ 166.3 (NCO), 165.9 (NCO), 163.3 (NHCHO), 159.2 (NHCHO), 137.6 (ipso), 136.6 (ipso), 133.2 (ipso), 132.1 (ipso), 129.7, 129.6, 129.3, 128.9, 128.7, 128.7, 128.4, 128.1, 127.3, 126.6, 126.2 (Ph), 74.3 (Ph*C*N), 73.8 (Ph*C*N), 70.3 (CH), 69.4 (CH), 27.1 (CH_3), 27.0 (CH_3); IR (film) ν 3263 (NH), 1759 (NCO), 1693 (NHCHO) cm^{-1}. High-resolution mass measurement (FAB M + 1) calcd for $C_{17}H_{17}N_2O_2$: 281.1290. Found: 281.1291±0.0006.

Preparation of α-Amino-β-lactam 19a. α-Formamido-β-lactam **18a** (70 mg, 0.23 mmol) was dissolved in MeOH (3 mL) under Ar, and the solution was cooled to 0 °C. PBr_3 (70 μL, 0.74 mmol) was added dropwise via syringe, and the reaction mixture was stirred for 40 min at 0 °C and for 3.5 h at room temperature. Elimination of the solvent on a rotary evaporator gave a residue, which was taken up in THF (3 mL). Et_3N (0.18 mL, 1.29 mmol) was added to the solution at 0 °C, and a white solid was immediately produced. After stirring the reaction mixture for an additional 1 h, the solid was filtered through Celite and the filtrate was concentrated under reduced pressure. The crude material was purified by column chromatography (hexane/AcOEt, 1/4) to give 29 mg (0.10 mmol, 45% yield) of α-amino-β-lactam **19a** as a colorless oil, which became a white solid upon refrigeration: mp 46–47 °C; ^{1}H-NMR δ 7.52 (m, 2H, Ph), 7.38–7.26 (m, 8H, Ph), 4.76 (d, 1H, J = 15.0 Hz, CH_2), 4.51 (s, 1H), 4.22 (d, 1H, J = 15.0 Hz, CH_2), 3.04 (s, 3H, OCH_3), 1.89 (bs, 2H, NH_2); ^{13}C-NMR δ 170.4 (CO), 135.7 (ipso), 135.2 (ipso), 128.8, 128.2, 128.1, 127.8, 127.0 (Ph), 93.6 (CH), 76.3 (Ph*C*N), 56.2 (OCH_3), 44.1 (CH_2); IR (film) ν 3363 (NH_2), 3299 (NH_2), 1755 (CO) cm^{-1}. MS (EI) *m/z* 282 (M^+, 2%), 150 (M^+ − $PhCH_2NCO$, 100%), 134 (M^+ − methyl *N*-benzylformimidate, 42%). High-resolution mass measurement calcd for $C_{17}H_{18}N_2O_2$: 282.1368. Found: 282.1359±0.000 66 (n = 7).

Acknowledgment. Support for this research by National Science Foundation Grant CHE-9224489 is gratefully acknowledged. Mass spectra were obtained on instruments supported by the National Institutes of Health shared instrumentation grant GM49631. I.M. would like to thank the Ministerio de Educación y Ciencia of Spain for a postdoctoral fellowship.

OM940979V

Generation of (μ-Ethynediyl)(methylalkoxycarbene)diplatinum Complexes from Reaction of *cis,trans*-[(OC)(C_6F_5)$_2$Pt(μ-η^2-C≡CSiMe$_3$)Pt(C≡CSiMe$_3$)L$_2$] with ROH (R = Et, Me)

Jesús R. Berenguer,[†] Juan Forniés,*[,‡] Elena Lalinde,*[,†] and Francisco Martínez[‡]

Departamento de Química, Universidad de la Rioja, 26001 Logroño, Spain, and Departamento de Química Inorgánica, Instituto de Ciencia de Materiales de Aragón, Universidad de Zaragoza, Consejo Superior de Investigaciones Científicas, 50009 Zaragoza, Spain

Received December 5, 1994[⊗]

Reaction of *cis*-[Pt(C_6F_5)$_2$(CO)(THF)] with *trans*-[Pt(C≡CSiMe$_3$)$_2$L$_2$], followed by reaction of the neutral μ-η^2-monoacetylide-bridged diplatinum intermediates *cis,trans*-[(OC)(C_6F_5)$_2$-Pt(μ-η^2-C≡CSiMe$_3$)Pt(C×ba≡CSiMe$_3$)L$_2$] (L = PPh$_3$ (**1**), PEt$_3$ (**2**)) with alcohols (EtOH, MeOH) yields the (μ-ethynediyl)(methylalkoxycarbene)diplatinum species *cis,trans*-[(OC)(C_6F_5)$_2$-Pt–C≡C–Pt{C(Me)OR}L$_2$] (L = PPh$_3$, R = Et (**3a**), Me (**3b**); L = PEt$_3$, R = Et (**4a**), Me (**4b**)), resulting from unexpected rearrangement chemistry involving bridging and terminal (trimethylsilyl)acetylide ligands. The X-ray molecular structure of the complex *cis,trans*-[(OC)(C_6F_5)$_2$Pt–C≡C–Pt{C(Me)OEt}(PEt$_3$)$_2$] (**4a**) has been determined. It crystallizes in the monoclinic system, space group $P2_1/c$ with a = 15.216(3) Å, b = 14.197(4) Å, c = 18.167(5) Å, β = 107.99(2)°, V = 3733(2) Å^3,, and Z = 4. The two coordination planes around the platinum atoms adopt an almost eclipsed arrangement (dihedral angle 6.7°) rather than the staggered form found in similar diplatinum complexes.

Introduction

There is considerable current interest in bimetallic complexes either bridged or connected by an organic group due to their possibly unique role in catalytic processes.[1] Particularly interesting are the ethynediyl connected complexes [L$_n$M–C≡C–M′L$_n$′], which comprise a relatively small but rapidly expanding group of compounds due not only to their potential catalytic activity but also to their role in new areas of electronic and material science.[2] In general, these types of complexes have been prepared:[2a,2b] (i) from metal halides or alkyl complexes and alkali-metal acetylides or alkyne complexes having acidic protons, (ii) from metal alkyls and acetylene, (iii) from dihaloacetylene and carbonylmetalate ions, and (iv) from lithiated metal alkynes and metal halides. Recently, it has been shown that cationic complexes containing μ-η^2-C≡CH bridges can also be easily deprotonated, yielding μ-ethynediyl compounds[2b,e,i,g,j] (eq. 1).

$$L_nM{-}C{\equiv}CH \underset{H^+}{\overset{\text{base}}{\rightleftharpoons}} L_nM{-}C{\equiv}C{-}M'L_n \qquad (1)$$
$$\downarrow$$
$$M'L_n$$

Here we wish to report that compounds with two different organometallic platinum fragments linked by a C_2 group can also be prepared from neutral complexes containing a μ-η^2-C≡CSiMe$_3$ bridging ligand.[3]

Results and Discussion

As part of our current research on polynuclear platinum complexes with bridging acetylide groups,[4] we recently reported the synthesis of the unusual zwitterionic complexes [(OC)(C_6F_5)$_2$Pt$^-$(μ-η^2-C≡CR)M$^+$L$_n$] by reacting *cis*-[Pt(C_6F_5)$_2$(CO)(THF)] with several metal

[†] Universidad de la Rioja.
[‡] Universidad de Zaragoza.
[⊗] Abstract published in *Advance ACS Abstracts,* April 1, 1995.

(1) For reviews of organometallic hydrocarbon-bridged complexes see: (a) Casey, C. P.; Audett, J. D. *Chem. Rev.* **1986,** *86,* 339. (b) Holton, J.; Lappert, M. F.; Pearce, R.; Yarrow, P. I. W. *Chem. Rev.* **1983,** *83,* 135. (c) Moss, J. R.; Scott, L. G. *Coord. Chem. Rev.* **1984,** *60,* 171.

(2) (a) Lang, H. *Angew. Chem., Int. Ed. Engl.* **1994,** *33,* 547. (b) Beck, W.; Niemer, B.; Wieser, M. *Angew. Chem., Int. Ed. Engl.* **1993,** *32,* 923 and references given therein. (c) Sünkel, K.; Birk, U.; Robl, C. *Organometallics* **1994,** *13,* 1679. (d) Koutsantonis, G. A.; Selegue, J. P. *J. Am. Chem. Soc.* **1991,** *113,* 2316. (e) Frank, K. G.; Selegue, J. P. *J. Am. Chem. Soc.* **1990,** *112,* 6414. (f) Davies, J. A.; El-Ghanam, M.; Pinkerton, A. A.; Smith, D. A. *J. Organomet. Chem.* **1991,** *409,* 367. (g) Akita, M.; Terada, M.; Oyama, S.; Moro-Oka, Y. *Organometallics* **1990,** *9,* 816; **1991,** *10,* 1561. (h) St. Clair, M.; Schaefer, W. P.; Bercaw, J. E. *Organometallics* **1991,** *10,* 525. (i) Appel, M.; Heidrich, J.; Beck, W. *Chem. Ber.* **1987,** *120,* 1087. Heidrich, J.; Steimann, M.; Appel, M.; Beck, W.; Phillips, J. R.; Trogler, W. C. *Organometallics* **1990,** *9,* 1296. (j) Beck, W.; Niemer, B.; Breimair, J.; Heidrich, J. *J. Organomet. Chem.* **1989,** *372,* 79. (k) Ogawa, H.; Joh, T.; Takahashi, S.; Sonogashira, K. *J. Chem. Soc., Chem. Commun.* **1985,** 1220. (l) Ogawa, H.; Onitsuka, K.; Joh, T.; Takahashi, S.; Yamamoto, Y.; Yamazaki, H. *Organometallics* **1988,** *7,* 2257. (m) Ramsden, J. A.; Weng, W.; Arif, A. M.; Gladysz, J. A. *J. Am. Chem. Soc.* **1992,** *114,* 5890; *Organometallics* **1992,** *11,* 3635. (n) Onitsuka, K.; Joh, T.; Takahashi, S. *Bull. Chem. Soc. Jpn.* **1992,** *65,* 1179. (o) Nast, R.; Schneller, P.; Hengefeld, A. *J. Organomet. Chem.* **1981,** *214,* 273. (p) Cross, R. J.; Davidson, M. F. *J. Chem. Soc., Dalton Trans.* **1986,** 411.

(3) The complex [Cp′$_2$Ti(μ-η^2-C≡CSiM$_3$)(σ:σ-C≡C)Cu]$_2$ is reported as the product of the reaction of [Cp′$_2$Ti(C≡CSiMe$_3$)$_2$] with [Cu(C≡CSiMe$_3$)]$_n$ in ref 14 in: Lang, H. *Angew. Chem., Int. Ed. Engl.* **1994,** *33,* 547. However, the reference given is an unpublished work.

(4) (a) Forniés, J.; Gómez-Saso, M. A.; Lalinde, E.; Martínez, F.; Moreno, M. T. *Organometallics* **1992,** *11,* 2873. (b) Berenguer, J. R.; Falvello, L. R.; Forniés, J.; Lalinde, E.; Tomás, M. *Organometallics* **1993,** *13,* 6. (c) Berenguer, J. R.; Forniés, J.; Martínez, F.; Cubero, J. C.; Lalinde, E.; Moreno, M. T.; Welch, A. J. *Polyhedron* **1993,** *12,* 1797. (d) Forniés, J.; Lalinde, E.; Martín, A.; Moreno, M. T. *J. Chem. Soc., Dalton Trans.* **1994,** 135. (e) Berenguer, J. R.; Forniés, J.; Lalinde, E.; Martínez, F.; Urriolabeitia, E.; Welch, A. J. *J. Chem. Soc., Dalton Trans.* **1994,** 1291.

0276-7333/95/2314-2532$09.00/0

Scheme 1[a]

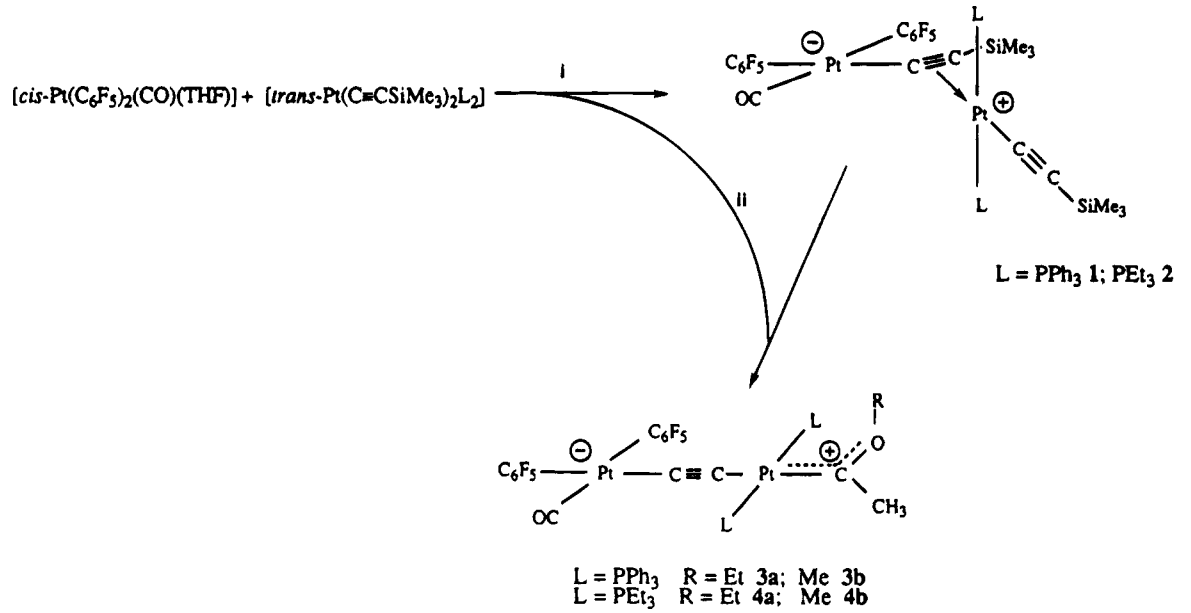

[a] Legend: (i) CH_2Cl_2, 1 h; (ii) CH_2Cl_2, 1 h; treatment with ROH (R = Me, Et; 1 h, L = PPh_3; 48 h, L = PEt_3).

alkynyl complexes $L_nMC{\equiv}CR$.[4e] These species arise from an unexpected alkynylation of the fragment "*cis*-$Pt(C_6F_5)_2(CO)$", probably brought about by the enhanced acidity of the metal center in *cis*-$[Pt(C_6F_5)_2(CO)(THF)]$.[4e] However, analogous reactions with the silylacetylide complexes rendered very soluble derivatives, which required a very long workup for crystallizing, and some other reactions, which were not explored at that moment, took place depending on the crystallizing solvents. In this paper we report on such processes which render the *cis,trans*-$[(OC)(C_6F_5)_2Pt(\mu\text{-}\eta^2\text{-}C{\equiv}CSiMe_3)Pt(C{\equiv}CSiMe_3)L_2]$ (L = PPh_3 (**1**), PEt_3 (**2**)) zwitterionic complexes and upon reaction of these species with alcohols (EtOH or MeOH), which give in moderate yield (μ-ethynediyl)(methylalkoxycarbene)diplatinum complexes (Scheme 1).

Reaction of *trans*-$[Pt(C{\equiv}CSiMe_3)_2L_2]$ (L = PPh_3, PEt_3) with *cis*-$[Pt(C_6F_5)_2(CO)(THF)]$ in CH_2Cl_2, at room temperature, affords first the expected *cis,trans* zwitterionic complexes **1** (L = PPh_3) and **2** (L = PEt_3), respectively (Scheme 1). Both complexes can be isolated (see Experimental Section) as air-stable microcrystalline white solids in low yields (29%, **1**; 25%, **2**), due to their high solubility in common organic solvents including hexane. Together with **1**, part of the starting material *trans*-$[Pt(C{\equiv}CSiMe_3)_2(PPh_3)_2]$ (25%) is also recovered (see Experimental Section). Both compounds **1** and **2** have been characterized by elemental analysis and IR and ^1H, ^{19}F, and ^{31}P NMR spectroscopic data. Thus, their IR spectra show three intense bands (2098, 2070 and 1928 cm^{-1} for **1** and 2089, 2062, and 1930 cm^{-1} for **2**) which are respectively assigned to the ν(CO) and terminal and bridging ν(C≡C) vibrations .[4e] As in previous observations,[4e] the ν(CO) bands (2098 cm^{-1} for **1** and 2089 cm^{-1} for **2**) are substantially lower in energy than that of *cis*-$[Pt(C_6F_5)_2(CO)(THF)]$ (2124 cm^{-1}), suggesting that the formation of the binuclear derivatives results in an increase of the electron density of the carbonyl platinum center (formal alkynylation of "$Pt(C_6F_5)_2(CO)$") in accord with the proposed structure. In addition, the shift of the terminal ν(C≡C) from 2041 cm^{-1} in *trans*-$[Pt(C{\equiv}CSiMe_3)_2(PPh_3)_2]$ or 2034 cm^{-1} in *trans*-$[Pt(C{\equiv}CSiMe_3)(PEt_3)_2]$ to 2070 cm^{-1} in **1** or 2062 cm^{-1} in **2** is consistent with the expected decrease of the electron density of this platinum center as a consequence of the reaction. Moreover, the $^{31}P\{^1H\}$ NMR spectra of **1** and **2** show a singlet with platinum satellites consistent with the *trans* arrangement of the $[Pt(C{\equiv}CSiMe_3)L_2]$ moiety and their ^{19}F NMR spectra exhibit two sets of three signals (2:1:2) in accord with the *cis* disposition of the C_6F_5 groups in the *cis*-$[Pt(C_6F_5)_2(CO)]$ fragment. Finally, two signals for the $SiMe_3$ protons in the ^1H NMR (δ −0.61 and −0.77 for **1** and δ 0.19 and 0.05 for **2**) support the proposed structure with terminal and bridging $C{\equiv}CSiMe_3$ groups.

When both reactions are monitored in $CDCl_3$ by ^{31}P NMR spectroscopy, it can be detected that the formation of complex **2** is complete in a few minutes (1 or 2 min) and that **2** is the only phosphine-containing compound present in solution. However, when a solution of *cis*-$[Pt(C_6F_5)_2(CO)(THF)]$ is added to a solution of *trans*-$[Pt(C{\equiv}CSiMe_3)_2(PPh_3)_2]$, ^{31}P NMR examination of the reaction mixture shows signals due to **1** and to the starting material *trans*-$[Pt(C{\equiv}CSiMe_3)_2(PPh_3)_2]$ in a ca. 2:1 molar ratio, plus one small signal at δ 17.9 indicating the presence of another product in very low concentration. Although the identity of the intermediate species remains uncertain due to its relatively low concentration, we tentatively suggest that this signal (δ 17.9 ppm) could be attributed to the initial formation of the binuclear acetylene complex *trans,cis*-$[(PPh_3)_2(Me_3SiC{\equiv}C)Pt(\mu\text{-}C{\equiv}CSiMe_3)Pt(C_6F_5)_2(CO)]$, which rearranges to the final complex **1** through an intramolecular $-C{\equiv}CSiMe_3$ migration between the platinum centers. On standing, this minor product disappears but, surprisingly, after ca. 4 h the ratio of **1** and *trans*-$[Pt(C{\equiv}CSiMe_3)_2(PPh_3)_2]$ remains practically unaltered. During our attempts to crystallize **1** with ethanol we observed that a subsequent reaction occurs, leading to the precipitation of a yellow microcrystalline solid. Therefore, we decided to investigate the behavior of the reaction mixtures toward EtOH and MeOH.

Treatment of the reaction mixture containing **2** in CH_2Cl_2 with EtOH and MeOH at room temperature results in the formation of pale yellow solids **4a** and **4b** (see Experimental Section) which according to the

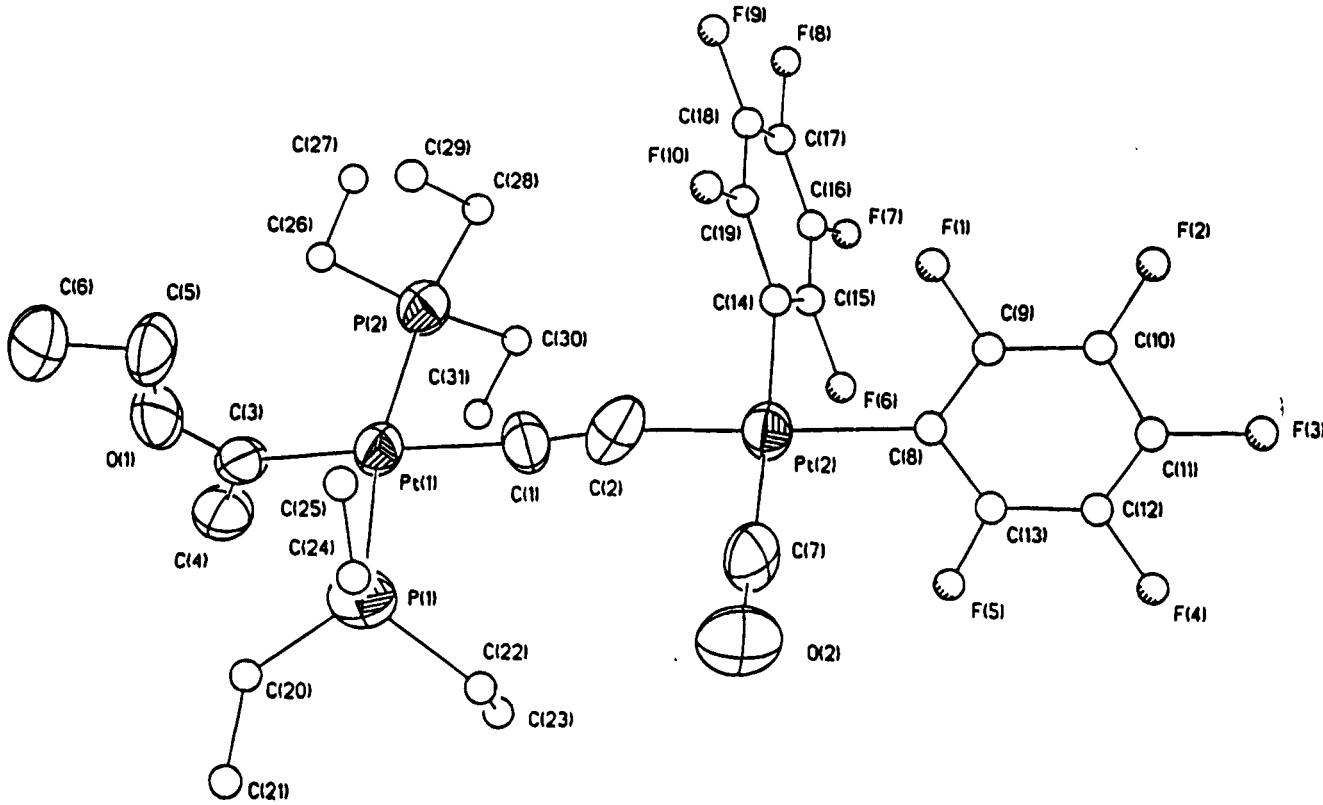

Figure 1. Molecular structure of *cis,trans*-[(OC)$(C_6F_5)_2$Pt−C≡C−Pt{C(Me)OEt}$(PEt_3)_2$] (**4a**).

Table 1. Selected Bond Lengths (Å) and Angles (deg) for Complex 4a

Pt(1)-P(1)	2.30(1)	Pt(1)-P(2)	2.31(1)
Pt(1)-C(1)	2.02(2)	Pt(1)-C(3)	2.00(3)
Pt(2)-C(2)	2.00(2)	Pt(2)-C(7)	1.83(2)
Pt(2)-C(8)	2.09(2)	Pt(2)-C(14)	2.05(2)
P(1)-C(20)	1.82(3)	P(1)-C(22)	1.89(4)
P(1)-C(24)	1.79(5)	P(2)-C(26)	1.88(3)
P(2)-C(28)	1.81(4)	P(2)-C(30)	1.88(3)
O(1)-C(3)	1.31(3)	O(1)-C(5)	1.47(4)
O(2)-C(7)	1.18(3)	C(1)-C(2)	1.22(3)
C(3)-C(4)	1.46(4)	C(5)-C(6)	1.50(4)
P(1)-Pt(1)-P(2)	169.6(3)	P(1)-Pt(1)-C(1)	86.3(6)
P(2)-Pt(1)-C(1)	83.3(6)	P(1)-Pt(1)-C(3)	94.4(6)
P(2)-Pt(1)-C(3)	96.0(6)	C(1)-Pt(1)-C(3)	175.6(11)
C(2)-Pt(2)-C(7)	88.9(10)	C(2)-Pt(2)-C(8)	177.5(9)
C(7)-Pt(2)-C(8)	93.4(10)	C(2)-Pt(2)-C(14)	87.7(8)
C(7)-Pt(2)-C(14)	176.4(10)	C(8)-Pt(2)-C(14)	90.0(8)
Pt(1)-P(1)-C(20)	116.2(9)	Pt(1)-P(1)-C(22)	115.6(13)
C(20)-P(1)-C(22)	107.4(17)	Pt(1)-P(1)-C(24)	113.1(16)
C(20)-P(1)-C(24)	103.4(25)	C(22)-P(1)-C(24)	99.1(26)
Pt(1)-P(2)-C(26)	113.7(9)	Pt(1)-P(2)-C(28)	114.5(10)
C(26)-P(2)-C(28)	108.2(14)	Pt(1)-P(2)-C(30)	109.9(11)
C(26)-P(2)-C(30)	104.1(13)	C(28)-P(2)-C(30)	105.6(15)
C(3)-O(1)-C(5)	120.1(20)	Pt(1)-C(1)-C(2)	174.6(19)
Pt(2)-C(2)-C(1)	171.7(23)	Pt(1)-C(3)-O(1)	127.2(21)
Pt(1)-C(3)-C(4)	124.9(18)	O(1)-C(3)-C(4)	107.7(22)
O(1)-C(5)-C(6)	108.9(25)	Pt(2)-C(7)-O(2)	178.5(17)
Pt(2)-C(8)-C(9)	125.0(19)	Pt(2)-C(8)-C(13)	121.2(21)
Pt(2)-C(14)-C(15)	123.9(21)	Pt(2)-C(14)-C(19)	125.3(16)

elemental analyses correspond apparently to 1:1 adducts of the desilylated starting material and the alcohols. Similar yellow solids were obtained with the reaction mixture containing **1** and *trans*-[Pt(C≡CSiMe_3)$_2$(PPh_3)], but in this case the products (**3a,b**) crystallize with solvent, which is supported by elemental analysis and ^{1}H NMR spectroscopy. The IR and ^{1}H, ^{19}F, and ^{31}P-{^{1}H} NMR spectra of these solids suggest that the complexes obtained from these reactions are the *cis,trans*-(μ-ethynediyl)(methylalkoxycarbene)diplatinum complexes **3** and **4** (Scheme 1).

The IR spectra in Nujol show one strong absorption between 2074 and 2064 cm^{-1} and a medium band between 2030 and 2019 cm^{-1} which can be assigned to the ν(CO) and ν(C≡C) frequencies, respectively. Moreover, the two absorptions observed in the 794−778 cm^{-1} region due to the IR-active vibrations of the x-sensitive modes of the C_6F_5 moiety indicate that both groups are mutually *cis*[5] (this fact is also confirmed by ^{19}F NMR spectroscopy).

The absence of silyl groups and the presence of a methylalkoxycarbene ligand is inferred from the ^{1}H NMR spectra, which do not contain SiMe_3 proton resonances, showing the usual signals attributable to :C(CH_3)OR (R = CH_2CH_3 (**3a**, **4a**), CH_3 (**3b**, **4b**)) ligands (see Experimental Section for data). The ^{31}P{^{1}H} NMR spectra exhibit a singlet with platinum satellites, indicating that the two phosphine ligands are equivalent, the magnitude of ^1J(^{195}Pt−^{31}P) (2357−2669 Hz) being typical of mutually *trans* phosphine groups.[6]

The definitive characterization of **3** and **4** as (μ-ethynediyl)(methylalkoxycarbene)diplatinum compounds came from a single-crystal X-ray diffraction study on complex **4a**. A view of the molecular geometry of this complex is shown in Figure 1. Selected interatomic distances and angles are given in Table 1.

This study confirms the presence of two organometallic moieties "Pt(2)$(C_6F_5)_2$(CO)" and "Pt(1){C(Me)OEt}-$(PEt_3)_2$" connected by the ethynediyl group (−C(1)≡C-(2)−). The most striking feature of this structure is that the two coordination planes around the platinum atoms are almost coplanar (dihedral angle 6.7°). This fact is in contrast with the staggered geometry found in the only two other (μ-ethynediyl)diplatinum complexes struc-

(5) Maslowsky, E., Jr. *Vibrational Spectra of Organometallic Compounds;* Wiley: New York, 1982, p 2449.
(6) Pregosin, P. S.; Kunz, R. W. *^{31}P and ^{13}C NMR of Transition Metal Phosphine Complexes;* Springer-Verlag: New York, 1979.

turally characterized. In the structure of $I(Me_3P)_2Pt-C\equiv C-Pt(PMe_3)_2I$, reported by Takahashi et al. several years ago,[2l] this angle is 89.8(3)°, and in $Cl(PPh_3)_2Pt-C\equiv C-Pt(PPh_3)_2Cl$, recently reported by Sünkel et al.,[2c] this angle is 82°. An ideal eclipsed conformation has been also found in the dinuclear $(OC)_5ReC\equiv CRe(CO)_5$ complex.[2i] The Pt(1)–C(1) (2.02(2) Å), Pt(2)–C(2) (2.00(2) Å), and C(1)–C(2) (1.22(3) Å) bond lengths of the fragment Pt(1)–C(1)≡C(2)–Pt(2) are similar to those found in $XL_2PtC\equiv CPtL_2X$ (X = I, L = PMe_3;[2l] X = Cl, L = PPh_3[2c]) and compare well with those of other μ-ethynediyl complexes.[2b]

The Pt(1)–C(1)–C(2) (174.6(19)°) and C(1)–C(2)–Pt(2) (171.7(23)°) angles indicate, as expected, a nearly linear sp hybridization at C(1) and C(2).

Each of the two moieties also shows the expected structural features. Thus, the Pt(2)–C(pentafluorophenyl) (2.05(2) and 2.09(2) Å) and carbonyl (Pt(2)–C(7) = 1.83(2) Å) distances are similar to those found in *cis,trans*-$[(OC)(C_6F_5)_2Pt(\mu\text{-}C\equiv CPh)Pt(C\equiv CPh)(PPh_3)_2]$[4e] and the Pt(1)–P distances (2.31(1) and 2.30(1) Å) are similar to those found in the related *trans*-Pt(II) phosphine complexes.[2c,l] Finally, the structural data of the carbene group formed are typical of platinum(II)–carbene complexes. Thus, the carbene ligand is oriented essentially perpendicular to the local coordination plane of Pt(1) (the dihedral angle formed by the fragment C(3)C(4)O(1) and the Pt(1) coordination plane is 88.17(2)°), as found in related platinum(II)–carbene complexes.[7] In addition, the Pt–C(carbene) distance (2.00(3) Å) is comparable to distances found in other platinum carbene complexes.[7] The high standard deviations in the C–O bond distances in the carbene group preclude any meaningful comparison between them. As is observed in Figure 1, the ethoxy and methyl substituents are anti to one another with the former bent away from Pt(1).

The formation of complexes **3** and **4** can be rationalized according to the mechanism outlined in Scheme 2.

Taking into account that C–Si bonds can easily be cleaved by proton sources[8] (even with traces of H_2O or alcohol[9]), it seems sensible to assume that the addition of alcohol to **1** or **2** would promote the desilylation of the $\mu\text{-}\eta^2\text{-}C\equiv CSiMe_3$ group as the first step (i), yielding similar derivatives containing $\mu\text{-}\eta^2$-ethynyl bridges (**A**). Then, in analogy to the known reactivity of $\mu\text{-}\eta^2\text{-}C\equiv CH$ dinuclear species toward bases[2b,e,g,i,j,10] and that of terminal acetylide toward acids,[11] the resulting intermediates (**A**) could undergo a sequence of two successive steps, deprotonation (ii)/protonation (iii), yielding the zwitterionic μ-ethynediyl vinylidene species type **C**. Finally, nucleophilic addition of ROH across the vinylidene carbon–carbon double bond, which is a very common process,[11a-c,12] could produce the resulting (μ-ethynediyl)(methylalkoxycarbene)diplatinum complexes **3** and **4**. The desilylation of the terminal $C\equiv CSiMe_3$ ligand could have taken place at some point during the three initial steps. In favor of the mechanism, we have to point out that Chisholm et al. have previously proposed the formation of similar vinylidene cations or carbocations $[Pt-C\equiv CHR]^+ \leftrightarrow [Pt-C^+=CHR]$ as intermediates in the formation of cationic alkoxycarbene complexes by treatment of alkynylplatinum compounds with acids in alcohols.[13]

Experimental Section

All manipulations were carried out under a nitrogen atmosphere. Solvents were dried by standard procedures and distilled under dry N_2 before use. The C, H, and N analyses and IR spectra were obtained as described elsewhere.[4] Proton, ^{13}C, ^{19}F, and ^{31}P NMR spectra were recorded on either a Varian Unity 300 or a Bruker ARX 300 spectrometer. Chemical shifts are reported in ppm relative to external standard ($SiMe_4$, $CFCl_3$, and 85% H_3PO_4). *cis*-$[Pt(C_6F_5)_2(CO)(THF)]$[14] and *trans*-$[Pt(C\equiv CSiMe_3)_2(PPh_3)_2]$[4c] were prepared according to literature procedures. *trans*-$[Pt(C\equiv CSiMe_3)_2(PEt_3)_2]$[15] was prepared by reacting *cis*-$[PtCl_2(PEt_3)_2]$ with $LiC\equiv CSiMe_3$.

***cis,trans*-[(OC)(C$_6$F$_5$)$_2$Pt(μ-C≡CSiMe$_3$)Pt(C≡CSiMe$_3$)(PPh$_3$)$_2$] (1).** To a solution of *trans*-$[Pt(C\equiv CSiMe_3)_2(PPh_3)_2]$ (0.16 g, 0.17 mmol) in CH_2Cl_2 (15 mL) was added *cis*-$[Pt(C_6F_5)_2(CO)(THF)]$ (0.107 g, 0.17 mmol), and the mixture was stirred at room temperature for 2 h. Evaporation of the resulting yellow solution to dryness and addition of Et_2O (10 mL) cause the precipitation of a white solid, which was identified by IR spectroscopy as the starting material *trans*-$[Pt(C\equiv CSiMe_3)_2(PPh_3)_2]$ (25% yield).

The resulting filtrate was evaporated to dryness, and after addition of *n*-hexane (4 cm^3), compound **1** was obtained as a white solid, yield 29%. Anal. Calcd for $C_{59}F_{10}H_{48}OP_2Pt_2Si_2$: C, 48.16; H, 3.29. Found: C, 47.96; H, 3.38. IR (cm^{-1}): ν(CO) 2098 (s); ν(C≡C) 2070 (s), 1928 (s); $\nu(C_6F_5)_{x\text{-sens}}$ 800(s), 787 (s).[5] ^1H NMR (δ; $CDCl_3$): 7.72, 7.41 (m, 30 H, PPh_3); −0.61 (s, 9 H, $SiMe_3$); −0.77 (s, 9 H, $SiMe_3$). ^{19}F NMR (δ; $CDCl_3$): −116.8 (dm, F_{ortho}, $^3J(Pt-F_{ortho})$ = 371 Hz); −117.6 (dm, F_{ortho}, $^3J(Pt-F_{ortho})$ = 325 Hz); −161.3 (t, F_{para}); −161.6 (t, F_{para}); −164.5 (m, F_{meta}); −165.0 (m, F_{meta}). ^{31}P NMR (δ; $CDCl_3$): 16.6 ($^1J(^{195}Pt-P)$ = 2510 Hz).

***cis,trans*-[(OC)(C$_6$F$_5$)$_2$Pt(μ-C≡CSiMe$_3$)Pt(C≡CSiMe$_3$)(PEt$_3$)$_2$] (2).** *cis*-$[Pt(C_6F_5)_2(CO)(THF)]$ (0.15 g, 0.24 mmol) was added to a solution of *trans*-$[Pt(C\equiv CSiMe_3)_2(PEt_3)_2]$ (0.15 g, 0.24 mmol) in CH_2Cl_2 (8 mL), and the mixture was stirred for

(7) (a) Hartley, F. R. In *Comprehensive Organometallic Chemistry;* Pergamon: Oxford, U.K., 1982, *Vol. 6*, p 508. (b) Michelin, R. A.; Ros, R.; Guadalupi, G.; Bombieri, G.; Benetollo, F.; Chapuis, G. *Inorg. Chem.* **1989**, *28*, 840.

(8) (a) Werner, H.; Baum, M.; Schneider, D.; Windmüller, B. *Organometallics* **1994**, *13*, 1089 and references given therein. (b) Espuelas, J.; Esteruelas, M. A.; Lahoz, F. J.; Oro, L. A.; Ruiz, N. *J. Am. Chem. Soc.* **1993**, *115*, 4683.

(9) (a)Höhn, A.; Otto, H.; Dziallas, M.; Werner, H. *J. Chem. Soc., Chem. Commun.* **1987**, 852. (b) Knaup, W.; Werner, H. *J. Organomet. Chem.* **1991**, *411*, 471. (c) Rappert, T.; Nürnberg, O.; Werner, H. *Organometallics* **1993**, *12*, 1359.

(10) Akita, M.; Takabuchi, A.; Terada, M.; Ishii, N.; Tanaka, M.; Moro-Oka, Y. *Organometallics* **1994**, *13*, 2516.

(11) (a) Bruce, M. I. *Chem. Rev.* **1991**, *21*, 197. (b) Davies, S. G.; McNally, J. P.; Smallridge, A. J. *Adv. Organomet. Chem.* **1990**, *30*, 1. (c) Miller, D. C.; Angelici, R. J. *Organometallics* **1991**, *10*, 79. (d) Gamasa, M. P.; Gimeno, J.; Lastra, E.; Martin, B. M.; Anillo, A.; Tiripicchio, A. *Organometallics* **1992**, *11*, 1373. (e) Bianchini, C.; Peruzzini, M.; Vacca, A.; Zanobini, F. *Organometallics* **1991**, *10*, 3697. (f) Bianchini, C.; Innocenti, P.; Meli, A.; Peruzzini, M.; Zanobini, F.; Zanello, P. *Organometallics* **1990**, *9*, 2514. (g) Adams, J. S.; Bitcon, C.; Brown, J. R.; Collison, D.; Cunningham, M.; Whiteley, M. W. *J. Chem. Soc., Dalton Trans.* **1987**, 3049. (h) Senn, D. R.; Wong, A.; Patton, A. T.; Marsi, M.; Strouse, C. E.; Gladysz, J. A. *J. Am. Chem. Soc.* **1988**, *110*, 6096. (i) Kolobova, N. E.; Skripkin, V. V.; Rozantseva, T. V.; Struchkov, Yu. T.; Aleksandrov, G. G.; Andrianov, V. G. *J. Organomet. Chem.* **1981**, *218*, 351.

(12) (a) Bruce, M. I.; Swincer, A. G. *Aust. J. Chem.* **1980**, *33*, 1471. (b) Bruce, M. I.; Swincer, A. G. *Adv. Organomet. Chem.* **1983**, *22*, 60. (c) Gamasa, M. P.; Gimeno, J.; Lastra, E.; Lanfranchi, M.; Tiripicchio, A. *J. Organomet. Chem.* **1992**, *430*, C39. (d) Werner, H.; Knaup, W.; Schulz, M. *Chem. Ber.* **1991**, *124*, 1121. (e) Boland-Lussier, B. E.; Hughes, R. P. *Organometallics* **1982**, *1*, 635. (f) Bullock, R. M. *J. Chem. Soc., Chem. Commun.* **1989**, 165.

(13) Bell, R. A.; Chisholm, M. H.; Couch, D. A.; Rankel, L. A. *Inorg. Chem.* **1977**, *16*, 677.

(14) Usón, R.; Forniés, J.; Espinet, P.; Fortuño, C.; Tomás, M.; Welch, A. J. *J. Chem. Soc., Dalton Trans.* **1988**, 3005.

(15) Sebald, A.; Fritz, P.; Wrackmeyer, B. *Spectrochim. Acta* **1985**, *41A*, 1405.

Scheme 2[a]

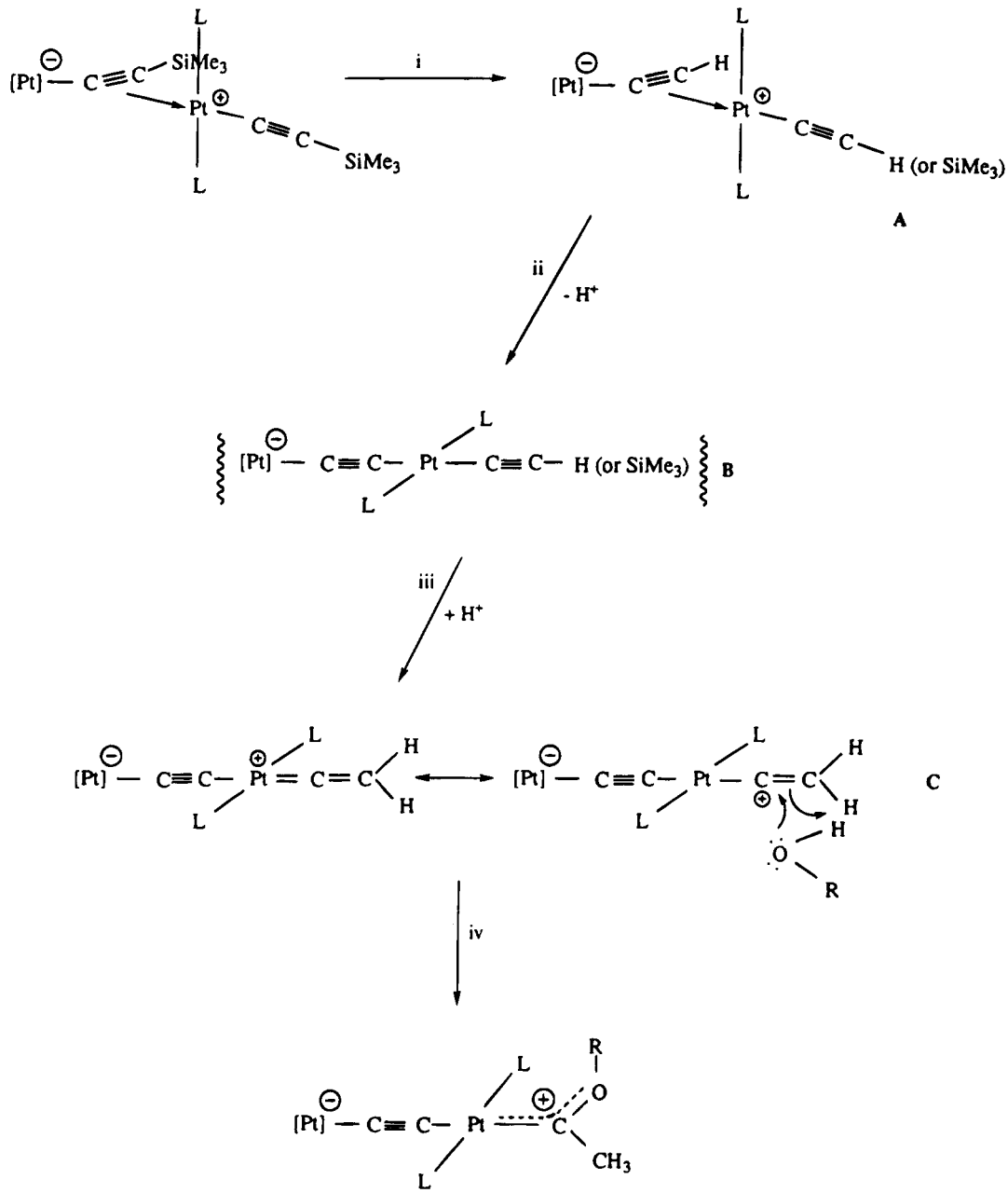

[a] [Pt] = *cis*-Pt(C_6F_5)$_2$(CO); L = PPh_3, PEt_3; ROH = EtOH, MeOH.

1 h. The resulting yellow solution was filtered through Kieselguhr and evaporated to dryness. By addition of *n*-hexane (5 mL) and standing overnight at −30 °C, a white solid, identified as complex **2**, separated; yield 25%. Anal. Calcd for $C_{35}F_{10}H_{48}OP_2Pt_2Si_2$: C, 35.53; H, 4.1. Found: C, 35.64; H, 3.81. IR (cm^{-1}): ν(CO) 2089 (vs); ν(C≡C) 2062 (vs), 1930 (vs); $\nu(C_6F_5)_{x\text{-sens}}$ 799 (s), 787 (s).[5] ^{1}H NMR (δ; $CDCl_3$): 2.03 (m, 12 H, CH_2, PEt_3); 1.13 (m, 18 H, CH_3, PEt_3); 0.19 (s, 9 H, $SiMe_3$); 0.05 (s, 9 H, $SiMe_3$). ^{19}F NMR (δ; $CDCl_3$): −117.7 (dd, F_{ortho}, ^3J(Pt−F_{ortho}) = 359 Hz); −118.4 (dm, F_{ortho}, ^3J(Pt−F_{ortho}) = 358 Hz); −160.2 (t, F_{para}); −161.2 (t, F_{para}); −163.5 (m, F_{meta}); −164.3 (m, F_{meta}). ^{31}P NMR (δ; $CDCl_3$): 11.26 (^1J(^{195}Pt−P) = 2309 Hz).

***cis,trans*-[(OC)(C_6F_5)$_2$Pt−C≡C−Pt{C(CH_3)(OEt)}(PPh_3)$_2$]·2Me_2CO (3a·2Me_2CO).** To a CH_2Cl_2 (10 mL) solution of *trans*-[Pt(C≡C$SiMe_3$)$_2$(PPh_3)$_2$] (0.18 g, 0.2 mmol) was added *cis*-[Pt(C_6F_5)$_2$(CO)(THF)] (0.125 g, 0.2 mmol). The mixture was stirred for 1 h, and the resulting yellow solution was concentrated to ~5 mL. By addition of EtOH (2 mL) and stirring for 2 h, a yellow solid separated. Subsequent recrystallization from Me_2CO−hexane gave complex **3** as a yellow microcrystalline solid. Under these conditions, **3** crystallizes with two molecules of Me_2CO (observed by ^{1}H NMR); yield 30%. Anal. Calcd for $C_{61}F_{10}H_{50}O_4P_2Pt_2$: C, 49.20; H, 3.38. Found: C, 49.36; H, 3.08. IR (cm^{-1}): ν(CO) 2071 (vs); ν(C≡C) 2026 (m); $\nu(C_6F_5)_{x\text{-sens}}$ 792 (m), 778 (m).[5] ^{1}H NMR (δ; $CDCl_3$): 7.72, 7.42 (m, 30 H, PPh_3); 4.64 (q, 2H,:CMeOCH_2Me, ^3J(H−H) = 7.2 Hz); 2.15 (s, 12 H, CO(CH_3)$_2$); 1.43 (s, 3H,:C(CH_3)OCH_2Me); 1.10 (t, 3H,:CMeOCH_2CH_3, ^3J(H−H) = 7.2 Hz). ^{19}F NMR (δ; $CDCl_3$): −116.8 (dd, F_{ortho}, ^3J(Pt−F_{ortho}) = 294 Hz); −117.9 (dd, F_{ortho}, ^3J(Pt−F_{ortho}) = 412 Hz); −164.3 (t, F_{para}); −166.2 (t, F_{para}); −165.9 (m, F_{meta}); −166.9 (m, F_{meta}). ^{31}P (δ; $CDCl_3$): 14.1 (^1J(^{195}Pt−P) = 2669 Hz).

***cis,trans*-[(OC)(C_6F_5)$_2$Pt−C≡C−Pt{C(CH_3)(OMe)}(PPh_3)$_2$]·2CH_2Cl_2 (3b·2CH_2Cl_2).** This complex was prepared from *trans*-[Pt(C≡C$SiMe_3$)$_2$(PPh_3)$_2$] (0.16 g, 0.17 mmol) and *cis*-[Pt(C_6F_5)$_2$(CO)(THF)] (0.11 g, 0.17 mmol) as described for **3a**, except MeOH was used instead of EtOH. Under these conditions, **3b** crystallizes with two molecules of CH_2Cl_2; yield 26%. Anal. Calcd for $C_{56}Cl_4F_{10}H_{40}O_2P_2Pt_2$: C, 44.00; H, 2.64. Found: C, 44.42; H, 2.60. IR (cm^{-1}): ν(CO) 2068 (vs); ν(C≡C) 2030 (m); $\nu(C_6F_5)_{x\text{-sens}}$ 793 (s), 779 (s).[5] ^{1}H NMR (δ; $CDCl_3$): 7.74, 7.45 (m, 30 H, PPh_3); 4.33 (s, 3H,:CMeOCH_3); 1.42 (s, 3H,:C(CH_3)OMe). ^{19}F NMR (δ; $CDCl_3$): −116.3 (dd, F_{ortho},

Table 2. Crystallographic Data for Complex 4a

formula	$C_{31}H_{38}O_2F_{10}P_2Pt_2$
fw	1084.7
color	yellow
cryst size, mm	0.17 × 0.28 × 0.30
space group	$P2_1/c$
a, Å	15.216(3)
b, Å	14.197(4)
c, Å	18.167(5)
β, deg	107.99(2)
V, Å^3	3773(2)
temp, °C	20 ± 1
data collected	$\pm h,+k,+l$
Z	4
density (calcd), g cm^{-3}	1.93
$F(000)$	2064
abs coeff, cm^{-1}	76.47
total no. of rflns collected	4687 + 216 ψ scan
2θ range, deg	3.0−43.0
no. of indep rflns	4295
no. of obsd rflns	2645 ($F > 4.0\sigma(F)$)
final R indices (obsd data)	$R = 0.0504$, $R_w = 0.0587$
weighting scheme	$w^{-1} = \sigma^2(F) + 0.0017F^2$
largest shift/esd	0.001
largest diff peak, e Å^{-3}	0.77
transmissn factors: min, max	0.468, 1.000
no. of params refined	424

^3J(Pt−F_{ortho}) = 310 Hz); −117.3 (dm, F_{ortho}, ^3J(Pt−F_{ortho}) = 419 Hz); −164.0 (t, F_{para}); −165.5 (m, overlap of a signal due to a F_{para} and a F_{meta}); −166.3 (m, F_{meta}). ^{31}P NMR (δ; $CDCl_3$): 14.1 ($^1J(^{195}Pt-P)$ = 2656 Hz, $^4J(^{195}Pt-P)$ = 14.4 Hz).

***cis,trans*-[(OC)(C_6F_5)$_2$Pt−C≡C−Pt{C(CH_3)(OEt)}(PEt_3)$_2$] (4a).** To a solution of *trans*-[Pt(C≡C$SiMe_3$)$_2$(PEt_3)$_2$] (0.156 g, 0.24 mmol) in CH_2Cl_2 (6 mL) was added *cis*-[Pt(C_6F_5)$_2$(CO)(THF)] (0.15 g, 0.24 mmol), and the mixture was stirred for 30 min. The resulting yellow solution was treated with EtOH (4 mL), stirred for 48 h, and evaporated to dryness. The addition of Et_2O (5 mL) afforded **4a** as a pale yellow solid, yield 54%. Anal. Calcd for $C_{31}F_{10}H_{38}O_2P_2Pt_2$: C, 34.33; H, 3.53. Found: C, 34.41; H, 3.44. IR (cm^{-1}): ν(CO) 2066 (vs); ν(C≡C) 2021 (m); $\nu(C_6F_5)_{x\text{-sens}}$ 792 (s), 781 (s).[5] ^{1}H NMR (δ; $CDCl_3$): 5.07 (q, 2H, :CMeOCH_2Me, ^3J(H−H) = 7.2 Hz); 2.45 (s, 3H, :C(CH_3)OCH_2Me); 1.93 (m, 12 H, CH_2, PEt_3); 1.59 (t, 3H, :CMeOCH_2CH_3, ^3J(H−H) = 7.2 Hz); 1.07 (m, 18H, CH_3, PEt_3). ^{13}C NMR (δ; $CDCl_3$): 309.8 (t, ^2J(P−C) = 7.3 Hz, Pt=C); 173.3 (t, ^2J(P−C) = 4.5 Hz, C=Pt−*C*≡C); 149−133 (m, C_6F_5); 80.2 (s, ^3J(Pt−C) = 77 Hz, OCH_2CH_3); 43.7 (s, ^2J(Pt−C) = 98.5 Hz, *C*H_3C=Pt); 16.0 (^1J(P−C) + ^3J(P−C) ≈ ^2J(Pt−C) ≈ 37 Hz, PCH_2); 13.9 (s, OCH_2CH_3); 7.94 (s, ^3J(Pt−C) = 25 Hz, PCH_2CH_3). ^{19}F NMR (δ; $CDCl_3$): −116.1 (d, F_{ortho}, ^3J(Pt−F_{ortho}) = 311 Hz); −117.3 (d, F_{ortho}, ^3J(Pt−F_{ortho}) = 416 Hz); −163.2 (t, F_{para}); −164.6 (t, F_{para}); −164.9 (m, F_{meta}); −166.0 (m, F_{meta}). ^{31}P NMR (δ; $CDCl_3$): 14.7 ($^1J(^{195}Pt-P)$ = 2373 Hz).

***cis,trans*-[(OC)(C_6F_5)$_2$Pt−C≡C−Pt{C(CH_3)(OMe)}(PEt_3)$_2$] (4b).** This complex was prepared as a pale yellow solid by a method similar to that for **4a**, but MeOH was used instead of EtOH; yield 26%. Anal. Calcd for $C_{30}F_{10}H_{36}O_2P_2Pt_2$: C, 33.66; H, 3.39. Found: C, 33.57; H, 3.45. IR (cm^{-1}): ν(CO) 2074 (vs); ν(C≡C) 2019 (m); $\nu(C_6F_5)_{x\text{-sens}}$ 794 (s), 782 (s).[5] ^{1}H NMR (δ; $CDCl_3$): 4.71 (s, 3H, :CMeO*CH*$_3$); 2.46 (s, 3H, :C(CH_3)OMe); 1.93 (m, 12 H, CH_2, PEt_3); 1.07 (m, 18H, CH_3, PEt_3). ^{19}F NMR (δ; $CDCl_3$): −116.6 (dm, F_{ortho}, ^3J(Pt−F_{ortho}) = 310 Hz); −117.8 (dm, F_{ortho}, ^3J(Pt−F_{ortho}) = 416 Hz); −163.6 (t, F_{para}); −165.1 (t, F_{para}); −165.4 (m, F_{meta}); −166.5 (m, F_{meta}). ^{31}P NMR (δ; $CDCl_3$): 15.35 ($^1J(^{195}Pt-P)$ = 2357 Hz).

Crystal Structure Determination of the Complex *cis,trans*-[(OC)(C_6F_5)$_2$Pt−C≡C−Pt{C(CH_3)(OEt)}(PEt_3)$_2$] (4a). Suitable crystals of **4a** for X-ray studies were obtained by slow diffusion of *n*-hexane into a THF solution of **4a** at −30 °C.

Crystallographic data were collected by Crystalytics (Lincoln, NE) on a four-circle Nicolet (Siemens) autodiffractometer using graphite-monochromated Mo Kα X-radiation (0.710 731 Å). Crystallographic details are summarized in Table 2. Cell constants were refined from 2θ values of 15 reflections including Friedel pairs (2θ > 25°). An absorption correction based on ψ scans was applied. Six standard reflections were measured every 300 reflections but showed no decay. The structure was solved by Patterson synthesis and subsequent difference Fourier maps (SHELXTL-PLUS[16]). All non-hydrogen atoms were refined anisotropically. All calculations were done on a Local Area VAX Cluster/VMS V.5.5. Positional parameters are given in Table 3.

Table 3. Atomic Coordinates (×10^4) for Complex 4a

	x	y	z
Pt(1)	2983(1)	1227(1)	2047(1)
Pt(2)	2867(1)	4480(1)	3372(1)
P(1)	4269(5)	894(5)	3075(4)
P(2)	1682(5)	1812(4)	1135(4)
O(1)	2652(13)	−749(11)	1475(10)
O(2)	4616(14)	3874(14)	4585(10)
C(1)	2940(17)	2469(16)	2581(14)
C(2)	2838(18)	3222(16)	2866(13)
C(3)	3072(16)	50(17)	1466(14)
C(4)	3582(18)	−36(18)	910(17)
C(5)	2049(21)	−861(16)	1966(17)
C(6)	1979(23)	−1886(18)	2133(22)
C(7)	3931(20)	4121(16)	4116(14)
C(8)	2866(18)	5818(15)	3854(14)
C(9)	2187(19)	6159(17)	4139(13)
C(10)	2189(21)	7025(21)	4486(14)
C(11)	2940(26)	7594(18)	4513(18)
C(12)	3594(19)	7300(16)	4244(14)
C(13)	3572(19)	6441(18)	3916(13)
F(1)	1463(11)	5570(10)	4120(10)
F(2)	1500(13)	7286(12)	4750(11)
F(3)	2944(13)	8452(11)	4866(13)
F(4)	4321(12)	7892(10)	4312(11)
F(5)	4279(11)	6221(10)	3676(9)
C(14)	1690(17)	4814(14)	2497(12)
C(15)	1673(22)	5394(18)	1894(17)
C(16)	929(30)	5626(22)	1264(21)
C(17)	110(30)	5235(24)	1254(16)
C(18)	23(19)	4684(21)	1810(19)
C(19)	782(15)	4458(16)	2419(15)
F(6)	2510(13)	5794(10)	1886(9)
F(7)	980(16)	6220(14)	723(10)
F(8)	−688(14)	5464(15)	667(11)
F(9)	−801(12)	4289(14)	1807(11)
F(10)	705(11)	3900(11)	2973(9)
C(20)	4950(22)	−113(19)	2960(16)
C(21)	5803(22	−388(23)	3675(23)
C(22)	5093(26)	1908(31)	3437(28)
C(23)	5416(31)	2242(36)	2868(33)
C(24)	4001(36)	631(53)	3948(21)
C(25)	3197(32)	486(31)	4023(18)
C(26)	1155(21)	973(21)	312(16)
C(27)	345(21)	1391(21)	−296(18)
C(28)	782(22)	2199(20)	1521(18)
C(29)	523(23)	1440(24)	2039(21)
C(30)	1993(25)	2874(20)	651(17)
C(31)	2715(31)	2626(27)	226(22)

Acknowledgment. We thank the Spanish Comisión Interministerial de Ciencia y Tecnología (CICYT) for financial support (Project PB92-0364) and for a research grant to J.R.B.

Supplementary Material Available: Tables of bond distances, bond angles, and isotropic and anisotropic thermal parameters (5 pages). Ordering information is given on any current masthead page.

OM940924T

(16) SHELXTL-PLUS, Release 4.21/v; Siemens Analytical X-ray Instruments, Inc., 1990.

Structural Study of (Oxodimethylenemethane)palladium and -platinum Complexes

Akihiro Ohsuka, Toshikazu Hirao, Hideo Kurosawa,* and Isao Ikeda*

Department of Applied Chemistry, Faculty of Engineering, Osaka University, Suita, Osaka 565, Japan

Received October 26, 1994[⊗]

Structures of (oxodimethylenemethane)palladium and -platinum complexes in solution and in crystalline states were investigated by ^{1}H NMR, IR, and X-ray crystallographical analyses. The following features are disclosed: the structures consisted of contributions from π-allylic and metallacyclobutanone canonical forms; the palladium complex has a larger contribution of π-allylic character than the platinum complex in both states; the degree of contribution of π-allylic character increased upon the increment of solvent polarity and the addition of protic solvent.

Introduction

Oxodimethylenemethane–transition metal complexes, which are important as the key intermediate in organic synthesis,[1] are very interesting in point of the correlation of structure and reactivity. There were several reports on structures of substituted (oxodimethylenemethane)palladium and -platinum complexes.[2,3] We have reported a preliminary, novel synthesis of unsubstituted (oxodimethylenemethane)palladium and -platinum complexes.[4] In this report, we studied the structures of oxodimethylenemethane complexes in solution and in crystalline states using NMR, IR, and X-ray crystallographical analyses.

Results and Discussion

Oxodimethylenemethane complexes were synthesized as shown in Scheme 1. Thus, π-allyl complexes **3** were treated with KOH dissolved in 2-propanol at 0 °C, to afford oxodimethylenemethane complexes **4**.

As shown in Table 1, the ^{1}H NMR signals[5] of the methylene protons of the complexes **4** coalesced, showing the inversion of the metallacyclobutanone ring (Scheme 2). The ring inversion rates[6] of oxodimethylenemethane **4** at the coalescence temperatures were calculated from the chemical shift separation[7] measured at the lower temperature. When the inversion rates of the two complexes are compared at any temperature in a given solvent through extrapolation of the data in Table 1, it is apparent that the palladium complex **4a**

Scheme 1

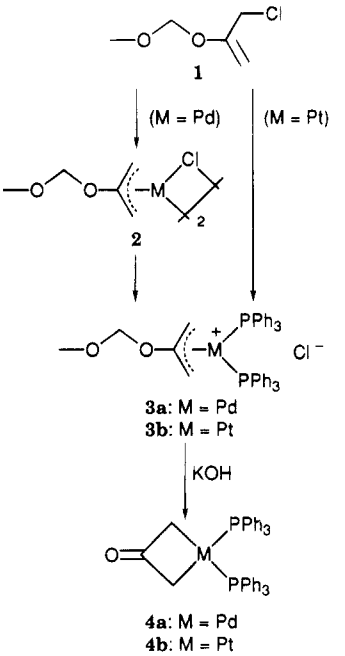

Table 1. Ring Inversion Rate of Oxodimethylenemethane Complexes 4 at Coalescence Temperature

	ring inversion rate (s^{-1}) (coalescence temp (°C))		
compd	CD_2Cl_2	$CDCl_3$	CD_2Cl_2/CD_3OD (v/v = 4/1)
4a (M = Pd)	240 (5)[a]	346 (28)[a]	364 (>60)[a]
		234 (24)[b]	246 (>40)[b]
4b (M = Pt)	160 (<−80)[a]	266 (−60)[a]	284 (−20)[a]
	240 (−60)[c]		192 (−29)[b]

[a] Measured by 400 MHz NMR instrument. [b] Measured by 270 MHz NMR instrument. [c] Measured by 600 MHz NMR instrument.

[⊗] Abstract published in *Advance ACS Abstracts,* March 15, 1995.

(1) Trost, B. M.; Schneider, S. *J. Am. Chem. Soc.* **1989**, *111*, 4430.

(2) Unsubstituted Pt complex: (a) Jones, M. D.; Kemmitt, R. D. W.; Fawcett, J.; Russell, D. R. *J. Chem. Soc., Chem. Commun.* **1986**, 427. (b) Fawcett, J.; Henderson, W.; Jones, M. D.; Kemmitt, R. D. W.; Russell, D. R.; Lam, B.; Kang, S. K.; Albright, T. A. *Organometallics* **1989**, *8*, 1991. (c) Ohe, K.; Matsuda, H.; Morimoto, T.; Ogoshi, S.; Chatani, N.; Murai, S. *J. Am. Chem. Soc.* **1994**, *116*, 4125. (d) Huang, T.-M.; Hsu, R.-H.; Yang, C.-S.; Chen, J.-T.; Lee, G.-H.; Wang, Y. *Organometallics* **1994**, *13*, 3657.

(3) Substituted Pd, Pt complexes: (a) Clarke, D. A.; Kemmitt, R. D. W.; Mazid, M. A.; McKenna, P.; Russell, D. R.; Schilling, M. D.; Sherry, L. J. S. *J. Chem. Soc., Dalton Trans.* **1984**, 1993. (b) Kemmitt, R. D. W.; McKenna, P.; Russell, D. R.; Sherry, L. J. S. *J. Chem. Soc., Dalton Trans.* **1985**, 259. (c) Imran, A.; Kemmitt, R. D. W.; Markwick, A. J. W.; McKenna, P.; Russell, D. R.; Sherry, L. J. S. *J. Chem. Soc., Dalton Trans.* **1985**, 549. (d) Chiu, K. W.; Henderson, W.; Kemmitt, R. D. W.; Prouse, L. J. S.; Russell, D. R. *J. Chem. Soc., Dalton Trans.* **1988**, 427. (e) Kemmitt, R. D. W.; McKenna, P.; Russell, D. R.; Prouse, L. J. S. *J. Chem. Soc., Dalton Trans.* **1989**, 345.

(4) Ohsuka, A.; Fujimori, T.; Hirao, T.; Kurosawa, H.; Ikeda, I. *J. Chem. Soc., Chem. Commun.* **1993**, 1039.

(5) ^{1}H NMR (25 °C, 399.78 MHz) signals of methylene protons are as follows. Pd complex: in CD_2Cl_2, δ 2.39 (s, br, 4 H) ppm; in $CDCl_3$, δ 2.71 (s, br, 2 H, *anti*), 2.43 (s, br, 2 H, *syn*) ppm; in CD_2Cl_2/CD_3OD (v/v = 4/1), δ 2.77 (s, 2 H, *anti*), 2.37 (s, 2 H, *syn*) ppm. Pt complex: in CD_2Cl_2, δ 2.19 (s, 4 H, J(PtH) = 48 Hz) ppm; in $CDCl_3$, δ 2.36 (d, 4 H, J(PtH) = 46 Hz, J(PH) = 3 Hz) ppm; in CD_2Cl_2/CD_3OD (v/v = 4/1), δ 2.34 (s, 4 H, J(PtH) = 40 Hz) ppm.

(6) Gutowsky, H. S.; Holm, C. H. *J. Chem. Phys.* **1956**, *25*, 1228.

0276-7333/95/2314-2538$09.00/0

Scheme 2

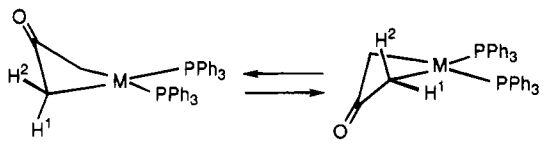

Scheme 3

Table 2. Chemical Shift of $^{13}C{=}O$ in Oxodimethylenemethane Complexes 4

	chem shift (ppm)		
compd	CD_2Cl_2	$CDCl_3$	CD_2Cl_2/CD_3OD (v/v = 4/1)
4a (M = Pd)	175.6	174.9	172.8
4b (M = Pt)	181.4	180.6	177.6

Table 3. ^{31}P NMR of Oxodimethylenemethane Complexes 4

	chem shift (ppm) (J(PtP) (Hz))		
compd	CD_2Cl_2	$CDCl_3$	CD_2Cl_2/CD_3OD (v/v = 4/1)
4a (M = Pd)	28.1	28.1	27.9
4b (M = Pt)	23.4 (2934)	23.5 (2972)	22.0 (3207)

always possesses the smaller rate than the platinum complex **4b**. One of the reasons for this difference can be traced to the larger contribution of the π-allyl structure in **4a** than **4b** (Scheme 3), which will be reinforced by other spectral and structural evidence, as discussed below.

Both complexes **4** exhibited an interesting solvent effect. Table 1 indicates that in order for each complex to attain a given inversion rate, a higher temperature is required in a CD_2Cl_2/CD_3OD solution than in a CD_2Cl_2 solution. In other words, the inversion in CD_2Cl_2/CD_3OD is slower than that in CD_2Cl_2, suggesting that the contribution of the π-allylic character increases in a polar solvent.

These results can be explained by assuming that hydrogen bonding of the carbonyl oxygen with a protic solvent molecule is also important in stabilizing the π-allylic structure, especially in palladium complex **4a**. This fact is in line with the finding that complexes **4** showed basicity in aqueous solution, and palladium complex **4a** showed a larger pK_a value.[8]

On increasing the polarity of the solvent, upfield shifts of $C{=}O$ in ^{13}C NMR occurred for both palladium and platinum complexes **4** (Table 2). The chemical shift value for $C{=}O$ of platinum complex **4b** was larger than that of palladium complex **4a** in the same solvent.

In ^{31}P NMR (Table 3), the J(PtP) value of platinum complex **4b** (2934–3207 Hz) was in the middle of those of the (π-allyl)platinum complex (J(PtP) = 3933 Hz,[9] 3634 Hz[10]) and dialkylplatinum complex (J(PtP) = 1899 Hz[11]) where all of these J(PtP) values correspond to the PR_3 ligand located *trans* to the carbon ligands. The J(PtP) value changed as the solvent polarity changed. Thus, the J(PtP) value in the polar solvent moved to the direction of that of the (π-allyl)platinum complex.

In the IR spectrum (KBr), the carbonyl stretching vibration of palladium complex **4a** absorbed at a smaller wavenumber region (1526 cm^{-1}) than platinum complex **4b** (1593 cm^{-1}), meaning that the contribution of the π-allyl canonical form was larger in the palladium complex **4a** than in the platinum complex **4b**.

The structure of (oxodimethylenemethane)palladium complex **4a**·CH_2Cl_2 was established by X-ray crystallographical analysis (Figure 1, Table 5). Concerning the structural parameters, palladium complex **4a** was similar to platinum complex **4b**[2b] except for angles θ and θ' (Table 4). The fold angle θ between the C(1)–M–C(3) and C(1)–C(2)–C(3) planes and dihedral angle θ' between the P(1)–M–P(2) and C(1)–C(2)–C(3) planes[12] of both the palladium and the platinum complexes are in the middle of those of the cyclobutanone,[13a] platinacyclobutane,[13b–d] and π-allyl complexes,[14] consistent with the suggestion that both complexes **4** have contributions from cyclobutanone and π-allylic characters. It is notable, however, that the angles θ,θ' of palladium complex **4a** are closer to those of typical π-allyl complexes than those of platinum complex **4b**. This trend is again in line with the results obtained by NMR and IR spectra, as well as the fact that the basicity of palladium complex **4a** is larger than that of platinum complex **4b**.

Conclusion

The X-ray structure, as well as the results from ^1H, $^{13}C\{^1H\}$, and $^{31}P\{^1H\}$ NMR and IR spectra, indicates that (oxodimethylenemethane)palladium complex **4a** possesses a larger contribution of the π-allylic canonical form than the corresponding platinum complex **4b** does in both solution and crystalline states.

Experimental Section

General Methods. Melting points were recorded in air on a Yanagimoto Yanaco Model MP-3. Infrared spectra were recorded as KBr disks on a JEOL JIR-AQS 20M. ^1H NMR spectra were recorded on JEOL GSX-270, JEOL JNM-GSX-400, and Bruker AM600 spectrometers at 269.73, 399.78, and 600.14 MHz with $SiMe_4$ (0.0 ppm) as an internal reference. $^{13}C\{^1H\}$ NMR spectra were recorded on a JEOL JNM-GSX-400 spectrometer at 100.53 MHz with $SiMe_4$ (0.0 ppm) as an internal reference. $^{31}P\{^1H\}$ NMR spectra were recorded on a JEOL JNX-GSX-400 spectrometer at 161.86 MHz with H_3PO_4(aq) (85%) as an external reference. Elemental analyses were carried by a Perkin-Elmer 240C.

(7) The chemical shift separations are as follows. Pd complex: in CD_2Cl_2 (−40 °C, 400 MHz), 0.27 ppm (δ 2.30, 2.57 ppm); in $CDCl_3$ (−30 °C, 400 MHz), 0.39 ppm (δ 2.38, 2.77 ppm); in CD_2Cl_2/CD_3OD (v/v = 4/1) (25 °C, 400 MHz), 0.41 ppm (δ 2.35, 2.76 ppm). Pt complex: in CD_2Cl_2 (−80 °C, 600 MHz), 0.18 ppm (δ 2.04, 2.22 ppm); in $CDCl_3$ (−70 °C, 400 MHz), 0.30 ppm (δ 2.19, 2.49 ppm); in CD_2Cl_2/CD_3OD (v/v = 4/1) (−40 °C, 400 MHz), 0.32 ppm (δ 2.18, 2.50 ppm).

(8) See ref 4. Oxodimethylenemethane complex **4** (0.01 mmol) showed basicity in acetone/H_2O (0.9 mL/0.1 mL) solution (Pd complex **4a**, pH = 9.7; Pt complex **4b**, pH = 8.6).

(9) ^{31}P NMR of [Pt(η^3-CH_2CHCH_2)(PPh_3)$_2$](BF_4): Boag, N. M.; Green, M.; Spencer, J. L.; Stone, F. G. A. *J. Chem. Soc., Dalton Trans.* **1980**, 1208.

(10) ^{31}P NMR of [Pt(η^3-$CH_2C(OH)CH_2$)(PPh_3)$_2$](BF_4): See ref 2d.

(11) ^{31}P NMR of *cis*-[Pt(CH_3)$_2$(PPh_3)$_2$]: Eaborn, C.; Odell, K. J.; Pidcock, A. *J. Chem. Soc., Dalton Trans.* **1979**, 758.

(12) Dihedral angle θ' of **4b** was not shown in ref 2b and was calculated from atomic coordinates tabulated in ref 2b.

(13) Cyclobutanone (θ = 10°): (a) Riche, C. *Acta Crystallogr., Sect. B* **1974**, *B30*, 587. Platinacyclobutanes (θ = 0–30°): (b) Puddephatt, R. J. *Coord. Chem. Rev.* **1980**, *33*, 149. (c) Ibers, J. A.; DiCosimo, R.; Whitesides, G. M. *Organometallics* **1982**, *1*, 13. (d) Klinger, R. J.; Huffman, J. C.; Kochi, J. K. *J. Am. Chem. Soc.* **1982**, *104*, 2147.

(14) (π-allyl)Pd and -Pt complexes (θ = 61–72°): (a) Mason, R.; Wheeler, A. G. *J. Chem. Soc. A* **1968**, 2549. (b) Hartley, F. R. In *Comprehensive Organometallic Chemistry*; Wilkinson, G., Stone, F. G. A., Abel, E. W. Eds.; Pergamon: Oxford, U. K., **1982**; Vol. 6, p 721.

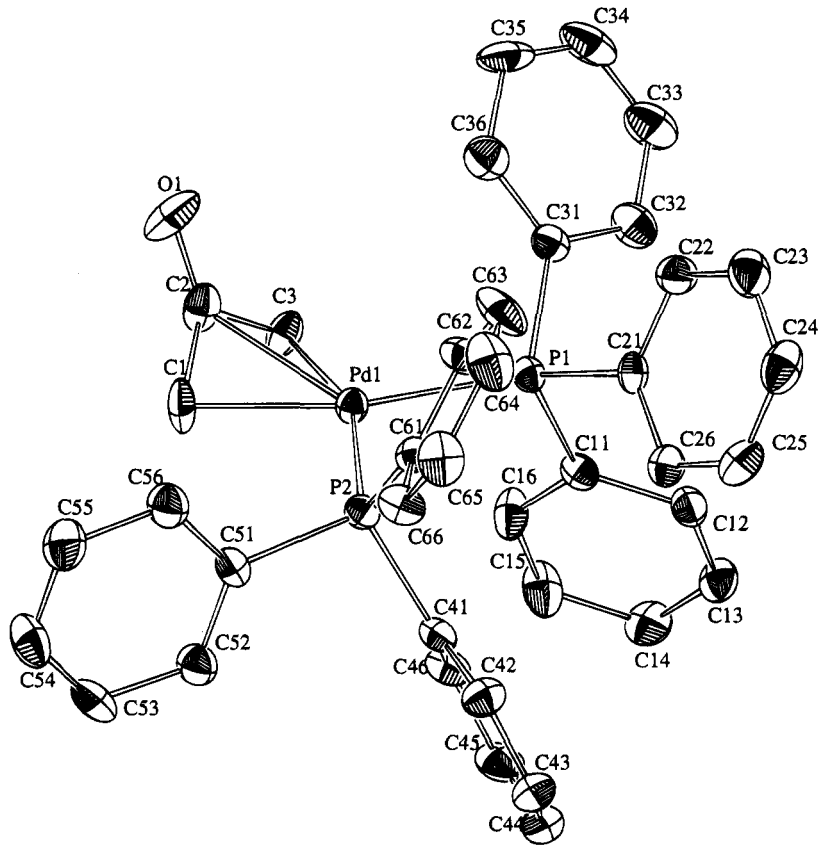

Figure 1. ORTEP drawing of the (oxodimethylenemethane)palladium complex with thermal ellipsoids shown at the 30% probability level. Hydrogen atoms and included solvent (CH_2Cl_2) are omitted. Selected bond distances and bond angles are in Table 5.

Table 4. Structural Parameters (Å, deg) of 4·CH_2Cl_2

structural param	4a	4b[a]
M–P	2.3385(30)	2.294(3)
M–C(1)	2.135(10)	2.132(14)
M–C(2)	2.40(1)	2.422(12)
C(1)–C(2)	1.47(1)	1.484(20)
C(2)–O	1.24(1)	1.257(15)
P(1)–M–P(2)	105.1(1)	103.6(1)
C(1)–C(2)–C(3)	105(1)	107.7(10)
θ	56.9	51.0
θ'	51.3	[45.6][b]

[a] See ref 2b. [b] Calculated from atomic coordinates tabulated in ref 2b. θ: fold angle between the C(1)–M–C(3) and C(1)–C(2)–C(3) planes. θ': dihedral angle between the P(1)–M–P(2) and C(1)–C(2)–C(3) planes.

Table 5. Selected Bond Lengths (Å) and Bond Angles (deg) for 4a·CH_2Cl_2

P(1)–Pd(1)	2.340(3)	P(2)–Pd–P(1)	105.1(1)
P(2)–Pd(1)	2.337(3)	C(1)–Pd–P(1)	160.3(3)
C(1)–Pd(1)	2.13(1)	C(1)–Pd–P(2)	94.5(3)
C(2)–Pd(1)	2.40(1)	C(2)–Pd–P(1)	124.7(3)
C(3)–Pd(1)	2.14(1)	C(2)–Pd–P(2)	128.3(3)
C(2)–C(3)	1.43(1)	C(2)–Pd–C(1)	37.3(4)
C(1)–C(2)	1.47(1)	C(3)–Pd–P(1)	95.0(3)
O(1)–C(2)	1.24(1)	C(3)–Pd–P(2)	158.6(3)
C(11)–P(1)	1.83(1)	C(3)–Pd–C(1)	65.3(4)
C(21)–P(1)	1.83(1)	C(3)–Pd–C(2)	36.1(4)
C(31)–P(1)	1.85(1)	C(3)–C(2)–C(1)	105(1)
C(41)–P(2)	1.84(1)	O(1)–C(2)–C(1)	126(1)
C(51)–P(2)	1.84(1)	O(1)–C(2)–C(3)	125(1)
C(61)–P(2)	1.82(1)		

Preparation of [Pd(η^3-$CH_2C(OCH_2OCH_3)CH_2$)(μ-Cl)]$_2$ (2). $Pd_2(dba)_3$·$CHCl_3$[15] (dba = dibenzylideneacetone) (522.6 mg, 0.5 mmol) and 2-(chloromethyl)-3,5-dioxahexene-1 (**1**)[16] (163.8 mg, 1.2 mmol) in acetone (50 mL) were stirred for 3 h at room temperature. The deep purple color on dissolution turned to yellow Then the precipitate was filtered off. The yellow solution was evaporated to dryness and the residue was washed with diethyl ether until the washings were no longer colored. The purification was made by recrystallization from dichloromethane/hexane (v/v = 1/10). Yellow needles formed. Yield: 199.3 mg (82%). Mp: 149–152 °C. NMR spectra ($CDCl_3$, 25 °C): ^{1}H NMR, δ 4.99 (s, 4 H, OCH_2O), 3.78 (d, 4 H, J(HH) = 2.4 Hz, *anti*-CH_2), 3.55 (s, 6 H, OCH_3), 2.61 (d, 4 H, J(HH) = 2.4 Hz, *syn*-CH_2) ppm; $^{13}C\{^1H\}$ NMR, δ 147.9 (s,

Table 6. Data for X-ray Diffraction Analysis of [Pd(η^3-$CH_2C(O)CH_2$)(PPh_3)$_2$] (4a·CH_2Cl_2)

A. Crystal Data	
cryst system	monoclinic
space group	$P2_1/c$
a, Å	13.907(3)
b, Å	17.554(3)
c, Å	15.567(2)
β, deg	110.15(1)
V, Å^3	3567(2)
fw	771.98
d(calcd), g/cm^3	1.437
Z	4
μ, cm^{-1}	7.82
λ(Mo Kα), Å	0.710 69
B. Data Collection and Analysis Summary	
cryst dimens, mm	0.30 × 0.30 × 0.30
2θ range for centered reflcns	27.1 ≤ 2θ ≤ 27.5
tot. no. refcns measd	8809
no. of unique data used	8473
max transm factor	0.9982
min transm factor	0.8351
R	0.058
R_w	0.074
F(000)	1576

Table 7. Fractional Atomic Coordinates for [Pd(η^3-$CH_2C(O)CH_2$)(PPh_3)$_2$] (4a·CH_2Cl_2)

atom	x	y	z	atom	x	y	z
Pd(1)	0.18203(6)	0.00234(6)	0.16051(5)	C(32)	0.1315(9)	−0.0294(7)	0.4471(8)
Cl(1)	0.5897(4)	0.1523(3)	−0.0410(4)	C(33)	0.137(1)	−0.0880(9)	0.5059(9)
Cl(2)	0.5259(5)	0.1393(4)	−0.2377(5)	C(34)	0.181(1)	−0.1546(9)	0.4994(9)
P(1)	0.1782(2)	0.0421(2)	0.3028(2)	C(35)	0.224(1)	−0.1651(7)	0.431(1)
P(2)	0.2771(2)	0.0954(2)	0.1179(2)	C(36)	0.2204(9)	−0.1053(7)	0.3726(8)
O(1)	0.1871(7)	−0.1826(5)	0.1195(7)	C(41)	0.2212(8)	0.1905(7)	0.1160(7)
C(1)	0.1510(10)	−0.0623(7)	0.0382(8)	C(42)	0.2729(9)	0.2581(7)	0.1191(8)
C(2)	0.1372(9)	−0.1229(7)	0.0982(8)	C(43)	0.221(1)	0.3265(7)	0.1117(8)
C(3)	0.0764(8)	−0.0898(6)	0.1458(8)	C(44)	0.122(1)	0.3296(8)	0.1035(8)
C(4)	0.588(1)	0.1921(9)	−0.145(1)	C(45)	0.0696(10)	0.2636(9)	0.1020(8)
C(11)	0.0652(8)	0.0992(6)	0.2942(7)	C(46)	0.1191(9)	0.1937(7)	0.1085(7)
C(12)	0.0666(8)	0.1596(6)	0.3556(7)	C(51)	0.2754(8)	0.0869(6)	−0.0006(7)
C(13)	−0.0203(9)	0.1998(7)	0.3430(8)	C(52)	0.2015(9)	0.1230(7)	−0.0717(8)
C(14)	−0.1097(9)	0.1855(7)	0.2736(9)	C(53)	0.196(1)	0.1106(8)	−0.1619(8)
C(15)	−0.1130(9)	0.1259(8)	0.2145(8)	C(54)	0.265(1)	0.0647(9)	−0.1793(8)
C(16)	−0.0262(9)	0.0843(7)	0.2259(8)	C(55)	0.338(1)	0.0284(7)	−0.1102(10)
C(21)	0.2851(8)	0.0989(6)	0.3774(7)	C(56)	0.3449(9)	0.0390(7)	−0.0193(8)
C(22)	0.3600(9)	0.0654(6)	0.4532(8)	C(61)	0.4138(8)	0.1046(6)	0.1805(7)
C(23)	0.4450(9)	0.1069(8)	0.5049(8)	C(62)	0.4577(9)	0.0665(7)	0.2628(8)
C(24)	0.4559(9)	0.1815(8)	0.4847(9)	C(63)	0.562(1)	0.0722(9)	0.3102(8)
C(25)	0.3817(10)	0.2150(7)	0.4111(9)	C(64)	0.6236(9)	0.1142(9)	0.2781(9)
C(26)	0.2981(8)	0.1741(6)	0.3573(7)	C(65)	0.5824(9)	0.1523(8)	0.1980(9)
C(31)	0.1748(9)	−0.0375(6)	0.3793(7)	C(66)	0.4797(8)	0.1470(7)	0.1486(8)

$OC(CH_2)_2$), 93.9 (s, OCH_2O), 56.7 (s, CH_3), 47.1 (s, $OC(CH_2)_2$) ppm. Anal. Calcd for $C_{10}H_{18}O_4Cl_2Pd_2$: C, 24.71; H, 3.73; Cl, 14.59. Found: C, 25.06; H, 4.06; Cl, 14.45.

Preparation of [Pt(η^3-$CH_2C(OCH_2OCH_2)CH_3$)(PPh_3)$_2$]-Cl (3b). $Pt(PPh_3)_4$[17] (248.8 mg, 0.20 mmol) was dissolved in benzene (6 mL) to give an orange solution. Into the solution was added **1** (32.4 mg, 0.24 mmol), and the solution was stirred at room temperature. After the solution became colorless (about 10 min), hexane (100 mL) was added. The precipitated compound (white powder) was collected by filtration and dried *in vacuo*. The crude compound (155.6 mg) included (oxodimethylenemethane)platinum complex **4b** (33%, estimated by ^{1}H NMR). The mixture including **4b** was used for further process to prepare **4b**.

Preparation of [Pd(η^3-$CH_2C(O)CH_2$)(PPh_3)$_2$] (4a). Into a suspension of **2** (243.0 mg, 0.50 mmol) in THF (10 mL) at 0 °C was added PPh_3 (550.8 mg, 2.10 mmol) in THF (10 mL). After the solution became homogeneous, potassium hydroxide dissolved in 2-propanol (0.1 M) (12 mL, 1.2 mmol) was added to the solution. After the temperature was held at 0 °C for 1 h, the solution was evaporated to dryness and the residue was washed with hexane. The product was purified by recrystallization from dichloromethane/hexane (v/v = 1/6). A yellow powder formed. Yield: 538.8 mg (78%). Mp: 165 °C dec. IR: ν(CO) 1526 cm^{-1}. NMR spectra ($CDCl_3$, 25 °C): ^{1}H NMR, δ 7.31−7.18 (m, 30 H, Ph), 2.71 (s, br, 2 H, *anti*-CH_2), 2.43 (s, br, 2 H, *syn*-CH_2) ppm; $^{13}C\{^1H\}$ NMR, δ 175.1 (s, *C*=O), 133.9 (t, $|^2J(PC) + {}^2J(PC)| = 13.7$ Hz), 133.1 (m, $|^1J(PC) + {}^3J(PC)| = 48.9$ Hz), 129.9 (s), 128.3 (t, $|^3J(PC) + {}^5J(PC)| = 9.9$ Hz), 58.8 (m, $|^2J(PC) + {}^2J(PC)| = 42.7$ Hz, CH_2) ppm; $^{31}P\{^1H\}$ NMR, δ 28.1 (s, PPh_3) ppm. Anal. Calcd for $C_{39}H_{34}OP_2Pd$: C, 68.18; H, 4.99. Found: C, 68.37; H, 5.26.

Preparation of [Pt(η^3-$CH_2C(O)CH_2$)(PPh_3)$_2$] (4b). Potassium hydroxide dissolved in 2-propanol (0.1 M) (2.0 mL, 0.2 mmol) was added to the crude **3b** containing **4b** (ca. 33%) (155.6 mg) in THF (4 mL). After the temperature was held at 0 °C for 1 h, the solution was evaporated to dryness and the residue was washed with hexane. The product was purified by recrystallization from dichloromethane/hexane (v/v = 1/6). A white powder was isolated. Yield: 118.0 mg (76% based on $Pt(PPh_3)_4$). Mp: 222 °C dec. IR: ν(CO) 1593 cm^{-1}. NMR spectra ($CDCl_3$, 25 °C): ^{1}H NMR, δ 7.29−7.16 (m, 30 H, Ph), 2.36 (d, 4 H, J(PtH) = 46 Hz, J(PH) = 3 Hz, CH_2) ppm; $^{13}C\{^1H\}$ NMR, δ 180.5 (s, J(PtC) = 138.9 Hz, *C*=O), 134.0 (m, $|^2J(PC) + {}^2J(PC)| = 12.2$ Hz), 133.0 (d, J(PtC) = 26.7 Hz, J(PC) = 49.6 Hz), 130.0 (s), 128.0 (m, $|^3J(PC) + {}^5J(PC)| = 9.2$ Hz), 51.0 (dd, J(PtC) = 244.1, J(*trans*-PC) = 55.2 Hz, J(*cis*-PC) = 5.1 Hz, CH_2) ppm; $^{31}P\{^1H\}$ NMR, δ 23.5 (s, J(PtC) = 2972 Hz, PPh_3) ppm.

NMR Study of Oxodimethylenemethane Complexes 4. The measurement of coalescence temperature and chemical shift separation was carried out using **4** (0.01 mmol) in solvent (0.5 mL) in a sealed tube with a 270, 400, or 600 MHz NMR instrument.

X-ray Data Collection and Structure Analysis of 4a·CH_2Cl_2. An orange plate crystal of **4a**·CH_2Cl_2 was obtained by recrystallization from dichloromethane/hexane (v/v = 1/5) in a refrigerator. The crystal was mounted on a glass fiber which was soaked in the **4a**-saturated solution in a glass tube sealed with wax. All measurements were made on a Rigaku AFC5R diffractometer with graphite monochromated Mo Kα radiation and a 12 kW rotating anode generator. Cell constants and an orientation matrix for data collection were obtained from a least-squares refinement using the setting angles of 25 centered reflections in the range $27.34 < 2\theta < 27.49$ which corresponded to a primitive monoclinic cell. The data were collected at a temperature of 23 ± 1 °C using the ω−2θ scan technique to a maximum 2θ value of 55.0°. The ω scan of several intense reflections, made prior to data collection, had an average width at half-height of 0.32° with a take-off angle of 6.0°. Scans of (1.21 + 0.35 tan θ)° were at a speed of 16.0°/min (in ω). Totals of 8809 independent reflections were obtained, and 8473 were unique (R_{int} = 0.034). The intensities of three representative reflections were measured after every 150 reflections. The data were corrected for Lorentz and polarization effects. The structure was solved by direct methods[18] and expanded using Fourier techniques.[19] The non-hydrogen atoms were refined anisotropically, and hydrogen atoms were included but not refined. The final cycle of full-matrix least-squares refinement was based on 4028 observed reflections ($I > 3\sigma(I)$). All the positions of hydrogen atoms were calculated by stereochemical considerations. The crystal data and other collection parameters are summarized

(15) Ukai, T.; Kawazura, H.; Ishii, Y. *J. Organomet. Chem.* **1974**, *65*, 253.
(16) Gu, X.-P.; Nishida, N.; Ikeda, I.; Okahara, M. *J. Org. Chem.* **1987**, *52*, 3192.
(17) Ugo, R.; Cariati, F.; La Monica, G. *Inorg. Synth.* **1968**, *11*, 105.
(18) SAPI91: Fan Hai-Fu (1991). Structure Analysis Programs with Intelligent Control, Rigaku Corp., Tokyo, Japan.
(19) DIRDIF92: Beurskens, P. T.; Admiraal, G.; Beurskens, G.; Bosman, W. P.; Garcia-Granda, S.; Gould, R. O.; Smits, J. M. M.; Smykalla, C. The DIRDIF program system, Technical Report of the Crystallography Laboratory, University of Nijmegen, The Netherlands, 1992.

in Table 6, and values for the refined positional parameters for all of the atoms are provided in Table 7.

Acknowledgment. Thanks are due to the Analytical Center, Faculty of Engineering, Osaka University, for the use of the NMR instruments. This work was supported by Grants-in-Aid for Scientific Research on Priority Area of Reactive Organometallics No. 05236104 from the Ministry of Education, Science, and Culture of Japan.

Supplementary Material Available: Tables of atomic coordinates and B_{eq} anisotropic displacement parameters, bond lengths and bond angles, and least-squares planes for **4a**·CH_2Cl_2 (20 pages). Ordering information is given on any current masthead page.

Registry Numbers (supplied by author): **1**, 105104-40-3; **4a**, 151344-42-2; **4b**, 105302-65-6; **4b**·CH_2Cl_2, 121443-75-2; $Pd_2(dba)_3$·$CHCl_3$, 52522-40-4; $Pt(PPh_3)_4$, 14221-02-4.

OM9408167

Generation and Reactivity of Cp*W(NO)(CH_2SiMe_3)H, a 16-Valence-Electron Alkyl Hydride Complex

Jeff D. Debad, Peter Legzdins,* and Sean A. Lumb

Department of Chemistry, The University of British Columbia, Vancouver, British Columbia, Canada V6T 1Z1

Raymond J. Batchelor and Frederick W. B. Einstein*

Department of Chemistry, Simon Fraser University, Burnaby, British Columbia, Canada V5A 1S6

Received January 17, 1995[⊗]

Treatment of solutions of Cp*W(NO)(CH_2SiMe_3)$_2$ with H_2 generates in situ the reactive 16-valence-electron alkyl hydride Cp*W(NO)(CH_2SiMe_3)H, formed by hydrogenolysis of one of the W–C σ-bonds of the dialkyl reactant. The Lewis-acidic hydride complex has not yet been isolated, but its existence has been inferred on the basis of the varied chemical reactions that it undergoes when generated in the presence of reactive substrates. PPh_3 affords the orthometalated complex Cp*W(NO)(H)($PPh_2C_6H_4$) as a yellow crystalline solid probably via the 18-electron adduct Cp*W(NO)(CH_2SiMe_3)(PPh_3)H. Consistently, the same reaction effected with PPh_3-d_{15} results in complete deuteration of the hydride position in the product. Acyclic, conjugated dienes such as butadiene or 2,3-dimethyl-1,3-butadiene afford Cp*W(NO)(η^4-*trans*-diene) complexes. The characteristic chemistry of Cp*W(NO)(CH_2SiMe_3)H is, however, dominated by the ability of its W–H link to insert unsaturated linkages, the regioselectivity of the insertions indicating that the hydride ligand is hydridic in nature. For instance, insertion of acetonitrile affords the ethylideneamido complex Cp*W(NO)(CH_2SiMe_3)(N=CHMe), which is isolable as a diastereomeric pair. Similarly, insertions of organic reagents containing carbonyl (O=C) or imine (HN=C) functional groups produce the corresponding alkyl alkoxide or alkyl amide products, respectively, in virtually quantitative yields. Phenylacetylene affords the novel alkyl alkenyl compound Cp*W(NO)(CH_2SiMe_3)(CPh=CH_2), which is thermally unstable and isolable in only low yields. Insertions into the W–H bond by other olefinic substrates are successful only if the unsaturated hydrocarbon also contains a Lewis-base functional group. Thus, propargylamine and allylamine produce the related metallacyclic complexes Cp*W(NO)(CH_2SiMe_3)(NH_2CH_2CHCH) and Cp*W(NO)(CH_2SiMe_3)($NH_2CH_2CH_2CH_2$), respectively. Treatment of Cp*W(NO)(CH_2SiMe_3)$_2$ with H_2 in the presence of allyl alcohol does not produce an oxometallacycle, but rather affords the allylalkoxo complex resulting from the alcohol simply functioning as a protonic acid toward the dialkyl reactant. The solid-state molecular structures of Cp*W(NO)(CH_2SiMe_3)(N=CHMe) and Cp*W(NO)(CH_2SiMe_3)($NH_2CH_2CH_2CH_2$) have been established by single-crystal X-ray crystallographic analyses. Crystals of Cp*W(NO)(CH_2SiMe_3)(N=CHMe) are monoclinic of space group $P2_1/n$: a = 9.515(2) Å; b = 21.946(3) Å; c = 9.552(2) Å; Z = 4; V = 1946.8 Å^3; T = 200 K; R_f = 0.029 for 2035 data ($I_o \geq 2.5\sigma(I_o)$) and 106 variables. Crystals of Cp*W(NO)(CH_2SiMe_3)($NH_2CH_2CH_2CH_2$) are orthorhombic of space group $P2_12_12_1$: a = 11.417(4) Å; b = 13.178(2) Å; c = 13.804(4) Å; Z = 4; V = 2076.9 Å^3; T = 200 K; R_f = 0.020 for 2420 data ($I_o \geq 2.5\sigma(I_o)$) and 208 variables.

Introduction

Current interest in the synthesis, characterization, and properties of organotransition-metal hydride complexes continues unabated, primarily because many important stoichiometric and catalytic chemical conversions have been demonstrated to involve metal–hydrogen linkages at key stages.[1] In particular, M–H bonds play an important role in organometallic chemistry because many can insert a variety of unsaturated substrates.[2] In this regard, however, relatively little is known presently about the physical and chemical properties of such linkages in organometallic nitrosyl complexes.[3] Consequently, we have been endeavoring for some time to develop new synthetic routes leading to such compounds.

[⊗] Abstract published in *Advance ACS Abstracts,* March 15, 1995.

(1) Collman, J. P.; Hegedus, L. S.; Norton, J. R.; Finke, R. G. *Principles and Applications of Organotransition Metal Chemistry*; University Science Books: Mill Valley, CA, 1987.
(2) Crabtree, R. H. *The Organometallic Chemistry of the Transition Metals,* 2nd ed.; Wiley-Interscience: Toronto, 1994.
(3) Legzdins, P.; Richter-Addo, G. B. *Metal Nitrosyls*; Oxford University Press: New York, 1992.

0276-7333/95/2314-2543$09.00/0

Our early efforts in this area involved the preparation of several hydrido nitrosyl complexes of tungsten containing the CpW(NO) [Cp = η^5-C_5H_5] fragment by treatment of appropriate halide precursors with main-group hydride reagents.[4] More recently, our investigations have centered on the synthesis of hydride compounds via hydrogenation of alkyl complexes. For example, we have discovered that reaction of the dialkyl species Cp*W(NO)(CH_2SiMe_3)$_2$ [Cp* = η^5-C_5Me_5] with dihydrogen affords the bimetallic hydride and alkyl hydride complexes [Cp*W(NO)(H)]$_2$[μ-H]$_2$ and [Cp*W(NO)(CH_2SiMe_3)](μ-H)$_2$[Cp*W(NO)(H)].[5] More importantly, however, we have found that when the hydrogenation of Cp′W(NO)(CH_2SiMe_3)$_2$ [Cp′ = Cp or Cp*] is performed in the presence of a Lewis base (L) such as a small phosphine or phosphite, the 18-valence-electron adducts, Cp′W(NO)(CH_2SiMe_3)(L)H [L = PMe_3, $P(OPh)_3$, $PMePh_2$], can be isolated in good yields.[5] These alkyl hydride adducts exhibit some interesting thermal chemistry in their own right. For example, Cp*W(NO)(CH_2SiMe_3)(PMe_3)H undergoes reductive elimination of $SiMe_4$ upon heating. When this thermolysis is performed in benzene, subsequent activation of the solvent results in the formation of the aryl hydrido complex Cp*W(NO)(Ph)(PMe_3)H. The phosphite analogue, CpW(NO)(CH_2SiMe_3)[$P(OPh)_3$]H, similarly liberates $SiMe_4$ when heated and then orthometalates one of the phenyl groups on the phosphite ligand to produce CpW(NO)[$P(OPh)_2OC_6H_4$]H as the final product.

The isolation of the original Cp′W(NO)(CH_2SiMe_3)(L)H adducts suggests that the 16-valence-electron alkyl hydride compounds, Cp′W(NO)(CH_2SiMe_3)H, are the initial species formed by treatment of the Cp′W(NO)(CH_2SiMe_3)$_2$ precursors with H_2. By analogy to their dialkyl precursors, the Cp′W(NO)(CH_2SiMe_3)H compounds are expected to possess a metal-centered LUMO lying between the hydride and the alkyl ligands and trans to the nitrosyl ligand as shown below.[6]

This LUMO renders these 16-valence-electron complexes Lewis acidic and is the site of attack by Lewis bases. Consistent with this view is the fact that all of the Cp′W(NO)(CH_2SiMe_3)(L)H adducts isolated to date possess the expected four-legged piano-stool molecular structures with the L and the NO groups occupying mutually trans positions. We therefore decided to investigate the reactions of the Cp′W(NO)(CH_2SiMe_3)H intermediates with other Lewis bases, particularly those that might be capable of effecting insertion of L into W−H bonds of the Cp′W(NO)(CH_2SiMe_3)(L)H adducts since these adducts possess the requisite cis orientation of the L and H ligands. The trans orientation of the alkyl and hydride ligands in these adducts also renders them stable with respect to reductive elimination of alkane. In this paper we report the results of our detailed studies in this regard with the pentamethylcyclopentadienyl complex Cp*W(NO)(CH_2SiMe_3)H. Portions of this work have been communicated previously.[7,8]

Experimental Section

All reactions and subsequent manipulations were performed under anaerobic and anhydrous conditions using an atmosphere of dinitrogen or argon. General procedures routinely employed in these laboratories have been described in detail previously.[9] The requisite organometallic reagents, Cp*W(NO)Cl_2[10] and Cp*W(NO)(CH_2SiMe_3)$_2$,[11] were prepared by established procedures. Phenylacetylene (MCB) was passed through a short column of activated alumina before use, benzaldehyde (Fisher) was dried over P_2O_5 and filtered through Celite, PPh_3 (Strem) was recrystallized from hexanes, 2,3-dimethyl-1,3-butadiene (Aldrich) was dried over molecular sieves, allylamine (Aldrich) was dried over Na_2CO_3 and vacuum-transferred, and allyl alcohol (Aldrich) was likewise dried over K_2CO_3 and vacuum-transferred. Dihydrogen (Linde, extra dry), butadiene (Matheson), PPh_3-d_{15}, propargylamine, 4-phenyl-3-penten-2-one, and benzophenoneimine (Aldrich) were all used as received.

Preparation of Cp*W(NO)($PPh_2C_6H_4$)H (1). Cp*W(NO)(CH_2SiMe_3)$_2$ (0.48 g, 0.92 mmol) and PPh_3 (0.29 g, 1.1 mmol) were combined in a large thick-walled bomb equipped with a Kontes stopcock (500 mL capacity) and then dissolved in pentane (30 mL). The vessel was then charged with H_2 (18 psig), and the solution was stirred for 5 h, during which time the product was deposited as a yellow precipitate and the originally purple solution became red-brown in color. Approximately half of the solvent was then removed under vacuum, and the precipitate was allowed to settle to the bottom of the vessel. The supernatant solution was removed via a cannula, and the remaining solid was washed with pentane (20 mL). The powder that remained was recrystallized from Et_2O at −15 °C to obtain bright yellow crystals of the product (0.24 g from three fractions, 43% yield).

Anal. Calcd for $C_{28}H_{30}NOPW$: C, 55.18; H, 5.02; N, 2.24. Found: C, 55.00; H, 4.95; N, 2.29. IR (Nujol) ν_{NO} 1545 cm^{-1}, ν_{WH} 1929 cm^{-1}; ^{1}H NMR (C_6D_6) δ 8.09 (d, $^3J_{HH}$ = 8.0 Hz, 1 H, H_{aryl}), 7.95 (m, 2 H, H_{aryl}), 7.55 (m, 3 H, H_{aryl}), 7.20 (m, 4 H, H_{aryl}), 6.95 (m, 4 H, H_{aryl}), 3.99 (d, $^2J_{PH}$ = 10.2 Hz, $^2J_{WH}$ = 101 Hz, 1 H, W*H*), 1.79 (s, 15 H, C_5Me_5); ^{13}C{^{1}H} NMR (C_6D_6) δ 171.75 (d, J_{CP} = 5.1 Hz, C_{ortho}), 149.23 (d, J_{CP} = 54.6 Hz, C_{ipso}), 1.44 (d, J_{CP} = 33.7 Hz, C_{ipso}), 134.3, 134.2, 133.4, 133.3, 132.2, 132.2, 130.7, 130.7, 129.9, 129.9, 128.9, 128.9, 128.8, 128.8, 128.7, 128.6, 129.5, 128.4 (C_{aryl}), 127.4 (d, J_{CP} = 9 Hz, *Caryl*), 105.5 (C_5Me_5), 10.8 (C_5Me_5); ^{31}P{^{1}H} NMR (C_6D_6) δ 49.21; low-resolution mass spectrum (probe temperature 150 °C); m/z 611 [P$^+$, ^{184}W].

Preparation of Cp*W(NO)(η^4-diene) Complexes 2 and 3. Both of these complexes were prepared in an identical manner, except that 1 equiv of 2,3-dimethyl-1,3-butadiene was weighed into the reaction vessel during the synthesis of complex **3**, whereas butadiene was condensed in excess into

(4) Legzdins, P.; Martin, J. T.; Oxley, J. C. *Organometallics* **1985**, *4*, 1263.
(5) (a) Legzdins, P.; Martin, J. T.; Einstein, F. W. B.; Jones, R. H. *Organometallics* **1987**, *6*, 1826. (b) Martin, J. T. Ph.D. Dissertation, University of British Columbia, 1987.
(6) Legzdins, P.; Rettig, S. J.; Sánchez, L.; Bursten, B. E.; Gatter, M. G. *J. Am. Chem. Soc.* **1985**, *107*, 1411.
(7) Legzdins, P.; Veltheer, J. E. *Acc. Chem. Res.* **1993**, *26*, 41.
(8) (a) Debad, J. D.; Legzdins, P.; Batchelor, R. J.; Einstein, F. W. B. *Organometallics* **1992**, *11*, 6. (b) Debad, J. D.; Legzdins, P.; Young, M. A.; Batchelor, R. J.; Einstein, F. W. B. *J. Am. Chem. Soc.* **1993**, *115*, 2051.
(9) Dryden, N. H.; Legzdins, P.; Rettig, S. J.; Veltheer, J. E. *Organometallics* **1992**, *11*, 2583.
(10) Dryden, N. H.; Legzdins, P.; Batchelor, R. J.; Einstein, F. W. B. *Organometallics* **1991**, *10*, 2077.
(11) Veltheer, J. E.; Legzdins, P. In *Handbook of Preparative Inorganic Chemistry*, 4th ed.; Herrmann, W. A., Ed.; in press.

the vessel during the synthesis of **2**. The preparation of the butadiene complex, **2**, is described as a representative example.

$Cp^*W(NO)(CH_2SiMe_3)_2$ (0.40 g, 0.76 mmol) was placed in a 300-mL thick-walled bomb. The vessel was evacuated and then refilled with butadiene gas (1 atm). The bomb was then cooled to −178 °C to condense the butadiene gas. Pentane (60 mL) was added slowly so that it froze on the sides of the vessel as it was added. The atmosphere was again removed under vacuum and was replaced with H_2 (15 psig). The vessel was warmed to room temperature, and the solution was stirred overnight. The solvent was removed in vacuo from the final yellow solution to obtain an orange powder which was washed with cold pentane (2 × 10 mL). The remaining powder was recrystallized from hexanes at −30 °C to obtain yellow crystals of **2** (0.17 g, 32% yield) which were isolated by removing the supernatant solution by cannulation. Complex **3** was also isolated as yellow crystals in a similar manner in 31% yield.

Anal. Calcd for $C_{14}H_{21}NOW$ (**2**): C, 41.70; H, 5.25; N, 3.47. Found: C, 41.73; H, 5.43; N, 3.48. IR (Nujol) ν_{NO} 1563 cm^{-1}; ^1H NMR (C_6D_6) δ 3.56 (m, 1 H, C*H*), 3.37 (dd, J = 5.4, 4.2 Hz, 1 H, C*H*), 2.95 (dd, J = 13.8, 3.6 Hz, 1 H, C*H*), 2.40 (dd, J = 6.3, 3.6 Hz, 1 H, C*H*), 1.63 (s, 15 H, C_5Me_5), 1.29 (m, 1 H, C*H*), 1.00 (dd, J = 12.0, 4.2 Hz, 1H, C*H*); $^{13}C\{^1H\}$ NMR (C_6D_6) δ 104.20 (C_5Me_5), 91.8 (*C*H), 85.0 (*C*H), 54.3 (CH_2), 51.5 (CH_2), 10.4 (C_5Me_5); low-resolution mass spectrum (probe temperature 150 °C), m/z 403 [P^+, ^{184}W].

Anal. Calcd for $C_{16}H_{25}NOW$ (**3**): C, 44.56; H, 5.84; N, 3.25. Found: C, 44.83; H, 5.89; N, 3.14. IR (Nujol) ν_{NO} 1574 cm^{-1}; ^1H NMR (C_6D_6) δ 3.35 (dd, J = 4.5, 0.9 Hz, 1 H, C*H*), 3.25 (d, J = 3.6 Hz, 1 H, C*H*), 2.49 (dd, J = 3.6, 1.2 Hz, 1 H, C*H*), 2.41 (br, 1 H, C*H*), 2.15 (s, 3 H, *Me*), 1.71 (s, 15 H, C_5Me_5), 1.20 (s, 3 H, *Me*); $^{13}C\{^1H\}$ NMR (C_6D_6) δ 104.6 (C_5Me_5), 103.45 (=CH_2), 95.5 (=CH_2), 54.3 (CH_2), 52.3 (CH_2), 21.92 (*Me*), 21.7 (CH_3), 10.6 (C_5Me_5); low-resolution mass spectrum (probe temperature 180 °C), m/z 431 [P^+, ^{184}W].

Preparation of Cp*W(NO)(CH_2SiMe_3)(N=CHMe) (4). Purple $Cp^*W(NO)(CH_2SiMe_3)_2$ (1.9 g, 3.6 mmol) was dissolved in acetonitrile (30 mL), and the solution was transferred to a 500-mL Fisher-Porter vessel. The atmosphere in the vessel was replaced with H_2 (12 psig), and the solution was stirred overnight at room temperature. The final red-orange solution was taken to dryness in vacuo, and the residue was washed with cold pentane (3 × 10 mL). The remaining yellow powder was recrystallized from hexanes at −30 °C to obtain yellow crystals (1.3 g, 78% yield) of analytically pure **4**.

Anal. Calcd for $C_{16}H_{30}SiN_2OW$: C, 40.17; H, 6.32; N, 5.86. Found: C, 40.50; H, 6.34; N, 5.99. IR (Nujol) ν_{NO} 1615 cm^{-1}, ν_{CN} 1652 cm^{-1}; ^1H NMR (C_6D_6), diastereomer 1 δ 7.20 (m, 1 H, C*H*), 1.71 (s, 15 H, C_5Me_5), 1.45 (d, $^3J_{HH}$ = 5.4 Hz, 3 H, N=CH*Me*), 0.43 (s, 9 H, $SiMe_3$), 0.10 (m, 2 H, CH_2), diastereomer 2 δ 6.48 (m, 1 H, C*H*), 1.66 (s, 15 H, C_5Me_5), 1.62 (d, $^3J_{HH}$ = 5.5 Hz, 3 H, N=CH*Me*), 0.50 (s, 9 H, $SiMe_3$), 0.25 (m, 2 H, CH_2); $^{13}C\{^1H\}$ NMR (C_6D_6), diastereomer 1 δ 158.77 (N=*C*HMe), 109.55 (C_5Me_5), 21.57 (*Me*), 19.05 (CH_2), 10.00 (C_5Me_5), 2.85 ($SiMe_3$), diastereomer 2 δ 158.35 (N=*C*HMe), 109.00 (C_5Me_5), 20.76 (*Me*), 19.15 (CH_2), 9.54 (C_5Me_5), 3.10 ($SiMe_3$); low-resolution mass spectrum (probe temperature 150 °C), m/z 478 [P^+, ^{184}W].

Preparation of Cp*W(NO)(CH_2SiMe_3)($OCHMe_2$) (5). $Cp^*W(NO)(CH_2SiMe_3)_2$ (0.38 g, 0.72 mmol), acetone (0.5 mL, 7 mmol), and hexanes (10 mL) were placed in a thick-walled bomb (300 mL). The vessel was then charged with H_2 (~18 psig), and the reaction mixture was stirred for 5 h at ambient temperature. After this time, the solvent was removed under vacuum to leave a red powder. The powder was recrystallized from a minimum amount of pentane at −30 °C to obtain **5** as deep red crystals, which were isolated by removing the mother liquor via a cannula. A second crop of crystals was obtained from the supernatant solution by further concentration and cooling (total of 0.28 g, 79% yield).

Anal. Calcd for $C_{17}H_{33}NO_2SiW$: C, 40.58; H, 6.52; N, 2.48. Found: C, 41.21; H, 6.71; N, 2.83. IR (Nujol) 1568, 1541 cm^{-1}; ^1H NMR (C_6D_6) δ 5.22 (sept, $^3J_{HH}$ = 6.3 Hz, 1 H, OC*H*Me_2), 1.61 (s, 15 H, C_5Me_5), 1.27 (d, $^3J_{HH}$ = 6 Hz, 3 H, *Me*), 1.21 (d, $^3J_{HH}$ = 6 Hz, 3 H, *Me*), 0.73 (d, $^2J_{HH}$ = 12 Hz, 1 H, CH_2), 0.52 (d, $^2J_{HH}$ = 12 Hz, 1 H, CH_2), 0.35 (s, 9 H, $SiMe_3$); $^{13}C\{^1H\}$ NMR (C_6D_6) δ 111.8 (C_5Me_5), 82.3 (O*C*HMe$_2$), 31.9 (J_{WC} = 109 Hz, CH_2), 27.9, 26.5 (*Me*), 9.8 (C_5Me_5), 2.4 ($SiMe_3$); low-resolution mass spectrum (probe temperature 180 °C), m/z 495 [P^+, ^{184}W].

Preparation of Cp*W(NO)(CH_2SiMe_3)(OCH_2Ph) (6). $Cp^*W(NO)(CH_2SiMe_3)_2$ (0.32 g, 0.61 mmol) was dissolved in hexanes (15 mL) in a thick-walled bomb. Benzaldehyde (0.06 g, 0.65 mmol) was added, and the atmosphere in the bomb was replaced with H_2 (~18 psig). The reaction mixture was stirred for 16 h, during which time its color changed from purple to deep orange. The solvent was removed in vacuo to leave a red-orange powder which was recrystallized in two crops from pentane at −30 °C to obtain red crystals (0.28 g total, 83% yield) of **6**.

Anal. Calcd for $C_{21}H_{33}NO_2SiW$: C, 46.38; H, 6.15; N, 2.40. Found: C, 46.41; H, 6.12; N, 2.58. IR (Nujol) ν_{NO} = 1545 cm^{-1}; ^1H NMR (C_6D_6) δ 7.41 (d, $^3J_{HH}$ = 6.9 Hz, 2 H, H_{ortho}), 7.1 (m, 3 H, H_{aryl}), 5.97 (d, $^2J_{HH}$ = 10.8 Hz, 1 H, OCH_2), 5.88 (d, $^2J_{HH}$ = 10.8 Hz, 1 H, OCH_2), 1.44 (s, 15 H, C_5Me_5), 0.82 (s, 2 H, CH_2), 0.36 (s, 9 H, $SiMe_3$); $^{13}C\{^1H\}$ NMR (C_6D_6) δ 141.7 (C_{ipso}), 129.6, 128.6, 128.0 (C_{aryl}), 111.9 (C_5Me_5), 85.5 (OCH_2), 35.1 ($^1J_{WC}$ = 119 Hz, SiCH_2), 9.5 (C_5Me_5), 2.3 ($SiMe_3$); low-resolution mass spectrum (probe temperature 120 °C), m/z 543 [P^+, ^{184}W].

Preparation of Cp*W(NO)(CH_2SiMe_3)(OCHMeCH=CHPh) (7). $Cp^*W(NO)(CH_2SiMe_3)_2$ (0.09 g, 0.17 mmol) was dissolved in hexanes (10 mL) in a small, thick-walled bomb. 4-Phenyl-3-buten-2-one (0.025 g, 0.17 mmol) was added, and the vessel was charged with H_2 (18 psig). After being stirred for 5 h, the solvent was removed in vacuo from the final reaction solution, which had developed a deep red color. The red residue was recrystallized in two crops from a minimum amount of pentane at −30 °C to obtain **7** as analytically pure red crystals (0.80 g total, 80% yield).

Anal. Calcd for $C_{24}H_{37}NO_2SiW$: C, 49.43; H, 6.45; N, 2.32. Found: C, 49.40; H, 6.39; N, 2.40. IR (Nujol) ν_{NO} = 1549 cm^{-1}; ^1H NMR (C_6D_6), major isomers δ 7.4 (m, 5 H, H_{aryl}), 6.68 (d, $^3J_{HH}$ = 15.6 Hz, 1 H, PhC*H*CH), 6.25 (dd, J_{HH} = 8.1, 15.6 Hz, 1 H, PhCHC*H*), 5.64 (m, 1 H, OC*H*), 1.86 (s, 15 H, C_5Me_5), 1.44 (d, J_{HH} = 6.3 Hz, 3 H, *Me*), 0.84 (d, $^2J_{HH}$ = 11.7 Hz, 1 H, CH_AH_B), 0.70 (d, $^2J_{HH}$ = 11.7 Hz, 1 H, CH_AH_B), 0.11 (s, 9 H, $SiMe_3$), minor isomers 7.4 (m, 5 H, H_{aryl}), 6.48 (d, $^2J_{HH}$ = 15.6 Hz, 1 H, PhC*H*CH), 6.23 (dd, J_{HH} = 6.3, 15.6 Hz, 1 H, PhCHC*H*), 5.64 (m, 1 H, OC*H*), 1.95 (s, 15 H, C_5Me_5), 1.50 (d, $^3J_{HH}$ = 6.3 Hz, 3 H, *Me*), 0.81 (d, $^2J_{HH}$ = 12.0 Hz, 1 H, CH_AH_B), 0.66 (d, $^2J_{HH}$ = 12.0 Hz, 1 H, CH_AH_B), 0.06 (s, 9 H, $SiMe_3$); $^{13}C\{^1H\}$ NMR (C_6D_6) (all isomers) δ 137.0, 136.8 (PhCHCH), 134.2, 134.03 (PhCHCH), 131.2, 129.3, 128.7, 128.5, 127.7, 127.6, 126.7, 126.6 (C_{aryl}), 112.63, 112.5 (C_5Me_5), 87.9, 86.4 (OC), 35.2, 35.2 (CH_2), 26.7, 24.4 (*Me*), 10.1, 10.0 (C_5Me_5), 2.0, 1.91 ($SiMe_3$); low-resolution mass spectrum (probe temperature 150 °C), m/z 583 [P^+, ^{184}W].

Preparation of Cp*W(NO)(CH_2SiMe_3)($NHCHPh_2$) (8). $Cp^*W(NO)(CH_2SiMe_3)_2$ (0.28 g, 0.53 mmol) and benzophenoneimine (0.10 g, 0.55 mmol) were dissolved in hexanes (10 mL) contained in a thick-walled bomb which was then charged with H_2 (18 psig). After the mixture had been stirred for 8 h, the solvent was removed under vacuum to obtain a yellow solid. This solid was recrystallized from CH_2Cl_2/hexanes to obtain analytically pure product (0.16 g, 49% yield).

Anal. Calcd for $C_{27}H_{38}N_2OSiW$: C, 52.18; H, 6.24; N, 4.47. Found: C, 52.43; H, 6.19; N, 4.53. IR (Nujol) ν_{NO} 1514 cm^{-1}, ν_{NH} 3249 cm^{-1}; ^1H NMR (C_6D_6) δ 7.75 (br, 1 H, N*H*), 7.6 (m, 6 H, H_{aryl}), 7.4 (m, 4 H, H_{aryl}), 6.72 (d, J_{HH} = 11.4 Hz, 1 H, CPh_2H), 1.71 (s, 15 H, C_5Me_5), −0.030 (d, J_{HH} = 2.7 Hz, 2 H, CH_2), −0.085 (s, 9 H, $SiMe_3$); $^{13}C\{^1H\}$ NMR (C_6D_6) δ 146.3, 143.3 (C_{ipso}), 128.8, 128.1, 128.0 (C_{aryl}), 126.9, 126.6, 126.5 (C_{aryl}), 78.9 (C_5Me_5), 24.7 ($^1J_{WC}$ = 104 Hz, CH_2), 9.7 (C_5Me_5),

2.0 ($SiMe_3$); low-resolution mass spectrum (probe temperature 120 °C), m/z 618 [P^+, ^{184}W].

Preparation of Cp*W(NO)(CH_2SiMe_3)(CPh=CH_2) (9). Cp*W(NO)(CH_2SiMe_3)$_2$ (0.50 g, 0.95 mmol) and phenylacetylene (0.15 g, 1.5 mmol) were dissolved in hexanes (30 mL), and the solution was transferred to a 300-mL thick-walled bomb. H_2 (18 psig) was introduced into the vessel, and the mixture was stirred for 5 h, whereupon it turned a dark brown color. The solvent was then removed under vacuum, the residue was dissolved in Et_2O (3 mL), and the solution was placed on the top of a chromatography column (Florisil, 10 × 2 cm) made up in hexanes. Elution of the column with Et_2O/hexanes (1:2) developed first a yellow band, which was eluted, and then a red band, which was collected. The red eluate was taken to dryness in vacuo, and the residue was recrystallized from pentanes at −30 °C to obtain a small amount of complex **9** as red crystals.

Anal. Calcd for $C_{22}H_{33}NOSiW$: C, 49.30; H, 6.29; N, 2.52. Found: C, 48.98; H, 6.17; N, 2.60. IR (Nujol) ν_{NO} 1539 cm^{-1}; ^{1}H NMR (C_6D_6) δ 7.87 (dd, J_{HH} = 8.0, 1.2 Hz, 2 H, H_{ortho}), 7.29 (t, J_{HH} = 8.0, 2 H, H_{meta}), 7.11 (t, J_{HH} = 8.0, 1 H, H_{para}), 3.88 (dd, J_{HH} = 5.4, 1.4 Hz, 1 H, C=CH_AH$_B$), 3.56 (dd, J_{HH} = 5.4, 1.1 Hz, 1 H, C=CH$_A$$H_B$), 1.50 (s, 15 H, C_5Me_5), 0.692 (d, J_{HH} = 12.6 Hz, 1 H, CH_AH$_B$), 0.214 (d, J_{HH} = 12.6 Hz, 1 H, CH$_A$$H_B$); ^{13}C{^{1}H} NMR ($C_6D_6$) δ 227.9 (W*C*Ph=CH$_2$), 145.3 (C_{ipso}), 137.44 (C_{ortho}), 129.6, 128.8 (C_{aryl}), 109.6 (C_5Me$_5$), 83.1 (WCPh=*C*H$_2$), 35.5 ($^1J_{WC}$ = 90.1 Hz, W*C*H$_2$), 9.5 (C_5Me_5), 3.4 ($SiMe_3$); low-resolution mass spectrum (probe temperature 120 °C), m/z 539 [P^+, ^{184}W].

Preparation of Cp*W(NO)(CH_2SiMe_3)($NH_2CH_2CH_2CH_2$) (10). Cp*W(NO)(CH_2SiMe_3)$_2$ (0.524 g, 1.00 mmol) was placed in a 100-mL-capacity thick-walled bomb, and hexanes (20 mL) were added. An excess of allylamine was vacuum-transferred into the bomb. The bomb was then charged with H_2 (18 psig), and the reaction mixture was stirred at room temperature. After 6 h, the initially purple solution had become reddish-brown and a finely divided precipitate had appeared. The brown supernatant solution was removed by cannula, and the remaining yellow solid was washed with cold hexanes (2 × 10 mL) and dried under vacuum to obtain a yellow powder (0.231 g, 0.467 mmol). Recrystallization of this powder from CH_2Cl_2/hexanes in two crops afforded pure crystals of **10** in the form of yellow cubes (0.18 g total, 37% yield).

Anal. Calcd for $C_{17}H_{34}N_2OSiW$: C, 41.30; H, 6.92; N, 5.67. Found: C, 41.34; H, 6.80; N, 5.54. IR (Nujol) ν_{NO} 1497 cm^{-1}; ^{1}H NMR ($CDCl_3$) δ 3.18 (br s, 2 H, NH_2CH$_2$CH$_2$CH$_2$W), 2.73 (m, 1 H, NH$_2$CH_AH$_B$CH$_2$CH$_2$W), 2.46 (m, 1 H, NH$_2$CH$_A$$H_BCH_2CH_2$W), 1.96 (m, 1 H, NH$_2CH_2CH_AH_BCH_2$W), 1.83 (m, 1 H, NH$_2CH_2CH_A$$H_BCH_2$W), 1.78 (s, 15 H, C_5Me_5), 1.58 (m, 1 H, NH$_2$CH$_2$CH$_2$CH_AH$_B$W), 0.77 (m, 1 H, NH$_2$CH$_2$CH$_2$CH$_A$$H_B$W), 0.38 (s, 9 H, CH$_2SiMe_3$), −0.78 (d, $^2J_{HH}$ = 15 Hz, 1 H, CH_AH$_B$SiMe$_3$), −1.39 (d, $^2J_{HH}$ = 15 Hz, 1 H, CH$_A$$H_B$SiMe$_3$); ^{13}C{^{1}H} NMR ($CDCl_3$) δ 102.9 (C_5Me$_5$), 43.9, 31.4, 30.5 (NH$_2$*C*H$_2$*C*H$_2$*C*H$_2$W), 10.3 (C_5Me_5), 5.9 (*C*H$_2$SiMe$_3$), −0.9 (CH$_2$SiMe_3); low-resolution mass spectrum (probe temperature 180 °C), m/z 494 [P^+, ^{184}W].

Preparation of Cp*W(NO)(CH_2SiMe_3)(NH_2CH_2CH=CH) (11). Cp*W(NO)(CH_2SiMe_3)$_2$ (0.262 g, 0.500 mmol) and hexanes (30 mL) were placed in a 100-mL thick-walled bomb, an excess of propargylamine in hexanes (10 mL) was added, and the bomb was pressurized with H_2 (18 psig). After being stirred for 8 h, the reaction mixture consisted of an orange precipitate and a brown supernatant solution. The orange solid was isolated by cannulation, washed with cold hexanes (2 × 10 mL), and dried under vacuum to obtain an orange powder (0.167 g). Recrystallization of this powder from CH_2Cl_2/hexanes afforded analytically pure crystals of **11** in the form of orange cubes (0.10 g, 42% yield).

Anal. Calcd for $C_{17}H_{32}N_2OSiW$: C, 41.47; H, 6.86; N, 5.69. Found: C, 41.51; H, 6.89; N, 5.70. IR (Nujol) ν_{NO} = 1501 cm^{-1}; ^{1}H NMR ($CDCl_3$) δ 7.23 (d, $^2J_{HH}$ = 18 Hz, 1 H, NH_AH$_B$), 6.47 (d, $^2J_{HH}$ = 18 Hz, 1 H, NH_AH$_B$), 3.48 (m, 3 H, NH$_2$CH_A-H_BCH=C*H*), 2.39 (m, 1 H, NH$_2$CH$_2$C*H*=CH), 1.80 (s, 15 H, C_5Me_5), 0.80 (s, 9 H, CH$_2$SiMe_3), −0.78 (d, $^2J_{HH}$ = 15 Hz, 1 H, CH_AH$_B$SiMe$_3$), −1.17 (d, $^2J_{HH}$ = 15 Hz, 1H, CH$_A$$H_B$SiMe$_3$); ^{13}C{^{1}H} NMR ($CDCl_3$) δ 175.1 (NH$_2CH_2$CH=*C*H), 131.2 (NH$_2$-CH$_2$*C*H=CH), 107.2 (C_5Me$_5$), 53.1 (NH$_2$*C*H$_2$CH=CH), 14.8 (*C*H$_2$SiMe$_3$), 9.8 (C_5Me_5), 3.1 (CH$_2$SiMe_3); low-resolution mass spectrum (probe temperature 100 °C), m/z 492 [P^+, ^{184}W].

Preparation of Cp*W(NO)(CH_2SiMe_3)(OCH_2CHCH_2) (12). Cp*W(NO)(CH_2SiMe_3)$_2$ (0.262 g, 0.500 mmol) and hexanes (25 mL) were placed in a small thick-walled bomb, an excess of allyl alcohol was added, and the bomb was pressurized with H_2 (18 psig). Stirring of the reaction mixture for 2 h resulted in it becoming dark red and in the deposition of an orange precipitate. The solvent was removed in vacuo, and the remaining red oil was extracted with pentane (15 mL). The red extracts were filtered through Celite (1 × 2 cm), and solvent was removed from the filtrate under vacuum to obtain a dark red oil (0.20 g). The oil was dissolved in a minimum volume of hexanes, and slow evaporation of this solution at −30 °C afforded dark red needles of **13** (0.08 g, 32% yield).

Anal. Calcd for $C_{17}H_{31}NO_2SiW$: C, 41.39; H, 6.33; N, 2.84. Found: C, 39.93; H, 6.25; N, 2.45. IR (Nujol) ν_{NO} = 1576 cm^{-1}; ^{1}H NMR (C_6D_6) δ 5.96 (m, $^3J_{HH}$ = 6.0, 6.5, 10, 17 Hz, 1 H, OCH$_2$C*H*=CH$_2$), 5.43 (m, $^2J_{HH}$ = 1.0 Hz, $^3J_{HH}$ = 6.0, 6.5 Hz, $^4J_{HH}$ = 0.9, 1.2, 1.5, 1.8 Hz, 2 H, OC$H_A$$H_B$CH=CH$_2$), 5.19 (d of m, $^2J_{HH}$ = 0.9 Hz, $^3J_{HH}$ = 17 Hz, $^4J_{HH}$ = 0.9, 1.2 Hz, 1 H, OCH$_2$-CH=CH_AH$_B$), 5.02 (d of m, $^2J_{HH}$ = 0.9 Hz, $^3J_{HH}$ = 10 Hz, $^4J_{HH}$ = 1.5, 1.8 Hz, 1 H, OCH$_2$CH=CH$_A$$H_B$), 1.60 (s, 15 H, C_5Me_5), 0.89 (d, $^2J_{HH}$ = 12.0 Hz, 1 H, CH_AH$_B$SiMe$_3$), 0.82 (d, $^2J_{HH}$ = 12.0 Hz, 1 H, CH$_A$$H_B$SiMe$_3$), 0.37 (s, 9 H, CH$_2SiMe_3$); ^{13}C{^{1}H} NMR ($C_6D_6$) δ 138.6 (OCH$_2$*C*H=CH$_2$), 116.5 (OCH$_2$CH=*C*H$_2$), 111.8 (C_5Me$_5$), 83.6 (O*C*H$_2$CH=CH$_2$), 35.4 (*C*H$_2$SiMe$_3$), 9.7 (C_5Me_5), 2.2 (CH$_2$SiMe_3); low-resolution mass spectrum (probe temperature 120 °C), m/z 493 [P^+, ^{184}W].

X-ray Crystallographic Analysis of Cp*W(NO)(CH_2-SiMe$_3$)(N=CHMe) (4). An amber-red crystal of **4** was mounted in a Lindemann capillary tube under argon. Intensity data (Mo Kα/graphite monochromator) were collected at 200 K with an Enraf Nonius CAD-4F diffractometer equipped with an extensively in-house modified low-temperature attachment. Two intensity standards were measured every hour of aquisition time and showed no significant variations during the course of data acquisition. The data were corrected for absorption by the Gaussian integration method.[12] Data reduction included intensity scaling and Lorentz and polarization corrections.

The position of the W atom was determined from a Patterson map. Subsequent Fourier synthesis revealed the non-hydrogen atoms of the NO, CH_2SiMe_3, and Cp* groups. An electron density difference map displayed peaks attributable to a disordered ligand, N=CHMe, presumably derived from acetonitrile being coordinated to the precursor tungsten hydride complex (vide infra). This disorder was modeled with two fractionally occupied isotropic sites and a single isotropic thermal parameter for each of the three non-hydrogen atoms of the ligand. A single parameter was refined for the split sites of this group such that the total N=CHMe occupancy was 1. Soft restraints were applied to the bond distances of the disordered ligand such that the lengths of the pairs of chemically equivalent bonds and the two N−C−C angles were restrained toward their respective mean values. The final full-matrix, least-squares refinement of 1056 parameters for 2035 observed data and 8 restraints included anisotropic thermal parameters for W and Si. Hydrogen atoms were placed in calculated positions and assigned anisotropic thermal parameters initially 10% larger than those for the corresponding carbon atoms. Those of the disordered ligand were given the appropriate fractional occupancies. The calculated rotational conformation of the methyl group in either conformation of

(12) Demeulenaer, J.; Tompa, H. *Acta Crystallogr.* **1965**, *19*, 1014.

Table 1. Crystallographic Data for Complexes Cp*W(NO)(CH$_2$SiMe$_3$)(N=CHMe) (4) and Cp*W(NO)(CH$_2$SiMe$_3$)(NH$_2$CH$_2$CH$_2$CH$_2$) (10)

	4	10
formula	$WSiON_2C_{16}H_{30}$	$WSiON_2C_{17}H_{34}$
fw	478.36	494.40
crystal system	monoclinic	orthorhombic
space group	$P2_1/n$	$P2_12_12_1$
a, Å[a]	9.515(2)	11.417(4)
b, Å	21.946(3)	13.178(2)
c, Å	9.522(3)	13.804(4)
β°	102.57(2)	
V, Å^3	1946.8	2076.9
Z	4	4
ϱ_{calcd}, g/cm^3	1.632	1.581
λ(Mo Kα), Å	0.70930 (Kα$_1$)	0.70930 (Kα$_1$)
μ(Mo Kα), cm^{-1}	61.22	57.4
temp, K	200	200
trans factors[b]	0.260–0.392	0.181–0.261
min–max 2θ, deg	4–48	4–54
reflns with $I \geq 2.5\sigma(I)$	2035	2420
no. of variables	106	208
R_f[c]	0.029	0.020
R_w[d]	0.028	0.025
GoF[e]	1.23	1.53

[a] Unit cell dimensions were determined for compounds **4** and **10** from 25 reflections (34° < 2θ < 44° and 43° < 2θ < 50°, respectively). [b] The data were corrected for the effects of absorption by the Gaussian integration method. [c] $R = \sum||F_o| - |F_c||/\sum|F_o|$ for $I_o \geq 2.5\sigma(I_o)$. [d] For compound **4**, $R_w = \sum w(|F_o| - |F_c|)^2/\sum wF_o^2$, where $w = [4.214t_0(x) + 4.849t_1(x) + 3.163t_2(x)]^{-1}$, $x = |F_o|/F_{max}$, and t_n are the polynomial functions of the Chebyshev series.[14] For compound **10**, $R_w = [\sum w(|F_o| - |F_c|)^2/\sum wF_o^2]^{1/2}$, where $w = [\sigma(F_o)^2 + 0.0001(F_o)^2]^{-1}$. [e] $GoF = [\sum w(|F_o| - |F_c|)^2/\text{degrees of freedom}]^{1/2}$.

this ligand was chosen such that a hydrogen atom eclipses the corresponding nitrogen atom when viewed along the C–C bond. While alternate conformations of these methyl groups did not significantly increase the least-squares residual, the one chosen produced a flatter electron density difference map, resulted in a slightly more stable refinement of the parameters of the ligand, and is chemically reasonable. Coordinate shifts equivalent to those of their respective carbon atoms were applied to the hydrogen atoms, and their temperature factors were refined as a single parameter. An empirical weighting scheme was applied such that $\langle w(|F_o| - |F_c|)^2\rangle$ was near constant as a function of both $|F_o|$ and sin θ/λ.

Complex scattering factors for neutral atoms[13] were used in the calculation of structure factors. The programs used for data reduction, structure solution, and initial refinement were from the NRCVAX Crystal Structure System.[14] The program suite CRYSTALS 5[15]was employed in the final refinement. All computations were carried out on a MicroVAX-II computer. Crystallographic data are found in Table 1. Fractional atomic coordinates are located in Table 2, and selected bond lengths and angles are provided in Table 3. A view of the solid-state molecular structure of **4** is shown in Figure 1. Tables of the coordinates for the hydrogen atoms and the anisotropic temperature factors for **4** are deposited as supplementary material.

X-ray Crystallographic Analysis of Cp*W(NO)(NH$_2$CH$_2$CH$_2$CH$_2$)(CH$_2$SiMe$_3$) (10). A crystal of **10** was prepared for X-ray structure determination in a manner similar to that described in the preceding section for **4**. Data were also recorded at 200 K with the same instrument and were processed analogously. Two standard reflections which were measured every hour of exposure time declined in intensity by ~8% during the course of the measurements. One complete octant of data ($+h$, $+k$, $+l$; 4° < 2θ < 54°) was measured.

Coordinates and anisotropic thermal parameters for all non-hydrogen atoms were refined. The hydrogen atoms were placed in calculated positions and were assigned isotropic temperature factors initially proportionate to the equivalent isotropic temperature factors of the corresponding C or N atom. In subsequent cycles of refinement, the coordinate shifts for the hydrogen atoms were linked with those for the atoms to which they were bound. Mean isotropic temperature factors were refined for the hydrogen atoms of each of the two chemically distinct types of methyl group and each CH_2 or NH_2 group, and the shifts were applied to the individual values.

All eight symmetry- and Friedel-related reflections were measured for each of 25 sets of indices, for which $|F_c^+| - |F_c^-|$ was calculated to be most significant in terms of $\sigma(F_o)$ (ranging

Table 2. Coordinates (×10^4) and Isotropic or Equivalent Isotropic Temperature Factors (Å^2 × 10^3) for the Non-Hydrogen Atoms of Cp*W(NO)(CH$_2$SiMe$_3$)(N=CHMe) (4) at 200 K

atom	x/a	y/b	z/c	U(iso)
W	1404.6(3)	810.5(2)	2472.3(4)	30
Si	−214(3)	2110(1)	3310(3)	45
O(1)	−1343(7)	119(3)	2225(7)	56(2)
N(1)	−263(7)	443(3)	2277(7)	42(2)
C(1)	3945(8)	882(4)	3436(8)	36(2)
C(2)	3326(9)	534(4)	4463(9)	37(2)
C(3)	2724(8)	6(4)	3753(8)	33(2)
C(4)	2921(9)	13(4)	2338(9)	40(2)
C(5)	3723(9)	545(4)	2160(9)	41(3)
C(10)	4740(10)	1478(4)	3753(10)	48(3)
C(20)	3494(9)	683(4)	6031(9)	46(3)
C(30)	1988(10)	−499(5)	4416(10)	51(3)
C(40)	2541(10)	−496(5)	1260(10)	52(3)
C(50)	4307(9)	703(4)	861(9)	47(3)
C(6)	956(9)	1457(4)	4033(9)	37(2)
C(7)	898(13)	2691(6)	2619(13)	77(4)
C(8)	−1830(12)	1891(5)	1898(12)	67(3)
C(9)	−904(14)	2463(6)	4829(14)	83(4)
N(2)[a]	1076(13)	1134(5)	614(8)	30(3)
C(11)[a]	934(14)	1244(5)	−674(10)	39(3)
C(12)[a]	442(17)	1836(6)	−1395(15)	57(4)
N(20)[b]	38(20)	1331(7)	828(12)	30(3)
C(110)[b]	873(22)	1622(7)	−315(13)	39(3)
C(120)[b]	1003(27)	1381(11)	−1752(16)	57(4)

[a] Occupancy = 0.60(2). [b] Occupancy = 0.40.

Table 3. Selected Intramolecular Distances (Å) and Angles (deg) for Cp*W(NO)(CH$_2$SiMe$_3$)(N=CHMe) (4) at 200 K

W–N(1)	1.753(7)	Si–C(6)	1.853(8)
W–Cp[a]	2.03	Si–C(7)	1.87(1)
W–C(6)	2.167(8)	Si–C(8)	1.87(1)
W–N(2)	1.87[b]	Si–C(9)	1.88(1)
W–N(20)	1.91[b]	O(1)–N(1)	1.242(9)
N(2)–C(11)	1.23[b]	N(20)–C(110)	1.25[b]
C(11)–C(12)	1.50[b]	C(110)–C(120)	1.50[b]
N(1)–W–Cp	123.8	C(7)–Si–C(6)	108.6(5)
N(2)–W–Cp	117.3	C(8)–Si–C(6)	113.7(5)
N(20)–W–Cp	123.3	C(8)–Si–C(7)	111.1(5)
C(6)–W–Cp	110.2	C(9)–Si–C(6)	108.2(5)
C(6)–W–N(1)	93.7(3)	C(9)–Si–C(7)	108.1(6)
N(2)–W–N(1)	96.5(4)	C(9)–Si–C(8)	106.9(6)
N(20)–W–N(1)	100.9(6)	Si–C(6)–W	116.3(4)
N(2)–W–C(6)	112.7(4)	C(11)–N(2)–W	168.4(9)
N(20)–W–C(6)	98.4(6)	C(12)–C(11)–N(2)	126[b]
O(1)–N(1)–W	171.7(6)	C(110)–N(20)–W	173.0(13)
		C(120)–C(110)–N(20)	127[b]

[a] Cp represents the center of mass of the ring carbon atoms of the pentamethylcyclopentadienyl group. [b] These parameters were subject to soft restraints during refinement such that the pairs of chemically equivalent values were restrained toward their respective means.

(13) *International Tables for X-ray Crystallography*; Kynoch Press: Birmingham, England, 1975; Vol. IV, p 99.
(14) Gabe, E. J.; LePage, Y.; Charland, J.-P.; Lee, F. L.; White, P. S. NRCVAX—An Interactive Program System for Structure Analysis. *J. Appl. Crystallogr.* **1989**, *22*, 384.
(15) Watkin, D. J.; Carruthers, J. R.; Betteridge, P. W. CRYSTALS. Chemical Crystallography Laboratory, University of Oxford, Oxford, England, 1984.

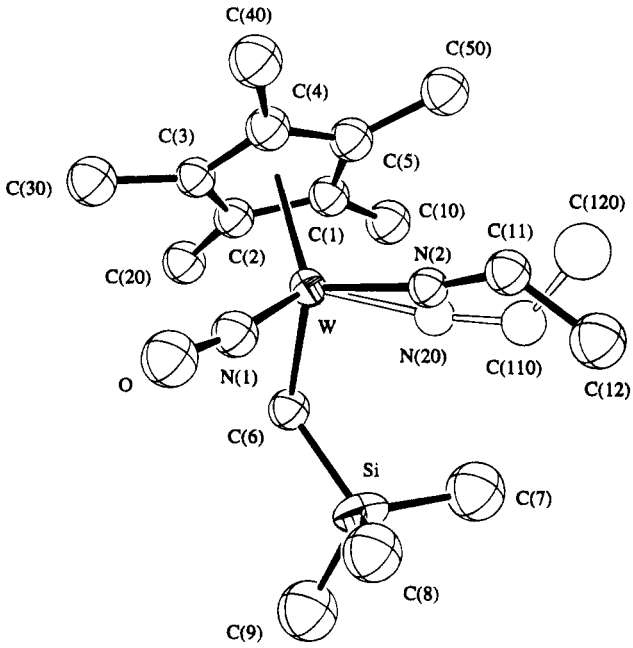

Figure 1. Molecular structure of Cp*W(NO)(CH_2SiMe_3)(N=CHMe) (**4**) at 200 K. The 50% probability displacement ellipsoids or spheres are shown for the non-hydrogen atoms. Both orientations of the disordered ethylideneamido ligand are shown with the minor orientation represented by the open spheres and unshaded bonds.

down from ~68σ (F_o)). After absorption corrections and data reduction (R_{merge} = 0.032), the resultant $|F_c^+| - |F_c^-|$ values were all very small and showed only a slight preference for the polarity represented by the structural coordinates reported here. The Flack enantiopole parameter,[16] included in the full-matrix least-squares refinement of the structure against the (4−54°:2θ) octant of data, refined to 0.50(2). This implies oriented twinning or microtwinning involving nearly equal domains of either hand within the sample.

A weighting scheme based on counting statistics was applied such that $\langle w(|F_o| - |F_c|)^2 \rangle$ was nearly constant as a function of both $|F_o|$ and sin θ/λ. Final full-matrix least-squares refinement of 208 parameters (including an extinction parameter)[17] for 2420 data ($I_o \geq 2.5\sigma(I_o)$) converged at R_f = 0.020. As for complex **4**, all computations were carried out on MicroVAX-II and 80486 computers utilizing the programs specified in the previous section. Crystallographic details are summarized in Table 1. Final fractional atomic coordinates for the non-hydrogen atoms are listed in Table 4, and selected bond lengths and angles are summarized in Table 5. A view of the solid-state molecular structure of **10** is shown in Figure 2. Tables of supplementary crystallographic data, the coordinates for the hydrogen atoms, and the anisotropic temperature factors for **10** are deposited as supplementary material.

Results and Discussion

Generation of the Transient Alkyl Hydride Complex, Cp*W(NO)(CH_2SiMe_3)H. Treatment of solutions of Cp*W(NO)(CH_2SiMe_3)$_2$ with molecular dihydrogen generates in situ the reactive 16-valence-electron alkyl hydride, Cp*W(NO)(CH_2SiMe_3)H, formed by hydrogenolysis of one of the W−C σ-bonds of the dialkyl reactant. The Lewis-acidic hydride complex has not yet been isolated (or spectroscopically characterized) as such, but it can be trapped by small Lewis bases, L, as the Cp*W(NO)(CH_2SiMe_3)(L)H adducts.[5] More importantly, if the coordinatively unsaturated hydride is

(16) Flack, H. *Acta Crystallogr., Sect. A* **1983**, *39*, 876.
(17) Larson, A. C. In *Crystallographic Computing*; Munksgaard: Copenhagen, 1970; p 293.

Table 4. Fractional Atomic Coordinates and Equivalent Isotropic Temperature Factors (Å^2) for the Non-Hydrogen Atoms of Cp*W(NO)(CH_2SiMe_3)($NH_2CH_2CH_2CH_2$) (10) at 200 K

atom	*x*	*y*	*z*	U_{eq}[a]
W	0.936459(16)	0.966499(14)	0.784514(14)	0.0231
Si	1.24225(13)	1.00669(13)	0.80671(12)	0.0316
O	1.0610(4)	0.7674(3)	0.7807(4)	0.043
N(1)	1.0168(4)	0.8545(4)	0.7771(4)	0.032
N(2)	0.9944(4)	1.0666(4)	0.6602(4)	0.031
C(16)	0.8453(6)	0.9147(6)	0.6505(5)	0.038
C(17)	0.9221(7)	0.9318(6)	0.5614(5)	0.041
C(18)	0.9498(7)	1.0429(6)	0.5617(5)	0.043
C(6)	1.0943(5)	1.0555(4)	0.8336(5)	0.029
C(7)	1.2669(6)	0.9645(7)	0.6777(5)	0.048
C(8)	1.2760(6)	0.8957(6)	0.8859(5)	0.044
C(9)	1.3541(6)	1.1067(6)	0.8345(7)	0.053
C(1)	0.8035(6)	0.8945(5)	0.8923(4)	0.033
C(2)	0.7318(5)	0.9545(5)	0.8320(4)	0.029
C(3)	0.7643(5)	1.0572(5)	0.8453(5)	0.032
C(4)	0.8521(6)	1.0613(5)	0.9176(5)	0.036
C(5)	0.8798(5)	0.9591(5)	0.9455(4)	0.030
C(11)	0.7936(6)	0.7806(5)	0.9042(6)	0.042
C(12)	0.6272(5)	0.9166(6)	0.7772(6)	0.042
C(13)	0.7070(6)	1.1491(5)	0.7985(6)	0.043
C(14)	0.8978(7)	1.1584(5)	0.9624(6)	0.045
C(15)	0.9596(7)	0.9255(7)	1.0245(5)	0.048

[a] U_{eq} is the cube root of the product of the principal axes of the thermal ellipsoid.

Table 5. Selected Intramolecular Distances[a] (Å) and Angles (deg) for Cp*W(NO)(CH_2SiMe_3)($NH_2CH_2CH_2CH_2$) (10) at 200 K

W−N(1)	1.741(5)	O−N(1)	1.255(6)
W−N(2)	2.263(5)	N(2)−C(18)	1.485(8)
W−C(6)	2.255(5)	C(16)−C(17)	1.528(8)
W−C(16)	2.230(6)	C(17)−C(18)	1.497(10)
W−C(1)	2.328(6)	C(1)−C(2)	1.410(8)
W−C(2)	2.432(5)	C(1)−C(5)	1.423(8)
W−C(3)	2.449(6)	C(2)−C(3)	1.415(7)
W−C(4)	2.422(6)	C(3)−C(4)	1.416(9)
W−C(5)	2.316(5)	C(4)−C(5)	1.436(9)
W−*Cp*[b]	2.062	C(1)−C(11)	1.513(8)
Si−C(6)	1.845(5)	C(2)−C(12)	1.499(8)
Si−C(7)	1.886(7)	C(3)−C(13)	1.521(8)
Si−C(8)	1.865(7)	C(4)−C(14)	1.513(8)
Si−C(9)	1.874(7)	C(5)−C(15)	1.488(8)
N(1)−W−N(2)	107.2(2)	N(1)−W−C(6)	92.1(2)
N(1)−W−C(16)	86.4(2)	N(2)−W−C(6)	72.0(2)
N(2)−W−C(16)	71.7(2)	C(16)−W−C(6)	141.4(2)
N(1)−W−*Cp*	121.5	C(16)−W−*Cp*	105.5
N(2)−W−*Cp*	131.2	C(6)−W−*Cp*	108.0
C(6)−Si−C(7)	115.4(3)	C(6)−Si−C(9)	109.7(3)
C(6)−Si−C(8)	110.2(3)	C(7)−Si−C(9)	107.4(4)
C(7)−Si−C(8)	106.9(3)	C(8)−Si−C(9)	106.9(3)
W−N(2)−C(18)	118.1(4)	W−C(6)−Si	119.3(3)
W−C(16)−C(17)	110.8(4)	W−N(1)−O	170.1(4)
C(16)−C(17)−C(18)	105.3(5)	C(2)−C(3)−C(4)	108.3(5)
N(2)−C(18)−C(17)	106.3(5)	C(2)−C(3)−C(13)	126.4(6)
C(2)−C(1)−C(5)	108.9(5)	C(4)−C(3)−C(13)	125.0(5)
C(2)−C(1)−C(11)	125.3(6)	C(3)−C(4)−C(5)	108.0(5)
C(5)−C(1)−C(11)	125.6(6)	C(3)−C(4)−C(14)	124.4(6)
C(1)−C(2)−C(3)	107.9(5)	C(5)−C(4)−C(14)	127.4(6)
C(1)−C(2)−C(12)	124.9(5)	C(1)−C(5)−C(4)	106.8(5)
C(3)−C(2)−C(12)	126.4(5)	C(1)−C(5)−C(15)	125.1(6)

[a] Distances are not corrected for thermal motion and may thus be underestimated by from 0.004 to 0.007 Å on the basis of the results of a rigid-body analysis of the thermal parameters. [b] *Cp* denotes the center of mass of the ring-carbon atoms of the pentamethylcyclopentadienyl group.

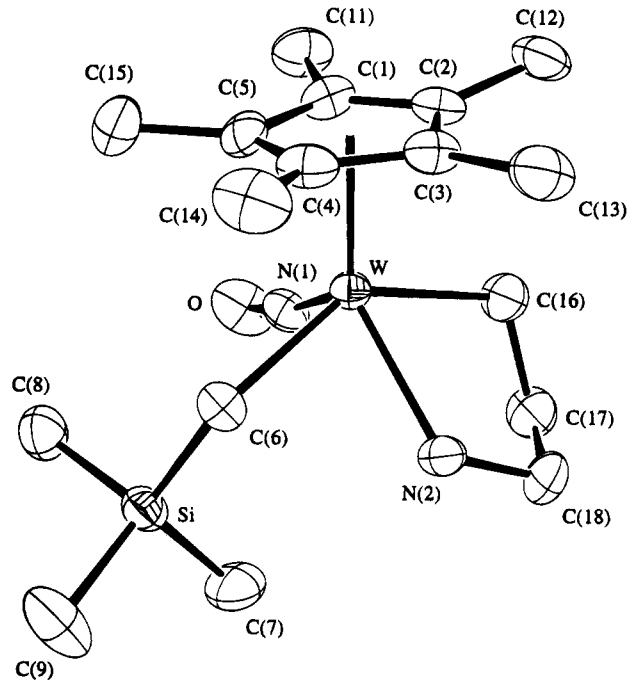

Figure 2. Molecular structure of Cp*W(NO)(CH$_2$SiMe$_3$)-(NH$_2$CH$_2$CH$_2$CH$_2$) (**10**) at 200 K. The 50% probability displacement ellipsoids are shown for the non-hydrogen atoms.

generated in the presence of a reactive substrate, some interesting chemical transformations occur. This paper describes a series of such reactions that detail the characteristic chemical properties of the transient alkyl hydride complex. The only caveat of which one must be mindful while exploring this rich chemistry is that the reactive substrates must not react with the dialkyl starting material, a fairly potent Lewis acid in its own right,[18] since Cp*W(NO)(CH$_2$SiMe$_3$)$_2$(substrate) adducts, once formed, are unreactive toward molecular dihydrogen. The discussion that follows is grouped in terms of the different types of substrates to which Cp*W(NO)(CH$_2$SiMe$_3$)H has been exposed.

Reaction with Triphenylphosphine. Treatment of Cp*W(NO)(CH$_2$SiMe$_3$)$_2$ with dihydrogen (1 atm) in the presence of 1 equiv of PPh$_3$ affords the orthometalated complex Cp*W(NO)(PPh$_2$C$_6$H$_4$)H (**1**), which is isolable in moderate yields as a yellow crystalline solid (eq 1).

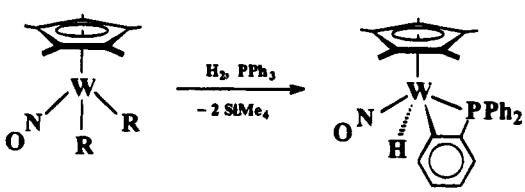

(1)

R = CH$_2$SiMe$_3$

1

The identity of **1** has been established by standard spectroscopic methods. Its IR spectrum as a Nujol mull clearly exhibits a W–H stretching band at 1929 cm^{-1}, and its ^{1}H NMR spectrum in C$_6$D$_6$ displays the hydride resonance as a doublet at δ 3.99 ($^2J_{PH}$ = 10 Hz). The latter signal is accompanied by small satellite peaks due to ^{183}W coupling ($^1J_{WH}$ = 104 Hz), which is also indicative of a W–H linkage. The orthometalated nature of the phosphine ligand is evident from the large number of peaks in the aryl region of both the ^{1}H and ^{13}C{^{1}H} NMR spectra of **1**.

The first step in the formation of complex **1** is undoubtedly the trapping of the transient 16-electron alkyl hydride compound with PPh$_3$ to form the intermediate 18-electron species, Cp*W(NO)(CH$_2$SiMe$_3$)-(PPh$_3$)H. As noted above, compounds of this type have been isolated from related reactions involving smaller Lewis bases. Reductive elimination of Me$_4$Si from this intermediate, followed by orthometalation of one of the phenyl groups on the PPh$_3$ ligand, would then produce the final product. Some support for this view of the mechanism is provided by the same reaction effected with PPh$_3$-d_{15}, which results in complete deuteration of the hydride position in the product. The W–D stretch in the IR spectrum expected at 1380 cm^{-1} (ν_{calcd})[19] for this complex is unfortunately obscured by a Nujol band. This observation indicates that the hydride ligand in **1** originates on the PPh$_3$ and that the reductive elimination of alkane occurs before the orthometalation step. This reductive elimination is evidently quite facile at ambient temperatures for this system. Such is not the case for other analogous complexes. For instance, Cp*W(NO)(CH$_2$SiMe$_3$)(PMe$_3$)H and CpW(NO)(CH$_2$-SiMe$_3$)[P(OPh)$_3$]H require heating to 40 and 50 °C, respectively, to induce such reactivity.[20] The facile reorganization of NO and triphenylphosphine from a trans to a cis orientation in Cp*W(NO)(CH$_2$SiMe$_3$)-(PPh$_3$)H is probably a result of the large steric interaction between the trimethylsilylmethylene ligand and the triphenylphosphine ligand, as compared to the smaller trimethylphosphine and triphenylphosphite ligands. That the NO and phosphine ligands are now cis places the alkyl ligand and hydride cis as well, affording reductive elimination, followed by orthometalation. Thus it appears that the steric bulk of the PPh$_3$ ligand facilitates the elimination of the bulky alkyl ligand and the replacement of a tungsten–alkyl link by a stronger tungsten–aryl bond in **1**.

Reaction with Dienes. When Cp*W(NO)(CH$_2$-SiMe$_3$)$_2$ is reacted with dihydrogen in the presence of butadiene or 2,3-dimethyl-1,3-butadiene, η^4-diene complexes of the type Cp*W(NO)(η^4-*trans*-diene) are formed (complexes **2** and **3**, respectively, eq 2). The spectroscopic properties of **2** resemble those exhibited by related molybdenum species whose solid-state molecular structures we have previously established.[21] Hence, it is likely that both of these tungsten compounds are

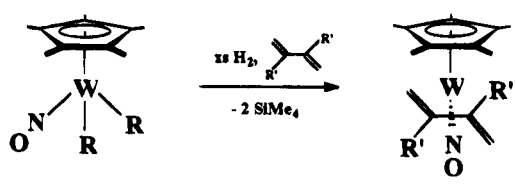

(2)

R = CH$_2$SiMe$_3$

2 R' = H
3 R' = Me

(18) Legzdins, P.; Rettig, S. J.; Sánchez, L. *Organometallics* **1988**, *7*, 2394.

(19) Debad, J. D. Ph.D. Dissertation, The University of British Columbia, 1994.

(20) Debad, J. D. Unpublished observations.

Scheme 1

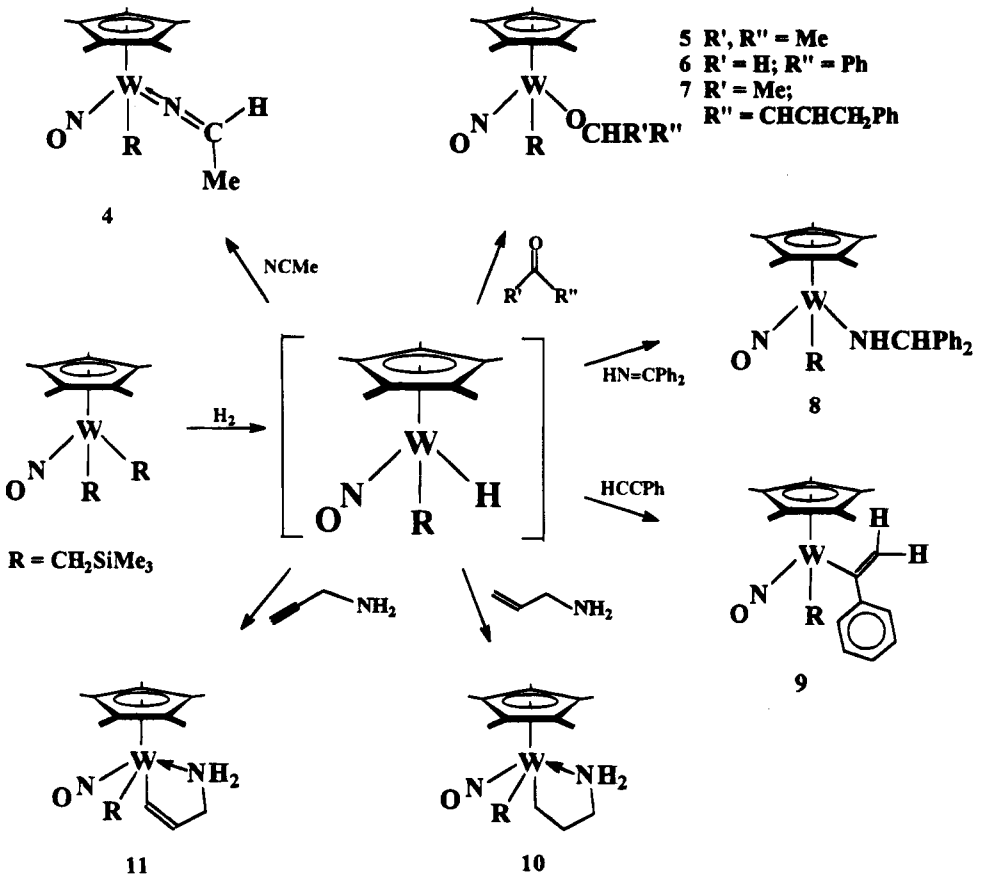

isostructural and contain the diene ligands attached to the metal centers in a twisted, transoidal fashion.[22] Mechanistically, conversions 2 probably resemble the PPh_3 metalation reaction (vide supra). Hydrogenolysis of one of the W–C bonds of $Cp^*W(NO)(CH_2SiMe_3)_2$ generates the alkyl hydride intermediate, and coordination of one double bond of the diene in an η^2-fashion produces the 18-electron complex, $Cp^*W(NO)(CH_2SiMe_3)(\eta^2\text{-diene})H$. Elimination of Me_4Si from this intermediate with concerted coordination of the dangling double bond of the diene to the tungsten center would then produce complexes **2** and **3**. Since the proposed η^2-diene-trapped intermediate is not observable spectroscopically, the elimination of the alkane from it must be rapid once this intermediate is formed. Since Me_4Si elimination after coordination of the diene requires a cis orientation of the alkyl ligand and the hydride ligand, an insertion/de-insertion isomerization process between the coordinated diene and the hydride complex must be occurring, since the diene would coordinate initially between the alkyl and hydride ligands. We have also monitored the reaction to form $Cp^*W(NO)(\eta^4\text{-}trans\text{-}2,3\text{-dimethyl-}1,3\text{-butadiene})$ (**3**) by ^1H NMR spectroscopy. The spectroscopic yield of the reaction is approximately 90%, and no evidence for organic products resulting from diene hydrogenation is detectable. There is also no evidence for organometallic products resulting from insertion of one of the diene double bonds into the W–H linkage of the 16-electron alkyl hydride intermediate in the manner found for the substrates considered in the next section.

Reactions with Substrates That Insert into the W–H Bond. A number of unsaturated molecules have been reacted with the transient alkyl hydride complex to investigate the insertion chemistry of its tungsten–hydrogen bond. The chemistry that we have discovered during the present study is summarized in Scheme 1. Each reaction shown in this scheme was also monitored by NMR spectroscopy to determine the spectroscopic yields of the conversions and to detect and identify any byproducts formed.

(a) Acetonitrile. When $Cp^*W(NO)(CH_2SiMe_3)_2$ is reacted with dihydrogen in the presence of acetonitrile, the ethylideneamido compound, $Cp^*W(NO)(CH_2SiMe_3)(N{=}CHMe)$ (**4**), is formed in quantitative spectroscopic yield (Scheme 1). The product arises from insertion of the N≡C bond of the acetonitrile into the W–H bond of the transient alkyl hydride.[8a] The solid-state molecular structure of **4** reveals an ethylideneamido ligand attached via a W=N link which is disordered, as depicted in the ORTEP diagram in Figure 1. The parameters of the disordered ligand (occupancy ratio 60:40, N(2)–C(11)–C(12):N(20)–C(110)–C(120)) are consistent with its formulation as ethylideneamide (N=CHMe) doubly bonded via nitrogen to tungsten in two diastereomeric orientations. Other formulations for this group do not appear to be reasonable in terms of the observed electron density distribution and in light of the other chemical and spectroscopic evidence (vide infra). The

(21) (a) Christensen, N. J.; Hunter, A. D.; Legzdins, P. *Organometallics* **1989**, *8*, 930. (b) Christensen, N. J.; Legzdins, P.; Einstein, F. W. B.; Jones, R. H. *Organometallics* **1991**, *10*, 3070. (c) Christensen, N. J.; Legzdins, P.; Trotter, J.; Yee, V. C. *Organometallics* **1991**, *10*, 4021. (d) Christensen, N. J. Ph.D. Dissertation, The University of British Columbia, 1990.

(22) (a) Erker, G.; Krüger, C.; Müller, G. *Adv. Organomet. Chem.* **1985**, *24*, 1. (b) Yasuda, H.; Tatsumi, K.; Nakamura, A. *Acc. Chem. Res.* **1985**, *18*, 120.

weighted mean N−C bond distance for **4** (1.24 Å) compares well with that of $[Ru(tpy)(bpy)(N{=}CMe_2)][ClO_4]_3{\cdot}H_2O$ (1.26(2) Å)[23] and other ethylideneamido-containing complexes[24] and implies multiple-bond character of this bond comparable with or greater than that extant in the corresponding Ru−N bond distance.

The existence of two sets of signals in the ^1H and $^{13}C\{^1H\}$ NMR spectra of **4** in C_6D_6 (see Experimental Section) indicates that these isomers also persist in solution in approximately the same ratio. The presence of the two diastereomers can be attributed to the existence of a large rotational barrier about the W=N bond. This observation, along with the essentially linear W−N−C angles (168.4 and 171.7°), is consistent with the views that the ethylideneamide functions as a formal 3-electron donor and that **4** is an 18-valence-electron complex.

(b) Organic Carbonyls. The transient alkyl hydride has also been generated in the presence of a number of organic reagents that contain a carbonyl functionality. Acetone, benzaldehyde, and 4-phenyl-3-buten-2-one all insert their carbonyl group into the W−H bond to produce an alkyl alkoxide product (complexes **5**, **6**, and **7**, respectively, in Scheme 1) in quantitative yield, as judged by NMR spectroscopy. Interestingly, the α,β-unsaturated ketone, 4-phenyl-3-buten-2-one, exhibits only this mode of reactivity even though, in principle, it could undergo insertion of its C=C linkage into the W−H bond or it could function like the diene reagents already discussed and coordinate to the metal center in an η^4-fashion following alkane elimination from the transient alkyl hydride compound. We have previously obtained alkyl alkoxide complexes of the type Cp*M(NO)(R)OR′ [M = Mo, W] by treatment of the Cp*M(NO)(R)Cl precursors with alkoxide anions.[25]

The spectroscopic properties of complexes **5** and **6** are consistent with their possessing three-legged piano-stool molecular structures. However, the NMR data for the unsaturated ketone insertion product **7** are quite complicated and indicate the presence of two isomers that are formed in a ratio of approximately 3:2. The resonances can be attributed to the two diastereomeric pairs of enantiomers formed by addition of the racemic hydride to different faces of the ketone, i.e. (*RS* and *SR*) and (*SS* and *RR*) isomeric pairs. This mode of addition is reminiscent of the enantiofacial binding of unsaturated organic substrates to the $Cp^*Re(NO)(PPh_3)$ cation studied by Gladysz and co-workers.[26] Interestingly, the reaction to form **7** is slightly stereoselective and does produce one set of enantiomers in excess. Presumably the reaction proceeds through an intermediate that has the ketone coordinated to the unsaturated alkyl hydride at its Lewis-acid site between the alkyl and hydride ligands.[6,7,27] The different product isomers would then be formed by addition of the hydride to either face of the ketone. In this case, the sterically preferred mode of coordination of the ketone would be with the smaller substituent, the methyl group, pointing upward toward the more sterically demanding Cp* ligand. Upon insertion, these conformations would produce the *SS* or *RR* configuration, depending upon the configuration of the hydride enantiomer. Hence, the major isomers formed during the hydrogenation−insertion reaction are expected to be those displaying *RR* and *SS* configurations. The different integrations of the ^1H NMR resonances allow the signals due to each pair of enantiomers of complex **7** to be assigned, although it is not possible to assign the two sets of signals to any one absolute configuration. A ^1H NMR spectrum taken after complex **7** was recrystallized revealed that one of the enantiomer pairs had been enriched by approximately 50% from one crystallization, thereby indicating that the two sets of enantiomers are separable by fractional crystallization.

(c) Benzophenoneimine. Hydrogenation of $Cp^*W(NO)(CH_2SiMe_3)_2$ in the presence of benzophenoneimine demonstrates that the alkyl hydride intermediate is also able to insert imine functionalities (Scheme 1). The product of this reaction, **8**, has been characterized as the alkyl amido complex $Cp^*W(NO)(CH_2SiMe_3)(NHCHPh_2)$. The ^1H NMR spectrum of this complex contains a broad peak at δ 7.6 assignable to the NH proton, and its IR spectrum exhibits a strong ν_{NH} at 3249 cm^{-1}. We have recently synthesized many alkyl and aryl amide complexes similar to **8** by metathesis reactions of appropriate alkyl chloride or amide chloride precursors.[28]

(d) Phenylacetylene. Hydrogenation of $Cp^*W(NO)(CH_2SiMe_3)_2$ in the presence of phenylacetylene results in the formation of the alkyl alkenyl compound $Cp^*W(NO)(CH_2SiMe_3)(CPh{=}CH_2)$ (**9**) via insertion of the substrate into the W−H bond of the transient alkyl hydride compound (Scheme 1). Complex **9** is only isolable in very low yield because it is prone to undergo further reactions during its synthesis. First and foremost, **9** is thermally unstable, and its thermal chemistry is dominated by its facile activation of alkane C−H bonds in a unique manner.[29] Second, the alkenyl product is sensitive to dihydrogen to the extent that an authentic sample of the complex decomposes slowly when exposed to the pressures of H_2 used during its synthesis.

The spectroscopic properties of **9** are consistent with its possessing the 16-valence-electron molecular structure shown in Scheme 1. The ^1H and $^{13}C\{^1H\}$ NMR spectra of complex **9** also suggest the existence of a weak interaction between the Lewis-acidic tungsten center and the π-electron density of the alkenyl group, though not to the extent customarily exhibited by an authentic η^2-alkenyl ligand (vide infra). For example, the ^1H NMR spectrum of **9** shows some unexpected coupling patterns. Both of the alkenyl protons are weakly coupled to one of the methylene protons of the trimethylsilylmethyl ligand (J_{HH} = 1.4 and 1.1 Hz), a surprising coupling through five bonds and four atoms. In addition, there are tungsten satellites observable on both of the alkenyl proton signals, one coupling constant being much greater than the other (J_{WH} = 10 and 5.1 Hz). Consistently, the $^{13}C\{^1H\}$ NMR spectrum of **9** in C_6D_6 displays the

(23) Adcock, P. A.; Keene, F. R.; Smythe, R. S.; Snow, M. R. *Inorg. Chem.* **1984**, *23*, 2336.
(24) (a) Werner, H.; Knaup, W.; Dziallas, M. *Angew. Chem., Int. Ed. Engl.* **1987**, *26*, 248. (b) Wilkinson, G. *J. Chem. Soc., Dalton Trans.* **1987**, 471.
(25) Legzdins, P.; Lundmark, P. L.; Rettig, S. J. *Organometallics* **1993**, *12*, 3545.
(26) Peng, T.; Pu, J.; Gladysz, J. A. *Organometallics* **1994**, *13*, 929 and references cited therein.
(27) Debad, J. D.; Legzdins, P.; Rettig, S. J.; Veltheer, J. E. *Organometallics* **1993**, *12*, 2714.
(28) Legzdins, P.; Rettig, S. J.; Ross, K. J. *Organometallics* **1993**, *12*, 2103.
(29) Debad, J. D.; Legzdins, P.; Lumb, S. A. *J. Am. Chem. Soc.* **1995**, *117*, 3288.

alkenyl carbon resonances at 228 and 83 ppm, ^{184}W satellites being evident on both the α carbon ($^1J_{WC}$ = 99 Hz) and the β carbon ($^2J_{WC}$ = 13 Hz) signals. Authentic η^1-alkenyl complexes usually display C_α resonances around 160 ppm and C_β resonances around 130 ppm,[30] whereas most tungsten η^2-alkenyl compounds exhibit these signals between 230 and 270 ppm and between 20 and 40 ppm, respectively.[31,32] Clearly, the alkenyl ligand of **9** is interacting with the tungsten center in a manner intermediate to that of the limiting η^1 and η^2 forms.

The regioselectivity of insertion, i.e. whether the unsymmetrical acetylene undergoes addition of the metal at the α or β carbon, is difficult to predict a priori for these types of insertion processes since both steric and electronic factors are operative. For example, $W(H)(CO)_2(NO)(PMe_3)_2$[32] and $Co(H)[N(CH_2CH_2PPh_2)_3]$[33] insert the activated acetylene HC≡CC{O}OMe to give alkenyl complexes of the type [M]C(C{O}OMe)=CH_2, whereas $CpRe(CO)(NO)(H)$[34] affords the other regioisomer, namely [M]CH=CH(C{O}OMe). On the other hand, the osmium complex $[Os(H)(acetone)(CO)_2(P^iPr_3)_2]BF_4$ is known to undergo both modes of insertion.[35] In the case of $Cp^*W(NO)(CH_2SiMe_3)H$, its reactions with organic substrates of the type ER [E = N≡, NH=, O=] afford complexes **4**–**8**, which are the expected product both sterically and electronically. In other words, the evidently hydridic hydride adds to the electropositive carbon center, and the metal binds the heteroatom such that the least sterically crowded ligand results. In addition, the preferential formation of a strong W–E bond (over a W–C bond) provides a thermodynamic driving force for these processes. In contrast, the formation of complex **9** seems to be primarily under electronic control, the hydride of $Cp^*W(NO)(CH_2SiMe_3)H$ adding to the unsubstituted, electropositive terminus of the acetylene. Interestingly, Schwartz's reagent exhibits the opposite regiochemistry toward phenylacetylene to produce the least sterically crowded insertion product.[36]

Hydrogenation of the dialkyl complex, $Cp^*W(NO)(CH_2SiMe_3)_2$, in the presence of diphenylacetylene or 1-pentyne does not yield any isolable products, and monitoring of these reactions by NMR spectroscopy gives no evidence for the formation of alkenyl products similar to **9**. Insertion of symmetric acetylenes is unlikely due to the apolar nature of the unsaturation. Likewise, the products of simple alkyne insertion into the W–H bond of the transient hydride complex are presumably unstable because they contain β hydrogens and are thus prone to elimination and subsequent decomposition. Complex **9** is no exception. This alkenyl compound is, in fact, the only 16-valence-electron species of the type Cp'M(NO)(R)R' in which one of the alkyl groups contains β hydrogens that we have yet been able to isolate. Nevertheless, as noted above, it does slowly decompose in solutions at ambient temperatures, presumably via a β-H elimination pathway. The next section details our discovery of how such olefin and acetylene insertion products may be stabilized.

(e) Allylamine and Propargylamine. Allylamine and propargylamine were chosen as potentially useful olefins for the study of their insertion chemistry into the W–H link of $Cp^*W(NO)(CH_2SiMe_3)H$ on the grounds that their pendant amine functionalities would stabilize otherwise coordinatively unsaturated and highly reactive 16-valence-electron products containing β-hydrogens. Gratifyingly, this expectation has been realized. Both amines undergo insertion of their unsaturated carbon–carbon link into the W–H bond, and following insertion, the pendant amine group coordinates to the metal to stabilize the complexes toward β-hydride elimination (Scheme 1). Both reactions are quantitative by ^1H NMR spectroscopy, and the azametallacyclic products are isolable in moderate yields. Specific details of each conversion are presented in the following paragraphs.

(1) Allylamine. When $Cp^*W(NO)(CH_2SiMe_3)_2$ is reacted with dihydrogen in the presence of allylamine, $Cp^*W(NO)(CH_2SiMe_3)(NH_2CH_2CH_2CH_2)$ (**10**) is the product obtained as a yellow crystalline solid. The lower yield results from the difficulty in isolating and recrystallizing this compound. The olefin insertion reaction that results in the formation of **10** is unprecedented for our tungsten hydride systems. Complex **10** was initially characterized by standard spectroscopic methods. Interestingly, the amine H signals in the ^1H NMR spectrum of the complex in $CDCl_3$ are observed at high field as a broad singlet at δ 3.18. The fact that only a broad singlet is observed for the two amine protons and not an AB quartet pattern as expected for diastereotopic protons is perhaps indicative of the existence of some exchange process. Regrettably, variable temperature NMR spectroscopy of complex **10** from 25 °C to the $CDCl_3$ solvent limit of −50 °C failed to bring about resolution of the individual signals. The six alkyl protons of the metallacycle give rise to multiplets integrating for one proton each, as expected for sets of diastereotopic protons. A ^1H COSY experiment revealed the three sets of diastereotopic protons, thereby allowing their assignment (see Experimental Section). The internuclear couplings between these protons are indeterminable, however, due to the broadening displayed by the signals.

Another notable spectroscopic feature of complex **10** is the nitrosyl-stretching band at 1497 cm^{-1} in its IR spectrum. This is a very low value for ν_{NO} and reflects the considerable weakening of the N–O bond that results from a large degree of back-donation of electron density from the metal to the nitrosyl ligand. This increased back-donation is, in turn, a manifestation of the increased electron density at the metal center afforded by the dative bond from the amine nitrogen atom's lone pair of electrons to the tungsten center. The existence of this latter bonding interaction has been confirmed by a single-crystal X-ray crystallographic analysis of **10**. The solid-state molecular structure of compound **10** is shown in Figure 2. The only significant intermolecular interaction is a hydrogen bond of 2.841(6) Å involving O–HN(2)', where ' indicates $2 - x$, $-1/2 + y$, $3/2 - z$. The C(16)–C(17) bond length of 1.528(8)

(30) Herberich, G. E.; Mayer, H. *Organometallics* **1990**, *9*, 2655.
(31) Feng, S. G.; Templeton, J. L. *Organometallics* **1992**, *11*, 2168.
(32) van der Zeijden, A. A. H.; Bosch, H. W.; Berke, H. *Organometallics* **1992**, *11*, 563.
(33) Bianchini, C.; Innocenti, P.; Masi, D.; Meli, A.; Sabat, M. *Organometallics* **1986**, *5*, 72.
(34) Labonova, I. A.; Zdanovich, V. I.; Kolobova, N. E.; Kalinin, V. N. *Metallorg. Khim.* **1990**, *3*, 916.
(35) Esteruelas, M. A.; Fernando, J. L.; Lopez, J. A.; Oro, L. A.; Schlunken, C.; Valero, C.; Werner, H. *Organometallics* **1992**, *11*, 2034.
(36) Hart, D. W.; Blackburn, T. F.; Schwartz, J. *J. Am. Chem. Soc.* **1975**, *97*, 679.

Å indicates the existence of a single C–C bond and confirms that the original allylic moiety of the amine has been hydrogenated. In all other aspects the intramolecular dimensions of **10** are comparable to those exhibited by related Cp*W(NO)-containing four-legged piano-stool molecules.[5]

The mechanism of formation of the azametallacycle in **10** probably proceeds via insertion of the C=C link of the allylamine into the W–H bond of Cp*W(NO)(CH_2SiMe_3)H. The 16-valence-electron complex so formed is stabilized by the subsequent coordination of the pendant amine group to the metal center through a dative bond, thereby resulting in the stable 18-valence-electron complex **10**. That olefin insertion occurs before coordination of the pendant Lewis-base site in this system is supported by the fact that saturated amines such as *tert*-butylamine fail to trap the transient tungsten hydride complex as an isolable adduct. In addition, if the amine functionality were to coordinate first, then the open coordination slot of the alkyl hydride complex would be occupied, eliminating the possibility of insertion of the olefinic moiety into the W–H bond. This would lead to decomposition of the complex, as is observed for the reaction with saturated amines. If coordination of amine functionality and olefin moiety is viewed as a competitive process, then the lower yields of allylamine insertion product, as compared to the products of the reactions with the polar, unsaturated organic substrates, are rationalized. This view of the mechanism in the tungsten case contrasts with the recent findings of Hiraki and co-workers during their studies of the analogous reactions of Ru(Cl)(CO)-(PPh_3)$_3$H with primary and secondary amines.[37] They find that the hydrido ligand labilizes the *trans*-PPh_3 ligand to substitution by allylamine. The ligand is purported to coordinate via the amine site first and then to undergo olefin insertion into the Ru–H bond.

The regioselectivity of the olefin insertion into the W–H linkage is identical to that displayed by Schwartz's reagent during the hydrozirconation of functionalized olefins.[36] The Cp*W(NO)(CH_2SiMe_3)H complex adds across the olefin link in such a manner that the metal ends up on the least hindered carbon center. There is no evidence for the formation of the congeneric metallacyclobutane species in this system. In contrast to phenylacetylene and the other carbonyl-, nitrile-, and imine-functionalized substrates (vide supra), polarization of the olefin moiety by the pendant amine function is probably a minor factor due to its distal relationship to the olefin link. The regioselectivity observed during the olefin insertion is thus probably determined to a greater extent by steric requirements within the olefin-inserted intermediate rather than by electronic factors within the substrate.

(2) Propargylamine. Reaction of Cp*W(NO)(CH_2-$SiMe_3$)H with propargylamine produces complex **11** which contains an azametallacyclopentene group (Scheme 1). The product is obtained in a yield comparable to **10**, and its mechanism of formation is assumed to be similar to that proposed for **10** in the preceding paragraph. The spectroscopic properties of **11** confirm its identity. For instance, the NO stretching band in its Nujol mull IR spectrum occurs at 1501 cm^{-1}, the same region as found for **10**. The diastereotopic amine proton signals are clearly visible as doublets at δ 7.23 and 6.47 with a two-bond coupling of 18 Hz in the one-dimensional ^{1}H NMR spectrum of **11** in $CDCl_3$. These doublets also display fine structure resulting from coupling to the α-methylene protons in the ring. Likewise, the diastereotopic methylene protons in the ring give rise to signals that are evident as a virtual quartet centered about δ 3.48. This virtual quartet is superimposed on the signal of the allylic proton α to the metal center, with the entire multiplet integrating for three protons. The remaining allyl proton, which couples to both the methylene protons and the α-allyl proton, produces the broad multiplet at δ 2.39. The ^{1}H COSY spectrum of **11** confirms these assignments. Definitive evidence for the allylic moiety is also found in the ^{13}C NMR spectrum of the complex, the allylic carbon signals at δ 175.1 and 131 being characteristic of the metal-bound allylic functionality.[38]

Closer inspection of the methyl signals in the Cp* region of the one-dimensional ^{1}H NMR spectrum of **11** reveals the existence of a second species in the ratio of 1:5 relative to the major isomer, **11**. Downfield there also exist two broad singlets integrating as 1H each at δ 6.04 and 5.38, which exhibit fine structure and are attributable to amine protons. Slightly upfield are two broad doublets at δ 5.09 and 4.29, which also exhibit fine structure and integrate as one proton each, and these are indicative of the presence of vinyl protons.[20] Diastereotopic methylene signals attributable to the Me_3SiCH_2 ligand of a minor isomer are also evident in the same region as those of the major isomer, **11**.

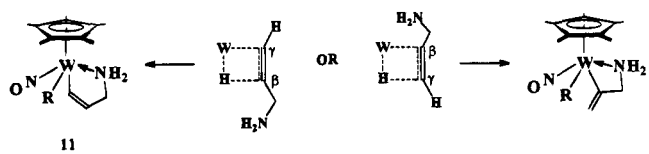

11

If one acknowledges that hydrogenation of the allyl moiety can occur at either the β or γ position relative to the pendant amine functional group, then it is possible that the minor isomer is a complex containing a vinyl metallacyclobutane ligand as shown above. Indeed, this view is supported by the ^{1}H COSY spectrum of **11**, which shows signals attributable to the vinyl protons displaying a weak mutual coupling. More importantly, partially obscured beneath the analogous methylene signal for the major isomer **11**, a three-bond coupling of the vinyl protons in the vinyl metallacyclobutane to a set of diastereotopic methylene protons is evident. At the same time, a long range coupling between the amine broad singlets and the same methylene signals of the vinyl metallacyclobutane is also clearly discernible. The relative preponderance of this complex containing the five-membered azametallacycle over that with the four-membered isomer is consistent with the well-known preferential formation of a five-membered ring over a four-membered ring. Interestingly, such a four-membered metallacyclic isomer is not observed for the saturated analogue, **10**.

Allyl Alcohol. While studying the olefin insertion resulting in the formation of the amine azametallacycle

(37) Hiraki, K.; Matsunaga, T.; Kawano, H. *Organometallics* **1994**, *13*, 1878.

(38) Mann, B. E.; Taylor, B. F. *^{13}C NMR Data for Organometallic Compounds*; Academic Press: New York, 1982.

in **10**, we decided to investigate whether the O analogue of **10** could be formed by utilizing allyl alcohol in place of allylamine in the hydrogenation reaction. However, instead of isolating the metallacyclic complex from the final reaction mixture, we obtained instead a red oil which was characterized as the allyl alkoxide complex, **12** (eq 3).

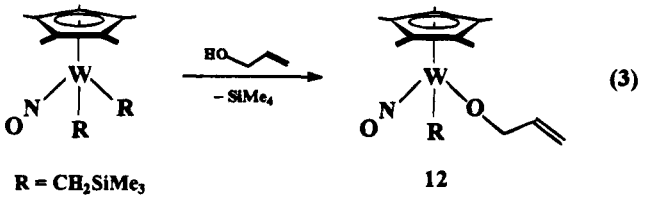

(3)

R = CH_2SiMe_3 **12**

Characterization of **12** was made facile by the presence of the allyl signals in both the ^1H and the ^{13}C NMR spectra. The allyl signals in the one-dimensional ^1H NMR spectrum are qualitatively identical to those exhibited by Cp*Mo(NO)($NHCH_2CH{=}CH_2$)Cl, an allylamido complex studied by our group recently.[39] Like this molybdenum complex, the allylic protons in **12** do not show the characteristic allyl splitting pattern,[40] since incorporation of the alcohol into the complex as an alkoxide ligand renders the methylene protons diastereotopic. The most notable feature of this spectrum is the resonance of the internal allyl proton, a 10-line multiplet at 5.96 ppm consisting of an overlapping doublet of doublets of doublets of doublets ($^3J_{HH}$ = 6.0, 6.5, 10, 17 Hz). The two largest couplings are consistent with cis and trans alkene coupling, and the two smaller couplings result from coupling to the two diastereotopic methylene protons. The nitrosyl band in the Nujol mull IR spectrum of **13** occurs at 1576 cm^{-1}, a region characteristic of such mixed alkyl alkoxide species.[25] The percent carbon in the elemental analysis of **12** was lower than expected due to the impurity of the sample. These types of complexes are difficult to obtain in pure crystalline form and **12** is no exception.

The probable mechanism of formation of **12** is simple protonolysis of the dialkyl reactant by allyl alcohol resulting in loss of Me_4Si followed by coordination of the allyl alkoxide. This view is supported by the fact that complex **12** is produced by the reaction of allyl alcohol with Cp*W(NO)(CH_2SiMe_3)$_2$ even in the absence of H_2. We have also shown that complex **12** can be prepared by the reaction of the lithium salt of allyl alcohol with the alkyl chloride, Cp*W(NO)(CH_2SiMe_3)Cl,[41] a methodology that has been employed to synthesize other alkyl alkoxide complexes studied by our group recently.[25] Unfortunately, complex **12** is inert to H_2, and the desired metallacycle cannot be obtained in this manner. Alternate synthetic routes that will lead to such metallacyclic complexes are currently being pursued.

Stability of the Insertion Products. All of the insertion products outlined in Scheme 1 and discussed above contain one common feature that raises an important question concerning their electronic nature. Each complex contains an alkyl ligand possessing a β-hydrogen atom and yet is an isolable species. In contrast, the isolable bis(hydrocarbyl) complexes, Cp′M(NO)R_2 [Cp′ = Cp or Cp*, M = Mo, W, R = alkyl or aryl], are devoid of β-hydrogens. The fundamental difference between the two classes of complexes is that the insertion products **4**–**11** attain a degree of electronic sufficiency at their metal centers, whereas the Cp′M(NO)R_2 species remain as 16-valence-electron entities. Electronic sufficiency in **4**–**11** can arise in the three different ways shown below.

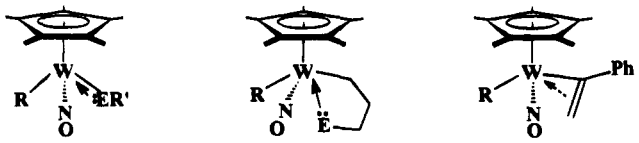

I II III

The first mode of electronic stabilization, namely that observed for complexes **4**–**8** and depicted as case I, involves dative bond formation between the heteroatom E [E = N=, O–, or HN–] and the tungsten through donation of electron density from the lone pair on E into the LUMO that lies between the alkyl ligands and trans to the nitrosyl ligand (vide supra). Case II depicts the second mode of stabilization resulting from the coordination of a pendant Lewis-base moiety, as occurs in complexes **10** and **11**, and the transfer of electron density to the LUMO. Finally, as shown in case III, stabilization results from donation of electron density from the alkenyl π system of the phenyl alkenyl ligand into the LUMO of **9**. As demonstrated by the work reported in this paper, the electronic stabilization is least in case III, thereby resulting in complex **9** being the most thermally sensitive and reactive insertion product.

Summary. The title compound, Cp*W(NO)(CH_2SiMe_3)H, has not been directly observed, but its production in situ by the hydrogenation of Cp*W(NO)(CH_2SiMe_3)$_2$ has been indicated by subsequent reactivity of this putative hydride intermediate. This compound has been useful for synthesizing in high yields a number of mixed-ligand compounds such as alkyl alkoxide, alkyl amide, and alkyl alkenyl species, as well as producing *trans*-diene complexes that cannot be produced by other routes. As determined by the regioselectivity of its insertions of polar substrates, the hydride ligand is hydridic in nature. This feature is best demonstrated by the product of phenylacetylene insertion, during which process only one regioisomer is formed. Furthermore, this isomer is the one in which the hydride has added to the more positive end of the unsaturated linkage, even though this mode of addition forms the more sterically demanding isomer.

Reaction of the intermediate hydride complex with olefins and acetylenes leads to insertion products which are usually not thermally stable since they contain β-hydrogens. Such is the case for phenylacetylene insertion, which affords a thermally sensitive complex that has been isolated only in low yield. Interestingly, these insertion products can be stabilized by pendant Lewis-base functional groups. Thus, the hydrido intermediate combines with allylamine, and the resulting insertion product, although containing β-hydrogens, is

(39) Legzdins, P.; Rettig, S. J.; Ross, K. J. *Organometallics* **1993**, *12*, 2103.
(40) See, for example: Matta, E.; Du, Y. *J. Am. Chem. Soc.* **1988**, *110*, 8249.
(41) Lumb, S. A. Unpublished observations.

stabilized to decomposition by coordination of the pendant amine group. Similar reactivity is observed with propargylamine, a conversion that results in the formation of a base-stabilized alkenyl complex.

Acknowledgment. We are grateful to the Natural Sciences and Engineering Research Council of Canada for support of this work in the form of grants to P.L. and F.W.B.E. and postgraduate scholarships to J.D.D. and S.A.L.

Supplementary Material Available: Tables of supplementary crystallographic data, the coordinates for the hydrogen atoms, and the anisotropic temperature factors for complexes **4** and **10** (8 pages). Ordering information is given on any current masthead page.

OM950031G

Palladium-Catalyzed Disilane Metathesis Reactions of 1,2-Disilacyclobutanes

Takahiro Kusukawa, Yoshio Kabe, Bernd Nestler, and Wataru Ando*

Department of Chemistry, University of Tsukuba, Tsukuba, Ibaraki 305, Japan

Received November 21, 1994[⊗]

3,4-Bis(isopropylidene)-1,1,2,2-tetraalkyldisilacyclobutanes (**1**) were prepared by intramolecular reductive coupling of the corresponding 3,4-bis(chlorodialkylsilyl)-2,5-dimethyl-2,4-hexadiene. In the presence of a Pd catalyst, 3,4-bis(isopropylidene)-1,1,2,2-tetramethyl-1,2-disilacyclobutane (**1a**) afforded 3,4,7,8-tetrakis(isopropylidene)-1,1,2,2,5,5,6,6-octamethyl-1,2,5,6-tetrasilacyclooctane (**2a**) as the disilane metathesis product in 93% yield. A highly selective cross-metathesis occurred between **1a** and 3,4-benzo-1,1,2,2-tetramethyl-1,2-disilacyclobutene (**1c**) and gave 3,4-benzo-7,8-bis(isopropylidene)-1,1,2,2,5,5,6,6-octamethyl-1,2,5,6-tetrasilacyclooct-3-ene (**3**) accompanied by only small amounts of homo-disilane metathesis products **2a** and **2c**. The structures of the products (**2a**, **2c**, and **3**) and **11** were characterized by X-ray diffraction studies.

Introduction

Transition metal-catalyzed double silylation of the C–C multiple bond with disilanes is an important development of organosilicon chemistry, and numerous reports have dealt with this topic (Scheme 1).[1-3]

Nevertheless, only a few examples are known of the related disilane metathesis reaction in which, formally, a Si–Si bond is doubly silylated; to the best of our knowledge only two examples of this have been reported.[1b,f]

In this paper, we present our results on Pd- and Pt-catalyzed reactions of bis(isopropylidene)disilacyclobutane[4] and benzo-1,2-disilacyclobutenes and show that these substrates efficiently undergo disilane metathesis. Interestingly, in conversions of mixtures of two different disilanes predominant formation of cross-metathesis products is observed.

Results and Discussion

Synthesis of Bis(isopropylidene)disilacyclobutanes (1). The novel disilacyclobutanes (**1a,b**) were synthesized by a method similar to the preparation of benzo derivative **1c** reported by Shiinia (Scheme 2).[5] Thus, treatment of dilithiated tetramethylbutatriene with the appropriate halosilane gave bis(silanes) that were chlorinated with $PdCl_2/CCl_4$. Reductive coupling of the resulting bis(chlorosilanes) with sodium in toluene afforded the desired disilacyclobutane **1a** and **1b** as oxygen and moisture sensitive liquids. While **1a** is readily polymerized and has to be stored in dilute solution to avoid decomposition, **1b** is stable at room temperature for several months even in neat form.

Disilane Metathesis Reaction of Bis(isopropylidene)disilacyclobutanes (1a) and 3,4-Benzo-1,2-disilacyclobutenes (1c,d). Attempted thermal or photochemical conversions of the disilacyclobutanes **1** into the corresponding metathesis products (**2**) were unsuccessful and led to the formation of insoluble polymeric materials. Only in the case of **1a**, after a dilute toluene solution of this compound was stored for 3 weeks at room temperature, could a trace amount of tetrasilacyclooctane **2a** (<1%) be detected. On the other hand, in the presence of a catalytic amount of $Pd(PPh_3)_4$, compound **1a** was cleanly converted into **2a** within 30 min (isolated yield: 93%) (Scheme 3). The latter was obtained as a 1:1 mixture of two conformational isomers that do not interconvert at room temperature.[7,8] One of these isomers was separated and identified as the chair conformer by X-ray structure analysis (Figure 1). Selected crystallographic data are listed in Table 1, interatomic distances and angles are listed in Table 2, and final atomic positional parameters are listed in Table 3. Besides $Pd(PPh_3)_4$, $PdCl_2(PhCN)_2$ also catalyzes the disilane metathesis reaction, although with lower yields, while $Pt(CH_2{=}CH_2)(PPh_3)_2$ did not exhibit

[⊗] Abstract published in *Advance ACS Abstracts,* April 15, 1995.

(1) (a) Okinoshima, H.; Yamamoto, K.; Kumada, M. *J. Organomet. Chem.* **1975**, *86*, C27. (b) Tamao, K.; Hayashi, T.; Kumada, M. *J. Organomet. Chem.* **1976**, *114*, C19. (c) Tamao, K.; Okazaki, S.; Kumada, M. *J. Organomet. Chem.* **1978**, *146*, 87. (d) Sakurai, H.; Kamiyama, Y.; Nakadaira, Y. *J. Am. Chem. Soc.* **1975**, *97*, 931. (e) Sakurai, H.; Kamiyama, Y.; Nakadaira, Y. *Chem. Lett.* **1975**, 887. (f) Sakurai, H.; Kamiyama, Y.; Nakadaira, Y. *J. Organomet. Chem.* **1977**, *131*, 147.

(2) (a) Tanaka, M.; Uchimaru, Y.; Lautenschlager, H. J. *Organometallics* **1991**, *10*, 16. (b) Uchimaru, Y.; Lautenschlager, H. J.; Wynd, A. J.; Tanaka, M.; Goto, M. *Organometallics* **1992**, *11*, 2639. (c) Uchimaru, Y.; Brandl, P.; Tanaka, M.; Goto, M. *J. Chem. Soc., Chem. Commun.* **1993**, 744. (d) Ito, Y.; Suginome, M.; Murakami, M. *J. Org. Chem.* **1991**, *56*, 1948. (e) Murakami, M.; Oike, H.; Sugawara, M.; Suginome, M.; Ito, Y. *Tetrahedron* **1993**, *49*, 3933.

(3) Disilacyclobutanes: (a) Seyferth, D.; Goldman, E. W.; Escudié, J. *J. Organomet. Chem.* **1984**, *271*, 337. Disilacyclobutenes: (b) Sakurai, H.; Kobayashi, T.; Nakadaira, Y. *J. Organomet. Chem.* **1978**, *162*, C43. (c) Ishikawa, M.; Sakamoto, H.; Okazaki, S.; Naka, A. *J. Organomet. Chem.* **1992**, *439*, 19. (d) Ishikawa, M.; Naka, A.; Okazaki, S.; Sakamoto, H. *Organometallics* **1993**, *12*, 87. (e) Ishikawa, M.; Naka, A.; Ohshita, J. *Organometallics* **1993**, *12*, 4987.

(4) Preliminary results were communicated in: Kusukawa, T.; Kabe, Y.; Ando, W. *Chem. Lett.* **1993**, 985.

(5) (a) Shiina, K. *J. Organomet. Chem.* **1986**, *310*, C57. (b) Ishikawa, M.; Sakamoto, H.; Tabuchi, T. *Organometallics* **1991**, *10*, 3173.

(6) Maercker, A.; Dujardin, R. *Angew. Chem., Int. Ed. Engl.* **1985**, *24*, 571.

(7) Strain energies (kcal/mol) of 1,2,5,6-tetrasilacyclooctanes are calculated by MMP2 as follows: **2a**-chair, 10.2; **2a**-twist, 10.2; **2c**-chair, 4.0; **2c**-boat, 3.0; **3**-chair, 5.9; **3**-boat, 12.3. Relatively high strain energy and both chair and twist conformations gave the same value, which are consistent with the 1:1 product ratio of **2a**. In the case of **1c**, the energy difference of the chair and boat conformers is very small. In the case of **3**, the energy difference of the chair and boat conformers is very large. (Acknowledgment: We thank Dr. T. Hagiwara, Whetten at Teijin IMS Ltd. for the MMP2 calculations.)

0276-7333/95/2314-2556$09.00/0

Scheme 1

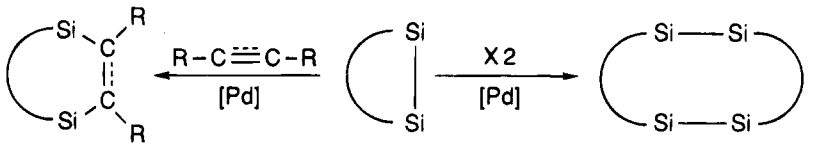

Scheme 2

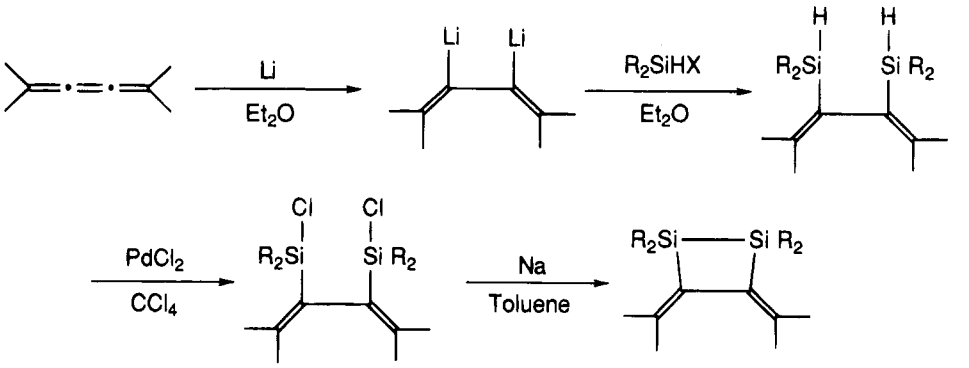

1
a: R = Me
b: R = Et

Scheme 3

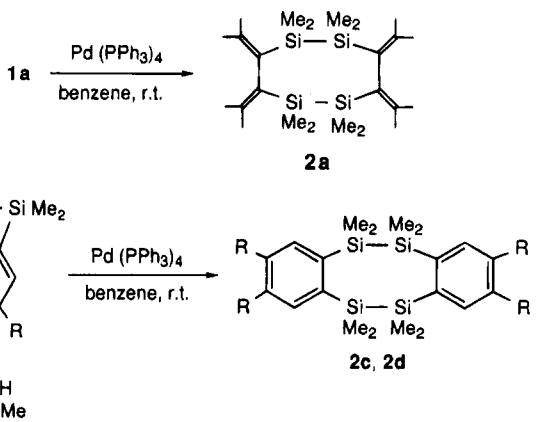

1
c: R = H
d: R = Me

any catalytic activity. In a similar manner, **1c** and **1d** were transformed into the corresponding metathesis products **2c** and **2d** in 83 and 70% yields, respectively. The structure of **2c** was assigned by X-ray structure analysis (Figure 2). However, it was not possible to convert **1b** even when more drastic conditions were employed (80 °C, 12 h). Presumably, steric shielding of the Si—Si bond by the ethyl substituents on the silicon atoms is responsible for this behavior.

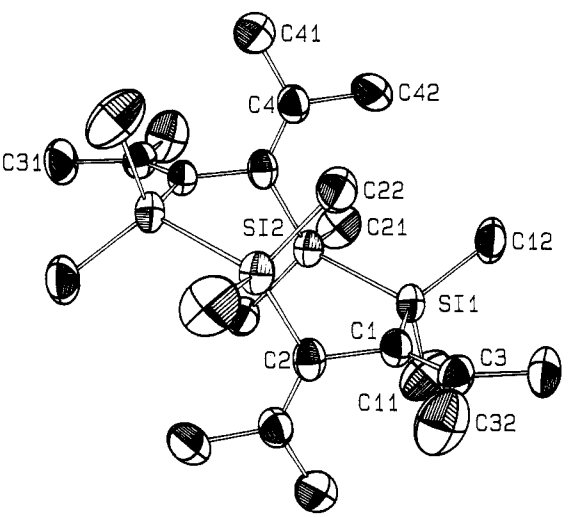

Figure 1. X-ray-determined structure of **2a**-chair.

Cross-Metathesis Reactions. When an equimolar mixture of **1a** and benzo derivatives **1c** or **1d** was treated with a catalytic amount of $Pd(PPh_3)_4$, the corresponding cross-metathesis products **3** and **4** were obtained, respectively, with high selectivity besides minor amounts of homo-metathesis products **2** (Table 4). The structure of **3** was unequivocally assigned by X-ray structure analysis (Figure 3).[6]

Favored formation of the cross-metathesis product **5** also was observed in the conversion of a mixture of **1c** and **1d**, however with a lower degree of selectivity.

The reason for this selectivity is unclear at the present moment.

Transition Metal Complex-Catalyzed Double Silylation of 1. When a benzene solution of **1a** and an excess of an alkyne in the presence of a catalytic amount of $Pd(PPh_3)_4$ was stirred at room temperature, double

(8) (a) Maercker, A.; Brauers, F.; Brieden, W. *J. Organomet. Chem.* **1989**, *377*, C45. (b) Maercker, A.; Brieden, W.; Kastner, F.; Mannschreck, A. *Chem. Ber.* **1989**, *124*, 2033. According to this precedent X-ray analysis, **2a** and **11** were assigned to chair conformational isomers as follows:

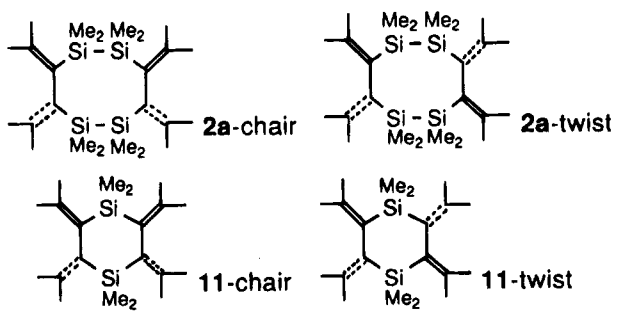

Table 1. Crystallographic Data for Diffraction Studies

compd	**2a**-chair	**2c**	**3**	**11**-chair
mol formula	$C_{24}H_{48}Si_4$	$C_{20}H_{32}Si_4$	$C_{22}H_{40}Si_4$	$C_{20}H_{36}Si_2$
fw	448.99	384.82	416.91	332.68
cryst syst	triclinic	orthorhombic	triclinic	triclinic
lattice params				
a, Å	8.438(4)	20.148(1)	9.046(1)	7.813(1)
b, Å	9.731(3)	13.345(2)	9.523(1)	8.694(1)
c, Å	10.188(4)	34.373(2)	17.504(2)	8.755(1)
α, deg	99.11(3)		77.07(1)	107.74(1)
β, deg	110.60(3)		89.23(1)	90.90(1)
γ, deg	106.75(3)		65.03(1)	103.97(1)
V, Å^3	717.7	9242.2	1326.7	547.1
space group	$P\bar{1}$ (No. 2)	$Pbca$ (No. 61)	$P\bar{1}$ (No. 2)	$P1$ (No. 1)
Z value	1	16	2	1
ϱ(calcd), g/cm^3	1.04	1.11	1.04	1.01
F(000)	248	3328	456	184
μ(Mo Kα), cm^{-1}	2.1	2.5	2.2	1.5
t, °C	23	23	23	23
$2\theta_{max}$, deg	50	50	50	50
no. of observns ($I > 3\sigma(I)$)	1098	4786	3220	1622
no. of variables	200	433	235	196
residuals: R; R_w	0.049; 0.054	0.074; 0.089	0.066; 0.098	0.073; 0.089
goodness of fit indicator	0.98	5.03	1.45	0.83
max shift in final cycle	0.07	0.07	0.01	0.03
largest/lowest peak in final diff map, e/Å^3	0.31/−0.14	0.47/−0.21	0.48/−0.14	0.35/−0.19

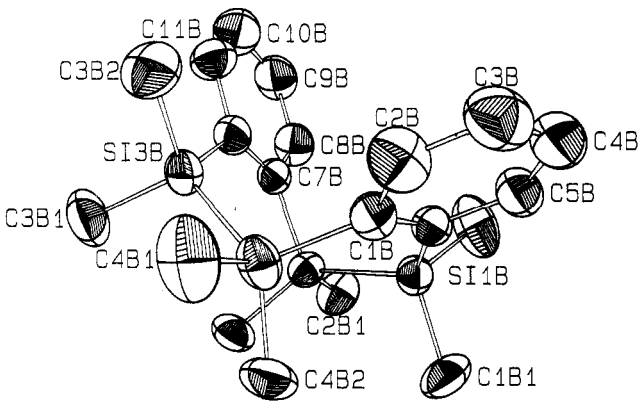

Figure 2. X-ray-determined structure of **2c**.

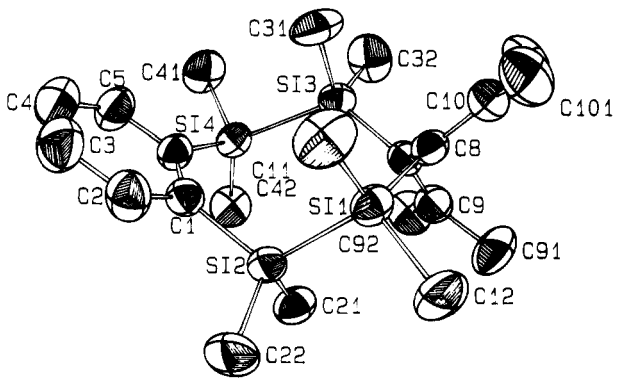

Figure 3. X-ray-determined structure of **3**.

silylation and disilane metathesis products (**2a**) were obtained, as shown in Scheme 4 and Table 5.

As seen in Table 5, in the case of $MeO_2CC{\equiv}CCO_2Me$ (DMAD) no disilane metathesis products were formed and only DMAD-incorporated products **6e** (mono-adduct) and **7e** (di-adduct) (run 1) were obtained. The yield of **7e** relative to **6e** was increased, if the catalyst was changed from $Pd(PPh_3)_4$ to $PdCl_2(PhCN)_2$ (run 2). In the case of diphenylacetylene, disilane metathesis and double silylation product formation were observed with moderate selectivity (run 5). The yield of **6f** relative to **2a** was increased, if the catalyst changed from $Pd(PPh_3)_4$ to $PdCl_2(PhCN)_2$ (run 6). In the case of phenylacetylene, the acetylene insertion product was produced and only $Pd(PPh_3)_4$ was used as catalyst. The product distribution of disilane metathesis **2a** and acetylene insertion appears to depend on the electrophilicity of the acetylenes themselves, since in the case of dimethylacetylenedicarboxylate the mono- and di-adduct are obtained and in the case of phenylacetylene only the mono-adduct is formed in the presence of $Pd(PPh_3)_4$ catalyst. On the other hand, (η^2-ethylene)bis(triphenylphosphine)platinum(0)-catalyzed reactions in all cases produced only acetylene insertion products (Table 5, runs 4 and 8). Similarly, compound **1b** only produced acetylene insertion products even when $Pd(PPh_3)_4$ was used as catalyst, probably because of the steric hindrance at the silicon atoms (Table 5, runs 3 and 7).

Competitive reactions of **1a** with other types of unsaturated compounds (Scheme 5) were examined. 2,3-Dimethyl-1,3-butadiene and benzaldehyde were not successful in competing with the disilane metathesis reaction even if 5 equiv of the unsaturated compound was employed in the presence of $Pd(PPh_3)_4$ at room temperature for 30 min. Only **2a** was obtained in 74 and 80% yields, respectively. In contrast, the $Pt(CH_2{=}CH_2)(PPh_3)_2$ catalyst (80 °C, 3 h) promoted double silylation to give **8** (41%), **9** (10%), and **10** (60%). In addition, the ethylene ligand of the Pt catalyst (10 mol % for **1a**) also participated, resulting in the formation of compound **9** (Scheme 5).

Of special interest, tetramethylbutatriene moderately inhibited the disilane metathesis reaction to give **2a** (15%) and 2,3,5,6-tetrakis(isopropylidene)-1,1,4,4-tetramethyl-1,4-disilacyclohexane (**11**, 68%) in the presence of $Pd(PPh_3)_4$ at room temperature while stirring for 30 min. The latter was obtained as a 3:1 mixture of two conformational isomers which do not interconvert at room temperature. The structure **11** was determined by X-ray analysis and is depicted in Figure 4.[7,8] *tert*-Butylallene inhibited disilane metathesis to give compound **12** (yield: 85%) in the presence of $Pd(PPh_3)_4$ at room temperature for 30 min.

From these findings, it is evident that this competition reaction involves a common intermediate with the

Table 2. Bond Lengths (Å) and Bond Angles (deg)

Bond Lengths

Compound **2a**

Si(1)–Si(2)	2.372(3)	Si(1)–C(1)	1.88(1)	Si(1)–C(11)	1.91(1)	Si(1)–C(12)	1.92(1)
Si(2)–C(2)	1.89(1)	Si(2)–C(21)	1.91(1)	Si(2)–C(22)	1.90(1)	C(1)–C(3)	1.36(1)
C(2)–C(4)	1.37(2)	C(3)–C(31)	1.53(1)	C(3)–C(32)	1.52(2)	C(4)–C(41)	1.52(1)
C(4)–C(42)	1.55(1)						

Compound **2c**

Si(1A)–Si(2A)	2.373(3)	Si(1A)–C(1A1)	1.91(1)	Si(1A)–C(12A)	1.895(8)	Si(1A)–C(1A2)	1.913(9)
Si(2A)–C(6A)	1.901(8)	Si(2A)–C(2A1)	1.90(1)	Si(2A)–C(2A2)	1.904(9)	Si(3A)–Si(4A)	2.362(3)
Si(3A)–C(7A)	1.914(8)	Si(3A)–C(3A1)	1.91(1)	Si(3A)–C(3A2)	1.92(1)	Si(4A)–C(1A)	1.884(7)
Si(4A)–C(4A1)	1.901(9)	Si(4A)–C(4A2)	1.888(8)	C(1A)–C(2A)	1.42(1)	C(1A)–C(6A)	1.41(1)
C(2A)–C(3A)	1.42(1)	C(3A)–C(4A)	1.39(2)	C(4A)–C(5A)	1.40(1)	C(5A)–C(6A)	1.43(1)
C(7A)–C(8A)	1.43(1)	C(7A)–C(12A)	1.39(1)	C(8A)–C(9A)	1.43(1)	C(9A)–C(10A)	1.35(1)
C(10A)–C(11A)	1.41(1)	C(11A)–C(12A)	1.44(1)				

Compound **3**

Si(1)–Si(2)	2.354(3)	Si(1)–C(8)	1.887(5)	Si(1)–C(11)	1.909(8)	Si(1)–C(12)	1.910(8)
Si(2)–C(1)	1.911(8)	Si(2)–C(21)	1.898(7)	Si(2)–C(22)	1.906(6)	Si(3)–Si(4)	2.359(3)
Si(3)–C(7)	1.896(7)	Si(3)–C(31)	1.909(8)	Si(3)–C(32)	1.912(7)	Si(4)–C(6)	1.895(5)
Si(4)–C(41)	1.912(8)	Si(4)–C(42)	1.906(8)	C(1)–C(2)	1.406(9)	C(1)–C(6)	1.421(7)
C(2)–C(3)	1.40(1)	C(3)–C(4)	1.37(1)	C(4)–C(5)	1.407(9)	C(5)–C(6)	1.41(1)
C(7)–C(8)	1.508(7)	C(7)–C(9)	1.35(1)	C(8)–C(10)	1.331(9)	C(9)–C(91)	1.52(1)
C(9)–C(92)	1.520(9)	C(10)–C(101)	1.54(1)	C(10)–C(102)	1.535(8)		

Compound **11**

Si(1)–C(3)	1.896(8)	Si(1)–C(5)	1.89(1)	Si(1)–C(11)	1.79(1)	Si(1)–C(12)	1.88(1)
Si(2)–C(4)	1.910(9)	Si(2)–C(6)	1.88(1)	Si(2)–C(21)	2.01(1)	Si(2)–C(22)	1.93(1)
C(3)–C(4)	1.56(1)	C(3)–C(7)	1.35(1)	C(4)–C(8)	1.27(1)	C(5)–C(6)	1.50(1)
C(5)–C(9)	1.43(2)	C(6)–C(10)	1.37(1)	C(7)–C(71)	1.57(1)	C(7)–C(72)	1.49(2)
C(8)–C(81)	1.62(2)	C(8)–C(82)	1.52(2)	C(9)–C(91)	1.46(2)	C(9)–C(92)	1.56(2)
C(10)–C(101)	1.50(2)	C(10)–C(102)	1.64(2)				

Bond Angles

Compound **2a**

Si(2)–Si(1)–C(1)	113.5(3)	Si(2)–Si(1)–C(11)	103.1(3)	Si(2)–Si(1)–C(12)	110.4(3)
C(1)–Si(1)–C(11)	108.5(6)	C(1)–Si(1)–C(12)	114.2(5)	C(11)–Si(1)–C(12)	106.2(6)
Si(1)–Si(2)–C(2)	120.0(3)	Si(1)–Si(2)–C(21)	104.4(3)	Si(1)–Si(2)–C(22)	108.4(3)
C(2)–Si(2)–C(21)	109.7(5)	C(2)–Si(2)–C(22)	108.0(4)	C(21)–Si(2)–C(22)	105.6(6)
Si(1)–C(1)–C(3)	126.7(8)	Si(2)–C(2)–C(4)	125.0(7)	C(1)–C(3)–C(31)	123(1)
C(1)–C(3)–C(32)	123.9(9)	C(31)–C(3)–C(32)	113.4(8)	C(2)–C(4)–C(41)	124.0(9)
C(2)–C(4)–C(42)	122.0(9)	C(41)–C(4)–C(42)	114(1)		

Compound **2c**

Si(2A)–Si(1A)–C(1A1)	103.3(3)	Si(2A)–Si(1A)–C(12A)	111.9(2)	Si(2A)–Si(1A)–C(1A2)	119.4(3)
C(1A1)–Si(1A)–C(12A)	108.6(4)	C(1A1)–Si(1A)–C(1A2)	102.2(5)	C(12A)–Si(1A)–C(1A2)	110.2(4)
Si(1A)–Si(2A)–C(6A)	120.6(3)	Si(1A)–Si(2A)–C(2A1)	102.0(3)	Si(1A)–Si(2A)–C(2A2)	110.0(3)
C(6A)–Si(2A)–C(2A1)	107.4(4)	C(6A)–Si(2A)–C(2A2)	110.1(4)	C(2A1)–Si(2A)–C(2A2)	105.4(4)
Si(4A)–Si(3A)–C(7A)	120.5(3)	Si(4A)–Si(3A)–C(3A1)	101.5(4)	Si(4A)–Si(3A)–C(3A2)	110.6(3)
C(7A)–Si(3A)–C(3A1)	107.3(4)	C(7A)–Si(3A)–C(3A2)	109.8(4)	C(3A1)–Si(3A)–C(3A2)	105.8(5)
Si(3A)–Si(4A)–C(1A)	110.6(2)	Si(3A)–Si(4A)–C(4A1)	102.0(3)	Si(3A)–Si(4A)–C(4A2)	118.9(3)
C(1A)–Si(4A)–C(4A1)	108.6(4)	C(1A)–Si(4A)–C(4A2)	111.9(4)	C(4A1)–Si(4A)–C(4A2)	103.7(4)
Si(4A)–C(1A)–C(2A)	115.3(6)	Si(4A)–C(1A)–C(6A)	125.1(6)	C(2A)–C(1A)–C(6A)	119.5(7)
C(1A)–C(2A)–C(3A)	121.1(9)	C(2A)–C(3A)–C(4A)	118.5(9)	C(3A)–C(4A)–C(5A)	120.9(8)
C(4A)–C(5A)–C(6A)	121.1(9)	Si(2A)–C(6A)–C(1A)	127.6(5)	Si(2A)–C(6A)–C(5A)	113.7(6)
C(1A)–C(6A)–C(5A)	118.7(7)	Si(3A)–C(7A)–C(8A)	113.0(6)	Si(3A)–C(7A)–C(12A)	127.4(6)
C(8A)–C(7A)–C(12A)	119.6(7)	C(7A)–C(8A)–C(9A)	119.1(8)	C(8A)–C(9A)–C(10A)	121.2(8)
C(9A)–C(10A)–C(11A)	120.1(8)	C(10A)–C(11A)–C(12A)	120.5(9)	Si(1A)–C(12A)–C(7A)	126.1(6)
Si(1A)–C(12A)–C(11A)	114.5(6)	C(7A)–C(12A)–C(11A)	119.4(7)		

Compound **3**

Si(2)–Si(1)–C(8)	115.2(2)	Si(2)–Si(1)–C(11)	104.9(3)	Si(2)–Si(1)–C(12)	105.7(3)
C(8)–Si(1)–C(11)	112.4(3)	C(8)–Si(1)–C(12)	109.0(3)	C(11)–Si(1)–C(12)	109.3(4)
Si(1)–Si(2)–C(1)	110.0(2)	Si(1)–Si(2)–C(21)	114.5(2)	Si(1)–Si(2)–C(22)	104.3(3)
C(1)–Si(2)–C(21)	115.5(3)	C(1)–Si(2)–C(22)	106.9(3)	C(21)–Si(2)–C(22)	104.5(3)
Si(4)–Si(3)–C(7)	120.1(2)	Si(4)–Si(3)–C(31)	102.4(3)	Si(4)–Si(3)–C(32)	109.9(3)
C(7)–Si(3)–C(31)	107.6(3)	C(7)–Si(3)–C(32)	109.5(4)	C(31)–Si(3)–C(32)	106.3(4)
Si(3)–Si(4)–C(6)	108.0(2)	Si(3)–Si(4)–C(41)	101.4(3)	Si(3)–Si(4)–C(42)	120.6(3)
C(6)–Si(4)–C(41)	107.8(3)	C(6)–Si(4)–C(42)	113.4(3)	C(41)–Si(4)–C(42)	104.2(4)
Si(2)–C(1)–C(2)	113.4(5)	Si(2)–C(1)–C(6)	128.2(5)	C(2)–C(1)–C(6)	118.4(7)
C(1)–C(2)–C(3)	122.4(6)	C(2)–C(3)–C(4)	119.2(6)	C(3)–C(4)–C(5)	119.9(8)
C(4)–C(5)–C(6)	121.9(6)	Si(4)–C(6)–C(1)	127.3(5)	Si(4)–C(6)–C(5)	114.3(4)
C(1)–C(6)–C(5)	118.2(5)	Si(3)–C(7)–C(8)	114.4(5)	Si(3)–C(7)–C(9)	123.5(4)
C(8)–C(7)–C(9)	122.1(6)	Si(1)–C(8)–C(7)	114.1(4)	Si(1)–C(8)–C(10)	125.2(4)
C(7)–C(8)–C(10)	120.7(4)	C(7)–C(9)–C(91)	122.4(6)	C(7)–C(9)–C(92)	123.1(7)
C(91)–C(9)–C(92)	114.5(7)	C(8)–C(10)–C(101)	123.2(5)	C(8)–C(10)–C(102)	122.9(6)
C(101)–C(10)–C(102)	113.9(6)				

Table 2 (Continued)

		Compound **11**			
C(3)–Si(1)–C(5)	100.5(4)	C(3)–Si(1)–C(11)	108.9(4)	C(3)–Si(1)–C(12)	119.9(4)
C(5)–Si(1)–C(11)	109.9(4)	C(5)–Si(1)–C(12)	117.0(5)	C(11)–Si(1)–C(12)	100.5(6)
C(4)–Si(2)–C(6)	103.7(5)	C(4)–Si(2)–C(21)	106.7(5)	C(4)–Si(2)–C(22)	116.2(5)
C(6)–Si(2)–C(21)	107.6(5)	C(6)–Si(2)–C(22)	114.8(4)	C(21)–Si(2)–C(22)	107.4(7)
Si(1)–C(3)–C(4)	108.7(5)	Si(1)–C(3)–C(7)	128.6(7)	C(4)–C(3)–C(7)	122.7(8)
Si(2)–C(4)–C(3)	106.3(6)	Si(2)–C(4)–C(8)	130.6(7)	C(3)–C(4)–C(8)	122.9(8)
Si(1)–C(5)–C(6)	112.5(7)	Si(1)–C(5)–C(9)	127.6(8)	C(6)–C(5)–C(9)	119(1)
Si(2)–C(6)–C(5)	109.4(6)	Si(2)–C(6)–C(10)	134(1)	C(5)–C(6)–C(10)	116(1)
C(3)–C(7)–C(71)	121.2(8)	C(3)–C(7)–C(72)	129.6(9)	C(71)–C(7)–C(72)	109.1(7)
C(4)–C(8)–C(81)	124.3(9)	C(4)–C(8)–C(82)	121.9(9)	C(81)–C(8)–C(82)	113.6(9)
C(5)–C(9)–C(91)	119(1)	C(5)–C(9)–C(92)	128(1)	C(91)–C(9)–C(92)	113(1)
C(6)–C(10)–C(101)	125(1)	C(6)–C(10)–C(102)	115(1)	C(101)–C(10)–C(102)	120(1)

Table 3. Positional Parameters and *B*(eq) Values

atom	*x*	*y*	*z*	*B*(eq) (Å²)	atom	*x*	*y*	*z*	*B*(eq) (Å²)
				Compound **2a**					
Si(1)	0.2568(4)	0.2329(3)	0.9197(3)	3.50(7)	Si(2)	0.5154(4)	0.3801(3)	1.1415(3)	3.33(6)
C(1)	0.256(1)	0.304(1)	0.758(1)	3.4(2)	C(2)	0.560(1)	0.585(1)	1.2182(9)	3.4(2)
C(3)	0.112(1)	0.262(1)	0.626(1)	4.1(3)	C(4)	0.447(1)	0.637(1)	1.261(1)	3.9(3)
C(11)	0.281(2)	0.042(1)	0.889(1)	5.6(3)	C(12)	0.037(1)	0.201(1)	0.948(1)	5.4(3)
C(21)	0.489(2)	0.275(1)	1.281(1)	5.6(3)	C(22)	0.726(1)	0.368(1)	1.121(1)	4.5(3)
C(31)	−0.076(1)	0.146(1)	0.590(1)	5.7(4)	C(32)	0.123(2)	0.322(1)	0.499(1)	5.9(4)
C(41)	0.492(1)	0.801(1)	1.332(1)	5.1(3)	C(42)	0.258(1)	0.531(1)	1.239(1)	5.4(3)
				Compound **2c**					
Si(1A)	0.6505(1)	0.1456(2)	0.06581(7)	3.80(5)	Si(2A)	0.7679(1)	0.1473(2)	0.07153(6)	3.54(4)
Si(3A)	0.6459(1)	0.1378(2)	−0.04090(7)	3.75(5)	Si(4A)	0.7435(1)	0.0472(2)	−0.02634(6)	3.49(4)
C(1A)	0.8120(3)	0.1348(6)	−0.0109(2)	3.5(2)	C(2A)	0.8570(4)	0.1631(7)	−0.0409(3)	5.1(2)
C(3A)	0.9131(5)	0.2245(7)	−0.0328(3)	6.0(2)	C(4A)	0.9242(4)	0.2544(7)	0.0054(3)	6.0(2)
C(5A)	0.8799(4)	0.2284(6)	0.0351(3)	4.9(2)	C(6A)	0.8222(4)	0.1699(5)	0.0272(2)	3.4(2)
C(7A)	0.6174(4)	0.2451(6)	−0.0080(3)	3.7(2)	C(8A)	0.5928(4)	0.3291(6)	−0.0292(3)	4.7(2)
C(9A)	0.5713(4)	0.4163(6)	−0.0083(3)	5.5(2)	C(10A)	0.5744(4)	0.4204(7)	0.0310(3)	5.2(2)
C(1A1)	0.6211(5)	0.1732(8)	0.1175(3)	6.5(3)	C(11A)	0.5972(4)	0.3371(6)	0.0523(3)	4.8(2)
C(12A)	0.6194(3)	0.2485(6)	0.0325(2)	3.5(2)	C(1A2)	0.6061(4)	0.0223(6)	0.0545(3)	5.2(2)
C(2A1)	0.7820(5)	0.2560(7)	0.1064(3)	6.5(2)	C(2A2)	0.7972(5)	0.0311(7)	0.0987(3)	5.5(2)
C(3A1)	0.6678(6)	0.1948(8)	−0.0903(3)	6.4(3)	C(3A2)	0.5732(5)	0.0481(7)	−0.0504(3)	6.2(2)
C(4A1)	0.7659(5)	−0.0084(7)	−0.0756(2)	5.6(2)	C(4A2)	0.7376(4)	−0.0657(6)	0.0066(3)	4.3(2)
				Compound **3**					
Si(1)	0.5669(2)	0.0367(2)	0.2177(1)	3.96(4)	Si(2)	0.4971(2)	0.0487(2)	0.3468(1)	3.99(4)
Si(3)	0.2564(2)	0.4802(2)	0.1958(1)	4.17(4)	Si(4)	0.2569(2)	0.4881(2)	0.3296(1)	4.10(4)
C(1)	0.5647(7)	0.1903(6)	0.3821(4)	3.9(1)	C(2)	0.7297(8)	0.1178(8)	0.4127(4)	5.3(2)
C(3)	0.8048(8)	0.2024(9)	0.4396(5)	6.2(2)	C(4)	0.7145(9)	0.3604(8)	0.4374(5)	6.4(2)
C(5)	0.5488(8)	0.4368(7)	0.4074(4)	5.4(2)	C(6)	0.4717(7)	0.3553(6)	0.3783(4)	3.9(1)
C(7)	0.2550(7)	0.3008(6)	0.1664(3)	3.9(1)	C(8)	0.4130(6)	0.1983(6)	0.1374(3)	3.8(1)
C(9)	0.1229(7)	0.2691(7)	0.1681(4)	4.8(2)	C(10)	0.4365(8)	0.2262(7)	0.0613(4)	5.1(2)
C(11)	0.7767(8)	0.0395(9)	0.2148(5)	6.3(2)	C(12)	0.588(1)	−0.1660(7)	0.2068(5)	6.7(2)
C(21)	0.2785(7)	0.0803(7)	0.3633(4)	5.1(2)	C(22)	0.629(1)	−0.1608(8)	0.4087(5)	6.4(2)
C(31)	0.4565(8)	0.4913(8)	0.1678(5)	6.4(2)	C(32)	0.084(1)	0.6709(9)	0.1349(5)	7.3(3)
C(41)	0.218(1)	0.7046(7)	0.3217(5)	6.6(2)	C(42)	0.0904(8)	0.4626(8)	0.3910(4)	5.8(2)
C(91)	0.1211(8)	0.1313(8)	0.1385(5)	7.0(2)	C(92)	−0.0351(8)	0.3661(9)	0.2003(5)	6.3(2)
C(101)	0.5970(9)	0.130(1)	0.0285(4)	6.9(2)	C(102)	0.306(1)	0.360(1)	−0.0015(4)	7.0(3)
				Compound **11**					
Si(1)	0.997	0.611	0.159	4.47(6)	Si(2)	0.9863(5)	0.9079(3)	−0.0228(4)	4.28(6)
C(3)	0.905(1)	0.5691(9)	−0.0558(9)	3.4(2)	C(4)	1.027(1)	0.6941(9)	−0.128(1)	3.6(2)
C(5)	0.962(1)	0.826(1)	0.258(1)	4.3(2)	C(6)	1.069(1)	0.955(1)	0.193(1)	4.7(2)
C(7)	0.757(1)	0.456(1)	−0.139(1)	3.3(2)	C(8)	1.136(1)	0.652(1)	−0.228(1)	3.7(2)
C(9)	0.833(2)	0.869(2)	0.366(1)	6.0(3)	C(10)	1.218(2)	1.059(1)	0.288(2)	7.4(4)
C(11)	1.229(1)	0.623(1)	0.162(1)	4.5(2)	C(12)	0.921(2)	0.450(1)	0.263(1)	6.9(4)
C(21)	0.722(2)	0.875(2)	−0.033(2)	6.6(4)	C(22)	1.083(2)	1.082(1)	−0.115(1)	6.5(3)
C(71)	0.700(1)	0.442(1)	−0.316(1)	4.2(2)	C(72)	0.621(2)	0.336(1)	−0.085(1)	6.3(3)
C(81)	1.165(2)	0.466(1)	−0.294(1)	6.2(3)	C(82)	1.264(2)	0.779(1)	−0.286(1)	6.1(3)
C(91)	0.819(2)	1.041(1)	0.421(1)	6.9(3)	C(92)	0.707(2)	0.755(2)	0.446(2)	7.7(4)
C(101)	1.277(2)	1.052(2)	0.449(1)	8.0(4)	C(102)	1.339(2)	1.194(2)	0.211(2)	8.2(4)

double silylation reaction, i.e., a bis(silyl)palladium(II) complex (Scheme 6).[9] Insertion of unsaturated compounds into this intermediate then follows. This pathway also competes with the disilane metathesis reaction. The selectivity of these pathways depends on the relative reactivity of unsaturated compounds.

In conclusion, bis(isopropylidene)disilacyclobutane (**1a**) and benzodisilacyclobutenes afforded the disilane metathesis products in the presence of a Pd catalyst. A highly selective cross-metathesis occurred between **1a**

Table 4. Palladium Complex-Catalyzed Cross-Disilane Metathesis Reaction[a]

disilacyclobutane	cross-products (%)[b]	homo-prduct (%)[b]
1a, **1c**	**3** (73)	**2a** (1), **2c** (3)
1a, **1d**	**4** (68)	**2a** (1), **2d** (2)
1c, **1d**	**5** (51)	**2c** (8), **2d** (12)

[a] Condition: disilacyclobutane (0.89 mmol), $Pd(PPh_3)_4$ (0.09 mmol), benzene (10 mL), room temperature, 30 min. [b] Isolated yield.

(9) Stable bis(silyl)palladium complexes were isolated: Pan, Y.; Mauge, J. T.; Fink, M. J. *Organometallics* **1992**, *11*, 3495.

Chart 1

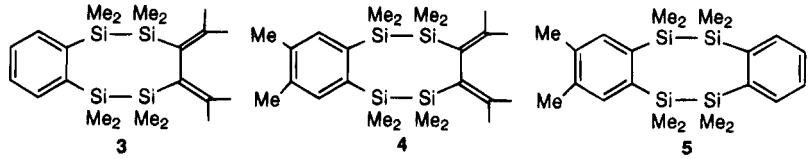

Scheme 4

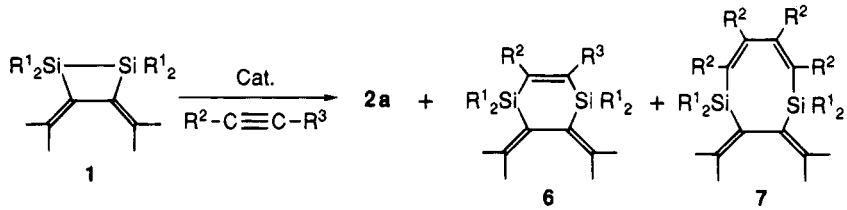

e: R^1= Me, R^2= R^3= CO_2Me; **f**: R^1= Me, R^2= R^3= Ph; **g**: R^1= Me, R^2= Ph, R^3= H;
h : R^1= Et, R^2= R^3= CO_2Me; **i** : R^1= Et, R^2= R^3= Ph

Table 5. Transition Metal Complex-Catalyzed Double Silylation of 1[a]

		reactant					product and yield/%[b]		
run	substrate R^1	R^2	R^3	temp	time/h	catalyst	**2a**	**6**	**7**
1	Me	CO_2Me	CO_2Me	rt[c]	0.5	$Pd(PPh_3)_4$		68	18
2	Me	CO_2Me	CO_2Me	rt	0.5	$PdCl_2(PhCN)_2$		30	47
3	Et	CO_2Me	CO_2Me	rt	10	$Pd(PPh_3)_4$		77	
4	Me	CO_2Me	CO_2Me	reflux	12	$Pt(CH_2{=}CH_2)(PPh_3)_2$		71	
5	Me	Ph	Ph	rt	0.5	$Pd(PPh_3)_4$	61	31	
6	Me	Ph	Ph	rt	0.5	$PdCl_2(PhCN)_2$	24	51	
7	Et	Ph	Ph	rt	10	$Pd(PPh_3)_4$		87	
8	Me	Ph	Ph	reflux	3	$Pt(CH_2{=}CH_2)(PPh_3)_2$		82	
9	Me	Ph	H	rt	0.5	$Pd(PPh_3)_4$		80	
10	Me	Ph	H	rt	0.5	$PdCl_2(PhCN)_2$	18	59	

[a] Condition: **1** (0.89 mmol), reactant (4.4 mmol), catalyst (0.09 mmol), benzene (10 mL). [b] Isolated yield. [c] Room temperature.

Scheme 5

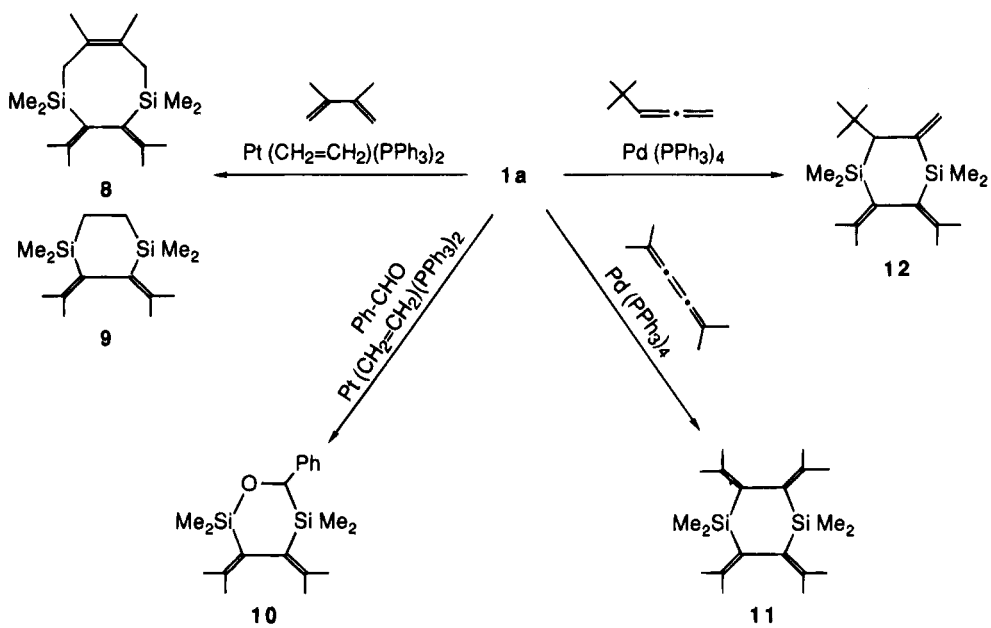

and **1c**. However, in the presence of unsaturated compounds, this disilane metathesis was inhibited to give doubly silylated compounds. The yields of disilane metathesis and doubly silylated products depend on the relative reactivity of unsaturated compounds.

Experimental Section

General Procedure. Melting points were determined with a Yanaco micro melting point apparatus and are uncorrected. ^1H, ^{13}C, and ^{29}Si NMR spectra were recorded on Bruker AM500 (500 and 125 MHz), AC400 (400, 100, and 80 MHz), and JEOL JNM-EX90 (90, 22, and 19 MHz) instruments. Infrared spectra were measured on a JASCO FT/IR-5000 spectrometer. Mass spectra were obtained on Shimadzu QP-2000 and JEOL JMS SX102A mass spectrometers. Elemental analyses were carried out by the Chemical Analytical Center of the University of Tsukuba. For column chromatography Kieselgel 60 (Merck, Art. 7734) was used. Gel permeation chromatography (GPC) was performed on a LC 908 instrument (Japan Analyti-

Scheme 6

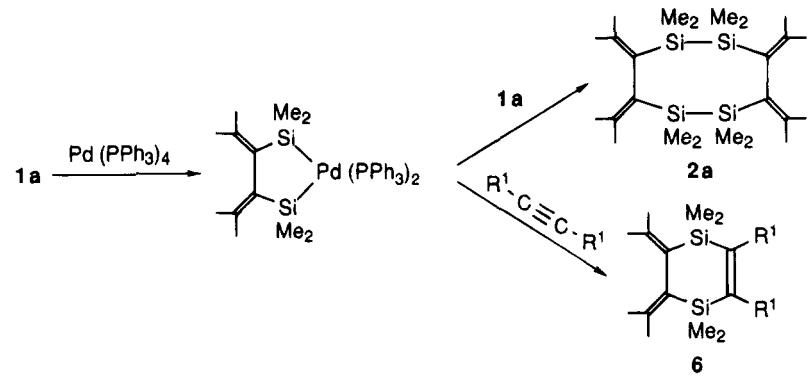

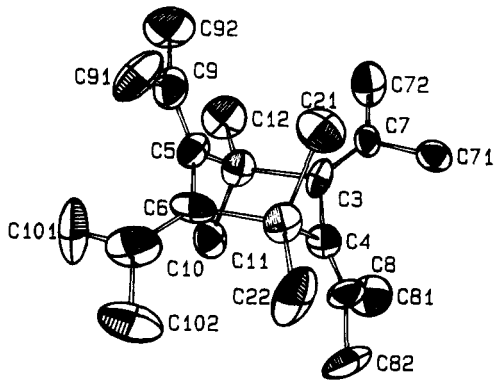

Figure 4. X-ray-determined structure of **11**-chair.

cal Industry Co. Ltd.) with a series of Jaigel 1H and 2H columns and toluene as eluent. All solvents and reagents were purified according to standard procedures. 2,5-Dimethyl-2,3,4-hexatriene was prepared by the published procedure.[10]

Preparation of 3,4-Bis(isopropylidene)-1,2-disilacyclobutanes (1). General Procedure A: Preparation of 3,4-Bis(dimethylsilyl)-2,5-dimethyl-2,4-hexadiene. To a mixture of 2.60 g of Li sand (375 mmol), 400 mg of sodium (17.4 mmol), and 20 mL of Et_2O was added a solution of 2,5-dimethyl-2,3,4-hexatriene,[10] generated from 10.0 g of 2,5-dichloro-2,5-dimethyl-3-hexyne (55.8 mmol) over a period of 1.5 h at room temperature. After stirring for 2 h, a solution of 13.0 g of dimethylchlorosilane (137 mmol) in 30 mL of Et_2O was introduced within 1 h. All solids were removed by filtration, the solvent was evaporated, and the residue was fractionally distilled under reduced pressure to give 4.62 g (37%) of 3,4-bis(dimethylsilyl)-2,5-dimethyl-2,4-hexadiene as a colorless liquid, bp 98–102 °C/20 Torr. ^{1}H NMR (90 MHz, $CDCl_3$): δ 0.13 (d, 6H, J = 4.1 Hz), 0.14 (d, 6H, J = 4.1 Hz), 1.57 (s, 6H), 1.88 (s, 6H), 4.21 (sept, 2H, J = 4.1 Hz). ^{13}C NMR (22 MHz, $CDCl_3$): δ −2.9 (q), −2.6 (q), 22.6 (q), 23.6 (q), 135.9 (s), 141.3 (s). ^{29}Si NMR (80 MHz, $CDCl_3$): δ −25.4. MS: *m/e* 226 (M^+). HRMS Calcd for $C_{12}H_{26}Si_2$: 226.1573. Found: 226.1595. Anal. Calcd for $C_{12}H_{26}Si_2$: C, 63.63; H, 11.57. Found: C, 63.48; H, 11.48. IR (neat): 2080 cm^{-1}.

3,4-Bis(diethylsilyl)-2,5-dimethyl-2,4-hexadiene was prepared from 10.0 g of 2,5-dichloro-2,5-dimethyl-3-hexyne (55.8 mmol) according to method A, giving 15.7 g (48%) of colorless liquid, bp 120–125 °C/2 Torr (Kugelrohr). ^{1}H NMR (90 MHz, $CDCl_3$): δ 0.5–1.1 (m, 20H), 1.55 (s, 6H), 1.83 (s, 6H), 3.88 (quint, 2H, J = 3.2 Hz). ^{13}C NMR (22 MHz, $CDCl_3$): δ 3.0 (t), 4.7 (t), 8.9 (q), 9.2 (q), 22.4 (q), 24.2 (q), 135.7 (s), 141.4 (s). ^{29}Si NMR (80 MHz, $CDCl_3$): δ −10.6. MS: *m/e* 282 (M^+). HRMS Calcd for $C_{16}H_{34}Si_2$: 282.2199. Found: 282.2189. Anal. Calcd for $C_{16}H_{34}Si_2$: C, 68.00; H, 12.13. Found: C, 68.28; H, 12.29. IR (neat): 2112 cm^{-1}.

(10) Gotthardt, H.; Jung, R. *Chem. Ber.* **1985**, *118*, 3438.

General Procedure B: Preparation of 3,4-Bis(chlorodimethylsilyl)-2,5-dimethyl-2,4-hexadiene. A solution of 3.40 g of 3,4-bis(dimethylsilyl)-2,5-dimethyl-2,4-hexadiene (15.0 mmol) in 10 mL of CCl_4 was added to 200 mg of $PdCl_2$ (1.13 mmol) over a period of 15 min at room temperature. Stirring was continued for 2 h, then the Pd catalyst was filtered, and the filtrate was Kugelrohr-distilled to afford 3.92 g (89%) of 3,4-bis(chlorodimethylsilyl)-2,5-dimethyl-2,4-hexadiene as a waxy solid, bp 98–102 °C/1.5 Torr (Kugelrohr). ^{1}H NMR (90 MHz, C_6D_6): δ 0.466 (s, 6H), 0.473 (s, 6H), 1.52 (s, 6H), 1.82 (s, 6H). ^{13}C NMR (22 MHz, C_6D_6): δ 4.2 (q), 4.5 (q), 23.3 (q), 24.2 (q), 135.4 (s), 147.1 (s). ^{29}Si NMR (18 MHz, C_6D_6): δ 15.2. MS: *m/e* 294 (M^+). Anal. Calcd for $C_{12}H_{24}Si_2Cl_2$: C, 48.79; H, 8.19. Found: C, 48.88; H, 8.24.

3,4-Bis(chlorodiethylsilyl)-2,5-dimethyl-2,4-hexadiene was prepared from 8.0 g of 3,4-bis(diethylsilyl)-2,5-dimethyl-2,4-hexadiene (28.3 mmol) according to method B, giving 7.90 g (97%) of colorless liquid, bp 130–140 °C/0.8 Torr (Kugelrohr). ^{1}H NMR (90 MHz, $CDCl_3$): δ 0.8–1.1 (m, 20H), 1.64 (s, 6H), 1.98 (s, 6H). ^{13}C NMR (22 MHz, $CDCl_3$): δ 7.4 (q, two carbon), 10.1 (t), 10.2 (t), 23.4 (q), 24.7 (q), 134.2 (s), 147.3 (s). MS: *m/e* 350 (M^+). HRMS Calcd for $C_{16}H_{32}Cl_2Si_2$: 350.1420. Found: 350.1431. Anal. Calcd for $C_{16}H_{32}Cl_2Si_2$: C, 54.67; H, 9.18. Found: C, 54.40; H, 9.15.

General Procedure C: Preparation of 3,4-Bis(isopropylidene)-1,1,2,2-tetramethyldisilacyclobutane, 1a. A solution of 3.60 g of 3,4-bis(chlorodimethylsilyl)-2,5-dimethyl-2,4-hexadiene (12.2 mmol) in 10 mL of toluene was added to 1.00 g of sodium (43.5 mmol), and the mixture was heated to reflux for 24 h. The precipitate was removed by filtration, and the solvent was evaporated. The residue consisted mainly of 3,4-bis(isopropylidene)-1,1,2,2-tetramethyldisilacyclobutane (1.82 g, 67% yield) and was contaminated with a small amount of corresponding siloxane (10%). The purity was determined by ^{1}H NMR spectroscopy (integration of the allylic methyl protons of the disilacyclobutane at δ = 1.62 ppm and the corresponding resonances of the siloxane at δ = 1.60 ppm). Attention: 3,4-Bis(isopropylidene)-1,1,2,2-tetramethyldisilacyclobutane is unstable and should be prepared immediately prior to use. ^{1}H NMR (90 MHz, C_6D_6): δ 0.37 (s, 12H), 1.62 (s, 6H), 1.80 (s, 6H). ^{13}C NMR (22 MHz, C_6D_6): δ 23.4 (q), 25.9 (q), 137.5 (s), 143.9 (s). ^{29}Si NMR (18 MHz, C_6D_6): δ −16.5. MS: *m/e* 224 (M^+). HRMS Calcd for $C_{12}H_{24}Si_2$: 224.1417. Found: 224.1395.

3,4-Bis(isopropylidene)-1,1,2,2-tetraethyldisilacyclobutane (1b) was prepared from 7.90 g of 3,4-bis(chlorodiethylsilyl)-2,5-dimethyl-2,4-hexadiene (22.5 mmol) according to method C; 6.01 g (95%) of colorless liquid was obtained, bp 85–90 °C/2 Torr (Kugelrohr). ^{1}H NMR (90 MHz, C_6D_6): δ 0.8–1.2 (m, 20H), 1.64 (s, 6H), 1.81 (s, 6H). ^{13}C NMR (22 MHz, C_6D_6): δ 5.7 (t), 9.6 (q), 23.2 (q), 26.3 (q), 137.2 (s), 142.9 (s). ^{29}Si NMR (18 MHz, C_6D_6): δ −4.5. MS: *m/e* 280 (M^+). HRMS Calcd for $C_{16}H_{32}Si_2$: 280.2043. Found: 280.2045. Anal. Calcd for $C_{16}H_{32}Si_2$: C, 68.49; H, 11.49. Found: C, 68.62; H, 11.29.

1,2-Bis(dimethylsilyl)-4,5-dimethylbenzene was prepared from 20.0 g of 4,5-dibromo-*o*-xylene (75.8 mmol) accord-

ing to a published procedure for a similar compound.[5] A colorless liquid (5.35 g, 32%) was obtained, bp 110 °C/14 Torr. ^{1}H NMR (400 MHz, C_6D_6): δ 0.37 (d, 12H, J = 3.8 Hz), 2.07 (s, 6H), 4.91 (sept, 2H), 7.36 (s, 2H). ^{13}C NMR (100 MHz, C_6D_6): δ −2.3 (q), 19.5 (q), 136.3 (d), 136.8 (s), 141.3 (s). ^{29}Si NMR (80 MHz, C_6D_6): δ −19.7. MS: *m/e* 222 (M^+). HRMS Calcd for $C_{12}H_{22}Si_2$: 222.1260. Found: 222.1252. Anal. Calcd for $C_{12}H_{22}Si_2$: C, 64.78; H, 9.97. Found: C, 64.28; H, 9.69. IR (neat): 2128 cm^{-1}.

1,2-Bis(chlorodimethylsilyl)-4,5-dimethylbenzene was prepared from 3.50 g of 1,2-bis(dimethylsilyl)-4,5-dimethylbenzene (15.8 mmol) according to method B. A colorless liquid (3.75 g, 82%) was obtained, bp 120−130 °C/2 Torr (Kugelrohr). ^{1}H NMR (400 MHz, $CDCl_3$): δ 0.80 (s, 12H), 2.30 (s, 6H), 7.63 (s, 2H). ^{13}C NMR (80 MHz, $CDCl_3$): δ 5.3 (q), 19.8 (q), 137.3 (d), 138.0 (s), 138.7 (s). MS: *m/e* 290 (M^+). HRMS Calcd for $C_{12}H_{20}Cl_2Si_2$: 290.0481. Found: 290.0479. Anal. Calcd for $C_{12}H_{20}Cl_2Si_2$: C, 49.47; H, 6.92. Found: C, 49.28; H, 6.61.

3,4-Bis(4,5-dimethyl-*o*-phenylene)-1,1,2,2-tetramethyl-1,2-disilacyclobutene (1d) was prepared from 3.75 g of 1,2-bis(chlorodimethylsilyl)-4,5-dimethylbenzene (12.9 mmol) according to method C; 26.7 mg (9.4%) of **4b** was obtained. The obtained liquid was contaminated with a siloxane (50%) derived from the starting material. The purity of the product was determined by ^{1}H NMR spectroscopy (integration of the methine protons of the benzene ring at δ = 7.24 ppm and the corresponding resonances of the siloxane at 7.30 ppm); 60−70 °C/1.5 × 10^{-5} Torr (Kugelrohr). ^{1}H NMR (400 MHz, C_6D_6): δ 0.44 (s, 12H), 2.09 (s, 6H), 7.24 (s, 2H). ^{13}C NMR (100 MHz, C_6D_6): δ −1.7 (q), 20.1 (q), 133.0 (d), 138.2 (s), 153.8 (s). ^{29}Si NMR (80 MHz, C_6D_6): δ −1.5. MS: *m/e* 220 (M^+). HRMS Calcd for $C_{12}H_{20}Si_2$: 220.1104. Found: 220.1108.

General Procedure for the Palladium- and Platinum-Catalyzed Reactions. A solution of the appropriate disilacyclobutane or disilacyclobutene (0.89 mmol), the catalyst (0.09 mmol), and the unsaturated compounds (4.4 mmol) in 10 mL of benzene was stirred for 30 min at room temperature. The solvent was evaporated, and the residue was purified by TLC (silica gel, *n*-hexane) or GPC.

3,4,7,8-Tetrakis(isopropylidene)-1,1,2,2,5,5,6,6-octamethyl-1,2,5,6-tetrasilacyclooctane, 2a. (The product consists of a 1:1 mixture of the twist and chair conformers; the latter can be separated by fractional recrystallization from hexane.) Chair conformer: mp 215−216 °C; ^{1}H NMR (90 MHz, C_6D_6) δ 0.23 (s, 12H), 0.46 (s, 12H), 1.59 (s, 12H), 1.79 (s, 12H); ^{13}C NMR (22 MHz, C_6D_6) δ −0.9 (q), 1.3 (q), 23.2 (q), 24.9 (q), 139.3 (s), 140.5 (s); ^{29}Si NMR (18 MHz, C_6D_6) δ −26.5; MS *m/e* 448 (M^+). HRMS Calcd for $C_{24}H_{48}Si_4$: 448.2833. Found: 448.2846. Anal. Calcd for $C_{24}H_{48}Si_4$: C, 64.20; H, 10.78. Found: C, 64.31; H, 10.72. Twist conformer: ^{1}H NMR (90 MHz, C_6D_6) δ 0.32 (s, 12H), 0.39 (s, 12H), 1.59 (s, 12H), 1.84 (s, 12H); ^{13}C NMR (23 MHz, C_6D_6) δ −0.06 (q), 0.11 (q), 23.0 (q), 24.7 (q), 139.4 (s), 139.7 (s); ^{29}Si NMR (18 MHz, C_6D_6) δ −27.4.

3,4,7,8-Dibenzo-1,1,2,2,5,5,6,6-octamethyl-1,2,5,6-tetrasilacycloocta-3,7-diene, 2c, and 3,4,7,8-Tetrakis(4,5-dimethyl-*o*-phenylene)-1,1,2,2,5,5,6,6-octamethyl-1,2,5,6-tetrasilacycloocta-3,7-diene, 2d. All spectral data obtained for **2c** and **2d** were identical with those of the authentic sample.[11]

3,4-Benzo-7,8-bis(isopropylidene)-1,1,2,2,5,5,6,6-octamethyl-1,2,5,6-tetrasilacyclooct-3-ene, 3: colorless prisms; mp 74−75 °C; ^{1}H NMR (400 MHz, C_6D_6) δ 0.11 (s, 6H), 0.31 (s, 6H), 0.46 (s, 6H), 0.48 (s, 6H), 1.54 (s, 6H), 1.77 (s, 6H), 7.18 (dd, 2H, J = 5.6, 3.2 Hz), 7.63 (dd, 2H, J = 5.6, 3.2 Hz); ^{13}C NMR (100 MHz, C_6D_6) δ −0.8 (q), −0.5 (q), 0.7 (q), 1.6 (q), 22.5 (q), 24.7 (q), 127.8 (d), 135.7 (d), 139.0 (s), 139.8 (s), 146.1 (s); ^{29}Si NMR (80 MHz, C_6D_6) δ −27.0, −19.1. HRMS Calcd for $C_{16}H_{30}O_2Si_2$: 416.2207. Found: 416.2218. Anal. Calcd for $C_{22}H_{40}Si_4$: C, 63.38; H, 9.67. Found: C, 62.92; H, 9.62.

(11) Sakurai, H.; Nakadaira, Y.; Hosomi, A.; Eriyama, Y. *Chem. Lett.* **1982**, 1971.

3,4-Bis(isopropylidene)-7,8-bis(4,5-dimethyl-*o*-phenylene)-1,1,2,2,5,5,6,6-octamethyl-1,2,5,6-tetrasilacyclooct-7-ene, 4: colorless prisms; mp 82−83 °C; ^{1}H NMR (500 MHz, C_6D_6) δ 0.15 (s, 6H), 0.35 (s, 6H), 0.52 (s, 6H), 0.54 (s, 6H), 1.56 (s, 6H), 1.79 (s, 6H), 2.08 (s, 6H), 7.50 (s, 2H); ^{13}C NMR (125 MHz, C_6D_6) δ −0.8 (q), −0.6 (q), 0.8 (q), 1.7 (q), 19.6 (q), 22.5 (q), 24.7 (q), 135.7 (s), 137.4 (d), 139.2 (s), 139.6 (s), 142.9 (s); ^{29}Si NMR (80 MHz, C_6D_6) δ −27.3, −19.8. HRMS Calcd for $C_{24}H_{44}Si_4$: 444.2520. Found: 444.2516. Anal. Calcd for $C_{24}H_{44}Si_4$: C, 64.78; H, 9.97. Found: C, 65.06; H, 9.87.

3,4-Benzo-7,8-bis(4,5-dimethyl-*o*-phenylene)-1,1,-2,2,5,5,6,6-octamethyl-1,2,5,6-tetrasilacycloocta-3,7-diene, 5: colorless needles; mp 72−73 °C; ^{1}H NMR (400 MHz, C_6D_6) δ 0.465 (s, 12H), 0.490 (s, 12H), 2.01 (s, 6H), 7.12 (dd, 2H, J = 5.2, 3.9 Hz), 7.41 (s, 2H), 7.58 (dd, 2H, J = 5.2, 3.9 Hz); ^{13}C NMR (100 MHz, C_6D_6) δ 1.0 (q), 1.1 (q), 19.6 (q), 128.2 (d), 134.7 (d), 136.2 (s), 136.4 (d), 142.3 (s), 145.7 (s); ^{29}Si NMR (80 MHz, C_6D_6) δ −19.8, −19.3. HRMS Calcd for $C_{22}H_{36}Si_4$: 412.1894. Found: 412.1921. Anal. Calcd for $C_{22}H_{36}Si_4$: C, 64.00; H, 8.79. Found: C, 64.28; H, 8.40.

2,3-Bis(isopropylidene)-5,6-bis(methoxycarbonyl)-1,1,4,4-tetramethyl-1,4-disilacyclohex-5-ene, 6e: colorless prisms; mp 86−87 °C; ^{1}H NMR (90 MHz, C_6D_6) δ 0.42 (s, 6H), 0.51 (s, 6H), 1.57 (s, 6H), 1.77 (s, 6H), 3.53 (s, 6H); ^{13}C NMR (22 MHz, C_6D_6) δ −1.3 (q), 0.7 (q), 23.2 (q), 23.5 (q), 51.2 (q), 133.7 (s), 144.1 (s), 154.6 (s), 170.3 (s); ^{29}Si NMR (18 MHz, C_6D_6) δ −11.7. HRMS Calcd for $C_{18}H_{30}O_4Si_2$: 366.1683. Found: 366.1696. Anal. Calcd for $C_{18}H_{30}O_4Si_2$: C, 58.97; H, 8.25. Found: C, 59.01; H, 8.36. IR (KBr) 1711 cm^{-1}.

2,3-Bis(isopropylidene)-5,6-diphenyl-1,1,4,4-tetramethyl-1,4-disilacyclohex-5-ene, 6f: colorless prisms; mp 118−119 °C; ^{1}H NMR (90 MHz, C_6D_6) δ 0.24 (s, 6H), 0.38 (s, 6H), 1.66 (s, 6H), 1.84 (s, 6H), 6.8−7.0 (m, 10H); ^{13}C NMR (22 MHz, C_6D_6) δ −0.9 (q), 1.8 (q), 23.3 (q), 23.7 (q), 125.2 (d), 127.8 (d), 128.4 (d), 136.2 (s), 141.5 (s), 144.5 (s), 158.6 (s); ^{29}Si NMR (18 MHz, C_6D_6) δ −14.1. HRMS Calcd for $C_{26}H_{34}Si_2$: 402.2199. Found: 402.2190. Anal. Calcd for $C_{26}H_{34}Si_2$: C, 77.54; H, 8.51. Found: C, 77.14; H, 8.55.

2,3-Bis(isopropylidene)-5-phenyl-1,1,4,4-tetramethyl-1,4-disilacyclohex-5-ene, 6g: colorless oil; ^{1}H NMR (90 MHz, C_6D_6) δ 0.20 (s, 3H), 0.33 (s, 3H), 0.35 (s, 3H), 0.40 (s, 3H), 1.59 (s, 3H), 1.62 (s, 3H), 1.76 (s, 3H), 1.82 (s, 3H), 6.59 (s, 1H), 7.0−7.3 (m, 5H); ^{13}C NMR (22 MHz, C_6D_6) δ −1.5 (q), 0.3 (q), 2.2 (q), 2.5 (q), 23.0 (q), 23.4 (q), 23.7 (q), 23.8 (q), 126.4 (d), 126.7 (d), 128.4 (d), 136.2 (s), 136.6 (s), 141.3 (s, two carbon), 148.0 (d), 148.3 (s), 163.8 (s); ^{29}Si NMR (18 MHz, C_6D_6) δ −12.8, −16.0. HRMS Calcd for $C_{20}H_{30}Si_2$: 326.1886. Found: 326.1882. Anal. Calcd for $C_{20}H_{30}Si_2$: C, 73.55; H, 9.26. Found: C, 73.34; H, 9.48.

2,3-Bis(isopropylidene)-5,6-bis(methoxycarbonyl)-1,1,4,4-tetraethyl-1,4-disilacyclohex-5-ene, 6h: colorless oil; ^{1}H NMR (90 MHz, C_6D_6) δ 0.9−1.1 (m, 20H), 1.53 (s, 6H), 1.74 (s, 6H), 3.43 (s, 6H); ^{13}C NMR (22 MHz, C_6D_6) δ 6.4 (t), 6.9 (t), 7.4 (q), 8.1 (q), 23.2 (q), 23.7 (q), 51.2 (q), 133.1 (s), 144.3 (s), 155.0 (s), 170.6 (s); ^{29}Si NMR (18 MHz, C_6D_6) δ −7.6. HRMS Calcd for $C_{22}H_{38}O_4Si_2$: 422.2309. Found: 422.2281. Anal. Calcd for $C_{22}H_{38}O_4Si_2$: C, 78.53; H, 9.23. Found: C, 78.78; H, 9.28. IR (NaCl): 1717 cm^{-1}.

2,3-Bis(isopropylidene)-5,6-diphenyl-1,1,4,4-tetraethyl-1,4-disilacyclohex-5-ene, 6i: colorless prisms; mp 86−87 °C; ^{1}H NMR (90 MHz, C_6D_6) δ 0.7−1.1 (m, 20H), 1.69 (s, 6H), 1.88 (s, 6H), 6.8−7.0 (m, 10H); ^{13}C NMR (22 MHz, C_6D_6) δ 6.4 (t), 6.7 (t), 7.7 (q), 8.4 (q), 23.4 (q), 23.9 (q), 125.1 (d), 127.6 (d), 128.6 (d), 135.4 (s), 141.7 (s), 144.7 (s), 159.2 (s); ^{29}Si NMR (18 MHz, C_6D_6) δ −9.8. HRMS Calcd for $C_{30}H_{42}Si_2$: 458.2825. Found: 458.2847. Anal. Calcd for $C_{30}H_{42}Si_2$: C, 78.53; H, 9.23. Found: C, 78.78; H, 9.28.

2,3-Bis(isopropylidene)-5,6,7,8-tetrakis(methoxycarbonyl)-1,1,4,4-tetramethyl-1,4-disilacycloocta-5,7-diene, 7e: colorless prisms; mp 195−196 °C; ^{1}H NMR (90 MHz, C_6D_6) δ 0.29 (s, 6H), 0.56 (s, 6H), 1.54 (s, 6H), 1.76 (s, 6H), 3.28 (s, 6H), 3.59 (s, 6H); ^{13}C NMR (22 MHz, C_6D_6) δ −1.6 (q),

1.4 (q), 22.7 (q), 24.0 (q), 51.3 (q), 51.9 (q), 135.2 (s), 138.7 (s), 143.4 (s), 155.0 (s), 164.1 (s), 170.4 (s); ^{29}Si NMR (18 MHz, C_6D_6) δ −12.2. HRMS Calcd for $C_{24}H_{36}O_8Si_2$: 508.1949. Found: 508.1953. Anal. Calcd for $C_{24}H_{36}O_8Si_2$: C, 56.67; H, 7.13. Found: C, 57.15; H, 7.16. IR (KBr): 1729 cm^{-1}.

2,3-Bis(isopropylidene)-6,7-dimethyl-1,1,4,4-tetramethyl-1,4-disilacyclooct-6-ene, 8: colorless oil; ^{1}H NMR (90 MHz, C_6D_6) δ 0.10 (s, 6H), 0.38 (s, 6H), 1.55 (s, 6H), 1.72 (br, 10H), 1.77 (s, 6H); ^{13}C NMR (22 MHz, C_6D_6) δ −0.3 (q), 1.4 (q), 22.8 (q), 23.1 (q), 24.0 (q), 26.3 (t), 123.5 (s), 139.1 (s), 139.9 (s); ^{29}Si NMR (18 MHz, C_6D_6) δ −10.8. HRMS Calcd for $C_{18}H_{34}Si_2$: 306.2199. Found: 306.2172. Anal. Calcd for $C_{18}H_{34}Si_2$: C, 70.51; H, 11.18. Found: C, 70.22; H, 11.35.

2,3-Bis(isopropylidene)-1,1,4,4-tetramethyl-1,4-disilacyclohexane, 9: colorless oil; ^{1}H NMR (400 MHz, C_6D_6) δ 0.10 (s, 6H), 0.34 (s, 6H), 0.69 (d, 2H, J = 11.1 Hz), 0.80 (d, 2H, J = 11.1 Hz), 1.58 (s, 6H), 1.79 (s, 6H); ^{13}C NMR (100 MHz, C_6D_6) δ −1.7 (q), 1.3 (q), 9.6 (t), 22.8 (q), 24.0 (q), 137.3 (s), 141.8 (s); ^{29}Si NMR (18 MHz, C_6D_6) δ −4.7. HRMS Calcd for $C_{14}H_{28}Si_2$: 252.1730. Found: 252.1734. Anal. Calcd for $C_{14}H_{28}Si_2$: C, 66.58; H, 11.18. Found: C, 66.43; H, 11.36.

5,6-Bis(isopropylidene)-3-phenyl-1,1,4,4-tetramethyl-1,4-disila-2-oxacyclohexane, 10: colorless oi; ^{1}H NMR (90 MHz, C_6D_6) δ 0.61 (s, 3H), 0.15 (s, 3H), 0.28 (s, 3H), 0.43 (s, 3H), 1.57 (s, 3H), 1.62 (s, 3H), 1.71 (s, 3H), 1.76 (s, 3H), 4.85 (s, 1H), 7.2−7.4 (m, 5H); ^{13}C NMR (22 MHz, C_6D_6) δ −3.6 (q), −3.3 (q), −0.6 (q), 2.6 (q), 22.5 (q), 22.7 (q), 24.2 (q), 24.6 (q), 69.9 (d), 124.6 (d), 125.3 (d), 128.3 (d), 135.6 (s), 136.8 (s), 143.0 (s), 144.2 (s), 144.3 (s); ^{29}Si NMR (18 MHz, C_6D_6) δ −6.0, 8.8. HRMS Calcd for $C_{19}H_{30}OSi_2$: 330.1835. Found: 330.1808. Anal. Calcd for $C_{19}H_{30}OSi_2$: C, 69.03; H, 9.15. Found: C, 69.25; H, 9.33.

2,3,5,6-Tetrakis(isopropylidene)-1,1,4,4-tetramethyl-1,4-disilacyclohexane, 11. (The product consists of a 3:1 mixture of the twist and chair conformers; the latter can be separated by fractional recrystallization from hexane.) Twist conformer: colorless prisms; ^{1}H NMR (90 MHz, C_6D_6) δ 0.42 (s, 12H), 1.61 (s, 12H), 1.78 (s, 12H); ^{13}C NMR (22 MHz, C_6D_6) δ 1.7 (q), 23.0 (q), 23.7 (q), 138.4 (s), 140.0 (s); ^{29}Si NMR (18 MHz, C_6D_6) δ −16.1. Chair conformer: ^{1}H NMR (90 MHz, C_6D_6) δ 0.03 (s, 6H), 0.71 (s, 6H), 1.61 (s, 12H), 1.89 (s, 12H); ^{13}C NMR (22.4 MHz, C_6D_6) δ −1.2 (q), 6.0 (q), 23.4 (q), 23.7 (q), 138.0 (s), 138.6 (s); ^{29}Si NMR (17.6 MHz, C_6D_6) δ −14.7. HRMS Calcd for $C_{20}H_{36}Si_2$: 332.2356. Found: 332.2383. Anal. Calcd for $C_{20}H_{36}Si_2$: C, 72.35; H, 10.84. Found: C, 72.21; H, 10.91.

5,6-Bis(isopropylidene)-2-*tert*-butyl-3-ethylidene-1,1,4,4-tetramethyl-1,4-disilacyclohexane, 12: colorless prisms; mp 82−83 °C; ^{1}H NMR (500 MHz, C_6D_6) δ 0.12 (s, 3H), 0.33 (s, 3H), 0.37 (s, 3H), 0.51 (s, 3H), 1.04 (s, 9H), 1.15 (s, 1H), 1.54 (s, 6H), 1.74 (s, 3H), 1.77 (s, 3H), 5.38 (d, 1H, J = 3.3 Hz), 5.59 (s, 1H, J = 3.3 Hz); ^{13}C NMR (125 MHz, C_6D_6) δ −0.7 (q), 1.5 (q), 3.8 (q), 4.5 (q), 22.8 (q), 23.1 (q), 23.9 (q), 24.2 (q), 32.1 (q), 33.8 (s), 58.0 (d), 128.6 (t), 137.1 (s), 137.7 (s), 140.9 (s), 142.9 (s), 153.6 (s); ^{29}Si NMR (18 MHz, C_6D_6) δ −15.6, −9.4. HRMS Calcd for $C_{19}H_{36}Si_2$: 320.2356. Found: 320.2352. Anal. Calcd for $C_{19}H_{36}Si_2$: C, 71.17; H, 11.32. Found: C, 71.28; H, 11.29.

Crystallographic Analysis. Crystals suitable for X-ray analysis of the following dimensions were prepared by slowly cooling hexane solutions: 0.2 × 0.4 × 0.4 mm for **2a**-chair, 0.2 × 0.2 × 0.1 mm for **2c**, 0.2 × 0.4 × 0.4 mm for **3**, and 0.2 × 0.4 × 0.8 mm for **11**-chair. Diffraction measurements were made on an Enraf-Nonius CAD4 computer-controlled Kappa axis diffractometer by using graphite-monochromatized Mo Kα radiation. The unit cells were determined and refined from 25 randomly selected reflections obtained by using the CAD4 automatic search, center, index, and least-squares routines. Crystal data and data collection parameters and the results of the analyses are listed in Table 1. All data processing was performed on a VAX 4000 computer by using the MOLEN structure solving program (Enraf Nonius Corp., Delft Netherlands). All intensities were corrected for Lorentz and polarization corrections. Neutral atom scattering factors were calculated by the standard procedures.[12a] An anomalous dispersion correction was applied to all non-hydrogen atoms.[12b] Full-matrix least-squares refinements minimized the function $\sum w(|F_o| - |F_c|)^2$, $w = 1$.

Compound 2a-chair crystallized in the triclinic crystal system. The $\omega-2\theta$ scan technique was adopted by varying the ω scan width as function of θ (ω scan width = 0.6 + 1.260 tan θ). Removal of redundant data left 2700 unique data in the final data set. The structure was solved by direct methods (MULTAN) and refined via standard least-squares and difference Fourier techniques. Hydrogen atoms were located and added to the structure factor calculations, but their positions were not refined.

Compound 2c crystallized in the orthorhombic crystal system. The $\omega-2\theta$ scan technique was adopted by varying the ω scan width as function of θ (ω scan width = 0.5 + 0.54 tan θ). Removal of systematically absent and redundant data left 8890 unique data in the final data set. The structure was solved by direct methods (SIR) and refined via standard least-squares and difference Fourier techniques. Hydrogen atoms were located and added to the structure factor calculations, but their positions were not refined.

Compound 3 crystallized in the triclinic crystal system. The $\omega-2\theta$ scan technique was adopted by varying the ω scan width as function of θ (ω scan width = 0.4 + 0.470 tan θ). Removal of redundant data left 4664 unique data in the final data set. The structure was solved by direct methods (MULTAN) and refined via standard least-squares and difference Fourier techniques. Hydrogen atoms were located and added to the structure factor calculations, but their positions were not refined.

Compound 11-chair crystallized in the triclinic crystal system. The $\omega-2\theta$ scan technique was adopted by varying the ω scan width as function of θ (ω scan width = 0.6 + 0.75 tan θ). Removal of redundant data left 2077 unique data in the final data set. The structure was solved by direct methods (MULTAN) and refined via standard least-squares and difference Fourier techniques. Hydrogen atoms were located and added to the structure factor calculations, but their positions were not refined.

Acknowledgment. This work was supported by a Grant-in-Aid for Scientific Research from the Ministry of Education, Science, and Culture of Japan.

Supplementary Material Available: Detailed information of the X-ray crystal analysis of **2a**-chair, **2c**, **3**, and **11**-chair including structure diagrams, a textual presentation of the details of data collection, reduction, and structure solution and refinement, and tables of experimental details, positional and thermal parameters, general temperature factor expressions, root-mean-square amplitudes of thermal vibration, and bond distances and angles (52 pages). Ordering information is given on any current masthead page.

OM940888Y

(12) (a) *International Tables for X-ray Crystallography*; The Kynoch Press: Birmingham, England, 1975; Vol. IV, Table 2.2B, pp 99−101. (b) *International Tables for X-ray Crystallography*; The Kynoch Press: Birmingham, England, 1975; Vol. IV, Table 2.3.1, pp 149−150.

The Ru(η^6-naphthalene)(η^4-cycloocta-1,5-diene)/ Acetonitrile System in the Selective Dimerization of Methyl Acrylate to *trans*-Dimethyl-2-hexenedioate

Paolo Pertici,* Valter Ballantini, and Piero Salvadori

Centro di Studio del CNR per le Macromolecole Stereordinate ed Otticamente Attive, Dipartimento di Chimica e Chimica Industriale, University of Pisa, via Risorgimento 35, 56100 Pisa, Italy

Martin A. Bennett

Research School of Chemistry, Australian National University, Canberra, ACT 0200, Australia

Received September 29, 1994[⊗]

The complex Ru(η^6-naphthalene)(η^4-cycloocta-1,5-diene), **I**, in the presence of acetonitrile, selectively catalyzes the tail-to-tail dimerization of methyl acrylate to *trans*-dimethyl-2-hexenedioate at 140 °C. An examination of the stoichiometric reaction between **I** and methyl acrylate shows that acetonitrile promotes removal of the dimer from the coordination sphere of ruthenium. Using tetrahydrofuran or *N*-methyl-2-pyrrolidinone as solvents, a long-lived catalyst is obtained which can be re-used without appreciable loss of activity.

Introduction

The selective tail-to-tail dimerization of substituted alkyl acrylates is a useful method for synthesizing important intermediates in fine and industrial chemistry. Tail-to-tail dimers of methyl acrylate **1a**, **1b** and **2a**, **2b** (Scheme 1) are potential precursors to adipic acid,[1] and one of them, *trans*-dimethyl-2-hexenedioate, **1b**, is a starting material for the preparation of biologically active compounds.[2]

A variety of transition metal-based systems of rhodium, palladium, nickel, and ruthenium catalyze acrylate dimerization.[3] So far, the most active of these catalyst is the agostic cation $[Cp^*(C_2H_4)\overline{RhCH_2CH_2\text{-}\mu\text{-}H}]^+$ obtained by protonation of $Cp^*Rh(C_2H_4)_2$.[3,4] Unlike most systems, this operates between room temperature and 60 °C with high selectivity for tail-to-tail coupling, although it requires the presence of H_2 (1 bar) to maintain catalyst lifetime. Ruthenium trichloride in methanol is active only at fairly high temperatures (210 °C),[5] but good conversion can be obtained at 125 °C by adding reducing agents, especially zinc.[6] The zerovalent metal complexes Ru(η^6-C_6H_6)(η^4-1,3-cyclohexadiene) and Ru(η^6-C_6H_6)(η^2-CH_2=$CHCO_2Me$)$_2$ have also been used as catalysts for acrylate dimerization, and high conversions to **1a**/**1b** have been obtained by addition of sodium naphthalide, suggesting that the active catalysts may be anionic ruthenium species.[7] Other ruthenium-based catalysts for methyl acrylate dimerization are $Ru_3(CO)_{12}$ in the presence of tertiary phosphines[8] and RuHCl(CO)-(PPr^i_3)$_2$ to which equiv of CF_3SO_3Ag has been added.[9]

Scheme 1. Tail-to-Tail Dimerization of Methyl Acrylate

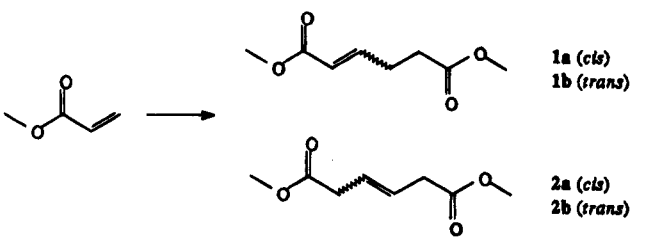

We recently reported that the complex Ru(η^6-naphthalene)(η^4-COD), **I** (COD = cycloocta-1,5-diene), in the presence of acetonitrile, shows a high catalytic activity in the isomerization and hydrogenation of unsaturated compounds.[10,11] We observed that the monocyclic arene complexes Ru(η^6-arene)(η^4-COD) (arene = benzene, *p*-cymene) are less reactive than **I** in these reactions, and we attributed this behavior to the greater lability of the naphthalene–ruthenium bond: polynuclear arenes are generally less firmly bonded than mononuclear arenes to transition metals.[12] In reactions catalyzed by **I**, naphthalene can be easily removed from the metal, thus making available coordination sites that are required for catalytic processes. The interesting catalytic properties of **I** deriving from the lability of the naphthalene–Ru bond prompted an investigation of its catalytic activity in other reactions. We describe here the results obtained in the dimerization of methyl acrylate.

[⊗] Abstract published in *Advance ACS Abstracts,* April 1, 1995.

(1) McKinney, R. J. U.S. Patent 4 504 674, 1985.
(2) (a) Nugent, W. A.; Hobbs, F. W. *J. Org. Chem.* **1983**, *48*, 5364. (b) A. Mitra In *The Synthesis of Prostaglandins*; Wiley: New York, 1979; pp 337–352.
(3) Brookhart, M.; Sabo-Etienne, S. *J. Am. Chem. Soc.* **1991**, *113*, 2777 and references cited therein.
(4) (a) Brookhart, M.; Hauptman, E. *J. Am. Chem. Soc.* **1992**, *114*, 4437. (b) Hauptman, E.; Sabo-Etienne, S.; White, P. S.; Brookhart, M.; Garner, J. M.; Fagan, P. J.; Calabrese, J. C. *J. Am. Chem. Soc.* **1994**, *116*, 8038.
(5) (a) Alderson, T. U.S. Patent 3 013 066, 1961. (b) Alderson, T.; Jenner, E. L.; Lindsay, R. V. *J. Am. Chem. Soc.* **1965**, *87*, 5638.
(6) McKinney, R. J.; Colton, M. C. *Organometallics* **1986**, *5*, 1080.
(7) McKinney, R. J. *Organometallics* **1986**, *5*, 1752.
(8) Ren, C. Y.; Cheng, W. C.; Chan, W. C.; Yeung, C. H.; Lau, C. P. *J. Mol. Catal.* **1990**, *59*, L1.
(9) Sustmann, R.; Hornung, H. J.; Schupp, T.; Patzke, B. *J. Mol. Catal.* **1993**, *85*, 149.
(10) Pertici, P.; Uccello Barretta, G.; Burzagli, F.; Salvadori, P.; Bennett, M. A. *J. Organomet. Chem.* **1991**, *413*, 303.
(11) Bennett, M. A.; Neumann, H.; Thomas, M.; Wang, X-q; Pertici, P.; Salvadori, P.; Vitulli, G. *Organometallics*, **1991**, *10*, 3237.
(12) See for example: Muetterties, E. L.; Bleeke, J. R.; Wucherer, E. J.; Albright, T. A. *Chem. Rev.* **1982**, *82*, 499.

0276-7333/95/2314-2565$09.00/0

Table 1. Catalytic Dimerization of Methyl Acrylate with Ru(η^6-naphthalene)(η^4-COD),[a] I

run	solvent	time (h)	conv (%)	reacn products[b] linear dimers (l)	1b/l	TO[c]
1	THF	4	70	70	80	181
		8	80	70	80	207
		24	100	75	75	278
2[d]	THF	8	50	65	70	120
3[e]	THF	8	30	70	70	78
4[f]	THF	8	5			
5	NMP	4	75	70	70	194
		8	90	70	70	233
		24	100	75	80	278
6[g]	reaction mixture of run 1	24	100	75	75	278
7[g]	reaction mixture of run 5	24	100	75	80	278
8[h]	NMP	8	65	45	80	108
9[i]	THF	8	80	70	80	207

[a] Reaction conditions: **I** [0.02 g (0.06 mmol)], acetonitrile [0.063 mL (1.2 mmol)], solvent (5 mL), methyl acrylate [2 mL (22.2 mmol)], heated at 140 °C in a thick-walled Carius tube. Decane was used as internal standard. [b] The other reaction products are branched dimers (ca. 5%) and trimers (20–30%). [c] Turnover number = mol of linear dimers produced per mol of Ru. [d] Heated at 100 °C. [e] Carried out without acetonitrile. [f] Catalytic precursor: Ru(η^6-*p*-cymene)(η^4-COD), 0.021 g (0.06 mmol). [g] Fresh methyl acrylate (2 mL) has been added. [h] Sodium naphthalide (0.12 mmol) in THF has been added. The reaction products are linear dimers (45%), branched dimers (5%), and trimers (50%). [i] Under hydrogen atmosphere.

Results

The results obtained in the dimerization of methyl acrylate are reported in Table 1. In all the runs *trans*-dimethyl-2-hexenedioate, **1b**, was the predominant product. After 4 h at 140 °C in THF the conversion was 70% and after 24 h was quantitative (run 1). The reaction also proceeded at 100 °C (run 2) with a similar chemoselectivity but a lower rate. The presence of acetonitrile is very important to achieve high catalytic activity: after 8 h in the absence of acetonitrile at 140 °C only 30% of methyl acrylate was converted into products (run 3). Using Ru(η^6-*p*-cymene)(η^4-COD) as catalytic precursor, only 5% conversion was obtained after 8 h (run 4).

A slight increase in conversion, without change in selectivity, was obtained in *N*-methyl-2-pyrrolidinone (NMP) as solvent (run 5). At the end of the reaction the THF or NMP solutions were clear red-brown and contained no suspended solids. These solutions maintained their activity unchanged, additional methyl acrylate being dimerized at the same rate as that observed during the previous reaction (compare runs 6 and 7 with runs 1 and 5, respectively). In order to obtain information on the function of acetonitrile and on the reaction mechanism, the reaction between **I** and methyl acrylate (molar ratio 1:2) has been examined in detail, both without and with acetonitrile.

Without Acetonitrile. A 2 equiv amount of methyl acrylate and 1 equiv of **I** were dissolved in toluene-d_8 at −70 °C, and the reaction was followed by ^{1}H-NMR spectroscopy at various temperatures. Reaction began only at −30 °C. At this temperature two multiplets at δ 7.35 ppm and 7.75 ppm, due to free naphthalene, and two singlets at δ 3.34 ppm and 3.37 ppm, assignable to

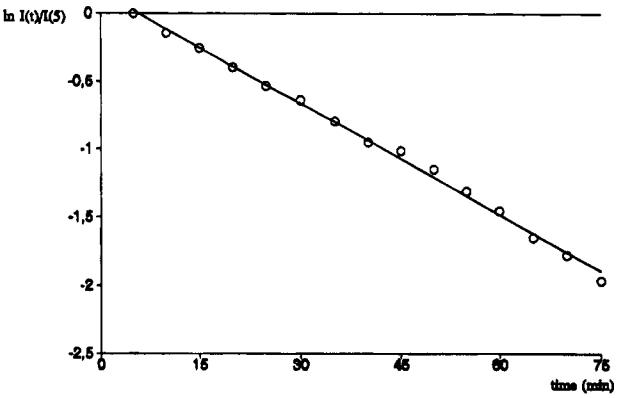

Figure 1. First-order plot for the reaction of Ru(η^6-$C_{10}H_8$)(η^4-COD), **I**, with methyl acrylate in toluene-d_8 at −30 °C.

−COOMe (see below), appeared, while the intensity of the resonances due to **I** decreased.

Some information about the kinetics of replacement of naphthalene in **I** by methyl acrylate at −30 °C was obtained by recording the extent of decrease of **I** at different times, determined by integrating the $C_{10}H_8$ protons (multiplet at δ 4.1 ppm of AA′ system).[11] The plot, displayed in Figure 1, shows the reaction is first-order, with a rate constant of 2.74×10^{-2} sec^{-1}.

When there was no further change in the intensity of the signals in two successive 5-min-intervals, a 2D-COSY NMR experiment was carried out in an effort to learn about the species present in solution (Figure 2). Cross-peak analysis shows that two systems of three protons are present, in which each proton is correlated to only two others. They correspond to the signals at δ 4.95, 3.85, 2.15, ppm and 3.95, 3.65, and 2.85 ppm. The fact that the spectrum also shows two singlets at δ 3.37 and 3.34 ppm assignable to COOMe resonances suggests that at least two molecules of methyl acrylate are attached to ruthenium. The other signals, to which the off diagonal peaks correspond, do not belong to a simple three proton system. The signal at δ 4.5 ppm is related to the signals at δ 3.7 and 2.85 ppm. The latter is related to the signals at δ 2.15 and 1.7 ppm, and they form cross-peaks with other signals. We think that these resonances are due to COD, or to a C_8 fragment derived from COD, which is not symmetrically bonded to ruthenium.

When the solution was kept at 25 °C for 24 h, two new resonances appeared at δ 5.4 and 0.9 ppm as double doublets, which were coupled, as shown by spin decoupling experiments. Comparison with literature data on the isolated complex Ru(MUC)$_2$[P(OMe)$_3$] (MUC = dimethyl muconate)[6] allows these signals be assigned to the olefinic protons of MUC bound to ruthenium. Other coupled signals are a quartet at δ 2.05 ppm and a triplet at δ 1.05 ppm that can be assigned to methyl propionate, which could be formed as shown in Scheme 2.

Scheme 2

$$2CH_2{=}CHCOOMe \xrightarrow{cat} MeOOCCH{=}CHCH{=}CHCOOMe + H_2$$

$$CH_2{=}CHCOOMe + H_2 \xrightarrow{cat} CH_3CH_2COOMe$$

Interestingly, neither methyl acrylate nor free dimers were present in the solution at this time and the NMR spectrum did not change after 3 days at room temper-

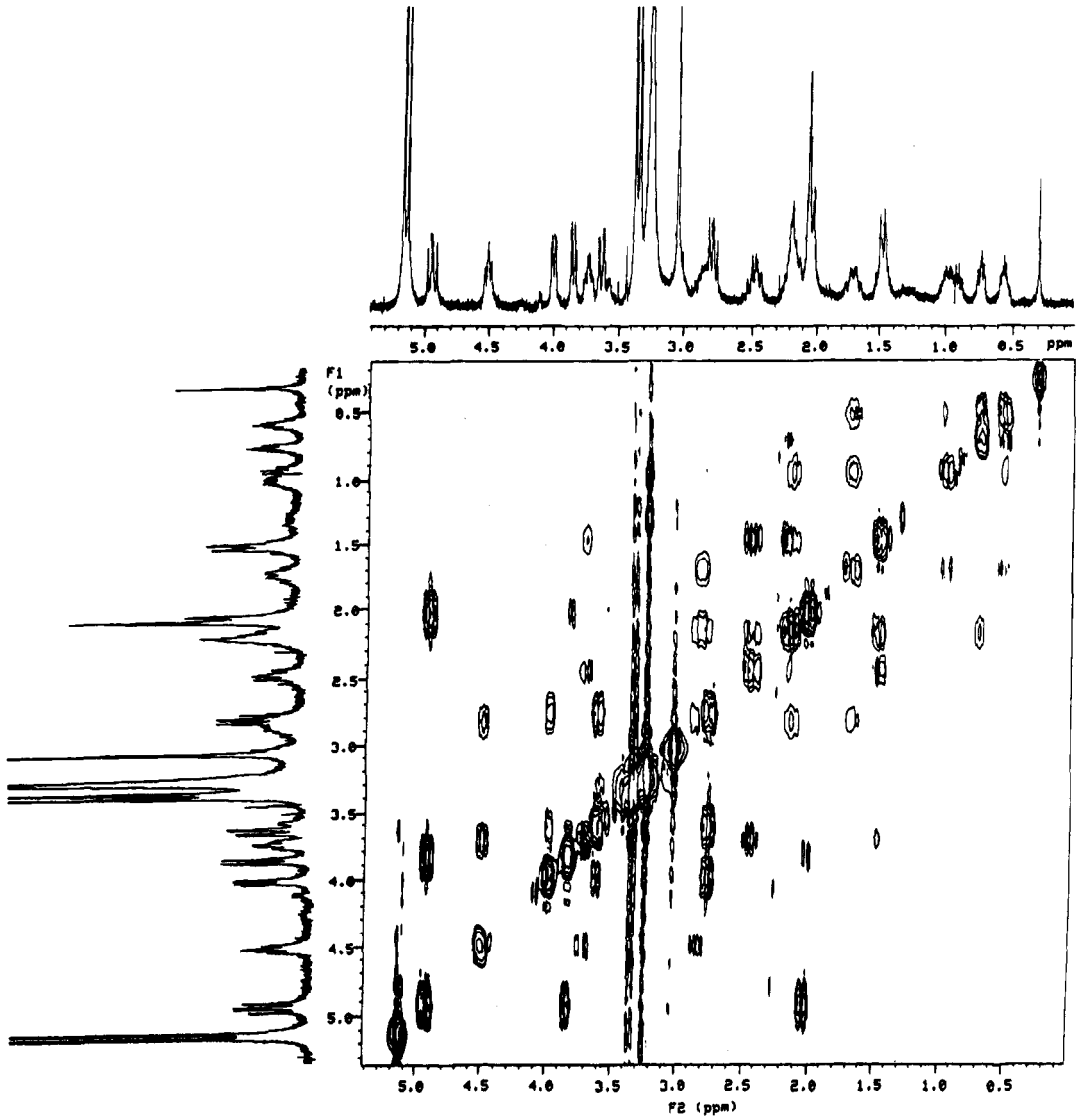

Figure 2. 2D-COSY spectrum for the reaction between Ru(η^6-$C_{10}H_8$)(η^4-COD), **I**, and methyl acrylate at −30 °C. Below 5 ppm, resonances due to known species are present.

Scheme 3

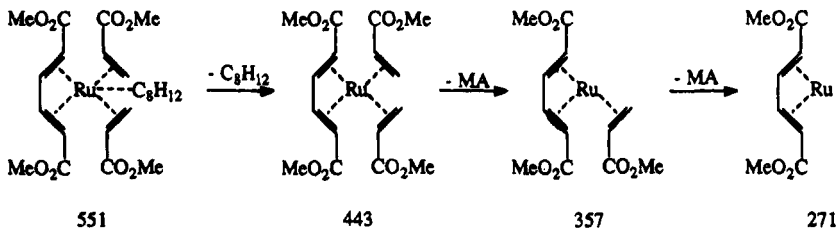

ature. The mass spectrum of the residue, after removal of the solvent, showed a peak at $m/e = 551.7$ and other peaks at 443.7, 357.8 and 271.8. These data are consistent with a species of empirical formula Ru(MUC)-(CH_2=$CHCO_2Me$)$_2$(C_8H_{12}) ($m/e = 551.7$) that fragments as shown in Scheme 3. These results show that, even in the absence of acetonitrile, methyl acrylate removes naphthalene from ruthenium in **I**, the final product being a compound containing methyl acrylate, MUC, and C_8H_{12}. Attempts to isolate the compound in a pure state have not been successful so far. Dimethyl-2-hexenedioate or other dimers do not form even after a long period at room temperature, as shown by ^{1}H-NMR spectroscopy.

With Acetonitrile. The behavior of the reaction of **I** and methyl acrylate in the presence of acetonitrile-d_3 (2 mol/mol of **I**) is completely different. The ^{1}H-NMR spectrum of this reaction mixture, recorded after 5 h at room temperature, clearly shows multiplets at δ 6.86 and 5.76 ppm due to the olefinic protons of free dimethyl *trans*-2-hexenedioate, together with peaks due to a trace of methyl propionate.

It is also worth noting that resonances due to ruthenium−hydride species were never observed, either in the presence or absence of acetonitrile.

Comparison of the results of these two reactions shows that **1b** is formed only in the presence of acetonitrile.

Discussion

The results do not suffice to give a detailed mechanistic scheme for the dimerization of methyl acrylate catalyzed by **I**/CH_3CN, but some general conclusions can be drawn.

(1) The system based on Ru(η^6-$C_{10}H_8$)(η^4-COD)/MeCN is far more active than that based on Ru(η^6-*p*-cymene)-(η^4-COD)/MeCN, as is true also for catalyzed hydrogenation and isomerization of olefins. This is because of the greater stability of the mononuclear arene–metal bond.[12]

(2) In contrast to the latter processes, the function of the acetonitrile is not to promote the η^6 to η^4 transformation of naphthalene, since methyl acrylate readily displaces naphthalene from **I**, even in the absence of acetonitrile. Instead, as a consequence of its high affinity for ruthenium,[10] it may help to eliminate **1b** from the coordination sphere after hydrogen transfer has taken place.

(3) In contrast to the behavior of Ru(η^6-C_6H_6)(η^2-CH_2=$CHCO_2Me$)$_2$ as catalyst precursor,[7] addition of sodium naphthalide does not increase the catalytic activity of **I**/CH_3CN (run 8). Hence intervention of an anionic ruthenium complex seems unlikely, although such a species might not be stable in the presence of CH_3CN. However, studies of the chemistry of **I** in the presence of THF[11] have given no indication of disproportionation into ionic fragments containing Ru(II) and Ru(−I) or Ru(−II). Thus, the simplest assumption is that the catalyst precursor is a neutral ruthenium(0) species of the type Ru(CH_2=$CHCO_2Me$)$_x$($NCMe$)$_y$ formed by complete displacement of COD and naphthalene from **I**. Several mechanisms for dimerization based on such a catalyst can be considered.[13] One possible cycle starts with vinylic C–H oxidative addition of methyl acrylate to Ru(0) to generate a hydrido(vinyl)ruthenium(II) species (Scheme 4a). Insertion of a second molecule of methyl acrylate into the Ru–H bond and acetonitrile-promoted elimination of the two Ru–C σ-bonds gives **1b**, thus completing the cycle. Models for these steps are provided by the reaction of ethyl methacrylate with Ru(C_2H_4)(PPh_3)$_3$ (eq 1)[14] and by the reaction of methyl acrylate with [RuCl(CO)H(PPh_3)$_3$] (eq 2).[15]

$$Ru(C_2H_4)(PPh_3)_3 + CH_2{=}C(Me)CO_2Et \rightarrow \overline{RuH\{CH{=}C(Me)COOEt\}}(PPh_3)_3 \quad (1)$$

$$RuCl(CO)H(PPh_3)_3 + CH_2{=}CHCO_2Me \rightarrow \overline{Ru\{CH_2CH_2COOMe\}}Cl(CO)(PPh_3)_2 + PPh_3 \quad (2)$$

A second possibility is the initial coupling of two MA units at ruthenium(0) to form a ruthenacyclopentane, which then undergoes β-hydride elimination to form a hydrido η^3- allyl complex. Transfer of hydride to the carbon atom bearing the CO_2Me group, which may be assisted by acetonitrile, completes the cycle (Scheme 4b). This type of mechanism has been proposed for the linear dimerization of methyl acrylate catalyzed by [Pd(acac)-(solv)$_2$]BF_4.[16] A model for the first step is provided by the formation of the ferracycle $(OC)_4\overline{FeCH(CO_2Me)C-H_2CH(CO_2Me)}$ in the photochemical reaction of methyl acrylate with $Fe(CO)_5$.[17] The corresponding reaction with $Ru_3(CO)_{12}$ gives only the bis(olefin) complex Ru-$(CO)_3$(η^2-CH_2=$CHCO_2Me$)$_2$, although this does form a ruthenacyclopentane on treatment with dimethyl 3-cyclobutene-*cis*-1,2-dicarboxylate.[18]

In conclusion, the Ru(η^6-naphthalene)(η^4-COD)/acetonitrile system represents a new catalyst for the selective tail-to-tail dimerization of methyl acrylate. The turnover numbers are better than or comparable with those achieved with other ruthenium-based catalysts such Ru-(η^6-C_6H_6)$(MA)_2$. The system is also longer-lived than

Scheme 4. Proposed Catalytic Cycles for the Dimerization of Methyl Acrylate (MA) by Ru(η^6-$C_{10}H_8$)(η^4-COD), I, in the Presence of CH_3CN[a]

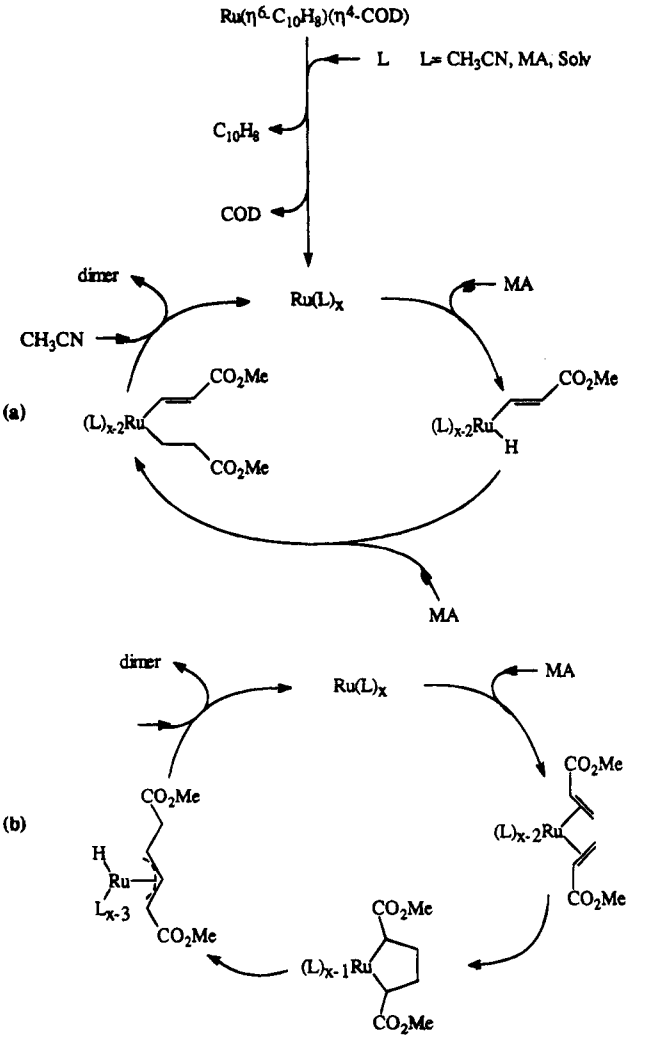

[a] The upper part of this scheme represents the catalyst activation, and the lower parts (a) and (b) represent the cycles themselves.

(13) Parshall, G. W.; Ittel, S. D. In *Homogeneous Catalysis: The Applications and Chemistry of Soluble Transition Metal Complexes*; Wiley: New York, 1992; pp 83–84.
(14) Komiya, S.; Ito, T.; Cowie, M.; Yamamoto, A.; Ibers, J. A. *J. Am. Chem. Soc.* **1976**, *98*, 3874.
(15) Hiraki, K.; Ochi, N.; Sasada, Y.; Hayashida, H.; Fuchita, Y.; Yamanaka, S. *J. Chem. Soc., Dalton Trans.* **1985**, 873.
(16) Guibert, I.; Neibecker, D.; Tkatchenko, I. *J. Chem. Soc., Chem. Commun.* **1989**, 1850.
(17) Grevels, F-W.; Schulz, D.; Koerner von Gustorf, E. *Angew. Chem., Int. Ed. Engl.* **1974**, *13*, 534.
(18) Grevels, F-W.; Reuvers, J. G. A.; Takats, J. *Angew. Chem., Int. Ed. Engl.* **1981**, *20*, 452.

that derived from the somewhat more active catalyst $RuHCl(CO)(P^iPr_3)_2/AgOTf$[9] and does not show the complications arising from tertiary phosphine-catalyzed dimerization of MA. It is, however, less active and somewhat less selective toward linear dimers than recently described systems based on rhodium(III)[3,4] and palladium(II),[19] but, in contrast to the former, it does not require the presence of hydrogen to mantain catalyst lifetime. Further investigations of the mechanism of dimerization are planned.

Experimental Section

The complex Ru(η^6-*p*-cymene)(η^4-COD) was made from [$RuCl_2(\eta^6$-*p*-cymene)]$_2$, COD, and Na_2CO_3 in propan-2-ol[20] and identified by comparison of its ^{1}H NMR spectrum with authentic material.[21] The complex Ru(η^6-naphthalene)(η^4-COD), **I**, was prepared as already described.[11]

All catalytic experiments were carried out in thick-walled Carius tubes under nitrogen atmosphere. THF was dried by refluxing over Na/K alloy before distillation. *N*-methyl-2-pyrrolidinone (Aldrich product), stored under nitrogen, was used directly. Methyl acrylate was degassed and kept under nitrogen before use. Acetonitrile was purified by distillation from P_4O_{10} under nitrogen. In a typical experiment **I** (20 mg, 0.06 mmol) was placed in a tube and dissolved in the appropriate solvent (5 mL). Acetonitrile (0.063 mL, 1.2 mmol) was introduced, and the solution was stirred at room temperature for a few minutes. Methyl acrylate (2 mL, 22.2 mmol) was added. The solution was heated at 140 °C in a constant-temperature bath (±0.2 °C). The reaction mixture was analysed by gas chromatography using a Perkin-Elmer 8500 apparatus equipped with a 12 m × 0.22 BP1 capillary column, using helium as carrier gas. The dimers were characterized by GC–MS, ^{1}H-NMR, and ^{13}C-NMR and by comparison with authentic samples. Some trimers that are also formed were not characterized.

Proton NMR spectroscopic studies were carried out on solutions of **I** in toluene-d_8 or benzene-d_6 in a 5 mm o.d. NMR tube to which methyl acrylate or a mixture of methyl acrylate and acetonitrile was added. The growth of the signals of the products was monitored on a Varian VXR-300 spectrometer at various probe temperatures in the range −70 to 25 °C.

Acknowledgment. This work was supported by the CNR research program Progetto Finalizzato per la Chimica Fine II.

OM940755C

(19) Grenouillet, P.; Neibecker, D.; Tkachenko, I. Fr. Patent 2 596 390, 1987.
(20) Bennett, M. A.; McMahon, I. J.; Pelling, S.; Brookhart, M.; Lincoln, D. M. *Organometallics* **1992**, *11*, 127.
(21) Pertici, P.; Bertozzi, S.; Lazzaroni, R.; Vitulli, G.; Bennett, M. A. *J. Organomet. Chem.* **1988**, *354*, 117.

Investigation of Organolithium Dimerization on Irradiated CdS Powder

Michael Lorenz and Timothy Clark*

Computer-Chemie-Centrum des Institutes für Organische Chemie der Friedrich-Alexander-Universität Erlangen-Nürnberg, Nägelsbachstrasse 25, D-91052 Erlangen, Germany

Received January 18, 1995[⊗]

Irradiation of CdS powder suspended in ethereal solutions of organolithium compounds, RLi, yields elemental Cd and the photooxidation products R-R. The mechanism is shown to be a radical one, the products R-R at least partly resulting from intraaggregate dimerization of radicals R• if the parent RLi is aggregated. Free solution-phase radicals have not been detected. The configuration of a benzyl anion adsorbate has been investigated using AM1 semiempirical molecular orbital calculations on a ZnS model surface. These suggest that η^1- and η^7-bound species compete with each other. A comparison of the reactivity of $PhCH_2$-Li and two alkyl-substituted, sterically hindered derivatives shows that the substituted benzylic species, which are η^1-bound, react faster than $PhCH_2Li$. We therefore propose that $PhCH_2Li$ prefers a η^7 configuration on the active CdS surface.

Considerable interest has been focused on the use of semiconductors in photovoltaic cells and in photoelectrosynthesis of potential fuels.[1] Their application in synthetic organic chemistry is, however, less common, often because of high demands on reaction conditions and photocatalysts. Only few examples of photoassisted syntheses on semiconductors are known that compete successfully with classical synthetic methods (e.g. the photo-Kolbe reaction[2] and olefin oxidation[3]) or lead to formerly unknown organic molecules (synthesis of bidihydrofuryls[4]). However, the synthetic use of such reactions is often less important than their significance as probes into the mechanisms of heterogeneous electron transfer and subsequent surface reactions or into microscopic characteristics of photosemiconductors.[5] Our studies on the photooxidation of simple organolithium compounds of CdS powder should be viewed thus. Competitive reactions of sterically different organolithium adsorbates and supporting semiempirical calculations provide information about important features of this type of heterogeneous reaction and on adsorption equilibria and mass transfer.

With the exception of certain dilithio compounds[6] that can be oxidized directly to their radical anions by irradiation, many organolithiums are photooxidized only in the presence of a suitable electron acceptor.[7] One might expect photosemiconductors to be well-suited for this purpose because of reduced back electron transfer and their chemical inertness in dark reactions. Fox and Owen were the first to take up this idea. Using a doped single-crystal TiO_2 electrode, they succeeded in photooxidizing fluorenyllithium and (tetraphenylcyclopentadienyl)lithium in a photoelectrochemical cell.[8]

Results and Discussion

Mechanism. The photooxidation of organolithiums can be achieved with commercially available hexagonal CdS powder and leads to dimeric products and metallic Cd (eq 1). The formation of metallic cadmium is a well-

$$2RLi + CdS \xrightarrow{h\nu} R\text{-}R + Cd + Li_2S \qquad (1)$$

$$R = PhCH_2,\ n\text{-Bu},\ Ph$$

known photocorrosion process in the absence of oxygen.[9] Overall, yields are moderate (Table 1), although the reaction is hampered by a continuous blackening of the sulfide powder. After 6−12 h of irradiation the reaction stops and unconsumed RLi remains. The 3−9% conversion obtained, however, is adequate for our purposes and so no attempt to increase the yield was made. Care was taken to find reaction conditions that preclude all possible reactions except that described by eq 1. First, photostability of BuLi and PhLi without CdS was ensured by using filters, and second, the reaction mixture was cooled.[10] The photoinduced electron trans-

[⊗] Abstract published in *Advance ACS Abstracts,* April 1, 1995.

(1) (a) Fujishima, A.; Honda, K. *Nature* **1972**, *238*, 37. (b) Memming, R. *Top. Curr. Chem.* **1988**, *143*, 79 and references therein. (c) Fox, M. A. *Acc. Chem. Res.* **1983**, *16*, 314 and references therein.

(2) Kraeutler, B.; Bard, A. J. *J. Am. Chem. Soc.* **1977**, *99*, 7729; **1978**, *100*, 5985.

(3) Kanno, T.; Oguchi, T.; Sakuragi, H.; Tokumaru, K. *Tetrahedron Lett.* **1980**, *21*, 467.

(4) Zeug, N.; Buecheler, J.; Kisch, H. *J. Am. Chem. Soc.* **1985**, *107*, 1459.

(5) (a) Fox, M. A.; Chen, C.-C. *J. Am. Chem. Soc.* **1981**, *103*, 6757. (b) Hetterich, W.; Kisch, H. *Chem. Ber.* **1988**, *121*, 15. (c) Henglein, A. *Top. Curr. Chem.* **1988**, *143*, 113.

(6) (a) Wilhelm, I.; Courtneidge, J. L.; Clark, T.; Davies, A. G. *J. Chem. Soc., Chem. Commun.* **1984**, 810. (b) Lorenz, M.; Clark, T.; Schleyer, P. v. R.; Neubauer, K.; Grampp, G. *J. Chem. Soc., Chem. Commun.* **1992**, 719.

(7) (a) Winkler, H. J. S.; Winkler, H. *J. Org. Chem.* **1967**, *32*, 1695. (b) Fox, M. A.; Ranade, A. C.; Madany, I. *J. Organomet. Chem.* **1982**, *239*, 269.

(8) Fox, M. A.; Owen, R. C. *J. Am. Chem. Soc.* **1980**, *102*, 6559.

(9) See, for instance: Meissner, D.; Memming, R.; Kastening, B. *J. Phys. Chem.* **1988**, *92*, 3476. Henglein, A. *Top. Curr. Chem.* **1988**, *143*, 113.

(10) (a) Photodecomposition of organolithiums: van Tammelen, E. E.; Braumann, J. I.; Ellis, L. E. *J. Am. Chem. Soc.* **1865**, *87*, 4964. Glaze, W. H.; Brewer, T. L. *J. Am. Chem. Soc.* **1980**, *91*, 6559. (b) $PhCH_2Li$ slowly decomposes in the dark at room temperature but not at −30 °C.

0276-7333/95/2314-2570$09.00/0

Table 1. Consumption and Reaction Conditions for Different RLi Species

RLi	consumption[a] (%)	conditions[b]
$PhCH_2Li$	9	6 h, $\lambda > 340$ nm
n-BuLi	5	6 h, $\lambda > 340$ nm
PhLi	3	10 h, $\lambda > 410$ nm

[a] The fraction of RLi that reacts to give R—R. [b] 150 W high-pressure mercury lamp, temperature −30 °C, Et_2O.

fer from RLi to CdS profits from an enormous electromotive force, and the ratio of the yields in Table 1 is due partly to a lower RLi oxidation potential on going from $PhCH_2Li$ (−1.43 V) and BuLi (−1.41 V) to PhLi (−0.34 V).[11]

In the cases of R = Bu, Ph we propose the mechanism given in Scheme 1. With light of wavelengths longer

Scheme 1

$$CdS \xrightarrow{h\nu} h^+_{vb} + e^-_{cb} \quad (2)$$

$$RLi_{ad} + h^+_{vb} \rightarrow [RLi^{\bullet+}_{ad}] \rightarrow R^\bullet_{ad} + Li^+ \quad (3)$$

$$2R^\bullet_{ad} \rightarrow R{-}R_{ad} \quad (4)$$

$$CdS + 2e^-_{cb} + 2Li^+ \rightarrow Cd + Li_2S \quad (5)$$

than 340 and 410 nm, respectively, the initial process must be the creation of electron-hole pairs in the semiconductor followed by the oxidation of RLi by the positive holes. The primary oxidation products, $RLi^{\bullet+}$, have been investigated previously. Ab initio calculations suggest that the *n*-propyllithium radical cation is a quite stable intermediate in the gas phase, Li^+ dissociation being endothermic by 23.3 kcal/mol.[12] However, taking into account that Li^+ is much better stabilized by solvation than by complexation with R•, we cannot regard $RLi^{\bullet+}$ as a stable species in solution. It dissociates immediately, and, as a consequence, radicals R• are involved in the subsequent reactions. This is shown by the fact that traces of the coupling products **1** and **2** were found for R = Bu. Their formation can only be explained if one assumes a radical H abstraction from Et_2O by R• as a side reaction (eq 6). *n*-Butane was not observed directly. No byproducts were found when the reaction was performed in *n*-hexane.

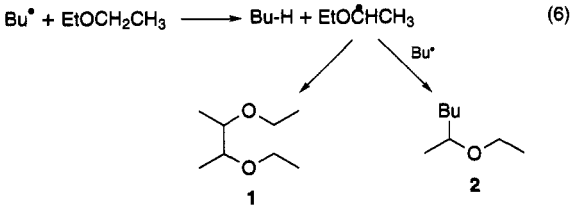

The final products R-R result from a simple dimerization of R• (eq 4). However, the R• concentration in solution is low and an excess of RLi is present throughout the reaction, and so an alternative route initiated by radical attack on RLi is conceivable (Scheme 2). If

(11) The values for PhLi and BuLi are not very reliable because of electrode-fouling effects, but the tendency should be described correctly. See: Jaun, B.; Schwarz, J.; Breslow, R. *J. Am. Chem. Soc.* **1980**, *102*, 5741.

(12) Clark, T. *J. Chem. Soc., Chem. Commun.* **1986**, 1774.

Scheme 2

$$R^\bullet_{ad/solv} + RLi_{ad/solv} \rightarrow R{-}R + Li \quad (7)$$

$$2Li + CdS \rightarrow Li_2S + Cd \quad (8)$$

reaction 7 proceeds on the surface, it would be facilitated by a reduced carbon−lithium binding energy of adsorbed RLi. To distinguish between the two possibilities (eqs 4/5 versus eqs 7/8), we performed a competitive reaction using $PhCH_2Li$ and BuLi in a molar ratio of 1.0:2.5. In this case, nearly equal amounts of benzyl and butyl radicals were formed, as can be deduced from the quantitative analysis of the three reaction products bibenzyl, 1-phenylpentane, and *n*-octane, which occurred in a molar ratio of 1.2:1.0:1.3 (Scheme 3).[13] If the

Scheme 3

$$PhCH_2Li + BuLi \xrightarrow[CdS]{h\nu} PhCH_2^\bullet + Bu^\bullet \rightarrow PhCH_2CH_2Ph + PhCH_2Bu + Bu{-}Bu$$

dimeric products R-R (R-R′) resulted from radical attack on RLi (eq 7), one would have expected that butyl and benzyl radicals would preferably attack excess BuLi with *n*-octane and 1-phenylpentane as the main products, unlike the experimental results. Hence, it follows that the reactions shown in Scheme 2 do not contribute significantly to the overall reaction. Surprisingly, the product ratio does not fit the statistical distribution of 1:2:1. This is approximately expected for a simple solution-phase recombination of the butyl and benzyl radicals, which are known to self-terminate by diffusion control.[14] A possible explanation is that the products R-R (R-R′) are formed, at least partly, by radical recombination on the CdS surface. Assuming that BuLi exists predominantly as a tetramer, as in its pure Et_2O solution,[15] it is possible that a portion of the butyl radicals formed does not escape from the adsorbed aggregate and is quenched on the surface by intraaggregate dimerization with a second butyl radical. As a consequence, the mixed dimer 1-phenylpentane is not the main product. In contrast, mixtures of $PhCH_2Li$ and *m*-alkyl-substituted benzyllithiums, which are both monomers in Et_2O,[16] do not show this aggregation effect and give high yields of the corresponding mixed dimers, as expected. These reactions will be discussed in detail below. We tested for free solution-phase radicals R• by adding an excess of tetramethylethylene (TME), which is capable of quenching radicals[17] but is unreactive toward organolithiums. The reaction mixture RLi/TME/CdS behaves as if no olefin were present when exposed to light. GC analysis gives no indication of olefin addition products. Although radical addition is slower than self-termination by 10^5−10^6, radical addition to TME should be able to compete if a significant amount

(13) Using a 1:1 mixture of $PhCH_2Li$ and BuLi, the products based on the butyl radical are slightly reduced.

(14) Self-termination rates: $2k_t$(benzyl) = 4.0×10^9 M^{-1} s^{-1}; $2k_t$(*n*-propyl) = 3.4×10^9 M^{-1} s^{-1}. Values from: Ingold, K. U. In *Free Radicals*; Kochi, J. K., Ed.; Wiley: New York, 1973; Vol. I, p 37.

(15) Seebach, D.; Hässig, R.; Gabriel, J. *Helv. Chim. Acta* **1983**, *66*, 308.

(16) West, P.; Waack, R. *J. Am. Chem. Soc.* **1967**, *89*, 4395.

(17) Rate constant k for CH_3• addition to TME: $k = 0.9 \times 10^4$; see: Tedder, J. M.; Walton, J. C. *Adv. Phys. Org. Chem.* **1978**, *16*, 51.

of R• desorbs from the surface. The absence of a reaction between R• and TME, therefore, indicates that free solution-phase radicals do not play an important role.[18]

For R = $PhCH_2$, Scheme 1 may be extended by a further mechanism, which takes into account that both CdS and $PhCH_2Li$ absorb in the blue region. Initially, $PhCH_2Li$ is excited to its S_1 state, a potent reductant, which transfers an electron to CdS (Scheme 4).[19] A

Scheme 4

$$PhCH_2Li \xrightarrow{h\nu} PhCH_2Li^* \quad (9)$$

$$2PhCH_2Li^* + CdS \rightarrow 2PhCH_2^\bullet + Cd + Li_2S \quad (10)$$

remaining radical dimerizes as described. If we keep in mind that the higher radical yield for $PhCH_2Li$ in comparison with that for BuLi presumably does not ensue from a very different electromotive force (Table 1), the operation of an alternative mechanism for $PhCH_2Li$ according to Scheme 4 may provide an explanation for the different reactivity. So far, a decision in favor of one of the routes discussed for $PhCH_2Li$ (Scheme 1 versus Scheme 4) is not possible.

Semiempirical Adsorbate Model. Little is known about the steric arrangement of anionic organic adsorbates. Benzylic species prefer a η^7 configuration on Pt(111)[20] and on a Ru_8 cluster.[21] Here, semiempirical calculations may shed some light on the configuration of the benzyl anion/CdS adsorbate. Problems arise in the search for a model surface which fits reality best. PM3,[22] the only semiempirical method with Cd parameters, was not suitable, because it shows no tendency to bind the benzyl anion in a η^7 way to a model surface; therefore, we chose AM1[23] and contented ourselves with a stable surface of the isomorphous ZnS, the (1010) layer of hexagonal wurzite. Zn_xS_x clusters have already been investigated using ab initio MO theory in order to find a suitable surface model for $ZnCl_2$ chemisorption.[24] We preferred a cluster with a suitable charge distribution in the vicinity of the site of adsorption. Therefore, all metal ions were 3-fold coordinated with sulfur ions. This made it necessary to consider a second layer and saturate with H_2S molecules (Figure 1). Unfortunately, AM1 optimization strongly distorted the chosen cluster; therefore, we used experimental values for the lattice parameters[25] instead of optimized data. According to the rigid lattice model,[26] the lattice parameters were

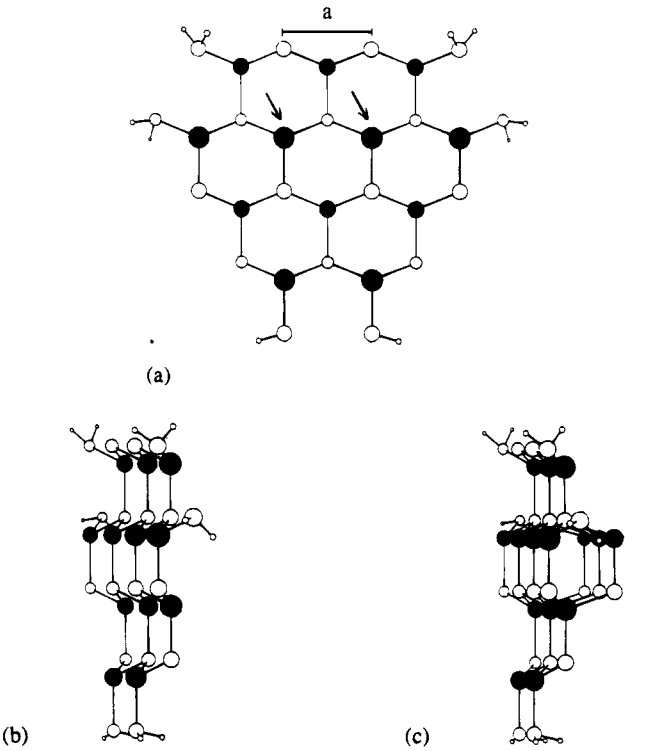

Figure 1. The (1010) surface model molecule Zn_n-S_n·$6H_2S$: (a) from above; (b) from the side with two layers ($n = 12$); (c) from the side with three layers ($n = 15$). Metal ions are black, and the sites of adsorption are marked. For wurzite, the lattice constant $a = 3.84$ Å, and for α-CdS, $a = 4.14$ Å.

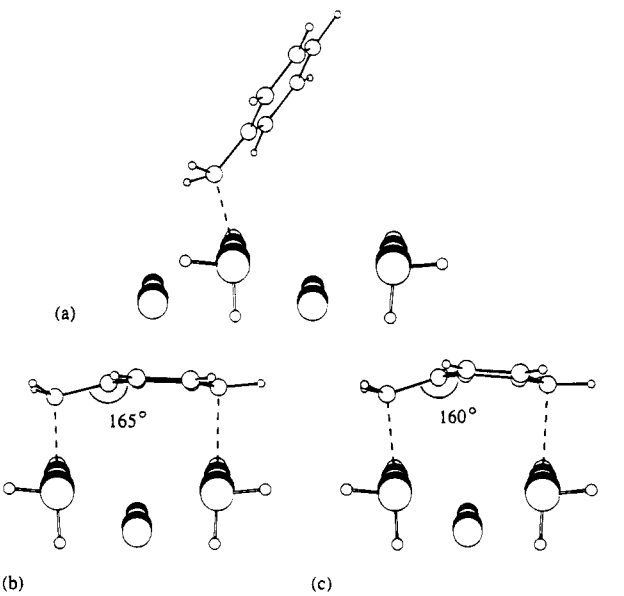

Figure 2. Details of the AM1-optimized η^1 and η^7 configurations of $PhCH_2^-/Zn_{12}S_{12}$·$6H_2S$: (a) η^1, $a = 4.14$ Å (for $a = 3.84$ Å, the benzyl anion structure is nearly identical); (b) η^7, $a = 4.14$ Å; (c) η^7, $a = 3.84$ Å.

also held constant during the optimization of the adsorbed benzyl anion.

The difference between the calculated adsorption energies of the η^1 and η^7 configurations[27] (Figure 2) of the benzyl anion/Zn_nS_n·$6H_2S$ complex is a function of the number of layers and of the lattice constant a (Table

(18) In addition, Kisch and Künneth recently suggested that the photodimerization of dihydrofurans also proceeds on the semiconductor surface. See: Kisch, H.; Künneth, R. In *Photochemistry and Photophysics*; Rabek, J. F., Ed.; CRC Press: Boca Raton, FL, 1991; Vol. IV, p 131.

(19) Photoinduced electron transfer from excited adsorbates to CdS has already been described by: Watanabe, T.; Takizawa, T.; Honda, K. *J. Phys. Chem.* **1977**, *81*, 1845.

(20) Avery, N. *J. Chem. Soc., Chem. Commun.* **1988**, 153.

(21) Bullock, L. M.; Field, J. F.; Haines, R. J.; Minshall, E.; Smit, D. N. *J. Organomet. Chem.* **1986**, *310*, C47.

(22) Stewart, J. J. P. *J. Comput. Chem.* **1989**, *10*, 209, 221.

(23) Dewar, M. J. S.; Zoebisch, E. G.; Healy, E. F.; Stewart, J. J. P. *J. Am. Chem. Soc.* **1985**, *107*, 3902.

(24) Lindblad, M.; Pakkanen, T. A. *J. Comput. Chem.* **1988**, *9*, 581.

(25) *Gmelins Handbuch der Anorganischen Chemie*; Verlag Chemie: Weinheim, Germany, 1959; Cd Suppl., p 595. *Ibid.*, Zn Suppl., p 916.

(26) Somorjai, G. A. In *Bonding Energetics in Organometallic Compounds*; American Chemical Society: Washington, DC, 1990; p 218.

(27) η^7 means that $PhCH_2^-$ lies flat over the surface; strictly speaking, the calculated "η^{7n} structure has a $\eta^1(\sigma)$:$\eta^1(\pi)$ configuration.

Table 2. AM1-Calculated Difference of η^1 and η^7 Adsorption Energies of the Model Adsorbate Complex Benzyl Anion/Zn_nS_n·$6H_2S$ as a Function of Lattice Constant *a* and Number of Layers

lattice params[a]	$E_{ad}(\eta^7) - E_{ad}(\eta^1)$ (kcal)[b]
a = 3.84 Å (wurzite) n = 12 (two layers)	11.1
a = 4.14 Å (α-CdS) n = 12 (two layers)	3.0
a = 4.14 Å (α-CdS) n = 15 (three layers)	0.4

[a] See Figure 1. [b] All calculated adsorbate complexes are (at least local) minima on the energy surface. For positive values, η^1 is more strongly bound than η^7.

Table 3. AM1 Adsorption Energies of Alkyl-Substituted Benzyl Anion Adsorbate Complexes Referred to the Unsubstituted η^1 Species

m-(X,X′)-$PhCH_2^-$/$Zn_{15}S_{15}$·$6H_2S$ (a = 4.14 Å)	rel E_{ad} (kcal)[a]	
	η^1 config	η^7 confign
X = X′ = H	0	0.4
X = X′ = Me (**3**)	0.3	11.2
X = Me, X′ = *t*-Bu (**4**)	−0.2	no minimum found

[a] For negative values, the anion is bound more strongly to the model surface than the unsubstituted benzyl anion.

2). The η^7 configuration is more favorable because of reduced strain if the distance between the two binding metal ions is increased. In this case, the angle between the benzylic CH_2 group and the plane of the aromatic ring is also increased, as can be seen in Figure 2. The artificial procedure of extending the Zn_nS_n·$6H_2S$ molecule to the lattice constant of α-CdS therefore reduces the difference between η^1 and η^7 adsorption energies considerably. The further addition of a third layer renders the two configurations nearly equal in energy. Finally, one should consider that the rigid lattice model will underestimate the stability of the η^7 complex, because this configuration is likely to be more susceptible to the flexibility of the surface than η^1. Therefore, a preponderance of the η^7-benzyl anion adsorbate seems to be probable on the surface in question.[28] Whether these results apply to the reactive surface as well may be deduced from a competitive experiment using $PhCH_2$-Li and an alkyl-substituted, sterically hindered derivative.

Steric Effects. Bulky substituents force a benzyl anion to adopt a η^1 configuration and offer the opportunity to compare the reactivity of a η^1-bound species with that of the unsubstituted benzyl anion. Alkyl groups in the *meta* position are very suitable to investigate steric effects, because they have negligible influence on the electronic structure of the benzyl anion. In order to estimate the adsorption energies of the two *meta*-substituted derivatives *m*-(X,X′)-$PhCH_2^-$ (**3**, X = X′ = Me; **4**, X = Me, X′ = *t*-Bu), we performed semiempirical calculations and compared the results to those for the unsubstituted benzyl anion adsorbate complex (Table 3). Interestingly, for **3** we also found a η^7 adsorbate complex that is a local minimum and lies about 11 kcal above the η^1 minimum, whereas **4** only exists in a η^1 configuration as expected.

Irradiating a 1:1 mixture of $PhCH_2Li$ and **4**-Li, which is definitely a η^1-bound species, with CdS gives a product distribution which indicates that about twice as many radicals are formed from **4** than from benzyllithium (eq 11). Furthermore, when the two mixtures

Scheme 5

$$\underset{1.0:1.0}{PhCH_2Li + \mathbf{4}\text{-Li}} \rightarrow \underset{1.0:1.8}{PhCH_2^{\bullet} + \mathbf{4}^{\bullet}} \rightarrow \text{dimeric products} \quad (11)$$

$$\underset{1.0:1.0}{PhCH_2Li + \mathbf{3}\text{-Li}} \rightarrow \underset{1.0:2.0}{PhCH_2^{\bullet} + \mathbf{3}^{\bullet}} \rightarrow \text{dimeric products} \quad (12)$$

$$\underset{1.0:1.0}{\mathbf{3}\text{-Li} + \mathbf{4}\text{-Li}} \rightarrow \underset{1.0:0.8}{\mathbf{3}^{\bullet} + \mathbf{4}^{\bullet}} \rightarrow \text{dimeric products} \quad (13)$$

$PhCH_2Li$/**3**-Li and **3**-Li/**4**-Li are irradiated under the same conditions, radical ratios of 1:2.0 (eq 12) and 1:0.8 (eq 13) (Scheme 5) are found. These results clearly indicate that *meta* alkyl substitution increases the reactivity of benzyllithiums toward CdS and that methyl and *tert*-butyl groups behave nearly equivalently. It seems reasonable (also with the AM1 results in mind) to accept a η^1 configuration for both **3** and **4**. Probably, the small difference in the radical yields of eq 13 can be explained by a somewhat lower adsorption energy of **4** because of the stronger repulsive effect of the *tert*-butyl group.[29]

The results of eqs 11 and 12 are less easy to explain. Assuming that both the benzyl anion and its *m*-alkyl-substituted derivatives are η^1-bound, it is difficult to see why the latter should react so much better. Alternatively, the benzyl anion differs from **3** and **4** in that it adopts a η^7 configuratino on the surface. We are then forced to assume that a η^1-bound benzylic species is more reactive than a η^7-bound one. As a possible clue to the problem, it should be noted that the metal ions of the surface have a strong polarizing effect on the electron density of the anion. A η^7-benzylic anion is both σ- and π-bound to metal ions and resembles a naked anion with a more diffuse electron density, whereas a η^1 species is strongly influenced by one σ-bound counterion, leading to a charge concentration on the benzylic carbon atom, which therefore should be oxidized more easily. However, AM1 calculations do not show significant differences in the charge distribution of the η^1- and η^7-bound benzyl anions. Possibly the rigid 1010 ZnS surface is not the best choice to test for this effect. Calculations on the benzyl anion adsorption on different ZnS surfaces are under way and will be discussed in the future.

Conclusion

The photoredox reaction between organolithium compounds RLi and CdS powder is somewhat unusual within the increasing class of chemical conversions with irradiated semiconductors in that in lacks a reducible solution-phase species. The semiconductor acts both as

(28) Here we emphasize that we intended to investigate whether a η^7 adsorbate is energetically feasible on a *certain* surface. We are not aware which surface plays the active part in the photoreaction.

(29) This effect is not reflected by the AM1 results in Table 3, because the model surface is flat, and even *meta tert*-butyl groups of a η^1 adsorbate do not interfere with the surface. However, this is surely not valid for rough surfaces or surfaces with impurities, which prevail in reality.

a sensitizer (at least in the reaction with BuLi and PhLi) and as a reactant, decomposing to elemental Cd in the course of the reaction. This complicates investigations on mass transfer or adsorption equilibrium because the surfaces are gradually decomposed to, or poisoned with, Cd metal. Nevertheless, we can conclude that radicals R• dimerize preferably on the semiconductor surface and that intraaggregate dimerization of R• dominates if the parent compound RLi is aggregated.

The interesting result that alkyl substitution in the *meta* position of $PhCH_2Li$ increases the reactivity can be explained by assuming two different adsorption configurations. We believe that bulky groups in the *meta* position force the benzyl anion to switch from a η^7 to a η^1 configuration and that the latter is more reactive because of a higher oxidation potential.

Experimental Section and Calculational Methods

All irradiations were carried out in an acetone bath with a Schlenk tube and the cooling jacket of a high-pressure mercury lamp (Hanau TQ 150 W) placed at a distance of 10 mm. The reaction mixture in the Schlenk tube was stirred with a magnetic stirrer. An Ultra Cryomat (Lauda K 120 W) was connected to the cooling jacket, both cooling the lamp and tempering the acetone bath (between room temperature and −70 °C). An immersion lamp apparatus was less suitable because Cd metal deposited on the glass in the region of the highest radiation density.

All products were detected by GC analysis (HP 5890; SE54, 25 m, 0.23 mm) and identified by comparison with an authentic sample and/or GC−MS (Finnigan MAT 90). Quantitative evaluations were carried out by adding a suitable GC standard to the reaction mixture.

CdS (99.999%, Strem Chemicals, hexagonal by powder diffraction) was degassed, dried in a drying apparatus for 5 h at 0.05 Torr and 100 °C, and kept under argon. Its suspension in Et_2O was activated in an ultrasonic unit for 15 min immediately before it was used. Benzyllithium and its alkyl-substituted derivatives **3**-Li and **4**-Li were obtained as orange, crystalline products by the method of Boche et al.[30] The ethereal solutions should be stored at −78 °C and used fresh, because small amounts of the corresponding bibenzylic species gradually emerged after several days. For determinations of the anion concentration and tests for decomposition products, small amounts of the benzyllithium solutions were quenched with trimethylchlorosilane ((TMS)Cl) and washed with water and a GC standard was added for quantitative GC analysis. PhLi was obtained by the method of Seebach and Bauer,[31] and *n*-BuLi was purchased as a 1.6 N solution from Aldrich. Et_2O was refluxed over Na−K alloy under argon before it was used, and all reactions were performed under an argon atmosphere.

Photostability without CdS. A 20 mL portion of an ethereal RLi solution (R = $PhCH_2$, Bu; 0.05 m) was irradiated at −30° in an acetone bath ($\lambda \geq 340$ nm). For PhLi a solution of $NaNO_2$ (1 *m*) in $MeOH/H_2O$ (1:1) was used ($\lambda \geq 410$ nm) instead of acetone. After 6 h of irradiation the solutions were quenched with (TMS)Cl and washed with water. GC analysis shows no consumption of the corresponding RLi.

Stability against CdS in the Dark. The organolithium solutions in question were mixed with an excess of CdS and stirred for 6 h at −30 °C in the dark. Again, no reaction was detectable.

Photodimerization of RLi. Into 30 mL of a cooled, ethereal suspension of 200 mg of CdS (1.4 mmol) in a 100 mL Schlenk tube was syringed 1.4 mmol of RLi (as a solution in Et_2O or hexane) under argon. After 6 h of irradiation (10 h for PhLi) at −30 °C the black suspension was cooled to −78 °C and an excess of (TMS)Cl was added. The cooling bath was removed, and the mixture was stirred for ½ h. After washing with water and separating the organic layer, a fixed amount of a GC standard was added and the products were submitted to GC analysis. Yields: 0.120 mmol of bibenzyl for R = $PhCH_2$, 0.073 mmol of *n*-octane for R = Bu, and 0.034 mmol of biphenyl for R = Ph. In the case of R = Bu, traces of **1** and **2** were detected by GC−MS. Cadmium metal was detected by filtering off the solids after quenching and washing with water. Treatment with dilute $NaHSO_4$ solution led to gas development, and the black suspension became yellow. The solution was filtered off and treated with dilute Na_2S solution to give a yellow CdS suspension.

Irradiation with Tetramethylethylene (TME). To a mixture of 1.4 mmol of CdS, 0.7 mmol of $PhCH_2Li$, and 30 mL of Et_2O was added 0.5 mL (4.2 mmol) of TME. Half of the suspension was quenched before and the other half after 6 h of irradiation at −30 °C. GC analysis showed that both samples contained equal amounts of TME. Bibenzyl was the only reaction product detected.

Competitive Reaction between $PhCH_2Li$ and BuLi. A suspension of 0.4 mmol of $PhCH_2Li$, 1.0 mmol of BuLi, and 1.4 mmol of CdS in 30 mL of Et_2O was irradiated under the conditions described. The product mixture consisted of 0.12 mmol of bibenzyl, 0.10 mmol of 1-phenylpentane, and 0.13 mmol of octane.

Competitive Reaction between Benzylic Species. As an example, reaction 11 is described: a mixture of 0.9 mmol of $PhCH_2Li$, 0.9 mmol of **4**-Li, 1.4 mmol of CdS, and 30 mL of Et_2O yielded, when irradiated for 6 h at −30 °C, 0.012 mmol of bibenzyl, 0.042 mmol of 1-(3-*tert*-butyl-5-methylphenyl)-2-phenylethane, and 0.039 mmol of 1,2-bis(3-*tert*-butyl-5-methylphenyl)ethane.

Calculations. Semiempirical calculations used the AM1 Hamiltonian with the VAMP 4.3 program[32] on a Convex C220. Zn parameters were those of Dewar and Merz.[33] Adsorption energies E_{ad} were obtained from the calculated heat of formation of the absorbate complex minus the sum of the heats of formation of the described model surface and of the corresponding free gas-phase anion. As solvation effects were omitted, we confined ourselves to present relative values of E_{ad} only.

Acknowledgment. We are indebted to Prof. H. Kisch and R. Künneth for helpful discussions and to D. Schaefer for carrying out all GC−MS analyses.

OM950038Y

(30) Zarges, W.; Marsch, M.; Harms, K.; Boche, G. *Chem. Ber.* **1989**, *122*, 2303.
(31) Bauer, W.; Seebach, D. *Helv. Chim. Acta* **1984**, *67*, 1972.
(32) Based on AMPAC (QCPE 539); vectorized and adopted to Convex C220, written by T. Clark.
(33) Dewar, M. J. S.; Merz, K. M. *Organometallics* **1988**, *7*, 522.

Synthesis and Chemistry of Chiral Tetraphenylcyclopentadienes: X-ray Structures of $Rh(\eta^5\text{-}C_5Ph_4R^*)(\eta^4\text{-}C_8H_{12})$ (R* = Menthyl, Neomenthyl)

James A. Ramsden, David J. Milner,[1] Harry Adams, Neil A. Bailey, Arnold J. Smith, and Colin White*

Department of Chemistry, The University, Sheffield S3 7HF, England

Received August 4, 1994[⊗]

The syntheses of the homochiral cyclopentadienes $C_5Ph_4R^*H$ (R* = menthyl; R* = neomenthyl) are reported together with those of the corresponding rhodium complexes $Rh(C_5Ph_4R^*)(COD)$ (**2a**, R* = menthyl; **2b**, R* = neomenthyl). Both complexes react with bromine to give the corresponding species $[Rh(C_5Ph_4R^*)Br_2]_2$ (**3a**, R* = menthyl; **3b**, R* = neomenthyl). The X-ray structures of $Rh(C_5Ph_4menthyl)(COD)$ and $Rh(C_5Ph_4neomenthyl)(COD)$ have been determined at room temperature with use of Mo Kα radiation (λ = 0.710 69 Å). Compound **2a** crystallizes in the orthorhombic space group $P2_12_12_1$ (D_2^4, No. 19) with a = 12.762(35) Å, b = 17.953(39) Å, c = 31.91(14) Å, V = 7311(42) Å^3, Z = 8, and D_c = 1.306 g cm^{-3} and was refined to R = 0.1349 on the basis of 1267 independent reflections. The analogous neomenthyl compound **2b** crystallizes in the hexagonal space group $P6_2$ (C_6^4, No. 171) with a = 27.034(78) Å, c = 9.540(19) Å, V = 6041(27) Å^3, Z = 6, and D_c = 1.246 g cm^{-3} and was refined to R = 0.0671 on the basis of 2310 independent reflections. A correlation between the CD spectra of **2a** and **2b** and their solid-state structures is discussed.

Introduction

Metal complexes containing a chiral cyclopentadienyl ligand have attracted considerable interest in recent years.[2] In part this is because of their potential in catalytic enantioselective synthesis; chiral cyclopentadienyl ligands are spatially and electronically very different from chiral bis(phosphine) ligands, and hence they are attractive alternatives in cases where chiral bis(phosphine) ligands give poor results. For example, nonfunctionalized alkenes are typically hydrogenated in ≤30% ee with rhodium(I)/bis(phosphine) catalysts,[3] whereas chiral bis(cyclopentadienyl)metal complexes give up to 96% ee.[4] To date, however, high optical yields (i.e. >80% ee) have only been achieved with chiral cyclopentadienyl ligands using bis(cyclopentadienyl)-metal complexes,[5] especially those having the cyclopentadienyl ligands linked together,[4,6] In contrast, chiral monocyclopentadienyl complexes have given at best modest optical yields.[7,8] There are several obvious reasons for this; for example in a mono- rather than a bis(cyclopentadienyl) complex it is clearly easier for the substrate to avoid interaction with a bulky chiral substituent. Further, in contrast to linked bis(cyclopentadienyl) ligands, rotation about the metal–cyclopentadienyl bond reduces the chiral directing influence of the mono(cyclopentadienyl) ligand. There are, however, a number of attractive mono(cyclopentadienyl) catalysts known. For example, whereas hydrogenation catalysts of the type $Ti(Cp')_2Cl_2$ need to be activated by the controlled addition of a reducing agent, are only really effective for the reduction of C=C bonds, have a limited turnover number, and are very sensitive to moisture and reaction conditions,[9] $[Rh(C_5Me_5)Cl_2]_2$ suffers from none of these disadvantages.[10] We therefore set out to synthesize an effective chiral mono(cyclopentadienyl) ligand in order to develop chiral analogues of $[Rh(C_5Me_5)Cl_2]_2$ and other attractive catalysts.

With this objective in mind, we considered the fact that a wide variety of chiral bis(phosphines) of the type $(Ar)_2P^{\frown}P(Ar)_2$ are successful despite the fact that the chiral center is often remote from the metal center. This is because the chiral center dictates the conformation of the chelate phosphorus ring, which in turn dictates the orientation of the propeller arrangement of the aryl groups on the phosphorus atoms; in this way the chirality is transmitted to the environment around the metal.[11] In a pentaphenylcyclopentadienyl ligand the five phenyl rings cannot lie coplanar and must adopt a

⊗ Abstract published in *Advance ACS Abstracts,* December 15, 1994.

(1) Present address: Zeneca Specialties, P.O. Box 42, Hexagon House, Blackley, Manchester M9 3DA, England.

(2) Halterman, R. L. *Chem. Rev.* **1992**, *92*, 965.

(3) (a) Dumont, W.; Poulin, J. C.; Dang, T. P.; Kagan, H. B. *J. Am. Chem. Soc.* **1973**, *95*, 8295. (b) Hayashi, T.; Tanaka, M.; Ogata, I. *Tetrahedron Lett.* **1977**, 295. (c) Samuel, O.; Couffignal, R.; Lauer, M.; Zhang, S. Y.; Kagan, H. B. *Nouv. J. Chim.* **1981**, *5*, 15.

(4) Conticello, V. P.; Brard, L.; Giarrdello, M. A.; Tsuji, Y.; Sabat, M.; Stern, C. L.; Marks, T. J. *J. Am. Chem. Soc.* **1992**, *114*, 2761.

(5) (a) Halterman, R. L.; Vollhardt, K. P. C.; Welker, M. E.; Blaser, D.; Boese, R. *J. Am. Chem. Soc.* **1987**, *109*, 8105.

(6) (a) Pino, P.; Cioni, P.; Wei, J. J. *J. Am. Chem. Soc.* **1987**, *109*, 6189. (b) Chen, Z.; Haltermann, R. L. *J. Am. Chem. Soc.* **1992**, *114*, 2276.

(7) (a) Schofield, P. A.; Adams, H.; Bailey, N. A.; Cesarotti, E.; White, C. *J. Organomet. Chem.* **1991**, *412*, 273. (b) Adams, H.; Bailey, N. A.; Colley, M.; Schofield, P. A.; White, C. *J. Chem. Soc., Dalton Trans.* **1994**, 1445.

(8) One exception is the Zr(dibornaCp)Cl_3 complex, which catalyzes the coupling of 1-naphthol with ethyl pyruvate in ≤80% ee: Erker, G.; van der Zeijden, A. A. H. *Angew. Chem., Int. Ed. Engl.* **1990**, *29*, 512.

(9) Kagan, H. B. In *Comprehensive Organometallic Chemistry*; Wilkinson, G., Stone, F. G. A., Abel, E. W., Eds.; Pergamon: Oxford, U.K., 1982; Vol. 8, p 479.

(10) (a) Russell, M. J. H.; White, C.; Maitlis, P. M. *J. Chem. Soc., Chem. Commun.* **1977**, 427. (b) Gill, D. S.; White, C.; Maitlis, P. M. *J. Chem. Soc., Dalton Trans.* **1978**, 617.

(11) (a) Knowles, W. S.; Vineyard, B. D.; Sabacky, M. J.; Stuls, B. R. In *Fundamental Research in Homogeneous Catalysis*; Ishii,Y., Tsutsui, M., Eds.; Plenum: New York, 1979; Vol. 3, p 537. (b) MacNeil, P. A.; Roberts, N. K.; Bosnich, B. *J. Am. Chem. Soc.* **1981**, *103*, 2273.

0276-7333/95/2314-2575$09.00/0

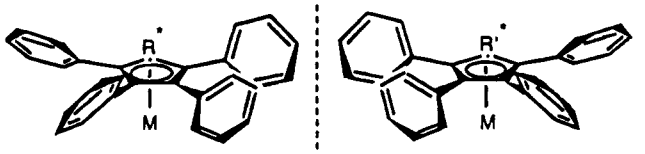

Figure 1. Chiral arrays of tetraphenyl substituents.

1a **1b**

Figure 2.

chiral array; further, we and others have shown that in metal–pentaphenylcyclopentadienyl compounds rotation about the phenyl–cyclopentadienyl bonds is sufficiently restricted that this chiral array can, in the presence of another chiral center, give rise to diastereoisomers.[12,13] We therefore wondered whether with a chiral tetraaryl cyclopentadienyl ligand it would be possible to mimic bis(phosphine) ligands by having a bulky chiral group which dictated the chiral orientation of the four aryl groups (Figure 1). This would produce a chiral "umbrella" over the metal and in this way transmit the chirality to the metal environment.

To our knowledge the only chiral tetraarylcyclopentadienyl compounds reported to date are those reported by us several years ago containing an (−)-*O*-methyl mandelate group as the chiral directing unit, i.e. $[M\{C_5Ph_4OCOCH(OMe)Ph\}]_n$ (where $n = 1$, M = $Rh(CO)_2$ or $Ru(CO)_2Cl$; $n = 2$, M = $RhCl_2$).[14] In these cases, however, the chiral center is too remote to have any significant effect upon the orientations of the four phenyl substituents and we reasoned that to do this it was necessary to locate the chiral center immediately adjacent to the cyclopentadienyl ring. We report herein the synthesis of such ligands, namely menthyltetraphenylcyclopentadiene (**1a**) and neomenthyltetraphenylcyclopentadiene (**1b**) (Figure 2) together with the synthesis and X-ray structures of their rhodium complexes.

Results and Discussion

Ligand Syntheses. The synthetic route to the chiral ligands involved the reaction of menthyl or neomenthyl tosylate with lithium tetraphenylcyclopentadienide (eq 1). This procedure has several attractive features: not

$$Li[C_5Ph_4H] + R^*Ts \rightarrow C_5Ph_4HR^* + LiTs$$

$$R^* = \text{menthyl, neomenthyl} \qquad (1)$$

only is it straightforward but also the tetraphenylcyclopentadiene[15] and the chiral tosylates[16,17] are readily available and the stereochemical course of the reaction is well defined with the addition proceeding with inversion of configuration at the chiral carbon center. Thus, the chiral unit is introduced in one step so that multigram quantities of the optically pure ligands can readily be prepared and *no resolution is required at any stage.*

The products were purified by liquid chromatography and found to be a mixture of the 1,3-, 2,4-, and 3,5-dienes. The yield of neomenthyltetraphenylcyclopentadiene (**1b**; 16%) was significantly lower than that obtained in the menthyl analogue **1a** (64%); this can be rationalized by the relative ease of the S_N2 displacement of the tosylate group. Neomenthyl tosylate can adopt a chair conformation where the leaving group is axial and the approach of the nucleophile is not hindered by any of the other substituents on the cyclohexyl ring. Menthyl tosylate can also adopt a conformation with an axial leaving group, but the approach of the bulky tetraphenylcyclopentadienide nucleophile is then hindered by the adjacent isopropyl group. The increased reactivity of neomenthyl tosylate over menthyl tosylate with respect to S_N2 displacement is also reflected in the relative rates of hydrolysis of these tosylates.[17]

Rhodium Complexes. Reaction of $Li(C_5Ph_4R^*)$ (R* = menthyl(men), or neomenthyl(neomen)) with $[Rh(COD)Cl]_2$ in xylene at 125–135 °C yielded the corresponding $Rh(C_5Ph_4R^*)(COD)$ complex (**2a**, R* = menthyl; **2b**, R* = neomenthyl) in near-quantitative yield. No product was observed when the same reaction was carried out in boiling tetrahydrofuran, dioxane, or toluene. Presumably, the high reaction temperature necessary reflects the considerable steric hindrance experienced by the ligand. Both **2a** and **2b** are air-stable compounds which have been fully characterized and whose X-ray crystal structures and CD spectra are reported below.

In an attempt to synthesize $Rh(C_5Ph_4neomen)(COD)$ (**2b**) under milder conditions, neomenthyltetraphenylcyclopentadiene and $[Rh(COD)Cl]_2$ were heated under reflux in methanol in the presence of sodium carbonate; this is the procedure reported for the synthesis of the corresponding $Rh(\eta^5\text{-}C_5H_5)(COD)$ complex.[18] In the case of neomenthyltetraphenylcyclopentadiene, however, no cyclooctadiene complex was obtained but a blue compound was isolated in low yield (4%). The infrared spectrum of the product contains a strong signal at 1735 cm^{-1} indicative of a bridging carbonyl ligand, and positive ion FAB mass spectroscopy indicated the presence of the $[Rh(C_5Ph_4neomen)(CO)]^+$ moiety. The compound proved to be unstable as a solid and in solution, but it has been tentatively assigned as bis(μ-carbonyl)-bis(η^5-neomenthyltetraphenylcyclopentadienyl)dirhodium. It is pertinent to note that the analogous C_5Me_5 complex[19] is also blue with ν_{CO} at 1732 cm^{-1} and

(12) Adams, H.; Bailey, N. A.; Browning, A. F.; Ramsden, J. A.; White, C. *J. Organomet. Chem.* 1990, *387*, 305

(13) Li, L.; Decken, A.; Sayer, B. G.; McGlinchey, M. J.; Brégaint, P.; Thépot, J.-Y.; Toupet, L.; Hamon, J.-R.; Lapinte, C. *Organometallics* **1994**, *13*, 682.

(14) Bailey, N. A.; Jassel, V. S.; Vefghi, R.; White, C. *J. Chem. Soc., Dalton Trans.* **1987** 2815.

(15) (a) Castellani, M. P.; Wright, J. M.; Geib, S. J.; Rheingold, A. L.; Trogler, W. C. *Organometallics* **1986**, *5*, 1116. (b) Cava, M. P.; Narashiman, K. *J. Org. Chem.* **1969**, *34*, 3641.

(16) Phillips, H. *J. Chem. Soc.* **1925**, *127*, 2566.

(17) Winstein, S.; Morse, B. K.; Grunwald, E.; Jones, H. W.; Corse, J.; Trifan, D.; Marshall, H. *J. Am. Chem. Soc.* **1952**, *74*, 1127 and references therein.

(18) Kang, J. W.; Moseley, K.; Maitlis, P. M. *J. Am. Chem. Soc.* **1969**, *91*, 5970.

(19) Nutton, A.; Maitlis, P. M. *J. Organomet. Chem.* **1979**, *166*, C21.

that $[Rh(C_5Ph_5)(CO)]_2$, which has been isolated as an impure solid, is dark green with ν_{CO} at 1767 cm^{-1} (CH_2Cl_2).[20]

There are two possible sources of the carbonyl ligand in $[Rh(C_5Ph_4neomen)(CO)]_2$. One is from the sodium carbonate used in the reaction as a base, but we know of no precedent for carbonate acting as a source of carbon monoxide for the formation of a metal carbonyl. However, under acidic conditions carbonate gives rise to water and carbon dioxide and the latter is known to be a source of carbon monoxide.[21] An alternative source of carbon monoxide is from decarbonylation of the solvent methanol, and we tend to prefer this explanation given that complexes such as $[Rh(C_5Me_5)Cl_2]_2$ are known to catalyze methanol decarbonylation.[22]

The complexes $Rh(C_5Ph_4R^*)(COD)$ (**2a**, R* = menthyl; **2b**, R* = neomenthyl) readily reacted with bromine to displace the COD ligand and to give the corresponding $[Rh(C_5Ph_4R^*)Br_2]_2$ (**3a**, R* = menthyl; **3b**, R* = neomenthyl). Again, these are both air-stable solids which have been stored at room temperature for months with no apparent change. One beneficial effect of the large chiral substituent is that they appear to be more soluble in a wide range of solvents compared to $[Rh(C_5Ph_5)Br_2]_2$.[20] The analogous compound $[Rh(C_5Me_5)Br_2]_2$ is an active hydrogenation catalyst,[10] and preliminary experiments indicate that the complexes **3a** and **3b** also catalyze alkene hydrogenation. Their ability to catalyze enantioselective reductions is being actively investigated.

X-ray Crystallographic Structures of 2a and 2b. The unit cell of $Rh(C_5Ph_4menthyl)(COD)$ (**2a**) consists of two crystallographically independent molecules which are illustrated in Figure 3. Tables 2 and 3 give bond lengths and angles with estimated standard deviations.

If the menthyl unit is disregarded, the remainder of the molecule is almost centrosymmetrically related through the origin of the unit cell. In contrast to the normal conformation adopted by a phenyl-substituted cyclopentadienyl,[12,13,14,23] the phenyl groups do not adopt a propeller arrangement. The two phenyls adjacent to the menthyl site are tilted in opposite directions to form an asymmetric "cup" with its open side directed away from the metal; within this cup is encapsulated the menthyl substituent, the bulky isopropyl group of which is situated on the side of the cyclopentadienyl away from the rhodium. The four phenyl groups in this cup arrangement still form a chiral array. The orientational change from propeller to cup is due to the fact that one of the two remote phenyl substituents lies almost perpendicular to the cyclopentadienyl ring; i.e., the interplanar angles between the phenyl rings and the cyclopentadienyl ring are 55° (C(1)–phenyl), 51° (C(2)–phenyl), 90° (C(3)–phenyl), and 112° (C(4)–phenyl) for molecule 1 and 78° (C(51)–phenyl), 36° (C(52)–phenyl), 91° (C(53)–phenyl), and 129° (C(54)–phenyl) for molecule 2. Both menthyl units adopt the chair conformation with three equatorial substituents, and in the two forms, the menthyl groups only differ in a slight twist in the torsion angle between the menthyl group and the cyclopentadienyl ring; torsion angles C(1)–C(5)–C(30)–C(31), C(4)–C(5)–C(30)–C(31), C(51)–C(55)–C(80)–C(81), and C(54)–C(55)–C(80)–C(81) are −44, +120, +136, and −32°, showing that equivalent (but *not* pseudo-symmetry-related) torsion angles differ by only about 14°. The cyclopentadienyl rings are planar (rms deviations 0.014 and 0.008 Å) and display no loss of aromaticity; the rhodium atoms lie 1.92 and 1.99 Å from these planes for molecules 1 and 2, respectively.

The X-ray crystal structure of $Rh(C_5Ph_4neomen)(COD)$ (**2b**; Figure 4) shows that the neomenthyl group is much bulkier than the menthyl group. The C_6 ring adopts a chair conformation with two of the substituents, methyl and isopropyl, occupying axial positions, while the bulkier tetraphenylcyclopentadienyl group is in an equatorial position. This conformation contrasts with that found in the less sterically hindered complexes $[Ru(C_5H_4neomen)(CO)(PPh_3)L]^{n+}$ (n = 0, L = I,[24] L = Me, SO_2Me;[25] n = 1, L = NCMe[26]) and $[Rh(C_5H_4neomen)Cl_2]_2$,[7a] where the methyl and isopropyl substituents are equatorial and the cyclopentadienyl group is in an axial position.

Also, in contrast to the menthyl analogue, the phenyl groups in **2b** adopt a propeller array (left-hand screw) around the cyclopentadienyl ring and are inclined to the plane of the C_5 ring by 56.7° (C(9)–phenyl), 48.7° (C(13)–phenyl), 45.1° (C(12)–phenyl), and 74.7° (C(11)–phenyl). Clearly the steeper pitch of the C(11)–phenyl ring is a result of the adjacent neomenthyl group. The cyclopentadienyl ring shows no loss of aromaticity, and the bond lengths (Table 2b) and bond angles (Table 3b) are unexceptional.

The X-ray crystal structures can only give an approximate guide to the conformational behavior of the ligand. The solution behavior of the complexes can, however, be probed by means of circular dichroism spectroscopy.

Circular Dichroism. Comparison of the CD spectra of $Rh(\eta^5\text{-}C_5R_4neomen)(COD)$ (R= H, Ph) (Figure 5) reveals that although both complexes display Cotton effects, they are clearly very different. The most intense maximum observed in the CD spectrum of $Rh(\eta^5\text{-}C_5H_4neomen)(COD)$ is associated with a strong UV absorption at 239 nm, whereas the CD spectrum of $Rh(\eta^5\text{-}C_5Ph_4neomen)(COD)$ (**2b**) shows a considerably more intense maximum at 287 nm ($\Delta\epsilon$ = 42.1) and a shoulder at 258 nm which are associated with the maxima at 285 and 248 nm, respectively, in the UV spectrum for the metal complex **2b**. *Clearly, therefore, these intense Cotton effects for* **2b** *are associated with the presence of the four phenyl substituents.* They are also probably associated with metal–ligand charge–transfer transitions, since the absorptions at 248 and 285 nm are absent in the UV spectrum of the free ligand $C_5Ph_4(neomen)H$ (Figure 6). The free ligand $C_5Ph_4(neomen)H$ does have a large positive Cotton effect at 242 nm ($\Delta\epsilon$ = +28), which is associated with a UV transition at 239 nm (ϵ = 42 000). This transition is

(20) Connerley, N. G.; Raven, S. J. *J. Chem. Soc., Dalton Trans.* **1986**, 1613.
(21) Sneeden, R. P. A. In *Comprehensive Organometallic Chemistry*; Wilkinson, G., Stone, F. G. A., Abel, E. W., Eds.; Pergamon: Oxford, U.K., 1982; Vol. 8, pp 262–265.
(22) Smith, T. A.; Maitlis, P. M. *J. Organomet. Chem.* **1985**, *166*, 385.
(23) Baghdadi, J.; Bailey, N. A.; Dowding, A. S.; White, C.,*J. Chem. Soc., Chem. Commun.*, **1992**, 170.
(24) Cesarotti, E.; Chiesa, A.; Ciani, G. F.; Sironi, A.; Vefghi, R.; White, C. *J. Chem. Soc., Dalton Trans.* **1984**, 653.
(25) Lindsay, C.; Cesarotti, E.; Adams, H.; Bailey, N. A.; White, C. *Organometallics* **1990**, *9*, 2594.
(26) Cesarotti, E.; Angoletta, M.; Walker, N. P. C.; Hursthouse, M. B.; Vefghi, R.; White, C. *J. Organomet. Chem.* **1985**, *286*, 343.

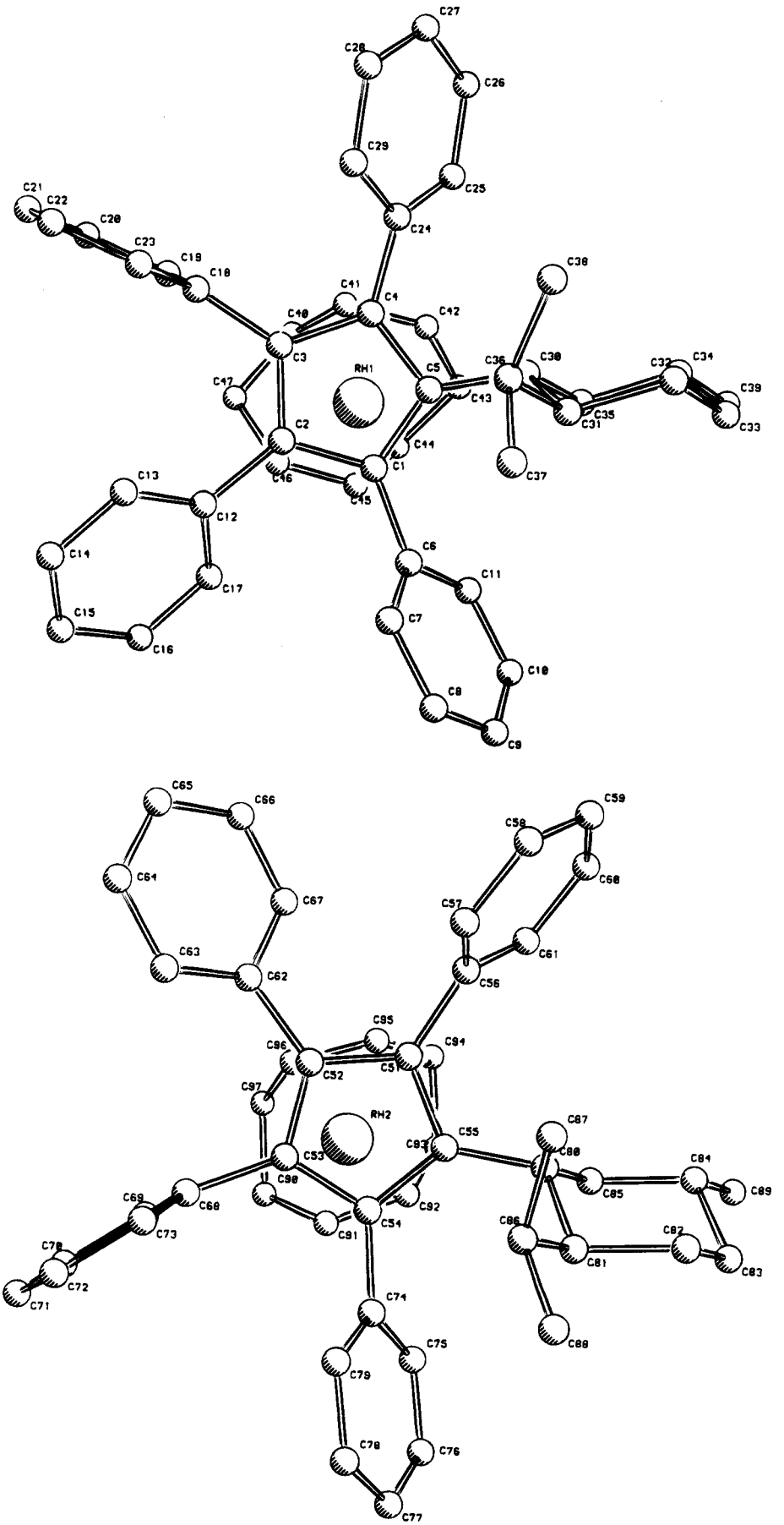

Figure 3. Structures of the two crystallographically independent molecules of $Rh(C_5Ph_4men)(COD)$ (**2a**).

Table 1. Atom Coordinates ($\times 10^4$) and Temperature Factors ($Å^2 \times 10^3$)

atom	x	y	z	U_{eq}[a]	atom	x	y	z	U_{eq}[a]
				(a) Rh(C_5Ph_4men)(COD) (**2a**)					
Rh(1)	142(6)	1461(5)	1707(2)	42(1)*	C(47)	1514(31)	2449(11)	2194(22)	52(6)
Rh(2)	−216(6)	−1323(5)	−1767(2)	42(1)*	C(51)	−492(14)	−415(11)	−1275(6)	26(6)
C(1)	280(12)	551(6)	1154(5)	26(6)	C(52)	−1011(14)	−1082(11)	−1149(6)	26(6)
C(2)	831(12)	1208(6)	1036(5)	26(6)	C(53)	−234(14)	−1627(11)	−1056(6)	26(6)
C(3)	101(12)	1811(6)	1039(5)	26(6)	C(54)	769(14)	−1299(11)	−1122(6)	26(6)
C(4)	−885(12)	1530(6)	1179(5)	26(6)	C(55)	606(14)	−556(11)	−1265(6)	26(6)
C(5)	−779(12)	747(6)	1239(5)	26(6)	C(56)	−952(23)	354(13)	−1269(10)	45(6)
C(6)	760(21)	−198(9)	1232(9)	45(6)	C(57)	−1197(23)	695(13)	−889(10)	49(7)
C(7)	1272(21)	−564(9)	905(9)	49(7)	C(58)	−1473(23)	1447(13)	−880(10)	54(8)
C(8)	1641(21)	−1288(9)	962(9)	54(8)	C(59)	−1504(23)	1857(13)	−1251(10)	58(8)
C(9)	1499(21)	−1647(9)	1345(9)	58(8)	C(60)	−1258(23)	1516(13)	−1631(10)	54(8)
C(10)	987(21)	−1282(9)	1672(9)	54(8)	C(61)	−982(23)	764(13)	−1640(10)	49(7)
C(11)	617(21)	−557(9)	1616(9)	49(7)	C(62)	−2181(15)	−1134(18)	−1098(11)	21(5)
C(12)	1987(13)	1235(16)	950(10)	21(5)	C(63)	−2598(15)	−1506(18)	−753(11)	23(5)
C(13)	2339(13)	1575(16)	583(10)	23(5)	C(64)	−3643(15)	−1398(18)	−641(11)	25(6)
C(14)	3409(13)	1608(16)	496(10)	25(6)	C(65)	−4273(15)	−918(18)	−875(11)	27(6)
C(15)	4128(13)	1300(16)	776(10)	27(6)	C(66)	−3856(15)	−546(18)	−1221(11)	25(6)
C(16)	3776(13)	959(16)	1143(10)	25(6)	C(67)	−2810(15)	−654(18)	−1333(11)	23(5)
C(17)	2706(13)	927(16)	1230(10)	23(5)	C(68)	−448(23)	−2393(12)	−887(9)	45(7)
C(18)	333(23)	2584(9)	887(9)	45(7)	C(69)	−509(23)	−2992(12)	−1165(9)	50(7)
C(19)	733(23)	3104(9)	1169(9)	50(7)	C(70)	−614(23)	−3716(12)	−1012(9)	55(8)
C(20)	1019(23)	3812(9)	1030(9)	55(8)	C(71)	−658(23)	−3841(12)	−581(9)	59(9)
C(21)	906(23)	3999(9)	608(9)	59(9)	C(72)	−596(23)	−3243(12)	−303(9)	55(8)
C(22)	505(23)	3478(9)	326(9)	55(8)	C(73)	−491(23)	−2519(12)	−456(9)	50(7)
C(23)	219(23)	2771(9)	465(9)	50(7)	C(74)	1798(17)	−1680(18)	−1049(11)	50(7)
C(24)	−1910(15)	1910(16)	1082(9)	50(7)	C(75)	2552(17)	−1707(18)	−1365(11)	55(7)
C(25)	−2620(15)	2054(16)	1404(9)	55(7)	C(76)	3463(17)	−2125(18)	−1308(11)	60(8)
C(26)	−3584(15)	2383(16)	1314(9)	60(8)	C(77)	3620(17)	−2515(18)	−936(11)	65(9)
C(27)	−3839(15)	2566(16)	902(9)	65(9)	C(78)	2866(17)	−2488(18)	−620(11)	60(8)
C(28)	−3129(15)	2421(16)	579(9)	60(8)	C(79)	1955(17)	−2071(18)	−677(11)	55(7)
C(29)	−2165(15)	2093(16)	670(9)	55(7)	C(80)	1412(19)	31(15)	−1318(7)	50(5)
C(30)	−1691(14)	239(11)	1277(7)	50(5)	C(81)	2343(19)	15(15)	−1016(7)	55(6)
C(31)	−1746(14)	−368(11)	946(7)	55(6)	C(82)	2988(19)	736(15)	−1069(7)	60(6)
C(32)	−2790(14)	−795(11)	977(7)	60(6)	C(83)	3386(19)	793(15)	−1524(7)	65(7)
C(33)	−2908(14)	−1130(11)	1419(7)	65(7)	C(84)	2449(19)	801(15)	−1827(7)	60(6)
C(34)	−2890(14)	−500(11)	1746(7)	60(6)	C(85)	1804(19)	81(15)	−1772(7)	55(6)
C(35)	−1840(14)	−80(11)	1717(7)	55(6)	C(86)	1957(19)	−48(15)	−562(7)	60(6)
C(36)	−1613(14)	−47(11)	504(7)	60(6)	C(87)	1442(56)	685(25)	−421(12)	65(7)
C(37)	−1291(57)	−673(18)	200(9)	65(7)	C(88)	2887(27)	−229(43)	−272(9)	65(7)
C(38)	−2646(27)	307(38)	355(12)	65(7)	C(89)	2846(19)	855(15)	−2281(7)	65(7)
C(39)	−3015(14)	−831(11)	2188(7)	65(7)	C(90)	−271(16)	−2728(10)	−2306(15)	52(6)
C(40)	454(33)	2568(25)	2404(15)	52(6)	C(91)	483(21)	−2213(12)	−2106(7)	43(5)
C(41)	−421(31)	2286(15)	2137(11)	43(5)	C(92)	772(18)	−1533(10)	−2280(7)	43(5)
C(42)	−883(19)	1594(20)	2223(9)	43(5)	C(93)	427(32)	−1309(25)	−2708(9)	52(6)
C(43)	−539(18)	1157(22)	2601(11)	52(6)	C(94)	−590(28)	−861(32)	−2690(16)	52(6)
C(44)	661(15)	1153(31)	2628(9)	52(6)	C(95)	−1133(33)	−971(11)	−2281(13)	43(5)
C(45)	1121(26)	1076(10)	2198(10)	43(5)	C(96)	−1470(26)	−1667(13)	−2148(11)	43(5)
C(46)	1583(28)	1690(16)	2003(8)	43(5)	C(97)	−1316(19)	−2353(12)	−2402(14)	52(6)
				(b) Rh(C_5H_4neomen)(COD) (**2b**)					
Rh(1)	8079(1)	2090(1)	0	42(1)*	C(32)	8911(4)	2253(4)	2820(11)	43(5)*
C(1)	7622(4)	1938(4)	−1925(11)	59(6)*	C(33)	9394(4)	2765(4)	2397(12)	57(6)*
C(2)	7844(5)	1590(4)	−1896(11)	62(6)*	C(34)	9922(5)	2931(5)	2943(14)	73(8)*
C(3)	8368(5)	1683(5)	−2654(14)	96(9)*	C(35)	9991(5)	2584(5)	3915(16)	81(8)*
C(4)	8910(4)	2213(5)	−2331(14)	85(7)*	C(36)	9512(5)	2075(5)	4329(15)	83(8)*
C(5)	8885(4)	2523(4)	−1056(11)	60(7)*	C(37)	8997(4)	1920(4)	3787(11)	54(6)*
C(6)	8665(4)	2866(4)	−1045(12)	66(6)*	C(38)	8352(4)	3057(4)	2547(12)	45(6)*
C(7)	8379(6)	2962(6)	−2290(13)	89(9)*	C(39)	8276(4)	3428(4)	1743(14)	57(6)*
C(8)	7863(5)	2463(5)	−2803(15)	91(9)*	C(40)	8469(5)	3988(4)	2112(13)	74(7)*
C(9)	7517(4)	2105(4)	1717(13)	41(5)*	C(41)	8733(5)	4183(4)	3374(15)	79(7)*
C(10)	7406(4)	1527(4)	1512(10)	29(4)*	C(42)	8810(4)	3814(5)	4249(13)	67(7)*
C(11)	7921(4)	1514(4)	1863(12)	42(5)*	C(43)	8598(4)	3253(4)	3832(11)	53(6)*
C(12)	8335(4)	2084(4)	2260(11)	36(5)*	C(44)	6114(4)	334(4)	−1457(12)	72(6)*
C(13)	8092(4)	2446(4)	2185(11)	40(5)*	C(45)	6453(4)	669(4)	3684(10)	43(5)*
C(14)	7073(4)	2283(4)	1761(14)	40(5)*	C(46)	6857(4)	1164(4)	4605(10)	54(6)*
C(15)	6986(4)	2509(4)	2961(14)	59(7)*	C(47)	5899(4)	308(4)	4509(11)	62(7)*
C(16)	6585(4)	2675(4)	3013(15)	81(8)*	C(51)	1054(55)	1179(53)	308(120)	212(17)
C(17)	6247(5)	2607(4)	1890(15)	84(7)*	C(52)	669	933	1607	179(14)
C(18)	6321(5)	2380(4)	692(15)	77(7)*	O(1)	524	1343	2114	163(13)
C(19)	6742(4)	2225(4)	576(13)	57(6)*	C(53)	93	1076	3166	179(14)
C(20)	6816(3)	1044(4)	1154(11)	38(5)*	C(54)	200	648	3990	212(17)
C(21)	6354(4)	896(4)	2305(11)	36(5)*	C(61)	1507(37)	977(52)	−608(107)	212(17)
C(22)	5780(4)	503(4)	1569(12)	44(5)*	C(62)	1089	751	640	179(14)
C(23)	5738(4)	−38(4)	973(11)	56(6)*	O(2)	683	941	501	163(13)
C(24)	6199(4)	94(4)	−63(12)	47(5)*	C(63)	573	1086	1860	179(14)
C(25)	6787(4)	494(4)	629(11)	42(5)*	C(64)	238	536	2729	212(17)
C(26)	8013(4)	1023(4)	1911(13)	45(5)*	C(71)	561(41)	1762(32)	3509(84)	212(17)

Table 1 (Continued)

atom	x	y	z	U_{eq}[a]	atom	x	y	z	U_{eq}[a]
(b) Rh(C_5H_4neomen)(COD) (**2b**) (Continued)									
C(27)	7797(4)	623(4)	2972(12)	50(6)*	C(72)	451	1154	3242	179(14)
C(28)	7899(5)	184(5)	3065(16)	90(8)*	O(3)	86	919	2050	163(13)
C(29)	8240(6)	140(5)	2096(17)	103(10)*	C(73)	210	518	1389	179(14)
C(30)	8452(6)	510(6)	1026(17)	102(11)*	C(74)	5	435	−142	212(17)
C(31)	8359(5)	971(5)	971(13)	74(7)*					

[a] Asterisks denote equivalent isotropic U values defined as one-third of the trace of the orthogonalized $\mathbf{U}_{ij}$ tensor.

Table 2. Selected Bond Lengths (Å) with Estimated Standard Deviations (Esd's)

(a) Rh(C_3H_4men)(COD) (**2a**)			
Molecule 1			
Rh(1)−C(1)	2.411(18)	Rh(1)−C(2)	2.358(19)
Rh(1)−C(3)	2.225(19)	Rh(1)−C(4)	2.139(19)
Rh(1)−C(5)	2.293(18)	Rh(1)−Cp(1)	1.92
Rh(1)−C(41)	2.143(33)	Rh(1)−C(42)	2.116(29)
Rh(1)−C(45)	2.119(32)	Rh(1)−C(46)	2.107(35)
C(1)−C(2)	1.425(4)	C(1)−C(5)	1.422(4)
C(2)−C(3)	1.427(4)	C(3)−C(4)	1.428(4)
C(4)−C(5)	1.424(4)		
Molecule 2			
Rh(2)−C(51)	2.289(22)	Rh(2)−C(52)	2.260(21)
Rh(2)−C(53)	2.333(21)	Rh(2)−C(54)	2.412(21)
Rh(2)−C(55)	2.358(22)	Rh(2)−Cp(2)	1.99
Rh(2)−C(91)	2.126(26)	Rh(2)−C(92)	2.103(24)
Rh(2)−C(95)	2.112(41)	Rh(2)−C(96)	2.103(35)
C(51)−C(52)	1.426(4)	C(51)−C(55)	1.424(4)
C(52)−C(53)	1.425(4)	C(53)−C(54)	1.425(4)
C(54)−C(55)	1.426(4)		
(b) Rh(C_5Ph_4(neomen)(Cod) (**2b**)			
Rh(1)−C(1)	2.136(11)	Rh(1)−C(2)	2.156(10)
Rh(1)−C(5)	2.140(10)	Rh(1)−C(6)	2.138(9)
Rh(1)−C(9)	2.249(12)	Rh(1)−C(10)	2.222(8)
Rh(1)−C(11)	2.260(11)	Rh(1)−C(12)	2.270(10)
Rh(1)−C(13)	2.292(11)	C(1)−C(2)	1.343(21)
C(1)−C(8)	1.489(17)	C(2)−C(3)	1.497(19)
C(3)−C(4)	1.479(13)	C(4)−C(5)	1.499(18)
C(5)−C(6)	1.327(20)	C(6)−C(7)	1.510(19)
C(7)−C(8)	1.455(16)	C(9)−C(10)	1.449(14)
C(9)−C(13)	1.424(13)	C(10)−C(11)	1.448(15)
C(11)−C(12)	1.428(12)	C(12)−C(13)	1.429(19)

Table 3. Selected Bond Angles (deg) with Estimated Standard Deviations (Esd's)

(a) Rh(C_5Ph_4men)(COD) (**2a**)			
Molecule 1			
Bond Angles			
C(2)−C(1)−C(5)	108.3(2)	C(1)−C(2)−C(3)	107.7(2)
C(2)−C(3)−C(4)	108.1(2)	C(3)−C(4)−C(5)	107.8(2)
C(1)−C(5)−C(4)	108.0(2)		
Torsion Angles			
C(1)−C(5)−C(30)−C(31)	−44	C(4)−C(5)−C(30)−C(31)	120
C(5)−C(1)−C(6)−C(11)	−48	C(1)−C(2)−C(12)−C(17)	−49
C(2)−C(3)−C(18)−C(19)	−90	C(3)−C(4)−C(24)−C(25)	−130
Molecule 2			
Bond Angles			
C(52)−C(51)−C(55)	107.6(2)	C(51)−C(52)−C(53)	108.2(2)
C(52)−C(53)−C(54)	108.1(2)	C(53)−C(54)−C(55)	107.6(2)
C(51)−C(55)−C(54)	108.4(2)		
Torsion Angles			
C(51)−C(55)−C(80)−C(81)	136	C(54)−C(55)−C(80)−C(81)	−32
C(55)−C(51)−C(56)−C(61)	80	C(51)−C(52)−C(62)−C(67)	27
C(52)−C(53)−C(68)−C(69)	96	C(53)−C(54)−C(74)−C(75)	127
(b) Rh(C_5Ph_4(neomen)(COD) (**2b**)			
C(2)−C(1)−C(8)	122.8(11)	C(1)−C(2)−C(3)	126.1(10)
C(2)-C(3)-C(4)	117.1(11)	C(3)−C(4)−C(5)	114.4(10)
C(4)−C(5)−C(6)	123.9(11)	C(5)−C(6)−C(7)	124.0(11)
C(6)−C(7)−C(8)	116.2(11)	C(1)−C(8)−C(7)	116.9(12)
C(10)−C(9)−C(13)	108.1(10)	C(9)−C(10)−C(11)	108.1(7)
C(10)−C(11)−C(12)	106.2(10)	C(11)−C(12)−C(13)	110.2(9)
C(9)−C(13)−C(12)	107.3(8)	C(21)−C(20)−C(25)	109.6(7)
C(20)−C(21)−C(22)	104.9(8)	C(20)−C(21)−C(45)	115.6(9)
C(22)−C(21)−C(45)	115.6(7)	C(21)−C(22)−C(23)	113.4(9)
C(22)−C(23)−C(24)	111.7(7)	C(23)−C(24)−C(25)	109.0(9)
C(23)−C(24)−C(44)	113.0(10)	C(25)−C(24)−C(44)	112.9(7)
C(20)−C(25)−C(24)	110.6(9)	C(21)−C(45)−C(46)	109.9(8)
C(21)−C(45)−C(47)	112.8(9)	C(46)−C(45)−C(47)	107.9(8)

also visible in the CD spectrum of the metal complex **2b**, although it has the opposite sign and is less intense.

Inspection of the CD spectra of Rh($C_5Ph_4R^*$)(COD) complex (**2a**, R* = menthyl; **2b**, R* = neomenthyl) shows that they exhibit pseudoenantiomorphic CD spectra (Figure 7). A simplistic explanation for this is that it reflects the fact that **2a** contains a menthyl substituent, whereas **2b** contains a neomenthyl substituent. Given, however, that it has been demonstrated above that the intense CD maxima of Rh($C_5Ph_4R^*$)(COD) (**2a**, R* = menthyl; **2b**, R* = neomenthyl) are associated with the four phenyl substituents, this is obviously not the total explanation. Clearly the two arrangements of the phenyl groups, i.e. the asymmetric cup of the menthyl complex and the propeller arrangement of the neomenthyl complex, are not mirror images. The arrangement adopted is, however, determined by the nature of the chiral fifth substituent in the cyclopentadienyl ring, and therefore in this sense the arrangements do reflect the chirality of this substituent. The enantiomorphic CD spectra of **2a** and **2b** suggests that the different chiral orientations of these four phenyl substituents are maintained in solution and that these different chiral orientations convey the epimeric relationship between the menthyl and neomenthyl substituents. In terms of developing chiral cyclopentadienyl ligands which are effective in enanantioselective synthesis, this is a promising result, suggesting that the influence of the chiral substituent is transmitted *via* the phenyl groups to the whole region around the cyclopentadienyl group.

Experimental Section

All reactions of moisture-sensitive reagents were performed under nitrogen. THF was heated under reflux over sodium benzophenone ketyl and distilled under nitrogen. Xylene and diethyl ether were heated under reflux over sodium and distilled under nitrogen, whereas methanol was used without purification. 1,2,3,4-Tetraphenylcyclopenta-1,3-diene,[15] [Rh(COD)Cl]$_2$,[27] and [Rh(C_5H_4neomen)I$_2$]$_2$[7a] were all prepared by literature procedures.

NMR spectra were recorded on a Bruker AM250 spectrometer. Low-resolution mass spectra were obtained on a Kratos MS80 fitted with a FAB source operating through a DS55 data

(27) Giordano, G.; Crabtree, R. H. *Inorg. Synth.* **1990**, *28*, 88.

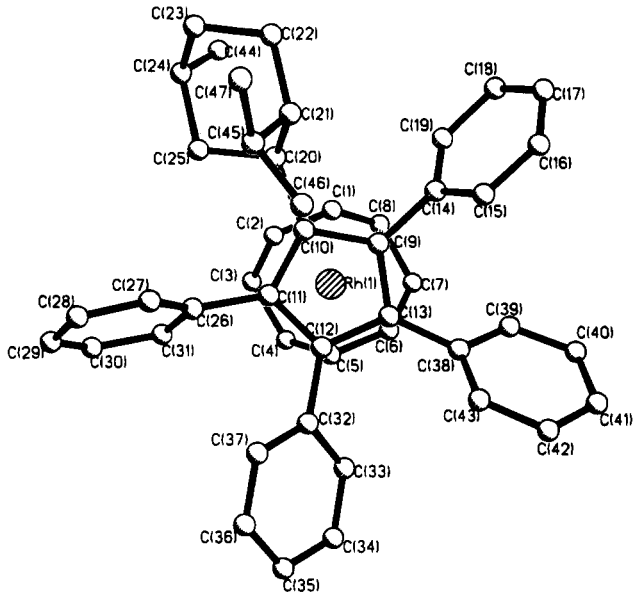

Figure 4. Structure of Rh(C_5Ph_4neomen)(COD) (**2b**).

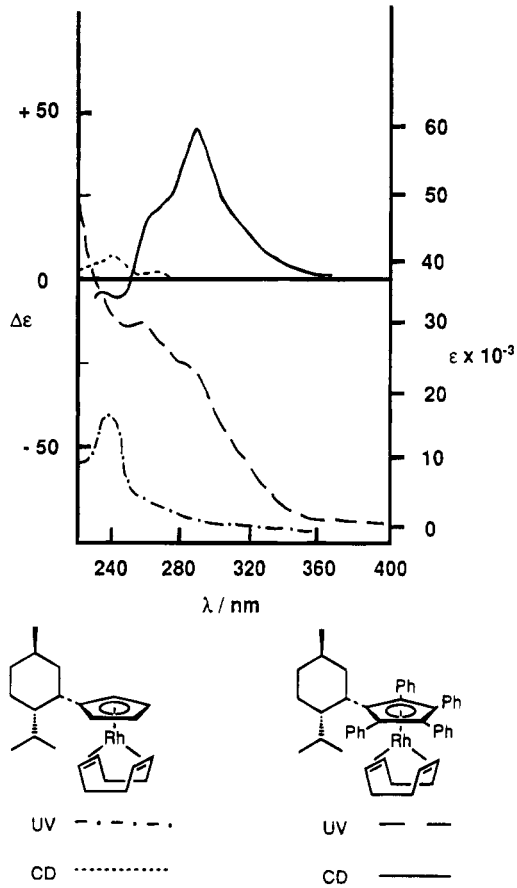

Figure 5. Rh(C_5Ph_4neomen)(COD) (**2b**): (—) CD spectrum; (— —) UV spectrum. Rh(C_5H_4neomen)(COD): (- - -) CD spectrum; (— • —) UV spectrum.

system; EI denotes electron impact, CI, chemical ionization; and +FAB (argon), positive fast atom bombardment with argon. IR spectra were recorded on a Perkin-Elmer 1710 IRFT spectrometer and UV spectra on a Perkin-Elmer 559 UV/vis spectrophotometer. Optical rotations were measured on a Perkin-Elmer 141 polarimeter, and CD spectra were obtained by the National CD Service, SERC, Birkbeck College, University of London. Elemental analyses were performed by the University of Sheffield Microanalysis Service.

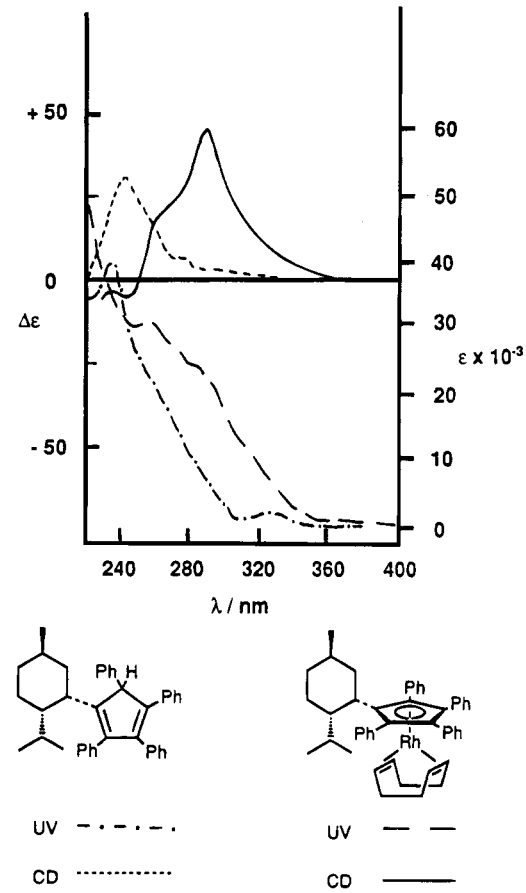

Figure 6. Rh(C_5Ph_4neomen)(COD) (**2b**): (—) CD spectrum; (— —) UV spectrum. C_5Ph_4H(neomen): (- - -) CD spectrum; (— • —) UV spectrum.

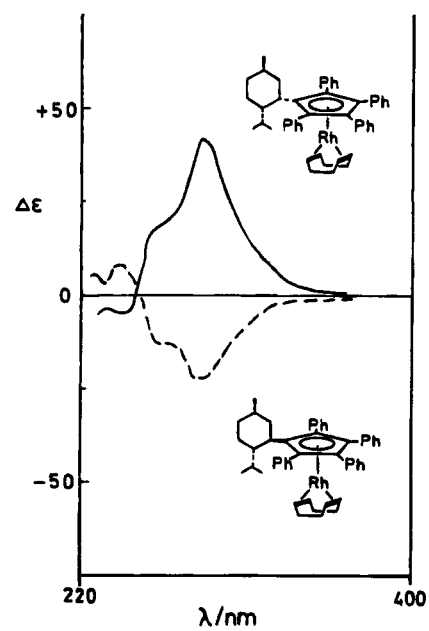

Figure 7. CD spectra of Rh(C_5Ph_4men)(COD) (**2a**) (—) and Rh(C_5Ph_4neomen)(COD) (**2b**) (- - -).

(−)-Menthyl Tosylate [(1*R*,2*S*,5*R*)-(−)-2-Isopropyl-5-methylcyclohexyl *p*-Toluenesulfonate]. This was prepared by the literature method.[16] Anal. Calcd for $C_{17}H_{26}O_3S$: C, 65.8; H, 8.4; S, 10.3. Found: C, 65.6; H, 8.3; S, 10.5. $[\alpha]_D$ (20 °C, l = 1.0, *c* = 2.45, EtOH): −66.71°. ^{1}H NMR ($CDCl_3$): δ 0.57 (d, J_{HH} 7 Hz, 3 H, CH_3), 0.78 (d, J_{HH} 7 Hz, 3 H, CH_3), 0.82 (d, J_{HH} 7 Hz, 3 H, CH_3), 0.65−2.17 (m, 9 H, CH_2, CH menthyl), 2.38 (s, 3 H, CH_3Ar), 4.37 (m, 1 H, CHOTs), 7.33

and 7.81 (m, 4 H, CH aromatic). ^{13}C NMR ($CDCl_3$): δ 15.0, 20.5, and 21.1 (CH_3), 22.7, 33.4, and 41.6 (CH_2), 21.5, 25.1, 31.2, and 47.3 (CH menthyl), 83.1 (CH_3Ar), 127.2 and 129.3 (CHAr), 134.6 and 144.0 (CAr).

(+)-Neomenthyl Tosylate [(1*S*,2*S*,5*R*)-(+)-2-Isopropyl-5-methylcyclohexyl *p*-Toluenesulfonate]. This was prepared by the following modification of the literature procedure.[17] Powdered toluenesulfonyl chloride (32.5 g, 0.17 mol) was added over 5 min to a solution of (+)-neomenthol (25.0 g, 0.16 mol) in pyridine (35 cm^3) in an ice–water bath and the mixture stored at 10 °C for 14 days but shaken daily. The mixture was then shaken with ice water (500 cm^3) and left to stand at 10 °C for a further 7 days; during this time large crystals formed. The crystals were filtered off and recrystallized from light petroleum ether to give (+)-neomenthyl tosylate (24 g, 52%). Anal. Calcd for $C_{17}H_{26}O_3S$: C, 65.8; H, 8.4; S, 10.3. Found: C, 65.7; H, 8.6; S, 10.4. $[\alpha]_D$ (20 °C, l = 1.0, c = 2.57, $CHCl_3$) +20.6°. ^1H NMR ($CDCl_3$): δ 0.68 (d, J_{HH} 7 Hz, 3 H, CH_3), 0.74 (d, J_{HH} 7 Hz, 3 H, CH_3); 0.77 (d, J_{HH} 7 Hz, 3 H, CH_3), 0.70–2.04 (m, 9 H, CH_2, CH neomenthyl), 2.38 (s, 3 H, CH_3Ar), 4.98 (s (br), 1 H, CHOTs), 7.32 and 7.81 (m, 4 H, CH aromatic).

(+)-1-Neomenthyl-2,3,4,5-tetraphenylcyclopenta-2,4-diene (1b). A solution of *n*-butyllithium (2.5 M in hexanes) (64 mmol) was added under nitrogen to a solution of 1,2,3,4-tetraphenylcyclopenta-1,3-diene (21.6 g, 60 mmol) in dry THF (240 cm^3) over 30 min at room temperature. This solution of lithium 1,2,3,4-tetraphenylcyclopentadienide was transferred to a pressure-equalized dropping funnel under nitrogen and then added drop-wise to a solution of (−)-menthyl tosylate (19.2 g, 60 mmol) in dry THF (100 cm^3). The mixture was heated under reflux under nitrogen for 17 h and then cooled to room temperature. After THF was removed *in vacuo*, the solid was extracted into petroleum ether (bp 60–80 °C) at room temperature. The petroleum ether was removed *in vacuo* to give a red oil, and chromatography (silica, petroleum ether bp 60–80 °C) yielded a white powder (4.5 g, 16%), mp 50–56 °C. Anal. Calcd for $C_{39}H_{40}$: C, 92.1; H, 7.9. Found: C, 91.6; H, 8.3. $[\alpha]$ (20 °C, l = 1.0, c = 1.055, $CHCl_3$): (589 nm) +239.8°, (578 nm) +256.9°, (546 nm) +295.7°, (436 nm) +601.9°; $C_{39}H_{40}$, m/e 508 (M^+). MS (EI): m/e 508 [$(M)^+$, 100%], 370 [$(M - C_{10}H_{19})^+$, 87%]. ^1H NMR ($CDCl_3$): δ 0.33–2.38 (m, 18 H, menthyl), 3.27–3.38 (m, 1 H, menthyl), 4.84 (s, 1 H, cyclopentadiene), 6.58–7.51 (m, 20 H, aromatic). ^{13}C NMR ($CDCl_3$): δ 21.0, 22.8, 27.0, 30.2, 37.0, 48.7, and 62.4 (CH/CH_3 nonaromatic), 26.3, 35.3, and 42.3 (CH_2), 125.9–130.2 (CH aromatic), 135.7, 136.3, 136.9, 138.5, 140.7, 147.4, 148.2, and 151.1 (C aromatic and olefinic).

(−)-1-Menthyl-2,3,4,5-tetraphenylcyclopenta-2,4-diene (1a). This was prepared in 64% yield by a procedure similar to that used for the neomenthyl analogue, except that the product was extracted from the reaction mixture using diethyl ether. The product was isolated after chromatography as a clear oil which solidified upon drying under vacuum: mp 58–61 °C. Anal. Calcd for $C_{39}H_{40}$: C, 92.1; H, 7.9. Found: C, 92.1; H, 8.2. $[\alpha]$ (20 °C, l = 0.1, c = 1.025, $CHCl_3$): (589 nm) −137.6°, (578 nm) −147.3°, (546 nm) −167.8°, (436 nm) −319.0°, $C_{39}H_{40}$, m/e 508 (M^+). MS (EI): m/e 508 [$(M)^+$, 100%], 370 [$(M - C_{10}H_{19})^+$ 96%]. ^1H NMR ($CDCl_3$) δ 0.18–2.66 (m, 19 H, menthyl), 4.50–5.29 (m, 1 H, cyclopentadienyl), 6.7–7.9 (m, 20 H, aromatic). ^{13}C NMR ($CDCl_3$): δ 14.1–16.0, 20.9–22.8, 26.5–28.3, 32.6–33.2, 40.4–43.6, and 61.3–62.6 (CH/CH_3 menthyl), 24.1–24.5, 34.9–35.3, and 42.8–44.6 (CH_2 menthyl), 125.8–130.5 (CH aromatic), 135.5–139.1, 144.6–147.8, and 151.5–152.3 (C aromatic).

(−)-(η^4-Cycloocta-1,5-diene)[η^5-1-menthyl-2,3,4,5-tetraphenylcyclopentadienyl]rhodium (2a). 1-((−)-Menthyl)-2,3,4,5-tetraphenylcyclopenta-2,4-diene (210 mg, 0.4 mmol) was dissolved in dry xylene (18 cm^3) and heated to 125 °C under nitrogen. *n*-Butyllithium solution (2.5 M in hexanes, 0.84 mmol) was added dropwise and the mixture stirred at 120–135 °C for 2 h. Bis(μ-chloro)bis(cycloocta-1,5-diene)-dirhodium (500 mg, 2 mmol) was added against a stream of nitrogen, and after it was stirred for 1 h at 125 °C, the mixture was cooled to room temperature and filtered. Removal of the xylene *in vacuo* gave a yellow powder. Chromatography (alumina, petroleum ether bp 40–60 °C followed by ether) gave the product as a bright yellow powder (290 mg, 98%), mp >240 °C. Anal. Calcd for $C_{47}H_{51}Rh$: C, 78.5; H, 7.2. Found: C, 78.4; H, 7.5. $[\alpha]$ (20 °C, l = 0.1, c = 1.230, $CHCl_3$): (589 nm) −340.7°, (578 nm) −360.1°, (546 nm) −425.2°, (436 nm) −865.9°; $C_{47}H_{51}Rh$, m/e 718 (M^+). MS (FAB argon): m/e 718 [$(M)^+$, 100%], 608 [$(M - COD)^+$, 54%]. ^1H NMR ($CDCl_3$): δ 0.2–2.6 (m, 27 H, menthyl and COD), 3.73–3.95 (m, 4 H, olefinic COD), 6.75–7.44 (m, 20 H, CH aromatic). ^{13}C NMR ($CDCl_3$): δ 15.7, 21.4, and 22.7 (CH_3), 24.7, 34.9, and 48.8 (CH_2 menthyl), 31.4 and 33.0 (CH_2 COD), 27.6, 33.8, 39.2, and 44.5 (CH menthyl), 71.6 and 72.4, (J_{C-Rh} 14 Hz, CH COD), 102.8, 105.7, 106.0, 106.3, and 114.2, (J_{C-Rh} 13.4 Hz, C cyclopentadienyl), 125.7–127.3 and 132.0–133.0 (CH aromatic), 134.5–135.8 (C aromatic).

(+)-(η^4-Cycloocta-1,5-diene)[η^5-1-neomenthyl-2,3,4,5-tetraphenylcyclopentadienyl]rhodium (2b). This was prepared as a bright yellow powder in 88% yield by the procedure described above for the menthyl analogue but with 1-neomenthyl-2,3,4,5-tetraphenylcyclopenta-2,4-diene (800 mg, 1.6 mmol). Mp: 168–171 °C. Anal. Calcd for $C_{47}H_{51}Rh$: C, 78.5; H, 7.2. Found: C, 78.5; H, 7.1. $[\alpha]$ (20 °C, l = 0.1, c = 1.175, $CHCl_3$): (589 nm) +612.8°, (578 nm) +644.2°, (546 nm) +761.7°, and (436 nm) +1600.0°; $C_{47}H_{51}Rh$, m/e 718 (M^+). MS (FAB argon): m/e 719 [$(M)^+$, 100%], 608 [$(M - COD)^+$, 40%], 580 [$(M - C_{10}H_{19})^+$, 40%]. ^1H NMR ($CDCl_3$): δ 0.5–1.8 (m, 22 H, neomenthyl), 1.8–2.2 and 2.3–2.6 (m, 8 H, methylene COD), 2.93 (m, 1 H, methine neomenthyl), 3.7 (m, 4 H, olefinic COD), 6.9–7.3 (m, 20 H, aromatic). ^{13}C NMR ($CDCl_3$): δ 17.9, 21.6, 24.6, 24.7, 27.6, 34.2, and 42.4 (CH_3 and CH neomenthyl), 23.8, 26.8, and 32.8 (CH_2 neomenthyl), 31.7 and 33.1 (CH_2 COD), 72.4 and 73.2 (J_{Rh-C} 14 Hz, COD), 106.8, 106.9, 107.6, 109.0, and 109.1 (C cyclopentadienyl), 125–133 (CH aromatic), 133.9, 134.1, 136.5, and 136.7 (C aromatic).

(−)-Bis(μ-bromo)dibromobis(η^5-1-menthyl-2,3,4,5-tetraphenylcyclopentadienyl)dirhodium (3a). (−)-(η^4-Cycloocta-1,5-diene)[η^5-1-menthyl-2,3,4,5-tetraphenylcyclopentadienyl]rhodium (215 mg, 0.3 mmol) was dissolved in ether (15 cm^3), and a solution of bromine in ether (0.035 M, 10 cm^3, 0.35 mmol) was added dropwise to give the product as a deep red precipitate. The product was filtered off, and the filtrate was evaporated to dryness *in vacuo* and redissolved in the minimum amount of dichloromethane; addition of pentane gave additional product (total yield 190 mg, 82%). Anal. Calcd for $C_{78}H_{78}Br_4Rh_2$: C, 60.8; H, 5.1; Br, 20.7. Found: C, 60.2; H, 5.1; Br, 20.0. $[\alpha]$ (20 °C, l = 0.1, c = 0.0948, $CHCl_3$): (589 nm) −316.5°, (578 nm) −295.4°, (546 nm) −200.4°, (436 nm) −1054.9°. ^1H NMR ($CDCl_3$): δ −0.07 (6 H, d, J_{HH} 7 Hz, CH_3), 0.76 (12 H, d, J_{HH} 7 Hz, CH_3), 0.32–1.56 (16 H, m, CH_2 and CH menthyl), 2.41–2.53 (2 H, m), 2.65–2.75 (1 H, m), 6.91–7.13 and 7.22–7.51 (40 H, m, aromatic). ^{13}C NMR ($CDCl_3$): δ 15.4, 21.4, and 22.1 (CH_3), 24.3, 34.3, and 41.8 (CH_2), 29.2, 32.9, 38.6, and 43.9 (CH), 101.3, 102.0, and 106.4 (C cyclopentadienyl), 126.9–127.3 (C aromatic), 127.7–132.6 (CH aromatic).

(+)-Bis(μ-bromo)dibromobis[η^5-1-neomenthyl-2,3,4,5-tetraphenylcyclopentadienyl]dirhodium (3b). This was prepared from (η^4-cycloocta-1,5-diene)[η^5-1-((+)-neomenthyl)-2,3,4,5-tetraphenylcyclo-pentadienyl]rhodium (100 mg, 0.14 mmol) as a red powder in 75% yield using the procedure described above for the menthyl analogue. Mp: 230–234 °C. Anal. Calcd for $C_{78}H_{78}Br_4Rh_2$: C, 60.8; H, 5.1; Br, 20.7. Found: C, 59.4; H, 5.5; Br, 20.1. $[\alpha]$ (20 °C, l = 0.1, c = 0.118, $CHCl_3$): (589 nm) +99.3°, (578 nm) +36.1°, (546 nm) −54.2°, (436 nm) +2400.7°. MS (+FAB argon): m/e 1461 [$(M - Br)^+$, 57%], 1383 [$(M - 2Br)^+$, 8%], 691 [$(CpRhBr)^+$, 16%], and 609

Table 4. Crystallographic Data for Diffraction Studies of Rh($C_5Ph_4R^*$)(COD) (2a, R* = Menthyl; 2b, R* = Neomenthyl)

	2a	2b
	(A) Crystal Parameters	
empirical formula	$C_{47}H_{51}Rh$	$C_{47}H_{51}Rh{\cdot}0.5C_4H_{10}O$
mol wt	718.8	755.89
color	yellow	yellow
solvent	dichloromethane/pentane	dichloromethane/pentane/diethyl ether
cryst size, mm	0.25 × 0.25 × 0.06	0.3 × 0.3 × 0.5
habit	diamond plates	plates
cryst syst	orthorhombic	hexagonal
space group	$P2_12_12_1$ (D_2^4, No. 19)	$P6_2$ (C_6^4, No. 171)
a, Å	12.762(35)	27.034(78)
b, Å	17.953(39)	
c, Å	31.91(14)	9.540(19)
V, Å^3	7311(42)	6041(27)
Z	8	6
D(calcd), g cm^{-3}	1.306	1.246
μ, cm^{-1}	4.89	4.48
F(000)	3023.66	2393.73
	(B) Intensity Data	
diffractometer	Nicolet R3 4-circle	Nicolet R3 4-circle
λ(Mo K$_\alpha$ radiation), Å	0.710 69	0.710 69
monochromator	graphite, incident beam	graphite, incident beam
rflns measured	$+h,+k,+l$	$+h,+k,+l$
2θ range, deg	3.5−50	3.5−48
temp, °C	20	20
scan type	ω	ω
scan range, deg	2.0	2.0
bkgd measurement	50% of scan time	50% of scan time
std rflns	1 check every 200 rflns, no decay cor necessary	1 check every 200 rflns, no decay cor necessary
no. of rflns collected	7069	4071
no. of rflns used	1267	2310
acceptance criterion	$\|F\|/\sigma(\|F\|) > 4.0$	$\|F\|/\sigma(\|F\|) > 3.0$
min transmissn coeff	0.699	0.867
max transmissn coeff	0.792	0.942
abs method	empirical, ψ scans (5 rflns, 180 measurements)	empirical, ψ scans (10 rflns, 360 measurements)
	(C) Structure Solution	
method	Patterson/Fourier	Patterson/Fourier
progams	SHELXTL[a]	SHELXTL[a]
computer	Data General Nova 3	Data General Nova 3
scattering factors	ref 28	ref 28
R	0.1349	0.0671
R_w		0.0491
weighting scheme	unit weights	$w = [\sigma^2(F) + 0.0002F^2]^{-1}$
H refinement	riding mode	riding mode

[a] Sheldrick, G. M. SHELXTL: An integrated System for Solving, Refining and Displaying Crystal Structures and Diffraction Data; University of Gottingen, Gottingen, Germany, 1978; revision 4.1, Aug 1983.

[(CpRh)$^+$, 100%]. ^{1}H NMR ($CDCl_3$): δ 0.7−2.3 (m, 36 H, menthyl), 3.3−3.5 (m, 2 H, menthyl), 7.0−8.9 (m, 40 H, aromatic).

Bis(μ-carbonyl)bis[η^5-1-((+)-neomenthyl)-2,3,4,5-tetraphenylcyclopentadienyl]dirhodium. Bis(μ-chloro)bis(η^4-cycloocta-1,5-diene)dirhodium (200 mg, 0.4 mmol), anhydrous sodium carbonate (200 mg, 2 mmol), and 1-neomenthyl-2,3,4,5-tetraphenylcyclopenta-2,4-diene (410 mg, 0.8 mmol) were heated under reflux together in methanol (20 cm^3) for 66 h under nitrogen. Extensive decomposition in the mixture was apparent. After the mixture was cooled, a black solid was filtered off and then extracted into THF to give a pale blue solution. The solvent was removed *in vacuo*, and chromatography (alumina, petroleum ether bp 60−80 °C followed by ether) gave a blue glassy solid (20 mg, 4%). Ms (FAB): *m/e* 638 [(M/2)$^+$, 12%], 608 [(M/2 − CO)$^+$, 100%]. IR (KBr, cm^{-1}): ν_{CO} 1765. ^{13}C NMR ($CDCl_3$): δ 14.1, 21.0, 22.7, 23.1, 27.0, 30.2, 30.4, 37.0, 48.7, and 62.4 (CH/CH_3), 26.3, 29.7, 35.3, and 42.3 (CH_2), 125.5−131.2 and 135.8−151.1 (CH aromatic). The carbonyl and cyclopentadienyl nuclei were not visible.

(+)-(η^4-Cycloocta-1,5-diene)(η^5-neomenthylcyclopentadienyl)rhodium. A mixture of [Rh(C_5H_4neomen)I_2]$_2$ (0.08 g, 0.071 mmol), cycloocta-1,5-diene (0.5 cm^3, 4.15 mmol), and sodium carbonate (0.20 g, 1.89 mmol) in ethanol (95%) was heated under reflux for 1 h. After the mixture was cooled to room temperature, solvent was removed *in vacuo* and the residue chromatographed (alumina, hexane) to yield a yellow oil which solidified on standing (50 mg, 85%). Anal. Calcd for $C_{23}H_{35}Rh$: C, 66.7; H, 8.5. Found: C, 66.6; H, 8.5. ^{1}H NMR ($CDCl_3$): δ 0.71 (3 H, d, J_{HH} 7 Hz, CH_3), 0.86 (3 H, d, J_{HH} 7 Hz, CH_3), 0.90 (3 H, d, J_{HH} 7 Hz, CH_3), 1.04−1.87 (8 H, m, CH_2 and CH neomenthyl), 1.89 (4 H, m, COD CH_2), 2.20 (4 H, m, COD CH_2), 2.37 (1 H, m, neomenthyl), 2.83 (1 H, m, neomenthyl), 3.88 (4 H, m, COD CH), 4.10 (1 H, m), 4.98 (2 H, m), 5.22 (1 H, m) [Cp].

Crystal Structure Determinations. Experimental details of X-ray data collection and solution and refinement of the structures are summarized in Table 4. Unfortunately, despite several attempts at growing crystals, only poor-quality crystals were obtained for the menthyl derivative **2a** and this limited the accuracy of this structure. The data for **2a** were corrected for Lorentz and polarization effects and for absorption by analysis of azimuthal scans. The positions of the rhodium atoms were determined by standard Patterson techniques and were found to be consistent with space group *Pbca* (of which $P2_12_12_1$ is a subgroup). Initially, structure solution was continued in this higher symmetry space group, since the positions of the phenyl groups, and of the cycloocta-1,5-diene seemed also to be essentially consistent with it. At this stage,

(28) *International Tables for X-ray Crystallography*; Kynoch Press: Birmingham, U.K., 1974; Vol. 4.

the atoms of the chiral menthyl group were ill-defined, but an acceptable model was derived which accounted well for the electron density and showed disorder of the two optical isomers in different rotational conformations about the bond linking the group to the cyclopentadienyl ring. The geometries of the menthyl groups were idealized with only the isopropyl substituent given some rotational freedom. The space group symmetry was lowered to the non-centrosymmetric $P2_12_12_1$, and two independent (COD)Rh(men-cp) fragments, each containing a menthyl of the correct chirality, were inserted. The omitted phenyl rings were redetermined from difference electron density syntheses: their positions were little changed. The overall structure still possessed approximate *Pbca* symmetry with the two crystallographically independent molecules approximately centrosymmetrically related, and correlation coefficients were very high. Sensible and controlled refinement could only be achieved after all phenyl groups had been given constrained D_{6h} symmetry and the geometries of the cyclopentadienyl ring and the cycloocta-1,5-diene ligands had also been restricted in terms of both bond lengths and angles. Refinement then proceeded by blocked-cascade least-squares methods. Hydrogen atoms were placed in predicted positions and refined in the riding mode, with isotropic thermal parameters related to those of the supporting carbon atoms. Refinement converged at a final $R = 0.1349$ with allowance for coupled anisotropic thermal motion of rhodium atoms only and related isotropic thermal parameters for each pseudo-centrosymmetrically related pair of ligands.

The crystal of **2b** contained a disordered half-molecule of solvent, Et_2O; the most successful model has this solvent disordered over three sets of positions.

Acknowledgment. We thank the SERC for a postgraduate studentship (to J.A.R.) and for the purchase of the diffractometer. Financial support from ICI Specialties is gratefully acknowledged, and we are indebted to Dr. Alex F. Drake and colleagues at the SERC Chiroptical Spectroscopy service for recording the CD spectra.

Supplementary Material Available: Tables of complete bond lengths and angles, thermal parameters, and hydrogen atom positional parameters for **2a** and **2b** and a table of least-squares planes and interplanar angles for **2b** (13 pages). Ordering information is given on any current masthead page.

OM9406207

Notes

Preparation and Structures of Arylmolybdenum(6+) Nitrido Compounds: $(2,4,6\text{-}Me_3C_6H_2)_3Mo{\equiv}N$ and $(2\text{-}Me_2NCH_2C_6H_4)_2(^tBuO)Mo{\equiv}N$

Kenneth G. Caulton,* Malcolm H. Chisholm,* Simon Doherty, and Kirsten Folting

Department of Chemistry and Molecular Structure Center, Indiana University, Bloomington, Indiana 47405

Received September 20, 1994[⊗]

*Summary: $(^tBuO)_3Mo{\equiv}N$, **1**, and the mesityl Grignard, MesMgBr, react in diethyl ether to give green solutions from which amber crystals of $(Mes)_3Mo{\equiv}N$, **2**, were obtained by crystallization from pentane/ether. In a related reaction **1** and $LiC_6H_4CH_2NMe_2$ (2 equiv) were found to yield $(^tBuO)(C_6H_4CH_2NMe_2)_2Mo{\equiv}N$, **3**, which was also isolated as dark amber crystals from ether/pentane. Compounds **2** and **3** have been crystallographically characterized. In **2** there is a central pyramidal $C_3Mo{\equiv}N$ moiety with Mo–N = 1.649(4) Å, Mo–C = 2.125(5) Å (av), and N–M–C = 100°. In **3** the coordination at molybdenum is that of a distorted octahedron with Mo≡N = 1.620(22) Å. The chelate $C_6H_4CH_2NMe_2$ ligand forms five-membered rings and the N–Mo distance trans to the Mo≡N bond is longer, cf. 2.742(2) Å vs 2.434(2) Å. These are the first crystallographically characterized metal nitrides supported by hydrocarbyl ligands for a group 6 element and contrast with the recently reported $(^tBuCH_2)_3Mo{\equiv}N$ that was proposed to be polymeric [Herrmann; et al. J. Am. Chem. Soc. **1994**, 116, 4989].*

Introduction

The recent communication by Herrmann and coworkers[1] on the preparation and reactivity of $(^tBuCH_2)_3Mo{\equiv}N$ prompts us to report on our synthesis of related hydrocarbyl-supported molybdenum(VI) nitrides together with their structural characterization and some initial comments on the reactivity of the Mo–C bonds.[2]

Results and Discussion

Treatment of a ether solution of $Mo(N)(O^tBu)_3$, **1**, at −78 °C with 3 equiv MesMgBr (Mes = mesityl) followed by gradual warming to room temperature gave a deep green solution from which $(Mes)_3Mo{\equiv}N$, **2**, could be isolated after filtration and extraction into pentane. The absence of structural data for σ-carbon-supported metal nitrido complexes of group 6 prompted us to undertake a single-crystal X-ray analysis. X-ray quality crystals of **2** were obtained as deep amber prisms by cooling a pentane-layered ether solution at −20 °C overnight.

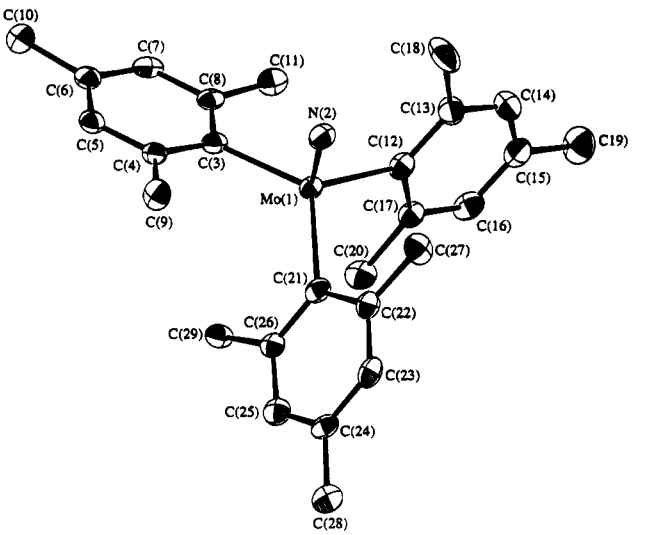

Figure 1. ORTEP diagram of $(Mes)_3Mo{\equiv}N$, **2**, illustrating the trigonal pyramidal environment of molybdenum. Selected bond distances (Å) and angles (deg): Mo(1)–N(2) = 1.649(4), Mo(1)–C(3) = 2.142(4), Mo(1)–C(12) = 2.100(5), Mo(1)–C(21) = 2.133(5); N(2)–Mo(1)–C(3) = 97.52(17), N(2)–Mo(1)–C(12) = 102.31, N(2)–Mo(1)–C(21) = 99.93-(18), C(3)–Mo(1)–C(12) = 118.88(17), C(3)–Mo(1)–C(21) = 122.24(17), C(12)–Mo(1)–C(21) = 110.26(17).

The ^1H NMR data of **2**, reveal three resonances assignable to the aromatic mesityl (δ = 6.63 ppm, 6H) and methyl (δ = 2.66 ppm, 18H; δ = 2.02 ppm, 9H) protons. We observed no significant line broadening in the low-temperature ^1H NMR spectrum of **2**, confirming that rotation about the Mo–C(sp^2) bonds is still rapid at these temperatures. We assign the Mo≡N stretch to an absorption band at 1041 cm^{-1} in the IR spectrum (KBr) which is some 40 cm^{-1} higher than that reported for $(^tBuCH_2)_3Mo{\equiv}N$, consistent with the absence of Mo≡N to Mo dative bonding in **2**.

Unlike $(^tBuCH_2)_3Mo{\equiv}N$, which is presumed to be polymeric in the solid state, compound **2** is monomeric and shows interesting stacking, as shown in Figures 1 and 2, respectively. In contrast to $(RO)_3Mo{\equiv}N$ compounds which are linear polymers with alternating short

[⊗] Abstract published in *Advance ACS Abstracts,* March 15, 1995.

(1) Herrmann, W. A.; Bogdanovic, S.; Poli, R.; Priermeier, T. *J. Am. Chem. Soc.* **1994**, *116*, 4989.

(2) For osmium nitride complexes see: (a) Marshman, R. W.; Shapley, P. A. *J. Am. Chem. Soc.* **1990**, *112*, 8369. (b) Shapley, P. A.; Kim, H. S.; Wilson, S. R. *Organometallics* **1988**, *7*, 928. (c) Marshman, R. W.; Shusta, J. M.; Wilson, S. R.; Shapley, P. A. *Organometallics* **1991**, *10*, 1671.

0276-7333/95/2314-2585$09.00/0

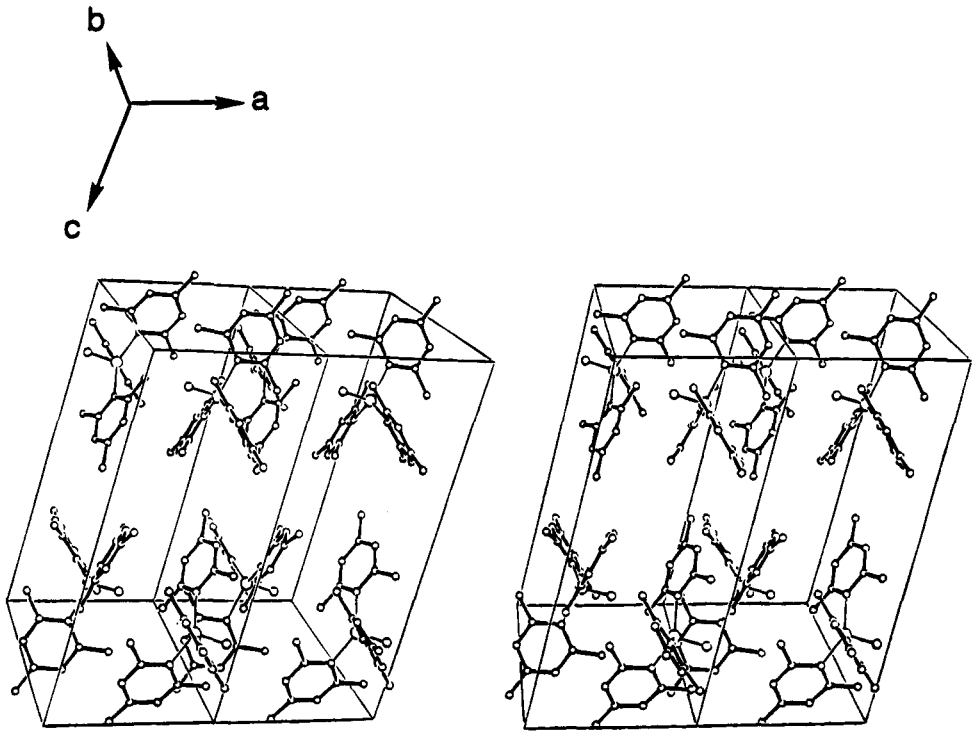

Figure 2. Stereoscopic view of the unit cell of $(Mes)_3Mo{\equiv}N$, **2**. Two cells along *a* show the intermolecular stacking between the mesityl rings.

and long Mo—N distances,[3] the shortest intermolecular Mo—N distance in **2** is 6.63 Å. The local trigonal C_3-Mo≡N geometry is as might have been expected with C—Mo—N angles close to 100°. The close intermolecular interactions of the "stacked" aromatic rings average 3.76 Å. Their nonparallel arrangement is reflected in an angle of 26° between the least squares planes defining their rings.

Treatment of a benzene solution of $Mo(N)(O^tBu)_3$ (**1**) with 2 mol equiv of $Li[C_6H_4CH_2NMe_2]$ resulted in smooth metathesis and replacement of two *tert*-butoxide ligands to afford $(^tBuO)(C_6H_4NMe_2)_2Mo{\equiv}N$ (**3**). The ^1H NMR spectrum of **3** consists of a single resonance corresponding to the ^tBuO ligand, an appropriate number of signals consistent with the presence of diasterotopic methylene protons, and broad resonances for the dimethylamino substituents. A single-crystal X-ray study of **3** was undertaken, revealing a pseudooctahedral geometry at molybdenum, as shown in Figure 3. A dimethylamino substituent occupies the site *trans* to the nitrido ligand [N(2)—Mo(1)—N(25) = 166.86(9)°]. The elongated metal nitrogen—amine bond [Mo(1)—N(25) = 2.742(2) Å] reflects the strong *trans* influence of the nitrido ligand[4] compared with the alkoxide [Mo(1)—N(15) = 2.434(2) Å]. Similar *trans* bond lengthening effects have been observed for high-valent imido- and oxo-containing group 6 complexes. The Mo—C(*ipso*) distances [Mo(1)—C(8) = 2.188(3) Å, Mo(1)—C(18) = 2.176(2) Å] are within the range expected for high-valent

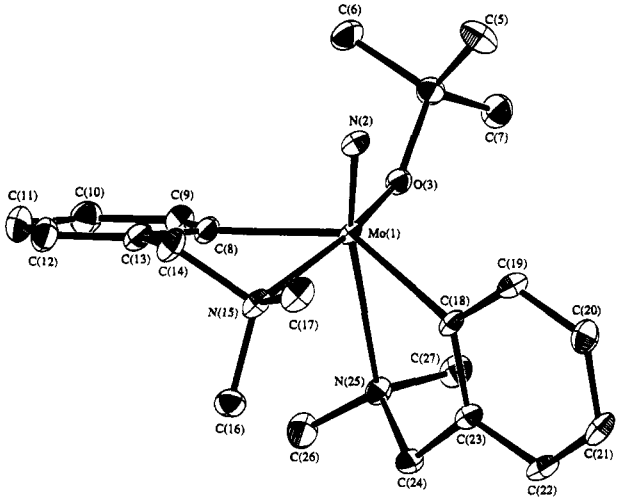

Figure 3. ORTEP diagram of $(^tBuO)(C_6H_4CH_2NMe_2)_2$-Mo≡N, **3**, illustrating the *trans* arrangement of the nitrido and elongated dimethylamino chelate substituent. Selected bond distances (Å) and angles (deg): Mo(1)—O(3) = 1.886(2), Mo(1)—N(2) = 1.663(2), Mo(1)—N(15) = 2.434(2), Mo(1)—N(25) = 2.742(2), Mo(1)—C(8) = 2.188(3), Mo(1)—C(18) = 2.176(2); O(3)—Mo(1)—N(2) = 104.00(9), O(3)—Mo(1)—N(15) = 167.04(8), O(3)—Mo(1)"bdN(25) = 77.64(7), O(3)—Mo(1)—C(8) = 95.94(9), O(3)—Mo(1)—C(18) = 109.63(9), N(2)—Mo(1)—N(15) = 82.55(9), N(2)—Mo(1)—N(25) = 166.86(9), N(2)—Mo(1)—C(8) = 102.93(10), N(2)—Mo(1)—C(18) = 97.32(10), N(15)—Mo(1)—N(25) = 98.58(7), N(15)—Mo(1)—C(8) = 71.51(9), N(15)—Mo(1)—C(18) = 80.13(8), N(25)—Mo(1)—C(8) = 89.77(8), N(25)—Mo(1)—C(18) = 142.30(10).

Mo—C(sp^2) bonds of chelate-supported aryl ligands.[5] The Mo≡N length [Mo(1)—N(2) = 1.663(2) Å] is similar to

(3) (a) Chisholm, M. H.; Huffman, J. C.; Hoffman, D. M. *Inorg. Chem.* **1983**, *22*, 2903. (b) Chan, D. M.-T.; Chisholm, M. H.; Folting, K.; Huffman, J. C.; Marchant, N. S. *Inorg. Chem.* **1986**, *25*, 4170.

(4) Nugent, W. A.; Mayer, J. M. *Metal Ligand Multiple Bonds: The Chemistry of Transition Metal Complexes Containing Oxo, Nitrido, Imido, Alkylidene, or Alkylidyne Ligands;* Wiley: New York, 1988; p 156. (b) Shustorovich, E. M.; Pora-Koshits, M. A.; Buslaev, Yu. A. *Coord. Chem. Rev.* **1975**, *17*, 1.

(5) (a) Sullivan, A. C.; Wilkinson, G.; Matevallil, M.; Hursthouse, M. B. *J. Chem. Soc., Dalton Trans.* **1988**, 53. (b) Lai, R.; Mabille, S.; Croux, A.; LeBot, S. *Polyhedron* **1991**, *10*, 463.

Table 1. Fractional Coordinates and Isotropic Thermal Parameters for Compound 2

atom	10^4x	10^4y	10^4z	$10B_{iso}$
Mo(1)	7530.6(4)	4553.3(2)	2414.1(2)	15
N(2)	5483(5)	4625(2)	2148(2)	21
C(3)	7592(5)	3583(3)	3235(2)	18
C(4)	7011(5)	3762(3)	3892(2)	18
C(5)	6970(6)	3124(3)	4409(3)	19
C(6)	7439(5)	2298(3)	4286(2)	21
C(7)	7976(6)	2131(3)	3635(3)	20
C(8)	8090(5)	2751(3)	3110(2)	17
C(9)	6329(7)	4621(3)	4026(3)	24
C(10)	7245(8)	1600(4)	4823(3)	28
C(11)	8646(7)	2484(3)	2408(3)	22
C(12)	8261(6)	4254(3)	1412(3)	19
C(13)	7254(6)	3986(3)	729(3)	22
C(14)	8010(7)	3806(3)	135(3)	27
C(15)	9722(6)	3871(3)	181(3)	24
C(16)	10695(6)	4121(3)	853(3)	23
C(17)	10019(5)	4319(3)	1467(2)	19
C(18)	5392(7)	3868(5)	623(3)	36
C(19)	10495(8)	3661(4)	−474(3)	35
C(20)	11167(6)	4598(4)	2179(3)	24
C(21)	8121(6)	5839(3)	2709(2)	18
C(22)	7309(5)	6513(3)	2269(2)	19
C(23)	7719(6)	7339(3)	2487(3)	21
C(24)	8884(5)	7539(3)	3122(3)	19
C(25)	9695(6)	6867(3)	3542(3)	22
C(26)	9341(5)	6028(3)	3349(2)	17
C(27)	5983(7)	6362(4)	1576(3)	25
C(28)	9260(7)	8443(3)	3354(3)	25
C(29)	10307(6)	5362(3)	3850(3)	21

Table 2. Fractional Coordinates and Isotropic Thermal Parameters for Compound 3

atom	10^4x	10^4y	10^4z	$10B_{iso}$
Mo(1)	7051.5(3)	2758.2(1)	2691.7(3)	9
N(2)	7934(3)	3502(1)	1863(3)	12
O(3)	8200(2)	1718(1)	2604(2)	12
C(4)	9469(3)	1432(2)	1943(3)	15
C(5)	10218(4)	668(2)	2937(4)	18
C(6)	8792(4)	1108(2)	155(4)	20
C(7)	10630(4)	2190(2)	2081(4)	21
C(8)	5051(3)	2307(2)	688(3)	12
C(9)	4757(3)	1414(2)	75(3)	14
C(10)	3468(3)	1170(2)	−1229(4)	18
C(11)	2458(3)	1809(2)	−1944(4)	20
C(12)	2722(3)	2695(2)	−1355(3)	18
C(13)	4014(3)	2937(2)	−63(3)	14
C(14)	4405(3)	3883(2)	613(3)	15
N(15)	5088(3)	3891(1)	2418(3)	13
C(16)	3817(3)	3722(2)	3182(4)	16
C(17)	5748(4)	4798(2)	2996(4)	17
C(18)	7675(3)	3385(2)	5162(3)	11
C(19)	8858(3)	4052(2)	5630(3)	14
C(20)	9416(3)	4402(2)	7235(3)	16
C(21)	8796(3)	4086(2)	8431(3)	16
C(22)	7636(3)	3430(2)	8017(3)	15
C(23)	7067(3)	3076(2)	6403(3)	12
C(24)	5826(3)	2356(2)	6023(3)	13
N(25)	6023(3)	1708(1)	4714(3)	12
C(26)	7297(4)	1123(2)	5425(4)	16
C(27)	4595(3)	1161(2)	4069(4)	18

that observed in **2** [1.648(4) Å] and other nitrido-containing complexes,[3,6] reflecting the retention of Mo—N triple bond character upon increasing the coordination from 4 to 6 in **2** and **3**, respectively.

Our preliminary studies of the reactivity of **2** reveal significant differences from that recently reported for the neopentyl complex $(CH_2{}^tBu)_3Mo{\equiv}N$, the chemistry of which is dominated by addition across the Mo≡N bond to yield imido (NH) complexes of increased coordination number and by α-C—H activation. These will be described in detail at a later time.

(6) (a) Kim, J. C.; Rees, W. S.; Geodken, V. L. *Inorg. Chem.* **1994**, *33*, 3191. (b) Herrmann, W. A.; Bogdanovic, S.; Behm, J.; Denk, M. *J. Organomet. Chem.* **1992**, *430*, C33. (c) Schmitte, V. J.; Friebel, C.; Weller, F.; Dehnicke, K. Z. *Anorg. Allg. Chem.* **1982**, *495*, 149. (d) Dehnicke, K.; Kruger, N.; Kujanek, R.; Weller, F. *Z. Kristallogr.* **1980**, *153*, 181.

Table 3. Selected Crystal Data for Compounds 2 and 3

	compd **2**	compd **3**
empirical formula	$C_{27}H_{33}MoN$	$C_{22}H_{33}N_3MpC$
color of cryst	dark amber	pale yellow/ colorless
cryst dimens	0.10 × 0.25 × 0.35	0.08 × 0.16 × 0.30
space group	$P2_1/a$	$P\bar{1}$
cell dimens		
temp (°C)	−173	−168
a (Å)	8.184(2)	8.929(2)
b (Å)	15.814(3)	15.054(3)
c (Å)	18.318(4)	8.533(1)
α (deg)		94.11(1)
β (deg)	102.00(1)	105.21(1)
γ (deg)		90.43(1)
Z (molecules/cell)	4	4
vol (Å^3)	2319.06	1103.44
calc dens (g/cm^3)	1.339	1.359
wavelength (Å)	0.710 69	0.710 69
mol wt	467.50	451.46
linear abs coeff	5.631	5.944
detector to sample dist (cm)	22.5	22.5
sample to source dist (cm)	23.5	23.5
av ω scan width at half-height (deg)	0.25	0.25
scan speed (deg/min)	8.0	8.0
scan width (deg + dispersion)	2.0	2.0
individual background (s)	4	4
aperture size (cm)	3.0 × 4.0	3.0 × 4.0
2θ range (deg)	6−45	6−55
total no. of reflns collcd	5625	7836
no. of unique intensities	3048	5092
no. with $F > 0.0$	2884	4887
no. with $F > 3^*\sigma(F)$	2652	4627
$R(F)$	0.0332	0.0341
$R_w(F)$	0.0349	0.0348
goodness of fit for the last cycle	1.092	1.010
max δ/σ for last cycle	0.02	0.03

Experimental Section

$(Mes)_3Mo{\equiv}N$, 2. To a diethyl solution of $Mo(N)(O^tBu)_3$ (2.75 g, 8.36 mmol) at −78 °C was added a solution of MesMgBr (25.0 mL, 25 mmol) dropwise over a period of 1 h. The reaction mixture was left to stir for 3 h, during which time a precipitate formed and a deep green coloration appeared. After warming to room temperature, filtration afforded a clear green solution. The solvent was removed *in vacuo* and the residue extracted with 6 × 50 mL of pentane to afford spectroscopically pure **2** in 45% (1.70 g) yield as a yellow brown solid. Crystallization from ether/pentane afforded deep amber prisms suitable for X-ray analysis. Selected data for **2** follow. Anal. Calcd for $C_{27}H_{33}NMo$: C, 69.35; H, 7.11; N, 3.00. Found: C, 67.94; H, 6.91; N, 3.02. ^1H NMR (300 MHz, C_6D_6, δ): 6.62 (br, s, 6H), 2.66 (s, 18H, *o*-Me), 2.02 (s, 9H, *p*-Me). $^{13}C\{^1H\}$ NMR (75 MHz, C_6H_6, δ): 192.94 (*ipso*), 141.51 (*para*), 128.60 (*ortho*), 127.0 (*meta*), 25.02 (CH_3), 21.35 (CH_3). IR (KBr, cm^{-1}): 3011 (m), 2950 (m), 2914 (m), 1591 (s), 1448 (br, s), 1398 (m), 1280 (s), 1041 (s), 846 (s), 702 (w), 584 (m).

$(2\text{-}Me_2NCH_2C_6H_4)_2(^tBuO)Mo{\equiv}N$, 3. To an ether solution of $Mo(N)(O^tBu)_3$ (0.250 g, 0.76 mmol) was added a suspension of $Li[C_6H_4CH_2NMe_2]$ (0.214 g, 1.52 mmol) with rapid stirring. The reaction mixture was stirred overnight and the solvent removed to leave a gummy yellow oil. Extraction with pentane afforded a clear yellow solution and a white precipitate was filtered out. Crystallization from pentane/ether afforded **3** as pale yellow crystals in 67% yield (0.21 g). Selected data for **3** follow. Anal. Calcd for $C_{22}H_{33}N_3MoO$: C, 58.33; H, 7.37; N,

9.31. Found: C, 58.46; H, 7.36; N, 9.47. ^{1}H NMR (300 MHz, C_6H_6, δ): 9.32 (d, 1H, $^2J_{HH}$ = 7.42 Hz, C_6H_4), 7.98 (dd, 1H, $^2J_{HH}$ = 5.8 Hz, 2.7 Hz, C_6H_4), 7.31 (t, 1H, $^2J_{HH}$ = 6.6 Hz, C_6H_4), 7.15–7.25 (m, 4H, C_6H_4), 6.98 (d, 1H, $^2J_{HH}$ = 8.4 Hz), 4.75 (d, 1H, $^2J_{HH}$ = 12.3 Hz, CH_2), 3.46 (d, 1H, $^2J_{HH}$ = 14.7 Hz, CH_2), 2.96 (d, 1H, $^2J_{HH}$ = 12.3 Hz, CH_2), 2.85 (d, 1H, $^2J_{HH}$ = 14.7 Hz, CH_2), 2.6 (br, 6H, NMe_2), 1.99 (s, 6H, NMe_2), 1.55 (s, 9H, $C(CH_3)_3$).

Crystallographic Studies. General operating procedures and a listing of programs have been previously given.[7] Atomic coordinates for compounds **2** and **3** are given in Tables 1 and 2, respectively, and a summary of the crystal data and procedures is given in Table 3.

(Mes)$_3$Mo≡N, 2. Dark amber prisms of **2** were grown by slow cooling of a ether/pentane solution at −20 °C overnight. Crystals of Mo(N)(Mes)$_3$ are monoclinic, space group $P2_1/a$ with unit cell constants a = 8.184(2) Å, b = 15.814(3) Å, c = 18.318(4) Å, β = 102.00(1)°, T = 173 °C, V = 2319.06 Å^3, d_{calcd} = 1.339 g/cm^3, and Z = 4. Data were collected by using the standard moving crystal–moving detector technique in the 2θ range 6.0–45.0°. A total of 3048 unique reflections were collected of which 2652 were observed ($F > 3\sigma(F)$). The structure was solved using a combination of direct methods and difference Fourier methods and refined by full matrix least-squares techniques. Refinement converged at $R(F)$ 0.033 and $R_w(F)$ = 0.035.

(2-Me$_2$NCH$_2$C$_6$H$_4$)$_2$(^{t}BuO)Mo≡N, 3. Pale yellow crystals of **3** were grown by the slow cooling of an ether/pentane solution at −20 °C overnight. Crystals of (^{t}BuO)C$_6$H$_4$CH$_2$NMe$_2$)$_2$Mo≡N are triclinic, space group $P\bar{1}$ with unit cell constants a = 8.929(2) Å, b = 15.054(3) Å, c = 8.533(1) Å, α = 94.11(1)°, β = 105.21(1)°, γ = 90.43(1)°, T = −168 °C, V = 1103.44 Å^3, d_{calcd} = 1.359 g cm^3, and Z = 2. Data were collected by using the standard moving crystal–moving detector technique in the 2θ range 6.0–55.0°. A total of 5092 unique reflections were collected of which 4627 were observed ($F > 3\sigma(F)$). The structure was solved by using a combination of direct methods (MULTAN-78) and difference Fourier techniques. The full matrix least-squares refinement was completed with anisotropic thermal parameters on all nonhydrogen atoms. Refinement converged at $R(F)$ = 0.0341 and $R_w(F)$ = 0.0348. The final difference map was essentially featureless, the largest peak was 0.61 e Å^{-3} in the vicinity of the molybdenum atom. The deepest hole was −0.87 e Å^3.

Acknowledgment. We thank the National Science Foundation for financial support.

Supplementary Material Available: For compounds **2** and **3**, listing of atomic coordinates, thermal parameters, bond distances, and bond angles (11 pages).

OM940732Y

(7) Chisholm, M. H.; Folting, K.; Huffman, J. C.; Kirkpatrick, C. C. *Inorg. Chem.* **1984**, *23*, 1021.

Transmetalation Reactions of Sterically Encumbered Gallium and Indium Halides with Tetrahydrometalates. Synthesis and Structure of a Base-Free Monomeric Aluminum Hydride

Alan H. Cowley,* Harold S. Isom, and Andreas Decken

Department of Chemistry and Biochemistry, The University of Texas at Austin, Austin, Texas 78712

Received December 27, 1994[⊗]

*Summary: The reaction of $(Ar^*)_2GaCl$ or $(Ar^*)_2InCl$ (Ar^* = 2,4,6-t-$Bu_3C_6H_2$) with $LiAlH_4$ resulted in transmetalation and formation of $(Ar^*)_2AlH$ (**6**), the first example of a structurally authenticated monomeric base-free aluminum hydride. An X-ray crystallographic study revealed that the monomeric nature of the new hydride is due to the shielding of the Al–H moiety by o-t-Bu groups of the aryl ligands. Crystal data for **6**: space group $P2_1/c$, a = 10.024(2) Å, b = 29.745(4) Å, c = 11.459(1) Å, β = 94.87(1)°, V = 3404(2) Å^3, Z = 4. The X-ray crystal structure of $(Ar^*)_2InCl$ (**5**) has also been determined. Crystal data for **5**: space group $P2_1/c$, a = 10.328(2) Å, b = 22.924(2) Å, c = 16.091(1) Å, β = 107.34(1)°, V = 3636.6(8) Å^3, Z = 4.*

Introduction

In part, our interest in the organometallic chemistry of the heavier group 13 hydrides stems from the fact that AlH_n and GaH_n entities have been detected on surfaces during film growth from organoaluminum[1] and organogallium[2] precursors. In order to learn more about the fundamental chemistry of these surface-bound hydrides, it would be desirable to have in hand neutral monomeric species of the types RMH_2 and R_2MH (M = Al, Ga). A second motivation for preparing these classes of compounds is related to the possibility that they might serve as sources of the corresponding univalent organometallics *via* reductive elimination of hydrogen or alkane. Thirdly (and somewhat optimistically), we were interested in the possibility of preparing neutral organoindium hydrides.

For both the organoaluminum and organogallium hydrides there is a pronounced tendency toward oligomerization on account of the coordinative unsaturation at the metal center. Until recently, therefore, all structurally authenticated examples were dimeric or, in some cases, oligomeric.[3,4] Information concerning indium hydrides is particularly sparse.[5] With the exception of an unstable ether adduct of composition $[(InH_3)_x{\cdot}nEt_2O]$ all other indium hydrides are anionic.

In order to maximize the chance of obtaining monomeric hydride derivatives, we opted to employ the bulky aryl group 2,4,6-t-$Bu_3C_6H_2$ as the other group 13 substituent. Herein we report (i) the synthesis and first structural characterization of a base-free monomeric organoaluminum hydride and (ii) facile transmetalation reactions.

Results and Discussion

The deployment of sterically demanding ligands can have dramatic effects, not only on the stabilities of main-group species but also on their patterns of reactivity. In the context of group 13 hydrides, it was discovered recently[6] that Ar^*GaH_2 (1; Ar^* = 2,4,6-t-$Bu_3C_6H_2$), the

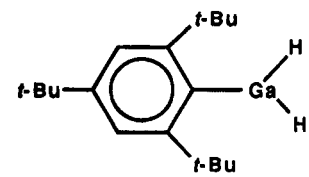

1

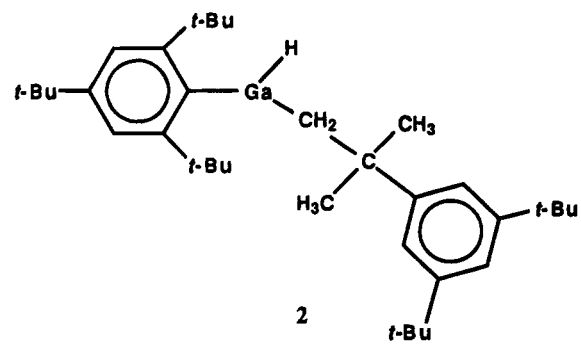

2

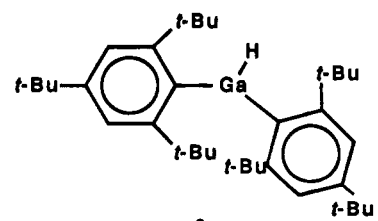

3

first monomeric organogallium hydride, could be isolated from the reaction of Ar^*GaCl_2 with $LiGaH_4$. Interestingly, the product of the reaction of the corre-

[⊗] Abstract published in *Advance ACS Abstracts,* April 1, 1995.

(1) Bent, B. E.; Nuzzo, R. G.; Dubois, L. H. *J. Am. Chem. Soc.* **1989**, *111*, 1634.

(2) Zanella, P.; Rossetto, G.; Brianses, N.; Ossola, F.; Porchia, M.; Williams, J. O. *Chem. Mater.* **1991**, *3*, 275. Butz, K. W.; Elms, F. M.; Raston, C. L.; Lamb, R. N.; Pigram, P. J. *Inorg. Chem.* **1993**, *32*, 3985.

(3) *Chemistry of Aluminum, Gallium and Indium*; Downs, A. J., Ed.; Blackie-Chapman Hall: London, 1993. Downs, A. J.; Pulham, C. R. *Chem. Soc. Rev.* **1994**, *23*, 175.

(4) *Gmelin Handbook of Inorganic and Organometallic Chemistry: Organogallium Compounds*; Springer-Verlag: Berlin, 1987; Part 1.

(5) *Gmelin Handbook of Inorganic and Organometallic Chemistry: Organoindium Compounds*; Springer-Verlag: Berlin, 1991; Part 1.

(6) Cowley, A. H.; Gabbaï, F. P.; Isom, H. S.; Carrano, C. J.; Bond, M. R. *Angew. Chem., Int. Ed. Engl.* **1994**, *33*, 1253.

0276-7333/95/2314-2589$09.00/0

Scheme 1

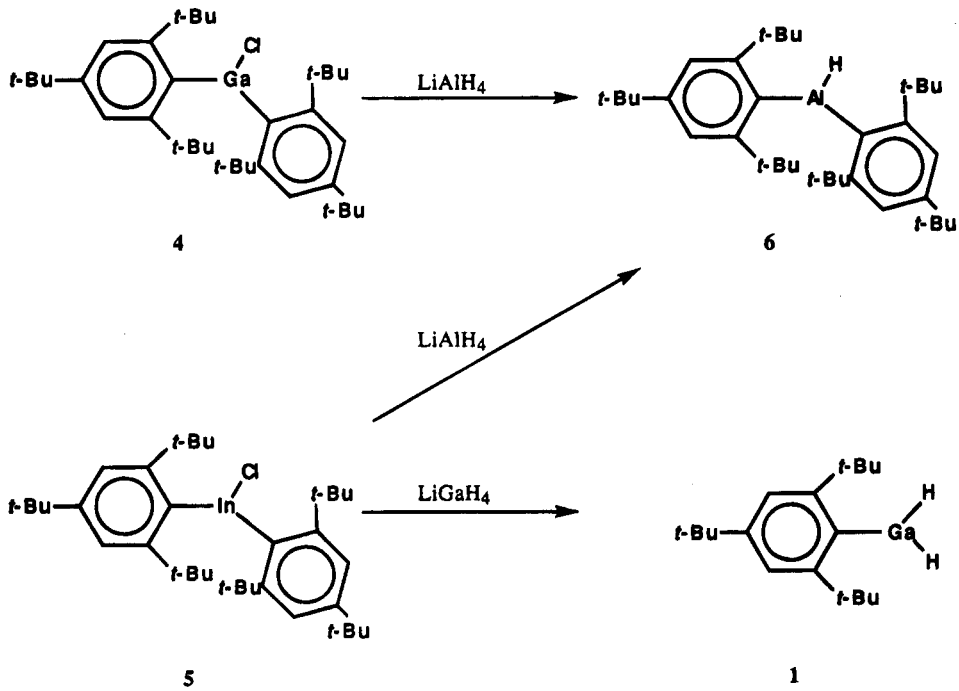

sponding monochloride $(Ar^*)_2GaCl$ with $LiGaH_4$ was the "aryl-rotated" product **2** rather than the anticipated monohydride $(Ar^*)_2GaH$ (**3**).[6] Compound **3** has been prepared subsequently by Power *et al.*[7] via the reaction of $(Ar^*)_2GaCl$ with *t*-BuLi.

As indicated in Scheme 1, treatment of $(Ar^*)_2GaCl$ (**4**)[8] with $LiAlH_4$ in Et_2O solution afforded an 80% yield of $(Ar^*)_2AlH$ (**6**) via a transmetalation reaction. The IR spectrum of **6** features a single, sharp absorption at 1869 cm^{-1}, which is close to the terminal Al–H stretching frequency reported[9] for the matrix-isolated monomer $(TMP)_2AlH$ (TMP = 2,2,6,6-tetramethylpiperidinyl). Further support for the monomeric nature of **6** stems from the CI mass spectrum, which exhibits a sharp cutoff at *m/z* 517 ($M^+ - H$), and from the detection of a proton resonance at δ 5.72, which corresponds to an Al–H moiety. It was, however, necessary to appeal to X-ray crystallography in order to establish the degree of oligomerization definitively. The crystalline state of **6** consists of individual monomers, and there are no conspicuously short intermolecular contacts. The structure is illustrated in Figure 1 along with the atom-numbering scheme, and selected bond distances and angles appear in Table 1. The significance of **6** is that this compound represents the first example of a structure of a base-free aluminum hydride monomer. Heretofore all structurally authenticated aluminum hydrides featured bridging hydride entities. Examples include $[Ar^*(H)Al(\mu\text{-}H)]_2$[10] and species with two sterically demanding substituents, *viz.* $[(TMP)_2Al(\mu\text{-}H)]_2$[9] and $[(t\text{-}Bu)_2Al(\mu\text{-}H)]_3$.[11] An indication of the cause of the monomeric nature of **6** stems from the observation that the *o*-*t*-Bu groups partially shield the terminal Al–H bond, thus thwarting the formation of Al–H–Al bridges. Within experimental error the geometry at aluminum is trigonal planar (sum of bond angles 359.1(3)°). However, the C–Al–C angle is unusually wide (131.7(3)°), thus furnishing evidence for the existence of strain in this molecule. Power *et al.*[7] have reported a similarly wide angle (131.9(1)°) for the analogous monomeric gallane **3**. Steric strain is also evident in the conformation of **6**. Thus, there is an angle of 35.7° between the Al–C(21) and C(21)···C(24) vectors, while in the other ring, which is approximately at right angles, the corresponding tilt angle is close to zero (1.8°). The conformation of **3**[7] is virtually identical with that of **6**;

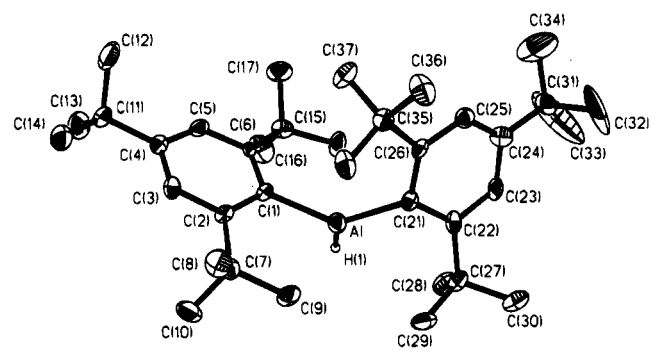

Figure 1. View of $(Ar^*)_2AlH$ (**6**) showing the atom-labeling scheme. Thermal ellipsoids are scaled to the 30% probability level. All hydrogens are omitted for clarity except the alane hydrogen.

Table 1. Selected Bond Distances (Å) and Bond Angles (deg) for $(Ar^*)_2InCl$ (5) and $(Ar^*)_2AlH$ (6) ($Ar^* = 2,4,6\text{-}t\text{-}Bu_3C_6H_2$)

	Compound **5**		
In–Cl	2.523(2)	Cl–In–C(1)	113.2(3)
In–C(1)	2.161(11)	Cl–In–C(19)	99.6(3)
In–C(19)	2.148(10)	C(1)–In–C(19)	144.2(5)
	Compound **6**		
Al–H(1)	1.53(4)	H(1)–Al–C(1)	114.3(14)
Al–C(1)	1.976(6)	H(1)–Al–C(21)	113.1(14)
Al–C(21)	2.007(6)	C(1)–Al–C(21)	131.7(3)

(7) Wehmschulte, R. J.; Ellison, J. J.; Ruhlandt-Senge, K.; Power, P. P. *Inorg. Chem.* **1994**, *33*, 6300.
(8) Meller, A.; Pusch, S.; Pohl, E.; Häming, L.; Herbst-Irmer, R. *Chem. Ber.* **1993**, *126*, 2255.
(9) Klein, C.; Nöth, H.; Tacke, M.; Thomann, M. *Angew. Chem., Int. Ed. Engl.* **1993**, *32*, 886.
(10) Wehmschulte, R. J.; Power, P. P. *Inorg. Chem.* **1994**, *33*, 5611.
(11) Uhl, W. *Z. Anorg. Allg. Chem.* **1989**, *570*, 37.

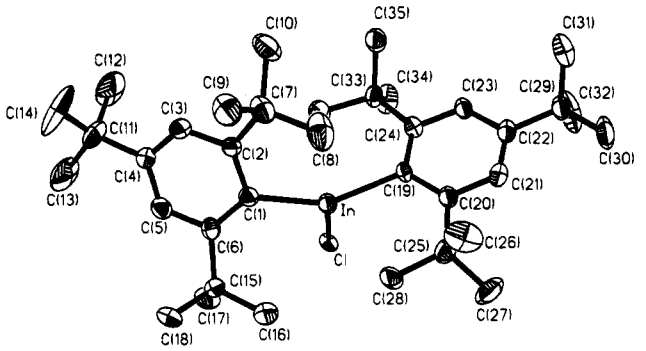

Figure 2. View of $(Ar^*)_2InCl$ (**5**) showing the atom-labeling scheme. Thermal ellipsoids are scaled to the 30% probability level. All hydrogens are omitted for clarity.

in this case the tilt angle of one of the rings is 33.6°. A further consequence of steric crowding is the presence of relatively short contacts between aluminum and some *o-tert*-butyl hydrogens, e.g. Al···H (9 B) = 2.33 Å and Al···H (9 C) = 2.24 Å. The Al–H bond distance of 1.53(4) Å is comparable to those in hydroaluminates such as $[HAl(NMe_2)_3]^-$ (1.52(2) Å)[12] but shorter than those in compounds with Al–H–Al bridge bonding such as $[Me_2Al(\mu\text{-}H)]_2$ (1.68(2) Å).[11] The Al–C bond distances, which average 1.991(6) Å, are similar to that in the recently reported dimer $[Ar^*(H)Al(\mu\text{-}H)]_2$ (1.966(3) Å)[10] and to those for the Ga–Ar* bonds[13] in **1** (1.942(7) Å)[6] and **2** (1.983(17) Å).[6]

Our reasons for investigating the reactivity of **5** toward tetrahydrometalates were twofold. The major motivation was to explore the possibility that the extensive steric blockade represented by two Ar* groups might permit isolation of the first example of a neutral indium hydride.[3,5] A second objective was to explore whether an "aryl-rotation" process would occur as observed in the formation of **2**. It was found that the reaction of **5** with $LiAlH_4$ proceeded in a fashion analogous to that for **4** (Scheme 1) and resulted in transmetalation and formation of the monomeric aluminum hydride **6**. Transmetalation was also observed in the reaction of **5** with $LiGaH_4$ (Scheme 1); however, in this case it was accompanied by cleavage of an aryl group and production of **1**. The fact that no aryl cleavage was observed in the formation of **6** is consistent with the order of bond enthalpies Al–C > Ga–C > In–C. Finally, we note that the aryl cleavage has been postulated[6] as a component of the mechanism of "aryl rotation".

Finally, we report the X-ray crystal structure of $(Ar^*)_2InCl$ (**5**). We have prepared this compound earlier.[6] However, at that time we were not able to isolate suitable crystals of this compound. In the interim, Oliver *et al.*[14] have reported the X-ray crystal structure of the corresponding bromide $(Ar^*)_2InBr$ (**7**). The solid state of **5** consists of isolated molecules, and there are no abnormally short intermolecular contacts. The molecular structure is illustrated in Figure 2, and a listing of bond distances and angles appears in Table 1. With the exception of the indium–halogen bond lengths, the metrical parameters for **5** and **7** are almost identical.

(12) Linti, G.; Nöth, H.; Rahm, P. *Z. Naturforsch., B* **1988**, *43*, 1101.
(13) Incomplete shielding by Ga(3d) electrons renders the covalent radii of Al and Ga virtually identical.
(14) Rahbarnoohi, H.; Heeg, M. J.; Oliver, J. P. *Organometallics* **1994**, *13*, 2123.

Table 2. Crystal Data, Details of Intensity Measurement, and Structure Refinement for $(Ar^*)_2InCl$ (5) and $(Ar^*)_2AlH$ (6) (Ar^* = 2,4,6-*t*-$Bu_3C_6H_2$)

	5	6
formula	$C_{36}H_{58}ClIn$	$C_{36}H_{59}Al$
fw	640.5	518.8
cryst dimens mm	0.17 × 0.21 × 0.42	0.34 × 0.44 × 0.44
cryst syst	monoclinic	monoclinic
space group	$P2_1/c$	$P2_1/c$
a, Å	10.328(2)	10.024(2)
b, Å	22.924(2)	29.745(1)
c, Å	16.091(1)	11.459(1)
α, deg	90	90
β, deg	107.34(1)	94.87(1)
γ, deg	90	90
V, Å^3	3636.6(8)	3404.3(9)
d(calc), g cm^{-3}	1.171	1.012
Z	4	4
radiation	Mo Kα	Mo Kα
total no. of rflns	7054	6344
no. of obsd rflns	6327	5944
no. of ref params	364	339
wR2/R1	0.2067/0.0882	0.1410/0.1065
GOF on F^2	1.096	1.174

Moreover, the conformations of **5** and **7** are similar in the sense that one of the aryl rings exhibits a pronounced tilt (angle between the In–C(1) and C(1)···C(4) vectors 34.0°) and the two aryl rings are close to orthogonal.

Experimental Section

General Considerations. All reactions were performed under oxygen-free argon or under vacuum using standard Schlenk line or drybox techniques. All solvents were dried over sodium and distilled from sodium benzophenone under argon before use. The starting materials $(Ar^*)_2GaCl$,[8] $(Ar^*)_2InCl$,[6] and $LiGaH_4$[15] were prepared according to the literature methods; $LiAlH_4$ was procured commerically and used without further purification.

Physical Measurements. IR spectra were obtained as KBr pellets on a Bio-Rad FTS-40 spectrometer. Mass spectra (CI) were run on a Bell and Howell 21-491 instrument, and NMR spectra were measured on a GE QE-300 spectrometer (^1H, 300.17 MHz; ^{13}C, 75.48 MHz). NMR spectra are referenced to C_6D_6 which was dried over Na/K alloy and distilled prior to use. All chemical shifts are reported relative to TMS (0.00 ppm). Melting points (uncorrected) were obtained in sealed capillaries under argon (1 atm), and elemental analyses were performed by Atlantic Microlab, Norcross, GA.

Reaction of $(Ar^*)_2GaCl$ (4) with $LiAlH_4$. A 100 mL capacity Schlenk flask was charged with 320 mg of **4** (0.54 mmol) and 21 mg of $LiAlH_4$ (0.54 mmol). The solids were dissolved in 25 mL of Et_2O at −78 °C, and the stirred reaction mixture was warmed immediately to ambient temperature. After 1 h the volatiles were removed under reduced pressure and the resulting solid was extracted with toluene (3 × 20 mL). After filtration, the volume of the filtrate was reduced by ~50%. Storage of the concentrated solution at −20 °C overnight afforded 210 mg (80% yield) of colorless crystalline **6** (mp 144–146 °C). Spectroscopic data for **6** are as follows: IR (KBr, cm^{-1}) 1869 (ν_{Al-H}, terminal); ^1H NMR (300 MHz, C_6D_6, 25 °C; δ (ppm)) 1.34 (s, 9H, *p*-Me), 1.45 (s, 18H, *o*-Me), 5.72 (s, 1H, Al–H), 7.46 (s, 2H, ring); $^{13}C\{^1H\}$ NMR (75.5 MHz, C_6D_6, 25 °C; δ (ppm)) 31.47 (*p*-Me), 34.72 (*para* quaternary), 33.03 (*o*-Me), 38.66 (*ortho* quaternary), 121.65 (CH, ring), 150.54 (C, ring), 159.65 (C, ring), *ipso* carbon not observed; CIMS (CH_4): m/z 517 (M^+ − H), 273 (M − Ar*), 246 (Ar* +

(15) Shirk, A. E.; Shriver, D. F. *Inorg. Synth.* **1977**, *17*, 45.

Table 3. Atomic Coordinates ($\times 10^4$) and Equivalent Isotropic Displacement Parameters ($Å^2 \times 10^3$) for $(Ar^*)_2InCl$ (5) and $(Ar^*)_2AlH$ (6) (Ar^* = 2,4,6-*t*-$Bu_3C_6H_2$)

atom	*x/a*	*y/b*	*z/c*	*U*(eq)	atom	*x/a*	*y/b*	*z/c*	*U*(eq)
				Compound **5**					
In	3350(1)	2583(1)	5352(1)	44(1)	C(18)	4296(14)	518(5)	6288(9)	69(4)
Cl	5381(2)	2529(1)	4789(2)	37(1)	C(19)	3124(12)	3513(4)	5389(8)	41(3)
C(1)	2301(11)	1760(5)	5277(7)	43(3)	C(20)	3621(12)	3830(5)	6174(8)	47(3)
C(2)	874(11)	1760(5)	4911(8)	48(3)	C(21)	3466(13)	4438(5)	6156(8)	54(3)
C(3)	272(13)	1300(6)	4354(9)	63(4)	C(22)	2893(12)	4748(5)	5420(8)	48(3)
C(4)	980(14)	839(5)	4174(9)	57(3)	C(23)	2417(12)	4432(5)	4653(8)	45(3)
C(5)	2345(14)	809(5)	4645(8)	53(3)	C(24)	2499(12)	3822(5)	4616(7)	39(3)
C(6)	3011(12)	1250(5)	5206(8)	46(3)	C(25)	4357(16)	3550(6)	7077(9)	69(4)
C(7)	−140(13)	2171(6)	5163(10)	65(4)	C(26)	3327(26)	3664(11)	7676(13)	95(8)
C(8)	545(16)	2658(7)	5774(12)	108(6)	C(27)	5721(29)	3890(12)	7521(19)	108(11)
C(9)	−904(15)	1796(6)	5671(10)	84(5)	C(28)	4589(29)	2909(9)	7114(13)	82(9)
C(10)	−1249(15)	2435(6)	4368(11)	101(5)	C(26A)	5828(65)	3273(29)	6920(33)	95(8)
C(11)	294(18)	379(7)	3476(11)	90(5)	C(27A)	3796(78)	3025(35)	7299(48)	108(11)
C(12)	−266(41)	695(12)	2605(16)	136(13)	C(28A)	5009(84)	3939(28)	7762(40)	82(9)
C(13)	1275(33)	−105(15)	3435(26)	153(15)	C(29)	2763(14)	5415(5)	5398(9)	57(3)
C(14)	−976(40)	124(18)	3731(24)	160(16)	C(30)	3160(21)	5682(6)	6270(10)	118(7)
C(12A)	436(150)	−247(46)	3834(55)	136(13)	C(31)	1339(19)	5601(6)	4980(13)	118(7)
C(13A)	−1217(109)	453(49)	2990(94)	153(15)	C(32)	3590(21)	5669(6)	4853(12)	121(8)
C(14A)	1256(116)	448(55)	2742(65)	160(16)	C(33)	1904(13)	3562(5)	3695(8)	48(3)
C(15)	4449(13)	1078(5)	5771(8)	55(3)	C(34)	2687(16)	3789(6)	3094(9)	77(4)
C(16)	5116(14)	1521(6)	6478(8)	67(4)	C(35)	434(14)	3755(5)	3334(8)	68(4)
C(17)	5376(13)	951(6)	5220(9)	67(4)	C(36)	1858(14)	2898(5)	3635(8)	63(4)
				Compound **6**					
Al	3589(2)	6271(1)	1467(2)	46(1)	C(21)	4098(6)	5880(2)	2861(5)	40(2)
C(1)	1937(6)	6610(2)	992(5)	38(2)	C(22)	5499(6)	5800(2)	3100(5)	40(2)
C(2)	961(6)	6446(2)	122(5)	37(2)	C(23)	6056(6)	5821(2)	4271(6)	48(2)
C(3)	−233(6)	6677(2)	−144(5)	39(2)	C(24)	5321(6)	5874(2)	5225(5)	43(2)
C(4)	−504(6)	7082(2)	359(5)	37(2)	C(25)	3960(6)	5874(2)	4978(5)	48(2)
C(5)	486(6)	7257(2)	1146(5)	43(2)	C(26)	3328(6)	5862(2)	3855(5)	39(2)
C(6)	1677(6)	7034(2)	1476(5)	35(2)	C(27)	6469(6)	5678(2)	2161(6)	46(2)
C(7)	1144(7)	6021(2)	−612(6)	48(2)	C(28)	7362(6)	6079(2)	1926(5)	70(2)
C(8)	24(6)	5683(2)	−535(5)	67(2)	C(29)	5776(6)	5502(2)	1016(5)	68(2)
C(9)	2483(6)	5786(2)	−299(5)	64(2)	C(30)	7398(6)	5292(2)	2644(5)	66(2)
C(10)	1174(6)	6162(2)	−1900(5)	71(2)	C(31)	6002(7)	5904(3)	6438(6)	53(2)
C(11)	−1807(6)	7342(2)	62(6)	43(2)	C(32)	6240(10)	5460(3)	6928(7)	198(6)
C(12)	−2462(6)	7444(2)	1183(6)	80(3)	C(33)	7283(9)	6118(4)	6513(7)	239(8)
C(13)	−1511(6)	7784(2)	−515(5)	73(2)	C(34)	5237(9)	6133(4)	7251(7)	246(8)
C(14)	−2815(6)	7084(2)	−742(5)	65(2)	C(35)	1784(6)	5816(2)	3775(6)	42(2)
C(15)	2705(7)	7302(2)	2290(6)	45(2)	C(36)	1385(6)	5472(2)	4685(5)	75(2)
C(16)	3322(7)	7662(2)	1559(6)	87(3)	C(37)	1100(6)	6258(2)	4028(5)	72(2)
C(17)	2068(6)	7424(2)	3296(5)	76(2)	C(38)	1167(6)	5638(2)	2595(5)	60(2)
C(18)	3860(6)	7024(2)	2828(5)	68(2)					

H). Anal. Calcd for $C_{36}H_{59}Al$ (**5**): C, 83.40; H, 11.40. Found: C, 82.23; H, 11.16.

Reaction of $(Ar^*)_2InCl$ (5) with $LiAlH_4$. A 100 mL capacity Schlenk flask was charged with 350 mg of **5** (0.55 mmol) and 19 mg of $LiAlH_4$ (0.54 mmol). The solids were dissolved in 25 mL of Et_2O at −78 °C, and the stirred reaction mixture was warmed immediately to ambient temperature. After 1 h the volatiles were removed under reduced pressure and the resulting solid was extracted with toluene (3 × 20 mL). After filtration, the volume of the filtrate was reduced by ~50%. Storage of the concentrated solution at −20 °C overnight afforded 180 mg (69% yield) of colorless crystalline **6**, which was identified on the basis of NMR and mass spectroscopy (see above).

Reaction of $(Ar^*)_2InCl$ (5) with $LiGaH_4$. A 100 mL capacity Schlenk flask was charged with 350 mg of **5** (0.55 mmol) and a solution of $LiGaH_4$ (10 mmol) in 25 mL of Et_2O at −78 °C. The stirred reaction mixture was warmed immediately to ambient temperature. After 1 h the volatiles were removed under reduced pressure and the resulting solid was extracted with toluene (3 × 20 mL). After filtration, the volume of the filtrate was reduced by ~50%. Storage of the concentrated solution at −20 °C overnight afforded 140 mg (88% yield) of colorless crystalline **1**, which was identified on the basis of published[6] NMR and mass spectroscopic data.

X-ray Crystallography. Details of the crystal data and summary of intensity data collection parameters for **5** and **6** are presented in Table 2. Atomic coordinates and equivalent isotropic thermal parameters for **5** and **6** are listed in Table 3. The crystals were mounted in thin-walled glass capillaries and sealed under argon. Both data sets were collected at 25 °C on an Enraf-Nonius CAD-4 diffractometer. The unit cell parameters were obtained by centering 25 reflections having 2θ values between 16 and 24°. For both structures, the data were corrected for Lorentz and polarization effects. The structures were solved by least-squares refinements. All calculations were performed using SHELXL[16] and the Siemens SHELXTL PLUS[17] software package.

Acknowledgment. We thank the National Science Foundation and the Robert A. Welch Foundation for generous financial support.

Supplementary Material Available: For **5** and **6**, tables of crystallographic data, anisotropic thermal parameters, bond lengths and angles, and hydrogen atom parameters (12 pages). Ordering information is given on any current masthead page.

OM9409884

(16) Sheldrick, G. M. SHELXL-93; University of Göttingen, Göttingen, Germany, 1993.
(17) Sheldrick, G. M. SHELXTL-Plus (PC) [4.2]; Siemens Analytical X-ray Instruments, Inc., 1990.

Coupling of the Triphenylphosphine Moiety to Water-Soluble Polymers: A New Method To Achieve Water-Soluble Metal Phosphine Complexes

Torsten Malmström, Hagen Weigl,† and Carlaxel Andersson*

Inorganic Chemistry 1, Chemical Center, University of Lund, P. O. Box 124, S 221 00 Lund, Sweden

Received December 22, 1994®

Summary: Coupling of methyl[4-(diphenylphosphino)-benzyl]amine to poly(acrylic acid) and 4-(diphenylphosphino)benzaldehyde to polyethylenimine demonstrates a new method of preparing water-soluble phosphine ligands. The feasability of these polymeric ligands in complex formation is demonstrated by the preparation and characterization of water-soluble cobalt carbonyl complexes.

Catalysis in biphasic media has emerged as an important method for achieving easier separation and reuse of homogeneous metal catalysts[1] and its feasibility has been demonstrated by the Rhone-Poulenc/Ruhrchemie hydroformylation process.[2] The key prerequisite for carrying out homogeneous catalysis in aqueous solution is the use of a water-soluble ligand, a property usually achieved by functionalization of parent chiral or achiral, mono- or bidentate ligands with polar substituents, *e.g.* $-OH$, $-COO^-$, $-SO_3^-$, and $-NR_3^+$. While monosulfonated triphenylphosphine (TPPMS) marks a starting point in the development[3] and application[4] of water-soluble phosphine ligands, trisulfonated triphenylphosphine (TPPTS), with its extremely high water solubility,[5] can be regarded as the prototypical ligand in the field. Concomitant with improvements[6] in the synthesis and purification of TPPTS, the coordination chemistry, as well as the catalytic chemistry, of TPPTS has progressed.[7] With respect to catalysis and coordination chemistry TPPTS complexes and their triphenylphosphine counterparts usually show similar characteristics. A slightly higher propensity for oxidation[8] and somewhat higher steric requirements[7] for TPPTS are the main differences observed.

The preparation of the 1,3,5-triaza-7-phosphaadamantane (PTA) ligand[9] or a diphenylalkylphosphine with a polar group at the end of the alkyl chain[10] and the coupling of various charged moieties to bis[2-(diphenylphosphino)ethyl]amine[11] demonstrates other means of obtaining water-soluble phosphines. Somewhat in resemblance to the latter method, the coupling of methyl[4-(diphenylphosphino)benzyl]amine to poly(acryloyl chloride) grafted onto poly-TRIM (poly(trimethylolpropane trimethacrylate) particles have been shown to give support particles well-suited for the preparation of heterogeneous metal complex catalysts.[12] In this particular case the insoluble porous poly-TRIM particle provides functionality *vis à vis* an intended application in heterogeneous catalysis. In the present study we show that functionality *vis `a vis* aqueous solvent can be achieved by using water-soluble polymers as coupling partners.

To enable water solubility under basic as well as acidic conditions, couplings to two different water-soluble polymers have been studied, *viz.* poly(acrylic acid) and polyethylenimine.

As outlined in the Scheme 1, the reaction of methyl-[4-(diphenylphosphino)benzyl]amine[13] and poly(acrylic acid) using dicyclohexylcarbodiimide (DCC) as the coupling agent affords, after workup, phosphinated poly-(acrylic acid) (PAA-PNH). The yield in the coupling reaction is virtually quantitative, provided that the coupling is carried out under strict exclusion of oxygen. The ^{31}P NMR spectrum of the resulting polymer shows only the resonanace of the free phosphine at -6.1 ppm; no traces of phosphine oxide or other side products are seen. The proportion of phosphine groups relative to carboxylate groups can, in principle, be varied in order to affect the solubility properties of the phosphinated polymer. To ensure a high degree of water solubility a

* To whom correspondence should be addressed. E-mail: Carlaxel.Andersson@inorgk1.lu.se

† Present address: University of Heidelberg, Heidelberg, Germany.

® Abstract published in *Advance ACS Abstracts,* March 15, 1995.

(1) (a) Joo, F.; Toth, Z. *J. Mol. Catal.* **1980,** *8,* 369. (b) Kalck, P.; Monteil, F. *Adv. Organomet. Chem.* **1992,** *34,* 219. (c) Herrman, W. A.; Kohlpaintner, C. W. *Angew. Chem., Int. Ed. Engl.* **1993,** *32,* 1524. (d) Gladysz, J. A. *Science* **1994,** *55,* 266.

(2) (a) Kuntz, E. *Chem. Tech.* **1987,** 571. (b) Bahrmann, H.; Bach, H. *Phosphorus Sulfur Relat. Elem.* **1987,** *30,* 611.

(3) (a) Ahrland, S.; Chatt, J.; Davies, N. R.; Williams, A. A. *J. Chem. Soc.* **1958,** 1403. (b) Ahrland, S.; Chatt, J.; Davies, N. R. *Q. Rev., Chem. Soc.* **1958,** *12,* 265. (c) Ahrland, S.; Chatt, J.; Davies, N. R.; Williams, A. A. *J. Chem. Soc.* **1958,** *264,* 276.

(4) (a) Borowski, A. F.; Cole-Hamilton, D. J.; Wilkinson, G. *Nouv. J. Chem.* **1977,** *2,* 137. (b) Joo, F.; Toth, Z.; Beck, M. T. *Inorg. Chim. Acta* **1977,** *25,* L61. (c) Casalnuovo, A. L.; Calabrese, J. C. *J. Am. Chem. Soc.* **1990,** *112,* 4324.

(5) The solubility of TPPTS is 1100 g/L of water.

(6) (a) Herrman, W. A.; Kulpe, J. A.; Kellner, J.; Riepl, H.; Bahrmam, H.; Konkol, W. *Angew. Chem., Int. Ed. Engl.* **1990,** *29,* 391. (b) Herrman, W. A.; Kulpe, J. A.; Konkol, W.; Bahrman, H. *J. Organomet. Chem.* **1990,** *389,* 85. (c) Herrman, W. A.; Kellner, J.; Riepl, H. *J. Organomet. Chem.* **1990,** *389,* 103.

(7) (a) Fache, E.; Santini, C.; Senocq, F.; Basset, J. M. *J. Mol. Catal.* **1992,** *72,* 331. (b) Fache, E.; Santini, C.; Senocq, F.; Basset, J. M. *J. Mol. Catal.* **1992,** *72,* 337. (c) Grosselin, J. M.; Mercier, C.; Allmang, G.; Grass, F. *Organometallics* **1991,** *10,* 2126. (d) Horvath, I. T.; Kastrup, R. V.; Oswald, A. A.; Mozeleski, E. J. *Catal. Lett.* **1989,** 85. (e) Darensbourg, D. J.; Bischoff, C. J.; Reibenspies, J. H. *Inorg. Chem.* **1991,** *30,* 1144. (f) Darensbourg, D. J.; Bischoff, C. J. *Inorg. Chem.* **1993,** *32,* 47.

(8) (a) Larpent, C.; Patin, H. *J. Organomet. Chem.* **1987,** *335,* C13. (b) Larpent, C.; Dabard, R.; Patin, H. *Inorg. Chem.* **1987,** *26,* 2922. (c) Larpent, C.; Dabard, R.; Patin, H. *New J. Chem.* **1988,** *12,* 907.

(9) Darensbourg, D. J.; Joo, F.; Kannisto, M.; Katho, A.; Reibenspies, J. H.; Daigle, D. J. *Inorg. Chem.* **1994,** *33,* 200.

(10) Manassen, J.; Dror, Y. *U.S. Patent* 4415500, 1983.

(11) (a) Wilson, M. E.; Nuzzo, R. G.; Whitesides, G. M. *J. Am. Chem. Soc.* **1978,** 100, 2269. (b) Nuzzo, R. G.; Feitler, D.; Whitesides, G. M. *J. Am. Chem. Soc.* **1979,** *101,* 3683. (c) Nuzzo, R. G.; Haynie, S. L.; Wilson, M. E.; Whitesides, G. E. *J. Org. Chem.* **1981,** *46,* 2861.

(12) Reinholdsson, P.; Hargitai, T.; Isaksson, R.; Nikitidis, A.; Andersson, C. *React. Polym.* **1992,** *17,* 175.

(13) Nikitidis, A.; Andersson, C. *Phosphorus, Sulfur Silicon Relat. Elem.* **1993,** *78,* 141.

0276-7333/95/2314-2593$09.00/0

Scheme 1. Preparation of PAA-PNH and PEI-PNH[a]

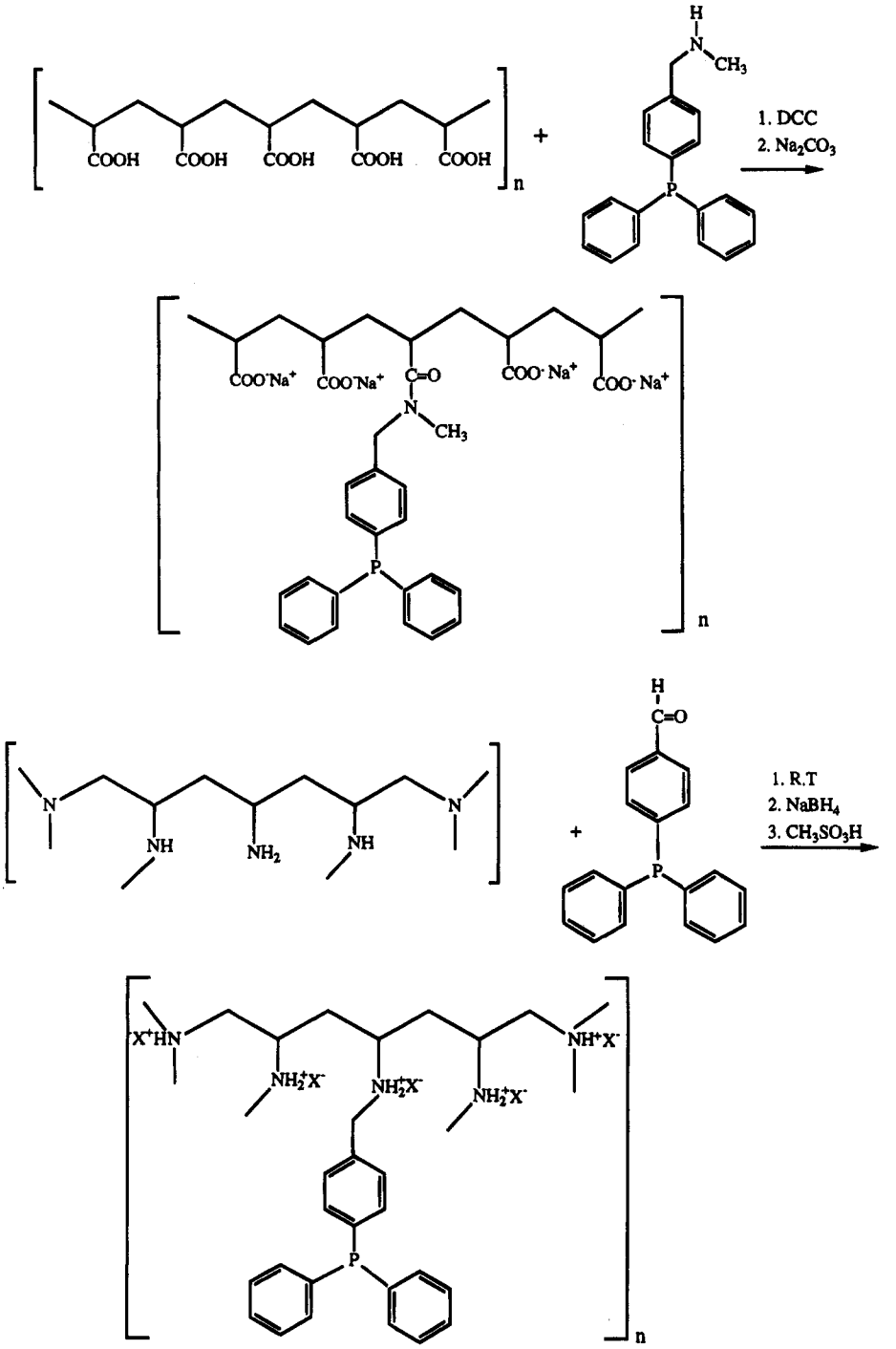

[a] The representation of PEI is schematic.

COO^-/P ratio around 5 has been kept throughout the present study, leading to a polymer with a phosphorus content of 3.2% and a water solubility of 165 mg/ml, which corresponds to a 0.17 M phosphine concentration and pH 8 for the solution. The solubility is pH-dependent and pH $\geq$7.0 must be kept to attain a reasonable solubility, although the phosphine is somewhat soluble at lower pH. Even after careful drying of the isolated solid, the elemental and thermogravimetric analyses are consistent with a water content of ~16%, indicating strong hydrogen bonding between water and the carboxylate groups in the polymer. Hydrolysis of the amide bond linking the phosphine group to the polymer has not been observed.

A similar coupling between polyethylenimine[14] and (4-carboxyphenyl)diphenylphosphine[15] using DCC as a coupling agent should, in principle, yield a polymeric ligand which is soluble under acidic conditions. All attempts to achieve this coupling reaction have, however, been unsuccessful, the reason probably being related to the polymer as such; similar reactions using nonpolymeric amines have been successfully applied previously.[16] To overcome this problem, the two-step procedure outlined in the Scheme 1 was applied.

(14) Polyethylenimine (average MW 1800) purchased from Polysciences, Inc.
(15) Hoots, J. E.; Rauchfuss, T. B.; Wrobleski, D. A. *Inorg. Synth.* **1982**, *21*, 178.

No attempts to isolate the imine intermediate have been made, but the reduction with sodium borohydride has been carried out *in situ*. The polymer can be isolated as its ammonium salt by addition of acids, and with regard to metal complex formation and catalysis, an acid with a weakly coordinating anion is preferably used. By addition of methanesulfonic acid and diethyl ether to the reaction mixture the methanesulfonic salt of phosphinated polyethylenimine (PEI-PNH) precipitates.

The yield in the overall reaction is lower than that observed in the case of PAA-PNH (*vide infra*), probably because the initial condensation reaction is an equilibrium reaction requiring water removal for completion. The polyethylenimine used in the present study is not well-defined with regard to the distribution between primary, secondary, and tertiary amine groups, although this can be quantified by ^{13}C NMR.[17] Consequently, the elemental analysis of the resulting polymer varies from batch to batch, typically giving a phosphorus content in the range of 2.6% and a nitrogen to phosphorus ratio around 7. At room temperature the solubility of PEI-PNH is 0.26 g/mL of water. The pH of the resulting solution is 3 and phosphine concentration 0.21 M, well in the range of interest for catalytic applications. As for PAA-PNH, the solubility of PEI-PNH is pH-dependent and reasonable solubility is attained at pH ≤ 6. The ^{31}P NMR shows only one resonance at -6.2 ppm, indicating that the coupling reaction and workup procedure do not give formation of phosphine oxide or other side products.

CO/phosphine exchange reactions in the complex $Co_2(CO)_8$ have been used to monitor the complex-formation properties of PAA-PNH and PEI-PNH. This type of reaction has been well studied in organic solvents for a great number of different phosphines[18] and additionally also studied in aqueous solution.[19,20] The initial product in the substitution reaction is the dimer $Co_2(CO)_7L$ (L = phosphine ligand) (**1**). This complex is thermodynamically very unstable and transforms to $[Co(CO)_3L_2]^+[Co(CO)_4]^-$ (**2**) and $Co_2(CO)_6L_2$ (**3**); the relative proportion between **2** and **3** is dependent on the nature of L, solvent polarity, and temperature. The three complexes can be identified by IR spectroscopy, where they all have characteristic absorptions in the CO-stretching region.[18] The ^{31}P NMR spectrum (D_2O) of the brown product, isolated after reacting PAA-PNH with $Co_2(CO)_8$ at ambient temperature for 24 h in a biphasic mixture of toluene and water, exhibited two resonances, a major one at 55.2 ppm (95%) and a minor one at 66.0 ppm (5%). In combination with the IR spectrum (Nujol/CsI) of the same sample, which contained a strong band at 1880 cm^{-1} characteristic of the $[Co(CO)_4]^-$ anion, bands at 2002 (m), 2013 (m), and 2077 (vw) cm^{-1} characteristic of the $[Co(CO)_3L_2]^+$ cation, and a weak band at 1950 cm^{-1} characteristic of **3**, it can be concluded that the substitution under these conditions led to the formation of two complexes, *viz.* **2** and **3**, in a 95/5 ratio according to ^{31}P NMR. Interestingly, the ionic compound **2** in the present case is stable enough to withstand isolation, while in a previous study[19] using the TPPTS ligand, a conversion to the disubstituted dimer **3** occurred on attempted isolation. As is evident by running the same reaction at elevated temperature (70 °C), the ionic complex **2** is, however, not completely thermodynamically stable. The product isolated after reaction at 70 °C showed the same IR stretching frequences and the same ^{31}P NMR resonances as those observed by reaction at ambient temperature, but when the phosphorus resonances are integrated, complexes **2** and **3** are found to exist in a 40/60 ratio in this case.

As a reflection of the change in pH, slight quantitative and qualitative differences in the product composition are observed when the same type of reactions are carried out using PEI-PNH instead of PAA-PNH. The ^{31}P NMR spectrum of the product isolated after 24 h reaction at ambient temperature shows two resonances at 65.6 and 54.2 ppm in a 57/43 ratio. The shifts in these two resonances are the same as those observed in the case of the PAA-PNH ligand, but the intensity ratio is drastically different. The IR spectrum of the product (ν(CO) 1950 (s), 1979 (m), 2002 (m) 2013 (m, sh) and 2077 (vw) cm^{-1}) is consistent with the coexistence of two different species, *viz.* the disubstituted dimer **3** and the cation $[Co(CO)_3L_2]^+$, but no peak corresponding to the anion $[Co(CO)_4]^-$ is present. The PEI-PNH polymer is acidic (pH ~3), and protonation of the anion $[Co(CO)_4]^-$ to give the corresponding hydride $HCo(CO)_4$ is a well-established reaction.[21] Once formed, this hydride is highly soluble in organic solvents and also thermally unstable, decomposing to H_2 and $Co_2(CO)_8$, its presence in substantial amounts in the product recovered from the water phase is therefore highly unlikely. In the hydrido complex $HCo(CO)_3TPPTS(H)$, which by spectroscopic methods has been shown to exist in aqueous solution,[18] ν(CO) was observed at 2053 (m) and 1980 (s) cm^{-1}. In support for the proton transfer suggested above, the weak peak at 1979 cm^{-1} in the IR spectrum of our product can thus be interpreted as originating from phosphine/CO exchange in the complex $HCo(CO)_4$. Since no trace of resonances other than the two given above are visable in the ^{31}P NMR spectrum, the amount of a supposed $HCo(CO)_3L$ complex in the isolated product must be very small.

Raising the reaction temperature to 70 °C in the case of PEI-PNH causes changes in the product composition qualitatively similar to those observed for PAA-PNH. Thus, the content of **3** increases at the expense of the other complex, leading to a product containing complex **3** and the cation $[Co(CO)_3L_2]^+$ in an 85/15 ratio. The quantitative difference (ratios 85/15 and 60/40 for PEI-PNH and PAA-PNH, respectively) might be caused by the difference in anions, the ion pair $[Co(CO)_4]^-$-$[Co(CO)_3L_2]^+$, in such a case, being more stable than the $[CH_3SO_3]^-[Co(CO)_3L_2]^+$ ion pair.

(16) Hedden, D. H.; Roundhill, D. M. *Inorg. Chem.* **1985**, *24*, 4152.
(17) Lukovkin, G. M.; Pshezhetsky, V. S.; Murtazaeva, G. A. *Eur. Polym. J.* **1973**, *9*, 559.
(18) (a) Szabo, P.; Fekete, L.; Bor, G.; Nagy-Magos, Z.; Marko, L. *J. Organomet. Chem.* **1968**, *12*, 245. (b) Wohler, O. *Chem. Ber.* **1958**, 1235. (c) Kemmit, R. D. E.; Russel, D. R. In *Comprehensive Organometallic Chemistry;* Wilkinson, G., Stone, F. G. A., Abel, E. W., Eds.; Pergamon Press: Oxford, U.K., 1982; Vol. 5, p 4. (d) Atwood, J. D. *Inorg. Chem.* **1987**, *26*, 2918.
(19) Bartik, T.; Bartik, B.; Hanson, B. E.; Whitmire, K. H.; Guo, I. *Inorg. Chem.* **1993**, *32*, 5833.
(20) Ding, H.; Hanson, B. E.; Bartik, T.; Bartik, B. *Organometallics* **1994**, *13*, 3761. Bartik, T.; Bartik, B.; Guo, I.; Hanson, B. E. *J. Organomet. Chem.* **1994**, *480*, 15.
(21) Sternberg, H. W.; Wender, I.; Orchin, M. *Inorg. Synth.* **1957**, *5*, 192.

Experimental Section

All reactions were carried out under an oxygen-free atmosphere. Solvents were degassed and flushed with argon before use. Organic solvents of p.A. quality were used without further purification. $Co_2(CO)_8$ was purchased from Strem Chemicals and used as received. ^{31}P NMR spectra were recorded on a Varian Unity 300 at an observation frequency of 121.426 MHz. Chemical shifts are referenced to external 85% H_3PO_4 with positive values downfield. FT-IR spectra were recorded on a Nicolet 20 SCX spectrometer. Elemental analyses were done by AB Mikrokemi, Uppsala, Sweden.

Preparation of PAA-PNH. An 8.0 g amount of poly(acrylic acid) (Jansen Chimica, 63% water solution) is dissolved in 200 mL of a 1/5 water/THF mixture. A 5.0 g amount of methyl[4-(diphenylphosphino)benzyl]amine (16.4 mmol) in 70 mL of THF is added in one portion and the solution degassed. A 4.3 g portion of dicyclohexylcarbodiimide (20.9 mmol) in 50 mL of THF is then added over a period of 20 min. After the mixture is stirred overnight, the THF is evaporated and the pH of the water solution is adjusted to 8 with a 0.5 M Na_2CO_3 solution, leaving dicyclohexylurea (DHU) as a white precipitate. After removal of DHU the remaining water solution is added to 2000 mL of absolute ethanol (99.5%), whereby PAA-PNH precipitates. Collection and drying of the precipitate gives 9.5 g of a white powder. ^{31}P NMR (D_2O): δ, −6.1 (s). Anal. Calcd for $[CH_2CHCOONa]_{4.1}[CH_2CHC(O)N(CH_3)CH_2(C_6H_4)P(C_6H_5)_2][\ H_2O]_{7.8}$: C, 47.9; H, 5.6; N, 1.6; P, 3.5. Found: C, 47.9, H, 4.7; N, 1.6; P, 3.2.

Preparation of PEI-PNH. A 2.1 g amount of polyethylenimine (Polysciences, Inc., average MW 1800) is dissolved in 100 mL of methanol. A 2.6 g portion of 4-(diphenylphosphino)-benzaldehyde (9.0 mmol) in 40 mL of THF is added slowly over a period of 30 min, and the solution is stirred at room temperature for 4 h. The solution is cooled to 0 °C, and 470 mg of sodium borohydride (12 mmol) is added. The reaction mixture is allowed to reach room temperature and is stirred overnight. A 10 mL portion of water is added, and the pH is adjusted to 3 with methanesulfonic acid. Addition of diethyl ether causes precipitation of PEI-PNH. The product is collected on a filter, washed three times with diethyl ether, and finally dried in vacuo. ^{31}P NMR (D_2O): δ −6.23 (s). Anal. Calcd for $[CH_2CHNH_3^+CH_3SO_3^-]_{5.5}[CH_2CHN(H_2^+CH_3SO_3^-)CH_2(C_6H_4)P(C_6H_4)_2][H_2O]_{7.2}$: C, 35.3; H, 6.7; N, 7.0; P, 2.4. Found: C, 38.7, H, 5.6, N, 7.0, P, 2.6.

Reactions with $Co_2(CO)_8$. Degassed solutions of $Co_2(CO)_8$ (1 equiv) in toluene and the ligand (2 equiv of phosphine) in water were mixed and vigorously stirred under argon at given temperatures. Phase separation after a given time, washing of the aqueous phase, and evaporation of the water afforded the products as brown powders.

Acknowledgment. Financial support from the TFR (Swedish Research Council for Engineering Sciences) and NUTEK (Swedish National Board for Industrial and Technical Development) is gratefully acknowledged.

Supplementary Material Available: Figures giving IR spectra for reaction mixtures of $Co_2(CO)_8$ and PAA-PNH or PEI-PNH at both room and reflux temperatures (4 pages). Ordering information is given on any current masthead page.

OM9409783

Equilibrium between Ylidene and Isocyanide Complexes: Synthesis and Crystal Structure of cis-(N-Methyl-1,2-dihydrobenzoxazol-2-ylidene)(triphenylphosphine)tetracarbonyltungsten

F. Ekkehardt Hahn, and Matthias Tamm

Organometallics, **1995**, 14 (5), 2597-2600• DOI: 10.1021/om00005a069 • Publication Date (Web): 01 May 2002

Equilibrium between Ylidene and Isocyanide Complexes: Synthesis and Crystal Structure of *cis*-(*N*-Methyl-1,2-dihydrobenzoxazol-2-ylidene)-(triphenylphosphine)tetracarbonyltungsten

F. Ekkehardt Hahn* and Matthias Tamm

Institut für Anorganische and Analytische Chemie, Freie Universität Berlin, Fabeckstrasse 34-36, D-14195 Berlin, Germany

Received November 1, 1994®

*Summary: Reaction of 2-(trimethylsiloxy)phenyl isocyanide (**1**) with [W(THF)(CO)$_5$] gives the complex [W(**1**)(CO)$_5$] (**2a**). Hydrolysis of the Si–O bond leads to the formation of an equilibrium between complexes with a 2-hydroxyphenyl isocyanide (**3a**) or a 1,2-dihydrobenzoxazol-2-ylidene ligand (**4a**), which lies mostly on the side of the ylidene complex **4a**. Substitution of one cis-CO ligand in **2a** for P(C$_6$H$_5$)$_3$ enhances metal-to-ligand (d → p)π-back-bonding and shifts the equilibrium toward the isocyanide complex **3e**. The equilibrium can again be shifted toward the ylidene complex by deprotonation and alkylation of the ylidene nitrogen to give (N-methyl-1,2-dihydrobenzoxazol-2-ylidene)(triphenylphosphine)tetracarbonyltungsten (**4f**) which was characterized by single-crystal X-ray structure analysis.*

Introduction

Reaction of coordinated isocyanides with nucleophiles constitutes the oldest method for the preparation of heteroatom-stabilized carbene complexes,[1] and many examples for this reaction can be found in the literature.[2] However, this reaction normally only works with isocyanides that are coordinated to late or oxidized transition metals. In this case the isocyanide carbon is not deactivated for nucleophilic attack by (d → p)π-back-bonding from the metal center. The isocyanide carbon in [W(CNCH$_2$CH$_5$OH)(CO)$_5$], for example, is stabilized against intramolecular nucleophilic attack by the hydroxyl oxygen,[3] while the same ligand reacts spontaneously to give complexes with the oxazolidin-2-ylidene ligand when coordinated to Pd(II).[4]

Results and Discussion

Different behavior was observed for the aromatic ligand 2-(trimethylsiloxy)phenyl isocyanide[5] when coordinated to a W(CO)$_5$ or Fe(CO)$_4$ fragment (Scheme 1). Complexes of type **2** react after hydrolysis of the Si–O bond to give a mixture of isocyanide complexes, **3** and complexes with a 1,2-dihydrobenzoxazol-2-ylidene ligand, **4**.[6,7] The equilibrium between complexes **3** and **4** resides mostly on the side of the ylidene complexes **4**. Driving force for the enhanced ylidene formation, compared to the aliphatic ligand 2-hydroxyethyl isocyanide,[3] is the high stability of the formed ylidene ligand with an aromatic five-membered ring.[6] In this contribution we report an example for the selective shift of the equilibrium between isocyanide and ylidene complexes to the side of the isocyanide complex by changing of the electronic properties of the metal center or to the side of the ylidene by a reaction at the coordinated ligand.

Scheme 1. Equilibrium between Isocyanide and 1,2-Dihydrobenzoxazol-2-ylidene Complexes in Coordination Compounds of 2-Hydroxyphenyl Isocyanide

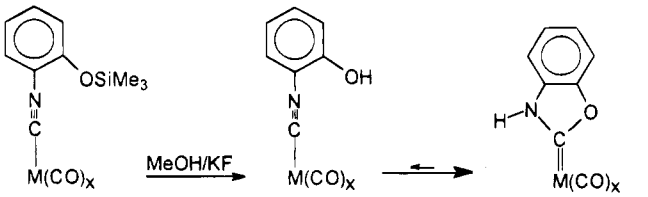

2

2a, M = W, x = 5
2b, M = Mo, x = 5
2c, M = Cr, x = 5
2d, M = Fe, x = 4

3

3a, M = W, x = 5
3b, M = Mo, x = 5
3c, M = Cr, x = 5

4

4a, M = W, x = 5
4b, M = Mo, x = 5
4c, M = Cr, x = 5
4d, M = Fe, x = 4

In a mixture of complexes **3** and **4**, the isocyanide complexes **3** can be identified by the N≡C IR absorption ($\tilde{\nu}_{NC}$ = 2132–2169 cm^{-1}) while complexes of type **4** show a strong IR absorption for the N–H bond around $\tilde{\nu}$ = 3430 cm^{-1}. The O*H* resonance for complexes of type **3** is found between 5.6 and 6.1 ppm in the ^{1}H NMR spectrum, while the N*H* resonance for complexes of type **4** appears around 10.5 ppm. Comparison of the integrals for these two resonances allows to determine the relative abundance of the components in a mixture of complexes of types **3** and **4**. Spectroscopic data for some complexes of the types **3** and **4** are summarized in Table 1.

The reactivity of coordinated carbonyl or isocyanide ligands can be related to the IR absorption frequencies or the force constants of the CO or CN bonds.[8] The force constant can be directly correlated with the positive

® Abstract published in *Advance ACS Abstracts,* March 15, 1995.

(1) Tschugajeff, L.; Skanawy-Grigorjewa, M.; Posnack, A. *Z. Anorg. Allg. Chem.* **1925**, *148*, 37.

(2) (a) Dötz, K. H.; Fischer, H.; Hofmann, P.; Kreissl, F. R.; Schubert, U.; Weiss, K. *Transition Metal Carbene Complexes*; VCH: Weinheim, 1983. (b) Crociani, B. In *Reactions of Coordinated Ligands, Vol. 1*; Braterman, P. S., Ed.; Plenum Press: New York, 1985. (c) Chatt, J.; Richards, R. L.; Royston, G. H. D. *J. Chem. Soc., Dalton Trans.* **1973**, 1433.

(3) Fehlhammer, W. P.; Bartel, K.; Weinberger, B.; Plaia, U. *Chem. Ber.* **1985**, *118*, 2220.

(4) Fehlhammer, W. P.; Bartel, K.; Plaia, U.; Völkel, A.; Liu, A. T. *Chem. Ber.* **1985**, *118*, 2235.

(5) Jutzi, P.; Gilge, U. *J. Organomet. Chem.* **1983**, *246*, 159.

(6) Hahn, F. E.; Tamm, M. *J. Organomet. Chem.* **1993**, *456*, C11.

(7) Hahn, F. E.; Tamm, M. *J. Chem. Soc., Chem. Commun.* **1993**, 842.

(8) (a) Singh, M. M.; Angelici, R. J. *Inorg. Chem.* **1984**, *23*, 2691. (b) *Ibid.* **1984**, *23*, 2699. (c) Darensbourg, D. J.; Darensbourg, M. Y. *Inorg. Chem.* **1970**, *9*, 1691. (d) Angelici, R. J.; Black, L. J. *Inorg. Chem.* **1972**, *11*, 1754.

0276-7333/95/2314-2597$09.00/0

Table 1. Physical and Spectral Data for Mixtures of Complexes 3 and 4

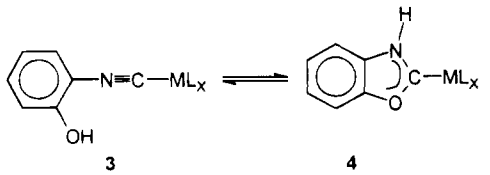

3 4

ML_x	complex	ratio, % isocyanide 3	ratio, % ylidene 4	^{1}H NMR, δ OH	^{1}H NMR, δ NH	IR, ν, cm^{-1}	k(CN), N m^{-1}
$W(CO)_5$	**3a/4a**	15	85	5.63	10.43	2141	1746
$Mo(CO)_5$	**3b/4b**	24	76	6.08	10.64	2137	1739
$Cr(CO)_5$	**3c/4c**	29	71	5.85	10.44	2132	1731
$Fe(CO)_4$	**4d**	0	100		10.95	2169[a]	1791
cis-[$W(CO)_4$-PPh_3]	**3e**	100	0	6.50		2117	1706

[a] Wave number for the 2-(trimethylsiloxy)phenyl isocyanide derivative **2d**; the 2-hydroxyphenylisocyanide derivative of type **3** was not isolated (Scheme 1).

charge on the carbon atom, e.g., with its susceptibility for nucleophilic attack.[9] In the series of the pentacarbonyl complexes **3a–c**, the N≡C stretching absorption is found at the lowest wavenumber for the chromium complex **3c** (Table 1). The force constant for the N≡C bond was calculated according to the method of Cotton[10] with corrections for the mass difference of CO vs CN. The lowest force constant was calculated for **3c** indicating that this isocyanide complex is partly stabilized by metal-to-ligand (d→p)π-back-bonding against intramolecular nucleophilic attack. Thus the chromium complex shows the smallest ylidene:isocyanide ratio (2:1). A slightly larger force constant was calculated for the tungsten complex **3a**. This difference is sufficient to cause a much stronger tendency of the coordinated isocyanide ligand to give the ylidene complex **4a** (ylidene:isocyanide ratio 6:1). In contrast to the aliphatic 2-hydroxyethyl isocyanide [k(NC) ≥ 1800 N m^{-1} for intramolecular ylidene formation[11]], a much stronger tendency for ylidene formation is observed with the aromatic 2-hydroxyphenyl isocyanide. Intramolecular nucleophilic attack is dominant at force constants as low as 1731 N m^{-1} (Table 1), which shows again that not only the activation of the isocyanide carbon—indicated by the N≡C force constant—but also the stability of the resulting ylidene determine the course of the reaction.[6,7]

No isocyanide complex of type **3** was detected by IR or ^{1}H NMR spectroscopy upon hydrolysis of the Si–O bond in the iron complex **2d**. Only formation of the ylidene complex **4d** was observed. This becomes plausible if the force constant for the 2-(trimethylsiloxy)-phenyl isocyanide complex **2d** [k(NC) = 1791 N m^{-1}] is considered. This force constant should not change significantly upon hydrolysis of the Si–O bond. It is significantly higher than the value calculated for **3a** (1746 N m^{-1}) which already reacts mostly to give the ylidene complex **4a**.

Not only the type of transition metal but also its electronic properties as determined by the coordinated ligands influence the position of the equilibrium between isocyanide and ylidene complexes. The stability of the coordinated isocyanide ligand in complex **3a** is greatly enhanced by substitution of a good π-acceptor (CO) for a good σ-donor (PPh_3) at the tungsten atom. The complex **2e** (Scheme 2) reacts after hydrolysis of the Si–O bond almost exclusively to give the isocyanide complex **3e**. The ylidene complex **4e** could not be detected by IR or ^{1}H NMR spectroscopy. The introduction of a σ-donor leads to enhanced (d → p)π-back-bonding, and the force constant for the N≡C bond in **3e** shrinks to 1706 N m^{-1} (Table 1). This low value indicates a complete deactivation of the isocyanide carbon in **3e** for intramolecular nucleophilic attack and explains why no ylidene complex **4e** could be identified spectroscopically.

Even the electronically stabilized isocyanide complex **3e** can be converted into a ylidene derivative. This requires removal of the trace amounts of **4e** from the reaction mixture which will cause the equilibrium to shift to the right side (Scheme 2). Removal of **4e** is best achieved by alkylation of the ylidene nitrogen[6,7] (Scheme 2). This alkylation prevents the back-reaction of the ylidene to the isocyanide complex and shifts the equilibrium completely to the side of the N-alkylated ylidene complex **4f**. However, an alternative mechanism is conceivable for the reaction of a mixture of **3e/4e** with strong bases and MeI. First, the strong base deprotonates the hydroxyl group in **3e**. Now the phenolate oxygen attacks the isocyanide carbon atom under formation of a coordinated iminoacyl. This ligand is then alkylated with MeI to give **4f**. In both cases the reaction product is the same. An electronically stabilized complex with a 2-hydroxyphenyl isocyanide ligand is completely converted into a complex with an N-methylated 1,2-dihydrobenzoxazol-2-ylidene ligand.

The molecular structure of **4f** was established by X-ray diffraction analysis. Scheme 2 shows an ORTEP diagram of **4f**. The tungsten atom is coordinated in a distorted octahedral fashion by one ylidene, four CO carbons, and a triphenylphosphine ligand. Bond distances and angles in **4f** compare well with equivalent parameters in **4a**[6] and its N-methylated derivative.[6]

In summary, we present an aromatic isocyanide ligand with a strong tendency to form ylidene complexes by intramolecular nucleophilic attack when attached to electron-poor transition metal fragments. Coordination to electron-rich transition metal fragments prevents the ylidene formation and leads to electronically stabilized complexes with the 2-hydroxyphenyl isocyanide ligand. The isocyanide complex can be converted into ylidene complexes by reaction with strong bases followed by alkylation of the ylidene nitrogen atom. These reactions might prove useful for the synthesis of ylidenes of early transition metals, e.g., Ti(IV), from isocyanide complexes, and corresponding investigations are under way.

Experimental Section

General Comments. All manipulations were performed in an atmosphere of dry argon using standard Schlenk techniques. Solvents were dried by standard methods and freshly distilled prior to use. ^{1}H and ^{13}C NMR spectra were recorded on a Bruker AM 270 spectrometer. Infrared spectra were taken in KBr on a Perkin-Elmer 983 instrument. Elemental analyses (C,H,N) were performed at the Freie Universität Berlin on a Heraeus CHN-rapid elemental analyzer. Mass spectra (EI, 70 eV) were recorded on a Varian

(9) Sarapu, A. C.; Fenske, R. F. *Inorg. Chem.* **1975**, *14*, 247.
(10) Cotton, F. A.; Kraihanzel, C. S. *J. Am. Chem. Soc.* **1962**, *84*, 4432.
(11) Fehlhammer, W. P.; Plaia, U. *Z. Naturforsch. Teil B* **1986**, *41*, 1005.

Scheme 2. Stabilization of 2-Hydroxyphenyl Isocyanide on a *cis*-[W(CO)$_4$(PPh$_3$)] Fragment and Molecular Structure of 4f[a]

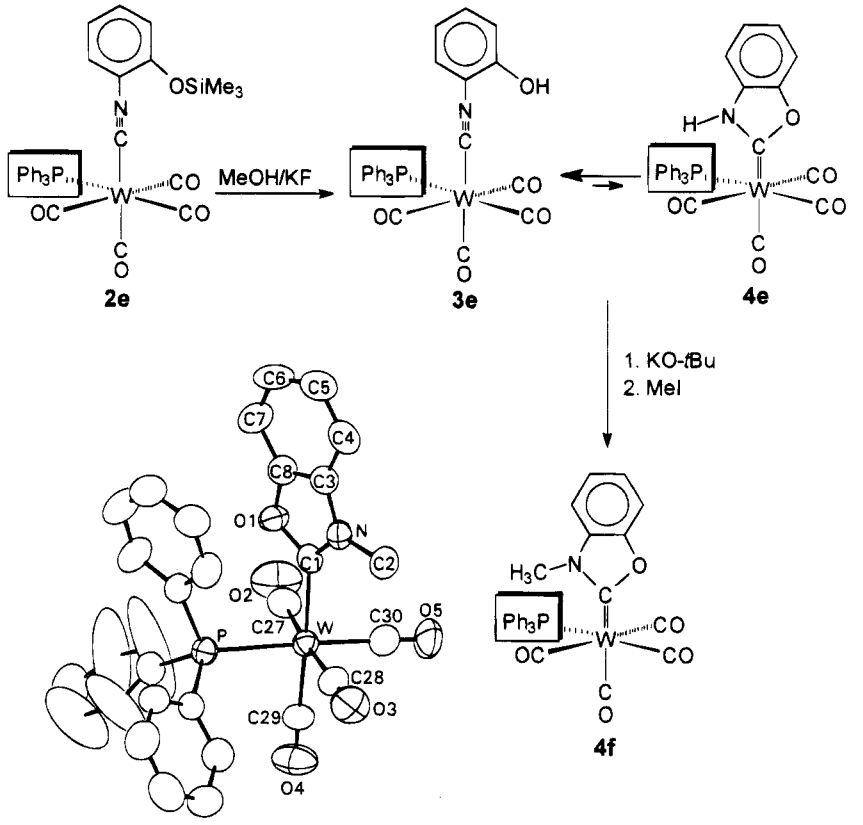

[a] Selected bond distances (Å) and angles (deg): W–P, 2.542(2); W–C1, 2.196(6); W–C27, 2.029(8); W–C28, 2.005(8); W–C29, 1.986(7); W–C30, 1.998(8); O1–C1, 1.373(8); O1–C8, 1.381(8); N–C1, 1.334(9), N–C2, 1.467(8); N–C3, 1.387(8); P–W–C1, 88.8(2); P–W–C27, 94.8(2); P–W–C28, 90.2(2); P–W–C29, 89.7(2); P–W–C30, 179.0(2); C1–W–C27, 84.8(3); C1–W–C28, 93.9(3); C1–W–C29, 176.1(2); C1–W–C30, 92.2(3); C27–W–C28, 174.9(3); C27–W–C29, 91.7(3); C27–W–C30, 85.4(3); C28–W–C29, 89.7(3); C28–W–C30, 89.7(3); C29–W–C30, 89.3(3); C1–O1–C8, 109.8(5); C1–N–C2, 124.5(6); C1–N–C3, 112.3(5); C2–N–C3, 123.2(6); W–C1–O1, 119.8(4); W–C1–N, 135.2(5); O1–C1–N, 105.1(5).

MAT 711 instrument. 2-(Trimethylsiloxy)phenyl isocyanide (**1**) was synthesized as previously described.[5] The syntheses of the tungsten complexes **2a**–**4a**[6] and the iron complexes **2d**–**4d**[7] have been described. The molybdenum and chromium complexes **2b**–**4b** and **2c**–**4c**, respectively, were prepared in an analogous manner. Selected spectroscopic data for these complexes are summarized in Table 1.

Synthesis of {W(CNC$_6$H$_4$-2-OH)[P(C$_6$H$_5$)$_3$](CO)$_4$} (3e). *cis*-[N(C$_2$H$_5$)$_4$]{WBr[P(C$_6$H$_5$)$_3$](CO)$_4$}[12] (8.03 g, 10.5 mmol) was dissolved in 200 mL of dry ethanol under argon. To this solution was added 2.0 g (10.5 mmol) of 2-(trimethylsiloxy)-phenyl isocyanide (**1**), and the yellow reaction mixture was stirred for 12 h under argon as described by Rommel.[13] The presumably formed 2-(trimethylsiloxy)phenyl isocyanide complex **2e** could not be isolated since this reaction was carried out in ethanol and partial hydrolysis of the Si–O bond of the ligand already occurred under these conditions. A catalytic amount of KF (100 mg) was added, and the reaction mixture was stirred at room temperature for an additional 18 h. Then all solvents were removed *in vacuo*, and the solid yellow residue was purified by column chromatography (neutral Al$_2$O$_3$, eluent CH$_2$Cl$_2$/hexane, 1:2, v:v). Complex **3e** was isolated as a yellow powder in 42% yield. Anal. Calcd for C$_{29}$H$_{20}$NO$_5$PW (M$_r$ = 677.31): C, 51.43; H, 2.98; N, 2.07. Found: C, 50.35; H, 3.18; N, 2.53. ^{1}H NMR (270 MHz, CDCl$_3$): δ 7.62–6.64 (m, 19H, Ar-*H*), 6.50 (s, br, 1H, O*H*). ^{13}C[^{1}H] NMR (67.89 MHz, CDCl$_3$): δ 203.5 (d, $^2J_{PC}$ = 24 Hz, *CO trans* to P), 202.9 (d, $^2J_{PC}$ = 7 Hz, *CO trans* to isocyanide), 199.7 (d, $^2J_{PC}$ = 7 Hz, $^1J_{WC}$ = 126 Hz, *CO trans* to CO), 163.8 (d, $^2J_{PC}$ = 9 Hz, Ar-N*C*), 152.27 (*C*-OH), 135.7 (d, $^1J_{PC}$ = 39 Hz, P-*C*), 133.1 (d, $^2J_{PC}$ = 12 Hz, P-C-*C*), 129.8 (P-C-C-C-*C*), 128.3 (d, $^3J_{PC}$ = 9 Hz, P-C-C-*C*), 128.0, 126.6, 120.1, 116.7 (Ar-*C*), 116.2 (Ar-*C*-NC). IR ($\tilde{\nu}$): 2117 (m, CN), 2009 (s, CO), 1895 (vs, br, CO). LRMS (*m*/*z*, rel intensity): 677 (M$^{\bullet+}$, 7.1), 649 (M$^{\bullet+}$ – CO, 4.3), 621 (M$^{\bullet+}$ – 2 CO, 5.9), 593 (M$^{\bullet+}$ – 3 CO, 9.7), 565 (M$^{\bullet+}$ – 4 CO, 3.0), 558 (M$^{\bullet+}$ – CNC$_6$H$_4$-2-OH, 4.5), 262 [P(C$_6$H$_5$)$_3$$^{\bullet+}$, 100].

Synthesis of {W[CN(CH$_3$)C$_6$H$_4$-2-O][P(C$_6$H$_5$)$_3$](CO)$_4$} (4f). **3e** (1.0 g, 1.5 mmol) was dissolved in 50 mL of dry DMF under argon. The solution was cooled to –40 °C, and 190 mg (1.7 mmol) of KO-*t*-Bu was added as a solid. The reaction solution was stirred for 3 h at –40 °C, and then 92 μL (1.5 mmol) of MeI was added via a syringe. The reaction mixture was allowed to warm up to room temperature and stirred at this temperature for 3 h. Then the DMF was removed *in vacuo*, and the yellow residue was recrystallized from CH$_2$Cl$_2$ to give 0.91 g (89%) of **4f** as bright yellow, slightly air-sensitive crystals. ^{1}H NMR (270 MHz, CDCl$_3$): δ 7.72–7.01 (m, br, 19H, Ar-*H*), 3.67 (s, 3H, N-C*H*$_3$). ^{13}C[^{1}H] NMR (67.89 MHz, CDCl$_3$): δ 221.8 (d, $^2J_{PC}$ = 9 Hz, N*C*O), 208.9 (d, $^2J_{PC}$ = 5 Hz, *CO trans* to ylidene), 207.1 (d, $^2J_{PC}$ = 25 Hz, *CO trans* to P), 202.7 (d, $^2J_{PC}$ = 8 Hz, *CO trans* to CO), 152.1 (Ar-*C*), 136.1 (d, $^1J_{PC}$ = 37 Hz, P-*C*), 133.0 (d, $^2J_{PC}$ = 12 Hz, P-C-*C*), 129.3 (Ar-*C* and P-C-C-C-*C*), 128.0 (d, $^3J_{PC}$ = 9 Hz, P-C-C-*C*), 124.4, 124.1, 110.3, 109.7 (Ar-*C*). IR ($\tilde{\nu}$): 2067 (m, CO), 1893 (s, CO), 1869 (vs, CO), 1847 (s, CO). LRMS (*m*/*z* rel intensity): 691 (M$^{\bullet+}$, 3.3), 663 (M$^{\bullet+}$ – CO, 2.7), 635 (M$^{\bullet+}$ – 2 CO, 5.6), 607 (M$^{\bullet+}$ – 3 CO, 4.4), 262 [P(C$_6$H$_5$)$_3$$^{\bullet+}$, 100].

X-ray Crystallographic Analysis of 4f. Yellow platelike

(12) Schenk, W. A. *J. Organomet. Chem.* **1979**, *179*, 253.
(13) Rommel, J. S.; Weinrach, J. B.; Grubisha, D. S.; Bennett, D. W. *Inorg. Chem.* **1988**, *27*, 2945.

crystals of **4f** were grown from CH_2Cl_2 at −26 °C. Selected crystallographic details: size of data crystal, 0.62 × 0.38 × 0.18 mm; formula, $C_{30}H_{22}NO_5PW$; M = 691.34 amu; triclinic, space group $P\bar{1}$; a = 10.032(2) Å, b = 10.258(2) Å, c = 16.580(4) Å; α = 79.12(2)°, β = 78.78(2)°, γ = 64.57(2)°; V = 1500.8(6) Å^3; ϱ_{exp} = 1.55 g/cm^3, ϱ_{calc} = 1.530 g/cm^3; Mo Kα radiation (λ = 0.71073 Å, monochromator graphite), μ(Mo Kα) = 40.18 cm^{-1}; 3908 symmetry independent diffraction data were measured at 20(3) °C in the 2θ range 2−45°; structure solution with Patterson and Fourier methods; refinement of positional parameters of all non-hydrogen atoms with anisotropic thermal parameters; hydrogens on calculated positions [d(C−H) = 0.95 Å] with $B_{eq(H)} = 1.3B_{eq(C)}$; R = 3.32, R_w = 4.75 for 3501 absorption-corrected (correction range 1.0/0.723) structure factors $F_o^2 \geq 3\sigma(F_o^2)$ and 343 refined parameters. Neutral atomic scattering factors[14] were used, and all scattering factors were corrected for anomalous dispersion.[14] All calculations were carried out with the MolEn program package.[15]

Acknowledgment. We thank the Deutsche Forschungsgemeinschaft and the Fonds der Chemischen Industrie for financial support. M.T. wishes to acknowledge BASF AG for a predoctoral grant.

Supplementary Material Available: Listings of X-ray data collection and refinement data, positional and thermal parameters, and bond lengths and angles for **4f** (8 pages). Ordering information is given on any current masthead page.

OM940830J

(14) *International Tables for X-Ray Crystallography*; Kynoch Press: Birmingham, England, 1974; Vol. I, Tables 2.2B and 2.3.1.
(15) *MolEN: Molecular Structure Solution Procedures. Program Description*; Enraf-Nonius: Delft, The Netherlands, 1990.

Novel Chiral *ansa*-Metallocene Complexes of Titanium and Zirconium with a Semirigid Bridge

Lev Atovmyan, Shaen Mkoyan, and Igor Urazowski*

Laboratory of Crystallochemistry, Institute of Chemical Physics, Russian Academy of Science, Chernogolovka, Moscow Region 142432, Russia

Roland Broussier, Serge Ninoreille, Patrice Perron, and Bernard Gautheron*

Laboratoire de Synthèse et d'Électrosynthèse Organométalliques (URA CNRS 1685), Université de Bourgogne, 6 Boulevard Gabriel, 21000 Dijon, France

Received November 28, 1994[⊗]

Summary: 3-tert-Butyl-6,6-dimethylfulvene undergoes smooth dimerization to give 1-(3-tert-butylcyclopentadienyl)-5-tert-butyl-1,3,3-trimethyltetrahydropentalene which is the precursor of novel chiral ansa-metallocene complexes of titanium and zirconium.[1] *For two representative compounds the crystal and molecular structures were determined: (R,R,S)(S,S,R)-[1,2,1'-(4-methylpentane-2,2,4-triyl)-4,3'-di-tert-butylbis(η^5-cyclopentadienyl)]-$TiCl_2$, space group $P2_1/n$, $Z = 4$, $a = 17.713(9)$ Å, $b = 9.440(5)$ Å, $c = 14.243(9)$ Å, $\gamma = 91.65(2)°$, $V = 2380.9$ Å^3, $R = 0.038$, $R_w = 0.042$ on the basis of 1403 reflexions with $I > 3\sigma$; (R,R,R)(S,S,S)-[1,2,1'-(4-methylpentane-2,2,4-triyl)-4,3'-di-tert-butylbis(η^5-cyclopentadienyl)]-$ZrCl_2$, space group $P2_1/n$, $Z = 4$, $a = 9.353(9)$ Å, $b = 12.398(9)$ Å, $c = 20.718(6)$ Å, $\gamma = 81.68(2)°$, $V = 2377.1$ Å^3, $R = 0.059$, on the basis of 2144 reflexions with $I > 3\sigma$.*

Introduction

Novel chiral *ansa*-metallocene complexes of the group 4 metals are of interest because of their conceivable application in stereoregular α-olefin polymerization processes[2] and asymmetric organic synthesis.[3] It was in 1982 that the synthesis of 1-cyclopentadienyl-1,3,3-trimethyltetrahydropentalene (**1**), a dimer of 6,6-dimethylfulvene[4] was reported; still there is no evidence in literature that this chiral chelating dicyclopentadienyl hydrocarbon or its derivatives were ever employed for the synthesis of chiral *ansa*-metallocenes. On the other hand, reductive coupling of β-substituted 6,6-dimethylfulvene gave after the appropriate reaction sequence chiral *ansa*-metallocene derivatives.[5]

Results and Discussion

We found that 3-*tert*-butyl-6,6-dimethylfulvene undergoes smooth dimerization in the presence of sodium cyclopentadienide to give 1-(3-*tert*-butylcyclopentadienyl)-5-*tert*-butyl-1,3,3-trimethyltetrahydropentalene (**2**) (Scheme 1a). Treatment with organolithium reagent resulted in the formation of the dilithium derivative (**4**). This salt may be also obtained from 1-cyclopentadienyl-1,3,3-trimethyltetrahydropentalene (**1**) (Scheme 1b). **4** is the precursor of a family of two racemic pairs of *ansa*-metallocene dichlorides of titanium and zirconium (**5a/5b**) and (**6a/6b**) (Scheme 1c). We isolated in pure state three of the four racemic pairs, **5a**, **6a**, and **6b**, and for **5a** and **6b** the crystal and molecular structures have been determined by X-ray analysis (Figures 1 and 2).

In accordance with our numbering, racemic **5a** should be assigned (11*R*,1*R*,2*S*)/(11*S*,1*S*,2*R*), and **6b** (11*R*,1*R*,2*R*)/(11*S*,1*S*,2*S*) configurations. The most important bond distances and valence angle values are given in Tables 1 and 2. The geometry of the sandwiches is featured in Table 3, in comparison with their close analogs, *anti*-[1,1'-isopropylidene-3,3'-di-*tert*-butylbis-(η^5-cyclopentadienyl)]$TiCl_2$[6] (**7**) and *syn*-[1,1'-isopropylidene-3,3'-di-*tert*-butylbis(η^5-cyclopentadienyl)]-$ZrCl_2$[6] (**8**).

The difference in the geometries is more pronounced in the zirconium pair **6b/8**. E.g. the angle between the Cp planes, δ, is 76.2° for **6b** and 73.4° for **8**; the angle C(2)C(1)C(11) by the bridging atom C(1), θ, is 101 and 99°, respectively. The mean Zr–C(Cp) distance, *d*, is 2.55 and 2.52 Å, respectively. The intramolecular contacts between the Cl ligands and the carbon atoms of the tBu substituents, *r* and *l*, are significantly shorter for **6b** (Table 3). In contrast to zirconium complexes, the difference in the sandwich geometries of the titanium analogs, **5a** and **7**, is insignificant. It is evident that the introduction of the condensed cyclopentene system, transition from **5a** to **7**, and from **6b** to **8**,

* To whom the correspondence should be addressed.

[⊗] Abstract published in *Advance ACS Abstracts,* April 15, 1995.

(1) Presented in part during the 1st Journal of Organometallic Chemistry Conference on Applied Organometallic Chemistry, dedicated to Professor Ernst Otto Fischer, München, Germany, November 4–5, 1993.

(2) For a recent review, see: Möhring, P. C.; Coville, N. J. *J. Organomet. Chem.* **1994**, *479*, 1.

(3) See, for example: (a) Halterman, R. L.; Ramsey, T. H.; Chen, Z. *J. Org. Chem.* **1994**, *59*, 2642. (b) Hong, Y.; Kuntz, B. A.; Collins, S. *Organometallics* **1993**, *12*, 964. (c) Morken, J. P.; Didiuk, M. T.; Hoveyda, A. H. *J. Am. Chem. Soc.* **1993**, *115*, 6997. (d) Broene, R. D.; Buchwald, S. L. *J. Am. Chem. Soc.* **1993**, *115*, 12569. (e) Collins, S.; Kuntz, B. A.; Hong, Y. *J. Org. Chem.* **1989**, *54*, 4154 and references therein.

(4) Kronig, P.; Slongo, M.; Neuenschwander, M. *Makromol. Chem.* **1982**, *183*, 359.

(5) (a) Gutmann, S.; Burger, P.; Hund, H. U.; Hofmann, J.; Brintzinger, H.-H. *J. Organomet. Chem.* **1989**, *369*, 343. (b) Burger, P.; Hund, H. U.; Evertz, K.; Brintzinger, H.-H. *J. Organomet. Chem.* **1989**, *378*, 153.

(6) These structures have been presented during the Xth FECHEM Conference on Organometallic Chemistry, September 5–10, 1993, Agia Pelegia, Crete, Greece. [1,1'-isopropylidene-3,3'-di-*tert*-butylbis(η^5-cyclopentadienyl)]$TiCl_2$ and -$ZrCl_2$ were synthesized from 2,2-dicyclopentadienylpropane or 3-*tert*-butyl-6,6-dimethylfulvene and obtained as a mixture of *anti*- and *syn*-isomers. **7** and **8** are the close analogs of **5a** and **6b**, respectively: *anti*-isomer for Ti and *syn*-isomer for Zr. Details of the synthesis and crystal structures will be published elsewhere.

0276-7333/95/2314-2601$09.00/0

Scheme 1[a]

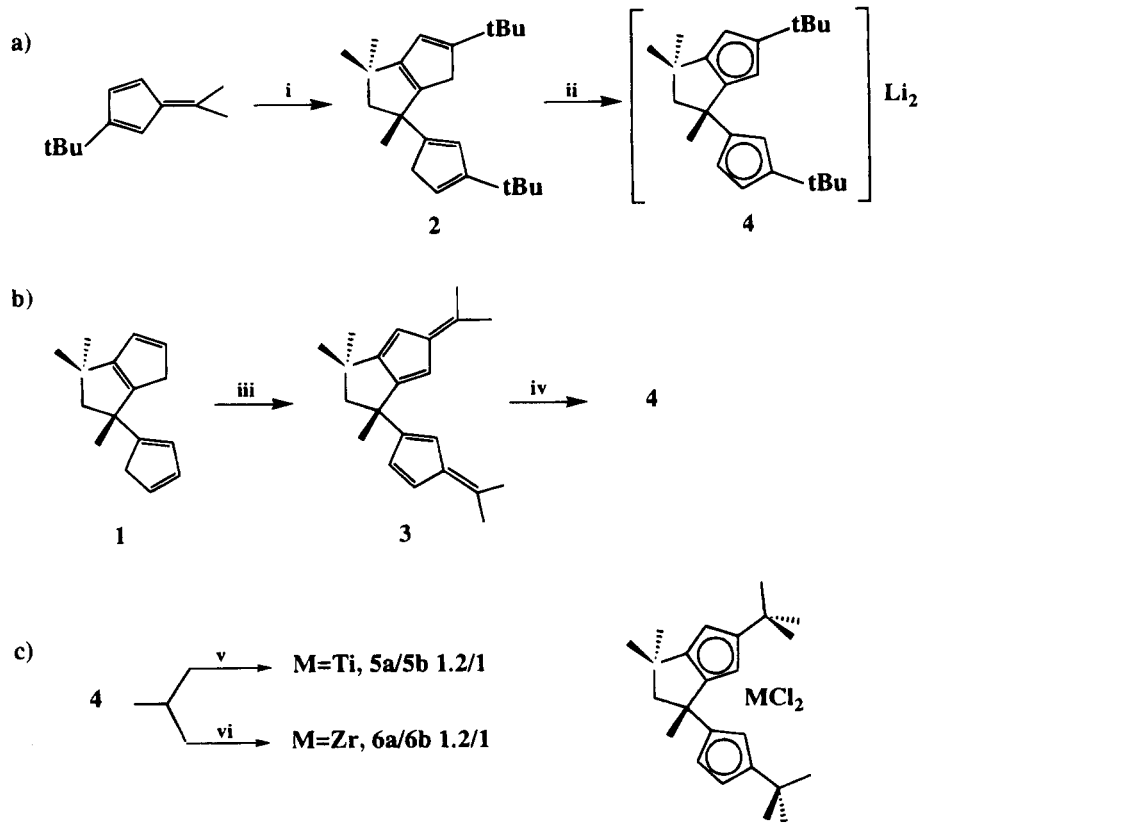

[a] Key: (i) THF, CpNa (catalyst), 1 mol %, reflux, 48 h, 80%; (ii) BuLi (2 equiv), diethyl ether, 0–25 °C, 12 h, 80%; (iii) acetone (2 equiv), methanol, pyrrolidine, 24 h, 90%; (iv) MeLi (2 equiv), diethyl ether/hexane, 0–25 °C, 12 h, 100%; (v) [(1) then (2)] (1) $TiCl_3$, diethyl ether/toluene, 0–50 °C, 12 h, (2) hexane, HCl/diethyl ether, isolable yield **5a** = 35%; (vi) $ZrCl_4$, diethyl ether/toluene, 0–50 °C, 12 h, isolable yield **6a** = 35%, **6b** = 20%.

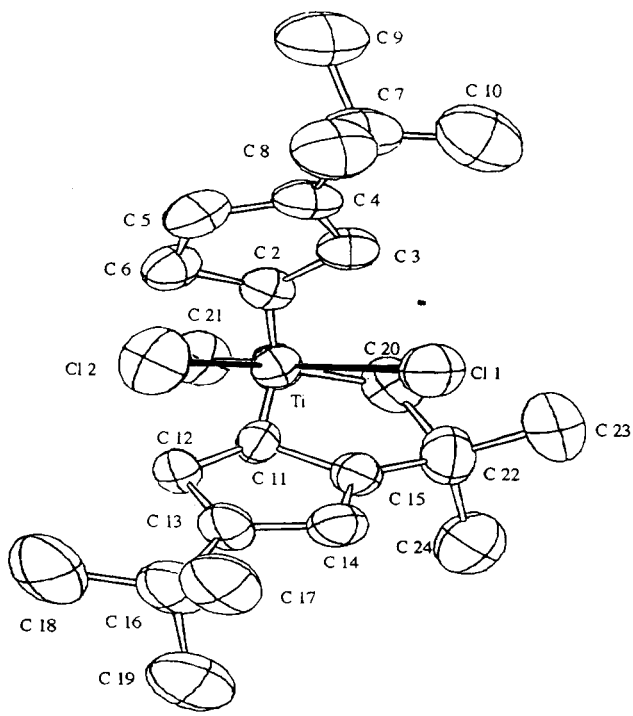

Figure 1. ORTEP diagram of **5a**, with probability ellipsoids drawn at the 30% level.

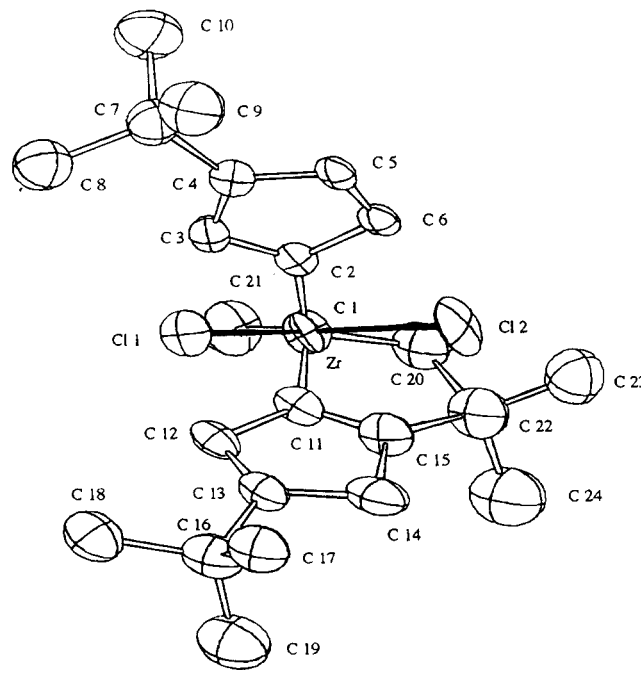

Figure 2. ORTEP diagram of **6b**, with probability ellipsoids drawn at the 30% level.

induces chirality by the C(1) bridging atom but does not affect severely the geometry of the bent sandwiches of the *ansa*-metallocenes. Other structural parameters can be compared to those of analogous *ansa*-metallocene complexes.[5a,7] Structural similarities are observed for out of plane bendings of the C–CtBu (ψ) and of the C(Cp)–C(bridging) (φ) bonds. The displacement of the central metal atom from the ideal position, which is also quite typical of this structural class, is measured in this paper by both τ (displacement angle) and n (normal distance).

Table 1. Important Bond Distances (Å)

	5a	6b
M−Cl(1)	2.339(2)	2.404(3)
M−Cl(2)	2.321(2)	2.407(3)
M−C(2)	2.307(5)	2.40(1)
M−C(3)	2.351(5)	2.45(1)
M−C(4)	2.525(5)	2.65(1)
M−C(5)	2.465(7)	2.55(1)
M−C(6)	2.337(6)	2.45(1)
M−C(11)	2.315(5)	2.40(1)
M−C(12)	2.321(5)	2.43(1)
M−C(13)	2.490(5)	2.58(1)
M−C(14)	2.490(6)	2.70(2)
M−C(15)	2.401(5)	2.48(2)
C(1)−C(2)	1.522(7)	1.45(2)
C(1)−C(11)	1.518(7)	1.55(2)
C(1)−C(20)	1.541(8)	1.58(2)
C(1)−C(21)	1.508(8)	1.58(2)
C(2)−C(3)	1.401(8)	1.49(2)
C(2)−C(6)	1.417(8)	1.40(2)
C(3)−C(4)	1.388(7)	1.43(2)
C(4)−C(5)	1.408(8)	1.38(2)
C(5)−C(6)	1.403(8)	1.36(2)
C(4)−C(7)	1.517(8)	1.54(2)
C(11)−C(12)	1.392(7)	1.44(2)
C(11)−C(15)	1.394(8)	1.34(2)
C(12)−C(13)	1.441(8)	1.39(2)
C(13)−C(14)	1.406(8)	1.47(2)
C(14)−C(15)	1.400(7)	1.48(2)
C(13)−C(16)	1.510(8)	1.54(2)
C(15)−C(22)	1.518(8)	1.52(2)
C(20)−C(22)	1.556(8)	1.60(2)
C(22)−C(23)	1.510(9)	1.54(2)
C(22)−C(24)	1.530(9)	1.51(3)

Table 2. Important Bond Angles (deg)

	5a	6b
Cl(1)−M−Cl(2)	97.09(7)	97.2(1)
C(2)−C(1)−C(11)	96.9(4)	101(1)
C(3)−C(2)−C(6)	105.4(5)	104(1)
C(2)−C(3)−C(5)	111.4(5)	111(1)
C(3)−C(4)−C(5)	105.9(5)	105(1)
C(4)−C(5)−C(6)	108.8(5)	111(1)
C(2)−C(6)−C(5)	108.4(5)	108(1)
C(12)−C(11)−C(15)	108.5(5)	110(1)
C(11)−C(12)−C(13)	108.1(5)	106(1)
C(12)−C(13)−C(14)	106.0(5)	111(1)
C(13)−C(14)−C(15)	109.0(5)	102(1)
C(11)−C(15)−C(14)	108.2(5)	111(1)
C(11)−C(1)−C(20)	101.7(4)	98(1)
C(1)−C(11)−C(15)	109.6(5)	113(1)
C(11)−C(15)−C(22)	111.9(5)	112(1)
C(1)−C(20)−C(22)	110.4(4)	110(1)
C(15)−C(22)−C(20)	100.9(4)	100(1)

Experimental Section

All experimental procedures were performed under argon or in a vacuum. All the solvents were purified and dried by standard procedures and saturated with Ar at room temperature. The ^{1}H NMR spectra were registered on a Bruker AC-200 instrument in $CDCl_3$ at room temperature, if not stated otherwise. Elemental analyses were performed by the Service Central d'Analyses du CNRS, Vernaison.

X-ray Structure Determination Technique. Crystal data and details of data collection are listed in Table 4. The absorption was corrected by the DIFABS program.[8] The weighting scheme for **5a** is $w = 1/(\sigma^2F_o + 0.003544F_o^2)$, and for **6b**, $w = 9.1233/(\sigma^2F_o + 0.000216F_o^2)$

1-(3-*tert*-Butylcyclopentadienyl)-5-*tert*-butyl-1,3,3-trimethyltetrahydropentalene (2). To the solution of 3-*tert*-butyl-6,6-dimethylfulvene (81 g, 500 mmol) in 200 mL of THF was added 5 mmol of CpNa. Vigorous stirring and reflux were maintained for 48 h. Then the mixture was quenched with 100 g of an ice/water mixture, and the organic layer was separated, washed with two portions of 100 mL of water, dried over sodium sulfate, and fractionally distilled under vacuum. The main fraction was collected (bp 108−110 °C/0.05 Torr). Yield: 65 g (80%). Recrystallization from 95% ethanol, at −10 °C, gave crystalline samples, mp 56 °C. Anal. Calcd for $C_{24}H_{36}$: C, 88.82; H, 11.18. Found: C, 88.64; H, 10.83.

^{1}H NMR reveals that **2** is a mixture of the six double bond shift isomers, δ (ppm): 6.12 − 5.69 (several multiplets, 3H), 2.90−2.71 (several multiplets, 4H), 2.40−2.28 (1H) and 2.16−1.98 (1H, superposition of six pairs of geminal doublets, J_{HH} = 10 Hz), 1.40−1.10 (superposition of several singlets, 27H).

1-(3-Isopropylidenecyclopentadien-1,4-yl)-1,3,3-trimethyl-5-isopropylidenetetrahydropentalene (3). A suspension of 1-cyclopentadienyl-1,3,3-trimethyltetrahydropentalene[4] (1) (18.9 g, 89 mmol) in 80 mL of reagent grade methanol was treated with reagent grade acetone (32 mL, 440 mmol) and pyrrolidine (25 mL, 300 mmol) at room temperature. The reaction mixture warmed spontaneously. It was refluxed for 5 min and left for 24 h at ambient conditions. Then

Table 3. Sandwich Geometry Characteristics in 5a, 6b, 7,[6] and 8[6]

	δ[a]	θ[b]	ϕ[c]	ψ[d]	d[e]	n[f]	τ[g]	r[h]	l[i]
5a	71	97	−14	8	2.40	2.08	6.4	3.65	3.53
							5.8	3.52	
7	70.3	98	−12.6	8	2.42	2.08	6.5	3.55	3.52
	70.4	96	−13.9	10			7.0	3.6	
			−14	11					
6b	76.2	101	−12	8.7	2.55	2.19	7.0	3.60	3.53
			−14	10			7.2	3.70	
8	73.4	99	−12.7	10	2.52	2.22	5.1	3.66	3.59
			−13				6.1	3.68	

[a] δ (deg) = angle between the mean least squares plane (mlsp) of the Cp rings. [b] θ (deg) = angle C(Cp)−C(bridging)−C(Cp'). [c] ϕ (deg) = deviation of the vector of the exocyclic C−C bond by the bridgehead C(Cp) atom from the mlsp of the corresponding Cp rings; the minus sign indicates endo deviation with regard to the metal atom. [d] ψ (deg) = deviation of the vector of the exocyclic C−C bond of the tBu groups from the mlsp of the corresponding Cp rings. [e] d (Å) = mean metal−C(Cp) distance. [f] n (Å) = metal−mlsp of Cp ring distance (normal vector). [g] τ (deg) = angle between the vector metal−centroid Cp and the normal vector from metal mlsp of the Cp rings. [h] r (Å) = distance between the key C atom of the tBu group and the nearest Cl. [i] l (Å) = mean distance between the Cl atoms and the nearest of the methyl (tBu) groups.

Table 4. Crystallogrpahic Data for 5a and 6b

formula	$C_{24}H_{34}TiCl_2$	$C_{24}H_{34}ZrCl_2$
dimens (mm)	0.2 × 0.2 × 0.4	0.25 × 0.22 × 0.5
a (Å)	17.713(9)	9.353(9)
b (Å)	9.440(5)	12.398(9)
c (Å)	14.243(9)	20.718(6)
γ (deg)	91.65(2)	81.68(2)
V (Å^3)	2380.9	2377.1
MW	441.4	485.1
d (g/cm^3)	1.23	1.354
Z	4	4
spacegroup	$P2_1/n$	$P2_1/n$
T (K)	298	298
no. of indt reflns with $I > 3\sigma$	1408	2144
no. of params refined	381	381
diffractometer	KM-4	DAR-UM
radiation	Mo Kα graphite	Cu Kα graphite
linear abs coeff (cm^{-1})	5.49	26.31
scan range (deg)	$5 < \theta < 25$	$6 < \theta < 44$
soln method	direct	Patterson
refinement	full matrix anisotropic	
R	0.038	0.059
R_w	0.042	0.061
godness-of-fit	1.2	1.63

(7) (a) Wiesenfeldt, H.; Reinmuth, A.; Barsties, E.; Evertz, K.; Brintzinger, H.-H. *J. Organomet. Chem.* **1989**, *369*, 359. (b) Nifant'ev, I. E.; Churakov, A. V.; Urazowski, I. F.; Mkoyan, Sh. G.; Atovmyan, L. O. *J. Organomet. Chem.* **1992**, *435*, 37.
(8) Walker, N.; Stuart, D. *Acta Crystallogr.* **1983**, *A39*, 158.

the mixture was treated with 500 mL of water and 100 mL of diethyl ether and shaken, and the organic layer separated, was washed two times with 100 mL of 1% acetic acid and then two times with 300 mL of water, and dried over sodium sulfate. After removal of the solvent, a bright yellow oil resulted which turned crystalline in the refrigerator. Recrystallization from a minimum amount of methanol gave analytically pure **3**. Yield: 23 g (90%), mp 62 °C. Anal. Calcd for $C_{22}H_{28}$: C, 90.35; H, 9.65. Found: C, 90.30; H, 9.51.

^{1}H NMR, δ (ppm): 6.58–6.02 (several multiplets, 5H), 2.46 (d, 1H), 2.09 (d, 1H, J_{HH} = 12 Hz), 2.16 (s, 6H), 2.15 (s, 3H), 2.14 (s, 3H), 1.52 (s, 3H), 1.32 (s, 3H), 1.17 (s, 3H).

[1,2,1′-(4-Methylpentane-2,2,4-triyl)-4,3′-di-*tert*-butylbis-(η^5-cyclopentadienido)]Li_2 (4). (a) From 2. A solution of **2** (3.25 g, 10 mmol) in 50 mL of diethyl ether was treated with 10 mL of *n*-BuLi (2 M in hexane, 20 mmol) dropwise at 0 °C, under vigorous stirring. Then the reaction mixture was left to warm and stirred at ambient conditions for 12 h. The solvent was removed in vacuum at 0 °C, and a white crystalline powder of **4** resulted. Yield: 3.6 g (100%). ^{1}H NMR, THF-d_8, δ (ppm): 5.67 (m, 1H), 5.52 (m, 1H), 5.41 (m, 1H), 5.31 (d, 1H), 5.11 (d, 1H), 2.80 (d, 1H), 2.06 (d, 1H, $J_{HH'}$ = 12.2 Hz), 1.49 (s, 3H), 1.24 (s, 3H), 1.20 (s, 9H), 1.19 (s, 9H), 1.17 (s, 3H), cocrystallized diethyl ether 3.39 (q, 2.7H), 1.12 (t, 4H).

(b) From 3. A solution of **3** (2.92 g, 10 mmol) in 50 mL of diethyl ether was treated at 0 °C with 10 mL of a solution of MeLi (2 M in diethyl ether, 20 mmol) dropwise under vigorous stirring. After all of the MeLi had been added, the cooling bath was removed and the reaction mixture was left to warm. The yellow color of the fulvene slowly disappeared during the next 24 h at room temperature, and colorless crystals precipitated. The solution was concentrated to 10 mL, and the crystals separated. Yield: 2.9 g (80% calcd for $C_{24}H_{34}Li_2 \cdot {}^2/_3Et_2O$).

***(R,R,S)*(*S,S,R*)-[1,2,1′-(4-Methylpentane-2,2,4-triyl)-4,3′-di-*tert*-butylbis(η^5-cyclopentadienyl)]$TiCl_2$ (5a).** A suspension of **4** (3.6 g 10 mmol) in 50 mL of diethyl ether was added by small portions to a vigorously stirred suspension of $TiCl_3$ (1.54 g, 10 mmol) in 50 mL of toluene at 0 °C, during 1 h. Then the reaction mixture was vigorously stirred for 12 h at 50 °C. The solid residue separated, and a clear blackish green solution was dried to give an almost black solid. It was dissolved in 200 mL of hexane, and the resulting solution was treated at room temperature with an excess of saturated ethereal solution of HCl, about 50 mL. The solvent was removed in vacuum, and the resulting deep green solid, by ^{1}H NMR a 1.2:1 mixture[9] of **5a/5b**, was recrystallized from a minimum of hexane to give 1.7 g (yield 35%) of dark green plates of **5a**, mp 228 °C. Anal. Calcd for $C_{24}H_{34}TiCl_2$: C, 65.32; H, 7.77. Found: C, 65.11; H, 7.79. ^{1}H NMR, δ (ppm): 6.80 (m, 1H), 6.46 (d, 1H), 5.62 (m, 1H), 5.33 (m, 1H), 5.01 (d, 1H), 2.72 (d, 1H), 2.35 (d, 1H, $J_{HH'}$ = 14.2 Hz), 1.91 (s, 3H), 1.37 (s, 9H), 1.34 (s, 9H), 1.24 (s, 3H), 1.18 (s, 3H).

***(R,R,R)*(*S,S,S*)-[1,2,1′-(4-Methylpentane-2,2,4-triyl)-4,3′-di-*tert*-butylbis(η^5-cyclopentadienyl)]$ZrCl_2$ (6a/6b).** An analogous reaction between **4** and $ZrCl_4$ was performed. Fractional crystallization of the crude 1.2:1 mixture of **6a/6b**, from heptane/toluene 2:1, gave pure **6a** as bright yellow cubes (yield 1.7 g, 35%), mp 215 °C. Anal. Calcd for $C_{24}H_{34}ZrCl_2$: C, 59.48; H, 7.07. Found: C, 59.23; H, 7.08. ^{1}H NMR, δ (ppm): 6.60 (m, 1H), 6.18 (d, 1H), 5.70 (m, 1H), 5.54 (m, 1H), 5.19 (d, 1H), 2.77 (d, 1H), 2.35 (d, 1H, $J_{HH'}$ = 14.2 Hz), 1.85 (s, 3H), 1.32 (s, 9H), 1.31 (s, 3H), 1.29 (s, 9H), 1.27 (s, 3H).

The mother solution was dried, and the residue was dissolved with 5 mL of hexane. After 24 h orange-yellow crystals of **6b** separated, 1 g (yield 20%), mp 230 °C with decomposition. Anal. Found: C, 59.13; H, 7.50. ^{1}H NMR, δ (ppm): 6.28 (m, 1H), 6.10 (d, 1H), 5.64 (m, 1H), 5.50 (m, 1H), 5.16 (d, 1H), 2.76 (d, 1H), 2.36 (d, 1H, $J_{HH'}$ = 14.2 Hz), 1.85 (s, 3H), 1.33 (s, 3H), 1.29 (s, 9H), 1.27 (s, 3H), 1.26 (s, 9H).

Acknowledgment is due to the Conseil Régional de Bourgogne for a postdoctoral scholarship kindly offered to I.U. Authors of Université de Bourgogne wish to thank Mrs. G. Delmas for her technical assistance.

Supplementary Material Available: Tables of crystal data, atomic positional parameters, hydrogen atom parameters, anisotropic thermal parameters, and all bond lengths and bond angles of **5a** and **6b** (14 pages). Ordering information is given on any current masthead page.

OM940898Z

(9) We did not isolate **5b** in an analytically pure state; the identification was made by its ^{1}H NMR spectrum in a **5a/5b** mixture, only proton (Cp) resonances were discerned: 6.49 (m, 1H), 6.27 (d, 1H), 5.58 (m, 1H), 5.39 (m, 1H), 4.95 (d, 1H).

Photochemistry of Indenyliron Dicarbonyl Disilanes, $(\eta^5\text{-}C_9H_7)Fe(CO)_2Si_2Me_2Ph_3$, Involving Isomerization, e.g. $(\eta^5\text{-}C_9H_7)Fe(CO)_2SiMe_2SiPh_3 \rightarrow (\eta^5\text{-}C_9H_7)Fe(CO)_2SiMePhSiMePh_2$, Prior to Silylene Elimination

Ziying Zhang, Ruth Sanchez, and Keith H. Pannell*

Department of Chemistry, University of Texas at El Paso, El Paso, Texas 79968

Received January 19, 1995[⊗]

Summary: A series of triphenyl(dimethyl)disilane isomers substituted with indenyliron dicarbonyl, $(\eta^5\text{-}C_9H_7)Fe(CO)_2Si_2Me_2Ph_3$, have been synthesized and characterized. Photochemical treatment of the complexes in inert hydrocarbon solvents ultimately resulted in the formation of the appropriate monosilyl complexes, $(\eta^5\text{-}C_9H_7)Fe(CO)_2SiMe_nPh_{3-n}$ ($n = 0-2$) via the elimination of silylene fragments. However, contrary to the results previously obtained with the cyclopentadienyl analogs, $(\eta^5\text{-}C_5H_5)Fe(CO)_2Si_2Me_nPh_{5-n}$, isomerization of the disilanes was observed prior to silylene elimination. The chemistry, which takes place via equilibrating intermediate silyl(silylene)iron complexes, e.g. $(\eta^5\text{-}C_9H_7)Fe(CO)(=SiMe_2)SiPh_3$, indicates that silylene elimination, a photochemical event, is extremely sensitive to the nature of the ligands bonded to the transition metal. 1,3-Alkyl(aryl) shifts coupled with the recombination of the silicon–silicon bond that lead to isomerization occur more rapidly than the silylene elimination in the indenyliron complexes.

Introduction

The chemistry of the silicon–silicon bond in transition metal-substituted oligosilanes has recently received considerable attention.[1-5] Isomerizations,[2a,c,e,5] migrations to ancilliary ligands,[2b] and silylene eliminations have been observed.[2f,3a,5] Using chemical substitutions to investigate the mechanism in the case of oligosilane complexes of the $(\eta^5\text{-}C_5H_5)Fe(CO)_2$, Fp, system, such chemistry was proposed to occur *via* a series of equilibrating silyl(silylene)iron intermediates formed upon photoelimination of CO and by undergoing a series of 1,3-methyl, -aryl, or -silyl, migrations.[2b-f] Using alkoxy- and amine-substituted disilanes, the Ogino/Tobita group isolated stable examples of this system,[3] and the Turner group spectroscopically observed the intermediate $(\eta^5\text{-}C_5H_5)Fe(CO)(=SiMe_2)SiMe_3$, using low-temperature matrix isolation and flash photolysis techniques.[4] Recently, the silylene elimination from, and isomerization of, oligosilanes was effected using $FpSiMe_3$ and $(\eta^5\text{-}C_5H_5)Fe(CO)(PPh_3)SiMe_3$ complexes as catalytsts.[5]

Since the initial studies on the Fp systems, related 1,3-alkyl migrations in silyl(silylene) tungsten complexes have been observed by Pestana et al.,[6] and Fink and co-workers have observed similar chemistry occurring for platinum disilanes.[7]

In the case of the oligosilanes with a single Fp substituent, recombination of the Si–Si bond in the silyl(silylene)iron intermediates occurred only in the case of the oligosilanes containing at least three silicon atoms;[2c,e] however, recombination did occur upon photolysis of the bimetallic complex $FpSiMe_2SiMe_2Fp$ to form initially $[(\eta^5\text{-}C_5H_5)Fe(CO)]_2(\mu\text{-}CO)(\mu\text{-}SiMeSiMe_3)$.[2g,3g] In an extension of the oligosilane chemistry to the analogous indenyliron complexes, $(\eta^5\text{-}C_9H_7)Fe(CO)_2$-oligosilane, we reported that the photochemical reaction between $(\eta^5\text{-}C_9H_7)Fe(CO)_2SiMe_2SiMe_3$ and PPh_3 resulted in phosphine substitution with no de-oligomerization, eq 1; similar treatment of the related trisilane resulted in isomerization and phosphine substitution, eq 2.[8]

In neither case was $SiMe_2$ elimination observed; therefore the results suggested that the indenyl ligand profoundly altered the photochemistry of the system. Since the disilane used was permethylated, isomerization was impossible to observe. On the basis of a preliminary observation of the chemistry of $(\eta^5\text{-}C_9H_7)Fe(CO)_2SiMe_2SiMe_2Ph$,[2g] we now report the synthesis of a series of isomeric disilane complexes $(\eta^5\text{-}C_9H_7)Fe(CO)_2Si_2Me_2Ph_3$ and the results obtained upon photochemical irradiation in inert hydrocarbon solvents.

Experimental Section

The syntheses of the isomeric complexes $(\eta^5\text{-}C_9H_7)Fe(CO)_2Si_2Me_2Ph_3$, [$(\eta^5\text{-}C_9H_7)Fe(CO)_2SiMe_2SiPh_3$ (**1**); $(\eta^5\text{-}C_9H_7)Fe(CO)_2SiMePhSiMePh_2$ (**2**); and $(\eta^5\text{-}C_9H_7)Fe(CO)_2SiPh_2SiMe_2Ph$ (**3**)] and the monosilane complexes $(\eta^5\text{-}C_9H_7)Fe(CO)_2SiMe_2Ph$ (**4**), $(\eta^5\text{-}C_9H_7)Fe(CO)_2SiMePh_2$ (**5**), and $(\eta^5\text{-}C_9H_7)Fe(CO)_2SiPh_3$ (**6**)

[⊗] Abstract published in *Advance ACS Abstracts,* April 15, 1995.

(1) Sharma, H. K.; Pannell, K. H. *Chem. Rev.*, in press.

(2) (a) Pannell, K. H.; Rice, J. R. *J. Organomet. Chem.* **1974**, *78*, C35. (b) Pannell, K. H.; Cervantes, J.; Hernandez, C.; Cassias, J.; Vincenti, S. *Organometallics* **1986**, *5*, 1056. (c) Pannell, K. H.; Wang, L.-J.; Rozell, J. M. *Organometallics* **1989**, *8*, 550. (d) Pannell, K. H.; Rozell, J. M.; Hernandez, C. *J. Am. Chem. Soc.* **1989**, *111*, 4482. (e) Hernandez, C.; Sharma, H. K.; Pannell, K. H. *J. Organomet. Chem.* **1993**, *462*, 259. (f) Jones, K. L.; Pannell, K. H. *J. Am. Chem. Soc.* **1993**, *115*, 11336. (g) Pannell, K. H.; Sharma, H. *Organometallics* **1991**, *10*, 954.

(3) (a) Tobita, H.; Ueno, K.; Ogino, H. *Bull. Chem. Soc. Jpn.* **1988**, *61*, 2979. (b) Ueno, K.; Tobita, H.; Shimoi, M.; Ogino, H. *J. Am. Chem. Soc.* **1988**, *110*, 4092. (c) Tobita, H.; Ueno, K.; Shimoi, M.; Ogino, H. *J. Am. Chem. Soc.* **1990**, *112*, 3415. (d) Ueno, K.; Tobita, H.; Ogino, H. *Chem. Lett.* **1990**, 369. (e) Tobita, H.; Wada, H.; Ueno, K.; Ogino, H. *Organometallics* **1994**, *13*, 2545. (f) Ueno, K.; Ito, S.; Endo, K.; Tobita, H.; Inomata, S.; Ogino, H. *Organometallics* **1994**, *13*, 3309. (g) Ueno, K.; Hamashima, N.; Shimoi, M.; Ogino, H. *Organometallics* **1991**, *10*, 959.

(4) Haynes, A.; George, M. W.; Haward, M. T.; Poliakoff, M.; Turner, J. J.; Boag, N. M.; Green, M. *J. Am. Chem. Soc.* **1991**, *113*, 2011.

(5) Pannell, K. H.; Brun, M-C.; Sharma, H. K.; Jones, K.; Sharma, S. *Organometallics* **1994**, *13*, 1075.

(6) Pestana, D. C.; Koloski, T. S.; Berry, D. H. *Organometallics* **1994**, *13*, 4173.

(7) Fink, M. J. Personal communication.

(8) Pannell, K. H.; Lin, S-H.; Kapoor, R. N.; Cervantes-Lee, F.; Pinon, M.; Párkányi, L. *Organometallics* **1990**, *9*, 2454.

0276-7333/95/2314-2605$09.00/0

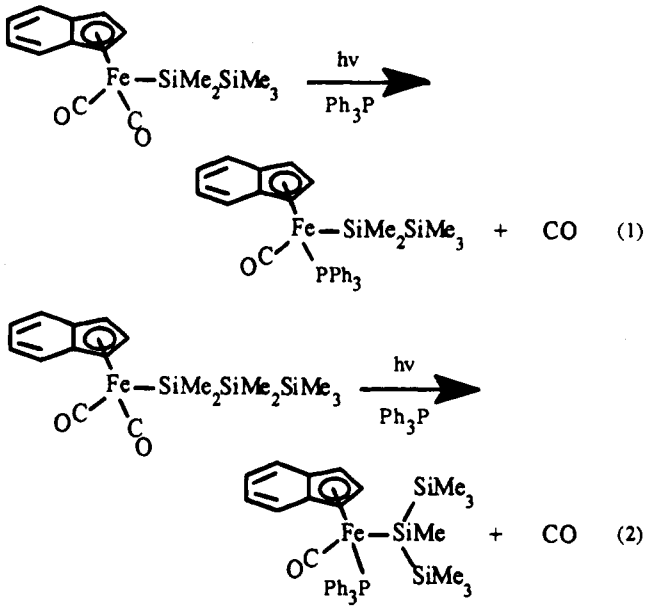

were performed using the same general procedure used for the cyclopentadienyl analogs, substituting $[(\eta^5\text{-}C_9H_7)Fe(CO)_2]_2$ for $[(\eta^5\text{-}C_5H_5)Fe(CO)_2]_2$.[8] A typical synthetic procedure is outlined below, and the spectroscopic and analytical data for the new complexes are recorded in Table 1.

Synthesis of $(\eta^5\text{-}C_9H_7)Fe(CO)_2SiPh_2SiMe_2Ph$. Into a 250 mL round-bottomed flask equipped with a side arm was placed 4 mL of Hg and 0.15 g of freshly cut Na metal. To this amalgam was added 1.0 g (2.2 mmol) of $[(\eta^5\text{-}C_9H_7)Fe(CO)_2]_2$ in 60 mL of THF. After vigorous shaking for 1 h the violet solution changed to orange and infrared spectroscopy indicated the presence of the required salt $[(\eta^5\text{-}C_9H_7)Fe(CO)_2]^-Na^+$, ($\nu$-(CO) 1883, 1866, 1815, 1780 cm^{-1}). Excess amalgam was drained *via* the side arm, and a solution of $ClSiPh_2SiMe_2Ph$ (1.47 g, 4.2 mmol, in 5 mL of THF) was added slowly to the stirred salt solution at 0 °C over a 30 min period. The solution was permitted to warm to room temperature and stirred for 3 h. Infrared spectroscopy at this time indicated complete removal of the salt and the appearance of new carbonyl bands at 1997 and 1947 cm^{-1} indicative of a silicon–iron complex.[9] The solvent was removed *in vacuo*, and the resulting oil was dissolved in 60 mL of a hexane/methylene chloride (9:1) solvent mixture. This solution was concentrated to 5 mL and placed upon a 2.5 x 15 cm silica gel column (MCB Reagents, grade 950, 60–200 mesh). Elution with hexane resulted in the development of a yellow band that was collected and (subsequent to the removal of the solvent and recrystallization of the resulting residue from hexane) yielded 0.64 g (1.2 mmol, 28%) of $(\eta^5\text{-}C_9H_7)Fe(CO)_2SiPh_2SiMe_2Ph$, **3**, mp 121.5–122.5 °C.

Photolysis and Product Analysis of a C_6D_6 Solution of $(\eta^5\text{-}C_9H_7)Fe(CO)_2SiPh_2SiMe_2Ph$. This was performed using two different experimental setups, and an example of each is detailed below. We made no general attempt to recover, separate, and purify the photoproducts and starting materials in such reactions. In a single experiment, of type A below, after 5 h of irradiation of **1** and subsequent to column chromatography as outlined in the syntheses described above using a 1 × 6 cm column, we recovered 75% of the material as a mixture of **1**–**6**.

A. A solution of 0.1 g of **3** in C_6D_6 (0.6 mL) was sealed into a Pyrex NMR tube *in vacuo*. The solution was irradiated by a Hanovia 450 W medium pressure lamp, at a distance of 10 cm and was monitored by ^1H, ^{13}C, and ^{29}Si NMR spectroscopy. After 1 h of irradiation, in addition to the ^{29}Si resonances at 25.4 ppm (Fe–**Si**–Si) and −16.7 ppm (Fe–Si–**Si**) due to the starting material, two new resonances were observed due to the formation of $(\eta^5\text{-}C_9H_7)Fe(CO)_2SiMePhSiMePh_2$ (**2**), 19.0 ppm (Fe–**Si**–Si) and −18.9 ppm (Fe–Si–**Si**). As irradiation continued, the resonances associated with the starting material became progressively less intense, while those of isomer **2** became dominant. Subsequently, after 5 h of irradiation, the appearance of a resonance indicative of $(\eta^5\text{-}C_9H_7)Fe(CO)_2SiMePh_2$ (39.6 ppm) was observed. At this stage the solution was analyzed by high-pressure liquid chromatography (Beckmann 110B with UV detector at 254 nm) using a C_{18} reversed phase column (Beckmann Ultrasphere 23529, 4.6 mm × 25 cm) using a solvent mixture of 80:20 (v/v) CH_3CN/H_2O, with a flow rate of 2.5 mL/min. This analysis exhibited the presence of all three isomers of the starting disilane, and each of the three possible monosilane complexes, $(\eta^5\text{-}C_9H_7)Fe(CO)_2R$, R = $SiMe_2Ph$ (**4**), $SiMePh_2$ (**5**), and $SiPh_3$ (**6**). The relative amounts of the six complexes from this reaction, and from separate photochemical reactions of the other isomers **2** and **3**, are presented in Table 2.

Table 1. Spectral and Analytical Properties of New Complexes[a]

	$(\eta^5\text{-}C_9H_7)Fe(CO)_2SiMe_2SiPh_3$, **1**: mp 141–142 °C.
	Calcd (found): C, 68.37 (68.30); H, 5.18 (5.23)
^{29}Si	23.9, −17.6
^{13}C	6.30 (SiMe); 72.5, 90.0, 105.5, 124.5, 127.2, 128.3, 129.3, 136.7, 137.2 (C_9H_7, Ph); 215.0 (CO)
^1H	0.52 (SiMe); 4.50, 4.61, 7.1–7.7 (C_9H_7, Ph)
IR	1996, 1946
UV/vis	392 (2130), 322 (14 800)
	$(\eta^5\text{-}C_9H_7)Fe(CO)_2SiPhMeSiPh_2Me$, **2**: Oil.
	Calcd (found): C, 68.37 (68.61); H, 5.18 (5.23)
^{29}Si	19.0, −18.9
^{13}C	−2.67, 2.61 (SiMe); 72.2, 72.6, 90.9, 105.0, 105.4, 124.1, 124.2, 127.0, 127.5, 127.7, 128.7, 134.1, 135.1, 138.1, 138.5, 144.9 (C_9H_7, Ph); 214.3, 214.5 (CO)
^1H	0.86, 0.92 (SiMe); 4.29, 4.55, 6.7–7.7 (C_9H_7, Ph)
IR	1999, 1949
UV/vis	404 (1860), 324 (11 100)
	$(\eta^5\text{-}C_9H_7)Fe(CO)_2SiPh_2SiPhMe_2$, **3**: mp 121.5–122.5 °C.
	Calcd (found): C, 68.37 (68.31); H, 5.18 (5.21)
^{29}Si	25.4, −16.7
^{13}C	−1.20 (SiMe), 74.2, 93.0, 105.7, 124.8, 127.7, 128.0, 128.1, 128.4, 128.9, 134.9, 135.9, 140.8, 143.3 (C_9H_7, Ph); 215.5 (CO)
^1H	0.51 (SiMe), 4.29, 4.52, 6.8–7.8 (C_9H_7, Ph)
IR	1997, 1947
UV/vis	402 (3510), 336 (17 700)
	$(\eta^5\text{-}C_9H_7)Fe(CO)_2SiPhMe_2$, **4**: mp 70–71 °C.
	Calcd (found): C, 62.99 (63.23); H, 5.08 (4.95)
^{29}Si	41.3
^{13}C	5.55 (SiMe); 72.7, 93.2, 105.6, 124.4, 127.0, 128.6, 133.1, 133.5, 147.1 (C_9H_7, Ph); 215.3 (CO)
^1H	0.68 (SiMe); 4.26, 6.8–7.7 (C_9H_7, Ph)
IR	1995, 1944
UV/vis	376 (3970), 296 (22 800)
	$(\eta^5\text{-}C_9H_7)Fe(CO)_2SiPh_2Me$, **5**: mp 82–84 °C.
	Calcd (found): C, 67.99 (68.41), H, 4.75 (5.10)
^{29}Si	39.6
^{13}C	5.48 (SiMe); 73.7, 92.8, 105.8, 124.7, 127.5, 128.0, 128.6, 134.5, 144.0 (C_9H_7, Ph); 215.0 (CO)
^1H	0.91 (SiMe); 4.39, 4.46, 6.8–7.8(C_9H_7, Ph)
IR	1998, 1948
UV/vis	378 (2010), 292 (16 400)
	$(\eta^5\text{-}C_9H_7)Fe(CO)_2SiPh_3$, **6**: mp 166–167 °C.
	Calcd (found) C, 71.61 (71.87); H, 4.56 (4.87)
^{29}Si	40.1
^{13}C	74.4, 92.6, 105.9, 124.8, 128.0, 128.7, 130.1, 135.8, 142.4 (C_9H_7, Ph); 215.5 (CO)
^1H	4.82, 7.3, 7.5 (C_9H_7, Ph)
IR	2001, 1951
UV/vis	378 (2140), 300 (14 100)

[a] Melting points are uncorrected; NMR spectra (ppm) were recorded in C_6D_6; IR (cm^{-1}) and UV [nm (ϵ)] spectra were recorded in *n*-hexane; analyses were performed by Galbraith Laboratories.

(9) Pannell, K. H.; Wu, C. C.; Long, G. J. *J. Organomet. Chem.* **1980**, *186*, 85.

Table 2. Relative Yields of Photoproducts, HPLC Analysis, after 5 h

reagent	product 1	2	3	4	5	6	2:3
$(\eta^5\text{-}C_9H_7)Fe(CO)_2SiMe_2SiPh_3$	2	13	7	19	2	1	1.8:1
$(\eta^5\text{-}C_9H_7)Fe(CO)_2SiMePhSiMePh_2$	1	20	12	33	3	1	1.7:1
$(\eta^5\text{-}C_9H_7)Fe(CO)_2SiPh_2SiMe_2Ph$	1	25	14	35	5	1	1.8:1

B. A solution similar to that described above was irradiated in a 5 mL Pyrex flask and monitored directly *via* HPLC, and the relative amounts of the isomers and products were determined. Under the HPLC conditions noted above, the retention times observed for the six complexes were such that a perfect analytical separation could be observed. The retention times (min) were as follows: $(\eta^5\text{-}C_9H_7)Fe(CO)_2SiMe_2Ph$ (**4**), 5.04; $(\eta^5\text{-}C_9H_7)Fe(CO)_2SiMePh_2$ (**5**), 5.53; $(\eta^5\text{-}C_9H_7)Fe(CO)_2SiPh_3$ (**6**), 6.88; $(\eta^5\text{-}C_9H_7)Fe(CO)_2SiMePhSiMePh_2$ (**2**), 12.8; $(\eta^5\text{-}C_9H_7)Fe(CO)_2SiPh_2SiMe_2Ph$ (**3**), 14.3; $(\eta^5\text{-}C_9H_7)Fe(CO)_2SiMe_2SiPh_3$ (**1**), 15.8.

Results and Discussion

The syntheses of the new complexes were readily achieved in moderate yields *via* the standard salt-elimination reaction illustrated in eq 3.

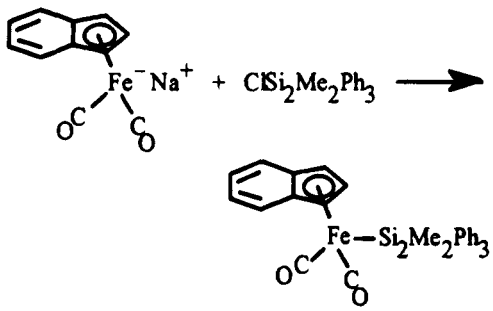

(3)

The spectroscopic and analytical data, in accord with the assigned structures, are recorded in Table 1. The ^{29}Si NMR data follow the same pattern exhibited by the corresponding cyclopentadienyl complexes when compared to their respective methyl analogs. Thus, the Si atoms bonded directly to the Fe atom, Si_α, exhibit significant low-field shifts (45–35 ppm) compared to the methyl analog, while those in the β-position exhibit lesser shifts (12 ppm).

Photochemical treatment of the disilane complexes ultimately resulted in chemistry identical to that noted for the cyclopentadienyl analogs, i.e. formation of the various monosilyl complexes $(\eta^5\text{-}C_9H_7)Fe(CO)_2SiR_3$, SiR_3 = $SiMe_2Ph$ (**4**), $SiMePh_2$ (**5**), $SiPh_3$ (**6**). The average ratio of the three complexes formed, independent of which isomer was photolyzed, was **4**:**5**:**6** = 1:30:4. The rate of formation of these final photoproducts was slower than that observed for the cyclopentadienyl analogs, and prior to their formation, and loss of the silylene fragment, we observed the isomerization of each of **1**, **2**, or **3** into a photostationary mixture of all three isomers, i.e. eq 4 and Scheme 1. The average isomer ratio after 5 h of irradiation was **1**:**2**:**3** = 1:15:8.

The substitution of the cyclopentadienyl group by the indenyl group altered the progress of the reaction by retarding the elimination of the silylene fragments from the equilibrating silyl(silylene) intermediates $(\eta^5\text{-}C_9H_7)Fe(CO)(=SiR_2)SiR_3$. This permits the recoordination of CO to cause the re-formation of the Si–Si bond, i.e. isomerization. Since the Turner group demonstrated

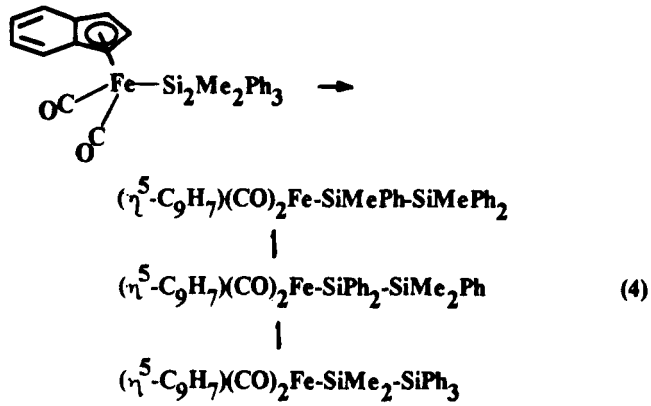

(4)

that the silylene expulsion is a photochemical event, it seems that even minor changes can reduce the photoefficiency of this process. The electronic spectra of the complexes in the range 230–450 nm do not yield any unusual features for the indenyl cf. cyclopentadienyl complexes that might account for the photochemical distinction.

It is possible that other aspects of the indenyl ligand facilitate the observed isomerization. The Cutler group has demonstrated the capacity of $(\eta^5\text{-}C_9H_7)Fe(CO)_2Me$ to facilitate CO coordination *via* an η^5 to η^3 ring slippage mechanism, forming $(\eta^3\text{-}C_9H_7)Fe(CO)_3Me$. This intermediate greatly enhances the migration of the methyl group to CO to produce the so-called CO insertion product $(\eta^5\text{-}C_9H_7)Fe(CO)_2(COMe)$.[10] In the present case a similar η^5 to η^3 slippage in the silyl(silylene) intermediate could facilitate CO coordination, forming a new intermediate that promotes the silyl migration to the silylene, i.e. re-formation of the Si–Si bond, in a manner analogous to the CO insertion reaction, eq 5. In this manner the recombination of the Si–Si bond can compete with the photochemical silylene expulsion.

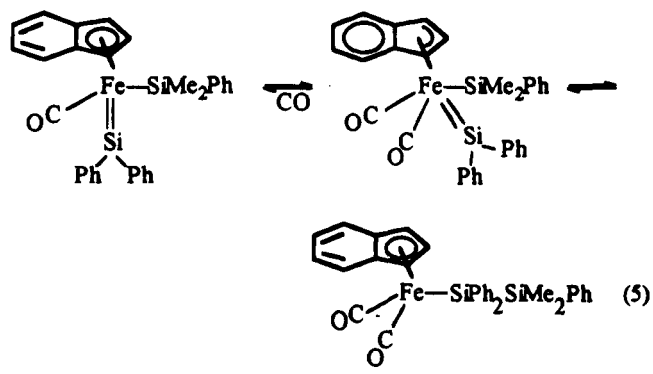

(5)

With respect to the relative amounts of the three monosilane complexes produced, the results are very similar to those reported from photochemical treatment of the Fp analogs, greatly favoring the formation of the Ph_2MeSi complex, least favoring the $PhMe_2Si$ complex. Such results suggest that the phenyl(methyl)silylene iron intermediate is significantly favored over the dimethyl and diphenyl forms.

$$PhMeSi{=}Fe \gg Me_2Si{=}Fe \geq Ph_2Si{=}Fe$$

(10) Forschner, T. C.; Cutler, A. R.; Kullnig, R. K. *Organometallics* **1987**, *6*, 889.

Scheme 1. Photochemical Reactivity of Complexes 1–3

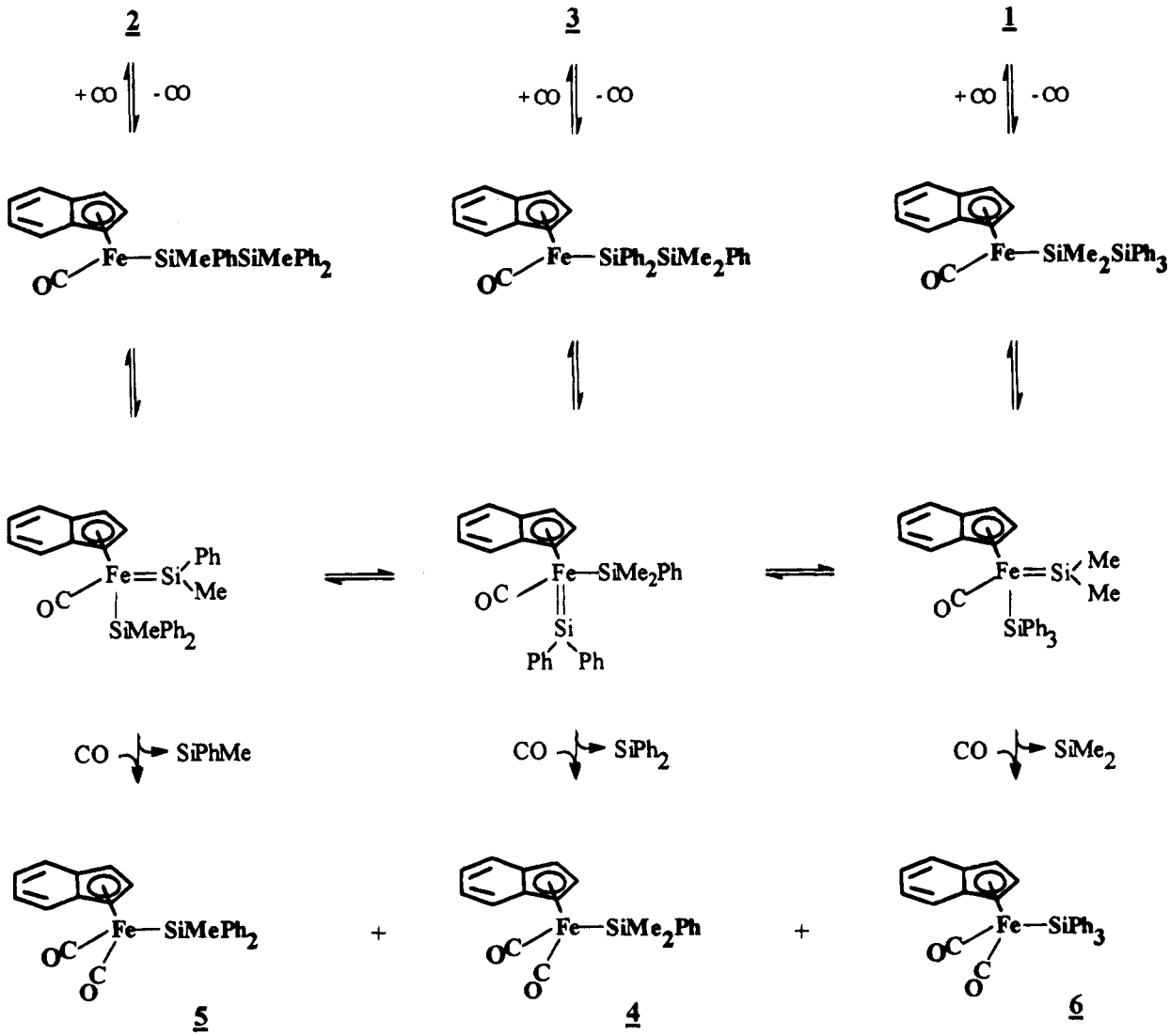

The relative amounts of the isomeric starting disilanes also reflect this stability, since the isomer derived from recombination of the silicon atoms in the PhMeSi=Fe complex, i.e. (η^5-C_9H_7)Fe(CO)$_2$SiMePhSiMePh$_2$ (**2**), strongly predominates in the equilibrium mixture. Whereas the isomer ratios **1**:**2**:**3** are not precisely equivalent to the monosilane photoproduct ratios **4**:**5**:**6**, the relative amounts fit into the above silylene stability ranking, i.e. **1**, **3** ≪ **2** and **4**, **6** ≪ **5**. Since we have previously shown that there is a considerable charge separation in the iron—silylene linkage (R_2Si=Fe ↔ R_2Si^+—Fe^-),[2f] it seems that, as usual, a combination of steric and electronic factors is responsible for these results. A phenyl group stabilizes the buildup of positive charge on the silylene; however, two phenyl groups provide a large and relatively unacceptable steric challenge.

The disilane isomerizations reported here are related to those occurring during the thermal disilane isomerization using (η^5-C_5H_5)Fe(CO)(PPh_3)R, R = Me_3Si, Me, as catalyst, eq 6.[5]

$$PhMe_2SiSiMe_2H \rightleftharpoons Me_3SiSiMePhH \qquad (6)$$

The distinction is that photochemical irradiation ultimately, with varying efficiencies, leads to silylene elimination, whereas thermal treatment does not.

Acknowledgment. Support of this research by the R. A. Welch Foundation, Houston, TX (AH-546), and the NIH-MARC Program (Grant No. GM-08048) is gratefully acknowledged.

OM9500432

Stereoselective Redox Reaction of Isodicyclopentadiene with the Bis(tetrachloroaluminato)(benzene)titanium(II) Complex

Karel Mach,*,† Jörg Hiller,‡ Ulf Thewalt,‡ Mark R. Sivik,§ Eugene I. Bzowej,§ Leo A. Paquette,§ Florence Zaegel,|| Philippe Meunier,|| and Bernard Gautheron||

J. Heyrovský Institute of Physical Chemistry, Academy of Sciences of the Czech Republic, Dolejškova 3, 182 23 Prague 8, Czech Republic, Universität Ulm, Sektion für Röntgen- und Elektronenbeugung, D-89069 Ulm, Germany, Evans Chemical Laboratories, The Ohio State University, Columbus, Ohio 43210, and Laboratoire de Synthèse et d'Electrosynthèse Organométalliques (URA CNRS No. 1685), Université de Bourgogne, BP 138, 21004 Dijon, France

Received November 16, 1994®

*Summary: Redox reaction of isodicyclopentadiene (isodiCpH, tricyclo[5.2.1.0^{2,6}]deca-2,5-diene) with the (benzene)Ti^{II} complex (η^6-C_6H_6)Ti[(μ-Cl)$_2$AlCl$_2$]$_2$ (**1**) affords exclusively the exo-faced (isodicyclopentadienyl)Ti^{III} complex (η^5-$C_{10}H_{11}$)Ti[(μ-Cl)$_2$AlCl$_2$]$_2$ (**2**). The X-ray crystal analysis of **2** (monoclinic, $P2_1/m$, No. 11, a = 7.006(1) Å, b = 17.351(3) Å, c = 8.346(2) Å, β = 100.30(1)°, Z = 2) revealed a square pyramidal coordination around the Ti(III) atom with four bridging chlorine atoms forming the pyramid base and an η^5-coordinated isodiCp at its apex. The molecular plane of symmetry is perpendicular to the plane containing the Ti atom and both Al atoms and bisects the isodiCp ligand.*

The isodicyclopentadienide (isodiCp) ligand (tricyclo-[5.2.1.0^{2,6}]deca-2,5-dienyl anion) coordinates to $TiCl_3$ or Cp′$TiCl_2$ (Cp′ = alkylcyclopentadienyl) fragments highly selectively, depending upon the temperature of the reaction.[1] Endo-faced coordination has been observed generally at low temperatures whereas exo-faced coordination operates at ambient temperature. Thus, bis(*exo,exo*-isodiCp)titanium dichloride was obtained by reaction of lithium isodicyclopentadienide (Li(isodiCp)) with $TiCl_3$·3THF in THF at room temperature and bis(*endo,endo*-isodiCp)titanium dichloride was obtained with 91% selectivity when the same reaction was carried out at −64 °C.[1a] The *endo,exo*-isomer was prepared by reacting Li(isodiCp) with (*exo*-isodiCp)$TiCl_3$ at low temperatures.[1b] The latter was stereoselectively obtained from *endo*-(trimethylsilyl)isodicyclopentadiene and $TiCl_4$.[2] The endo-faced coordination of the isodiCp anion is favored at low temperatures, probably as a consequence of the prevailing dimeric form of Li(isodiCp) at this temperature. At room temperature, the monomeric Li(isodiCp) with exo-faced π-bonded lithium is believed to be responsible for the selective formation of exo-faced titanium derivatives.[3]

In the present paper, the stereoselectivity associated with the involvement of the isodiCp ligand in the fast redox reaction between isodicyclopentadiene (isodiCpH) and the (arene)Ti^{II} complex (η^6-C_6H_6)Ti[(μ-Cl)$_2$AlCl$_2$]$_2$ has been examined.

Experimental Section

Chemicals. Solvents benzene, hexane, and toluene were refluxed over $LiAlH_4$, degassed, and stored as solutions of dimeric titanocene,[4] (μ-η^5:η^5-$C_{10}H_8$)[(η^5-C_5H_5)Ti(μ-H)]$_2$, on a vacuum line. (η^6-C_6H_6)Ti($AlCl_4$)$_2$ (**1**) was prepared as described earlier[5] and was purified by precipitation with hexane from benzene solution. Crystalline **1** was dissolved in benzene to give a 0.04 M solution. Crude isodicyclopentadiene (isodiCpH) (0.8 mL) was purified by slow distillation in vacuum at room temperature. The colorless distillate (0.6 mL) was perfectly dried by repeatedly adding a small portion of solid green dimeric titanocene, until the mixture remained green after standing for 2 days. isodiCpH (0.35 mL) was distilled in vacuum at ambient temperature into a calibrated capillary and diluted by benzene to give 21 mL of 0.1 M solution.

Reaction of isodiCpH with 1. A benzene solution of **1** (0.04 M, 10 mL) was mixed with 4 mL of 0.1 M solution of isodiCpH in a three-necked ampule equipped with breakable seals. A dirty yellow-green solution was immediately formed, slowly precipitating a rusty-brown sediment. The yellow-green solution was separated from the solid and was evaporated to dryness in vacuum. The residue was then extracted with 10 mL of hexane to give a green solution. The hexane was distilled to an attached ampule, and the residue was extracted with condensing vapors of hexane. A yellow impurity, very soluble in hexane, was removed from a green crystalline product into an attached ampule. The product was recrystallized from hexane to give 0.25 g of green crystalline **2** (50% of theory). Approximately the same yield was obtained in a reproduced experiment. The hexane solution of **2** was used for ESR and UV–vis measurements and for fractional crystallization of **2**.

Reaction of isodiCpH with 1 in the Presence of Et_3Al. The benzene solution of **1** (0.04 M, 4 mL) was mixed with that of isodiCpH (0.1 M, 1.6 mL), and immediately a 0.1 M solution of Et_3Al in benzene was added in quantities 0.8, 2.4, and 6.4 mL to reach Et_3Al:**1** molar ratios of 0.5, 1.5, and 4.0, respectively. The solutions were examined by EPR spectroscopy in order to establish the approximate composition of ethyl deriva-

* To whom correspondence should be addressed.
† J. Heyrovský Institute.
‡ University of Ulm.
§ The Ohio State University.
|| Université de Bourgogne.

® Abstract published in *Advance ACS Abstracts,* March 15, 1995.

(1) (a) Gallucci, J. C.; Gautheron, B.; Gugelchuk, M.; Meunier, P.; Paquette, L. A. *Organometallics* **1987**, *6*, 15–19. (b) Sornay, C.; Meunier, P.; Gautheron, B.; O'Doherty, G. A.; Paquette, L. A. *Organometallics* **1991**, *10*, 2082–2083. (c) Paquette, L. A.; Moriarty, K. J.; Meunier, P.; Gautheron, B.; Sornay, C.; Rogers, R. D.; Rheingold, A. L. *Organometallics* **1989**, *8*, 2159–2167. (d) Paquette, L. A.; Moriarty, K. J.; Meunier, P.; Gautheron, B.; Crocq, V. *Organometallics* **1988**, *7*, 1873–1875.

(2) Paquette, L. A.; Sivik, M. R. *Organometallics* **1992**, *11*, 3503–3505.

(3) (a) Paquette, L. A.; Bauer, W.; Sivik, M. R.; Bühl, M.; Feigel, M.; Schleyer, P. v. R. *J. Am. Chem. Soc.* **1990**, *112*, 8776–8789. (b) Zaegel, F.; Gallucci, J. C.; Meunier, P.; Gautheron, B.; Sivik, M. R.; Paquette, L. A. *J. Am. Chem. Soc.* **1994**, *116*, 6466–6467.

(4) Antropiusová, H.; Dosedlová, A.; Hanuš, V.; Mach, K. *Transition Met. Chem.* **1981**, *6*, 90–93.

(5) Antropiusová, H.; Mach, K.; Zelinka J. *Transition Met. Chem.* **1978**, *3*, 127–130.

0276-7333/95/2314-2609$09.00/0

Table 1. Crystallographic Data for 2

formula	$C_{10}H_{11}Al_2Cl_8Ti$
fw	516.66
cryst, color, habit	green, irregular
cryst dimens (mm)	0.5 × 0.6 × 0.7
cryst syst	monoclinic
space group	$P2_1/m$, No. 11
a, Å	7.006(1)
b, Å	17.351(3)
c, Å	8.346(2)
β, deg	100.30(1)
Z	2
V, Å^3	998.2(5)
D_{calc}, g·cm^{-3}	1.72
μ(Mo Kα), cm^{-1}	14.71
$2\theta_{max}$, deg	50
total no. of reflns	1828
no. of unique reflns	1717
reflns with $F_o \geq 2\sigma(F_o)$	1522
no. of params refined	103
residuals: R, R_w[a]	0.045, 0.054

[a] For the 1522 reflections with $F_o \geq 2\sigma(F_o)$; $2\theta < 50°$.

tives of **2** from the line width of the EPR signal. Alternatively, the same EPR spectra were obtained from mixtures of 0.1 M benzene solutions of **2** and Et_3Al in adequate molar ratios. In this case much purer products were obtained and their UV–vis spectra were also measured.

X-ray Single Crystal Analysis of 2. A crystal fragment was mounted into a Lindemann glass capillary under purified nitrogen in a glovebox (Braun) and was sealed by wax. The X-ray measurement was carried out on a Phillips PW 1100 four circle diffractometer equipped with a STOE electronic control system. Intensity data were collected by the $\theta/2\theta$ method using graphite-monochromated Mo Kα radiation (λ = 0.710 69 Å) at room temperature.

The positions of the heavy atoms (Ti, Al, and Cl) were determined by the Patterson method. Atomic coordinates and anisotropic thermal parameters of all non-hydrogen atoms were refined by the least-squares method. Hydrogen atoms were included at their optimized positions. The PC ULM package[6] was used for all calculations. Crystallographic data for **2** are listed in Table 1. Atomic coordinates of non-hydrogen atoms in **2** are given in Table 2.

Spectroscopic Methods. EPR spectra were recorded on an ERS-220 spectrometer (German Academy of Sciences, Berlin) at room temperature in the X-band. Quantitative evaluation of the signal intensity was carried out by comparing the integrated signal with that of a standard ($(C_5H_5)_2Ti(AlCl_3$-Et), 5.275×10^{-3} M in benzene). The g values were calibrated relative to the signal of a Mn^{2+} ($M_I = -1/2$ line) standard at g = 1.9860. Magnetic fields were measured with a MJ 110-R magnetometer equipped with a proton NMR probe (Radiopan, Poznan, Poland). UV–vis spectra were measured on a Varian Cary 17 D spectrometer in the range 270–2000 nm using all-sealed quartz cells (Hellma, d = 0.1 and 1.0 cm).

Results and Discussion

Tricyclo[5.2.1.0^{2,6}]deca-2,5-diene (isodicyclopentadiene, isodiCpH) reacts rapidly with bis(tetrachloroaluminato)(η^6-benzene)titanium(II) (**1**) to give bis(tetrachloroaluminato)(isodiCp)titanium(III) (**2**) in a redox reaction (eq 1).

Redox reactions of this type proceed with all methyl-substituted cyclopentadienes at a rate that has been immeasurably fast even with the least acidic pentamethylcyclopentadiene.[7] Compound **2** in hexane solution affords an eleven-line EPR spectrum due to interaction of the Ti(III) unpaired electron with two equivalent aluminum nuclei (I_{Al}) = 5/2), resembling the spectra of methyl-substituted $Cp'Ti(AlCl_4)_2$ ($Cp' = C_5H_{5-n}Me_n$; n = 0–5) compounds (Table 3). In the latter compounds g values decreased (1.9726–1.9696) on going from C_5H_5 to C_5Me_5 whereas the a(Al) coupling constant decreased only marginally (0.580–0.575 G).[7b] The observed parameters of **2** are controversial as g = 1.9730 points to a more acidic Cp′ ligand and a(Al) = 0.55 G to a more basic Cp′ ligand, both values being outside the range observed for the methyl-substituted complexes. The UV–vis spectrum of **2** resembles the spectra of the $Cp'Ti(AlCl_4)_2$ compounds, but the positions of two CT bands and one d–d transition do not fit to any of the Cp′ compounds. It shows that the effect of a cage substituent in isodiCp cannot be compared to the effect of a certain number of Me groups at the Cp′ ligands in the $Cp'Ti(AlCl_4)_2$ series using these methods. Experiments demonstrating the influence of Et groups introduced into outer positions of the $AlCl_4$ ligands of **2** by adding Et_3Al indicated the regular behavior known for the series of $Cp'TiAl_2Cl_{8-x}Et_x$ (x = 0–4) complexes,[7] i.e., the increase in g value, the decrease in a(Al) as observed in the narrowing of the EPR signal, the decrease in wavelengths of two CT bands, and the increase in the wavelength of the d–d transition band (Table 3).

Crystalline green **2** was obtained from concentrated hexane solution by slow cooling in 50% yield. The X-ray single crystal analysis of a suitable crystal from the first crop of crystals confirmed the expected overall trinuclear structure of the inorganic skeleton common to the $(C_5H_5)Ti(AlCl_4)_2$ or $(C_5Bz_5)Ti(AlCl_4)_2$ complexes[8] as well

Table 2. All Calculated Atomic Coordinates and Equivalent Isotropic Temperature Factors for Complex 2[a]

atom	x	y	z	U_{eq}/U_{iso}, Å^2
Ti(1)	0.2253(1)	0.2500	−0.1676(1)	0.035(1)
Cl(1)	0.0205(1)	0.3458(1)	−0.0471(1)	0.058(1)
Cl(2)	0.1431(2)	0.3460(1)	−0.4000(1)	0.053(1)
Cl(3)	0.2468(2)	0.5115(1)	−0.1539(2)	0.114(1)
Cl(4)	−0.2382(2)	0.4700(1)	−0.3468(2)	0.068(1)
Al(1)	0.0357(2)	0.4298(1)	−0.2411(2)	0.051(1)
C(1)	0.4663(6)	0.3158(2)	0.2173(4)	0.052(2)
H(1)	0.4189(6)	0.3744(2)	0.2303(4)	0.09(2)
C(2)	0.4771(4)	0.2907(2)	0.0470(4)	0.038(2)
C(3)	0.5153(5)	0.3168(2)	−0.1042(4)	0.050(2)
H(3)	0.5259(5)	0.3760(2)	−0.1417(4)	0.18(2)
C(4)	0.5368(7)	0.2500	−0.1973(7)	0.059(5)
H(4)	0.6417(7)	0.2180	−0.2509(7)	0.18(2)
C(5)	0.6692(7)	0.2959(3)	0.3152(5)	0.054(3)
H(5a)	0.7820(7)	0.2697(3)	0.2606(5)	0.29(3)
H(5b)	0.7339(7)	0.3263(3)	0.4244(5)	0.29(3)
C(6)	0.3438(9)	0.2500	0.2696(6)	0.059(5)
H(6a)	0.4053(9)	0.2040	0.3496(6)	0.29(3)
H(6b)	0.1918(9)	0.2562	0.2753(6)	0.29(3)

[a] Atoms Cl(1′), Al(1′), etc. are related to atoms Cl(1), Al(1), etc., respectively, by the symmetry operation x, $1/2 - y$, z. Hydrogen atoms were included in optimized positions.

$$\text{isodiCpH} + \underset{\mathbf{1}}{(\eta^6\text{-}C_6H_6)Ti(AlCl_4)_2} \rightarrow \underset{\mathbf{2}}{(\text{isodiCp})Ti(AlCl_4)_2} + C_6H_6 + H^{\bullet} \quad (1)$$

(6) Brüggemann, R.; Debaerdemaeker, T.; Müller, B.; Schmid, G.; Thewalt, U. ULM-Programmsystem (1. Jahrestagung der Deutschen Gesellschaft für Kristallografie, Mainz, June 9–12, 1992; Abstracts, p 33) which includes the SHELX-76 Program for Crystal Structure Determination (G. M. Sheldrick, University of Cambridge, Cambridge, England, 1976).

(7) (a) Mach, K.; Antropiusová H.; Poláček, J. *J. Organomet. Chem.* **1980**, *194*, 285–295. (b) Mach, K.; Varga, V.; Antropiusová, H.; Poláček, J. *J. Organomet. Chem.* **1987**, *333*, 205–215. (c) Mach, K.; Antropiusová, H.; Poláček, J. *J. Organomet. Chem.* **1990**, *385*, 335–344.

Table 3. EPR and UV−Vis Spectra of the 1 + isodiCp + nEt$_3$Al Systems[a]

Et$_3$Al n[a]	g	a_{Al} or ΔH, mt	UV-vis (nm) CT		d−d
0	1.9730	0.55 (a_{Al})	375	415	662
0.5	1.9732	1.6	372	407	675
1.5	1.9733	1.2	370	405	680
4.0	1.9734	0.9	360	395	705

[a] Additions of n Et$_3$Al equivalents to **1** and Cp'H afforded Cp'TiAl$_2$Cl$_{8-x}$Et$_x$ complexes containing x = 1.0, 2.0, and 4.0.[7b] Since the value of x was independent of Cp', a very similar or identical composition of the aluminate groups is assumed in the isodiCp complexes.

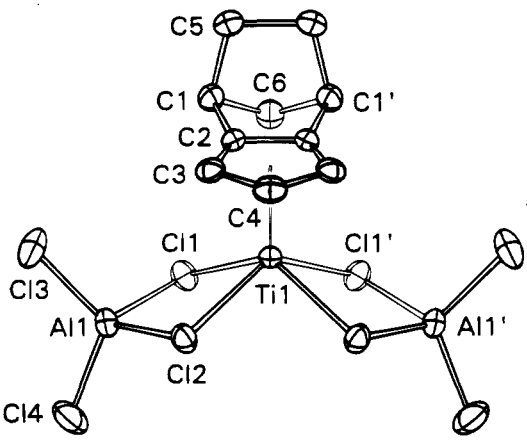

Figure 1. ORTEP drawing of **2**, with ellipsoids drawn at the 50% probability level. Atoms Cl(1'), Al(1'), etc. are related to atoms Cl(1), Al(1), etc., respectively, by the symmetry operation x, $^1/_2 - y$, z.

as to (arene)Ti^{II} complexes (benzene)Ti(AlX$_4$)$_2$ (X = Cl,[9ab] Br[9c]), (hexamethylbenzene)Ti(AlCl$_4$)$_2$,[9d] (durene)TiAl$_2$Cl$_{8-3.25}$I$_{3.25}$,[9e] and (hexamethylbenzene)Ti(AlCl$_3$Et)$_2$.[9f] All such complexes show a square pyramidal coordination around the titanium atom: four bridging halogen atoms form the pyramid base and one π-bonded organic ligand its apex. The ORTEP drawing of **2** with atoms drawn at 50% probability thermal ellipsoids is shown in Figure 1. The isodiCp ligand is bonded to titanium by its exo-face (methano bridge toward titanium) and is oriented perpendicular to the plane of the inorganic skeleton containing the titanium and both aluminum atoms. The η^5-cyclopentadienyl moiety of isodiCp forms a least-squares plane with maximum deviation of 0.005 Å. The molecule of **2** is symmetrical with respect to the plane which contains Ti(1) and the methano bridge C(6) atom and bisects the isodiCp ligand. In the inorganic skeleton, one pair of bridging chlorine atoms (Cl(2), Cl(2')) exerts longer bonding distances to both Ti and Al atoms than the other one; however, the plane of bridging chlorine atoms is perpendicular to the Ti−CE (CE = centroid of the Cp ring of isodiCp) line within 0.1°. The outer AlCl$_2$ groups contain two equivalent Al−Cl bonds. All the bond distances in the inorganic segment and the Ti−CE bond do not differ from those of (C$_5$H$_5$)Ti(AlCl$_4$)$_2$ or (C$_5$Bz$_5$)Ti(AlCl$_4$)$_2$ complexes[8] by more than 0.02 Å. The bond distances and selected valence angles determined for **2** are listed in Table 4. The chlorine bridging bonds are folded. The dihedral angle between the planes defined by Ti(1), Cl(1), and Cl(2) atoms and by Al(1), Cl(1), and Cl(2) atoms amounts to 19.0°. As a result, the aluminum atoms are only 0.330 Å below the plane of bridging chlorine atoms whereas the titanium atom is at a distance of 1.030 Å above it. The cyclopentadienyl ring of isodiCp is tilted with respect to the plane of bridging chlorine atoms by 4.1°; the carbon atoms bearing the norbornane moiety (C(2), C(2')) are by about 0.1 Å farther away from Ti than the C(4) atom. That carbon atoms bearing substituents at partly substituted Cp rings are more distant from the metal than those bearing hydrogen atoms seems to be a general phenomenon.[10] The isodiCp ligand is bent about the C(2)-C(2') bond so that the norbornane moiety is tilted from the cyclopentadienyl plane to the endo-face, farther away from the titanium atom. The dihedral angle between the plane of the cyclopentadienyl ring and the plane defined by the C(2), C(2'), C(1), and C(1') atoms is 171.9°. This is close to the angles 168.1 and 169.3° found in bis(*exo,exo*-isodiCp)$_2$TiCl$_2$ for two nonequivalent molecules in a unit cell.[1a] It has to be mentioned that the isodiCp ligand is generally bent to the face opposite the coordinated face. For instance, in (C$_5$H$_4$Me)(*endo*-isodiCp)TiCl$_2$ the bending to the exo-face yielded a dihedral angle as large as 165.5°.[1b] In **2**, the isodiCp bending enlarges the coordination space on the *exo*-face as the methano bridge C(6) is placed only 0.513 Å below the plane of Cp ring whereas the *syn*-ethano bridge C(5) and C(5') atoms are 1.683 Å above this plane.

Table 4. Bond Distances (Å) and Angles (deg) for 2[a]

Bond Distances			
Ti(1)−Cl(1)	2.520(1)	Ti(1)−Cl(2)	2.543(1)
Cl(1)−Al(1)	2.194(1)	Cl(2)−Al(1)	2.190(2)
Cl(3)−Al(1)	2.084(2)	Cl(4)−Al(1)	2.084(2)
Ti(1)−CE	1.995(3)	Ti(1)−C(2)	2.385(3)
Ti(1)−C(3)	2.317(4)	Ti(1)−C(4)	2.240(3)
C(1)−C(2)	1.502(5)	C(1)−C(5)	1.547(6)
C(1)−C(6)	1.538(5)	C(5)−C(5')	1.592(6)
C(2)−C(3)	1.411(5)	C(2)−C(2')	1.411(5)
C(3)−C(4)	1.418(5)		
Bond Angles			
Cl(1)−Ti(1)−Cl(2)	78.7(0)	Cl(1)−Ti(1)−Cl(1')	82.6(0)
Cl(1)−Ti(1)−Cl(2')	107.0(1)	Cl(2)−Ti(1)−Cl(2')	81.8(0)
Ti(1)−Cl(1)−Al(1)	92.2(0)	Ti(1)−Cl(2)−Al(1)	91.6(0)
Cl(1)−Al(1)−Cl(2)	94.2(1)	Cl(1)−Al(1)−Cl(3)	108.6(1)
Cl(1)−Al(1)−Cl(4)	111.9(1)	Cl(2)−Al(1)−Cl(3)	111.4(1)
Cl(2)−Al(1)−Cl(4)	110.8(1)	Cl(3)−Al(1)−Cl(4)	117.5(1)
C(2)−C(1)−C(5)	103.7(3)	C(2)−C(1)−C(6)	100.2(3)
C(1)−C(2)−C(3)	143.4(3)	C(1)−C(2)−C(2')	106.9(3)
C(1)−C(5)−C(5')	102.9(3)	C(1)−C(6)−C(1')	95.9(3)
C(2)−C(3)−C(4)	106.4(3)	C(3)−C(4)−C(3')	109.6(3)

[a] All C−H distances were adjusted to be 1.08 Å.

The evidence for the exclusive exo-face coordination of isodiCp is based on X-ray single crystal measurements. No disorder was observed in the positions of the carbon atoms C(6), C(5), and C(5') which would stem from a mixture of molecules with exo- and endo-coordinated isodiCp ligands. The effect of a preference fractional crystallization of one isomer in the crystals of the first crop was excluded by the X-ray examination

(8) Schmid, G.; Thewalt, U.; Troyanov, S. I.; Mach, K. *J. Organomet. Chem.* **1993**, *453*, 185−191.

(9) (a) Thewalt. U.; Stollmaier, F. *J. Organomet. Chem.* **1982**, *228*, 149−152. (b) Troyanov, S. I.; Furkalyuk, M. Yu.; Rybakov, V. B. *Metalloorg. Khim.* **1988**, *1*, 298−300. (c) Troyanov, S. I.; Rybakov, V. B. *Metalloorg. Khim.* **1988**, *1*, 1280−1284. (d) Thewalt, U.; Österle, F. *J. Organomet. Chem.* **1979**, *172*, 317−324. (e) Troyanov, S. I.; Mach, K. *J. Organomet. Chem.* **1990**, *389*, 41−46. (f) Troyanov, S. I.; Poláček, J.; Antropiusová, H.; Mach, K. *J. Organomet. Chem.* **1992**, *430*, 317−325.

(10) Howie, R. A.; McQuillan, G. P.; Thompson, D. W.; Lock, G. A. *J. Organomet. Chem.* **1986**, *303*, 213−220.

of one of the crystals of the last crop. The unit cell parameters were identical with those of the fully analyzed crystal from the first crop. In contrast to previous examples of stereoselective coordination of the isodiCp ligand in titanium complexes, which turned out to be induced by the structure of Li(isodiCp) compounds,[3] the reason for the high stereoselectivity of the redox reaction (eq 1) is to be sought in a more accessible exo face of isodiCpH in the act of replacing benzene by isodiCpH and the electron transfer from Ti(II) to isodiCpH followed by elimination of a hydrogen atom.

Acknowledgment. This investigation was supported by the Grant Agency of the Academy of Sciences of the Czech Republic (Grant No. 440403). M.R.S. was both a National Fellow (1989–1990) and an Amoco Foundation Fellow (1991). E.I.B. is the holder of an NSERC Postdoctoral Fellowship (1994–1995). The work at The Ohio State University was supported by the National Science Foundation.

Supplementary Material Available: Tables of atomic coordinates, anisotropic thermal parameters, bond distances, valence angles, least-squares planes and atomic deviations therefrom, and important intermolecular contacts and views of the unit cell (12 pages). Ordering information is given on any current masthead page.

OM940871F